

Proceedings of the 2010 World Molecular Imaging Congress Kyoto, Japan September 8-11, 2010

For a fully searchable and indexed HTML version, visit
<http://www.wmicmeeting.org/2010/Abstracts/Start.htm>

Presentation Number **0001**

Educational Workshop 1: The Hallmarks of Cancer

Targeting the Hallmarks of Cancer: Survival of the Fittest

Robert Gillies, Moffitt Cancer Center, Tampa, FL, USA. Contact e-mail: robert.gillies@moffitt.org

Cancers are complex, dynamic, evolving, multiscale ecosystems that are characterized by profound spatial and temporal heterogeneity. The conversions from genome to the anatome are non-linear processes that are affected by genetic and epigenetic events, and their interaction with the microenvironment. In toto, these processes form an "adaptive landscape" that dictates the rate and direction of Darwinian dynamics. A fundamental outstanding problem in modern biology is how to directly link genetic data cellular phenotypes. These complex interactions between intra- and extracellular processes give rise to complex intra-tumoral heterogeneity that can arise even from a limited set of cell-environment interactions. **Nature selects for phenotype, not genotype.** Thus, tumors can have similar phenotypes (i.e. the "hallmarks" of cancer, yet have variable underlying genotypes. Furthermore, intratumoral heterogeneity confounds our ability to study in-vivo cancers by molecular diagnostics. Typical molecular characterizations such as expression arrays measure the transcriptome in a large number of cells. The relevance of this single, average measurement in a variable population is limited. In such studies, the impact of heterogeneity can only be appreciated with large data sets from a large study population, i.e. "systems biology". Consequently, the applicability of these data to individual patients may be limited. Phenotypic heterogeneity is the most significant factor underlying evolutionary rates. Thus, heterogeneous tumors are more readily adaptable to perturbations such as chemotherapy and can readily develop chemoresistance. An unpopular concept to come from this Darwinian approach is that targeted therapies will have only limited success. An emerging alternative approach is to target the hallmarks and their sequelae themselves. One targetable hallmark is angiogenesis, which results in a chaotic and inefficient vasculature. This leads to poor perfusion and tumor hypoxia and acidosis. Hypoxia in early cancers leads to selection of cells with a glycolytic phenotype. This phenotype is maintained in metastatic cancers because it produces acid, which provides a selective advantage of the tumor cells over stroma. Hypoxia and acidosis are therapeutic targets that may have application over a wide variety of solid tumors. We have shown that inhibiting the acid with oral buffers can prevent experimental metastasis, and this is in clinical trials.

Presentation Number **0002**
Educational Workshop 2: Animal Imaging in Translational Medicine

Animal Imaging in Drug Discovery and Development

Raymond E. Gibson¹, Christopher T. Winkelmann², Elaine Jagoda³, Shailendra Patel², ¹Gibson Imaging Apps, LLC, Holland, PA, USA; ²Merck, Whitehouse Station, NJ, USA; ³NIH, Bethesda, MD, USA. Contact e-mail: raymond_gibson@comcast.net

With the desire to develop novel drugs faster and more cost-effectively, drug companies are searching for clear strategies to manage the complex drug discovery process in terms of balancing costs, time, product value and possibility of success. To this end, pharmaceutical companies have turned to imaging, be it radiotracer imaging (PET and SPECT), magnetic resonance techniques (MRI, fMRI, and MRS), CT, ultrasound and optical imaging, as the means to determine the efficacy of drugs more quickly. Alternatively, imaging techniques may generate biomarkers that can demonstrate target engagement, important for the proof-of-principle studies that encourage further development of the putative drug entity. We have used all of these technologies, with an emphasis on radiotracer imaging, and will provide examples of the preclinical uses of each. A key feature of drug development is hypothesis testing: at an appropriate dose, does the putative drug provide the desired therapeutic effect? This dose may be predicted by determining the maximum dose that can be given without side-effects, or estimated from animal studies where target-site occupancy is determined via post-mortem sampling. A more satisfying approach is to determine the fractional site occupancy, as a function of plasma concentration of drug, via blockade of in vivo radiotracer binding. Currently approved radiopharmaceuticals, e.g., FDG, may provide measures of target engagement or even an indication of efficacy. A key feature of these imaging methods is that the methods can be tested in preclinical models, often becoming a primary method for assessing efficacy, which can subsequently be translated to the clinic. The continued success in developing novel pharmaceuticals in an environment of continually increasing costs is to be inventive in the potential uses of all technologies available to the industry, particularly imaging technologies.

Presentation Number **0003**
Educational Workshop 2: Animal Imaging in Translational Medicine

Translational Molecular Imaging: Large Animal Imaging

Mei Tian, *Exp. Diagnostic Imaging, MD Anderson Cancer Center, Houston, TX, USA. Contact e-mail: Mei.Tian@mdanderson.org*

Molecular imaging is a rapidly developing research field of biomedical science, which has been used to directly or indirectly monitor and record the spatiotemporal distribution of molecular or cellular processes for biochemical, biologic, diagnostic or therapeutic applications. In the past few decades, there has been sufficient experience with specifically targeted therapeutic or diagnostic imaging agents that we have to begin moving them from bench to bedside. From the translational perspective, molecular imaging research in large animals is an ideal preclinical setting for establishing the relationship between disease, treatment, and imaging endpoint. A well designed preclinical imaging plan can address the some critical questions, i.e., what technology or biomarker to scan with, what parameters to measure, the optimal scanning protocol, etc. Proper large animal imaging research environment not only provide critical clinical planning data, but also firmly established a link between the preclinical safety/efficacy database and early clinical data. During this educational lecture, I will introduce the history and current status of our translational large animal imaging program, discuss the preclinical practice of large animals in drug development, in vivo T-cell and stem cell trafficking, and the other critical questions.

Presentation Number **0004**
Educational Workshop 3: Basics of Small Animal MRI

Basics of Small Animal MRI

Stefan Zwick, *Dept. of Radiology, Medical Physics, University Hospital Freiburg, Freiburg, Germany. Contact e-mail: stefan.zwick@uniklinik-freiburg.de*

The lecture focuses on all basics required to perform a small animal imaging experiment using a MRI system. In addition to basic MR theory, animal handling and monitoring will be part of this lecture. Participants interested in the basics of pre-clinical MRI are encouraged to attend. Together we will cover the long way from a single spin to a highly resolved MRI image - including the phenomenon of relaxation, contrast generation and the basic sequences like Spin-Echo and Gradient-Echo. Furthermore, the hardware components of a MRI system will be explained and references for specific applications will be given. To execute an efficient pre-clinical study, unwanted bias must be reduced as much as possible. Therefore, handling of animals has to be done carefully and standardized operating procedures should be established. The lecture will give a detailed look into animal handling before and during the measurement (for example: anesthesia, placement of catheter, monitoring of vital signs and general hints). The lecture is not designed as a monolog. Feel free to ask questions whenever they occur. If you are interested in more specific information about special applications please join the lecture "Advanced animal MRI: from anatomy to function".

Presentation Number **0005**
Educational Workshop 4: Grantsmanship (NIH)

Grantsmanship in an Era of Budget Retrenchment

Barbara Croft, *Cancer Imaging Program, National Institutes of Health, Bethesda, MD, USA. Contact e-mail: Barbara_Croft@nih.gov*

There will be an emphasis on funding by the National Institutes of Health in this course on research funding by the government and other agencies, in this era of change and stimulus funding. It is intended for those interested in learning about the government funding process and in finding funding sources for their own research projects. Special points will be made for new investigators. NIH funding of imaging research will be described in some detail. The identification of agencies, the preparation and submission of the application, the assignment of those applications to review panels, and the review process will be treated in some depth. There will be ample time for questions from attendees. Speakers will be available after the session to answer more specific questions from individuals. Learning Objectives; Upon completion of this session, attendees will be able to: 1. Identify government and other funding sources for nuclear medicine and imaging research. 2. Discover the sources of special funding initiatives and discover how to take advantage of them. 3. Learn how to take best advantage of the grant application and review process for the funding agencies. 4. Find out how the 2010 and 2011 changes in the review process and the application format affect the applicant. 5. Place the applicant in the New Investigator, Early Investigator or not scheme.

Presentation Number **0006**

Educational Workshop 5: "Imaging Technology & Protocols: Optical, Ultrasound & CT"

Illuminating Biomedical Discovery with Advanced Optical and Opto-acoustic Imaging

Vasilis Ntziachristos, *Institute for Biological and Medical Imaging, Technical University of Munich, Munich, Germany. Contact e-mail: v.ntziachristos@tum.de*

Optical imaging is unequivocally the most versatile and widely used visualization modality in clinical practice and life sciences research. In recent years, advances in optical and opto-acoustic technologies and image formation methods have received particular attention in biological research and the drug discovery process for non-invasively revealing information on the molecular basis of disease and treatment. An increasing availability of endogenous reporters such as fluorescent proteins, probes and photo-absorbing probes with physiological and molecular specificity enable insights to cellular and sub-cellular processes through entire small animals, embryos, fish and insects and have revolutionized the role of imaging on the laboratory bench, well beyond the capability of conventional microscopy. This talk describes current progress with instruments and methods for in-vivo photonic tomography of whole intact animals and model biological organisms. We show how new tomographic concepts are necessary for accurate and quantitative molecular investigations in tissues and why it could be potentially a valuable tool for accelerated investigations of therapeutic efficacy and outcome. We further demonstrate that cellular function and bio-chemical changes can be detected in-vivo, through intact tissues at high sensitivity and molecular specificity. Examples of imaging enzyme up-regulation, carcinogenesis and gene-expression are given. The potential for clinical translation is further outlined. Limitations of the method and future directions are also discussed.

Presentation Number **0007**

Educational Workshop 5: "Imaging Technology & Protocols: Optical, Ultrasound & CT"

Ultrasound and Ultrasound Probes

Fabian Kiessling, *Experimental Molecular Imaging, RWTH-Aachen University, Aachen, Germany. Contact e-mail: fkiessling@ukaachen.de*

Ultrasound imaging is the mostly used imaging modality in the clinics and also increasingly popular in preclinical research. In particular high frequency ultrasound devices, which are mostly used for small animal imaging, enable to image tissue morphology in a superb resolution and with an excellent tissue contrast. Doppler ultrasound enables to assess tissue vascularisation and blood velocity without the need for administering contrast agents. Unfortunately, Doppler ultrasound imaging is not capable of capturing the slow blood flow in very small vessels. In this context the use of microbubbles as contrast agents is mandatory. Microbubbles can be detected by ultrasound with a very high sensitivity and specificity by either destructive or non destructive imaging methods or by a combination thereof. By conjugating antibodies or peptides to microbubbles molecular probes are generated. Most endovascular targets can be targeted. Two important strategies of detecting molecular ultrasound probes will be presented. Beside these previously mentioned capabilities an outlook will be given on new imaging strategies including nanobubbles and smart hybrid imaging agents.

Presentation Number **0008**

Educational Workshop 5: "Imaging Technology & Protocols: Optical, Ultrasound & CT"

Computed Tomography

Fabian Kiessling, *Experimental Molecular Imaging, RWTH-Aachen University, Aachen, Germany. Contact e-mail: fkiessling@ukaachen.de*

Computed tomography plays a crucial role in patient management but also in preclinical research. The option to image organisms with high resolution and good tissue contrast makes it highly complementary to imaging modalities with high sensitivity for molecular probes like PET, SPECT and optical imaging. However, there are some simple facts that should be considered when dealing with μ CT imaging: 1) The higher the resolution, the higher will be the x-ray dose 2) The higher the resolution, the longer will be the scan time (at comparable CNR) Thus, a compromise has always to be made if CT-imaging is performed in vivo, which particularly holds true if contrast agents are used. Highly resolving μ CT-systems usually do not have a 360° freely rotating gantry and are mostly suited for imaging tissue samples like biopsies with microcalcifications, bone, or cast fixated microvessels in tissues. Gantry based μ CT-systems with volume detectors such as flat panels enable the acquisition of larger volumes in a considerably short time. For studies on contrast agent kinetics or for μ -angiography studies these μ CT-scanners are preferable. The high temporal and spatial resolution also enables functional cardio-respiratory studies and it was shown that quantitative parameters of heart and lung can reliably be assessed in mice and rats using retrospective intrinsic and extrinsic gating methods. PET- and SPECT-scanners have been hybridized with gantry based CT-systems and are commercially available. Also data of optical reflectance imaging and diffuse optical tomography often is fused with CT imaging data. In this context, we will demonstrate that the information from the CT does not only provide anatomical landmarks but even can be used to improve the optical raw data reconstruction. In summary, in this talk you will hear about different CT-scanner types and their use for different research purposes including imaging at the microscopic and macroscopic level, functional imaging and hybrid-imaging. Also novel contrast agent concepts will be discussed.

Presentation Number **0009**
Educational Workshop 6: Novel Probes & Targets

Radiolabeled Antibodies and Peptides as Targeted Molecular Imaging Agents

Julie L. Sutcliffe, ¹*Biomedical Engineering, UC Davis, Davis, CA, USA;* ²*Hematology-Oncology, UC Davis, Davis, CA, USA.* Contact e-mail: jsutcliffe@ucdavis.edu

Over the decades radiolabeled biomolecules such as antibodies and peptides have emerged as important tools for imaging, particular for the detection of human cancers. As many cancers have demonstrated overexpression of a variety of receptors these cell surface receptors have become of huge interest as molecular imaging targets. Numerous radiolabeled peptides and antibodies are therefore under investigation as molecular probes to target receptor expression in vivo. It is therefore critical that fast, reproducible radiolabeling approaches are developed and optimized for the labeling of such biomolecules allowing these agents to be synthesized rapidly and screened both in vitro and in vivo to assess their efficacy. This presentation will identify some of the current approaches that have been developed for the design, synthesis and in vivo evaluation of both radiolabeled antibodies and peptides. Recent advances in radiolabeling methods, such as site specific radiolabeling and automation will be described. Problems associated with modifying peptides and antibodies for radiolabeling will be described. Finally, a number of clinically relevant disease specific biomarkers that are currently being investigated using radiolabeled peptides and antibodies will be discussed.

Presentation Number **0010**
Educational Workshop 6: Novel Probes & Targets

Aptamers and Oligonucleotides

Bertrand Tavitian, ¹*European Molecular Imaging Labs, Atomic Energy Commission, Orsay, France;* ²*Inserm U1023, CEA, Orsay, France. Contact e-mail: bertrand.tavitian@cea.fr*

Nucleic acids can form a myriad of three-dimensional structures, some of which possess a catalytic activity or interact with proteins or other partners. This property is the basis for combinatorial approaches designed to create artificial nucleic acids that bind to specific targets by virtue of their 3D structure. The nucleic acid-based ligands found by this technique are called aptamers, from the Latin “aptus,” meaning “to fit,” and the method is known as Systematic Evolution of Ligands by Exponential Enrichment (SELEX). Due to their unique recognition capacities, aptamers rival antibodies in terms of affinity and specificity for their targets and have entered the fields of medical diagnosis and therapy. The way aptamers engage their target molecules is different from that of antibodies and renders them unique as recognizing agents. Aptamers can be selected against targets that are too toxic to be used as antigens for raising antibodies in a living organism, as well as against targets that do not elicit antibody response. They have shown little or no toxicity or immunogenicity and capable to address a very wide range of targets. Aptamers can be conjugated to a wide array of labels or other molecules and many possibilities are available to introduce changes in oligonucleotidic structure through defined chemical modifications. This allows testing a large number of modifications designed to improve their pharmacokinetics or binding properties. As drugs, several aptamers have reached the clinical development stage; “escort” aptamers can be used to deliver an active drug, radionuclide, toxin, or cytotoxic agent to a desired organ for therapy. The discrimination and targeting capacities of aptamers render them attractive as imaging agents for noninvasive diagnostic procedures. Current developments of aptamers as imaging agents concern improved in vivo stability, improvement in their binding affinity, increasing circulation times and extravasation in order to access diseased tissues or the interior of tumors. With the rapidly increasing spectrum of targets accessible for imaging, there is growing interest for the improvement of aptamers as “nucleic acid biotools” for in vivo molecular imaging.

Presentation Number **0011**
Educational Workshop 6: Novel Probes & Targets

Gamma Counting and Autoradiography

David Stout, *M&M Pharmacology, UCLA Crump Institute, Los Angeles, CA, USA. Contact e-mail: dstout@mednet.ucla.edu*

This seminar will explain the principles of both gamma counters and autoradiography methods, along with examples of how they are used in conjunction with in-vivo imaging systems. Calibration and quantitation of in-vivo PET and SPECT imaging data requires the use of a gamma counter to accurately determine radioactivity amounts. Gamma counters are specifically designed to measure very small amounts of radiation, such as those in blood samples taken from subjects being imaged in PET or SPECT systems. Autoradiography is an ex-vivo imaging method sometimes conducted following a nuclear medicine based experiment, or may make use of longer lived isotopes such as C-14 or tritium. The limited spatial resolution of in-vivo methods cannot determine the exact location of the imaging probes, thus autoradiography can be used to obtain high resolution images from ex-vivo tissue sections. The talk will include examples of how gamma counters are frequently used within imaging centers and how autoradiography is commonly used in the development of nuclear medicine based imaging probes.

Presentation Number **0012**

Educational Workshop 7: Translation of Molecular Imaging into the Clinic - What Does it Take? - I

Filing eIND/IND for Molecular Imaging Agents*King Li, Radiology, The Methodist Hospital, Houston, TX, USA. Contact e-mail: kli@tmhs.org*

Moving molecular imaging agents from the academic laboratory in the clinic requires going through many processes that are unfamiliar to most researchers. The purpose of this presentation is to give some information on the Investigational New Drug (IND) Application and more importantly the exploratory Investigational New Drug (e-IND) Application process which may facilitate the clinical translation of molecular imaging agents. In general, medical imaging agents are governed by the same regulations as drugs or biological products. However, medical imaging agents may be used in much lower doses and in much less frequency. The Food and Drug Administration (FDA) has an alternative e-IND process which may be well suited for development of medical imaging agents. Exploratory IND study is intended to describe a clinical trial that is conducted early in phase 1, involves very limited exposure, and has no therapeutic or diagnostic intent. Microdose studies are designed to evaluate pharmacokinetics or imaging of specific targets without inducing pharmacologic effects so the associated risk is very limited. A microdose is defined as less than 1/100th of the dose required to cause a pharmacologic effect with a maximum dose of <100 micrograms. For e-IND applications FDA currently accepts the use of extended single-dose toxicity studies in animals to support single-dose studies in humans. Routine genetic toxicology testing is not needed and safety pharmacology studies are also not recommended. So, the preclinical testing programs for e-IND studies can be less extensive than traditional IND studies. e-IND allows testing of radiotracers in a small number of human subjects (approx. 30-50) without toxicology. Further studies in human subjects will require a full IND with a complete toxicology package. With the added flexibility of the e-IND application process it is hoped that more and more molecular imaging agents will be able to be translated into the clinic.

Presentation Number **0013**

Educational Workshop 7: Translation of Molecular Imaging into the Clinic - What Does it Take? - I

Translation of Optical Imaging Agents to the Clinic**Ching-Hsuan Tung**, *The Methodist Hospital Research Institute, Houston, TX, USA. Contact e-mail: ctung@tmhs.org*

During the past decade, many optical contrast agents have been developed, and tested in various diseases models. However, translating these promising contrast agents to the clinic is still some distance away. Under specific excitation light, the applied contrast agent would emit fluorescent signal to report the location and statue of the diseases. Since the fluorescence signal can be detected by naked eyes or through a sensitive camera, the optical imaging technology could be extremely helpful in guiding surgical procedure. Fluorochrome is the key component of the optical contrast agents, whereas a safe fluorochrome with appropriate optical property is still waiting to be determined. Once a suitable fluorochrome was identified, speedy translation of the optical imaging technology can be expected. In conjunction with many newly developed imaging devices and systems, the optical imaging technology could revolutionize current clinical practice in many ways, such as disease detection, screening, diagnosis, surgery, and treatment evaluation.

Presentation Number **0014**

Educational Workshop 8: Advanced Animal MRI: From Anatomy to Function

Advanced Animal MRI: From Anatomy to Function

Jan-Bernd Hövener, *Medical Physics, Dept. of Radiology, University Hospital of Freiburg, Freiburg, Germany. Contact e-mail: jan.hoevener@uniklinik-freiburg.de*

Beyond relaxivity contrast - The amount of information available by non-invasive MR methodologies nowadays is unprecedented; its potential, however, is immense and just beginning to be realized in the clinic. Currently, modern high-field animal MR methods deliver "anatomical" maps using relaxivity contrast at the micrometer resolution; yet a new focus is being given to the assessment of physically functional parameters, such as diffusion (of liquids along structures), perfusion (of blood in organs), oxygen consumption (in the brain) and venous blood flow. Ideally, these "physical parameters" translate to "diagnostic parameters" such as the distribution of nervous fiber bundles or lipid-content of the liver. In this session, both present and future MR methodologies are presented, including diffusion weighted / tensor imaging, MR-spectroscopy, vessel-size imaging and hyperpolarization. Examples of current research will be provided, and the potential of MR for molecular imaging discussed. While special attention is paid to a deductive approach for a broad audience, please note that the attendee is advised to participate in the preceding "basics of small animal MRI" course.

Presentation Number **0015**
Educational Workshop 9: Basic Principles of Tracer Kinetic Modeling

Tracer Kinetic Modeling

Adriaan A. Lammertsma, *Department of Nuclear Medicine and PET Research, VU University Medical Center, Amsterdam, Netherlands. Contact e-mail: aa.lammertsma@vumc.nl*

Positron emission tomography (PET) is a tomographic imaging technique, which allows for accurate non-invasive in vivo measurements of a wide range of molecular processes and interactions in man. Based on its unrivalled sensitivity (picomolar level), the use of PET in imaging and measuring pre- and post-synaptic receptor density and affinity, neurotransmitter release, enzyme activity, and drug delivery and uptake is particularly interesting. Accurate quantification is based on the detection principles of PET. In particular, the capacity to accurately correct for tissue attenuation is a major asset compared with single photon techniques. Nevertheless, it should be noted that PET only measures the (temporal) distribution of radioactivity. Although imaging the distribution of a tracer at a certain time after intravenous injection may provide useful information, especially when uptake can be related to that in a reference region without specific signal (i.e. without receptors), it can also be misleading, as uptake depends on a number of factors of which specific binding is only one. For true quantification of a molecular process a tracer kinetic model is essential. A tracer kinetic model is a mathematical description of the fate of a tracer in the body, with emphasis on the organ of interest. Using such a model, observed tissue uptake and clearance of the tracer can be related to various model parameters, provided the input function is also known. As most tracers are injected intravenously, they reach tissue through the bloodstream. Consequently, in most cases, measurement of the arterial concentration over time is also needed. Although other types of models have also been proposed, in practice compartmental models are used. In these models, the distribution of activity is allocated to a number of (not necessarily physical) discrete compartments. The resulting operational equation primarily contains (unknown) rate constants, describing the rate of exchange of tracer between the various compartments, which are estimated by fitting the measured PET data. The series of tutorials will address the following issues: 1. Basic principles. 2. Structure of the most commonly used compartment models. 3. Reference tissue models. 4. Practical issues. 5. Linearised methods. 6. Parametric imaging. 7. Model selection for a new tracer. 8. Specific issues for small animal studies. The aim of the tutorials is to provide participants with a basic understanding of tracer kinetic modelling and its use in quantitative PET studies.

Presentation Number **0016**
Educational Workshop 10: Quantitative Nuclear Imaging

PET and SPECT Systems

Jae Sung Lee, *Department of Nuclear Medicine, Seoul National University, Seoul, Republic of Korea. Contact e-mail: jaes@snu.ac.kr*

PET and SPECT systems, which enable quantitative measurements of physiological characteristics by the in-vivo imaging of biochemical substances, are used to investigate biochemical and pathological phenomena, diagnose disease, and to determine prognosis after treatment. The course will cover the fundamental principles in PET, SPECT and related hybrid imaging, such as PET/CT and PET/MRI, and overview of modern hardware systems and their applications.

Presentation Number **0017**
Educational Workshop 10: Quantitative Nuclear Imaging

Image Reconstruction and Correction

Jinyi Qi, ¹*University of California at Davis, Davis, CA, USA;* ²*Lawrence Berkeley National Laboratory, Berkeley, CA, USA.* Contact e-mail: qi@ucdavis.edu

Image reconstruction plays an important role in quantitative nuclear imaging. It translates convolved raw data into three-dimensional images from which quantitative information of spatial and temporal tracer distribution can be extracted. The course will start with fundamental issues of image reconstruction, including the modeling of imaging physics and measurement noise, regularization, and optimization algorithms. It will then discuss specific issues in quantitative imaging and related correction methods.

Presentation Number **0018**
Educational Workshop 11: Reporter Gene & Vascular Imaging

Nuclear and Optical Imaging of Reporter Probes

David Piwnica-Worms, *Washington University School of Medicine, St. Louis, MO, USA. Contact e-mail: piwnica-wormsd@mir.wustl.edu*

Genetically-encoded imaging reporters introduced into cells and transgenic animals enable noninvasive, longitudinal studies of dynamic biological processes in intact cells and living animals. The most common reporters include firefly luciferase (bioluminescence imaging), green fluorescence protein (fluorescence imaging), Herpes Simplex Virus-1 thymidine kinase (positron emission tomography) and variants with enhanced spectral and kinetic properties optimized for use in vivo. When cloned into promoter/enhancer sequences or engineered into fusion proteins, imaging reporters enable fundamental processes such as transcriptional regulation, signal transduction cascades, protein-protein interactions, oncogenic transformation, immunologic response and targeted drug action to be temporally and spatially registered in vivo. Spying on biology with genetically-encoded imaging reporters provides new insight into cell-specific molecular and regulatory machinery within the contextual environment of the whole animal.

Presentation Number **0019**
Educational Workshop 11: Reporter Gene & Vascular Imaging

In Vivo Optical Fluorescence Imaging from the Animal to the Cellular Level

Yoseph Addadi, *Biological Regulation, Weismann Institute, Rehovot, Israel. Contact e-mail: yosepha@weizmann.ac.il*

Biological processes are characterized by fast changes and high heterogeneity, therefore continuous follow-up of processes in vivo by imaging can lead to better understanding of the process of interest. Fluorescence optical intravital imaging offers us the ability to follow specific sites of interest at high spatial and temporal resolution with high sensitivity. Summing together the wide labeling possibilities, using different fluorescent proteins and markers, together with a wide range of modalities, enable us to choose and tailor the right system to answer a specific question. The available optical fluorescent imaging applications cover a wide range, from the whole animal level down to the sub-cellular level, the main limitation of fluorescence optical imaging is in the depth penetration, as photons are absorbed and scattered by the tissue. Using two-photon microscopy, penetration depth is increased together with reduced noise and lower off-target toxicity, opening the possibility for in vivo imaging at high resolution. Several optical fluorescence imaging methods will be presented and the considerations that should be thought of when choosing the proper model.

Presentation Number **0020**
Educational Workshop 11: Reporter Gene & Vascular Imaging

Angiogenesis and Vascular Imaging

Michal Neeman, Weizmann Institute, Rehovot, Israel. Contact e-mail: michal.neeman@weizmann.ac.il

Expansion of blood vessels, through angiogenesis, namely the sprouting of new capillaries from existing vessels, is an integral component of growth of any large multicellular tissue. Thus, angiogenesis accompanies fetal and postnatal development and is critical for adaptive maintenance of tissue homeostasis in face of growing needs for oxygen and nutrients. Similarly, growth of solid tumors requires active vasculature which can be provided either through co-option of existing vessels or through activation of sprouting angiogenesis. Non invasive imaging provides important tools for detection of the activation of proangiogenic signaling pathways, activation of acute vascular adaptation mechanisms in existing vessels, including vasoreactivity and vascular permeability, and detection of sprouting angiogenesis. In addition to mapping of blood volume, blood flow, vessel permeability and vasoreactivity, molecular markers can be used for detection of activated endothelial cells. The most prominent molecular marker is the integrin $\alpha V \beta 3$ which is highly expressed by endothelial cells during angiogenesis. Smart contrast media can be used for detection of changes in the extracellular matrix during angiogenesis. Key enzymes include matrix metallo proteinases, transglutaminases and hyaluronidases. Methods for cell tracking can be used for imaging the recruitment of endothelial and perivascular cells to sites of angiogenesis. Collectively, these tools help in analysis of the complex process of constructing new vessels.

Presentation Number **0021**

Educational Workshop 12: Translation of Molecular Imaging into the Clinic - What Does it Take? - II

Radiogenomics: Optimizing Clinical Information Yield of MRI Imaging Agents to Enable Molecular Imaging

Michael Kuo, UCLA, Los Angeles, CA, USA. Contact e-mail: michaelkuo@mednet.ucla.edu

Over the past twenty years, there has been tremendous growth in the power of medical imaging tools such as magnetic resonance imaging (MRI) to non-invasively diagnose and characterize disease and to guide clinical management. However, while clinically widespread much of this work has been focused on improved structural and functional characterization of disease with an associated perception of poor molecular resolution. In parallel, the sequencing of the human genome has provided powerful methods for dissecting the molecular basis of disease. One of the current limitations of these existing diagnostic tools conversely, continues to be the difficulty of translating molecular findings into clinically useful assays or interventions. Radiogenomics, the systematic integration of large-scale biological data with medical imaging data obtained from existing imaging methods, provides a unique opportunity for bringing molecular imaging to the clinic. In this talk I will discuss the field of radiogenomics and how, by leveraging MR imaging contrast agents, expanding computational power, and improved understanding of disease biology, it is becoming increasingly feasible to extract clinically meaningful large-scale molecular detail of a given disease from existing MRI scans.

Presentation Number **0022**

Educational Workshop 12: Translation of Molecular Imaging into the Clinic - What Does it Take? - II

Translation of Microbubbles to the Clinic*Evan C. Unger, University of Arizona, Tucson, AZ, USA. Contact e-mail: evanunger@comcast.net*

How can new USCA for molecular imaging be developed and translated into clinical studies? Contrast agents are regulated by the FDA as drugs. In order to enter clinical testing USCA must file an investigational new drug (IND) application. Generally after filing an IND the FDA will respond in 30 days. For a successful IND submission the USCA must be manufactured according to good manufacturing (cGMP) practice guidelines, undergo chemistry, manufacturing, characterization and stability studies. USCA must also undergo extensive preclinical pharmacology and toxicology testing completed according to good laboratory practice guidelines. Before the first patient can be studied with the USCA it will generally cost at least several million dollars to complete such studies and take a year or more to complete the studies after initial cGMP manufacturing has been completed. Generally, contrast agents (drugs) enter phase I clinical trials in which patients or normal volunteers are exposed as cohorts to ascending doses of the agent to assess safety. Then in Phase II trials dosing is performed in larger cohorts of patients to assess dose response and efficacy and to determine the optimal dose of agent for definitive Phase III clinical trials. Generally, a single dose or limited doses are selected for Phase III clinical trials which are designed to show efficacy in meeting a primary end-point at a significant level, i.e. $p < .05$. Usually two Phase III clinical trials are required to show efficacy for a primary end-point in order for the FDA to approve the agent for sale and clinical use. Recently a new pathway designed to potentially more rapidly introduce drugs into the early clinical studies has been exploited. Phase 0 clinical study can be performed in a limited number of subjects to assess target validation. In such studies, the dose of agent used must be less than 1/50th the no effect level determined from pre-clinical acute toxicity studies. Under the Phase 0 pathway limited preclinical studies need to be performed prior to first human studies than with the classic approach to entering phase I studies, potentially saving time and money. This approach has been taken for some nuclear medicine agents to enter early human testing.

Presentation Number **0023**

Educational Workshop 12: Translation of Molecular Imaging into the Clinic - What Does it Take? - II

Translation of SPECT/PET Agents to the Clinic

H. William Strauss, Nuclear Medicine Service, Memorial Sloan Kettering Cancer Center, New York, NY, USA. Contact e-mail: straussh@mskcc.org

To extend observations made in the molecular imaging laboratory to the clinic may require the development of unique instrumentation, and may utilize existing or new radiopharmaceuticals. For example, advances in understanding the etiology of major acute coronary events (MACE) suggests that individual coronary lesions must be evaluated to identify those likely to cause a clinical event. In addition to the known clinical risk factors for coronary disease, such as diabetes, hypercholesterolemia, and hypertension, new data has demonstrated a correlation between specific genetic mutations, such as changes in 9q21, which is associated with a doubling of the risk of heart attack before the age of 60. Although the risk is doubled, the actual chances of clinical event remain small. Current clinical practice utilizes a combination of clinical history, serum biomarkers, anatomic information from coronary CT angiography and information about tissue perfusion at rest and stress from radionuclide studies to evaluate patients at risk for MACE. However, even in patients with extensive myocardial ischemia and severe coronary artery disease, the likelihood of a clinical event is only about 15%/year. This observation suggests that other factors must play a significant role in causation of MACE. Coronary histopathology in patients dying from MACE has identified two major processes that lead to the formation of a coronary thrombus. A. Plaque rupture, where the atheroma sustains an intraplaque hemorrhage, causing the lesion cap to rupture, exposing highly thrombogenic material into the flowing blood leading to thrombus formation; and B. Plaque erosion, where endothelial cells covering the lesion die, exposing the underlying thrombogenic collagen to flowing blood, leading to formation of a thrombus. Plaque rupture causes more than two-thirds of coronary events. Atheroma vulnerable to rupture share features of a thin cap, larger size, and the presence of numerous inflammatory cells. Molecular imaging studies confirmed that inflammatory cells in atheroma consume exogenous glucose as a major source of energy. Autoradiographic studies demonstrate high uptake of the glucose analog, ¹⁸F-FDG, in the lesions. These observations led to the use of FDG PET-CT imaging to characterize the degree of inflammation in human atheroma in large vessels, such as the carotid arteries. Serial FDG PET-CT images revealed that therapy with statins reduced the glucose consumption in the lesions, suggesting a decrease in lesion inflammation.

Presentation Number **0024**

Educational Workshop 13: Approaches and Methods in MRI Probe Design

Gd-based Probes; Lipidic Nanoparticles*Klaas Nicolay, Biomedical Engineering, Eindhoven University, Eindhoven, Netherlands. Contact e-mail: k.nicolay@tue.nl*

Magnetic Resonance (MR) offers a diversity of non-invasive readouts that find extensive use in biomedical research and clinical diagnostics. PET and SPECT, however, have a much higher sensitivity than MR. Therefore, these techniques are presently preferred for the visualization of sparse molecular markers. Making MR suitable for molecular imaging applications, is a challenging task. Several approaches are explored to allow in vivo detection of low-level molecular markers with MR. One widely employed strategy involves the use of nano-particles, as these can readily be equipped with a high payload of MRI contrast agent. Four main types of nanoparticles are used: (i) nano-particles loaded with Gd³⁺-chelates for T1 shortening¹; (b) FeO nano-crystals for T2-detection²; (c) fluorinated nano-emulsions for F-19 MR³; (d) nano-particles incorporating CEST agents⁴. Nano-particles also offer attractive features for multimodality imaging and incorporation of drugs for image-guided therapy. Nano-particles are primarily used for targeting of intravascular markers and of extravascular markers in case of enhanced vascular permeability, such as occurring in tumors, atherosclerosis and myocardial infarction. The presentation will focus on the design and characterization of lipid-based nanoparticulate contrast agents that are equipped with a high payload of Gd for MRI contrast. Examples on their use will be drawn from preclinical imaging studies on animal models of disease. References 1. Mulder W.J.M. et al., NMR Biomed, 19, 142 - 164 (2006) 2. Laurent S, Curr Med Chem, 16, 4712 - 4727 (2009) 3. Janjic J.M. et al, Wiley Interdiscip Rev Nanomed Nanobiotechnol, 1, 492 - 501 (2009) 4. Aime S. et al., Acc Chem Res, 42, 822 - 831 (2009) Acknowledgements: The author's research on this topic was funded in part by the Integrated EU Project MEDITRANS (FP6-2004-NMP-NI-4/IP 026668-2), the European Community EC-FP6-project DiMI, LSHB-CT-2005- 512146 and by the BSIK program entitled Molecular Imaging of Ischemic Heart Disease (project number BSIK03033). This study was performed in the framework of the European Cooperation in the field of Scientific and Technical Research (COST) D38 Action Metal- Based Systems for Molecular Imaging Applications.

Presentation Number **0025**

Educational Workshop 13: Approaches and Methods in MRI Probe Design

Approaches and Methods in MRI Probe Design: Iron Oxides

Jeff W. Bulte, Dept. of Radiology, Johns Hopkins University School of Medicine, Baltimore, MD, USA. Contact e-mail: jwmbulte@mri.jhu.edu

Jeff W.M. Bulte, Ph.D. Department of Radiology, Division of MR Research, The Johns Hopkins University School of Medicine, Baltimore, MD, USA. jwmbulte@mri.jhu.edu The physicochemical properties of superparamagnetic iron oxide nanoparticles have been studied in detail for more than 60 years. Many different methods exist that can produce particles under “the critical domain size” (required for superparamagnetism), i.e., iron oxides with a crystal core diameter no larger than about 50 nm. The particles have an additional coating that can take the total diameter to well above 100 nm. There are many different coatings that can be used to prepare stable iron oxide colloid formulations, e.g., dextran, carboxydextran, silica, lipids, citrate, amino acids, peptides, and dendrimers, to name a few. Initially, dextran-coated iron oxides were developed in the 1980s for clinical imaging of macrophages, with liver and lymph node imaging as the main application that was later extended to contrast-enhanced imaging of plaques occurring in multiple sclerosis and arteries. The particle surface charge is a major determinant of non-specific uptake and overall blood half-life, and dependent on the intended application, the proper particle formulation needs to be selected. For instance, for cell labeling before transplantation or infusion, larger charged (cationic) particles are more efficient, while for targeted molecular imaging of epitopes in vivo neutrally charged, smaller particles are preferred. Methods for labeling for cell tracking include the use of transfection agents or cationic peptides/dendrimers as secondary coatings, or magneto-electroporation or -sonoporation based instant labeling techniques. Approaches for conjugating targeting ligands for molecular imaging vary and are dependent on the particle coating. Conventional sulfo-NHS conjugation, periodate-oxidation/borohydrate-reduction (with Schiff's base intermediates), avidin-biotin linkage, etc. may produce the desired specificity. As for clinical use and safety concerns, the human adult has about 4 grams of total iron in the body and any given iron oxide contrast formulation will be in the microgram dosing range. This natural abundance, together with the biocompatibility and the ability of the body to recycle the injected iron, makes iron oxide particles one of the safest contrast agents available for molecular and cellular imaging.

Presentation Number **0026**

Educational Workshop 13: Approaches and Methods in MRI Probe Design

MRI Probe Design: CEST and PARACEST Agents

Silvio Aime, Department of Chemistry, IFM/ Center of Molecular Biotechnology, University of Torino, Torino, Italy. Contact e-mail: silvio.aime@unito.it

Contrast in magnetic resonance imaging (MRI) arises from changes in the intensity of the proton signal of water between voxels. Differences in intervoxel intensity can be significantly enhanced with chemicals that alter the nuclear magnetic resonance (NMR) intensity of the imaged spins. Paramagnetic lanthanide(III) complexes are used in two major classes of MRI contrast agents; namely, the well-established class of Gd-based agents and the emerging class of chemical exchange saturation transfer (CEST) agents. A Gd-based complex increases water signal by enhancing the longitudinal relaxation rate of water protons, whereas CEST agents decrease water signal as a consequence of the transfer of saturated magnetization from the exchangeable protons of the agent. Unlike the Gd(III) complexes, the presence of a CEST agent is visualized in an MRI image only if, following the application of a suitable radiofrequency field, the resonance corresponding to the exchangeable protons is saturated (1). To maximize magnetization transfer it is necessary that the exchange rate between the resonance of the mobile protons on the CEST agent and the bulk water resonance has an optimal value. Too high values are not usable since these result in the coalescence of the two signals. Therefore, to get high exchange rates without signal coalescence, the use of paramagnetic systems in which there is a large shift of the mobile proton signal has been suggested. This type of CEST agents has been termed PARACEST. Moreover a further, dramatic improvement in sensitivity has been attained with the use of liposomes loaded with paramagnetic Lanthanide chelates (LIPOCEST). In these systems the exchangeable pool of protons is represented by the whole ensemble of water molecules contained in the inner aqueous cavity of the vesicles. The chemical shift of the inner water resonance is made different from the "bulk" water through the entrapment in the liposome of a paramagnetic shift reagent. The chemical shift separation between the water signals in the inner and external compartment can be markedly increased by passing from spherical to non-spherical liposomes and by entrapping polynuclear paramagnetic shift reagents. A large array of PARACEST agents is now available that can be selectively "interrogated" to report about different targets in the same MR image (2). 1)Terreno E, DelliCastelli D., Viale A, Aime S. CHEMICAL REVIEWS, 110,3019-3042,2010 2)Terreno E, DelliCastelli D, Aime S. CONTRAST MEDIA & MOLECULAR IMAGING,5, 78-98,2010

Presentation Number **0027**

Educational Workshop 14: Advanced Issues in Modeling and Application to Small Animal PET

Tracer Kinetic Modeling

Adriaan A. Lammertsma, *Department of Nuclear Medicine and PET Research, VU University Medical Center, Amsterdam, Netherlands. Contact e-mail: aa.lammertsma@vumc.nl*

Positron emission tomography (PET) is a tomographic imaging technique, which allows for accurate non-invasive in vivo measurements of a wide range of molecular processes and interactions in man. Based on its unrivalled sensitivity (picomolar level), the use of PET in imaging and measuring pre- and post-synaptic receptor density and affinity, neurotransmitter release, enzyme activity, and drug delivery and uptake is particularly interesting. Accurate quantification is based on the detection principles of PET. In particular, the capacity to accurately correct for tissue attenuation is a major asset compared with single photon techniques. Nevertheless, it should be noted that PET only measures the (temporal) distribution of radioactivity. Although imaging the distribution of a tracer at a certain time after intravenous injection may provide useful information, especially when uptake can be related to that in a reference region without specific signal (i.e. without receptors), it can also be misleading, as uptake depends on a number of factors of which specific binding is only one. For true quantification of a molecular process a tracer kinetic model is essential. A tracer kinetic model is a mathematical description of the fate of a tracer in the body, with emphasis on the organ of interest. Using such a model, observed tissue uptake and clearance of the tracer can be related to various model parameters, provided the input function is also known. As most tracers are injected intravenously, they reach tissue through the bloodstream. Consequently, in most cases, measurement of the arterial concentration over time is also needed. Although other types of models have also been proposed, in practice compartmental models are used. In these models, the distribution of activity is allocated to a number of (not necessarily physical) discrete compartments. The resulting operational equation primarily contains (unknown) rate constants, describing the rate of exchange of tracer between the various compartments, which are estimated by fitting the measured PET data. The series of tutorials will address the following issues: 1. Basic principles. 2. Structure of the most commonly used compartment models. 3. Reference tissue models. 4. Practical issues. 5. Linearised methods. 6. Parametric imaging. 7. Model selection for a new tracer. 8. Specific issues for small animal studies. The aim of the tutorials is to provide participants with a basic understanding of tracer kinetic modelling and its use in quantitative PET studies.

Presentation Number **0028**

Educational Workshop 15: Perspectives of Cardiovascular Molecular Imaging (Co-organized with JSNM)

Practical and Reliable Assessment of Myocardial Blood Flow*Hidehiro Iida, National Cerebral Cardiovascular Center, Suita City, Japan. Contact e-mail: iida@ri.ncvc.go.jp*

Regional myocardial blood flow is a key parameter for characterizing the pathos-physiological status of the ischemic heart disease. Among a number of techniques, PET is recognized a gold standard, and can provide absolute quantitation both at rest and during stress conditions in clinical settings. Recent reports demonstrated that the quantitation of regional myocardial blood flow can reform the detection of coronary artery disease, particularly in patients with multiple vessel disease and/or various risk factors. Physics contribution to ensure the quantitative accuracy with regard to corrections for scatter and attenuation, as well as various mathematical approaches to model the kinetics of each tracer was shown to be key issues. Extent of water-perfusible tissue in the cell-transplanted regions is the direct marker of tissue regeneration that established the normal capillary structures. Regional perfusion and flow reactivity are also of a potential use for functional outcome after various therapeutic trials. Other works also demonstrated the improvement of SPECT technique to provide absolute quantitative of regional blood flow at rest and after stress from a single session of a SPECT scan. Of the uniqueness is the applicability of SPECT devices for large scale clinical studies, attributed not only to the availability of the system, but also to the intrinsic feature the scatter and attenuation not being dependent on the geometric design of this device. Thus, once a protocol is established for quantitative functional imaging, the technique can be extended to all SPECT systems installed in various clinical institutions. There could be a number of application fields for evaluating new therapeutic trials in clinical institutions.

Presentation Number **0029**

Educational Workshop 15: Perspectives of Cardiovascular Molecular Imaging (Co-organized with JSNM)

Detection of Ischemia and Apoptosis in the Diseased Myocardium*Junichi Taki, Nuclear Medicine, Kanazawa University Hospital, Kanazawa, Japan. Contact e-mail: taki@med.kanazawa-u.ac.jp*

Severe myocardial ischemia results in a substantial loss of cardiomyocytes through apoptosis followed by necrosis. Commonly used imaging approach for the detection of apoptosis has been to target the phosphatidylserine, which externalizes on the outer cell membrane in the early process of apoptosis. ^{99m}Tc -Annexin-V (Tc-AV) imaging has been proved to be feasible to detect apoptotic cells. In a rat model of 20min ischemia and reperfusion, Tc-AV accumulation peaked at 30min after reperfusion followed by rapid reduction until 24 hr and gradual decrease until 3 days after reperfusion. Interestingly, significant uptake of Tc-AV was observed in shorter period of ischemia, which induced no histological change and minimal TUNEL-positivity, suggested reversibility of apoptosis upon removal of mild ischemia. Tc-AV is feasible to monitor apoptotic process not only after myocardial infarction but also to detect transient myocardial ischemia shortly after the episode. After myocardial cell death, inflammatory signals start to recruit leucocytes within 24 hr, and during the repair process, extracellular matrix constituents are also reorganized. Tenascin-C, an extracellular matrix glycoprotein, could provide important biologic signaling that influences cell motility, proliferation, differentiation, survival, or apoptosis via cellular-extracellular matrix interaction during tissue remodeling. After infarction ^{125}I -anti-tenascin C antibody can detect tenascin-C expression. It's intense accumulation lasted around 1 week after reperfusion, followed by gradual decline until 4 weeks, suggesting the ^{125}I -anti-tenascin C antibody imaging may be a way to monitor myocardial injury and its repair process.

Presentation Number **0030**

Educational Workshop 15: Perspectives of Cardiovascular Molecular Imaging (Co-organized with JSNM)

Detection and Assessment of Vulnerable Plaque*Yuji Kuge, Graduate School of Medicine, Hokkaido University, Sapporo, Japan. Contact e-mail: kuge@med.hokudai.ac.jp*

Thrombus formation triggered by plaque rupture is the most important mechanism leading to the onset of acute arterial disease and ischemic sudden death. Accordingly, various invasive and noninvasive imaging methods are used to obtain morphological and functional information necessary for the identification of atherosclerotic plaques with a risk of rupture (vulnerable plaques). It may be possible for molecular imaging, such as PET and SPECT, to visualize the determining factors of plaque vulnerability based on cellular and biological changes, surpassing morphological information. As inflammation and apoptosis are important components of plaque vulnerability, ^{18}F -FDG (a marker of inflammation) and $^{99\text{mTc}}$ -annexin A5 (a marker of ongoing apoptotic cell death) are expected for the evaluation of plaque vulnerability. The development of new probes capable of more specifically detecting vulnerable plaques is also a matter of great concern in the molecular imaging of atherosclerosis. In these regards, we recently investigated the potentials of ^{18}F -FDG, $^{99\text{mTc}}$ -annexin A5, and probes that target oxidized LDL receptor-1 (LOX-1), membrane type-1 matrix metalloproteinase (MT1-MMP), and tissue factor (TF) for imaging of vulnerable atherosclerotic plaque. In this session, I will introduce recent topics on PET and SPECT imaging of atherosclerotic plaque vulnerability, mainly focused on our recent studies in mouse and rabbit models of spontaneous atherosclerosis.

Presentation Number **0040**
Plenary Session 1: Keynote Presentation

Innate Immunity and Pathogen Recognition

Shizuo Akira, *WPI Immunology Frontier Research Center, Osaka University, Osaka, Japan. Contact e-mail: sakira@biken.osaka-u.ac.jp*

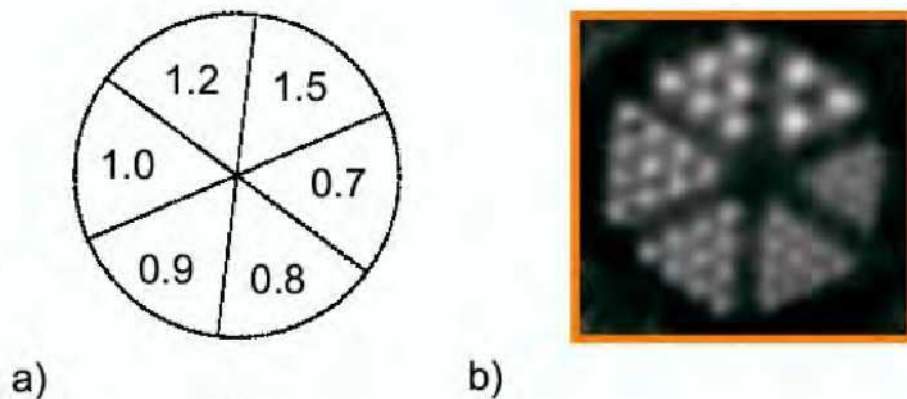
Immune response is broadly categorized into innate and acquired immunity. Acquired immunity is mediated by T and B cells, both of which generate their receptors through DNA rearrangement and respond to a wide range of potential antigens. This highly sophisticated system is observed only in vertebrates and has been the subject of considerable study. On the other hand, innate immunity was formerly considered as non-specific because the major work of this system is to digest pathogens and present the antigen to the cells involved in acquired immunity. Therefore, the study on innate immunity has been for a long time discarded and not appreciated. However, recent studies showed that innate immunity is not non-specific but specific enough to discriminate self and pathogens through evolutionarily conserved receptors, named Toll-like receptors (TLRs) and play a crucial role in early host defense against invading pathogens. Furthermore, accumulating evidence indicates that activation of innate immunity is prerequisite to induction of acquired immunity. This paradigm shift is now changing our thinking on pathogenesis and treatment of infectious diseases, immune diseases, allergic diseases, and cancers. Besides TLRs, recent findings have shown the presence of cytosolic detector system of invading pathogens. Two DExD/H box RNA helicases, retinoic acid inducible protein-I (RIG-I) and melanoma differentiation-associated gene 5 (mda-5) are involved in anti-viral responses by recognizing RNA in the cytoplasm. RIG-I and mda-5 recognize distinct RNA viruses. Bacterial components are also recognized by NOD-like receptors (NLRs) in the cytoplasm. I will review the pathogen recognition by TLRs and cytoplasmic receptors.

Presentation Number **0041**
Scientific Session 1: PET/SPECT/CT Instrumentation & Methodology

Simultaneous Sub-millimetre PET and SPECT with a Dedicated Multi-pinhole Geometry

Frederik J. Beekman^{1,3}, **Frans van der Have**^{1,3}, **Rob Kreuger**¹, **Marlies C. Goorden**^{1,2}, ¹*Radiation, Detection & Medical Imaging, TU Delft, Delft, Netherlands;* ²*Image Sciences Institute and Rudolf Magnus Institute, University Medical Centre Utrecht, Utrecht, Netherlands;* ³*Molecular Imaging Laboratories, Utrecht, Netherlands.* Contact e-mail: f.j.beekman@tudelft.nl

Here we present a new imaging option for U-SPECT-II (MILabs, The Netherlands), which is now capable of simultaneous and quantitative sub-mm resolution imaging of positron emitters and single photon emitters. To this end a novel collimator optimized for high energy gamma photons was developed with clustered multi-pinholes (CMP). The narrow opening angle of each pinhole reduces resolution loss due to the strong pinhole edge penetration of 511 keV annihilation photons. The CMP collimator contains 48 clusters that consist of four pinholes each with diameters of 0.7 mm. The peak geometric sensitivity of the collimator was 1.3% for F-18. The CMP collimator was placed in the triangular stationary detector set-up of the U-SPECT-II system. Image resolution was determined with a Jaszczak hot capillary resolution phantom. Images were obtained using pixel-based OS-EM that correct blurring due to limited system resolution and positron range. For F-18 and Tc-99m the smallest rods that could be resolved in the reconstructed images have a diameter of 0.8 mm and 0.5 mm respectively. Experiments are being conducted to see if CMP is capable to resolve structures in tumours and the brain and that can not be resolved with coincidence PET. Additional capabilities of CMP include high resolution imaging of other high-energy single-photon emitters such as I-131. We conclude that CMP is a cost-effective alternative to systems that combine coincidence PET and pinhole SPECT with unique imaging capabilities.



Hot rod phantom with capillary diameters of 0.7, 0.8, 0.9, 1.0, 1.2 and 1.5 mm (a) reconstructed with FDG (b) (75 MBq, 4h scan time).

Presentation Number **0042**
Scientific Session 1: PET/SPECT/CT Instrumentation & Methodology

Development of a Si-PM Based High Resolution DOI-PET System for Small Animals

Seiichi Yamamoto¹, **Masao Imaizumi**², **Tadashi Watabe**², **Hiroshi Watabe**², **Yasukazu Kanai**², **Eku Shimosegawa**², **Jun Hatazawa**²,
¹Kobe City College of Technology, Kobe, Japan; ²Osaka University Graduate School of Medicine, Osaka, Japan. Contact e-mail: s-yama@kobe-kosen.ac.jp

Geiger-mode avalanche photodiode (Si-PM) is a promising photo-detector for PET, especially for the use in a magnetic resonance imaging (MRI) system because it is less sensitive to static magnetic field. However Si-PM has temperature dependent gain and relatively high noise that may be problems for development of a PET system. In addition it is not clear the Si-PM based PET system can be used in a MRI system. Thus we developed a Si-PM based depth-of-interaction (DOI) PET system for small animals and tested its performance. We also tested the Si-PM based PET system in MRI. Hamamatsu 4x4 Si-PM arrays (S11065-025P) were used for the detector blocks of the PET system. Two types of LGSO scintillator of 0.75 mol% Ce (decay time:~45ns: 1.1mm x 1.2mm x 5mm) and 0.025 mol% Ce (decay time:~31ns: 1.1mm x 1.2mm x 6mm) were optically coupled in DOI direction to form a DOI detector, arranged in 11 x 9 matrix and optically coupled to the Si-PM array. Pulse shape analysis was used for the DOI detection of these two types of LGSOs. Sixteen detector blocks were arranged in a 68mm diameter ring to form the PET system. The signals from each block detector is weighted summed and is fed to 100MHz analog to digital (A-D) converters of the data acquisition system and signals are integrated with two different integration times (120ns and 320ns), calculated the position using the Anger principle by FPGA. Also coincidence is measured digitally among eight groups (2 block detectors for 1 group) and stored in list mode to a personal computer (PC). Temperature was monitored and correction factor was applied for variable gain amplifiers of the front-end circuit for the temperature dependent gain compensation of the Si-PM. The number of slices of the developed PET system was 17 and the axial FOV was 11.7mm. Radial resolution was 1.5mmFWHM at center and 2.2mmFWHM at 15 mm off center. Sensitivity was 0.8% at the center of the axial FOV. High resolution mice and rats images were successfully obtained using the PET system. The temperature dependent gain control system can reduce its gain variations of the Si-PM based detectors. Developed PET system was also tested in a 0.3T permanent magnet MRI and we found that no change in PET images and count rate, and some S/N degradation for MRI images probably due to the electronics noises from the PET detectors. We confirmed that the developed Si-PM based DOI PET system is promising for molecular imaging researches.

Presentation Number **0043**
Scientific Session 1: PET/SPECT/CT Instrumentation & Methodology

Detector Development Toward a Dedicated Mouse Brain PET Scanner with High Spatial Resolution and High Sensitivity

Yongfeng Yang¹, **Yibao Wu**¹, **Sara St. James**¹, **Julien Bec**¹, **Kun Di**¹, **Jinyi Qi**¹, **Richard Farrell**², **Purushottam A. Dokhale**², **Kanai Shah**², **Simon R. Cherry**¹, ¹*Department of Biomedical Engineering, UC Davis, Davis, CA, USA;* ²*Radiation Monitoring Devices Inc, Watertown, MA, USA. Contact e-mail: yfyang@ucdavis.edu*

The performance of available small animal positron emission tomography (PET) scanners continues to be detector rather than physics limited. Significant improvements in the sensitivity and spatial resolution would not only improve the quantification of signals that we are currently able to visualize but would also open up important new applications that are beyond the reach of contemporary animal PET systems. Depth of interaction (DOI) is the major factor that limits the simultaneous achievement of high spatial resolution and high sensitivity for small animal PET scanners since long crystals are required to achieve a high sensitivity, but meanwhile the spatial resolution is degraded due to DOI if long crystals are used. We have been developing depth-encoding PET detectors by using dual-ended readout of finely pixelated lutetium oxyorthosilicate (LSO) scintillator arrays with position sensitive avalanche photodiodes (PSAPDs). Tapered LSO arrays were developed to further increase the sensitivity of a PET scanner by minimizing the gaps between detector modules. Tapered LSO arrays with different crystal surface and inter-crystal reflectors were manufactured and evaluated to find the best compromise between crystal identification and DOI resolution. The results showed that with proper crystal surface and reflector, all crystals in the arrays can be clearly resolved and a DOI resolution of ~ 2 mm can be obtained for a LSO array of 20 mm depth with a crystal size of as small as 0.5 mm. The intrinsic spatial resolution and efficiency were measured for a traditional cuboid LSO array (13×13 crystals, crystal size: 0.514×0.514×20 mm³) and a tapered LSO array (13×13 crystals, crystal size: 0.514×0.514 mm² at front and 0.514×0.914 mm² at back, 20 mm long). The measured intrinsic spatial resolutions are 0.67 mm and 0.74 mm for the cuboid and tapered arrays respectively. The increase of sensitivity for the tapered array as compared with the cuboid array is 43%. The flood histogram of the tapered array is better compared with a cuboid array with the same crystal dimensions as the front of the tapered array. A dedicated mouse brain PET scanner is under development using the tapered depth encoding detectors. The scanner consists of 4 detector rings and 16 detectors per ring. The scanner has an axial field of view (FOV) of 41 mm and a transverse FOV of 40 mm. Monte Carlo simulations show the scanner has a sensitivity of ~ 17% at the center of the FOV and a spatial resolution approaching 0.5 mm across the whole FOV.

Presentation Number **0044**
Scientific Session 1: PET/SPECT/CT Instrumentation & Methodology

Derivation of a Respiration Trigger Signal in Small Animal Listmode PET Based on Respiration-induced Variations of the ECG Signal

Andrei Todica, Erik Mille, Peter Bartenstein, Marcus Hacker, Guido Boening, Dept. of Nuclear Medicine, Ludwig-Maximilians University of Munich, Munich, Germany. Contact e-mail: Andrei.Todica@med.uni-muenchen.de

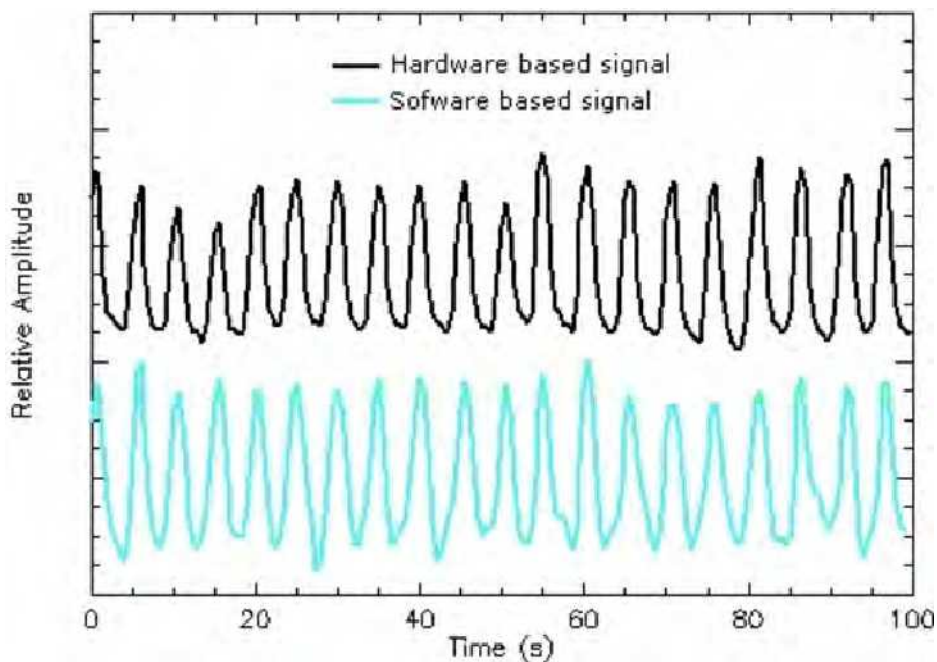
In molecular imaging of small animals the collection of physiological information is important to monitor the animal's status and to allow for advanced processing techniques such as the reconstruction of gated images. A major source of physiological information is the electro-cardiogram (ECG), which is obtained by attaching electrodes to the subject. Furthermore, respiration can be registered by using stretchable belts or cushions. This work proposes a method to calculate respiratory trigger signals from ECG data to which can be inserted into PET listmode data. While respiratory motion alters the amplitude of the ECG signal, respiratory sinus arrhythmia modulates the length of the heart cycle. A respiratory trigger signal can be detected from these respiration-induced variations. We analyzed 500 s ECG and respiratory cushion recordings (BioVet, m2m Imag. Corp.) of ten rats (Sprague Dawley, 226.8 ± 7.5 g). ECG trigger events were determined by a robust search for the R-peaks. The reference respiratory (RR) trigger events were determined by searching for peaks in the respiratory recording after applying a moving average filter (50 ms). The ECG-based respiratory curve was generated by combining the spline interpolation of the amplitudes of the ECG trigger points and the spline interpolation of the respiratory cycle length. The peaks in the resulting function were detected and defined as ECG-based respiratory (ER) trigger points. The mean heart rate of all measurements was 368 ± 31 bpm. The mean RR duration was 1577 ± 159 ms with a mean intra-subject standard deviation of 65 ms. No difference to the mean ER duration (1577 ± 159 ms) was observed although a slight increase in intra-subject standard deviation (70 ms) occurred. In average, the ER trigger points were detected 34 ± 12 ms later than the RR trigger point which indicates a systematic phase shift caused by the two different triggering techniques. A direct comparison of each individual RR and ER duration showed increased noise due to the reduced sampling rate of ER (defined by the ECG trigger points). This noise was reduced by a factor of 7 when a moving average filter over 8 samples was applied to the ER durations, as it is the case in many online ECG and respiratory triggering systems. Insertion of RR and ER trigger points into a rat's listmode file showed no difference in respiratory motion which was estimated by tracking the upper liver boundary. The good agreement of RR and ER trigger detection allows ECG based respiratory monitoring and triggering of PET listmode data.

Presentation Number **0045**
Scientific Session 1: PET/SPECT/CT Instrumentation & Methodology

Reading between the Listmode Lines - A Method for Fast Extraction of Respiratory Signal from Raw PET Data and its Comparison to Other Methods

Adam L. Kesner¹, **Claudia Kuntner**², ¹Human Health, IAEA, Vienna, Austria; ²Molecular Medicine, AIT Austrian Institute of Technology GmbH, Seibersdorf, Austria. Contact e-mail: a.kesner@iaea.org

Introduction: Respiratory motion causes image degradation in PET thorax imaging, and techniques for addressing this problem using respiratory gating have been in development over the last decade. One obstacle for practically implementing respiratory gating in routine clinical protocols is the extra hardware, time, and efforts necessary for implementation. In this work, an automated software based algorithm is presented for extracting respiratory information from raw PET data in a manner requiring less time than the real time acquisition, and compared with other approaches using the same set of data. **Methods:** The presented algorithm is based upon a principle of rebinning sinogram data into smaller, more manageable data structures, and then analyzing the time activity behavior in the elements of these structures. Respiratory signal was extracted from a collection of 22 clinical PET scans, using this method as well as several other software based methods, and all were compared to hardware based measurements. **Results:** The method presented required approximately nine minutes of processing time for a 10 minute scan (single 2.67 GHz processor), and can be potentially be integrated with PET systems to produce a trace in real time. The mean/median/range of correlations for the set of scans when using the optimal parameters was found to be 0.56/0.59/0.11-0.84. The speed of this method compared well with the fastest previously presented data based algorithm while the accuracy compared well with the most accurate of the previously presented algorithms. **Conclusion:** Raw PET listmode data contains information about respiratory motion in a large percentage of scans, which can be extracted in a fully automated and fast manner. Such methods can be expected to improve with better hardware and methodological improvements, and lay the groundwork for an easy implementation of respiratory gating in routine clinical PET.



An example of the correlating hardware and software based respiratory signals for a patient FDG PET scan. The correlation illustrates the potential for extracting the signal directly from the data.

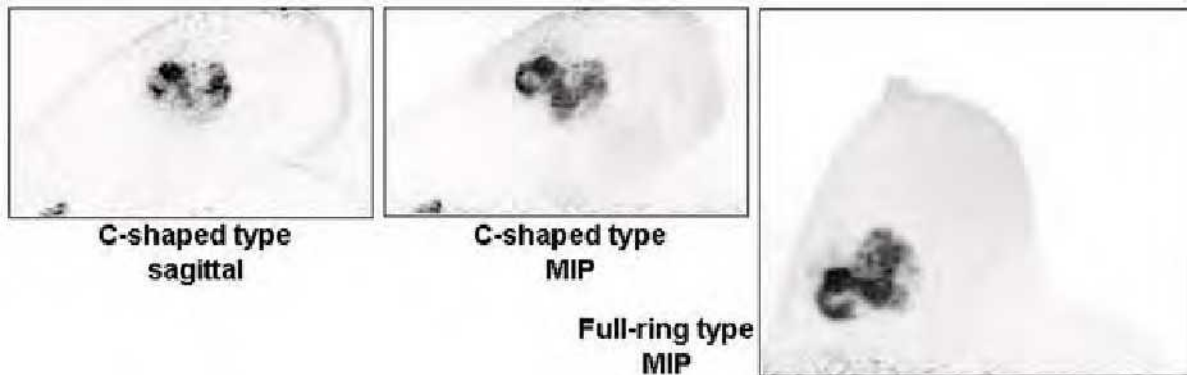
Presentation Number **0046**

Scientific Session 1: PET/SPECT/CT Instrumentation & Methodology

First Clinical Trials of Dedicated Breast PET Scanners

Junichi Ohi¹, **Keishi Kitamura**¹, **Masanobu Sato**¹, **Masafumi Furuta**¹, **Yuji Nakamoto**², **Shotaro Kanao**², **Koichi Ishizu**², **Kanae K. Miyake**², **Kaori Togashi**², ¹*Technology Research Laboratory, SHIMADZU Corporation, Kyoto, Japan;* ²*Diagnostic Imaging and Nuclear Medicine, Kyoto University, Kyoto, Japan. Contact e-mail: ohi@shimadzu.co.jp*

We have developed two prototypes (C-shaped type and Full-ring type) of dedicated breast PET scanners capable of high-resolution three-dimensional imaging throughout the entire field-of-view (FOV). The C-shaped type was designed so that the whole breast including axillary area at the chest-wall edge can be fully scanned. The full-ring type was developed to compare the performance with the C-shaped scanner, and to make image fusion with MR in a prone position. Compression of the breast is not required during the scanning. We present a basic performance of these scanners and demonstrate initial clinical images. Method: The detector consists of four-layer of 32×32 Lu1.8Gd0.2SiO5 (LGSO) crystal array, a light guide and a 64ch flat panel type photomultiplier tube (H8500), and the size of crystal element is 1.45 mm \times 1.45 mm \times 4.5 mm. The C-shaped type consists of 24 detector modules arranged in a 2-ring configuration with a diameter of 216 mm and an axial extent of 105 mm. The full-ring type consists of 36 detector modules arranged in a 3-ring configuration with a diameter of 183 mm and an axial extent of 155.5 mm. Acquisition data were reconstructed with a PSF (point spread function) corrected list-mode 3D-DRAMA (dynamic row-action maximum likelihood algorithm). Result: We evaluated the image quality of each prototype with an original breast-like phantom containing hot spheres and back ground area. The high resolution of approximately 1 mm FWHM allowed us to visualize a 3-mm diameter sphere having 4x background activity concentration, except for only near the open end of the C-shaped type. For clinical application, patients with known or suspected breast cancer underwent a whole body PET/CT scan at one hour post-injection of 18F-fluorodeoxyglucose, followed by breast scanning for 10 min using these dedicated breast scanners. All viable tumors were clearly depicted, although some lesions were out of scanning range due to the positioning problems. Conclusion: Preliminary clinical results demonstrate that the high-resolution breast PET scanners can provide functional imaging of small lesions. We are now assessing a clinical utility of two types of dedicated breast PET scanner through the patient clinical images comparing with other modalities, such as X-ray mammography, MRI, US and whole body PET/CT.



Presentation Number **0047**

Scientific Session 2: Multimodality Imaging of Small Animal Models in Oncology

Simultaneous Real-Time Color-Coded Imaging of Interacting Cancer-Stem and Non-Stem Cells

*Atsushi Suetsugu^{1,3}, Yosuke Osawa³, Masahito Nagaki³, Hisataka Moriwaki³, Michael Bouvet², **Robert M. Hoffman**^{1,2}, ¹AntiCancer, Inc., San Diego, CA, USA; ²Department of Surgery, University of California, San Diego, CA, USA; ³Department of Surgical Oncology, Gifu University Graduate School of Medicine, Gifu, Japan. Contact e-mail: all@anticancer.com*

We have developed color-coded simultaneous imaging of tumor growth, metastasis and drug resistance of co-implanted cancer stem cells (CSC) and non stem cancer cells (NSCC). In this study, CD 133+ Huh-7 human hepatoma cells were considered as liver cancer CSC, and CD133- Huh-7 cells were considered liver cancer NSCC. CD133+ cells were isolated by magnetic bead sorting. CSC were labeled with GFP and NSCC were labeled with RFP using retroviruses. The same number of GFP CSC and the RFP NSCC were mixed and co-cultured or injected subcutaneously or in the spleen of nude mice. CSC had higher proliferative potential compared with NSCC in vitro. Dual-color imaging demonstrated that CSC were more tumorigenic and more resistant to chemotherapy in vivo than NSCC. To compare the effect of CSC and NSCC on stromal cells or blood vessels in tumors, non-colored CSC or NSCC along with RFP stromal cells were implanted into nestin driven (ND)-GFP transgenic nude mice which express ND-GFP in nascent blood vessels. Extensive RFP-expressing stromal and GFP-expressing nascent blood vessels cells were imaged in the tumors formed from CSC. Tumors formed from NSCCs had less GFP-expressing nascent blood vessels and RFP-expressing stromal cells suggesting that more stromal cells and blood vessels were induced by CSC than NSCC. Thus, liver cancer CSC have more malignant characteristics such as higher proliferation, more resistance to chemotherapy, and induction of stromal cells and blood vessels compared with NSCC. Color-coded imaging of CSC and NSCC is a powerful tool to investigate the characteristics and roles of CSC and NSCC in tumor progression.

Presentation Number **0048**

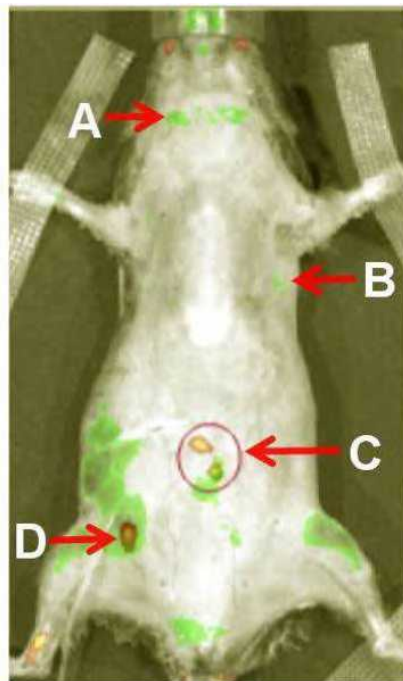
Scientific Session 2: Multimodality Imaging of Small Animal Models in Oncology

Metastatic Breast Carcinoma Cells are Attracted to the Distant Sites of Inflammation, Engraft and Develop Metastatic Lesions

Partick Gillespie, Juri G. Gelovani, Experimental Diagnostic Imaging, MD Anderson Cancer Center, Houston, TX, USA. Contact e-mail: patrick.gillespie@mdanderson.org

Background: Inflammation is part of tumor micro-environment and stimulates EMT, proliferation and survival of malignant cells, angiogenesis, cancer cell invasion and intravasation, followed by formation metastases in distant organs and tissues. Our hypothesis is that distant sites of inflammation and/or injury may produce chemoattractants, cytokines, growth factors, and suitable inflammatory microenvironment for engraftment of circulating metastatic tumor cells and development of a metastatic lesion. Therefore, we developed a transgenic mouse model for in vivo optical imaging of monocytes, mature macrophages, and granulocytes during injury and inflammation and to investigate their role during the development of tumor metastatic lesions in the remote sites of inflammation.

Methods: Mice, B6.129P2-Lyz2^{tm1(Cre)lf0}/J, express Cre recombinase from the endogenous Lyz2 locus. When crossed with a strain containing lox P site flanked sequence of interest, Cre-mediated recombination results in deletion of the targeted gene in monocytes, mature macrophages, and granulocytes. Mice, FVB.129S6(B6)-Gt(ROSA)26Sor^{tm1(Luc)Kael}/J, contain the firefly luciferase (luc) gene inserted into the Gt(ROSA)26Sor locus. When crossed with Cre recombinase-expressing strain, successful Cre-mediated excision produced Luc expression. 4T1-tdTomato Red Ultra cells (Caliper Life Science) 5 x 10⁵ cells were implanted orthotopically into the mammary fat pad of 8 week old female F1 progeny. BLI and fluorescence imaging was performed twice/week using IVIS200 (Caliper). BL images were acquired at 10 min post D-luciferin injection (160 mg/kg 100ul i.p.) followed by fluorescence imaging to co-localize Luc (macrophages) and dtTomato (tumor cells) reporter gene expression. **Results:** At 2 weeks post-injection, barely palpable tumor burdens were easily detected at the sites of injection. A small injury in the contralateral mammary fat pad was inflicted by incision. At 8 weeks, a contralateral mammary fat pad metastasis was detected and, by thirteen weeks, metastases to lymph nodes were detectable. In most cases the tdTomato signals co-localized with the Luc signals. **Conclusions:** We have developed a novel transgenic mouse model that allows for non-invasive monitoring of spatial and temporal dynamics of monocytes, mature macrophages, and granulocytes. Using this new transgenic mouse model, we demonstrated that metastatic murine breast carcinoma cells are recruited to the sites of inflammation and develop metastatic tumor lesions. The results of this study suggest that anti-inflammatory therapies should be explored for prevention and control of development and progression of metastases.



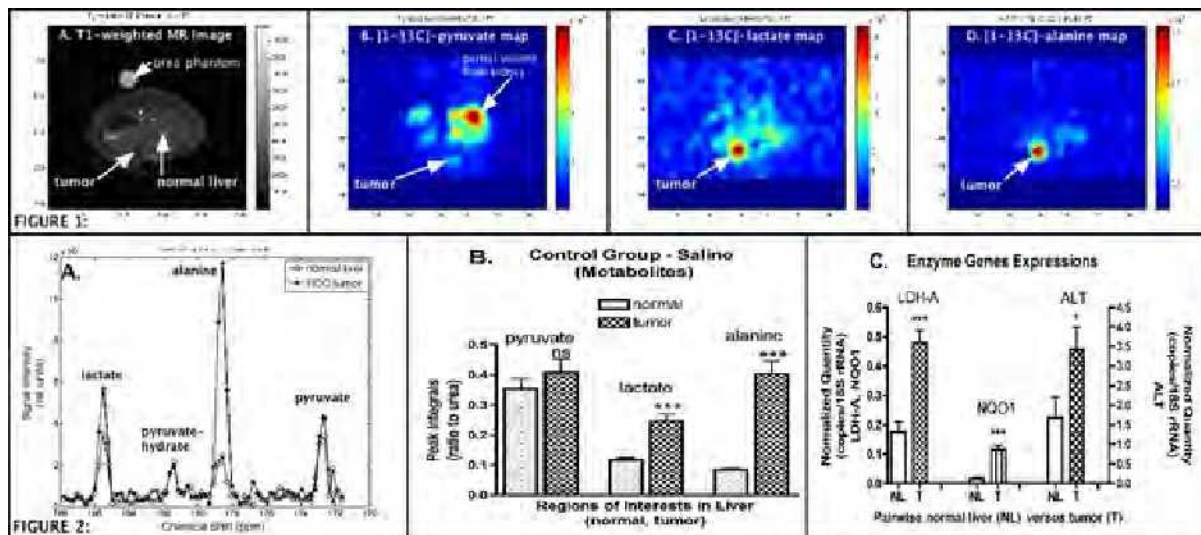
Bioluminescence (green) and fluorescence (red) imaging of co-localization of inflammatory cells (green) and metastatic tumor cells (red) in a novel transgenic mouse model. Cervical lymph nodes (A); axillary lymph node (B); co-localized tumor and inflammatory cells in the site of tumor implantation (C) and in the inguinal lymph node (D).

Presentation Number **0049**
 Scientific Session 2: Multimodality Imaging of Small Animal Models in Oncology

In Vivo Metabolic Imaging of Hyperpolarized [1-13C]-Pyruvate in Orthotopic Hepatocellular Carcinoma

Moses M. Darpolor¹, Yi-Fen Yen², Mei-Sze Chua³, Lei Xing⁴, Regina Clarke-Katzenberg¹, Wenfang Shi³, Dirk Mayer^{1,5}, Sonal Josan^{1,5}, Ralph E. Hurd², Adolf Pfefferbaum⁵, Lasitha Senadheera⁴, Samuel So³, Lawrence "Rusty" Hofmann¹, Gary Glazer¹, Daniel M. Spielman¹, ¹Radiology, Stanford University, Stanford, CA, USA; ²Global Applied Science Laboratory, GE Healthcare, Menlo Park, CA, USA; ³Surgery, Stanford University, Stanford, CA, USA; ⁴Radiation Oncology-Physics, Stanford University, Stanford, CA, USA; ⁵Neuroscience, SRI International, Menlo Park, CA, USA. Contact e-mail: mdarpolor@gmail.com

In the present study, we implemented a three-dimensional double-spin-echo echo-planar spectroscopic imaging (3D DSE-EPSI) pulse sequence to investigate potential hallmarks of cellular carbon metabolism in rat liver bearing orthotopic hepatocellular carcinoma (HCC). In addition, gene expression analysis was performed for lactate dehydrogenase A (LDH-A), NAD(P)H dehydrogenase quinone 1 (NQO1), and alanine transaminase (ALT) using quantitative real-time PCR. Hyperpolarized 13C MRS imaging experiments were performed on 7 rats in a 3.0 Tesla clinical system as previously described [1,2]. Metabolic maps of [1-13C]-pyruvate, [1-13C]-lactate, and [1-13C]-alanine of one of the rats are shown (Fig. 1A-D) color-coded with values ranging from minimum (blue) to maximum (red). Spectra from voxels in tumor and normal liver are shown (Fig. 2A). Difference in the means of normal liver and tumor (Fig. 2B) were statistically significant for [1-13C]-lactate ($p < 0.0001$) and [1-13C]-alanine ($p < 0.0001$), but not significant for [1-13C]-pyruvate ($p = 0.3428$). All three enzymes, LDH-A ($p < 0.0001$), NQO1 ($p < 0.0001$), and ALT ($p = 0.0173$) were significantly elevated in HCC tumors than normal liver tissues (Fig.2C). The data herein suggest that the conversion of exogenous [1-13C]-pyruvate to [1-13C]-lactate and [1-13C]-alanine is a characteristic marker of this HCC model in vivo. Coupled to this finding, the associated enzymes (LDH-A, NQO1, and ALT) are significantly elevated in this HCC model as compared to normal liver. Such molecular signatures of HCC should serve as an impetus to developing novel enzyme inhibitors as therapeutic agents. As such, hyperpolarized 13C 3D MRSI may be a diagnostic tool for detection of HCC and a potentially useful imaging tool as a surrogate marker or endpoint for drug activity targeting these specific enzymatic pathways. References: [1] Yen, Y-F et al MRM 2009; [2] Yen, Y-F et al NMR Biomed 2010.



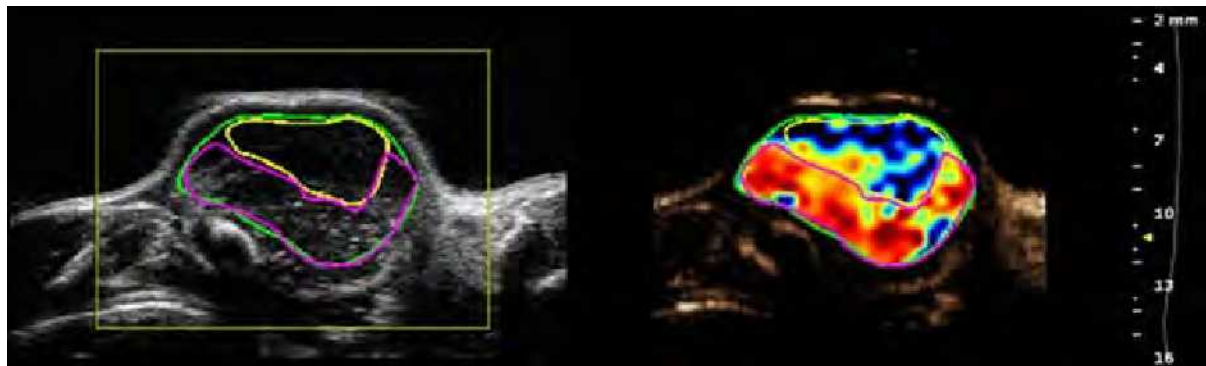
Presentation Number **0050**

Scientific Session 2: Multimodality Imaging of Small Animal Models in Oncology

Micro-ultrasound in Single and Combined Drug Studies of Cancer in Mice

F. Stuart Foster¹, **John Sun**¹, **Carolyn E. Cesta**¹, **Giulio Francia**¹, **Andrew Needles**², **Desmond Hirson**², **Robert S. Kerbel**¹, ¹*Medical Biophysics, Sunnybrook Health Sciences Centre and University of Toronto, Toronto, ON, Canada;* ²*VisualSonics Inc., Toronto, ON, Canada.* Contact e-mail: stuart.foster@sw.ca

The development of new targeted antiangiogenic therapeutics for cancer therapy has been complicated by acquired resistance effects that appear to reduce the expected clinical gains. Recent high profile papers have even suggested that antiangiogenic mono therapies may increase the aggressiveness of disease by accelerating metastasis and angiogenesis independent growth patterns. In this paper, tumor growth in the mouse is studied using micro-ultrasound to investigate the differences between mono and combination therapy with an emphasis on functional flow biomarkers. Imaging was performed with a VisualSonics 2100 scanner using Micromarker contrast agents as described previously. An orthotopic breast tumor model 231/LM2-4LUC+ was studied with 2 receptor tyrosine kinase inhibitors (RTKI's) alone or in combination with low dose "metronomic" chemotherapy (cyclophosphamide, CTX). Treatment was performed daily over a 1 week interval while imaging was performed before the start of treatment, at the end of treatment, and 1 and 2 weeks post treatment. Imaging data were analyzed using a new parametric mode of image display and analysis developed in collaboration with Bracco (Vevo CQ, see figure 1). The parametric maps of contrast wash-in and wash-out of US contrast graphically demonstrate tumor heterogeneity in terms of relative perfusion and blood volume. One of the RTKI mono therapies showed a significant functional "rebound" indicative of the resistance phenotype (n = 8 treated, 8 control). Combined RTKI and metronomic chemotherapy also exhibited a significant additive effect. While CTX treatment alone showed significant reductions in both blood volume and overall perfusion, a second metronomic study with a novel chemotherapeutic agent showed significant increases in tumor blood flow even in the presence of marked tumor shrinkage (n= 5 treated, 5 control). The results show the ability of contrast ultrasound to monitor the functional microvascular status of tumors in mono and combination therapies. Further studies are warranted to better understand the complex biology associated with resistance mechanisms in angiogenesis and to mitigate these effects in combination strategies.



Micro-ultrasound B-scan image (left) and parametric blood volume image (right) of tumor.

Presentation Number **0051**

Scientific Session 2: Multimodality Imaging of Small Animal Models in Oncology

Expression of LAT1 and Analysis of Iodine-123-Methyltyrosine Tumor Uptake in a Pancreatic Xenotransplantation Model Using Fused High-Resolution-Micro-SPECT-MRI

Corinna von Forstner², Maaz Zuhayra², Ole Ammerpoh³, Yi Zhao², Sanjay Tiwari¹, Olav Jansen⁴, Eberhard Henze², Jan-Hendrik Egberts⁵, **Holger Kalthoff**¹, ¹Molecular Oncology, Institute for Experimental Cancer Research, Kiel, Germany; ²Nuclear Medicine, University Hospital of Schleswig-Holstein, Kiel, Germany; ³Human Genetics, University Hospital of Schleswig-Holstein, Kiel, Germany; ⁴Neuroradiology, University Hospital of Schleswig-Holstein, Kiel, Germany; ⁵General Surgery and Thoracic Surgery, University Hospital of Schleswig-Holstein, Kiel, Germany. Contact e-mail: hkalthoff@email.uni-kiel.de

Aim: Pancreatic cancer generally has a poor outcome, which is due to the fact that it is most frequently only recognized at an advanced stage of disease. Imaging with ¹⁸F-FDG -PET has shown to be useful, however the specificity in discriminating pancreatitis is limited and moreover it is not widely available. Therefore substitution with a more commonly used tracer in nuclear medicine like iodine-123-Methyltyrosine (123I-IMT) for imaging of pancreatic cancer would be helpful. The aim of the underlying study was to examine tumor uptake of 123I-IMT in a fused high-resolution- micro-SPECT-(Hi-SPECT)-MRI in xenotransplantation models of pancreatic carcinoma in mice harboring subcutaneous and orthotopic tumors. To further elucidate the utility of (123I-IMT) in pancreatic tumor imaging gene expression level of L amino acid transport system 1 (LAT1) was analysed and correlated with tumor uptake. **Methods:** 123I-IMT was synthesized in accordance with the method described by Meier. The pancreatic cancer cell line Colo357 was transplanted orthotopically (n=4) and subcutaneously (n=4) in SCID-beige-mice which received 15 MBq of 123I-IMT for imaging. Two hours after injection combined imaging was performed with Hi-SPECT (Scivis, Siemens-ECAM) and a 3T MR scanner using a dedicated mouse coil. Tumor uptake analysis was based on ROI interpretation using a Tumor/Background ratio (T/B) with adjacent visceral region designated to be background. We also compared the tracer uptake to the gene expression profile of the LAT1. **Results:** In all of the eight mice a significantly higher uptake into tumor tissue could be elicited. After subcutaneous xenotransplantation the tumor to background ratio (T/B) was 10.26 (2.88-17.95) and after orthotopic xenotransplantation it was 8.51 (2.57-16.61). Fusion with MRI enabled good correlation of the anatomical site of the tumor with 123I-IMT uptake. In Colo357 cells LAT1 expression was increased compared to other PDAC cell lines or non malignant controls. **Conclusion:** A high 123I-IMT uptake in pancreatic tumor was shown in all eight mice. Accordingly, the cell line Colo357 showed an increased LAT1 expression. If these findings are also applicable to tumors derived from other human pancreatic cancer cells, imaging with IMT would be an additional option for the diagnosis of pancreatic cancer. Since amino acids play a minor role in metabolism of inflammatory cells, the potential for application of 123I-IMT to distinguish pancreatic tumor from inflammatory pancreatitis warrants further investigation.

Presentation Number **0052**

Scientific Session 2: Multimodality Imaging of Small Animal Models in Oncology

Real-time Multispectral Near Infrared Fluorescence (NIRF) Intra-operative Imaging in Cancer by Using an $\alpha v\beta 3$ - Integrin Targeted Fluorescence Agent

Niels J. Harlaar^{1,2}, Wendy Kelder², Athanasios Sarantopoulos¹, Joost Bart⁴, Gooitzen M. van Dam^{2,3}, George Themelis¹, Vasilis Ntziachristos¹, ¹Institute for Medical and Biological Imaging, Technische Universität München and Helmholtz Zentrum München, Munich, Germany; ²Surgery, University Medical Center Groningen, Groningen, Netherlands; ³BioOptical Imaging Center Groningen, University Medical Center Groningen, Groningen, Netherlands; ⁴Pathology, University Medical Center Groningen, Groningen, Netherlands. Contact e-mail: n.j.harlaar@hotmail.com

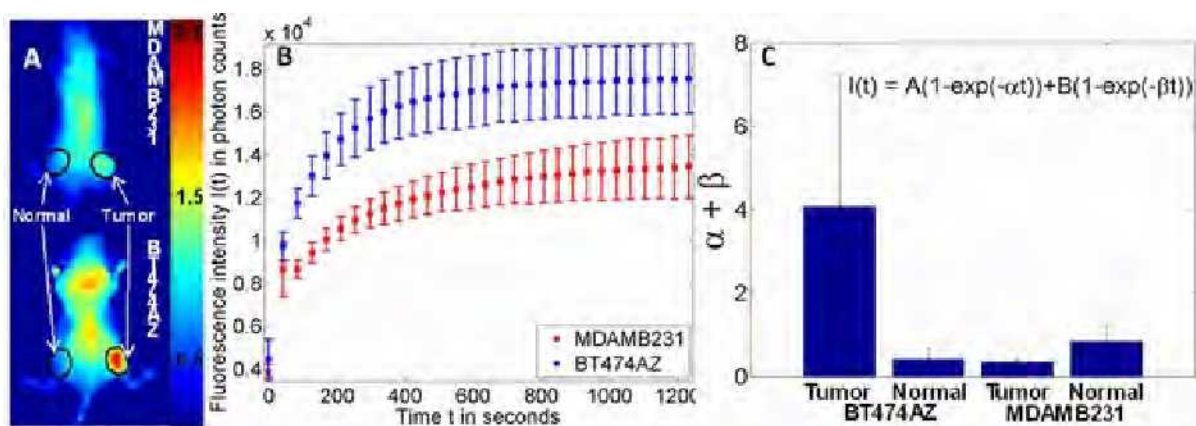
Introduction: Surgical excision of cancer is often confronted with difficulties in the identification of cancer spread and the accurate delineation of tumor margins. Currently, the assessment of tumor is done by post-operative pathology or intraoperative frozen sectioning which is less reliable and time consuming. Fluorescence imaging is a natural modality for intra-operative use, since it relates directly to the surgeon's vision and offers attractive characteristics such as high-resolution, sensitivity and portability. A targeted fluorescent probe which is tumor specific can lead to significant improvements in surgical procedures and outcome. We describe the use of an $\alpha v\beta 3$ integrin targeted probe for intra-operative tumor detection with multispectral near-infrared fluorescence imaging. **Methods:** Mice bearing xenograft human ovarian and breast cancer were injected with an $\alpha v\beta 3$ -integrin receptor targeted fluorescent probe and in vivo visualized using a novel real-time multi-spectral fluorescence imaging system. Histopathology results, scored by a pathologist blinded for the imaging results, were used to validate the in vivo findings and to estimate the sensitivity and specificity of the imaging system and targeted probe. **Results:** Fluorescence imaging successfully guided radical tumor excision by detecting small tumor residuals, which occasionally were missed by the surgeon. Tumor tissue exhibited a Target to Background Ratio (TBR) of ~4.0 which was significantly higher compared to white-light (WL) images representing the visual contrast ($p < 0,01$). Histopathology (n=58 samples) confirmed the capability of the method to identify intra-abdominal tumor deposits with high specificity (100%) and sensitivity (95%). **Conclusion:** Real-time multispectral near-infrared fluorescence imaging using an $\alpha v\beta 3$ integrin targeted probe provides detection of tumor tissue intra-operatively with high specificity and sensitivity. It improves diagnostic accuracy compared to visual inspection alone. This approach that is based on real time feedback to the surgeon in the theatre, warrants further (pre-) clinical development to eventually accomplish clinical application in patients with ovarian cancer and breast cancer.

Presentation Number **0053**
 Scientific Session 3: Probes for Imaging Breast and Brain Tumors

Dynamic Pharmacokinetic Analysis of Multimodal Nanoplatforms for Breast Cancer Theranostics

Marc Bartels¹, Wenxue Chen^{1,2}, Rizia Bardhan³, Rachel Schiff⁴, Naomi J. Halas^{3,5}, **Amit Joshi**¹, ¹Department of Radiology, Baylor College of Medicine, Houston, TX, USA; ²Department of Obstetric & Gynecology, Fourth Hospital of Hebei Medical University/Hebei Province Tumor Hospital, Shijiazhuang, China; ³Department of Chemistry, Rice University, Houston, TX, USA; ⁴Lester and Sue Smith Breast Center, Baylor College of Medicine, Houston, TX, USA; ⁵Department of Electrical and Computer Engineering, Rice University, Houston, TX, USA. Contact e-mail: marc.bart@gmx.de

The understanding of pharmacokinetics of emerging nanomedicine agents is an essential step towards FDA clearance for personalized cancer theranostics. We demonstrate that dynamic NIR imaging with sensitive instrumentation capable of sub-second temporal resolution, coupled with compartmental pharmacokinetic modeling can provide information about relative performance of EPR based passive tumor targeting vs antibody mediated active targeting for a new class of magnetofluorescent gold nanostructures developed for breast cancer theranostics. **METHODS:** Silica core gold nanoshells (GNS) resonant at 810 nm were encapsulated in silica epilayers doped with super-paramagnetic iron oxide (SPIO) and NIR dye Indocyanine Green, and conjugated with antibodies targeting HER2 receptors resulting in a superbright and stable targeted NIR/MR probe with photothermal action. HER2[±] xenografts were created with BT474AZ and MDAMB231 cell lines, respectively. Approximately 1 million nanoshells in 200 μ l were injected into tail vein under NIR image guidance. Mice were imaged with 800 ms exposure continuously for 20 min by a homebuilt EMCCD system and NIR laser diode based illumination with peak excitation/emission (785/830) nm. A three-compartmental model was fitted to spatially averaged tumor and normal ROI intensities in both sets of mice (Fig. B). The sum of constants $\alpha + \beta$ quantifying the uptake rate into tumor compartment was estimated using non-linear Levenberg-Marquard regression (Fig. C). The uptake in HER2⁻ negative mice was due to EPR effect, while the uptake in HER2⁺ mice was due to antibody binding in addition to EPR. **RESULTS:** HER2 overexpressing BT474AZ had a ~30% greater uptake of the contrast agent than MDAMB231 with low HER2 expression (Fig. B). The sum of uptake rate constants $\alpha + \beta$ was 4 times higher for HER2⁺ tumor indicating the relative impact of antibody based targeting over EPR (Fig. C). The image contrast between the two tumors sustained with time and peaked at 4 h (Fig. A) at ~50%.

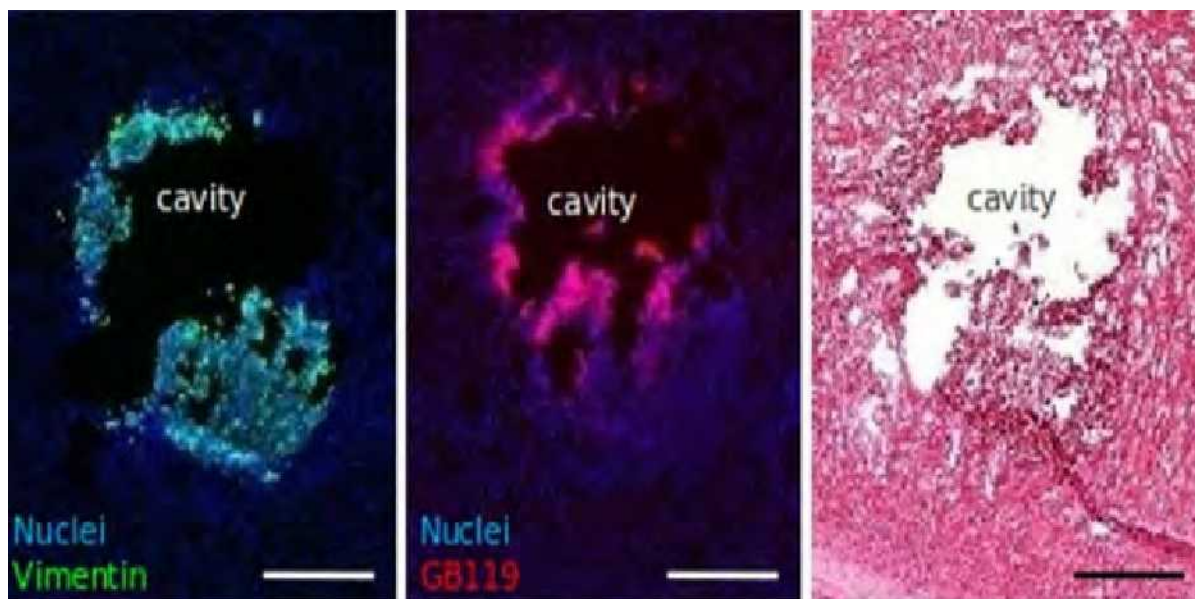


Presentation Number **0054**
 Scientific Session 3: Probes for Imaging Breast and Brain Tumors

Topical Application of Activity Based Probes for Real-time Identification of Infiltrating Brain Tumor Cells

Nicolas Salem¹, Jennifer L. Cutter¹, Jing Wang¹, Andrew E. Sloan³, Mark Schluchter⁴, Galia Blum⁵, Matthew Bogoy^{5,6}, James Basilion^{1,2}, ¹Radiology, Case Western Reserve University, Cleveland, OH, USA; ²Biomedical Engineering, Case Western Reserve University, Cleveland, OH, USA; ³Neurological Surgery, University Hospitals Case Medical Center, Cleveland, OH, USA; ⁴Epidemiology and Biostatistics, Case Western Reserve University, Cleveland, OH, USA; ⁵Pathology, Stanford University, Stanford, CA, USA; ⁶Microbiology and Immunology, Stanford University, Stanford, CA, USA. Contact e-mail: nxs90@case.edu

Several investigators have shown the utility of systemically delivered optical imaging probes to image tumor proteases in small animal models of cancer. Here we demonstrate an innovative method for real-time imaging of brain tumor associated cathepsin proteases during surgery. Specifically, we show that topically applied optical imaging probes rapidly differentiate between normal and disease-associated tissues in athymic nude mice with Gli36Δ5 xenograft tumors. In contrast to systemic delivery of optical imaging probes that label tumors uniformly over time, topical probe application results in robust probe activation that is detectable as early as 5 minutes after application and identifies infiltrative cells that are missed by systemic agents such as 5-ALA. This technique is currently being applied in animal models of CD133⁺ glioma stem cells-derived xenograft brain tumors. This technology provides a means for real-time intraoperative visualization of tumor margins and infiltrating cells and has potential use for directed surgical excision of tumor tissues. Furthermore, this technology is not limited to brain tumors and could find use in surgical resections for any tumors having differential regulation of cysteine cathepsin proteases.



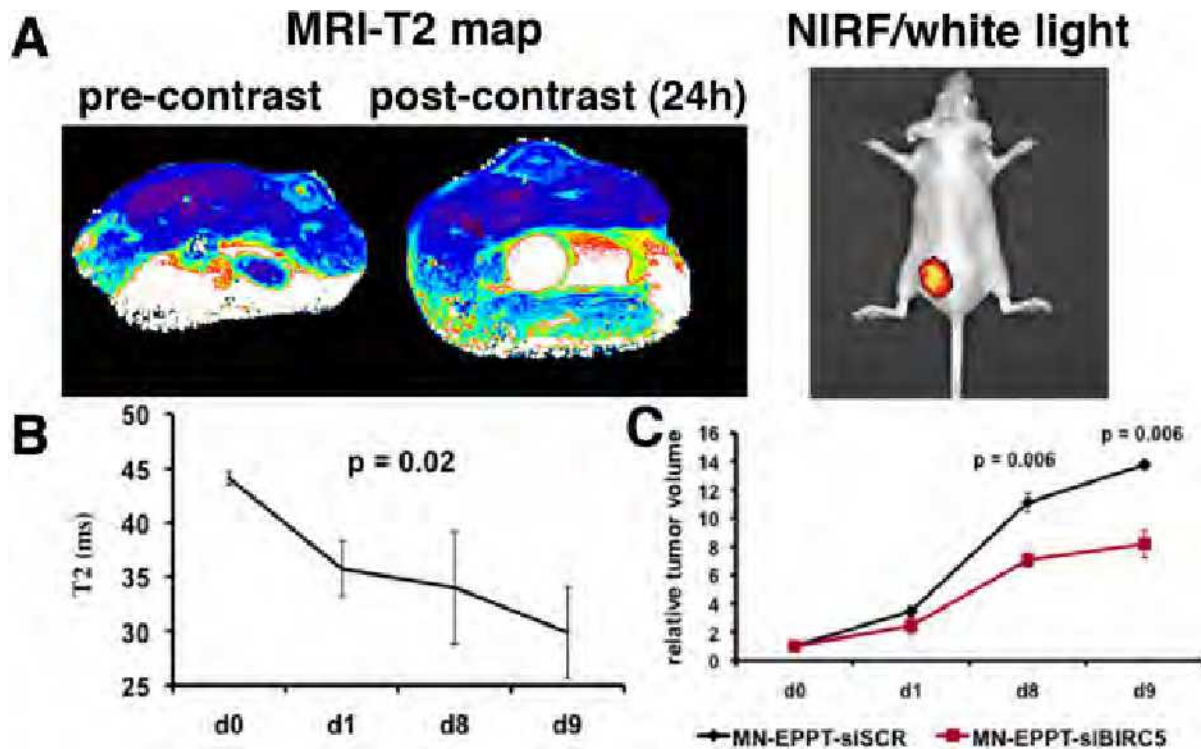
A Gli36Δ5 xenograft tumor was partially resected before applying the cysteine cathepsin-activated optical probe (GB119). After imaging, the brain tissues were processed for immunohistochemistry. (Left) Human cancer cells remaining around the surgical cavity are labeled with vimentin and cell nuclei, with DAPI (Center) Cancer-associated tissues are labeled by GB119 (Red). (Right) Corresponding H&E section.

Presentation Number **0055**
 Scientific Session 3: Probes for Imaging Breast and Brain Tumors

Target-specific Imaging and Delivery of siRNA to Breast Tumors

Mohanraja Kumar, Mehmet V. Yigit, **Anna Moore**, Zdravka Medarova, Radiology, Massachusetts General Hospital, Charlestown, MA, USA. Contact e-mail: amoores@helix.mgh.harvard.edu

RNA interference (RNAi) is an emerging form of molecular therapy characterized by both a broad applicability and exquisite specificity. The main impediment to the application of RNAi *in vivo* is the difficulty in achieving efficient delivery of the siRNA to target organs. In addition, it is very important to monitor the bioavailability of the siRNA following *in vivo* administration as well as the associated therapeutic effect, since this will help develop more successful delivery strategies. In this regard, non-invasive imaging plays an important role, as a technology that permits the *in vivo* monitoring of siRNA delivery. Here, we describe the application of a dual-purpose nanoparticle probe for the concurrent tumor-antigen targeted imaging and delivery of siRNA to tumors. The probe (MN-EPPT-siBIRC5) consists of magnetic nanoparticles (MN for magnetic resonance imaging, MRI), labeled with the near-infrared dye Cy5.5 (for near infrared optical imaging, NIRF) and conjugated to a peptide (EPPT), which specifically targets the tumor-specific antigen, uMUC-1, as well as to siRNA against the anti-apoptotic gene, birc5, which encodes Survivin. Flow cytometry demonstrated that 97.8±0.8 % of tumor cells incubated with the probe *in vitro* took up the complex. This resulted in significant down-regulation of birc5 ($p = 0.004$). *In vivo*, intravenous injection of the probe into tumor-bearing animals resulted in a significant shortening of the T2 relaxation times of the tumors and a concomitant NIR fluorescent enhancement (Fig. 1A). Serial assessment of T2 relaxation times revealed a continued accumulation of the probe in tumor tissue throughout the course of treatment (Fig. 1B). Probe uptake into tumor cells after injection was confirmed by *ex vivo* microscopy. This resulted in a significant reduction in tumor growth rate (Fig. 1C). Our studies illustrate the value of iron oxide nanoparticles as a backbone for combined imaging and siRNA therapy probes.



Presentation Number **0056**

Scientific Session 3: Probes for Imaging Breast and Brain Tumors

Non-invasive Detection of Breast Cancer in Lymph Nodes

Narges K. Tafreshi¹, Kellsey Bishop¹, Steven Enkemann², Dominique Abrahams³, Monica Torres³, Robert Gillies¹, Stephen R. Grobmyer⁴, **David L. Morse¹**, ¹Molecular and Functional Imaging, H. Lee Moffitt Cancer Center & Research Institute, Tampa, FL, USA; ²Microarray Core, H. Lee Moffitt Cancer Center & Research Institute, Tampa, FL, USA; ³Comparative Medicine, University of South Florida, Tampa, FL, USA; ⁴Surgery, University of Florida, Gainesville, FL, USA. Contact e-mail: david.morse@moffitt.org

Lymph node (LN) status is the most important prognostic factor in breast cancer and LNs are routinely excised for evaluation. Our aim is to develop an imaging platform for non-invasive LN assessment which could eliminate the need for surgery in many patients and aid in treatment planning. Mammaglobin is expressed in malignant breast tissues and is not expressed in normal LN or skin, as determined by DNA and tissue microarray. In this work, we have developed a mammaglobin targeted imaging probe. Three monoclonal antibodies (mAbs) were compared by immunostaining of cells, tissues and Western analysis. One highly specific mAb was conjugated to a near-infrared dye (VivoTag 680, VisEn) and intravenously injected into nude mice bearing bilateral mammary fat pad (MFP) tumors of mammaglobin-positive (ZR-75.1) and -negative (MDA-mb-231) cells. In vivo fluorescence imaging showed agent was retained only in ZR-75.1 tumors. Selectivity for positive LNs was determined by implanting ZR-75.1/luc cells in the axillary LN using ultrasound guidance (Fig. 1A) and monitoring by bioluminescence (1B). Labeled mAb was delivered by MFP injection and traversed to LN (1C). Label was retained in mammaglobin-positive LNs (1D) long after clearance from the MFP and negative LNs. To identify more targets, 3800 cell surface genes were curated from Gene Bank and used to filter DNA microarray data from 304 breast tumors (38 node positive), 111 normal breast tissues, 15 LNs, and 189 samples from 6 unaffected organ sites in the area surrounding the LNs and involved in clearance and toxicity. Of all genes, carbonic anhydrases -9 and -12 were seen to be highly expressed in breast and LN-positive cancers but not in the normal tissues. Immunohistochemistry was performed on 50 normal breast tissues, 50 DCIS, 50 IDCs without metastasis, 50 IDCs with metastasis and 50 LN macrometastases. Nearly all (95%) of LN metastases expressed either CA-9 or -12. Thus, these CAs are valid targets for imaging of LN status for breast cancer.

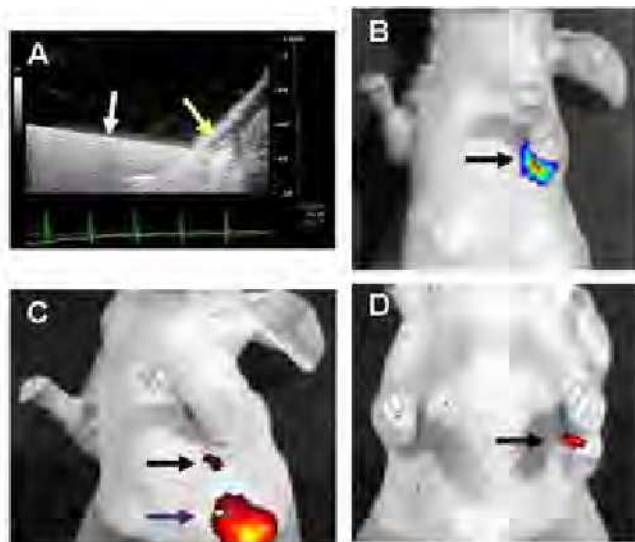


Figure 1. A) Ultrasound guided injection of cells into axillary node (yellow arrow). Needle is indicated by white arrow. B) Bioluminescence imaging of luciferase expressing cells in axillary node. C) Fluorescence image of agent injection site (blue arrow) and agent associated with node (black arrow) three days after injection. D) After 7 days, agent is retained in axillary node bearing mammaglobin expressing cells, but has cleared from injection site and other nodes.

Presentation Number **0057**
Scientific Session 3: Probes for Imaging Breast and Brain Tumors

In Vivo Imaging of Necrotic Breast Tumors in an Animal Model Using Novel Bacteriochlorophyll-RGD Derivatives

Liat Goldshaid¹, Yoram Salomon², Avigdor J. Scherz¹, ¹Plant Sciences, Weizmann Institute of Science, Rehovot, Israel; ²Biological Regulation, Weizmann Institute of Science, Rehovot, Israel. Contact e-mail: liat.goldshaid@weizmann.ac.il

Introduction: Necrosis at the tumor center is a common feature of aggressive cancers associated with poor prognosis. Selective accumulation of contrast agents in such tumors is imperative for their in vivo imaging and treatment strategy. Here we achieve this goal by covalent binding of bacteriochlorophyll-derivatives (Bchl-Ds) developed as photodynamic agents and fluorescent probes in our lab, to c(RGDfK) molecules. Non-covalent association of the Bchl-D moiety to serum albumin (SA) and ligation of the c(RGDfK) moiety to $\alpha V\beta 3$ integrin receptors, over-expressed in the tumor tissue, synergistically drive their preferential accumulation and over-days retention in necrotic tumors of the breast and other cancers. Methods: STL-6014, a c(RGDfK)-Bchl-D representative, was i.v. injected to CD-1, nude female mice orthotopically grafted (mammary pad) with necrotic or non-necrotic human MDA-MB-231-RFP breast tumors. The intrinsic and transfected fluorescence of the Bchl-Ds and RFP respectively, were monitored over 9 days after treatment by IVIS[®] imaging of whole body and excised tumor/tissue samples derived thereof. Complementary experiments included competitive inhibition of STL-6014 uptake by free c(RGDfK), as well as comparative pharmacokinetics of non-conjugated Bchl-D (STL-7012) and of two human SA (HSA) conjugates (HSA-STL-6014 and HSA-STL-7012). Tumor necrosis volumes were calculated and validated by histological approaches and correlated with tumor fluorescence in whole body fluorescence images. Computations were subjected to statistical analyses. Results: STL-6014, HSA-STL-7012 and HSA-STL-6014, selectively accumulated at similar rates in viable tumor regions over the first 8 h post administration. They then migrated into the necrotic tumor domain and presented tumor half lifetimes ($T_{1/2}$) in the range of days where $T_{1/2}$ for HSA-STL-6014 > STL-6014 > HSA-STL-7012. No accumulation of STL-7012 was observed. Pre-injection of c(RGDfK) excess, prevented the uptake of STL-6014 in non-necrotic tumors. Conclusion: Non-covalent association with SA in the circulation drives the preferential uptake of the c(RGDfK)-Bchl-D by the tumor tissue through the enhanced permeability and retention (EPR) effect, while ligation to the integrin receptors in the necrotic tumors results in their prolonged retention. Chelation of metal atoms in the central core of Bchl-D that was recently accomplished in our lab should enable other imaging applications such as MRI (Mn,Gd) and PET-scan (⁶⁴Cu). Supported in part by Steba Biotech, France, and The Susan Komen Foundation For The Cure.

Presentation Number **0058**

Scientific Session 3: Probes for Imaging Breast and Brain Tumors

Early Detection of Brain Metastasis Using Novel MRI Contrast Agent Targeting VCAM-1

Sebastien Serres¹, **Lukxmi Balathasan**¹, **Alastair Hamilton**¹, **Thomas Weissensteiner**¹, **Shawn Carbonell**¹, **Martina McAteer**², **Andrew Jefferson**², **Robin Choudhury**², **Daniel Anthony**³, **Ruth Muschel**¹, **Nicola Sibson**¹, ¹Gray Institute for Radiation, Oncology and Biology, University of Oxford, Oxford, United Kingdom; ²Department of Cardiovascular Medicine, University of Oxford, Oxford, United Kingdom; ³Department of Pharmacology, University of Oxford, Oxford, United Kingdom. Contact e-mail: sebastien.serres@rob.ox.ac.uk

Background: Contrast-enhanced magnetic resonance imaging (MRI) is currently the most sensitive method for brain metastasis detection, but relies on blood-brain barrier (BBB) compromise and, consequently, is sensitive to late-stage metastases only. We have developed an MRI-detectable contrast agent targeted specifically at the endothelial adhesion molecule VCAM-1 (VCAM-MPIO) and have shown that this agent enables detection of endothelial activation early in brain pathology [1]. Based on our recent findings that brain metastases develop in close association with existing brain vessels [2], we hypothesised that VCAM-1 is upregulated during metastasis development and that our VCAM-MPIO may enable early detection of brain metastases. Methods: Balb/c mice were injected intracardially with 100000 4T1 cells, a metastasising murine mammary carcinoma line. Purified monoclonal rat antibodies specific to mouse VCAM-1 (clone M/K2, Cambridge Bioscience) or control IgG-1 (clone Lo-DNP-1, Serotec) were conjugated to myOne tosylactivated MPIO (1- μ m diameter; iron content 26%; Invitrogen) as described previously [1]. Either 5, 10 and 13 days after 4T1 cell injection animals were anaesthetised and injected intravenously with either VCAM-MPIO or control IgG-MPIO. After 1h animals underwent MRI at 7T and a T2*-weighted 3D gradient-echo dataset was acquired. Post-gadolinium T1-weighted images were acquired to assess BBB integrity. T2*-weighted images were processed into a 3D isotropic dataset and the brain was manually masked to exclude extracerebral structures. Quantification of VCAM-MPIO binding (defined as focal hypointensities) was done using Image pro software and volumes are expressed in μ L. Results: Immunohistochemically, upregulation of VCAM-1 was co-localised to brain metastases. MRI revealed focal areas of signal hypointensity throughout the brain, indicating VCAM-MPIO accumulation. Also we demonstrated co-localisation of the MRI hypointensities with metastases. Quantitatively, the volume of hypointensities in the VCAM-MPIO injected animals was greater than in IgG-MPIO-injected animals (i.e. background) and was increasing with disease progression. None of the animals showed BBB breakdown. Conclusion: Upregulation of VCAM-1 during metastasis development enables earlier detection of metastases in the brain, using our novel VCAM-1-targeted contrast agent, than is currently possible clinically. Early detection of brain metastases may significantly alter patient prognosis. [1]. McAteer MA et al. Nat Med. 2007;13:1253-1258 [2]. Carbonell WS et al. PLoS One. 2009;4:e5857

Presentation Number **0059**
Scientific Session 4: Alzheimers and Parkinsons

In Vitro and In Vivo Testing of Curcumin Analogue as “Turn-on” Fluorescent Probe for Soluble and Insoluble Amyloid Beta Species

Chongzhao Ran, Anna Moore, Radiology, Massachusetts General Hospital, Charlestown, MA, USA. Contact e-mail: cran@nmr.mgh.harvard.edu

One of the major hurdles in the diagnosis of presymptomatic Alzheimer's disease (AD) is the lack of imaging probes capable of detecting early stage biomarkers. Amyloid β ($A\beta$) species, which include soluble monomers, dimers, oligomers, and insoluble fibrils and plaques, are widely believed to be important biomarkers for AD. Most of advances in the imaging of AD lesion have focused on the detection of insoluble fibrils and plaques, species present in the symptomatic stage. Our approach focuses on developing imaging probes for the detection of soluble $A\beta$ species, the likely early stage biomarkers, and may enable earlier AD detection. Here we report that the curcumin derivative, CRANAD-3, is able to detect a variety of $A\beta$ species, ranging from insoluble plaques to soluble monomers and even the core fragment (KLVFF) of $A\beta_{40/42}$. We also show that amino acid K16 of the $A\beta$ peptide is the hot spot for CRANAD-3 binding, and the diketone moiety of curcumin and its derivatives is crucial for the interaction. Two-photon imaging results demonstrate that CRANAD-3 is specific to $A\beta$ plaques and able to detect cerebral amyloid angiopathy (CAA) in vivo. Remarkably, in vivo near-infrared imaging (NIR) shows that CRANAD-3 is capable of differentiating between transgenic AD mice and wild-type. Furthermore, CRANAD-3 detects $A\beta$ species in young animals at the early stages of the disease. These data show the potential for CRANAD-3 to monitor the full course of amyloidosis in AD. We believe that CRANAD-3, along with its analogues modified to include ^{18}F or ^{11}C , will be valuable tools for early, presymptomatic diagnosis of AD and the assessment of AD therapies.

Presentation Number **0060**
Scientific Session 4: Alzheimers and Parkinsons

Molecular Imaging of Cell Death in Experimental Parkinson's Disease with a Novel Apoptosis-targeting Peptide

Kai Wang¹, **Min-Jeong Lee**², **Bodhraj Acharya**¹, **In-San Kim**¹, **Hyung-Soo Han**², **Byung-Heon Lee**¹, ¹*Department of Biochemistry, School of Medicine, Kyungpook National University, Korea, Daegu, Republic of Korea;* ²*Physiology, School of Medicine, Kyungpook National University, Daegu, Republic of Korea. Contact e-mail: kiki572125@hotmail.com*

During the development of Parkinson's disease (PD), the second most common human neurodegenerative disorder after Alzheimer's disease, apoptosis plays an important role in the selective loss of dopaminergic neurons in the substantia nigra pars compacta (SNC). Noninvasive imaging of apoptosis therefore may help in the diagnosis of the disorder as well as in the prognosis and assessment of treatment response. Using phage display technology, we have previously identified a 6-mer peptide ligand that targets apoptotic cell and named it ApoPep-1 (Apoptosis-targeting Peptide-1). When injected intravenously into Parkinson's disease mouse induced by injection of MPTP (1-methyl-4-phenyl-1,2,3,6-tetrahydropyridine), fluorescein-conjugated ApoPep-1 selectively targeted to apoptotic cells at SNC and substantia nigra pars reticulata (SNR) area in mouse brain, which was demonstrated by tyrosine hydroxylase and caspase-3 antibody staining. To image apoptosis in vivo in PD model, Cy7.5 labeled ApoPep-1 was injected intravenously to 1 - 3 week-old mice after MPTP treatment. Peptides were allowed to circulate and optical imaging was taken at 2 h. In contrast to control mouse or control peptide group, Cy7.5-ApoPep-1 in PD group showed significant signals from brain, interestingly, the signal was increasing from 1 - 3 weeks of MPTP treatment. Similar results were observed by ex vivo imaging. These results suggest that ApoPep-1 is a useful probe for imaging apoptosis and diagnosis of Parkinson's diseases as well as the assessment of prognosis and treatment response.

Presentation Number **0061**
Scientific Session 4: Alzheimers and Parkinsons

Non-invasive Detection of Amyloid Plaques by Combined Near-infrared Optical and PET/MR Imaging Using an Oxazine Derivative Probe and [¹¹C]PIB in Transgenic Mouse Models of Alzheimers Disease

Florian C. Maier¹, Hans F. Wehr¹, Andreas Schmid¹, Jörg Odenthal², Gerald Reischl³, Stefan Wiehr¹, Julia G. Mannheim¹, Detlef Stiller⁴, Bernd J. Pichler¹, ¹Department of Radiology, Laboratory for Preclinical Imaging and Imaging Technology of the Werner Siemens-Foundation, Tuebingen, Germany; ²Cell Biology of Neurological Disorders, Hertie Institute for Clinical Brain Research, Tuebingen, Germany; ³Department of Radiology, Radiopharmacy, Tuebingen, Germany; ⁴Drug Discovery Support, Boehringer Ingelheim Pharma GmbH & Co. KG, Ingelheim, Germany. Contact e-mail: florian.maier@med.uni-tuebingen.de

Current biomarkers for imaging amyloid plaque deposition are not yet fully understood, thus our aim was the quantification of amyloid plaques in different mouse models of Alzheimers Disease using AOI987 - a near infrared optical imaging agent - and [¹¹C]PIB. APPPS1 tg mice and Tg2576 mice with respective littermate controls were i.v. injected with 7.6 ± 2.8 MBq [¹¹C]PIB (specific activity > 50 GBq/ μ mol) and with 0.1 mg/kg AOI987. Mice were anesthetised with 1.5% isofluran in 100% oxygen and the body temperature was kept constant at 37 ± 0.1 °C during scans. Dynamic small animal PET scans were performed for 1h p.i. while static optical imaging scans were acquired 30, 60 and 120min p.i. In addition, 3D MR images were acquired. Relative fluorescence intensities (Irel) and specific binding ($B_{sp} = \frac{Irel(tg) - Irel(co)}{Irel(co)}$) of AOI987 was determined for the entire forebrain. The co-registered PET/MR images were analysed using frontal cortex and hippocampus as target regions and the cerebellum as internal reference. The obtained time activity curves were processed with the Logan Plot and the simplified reference tissue model (SRTM). AOI987 showed significant binding 120min p.i. in 12month old transgenic APPPS1 mice ($B_{sp}^{**} = 0.12 \pm 0.02$), while there was no specific binding observable in 2month old APPPS1 mice ($B_{sp}^{**} = 0.01 \pm 0.02$). In addition, the detection of transgenic animals was already possible at the age of 5 months ($B_{sp}^* = 0.03 \pm 0.03$, $n=4$, $*p < 0.05$, $**p < 0.01$). In 1.5months old APPPS1 mice, the binding potential (BP) of [¹¹C]PIB in cortical regions was comparable to littermate controls (tg 0.00 ± 0.02 ; co 0.00 ± 0.01), reached 0.17 ± 0.09 in 8.5months old transgenic animals and 0.26 ± 0.16 in 10months old animals. Surprisingly, 12-16.5 months old transgenic animals did not show higher BP (0.22 ± 0.06 , $n=4$, $p=0.65$). Most importantly, 5months old transgenic animals could not be detected with [¹¹C]PIB (tg 0.03 ± 0.06 ; co 0.01 ± 0.03 , $n=8$, $p=0.17$). In sharp contrast, transgenic Tg2576 mice (Logan 0.05 ± 0.01 ; SRTM 0.02 ± 0.02) could neither be differentiated from age matched controls using [¹¹C]PIB (Logan 0.06 ± 0.02 ; SRTM 0.01 ± 0.01 , $n=4$, 18 months old) nor with AOI987. These results clearly elucidate the potential of AOI987 and [¹¹C]PIB for imaging amyloid plaques in APPPS1 mice but not in Tg2576 mice and also show that monitoring of disease progression regarding amyloid plaque-load after 10 months is not possible using [¹¹C]PIB. If the same issue applies to clinical observations, this could lead to critical misinterpretation of patient data.

Presentation Number **0062**
Scientific Session 4: Alzheimers and Parkinsons

Assessment of Cerebral Hemodynamics with Acetazolamide Tc-99m ECD Brain SPECT in Patients with CADASIL

Soon-Ah Park¹, Chung-Yong Yang², Hyun-Young Park³, Woo Hyoung Kim¹, ¹nuclear medicine, wonkwang university college of medicine, Iksan, Republic of Korea; ²Physical Medicine and Rehabilitation, wonkwang university college of medicine, Iksan, Republic of Korea; ³Neurology, wonkwang university college of medicine, Iksan, Republic of Korea. Contact e-mail: nmbach@wonkwang.ac.kr

Purpose: Cerebral autosomal dominant arteriopathy with subcortical infarcts and leukoencephalopathy (CADASIL) is a hereditary, monogenic form of small-vessel disease caused by mutations in the Notch3 gene on chromosome 19. The aim of this study is the evaluation of cerebral hemodynamics including cerebral blood flow (CBF) and cerebrovascular reactivity (CVR) after administration of acetazolamide (ACZ) on Tc-99m ECD brain SPECT in patients with CADASIL. Methods: Two CADASIL patients from two families (1 male/1 female: age 37/45 years, respectively) were enrolled in the study. In all patients, the diagnosis had been confirmed by the identification of a mutation in the Notch3 gene. A detailed medical history was taken, and a neurological examination was performed for correlation analyses with imaging studies. All subjects were examined with cranial magnetic resonance imaging (MRI) and Tc-99m ECD brain SPECT. The SPECT was performed twice, once before and once after administration of ACZ. Results: Chief clinical features were isolated cranial nerve palsy and stroke. MRI demonstrated diffuse white matter, T2-signal hyperintensities and lacunes infarctions. Brain SPECT showed decreased cerebral blood flows in whole brain involving bilateral temporal, frontal, parietal lobes, thalamic and periventricular white matter but cerebral blood flow increased dramatically after the administration of acetazolamide in the cerebral cortex. Conclusions: Tc-99m ECD Brain SPECT provided functional information that both CBF and CVR were reduced in CADASIL and ACZ infusion induces a significant increase in cerebral perfusion. These findings suggest that dysfunction of autoregulation of small-vessel play an essential role in the pathogenic mechanisms in CADASIL, and ACZ might be a promising treatment for CADASIL patients.

Presentation Number **0063**
Scientific Session 4: Alzheimers and Parkinsons

Pharmacokinetics of a New ^{18}F -labeled Amyloid Imaging Agent, [^{18}F]FACT, in Alzheimer's Disease Patients

Manabu Tashiro¹, Nobuyuki Okamura³, Shoichi Watanuki¹, Shozo Furumoto^{2,3}, Katsutoshi Furukawa⁴, Yoshihito Funaki², Ren Iwata², Yukitsuka Kudo⁵, Hiroyuki Arai⁴, Kazuhiko Yanai^{1,3}, ¹Division of Cyclotron Nuclear Medicine, Tohoku University Cyclotron and Radioisotope Center, Sendai, Japan; ²Division of Radiopharmaceutical Chemistry, Tohoku University Cyclotron and Radioisotope Center, Sendai, Japan; ³Department of Pharmacology, Tohoku University Graduate School of Medicine, Sendai, Japan; ⁴Department of Geriatrics and Gerontology, Institute of Development, Aging and Cancer, Tohoku University, Sendai, Japan; ⁵Innovation of New Biomedical Engineering Center, Tohoku University Hospital, Sendai, Japan. Contact e-mail: mtashiro@m.tains.tohoku.ac.jp

In vivo detection of amyloid deposition is important for early diagnosis of Alzheimer's disease (AD) and for prediction of potential conversion from mild cognitive impairment (MCI) to AD. Purpose of the present study is to examine the pharmacokinetic property of our new fluorine-labeled amyloid imaging probe, [^{18}F]Fluorinated Amyloid imaging Compound of Tohoku university ([^{18}F]FACT). For the study subjects, ten AD patients (mean age: 74.5 y.o.) and nine healthy controls (mean age: 68.3 y.o.) were studied in the present study. Regions of interest (ROIs) were placed on various cortical and subcortical regions in dynamic PET images of 60-min- and 90-min-long duration, based on the coregistered MRI T1 images. Results of quantification using arterial inputs were compared to those calculated by Logan graphical analysis with arterial data (LGA) and with the reference data (LGAR), and to those calculated by full kinetic analysis based on 1- and 2-tissue compartmental models (1TM and 2TM). These results were compared to the ratio of standardized uptake values (SUV) in the cortex to that in the cerebellum, as well. [^{18}F]FACT displayed significantly higher distribution volume ratio (DVR) values in AD patients than in controls in various cortical regions such as the cingulate, temporal and occipital regions, especially in the temporo-occipital regions. 2TM demonstrated better fitting result compared to 1TM. The correlation of distribution volume ratio (DVR) values calculated by LGA and LGAR to those by 2TM was very good. In addition, these values correlated well to the SUV values. These findings have demonstrated that [^{18}F]FACT is a promising PET probe and that DVR values based on LGA, LGAR and SUVR can be good indices of amyloid deposition in AD patients and MCI. The preliminary results of the present quantitative analysis of [^{18}F]FACT have shown nearly the same findings as those of [^{11}C]BF-227. Considering the longer half-life of ^{18}F -nuclide (110 min) than that of ^{11}C -nuclide (20 min), this [^{18}F]FACT may be more useful [^{11}C]BF-227 than as a radiotracer for conducting routine diagnosis of AD and for delivery to satellite PET facilities.

Presentation Number **0064**
Scientific Session 4: Alzheimers and Parkinsons

⁶²Cu-ATSM PET Demonstrates Increase of Striatal Oxidative Stress in Living Patients with Parkinson's Disease

Masamichi Ikawa¹, Hidehiko Okazawa², Takashi Kudo², Masaru Kuriyama¹, Yasuhisa Fujibayashi², Makoto Yoneda¹, ¹Neurology, University of Fukui, Fukui, Japan; ²Biomedical Imaging Research Center, University of Fukui, Fukui, Japan. Contact e-mail: iqw@u-fukui.ac.jp

While many investigations of postmortem brains or animal models have demonstrated enhancement of oxidative stress and impairment of mitochondrial function in the nigrostriatal system in Parkinson's disease (PD), the effect of these factors on neurodegeneration in the pathogenic process of PD in living patients remains obscure. To clarify the relation of these factors to disease progression and the pathogenesis of Parkinson's disease, we performed PET with [⁶²Cu]-diacetyl-bis(*N*⁴-methylthiosemicarbazone) (⁶²Cu-ATSM). ⁶²Cu-ATSM PET enables imaging of regional oxidative stress due to mitochondrial dysfunction in the patient's brain by a redox trapping mechanism. Fifteen patients with PD and 6 healthy volunteers as normal controls underwent PET with ⁶²Cu-ATSM. The patients had presented with lateral dominant symptoms at onset, and the severity of symptoms was evaluated by the Unified Parkinson's Disease Rating Scale (UPDRS). Twenty-min dynamic PET data acquisition was started after the injection of 555 MBq ⁶²Cu-ATSM with time frames of 10 sec x 12, 60 sec x 8 and 10 min x 1. Delayed phase images of ⁶²Cu-ATSM were obtained by average of the dynamic data for the last frame, and standardized uptake values (SUV) of ⁶²Cu-ATSM was measured by means of region of interest (ROI) analysis. The striatum-to-cerebellum SUV ratio (S/C ratio) was obtained from the ratio of the SUV of the striatum to the SUV of the cerebellar cortex. The mean S/C ratio of the bilateral striatum in patients (1.15 ± 0.10) was significantly increased compared with that in the controls (1.08 ± 0.02) ($P < 0.05$). In the patients, the S/C ratio of the bilateral striatum showed a positive correlation with the UPDRS ($r = 0.52$, $P < 0.05$), and the S/C ratio of the striatum contralateral to the initially affected body side showed a strong positive correlation with the UPDRS ($r = 0.62$, $P < 0.05$). In the present study, ⁶²Cu-ATSM PET enabled to delineate regional oxidative stress on the nigrostriatal system in living patients with PD. ⁶²Cu-ATSM PET images clearly demonstrated that in patients with PD, striatal oxidative stress is enhanced compared with that in controls, and is increased with the progression of disease severity, particularly in the striatum contralateral to the initially affected body side. These findings present the first in vivo evidence that oxidative stress due to mitochondrial dysfunction plays a causal role in the progression of neurodegeneration in PD.

Presentation Number **0065**
Scientific Session 5: Monitoring Therapy

In Vivo Imaging to Monitor Anti-angiogenesis and Re-oxygenation on Radio-sensitivity in Pancreatic Cancer Xenografts

Ning Cao¹, **Ling Chen**^{1,5}, **Teimour Maleki**⁴, **Michael Shaffer**¹, **Bo Liu**¹, **Babak Ziaie**⁴, **Song-Chu Ko**³, **Keith Stantz**^{1,2}, ¹*School of Health Sciences, Purdue University, West Lafayette, IN, USA;* ²*Radiology, Indiana University, School of Medicine, Indianapolis, IN, USA;* ³*Clinical Radiation Oncology, Indiana University, School of Medicine, Indianapolis, IN, USA;* ⁴*Electrical and Computer Engineering, Purdue University, West Lafayette, IN, USA;* ⁵*School of Life Science and Biotechnology, Shanghai Jiaotong University, Shanghai, China. Contact e-mail: ncao@purdue.edu*

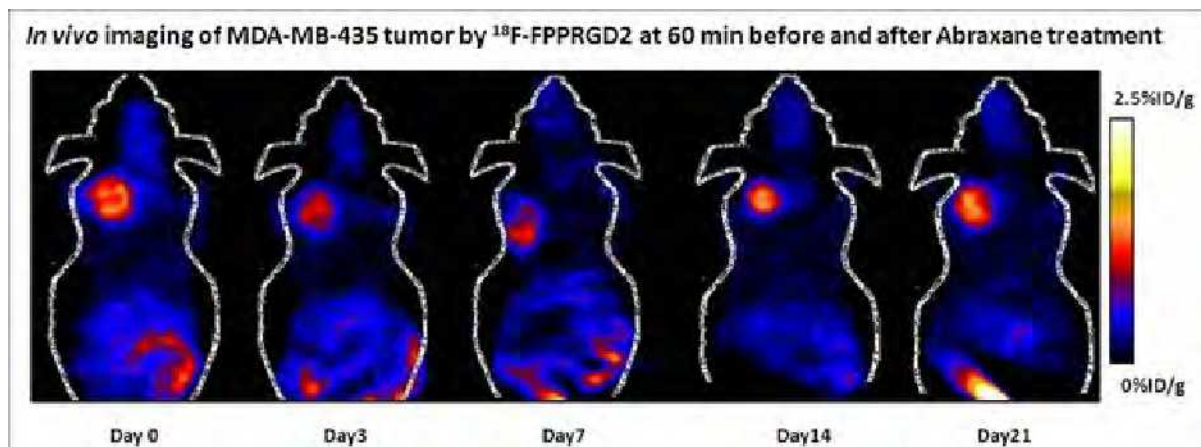
Purpose: The objective is to longitudinally monitor and evaluate the physiology and oxygenation status of pancreatic tumor xenografts after anti-angiogenic treatment (AAT) or Implantable Micro Oxygen Generator (IMOG, excited by wireless waves from the ultrasonic supply power to produce O₂). In vivo imaging of tumor hemodynamics will define a suitable time window for further radiotherapy (RT). **Introduction:** Hypoxia plays an essential role in tumor angiogenesis. Intra-tumor angiogenic heterogeneity and hypoxia promote tumor progression and metastasis and decrease cellular response to cytotoxic treatments. High levels of hypoxia and angiogenesis are major causes for the extremely low survival rate of pancreatic cancer patients. Thus, targeting the abnormal vascular structure by AAT or increasing the overall tumor oxygenation with IMOG will synergize radiotherapy if applied in a suitable time period. **Molecular and dynamic imaging of tumor hemodynamics, e.g. Photoacoustic Computed Tomography Spectroscopy (PCT-S, measuring hemoglobin concentration and SaO₂) and Dynamic Contrast-Enhanced CT (DCE-CT, measuring vascular physiological parameters, e.g. perfusion, permeability, fractional plasma volume and interstitial space), will be used to monitor both vascular physiology and morphology changes. Material and Methods:** A cohort of athymic mice bearing BxPC-3 pancreatic tumors was divided into three groups: control group (non-specific, rat immunoglobulin IgG1, i.p.), anti-angiogenic therapeutic group (40 mg/kg DC101, i.p.), and IMOG treated group. For control and DC101 group, DCE-CT and PCT-S scans were acquired at baseline, 2 days, 1 week, and 2 weeks post treatment. The fluorescence-based optical O₂ sensor (NeoFox Phase Measurement system, Ocean Optics Inc., FL) was used to measure tumor oxygen change in response to IMOG initiation. These results were compared to pimonidazole stained tissue sections to evaluate hypoxia status in treated and control tumors. **Results:** Pimonidazole staining showed severe hypoxia status in pancreatic tumors. DCE-CT and PCT-S results demonstrated that AAT by DC101 normalized the abnormal vascular structure and increased the oxygenation in pancreatic tumor. IMOG was confirmed to significantly increase local tumor oxygenation in vivo. **Conclusions:** DCE-CT and PCT-S provide a unique ability to monitor tumor physiology and oxygenation changes in response to AAT. We believe that applying radiotherapy in the "normalization window" after AAT or during IMOG initiation period will greatly augment treatment outcomes for pancreatic tumor.

Presentation Number **0066**
Scientific Session 5: Monitoring Therapy

18F-FPPRGD2 and 18F-FDG PET Imaging of Abraxane Therapy Response

Xilin Sun^{1,2}, **Yongjun Yan**¹, **Shuanglong Liu**³, **Gang Niu**¹, **Qizhen Cao**³, **Xiaoyuan Chen**¹, ¹Laboratory of Molecular Imaging and Nanomedicine (LOMIN), National Institute of Biomedical Imaging and Bioengineering (NIBIB), National Institutes of Health (NIH), Bethesda, MD, USA; ²Department of Medical Imaging and Nuclear Medicine, the 4th Affiliated Hospital, Harbin, China; ³The Molecular Imaging program at Stanford (MIPS), Department of radiology, Stanford University School of Medicine, Stanford, CA, USA. Contact e-mail: sunxilin@yahoo.com.cn

Purpose: Abraxane is a FDA approved anti-cancer drug. However, the mechanism of the action of Abraxane is complex and no established biomarker is available to accurately monitor the treatment outcome. The aim of this study was to investigate whether integrin specific PET tracer 18F-FPPRGD2 (eIND 104150) can be utilized to monitor Abraxane therapy response. **Methods:** Orthotopic MDA-MB-435 breast cancer mice were treated with Abraxane (25 mg/kg every other day, 3 doses) or PBS. Tumor volume was monitored by caliper measurement. PET scans were performed before and at different time points after treatment was started (Day 0, 3, 7, 14 and 21) using 18F-FPPRGD2 and ¹⁸F-FDG. The tumoricidal effect was also assessed ex vivo by immunohistochemistry and Western blot. **Results:** Abraxane treatment inhibited the tumor growth and the significant difference in tumor volume can be identified at day 7 after the initiation of treatment. However, regrowth of tumor was observed at day 14 after the treatment was halted. 18F-FPPRGD2 tumor uptake and tumor/muscle ratio in Abraxane treated group were both significantly lower than the baseline on day 3 and day 7, but restored to the baseline level at day 14 and day 21. No significant change of 18F-FPPRGD2 uptake in the PBS control group was observed throughout the study. In the contrary, no significant change of ¹⁸F-FDG uptake was found between the treated and control tumors. Immunohistological staining and western blot confirmed that the change of 18F-FPPRGD2 uptake corroborates with the variation of integrin $\alpha\beta3$ level in the tumor vasculature induced by Abraxane treatment. **Conclusion:** Abraxane treatment downregulation of integrin $\alpha\beta3$ expression, especially those on tumor endothelial cells can be quantitatively visualized by PET. Consequently, 18F-FPPRGD2 PET is superior to FDG-PET in monitoring early response to the treatment, substantiating its potential clinical translation.



Presentation Number **0067**
Scientific Session 5: Monitoring Therapy

Longitudinal Imaging of the Response to Dasatinib® Treatment in PC-3 Prostate Tumor-bearing Nude Mice Assessed by 68Ga-AMBA and ¹⁸F-FDG

Antonietta Bartoli¹, **Giovanna Esposito**¹, **Luca D'Angeli**¹, **Azzurra Filannino**², **Lorenza Fugazza**², **Donato Barbato**², **Claudia Cabella**³, **Luigi Miragoli**³, **Cristina Neira**³, **Vito Lorusso**⁴, **Laura E. Lantry**⁵, **Aldo Cagnolini**⁵, **Adrian D. Nunn**⁵, ¹Molecular Biotechnology Center, University of Turin, Torino, Italy; ²Research & Development Radiochemistry, Advanced Accelerator Applications - S.r.l., Collettero Giacosa (To), Italy; ³Centro Ricerche Bracco, Bracco Imaging SpA, Collettero Giacosa (To), Italy; ⁴EPHORAN - Multi Imaging Solutions, Collettero Giacosa (To), Italy; ⁵Ernst Felder Laboratories, Bracco Research USA INC, Princeton, NJ, USA. Contact e-mail: bartoli@df.unipi.it

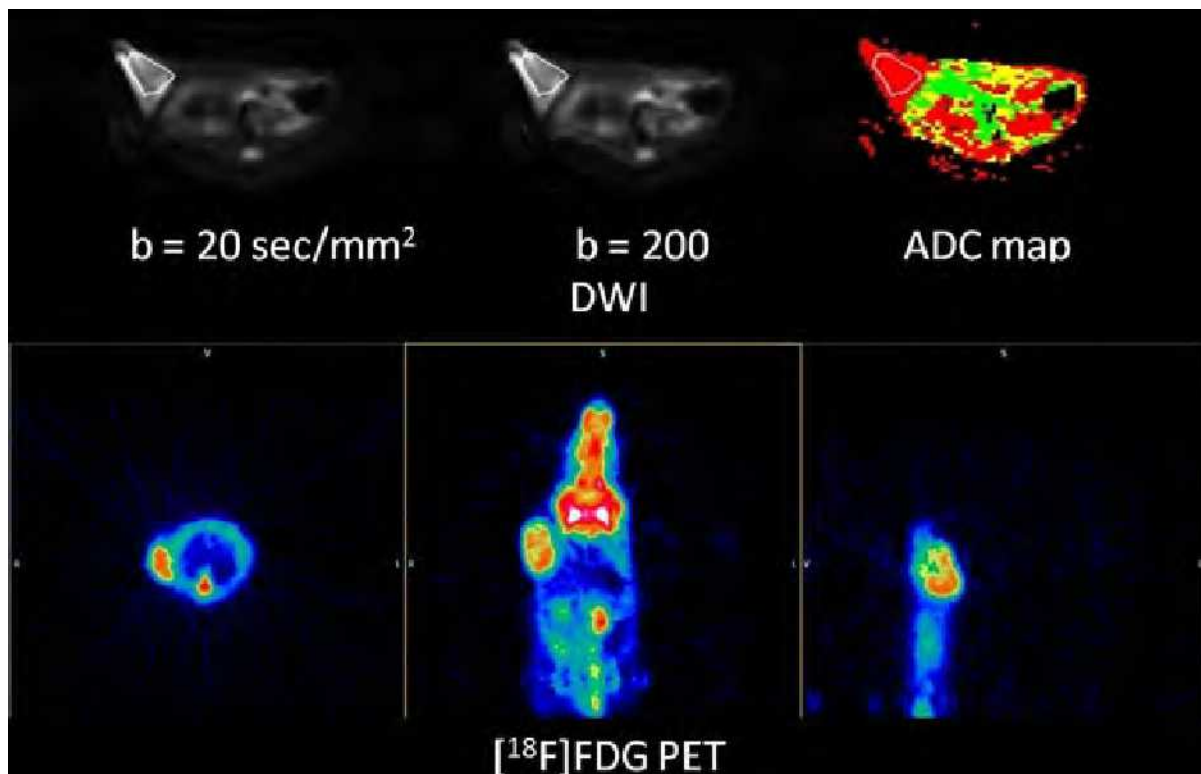
Aims: The objective of the study is to assess the capability of 68Ga-AMBA and ¹⁸F-FDG longitudinal PET imaging for monitoring the response to Dasatinib® treatment in prostate tumor-bearing nude mice (xenograft, PC-3). **Materials and Methods:** 68Ga-AMBA is a radiolabeled bombesin derivative that is bound and internalized by cells expressing the G-protein-coupled gastrin-releasing peptide receptor (GRP-R). GRP-R are up regulated in many cancers, including prostate. (Preparation and in vitro binding of 67Ga-AMBA, comparison to 177Lu-AMBA. Chen L et al, J Nucl Med. 2007; 48 Sup 2, 306P). Five million PC-3 cells were suspended in 0.1 mL PBS and injected subcutaneously in the right flank of 5 week old male athymic Nu/Nu mice. The animals were divided in two groups: the control (n=8) and the treated one (n=8). In both groups tumor growth was monitored by caliper measurement twice a week. In the treated group, a first ¹⁸F-FDG acquisition was performed when the tumor size reached a volume of ~ 200 mm³. One-two days later, a first 68Ga-AMBA acquisition (scan #1) was performed. The day after the 68Ga-AMBA imaging, Dasatinib® treatment was started by administering orally a dose of 50 mg/kg, once a day, 5 days on/2 off. 68Ga-AMBA scan #2 and scan #3 were performed 2 and 4 weeks after the beginning of Dasatinib® treatment, respectively. One-two days after scan #3 a final ¹⁸F-FDG scan was performed. Intravenous doses of 250-350 µCi ¹⁸F-FDG or 350-400 µCi 68Ga-AMBA were used and acquisitions were initiated after uptake times of 45 min or 60 min respectively. Static PET acquisitions were performed by acquiring 80 M events for ¹⁸F-FDG or 40 M events for 68Ga-AMBA. **Results:** In all mice treated with Dasatinib® tumor growth was inhibited (the tumors maintained approximately the same volume) while, in the control group, the tumors continued growing almost exponentially. Uptake in the tumors was lower for ¹⁸F-FDG (%ID/g ~ 2%) than for 68Ga-AMBA (%ID/g scan #1 between 5 and 7%). In most cases 68Ga-AMBA tumor uptake (%ID/g or SUV) changed on treatment despite the tumours maintaining their volume. In contrast, uptake of ¹⁸F-FDG was comparable pre and post treatment. **Conclusions:** Dasatinib® treatment at a dose of 50 mg/kg inhibits the growth of prostate cancer in this model of tumor-bearing nude mice (xenograft, PC-3). 68Ga-AMBA uptake changes soon after treatment begins and may provide an indication of response to treatment whereas ¹⁸F-FDG provided a lower signal with little change. Imaging with 68Ga-AMBA may provide a useful indicator of the response to Dasatinib® treatment.

Presentation Number **0068**
Scientific Session 5: Monitoring Therapy

Monitoring of Antiangiogenic Therapy with Anticalins in a Preclinical Sarcoma Model Using DWI and FDG-PET

Reinhard Meier¹, Rickmer Braren¹, Andreas Steingötter¹, Yvonne Kosanke¹, Hendrik Gille³, Ernst J. Rummeny¹, Markus Schwaiger², Ambros J. Beer², ¹Department of Radiology, Klinikum rechts der Isar, Technische Universität München, Munich, Germany; ²Department of Nuclear Medicine, Klinikum rechts der Isar, Technische Universität München, Munich, Germany; ³Pieris AG, Freising, Germany. Contact e-mail: reinhardt.meier@gmail.com

Purpose: To compare the performance of DWI and FDG-PET for monitoring early response to a novel antiangiogenic therapy directed to VEGF with the anticalin PRS-050. **Method and Materials:** Anticalins are a novel class of targeted protein therapeutics based on human liopcalin protein scaffolds. The PEGylated Anticalin Angiocal (PRS-050-PEG40) is directed against VEGF-A. 24 mice were implanted subcutaneously A673 rhabdomyosarcoma xenografts and underwent DWI-MR and FDG-PET imaging before and 2 days after i.p. injection of Angiocal (n=13) or PBS (n=11). Tumor size was measured manually with a caliper and by MRI. MRI scans were performed on a 1.5 T clinical MR system (1.5T Achieva, Philips Medical Systems, Best, The Netherlands) using a dedicated surface coil. Following a survey scan, a multi-slice T2-weighted TSE sequence was applied for tumor detection. DWI data were collected with a standard spin echo sequence with 3 b-factors (20, 200 and 600). FDG-PET was performed with a Micro-PET Scanner using ¹⁸F-FDG with approximately 3,7 MBq per animal. ROI analysis was performed comparing initial and follow up MRI and PET scans. Results were compared between therapeutic and control groups. Differences were tested for significance with analysis of variance (p<0.05). **Results:** Tumor size was not significantly different in the therapeutic compared to the control group (p=0,977) on day 2 after therapy onset. The FDG-PET Signal increased only slightly (3±7%) in the therapeutic group; controversially there was a significant increase in FDG signal in the control group (60±17%) (p<0.05). The therapeutic group showed a significant increase in ADC value (16±8%), while the control group showed a slight decrease (12±12%) (p<0.05). **Conclusion:** Although tumor size was not substantially influenced by Angiocal therapy on day 2 after therapy onset, both FDG-PET signal and ADC value showed significant changes in the therapy versus control group as early as two days after treatment. Therefore both modalities are promising for monitoring early response of antiangiogenic therapy using Anticalins.



Presentation Number **0069**
Scientific Session 5: Monitoring Therapy

The Role of HDAC Activation in Chemotherapy-induced Neurotoxicity and Protective Effects of HDAC Inhibitors in Rats Demonstrated Using PET/CT with ^{18}F -FAHA and ^{18}F -FDG.

Nobuyoshi Fukumitsu, Hsin-Hsien Yeh, Leo G. Flores, Suren Soghomonyan, Uday Mukhopadhyay, Daniel Young, Mian M. Alauddin, William Tong, Juri G. Gelovani, Experimental Diagnostic Imaging, MD Anderson Cancer Center, Houston, TX, USA. Contact e-mail: fukumitsun@yahoo.co.jp

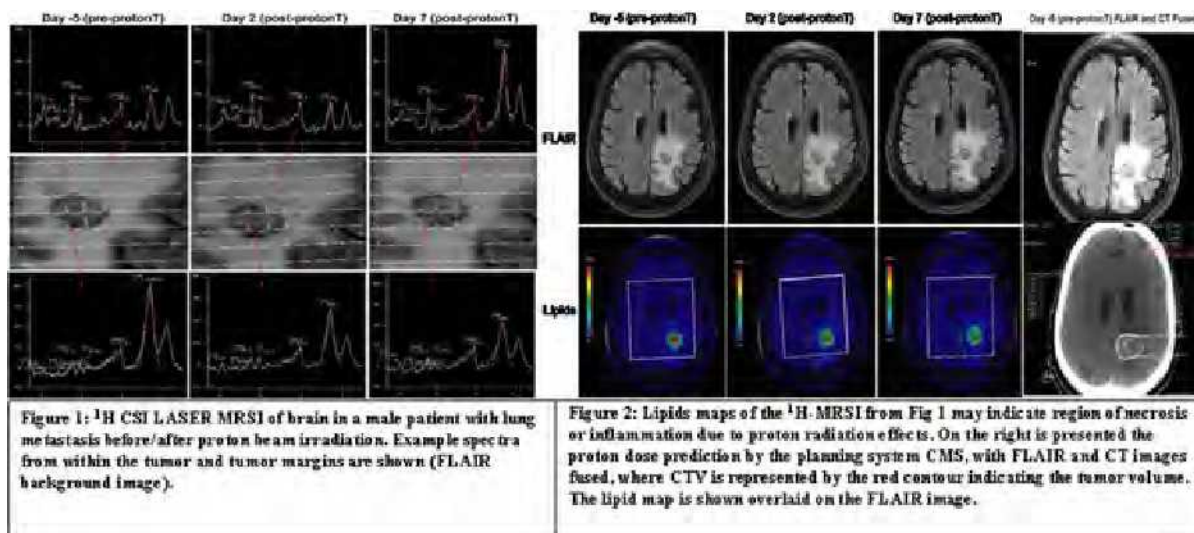
Objectives: There is increasing evidence that administration of histone deacetylase (HDAC) inhibitors can exert neuroprotective effects by a variety of mechanisms. Therefore, we aimed to assess the role of HDACs in the mechanism of cisplatin-induced neurotoxicity and to explore the therapeutic potential of HDAC inhibitors. **Methods:** Eight week old male nu/nu mice were studied in three groups (N=8/groups). To induce acute neurotoxicity, the mice received: Group A, 2 doses of 2 mg/kg cisplatin; Group B, 2 doses of 4 mg/kg cisplatin; Group C, 2 doses of 4 mg/kg cisplatin. Cisplatin doses were administered 12 hours apart. Group C was pre-treated with SAHA (300 mg/kg / twice day) starting two days prior to and continuing after cisplatin administration for 2 days. PET/CT with [^{18}F]FAHA (dynamic) and [^{18}F]FDG (static) studies were performed on subsequent days at baseline and after therapy with different doses of cisplatin or cisplatin+SAHA. Brain metabolic activity (%ID/g [^{18}F]FDG) and HDACs activity (Ki [^{18}F]FAHA) were calculated and compared before and after therapy. In parallel, the mice underwent a series of neurobehavioral tests before and after therapy. To validate in vivo imaging results, mice were sacrificed, brains sampled and stained with IHC for the degree of acetylation of different histone core proteins in various brain structures. **Results:** Brain glucose metabolism (%ID/g [^{18}F]FDG) was significantly decreased ($p < 0.05$, paired T-test) but the activity of HDACs was significantly increased (Ki [^{18}F]FAHA) after cisplatin treatment in both groups A and B ($p < 0.05$, paired T-test). Neurobehavioral tests demonstrated that mice in Group B treated with higher dose of cisplatin developed more neurotoxicity than mice in Group A. In contrast, treatment with SAHA prevented the development of neurotoxicity in Group C was, which manifested by minimal inhibition of cognitive and motor functions, no changes in brain glucose metabolism and inhibition of HDACs activity in the brain, based on the results of PET/CT with [^{18}F]FDG and [^{18}F]FAHA, respectively. In situ IHC analyses of brain tissue sections confirmed the in vivo imaging results: in Groups A and B, significant deacetylation of H2A, H3 and H4 histone core proteins was observed in hippocampus and, especially, of H3 in cortex. In contrast, in Group C, HDACs inhibition with SAHA resulted in some hyperacetylation of these histone core proteins. **Conclusions:** Quantitative PET/CT imaging with [^{18}F]FAHA could be used for monitoring HDAC-mediated epigenetic regulation during the development of neurotoxicity and for the assessment of novel HDAC inhibitors. Combination therapy with HDAC inhibitors can prevent the development of cisplatin-induced neurotoxicity and should be explored in the clinic.

Presentation Number **0070**
 Scientific Session 5: Monitoring Therapy

In Vivo Assessment of Proton Beam Therapy of Brain Tumors

Joao C. Seco³, Ravi T. Seethamraju¹, Helen A. Shih³, Dominique L. Jennings⁴, Ovidiu C. Andronesi⁴, Gregory A. Sorensen^{2,4}, Mukesh G. Harisinghani², ¹MR R and D, Siemens Medical Solutions, USA Inc., Malden, MA, USA; ²Radiology, Massachusetts General Hospital, Boston, MA, USA; ³Radiation Oncology, Massachusetts General Hospital, Boston, MA, USA; ⁴Radiology, Massachusetts General Hospital, Charlestown, MA, USA. Contact e-mail: ravi.seethamraju@siemens.com

The advantage of proton radiation over other methods of radiation therapy is the significant sparing of dose delivered to healthy organs surrounding a tumor while delivering a high target dose, because 75% of the dosage is very close to the end-of-range (EOR) or Bragg peak. However, the delivery precision is affected by organ motion, setup error and tissue heterogeneity. Accuracy of treatment delivery is crucial to tumor control as the beam EOR aims complete coverage of the at-risk volume while sparing normal tissue. Under-treatment of a 1% sub-volume may decrease the efficacy by nearly 20%. Previously in phantom experiments [1] it was shown MRI can precisely determine EOR. The hypothesis is that proton beam therapy produces alterations at multiple levels (membranes, DNA, proteins) in the cell structure which will trigger metabolic and bio-chemical changes that can be observed by 1H MRSI (CSI LASER sequence [2]). In a cohort of 5 patients treated with high energy protons in the range of 100-220 MeV, 1H-MRS was performed pre and post proton irradiation approximately 1-2 day, 1 week and 1 month after irradiation. A total dose of 10-15 Gy(RBE) was delivered to each patient in single fraction stereotactic treatment. Lipids and myo-inositol changes pre and post proton therapy were used as biomarkers to ascertain the early effects of irradiation (fig 1). There was an increase in both these markers 1 week post-treatment. Lipid density changes correlated directly with biochemical changes due to radiation treatment (fig 2). Increase in Myo-Inositol indicates better exchange of K⁺ and Na⁺ ions between tumor region and surrounding areas after irradiation. In both figures the concentration of lipids in and around the tumor site has changed. We speculate that the lipid change would be a good marker to identify early biochemical changes due to proton radiation effects, and therefore be used to indicate the initial planned proton dose distribution. The preliminary results at 3T indicate that MRS can be used for proton beam therapy to provide quantitative and qualitative information on proton irradiation. References: 1. Seco J., et al., The Application of MRI Pulse Sequences in the Verification of Proton Beam Radiotherapy, ISMRM 2009, 594 2. Andronesi O.C. et al, JMR 2010;203(2):283-293.



Presentation Number **0071**
Plenary Session 2: Translational Molecular Imaging

Translational Molecular Imaging

Robert J. Gropler, Radiology, University of Washington, St. Louis, MO, USA. Contact e-mail: groplerr@mir.wustl.edu

Molecular imaging holds much promise for the diagnosing of disease at its earliest stages and monitoring its progression and response to specific therapies. Indeed, it is envisioned to be a key component in our armamentarium for the application of personalized medicine. Moreover, molecular imaging is also expected to play an increasingly important role in drug discovery and development. However numerous challenges must be overcome for molecular imaging to fulfill these promises and expectations. Examples include current academic research paradigms that are not optimized for the development of molecular imaging contrast agents and detection schemes, the economics of contrast agent development particularly for “niche” markets, and a restrictive regulatory/reimbursement environment. In this talk these and other challenges and potential strategies to overcome them will be discussed.

Presentation Number **0072**
Scientific Session 6: Cancer Therapy

Shedding Light on ER α -coregulator Interactions

Madryn Lake¹, Quang-De Nguyen^{1,2}, Simak Ali¹, Eric O. Aboagye^{1,2}, ¹Oncology, Imperial College, London, United Kingdom; ²Molecular Therapy, Medical Research Council, London, United Kingdom. Contact e-mail: m.lake07@imperial.ac.uk

Over a million women are diagnosed with breast cancer each year, resulting in over 410,000 deaths annually. Estrogen (E2) regulates breast cancer growth through the action of the estrogen receptors ER α and ER β . Anti-estrogens, in particular tamoxifen (TAM), combined with surgery or as a prophylactic in high risk women, have contributed greatly to the reduction in breast cancer mortality. TAM is a tissue selective anti-estrogen; it is anti-estrogenic in the breast but estrogenic in other tissues, thereby enabling it to promote the beneficial effects of E2, such as healthy bone density. However, like E2, TAM also promotes endometrial cancer, and so there is an impetus for the development of novel tissue selective ER α ligands. Depending upon the ligand and cell context, ER α can stimulate or inhibit gene expression by recruiting coactivator (CoA) or corepressor (CoR) proteins. In breast cancer, ER α -CoA interaction are associated with tumour progression while ER α -CoR interaction are associated with receptor antagonism and a therapeutic block of ER α signalling. This work aims to image transient ER α :coregulator interactions in vivo using a luciferase fragment complementation (LFC) assay. Elucidation of these interactions will enable a greater appreciation of the tissue selective actions of ER α ligands and aid in the screening of novel ER α antagonists. Luciferase fragment fusion proteins have been produced for ER α , the CoA AIB1, and the CoR SMRT. Transient transfection of ER α and AIB1 luciferase fusion proteins have shown an E2 induced increase in LFC which can be modulated by the anti-estrogens TAM and Faslodex (FAS). The ER α -AIB1 mediated LFC observed correlates with ER α transcriptional activity, as assessed by comparison with an MCF7-estrogen responsive luciferase reporter, and is independent of changes in protein expression. The specificity of the observed LFC has been further validated by L539/540A and Y537S ER α fusion protein mutants; mutations which prevent or induce ER α interaction with AIB1, respectively. Using the competitive inhibitor TAM, the potential for imaging dynamic interactions has been demonstrated. Using xenograft models, E2 induced LFC mediated by ER α -AIB1 fusion proteins has been demonstrated in vivo. Transient transfection of ER α and SMRT luciferase fusion proteins have shown increased LFC with TAM and FAS compared with E2, consistent with the notion that the ER α -SMRT interaction is characteristic of ER α antagonism. Results suggest that LFC is an effective means of imaging ER-coregulator interaction.

Presentation Number **0073**
Scientific Session 6: Cancer Therapy

Ligand-directed Delivery Through the Blood-brain Barrier: A Translational Approach for Detection and Treatment of Brain Tumors

*Fernanda I. Staquicini¹, Michael G. Ozawa¹, Catherine Moya¹, Wouter H. Driessen¹, Suren Soghomonyan², Leo G. Flores², Mian M. Alauddin², Juri G. Gelovani², Richard L. Sidman³, Webster K. Cavenee⁴, Renata Pasqualini¹, **Wadiah Arap¹**, ¹David H. Koch Center, The University of Texas M. D. Anderson Cancer Center, Houston, TX, USA; ²Department of Diagnostic Imaging, The University of Texas M. D. Anderson Cancer Center, Houston, TX, USA; ³Beth Israel Deaconess Medical Center, Boston, MA, USA; ⁴Ludwig Institute for Cancer Research, La Jolla, CA, USA. Contact e-mail: warap@mdanderson.org*

Treatment for diseases of the central nervous system (CNS) is limited by the blood-brain barrier (BBB), a selective interface that restricts passage of most molecules from blood into brain. Thus, development of effective delivery strategies for this sanctuary site calls for identification of molecular targets that permit appropriate exposure of the CNS to various drugs, viruses, and imaging agents. Here we used the in vivo phage display technology to isolate peptide-targeted phage particles that can cross the BBB under normal and pathological conditions. We demonstrate that peptide-targeted phage particles cross the BBB, under both normal and pathological conditions. Moreover, such intrinsic properties were further explored for the development of an integrated targeted molecular-genetic imaging and treatment (so called "see-and-treat") of intracranial tumors. We used a vector with genomic cis-elements of adeno-associated virus (AAV) and of M13-derived phage (termed AAV phage; AAVP) to display the brain tumor-targeted peptide. We show that the targeted AAVP-HSVtk, when systemically delivered into brain tumor-bearing mice, (i) provides molecular imaging of a reporter transgene, (ii) enables serial non-invasive monitoring of intracranial tumors in a preclinical setting and (iii) allows ligand-directed targeting and vascular ablation of human malignant glioma xenografts through a suicide gene approach. Together, these findings have potential translational applications for systemic therapy of malignant gliomas.

Presentation Number **0074**
Scientific Session 6: Cancer Therapy

Potential of PET Imaging to Predict the Response to Anti-HER2 Therapy in Breast Cancer

Gabriela Kramer-Marek¹, Dale O. Kiesewetter², Merel Gijzen³, Anthony Kong³, Jacek Capala¹, ¹NCI/NIH, Bethesda, MD, USA; ²NIBIB/NIH, Bethesda, MD, USA; ³University of Oxford, Oxford, United Kingdom. Contact e-mail: marekg@mail.nih.gov

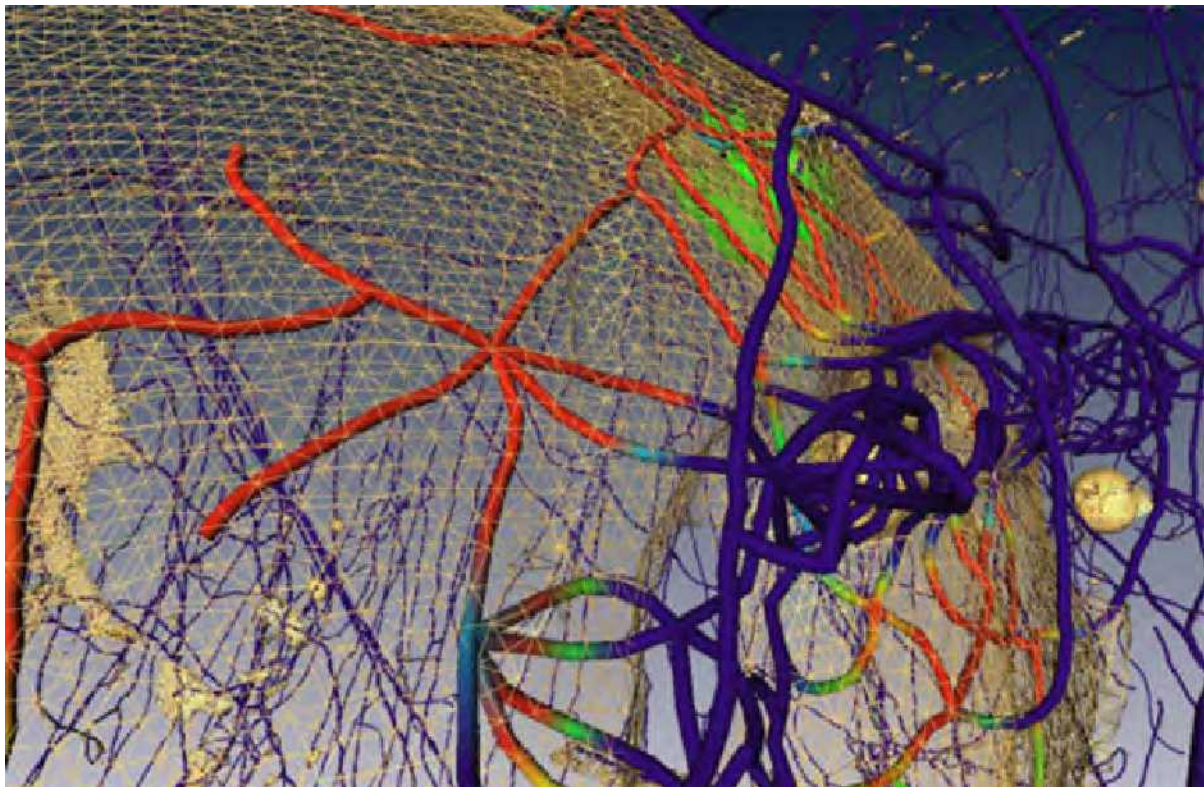
Overexpression of HER2 is associated with resistance to standard therapies and, consequently, poor prognosis. The most successful of HER2-targeted therapies uses trastuzumab - a recombinant, humanized anti-HER2 monoclonal antibody. Currently, alteration of gross tumor volume is used to assess the response to trastuzumab. But, this approach provides only a late indicator of the response. The ex vivo assays of tissue samples are potentially valuable, but their procurement through biopsies is invasive and might be biased by tumor heterogeneity. We studied the feasibility of PET imaging to quantify changes in HER2 expression and to predict the response to trastuzumab in breast cancer xenografts model using 18F-ZHER2-Affibody molecule as a tracer. We administered the tracer to mice bearing subcutaneous BT474 tumors (high HER2 expression). The tumor volume was monitored twice weekly by caliper measurements. Trastuzumab (50 mg/kg loading dose, 25 mg/kg maintenance dose) was given i.p. twice a week for a total of 5 doses. Animals were scanned before the treatment, 48h and two weeks post the beginning of therapy. Immediately after the last scan, animals were euthanized and pieces of tumors were fixed and/or frozen for further analysis. The HER2 expression and activation of HER2 signaling pathways in the tumor samples were assessed by Western blot, IHC and ELISA. Quantitative analysis of PET images indicated decrease of HER2 expression, associated with significant tumor regression (>30% volume reduction), in 8 of 21 treated tumors. Only negligible changes in HER2 expression and stable disease were found in the remaining treated mice. No changes in HER2 expression and intensive growth of the tumors (increase more than 100% of tumor volume) were observed in the control group. These results were confirmed by ex vivo analysis showing dramatic decrease of total HER2 level in responding tumors. Despite the reduction of HER2 levels, there was also persistent HER2 phosphorylation. As previously shown, it might be due to activation of alternative HER receptors as a result of ADAM17-mediated autocrine ligand release. Tissue analysis indicated higher levels of ADAM17 and heregulin in treated xenografts compared to the untreated mice. Other mechanisms that might account for the observed difference between the responders and the non-responders are currently investigated. Our results suggest that monitoring of changes in HER2 expression after five doses of trastuzumab allows predicting the tumor response and identifying mice that would not fully benefit from the treatment.

Presentation Number **0075**
Scientific Session 6: Cancer Therapy

Multimodality Approach in the Study of Tumor Angiogenesis: Magnetic Resonance Imaging (MRI), Synchrotron Radiation Based Micro-CT (SR μ CT), Positron Emission Tomography (PET) and Pattern Analysis to Follow the Vessel Formation

Marco Dominietto¹, **Steffi Lehmann**¹, **Ruth Keist**¹, **Sabrina Lang**², **Bert Müller**², **Markus Rudin**¹, ¹*Institute for Biomedical Engineering, ETHZ, Zurich, Switzerland;* ²*Biomaterials Science Center, University of Basel, Basel, Switzerland.* Contact e-mail: dominietto@biomed.ee.ethz.ch

Several imaging techniques are available to study neovasculature in tumors. MRI provides information on tumor morphology, blood volume (TBV), blood flow (TBF), vascular permeability, and on the average diameter of tumor vessels (vessel size index, VSI), while PET enables analysis of tumor hypoxia. While these in vivo imaging methods provide indirect readouts on neovasculature at a macroscopic resolution, validation of these techniques requires for 3D analysis of the vessel architecture at a capillary level (5-10 μ m). Methods such as ex-vivo synchrotron radiation based μ CT (SR μ CT) are attractive in this context. In addition, it has been found that due to the high biological variability standard statistical image analysis is not sensitive in picking up differences between different groups of animals. To overcome such a problem pattern analysis has been introduced. The aim of this work is to characterize vessel formation in tumors using these imaging modalities in combination with pattern analysis, in order to elucidate multiple aspects of the angiogenic process. The MRI protocol comprised high-resolution measurements of tumor morphology, TBV, TBF, VSI and permeability every three days. Seven days following tumor inoculation a PET experiment was performed using [¹⁸F]-FMISO as hypoxia radiotracer, which has been shown to accumulate in hypoxic cells. Finally, at day twelve post-inoculation, the mice were sacrificed and the tumor was explanted and fixed for (SR μ CT) analysis. Significant tissue heterogeneity in the growing tumor has been found. Pattern analysis has quantified the differences with regard to morphological appearance, physiological behaviour and regarding the degree of hypoxia. Images from SR μ CT showed a chaotic structure of the vessel architecture in line with the in vivo findings at day 12. By using complementary imaging modalities it is possible to non-invasively investigate various aspects of the vessel network formation in tumor tissue in a longitudinal manner, which might be relevant for mechanistic insight.



SR μ CT showing the chaotic vessel network surrounding a perfused region of the tumor

Presentation Number **0076**
Scientific Session 6: Cancer Therapy

Evaluation of Chemotherapy Response in VX2 Rabbit Lung Cancer with 18F-Labeled C2A Domain of Synaptotagmin I

Feng Wang, Nuclear medicine, Nanjing first hospital, Nanjing Medical University, Nanjing, China. Contact e-mail: fengwangcn@hotmail.com

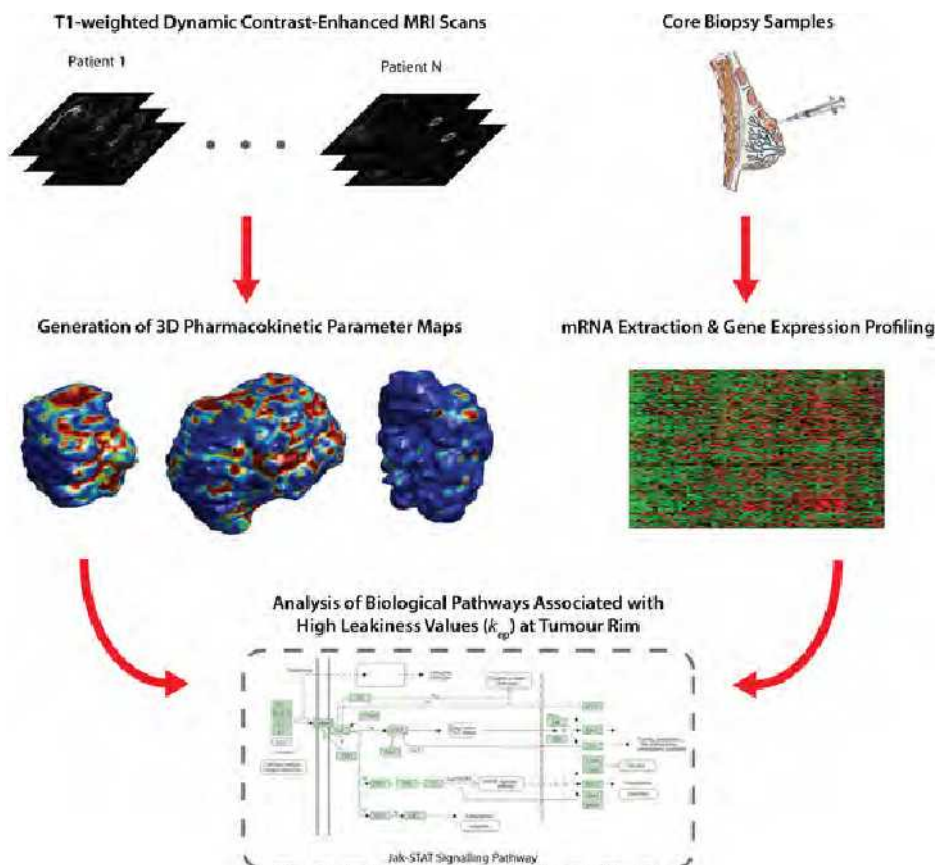
The C2A domain of synaptotagmin I can target apoptotic cell by binding to exposed anionic phospholipids. The goal of this study is to synthesize and evaluate F-18-labeled C2A domain of synaptotagmin (18F-C2A-GST) for the detection of apoptosis. Methods: 18F-C2A-GST was prepared by labeling C2A-GST with N-succinimidyl 4-18F-fluorobenzoate (18F-SFB). The radioactive products were confirmed by SDS-PAGE and high performance liquid chromatography (HPLC), respectively. The binding of 18F-C2A-GST toward apoptosis were validated in vitro using camptothecin-induced Jurkat cells. In vivo bio-distribution of 18F-C2A-GST was determined in mice by dissection method and micro PET dynamics imaging. Apoptosis was induced by paclitaxel in VX2 rabbit tumor model. ¹⁸F-FDG PET was performed before paclitaxel inducement, 18.5~37 MBq(0.5~1.0mCi) was injected by tail vein 72h after chemotherapy, PET/CT was performed 1h post-injection. SUV(standard uptake value) was calculated respectively. VX2 rabbits were sacrificed, Tumor tissue was analyzed with HE staining and activated Caspase 3 to confirm the presence of apoptosis. Results: 18F-C2A-GST was labeled by conjugating the corresponding proteins with 18F-SFB. After purification, the radiochemical purity was higher than 95%. During the synthesis, no degradation of C2A-GST was found. 18F-C2A-GST bound apoptotic cells specifically. Bio-distribution in the mice showed that 18F-C2A-GST had the highest uptake in the kidney, relatively low uptake in the liver, spleen, and a rapid blood clearance. ¹⁸F-FDG PET showed intense uptake was visualized in primary tumor site, whereas no significant accumulation of 18F-C2A-GST was found in the tumor before paclitaxel treatment. 72h after treatment, high focal uptake of 18F-C2A-GST was visualized in tumor sites. HE staining and activated caspase-3 confirmed a large number of apoptosis was presented, after treatment, whereas no significant apoptosis was observed before inducement. Conclusion: 18F-C2A-GST can be easily prepared with conjugation of 18F-SFB. Due to its rapid blood clearance and low uptake in abdomen organ, it holds prospects in the detection of apoptosis. It might serve as a potential early surrogate marker of therapeutic efficacy in tumor therapy. Further study is warranted .

Presentation Number **0077**
 Scientific Session 6: Cancer Therapy

Uncovering the Molecular Correlates of Dynamic Contrast-Enhanced MRI in Breast Cancer Using 3D Pharmacokinetic Mapping and Gene Expression Profiling

Nicholas P. Hughes^{1,4}, **Shaveta Mehta**², **Francesca M. Buffa**², **Rosemary F. Adams**³, **Sanjiv S. Gambhir**^{1,5}, **Adrian L. Harris**²,
¹Radiology, Molecular Imaging Program at Stanford (MIPS), Bio-X, Stanford University, Stanford, CA, USA; ²Weatherall Institute of Molecular Medicine, University of Oxford, Oxford, United Kingdom; ³Oxford Breast Imaging Centre, Churchill Hospital, Oxford, United Kingdom; ⁴Institute of Biomedical Engineering, University of Oxford, Oxford, United Kingdom; ⁵Bioengineering, Stanford University, Stanford, CA, USA. Contact e-mail: nhughes@stanford.edu

Dynamic contrast-enhanced MRI (DCE-MRI) is a widely used functional imaging modality for the management of patients with breast cancer. Unlike molecular imaging modalities however, there is little understanding at present of how imaging patterns on DCE-MRI relate to the genes and pathways that drive tumor growth. To address this problem, we performed a retrospective study of 65 patients with primary breast cancer, for whom DCE-MRI scans and core biopsies were available prior to neoadjuvant chemotherapy. We used pharmacokinetic modeling with a population-based arterial input function to quantify the rate constant (k_{ep}) governing contrast agent washout from the tumor extravascular extracellular space, which simulations showed could be estimated reliably from our low temporal resolution DCE-MRI data. The resulting voxel-wise pharmacokinetic parameters were then used to generate a tumor surface leakiness score by computing the mean k_{ep} within a thin shell at the surface boundary of each tumor (see Figure 1). We extracted RNA from formalin fixed paraffin embedded cores and measured gene expression using Affymetrix whole genome arrays. Following normalization and pre-processing, we used permutation tests to determine which genes were significantly correlated with the mean k_{ep} value at the tumor rim. Setting the False Discovery Rate to 5% gave a total of 538 genes that were all significantly positively correlated with tumor surface leakiness. We then used pathway analysis to determine which pathways and biological processes were significantly represented in the gene list. This analysis revealed that the immune response ($P < 1e-15$), inflammatory response ($P < 1e-9$) and Jak-STAT signalling ($P < 1e-3$) pathways were all significantly associated with the degree of tumor surface leakiness. These results illustrate how the combination of non-invasive imaging and gene expression profiling can reveal the molecular correlates of radiological features, and help bring physiological imaging modalities such as DCE-MRI into the realm of molecular imaging.



Presentation Number **0078**

Scientific Session 7: Translational Molecular Imaging (Co-organized with SNM)

In Vivo Assessment of the Induction of Pulmonary Intravascular Macrophages Using Bimodal SPECT and Fluorescence Probes

Stéphanie Lerondel¹, Guillaume Réveillon¹, Julien Sobilo¹, Sabrina Pesnel¹, Alain Le Pape^{1,2}, ¹CIPA - TAAM UPS44, CNRS, Orléans, France; ²INSERM U618, Tours, France. Contact e-mail: lepape@med.univ-tours.fr

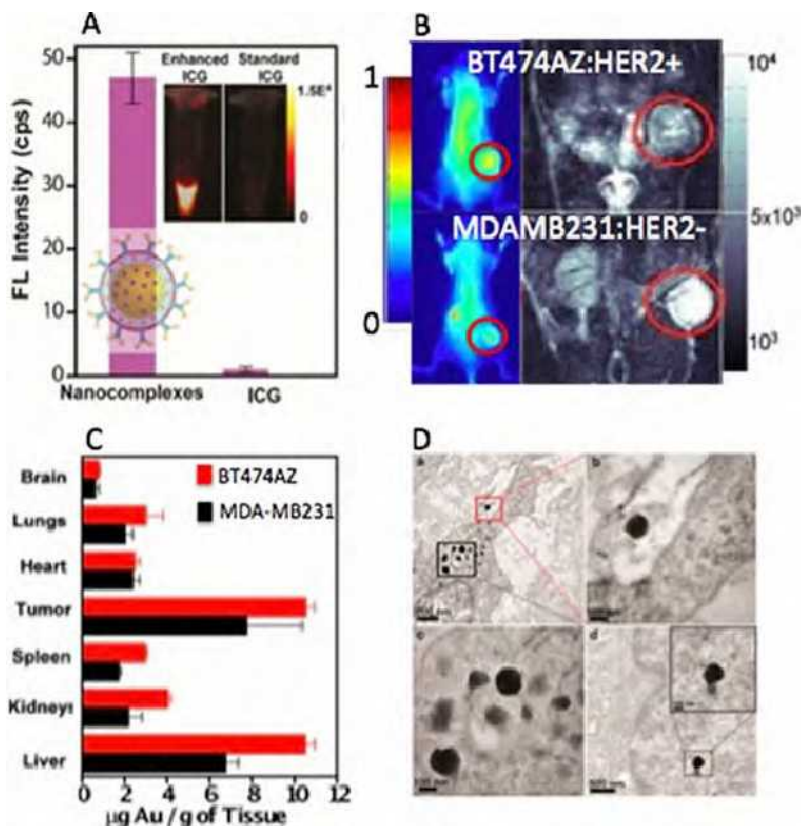
Pulmonary Intravascular Macrophages (PIMs) are large mononuclear cells different from interstitial and alveolar macrophages that develop from circulating monocytes in the pulmonary capillaries or arteriols. In humans, rats, dogs and monkeys lung does not contain PIMs under normal conditions. However, many cases of lung uptake of colloidal radiopharmaceuticals have been reported in patients with liver pathologies, infections or some cancers. Phagocytosis triggered by iv infusion of colloidal or nano-formulations could result in serious side effects including cardiopulmonary distress. Rats are very sensitive to PIMs induction following experimental biliary cirrhosis or repeated infusion of lipid formulations, peptides or new therapies from biotechnology. Using this model we have developed sensitive bimodal imaging probes (^{99m}Tc and fluorochrome labelled) for both exploration of activated macrophages recruitment and phagocytosis. For imaging recruitment of activated cells from the monocyte-macrophage lineage, in vivo targeting was achieved using an Acylated-Poly-Galactoside (APG) from bacterial origin via specific interactions with CD14, CD18 and CD11b. Fluorescent labeling was performed from the carbohydrate part of the molecule and reduced ^{99m}Tc was chelated thanks to the APG Pyrophosphate group. SPECT imaging was performed 2hours following iv infusion of 25µg APG (7.4MBq). Phagocytosis imaging was performed using fluorescent (FITC or Nile red) microsphere (1µm) functionalized for direct labeling with tin reduced ^{99m}Tc. SPECT was achieved 20 minutes after iv infusion (7.4MBq). To follow the development of the pathology, after induction (bile duct ligation or xenobiotic injection) imaging was performed 2 times a week over 40 days. The ratio between lung and liver+lung activity was determined. A ratio higher than 5% results in a significant PIMs induction that was histologically validated. Following in vivo imaging, lung was excised for fluorescence microscopy to document PIMs localization within capillaries and arteriols. The combination of SPECT and fluorescence allows to demonstrate that PIMs induction starts as punctual foci in the capillaries then spread to all of them and at the end to the endothelium of arteriols. Such PIMs have a long life time (40-60 days) as demonstrated by green and red microspheres administered at various time intervals. This approach provides new arguments to reconsider the patho-physiological involvement of this cell population for preclinical safety pharmacology studies of new drugs and more especially nanomedicines.

Presentation Number **0079**
 Scientific Session 7: Translational Molecular Imaging (Co-organized with SNM)

In Vivo Imaging and Bio-distribution of NIR Fluorescence and MR Contrast Enhancing Theranostic Nanostructures Targeted to Breast Cancer

Wenxue Chen^{1,2}, Rizia Bardhan³, Marc Bartels¹, Carlos J. Perez-Torres⁴, Maria F. Botero⁵, Robin Ward⁵, Rachel Schiff⁵, Robia G. Pautler⁴, Naomi J. Halas^{3,6}, **Amit Joshi**¹, ¹Radiology, Baylor College of Medicine, Houston, TX, USA; ²Obstetric & Gynecology, The Fourth Hospital of Hebei Medical University/Hebei Province Tumor Hospital, Shijiazhuang, China; ³Chemistry, Rice University, Houston, TX, USA; ⁴Molecular Physiology and Biophysics, Baylor College of Medicine, Houston, TX, USA; ⁵Lester and Sue Smith Breast Center, Baylor College of Medicine, Houston, TX, USA; ⁶Electrical and Computer Engineering, Rice University, Houston, TX, USA. Contact e-mail: wenxuec@bcm.edu

We report on (i) the temporal/spatial variation of NIR/MR contrast achieved via novel magnetofluorescent and photothermally active gold nanostructures in HER2+/- expressing breast cancer xenografts, and (ii) Biodistribution of theranostic nanoparticles in internal organs/tumors via ICP-MS analysis. Methods: Gold nanoshells (GNS) with plasmon resonance at 810nm were encapsulated in silica epilayers doped with superparamagnetic iron oxide (SPIO) nanoparticles and FDA cleared dye ICG, and conjugated with anti-HER2. In vivo experiments were conducted on BT474AZ (HER2+), and MDA-MB231 (HER2-) xenografts. Animals were imaged at 0.3, 2, 4, 24, 48, 72 hours post injection via both NIR and T2 weighted MR imaging. Organs/tumors harvested at 72 hours were analyzed for gold content with Inductively Coupled Plasma-Mass Spectrometry (ICP-MS). TEM imaging was used to determine the intracellular location and nanoparticle structural integrity on extracted tumor tissue. Results: GNS-Iron oxide-ICG complex enhanced fluorescent intensity 50X compared to free dye (Fig.A), while providing a specific r2 relaxivity of 390 mM⁻¹s⁻¹. Best contrast between HER+/- tumors was obtained at 4hrs for NIR imaging (Fig.B, left column), and at 24hrs for MR imaging (B, right column). SPIO in nanoshells caused darkening of tumor interior in T2 weighted imaging thus confirming antibody mediated internalization in HER2+ tumors. ICP-MS analysis (Fig.C) confirmed that tumors and liver exhibited maximal uptake of nanoparticles, with a 40% higher uptake of the agent in HER+ tumors. TEM images (Fig.D) confirmed that nanoparticles remained intact in vivo and were bound on cell membranes as well as internalized in the cytoplasm of tumor cells. We have previously demonstrated photothermal efficacy of GNS. With complementary abilities of NIR and MR imaging, the biodistribution of these theranostic nanoparticles can be accessed, and it can potentially provide tracking capabilities before, during and after treatment.



Presentation Number **0080**

Scientific Session 7: Translational Molecular Imaging (Co-organized with SNM)

Fluorescent Molecular Imaging and Microdosing in Humans

Milton V. Marshall¹, John C. Rasmussen¹, I-Chih Tan¹, Melissa B. Aldrich¹, Kristen E. Adams¹, Chinmay D. Darne¹, Caroline E. Fife^{2,1}, Latisha A. Smith^{2,1}, Erik A. Maus^{2,1}, Sunday Hoy³, Eva Sevick¹, ¹Institute of Molecular Medicine, Univ. of TX Health Sci. Ctr. Houston, Houston, TX, USA; ²Lymphedema and Wound Healing, Memorial Hermann Hospital, Houston, TX, USA; ³Tactile Systems, Inc., Minneapolis, MN, USA. Contact e-mail: M_Marshall@msn.com

Near-infrared (NIR) fluorescence molecular imaging depends upon the development of instrumentation sensitive enough to detect signals deep within tissues. We have developed a gain-modulated, image intensified camera and have employed it in IRB-approved human studies using a dim, non-specific dye, indocyanine green (ICG) administered at microdosing levels (<100 µg) in an off-label use to identify lymphatic diseased states, direct therapy, and determine treatment efficacy. After informed consent, ICG was administered intradermally and tissues were illuminated with <1.9 mW/cm² 785 nm excitation light. The emitted fluorescent light at 830 nm and over a >1500 cm² field of view was collected with integration times of 200 milliseconds. In over 130 human subjects we visualized normal and diseased lymphatic structures and function including propulsion of lymph through normal lymphatic vessels, dilated lymphatic vessels, lymph drainage into the abdomen, lymph nodes, tortuous lymphatic vessels presumably associated with lymphangiogenesis, lymph "reflux," and distal rather than normal proximal lymph flow. In addition, the utility of the new imaging approach was demonstrated in a compassionate use case in which the method was used to direct therapy in a head and neck cancer patient who suffered from severe lymphedema (LE). Lymphatic channels were identified by the imaging procedure, targeted for manual lymph drainage (MLD) therapy, and volume reduction was observed in edematous areas identified as being drained by functional lymph vessels. Because NIR fluorescence imaging enables real time quantification of lymph propulsion, we also used it to directly image the lymphatic response to MLD and a compression device that mimics MLD. Specifically, our studies demonstrate the potential use of NIR fluorescence imaging to detect subclinical lymphatic disease and enable evaluation of treatments that target the lymphatics. Given that ICG is approximately 10-30 times less bright than emerging new NIR fluorescent dyes with reactive group for conjugation, the opportunities for NIR fluorescence molecular imaging are bright. Supported by grants NIH R01 CA128919, R01 HL092923; RSG-06-213-01-LR from the American Cancer Society; and Tactile Systems, Inc.

Presentation Number **0081**

Scientific Session 7: Translational Molecular Imaging (Co-organized with SNM)

Prediction of Ischemic Bowel Viability Using Near-Infrared Fluorescence Angiography

Aya Matsui^{1,2}, **Joshua H. Winer**³, **Rita Laurence**¹, **John V. Frangioni**¹, ¹*Beth Israel Deaconess Medical Center, Boston, MA, USA;* ²*Division of Cancer Diagnostics and Therapeutics, Hokkaido University Graduate School of Medicine, Sapporo, Japan;* ³*Department of Surgery, Brigham & Women's Hospital, Boston, MA, USA. Contact e-mail: a_ma.sur@hotmail.co.jp*

Background: Assessing the viability of ischemic bowel is challenging. Presently, surgeons estimate viability by clinical inspection; however, the accuracy of clinical assessment is unknown. Previously, we have demonstrated that near-infrared (NIR) fluorescence angiography provides qualitative and quantitative measurement of tissue perfusion. In this study, we hypothesized that perfusion measured intraoperatively correlates with post-operative survival of the bowel, and we investigated whether NIR fluorescence angiography could predict viability of ischemic bowel. Material and Methods: Female Yorkshire pigs (n = 24) and Sprague-Dawley rats (n = 60) were enrolled. In pigs, bowel perfusion was imaged using the FLARE™ system and intravenously injected indocyanine green (ICG; 0.05 mg/kg). Three different lengths of ischemia were created in the imaged bowel by mesenteric vascular occlusion, and the bowel was re-imaged. Regions of interest were placed at equal intervals in the imaged bowel and fluorescence intensity was quantified over time via custom software. Contrast-to-background ratio (CBR) was obtained and graphical patterns of CBR curves were analyzed. Rat bowels were imaged by intravenous injection of 0.5 mg ICG 0.5 to 4 h after strangulation (n = 50) or without strangulation (n = 10). Animals were allowed to recover for 3 days and the bowel was then re-explored. Findings by clinical assessment and NIR fluorescence angiography on the day of surgery were checked for correlation with animal survival, histological grade of ischemic injury, and visible necrosis at postoperative day (POD) 3. Results: The pig study revealed that the CBR curve of non-ischemic bowel was characterized by an inflow peak, while the CBR curve of ischemic bowel lacked an inflow peak as a function of distance from normal bowel. In rat strangulation models, clinical assessment was found to have high specificity but low sensitivity. Existence of the inflow peak in the CBR curve and a filling defect in the NIR fluorescence angiography permitted prediction of animal survival and appearance of necrosis on POD 3 with high accuracy (90% and 92%, respectively). Both also showed high accuracy (85%) for prediction of the worst histological grade. Conclusion: NIR fluorescence angiography can not only assess bowel perfusion, but also predict bowel survival, with considerable accuracy. This technology could potentially help avoid unnecessary resection of the bowel.

Presentation Number **0082**

Scientific Session 7: Translational Molecular Imaging (Co-organized with SNM)

Metabolic Response to Chemotherapy in Multicentric Canine Lymphoma by Biopsy-based Nuclear Magnetic Resonance (NMR) Spectroscopy

Susan Kraft¹, Susan Lana², Eugene Ehrhart³, Kelly Carlsten², Andrea Merz⁴, Kalie Petefish¹, Natalie J. Serkova⁴, ¹*Environmental and Radiological Health Sciences, Colorado State University, Fort Collins, CO, USA;* ²*Clinical Sciences, Colorado State University, Fort Collins, CO, USA;* ³*Microbiology, Immunology, Pathology, Colorado State University, Fort Collins, CO, USA;* ⁴*Anesthesiology, University of Colorado, Aurora, CO, USA. Contact e-mail: skraft@colostate.edu*

Introduction and objectives: Lymphoma is a common naturally-occurring cancer in dogs that serves as an excellent translational model for human non-Hodgkin's lymphoma. We established metabolite profiles of canine lymphoma before and 24 hrs after first induction dose of chemotherapy using high-resolution nuclear magnetic resonance (NMR) of canine biopsies. Our working hypothesis was that we could detect metabolic biomarker(s) that predict initial cell response to treatment. The ultimate goal is to identify biologically-relevant metabolic biomarkers to guide development of novel targeted imaging agents for early assessment of response to therapy in vivo. **Methods:** Lymph node biopsies were obtained from 25 dogs with multicentric lymphoma just before (baseline), and 24 hours after, initial dose of induction chemotherapy. Samples were immediately snap-frozen in liquid nitrogen and processed by acid extraction to separate water- and lipid-soluble metabolites. High-resolution ¹H-NMR spectra were obtained in a 500 MHz NMR spectrometer using a 1-mm QNP ¹H/¹³C/¹⁹F microprobe (Bruker). Peaks of 30 metabolites were integrated and quantified using 1D WINNMR program. Immediate measures of biological response included lymph node size (RECIST) and biopsy-derived apoptosis score by caspase 3 immunohistochemistry. Two-sample t-tests were run for statistical differences before and after treatment. **Results:** Mean polyunsaturated fatty acids (PUFA), its ratio with monounsaturated fatty acids (MUFA), and acetate more than doubled after first induction dose of chemotherapy (p<0.05). The mean ratio of phosphocholine to glycerophosphocholine (PCho/GPC) decreased in half (p<0.01). Mean lactate increased slightly. Mean apoptosis score doubled (p<0.01), and mean lymph node size decreased by 20% (p < 0.01). **Conclusions:** The increased PUFA/MUFA after induction chemotherapy is consistent with apoptosis, and increased acetate and decreased PCho/GPC consistent with decreased fatty acid synthesis and cell membrane turnover respectively. Metabolic changes were associated with reduced lymph node size and increased apoptosis. Cancer metabolomic changes were documented 24 hrs immediately after first induction dose of chemotherapy demonstrating its use as an early indicator of biological response. Ultimately, we will use ongoing assessment of long term survival to identify metabolic biomarkers that discriminate between responders and non-responders.

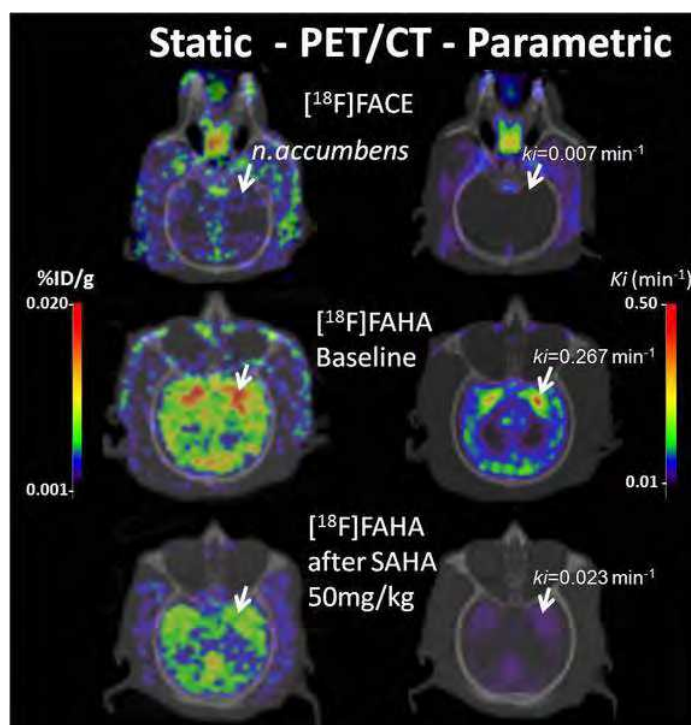
Presentation Number **0083**

Scientific Session 7: Translational Molecular Imaging (Co-organized with SNM)

Quantification of HDAC Activity in the Forebrain, N.accumbens, and Cerebellum in Non-human Primates Using ^{18}F -FAHA PET/CT and an Optimized Pharmacokinetic Model

Hsin-Hsien Yeh¹, Rainer Hinz², Suren Soghomonyan¹, Julius A. Balatoni¹, Uday Mukhopadhyay¹, Leo G. Flores¹, Asutosh Pal¹, Hwan Jeong¹, Rajesh Uthamanthil¹, James Jackson¹, William Tong¹, Mei Tian¹, Mian M. Alauddin¹, Karl Herholz², Juri G. Gelovani¹,
¹Experimental Diagnostic Imaging, MD Anderson Cancer Center, Houston, TX, USA; ²Wolfson Molecular Imaging Center, University of Manchester, Manchester, United Kingdom. Contact e-mail: HsinHsien.Yeh@mdanderson.org

Objective: Molecular imaging of epigenetic regulation by histone deacetylases (HDACs) using [^{18}F]FAHA PET/CT is a novel important area of research. In this study, we aimed to optimize the pharmacokinetic model of [^{18}F]FAHA-derived radioactivity accumulation in the brain in non-human primates for quantification of HDACs activity. **Methods:** Three PET imaging studies were performed in anesthetized rhesus macaques (N=2): 1) baseline study with [^{18}F]fluoroacetate ([^{18}F]FACE) - the major metabolite of [^{18}F]FAHA; 2) baseline study with [^{18}F]FAHA; and 3) repeat study with [^{18}F]FAHA after treatment with HDAC inhibitor SAHA (50 mg/kg i.v. infusion 1h prior to PET). Dynamic PET images of the brain were acquired for 30 minutes post i.v. injection of each radiotracer (6.07±0.75 mCi/5ml) and multiple blood samples were obtained for the analysis of metabolites ([^{18}F]FACE and [^{18}F]fluoride). The intracerebral influx rate constants (k_i) were calculated for each radiotracer using Patlak graphical analysis with corrections for radiolabeled metabolites and subtraction of [^{18}F]FACE-derived radioactivity contribution from the total brain radioactivity produced due to systemic catabolism of [^{18}F]FAHA. **Results:** Parametric PET images of [^{18}F]FAHA K_i were developed using PMOD (PMOD Technologies, Switzerland), which demonstrated predominant localization of HDAC activity in cerebellum, vermis, caudate-putamen, n.accumbens and amygdalae. The K_i of [^{18}F]FAHA in the brain (0.125 min⁻¹) was more than 12-fold higher than that of [^{18}F]FACE (0.007 min⁻¹). In n.accumbens, the K_i of [^{18}F]FAHA (0.267 min⁻¹) was 2-fold higher than in the surrounding forebrain structures and almost 40-fold higher than K_i of [^{18}F]FACE. After pre-treatment with SAHA, a significant increase in blood input function of [^{18}F]FAHA was observed, presumably due to inhibition of HDACs-mediated degradation of [^{18}F]FAHA in the periphery. However, the K_i of [^{18}F]FAHA in the brain was significantly decreased in n.accumbens (0.023 min⁻¹) and in the surrounding forebrain (0.005 min⁻¹), consistent with the inhibition of HDACs activity in CNS. Similar values for K_i and k_3 of [^{18}F]FAHA were obtained using a three-compartmental model with correction for the influx and efflux rate of [^{18}F]FACE, which was minimal and could be ignored. **Conclusions:** Using the optimized Patlak graphical analysis with correction for influx rate of radiolabeled metabolites (i.e., [^{18}F]FACE), the calculated K_i rate constant for [^{18}F]FAHA accumulation in the brain reflects the expression-activity of HDACs in the brain. PET/CT with [^{18}F]FAHA could be used reliably for non-invasive assessment of pharmacodynamics of novel HDAC inhibitors in CNS.



Presentation Number **0084**
Scientific Session 8: Probes for Brian Disease

Non-Conjugated Small Molecule FRET Pair: An Application for Differentiating Amyloid Beta Monomers from Higher Molecular-weight Species

Chongzhao Ran, Anna Moore, Radiology, Massachusetts General Hospital, Charlestown, MA, USA. Contact e-mail: cran@nmr.mgh.harvard.edu

Differentiating amyloid beta monomers from higher molecular weight species with known toxic effects is tremendously important in Alzheimer's disease (AD) research. Here we demonstrated that a small molecule FRET (Förster resonance energy transfer) pair was able to distinguish monomers from high molecular weight species in solution. Although FRET is widely used in biological studies, previous applications of the technique have required tedious construction of a FRET pair by chemical conjugation. In contrast, our approach involves the use of a non-conjugated, non-bioengineered FRET technique in which amyloid beta (A β) aggregates are used as intrinsic platforms for FRET pair assembly. Mixture of two structurally-similar curcumin derivatives with A β 40 aggregates resulted in FRET signal in solution, a signal that was absent when derivatives were placed in solution with A β 40 monomers. We believe that this FRET technique could potentially be used as a tool for differentiation of A β species in biofluids, such as cerebrospinal fluid (CSF) or serum, of Alzheimer's disease patients. In addition, we believe that this concept could be generalized to other misfolded proteins/peptides in disease, including amyloid in diabetes, prion in Bovine Spongiform Encephalopathy, tau protein in AD, and α -synuclein in Parkinson disease.

Presentation Number **0085**
Scientific Session 8: Probes for Brian Disease

Protein-based MRI Probes for Functional Neuroimaging

Alan Jasanoff¹, Eric Brustad², Victor S. Lelyveld¹, Fay Bi², Taekwan Lee¹, Gil G. Westmeyer¹, Frances H. Arnold², ¹Massachusetts Institute of Technology, Cambridge, MA, USA; ²California Institute of Technology, Pasadena, CA, USA. Contact e-mail: jasanoff@mit.edu

Functional MRI with contrast agents sensitive to neural activity would combine noninvasive whole-brain coverage with molecular level specificity for neuronal events. Protein-based contrast agents are of particular interest because of the possibility of gene-based brain delivery strategies, and the availability of protein engineering techniques that leverage knowledge gleaned from structural biology. We have used protein engineering to create macromolecular responsive MRI probes that detect events including neurotransmitter release and that are designed for functional brain imaging. First-generation sensors derived from the bacterial cytochrome P450 BM3 were prepared using directed evolution and shown to detect dopamine release in cell culture and in living rat brains. The protein engineering technique was adapted to produce P450-based sensors for serotonin, another monoamine transmitter. Longitudinal relaxivity of the sensors was substantially improved through a transmetallation technique, potentially facilitating more sensitive in vivo measurements and reduced tendency for analyte buffering. Ongoing work involves applying the sensors to map neurotransmitter release profiles during behaviorally salient stimulation in rats. In addition, we are experimenting with alternative protein-based sensing platforms that may offer further increases in MRI detection sensitivity or access to additional neurochemical analytes.

Presentation Number **0086**
Scientific Session 8: Probes for Brain Disease

Plaque Detection with a Novel PET Amyloid Imaging Agent, [¹⁸F]AV-45 in a Transgenic Mouse Model

Chi-Chang Weng¹, Kun-Ju Lin^{1,2}, James Che-Kun Shen³, Kuen-Jer Tsai^{3,4}, Tzu-Chen Yen², Daniel M. Skovronsky^{5,6}, Shiaw-Pyng Wey^{1,2}, Mei-Ping Kung^{2,6}, ¹Department of Medical Imaging and Radiological Sciences, Chang Gung university, Taoyuan, Taiwan; ²Molecular Imaging Center, Department of Nuclear Medicine, Chang Gung Memorial Hospital, Taoyuan, Taiwan; ³Institute of Molecular Biology, Academia Sinica, Taipei, Taiwan; ⁴Institute of Clinical Medicine, College of Medicine, National Cheng Kung University, Tainan, Taiwan; ⁵Avid Radiopharmaceuticals Inc, Philadelphia, PA, USA; ⁶Department of Radiology, School of Medicine, University of Pennsylvania, Philadelphia, PA, USA. Contact e-mail: b9003223@stmail.cgu.edu.tw

Purpose: Florbetapir F 18 ([¹⁸F]AV-45) is a selective positron emission tomography (PET) tracer currently in clinical trials for detection of β -amyloid (A β) pathology. This study was to evaluate the feasibility of detecting A β plaques with [¹⁸F]AV-45 in the Tg2576 mouse model of Alzheimer's disease (AD) with small animal PET imaging. Methods: PET imaging was performed with an Inveon™ small animal scanner in three Tg2576 mice (Tg, age 24.80 \pm 0.85 months; BW 25.33 \pm 4.07 g) and three age-matched wild-type mice (WW, age 25.37 \pm 0.58 months; BW 37.57 \pm 0.95 g). The dynamic PET scan was performed for 60 min in each isoflurane-anesthetized mouse after a bolus injection of 11-22 MBq of [¹⁸F]AV-45. On the coronal PET image, regions of interest (ROIs) were placed on frontal lobe (FL) and cerebellum (CB), guided by a mouse stereotaxic atlas. Time-activity curves (TACs) (expressed as percent injected dose per gram normalized to body weight: %ID/kg/g) were obtained for FL and CB. Standard uptake value ratio (SUVr) of FL-to-CB was also calculated. After PET scan, the mice were sacrificed for ex vivo and in vitro autoradiography, and the same or adjacent sections were stained with thioflavin-S to confirm the A β -plaque deposition. Results: [¹⁸F]AV-45 in all ROIs peaked early (at 2 min), with the radioactivity washing out quickly in both Tg and WW mice. Peak uptakes in all regions were significantly lower in Tg mice than in WW mice due to the lower body weights. The TAC corrected for body weight (%ID/kg/g) in Tg mice resembled to the WW mice for the CB region; whereas Tg mice exhibited increased radioactivity retentions in the FL region. During the later part of the washout phase (20-40 min), the mean FL/CB was higher in Tg than WW mice (1.26 \pm 0.07 vs. 0.98 \pm 0.06). Ex vivo, in vitro autoradiography and fluorescent staining with thioflavin-S all clearly revealed widespread deposition of A β plaques in FL, but not in CB of Tg mice or in the brain regions of WW mice. Conclusion: [¹⁸F]AV-45 showed a higher retention in the FL region in Tg mouse brain as compared to the WW mouse brain (1.26 vs. 0.98), reflected to the 30% FL-to-CB SUVr difference. The high retention correlated to the plaque accumulation evidenced by autoradiography and fluorescent staining. With the power of animal PET technology in pursuit of amyloidogenesis and evaluation of emerging anti-amyloid treatments, [¹⁸F]AV-45 may provide an opportunity to detect the A β plaque load change in drug-treated Tg2576 mice, and it could be helpful to screen the new therapeutic drugs for AD.

Presentation Number **0087**
Scientific Session 8: Probes for Brain Disease

¹¹C-Ketoprofen-methyl Ester as a Novel Cyclooxygenase-1 Specific PET Probe for Imaging of Neuroinflammation

Miho Shukuri¹, Misato Takashima-Hirano¹, Keiko Tokuda¹, Kiyoshi Matsumura², Miki Goto¹, Hisashi Doi¹, Masaaki Suzuki¹, Yasuyoshi Watanabe¹, Hirotaka Onoe¹, ¹Center for Molecular Imaging Science, RIKEN, Kobe, Japan; ²Faculty of Information Science and Technology, Osaka Institute of Technology, Hirakata, Japan. Contact e-mail: shukuri@riken.jp

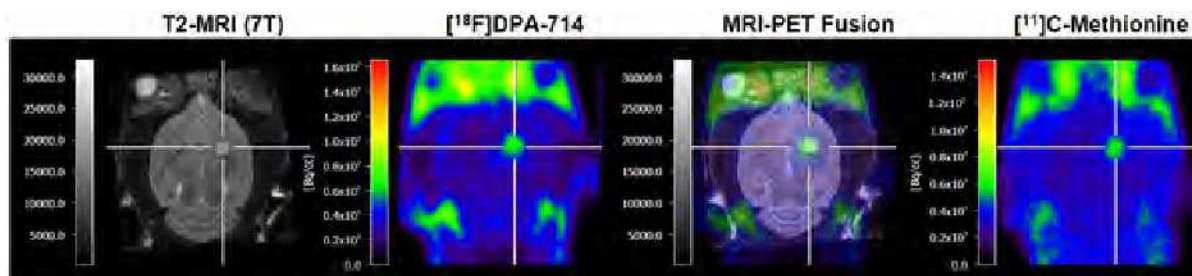
Neuroinflammation is critically involved in the pathological processes of neurodegenerative disorders, such as multiple sclerosis, Parkinson's disease, and Alzheimer's disease. Cyclooxygenase (COX), the prostanoid-synthesizing enzyme, plays an important role for the regulation of neuroinflammatory process in brain. Recently, we have developed PET probes targeting COX using several nonsteroidal anti-inflammatory drugs (NSAIDs) to detect neurodegenerative disorders with neuroinflammation. Among more than 10 NSAIDs derivatives examined, ¹¹C labeled ketoprofen-methyl ester (¹¹C-KTP-Me) has the most suitable characteristics as a PET probe for imaging of neuroinflammation. Two distinct isoforms, COX-1 and COX-2, are known as a constitutive and an inducible form, respectively, and ketoprofen is reported to be rather specific to COX-1 than COX-2. Though, COX-2 is thought to be a key isoform induced in the activated microglia during neuroinflammation, isoform responsible for ¹¹C-KTP-Me under in vivo imaging condition has not been verified yet. In order to characterize the specificity of ¹¹C-KTP-Me to each COX isoform in the brain, we performed ex vivo autoradiography and in vivo PET studies with ¹¹C-KTP-Me using COX-1 deficient (COX-1^{-/-}) and COX-2 deficient (COX-2^{-/-}) mice. In addition, changes of COX expression and localization in inflamed stimuli were examined by immunohistochemical study. Ex vivo autoradiography and PET imaging of COX-deficient mice have revealed that COX-1^{-/-} mice showed significantly lower accumulation of ¹¹C-KTP-Me in all brain regions (P<0.01) than wild type mice. In contrast, COX-2^{-/-} mice showed the same accumulation level as compared with wild type mice. Intraatrial injection of lipopolysaccharide (LPS) in rats caused high accumulation of ¹¹C-KTP-Me at the early time points, 6 hours and 1 day, with the activation of microglia demonstrated by accumulation of ¹¹C-PK11195, a PET probe for imaging of activated microglia. In addition, immunohistochemical study has shown that activated microglia/monocyte was identified to express COX-1 but not COX-2 at the early phase. These results strongly indicate that ¹¹C-KTP-Me is a COX-1 selective PET probe, and provides a new evidence for the specific action of COX-1 in the neuroinflammatory process.

Presentation Number **0088**
 Scientific Session 8: Probes for Brain Disease

The TSPO-ligand [¹⁸F]DPA-714 Images Glioma In Vivo

Alexandra Winkeler^{1,2}, **Raphael Boisgard**^{1,2}, **Albertine Dubois**^{1,2}, **Ali R. Awde**^{1,2}, **Jinzi Zheng**^{1,2}, **Luisa Ciobanu**³, **Karine Siquier-Pernet**^{1,2}, **Frederic Dolle**², **Thomas Viel**⁴, **Andreas H. Jacobs**⁴, **Bertrand Tavitian**^{1,2}, ¹Inserm, U1023, Laboratoire d'Imagerie Moléculaire Expérimentale; Université Paris Sud, Orsay, France; ²CEA, DSV, I2BM, SHFJ, Orsay, France; ³CEA, DSV, I2BM, NeuroSpin, LRMN, Gif sur Yvette, France; ⁴MPI for Neurological Research, Koln, Germany. Contact e-mail: alexandra.winkeler@cea.fr

Introduction: In the last years there has been an enormous increase in the development of radioligands targeted against the translocator protein (TSPO). TSPO expression is well documented in activated microglia and serves as a biomarker for imaging neuroinflammation. In addition, TSPO has also been reported to be over-expressed in a number of cancer cell lines and human tumors including glioma. Here, we investigate the use of [¹⁸F]DPA-714, a TSPO PET radioligand as new marker to image glioma in vivo. **Methods:** 9L rat glioma cells were stereotactically implanted in the striatum of Fisher, Wistar and Sprague Dawley rats. To monitor tumor growth T2w-MRI and/or [¹¹C]Methionine PET were performed prior to [¹⁸F]DPA-714 PET imaging. Dynamic [¹⁸F]DPA-714 PET scans were acquired 11-14 days post-inoculation. The injected dose was 1.24 ± 0.30 mCi (mean ± sd). For qualitative and quantitative analysis, [¹⁸F]DPA-714 PET images were co-registered to the corresponding MRI and a volume-of-interest (VOI) analysis was performed on both the kinetic and summed image data sets. A VOI was manually delineated on the tumor and a mirror VOI was copied and symmetrically pasted into the contralateral hemisphere. In addition, the expression of TSPO in 9L rat glioma cells was investigated using Western Blot and immunohistochemistry. **Results:** 9L glioma cell inoculation resulted in tumor growth in all strains. Tumors developed in Fisher and Wistar rats were evidenced by MRI. Gliomas grown in Fisher (n=5), Wistar (n=4) and Sprague Dawley (n=6) rats were detected by [¹⁸F]DPA-714 PET. All rats showed [¹⁸F]DPA-714 PET accumulation at the site of tumor implantation compared to the contralateral site (Figure). Calculations of %ID/cc showed significant differences between tumor and control VOIs in Fisher, Wistar and Sprague Dawley rats (Table). TSPO expression in tumors was also confirmed by Western Blot of 9L cells *in vitro* and by immunohistochemistry *ex vivo*. **Conclusion:** This study demonstrates the feasibility of using the TSPO-radioligand [¹⁸F]DPA-714 to characterize 9L glioma *in vivo* in different rat models with PET imaging, supporting further assays of [¹⁸F]DPA-714 for imaging human glioma.



Figure

	%ID/cc contralateral (mean ± sd)	%ID/cc tumor (mean ± sd)
Fisher	0.13 ± 0.02	0.49 ± 0.05
Wistar	0.13 ± 0.06	0.31 ± 0.09
Sprague Dawley	0.11 ± 0.05	0.26 ± 0.06

Presentation Number **0089**
Scientific Session 8: Probes for Brain Disease

Study on Scanning Time Window of a Novel PET Tracer 18F-AV-133 for VMAT2 Imaging

Chia-Ju Hsieh¹, **Ing-Tsung Hsiao**^{1,2}, **Kun-Ju Lin**^{1,2}, **Wey-Yil Lin**³, **Yi-Hsin Weng**³, **Chin-Song Lu**³, **Shiaw-Pyng Wey**^{1,2}, **Mei-Ping Kung**⁴, **Daniel M. Skovronsky**⁵, **Tzu-Chen Yen**^{1,2}, ¹*Medical Imaging and Radiological Sciences, Chang Gung University, Tao-Yuan, Taiwan;* ²*Nuclear Medicine and Molecular Imaging Center, Chang Gung University and Memorial Hospital, Tao-Yuan, Taiwan;* ³*Neurology, Chang Gung Memorial Hospital, Tao-Yuan, Taiwan;* ⁴*Radiology, University of Pennsylvania, PA, PA, USA;* ⁵*Avid Radiopharmaceuticals, PA, PA, USA. Contact e-mail: funnybobo@gmail.com*

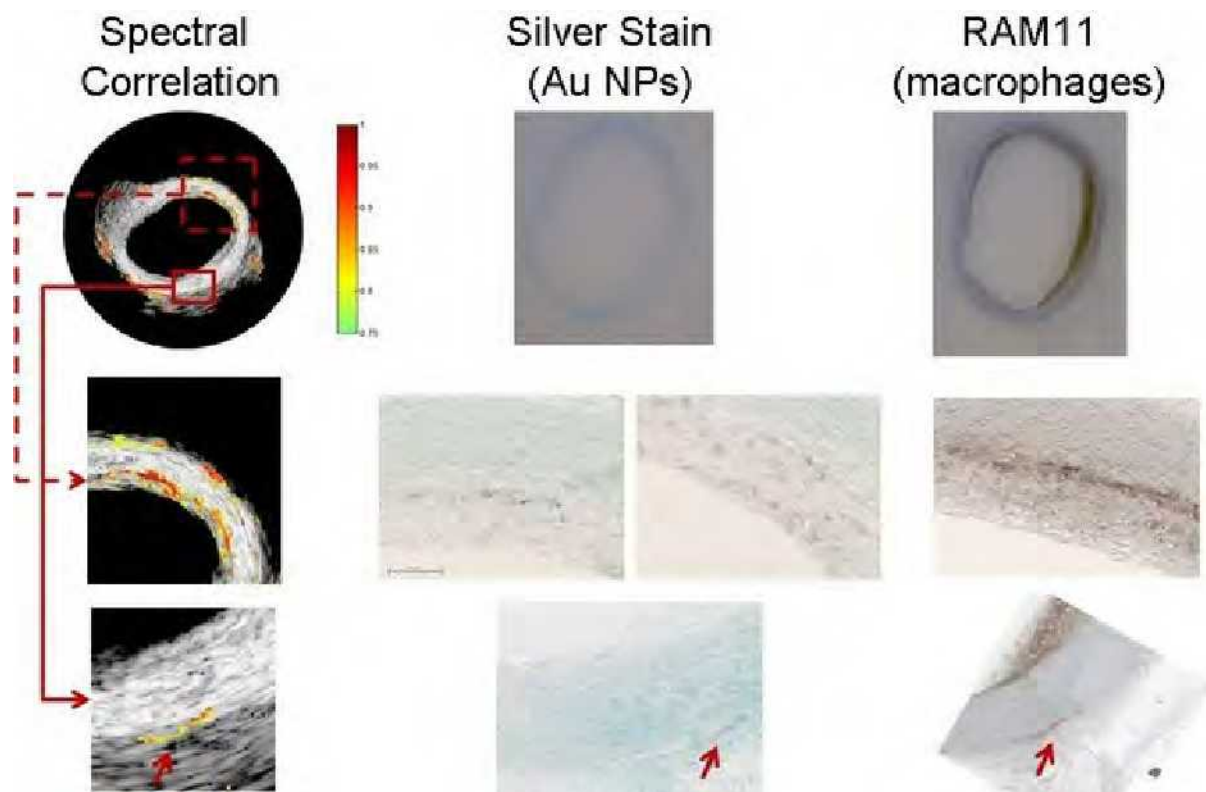
Objectives: 18F-AV-133 ([F-18]9-fluoropropyl-DTBZ) is a novel PET tracer for imaging the vesicular monoamine transporter II (VMAT2) in dopaminergic neuron degeneration of Parkinson diseases (PD). Initial studies were performed for optimizing imaging time window in calculating SUVR (specific uptake value ratio) with correlation to DVR (distribution volume ratio), and in differentiating PD from normal controls. **Methods:** With the written informed consent, a total of 13 dynamic AV-133 PET studies were conducted on 4 healthy controls, and 9 PD patients with Hoehn and Yahr stages 2-3 (10 mCi; dynamic scan of 0-30, 50-140 and 160-180 min). Volume of interest (VOIs) of left and right putamen (PL, PR), left and right caudate (CL, CR), and occipital cortex (OC) were drawn according to each subject's MRI and early-time PET images. SUVR from mean uptake value in VOI to that of OC was computed for 14 of 10-min, and 10 of 20-min window from the 180-min scanning period. The values of DVR were also computed from Logan graphic analysis by using primary visual cortex as input. The performance of SUVRs was evaluated based on the correlation of regional SUVR to DVR, as well as the Cohen effect size (group-mean difference / pooled STD) between PD and control groups. **Results:** Consistent higher correlations of SUVRs to DVR for all VOIs were observed at later time window (> 20min after injection), and the maximal correlations of 0.9849 and 0.9826 were achieved at 90-100 min and 80-100 min for 10- and 20- min time window, respectively. The group-mean differences and pooled STD between control and PD groups across different VOIs reached relatively stable values after 90 min. The resulted effect size for all VOIs was stable across different time windows (except for CR) and with the largest value around the 90~100 min time window. **Conclusion:** The SUVRs of the AV-133 displayed strong correlation to DVR for imaging both control and PD groups. In particular, the results also consistently showed good differentiation between these two groups. In terms of clinical feasibility across healthy controls and PD patients for all VOIs, the 10-min scanning time of 90-100 min is considered as the optimal time window.

Presentation Number **0090**
 Scientific Session 9: Tracking Immune Cells

Spectroscopic Intravascular Photoacoustic Imaging of Macrophages in Atherosclerotic Plaques

Bo Wang¹, Pratixa P. Joshi¹, Richard Smalling², Konstantin Sokolov¹, **Stanislav Y. Emelianov¹**, ¹Biomedical Engineering, University of Texas at Austin, Austin, TX, USA; ²Cardiology, University of Texas Health Science Center - Houston, Houston, TX, USA. Contact e-mail: emelian@mail.utexas.edu

The rupture of the atherosclerotic plaques may cause life threatening consequences such as stroke or heart failure. Macrophage is a critical cell type that positively contributes to the development and rupture of the atherosclerotic plaques. The ability to image the distribution of macrophages in plaques will benefit disease diagnosis and treatment. We have developed a technique to visualize active macrophages in atherosclerotic plaques using intravascular photoacoustic (IVPA) imaging augmented with targeted plasmonic nanoparticles. The experiments were performed using a rabbit model of atherosclerosis. The animals were injected intravenously with targeted 20 nm spherical gold nanoparticles (Au NPs). These nanoparticles entered the atherosclerotic region of the vessel through the leaky endothelium, and labeled the macrophages located in the thickened intimal layer of the artery. The rabbit was sacrificed 29 hours after the injection of Au NPs. Excised samples of rabbit aorta were imaged using a bench-top system capable of simultaneous IVPA and intravascular ultrasound (IVUS) imaging. The imaging system consisted of a tunable (700-950 nm) pulsed (4-6 ns) laser, a 40 MHz intravascular ultrasound (IVUS) imaging catheter, and a data acquisition system. Multi-wavelength IVPA images were acquired in the 700-760 nm spectral region where the optical absorption spectrum of macrophages labeled with Au NPs was elevated due to plasmon resonance coupling phenomena. Utilizing this change in optical properties of Au NPs, an image processing method was developed to identify the regions in the artery that contained Au NPs labeled macrophages. Spectral analysis of IVPA signals revealed regions containing aggregated Au NPs in the aorta. Silver stain of the vessel confirmed the distribution of Au NPs in the combined IVUS and spectroscopic IVPA image. Furthermore, RAM11 staining of the vessel indicated a strong correlation between the location of Au NPs and macrophages within the atherosclerotic plaque. Therefore, our results demonstrated that spectroscopic IVPA imaging can detect Au NP labeled macrophages in atherosclerotic plaques.



Presentation Number **0091**
Scientific Session 9: Tracking Immune Cells

Preliminary Intravital Microscopic Analysis Reveals Macrophage Uptake of Circulating Nanotubes and RGD-dependent Delivery into Tumor

Bryan R. Smith¹, **Harikrishna Rallapalli**¹, **Jennifer Prescher**¹, **Cristina Zavaleta**¹, **Jarrett Rosenberg**¹, **Zhuang Liu**², **Hongjie Dai**², **Sanjiv S. Gambhir**¹, ¹*Radiology/Molecular Imaging, Stanford University, Stanford, CA, USA;* ²*Chemistry, Stanford University, Stanford, CA, USA. Contact e-mail: brsmith@stanford.edu*

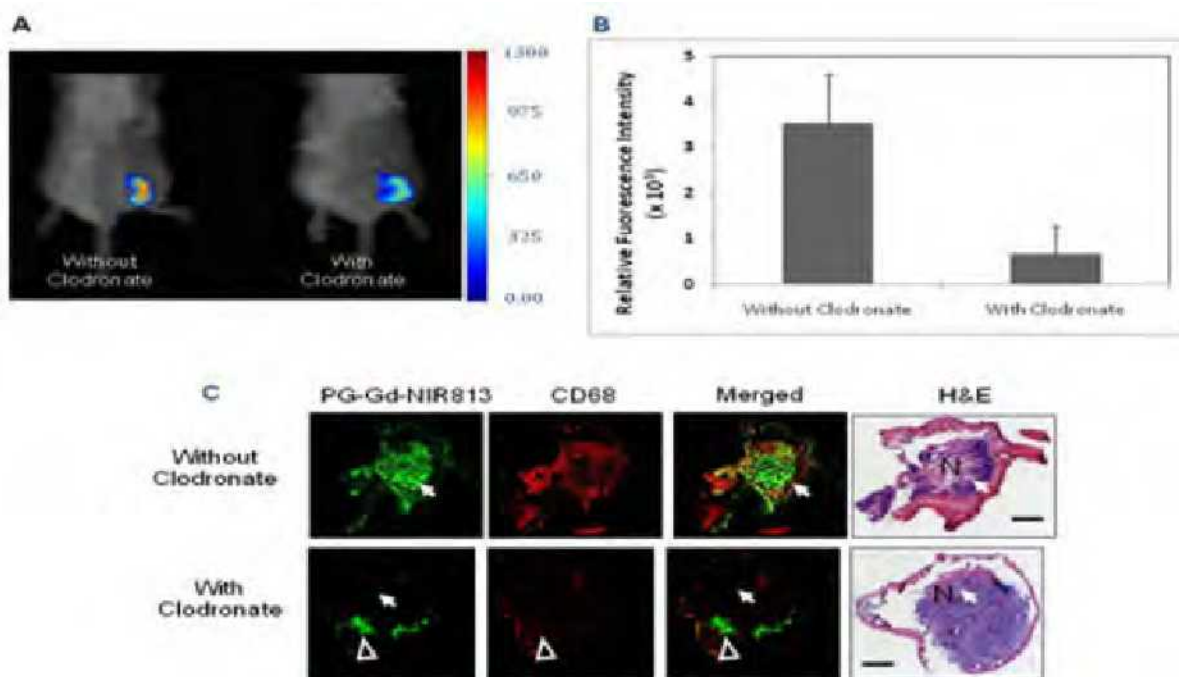
Molecular targeting of nanoparticles (nps) is known to increase tumor uptake, but is believed to do so via a direct np ligand-receptor binding mechanism. It is also well-known that macrophages (macs) tend to accumulate in tumor. The present work unexpectedly suggests that circulating macs can be programmed by molecularly-targeted nps to increase preferential deposition into tumor. We used intravital microscopy (IVM) to visualize U87MG tumor (EGFP) in a dorsal window chamber mouse model (n=25 mice) as we IV injected single-walled carbon nanotubes (SWNTs) conjugated to cy5.5 dye. In real time, we visualized uptake of SWNTs into circulating macrophages (identified via flow cytometry) and their behavior within tumor interstitium. We also used the intrinsic Raman signature of SWNTs to quantify overall tumor uptake. SWNTs were conjugated to RGD which binds integrin $\alpha v \beta 3$ RAD peptide and unconjugated SWNTs (plain) were controls. We observed rapid uptake (< 1 min) of SWNTs into macs with plain SWNTs, compared with several hours for peptide-conjugated SWNT uptake. Macs observed in vasculature were categorized as 1) non-interacting (free-flowing) 2) interacting cells (crawling along the luminal surface). At one day p.i., we observed more non-interacting macs containing plain SWNTs than those with RAD, and more RAD than RGD (p=0.0001). However, interacting macs displayed the reverse trend (0.0057), suggesting that having peptides linked to SWNTs encouraged mac interaction with the endothelium. Last, across the first week p.i., we found more non-interacting macs in the plain condition than in the RGD-SWNT condition (p<0.0001), with no difference between RAD and plain SWNTs. We observed (1) SWNT-laden macs in tumor interstitium and (2) total SWNTs in tumor increased over the first week p.i. for RGD/RAD, but only for the first 3 days p.i. for Cy5.5. Together with the above results, the data imply SWNT delivery into tumor via the mac "Trojan Horse." Our data thus indicate that RGD may encourage not only typical np ligand-recptor binding routes, but also indirect uptake into (and perhaps on the surface of) macrophages. These RGD-SWNT laden macrophages appear to be preferentially taken up into tumor compared with SWNTs without RGD. In conclusion, these results could (1) lead to improved np design to increase mac delivery, (2) transform non-specific tumor macs into specific delivery vehicles, and (3) may explain the high tumor uptake displayed by SWNTs.

Presentation Number **0092**
 Scientific Session 9: Tracking Immune Cells

Targeted Imaging of Tumor-Associated M2 Macrophages Using a Macromolecular Contrast Agent PG-Gd-NIR813

Marites P. Melancon^{2,1}, **Wei Lu**¹, **Qian Huang**¹, **Prakash Thapa**³, **Dapeng Zhou**³, **Chaan S. Ng**⁴, **Chun Li**¹, ¹*Experimental Diagnostic Imaging, UT-MD Anderson Cancer Center, Houston, TX, USA;* ²*Imaging Physics, UT-MD Anderson Cancer Center, Houston, TX, USA;* ³*Melanoma and Medical Oncology, UT-MD Anderson Cancer Center, Houston, TX, USA;* ⁴*Radiology, UT-MD Anderson Cancer Center, Houston, TX, USA.* Contact e-mail: mmelancon@di.mdacc.tmc.edu

Objectives: Tumor-associated macrophages (TAMs) are diverse population containing multiple subtypes. Based on their immunological functions, subtypes of M1 and M2 have been proposed. The purpose of this study was to evaluate whether PG-Gd-NIR813, a dual magneto-optical imaging probe based on poly(L-glutamic acid) (PG) backbone conjugated with DTPA-Gd and a near-infrared dye (NIR813) could be used for dual modal imaging of TAMs after intravenous injection. **Methods:** PG-Gd-NIR813 was synthesized and characterized with regard to molecular weight, Gd and dye payload, and relaxibility. PG-Gd-NIR813 was evaluated for noninvasive assessment of TAMs after intravenous injection. **Results:** PG-Gd-NIR813 injected in nude rats bearing C6 tumors showed tumor-specific uptake of the polymeric contrast agent at 1 and 48 h after injection both in vivo and ex vivo optical imaging. T1-weighted MR imaging results showed accumulation of PG-Gd-NIR813 into the tumor necrotic area, which was confirmed by TUNEL staining of resected tumors. The uptake of PG-Gd-NIR813 within tumor necrosis decreased after animals were treated by the macrophage depleting agent. Immunohistochemical staining demonstrated that PG-Gd-NIR813 colocalized with CD68 (marker for macrophages) and CD169 (marker for activated macrophages), but not with CD163 (residential macrophages). Using combined near-infrared fluorescence imaging and MRI, we demonstrated that the accumulation of PG-Gd-NIR813 in tumors was mediated through M2 TAMs, a macrophage subtype that secrete a wide range of proangiogenic factors and growth factors and promote tumor growth and metastasis. **Conclusions:** Poly(L-glutamic acid) based reagents could be potentially used to image response to antitumor therapies targeted at M2 TAMs. Poly(L-glutamic acid) may also be a promising carrier for candidate immunotherapeutics targeting M2 TAMs.



Presentation Number **0093**
Scientific Session 9: Tracking Immune Cells

Optical Imaging and PET-investigations of Intra-venous or Intra-peritoneal Administered IFN-gamma Producing CD4+ T Cells (Th1) Confirmed Significant Differences in Homing and Biodistribution

Christoph M. Griessinger¹, Daniel Bukala¹, Kerstin Fuchs³, Ivana Glocova³, Walter Ehrlichmann², Martin Röcken³, Bernd J. Pichler¹, Manfred Kneilling³, ¹Department of Radiology, Eberhard Karls University Tübingen, Laboratory for Preclinical Imaging and Imaging Technology of the Werner Siemens-Foundation, Tübingen, Germany; ²Radiopharmacy, Eberhard Karls University Tübingen, , Tübingen, Germany; ³Department of Dermatology, Eberhard Karls University Tübingen, , Tübingen, Germany. Contact e-mail: christoph.griessinger@med.uni-tuebingen.de

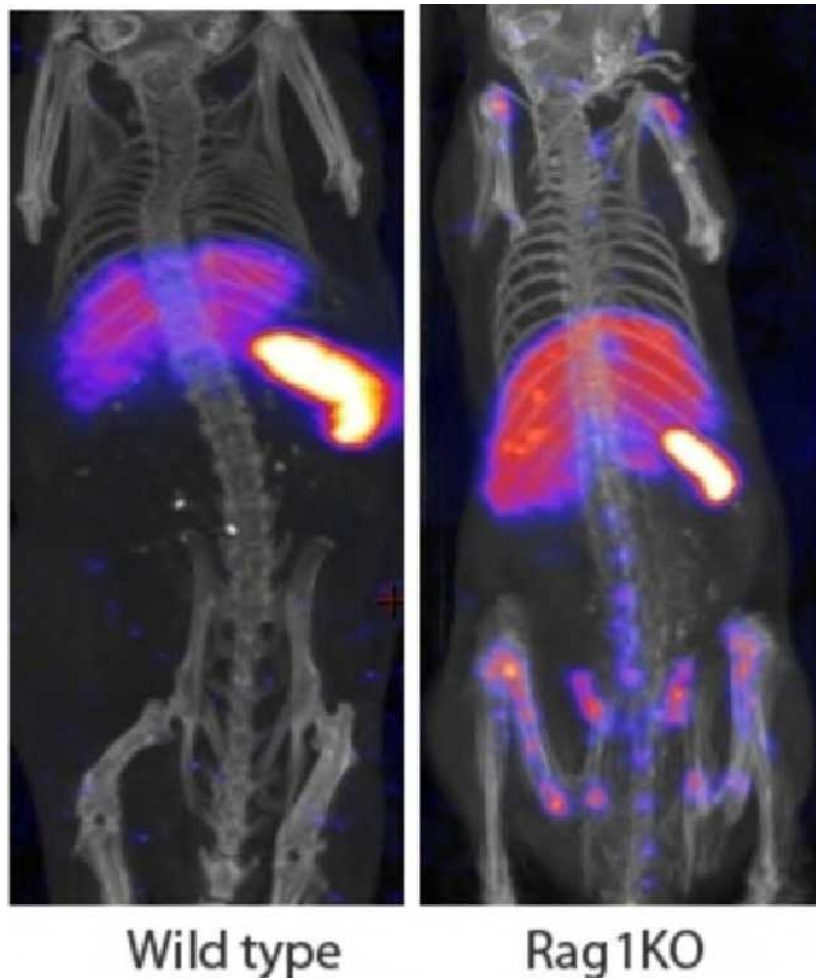
Specific T cell based immunotherapy for cancer or autoimmune diseases require suitable administration routes to ensure T cell homing to the target site. The aim of our study was to analyse differences in Th1 cell homing after intra-peritoneal (i.p.), intra-venous (i.v.), and retro-bulbar venous plexus (r.b.) administration by small animal positron emission tomography (PET) and optical imaging (OI). Ovalbumin (OVA)-T cell receptor (TCR) transgenic CD4+ T cells were isolated from spleens and lymph nodes of DO.11.10 mice, and cultured together with irradiated antigen presenting cells, OVA peptide, CpG oligonucleotide 1668, anti-IL-4, and IL-2 for 12-14 days to generate a Th1 phenotype. OVA-Th1 cells were labelled intracellularly with [64Cu]PTSM or with Cy5 vibrant dye solution. [64Cu]PTSM labelled OVA-Th1 cells were tracked in vivo for up to 48 hours, and Cy5-labelled OVA-Th1 cells for up to 4 weeks. We injected 1E+7 [64Cu]PTSM- or Cy5-labelled OVA-Th1 cells (i.p., i.v. or r.b.) into naive BALB/c mice and analysed their migration properties using PET/CT and OI. Additionally, we investigated [64Cu]PTSM-/Cy5-labelled OVA-Th1 cells ex vivo by biodistribution and flow cytometry (FACS) analysis 48 hours ([64Cu]PTSM) and 1, 2, and 4 weeks (Cy5) after administration. After i.p. injection OVA-Th1 cells accumulated into the thymus, inguinal-, and axillary lymph nodes, as well as into the mesenteric lymphatic tissue (mesenteric-, pancreatic lymph nodes, omentum majus). After i.v. and r.b. administration OVA-Th1 cell migrated predominantly into the heart, lung, liver and spleen. One week after i.v. and r.b., but not after i.p. administration of OVA-Th1 cells, we detected migration into the bone marrow by OI and FACS analysis. However, we could detect a strong accumulation of i.p. administered but not i.v. administered OVA-Th1 cells into the lymph nodes by OI. PET and OI data were confirmed by FACS-analysis, OI and biodistribution. Comparison of OI-imaging (Cy5) and PET-imaging ([64Cu]PTSM) revealed that OI fits very well for longitudinal studies for up to four weeks and PET is best for quantitative high resolution imaging for up to 48 hours. The main disadvantage for OI is the missing option for exact quantification and for PET the loss of T cell functioning after 48 hours due to the radiolabel [64Cu]PTSM. Thus, we detected significant differences in T cell migration and biodistribution between i.v. and i.p. administration by PET and OI which might be relevant for T cell based specific immunotherapy.

Presentation Number **0094**
Scientific Session 9: Tracking Immune Cells

In Vivo Imaging Revealed Trafficking of T Cells to Bone Marrow for Homeostatic Proliferation

Noriko Sato, Karen J. Wong, Peter Choyke, Molecular Imaging Program, National Cancer Institute, Bethesda, MD, USA. Contact e-mail: saton@mail.nih.gov

Peripheral lymphocytes undergo homeostatic proliferation to maintain their number when they are in lymphopenic conditions. However, in which organ this proliferation takes place has not been well investigated. To examine the migration of lymphocytes under lymphopenic condition, we tracked purified CD8 T cells labeled with In-111 oxine after adoptive transfer to lymphopenic mice using a small animal SPECT imager. CD8 T cells were purified from C57/B6 mice or OT1 T cell receptor transgenic mice using magnetic beads. The purified CD8 T cells were labeled with In-111 oxine. The average specific activity was 395×10^{-4} Bq/cell. Rag1 knockout (Rag1KO) mice and C57/B6 wild type mice (control) were transferred with 3 million In-111 oxine labeled CD8 T cells via the tail vein. Fifteen hours after the transfer, the recipient mice underwent SPECT imaging using nanoSPECT (Bioscan). In wild type mice, the transferred CD8 T cells migrated to the spleen and the liver. However, interestingly, in lymphopenic Rag1KO mice, the CD8 T cells migrated to the bone marrow of various area including, femur, tibia, pelvic bones, spines (especially lumbar spines), and the head of humerus, in addition to the spleen and the liver. Homeostatic proliferation in these organs was confirmed by transferring CMFDA labeled CD8 T cells and analyzing the proliferation of the cells collected from the spleen and the bone marrow (femurs) 5 days after the transfer using a flowcytometry. These results would suggest that the bone marrow, which is an organ for hematopoiesis, in fact, provides an important microenvironment for homeostatic proliferation of matured peripheral T cells. *In vivo* whole body imaging would provide useful information on the systemic distribution of the T cells and could benefit to investigations of the environmental factors involved in the T cell homing.

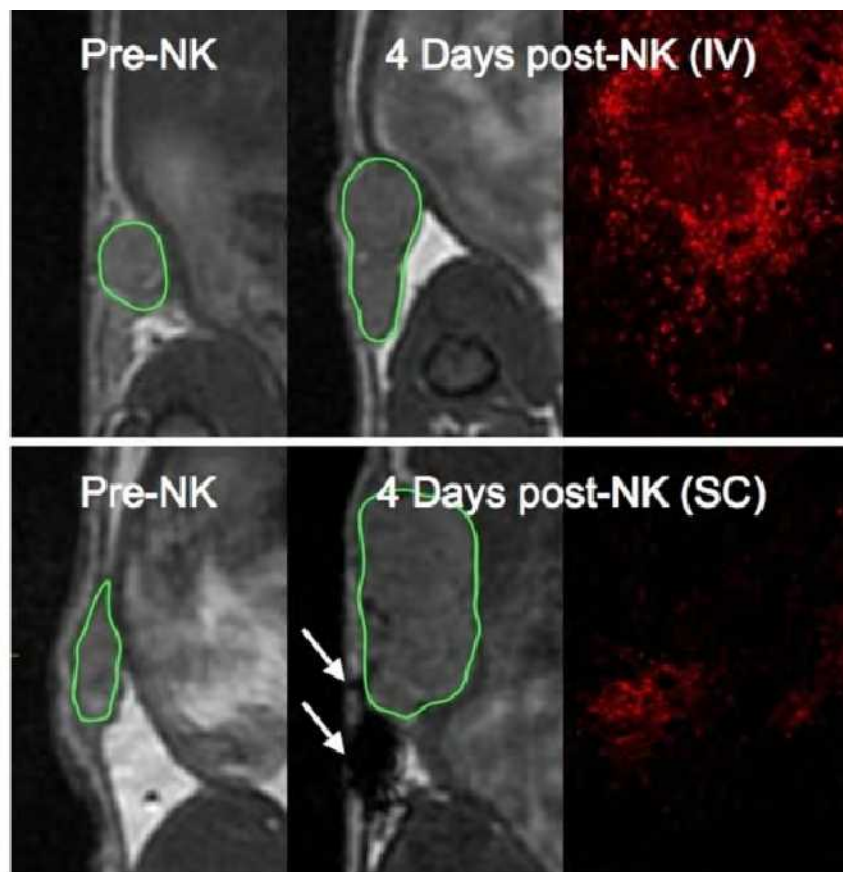


Presentation Number **0095**
 Scientific Session 9: Tracking Immune Cells

Human Natural Killer Cells Labeled with Dual Iron/Fluorescent Agent Tracked to Subcutaneous Prostate Tumors in Nude Mice after Both Intravenous and Subcutaneous Administration

Christiane Mallett^{1,2}, Catherine Ramsay¹, Paula Foster^{1,2}, ¹Imaging Research Laboratories, Robarts Research Institute, London, ON, Canada; ²Department of Medical Biophysics, The University of Western Ontario, London, ON, Canada. Contact e-mail: cmall@imaging.robarts.ca

Natural killer (NK) cells are currently being investigated in clinical and pre-clinical trials as a cancer therapy. This is the first demonstration of the ability to image the recruitment of non-targeted NK cells to tumors *in vivo*. We have labeled a highly cytotoxic human NK cell line (KHYG-1) with a dual iron/fluorescent probe and detected their accumulation in prostate tumors after intravenous (IV) and subcutaneous (SC) injection using MRI and fluorescence microscopy. Human KHYG-1 NK were labeled with Molday-Rhodamine ION. Two million PC-3M human prostate cancer cells were injected SC into the right flank of 6 nude mice. 8 days after injection of tumor cells mice were injected with Molday-labeled NK cells. 3 mice received 10 million NK cells IV (tail vein) and 3 received 2 million NK cells SC ~1 cm caudal of the tumor. Mice were imaged on days 2 and 7 post-tumor injection and on days 1 and 4 post-NK injection. Imaging was performed on a 3T GE MRI scanner with a custom gradient insert coil. CNR was measured as the difference in SNR between the tumor and the contralateral leg muscle. Tumors were removed and sections examined by fluorescence microscopy. In mice that received NK cells IV, the tumor contrast was decreased over the tumor volume at day 4 post NK cell injection; CNR decreased by 23-38%. In mice that received NK cells SC, a region of signal void was observed extending toward the tumor at day 1 post NK cell injection and reaching the margin of the tumor by day 4 post NK cell injection. The presence of Molday+ NK cells in the tumors was validated by fluorescence microscopy. A widespread distribution of red fluorescence was seen in a tumor from a mouse that received NK IV and a concentrated distribution of red fluorescence at the lobe of the tumor closest to the site of NK injection for a mouse that received NK SC.



MRI images of accumulation of iron-labeled natural killer cells in tumours with corresponding fluorescence images. Arrows show voids from infiltration of labeled NK cells.

Presentation Number **0096**
Scientific Session 10: MRI Methods (Co-organized with ISMRM)

A Spectrometer Using Oscillating and Static Fields to Measure the Suitability of Super-Paramagnetic Nanoparticles for Magnetic Particle Imaging

Sven Biederer, Timo F. Sattel, Stefanie Kren, Marlitt Erbe, Tobias Knopp, Kerstin Luedtke-Buzug, Thorsten M. Buzug, Institute of Medical Engineering, University of Luebeck, Luebeck, Germany. Contact e-mail: biederer@imt.uni-luebeck.de

Magnetic particle imaging (MPI) is a new tomographic imaging modality to measure the spatial distribution of super-paramagnetic iron oxide nanoparticles (SPIOs). MPI applies a sinusoidal oscillating magnetic field to the SPIOs. Due to their nonlinear magnetization behaviour, the magnetization response contains harmonics of the excitation field frequency. The temporal changes of the magnetization response can be measured by receive coils. By superimposing the excitation field with a static gradient field, spatial encoding is achieved. The SPIOs currently used in MPI have been originally designed for magnetic resonance imaging (MRI) and not for MPI. Thus, there was no aim during particle syntheses to fulfil particular requirements for MPI. It is assumed that optimal SPIOs could increase the sensitivity of MPI by more than a factor of 100. To measure the SPIO performance during the syntheses process, a magnetic particle spectrometer (MPS) is an essential monitoring tool. MPS so far presented, consist of a homogeneous oscillating excitation field. This allows only for analysing the magnetization response of particles at the so-named field-free-point (FFP) of the field-of-view (FOV), where the gradient field is zero. In this contribution, an MPS is presented that additionally applies a static offset field, such that the magnetization response of particles outside the FFP can be measured as well. This enables a new dimension of particle analysis. The presented MPS consists of a Helmholtz coil pair for generating the oscillating and the static field. Both can be set to a maximum field amplitude of 40 mT allowing for covering a large range of the SPIO magnetization curve. In figure 1, the measured spectral magnetic moment of the MRI contrast agent Resovist® is shown for an oscillating field amplitude sweep between 1 and 20 mT. At the left, no offset field and at the right an offset field of 5 mT is applied. It can be seen that without offset, only odd harmonics are intensified, while when using an offset field, also the even harmonics rise, which improves the sensitivity of the spectrometer for tracer analysis.

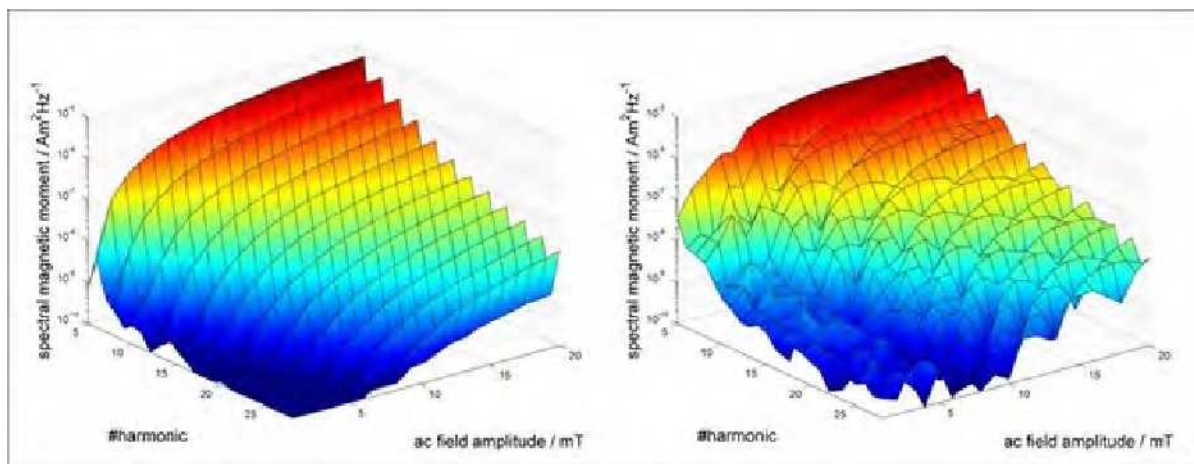


Fig 1.: Spectral magnetic moment of an oscillating field sweep without static offset field (left) and with a static offset field of 5 mT (right)

Presentation Number **0097**
Scientific Session 10: MRI Methods (Co-organized with ISMRM)

Molecular-based Image Contrast Using Fast Field-Cycling MRI

Lionel M. Broche, Saadiya Ismail, Nuala A. Booth, Henning Wackerhage, David J. Lurie, School of Medical Sciences, University of Aberdeen, Aberdeen, United Kingdom. Contact e-mail: l.broche@abdn.ac.uk

Conventional MRI is performed at a fixed, high magnetic field in order to obtain high signal-to-noise ratio. Fields such as 3 T or even 7 T are common nowadays. However, proton MRI at such magnetic strengths is known to give results related mostly to free water, hence providing little information about water-protein interactions. One way to solve this issue is to use a scanner with the ability to change its main magnetic field and collect information at a range of fields: this is the principle of fast field-cycling MRI (FFC-MRI). Our work consists of developing a fast field-cycling MRI scanner together with new techniques to create protein-dependent contrast in MRI images. In particular, we are investigating the use of the ^1H - ^{14}N quadrupolar cross-relaxation process, which occurs when a sufficiently immobilised NH entity is in contact with low-mobility water molecules. Under such conditions, a magnetisation transfer occurs between the bulk water and the ^{14}N nuclei, which act as a sink. This generates bell-like features in the dispersion curve (R_1 versus magnetic field), called 'quadrupolar peaks', at well-defined field strengths (16, 49 and 65 mT) where the ^{14}N nuclear quadrupole resonance and ^1H NMR frequencies coincide. A preliminary validation was conducted using FFC-NMR relaxometry on the fibrinogen/fibrin (blood clotting) system in vitro. We have measured the amplitude of the quadrupolar peaks at different fibrin concentrations and have shown that the peak amplitude increases linearly with fibrin concentration, as expected. It was also shown that soluble and thus mobile fibrinogen did not exhibit a quadrupolar signal. Proof-of-concept FFC-MRI experiments have been conducted on volunteers' legs to detect the quadrupolar relaxation in vivo. This relaxation process was used to create protein-dependent contrast using the NH_2 groups from actin/myosin filaments in the muscles. A series of images was obtained at different magnetic fields using a field-cycling pulse sequence, which successfully provided an image with a linear, muscle-dependant contrast. This technique can potentially lead to a novel way to measure changes in the concentration of immobilised muscle protein possibly during hypertrophy/atrophy and muscle damage/injury, and is likely to be used for the detection of other types of tissue and protein gels and agglomerates. Furthermore, FFC-MRI used with tailored contrast agents can significantly increase detection sensitivity.

Presentation Number **0098**
 Scientific Session 10: MRI Methods (Co-organized with ISMRM)

Design and Implementation of Active Feedback Device for Feedback-Enhanced MR Imaging

Dennis W. Hwang¹, **Chao-Hsiung Hsu**^{2,4}, **Hsing-Wei Chang**², **Yung-Ya Lin**³, **Lian-Pin Hwang**^{2,4}, ¹*Dept. of Chemistry & Biochemistry, National Chung Cheng University, Chiayi, Taiwan;* ²*Dept of Chemistry, National Taiwan University, Taipei, Taiwan;* ³*Department of Chemistry and Biochemistry, University of California, Los Angeles, Los Angeles, CA, USA;* ⁴*Institute of Atomic and Molecular Sciences, Academia Sinica, Taipei, Taiwan. Contact e-mail: chedwh@ccu.edu.tw*

MRI is one of the most important noninvasive methods in modern clinical diagnosis, and contrast improvement is a crucial issue. Feedback fields such as radiation damping (RD) have demonstrated their potential in contrast enhancement and highlighting structures not visible in conventional imaging. Nevertheless, for most scanners, the sensitivity of the RF receiver coil is not high enough to induce a strong RD field. Utilizing an external electronic device can significantly enhance the RD feedback field. In this work, we demonstrate an active RF feedback loop to amplify and control the feedback field. To integrate this external feedback device with conventional MR scanners, we can create a quasi-real time feedback signal. In addition, the phase and gain of the feedback field is also controllable, which allows for the design of new pulse sequences. To validate the efficacy of active feedback, tumor detection in *in vivo* mice was investigated. The mice were injected subcutaneously with human colon tumor cell line. The resulting active feedback-enhanced image showed strong contrast and highlighted boundaries in an early stage tumor [Fig. 1(b)]. These features were barely distinct in the corresponding conventional proton density, T1-weighted, T2-weighted, and T2*-weighted images [Figs. 1(a), (c)-(e), respectively]. Moreover, the tumor size observed in the active RD feedback-enhanced image was consistent with that measured by the histology [Fig. 1(f)]. To verify the mechanism of the contrast, detailed molecular dynamics were also investigated. In summary, differential excitation under the feedback field distinguishes tissues and enhances contrast at the tissue boundaries, especially for abnormal tissues, e.g. tumor. The development of an active feedback circuit to amplify the RD field thus enables improved differentiation of neighboring normal and abnormal tissues at low fields using conventional receiver coils.

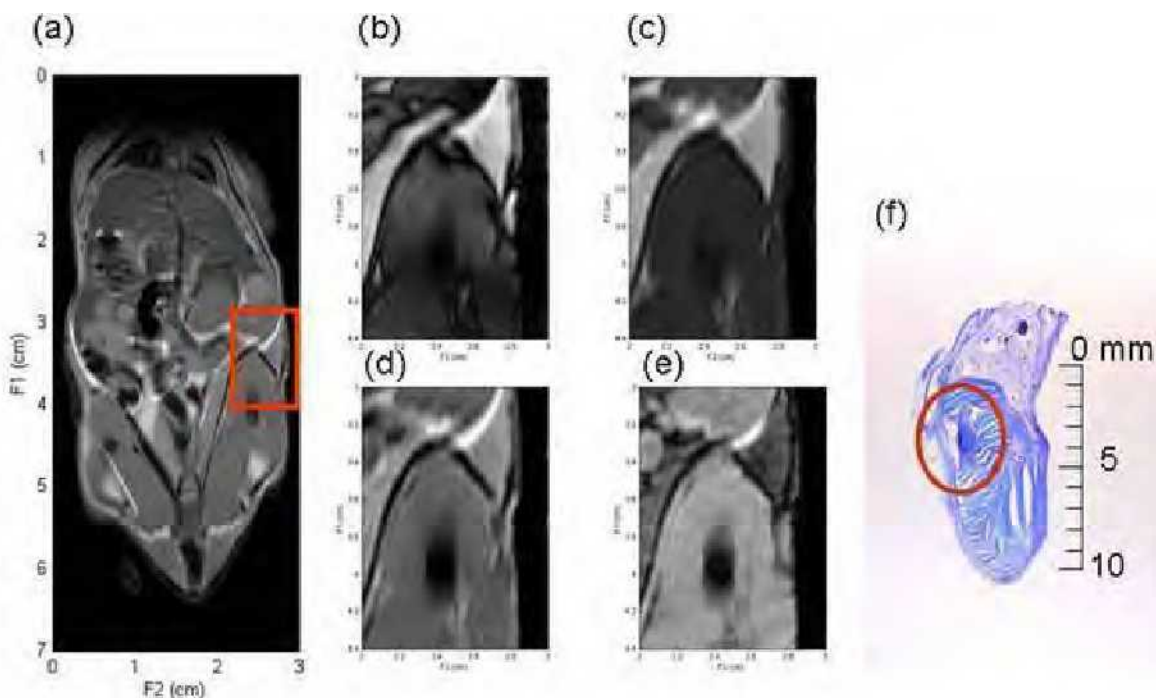


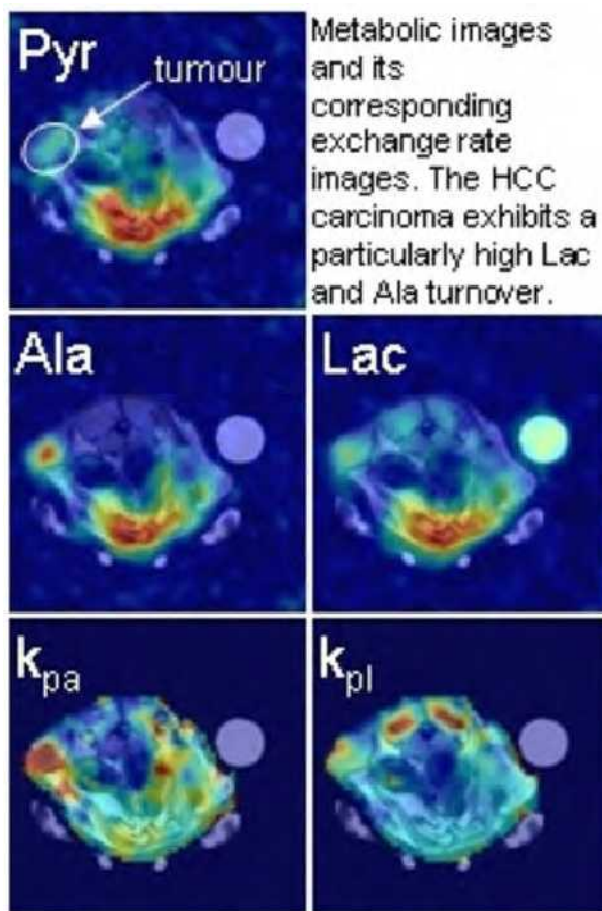
Figure 1. Tumor of mice *in vivo*. (a) Proton density image. (b) Active feedback-enhanced image. (c) T1-weighted image (d) T2-weighted image. (e) T2*-weighted image. (f) Histology.

Presentation Number **0099**
 Scientific Session 10: MRI Methods (Co-organized with ISMRM)

Saturation-Recovery Metabolic Imaging of Hyperpolarised [1-13C]Pyruvate

Rolf F. Schulte¹, Marion I. Menzel¹, Eliane Weidl², Martin Janich^{1,3}, Markus Schwaiger², Florian Wiesinger¹, ¹GE Global Research, Munich, Germany; ²Nuclear Medicine, Technische Universität München, Munich, Germany; ³Chemistry, Technische Universität München, Munich, Germany. Contact e-mail: rolf.schulte@research.ge.com

Metabolic imaging with hyperpolarised [1-13C]pyruvate (Pyr) enables the real-time detection of metabolism¹. It requires encoding of typically 5 dimensions (3 spatial, 1 spectral, 1 temporal) in <1 minute, which can be efficiently achieved with spectral-spatial (SPSP) excitation in combination with spiral imaging readout². Goal was to directly acquire spatially resolved metabolic exchange rate images by saturation-recovery with a SPSP sequence. Pyr is intracellularly converted into lactate (Lac) and alanine (Ala) according to a simplified model $dM_X/dt = k_{PX}M_P - 1/T_{1eff}M_X$ (M =magnetisation; P =Pyr; X =Lac/Ala; k_{PX} =metabolic conversion rates; T_{1eff} =effective decay time). Normally depletion dominates build-up (ie $T_{1eff} < 1/k_{PX}$), but can be neglected for short build-up times ($\tau < 5s$). Hence, after crushing all existing metabolite polarisation M_X and waiting a suitable time τ , one will get predominantly signal S governed by $k_{PX} = S_X \sin \alpha_P / (\tau S_P \sin \alpha_X)$ (α =flip angle). The validity of this assumption was verified by simulations with typical k_{PX} and T_{1eff} values. A SPSP pulse was designed (BW=90Hz, 15 lobes, duration=26ms) and implemented on a GE HDx 3T scanner in a pulse-and-acquire sequence (TR=4s, t=3.5s) with single-shot spiral readout (FOV=8cm, resolution 38x38). The excitation band was shifted between Lac, Ala, Pyr ($\alpha=90^\circ, 90^\circ, 7^\circ$) to crush Lac, Ala but not Pyr. 2.5ml/kg of 80mM hyperpolarised Pyr solution was injected into the tail vein of healthy rats and one with a subcutaneous hepato-cellular carcinoma. SPSP excitation in combination with 2D spatial in-plane encoding considerably accelerates image encoding and simplifies reconstruction. Using 90° excitation for Lac/Ala results in higher signal levels than small flip angle excitation, with the additional advantage of simplified biological interpretation. Saturation-recovery metabolic imaging describes a novel method for the direct assessment of spatially-resolved metabolic rate constants k_{PX} . References: ¹PNAS2003,100,10435. ²JMR2008,193,139. BMBF grant #01EZ0827.

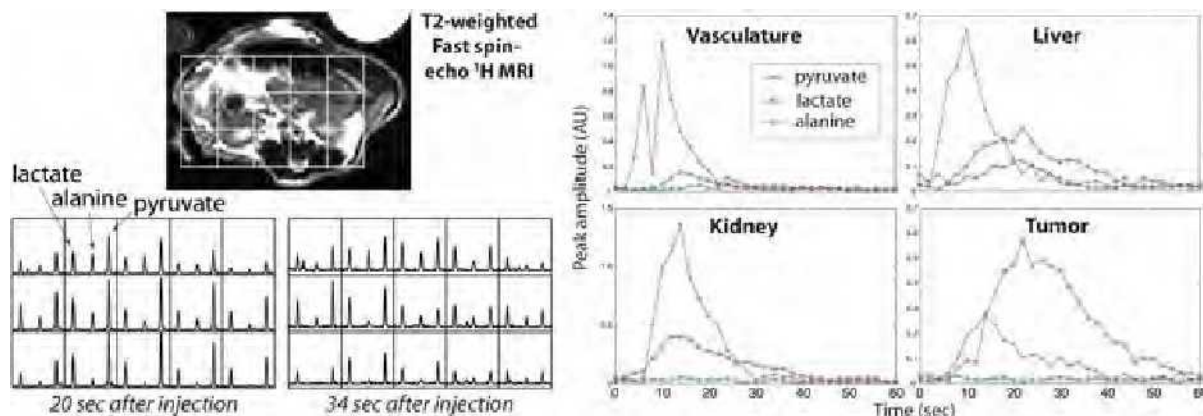


Presentation Number **0100**
 Scientific Session 10: MRI Methods (Co-organized with ISMRM)

A Rapid, 3D Dynamic MRI Method for Hyperpolarized Carbon-13 Metabolic Imaging

Peder E. Larson¹, **Simon Hu**¹, **Michael Lustig**², **Adam B. Kerr**³, **Sarah Nelson**¹, **John Kurhanewicz**¹, **John M. Pauly**³, **Daniel B. Vigneron**¹, ¹Radiology and Biomedical Imaging, University of California - San Francisco, San Francisco, CA, USA; ²Electrical Engineering and Computer Science, University of California - Berkeley, Berkeley, CA, USA; ³Electrical Engineering, Stanford University, Stanford, CA, USA. Contact e-mail: peder.larson@radiology.ucsf.edu

We present a new method for rapidly acquiring 3D MR spectroscopic imaging (MRSI) with hyperpolarized carbon-13 substrates for dynamic metabolic imaging. Following injection of hyperpolarized [1-13C]pyruvate, we are able to image an entire animal every 2 sec, allowing for observation of uptake and perfusion as well as the dynamic conversion of [1-13C]pyruvate to [1-13C]lactate and [1-13C]alanine. The high temporal resolution and dynamic metabolite imaging is facilitated by a compressed sensing (CS) acquisition and reconstruction for high accelerations [1,2] and a multiband excitation pulse to efficiently utilize the hyperpolarized magnetization [3]. The CS uses gradient blips during an echo-planar spectroscopic imaging (EPSI) readout to create a random sampling pattern, and this is varied across images. In the CS reconstruction [1], a wavelet-in-time (across the images) is used as the sparsifying transform, since it can capture the relatively smooth temporal dynamics with very few coefficients. This facilitates an overall 18-fold acceleration in speed in our acquisition of a 12x12x16 spatial grid. The multiband pulse applies varying excitations to the various metabolites based on the expected approximate concentrations, which enables more efficient magnetization usage [3]. A smaller flip angle of 1.75 degrees was applied to [1-13C]pyruvate, since it is observed in larger concentrations than the metabolic products of [1-13C]lactate and [1-13C]alanine, which were given a 12 degree flip to improve their relative SNR. We have validated this method in simulations, and in vivo results at 3.5x3.5x5.4 mm resolution (0.067 cc voxels) have shown variable perfusion of pyruvate between organs and across heterogeneous prostate tumors in the transgenic adenocarcinoma of mouse prostate (TRAMP) model. These tumors have also shown distinctly longer lactate conversion dynamics, facilitated by this new rapid imaging method. References: [1] Lustig M, et al. MRM. 2008; 58: 1182-1195. [2] Hu S, et al. MRM 2010; 63: 312-321. [3] Larson PEZ, et al. JMR 2008; 194:121-127.



Typical in vivo 3D dynamic metabolic imaging results with 2 sec temporal resolution. The kidney and vasculature dynamics show early high pyruvate, while the lactate is the largest and the longest in the TRAMP tumor.

Presentation Number **0101**
 Scientific Session 10: MRI Methods (Co-organized with ISMRM)

Positive Contrast for Imaging of EGFR Targeted Magnetic Nanoparticles in the Orthotopic Pancreatic Cancer Xenograft Model Using Ultrashort Echo Time MRI

Hui Mao^{1,2}, **Lily Yang**^{3,1}, **Weiping Qian**³, **Liya Wang**^{1,2}, **Xiaodong Zhong**⁴, **Longjiang Zhang**^{1,5}, **Hongwei Chen**^{1,2}, **Julie Yeh**^{1,2},
¹Radiology, Emory University, Atlanta, GA, USA; ²Center for Systems Imaging, Emory University, Atlanta, GA, USA; ³Surgery, Emory University, Atlanta, GA, USA; ⁴MRI Research and Development, Siemens Healthcare, Atlanta, GA, USA; ⁵Radiology, Nanjing University College of Clinical Medicine, Nanjing, China. Contact e-mail: hmao@emory.edu

Magnetic iron oxide nanoparticles (IONPs) are used for developing molecular MRI probes because of their superb ability in shortening T2 and T2* of the tissue that leads to a strong signal decrease in target organs when using T2 weighted imaging. However, the typical drawback of the negative contrast is poor contrast to noise ratio (CNR) when used to study areas with low background signals from surrounding organs. We reported that bright or “positive” contrast from the receptor targeted IONP probe can be obtained using ultrashort echo time (UTE) imaging in vitro and in vivo. MRI experiments were carried out using T2 relaxometry mapping, T2-weighted fast spin echo and 3D UTE (TE=0.07ms) imaging on a 3T MRI scanner. UTE imaging of IONPs with different core size and different concentrations showed that signal intensities are proportional to the sizes and concentrations of IONPs, suggesting potential capability of UTE imaging in quantifying IONPs (Fig 1). The CNRs of UTE images were 3 to 4 times higher than those of conventional T2 weighted images. Positive contrast was also evident in animals (N=6) bearing pancreatic cancer xenograft tumors 24 hours after intravenous administration of EGFR targeted IONP probes prepared from conjugating single chain antibody ScFvEGFR with a near infrared tag NIR-830 to the IONP. Orthotopic pancreatic tumors showed signal drops in T2-weighted MRI due to the accumulation of ScFvEGFR-IONPs. In contrast, same tumors were bright in UTE imaging. The “positive” contrast from the UTE imaging correlated well with primary pancreatic tumor and metastatic lesions detected optical imaging. The localizations of tumor and metastatic lesions by UTE imaging were confirmed by the postmortem analysis. Prussian blue stained tumor tissue sections revealed the presence of Fe positive cells bound and internalized with EGFR targeted IONPs.

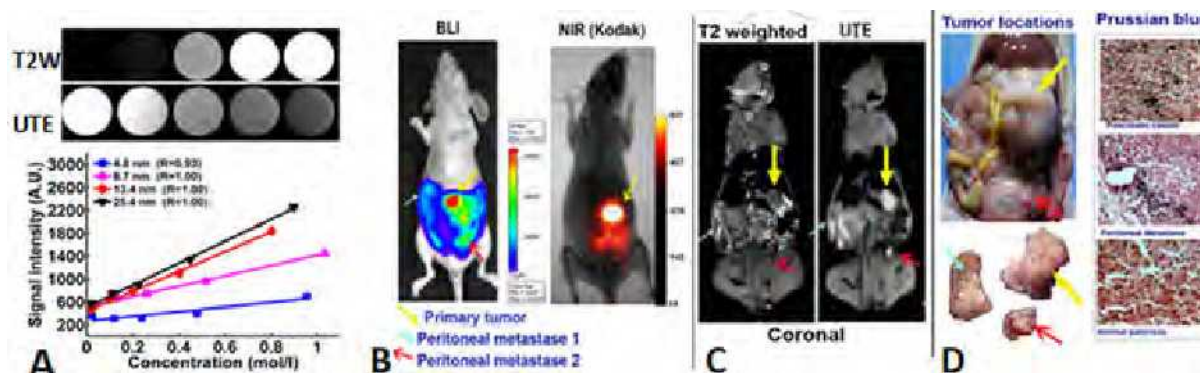


Fig 1. (A) IONPs (10 nm) with different concentrations show signal decrease in T2 weighted imaging and signal increase in UTE imaging (top). The size and concentration of IONPs are correlated to the signal intensity in UTE imaging; (B) BLI and NIR imaging showed the presence of the tumors and accumulation of ScFvEGFR-IONP-NIR850 probe; (C) Pancreatic tumors (arrows) were shown in T2 weighted and UTE images with different contrast; (D) Pathology and Prussian blue staining confirmed the location of tumors and presence of EGFR targeted IONPs.

Presentation Number **0102**
Plenary Session 3: Hyperpolarized ^{13}C -Labelled Cell Substrates

Imaging Tumour Metabolism Using Hyperpolarized ^{13}C Magnetic Resonance Spectroscopic Imaging

Kevin M. Brindle, Department of Biochemistry, University of Cambridge, Cambridge, United Kingdom. Contact e-mail: kmb1001@cam.ac.uk

Patients with similar tumour types can have markedly different responses to the same therapy. The development of new treatments would benefit significantly, therefore, from the introduction of imaging methods that allow an early assessment of treatment response in individual patients, allowing rapid selection of the most effective treatment (1). Treatment response is frequently assessed from measurements of decreases in tumour size, however imaging changes in tumour metabolism can give a much earlier indication of whether a tumour is responding to treatment. Nuclear spin hyperpolarization techniques, which can increase sensitivity in the MR experiment by >10,000x (2) have offered us a new way with which to image tissue metabolism (3). Using this technique we are able to image the location of an injected hyperpolarized ^{13}C -labelled cell substrates and, more importantly, its metabolic conversion into other cell metabolites. In this lecture I will review the ways in which we, and others, have used this approach to image various aspects of tumour metabolism, with a focus on detecting early evidence of response to treatment. **References:** 1. Brindle, K. New approaches for imaging tumour responses to treatment. *Nature Rev. Cancer* 8, 1-14 (2008). 2. Ardenkjaer-Larsen, J.H., et al. Increase in signal-to-noise ratio of > 10,000 times in liquid-state NMR. *Proc. Natl. Acad. Sci. U. S. A.* 100, 10158-10163 (2003). 3. Gallagher, F., Kettunen, M. & Brindle, K. Biomedical applications of hyperpolarized ^{13}C magnetic resonance imaging. *Prog. NMR Spectrosc.* 55, 285-295 (2009). **Acknowledgements** The work on hyperpolarization in my laboratory is supported by a Cancer Research UK Programme grant (C197/A3514), by a Translational Research Program Award from The Leukemia & Lymphoma Society and by GE Healthcare.

Presentation Number **0103**
Scientific Session 11: Novel Probes for Cancer Detection

Development of Novel Near-infrared Fluorophore Encapsulated Nanocarriers for In Vivo Tumor Imaging

Yoichi Shimizu¹, **Takashi Temma**¹, **Isao Hara**², **Hideki Minematsu**³, **Takayuki Otani**³, **Ryo Yamahara**², **Masahiko Hiraï**³, **Eiichi Ozeki**², **Masahiro Ono**¹, **Hideo Saji**¹, ¹Graduate School of Pharmaceutical Sciences, Kyoto University, Kyoto, Japan; ²Technology Research Laboratory, Shimadzu Corporation, Kyoto, Japan; ³R&D Division, Katayama Chemical Industries Corporation, Osaka, Japan. Contact e-mail: shimizuyoichi@t03.mbox.media.kyoto-u.ac.jp

Objectives: Optical imaging is a useful and sensitive technology for *in vivo* imaging. Near-infrared (NIR) fluorescence (700-900 nm) probes can provide improved photon penetration through tissue and minimize tissue autofluorescence effects. Furthermore, signal switchable probes are useful for imaging targeted molecules having a high target-to-background signal ratio. Here, we aimed to achieve highly sensitive tumor detection *in vivo* by employing tumor-specific signal activation systems using an NIR fluorophore. We developed a novel NIR fluorophore, IC7-1, and encapsulated it in an amphiphilic polydepsipeptide micelle "lactosome" at high concentrations to obtain the self-quenching form (IC7-1 lactosome). To conjugate a targeting moiety, we then encapsulated self-quenched IC7-1 lactosomes in liposomes for evaluation of their use as an activatable probe for tumor imaging by self-quenching mechanism. **Methods:** IC7-1 was synthesized in three steps and encapsulated in lactosomes at varying IC7-1 concentrations (1-20 mol%). The excitation and emission spectra of IC7-1 lactosomes were then evaluated in water and 5% sodium dodecyl sulfate (SDS). The quantum yield (Φ) and molar extinction coefficient (ϵ) of IC7-1 lactosomes (1 mol% of IC7-1) were also measured in water. IC7-1 lactosomes (20 mol% of IC7-1) were encapsulated in liposomes by cholates dialysis (IC7-1 lactosome/liposome). IC7-1 lactosome/liposomes were added to tumor cells and fluorescence images were obtained after incubation at 37 °C or 4 °C for 6 hr. **Results:** IC7-1 lactosomes (1 mol% of IC7-1) had a maximum excitation and emission wavelength at 824 nm and 840 nm, respectively, and $\Phi = 0.059$ and $\epsilon = 2.2 \times 10^5$ ($M^{-1} \text{ cm}^{-1}$), which are suitable for *in vivo* imaging. The fluorescence intensity of IC7-1 lactosomes decreased as the IC7-1 concentration in lactosomes decreased. The IC7-1 lactosome (20 mol% IC7-1) fluorescence intensity was similar to background levels in water and increased following treatment with 5% SDS. Upon incubation at 37 °C, but not at 4 °C, the addition of IC7-1 lactosome/liposomes in a self-quenched form significantly increased the fluorescence intensity of cells in a time-dependent manner. **Conclusion:** IC7-1 lactosomes show appropriate properties for *in vivo* imaging, and IC7-1 at high concentrations is self-quenched. IC7-1 encapsulated in lactosome/liposomes exists in a self-quenched form and can be dequenched in tumor cells to emit optical signals. These results suggest that IC7-1 lactosome/liposomes would be an activatable-type probe for tumor-specific imaging *in vivo*.

Presentation Number **0104**
Scientific Session 11: Novel Probes for Cancer Detection

Imaging Liver Cancer in Mice with Multi-Target-Specific Agents

Wei Wang, Arlin G. Cameron, Michel E. Mawad, Shi Ke, Radiology, Baylor College of Medicine, Houston, TX, USA. Contact e-mail: shik@bcm.tmc.edu

Background: Liver cancer is the fifth most common cancer caused deaths worldwide and its incidence is increasing. For diagnosis of liver cancer 50% of patients require invasive biopsies. In fact, histological confirmation of liver cancer from a limited sample remains a complex undertaking, and is often impossible. Furthermore, the cellular heterogeneity of the disease reduces the accuracy of diagnostic assays. Recent developments in molecular imaging provide technologies to study disease noninvasively and permit the analysis of disease status at the level of the entire body or individual lesion, as well as at the cellular level. These approaches can be used to study different components of a disease in whole body to provide a comprehensive disease picture and enhance the diagnose accuracy. **Aims:** To use multiple target-specific molecular imaging agents and multiple imaging modalities to study liver cancer both in vitro and in vivo. **Methods:** Two target-specific MMP and RGD peptides imaging agents were synthesized for this study. Imaging studies were performed in cancer cells and xenograft models. Cell study was carried out by confocal microscopy. In vivo imaging studies (n=10) were performed with peptide imaging agents and ^{18}F fluoro-deoxy-glucose (^{18}F -FDG) using optical, CT and PET scanning. **Results:** The MMP peptide imaging agent, but not the free dye, bound to liver tumor cells in vitro and was internalized into the cells. Both cell and animal data confirmed that MMP imaging agent is taken up by liver cancer cells. RGD imaging agent was used to display blood vessel formation in the tumor regions. ^{18}F -FDG PET imaging exhibited glucose metabolic stage in the disease site. It is found that the molecular imaging agents had different distributions in the body and differentially internalized into liver cancer cells. All target-specific agents yielded high tumor-to-background ratios after injection. **Conclusions:** Target-specific molecular imaging agents can be used to study liver cancer in vitro and in vivo. Noninvasive imaging with multi-target-specific molecular imaging agents could provide a tool for simultaneously studying multiple disease components.

Presentation Number **0105**
 Scientific Session 11: Novel Probes for Cancer Detection

Optoacoustic Tomography of Cancer Receptors in Mouse Models Using Targeted Gold Nanorods

Raghuraman Kannan¹, Richard Su³, Sergey A. Ermilov³, Hans-Peter F. Brecht³, Andre Conjusteau³, Vyacheslav Nadvoretzky³, Nripen Chanda¹, Ravi Shukla¹, Ajit Zambre¹, Kattesh V. Katti¹, Alexander A. Oraevsky^{3,2}, ¹Radiology, University of Missouri-Columbia, Columbia, MO, USA; ²Biomedical Engineering Department, University of Houston, Houston, TX, USA; ³TomoWave Laboratories, Houston, TX, USA. Contact e-mail: kannanr@health.missouri.edu

Recently we developed a 3D optoacoustic tomography (OAT) system combining advantages of pulsed optical spectroscopy and high-resolution ultrasonic detection, characterized and shown to produce high-contrast 3D maps of optical absorbance through the whole body of an animal with resolution better than 0.5 mm. Much smaller tissue structures and microvessels can be visualized in case of sufficient contrast. An ultrawide-band of ultrasonic frequencies present in optoacoustic signals contains wealth of information, which can be revealed through proper filtering and post-processing. We demonstrated that either larger anatomy, such as organs or major vessels, or the smaller structures (kidney medullas, ovarian arteries) and even microvasculature can be visualized depending on methods of signal and image processing (See Figure 1). This system was employed to generate molecular images of malignancy-related protein receptors in cancer cells. An orthotopic model of human pancreatic cancer and a subcutaneous xenograft model of breast cancer in a nude mouse model were generated and used to test the system capability for molecular imaging. Acquisition of these images was facilitated by the use of gold nanorods (GNR) as optoacoustic (OA) contrast agent. We developed techniques of covalent conjugation of gold surface of nanorods to specific anticancer vectors such as monoclonal antibodies (MAB) or EGFR-avid peptides. Breast cancer was targeted with Herceptin MAB. High sensitivity of our 3D OAT system to changes in the optical absorption enabled high contrast imaging. Pancreatic cancer in our preclinical model was targeted with GNR conjugated with GE11 peptides that selectively target EGF receptors of cancer cells. As shown in Figures c and d 3D optoacoustic tomography enhanced with gold nanorods has the potential to become a useful molecular imaging modality for preclinical research. Translation of the developed system to clinical applications will be also discussed.

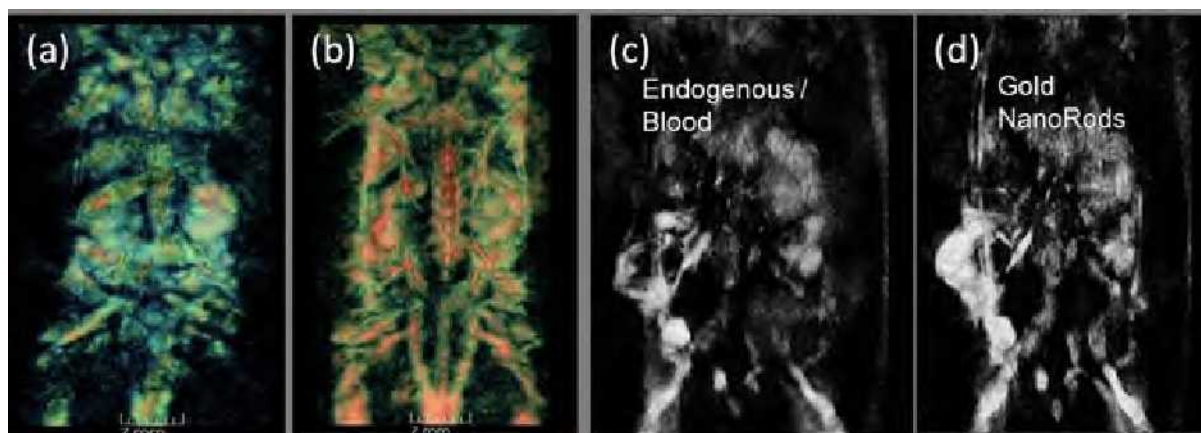


Figure 1. 3D optoacoustic tomography images of a live nude mice showing (a,b) internal organs, vasculature and spine and (c,d) xenograft tumor grown from BT474 breast cancer cells. Panels (a) and (c) display images before injection of GNR contrast. Panel (b) shows OA image 24 hrs after iv injection of 600 µL GNR-PEG. Panel (d) shows OA mouse image 24 hrs after iv injection of GNR-PEG-Herceptin.

Presentation Number **0106**
Scientific Session 11: Novel Probes for Cancer Detection

Improved Detection of Cancer-specific Enzyme Activity Using Fluorescence Lifetime Contrast

Walter J. Akers, Wilson B. Edwards, Mikhail Y. Berezin, Hyeran Lee, Samuel Achilefu, Radiological Sciences, Washington University School of Medicine, St. Louis, MO, USA. Contact e-mail: akersw@mir.wustl.edu

Preclinical optical imaging with fluorescent contrast agents has become prominent in recent years due to the high sensitivity and high throughput of this technique. Fluorescent molecular probes can be administered for rapid detection of disease throughout the body of mice and rats, economically and without ionizing radiation. Activatable fluorescent probes, those that are initially non-fluorescent until activated by specific molecular events, may improve target contrast relative to “always on” fluorescent molecular probes. Spectral unmixing may also improve target contrast by eliminating background signal or separating multiple reporter signals based on excitation and/or emission spectral differences. Still, fluorescence imaging techniques are limited, in part, by the semi-quantitative nature of fluorescence intensity. In general, fluorescence intensity is directly related to the concentration of the dye and the excitation power. In many cases, this relationship can be altered by changes in fluorophore environment such as pH, oxygenation or quenching. These changes may change the quantum yield of fluorescence and affecting signal interpretation. Fluorescence lifetime is a characteristic property of each fluorophore that is independent of dye concentration but may be sensitive to environmental conditions similar to intensity. Simultaneous measurement of fluorescence lifetime with intensity can add significant information to optical imaging studies and improve image interpretation. We report recent applications of fluorescence lifetime imaging in preclinical cancer models using activatable fluorescent probes. We demonstrate that fluorescence intensity can report the relative concentration of molecular probes within different regions of the body while fluorescence lifetime provides specific evidence of activation by cancer-specific enzymes. Quenching of the fluorescent reporters results in shortening of the molecular probe’s fluorescence lifetime, which is subsequently restored upon activation. Indeed, the fluorescence lifetimes of the enzyme-activatable molecular probe immediately after injection and 24 hours later corresponded to values determined in vitro before and after activation, respectively. The fluorescence lifetime maps created from in vivo measurements demonstrated improved tumor-specific contrast, aiding in tumor identification and interpretation of fluorescence data. These results show that fluorescence lifetime contrast is a powerful addition to preclinical imaging and has translational potential.

Presentation Number **0107**
 Scientific Session 11: Novel Probes for Cancer Detection

Chemically Conjugated Affibody-HSA for PET Imaging of HER2-Expressing Tumors

Susan Hoppmann, Zheng Miao, Shuanglong Liu, Hongguang Liu, Zhen Cheng, Radiology, Stanford University, Stanford, CA, USA.
 Contact e-mail: hoppmann@stanford.edu

Radiolabeled anti-human epidermal growth factor receptor type 2 (HER2) Affibodies have shown excellent and specific tumor localizations in recent PET and SPECT studies. However, radiometal labeled Affibodies display extremely high kidney uptakes (> 100 % ID/g), which is unfavorable for the detection of tumors adjacent to the kidneys and also represents a concern for high radiation doses to the radiation sensitive kidneys. Therefore, the purpose of this study is to explore a simple and generalizable method to chemically conjugate Affibody and human serum albumin (HSA), and to use the resulting Affibody-HSA bioconjugate for microPET imaging of HER2-expressing tumors. First, human serum albumin (HSA) was modified by a site-specific conjugation with DOTA-NHS ester and the bifunctional crosslinker Sulfo-SMCC, respectively. The HER2 Affibody analog Ac-Cys-ZHER2:342 was then covalently conjugated with the HSA, and the resulting bioconjugate DOTA-HSA-ZHER2:342 was further radiolabeled with ^{64}Cu in sodium acetate buffer (0.1 N, pH=5.0) at 37 °C for 1 h. ^{64}Cu -DOTA-HSA-ZHER2:342 (Fig. 1A) was subjected to in vitro cell uptake studies using SKOV3 cells to evaluate its feasibility as a tumor targeting probe with and without pre-incubation of Ac-Cys-ZHER2:342 for blocking (n=6). MicroPET imaging was performed in SKOV3 tumor-bearing nude mice at 1, 4, 24 and 48 h post-injection (p.i.) (n=3). It was found that up to four Affibody molecules were covalently conjugated onto one HSA molecule as identified by MALDI-TOF-MS. Radiolabeling with ^{64}Cu resulted in high radiochemical yields (> 75 %). The radiolabeled probe displayed a significant (1.52 % at 2 h) and specific in vitro cell uptake. MicroPET experiments showed very high tumor uptake values (> 10 % ID/g at 4 h and 24 h, respectively) and high liver while very low kidney accumulations (Fig. 1B). In conclusion, ^{64}Cu -labeled HSA modified Affibody is a promising probe for molecular imaging. The concept of using HSA to alternate the pharmacokinetic and biodistribution of biomolecules such as Affibodies indicates a broader application in the design of many other PET probes.

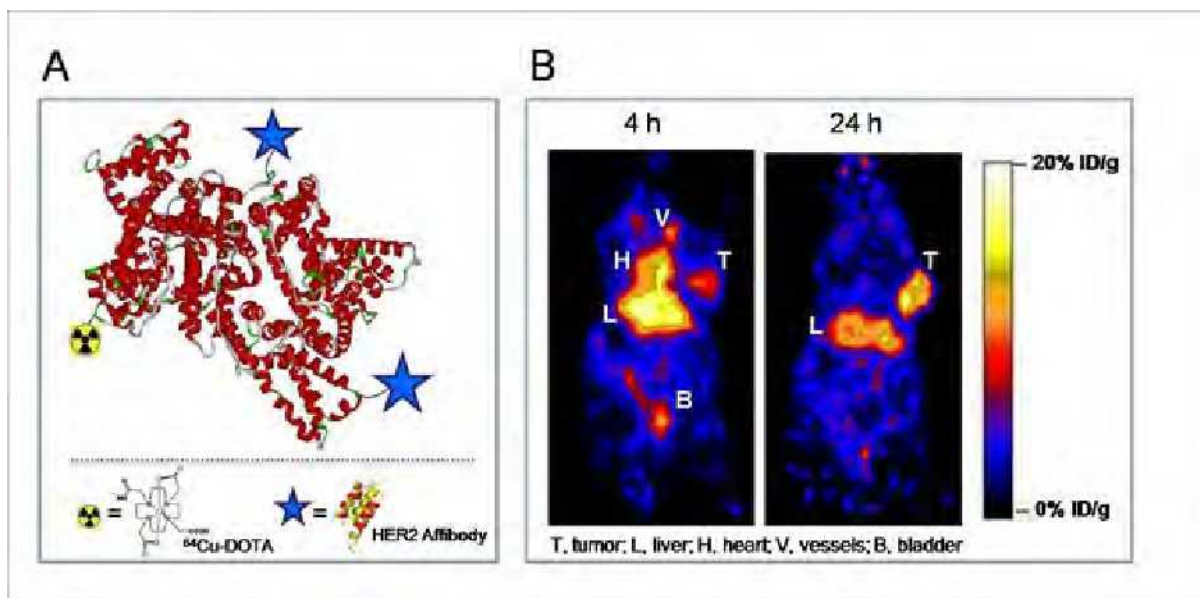


Fig 1: (A) Illustration of ^{64}Cu -DOTA-HSA-ZHER2:342. (B) MicroPET coronal image of a mouse bearing a SKOV3 tumor at 4 h and 24 h p.i. of ^{64}Cu -DOTA-HSA-ZHER2:342.

Presentation Number **0108**
Scientific Session 11: Novel Probes for Cancer Detection

Evaluation of a Novel Human Anti-EGFR Monoclonal Antibody as an Imaging Probe

Chizuru Sogawa¹, **Atsushi B. Tsuji**¹, **Takako Furukawa**¹, **Misturu Koizumi**¹, **Yoshinori Uka**², **Gene Kurosawa**², **Yoshikazu Kurosawa**², **Tsuneo Saga**¹, ¹*Diagnostic Imaging Group, Molecular Imaging Center, National Institute of Radiological Science, Chiba, Japan;* ²*Division of Antibody Project, School of Medicine, Fujita Health University, Aichi, Japan. Contact e-mail: c-sogawa@nirs.go.jp*

The epithelial growth factor receptor (EGFR) is over-expressed in many epithelial cancers, and is an attractive target for cancer imaging and therapy. Here we report a novel anti-EGFR human monoclonal antibody which was isolated from a human phage-display antibody library by comprehensive screening using living cancer cells. In this study, we selected one antibody from nine anti-EGFR antibody clones by cell binding assay and further assessed the selected antibody in vitro and in vivo regarding the potential as an imaging probe. [Material and Methods] Nine anti-EGFR antibodies and cetuximab, a well-defined anti-EGFR antibody, were radiolabeled with ¹²⁵I using chloramine-T method. Cell binding assay using human epidermal cancer cell line A431 highly expressing EGFR was performed to select an antibody showing the highest binding. The selected antibody was further radiolabeled with ¹¹¹In by conjugating antibody with a bifunctional chelate, N-[(R)-2-Amino-3-(p-isothiocyanato-phenyl)propyl]-trans-(S,S)-cyclohexane-1,2-diamine-N,N',N'',N'''-pentaacetic acid (CHX-A"-DTPA), and assessed by in vitro cell binding, competitive inhibition and internalization assays. The xenografted tumor was made by subcutaneous inoculation of 2x10⁶ A431 cells into BALB/c-nu/nu mice, and in vivo biodistribution study, planar imaging and SPECT were performed after intravenous administration of ¹¹¹In-labeled selected antibody. [Results] The monoclonal antibody (048-006) was selected showing the highest binding to A431 cells among seven antibodies tested. ¹²⁵I- and ¹¹¹In-labeled 048-006 showed almost equivalent affinity constant to ¹²⁵I- and ¹¹¹In-labeled cetuximab (3.8x10⁹M⁻¹ and 1.8x10⁹M⁻¹ for 048-006 vs. 3.3x10⁹M⁻¹ and 2.3x10⁹M⁻¹ for cetuximab, respectively), and both antibodies were internalized after binding. ¹¹¹In-048-006 showed high uptake in A431 tumors (highest tumor uptake of 15.98±3.65 %ID/gram obtained at 48 hours after injection), and the xenografted tumor was clearly visualized by planar and SPECT using ¹¹¹In-048-006. [Conclusion] Radiolabeled human anti-EGFR monoclonal antibody 048-006 would be promising for the imaging tumors with EGFR over-expression.

Presentation Number **0109**
 Scientific Session 12: Novel Hybrid Molecular Imaging Technology

Quantitative High-resolution Optical Spectroscopy in Deep Tissues by Combining Photoacoustic Tomography with Diffuse Optical Tomography

Adam Q. Bauer¹, Ralph Nothdurft¹, Changhui Li², Lihong V. Wang², Joseph P. Culver¹, ¹Radiology, Washington University in Saint Louis, Saint Louis, MO, USA; ²Biomedical Engineering, Washington University in Saint Louis, Saint Louis, MO, USA. Contact e-mail: abauer@hbar.wustl.edu

Accurate and rapid imaging of functional and molecular processes in vivo are vital for elucidating the cause of diseases, preventing the progression or onset of diseases, and rapidly implementing a tailored therapeutic regimen. Photoacoustic tomography (PAT) has the potential to image biological tissue with simultaneous high contrast and high spatial resolution. PAT has been used to visualize brain structure, brain lesions, and map functional organization of the cerebral cortex. PAT also has the potential for molecular imaging through spectral identification of absorbing contrast agents such as bioconjugated, tunable, gold nanoparticles. Quantitative spectral PAT remains challenging due to the nature of the photoacoustic signal, which is the product of tissue absorption and light fluence. The fluence can depend on wavelength which can corrupt spectral interpretation. The fluence also has strong spatial variability - objects in the optical path, but out of the field of view of the PAT image, can cause artifacts in reconstructed PAT images possibly leading to an under- or overestimation of optical absorption and therefore chromophore concentration. For quantitative spectroscopy, the fluence would preferably be measured in situ. A potential noninvasive solution is to combine PAT with diffuse optical tomography (DOT). DOT is able to reconstruct quantitative images of optical properties while also providing high contrast due to the strong optical absorption of the endogenous chromophores oxy- and deoxy- hemoglobin, water, and fat in the near-infrared regime. We performed DOT and PAT measurements on a phantom that produced inhomogeneous fluence in a region with two targets having identical optical properties. We were able to reduce fluence-related artifacts in the PAT image by accounting for the fluence throughout the phantom. Preliminary results of this study motivate the development of integrated PAT/DOT systems to provide quantitative spectroscopy for improved functional and molecular PAT imaging.

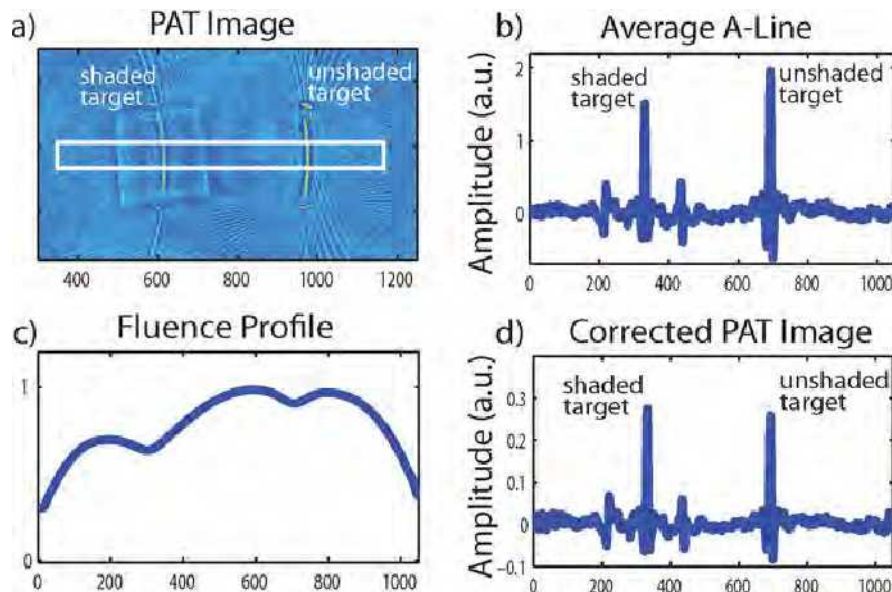


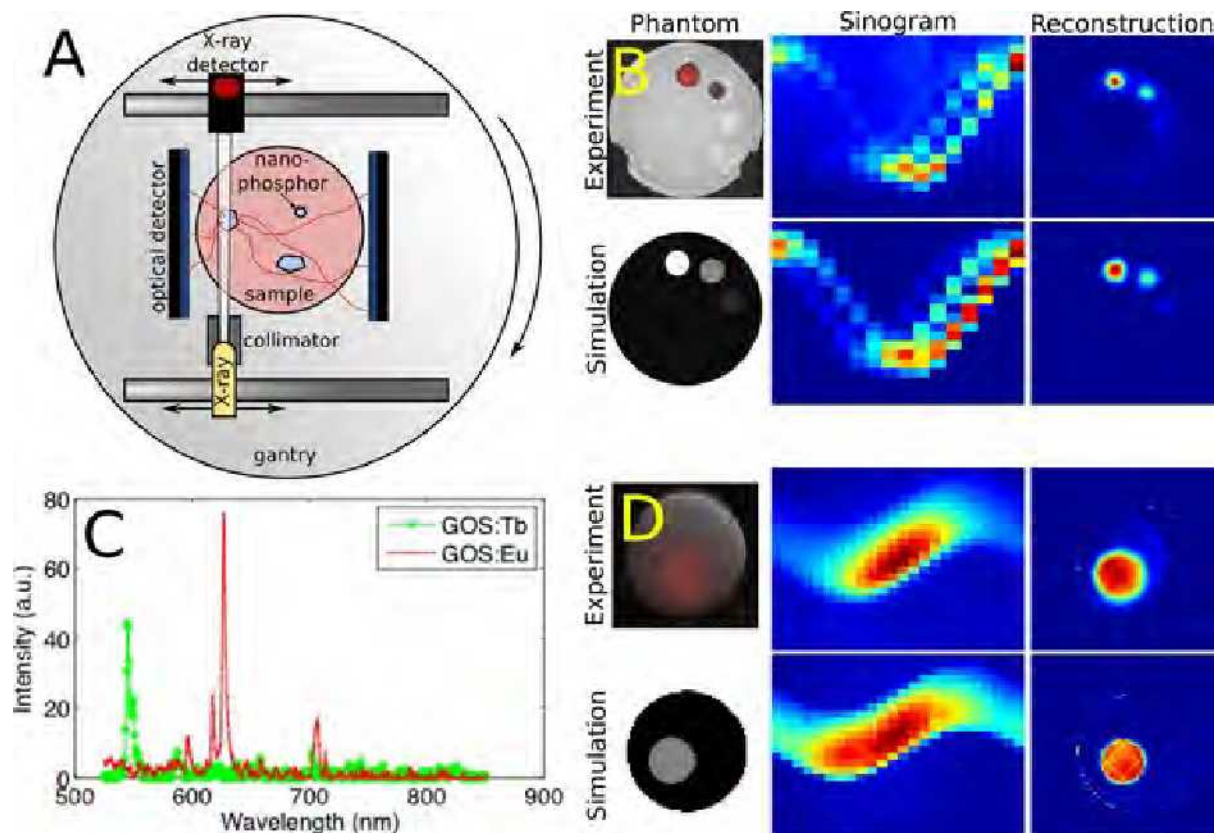
Figure 1: a) PAT image of the phantom b) Average of 60 RF A-lines within white box of a). This line profile suggests that the absorption of these two objects differs by 25%. DOT reconstructions of the optical properties of this phantom do not suffer from this artifact and were used to calculate the fluence everywhere in the phantom. c) The recovered fluence distribution from DOT measurements at the depth of the two targets. d) Corrected PAT image showing that the artifact in the PAT image has been reduced by a factor of 5. A pressure-to-voltage calibration of the PAT system would allow this hybrid imaging technique to produce absolute maps of the absorption coefficient.

Presentation Number **0110**
 Scientific Session 12: Novel Hybrid Molecular Imaging Technology

Simultaneous Anatomical and Molecular Tomographic Imaging using X-Ray-Excitable Nanoparticles

Guillem Pratx¹, Colin M. Carpenter¹, Conroy Sun¹, Padmanabha R. Ravilisetty², Lei Xing¹, ¹Radiation Oncology, Stanford University School of Medicine, Stanford, CA, USA; ²SRI International, Menlo Park, CA, USA. Contact e-mail: pratx@stanford.edu

X-ray luminescence computed tomography (XLCT) is proposed as a new molecular imaging modality for imaging X-ray-excitable phosphorescent nanoparticles three-dimensionally, in small animals. Some of these nano-sized particles can emit near-infrared (NIR) light when excited with X-rays and be functionalized to target specific biological processes in vivo. XLCT enables anatomical images to be acquired simultaneously with molecular images via standard X-ray computed tomography (CT). The imaging mechanism used in XLCT consists in irradiating the subject using a sequence of X-ray beams while sensitive photo-detectors measure the light diffusing out of the subject. For each beam position, the production of light is constrained to the narrow volume of the beam, hence, the collection of optical measurements forms parallel-beam projections. An XLCT system was simulated using Monte-Carlo. Preliminary experiments were also conducted in phantoms using a 50 kvP treatment X-ray generator and an EM-CCD camera. Images were reconstructed using a maximum-likelihood iterative algorithm. From simulations, tracer uptake in 2 mm-diameter targets can be detected and quantified with sub-picomolar sensitivity with less than 1 cGy of average radiation dose. Provided sufficient signal-to-noise ratio, the spatial resolution of the system can be made arbitrarily small by narrowing the beam aperture. In particular, 1 mm uniform spatial resolution was achieved for a 1 mm-wide X-ray beam. Images reconstructed from experimental XLCT measurements showed good agreement with the simulation model. In particular, the reconstructed signal was linear with phosphor concentration. Preliminary simulations and experiments show that XLCT is a feasible approach for imaging small animals or dedicated organs. With the next version of our experimental set-up, we expect improved spatial resolution and molecular sensitivity.



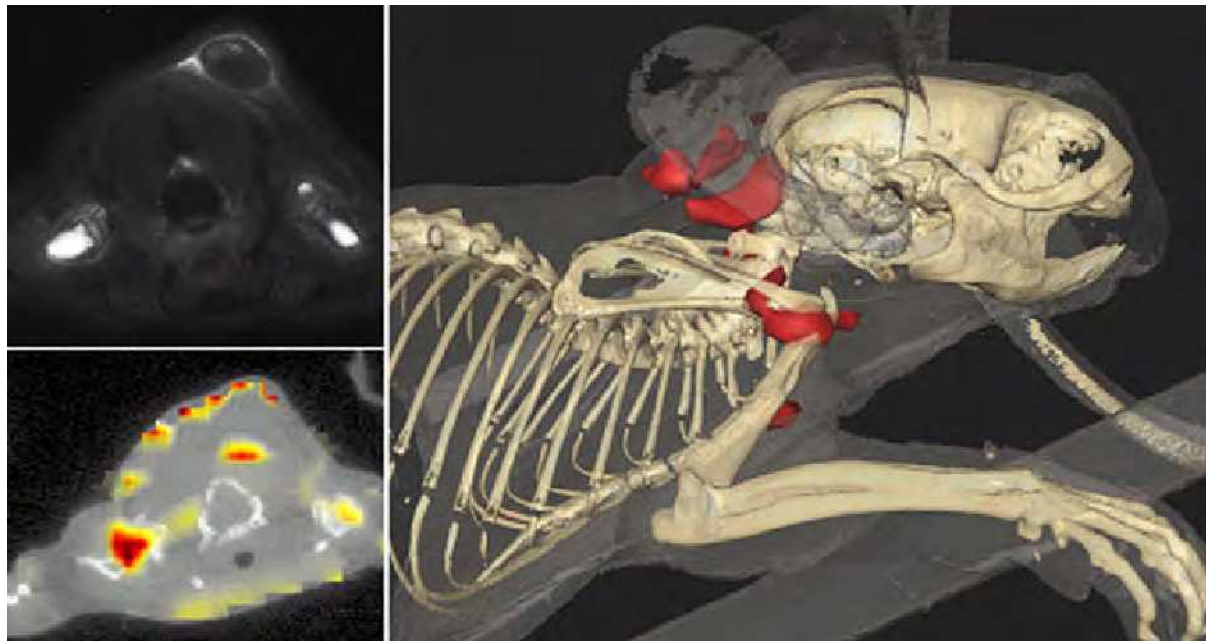
A: Proposed design for an XLCT system. B: Gradient phantom. C: Nanophosphor X-ray-stimulated emission spectrum. D: Optically diffusive phantom.

Presentation Number **0111**
Scientific Session 12: Novel Hybrid Molecular Imaging Technology

In Vivo Tumor Imaging Using a Hybrid Fluorescence Molecular Tomography - X ray Computed Tomography System with Prior Based Reconstruction

Angelique Ale, Ralf B. Schulz, Athanasios Sarantopoulos, Vasilis Ntziachristos, Institute for Biological and Medical Imaging, Helmholtz Zentrum Muenchen and Technische Universitaet Muenchen, Neuherberg, Germany. Contact e-mail: angelica.ale@helmholtz-muenchen.de

Fluorescence Molecular Tomography (FMT) is an emerging imaging technique for non-invasive three-dimensional image reconstruction of fluorescence biodistribution in-vivo. Recent developments in this field include the development of a hybrid FMT and X-ray computed tomography (XCT) system, which allows 360 degree projection viewing for both FMT and XCT and uses CCD-cameras for photon detection. The combination of these two imaging modalities in one hybrid system improves visualization possibilities as a result of the seamless co-registration of images. The anatomical structures obtained from the XCT volume can be overlaid with molecular information from FMT. Additionally, the anatomical information can be used to guide the FMT reconstruction in the form of priors. In this work, the anatomical information was used 1) to assign appropriate attenuation coefficients to the different anatomical regions and 2) as structural prior information. We investigated the performance of previously developed schemes and alternative methods for improving the FMT imaging performance using priors. Results from simulations, as well as measurements of a lung inflammation animal model and an in-vivo tumor model demonstrated significant improvements in the reconstructions when prior information from XCT was used. Results were compared against tissue slices obtained after cryo-slicing the mice that were frozen in a position similar to the position they were imaged in by the FMT-XCT system. Figure 1 shows the result of an in-vivo tumor model experiment. The mouse had a subcutaneous 4T1 tumor, and was intravenously injected with ProSense 680. The fluorescent signal visible in the cryoslice shown in the upper left image corresponds well with the prior based reconstruction shown in the lower left image. Accurate reconstructions, in combination with hybrid 3D visualization, as shown in the right image, can greatly improve our understanding of molecular processes in-vivo.



Presentation Number **0112**
 Scientific Session 12: Novel Hybrid Molecular Imaging Technology

Towards Combined Functional Imaging Using [^{15}O]Water PET and BOLD fMRI

Hans F. Wehr¹, **Martin S. Judenhofer**¹, **Florian C. Maier**¹, **Alexander Sauter**¹, **Petros Martirosian**², **Gerald Reischl**³, **Fritz Schick**², **Bernd J. Pichler**¹, ¹University of Tuebingen, Laboratory for Preclinical Imaging and Imaging Technology of the Werner Siemens-Foundation, Tuebingen, Germany; ²University of Tuebingen, Section on Experimental Radiology, Tuebingen, Germany; ³University of Tuebingen, Radiopharmacy and PET-Center, Tuebingen, Germany. Contact e-mail: wehr@gmx.de

In this work we present two novelties in small animal neuroimaging: Brain activation in rats is tracked by [^{15}O]water PET and confirmed by BOLD fMRI. Moreover we show in vivo BOLD data from our PET/MR system. Male rats (n=3) were anesthetized (0.8% Isoflurane in air) and an electrode pair was used to stimulate unilateral the vibrissae of the animals (3Hz/8Hz). Animals were placed in a microPET scanner, and a [^{15}O]water infusion (163MBq, duration 40s) was started. For each animal 3 activation and 3 baseline scans were obtained. Animals were moved to a 7T MRI and BOLD fMRI was performed (EPI GE, TR=2s, TE=18ms, block design). PET images were summed, coregistered, normalized, thresholded and smoothed. Baseline images were subtracted from activation images. Linear modeling was used to evaluate the fMRI images. Data were validated by statistical testing and comparison of the activated areas from PET and fMRI images by correlating them to a rat brain atlas. Analysis of the PET subtraction images in the barrel field cortex, showed on average (n=9), that the ipsilateral side had a slight decrease in perfusion ($-4\pm 23\%$), the contralateral side had an increase of ($26\pm 20\%$), the difference ($30\pm 16\%$) during stimulation between the two sides was significant ($p<0.01$). BOLD maps showed activation ($p<0.01$) in the contralateral barrel field, corresponding to the regions found in PET (figure 1). The average increase of the BOLD signal was ($1.3\pm 0.8\%$), range (0.2-5.7)%. In addition fMRI stability tests were performed when the PET was installed. BOLD data from animals were obtained within the PET/MR system during forepaw and whisker stimulation. With the PET/MR system we found a BOLD signal stability of 0.07% (n=30), and were able to observe in vivo BOLD activation. We demonstrated for the first time that: [^{15}O]water PET can be used to rapidly map brain activation in rats allowing a comparison with BOLD. Also small animal fMRI can be performed inside a PET/MR system, opening the realm for simultaneous PET/fMRI studies.

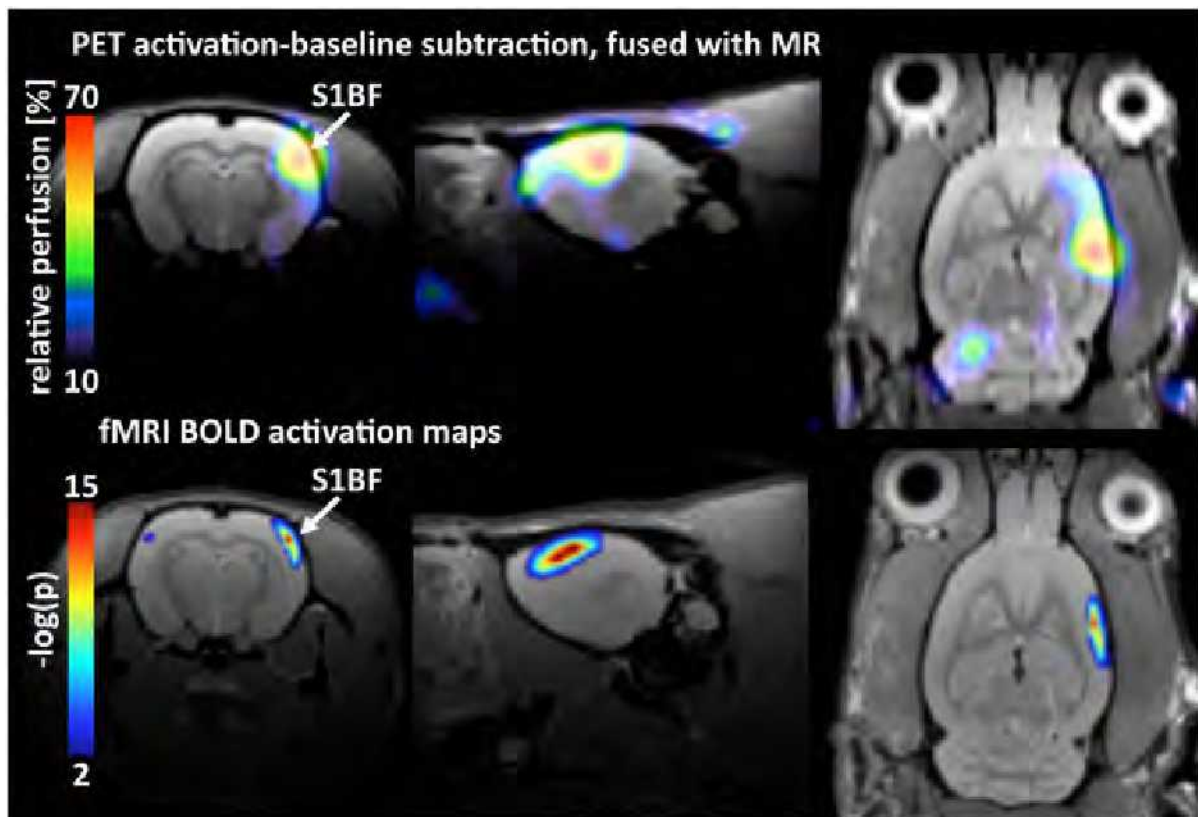


Figure 1: PET subtraction maps and corresponding fMRI BOLD activation maps, show activation in the right primary somatosensory cortex (S1BF), after stimulation of the left vibrissae.

Presentation Number **0113**
Scientific Session 12: Novel Hybrid Molecular Imaging Technology

A DOI-capable MR-compatible PET Insert for Simultaneous PET/MRI Imaging

Yibao Wu, Yongfeng Yang, Julien Bec, Simon R. Cherry, Department of Biomedical Engineering, University of California, Davis, Davis, CA, USA. Contact e-mail: ybwu@ucdavis.edu

Previously, we developed a magnetic resonance (MR) compatible positron emission tomography (PET) insert in our laboratory for small-animal imaging. A next generation system is now under development and will fit inside a 7-T Bruker MRI scanner which has magnet with inner diameter of 30 cm and a gradient set with inner diameter of 20 cm. The PET system will be able to accept gating signals and can be synchronized with the MRI scanner. The PET insert will have far superior performance, including improved spatial resolution with finely pixelated detector elements, a larger axial field of view, and greater than an order of magnitude increase in sensitivity by utilizing 20 mm thick scintillator crystal elements with excellent stopping power. To overcome the resolution-degrading parallax errors associated with such thick detectors, a detector module based on position sensitive avalanche photodiode (PSAPD) read out with depth-of-interaction encoding was designed. Two PSAPDs are used to readout the detector, one from each end. A flexible circuit board was used to deliver the high bias voltage and route the signal in the confined geometry, a new electronics system was adapted to accommodate the large number (~100) of detectors and a new shaping circuit was designed to adapt the signal to the electronics system. Non-magnetic components were chosen for the circuit boards and connectors used inside the MRI and non-magnetic coaxial cable bundles were used to transmit the signals from inside the MRI to the outside electronics. Optimized shielding was used to reduce the radiofrequency interference between the PET and MRI systems. The new system design also features a system for uniformly cooling the PSAPDs, thermal insulation, shielding material, structural support, and easy replacement of defective detector modules. Testing of single PET detector modules (9x9 array of 1.3x1.3x20 mm³ LSO scintillator crystals coupled to two 14x14 mm² PSAPDs) showed no obvious interference with the MRI system. The flood histograms of PET detector showed no significant difference outside the MRI scanner, inside the MRI scanner, nor when typical MR sequences were running. The energy spectra showed no obvious difference either. The MR images of a structured phantom acquired with typical Gradient Echo and Spin Echo sequences were unaffected by the presence of the PET detector. New tapered LSO arrays also are being pursued to further improve the sensitivity.

Presentation Number **0114**
Scientific Session 12: Novel Hybrid Molecular Imaging Technology

The Development of SPECT-MR Instrumentation and Techniques for Preclinical Small Animal Imaging

Benjamin M. Tsui¹, Si Chen¹, Jingyan Xu¹, Jianhua Yu¹, Dirk Meier², James W. Hugg², Douglas J. Wagenaar², Bradley E. Patt²,
¹Radiology, Johns Hopkins University, Baltimore, MD, USA; ²Gamma Medica-Ideas, Northridge, CA, USA. Contact e-mail: btsui1@jhmi.edu

The goal is to develop instrumentation and techniques for simultaneous SPECT-MR imaging of small animals (SA). A prototype MR-compatible SA SPECT subsystem was previously constructed to allow simultaneous SPECT-MR data acquisition in a MRI system with a minimum bore size of 12 cm. It consists of 3 angularly offset rings of 8 2.54x2.54 cm² CdZnTe detectors each having 16x16 pixels. A cylindrical multi-pinhole (MPH) collimator sleeve was designed to obtain pinhole projection of a 25 mm diameter volume-of-view on each of the 24 detectors. It is made of a tungsten compound material that does not support eddy current and is transparent to RF signals of an encompassing birdcage coil for MRI. The effects of the SPECT subsystem on MR images and of the MRI system on SPECT images were evaluated. The detector uniformity and system resolution and geometric efficiency with different pinhole aperture sizes were determined. We developed a statistical ML-EM reconstruction method for sparse projection views. The method included accurate models of the point response functions of the 24 pinhole-detector pairs that were measured from scanning point-source experiments. The imaging performance of the stationary SPECT subsystem was evaluated using simulation and experimental phantom studies and its dynamic imaging capability was evaluated through a mouse renal kinetics study using Tc-99m DTPA. Minimal effects were found on the SPECT and MR images in simultaneous SPECT-MR imaging using the prototype SPECT subsystem in a 3T clinical MRI system. After pre-processing to correct for the Lorentz shift in the acquired data, artifact-free SPECT images were obtained with 24 projections using the new sparse-view image reconstruction method. The image quality was similar to that obtained using additional projection views by rotating the collimator sleeve. The measured system resolutions were 3.3 mm and 4.7 mm and geometric efficiencies 0.5% and 1.2% for pinhole aperture sizes of 1.3 mm and 2.0 mm, respectively. The SPECT renal kinetics study demonstrates the ability to acquire fast dynamic data with time intervals down to 3 seconds. Our results demonstrate the feasibility of SPECT-MR imaging using the prototype MR-compatible SPECT instrumentation. The new sparse-view SPECT image reconstruction method allows fast dynamic data acquisition from the stationary SPECT subsystem in kinetics studies. Also, the feasibility study provides important data in the current development of a high-resolution SPECT subsystem for SPECT-MR imaging of SA and the human brain.

Presentation Number **0115**
Scientific Session 13: Stem Cells

Role of Cancer Stem Cells in [¹⁸F]FDG Uptake and Therapy Response in Osteosarcoma

Celia M. Gomes¹, Sara R. Neves¹, Aurio O. Lopes¹, Antero J. Abrunhosa², Paulo C. Simões³, Artur A. Paiva⁴, Maria F. Botelho¹,
¹Institute of Biophysics/Biomathematics, IBILI - Faculty of Medicine - University of Coimbra, Coimbra, Portugal; ²Institute for Nuclear Sciences Applied to Health, ICNAS - University of Coimbra, Coimbra, Portugal; ³Radiotherapy Service, University Hospital of Coimbra, Coimbra, Portugal; ⁴Histocompatibility Centre, University Hospital of Coimbra, Coimbra, Portugal. Contact e-mail: cgomes@ibili.uc.pt

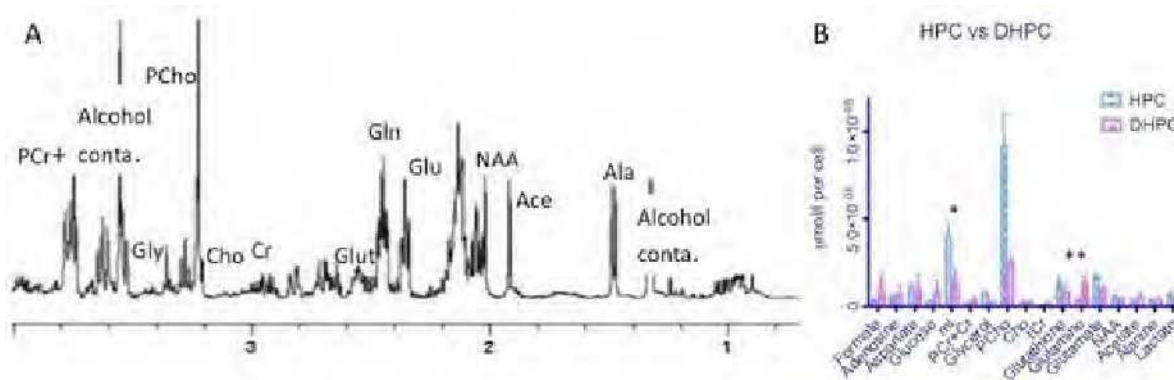
Aim: There is growing evidence that human tumors contain a subset of cells with stem-like properties that are responsible for sustaining tumor growth and relapse after therapy. We aimed to identify the presence of putative stem-like cells in osteosarcoma (OS) and to establish their relevance on [¹⁸F]FDG uptake and responsiveness to conventional therapies. **Methods:** Cancer stem cells (CSC) were isolated from an human OS cell line (MNNG) using the sphere formation assay (serum-free medium, non-adherent surfaces) and characterized for the expression of mesenchymal stem cell (MSC) markers (CD90+, CD105+, CD73+) by flow cytometry. The metabolic activity of both MNNG and CSC was measured based on cellular uptake of [¹⁸F]FDG. To investigate whether CSC can account for the poor response of OS to conventional therapies, we evaluated the sensitivity of both cell types to radiotherapy and to common chemotherapeutic drugs (DOX+CIS). This included irradiation of the cells with an X-ray linear accelerator at different doses (0-20Gy) and incubation for 48h with different concentrations of the drugs (0-80µM). Response to the treatments was analysed by MTT colorimetric cell proliferation assay. **Results:** A subset of MNNG cells formed spherical clones with stem-like properties. These cells proliferated in serum-starved conditions and were positive for MSC markers. [¹⁸F]FDG uptake in CSC (2.94±0.12%) was significantly lower (p<0.05) than in MNNG cells (12.5±1.4%). CSC were found to be more resistant to both radio- and chemotherapy when compared with MNNG cells. The mean lethal dose (LD50) obtained from radiosensitivity studies in CSC (6.8±1.5Gy) was significantly higher than that in MNNG cells (3.4±0.6Gy, p<0.05). Accordingly, the half maximal inhibitory concentrations (IC50) of DOX (0.9±0.1µM) and CIS (13.9±1.1µM) were significantly higher (p<0.05) than those calculated in MNNG cells (DOX: 0.3±0.1µM; CIS: 8.1±3.7µM). **Conclusions:** OS contains a subset of tumour cell with stem-like properties that are relatively resistant to radiation and to conventional chemotherapeutic agents. This relative resistance of CSC to therapy appears to be related with the metabolically quiescent status of CSC, as indicated by the lower accumulation of [¹⁸F]FDG in these cells. These findings suggest that conventional therapies may not address this subset of CSC, resulting in subsequent regrowth of the tumour after therapy. This has important clinical implications when assessing tumour response to therapy with PET-FDG since residual viable CSC do not accumulate [¹⁸F]FDG.

Presentation Number **0116**
 Scientific Session 13: Stem Cells

Characterisation of a Human Neural Stem Cell Biomarker Using ¹H Magnetic Resonance Spectroscopy

Bhavana S. Solanky¹, Yuen-Li Chung², Harry Parkes³, Martin O. Leach², Po-Wah So¹, Michel Modo¹, ¹Institute of Psychiatry, Kings College London, London, United Kingdom; ²Institute Of Cancer Research, London, United Kingdom; ³Institute of Child Health, University College London, London, United Kingdom. Contact e-mail: bhavana.solanky@kcl.ac.uk

Neural stem cells (NSCs) have been identified as a potential therapeutic solution for many neurodegenerative diseases. However, their transition from NSCs to mature functioning cells is poorly documented, but essential if therapy is to be effective. We explored high-resolution magnetic resonance spectroscopy (MRS) to identify and quantify specific metabolites that are present in undifferentiated and differentiated human NSCs to elucidate potential biomarkers for each state. Aqueous soluble extracts of hippocampal (HPC) and striatal (STR) neural stem cell lines were scanned with a Bruker 11.74T NMR system (500 MHz) using a water pre-saturation sequence. The HPC line was differentiated (DHPC) and also underwent MRS. MRS showed stem cell lines differed by reduced formate, PCr+Cr and acetate in addition to increased myo-inositol (mI) in the HPC samples. Trends showing decreased adenosine and higher glutathione levels in HPC samples relative to STR were also noted. Metabolite levels for HPCs relative to DHPCs were generally higher across the spectrum. Significant differences were only noted in the glutamine region, this change was probably due to the higher glutamate-containing DHPC basal media. Trends were seen in increased mI and PCho in the HPCs. The highly proliferative nature of stem cells is likely to be responsible for the higher PCho in HPCs compared to DHPCs. These metabolite differences provide a potential way to follow differentiation in vivo at high fields using CSI.



Presentation Number **0117**
Scientific Session 13: Stem Cells

In Vivo Bioluminescence Monitoring of Mouse Mesenchymal Stem Cell Engraftment and Proliferation within In Situ Forming Hydrogel

Hye-kyung Shim¹, **Do Won Hwang**¹, **So Won Oh**¹, **Hyewon Youn**^{1,2}, **Yoon Ki Joung**³, **Ki Dong Park**³, **Dong Soo Lee**^{1,4}, ¹*Department of Nuclear Medicine, Seoul National University College of Medicine, Seoul, Republic of Korea;* ²*Institute of Radiation Medicine, Seoul National University Medical Research Center, Seoul, Republic of Korea;* ³*Department of Molecular Science and Technology, Ajou University, Suwon, Republic of Korea;* ⁴*Department of Molecular Medicine and Biopharmaceutical Science, Seoul National University WCU Graduate School of Convergence Science and Technology, Seoul, Republic of Korea. Contact e-mail: shimhk@naver.com*

Background: Hydrogel scaffolds, possessing similarities to biological tissue environment, have been widely used in regenerative medicine to provide biomechanical support for stem cells and to fill up lost tissue space together with stem cells. We evaluated survival and proliferative characteristics of mouse mesenchymal stem cell (mMSC) incorporated with in situ forming hydrogel based on tyramine conjugated 4-arm-PPO-PEO. Material and Method: To evaluate the characteristics of mMSC within the hydrogel, stable cell line retrovirally transduced with an enhanced firefly luciferase (mMSC-effLuc) was used. The hydrogel was prepared using a Tet-SA-TA solution in the presence of horseradish peroxidase and hydrogen peroxide, and then mMSC-effLuc was injected through a dual syringe system after mixing with the Tet-SA-TA solution. For in vitro characterization, luciferase activity was measured at various conditions; different cell numbers (1x10⁴, 5x10⁴, 1x10⁵, 5x10⁵ cells) using 100 μ L of the hydrogel per each well in a 96-well plate, and physical strengths of the hydrogel (200,400,800 Pa) using 1x10⁴ cells per each well. For in vivo characterization, mMSC-effLuc with different numbers (1x10⁵, 5x10⁵, 1x10⁶ cells/each site) was subcutaneously injected onto BalB/C mice using the 200 Pa hydrogel (100 μ L/each site), and they were followed by bioluminescence imaging. As control group, mMSC-effLuc without hydrogel was examined in both in vivo and in vitro experiments. Results: In vitro luciferase activity was linearly correlated with the cell number (p=0.002). In the mMSC-effLuc within the hydrogel group, peak values of in vitro luciferase activity were seen at a later time (20 min vs. 10 min after luciferin substrate injection), and the intensities was smaller than those of the controls (8x10⁵ vs 1.9x10⁶ RLU, p<0.001) On in vivo bioluminescence imaging, a signal peak in the mMSC-effLuc within the hydrogel as well as the control group was seen at 20 min after luciferin substrate injection. In vivo bioluminescence activity of mMSC-effLuc with the hydrogel gradually increased upto 33.2% in average on day 15, whereas that of the control group gradually decreased and nearly disappeared. Conclusion: We successfully monitored the survival and proliferation pattern of mMSC-effLuc within the hydrogel. We expect that in vivo monitoring system could provide a powerful tool to evaluate the characteristics of stem cells within the hydrogel system.

Presentation Number **0118**
Scientific Session 13: Stem Cells

Hepatic Ischemia/Reperfusion Injury Promotes Lung Metastasis After Major Hepatectomy by Mobilization of Circulating Endothelial Progenitor Cells (EPCs) - Application of Optical Imaging System in Rat and Mouse Models with Orthotopic Liver Cancer

Kwan Man¹, Kevin TP Ng¹, Xiao Bing Liu¹, Chung Mau Lo¹, Sheung Tat Fan¹, ¹Department of Surgery, The University of Hong Kong, Hong Kong, China; ²Surgery, UCLA, Los Angeles, CA, USA. Contact e-mail: kwanman@hkucc.hku.hk

Objective We aim to explore the precise mechanism of tumor metastasis under surgical stress by investigating the impact of hepatic I/R injury on mobilization of circulating endothelial progenitor cells and regulatory T cells. **Methods** Orthotopic rat liver tumor model was established in male Buffalo rats with cirrhotic liver. Major hepatectomy was performed at 3 weeks after tumor implantation in the left lobe with (I/R injury group) or without (Control group) partial hepatic ischemia/reperfusion (I/R injury - 20/20 minutes duration on right and median lobes). The tumor growth and metastases were longitudinally monitored by Xenogen in vivo imaging system (IVIS) in live animals by detection of luminance signals from tumor cells, which stably labeled with luciferase gene. Blood samples were taken at day0, 3, 7, 17, 21 and 28 after hepatectomy for detection of circulating endothelial progenitor cells (CD133+CD34+CXCR4+). Intra hepatic and circulating gene/protein markers linking to I/R injury and lung metastasis were identified. To further validate the role of EPCs with inflammatory chemokine IP10 treatment on liver tumor growth and metastasis, the EPCs with or without IP10 treatment from a rat model with green fluorescence protein (GFP) labeling were further injected into an orthotopic nude mice liver cancer model. The liver tumor growth and metastasis in nude mice were longitudinally monitored by IVIS system. The EPCs were also traced with their GFP signals. **Results** Significant high incidence of lung metastasis was present in I/R injury group (50%, 16/32) compared to the control group (10%, 2/20; p=0.000) at 4 weeks after major hepatectomy. The early occurrence of lung metastasis was found in I/R injury group at 2 weeks after operation detected by IVIS. Significant higher levels of IP10/CXCR4/VEGF induced by hepatic I/R injury subsequently mobilized more bone marrow derived endothelial progenitor cells (CD133+CD34+CXCR4+) to circulation compared to the control group (day14: 12.21% vs 7.73%, p=0.002; day21: 12.25% vs 4.47%, p=0.004; day28: 9.64% vs 2.27%, p=0.004). The circulating protein marker linking to hemopoietic progenitor cell - myelin basic protein (MBP) was also over-expressed in I/R injury group. IP10 treated EPCs has greater potential to promote liver tumor growth and metastasis via increasing angiogenesis in the orthotopic nude mice liver tumor model. **Conclusion** Hepatic ischemia/reperfusion injury promoted lung metastasis after major hepatectomy by mobilization of circulating endothelial progenitor cells.

Presentation Number **0119**
 Scientific Session 13: Stem Cells

Multimodality Molecular Imaging of Adipose-derived Mesenchymal Stem Cells in Hindlimb Ischemia Mice

Weiwei Fan¹, **Feng Cao**¹, Junting Liu², Shuang Li¹, Jie Tian², ¹Cardiology, Xijing Hospital, Fourth Military Medical University Molecular Imaging Center, Xian, China; ²School of Life Sciences and Technology, Xidian University, Xian, China. Contact e-mail: wind8828@gmail.com

Background Peripheral arterial disease (PAD) is highly prevalent and particularly in patients with atherosclerosis. Stem cell transplantation offers promising approaches for therapeutic angiogenesis and tissue repair. In this study we try to use in vivo multimodality molecular imaging strategies to investigate adipose tissue-derived mesenchymal stem cells (MSCs) survival, function and relative mechanism. Method MSCs were isolated from transgenic mice which carried double reporter genes: firefly luciferase (Fluc) and enhanced green fluorescent protein (eGFP). Hindlimb ischemia mice model was created by ligating the proximal and distal femoral artery. MSCs (1×10^5) along with/without VEGF (0.4 ng) were transplanted into ischemic hindlimb. The animals were subjected to be imaged by bioluminescence and CT scan. Laser doppler perfusion imaging (LDPI) were used to show blood perfusion. Micro-CT, histological and molecular analysis were tested to confirm the cells' location and angiogenesis. Result On day 3 after transplantation, the bioluminescence signals in MSCs with VEGF group were $4.6 \times 10^6 \pm 2.5 \times 10^5$ photons/s/cm²/sr, while in MSCs group were $2.8 \times 10^6 \pm 3.1 \times 10^5$ photons/s/cm²/sr, respectively ($P < 0.01$ versus control). The signals of bioluminescence increased gradually from POD 3 to day 28, which proved survival and proliferation of the MSCs in the host. The group treated with MSCs and VEGF showed higher signals than that injected by MSCs only, which indicated the reinforcement of VEGF. The color-coded index of LDPI was significantly higher in the MSCs-transplanted group than that in the control group from day 3 to 28 post cell transplantation. Micro-CT angiography demonstrated more angiogenesis in the hindlimbs of the treated mice on day 21, which were also confirmed by molecular analysis. Conclusion: Bioluminescence fusion with CT scan provides higher detailed 3D imaging for monitoring MSCs in vivo. Angiogenesis activator VEGF might promote MSCs' beneficial function for hindlimb ischemia therapy.

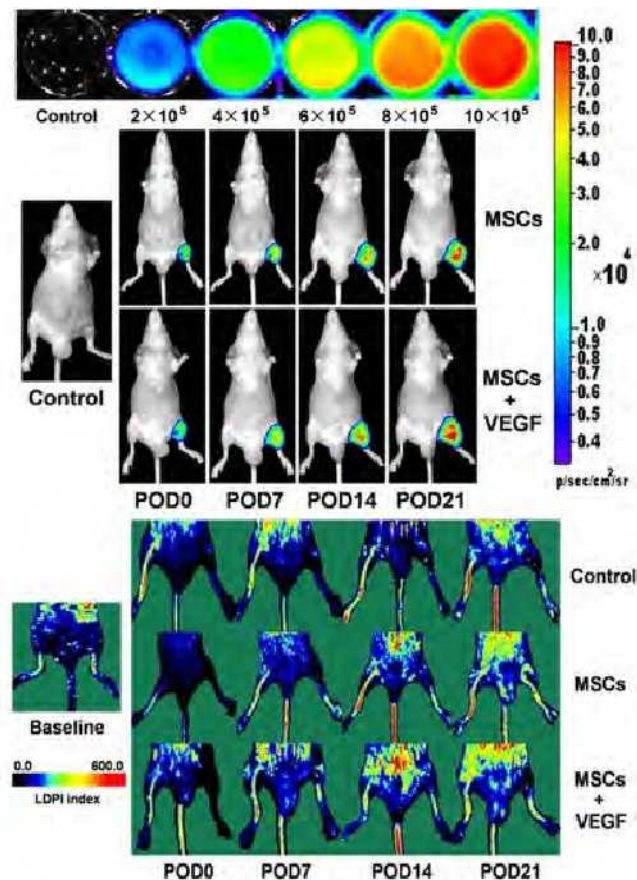


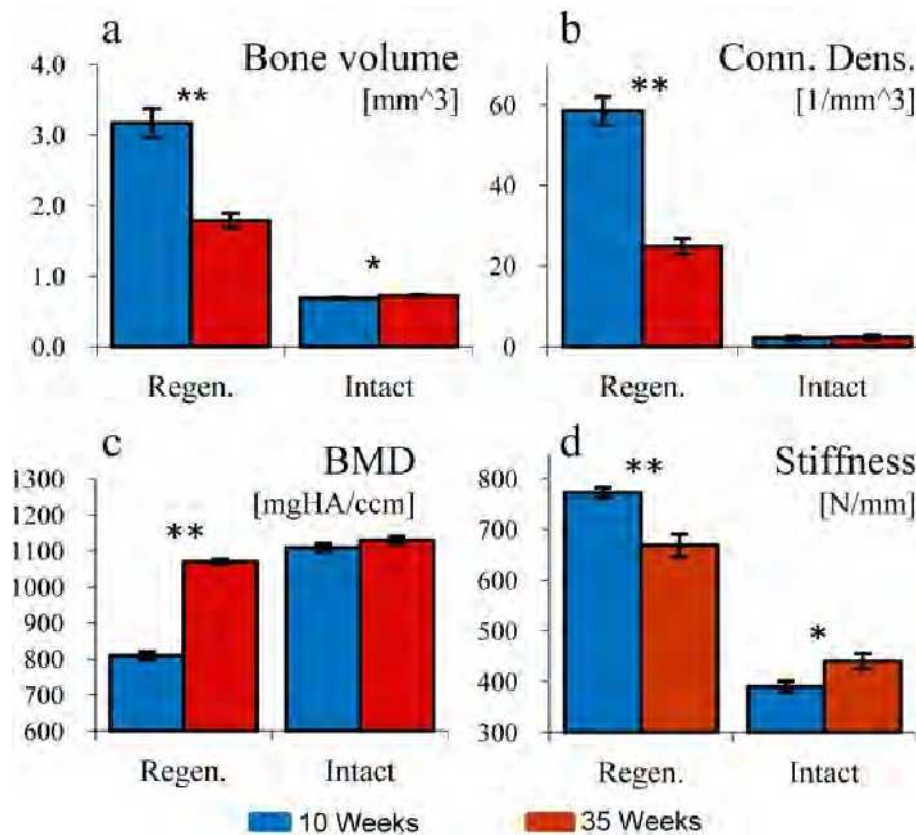
Figure Bioluminescence and LDPI of the MSCs-transplanted Hindlimb Ischemia Mice

Presentation Number **0120**
 Scientific Session 13: Stem Cells

Micro CT Imaging and Finite Element Analysis of Nonunion Fracture Repaired by Genetically Engineered Mesenchymal Stem Cells

Wafa Tawackoli^{1,2}, **Gadi Pelled**^{2,3}, **Ilan Kallai**³, **Davide Ruffoni**⁴, **Yoram Zilberman**³, **Harry van Lenthe**⁵, **Dan Gazit**^{2,3}, ¹*Biomedical Sciences, Cedars-Sinai Medical Center, Los Angeles, CA, USA;* ²*Surgery, Cedars-Sinai Medical Center, Los Angeles, CA, USA;* ³*Hebrew University of Jerusalem, Jerusalem, Israel;* ⁴*Institute for Biomechanics, ETH Zürich, Zürich, Switzerland;* ⁵*Biomechanics and Engineering Design, K.U.Leuven, Leuven, Belgium. Contact e-mail: Wafa.Tawackoli@cshs.org*

Stem cell-mediated gene therapy for fracture repair utilizes genetically engineered mesenchymal stem cells (MSCs) for the induction of bone growth and is considered a promising approach in skeletal tissue regeneration. Previous studies have shown that murine nonunion fractures can be repaired by implanting MSCs over-expressing recombinant human bone morphogenetic protein-2 (rhBMP-2). However, the structural and biomechanical properties of the regenerated bone after a prolonged period of time remained unknown. We hypothesized that the new bone tissue formed by BMP-engineered MSCs in a critical-size bone defect, remodels and provides biomechanical competence over time. We utilized a novel image-based system for the biomechanical analysis of murine radius bones. Cultured rhBMP-2-expressing MSCs were loaded onto a collagen sponge and implanted into segmental defects created in the mice radii. High resolution micro computed tomography was performed 10 and 35 weeks post MSC implantation, followed by micro finite element analysis. Quantitative analysis of the newly formed bone showed that the structural indices of the regenerated bones, at 35 weeks, were more similar to the indices of the intact untreated bones, than the indices at 10 weeks (Fig 1). These results show that the regenerated bone tissue remodels over time, as indicated by a significant decrease in bone volume and connectivity density combined with an increase in mineral density. In addition, the axial stiffness of limbs repaired with MSCs was 2 to 1.5 times higher compared to the contra lateral intact limbs, at 10 and 35 weeks post treatment. These results could be attributed to the fusion that occurred between in the ulna and radius bones. In conclusion, although MSCs induce bone formation, significant remodeling of the repair callus occurs over time. In addition, limbs treated with an MSC graft demonstrated superior biomechanical properties, which could indicate the clinical benefit of future MSC application in nonunion fracture repair.



Presentation Number **0121**
Scientific Session 14: Metabolism and Hypoxia

A Novel High Throughput System for In Vitro and In Vivo Screening and Evaluation of Novel Inhibitors of HIF1 - HIF1 Interaction

Yun-Chen Chiang, Amer M. Najjar, Brian Rabinovich, Juri G. Gelovani, Experimental Diagnostic Imaging, MD Anderson Cancer Center, Houston, TX, USA. Contact e-mail: yunchen.chiang@gmail.com

Background: Tumor growth can often outpace the vascularization process leading to the development of a hypoxic tumor environment. In response, an intracellular hypoxia survival pathway is initiated by the heterodimerization of hypoxia induced factor-1 α (HIF-1 α) and HIF-1 β , enhancing the survival of tumor cells in the oxygen-deprived environment. These hypoxic tumor regions are associated with resistance to various classes of chemotherapeutic agents, such as doxorubicin, etoposide, and mitoxantrone. In an attempt to reverse tumor chemoresistance, drug therapy coupled with disruptors of HIF-1 α / β dimerization is being considered as therapeutic strategy. To this end, we have designed a high-throughput screening system based on firefly luciferase complementation to assay small molecule libraries for inhibitors of HIF-1 α / β PAS AB domain heterodimerization. **Methods:** The interacting PAS AB domains of HIF-1 α and HIF-1 β were fused with the N-terminal (Nluc) and C-terminal (Cluc) domains of firefly luciferase, respectively. Fusions were created using a lentiviral expression plasmid with dual Gateway sites designed to express the inserted domains in frame. A total of four fusion genes were created (Nluc-HIF1 α , HIF1 α -Nluc, Cluc- HIF1 β , and HIF1 β -Cluc). U87 cells were co-transfected with the four possible plasmid pair combinations to determine the optimal orientation for luciferase complementation. **Results:** Paired fusion genes expressing the luciferase domains on same side of HIF (N- or C-terminus) yielded the highest luciferase complementation signals. Thus, Nluc-HIF1 α and HIF1 α -Nluc combined with Cluc-HIF1 β and HIF1 β -Cluc, respectively, produced the highest detectable luminescent signals. Consequently, U87 cells were transduced with these complimentary pairs to produce stable cell lines for high-throughput drug screening. **Conclusion:** The constitutive expression PAS AB domains of HIF-1 α and HIF-1 β fused with complementary luciferase domains results in reconstitution of the luciferase activity instigated by the PAS AB domain interaction. A stable cell line highly enriched for stable expression of this reporter system will facilitate high-throughput screening of drug candidates for inhibitors of this interaction.

Presentation Number **0122**
Scientific Session 14: Metabolism and Hypoxia

Pharmacodynamic Effects of Fatty Acid Synthase Inhibition by Orlistat on the Uptake of [¹⁸F]FDG, [³H]Acetate and [¹⁴C]Fluoroacetate in Non Small Cell Lung Carcinoma Cells In Vitro

Madhuri Sankaranarayanapillai, Juri G. Gelovani, Experimental Diagnostic Imaging, MD Anderson Cancer Center, Houston, TX, USA. Contact e-mail: madhuri.pillai@mdanderson.org

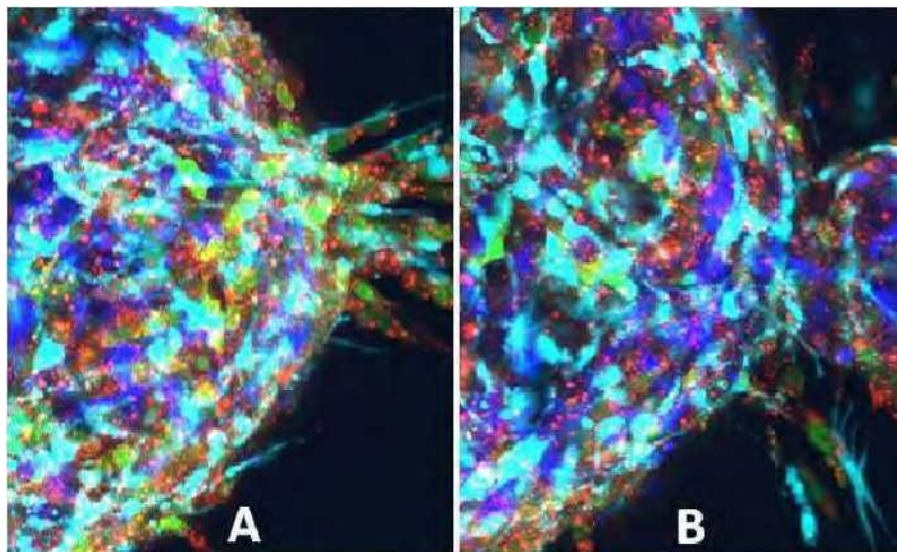
Introduction: Fatty acid synthase (FAS) is a multifunctional enzyme that plays a key role in catalysis of fatty acid biosynthesis. FAS is specifically upregulated in many cancers including cancer of prostate, breast and lung. Orlistat is a novel and rather selective inhibitor of FAS in tumor cells. This drug inhibits the thioesterase function of the enzyme, interferes with cellular fatty acid synthesis, and can halt tumor cell proliferation and induce tumor cell apoptosis. This study was aimed to investigate the pharmacodynamic effects of FAS inhibition by Orlistat on the cellular uptake of [¹⁸F]FDG, [³H]Acetate and [¹⁴C]Fluoroacetate in non small cell lung carcinoma (NSCLC) cells in vitro. **Methods:** Two human NSCLC cells, H441 and H1975 were treated for 24 hrs with 30μM of Orlistat; controls were treated with vehicle (DMSO). To initiate in vitro cell uptake study, culture medium was replaced with fresh medium containing 100 μCi of [¹⁸F]FDG, 0.1 μCi/ml of [³H]Acetate and 0.01 μCi/ml of [¹⁴C]Fluoroacetate, in the presence of Orlistat/DMSO for experimental and control groups respectively. Incubation was terminated at various time points (15, 30, 60 and 120 min.) and cells were collected by scraping and centrifugation. Samples of culture media and cell pellets were collected and weighed. Radioactivity of [¹⁸F]FDG was quantified by gamma counter and that of [³H]Acetate and [¹⁴C]Fluoroacetate by scintillation counting. Cellular uptake data was expressed as the ratio of accumulation in cell-to-medium and normalized to cell/medium weight. **Results:** In both H441 and H1975 cells, the upake of [³H]Acetate was the maximum and the uptake of [¹⁸F]FDG was the least, in both control and Orlistat treated groups. In H441 cells, the rate of uptake of [³H]Acetate, [¹⁴C]Fluoroacetate and [¹⁸F]FDG decreased significantly by 200%, 192% and 365% following Orlistat treatment. In H1975 cells, the rate of uptake of [³H]Acetate, [¹⁴C]Fluoroacetate and [¹⁸F]FDG decreased significantly by 145%, 160% and 230% in Orlistat treated cells, compared to control group. **Conclusions:** The observed results of radiotracer uptake in H441 and H1975 cells clearly demonstrate the potential of this technique as a promising pharmacodynamic marker of FAS inhibition by novel FAS inhibitors such as Orlistat. Further studies to understand the mechanisms underlying the observed results, to find the correlation between FAS inhibition, glycolytic activity and EGFR expression, are in progress.

Presentation Number **0123**
Scientific Session 14: Metabolism and Hypoxia

A Novel Organotypic Multi-cellular Tumor Spheroid Model for High-content Screening of HIF1 Signaling and Metastasis Inhibitors

Andrei Volgin, Lucia LeRoux, Brian Rabinovich, Juri G. Gelovani, *Experimental Diagnostic Imaging, MD Anderson Cancer Center, Houston, TX, USA. Contact e-mail: andrei.volgin@mdanderson.org*

Objective: The aim of this study was to investigate spatial and temporal interactions and cooperation of tumor and stromal cells during hypoxia-induced motility and invasion in a well controlled in vitro model of organotypic multi-cellular tumor spheroids. We also assessed whether this in vitro model could be used for high content screening of novel HIF1 signaling inhibitors. **Methods:** Multicellular organotypic lung tumor spheroids were developed by micro-extrusion in a matrix of heat-inactivated Matrigel followed by placement onto the collagen matrix: a) Lewis lung carcinoma tumor cells (3LL LM) transduced with HIF1-inducible GFP (peak emission of 507 nm) below 10% oxygen in the atmosphere and constitutively expressed RFP (peak emission of 590 nm) reporters b) murine tsA58 (H-2Kb) pulmonary fibroblasts (FBs) transduced with eBFP2 (peak emission of 478 nm) c) murine endothelial cells (ECs) transduced with mKateS158A (peak emission of 620 nm) **Results:** These 3D spheroids form tumor stromal microarchitecture characterized by vascular tubulo-genesis with an organized network of FBs & ECs. Under normoxic conditions, dynamic confocal fluorescence microscopy revealed an organized network of fibroblasts and ECs surrounding the eGFP+ hypoxic tumor core. However, under hypoxic conditions, a distinct migration of all 3 cell types out of tumor and into the matrix was observed. Notably, cellular migration and invasion into the surrounding collagen matrix is organized such that FBs escape first, followed by tumor cells (Fig. A) and finally by ECs (Fig. B). We termed this observation an “invasion complex” or “invasion triad”. The formation of characteristic tumor-stromal microarchitecture and the formation of “invasion complexes” was diminished when hypoxic spheroids were cultured in the presence of known inhibitors of HIF1 signal transduction (YC-1 and Px-478). Generation of spheroids with 3LL LM and skin instead of tissue-matched pulmonary FBs and ECs resulted in neither an organized multicellular morphology nor hypoxia induced formation of “invasion complexes”. **Conclusions:** This study suggests that hypoxic conditions contribute to a tumor invasion into the surrounding tissue, which is spatially and temporally coordinated between hypoxic tumor cells and tumor stromal cells (fibroblasts and endothelial cells) that form an “invasion complex” and move in a particular sequence: fibroblast, tumor cell, and endothelial cell. Inhibition of HIF1-signaling disrupts the cooperative signaling between tumor and stromal cells, prevents the formation of “invasion complexes” and inhibits tumor invasion. This novel spheroid model provides an in vitro system for high throughput screening of compounds which modulate HIF1 signaling or may affect tumor invasion and metastasis.



- **Normoxic 3LL cells**
- **Hypoxic 3LL cells**
- **Endothelial cells (ECs)**
- **Fibroblasts (FBs)**

Presentation Number **0124**
Scientific Session 14: Metabolism and Hypoxia

HIF-1 α Silencing in MDA-MB-231 Human Breast Cancer Cells Alters Choline Phospholipid Metabolism

Tariq Shah, Balaji Krishnamachary, Flonné B. Wildes, Zaver M. Bhujwalla, Radiology, Johns Hopkins University, Baltimore, MD, USA.
Contact e-mail: tariq196@yahoo.com

Hypoxia-inducible factor-1 α (HIF-1 α) over-expression is associated with increased patient mortality in several cancers. We studied the effect of HIF-1 α silencing on the choline phospholipid metabolism of MDA-MB-231 human breast cancer cells using a magnetic resonance (MR) compatible cell perfusion assay. Increased expression of choline kinase (Chk), the enzyme that converts choline to phosphocholine (PC) is typically associated with a more aggressive breast cancer phenotype. MDA-MB-231 cells were transduced with a HIF-1 α shRNA lentivirus vector containing a GFP reporter and validated for HIF-1 α knock-down by western blots and quantitative RT-PCR. ^1H and ^{31}P MR spectra were obtained from intact perfused cells. High-resolution spectra from cell extracts were acquired to further characterize metabolic changes. Immunoblots detected reduced expression of Chk in HIF-1 α silenced cells compared to parental cells. Expression of Chk was intrinsically lower in HIF-1 α silenced cells compared to parental cells, and following treatment with the hypoxia mimetic CoCl_2 . Representative ^1H and ^{31}P MR spectra, shown in Figure 1, demonstrate a decrease of total choline (tCho) and PC in intact silenced cells. Quantitative data from ^1H and ^{31}P MR spectra of these intact perfused cells revealed significantly reduced levels of tCho ($p < 0.05$) and PC ($p < 0.01$) in HIF-1 α silenced cells compared to parental cells, confirming that HIF-1 α silencing reduced PC by reducing Chk expression. High-resolution cell extract data further confirmed these changes. We previously observed that Chk is up regulated under hypoxia, and identified HIF-1 binding sites on the Chk promoter. The reduction of choline metabolites in HIF-1 α silenced cells further confirms the role of HIF-1 α in the regulation of Chk. The reduction of Chk, tCho and PC levels in HIF-1 α silenced cells are also typical of a less aggressive metabolic phenotype.

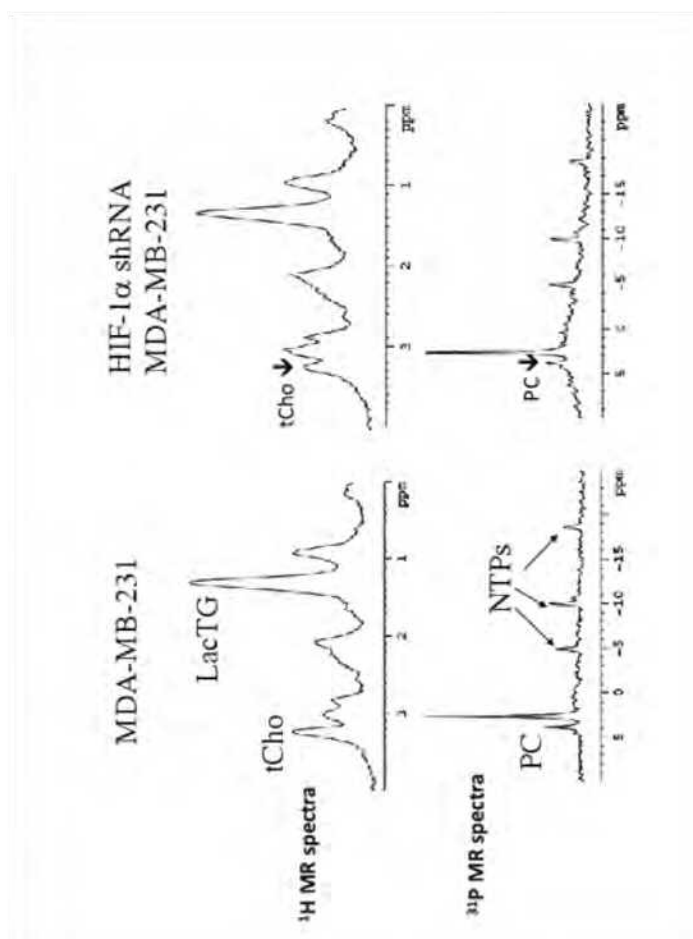


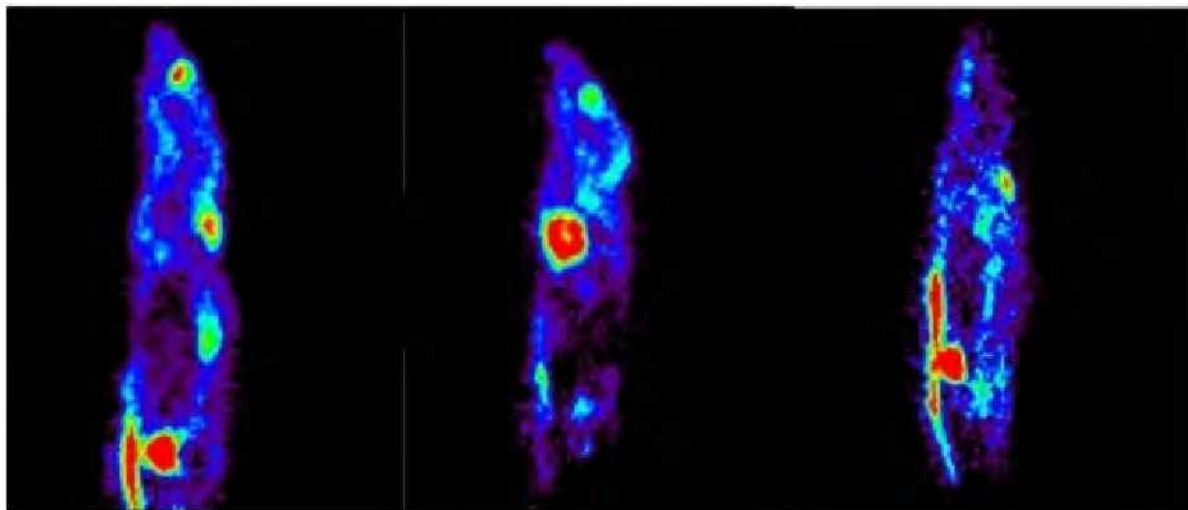
Figure 1. Representative ^1H and ^{31}P spectra from MDA-MB-231 and HIF1 α shRNA MDA-MB-231 cells.

Presentation Number **0125**
 Scientific Session 14: Metabolism and Hypoxia

A MicroPET Study of Brown Adipose Tissue Uptake of ¹⁸F-FDG in an Obesity Mouse Model Taking Weight Loss Treatment

Wuying Cheng¹, Fengying Gong², Zhaohui Zhu¹, Huijuan Zhu², Chenxi Wu¹, Kun Zheng¹, Hui Pan², Fang Li¹, ¹Nuclear Medicine, Peking Union Medical college hospital, Beijing, China; ²Endocrinology, Peking Union Medical College Hospital, Beijing, China. Contact e-mail: chengwuying@sohu.com

Objective: This study aimed to investigate the ¹⁸F-FDG uptake in brown adipose tissue (BAT) of an obesity mouse model taking weight loss treatment. **Methods:** Eighteen "Inprinting Control Region" (ICR) mice (4 weeks old) were randomly divided into 3 groups: the obesity group (n=7) was bred with special high-fat food for 16 weeks; the treatment group (n=6) was also bred with the high-fat food, but was additionally treated with Sibutramine Hydrochloride (7mg/kg) via gastrogavage daily 9 weeks later; the control group (n=5) was bred only with the normal food. After a BAT activation at 7 degree centigrade one hour per day for two days, a microPET scan was underwent 40 minutes after intraperitoneal injection of 3.7 MBq ¹⁸F-FDG using a Siemens Inveon system. The standardized uptake value (SUV) of BAT at the shoulder region was measured, and the ratio to SUV of Brain (R) of each mouse was used to compare the BAT uptake among the three groups. Finally, the BAT at the shoulder region of each mouse was surgically removed and weighted, and the percentage to body weight of the same mouse was calculated. **Results:** The weight of obesity model group (55.60±5.73 g) was significantly higher than that of the control group (44.20±2.08 g, P=0.002), and the weight decreased to some extent in the treatment group (50.88±3.81 g, P=0.115). MicroPET scans revealed significantly elevated ¹⁸F-FDG uptake in the BAT of the treatment group (R=3.25±1.58) than that of the obesity model group (R=1.85±1.25, P=0.03). Lesser uptake was also observed in the obesity model group than the control group (R=2.03±0.6), but without significance. The percentage of shoulder BAT of the control, obesity and treatment group was 0.46%±0.13%, 0.36%±0.13%, and 0.39%±0.18%, respectively (P>0.05 among the groups). **Conclusion:** The mouse taking a weight loss treatment using Sibutramine Hydrochloride is more ready for the activation of BAT, and ¹⁸F-FDG PET is a promising method for evaluation of BAT activation.



¹⁸F-FDG microPET imaging(from left to right):control,obesity,and treatment group.

Data of 3 groups

	Weight	BAT%	Rat
control group	44.20±2.08	0.46%±0.13%	2.03±0.6
obesity group	55.60±5.73	0.36%±0.13%	1.85±1.25
treatment group	50.88±3.81	0.39%±0.18%	3.25±1.58

Presentation Number **0126**
 Scientific Session 14: Metabolism and Hypoxia

Fluorescence Imaging of Glycan Sialylation in Tumors

Andre Neves¹, **Henning Stoeckmann**^{1,2}, **Rebecca Harmston**¹, **Scott K. Lyons**¹, **Finian J. Leeper**², **Kevin M. Brindle**^{1,3}, ¹Cambridge Research Institute, Cancer Research UK, Cambridge, United Kingdom; ²Department of Chemistry, University of Cambridge, Cambridge, United Kingdom; ³Department of Biochemistry, University of Cambridge, Cambridge, United Kingdom. Contact e-mail: andre.neves@cancer.org.uk

Altered glycosylation is a characteristic of tumor cells that is related to malignancy. Consequently, the ability to image the alterations in glycosylation that occur in the tumor microenvironment has the potential to provide novel methods for monitoring disease progression. N-acetylneuraminic (sialic) acid (Neu5Ac) is a monosaccharide that frequently terminates cellular glycoproteins and/or glycolipids. Heavily sialylated glycoproteins, commonly overexpressed in cancer cells, mediate the processes of invasion and metastasis, by interacting with selectin adhesion receptors on stromal cells. We show here that sialic acid can be imaged *in vivo* in tumors, using a bio-orthogonal reporter strategy^[1]. The method was demonstrated in a mouse model of lung carcinoma, using planar fluorescence imaging. We have used a sequential, three-probe based, labelling approach. In the first step, animals were pulsed with the azido-labelled metabolic precursor of sialic acid, peracetylated N-azidoacetyl-mannosamine (Ac₄ManNAz), and subsequently detected *in vivo*, by Staudinger ligation, using a biotinylated phosphine (bPP). In the second step, a deglycosylated, neutral avidin, labelled with a far-red fluorophore (NADyL647), was used to detect the biotinylated phosphine probe. Significantly higher labelling of sialic acid was observed in the tumor environment, compared to surrounding tissue (P<0.0005, n=8). Given the prognostic indications of aberrant sialic acid expression in tumors, variants of this technique, particularly with radiolabelled probes, may be translatable to a clinical setting, where they could be used for monitoring cancer progression. ^[1] Prescher JA et al. (2004) *Nature* 430:873-7.

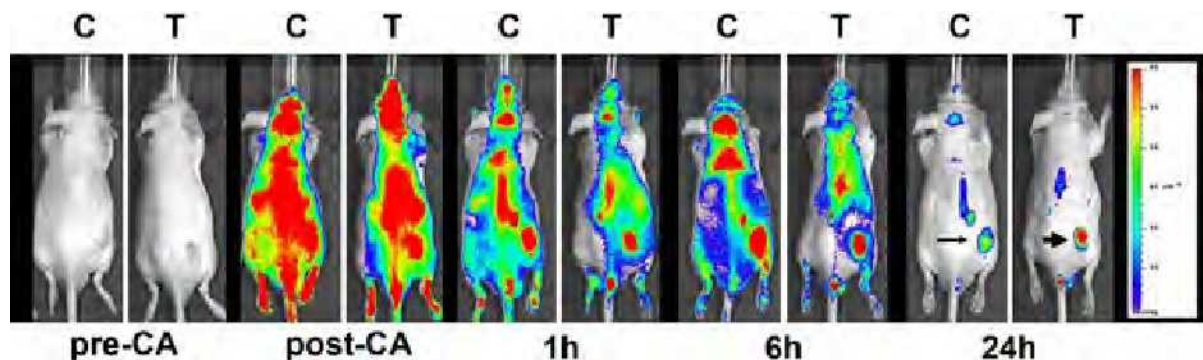


Figure 1 - Non-invasive imaging of glycan sialylation in tumors. A subcutaneous lung carcinoma model was setup in nude mice. The experimental test group (T) was pulsed with Ac₄ManNAz over 7 days (i.p.); the control group (C) was pulsed with vehicle only; both experimental groups were subsequently treated with bPP (i.p.) on the 8th day; 2h after bPP injection, both groups were injected with NADyL647 (i.v.). Contrast agent distribution was imaged over a period of 24h. Significantly more labeling (+50%) was detected in test (thick arrow), compared with control (thin arrow) tumors (n=8/group, p=0.0004); vertical scale in fluorescence efficiency units.

Presentation Number **0127**
Scientific Session 15: Cardiovascular Diseases

Photodynamic Therapy as a Tool of Theranostics to Detect and Treat Atherosclerotic Plaques

Dong Kun Lee¹, **Yongdoon Choi**², **Soo-Min Shon**¹, **Jin Eok Park**¹, **Jeong-Yeon Kim**¹, **Dawid Schellingerhout**³, **Dong-Eog Kim**¹,
¹Neurology, Dongguk University Ilsan Hospital, Goyangsi, Republic of Korea; ²Molecular Imaging and Therapy Branch, National Cancer Center, Goyang, Republic of Korea; ³Radiology and Experimental Diagnostic Imaging, The University of Texas M.D. Anderson Cancer Center, Houston, TX, USA. Contact e-mail: leeinkr@naver.com

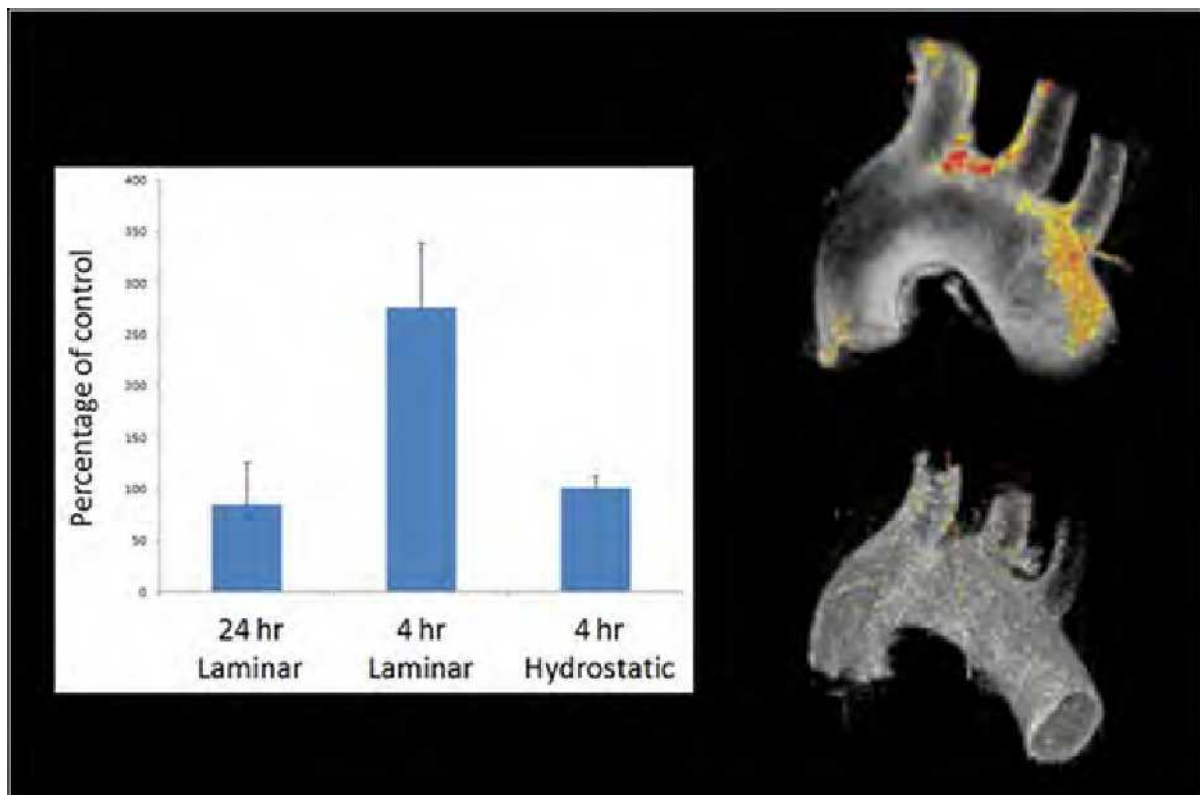
Purpose: Photodynamic therapy (PDT) has been applied to eliminate undesired cells by using photosensitizers and light to form short-lived reactive oxygen species (ROS) that locally destroys cells. PDT for atherosclerosis, based on the preferential accumulation of photosensitizers in lipophilic atherosclerotic plaques, to eliminate inflammatory macrophages in unstable atherosclerotic plaques is most desirable. Methods & Results: To accommodate preferential activation of a photosensitizer in inflammatory macrophages which are enriched with cathepsin B, a cathepsin B-activatable photosensitizer L-SR15 with multiple Ce6 molecules coupled onto a poly-L-lysine backbone (Choi et al., Cancer Res 66:7225-9) was used. Resonance energy transfer between Ce6 groups in L-SR15 due to close geometry of Ce6 prohibits generation of ROS and fluorescence even upon illumination. Digestion of poly-L-lysine backbone with cathepsin B releases quenching effect and generates ROS upon illumination of light. D-SR15 with Ce6 molecules on a poly-D-lysine backbone was used as a control. Aortas from ApoE knockout mice fed on western diet were incubated in DMEM media containing 4 micromolar L-SR15 or D-SR15 for 24 hr, washed with PBS, analyzed for fluorescence reflectance imaging, illuminated with light (non-ionizing and non-thermal) at 8J/cm² for 50 sec, further incubated for 1 day, and processed for immunohistochemical staining. Near-infrared fluorescence signal (Cy5) was detected in atherosclerotic plaques of aorta incubated with L-SR15, but not with D-SR15. This result indicates that digestion of L-SR15 backbone with cathepsin B turns on the photosensitizer L-SR15 for fluorescence and generation of ROS. Immunohistochemical staining (Mac-3) of aortas showed that selective destruction of macrophages in atherosclerotic plaques of aorta incubated with L-SR15, but not with D-SR15. Conclusion: These results indicate that protease-activatable photosensitizer is able to serve as an imaging-based molecule with capacity of both therapy and diagnosis (theranostics) of atherosclerotic plaques.

Presentation Number **0128**
Scientific Session 15: Cardiovascular Diseases

A Novel Molecular Marker for Hemodynamic Stress

Xiangyang Bai¹, Jeffrey A. LaMack², Andrew S. Nencka¹, Zhixin Li¹, **Ming Zhao**¹, ¹Biophysics, medical college of wisconsin, Milwaukee, WI, USA; ²Electrical Engineering and Computer Science, Milwaukee School of Engineering, Milwaukee, WI, USA. Contact e-mail: mzhao@mcw.edu

Aberrant blood flow patterns are associated with vascular anomalies. Molecular markers that reflect hemodynamics stress will provide critical information on vascular health and diseases. Emerging evidence indicates that endothelial cells externalize phosphatidylethanolamine (PE) in response to hemodynamic stress, and that this phenomenon has implications in the thrombo- and athero-protective functions of the endothelium. The objective is to investigate the hemodynamic factors that contribute to the upregulation of vascular PE. Methods: Three-dimensional, T1-weighted molecular MRI (80 micron isotropic resolution) was acquired on the rat aortic arch, using gadolinium-labeled Duramycin as a PE-specific molecular probe on a 9.4T Bruker scanner. The data were correlated to the hemodynamic profile of the vessel obtained by computed simulation. Various flow chambers were used to replicate different hemodynamic stimuli experienced by the endothelium. Cultured human aortic endothelial cells were subject to laminar shear stress, hydrostatic pressure, or blunt flow impact. The surface expression of PE was measured using radiolabeled Duramycin. Results: According to the MRI data, vascular PE is present in high concentration at regions correlated with flow patterns that have a strong blunt impact component, whereas the PE level is relatively low in areas of laminar shear stress and the inner curvatures. In vitro flow chamber studies indicate that laminar shear stress induced a low to moderate upregulation of surface PE, which diminishes over time. No difference was induced by hydrostatic pressure. In contrast, blunt flow impact resulted in a prominent upregulation of PE at the endothelial surface. Conclusions: The greater presence of PE at the luminal endothelial surface in major conduit arteries reflects regions of high impact stress. While the exact regulatory molecular signal transduction mechanism warrants further investigation, this phenomenon may provide a novel molecular marker for vascular hemodynamics.

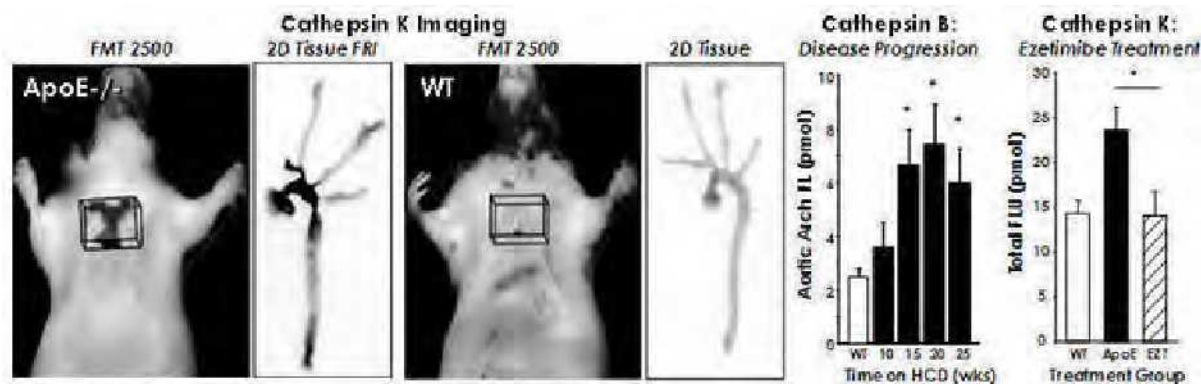


Presentation Number **0129**
 Scientific Session 15: Cardiovascular Diseases

Non-Invasive, In Vivo Optical Tomographic Imaging and Quantification of Atherosclerosis Progression in ApoE Deficient Mice

Bagna Bao, Jeff Morin, Kevin Groves, Jun Zhang, Milind Rajopadhye, Karen Madden, Wael Yared, David Z. Gao, **Jeffrey D. Peterson**, VisEn Medical, Bedford, MA, USA. Contact e-mail: jpeterson@visenmedical.com

Current non-invasive tools to assess preclinical models of atherosclerosis and treatment efficacy rely almost entirely on structural and anatomic features of atherosclerotic lesions. A robust means of non-invasive molecular imaging of atherosclerosis would enable a quantitative, biologically-targeted approach to measure disease progression and to evaluate the effects of therapy in vivo. We report the utility of a panel of near infrared (NIR) imaging agents (detecting multiple cathepsins, cathepsin B, cathepsin K, and $\alpha\beta3$ integrin), in non-invasive fluorescence molecular tomography (FMT) imaging to quantify atherosclerosis in apolipoprotein (apo) E-deficient mice. Using ProSense750 (multiple cathepsins) - or Cat B 750 FAST (selective for cathepsin B) - as imaging agents, significant disease could be detected and quantified by FMT in the aortic arch region in living animals. These agents quantified increases in disease as early as 15-20 weeks following the start of high fat diet, and in-life FMT imaging yielded ranges of values in good agreement with ex vivo assessment of aortic arches by reflectance imaging or tissue lipid staining (Oil Red O). The efficacy of prophylactic ezetimibe and atorvastatin treatments (20 to 25 weeks) were quantified using Cat K 680 FAST (cathepsin K) and ProSense750 imaging agents, respectively, and the decreased FMT fluorescence signals in vivo correlated with plasma cholesterol, ex vivo tissue fluorescence reflectance imaging and tissue lipid staining. These studies demonstrate the ability of FMT-based optical tomography of NIR fluorescent agents to non-invasively visualize and quantify the biological progression of inflammation in atherosclerotic lesions in vivo.



Presentation Number **0130**
 Scientific Session 15: Cardiovascular Diseases

Assessment of Microstructure Variability in the Hypertrophied Myocardium using Diffusion Tensor MRI and the Log-Euclidean Computational Framework

Archontis Giannakidis¹, **Osama Mahmoud Abdullah**², **Kathleen M. Brennan**¹, **Edward W. Hsu**², **Grant T. Gullberg**^{1,3}, ¹*Radiotracer Development & Imaging Technology, Lawrence Berkeley National Laboratory, Berkeley, CA, USA;* ²*Bioengineering, University of Utah, Salt Lake City, UT, USA;* ³*Radiology, University of California San Francisco, San Francisco, CA, USA.* Contact e-mail: AGiannakidis@lbl.gov

Purpose: The objective of this study is to quantify changes in cardiac fiber architecture that are associated with hypertrophy development. We seek to explore the mechanism behind the progressive deterioration in myocardial function that is characteristic of hypertrophy. **Materials and Methods:** To examine the relationship between temporal evolution of hypertrophy and cardiac microstructure, we studied 6 spontaneous hypertensive rats (SHR), born with high blood pressure, and 4 age-matched Wistar Kyoto (WKY) rats, that served as control. We characterized the rat hearts ex vivo by applying diffusion tensor magnetic resonance imaging (DT-MRI), a non-destructive tool that has made it easy to determine the fiber arrangement. Heart excision times varied from 6 to 18 ½ months after birth. To extract the variability of myocardial fiber architecture, we relied on Log-Euclidean metrics, which are consistent with the Riemannian nature of the tensor space and also lead to fast and simple solution. **Results:** Compared with controls, the hypertrophied hearts exhibited increased dispersion in the orientation of microstructural components of myocardium. The trend became more predominant as the disease progressed and it was more pronounced in the laminar sheet orientations. The hypertrophy in SHR was confirmed by measurements of the myocardial mass normalized to the entire body weight. The results are summarized in Fig. 1. **Conclusions:** DT-MRI together with the Log-Euclidean computational framework is favorable for assessing changes in the myocardial structure that occur at the cellular level at various stages of cardiac hypertrophy. The increase in derangement of normal spatial patterns, that takes place in the time course of hypertrophy and was evaluated in this study, may be the cellular mechanism responsible for the observed gradual decline in cardiac performance.

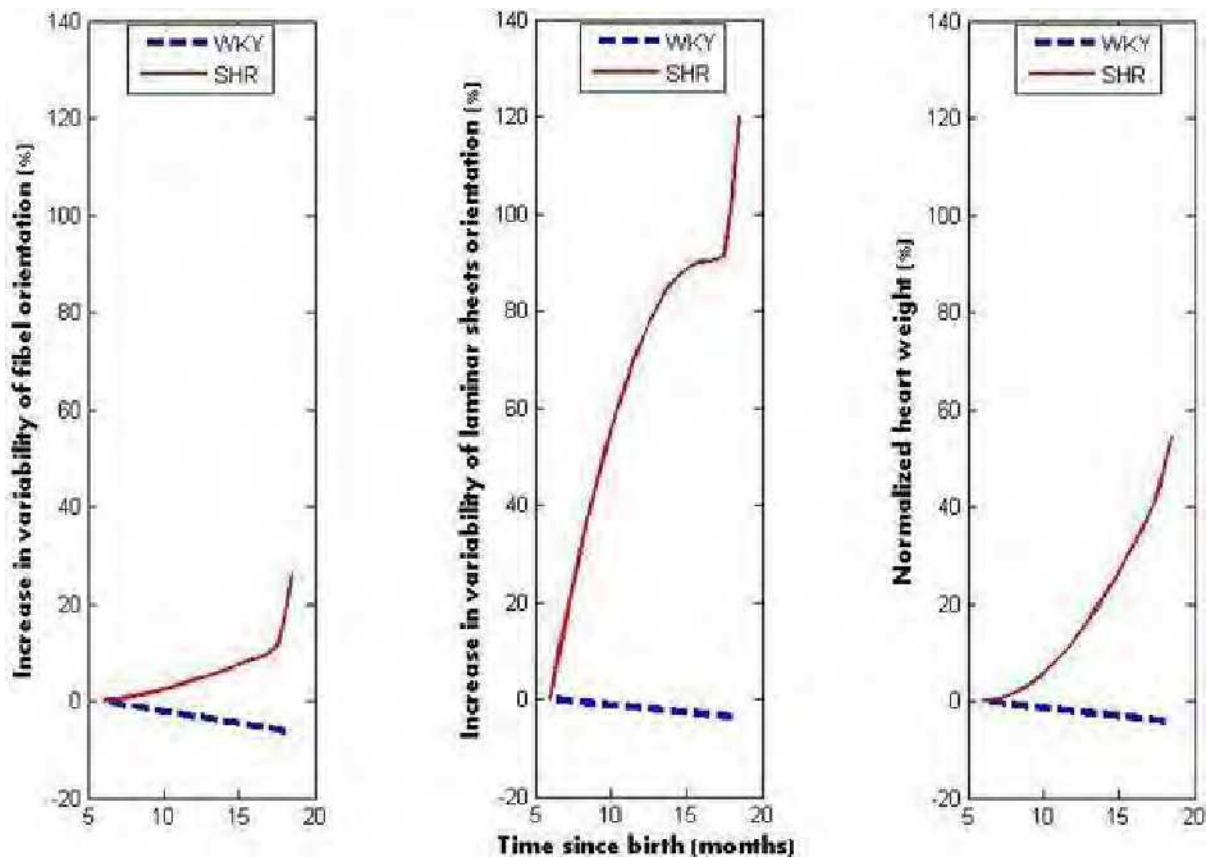


Fig. 1: Time course of the increase in variability of myocardial tissue and the normalized heart weights for the two groups of rats.

Presentation Number **0131**
 Scientific Session 15: Cardiovascular Diseases

Near-infrared Fluorescence Intravascular Catheter System for Two-Dimensional Molecular Imaging of Atherosclerosis

Amir Rosenthal^{1,2}, Marcella A. Calton¹, Georgios Mallas¹, R. Nika Razansky², Adam Mauskopf¹, Farouc A. Jaffer¹, Vasilis Ntziachristos², ¹Cardiovascular Research Center (CVRC) and Cardiology Division, Massachusetts General Hospital and Harvard Medical School, Boston, MA, USA; ²Institute for Biological and Medical Imaging (IBMI), Helmholtz Zentrum München, Neuherberg, Germany. Contact e-mail: eeamir@gmail.com

Detection of high-risk coronary arterial plaques prior to rupture remains an unmet clinical challenge, in part due to the stringent resolution and sensitivity requirements. To address this need, we have developed a near-infrared fluorescence (NIRF) catheter system for 2D intravascular molecular imaging of inflamed atherosclerotic plaque, based on the scheme developed in Ref. [1]. A schematic description of the catheter is shown in Fig. 1. The catheter is based on an optical fiber that guides exciting laser light (750 nm) to the tissue and collects the subsequent fluorescent emission. The fiber is rotated and translated using mechanical stages. The fiber tip is slanted with a 45-degree angle to reflect the guided laser light to the wall of the blood vessel and excite targeted fluorochromes within the vessel wall. A portion of the fluorescence is collected by the fiber and is guided back to the system. A dichroic mirror and a set of filters selectively transmit the fluorescent light to a photomultiplier tube (PMT). The voltage produced by the PMT is used to form a 2D image of the fluorescent probe within the blood vessel. The system was tested in vivo in the abdominal aorta of six hyperlipidemic, balloon-injured atherosclerotic rabbits. The rabbits were injected with a cysteine protease-activable NIRF imaging agent targeting inflammatory cysteine proteases in plaque (VM110, ex/em 750/770nm). The aorta was imaged in vivo using both the intravascular 2D NIRF imaging catheter, and intravascular ultrasound (IVUS) for anatomical co-registration. The aorta was sequentially imaged ex vivo using fluorescence reflectance imaging (FRI). In vivo enhanced NIRF signal in plaques coincided with the ex-vivo FRI data. The results demonstrate the high dynamic range of the NIRF catheter in imaging inflammation in plaques, and offer a coronary artery-targeted translatable approach to detect biologically high-risk plaques. References: 1) F. Jaffer et al. *Circulation*, 28, 1802-09 (2008).

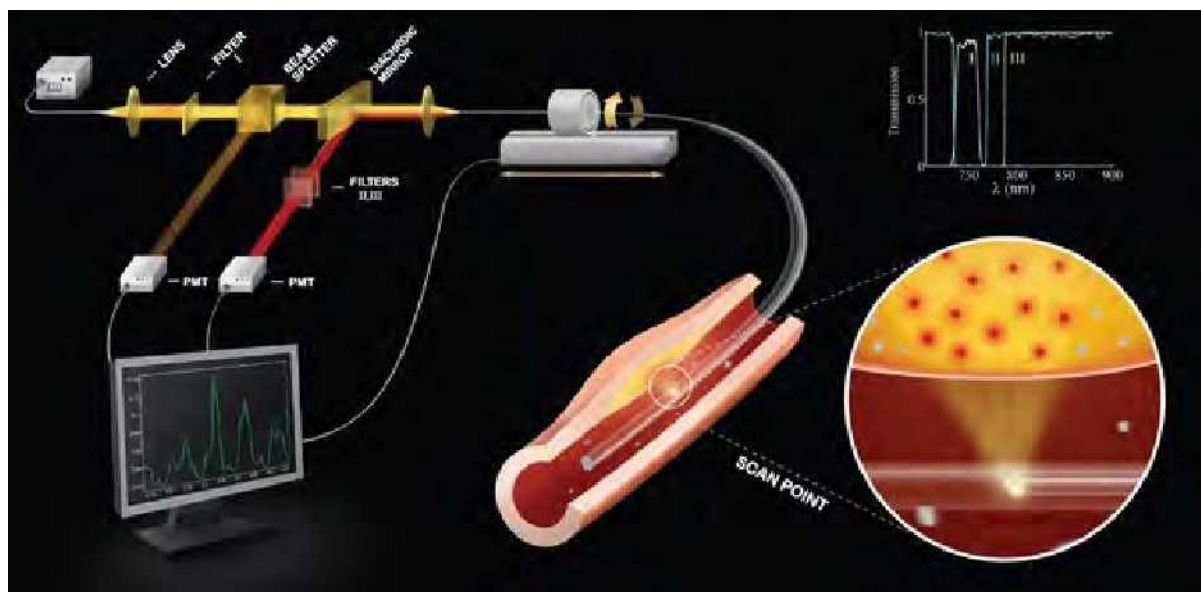


Fig. 1. A schematic description of the NIRF imaging catheter. The inset shows the transmission spectrum of the filters used.

Presentation Number **0132**
 Scientific Session 15: Cardiovascular Diseases

Multimodality Imaging of Myocardial $\alpha\beta3$ Expression, Blood Flow and Infarct Size in Patients after Acute Myocardial Infarction

Ambros J. Beer¹, Marcus R. Makowski¹, Alexandra Keithahn¹, Ullrich Ebersberger², Stephan G. Nekolla¹, Markus Schwaiger¹,
¹Department of Nuclear Medicine, Technische Universität München, Klinikum rechts der Isar, Munich, Germany; ²Cardiology, Klinikum Bogenhausen, Munich, Germany. Contact e-mail: ambros.beer@tum.de

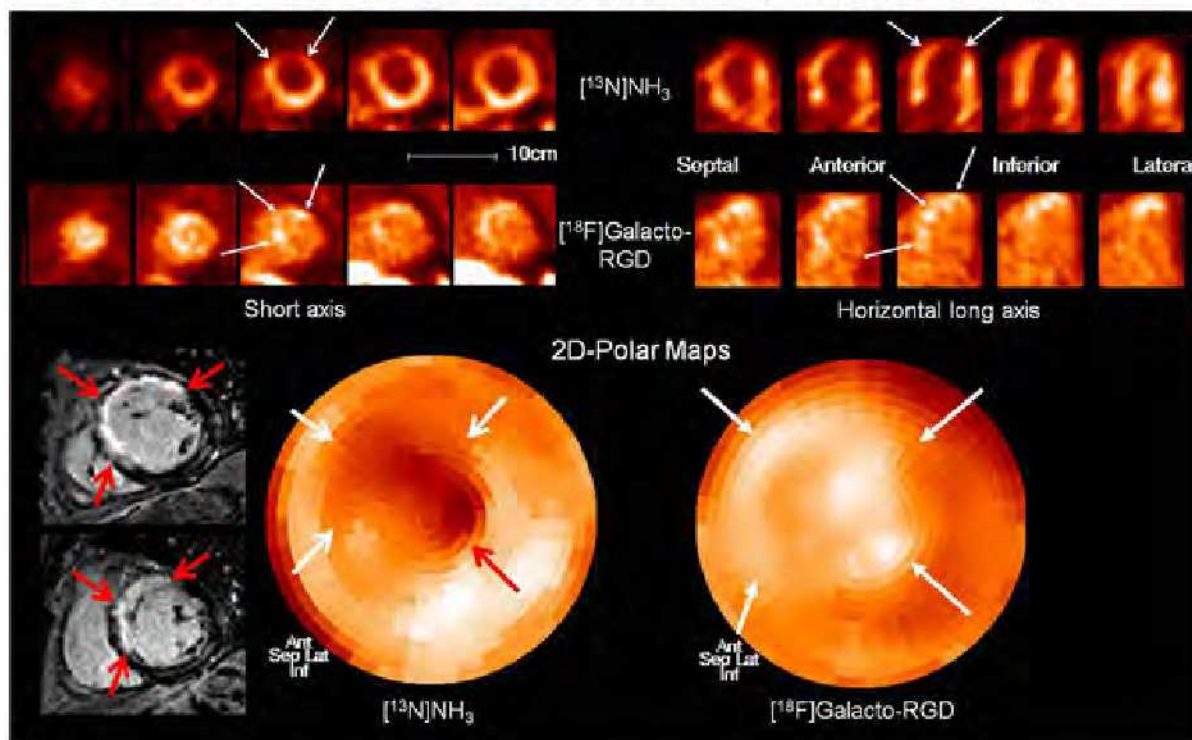
Purpose: The $\alpha\beta3$ integrin may be an important target associated with myocardial repair after ischemic injury. We thus evaluated whether [¹⁸F]Galacto-RGD PET/CT can demonstrate $\alpha\beta3$ expression in patients after myocardial infarction and to what extent tracer uptake correlates with myocardial blood flow and infarct size. **Methods:** 12 patients were examined 31±14 days after myocardial infarction with PET/CT using [¹³N]NH₃ and [¹⁸F]Galacto-RGD (120 min. after injection) and with cardiac MRI including late enhancement. Normal myocardium (remote) and areas of infarction (lesion) were identified on the [¹⁸F]Galacto-RGD PET/CT images by correlation with the late enhancement MRI studies and [¹³N]NH₃. Polar maps were subsequently created. Regions of interest were drawn in normal myocardium, lesions, liver and blood pool and lesion/liver-, lesion/blood- and lesion/remote-ratios were calculated. Blood flow and [¹⁸F]Galacto-RGD uptake were quantified and correlated for each segment of the myocardium using a 17 segment model. **Results:** [¹⁸F]Galacto-RGD uptake could be demonstrated in 5 patients, either adjacent to and/or in the infarcted areas with a mean signal increase compared to myocardium of 46% (26-83%; lesion/blood 1.15±0.06; lesion/liver 0.61±0.18). In the residual patients, uptake was only faint or lower than in myocardium (mean -13%±22%; lesion/blood 0.82±0.25; lesion/liver 0.32±0.06). [¹⁸F]Galacto-RGD uptake correlated significantly with infarct size (R=0.730;p=0.016). Moreover it correlated significantly with restricted blood flow for all myocardial segments (r=-0.385;p<0.0001) and even stronger in infarct areas (r=-0.750;p<0.0001). **Conclusions:** [¹⁸F]Galacto-RGD PET can successfully demonstrate tracer uptake in a subset of patients after myocardial infarction suggesting elevated myocardial $\alpha\beta3$ expression in this group. The data suggest that $\alpha\beta3$ expression is more intense in larger infarcts and in areas with more impaired blood flow. Follow up studies have to show, whether [¹⁸F]Galacto-RGD PET might be of value for prediction of prognosis and ventricular remodelling.

Technische Universität München, Department of Nuclear Medicine



Patient with MI of anterior, anteroseptal wall and apex

[¹⁸F]Galacto-RGD uptake in the [¹³N]NH₃ perfusion defect but also extending to areas of preserved [¹³N]NH₃ perfusion



Presentation Number **0133**
Plenary Session 4: Stem Cell Imaging

Brain Imaging in Stem Cell Therapy for Primate Parkinson's Disease Models

Jun Takahashi^{1,2,3}, **Daisuke Doi**^{1,2,3}, **Tetsuhiro Kikuchi**^{2,3}, **Hirotaaka Onoe**⁴, **Takuya Hayashi**⁴, **Asuka Morizane**^{1,2}, ¹*Department of Cell Growth and Differentiation, Center for iPS Cell Research and Application, Kyoto, Japan;* ²*Department of Biological Repair, Institute for Frontier Medical Sciences, Kyoto, Japan;* ³*Department of Neurosurgery, Kyoto University Graduate School of Medicine, Kyoto, Japan;* ⁴*Functional Probe Research Laboratory, RIKEN Center for Molecular Imaging Science, Kobe, Japan. Contact e-mail: jbtaka@frontier.kyoto-u.ac.jp*

Considering cell therapy with embryonic stem cells (ESCs) and induced pluripotent stem cells (iPSCs) for Parkinson's disease into clinical application, formation of a graft cell-derived tumor is a major concern about safety of the therapy. So, it is critical to evaluate the tumorigenicity of human ES cell-derived neural cells in primates. We induced neural progenitor cells (NPCs) from human ESC lines by the modified SDIA (stromal cell-derived inducing activity) method. The cells were cultured on Matrigel in conditioned medium of PA6 cells for one week, and transferred to sphere culture in the presence of FGF-2 for one or three weeks; 14day- and 28day-spheres, respectively. Then, the cells were transplanted into the bilateral striatum of monkey models of Parkinson's disease. The survival and differentiation of the grafted NPCs were monitored by MRI and PET scans, and histological studies were performed after the animals were sacrificed in nine months. In case of the monkey with 14day-spheres which still contained undifferentiated ESCs, MRI scan revealed tumor-like growth of the cells with perifocal edema. PET scan showed increase of glucose metabolism ($[^{18}\text{F}]\text{FDG-PET}$) and uptake of fluoro-thymidine ($[^{18}\text{F}]\text{FLT-PET}$) in this region. Histological studies also revealed intense proliferation of undifferentiated cells, and positive staining for Oct3/4. The study also showed existence of nestin- or tyrosine hydroxylase (TH)-positive cells, but there was no complete evidence for teratoma formation such as bones, skins, guts, muscles etc. Other two monkeys with 28day-spheres which contained no ESCs showed slight expansive growth of the cells, but Oct3/4+ cells were not found. Small amount of Ki67+ cells were observed sporadically, and most of them were also immunoreactive for nestin. Next, we induced NPCs from a human iPSC line, and transplanted them into the striatum of a monkey model. We could monitor the dopaminergic function of the grafted NPCs by PET studies; $[^{18}\text{F}]\text{DOPA}$ for dopamine synthesis, $[^{11}\text{C}]\text{DTBZ}$ for vesicle transport, and $[^{11}\text{C}]\text{PE2I}$ for dopamine re-uptake. Thus, MRI and PET studies were useful for the evaluation of the survival, proliferation, and differentiation of the ESC- or iPSC-derived NPCs, and can be expected for a clinical use.

Presentation Number **0134**
Scientific Session 16: Cancer Detection

Detection of MMP Activity in FCCC^{Apc+/Min} Mouse Colorectal Adenomas Using an Enzymatically Activated Probe

Harry Cooper, **Harvey Hensley**, Wen-chi Chang, Karthik Devarajan, Christina Ferrara, Clapper Margie, Fox Chase Cancer Center, Philadelphia PA, PA, USA. Contact e-mail: harvey.hensley@fcc.edu

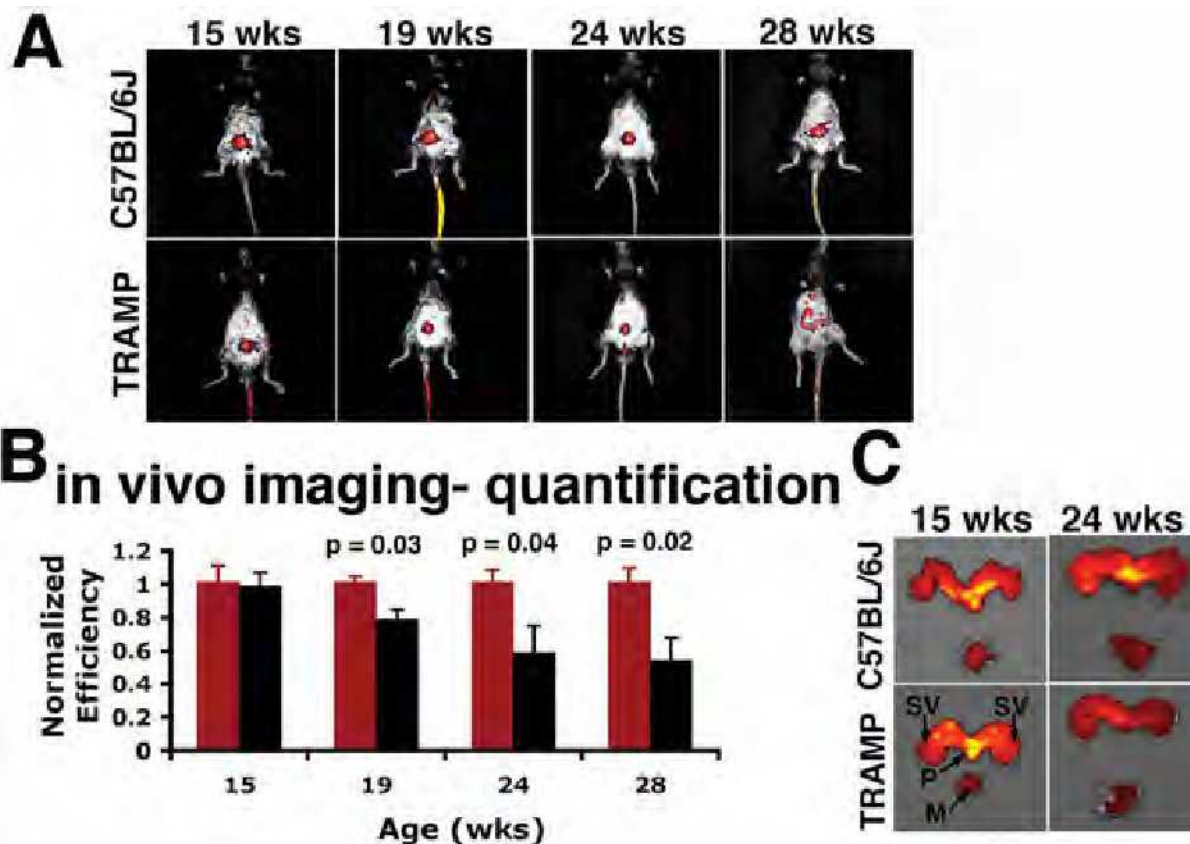
Matrix metalloproteinases (MMPs), a large family of enzymes that degrade the extracellular matrix, participate in all stages of colorectal carcinogenesis including the formation of early adenomas. Previous work has shown that expression of MMP-7, an epithelial cell-specific MMP, is elevated substantially in colorectal adenomas from a unique strain of C57Bl/6J Min mice (FCCC^{Apc+/Min}) that spontaneously develop multiple colorectal adenomas. The advent of a bioactivatable probe (MMPSense 680, VisEn Medical) that emits a near-infrared fluorescent signal when cleaved by MMPs provides new opportunities for monitoring this early molecular event in vivo. The goal of this experimentation was to determine if MMPSense 680 can be used to detect colorectal adenomas reliably in FCCC^{Apc+/Min} mice. Colonoscopic exams were performed using a rigid bore endoscope (Karl Storz Veterinary Endoscopy, Inc.), and the cross-sectional area of detectable lesions was measured. Mice were subsequently injected retroorbitally with a single dose of MMPSense (2 nmol in PBS) generously provided by VisEn Medical. At 60 hours post-injection, the mice were euthanized, and the excised colons were imaged using an IVIS Spectrum In Vivo Imaging System (Caliper Life Sciences). The multiplicity of gross colorectal adenomas ranged from 1 to 13. Following overnight fixation in formalin, the entire colon was cut at 2 mm intervals, and each segment was placed in an individual cassette for histopathological evaluation. A training set was constructed from 6 animals and used to inform the observer of the presence or absence of fluorescent signal in areas of known pathological diagnosis. Following this training, two independent observers scored each ROI in the fluorescent images (dichotomized as positive vs. negative) from 10 colons, and the scores were subsequently correlated with the presence of histopathologically confirmed neoplasia. Receiver operating characteristic (ROC) curves for Observer A had an AUC of 0.859 with 95% C.I.=(0.747,0.971), specificity = 0.933, sensitivity = 0.762. The ROC curve for Observer B was similar, with AUC=0.829, 95% C.I.=(0.71,0.949), specificity = 0.923, sensitivity=0.696. The median inter-observer correlation was 0.90. These data indicate that MMPSense can detect colorectal adenomas with high sensitivity and specificity and support its further development for the early detection of colorectal tumors. A significant percentage of colorectal tumors remain undetected during colonoscopic examination in humans.

Presentation Number **0135**
 Scientific Session 16: Cancer Detection

In Vivo Imaging of Zinc Levels in Prostate Cancer

Subrata K. Ghosh¹, Xiao-an Zhang², Stephen J. Lippard², Zdravka Medarova¹, **Anna Moore**¹, ¹Radiology, Massachusetts General Hospital, Charlestown, MA, USA; ²Department of Chemistry, Massachusetts Institute of Technology, Cambridge, MA, USA. Contact e-mail: amoore@helix.mgh.harvard.edu

Prostate cancer causes no symptoms in its early curable stage. Consequently, the ability to diagnose prostate cancer early, before it has spread beyond the confines of the organ, could offer the only possibility of a cure to patients at risk for aggressive disease. Over half a century of research has identified zinc as a potential diagnostic biomarker. The healthy prostate contains the highest concentrations of mobile zinc of all soft tissues in the body. These levels decrease dramatically during the development of prostate cancer. Here, we describe a novel method to image prostatic mobile zinc using a new fluorescent zinc sensor (ZPP1), which has a unique turn-on response to zinc and a low fluorescence background, 10-fold lower than in the zinc-saturated state¹. We demonstrate that ZPP1 can distinguish between nonmalignant and malignant prostate cell lines, based on the marked reduction of zinc uptake by the adenocarcinoma cells. We apply in vivo fluorescence optical imaging to detect prostatic zinc in mice and apply this method for the monitoring of prostate cancer development in a transgenic mouse model of prostate adenocarcinoma (TRAMP). Specifically, in the TRAMP model we observe a loss of fluorescence signal with disease progression beginning at 19 weeks of age, which is the age representative of well-differentiated localized carcinoma (Fig. 1A and B). By 28 weeks of age, the signal associated with the TRAMP prostate is reduced 2-fold, compared to the healthy age-matched controls ($p = 0.03$, $n = 4$; Fig. 1A and B). These observations are confirmed by ex vivo optical imaging (Fig. 1C). Overall, we are confident that the described studies clearly illustrate the value of zinc-based prostate-cancer diagnostics. 1. Zhang, X.A., Hayes, D., Smith, S.J., Friedle, S. & Lippard, S.J. New strategy for quantifying biological zinc by a modified zinpyr fluorescence sensor. *J Am Chem Soc* 130, 15788-15789 (2008).



Presentation Number **0136**
Scientific Session 16: Cancer Detection

Application of Carboxymethyl Mannan-coated MR Contrast Agent for Detecting Micro-metastasis in Lymph Node

Hieu Vu-Quang^{1,2}, Sangjoon Lee^{1,5}, Hwa Jeong Lee^{1,5}, Hui Lian Che^{1,2}, Myeong Ju Moon³, Mi Kyong Yoo⁴, Chong Su Cho⁴, Yong Yoen Jeong³, In-Kyu Park^{1,5}, ¹Department of Biomedical Sciences, Chonnam National University Medical School, Gwangju, Republic of Korea; ²Clinical Vaccine R&D center, Chonnam National University, Hwasun, Republic of Korea; ³Department of Radiology, Chonnam National University Medical School, Gwangju, Republic of Korea; ⁴School of Agricultural Biotechnology, Seoul National University, Seoul, Republic of Korea; ⁵BioImaging Research center, GIST, Gwangju, Republic of Korea. Contact e-mail: vuquanghieu86@gmail.com

Metastatic lymph node (LN) cancer originated from primary cancer cells that break away and enter the lymphatic system may be diagnosed by magnetic resonance imaging (MRI). However, distinguishing between normal and metastatic LNs by MRI is difficult because evaluated images mostly rely on the size and shape of LNs. To overcome this problem, many contrast agents have been developed to increase the contrast level of metastatic LNs compared to the normal LNs, such as Gadoflurine M, Combidex, Endorem, etc. Carboxymethyl (CM) Mannan is synthesized by chemical modification with iodoacetic acid from Mannan, a water soluble polysaccharide, having high content of D-Mannose residues and recognized by mannose receptors of antigen presenting cells (APCs) such as dendritic cells or macrophages, then presented to lymphocytes in LNs. We supposed that CM-Mannan is less toxic and less trapped by circulation system. Therefore, CM-Mannan-coated super paramagnetic iron oxide nanoparticles (CM-Mannan-SPIONs) have been developed with the assumption that it will be taken up by APCs in order to trace the metastatic LNs. Mannan-SPIONs, CM-Mannan-SPIONs, Dextran-SPIONs, PVA-SPIONs have been injected to rats and metastatic mouse models intravenously. Compared to the positive control, Dextran-SPIONs and PVA-SPION, CM-Mannan-SPIONs have been quickly taken up one hour after the intravenous injection and the signal intensities in lymph nodes after the administration of CM-Mannan-SPIONs have decreased to 25% lower than 60% with the positive control. After 24 hours, the signal intensities in LNs of CM-Mannan-SPIONs reached to plateau at 30 % which is the same as positive control. From the results, CM-Mannan-SPIONs have greatly demonstrated its potential to enhance contrast level and detect the lymph nodes. Now another test is under way to detect the metastatic lymph nodes with CM-Mannan-SPION.

Presentation Number **0137**
Scientific Session 16: Cancer Detection

Dual c-MET and Gastrin Releasing Peptide Receptor Targeted Pancreas Tumor Imaging Using c-MET Binding Peptide-Bombesin Heterodimer

Su-Jin Cheong, Chang-Moon Lee, Eun-Mi Kim, Sun-Hee Kim, DooRye Jang, Min-Hee Jeong, Hwan-Jeong Jeong, Seok Tae Lim, Myung-Hee Sohn, Department of Nuclear Medicine, Chonbuk National University Medical School, "Geumam-dong, Dukjin-gu, Jeonju, Jeonbuk", Republic of Korea. Contact e-mail: thinkfamily99@daum.net

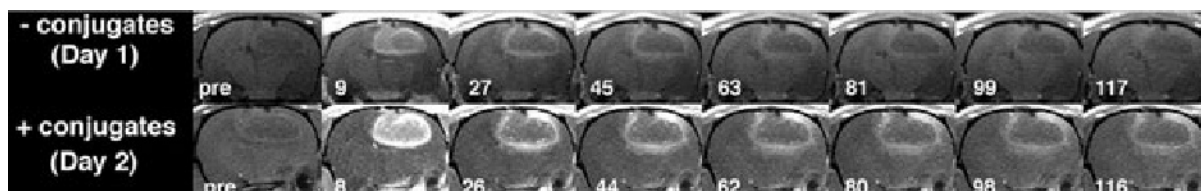
Mesenchymal-epithelial transition factor receptor (c-MET) binding peptide (cMBP) has been extensively investigated for c-Met expression imaging in various tumors. Bombesin (BBN) shows high affinity for gastrin-releasing peptide receptor (GRPR) overexpressed in tumors. Recently, we designed cMBP-BBN heterodimeric peptide for dual target tumor imaging. The goal of this study was to investigate the possibility of dual receptor-targeting for tumor imaging. The cMBP-BBN peptide was coupled with Cy5.5. The cellular binding of Cy5.5-conjugated cMBP-BBN was tested in Miapaca-2 cells by confocal fluorescent microscopy and the binding quantification was measured using an IVIS optical imaging system. In vivo tumor targeted imaging studies of Cy5.5-conjugated cMBP-BBN was performed with firefly luciferase gene transfected human pancreatic tumor (Miapaca-2-Fluc)-bearing orthotopic mice. For the in vitro and in vivo blocking study, Cy5.5-conjugated cMBP-BBN was co-treated with free cMBP, BBN or cMBP-BBN without Cy5.5 conjugation. Confocal fluorescence imaging for cellular binding in vitro show that Cy5.5-conjugated cMBP-BBN peptide bound to cell surface and that the peptide binding was significantly inhibited by free cMBP, BBN or cMBP-BBN treatment. Quantification results for cellular binding show that Cy5.5-conjugated cMBP-BBN-treated cells had a high signal intensity and in the blocking studies, the cellular binding of Cy5.5-conjugated cMBP-BBN was reduced by co-treating free cMBP, BBN, or cMBP-BBN, which indicates that the cMBP-BBN peptide shows the specific binding to their receptors on the cells. In the in vivo animal study, orthotopic Miapaca-2-Fluc pancreas tumors were effectively visualized with Cy5.5-conjugated cMBP-BBN. The tumor-to muscle ratio for Cy5.5-conjugated cMBP-BBN was 7.45 ± 0.9 . In contrast, the mice co-injected with free peptides (cMBP, BBN or cMBP-BBN) exhibited lower signal in the pancreas tumor area compared to the Cy5.5-conjugated cMBP-BBN. These results demonstrate that Cy5.5-conjugated cMBP-BBN heterodimeric peptide shows the high tumor targetability in mice bearing pancreas tumor cells and suggest that Cy5.5-conjugated cMBP-BBN may be useful for pancreas cancer imaging.

Presentation Number **0138**
 Scientific Session 16: Cancer Detection

Imaging EGF Receptor Expression in Gli36 Tumor Xenografts Using Targeted MR Signal-Amplifying Enzymes

Alexei A. Bogdanov¹, Mohammed S. Shazeeb², Christopher H. Sotak², ¹Radiology, UMASS Medical School, Worcester, MA, USA; ²Biomedical Engineering, Worcester Polytechnic Institute, Worcester, MA, USA. Contact e-mail: alexei.bogdanov@umassmed.edu

Aggressive gliomas commonly overexpress 170kD epidermal growth factor receptor (EGFR). We used humanized anti-EGFR monoclonal antibody (mAb EMD72000) for targeted delivery of a self-complementing enzymatic magnetic resonance (MR) signal amplification system. The substrate for the key reaction catalyzed by peroxidase (HRP) conjugated to mAb was supplied by the second conjugate of mAb and glucose oxidase (GO). Our goal was to explore enzyme-mediated paramagnetic tagging of cells as a strategy for specific retention of a molecular probe at the sites of anti-EGFR expression. Methods: Conjugates were synthesized by covalently linking HRP or GO to mAb and characterized in human Gli36ΔEGFR cell culture as well as in a glioma model. diTyr-GdDTPA, a paramagnetic HRP substrate, was injected I.V. at a dose of 0.1 mmol/kg. T1-weighted 3T MR imaging was performed sequentially in the same animals: Day 1: pre- and post-injection of diTyr-GdDTPA; Day 2: targeted mAb conjugates were initially injected IV; MRI pre- and post-injection of diTyr-GdDTPA was performed 4 h later. T1-weighted 3T MR imaging was performed in animals before and after I.V. injection of diTyr-GdDTPA (0.1 mmol/kg). On the following day, animals were preinjected with targeted mAb conjugates, and 4 hours later, MR images were again obtained before and after the injection of diTyr-GdDTPA. Results: T1wt MR images showed strong initial enhancement of the tumor within minutes after the administration of diTyr-GdDTPA. A significantly longer substrate retention in tumors was observed on Day 2 (Figure). Temporal MR signal decay for Day 1 was monoexponential whereas on Day 2 a biexponential signal decay was observed. The washout time constants (WTCs) on Day 1 and short WTCs on Day 2 were attributed to free substrate elimination and they were significantly different in tumor rim and core regions. Conclusion: our experiments demonstrated the effect of local MR signal increase and retention as a consequence of EGFR targeted enzyme co-delivery to gliomas in vivo.



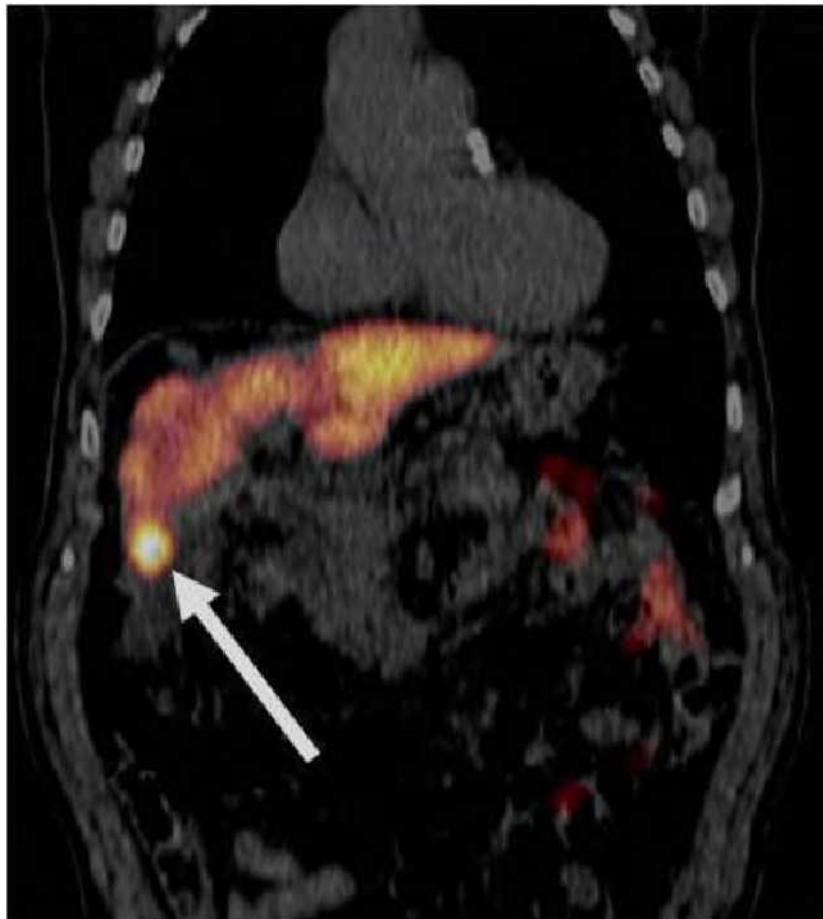
T1-weighted sequential MR images depicting Gli36 glioma tumor xenografts. Top row – images showing temporal washout of diTyr-GdDTPA with no anti-EGFR conjugate pre-injection (Day 1). Bottom row – images showing temporal washout of diTyr-GdDTPA at 4 h following pre-treatment with anti-EGFR conjugates (Day 2) in the same slice for the same animal. Time intervals (in min) after the injection of diTyr-GdDTPA are shown for each image.

Presentation Number **0139**
Scientific Session 16: Cancer Detection

[¹⁸F]Fluoro-2-deoxy-2-galactose has Great Potential as a PET Tracer for Detection of Hepatocellular Carcinoma: A Prospective, Consecutive Study in 40 Patients

Michael Sørensen^{1,2}, **Kim Frisch**¹, **Dirk Bender**¹, **Susanne Keiding**^{1,2}, ¹*PET Centre, Aarhus University Hospital, Aarhus, Denmark;*
²*Department of Medicine V, Aarhus University Hospital, Aarhus, Denmark. Contact e-mail: michael@pet.auh.dk*

Background and Aim Hepatocellular carcinoma, HCC, remains difficult to diagnose at an early stage, at which time it may still be curable. [¹⁸F]fluoro-2-deoxy-2-galactose, FDGal, is a hepatocyte specific positron emitting tracer which in a preliminary study showed potential as a positron emission tomography, PET, tracer for detection of HCC. In the present study we tested the potential use of FDGal as PET tracer for HCC in a larger group of patients. **Subjects and Methods** Forty patients were enrolled in a consecutive, prospective study. As part of standard clinical management, the patients were offered an FDGal PET/CT scan. The FDGal PET images were analyzed blinded before comparison with other imaging modalities and without knowledge of any clinical information. All patients had a multi-phase, contrast enhanced CT (ceCT) performed. Diagnosis of HCC was based on internationally approved criteria. **Results** Of the 40 patients included, 23 were diagnosed with HCC, nine patients had previously been treated for HCC and were now suspected to have relapse, and eight patients were suspected to have HCC, but the diagnosis was rejected. The sensitivity of FDGal PET/CT was 96%, which was similar to that of ceCT (also 96%). All patients without HCC had negative FDGal PET/CT yielding a specificity of 100%. Nine patients had extra-hepatic disease, which in eight of the patients was detected by FDGal PET/CT as a novel finding. FDGal PET/CT also seemed to be able to determine the effect of local treatment of HCC. **Conclusion** We conclude that FDGal has great potential as a PET tracer for detection of HCC including extra-hepatic lesions. The present study allowed us to assess both the general sensitivity and specificity of FDGal PET/CT, but the value of FDGal PET/CT in detection of early HCC needs to be confirmed in a larger trial including patients undergoing surveillance for HCC.



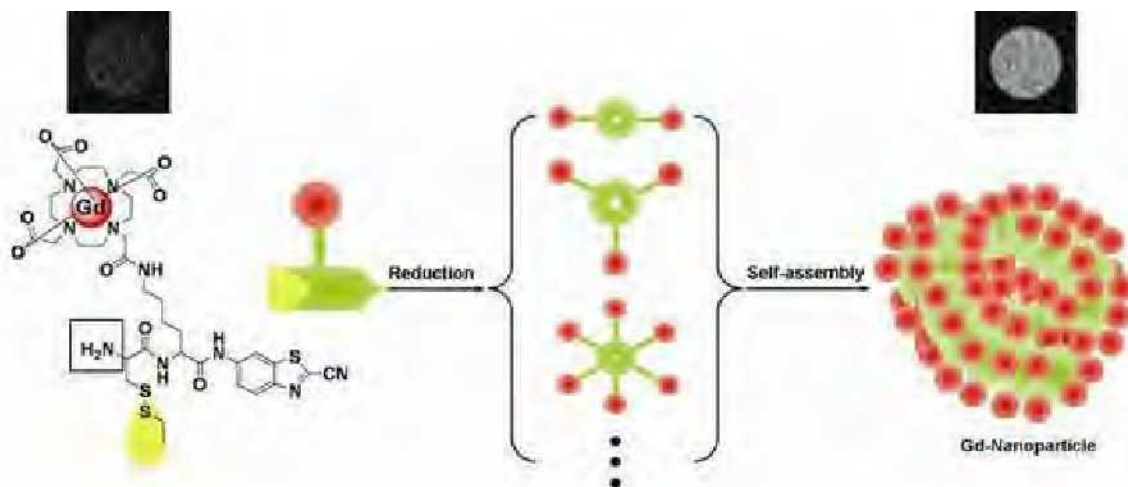
The image shows an FDGal PET/CT positive HCC lesion in the caudal part of the right liver lobe (arrow).

Presentation Number **0140**
 Scientific Session 17: Smart Probes

Controlled Self-assembly of Nanoparticles: A General Template for Developing “Smart” MRI Contrast Agents

Jianghong Rao¹, **Brian K. Rutt**¹, **Gaolin Liang**^{1,3}, **Nan Ma**¹, **Yuanxin Chen**², **Deju Ye**¹, **Man Lung Ma**¹, **John A. Ronald**¹, ¹Stanford University School of Medicine, Palo Alto, CA, USA; ²Robarts Research Institute, University of Western Ontario, London, ON, Canada; ³Chemistry, University of Science and Technology, Hefei, China. Contact e-mail: jrao@stanford.edu

Significant efforts have been dedicated to the development of “smart” magnetic resonance imaging (MRI) contrast agents. A common strategy involves a T1 relaxivity change in response to the presence of the intended target. However, there is still an important need for a general molecular template within this class of MRI probes which through simple chemical modifications can generate unique probes specifically targeted to different molecular targets. Our strategy is based on a system we recently developed [ref 1] based on the condensation reaction between two chemical groups -- 1,2-aminothiol and 2-cyanobenzothiazole. We have demonstrated that this condensation chemistry can lead to the formation and assembly of nanoparticles in vitro and in living cells under the control of pH, disulfide reduction and/or enzymatic cleavage. For example, a small molecule probe Cys(SEt)-Lys(DOTA-Gd)-CBT (1), as shown in Scheme 1, comprising these two chemical groups and a Gd³⁺ chelate, will condense to form oligomers upon disulfide reduction that generates the free 1,2-aminothiol. These oligomers will further aggregate and assemble into nanoparticles through hydrophobic interactions. The change of the chemical form of the probe from single monomers to assembled nanoparticles results in an increase in the T1 relaxivity of Gd. A series of such compounds was prepared, and T1 relaxivity vs field strength measurements were made between 0 and 3T. These measurements show that the as-formed Gd-nanoparticle exhibits an overall increased relaxivity in comparison to that of its monomeric precursor, as well as a distinct change in shape of the NMRD profile in the range 0.5T - 3T. For the probe 1 in Scheme 1, the T1 relaxivity increase is 2.64 fold at ~21MHz (0.5T) and 2.14 fold at 64 MHz (1.5T). These probes are efficiently taken up by cells, and T1 measurements of loaded cell pellets demonstrate good intracellular T1 relaxivity. By varying reactive groups used to mask the presence of the free 1,2-aminothiol, a class of “smart” MRI contrast agents can be similarly developed to sense and image a variety of molecular targets.



Scheme 1. An example of “smart” MRI contrast agents that can form Gd-nanoparticles through multiple condensation reactions and assembly upon reduction and show an increased relaxivity. The amine group (in box) may also be modified to make the agent reactive to various enzymes.

Presentation Number **0141**
 Scientific Session 17: Smart Probes

Divalent Metal Transport Protein, DMT1: A Novel MRI Reporter

Benjamin B. Bartelle, Kamila U. Szulc, Daniel H. Turnbull, *Structural Biology, Skirball Institute for Biomolecular Medicine, New York, NY, USA. Contact e-mail: Ben.Bartelle@nyumc.org*

Divalent Metal Transport Protein, DMT1: A Novel MRI Reporter Benjamin B. Bartelle, Kamila U. Szulc and Daniel H. Turnbull
Motivation and Background The development of effective genetic reporters for MRI has long been an elusive goal. Based on the observed correlation between expression of the divalent metal transporter DMT1 and contrast-enhanced regions of the mouse brain on manganese (Mn)-enhanced MRI (MEMRI) images, we tested DMT1 as a potential T1-based MRI reporter. Results We characterized DMT1-related contrast first by expressing the protein in a cell culture model. Relaxometry showed that HEK cells stably expressing DMT1 had significantly reduced T1 relaxation time (-450ms) compared to control cells, both supplemented with 100 μ M MnCl₂ for 1hr (n=12; p=0.0000003). Based on these data, we tested DMT1 in vivo, using electroporation for ectopic expression of DMT1 in the cortex of neonatal mice. Postnatal day (P)0 neonatal mice were electroporated with pCAGG-DMT1-IRES-eGFP to co-express both DMT1 and eGFP. At P2, neonates were screened for eGFP with a fluorescence dissection microscope. At P5 the mother mouse was administered an intraperitoneal injection of MnCl₂ (80mg/kg body weight). T1-weighted images (3D gradient echo: TE=3.1ms; TR=50ms; Flip angle=45°; 100 μ m isotropic resolution data acquired in 2h) were acquired 8h after injection of MnCl₂, revealing unilateral cortical enhancement on the eGFP-expressing side of the electroporated mice (Figure). To further validate these results, brains were cryosectioned and analyzed with immunohistology, showing correlation between DMT1-expression and cortical MEMRI enhancement. **Discussion and Conclusion** Applications for a T1 MRI reporter include in vivo imaging of gene expression patterns and long-term cell labeling and tracking in transfected or transgenic animals. The current data are very promising and warrant future studies to determine the full efficacy of DMT1 as an MRI reporter.

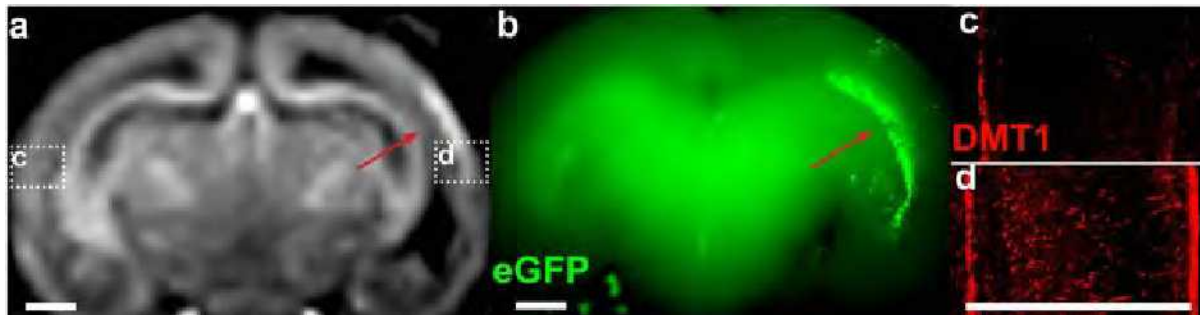


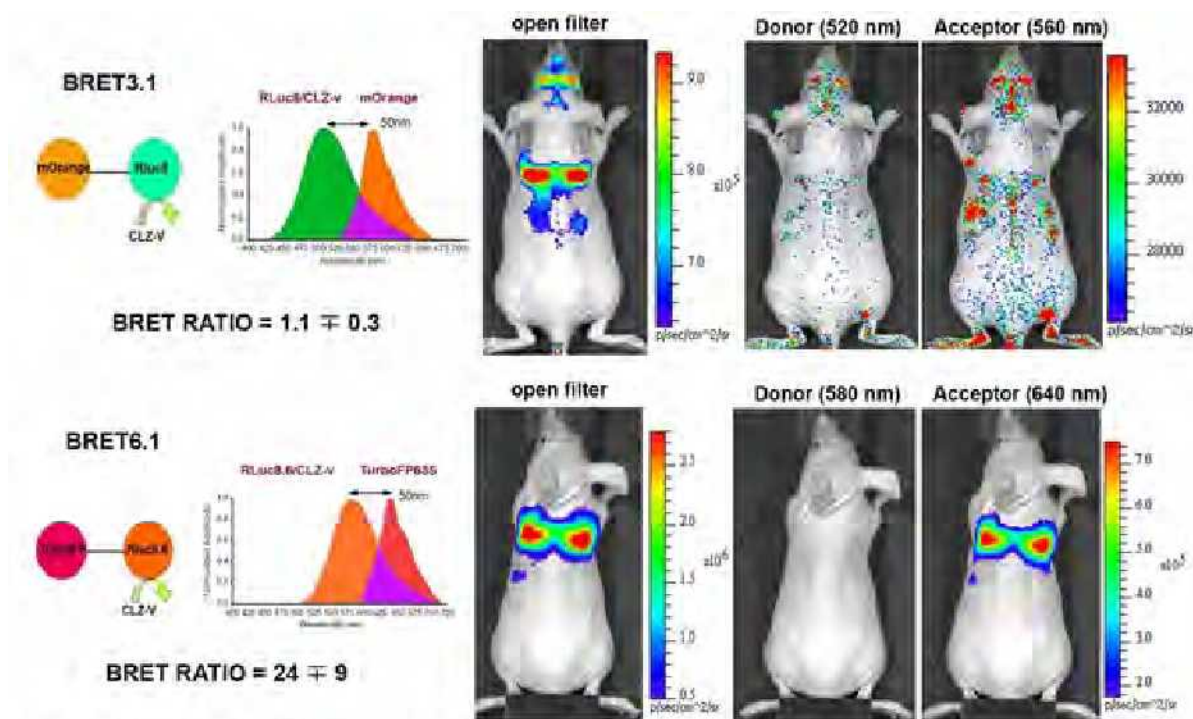
Figure: Coronal sections of a P5 mouse brain after electroporation at P0. (a) MEMRI shows a focal pattern of cortical enhancement on the electroporated side (arrow). (b) Fluorescence microscopy of a coronal slice shows focal expression of eGFP on the same side as the MEMRI enhancement. Immunostaining shows DMT1 expression only on the electroporated side of the brain (c,d).

Presentation Number **0142**
 Scientific Session 17: Smart Probes

Bioluminescence Resonance Energy Transfer (BRET): Marked Enhancement of In Vivo Protein-protein Interaction Imaging Based on Red-light Emitting Proteins

Anca Dragulescu-Andrasi¹, Carmel T. Chan¹, Abhijit De³, Sanjiv S. Gambhir^{1,2}, ¹Department of Radiology, Molecular Imaging Program at Stanford (MIPS), and Bio-X Program, Stanford University School of Medicine, Stanford, CA, USA; ²Division of Nuclear Medicine and Department of Bioengineering, Stanford University School of Medicine, Stanford, CA, USA; ³Tata Memorial Centre, ACTREC, Navi Mumbai, India. Contact e-mail: ancad@stanford.edu

Mapping protein-protein interactions is essential for attaining a molecular understanding of diseases and developing target-specific approaches for their therapeutic management. Current optical methods for noninvasive assessment of protein-protein interactions in small animal orthotopic disease models often lack sensitivity because of extensive tissue signal attenuation and scattering. Bioluminescence based methods have a particular potential for imaging protein-protein interactions in small living subjects because of minimal background signal. Fusion constructs of luciferases and fluorescent proteins can provide responsive turn-on signals based on bioluminescence resonance energy transfer (BRET). Here we describe the development of the first red-light emitting BRET systems that enable deep-tissue imaging studies in small animals with high sensitivity. These systems, named from BRET4 to BRET6.1, consist of novel red-shifted *Renilla reniformis* luciferase variants as BRET donors paired with mutant red fluorescent proteins as acceptors. The generated BRET fusion proteins were tested in living mice for bioluminescence deep-tissue imaging. Cancer cells stably expressing each system were injected intravenously to promote lung trapping. The BRET6.1 system was the most sensitive in detecting trapped cells with 24-fold higher BRET ratio ($n=10$, $P=7.7 \times 10^{-9}$) than the current system BRET3.1 (see Figure). Additionally, we tested the BRET6 system for monitoring rapamycin-mediated FRB/FKBP12 association in mice by fusing the luciferase donor to FRB and the acceptor to FKBP12. The BRET6 system successfully reported the FRB/FKBP2 interaction showing a higher BRET ratio in rapamycin treated mice than in carrier-control mice ($P < 0.01$). These novel red-light emitting BRET systems have great potential for monitoring protein-protein interactions in the context of drug screening and validation, directly from cell culture to deep tissues of small animal disease models.



Bioluminescence imaging of HT1080 cells stably expressing either mOrange-RLuc8 (BRET3.1) or TurboFP635-RLuc8.6 (BRET6.1) fusion proteins in nude mice. Cells (3×10^6) were injected via tail vein, resulting in significant trapping in the lungs. The mice were injected with luciferase substrate coelenterazine-v at 75 min. after cell injection and imaged for 1 min. with each set of filters. Representative mice from BRET3.1 ($n = 10$) and BRET6.1 ($n = 10$) groups are shown. Average radiance from the thorax region was measured, and substrate-only control mice were used for background subtraction.

Presentation Number **0143**
Scientific Session 17: Smart Probes

Targeting of Myocardial Necrosis and Apoptosis Using a Novel Small Molecular Probe, Bis(zinc(II)-dipicolylamine) Complex (Zn-DPA)

Leonie Wyffels¹, Zhonglin Liu¹, Christy Barber¹, Harrison H. Barrett¹, Bradley D. Smith², Jeffrey A. Mattis³, Brian Gray³, Koon Y. Pak³,
¹Radiology Department, University of Arizona, Tucson, AZ, USA; ²Chemistry and Biochemistry Department, University of Notre Dame, Notre Dame, IN, USA; ³Molecular Targeting Technologies Inc, West Chester, PA, USA. Contact e-mail: lwyffels@email.arizona.edu

Objective. This study was designed to investigate the feasibility of a rationally-designed small molecule probe, bis(zinc(II)-dipicolylamine) coordination complex (Zn-DPA), for targeting apoptosis and necrosis indicative of a recent myocardial ischemic insult based on cell membrane anionic phosphatidylserine content. **Methods.** The targeting properties of Zn-DPA were first investigated using ex vivo fluorescent imaging. An ischemic-reperfused rat heart model was created by ligation of the left coronary artery followed by reflow. The fluorescent-labeled Zn-DPA was intravenously injected in rats subjected to 30-min and 5-min myocardial ischemia followed by 2-hr reperfusion. 90 minutes post-injection, the rat hearts were excised and sectioned for postmortem analysis and imaging. ^{99m}Tc labeling of Zn-DPA was carried out with a preformed ^{99m}Tc(I) tricarbonyl complex cation [^{99m}Tc(CO)₃(H₂O)₃]⁺ by exchange of the water molecules in the precursor for the aromatic N-heterocyclic nitrogens in DPA. In vivo and ex vivo cardiac images of ^{99m}Tc-labeled Zn-DPA (^{99m}Tc-Zn-DPA) were acquired using a high-resolution SPECT imager called FastSPECT II and autoradiography in the ischemic-reperfused rat hearts. Myocardial ischemic area, infarction, and apoptosis were evaluated by histological and immunochemical assay. **Results.** Zn-DPA was successfully labeled with ^{99m}Tc and a consistent production with radiochemical purity greater than 95% was obtained. Myocardial infarction was clearly observed in the rat hearts with 30 minutes ischemia and 2-hours reperfusion, but not in the hearts with 5-minute ischemia. In vivo hot spot uptake of ^{99m}Tc-Zn-DPA was detected in the ischemic rat hearts. Postmortem autoradiography and fluorescent imaging showed that Zn-DPA accumulated not only in infarcted myocardium, but also in ischemic viable myocardium. The uptake of Zn-DPA was related to myocardial cell death including necrosis and apoptosis. **Conclusions.** We have preliminarily demonstrated the usefulness of fluorescent and ^{99m}Tc labeled Zn-DPA for hot-spot detection of recent myocardial ischemic insults. This novel small molecule probe might have a promising potential for imaging of apoptosis with unique radiopharmaceutical characteristics, including more favorable blood clearance and biodistribution for imaging than a protein, and capability of radiolabeling with ^{99m}Tc, a radionuclide with broad clinical utility.

Presentation Number **0144**
 Scientific Session 17: Smart Probes

Red and Green Emitting Luciferases for Simultaneous Monitoring of Tumor Growth and NF- κ B Signalling by Bioluminescence Imaging

Laura Mezzanotte^{1,2}, **Elisa Michelini**¹, **Eric Kaijzel**², **Ivo Que**², **Francoise Carlotti**³, **Rob C. Hoeben**³, **Aldo Roda**¹, **Clemens Lowik**²,
¹Dept. of Pharmaceutical Sciences, University of Bologna, Bologna, Italy; ²Dept. of Endocrinology, Leiden University Medical Center, Leiden, Netherlands; ³Dept. of Molecular Cell Biology, Leiden University Medical Center, Leiden, Netherlands. Contact e-mail: laura.mezzanotte2@unibo.it

Amongst the numerous luciferase reporter genes cloned from different animal species and mutated to achieve different emission properties, only a few have been employed for in vivo bioluminescence imaging (BLI). Good thermostability, high and stable photon emission and codon optimization of the luciferase gene are required. Recently, spectral unmixing methodologies have been employed to quantify signals from BLI images obtained using luciferases with different emission spectra. Here we investigated the combined use of green click beetle luciferase (CBG99, max. emission 537 nm) and a red codon-optimized mutant of *P. pyralis* (Ppy-RE8, max emission 618 nm) for in vivo monitoring of tumor progression and NF- κ B signalling. Both in vitro and in vivo studies were carried out to characterize the different luciferases. Lentiviruses expressing Ppy-RE8 and CBG99 luciferase reporter genes constitutively or under the control of NF- κ B promoter were generated and human embryonic kidney (Hek293T) cells were subsequently transfected to express luciferases. Validity of spectral unmixing for the quantitation of the different luciferases was assessed using both a luminometer with appropriate bandpass filters (535nm and 628nm) and the IVIS Spectrum system (Caliper LS). These luciferase variants demonstrated to be a good couple for dual luciferase applications employing the same substrate luciferin, even in presence of an unpaired expression of the genes due to different promoter activity. Then, confirmative results were obtained when the cells expressing Ppy-RE8 or Green CBG99 were injected subcutaneously into immunodeficient mice and BLI imaging was performed in vivo using the same system. Signals from the two luciferases were unmixed using Living Image 3.2 software and images composed by the signals of the two different luciferases were obtained. Preliminary in vivo data envisage the future application of these couple of luciferases for monitoring of multiple events simultaneously by means of BLI.

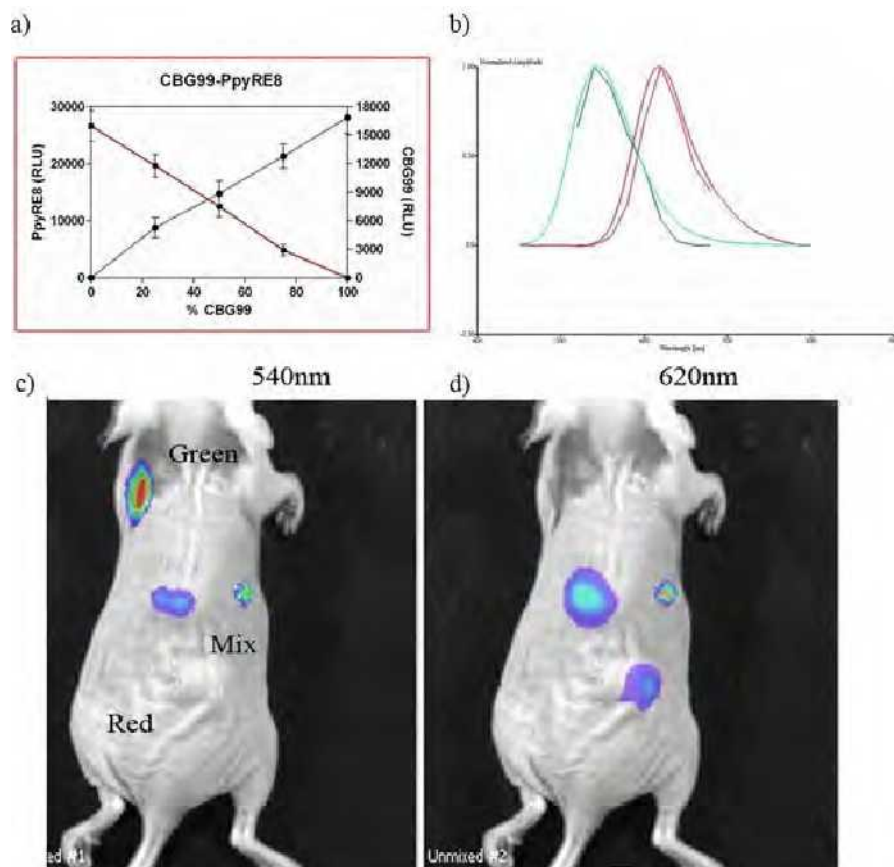


Fig 1. CBG99 and PpyRE8 expressing cellswere mixed in different ratios and measured in vitro (a) and in vivo at 540nm (c) and 620nm (d). The graph (b) shows the max emission peaks of the different luciferases.

Presentation Number **0145**
 Scientific Session 17: Smart Probes

Hybrid Superparamagnetic Iron Oxide Nanoparticles for Tumor Imaging and Therapy In Vivo

DooRye Jang, Chang-Moon Lee, Hwan-Jeong Jeong, Su-Jin Cheong, Eun-Mi Kim, Sun-Hee Kim, Min-Hee Jeong, Seok Tae Lim, Myung-Hee Sohn, Department of Nuclear Medicine, Chonbuk National University Medical School and Hospital, Jeonju, Republic of Korea. Contact e-mail: drth282@nate.com

Development of novel hybrid nanoparticles for both tumor imaging and therapy is an area of significant research interest. In this study, the ability of our hybrid superparamagnetic iron oxide nanoparticles (SPIONs) on tumor-targeted imaging and therapy was investigated and evaluated for animal models. SPIONs were synthesized using a co-precipitation method and surface-modified to avoid the uptake by RES. Further, a vascular endothelial growth factor receptor (VEGFR)-targeted antibody having antiangiogenic effect was conjugated to the SPIONs using a bifunctional linker and Cy5.5 was labeled to the nanoparticles. Tumor-targeted imaging of nude mice bearing MDA-MB231 breast tumors was performed using an animal optical imaging system. For anti-tumor efficacy studies, anti-VEGFR antibody-conjugated SPIONs (80 μ g antibody, 13 mg Fe/kg) were injected intravenously to MDA-MB231 bearing mice (n=5 per group) at every third day. Accumulation of the nanoparticles was assessed using Prussian blue staining. To further analyze the antiangiogenic effects of anti-VEGFR antibody-conjugated SPIONs, immunohisto-chemistry analysis on tumor tissues was performed. The SPIONs were a core size of 12 nm and showed superparamagnetic behavior. Anti-VEGFR antibody-conjugated SPIONs exhibited VEGFR-selective cell binding properties on confocal fluorescent microscopy. Prominent accumulation of anti-VEGFR antibody-conjugated SPIONs in tumor was visualized by animal optical imaging studies. In addition, ex vivo imaging and Prussian blue staining of the harvested tumors further confirmed the accumulation of the SPIONs within the tumor. In tumor growth studies, significant decreases of tumor volumes were found in mice treated with anti-VEGFR antibody-conjugated SPIONs ($p < 0.005$ for all). Concomitant decreases of blood-vessel density (CD31) were found in tumor tissues from anti-VEGFR antibody-conjugated SPIONs-treated mice. In this study, we propose that the hybrid SPIONs could be potentially used for both tumor imaging and therapy.

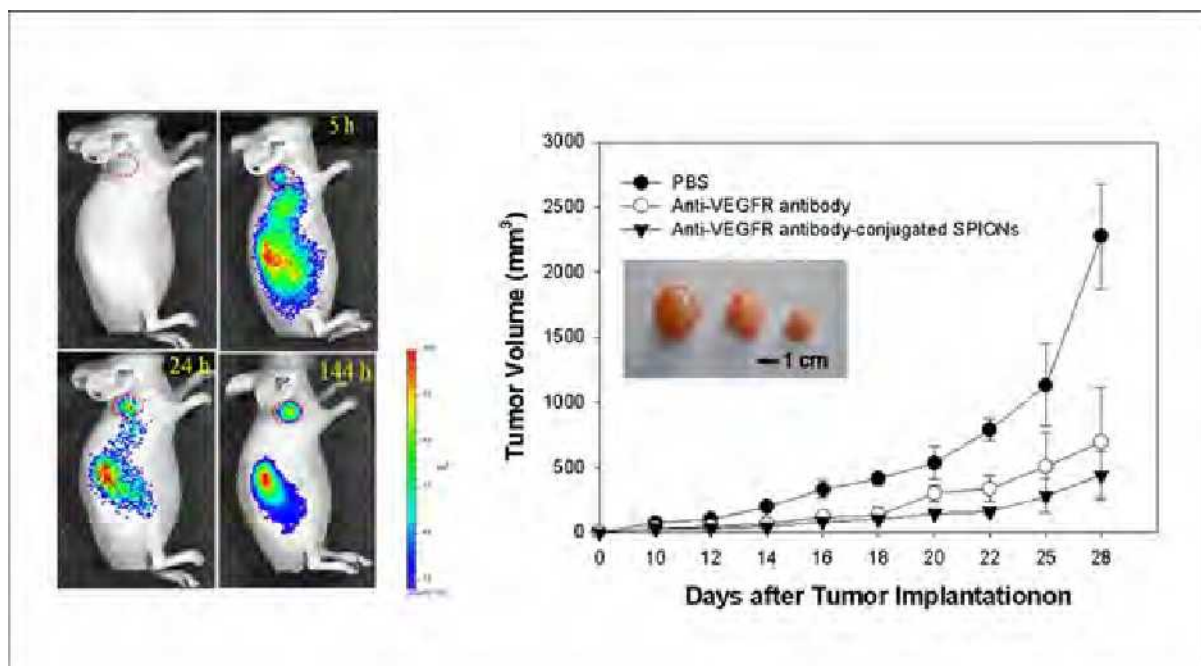


Figure 1. The optical images (left) of MDA-MB231 bearing mice injected with anti-VEGFR antibody-conjugated SPIONs and tumor growth inhibition results (right) from PBS, anti-VEGFR antibody, or anti-VEGFR antibody-conjugated SPIONs-treated mice.

Presentation Number **0146**

Scientific Session 18: SPECIAL SESSION: Close to Clinical Cell Therapies

Cell Tracking for Cartilage Repair Using Superparamagnetic Iron Oxides: Clinical Feasibility

Gerben M. van Buul^{1,2}, Gyula Kotek¹, Piotr A. Wielopolski¹, Eric Farrell^{2,3}, Pieter K. Bos², Harrie Weinans², Jan A. Verhaar², Gabriel P. Krestin¹, Gerjo J. van Osch^{2,3}, **Monique R. Bernsen¹**, ¹Radiology, Erasmus MC, Rotterdam, Netherlands; ²Orthopaedic, Erasmus MC, Rotterdam, Netherlands; ³Otorhinolaryngology, Erasmus MC, Rotterdam, Netherlands. Contact e-mail: m.bernsen@erasmusmc.nl

Purpose: Cell tracking is a useful tool to optimize the use of human bone marrow stromal cells (hBMSCs) for cartilage repair. Cell labeling using superparamagnetic iron oxides (SPIOs) enables non-invasive in vivo cell tracking using MRI. We investigated the safety, intra-articular MRI traceability and possible SPIO re-uptake of this cell tracking technique. **Materials & Methods:** *Safety:* hBMSCs (triplicate samples for 3 donors) were labeled with SPIO (ferumoxides-protamine sulfate) in a dose range of 0 - 250 µg/ml. Cell viability was assessed and cell activity was quantified up to 7 days. *Intra-articular imaging:* SPIO-labeled hBMSCs were injected in pig knees ex vivo and seeded in cartilage defects in vitro. Scanning was performed on a clinical 3.0 T MRI scanner. *SPIO re-uptake:* To show possible SPIO re-uptake by synovial cells, viable and dead GFP⁺-SPIO⁺ chondrocytes were co-cultured on human synovium explants. Samples were analyzed using fluorescence- and light microscopy. **Results:** *Safety:* SPIO labeling resulted in labeling efficiencies of ± 95% and did not impair cell viability or subsequent cell activity at any dose. *Intra-articular imaging:* All SPIO-labeled cell dosages, both intra-articular injected or seeded in cartilage defects, were visualized by MRI (Fig. 1). Cells could be clearly differentiated from anatomical structures. SPIO-labeled cells seeded in cartilage defects were additionally quantified using a T2* mapping MRI technique. *SPIO re-uptake:* GFP⁺-SPIO⁺ cells, indicating originally seeded cells, were seen in samples containing live cells. GFP⁻-SPIO⁺ cells, indicating SPIO re-uptake by synovial cells, were found in samples containing dead cells. **Conclusion:** We showed promising results for the use of SPIO labeling for cell tracking in clinical cartilage repair, although possible SPIO re-uptake by host cells has to be taken into account. This approach provides the extra advantage to simultaneously track cells and evaluate cartilage repair in one MRI session.

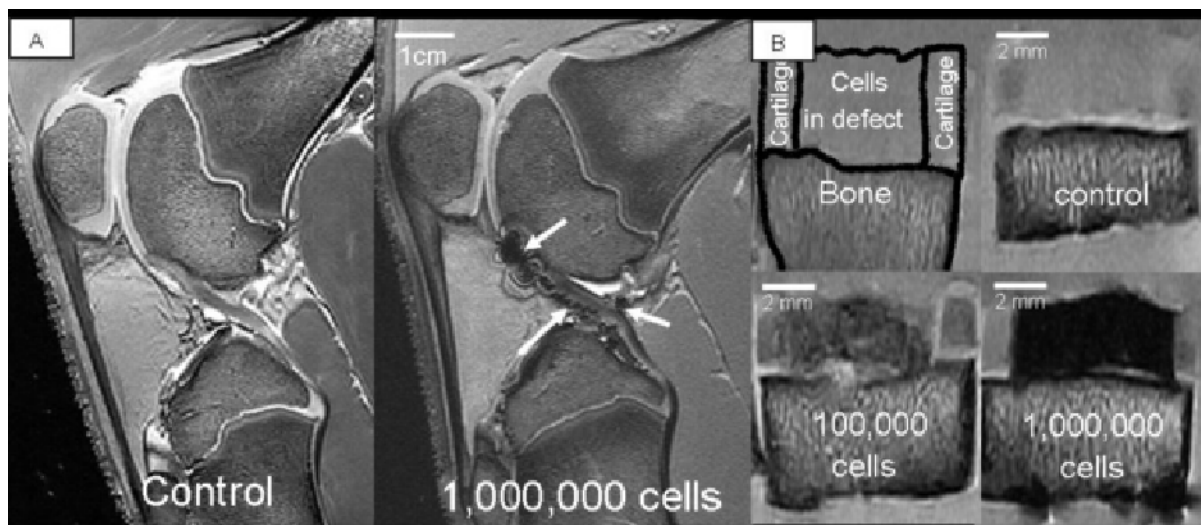


Fig. 1: Intra-articular injected SPIO-labeled cells (1A) and cells seeded in circular cartilage defects in a volume of 75 µl (1B) were accurately visualized by MRI. The amount and intensity of signal voids was related to cell number used.

Presentation Number **0147**

Scientific Session 18: SPECIAL SESSION: Close to Clinical Cell Therapies

Imaging of Rosuvastatin on Survival and Function of Implanted Adipose Tissue-derived Mesenchymal Stem Cells in Mice Infarcted Hearts

Shuang Li, Feng Cao, Weiwei Fan, Xijing Hospital, Xian, China. Contact e-mail: wind8828@gmail.com

Background Adipose-derived stromal/stem cells (ASCs) have been extensively studied for their therapeutic potential for myocardial infarction (MI) due to abundant source and pluripotency. However, the harsh environment in the cardiac tissue after MI, which was characterized by local inflammation and ischemia, induced substantial loss of transplanted ASCs. HMG-CoA reductase inhibitors have been shown to suppress inflammation and promote survival of stem cells, so we postulate that the combination of ASCs transplantation and Rosuvastatin administration may result in a synergistic effect on myocardial repair and functional improvement. Methods and results ASCs were cultured from adipose tissue from transgenic mice, which stably expressed firefly luciferase and enhanced green fluorescence protein (Fluc-eGFP). Myocardial infarction was created in inbred mice by coronary LAD ligation. ASCs were transplanted into the hearts of MI mice with or without Rosuvastatin pretreatment. Transplanted ASCs were tracked by longitudinal bioluminescence imaging. Four weeks after transplantation, cardiac function and left ventricular remodeling were evaluated by serial echocardiography and histology. Rosuvastatin and ASCs treated mice consistently exhibited better cardiac function than control mice evaluated by small animal echocardiography. Increased survival and differentiation of implanted ASCs and decreased infarct area were observed in the Rosuvastatin+ASC group. In the absence of Rosuvastatin, ASC transplantation only achieved a modest improvement in perfusion and morphology. The combined treatment with Rosuvastatin and ASCs also significantly inhibited cardiac cell apoptosis, reduced ROS production, and suppressed expression of TNF α and IL6 in the post-infarct myocardium. Conclusion Noninvasive imaging could be a valuable tool for monitoring stem cell treatment. Rosuvastatin treatment may protect the myocardium undergoing acute infarction by creating a better environment for the survival and differentiation of implanted ASCs.

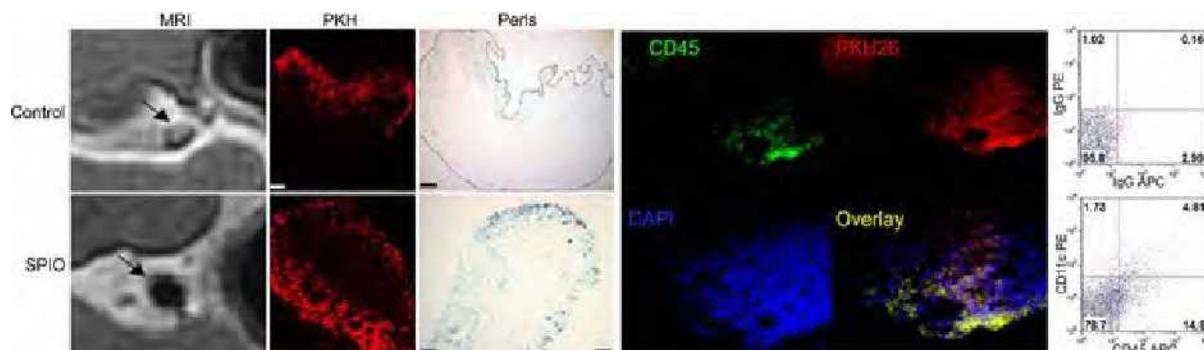
Presentation Number **0148**

Scientific Session 18: SPECIAL SESSION: Close to Clinical Cell Therapies

An In Vivo MRI Assay for Human Dendritic Cell Migration in the CB17 SCID Mouse

Gregory A. Dekaban¹, Xizhong Zhang¹, Roja Rohani¹, Jennifer C. Noad¹, Vasiliki Economopoulos¹, Megan Levings², Ronan Foley³, Paula Foster¹, ¹Imaging, Robarts Research Institute, London, ON, Canada; ²Surgery, University of British Columbia, Vancouver, BC, Canada; ³Pathology, McMaster University, Hamilton, ON, Canada. Contact e-mail: pfoster@imaging.robarts.ca

In cancer immunotherapy DC will come from the patients blood, be prepared ex vivo and then re-administered, in an autologous transfer. This is the first study which compares the impact of iron labeling, and the migration efficiency for DC from healthy volunteers versus cancer patients. Our data shows that DC from cancer patients can be labeled with iron and their migration can be detected, monitored and quantified by MRI. Methods: DC were labeled with FeREX and a red fluorescent membrane dye, and then matured. Flow cytometry was used to measure the expression of cell surface receptors for antigen presentation (HLA), co-stimulation (CD80, CD83, CD86), migration (CD86, CCR7) and activation (CD40). Cytokine levels were measured in the supernatants. Interactions of DC with T cells was assessed by mixed lymphocyte reaction assays. Endocytosis of dextran FITC was evaluated. One million iron+ DC were injected into left footpad of CB17 scid mice (n=32) for MRI. Whole mouse body 3D balanced steady state free precession (bSSFP) images were acquired at 1.5T. The presence of human DC were identified in lymph node sections by PKH26 fluorescence, Perl's Prussian blue and human CD45. Results: Iron labeling did not affect the phenotype or functionality of DC in vitro for either healthy donor DC or DC from cancer patients; viability, cell surface receptors, cytokine release, T cell proliferation and endocytosis were not different for labeled versus unlabeled DC from both donors. Both types of donor DC migrated to the popliteal lymph node in CB17 scid mice. Nodes contained cells that were PKH26+huCD45+ (Figure).



MRI shows signal void in right lymph node reflecting accumulation of iron labeled DC. Red fluorescence indicates accumulation of PKH positive DC at periphery of node which is confirmed by Perls staining (PPB) of same sections. Further confirmation is given by anti human CD45 antibody staining for human DC which corresponds well with red PKH. Dapi cell staining and the overlay of the fluorescence images is also shown.

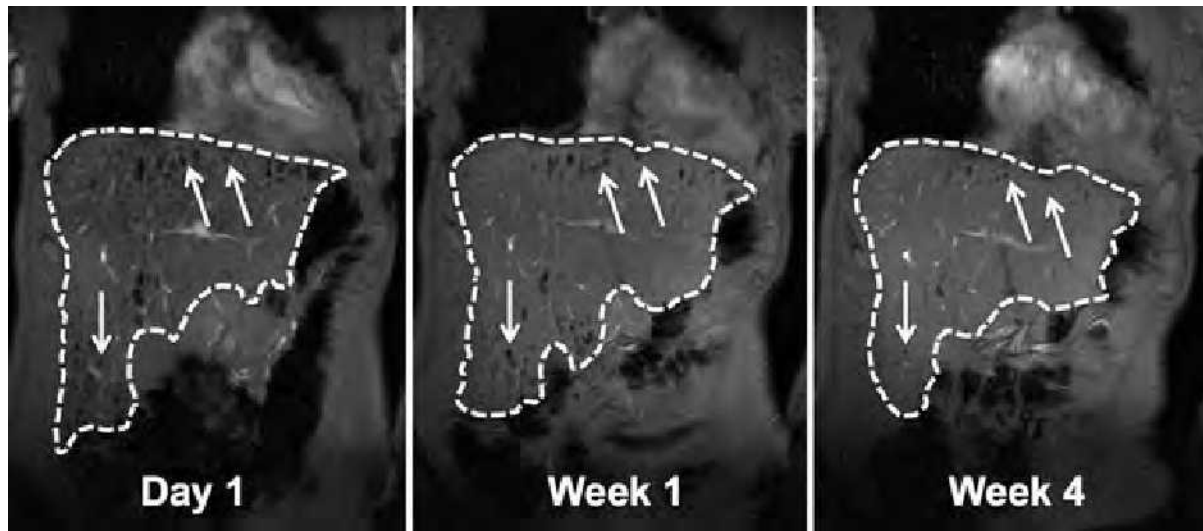
Presentation Number **0149**

Scientific Session 18: SPECIAL SESSION: Close to Clinical Cell Therapies

Monitoring the Survival of Pancreatic Islet Transplants by MR: A Pilot Clinical Trial

Daniel Jirak^{1,2}, **Peter Girman**³, **Vit Herynek**^{1,2}, **Klara Zacharovova**³, **Monika Dezortova**^{1,2}, **Jan Peregrin**¹, **Lenka Pektorova**³, **Frantisek Saudek**³, **Milan Hajek**^{1,2}, ¹Department of Diagnostic and Interventional Radiology, Institute for Clinical and Experimental Medicine, Prague, Czech Republic; ²Center for Cell Therapy and Tissue Repair, 2nd Medical faculty, Charles University, Prague, Czech Republic; ³Diabetes Center, Institute for Clinical and Experimental Medicine, Prague, Czech Republic. Contact e-mail: daji@ikem.cz

Labeling of pancreatic islets (PI) with superparamagnetic nanoparticles enables their direct posttransplant visualization by magnetic resonance (MR) as hypointense areas. It might help to study the posttransplant islet distribution and survival. We present the first results of a pilot clinical trial where we monitored the fate of transplanted PI in type-1 diabetic islet recipients. Freshly isolated PI (280 - 480 ths islet equivalents) were in vitro labeled with a clinically approved MR contrast agent ferucarbotran (6-48 hours), washed and transplanted into the portal vein in 8 C-peptide negative recipients (6 nonuremic, 2 after kidney transplants). The liver imaging was performed on a 3T MRI scanner using a standard and fully refocused (steady-state free precession) gradient-echo sequences on days 1, 7 and 28 after PI transplantation. Hypointense islet spots were counted manually. Their total number 1 day post transplant was rated as 100% and subsequent measurements of signal loss regions were recalculated as relative numbers. In all recipients, C-peptide levels > 0.5 pmol/ml and near-normal HbA1c values were achieved with insulin dose reduction of 50-80%. PI represented by hypointense spots were detected in all recipients. During the first week after transplantation we observed a substantial decrease of PI (45%). Then the decline slowed down (between 7-28 days: 9%) (see Figure). MR confirmed the technical success of PI transplantation in all recipients and enabled their posttransplant PI detection correlated with sustained C-peptide production. A dramatic loss of PI spots occurred in the 1st week suggesting an early destruction or impaired engraftment. Then the PI spot numbers stabilized. It is in accordance with data obtained in an animal model [1]. Our data suggest that posttransplant MR monitoring might be of importance for assessment of the islet fate following clinical transplantation. The study was supported by grants: ENCITE-201842, MZ0IKEM2005. 1) Jirak D et al. Magn Reson Mater Phy 2009;22:257-265



Coronal liver MR images 1 day, 1 week and 4 weeks after PI transplantation. PI were detected on MR images as dark spots of varying size mainly at the periphery of the portal vasculature. Note the substantial loss of islet signals at 1 week with subsequent stabilization.

Presentation Number **0150**

Scientific Session 18: SPECIAL SESSION: Close to Clinical Cell Therapies

In Vivo Monitoring of the Aromatic L-Amino Acid Decarboxylase Gene Expression by PET in a Phase 1 Gene Therapy Study for Parkinson's Disease

Sayaka Asari¹, Ken-ichi Fujimoto¹, Seiya Kato², Toshihiko Sato⁴, Hiroaki Mizukami³, Kunihiko Ikeguchi¹, Tadataka Kawakami¹, Masashi Urabe³, Akihiro Kume³, Eiju Watanabe², Keiya Ozawa³, Imaharu Nakano¹, Shin-ichi Muramatsu¹, ¹Neurology, Jichi Medical University, Shimotsuke, Japan; ²Neurosurgery, Jichi Medical University, Shimotsuke, Japan; ³Genetic Therapeutics, Jichi Medical University, Shimotsuke, Japan; ⁴Radiology, Utsunomiya Central Clinic, Utsunomiya, Japan. Contact e-mail: sasari@jichi.ac.jp

Parkinson's disease (PD) is a common movement disorder marked by the degeneration of the nigral dopaminergic neurons that project to the striatum. A severe loss of the nerve terminals in advanced PD is associated with an 80-95% depletion of aromatic L-amino acid decarboxylase (AADC). Researchers including us have so far demonstrated that the recombinant adeno-associated virus (AAV) vector-mediated gene transfer of AADC into the striatal neurons in combination with the oral administration of L-dopa has led to the behavioral recovery in primate models of PD. A non-catecholic tracer, 6-[¹⁸F]fluoro-L-*m*-tyrosine (FMT), for positron emission tomography (PET) is a good substrate for AADC since it is not metabolized by catechol-O-methyl-transferase, and it therefore has a better sensitivity than the more commonly used 6-[¹⁸F]fluoro-L-dopa. We herein performed FMT-PET to evaluate the expression of the transgene in a phase 1 clinical trial of AADC gene therapy. Six patients, ranging from 51 to 68 years of age, comprising 4 men and 2 women, and presenting with moderate to advanced PD (Hoehn & Yahr Stage IV), received AAV vectors expressing human AADC (3×10^{11} vector genome) via bilateral intraputamenal infusions. They were evaluated at baseline pre-operative and thereafter monthly post-operatively for 6 months, using multiple measures, including the Unified Parkinson's Disease Rating Scale (UPDRS), motor state diaries, and FMT PET. For PET assessment, all patients stopped taking dopaminergic medications at least 6 h before and all took an oral peripheral AADC inhibitor, 1 h before the FMT injection. The radioactivities within the volumes of interest drawn in the putamen and occipital lobe were calculated between 80 and 90 min after the tracer injection. Six months after surgery, the motor functions in the off medication state improved an average of 46% based on the UPDRS scores. Motor diaries showed increased "on-state" even though the dose of L-dopa was not observed to increase. The FMT activity increased at 4 weeks postoperatively. The mean increase in the FMT uptake from baseline in the combined (right and left) putamen at 6 months was 56%. Three patients who underwent PET scans 96 weeks after surgery showed a persistently increased FMT uptake. FMT-PET is therefore considered to be a valuable technique to image the AADC distribution in PD. The expression of the AADC transgene has herein been monitored as part of the assessment of long-term *in vivo* gene therapy.

Presentation Number **0151**

Scientific Session 18: SPECIAL SESSION: Close to Clinical Cell Therapies

Achieving a Preserved Differentiation Capacity and Significant MR Effects of SPIO-Labeled Human Embryonic Stem Cell Derived Cardiomyocytes: The Optimal Timing, Dose and Technique

Rosalinda T. Castaneda, Sophie E. Boddington, Michael F. Wendland, Tobias D. Henning, Lydia Mandrussow, Heike E. Daldrup-Link, University of California, San Francisco, San Francisco, CA, USA. Contact e-mail: rosalinda.castaneda@radiology.ucsf.edu

Purpose: To optimize a labeling protocol for human embryonic stem cell derived cardiomyocytes (hESC-CMs) with FDA-approved Ferumoxides for tracking with MR imaging. **Materials and Methods:** hESCs were labeled with Ferumoxides (50 µg Fe/ml) by simple incubation for 24 hr either (I) before differentiation into beating CMs or (II) after CM differentiation to compare the feasibility and signal yield of these labeling protocols. Triplicate samples from each group underwent MR imaging on a 7T MR scanner using T2-weighted multi-echo spin-echo sequences. Endpoints included a successful CM differentiation, unimpaired function, and a significant MR signal. Trypan Blue assays were performed to assess viability. Sample T2 relaxation rates and iron content, as measured by inductively coupled plasma atomic emission spectrometry, were compared between the non-labeled control and two labeled groups, using statistical t-test. **Results:** hESCs labeled before differentiation successfully differentiated into beating CMs and demonstrated both significant iron uptake (1.4 pico grams Fe/cell) and shortened T2-relaxation times (59.8 ms +/- 1.24) compared to controls (0 pico grams Fe/cell and 100.2 ms +/- 4.20, respectively). CM labeled after differentiation showed no significant iron uptake and no significant change in T2-relaxation times (100.3 ms +/- 1.96) compared to controls. All groups showed normal morphology, beating pattern and beating rate post-labeling. **Conclusion:** Labeling of hESCs with Ferumoxides prior to CM differentiation was determined the optimal approach. Undifferentiated stem cells spontaneously phagocytose iron oxide nanoparticles, retain particles through differentiation, and provide a persistent MR effect without impairment to CM function. Labeling after CM differentiation demonstrated not possible via simple incubation.

Presentation Number **0152**
Scientific Session 19: Antibodies and Immunology

In Vivo Fluorescence Imaging of T Cells: A Comparison of Nanobodies and Conventional Monoclonal Antibodies

Peter Bannas¹, Björn Rissiek², Sonja Schrepfer³, Frieder Haag², Gerhard Adam¹, Harald Ittrich¹, Friedrich Koch-Nolte², ¹Diagnostic and Interventional Radiology, University Medical Center Hamburg-Eppendorf, Hamburg, Germany; ²Institute of Immunology, University Medical Center Hamburg-Eppendorf, Hamburg, Germany; ³Transplant and Stem Cell Immunobiology Lab, University Heart Center Hamburg, Germany, Hamburg, Germany. Contact e-mail: p.bannas@uke.de

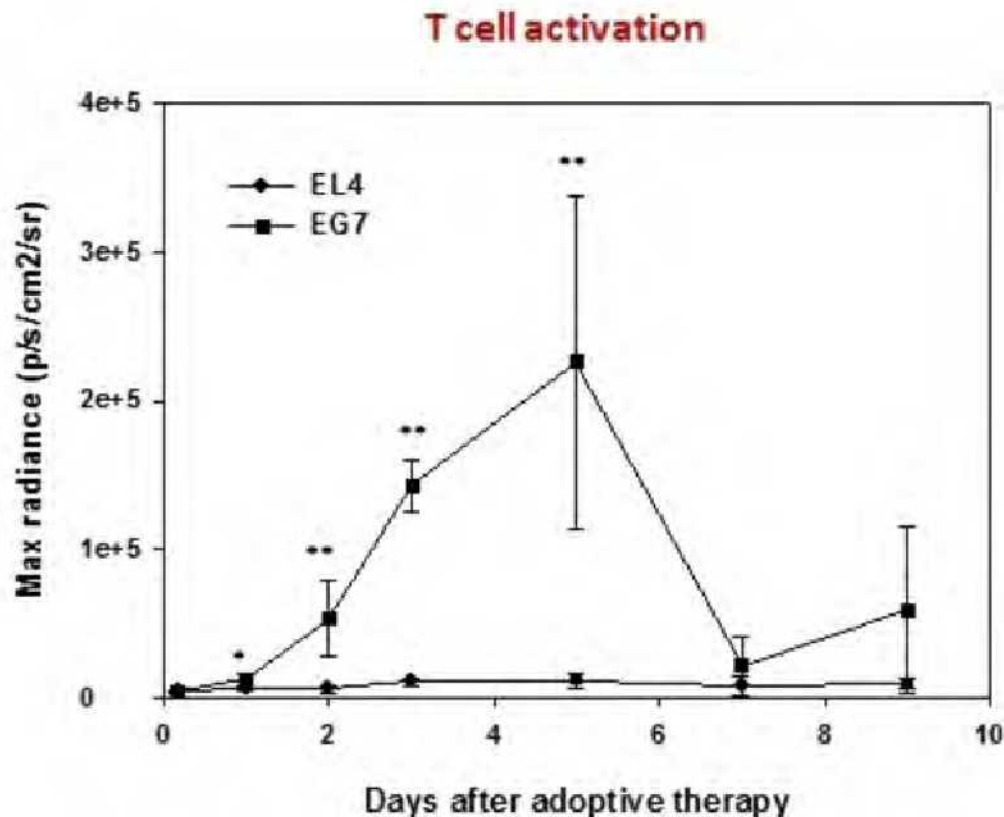
Purpose: The ecto-enzyme ADP-ribosyltransferase 2 (ART2) on T cells can apoptotically delete various T-cell subsets, a mechanism that can be blocked by inhibitory nanobodies in vitro and in vivo. The objective of our study was to noninvasively monitor the pharmacokinetic, biodistribution and efficacy of fluorochrome-conjugated ART2 inhibitory nanobodies with conventional monoclonal antibodies by in vivo fluorescence imaging. **Methods:** We used three different types of ART2-specific antibody molecules: a llama derived recombinant single-domain antibody (nanobody s+16), a modified version of s+16 incorporating the murine IgG1 Fc tail (s+16-Fc) and a conventional rat IgG2a monoclonal antibody (Nika102) as targeting agents and labeled them with Alexa-Fluor dyes. The resulting conjugates were characterized in vitro by flow cytometry and confocal microscopy for labeling efficacy and enzymatic inhibition of ART2. Semiquantitative in vivo fluorescence imaging was carried out using ART-deficient, wildtype and ART2-overexpressing transgenic mice with subsequent comparative FACS-analysis of cells prepared from lymphatic organs. **Results:** Binding specificities of the antibody-constructs to ART2 were unchanged by conjugation to Alexa-Fluor dyes. In vivo imaging confirmed specific labeling of lymph nodes in ART2-expressing wildtype and ART2-transgenic mice but not in ART2-deficient mice. Pharmacokinetics and biodistribution studies showed the s+16-Alexa-Fluor conjugate to be an optimal probe for fluorescence imaging and monitoring of ART2 in vivo. **Conclusions:** Inhibitory nanobody-Alexa-Fluor conjugates can be used as specific fluorescence imaging probes for noninvasive inhibition and imaging of ART2 on T cells. These results demonstrate the feasibility of non-invasive monitoring of a new class of immuno-modulating drugs in vivo.

Presentation Number **0153**
 Scientific Session 19: Antibodies and Immunology

Monitoring the Dynamics of CD8+ T Cell Responses in the Small Animal Model

Ya-Fang Chang^{1,2}, **Manishkumar Patel**³, **Jeng-Jong Hwang**¹, **Sanjiv S. Gambhir**^{2, 1} *Department of Biomedical Imaging and Radiological Sciences, National Yang-Ming University, Taipei, Taiwan;* ²*Radiology, Stanford University, Stanford, CA, USA;* ³*Imaging Department, Merck, West point, PA, USA. Contact e-mail: d49520006@ym.edu.tw*

Adoptive therapy using tumor-specific T cells may eventually play an important role in cancer treatment. Noninvasive and sensitive imaging techniques are required for monitoring T cell localization and activation after delivery. The aim of this study was to develop novel imaging reporters that could be activated when targets are recognized by T cells via the T-cell receptor. After ex vivo expansion of CD8+ T cells with chicken ovalbumin peptide-specific T cell receptors, the specificity and cytolytic activity of T cells toward the targets were determined by co-culture with EL4 and E.G7-OVA cells. T cells were genetically modified to express firefly luciferase (Fluc) gene driven by the Granzyme B promoter or red-shift renilla luciferase (Rluc8.6) gene driven by the Ubiquitin promoter as reporters to follow T cell survival and activation, respectively using lentiviral transduction. For small animal experiments, 5×10^6 CD8+ T/luc and 5×10^6 CD8+ T/Rluc8.6 cells were tail-vein injected into the same recipient mice (N=5/group) bearing subcutaneous EL4 and E.G7 mouse lymphomas. The BLI indicated that CD8+ T cells preferentially accumulated and proliferated in E.G7 tumors. The bioluminescent signal from the E.G7 peaked on day 3 after adoptive transfer, and was significantly higher than that from the EL.4 ($P < 0.01$). We also observed the peak signal intensity from the E.G7 coincided with tumor regression. In conclusion, these results suggest that this system may not only be a promising tool for tracking T cell migration and activation in living subjects, but also facilitate the development of other effective adoptive therapies.



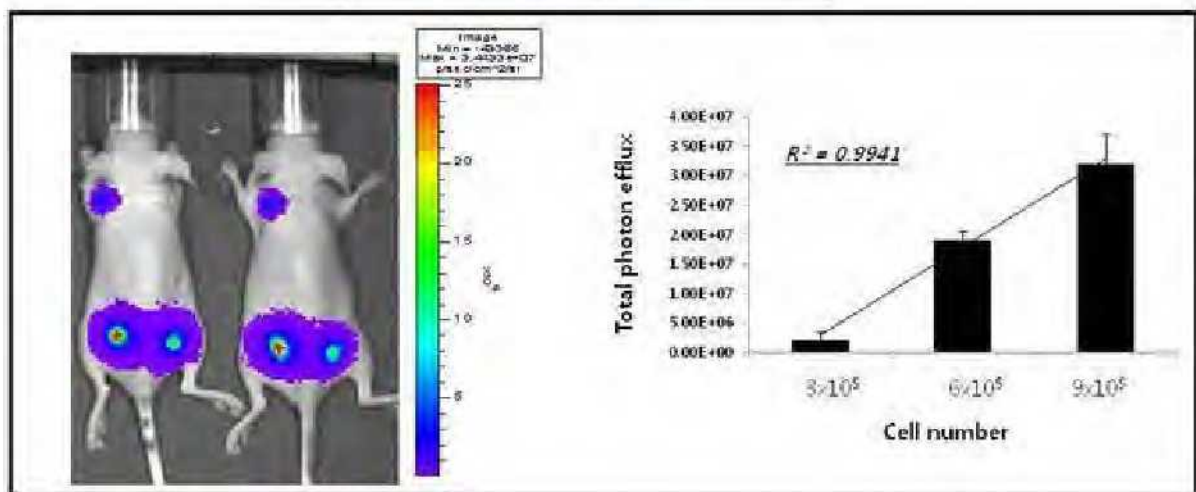
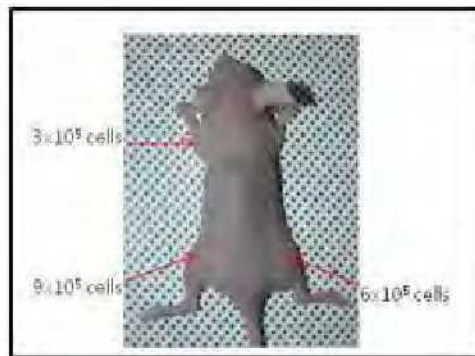
The kinetics of T cell activation in tumor-bearing mice after adoptive therapy (n = 5; *p < 0.05, **p < 0.01). This figure showed the quantitative analysis of ROIs on EL4 and E.G7 from BLI.

Presentation Number **0154**
 Scientific Session 19: Antibodies and Immunology

Development of Dual Reporter Macrophage to Monitor Macrophage Migration Using a Human Sodium Iodide Symporter and Firefly Luciferase

Ho Won Lee¹, Yong Hyun Jeon¹, Jung Eun Kim¹, Mi-hye Hwang¹, Shin Young Jeong¹, Sang-Woo Lee¹, Byeong-Cheol Ahn¹, Jeoung-Hee Ha², Jaetae Lee¹, ¹*Nuclear Medicine, School of Medicine, Kyungpook National University, Daegu, Republic of Korea;*
²*Pharmacology, School of Medicine, Kyungpook National University, Daegu, Republic of Korea. Contact e-mail: shaeni@nate.com*

Objective: The aim of this study is to develop macrophage co-expressing a human sodium iodide symporter and firefly luciferase to visualize macrophage migration toward inflammation tissue in nude mouse model. **Methods:** Murine macrophage cell line (Raw264.7) was co-transduced with lentivirus expressing hNIS or Fluc under PGK promoter, referred as a Raw264.7/NF cells. In vitro I-125 uptake and Fluc assay was performed to determine the functional activity of hNIS and Fluc protein. For in vivo imaging study, 3×10^5 , 6×10^5 , and 9×10^5 Raw264.7/NF cells were subcutaneously inoculated in left thigh of fore leg, right and left thighs of hind leg of nude mice, respectively. Bioluminescent imaging was acquired at 1 day after cell inoculation. To quantify the bioluminescent signals, regions of interest (ROIs) were drawn over injection sites. **Results:** I-125 uptake and Fluc signal were about 67- and 352-fold higher in Raw264.7/NF cells than parental Raw264.7 cells, respectively. In vivo bioluminescent imaging showed the well correlated between bioluminescent signal and inoculated cell number (3×10^5 , 6×10^5 , and 9×10^5 Raw264.7/NF cells, $2.16 \times 10^6 \pm 1.0 \times 10^6$, $1.91 \times 10^7 \pm 2.0 \times 10^6$, and $3.20 \times 10^7 \pm 5.0 \times 10^6$, respectively, $r^2=0.994$). **Conclusions:** We successfully established macrophage cells co-expressing hNIS and Fluc genes to visualize macrophage migration with nuclear and optical molecular imaging. These dual reporter gene expressing macrophages could be used as a useful tool to monitor the macrophage migration or proliferation from early to late time point in pre-clinical mouse model.



In vivo bioluminescence imaging of nude mice with Raw264.7/NF

Presentation Number **0155**
Scientific Session 19: Antibodies and Immunology

In Vivo Monitoring Therapeutic Response of Combined Dendritic Cell (DC)-based Immunotherapy and hNIS Radioiodine Gene Therapy for Cervical Cancer in Nude Mice

Yong Hyun Jeon¹, **Ho Won Lee**¹, **Lee You La**¹, **Jung Eun Kim**¹, **Mi-hye Hwang**¹, **Shin Young Jeong**¹, **Sang-Woo Lee**¹, **Byeong-Cheol Ahn**¹, **Jeoung-Hee Ha**², **Jaetae Lee**¹, ¹*Nuclear Medicine, School of Medicine, Kyungpook National University, Daegu, Republic of Korea;* ²*Pharmacology, School of Medicine, Kyungpook National University, Daegu, Republic of Korea. Contact e-mail: jeon9014@empal.com*

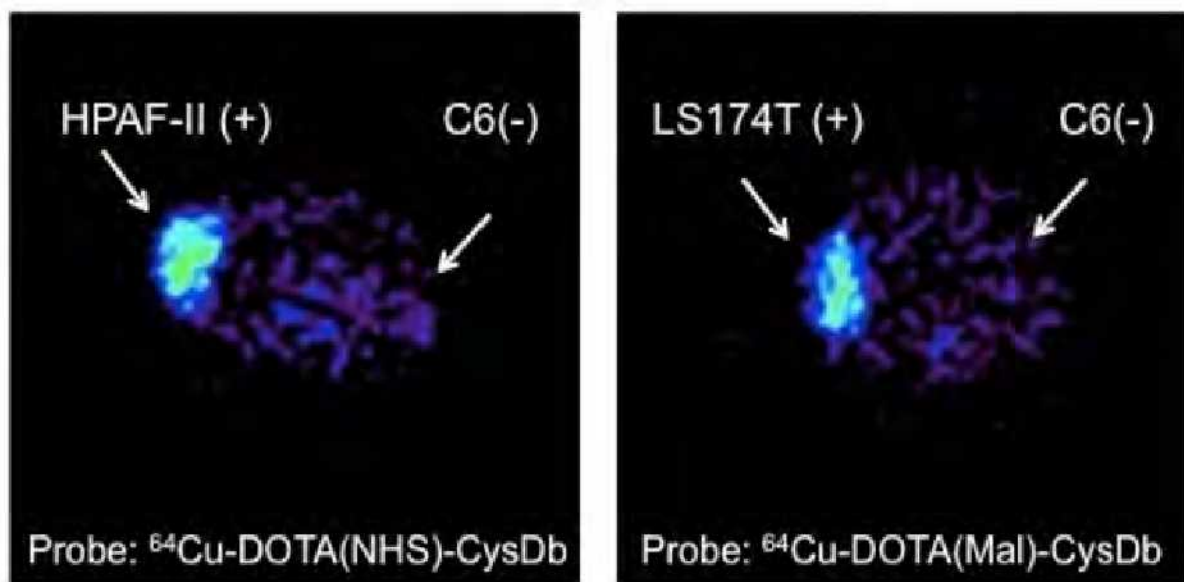
Objective: The aim of this study is to investigate the therapeutic potential of combined DC-based vaccination and hNIS radionuclide gene therapy in immunocompromised mouse having cervical cancer xenograft. **Methods:** Control DC cell(DC-no insert), DC cells expressing E7 antigen (DC-E7), uterine cervical cancer cells co-expressing E7 antigen and firefly luciferase gene (TC-1/Fluc) were prepared for this study. TC-1/Fluc cells were stably transduced with retrovirus co-expressing hNIS and EGFP gene under PGK promoter (TC-1/Fluc-hNIS-EGFP, TC-1/FNG cells). In vitro I-125 uptake was performed to assess the functional activity of hNIS protein. The survival rates (%) of TC-1/FNG cells were determined using clonogenic assay after 1mCi I-131 treatment. Immunocompromised C57Balb/c mice were divided into five groups (PBS, DC-no insert, DC-E7, 1mCi I-131, DC-E7+ 1mCi I-131 groups, 6 mice per group) for in vivo cancer therapy and 1×10^5 TC-1/FNG cells were subcutaneously challenged into right hind limb of each mouse. On 4th and 11th day, mice were intramuscularly immunized with 1×10^6 DC-no insert cells or DC-E7 cells and subsequently injected with 1mCi I-131 at 14 days after tumor challenge. Tumor growth was assessed with bioluminescent imaging and size measurement with caliper at designated days. **Results:** I-125 uptake was 71- fold higher in TC-1/FNG cells than TC-1/Fluc cells. The survival rates of TC-1/FNG cells were markedly reduced to $38 \pm 5\%$ with I-131 treatment compared to parental cells ($P < 0.001$). In mice treated with either DC-E7 or I-131 alone, there was a slight delay in tumor growth as compared to non-treated groups (PBS and DC-no insert) but not statistically significant. However, combination therapy with DC-E7 and I-131 resulted in significant inhibition of tumor growth compared to other single therapy such as DC-no insert, DC-E7, and 1mCi I-131 treatment ($P < 0.05$). **Conclusions:** Enhanced therapeutic response was achieved with combined DC-based vaccination and hNIS radioiodine gene therapy in mouse model with cervical cancer xenograft, and anti-tumor effects were successfully visualized using a bioluminescent imaging. Combination of DC-based immunotherapy and hNIS radioiodine gene therapy could be used as a potential therapeutic method to generate E7-specific immune response in cervical cancer animal model.

Presentation Number **0156**
Scientific Session 19: Antibodies and Immunology

An Engineered Cysteine-modified Diabody for PET Imaging of ALCAM-positive Pancreatic and Colorectal Tumor Models

Katelyn E. McCabe¹, Bin Liu², James D. Marks², Anna M. Wu¹, ¹Crump Institute for Molecular Imaging, Molecular and Medical Pharmacology, UCLA, Los Angeles, CA, USA; ²Anesthesia, UCLA, Los Angeles, CA, USA. Contact e-mail: kmccabe@ucla.edu

Activated leukocyte cell adhesion molecule (ALCAM/CD166) is a transmembrane protein that has been found to be upregulated in several malignancies. In pancreatic adenocarcinoma and colorectal carcinoma, overexpression of ALCAM has been identified as a prognostic marker that correlates with a lower survival rate. This expression pattern and clinical relevancy make ALCAM a potentially useful imaging biomarker. To examine this possibility, an anti-ALCAM cysteine-modified diabody was engineered from an existing scFv to create an antibody-based PET probe. Biochemical characterization by SDS-PAGE, size exclusion chromatography, and MALDI-TOF mass spectrometry confirmed production of a covalent dimer of approximately 51 kDa, and specific binding to ALCAM-positive cells was determined by flow cytometry and immunofluorescence binding studies. The CysDb demonstrated an affinity of about 2 nM, as determined by flow cytometry. To create the PET probe, the CysDb was either randomly conjugated with DOTA-NHS-ester or reduced for site-specific conjugation with maleimide-mono-amide-DOTA, and subsequently labeled with the positron-emitter ⁶⁴Cu. Radiometal labeling efficiency was 77% for the randomly DOTA-conjugated CysDb and 68% for the site-specifically DOTA-conjugated CysDb. Mice bearing either an ALCAM-positive human pancreatic adenocarcinoma tumor (BxPC-3 or HPAF-II) or an ALCAM-positive colorectal carcinoma tumor (LS174T), as well as an ALCAM negative control tumor (C6; rat glioma) were imaged at 4 h post-injection of ⁶⁴Cu-DOTA-CysDb. MicroPET images show high activity in the positive tumor compared to the negative tumor (see Figure). Positive tumor-to-negative tumor and positive tumor-to-blood ratios (ranging from 1.8-3.7 and 2.6-3.9, respectively) calculated from ex vivo biodistribution data confirmed specific targeting of the tracers. Demonstration of successful imaging in pancreatic and colorectal tumor models suggests that ALCAM has potential as a cancer imaging biomarker.



Presentation Number **0157**
Scientific Session 19: Antibodies and Immunology

HER1-targeted 86Y-panitumumab has Better Targeting Characteristics Than 86Y-cetuximab for PET Imaging of Human Malignant Mesothelioma Tumors Xenografts

Tapan K. Nayak, Kayhan Garmestani, Diane Milenic, Kwamena E. Baidoo, Martin Brechbiel, NCI/NIH, Bethesda, MD, USA. Contact e-mail: tapann@gmail.com

Malignant mesothelioma (MM) is a rare form of cancer that is often associated with previous exposure to fibrous minerals such as asbestos. Asbestos exposure increases HER1-activity and expression in preclinical models. Therefore, in this study we explored the utility of HER1-targeting chimeric IgG1, cetuximab and human IgG2, panitumumab radiolabeled with 86Y for PET imaging and detection of MM. Radioimmunoconjugates of cetuximab and panitumumab were prepared by the conjugation of CHX-A''-DTPA to the mAbs followed by radiolabeling with 86Y. The HER1 expression of NCI-H226, NCI-H2052, NCI-H2452 and MSTO-211H human mesothelioma cells were characterized by flow cytometry. In vivo biodistribution, pharmacokinetic analysis and PET imaging was performed in tumor bearing athymic mice. In vivo studies demonstrated high HER1 tumor uptake of both radioimmunoconjugates. Significant reduction in tumor-uptake was observed in mice co-injected with excess mAbs (0.1 mg), demonstrating uptake in the tumor was receptor specific. Significant differences were observed in the in vivo characteristics of the RICs. The blood clearance α -half-life of 86Y-cetuximab (0.9-1.1h) was faster than 86Y-panitumumab (2.6-3.1h). The tumor AUC to liver AUC ratios of 86Y-panitumumab were 1.5 to 2.5 times greater than 86Y-cetuximab as observed by the differences in PET tumor to background ratios, which could be critical when imaging orthotopic tumors. This study demonstrates the superiority of 86Y-panitumumab over 86Y-cetuximab for non-invasive staging and assessment of the HER1 status of MM by PET imaging due to its favorable pharmacokinetics and imaging characteristics.

Presentation Number **0158**
 Scientific Session 20: Image Guided Therapy

Temperature Sensitive Liposomes for Focused Ultrasound-induced Drug Delivery under MRI Guidance

Holger Gruell^{1,2}, **Mariska de Smet**², **Nicole Hijnen**², **Edwin Heijman**¹, **Jochen Keupp**³, **Sander Langereis**^{1, 1} *Biomolecular Engineering, Philips Research, Eindhoven, Netherlands;* ²*Biomedical NMR, Eindhoven University of Technology, Eindhoven, Netherlands;* ³*Tomographic Imaging, Philips Research, Bethesda, MD, USA. Contact e-mail: holger.gruell@philips.com*

Locally induced hyperthermia using focused ultrasound combined with temperature sensitive liposomes (TSL) that release a drug are enabling new local image guided therapies. Loading these TSLs with MRI contrast agents allows to simultaneously monitor and quantify the drug delivery with MRI. Here, we will present a new approach to MR-guided drug delivery using T1-MRI contrast agents that are co-released with doxorubicin (dox) from the lumen of TSLs¹. The challenge is to find TSL systems that stably encapsulate dox and the contrast agent at body temperature (310 K), while rapidly releasing both under hyperthermia (T=315 K). Different TSLs filled with dox and 250 mM solution of a T1 agent (GdHPDO3A) are prepared. The release kinetics of dox and GdHPDO3A upon heating is studied in vitro¹ and in gel phantoms using MRgHIFU. Biodistribution of the TSLs and dox are assessed in 9L glioma rat model using radiolabeling and dox extraction from tissues. Subtle changes in the nature of the lipids and the relative composition of the lipid bilayer strongly affect dox leakage at T=310 K and release kinetic at T=315 K. Surprisingly, the MRI contrast generation assessed in gel phantom experiments seems to depend more on peculiarities of the head group rather than the bilayer thickness. Blood kinetic of the TSLs shows biphasic behaviour but different blood half lives though all systems were PEGylated to the same degree. Gel phantom experiments show a strong change in T1 upon heating TSLs with HIFU (Fig. 1a). MRgHIFU allows to maintain hyperthermia inside the tumor at e.g. T=313K +/- 1K for 15 min. (Fig. 1b,c). A proof of concept for temperature induced drug delivery using MRgHIFU will be shown. Reference: 1) De Smet M et al, J. Controlled Rel, 143,120(2010). This research is part of FP7 European Project Sonodrugs (ref. 213706).

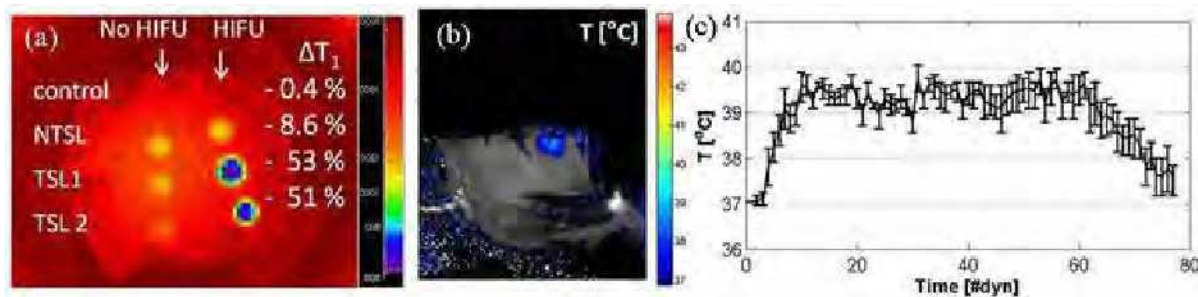


Figure 1: (a) T1 map of non-temp. sens. liposomes (NTSL) and TSLs before and after heating in gel phantoms. (b) MR temp. map during ultrasound heating of a rat tumor, (c) average temperature inside the tumor as function of dyn. scan number (total acq. time: 15 min.).

Presentation Number **0159**
 Scientific Session 20: Image Guided Therapy

Delivery of Diagnostic and Therapeutic Agents to Tumors by Multifunctional Nanoparticles

Anita Gianella^{1,2}, Peter A. Jarzyna¹, Venkatesh Mani¹, Sarayu Ramachandran¹, Claudia Calcagno¹, Gert Storm³, David P. Cormode¹, Victor L. Thijssen⁴, Arjan Griffioen⁴, Zahi Fayad¹, Willem J. Mulder¹, ¹Translational and Molecular Imaging Institute, Mount Sinai School of Medicine, New York, NY, USA; ²Cardiology Monzino Center, Milano, Italy; ³Utrecht Institute of Pharmaceutics, Utrecht, Netherlands; ⁴Angiogenesis Laboratory, Dept. of Medical Oncology, VUMC - Cancer Center, Amsterdam, Netherlands. Contact e-mail: anita.gianella@gmail.com

Background and aim: Multifunctional nanomaterials are useful for combined therapy and diagnosis (theranostics) of pathologies. The aim of the current study is to develop a multifunctional nanoparticle that can be applied for cancer therapy and diagnosis. The potential of this platform for targeting, imaging and treating tumors was evaluated in a mouse model. Methods and Results: Oil-in-water emulsions were loaded with iron oxide nanocrystals (FeO) for MR imaging as well as prednisolone acetate valerate (PAV) for therapeutic purposes. These nanoemulsions, 50-60 nm in diameter, were stabilized by PEGylated, ordinary and near infrared fluorescent (NIRF) Cy7 labeled phospholipids (Fig. 1A). LS174T tumors were grown in nude mice. When tumors were palpable (n=8 per group) mice were iv injected at day 1, 3 and 6 with: saline, free PAV, control nanoparticles, PAV-nanoparticles, RGD-PAV-nanoparticles, FeO-nanoparticles and FeO+PAV-nanoparticles. The nanoemulsions were dosed at 30 mg Fe/kg and 10 mg PAV/kg. At day 8, mice were imaged using 3T MRI and NIRF imaging. A significant accumulation of the FeO loaded nanoparticles was observed by MRI (Fig. 1B), while the tumor accumulation of Cy7 labeled nanoemulsions was visualized by NIRF imaging (Fig. 1C). The accumulation of the non-functionalized nanoemulsions in the tumor interstitial space occurred via the enhanced permeability and retention effect, while the RGD peptide functionalized nanoemulsions targeted the angiogenic endothelial cells in tumors due to their affinity for $\alpha v\beta 3$ -integrin. Finally, tumor growth profiles (Fig. 1D) revealed a significant inhibition effect for all the PAV-nanoemulsions treated animals as compared to the ones treated with control nanoemulsions, free drug or saline. Conclusion: This comprehensive study showed our nanoemulsion platform, loaded with PAV, iron oxide nanocrystals and Cy7, to accumulate in tumors and effectively inhibit tumor growth. Further biochemical experiments are performed to unravel the mechanism of action.

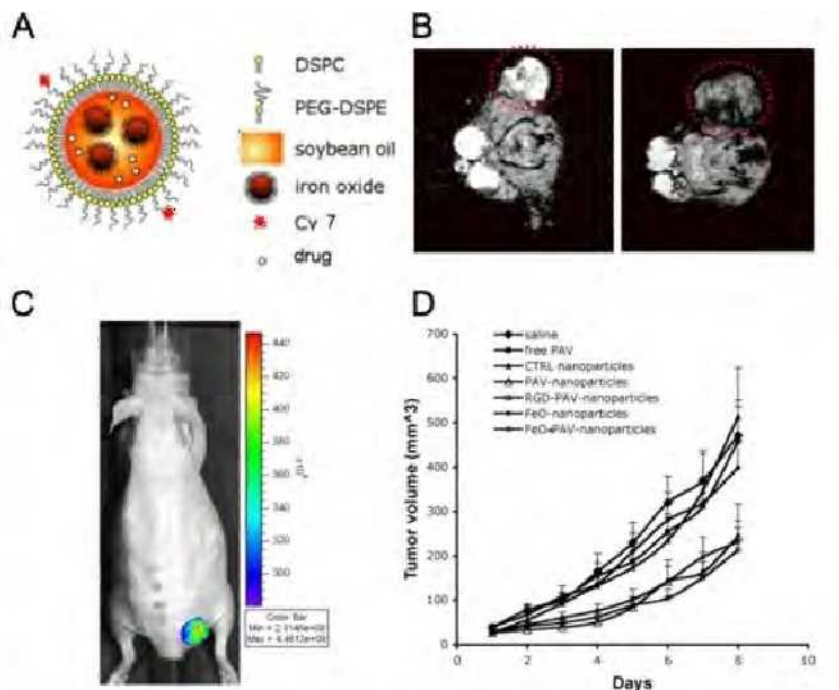


Fig.1 A) Nanoemulsion schematic, B) T2*-weighted MRI comparison of CTRL nanoemulsion injected mouse (left) and FeO-nanoemulsion injected mouse (right), signal attenuation (right image) shows nanoparticle accumulation in the tumor, C) Nanoparticle accumulation in tumor visualized by NIRF, D) Tumor growth profiles show a significant inhibition effect ($P < 0.001$) of all the PAV-nanoemulsions compared to CTRL nanoemulsions, free PAV and saline

Presentation Number **0160**
Scientific Session 20: Image Guided Therapy

Preclinical SPECT Imaging of VEGF Receptors in Tumor Vasculature in the Course of Treatment with Pazopanib, a Small Molecule TKI

Francis G. Blankenberg², Zoia Levashova², Susanta K. Sarkar³, Marina Backer¹, Joseph M. Backer¹, ¹SibTech, Inc., Brookfield, CT, USA; ²Department of Pediatrics & Division of Nuclear Medicine/Department of Radiology, Stanford University, Stanford, CA, USA; ³Medicines Development, Oncology R&D, GlaxoSmithKline, Collegeville, PA, USA. Contact e-mail: jbacker@sibtech.com

Signaling via receptors for vascular endothelial growth factor (VEGFR) drives tumor angiogenesis, and therefore these receptors are the targets for several blockbuster and many experimental anti-angiogenic drugs. Unfortunately, the benefit to a large percentage of patients from these targeted drugs treatments is still limited. According to current understanding, VEGFR inhibitors induce initial vascular regression that leads to tumor growth delay and/or shrinkage and, hence, increased progression-free survival. Recent preclinical studies (1, 2) suggest that the initial vascular regression may be followed by vascular rebound, which is resistant to anti-angiogenic drugs. These complexities and, particularly, the opposing processes of vascular regression and rebound, bring a critical need in imaging-based guidance for optimization and management of anti-angiogenic therapy. To image the target of these inhibitors, we have recently developed a molecular imaging tracer, scVEGF/99mTc, engineered single chain (sc) form of VEGF site-specifically radiolabeled with 99mTc for SPECT imaging. The tracer binds to and is internalized by VEGF receptors overexpressed in angiogenic vasculature in tumor and inflammatory diseases and can be used for monitoring changes in VEGFR prevalence in response VEGFR inhibitors. Pazopanib is a recently approved small molecule tyrosine kinase inhibitor targeting VEGFR, PDGFR and c-Kit. Longitudinal SPECT imaging of VEGFR in HT29 tumor-bearing mice in the course of pazopanib treatment revealed rapid decline in tracer uptake by Day 5. However, this decline is followed by the increase in tracer uptake by Day 15, particularly at the tumor edges. Immunohistochemical analysis of endothelial markers indicates, that these changes are due to depletion and resurgence of VEGFR-2+/CD31+ cells associated with vascular regression and revascularization. Thus, potentially, VEGFR-2 imaging might identify patients that respond to pazopanib and similar drugs with effective depletion of VEGFR-2+/CD31+, and to help to optimize combination regimens that prevent resurgence of such cells and revascularization. Experiments are in progress to establish how to use VEGFR imaging for optimization of regimens combining VEGFR inhibitors and chemotherapeutic drugs. Reference 1. J. M. Ebos et al, Cancer Cell, 15, 232-239, 2009 2. M. Paez-Ribes et al, Cancer Cell, 15, 220-231, 2009

Presentation Number **0161**
Scientific Session 20: Image Guided Therapy

Targeting Pc 4 Conjugated Gold Nanoparticles to Tumors Improves Drug Accumulation and PDT Efficacy

Ann-Marie Broome^{1,2}, Yu Cheng³, Joseph D. Meyers^{1,2}, Richard S. Agnes^{1,2}, Clemens Burda³, James Basilion^{1,2}, ¹Biomedical Engineering, Case Western Reserve University, Cleveland, OH, USA; ²National Foundation for Cancer Research, Case Western Reserve University, Cleveland, OH, USA; ³Chemistry, Case Western Reserve University, Cleveland, OH, USA. Contact e-mail: Ann-Marie.Broome@case.edu

Malignant gliomas are among the most lethal cancers with a median survival expectancy of only 6-12 months. Surgical resection is the mainstay of treatment. However, curative resection is often not possible due to infiltrating growth of the tumor into normal brain. Photodynamic therapy (PDT) has been suggested as an additional therapy to guide tumor resections and enhance the effect of surgery via photoreactive treatment during or at the cessation of surgical intervention. The most difficult challenge in treating malignant brain tumors may be delivering targeted therapies that preserve healthy tissue while effectively eradicating the cancer. Therefore, improving drug delivery rate and tumor selectivity of the photosensitizing agent will dramatically reduce systemic toxicity and enhance the success of PDT. EGFR amplification is the most common genetic alteration in gliomas and plays a critical role in stimulating glioma progression, making it an ideal target. Consequently, we have developed a highly efficient EGFR-targeted gold-nanoparticle (EGF-Au NP) to improve delivery of PDT cancer drugs to tumors in vivo. EGF peptides attached to PEGylated Au NPs deliver hydrophobic PDT drug, Pc 4, to brain tumors overexpressing EGFR better than either the non-targeted Au NPs or Pc 4 alone. The drug rapidly releases and penetrates deep within tumors within 1-4 hrs. In vivo small animal imaging experiments show targeted delivery of Pc 4 to tumor sites. Ex vivo imaging of the tumors confirmed as much as a 4-fold increase in the intrinsic fluorescence of Pc 4 over non-targeted conjugates after systemic administration. Moreover, in vitro experiments show a higher concentration of Pc 4 uptake per Au NP over non-targeted Au NPs per cancer cell. Histological analysis shows that after targeting the delivered Pc 4 localizes in the endosomes of the cancer cells. Localization within the endosomal pathway is shown to be more effective and produce less phototoxicity than free Pc 4, which preferentially accumulates in mitochondria. Further, glioma cells treated for 4 hrs with EGF-targeted Au NP-Pc 4 and then exposed to PDT show an enhanced killing effect, especially when compared to either non-targeted Au NP-Pc 4 or free Pc 4 controls. Systemic delivery of EGF-Au NP-Pc 4 to heterotopic brain tumors reveals increasing tumor necrosis after PDT. Biodistribution experiments also show that the Au NPs and Pc 4 are effectively excreted over time. This study suggests that the EGFR-targeted Au NPs improve drug delivery to tumors for PDT and are removed from the body safely after treatment.

Presentation Number **0162**
Scientific Session 20: Image Guided Therapy

Induction of Leukocyte Accumulation by Image-Guided Ultrasound Tumor Therapy: Monitoring by Ultrasound Contrast Molecular Imaging

Alexander L. Klibanov¹, **Talent Shevchenko**¹, **Zhongmin Du**¹, **Bijoy K. Kundu**², **Ralf Seip**³, **Balasundar I. Raju**³, **Chien Ting Chin**³,
¹Dept. of Medicine, Cardiovascular Div., University of Virginia, Charlottesville, VA, USA; ²Radiology, University of Virginia, Charlottesville, VA, USA; ³Philips Research North America, Briarcliff Manor, NY, USA. Contact e-mail: sklib1@gmail.com

Image-guided therapeutic ultrasound is gaining attention as a targeted, non-invasive intervention modality. Ultrasound can be focused at tumors deep in the body. Tumors can be sensitized to ultrasound bioeffects by microbubble (MB) agents. We investigated the mechanism of tumor therapy by ultrasound-mediated MB destruction in the tumor vasculature. We used leukocyte-targeted ultrasound contrast molecular imaging to check whether insonation induces inflammatory response. MBs were prepared by sonication of aqueous micellar emulsion in decafluorobutane atmosphere. MB shell consisted of phosphatidylcholine (PC) and PEG stearate. A formulation for leukocyte targeting included phosphatidylserine (PS) at 3:20 PS:PC ratio. MC38 murine adenocarcinoma (J Schlom, NIH) was used for hind leg tumor model in C57BL/6 mice. PC MBs (50 million) were injected i.v. in anesthetized mice. Under ultrasound imaging guidance (harmonic mode, L15-7 probe), tumors were immediately treated by focused ultrasound (3 MPa, 1.2 MHz, 30 pulses, 0.1 s, 1 Hz) with TIPS System (Philips). One hour or one day after TIPS treatment, 50 million PS or PC MBs were administered i.v., and ultrasound imaging of leukocyte-targeted MB in hindlimb vasculature was performed using MB-specific CPS mode (15L8 probe). After euthanasia, tissue samples were obtained for histology. MB destruction in tumor vasculature by TIPS treatment caused transient cessation of tumor blood flow; it resumed in minutes. Repeated (twice daily) treatments over two week period suppressed tumor growth. MicroPET study showed significant FDG uptake in the insonated hind leg, supporting inflammatory response hypothesis. Leukocyte-specific imaging with PS MB performed an hour after TIPS treatment showed strong signal in the insonated tissues, and not in untreated controls. PS MB signal was observed 30 minutes following MB administration, which supports the idea of PS MB internalization by leukocytes adhered to vessel wall. PS MB uptake was significantly lower next day after TIPS treatment. Control PC MB did not significantly accumulate in any setting. Immunohistology (Gr1 and 7-4 markers) confirmed leukocyte (neutrophil) accumulation in TIPS-treated tissues an hour after insonation; the following day even higher leukocyte numbers were observed. In summary, leukocyte-targeted ultrasound contrast molecular imaging, validated by histology, confirmed accumulation of leukocytes in the tissue as a primary response to microbubble destruction in the vasculature. This induced inflammatory response may be responsible for antitumor effects.

Presentation Number **0163**
Scientific Session 20: Image Guided Therapy

Incorporating Four-Dimensional (4D) PET Information into Treatment Planning of Thoracic Stereotactic Radiosurgery

Lei Xing¹, Guillem Pratx¹, Tae Suk Suh², Jina Chang², ¹Radiation Oncology, Stanford University, Stanford, CA, USA; ²Biomedical Engineering, The Catholic University of Korea, Seoul, Republic of Korea. Contact e-mail: lei@stanford.edu

A number of clinical trials have shown the efficacy of stereotactic body radiosurgery (SBRT), for treatment of lung, liver and other cancers. Lung SBRT, for example, achieved 96.7% of local tumor control rate. However, toxicity is significant. An effective use of emerging 4D PET image information in treatment planning provides a significant opportunity to reduce the tumor margin and radiation side effects while maintaining the excellent tumor local control rate of the treatment. We report a 4D PET image reconstruction method to solve the unmet problem of temporo-spatio resolution competition in 4D PET imaging and describe a method of integrating the 4D PET data into respiration-gated SBRT planning. During the processes of forward- and backward-projection in the ML-EM iterations, all projection data acquired at different phases are combined together to update the emission map with the aid of deformable model, the statistics is therefore greatly improved. Liver, lung and pancreatic patients were acquired via the gated PET mode. A single-bed FOV PET scan typically requires several minutes to acquire adequate data for reconstruction, necessarily spanning several respiratory cycles and smearing the radiotracer signal within a given lesion over an increased volume. Although prospective or retrospective gating captures the PET image at a single point in the respiratory cycle, restricting the data to events within the gating interval increases the SNR. We developed a 4D Pet reconstruction method to combine the data from the entire respiratory cycle through deformable registration. The exhale or inhale phase was selected as the gating phase for SBRT planning. The residual motion inside a selected gating widow is considered by measuring the motion range in the 4D PET images. A gated IMRT inverse planning was then carried out with 4D PET defined tumortarget. We found that the performance of 4D PET was significantly improved by the proposed reconstruction with the SNR increased by ~6 folds over conventional PET. Using 4D PET, 35%~48% reduction in target volumes was observed, which leads to significant reduction in radiation toxicity and makes it possible for patients to truly benefit from the modern SBRT treatment.

Presentation Number **0164**

Plenary Session 5: Realizing the Power of Imaging in the Fight against Cancer

Realizing the Power of Imaging in the Fight against Cancer

Gregory M. Lanza¹, *Keyvan Farahani*³, *Chrit Moonen*², ¹*Cardiology, Washington University, St. Louis, MO, USA;* ²*University Victor Segalen, Bordeaux, France;* ³*NCI-Cancer Imaging Program, Washington, DC, USA. Contact e-mail: greg.lanza@mac.com*

While the concept of targeted drug delivery to improve the safety and efficacy of pharmaceuticals by optimizing therapeutic release at the site of disease is not new concept, the critical role of imaging to enable a more personalized strategy for medical management has recently been appreciated. Imaging offers the potential to noninvasively detect and biochemically characterize disease earlier, which is expected to lead to better risk stratification and more finely tuned patient management options. Imaging modalities can guide and deliver therapy through the deposition of energy to ablate tumors directly or locally release drug from circulating particles. Molecular imaging agents combined with drugs can home to distinctive tumor biomarkers and deliver higher local levels of therapy with lower total body exposure. Imaging provides the essential tool that allows us to assess treatment response based on early biochemical changes, which enables timely re-intervention before clinical manifestations recrudescence, if needed. Although great technological progress has been made in recent years, the clinical implementation of image-guided drug delivery (IGDD) strategies has been rather slow. In this presentation, a consensus opinion of challenges and recommendations for accelerating the translation of these technologies will be presented.

Presentation Number **0165**
Scientific Session 21: Probes for Imaging the Tumor Microenvironment

Fast-responding and Sensitive Fluorescence In Vivo Imaging of Cancer by Using a Novel Protease Probe for Gamma-glutamyltransferase

Masayo Sakabe^{1,5}, Nobuyuki Kosaka², Makoto Mitsunaga², Mikako Ogawa³, Peter Choyke², Daisuke Asanuma^{1,5}, Mako Kamiya⁴, Tetsuo Nagano^{1,5}, Hisataka Kobayashi², Yasuteru Urano⁴, ¹Pharmaceutical Sciences, The University of Tokyo, Tokyo, Japan; ²Molecular Imaging Program, NCI/NIH, Bethesda, MD, USA; ³Photon Medical Research Center, Hamamatsu University School of Medicine, Shizuoka, Japan; ⁴Medicine, The University of Tokyo, Tokyo, Japan; ⁵JST CREST, , Tokyo, Japan. Contact e-mail: ff097011@mail.ecc.u-tokyo.ac.jp

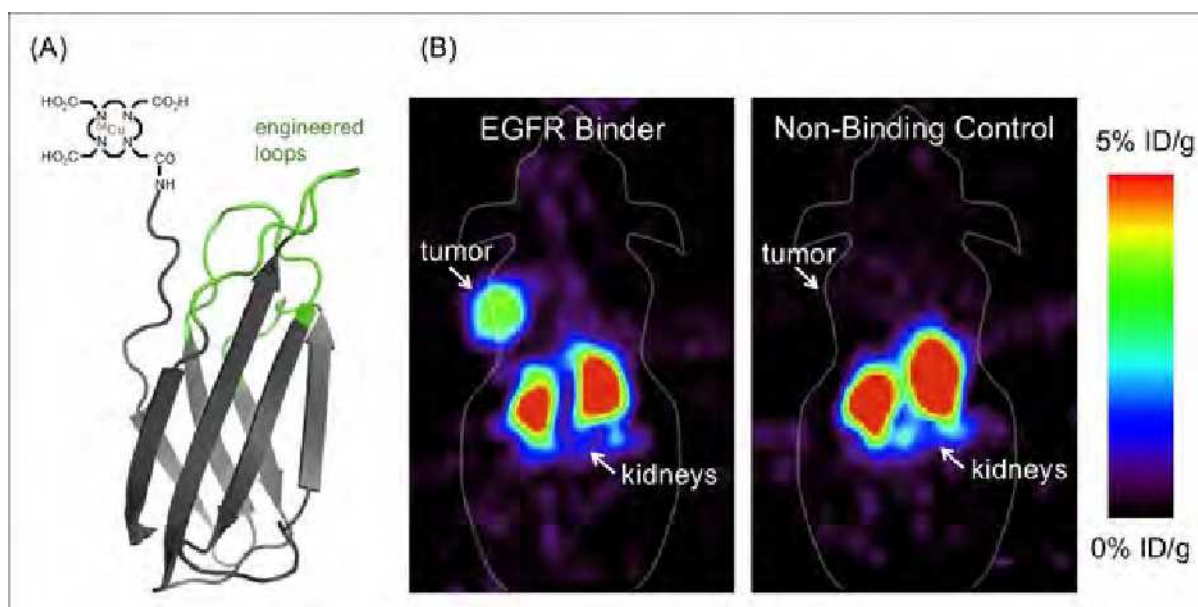
Proteases play essential roles in cancer, inflammation and vascular disease, as well as in the generation of amino acids for protein synthesis. Sensitive and selective protease detection systems become a crucial tool for the early diagnosis of diseases. To detect the activity of protease, Rhodamine Green (RG) derivatives based fluorescence probes have been widely used. However, since these substrates have two reactive sites, two-step enzymatic reactions are necessary to yield strongly fluorescent products, which leads to decrease in the rate of fluorescence manifestation. Recently, we reported that a series of tetramethylrhodamine derivatives bearing a hydroxymethyl or mercaptomethyl group instead of original carboxy group showed unique intramolecular spirocyclization. Based on these findings, we synthesized a novel series of hydroxymethyl-Rhodamine Green (HMRG) derivatives. HMRG was strongly fluorescent in aqueous solution at pH7.4, while a HMRG derivative, which is mono-acetylated at its amino group, was colorless and non-fluorescent. This result suggested that we can regulate fluorescence by controlling intramolecular spirocyclization at one reactive site. Based on this finding, we developed a novel protease probe (gGlu-HMRG) for gamma-glutamyltransferase. Gamma-glutamyltransferase (GGT) plays a central role in the metabolism of glutathione and its overexpression is often observed in human cancers including ovarian, lung and breast cancers. Our probe could detect the activity of GGT in the cuvette more sensitively, quickly and quantitatively than (gGlu)2-RG which has two reactive sites. Next, we tried to visualize cancer cells with this probe. gGlu-HMRG showed a large fluorescence increase in both most cancer cell lines, such as SHIN3 and A549, but not in HUVEC, a normal cell line. Finally, we performed imaging of cancer in a mouse model of peritoneal metastases. Cancer cells in peritoneal cavity were successfully visualized with gGlu-HMRG even at a few minutes i.p.-injection. gGlu-HMRG will be a powerful tool as an imaging guidance for the diagnosis of the cancer site.

Presentation Number **0166**
 Scientific Session 21: Probes for Imaging the Tumor Microenvironment

^{64}Cu -Labeled Fibronectin Domain for PET Imaging of EGFR+ Tumors

Benjamin J. Hackel, Richard Kimura, Sanjiv S. Gambhir, Radiology, Stanford University, Palo Alto, CA, USA. Contact e-mail: bhackel@stanford.edu

The fibronectin domain (Fn) is a beta-sandwich protein that has been utilized as a scaffold for engineering molecular recognition domains but has yet to be demonstrated for use in molecular imaging. A 98-amino acid Fn, engineered with picomolar affinity for epidermal growth factor receptor (EGFR), is site-specifically conjugated to 1,4,7,10-tetraazadodecane-N,N',N'',N'''-tetraacetic acid and labeled with ^{64}Cu with modest specific activity (36 mCi/mg). The ^{64}Cu -Fn tracer exhibits EGFR-specific binding to A431 epidermoid carcinoma cells in culture. The tracer is stable as it exhibits an unchanged HPLC chromatogram after 24h in 50% mouse serum at 37°. The ^{64}Cu -Fn (~50 μCi injected via tail-vein) was used for positron emission tomography of EGFR-overexpressing A431 xenografts (~5-10 mm diameter) in mice (n=5). The tracer exhibits good tumor localization (2.6 ± 0.8 %ID/g at 1h), retention (2.1 ± 0.5 %ID/g at 24h), and specificity (5.1 ± 1.2 tumor:muscle at 2h). Specific targeting is statistically significant as verified by low localization to a tumor with low EGFR expression (0.7 ± 0.1 %ID/g, $P < 0.005$); specificity is further demonstrated as a non-binding wild-type control fibronectin has low localization to the EGFR-overexpressing A431 xenograft (0.7 ± 0.1 %ID/g at 1h, $P < 0.005$). These results are corroborated by ex vivo gamma counting analysis of dissected tissues. These data represent the first reported use of the fibronectin domain for in vivo imaging and demonstrate the potential for this domain to serve as a robust scaffold for the development of other molecular imaging agents.



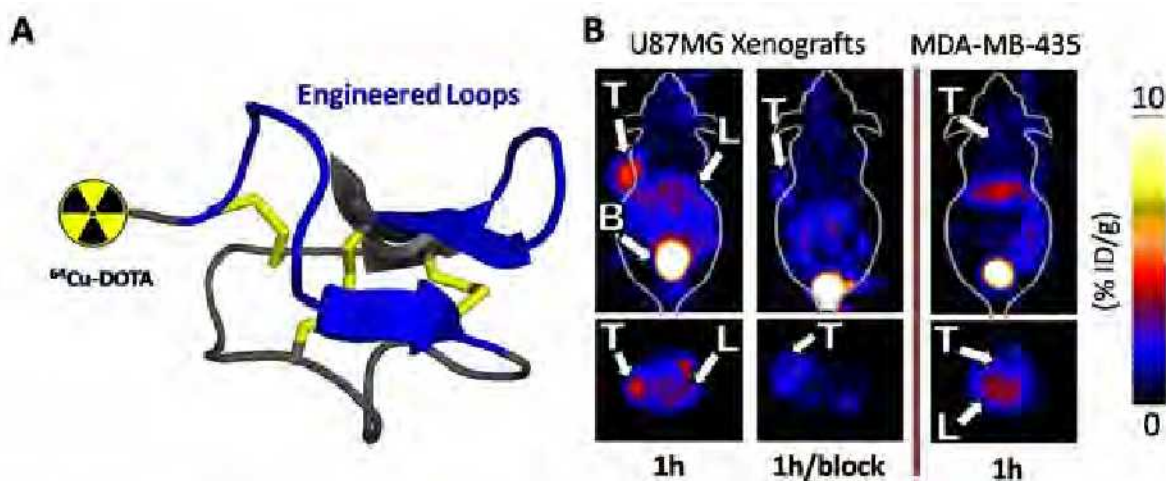
(A) Schematic of labeled protein. The fibronectin domain (depicted as the NMR solution structure of wild-type fibronectin domain (PDB code: 1TTG)) was engineered (mutated residues in green) for binding to EGFR. DOTA was conjugated to the sole primary amine (the N-terminus) and used to chelate ^{64}Cu . (B) PET imaging. A431 epidermoid carcinoma cells were xenografted into nude mice. ^{64}Cu -Fn3 (EGFR binder D' or non-binding control WT') was injected via the tail vein. 5 min. static scans were acquired at 1h post-injection.

Presentation Number **0167**
 Scientific Session 21: Probes for Imaging the Tumor Microenvironment

Development of a Multivalent Dual-RGD Knottin Peptide: Engineering Higher Affinity Translates to Slower Tumor Clearance Rates In Vivo

Richard Kimura¹, Douglas Jones², Lei Jiang³, Zheng Miao¹, Sanjiv S. Gambhir^{1,2}, Zhen Cheng¹, Jennifer R. Cochran², ¹Radiology, Molecular Imaging Program at Stanford, Canary Center, Stanford University, Palo Alto, CA, USA; ²Bioengineering, Bio-X, Stanford University, Palo Alto, CA, USA; ³Nuclear Medicine, Shanghai Ruijin University Hospital, Shanghai, China. Contact e-mail: rkimura1@stanford.edu

Knottins are small (~3-4kDa) highly structured peptides that are stabilized by a core network of three intertwined disulfide bonds which form a molecular knot. This knotted structure allows for the formation of several looped regions upon which molecular recognition elements may be engineered. Here, we present molecular imaging studies of living animals injected with ~ 50uCi ⁶⁴Cu-DOTA knottin radiotracer (~100uCi/ug) containing two RGD integrin-binding motifs. Compared to the parental single-RGD knottin (IC₅₀ = 19±6 nM), this higher affinity dual-RGD knottin (IC₅₀ = 7.5±1.4 nM) demonstrates significantly slower tumor clearance rates from U87MG tumors leading to excellent contrast and high tumor retention of radioactivity at late times post injection. Tumor uptake is high, rapid and specific (3.5±0.8 ID/g, tumor-to-muscle (t/m) ratio = 10.3±4.5, n=3, at 1 hr p.i.) and tumor washout is slow (0.07±0.03 %ID/g/hr for dual-RGD vs. 0.13±0.04 %ID/g/hr single-RGD parent). Specificity of the radiotracer was determined using a low integrin-expressing MDA-MB-435 xenograft model where tumor uptake was significantly lower (1 hr, 0.82±0.05 % ID/g tumor, n=3, p<0.05). Radiotracer was also blocked with a coinjection of a molar excess of unlabeled peptide in higher integrin-expressing U87MG xenografts (1h/block, 0.53 ± 0.03 %ID/g tumor, n=3, p<0.05). Importantly, this extensively engineered knottin demonstrates low uptake in non-targeted organs and rapid renal clearance (1 hr and 24 hr, 2.2±0.5 and 2.6±0.4 %ID/g liver, 10.6±1.2 and 3.3±0.8 %ID/g kidney). Collectively, these studies demonstrate that knottin radiotracers are effective cancer imaging agents.



Abstract Figure: (A) Structural Representation of the Dual-RGD Knottin Peptide based on EETI-II (PDB: 2ETI). Wildtype backbone residues are shown in gray, while engineered loops are shown in blue. Yellow represents the three knotted disulfide bonds which stabilize the core cystine knot motif. The N-terminus was conjugated to DOTA and radiolabeled with Cu-64. **(B) MicroPET Imaging with ⁶⁴Cu-DOTA-Dual-RGD Knottin.** Images were acquired 1 hour post injection in U87MG xenografts (left), which express ~100K integrin $\alpha_v\beta_3$ /cell and MDA-MB-436 xenografts (right), which express ~20K integrin $\alpha_v\beta_3$ /cell. Radiotracer specificity was also determined with a coinjection of a molar excess of cold competitor (1h/block). Tumor

Presentation Number **0168**
 Scientific Session 21: Probes for Imaging the Tumor Microenvironment

Molecular MR Imaging of U87 Brain Tumor Angiogenesis Using a Novel RGD Gd-based Emulsion: In Vitro and In Vivo Validation

Benjamin Marty¹, Françoise Geffroy¹, Julien Flament¹, Céline Giraudeau¹, Caroline Robic², Marc Port², Philippe Robert², Denis Le Bihan¹, Julien Valette¹, Fawzi Boumezbeur¹, Franck Lethimonnier¹, Sébastien Mériaux¹, ¹CEA/DSV/I2BM/Neurospin, Gif-Sur-Yvette, France; ²Research Division, Guerbet, Roissy-Charles de Gaulle, France. Contact e-mail: benjamin.marty@cea.fr

INTRODUCTION. Molecular magnetic resonance (MR) imaging is an increasingly used tool to investigate tumors angiogenic activity. In this study we used a Gd-based emulsion (30000Gd/droplet) grafted with RGD peptides to target $\alpha v\beta 3$ protein over-expressed during brain tumor angiogenesis in a mouse model. **MATERIALS AND METHODS.** The binding and internalization of RGD-emulsions were studied in vitro using U87 (human glioma) cells incubated for 1 hour with RGD labeled and unlabeled emulsion. In vivo experiments were carried out on nude mice with brain tumor induced by intra-cerebral injection of U87 cells. MRI experiments were performed 14 days after tumor induction on a 7T preclinical scanner using a 2.8cm home made birdcage 1H coil. Quantitative T1 maps were acquired before and every 10 minutes after intra-venous injection of contrast agent using an IR-TurboFLASH sequence (TE/TR=2.4/4.8ms, 30 inversion times spaced by 96.6ms) to produce concentration maps of the emulsion. **RESULTS.** The in vitro study (Fig. 1) reveals that after 1h of incubation, both emulsions are almost completely internalized in U87 cells (no significant T1 decrease between tubes 1, 2 and 3). In the case of lysed cells (tubes 4 and 5), the T1 decrease is more important for the labeled emulsion (9%) than for the unlabeled emulsion (4%), indicating a higher contrast agent concentration due to the RGD binding. In vivo experiments (Fig 2-3) show that the uptake of contrast agent in the rim of the tumor is 2.6 times higher for the labeled emulsion compared to the unlabeled emulsion and does not seem to follow the vascular uptake. This result confirms the binding observed in vitro and seems to indicate a higher angiogenic activity in the rim of the tumor compared to the necrotic centre. **DISCUSSION AND CONCLUSION.** This study shows that molecular MR imaging dedicated to brain tumor angiogenesis detection is possible using an appropriate targeted Gd-based contrast agent combined with quantitative T1 MR imaging. A proof of concept of its binding was realized both in vitro and in vivo using U87 tumor cells expressing $\alpha v\beta 3$ protein.

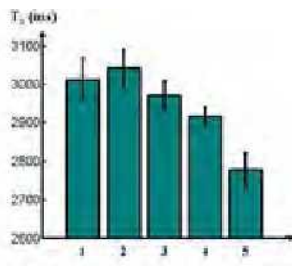


Fig. 1 In vitro study. Tube 1 - Reference; Tube 2 - Unlabeled emulsion, lysed cells; Tube 3 - Unlabeled emulsion, lysed cells; Tube 4 - Labeled emulsion, lysed cells; Tube 5 - Labeled emulsion, lysed cells.

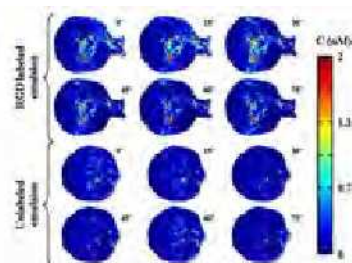


Fig. 2 In vivo dynamic concentration maps of the labeled and unlabeled emulsions after IV injection in U87 mice. The rim of the tumor is indicated in red dashes.

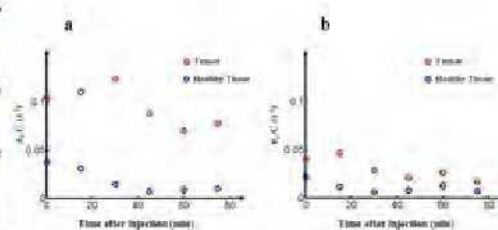


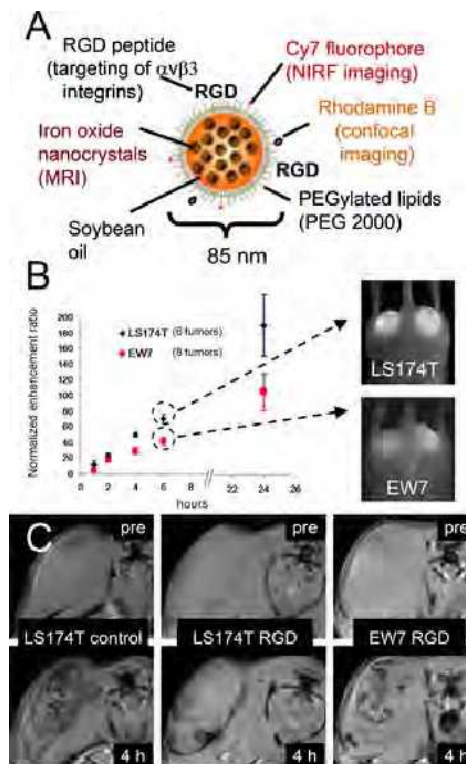
Fig. 3 Normalized emulsion concentration during the 2 hours experiments in 2 regions of interest: tumor rim and healthy tissue. a) Labeled emulsion; b) Unlabeled emulsion.

Presentation Number **0170**
 Scientific Session 21: Probes for Imaging the Tumor Microenvironment

Targeted Nanoemulsions as Contrast Agents for Tumor Angiogenesis Imaging and Phenotyping

Peter A. Jarzyna¹, Lisette H. Deddens², Wei Chen¹, Rick M. Dijkhuizen², Arjan Griffioen³, Zahi Fayad¹, Willem J. Mulder¹,
¹Translational and Molecular Imaging Institute, Radiology, Mount Sinai School of Medicine, New York City, NY, USA; ²Department of Medical Imaging, Image Sciences Institute, University Medical Center Utrecht, Utrecht, Netherlands; ³Angiogenesis Laboratory, Department of Medical Oncology, VUmc-Cancer Center Amsterdam, VU University Medical Center, Amsterdam, Netherlands. Contact e-mail: peter.jarzyna@mountsinai.org

Angiogenic activity is an important parameter for the evaluation of tumor aggressiveness and angiostatic therapy. Non-invasive imaging methods to assess tumor angiogenesis are increasingly explored. We developed a biodegradable nanoparticle system based on oil-in-water emulsions with a tunable average particle size (30-100 nm) that allows tumor imaging with magnetic resonance (MR) and optical methods. The aim of the current study is to apply this nanoparticle for phenotyping of tumors with different microvessel densities (MVDs) by imaging. To that end, the nanoparticles were functionalized with $\alpha v\beta 3$ integrin specific RGD peptides. To enable their visualization by near infrared fluorescence (NIRF) imaging, Cy7 was linked to the surface of the particles (85 nm mean size), while oleic acid capped iron oxide nanocrystals were included in the soybean oil core for MRI (Fig. A). Two subcutaneous swiss nude mice tumor models with different MVDs (human Ewing's Sarkoma; low MVD vs human colon cancer LS174T; high MVD) were chosen to examine the accumulation kinetics in the tumors by MRI (36 Fe mg/kg) and optical imaging (without Fe). Accumulation kinetics of the targeted nanoparticles at 1 h, 2 h, 4 h, and 6 h post administration revealed statistically significant differences ($p < 0.05$) between the two different tumor models as shown by in vivo NIRF imaging (Fig. B). Ex vivo confocal laser scanning microscope images of the tumors showed the RGD conjugated particles to be associated with tumor endothelial cells. The in vivo MRI data revealed a different pattern of signal attenuation within the different tumor types (Fig. C). The signal loss in the T_2^* images of the targeted LS174T group was primarily confined to the tumor periphery, while the EW7 group showed attenuation throughout the entire tumor, similar to the control LS174 group (non-functionalized nanoparticles). In summary we have shown our nanoparticle platform to be of great value for non-invasive tumor phenotyping by molecular MRI and NIRF imaging.



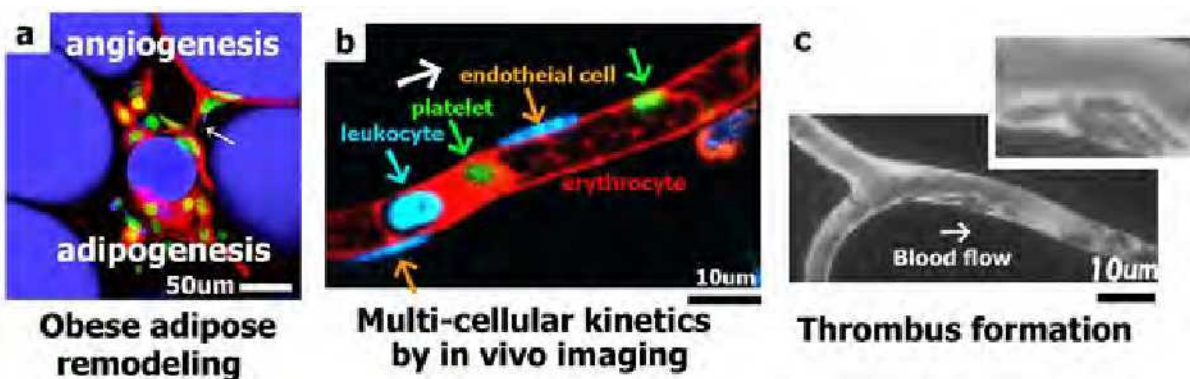
A) Nanoparticle carrier (oil-in-water emulsion). B) NIRF imaging demonstrated difference in tumor accumulation (LS174T vs EW7). C) MR images (T_2^*) showed a distinct pattern of signal loss in the two tumor models 4 h after injection.

Presentation Number **0171**
 Scientific Session 22: In Vivo Animal Models

In Vivo Molecular Imaging Reveals Parenchymal and Interstitial Cell Cross-talks in Chronic Inflammatory Diseases

Satoshi Nishimura^{1,3}, **Mika Nagasaki**^{1,4}, **Ichiro Manabe**^{1,3}, **Koji Eto**², **Ryozo Nagai**¹, ¹*Department of Cardiovascular Medicine, The University of Tokyo, Tokyo, Japan;* ²*Center for Stem Cell Biology and Regenerative Medicine, The Institute of Medical Science, The University of Tokyo, Tokyo, Japan;* ³*PRESTO, Japan Science and Technology Agency, Tokyo, Japan;* ⁴*Computational Diagnostic Radiology and Preventive Medicine, The University of Tokyo, Tokyo, Japan.* Contact e-mail: snishi-tyk@umin.ac.jp

Metabolic syndrome is a major risk factor of cardiovascular events, and adipose tissue obesity based on chronic inflammation play a central role. To assess dynamic interplay between multiple cell-types in inflammatory diseases, in vivo imaging technique based on single- and multi-photon microscopy was developed. Imaging revealed close spatial and temporal interrelationships between angiogenesis and adipogenesis in obese adipose (Fig a, 2007 Diabetes). In addition, increased leukocyte-platelet-endothelial cell interactions in the microcirculation of obese adipose were observed, a hallmark of inflammation (2008 JCI). We also found that large numbers of CD8+ effector T cells infiltrated into obese adipose. Infiltration by CD8+ T cells is essential for the initiation and development of adipose inflammation (2009 NatMed). By our in vivo imaging technique, multiple cell types are specifically visualized (b), and thrombus formation was induced by laser irradiation which cause ROS production inside the blood vessel (c). Using this technique, we revealed Lnk/Sh2b3 regulates integrin alpha-IIb-beta-3 outside-in signaling in platelets leading to stabilization of developing thrombus in vivo (2010 JCI). In addition, we established human iPS-derived platelets, and tracked them in mice to elucidate its function in vivo. We confirmed injected platelets circulate, and contributed to the thrombus formation in vivo, indicating the clinical usefulness of this strategy for future. Our results clearly demonstrated the power of our imaging technique to analyze complex cellular interplays in inflammatory diseases, especially parenchymal and stromal cell cross talks, and to evaluate new therapeutic interventions against them.



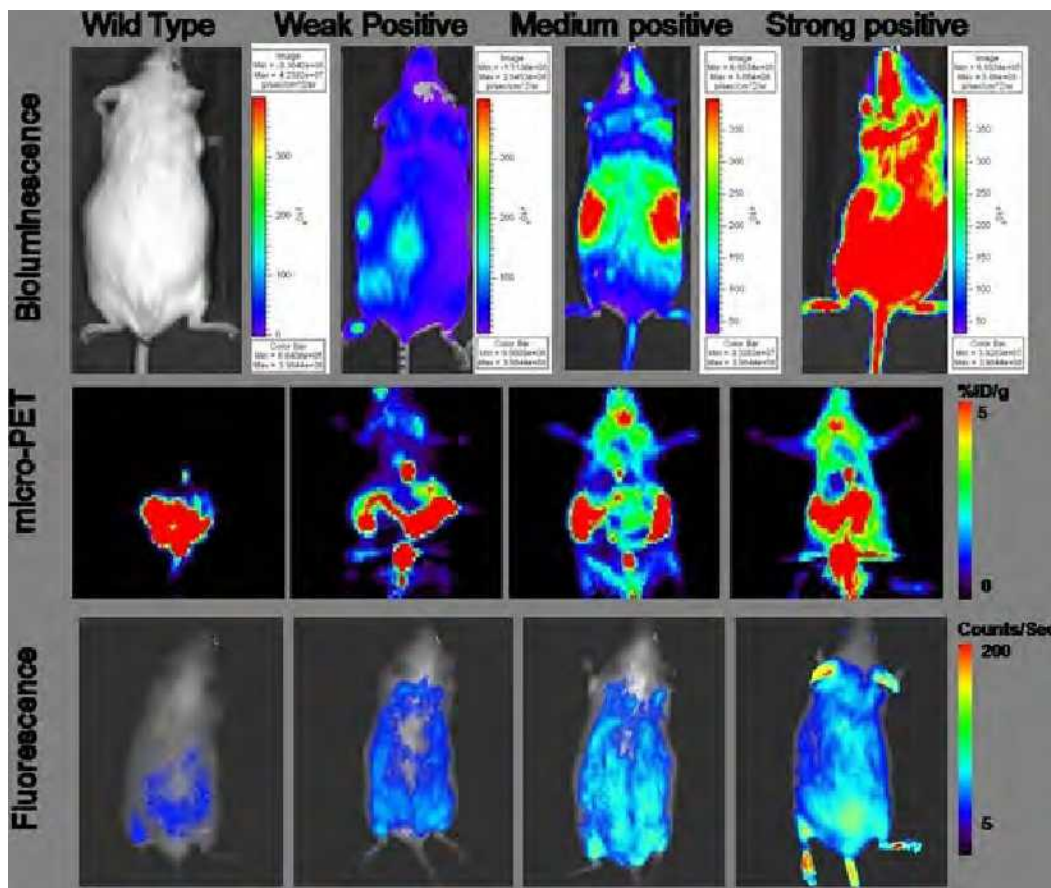
(a) Adipose tissue remodeling in obesity including adipogenesis and angiogenesis (b) Multi-cellular kinetics visualized by novel in vivo imaging technique (c) Thrombus formation and single platelet kinetics revealed by in vivo imaging

Presentation Number **0172**
 Scientific Session 22: In Vivo Animal Models

The Mighty Mouse: Ubiquitous Expression of a Tri-Fusion (Bioluminescence, Fluorescence, PET) Reporter Gene in a Transgenic Mouse Model

Xinrui Yan¹, **Pritha Ray**¹, **Ricky Tong**¹, **Ataya Sathirachinda**¹, **Sanjiv S. Gambhir**^{1,2}, ¹Radiology and Molecular Imaging Program, Stanford University, Palo Alto, CA, USA; ²Bio-X, Stanford University, Palo Alto, CA, USA. Contact e-mail: xryan@stanford.edu

Reporter genes are extremely useful in following the gene expression and cellular behavior in development and disease studies in mice. We have created a transgenic mouse that expresses the tri-fusion reporter gene with pcAGGS-fluc2-tdTomato-ttk vector which is driven by the chicken β -actin promoter carrying an improved bioluminescent (fluc2), an improved red fluorescent protein (tdTomato) and a truncated herpes simplex virus type 1 sr39 thymidine kinase (tkk) reporter genes. This allows one to image any cell from the donor mouse using bioluminescent, fluorescent, and PET imaging (with [¹⁸F]FHBG) techniques. Mice (N=15) with different expression levels of the tri-fusion reporter were scanned, and multimodality imaging results show that the expression level of all three genes are correlated with each other (Figure 1). In vitro luciferase assay, fluorescent assay and TK assay were performed with cell lysates from the tail of those mice, the signal levels of fluc2 (8364-5,212,160 RLU/ μ g), tdTomato (0.2-20.5 FI/ μ g) and tkk (2055.6-281,836.5 dpm) are correlated to each other (R²=0.99), and the results from in vitro experiments are correlated to those from in vivo imaging. Organs from transgenic mice with high expression level of reporter gene were harvested and tested using in vitro assays. Muscle, heart, tail, pancreas and bladder have statistically higher expression (P<0.05) of reporter gene than other tissues, while the liver and intestine have less expression. To date, the signals from strong positive mice persist for 4 generations, and no developmental abnormalities/toxicity has been observed. To monitor MSC (mesenchymal stem cell) survival, FVB mice acute myocardial infarction were induced by coronary ligation with subsequent intramyocardial injection of MSC (mesenchymal stem cell) isolated from the bone marrow of the transgenic mice. Bioluminescence imaging results showed MSC signal decreased and became undetectable after 9 days. This mighty mouse will serve as an important tool in multiple fields such as stem cells and transplant biology.



Presentation Number **0173**
 Scientific Session 22: In Vivo Animal Models

In vivo MRI studies of *Crim1* mutant mice: a model of abnormal renal vascular disease

Nyoman D. Kurniawan¹, Lorine Wilkinson², Melissa H. Little², ¹Centre for Advanced Imaging, University of Queensland, Brisbane, QLD, Australia; ²Institute for Molecular Biology, University of Queensland, Brisbane, QLD, Australia. Contact e-mail: n.kurniawan@uq.edu.au

Background: *Crim1* is a transmembrane protein that is essential for delivery of VEGFA from podocytes to the developing glomerular endothelium. Mutant *Crim1* hypomorphic mice develop chronic and progressive kidney disease, characterized by leaky renal vasculature, abnormal glomerular capillaries, glomerular cysts, fibrosis and low glomerular flow rate. **Method:** Hypomorphic *Crim1*^{KST264/KST264} CD1 mice were studied using *in vivo* MRI. A suite of MR imaging experiments was performed using 16.4T Bruker NMR scanner, including: 2D fast spin echo *T*₂-weighted imaging, time-of-flight angiography and kinetic clearance of Gd-DTPA to assess renal physiology. This study was performed using 8 littermate pairs of wild type and mutant mice age 5 -37 weeks. 4 pairs were serially imaged between 4-28 weeks of age. **Results:** *T*₂-weighted MRI showed clear delineation of renal morphology of the cortex, medulla, inner medulla and papilla and ureter. Unlike in tubular cystic diseases, the kidneys of *Crim1* mutant mice appeared smaller compared to the littermates and developed cysts (0.15-1.5 mm) in the cortical region. Serial MR imaging revealed that the cysts in hydronephrotic *Crim1* mutant mice were stable (visible) throughout the timeline of the study, but were transient in non-hydronephrotic *Crim1* mice. Hydronephrotic *Crim1* kidneys may unable to drain accumulated fluid leading to fibrosis of the parietal epithelium in glomerular cysts and stabilization of the cysts.

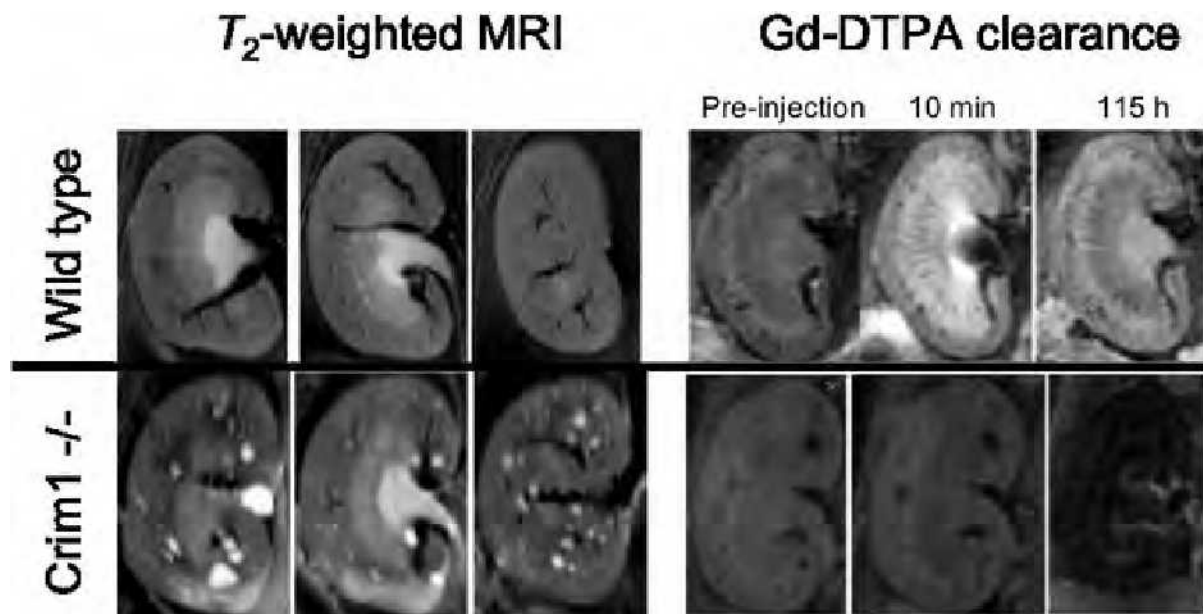


Figure 1. *Crim1* mutant mice developed cysts in the cortical areas of the kidney and impaired Gd-DTPA clearance.

Presentation Number **0174**
Scientific Session 22: In Vivo Animal Models

Integrating Molecular Imaging and Behavioral Neuroscience: Seeing Animal Models in a New Light

Wynne Schiffer^{1,2}, Joseph Carrion¹, David Eidelberg¹, Jonathan D. Brodie², ¹Feinstein Institute for Medical Research, North Shore University Health System, Manhasset, NY, USA; ²Psychiatry Department, New York University Medical Center, New York, NY, USA; ³Medical Department, Brookhaven National Laboratory, Upton, NY, USA. Contact e-mail: wschiffer@nshs.edu

We will describe the development and validation of a new paradigm in which PET and a host of receptor specific radiotracers can be used to capture dynamic molecular events in behaving animals. Key to our paradigm, radiotracer uptake occurs while animals move freely in a range of test environments, followed by anesthesia and scan. Using 11C-raclopride (11C-rac) as a prototypical probe whose displacement reflects changing dopamine, we validated this paradigm with drug challenges designed to directly perturb 11C-rac (loading doses of cold rac) or indirectly change 11C-rac by changing dopamine (METH to increase and AMPT to decrease dopamine). Systematic variations in uptake duration, type and presence of anesthetic, route of 11C-rac administration and image acquisition methods were used to optimize the protocol. For these validations, paired scans were performed where uptake occurred in the awake state, followed by anesthesia and scanning. While still in the gantry, a second scan gave full time activity data from the same animal. Comparing these data allowed us to validate derivations of binding potential used to quantitate awake uptake. All awake studies were videoed and analyzed with behavioral phenotyping software. With this information, individual behaviors were directly related changes in 11C-rac binding. Behavioral challenges revealed striking parallels analogous to human PET studies. First, stress decreased 11C-rac binding, an effect that significantly correlated with behavior and was similar in magnitude to that following METH. Second, cue exposure in cocaine-addicted animals significantly decreased 11C-rac, and this decrease correlated with individual measures of craving using the CPP model. The magnitude was similar to the decrease in 11C-rac from an acute dose of cocaine. Microdialysis data revealed that cue exposure produces lower but sustained increases in dopamine, while cocaine produces large, rapid increases that quickly return to baseline. Comparable decreases in 11C-rac in behavioral and drug challenge studies have recently been raised in clinical PET studies. Perhaps the most important message, individual changes in 11C-rac are associated with individual differences in behavior in each model. Animals with little genetic variation and no difference in rearing will, for example, respond uniquely to stress and this response closely reflects 11C-rac. This mimics the inherent variability commonly observed in clinical PET which, in animals, can be obscured by examining group responses in single-focus behavioral or biological experiments.

Presentation Number **0175**
 Scientific Session 22: In Vivo Animal Models

In Vivo Ultrasound Imaging of Cerebral Ischemia Using Shear Wave Imaging and Ultrafast Doppler

Abraham Martin^{1,2}, **Emilie Mace**³, **Mickael Tanter**³, **Bertrand Tavitian**^{1,2}, ¹CEA, DSV, I2BM, SHFJ, Orsay, France; ²Inserm, U1023 ; Université Paris Sud, Orsay, France; ³Institut Langevin, ESPCI Paris Tech, Paris, France. Contact e-mail: abraham.martin-munoz@cea.fr

Introduction: Stroke is the third leading cause of death in industrialized countries and the most frequent cause of permanent disability in adults worldwide. So far, neuroimaging methods have been indispensable to understand the different pathological processes underlying ischemic stroke in both the laboratory and clinic. Here, we investigated the potential of ultrafast ultrasound imaging to provide new findings on stroke research. **Methods:** Shear Wave Imaging and an Ultrafast Doppler scan were performed in control animals and at 1, 2, 4 and 7 days after a 2-hour middle cerebral ischemia in rats. Rats were trepanned and scans performed using an ultrafast ultrasound scanner. Shear Wave Imaging consists of generating a shear wave and tracking its propagation to map local brain stiffness. Ultrafast Doppler provides very high sensitivity maps of cerebral blood flow from the Doppler analysis of plane wave compounded images acquired at 1 kHz. **Results:** The ischemic lesion was found to be very soft (mean value < 7 kPa) compared to healthy brain tissues (mean value 12 kPa, ranging from 2 to 25 kPa in different regions). From 1 to 7 days after occlusion, the soft part of the lesion increased in size and the mean value decreased. Ultrafast Doppler revealed an important increase in the power Doppler intensity in the ischemic hemisphere compared to the healthy hemisphere. This difference peaked at day 1 after the occlusion (+30% with respect to control) and then decreased until day 7 (+10%). Local analysis of the blood flow modifications with a high spatial resolution showed different time courses of the Doppler signal in the cortex and in the striatum. **Conclusions:** Ultrafast imaging explores previously undescribed neurophysiological parameters of cerebral ischemia in rodents. Stiffness appears to be a relevant parameter for monitoring the evolution of cerebral ischemia over time, while Ultrafast Doppler provides high spatial resolution imaging of cerebral blood flow changes after the stroke.

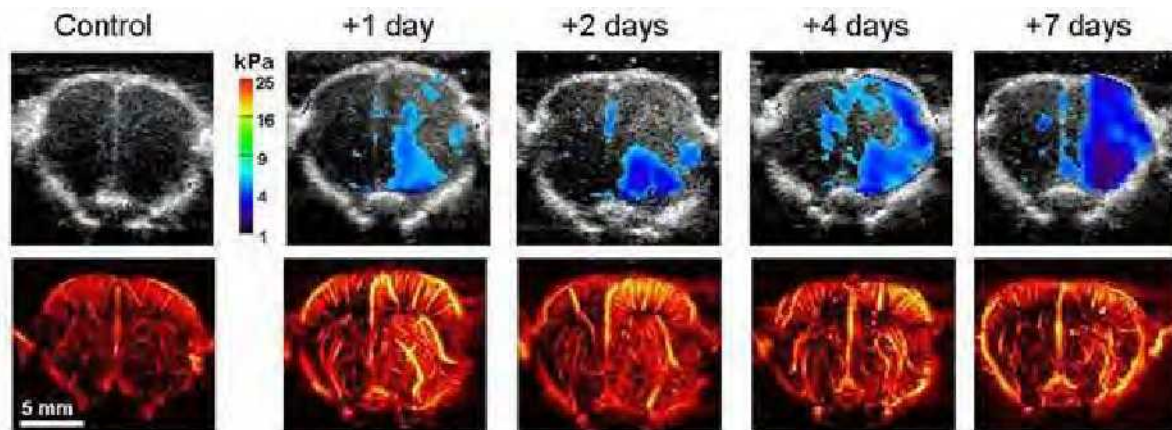


Figure: Evolution of stiffness and blood flow in the ischemic lesion over time for a selected coronal slice of the rat brain. The ischemic hemisphere is on the right.

(Top) Elasticity map superposed on the Bmode image (only values < 6.25 kPa shown).

(Bottom) Ultrafast Power Doppler image.

Presentation Number **0176**
Scientific Session 22: In Vivo Animal Models

Tracer Input for Kinetic Modeling of Liver Physiology by PET in Pigs Determined without Sampling Portal Venous Blood

Michael Winterdahl, **Susanne Keiding**, Michael Sørensen, Frank V. Mortensen, Aage K. Olsen, Ole L. Munk, Aarhus University Hospital, Aarhus, Denmark. Contact e-mail: susanne@pet.auh.dk

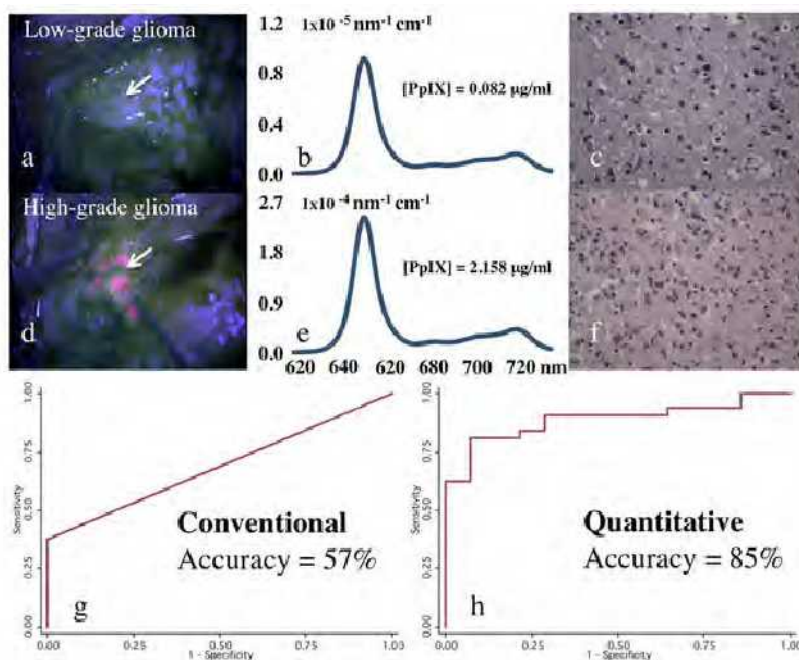
Positron emission tomography (PET) provides unique possibilities for quantifying hepatic metabolism *in vivo*, but this requires measurement of tracer input from both the hepatic artery (HA) and the portal vein (PV). As blood sampling from the PV is impracticable in humans, we decided to develop a method for estimating the dual tracer input without the necessity to sample PV blood. We used a previously developed PV-model for the transfer of tracer through the splanchnic vascular bed from the arteries to the PV, which includes a single tracer-specific parameter β (min) that reflects the splanchnic mean transit time of the tracer. **Methods:** 40-kg pigs were administered bolus doses of $C^{15}O$, [^{18}F]fluoro-2-deoxyglucose (^{18}FDG), [^{11}C]methylglucose (^{11}C -MG), [^{18}F]fluoro-2-deoxygalactose ($^{18}FDGal$) or $H_2^{15}O$ (n=36). Tracer concentration time courses (3 min) were measured in the femoral artery and the PV by blood sampling and the blood flow was measured in the HA and PV using surgically positioned flowmeters. β was estimated for each tracer administration and by using tracer-specific population means of β , the individual PV-modeled tracer concentration time course in the PV was calculated from the measured arterial concentration. Next the dual-input was calculated from the modeled PV concentration and the mean HA flow fraction (= 0.25). The use of the modeled dual-input for the assessment of hepatic tracer kinetics was validated by using a simulated tracer concentration time courses in liver tissue, calculated from the measured dual-input and a compartmental model of the hepatic tracer kinetics with a fixed "true" K_1^{true} , i.e. clearance of tracer from blood to liver cells = 1 mL blood/mL liver tissue/min. An estimated K_1^{est} was calculated using the model-derived dual-input. **Results:** The rank order of the population means of β was $C^{15}O < ^{18}FDG \approx ^{11}C$ -MG $< ^{18}FDGal < H_2^{15}O$, reflecting the different splanchnic mean transit times. Estimated tracer concentrations in the PV and the dual-input compared well with the respective measured concentrations. The mean K_1^{est} based on the model-derived dual-input was not significantly different from the K_1^{true} . Thus the simulated tracer concentration time courses in liver tissue were estimated with good accuracy using the model-derived dual-input. **Conclusion:** The hepatic dual tracer input from the HA and PV can be determined in pigs without PV blood sampling and measurement of hepatic blood flow; only arterial blood sampling is needed, a finding of great potential for quantitative PET of liver physiology in man.

Presentation Number **0177**
 Scientific Session 23: Clinical Studies (Co-organized with RSNA)

Sensitive Intraoperative In Vivo Detection of Endogenous Biomarker Fluorescence From Gliomas to Maximize Brain Tumor Resection

Pablo A. Valdes^{1,2}, Frederic Leblond¹, Anthony Kim³, Brian C. Wilson³, Brent T. Harris^{2,4}, Keith D. Paulsen^{1,5}, David W. Roberts^{2,6},
¹Thayer School of Engineering, Dartmouth College, Hanover, NH, USA; ²Dartmouth Medical School, Dartmouth College, Hanover, NH, USA; ³University of Toronto, Ontario Cancer Institute/University Health Network, Toronto, ON, Canada; ⁴Pathology, Dartmouth-Hitchcock Medical Center, Lebanon, NH, USA; ⁵Norris Cotton Cancer Center, Dartmouth-Hitchcock Medical Center, Lebanon, NH, USA; ⁶Neurosurgery, Dartmouth-Hitchcock Medical Center, Lebanon, NH, USA. Contact e-mail: pablo.a.valdes@dartmouth.edu

Background: Gliomas account for more than 70% of all brain tumors, with median survival times as low as 1 year. Studies show a correlation between maximization of tumor resection and survival/quality of life in this patient population. As such, our group is developing an imaging platform for fluorescence-guided resection (FGR) with the ultimate goal of maximizing tumor removal. Methods: Patients are administered an oral dose of δ -aminolevulinic acid (ALA) prior to surgery, inducing selective accumulation in tumor tissue of the endogenous fluorophore, protoporphyrin IX (PpIX), as a result of metabolic and proliferative changes that differ significantly between normal and tumor tissue. Conventional intraoperative *in vivo* FGR technologies are not sufficiently sensitive to detect low levels of PpIX fluorescence in low- and high-grade gliomas, thus leaving tumor tissue undetected. Further, in low-grade gliomas, ALA-PpIX FGR has shown no significant value as an imaging modality for surgical guidance, but in this tumor type maximization of tumor removal could have the most significant impact on survival/quality of life. Results: We show the use of a light-transport modeling spectroscopic approach for sensitive intraoperative *in vivo* quantification down to the ng/ml concentrations of PpIX for real-time (i.e., <0.5 s) FGR of gliomas. Receiver-operating characteristic (ROC) analysis for low- and high-grade glioma cases ($n=5$) in our clinical study was performed to compare the conventional approach using a fluorescence imaging surgical microscope and our fiber-optics quantitative approach. Our results show significantly improved diagnostic capabilities for tumor tissue detection of our quantitative approach. Conclusions: We show sensitive and quantitative fluorescence detection of PpIX biomarker for real-time *in vivo* tumor margin delineation in gliomas, as part of an intraoperative imaging platform for FGR of brain tumors with the goal of providing improved surgical guidance technologies to the neurosurgeon.



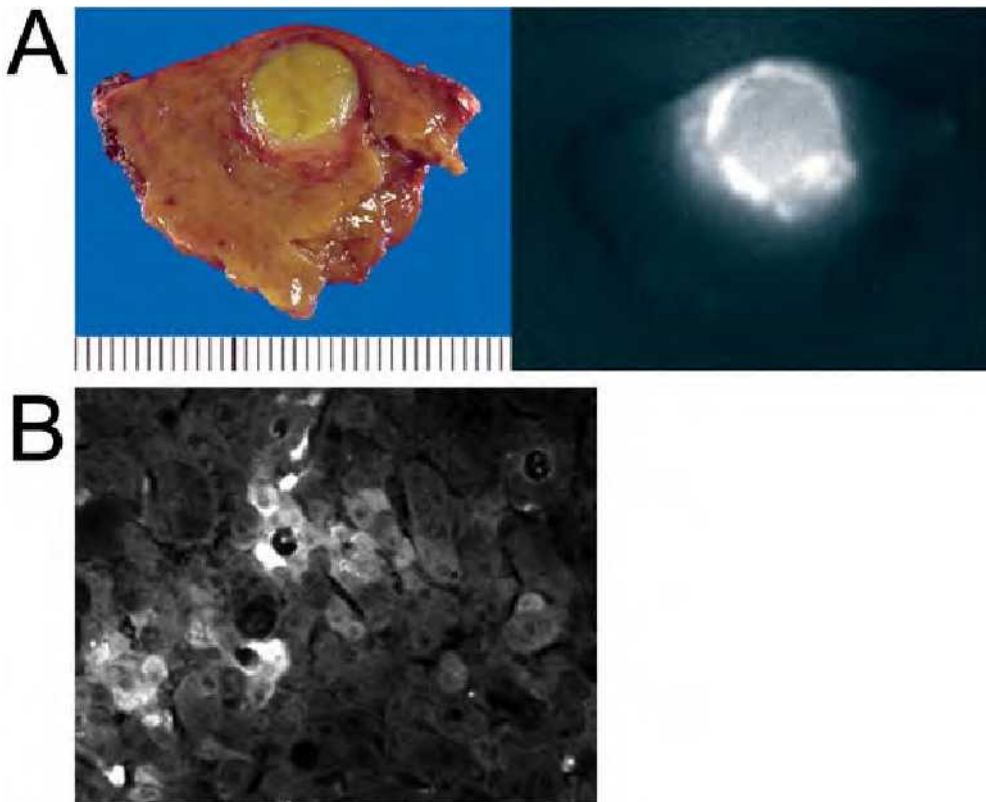
In vivo fluorescence-guided surgery of brain tumors. Intraoperative surgical microscope fluorescent images (a,d) with white arrows at the location where quantitative probe measurements (b,e) and biopsies were acquired for a low- (c) and high-grade (f) glioma case, respectively. ROC curves for conventional fluorescence imaging (g) and our quantitative approach (g), with diagnostic accuracies of 57% and 85%, respectively.

Presentation Number **0178**
Scientific Session 23: Clinical Studies (Co-organized with RSNA)

Indocyanine Green-fluorescent Imaging for Identifying Hepatocellular Carcinoma During Liver Resection

Takeaki Ishizawa¹, **Koichi Masuda**¹, **Shoichi Satou**¹, **Junichi Kaneko**¹, **Taku Aoki**¹, **Yoshifumi Beck**¹, **Kiyoshi Hasegawa**¹, **Yasuhiko Sugawara**¹, **Junji Shibahara**², **Masashi Fukayama**², **Norihiro Kokudo**¹, ¹Hepato-Biliary-Pancreatic Surgery Division, Department of Surgery, Graduate School of Medicine, University of Tokyo, Bunkyo-ku, Japan; ²Department of Pathology, Graduate School of Medicine, University of Tokyo, Tokyo, Japan, Hongo, Bunkyo-ku, Japan. Contact e-mail: tish-tky@umin.ac.jp

Background: Recently, fluorescent imaging using indocyanine green (ICG) has been developed to identify liver cancers during surgery, through allowing visualization of the disordered biliary excretion of ICG in the cancer tissues and the surrounding non-cancerous liver tissues. Methods: ICG (0.5 mg/kg) had been intravenously injected for a routine liver function test in 136 patients with hepatocellular carcinoma (HCC). Resected specimens were sliced and all of the cut surfaces were examined using the fluorescent imaging system in the OR. Any fluorescing lesions (≥ 5 mm) were marked for subsequent microscopic examination. Results: ICG-fluorescent imaging identified 240 out of the 243 (99%) microscopically-confirmed HCCs. The fluorescent patterns of the 240 HCCs were classifiable into a total fluorescent type (the cancer tissues showed a uniform fluorescence, $n = 109$), a partial fluorescent type ($n = 105$), and a rim fluorescent type (only the surrounding liver parenchyma showed fluorescence, $n = 26$). Forty-nine of the 57 well-differentiated HCCs (86%) showed a total fluorescence, while 17 of the 22 poorly differentiated HCCs (77%) appeared as rim-fluorescing lesions. Fluorescent imaging detected 37 grossly-unidentifiable lesions: 21 were microscopically diagnosed as HCC and the remaining 16 were non-cancerous lesions. The 21 grossly-unidentifiable HCCs had larger tumor diameter and higher fluorescent intensity compared with those of the 16 non-cancerous lesions (median [range], 7[5-12]mm vs 5[5-7]mm; $P=0.001$, and 194[135-255] vs 112[30-193]; $P<0.001$, respectively). Fluorescent microscopy confirmed the presence of fluorescence in the cytoplasm and pseudoglands of well-differentiated HCC tissues and in the non-cancerous liver parenchyma compressed by HCCs (Figure). Conclusion: ICG-fluorescent imaging enables the highly-sensitive identification of HCC during surgery. The tumor size and fluorescent intensity may be useful to differentiate HCCs from non-cancerous lesions. (Figure legends) A: Macroscopic view (left) and its fluorescent image (right) of a well-differentiated HCC. B: Fluorescent microscopy of a well-differentiated HCC.

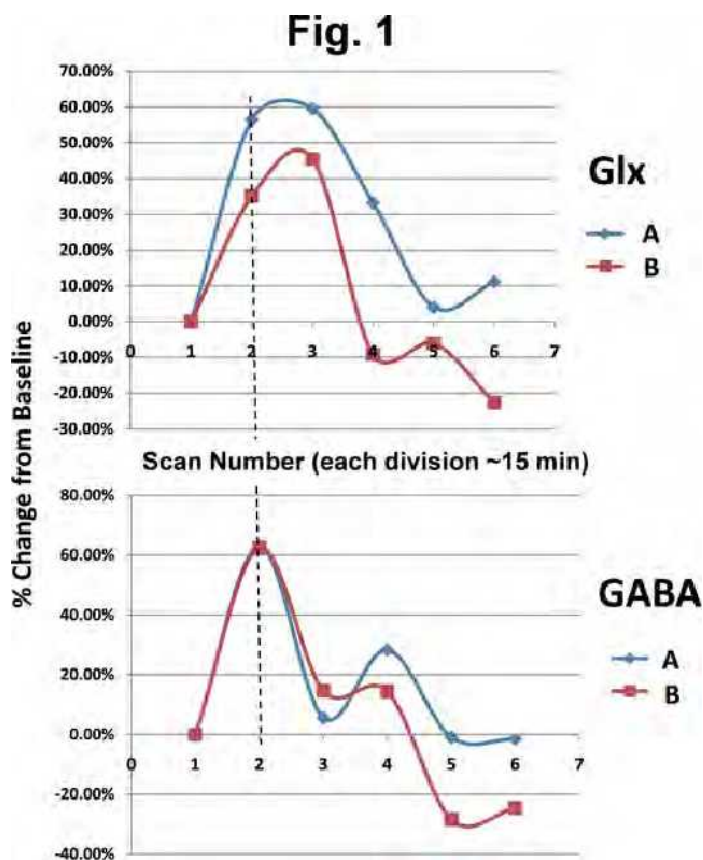


Presentation Number **0179**
 Scientific Session 23: Clinical Studies (Co-organized with RSNA)

In Vivo Human Brain ¹H MRS Monitoring of Dynamic Amino Acid Neurotransmitter Response to Acute Administration of Ketamine

Dikoma C. Shungu^{1,2}, **Matthew S. Milak**², **Lawrence S. Kegeles**^{2,3}, **Caitlin J. Proper**², **Xiangling Mao**¹, **J. J. Mann**^{2,3}, ¹Radiology, Weill Cornell Medical College, New York, NY, USA; ²Psychiatry, College of Physicians and Surgeons of Columbia University, New York, NY, USA; ³Radiology, College of Physicians and Surgeons of Columbia University, New York, NY, USA. Contact e-mail: dcs7001@med.cornell.edu

BACKGROUND. Acute intravenous administration of single sub-anesthetic doses of ketamine (KET) has been recently investigated as a potentially fast-acting treatment for major depressive disorder (MDD). The near immediate anti-depressant effects of KET, a noncompetitive glutamate (Glu) NMDA receptor antagonist, are postulated to involve the drug's stimulation of a rapid increase in brain Glu that may then enhance transmission at metabotropic Glu receptor subtypes. Here, we report the results of a pilot *in vivo* human brain ¹H MRS study that aimed to dynamically monitor Glu changes following acute intravenous administration of KET. **METHODS.** Five patients with MDD received 0.5 mg/kg of KET intravenously over a period of 40 min, while in the MRI scanner. Prior to and approximately every 15 min during and following infusion of the drug, six serial ¹H MR spectra were recorded with the J-editing technique on a 3T GE MR system to measure the levels of glutamate+glutamine (Glx) from their combined resonances in a 25x25x30 mm³ medial prefrontal cortex voxel. In addition to Glx, the J-editing method achieved simultaneous detection of the major inhibitory neurotransmitter γ -aminobutyric acid (GABA), which has also been implicated in the pathophysiology of MDD. **RESULTS AND CONCLUSION.** Time-course curves describing the dynamic response of Glx and GABA to a single acute dose of KET are shown in Fig. 1 for two of the subjects (A and B). Both Glx and GABA increased rapidly, reaching values of up to 60% above baseline within 20 min. In both cases, the rise of GABA was more rapid and bimodal, peaking slightly ahead of Glx, with a second lower peak occurring approximately 30 min after the initial maximum. Notably, end Glx and GABA values for subject B fell below baseline, suggesting a heterogeneous response. In summary, we have reported what may be the first observation of robust *in vivo* human brain Glx and GABA changes following KET administration, in support of the postulated mechanism of action of the drug.



Presentation Number **0180**
Scientific Session 23: Clinical Studies (Co-organized with RSNA)

Comparison between F-18 FDG PET/CT and MR for Monitoring Preoperative Chemoradiation Therapy in Rectal Cancer

Ari Chong, Ho-chun Song, Hee-Seung Bom, Ja-Hye Kim, Su-Ung Yoo, Jong-Ryool Oh, Jung-Min Ha, Byung Hyun Byun, Sun-pyo Hong, Jung-Joon Min, Nuclear medicine, Chonnam National University Hospital, Gwang-ju, Republic of Korea. Contact e-mail: aricori@naver.com

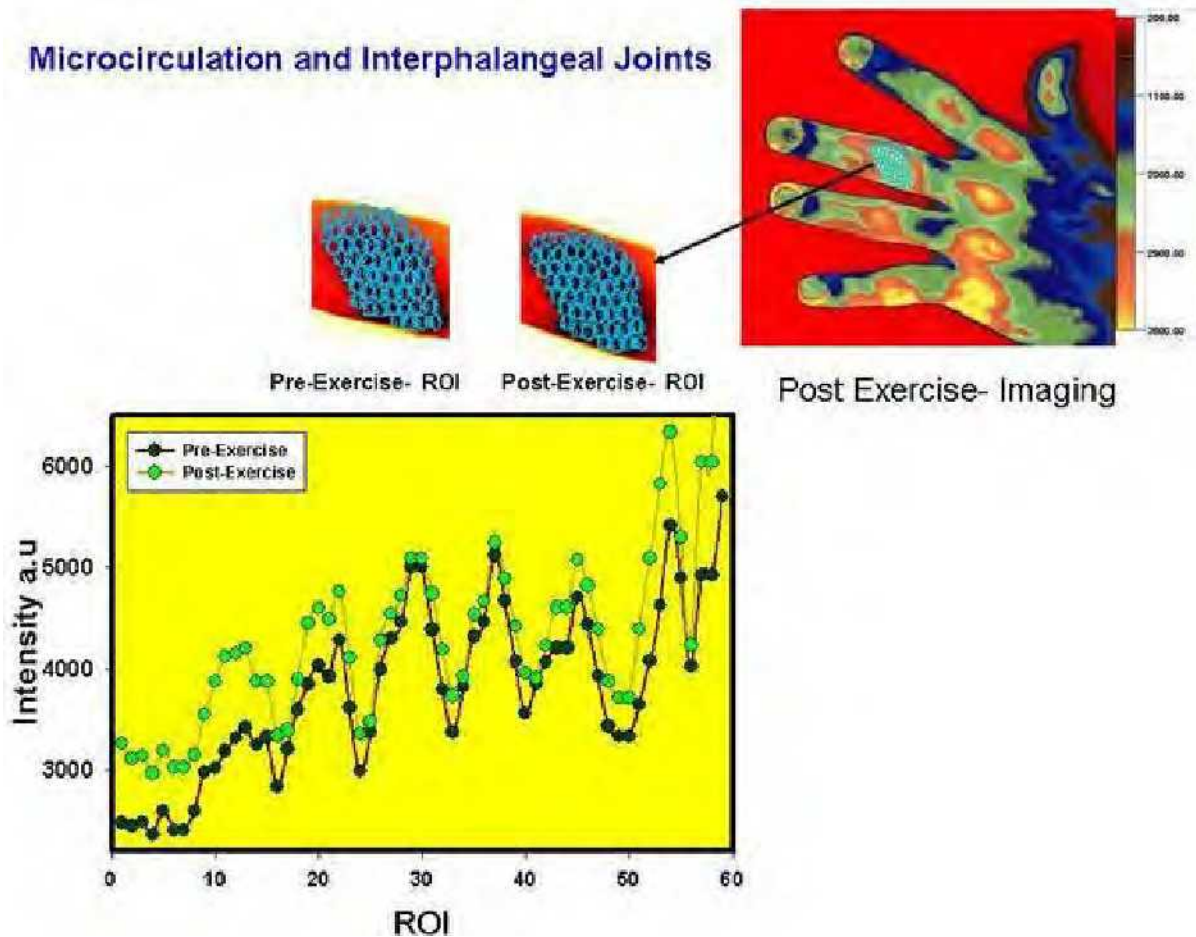
Purpose: To compare F-18 FDG PET/CT (PET) with magnetic resonance imaging (MR) in predicting tumor response to chemoradiation therapy (CRT) in patients with rectal cancer **Methods:** Twenty-five patients with rectal cancer underwent PET and MR before and after CRT. The maxSUV (at restaging), SR (SUV reduction rate=(stagingSUV-restagingSUV)/stagingSUV) and deltaSUV (differences of SUV between staging and restaging) were calculated on PET, and MVR (MR volume reduction ratio), deltaMvol (differences of MR volume between staging and restaging) on MR. Responders (n=16) and non-responders (n=9) were determined by pathologic tumor regression degree (TRG). Threshold of each parameters was analyzed using ROC curve to detect non-responders. **Results:** Only SR (rho=0.48, p=0.0183) and maxSUV (rho=-0.55, p=0.0068) showed significant relationship with TRG. Between responder and non-responder groups, all three PET parameters showed significant differences (maxSUV: p=0.0445, SR: p=0.0149, deltaSUV: p=0.0315). Two MR volume parameters didn't show significant differences between two groups. In detecting non-responders, all PET parameters showed better results than MR parameters: SR (AUC: 0.799, p=0.073), deltaSUV (AUC: 0.764, p=0.045), maxSUV (AUC: 0.747, p=0.047) vs MVR (AUC: 0.493), DeltaMvol (AUC: 0.562). Threshold for non-responders were SR<=0.45 (sen 66.7, spe 87.5), maxSUV >5.5 (sen 55.6, spe:93.8), deltaSUV <=5.1 (sen: 77.8, spe: 81.3). **Conclusion:** PET parameters are superior to MR volume parameters in determining tumor response after preoperative CRT in rectal cancer.

Presentation Number **0181**
 Scientific Session 23: Clinical Studies (Co-organized with RSNA)

Optical Imaging of Human Interphalangeal Joints and Microcirculation

Rao V. Papineni, William McLaughlin, Douglas Vizard, Sean P. Orton, Carestream Molecular Imaging, Carestream Health, Inc., Woodbridge, CT, USA. Contact e-mail: rao.papineni1@carestreamhealth.com

Rheumatoid arthritis (RA) is the most chronic inflammatory joint disease with an incidence rate of approximately 1% in most populations around the world. Sensitive and specific methods for noninvasive detection of early stages of synovitis in RA and other inflammatory joint diseases are becoming essential, and may well assist in the delaying the onset of the destructive changes to the affected joints of RA. An optical clinical imaging set up capable of imaging the metacarpophalangeal joints and microcirculation using autofluorescence, or fluorescent molecular probes, is described here. In this work, noninvasive autofluorescence imaging of the perfusion at the interphalangeal joints was performed on healthy human volunteers. Significant changes in the microcirculation were observed when challenged with a 10 min simple hand exercise routine (Figure below). Perfusion patterns in conditioned athletes, non athletes, along with age related differences observed signifies the sensitivity of the system. These results also present the opportunity in early detection of the inflammatory activity associated with the interphalangeal joints in RA. Further, provides a potential role in microvascular dynamic analysis, testing endothelial function in clinical studies.



Presentation Number **0182**
Scientific Session 23: Clinical Studies (Co-organized with RSNA)

Regional Distribution of High and Low-affinity States of Dopamine D2/3 Receptor Binding in Humans: A PET Study Using [¹¹C]MNPA and [¹¹C]raclopride

Fumitoshi Kodaka, Hiroshi Ito, Harumasa Takano, Hidehiko Takahashi, Ryosuke Arakawa, Saori Fujie, Takeshi Sasaki, Tetsuya Suhara, Molecular Imaging Center, National Institute of Radiological Sciences, Chiba, Japan. Contact e-mail: kodaka@nirs.go.jp

Dopaminergic neurotransmission is of major interest in the pathophysiology of schizophrenia. Early in vitro studies indicated that dopamine D2/3 receptor has two interconvertible states, that is, high-affinity state (D2/3H) and low-affinity state (D2/3L). D2/3H reflects a functional state of endogenous dopamine. The sum of bindings of both D2/3H and D2/3L in these regions can be measured by the use of dopamine D2/3 antagonist radioligands such as [¹¹C]raclopride. D2/3H binding can be measured with dopamine D2/3 agonist radioligands such as [¹¹C]MNPA. However, little is known about the regional differences in distribution between D2/3H and D2/3L bindings. In the present study, we measured D2/3H binding and the sum of bindings of D2/3H and D2/3L using [¹¹C]MNPA and [¹¹C]raclopride in same human subjects. The respective regional bindings of [¹¹C]MNPA and [¹¹C]raclopride were compared. Thirty-three male volunteers participated in the study (20-39 years). Both PET studies with [¹¹C]MNPA and [¹¹C]raclopride were performed for each of the subjects. Binding potential (BPND) values were calculated by the reference tissue model method on a voxel-by-voxel basis using the cerebellum as reference brain region. Volumes of interest (VOIs) were defined for the putamen, caudate head, globus pallidus (GP), nucleus accumbens (NAcc), ventral tegmental area (VTA), substantia nigra (SN), and thalamus and its subregions including the anterior nuclei (AN), dorsomedial nucleus (DN), and pulvinar (PUL). To evaluate the regional differences of BPND among different radioligands, percentage of BPND values of the putamen was calculated. Significant positive correlations of BPND between [¹¹C]raclopride and [¹¹C]MNPA were observed in all VOIs ($r=0.83$, $P=0.00$). The percentage of putaminal BPND was $38.8 \pm 0.1\%$ for [¹¹C]MNPA and $14.9 \pm 0.0\%$ for [¹¹C]raclopride in the thalamus. The percentages of putaminal BPND with [¹¹C]MNPA in the thalamus and its subregions (AN, DN, PUL), VTA, and SN were significantly higher than those with [¹¹C]raclopride. Meanwhile, there were no significant differences in the caudate nuclei ($71.2 \pm 0.2\%$ for [¹¹C]MNPA and $75.3 \pm 0.1\%$ for [¹¹C]raclopride) and NAcc. Higher D2/3H bindings in the GP, thalamus, its subregions, and VTA than the sum of bindings of D2/3H and D2/3L could indicate a higher proportion of D2/3H to dopamine D2 receptors including D2/3H and D2/3L compared with other brain regions such as the caudate nuclei and NAcc. This might indicate that there exist regional differences in the proportion of D2/3H in the dopaminergic neural system.

Presentation Number **0183**
Scientific Session 24: Ultrasound

Real-time Approach to Selective Molecular Imaging, Local Drug Delivery and Interventional Guidance of Catheters in Large Blood Vessels

Abhay V. Patil¹, Joseph P. Kilroy¹, Bryce T. Lowrey¹, Alexander L. Klibanov², John A. Hossack¹, ¹Biomedical Engineering, University of Virginia, Charlottesville, VA, USA; ²Cardiovascular Medicine, University of Virginia, Charlottesville, VA, USA. Contact e-mail: avp2b@virginia.edu

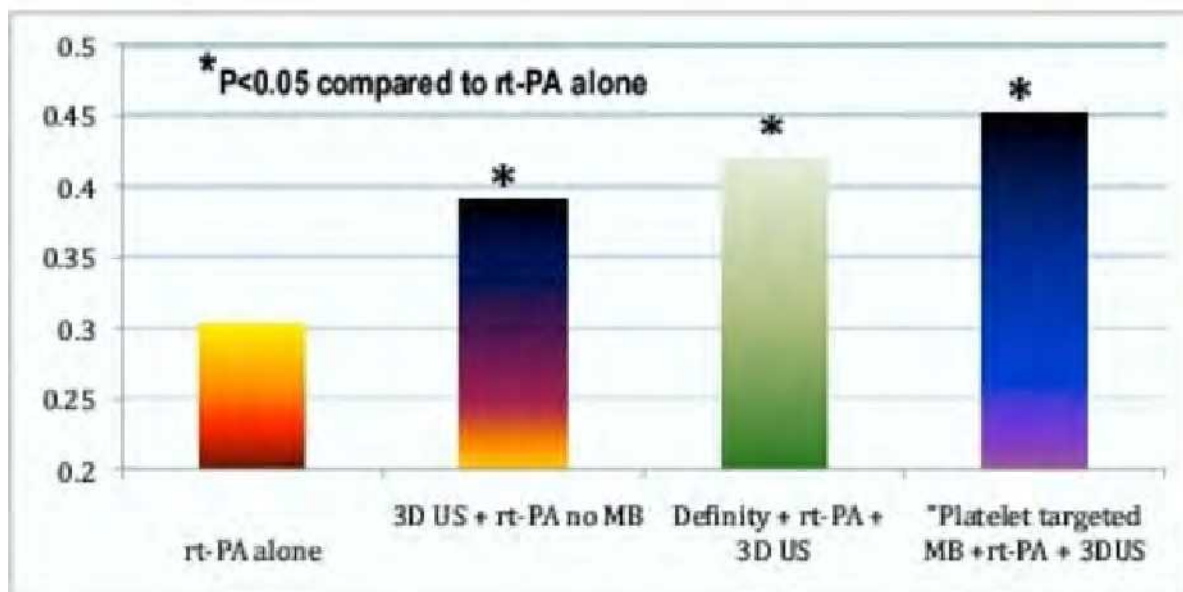
Atherosclerosis of arterial vessels is a leading cause of death in the developed world. A sensitive molecular imaging technique that can identify the early markers of atherosclerosis may assist clinicians in determining the presence or extent of the disease and may also play a critical role in real-time guidance of local drug delivery. In this work, we present a resonance stimulation pulse inversion (RSPI) technique that performs real-time selective molecular imaging, mediates local drug delivery and provides interventional guidance to intravascular ultrasound (IVUS) catheters. The RSPI method uses a dual frequency excitation approach for simultaneously guiding and imaging microbubbles, followed by destruction pulses for mediating targeted drug delivery. The method is implemented on an Ultrasonix RP programmable scanner. The RSPI sequence (5 MHz, 20 cycle pushing pulse, 8 MHz single cycle pulse inversion pulses) was applied to a wall-less flow phantom to assess the effect of varying blood hematocrit on translational motion and adhesion of microbubbles to the distal arterial vessel wall. For constant acoustic, flow and microbubble parameters, it was found that the stationary (or adherent) microbubble signal in 40 % hematocrit blood decreased by 15 dB when compared with normal saline. In vitro Opticell experiments conducted on rat brain endothelial cells confirmed local Dil (dye) delivery in the insonated region without any destruction of the endothelial cells. RSPI sequence was applied to ex vivo swine carotid arteries of 2 and 5 mm (10 cm/s flow velocity, 20 million bubbles/ml) cross-sectional diameter. The adhered microbubbles were destroyed using high mechanical index (MI) pulses (20 cycle, 5 MHz, PRF= 42 kHz, MI= 1) at the end of the RSPI sequence. A high degree of correspondence was found between the ultrasound images of the arterial wall and the fluorescent images of the excised arterial cross-sections confirming local Dil delivery. Finally, in vitro wall-less phantom experiments were conducted to assess the performance of an IVUS drug delivery catheter. Similar modified IVUS catheters may play a vital role in enhancing drug delivery in coronary arteries where mediating drug delivery using transcutaneous ultrasound may prove challenging.

Presentation Number **0184**
 Scientific Session 24: Ultrasound

In Vitro Studies of Sonothrombolysis Using Targeted Microbubbles

Evan C. Unger¹, Terry O. Matsunaga¹, Feng Xie², John Lof², Jennifer L. Johnson³, Steve Morehead³, Arthur Kerschen³, Thomas Porter², ¹University of Arizona, Tucson, AZ, USA; ²Cardiology, University of Nebraska Medical Center, Tucson, NE, USA; ³NuvOx Pharma, Tucson, AZ, USA. Contact e-mail: evanunger@comcast.net

The purpose of this research is to determine if targeted microbubbles (MB) are more effective than non-targeted MB for sonothrombolysis. Targeted MB were prepared to bind activated GPIIb/IIIa in platelets and fibrin. Bioconjugates were prepared from an anchor lipid, a PEG spacer, a cyclized RGD analog and fibrin-binding peptide. Bioconjugates were isolated by HPLC and characterized by Mass Spec. Lipids comprising DPPC, DPPA and DPPE-PEG-2000 (with bioconjugates for targeted MB) were suspended in aqueous solution in vials. The headspace of the vials was replaced with fluorocarbon gas; vials were shaken for 45 seconds on a modified dental amalgamator at 4,500 cps. Resulting MB were sized by quasi-elastic light scattering. Clots were prepared from whole pig blood and aged for 6 hours prior to testing. They were placed in 10% fresh pig plasma in a closed flow system; flow rate was 20 mL/min. In studies with non-targeted MB and platelet targeted MB, the drug, rt-PA (330 ug), was also injected into the flow through system. MB was diluted to 0.5% concentration were infused at 1.0 mL/min during ten minutes treatment time. A 10 centimeter thick tissue mimicking phantom was placed between the ultrasound probe and the acoustically transparent tube containing the thrombus and ultrasound was applied for 10 minutes using a 3D ultrasound system (Philips Medical Systems). Clots were weighed pre and post treatment. Ultrasound significantly increased the degree of clot weight loss compared to t-PA alone. Platelet-targeted MB appeared to be more effective than fibrin-targeted MB, which in turn appeared to be more effective than non-targeted MB. Additional work is currently in progress to test an additional fibrin-binding bioconjugate and MB containing both anti-GPIIb/IIIa and anti-fibrin bioconjugates. GPIIb/IIIa-targeted MB appear to be more effective than non-targeted MB at decreasing clot weight in sonothrombolysis. These findings need to be confirmed in in vivo studies.

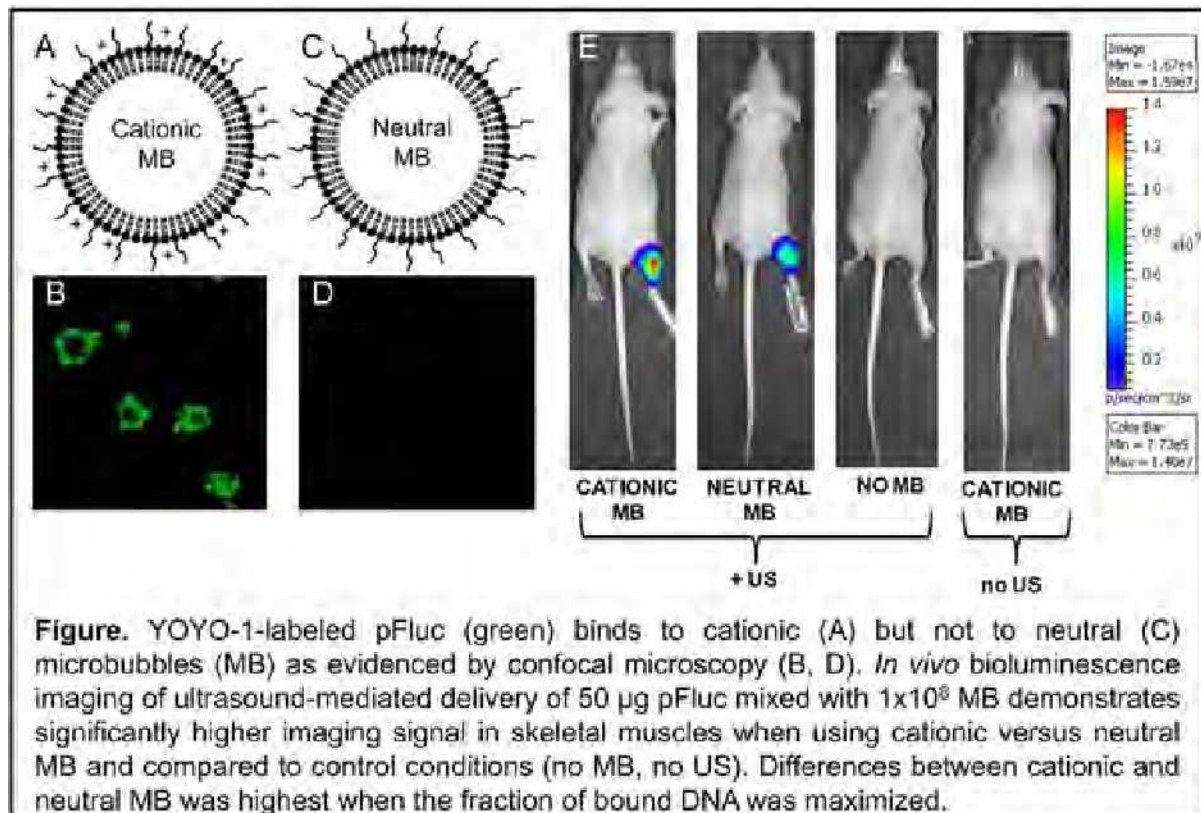


Presentation Number **0185**
 Scientific Session 24: Ultrasound

In Vivo Ultrasound-mediated Gene Delivery with Cationic and Neutral Microbubbles: Effect of Varying Microbubble and DNA Doses

Cedric Panje¹, Marybeth A. Pysz¹, David S. Wang¹, Ying Ren¹, Michel Schneider², Juergen K. Willmann¹, ¹MIPS, Radiology, Stanford University, Stanford, CA, USA; ²Bracco Research, Geneva, Switzerland. Contact e-mail: mpysz@stanford.edu

Ultrasound (US) mediated sonoporation using contrast microbubbles (MB) is a promising strategy for therapeutic gene delivery. The purpose was to assess the influence of different MB and DNA doses on in vivo gene delivery to skeletal muscles in mice using novel cationic and neutral MB. Cationic and neutral MB were characterized for their charge and amount of bound plasmid DNA encoding Firefly luciferase (pFluc). Protective effects of cationic MB in binding DNA were tested by incubating pFluc-MB mixtures with DNase and assessing the extent of degraded DNA. US-mediated gene delivery of 4 μ g pFluc to endothelial cells with 5E7 cationic or neutral MB was performed and quantified using the luciferase assay kit. US-mediated in vivo gene delivery to hindlimb skeletal muscle was performed with varying cationic and neutral MB (1E7, 5E7, 1E8, or 5E8 with 50 μ g pFluc) or pFluc doses (10, 17.5, 25, 37.5, or 50 μ g with 1E8 MB), which were injected intravenously in 48 mice. Bioluminescence imaging was performed every 24h post-transfection (total 168 h) to compare each dose and to compare to negative control conditions (no MB or no US). pFluc binding of cationic (zeta potential=28.4 mV) MB was significantly ($P<0.01$) higher and more protective to DNase degradation than neutral MB. Fluc activity using cationic MB was significantly higher both in cell culture ($P<0.01$) and in vivo ($P<0.006$) experiments and was significantly lower in negative controls ($P<0.002$; Figure). The magnitude of in vivo gene delivery using cationic compared to neutral MB increased linearly ($R^2=0.9$) with the amount of bound pFluc ($P<0.05$). Cationic MBs bound with 10 μ g pFluc (30% bound fraction) resulted in 3.4-fold higher gene delivery compared to neutral MB. In contrast, cationic MB mixed with 50 μ g pFluc (6% bound fraction) resulted in only 1.3-fold higher gene delivery compared to neutral MB. US-mediated gene delivery is more efficient with cationic compared with neutral MBs when the fraction of bound DNA is maximized. Optimizing the doses of MB and DNA are important requisites to translate MB as a promising theranostic strategy for both imaging and efficient US-mediated delivery of therapeutic genes in the clinic.

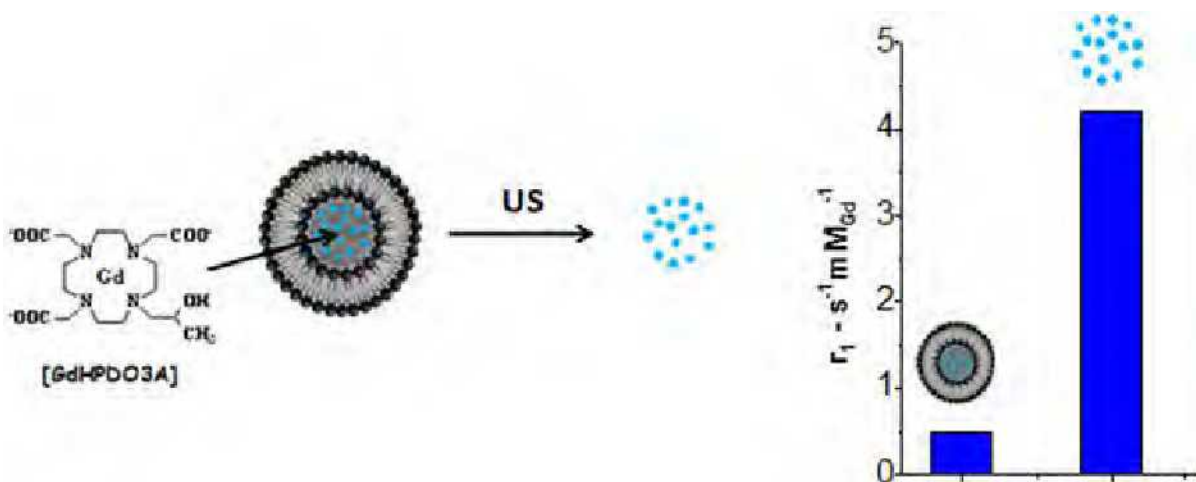


Presentation Number **0186**
 Scientific Session 24: Ultrasound

Ultrasounds Triggered Release from Paramagnetic Liposomes for the Development of MRI-guided Drug Delivery Protocols

Enzo Terreno, Daniela Delli Castelli, Pierangela Giustetto, Cinzia Boffa, Silvio Aime, Molecular Imaging Center, University of Torino, Torino, Italy. Contact e-mail: enzo.terreno@unito.it

The non invasive in vivo visualization of drug release triggered by externally applied ultrasounds (US) is an emerging topic in molecular imaging field. Most of the reported studies were performed using nano- or micro-bubbles in which the presence of the gas-filled core makes cavitation (and US detection) possible. However, the use of imaging modalities with an improved spatial resolution and wider diagnostic/therapeutic potential like MRI would be very useful. Liposomes, nanovesicles endowed with an aqueous core, are extensively used as drug delivery nanocarriers and are also under intense scrutiny in the field of MRI contrast agents where they represent one of the most promising nanoplatform for designing highly-sensitive probes. The most straightforward approach to design liposomal MRI probes whose image contrast can report about the US-induced cavitation of the nanocarrier is the encapsulation of a large amount (100-200 mM) of a clinically approved Gd(III) agent in the vesicle. The ability of the encapsulated agent to generate a good T1 contrast is strongly limited by the water permeability of the vesicle membrane. Upon the probe release, the T1 "quenching" is removed and a contrast enhancement can be observed. In this contribution, we demonstrate that low frequency US (20 kHz) can induce a probe release much more efficiently than using high frequency waves (3 MHz). The evaluation of the probe release, monitored in vitro at 0.5 T on a fixed frequency relaxometer, was performed at different US frequencies, power, application times, liposome size and chemical composition of the membrane, thus allowing the development of a model to predict the efficiency of the release mechanism. The in vitro work was followed by an ex vivo and in vivo (on a xenografted B16 melanoma mouse model) MRI study that successfully demonstrated the potential of this approach to visualize the probe release following a local US application.



Presentation Number **0187**
 Scientific Session 24: Ultrasound

In Vivo SPECT/CT Imaging of Focused Ultrasound Induced Extravasation

Holger Gruell^{1,2}, **Pedro Sanches**², **Raffaella Rossin**¹, **Marcel Bohmer**¹, **Klaus Tiemann**³, ¹Biomolecular Engineering, Philips Research, Eindhoven, Netherlands; ²Cardiology, University Hospital Münster, Münster, Germany; ³Biomedical NMR, Eindhoven University of Technology, Eindhoven, Netherlands. Contact e-mail: holger.gruell@philips.com

Focused ultrasound (FU) induced drug delivery has potential to solve the delivery dilemma of macromolecular drugs such as siRNA or pDNA, by promoting drug extravasation across endothelial layers and potentially uptake in cells. The bursting of microbubbles upon FU exposure leads to transient openings in the vascular endothelium and pores in cell membranes facilitating the extravasation of drugs otherwise confined to the vascular system. So far, little quantitative information is available to correlate ultrasound settings, bubble characteristics and treatment schemes with the induced effects in vivo. We have developed a method to image and quantify the extent and duration of this effect in vivo by using a radiolabeled model drug, ¹¹¹In-DTPA-BSA, employing dynamic SPECT/CT measurements. Swiss mice were intravenously injected with polymer microbubbles and treated with FU in the hind limb muscle. Shortly after, the animals were transferred to the SPECT/CT and injected with ¹¹¹In-DTPA-BSA (ca. 30µg, 30MBq), (fig. 1 (b)). Dynamic acquisitions up to 60min post-injection showed increased drug extravasation and quantitative data from SPECT (7 %ID/cm³ treated; 0.4% ID/cm³ control muscle, fig. 1 (a,c)) was calculated and confirmed by biodistribution. Tissue damage is assessed in pathology. Above approach can be used to mediate drug extravasation into the interstitial space and potentially also cellular uptake. These findings have important implications to therapies based on siRNA and pDNA. References: 1. Ferrara, KW, Adv Drug Delivery Rev 2008, 60 (10). This research is part of FP7 European Project Sonodrugs (ref. 213706).

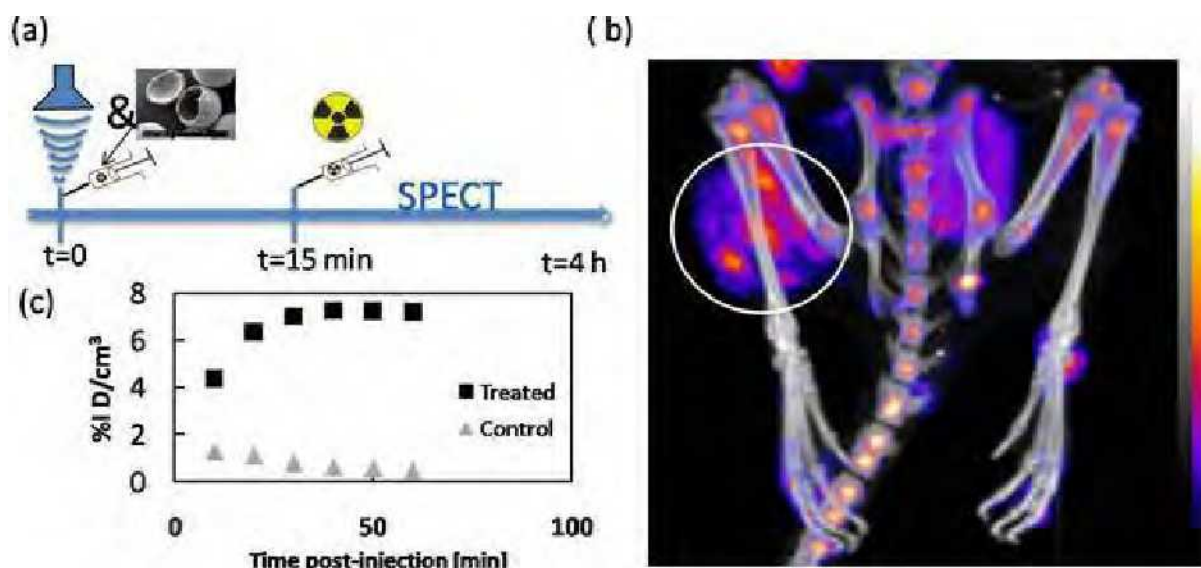


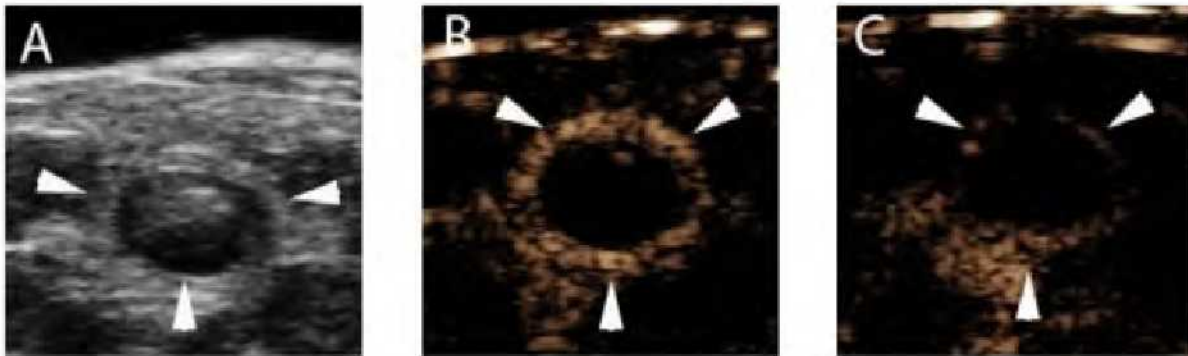
Figure 1: (a) treatment scheme of the experiment, (b) SPECT image of the treated hind limb muscle (white circle shows treatment zone), (c) extravasated amount in treated muscle area quantified with SPECT

Presentation Number **0188**
Scientific Session 24: Ultrasound

Quantification of Inflammation in Inflammatory Bowel Disease by Molecular Ultrasound Imaging

Nirupama Deshpande¹, Ying Ren¹, Kira Foygel¹, Michel Schneider², Pankaj J. Pasricha³, Juergen K. Willmann¹, ¹Molecular Imaging Program/Radiology, Stanford university, Stanford, CA, USA; ²Bracco Research SA, Geneva, Switzerland; ³Division of Gastroenterology and Hepatology, Stanford Medical Center, Stanford, CA, USA. Contact e-mail: niru@stanford.edu

The goal of our study was to assess the potential of molecular ultrasound (US) imaging using microbubbles (MB) targeted to the inflammation marker P-selectin (MB-Pselectin) to quantify inflammation and to predict remission of inflammation following treatment in a chemically-induced colitis mouse model. Binding affinity and specificity of MB-Pselectin was tested in a flow chamber under flow shear stress conditions (at 100 sec⁻¹). In vivo binding specificity of MB-Pselectin to P-selectin was tested in 10 mice with colitis (induced by rectal administration of TNBS) and in 10 control mice without colitis using non-linear in vivo US imaging (25 MHz). Furthermore, in vivo molecular US imaging signal in treated (n=6; prednisolone therapy) versus non-treated (n=6; saline only) mice was compared over 3 subsequent treatment days. Attachment of MB-Pselectin was significantly ($p=0.01$) higher to P-selectin positive (stimulated by TNF-alpha) than unstimulated endothelial cells and compared to MB-Control ($p=0.003$). Attachment of MB-Pselectin correlated ($R^2 >0.8$, $p=0.01$) with expression levels of P-selectin on endothelial cells as quantified by flow cytometry. In vivo US signal of colitis was significantly higher ($p=0.0003$) with MB-Pselectin compared with MB-Control (Figure), and dropped by 53% ($p=0.01$) following injection of blocking antibodies. In treated animals, in vivo US imaging signal ($p=0.03$) decreased during the course of treatment while in non-treated mice US signal in the colon wall remained elevated. In vivo US imaging signal correlated ($R^2 >0.6$; $p=0.04$) with P-selectin expression levels as assessed by ex vivo assays (WB and IF). In conclusion, molecular US using MB-Pselectin allows non-invasive in vivo quantification and monitoring of inflammation at the molecular level in a chemically-induced colitis mouse model. This study lays the foundation for an eventual future clinical translation of molecular US imaging for monitoring inflammation in IBD.



(A) Transverse B-mode image of the colon wall (white arrows) in a mouse with TNBS-induced colitis using a high-resolution US scanner. Molecular ultrasound imaging signal in colon wall (arrows) following injection of MB-Pselectin (B) was significantly higher compared to control conditions following injection of MB-Control (C), suggesting binding specificity of MB-Pselectin to P-selectin in inflamed colon wall.

Presentation Number **0189**
Scientific Session 25: Gene Expression and Reporters

Histone Deacetylase Inhibitor Inducible Reporter Gene Expression for Drugs Screening and Suicide Gene Therapy

Yi-Chieh Chen¹, Luen Hwu¹, Kuan-Hung Lin¹, Hsin-Ell Wang¹, Ren-Shyan Liu^{1,2}, ¹MAGIC/NRPGM, Nuclear Medicine, Faculty of Medicine, National Yang-Ming University, Taipei, Taiwan; ²NPCC, Taipei Veterans General Hospital, Taipei, Taiwan. Contact e-mail: zambia3@hotmail.com

Objectives: The dietary histone deacetylase inhibitor (HDACI) has been shown to alter the status of histone acetylation and activate the silenced gene expressions. The expression of p21 gene could be mostly induced by HDACI to cause cell cycle arrest and inhibit cancer cell proliferation. This study aimed to use the established HDACI screening platform by indirectly examination of the p21 gene up-regulation with dietary HDACI treatment. **Methods:** Trichostatin A (TSA) was applied into the NSCLC H1299 cells that stably expressed the p21promoter-driven triple fusion reporter (luciferase, DsRed monomer and truncated HSV-1 thymidine kinase SR39 mutant gene). The reporter's activities were determined by confocal laser scanning microscopy, luciferase assay and ³H-FEAU uptake. In addition, the p21 gene induction effects by TSA were also assessed by optical imaging system and micro-PET with ¹⁸F-FEAU in vivo. The MTT assays were performed to evaluate the effect of combinational therapy by treatment with TSA and GCV prodrug. Furthermore, the dietary HDACI, curcumin and sulforaphane, were also applied into this established drug screening platform to examine their p21 induction effects. **Results:** The stably expressed p21-driven reporter H1299 cells with TSA treatment have shown that remarkable up-activation of p21 gene expression both in vitro and in vivo. The MTT assays showed more significant therapeutic effect by co-treatment with TSA and GCV prodrug at lower concentration than individual/singular treatment. The dietary HDACI, curcumin and sulforaphane, were also up-regulated the p21-driven reporter gene expression in this sensitive, quantitative high-throughput HDACI drug testing platform. **Conclusions:** The stably expressed p21-driven triple fusion reporter cells are TSA inducible. These clones could be used for new HDACI drugs screening and other chemotherapy drugs that activate p21. Furthermore, this p21-driven triple fusion reporter construct might be useful for suicide gene therapy of cancer by combined TSA and gangcyclovir (GCV) prodrug treatment.

Presentation Number **0190**
Scientific Session 25: Gene Expression and Reporters

A Novel NesTK:IFP1.4 Fusion Reporter Gene for Imaging of Temporal Dynamics and Spatial Heterogeneity of MDR1 Transcriptional Activation Mediating Tumor Microenvironment in Living Mice

Yu-jung Lin¹, **Yi-Jang Lee**², **Chia-Hung Hsieh**¹, ¹*Graduate Institute of Basic Medical Science, China Medical University, Taichung, Taiwan;* ²*Department of Biomedical Imaging and Radiological Sciences, National Yang-Ming University, Taipei, Taiwan. Contact e-mail: chiahung2004@msn.com*

Abstract P-glycoprotein (Pgp), coded for by the MDR1 gene, is one of the ABC transporters held responsible for the phenomenon of multidrug resistance (MDR), which is reflected by a rapidly escalating failure of chemotherapy with different classes of cytotoxic agents. However, the lack of technologies for quantitative noninvasive imaging of the dynamics and spatial heterogeneity of the transcriptional activation of MDR1 in experimental tumor models in vivo is a significant impediment for investigating its relationship to tumor microenvironment and drug response. The purpose of this study was to create a novel dual reporter gene, herpes simplex virus type 1 thymidine kinase/ infrared fluorescent protein (NesTK:IFP1.4) for monitoring temporal dynamics and spatial heterogeneity of MDR1 transcriptional activation and investigate tumor microenvironment on its transcriptional activation in living U87 glioma-bearing mice. In this study, the NesTK:IFP1.4 was created by the addition of a nuclear export signal (NES) in the N-terminal end of HSV1-TK and fusing the Infrared fluorescent protein (IFP1.4) to the C-terminal end. The reporter function of NesTK:IFP1.4 in living 293 TF cells was determined by HSV1-TK enzyme activity assay and flow cytometry analysis, respectively. To determine the impact of tumor microenvironment on MDR1 transcriptional activation, U87 glioma cells were stably transfected with a lentiviral vector bearing a 2028 bp MDR1 promoter driven NesTK:IFP1.4 reporter gene that allowed for dynamic monitoring of the transcriptional activation of MDR1 in vitro and in vivo. Our result indicated that NesTK:IFP1.4 could be able to act a novel transcription reporter for monitoring MDR1 transcriptional activation in vitro and in vivo using optical imaging and nuclear imaging system. In vitro and in vivo studies demonstrated that cycling hypoxia could induce and prolong higher transcriptional activation of MDR1 than could chronic hypoxia. HIF-1 blockade in vitro and in vivo inhibited cycling hypoxia-mediated MDR1 transcriptional activation. These results have potentially important clinical implications and suggest that cycling hypoxia plays a virtual role in the tumor microenvironment-mediated MDR1 induction and HIF-1 blockade before drug administration and concurrent with chemotherapy may be an effective approach by which to suppress cycling hypoxia-induced MDR1 induction and further improve the treatment efficacy of chemotherapy.

Presentation Number **0191**
Scientific Session 25: Gene Expression and Reporters

PET Visualization of Na/I Symporter Gene Expression after Delivery by Nanobubbles and Ultrasound

Yukiko Watanabe¹, Sachiko Horie¹, Yoshihito Funaki², Youhei Kikuchi³, Hiromichi Yamazaki², Keizo Ishii^{3,2}, Shiro Mori⁴, Georges Vassaux⁵, Tetsuya Kodama¹, ¹Graduate School of Biomedical Engineering, Tohoku University, Sendai, Japan; ²Cyclotron and Radioisotope Center, Tohoku University, Sendai, Japan; ³Graduate School of Engineering, Tohoku University, Sendai, Japan; ⁴Maxillofacial Surgery, Tohoku University Hospital, Sendai, Japan; ⁵Institut des Maladies de l'Appareil Digestif, CHU Hôtel Dieu, Nantes, Nantes, France. Contact e-mail: yukiko-watanabe@bme.tohoku.ac.jp

In gene therapy, reporter gene is important to detect gene expression. Na/I symporter (NIS), one of the membrane glycoprotein, has an iodine uptake function. The NIS gene has been proposed as a valid reporter gene for positron emission tomography (PET) imaging using ¹²⁴I. The development of non-viral gene delivery systems is essential in gene therapy, and the utilization of minimally-invasive imaging methodology can provide important clinical endpoints. In the present study, we present a new methodology for gene therapy: a delivery system by using nanobubbles (NB) and ultrasound (US) as a non-viral gene delivery method (sonoporation). Here, we evaluated whether NIS gene expression mediated by US and NB could be detected by the practical semiconductor animal PET with a CdTe detector (Fine Structure Imaging PET: Fine-PET) in mice by using ¹²⁴I as radiotracer. Two kinds of reported vectors [Luciferase and human NIS (hNIS)] were transfected or cotransfected into the tibialis anterior (TA) muscles of normal mice (BALB/c) by sonoporation. The kinetics of luciferase gene expression was analyzed by using in vivo bioluminescence imaging system. At the peak of gene transfer, PET imaging of hNIS expression was performed by using the Fine-PET, following by injection of ¹²⁴I. The imaging data were confirmed using RT-PCR amplification, biodistribution, and blocking study. The imaging potential of the two methodologies was evaluated in two mice models of human pathology (McH/lpr-RA1 mice showing vascular disease, and C57BL/10-mdx Jic mice showing muscular dystrophy). Peak luciferase gene activity was observed in the TA muscle 4 days after transfection. Two days after hNIS and luciferase cotransfection, the expression of these genes was confirmed by RT-PCR on a muscle biopsy. PET imaging of the hNIS gene, biodistribution, the blocking study, and autoradiography were carried out on day 4 after transfection, and it was indicated that hNIS expression was restricted to the transfection site (TA muscle). Similar localized PET imaging and ¹²⁴I accumulation were successfully obtained in the disease-model mice. The hNIS gene was delivered into the TA muscle of the normal and disease model mice using sonoporation, and gene expression was successfully visualized with the Fine-PET. The combination of sonoporation gene transfer and PET imaging may be applied to clinical protocols of gene therapy.

Presentation Number **0192**
Scientific Session 25: Gene Expression and Reporters

Delivery of a Bioluminescent Transgene to a Tumor via Bone Marrow Engraftment and Local Control of Gene Expression by Non-invasive Local Hyperthermia

Pierre-Yves Fortin, Matthieu Lepetit-Coiffe, Coralie Genevois, Christelle Debeissat, Bruno Quesson, Chrit Moonen, Franck Couillaud, CNRS, UMR 5231, Laboratory for Molecular and Functional Imaging (IMF), Bordeaux, France. Contact e-mail: py.fortin@imf.u-bordeaux2.fr

Introduction: The success of a gene therapy strategy depends on several parameters including the right choice of therapeutic gene, an efficient delivery method and a reliable control of gene expression. In the present study, we investigate an in vivo strategy to deliver a transgene around a tumor and to control transgene expression. This strategy includes bone marrow engraftment of genetically engineered cells to create a chimera with nucleated circulating blood cells (CBCs) expressing the firefly luciferase (lucF) under the transcriptional control of a thermosensitive promoter. Later on, a subcutaneous tumor is induced. Finally, lucF expression detected by bioluminescence imaging (BLI) is induced "on demand" by local hyperthermia using MR guided high-intensity focused ultrasound (MRgHIFU). Methods: Bone marrow cells (BMCs) were obtained from homozygote C57/BL6 (CD45.2) transgenic mice containing the lucF transgene under Hsp70. BMCs were transplanted into a congenic mouse (CD45.1) pre-treated with Busilvex®, (2 IP injections, 25 mg/Kg) to induce medullar aplasia. The level of engraftment was measured 2 months later by measuring CD45.1/CD45.2 ratio using Fluorescence Activated Cell Sorting (FACS). Carcinoma Mouse Tumor 93 (CMT-93) cells were implanted subcutaneously to generate a tumor on the left leg. Tumors were heated (44°C, 8 min) for local gene activation using either a water bath or MRgHIFU. LucF expression was evaluated in vivo 6 hours post heating by BLI. Results: After 2 months, about 80% of engrafted mice exhibited more than 65% of donor CBCs. CMT-93 cells formed tumors ranging from 5 and 10 mm in one month. Tumors heated (44°C, 8 min) by dipping the tumor-bearing leg into a water bath, in mice exhibiting more than 65% of engraftment, induced lucF activation and transient light emission 6 hours later. Light emission was found in and around the tumor, for about 50% of the mice. A week later light-emitting mice did not produce light anymore. They were heated again (44°C, 8 min) but using the MRgHIFU device. Six hours later, light emission was found around tumors (n = 15). Light emission was also detected to head region of bone both on ipsi (n = 15) and contralateral legs (n = 6). Conclusions: The bioluminescent chimera mice express the lucF reporter in hematopoietic cells. This model allows for studying gene delivery to tumor using circulating blood cells. Local gene expression was induced "on demand" by local hyperthermia. Acknowledgement: This work was supported in part by Diagnostic Molecular Imaging and the Conseil Régional d'Aquitaine.

Presentation Number **0193**
 Scientific Session 25: Gene Expression and Reporters

A Novel Paradigm to Markedly Enhance the Specificity of Gene Expression in Hepatocellular Carcinoma Using MicroRNAs

John A. Ronald^{1,2}, Regina H. Katzenberg^{1,3}, Carsten H. Nielsen^{1,4}, Hwan Jun Jae^{1,3}, Lawrence V. Hofmann^{1,3}, Sanjiv S. Gambhir^{1,2},
¹Molecular Imaging Program at Stanford, Stanford University, Stanford, CA, USA; ²Radiology, Stanford University, Stanford, CA, USA;
³Interventional Radiology, Stanford University, Stanford, CA, USA; ⁴Cluster for Molecular Imaging & Department of Clinical Physiology, Nuclear Medicine and PET, Rigshospitalet, University of Copenhagen, Copenhagen, Denmark. Contact e-mail: jronald1@stanford.edu

In cancer gene therapy potent, tumor-specific expression is of utmost importance to improve outcome and ensure safety. Tumor-specific promoters may be used but often promote weak tumor and “leaky” non-tumor expression. Hence, novel strategies for specific, yet robust, expression are needed. MicroRNAs (miRNAs) are short, endogenous RNAs that inhibit translation by binding to complementary sequences (miRTs) in target mRNAs. Here we explore the ability to achieve the coveted tumor-on/liver-off expression profile in a rat hepatocellular carcinoma (HCC) model by engineering potent vectors regulated by miRNAs. The levels of 11 miRNAs downregulated in human HCC were compared in both rat HCC (n=5) and liver (n=8) by qRT-PCR. 7 miRNAs were reduced (p<0.05; range 3 to 16-fold) in rat HCC including, miR-26a, miR-101a, miR-122, miR-125a-5p, miR-125b, miR-139-5p and miR-150. The robustness of miRNA repression in vitro and in vivo was explored by constructing 3 vectors all expressing firefly luciferase (Fluc2) driven by the strong CMV promoter (pcDNA3.1) either with no miRTs (pCMV-Fluc2), or 4 tandem sense or 4 anti-sense miRTs (miRT and anti-miRT, respectively) for the liver-specific miR-122 inserted in the 3' untranslated region. HUH-7 (miR-122 +ve) cells were transfected and Fluc2 activity 24 hours later was decreased ~80% (p<0.05) for the miRT versus the 2 control vectors. Each vector was then hydrodynamically injected via the tail-vein of Balb/c mice (n=3 per group) to assess the degree of repression in liver. Importantly, average radiance (p/sec/cm²/sr) in bioluminescent images taken 48 hours post-injection was markedly reduced (~100-fold; p<0.05) with the miRT (4.7e6 ± 5.2e5) versus the control vectors (pCMV-Fluc2=4.1e8 ± 1.0e8; anti-miRT=3.2e8 ± 1.8e8) (Figure). Based on these exciting results current work focuses on generating additional vectors regulated by one or more miRNAs and expressing a reporter gene fused to a therapeutic gene for testing in tumor-bearing rats. This is the first work to explore the use of miRNAs to control transgene expression in HCC and should have broad applicability for other cancers and imaging across cell lineages.

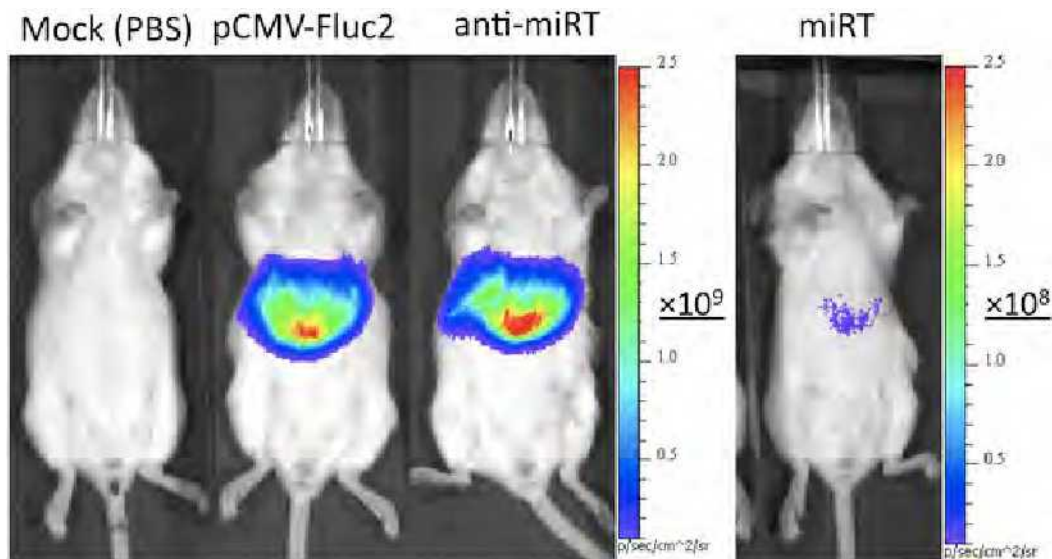


Figure: *In vivo* miRNA-regulated gene expression. Inclusion of miRTs for the liver-specific miR-122 into expression vector significantly reduces (by approximately two log-orders) Fluc2 liver activity following hydrodynamic delivery in mice.

Presentation Number **0194**
 Scientific Session 25: Gene Expression and Reporters

Noninvasive Assessment of Lymph Node Metastasis of Melanoma Using Molecular MR Reporter Gene of Ferritin

Hye Rim Cho¹, Seung Hong Choi¹, Hoe Suk Kim¹, Woo Kyung Moon¹, Hyeonjin Kim², ¹Departement of Radiology, Seoul National University Hospital, Seoul, Republic of Korea; ²Lee Gil Ya Cancer and Diabetes Institute, Gacheon Univeristy of Medicine and science, Seoul, Republic of Korea. Contact e-mail: hyerimcho1030@gmail.com

We aim to develop genetically-based technique for molecular imaging of the MRI gene reporter ferritin to enable noninvasive assessment of lymph node metastasis of cancer cells after transplantation into subcutaneous area of mice. Materials and Methods Lentiviral vector was used to simultaneously generate MRI and fluorescent imaging via expression of both human ferritin H-subunit (hFTH) and enhanced green fluorescent protein (GFP). The transgene construct was stably transfected into B16F10 cell. Expression of ferritin and GFP was monitored by Western blot analysis using monoclonal mouse hFTH-antibody. B16F10 cells were incubated with 100 mM and 200 mM ferric citrate in DMEM for 5 days. We measures the transverse relaxation rate (T2*) of the cell pellet of 1 x 10⁷ using a 1.5 T MR scanner. For the in vivo MRI we injected 1 x 10⁶ B16F10 cells expressing hFTH/GFP into the dorsal subcutaneous area of Balb/c nuce mice (n = 6) to induce metastasis in the lymph node. In addition, normal B16F10 cells of 1 x 10⁶ were also inoculated in the mice (n = 6). We also measured the transverse relaxation rate (T2*) of the main mass, and the brachial and axillary lymph nodes using a 9.4 T MR scanner. After MR imaging, in vivo and ex vivo fluorescent imaging of the main tumor and lymph nodes was obtained using optical imaging analyzer. To confirm lymph node metastasis of B16F10 cells and transgene expression, immunohistochemistry (IHC) and hematoxylin/eosin staining were performed. Results and Discussion The expression of GFP and hFTH was confirmed by Western blot analysis. B16F10 cells expressing hFTH/GFP showed significantly lower T2* relaxation rate than control cells . Main tumor with hFTH/GFP also showed significantly lower T2* relaxation rate than control, and the metastatic cells with hFTH/GFP revealed significantly lower T2* relaxation rate than control. However, the only main tumor with hFTH/GFP was demonstrated on in vivo optical imaging, and ex vivo optical imaging could demonstrate the lymph node metastasis with hFTH/GFP. Our study shows that hFTH/GFP transgene is a feasible modality for the investigation of cancer cell fate.

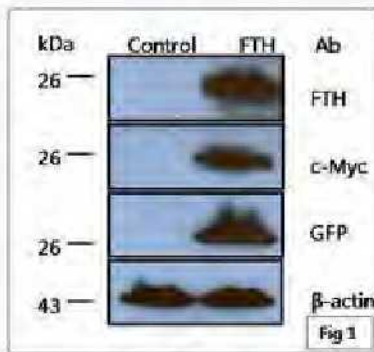


Fig 1. Western blot analysis with mouse monoclonal antibodies indicates the expression of FTH, c-Myc, and GFP. C-Myc is conjugated with FTH.

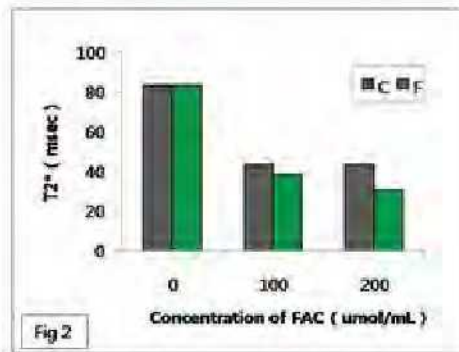


Fig 2. B16F10 cells expressing hFTH/GFP showed significantly lower T2* relaxation rate than control cells.

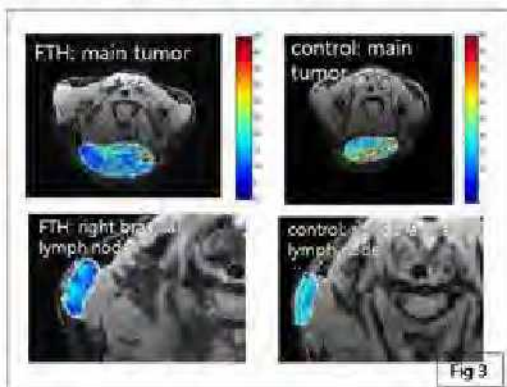


Fig 3



Fig 4

Fig 3. Main tumor with hFTH/GFP also showed significantly lower T2* relaxation rate than control, and the metastatic cells with hFTH/GFP in the right brachial lymph node revealed significantly lower T2* relaxation rate than control. Fig 4. The only main tumor with hFTH/GFP was demonstrated on in vivo optical imaging, and ex vivo optical imaging could demonstrate the lymph node metastasis with hFTH/GFP.

Presentation Number **0195**
Plenary Session 6: Gene Imaging

Imaging of Signal Transduction at High Throughput: From Single Molecules to Living Organisms

Herman P. Spaink¹, **Marcel J. Schaaf**¹, **Thomas Schmidt**², **Michel Orrit**², **Annemarie H. Meijer**¹, ¹*Cell Biology, Leiden University, Leiden, Netherlands;* ²*Biophysics, Leiden University, Leiden, Netherlands.* Contact e-mail: h.p.spaink@biology.leidenuniv.nl

Various technological advances will be presented that enable imaging molecular signal transduction processes in living organisms at high throughput. At the molecular level we have made use of highly sensitive fluorescence spectroscopy techniques to visualize single molecules at the nanometer and millisecond scale. We have also performed high throughput imaging of molecular interactions using thermo-optical detection of gold particles, which is highly sensitive and not subject to bleaching. At the organism level we make use of the zebrafish embryo system, which is a highly versatile imaging model for following signal transduction in vivo. Zebrafish embryos are small and transparent and through genetic engineering technology fusion proteins labeled with different fluorescent labels can be expressed. Using total internal reflection microscopy is even possible to follow the dynamics of single molecule behavior in membranes of an intact living embryo. By means of this technology a better understanding of the biological function of membrane sub-domains in many developmental and disease processes is within reach. Finally, it is shown that by using a robotic injection system in combination with our high throughput imaging technology we can perform biomedical screening assays leading to the discovery of new medicines for diseases such as tuberculosis.

Presentation Number **0196**
Scientific Session 26: SPECIAL SESSION: Close to Clinical Probes

Intracellular Coalescence of Nanoscale Perfluorocarbon Droplets for Enhanced Size-dependent Ultrasound Conversion

Amanda L. Martin¹, Farnaz Niroui¹, Ross Williams¹, Grace Belayneh¹, Ivan Gorelikov¹, Peter N. Burns^{1,2}, F. Stuart Foster^{1,2}, Naomi Matsuura^{1,2}, ¹Imaging Research, Sunnybrook Health Sciences Centre, Toronto, ON, Canada; ²University of Toronto, Toronto, ON, Canada. Contact e-mail: matsuura@sri.utoronto.ca

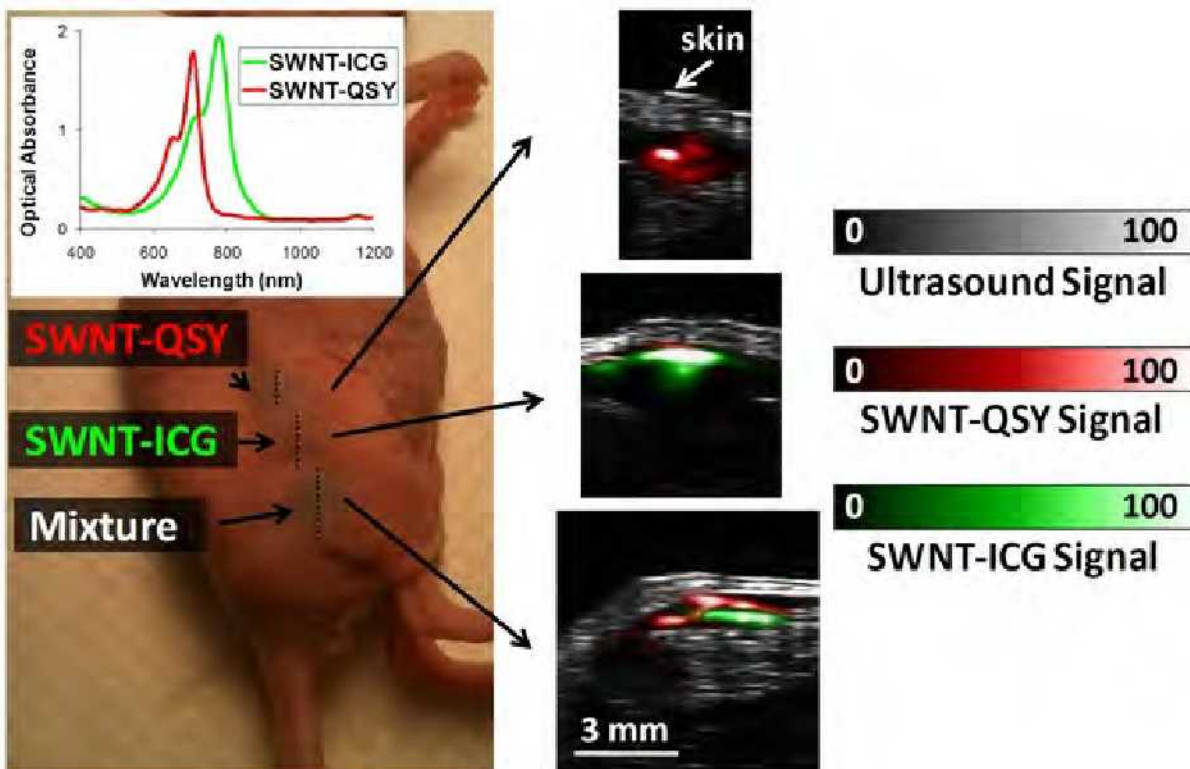
Introduction. Liquid perfluorocarbon (PFC) droplets can be vaporized to form highly echogenic microbubbles *in situ* following ultrasound (US) exposure for imaging or therapy. Due to their small size and *in vivo* stability, nanoscale PFC droplets (100-300 nm) can accumulate in diseased tissues with characteristic leaky vasculature prior to their conversion to bubbles. However, the energy required to convert PFC droplets is size-dependent, and nanoscale PFC droplets require significantly greater pressures for conversion compared to micron-scale droplets. Here, we investigate if nanoscale PFC droplets can be designed to coalesce into larger droplets within cells to lower their US conversion threshold to clinically relevant pressures. **Methods.** Nanoscale (100-300 nm) and micron-scale (1-3 μm) PFC (perfluoropentane and perfluorohexane) droplets were monitored for uptake and coalescence in macrophage cells as a function of incubation time, surface charge and initial size. The integration of fluorescent quantum dot nanoparticles within the droplets allowed for the optical assessment of single droplet interactions with cells. US experiments to measure droplet conversion at low frequency were performed at 1 MHz with passive detection at 500 kHz; and at high frequency were performed using high-power US bursts with low-power pulse-echo detection at 18 MHz. **Results.** *In vitro* experiments demonstrated that the cavitation and vaporization pressure thresholds in cells can be controlled by incubation time, droplet composition and size. The time-dependent uptake and coalescence of droplets was found to be strongly dependent on their surface charge, with 50% less uptake of non-ionic PFC droplets compared to anionic droplets after 2 hours. Uptake for anionic PFC agents occurred after as little as 5-15 minutes incubation. Over time (up to 4 hours), coalescence of the droplets in cells (from ~ 200 nm up to >2 μm , with droplets as large as 7 μm) was observed. After exposure to US pulses at both 1 and 18MHz, cells containing larger droplets were destroyed due to PFC droplet conversion, while cells containing only smaller ($<2\mu\text{m}$) droplets remained intact. **Conclusions.** Initial *in vitro* experiments demonstrate that nanoscale PFC droplets coalesce within macrophage cells to form easily US-convertible, micron-scale droplets. The concept of intracellular droplet coalescence merits further investigation to determine if similar effects can be observed in cancer cells and at high concentrations within diseased tissue *in vivo*.

Presentation Number **0197**
 Scientific Session 26: SPECIAL SESSION: Close to Clinical Probes

Family of enhanced photoacoustic imaging agents for high sensitivity and multiplexing studies in living mice

Adam de la Zerda^{1,2}, Sunil Bodapati², Robert Teed², Scott Tabakman⁴, Zhuang Liu^{5,4}, Butrus Khuri-Yakub¹, Xiaoyuan Chen^{6,2}, Hongjie Dai⁴, Sanjiv S. Gambhir^{2,3}, ¹Electrical Engineering, Stanford University, Stanford, CA, USA; ²Radiology Department and the Molecular Imaging Program at Stanford, Stanford University, Stanford, CA, USA; ³Bioengineering, Stanford University, Stanford, CA, USA; ⁴Chemistry, Stanford University, Stanford, CA, USA; ⁵Functional Nano & Soft Materials, Soochow University, Jiangsu, China; ⁶Laboratory for Molecular Imaging and Nanomedicine, National Institute of Biomedical Imaging and Bioengineering, NIH, Bethesda, MD, USA. Contact e-mail: adlz@stanford.edu

Photoacoustic molecular imaging of living subjects offers high spatial resolution at increased tissue depths compared to optical imaging. We have recently shown that intravenously injected single walled carbon nanotubes (SWNTs) can be used as targeted photoacoustic imaging agents in living mice. We have synthesized two new photoacoustic imaging agents based on SWNT conjugated to either QSY₂₁ (SWNT-QSY) or to Indocyanine Green (SWNT-ICG) through strong pi-pi stacking interactions with the nanotubes. The particles were conjugated to cyclic Arg-Gly-Asp (RGD) peptides to molecularly target the $\alpha_v\beta_3$ integrins, which are associated with tumor angiogenesis. Control particles were conjugated to the RAD peptide (which does not bind to $\alpha_v\beta_3$). We verified both particles are stable in serum and can target $\alpha_v\beta_3$ integrin through cell uptake studies with U87 cells. We found the photoacoustic signal to be highly linear to the particles' concentration both in phantom studies ($R^2 = 0.99$, $R^2 = 0.98$) as well as in living mice injected subcutaneously with the particles ($R^2 = 0.96$, $R^2 = 0.97$ for SWNT-QSY and SWNT-ICG respectively). We measured the detection sensitivity of SWNT-QSY and SWNT-ICG in living mice ($n = 3$) to be 450 pM and 170 pM respectively, which represents 110-fold and 300-fold improvement compared to plain SWNTs respectively ($p < 0.05$). U87 tumor-bearing mice were injected via the tail-vein with RGD-targeted SWNT-QSY or SWNT-ICG. At 2 hours post-injection, mice injected with the RGD-targeted particles showed significantly higher photoacoustic signal in the tumor compared to mice injected with the control RAD-labeled particles ($p < 0.05$ for both particles, $n = 4$ per group). While overlapping, the optical absorption spectra of SWNT-QSY and SWNT-ICG are different, which allowed us to spectrally separate their photoacoustic signals both in a phantom as well as in living mice (see Figure). This is the first demonstration of true multiplexing of photoacoustic imaging agents that were also shown to target tumors in living mice.



SWNT-QSY (red) and SWNT-ICG (green) were multiplexed in subcutaneous injections in living mice with our photoacoustic instrument, despite their overlapping spectra.

Presentation Number **0198**
 Scientific Session 26: SPECIAL SESSION: Close to Clinical Probes

Multi-compound Hyperpolarized ¹³C Spectroscopy

David M. Wilson¹, Kayvan R. Keshari¹, Peder E. Larson¹, Albert P. Chen³, Simon Hu¹, Mark Van Criekinge¹, Robert Bok¹, Sarah Nelson¹, Jeffrey Macdonald², Daniel B. Vigneron¹, John Kurhanewicz¹, ¹Department of Radiology and Biomedical Imaging, University of California, San Francisco, San Francisco, CA, USA; ²Department of Biomedical Engineering, University of North Carolina, Chapel Hill, Chapel Hill, NC, USA; ³GE Healthcare, Menlo Park, CA, USA. Contact e-mail: dmeybin@gmail.com

INTRODUCTION: Hyperpolarized ¹³C MR spectroscopy has emerged as a powerful new imaging modality, with a rapidly expanding arsenal of endogenous ¹³C probes including pyruvate, bicarbonate, and fumarate [1-3]. The ability to probe multiple pathways simultaneously may provide valuable metabolic signatures associated with specific types of diseased tissue. As a proof of concept, four ¹³C substrates were copolarized, namely [1-¹³C] pyruvate, ¹³C bicarbonate, [1,4-¹³C] fumarate, and ¹³C urea, potentially providing information on glycolysis, pH, necrosis and perfusion in a single imaging experiment. **METHODS:** ¹³C agents (Isotec, Miamisburg, OH) were polarized on the Hypersense (Oxford Instruments) as published previously [4]. T1 and %pol were quantified on a 11.7T Varian INOVA spectrometer. ¹³C spectroscopic imaging was performed in a Transgenic Adenocarcinoma of Mouse Prostate (TRAMP) model at 3T [5]. **RESULTS:** Calculated T1's and %pol in the multi-metabolite case were similar to those recorded for ¹³C probes polarized individually (Table 1). Resolution of all four metabolites in vivo was demonstrated at high SNR (Figure 1). **DISCUSSION:** Multi-metabolite polarization is intended to circumvent one of the main drawbacks of DNP, namely its long polarization times, by polarizing several precursors at the same time, and then developing a biological scenario whereby the inevitably very complex metabolic data in vivo can be analyzed. This approach will be increasingly useful as ¹³C probes continue to proliferate. **REFERENCES:** [1] Golman K et al. Cancer Res 2003; 100(18): 10435-10439. [2] Gallagher F et al. Nature 2008; 453(7197): 940-943. [3] Gallagher F et al. PNAS 2009; 106(47): 19801-19806. [4] Ardenkjaer-Larsen J et al. PNAS 2003; 100(18): 10158-10163. [5] Cunningham C et al. J Magn Reson 2007; 187(2): 357-362.

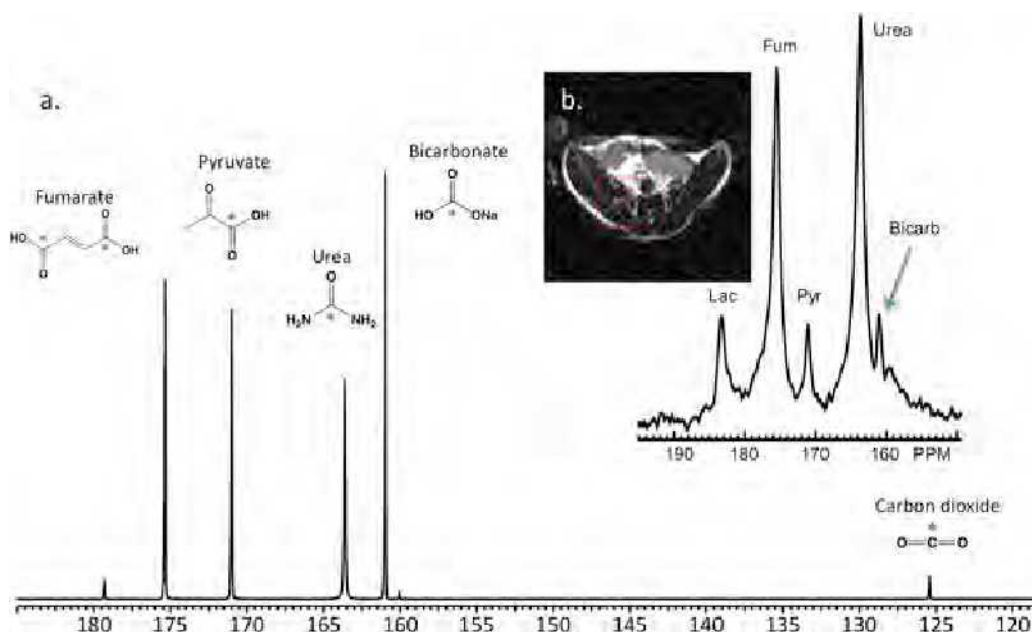


Figure 1. (a) Multi-compound polarization of fumarate, pyruvate, urea, and bicarbonate in vitro (b) Multi-compound polarization in vivo performed in a TRAMP mouse model at 3T.

Compound	T1 (s) multipol	T1 (s) alone	%pol multipol	%pol alone
¹³ C bicarbonate	43.3±1.2	45.7±0.6	10.3±1.3	12.7±1.9
[1- ¹³ C] pyruvate	48.3±1.5	48.3±0.6	17.5±1.4	17.4±1.5
[1,1- ¹³ C] fumarate	29.0±1.0	29.3±0.6	15.6±1.9	12.0±0.7
[1- ¹³ C] urea	43.0±1.0	44.0±0.3	11.6±2.5	12.4±0.4

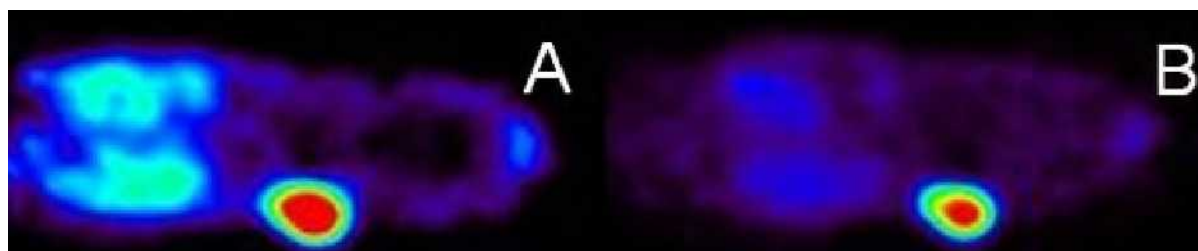
Table 1. T1 values, and % polarization achieved at 11.7T.

Presentation Number **0199**
 Scientific Session 26: SPECIAL SESSION: Close to Clinical Probes

⁶⁸Ga and ⁶⁴Cu -RGD-based PET Tracers for Imaging $\alpha_v\beta_3$ Expression: A Comparative Study

Rebecca A. Dumont¹, Helmut R. Maecke¹, Roland Haubner², Wolfgang A. Weber¹, Melpomeni Fani¹, ¹Nuclear Medicine, University of Freiburg, Freiburg, Germany; ²Nuclear Medicine, Medical University of Innsbruck, Innsbruck, Austria. Contact e-mail: rdumont@ucla.edu

Introduction: PET imaging with ¹⁸F-labeled RGD peptides can quantify $\alpha_v\beta_3$ integrin expression in patients, but radiolabeling is complex and image contrast can be limited in some tumor types. Development of a ⁶⁸Ga-RGD tracer would be of great utility given the convenience of ⁶⁸Ga production and radiolabeling. Labeling with ⁶⁴Cu allows for delayed imaging with potentially improved tumor-to-background ratios. We developed [⁶⁸Ga] and [⁶⁴Cu]NODAGA-c(RGDfK) and [⁶⁴Cu]CB-TE2A-c(RGDfK) for comparison with the previously described [⁶⁸Ga]DOTA-c(RGDfK). Methods: DOTA-, NODAGA- and CB-TE2A-c(RGDfK) were synthesised using modified protocols from the literature. Labeling was performed in acetate buffer at pH 4 for ⁶⁸Ga and pH 8 for ⁶⁴Cu. NODAGA-c(RGDfK) was labeled at room temperature with both radionuclides, while incubation at 95°C was used for the other two compounds. Small animal PET studies and tissue sampling were performed in mice bearing subcutaneous U87MG glioblastomas at 1h (⁶⁸Ga&⁶⁴Cu) and 18h (⁶⁴Cu) post-injection (0.5-0.6nmol/4-5MBq/mouse, 3 mice/group). Blocking studies were done with an excess of cold peptide. Results: The conjugates were labeled with radiochemical purity >97% and specific activities of 10MBq/nmol and 7MBq/nmol for ⁶⁸Ga and ⁶⁴Cu, respectively. While biodistribution in normal organs and tumor uptake did not significantly differ among ⁶⁸Ga and ⁶⁴Cu labeled compounds at 1h, all tumor:background ratios were several-fold improved at 18h for the ⁶⁴Cu-labeled conjugates compared to all conjugates at 1h. Additionally, [⁶⁸Ga]NODAGA-c(RGDfK) showed improved tumor:blood and tumor:kidney ratios compared to [⁶⁸Ga]DOTA-c(RGDfK) at 1h. Specificity of the tracers was demonstrated by successful blocking of tumor uptake with excess of cold peptide. PET studies demonstrated high contrast images of the U87MG tumors and quantitatively confirmed the ex-vivo biodistribution data. Conclusions: The studied ⁶⁸Ga and ⁶⁴Cu-RGD conjugates demonstrate similar biodistribution at 1h. However, the markedly improved tumor:background ratios of [⁶⁴Cu]NODAGA-c(RGDfK) and [⁶⁴Cu]CB-TE2A-c(RGDfK) at 18h are encouraging and warrant testing of [⁶⁴Cu] labeled RGD peptides in patients.



1h (A) & 18h (B) microPET images of ⁶⁴Cu-NODAGA-cRGDfK

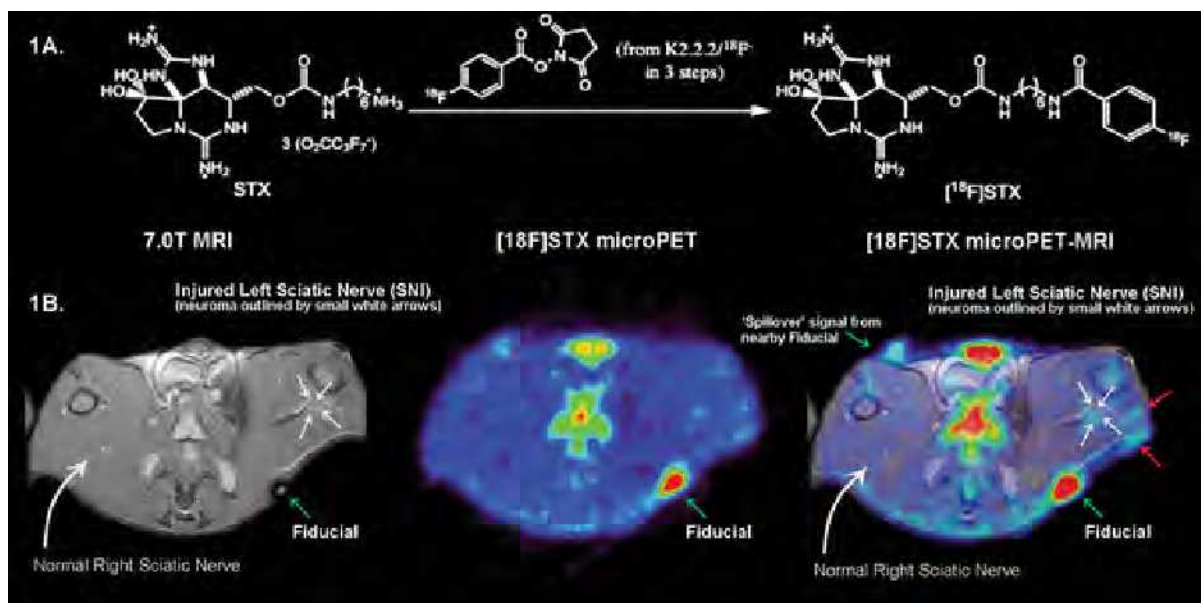
Ratio, 1h and 18h	[⁶⁸ Ga]DOTA-c(RGDfK)	[⁶⁸ Ga]NODAGA-c(RGDfK)	[⁶⁴ Cu]NODAGA-c(RGDfK)	[⁶⁴ Cu]CB-TE2A-c(RGDfK)
tumor:blood	9.24/na	27.67/na	10.15/1067	7.5/127.5
tumor:liver	2.25/na	2.75/na	2.67/164	2.38/0
tumor:kidney	1.57/na	2.64/na	1.72/333	1.1/2.7
tumor:muscle	12.57/na	12.80/na	12.16/3153	11.9/30.6

Presentation Number **0200**
 Scientific Session 26: SPECIAL SESSION: Close to Clinical Probes

[¹⁸F]Saxitoxin PET-MRI: A New PET-based Method for Imaging Pain in Living Subjects

Frederick T. Chin¹, Aileen Hoehne¹, William H. Parsons², Deepak Behera¹, Justin Du Bois², Sandip Biswal¹, ¹Radiology, Stanford University, Stanford, CA, USA; ²Chemistry, Stanford University, Stanford, CA, USA. Contact e-mail: chinff@stanford.edu

Purpose: The sensation of pain is dependent upon voltage-gated sodium channels (NaV), which are essential to generation of action potentials and nerve impulse conduction. NaV isoforms are known to be increased in peripheral sensory neurons in chronic and neuropathic pain. The radiofluorination of saxitoxin (STX), a non-protein neurotoxin that binds NaV channels with high affinity, and evaluation of [¹⁸F]STX in living rats using positron emission tomography-magnetic resonance imaging (microPET-MRI) can potentially be used to identify neuropathic changes in living subjects. **Methods:** N-succinimidyl 4-[¹⁸F]fluorobenzoate ([¹⁸F]SFB) was made via nucleophilic substitution using a commercially-available automated radiochemistry module. The conjugation of [¹⁸F]SFB with STX (synthesized in-house) afforded [¹⁸F]STX (Figure 1A) with a minimum specific radioactivity of 1.3 Ci/μmol (48 GBq/μmol) and radiochemical purity ≥93% in a total synthesis time of about 3.5 h from end of bombardment (n=3). In vivo biodistribution of [¹⁸F]STX was assessed via 60 minute dynamic imaging of neuropathic pain-model rats (Spared Nerve Injury (SNI) of the left sciatic nerve) using small animal PET-MRI (microPET-MRI). Biodistribution studies via radioactivity measurements in organs using a gamma counter was also performed (n=3). **Results:** MicroPET-MRI images and individual organ measurements showed accumulation of [¹⁸F]STX in the kidneys (10.7±8.9% ID/gm). No significant uptake was seen in bone (0.03±0.02% ID/gm). [¹⁸F]STX was observed in the injured left sciatic nerve region at 15 min p.i. (small white arrows; Figure 1B). Adjacent areas around the injured nerve also showed increased uptake (small red arrows). The control intact right sciatic nerve by comparison showed no significant uptake (large white arrow). **Conclusions:** [¹⁸F]STX shows tremendous potential as a specific radioligand for visualizing NaV channels in vivo. Since [¹⁸F]STX is the only reported radioligand targeting NaV channels to date, it is a valuable lead compound for future tracer development to image pain and facilitate future image-guided therapies for humans.

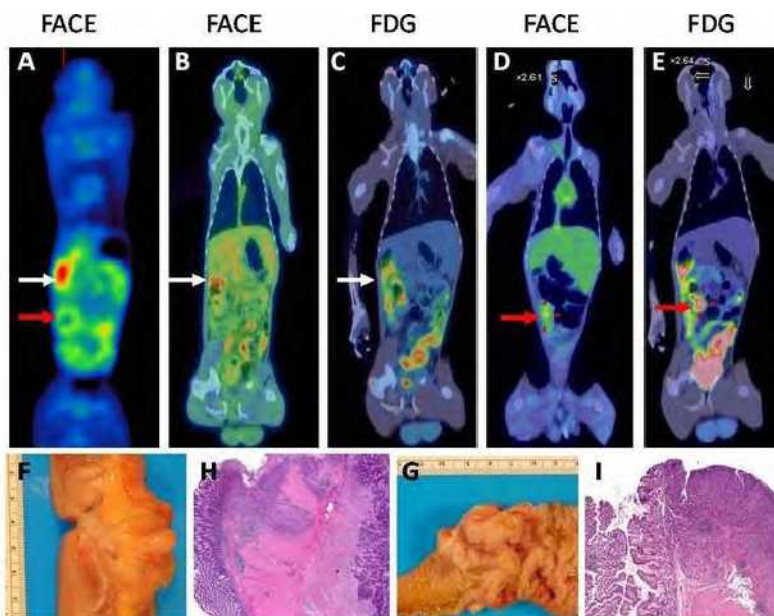


Presentation Number **0201**
 Scientific Session 26: SPECIAL SESSION: Close to Clinical Probes

Multi-tracer PET/CT and Endoscopy for Diagnosis and Characterization of Rhesus Macaques with Hereditary Non-Polyposis Colon Cancer Syndrome due to MLH1 gene mutation.

Mei Tian¹, David Brammer¹, Partick Gillespie¹, Daniel Young¹, Bruce Bernacky², Christian R. Abee², Manoop Bhutani³, Juri G. Gelovani¹, ¹Experimental Diagnostic Imaging, MD Anderson Cancer Center, Houston, TX, USA; ²Center for Comparative Medicine Research, MD Anderson Cancer Center, Houston, TX, USA; ³Gastroenterology, Hepatology and Nutrition, MD Anderson Cancer Center, Houston, TX, USA. Contact e-mail: Mei.Tian@mdanderson.org

Introduction: Colon cancer is one of the most common inherited cancer syndromes known in patients. Among the genes found to be involved in colorectal cancer patients are MLH, MSH2 and MSH6. We initially discovered multiple cases with colonic cancer in rhesus macaques. The aim of this study was to screen animals using MLH1, MSH2, and MSH6 gene sequencing; find the mutant gene in suspected colon cancer-bearing macaques, and evaluate the diagnostic potential of PET/CT imaging with [¹⁸F]Fluoroacetate ([¹⁸F]FACE) and [¹⁸F]-FLT, in comparison with [¹⁸F]FDG. **Methods:** PET/CT imaging studies were performed at 60 min after intravenous injection of 5 mCi of [¹⁸F]FACE, [¹⁸F]FLT, or [¹⁸F]FDG. The regional accumulations of the above radiopharmaceuticals were assessed by using ROI analyses. After PET imaging, tumors and enlarged lymph nodes were removed or biopsied by colonoscopy for histo- and immunohistochemical examinations. To identify germline mutations in MLH1, MSH2 and MSH6, all gene coding regions, exon/intron boundaries and core promoters were screened by polymerase chain reaction-single strand conformation polymorphism (PCR-SSCP) analysis. Pedigree analysis was performed for these rhesus families. **Results:** Tumors ranged from 1-3 cm in size and histopathologically were invasive adenocarcinomas of colon and ileo-cecum. Significantly elevated in the serum were: EGF, endothelin, IL-12p70, IL-7, IL-8, IGF-1 and PAI-1. Increased expression of IL-8, EGF, EGFR, VEGF and VEGFR was observed in tumors. [¹⁸F]FDG exhibited higher accumulation in the inflammatory tumor regions and peritumoral inflammatory colon, which correlated with histopathology and elevated inflammatory biomarkers. In contrast, [¹⁸F]FACE and [¹⁸F]FLT localized only in tumor tissue. Immunohistochemical staining revealed a deficiency in the expression of MHL1 in the colonic tumor. An analysis of the historic cases of colonic cancer from this rhesus monkey breeding colony and the pedigree of the monkeys revealed an inherited MLH1 mutation. **Conclusions:** MLH1 mutation is a dominant gene and essential for the colon cancer monkeys. [¹⁸F]FACE and [¹⁸F]FLT exhibit significantly less uptake in inflammatory regions, as compared to [¹⁸F]FDG. PET/CT with [¹⁸F]FACE could be used for detection and characterization of colon carcinomas. Therefore, colon cancer-bearing macaques represent an ideal animal model for testing the efficacy of molecular imaging agents prior to clinical Phase I trials.



A19-year-old male rhesus monkey with colonic adenocarcinoma. FACE-PET imaging found intensive radiotracer accumulation in the ascending colon and cecum at 24 months before the monkey developed clinical symptom (A). The follow-up PET images demonstrated the lesion in the colon (B, C) and ileocecal junction (D, E). Necropsy after euthanasia revealed the irregular stricture at the ascending colon (F) and cecum (G). Histological section depicted colonic adenocarcinoma, invasive with desmoplastic response, luminal necrosis with fibrinopurulent pseudomembrane containing myriads of bacteria (H) and cecal adenocarcinoma, invasive with desmoplastic response (I). White arrow: ascending colon; Red arrow: ileocecal junction.

Presentation Number **0202**
Scientific Session 27: Optical Imaging Methods

Ex Vivo FLIM-FRET Tomographic Reconstruction in Mouse

Daniel W. Stuckey¹, **James McGinty**², **Vadim Y. Soloviev**³, **Jospeh V. Hajnal**¹, **Simon R. Arridge**³, **Paul French**², **Alessandro Sardini**¹,
¹MRC Clinical Sciences Centre, Imperial College, London, United Kingdom; ²Imperial College Photonics, Imperial College, London, United Kingdom; ³Department of Computer Science, University College, London, United Kingdom. Contact e-mail: daniel.stuckey03@imperial.ac.uk

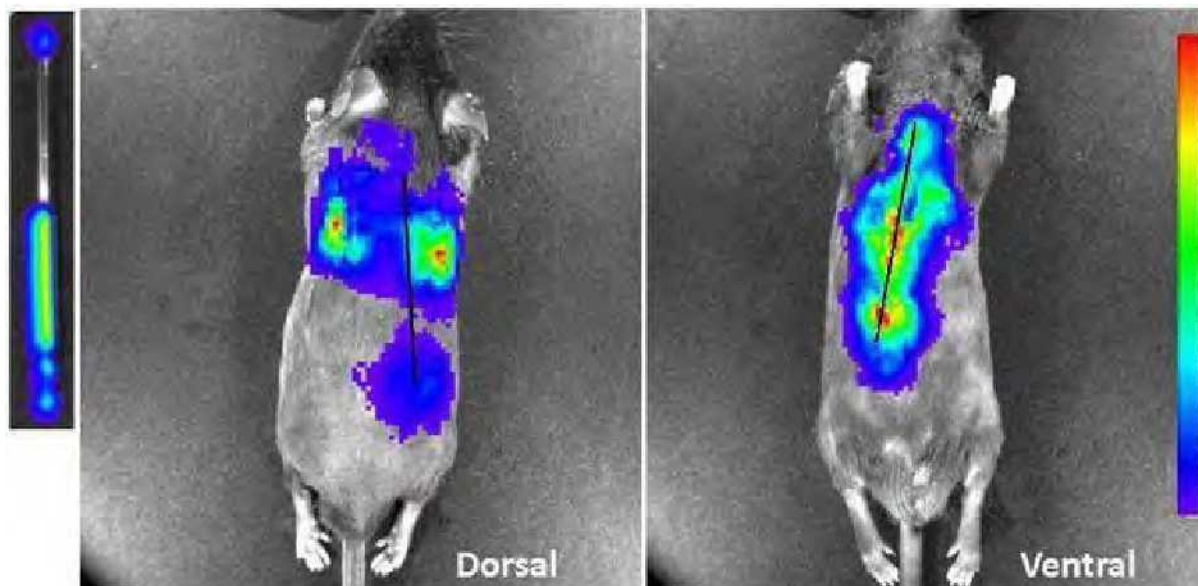
Intro Förster Resonance Energy Transfer (FRET) occurs when a donor fluorophore transfers energy to an acceptor fluorophore in close proximity by non-radiative dipole-dipole coupling. This can be read out via the reduced donor fluorescence lifetime. Applying lifetime measurements (FLIM) to whole animal imaging would allow non-invasive monitoring of molecular interactions *in vivo*. However, the ability to localise and reconstruct a FRET interaction in turbid media is currently limited by the diffusive nature of light transport and its absorption in biological tissue. **Aim** Tomographic reconstruction of FLIM-FRET interaction in highly scattering medium. **Methods** The genetically encoded sensor, TN-L15, comprises the calcium-binding Troponin C (TnC), flanked by CFP and citrine. In the presence of calcium ions, TnC changes conformation and brings the two fluorophores into close proximity, resulting in FRET. Cytosolic fractions from cells expressing TN-L15 were loaded in a highly scattering phantom, or glass capillaries inserted in the thigh of a euthanised mouse. FRET was induced by adding 10 mM CaCl₂ to the cytosol preparations. Samples were imaged tomographically over 360° rotation in transmission. A spectrally-filtered supercontinuum source provided picosecond excitation pulses; the fluorescence emission was detected by a time-gated optical intensifier and read out by CCD camera. The acquired series of wide-field time-gated images were fitted at each rotation angle to a single exponential fluorescence model. A 3D fluorescence lifetime distribution was reconstructed by back projection using the mouse dataset. The 3D distribution of fluorescence lifetime of the phantom dataset was also reconstructed using a more rigorous inverse scattering approach based on the diffusion approximation. This is intended for application to whole mouse imaging *in vivo*. **Results** Reconstructed donor lifetime values in the FRETing and non-FRETing capillaries inserted in the mouse thigh displayed a detectable contrast (2.13 ns and 2.36 ns respectively). The diffusion based reconstruction applied to the same FRET preparation embedded in a highly scattering phantom resulted in a reduction in quantum yield and lifetime value of 2.3 ns compared to 2.7 ns in the non-FRETing well. These values are comparable to those measured in a transparent phantom, validating the reconstruction methodology. **Conclusions** We have demonstrated tomographic FLIM-FRET reconstruction in a highly scattering phantom and *ex vivo*.

Presentation Number **0203**
Scientific Session 27: Optical Imaging Methods

Small Animal Cerenkov Luminescence Imaging

Ruby K. Gill, Gregory S. Mitchell, Changqing Li, **Simon R. Cherry**, Biomedical Engineering, University of California, Davis, Davis, CA, USA. Contact e-mail: srcherry@ucdavis.edu

Cerenkov radiation is a well-known phenomenon, in which optical photons are emitted when a charged particle moves faster than the speed of light in a medium. We propose and demonstrate a method, based on the detection of Cerenkov radiation, to noninvasively image beta-emitting radionuclides inside small animals. This imaging method is referred to as Cerenkov Luminescence Imaging (CLI). At present, there is no sensitive in vivo imaging method for monitoring the biodistribution of β^- emitting radionuclides used for radioimmunotherapy or other therapeutic treatments for cancer. CLI will allow in vivo imaging of the biodistribution of these radionuclides, such as Y-90 (end point energy 2.28 MeV, half life of 2.67 days) with high sensitivity. It can also be used as a low cost alternative to PET imaging for β^+ emitting radionuclides. We have verified that the spectral characteristics of the signal follow an inverse square relationship with wavelength as expected for Cerenkov light using a set of wavelength filters between 400-800 nm and a sensitive CCD camera (Xenogen IVIS 100 system). The optical photon intensity is proportional to the radionuclide activity. We have also successfully detected Cerenkov light from F-18 and Y-90 in small animals using reasonable injected doses of $\sim 200 \mu\text{Ci}$. An ex vivo mouse study using Y-90 where a capillary tube with 274 μCi of Y-90 was inserted down the esophagus is shown in the figure. The number of photons detected in the bare capillary tube was $\sim 7 \times 10^6$ photons/s/cm²/sr. In vivo, 1.9×10^4 and 2.3×10^5 photons/s/cm²/sr was detected from the dorsal and ventral sides, respectively. Based on GEANT4 Monte Carlo calculations for Y-90, we expect to observe ~ 70 visible light photons per decay. Currently, we are characterizing the intensity and optical emission spectra of Cerenkov radiation at different depths using tissue and agar phantoms. By measuring the emitted light from several views of the mouse, it is possible to reconstruct 3D images of the Cerenkov light distribution using analogous techniques to those used for bioluminescence tomography.



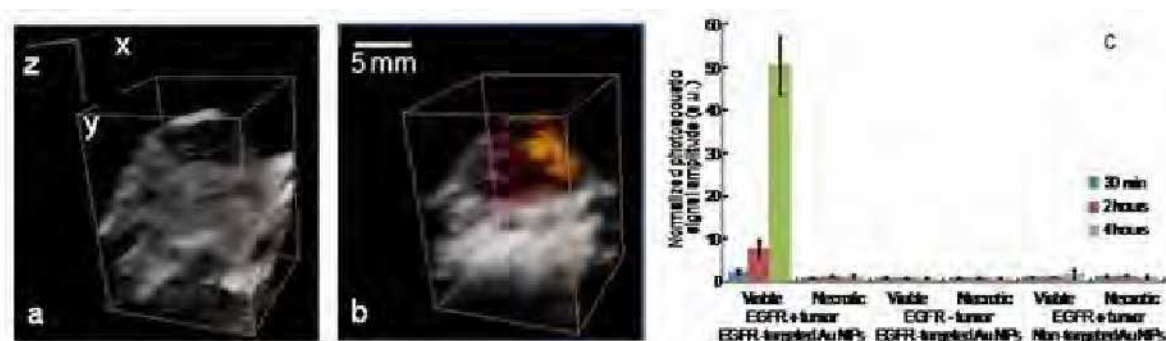
Luminescent dorsal and ventral images of 274 μCi of Y-90 in a capillary tube (left) inserted down a mouse esophagus post-mortem. Black line indicates approximate region of capillary tube.

Presentation Number **0204**
 Scientific Session 27: Optical Imaging Methods

Molecular Imaging of Tumors In Vivo Using Nanoparticle Augmented Ultrasound Guided Photoacoustic Imaging

Srivalleesha Mallidi, Seungsoo Kim, Pratixa P. Joshi, Konstantin Sokolov, **Stanislav Y. Emelianov**, Biomedical Engineering, University of Texas at Austin, Austin, TX, USA. Contact e-mail: emelian@mail.utexas.edu

An in-vivo imaging technique that can sense and monitor molecular events during various stages of tumor progression is required. When spherical gold nanoparticles (AuNPs) are functionalized to target cancer biomarkers such as epidermal growth factor receptor (EGFR), they undergo molecular specific aggregation at the site of active cancerous cells. This receptor mediated clustering of AuNPs leads to an optical red-shift of the plasmon resonance frequency. Capitalizing on this effect we present a 3D ultrasound (US) and molecular specific photoacoustic (PA) imaging technique to simultaneously obtain the anatomical and molecular map of tumor in-vivo. Subcutaneous tumor implantation of cells that overexpress EGFR (A431 cells) or cells that have low expression of EGFR (MDA-MB-435 cells) were performed in immunodeficient mice. Intravenous injection of EGFR targeted or PEGylated AuNPs was performed after the tumor reached ~8-10 mm in diameter. 3D ultrasound and multi-wavelength PA imaging of the tumor region was performed at various time points to observe the accumulation of AuNPs in the tumor. Intraclass correlation analysis was performed on multi-wavelength PA images to demarcate blood vessels and regions of AuNPs accumulation. H&E stain and silver stain were performed on the tumor tissue to validate the presence of AuNPs in viable region of tumor tissue. The combined US and PA images of A431 tumor obtained before and after the injection of AuNPs clearly showed heterogeneous contrast enhancement in the tumor region. Quantitative analysis of the PA signal amplitude in the viable and necrotic regions of the A431 tumor showed approximately five-fold increase in signal at 720 nm due to plasmon resonance coupling of the AuNPs with viable cells. In control mice, there was minimal variation in PA signal. In conclusion, multiplex labeling of AuNPs and PA imaging can help in understanding the complete molecular signature of cancers, thus aiding in developing, designing and implementing tumor specific therapeutic procedures.



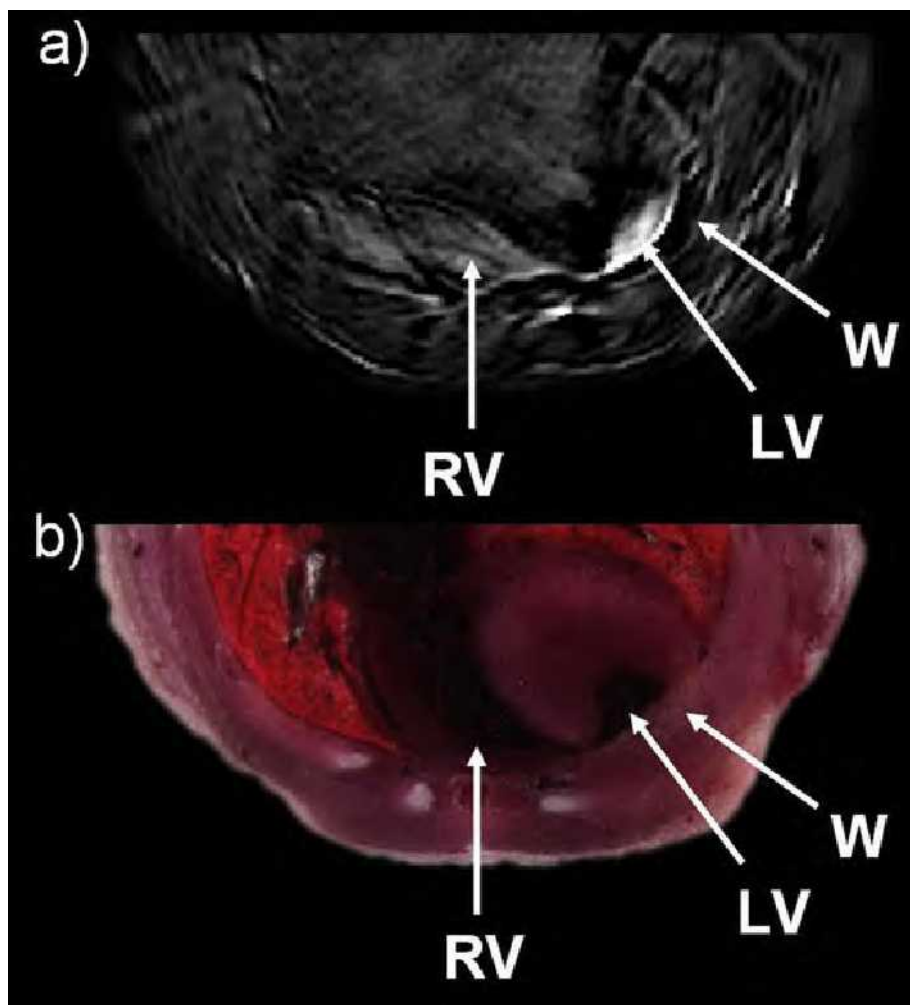
Three-dimensional (a) ultrasound and (b) photoacoustic images of tumor before and 4 hours after intravenous injection of EGFR targeted AuNPs. The orange color in represents the accumulation of AuNPs. (c) Photoacoustic signal amplitude (720 nm wavelength illumination) in the viable and necrotic regions of the tumors at different time points after intravenous administration of gold nanoparticles normalized to the photoacoustic signal before injection of AuNPs. The normalized photoacoustic signal strength 30 minutes, 2 hours and 4 hours after administration of AuNPs is shown in blue, red and green respectively.

Presentation Number **0205**
Scientific Session 27: Optical Imaging Methods

Multispectral Optoacoustic Tomography (MSOT) for Small Animal Imaging of the Heart

Adrian Taruttis^{1,2}, Niels J. Harlaar^{3,1}, Moritz Wildgruber⁴, Daniel Razansky^{1,2}, Vasilis Ntziachristos^{1,2}, ¹Institute for Biological and Medical Imaging, Technische Universität München, Munich, Germany; ²Institute for Biological and Medical Imaging, Helmholtz Zentrum München, Neuherberg, Germany; ³Department of Surgery, University Medical Center Groningen, Groningen, Netherlands; ⁴Department of Radiology, Klinikum Rechts der Isar, Munich, Germany. Contact e-mail: adrian.taruttis@helmholtz-muenchen.de

Optoacoustic tomography is emerging as a highly promising modality for high resolution macroscopic imaging of optical and molecular contrast. We show results from Multispectral Optoacoustic Tomography (MSOT) of the heart in healthy mice and in a model of myocardial infarction. Our newly developed experimental system is capable of real-time imaging, revealing cardiac structures previously unreported in optoacoustics and enabling dynamic imaging of contrast enhancement. Additionally, MSOT techniques allow for the specific separation of multiple chromophores, intrinsic to the tissue or exogenously administered, paving the way forward to molecular cardiac imaging. The system is based on laser excitation by a high near-infrared energy tunable laser and ultrasound detection by a 64-element transducer array, allowing for generation of a transverse slice tomographic image from a single laser pulse with an acquisition time of under 50 μ s. This is especially significant in the domain of in-vivo cardiac imaging, since the fast acquisition allows for images free of motion artifacts from the heartbeat or breathing. From these images it is possible to distinguish the heart wall from the blood pool inside heart chambers as well as identify different parts of the cardiac cycle in motion over time. By additionally varying the laser excitation wavelength, chromophores can be resolved based on their unique spectral signatures. We show the ability to thus multispectrally resolve hemoglobin oxygenation states and the distribution of exogenously administered contrast agents.



The figure shows a transverse slice through a mouse with a myocardial infarct. a) optoacoustic image; b) photograph of corresponding cryosection. LV: blood inside left ventricle; RV: right ventricle; W: heart wall.

Presentation Number **0206**
 Scientific Session 27: Optical Imaging Methods

Handheld Video Rate Fluorescence Diffuse Optical Tomography

Metasebya Solomon¹, **Brian R. White**³, **Ralph Nothdurft**², **Walter J. Akers**², **Adam Eggebrecht**², **Samuel Achilefu**^{2,3}, **Joseph P. Culver**^{2,3}, ¹Biomedical Engineering, Washington University in Saint Louis, Saint Louis, MO, USA; ²Radiology, Washington University in Saint Louis, Saint Louis, MO, USA; ³Physics, Washington University in Saint Louis, Saint Louis, MO, USA. Contact e-mail: solomonm@mir.wustl.edu

Fluorescence molecular tomography (FMT) is an emerging technology that can provide molecular contrast in deep tissues (> 3 mm). While FMT often images on the time scales of minutes to hours, the method also has the potential for imaging at higher speeds above the respiratory and cardiac fluctuations to capture pharmacokinetics and pharmacodynamics of diagnostic and therapeutic agents. Currently, most FMT systems are CCD-camera based and subsequently have inherent limitations of low dynamic range and slow scan times. Here, we demonstrate the feasibility of implementing a 30Hz APD-based (avalanche photodiodes) handheld fluorescence diffuse optical tomography (DOT) system with high dynamic range (106) and cross-talk rejection (10⁻⁶) build upon the platform of our high speed APD-DOT system (Zeff, 2007). The fiber-based video-rate fluorescence DOT imaging system is composed of a grid of alternating 12 sources (785nm and 830nm laser diodes) and 13 detectors. To maintain high temporal sampling, the system simultaneously acquires ratio-metric data by measuring frequency encoded fluorescent emission and reference transmission light levels at each detector through individualized bandpass filter optimized for fluorescence emission. The data is then reconstructed using the normalized Born approach with accurate depth localization and high sensitivity of fluorescent targets embedded in silicone phantom upto 22mm. We have also confirmed the high dynamic range and linear response of our system to varying ICG concentrations as measured by the resulting fluorescent yield. Handheld video-rate fluorescent DOT has the potential to become a powerful and practical tool for a broad array of imaging applications, ranging from sentinel lymph node mapping to monitoring cancer therapy progress.

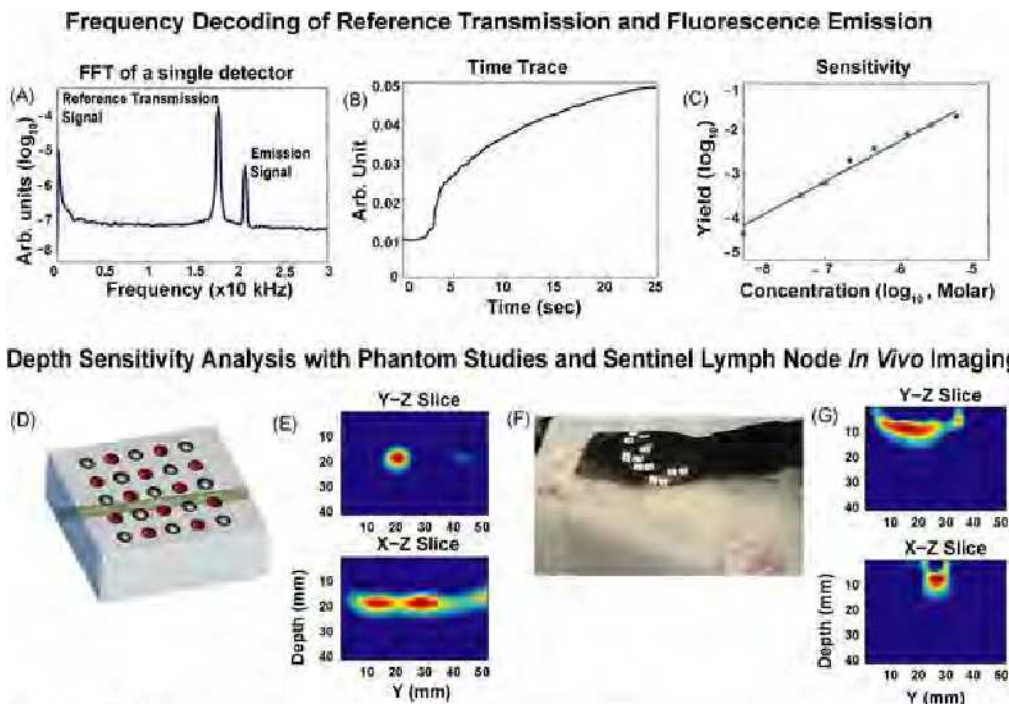


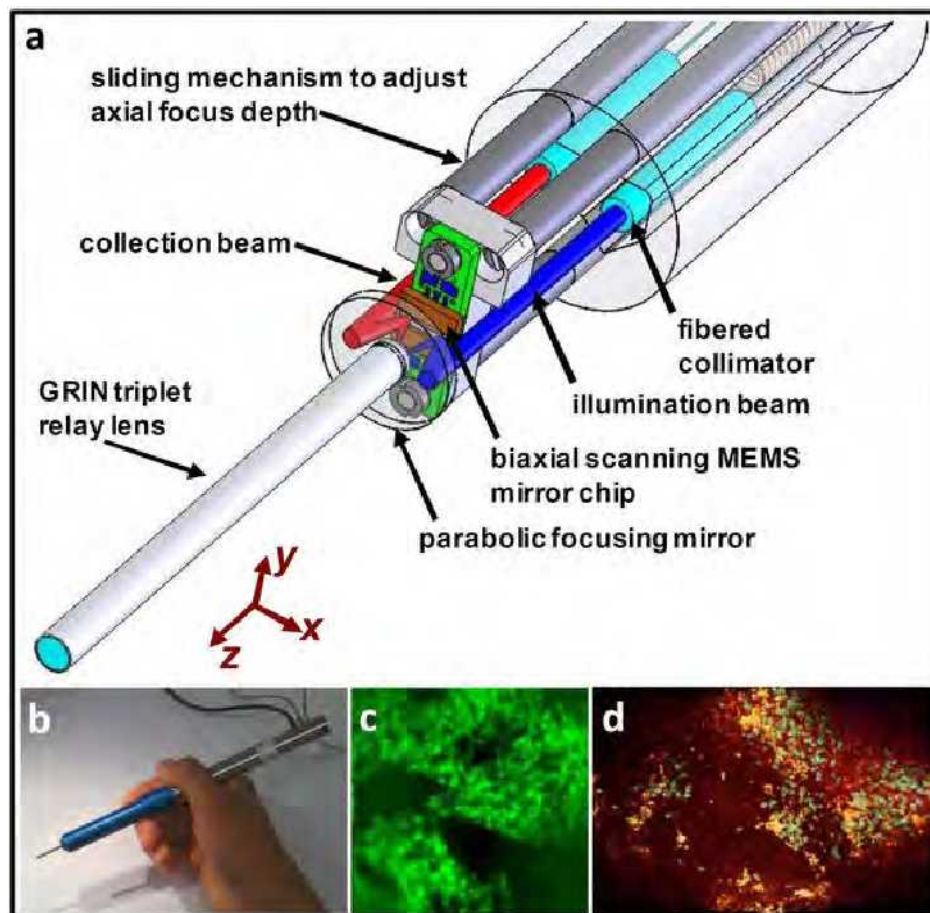
Figure 1: A) Fourier transform to demonstrate identification of transmission and emission signals from a single detector. (B) Time trace showing real time response of the system after addition of ICG in phantom after start of recording. (C) Titration of ICG from 10nM to 4uM concentrations in a 3mm tube shows the sensitivity of system. (D) Schematic of our experimental setup of a 3mm ICG tube embedded in silicone phantom with an imaging array. (E) Vertical x-z and y-z slices of reconstructed experimental data from a fluorescence 3mm tube target located at 19mm depth. (F) Picture showing the placement of fiber array on rats. (G) DOT reconstruction of fluorescent sentinel lymph node.

Presentation Number **0207**
 Scientific Session 27: Optical Imaging Methods

Miniature Optical-sectioning Microscopy for Molecular Image Guidance During Brain Tumor Resection

Jonathan T. Liu¹, Michael J. Mandella², Nathan O. Loewke², Hyejun Ra², Olav Solgaard³, Gordon S. Kino³, Christopher Contag²,
¹Biomedical Engineering, State University of New York (SUNY) at Stony Brook, Stony Brook, NY, USA; ²Pediatrics, Stanford University School of Medicine, Stanford, CA, USA; ³Electrical Engineering, Stanford University, Stanford, CA, USA. Contact e-mail: jonliu@stanfordalumni.org

There is a need for a real-time alternative to frozen-section pathology for accurate margin detection, allowing for complete tumor resection in the brain without the debilitating effects of over-aggressive resection. Confocal microscopy, if modified for deep tissue imaging, can achieve sub-surface imaging of cells that are in their undisturbed tissue microenvironment, where cell-surface biomarkers may accurately be labeled with molecular probes. We have developed a surgical microscope with a 2-mm diameter GRIN relay lens as a convenient form factor to guide brain tumor resection, utilizing a dual-axis confocal architecture to efficiently reject out-of-focus light for high-contrast optical sectioning within tissues. A biaxial MEMS scanning mirror is actuated at resonance along each axis to achieve a large field of view. An efficient method has been developed to decode the unstable Lissajous pattern that results from actuating the orthogonal axes of the MEMS mirror at disparate resonance frequencies. Ex vivo and in vivo imaging studies have been performed with tissues from transgenic mice (Ptc+/-p53-/- Math1-GFP) that spontaneously develop medulloblastoma with co-localized GFP expression. This mouse model has been used to validate exogenous contrast agents, including a fluorescent monoclonal antibody that targets VEGFR1. In particular, a ratiometric microscopy technique has been developed to quantify the specific vs. nonspecific binding of our fluorescent VEGFR1 mAb to tumor and normal tissues from our spontaneous mouse model. Furthermore, we demonstrate the feasibility of topical contrast-agent delivery, which may have significant advantages for circumventing the blood-brain barrier, reducing toxicity effects, and eliminating the need to introduce a contrast agent several hours prior to surgery.



a) Microscope schematic b) Photograph of microscope c) GFP-expressing tumor imaged with our miniature microscope d) Image fusion showing GFP-labeled tumor and fluorescent VEGFR1 mAb

Presentation Number **0208**

Scientific Session 28: Multimodality Approaches for Studying Inflammation and Infection

In Vivo Multi-color Endoscopic Fluorescence Imaging of Experimental Human Papillomavirus (HPV) Infection

Makoto Mitsunaga¹, Nobuyuki Kosaka¹, Rhonda C. Kines², Jeff Roberts², Douglas R. Lowy², John T. Schiller², Peter Choyke¹, Hisataka Kobayashi¹, ¹Molecular Imaging Program, CCR, NCI, NIH, Bethesda, MD, USA; ²Laboratory of Cellular Oncology, CCR, NCI, NIH, Bethesda, MD, USA. Contact e-mail: mitsunagam@mail.nih.gov

Human papillomavirus (HPV) is generally acquired by sexual contact, and more than 95% of cervical cancers are caused by HPV infection. The recently developed HPV vaccine is expected to reduce the risk of developing cervical cancer if the vaccination occurs prior to HPV exposure. In further developing vaccines for maximal potency, as well as exploring other methods of preventing HPV infection, either large numbers of animals or the ability to observe fewer numbers of animals over time will be needed. To aid in the study of HPV infections in mice, we established a multi-color endoscopic fluorescence imaging method based on HPV pseudovirus (PsV) infection that can be used to monitor experimental interventional procedures in the female genital tract of living mice. Female BALB/c or nude mice, pretreated with a vaginal spermicide containing 4% nonoxonyl-9, which transiently disrupts epithelial integrity, were intravaginally instilled with HPV PsV, which has an authentic viral capsid encapsidating green fluorescent protein (GFP) or tdTomato (RFP) fluorescent reporter gene. Fluorescence endoscopy, using a specially designed apparatus for the detection of GFP and RFP fluorescence, was performed on consecutive days in the same living animals after the PsV challenge. Expression of GFP or RFP was detected as early as 1 day after PsV challenge, and peaked after 2 or 3 days, decreasing thereafter. There was almost no background signal and no overlap of GFP and RFP fluorescent signals. A second PsV challenge, using the same PsV type but a different fluorescence reporter, revealed that there was no detectable fluorescence after the second PsV challenge in immunocompetent BALB/c mice, whereas the second fluorescent signal could be detected in immunodeficient nude mice. In addition, no fluorescence was detected in quadrivalent VLP vaccine-treated immunocompetent mice, even 2 days after PsV challenge, and a significantly weaker signal was detected when the mice received a topical pre-treatment of IFN alpha-2b compared with non-pretreated mice. These results indicate that the effects of the immunological response against HPV PsV can be monitored in a mouse model using multi-color fluorescence endoscopy. These results suggest that it is possible to follow these effects in a single living mouse over time as opposed to sacrificing many mice at different time intervals. Moreover, this technique could be generally used for investigating the effectiveness of various vaccine strategies in a broad range of viral challenges.

Presentation Number **0209**

Scientific Session 28: Multimodality Approaches for Studying Inflammation and Infection

P904 Magnetic Resonance Contrast Enhancement in Acute Inflammation is Stimulated by TNF- α in ApoE Knockout Mice

Marta Michalska^{1,2}, Wolfgang Rudolf Bauer¹, Peter Jakob², ¹Medizinische Klinik und Poliklinik I, Universitätsklinik Würzburg, Würzburg, Germany; ²Experimentelle Physik 5, Universität Würzburg, Würzburg, Germany. Contact e-mail: marta.michalska@physik.uni-wuerzburg.de

Background: Monocytes and macrophages play an active role in the initiation and progression of atherosclerosis. Visualization of these inflammatory cells is, therefore, a central challenge expected to contribute to deeper pathophysiologic understanding of the underlying processes. The aim of the current study was to characterize the inflammatory process stimulated by TNF- α treatment in the atherosclerotic plaque by use of the iron oxide contrast agent P904. Materials and methods: Female ApoE knockout mice and C57BL/6 control mice aged 10 months were investigated. ApoE knockout mice received western diet and were divided into two groups: mice in the first group received TNF- α (one dosis of 0.4 μ g IP), the second group served as a nontreated control. Six hours after cytokine treatment, all ApoE knockout mice received P904 (1000 μ mol iron/kg body weight) by intravenous injection. Three days after contrast agent delivery, mice were sedated and in vivo MRI was performed on a 17.6 T MR system. Images of the aorta and aortic arch were acquired in axial slice orientation using an ECG-triggered FLASH sequence. After the measurements, the internal organs, including heart and aorta, were excised and histologically investigated. The composition of the plaques, including lipids, and macrophages was demonstrated by oil red O staining and immunohistochemical staining. Iron contrast agent uptake from macrophages was determined by Prussian Blue staining. Validation of the contrast agent MRI characteristics was performed in the MRI animal ear model at 7 T MR using a Multi-Gradient-Echo sequence. Results: Histologically, ApoE knockout mice with TNF- α stimulation showed increased overall iron-positive macrophage content in comparison with nontreated ApoE knockout mice. MR imaging of atherosclerotic plaques revealed good visual correlation with the histologic findings, as demonstrated by a significant local T2*-weighted signal attenuation and a 4-fold increase in contrast-to-noise ratio associated with TNF- α treatment. No iron deposition was seen in aortas of the C57BL/6 control mice. The MR validation studies confirmed association of macrophage recruitment within the inflamed region after acute stimulation by TNF- α with a decrease in T2* from 11 to 4 ms. Conclusion: TNF- α -treated ApoE knockout mice develop higher macrophage deposition and iron content in atherosclerotic plaques than non-treated ApoE mice. MR imaging using P904 as contrast agent is a useful tool for non-invasive localization of the inflammatory process within atherosclerotic plaques.

Presentation Number **0210**

Scientific Session 28: Multimodality Approaches for Studying Inflammation and Infection

In Vivo Molecular MRI Targeting VCAM-1 Reveals Sub-clinical Disease and Provides an Assessment of Anti-IL-17 Treatment in Experimental Autoimmune Encephalomyelitis

Sebastien Serres¹, *Silvy Mardiguiian*², *Sandra J. Campbell*², *Martina McAteer*³, *Fay Saunders*⁴, *Gillian Watt*⁵, *Robin Choudhury*³, *Daniel Anthony*², *Nicola Sibson*¹, ¹*Gray Institute for Radiation, Oncology and Biology, University of Oxford, Oxford, United Kingdom;* ²*Department of Pharmacology, University of Oxford, Oxford, United Kingdom;* ³*Department of Cardiovascular Medicine, University of Oxford, Oxford, United Kingdom;* ⁴*Department of Antibody Biology, UCB, Slough, United Kingdom;* ⁵*Department of Pharmacology, UCB, Slough, United Kingdom. Contact e-mail: sebastien.serres@rob.ox.ac.uk*

Background: Multiple sclerosis (MS) is diagnosed clinically when contrast-enhancing lesions are visible using MRI, which represents relatively advanced disease and, thus, the potential of therapy is greatly reduced. The initial recruitment of leukocytes in MS takes place across an intact blood-brain barrier expressing vascular cell adhesion molecules such as VCAM-1. Identification and quantification of VCAM-1 is an attractive imaging target to accelerate diagnosis and to guide specific therapy in MS. Here, we have used anti-VCAM-1 antibodies conjugated to 1µm microparticles of iron oxide (MPIO) to detect in vivo VCAM-1 expression in the brain of pre-symptomatic EAE (experimental autoimmune encephalomyelitis) mice and to assess anti-IL-17 therapy in chronic relapsing EAE mice. Methods: 2 models were used: EAE SJL mice [1] and chronic relapsing (CR) EAE Biozzi ABH mice [2]. Animals were weighed daily and assessed for clinical signs. EAE SJL mice were imaged at day 8 (pre-symptomatic), day 12 and 15 after EAE induction. CR-EAE ABH mice were administered either with 400µL of anti-IL-17 or IgG (32 mg/kg, s.c.) following the acute phase of EAE at days 17, 24, 31 and 38 after EAE induction. Animals were imaged at day 28 and 42 after EAE induction. Isoflurane-anaesthetised animals were injected with VCAM-MPIO and 1h later underwent MRI at 7T using a 3D T2*-weighted gradient-echo sequence. Post-gadolinium T1-weighted images were acquired to assess BBB integrity. Quantification of VCAM-MPIO binding (defined as focal hypointensities) was performed using Image-Pro software and volumes were expressed in µL. Results: In EAE SJL mice, we showed that pre-symptomatic lesions can be visualized at a time when they are undetectable by conventional gadolinium (Gd)-enhancing MRI and when clinical symptoms are absent. VCAM-MPIO binding correlated with disease progression and increasing disability. During remission in CR EAE-ABH mice, VCAM-1 expression was significantly higher in IgG-treated mice than in anti-IL-17-treated mice. In the following relapse phase, we noticed significant reduction in clinical score in anti-IL-17-treated animals. Conclusion: Our results show that our targeted MRI contrast agent VCAM-MPIO provides a more sensitive tool for detection of early stage of MS disease and assessment of new therapies than clinical Gd-enhancing MRI. [1] Fridkis-Hareli, M. (2002) J. Clin. Invest. 109, 1635-1643. [2] Smith et al. Congress of the European Committee for Treatment and Research in Multiple Sclerosis. 2006. Poster 795.

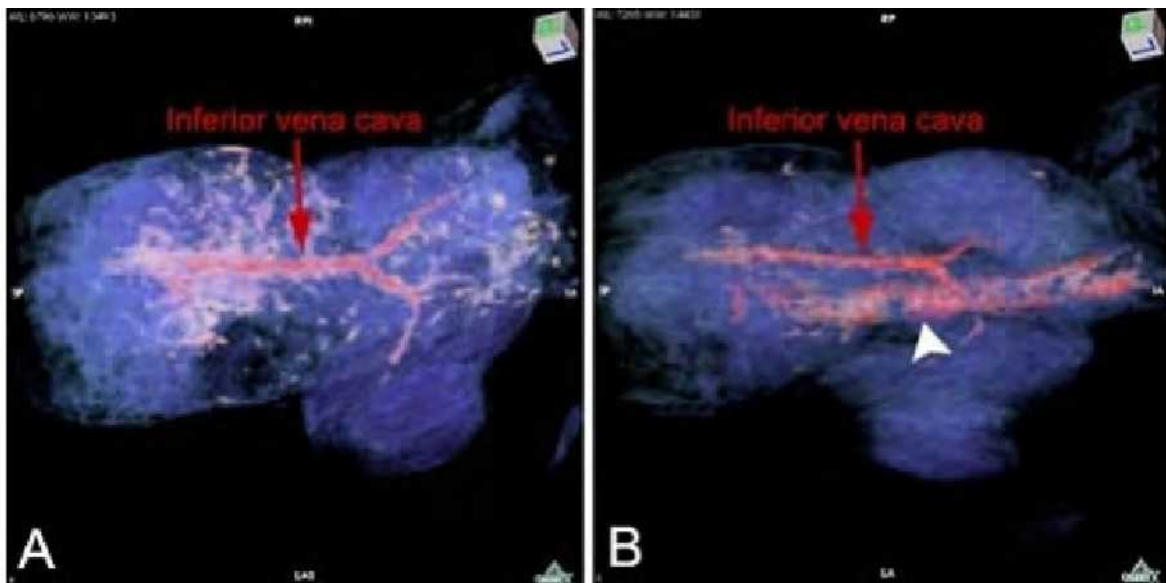
Presentation Number **0211**

Scientific Session 28: Multimodality Approaches for Studying Inflammation and Infection

Macromolecular Dynamic Contrast Enhanced (DCE) MRI Characterizes Hyperpermeability of the Intestinal Microvasculature in a Colitis model

Tegest Aychek¹, **Katrien Vandoorne**², **Michal Neeman**², **Jung Steffen**¹, ¹*immunology, Weizmann Institute of science, Rehovot, Israel;* ²*Biological Regulation, Weizmann Institute of science, Rehovot, Israel. Contact e-mail: tegest.aychek@gmail.com*

Inflammatory bowel diseases (IBD) are chronic inflammatory disorders of the gastrointestinal tract, among other things, results in alteration and dysfunction of the intestinal microvasculature. The goal of this work was to image and characterize blood vessels in the colon in an animal colitis model and to develop a protocol for detection of alterations of the microvasculature in colitis. After 7 days of exposure to DSS in the drinking water, the lower abdomen was imaged at 9.4T BioSpec (Bruker, Germany) before and sequentially for 30 minutes after iv injection of macromolecular Biotin-BSA-GdDTPA, as contrast agent. Subsequently, a few minutes before euthanasia, iv injected with BSA-ROX, as an early vascular marker. In the colon of the control mice, drinking regular water, contrast agent shows slow clearance, since blood vessels in the healthy colon are not leaky. The colon of mice with colitis showed enhanced accumulation rate of macromolecular contrast agent. The data are consistent with substantial extravasation of plasma proteins (such as the BSA-based contrast media) from colon vasculature. Post contrast, selective enhancement of the colon was observed in the mice with colitis compared to control animals, validated by staining of the contrast agent, with avidin-FITC. Thus, we showed with non-invasive macromolecular DCE-MRI, plasma protein leakage to the colon, highlighting the focal patches of colitis in post contrast 3D rendering. Macromolecular DCE-MRI demonstrated to be able to identify severe colitis and the loss of plasma proteins, validated by fluorescence microscopy. To further confirm and validate the data received with the MRI technique we included an additional in vivo imaging method. For this purpose, mice were treated with DSS as before afterwards, anesthetized mice received an intravenous injection of Dextran-FITC and the colon was imaged by a fibred confocal fluorescence microscope (Mauna Kea Technologies). Similar to the results obtained by the MRI technique, a highly distorted vascular pattern could be observed, demonstrated by increased Dextran-FITC leakage in the microvessels. Leakage of plasma proteins and deposition of a provisional matrix can support inflammation and stimulate remodeling of the colon vasculature.



Presentation Number **0212**

Scientific Session 28: Multimodality Approaches for Studying Inflammation and Infection

Quantitative Longitudinal Analysis of Inflammatory Bowel Disease Using Perfluorocarbon Emulsion and ^{19}F MRI

Deepak K. Kadayakkara, Won-Bin Young, **Eric Ahrens**, Department of Biological Sciences, Carnegie Mellon University, Pittsburgh, PA, USA. Contact e-mail: eta@andrew.cmu.edu

Introduction. Non-invasive diagnostic imaging and quantification of inflammatory bowel disease (IBD) can potentially aid in our understanding and treatment of this serious disease. In a mouse model, we demonstrate that quantitative and longitudinal monitoring of IBD is possible *in vivo* using ^{19}F MRI following perfluorocarbon (PFC) emulsion delivery intravenously (*i.v.*). The ^{19}F signal was highly specific to macrophage in the colon, with no background signal, and linearly proportional to inflammation severity. Results were validated using *ex vivo* MR microscopy, histology, and qRT PCR. **Methods.** IBD was induced in IL10^{-/-} mice (n=6) by feeding piroxicam-doped chow for 14 days. A PFC emulsion containing a trace amount of Dil fluorophore in the surfactant was injected *i.v.* via the tail vein. Anesthetized mice were longitudinally imaged on days 2, 9, 16, 23 and 30 post-injection. Multi-slice, 1H MRI data were acquired at 11.7 T through the abdomen, along with co-registered ^{19}F images. ^{19}F signal intensity in the colon was quantified relative to an external PFC reference capillary. Excised colon tissues were also imaged *ex vivo* using MR microscopy. Colon tissues were subjected to H&E histology, immunohistochemistry to look at macrophages (F4/80), neutrophils, monocytes (Ly6C) and endothelial cells (CD31), and RNA was extracted to measure macrophage load using qRT PCR. **Results and Conclusions.** A thickening of the colon wall was observed in 1H images, and patchy ^{19}F signals were observed (Figs. 1a-c). Longitudinal quantification of ^{19}F in the colon showed increasing ^{19}F signal from days 2 to 16 and then decreased thereafter. H&E staining displayed pancolitis with heavy mononuclear cell infiltration. Immunofluorescence of colon tissues showed that PFC was localized within macrophage exclusively (Fig. 1d). The qRT PCR revealed a linear correlation between macrophage RNA and ^{19}F signal in the same tissue samples.

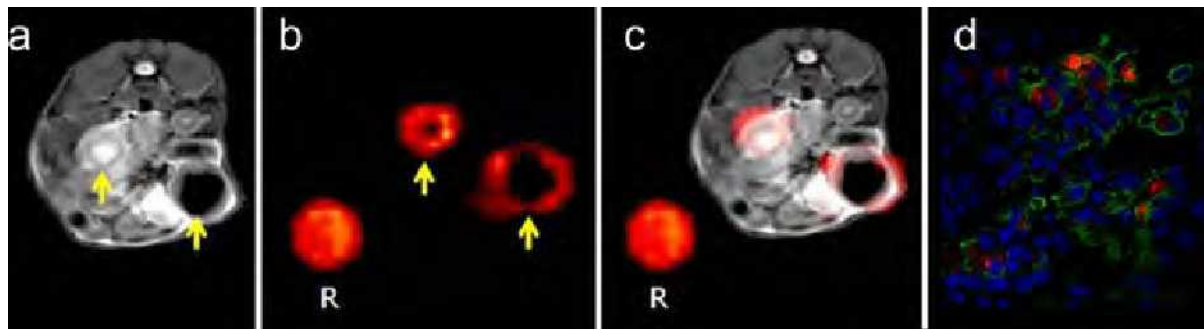


Fig. 1. (a) Axial 1H image through the abdomen showing ascending and descending colon (arrows). (b) Corresponding ^{19}F image (R is reference capillary). (c) $^{19}\text{F}/1\text{H}$ composite image. (d) Macrophages engulfing PFC-Dil (day 2, F4/80 macrophage is green, PFC-Dil is red, nuclei are blue).

Presentation Number **0213**

Scientific Session 28: Multimodality Approaches for Studying Inflammation and Infection

18FDG-Uptake and Gene Expression of Molecular Markers of Neoangiogenesis in Atherosclerotic Carotid Plaques

Sune F. Pedersen^{1,2}, **Martin Graebe**³, **Anne Mette F. Hag**^{1,2}, **Liselotte Hoejgaard**^{2,1}, **Henrik Sillesen**³, **Andreas Kjaer**^{1,2}, ¹Cluster for Molecular Imaging, Department of Biomedical Sciences, University of Copenhagen, Copenhagen, Denmark; ²Department of Clinical Physiology, Nuclear Medicine and PET, Rigshospitalet, University of Copenhagen, Copenhagen, Denmark; ³Department of Vascular Surgery, Rigshospitalet, University of Copenhagen, Copenhagen, Denmark. Contact e-mail: folke@mfi.ku.dk

Introduction & Aim: Inflammation and atherosclerosis are two inseparable entities. As such the advanced atherosclerotic lesion experiences a constant influx of macrophages. Neoangiogenesis is an important mechanism facilitating this influx which aggravates the disease by further enhancing plaque development and vulnerability. To uncover a correlation between molecular markers of neoangiogenesis and the imaging modality positron emission tomography (PET), we used the PET tracer 18FDG and real-time quantitative PCR. **Methods & Results:** A total of 17 patients with known atherosclerotic carotid disease and scheduled for carotid endarterectomy were included. Prior to operation an FDG PET scan was performed and SUVmean and SUVmax measured in plaques. Thereafter, plaques were removed and used for gene expression analysis by means of real-time qPCR. The gene expression of several key markers of neoangiogenesis were measured: The integrins αv and $\beta 3$ that together make up the dimer $\alpha v\beta 3$, cluster of differentiation-34 (CD34), a marker of micro vessel density (MVD) and vascular endothelial growth factor (VEGF) were measured. In addition, expression of the macrophage marker cluster of differentiation-68 (CD68) and of matrix metalloproteinase-9 (MMP9) was measured. Correlation analysis revealed, that in univariate analyses gene expression of CD34 correlated with both measures of 18FDG-uptake indicating a link between glucose metabolism and micro vessel density (MVD). Furthermore final models of multivariate regression demonstrated that gene expression of $\beta 3$ and CD34 offered independent information about 18FDG-uptake calculated as SUVmean as did gene expression of CD34 and VEGF for SUVmax (SUVmean: $R^2=0.13$; $p<0.0001$, SUVmax: $R^2=0.08$; $p<0.01$). In addition, multivariate regression models including αv , $\beta 3$, CD34 and VEGF gene expression had independent information about the gene expression of the macrophage marker cluster of differentiation-68 (CD68: $R^2=0.29$; $p<0.0001$) as did gene expression of $\beta 3$, CD34 and VEGF for matrix metalloproteinase-9 (MMP9: $R^2=0.31$; $p<0.0001$). **Conclusion:** Our data support that uptake of FDG in carotid atherosclerotic plaques are related to the level of neoangiogenesis and MVD. Furthermore, we found relation between neoangiogenesis and expression of CD68 and MMP9.

Presentation Number **0214**
 Scientific Session 29: Imaging Cell Death

Live Imaging of Bax Activation in Apoptotic Cells

Natalie Yivgi-Ohana, Michal Eifer, Yoseph Addadi, Atan Gross, Michal Neeman, Biological Regulation, Weizmann Institute of Science, Rehovot, Israel. Contact e-mail: nataliey@weizmann.ac.il

Non-invasive molecular imaging could provide a powerful tool to monitor apoptosis during physiological and pathological processes. Apoptosis imaging could also enable a specific and early measurement of drug-response in cancer patients. Several approaches to monitor apoptosis non-invasively have been developed, using probes that serve as substrates for caspase proteases and reagents with affinity to phosphatidyl serine. The aim of this work was to complement these tools by developing an imaging technique focusing on early intracellular events following the initial cellular commitment to undergo apoptosis. One of the major "hallmarks" of the apoptotic process is the translocation of Bax from the cytosol to the mitochondria and its oligomerization on the outer mitochondrial membrane, leading to membrane permeabilization and the release of intermembrane space proteins such as Cytochrome c (Cyt c). Our experimental strategy was based on monitoring Bax homodimerization at the mitochondria and the release of Cyt c using bimolecular fluorescence complementation (BiFC). Split yellow fluorescent protein (YFP) fragments were fused to Bax and Cyt c, expressed in MCF-7 cells and followed by live cell imaging techniques after apoptotic stimuli. Likewise, MCF-7 cells were transfected with Bax fused to the N or the C-terminus fragments of the YFP protein. Very low basal YFP signal was observed in healthy cells. Following an apoptotic signal, the YFP fluorescence was significantly increased at the mitochondria. The increased fluorescence correlated with a conformational change in Bax, its translocation and oligomerization on the mitochondria, allowing its close proximity with Cyt c and subsequently caspase activation. Similar constructs expressed *in vivo* by chicken embryonic cells (figure 1), mouse liver hepatocytes or by ovarian carcinoma cells demonstrated YFP fluorescence in apoptotic cells. YFP complementation could thus aid in high-throughput detection of apoptosis as well as in intravital imaging of apoptosis in preclinical animal models.

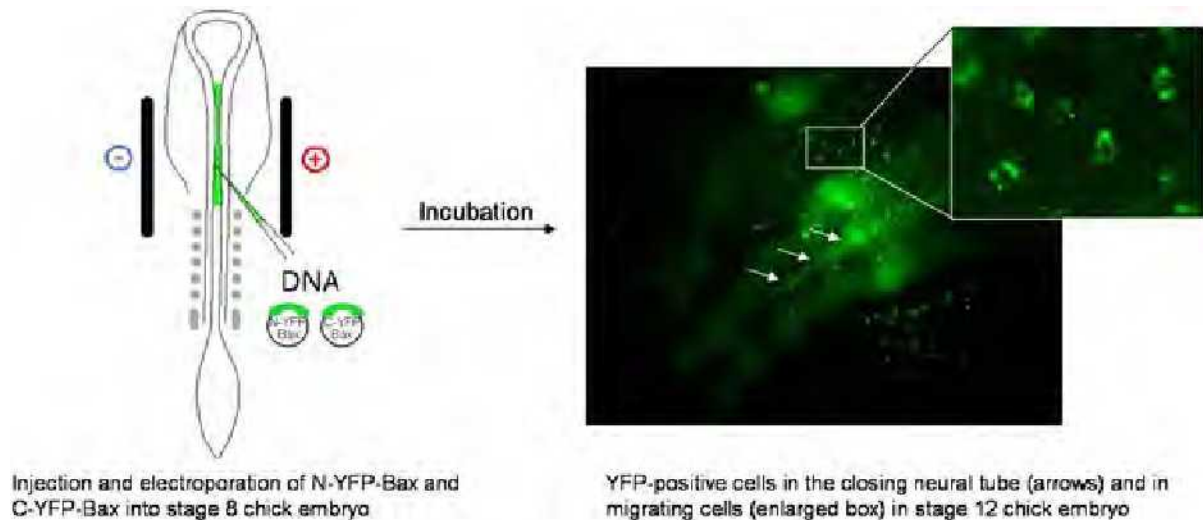


Figure 1: Neural tube closure as an apoptotic model in chicken embryo

Presentation Number **0215**
Scientific Session 29: Imaging Cell Death

The Role of cIAP2 in Atherosclerotic Lesion Development and the Use of ^{18}F -FDG to Detect Changes in Lesion Size

Lyne Sleiman, Stephanie Thorn, Martin Holcik, Jean N. DaSilva, Robert A. deKemp, Rob S. Beanlands, Stewart Whitman, PET biotesting and Vascular Biology, Ottawa Heart Institute, Ottawa, ON, Canada. Contact e-mail: lsleiman@ottawaheart.ca

Macrophages are a key component in the early stages of atherosclerosis, and the ability of these cells to evade apoptosis is an important means by which they accumulate lipids during their transformation into foam cells. Both anti- and pro-apoptotic mechanisms contribute to the development and progression of atherosclerosis. Cellular Inhibitor of Apoptosis 2 (cIAP2) belongs to the IAP gene family, the only recognized group of endogenous proteins that directly bind to and inhibit caspases, which are the terminal regulators of apoptosis. Methods: Inbred C57BL/6 mice of two different genotypes were used; cIAP2 $+/+$ x Apo E $-/-$ (WT, n = 13) and cIAP2 $-/-$ x Apo E $-/-$ (KO, n = 10) to examine the effect of cIAP2 protein on the progression of atherosclerosis. At 8 weeks of age, male mice from each group were put on a high-fat high-cholesterol diet for a period 12 weeks to induce late atherosclerotic lesions. Following the high-fat diet period, mice were sacrificed by pentobarbital overdose, and tissues were harvested. Analysis was focused on the aortic root, the aortic arch, the descending aorta, and the blood. The aortic root was serially sectioned into 90 sections, 10 μm apart. The sections were stained with SUDAN IV and lipid uptake and accumulation was quantified. The arch and descending aorta were examined by en face methodology and lesion surface area was quantified as percent of total surface. Blood was processed for FPLC and total cholesterol content. Mice were injected with 500 μCi ^{18}F -FDG intravenously and sacrificed 1 hr later. En face aorta were placed on glass slide and exposed to phosphor imaging film for 2 hrs. Results: Ex vivo results show a significant decrease in lesion area at the aortic arch KO mice vs. WT; $8.63\% \pm 1.1\text{SE}$ vs. $17.22\% \pm 1.72\text{SE}$ ($p = <0.001$), respectively. Results also show a decrease in aortic root lesion size in KO vs. WT; $0.2756 \text{ mm}^2 \pm 0.042\text{SE}$ vs. $0.505 \text{ mm}^2 \pm 0.123$ ($p = <0.05$), respectively. Total cholesterol assays and serum FPLC profiles between the two groups did not show any significant differences. Autoradiography techniques attempted using ^{18}F -FDG injected mice revealed significant uptake of the tracer in lesion areas. Conclusions: cIAP2 knock-out mice resulted in significantly reduced lesion development when compared to wild type mice. These results indicate a prominent role for cIAP2 in atherosclerotic lesion formation and suggest that cIAP2 may provide a novel target for therapeutic. ^{18}F -FDG can serve as a potential imaging tracer for atherosclerotic lesions and imaging protocols in micro PET are under development.

Presentation Number **0216**
Scientific Session 29: Imaging Cell Death

Characterization of a Water Soluble Z-DEVD-aminoluciferin Probe for the Non-invasive Bioluminescent Imaging of Apoptosis In Vivo

Jonathan Hickson¹, Thomas McGonigal¹, Anatol Oleksijew¹, Scott Ackler¹, Sally Schlessinger¹, Dieter H. Klaubert², Erwin R. Boghaert¹, David Frost¹, ¹Abbott, Abbott Park, IL, USA; ²Promega Biosciences Inc, San Luis Obispo, CA, USA. Contact e-mail: jonathan.hickson@abbott.com

Apoptosis, or programmed cell death, is essential for homeostasis of multicellular organisms. Dysregulation of apoptosis contributes to the development and progression of a variety of diseases including cancer, neurodegenerative disorders, and chronic heart failure. Quantitative non-invasive imaging of apoptosis in preclinical models would allow for dynamic longitudinal screening of candidate apoptosis restoring agents and facilitate a more rapid determination of therapeutic efficacy. We have recently reported the in vivo characterization of Z-DEVD-aminoluciferin, a modified firefly luciferase substrate that in apoptotic cells is cleaved by caspase-3 to liberate aminoluciferin, which can be consumed by luciferase to generate a luminescent signal. Z-DEVD-aminoluciferin was administered to tumor (SKOV3-luc or MDA-MB-231-luc-LN) bearing mice 24, 48 and 72 hours following treatment with docetaxel and bioluminescent images were acquired. Significantly more light was detected at all time points in the docetaxel-treated group compared to the vehicle-treated group. Here we report the development and characterization of an improved sodium salt version of Z-DEVD-aminoluciferin that is water soluble up to 500 mg/ml and stable for up to three days. This apoptosis probe presented a practical advantage over the original free acid that necessitated a complex formulation for in vivo delivery and aggregated within two hours. Using a human acute lymphoblastic leukemia cell line, RS4;11, that stably expresses the fusion construct of luc2, a firefly luciferase optimized for expression in mammalian cells, and mCherry, a far-red fluorescent protein, we evaluated apoptosis induction following treatment with ABT-263, a small molecule inhibitor of Bcl-2, Bcl-xL, and Bcl-w designed to restore apoptosis, currently in Phase II clinical trials. Four hours after treatment we were able to non-invasively detect ABT-263-induced apoptosis which remained elevated through 24 hours post treatment. Caspase-3 activation at these time points was confirmed by immunohistochemical techniques. Importantly, we were able to use a significantly lower dose of the water-soluble probe (150 mg/kg) compared to our previous work using the free acid (500 mg/kg) and still maintained a similar window of activity. Together, these data demonstrate that imaging of apoptosis in vivo with Z-DEVD-aminoluciferin provides a sensitive and rapid method for early detection of drug efficacy that could be utilized in numerous therapeutic disciplines.

Presentation Number **0217**
Scientific Session 29: Imaging Cell Death

Monitoring Autophagy and Apoptosis by In Vivo Imaging in tMCAO Model of Mice

Feng-Feng Tian, Kentaro Deguchi, Toru Yamashita, Yasuyuki Ohta, Nobutoshi Morimoto, Jingwei Shang, Xuemei Zhang, Ning Liu, Yoshio Ikeda, Koji Abe, Okayama University, Okayama, Japan. Contact e-mail: gmd20201@s.okayama-u.ac.jp

Abstract Recent study suggested that autophagy is involved in a pathway neural death after cerebral ischemia. In vivo detection of such autophagy may be important to evaluate ischemic neural cell damage for human stroke patients. With a novel green fluorescent protein (GFP) fused with microtubule-associated protein 1 light chain 3 (LC3) transgenic (Tg) mice, in vivo imaging of autophagy was performed at 1, 3 and 6 d after 60 min of transient middle cerebral artery occlusion (tMCAO). Ex vivo imaging of autophagy, Western blot, immunohistochemistry and terminaldeoxynucleotidyltransferase-mediated dUTP-digoxigenin nick end labeling (TUNEL), fluorescent analyses were also performed with brain sections after the tMCAO. In vivo fluorescent signal was detected over head of the ischemic hemisphere through skull bone at 1, 3 and 6 d after tMCAO with peak at 1d. The same results were obtained with ex vivo fluorescent imaging. These intrinsic GFP fluorescence signals were confirmed as autophagic LC3 signals with double immunofluorescent study with antibodies for LC3 and P62. Western blot analysis showed that the LC3-I and LC3-II levels reached maximum at 1 d after tMCAO, and fluorescent immunohistochemistry showed that GFP-LC3 positive cells were mainly neuronal cells but not astroglial or microglial cells. The number of GFP-LC3/TUNEL double positive cells were larger in the peri-ischemic area than in the core. This study provided evidence of in vivo detection of autophagy in live animal model after cerebral ischemia with a peak at 1d, and the source of the autophagic signal was mainly neuronal cells. This novel technique is important for monitoring autophagic process in vivo in live stroke patients, and also for clarifying the detailed role of autophagy not only in the ischemic brain but also in other neurological diseases.

Presentation Number **0218**
Scientific Session 29: Imaging Cell Death

A Critical Step Toward Noninvasively Quantifying Cell Death

Zhixin Li¹, Said Audi², **Ming Zhao**¹, ¹*Biophysics, medical college of wisconsin, Milwaukee, WI, USA;* ²*Biomedical Engineering, Marquette University, Milwaukee, WI, USA. Contact e-mail: mzhao@mcw.edu*

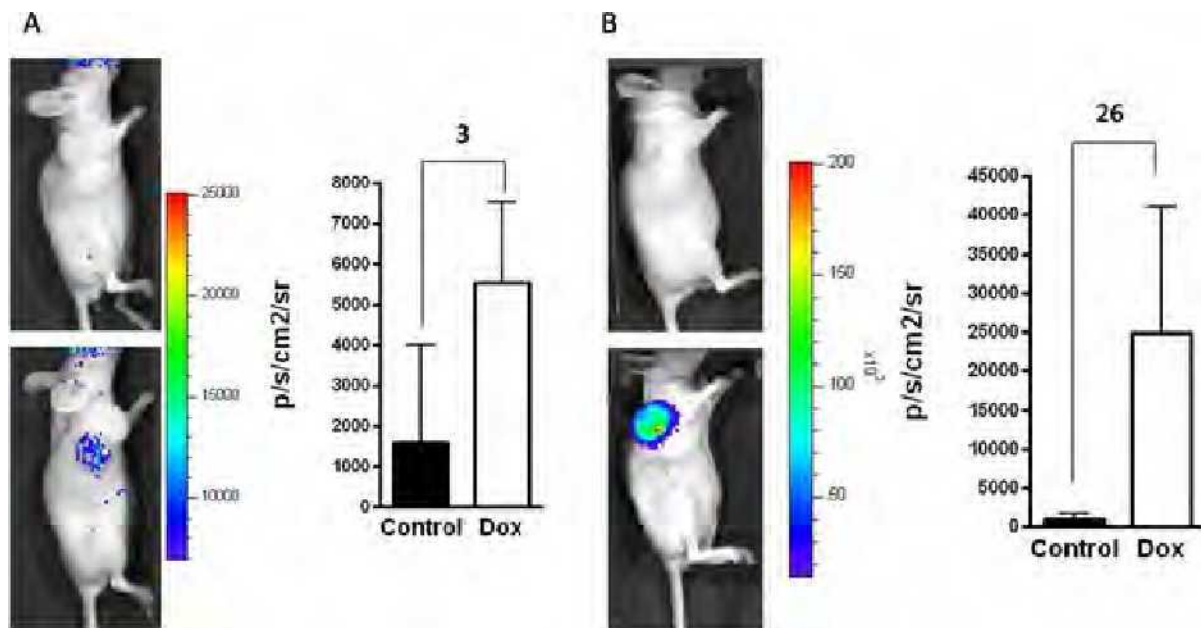
For imaging cell death at a given time, different techniques should arrive at a consistent level of apoptosis/necrosis in the target tissue regardless of the nature of the molecular probes. This rule is fundamental in the effort to quantify apoptosis and necrosis in vivo. The objective of this study is to quantitatively assess the level of cell death using two sets of completely different probe/target pairs. Methods: Acute cardiac cell death was induced in a rat model by 30 minutes of coronary ischemia followed by reperfusion. ^{99m}Tc-labeled C2A domain of Synaptotagmin I, which binds phosphatidylserine (PS) and phosphatidylinositides (PI), and ^{99m}Tc-Duramycin, which binds phosphatidylethanolamine (PE), are injected intravenously in separate groups of animals at 2 hr after reperfusion. The absolute radioactivity uptake in the ischemic myocardium, in terms of %ID/g, was determined by sacrificing the animals for gamma counting at different time points after injection. The total number of available PS/PI and PE for binding by either probe in the infarcted myocardium was quantified using compartment modeling. The findings were cross-validated by in vivo dynamic SPECT. Results: Quantitative analysis of tracer kinetics validated that the two molecular probes have markedly different behaviors in vivo, in terms of rate of clearance, biodistribution, transvascular diffusion, binding targets, binding affinity, and pharmacokinetics. Importantly, the number of total binding sites for PS/PI and PE corresponds to a consistent level of cell death in the infarct tissue independent of the probe used. Conclusion: Among the confounding factors in molecular imaging, target density, but not probe density or behaviors, reflects the true level of cell death. The data from the current study were a proof of concept where the level of cell death can be noninvasively quantified. The findings pave the way for clinical translation of quantitative apoptosis/necrosis imaging techniques.

Presentation Number **0219**
 Scientific Session 29: Imaging Cell Death

Molecular Imaging of the Dynamics of Doxorubicin Induced Apoptosis

Gang Niu^{1,2}, **Lei Zhu**², **Orit Jacobson**², **Yongjun Yan**², **Joseph A. Frank**¹, **Takeaki Ozawa**³, **Xiaoyuan Chen**², ¹Radiology and Imaging Sciences, Clinical Center and National Institute Biomedical Imaging and Bioengineering, National Institutes of Health, Bethesda, MD, USA; ²Laboratory of Molecular Imaging and Nanomedicine (LOMIN), National Institute of Biomedical Imaging and Bioengineering (NIBIB), National Institutes of Health, Bethesda, MD, USA; ³Department of Chemistry, the University of Tokyo and Japan Science and Technology Agency, Tokyo, Japan. Contact e-mail: niug@mail.nih.gov

Objectives: The early assessment of tumor response is of tremendous need to manage the patients in terms of quality of life versus intensive chemotherapy. This study aims to visualize the dynamics of apoptosis process with temporal molecular imaging. **Methods:** Both 22B human head and neck squamous carcinoma cells and 4T1 murine breast cancer cells were genetically modified with a caspase-3 specific cyclic firefly luciferase reporter gene (pcFluc-DEVD). Annexin V, a phosphatidylserine (PS) binding marker, was expressed and purified in E. Coli competent cells. The apoptosis induced by different concentrations of doxorubicin in the transfected cells was evaluated by both annexin V staining and bioluminescence imaging (BLI). At different time points after doxorubicin treatment, BLI was performed to evaluate apoptosis. Annexin V was conjugated with both Cy5.5 and 18F for optical fluorescence imaging and PET imaging. After imaging, DNA fragmentation in apoptotic cells was assessed in frozen tumor sections using TUNEL staining. **Results:** Doxorubicin induced apoptosis in both 22B and 4T1 cells as reflected by the photon intensity was determined by BLI and was found to be dose-dependent. The apoptotic cell ratio is consistent with FITC-Annexin V staining. At 24 and 48 hr after doxorubicin treatment at a dose of 10 mg/kg, a significant increase of BLI signal was visualized and photon intensity emitted by treated tumors was 3 and 26 fold respectively, compared with control tumors. On fluorescence imaging with Cy5.5-Annexin V and PET imaging with ¹⁸F-annexin V, only marginal increase of Annexin V signal was found until 48 h post treatment. **Conclusions:** Bioluminescence imaging of apoptosis with the cyclic firefly luciferase facilitates the determination of localization, extent and kinetics of apoptosis process over time in vitro and in vivo. Combination of BLI and PET imaging will be of great value for early response to cancer therapy.



BLI imaging of apoptosis in 22B tumor models at 24 hr (A) and 48 hr (B) after administration of 10 mg / kg dose of doxorubicin. The upper animals are from the control group and the lower animals from the treated group.

Presentation Number **0220**
Scientific Session 30: Novel Therapy

Development of Lutebodies: A New Class of Targeted Anti-cancer Agents for Radionuclide Therapy

Matthias D'huyvetter^{1,3}, An Aerts¹, Arnaud Campsteyn¹, Ilse Vaneycken³, Nick Devoogdt^{2,3}, Catarina Xavier³, Nathalie Impens¹, Sarah Baatout¹, Vicky Caveliers³, Tony Lahoutte³, ¹Molecular and Cellular Biology Expert Group, Radiobiology Unit, Belgian Nuclear Research Centre (SCK-CEN), Mol, Belgium; ²Laboratory of Cellular and Molecular Immunology, VIB, Brussels, Belgium; ³In vivo Cellular and Molecular Imaging Laboratory (ICMI), Free University Brussel, Brussels, Belgium. Contact e-mail: mdhuyvet@vub.ac.be

Introduction: Nanobodies are small (15kDa) antibody fragments, derived from heavy chain-only antibodies present in Camelidae. These proteins show favourable pharmacokinetic characteristics for tumor targeting. Nanobodies, labelled with a therapeutic radionuclide, may be used for the treatment of cancer. Within this project, we labeled nanobodies with the beta-gamma emitter ¹⁷⁷Lu. **Materials and methods:** In a first step the nanobody was conjugated with the bifunctional chelator 1,4,7,10-tetraazacyclododecane-1,4,7,10-tetraacetic acid N-hydroxysuccinimide (DOTA-NHS-ester), through a peptide-bound. Degree of conjugation was analysed with Mass Spectrometry (MS). In a second step ¹⁷⁷Lu was complexed during a moderate temperature (55°C at pH=5,5) labeling reaction. Purification was done by means of disposable gel filtration columns. Assessment of radiochemical purity was performed with Instant Thin Layer Chromatography (ITLC) on Silica gel Impregnated Glass fiber sheets using 0.2M citric acid as eluent. Subsequently, binding potential of the ¹⁷⁷Lu-labeled nanobody was evaluated in binding studies on target-expressing cancer cell lines. **Results:** MS results showed conjugation of 1 up to 4 DOTA molecules per nanobody. After labeling, ITLC showed a radiochemical purity >98%, suggesting a successful labeling procedure. Binding study results revealed nanomolar affinity of the ¹⁷⁷Lu-labeled nanobodies towards their target. **Conclusions:** We showed for the first time the successful labeling of cancer targeting nanobodies with ¹⁷⁷Lu through the DOTA chelator. After these chemical modifications, the lutebodies still exhibit nanomolar affinity towards their target. Stability studies and first in vivo data are now in progress. **Acknowledgement:** This work was supported by FWO-Vlaanderen (Research Project G.013910). The research at ICMI is funded by the Interuniversity Attraction Poles Program - Belgian State - Belgian Science Policy. Matthias D'huyvetter is funded by SCK-CEN/VUB.

Presentation Number **0221**
Scientific Session 30: Novel Therapy

Evaluation OF Immune Responses after Nanovectorized Internal Radiotherapy for Glioblastomas

Claire Vanpouille^{1,2}, Emmanuel Garcion^{1,2}, Franck Lacoeyille^{1,2}, Laurent Lemaire^{1,2}, Nicolas Lepareur^{3,4}, Jean-Jacques Le Jeune^{1,2}, Jean-Pierre Benoît^{1,2}, Olivier Couturier^{1,2}, François Hindré^{1,2}, ¹INSERM U646, Angers, France; ²University of Angers, Angers, France; ³Medical Imaging Department, CRLCC Eugene Marquis, Rennes, France; ⁴European University of Brittany, Rennes, France. Contact e-mail: claire_vanpouille@yahoo.fr

Objectives: Lipid nanocapsules loaded with rhenium-188 (LNC188Re-SSS), used for fractionated internal radiation in a glioblastoma rat model, led to important increase of survival with 83% of long-term survivors. As already observed with ionizing radiation, the development or potentiation of an immune response could explain these results. The aim of this study was therefore to characterize and better understand the various factors involved in this reaction. **Methods:** After stereotactic implantation of glioma 9L cells in the right striatum of fisher female rats, a local fractionated administration of LNC188Re-SSS (2.8 MBq) at D6 and D12 was realized. Two types of injection were used: bolus and convection-enhanced delivery (CED). The best results were obtained with the combination of these two types of injections, so two protocols were selected: CED + bolus (n=6) and bolus + CED (n=6). Each protocol was composed with three additional control groups: blank lipid nanocapsules (LNCB - n=4), 188Re-perrhenate solution (n=4) and saline solution (n=4). Peripheral immunostimulation was evaluated by plasmatic quantification of cytokines IL-2 (interleukin-2) and IFNg (interferon-g) at D8, D16 and D24 post 9L cells implantation. Meanwhile, recruitment and activation of inflammatory and immune cells were analyzed by immunostaining of brain sections at D15 (n=4), D24 (n=4) and D32 (n=4). Finally, the establishment of immune memory in long-term survivors was assessed after 9L cells implantation in the left hemisphere. **Results:** Results demonstrated increase of cytokine (IL-2 and IFNg) peripheral production after internal radiation. Recruitment of immune and inflammatory cells (dendritic cells, CD4, CD8, NK, macrophages, microglia) is observed into the tumoral site. Moreover, increased expression of MCH class I and MCH class II was also demonstrated. Finally, increase of survival up to 32% compares to control rats with 25% of long-term survivor after rechallenging showed an immunization process. **Conclusion:** Because of the brain immune privileged status, these results offers new prospects for therapy of malignant gliomas.

Presentation Number **0222**
Scientific Session 30: Novel Therapy

Molecularly-targeted Auger Electron Radiotherapy Using Nucleolin-Targeted ^{111}In -F3 Peptide

Bart Cornelissen, Carol Target, Andrew Waller, Veerle Kersemans, Sean Smart, Katherine A. Vallis, Gray institute for radiation oncology and biology, University of Oxford, Oxford, United Kingdom. Contact e-mail: bart.cornelissen@rob.ox.ac.uk

Background: The F3-peptide (KDEPQRRSARLSAKPAPPKPEPKPKKAPAKK), a fragment of the human high mobility group protein 2 (HMGN2), was discovered by phage display screening. It binds nucleolin, a protein usually expressed only in the nucleus. In some cancer cells, nucleolin is expressed on the membrane, and can be used as a target for SPECT imaging and radioimmunotherapy. Others have reported synthesis of a ^{213}Bi -labeled F3 dimer that binds cancer cells in vitro and in vivo, and causes tumour growth inhibition through alpha-particle radiation. We have radiolabeled the F3-peptide with ^{111}In , for molecularly targeted Auger electron radiotherapy. Methods and Results: F3 was conjugated with p-SCN-BnDTPA to enable ^{111}In labeling. Radiolabeling yield was >95%, resulting in specific activity of ≥ 8 MBq/ μg . MDA-MB-231/H2N cells (H2N) human breast cancer cells were used in fractionation studies to investigate binding, internalization and nuclear translocation of ^{111}In -F3. Membrane binding of F3 was observed (1.7% of added ^{111}In was bound to the membrane after 2h). Cytoplasmic and nuclear uptake of ^{111}In -F3 and FITC-F3 was limited (0.3% of added ^{111}In was internalized after 2h). FITC-F3 was used for confocal microscopy which confirmed that internalization of F3 is cell line-specific and modest in extent. There was, however, significant reduction in clonogenic survival in ^{111}In -F3 treated H2N cells ($46 \pm 4.1\%$) compared to untreated ($100 \pm 1.8\%$) or cold, unlabeled F3-treated cells ($132 \pm 7.7\%$). In biodistribution studies H2N xenograft-bearing mice received ^{111}In -F3 (1 μg , 10 MBq) i.v. Tumor uptake was 1% ID(Injected dose)/g, and muscle uptake was 0.5%ID/g at 4h post injection. Tumor accumulation of ^{111}In -F3 was visualized and quantified using nanoSPECT/CT imaging. Dynamic planar gamma-camera imaging was performed to generate time-activity curves for ^{111}In -F3 in tumor and other organs, to determine ^{111}In dosimetry, and confirmed uptake of 1%ID/g at 2h in the tumour. In tumor growth delay studies, groups of 7 mice received ^{111}In -F3 (10 MBq, 1 μg) i.v, on 4 consecutive days. Tumour growth was reduced 19-fold ($p = 0.023$) by day 34 in ^{111}In -F3-treated, compared to untreated or unlabeled F3-treated mice. Conclusion: The extent of cellular internalization and nuclear localization of ^{111}In -F3 peptide is modest. However, ^{111}In -F3 has a potent antitumor effect in mice bearing H2N xenografts. The mechanism of cytotoxicity of ^{111}In -F3 is being investigated.

Presentation Number **0223**
Scientific Session 30: Novel Therapy

A New Family of Cross Bridged Azamacrocycles for the Development of Robust ^{64}Cu -based Radiopharmaceuticals

Darpan N. Pandya¹, Jung Young Kim², Jeong Chan Park¹, Wonjung Kwak¹, Eun Kyung Wang¹, Yeong Su Ha¹, Gwang Il An², Jeongsoo Yoo¹, ¹Department of Molecular Medicine and Nuclear Medicine, Kyungpook National University School of Medicine, Daegu, Republic of Korea; ²Molecular Imaging Research Center, Korea Institute of Radiological and Medical Sciences, Seoul, Republic of Korea. Contact e-mail: darpan2147@gmail.com

Objectives: Earlier reports on the synthesis and modification of the framework of cyclen and cyclam derivatives to achieve a better bifunctional chelating agents for medical imaging and targeted radiotherapy have revealed that the ethylene-cross-bridged (ECB) macrocycles are superior in terms of kinetic stability and inertness to the metal ion loss in vivo. We have designed a novel route to synthesize a propylene cross-bridged (PCB) cyclam which may afford a better cavity shape and size as well as rigidity for the encapsulation of the metal ion in the framework and consequently leading to a better bifunctional chelators. **Methods:** The propylene cross-bridging of the non-adjacent nitrogens was achieved by refluxing trans-1,8-di(t-butyloxycarbonylmethyl)-cyclam with the ditosyl ester of 1,3-propane diol in toluene. The deprotection of the t-butyl ester was carried out with trifluoroacetic acid to afford PCB-TE2A as trifluoroacetic acid salt. Then, in order to evaluate the kinetic stabilities of the copper(II) complex (Cu-PCB-TE2A), acidic decomplexation in 5M HCl at 90°C was performed. Complexation of ^{64}Cu with PCB-TE2A was achieved by the addition of no-carrier added $^{64}\text{CuCl}_2$ to a solution of PCB-TE2A in 0.1 M ammonium acetate (pH 8) followed by 1 h incubation at 75°C. ^{64}Cu -labeled PCB-TE2A was subjected to biodistribution studies, and the organs of interest were collected at 24h post injection. PCB-TE2A was conjugated to a c(RGDyK) peptide by using standard EDC/SNHS conjugation method. PCB-TE2A-c(RGDyK) was then labeled with ^{64}Cu in 0.1 M NH_4OAc (pH 8) at 80 °C for 30 min and purified using HPLC. The microPET studies were performed by tail-vein injection of ^{64}Cu -PCB-TE2A-c(RGDyK) into the nude mice bearing U87MG tumor cells. **Results:** All the steps involved during the synthesis of PCB-TE2A are very high yielding to afford 62% overall yield. The half-life of Cu-PCB-TE2A in acidic decomplexation experiments was comparable with that of Cu complex of ECB-TE2A. Quantitative radiolabeling for ^{64}Cu -PCB-TE2A was achieved at 75°C, which was confirmed by radio-TLC. The biodistribution of ^{64}Cu -PCB-TE2A showed faster clearance from all organs than ^{64}Cu -TETA. Tumor was clearly visualized by ^{64}Cu -PCB-TE2A-c(RGDyK) at 1 h post injection. **Conclusions:** An efficient synthesis of novel propylene cross-bridged TE2A derived from cyclam have been developed. PCB-TE2A showed good potentials as a new bifunctional chelator for ^{64}Cu radiometals.

Presentation Number **0224**
Scientific Session 30: Novel Therapy

Preclinical Evaluation of the c-Met Inhibitor ZK 7003295 in a H746T Tumor Xenograft Model by Small Animal PET

Stefan Wiehr¹, **Oliver von Ahsen**², **Lars Röse**², **Julia G. Mannheim**¹, **Valerie S. Honndorf**¹, **Damaris Kukuk**¹, **Kerstin Fuchs**¹, **Kristina Fischer**¹, **Maren K. Koenig**¹, **Nadine Bauer**¹, **Gerald Reischl**³, **Bernd J. Pichler**¹, ¹Laboratory for Preclinical Imaging and Imaging Technology of the Werner Siemens-Foundation, Department of Radiology, Eberhard Karls University Tübingen, Röntgenweg 13, 72076 Tübingen, Germany; ²Bayer Schering Pharma AG, Global Drug Discovery, Biomarker Research, Berlin, Germany; ³Department of Radiopharmacy, Eberhard-Karls University Tuebingen, Röntgenweg 11, Tübingen, Germany. Contact e-mail: stefan.wiehr@med.uni-tuebingen.de

c-Met, an proto-oncogenic receptor tyrosine kinase, is a transmembrane protein with a wide range of biological activities including proliferation, survival and motility, all of which are often dysregulated in cancer. Hence, c-Met is an attractive target for therapeutic blockade in cancer. Here, we describe the novel, highly selective c-Met inhibitor ZK 7003295 in its efficacy to reduce tumor growth in a subcutaneous H746T xenograft mouse model using [¹⁸F]FDG and [¹⁸F]FLT small animal PET. The c-MET inhibitor ZK 7003295 or control vehicle was administered orally in H746T tumor bearing mice (n=5 per group) twice a day in different doses (control vehicle, 0.1, 0.3, 1, 3, 10 mg/kg). ZK 7003295 efficacy was evaluated with [¹⁸F]FDG and [¹⁸F]FLT small animal PET before the treatment, 48h and 96h after first treatment. PET data were compared to tumor growth curves and autoradiography. Biomolecular analysis of tumor tissue probes (% phosphorylation of c-Met, ERK and Cyclin D1) as well as Glut-1 and Ki67 stained sections of tumors were compared. ZK 7003295 reduces significantly tumor growth. [¹⁸F]FDG (3.83 %ID/cc ± 0.64 vehicle-group, 0.85 %ID/cc ± 0.5 96h post 10 mg/kg treated group) and [¹⁸F]FLT (3.1 %ID/cc ± 1.35 vehicle-group, 1.23 %ID/cc ± 0.21 48h post 10 mg/kg treated group) uptake in H746T tumors was significantly reduced in treated groups compared to the vehicle-group. No [¹⁸F]FLT uptake was seen 96h post treatment in tumors. Autoradiography confirmed the PET findings. Phosphorylation of c-Met, ERK and levels of Cyclin D1 and Ki67 were significantly reduced in tumor probes of treated mice. Membrane localization and expression levels of Glut-1 were dose dependently reduced. No influence of the c-MET inhibitor treatment was seen on the bodyweight und glucose levels. No adverse effects were observed in the animals. Our findings support application of the c-Met inhibitor ZK 7003295 for cancer therapy and the use of PET-imaging for early response monitoring.

Presentation Number **0225**
 Scientific Session 30: Novel Therapy

Focused-Ultrasound Induced Blood-Brain Barrier (BBB) Disruption to Enhance of Chemotherapeutic Drug Delivery for Glioblastoma Treatment

Hao-Li Liu^{1,2}, Mu-Yi Hua³, Pin-Yuan Chen⁴, Hung-Wei Yang³, Chiung-Yin Huang⁴, Jiun-Jie Wang⁵, Tzu-Chen Yen^{6,2}, Kuo-Chen Wei⁴,
¹Department of Electrical Engineering, Chang Gung University, Kweishan, Taoyuan,, Taiwan; ²Molecular Imaging Center, Chang-Gung Memorial Hospital, Taoyuan, Taiwan; ³Department of Chemical and Material Engineering, Chang-Gung University, Taoyuan, Taiwan; ⁴Department of Neurosurgery, Chang-Gung Memorial Hospital, Taoyuan, Taiwan; ⁵Department of Medical Image and Radiological Sciences, Chang-Gung University, Taoyuan, Taiwan; ⁶Department of Nuclear Medicine, Chang-Gung Memorial Hospital, Taoyuan, Taiwan. Contact e-mail: haoliliu@mail.cgu.edu.tw

Focused ultrasound can transiently and reversibly disrupt the blood-brain barrier (BBB) in a localized fashion, opening new frontiers for treating disorders of the central nervous system. The purpose of this study is to demonstrate the feasibility of using focused ultrasound (FUS) to enhance delivery of chemotherapeutic agent (BCNU) delivery for C6-glioma brain-tumor model treatment and determine if such an approach increases treatment efficacy. A focused ultrasound generator was used to transcranially disrupt the BBB in rat brains by delivering burst-tone ultrasonic energy under the presence of microbubbles. The process was monitored in vivo by magnetic resonance imaging (MRI). BCNU deposited in brains was quantified by high performance liquid chromatography, and brain tissues were examined histologically. MRI was used to evaluate the effects of tumor treatment longitudinally, including analysis of tumor progression and animal survival. Results showed that focused ultrasound significantly enhanced the penetration of BCNU through the BBB by >300% without causing brain damage, and Combining focused ultrasound with BCNU delivery improved treatment efficacy, significantly suppressing tumor growth and prolonging survival. This study strongly supports the feasibility of this treatment in a clinical setting, and provides a means of increasing localized chemotherapeutic drug delivery for brain tumor treatment.

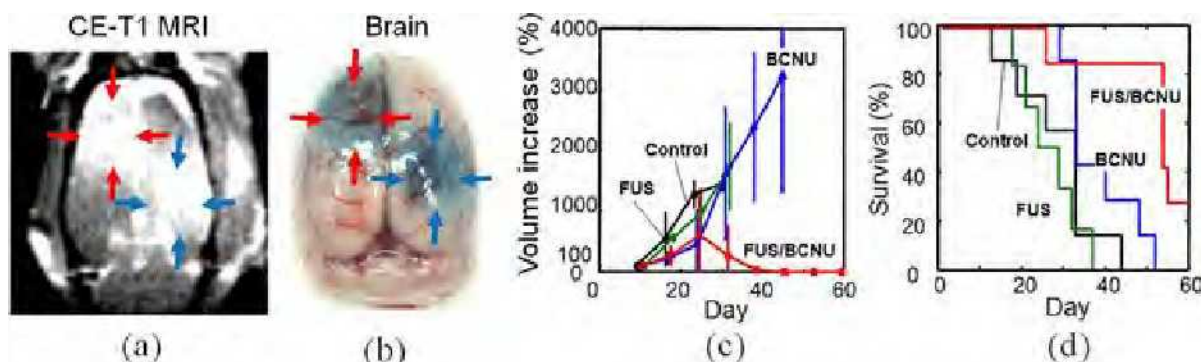


Figure. (a) Contrast-enhanced T1-weighted MRI of rat brains showing BBB disruption at two sonicated regions; (b) Blue-dye stained brains of the corresponding to (a); (c) tumor progression rate (in % relative to Day 10); (d) Kaplan-Meier animal survival (group 1 = control; group 2 = BCNU only; group 3 = FUS only; group 4 = combine BCNU with FUS).

Presentation Number **0953A**

Poster Session 2c: In Vivo Studies & Development/Novel Use of Imaging Probes

Gold Nanoparticles in PEGylated Dendrimer as a CT Contrast Agent for blood pool

Chie Kojima¹, Yasuhito Umeda², Mikako Ogawa³, Atsushi Harada², Yasuhiro Magata^{3,4}, Kenji Kono², ¹Nanoscience and Nanotechnology Research Center, Osaka Prefecture University, Sakai, Japan; ²Dept. of Applied Chemistry, Osaka Prefecture University, Sakai, Japan; ³Photon Medical Research Center, Hamamatsu University School of Medicine, Hamamatsu, Japan; ⁴Molecular Imaging Frontier Research Center, Hamamatsu University School of Medicine, Hamamatsu, Japan. Contact e-mail: c-kojima@21c.osakafu-u.ac.jp

X-ray computed tomography (CT) is a common in vivo imaging technique. The blood pool imaging is indispensable for diagnosis of heart, brain and vascular diseases. Commercially available contrast agents of blood pool, iodinated compounds, are rapidly excreted. Thus, it is difficult to perform the long term detection of blood pool. We have studied the application of unique macromolecules, dendrimers, to drug delivery system. And, polyethylene glycol (PEG)-attached dendrimers have been produced as a potential drug carrier with long blood circulation. In this paper, the PEGylated dendrimer was used as a carrier of gold nanoparticles (Au NPs) because they are a potential CT contrast agent. Au NPs were prepared in the PEGylated dendrimer by reducing gold ions inside the dendrimer ([1], Figure). To enhance the CT intensity, the Au NP was grown by adding gold ion and a reductant at various equivalents to the dendrimer solution. Diameter of the grown Au NPs increased, with increasing the amount of gold ions in the seeding growth. The X-ray attenuation of the Au-NPs also increased after the seeding growth of Au NPs. The Au NPs grown in the PEG-attached dendrimer at the maximum under our condition exhibited the similar CT value to a commercial iodine agent, iopamidol, in vitro. This Au NP-loaded PEGylated dendrimer was injected into mice, and the CT images were obtained after different times. In comparison of the Au NP-loaded dendrimer, iopamidol was also injected. The Au NP-loaded PEGylated dendrimer achieved a blood pool imaging, which was greater than a commercial iodine agent. Even though iopamidol was excreted after 1 min, the PEGylated dendrimer loading the grown Au NP was not essentially excreted even after 60 min. Instead, the Au NP encapsulated in the PEGylated dendrimer was accumulated in liver. In conclusion, the grown Au NPs-encapsulated dendrimers are useful for blood pool contrast agent of CT. (Reference) [1] Y. Haba, C. Kojima, A. Harada, T. Ura, H. Horinaka, K. Kono. *Langmuir*, 23, 5243-5246 (2007).

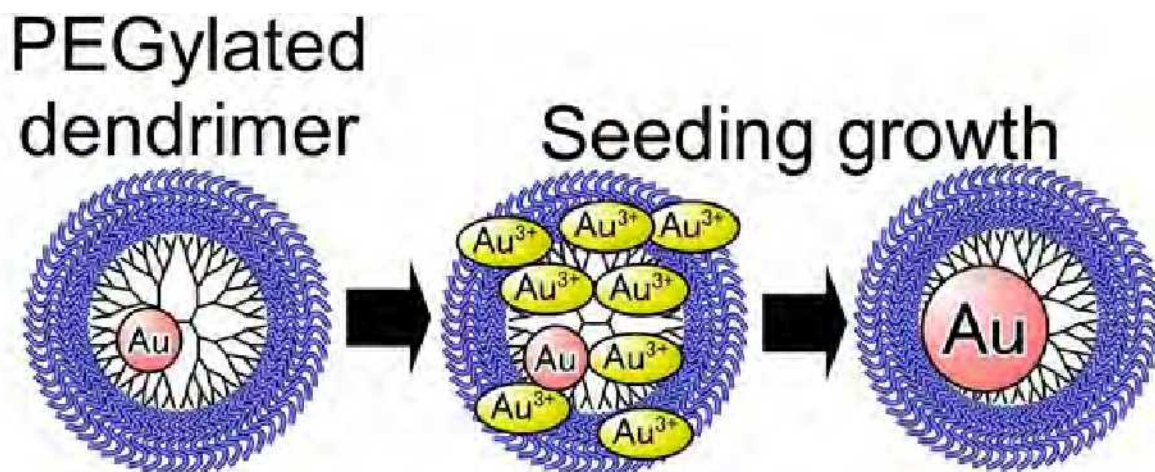


Figure 1. Preparation of gold nanoparticles in the PEGylated dendrimer.

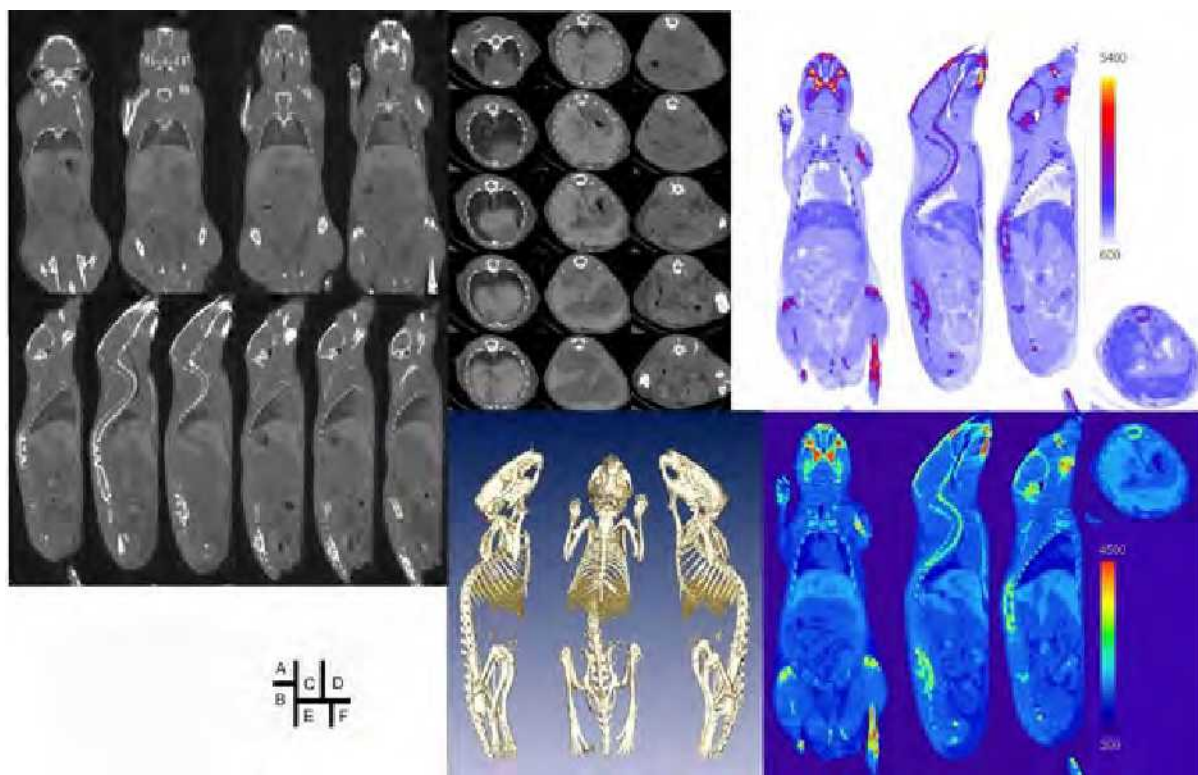
Presentation Number **0954A**

Poster Session 2c: In Vivo Studies & Development/Novel Use of Imaging Probes

In vivo CT imaging of Gold Nanoparticles: RES-Selective Contrast Enhancement

Adrian Chrastina, Jan Schnitzer, Proteogenomics Research Institute for Systems Medicine, San Diego, CA, USA. Contact e-mail: achrastina@prism-sd.org

Gold-based nanoparticle formulations have inherent X-ray attenuation capability (high atomic number and electron density) and therefore they might be suitable for development of radiographic contrast media. In this study, we performed analysis of in vivo tissue contrast enhancement after systemic administration of colloidal gold (30 nm) dispersion into mice. Nearly monodisperse gold nanoparticles sterically stabilized by grafting of hydrophilic polyethylene glycol (PEG) on the surface were prepared by reduction of chloroauric acid H₂AuCl₄ with sodium citrate following the Turkevich and Frens method with some modifications. Nanoparticles were characterized by spectral analysis and size was determined by dynamic light scattering and transmission electron microscopy. Mice received gold dispersion intravenously and computerized tomography (CT) scans were acquired using CT-SPECT second generation MicroSPECT® small animal imaging system. Tomographic acquisitions were reconstructed by standard filtered backprojection and further processed on the AMIRA system. Static X-ray scans and CT tomographic acquisitions revealed significant hepatic and splenic opacification already at 1h after administration. We have observed excellent demarcation of liver lobes from other internal organs not recognizable before injection. Selective contrast enhancement in tissues of reticuloendothelial system (RES; liver and spleen) was further verified and confirmed in dissected tissues samples and was found to be persistent over all analyzed time points up to 30 days. Our study provides useful insights in the biodistribution pattern, tissue deposition and in vivo stability of 30 nm gold particles and suggests further investigation of gold-nanoparticles as a potential radiographic contrast agents.



CT-images of balb/c mouse 1 h after iv injection of cAu nanoparticles (5 mg). Coronal (A); sagittal (B) and axial (C) projections. E; 3-D isosurface reconstruction of CT data. Physics (D) and temperature (F) scales were applied to further show contrast enhancement in liver and spleen.

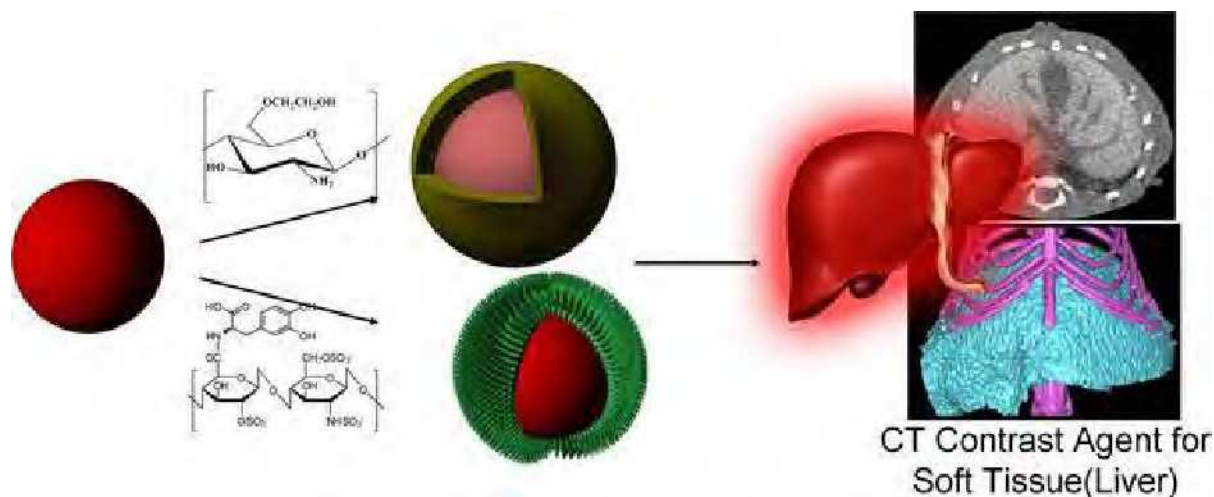
Presentation Number **0955A**

Poster Session 2c: In Vivo Studies & Development/Novel Use of Imaging Probes

Biocompatible Gold Nanoparticles for Liver-Specific CT Imaging

In-Cheol Sun¹, **Kuiwon Choi**¹, **Ick Chan Kwon**¹, **Cheol-Hee Ahn**², **Kwangmeyung Kim**¹, ¹*Biomedical Research Center, Korea Institute Science and Technology, Seoul, Republic of Korea;* ²*Department of Materials Science and Engineering, Seoul National University, Seoul, Republic of Korea. Contact e-mail: pfesun@gmail.com*

We developed a new method of encapsulating gold nanoparticles (AuNP) with biocompatible polymers. The stability and biocompatibility of AuNP were significantly enhanced due to the existence of polymer. Bio-distribution and tissue targeting properties were able to be controlled by changing polymers on the surface of AuNP. A different aspect of accumulation of AuNP in the tissue according to the surface property was observed. This targeting property was applied as a tissue specific CT contrast agent because X-ray absorption of concentrated AuNP is higher than that of iodine. CT images of tissues were acquired from micro-CT and the contrast enhancement was achieved using polymer-coated AuNP when they compared to one using commercial iodine based CT contrast agent. Those polymer coated AuNPs were characterized with TEM, UV-vis and zeta-potential measurement. Biocompatible AuNPs showed low toxicity, prolonged stability and enhanced contrast, which is suitable for the biomedical application such as molecular imaging probes.



Presentation Number **0956A**

Poster Session 2c: In Vivo Studies & Development/Novel Use of Imaging Probes

Multifunctional, Polymer-coated Gold Nanoparticles for CT Imaging of Cancer

Myeong Ju Moon¹, SangJoon Lee^{2,4}, Hwa Jeong Lee^{2,3}, Hieu Vu-Quang^{2,4}, Hui Lian Che^{2,3}, Jeong Hwa Shin¹, In-Kyu Park^{2,3}, Yong Yoen Jeong¹, ¹Radiology, Chonnam National University Medical School, Gwangju, Republic of Korea; ²Biomedical Sciences, Chonnam National University Medical School, Gwangju, Republic of Korea; ³Heart Research Center, Chonnam National University Hospital, Gwangju, Republic of Korea; ⁴Clinical Vaccine R&D Center, Chonnam National University, Gwangju, Republic of Korea. Contact e-mail: mjmoon2398@gmail.com

X-ray based computed tomography (CT), is among the most convenient imaging/diagnostic tools in hospitals today in terms of availability, efficiency and cost. However, in contrast to magnetic resonance imaging (MRI) and various nuclear medicine imaging modalities, CT is not considered a molecular imaging modality since targeted and molecularly specific contrast agents have not yet been developed. Gold induces a strong X-ray attenuation, and gold of nano-size have in addition, unique physical, chemical and biological properties, which make them an ideal candidate for CT contrast agents. Here we synthesized multifunctional gold nanoparticles (MFGNP) as a CT imaging agent. Their sizes were controlled under 20 nm enabled the targeted accumulation to tumor by the enhanced permeability and retention (EPR) effect. Their surface were coated PEG (poly ethylene glycol) for enhancing blood circulation time. At the same time, they were coated bPEI (branched poly ethylene imine) for conjugating targeting ligand and therapy materials. MFGNP were characterized size, shape and properties for Transmission Electron Microscopy (TEM), Dynamic Light Scattering Particle Size Analysis (DLS), Zeta-potential and Thermo Gravimetric Analysis (TGA). Thereafter, we observed endocytosis of MFGNP in CT-26 cell line in vitro, and analyzed in vivo biodistribution of MFGNP and cancer targeting effect in tumor-xenografted mice. In conclusion, the size and shape of MFGNP were observed to be around 20nm and spherical, respectively. Also, they were confirmed positive charge and water-soluble property. Through this result, we verified that it was coated two polymers (PEG, PEI) at gold nanoparticles. We confirmed intracellular uptake in vitro & vivo tumor model. MFGNP could be utilized as a molecular probe for early diagnosis of cancer or cell labeling. In addition, it will be easily developed with introduction of other bioactive agents such as an anticancer drug, genes, or an active tumor-targeting moiety for further biomedical explorations.

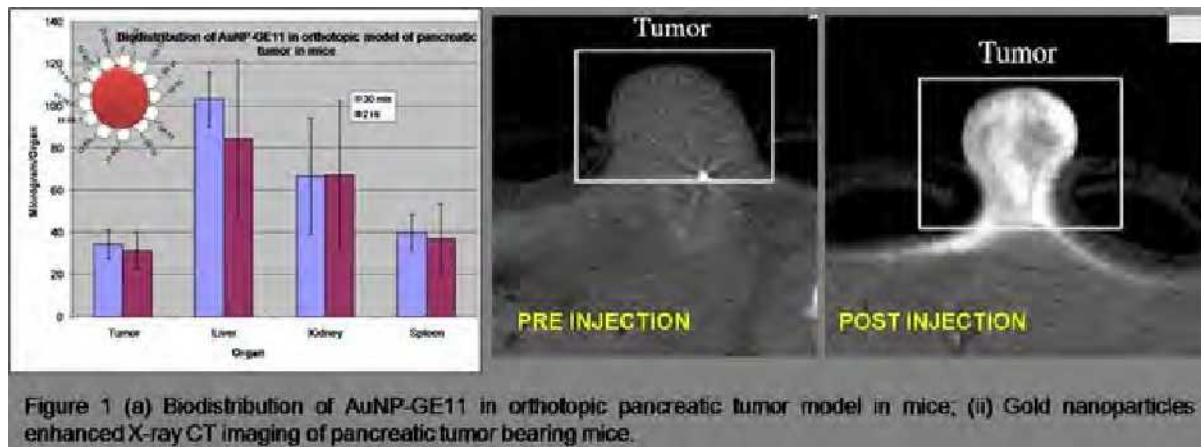
Presentation Number **0957A**

Poster Session 2c: In Vivo Studies & Development/Novel Use of Imaging Probes

TARGETED GOLD NANOCONJUGATES AS X-RAY CONTRAST ENHANCERS FOR MOLECULAR IMAGING OF PANCREATIC CANCER

Raghuraman Kannan¹, **Nripen Chanda**¹, **Ravi Shukla**¹, **Ajit Zambre**¹, **Evan J. Boote**¹, **Priyabrata Mukherjee**², **Debabrata Mukhopadhyay**², **Shamit K. Dutta**², **Jameel A. Khan**², **Kattesh V. Katti**¹, ¹Radiology, University of Missouri-Columbia, Columbia, MO, USA; ²Biochemistry and Molecular Biology, Mayo Clinic, Rochester, MN, USA. Contact e-mail: kannanr@health.missouri.edu

Over 95% of pancreatic cancer patients die within five years of detection. Early detection appears to be the key to survival for pancreatic cancer patients. Epidermal Growth Factor Receptor (EGFR) is over expressed in more than 95% of human pancreatic cancer patients. A number of peptides and monoclonal antibodies have been developed to target the EGFR in pancreatic cancer. Our research has focused on developing EGFR targeting biomolecule conjugated gold nanoparticles as X-ray contrast agents for CT imaging of pancreatic tumor. In this study, we synthesized a series of Antibody EGFR (monoclonal antibody -cetuximab) and EGFR-peptide (GE11) conjugated AuNPs. We investigated the in vivo EGFR targeting characteristics of these conjugates in orthotopic pancreatic tumor mice models. Our investigation establishes that the peptide conjugated AuNPs have high in vivo mobility and targets pancreatic tumor effectively. We have also established that EGFR-peptide -AuNP conjugates act as better X-ray contrast agents for early detection of pancreatic cancer in mice models. The details of this study will be presented in this poster.



Presentation Number **0896B**

Poster Session 3c: In Vivo Studies & Development/Novel Use of Imaging Probes

α V β 3 integrin targeted dynamic contrast enhanced MR imaging using Gd-DTPA loaded dendrimer conjugated with cyclic RGD in a mouse xenograft model

Wei-Tsung Chen^{1,2}, **Tiffany Ting-Fang Shih**^{2,3}, **Ching-Hsuan Tung**⁴, **Wen-Yuan Hsieh**⁶, **Ran-Chou Chen**⁵, **Hsing-Yang Tu**^{1, 1}, ¹Radiology, Taipei City Hospital, Ren Ai branch, Taipei, Taiwan; ²Radiology, School of Medicine, National Taiwan University, Taipei, Taiwan; ³Medical imaging, National Taiwan University Hospital, Taipei, Taiwan; ⁴Imaging Chemistry, Methodist Hospital Research Institute, Houston, TX, USA; ⁵Union Chemical Laboratory, Industrial Technology Research Institute, Hsinchu, Taiwan; ⁶Biomedical Imaging and Raiological Sciences, National Yang-Ming University Hospital, Taipei, Taiwan. Contact e-mail: wt2000.chen@msa.hinet.net

Purpose: To validate an α V β 3 integrin targeted dendrimer, PEG-G3-(Gd-DTPA)3-(cRGD-DTPA)2 (figure 1), for its ability to detect angiogenesis by using dynamic contrast enhance MRI. Procedures: α V β 3 integrin positive U87 cells, beta3 integrin siRNA knockdown U87cells, and α V β 3 integrin negative KB cells, were incubated with fluorescein-labeled dendrimer, and their cellular attachment ability was observed. Dynamic contrast enhanced MRI was performed on mice bearing U87 tumors by injecting PEG-G3-(Gd-DTPA)3-(cRGD-DTPA)2 or PEG-G3-(Gd-DTPA)3-(cRAD-DTPA)2, and the enhancement patterns and parameters were analyzed. Results: Green fluorescence was found in the U87 cells in the cellular attachment experiment, but was much less seen in β 3 integrin siRNA knockdown U87 cells and α V β 3 integrin negative KB cells. Decreased green fluorescence was also seen in 500X free RGD competition group. In the dynamic contrast enhanced MRI, the 30 minute contrast washout percentage was $-6\pm 12\%$ in the PEG-G3-(Gd-DTPA)3-(cRGD-DTPA)2 injection group (n=10) and $36\pm 23\%$ in the PEG-G3-(Gd-DTPA)3-(cRAD-DTPA)2 injection group (n=10). A 12% cut-off point gave a sensitivity of 94.4%, and a specificity of 93.8%. There exist statistically significant differential distribution of the enhancement patterns between the two contrast agents (p<0.001)(Table 1). Conclusions: We have demonstrated the α V β 3 integrin targeting ability of PEG-G3-(Gd-DTPA)3-(cRGD-DTPA)2 in vitro and in vivo. A 12% cut-off point for a 30 minute washout percentage can be used as a useful parameter for the detection of angiogenesis.

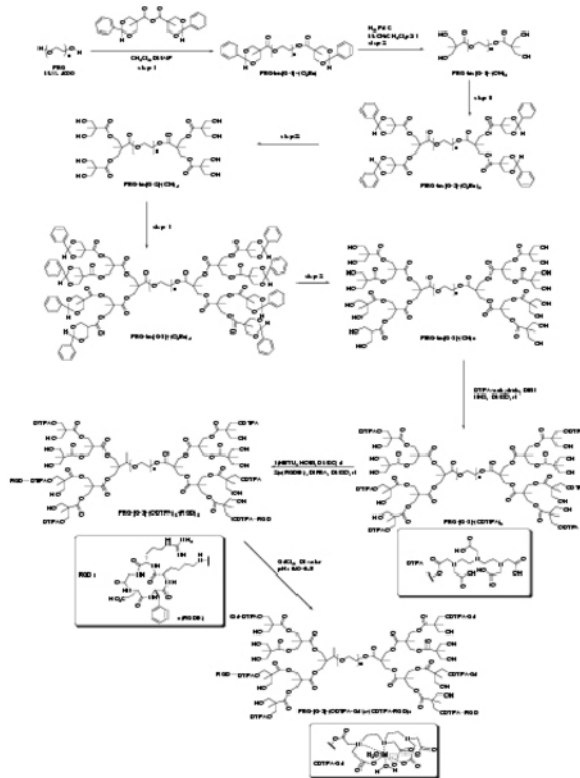


Figure 1 . The synthesis scheme of the PEG-G3-(Gd-DTPA)3-(cRGD-DTPA)2 dendrimer.

Distribution of the enhancement patterns in PEG-G3-(Gd-DTPA)3-(cRGD-DTPA)2 and PEG-G3-(Gd-DTPA)3-(cRAD-DTPA)2 injection groups

	type A	type B	type C
PEG-G3-(Gd-DTPA)3-(cRGD-DTPA)2 injection group	7	3	0
PEG-G3-(Gd-DTPA)3-(cRAD-DTPA)2 injection group	0	1	9

Presentation Number **0897B**

Poster Session 3c: In Vivo Studies & Development/Novel Use of Imaging Probes

Europium(II) complexes as potential contrast agents for MRI*Matthew J. Allen, Chemistry, Wayne State University, Detroit, MI, USA. Contact e-mail: mallen@chem.wayne.edu*

We present our progress toward stabilizing the Eu(II) ion from oxidation to study the influence of water-exchange rate on contrast enhancement at high field strengths. Although Gd(III)-based agents are good contrast agents at low field strengths (~1.5 T), they become less effective at high field strengths (≥ 7 T). At these high fields, Eu(II) is potentially an excellent contrast agent because of its near optimal water-exchange rate ($3 \times 10^8 \text{ s}^{-1}$). [1] The major barrier preventing the use of Eu(II) complexes as contrast agents is their propensity to oxidize. To increase the utility of Eu(II) as a contrast agent, it is desirable to increase the oxidative stability of the Eu(II) ion in aqueous solution. We are working toward increasing the oxidative stability of the Eu(II) ion by modifying the current most stable ligand for this electron-rich ion, 2,2,2-cryptand. Our strategy involves changing the electronic properties of the ligand, changing the ligand cavity size, increasing the steric bulk of the ligand, and optimizing the hard-soft acid-base chemistry of the ligand. Here, we present our efforts to overcome the obstacle of oxidative instability using coordination chemistry. We will present trends in oxidative stability of the Eu(II) complexes of our new ligands, which have resulted in the most oxidatively stable Eu(II) aqueous complex to date. Our Eu(II) cryptates are a step toward realizing the full use of the magnetic and optical properties of this ion, ultimately leading to air-stable Eu(II) complexes that could serve as powerful contrast agents for high field strength MRI. [1] Burai, L.; Scopelliti, R.; Tóth, É. Chem. Commun. 2002, 2366-2367.

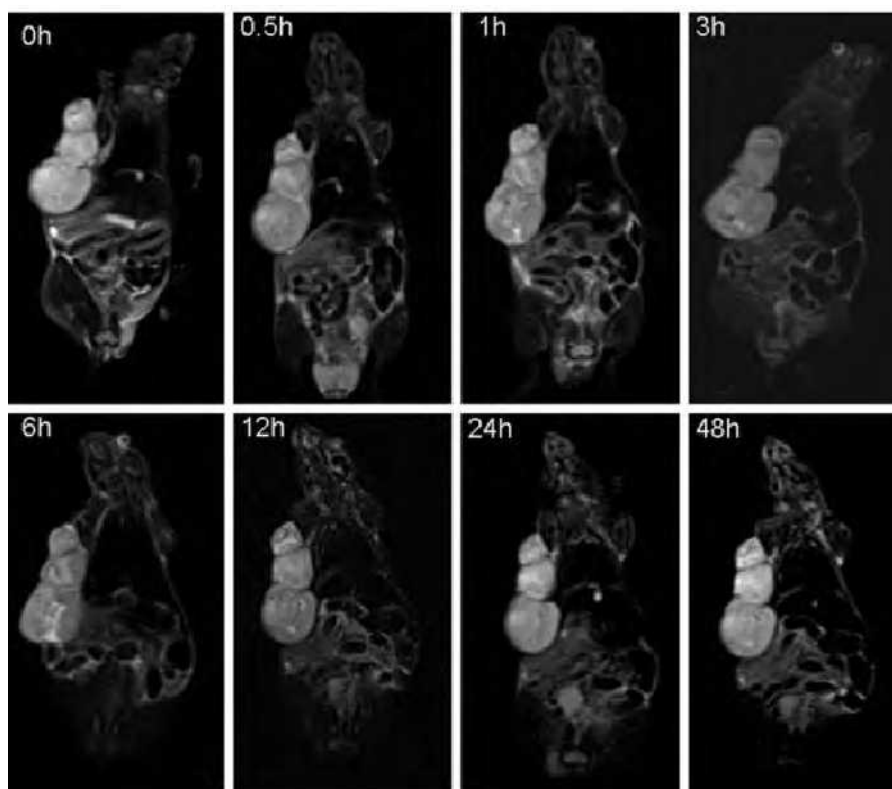
Presentation Number **0898B**

Poster Session 3c: In Vivo Studies & Development/Novel Use of Imaging Probes

Molecular MR imaging of colorectal carcinoma with novel superparamagnetic iron oxide loaded nanovesicles in a rodent model: in vitro and in vivo studies

Alex Ching¹, Shi Ting Feng², Hao Li³, Can Hui Sun², Hua Song Cai², Peng Xin Qiu⁴, Jian Zhou², Xin Tao Shuai³, Zi Ping Li², Qf Meng², ¹Insitut National des Science et Techniques Nuclearies, Commissariat a l'Energie Atomique, Saclay, France; ²Department of Radiology, The First Affiliated Hospital, Sun Yat Sen University, Guangzhou 510080, China; ³School of Chemistry and Chemical Engineering, Sun Yat-Sen University, Guangzhou 510275, China; ⁴Department of Pharmacology, Zhongshan Medical College, Sun Yat-Sen University, Guangzhou 510080, China. Contact e-mail: chingssc@hotmail.com

Objectives: We evaluate the uses of novel superparamagnetic iron oxide loaded polymeric nanovesicles (SPIOPN) in human colon adenocarcinoma cell LoVo by in vitro and in vivo MR imaging. **Methods:** New SPIOPN form PDLLA and PEG was prepared by a multiple emulsion/solvent evaporation techniques. The novel nanovesicles were loaded with hydrophobic and hydrophilic forms of SPIO. Human colorectal adenocarcinoma LoVo-6-luc-1 cells and human hepatic cells L-O2 were cultured in media containing different SPIOPN concentration. MR imaging of these two cell lines were performed with T2-weighted sequences. T2 relaxivities rate were measured using T2-weighted mapping software. The differences of T2 relaxivities rate between LoVo and L-O2 cells were compared. The growth ability of different cell lines was evaluated using MTT assay. BALB/C nude mice model with LoVo xenograft was made (n=18). Three equal numbered groups were received same SPIO concentration of 1) water-soluble SPIO particles, 2) hydrophobic and 3) hydrophilic SPIOPN i.v. injection respectively. Serial MR T2-weighted imaging was obtained and T2 relaxation time was measured in the tumour, liver and muscle by using T2 mapping software. **Results:** SPIOPN were more superparamagnetic than water-soluble SPIO. SPIOPN showed higher T2 relaxivity rate with LoVo cells than L-O2 cells. Hydrophilic SPIOPN showed higher T2 relaxivity rate than hydrophobic form. MTT assay revealed no significant difference in optical density by using different concentration of SPIOPN in the cell lines. In nude mice model, T2-weighted MR signal of the human colon adenocarcinoma LoVo xenografts was significantly decreased with SPIOPN (see figure). There was no significant difference in T2-weighted signal intensity in the groups with hydrophobic and hydrophilic SPIOPN. Histopathology confirmed the presence of SPIO in tumour cells. **Conclusions:** The feasibility to image human colonic adenocarcinoma LoVo with novel SPIOPN was shown on in vitro monitoring and in a rodent MR model.



Sequential whole body MR coronal T2W images of a mouse showed a gradual decrease in T2W signal intensity of LoVo xenograft after SPIOPN injection.

Presentation Number **0899B**

Poster Session 3c: In Vivo Studies & Development/Novel Use of Imaging Probes

Hyperpolarized ^{13}C MR Reporter Probe System with *Acy-1* Gene and $[1-^{13}\text{C}]$ N-acetyl-L-methionine

Albert P. Chen¹, **Ralph E. Hurd**², **Yi-ping Gu**³, **David M. Wilson**⁴, **Charles H. Cunningham**³, ¹GE Healthcare, Toronto, ON, Canada; ²GE Healthcare, Menlo Park, CA, USA; ³Medical Biophysics, Sunnybrook Health Sciences Centre, Toronto, ON, Canada; ⁴Radiology, UCSF, San Francisco, CA, USA. Contact e-mail: Albert.Chen@ge.com

Introduction: Indirect labeling of cells with reporter genes allows a stable beacon for assessment of their survival, proliferation, migration and function at the target site. Techniques to achieve highly polarized nuclear spins states via dynamic nuclear polarization (DNP) and retain the polarization in solution were recently developed, and excellent ^{13}C MRI and MRS data depicting endogenous enzyme mediated reactions have been obtained in vitro and in vivo. It may also be feasible to use a hyperpolarized substrate to target a reporter enzyme. In this study, a hyperpolarized ^{13}C MR reporter system is demonstrated in cells transfected with a reporter gene, aminoacylase-1 (*Acy-1*), using pre-polarized $[1-^{13}\text{C}]$ acetyl-methionine as the probe. **Methods:** $[1-^{13}\text{C}]$ N-acetyl-L-methionine was polarized using a Hypersense DNP polarizer. Plasmid DNA of human *Acy-1* gene was transfected to HEK293 cells. Dynamic MRS (GE 3T scanner, 64 transients, $\text{TR}=3\text{s}$, 10° RF pulse) experiments were performed on intact cells ($\sim 2.5 \times 10^8$ cells, 24 hours after transfection) mixed with polarized ^{13}C substrate in solution. Experiments were repeated using the cell lysate. Non-transfected cells were used as control. **Results:** After the transfected cells (or lysate) were added to the polarized substrate solution, an increase in $[1-^{13}\text{C}]$ methionine signal was observed as the result of de-acetylation of $[1-^{13}\text{C}]$ acetyl-methionine (Fig.1) by the *Acy-1* enzyme. No observable de-acetylation of the substrate was measured with control. Enzyme activities of 1.9U and 1.4U were estimated from two intact cell experiments, while 3.2U and 4.8U were measured from the corresponding cell lysate. This proposed system has potential for targeted MR imaging in vivo.

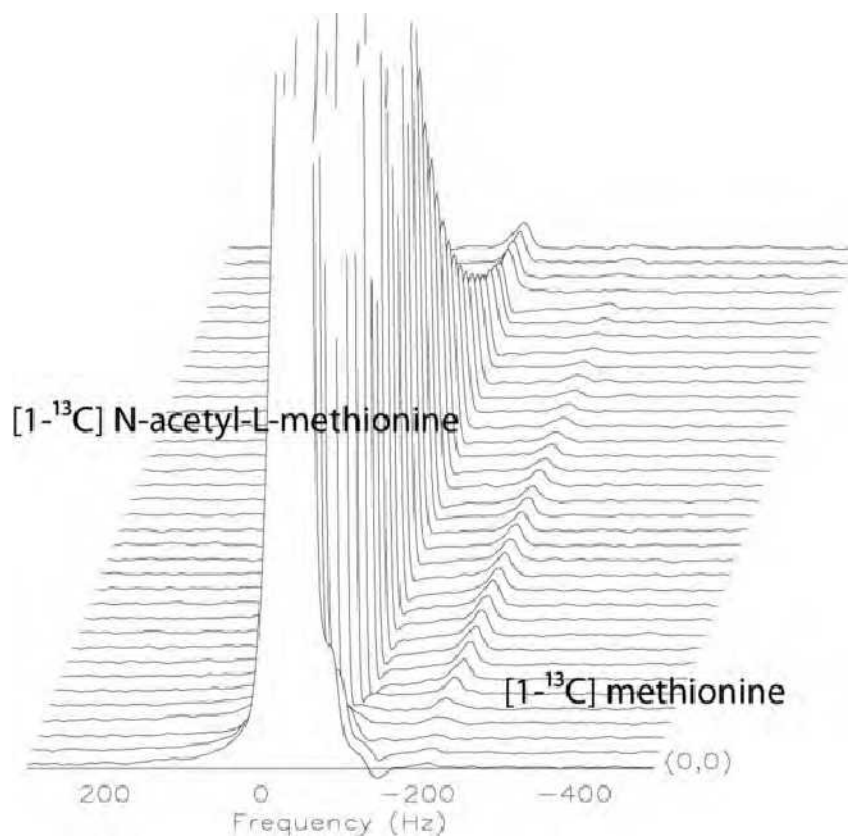


Figure 1. Representative dynamic MRS data from lysed cells that were transfected with the *Acy-1* reporter gene. The pre-polarized substrate $[1-^{13}\text{C}]$ N-acetyl-L-methionine was de-acetylated by the aminoacylase-1 enzyme and its product $[1-^{13}\text{C}]$ methionine was observed.

Presentation Number **0900B**

Poster Session 3c: In Vivo Studies & Development/Novel Use of Imaging Probes

Effect of Molecular Architecture on the Performance of ^{19}F MRI Imaging Agents

Hui Peng, Idriss Blakey, Kristofer J. Thurecht, **Andrew K. Whittaker**, The University of Queensland, Brisbane, QLD, Australia. Contact e-mail: a.whittaker@uq.edu.au

Recently there has been intense interest in the development of fluorinated molecules to allow tracking of therapeutic particles and cells.¹⁻⁴ An advantage of this imaging strategy is that specifically-labelled cells can be mapped in vivo, without any confounding endogenous background signal. The dynamic ^{19}F MR images can be superimposed on anatomical proton images acquired within the same imaging session. In this study we have examined in detail the effect of polymer composition, sequence distribution and architecture on the performance of candidate ^{19}F MRI imaging agents. Initially we prepared a series of amphiphilic diblock copolymers of acrylic acid with partially-fluorinated (meth) acrylate monomers using atom-transfer radical polymerization. The diblock copolymers could undergo spontaneous self-assembly in mixed and aqueous solvents to form stable micelles having a fluorine-rich core which provides a strong signal for MRI examinations. Significant differences in self-assembly and NMR properties were observed for block copolymers and for hyperbranched polymers. The NMR properties have been demonstrated to depend strongly on the composition of the hydrophobic block, and on the strengths of interactions between the fluorinated segments. Specifically the flexibility of the backbone and the polymer-solvent interaction parameters determine the details of molecular motion and hence averaging of the dipolar interactions between the fluorine spins. In this present paper the effects of polymer and particle structure on the spin-spin and spin-lattice relaxation times and, hence, ultimately on image intensity, are discussed. A detailed discussion of the relationships between polymer structure and the solution properties of assemblies of the copolymers and imaging performance will be given. References 1 Thurecht, K. J.; Blakey, I.; Peng, H.; Squires, O.; Hsu, S.; Alexander, C.; Whittaker, A. K. *Journal of the American Chemical Society* 2010, ASAP. 2 Peng, H.; Blakey, I.; Dargaville, B.; Rasoul, F.; Rose, S.; Whittaker, A. K. *Biomacromolecules* 2009, 10 (2), 374-381. 3 Janjic, J. M.; Srinivas, M.; Kadayakkara, D. K. K.; Ahrens, E. T. *Journal of the American Chemical Society* 2008, 130 (9), 2832-2841. 4 Du, W.; Nystrom, A. M.; Zhang, L.; Powell, K. T.; Li, Y.; Cheng, C.; Wickline, S. A.; Wooley, K. L. *Biomacromolecules* 2008, 9(10), 2826-2833.

Presentation Number **0901B**

Poster Session 3c: In Vivo Studies & Development/Novel Use of Imaging Probes

Visualization of Drug Accumulation and Release after Heating in Deep-Seated Tumor using Multimodal Thermo-sensitive Polymer-modified Liposome

Daisuke Kokuryo¹, Fuminori Ozaki², Iwao Kanno¹, Kenji Kono², Ichio Aoki¹, ¹*Biophysics Group, Molecular Imaging Center, National Institute of Radiological Sciences, Chiba, Japan;* ²*Graduate School of Engineering, Osaka Prefecture University, Sakai, Japan.* Contact e-mail: kokuryo@nirs.go.jp

Introduction: In previous work, our novel Multimodal Thermo-sensitive Polymer-modified Liposome (MTPL) containing a MR contrast agent, fluorescence dye and anticancer drug was shown to accumulate in the tumor area over 8 hours. Moreover, the MR signal intensity in the tumor region was observed to increase after localized heating. As a next step, we have applied our MTPL to a deep-seated tumor model with the aim of achieving localized drug release from the MTPL without side-effects. In this paper, we evaluated drug accumulation using quantitative MR imaging, and visualized the signal changes after heating. **Methods:** Our MTPL was composed of EYPC/DOPE/Cholesterol/PEG-2000-PE/EOEOVE-ODVE/Rhodamine-PE (23.4/15/54.6/4/2/1 mol%) enclosing MnSO₄ (300 mM) and doxorubicin (approximately 1.0 g/l). The average diameter of our MTPLs was approximately 120 nm. The structure of the MTPL changed from hydrophilic to hydrophobic at around 42.0 °C. Colon-26 cancer cells (2.0×10^5) were transplanted intramuscularly into nude female Balb/c mice. In order to evaluate the MTPL accumulation and to optimize the time that heat was applied after intravenous administration, T₁-mapping using a modified Look-Locker sequence (Chuang KH: Magn Reson Med., 2006) was performed on a 7.0 tesla horizontal MRI (Magnet: Kobelco + Jastec, Japan, Console: Bruker-biospin) with a 35 mm diameter volume coil. Heating (42.5 °C, 15 minutes) was applied using a high-power RF pulse with a 25 mm diameter surface coil (Takashima Seisakusho, Japan). **Results & Discussion:** R₁ (=1/T₁) values in tumor area increased for 4 hours after MTPL administration, and thereafter remained steady until 12 hours. At 24 hours, R₁ in the tumor area had decreased to 85% of the value at 4 hours. On the other hand, R₁ in the liver increased immediately after the MTPL administration but after 8 hours it began to decrease rapidly so that at 24 hours the value was similar to the one before administration. *Ex vivo* fluorescence imaging also showed that there was little signal in the liver area at 24 hours after administration. Therefore, the optimal time to apply heating and minimize side-effects was found to be between 12 and 24 hours. The signal intensity in the tumor after heating at 12-14 hours after the administration was higher than that before heating. The effects of treatment were also found to increase. This indicates that our MTPL is useful for 'theragnostic' imaging.

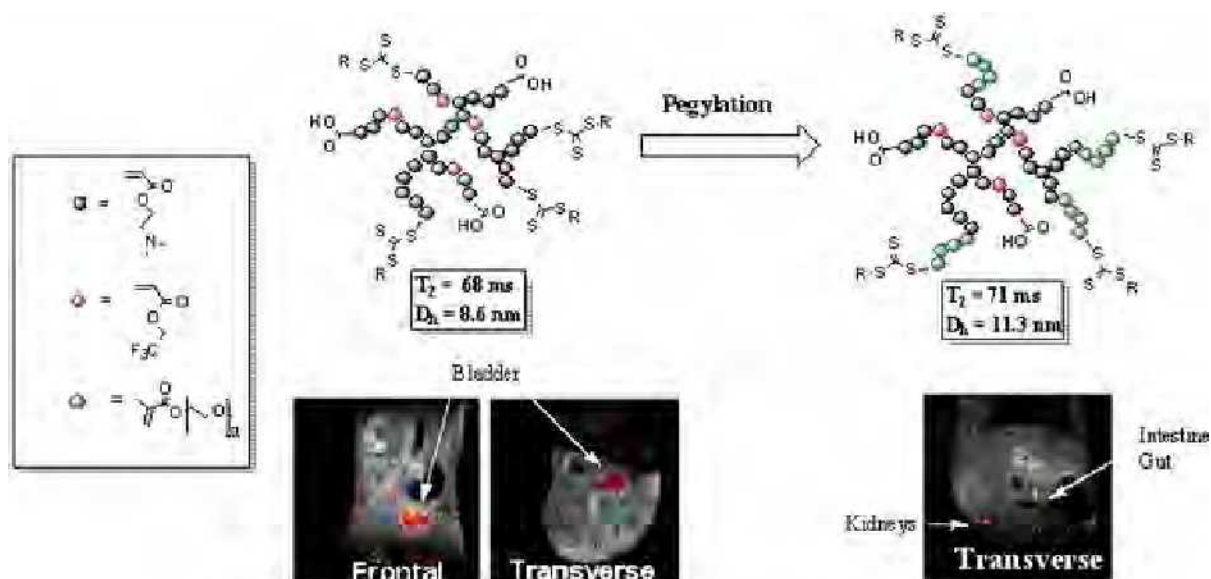
Presentation Number **0902B**

Poster Session 3c: In Vivo Studies & Development/Novel Use of Imaging Probes

Functional Hyperbranched Polymers: Towards Targeted in vivo ^{19}F Magnetic Resonance Imaging using Designed Macromolecules

Kristofer J. Thurecht¹, Idriss Blakey¹, Hui Peng¹, Oliver Squires¹, Steven H. Hsu¹, Cameron Alexander², Andrew K. Whittaker¹,
¹Australian Institute for Bioengineering and Nanotechnology and Centre for Advanced Imaging, The University of Queensland, Brisbane, QLD, Australia; ²School of Pharmacy, The University of Nottingham, Nottingham, United Kingdom. Contact e-mail: k.thurecht@uq.edu.au

Recent advances that facilitate control over polymer structure and functionality have led to the advent of polymer theranostics. Monitoring these devices in an in vivo clinical setting remains a significant scientific challenge, despite some elegant attempts to develop polymeric devices[1-3] or emulsions[4,5] for ^{19}F MRI. We report on the development of sensitive polymeric ^{19}F MRI contrast agents that combine controllable functionality, ability for cell-targeting and low cytotoxicity. Poor sensitivity in ^{19}F MRI of polymeric probes is attributed to three main factors: poor molecular mobility; association of fluorinated segments; and low fluorine content. To overcome such issues, we use hyperbranched polymers enabling high segmental molecular mobility while maintaining high fluorine content. Controlled functionality was introduced through specific chemistry and molecular mobility was conferred via low-T_g (acrylate) and polar repeat units. Random branching frustrates aggregation of the fluorinated segments allowing incorporation of up to 20 mol % fluoro-monomer. Hyperbranched polymers also facilitate orientation of functionality, such as cell-targeting agents, thus ensuring correct presentation for efficient biological recognition. Particle size and ^{19}F T₂ relaxation times (at 7 T) are presented for the first generation construct and the device following pegylation (Figure 1). Upon intravenous injection into mice, the first generation polymer quickly accumulated in the bladder suggesting rapid clearance from the body. The pegylated analogue, however, was located throughout many organs (kidneys, intestine and gut - Figure 1). This is undoubtedly due to the longer retention and circulation time for the pegylated species. This is the first example of polymeric devices being used for ^{19}F in vivo imaging and we show image times of less than 10 minutes. Such devices are ideal for developing the field of theranostics due to the high level of functionality within the polymers. 1 Nystrom, A. M. et al. J. Poly. Sci., Part A: Poly. Chem. 2009, 47, 1023-1037. 2 Du, W. et al. Biomacromolecules 2008, 9, 2826-2833. 3 Peng, H. et al. Biomacromolecules 2009, 10, 374-381. 4 Janjic, J. M. et al. J. Am. Chem. Soc. 2008, 130, 2832-2841. 5 Ahrens, E. T. et al. Nat. Biotechnol. 2005, 23, 983-987.



Presentation Number **0903B**

Poster Session 3c: In Vivo Studies & Development/Novel Use of Imaging Probes

Virus-capsid Based Nano-sized, High-relaxivity MRI Contrast Agents

Ankona Datta^{1,2}, Praveena D. Garimella³, Mauro Botta⁴, Matthew B. Francis^{3,5}, Kenneth N. Raymond³, ¹Prior Affiliation: Department of Chemistry, University of California, Berkeley, CA, USA; ²Current Affiliation: Department of Chemical Sciences, Tata Institute of Fundamental Research, Mumbai, India; ³Department of Chemistry, University of California, Berkeley, CA, USA; ⁴Dipartimento di Scienze dell'Ambiente e della Vita, Università del Piemonte Orientale "Amedeo Avogadro", Alessandria, Italy; ⁵Materials Sciences Division, Lawrence Berkeley National Labs, Berkeley, CA, USA. Contact e-mail: ankona@tifr.res.in

Magnetic Resonance Imaging (MRI) is widely used for medical imaging because of its high depth penetration and its ability to differentiate soft tissues. Although this technique can provide anatomical details it lacks the μM - nM sensitivity required for molecular imaging.¹ Paramagnetic agents are usually administered to improve the contrast in MRI. These agents are evaluated on the basis of their relaxivity, which is defined as the increase in the relaxation rate of water molecule protons per mM concentration of contrast agent applied. Current commercial agents have low relaxivity values ($4\text{-}5\text{ mM}^{-1}\text{s}^{-1}$) and hence gram quantities of Gd have to be injected to obtain significant contrast enhancement. According to theory, relaxivity values of up to $350\text{ mM}^{-1}\text{s}^{-1}$ can be achieved under current clinical field strengths (60-100 MHz) if the properties of the contrast agents (CAs) are optimized. CAs having such high relaxivity values would be useful both to reduce the amount of Gd to be injected and also to obtain the high sensitivities required for molecular imaging. Relaxivity values of CAs can be improved by slowing their tumbling rate provided the water residence time of the water molecules in the inner-sphere of the paramagnetic metal ion is optimum (10-20 ns). Gd-hydroxypyridonate (HOPO) based CAs have 2-3-fold higher relaxivity values than commercial agents due to the higher number of inner sphere water molecules and optimum water residence times. We have attached multiple Gd-HOPO based CAs to nano-sized virus capsids in order to optimize tumbling rates.² Strategies were developed to exclusively modify either the external or the internal surface of the capsids. Relaxivity values as high as $41.6\text{ mM}^{-1}\text{s}^{-1}$ (per Gd, at 30 MHz and 298 K) were achieved for the internally modified capsids. The results obtained from detailed relaxometric studies on these systems indicated that the rigidity of the linker attaching the CA to the macromolecule could be a crucial factor determining relaxivity values.³ In order to check this hypothesis Gd-HOPO based agents were attached to virus capsids by using a series of linkers with varying rigidity. The results indicate that although greater linker rigidity leads to higher relaxivity values the internal motions of the macromolecule (in this case the protein shell of the virus capsid) might be a limiting factor for the maximum relaxivity values that can be achieved in this system. 1. Datta and Raymond, Acc. Chem. Res., 2009, 938-947 2. Hooker et al., Nano Lett. 2007, 2207-2210 3. Datta et al., J. Am. Chem. Soc., 2008, 2546-2552

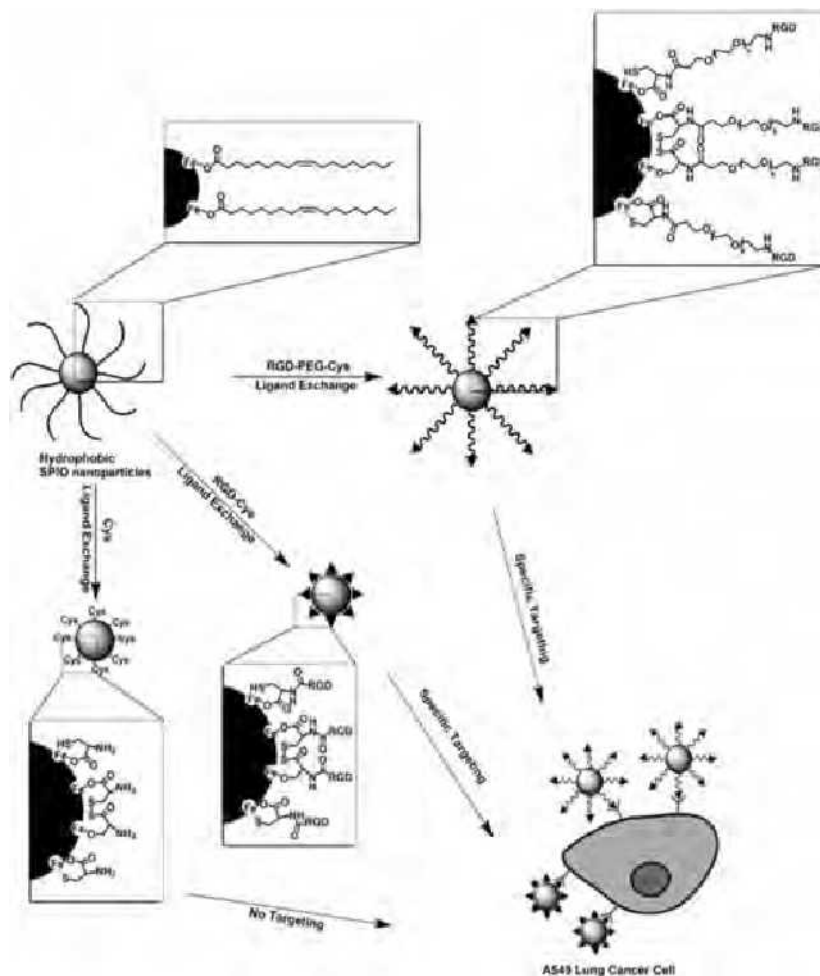
Presentation Number **0904B**

Poster Session 3c: In Vivo Studies & Development/Novel Use of Imaging Probes

Cysteine-terminated peptide replacement: a general strategy to fabricate MR molecular imaging probe for cancer detection

Chunfu Zhang, Med-X Research Institute, Shanghai Jiao Tong University, Shanghai, China. Contact e-mail: zchunfu@yahoo.com.cn

Introduction Due to the hydrophobic surface, the biological application of superparamagnetic iron oxide nano particles (SPIO) coated with oleic acid is limited. So, in this study, we developed a novel method to fabricate MR molecular imaging probes by direct replacing surface oleic acid with small peptides terminated with cysteine. **Materials and Methods** Oleic acid-coated SPIO was transferred into being hydrophilic one by surface replacing oleic acid with cysteine, RGD-Cys or RGD-PEG-Cys. The specificity of RGD-Cys-SPIO or RGD-PEG-Cys-SPIO in vitro was studied by co-culturing A549 cells with the probes using Cys-SPIO as control. Cell uptake of the probes was detected with Prussian blue staining and quantified by ICP-OES measurement. The specificity of the probes for tumor was evaluated by a 3T MRI scanner. **Results** The size of oleic acid-coated SPIO is 6.7 nm, which does not change after the surface ligand exchanges indicated by TEM images. The hydrodynamic size of Cys-, RGD- and RGD-PEG-Cys-SPIO are 10 nm, 11 nm and 13 nm, respectively. After ligand exchange, the T2 relaxivities of the water-soluble particles are 139.06 s⁻¹ mM⁻¹ for Cys-SPIO, 141.53 s⁻¹ mM⁻¹ for RGD-Cys-SPIO and 141.33 s⁻¹ mM⁻¹ for RGD-PEG-Cys-SPIO. Both RGD-Cys-SPIO and RGD-PEG-Cys-SPIO can specifically target $\alpha\beta3$ -expression cells (A549) in vitro, with RGD-Cys-SPIO more efficiently. Furthermore, MR imaging of A549 tumors receiving RGD-Cys-SPIO or RGD-PEG-Cys-SPIO demonstrate both probes can also address tumors, with RGD-PEG-Cys-SPIO more effectively. **Histological study** of tumor tissues show that the probes not only target tumor neovasculatures but also extravasate from vessels registering tumor cells. **Summary** We demonstrate a novel strategy to transfer the hydrophobic SPIO hydrophilic and fabricate MR molecular imaging probes by direct replacing oleic acid with cysteine-terminated small peptide.



Presentation Number **0905B**

Poster Session 3c: In Vivo Studies & Development/Novel Use of Imaging Probes

Development of novel stimuli-responsive MRI probes

Satoshi Okada¹, Shin Mizukami^{1,2}, Kazuya Kikuchi^{1,2}, ¹Graduate School of Engineering, Osaka University, Suita, Japan; ²Immunology Frontier Research Center, Osaka University, Suita, Japan. Contact e-mail: satoshi_okada@molpro.mls.eng.osaka-u.ac.jp

Magnetic resonance imaging (MRI) is anticipated as a next-generation molecular imaging technique because it provides information about deep tissues of living organisms noninvasively with high temporal and spatial resolution. There are various functional MRI probes developed by chemical modification of MRI contrast agents to image many types of biological reactions. However, molecular design principles to functionalize MRI probes are limited. Therefore, development of a new probe design strategy is strongly desired. We developed a novel MRI probe whose design strategy is robust in wide application. Stimuli-responsive polymers were adopted as molecular source. Many types of stimuli-responsive polymers have been reported, whose conformation can be responsive to external stimuli such as temperature changes, pH changes, and the addition of chemicals. We applied this stimuli-responsive conformational change as an on/off MRI signal switch, which has not been reported previously, to our knowledge. Clinically used MRI contrast agents were attached to a pH-responsive polymer in order to detect pH changes by MRI. Relaxivities of this novel probe were changed in a pH-dependent manner and thus proved to be useful as a pH-responsive MRI probe for detecting pathological tissues whose extracellular pH is lower than normal tissues. Moreover, we measured fluorescence spectra, lifetimes, and anisotropies, and calculated the rotational correlation time, which is a significant factor influencing the function of MRI probes. These experiments revealed that conformational changes of pH-responsive polymer functioned as an on/off MRI signal switch and pH sensor. This unique stimuli-responsive switch should become a new design strategy to variously functionalize MRI probes and lead to further development of functional MRI probes for monitoring many types of biological activities. Such probes should have the high capability to promote future molecular imaging studies.

Presentation Number **0906B**

Poster Session 3c: In Vivo Studies & Development/Novel Use of Imaging Probes

Development of ^{19}F MRI Probes for Imaging Gene Expression

Hisashi Matsushita¹, Shin Mizukami^{1,2}, Kazuya Kikuchi^{1,2}, ¹Graduate School of Engineering, Osaka University, Suita, Japan;
²Immunology Frontier Research Center, Osaka University, Suita, Japan. Contact e-mail: mtsthss@molpro.mls.eng.osaka-u.ac.jp

Reporter gene systems have been developed and applied to monitor gene expression in eukaryotic cells. Optical reporter systems using luciferase or GFP have advantages including noninvasiveness and feasible application to living cells. However, due to the limitation of visible light penetration into organs in deep regions, most of the current optical imaging systems are suitable for studying gene expressions in the internal organs of living animals. Therefore, we focused attention on magnetic resonance imaging (MRI) for visualizing *in vivo* gene expressions. β -Galactosidase and ferritin have been used as reporter genes in ^1H MRI-based reporter assay systems. However, high background ^1H MRI signals due to intrinsic protons in animal bodies prevent the sensitive detection of the target gene expression. In order to overcome this limitation, we utilized ^{19}F , which yields low background MRI signals in living bodies and has a high sensitivity comparable to ^1H . β -Lactamase and β -galactosidase were chosen as reporter genes and the chemical MRI probes as substrates for these enzymes were developed. β -Lactamase is a small monomeric enzyme (29 kDa), and efficiently hydrolyzes various β -lactam substrates. Although it does not exist in eukaryotes, it can be easily expressed in eukaryotic cells without any prominent toxicity. β -Galactosidase is an enzyme encoded by the *lacZ* gene of *Escherichia coli*; it catalyzes hydrolysis of β -D-galactosides and is widely utilized and wide variety of substrates were developed. We designed and synthesized several ^{19}F MRI probes detecting β -lactamase and β -galactosidase activities. The ^{19}F MRI contrasts of the probes were enhanced by the reaction with each target reporter enzyme. These probes should be applicable to *in vivo* imaging of gene expressions.

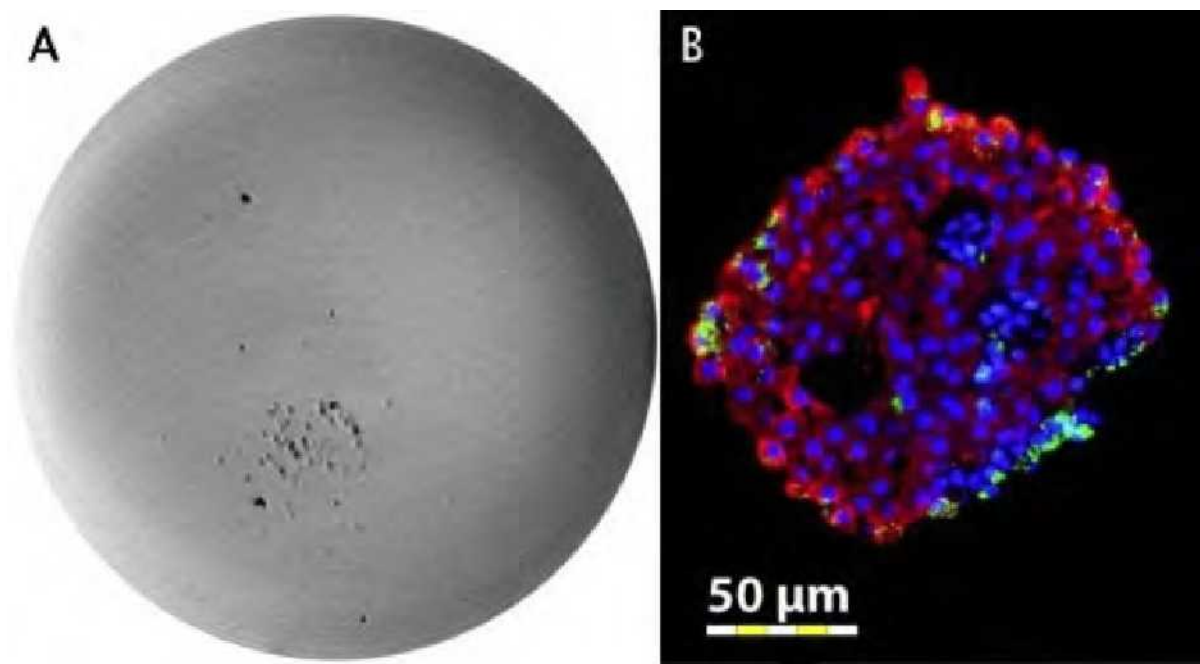
Presentation Number **0907B**

Poster Session 3c: In Vivo Studies & Development/Novel Use of Imaging Probes

New perovskite manganite based contrast agent for magnetic resonance imaging and fluorescence microscopy: example in pancreatic islets

Daniel Jirak^{1,2}, **Michal Kacemka**^{3,4}, **Vit Herynek**^{1,2}, **Ondrej Kaman**^{3,4}, **Klara Zacharovova**⁵, **Emil Pollert**⁴, **Zuzana Berkova**⁵, **Milan Hajek**^{1,2}, **Ivan Lukeš**³, ¹Department of Diagnostic and Interventional Radiology, Institute for Clinical and Experimental Medicine, Prague, Czech Republic; ²Center for Cell Therapy and Tissue Repair, 2nd Medical faculty, Charles University, Prague, Czech Republic; ³Department of Inorganic Chemistry, Faculty of Science, Charles University, Prague, Czech Republic; ⁴Institute of Physics, AS CR, Prague, Czech Republic; ⁵Diabetes Center, Institute for Clinical and Experimental Medicine, Prague, Czech Republic. Contact e-mail: daji@ikem.cz

Introduction: We developed and tested a new bimodal contrast agent (CA) dedicated for labeling and monitoring of pancreatic islets (PI) by MR and optical imaging. CA is based on the perovskite manganite nanoparticles coated by double silica with fluorescein moieties covalently attached to the inner layer. **Methods:** The relaxivity was measured at the 0.5 T Minispec and 4.7 T Biospec spectrometer (Bruker, Germany; 25 °C). The isolated rat PI were labeled by 24 hrs. incubation in culture media with CA (CA concentration in media: 0.11 mM(Mn)). Then the islet viability was tested (propidium iodide and acridine orange staining) and static insulin release was measured. In vitro MR imaging (PI in 4% gel phantom) was performed on a 4.7 T Biospec spectrometer using a standard CPMG multiecho and gradient echo sequences with resolution 0.2×0.2×0.6 mm³. The labeled islets were subjected to fluorescence microscopy (Olympus BX-41, USA). **Results:** The relaxometry performed at 0.5 and 4.7 T provided similar values of r₂ (580 and 540 s⁻¹ mM(Mn)⁻¹, respectively), far exceeding the relaxivities reported for the clinically used iron oxides nanoparticles. In vitro labeled PI were functional and the viability was comparable to non labeled PI. The labeled pancreatic islets were clearly visualized in gel phantom as hypointense areas on T2 and T2*-weighted MR images (Fig.1A). The fluorescein was detected inside the peripheral islet cells, it was incorporated into the different cell types including the beta-cells (Fig.1B). **Conclusion:** The developed bimodal nanoparticles based on perovskite manganite seem to be safe for islet labeling with extraordinarily high spin-spin relaxivity; their localization inside the cells was confirmed by fluorescence microscopy. The study was supported by grants ENCITE-201842, GACR 203/09/1242, ASCR KAN20020061, ASCR KAN201110651, M0538.



A: T2w MR image of the labeled PI in 4% gel phantom (petri dish 35 mm), B: colocalization of immunostained c-peptide indicating beta-cells (red), tested CA (green), and DAPI stained cell nuclei (blue).

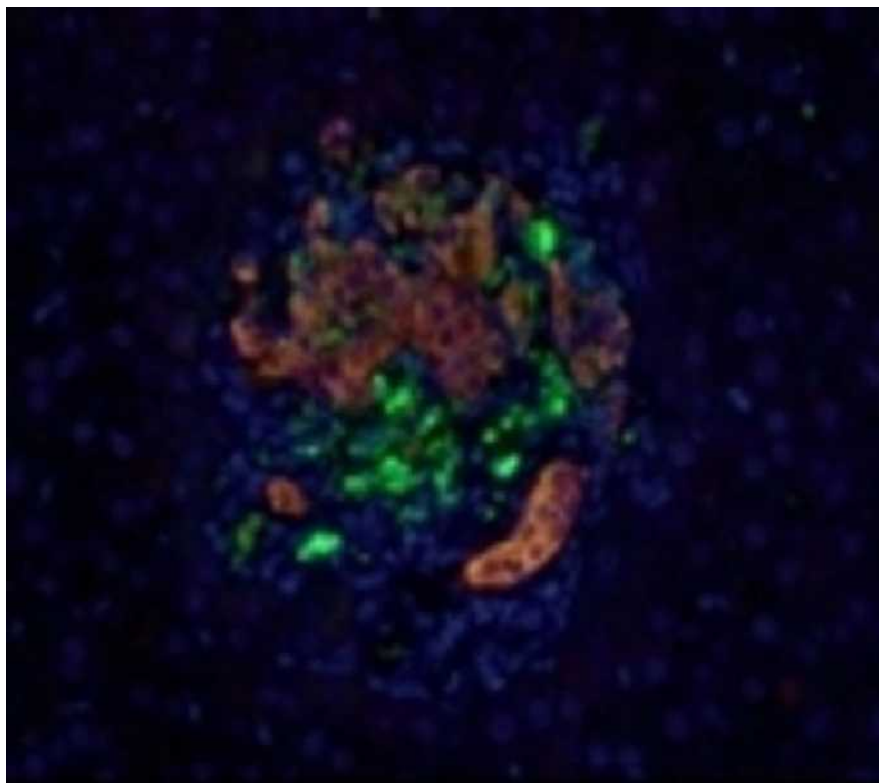
Presentation Number **0908B**

Poster Session 3c: In Vivo Studies & Development/Novel Use of Imaging Probes

New gadolinium based contrast agent for magnetic resonance imaging and fluorescence microscopy: example in pancreatic islets

Daniel Jirak^{1,4}, Zuzana Berkova², Zuzana Kotkova³, Klara Zacharovova², Vit Herynek^{1,4}, Jan Kotek³, Ivan Lukeš³, Frantisek Saudek^{2,4}, Milan Hajek^{1,4}, ¹Department of Diagnostic and Interventional Radiology, Institute for Clinical and Experimental Medicine, Prague, Czech Republic; ²Diabetes Center, Institute for Clinical and Experimental Medicine, Prague, Czech Republic; ³Department of Inorganic Chemistry, Faculty of Science, Charles University, Prague, Czech Republic; ⁴Center for Cell Therapy and Tissue Repair, 2nd Medical faculty, Charles University, Prague, Czech Republic. Contact e-mail: daji@ikem.cz

Magnetic resonance (MR) has recently been introduced as a promising method to monitor transplanted pancreatic islets (PI) labeled with not only superparamagnetic iron oxide nanoparticles but also with agents based on gadolinium (Gd) (1). We have tested the quality and MR properties of PI labeled with a new bimodal contrast agent (CA) containing fixed Gd complexes conjugated with fluorescein to betacyclodextrin ring. The relaxivity was measured at the 0.5T. The isolated rat PI were labeled for 1 day (CA concentration: 0.5mmol and 1.0mmol). After incubation we studied PI viability test and static insulin release. MR imaging (PI in 4% gel phantoms) was performed on a 4.7T, T1w spin echo sequence with resolution 0.2x0.2x0.6mm³ was used. The gel samples and liver tissue with transplanted PI were also processed for fluorescence microscopy. The relaxivity of new CA was 22 s⁻¹mmol⁻¹. The viability of the labeled PI was not impaired as compared with control PI. Static insulin release of the labeled PI did not differ between labeled and control PI. Labeled PI were visible on MR as hyperintense spots. The bound fluorescein was detected in syngeneic islets 3 days after transplantation into the liver. Specific staining for C-peptide and CD-68 demonstrated incorporation of the contrast agent into the beta cells and macrophages. Conclusions The newly developed bimodal gadolinium based CA for PI labeling did not show any signs of short-term islet toxicity and did not impair insulin secretion in vitro. Labeled PI were clearly visible as hyperintense spots on MR images, even single PI was detected. Their cellular localization was confirmed by fluorescence microscopy. The new CA containing Gd complexes conjugated with fluorescein molecule bound to betacyclodextrin seems to be highly stable and safe for PI labeling with excellent MR properties. 1. Biancone et al. NMR Biomed. 2007;20:40-8 The study was supported by ENCITE-201842



Immunofluorescence image of transplanted PI into the liver labeled. Fluorescein - green, C-peptide - red, nucleus - blue.

Presentation Number **0909B**

Poster Session 3c: In Vivo Studies & Development/Novel Use of Imaging Probes

PyroEGTA-Derived Metal Ion Responsive Probes for MRI

Anurag Mishra^{1,2}, David Parker², Nikos K. Logothetis^{1,3}, ¹Department for Physiology of Cognitive Processes, Max-Planck Institute for Biological Cybernetics, Tuebingen, Germany; ²Department of Chemistry, Durham University, Durham, United Kingdom; ³Imaging Science and Biomedical Engineering, University of Manchester, Manchester, United Kingdom. Contact e-mail: anurag.mishra@durham.ac.uk

For proper brain development and function, a critical relationship exists between the elements calcium, magnesium and zinc. Their deficiency or excess accumulation in the body may cause several diseases. Thus, in vivo determination of the distribution of these metal ions is extremely desirable. Recently, advances have been made in the design of responsive probes sensitive to certain metal ions.^{1,2} The use of MRI to detect fluctuations in the concentration of vital metal ions has recently received much attention. However, there is still a need to develop more sensitive and selective probes for biologically important metal ions. Here, we describe two structurally different pyro-EGTA derived lanthanide complexing DO3A probes, which respond to changes in Ca²⁺ and Zn²⁺ concentrations at physiological pH. The complex [LnL1] contains a LnDO3A moiety coupled to a carbomethoxy group of the pyroEGTA derivative [2,2'-(2-(2-(carboxymethoxy)phenoxy)ethylazanediyl)diacetic acid] via an amide bond. This complex possesses six coordination sites suitable for sensing small ionic radii (Zn²⁺, Mg²⁺) metal ions. The complex [LnL2] contains eight coordination sites, appropriate for larger ions such as Ca²⁺. Changes in relaxivity were monitored following addition of appropriate divalent metal ions. In vitro relaxivity measurements were performed at physiological pH in competitive aqueous media at 1.4T and 37°C. [GdL1] showed a 66% relaxivity change on addition of Zn²⁺. This molecule responded selectively to Zn²⁺ rather than Ca²⁺ and Mg²⁺. [GdL2] showed a relaxivity change of 64% upon addition of Ca²⁺ and was insensitive to other added divalent ions in the millimolar range. Parallel luminescence titrations were also undertaken with [EuL1] and [EuL2] in the presence and absence of various divalent ions. Changes in europium emission spectra and the modulation of q values were observed upon addition of Zn²⁺ and Ca²⁺ for [EuL1] and [EuL2], respectively. Thus, enhancements in hydration numbers were found were, in accord with the variations in relaxivity. 1. Que E. L. et al, Chem Soc Rev. 2010;39 (1):51-60. 2. Reany O. et al, J. Chem. Soc. Perkin. Trans. 2, 2000, 1819-1831.

Presentation Number **0910B**

Poster Session 3c: In Vivo Studies & Development/Novel Use of Imaging Probes

Preclinical Research on the Use of Thermally Cross-Linked Superparamagnetic Iron Oxide Nanoparticles (TCL-SPION)

Mulan Li^{1,2}, **YoonSeok Choi**^{1,2}, **Seung Hong Choi**², **Hoe Suk Kim**², **Mi Kyung Yu**³, **Yong Yeon Jeong**⁴, **Sangyong Jon**³, **Woo Kyung Moon**^{1,2}, ¹*Biomedical Sciences, Seoul National University, Seoul, Republic of Korea;* ²*Radiology, Seoul National University, Seoul, Republic of Korea;* ³*Life Science, Gwangju Institute of Science and Technology, Gwangju, Republic of Korea;* ⁴*Radiology, Chonnam National University Medical School, Gwangju, Republic of Korea. Contact e-mail: jinglian1981@gmail.com*

The TCL-SPION (20 - 30 nm size) is a novel T2 MRI contrast agent, which is anti-biofouling polymer coated, thermally cross-linked superparamagnetic iron oxide nanoparticle. First, we assessed the safety and effectiveness of TCL-SPION as a MRI contrast agent using a 1.5T clinical scanner and by comparing with clinically used T2 MRI contrast agents (Feridex and MION-47). The lower T2 value of same concentration of TCL-SPION solution was measured on 1.5T at 20°C as compared with those of Feridex and MION-47. Cellular toxicity was not observed when human fibroblast were incubated with TCL-SPION (25-1000 mg Fe/mL) for 72 hours. Amount of iron oxides within human fibroblast cells measured by Prussian blue stain and TEM was significantly lower when cells were incubated with TCL-SPION compared to Feridex and MION-47. We also used human blood serum to inspect and find that some of the human's protein in blood plasma stick to the surface of dextran coated Feridex only. Second, the in vivo contrast enhancing effects of TCL-SPION were evaluated in nude mice after intravenous injection of 12.5mg Fe/kg TCL-SPION into tail vein. The quantitatively analyzed T2-weighted image showed that the TCL-SPION accumulated in the liver, spleen, lymph node and kidney within 30 minutes like a MION-47. The TCL-SPION was stable in the blood stream for more than 3 hours. Next, we examined whether Dox@TCL-SPIONs are able to localize and accumulate in tumors by EPR effect as TCL-SPIONs did. In tumor-bearing mice, the excellent passive tumor targeting efficiency of TCL-SPION allowed detection of tumors by MR imaging and at the same time delivery of sufficient amounts of anticancer drugs that in turn were released from the nanoparticles to exhibit anticancer activity. We anticipate that the aforementioned TCL-SPIONs may be utilized in distinct ways to develop combined therapeutic and diagnostic modalities by incorporating other drugs such as siRNA and small molecular anticancer drugs. **Acknowledgements** This work was supported by a grant from the National R&D Program for Cancer Control, Ministry of Health & Welfare, Republic of Korea (0920030). M. Lee is fellowship awardees of the Brain Korea 21 (BK21, 2010).

Presentation Number **0911B**

Poster Session 3c: In Vivo Studies & Development/Novel Use of Imaging Probes

21 Tesla Rat Heart Magnetic Resonance Microimaging By Paramagnetic Anti-Troponin Bound Polyethylene Based Iron-Oxide Nanoparticles

Rakesh Sharma^{1,2}, **Ching J. Chen**², ¹Computer Science, TCC and Florida State University, Tallahassee, FL, USA; ²Center of Nanobiotechnology, Florida State university, Tallahassee, FL, USA. Contact e-mail: rksz2004@yahoo.com

AIM: Nanoparticle (SPIOT) of antitroponin coated and polyethylene encapsulated biotin-avidin-iron-oxide core in center was used in imaging of rat heart at 21 Tesla MR by rapid 3D fast low angle shot, 3D gradient echo flow compensated and multislice multiecho MR imaging techniques. **Hypothesis:** Antibody-troponin binding within muscle and generate dephasing heart maps due to iron-oxide paramagnetic character. **Microimaging** was done on 21T MR vertical bore imager. The imaging techniques were used: i. GE Flow compensated; ii. 3D FLASH pulse sequence; iii. Multislice multiecho spin echo sequence; iv. The diffusion-sensitizing bipolar gradients in six non-colinear directions using TE = 18 ms; TR = 10000 ms; time interval between gradient pulses = 5 ms; gradient pulse duration = 0.5 ms, gradient factor = 950 s/mm², b value 950 s/mm², in-plane resolution 35x35 μ m, slice thickness = 1 mm, slice gap = 0.5 mm, number of slices covering heart = 7[2]. **Results:** At 21 Tesla, 3D reconstruction using ImagePro 3D reconstructor program, 3D set of FLASH images display heart images in three planes [Fig 1]. The diffusion tensor imaging weighted (DTI) images with diffusion-sensitizing bipolar gradients showed six non-colinear directions displayed as tensor maps. Quantitative characterization showed contraction related fiber orientation at apex, midventricle, apex from primary eigenvector and sheet orientation by secondary and tertiary eigenvector offers an evaluation of radial myofiber shortening. **Segmentation:** It was iterative method to estimate maximum likelihood (correct classification). Delineation and measurement of feature mass showed vascular area and shape analysis showed cardiac features. **Conclusion:** The microimaging technique by 21T MRI is technical advancement suitable to labs to design functional imaging contrast agents. **Source:** Sharma R. (2009) US patent. <http://www.freepatentsonline.com/y2009/0220434.html>

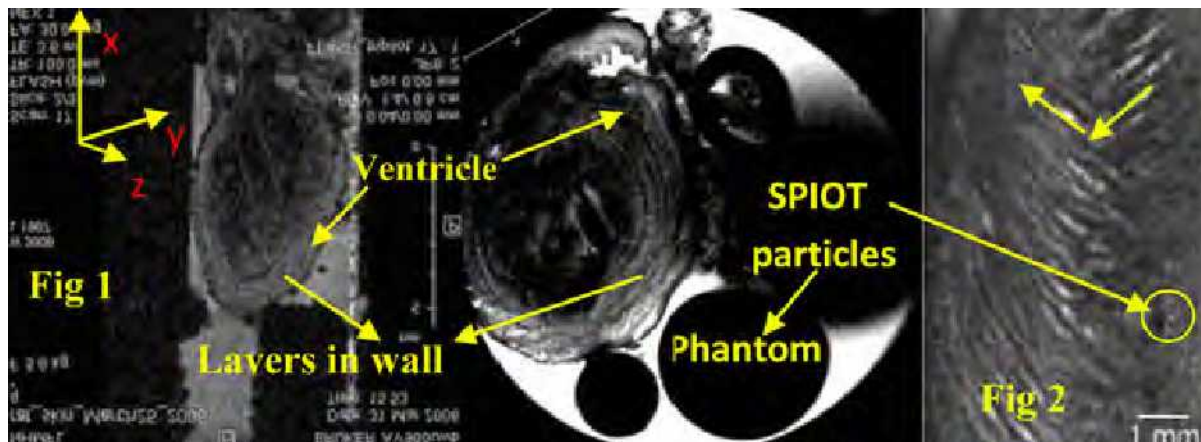


Fig 1: 21T MRI Heart image at TE/TR 8/100 ms (on left); On right, fiber orientation is shown with SPIOT particles trapped inside

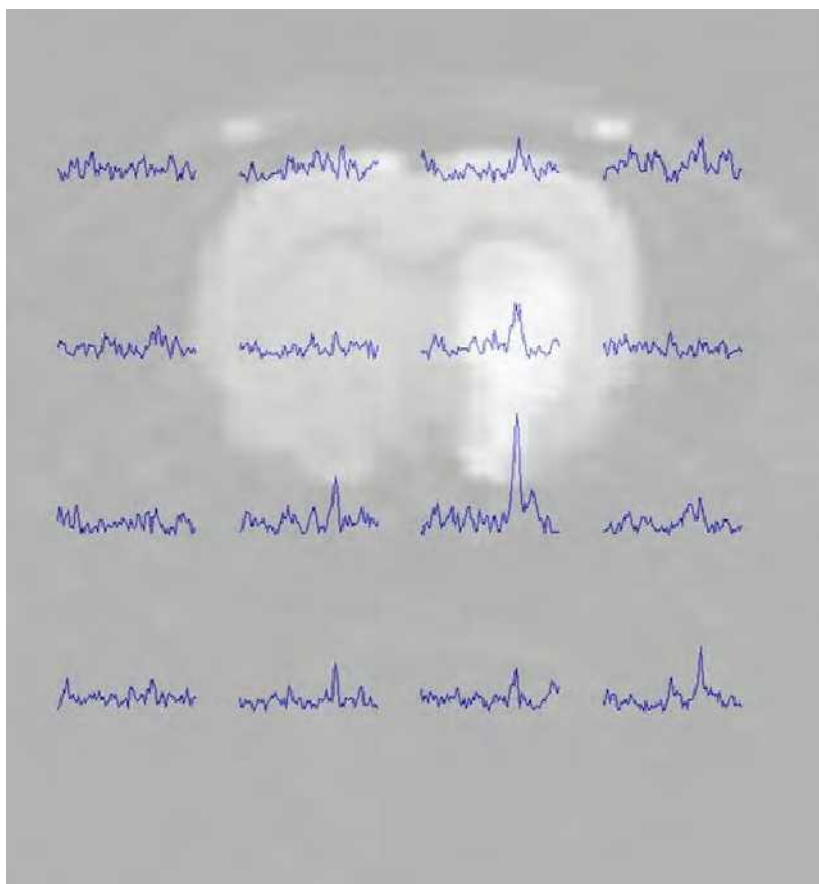
Presentation Number **0912B**

Poster Session 3c: In Vivo Studies & Development/Novel Use of Imaging Probes

Hyperpolarized ^{129}Xe spectra from transient ischemic tissue with delayed hyperperfusion in rat brain

Kazuhiro Nakamura, Yasushi Kondoh, Shigenori Mizusawa, Toshibumi Kinoshita, Radiology, Akita Research Institute for Brain and Blood Vessels, Akita, Japan. Contact e-mail: knam@akita-noken.jp

Introduction: Chemical shift of hyperpolarized ^{129}Xe is thought to reflect local structure. Previous reports have shown that strong hyperperfusion is observed in transient ischemic brain tissue 48 h after middle cerebral artery occlusion (MCAO). As numerous histological investigations have shown dramatic cell modifications in ischemic areas at two days after MCAO, we expected a change in the dissolved peak of Xe in ischemic brain tissue. To confirm spectral differences between normal and ischemic tissue, ^{129}Xe spectra were acquired from rats prepared with MCAO. **Methods:** Ischemic regions were induced by occluding the left middle cerebral artery with embolic thread for 60 min. At 48 h after reperfusion, an endotracheal tube was inserted into the trachea followed by a thinner tube. Animals were set in the bore of a 4.7-T Varian Inova magnetic resonance spectrometer with a 3 cm ^1H and ^{129}Xe dual-tuned surface coil placed over the head. Next, 25 ml of hyperpolarized, enriched ^{129}Xe gas (^{129}Xe 80% + N_2 20%) was produced in a commercially available polarizer (Toyoko-Kagaku, Japan). Spectra were acquired using a single hard-pulse sequence. Chemical shift imaging (CSI) with 8×8 voxels and 45 mm field of view was acquired within the 25 ml of hyperpolarized gas delivery. **Results:** Figure shows extracted CSI spectra of a 4×4 matrix in rat brain. Spectra were superimposed on proton diffusion-weighted imaging (DWI). A high signal was observed in the area represented as high intensity on DWI. Decay time did not differ significantly between MCAO rats (16.7 s, 12.6 s) and normal rats (mean 11.7 ± 1.8 s). **Discussion:** CSI shows hyperperfusion in the ischemic area, but this was not shown as either an additional peak in the spectra or a frequency shift in spectra from the whole brain. Spectra from the whole brain may not represent ischemic tissue alone. Spectra obtained from a much smaller region may be necessary to detect differences between ischemic and normal tissues.



Presentation Number **0913B**

Poster Session 3c: In Vivo Studies & Development/Novel Use of Imaging Probes

Cracked Iron Oxide Nanoparticles coated with DMSA for MRI T2 Contrast Agents

Min Kyung Chae¹, Jee H. Cho¹, Eunjoo Jang¹, Sangdoo Ahn², **Chulhyun Lee¹**, ¹Div. of Magnetic Resonance Research, Korea Basic Science Institute, Ochang, Republic of Korea; ²Dept. of Chemistry, Chung-Ang Univ., Seoul, Republic of Korea. Contact e-mail: chulhyun@kbsi.re.kr

Metal [Fe, Mn, Gd, and Co] oxide nanoparticles with small size and large surface provide magnetic resonance image with high sensitivity and specificity at low imaging-agent concentration. Metal oxide nanoparticles with hollow spheres can incorporate therapeutic agents into their payloads, enabling simultaneous MRI diagnosis and delivery of drugs to targeted sites. Iron oxide nanoparticles as T2 contrast agents are employed to image tumors, stem cell migration, and cancer metastases. Iron ions are usually safer than potentially toxic metal ions such as Gd³⁺ and Mn²⁺ in the body. Herein, we report a facile synthesis of nontoxic cracked iron oxide nanoparticles (CIONPs) from hydrophobic FeO nanoparticles (HIONPs) via 3 steps. With complex surface structure, CIONPs showed improved r₂ relaxivities compared to hydrophobic FeO nanoparticles (HIONPs). Besides, CIONPs coated with meso-2,3-dimercaptosuccinic acid (DMSA) have much stronger r₂ relaxivities than PEGylated CIONPs because coating thickness can significantly impact the r₂ relaxivities of CIONPs. We expect that CIONPs have the potential application as a drug or chemical delivery vehicle because of their cracked spheres. To examine the drug delivery potential, CIONPs were loaded with drug by DOX and evaluated cellular uptake by using HT-29 human colon carcinoma cells.



Synthetic pathway of CIONPs. Cracked iron oxides core made the relaxivities higher.
Relaxivities of DMSA-coated CIONPs at 4.7 T MRI

Nanoparticle	T2 (ms)	r ₂ (L/mole)
PEG-WIONPs	54	55.4
DMSA-WIONPs	13	167.5
PEG-CIONPs, pH 5.0	30	167.9
DMSA-CIONPs, pH 5.0	44	151.7
PEG-CIONPs, pH 2.0	40	216.4
DMSA-CIONPs, pH 2.0	27	345.7

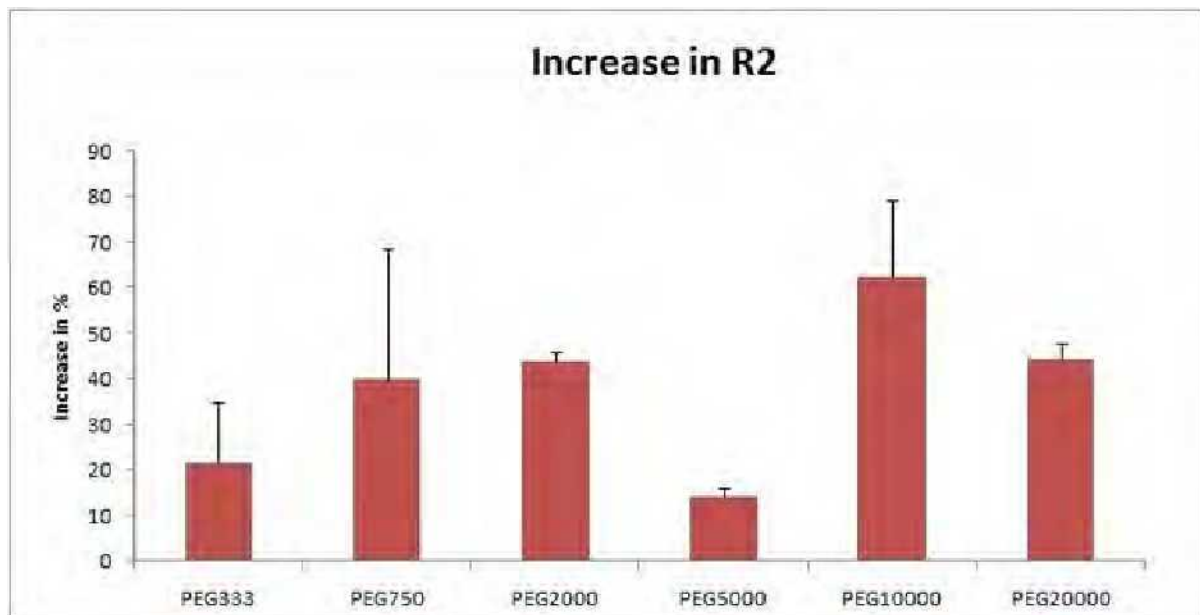
Presentation Number **0914B**

Poster Session 3c: In Vivo Studies & Development/Novel Use of Imaging Probes

Accumulation of magnetic nanoparticles with different sized PEG in mouse tumors

Esben Larsen¹, Thomas Wittenborn^{1,3}, Thomas Nielsen², Jørgen Kjems¹, ¹iNANO, Aarhus University, Aarhus, Denmark; ²Department of Neuroradiology, Aarhus University Hospital, Aarhus, Denmark; ³Department of Experimental Clinical Oncology, Aarhus University Hospital, Aarhus, Denmark. Contact e-mail: ekul@mb.au.dk

Here we present results regarding accumulation of iron oxide nanoparticles coated with different lengths of PEG (333-20.000da). The length of PEG influenced cell uptake, blood half-life and uptake in murine tumours. Iron oxide nanoparticles were coated with silane amine together with different lengths of NHS-PEG. The PEG coated nanoparticles had a hydrodynamic size range from 20 nm (333 da PEG) to 50nm (20.000da PEG). The zeta potential showed a decreasing trend corresponding to increasing lengths of PEG. In vitro experiment in cancer cell lines (Hela, RAW and J774a.1), showed a tendency for the particles coated with short PEG to be taken up more than particles coated with longer PEG, with 20.000da as an exception. The PEG length also influenced the half-life of the particles, as longer particles had a longer half-life in the mouse. In vivo experiments where the particles were injected into the tail vein of mice with a tumour implanted on the leg, showed that particles coated with longer PEG had a larger increase in the R2 value in the tumour, with PEG 5000da as an exception (figure 1). The length of PEG clearly influences the fate of the particles both in vitro and in vivo. The PEG coating makes the particles become more stealth and therefore, masking the particles towards elimination. The increased size of the particles could make the particles less prone to be filtered in the kidney, and the lower zeta size could decrease opsonization by the immune system. All these effects together probably create the higher contrast in the tumour. Particles coated with longer PEG length has a higher contrast increase in a murine tumour model, this highlights the importance of the coating when developing new contrast agents.



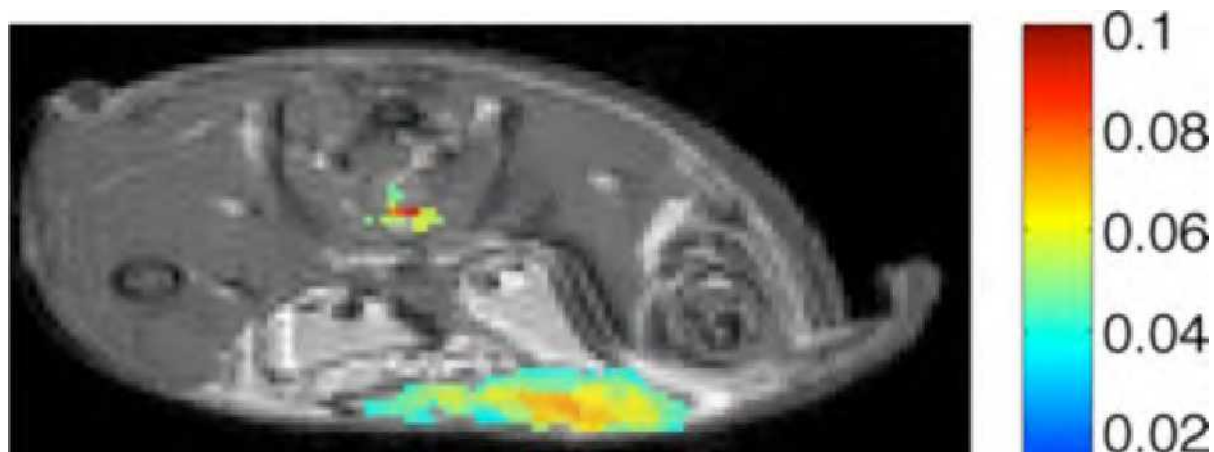
Presentation Number **0916B**

Poster Session 3c: In Vivo Studies & Development/Novel Use of Imaging Probes

New Diamagnetic Microcapsules for simultaneous immunoprotection of human pancreatic islet cells and remote MRI sensing of pH using Polycationic DIACEST peptides as crosslinkers

Dian R. Arifin^{2,3}, Kannie WY Chan^{1,2}, Guanshu Liu^{1,2}, Jeff W. Bulte^{1,2}, **Michael McMahon**^{1,2}, ¹F.M. Kirby Research Center, Kennedy Krieger Institute, Baltimore, MD, USA; ²Radiology, Johns Hopkins Univ SOM, Baltimore, MD, USA; ³Institute for Cell Engineering, Johns Hopkins Univ SOM, Baltimore, MD, USA. Contact e-mail: mcmahon@mri.jhu.edu

Cell transplantation is a potential treatment for various diseases such as type I diabetes, liver failures and arterial or cardiovascular disorders. Encapsulation of cells inside semi-permeable and biocompatible microcapsules offers immunoprotection for the cells and recipients, and the functional status of the cells once they are transplanted is a critical component to this therapy. Recently we have developed a library of CEST peptides which produce contrast in a pH responsive manner and could be used to crosslink alginate layers in these microcapsules. Using this library, we have produced novel biodegradable DIACEST microcapsules which can be visualized using CEST imaging. The contrast produced by these capsules is pH dependent, and can be used to monitor biological activities such as apoptosis and insulin release, which are accompanied by pH changes. This proof-of-concept was demonstrated in vitro by acquiring MR images of DIACEST microcapsules which encapsulated either functional or apoptotic pancreatic beta cells. Pancreatic cells were first encapsulated in alginate beads gelled by 20 mM Ba²⁺ and then cross-linked by addition of a polycationic DIACEST peptide solution and further cross-linked by addition of alginate. We experimented with multiple 12-residue polypeptides and compared the microcapsules produced to those generated using clinical-grade protamine (P). The MRI images were acquired on a 9.4T Bruker Avance system. $MTR_{asym} = (S - \Delta\omega - S + \Delta\omega) / S - \Delta\omega$ was computed and used to display the CEST contrast. Individual microcapsules could be visualized in vitro with the (KG)6 capsules possessing the highest contrast in the MTR_{asym} images. We varied the pH over a physiologically relevant range of 5.5-8.0, with the MTR_{asym} ranging from 5-33%. In addition, the MTR_{asym} for protamine microcapsules containing viable murine β TC6 insulinoma cells was ~15% higher than those containing 30-50% apoptotic cells and ~10% higher than empty microcapsules. Finally, we have acquired in vivo images using these capsules with a representative image displayed in Figure 1.



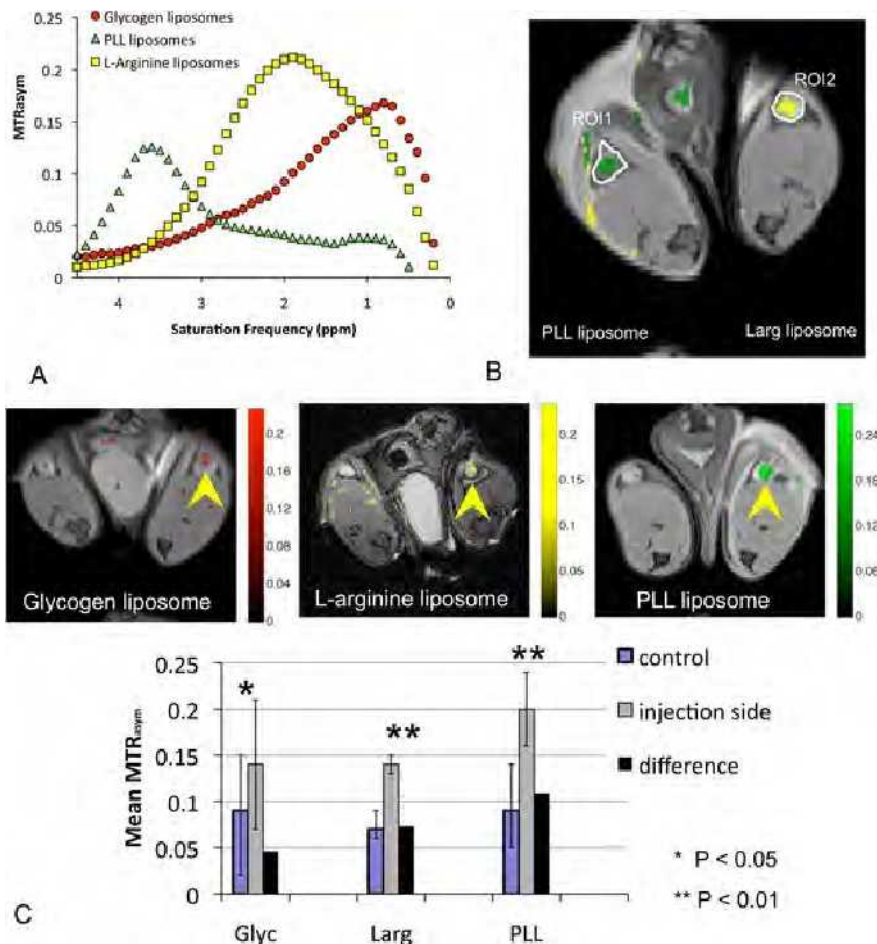
Presentation Number **0917B**

Poster Session 3c: In Vivo Studies & Development/Novel Use of Imaging Probes

Multi-Color in Vivo MR Imaging of Lymph Nodes using DIACEST Liposomes

Guanshu Liu^{1,2}, Matthew Moake¹, Assaf Gilad², Jeff W. Bulte², Peter C. van Zijl^{1,2}, **Michael McMahon**^{1,2}, ¹F.M. Kirby Research Center for Functional Brain Imaging, Kennedy Krieger Institute, Baltimore, MD, USA; ²radiology, Johns Hopkins University, Baltimore, MD, USA. Contact e-mail: mcmahon@mri.jhu.edu

As new MRI contrast mechanism, diamagnetic Chemical Exchange Saturation Transfer (DIACEST) has the capability of producing multi-color MR image, which is only demonstrated in vitro. Herein, three DIACEST liposomes have been produced with three artificial MR colors, i.e. blue for Glyc liposomes at 0.8ppm, red for Larg liposomes at 1.8ppm and green for PLL liposomes at 3.6ppm. We first determined the favorable condition for MRI detection of these DIACEST liposomes in popliteal lymph nodes using SPECT-CT, i.e. liposome size=100-200nm and post-injection time=24hours. The mice were tested with one-foot injection for the direct comparison of CEST signals in both nodes, with the node on non-injection side as the internal control. In studies on multiple mice (n=5 for PLL and Larg, and n=3 for Glyc), all three types of DIACEST liposomes displayed the ability to increase CEST contrast in the nodes on the injection side. We also tested the CEST detection of two-foot injection of Larg and PLL liposomes on multiple mice (n=3). The results clearly showed distinctive CEST contrast existing in the nodes on two injection sides, which enable the two-color MRI on the same animal model. The majority of these liposomes were found to be extra-cellular as revealed by immunohistological staining for anti-CD45 and liposomal rhodamines. In conclusion, we acquired the first in-vivo multi-color DIACEST MR images for visualizing lymphatic accumulation of liposomes, which will have great impact to many MRI applications, including the simultaneous visualization of the delivery multiple liposomes of anticancer drugs.



A) MTRAsym plots of three multi-color DIACEST liposomes (~30 nM) in in vitro (pH 7.3 and 37°C), with blue assigned to Glyc, red assigned to Larg and green assigned to PLL; B) The in-vivo demonstration of two-color DIACEST; C) three MTRAsym images showing for Glyc liposomes (red), Larg liposomes (yellow), and PLL liposomes (green), and the statistic analysis.

Presentation Number **0918B**

Poster Session 3c: In Vivo Studies & Development/Novel Use of Imaging Probes

Comparison of paramagnetic molecular imaging probes for the in vivo detection of oxidative epitopes

Karen Briley-Saebo^{1,2}, **Tuyen Hoang**^{1,3}, **Alexander Saeboe**¹, **Sung Kee Ryu**⁴, **Young Seok Cho**⁴, **Simone Green**⁴, **Venkatesh Mani**^{1,3}, **Stephen D. Dickson**^{1,3}, **Peter X. Shaw**⁴, **Joseph L. Witztum**⁴, **Zahi Fayad**^{1,3}, **Sotirios Tsimikas**⁴, ¹Radiology, Mount Sinai School of Medicine, New York, NY, USA; ²Cell and Molecular Medicine, Mount Sinai School of Medicine, New York, NY, USA; ³Translational Molecular Imaging Institute, Mount Sinai School of Medicine, New York, NY, USA; ⁴Vascular Medicine Program, University of California San Diego, La Jolla, CA, USA. Contact e-mail: ksaeb@gsi.com

Oxidized low density lipoproteins (OxLDL) have been identified a main factor in atherosclerotic plaque de-stabilization. Studies in sudden death victims show a strong correlation between lesion stage and oxLDL. We hypothesize that targeting of oxLDL may allow for in vivo detection of high risk lesions by MRI. Aim: To evaluate the in vivo efficacy of gadolinium (Gd) and manganese (Mn) micelles targeted to oxLDL in murine models of atherosclerosis. Methods: Thin film techniques were used to prepare untargeted and oxLDL targeted Gd and Mn micelles. The murine antibody MDA2 was used for oxLDL targeting. All formulations were characterized and vascular stability evaluated. Uptake and viability studies were performed in J7774A.1 macrophages. Biodistribution and pharmacokinetics were evaluated in ApoE^{-/-} mice. MR imaging was performed over 1 week interval at 9.4T using T1-weighted black blood TSE sequences. Results: Vascular transmetallation was observed for both Mn (1.5%) and Gd (3.5%) micelles. Uptake into macrophages was mediated and resulted in limited apoptosis for targeted Mn-micelles. Significant apoptosis was observed for targeted Gd-micelles. Targeting resulted in prolonged circulation times, relative to untargeted materials. Targeted Mn-micelles exhibited strong initial arterial wall uptake (half-life = 58 hrs). Initial uptake of Gd was lower and persisted for 1 week. Maximum MR signal enhancement was observed 48 hrs and 96 hrs after injection of targeted Mn-micelles and Gd-micelles, respectively (Fig.1). Conclusion: This study demonstrates that Mn based probes may be used for the in vivo detection of oxLDL. The bio-compatibility of Mn may facilitate clinical translation of this approach.

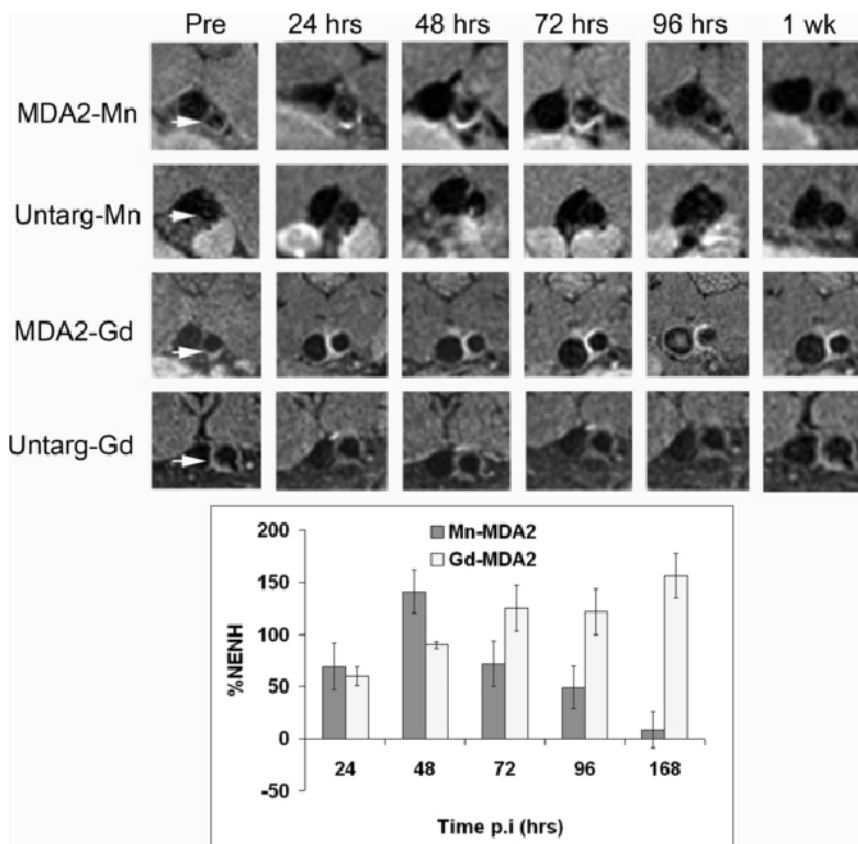


Fig.1: Representative MR images obtained in the abdominal aorta (arrow) of apoE^{-/-} mice following injection of Mn micelles (0.05 mmol Mn/Kg) or Gd micelles (0.075 mmol Gd/Kg). The percent normalized enhancement values (%NENH) represents the relative change in the contrast-to-noise ratios pre and post imaging.

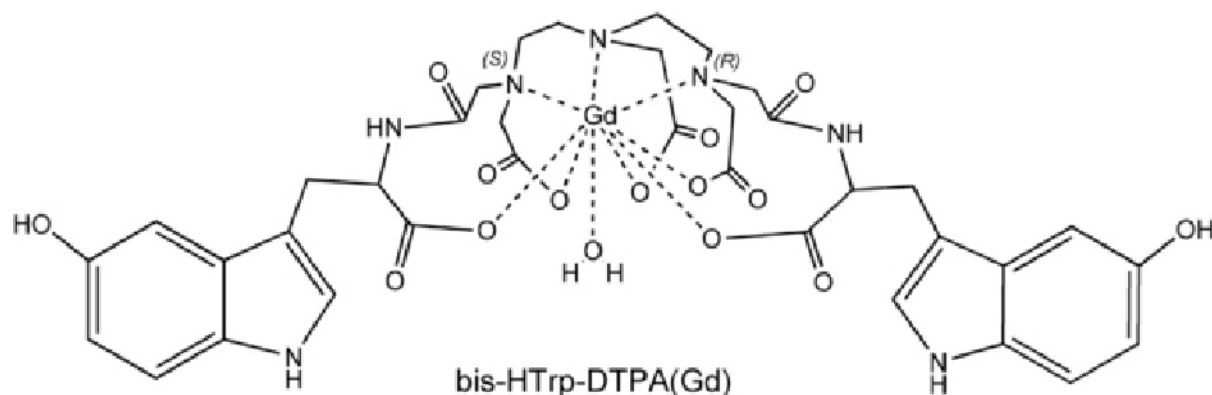
Presentation Number **0919B**

Poster Session 3c: In Vivo Studies & Development/Novel Use of Imaging Probes

The Synthesis and Characterization of a Novel Octadentate Myeloperoxidase Sensing Probe

Alexei A. Bogdanov, Yang Xie, Radiology, UMASS Medical School, Worcester, MA, USA. Contact e-mail: alexei.bogdanov@umassmed.edu

Myeloperoxidase (MPO) is one of the crucial imaging targets having an outcome- predictive value in numerous diseases such as atherosclerosis, cancer and several CNS pathologies. We previously synthesized and tested paramagnetic complexes of mono- and bis- amides of macrocyclic and linear chelates that “sense” MPO activity [1,2]. As a result of MPO catalysis, the sensors oligomerize and/or form covalent bonds with proteins resulting in increased molar relaxivity (r_1 and r_2). This enables MR imaging of MPO activity in vivo. Although the existing MPO sensors have very high kinetic stability [3]; the thermodynamic stability of bisamides is usually compromised. The goal of the current study was to synthesize and characterize a novel bifunctional MPO sensor with the same number of donor atoms as in DTPA (N3O5) in anticipation of improved thermodynamic stability and better solubility. We synthesized an octadentate ligand by reacting hydroxytryptophan, a naturally occurring amino acid, with DTPA dianhydride and characterized the obtained product (bis-HTrp-DTPA(Gd)) using ^1H , ^{13}C NMR and TI-MS. The initial in vitro efficacy testing involved comparing the MPO-mediated relaxivity increase to that of a standard substrate, bis-5HT-DTPA(Gd) [2] in the presence of a hydrogen peroxide source (glucose/glucose oxidase). Within 1 h we observed an enzyme-dependent increase of molar relaxivity from 4.9 to 8.6 mM $^{-1}$ (1.75 fold at 0.47T) as opposed to a 50% increase of relaxivity under the identical conditions in the case of bis-5HT-DTPA(Gd). Total r_1 increase was 2.2 times (MPO) and 2.5 times (HRP, positive control). Gradient SDS-PAGE analysis of MPO-catalyzed activation of bis-HTrp-DTPA(Gd) showed the formation of 10-20 kDa products. Hence, bis-HTrp-DTPA(Gd) is a novel MPO paramagnetic substrate which could potentially provide a more sensitive means of detecting MPO activity in vivo. References: 1. Chen JW et al MRM 52: 1021, 2004; 2. Querol M et al., Org Lett. 17, 1719, 2005; 3. Rodriguez E. et al. JACS 132:168, 2009.



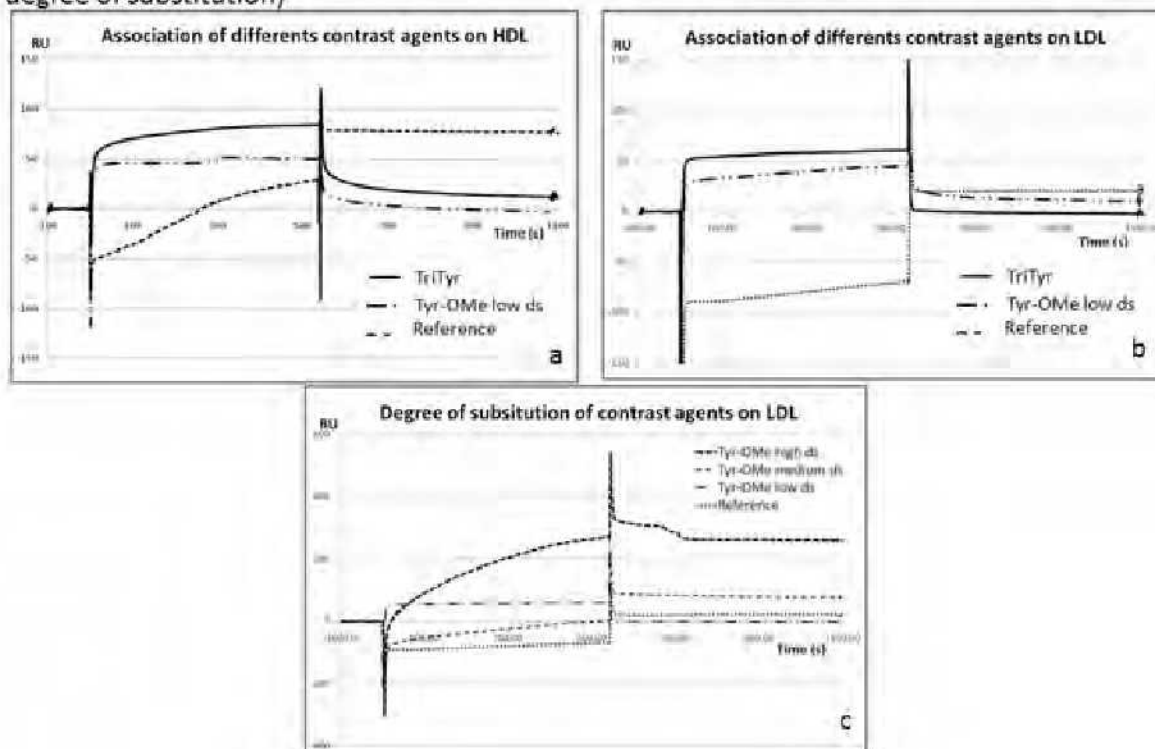
Presentation Number **0921B**
 Poster Session 3c: In Vivo Studies & Development/Novel Use of Imaging Probes

A new MRI polysaccharide based contrast agent for the detection of lipid core in atherosclerotic plaque

Anne Beilvert^{1,2}, Roger Vassy³, Eric Lancelot⁴, Claire Corot⁴, Didier Letourneur^{1,2}, Frédéric Chaubet^{1,2}, ¹Cardiovascular bio-engineering, INSERM U698, Paris, France; ²Institut Galilée, Université Paris 13, Villetaneuse, France; ³SMBH, Université Paris 13, Bobigny, France; ⁴Recherche et développement, Guerbet, Villepinte, France. Contact e-mail: anne.beilvert@inserm.fr

Objective: The aim of this study is the synthesis and the evaluation of a innovative MRI polysaccharide based contrast agent able to specifically target the lipid core in the atherosclerotic plaque. The starting contrast agent is a carboxymethyl dextran bearing GdDOTA residues (Chaubet et al., CMMI, 2007), grafted with tyrosine-OMe (Tyr-OMe) or trityrosine (TriTyr) which promote interactions with LDL and HDL (Beilvert et al., MRM, 2009) Methods: The contrast agent is a carboxymethyl dextran substituted with GdDOTA groups exhibiting a high longitudinal relaxivity (10.6 mM⁻¹(Gd).s⁻¹). A limited oxidation was performed with sodium periodate, and Tyr-OMe or TriTyr were linked to the dextran backbone. All derivatives have been characterized by UV spectroscopy, light scattering and elemental analysis. The affinity of the modified polysaccharides for LDL and HDL was evaluated by Surface Plasmon Resonance with a BIAcore® X100. Briefly, on a CM5 or a L1 chips LDL or HDL were immobilized as suggested by manufacturer's instructions. Lipoproteins have been covalently attached to the CM5 chips, whereas they have been immobilized on L1 chips by hydrophobic affinity. Different concentrations of modified polysaccharides were then injected in HBS-P buffer with EDTA to prevent the oxidation of lipoproteins. Affinities and kinetics were evaluated by comparison with the unmodified contrast agent (see Fig. 1). Results: Different degrees of substitution in Tyr-OMe and TriTyr have been achieved from 2 to 25 groups per polysaccharidic chain. Modified contrast agents have a different binding profile (affinity and specificity) regarding the immobilized ligand (Fig. 1 (a and b)). For the same ligand, contrast agents with the highest levels of substitution exhibited a higher affinity for LDL than unmodified one (Fig 1.c) Conclusions: In a near future, modified polysaccharides will be injected in ApoE^{-/-} mouse model to confirm the detection of atherosclerosis by MRI. Our strategy for targeting the lipid core will help the localization of atherosclerotic plaques.

Figure 1 : Association of different contrast agent according to immobilized ligand : HDL (a) or LDL (b), regarding the type of substitution of the contrast agent : different binding (affinity and specificity). Different binding profile regarding the degree of substitution (ds) on LDL (c). (ds : degree of substitution)



Presentation Number **0922B**

Poster Session 3c: In Vivo Studies & Development/Novel Use of Imaging Probes

Manganese Loaded Liposomes as Molecular Imaging Contrast Agents using Fast Field-Cycling MRI

Dara O Hogain¹, Lionel M. Broche, Simona Baroni², Silvio Aime³, David J. Lurie¹, ¹Bio-Medical Physics, University of Aberdeen, Aberdeen, United Kingdom; ²Invento S.r.l, Torino, Italy; ³Department of Chemistry, University of Torino, Torino, Italy. Contact e-mail: l.broche@abdn.ac.uk

Fast Field-Cycling MRI (FFC-MRI) switches between magnetic fields during a single pulse sequence, thus exploiting the different T1 dispersion behaviour of tissue and contrast agents, to optimise contrast between normal and pathological tissues. FFC-MRI allows access to a new contrast mechanism known as $\Delta R1$ imaging in which contrast depends on the change in R1 between different fields. A new contrast agent consisting of Mn[II] ions encapsulated within liposomes was designed as a molecular imaging probe for use with FFC-MRI. This agent shows large changes in R1 between fields which allow detection with much greater sensitivity in a $\Delta R1$ image compared with standard T1 weighted images. The liposomal membrane may also be manipulated to target specific tissue cells in vivo. The agent was first diluted to Mn[II] concentrations of; A: 0.15 mM, B: 0.1 mM, C: 0.08 mM, D: 0.06 mM, and E: 0.04 mM respectively. A sixth sample (F) containing 1.0 mM CuSO4 was also prepared in de-ionised water in order to provide comparison with the Mn[II] contrast agent, as CuSO4 unlike Mn[II] shows little change in R1 between field strengths. The samples were imaged using a home-built, whole-body FFC-MRI scanner with detection at B0 = 59 mT. T1 weighted images were acquired first at 59 mT then at 2 mT for a range of evolution times. Using these data, R1 maps were calculated for each pixel in both sets of images. R1 maps at 59 mT and 2 mT were then subtracted to give a $\Delta R1$ map for each sample. Figure 1 shows the ratio between the image intensities of the Mn[II] samples and the CuSO4 sample, comparing the $\Delta R1$ values to T1 weighted images at 2 mT, and at 59 mT. The $\Delta R1$ mapping technique resulted in higher contrast between the Mn[II] and the 1.0 mM CuSO4 samples compared with T1 weighted imaging. Typically normal tissue exhibits only a small change in R1 between 2.5 and 10 MHz, and as such, $\Delta R1$ mapping could be used to enhance contrast between regions containing contrast agent and surrounding areas of normal tissue. The observed $\Delta R1$ enhancements clearly indicate that this technique (FFC-MRI and reporting probe) is well suited for molecular imaging applications.

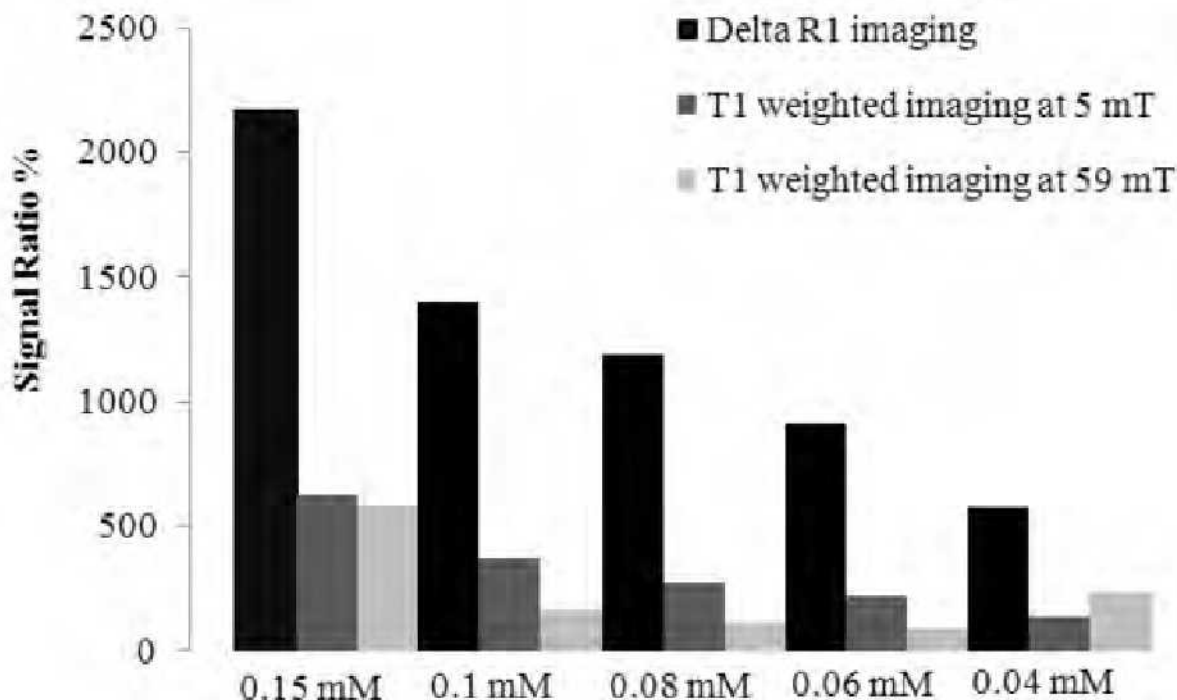


Figure 1

Presentation Number **0923B**

Poster Session 3c: In Vivo Studies & Development/Novel Use of Imaging Probes

DOTA Conjugated Tranexamic acid(ester) Gd-complexes: Fine Tuning to Increase Safety from NSF in MRI

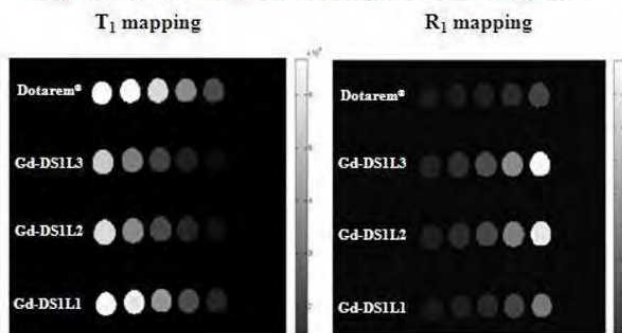
Sungwook Gu¹, Apuri Satyender¹, Ji-Ae Park², Tae-Jeong Kim¹, ¹Applied Chemistry, Kyungpook national university, Daegu, Republic of Korea; ²Korea institute of radiological & medical Sciences, Seoul, Republic of Korea. Contact e-mail: pivotman82@gmail.com

Gadolinium-based CAs employed in MRI has been reported to cause nephrogenic systemic fibrosis (NSF) disorder. Therefore the present study is directed toward the improvement of safety of MRI CAs and in this regard, we designed a new series of ligands derived from DOTA conjugated tranexamic acid (ester). The main focus was on 3 key factors: i) to enhance relaxivity for reducing Gadolinium ion administration by incorporating tranexamic acid (ester), ii) to increase thermodynamic and kinetic stability by introducing DOTA, iii) to synthesize lipophilic Gd-complexes for quick dual elimination *via* kidney and bile from patient body. Based on our ideology, a series of Gd(III) complexes of type [Gd(L)(H₂O)].nH₂O were synthesized and characterized. All the newly prepared Gd complexes exhibited enhanced R1 relaxivity compared with Gd-DOTA (Dotarem®, 3.67 mM⁻¹s⁻¹). Highest R1 was observed for [Gd(L3)(H₂O)] (9.54 mM⁻¹s⁻¹). The safety of Gd(III) complexes(**1-3**) toward NSF was investigated by measuring some relevant physicochemical properties such as (i) thermodynamic and conditional stability constants, (ii) the selectivity (pGd) of **1-3** for the Gd(III) ion over the endogenous metal ions like Zn(II), Ca(II), and Cu(III), (iii) transmetallic kinetics of GdL with Zn(II) ion. *In vivo* imaging for quick elimination and cell viability test (MTT) is under progress.

Table 1. Relaxivity data of DOTAREM®, DOTA conjugated of tranexamic acid, and its esters (B₀ = 1.5T at 25 °C)

	R ₁ (mM ⁻¹ s ⁻¹)	R ₂ (mM ⁻¹ s ⁻¹)
Dotarem®	3.67 ± 0.04	4.14 ± 0.21
Gd-DSIL1	3.87 ± 0.04	4.04 ± 0.12
Gd-DSIL2	8.59 ± 0.01	9.18 ± 0.23
Gd-DSIL3	9.54 ± 0.12	10.89 ± 0.03

Figure 1. *In vitro* MR phantom images of contrast agents



Stability constants, selectivity constants and pM^a value of Gd³⁺, Ca²⁺, Zn²⁺ and Cu²⁺ complex of DOTA conjugated of tranexamic acid and its esters

	DSIL2	DSIL3	STL3	DTPA-BMA	DOTA
Log K _{therm} (GdL)	22.07	21.32	20.53	16.53	21.6
Log K _{cond} (GdL)	19.70	18.47	18.15	14.54	19.3
Log K _{se} (Gd/Ca)	6.67	6.53	13.19	9.85	8.07
Log K _{se} (Gd/Zn)	3.42	3.91	5.25	4.31	4.23
Log K _{se} (Gd/Cu)	4.65	2.22	7.31	3.32	2.67
Log K _{se}	6.55	4.54	9.37	9.05	-
pGd	18.70	17.47	17.15	13.55	19.2
pCa	11.63	10.91	3.99	4.19	-
pZn	12.89	13.36	5.95	9.05	-
pCu	13.62	13.23	9.37	10.03	-

{log K(25°C), μ = 0.10 M(KCl)}

a: pM = -log[Mⁿ⁺]_{free} at pH 7.4

Presentation Number **0924B**

Poster Session 3c: In Vivo Studies & Development/Novel Use of Imaging Probes

Cell-released Microparticles: towards noninvasive detection using MRI

Achraf Al Faraj^{1,2}, Pierre-Emmanuel Rautou², Olivier Clément², Claire Wilhelm¹, Chantal Boulanger², Florence Gazeau¹, ¹University Paris 7, CNRS 7057, MSC, Paris, France; ²Paris Cardiovascular Research Center - PARCC, Université Paris 6, INSERM U970, Paris, France. Contact e-mail: achraf.al-faraj@univ-paris-diderot.fr

Microparticles (MP) are submicron vesicles shed from plasma membranes in response to cell activation, injury, and/or apoptosis. MP of different cellular origin, including endothelial, circulate in the blood. They are recently considered as key biological messengers and mediators of diseases progression. Therefore, their noninvasive detection opens fascinating prospects to investigate their role in biological processes like thrombosis, angiogenesis or cancer development. MRI has been demonstrated as a powerful technique for monitoring specific cell populations after their magnetic labeling using ultra-small particles iron oxide (USPIO). To minimally interfere with the biodistribution of MP, a labeling procedure which confines the USPIO to the inner of MP was elaborated. Murine endothelial cells were firstly labeled using anionic citrate-coated USPIO. Nanoparticles accumulated within intracellular endosomes progressively returned to the cell surface to be released within microvesicular structures in a serum-deprived medium. Shed iron loaded MP can be then isolated by either successive centrifugation steps to allow MP pelleting or on magnetic columns. To assess their in vivo biodistribution, a 1 week follow-up study was performed on a 4.7T magnet after i.v. injection of 10^6 labeled MP (FACS Annexin V-positive events) to a mice model. A positive control, injected with free USPIO (1 $\mu\text{mol/Kg}$), was also included in this study. MPs were only detected in the spleen with a 10% fold attenuation of signal assessed using susceptibility weighted gradient echo sequence however comparable signal loss was observed in both spleen and liver for free USPIO injected group. Signal attenuation gradually decreases with time to become like a control. Histological analysis performed on spleen, liver, kidneys and lungs confirm MRI readouts.

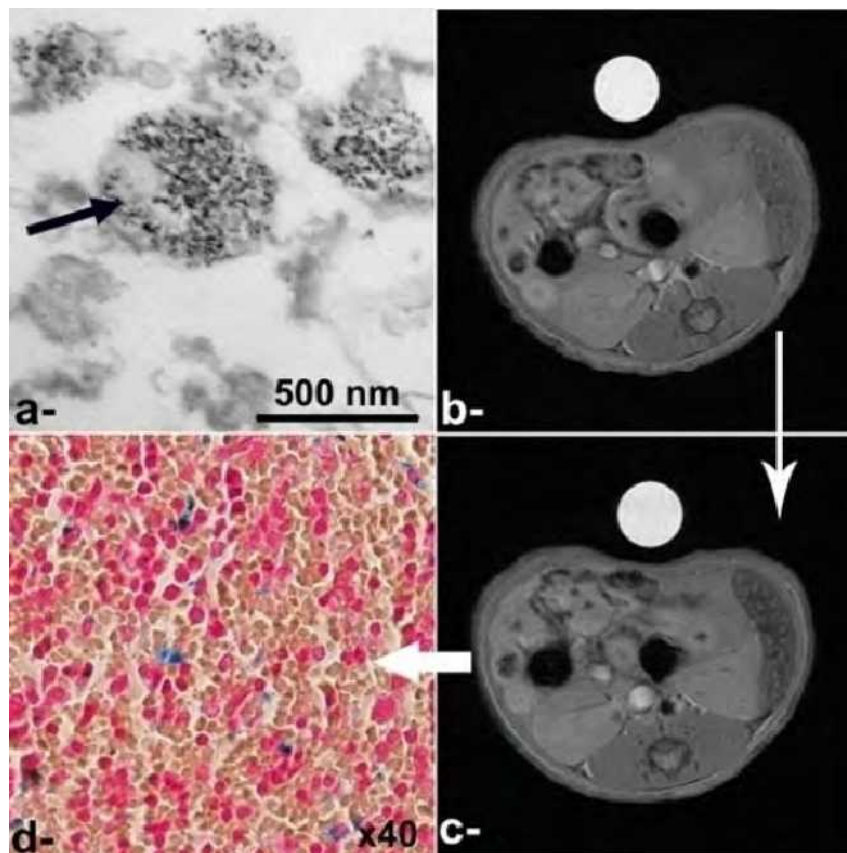


Figure1: a-TEM image of iron loaded MP. b- MR image showing the spleen before and c- after MP injection. d- Histological image showing the localization of MP in the spleen (Perts staining).

Presentation Number **0925B**

Poster Session 4c: In Vivo Studies & Development/Novel Use of Imaging Probes

Production and Preliminary Testing of Ultra-Stable Gadolinium-Benzyl-DOTA-Cholera Toxin B Conjugates as MRI Brain Circuitry Tracking Agents

Olga Vasalatiy, Sarah Cheal, Haitao Wu, Gary L. Griffiths, Agnieszka Sulima, NHLBI, NIH, Rockville, MD, USA. Contact e-mail: agnieszks@mail.nih.gov

Cholera toxin subunit B (CTB) is a useful agent for MRI imaging of brain circuitry by virtue of its transport properties. CTB labeled with gadolinium (Gd) may allow us to non-invasively image neuronal connections over extended time periods. Moreover it may have advantages over low molecular weight Gd complexes of DOTA-biotin, or over the toxic manganese chloride. Gd in chelated form, covalently attached to CTB by a bifunctional version of the macrocyclic chelating agent 1,4,7,10-tetraazacyclododecane-N,N',N'',N'''-tetraacetic acid (DOTA), should represent an optimum CTB contrast reagent useful for multi-day tracking, by virtue of its extreme in vivo stability. The Gd complex of the 4-isothiocyanatobenzyl-DOTA pre-activated bifunctional chelate was prepared and conjugated to CTB at Gd-chelate:CTB ratios ranging from 1.4 to 4.0, as we sought to balance maximum Gd content for ideal signal detection with maximum retention of CTB biological transport activity. Conjugates were comprehensively characterized for protein concentration and Gd content by MADLI-TOF, HPLC and ICP-MS, and the synthesis of the reagent and its physical and in vitro properties will be described.

Presentation Number **0926B**

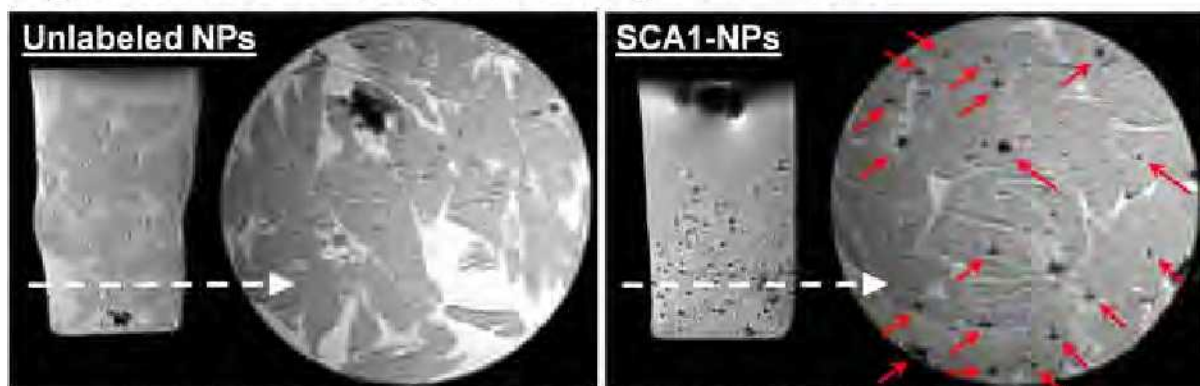
Poster Session 4c: In Vivo Studies & Development/Novel Use of Imaging Probes

Molecular imaging of pancreatic islets in mice with a newly developed beta-cell specific superparamagnetic contrast agent at the ultra high field of 16.4T

Sven Gottschalk, David Z. Balla, Rolf Pohmann, Joern Engelmann, Max-Planck-Institute for Biological Cybernetics, Tuebingen, Germany. Contact e-mail: sven.gottschalk@tuebingen.mpg.de

Despite of decade-long research currently no method exists that could either accurately or non-invasively determine beta-cell mass *in vivo*. However, quantification of beta-cells would allow to understand the pathophysiology of diabetes, to identify pre-diabetic patients and to follow up cellular therapies (e.g. islet transplantations). Here, we present *in vivo* and *ex vivo* MRI data of the murine pancreas at ultra high fields (16.4T) and the first attempt to visualize pancreatic islets with a newly developed targeted contrast agent (CA) based on a single chain antibody fragment (SCA1, kindly provided by S. Schneider, Bochum, Germany). **METHODS:** Beta-cell specific SCA1 was covalently coupled to superparamagnetic cobalt nanoparticles (NPs). C57BL/6J-mice were injected intravenously with PBS (control), unlabeled NPs or SCA1-NPs. Five hours later the animals were anaesthetized with isoflurane, a constant breathing rate was maintained and T2*-weighted MR-Images were recorded. Then, the mice were sacrificed, organs were taken out and MR-images were recorded overnight (fig. 1). **EX VIVO:** As expected, punctuate loss of signal intensity (sizes are consistent to average diameters of islets) in the excised pancreas of SCA1-NPs treated mice was seen. Binding of the prospective CA to the islets was also verified by immunofluorescence (data not shown). **IN VIVO:** All organs can be easily identified and accumulation of unlabeled NPs as well as SCA1-NPs was clearly visible in liver and spleen. However, the anticipated punctuate signal-loss in pancreatic tissue was not yet detectable *in vivo* (data not shown). **CONCLUSIONS:** For the first time we have demonstrated the feasibility of *in vivo* MRI of the mouse abdomen at 16.4T. This allowed MR-microscopic sensitivity for structures <100 μ m and anatomical details of the pancreas were identified. Despite of the high spatial resolution at this field strength the cellular architecture of the pancreas, i.e. the location or amount of islets of Langerhans remains difficult to assess. Furthermore, using a novel targeted CA *in vivo*, beta-cell containing islets of Langerhans were identified in excised pancreas. Financial support of the Max-Planck Society and German Ministry for Education and Research (BMBF, FKZ: 01EZ0813) is gratefully acknowledged.

Figure 1: Ex vivo T2*-weighted MR-Images of Pancreas



Longitudinal images: Surface coil, 3D-FLASH, 50x50x50 μ m³, TR/TE=15/4.25ms, α =5°
 Transversal images: Linear birdcage coil, 3D-FLASH, 50x50x50 μ m³, TR/TE=15/2.8ms, α =5°
 (Labeled islets are marked with a red arrow.)

Presentation Number **0927B**

Poster Session 4c: In Vivo Studies & Development/Novel Use of Imaging Probes

Synthesis of UDP-2-Ketogalactose and UDP-2-Ketoglucose for the Site-Specific Linkage of Biomolecules via Modified Glycan Residues using Glycosyltransferases

Andres E. Dulcey, Jeffrey Lamb, Gary L. Griffiths, Agnieszka Sulima, NHLBI, NIH, Rockville, MD, USA. Contact e-mail: agnieszks@mail.nih.gov

Structural information on glycosyltransferases previously revealed that the sugar-donor specificity of these enzymes can be broadened to include modified sugars with chemical handles that can be utilized for conjugation chemistry. The potential of wild-type and mutant glycosyltransferases to produce glycoproteins with modified sugar moieties has made it possible to insert orthogonally reactive groups at specific protein sites. This platform technology enables the preparation of a range of site-specifically modified agents for targeted drug delivery such as drug-bearing bio/nanoparticles, and for diagnostic imaging modalities such as for magnetic resonance imaging. The first series of orthogonal groups we targeted was insertion of a ketone group on glycoproteins as this functional group is not abundant/present in biological systems. The ketone group insertion would then allow further substitution via a mild Schiff base or aminoxy-modification strategy. The synthesis of UDP-2-ketogalactose was previously carried out, albeit with great difficulty and low efficiency and the principal investigator at NCI approached the IPDC for assistance with this agent and for synthesis of the heretofore non-described 2-ketoglucose analog. The synthetically modified approach developed by the IPDC for the synthesis of UDP-2-ketoglucose and UDP-2-ketogalactose has allowed improved access to the desired compounds. The UDP-2-ketoglucose analog was synthesized in 8 steps and 4.7% overall yield, and the UDP-2-ketogalactose analog was obtained in the same number of steps with an overall yield of 5.3%. The yield of the latter represents an approximately eight-fold improvement over the 1st generation literature synthesis, which involved 8 steps and an overall yield of 0.7%.

Presentation Number **0928B**

Poster Session 4c: In Vivo Studies & Development/Novel Use of Imaging Probes

Detection of Human Malignant Glioma in an Experimental Rat Model by PARACEST MRI

M. M. Ali¹, Asm Iskander¹, Nadimpalli Ravi S Varma¹, Branislava Janic¹, Guangliang Ding¹, Robert A. Knight¹, Marty Pagel², Ali S. Arbab¹, ¹Radiology, Henry Ford Health System, Detroit, MI, USA; ²Biomedical Engineering and Chemistry, University of Arizona, Tucson, AZ, USA. Contact e-mail: mesera@rad.hfh.edu

PARACEST (PARAMagnetic Chemical Exchange Saturation Transfer) MRI contrast agents have advantages relative to T1- or T2-relaxivity MRI contrast agents. However, a major problem for in vivo PARACEST applications is the sensitivity of the agent. We have recently reported that 1.62 and 1.43 mM of Eu-DOTA-Gly and Yb-DOTA-Gly are required to achieve a 3% CEST effect in solution which may limit in vivo application. To overcome this problem, small molecule, Eu-DOTA-Gly PARACEST agents have been conjugated to a G5 PAMAM dendrimer through EDC/NHS method. But, only 37% of the surface amines of a G5 dendrimer were conjugated with PARACEST agents. Here, we develop a new method to conjugate PARACEST agents with a G5 dendrimer through benzyl-thiourea linkage that achieves excellent synthesis yields and purities. G5-Eu PARACEST agent showed a tremendous improvement in sensitivity on a per-molecule basis. The solution study showed that 45 μ M G5-Eu is required to generate 3% of CEST effect. Besides, dendrimer-based MRI contrast agents passively target tumor tissues via the Enhanced Permeability and Retention (EPR) effect, which may further improve the detection of dendritic PARACEST agents within tumors. Here, we report the detection of U87 glioma by a dendritic PARACEST agent. Intracranial implanted U87 glioma was produced in nude rats and MRI was performed on day 35-37 following the implantation of the tumor. A series of RARE MRI experiments were conducted with presaturation applied at +55 ppm, 20 μ T and 2.2 sec to generate the PARACEST effect (4 sec TR, 64 sec/image). After acquiring five pre-injection images, 0.04 mmol/kg of G5-Eu in 800 μ L was injected via the tail vein catheter, and a series of images were acquired to monitor the dynamic pharmacokinetics of the agent for 50 minutes. Post-injection images were subtracted from pre-injection images to measure the PARACEST effect. The pharmacokinetics of G5-Eu was visualized in the rat glioma tumor. Administration of 800 μ L of PAMAM-G5-Eu to a rat glioma model of U87 human malignant glioma showed a dynamic change in the PARACEST effect, culminating in a 15% CEST effect 20 minutes after administration. The change in image contrast of the tumor was assigned to the accumulation of the PARACEST agents in the tumor. This assignment was supported by the lack of significant contrast changes before injection of the agents and the generation of significant contrast changes after injection. This is the first demonstration of detection of human malignant glioma in a rat model by PARACEST MRI.

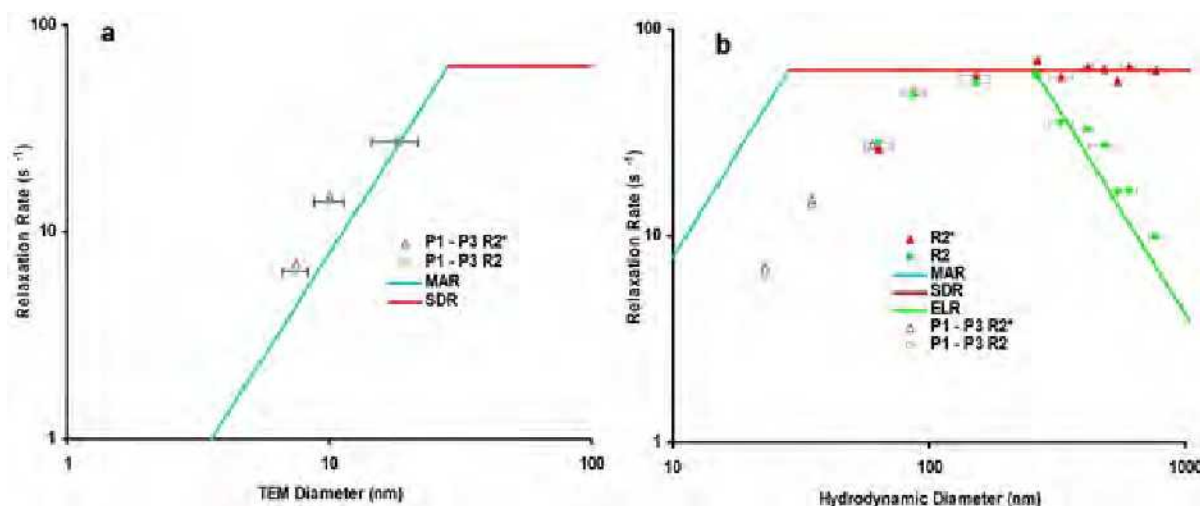
Presentation Number **0929B**

Poster Session 4c: In Vivo Studies & Development/Novel Use of Imaging Probes

Microgel Iron Oxide Nanoparticles in Studies of Magnetic Resonance Relaxation and Endothelial Progenitor Cell Labelling

Eddy Lee^{1,2}, Shuter Borys¹, Jerry Chan^{3,4}, Shih-Chang Wang⁵, ¹Diagnostic Radiology, Yong Loo Lin School of Medicine, National University of Singapore, Singapore, Singapore; ²UQCCR, University of Queensland, Herston, QLD, Australia; ³Experimental Fetal Medicine Group, Yong Loo Lin School of Medicine, National University of Singapore, Singapore, Singapore; ⁴Reproductive Medicine, KK Women's and Children's Hospital, Singapore, Singapore; ⁵Radiology, University of Sydney, Westmead, NSW, Australia. Contact e-mail: eddysmlee@gmail.com

In vivo tracking of stem cells after transplantation is crucial for understanding cell-fate and therapeutic efficacy. We previously described the synthesis of microgel iron oxide nanoparticle (MGIO) and demonstrated that they provide superior MRI tracking sensitivity over commercially available particles. Here, we report on MGIO morphology by transmission electron microscopy, crystallinity by electron diffraction, hydrodynamic diameters by light scattering, composition by thermogravimetric analysis, magnetization characteristics by vibrating sample magnetometry and SQUID, magnetic resonance relaxation and labelling of human endothelial progenitor cells (EPC). MGIO over a nine-fold range of diameters were synthesized (87 to 766nm) with iron oxide content of up to 82 wt%. TEM showed that they consisted of numerous sub-5nm primary iron oxide nanoparticles (PIO) structures held together by a polymer mesh, which is in agreement with the electron diffraction pattern that showed interplanar spacing typical of composite particles consisting of magnetite PIO. The low M_R/M_S ratio ($M_S = 52.9 \text{ Am}^2/\text{kg}$, $M_R = 0.061 \text{ Am}^2/\text{kg}$) and low $H_C (= 0.672 \text{ A/m})$ implied that the PIO within MGIO were moderately well separated. Their MR transverse relaxation rates ($R2^*$ and $R2$) are comparable to those of theoretical models and represent a correlation between model and real particles of varying diameters. The $R2$ and $R2^*$ of MGIO can be described as the distinct regimes of motional averaging (MAR), static dephasing (SDR) and echo limited (ELR). For small particles, the measured relaxation rates and TEM diameters (<30nm) are comparable to the MAR (Fig a). The $R2$ decrease for hydrodynamic diameters >250nm in correlation to the ELR (Fig b). In the intermediate region, the relaxation is independent of particle diameter as described by the SDR. A labelling study of EPC also confirms that MGIO is an efficient label regardless of cell type. The range of MGIO diameters makes it a useful tool for the studying of relaxation induced by magnetic particles and cellular tracking by MRI.



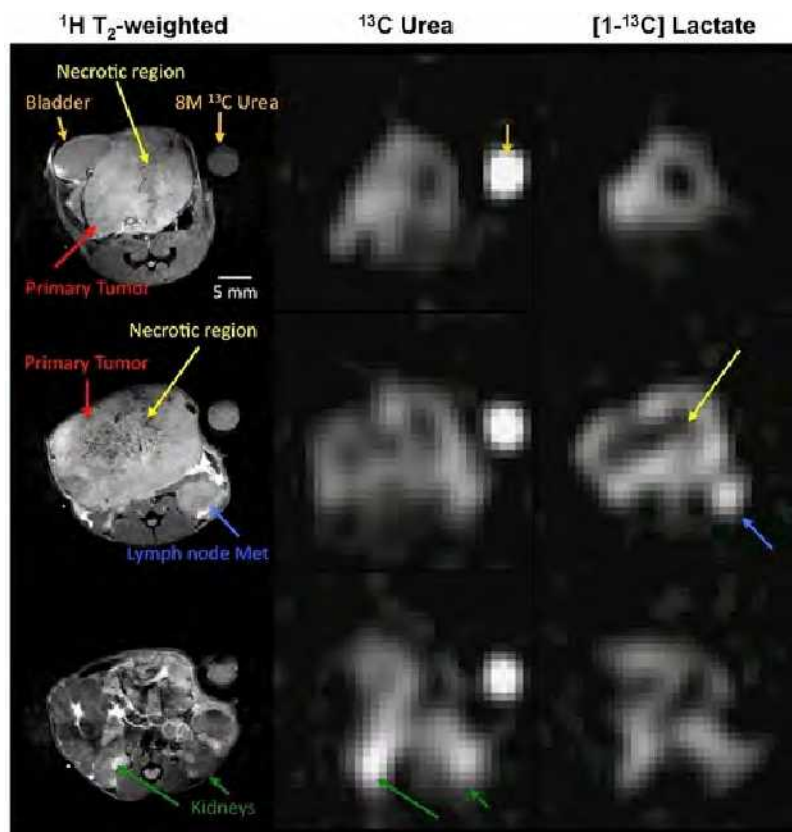
Presentation Number **0930B**

Poster Session 4c: In Vivo Studies & Development/Novel Use of Imaging Probes

Frequency Specific 3D imaging at 14T using hyperpolarized MR

Kayvan R. Keshari, Subramaniam Sukumar, David M. Wilson, Mark Van Criekinge, Robert Bok, Daniel B. Vigneron, John Kurhanewicz, Radiology and Biomedical Imaging, University of California, San Francisco, San Francisco, CA, USA. Contact e-mail: kayvan.keshari@radiology.ucsf.edu

Hyperpolarized ^{13}C magnetic resonance (MR) has emerged as an exciting new technique to investigate biochemical and physiologic processes in vivo. Signal enhancements are irreversibly lost due to spin relaxation (T_1), metabolism and RF saturation. Additionally, high field studies are hindered by increased chemical shift dispersion and T_2^* effects. The goal of this study was to develop a 3D frequency specific imaging sequence that could be used at high fields for molecular imaging. $[1-^{13}\text{C}]$ pyruvate and ^{13}C urea were prepared using the OX63 radical and polarized using an Oxford Hypersense. The experiments were performed on a 14T, 600WB micro-imaging spectrometer equipped with 100G/cm gradients (Varian Instruments). An echo planar imaging (EPI) based pulse sequence (below) was constructed using frequency specific pulses ($f = \text{pyruvate, lactate or urea}$) to generate a 3D image for each metabolite with an acquisition time of approximately 180ms. $[90_f - (180_f - \text{EPI}_n)N]_f$ n, N=12 180° pulses were implemented to minimize T_2^* related signal loss and artifacts. The imaging sequence was validated in solution experiments and then a transgenic model of prostate cancer (TRAMP) mouse was used to demonstrate the sequence in vivo. Representative ^1H T_2 -weighted images and hyperpolarized ^{13}C 3D EPI images after injection of copolarized $[1-^{13}\text{C}]$ pyruvate and ^{13}C urea (Figure) demonstrate the distribution of ^{13}C urea and $[1-^{13}\text{C}]$ lactate, produced from pyruvate. Good spatial correlation to both the primary TRAMP tumor and lymphnode metastasis including clear distinction from surrounding tissue is observed with minimal artifact. This method overcomes problems encountered with hyperpolarized ^{13}C at high fields related to the wide spectral dispersion and T_2^* . It can also be applied to both multiple frequencies as well as simultaneous time course measurements. Thus, the pulse sequence described here is well suited for obtaining chemical shift specific images from hyperpolarized ^{13}C studies at high field strengths in vivo.



T_2 -weighted images were acquired using a spin-echo sequence ($T_1=20\text{ms}, T_R=1.5\text{s}$). Representative axial slices from the 3D ^{13}C sequence have a FOV of 40mm isotropic ($16 \times 12 \times 12$) and zero-filled to a final resolution of 1.25mm isotropic (0.002 cc). Tumor pathology was verified by histology and immunohistochemistry.

Presentation Number **0931B**

Poster Session 4c: In Vivo Studies & Development/Novel Use of Imaging Probes

In vivo imaging with a cell-permeable porphyrin-based MRI contrast agent

Alan Jasanoff, Taekwan Lee, Xiao-an Zhang, Shanta Dhar, Henryk M. Faas, Stephen J. Lippard, MIT, Cambridge, MA, USA. Contact e-mail: jasanoff@mit.edu

Magnetic resonance imaging (MRI) with molecular probes offers the potential to monitor physiological parameters with comparatively high spatial and temporal resolution in living subjects. For detection of intracellular analytes, construction of cell-permeable imaging agents remains a challenge. Here we show that a porphyrin-based MRI molecular imaging agent, Mn-(DPA-C2)₂-TPPS₃, effectively penetrates cells and persistently stains living brain tissue in intracranially injected rats, without apparent toxic side effects. Chromogenicity of the probe permitted direct visualization of its distribution by histology, in addition to MRI. Distribution was concentrated in cell bodies after hippocampal infusion. Tissue fractionation and elemental analysis studies showed that the probe was primarily localized to cytosolic compartments in injected brain samples. Mn-(DPA-C2)₂-TPPS₃ binds Zn²⁺ ions with high affinity, and preliminary evidence of zinc-dependent uptake of the probe was provided by comparison of staining results obtained in brain regions containing different labile zinc concentrations. MRI-based molecular imaging with probes that accumulate in analyte-dependent fashion in vivo represents a novel and potentially generalizable approach distinct from strategies for sensing analytes via relaxivity changes. Membrane permeability, optical activity, and high relaxivity of porphyrin-based contrast agents offer exceptional functionality for in vivo imaging.

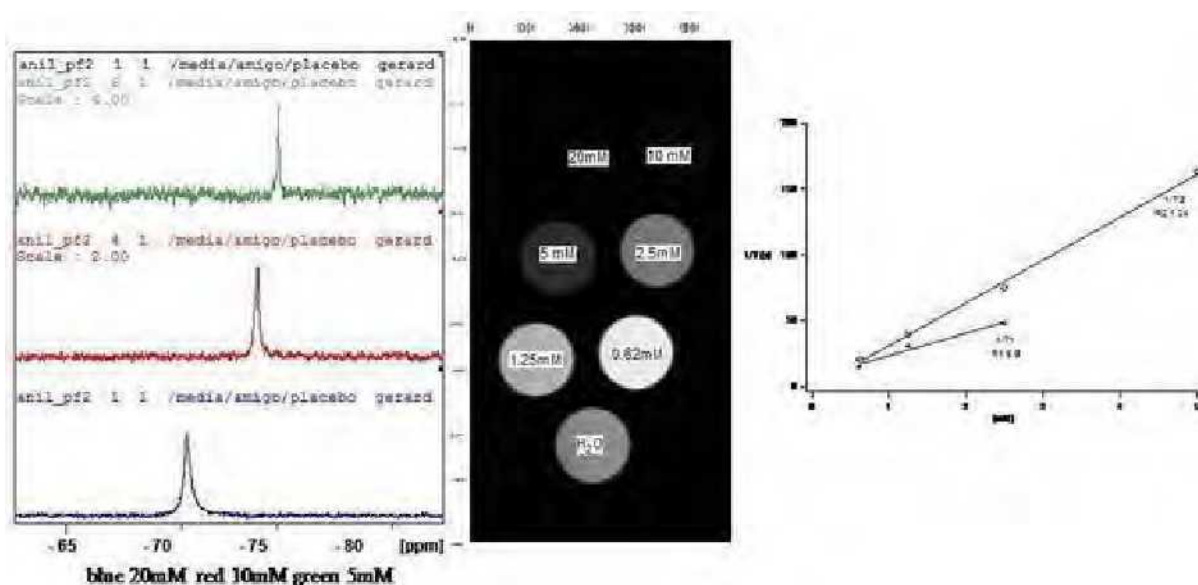
Presentation Number **0933B**

Poster Session 4c: In Vivo Studies & Development/Novel Use of Imaging Probes

Design and Synthesis of New Generation Bifunctional MR Contrast Agents Based on Gd(III) and ^{19}F for MR Molecular Imaging: DO3A-Ph-(PF)₂

Jasleen K. Uppal^{1,2}, Gerard Raffard³, Puja P. Hazari¹, Jean M. Franconi³, Michele Allard⁴, Jurgen Schulz³, Narender K. Kaushik², Anil K. Mishra^{1,3}, ¹DCRS, INMAS, Delhi, India; ²Department of chemistry, University of Delhi, Delhi, India; ³CRMSB, CNRS, University of Bordeaux, Bordeaux, France; ⁴University of Bordeaux, Bordeaux, France. Contact e-mail: akmishra@inmas.drdo.in

Introduction In addition to Gd(III)-assisted ^1H -MRI techniques, contrast agents based on ^{19}F are emerging as attractive alternatives. ^{19}F is one of the most promising nuclides for MRI and its significance ascribe to its exceptional characteristics, namely, high sensitivity of the ^{19}F chemical shift to the local microenvironment. In the present work, we have focussed on the synthesis of ^{19}F -labeled phenylalanine based macrocyclic chelating agents (DO3A) and the in-vitro MR relaxation changes caused due to variation in concentration of the chelate from ^1H as well as ^{19}F MRS experiments. **Synthesis** The ^{19}F labeling was performed by carrying out N, N-bis-alkylation of phenylalanine with pentafluorobenzyl bromide. The corresponding ^{19}F labeled derivative was subjected to hydrogenation followed by subsequent reaction with chloroacetyl chloride for conjugation to DO3A-tert butyl ester. **Methods** The gadolinium complexation was carried out with $\text{GdCl}_3 \cdot 6\text{H}_2\text{O}$ in water at 60°C . For measurements of the relaxivities r_1 , different concentrations ranging from 0.62 to 20mM of the CA were prepared. **Results and Discussion** All intermediates and the final compound DO3A-Ph-(PF)₂ were fully characterized by ^1H and ^{13}C NMR and mass spectroscopy. High Resolution ^{19}F NMR spectra have been acquired and inversion recovery for ^{19}F T₁. In T₁-weighted images ^1H , different MR image intensities at different concentrations were observed due to changes in the relaxation rates. $1/T_1$ values from sample at different concentration values were plotted and r_1 and r_2 relaxivity of the complex was determined to be 6.6 s⁻¹mM⁻¹ and 1.24 s⁻¹mM⁻¹ respectively. In conclusion, we have designed and developed a new generation bifunctional MR contrast agent which integrates ^1H and ^{19}F MRI and offers potential applications in the field of molecular imaging. Most important feature of this type of bifunctional MR contrast agent is that relaxivity changes in the presence and absence of Gd(III) ions. Secondly, even after cleavage of Gd-L from biological moiety it offers a powerful nuclei (^{19}F) to detect the site or dynamics of biomolecule by MRI which does not exist in literature till date.



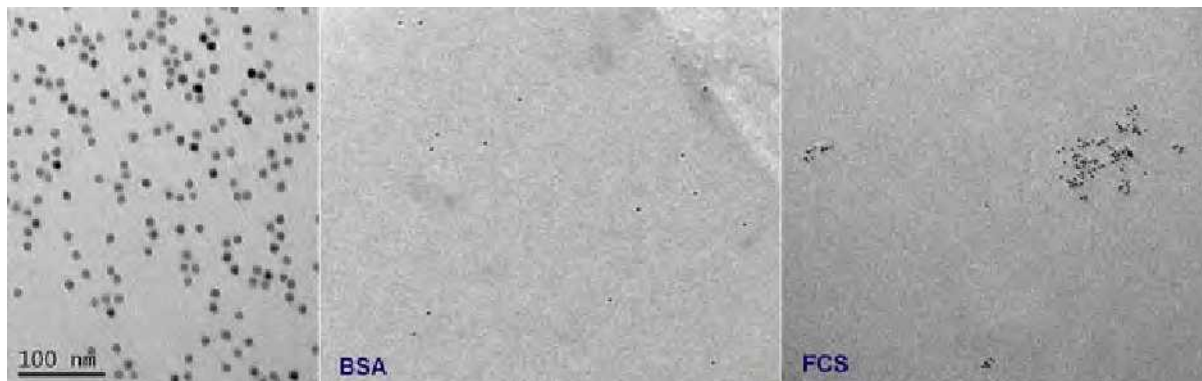
Presentation Number **0934B**

Poster Session 4c: In Vivo Studies & Development/Novel Use of Imaging Probes

Changes of transversal relaxivity of SPIO in different biological solutions at 3T: influence of protein binding

Harald Ittrich¹, **Nina Raabe**¹, **Evelyn Grabowski**¹, **Barbara Freund**², **Oliver T. Bruns**^{3,2}, **Markus Heine**⁴, **Michael G. Kaul**¹, **Gerhard Adam**¹, ¹Center for Radiology and Endoscopy, University Medical Center Hamburg-Eppendorf, Hamburg, Germany; ²Department of Biochemistry and Molecular Biology II, University Medical Center Hamburg-Eppendorf, Hamburg, Germany; ³Heinrich-Pette-Institute for Experimental Virology and Immunology, University of Hamburg, Hamburg, Germany; ⁴Department of Anatomy II: Experimental Morphology, University Medical Center Hamburg-Eppendorf, Hamburg, Germany. Contact e-mail: ittrich@uke.uni-hamburg.de

Background: Transversal relaxivity of superparamagnetic iron oxid nanoparticles (SPIO) is influenced not only by the composition and diameter of the iron core but also by their coating and aggregation in biological fluids caused by protein binding. Consequently development of quantitative in vivo MRI needs an accurate in vitro characterisation of SPIO before in vivo application. Therefore the purpose of this study was to characterise the relaxivities of monodisperse SPIO in different biofluids. Methods and materials: Monodisperse SPIO were synthesized in organic and transferred in water-soluble phase with a core of 10 nm (hydrodynamic diameter: 25 nm). SPIO were diluted in different biofluids (aqua, 1%, 3.6% and 8% bovine serum albumin (BSA) and fetal calf serum (FCS)). T2 and T2* were measured in vitro at 3T MRI (Philips Intera) and calculation of r2 and r2* was performed. Results were compared to those of the size exclusion chromatography (SEC). Iron measurement of the fractions of SEC was done by Bathophenanthrolin-assay. All samples were controlled by transmission electron microscopy (TEM). Results: r2 and r2* relaxivities ([in mM-1s-1] ± SD) showed no significant difference between H2O (55.5 ± 2.2; 60.0 ± 1.5), 1% BSA (58.61 ± 1.9; 64.6 ± 1.9), 3.6% BSA (60.7 ± 1.3; 66.9 ± 1.8) and 8% BSA (63.0 ± 4.16; 71.0 ± 1.4) but a significant increase of relaxivities for SPIO diluted in FCS (202.6 ± 12; 294.7 ± 17.2). Data of the SEC measurements revealed an agglomeration of SPIO after incubation in FCS with all iron in the exclusion fraction (> 70 nm), which correlated with SPIO agglomeration seen on TEM images without changes in core size or hydrodynamic diameter of single SPIO. Conclusion: r2 and r2* relaxivities dominantly depend on SPIO surrounding medium. The lack of relaxivity increase or changes in particle size in different concentrations of albumin shows that particle agglomeration seems to depend on specific serum proteins different from albumin. We conclude that an exact in vitro characterisation of SPIO in serum before in vivo application is necessary for reliable relaxivity measurements in quantitative MRI approaches as an essential tool for molecular MRI, e.g. targeted imaging using SPIO.



Presentation Number **0935B**

Poster Session 4c: In Vivo Studies & Development/Novel Use of Imaging Probes

Development of a Small Molecule Based MRI contrast agent for Atherosclerotic Plaques

Kenjiro Hanaoka^{1,2}, Takehiro Yamane^{1,2}, Kazuhisa Hirabayashi^{1,2}, Tetsuo Nagano^{1,2}, ¹Graduate School of Pharmaceutical Sciences, The University of Tokyo, Tokyo, Japan; ²JST CREST, Saitama, Japan. Contact e-mail: khanaoka@mol.f.u-tokyo.ac.jp

Atherosclerosis is the primary cause of heart disease and stroke, and it is also the underlying cause of about 50% of all deaths in westernized societies via its sequelae of myocardial infarction and stroke. This progressive disease is characterized by the accumulation of lipids and fibrous elements as an atherosclerotic plaque in the large arteries, and there are preferred sites of its lesion formation in the arteries because of differences in blood flow dynamics. Because of its high-risk, the early detection of atherosclerotic plaques would direct therapies to prevent its complications. Magnetic resonance imaging (MRI) is a noninvasive imaging technique that can provide images even deep inside the body, and MRI is used for clinical diagnosis. Moreover, there is considerable interest in MRI contrast agents, which can improve the resolution of MR images. Gadolinium ion (Gd^{3+})-based MRI contrast agents increase tissue contrast by increasing water proton relaxation, and are widely used in clinical diagnostics. Commonly used MRI contrast agents are mainly extracellular agents with nonspecific biodistribution. However, it is also possible to develop Gd^{3+} complexes with various chemical properties by means of appropriate ligand design for Gd^{3+} . Here, we designed and synthesized a novel small molecule based MRI contrast agent that targets atherosclerotic plaques. There have been some theoretic discussions of the likely limits to achieving molecular imaging with MRI, and these have highlighted the practical difficulties of achieving sufficiently high local concentrations of MRI contrast agents within tissue to be detectable, because simple low molecular weight chelates of Gd^{3+} such as those currently used in clinical MRI are considered too insensitive for most molecular imaging applications. Therefore, the challenge of this study is to accumulate low molecular weight Gd^{3+} chelates targeted to atherosclerotic plaques at the detectable level. We have paid attention to boron dipyrromethene (BDP), which is a fluorescent dye for lipid droplets of adipocytes, as a targeting moiety for atherosclerotic plaques. We have designed and synthesized novel MRI contrast agents by combining Gd^{3+} complexes and BDP derivatives, and have successfully visualized atherosclerotic plaques by MRI. We also confirmed their accumulation in atherosclerotic plaques by observing fluorescence ex vivo images of the aortic tree of ApoE^{-/-} mice.

Presentation Number **0936B**

Poster Session 4c: In Vivo Studies & Development/Novel Use of Imaging Probes

Bis(Gd³⁺-GlyMe-DOTA)-Contrast Agent for ¹⁹F-Molecular MR Imaging at 7T

Markus Plaumann¹, **Ekkehard Küstermann**², **Dieter Leibfritz**¹, ¹University of Bremen, Institute of Organic Chemistry, Bremen, Germany; ²University of Bremen, CAI, Bremen, Germany. Contact e-mail: mplauman@uni-bremen.de

Fluorinated Gd³⁺-DOTA-complexes are interesting as contrast agents for MRI. They permit recording ¹⁹F-images without any background signals and classical ¹H-MR images at the same time. The labeling of C6-cells with lanthanide-(Ln³⁺)-DTPA- or -DOTA-complexes of 3,5-bis(trifluoromethyl)benzyl derivatives is established in our group. Our aim was to characterize the influence of temperature and pH on the chemical shift of the fluorine NMR signal and T₁ time. Therefore, 4,4'-(hexafluoroisopropylidene)diphenol was selected to synthesize a bis-(Gd³⁺-GlyMe-DOTA)-complex (see figure 1). The new complex with two -CF₃ groups was compared with different 3,5-bis(trifluoromethyl)benzylamine- and 3,5-bis(trifluoromethyl)phenylhydrazine-Gd-GlyMeDOTA complexes. Tris-*t*-butyl-GlyMe-DOTA was activated with TBTU and DIPEA for reaction with 4,4'-(hexafluoroisopropylidene)diphenol at room temperature for 24h. The *t*-butyl esters were cleaved with trifluoroacetic acid. Ligand system was characterized with ESI-MS and NMR spectra. The Gd-complex was obtained by adding GdCl₃ in an aqueous/ethanol solution of the ligand and following neutralization with 0.1M NaOH. All complexes were purified by HPLC and characterized by ESI-MS. T₁-measurements were performed at 8.4T in 1mmol/L solutions. Measurements of pure 4,4'-(hexafluoroisopropylidene)diphenol have shown temperature dependency in the range of 295 K to 315K in CDCl₃ (blue) and in D₂O/DMSO (red) (see figure 2). Protic solvents have bigger influence. Furthermore, the sensitivity concerning to temperature and pH is bigger for the new 4,4'-(hexafluoroisopropylidene)diphenol-Gd-GlyMeDOTA-complex (i.e. 293.15K to 313.15K, Δδ=0.4ppm) in comparison to different 3,5-bis(trifluoromethyl)benzyl derivatives (i.e. 293.15K to 313.15K, Δδ=0.2ppm). It was shown that the ¹⁹F-MRI signal of the new Gd-complex is sensitive enough to be detected on a Biospec 7T MR scanner.

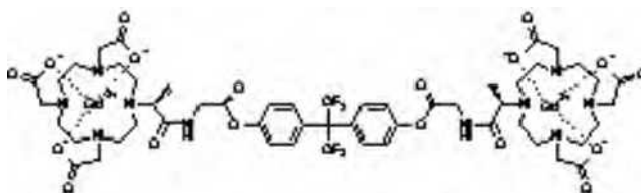


Figure 1: Structure of the 4,4'-(hexafluoroisopropylidene)diphenol-bis-(Gd³⁺-GlyMe-DOTA)-complex

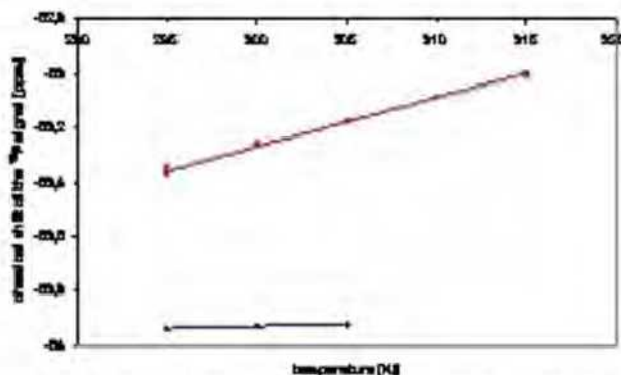


Figure 2: Temperature dependency of the ¹⁹F chemical shift of 4,4'-(hexafluoroisopropylidene)diphenol in CDCl₃ (blue) and in D₂O/DMSO (red).

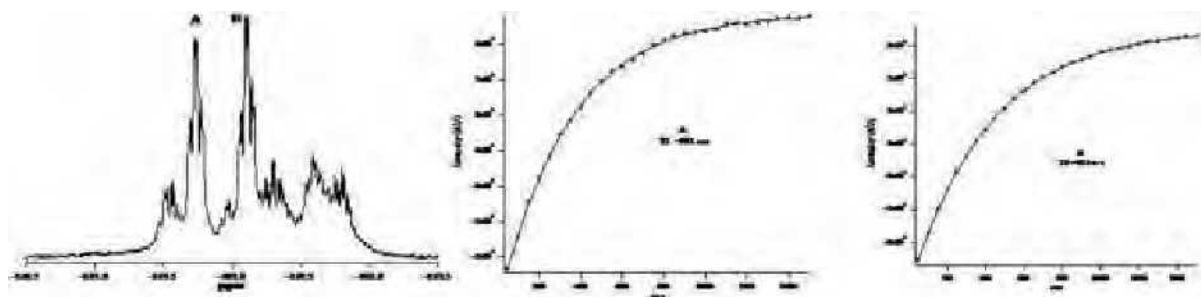
Presentation Number **0937B**

Poster Session 4c: In Vivo Studies & Development/Novel Use of Imaging Probes

Towards Rational Design, Synthesis and Relaxometric Studies of Non-Aqueous Target Specific ^{19}F Magnetic Resonance Imaging Agents

Jasleen K. Uppal^{1,2}, Puja P. Hazari¹, Gerard Raffard³, Jean M. Franconi³, Michele Allard⁴, Jurgen Schulz³, Narender K. Kaushik², Anil K. Mishra^{1,3}, ¹DCRS, INMAS, Delhi, India; ²Department of chemistry, University of Delhi, Delhi, India; ³CRMSB, CNRS, University of Bordeaux. France, Bordeaux, France; ⁴University of Bordeaux, Bordeaux, France. Contact e-mail: uppal.jasleen@gmail.com

Introduction Labeling biocompatible molecules with ^{19}F over short-lived radio-isotopes offers potential advantages in the field of molecular imaging. ^{19}F is a 100% naturally abundant nucleus with a high NMR sensitivity. It has a wide dispersion of isotropic chemical shifts as well as large chemical shift anisotropy which renders it a highly informative reporter of local structure. We have developed ^{19}F labeled choline derivatives to target the cell proliferation associated abnormal choline metabolism in tumor cells. Another significant aspect of our work focuses on the development of ^{19}F labeled methoxyphenylpiperazine (MPP) analogues as promising brain imaging agents targeting dopamine and 5HT receptors. **Synthesis** The ^{19}F labeling was performed by carrying out N, N-bis-alkylation of 2-bromoethylamine with pentafluorobenzyl bromide. The choline and MPP derivatives were prepared by reacting N, N-dimethylaminoethanol and methoxyphenylpiperazine respectively with above synthesized ^{19}F labeled synthon in acetonitrile. **Methods** ^{19}F -NMR spectra and spin-lattice relaxation times T1 were recorded on a Bruker (Wissembourg, France) DPX500 NMR apparatus (^{19}F frequency at 470.6 MHz) using an inversion recovery (IR) sequence. **Results and Discussion** All intermediates and the final compounds have been fully characterized by ^1H and ^{13}C NMR and mass spectroscopy. The intensity of peak A (ortho fluorine) and peak B (meta and para fluorine) in the compound has been plotted as a function of delay time with a theoretical best fit curve connecting the experimental points and time obtained corresponding to the null point on intensity axis was used to calculate the value of spin lattice relaxation time. T1 value corresponding to ortho fluorine and meta fluorine in the pentafluorophenyl ring in the compound was determined to be 341 and 416 ms respectively. In conclusion, we have optimized a facile approach towards synthesis and relaxometric studies of non-aqueous ^{19}F labeled biocompatible probes. Our initial results demonstrate a promising future of these fluorine label in the field of ^{19}F magnetic resonance imaging.



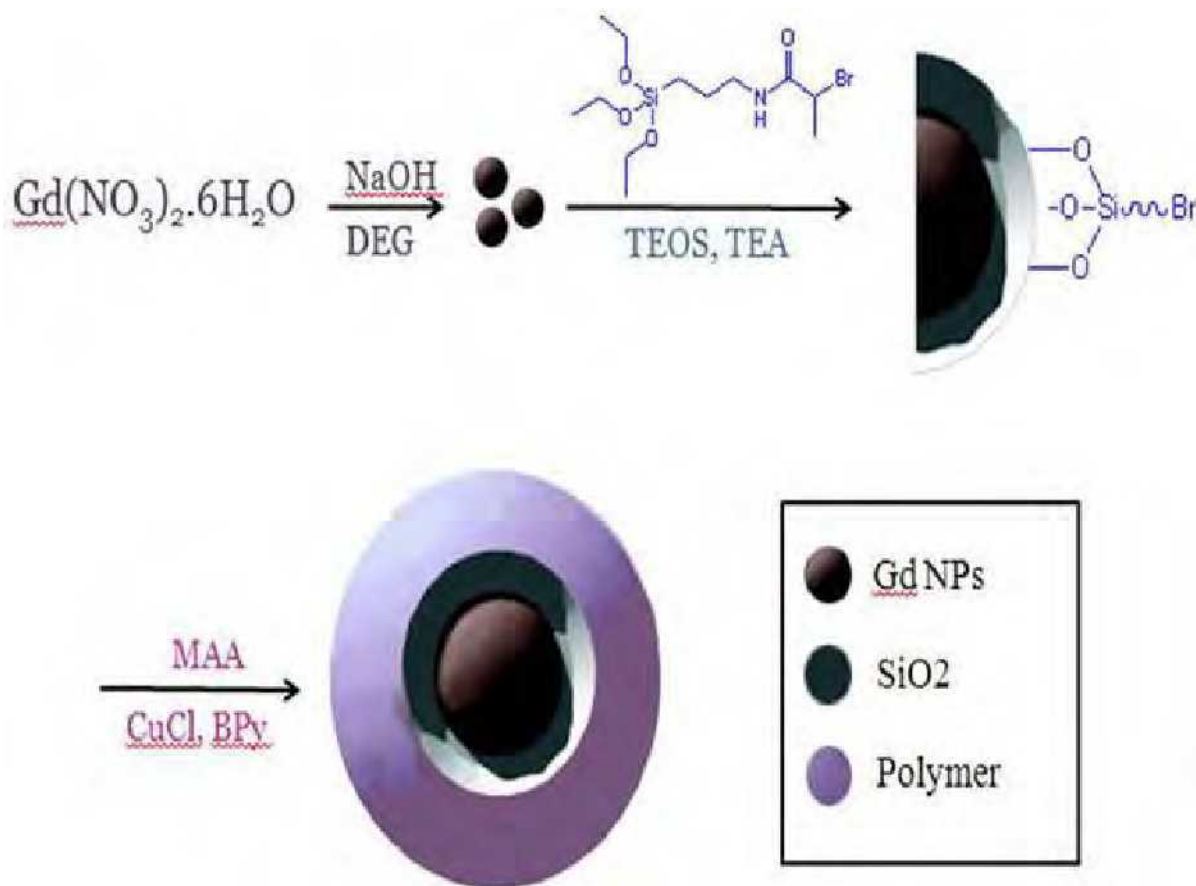
Presentation Number **0938B**

Poster Session 4c: In Vivo Studies & Development/Novel Use of Imaging Probes

Synthesis of polymer coated Gadolinium Oxide Nanoparticles for Magnetic Resonance Imaging

EunJi Yang¹, Hee Kyung Kim², Mehul A. Patel³, Tae-Jeong Kim³, InWoo Cheong³, ¹Department of Nano-science, Kyungpook National University, Daegu, Republic of Korea; ²Department of Medical & Biological Engineering, Kyungpook National University, daegu, Republic of Korea; ³Department of Applied Chemistry, Kyungpook National University, daegu, Republic of Korea. Contact e-mail: ejyang@knu.ac.kr

Magnetic resonance imaging (MRI) is a very important non-invasive technique that is used to diagnose diseases. The diagnosis of diseases through MRI is further improved by using the MRI contrast agent. In this work, polymers were grafted on the surface of gadolinium oxide (Gd₂O₃) nanoparticles, and which would be the most promising way to ensure the long-term stability and low toxicity of Gd₂O₃ nanoparticles in human body. The surface modified Gd₂O₃ nanoparticles provide enhanced relaxivity while the polymer prevents the aggregation of the nanoparticles.



Synthesis route of PMAA-grafted Gd₂O₃ nanoparticles by ATRP

Presentation Number **0939B**

Poster Session 4c: In Vivo Studies & Development/Novel Use of Imaging Probes

Assessment for therapeutic efficacy of new anti-cancer drug in melanoma animal model using ferritin as MRI reporter

Gunwoo Lee^{1,2}, Gyuman Park², Onseok Lee^{1,2}, Kwan S. Hong³, Hyeonseung Lee³, Young W. Choi⁴, Minwon Lee⁴, Chilhwan Oh^{1,5},
¹Biomedical Science of Brain Korea 21, Korea University College of Medicine, Seoul, Republic of Korea; ²Research Institute for Skin Image, Korea University Medical Center, Seoul, Republic of Korea; ³MRI Team, Korea Basic Science Institute(KBSI), Seoul, Republic of Korea; ⁴Department of Pharmaceutics, Chungang University College of Pharmacy, Seoul, Republic of Korea; ⁵Department of Dermatology, Korea University Guro Hospital, Seoul, Republic of Korea. Contact e-mail: pglgw@korea.ac.kr

Recently, many researchers have tried to develop new MRI contrast recipe for cell tracking. Generally, paramagnetic ion oxoide such as feridex® and resovist® are used as negative contrast agent in magnetic resonance image, but duration time of these contrast agents is very limited. Ferritin, which serves to store iron in cells as a non-toxic form, is one of the potential candidate for long-cellular imaging method for MRI. In this study we investigated potential of ferritin gene for inducing contrast enhancement in MRI. We infected human ferritin heavy chain (hFTH) expressing lentiviral vector in melanoma cell line (B16) and tested contrast ability of gene transduction. We compared the contrasting ability and duration time of ferritin expression with feridex®, which is generally used as T2 contrast agent. We found that tumor masses of ferritin-transduced B16 showed much more enhanced MR contrast from 7days than negative controls and cancer kept the enhanced contrast until mice death. Finally, we assessed B16/hFTH animal model for evaluating the therapeutic potential of new developed anti-cancer drug. After two weeks of cancer inoculation, dacabazine and oregonin were treated on tumors and monitored the therapeutic effects of drugs. We found that oregonin strongly suppressed the increase of tumor volume than dacabazine, and survival ratio of highly increase by oregonin treatment. We suggested that ferritin-transduced cancer animal models might be useful for longitudinal study for pharmacologic evaluation.

Presentation Number **0940B**

Poster Session 4c: In Vivo Studies & Development/Novel Use of Imaging Probes

Generation of a hyperpolarized ¹³C RGD peptide by secondary labeling using [1,1-¹³C] acetic anhydride

David M. Wilson¹, Kayvan R. Keshari¹, Mark Van Criekinge¹, Peder E. Larson¹, Jeffrey Macdonald², Daniel B. Vigneron¹, John Kurhanewicz¹, ¹Department of Radiology and Biomedical Imaging, University of California, San Francisco, San Francisco, CA, USA; ²GE Healthcare, Menlo Park, CA, USA. Contact e-mail: dmeybin@gmail.com

Introduction: As was shown in studies of n-acetyl lysine, cysteine and α-MSH small molecules and peptides can be labeled via [1,1-¹³C] acetic anhydride, and are potentially applicable as in vivo probes (1). The tripeptide Arginine-Glycine-Aspartate (RGD, MW 346.34) is another such peptide with a important in vivo application, binding cell surface integrins(2) which have been shown to upregulated in cancer (3,4). Thus, secondary labeling of RGD with [1,1-¹³C] acetic anhydride was investigated. **Methods:** 6.2μL of [1,1-¹³C] acetic anhydride preparation (2.12 x 10⁻⁴ mol) were polarized using the HyperSense DNP polarizer. Five mL of the following dissolution media were used: 6.1μL of 10N NaOH, 21mg of RGD peptide (12mM), 0.3mM EDTA in H₂O. This resulted in equimolar concentrations of labeled acetic anhydride and RGD. In a second experiment with analogous parameters, 6.2μL of [d6-1,1-¹³C] acetic anhydride (2.12 x 10⁻⁴ mol) were polarized. **Results:** Acetylation of RGD was accomplished in a basic solution containing the peptide during dissolution of the hyperpolarized acetic anhydride. The first pulse of the experiment (Figure 1) demonstrates the signal of the acetylated RGD at 11.7T, with T₁ of ~7s. In an attempt to increase the T₁ of acetylated RGD, the acetylation was carried out using per-deuterated [d6-1,1-¹³C] acetic anhydride. This yielded a T₁ of ~8s, only slightly longer than the protonated version. However, at 3T, deuteration significantly lengthens the acetylated RGD as compared to the protonated compound (to 30 secs). In the presence of 1.1 equivalents of base, only the primary amine was acetylated. **Discussion:** Acetylation of RGD with [1,1-¹³C] acetic anhydride to produce the hyperpolarized adduct confirms the possibility of performing hyperpolarized ¹³C imaging studies using complex biomolecules relevant to oncogenesis. Future studies will focus on optimizing hyperpolarized ¹³C labeling for in vivo applications. **References:** (1)Wilson PNAS 2009 (2)Ruoslahti Annu Rev Cell Dev Biol 1996 (3)Edick Mol Biol Cell 2007 (4)Goel Endocr Relat Cancer 2008

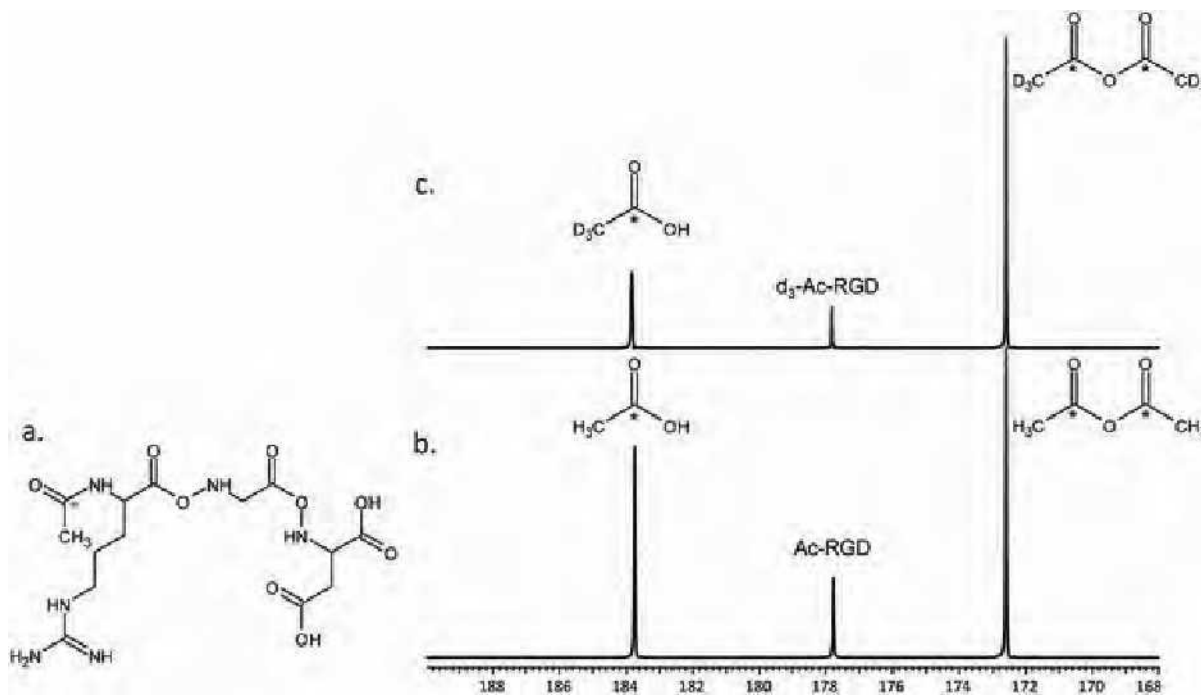


Figure 1. (a) Structure of Arg-Gly-Asp demonstrating the site of acetylation. Generation of hyperpolarized Ac-RGD (b) and d₃-Ac-RGD (c).

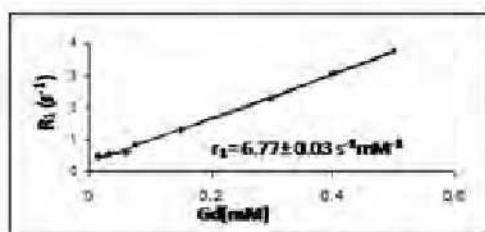
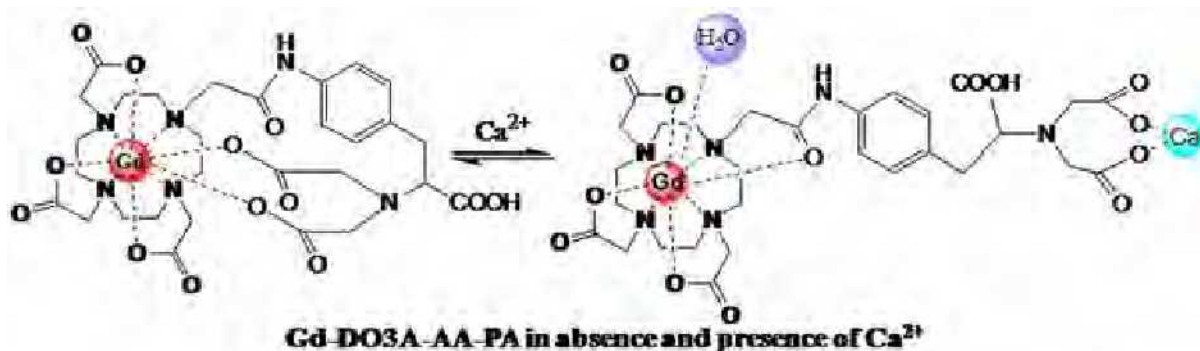
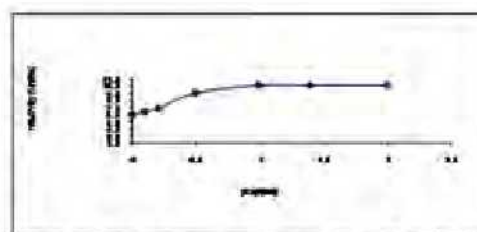
Presentation Number **0941B**

Poster Session 4c: In Vivo Studies & Development/Novel Use of Imaging Probes

Synthesis and Characterization of 'Smart Contrast Agent' for Calcium Sensing

Jyoti Tanwar^{1,2}, Anupama Datta¹, Anjani K. Tiwari¹, Thirumal Meganathan², Senthil S. Kumaran³, Anil K. Mishra¹, ¹Department of Cyclotron and Radiopharmaceutical Sciences, Institute of Nuclear Medicine and Allied Sciences, Delhi, India; ²Department of Chemistry, University of Delhi, Delhi, India; ³Department of NMR and MRI, All India Institute of Medical Sciences, New Delhi, India. Contact e-mail: anuabha@hotmail.com

Calcium plays important dual role as a carrier of electric current and as a second messenger in brain. Calcium concentration modulation both inside and outside cell is a considerable factor for nervous system function in normal and pathological conditions. MRI has potential for very high spatial resolution at molecular/ cellular level. Smart contrast agents enhance MRI applications to understand biological events. With objective of tracking the modulation of Ca²⁺ with high relaxivity response, a novel Ca-sensitive MRI contrast agent, Gd-DO3A-AA-PA, based on 1,4,7,10-tetraazacyclododecane and L-phenyl alanine was synthesized. Synthesis done in multistep from 1,4,7,10-tetraazacyclododecane and L-phenyl alanine with purification and characterization by NMR and mass. Relaxivity of Gd-DO3A-AA-PA was studied on 4.7 T Animal MR Scanner (Biospec, Bruker) in the presence and absence of calcium ion, in presence of Mg²⁺ and Zn²⁺ ions. T1 and T2 values were determined at various concentration of Gd-DO3A-AA-PA at pH 7.2, 27°C. Remarkable dependence of T1 on the concentration of calcium ions was exhibited. T1 value of Gd-DO3A-AA-PA in absence of Ca²⁺ ion is 6.77 mMol⁻¹s⁻¹ and an increase of 60% observed in presence of Ca²⁺ ions (1:1 stoichiometric ratio). Iminoacetate groups present on phenyl alanine backbone in Gd-DO3A-AA-PA acts as capping to Gd³⁺ ion of complex and prevent its interaction with water molecules in surrounding tissues. Because of this shield, relaxivity observed is low, however in presence of Ca²⁺ ions, rearrangement occurs and iminoacetate groups get bounded with calcium ions, allowing water molecules to interact directly with Gd³⁺. A maximum exposure of Gd³⁺ to bulk water occurs, thereby changing the relaxivity from weak to strong. No change in relaxation behaviour was observed in presence of Mg²⁺ and Zn²⁺. Smart Magnetic Resonance Imaging Contrast Agent sensitive to the presence of calcium, that is developed, has plausible application in neuronal imaging, for sensing brain disorder.

**r₁ measurements at pH 7.2, 2.1T, 27°C****Relaxivity enhancement profile with Ca²⁺ at pH 7.2, 27°C**

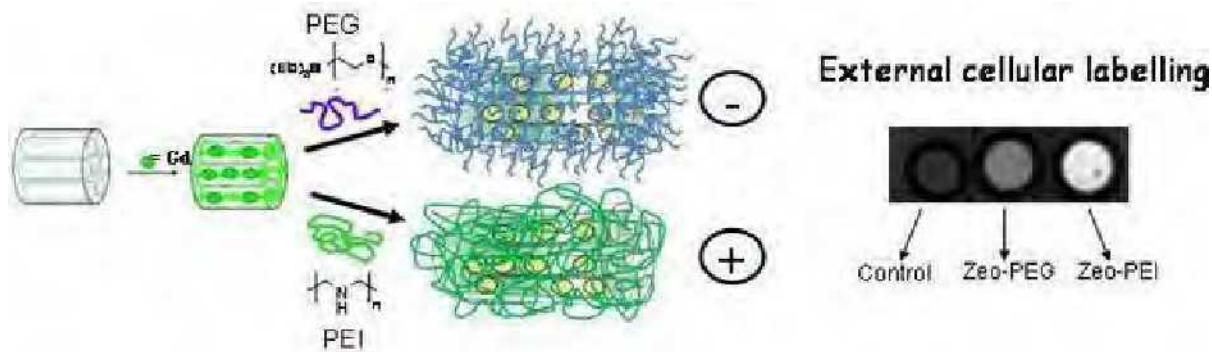
Presentation Number **0942B**

Poster Session 4c: In Vivo Studies & Development/Novel Use of Imaging Probes

New Gd-loaded Zeolites as nanoprobes for MR-Molecular Imaging applications

Eliana Gianolio¹, **Manuel Tsotsalas**², **Silvia Porto**¹, **Francesca Arena**¹, **Silvio Aime**¹, **Luisa De Cola**², ¹Chemistry IFM, University of Torino, Torino, Italy; ²Physics Institute and Center for Nanotechnology, University of Muenster, Muenster, Germany. Contact e-mail: eliana.gianolio@unito.it

Among the available imaging modalities MRI continues to be under intense scrutiny thanks to the superb anatomical resolution that can be attained in its images. However MRI is an intrinsically insensitive modality and therefore it requires large amounts of proton relaxation agents to affect the contrast in the corresponding images. Indicatively to get a 50% contrast enhancement in an MR image with the currently available commercial contrast agents one needs to reach a number of ca. 10^9 Gd centers per cell. Thus the development of MR-Molecular Imaging applications strongly relies on the search of procedures that allow to deliver a large number of imaging reporting units at the targeting site. Here we describe the synthesis, characterization and in vitro cellular labeling of rigid, nanosized particles obtained by loading Zeolite L scaffolds with Gd(III) ions. These particles are characterized by a cylindrical or discoidal shape (with length of 30-150 nm and diameters ranging from few tens to 120 nm). Two different approaches were followed in order to coat the particles with a polymer shell. In the first approach the particles have been coated with PEI (polyethylene imine) while in the second approach MPEG-Silane (polyethylene glycol) chains have been covalently bound to the surface of the particles. Several systems have been considered differing in surface functionalization, size, charge and shape (Fig. 1). Overall, Gd-loaded zeolites display good relaxivities and provide new routes for cellular labelling. For instance, by exploiting the positively charged surface of Gd-zeoPEI it has been possible to bind the paramagnetic nanoparticles on the outer membrane of NEURO2a cells. The attainable amount of paramagnetic loading is definitively higher than the threshold for MRI visualization (up to $3-4 \times 10^{10}$ Gd/cell). Viability tests indicate that this labeling procedures can be used to design novel molecular imaging applications.



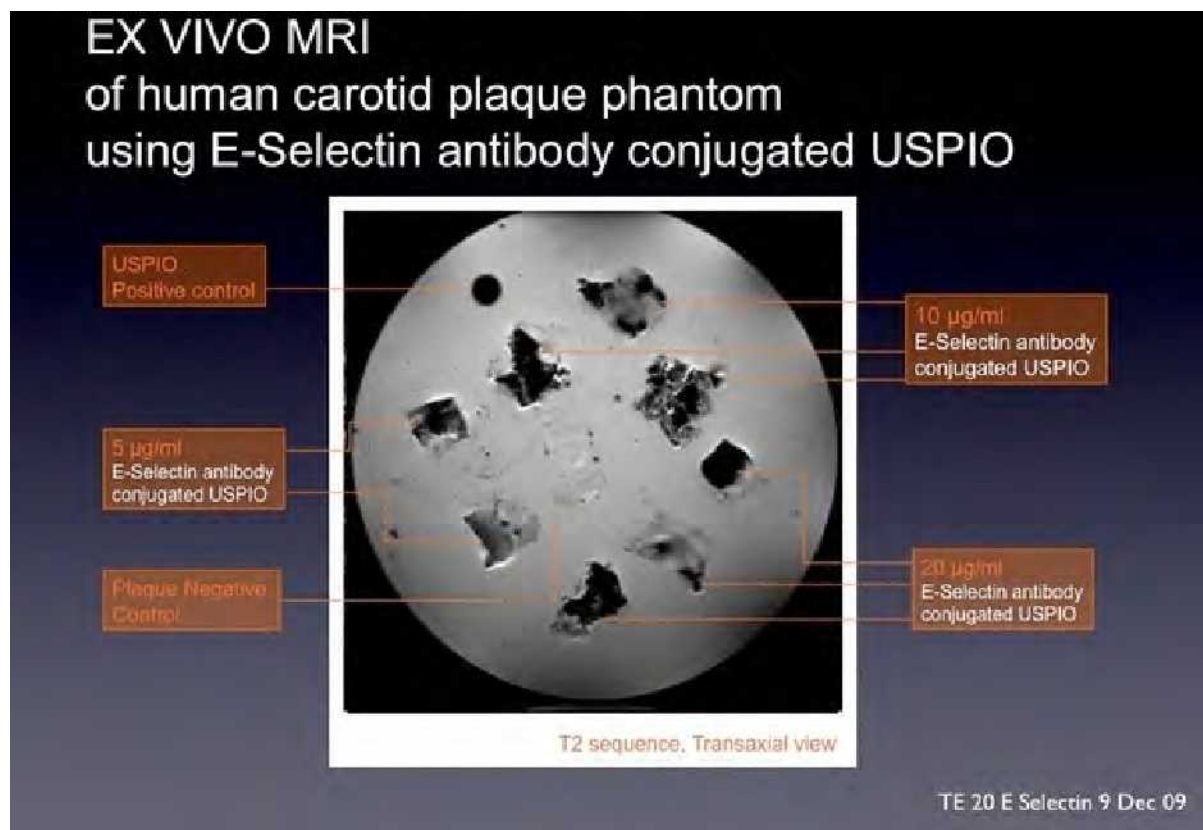
Presentation Number **0943B**

Poster Session 4c: In Vivo Studies & Development/Novel Use of Imaging Probes

MR Imaging of Vulnerable Carotid Plaques: Biological Targeting of Inflammation using Ultrasmall Superparamagnetic Particles of Iron Oxide (USPIO)

Joyce Chan¹, Claudia Monaco², Kishore Bhakoo³, Richard Gibbs¹, ¹Vascular Surgery unit, St Mary's Hospital, Imperial College Healthcare NHS Trust, London, United Kingdom; ²Cytokine Biology of Atherosclerosis, Kennedy Institute of Rheumatology, Imperial College, London, United Kingdom; ³Translational Molecular Imaging Group, Singapore Bioimaging Consortium, Agency for Science, Technology and Research (A*STAR), Singapore, Singapore. Contact e-mail: joyce.chan07@imperial.ac.uk

Introduction: Inflammation drives atherosclerotic plaque instability and acute thromboembolic events, such as stroke. There is currently no clinical imaging technique available to assess the degree of inflammation associated with plaques. This study aims at visualising and characterising atherosclerosis using targeted USPIO as an MRI probe for detecting inflamed endothelial cells and inflamed human carotid atherosclerotic plaques. **Method:** The initial in vitro feasibility study involved MRI detection of activated endothelial cells using anti-E-selectin antibody conjugated USPIO with confirmatory immunohistochemistry. In the ex vivo stage we have detected inflammatory markers on human atherosclerotic plaques harvested during carotid endarterectomy by anti-E-selectin antibody and anti-VCAM-1 antibody conjugated USPIO using MRI. **Results:** We have established an in vitro cellular model of endothelial inflammation induced with TNF-alpha. We confirmed the inflammation of endothelial cells with both immunocytochemistry and MRI. We are able to image inflammation of human atherosclerotic plaques by ex vivo MRI. We have demonstrated for the first time that ex vivo MRI of inflammatory markers, i.e. E-selectin or VCAM-1, on human atherosclerotic plaques using antibody conjugated USPIO. We also demonstrated that the signal void in the MR image of plaque phantom was dose-dependent on exposure to E-selectin or VCAM-1 antibody conjugated USPIO. **Conclusion:** We have successfully developed an in vitro model to detect and characterise inflamed endothelial cells by immunocytochemistry and MRI, and are able to image the degree of inflammation associated with atherosclerotic plaques by ex vivo MRI. This novel work will allow us to develop reagents and protocols for in vivo imaging of vascular inflammation in atherosclerosis. This provides a new biologically based imaging modality to identify the 'at risk' group with carotid plaque disease and aid decision making for appropriate clinical intervention.

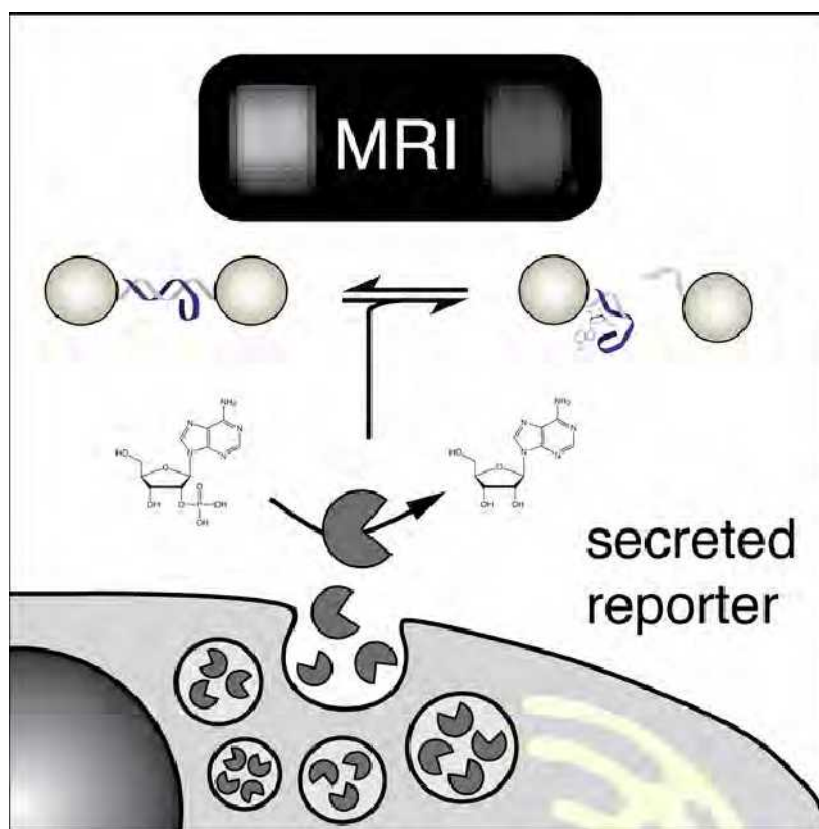


Presentation Number **0944B**

Poster Session 4c: In Vivo Studies & Development/Novel Use of Imaging Probes

Enzymatically amplified molecular MRI via a secreted reporter*Gil G. Westmeyer, Alan Jasanoff, M.I.T., Cambridge, MA, USA. Contact e-mail: gwestmey@mit.edu*

Molecular imaging with MRI has recently gained momentum with the advent of prototypical genetic and non-genetic contrast agent systems. Although MRI-based methods allows for non-invasive mapping of molecular events at relatively high spatial and temporal resolution, they have inherently low sensitivity. Signal amplification schemes are thus of great importance to shift the dynamic range of molecular MRI into the realm of nanomolar concentrations relevant for many analytes of interest. Here we present an enzymatic amplification strategy for a contrast system composed of superparamagnetic nanoparticles (SPIOs) that reversibly responds to the established gene reporter secreted alkaline phosphatase (SEAP). Once secreted out of the cell, SEAP catalyzes the generation of a "second messenger" molecule that actuates disaggregation of the SPIO sensor via specific binding and subsequent conformational change of a DNA aptamer. Contrast can be reversed by removal or enzymatic destruction of the second messenger molecule. By design, the system generates robust and reversible T2 MRI contrast without the need for cellular delivery or catalytic destruction of the SPIO sensor. In addition, ratiometric measurements are possible due to an analyte-independent T1 relaxation effect of the SPIO sensor. To enable cellular resolution, the MRI readout can be complemented with optical detection via available luminescent or fluorescent SEAP substrates. Application of this imaging system as a reversible reporter for gene expression in cell culture and for multimodal in vivo readout in rat brain will be presented.



Presentation Number **0945B**

Poster Session 4c: In Vivo Studies & Development/Novel Use of Imaging Probes

The Use of Gadolinium-based Contrast Agents for Molecular and Cellular MRI: Quantitative Considerations

Goran Angelovski¹, Ilgar Mamedov¹, Joern Engelmann², Sven Gottschalk², David Z. Balla², Rolf Pohmann², Nikos K. Logothetis¹,
¹Physiology of Cognitive Processes, MPI for Biological Cybernetics, Tuebingen, Germany; ²High-Field Magnetic Resonance Center,
MPI for Biological Cybernetics, Tuebingen, Germany. Contact e-mail: goran.angelovski@tuebingen.mpg.de

Magnetic resonance imaging (MRI) is a powerful tool in clinical diagnostics and is also used for the understanding of developmental and biological processes. It visualizes the differences in tissues and organs, as well as between normal and pathological states. Due to its noninvasive nature, excellent spatial resolution and tissue penetration, MRI became one of the preferential methods for molecular and cellular imaging. The specificity and sensitivity of MRI can be further enhanced by the introduction of contrast agents. Many of the currently existing contrast agents are restricted to the extracellular space, though novel approaches enforce generations of intracellular contrast agents that can be developed for targeted labeling of cells for the visualization of a specific biological process. However, the lower sensitivity of MRI as compared to other imaging techniques demands certain quantitative considerations for the rational design of these intracellular agents. Gadolinium complexes are the most frequent choice for T1-weighted MR-imaging. Besides having a high longitudinal relaxivity (r_1), these agents should also be delivered in a sufficient amount to target structures on the cell membrane or inside the cells. We have performed a study in an attempt to determine the minimum number of gadolinium ions needed for the efficient labeling of cells. The concentration dependent contrast enhancement of Gd-DOTA, Gd-DO3A or Gd-AAZTA in T1-weighted MR-images of phantoms with water only, cell culture medium containing serum, or in the presence of cells was followed at different, ultra-high magnetic fields (3T, 7T, 16.4T) and with the spatial resolution commonly used for in vivo measurements. The results suggest MRI detectability at low micromolar concentrations for all applied contrast agents, which correspond to the previously predicted number of metal atoms per cell [1]. However, this number is dependent on the r_1 of the contrast agent and the magnetic field of the imaging scanner. Financial support of the Max-Planck Society and German Ministry for Education and Research (BMBF, FKZ: 01EZ0813) is gratefully acknowledged. References: [1] E. Gianolio, G. B. Giovanzana, A. Ciampa, S. Lanzardo, D. Imperio, S. Aime, *ChemMedChem* 2008, 3, 60-62.

Presentation Number **0946B**

Poster Session 4c: In Vivo Studies & Development/Novel Use of Imaging Probes

Effective tumor targeting of polymeric micelle MRI contrast agent by a tumor vascular disrupting agent

Kouichi Shiraishi¹, Kumi Kawano², Yoshie Maitani², Katsuyoshi Hori³, Masayuki Yokoyama¹, ¹Research Center for Medical Science, Jikei University School of Medicine, Minato-ku, Japan; ²Institute of Medicinal Chemistry, Hoshi University, Shinagawa-ku, Japan; ³Tohoku University, Sendai, Japan. Contact e-mail: kshiraishi@jikei.ac.jp

Enhancement of targeting efficiency of contrast agent is a one of the attractive approach to obtain high signal intensity in the target tissues, as well as an anticancer drug targeting. Encapsulations of anticancer drugs in nanocarriers, such as liposomes and polymeric micelle have been developed as novel therapeutics for selective solid tumor targeting. These nano-sized carrier encapsulating anticancer drugs accumulated in solid tumor by the EPR effect. However, Hori et al reported nanocarrier did not accumulated in <2-3 mm diameter of solid tumor with no necrotic area. This suggests the nanocarrier systems for cancer chemotherapy may not achieve microtumor targeting by the EPR effect. We reported the observation of Cderiv effect on tumor permeability by the means of vital microscopic image system. We observed a vascular disrupting agent, combretastatin derivative (Cderiv, Tokyo Kasei Co.,Ltd), enables nanocarrier, such as polymeric micelle, to accumulate in microtumors. This Cderiv selectively interrupts tumor blood flow and disrupts tumor vessels. As a result, Cderiv causes necrosis in microtumor. We performed MRI study of Cderiv administrated mice, as well as the biodistribution after injection of our polymeric micelle MRI(T1) contrast agent. Our polymeric micelle MRI contrast agent showed high tumor accumulation at 24 h after the injection. The biodistribution including tumor accumulation was similar to doxorubicin encapsulated polymeric micelle system. The observation of biodistribution and MRI study (9.4T) indicated that administration of Cderiv at a dose of 20mg/kg enhanced the polymeric micelle MRI contrast agent to accumulate in tumor. This finding may greatly improve drug targeting efficacy by the use of the MRI contrast agent. Herein, we report the effect of the Cderiv administration on tumor targeting of polymeric micelle MRI contrast agent.

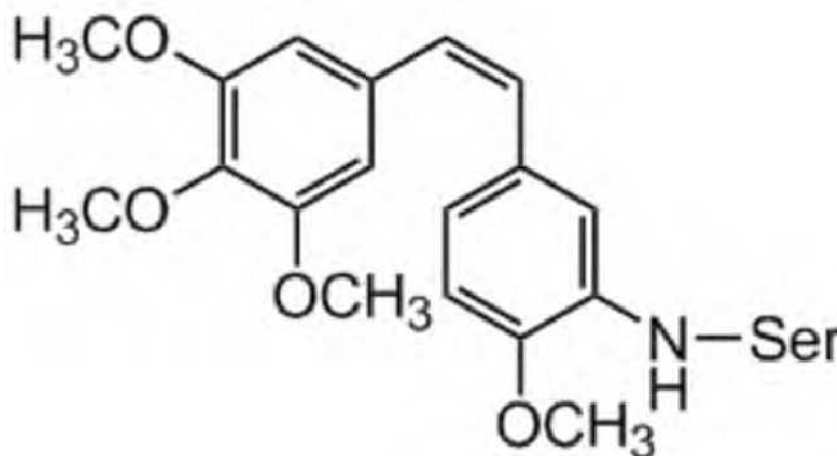


Figure 1. Structure of combretastatin derivative (Cderiv)

Presentation Number **0947B**

Poster Session 4c: In Vivo Studies & Development/Novel Use of Imaging Probes

Smart Gd(III)-loaded Liposomes as Enzyme Responsive MRI probes

Sara Figueiredo^{1,2}, **Evelina Cittadino**¹, **Enzo Terreno**¹, **João Nuno Moreira**³, **Carlos F. Geraldes**², **Silvio Aime**¹, ¹*Department of Chemistry IFM and Molecular Imaging Center, University of Turin, Turin, Italy;* ²*Department of Biochemistry, Faculty of Sciences and Technology and Center for Neurosciences, University of Coimbra, Coimbra, Portugal;* ³*Lab. of Pharmaceutical Technology, Faculty of Pharmacy and Center for Neuroscience and Cell Biology, University of Coimbra, Coimbra, Portugal. Contact e-mail: saharic@gmail.com*

When Magnetic Resonance is the imaging modality of choice it is necessary to design highly sensitive systems in order to overcome the relatively low sensitivity of such an imaging modality. One way to solve this problem is the use of nanosystems, such as liposomes, able to deliver a large number of imaging units to a given biological target. There is a great interest to design agents whose MRI response is sensitive to the presence of a specific enzyme. We have envisaged several approaches to design enzyme-responsive agents based on the use of Gd(III)-loaded liposomes. i) Liposomes exposing a peptide acting as a MMP substrate and encapsulating a clinically approved Gd(III) agent were prepared and tested in vitro by measuring the relaxivity over time in the presence of collagenase. We demonstrate that the enzyme triggers the release of the imaging probe through a destabilization of the liposome membrane, thus causing a relaxivity enhancement. Preliminary in vivo kinetic experiments following the intratumor injection of the lipopeptide-based liposome in a melanoma mouse model indicated a rapid washout of the imaging probe from the tumor. This finding is consistent with a release of the MRI probe in the extracellular tumor fraction, where MMPs accumulates. Suitable control liposomes do not show any relaxivity enhancement in the presence of the enzyme in vitro, whereas in vivo they showed a different kinetic that suggests a cellular uptake of the nanovesicles. As further goal, an anti-tumoral drug will be co-encapsulated with the MRI probe, allowing supervise the tumoral therapy. ii) The interaction of anionic liposomes and protamine yields to supramolecular aggregates with low relaxivity. The action of the serine protease trypsin causes the digestion of protamine and the consequent de-assembly of the aggregates that results in a relaxivity enhancement. An illustrative example of the possible use of this responsive agent consists of the entrapment of the aggregates in alginate vesicles that have been used as gaskets for in vivo transplantation of cells. In such a way, the enhancement in T1 contrast may act as a sensor of the protease activity in the biological environment in which the cells are located. Summarizing, we have prepared molecular probes that work as an enzymatic substrate in a particular microenvironment and able to enhance the MRI contrast as a function of enzymatic activity.

Presentation Number **0948B**

Poster Session 4c: In Vivo Studies & Development/Novel Use of Imaging Probes

Contrast- and Sensitivity-Enhanced MR Molecular Imaging by Supramolecular Magnetic Nanoparticles with Spin-Lock Detection

Zhao Li¹, Stephanie M. Wolahan¹, Yung-Ya Lin^{1,2}, ¹Chemistry and Biochemistry, UCLA, Los Angeles, CA, USA; ²California NanoSystem Institute, Los Angeles, CA, USA. Contact e-mail: zhaoli@chem.ucla.edu

I. Purpose. To improve the contrast and sensitivity of MR molecular imaging, a joint approach is demonstrated: with material chemistry to develop "supramolecular magnetic nanoparticles" (SMNP) MR contrast agents for improved imaging sensitivity and specificity, and with spin engineering to realize contrast amplification with continuous-wave radio-frequency spin-lock detection. II. Materials and Methods. (1) Material Chemistry. The framework of our new contrast agent is based on the size-controllable supramolecular magnetic nanoparticles (SMNP) [1], due to its structure flexibility, size controllability, and biocompatibility. Longitudinal relaxivity (r_1) agent (e.g., GdDOTA complex) or transverse relaxivity (r_2) agent (e.g., superparamagnetic iron oxide, SPIO) can be encapsulated into SMNP to form Gd-SMNP and SPIO-SMNP, respectively (Fig. 1). (2) Spin Engineering. The relaxivities of the Gd-SMNP and SPIO-SMNP in the rotating frame under continuous-wave radio-frequency spin-lock are then investigated theoretically and numerically. III. Results and Conclusion. Supramolecular magnetic nanoparticles (SMNP) with novel MR detection schemes have been developed for contrast- and sensitivity-enhanced MR molecular imaging. Results from (i) analytical formulation, (ii) numerical simulations, (iii) simple phantom experiments, and (iv) in vivo mice tumor imaging confirmed its scientific validity and demonstrated its applicability for (i) enhanced longitudinal relaxivity (r_1) by encapsulating gadolinium; (ii) enhanced transverse relaxivity (r_2) by encapsulating superparamagnetic nanoparticles; (iii) enhanced detection specificity with adjustable r_1 to r_2 ratios ($r_1:r_2$) by encapsulating both r_1 and r_2 nanoparticles with newly developed T1/T2-weighted imaging; and (iv) multicolor MR imaging by encapsulating chemical shift agents to frequency encode the exchange-able protons with chemical-exchange saturation-transfer (CEST) detection. Reference: [1] Jang J, et. al. Angew. Chem. Int. Ed. 2009; 48: 1234-1238.

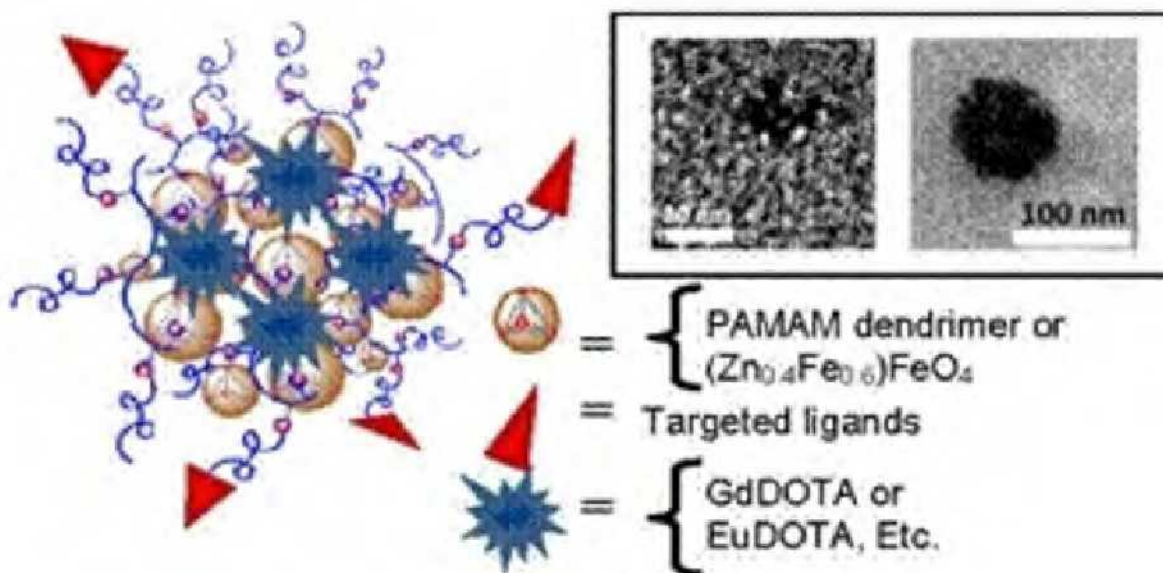


Fig. 1 Schematic diagram of supramolecular magnetic nanoparticles (SMNP). Box contains SEM images of 20 nm and 80 nm SMNP, as labeled. SMNP can be loaded with relaxation agents for contrast enhancement, chemical-shift agents for multi-color MR imaging, and cancer drugs for nano medicine.

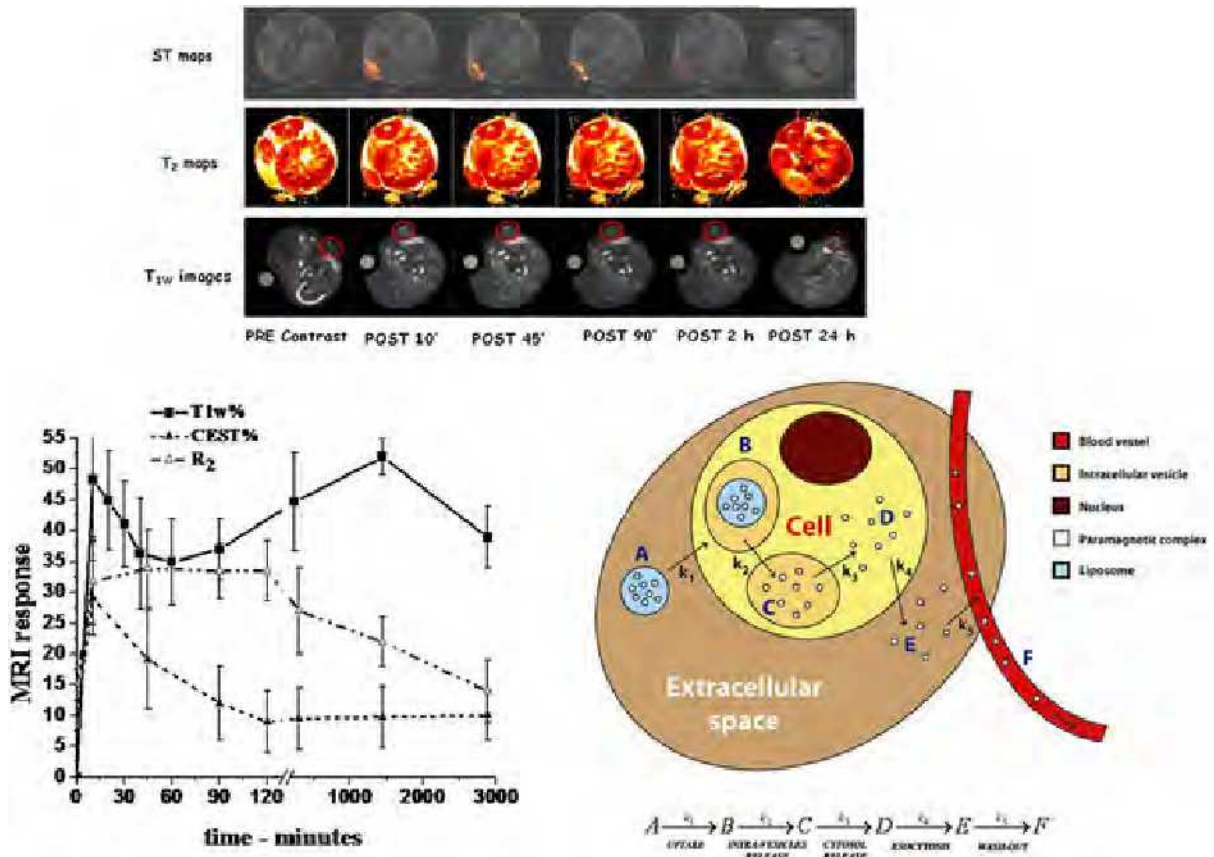
Presentation Number **0950B**

Poster Session 4c: In Vivo Studies & Development/Novel Use of Imaging Probes

Multicontrast proton MRI agents: an useful approach to assess the in vivo intratumor trafficking of paramagnetically labeled liposomes

Daniela Delli Castelli¹, Walter Dastrù¹, Enzo Terreno¹, Evelina Cittadino¹, Elena Torres¹, Francesco Mainini¹, Michela Spadaro², Silvio Aime¹, ¹Molecular Imaging Center, University of Torino, Torino, Italy; ²Molecular Biotechnology Center, University of Torino, Torino, Italy. Contact e-mail: daniela.dellicastelli@unito.it

Many nanocarriers have been explored in drug delivery, and liposomes have been often used mostly for their ability to load both hydrophilic and lipophilic molecules. In spite of the long history, extensive development, and proven therapeutic efficacy, the in vivo behaviour of such nanovesicles is still poorly understood. An improved knowledge is expected to result in better formulations not only for drug delivery but also for imaging-guided therapy, which is a new emerging field of theragnosis (therapy and diagnosis). Loading the vesicles with paramagnetic metal complexes resulted in new classes of MRI contrast agents that are under intense development, because they can overcome the intrinsic low sensitivity of the technique. In this contribution, we report a novel approach to obtain indirect evidence of in vivo intratumor trafficking of paramagnetic liposomes through monitoring the time evolution of different contrast modalities (T1, T2 and chemical exchange saturation transfer (CEST)). The study utilized two types of liposomes loaded with either [Gd-HPDO3A] complex (acting as T1 and T2 agent) or [Tm-DOTMA]- (acting as T2 and CEST agent). The bases for the approach used are: (i) the maximum of T1 contrast enhancement occurs when the nanovesicles lose their integrity to release their content; (ii) the maximum T2 contrast occurs when a contrast agent is concentrated, i.e., when the nanovesicles are intact or slightly diluted in intracellular organelles, and (iii) the maximum CEST contrast is observed when intact liposomes are free in the extracellular fluids. The data was analyzed through a kinetic model in which the overall process was analyzed using five consecutive kinetic steps corresponding to recruiting and cellular uptake, degradation or disassembling of liposomes, cytosolic release of imaging probes, cellular efflux of the probes, and washout of the probe from the tumor region to the blood stream. The model was validated by using liposomes known to have different stabilities.



Presentation Number **0951B**

Poster Session 4c: In Vivo Studies & Development/Novel Use of Imaging Probes

Host inflammatory response to SPIO-labeled RPE19 cells implanted into the rat brain

Joseph Flores¹, **Guangwei Du**², **Piotr Kozlowski**³, **Xuemei Huang**², **Doris J. Doudet**¹, ¹*Pacific Parkinson's Research Centre, University of British Columbia, Vancouver, BC, Canada;* ²*Hershey Brain Analysis Research Center, Penn State University Milton S. Hershey Medical Center, Hershey, PA, USA;* ³*High Field MRI Centre, University of British Columbia, Vancouver, BC, Canada.* Contact e-mail: joflores@interchange.ubc.ca

Introduction. There is increasing interest in the use of superparamagnetic iron oxide (SPIO) nanoparticles to label cells and follow their in vivo, post implant survival through magnetic resonance imaging (MRI). However, little evidence exists on the potential cytotoxic effects and accompanying immune response associated with released iron from dead SPIO-labeled cells in the host. In this study, SPIO-labeled and non-labeled cells were implanted in opposite hemispheres in the rat striatum and followed longitudinally in vivo with MRI. Iron presence and host immune response were assessed post mortem at the same time points used for MR imaging. **Methods.** RPE19 cells were labeled using ferumoxides (Feridex®) (50µg/ml) complexed to protamine sulfate (1.0µg/ml) (FePro), and attached to gelatin microcarriers to create a stable RPE19 suspension (RPE19-GM). Rats were implanted with 1) FePro-labeled RPE19-GM and 2) non-labeled RPE19-GM in opposite striata. All rats underwent MRI (T2-weighted FSE) at multiple time points up to 5 months post-implant using a 7T MR scanner. After each MRI session, one rat was randomly selected and sacrificed for a post-mortem histological representation of iron concentration and host immune response (CD68 for activated microglia and GFAP for astrocytes) at that specific time point. **Results and Conclusions.** In both striata, there was a progressive increase in MR signal over time suggesting loss of iron from label and/or hemosiderin. There was no difference in the rate of signal loss between FePro-labeled and non-labeled implants but there was an initial significant difference in signal intensity between the FePro and non-labeled RPE implants, which was maintained at every time point thereafter. Corresponding post-mortem histological examination demonstrated Prussian blue positive cells at the level of the implant at each time point, which suggests FePro-labeled RPE cell survival up to 5 months. There was, however, a significant qualitative difference in host inflammatory response between FePro-labeled and non-labeled RPE-GM sites: both CD68 and GFAP immunohistochemistry demonstrated widespread increase in microglial response and reactive astrogliosis in the entire striatum containing FePro-labeled cells compared to the contralateral, non-labeled cell-implanted side. This suggests a possible interaction between the iron released from dying SPIO-labeled cells and host inflammatory response that deserve further investigation if this method is to be used to assess cell fate and survival in future transplant studies.

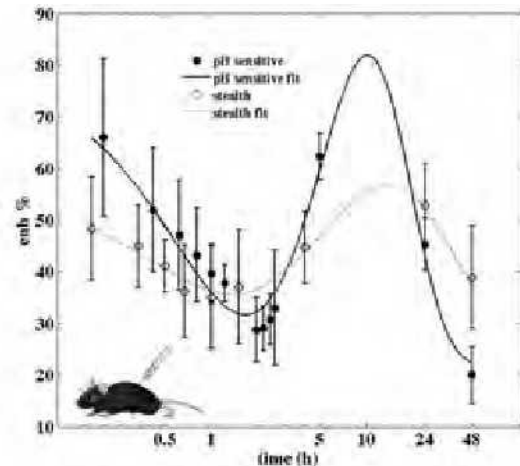
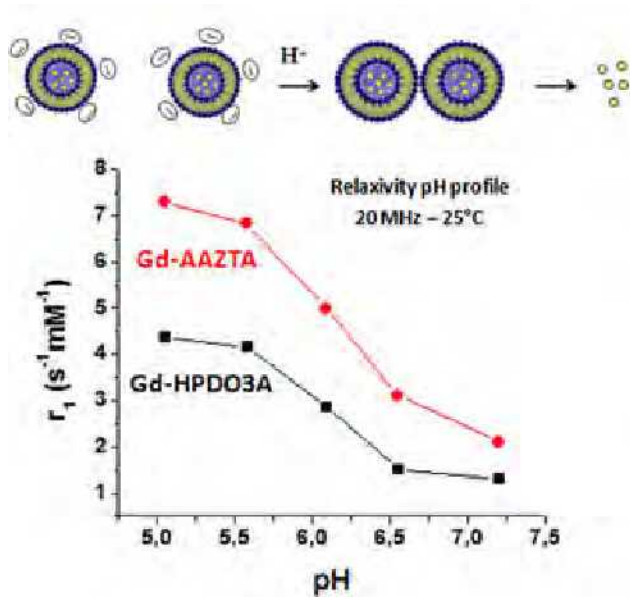
Presentation Number **0952B**

Poster Session 4c: In Vivo Studies & Development/Novel Use of Imaging Probes

Gd-loaded liposomes as MRI probes for the intratumor visualization of pH triggered drug release

Enzo Terreno¹, **Elena Torres**¹, **Evelina Cittadino**¹, **Roberta Cavalli**², **Franco Fedeli**³, **Roberta Napolitano**¹, **Silvio Aime**¹, ¹*Molecular Imaging Center, University of Torino, Torino, Italy;* ²*Department of Drug Sciences and Technology, University of Torino, Torino, Italy;* ³*Integrated Laboratory of Advanced Methodology, BioIndustry Park of Canavese, Colleretto Giacosa (TO), Italy. Contact e-mail: enzo.terreno@unito.it*

The development of nanometric drug carriers able to release their bioactive content through the action of specific triggering stimuli is an emerging topic in medical field. In addition to their use in therapy, nanoparticles have been also widely investigated in diagnosis, especially in MRI field, as highly sensitive probes. Among the nanoparticles that have been considered so far, liposomes occupy certainly a leading role being successfully used since a long time in pharmaceutical field as drug-delivery systems. The aim of this work was the preparation of suitably formulated liposomes that can release the entrapped material (imaging reporter + drug) as a consequence of a mildly pH reduction. In addition to report about drug delivery, there is a growing interest to design systems able to visualize the release process. Through the encapsulation of a Gd-complex into a liposome, the T1 contrast can be strongly reduced owing to the compartmentalization of the paramagnetic agent, and therefore the release of the probe from the nanocarriers leads to a detectable contrast enhancement. A novel formulation of pH sensitive liposomes based on POPE (palmitoyl-oleyl-phosphatidylcholine) and THS (α -tocopherol-hemisuccinate) was developed. The probe release is due to the aggregation and membrane destabilization of the vesicles following the protonation of THS moiety. The pH induced release from such vesicles of hydrophilic Gd(III) complexes with different size and relaxivities was tested in vitro and in vivo after intratumor injection on a xenografted B16 melanoma mouse model. It was found that the release kinetic is related to the size of the encapsulated agent. Furthermore, since the tumor accumulation after i.v. injection requires a prolonged blood circulation, stealth pH sensitive liposomes where PEG chains are linked to the vesicles through a degradable disulfide bond were prepared and tested.



pH sensitive liposomes release the imaging probe faster than conventional stealth liposomes

Presentation Number **0953B**

Poster Session 4c: In Vivo Studies & Development/Novel Use of Imaging Probes

Real time MR Imaging of lipoprotein uptake in liver with lipophilic USPIO at 3T

Harald Ittrich¹, Oliver T. Bruns^{2,3}, Kersten Peldschus¹, Michael G. Kaul¹, Ulrich Tromsdorf⁴, Rudolph Reimer³, Gerhard Adam¹, Jörg Heeren¹, ¹Center for Radiology and Endoscopy, University Medical Center Hamburg-Eppendorf, Hamburg, Germany; ²Department of Biochemistry and Molecular Biology II, University Medical Center Hamburg-Eppendorf, Hamburg, Germany; ³Heinrich-Pette-Institute for Experimental Virology and Immunology, University of Hamburg, Hamburg, Germany; ⁴Institute of Physical Chemistry, University of Hamburg, Hamburg, Germany. Contact e-mail: ittrich@uke.uni-hamburg.de

Purpose The aim of the study was to develop dynamic MRI methods for an in-vivo imaging of liver lipoprotein uptake and metabolism in a mice model and to detect lipoprotein metabolism disorders via MRI. **Material and Methods** Nanosomes were designed in vitro with a magnetic iron oxide core (USPIO) coated by a lipid layer with lipoproteins. Dynamic in vivo MRI using a T2*w 2D gradient echo sequence (TR/TE 20/6.9 ms, FA 20°, FoV 40×40 mm, eff. voxel volume 0.28×0.33×2mm, TA/image 5,5 sec.) was performed before, during, and after i.v. application of USPIO in apolipoprotein E (ApoE) deficient and wildtype mice (WT, control) using a clinical 3T scanner (Philips Intera) with a custom made small animal solenoid coil. Relaxometric R2* measurements were performed before (ba) and after (pa) USPIO application using a fat-saturated 3D multi-echo gradient echo sequence (TR 65 ms, FA 40°, inter echo time 2.8ms, FoV 50×50mm, eff. voxel volume 0.39×0.42×2mm). SNR in vena cava, aorta, portal vein, and liver as well as R2* of the liver were measured for estimation of lipoprotein clearance. Uptake kinetics and R2* of both animal groups were tested for statistical significance (t-test, p<0.05) and matched with histology (H&E, Prussian blue) and electron microscopy. **Results** In vivo measurements showed a two-phase exponential SNR decrease after application of nanosomes in order of vena cava, aorta, portal vein, and liver followed by an increase of SNR in all vessels, but stable SNR drop in the liver of WT (ba: 43.9±2.3, pa: 8.2±1.2). ApoE deficient animals showed a significantly delayed and reduced SNR decline of the liver (ba: 44.2±3.1, pa: 10.6±0.6; p<0.03). Correlating the R2* (in sec⁻¹) of WT showed a significantly higher increase (ba: 76.3±3.4 sec⁻¹, pa: 164.3±11.4 sec⁻¹) compared to ApoE mice (ba: 79.9±2.5 sec⁻¹; pa: 114.7±5.1 sec⁻¹, p<0.004). Corresponding to MR imaging histology and electron microscopy showed a predominantly accumulation of nanosomes in hepatocytes, but not in Kupffer cells. **Conclusions** Liver uptake of USPIO-marked lipoproteins can be monitored by real time in vivo MRI at a clinical 3T MR System. Defects in liver lipoprotein metabolism (e.g. apolipoprotein E) can be detected non-invasively by MRI. The study demonstrates the potential of realtime in vivo MRI for the enhancement of metabolic disorders in lipoprotein metabolism by USPIO-lipoprotein nanosomes.

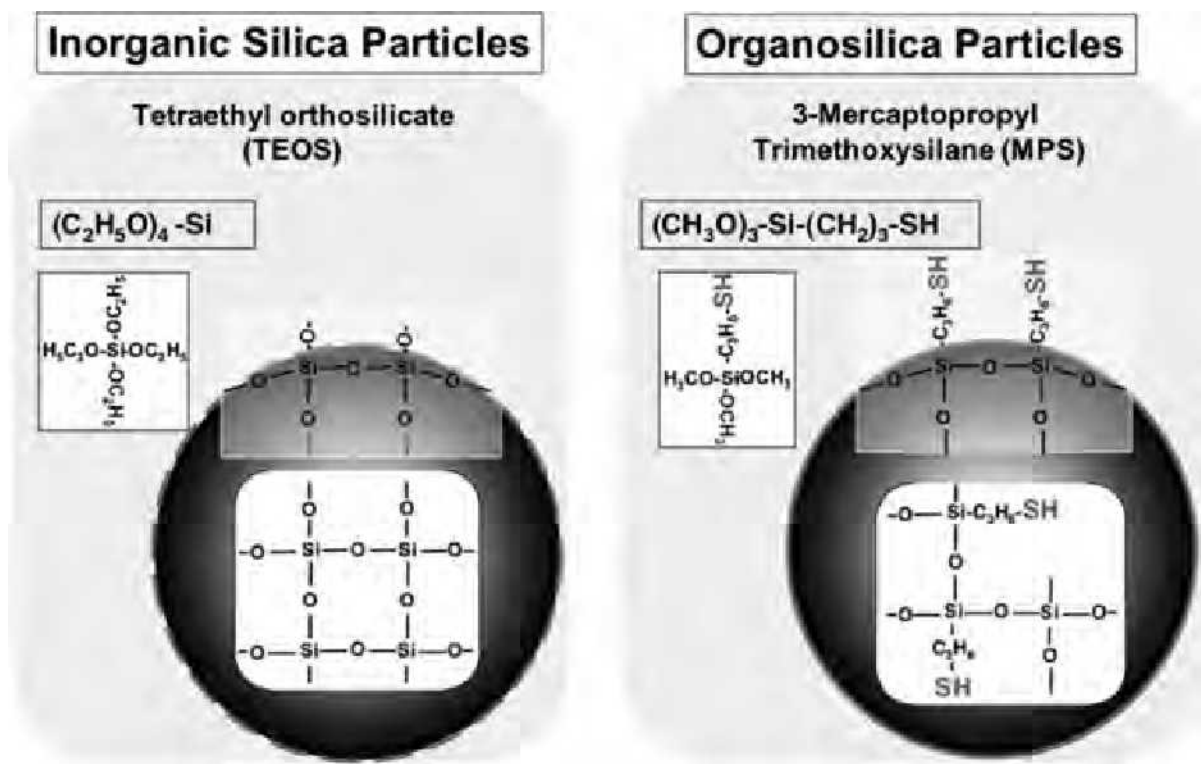
Presentation Number **0896A**

Poster Session 1c: In Vivo Studies & Development/Novel Use of Imaging Probes

Preparation of Novel Multimodal Imaging Nanoparticles using Organosilica Particles Technology

Michihiro Nakamura, Kazunori Ishimura, Department of Anatomy and Cell Biology, The University of Tokushima, Tokushima, Japan.
 Contact e-mail: michy@basic.med.tokushima-u.ac.jp

Organosilica nanoparticles comprising a single organosilicate were new materials for multimodal imaging. These organosilica particles are both structurally and functionally different from typical silica particles prepared from tetraethoxyorthosilicate because the organosilica particles contain both interior and exterior functionalities (Fig. 1). These organosilica nanoparticles allow for facile surface and internal functionalization, offering new opportunities to multifunctionalize nanoparticles. In addition, functional fusions of organosilica nanoparticles and other functional nanoparticles such as quantum dots, gold nanoparticles, and iron oxides were possible based on organosilica particles technology. Novel multimodal imaging nanoparticles were synthesized in a one-pot process using organosilica particle technology. Imaging particles such as iron oxide were encapsulated in organosilica layer, and the organosilica layer could be functionalized with fluorescent dyes. The multimodal imaging nanoparticles showed multimodal imaging signals in vitro and in vivo. Novel multimodal imaging nanoparticles synthesized using organosilica particle technology showed high potential for various applications in multimodal imaging in vitro and in vivo.



Presentation Number **0897A**

Poster Session 1c: In Vivo Studies & Development/Novel Use of Imaging Probes

Dendritic hybrid nanoparticles and macromolecular chelates for (ME)MRI and SPECT

Giuseppe Lamanna¹, Brice Basly¹, Jérôme Steibel², Sylvie Begin-Colin¹, **Cynthia Ghobril**, Delphine Felder-Flesch¹, ¹IPCMS, UMR CNRS-UdS 7504, Strasbourg, France; ²LINC, FRE 3289, Strasbourg, France. Contact e-mail: cynthia.ghobril@ipcms.u-strasbg.fr

The diagnosis of neurodegenerative diseases such as Alzheimer or Parkinson requires contrast agents able to reach the brain by first getting through the Blood Brain Barrier. Thus, the goal of our research is to adopt a polyfunctional strategy for the elaboration of brain-specific (Manganese Enhanced) MRI contrast agents and radiopharmaceuticals by means of chemical engineering and, in particular, a 'dendrimer' approach. For biological applications, dendrimers and especially the so-called "dendron" building blocks are very promising as the diversity of functionalization brought by the arborescent structure simultaneously solves the problems of biocompatibility, low toxicity, large in vivo stability and specificity. Moreover, in addition to the multifunctionalization of a low molecular weight molecule, the arborescent monodisperse building blocks allow a versatility of size (according to the generation) and of physicochemical properties (hydrophilic, lipophilic). The resulting effects on stability (dendrimer effect), contrast qualities, pharmacokinetics and biodistribution of the contrast agents can clearly be identified. In the field of tree-like molecules, our work is focused on the development of dendritic chelates based on a synthetic tripodal derivative able to complex ions such as Gd (III) (MRI) and Mn (II) (MEMRI) but also ^{99m}Tc for Single Photon Emission Computed Tomography (SPECT). The arborescent PEGylated structure grafted at the focal point of the chelate is polyfunctional as the groups grafted at its periphery are either body- (or receptor-) specific, or help the product to get through the BBB. We will first describe the synthesis, in vitro toxicity studies (on cerebellar neurons) and in vivo relaxivity measurements of dendritic polyfunctional Mn²⁺ chelates in regard to their potential application in (ME)MRI dedicated to brain imaging. We will also discuss the synthesis of stable dendritic ^{99m}Tc-based complexes for scintigraphy. In a second part dedicated to dendritic hybrid nanoparticles, the suspension stability as a function of the grafting rate and optimisation of grafting conditions leading to very stable suspensions of magnetite nanoparticles in water and physiological conditions will be discussed in details. The magnetic and relaxation properties of the colloidal suspensions were also studied in order to evaluate the possible use of these materials as efficient MRI CA. 1) Bioconjugate Chemistry 2009, 20, 760-767. 2) Dalton Trans. 2009, 4442-4449. 3) New J. Chem., 2010, 34, 267-275. 4) Chem. Comm. 2010, 46, 985-987.

Presentation Number **0899A**

Poster Session 1c: In Vivo Studies & Development/Novel Use of Imaging Probes

Multimodal OCT/FMI and multispectral optical imaging confirms carbohydrate expression via lectin targeting in the APC murine model of colorectal carcinoma

Celeste A. Roney¹, Biying Xu², Shuai Yuan³, Jeremiah Wierwille³, Chao-Wei Chen³, Jianwu Xie¹, Gary L. Griffiths², Yu Chen³, Ronald M. Summers¹, ¹Radiology and Imaging Sciences, National Institutes of Health, Bethesda, MD, USA; ²Imaging Probe Development Center, National Institutes of Health, Bethesda, MD, USA; ³Fischell Department of Bioengineering, University of Maryland, College Park, MD, USA. Contact e-mail: celesteroney@aol.com

Colorectal carcinoma (CRC), the 3rd most frequently diagnosed cancer in the US, is the 2nd leading cause of cancer-related deaths. Lesion detection assists disease prognosis and theragnosis. Mutated tumor suppressor APC genes (adenomatous polyposis coli) precede CRC. Polymerized liposomes were engineered to target, detect and image α -L fucose expression in the mucoglycoprotein layer of adenomatous polyps in the APCMin mouse. Rhodamine B optical contrast imaging agent (532 nm emission, 590-620 nm excitation) was incorporated within the liposomes for imaging. Protein conjugation of UEA-1 lectin (ulex europaeus agglutinin), which has fucose affinity, dictated polyp targeting. Surgically excised APCMin bowels were incubated with UEA-1-conjugated liposomes (N=12 polyps) or nonconjugated liposomes (N=16 polyps). The liposomes were characterized (45 nm average radii) by Dynamic Light Scattering (DLS) and Scanning Electron Microscopy (SEM). Multispectral Optical Imaging (MSI, 500 nm to 800 nm) verified binding to the mucinous polypoid surface coat with good specific binding of the fucose to the polyps, and detected any nonspecific binding to the normal mucosa. Carbohydrate expression, via glycoside bonds of the fucosyl hydroxyl with lectin, suggest α -L-fucose as a potential biomarker. High resolution optical coherence tomography (OCT) imaging exhibited polyp depth of 1 to 2.5 mm. Co-registration of the OCT with fluorescence molecular imaging (FMI) correlated the spatial distribution of contrast. The polyp-to-background ratio in the tissue incubated with targeted liposomes (Rh-UEA-1) was 1.45 ± 0.18 versus tissue incubated with non-conjugated liposomes (0.74 ± 0.16 ; $P < 0.01$). Novel Rh-UEA-1 were designed to specify the mucinous surface layer of adenomatous colon polyps; targeted detection permits imaging opportunities with multiple modalities, including dual OCT/FMI and MSI. Rh-UEA-1 liposomes have clinical relevance as prospective cancer imaging probes with potential to improve diagnostic accuracy in CRC detection.

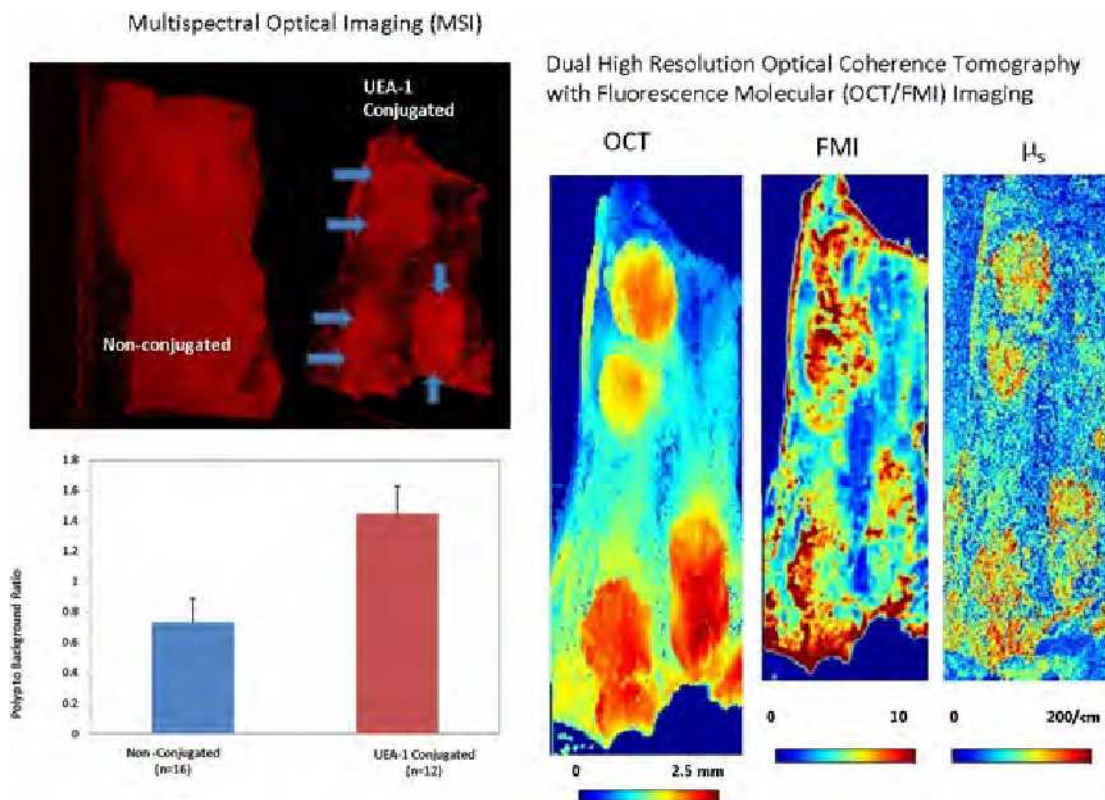


Figure 1. Rh-UEA-1 liposomes target, detect and image adenomatous colon polyps along the mucoglycoprotein surface layer in the APCMin mouse.

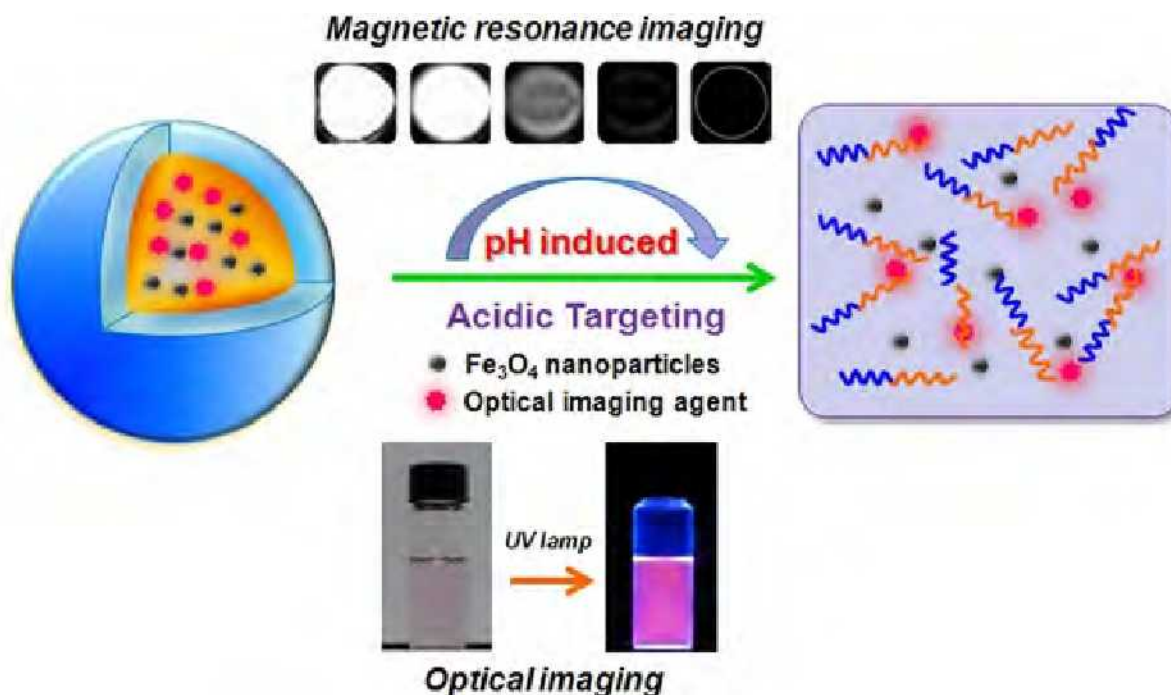
Presentation Number **0900A**

Poster Session 1c: In Vivo Studies & Development/Novel Use of Imaging Probes

pH-Triggered Degradable Polymer as Intelligent Vehicle for Dual-modality MR and Optical Imaging

GuangHui Gao¹, **Yi Li**¹, **Jung Hee Lee**², **Doo Sung Lee**¹, ¹*Polymer Science and Engineering, Sungkyunkwan University, Suwon, Republic of Korea;* ²*Department of Radiology, Samsung Medical Center, School of Medicine, Sungkyunkwan University, Seoul, Republic of Korea.* Contact e-mail: gao79@skku.edu

A dual-modality imaging probe was designed and developed for magnetic resonance imaging (MRI) and optical imaging, based on a magnetite-encapsulated pH-responsive degradable block copolymer, which was conjugated with a red fluorescent dye Sulforhodamine 101 (SR101). The block copolymer, containing methoxy poly(ethylene glycol) (PEG) as a hydrophilic segment and poly(β -amino ester) (PAE) with ionizable tertiary amine groups on its backbone as a pH-responsive segment, can be dissolved in response to an acidic pH environment, or form self-assembly micelles in aqueous media at the physiological pH (~ pH 7.4) due to the hydrophobic deionized PAE segment as a micellar core. The polymeric micelle conjugating SR101 was found to have a red-fluorescent emission at 612 nm, a sharp pH transition of pH 6.8~7.0, indicating that it can be an ideal pH-triggered carrier in response to the acidic biological environment. The confocal laser scanning microscopy observation demonstrated the cellular uptake of SR101-labeled polymeric micelles by breast cancer cells. The facile and powerful magnetite-encapsulated polymeric micelle was acted as an acidic pH-triggered agent without any targeting ligands for dual-modality MRI and optical imaging. In this investigation, we demonstrated its initial application to acidic disease rats subjected to middle cerebral artery occlusion, however, it is believed that more applications will be possible owing to its unique ability to target and simultaneously image the pH-stimuli pathologic environment.



A facile and powerful acidic pH-triggered magnetite-encapsulated polymeric micelle conjugated with a fluorescent dye for dual-modality MRI and optical imaging

Presentation Number **0901A**

Poster Session 1c: In Vivo Studies & Development/Novel Use of Imaging Probes

USPIO-PBCA Hybrid Microbubbles as Novel MR-Ultrasound Dual-Modal Contrast Agents

Zhe Liu, Fabian Kiessling, Jessica Gätjens, Department of Experimental Molecular Imaging (ExMI), RWTH Aachen University, Aachen, Germany. Contact e-mail: zhliu@ukaachen.de

Introduction: Magnetic resonance imaging (MRI) and ultrasonography (US) are non-invasive and widely-used modalities in various clinical and experimental applications. In particular, it is promising to design a single contrast agent which renders MR-US synergistic effects and to make them applicable to both modalities. Thus, physiochemical and biological processes will be detected more precisely and efficiently, and multifunctional applications such as US-mediated gene delivery, MR-guided drug release and hyperthermia therapy will be achievable simultaneously. Methods: USPIO (ultrasmall superparamagnetic iron oxide) nanoparticle-embedded PBCA (polybutylcyanoacrylate) microbubbles, abbreviated as UNEM, have been fabricated via a one-pot in-situ polymerization with the encapsulation of superparamagnetic nanoparticles in the shell structure to produce magnetic microbubbles. The size distribution and zeta potential were measured by particle sizing and dynamic light scattering (DLS), and the embedding structure was characterized by transmission electron microscopy (TEM). High-frequency ultrasound imaging was performed using a VEVO770 from VisualSonics. The relaxivities r_2 and r_1 were determined at room temperature using a clinical Philips Achieva 3T MR scanner. Results: The UNEM microbubbles exhibited a narrow size distribution (size range: 2.03-2.33 μm , mean diameter: 2.1 μm), and zeta potential analysis (varied from -24.8 to -41.8 mV) indicated a strong electrostatic repulsion between microbubbles leading to a good stability. The hybrid magnetic bubbles exhibited a strong contrast in ultrasonography and presented a high transverse relaxivity (r_2) in MR phantoms (up to 1447.3 $\text{s}^{-1}\text{mM}^{-1}$ for UNEM compared to 552.57 $\text{s}^{-1}\text{mM}^{-1}$ for pure USPIOs). Moreover, a significant increase in r_1 was observed after UNEM destruction when compared to undestroyed microbubbles. Conclusions: UNEM magnetic microbubbles may be a useful platform technology for dual-modality (MR and US) contrast agents. They may be further functionalized with targeting moieties to generate molecular probes and their changing MR-imaging characteristics recommend them as vehicles for US-mediated/MR-guided drug delivery in cancer and other diseases. Acknowledgment: This work was supported by the German Federal Ministry of Education and Research (BMBF-0315017).

Presentation Number **0902A**

Poster Session 1c: In Vivo Studies & Development/Novel Use of Imaging Probes

Title Dinuclear Heterometallic Lanthanide Complexes Exhibiting MRI and Luminescence Response

Ilgar Mamedov¹, **Tatjana Parac-Vogt**², **Nikos K. Logothetis**^{1,3}, **Goran Angelovski**¹, ¹*Department for Physiology of Cognitive Processes, Max Planck Institute for Biological Cybernetics, Tuebingen, Germany;* ²*Department of Chemistry, Laboratory of Molecular Design and Synthesis, Katholieke Universiteit Leuven, Leuven, Belgium;* ³*Imaging Science and Biomedical Engineering, University of Manchester, Manchester, United Kingdom. Contact e-mail: ilgar.mamedov@tuebingen.mpg.de*

Heteronuclear lanthanide complexes have gained an increased level of interest recently, due to their high potential for application in various molecular imaging techniques. They appear primarily as the most rational choice for agents to be used in multimodal imaging approaches.[1-2] Namely, due to their versatile physicochemical properties, they are widely used in MRI or luminescence imaging. Several lanthanide complexes have been reported recently with the potential to be used as multimodal agents. Depending on the approach the final ligand structure contained a single chelator for the lanthanide ion, or consisted of two chelating units, consequently bearing same or different Ln³⁺. Following these principles, we designed and synthesized a ligand containing two different chelators where the antenna acts not only as a linker between these two chelators, but also as an integral component in one of their structures. The macrocyclic, DOTA-type moiety of this ligand forms a stable complex with Eu³⁺ and Gd³⁺ which exhibit the expected luminescence emission and relaxometric characteristics, respectively. An aryl-containing acyclic chelator 5A-PADDTA (abbreviated from 5-aminoisophthalamide diethylenediaminetetraacid) of this ligand also forms complexes with lanthanides and their existence is confirmed by the means of luminescence and NMR spectroscopy. Depending on the choice of the metal ion (Gd³⁺, Tb³⁺, Eu³⁺, Nd³⁺, Yb³⁺ or Er³⁺), the system could act as a potential dual-modal (MRI / Vis or NIR luminescence imaging) or dual-emissive (luminescence imaging at various wavelengths in Vis/NIR region) contrast agent. [1] L. E. Jennings, N. J. Long, *Chemical Communications* 2009, 3511-3524. [2] L. Frullano, T. J. Meade, *Journal of Biological Inorganic Chemistry* 2007, 12, 939-949.

Presentation Number **0904A**

Poster Session 1c: In Vivo Studies & Development/Novel Use of Imaging Probes

Dual functional, Ultra Sensitive Fluorescent Magnetite-Nano Cluster (FMNC) Probe for Stem Cell Labeling and Tracking in Ischemia Mouse Brain*Chunfu Zhang, Med-X Research Institute, Shanghai Jiao Tong University, Shanghai, China. Contact e-mail: zchunfu@yahoo.com.cn*

Due to high spatial resolution and good soft tissue contrast, MRI is very suited for stem cell tracking in vivo. For MR stem cell tracking, multifunctional probe with ultra high MR sensitivity is highly desirable. In current study, we fabricated magnetic and fluorescent dual-functional probe based on magnetite cluster. The size of the probe was about 80 nm and the T2 relaxivity was $432 \text{ s}^{-1}/\text{sup>)} \text{ mM}^{-1}/\text{sup>)} .$ When used for mesenchymal stem cell (MSC) labeling, FMNC did not demonstrate cytotoxicity and had no inverse effects on cell differentiation into adipose cell, osteal cell and neuron cell. For cell labeling, cell ingestion of the particles showed dose- and time-dependent feature. Fluorescent imaging of labeled cells indicated that the probes were mainly distributed peri nucleus with some foci in cytoplasm. In addition, MR imaging manifested that small amount of labeled cells (3000 cells/mL, labeled at 0.05 mM iron concentration for 30 min) could be detected with 3 T MRI scanner. In vivo study indicated that the labeled cells ($5 \times 10^5/\text{sup>)} could be continuously detected for more than 30 days after implanting into the normal mouse brain. The cells mainly stayed in the injection site and part of them migrated into the ventricle of the counter side. Even more, after implanted into the normal hemisphere of brain ischemic mouse, the migration of the labeled cells toward and accumulation in the pathological zone could be observed and the labeled cells showed neuronal phenotype under the in vivo condition in short term, which were confirmed by histological study of the brain. Our study demonstrated that magnetite cluster based dual functional probe is highly sensitive tool that is suitable for small amount of stem cell labeling and tracking in vivo.$

Presentation Number **0905A**

Poster Session 1c: In Vivo Studies & Development/Novel Use of Imaging Probes

Molecular Beacon Induced Nanoparticle Aggregation for Imaging

Jonathan F. Lovell, Honglin Jin, Juan Chen, Gang Zheng, *Institute of Biomaterials and Biomedical Engineering, University of Toronto, Toronto, ON, Canada. Contact e-mail: jon.lovell@utoronto.ca*

DNA has proven to be a valuable tool for both detection and manipulation of biomolecules. Molecular beacons in particular are known for their ability to discriminate target sequences with single base precision. We developed a new solid phase synthesis approach that permitted the creation of a new class of molecular beacons that demonstrate excellent quenching and simplified purification. These hydrophobically modified beacons could efficiently insert into lipophilic nanoparticles. Remarkably, opening of these molecular beacons by incubation with a target nucleic acid sequence resulted in the dramatic and irreversible aggregation of the nanoparticles (Figure 1). This process discriminated single base mismatches and was modulated both by nanoparticle concentration and the number of beacons per nanoparticle. This new phenomena has potential to be a unique tool for activatable fluorescence and MRI imaging.

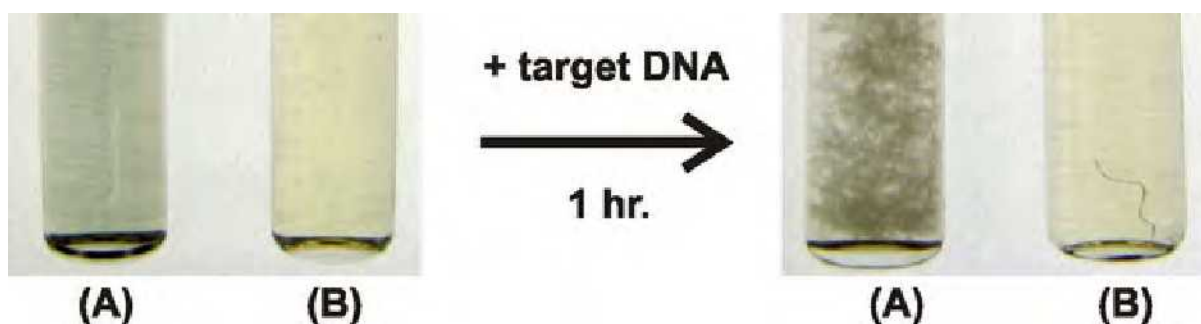


Figure 1: Molecular beacon induced nanoparticle aggregation. Lipophilic nanoparticles were incubated with modified photodynamic beacons or mock treated (A and B, left). A ten fold excess of target nucleic acid was added to both test tubes and heavy aggregation was observed (A and B, right).

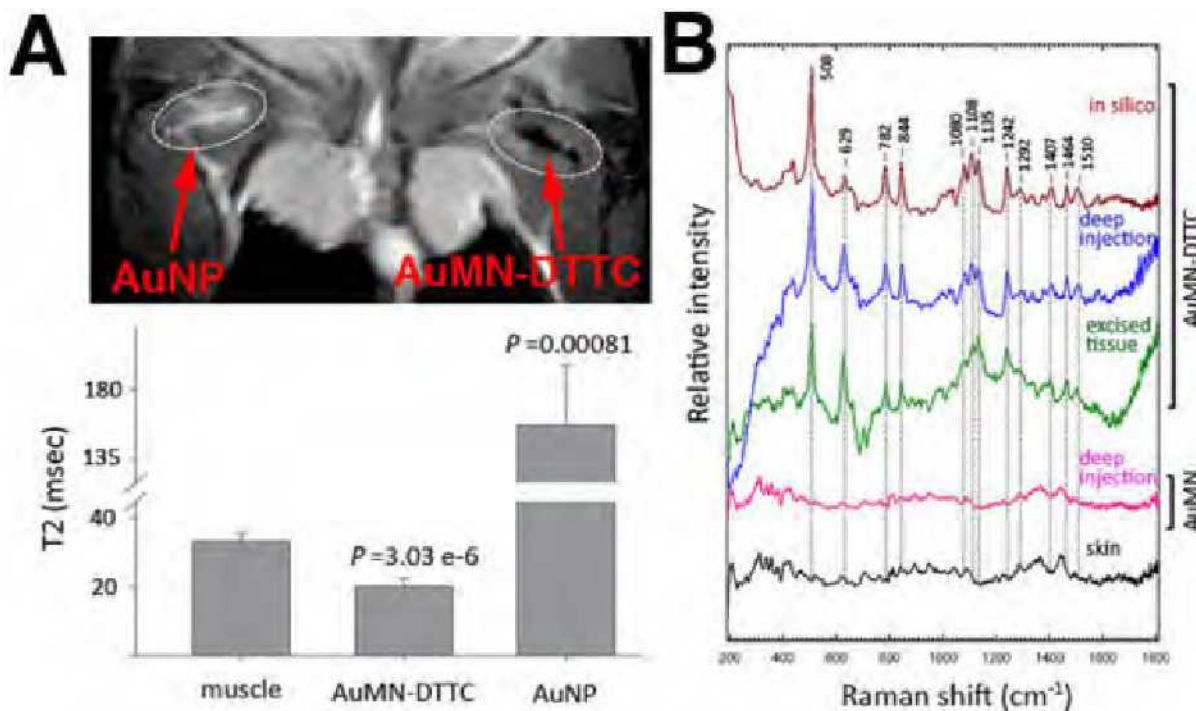
Presentation Number **0906A**

Poster Session 1c: In Vivo Studies & Development/Novel Use of Imaging Probes

A Novel Bimodal Contrast Agent for in Vivo MRI-SERS

Mehmet V. Yigit¹, Leyun Zhu², Marytheresa Ifediba¹, Kevin Carr², **Anna Moore**¹, Zdravka Medarova¹, ¹Radiology, Massachusetts General Hospital, Charlestown, MA, USA; ²Agiltron Corporation, Agiltron Corporation, Woburn, MA, USA. Contact e-mail: amoore@helix.mgh.harvard.edu

The enhancement of the Raman signal of reporter dye molecules adsorbed on the surface of gold nanoparticles has introduced surface enhanced Raman scattering (SERS) as an attractive biomedical imaging modality. SERS has potential applications in ultrasensitive optical detection and spectroscopy, due to its significant signal enhancement (two orders of magnitude brighter than quantum dots) and unique Raman signature. It has been shown that such materials can be used in vivo without toxic effects to gain biological information in living subjects. Despite this progress, there are very limited reports of the synthesis and in vivo application of multimodal contrast agents, which have SERS as a component modality. Here, we address this issue by describing a novel nanomaterial (AuMN-DTTC) that comprises gold nanoparticles deposited onto dextran-coated superparamagnetic iron oxide nanoparticles (MN). The gold component serves as a substrate for a Raman active dye molecule to generate a surface-enhanced Raman scattering effect. The contrast agent has a diameter of less than 100 nm. It is stable in serum, attesting to its in vivo applicability. The AuMN-DTTC complex has magnetic relaxivity values comparable to the parental MN probe and can be detected by T2 weighted MRI and SERS in silico. In vivo studies in mice revealed that the complex can also be visualized by MRI (Fig. 1A) and SERS (Fig. 1B), following injection into deep muscle. Toxicity studies suggested that AuMN-DTTC has no overt detrimental effects on animal health even at doses three times as high as those routinely used for imaging. Our studies illustrate the design and in vivo application of a bimodal contrast agent, whose component modalities include MRI and SERS. Considering the paucity of examples describing in vivo SERS-active probes and the importance of developing multimodal imaging strategies, we feel that the development of our agent is both timely and valuable as a new molecular imaging tool.



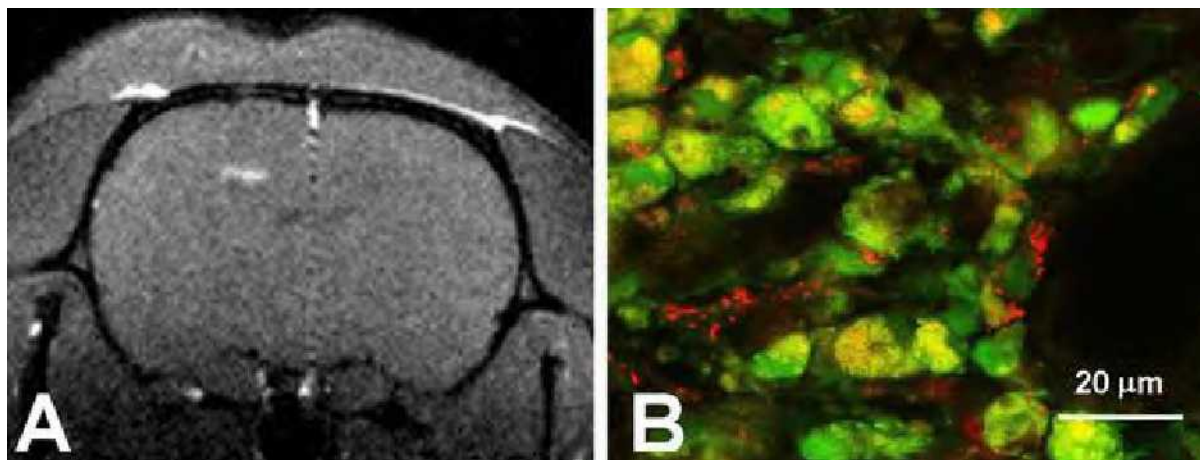
Presentation Number **0907A**

Poster Session 1c: In Vivo Studies & Development/Novel Use of Imaging Probes

Tracking of grafted cells using a gadolinium based marker with a bound fluorescein

Vit Herynek^{1,2}, **Pavla Jendelova**^{2,3}, **Karolina Turnovcova**^{2,3}, **Miroslava Kapcalova**^{2,3}, **Jan Kotek**⁴, **Zuzana Kotkova**⁴, **Daniel Jirak**^{1,2}, **Ivan Lukeš**⁴, **Eva Sykova**^{2,3}, **Milan Hajek**¹, ¹MR Unit, Department of Diagnostic and Interventional Radiology, Institute for Clinical and Experimental Medicine, Prague, Czech Republic; ²Center for Cell Therapy and Tissue Repair, 2nd Medical faculty, Charles University, Prague, Czech Republic; ³Institute of Experimental Medicine ASCR, Prague, Czech Republic; ⁴Department of Inorganic Chemistry, Charles University, Faculty of Science, Prague, Czech Republic. Contact e-mail: vit.herynek@medicon.cz

Introduction Magnetic resonance imaging (MRI) is a powerful tool for stem cell tracking in vivo. However, cell labeling is necessary for cell visualization. Usually iron oxide nanoparticles are used, but they produce hypointense signal, which can be confused with signal voids of different origin. Therefore we prepared and tested a novel bimodal contrast agent (CA) containing fixed Gd complexes conjugated with fluorescein to betacyclodextrin ring (Gd-F), which provides positive contrast on T1-weighted MR images and can be used also for optical imaging. **Methods** Experiments were performed with rat (rMSC) and human mesenchymal stem cells (hMSC). The cells were labeled by addition of Gd-F into the culture medium. In vitro tests consist of cell viability, relaxometry and MRI of labeled cells in a 4.7 T MR imager. In vivo T1-weighted MRI was performed on Sprague-Dawley rats after grafting of labeled hMSC into the cortex. After sacrificing the rats, the Gd-F marker was detected by fluorescence microscopy and the grafted hMSC were colocalized using a human mitochondrial marker MTCO2. **Results** T1 relaxivity of the CA was 20.1 s⁻¹/mM. Viability of the cells was not altered. MRI visualized cell suspensions in vitro as hyperintense spots. Grafted labeled hMSC in the rat cortex were visible as hyperintense spots in vivo (Fig A). The fluorescein was detected by fluorescence in the green part of the spectra on histological sections. Colocalization with a human mitochondrial marker MTCO2 proved presence of the grafted cells in the cortex as well as presence of the Gd-F inside the grafted cells (Fig. B). **Conclusion** The novel bimodal CA did not impair cell viability. Labeled cells were clearly visible as hyperintense spots on T1-weighted MR images both in vitro and in vivo. Colocalization of fluorescence with a mitochondrial marker proved that the grafted cells kept the label and remained viable. The bimodal CA is highly stable and safe for cell labeling with excellent MRI properties. **Grants:** GACR 203/09/1242, 309/08/H079, ASCR KAN201110651, MZ0IKEM2005, 1M0538, ENCITE-7th FW EU No.201842



MRI of the rat brain with grafted 50000 labeled cells (A) and colocalization of green CA fluorescence and red MTCO2 marker (B).

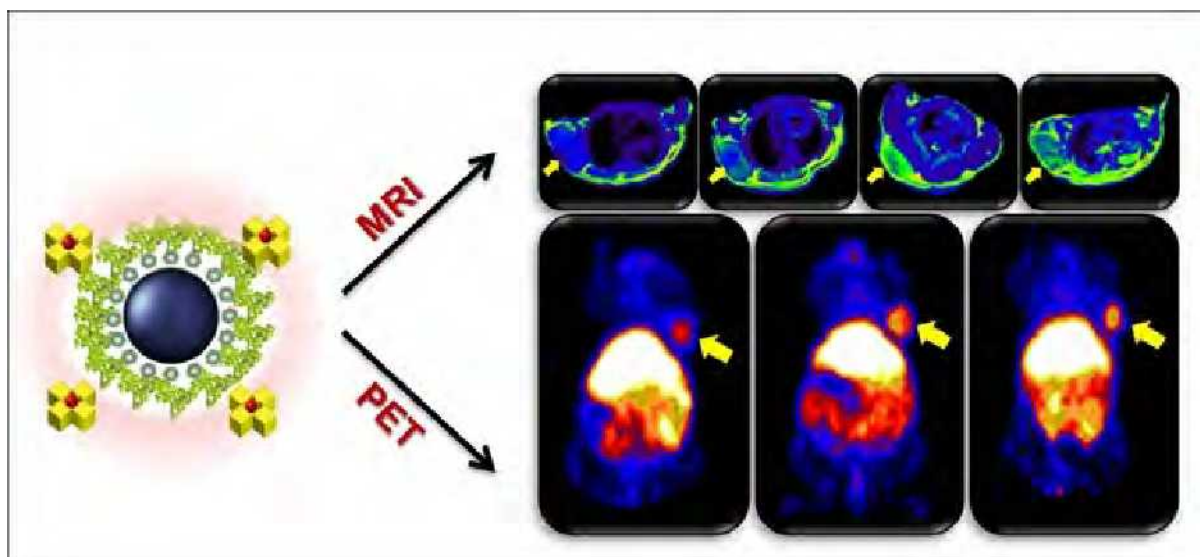
Presentation Number **0908A**

Poster Session 1c: In Vivo Studies & Development/Novel Use of Imaging Probes

HSA coated MnO nanoparticles with prominent MRI contrast for tumor imaging

Jin Xie^{1,2}, **Jing Huang**^{2,3}, **Kai Chen**², **Lihong Bu**^{2,4}, **Seulki Lee**^{1,2}, **Zhen Cheng**², **Xingguo Li**³, **Xiaoyuan Chen**^{1,2}, ¹National Institute of Biomedical Imaging and Bioengineering, National Institutes of Health, Bethesda, MD, USA; ²Department of Radiology and Bio-X Program, Stanford University, Stanford, CA, USA; ³College of Chemistry and Molecular Engineering, Peking University, Beijing, China; ⁴Department of Radiology, The Fourth Hospital of Harbin, Harbin, China. Contact e-mail: jin.xie@nih.gov

Inorganic magnetic nanoparticles have emerged as an important class of biomaterials and found a wide range of applications, such as serving as contrast agents for MRI. In contrast to the rapid pace of in T2 probe development, research progress in developing nanoparticle based T1 probes has so far been slow. Compared to the traditionally utilized metal-chelator complex, magnetic nanoparticles, each constructed with thousands of metal atoms, could potentially offer advantages such as possessing longer circulation half-life and better contrast. One reason that hampers their translation into practice, however, is the lack of a reliable surface coating technique that can render particles with sufficient stability while not compromising the contrast effect. Previously, the Hyeon group reported the use of MnO nanoparticles (MONPs) as T1 contrast agents for brain imaging. However, the T1 relaxivity from the resulted MONPs was relatively low, presumably due to the di-layered coating structure that prohibits effective water exchange. In the present study, we developed a facile, two-step surface modification strategy to produce physiologically stable MONPs. The yielded MONPs show T1 effect that is 5 times more prominent than the previously reported formula. We then coupled the MONPs with 64Cu-DOTA and administrated the probes into a U87MG glioblastoma xenograft model to evaluate their tumor targeting efficiency. MRI found a signal increase in tumor of $5.3 \pm 0.6\%$, $13.8 \pm 2.0\%$ and $9.7 \pm 2.1\%$ at 1, 4, 24 h p.i. Similar targeting pattern was also observed in PET results, showing uptake rate at 3.3 ± 0.4 , 4.7 ± 0.4 and $4.3 \pm 0.2\%$ at 1, 4, 24 h p.i. Such correlated dual-modality imaging results confirmed the efficient tumor targeting of the probes and suggested their role as a promising nanoplatform for tumor imaging and therapeutics.



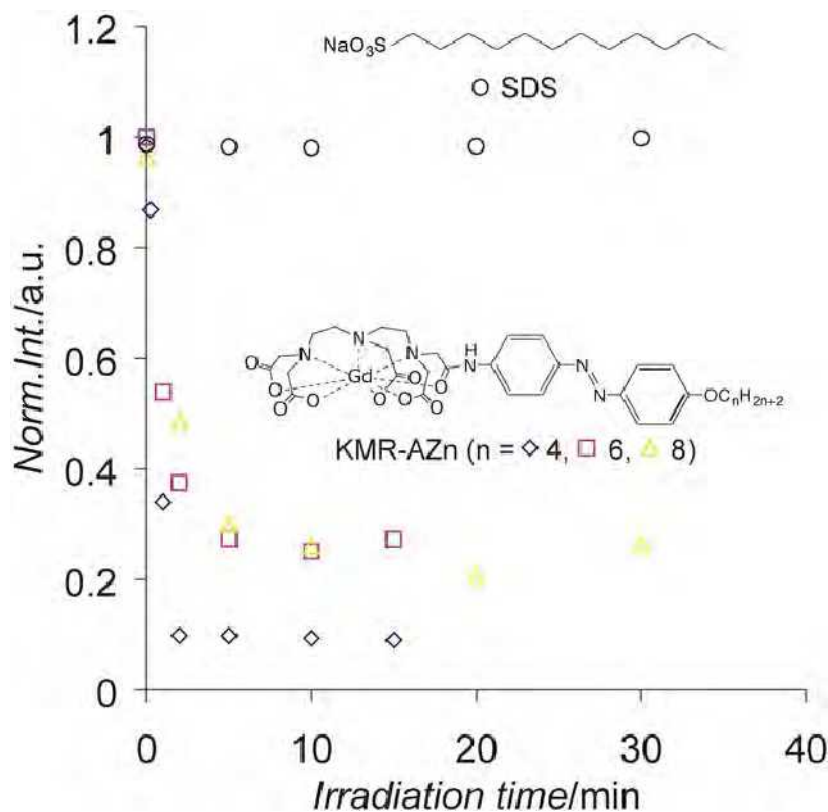
Presentation Number **0909A**

Poster Session 1c: In Vivo Studies & Development/Novel Use of Imaging Probes

Photochromic Micelles as a Potential Magnetic Resonance Imaging-Visible Drug Delivery Carrier

Yushi Heta¹, Kentaro Kumaki¹, Hiroki Hifumi¹, Daniel Citterio¹, Akihiro Tanimoto², Koji Suzuki¹, ¹Science and Technology, Keio University, Yokohama, Japan; ²School of Medicine, Keio University, Shinjuku, Japan. Contact e-mail: yushi@a3.keio.jp

Stimuli responsive amphiphilic compound aggregates such as micelles and liposomes have attracted much attention in the field of drug delivery systems and for the controlled release of drugs. Applying these materials *in vivo*, some kinds of imaging probes (fluorescence, luminescence, MRI) are attached to drug carriers allowing the monitoring of drug pharmacokinetics. In this study, we designed and synthesized novel micellar MRI contrast agents, which have a photochromic molecule incorporated into the hydrophobic chain. As the hydrophobic group, an azobenzene derivative, which undergoes photoisomerization from the *trans* to the *cis* configuration upon ultraviolet or visible light irradiation, was coupled to one carboxylic acid residue of a DTPA-Gd derivative, which acts as the hydrophilic group. Here, we report on the fundamental properties of a series of bifunctional (MRI and light-induced drug release) amphiphilic probes (KMR-AZn), which can assume the form of simplest low molecular weight micelles. A lipophilic fluorescent dye Nile Red (NR) was applied to the investigation of the critical micellar concentration and photosensitivity of KMR-AZn. The photosensitivity measurement of KMR-AZn micelles towards UV irradiation is shown in the figure. NR encapsulating micellar solutions were prepared with KMR-AZn concentrations above CMC. These solutions were irradiated with a halogen light and the emission of NR was observed as a function of irradiation time. The figure shows that the fluorescence of NR in KMR-AZn gradually decreases during photoirradiation, indicating the dye release from the inside of the hydrophobic environment of the KMR-AZn micelles into the aqueous medium. A comparison experiment performed with micelles formed from sodium dodecyl sulfate, which is not able to undergo photoisomerization, showed no decrease in emission for as long as 90 minutes of UV irradiation. In conclusion, we have introduced a simplest model of MRI visible DDS and they have high compatibility with with other materials.



Presentation Number **0910A**

Poster Session 1c: In Vivo Studies & Development/Novel Use of Imaging Probes

The development of hybrid nanoparticles as a CT/MRI dual contrast agent for in vivo hepatoma imaging

Dongkyu Kim¹, **Mi Kyung Yu**¹, **Yong Yeon Jeong**², **Sangyong Jon**¹, ¹*Life science, GIST, Gwangju, Republic of Korea;* ²*Diagnostic Radiology, Chonnam National University Medical School, Gwangju, Republic of Korea. Contact e-mail: dgkim@gist.ac.kr*

We recently developed a multimodal imaging agent, consisting of a SPION core (magnetite, Fe₃O₄) and a thin gold-layered shell that could be used for both MRI and CT. These core-shell nanoparticles showed high CT attenuation because of the presence of gold layers but had a much lower T₂ signal intensity in MRI than did normal SPIONs, presumably due to the embedding of SPIONs in the inner core, thus hampering in vivo application of such nanoparticles as a CT/MRI dual contrast agent. To overcome this limitation, we designed a new type of hybrid nanoparticle, in which several SPIONs were fused with a gold nanoparticle in a dumbbell-shaped manner as potential dual contrast agents for both computed tomography (CT) and magnetic resonance imaging (MRI). The hybrid nanoparticles were synthesized by thermal decomposition of mixtures of Fe-oleate and Au-oleylamine complexes. Using a nanoemulsion method, the nanoparticles were coated with amphiphilic poly(DMA-r-mPEGMA-r-MA) to impart water-dispersity and antibiofouling properties. An in vitro phantom study showed that the hybrid nanoparticles were of high CT attenuation, because of the constituent gold nanoparticles, and afforded a good MR signal, attributable to the contained iron oxide nanoparticles. Intravenous injection of the hybrid nanoparticles into hepatoma-bearing mice resulted in high contrast between the hepatoma and normal hepatic parenchyma on both CT and MRI. These results suggest that the hybrid nanoparticles may be useful as CT/MRI dual contrast agents for in vivo hepatoma imaging.

Presentation Number **0911A**

Poster Session 1c: In Vivo Studies & Development/Novel Use of Imaging Probes

The Imaging Probe Development Center at NIH: An Update of Activities from a Central Core Facility for the Production and Dissemination of Molecular Imaging Probes

Agnieszka Sulima, Falguni Basuli, Sarah Cheal, Andres E. Dulcey, Nalini Shenoy, Zhen-Dan Shi, Valerie J. Smith, Olga Vasalatiy, Haitao Wu, Biying Xu, Gary L. Griffiths, IPDC, NIH, Rockville, MD, USA. Contact e-mail: agnieszks@mail.nih.gov

The Imaging Probe Development Center (IPDC) was founded as part of the 2003 trans-NIH Roadmap for Medical Research initiative, with the aim of providing the essential synthetic chemistry support needed to advance molecular imaging technologies in interdisciplinary research from basic through translational to clinical levels. The IPDC laboratories are located in Rockville, MD with state-of-the-art equipment and scientists drawn from diverse backgrounds with expertise in synthetic, inorganic, radiochemical, and conjugation chemistries. The IPDC has a rolling solicitation system and NIH scientists are welcome at any time to enquire about obtaining a probe in which they are interested. The IPDC is currently working with principal investigators from more than a dozen different NIH Institutes along with some extramural collaborators. We supply requested imaging probes that are already known, but otherwise unavailable, or are completely novel, and they are used in all types of imaging modalities, including MRI, optical fluorescence and PET/SPECT. Examples of molecular imaging probes we have made include various complexes for MRI studies, fluorogenic enzyme substrates, fluorescent dyes and analogs, caged derivatives which become fluorescent upon uncaging, radio- and fluorescent-labeled antibodies and other proteins, radiolabeled low molecular weight compounds, liposomes, dendrimers and nanoparticles. A selection of several dozen recently made probes will be used to illustrate the scope and capabilities of the Center. For more information, or to make enquiries about probe availability you may also visit our website: <http://www.ipdc.nih.gov>.

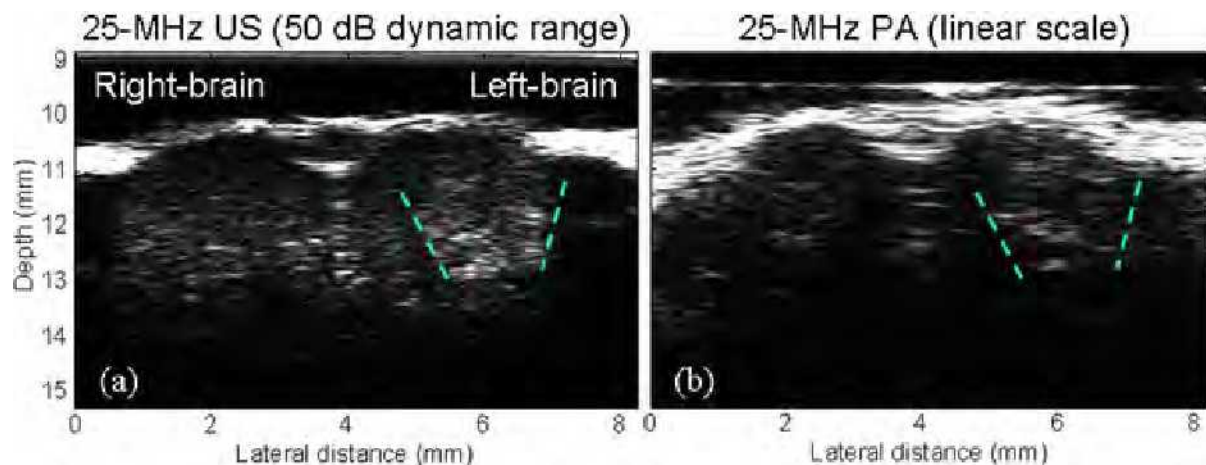
Presentation Number **0912A**

Poster Session 1c: In Vivo Studies & Development/Novel Use of Imaging Probes

Gold Nanorods as a Multi-modal - Ultrasound and Photoacoustic - Contrast Agent for *In Vivo* Imaging Focused-Ultrasound Induced Blood-Brain-Barrier Opening

Po-Hsun Wang¹, **Po-Hung Hsu**², **Hao-Li Liu**², **Chung-Ren C. Wang**³, **Pin-Yuan Chen**⁴, **Kuo-Chen Wei**⁴, **Tzu-Chen Yen**⁵, **Meng-Lin Li**¹,
¹Dept. of Electrical Engineering, National Tsing Hua University, Hsinchu, Taiwan; ²Dept. of Electrical Engineering, Chang Gung University, Taoyuan, Taiwan; ³Dept. of Chemistry and Biochemistry, National Chung Cheng University, Chiayi, Taiwan; ⁴Dept. of Neurosurgery, Chang-Gung Memorial Hospital, Taoyuan, Taiwan; ⁵Molecular Imaging Center and Dept. of Nuclear Medicine, Chang-Gung Memorial Hospital, Taoyuan, Taiwan. Contact e-mail: gnaw22@msn.com

For local drug delivery of cerebral-disease treatment, focused ultrasound (FUS) has been proven to be able to disrupt blood brain barrier (BBB) locally and reversibly. In this study, we report on the first demonstration of gold nanorods (AuNRs) as a multi-modal - ultrasound (US) and photoacoustic (PA) - contrast agent for imaging FUS-induced BBB opening *in vivo*. Due to their nano-scale size, AuNRs tend to extravasate and accumulate at BBB opening foci. AuNRs used here are with the mean size of 40 nm by 10 nm. Under this aspect ratio, AuNRs own peak near-infrared optical absorption at ~800 nm, turning out to be a good PA contrast agent. It has been reported that US contrast enhancement by smaller than 1000-nm solid nanoparticles is not significant. Nonetheless, via transmission electron microscopy, we found that after extravasating from cerebral vessels at FUS-applied regions, AuNRs tend to aggregate, forming micrometer-sized clusters which may serve as strong US scatterers and offer US contrast enhancement. In our *in vivo* experiments, localized BBB disruption at the rat's left brain parenchyma was achieved by delivering 1.5 MHz FUS energy in the presence of microbubbles. PEGylated AuNRs were then intravenously administered. 25-MHz ultrasound and photoacoustic imaging results (n = 8) showed that PA and US contrast at BBB disruption area in left brains could be enhanced by accumulated AuNRs while there were no changes observed in the right brains. In addition, in photoacoustic images, we observed higher local concentration of AuNRs at BBB opening foci than that in blood, which as well as the formation of AuNR clusters is inferred as the cause of US contrast enhancement. This discovered US contrast mechanism suggests that metallic nanoparticles smaller than 5 nm, which permits rapid and efficient renal clearance from the body, may potentially be used as a US contrast agent in such a study. In summary, from our results, AuNRs show the promise as a novel multi-modal - US and PA - contrast agent for identifying the location and variation of FUS based BBB opening and local drug delivery.



25-MHz gold nanorod contrast-enhanced ultrasound (a) and photoacoustic (b) B-mode images of the rat brain with focused-ultrasound induced blood-brain-barrier opening

Presentation Number **0913A**

Poster Session 1c: In Vivo Studies & Development/Novel Use of Imaging Probes

PET-Optical Dual Modality Imaging of Pancreatic Cancer Using Targeted Dendritic Nanoparticles

David M. Pham¹, Jinjin Feng¹, Elizabeth Allen², Venkata Ramana Kotamraju³, Kazuki N. Sugahara³, Tambat Teesalu³, Francis C. Szoka⁴, Jiang He¹, Erkki Ruoslahti³, Douglas Hanahan², Henry F. VanBrocklin¹, Ella F. Jones¹, ¹Radiology and Biomedical Imaging, University of California, San Francisco, CA, USA; ²Diabetes Center, University of California, San Francisco, CA, USA; ³Sanford-Burham Medical Research Institute, University of California, Santa Barbara, CA, USA; ⁴Biopharmaceutical Sciences, University of California, San Francisco, CA, USA. Contact e-mail: david.pham@radiology.ucsf.edu

Background: Pancreatic cancer strikes more than 42,000 Americans and claims over 35,000 lives every year. The overexpressed angiogenic markers such as α v-integrins in neovasculature are promising targets for early tumor detection. Herein, we demonstrate the utility of a new RGD peptide (iRGD:CRGDKGPDC) on a dendritic nanopatform that mediates the binding and internalization in pancreatic cancer cells. Methods: The pegylated 6th generation PAMAM dendrimer was conjugated with FAM, FAM-iRGD, Cy5.5 and/or [¹⁸F]-FBAM through step-wise coupling reactions using iodoacetic anhydride and protected cysteine. Mercaptoethanol was used to neutralize the remaining iodoacetyl groups to prevent undesirable in vivo reactions. The resulting probes were characterized by GPC, MS and fluorescence assays. PDAC cell lines derived from the pancreas of tumor-bearing KrasG12D p48-Cre Ink4a^{+/+} and KrasG12D p48-Cre p53^{+/-} mice were used for in vitro uptake studies. The initial biodistribution and in vivo PET and optical imaging studies were performed using transgenic PDAC mice. Results: The probe synthesized for biodistribution studies contains an average of 15 FAM-iRGD. Our results indicate that the multivalent FAM-(15)iRGD-dendrimer has tumor uptake >2 times higher than the native FAM-iRGD and FAM-dendrimer without iRGD (Figure 1). The PET-optical dual labeled probe comprises 15 FAM-iRDG, 1 Cy5.5 and 10 [¹⁸F]-FBAM. The PET imaging at 1 h showed significant uptake in the tumor. Despite the high background signal from blood and liver, in vivo optical imaging at 24 and 48 h showed specific accumulation in the tumor and washout from the other organs. The ex vivo results at 48 h showed significant tumor uptake compared to that of any other organs (Figure 2). Conclusions: The multivalent dendrimer with high payload of iRGD shows effective targeting to pancreatic cancer. Incorporation of multiple reporters allows for dual PET and optical imaging to characterize the probe's in vivo biodistribution from early to late time points.

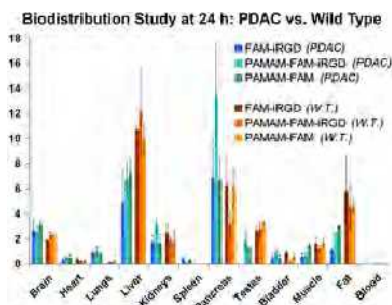


Figure 1. A preliminary biodistribution of the FAM-iRGD-dendrimer probe compared to two control probes, FAM-iRGD and FAM-dendrimer in both PDAC and wild type mouse models (n=4 for each group). PDAC transgenic mice are in blue (5FAM-iRGD), light blue (5FAM-iRGD-dendrimer) and green (5FAM-dendrimer); wild type mice are in red (5FAM-iRGD), orange (5FAM-iRGD-dendrimer) and yellow (5FAM-dendrimer). From this preliminary study, it is clear that the 5FAM-iRGD-dendrimer exhibits tumor uptake over 2 times higher than the control probes. Non-specific liver uptake is relatively low with tumor-to-liver ratio of 2:1 compared to 0.9-1.2 from the two control probes.

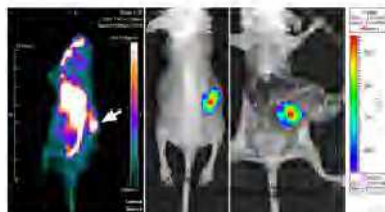


Figure 2. In vivo imaging studies of the PET-optical dual labeled probe in PDAC mice. a) In vivo PET image 1 h post injection; b) in vivo optical image 48 h post-injection; c) probe specificity to pancreatic cancer as confirmed by the post-mortem optical imaging study.

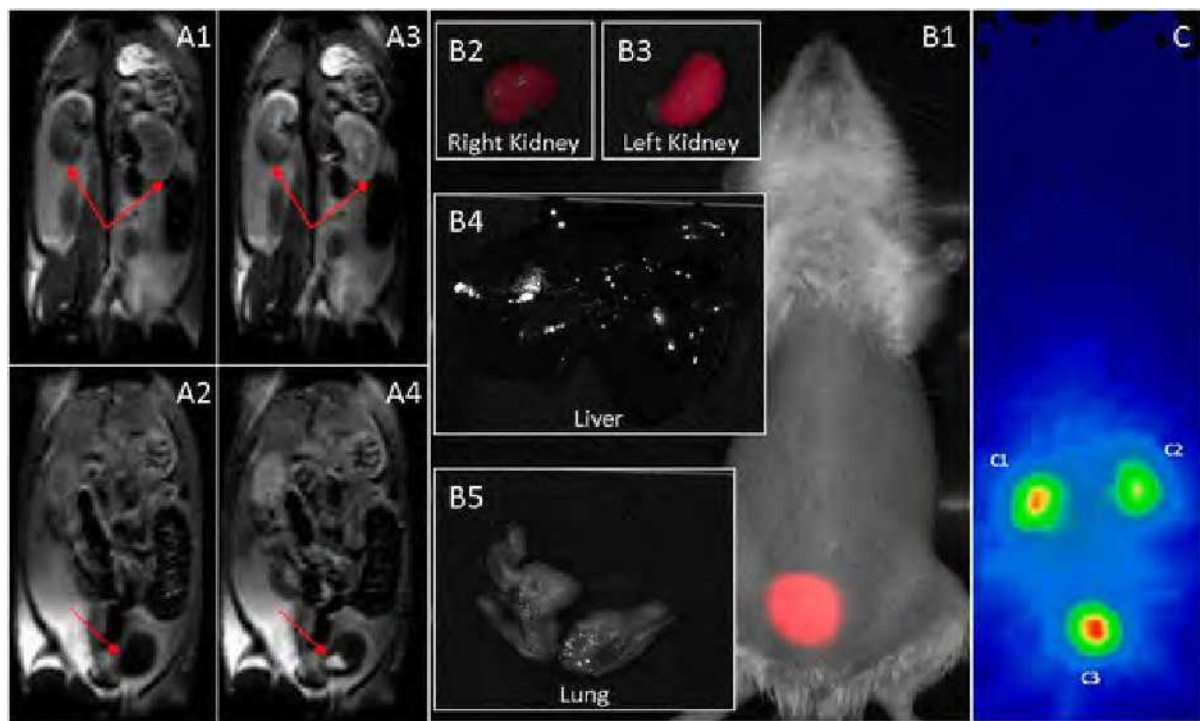
Presentation Number **0914A**

Poster Session 1c: In Vivo Studies & Development/Novel Use of Imaging Probes

In vivo biodistribution of hybrid gadolinium oxide nanoparticles as a multimodal imaging agent

David Kryza¹, **Jacqueline Taleb**¹, **Pierre Mowat**², **Emmanuel Deshayes**¹, **Marc F. Janier**¹, **Cedric Louis**³, **Laurence Marmuse**³, **Stephane Roux**², **Pascal Perriat**⁴, **Olivier Tillement**², **Claire Billotey**¹, ¹Université Claude Bernard Lyon 1, CREATIS, Hospices Civils de Lyon, Lyon, France; ²LPCML UMR 5620 CNRS, Université Claude Bernard Lyon 1, Villeurbanne, France; ³NanoH, Saint Quentin Fallavier, France; ⁴UMR 5510 CNRS-INSA de Lyon, Villeurbanne, France. Contact e-mail: david.kryza@chu-lyon.fr

Challenges in diagnostic imaging have lead to an explosion of interest in designing new medical imaging contrast agents that can permit multiple imaging applications using a single agent. Herein, we report the biodistribution of intravenously administered nanoparticles (mean diameter of 3-4 nm) obtained by encapsulating Gd₂O₃ cores within a polysiloxane shell which carries organic fluorophore (Cy 5) and derivatised by an hydrophilic carboxylic layer. Nanoparticles were labelled with Indium-111 at high radiochemical purity. The GadoSi nanohybrid nanoparticles were imaged in control Wister rats using MRI (7 T), optical fluorescent imaging and SPECT. A clear correlation could be observed between MRI, optical imaging and SPECT as demonstrated in the included figure. Rats were sacrificed at 30 min, 2h, 24h, 48h and 72h post injection (n=3 at each time) and organs of interest were collected, weighed and counted in a gamma scintillation counter. The tissue distribution was expressed as the percentage injected dose per gram tissue (% ID/g). Quantitative biodistribution data obtained from each organ revealed that these nanoparticles freely circulated in the blood pool and were rapidly eliminated by renal excretion without accumulation in liver and RES uptake. Multimodal and quantitative biodistribution of this new category of nanoparticles shows promising properties to develop them as targeted or non targeted contrast media or therapeutic agents.



A: in vivo MR images at 7T - T1w MR signal before and after intravenous injection of Gd₆Si at 100 mM Gd. A1 = Kidneys before injection, A2 = Bladder before injection, A3 = Kidney 15 min after injection, A4 = Bladder 15 min after injection B: in vivo and ex vivo optical fluorescence imaging. B1 = in vivo image 15 min after intravenous injection of Gd₆Si-Cy5 at 100mM Gd, B2 = ex vivo right kidney image, B3 = ex vivo left kidney image, B4 = ex vivo liver image, B5 = ex vivo lung image C: in vivo SPECT image 15 min after intravenous injection of Gd₆Si-111In (30 MBq). C1= right kidney, C2 = left kidney, C3 = bladder

Presentation Number **0915A**

Poster Session 1c: In Vivo Studies & Development/Novel Use of Imaging Probes

Combined MR and Optical Imaging of Head and Neck Tumor Xenografts using Gadolinium-labeled Phosphorescent Polymeric Nanomicelles

Jaimee M. Lockwood¹, Rajiv Kumar², Steve G. Turowski¹, Tymish Y. Ohulchansky², Mark E. Thompson³, Paras N. Prasad², Mukund Seshadri^{1,4}, ¹Cancer Biology, Roswell Park Cancer Institute, Buffalo, NY, USA; ²Institute for Lasers, Photonics and Biophotonics, University at Buffalo, Buffalo, NY, USA; ³Chemistry, University of Southern California, Los Angeles, CA, USA; ⁴Dentistry and Maxillofacial Prosthetics, Roswell Park Cancer Institute, Buffalo, NY, USA. Contact e-mail: mukund.seshadri@roswellpark.org

Radiologic techniques constitute an integral component of the diagnostic armamentarium in oncology. However, modalities such as magnetic resonance imaging (MRI), computed tomography (CT) and near-infrared (NIR) optical imaging vary in their limits of sensitivity and resolution. Therefore, the development of targeted imaging probes that can be utilized across multiple imaging platforms will not only provide complementary information on tumor biology but also enable cross-validation of data. Here, we report the use of polymeric phospholipid nanomicelles encapsulating a NIR phosphorescent dye Pt(II)-tetraphenyltetranaphthoporphyrin [Pt(TPNP)] and surface functionalized with gadolinium [Gd-Pt(TPNP)] for combined MR and optical imaging of tumors. The nanomicelles were ~100 nm in size and stable in aqueous suspension. In vitro MR relaxometry studies of Gd-Pt(TPNP) nanomicelles carried out in a 4.7T MR scanner revealed a T1 relaxivity of 10.4 mmol⁻¹.s⁻¹. Subsequently, in vivo experiments were carried out using nude mice bearing primary patient tumor-derived human head and neck squamous cell carcinoma xenografts. T1-enhancement characteristics and relaxation rate (R1=1/T1) measurements of tumor and blood (kidneys) were performed before, 1h, 4h and 24h after nanoparticle administration (35 μmol Gd/kg). Signal enhancement was visible immediately post nanoparticle injection, particularly in the tumor periphery and persisted upto 24 hours post administration. Kidneys also showed visible enhancement on T1-weighted images. Maximum intensity projections (MIPs) generated from 3D T1-weighted images showed visible enhancement in contrast within the tumor, liver and blood vessels. Measurement of T1 relaxation rates (R1=1/T1) showed peak enhancement in the tumor at 4 hours post injection. NIR optical imaging performed following completion of MRI (in vivo and ex vivo) at the 24h time point revealed high contrast phosphorescence signal and confirmed tumor localization of the nanoparticles. The large spectral separation between the Pt(TPNP) absorption (~700 nm) and phosphorescence emission (~900 nm) allowed for a dramatic decrease in the level of background autofluorescence. In conclusion, Gd-Pt(TPNP) nanomicelles exhibit a high degree of tumor-avidity and favorable imaging properties that allowed for combined MR and optical imaging of tumors. Further investigation into the potential of Gd-Pt(TPNP) nanomicelles for combined imaging and therapy of cancer is currently underway.

Presentation Number **0916A**

Poster Session 1c: In Vivo Studies & Development/Novel Use of Imaging Probes

AN ENHANCED PAIR OF NEXT GENERATION TRIPLE REPORTER GENES FOR SEQUENTIAL HIGH SENSITIVITY IMAGING OF TWO DISTINCT CELL POPULATIONS.

Brian Rabinovich, Amer M. Najjar, Juri G. Gelovani, *Experimental Diagnostic Imaging, MD Anderson Cancer Center, Houston, TX, USA. Contact e-mail: brian.rabinovich@gmail.com*

Objective: Live animal imaging is a valuable tool that eliminates the need to sacrifice multiple animals to track cell populations in vivo. Previous triple reporters have consisted of fusion proteins of a thymidine kinase (TK), a luciferase (luc) enzyme and a fluorescent protein (FP). Such constructs are hindered by diminished functional activity of each subunit due to the size and orientation of the resulting chimeric protein. Distinct triple reporters which can be used for sequential multicellular imaging have not been reported. Therefore, we generated two new constructs with distinct reporter genes engineered so that each component of the reporter is expressed as a separate protein. **Methods:** The first triple-reporter encodes wild type HSV1-tk, effLuc and eGFP, which phosphorylate ^{18}F -FEAU, catalyze D-luciferin and has a peak fluorescence emission at 610 nm, respectively. The second triple-reporter, encodes A168H mutant HSV1-tk, RLuc-8.6 535 and mKate S158A, which phosphorylates ^{18}F -FHBG (but not ^{18}F -FEAU), catalyzes coenterazine and has a peak fluorescence emission at 630 nm, respectively. Each reporter gene was enhanced via codon optimization and removal of cryptic splice sites. Each gene within the triple reporter was expressed as its own gene product by encoding aphthovirus based 2A ribosomal slippage sites between the TK, luc and FP. 293 cells transfected with each construct were studied. The constructs were generated within entry clones flanked by lambda phage recombination sites which allow for shuttling of the triple reporters into an expression vector of choice (e.g. lentiviral, adenoviral) in one hour. **Results:** The mean fluorescence intensities for eGFP and mKateS158A were similar (+/- 10%) to those for 293 cells expressing eGFP or mKateS158A alone >100 fold brighter than that observed for analogous fusion proteins (Fig. 1). Bioluminescence activity was measured as >14,000 photons/sec/cell for RLuc 8.6-535 and >8,000 photons/sec/cell for effLuc. Cell-to-media uptake ratios at 1 hour for HSV-TK (^3H -FEAU) and A168H-HSV1-TK (^3H -penciclovir) were 27 ± 2.0 and 6.5 ± 0.7 , respectively. Initial in vivo imaging experiments suggest that both triple reporters are sufficiently sensitive to detect <100 cells injected subcutaneously using BLI and fluorescence and < 5000 by PET. **Conclusions:** These next generation triple reporters could serve as valuable tools for tracking small numbers of multiple populations in-vivo and the translation of such results into the clinic.

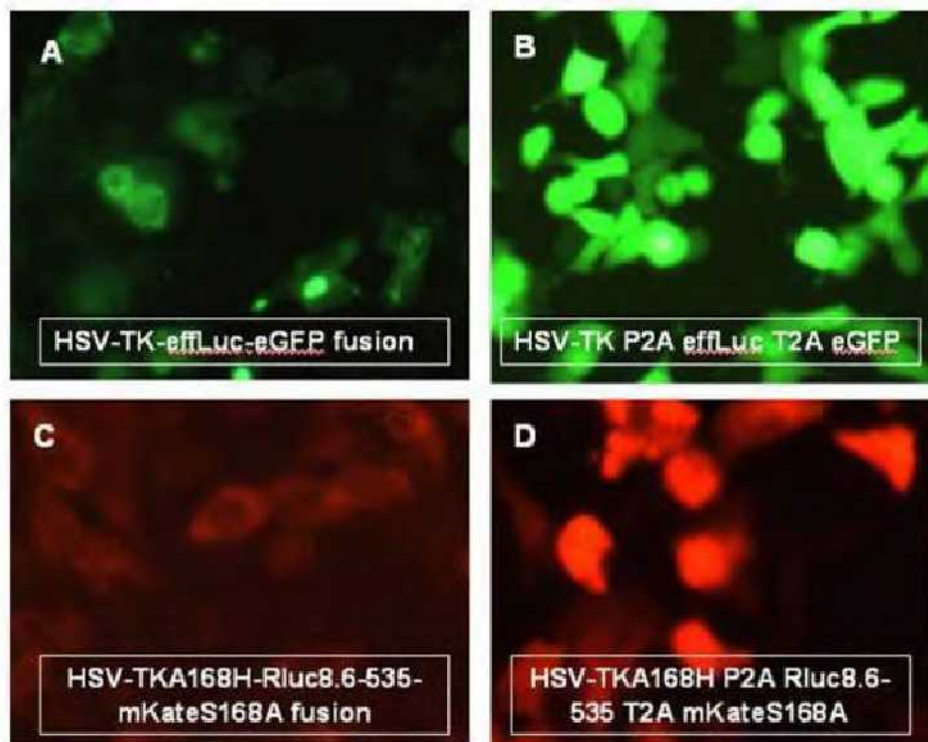


Figure 1. Comparison of the intensity of the fluorescent reporter component of fusion protein based versus ribosomal slippage site based triple reporter gene products. (A) 293 cells transfected with a fusion of HSV1-TK, effLuc and eGFP. (B) 293 cells transfected with HSV1-TK, effLuc and eGFP separated by 2A ribosomal slippage sites. (C) 293 cells transfected with a fusion of HSV1-TK-A168H, RLuc8.6-535 and mKate-S158A. (D) 293 cells transfected with HSV1-TK-A168H, RLuc8.6-535 and mKate-S158A separated by 2A ribosomal slippage sites.

Presentation Number **0917A**

Poster Session 1c: In Vivo Studies & Development/Novel Use of Imaging Probes

Development of radioisotope labelled NIR upconversion nanoprobe for clinical imaging

Rita Song¹, **Tae Sup Lee**², **Jiyoung Ryu**¹, **Hye-Young Park**¹, **Sukmin Hong**¹, **Keumhyun Kim**¹, **Heeyeon Kim**¹, **Gi Jeong Cheon**²,
¹Institut Pasteur Korea, Seongnam-si, Republic of Korea; ²Molecular Imaging Laboratory, Korea Institute of Radiological and Medical Sciences, Seoul, Republic of Korea. Contact e-mail: rsong@ip-korea.org

Synthesis of nanomaterials with multi-imaging modality is of great importance in clinical molecular imaging and diagnostics. Upconversion phosphors (UCP) such as NaREF₄:RE(Er, Y, Yb, Tm) use inexpensive and high power near-IR diode laser (980 nm). The near IR excitation allows deeper light penetration in tissue and has much higher signal to noise ratio due to the absence of autofluorescence and the reduction of light scattering. Furthermore, the lanthanide ions are inherently resistant to photo-bleaching and photochemical degradation, which bring additional advantages over organic dye for biological application. The challenging point of this project is to develop the methodology to label radioisotope (RI) on the UCP using appropriate chelate ligand modification. The RI labeled UCP will be tested for clinical diagnostics using SPECT or PET. This paper reports novel synthetic strategy to create upconversion nanoparticles with inherent magnetic properties due to Gd in the host material, showing potential to be used as contrast agent in MRI. By introducing simple precursors, NaGdF₄: Yb³⁺, Er³⁺ (Tm³⁺) with pure hexagonal crystalline structure has been created. (Figure 1) The NaGdF₄: Yb³⁺, Er³⁺ (Tm³⁺) nanoparticles exhibit strong upconversion optical properties and T₁ magnetic contrast effect (Figure 2). Highly bright and non-photobleaching upconversion nanoparticles have been prepared by introducing simple precursors, NaGdF₄: Yb³⁺, Er³⁺ (Tm³⁺) with various crystalline structure and shape. These nanoparticles were polymer-coated, PEGylated and bound to DOTA to label Cu-64. These nanoparticles were injected and determined their biodistribution pattern. In addition, DOTA-UCP-RGD conjugates were also prepared and the targeting properties for vEGFR in xenograft animal model were investigated.

Presentation Number **0918A**

Poster Session 1c: In Vivo Studies & Development/Novel Use of Imaging Probes

Multifunctional Nanomedicine for Near-Infrared Photothermal Cancer Therapy and MR Targeting Imaging in vivo

Chia-Hao Su¹, **Fong-Yu Cheng**², **Chen-Sheng Yeh**², ¹*Center for Translational Research in Biomedical Sciences, Chang Gung Memorial Hospital, Kaohsiung, Taiwan;* ²*Department of Chemistry, National Cheng Kung University, Tainan, Taiwan. Contact e-mail: chiralsu@gmail.com*

Due to the nanomedicine ability to simultaneously provide detection, diagnosis, and therapy in a single nanoparticle (NP), multifunctional nanomaterials have been intensively explored for promising applications in biomedicine. Recently, nanoparticles with photothermal therapeutic capabilities have attracted a great deal of attention in the photothermal treatment of tumor cells. Those near-infrared (NIR) resonant nanomaterials are chosen due to the optimal transmission to tissue in the NIR region. However, there are still some challenges existed for clinical applications. To overcome this limitation, chemotherapy by the photothermal-control drug release method could be incorporated with NIR therapy in the thermoresponsive polymers. The combination of chemotherapeutics and hyperthermia has been an emerging approach for cancer therapy. Recently, we have developed stabilizer-free Au NR/QD/Fe₃O₄/Taxol-loaded PLGA NPs, and they can be easily and directly made conjugation on the surface and the inner core can capsule drugs to potentially serve as multifunctional probe, and the nanomaterials hold the great potential to achieve localized treatments to the area of interest. In this work, we demonstrated the first example of nanosystems with the combination of chemotherapeutic and photothermal therapy in the mammalian cells and animal disease model. The stabilizer-free Taxol(paclitaxel)-loaded PLGA NPs were conjugated with amine-terminal Fe₃O₄ NPs (~6 nm) and QDs (~12 nm) obtained to QD/Fe₃O₄/Taxol-loaded PLGA NPs with optical and MR imaging functionalities. Subsequently, poly(styrenesulfonate) (PSS)-coated Au nanorods were introduced to attach to the QD/Fe₃O₄/Taxol-loaded PLGA NP surface. Because Au NRs can absorb NIR light and convert it to heat, spherical PLGA NPs can be destroyed to efficiently release encapsulated Taxol. Both in vitro and in vivo studies were conducted to evaluate therapeutic performance. For MR molecular imaging applications, the r1 and r2 relaxivities of Au NR/QD/Fe₃O₄/Taxol-loaded PLGA NPs were determined to be 0.19 and 14.05 s⁻¹mM⁻¹, respectively. The Au NR/QD/Fe₃O₄/Taxol-loaded PLGA NPs were further administrated to the A549 (lung cancer cells)-induced SCID mice. The administrated dosage of 0.1 mg/Kg as those used was intratumorally injected into mice. The T2-weighted images of A549-induced SCID mice before and after injection of Au NR/QD/Fe₃O₄/Taxol-loaded PLGA NPs, and the tumor area appeared darkened and imaging signal decreased about 24 %.

Presentation Number **0919A**

Poster Session 1c: In Vivo Studies & Development/Novel Use of Imaging Probes

Trafficking of a Dual Reporting Magnetic Resonance and Fluorescence Imaging Superparamagnetic Iron-Oxide Based Nanoprobe Developed for Sentinel Node Imaging

Ambika Bumb¹, Celeste Aida S. Regino², Jackson Egen³, Marcelino Bernardo², Ronald Germain³, Peter Choyke², Martin Brechbiel¹,
¹Radiation Oncology Branch, National Cancer Institute, Bethesda, MD, USA; ²Molecular Imaging Program, National Cancer Institute, Bethesda, MD, USA; ³Laboratory of Immunology, National Institute of Allergy and Infectious Diseases, Bethesda, MD, USA. Contact e-mail: Bumba@mail.nih.gov

Current methods for characterizing primary draining, or sentinel, lymph node (LN) of primary tumors rely on nodal size as the primary yardstick for differentiating benign from malignant LNs. Other parameters such as nodal shape, contour, and level of enhancement would also provide useful information. Two imaging agents are currently used for sentinel node imaging, a radiolabeled macromolecule such as ^{99m}Tc-albumin or sulfur colloid and the optical blue dye isosulfan. We have developed a dual-reporting nanoparticle by encasing ultrasmall superparamagnetic iron oxide nanoparticles in a thin ~3nm layer of silica containing conjugated fluorophore. During each phase of development, the nanoparticles have been characterized for size, surface charge, structure, optical response, and magnetic properties. With in vivo optical and magnetic resonance imaging, axillary LNs were visualized in athymic mice given front foot pad intracutaneous injections. Histology analysis on the dissected lymph nodes confirmed particle presence. To further analyze the mechanism of agent trafficking from the dermal injection site and then its localization in LN, transgenic mice models expressing fluorescent dendritic and myelomonocytic cells were given intracutaneous injections of the particle in hind foot pad. The lymphatic vessel to the popliteal LN was exposed and video taken at points pre-, during, and post-injection. The popliteal LNs were then harvested, stained for different cell types, and examined under confocal microscopy. The findings indicate that transport is primarily passive, not cell-mediated, and that particles did not localize in phagocytic dendritic cells or macrophages, as would be expected.

Presentation Number **0920A**

Poster Session 1c: In Vivo Studies & Development/Novel Use of Imaging Probes

Development of Superparamagnetic Iron Oxide Nanoparticles for NIRF/MRI Multi Modal Imaging

Eui-Joon Cha¹, **In-Cheol Sun**², **Kwangmeyung Kim**², **Ick Chan Kwon**², **Cheol-Hee Ahn**¹, ¹*Department of Materials Science and Engineering, Seoul National University, Seoul, Republic of Korea;* ²*Biomedical Research Center, Korea Institute of Science and Technology, Seoul, Republic of Korea. Contact e-mail: mage82@snu.ac.kr*

During the past decades, various nanostructures have been exploited and successfully employed as molecular imaging probes for disease detection. Superparamagnetic iron oxide nanoparticles (SPIONs) with appropriate surface chemistry are one of the famous candidates for numerous biomedical applications such as a contrast enhancing agent of magnetic resonance imaging (MRI), tissue repair, immunoassay, hyperthermia, drug delivery and cell separation. However, in vivo application of SPIONs is challenged by stability problems because of their hydrophobic surface, insufficient accumulation and retention within tumors due to limited specificity to the target, and an inability to traverse biological barriers. Therefore, numerous SPIONs with biocompatible surface chemistry have been developed for overcoming these problems. Recently, imaging probes have several imaging modalities are the focus of researchers in biomedical field, because single imaging modality has limitations to allow overall structural, functional, and molecular information. Since each imaging modality differs from another in terms of spatial and temporal resolution, anatomical and molecular details and imaging depth, it is advantageous to apply multiple complimentary imaging modalities for faster and more accurate prognosis on many occasions. Here, we describe the preparation of biocompatible multi functional SPIONs to combine MRI and near-infrared fluorescence (NIRF) imaging for cancer diagnosis using simple coating and coupling methods. Chemically modified biocompatible polymer with enhanced adhesive ability to nanoparticles was used as a biocompatible stabilizer for SPIONs and NIRF organic dyes were conjugated to polymer coating layer for optical imaging. The nanoprobe shows remarkable cancer specific NIRF and MR images. With the conjugation of various targeting ligands and the flexible conjugation chemistry for alternative diagnostic and therapeutic agents, this nanoprobe platform can be potentially used for the diagnosis and therapy of various tumor types.

Presentation Number **0921A**

Poster Session 1c: In Vivo Studies & Development/Novel Use of Imaging Probes

Photothermal Transfection of siRNA under the Guidance of PET/CT Imaging Using Hollow Gold Nanospheres

Wei Lu, Guodong Zhang, Rui Zhang, Leo G. Flores, Qian Huang, Juri G. Gelovani, **Chun Li**, Exp. Diagnostic Imaging, U.T. M. D. Anderson Cancer Center, Houston, TX, USA. Contact e-mail: cli@mdanderson.org

Objectives: Successful RNAi therapeutics is challenged by the need for efficient endo-lysosomal escape, dynamic control over activation of RNAi, and targeted in vivo delivery. Here, we present a novel strategy, "photothermal transfection", which selectively induces cytoplasmic delivery of small siRNA through photothermal effect mediated by hollow gold nanospheres upon near-infrared light irradiation. **Methods:** We constructed folate receptor-targeted hollow gold nanospheres carrying siRNA recognizing NF- κ B p65 subunit (F-PEG-HAuNS-siRNA). We conjugated 1,4,7,10-tetraazacyclododecane-1,4,7-tris(acetic acid)-10-[acetic acid-N-(2-(2-(2-aminoethoxy)ethoxy)ethyl)-lipoic acid mono amide] (DOTA-LA) to F-PEG-HAuNS-siRNA, which allowed labeling with ^{64}Cu for PET imaging. **Results:** μ PET/CT imaging revealed that the tumor uptake of F-PEG-HAuNS-siRNA(DOTA- ^{64}Cu) was significantly higher than that of nontargeted PEG-HAuNS-siRNA(DOTA- ^{64}Cu) at 6 h following i.v. injection into nude mice bearing s.c. HeLa cervical cancer xenografts. This was confirmed by biodistribution study, which showed 4.7-fold higher tumor uptake of F-PEG-HAuNS-siRNA(DOTA- ^{64}Cu) as compared to PEG-HAuNS-siRNA(DOTA- ^{64}Cu) ($5.26 \pm 1.25\% \text{ID/g}$ versus $1.11 \pm 0.50\% \text{ID/g}$). This resulted in efficient site-specific down-regulation of NF- κ B p65 in tumor xenografts irradiated with near-infrared light after i.v. injection of F-PEG-HAuNS-siRNA. Combined treatments with NF- κ B p65 siRNA photothermal transfection and irinotecan caused substantially enhanced tumor apoptosis and significant tumor growth delay compared with other treatment regimens. **Conclusions:** PET/CT imaging using ^{64}Cu can be an accurate imaging modality for the guidance of tumor targeted delivery of HAuNS-siRNA nanoconstructs, which is a key premise of the success in site-specific photothermal transfection of siRNA as well as chemo-sensitization.

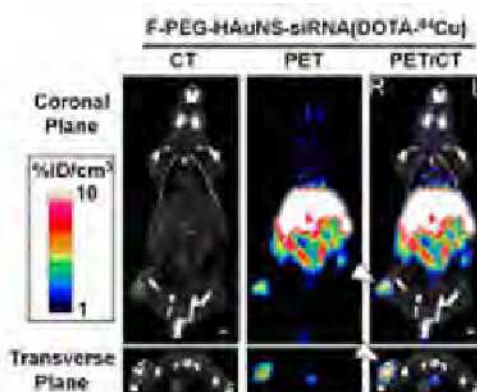


Figure 4. Tumor targeting of F-PEG-HAuNS-siRNA directed at folate receptor. Micro-PET/CT imaging of nude mice-bearing HeLa cervical cancer xenografts in right rear leg 6 h after i.v. injection of F-PEG-HAuNS-siRNA(DOTA- ^{64}Cu). Arrow, tumor.

Presentation Number **0898A**

Poster Session 1c: In Vivo Studies & Development/Novel Use of Imaging Probes

Affibody-based Nanoprobes for HER2-Expressing Cell and Tumor Imaging

Jinhao Gao¹, Kai Chen¹, Zheng Miao¹, Gang Ren¹, Sanjiv S. Gambhir^{1,2}, Zhen Cheng¹, ¹Radiology, Stanford University, Stanford, CA, USA; ²Bioengineering, Stanford University, Stanford, CA, USA. Contact e-mail: gaojh@stanford.edu

Herein we reported the Affibody-based nanoprobes specifically target and image HER2-expressing cells and tumors. The simple, robust, and precise structure of Affibody molecules are a promising class of cancer-specific ligands with high affinity. Using near-infrared (NIR) quantum dots (QDs) and iron oxide (IO) nanoparticles as two representative nanomaterials, we designed anti-HER2 Affibody molecules (ZHER2:342) with the C terminus cysteine residue and precisely conjugated Affibody with maleimide-functionalized nanoparticles to make nanoparticle-Affibody conjugates. The multivalent binding effect of nanoparticle-Affibody conjugates may further enhance the affinity and targeting because the collective binding in a multivalent interaction is much stronger than monovalent binding. The in vitro and in vivo study showed the nanoparticle-Affibody conjugates are highly specific to target and image HER2-expressing cells and tumors. These specific nanoparticle-based probes ensure that Affibody molecules are excellent candidates as targeting molecules to modify and functionalize various nanomaterials. In addition, the Affibody-based nanoprobes may open up new strategies for the development of novel molecular imaging probes in cancer early detection and diagnosis applications.

Presentation Number **0922A**

Poster Session 2c: In Vivo Studies & Development/Novel Use of Imaging Probes

Gold Nanoparticles as Potential Cancer Imaging and Therapeutic Agents

Agnieszka Sulima¹, **Biying Xu**¹, **Nalini Shenoy**¹, **Gary L. Griffiths**¹, **Jacek Capala**², **Gabriela Kramer-Marek**², ¹NHLBI, NIH, Rockville, MD, USA; ²NCI, NIH, Bethesda, MD, USA. Contact e-mail: agnieszs@mail.nih.gov

Nanoparticles, engineered as a platform for targeted drug delivery, diagnosis, therapy and imaging, have been actively pursued for biomedical applications in recent years. In particular, gold nanoparticles (GNP) are well suited for these applications. At the Imaging Probe Development Center (IPDC) (www.ipdc.nih.gov) we are developing multifunctional gold nanoparticle-based agents for cancer imaging and therapy. Preparation and characterization of multifunctional poly(ethylene glycol)-grafted gold nanospheres will be reported in detail along with a discussion of their potential use in molecular imaging and radiotherapy. The preparation of multifunctional GNP was initiated by the synthesis of colloidal gold with a well defined size. In order to enhance the biocompatibility of colloidal gold and suppress particle uptake by the reticuloendothelial system (RES), gold nanoparticles were grafted with thioctic acid functionalized poly(ethylene glycol), (TA-PEG5,000-OMe). In addition, bifunctional PEGs were used to facilitate the conjugation of targeting ligands and imaging labels to nanoparticles. For the targeted delivery of gold nanoparticles, Affibody Molecules® were conjugated to the GNP. The Affibody molecules employed in this study selectively bind the human epidermal growth factor receptor-2 (HER-2), which is overexpressed in certain breast and lung tumors. For fluorescence imaging purposes GNP were further functionalized with a NIR dye, IRDye®800CW. Biological evaluation of targeted versus non-targeted gold nanoparticles as well as biodistribution and imaging studies are currently ongoing at the National Cancer Institute. Application of multifunctional GNP in radiation and neutron therapies will be investigated in the near future.

Presentation Number **0923A**

Poster Session 2c: In Vivo Studies & Development/Novel Use of Imaging Probes

Active targeting liposomes as the multifunctional contrast agents

Takayuki Otani^{1,2}, Hideki Minematsu¹, Yoshie Hiramatsu¹, Masahiko Hirai¹, Katsuyuki Takashima⁴, Seiji Nakashima³, Shinki Iwashita¹, Hiroyuki Kitagawa¹, Kenji Kono³, Kazunori Oie¹, Masaharu Seno², Koichi Igarashi¹, ¹R&D division, Katayama Chemical Industries Co., Ltd., Minoh, Japan; ²Graduate school of Natural Science and Technology, Okayama University, Okayama, Japan; ³Graduate School of Engineering, Osaka Prefecture University, Sakai, Japan; ⁴DS Pharma Biomedical Co., Ltd., Suita, Japan. Contact e-mail: ta.otani@katayamakagaku.co.jp

Previously we reported that the liposomes with Sialyl Lewis X (SLX) on the surface, in which the fluorescent dye was encapsulated, were useful as in vivo active targeting fluorescent imaging reagent (Hirai et al., 2006). These SLX liposomes were prepared to mimic the behavior of leucocytes which accumulate in inflammation or tumor regions in vivo. Interaction of SLX present on the surface of leucocytes and the sugar chain recognizing proteins called selectin expressing on the endothelial cells in inflammation and tumor regions is well known. The SLX liposomes administered intravenously from mouse tail vein were accumulated significantly in inflammation or tumor regions. In order to develop these liposomes as the multifunctional active targeting contrast agents, we studied the targeting units for binding on the surface of the liposomes and also the various contrast agents to encapsulated into the liposomes as the detection unit, and combine these two units to prepare the most suitable detection system. As one of the targeting units, anti-E-selectin antibody was conjugated on the surface of liposomes encapsulating fluorescent dye, and it was demonstrated that these liposomes with antibody were accumulated in inflammation and tumor regions. Next, colloidal gold, magnetic iron or gadolinium is encapsulated into liposomes as the detection units for opt-acoustic imaging, electron microscopy, MRI and so on. These liposomes were injected intravenously from the tail vein of the tumor bearing mouse. At 24 to 48 hours after administration, we detected clearly colloidal gold in the surrounding vascular endothelial cells in tumor region by the observation with transmission electron microscopy, or T1 and T2 weighted images of tumor regions by MRI (1T). It is also possible to encapsulate other contrast agents such as for PET or CT into liposomes, or to encapsulated these plural agents simultaneously for obtaining multimodality. We suggest that these active targeting liposomes are useful as the multifunctional contrast agents for the research and also clinical diagnostics. We are now trying to encapsulate these contrast agents and pharmaceutical compounds together to carry out diagnosis and medical treatment simultaneously in the near future.

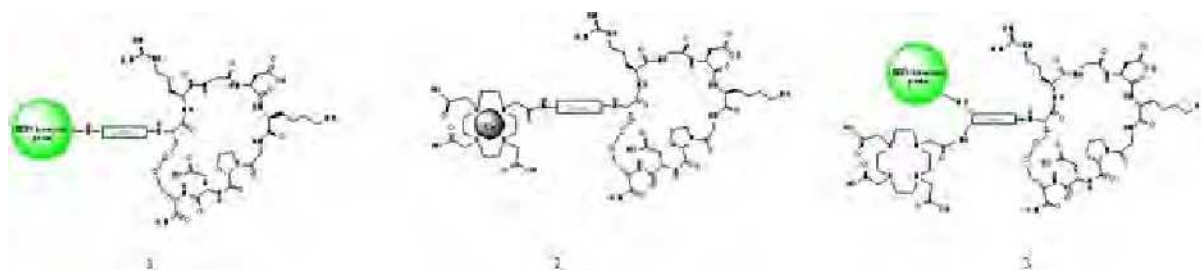
Presentation Number **0924A**

Poster Session 2c: In Vivo Studies & Development/Novel Use of Imaging Probes

Synthesis and Evaluation of iRGD Peptide Analogs for Tumor Optical and PET Imaging

Yunpeng Ye, Lei Zhu, Min Yang, Haokao Gao, Gang Niu, Ying Ma, Xiaoyuan Chen, Laboratory of Molecular Imaging and Nanomedicine, NIBIB/NIH, Bethesda, MD, USA. Contact e-mail: Yunpeng.Ye@nih.gov

Diverse tumor imaging agents have been discovered based on targeting integrin and some other receptors related to tumor angiogenesis, growth, and metastasis. Nevertheless, most of them lack deep tumor penetration. It was recently reported a cyclic tumor-penetrating peptide i.e. CRGDKGPDC (iRGD) binds to integrin $\alpha\beta_3$, followed by enzymatic hydrolysis to form an active CendR peptide that binds to neuropilin-1 and mediates an active transport system for extravasation and deep tumor penetration. This has inspired us to discover novel, innovative imaging agents based on iRGD which is different from the conventional cyclic penta-RGD peptide c(RGDfK) analogs in structure and function. This presentation will report several iRGD analogs coupled with different imaging agents via different linkers at the N-terminus of iRGD for optical and PET imaging. They include iRGD analogs with a near-infrared fluorescent probe (1) and macrocyclic chelator DOTA (2) as well as a dual labeling analog 3 of both DOTA and near-infrared fluorescent probe. The conjugations were performed in solution or on solid support. The final products were obtained by TFA cleavage, HPLC purification, and ES-MS identification. The DOTA conjugates were labeled with ^{64}Cu for PET imaging. All the compounds were evaluated by in vitro and in vivo studies including cell staining, cell binding assay, in vivo tumor imaging, and ex vivo validation. All the compounds showed remarkable tumor accumulation and retention in orthotopic MDA-MB-435 xenograft model as revealed by both optical and PET imaging modalities. Our results suggest that iRGD peptide may be a good ligand for integrin targeted tumor imaging. Further structural modification for molecular imaging is currently underway.



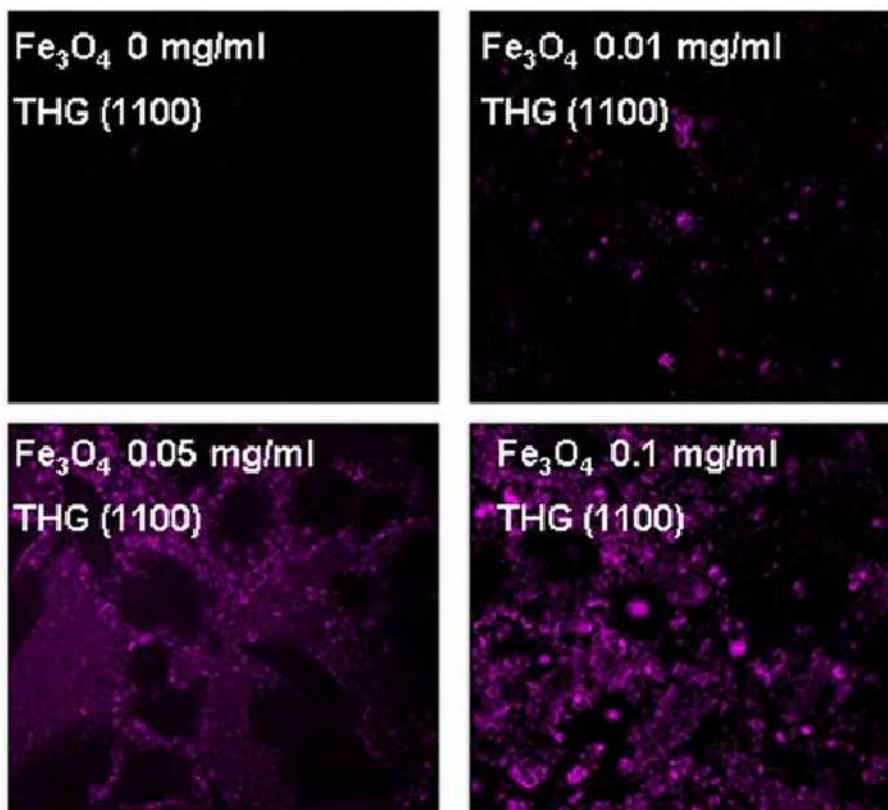
Presentation Number **0925A**

Poster Session 2c: In Vivo Studies & Development/Novel Use of Imaging Probes

Bifunctional Nanocontrast Medium for MR and Optical Targeting Imaging Applications

Chia-Hao Su¹, **Ching-Tang Chen**^{2,3}, **Jyh-Horng Chen**^{2,3}, ¹Center for Translational Research in Biomedical Sciences, Chang Gung Memorial Hospital, Kaohsiung, Taiwan; ²Department of Electrical Engineering, National Taiwan University, Taipei, Taiwan; ³NTU Research Center for Medical Excellence, Division of Genomic Medicine, National Taiwan University, Taipei, Taiwan. Contact e-mail: chiralsu@gmail.com

Molecular imaging has become an indispensable technology in cancer research and clinical use. Among various molecular imaging modalities, magnetic resonance imaging (MRI) provides high spatial resolution and soft-tissue contrast in global view and optical microscopy supplies excellent time and spatial resolution in local view. In the previous study, nano-sized Fe_3O_4 particles showed significantly negative contrast in the MR imaging, and highly fluorescence signals in multi-photon imaging system. Therefore, the goal of this study is to combine magnetic resonance imaging and optical imaging system with multifunctional contrast agent to detect xenograft non-small cell lung cancer (NSCLC) murine model. In the in vitro imaging experiments, Prussian blue staining imaging and fluorescence microscope imaging (Shown in Figure.) showed different targeting efficiency in CL1-0. In the in vivo imaging, T_2 and T_2^* MR imaging showed more than 30% signal decrease. And the change of the signal intensity in the two adjacent slices reveals similar tendency in the time intervals from 0 to 5 hours after injection. It was proved the dynamic contrast change caused by nano-probe targeting by using histological cytochemistry staining. We have demonstrated that multi-functional contrast enhancement of Fe_3O_4 and conjugated with anti-EGFR antibody were capable of probing NSCLC cells in vitro and in vivo. And we also have investigated the biodistribution, and cytotoxicity of the nanoparticles. Multifunctional nanocontrast agent could hopefully not only serve as cancer detection and treatment but also used to predict disease prognosis in the future. By recombining the desired targeting moiety and various functional nanoparticles through bioconjugation, this modularly designed platform has the capability of enhancing the efficiency of targeted diagnosis and therapies for a wide spectrum of biomedical applications.



The third-harmonic generation (THG) imaging of CL-1 cells that were targeted by Fe_3O_4 @anti-EGFR antibody.

Presentation Number **0926A**

Poster Session 2c: In Vivo Studies & Development/Novel Use of Imaging Probes

Development of a Transgenic Rat for Dual Modality Imaging of Cell, Tissue and Organ Transplantation

Lode Goethals^{1,2}, Isabel Remory¹, Marleen Keyaerts^{1,3}, Christian Vanhove^{1,3}, **Tony Lahoutte**^{1,3}, ¹*In Vivo Cellular and Molecular Imaging, Free university of Brussels, Brussel, Belgium;* ²*Departement of radiology, University Hospital Brussels, Brussels, Belgium;* ³*Department of nuclear medicine, University Hospital Brussels, Brussels, Belgium. Contact e-mail: tony.lahoutte@uzbrussel.be*

Introduction: We combined bioluminescence and SPECT/PET imaging techniques by developing a dual modality reporter gene incorporating red shifted firefly luciferase (fLuc) and rat sodium iodide symporter (rNIS). We aimed at maintaining the high sensitivity of the bioluminescence signal, in combination with the exact 3D localization of the SPECT/PET signal. Both genes are under control of an ubiquitous promoter (CAGGS). This dual modality reporter gene was used to develop a transgenic rat expressing reporter proteins in every cell. **Material & Methods:** Transgenic rats were developed through pronuclear DNA injection technology in the Sprague-Dawley strain. Validation of the transgene insertion is based on initial PCR genotyping, followed by Southern Blot analysis. Animals, transgenic on PCR and Southern Blot analysis, were then used to determine biodistribution of ^{99m}Tc. ROI's were drawn over the thyroid, thigh and thorax regions. ROI analysis was confirmed by counting of organs in a gamma well counter. Functional expression of fLuc was monitored after intravenous and intraperitoneal injection of luciferine. **Results:** ^{99m}Tc biodistribution was altered in transgenic animals: demonstrating a higher absolute thyroid uptake and a more intense stomach delineation with diffusely higher background values and significantly lower urinary activity compared to wild types. These ROI data were confirmed with gamma well counting, showing higher activity (in % injected activity per gram) for all samples, except urine. Highest increase in activity was noted in the thyroid and in the small and large intestine. After intravenous injection of 10mg/kg luciferine, diffuse light output was generated. This positive signal was confirmed after IP injection of luciferine. **Conclusion:** These results suggest functional expression of both rNIS and fLuc in a transgenic rat. These results will be confirmed on the cellular level in the near future to quantify in vitro uptake dynamics of transgenic cells. Future steps are to determine the feasibility of tracking organs and cells, isolated and characterized from this transgenic animal in wild type animals.

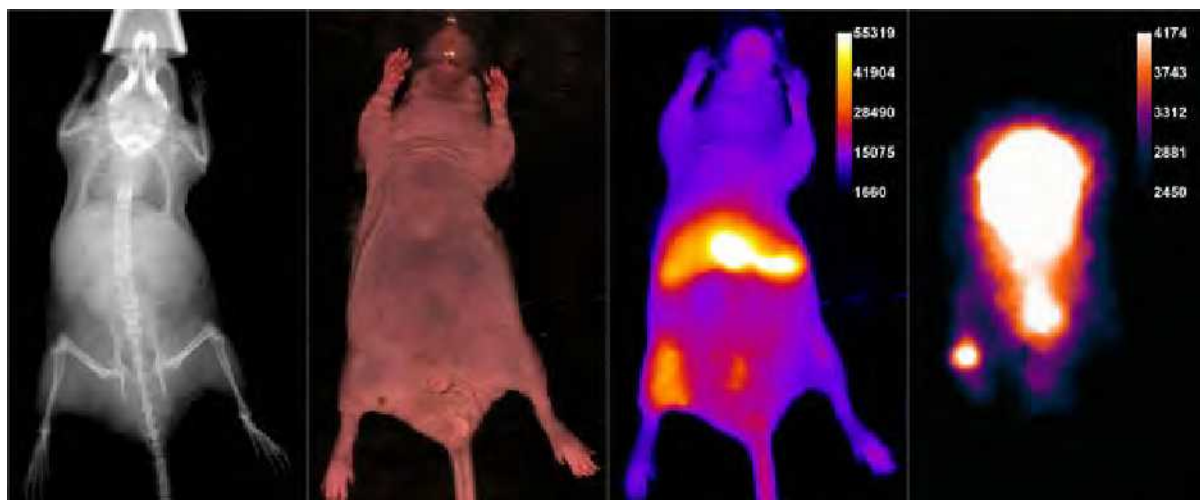
Presentation Number **0927A**

Poster Session 2c: In Vivo Studies & Development/Novel Use of Imaging Probes

Multimodal Imaging of Fluorescent and Radioisotopic Probes for *Staphylococcus aureus* Infection

Alexander White, Bradley D. Smith, **W. Matthew Leevy**, Chemistry and Biochemistry, University of Notre Dame, Notre Dame, IN, USA.
Contact e-mail: wleevy@nd.edu

Multimodal imaging is an effective strategy to maximize the information gathered from a given experimental mouse study. Usually, a single probe is used to gain molecular information, while a second image, like an X-ray, is acquired to provide anatomical information. The simultaneous use of multiple molecular probes is less common given the inherent challenge of matching their pharmacokinetic profiles and necessary imaging technology. The goal for this study was to validate that our fluorescent infection probes can be used in conjunction with FDG for in vivo multimodal imaging. Further, we wanted to validate that our equipment could perform this desired imaging task. We have recently synthesized and reported a second generation fluorescent probe for infection imaging known as SQR-DPA, which typically yields T/NT contrast ratios in excess of 5 within 3-6 hours. We hypothesized this would be compatible with FDG for the purposes of multimodal imaging. For this study, we co-injected a solution of SQR-DPA (8 nmol) and FDG (200 μ Ci) into a cohort of three mice bearing *S. aureus* infections (left leg). We subsequently acquired fluorescence and radioisotopic images in a continuous fashion for three hours at 10 minute intervals to simultaneously monitor the distribution of both probes. This was followed by an additional time point at 6 h. We observed significant co-registration of both the fluorescent and radioisotopic probes at the infection site as judged from image overlay analysis. In addition, we acquired images for anatomical information: an X-ray for gross anatomical changes in tissue or bone density, and an RGB composite for any surface indications of biological response. This work confirms that our fluorescent probe has a suitable optical clearance and targeting profile to be used in concert with FDG to image bacterial infection in a multimodal fashion. The use of multiple molecular probes is especially useful when anatomical imaging with X-ray, or surface detection of redness or swelling, provides limited insight into the biological process at hand.



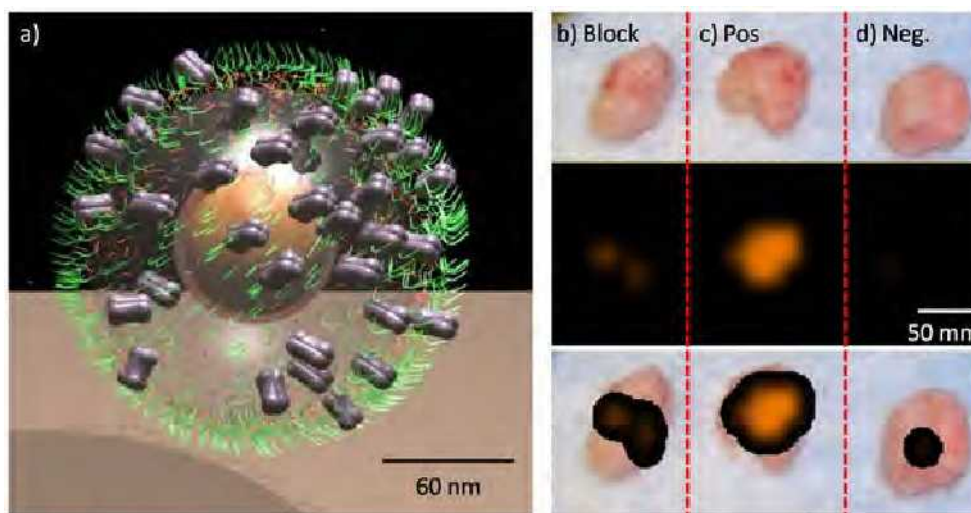
Presentation Number **0928A**

Poster Session 2c: In Vivo Studies & Development/Novel Use of Imaging Probes

Affibody-Functionalized, Multimodal Raman/Fluorescence Nanoparticles for Biomarker Profiling and Tumor Imaging

Jesse V. Jokerst¹, Zheng Miao¹, Cristina Zavaleta¹, Carmel T. Chan¹, Zhen Cheng^{1,2}, Sanjiv S. Gambhir^{1,2}, ¹Department of Radiology and Molecular Imaging Program at Stanford, Stanford University, Stanford, CA, USA; ²Department of Bioengineering and Bio-X, Stanford University, Stanford, CA, USA. Contact e-mail: jokerst@stanford.edu

Surface enhanced Raman spectroscopy (SERS) nanoparticles (NPs) offer picomolar sensitivity and extensive multiplexing in vivo. While these NPs' photo-physical properties are established, their use as biological probes requires further efforts. Here we report targeted hybrid NPs with tunable, multiplexed SERS signal, NIR fluorescence for high throughput cell assays, and selective binding to the cancer markers epidermal growth factor receptor (EGFR) and $\alpha\beta3$ integrin. The NPs contain a gold core/silica shell functionalized with affibodies—an intriguing ligand for molecular imaging purposes due to its small size, high affinity, and capacity to be rapidly reprogrammed to different biomarkers. These affibodies coat NPs via a hetero-bifunctional, PEG-based linker with controlled synthesis resulting in ~200 ligands per NP. The SERS NPs are optimized in cell culture via the fluorescence mode. For NP with EGFR-specific affibodies incubated with A431 cells, 6.3-fold greater signal was observed by flow cytometry versus isotype control NPs and 55-fold greater signal than non-targeted NPs. Blocking studies with free affibody (“cold probe”), followed by the targeted NP, decreased signal by 7.3-fold. NP detection in vivo after sub-cutaneous injection yielded detection limits of 30 pM and 6 pM via fluorescence and Raman, respectively. Next, the bioconjugated NPs labeled EGFR on A431 tumors excised from Nu/Nu mice. The SERS signal via EGFR-targeted NPs was 11 times higher than unlabeled particles ($n = 3$; $p < 0.05$). Tumors blocked with unlabeled affibody produced signal 6 times lower ($n = 3$; $p < 0.08$). Alternatively, the $\alpha\beta3$ integrins in U87MG cells were labeled via NPs with IgG antibody. Integrin signal (targeted NPs) to background (bare NPs) ratios of 25:1 and 13:1 were obtained for the particles via SERS and fluorescence, respectively. To the best of our knowledge, this is the first demonstration of affibody ligands deployed in tandem with multimodal SERS nanoparticles for biomarker identification. These results suggest that full utilization of SERS NPs will have significant potential for applications in living subjects.



a) The NP has a gold core and silica clad, fluorescent label (red), passivated by PEG (green), and covalently coated with EGFR-specific affibody (purple). This probe labeled A431 tumors *ex vivo*: b) tumor is blocked with free affibody prior to staining, which decreases Raman signal; c) EGFR labeling by NPs as indicated by Raman signal; d) untargeted NPs produce low non-specific binding.

Presentation Number **0929A**

Poster Session 2c: In Vivo Studies & Development/Novel Use of Imaging Probes

A Novel Scalable Multifunctional Nanoparticle for Drug Delivery, Targeting, and Imaging

Robert Prud'homme², Marian E. Gindy², Carlos N. Pacheco³, Carlos Rinaldi⁴, **Shahram Hejazi**¹, ¹Optimeos Life Science LLC, Radnor, PA, USA; ²Department of Chemical Engineering, Princeton University, Princeton, NJ, USA; ³Department of Chemistry, Princeton University, Princeton, NJ, USA; ⁴Department of Chemical Engineering, University of Puerto Rico, Mayaguez, Puerto Rico. Contact e-mail: hejasis@gmail.com

Nanoparticle materials present unique opportunities for improved medical imaging and diagnostics via optical fluorescence, and magnetic resonance imaging modalities as well as for in vivo imaging for drug discovery. The requirements of these applications are biocompatibility, high payload of contrast agent, precise control of particle size and robust surface functionality, which allow for selective localization of contrast agents at levels sufficient to provide enhanced detection in vivo. There are also significant commercial challenges in terms of reliable and cost effective manufacturing which would provide consistent functionality, especially in clinical setting. Here, we present a novel technology --Flash NanoPrecipitation - a controlled precipitation process that produces stable nanoparticles at high concentrations of encapsulated components using amphiphilic block copolymers to direct self-assembly. Uniform particles with tunable sizes from 25-500 nm can be prepared in an economical, scalable, and reliable manner. The key to the process is the control of time scales for micromixing, self-assembly, and nucleation and growth. The diffusion-limited assembly enables particles of complex composition to be formed. Using this technology, fluorescent imaging agents can be incorporated alone or in combination with drug compounds. A new class of fluorescent imaging compounds for long-wavelength fluorescent imaging is demonstrated that does not suffer from fluorescence quenching, thus enabling highly loaded, bright imaging nanoparticles. Pre-formed inorganic nanocrystals can be incorporated within biocompatible block copolymer core/shell-type Composite Nanoparticles (CNPs). Because the CNPs assemble spontaneously from solution by simultaneous desolvation of nanocrystals and amphiphilic copolymer components, explicit surface functionalization of the nanocrystals is not required, and the method can be applied to a variety of nanocrystals that lack appropriate conjugate surface chemistry. Examples of CNP formulations with superparamagnetic iron oxide nanocrystals as enhanced T2 contrast agents for magnetic resonance imaging will be presented. Also in vivo optical images of a novel fluorescent dye encapsulated inside the nanoparticle and its temporal biodistribution within mice will be presented. Finally, the functionalization CNP surfaces with disease-specific targeting ligands allows for directed delivery of the carriers. The technology provides a comprehensive and highly flexible platform for tailored preparation of multifunctional nanomaterials.

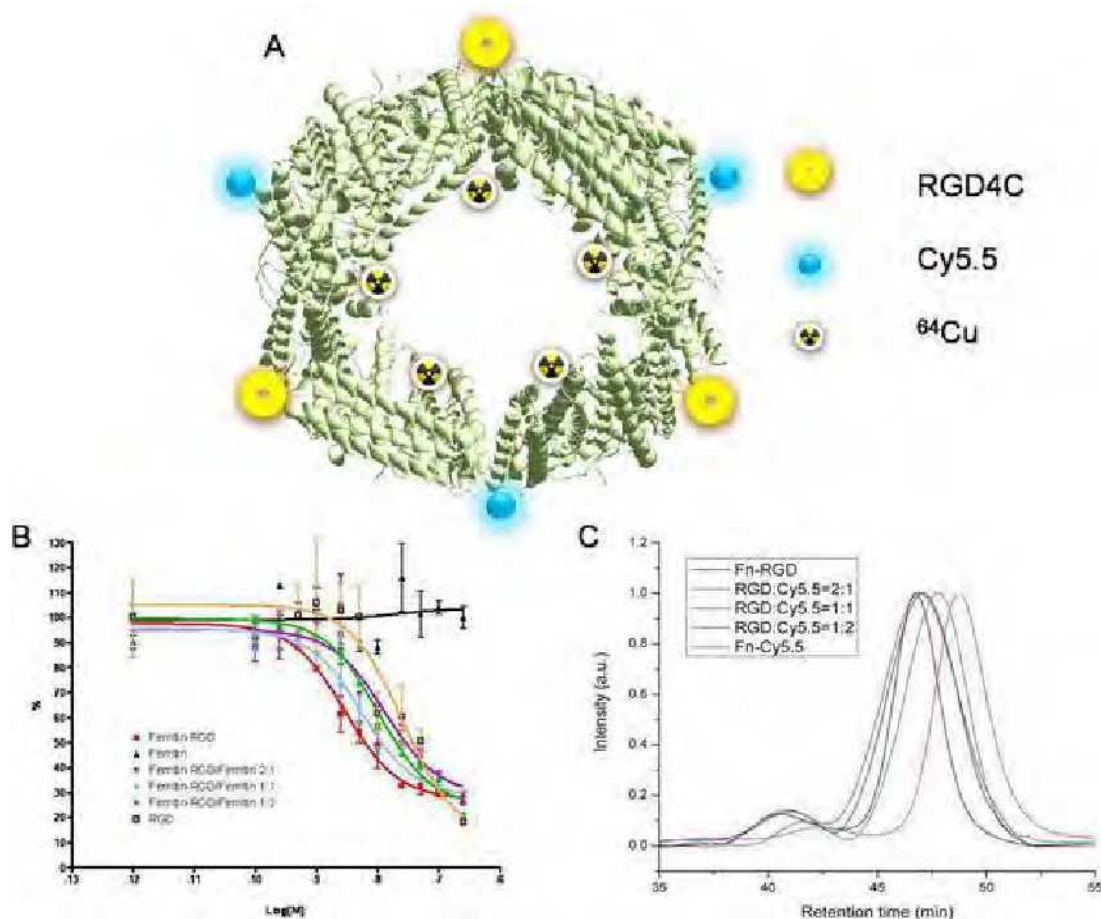
Presentation Number **0930A**

Poster Session 2c: In Vivo Studies & Development/Novel Use of Imaging Probes

Chimeric ferritin nanocages for NIRF/PET dualmodal imaging

Xin Lin, Jin Xie, Gang Niu, Gang Liu, Lei Zhu, Min Yang, Xiaoyuan Chen, National Institutes of Health, Bethesda, MD, USA. Contact e-mail: Lin.Xin@nih.gov

Ferritin is a multi-subunit protein with a hollow interior cavity. It is well-known for its ability to store iron in mammals, and has been investigated as reaction carriers to prepare a number of metal nanoparticles, such as iron oxide, Pd, Ag, Cu, Ni, Co, CoPt and Au/Pd bimetallic alloy. More recently, it was reported that ferritin cages can be broken down in acid environment and reassembled when neutral pH is restored. These interesting features make ferritin a powerful, capacious nanoplatform, with potential in a wide spectrum of applications, such as serving as multi-modality imaging probes. In the present study, we prepared a series of chimeric ferritin cages that are tagged with Cy5.5 and RGD motifs at various ratios. It was achieved by decomposing ferritin-Cy5.5 and ferritin-RGD4C fusion proteins at different ratios in acid environment, followed by self-resembling at neutral pH. The formation of chimeric nanocage was confirmed with size exclusion chromatography, and the binding affinities of the composite ferritin were evaluated with MDA-MB-435 cells using ¹²⁵I-echistatin as the competitive radioligand. More interestingly, the decomposing-reassembling strategy was found efficient to load ⁶⁴Cu into the inner cavity of the ferritin nanocages. The loaded ⁶⁴Cu is stable against leakage and transchelation in plasma and during circulation, making such approach a convenient yet reliable means to confer radioactivity to the ferritin nanoplatform. We then applied such ⁶⁴Cu-labeled composite ferritin to integrin positive MDA-MB-435 and U87MG tumor models and assessed the tumor targeting efficacy by both NIRF and PET imaging. Tumor uptake was observed in the U87MG model, which was attributed to its high integrin $\alpha\beta_3$ expression and its rich tumor vasculature.



A. Schematic structure of ⁶⁴Cu-labeled chimeric ferritin cage self-reassembled from ferritin-Cy5.5 and ferritin-RGD4C. B. Cell binding assay of peptide cyclo(RGDyk) and a series of composite ferritin with various ferritin and ferritin-RGD4C ratios. C. HPLC spectra of a series of composite ferritin with various ferritin-Cy5.5 and ferritin-RGD4C ratios.

Presentation Number **0931A**
 Poster Session 2c: In Vivo Studies & Development/Novel Use of Imaging Probes

The Use of Oleyl-Chitosan Nanoprobe to Encapsulate Iron Oxide Nanoparticles for Tumor Imaging In Vivo

Chang-Moon Lee, DooRye Jang, Hwan-Jeong Jeong, Su-Jin Cheong, Eun-Mi Kim, Sun-Hee Kim, Min-Hee Jeong, Dong Wook Kim, Seok Tae Lim, Myung-Hee Sohn, Department of Nuclear Medicine, Chonbuk National University Medical School, Jeonju, Republic of Korea. Contact e-mail: commy@hanmail.net

Oleic acid-conjugated chitosan (Oleyl-chitosan) is a powerful platform for encapsulating oleic acid-decorated iron oxide nanoparticles (IONs) and is a good MRI probe. In this study, we describe the usefulness of oleyl-chitosan as a stabilizer of IONs. Furthermore, we investigated tumor accumulation of IONs-oleyl-chitosan nanoparticles through the enhanced permeability and retention (EPR) effect in vivo. Oleyl-chitosan can self-assemble into core-shell structures in aqueous solution and provides an effective core compartment for loading IONs. IONs-oleyl-chitosan nanoparticles show enhanced MRI sensitivity on an MR scanner. Cy5.5 was coupled to the oleyl-chitosan conjugate for in vivo optical imaging. After intravenous injection of IONs-Cy5.5-oleyl-chitosan nanoparticles in U87MG tumor-bearing mice, both NIFR and MR imaging showed detectable signal intensity and enhancement in tumor tissues via EPR effect. Tumor accumulation of the nanoparticles was confirmed through ex vivo fluorescence imaging and Prussian blue staining of tumor tissues. We conclude that the IONs-Cy5.5-oleyl-chitosan nanoparticles are a highly effective imaging probe for detecting tumors in vivo.

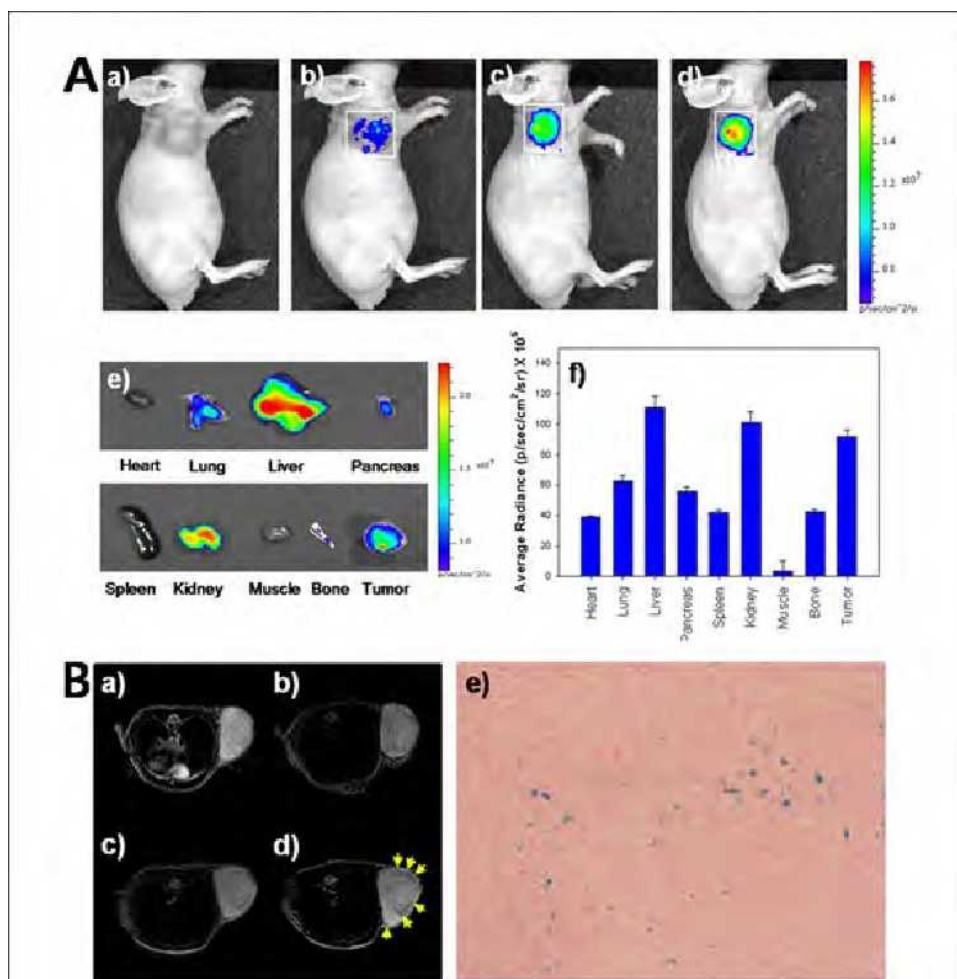


Figure A. In vivo NIFR images of U87MG-bearing mice (a) before injection and at (b) 1 h, (c) 3 h, and (d) 5 h after injection of ION-Cy5.5-oleyl-chitosan nanoparticles. (e) Ex vivo NIFR images of major tissues excised from the mice at 5 h post-injection. (f) A quantification of the ex vivo tissues was recorded as average radiance (p/s/cm²/sr). All data are represented as mean±S.D. (n=3). Figure B. In vivo T2-weighted MR images of U87MG-bearing mice (a) before and at (b) 1 h, (c) 2 h, and (d) 3.5 h after injection of ION-Cy5.5-oleyl-chitosan nanoparticles on a 1.5 T MR scanner. Yellow arrows in the dark area of the tumor tissue indicate accumulation of ION-Cy5.5-oleyl-chitosan nanoparticles. (e) Prussian blue staining image of tumor tissues at 5 h post-injection.

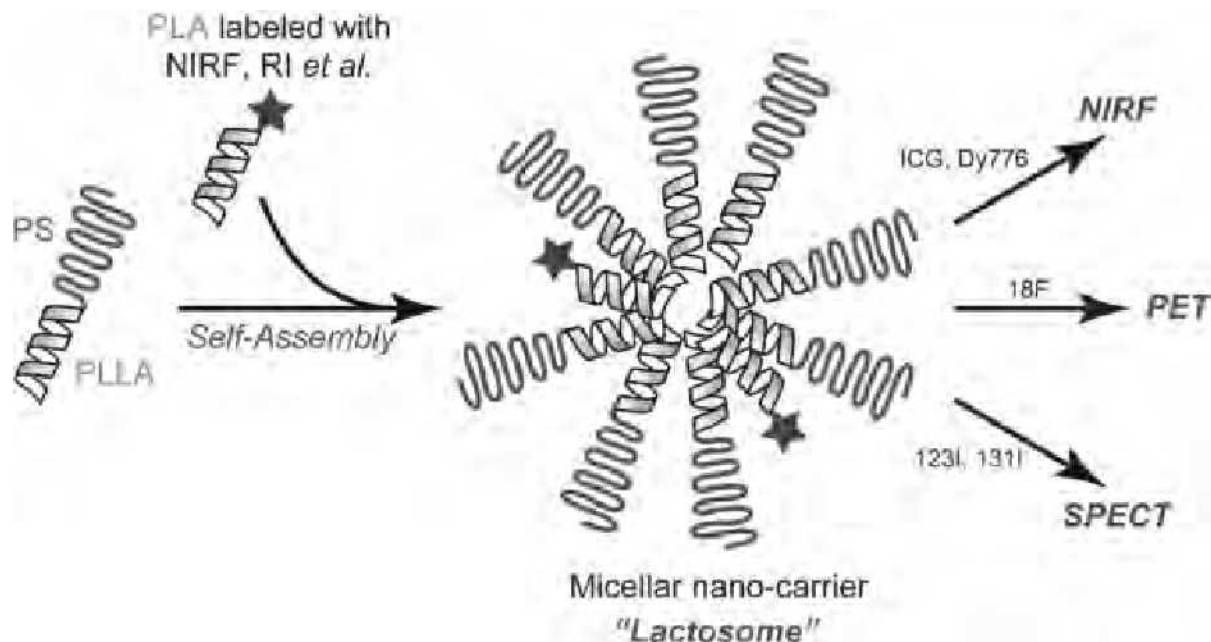
Presentation Number **0933A**

Poster Session 2c: In Vivo Studies & Development/Novel Use of Imaging Probes

“Lactosome” a potential nano-ordered carrier for molecular imaging composed of a poly(L-lactic acid)- *block* -poly(sarcosine) amphiphilic polydepsipeptide and poly(lactic acid) derivatives

Akira Makino^{1,2}, Ryo Yamahara¹, Isao Hara¹, Eri Takeuchi¹, Eiichi Ozeki¹, Kensuke Kurihara³, Shinae Kizaka-Kondoh⁴, Fumihiko Yamamoto^{3,5}, Akira Shimizu³, Shunsaku Kimura^{2,3}, ¹Technology Research Laboratory, Shimadzu Corporation, Kyoto, Japan; ²Department of Material Chemistry, Graduate School of Engineering, Kyoto University, Kyoto, Japan; ³Translational Research Center, Kyoto University, Kyoto, Japan; ⁴Department of Biomolecular Engineering, Graduate School of Bioscience and Biotechnology, Tokyo Institute of Technology, Yokohama, Japan; ⁵Department of Radiopharmacy, Tohoku Pharmaceutical University, Sendai, Japan. Contact e-mail: makino@peptide.polym.kyoto-u.ac.jp

“Lactosome” is a molecular assembly composed of hydrophobic helical poly(L-lactic acid) (PLLA) and hydrophilic poly(sarcosine) (PSar) amphiphilic block polydepsipeptide. By controlling the hydrophilic-hydrophobic balance of the polymer, molecular assembly having various morphologies can be prepared in aqueous buffered solution. Among these molecular assemblies, polymeric micelle having a diameter of 30 nm shows high escape ability, stealth property in other word, from reticuloendothelial system (RES), and accumulated to the tumor region by the enhanced permeation and retention (EPR) effect. This is because the high density of hydrophilic PSar chains so called polymer brush around the molecular assemblies contributes to the inhibition from RES recognition. Lactosome is normally prepared by using a “film method”. We revealed that lactosome labeled with various kinds of imaging agents can be prepared by only mixing a chemically modified poly(lactic acid) (PLA) chain to the film of PLLA-*block*-PSar, and diameter of the resulting lactosome also can be controlled by the mixing ratio. On this presentation, synthetic method of PLA labeled with near-infrared fluorescein (NIRF) compound or radioisotopes (RI), and preparation of the NIRF or RI labeled lactosome are discussed. Then, *in vivo* imaging of NIRF (indocyanine green) and RI (18F, 123I, and 131I *et al.*) labeled lactosomes was examined by using optical and PET/SPECT imaging techniques, respectively. As the result, these modified lactosomes keep high stealth property, and *in vivo* disposition of lactosome was not also influenced by the labeled imaging agents. PSar chain is considered to have advantages against poly(ethylene glycol) (PEG) on biodegradability and the equipped metabolic pathway for sarcosine. Therefore, lactosome is expected to be a potential nano-ordered carrier for drug and imaging agent delivery.



Presentation Number **0934A**

Poster Session 2c: In Vivo Studies & Development/Novel Use of Imaging Probes

A Novel Approach for Cell-penetration of Gd³⁺-based MRI Contrast Agents

Takehiro Yamane^{1,2}, **Kenjiro Hanaoka**^{1,2}, **Yasuaki Muramatsu**^{1,2}, **Tetsuo Nagano**^{1,2}, ¹*Graduate School of Pharmaceutical Sciences, The University of Tokyo, Tokyo, Japan;* ²*CREST, JST, Tokyo, Japan. Contact e-mail: ff087019@mail.ecc.u-tokyo.ac.jp*

MRI is a useful tool for medical care or in vivo imaging in research, because MRI can provide the three-dimensional images inside the body noninvasively with high resolution. On the other hand, gadolinium ion (Gd³⁺) complexes are commonly used as a MRI contrast agent, which enhance contrast of MR images. Recently, many researchers have challenged to image specific diseases or biological processes by functionalizing Gd³⁺-based MRI contrast agent. To achieve this purpose, one of approaches is to develop cell-permeable contrast agents, which accumulate target cells selectively and enable to image with high sensitivity on MRI. Some cell-permeation methods such as cell penetrating peptides (CPPs) have been reported, however, these methods still have some problems about uptake efficiency, leakage from cells, sensitivity in MRI, etc. To resolve these problems, we focused attention to fluorescent dyes. Because some fluorescent dyes can easily penetrate the cell membrane, fluorescent dyes are used widely for fluorescence imaging in living cells or animals. Therefore, we tried to internalize Gd³⁺ complexes into the cells by utilizing cell-permeable characteristics of fluorescent dyes. We carried out the screening of fluorescent dyes which can internalize Gd³⁺-DOTA (DOTA = 1,4,7,10-tetraazacyclododecane-1,4,7,10-tetraacetate) complex into the cells. Among these compounds, Gd³⁺ complex conjugated with boron dipyrromethene (**BDP-Gd**) and Cy7 dye (**Cy7-Gd**) showed the efficient uptake and significant enhancement of MR signal of HeLa cells in the T₁-weighted MR image. Furthermore, we compared the efficiency of cell uptake of **BDP-Gd** and **Cy7-Gd** with **R₈-Gd**, which is already reported cell-penetrate octaarginine-conjugated Gd³⁺ complex, by using ICP-MS. **BDP-Gd** showed almost same uptake in HeLa cells as that of **R₈-Gd**, and **Cy7-Gd** showed higher uptake compared with **R₈-Gd**. To examine the relationship between the chemical structure of dye-Gd conjugates and the cell-permeability, we synthesized various **Cy7-Gd** derivatives and the efficiency of cell-uptake was measured by FACS analysis. The results indicated that highly hydrophobic and non-anionic dyes should be suitable unit for the cell-penetration of Gd³⁺ complex. Furthermore, distribution and contrast effect of cell-permeable or cell-impermeable **Cy7-Gd** derivatives in mice were also investigated.

Presentation Number **0935A**

Poster Session 2c: In Vivo Studies & Development/Novel Use of Imaging Probes

A9 PSMA Aptamer Hybrid-Functionalized thermally cross-linked superparamagnetic iron oxide nanoparticles (TCL-SPION) for Combined Prostate Cancer Imaging and Therapy

Mi Kyung Yu¹, **Yong Yeon Jeong**², **Sangyong Jon**¹, ¹*Life science, Gwangju Institute of Science and Technology, Gwangju, Republic of Korea;* ²*Diagnostic Radiology, Chonnam National University, Gwangju, Republic of Korea.* Contact e-mail: [ymk@gist.ac.kr](mailto:y mk@gist.ac.kr)

We developed A9 prostate specific membrane antigen (PSMA) aptamer, a proficient targeting ligand for PSMA with low nanomolar affinity, functionalized superparamagnetic iron oxide nanoparticles (SPION) as combined prostate cancer imaging and therapeutic agent. We firstly coated DNA oligonucleotides onto the thermally cross-linked superparamagnetic iron oxide nanoparticles (TCL-SPION) and the aptamer capture oligonucleotide-derivatized TCL-SPION were then hybridized with CGA extended A9 PSMA aptamers. The prepared A9 PSMA aptamer-hybrid TCL-SPION indicated the mean hydrodynamic size of 74 nm and approximately 4.6 wt% of aptamers were incorporated onto the nanoparticles. Those nanoparticles exhibited preferential binding toward target cancer cells (LNCaP, PSMA+) compared to non-target cancer cells (PC3, PSMA-) analyzed by T2-weighted MR imaging (3T). To impart therapeutic ability, doxorubicin (Dox; anti-cancer drug) was loaded to the A9 PSMA aptamer-hybrid TCL-SPION by intercalating into double-stranded regions of the complementary sequences (CGA) or tertiary structure of the aptamers. The amount of Dox loaded onto the A9 PSMA aptamer-hybrid TCL-SPION was 1.5 wt%, determined by monitoring of fluorescence quenching process, and the loading efficiency was almost 95 %. The resulting Dox@A9 PSMA aptamer-hybrid TCL-SPION showed differential cytotoxicity in LNCaP cells compared to that incubated in PC3 cells. These results suggest that Dox@A9 PSMA aptamer-hybrid TCL-SPION have potential for use as targeted imaging and therapeutic agents for prostate cancer.

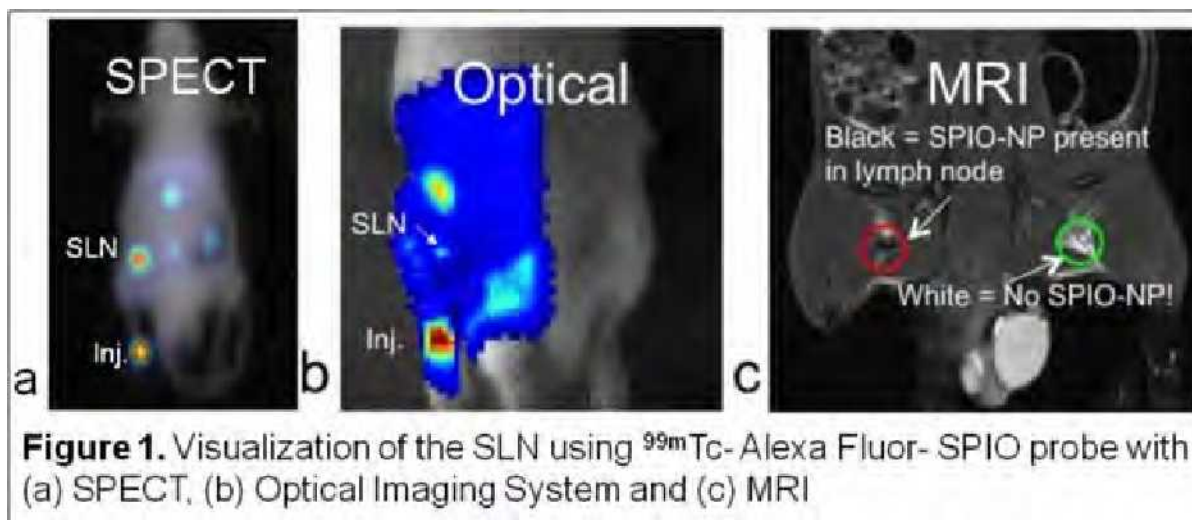
Presentation Number **0936A**

Poster Session 2c: In Vivo Studies & Development/Novel Use of Imaging Probes

99mTc- Alexa Fluor - SPIO aiming for SPECT, Optical and MR imaging of Sentinel Lymph Node in breast cancer and malignant melanoma

Renata Madru¹, Pontus Kjellman², Pontus Svenmarker³, Karin Wingårdh¹, Sarah Fredriksson², Anders Orborn¹, Stefan Andersson-Engels³, Christian Ingvar⁴, Linda Knutsson¹, Johan Olsrud⁵, Jimmy Latt⁵, Freddy Sthalberg¹, Sven-Erik Strand¹, ¹Medical Physics, Lunds University, Lund, Sweden; ²Genovis AB, , Lund, Sweden; ³Physics, Lunds University, Lund, Sweden; ⁴Surgery, Skane University Hospital, Lund, Sweden; ⁵Center for Medical Imaging and Physiology, Skane University Hospital, Lund, Sweden. Contact e-mail: renata.madru@med.lu.se

Purpose: Quantitative and high resolution imaging in hybrid systems is warranted. In order to meet this, a superparamagnetic iron oxide (SPIO) based probe with magnetic, radioactive and fluorescent properties has been developed in this study. The final aim is to be able to image SLN thereby guiding the surgeon to find SLN in breast cancer and malignant melanoma patients. **Material and Methods:** Synthesized SPIO:s with a diameter of 15-30nm were coated with polyethylene glycol containing primary amino groups and labeled with Alexa Fluor 647. Subsequently, the nanoparticles were labeled with ^{99m}Tc by stannous reduction. The labeling efficiency and stability of the probe was determined by instant thin layer chromatography. An amount of 0.07-0.1ml of the probe (40-65MBq, 3mgFe/ml) was injected subcutaneously in the back pad of Wistar rats. Four hours post injection the animals were sacrificed and imaged with SPECT, MR and optical imaging system. In order to study the biodistribution each animal was dissected and organs: lymph nodes, kidneys, spleen, liver and the back pad containing the injection site (IS) were removed, weighed and measured for radioactivity. The nanoparticles distribution within the SLN was studied by digital autoradiography. **Results:** The labeling efficiency of the SPIO-Alexa Fluor with ^{99m}Tc was found to be over 99% 6h after the labeling process. The SPECT, MR and Optical systems clearly showed the lymph nodes. About 6.5% of the injected probe leaved the IS whence 3.3% was found in SLN, 1.4% in 2:nd LN, 1.4% in liver and about 0.4% in kidneys. The autoradiography images show more activity in cortex of the SLN, also the place where metastases appear. **Conclusion:** SPECT offers high-sensitivity while MRI offers anatomical information and high resolution. The optical tag is used for fluorescent guided resection of the SLN. Combining functional and anatomical information can lead to new therapeutic strategies. The obtained results from our study showed that the probe is suitable for SNL imaging.



Presentation Number **0937A**

Poster Session 2c: In Vivo Studies & Development/Novel Use of Imaging Probes

Cu64-ATSM labeling and preclinical animal test

*Tsai-Yueh Luo, I-Chang Tang, Po-Ching Cheng, Wu-Jyh Lin, Lie-Hang Shen, **Chung-Hsin Yeh**, Isotope Application Division, Institution of Nuclear Energy Research, Longtan Township, Taoyuan County, Taiwan. Contact e-mail: ycha111@ms7.hinet.net*

This aim of study is to evaluate the ability of Cu64-ATSM accumulation in LL2 hypoxia tumor model. We designed several important methods to test the characteristics of Cu64-ATSM in hypoxia tissue, including autoradiography, bio-distribution, micro-PET image, micro-ultrasound, pathology section, immune immune-tissue stain examination, quantization of micro-PET image data. Our animal experimental results demonstrate that Cu64-ATSM could accumulate in hypoxia region of LL2-induced tumor. The quantization of micro-PET image data and immune immune-tissue stain examination data confirm the Cu64-ATSM that labeling in INER could accumulate in hypoxia tissue about 20~50 μ Ci/ml that quarter of total injection activity.

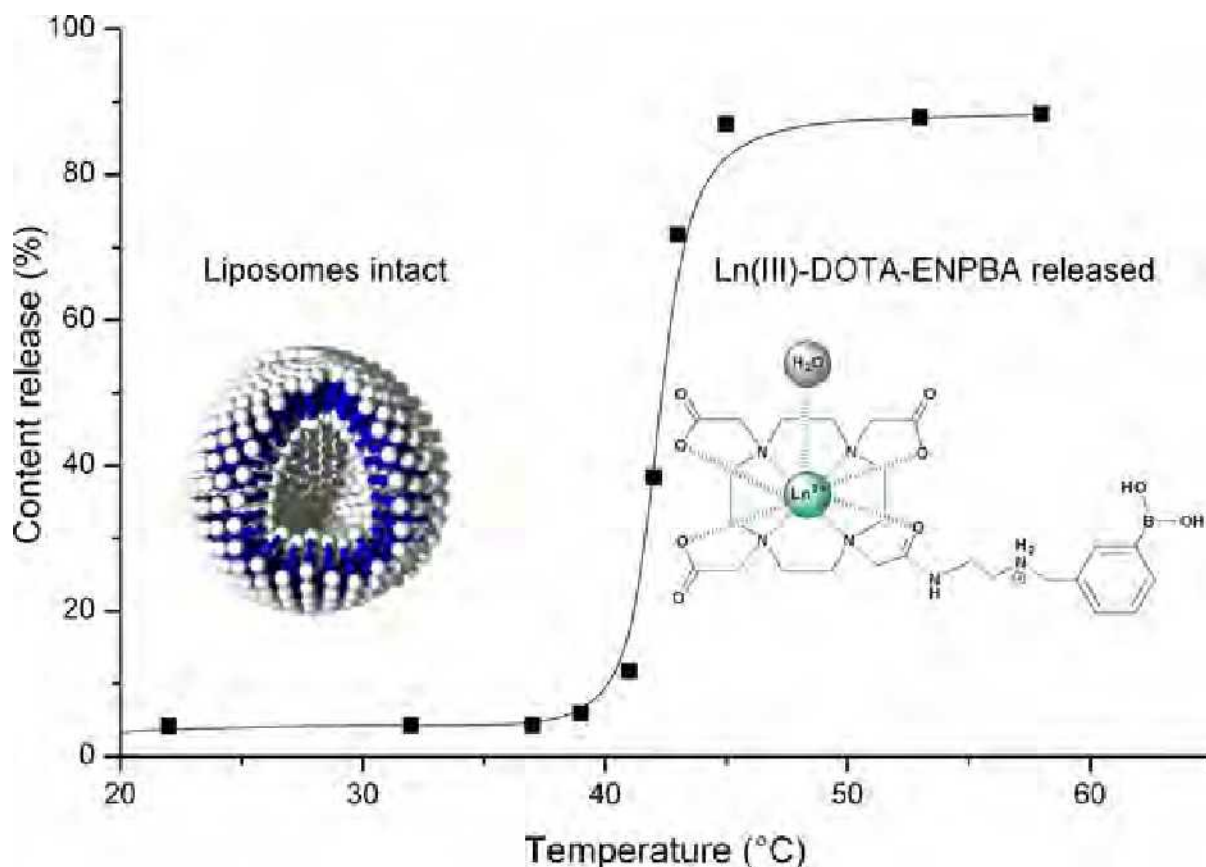
Presentation Number **0938A**

Poster Session 2c: In Vivo Studies & Development/Novel Use of Imaging Probes

Temperature-triggered liposomal delivery of a tumor targeting agent, Ln(III)-DOTA-phenylboronate

Kristina Djanashvili¹, **Timo ten Hagen**², **Blangé Roy**¹, **Debby Schipper**², **Joop A. Peters**¹, **Gerben A. Koning**², ¹*Department of Biotechnology, Delft University of Technology, Delft, Netherlands;* ²*Department of Surgery, Erasmus Medical Center, Rotterdam, Netherlands. Contact e-mail: k.djanashvili@tudelft.nl*

Liposomes, capable of temperature-triggered content release at the site of interest, can be of great importance for imaging and therapy of tumors. The delivery of imaging agents or therapeutics can be improved by application of liposomes with a gel-to-liquid phase transition temperature suitable for mild hyperthermia (41-43°), and by prolonging circulation time by incorporation of lipids containing polyethyleneglycol moieties. Still, the rapid wash out of the delivered material from the tumor tissue is a major obstacle for both imaging and therapy. In this study, we developed an optimized temperature sensitive liposomal system to be used with mild hyperthermia: highly stable at physiological temperature and with a sharp transition of the bilayer at 41.5 °C, with subsequent rapid release of entrapped compounds such as calcein or tumor cell-targeting contrast agents. Intravital microscopy on calcein/rhodamine containing liposomes was applied to demonstrate the applicability of this system in vivo. The calcein loaded liposomes were injected i.v. into nude mice with a human BLM melanoma tumor implanted in a dorsal skin chamber. Arrival of the liposomes at the tumor site and content release after temperature increase were monitored. The results demonstrated not only accumulation of the liposomes at the tumor site, but also a massive release of calcein after increase of temperature to 41 °C. Versatility of the thermosensitive liposomes was further demonstrated by encapsulation of tumor cell-targeting DOTA-phenylboronate conjugate and its release at elevated temperatures. The DOTA ligand in this system is able to chelate a variety of metals suitable for both diagnostic and therapeutic applications, whereas the phenylboronate function is able to target these specifically to tumor cells through a covalent binding with sialic acid moieties over-expressed on their surface upon heat-triggered release from the liposomal carrier.



Presentation Number **0939A**

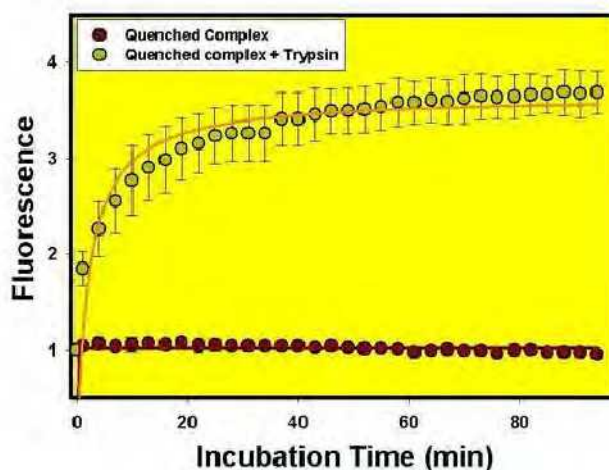
Poster Session 2c: In Vivo Studies & Development/Novel Use of Imaging Probes

Fluorescence Quenching of Near-IR dye by Neutravidin PEGylated Gold Nanoparticles

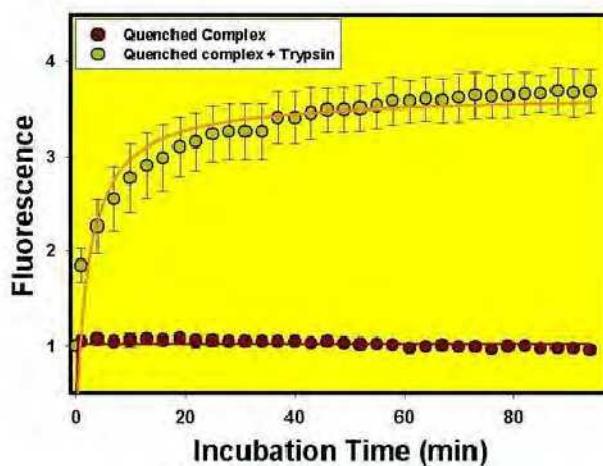
Rao V. Papineni, Hans F. Schmitthenner, Tao Ji, Jingyi Pan, Carestream Molecular Imaging, Carestream Health, Inc., Woodbridge, CT, USA. Contact e-mail: rao.papineni1@carestreamhealth.com

Activatable probes are rapidly becoming a smart and essential tool in optical imaging of in vivo molecular targets. Addition of multimodal reporting capability to the technology along with simpler chemistry to attach substrate moieties will augment the process of developing activatable probes for novel molecular targets and pathways. In pursuit of achieving this goal, we developed a system where an organic dye conjugate can be linked by a simple step of incubation with gold nanoparticles. Biotin was conjugated to a water soluble, near-infrared (NIR) tricyanocyanine, cyclic enamine-functionalized dye. Dose-dependent fluorescence quenching was observed when biotin-NIR dye was linked to monodispersed neutravidin PEGylated gold nanoparticle (20nm). This process is reversed by the enzymatic cleavage of neutravidin by trypsin. As expected, quenching was not observed when incubating the biotin-NIR dye complex with trypsin treated neutravidin PEGylated gold nanoparticle. The high biotin-binding affinity of this fluorescence activatable system can be exploited by incorporating novel peptide substrates to the biotin-dye complex. The resultant quenching and unquenching processes of the neutravidin PEGylated gold nanoparticle and biotin-dye conjugated substrates can be monitored in vivo by NIR fluorescence, computed tomography CT and planar bench top X-ray modalities. Further, to enhance the selectivity of the activatable probe a biotinylated targeting macromolecule can be linked along with the substrate-dye complex.

Quenched Complex of NIR Biotin-Dye & Neutravidin PEGylated Gold Nanoparticle



Quenched Complex of NIR Biotin-Dye & Neutravidin PEGylated Gold Nanoparticle



Presentation Number **0940A**

Poster Session 2c: In Vivo Studies & Development/Novel Use of Imaging Probes

DESIGN, SYNTHESIS AND EVALUATION OF NOVEL lacZ RESPONSIVE ENHANCED Gd-BASED 1H MRI AGENTS

Jian-Xin Yu, Ralph Mason, Radiology, The University of Texas Southwestern Medical Center at Dallas, Dallas, TX, USA. Contact e-mail: Jian-Xin.Yu@UTSouthwestern.edu

Gene therapy holds great promise for treating cancer and has been successfully exploited in several clinical trials. A major current obstacle to implementation is to establish a method of assessment of therapeutic gene expression in terms of heterogeneity and longevity in tissues. The lacZ gene encoding beta-galactosidase (beta-gal) has been well characterized and extensively used as reporter gene in immunosorbent assays, in situ hybridizations, classification of mycobacteria and gene expression studies. A variety of lacZ gene reporters has been developed, such as colorimetric, fluorescent, chemiluminescent, radiotracers for PET or SPECT, 19F MRS/MRI, and MRI probes, though most have only been utilized in vitro, with a very few successful applications in vivo so far. We now report the exploration of a novel approach to lacZ responsive Gd-based 1H MRI agents, generating high relaxivity by forming higher molecular weight and rigidity of the complexes. We anticipate that, following cleavage by beta-gal, the released and activated aglycone, which is an Fe³⁺-ligand will spontaneously trap endogenous Fe³⁺ at the site of enzyme activity forming a highly stable complex, exhibiting restricted motion of the Gd³⁺ chelates enhancing relaxivity and providing contrast based on gene (viz. enzyme) stimulated local accumulation. We will present the design, synthesis and evaluation of 2-[(beta-D-galactopyranosyl)oxy]-5-{N,N-bis[2-[N',N'-bis(carboxymethyl)amino]ethyl]benzene} benzaldehyde substituted benzoylhydrazones, and the characterization of these target molecules with beta-gal reaction, the Fe-complex formation, and the resulting relaxation changes.

Presentation Number **0941A**

Poster Session 2c: In Vivo Studies & Development/Novel Use of Imaging Probes

A “Click Chemistry” Approach for the Efficient Synthesis of lacZ Responsive Enhanced 1H MRI Agents

Jian-Xin Yu, Ralph Mason, Radiology, The University of Texas Southwestern Medical Center at Dallas, Dallas, TX, USA. Contact e-mail: Jian-Xin.Yu@UTSouthwestern.edu

In the last two decades, magnetic resonance imaging (MRI) has become one of the most powerful and widespread diagnostic technique in medicine, particularly, with the use of Gd-based contrast agents. Recently, many attempts have been made to utilize MRI to detect gene expression. The lacZ gene encoding beta-galactosidase (beta-gal) has been well characterized and extensively used with applications ranging from molecular biology to small animal investigations and to clinical trials including assays of clonal insertion, transcriptional activation, protein expression, and protein interaction. So far, a variety of reporters including colorimetric, fluorescence, chemiluminescence, radiotracers for positron emission tomography or single-photon emission computed tomography, MRI probes, and ¹⁹F-NMR approaches are already developed. We now report the exploration of a novel approach for detection of lacZ gene using 1H MRI agents, by click chemistry to introduce Gd³⁺ signal part to the prodrugs of galactose-conjugated iron-chelators, which are anticipated, trapping Fe³⁺ to form a highly stable complex, restricting motion of the Gd³⁺ chelates and providing local accumulation upon the reaction with beta-gal, then generating high relaxivity by forming higher molecular weight and rigidity of the complexes.

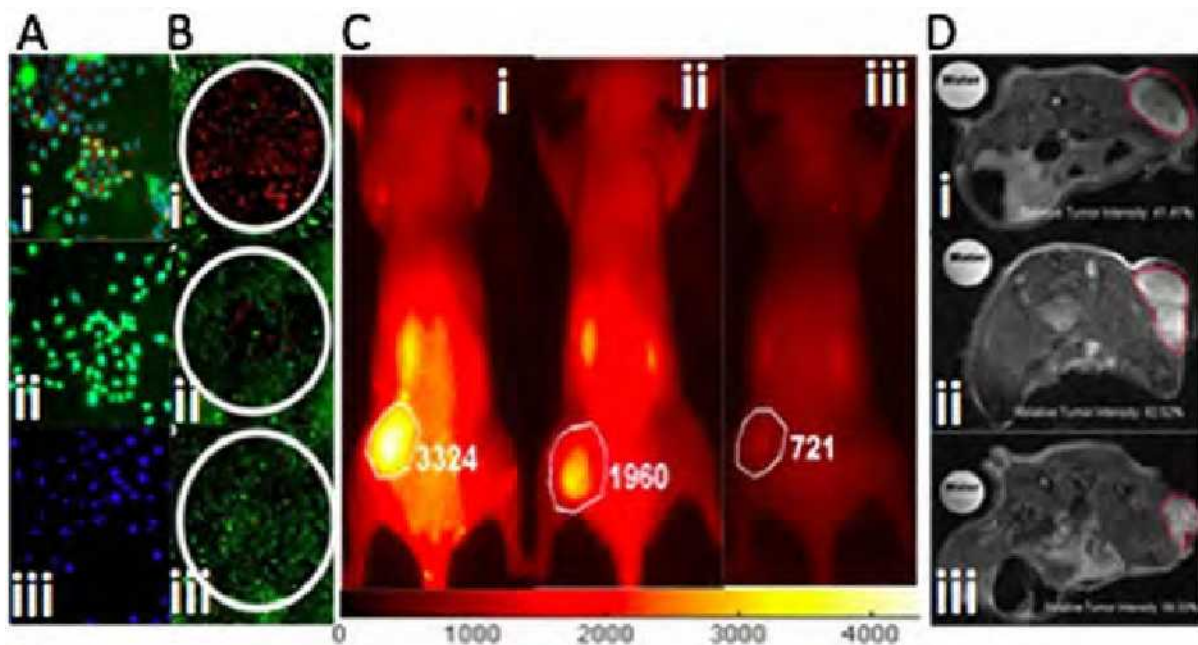
Presentation Number **0942A**

Poster Session 2c: In Vivo Studies & Development/Novel Use of Imaging Probes

Multimodal Theranostics of Pancreatic Cancer with Gold Nanostructures

Wenxue Chen^{1,2}, **Marc Bartels**¹, **Rizia Bardhan**³, **Carlos J. Perez-Torres**⁴, **Ciceron Ayala-Orozco**³, **Baoan Ji**⁵, **Robia G. Pautler**⁴, **Naomi J. Halas**^{3,6}, **Amit Joshi**¹, ¹Radiology, Baylor College of Medicine, Houston, TX, USA; ²Obstetric & Gynecology, The Fourth Hospital of Hebei Medical University/Hebei Province Tumor Hospital, Shijiazhuang, China; ³Chemistry, Rice University, Houston, TX, USA; ⁴Molecular Physiology and Biophysics, Baylor College of Medicine, Houston, TX, USA; ⁵Cancer Biology, The University of Texas MD Anderson Cancer Center, Houston, TX, USA; ⁶Electrical and Computer Engineering, Rice University, Houston, TX, USA. Contact e-mail: wenxuec@bcm.edu

Novel magnetofluorescent theranostic nanocomplexes for imaging/therapy of pancreatic cancer overexpressing Neutrophil gelatinase-associated lipocalin (NGAL) are reported. Methods: Silica core gold nanoshells (GNS) resonant at 810 nm were encapsulated in silica epilayers doped with iron oxide and NIR dye ICG, and conjugated with antibodies targeting NGAL. Human pancreatic cancer cells AsPC-1 were employed for in vitro and in vivo studies in nude mice xenografts. Three groups were: (i) Cells/mice treated with GNS-antiNGAL, (ii) Cells/mice blocked with pre-treatment with free anti-NGAL, (iii) Cells/mice treated with unconjugated GNS. Animals were imaged at 0.3, 2, 4, 24, 48, 72 hours post injection via both NIR and T2 weighted MR imaging. Results: We demonstrate for the first time that the GNS-conjugated-anti-NGAL can specifically image pancreatic cancer cells in vitro and in vivo, and obtain highly specific cancer cell death via NIR therapy. Results are summarized in Fig.1. GNS-anti-NGAL specific binding occurred predominantly around the cell membrane (A.i, shown in red color). The two controls: blocking NGAL with pretreatment with free antibody (A.ii), and incubation with unconjugated GNS (A.iii) confirm the specificity. After the photothermal therapy with 3.72 W/cm² power, Cell death was significantly observed in AsPC-1 cells labeled with GNS-conjugated-NGAL (Fig. B.i) with dead cells stained in red. Therapy had minimal effect in controls (B.ii, and B.iii). In Vivo NIR imaging of mice with xenografts (Fig. 1C) verifies maximal uptake of GNS in tumors when conjugated with anti-NGAL (C.i) compared to the two controls at 24 hrs post injection. T2 weighted MR imaging of tumor interior in Fig. 1D further demonstrates GNS-antiNGAL internalization (D.i) via the darkening of the image compared to water control. The T2 image intensity in tumor core drops to 41% from pre-injection image compared to 69% for bare GNS treatment (D.iii), and only 82% when receptors are blocked by pre-injecting free antibody (D.ii).



A: In vitro imaging, B. Photothermal therapy, C In vivo NIR imaging, and D. MR imaging with (i) GNS-antiNGAL, (ii) NGAL blocking, (iii) bare GNS.

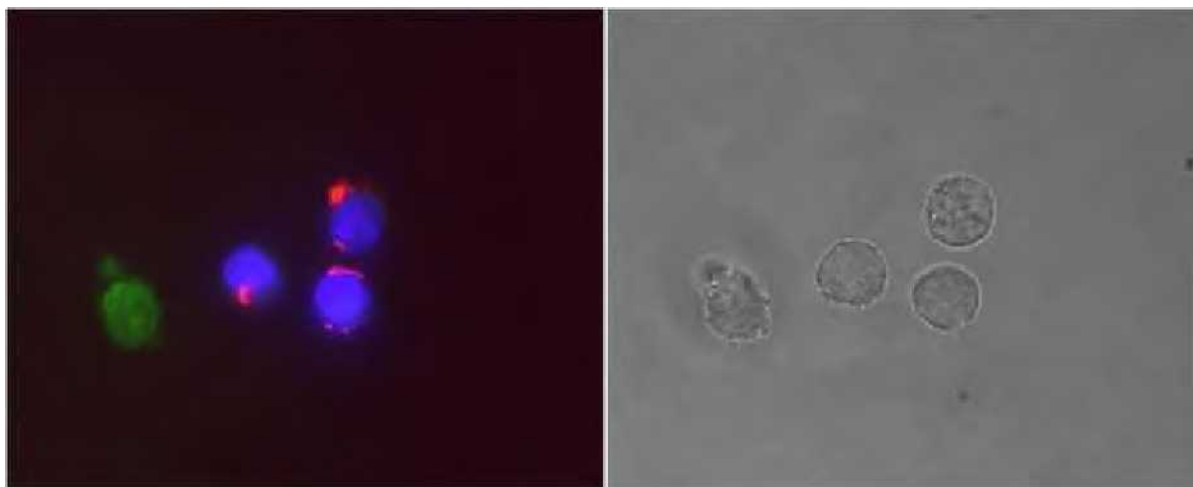
Presentation Number **0943A**

Poster Session 2c: In Vivo Studies & Development/Novel Use of Imaging Probes

Imaging sentinel lymph nodes using target specific superparamagnetic iron oxide nanoparticles

Pontus Kjellman^{1,2}, **Fredrik Olsson**², **Renata Madru**¹, **Karin Wingårdh**¹, **Rene in 't Zandt**², **Linda Andersson**², **Sarah Fredriksson**², **Freddy Ståhlberg**¹, **Sven-Erik Strand**¹, ¹Medical Physics, Lund University, Lund, Sweden; ²Genovis AB, Lund, Sweden. Contact e-mail: pontus.kjellman@genovis.com

Background: Examining the first lymph node that the tumor tissue drains into (the sentinel lymph node, SLN) tells whether the tumor has metastasized or not. Protein tyrosine phosphatase, receptor type C (PTPRC) or CD45 is a protein found on most differentiated hematopoietic cells. Since the lymph nodes contain large amounts of lymphocytes, CD45 is a good molecule to use for studying the ability to target the SLN. In this study, superparamagnetic iron oxide nanoparticles (SPION) with conjugated antibody fragments was used to target and image the SLN in rats using MRI. Materials and Methods: SPION:s with a NH₂-PEG coating were modified to contain maleimide groups and subsequently coupled to thiol groups of reduced anti-CD45 antibodies. Remaining free amino groups were conjugated to a fluorescent dye, DY647. The discriminating capability of the particles was tested in vitro on a mixture of CD45+ (THP-1) and CD45- (LADMAC) cells (Figure 1). In vivo the SPION:s were injected subcutaneously in the hind paw of rats. The retention of the particles in the lymphatic system was studied with MRI. Results: The image to the left in Figure 1 shows that the antibody conjugated SPION:s (red) have only attached to the CD45+ THP-1 cells (blue), while no binding to the CD45- LADMAC cells (green) can be detected. The image to the right in Figure 1 is the corresponding bright field image. This proves that the molecular design of the SPION was successful. Preliminary results from tail vein injection of nontargeted SPION:s show long circulation retention and low toxicity. As shown earlier by R. Madru et al (1), the nontargeted SPION behaved very stably when injected s.c. into the lymphatics. It is furthermore clearly advantageous to trace the SPION:s using MRI in combination with subsequent and parallel histology studies using the fluorescent marker to identify the SPIONs.. Conclusion: Studies have shown that the SPION:s designed for this study are biocompatible and stable both in vitro and in vivo. When injected into the lymphatic system the SPION will be retained for different periods of time, depending on the size and targeting effect of the particle. 1. Madru, R. et al. Preparation and characterization of 99mTc-labeled superparamagnetic iron oxide (IO) nanoparticles for multimodality imaging (MRI/SPECT) of SLN. ESMRMB 2009.



Presentation Number **0944A**

Poster Session 2c: In Vivo Studies & Development/Novel Use of Imaging Probes

Dual-labeled Cetuximab-based imaging agent for NIR Fluorescence and PET

Ralf K. Bergmann¹, **Martin Zenker**¹, **Martin Walther**¹, **Hans-Juergen Pietzsch**¹, **Frank Hofheinz**², **Joerg van den Hoff**¹, **Jens Pietzsch**¹, **Jörg Steinbach**¹, ¹Institute of Radiopharmacy, Forschungszentrum Dresden-Rossendorf, Dresden, Germany; ²ABX GmbH, Radeberg, Germany. Contact e-mail: r.bergmann@fzd.de

Cetuximab (C225) as a chimeric monoclonal antibody specifically targets the epidermal growth factor receptor (EGFR) that often is overexpressed in human malignancies. This phenotype is associated with tumor aggressiveness, treatment resistance, and biological heterogeneity with potential to bypass the blockade of the EGFR signaling pathways. The aim of this work was to prepare and characterize the C225 for near infrared fluorescence (NIRF) and PET imaging using a X-SIGHT Large Stokes Shift Dye (X-SIGHT 670 LSS Dye) and [⁶⁴Cu]Cu-NOTA as a prerequisite for combination of both imaging methods. C225 was conjugated with the bifunctional chelator 2-(p-isothiocyanatobenzyl)-1,4,7-triazacyclononane-1,4,7-triacetic acid (SCN-Bz-NOTA) and the X-SIGHT 670 Large Stokes Shift Dye, TFP Ester (XS670). The EGFR-affinity of the immunoconjugate resulted in 94% versus 100% of the unmodified C225 measured with specific enzyme-linked immunosorbent assay (ELISA) on EGFR-positive tumor cell line A431. C225-SCN-Bz-NOTA was labeled with ⁶⁴Cu within 30 min with high radiolabeling yield and radiochemical purity. The [⁶⁴Cu]Cu-NOTA-C225-XS670 showed high accumulation in xenotransplanted squamous cell carcinoma tumors in mice after 24 hours imaged with small animal PET and NIRF. The comparison of both methods in living animals showed the high signal intensity and accumulation of the probe in tumors; however only PET allowed the quantitative characterization of the probe distribution in vivo. The subsequent whole body cryosectioning of the animals into 40 µm sections permitted the direct comparison of the autoradiograms and NIRF images of the tissue cuts. The quantitative comparison of the autoradiograms and the NIRF images after coregistration of the corresponding images yielded a good correlation of the pixel intensities, but the different geometric resolution did not allow a pixel wise comparison. The NIRF images showed a higher differentiation than the autoradiograms. The dual-labeled C225 demonstrated the higher resolution and comparable concentration values of the antibody distribution in whole body cryosections of tumor bearing mice using the combination of ⁶⁴Cu-radioluminography and NIRF imaging. The dual-labeling of antibodies is a promising tool for quantitative evaluation of the long time distribution in animals using NIRF of cryosections beyond the decay of the radionuclide used. Acknowledgement: This project was partially supported by FP7 project "GIPIO", Project Reference: 223057

Presentation Number **0945A**

Poster Session 2c: In Vivo Studies & Development/Novel Use of Imaging Probes

PEG-coated BaYF₅:Eu³⁺ Nanophosphors for X-ray Excited Optical Luminescence Molecular Imaging

Conroy Sun, Colin M. Carpenter, Guillem Pratx, Lei Xing, Radiation Oncology - Physics, Stanford University School of Medicine, Stanford, CA, USA. Contact e-mail: conroys@stanford.edu

Molecularly targeted nanophosphors that produce X-ray excited optical luminescence (XEOL) enable unique multimodal imaging capabilities, such as combined optical/fluoroscopic or optical/CT imaging. Here we present the synthesis and characterization of a poly(ethylene glycol) (PEG)-coated BaYF₅ nanoparticle platform to serve as a XEOL probe. In this system, optical emission can be tuned by selection of lanthanide dopants, such as Eu³⁺. BaYF₅ core particles were synthesized by the thermal decomposition method using lanthanide trifluoroacetates, barium acetylacetonate, oleic acid and 1-octadecene. Uniform cubic (~10 nm) nanocrystals were obtained by this process and observed by transmission electron microscopy (TEM, Fig. 1A). A solvent exchange process using dicarboxyl functionalized PEG was then performed to produce hydrophilic and colloidal aqueous suspensions of the nanophosphors (Fig. 1B & C). Incorporating a biocompatible PEG coating bearing carboxyl functional groups, this nanophosphor platform possesses the ability to attach a variety of targeting and other biological ligands through conventional bioconjugate techniques. To evaluate the XEOL of these nanophosphors a suspension of the particles was irradiated at 50 kVp while an emission spectrum (Fig. 1D) was obtained by a spectrograph coupled to an EM-CCD. Strong peaks were observed at 590, 615 and 700 nm with the BaYF₅:Eu³⁺ nanophosphors. Of particular interest, emission at 700 nm in the near-infrared region provides significant tissue penetration necessary for in vivo applications. In summary, a PEG-coated nanophosphor was developed with physical and optical properties required to serve as a XEOL molecular imaging probe. Luminescent nanophosphors may enable multimodal x-ray/optical imaging, as well as a wide range of other applications in molecular imaging and nanomedicine.

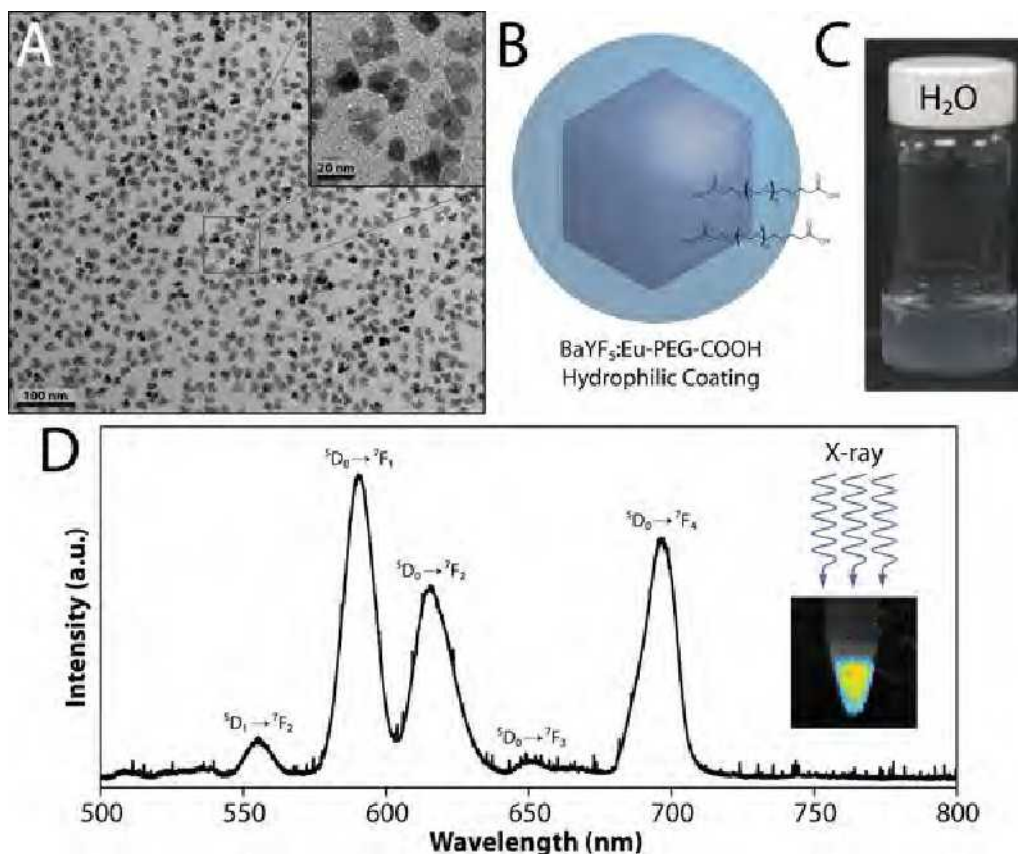


Figure 1 - (A) TEM of PEG-coated BaYF₅:Eu³⁺ nanophosphors. (B) Illustration of PEG-COOH functionalized nanophosphor for bioconjugation. (C) Dispersion of 1 mg/mL hydrophilic nanophosphors in water. (D) X-ray excited luminescence spectra.

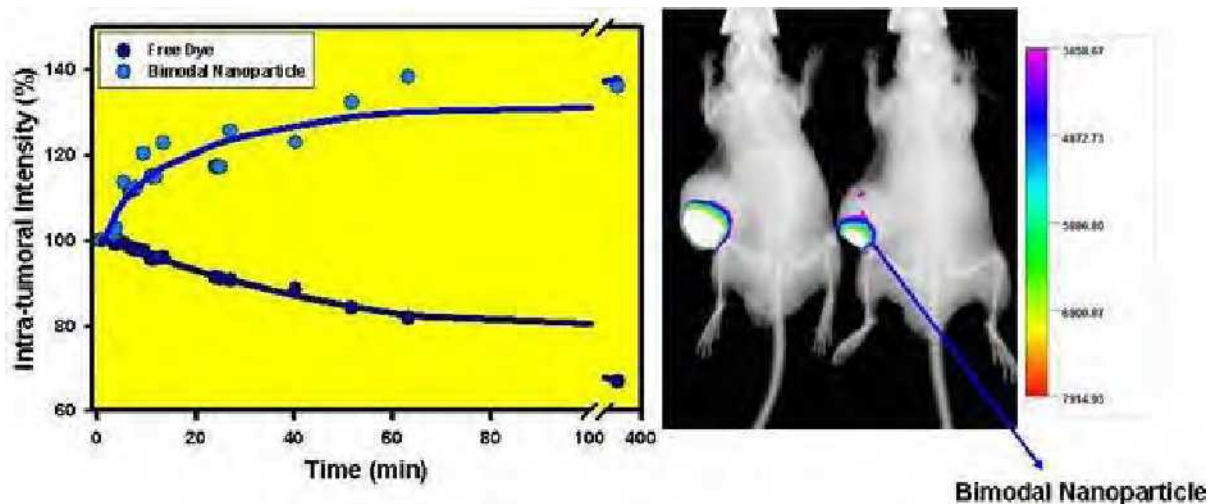
Presentation Number **0946A**

Poster Session 2c: In Vivo Studies & Development/Novel Use of Imaging Probes

Degradable Bimodal Nanoparticles with both Near-IR and Radio Contrast

Rao V. Papineni¹, **Sudharsan R. Gongati**², **Sean P. Orton**¹, **William McLaughlin**¹, **Jingyi Pan**¹, **Ram G. Reddy**², ¹Carestream Molecular Imaging, Carestream Health, Inc., Woodbridge, CT, USA; ²Next Generation Therapeutics, Inc., Plymouth, MI, USA. Contact e-mail: rao.papineni1@carestreamhealth.com

Multimodal imaging is rapidly becoming important tool in molecular imaging. Low energy X-ray imaging together with optical imaging modality complements each other in preclinical imaging. In combination, the two modalities compensate each other's deficiencies in the spatial resolution, sensitivity, and the depth detection. These advantages are maintained in imaging agents that harbor multimodal reporting capability. Here, we developed a multimodal nanoparticle that can be simultaneously be imaged by optical, and X-ray modalities. Encapsulation of radio contrast iodixanol and amine functionalization was performed in a one pot synthesis by microemulsion technique. The near-IR fluorescent (NIRF) dye was conjugated through standard succinimidyl chemistry. The hydrodynamic radii of nanoparticle and zeta potential were measured using Nicomp 380 zls particle sizer. We created a fibrosarcoma mouse model using human HT 1080 cell lines for the analysis of bimodal nanoparticles. Steady increase in the fluorescence intensity upon intratumoral injection is likely due to gradual degradation of the nanoparticles in the tumor environment, a useful property for the drug release mechanisms. In summary, we have described the development of a simple and efficient dynamic imaging multimodal nanoparticle to be used for NIRF and CT imaging.



Presentation Number **0947A**

Poster Session 2c: In Vivo Studies & Development/Novel Use of Imaging Probes

Manganese-Sarar: a new MRI agent with dual PET / MRI imaging capability

Suzanne V. Smith¹, **Mikko I. Kettunen**^{2,3}, **Gary Perkins**¹, **Tiago B. Rodrigues**^{2,3}, **Binh Pham**¹, **Eskender Mume**^{1,4}, **Kevin M. Brindle**^{2,3},
¹Centre of Excellence in Anti-matter Matter Studies, Australian Nuclear Science and Technology Organisation, Sydney, NSW, Australia;
²Cancer Research UK, Cambridge Research Institute, Cambridge, United Kingdom; ³Department of Biochemistry, University of
Cambridge, Cambridge, United Kingdom; ⁴Centre of Excellence in Anti-matter Matter Studies, The Australian National University,
Canberra, ACT, Australia. Contact e-mail: svs@ansto.gov.au

Sarar[1][2] is a versatile agent for use in Cu-64 PET imaging, it rapidly and quantitatively complexes Cu-64 at micromolar concentration over a wide range of pH. Here we report the synthesis of the manganese complex of sarar, its exceptional stability in the presence of excess Cu²⁺, Zn²⁺, Mg²⁺ and Ca²⁺ and its potential for use in MRI. Divalent manganese ion (Mn²⁺) has played an important role in the history of magnetic resonance. However, problems with toxicity has slowed its development as a routine MRI contrast agent. While manganese is an essential element, in excess it can cause neurological deficits, similar to Parkinson disease. Manganese dipyrroldiphosphate (MnDPDP) is approved for liver imaging. However, Mn²⁺ can be slowly released from the chelate via transmetallation with zinc. As the hexaza cage compound, diamsar, is known to form stable complexes with Cu²⁺ and Mn²⁺, we decided to investigate if the manganese complex of sarar possesses similar properties. The manganese complexes of sarar and its parent diamsar were prepared in a similar manner to that previously described.[1] Each complex was dissolved in water and in phosphate buffer. The T1 and T2 values of these solutions were determined using a 7 T horizontal magnet (Oxford Instruments, UK) equipped with actively shielded gradients (Magnex) interfaced to a VNMR5 (Varian Inc, Palo Alto, CA, USA) imaging console. Mn-sarar and Mn-diamsar complexes were also exposed to equimolar and excess (up to 100-fold) concentrations of competing metals ions such as Cu²⁺, Zn²⁺, Mg²⁺ and Ca²⁺ in acetate buffer. R1 value for Mn-diamsar in water was modest at 1.01 1/sec.1/mM, however R1 for Mn-sarar in water was significantly higher at 1.99 1/sec.1/mM. All complexes were stable in buffer at ambient temperature for long periods of time (up to 21 hours) and in presence of competing metal ions. References: 1. 1-N-(4-aminobenzyl)-3,6,10,13,16,19-hexaazabicyclo[6.6.6]icosane-1,8-diamine (sarar); 3,6,10,13,16,19-hexaazabicyclo[6.6.6]icosane-1,8-diamine (diamsar) 2. Nadine M. Di Bartolo, Alan M. Sargeson, Therese M. Donlevy and Suzanne V. Smith, J. Chem. Soc., Dalton Trans., 2001, 2303-2309 3. A.M. Sargeson, Coordination Chemistry Review, 151, (1996) 89-114.

Presentation Number **0800A**

Poster Session 1c: In Vivo Studies & Development/Novel Use of Imaging Probes

A Novel Near-Infrared Fluorescence Imaging Probe for in vivo Neutrophil Tracking

Li Xiao^{1,2}, **Yi Zhang**¹, **Lin Pu**², **Dongfeng Pan**¹, ¹Radiology, University of Virginia, Charlottesville, VA, USA; ²Chemistry, University of Virginia, Charlottesville, VA, USA. Contact e-mail: lx4c@virginia.edu

In a majority of inflammatory disorders, neutrophils, the most abundant class of white blood cells, migrate immediately to the site of injury and release reactive oxygen species and proteolytic enzymes which are responsible for the tissue damage associated with such inflammatory diseases. Therefore, imaging technologies that could enable specific visualization of neutrophil activation and infiltration non-invasively are highly desirable. Nuclear imaging is currently the gold standard technique for leukocyte tracking; however, many disadvantages, such as radioactive exposure, high cost, and laborious work, limit its application in research. To address these issues, three near-infrared (NIR) fluorescence peptide agents cFLFLF-PEG_n-Cy7 (1. n=0; 2. n=12; 3. n=76), with high binding affinity towards formyl peptide receptor (FPR) on leukocytes, have been developed. By measuring the partition coefficient constant (logP) of these probes in *n*-octanol and water, probe 3 was chosen for further study as it demonstrated the optimal blood solubility. In vivo fluorescence imaging was performed using a mouse model with phorbol 12-myristate 13-acetate (PMA) induced inflammation on left ears and right ears untreated as negative controls. Strong fluorescence signal of 3 was detected in left ears while much less signal was present in right ears (Fig. 1A). Moreover, in vivo specificity of 3 was determined by blocking FPR receptors with excess of non-fluorescence peptide cFLFLF-PEG₇₆ and imaging with a synthesized scrambled peptide probe 4 cLFFFL-PEG₇₆-Cy7. The signals from images acquired with the scrambled probe 4 (Fig. 1B) as well as from the blocking study (Fig. 1C) were significantly lower in the PMA-treated ears compared to images with probe 3 (Fig. 1A). Microscopic images of inflammatory ears confirmed that the fluorescence signal of 3 correlated well with antibody-stained neutrophils. In conclusion, the first neutrophil-specific probe for NIR fluorescence imaging of live animals was reported. In vivo neutrophil specificity of the NIR fluorescence probe was determined by correlation of the whole body imaging with the pathological microscopic imaging.

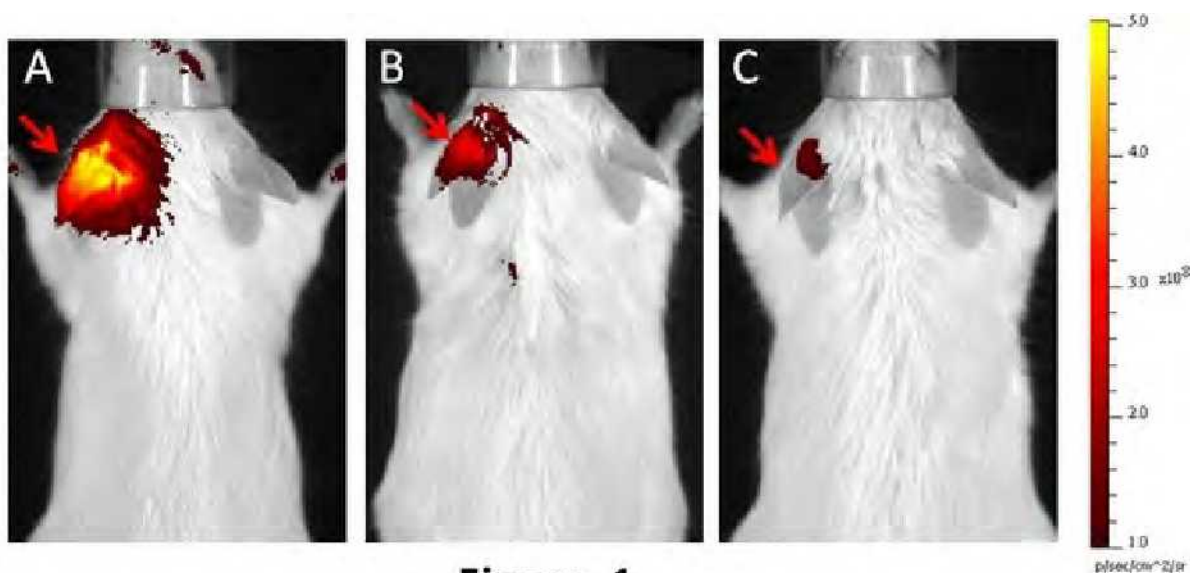


Figure. 1

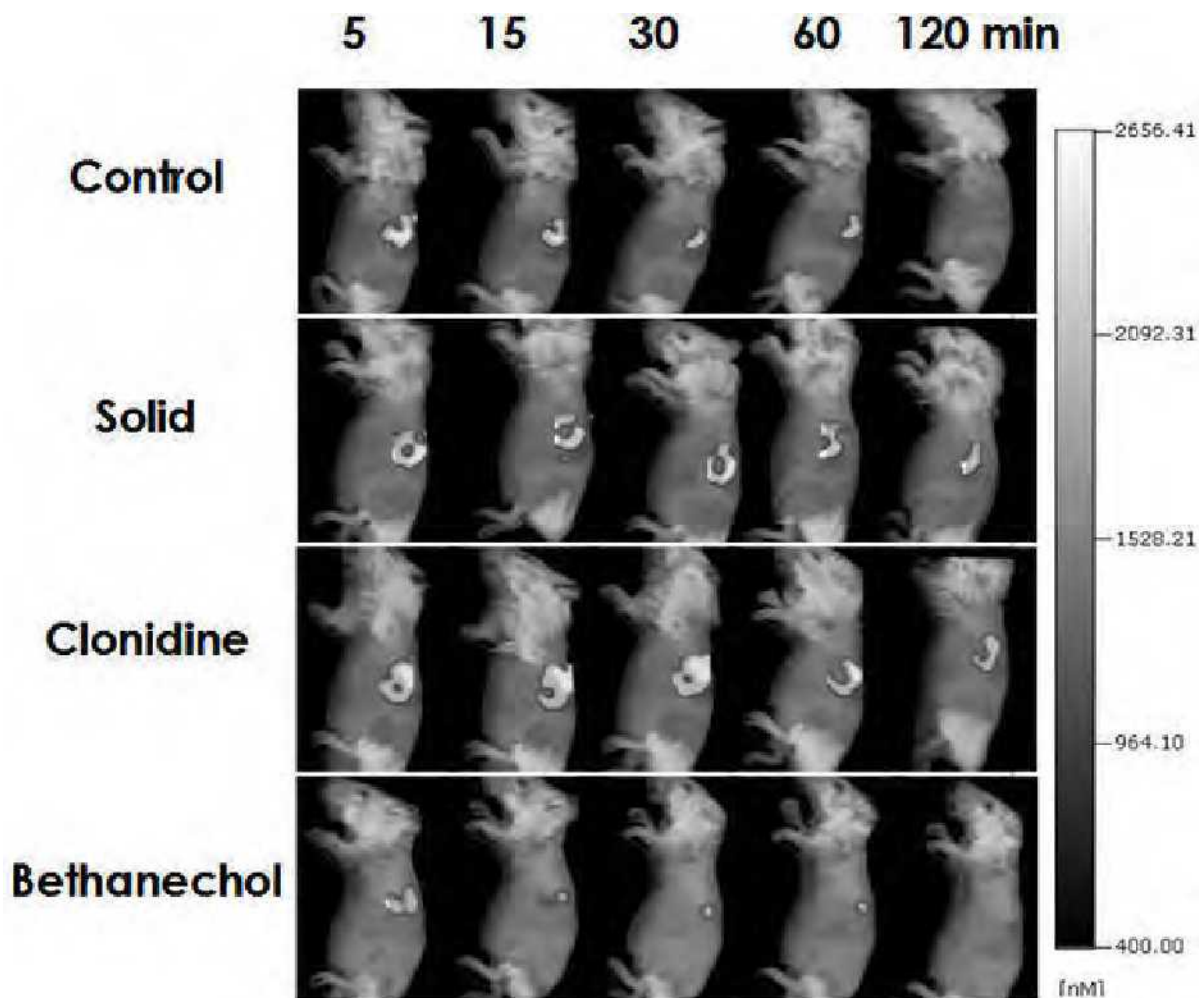
Presentation Number **0801A**

Poster Session 1c: In Vivo Studies & Development/Novel Use of Imaging Probes

Dynamics of Gastric Emptying Quantified by Near-Infrared Fluorescence Imaging In Vivo

Jeff Morin, Sylvie Kossodo, Emma Handy, Garry J. Cuneo, David Z. Gao, **Jeffrey D. Peterson**, Milind Rajopadhye, Kevin Groves, VisEn Medical, Bedford, MA, USA. Contact e-mail: jpeterson@visenmedical.com

The accurate quantification of gastric emptying is crucial for understanding the physiological, pathological and pharmacological mechanisms underlying gastric motility both clinically and in animal studies. Current methods used for determining gastric emptying rates in small animals are either terminal or involve radioactive tracers, incurring high financial and time cost. We have developed a novel, near-infrared fluorescent (NIRF) imaging agent, GastroSense 750, to monitor and quantify gastric emptying rates in murine models in vivo, non-invasively and in real time. The imaging agent is comprised of an acid-stable NIRF fluorophore conjugated to a non-absorbable pharmacokinetic modifier designed to be formulated in liquid or incorporated into a solid meal. Using female 8 week old BALB/c mice recipients, 0.25 nmol GastroSense 750 was orally gavaged in 0.5% methylcellulose/0.025% Tween 20 (Control) or in egg yolk, an experimental approach designed to better mimic changes in gastric emptying in the presence of solid diet. In vivo 3D fluorescent imaging and quantification using the FMT 2500 Fluorescence Molecular Tomography (FMT) system at multiple time points revealed a gastric half-life ($t_{1/2}$) of 25 ± 2.0 minutes for Control liquid meal and 65 ± 12.6 minutes ($p = 0.005$) for the solid meal (figure below.) To determine drug effects, mice fed with liquid meal were treated with either clonidine or bethanechol, known to delay or stimulate gastric emptying, respectively. Clonidine induced a 4-fold delay in gastric emptying ($t_{1/2} = 108 \pm 28.5$ min, $p = 0.009$), while bethanechol accelerated emptying 2-fold ($t_{1/2} = 11.5 \pm 0.3$ min, $p = 0.01$). Comparable results were seen in mice fed with GastroSense 750 mixed with solid diet. These findings reveal that GastroSense 750 and FMT 3D fluorescent in vivo imaging can be used successfully to quantify gastric emptying rates of both liquid and solid diets in small animals and measure pharmacological effects of drugs that affect gastric motility.



Presentation Number **0802A**

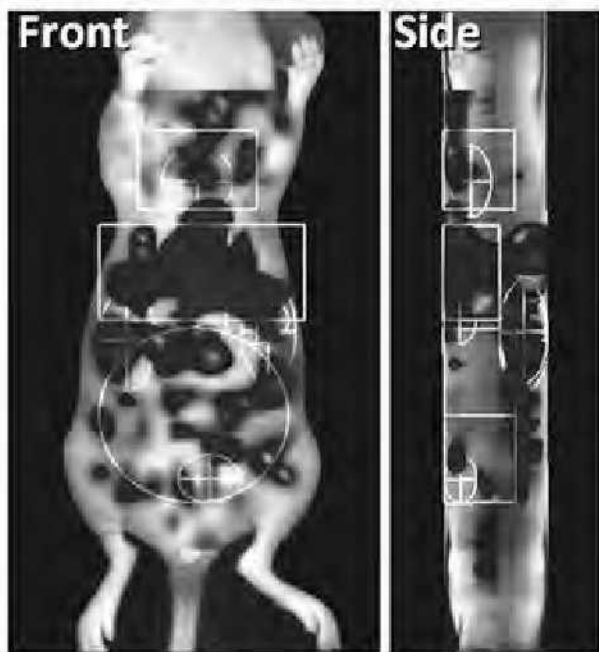
Poster Session 1c: In Vivo Studies & Development/Novel Use of Imaging Probes

Non-Invasive, In Vivo Optical Tomographic Imaging and Quantification of Whole Body Biodistribution

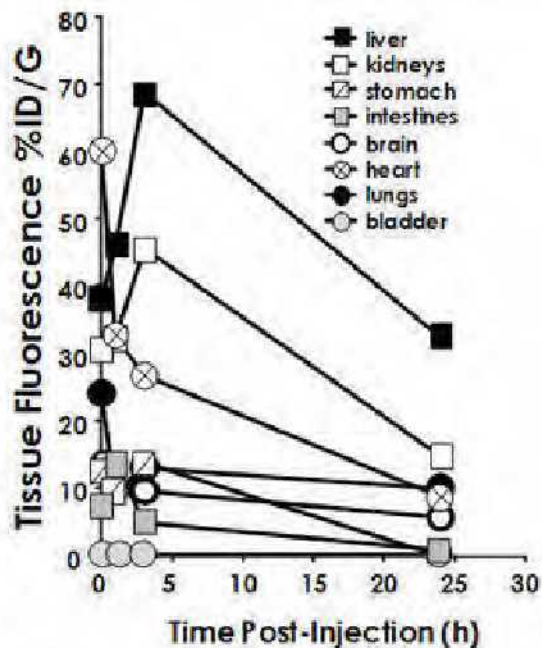
Kristine Vasquez, Chelsea S. Casavant, Jeffrey D. Peterson, VisEn Medical, Bedford, MA, USA. Contact e-mail: jpeterson@visenmedical.com

When proteins or small molecules are injected into live animals, their fate is influenced by pharmacokinetics, biodistribution, and routes of clearance/metabolism, and understanding these factors can be critical in developing therapeutics and other agents. Typically, biodistribution is assessed using radiolabeled agents with measurements in tissue conducted by live PET imaging or by ex vivo tissue assessment. Fluorescence molecular tomography (FMT), offers an alternative to using radioactivity, with the ability to detect and quantify fluorescence throughout the body in a wide variety of disease areas, including oncology, inflammation, and cardiovascular disease. This report describes the application of FMT imaging to quantitative biodistribution of near infrared (NIR) labeled molecules in vivo. FMT results correlated well with both fluorescence from tissue homogenates as well as with reflectance (2D) imaging of excised intact organs ($r^2 = 0.996$ and 0.969 , respectively). Further dynamic FMT imaging (multiple time points from 0 to 24h) was performed in live mice after the injection of four different NIR-labeled agents, including free fluorophore (VivoTag 680 XL), bovine serum albumin (BSA), a large molecular weight vascular imaging agent (AngioSense 750), and a small molecule integrin antagonist imaging agent (IntegriSense 680). These imaging agents showed clear differences in % of injected dose per gram of tissue (%ID/g) in liver, kidney, and bladder signal, with BSA favoring liver/kidney signal, IntegriSense and AngioSense showing mostly kidney and bladder signal, and VivoTag 680 XL showing rapid clearance through the bladder. These studies demonstrate the ability of quantitative fluorescence-based tomography of NIR agents to non-invasively visualize and quantify the biodistribution of different agents non-invasively over time, requiring very few animals to generate large temporal biodistribution datasets.

In Vivo FMT 2500 Imaging: BSA-VT680XL Biodistribution



In Vivo FMT Quantification



Presentation Number **0803A**

Poster Session 1c: In Vivo Studies & Development/Novel Use of Imaging Probes

Antibody-conjugated Polymer Nano-Particle as Molecular Probe for Photoacoustic Imaging

Fumio Yamauchi¹, Masato Minami¹, Atsushi Takahashi¹, Yoshinori Tomida¹, Satoshi Yuasa¹, Tetsuya Yano¹, Shinae Kizaka-Kondoh², Yasuo Mori³, Yoichi Shimizu⁴, Takashi Temma⁴, Masahiro Ono⁴, Hideo Saji⁴, Yasuhiko Tabata⁵, Satoshi Nitahara⁶, Hiroyuki Aoki^{6,7}, Shinzaburo Ito⁶, ¹Medical Imaging Project, CANON INC., Tokyo, Japan; ²Department of Biomolecular Engineering, Graduate School of Bioscience and Biotechnology, Tokyo Institute of Technology, Yokohama, Japan; ³Department of Synthetic and Biological Chemistry, Graduate School of Engineering, Kyoto University, Kyoto, Japan; ⁴Department of Patho-Functional Bioanalysis, Graduate School of Pharmaceutical Sciences, Kyoto University, Kyoto, Japan; ⁵Department of Biomaterials, Institute for Frontier Medical Sciences, Kyoto University, Kyoto, Japan; ⁶Department of Polymer Chemistry, Graduate School of Engineering, Kyoto University, Kyoto, Japan; ⁷Advanced Biomedical Engineering Research Unit, Kyoto University, Kyoto, Japan. Contact e-mail: yamauchi.fumio@canon.co.jp

The purpose of this study was to develop an antibody-conjugated polymer nano-particle as molecular probe for photoacoustic (PA) imaging of human epidermal growth factor receptor 2 (HER2)-overexpressing tumors. A polymer nano-particle (PNP) composed of a polymer matrix, near-infrared (NIR) fluorescent dyes, non-ionic surfactants, and functionalized PEG-modified phospholipids (PEG-PL) was prepared by a nano-emulsion method. To achieve specific targeting of PNP against HER2, anti-HER2 single-chain variable fragment (scFv) antibodies were covalently conjugated to a maleimide-activated PNP. The scFv-conjugated PNP (scFv-PNP) had an average hydrodynamic diameter of about 120 nm. The molar absorption coefficient per nanoparticle was approximately $10^{10} \text{ M}^{-1} \text{ cm}^{-1}$ at the absorption maximum (780 nm), which resulting in the efficient optical absorption of pulsed laser light and subsequent generation of acoustic waves. The scFv-PNP was tested in vitro to determine HER2 targeting efficacy. The result showed that the scFv-PNP could bind to HER2-positive cancer cells, but not HER2-negative cells. The biodistribution of an ¹¹¹In-labelled scFv-PNP (¹¹¹In-scFv-PNP) was further studied in tumor-bearing mice. Maximum tumor uptakes (%ID/g \pm SD) of the ¹¹¹In-scFv-PNP to HER2-positive and HER2-negative tumors were 6.2 ± 2.3 at 6 hr postinjection and 3.6 ± 0.5 at 3 hr postinjection, respectively, indicating the effective targeting of scFv-PNP to the HER2-positive tumor. As shown in Figure 1, the accumulation of scFv-PNP in tumors could be visualized with PA imaging following intravenous injection of scFv-PNP to mice. Our results demonstrate that the scFv conjugation of PNP, which is a powerful contrast agent for PA imaging, facilitates the specific targeting to tumors. Consequently, the scFv-PNP would be a promising molecular probe for PA imaging of HER2-overexpressing tumors such as breast cancer.

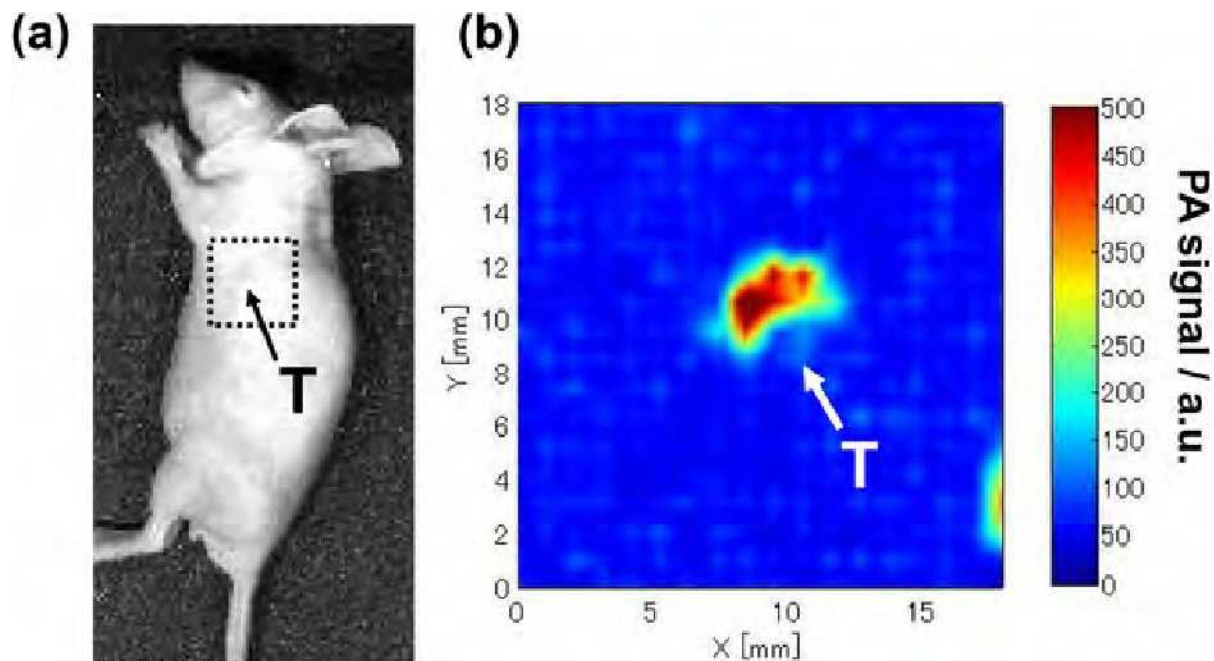


Figure 1. Photoacoustic (PA) imaging of a subcutaneously inoculated HER2-positive tumor in a nude mouse using a scFv-PNP. (a) Photograph of a nude mouse. (b) Two-dimensional PA imaging within the marked region in (a) at 1 day after intravenous injection of the scFv-PNP. T: tumor.

Presentation Number **0804A**

Poster Session 1c: In Vivo Studies & Development/Novel Use of Imaging Probes

In Vivo Pharmacokinetics of Tumor-targeting With a Fluorescently-labeled δ -Opioid Receptor-Targeted Probe

Amanda Shanks Huynh¹, David L. Morse¹, Jatinder S. Josan^{2,1}, Robert Gillies¹, ¹Molecular & Functional Imaging, H. Lee Moffitt Cancer Center & Research Institute, Tampa, FL, USA; ²Chemistry, University of Arizona, Tuscon, AZ, USA. Contact e-mail: amanda.huynh@moffitt.org

Fluorescence imaging can be applied to in vivo pharmacokinetic (PK) studies for development of novel cancer targeting agents. The PK of a fluorescent targeted probe is tracked in vivo by acquiring real-time images using a fluorescence imaging system. We evaluated the in vivo PK of a small peptidomimetic ligand conjugated with Cy5 dye, Dmt-Tic, over a time course of 0-168 h using fluorescence imaging. By solid-phase synthesis, this potent (3nM Ki) δ -opioid receptor (DOR)-antagonist was conjugated to Cy5 and retained high binding affinity and antagonist activity in vitro. To evaluate the PK, HCT116 DOR- and DOR+ engineered HCT116 cells (8×10^6) were bilaterally xenografted into flanks of nude mice. After 10 days tumors were >5 mm diameter, an optimized dose 4.5nmol/kg probe was injected IV and tracked by acquiring images over 0-168 h with the Caliper IVIS 200 Imaging System using the standard Cy5.5 fluorescence filter set. A dark chamber, dark covers, alfalfa-free food, special cage bedding were used to minimize photo-bleaching of the dye and autofluorescence resulting in 10-fold reduction in the the optimal dose concentration. The signals measured from DOR- and DOR+ tumors (Fig. 1A) were quantified and plotted over time from 0-168 h, the graph shows the maximum Dmt-tic uptake in the DOR+ tumor at 3 h (Fig.1B). Uptake by organs, kidney and liver, is present from 45m-24h and confirmed by ex-vivo imaging. The DOR-targeted probe exhibits long-lasting and specific signal in DOR+ xenografts and not in DOR- xenografts, demonstrating high binding specificity of Dmt-Tic for DOR. Signal enhancement (18-fold) at 24 h in DOR+ tumors relative to DOR- tumors was quantified following autofluorescence background subtraction. Future plans involve in vivo biodistribution studies to further this tumor-targeting study with the targeted probe,Dmt-Tic.

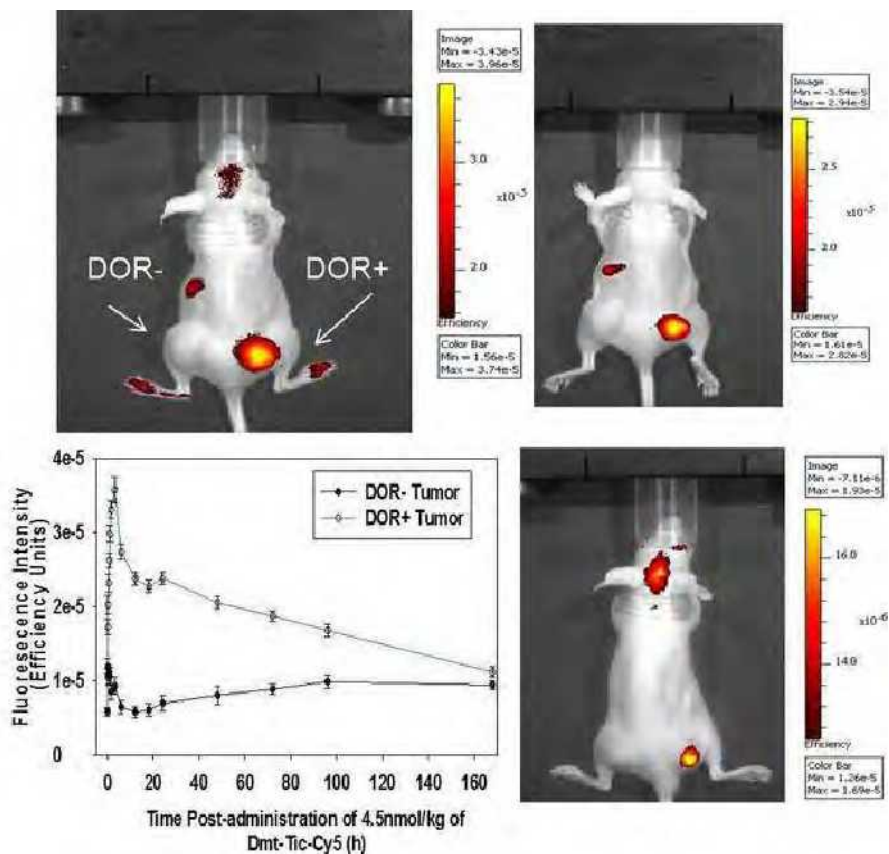


Figure 1 .A) In vivo fluorescence images acquired at 3h, 24h, 48h post-administration of 4.5nmol/kg Dmt-Tic B) Mean image-acquired fluorescence signal over time (0-168h).

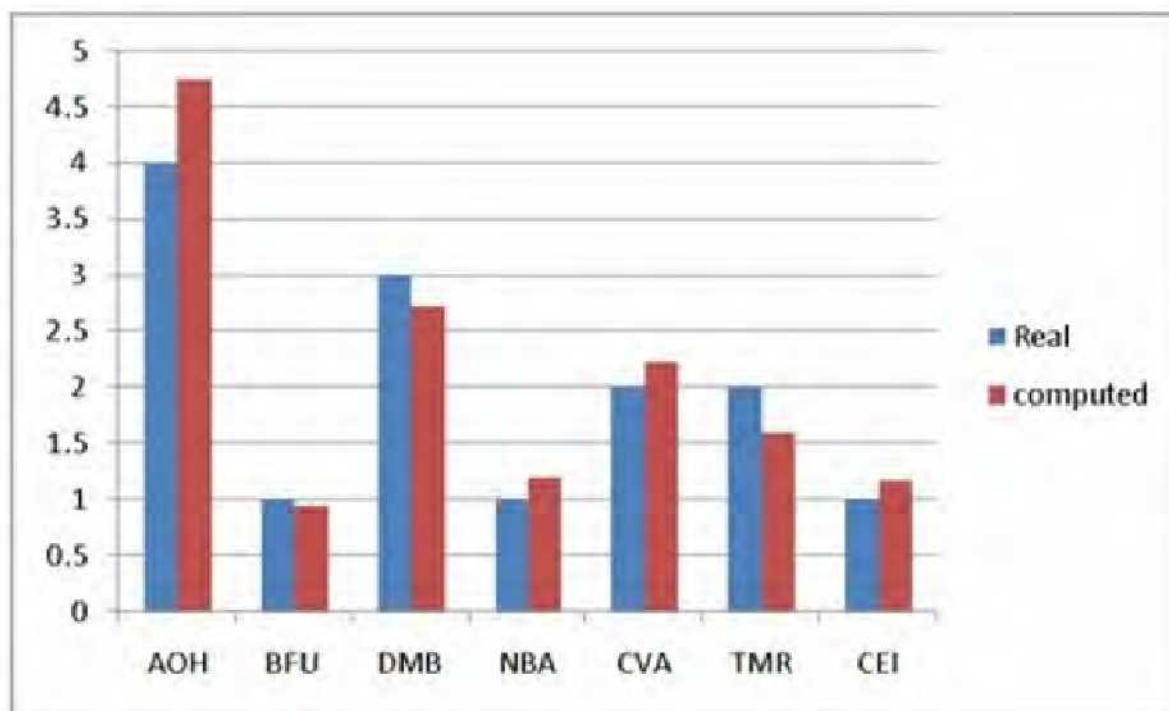
Presentation Number **0805A**

Poster Session 1c: In Vivo Studies & Development/Novel Use of Imaging Probes

Raman Labeled Nanoparticles for In-vivo Imaging: Characterization of Variability and Improved Method for Unmixing

Kranthi K. Kode¹, Catherine Shachaf³, Sailaja V. Elchuri³, Garry Nolan³, David Paik², ¹Computational and Mathematical Engineering, Stanford University, Stanford, CA, USA; ²Radiology, Stanford University, Stanford, CA, USA; ³Microbiology and Immunology, Stanford University, Stanford, CA, USA. Contact e-mail: kranthi@stanford.edu

Raman spectroscopy can differentiate the spectral fingerprint of many molecules, resulting in potentially high multiplexing capabilities. However, accurate quantitative unmixing of Raman spectra is challenging because of overlaps of the Raman peaks from each molecule as well sensitivity to variation across spectra of a given molecule. If not accounted for, these inconsistencies in the spectra produce significant error which will ultimately result in poor unmixing accuracy. The objective of our study was to develop and validate mathematical techniques using parametric models of the Raman spectra of nanoparticles to unmix the contributions from each nanoparticle to allow for simultaneous multiplexed quantitation of nanoparticle concentrations for tumor cell characterization with applications in in-vivo imaging. This study consists of two parts: 1) statistical characterization of the variations in individual spectra, and 2) an algorithm for quantitative unmixing of the spectra. The variation in the heights of individual peaks of spectra for Raman labeled composite organic inorganic nanoparticles (COINs) is upto 20% and the location of peaks shifted by 5cm⁻¹ to 10 cm⁻¹ which was as much as 50% of full width half max. These variations between the peaks are uncorrelated with R² ranging from 0.08 to 0.16. We modeled individual Raman peaks to accurately represent the Raman spectra of COINs and successfully unmixed up to 6 COINs after accounting for the spectral variations, achieving considerable improvement over the results obtained using direct linear least squares. The errors in estimation of the individual contributions of each nanoparticle using classical least squares were in the range of 20-70% while the error based on results from our model-based algorithm are in the range of 10-20% for unmixing of 6 COINs. To the best of our knowledge, we are reporting here for the first time, the quantitative unmixing up to 6 nanoparticles with maximum error less than 20%.



Unmixing results of 6 COIN multiplexing

Presentation Number **0806A**

Poster Session 1c: In Vivo Studies & Development/Novel Use of Imaging Probes

Auditory Display of Fluorescence Image Data in Living Tumor Model

Sheen-Woo Lee^{1,2}, **Woon Seung Yeo**³, **Zhen Cheng**⁴, **Jee Eun Kim**¹, **Sang Hoon Lee**², **Myung Jin Shin**², ¹Radiology, Gachon University, Incheon, Republic of Korea; ²Radiology, Asan Medical Center, Seoul, Republic of Korea; ³Graduate School of Culture Technology, Korea Advanced Institute of Science and Technology, Daejeon, Republic of Korea; ⁴Radiology, Stanford University, Stanford, CA, USA. Contact e-mail: leesw1@gmail.com

Auditory display is the use of non-speech audio to convey information for data interpretation, the Geiger counter as an example. In this study we aim to develop a molecular imaging strategy using auditory display, and test its feasibility in tumor imaging in-vivo using hyperspectral data of near-infrared fluorescence (NIRF). Mice with PC3 xenograft underwent fluorescence imaging after injection of cy5.5-glucose (N=6), and their raw spectral data was processed for auditory display. Typical computer maneuvers such as drag, scroll, and click specified the regions of interest (ROIs) in mouse on screen. Then selected spectral components in the ROI were parametrized to emphasized the NIRF range information, which were mapped to control parameters of a two-oscillator frequency modulation (FM) sound synthesizer. For statistical analysis, the signal to noise ratio (SNR) of the tumor area was compared with the body area without tumor ($p < 0.05$), with the injected tail as positive control. Figure 1 shows a sample spectral pattern and waveform; the tumor area resulted in sounds with higher spectral variation and heterogeneous waveform, compared to the no-tumor body area with more homogeneous spectral pattern and waveform. The SNR was higher in the tumor area than the no-tumor area (3.63 ± 8.41 vs 0.42 ± 0.085 , $p < 0.05$). The post-injection tail produced louder audio signal compared to the no-tumor area (10.39 ± 0.67 vs 0.28 ± 0.01 , $p < 0.05$). Sound from the tumor was perceived by the naked ear as harsh, noisy, and unpleasant. In conclusion, the auditory display has a strong potential as a new approach of molecular probe development, which can aid in translation of fluorescence imaging in early cancer evaluation.

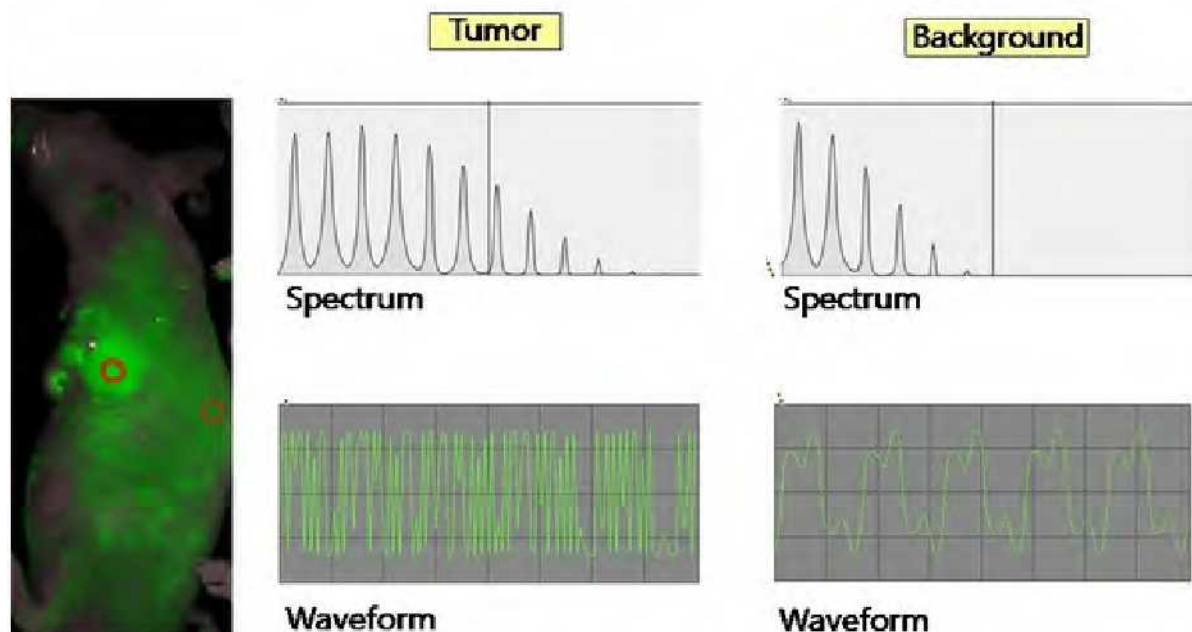


Figure 1. Tumor area (solid line) shows the soundwaves with heterogeneous spectrum and irregular waveform, compared to the no-tumor area (dotted line) with more homogeneous pattern.

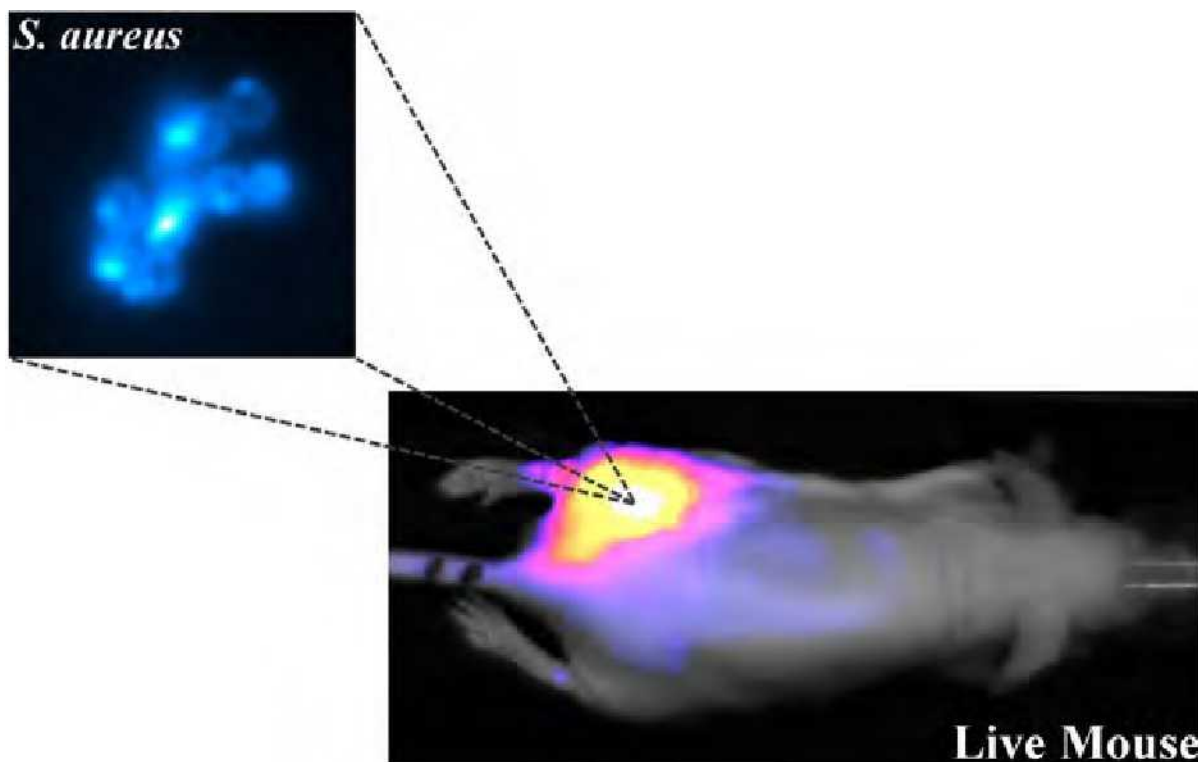
Presentation Number **0807A**

Poster Session 1c: In Vivo Studies & Development/Novel Use of Imaging Probes

Targeting of Bacterial Infection in Murine Models utilizing Zinc(II)-dipicolylamine Conjugated Squaraine Rotaxane Fluorescent Probes

Alexander White¹, **Bradley D. Smith**^{1,2}, ¹Chemistry and Biochemistry, University of Notre Dame, Notre Dame, IN, USA; ²Notre Dame Integrated Imaging Facility, University of Notre Dame, Notre Dame, IN, USA. Contact e-mail: awhite8@nd.edu

For years optical imaging of bacteria in vivo has been reliant upon the manipulation of genetic materials within the bacterial cell to produce optical light emitting materials. Such advances have been invaluable in the understanding of bacterial infection and the evaluation of antimicrobial therapies. However, such optimal conditions are not present in clinical bacterial infections. In this sense, the need for methods to evaluate a bacterial infection which mimics those seen in preclinical and clinical settings is high. We have discovered that the zinc(II)-dipicolylamine (Zn-DPA) organic ligand will associate with the anionic structures of the bacterial cell envelope. When linked to an organic fluorophore such as a far-red emitting squaraine rotaxane, these fluorescent probes can detect both Gram-positive and Gram-negative bacteria in vitro and in vivo. Here we compare two versions of Zn-DPA conjugated squaraine rotaxane probes and their ability to target bacterial cells in the living mouse. Clear association with the bacterial infection can be visualized within three hours of probe treatment followed by a clearance time of only a few hours. Biodistribution analysis of probe location indicates significant levels of probe in infected tissue. In addition to the infection site, probe is seen in the liver and kidneys indicating possible metabolic and excretory routes. Targeting of bioluminescent *Salmonella* shows exquisite overlay between luminescent signal from bacteria and fluorescent signal from the Zn-DPA associated probes which supports direct binding to the bacterial cell surface.



Presentation Number **0808A**

Poster Session 1c: In Vivo Studies & Development/Novel Use of Imaging Probes

ABC phenomenon with lactosome studied by *in vivo* NIRF imaging

Eri Takeuchi¹, **Isao Hara**¹, **Ryo Yamahara**¹, **Akira Makino**^{1,5}, **Kensuke Kurihara**², **Fumihiko Yamamoto**³, **Shinae Kizaka-Kondoh**⁴, **Akira Shimizu**², **Eiichi Ozeki**¹, **Shunsaku Kimura**^{2,5}, ¹Technology Research Laboratory, Shimadzu Corp., Kyoto, Japan; ²Translational Research Center, Kyoto University Hospital, Kyoto University, Kyoto, Japan; ³Tohoku Pharmaceutical University, Department of Radiopharmacy, Miyagi, Japan; ⁴Department of Biomolecular Engineering, Graduate School of Bioscience and Biotechnology, Tokyo Institute of Technology, Kanagawa, Japan; ⁵Department of Material Chemistry, Graduate School of Engineering, Kyoto University, Kyoto, Japan. Contact e-mail: takeuchi@kuhp.kyoto-u.ac.jp

Objectives: Repeated injections of PEGylated liposomes are known to evoke the accelerated blood clearance (ABC) phenomenon. In this study, the ABC phenomenon induced by amphiphilic polydepsipeptide micelle "lactosome" was studied by *in vivo* optical imaging of tumor-bearing mice. **Methods:** Micellar assemblies with a diameter of ca. 30 nm (lactosome) were prepared from a mixture of ICG-labeled poly(lactide) and the amphiphilic polydepsipeptide (poly(Sar)-*b*-poly(L-lactide)) by a film method. *In vivo* distribution of lactosome was studied by NIRF imaging with using BALB/c mouse, BALB/c nu/nu mouse, and SCID mouse. The production of anti-lactosome IgM was evaluated by ELISA. **Results:** The NIRF-labeled lactosome was shown to accumulate selectively in tumor at first intravenous injection. However, *in vivo* distribution of lactosome upon the second injection was changed to accumulate predominantly in liver (Fig.1). This type of the ABC phenomenon was not observed with using SCID mice. In the case of BALB/c nu/nu mice, anti-lactosome IgM was found in blood plasma to increase upon repeated injections of lactosome. **Conclusions:** The NIRF imaging is shown here to be an effective method for evaluation of the ABC phenomenon, which is induced generally by intravenous injection of nanocarriers.

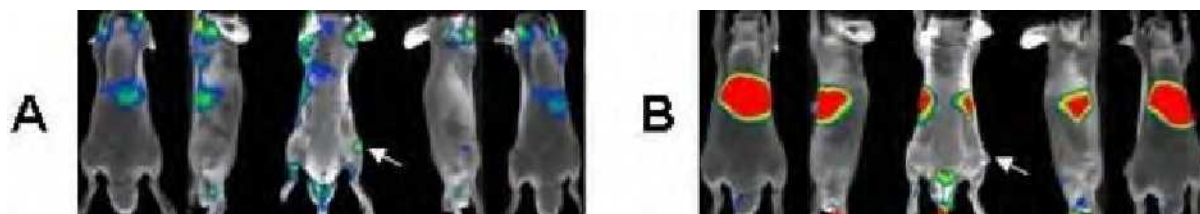


Fig1. The ABC phenomenon observed with a BALB/c nu/nu mouse by using ICG-lactosome. Arrows indicate the tumor regions. A: First injection B: Second injection after 8days from the first injection

Presentation Number **0809A**

Poster Session 1c: In Vivo Studies & Development/Novel Use of Imaging Probes

Novel Bright Near-Infrared Fluorescent Probes for in vivo Fluorescent Imaging

Keitaro Umezawa^{1,2}, Hiroko Yamamoto¹, Tomohiro Chiba³, Yuki Nakamura¹, Sadakazu Aiso³, Daniel Citterio¹, Kotaro Oka², Koji Suzuki¹, ¹Applied Chemistry, Keio University, Yokohama, Japan; ²Bioinformatics, Keio University, Yokohama, Japan; ³School of Medicine, Keio University, Tokyo, Japan. Contact e-mail: keitaro.umezawa@gmail.com

Bright and long-wavelength (red-NIR) fluorescent probes are recently required as new fluorescent probes and indicators for intracellular multicolor imaging, and as new contrast agents for in vivo imaging. While various long-wavelength fluorescent probes, as for example typified by cyanines (e.g. CyDye Fluor) have been developed, many of them suffer from certain insufficient optical characteristics such as a lack of brightness (fluorescence quantum yield) and photostability. Hence, alternative long-wavelength fluorescent probes are still required. In this presentation, we report a new series of bright fluorescent probes (Keio Fluors: KFL) which have sophisticated optical properties in the VIS-NIR region.[1,2] <p> The newly-synthesized KFL, which are based on boron-dipyromethene (BODIPY), have excellent optical properties: vivid colors in the wider spectral region (547-738 nm), extremely bright fluorescence, (quantum yield (QY): 56-98%), high extinction coefficients (140,000-288,000 M⁻¹cm⁻¹), and good photostabilities. The emission spectra can be tuned flexibly and finely by simple modifications of the KFL chromophore. The emission spectra of the KFL fluorophores are nearly identical to those of CyDye Fluor and Alexa Fluor. Furthermore, the emission spectral bands of KFL are extremely sharp, often even sharper than those of quantum dots (which are recognized as fluorescent materials with "sharp" emission spectra), and almost no spectral overlap between their emission bands is observed. These optical properties are totally superior to many of the existing fluorescent dyes such as rhodamines, cyanines or other BODIPY-based fluorescent probes. <p> In order to demonstrate in vivo imaging using KFL, labeling of KFL to biomolecules that can target specific lesion (e.g. antibodies, peptides) was performed. Labeling of NIR-emissive KFL to Herceptin (known as an anti-cancer antibody) and colivelin[3] (known as an anti-Alzheimer peptide) could be succeeded with retaining their bright emission (QY: ~86%). As far as we know, this is the brightest probe among the reported NIR fluorescent labeling ones. Finally, in vivo imaging using KFL could be achieved. In conclusion, KFL probes have sufficient potential to be applied for various bioimaging purposes such as intracellular multi-color imaging and in vivo NIR imaging. <p> [1] K. Umezawa et al. J. Am. Chem. Soc. 2008, 130, 1550-1551. [2] K. Umezawa et al. Chem. Eur. J. 2009, 15, 1096-1106. [3] T. Chiba et al. J. Neurosci. 2005, 25, 10252-10261.

Presentation Number **0810A**

Poster Session 1c: In Vivo Studies & Development/Novel Use of Imaging Probes

Protein-labeling technology based on a mutant β -lactamase and its functional substrates

Shin Mizukami^{1,2}, **Shuji Watanabe**¹, **Kazuya Kikuchi**^{1,2}, ¹*Graduate School of Engineering, Osaka University, Suita, Japan;*
²*Immunology Frontier Research Center, Osaka University, Suita, Japan. Contact e-mail: smizukami@mls.eng.osaka-u.ac.jp*

Protein labeling technology has attracted the increasing attention of life scientists, because protein labeling methods hold promise for overcoming the various limitations of fluorescent proteins in live cell imaging. This technology enables various functionalization of proteins with small molecules and is expected to lead to various protein assay methods. Fluorescence labeling techniques have contributed to several biological advances including, for example, characterization of the protein-protein interactions of the G protein-coupled receptor, trafficking of myoblasts, and cell cycle-regulated processes. We developed a novel protein labeling system based on a modified β -lactamase and its specific substrates. The active site of the tag protein was genetically engineered to reduce the substrate-leaving rate to attain covalent binding of the substrates. The labeling substrates can be designed such that the fluorescence increase can be triggered by the labeling step. Owing to the rational design of both the tag protein and the labeling substrates, this system enables us to simultaneously achieve specific and fluorogenic labeling of the target protein. We developed a series of longer-wavelength fluorescence labeling substrates and studied the broad applicability of this labeling technology to live cell imaging. New labeling probes employ a fluorescein or rhodamine chromophore for the practical applicability. These probes were specifically labeled on the β -lactamase tag. Also, orthogonality of the substrate specificity between our labeling technology and currently used protein labeling technology was verified. Then, our labeling technology can be exploited simultaneously with conventional protein labeling methods for investigating the specific labeling of two or more different proteins in single cells. We believe that our technology can be applied to more sophisticated imaging methods such as pulse-chase imaging, and that we can describe various protein-protein interactions identifiable by combining our method with fluorescent proteins and/or other protein labeling techniques.

Presentation Number **0811A**

Poster Session 1c: In Vivo Studies & Development/Novel Use of Imaging Probes

Development and Biological Application of a “Turn-on” Fluorescent Probe System for His-tagged Proteins

Atsushi Murata¹, **Yoon Su-In**^{2,3}, **Satoshi Arai**², **Masao Takabayashi**¹, **Miwako Ozaki**^{2,3}, **Shinji Takeoka**^{1,3}, ¹*Life Science and Medical Bioscience, Graduate School of Advanced Science and Engineering, Waseda University, TWIns, Tokyo, Japan;* ²*Comprehensive Research Organization, Waseda University, Tokyo, Japan;* ³*Waseda Bioscience Research Institute in Singapore (WABIOS), Singapore, Singapore. Contact e-mail: over-and-over@fuji.waseda.jp*

Fluorescence imaging is an excellent method to visualize bio-molecules under physiological conditions, because it is sensitive and has great temporal/spatial resolution. Labeling of the target protein with small chemical probes has the advantage of suppressing the movement obstruction of the target protein to minimum and being easy to be labeled. Hexahistidine (His6) has been widely used as an affinity tag for the purification of genetically engineered proteins by using affinity chromatography. Herein, we describe an approach to construct a novel “turn-on” probe system for His-tagged proteins using a small chemical probe and quencher-conjugated peptide. Because fluorogenic probes have the advantage that a washing step to remove the probe that is not bound to the His-tagged protein is not necessary, this system is expected to simplify the labeling procedure. As a His-tag targeting fluorescent probe, tetramethylrhodamine-conjugated tris-nitrilotriacetic acid (TMR-TriNTA) was synthesized. The NTA moieties of TMR-TriNTA would recognize the imidazole ring of histidine with coordination bonding via Ni²⁺ and makes a “turn-off” state by complexation with a Dabcyl-conjugated hexahistidine peptide (Dabcyl-His6). The recognition property of the TMR-TriNTA-3Ni²⁺ was analyzed with electrospray ionization mass spectrometry (ESI-MS), fluorescence correlation spectroscopy (FCS) and fluorescence intensity distribution analysis-polarization (FIDA-PO). The addition of Dabcyl-His6 decreased the fluorescence of the TMR-TriNTA-3Ni²⁺ solution to approximately 8% of its initial intensity. The fluorescence recovery efficiency was tested by adding either ubiquitin or His-tagged ubiquitin to a solution of Dabcyl-His6 and TMR-TriNTA-3Ni²⁺. Although there was no significant enhancement in fluorescence after addition of an equimolar amount of ubiquitin, the fluorescence increased ~3.1-fold when an equimolar amount of His-tagged ubiquitin was added. Additionally, TMR-TriNTA-3Ni²⁺ probe with or without Dabcyl-His6 were applied to Cos 7 cells expressing His-tagged membrane protein. By using TMR-TriNTA-3Ni²⁺ with Dabcyl-His6, non-specific background fluorescence was reduced. Therefore, this fluorescent probe was able to specifically recognize to His-tagged proteins with good resolution and has the additional advantage that a washing step is not required to remove fluorescent probe that is not bound to the His-tagged protein.

Presentation Number **0812A**

Poster Session 1c: In Vivo Studies & Development/Novel Use of Imaging Probes

Chemiluminescent probes for in-vivo imaging: Application to the detection of peptidases

Virgile Grandclaude^{1,2}, Jean-Alexandre Richard^{1,2}, Christophe Portal², Anthony Romieu¹, Marc Massonneau², Pierre-Yves Renard¹,
¹COBRA, University of Rouen, Mont Saint Aignan, France; ²Department of Chemistry, QUIDD, Saint Etienne du Rouvray, France.
Contact e-mail: virgile.grandclaude@gmail.com

Molecular imaging is of particular interest to detect biological disorders, provide accurate diagnosis and speed up drug development. Proteases play a fundamental role in most biological processes and diseases and thus constitute an attractive target. Luminescence spectroscopy happens to be a simple, low background noise, cheap and very sensitive technique. Chemiluminescence emission is the result of a chemical reaction allowing the generation of an excited molecule which emits light when coming back to the ground state and seems like a good prospect to improve signal to noise ratio and overcome problems related to radiative excitation. We proved the efficiency of the first chemiluminescent probe for the sensing of proteases(1,2). In particular, the activity of caspase-3 could be assessed with a promising detection limit of around 1 pmol. Current efforts are directed to the synthesis of 1,2-dioxetanes with enhanced light emission at wavelengths above 600 nm in order to allow in vivo imaging. The multistep synthesis of several new chemiluminescent species emitting in the NIR region will be described. Comparable emission levels were achieved for almost all structures prepared. Special attention was subsequently granted to the water compatibility of those luminophores. [1] Richard et al, Org. Lett., 2007, 9, 4853 [2] Richard et al, Org. Biomol. Chem., 2009, 7, 2941-2957



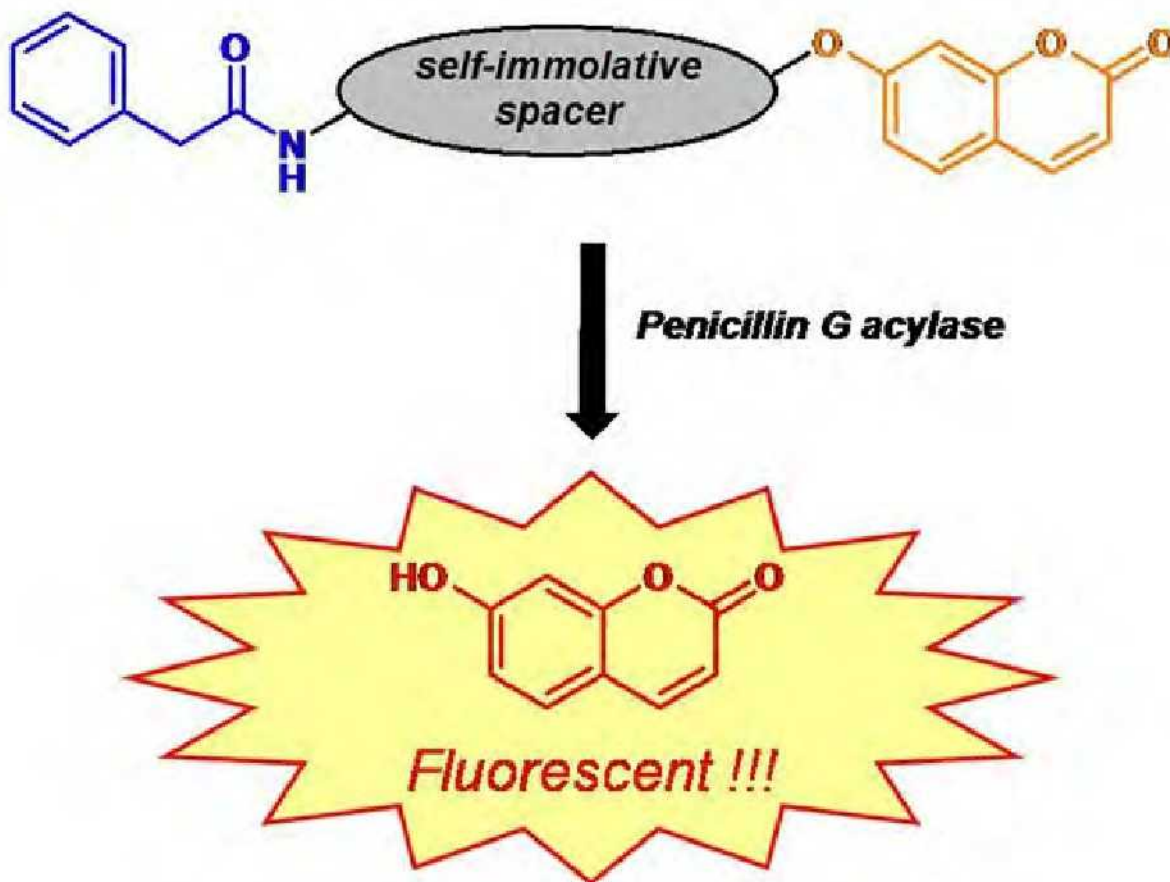
Presentation Number **0814A**

Poster Session 1c: In Vivo Studies & Development/Novel Use of Imaging Probes

A comparative study of the self-elimination of para-aminobenzyl alcohol and hemithioaminal-based linkers. Application to the design of Caspase-3 sensitive pro-fluorescent probes

Yves Meyer^{1,2}, Jean-Alexandre Richard^{1,2}, Bruno Delest², Anthony Romieu¹, **Pierre-Yves Renard**¹, Pauline Noack², Marc Massonneau², ¹COBRA, University of Rouen, Mont Saint Aignan, France; ²Department of Chemistry, QUIDD, Saint Etienne du Rouvray, France. Contact e-mail: pierre-yves.renard@univ-rouen.fr

Via general administration drugs may be delivered to undesired sites and this may lead to side effects. This issue may be addressed by increasing the specificity of action of the agent. A solution may be found with a prodrug strategy. More specificity of action is also an issue with activatable optical probes: in FRET-based activatable probes, the cleavage at the recognition site (peptide substrate for instance) gives rise to a modified signal but also any unspecific cleavage between the two partners of the FRET pair. A profluorescent approach may circumvent this problem as only the cleavage of one specific bond leads to a signal. In both approaches (prodrugs and profluorescence), a self-immolative linker is incorporated between the recognition moiety and the drug/fluorophore. In order to optimize this strategy, the disassembly-behavior of self-immolative pro-fluorescent linkers (via an enzyme-initiated domino reaction) under physiological conditions was studied (1). The targeted linkers are based on para-aminobenzylalcohol (PABA) (2) or hemithioaminal derivatives (3) of para-carboxybenzaldehyde or glyoxilic acid. We found that a fine tuning of the kinetic properties can be obtained through the modulation of the linker structure, giving either a fast signal response or customizable systems suitable for the design of protease-sensitive fluorogenic probes or prodrug systems (4). (1) R. Erez and D. Shabat, *Org. & Biomol. Chem.*, 2008, 15, 2669-2672. H. Y. Lee, X. Jiang and D. Lee, *Org. Lett.*, 2009, 11, 2065-2068. (2) C. Fossey, A.-H. Vu, A. Vidu, I. Zarafu, D. Laduree, S. Schmidt, G. Laumond and A.-M. Aubertin, *J. Enzyme Inhib. Med. Chem.*, 2007, 22, 591. C. Fossey, N.-T. Huynh, A.-H. Vu, A. Vidu, I. Zarafu, D. Laduree, S. Schmidt, G. Laumond and A.-M. Aubertin, *J. Enzyme Inhib. Med. Chem.*, 2007, 22, 608. (3) Y. Meyer, J. A. Richard, M. Massonneau, P. Y. Renard and A. Romieu, *Org. Lett.*, 2008, 10, 1517-1520. (4) Y. Meyer, J. A. Richard, B. Delest, P. Noack, P. Y. Renard and A. Romieu, *Org. & Biomol. Chem.*, 2010, 8, 1777-1780.



Presentation Number **0815A**

Poster Session 1c: In Vivo Studies & Development/Novel Use of Imaging Probes

D-Luciferin Based Bioluminescence Imaging Signal Dynamics is Affected by an Uptake Mechanism and ABCG2 Efflux Transporter Combined

Yimao Zhang¹, **Mrudula Pullambhatla**¹, **John Laterra**^{2,3}, **Martin Pomper**¹, ¹*Russell H. Morgan Department of Radiology, Johns Hopkins University, Baltimore, MD, USA;* ²*Department of Neurology, Johns Hopkins University, Baltimore, MD, USA;* ³*The Kennedy Krieger Institute, Baltimore, MD, USA. Contact e-mail: yzhang00@jhmi.edu*

Bioluminescence imaging (BLI) is used widely for imaging transgene expression in cell-based assays as well as in vivo in relevant preclinical models. BLI proceeds by detection of light generated by oxidation of substrates for a variety of luciferases. The most commonly used luciferase for in vivo applications is firefly luciferase (fLuc), with the intensity of signal output dependent upon the availability of its substrate, D-luciferin, to fLuc expressing cells. We have demonstrated previously that ABCG2 transporter efflux D-luciferin. Here we show that an uptake mechanism facilitates the uptake of D-luciferin, and BLI dynamics of different cell lines is affected by both ABCG2 efflux transporter and the uptake mechanism, with the uptake mechanism alone causing an initial high signal followed by continuously decreasing signal, and ABCG2 overexpression causing reduced but more stable signal dynamics. We show that the expression of SLC22A4 (OCTN1), a member of the organic cation/zwitterion uptake transporter family, is consistent with a role it may play in facilitating D-luciferin uptake. These findings provide insight into what contributes to the cellular uptake kinetics and in vivo biodistribution of D-luciferin, and may facilitate the improvement of BLI technique as a semi-quantitative imaging tool for more precise quantification.

Presentation Number **0816A**

Poster Session 1c: In Vivo Studies & Development/Novel Use of Imaging Probes

Biotin modification of living cell surface using mutant β -lactamase-tag technology

Akimasa Yoshimura¹, Shin Mizukami^{1,2}, Kazuya Kikuchi^{1,2}, ¹Graduate School of Engineering, Osaka University, Suita, Japan; ²Immunology Frontier Research Center, Osaka University, Suita, Japan. Contact e-mail: yoshimura@molpro.mls.eng.osaka-u.ac.jp

In order to visualize activities or localization of proteins of interest (POIs), specific protein labeling is important in the field of life science research. Most of the current strategies to achieve these objectives can be based on genetic fusion of POIs with a reporter protein such as fluorescent proteins (FPs). Although this technique is simple and is used by many scientists, several limitations remain in the current methods: for example, the modest fluorescence intensity, the scarce optical transparency to deep regions in living animals, etc. Recently, techniques for labeling POIs with small organic molecules have attracted the attention of many life scientists, because these techniques can extend the application range of natural FPs by appropriately using fluorescent dyes or functional molecules such as biotin. We focused on β -lactamases as the tag protein. β -Lactamases are monomeric bacterial enzymes that hydrolyze antibiotics containing a β -lactam structure and have no endogenous counterpart among eukaryotic organisms. A mutant β -lactamase was genetically modified to form a stable covalent adduct with the β -lactam compounds. We here report a general method for labeling POIs with biotin. If the POIs are biotinylated specifically, various streptavidin-conjugated functional molecules can be modified to POIs. As a ligand of β -lactamase-tag (BL-tag), a biotin-modified probe BHA was designed and synthesized. BHA consists with ampicillin and biotin, conjugated with a linker. By using BHA, POIs were able to be easily biotinylated. The specific labeling of BL-tag with BHA was confirmed by western blotting. Then, BL-tag was expressed on cell surface as a fusion protein with epidermal growth factor receptor (EGFR), and the fusion protein BL-EGFR was labeled with BHA. Biotinylated BL-EGFR was further functionalized by a streptavidin-conjugated quantum dots (saQDs). When the fluorescence of cells expressed with BL-tag were observed after addition of saQDs under a fluorescence microscope, fluorescence from saQDs was imaged on the cell surfaces. This labeling method should provide new imaging techniques for sensitive imaging and for functional regulation of POIs.

Presentation Number **0817A**

Poster Session 1c: In Vivo Studies & Development/Novel Use of Imaging Probes

Deeply Penetrating Photoacoustic Tomography in Biological Tissues Using CuS Nanoparticles and Hollow Gold Nanospheres (HAuNS) as Optical Contrast Agents

Geng Ku¹, Min Zhou¹, Meng Zhong¹, John D. Hazle², Juri G. Gelovani¹, Chun Li¹, ¹Exp. Diagnostic Imaging, U.T. M. D. Anderson Cancer Center, Houston, TX, USA; ²Imaging Physics, U.T. M. D. Anderson Cancer Center, Houston, TX, USA. Contact e-mail: cli@mdanderson.org

Objectives: Photoacoustic tomography (PAT) is a developing biomedical imaging modality that is based on the acoustical detection of the optical absorption of laser light by biomolecules. The purpose of this study was to evaluate new nanoparticles as a potential contrast agent for PAT. **Methods:** The semiconductor copper sulfide nanoparticles (CuS NP, ~11 nm in diameter) and hollow gold nanoshells (HAuNS, ~40 nm in diameter) were synthesized and characterized. The nanoparticles were dispersed with 10% polyacrylamide gelatin and used as an imaging object inside fresh chicken breast tissues. Near-infrared laser pulses 800-1064 nm were used to induce photoacoustic signals. PAT images were acquired with a prototype PAT device. **Results:** Objects containing a concentration of 1 mM of CuS NP and HAuNS could be clearly visualized at ~5 cm depth from the laser illuminating surface. Imaging resolution and sensitivity were estimated to be ~800 μm and ~6 nmol, respectively, at this depth. Significantly, PAT imaging of gels containing CuS NP at 7 cm was attainable under optimal data acquisition conditions. **Conclusions:** Both CuS NP and HAuNS nanoparticles were capable of transmitting and detecting photoacoustic signals. It is feasible to obtain deeply penetrating PAT images with high ultrasonic spatial imaging resolution in the presence of appropriate contrast agents.

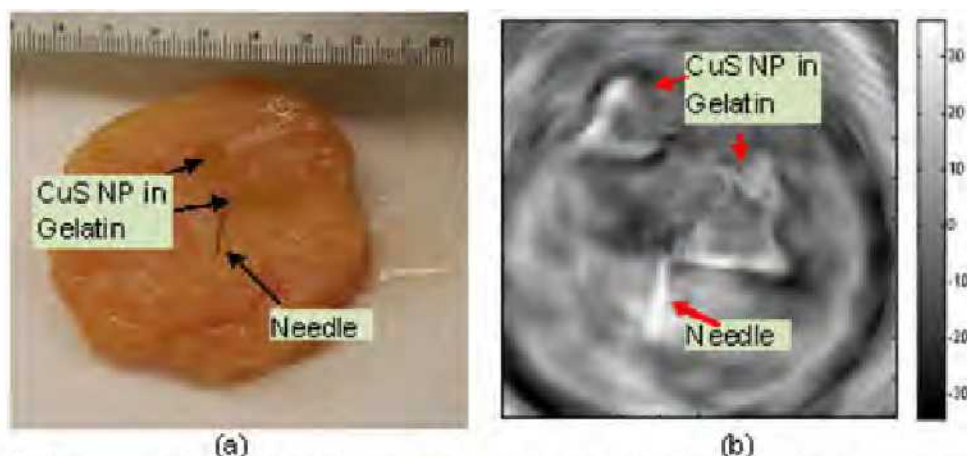


Figure PTA images of chick breast tissues with imbedded CuS NP-containing gels containing. (a) Photograph of the cross section of chicken breast tissue with gelatin objects containing CuS NP (1 mM) and a steel needle. (b) Two dimensional photoacoustic image at the depth of ~ 5 cm from laser illuminated surface.

Presentation Number **0818A**

Poster Session 1c: In Vivo Studies & Development/Novel Use of Imaging Probes

Comparison of In Vivo Molecular Imaging with Histology Samples for Lung Cancer Detection

Miguel Valdivia y Alvarado, Tian Cheng He, Zhong Xue, Stephen T. Wong, Kelvin Wong, Center of Bioinformatics, The Methodist Hospital Research Institute, Houston, TX, USA. Contact e-mail: kwong@tmhs.org

Introduction: Biopsies gives the ultimate diagnosis of cancer; however this practice has some delays due to sample preparation. In contrast, molecular imaging microscopy can provide in vivo cellular morphology and optical expression while guiding the biopsy procedure in real time. In this study we compared the detection of lung tumors using microendoscopic fluorescence reflectance imaging and validated it by histology. **Materials and Methods:** We conducted experiments in 6 nude mice where we inoculated A549 adenocarcinoma cell line in the lung and Indocyanine Green (ICG) was used for tumor vessel labeling. Mice were anesthetized with Ketamine/Xylazine, and ICG was administered via tail vein injection. After 15 minutes the chest was opened and the tumor was imaged using cellvizio 660 (Mauna Kea) using a 1mm O.D. fiberoptic probe. After imaging the mice were euthanized, and tumor samples were removed. The samples were fixed with 10% formalin and sectioned for H& E staining. **Results:** Using microendoscopy we can visualize zones with a high and low contrast uptake, which correspond to different level of angiogenesis inside the tumor. This was confirmed in the H& E slices. **Conclusion:** Microendoscopy fluorescence imaging can reliable detects tumors with leaky microvasculature and has the advantage to be performed in real time. **Discussion:** This technique allows detection of tumor vascularity. Upon injection, ICG binds to plasma protein, and it is confined to the vascular space. ICG acts as a blood tracer in normal capillaries, while it acts as a diffusible tracer in leaky capillary in tumor.

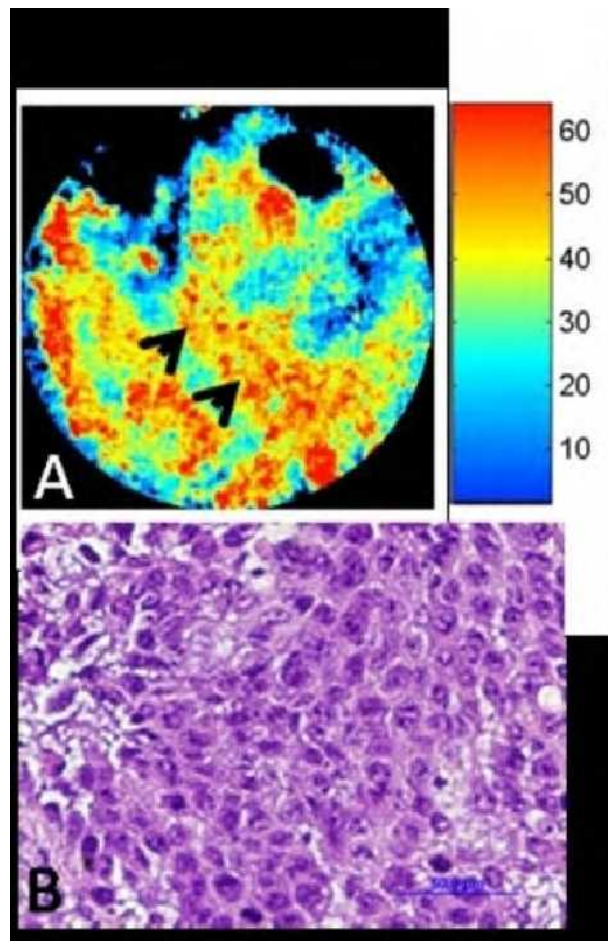


Fig. 1 A: Video sequence recorded from Cellvizio 660 microendoscope inside the tumor. In the top left we can see the original fluorescent image. The dark areas are necrotic zones due to hypoxia. The contrast uptake by the tumor is estimated using a signal intensity histogram. Black arrows denote the areas with high contrast uptake. B, H& E sample under optical microscopy at 40x showing adenocarcinoma cells .

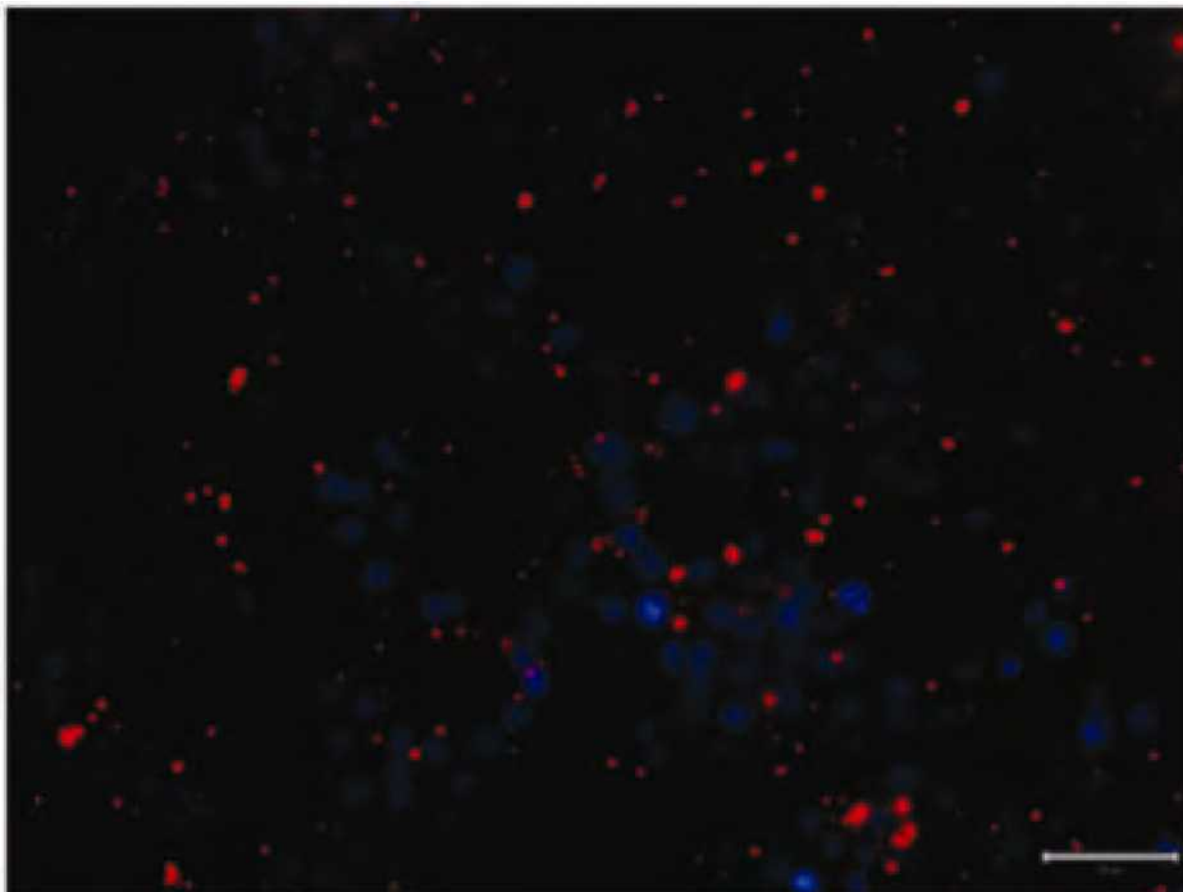
Presentation Number **0819A**

Poster Session 2c: In Vivo Studies & Development/Novel Use of Imaging Probes

Zinc sensors for imaging pancreatic beta-cell function

*Brahma Ghosh*¹, *Sujatha Thyagarajan*², *Sergei Vinogradov*², ***Anna Moore***¹, ¹*Radiology, Massachusetts General Hospital, Charlestown, MA, USA;* ²*Department of Biochemistry and Biophysics, University of Pennsylvania, Philadelphia, PA, USA. Contact e-mail: amoores@helix.mgh.harvard.edu*

Pancreatic islet beta cells contain a dynamic pool of mobile and chelatable zinc (Zn^{2+}), which acts as a mediator of insulin storage and secretion. A direct relationship between vesicular zinc ion content and insulin content has been demonstrated. It is, therefore, possible to evaluate beta-cell mass based on Zn^{2+} chelation by an imaging agent. In addition, Zn^{2+} and insulin are co-released by exocytosis. Consequently, the Zn^{2+} content of beta cells can serve as an indicator for insulin secretion, providing a way to not only detect beta-cell mass but also to directly evaluate beta-cell function. Further, there appears to be a complex relationship between Zn^{2+} and both type 1 and type 2 diabetes because several complications of diabetes may be mediated through oxidative stress, which is amplified in part by Zn^{2+} deficiency. This provides the impetus for the development of Zn^{2+} -specific imaging probes for detection of beta-cell mass during diabetes development. In this report we describe a family of dipyrrin-based chelating ligands that exhibit significant spectral change and extremely high fluorescence turn-on upon complexation with Zn^{2+} ; have their absorption and emission bands positioned in the near infrared region of the spectrum; and have fluorescence quantum yields (Φ) up to 0.7 in organic solvents—making them ideal for use as sensors for biological imaging of Zn^{2+} . Facile introduction of water-solubilizing groups led to derivatives with Zn^{2+} -binding constants in the micromolar range ($K_d \sim 2.5 \mu M$), which is compatible with concentrations of “free Zn^{2+} ” in several biological systems. In addition, the water-soluble analogs exhibit 100-fold higher affinity for Zn^{2+} over Ca^{2+} and Mg^{2+} in aqueous media. We demonstrate cellular uptake of membrane-permeable variants of this family of sensors using microscopy and report imaging/visualization of endogenous Zn^{2+} within secretory granules of RinM5f insulinoma cells (Figure 1). We also report detection of Zn^{2+} released upon glucose-stimulated insulin release from pancreatic beta-cells using the water-soluble derivatives.



Presentation Number **0820A**

Poster Session 2c: In Vivo Studies & Development/Novel Use of Imaging Probes

Development of Polymer Nano-Particle with Near-Infrared Absorption as Contrast Agent for Photoacoustic Tomography

Hiroyuki Aoki^{1,2}, Mayumi Nojiri², Hiroyuki Fujimoto², Shinzaburo Ito^{1,2}, Atsushi Takahashi³, Masato Minami³, Yoshinori Tomida³, Satoshi Yuasa³, Tetsuya Yano³, ¹Advanced Biomedical Engineering Research Unit, Kyoto University, Kyoto, Japan; ²Department of Polymer Chemistry, Kyoto University, Kyoto, Japan; ³Medical Imaging Project, Canon Inc., Tokyo, Japan. Contact e-mail: aoki@photo.polym.kyoto-u.ac.jp

The nano-particle of polymer materials was developed as a contrast agent for photoacoustic tomography (PAT). The polymer nano-particle (PNP) was prepared by a nano-emulsion method from a chloroform solution of polystyrene and silicon naphthalocyanine (SiNc). Since SiNc has an absorption band at 780 nm, it is suitable for the photoacoustic (PA) conversion in the near-infrared region. The SiNc moiety can be loaded up to 40 wt% in the particle, resulting in the molar absorption coefficient as large $10^{10} \text{ M}^{-1} \text{ cm}^{-1}$. The PA signal of the PNP containing SiNc (SiNc-PNP) was compared with the gold nano-rod (Au-NR, 75 x 25 nm), which is known as an efficient contrast agent for PAT. The SiNc-PNP with a diameter of 60 nm showed the PA intensity of 260 V/J (normalized by the excitation energy) in the solution with an absorbance of 1.0 (concentration of 1.4 nM), while that of the Au-NR solution was 490 V/J. This indicates that the PA conversion efficiency of PNP is comparable to that of the Au-NR. Moreover, while the PA signal from the gold nano-rod gradually decreased due to bleaching by the laser illumination, that from the SiNc-PNP was not altered after the repeated pulse irradiation. This indicates the high durability of the PNP against the photo-bleaching. For the demonstration of the in-vivo imaging, a PBS solution of SiNc-PNP at a concentration of 10 pM was subcutaneously injected into a thigh of a mouse. SiNc in PNP emits weak fluorescence at $> 780 \text{ nm}$; therefore, the spatial distribution can be observed in the fluorescence image as shown in Figure 1a, indicating the localization of the PNP at the thigh. Figure 1b shows the photoacoustic image. The photoacoustic signal from the PNP was greater than the background level due to the tissue chromophore such as hemoglobin in an in-vivo condition, and the spatial distribution of the PNP was clearly observed in this image. Thus the PNP would be a powerful contrast agent in PAT.

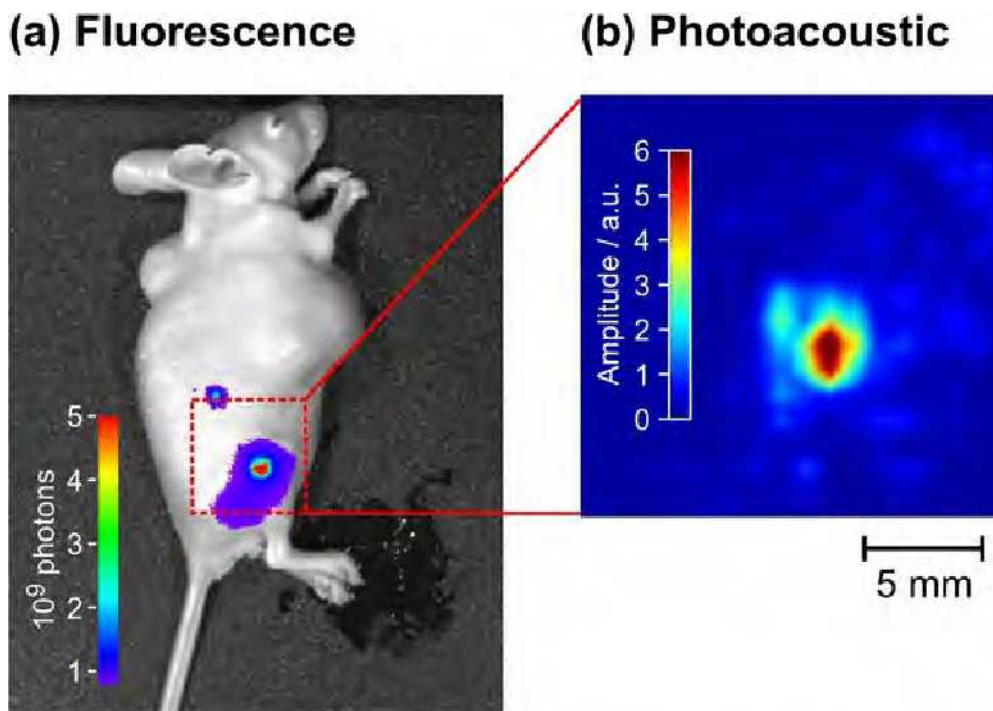


Fig 1. Fluorescence (a) and photoacoustic (b) images of PNP containing SiNc.

Presentation Number **0821A**

Poster Session 2c: In Vivo Studies & Development/Novel Use of Imaging Probes

Enhanced photoacoustic imaging efficacy of indocyanine green by the complexation with lipid-introduced gelatin derivatives

Jun-ichiro Jo¹, **Mie Morita**¹, **Masato Minami**², **Satoshi Yuasa**², **Tetsuya Yano**², **Yasuhiko Tabata**¹, ¹*Department of Biomaterials, Institute for Frontier Medical Sciences, Kyoto University, Kyoto, Japan;* ²*Molecular imaging Division, Medical Imaging Project, Corporate R&D Headquarters, Canon Inc., Tokyo, Japan. Contact e-mail: jo@frontier.kyoto-u.ac.jp*

Photoacoustic (PA) tomography is one of the promising imaging methods which play an important role in tumor diagnosis. Since the PA signal is generated through energy transfer from light to heat, various dyes with an ability of light absorption are used as the imaging agent. In this study, indocyanine green (ICG) was used for the PA imaging agent. It has been clinically used to diagnose hepatic functions. In addition, since the ICG absorbs light at a near-infrared wavelength, the PA imaging in the deep body site is highly expected. However, it is recognized that after intravenous injection, the absorbance of ICG decreases with time and the ICG is often accumulated in the liver, which are the drawbacks in terms of tumor imaging. Therefore, it is necessary to develop the technology of drug delivery system (DDS) to change the body distribution of ICG as well as enhance in vivo absorbance. For the DDS modification, gelatin was selected. Gelatin is a biocompatible material which has been clinically available while it has various functional groups to be chemically modified with ease. It has been reported that the ICG absorbance was enhanced and retained by binding to lipids present in the blood. Thus, to give gelatin a binding affinity for ICG, chemical modification with various lipids was performed for gelatin. Various amounts of cholesterol and distearoylphosphatidyl ethanolamine (DSPE) were chemically introduced to gelatin to obtain cholesterol-gelatins and DSPE-gelatins with different introduction extents, respectively. The gelatin derivatives (40 mg/ml) were simply mixed with the ICG (0.5 mg/ml) in aqueous solution to obtain various ICG-gelatin complexes. The absorbance was enhanced by the complexation with gelatin derivatives although it depended on the type of gelatin derivatives. The highest absorbance was observed for the ICG-DSPE gelatin complex. The intensity of PA signal was proportionally corresponded to that of ICG absorbance and enhanced by the complexation with gelatin derivatives. The complexation with gelatin derivatives enabled ICG to retain the absorbance at high levels, whereas the absorbance of ICG itself decreased after incubation in water with time. When intravenously injected to tumor-bearing mice, the ICG-gelatin complexes were accumulated to the tumor tissue to a great extent compared with the ICG solution. These results clearly indicate that the complexation with gelatin derivatives was effective in enhancing the PA imaging efficacy of ICG.

Presentation Number **0822A**

Poster Session 2c: In Vivo Studies & Development/Novel Use of Imaging Probes

Development of fluorescence activatable probes for β -galactosidase and their application as a diagnostic tool for the detection of peritoneal metastases of ovarian tumors in mouse models

Daisuke Asanuma¹, Mako Kamiya², Mikako Ogawa³, Nobuyuki Kosaka³, Yukihiro Hama³, Yoshinori Koyama³, Peter Choyke³, Hisataka Kobayashi³, Tetsuo Nagano¹, Yasuteru Urano², ¹Graduate School of Pharmaceutical Sciences, The University of Tokyo, Tokyo, Japan; ²Graduate School of Medicine, The University of Tokyo, Tokyo, Japan; ³Molecular Imaging Program, National Cancer Institute/NIH, Bethesda, MD, USA. Contact e-mail: ff087001@mail.ecc.u-tokyo.ac.jp

Peritoneal metastasis is an important cause of morbidity and mortality especially in ovarian cancer patients. The majority of patients with ovarian cancer have a poor prognosis because they already have advanced-stage disease with peritoneal metastasis at the time of diagnosis. Cytoreductive surgery followed by systemic or peritoneal chemotherapy is the standard of care for the patients. However, cytoreduction is often suboptimal due to the small size and location of the metastases and the poor visual contrast between tumor and normal tissue under the white-light conditions. For such operations, fluorescence activatable probes that become highly fluorescent in the lesion site have been attracting much attention. As for several ovarian tumor cells, we found high enzymatic activities of β -galactosidase that is often used as a reporter enzyme and is believed not to be expressed so much in normal mammalian cells. Therefore, we tried to visualize peritoneal metastases by the development and the application of β -galactosidase targeted fluorescence activatable probes satisfying the conditions as follows: (i) fluorescence activation after the target reaction by β -galactosidase, (ii) intracellular accessibility to the site of the target reaction, which is believed to be intralysosomal, and (iii) intracellular retention of their fluorescent products in the target cells. To fulfill these conditions, we adopted rhodol as a fluorophore and intramolecular spirocyclization reaction as an "OFF-ON" fluorescence switch for activatable probes. The properties of the developed activatable probes were evaluated in vitro, and subsequently, in ovarian tumor cells. These probes could be activated by β -galactosidase with over 100-times increase in fluorescence intensity and could detect intracellular β -galactosidase activity in live cell imaging. Then, we tried to visualize peritoneal metastases by intraperitoneal injection of the developed probes to several mouse models with ovarian tumor cells. At 1 hr post-injection, peritoneal metastases were successfully visualized in vivo as small as submillimeter in size by laparoscopic or endoscopic fluorescence imaging in all tested mouse models. Furthermore, unlike other fluorescence activatable probes such as 5-aminolevulinic acid, our activatable strategy targets rapid enzymatic reaction. Therefore, visualization of the lesions with the probes in the mouse models was achieved even at 10 min post-injection, indicating that our strategy could realize early fluorescence detection of peritoneal metastases in the imaging time course.

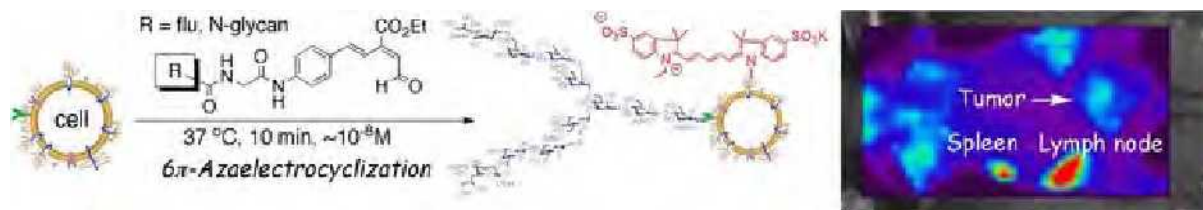
Presentation Number **0823A**

Poster Session 2c: In Vivo Studies & Development/Novel Use of Imaging Probes

Azaelectrocyclization-Based Labeling & Engineering Allow Non-Invasive Imaging of Cellular Trafficking and Tumor Targeting by Lymphocytes

Katsunori Tanaka¹, Kaori Minami¹, Tsuyoshi Tahara², Yohei Fujii¹, Eric Siwu¹, Satoshi Nozaki², Hirota Onoe², Satomi Yokoi³, Koichi Koyama³, Yasuyoshi Watanabe², Koichi Fukase¹, ¹Department of Chemistry, Graduate School of Science, Osaka University, Toyonaka, Japan; ²Center for Molecular Imaging Science, RIKEN, Kobe, Japan; ³Kishida Chemical Co., Ltd, Sanda, Japan. Contact e-mail: ktzenori@chem.sci.osaka-u.ac.jp

We recently developed the electrocyclization-based labeling of peptides and proteins with DOTA and fluorescent groups, and the method was applied to the efficient PET [1]. In this symposium, we report the labeling of a whole living cell through azaelectrocyclization; the present chemical method tightly anchors the fluorescence labels on the cell membranes under extremely diluted concentration of 10 nM [2]. Not only the fluorescence labels, but also the other functional groups, such as biotin or complex oligosaccharides, can be efficiently and covalently loaded onto cell surfaces by azaelectrocyclization [3]. Such a simple operation, namely, treatment of the living cells with electrocyclization probes in an appropriate buffer for a few minutes under physiological conditions, provides a promising opportunity for chemical labeling and chemical engineering of cell surfaces with broad and general applicability. An investigation of the non-invasive imaging of the fluorescence-labeled lymphocytes visualized the cellular trafficking into the immune-related organs with markedly high imaging contrasts [2]. The totally unexpected lymphocyte trafficking was also discovered by the cell surface engineering by the N-glycan; the engineered lymphocytes target the DLD-1 human colon carcinoma implanted in BALB/c nude mice [3]. [1] Tanaka, K.; Masuyama, T.; Hasegawa, K.; Tahara, T.; Mizuma, H.; Wada, Y.; Watanabe, Y.; Fukase, K. *Angew. Chem. Int. Ed.* 2008, 47, 102-105. [2] Tanaka, K.; Minami, K.; Tahara, T.; Fujii, Y.; Siwu, E. R. O.; Nozaki, S.; Onoe, H.; Yokoi, S.; Koyama, K.; Watanabe, Y.; Fukase, K. *ChemMedChem* in press. [3] Tanaka, K.; Minami, K.; Siwu, E. R. O.; Nozaki, S.; Watanabe, Y.; Fukase, K. *J. Carbohydr. Chem.* in press.



Presentation Number **0824A**

Poster Session 2c: In Vivo Studies & Development/Novel Use of Imaging Probes

Optical imaging probe for matrix metalloproteinases activity in malignant tumors

Tao Zhao^{1,2}, Hiroshi Harada^{1,2}, Yuji Teramura³, Shotaro Tanaka², Satoshi Itasaka², Akiyo Morinibu^{1,2}, Kazumi Shinomiya^{1,2}, Yuxi Zhu^{1,2}, Hirofumi Hanaoka^{4,5}, Hiroo Iwata³, Hideo Saji⁴, Masahiro Hiraoka², ¹Group of Radiation and Tumor Biology, Career-Path Promotion Unit for Young Life Scientists, Kyoto University, Kyoto, Japan; ²Department of Radiation Oncology and Image-applied Therapy, Graduate School of Medicine, Kyoto University, Kyoto, Japan; ³Institute for Frontier Medical Sciences, Kyoto University, Kyoto, Japan; ⁴Department of Patho-Functional Bioanalysis, Graduate School of Pharmaceutical Sciences, Kyoto University, Kyoto, Japan; ⁵Department of Bioimaging Information Analysis, Graduate School of Medicine, Gunma University, Maebashi, Japan. Contact e-mail: zhaotao@kuhp.kyoto-u.ac.jp

Matrix metalloproteinases (MMPs) are endopeptidases, which are responsible for degrading the extracellular matrix (ECM) and remodeling tissue in both physiological and pathological processes. MMP2 and membrane-type 1 MMP (MT1-MMP), two of the important members of MMPs, have been associated with tumor invasion, metastasis and angiogenesis; therefore, a molecular imaging strategy assessing their activity may help to predict the malignancy of tumors. Here, we successfully established a novel method of specifically tagging the surface of MMP2- and MT1-MMP-positive cells, and applied it to the development of an optical imaging probe. We constructed a protein-based probe composed of a glutathione-S-transferase (GST)-tag (Inhibitory [I]-domain), a polypeptide as a specific substrate for both MMP2 and MT1-MMP (Cleaved [C]-domain), a transmembrane domain of the epidermal growth factor receptor (Transmembrane [TM]-domain), and DsRed2 (Fluorescent [F]-domain). In vitro experiments clearly demonstrated that, after the probe was cleaved at the C-domain by the MMPs, the resultant TM-F-domain was inserted into the cellular membrane. Optical imaging experiments in vivo demonstrated that the probe was cleaved and specifically remained in tumor xenografts in a MMP-dependent manner. These results indicate that the release of the I-C-domain through the proteolytic cleavage of the C-domain by MMP2 and MT1-MMP triggers the tagging of cellular membranes with the TM-F-domain. The present feasibility study opens the door to the development of a novel imaging probe for tumor malignancy using positron emission tomography as well as an optical imaging device.

Presentation Number **0825A**

Poster Session 2c: In Vivo Studies & Development/Novel Use of Imaging Probes

In Vivo Ultra-low Background Optical Lymphatic Imaging Using Upconverting and BRET-QD Nanoparticles

Nobuyuki Kosaka, Mikako Ogawa, Makoto Mitsunaga, Peter Choyke, Hisataka Kobayashi, Molecular Imaging Program, National Cancer Institute / NIH, Bethesda, MD, USA. Contact e-mail: nobu.kosaka@gmail.com

Optical lymphatic imaging has advantages over other modalities, including portability, high spatial resolution, real-time display and absence of radiation. Thus it holds promise for preclinical and clinical applications. Previous studies have used conventional fluorescent agents, which need excitation light to induce fluorescence. However, excitation light also induces autofluorescence (background signal) from intrinsic fluorophores in the normal tissue, thereby lowering the signal-to-background ratio (SBR). Herein, we employed two unique nanoparticles; an upconverting nanoparticle (UCNP) and a self-illuminating bioluminescence resonance energy transfer quantum-dot (BRET-QD) nanoparticle for optical lymphatic imaging. These agents successfully eliminated autofluorescence resulting in higher SBR. UCNPs are unique nano-sized particles that are excited in the NIR but emit light at shorter wavelengths thus greatly reducing autofluorescence. By changing the composition of the doping metals, UCNPs can be designed to emit at multiple specific wavelengths. When UCNPs were injected into the chin of anesthetized mice, and excited at 950-nm, superficial neck lymph nodes were successfully depicted with no background signals in the visible-range (peak 550 nm) or NIR-range (peak 800 nm) in all mice. Furthermore, with serial injection of the visible and NIR-range UCNPs, simultaneous lymphatic imaging was achieved in two colors. The BRET-QD employs the substrate, coelenterazine, which reacts with luciferase conjugated on the BRET-QD. The bioluminescent blue light efficiently excites the NIR-QD, which emits photons in the NIR, thereby avoiding autofluorophore excitation. BRET-QD655, (QD655 in its core), was injected at different sites (chin, ear, forepaws, and hind paws) of anesthetized mice. After BRET-QD injection, coelenterazine was intravenously injected and imaging was performed without extrinsic excitation light. In all mice, each lymphatic basin were clearly visualized with ultra-low background signals, and lasted at least 30 min after coelenterazine injections. In conclusion, we demonstrate that optical imaging using two unique nanoparticles were able to depict lymphatic basins with minimal autofluorescence. This enables direct, real time lymphatic imaging without extensive post processing of the images. These two novel nanoparticles have the potential to be robust tools for in vivo lymphatic imaging.

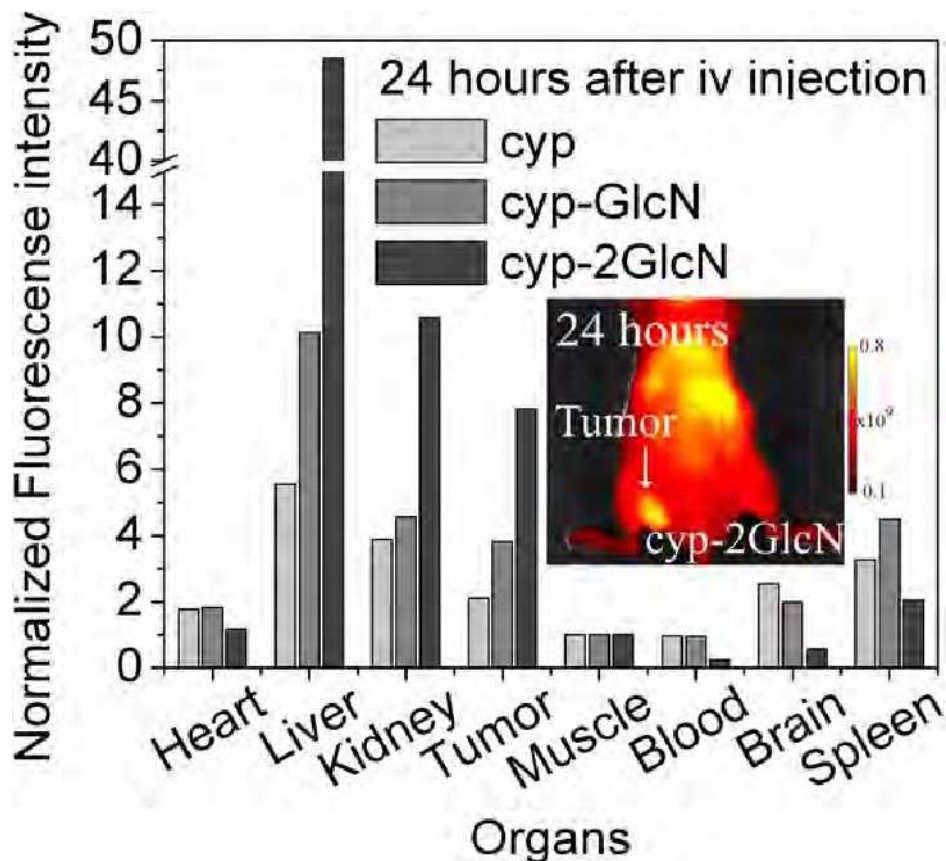
Presentation Number **0826A**

Poster Session 2c: In Vivo Studies & Development/Novel Use of Imaging Probes

Glucosamine Linked Near-infrared Fluorescent Probes for Noninvasive Imaging of Solid Tumor Xenografts

Alexandru V. Korotcov¹, Yunpeng Ye², Yue Chen¹, Rajagopalan Sridhar³, Samuel Achilefu², Paul C. Wang¹, ¹Molecular Imaging Laboratory, Department of Radiology, Howard University, Washington, DC, USA; ²Optical Radiology Laboratory, Department of Radiology, Washington University School of Medicine, St. Louis, MO, USA; ³Department of Radiation Oncology, Howard University, Washington, DC, USA. Contact e-mail: akorotcov@howard.edu

Background/Aims: The near-infrared fluorescence (NIRF) imaging is an attractive noninvasive technique for studying diseases at the molecular level, detecting small tumors, monitoring targeted drug delivery, and evaluating therapeutic efficacy. The goal of this study was to evaluate newly developed glucosamine linked NIRF probes for optical imaging in tumor cell culture and in solid tumor xenografts in nude mice. **Materials and Methods:** Cellular uptake of the probes (1 μmol) was investigated in monolayer cultures of PC-3-luc cells. The prostate tumors were established as subcutaneous xenografts using PC-3-luc cells in nude mice. NIRF imaging was performed using Caliper-Xenogen optical imaging system. The tumor, muscle and the major organs were collected for the ex vivo optical imaging study. The biodistribution and tumor targeting specificity of cypate (cyp), cypate conjugated to a single glucosamine molecule (cyp-GlcN), and cypate conjugated to two glucosamine molecules (cyp-2GlcN) were studied. **Results:** The tumor cell uptake of cyp-2GlcN was significantly higher than the uptake of the cyp-GlcN and cyp. For in vivo experiments the animals were given 10 nmol of NIRF probes via tail vein injection. The cyp-2GlcN demonstrated higher maximum fluorescence intensity and longer residence lifetime in tumors than cyp-GlcN and cyp. The ex-vivo biodistribution analyses revealed that tumor uptake of cyp-2GlcN and cyp-GlcN was 4 and 2-fold higher than that of cyp at 24 hours post injection. **Conclusions:** Both cyp-GlcN and cyp-2GlcN NIRF probes have demonstrated good tumor-targeting properties in prostate cancer cell culture and live mice. The cyp-2GlcN probe showed the highest uptake with excellent retention characteristics in vivo. The uptake of cyp-2GlcN and cyp-GlcN is likely mediated by glucose and/or glucose derivative transporters. The uptake mechanism is under investigation with a view to improve cypate-glucosamine based probes for optical imaging in cell culture and living subjects.



Presentation Number **0827A**

Poster Session 2c: In Vivo Studies & Development/Novel Use of Imaging Probes

Comparing NIRF imaging using a protease-activatable probe with narrow-band imaging for tumor detection in APCmin mice

Soon Man Yoon^{1,2}, Seung-Jae Myung^{1,2}, Byong Duk Ye^{1,2}, In-Wha Kim², Eun Ju Do², Ji Hye Kim², Ju Hee Ryu³, Kwangmeyung Kim³, Ick Chan Kwon³, Mi Jung Kim⁴, Dae Hyuk Moon^{2,5}, Dong-Hoon Yang¹, Kyung-Jo Kim¹, Jeong-Sik Byeon¹, Suk-Kyun Yang¹, Jin-Ho Kim¹, ¹Department of Internal Medicine, Asan Medcial Center, University of Ulsan College of Medicine, Seoul, Republic of Korea; ²Molecular Imaging Center, Asan Institute for Life Sciences, Seoul, Republic of Korea; ³Biomedical Research Center, Korea Institute of Science and Technology, Seoul, Republic of Korea; ⁴Department of Pathology, Asan Medcial Center, University of Ulsan College of Medicine, Seoul, Republic of Korea; ⁵Department of Nuclear Medicine, Asan Medcial Center, University of Ulsan College of Medicine, Seoul, Republic of Korea. Contact e-mail: sm6034@hanmail.net

Background/Aims: Evolving endoscopic technology has been advancing in order to produce more accurate tumor detection. Recently developed endoscopies such as narrow band imaging (NBI), however, still have limitations based on morphologic diagnosis. This study aims to investigate whether near-infrared fluorescence (NIRF) imaging using a protease-activatable probe is helpful in providing more accurate tumor detection by comparison of NIRF imaging and NBI. **Methods:** We first obtained the NIRF imaging in the intestines of APCmin mice. The probe used for the NIRF imaging was a matrix metalloproteinase (MMP)-sensing probe based on a polymeric nanoparticle platform. And then, NBI was performed immediately using an endoscopic imaging system (Olympus Medical Systems) in the same excised intestine. The intestines were evaluated by histological examination and MMP expression was analyzed by Western blotting and real time-PCR. **Results:** Numerous tiny polypoid lesions were observed in the intestines of aged APCmin mice. NIRF imaging using an MMP-activatable probe showed highly fluorescent in the adenomatous polyps. The tumor-to-background ratios of NIRF signal intensity by MMP-activatable probe and scramble control probe were 6.01 and 2.91, respectively ($p < 0.05$). The MMP expression of tumors was higher than in the adjacent normal mucosa. Sensitivity and specificity for tumor detection with NIRF imaging were 88.9% and 77.8%, respectively, whereas, those with NBI were 68.4% and 63.9%, respectively ($p < 0.05$). **Conclusions:** NIRF imaging using a protease-activatable probe could be helpful in tumor detection. The clinical application of this approach could significantly improve the endoscopic detection of colon tumors.

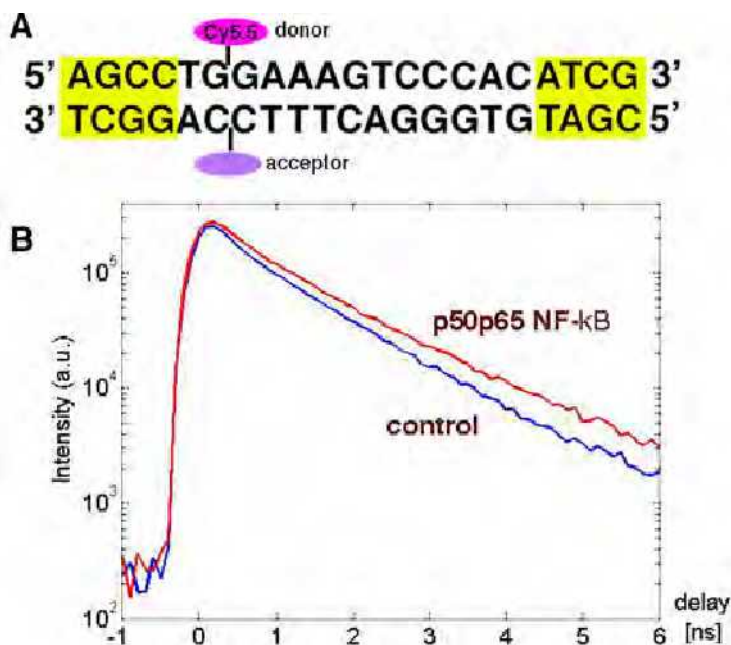
Presentation Number **0828A**

Poster Session 2c: In Vivo Studies & Development/Novel Use of Imaging Probes

Time-resolved fluorescence detection of NF-kappaB interaction using FRET oligonucleotide probes

Surong Zhang¹, Anand T. Kumar², Valeriy G. Metelev¹, Alexei A. Bogdanov¹, ¹Laboratory of Molecular Imaging Probes, UMASS Medical School, Worcester, MA, USA; ²A. Martinos' Center, Massachusetts General Hospital, Charlestown, MA, USA. Contact e-mail: alexei.bogdanov@umassmed.edu

We previously reported novel nucleoside linker chemistry designed for positioning covalently bound ligands between any nucleotides in a DNA or RNA duplex without interfering with Watson-Crick base pairing [1]. The goal of the current study was to investigate interactions of NF-kB p50/p65 transcription factor complex with near-infrared FRET DNA duplex probes based on the above chemistry by applying a time domain multiexponential analysis for resolving discrete fluorescence lifetimes (FL-TD) present within the sample mixture [2]. We used hybrid phosphorothioate-phosphodiester DNA duplexes with dyes linked to complementary strands to create an efficient trans-duplex FRET probe (FRET efficiency ~ 82%, Cy5.5 - donor/Cy7 or 800CW - acceptor) (Fig. A). Within the probe, the dye pair is sterically constrained and thus non-interacting so that quenching does not occur. Measurements of FL-TD sensitivity to the presence of FRET and non-FRET Cy5.5 populations correlated well with data obtained in phantoms consisting of a mixture of FRET (Cy5.5/Cy7) and non-FRET (Cy5.5) duplex probes. These results suggest that FL-TD can be used for detecting minor fractions of non-FRET duplexes in mixtures of fluorescent probes. The addition of p50 and p65 (3 fold molar excess over DNA) to the solution of FRET probe (100 nM) resulted in a measurable increase of Cy5.5 dye lifetime, which depended on acceptor (Cy7- 1.05 to 1.13 ns and 800CW - 1.1 to 1.25 ns). These results suggest interference of protein-DNA interactions with NIR FRET (Fig. B). In view of: 1) applicability of NIR fluorochromes for in vivo imaging; and 2) inherent advantages of the asymptotic FL-TD approach to fluorescence tomography when deconvoluting discrete lifetimes [2], we anticipate that further development of chemically stabilized NIR FRET probes will allow for direct imaging of transcription factor interactions in living systems using FL-TD approach. References: 1. Zhang, S. et al. PNAS 105:4156, 2008 2. Kumar, A.T.N. et al. Optics Lett 33:470, 2008.



A - the sequence of hybrid DNA FRET probe;
B - fluorescence decay curves showing differential fluorescence lifetimes.

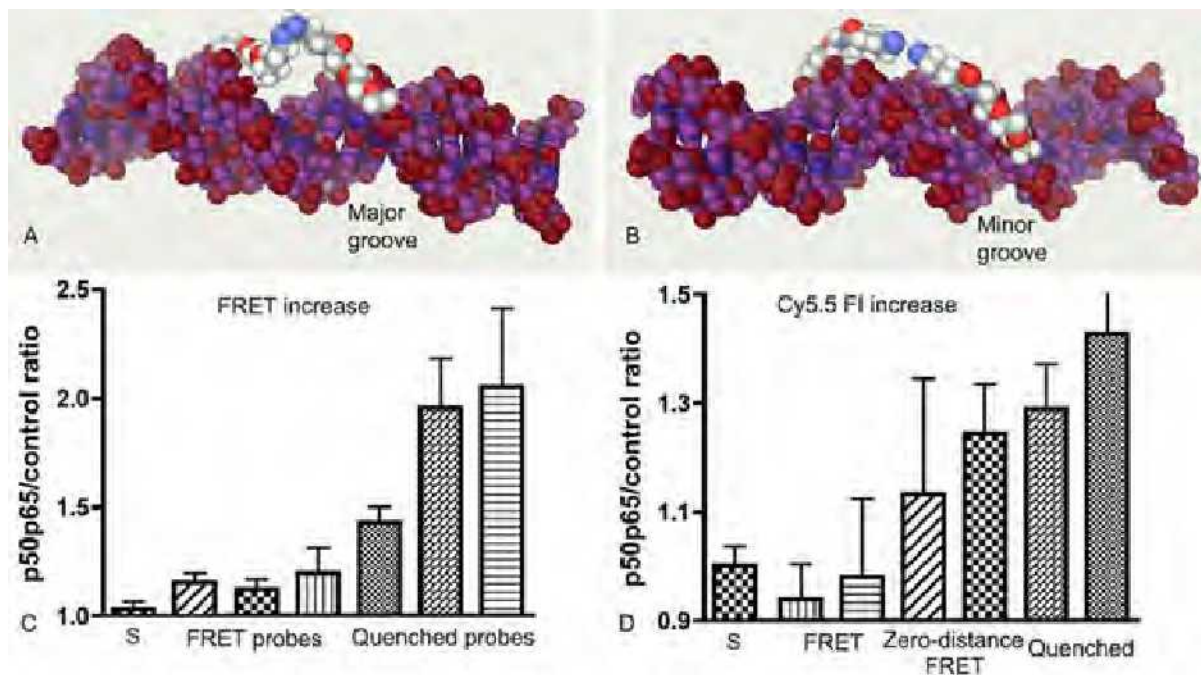
Presentation Number **0829A**

Poster Session 2c: In Vivo Studies & Development/Novel Use of Imaging Probes

Encoding of radiative and non-radiative fluorescence energy transfer in DNA duplex probes for NF- κ B imaging

Valeriy G. Metelev¹, Surong Zhang¹, Alexander M. Nikitin², Alexei A. Bogdanov¹, ¹Radiology, Laboratory of Molecular Imaging Probes, Worcester, MA, USA; ²Protein-DNA Recognition, Engelhardt Institute of Molecular Biology, Moscow, Russian Federation. Contact e-mail: alexei.bogdanov@umassmed.edu

We synthesized and characterized dual-NIRF dye NF- κ B binding DNA duplex probes with various inter-fluorochrome distances and positions along the complementary oligonucleotide sequences. We used novel nucleoside synthons with hydrophilic internucleoside triethylene glycol linkers for conjugating Cy5.5 (donor) and 800CW (acceptor) dyes to oligonucleotides. Exonuclease resistance was achieved by incorporating three phosphorothioates at the 3'- and 5'- ends of oligonucleotides during the synthesis. The formation of DNA duplexes resulted in 0-10 base pair distances between the dyes. We established that the distance alone does not determine the resultant fluorescence emission or quenching modes. For probes with the same 8-base pair inter-fluorochrome distance we observed either: 1) strong static quenching of NIR fluorescence if DNA- linked fluorochromes were separated by the major groove (Fig. A); or 2) an efficient FRET if the linked dyes were separated by the minor groove of the DNA duplex (Fig. B). 3D-modeling of the corresponding DNA duplexes showed high probability of dye contact (A) and low probability of dye interaction (B), respectively. We performed limited screening of these probes for NF- κ B-mediated activation in the presence of a p50/p65 complex by measuring FRET ($\lambda_{ex}=675$ nm/ $\lambda_{em}=800$ nm) as a result of dequenching of fluorochromes or, alternatively, the increase of donor fluorescence as a result of FRET decrease ($\lambda_{ex}=675$ nm/ $\lambda_{em}=700$ nm) in FRET probes. The highest experiment/control ratio of fluorescence signal change upon the addition of NF- κ B was observed when the quenched probes were used (Fig C). Zero-distance FRET probes showed an increase of Cy5.5 donor fluorescence, suggesting a protein-mediated change of the inter-fluorochrome distance and the decrease of FRET efficiency (Fig. D). Our results demonstrate for the first time that the choice of relative internucleoside linker positions on individual oligonucleotides is crucial in determining whether the resultant DNA duplex will fluoresce or not.



A - a model of a quenched duplex probe- linker nitrogens (blue) are in close proximity; B - FRET (non-quenched) probe; C - the increase of FRET in response to p50/p65 binding to DNA duplex probes; D - the increase of Cy5.5 fluorescence intensity. S- standard control duplex with a single 800CW acceptor dye.

Presentation Number **0830A**

Poster Session 2c: In Vivo Studies & Development/Novel Use of Imaging Probes

Determining potential targets for intra-operative cancer-specific fluorescent imaging (ICSFI) in colorectal peritoneal carcinomatosis

Marleen van Oosten¹, Lucia M. Crane¹, Niels J. Harlaar¹, Wijnand Helfrich¹, Klaas Havenga¹, Robert J. van Ginkel¹, Philip S. Low³, Barbara L. van Leeuwen¹, Gooitzen M. van Dam¹, Joost Bart², ¹Surgery, University Medical Center Groningen, Groningen, Netherlands; ²Pathology, University Medical Center Groningen, Groningen, Netherlands; ³Chemistry, Purdue University, West Lafayette, IN, USA. Contact e-mail: marleenvanoosten@hotmail.com

Introduction: Peritoneal carcinomatosis (PC) of colorectal origin is associated with poor prognosis. The median survival time of patients with untreated PC of colorectal origin is limited to 22 weeks with no 5 year survival. In selected patients with colorectal PC, treatment is possible with cytoreductive surgery in combination with hyperthermic intraperitoneal chemotherapy (HIPEC). In this procedure the abdominal cavity is flushed with a warmed chemotherapeutic agent after cytoreduction. With this treatment the 5 year survival raises to 30%, yet leaving ample room for improvement. It is known that radical tumor resection is correlated with a better prognosis, and that residual tumor is correlated with a worse prognosis. However, so far a reliable method for detecting minimal residual disease does not exist. Detection and surgical elimination of microscopic residual disease can possibly be improved by intra-operative cancer specific fluorescent imaging (ICSFI) for detection of microscopic disease, using labelled antibodies against proteins that are expressed by tumor cells. Potential targets for ICSFI could be hypoxia inducible factor-1alpha (HIF-1 α), folate receptor alpha (FR- α), CXCR4, vascular endothelial growth factor-A (VEGF-A), epidermal growth factor receptor (EGFR) and epithelial cell adhesion molecule (EpCAM). Methods: Of 21 patients who underwent the HIPEC procedure because of colorectal PC or pseudomyxoma peritonei, excised tumor tissue was immunohistochemically analysed for expression of HIF-1 α , FR- α , CXCR4, VEGF-A, EGFR and EpCAM, on slides of formalin fixed, paraffin embedded tissue. All tumor tissue sections were evaluated independently by one researcher and one pathologist. Results: Tumor tissue of all patients was strongly positive for VEGF-A (21/21) and EpCAM (21/21). 93% (15/16) of the tumors showed diffuse, but variable expression of CXCR4. 93% (15/16) of the tumors showed focal expression of HIF-1 α . 29% of the tumors (6/21) showed focal, weak to moderate expression of FR- α . None of the tumors showed expression of EGFR. Conclusion: VEGF-A, CXCR4 and EpCAM are promising proteins to develop cancer specific targeted agents for intra-operative visualization of residual colorectal PC and thereby improvement of surgical outcome. In addition, these proteins may potentially function as a target for innovative, relatively cancer-specific cytotoxic drugs, used in the HIPEC setting.

Presentation Number **0831A**

Poster Session 2c: In Vivo Studies & Development/Novel Use of Imaging Probes

SRFluor®: Superior NIR Dyes for Bioimaging

Arunkumar Easwaran¹, Brian Gray¹, Maria Kleinz¹, Jung-Jae Lee², Koon Y. Pak¹, Bradley D. Smith², ¹Molecular Targeting Technologies, Inc., West Chester, PA, USA; ²Chemistry and Biochemistry, University of Notre Dame, Notre Dame, IN, USA. Contact e-mail: cpak@mtarget.com

The need for bright and stable NIR dyes in optical imaging triggered the development of several new class of dyes in this decade. Among these, squaraine rotaxanes (SR) look quite promising as they are among the world's brightest and most stable fluorescent NIR dyes. However due to their poor solubility under aqueous conditions, their usefulness in biological applications remains a challenge. Therefore we have developed a new generation of water soluble SR dyes by incorporating multiple sulfonate groups and a carboxylic acid which can readily undergo conjugation with free amino groups. The new generation SR dyes retained sharp absorption and emission features in phosphate buffer unlike the commercially available cyanine (Cy5) dyes. We have successfully conjugated these new generation SR dyes to biomolecules such as IgG and streptavidin and carried out detailed investigation on their photophysical properties. The results show they are likely to become superior replacements for the Cy5 dyes and become extremely useful probes for both in vitro and in vivo imaging applications. Squaraine Rotaxane dyes are commercialized by MTTI under the name SRFluor®.

Presentation Number **0832A**

Poster Session 2c: In Vivo Studies & Development/Novel Use of Imaging Probes

PEGylated Molecular Beacons for Imaging Protease Expression In Vivo

Seulki Lee, Lei Zhu, Jin Xie, Xiaoyuan Chen, NIBIB, National Institutes of Health, Bethesda, MD, USA. Contact e-mail: seulki.lee@nih.gov

Many of the reported peptide-based molecular beacons, so called activatable probes, have demonstrated promising results both in vitro and in vivo. However, the inherent instability, short half-life, and nonspecific activation of peptides are still major obstacles for its in vivo application. Conjugation of macromolecules efficiently increases the stability and in vivo circulation, but typically decreases the sensitivity of the probe requiring longer circulation time to get high contrast images. Therefore, it is important to strike a balance between stability and sensitivity of the probe in vivo to enable quick screening of animals with enhanced target-to-background ratios. Here, we show that the PEGylated NIR molecular peptide probes can be used as an efficient optical contrast agent for imaging various protease-associated diseases. The probes consist of strongly quenched matrix metalloproteinase (MMP)-specific fluorogenic peptide and PEGs with different molecular weights (MWs). It was hypothesized that chemically labeled dark quenched MMP substrates with PEGs induce different specificity and sensitivity of the probe in vivo, since PEG can alter the stability, half-life, and enzyme susceptibility of the probe. To demonstrate our rationale, we prepared the MMP activatable probe, Cy5.5-GLGVRGK(BHQ-3)GG, labeled with PEGs of different sizes (molecular weight from 250 to 3,000 Da, MMP-Ps). The spectrofluorometry clearly demonstrates that significant time- and concentration-dependent recovery of the fluorescence signals occurred against MMPs (> 30-folds vs. without MMP). IV administration of the MMP-Ps in MMPs-positive UM-SCC-22B xenograft model verifies the MW-dependent enzyme specificity of the probe in vivo. An optimized formulation is able to achieve high fluorescent signal intensity in tumor bearing mice in 30 min. These results were further confirmed by ex vivo immunohistology. MMP-P is able to sense and image target proteases in a rapid and efficient fashion. This system permits reproducible constructs with accurate chemical structures and provides easy scale-up synthesis, handling, and storage. Moreover, the design platform is fine-tunable for a wide array of applications, such as detecting biomolecules, early diagnosis of disease, and monitoring therapeutic efficacy.

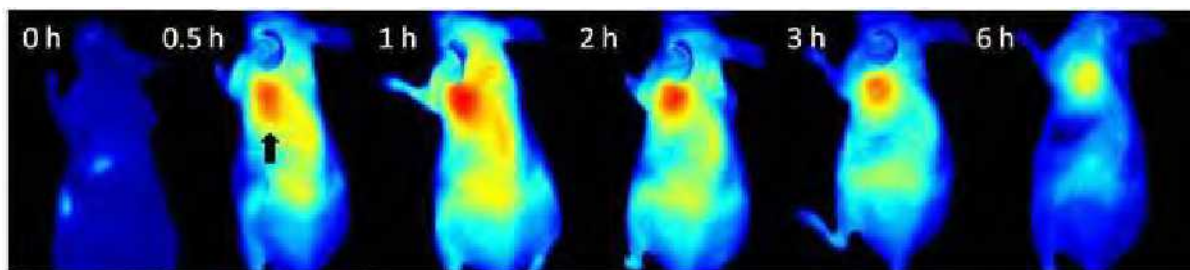


Figure 1. Serial NIR images of UM-SCC-22B tumor-bearing mice after intravenous injection of MMP-P. Arrow indicates the tumor.

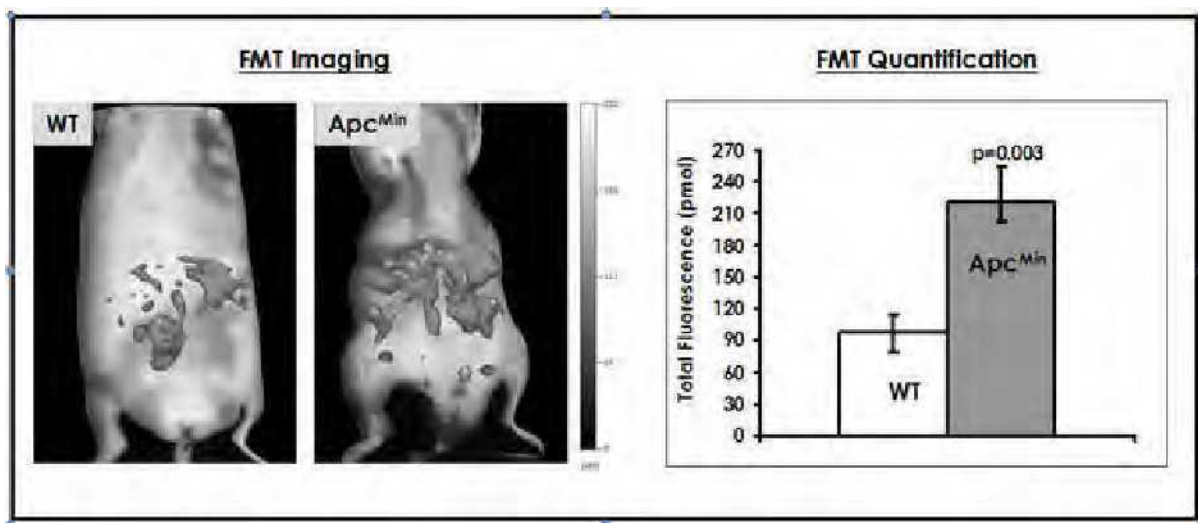
Presentation Number **0833A**

Poster Session 2c: In Vivo Studies & Development/Novel Use of Imaging Probes

Non-Invasive Near-Infrared Fluorescent Imaging and Quantification of MMP-Targeting of Intestinal Adenomas In Vivo

Jeff Morin, Garry J. Cuneo, **Jeffrey D. Peterson**, David Z. Gao, Sylvie Kossodo, VisEn Medical, Bedford, MA, USA. Contact e-mail: jpeterson@visenmedical.com

Colorectal cancer is the third leading cause of cancer-related deaths in the US. Matrix metalloproteinases (MMPs) are associated with colorectal cancers and their over-expression has been shown to correlate with disease staging and/or prognosis. Herein, we illustrate the use of MMPsense750 FAST, a near-infrared fluorescence MMP-activatable imaging agent, for detecting early cancers and adenomatous polyps in two relevant colorectal mouse models in vivo, non-invasively and in real time. Using quantitative fluorescence molecular tomography (FMT 2500), tumor fluorescence was measured in human HT-29 colorectal adenocarcinomas implanted into Nu/Nu mice and shown to peak 6h post-agent injection. Selective in vivo activation of MMPsense750 FAST by MMPs was confirmed by the significant inhibition of tumor fluorescence after mice were treated with a combination of the non-protein thiol N-acetyl-cysteine and a synthetic pan-MMP inhibitor. As early as day 1 of treatment, before affecting tumor size, this regimen decreased MMP signal in tumors by 88% ($p=0.0042$ as compared to vehicle-injected control mice). In vivo activation of the agent was also quantified in spontaneously-developing polyps in Apc^{Min} mice ($n=12$), which showed significantly higher abdominal signal (as a measure of tumor burden) compared to normal background signal in wild-type age-matched controls ($n=13$) (220.9±33 versus 96.9±18 pmoles respectively, $p=0.003$). Ex vivo imaging of excised HT-29 and gastrointestinal tracts confirmed this result, revealing MMP activity in tumors and polyps along the intestinal wall, suggesting that MMPsense750 FAST was effective at detecting early stages of colorectal cancer in preclinical models. Routine endoscopy has a high rate of missing adenomatous polyps especially on the right side colon in human, fluorescent imaging agents targeting cancer-specific MMPs can help improve early detection, specificity, diagnosis, staging, and stratification of patients with colorectal cancer or polyps.



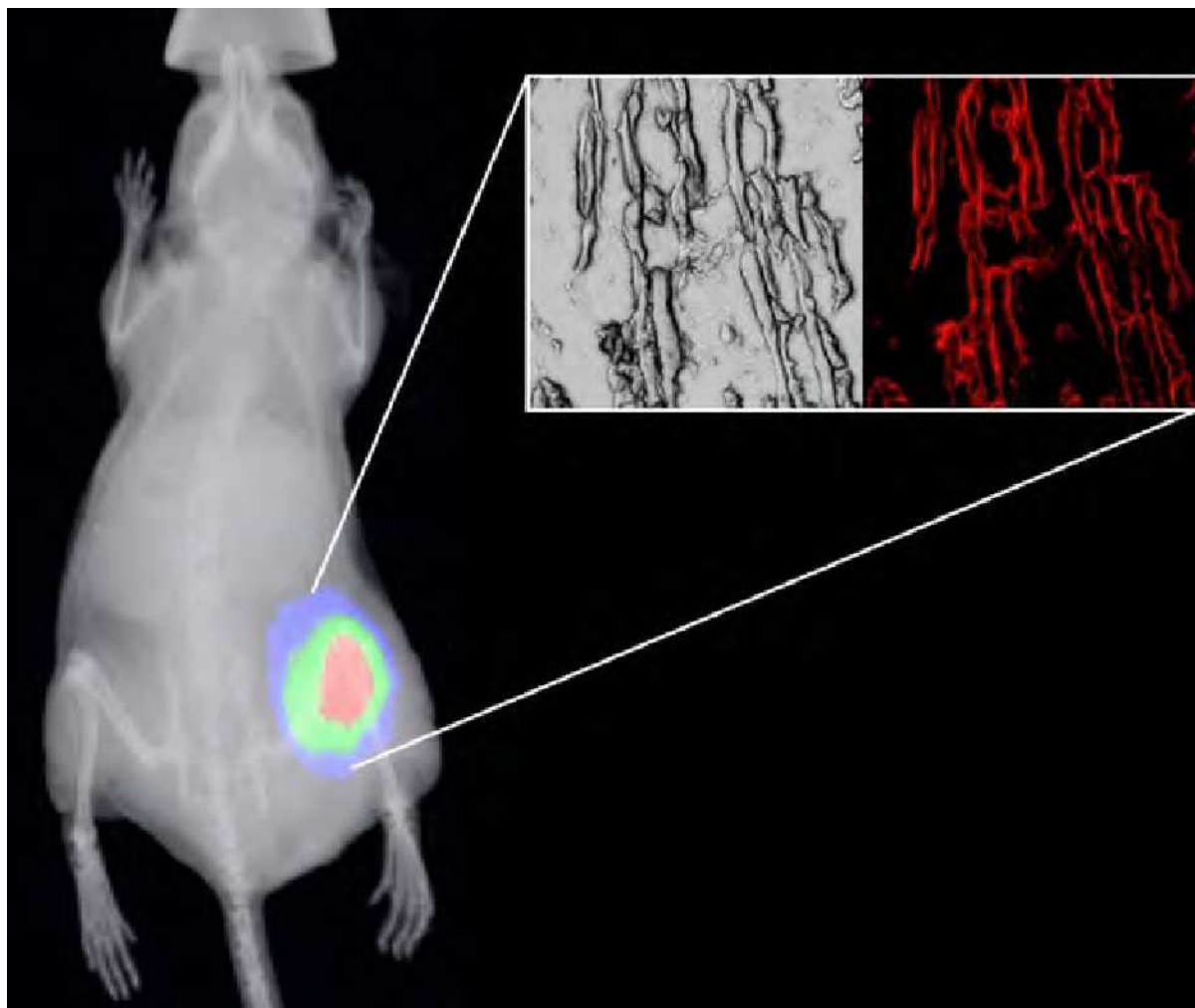
Presentation Number **0834A**

Poster Session 2c: In Vivo Studies & Development/Novel Use of Imaging Probes

In Vivo Optical Imaging of Cell Death Caused by Acute Tissue Damage Using a Near-Infrared Synthetic Zinc(II)-Dipicolylamine Probe

Bryan A. Smith, Shuzhang Xiao, Bradley D. Smith, W. Matthew Leevy, Notre Dame Integrated Imaging Facility, University of Notre Dame, Notre Dame, IN, USA. Contact e-mail: bsmith23@nd.edu

Imaging probes that can non-invasively monitor cell death in vivo will profoundly affect the clinical diagnosis and prognosis of malignant disorders as well as pre-clinical drug development. Numerous probes have been developed using proteins or peptide sequences to specifically target intracellular or extracellular biomarkers during cell death. Difficulties in optimizing the formulation and pharmacokinetic properties of these agents have limited their translation into humans. We have developed a fluorescent, small molecule mimic of the phosphatidylserine binding protein Annexin V. Our near-infrared probe contains a carbocyanine dye conjugated to a zinc (II)-2,2-dipicolylamine (Zn-DPA) coordination complex, which can bind to dead and dying cells both in biological media and in tumors (1). Here, we have expanded the use of our probe by selectively targeting and imaging acute tissue damage in living animals. Using mouse and rat models, the near-IR Zn-DPA probe localized to the site of tissue damage induced by both anesthetics and cytotoxins. Histological analysis confirmed binding of the probe to the myopathy. (1). Smith, B. A.; Akers, W. J.; Leevy, W. M.; Lampkins, A. J.; Xiao, S.; Wolter, W.; Suckow, M. A.; Achilefu, S.; Smith, B. D. J. Am. Chem. Soc. 2010, 132, 67-69.



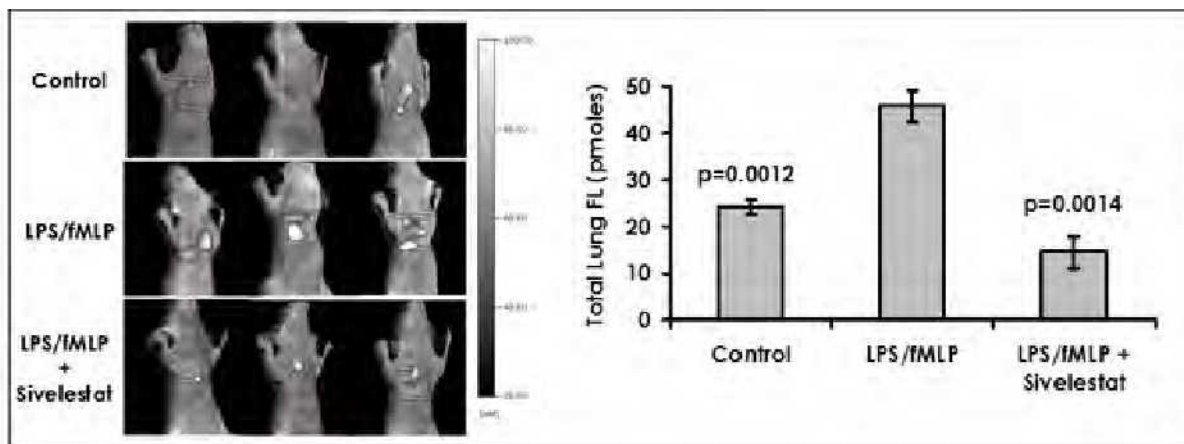
Presentation Number **0835A**

Poster Session 2c: In Vivo Studies & Development/Novel Use of Imaging Probes

A Novel and Selective Fluorescence Activatable Imaging Agent for In Vivo Quantification of Neutrophil Elastase Activity and Treatment Response in Acute Lung Injury

Jun Zhang, Kevin Groves, Garry J. Cuneo, Emma Handy, Jeff Morin, David Z. Gao, **Jeffrey D. Peterson**, Milind Rajopadhye, Sylvie Kossodo, VisEn Medical, Bedford, MA, USA. Contact e-mail: jpeterson@visenmedical.com

Of critical importance to the pathogenesis of acute lung injury (ALI) is the accumulation of activated neutrophils in the lungs and concomitant release of neutrophil elastase (NE). To date, it has not been possible to quantify NE activity in vivo with existing optical imaging technologies. This report shows for the first time the development of a NE-specific near-infrared fluorescence imaging agent, Neutrophil Elastase 680 FAST, using a selective NE peptide substrate, a polymer carrier and quenched fluorochromes. In vitro, the agent becomes highly fluorescent upon cleavage, with selective activation by human and mouse NE over cathepsins B, G, and MMP-9 (enzymes which often are present in the same neutrophil-infiltrated disease processes as NE). In vivo, the agent is activated in sites of neutrophil activation; FMT 2500 quantitative tomographic imaging showed significantly higher Neutrophil Elastase 680 FAST signal in mice with LPS/fMLP-induced ALI as compared to healthy controls (1.9 fold higher, $p=0.0012$). The fluorescent signal correlated with increases in the total number of bronchoalveolar lavage cells, neutrophils and fluid elastase activity using AAPV-AMC. The agent was significantly activated ex vivo by incubation with lung cryosections from ALI but not from control mice, and this activation was ablated by the NE-specific inhibitor Sivelestat. Most importantly, the agent was used as a mechanistic biomarker for quantifying specific NE inhibition efficacy in vivo: treatment with Sivelestat significantly reduced lung signal in LPS/fMLP-challenged mice (68%, $p=0.0014$ as compared to LPS/fMLP alone). These results underscore the unique ability of Neutrophil Elastase 680 FAST and FMT 2500 to quantify specific molecular processes such as NE activity in lung inflammatory diseases through non-invasive fluorescent-based imaging techniques, crucial for understanding the mechanisms underlying disease progression and for assessing and monitoring novel pharmacological interventions in vivo.



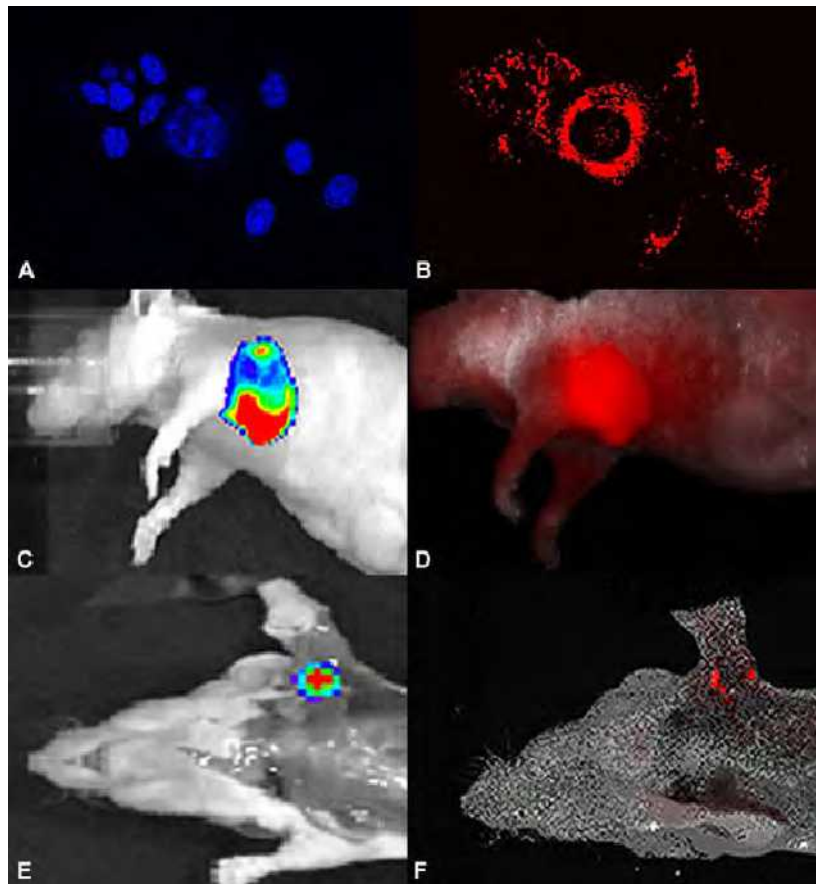
Presentation Number **0836A**

Poster Session 2c: In Vivo Studies & Development/Novel Use of Imaging Probes

Near-infrared fluorescence (NIRF) and bioluminescence imaging (BLI) of mouse breast cancer development and metastasis

Bang-Wen Xie¹, Isabel Mol¹, Thomas Snoeks¹, Pieter V. Driel¹, Stijn Keereweer², Eric Kaijzel¹, Clemens Lowik¹, ¹Endocrinology, Leiden University Medical Center, Leiden, Netherlands; ²Otorhinolaryngology Head and Neck Surgery, Erasmus Medical Center, Rotterdam, Netherlands. Contact e-mail: b.xie@lumc.nl

NIRF imaging improves photon penetration and minimizes tissue autofluorescence. Thus, it could be applied as real-time visualization for imaging-guided surgery, making radical removal of tumor tissues and local metastases possible. Four NIRF probes were assessed to detect progression and metastasis of mouse breast cancer cell line 4T1-luc2. BLI was used as an internal control to co-localize fluorescence imaging (FLI), as this cell line contains luciferase2 gene, sensitively indicating luciferase expression level in tumor areas. The probes are tumor-specific, either activated by matrix metalloproteinases, cathepsins (MMPsense680TM, ProSense680TM, VisEn Medical), or targeted to glucose transporter and to epidermal growth factor receptor (800CW 2-DGTM, EGFTM, LI-COR). In vitro, methods included cell-based fluorescent assay by Odyssey, flow cytometry, and visualization of probe uptake by confocal microscopy. In vivo, 20,000 4T1-luc2 cells were implanted into the upper mammary fat pad of nude mice. After time-dependent (Day 4, 11, 18) whole body BLI (IVIS-100TM, Caliper) and FLI (MaestroTM, CRI), thoracic cavities of mice bearing tumors were surgically opened and reimaged to reveal metastases of surrounding tissues. Tissues with positive signals were collected for histochemical analysis. In vitro data consistently showed that all probes have strong specificity for 4T1-luc2 cells, of which ProSense680TM was superior. In vivo data showed at Day 4, there was already detectable tumor progression in intact mice, both by BLI and FLI. After opening up the mice, clear lung and axial lymph node (LN) metastases could be detected (Figure). Using BLI as an internal control for FLI, we have shown NIRF imaging can detect breast cancer and metastases in lungs and axial LNs at an early stage, in vitro, in vivo and during open surgery. This pre-clinical study will pave the way for translation into clinic.



In vitro ProSense680TM uptake (A) nuclei (B) probe; In vivo tumor progression (C) BLI (D) FLI; Open surgery tumor metastases in LNs (E) BLI (F) FLI.

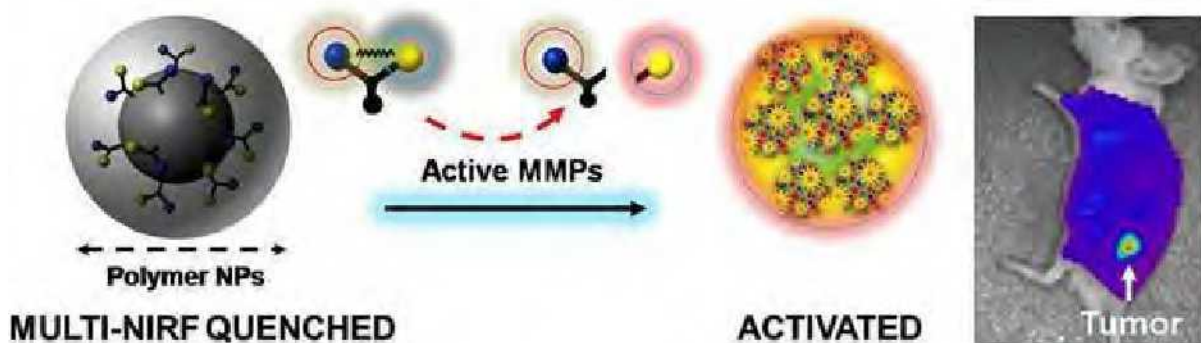
Presentation Number **0837A**

Poster Session 2c: In Vivo Studies & Development/Novel Use of Imaging Probes

Dark-quenched fluorogenic nanoprobe for MMPs activity in living animals

Ju Hee Ryu¹, **In-Cheol Sun**¹, **Soon Man Yoon**², **Dong-Eog Kim**³, **Kuiwon Choi**¹, **Ick Chan Kwon**¹, **Kwangmeyung Kim**¹, ¹*Biomedical Center, Korea Institute of Science and Technology, Seoul, Republic of Korea;* ²*Asan Medical Center, University of Ulsan College of Medicine, Seoul, Republic of Korea;* ³*Dongguk University Ilsan Hospital, Goyang, Republic of Korea.* Contact e-mail: jhryu@kist.re.kr

Proteases including MMPs are among the most studied enzyme families due to their involvement in regulation of diverse disease processes and their potential value as biomarkers and therapeutic targets. We developed the nanoprobe consisting of a self-assembled chitosan nanoparticle and activatable dark-quenched fluorogenic MMP peptide; Cy5.5 (NIR dye)-peptide substrate, which is quenched by the NIR dark quencher, BHQ-3. Polymeric nanoparticle platform-based protease activatable probe allowed noninvasive imaging of the specific MMPs of interest in vivo. The nanoprobe provided high NIR fluorescence signal in MMP-positive tumor-bearing mice and enabled clear visualization of tumors. Next, we studied imaging responses using a colon tumor mouse model and human atherosclerotic plaque. Colon tumor-bearing mice treated with azoxymethane were intravenously injected with the nanoprobe. The NIR ex vivo image demonstrated that all tumors obtained high fluorescence signals compared with adjacent mucosa. Human atherosclerotic plaque obtained at carotid endarterectomy was tissue-cultured in media containing MMP nanoprobe. Atherosclerotic plaque showed strong fluorescent signal, which reflects the pathophysiologic alterations of plaque inflammation. Overall, our data supports the notion that the nanoprobe can be used for NIR fluorescence imaging of MMP activity in a living animal.



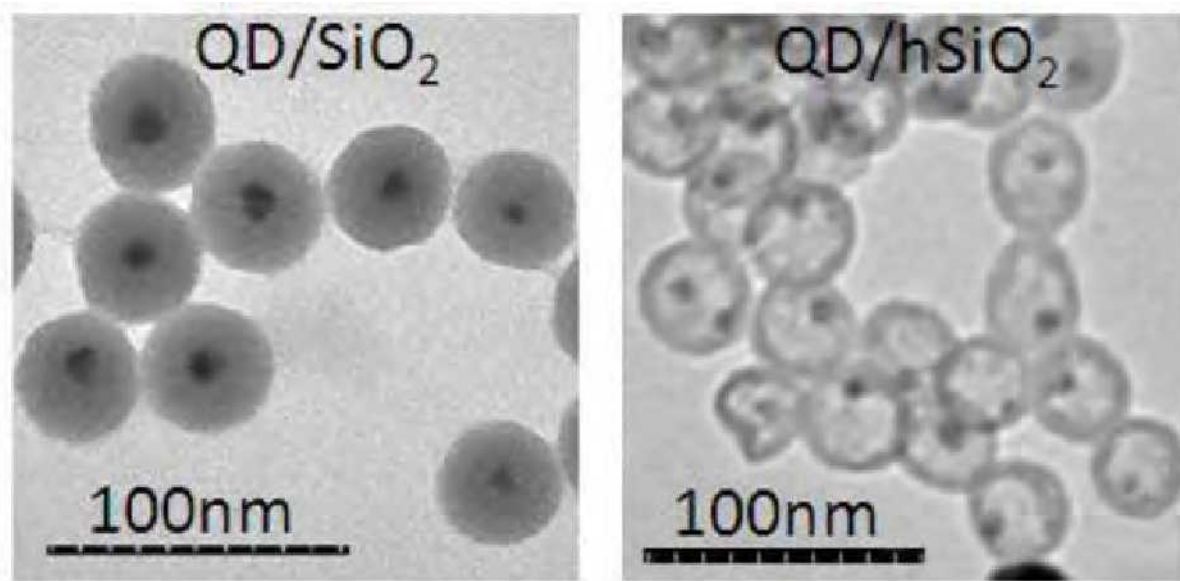
Presentation Number **0838A**

Poster Session 2c: In Vivo Studies & Development/Novel Use of Imaging Probes

Single moveable quantum dot in a hollow silica sphere by in-situ synthesis via QD/SiO₂ core-shell nanoparticles for bio-imaging application

Ching-Mao Huang, Leu-Wei Lo, Shih-Hsun Cheng, Medical Engineering Research, National Health Research Institutes, Miaoli County, Taiwan. Contact e-mail: chingmao@nhri.org.tw

Monodispersed CdSe/CdS/CdS_{0.5}Zn_{0.5}S/ZnS quantum dot/silica (QD/SiO₂) core-shell nanoparticles were prepared in the nonionic reverse microemulsions. QD/SiO₂ core-shell nanoparticles maintain high photoluminescence because of the passive and high band gap multishell. A fluorescent QD ($\lambda_{em}=650$ nm) encapsulated in a porous hollow silica (hSiO₂) nanoparticle with a diameter of 30-40 nm and thickness of approximately 5nm were synthesized by using QD/SiO₂ core-shell nanoparticles as the inorganic template. NaOH was used as catalyst for the hydrolysis of silica, etching initially forms porous structures in the interface of silica and QD. The results of whether core/shell nanoparticles or hollow spheres were governed by the concentration of NaOH and reaction duration. The nanostructure of QD/hSiO₂ yolk-shell nanoparticles were characterized by TEM and EDX analysis, indicating that QD/hSiO₂ were uniform spherical particles with good dispersion and had an empty space between QD core and silica shell. The photoluminescence property of QD/hSiO₂ yolk-shell nanoparticles were monitored during different reaction duration. Most important, the silica shells can be easily modified by silane groups with amine, thiol, or PEG chains for bioconjugation; besides, the hollow nanocontainer can be served as a drug carrier. The produced yolk-shell nanospheres are envisioned to have applications in areas ranging from medicine to pharmaceuticals, optical bio-imaging, and materials science.



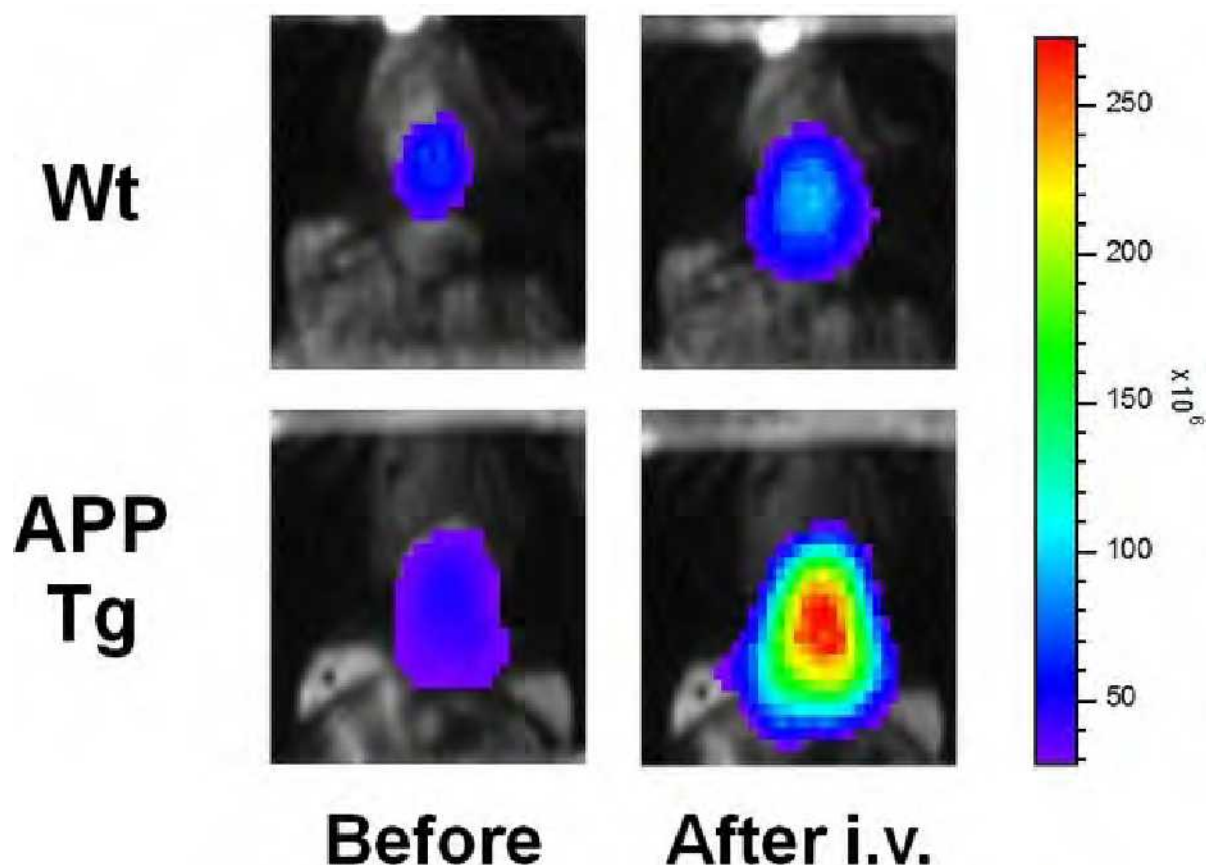
Presentation Number **0800B**

Poster Session 3c: In Vivo Studies & Development/Novel Use of Imaging Probes

Noninvasive detection of amyloid deposits using near-infrared fluorescence probe X50 in mice

Nobuyuki Okamura^{1,2}, Masanori Mori^{1,2}, Shozo Furumoto¹, Kazuhiko Yanai¹, Yukitsuka Kudo², ¹Department of Pharmacology, Tohoku University School of Medicine, Sendai, Japan; ²Innovation of New Biomedical Engineering Center, Tohoku University, Sendai, Japan. Contact e-mail: oka@mail.tains.tohoku.ac.jp

The neuropathological hallmark of Alzheimer's disease (AD) is the deposition of amyloid- β (A β) and hyperphosphorylated tau protein in the brain. The abnormal accumulation of A β deposits has been implicated as a critical event in the etiology and pathogenesis of AD and it precedes cognitive deterioration. Thus, near-infrared fluorescence (NIRF) imaging of amyloid- β (A β) deposits in the brain is expected to offer powerful method for screening presymptomatic AD patients. We developed a novel NIRF probe named X50 for in vivo detection of A β deposits in the brain. X50 showed excellent fluorescence properties as an NIRF agent. The maximal emission wavelength of X50 was greater than 700 nm and it showed high quantum yield and high molar absorption coefficients. A fluorescence binding assay demonstrated a hyperchromic effect in the binding of X50 to A β aggregates and showed its high binding affinity to A β fibrils. In addition, X50 clearly stained amyloid plaques in AD neocortical brain sections. Furthermore, X50 showed good permeability of the blood brain barrier. After intravenous administration of X50 in APP transgenic mice, amyloid deposits in the brain were clearly labeled with X50. Finally, we investigated whether X50 can noninvasively detect amyloid deposits in APP transgenic mice or not. As a result, we found significantly higher fluorescence intensity in the brains of APP transgenic mice compared to those of wild type mice. These findings suggest that X50 is a potential candidate as an NIRF imaging probe for noninvasive measurement of brain amyloid load.



In vivo detection of brain amyloid deposits using near-infrared fluorescence probe X50. Images from the brains of 22 month old wild type (Wt) and APP transgenic (APP Tg) mice before and after intravenous injection (i.v.) of X50 at a dose of 0.3 mg/kg.

Presentation Number **0801B**

Poster Session 3c: In Vivo Studies & Development/Novel Use of Imaging Probes

Functionalized, Crosslinked Nanostructures for Tandem Optical Imaging and Therapy

Nam S. Lee¹, Yun L. Lin¹, John Freskos², Jeng-Jong Shieh², Richard B. Dorshow², Karen L. Wooley¹, ¹Chemistry, Texas A&M University, College Station, TX, USA; ²Covidien Pharmaceuticals, Hazelwood, MO, USA. Contact e-mail: nam.lee@chem.tamu.edu

Optical imaging and detection is a robust method to illuminate important biological processes at the molecular level. For eventual in vivo pH determination, a unique pH-responsive photonic shell-crosslinked nanoparticle system has been developed. Fluorescent pyrazine dyes were utilized as the crosslinking chromophores to guarantee the structural integrity of the pH-responsive micelles, and also serve as the fluorescent reporting group. The fluorescence emission depends significantly on the local environment governed by the solution pH and the nanostructure morphology. Our nanoparticle system consists of pyrazine-shell-crosslinked nanoparticles (pyrazine-SCKs) self-assembled from poly(acrylic acid)-*b*-poly(*p*-hydroxystyrene) (PAA-*b*-PpHS). This system displays pH-responsive morphological changes which result in pH-responsive fluorescence emission. In addition, two different morphologies of fluorescent nanomaterials using these same constituents were evaluated as potential drug carriers. Interactions between the drug molecules (the payload) and the nanomaterial that is used as a vehicle (*i.e.*, ionic interactions, hydrophobicity, *etc.*) are essential properties to understand for optimal delivery. Also, the morphology of the nanostructure contributes an important role in drug loading and release behaviors. Herein, effects of ionic interactions and morphologies on drug loading and release using doxorubicin (DOX) as a model will be discussed. Both shell-crosslinked rods (SC-rods) and shell-crosslinked knedel-like nanoparticles (SCKs) were crosslinked with the fluorophore platform described above, and shown to yield distinct fluorescence emission profiles. **Acknowledgement.** Financial support from Covidien is gratefully acknowledged. This material is based upon work supported partially also by the National Heart, Lung and Blood Institute of the National Institutes of Health as a Program of Excellence in Nanotechnology (HL080729). N. S. Lee thanks GlaxoSmithKline for their financial support through the ACS Division of Organic Chemistry Graduate Fellowship.

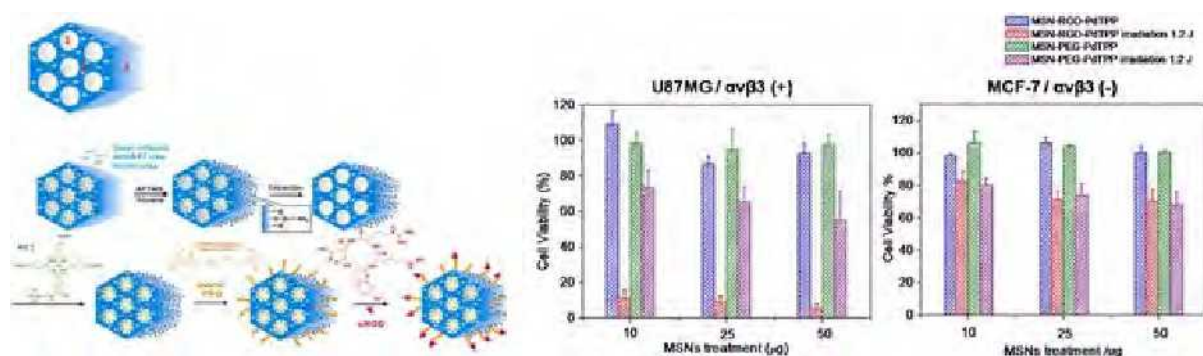
Presentation Number **0802B**

Poster Session 3c: In Vivo Studies & Development/Novel Use of Imaging Probes

Tri-Functionalization of Mesoporous Silica Nanoparticles for Diagnosis and Therapy

Jeffrey S. Souris¹, Shih-Hsun Cheng³, Meng-Chi Chen³, Chia-Hung Lee², Fan-Gang Tseng⁵, Chung-Shi Yang², Chung-Yuan Mou⁴, Chin-Tu Chen¹, Leu-Wei Lo³, ¹Department of Radiology, The University of Chicago, Chicago, IL, USA; ²Center for NanoMedicine Research, National Health Research Institutes, Zhunan, Taiwan; ³Division of Medical Engineering Research, National Health Research Institutes, Zhunan, Taiwan; ⁴Department of Chemistry, National Taiwan University, Taipei City, Taiwan; ⁵Department of Engineering and System Science, National Tsing Hua University, Hsinchu, Taiwan. Contact e-mail: sourisj@uchicago.edu

In this work we describe the development of the first tri-functionalized mesoporous silica nanoparticles (MSNs) for therapeutic and diagnostic (theranostic) use; with separate domains for the attachment of contrast agents for particle tracking, drug payloads for therapeutic intervention, and biomolecular ligands for targeted delivery. TEM studies of the MSNs revealed 90-100 nm diameter particles that possessed parallel, 3 nm diameter hexagonal pores that spanned each particle's width and communicated directly with the external environment. Nitrogen adsorption/desorption isotherm measurements of MSNs demonstrated enormous particle surface areas (>1000 m²/gm) and pore volumes (>1.0 cm³/gm). Sequential functionalization of domains proceeded first with incorporation of a bright near-infrared (NIR) fluorophore (ATTO647N) within the MSN's silica framework during sol-gel synthesis - to exploit the relative transparency of most tissues at NIR wavelengths and retain maximal MSN surface area for conjugation of therapeutic payloads and targeting ligands. Next an oxygen-sensing photosensitizer (palladium-porphyrin: PdTPP) was conjugated onto the inner surfaces of the MSN nanochannels - to enable the generation of singlet oxygen for photodynamic therapy (PDT). Finally cRGDyK peptides were attached to the MSNs' outermost surfaces - to permit the targeting of membrane-bound $\alpha_v\beta_3$ integrins that cancer cells commonly over-express and to ensure the internalization of the cytotoxic PdTPP. Various stages of functionalized MSNs were then evaluated for their targeting, uptake, toxicity, and PDT utility via a series of *in vitro* studies using a 532 nm diode laser (1.2 J/cm² dose) and human $\alpha_v\beta_3$ -integrin deficient (MCF-7 breast adenocarcinoma) or $\alpha_v\beta_3$ -integrin abundant (U87-MG glioblastoma) cells - for a variety of particle/cell incubation periods and dosages. Flow cytometry, confocal microscopy, and WST-1 assay revealed that the tri-functionalized MSNs exhibited high affinity for (and uptake by) integrin-expressing cells and potent PDT response; with relatively little collateral toxicity and very little non-specific binding.



Schematic of MSN topology and steps in functionalization (left). Effectiveness of tri-functionalized MSNs in PDT of integrin +/- cells, reflecting MSN targeting, toxicity, and lethality upon irradiation (right).

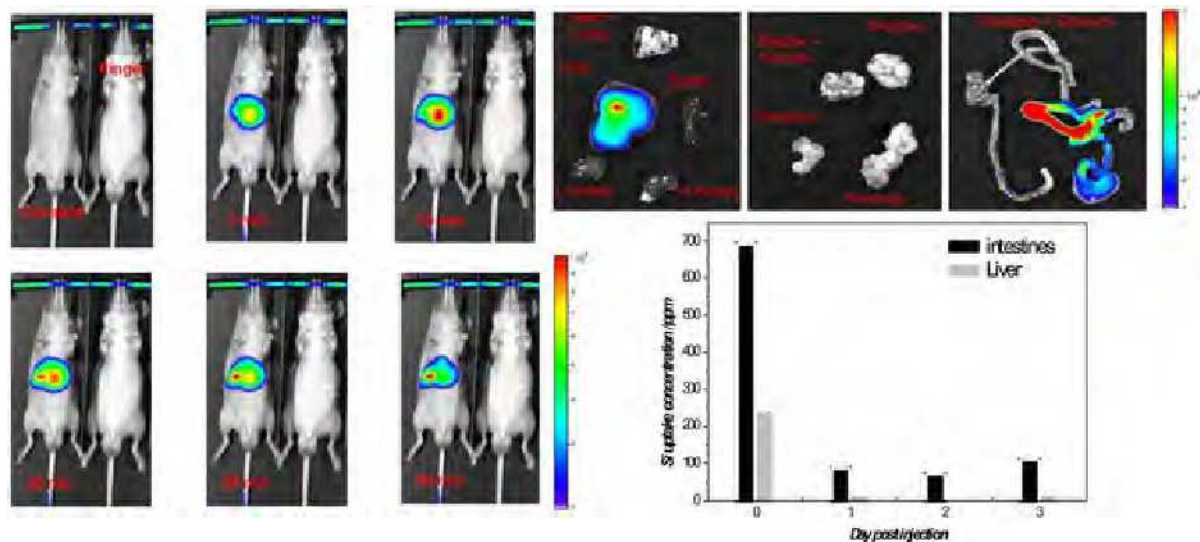
Presentation Number **0803B**

Poster Session 3c: In Vivo Studies & Development/Novel Use of Imaging Probes

Charge-Mediated Hepatobiliary Transport and Excretion of Fluorescent Mesoporous Silica Nanoparticles

Jeffrey S. Souris¹, Chia-Hung Lee², Shih-Hsun Cheng³, Chin-Tu Chen¹, Chung-Shi Yang², Ja-an Annie Ho⁴, Chung-Yuan Mou⁵, Leu-Wei Lo³, ¹Department of Radiology, The University of Chicago, Chicago, IL, USA; ²Center for NanoMedicine Research, National Health Research Institutes, Zhunan, Taiwan; ³Division of Medical Imaging Research, National Health Research Institutes, Zhunan, Taiwan; ⁴Department of Chemistry, National Tsing Hua University, Hsinchu, Taiwan; ⁵Department of Chemistry, National Taiwan University, Taipei City, Taiwan. Contact e-mail: sourisj@uchicago.edu

In this work we report on the synthesis of 80-100 nm diameter, mesoporous silica nanoparticles (MSNs) onto which we covalently conjugated the FDA-approved, near-infrared fluorophore indocyanine green (MSN-NH₂-ICG) - for comparison to our previous *in vitro* and *in vivo* studies of the same fluorophore ionically conjugated to the same nanoparticle (MSN-TA-ICG). Nitrogen adsorption-desorption isotherm measurements of unconjugated MSN-NH₂ demonstrated surface areas 50%, pore sizes 85%, and accessible pore volumes 29% those of unconjugated MSN-TA. At physiological pH - and slightly more acidic conditions, like those within endosomes - zeta potential measurements of MSN-NH₂-ICG revealed it to be considerably more charged than MSN-TA-ICG (e.g., +34.4 mV vs. -17.6 mV, at pH 7.4). *In vivo* and *ex vivo* fluorescence imaging of mice and their harvested tissues/excrement demonstrated markedly different patterns of nanoparticle elimination between the 2 formulations; with MSN-TA-ICG having high uptake and retention by the reticuloendothelial system in liver, but MSN-NH₂-ICG additionally undergoing rapid hepatobiliary transport and fecal excretion. Inductively Coupled Plasma Mass Spectroscopy of organs harvested 3 days after contrast agent injection further suggested the onset of MSN biodegradation into orthosilicic acid with possible renal excretion, although secondary confirmation could not be readily obtained due to inefficiencies in urine collection. While both MSN-TA-ICG and MSN-NH₂-ICG were found to undergo equally swift phagocytosis by Kupffer cells in the liver, we postulate that the latter nanoparticle's greater charge resulted in it becoming more highly opsonized by serum proteins and thus amenable to hepatobiliary transport. As such, judicious tailoring of the MSN's surface charge should enable pathology-relevant control of both MSN biodistribution and rate of excretion - for optimal, targeted drug delivery and minimal systemic toxicity. Current studies are aimed at manipulating MSN surface charge to selectively modulate the nanoparticle's behavior/fate following non-intravenous routes of administration.



Rapid transport of fluorescent MSNs in the intact animal, localization in liver and GI-tract 3 hours post-injection, and ICPMS of Si uptake in liver and intestines.

Presentation Number **0804B**

Poster Session 3c: In Vivo Studies & Development/Novel Use of Imaging Probes

Novel EPR-Based Fluorescent Probe for Tumour Imaging during Radiotherapy

Réjean Lebel^{1,3}, Heidi Ligeret³, Freddy Rivault³, Martin Lepage^{1,2}, Marc Massonneau³, ¹Département de Médecine Nucléaire et de Radiobiologie, Université de Sherbrooke, Sherbrooke, QC, Canada; ²Centre d'imagerie moléculaire de Sherbrooke, Sherbrooke, QC, Canada; ³Laboratoires Quidd, Saint Etienne du Rouvray, France. Contact e-mail: rejean.lebel@usherbrooke.ca

Introduction: Neoplastic tissues are known to possess hyperpermeable angiogenic vessels and to lack lymphatic drainage. These characteristics result in the enhanced permeability and retention effect (EPR), which is responsible for the accumulation of high molecular weight molecules inside tumours. The EPR phenomenon is commonly used to improve the targeting of tumours with imaging probes and therapeutic agents. The aim of our study is to evaluate the capability of a new EPR-based imaging compound, QEPR-1.8, to assess tumour growth and response to radiotherapy. **Method:** 10 million MC7-L1 cells (mouse mammary carcinoma) were inoculated over both dorsal hips of 12 female Balb/c mice. Tumour growth was monitored before and after radiotherapy (Gamma knife, 30 Gy, 1 dose) using a caliper, optical imaging (QOS optical imager) and magnetic resonance imaging (MRI). For optical imaging, 0.05 nmole/g of QEPR-1.8 was injected i.v. 24 h prior to imaging (Ex/Em: 685/707nm). Tumours reached 4mm size after 4 weeks, and the left tumours were irradiated (I) 6 days later. **Results and discussion:** Tumour size was monitored on days I-6, I-2, I+2, I+6, I+10, and I+15 (caliper, MRI, optical imaging). Accumulation of QEPR-1.8 was shown to increase with tumour growth and this was further increased in irradiated tumours and surrounding tissues. Spearman's tests revealed a significant correlation between fluorescence signal and caliper/MRI measurements (Spearman's $r = 0.57$ and 0.65 respectively, two-tailed $P < 0.0001$). Therefore, this study is in accordance with previous data showing that the EPR effect is more important after radiation; probably due to tissue inflammation and damage to blood vessels. **Conclusion:** QEPR-1.8 is a novel fluorescent optical probe which allows successful imaging of tumour growth and inflammation in a model of radiotherapy.

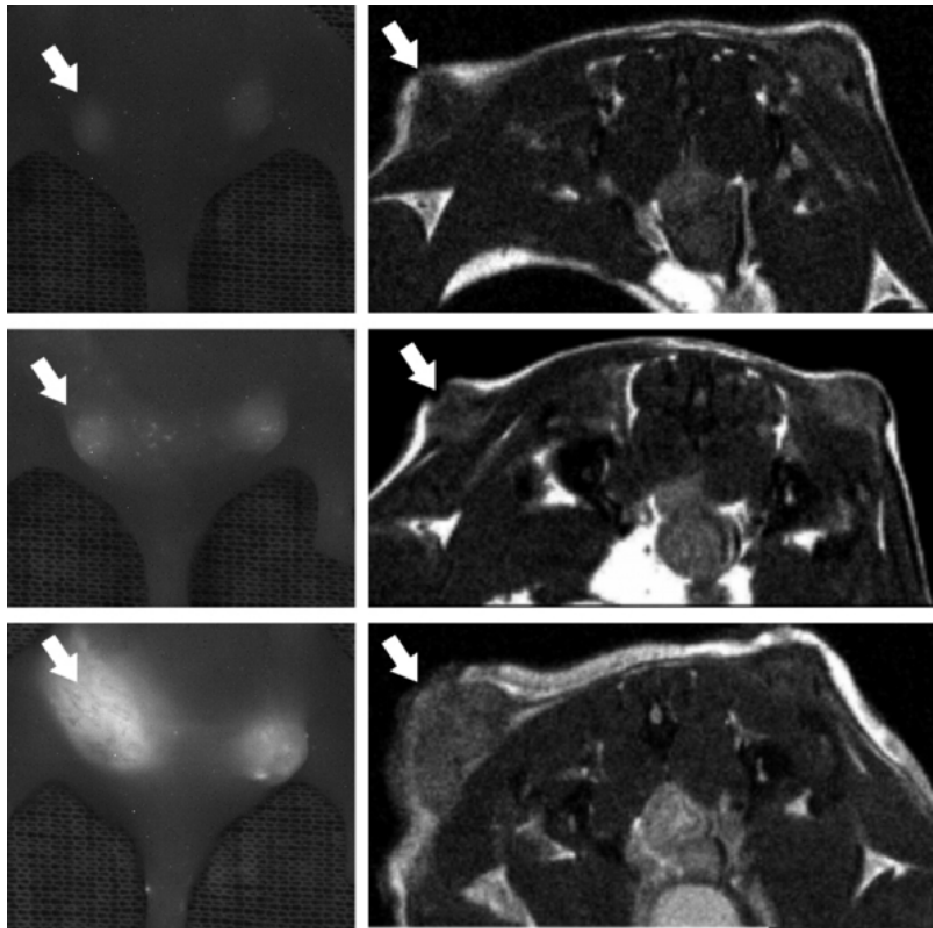


Figure 1. Optical (left) and MRI (right) imaging of tumours at days I-6 (top), I+2 (middle) and I+15 (bottom). Arrows point to the irradiated tumour.

Presentation Number **0805B**

Poster Session 3c: In Vivo Studies & Development/Novel Use of Imaging Probes

Dual Wavelength Imaging of a Novel Activatable Photoacoustic Probe

Jelena Levi¹, **Sri Rajasekhar Kothapalli**², **Te Jen Ma**³, **Butrus Khuri-Yakub**³, **Sanjiv S. Gambhir**^{2,1}, ¹Radiology, Canary Center at Stanford, Palo Alto, CA, USA; ²Molecular Imaging Program at Stanford, Department of Radiology and Bio-X Program, Stanford University, Palo Alto, CA, USA; ³Department of Electrical Engineering, Stanford University, Palo Alto, CA, USA. Contact e-mail: jlevi@stanford.edu

Photoacoustic tomography has the capability of providing images of high spatial resolution and high contrast at depths up to 5 cm. As the breadth of application for this modality grows, so does the need for probes with high specificity. We report here the design, synthesis and evaluation of an activatable probe that shows great promise in providing highly specific photoacoustic images. Before the activation by its target, matrix metalloprotease MMP-2, the probe, an activatable cell penetrating peptide labeled with two different chromophores, shows photoacoustic signal of similar intensity at the two wavelengths corresponding to the absorption maxima of the chromophores. After the cleavage, the dye associated with the cell penetrating part of the probe accumulates in the cells, resulting in photoacoustic signal seen only at one of the wavelengths. The subtraction of the photoacoustic images at two wavelengths reveals the location of the cleaved probe only, as the signals at two wavelengths for the non-activated probe cancel out. To evaluate our approach towards smart photoacoustic probes, we have incubated human fibrosarcoma cells, HT 1080, with three probes: non-activated, MMP-2 specific probe, BHQ3-ACPP-Alexa750; non-activated, MMP-2 non-specific probe, BHQ3-CPP-Alexa750; and cleaved probe BHQ3-CPP. The uptake of the cleaved probe was clearly distinguished from the accumulation of both non-activated probes by subtracting the photoacoustic images taken at two wavelengths corresponding to the absorption maxima of the two chromophores used, BHQ3(675nm) and Alexa750(750nm) (Figure 1 d,e). A great utility of our probe in combination with dual wavelength imaging lies in the possibility of detection of the cleaved probe in the presence of the high levels of non-activated probe, a challenging task to attain in an absorbance-based modality. This method could prove useful in pre-clinical models, photoacoustic guided surgical interventions, treatment efficacy evaluations, as well as many other applications.

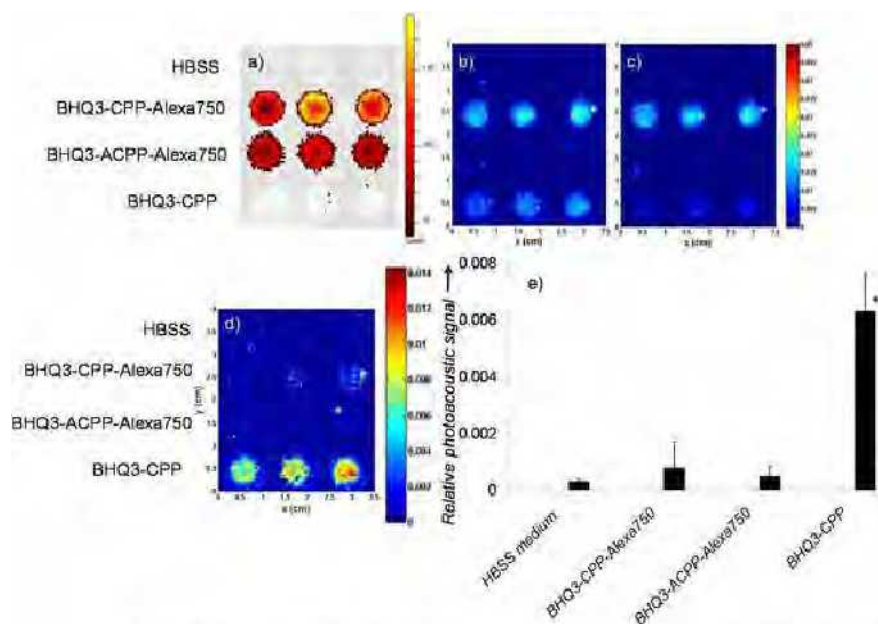


Figure 1. Photoacoustic imaging of the smart probe accumulation in cells. HT1080 cells were incubated with 150 μ L of 10 μ M solution of BHQ3-CPP-Alexa750, BHQ3-ACPP-Alexa750 or BHQ3-CPP for 10 minutes and embedded in triplicate in an agar phantom. (a) Fluorescence image (λ_{exc} 675 nm, ICG emission filter) of the agar phantom shows location of the cells as well as the uptake of BHQ3-CPP-Alexa750 and BHQ3-ACPP-Alexa750. Photoacoustic images of the agar phantom with embedded cells taken at two wavelengths: 675 nm (b) and 750 nm (c). Subtraction of the images taken at 675 nm and 750 nm resulted in an image with distinct signal coming from the cells incubated with the cleaved probe, BHQ3-CPP (d). The accumulation of different probes in the cells was quantified from the subtraction image using mean photoacoustic values for each well (e). Error bars represent the standard deviation of the mean of triplicates. Accumulation of BHQ3-CPP probe was significantly different ($p < 0.05$) from the accumulation of both BHQ3-ACPP-Alexa750 and BHQ3-CPP-Alexa750. Color bars represent relative photoacoustic signal intensity.

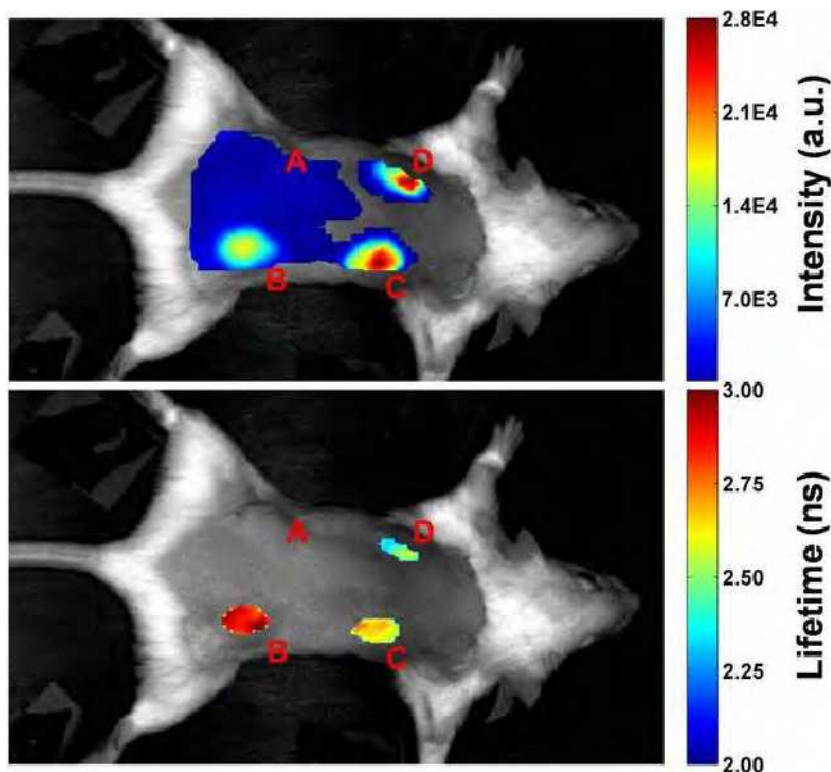
Presentation Number **0806B**

Poster Session 3c: In Vivo Studies & Development/Novel Use of Imaging Probes

Sensing pH in vivo using fluorescence lifetime

Guobin Ma, Dao Chao Huang, Nicolae Mincu, Muriel Jean-Jacques, Mario Khayat, ART Advanced Research Technologies, Inc., Montreal, QC, Canada. Contact e-mail: gma@art.ca

Detection of possible alterations of physiological parameters (e.g. pH and temperature) resulting from malignant transformation of tissue can be a powerful diagnostic tool for earlier cancer detection and prognosis. Fluorescent lifetime imaging (FLIM) of specifically targeted fluorescent labeled antibodies can be sensitive to such variations and provide functional images of the regions of interest. FLIM has been widely used using microscopy. We present a method of in vivo animal imaging to sense the local pH microenvironment by FLIM using a time-resolved fluorescence imaging platform. The imaging agent used in the study is a pH sensitive fluorescent dye, SNARF-1. In the preliminary study, SNARF-1 mixed with matrigel at different biological relevant pH levels were implanted in several mice. The mice were then imaged using a time-resolved imaging system. Shown in figure 1 are the result images. In location A, the matrigel-only sample is implanted; B, C, and D are respectively the locations of SNARF-1 matrigel mixtures with pH 6, 7, and 8. The intensities (top image) from the pH samples are slightly different while the signal from the matrigel-only is comparable to the tissue autofluorescence. However, the fluorescence lifetimes from the 3 pH varied samples are clearly different (bottom image and the table), ranging from 2.4 to 2.9 nanosecond. These results demonstrate that FLIM can be used in vivo to differentiate the local pH microenvironment that could find many applications in cancer research and other fields. Further studies using pathological models with varied pH microenvironment caused by physiological effect are under the way.



In vivo fluorescence intensity (top) and lifetime (bottom) images of a mouse implanted four samples with different pH values. The samples are clearly differentiated by FLIM attributed to pH.

Lifetime values of the 4 pH samples

Sample	pH	Lifetime (ns)
A	matrigel	11.1
B	6	2.86
C	7	2.62
D	8	2.39

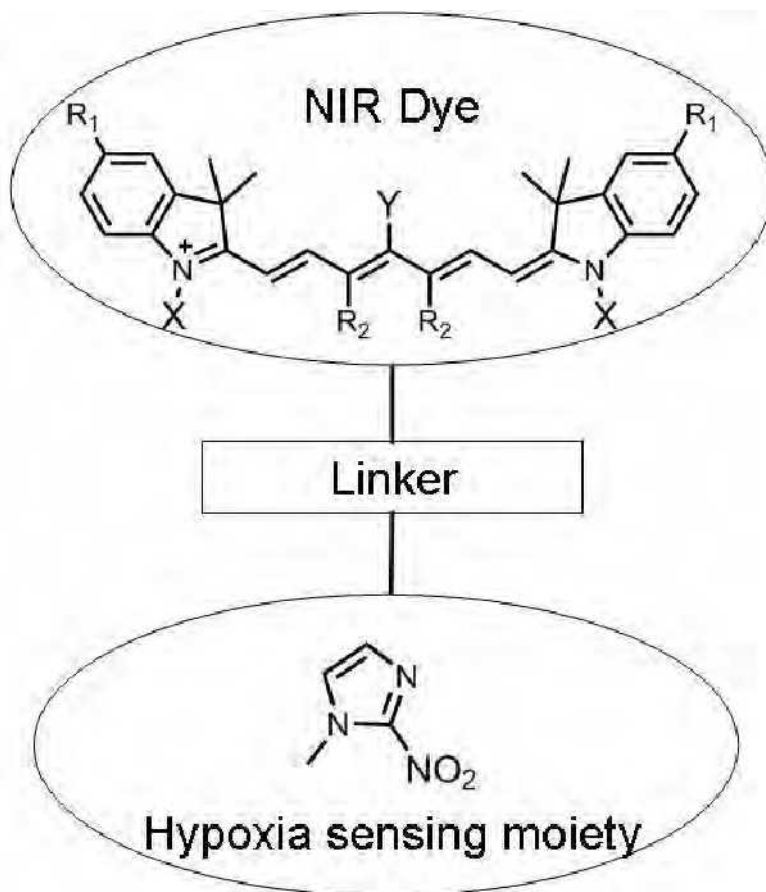
Presentation Number **0807B**

Poster Session 3c: In Vivo Studies & Development/Novel Use of Imaging Probes

Development of NIR fluorescent probe for non-invasive imaging of tumor hypoxia *in vivo*

Kensuke Okuda¹, Bahaa G. Yuossif¹, Takahiro Ueno¹, Tetsuya Kadonosono³, Shinae Kizaka-Kondoh^{2,3}, Hideko Nagasawa¹,
¹Laboratory of Medicinal & Pharmaceutical Chemistry, Gifu Pharmaceutical University, Gifu, Japan; ²School of Bioscience and Biotechnology, Tokyo Institute of Technology, Midori-ku, Japan; ³Graduate School of Medicine, Kyoto University, Sakyo-ku, Japan.
 Contact e-mail: okuda@gifu-pu.ac.jp

Tumor hypoxia has been attributed as an indicator of malignancy and adverse prognosis with increased metastatic potential and therapeutic resistance. Therefore there is an urgent need to develop non-invasive methods of detecting hypoxic regions for cancer diagnosis. Among imaging modalities, we focus on fluorescence imaging because of it can be safely performed with simple instruments and facilities with good resolution. Utilization of near-infrared (NIR) region fluorescence is especially fruitful because it is less absorbed by biomolecules and can penetrate deeply into tissues. There is also less autofluorescence in this region. In the present study, we are developing NIR fluorescence probes for non-invasive imaging of tumour hypoxia. We designed and synthesized novel NIR fluorescent probes for selective imaging of tumour hypoxia via bioreductive activation and labeling to cellular macromolecules. The molecular design depends on the conjugation of hypoxia targeting moiety such as 2-nitroimidazole and a NIR fluorescent dye (Cy7) through various linkers controlling hydrophilicity and pharmacokinetics. 2-Nitroimidazoles function as bioreductive hypoxia markers, whereby active species such as hydroxylamine derived by enzymatic reduction under hypoxia reacts with intracellular nucleophiles and are retained as bioconjugates. As our 1st generation probe, we prepared GPU-167 and 172 by usual chemical synthesis manner. *In vitro* evaluation using SUIT-2 cells indicated that both GPU-167 and 172 showed tendency to accumulate in the cells under hypoxic condition (O₂: 0.02%) selectively over aerobic condition at the concentration of 10 µg/ml. GPU-172 was incorporated into the cell more than GPU-167. This phenomenon reflects probably due to their hydrophobicity. *In vivo* result using SUIT-2 transplanted mouse showed that GPU-167 (10 nmol / mouse) had tumour selectivity but its clearance was too slow to put into practical use. Now we are pursuing various molecular modifications to accomplish fast clearance and sufficient hypoxia selectivity for *in vivo* imaging.



Presentation Number **0808B**

Poster Session 3c: In Vivo Studies & Development/Novel Use of Imaging Probes

Development of Near-Infrared Fluorescence Probes for *In Vivo* Tumor Imaging with Using an Amphiphilic Polydepsipeptide Micelle “Lactosome”

Isao Hara¹, **Ryo Yamahara**¹, **Eri Takeuchi**¹, **Akira Makino**¹, **Kensuke Kurihara**², **Fumihiko Yamamoto**³, **Shinae Kizaka-Kondoh**⁴, **Akira Shimizu**², **Eiichi Ozeki**¹, **Shunsaku Kimura**⁵, ¹Technology Research Laboratory, Shimadzu Corporation, Kyoto, Japan; ²Translational Research Center, Kyoto University Hospital, Kyoto University, Kyoto, Japan; ³Department of Radiopharmacy, Tohoku Pharmaceutical University, Miyagi, Japan; ⁴Department of Biomolecular Engineering, Graduate School of Bioscience and Biotechnology, Tokyo Institute of Technology, Kanagawa, Japan; ⁵Department of Material Chemistry, Graduate School of Engineering, Kyoto University, Kyoto, Japan. Contact e-mail: i-hara@shimadzu.co.jp

Near-infrared fluorescence (NIRF) *in vivo* imaging technique provides a high contrast tumor image without background fluorescence. It was observed that ICG-lactosome, which is a molecular assembly composed of hydrophobic helical poly(L-lactic acid)₃₁ (PLLA) and hydrophilic poly(sarcosine)₇₀ (PSar) amphiphilic block polydepsipeptide including indocyanine green (ICG) labeled PLLA₃₁ in the hydrophobic inner core, provides good tumor imaging without accumulation to liver. ICG-lactosome having a diameter of 30 nm shows high escape ability, stealth property in other word, from reticuloendothelial system (RES), and accumulated to the tumor region by the enhanced permeation and retention (EPR) effect. This is because the high density of hydrophilic PSar chains so called polymer brush around the molecular assemblies contributes to the inhibition from RES recognition. In this study, accumulation to tumor of ICG-lactosome with using various ICG-labeled poly(lactic acid) was examined to enhance tumor/background (T/B) ratio. *In vivo* imaging of tumors was performed on mice with subcutaneously implanted human cancer cells in leg. Images were obtained up to 48 hours after i.v. administration of ICG-lactosome. The T/B ratio was increased at 2-9 hour after i.v. administration with using the lactosome included ICG-labeled poly(D-lactic acid)₃₀. The lactosome included ICG-labeled poly(DL-lactic acid)₃₂ was accumulated to tumor and was exhibited rapid clearance from the body in bile. The T/B ratio with using the lactosome included ICG-PDLLA₃₂ at 48 hour after i.v. administration was higher than that of ICG-PLLA₃₁. These results indicate that the T/B ratio with using ICG-lactosome *in vivo* is controlled by the structure of ICG-labeled poly(lactic acid) in the lactosome. In addition, high contrast imaging of tumor was also achieved with using ICG-lactosome labeled cyclo(RGDyK) which is a ligand to bind to integrin receptor.

Presentation Number **0809B**

Poster Session 3c: In Vivo Studies & Development/Novel Use of Imaging Probes

Real-time reporting of drug release from smart probes for cancer theranostics

Ehud Segal¹, Roy Weinstain², Doron Shabat³, Ronit Satchi-Fainaro¹, ¹Physiology and Pharmacology, Sackler Faculty of Medical Sciences, Tel Aviv University, Tel Aviv, Israel; ²Pharmacology, University of California, San Diego, CA, USA; ³School of Chemistry, Raymond and Beverly Sackler Faculty of Exact Sciences, Tel Aviv University, Tel Aviv, Israel. Contact e-mail: ehudsega@post.tau.ac.il

Anti-angiogenic therapy combined with conventional treatment holds great potential for osteosarcoma management and metastatic risk reduction. We developed a new therapeutic strategy to target bone metastases and calcified neoplasms using combined polymer-bound angiogenesis inhibitors. Using a novel "living polymerization" technique, the reversible addition-fragmentation chain transfer (RAFT), we conjugated the aminobisphosphonate alendronate (ALN), and the potent anti-angiogenic agent TNP-470, with N-(2-hydroxypropyl)methacrylamide (HPMA) copolymer through a Glycine-Glycine-Proline-Norleucine linker, cleaved by cathepsin K, a cysteine protease overexpressed at resorption sites in bone tissues. Live-Imaging is revolutionizing the way in which disease progression can be monitored and how therapeutic intervention can be evaluated. Incorporation of a fluorescence drug-release reporting probe to our novel drug delivery system enables both tumor progression and drug release monitoring by the use of a non-invasive intravital fluorescence imaging systems. For this purpose we recently developed a preliminary prototype of a reporting drug-delivery system (RDDS). Coupling of latent fluorophore activation reporter with a drug release event allows continuous monitoring of the cargo release through an ON-OFF fluorescent signal, which can be detected by non-invasive intravital fluorescent imaging techniques. The design of our RDDS was based on a 7-hydroxycoumarin linker with a hydroxymethyl substituent. When the trigger is attached, no fluorescence is emitted. However, when the system undergoes specific activation, the end-unit is released and fluorescence is generated through formation of coumarin. We showed that our RDDS signal cytotoxic activity toward human T-lineage acute lymphoblastic leukemia MOLT-3 and endothelial cells, by emitting fluorescence. This allowed us to monitor in real-time the drug release. We observed a strong direct correlation between tumor cell growth inhibition activity and emitted fluorescence in MOLT-3 cells. Using confocal microscopy, we showed that the drug release event in endothelial cells occurred in the cytoplasm. The amount of drug release can be calculated by quantifying the emitted fluorescence thus allowing prediction of a DDS's therapeutic effect and potential side effects. We are currently integrating the RDDS with HPMA copolymer-ALN-TNP-470 conjugate to generate the first targeted therapeutic RDD combined polymeric system.

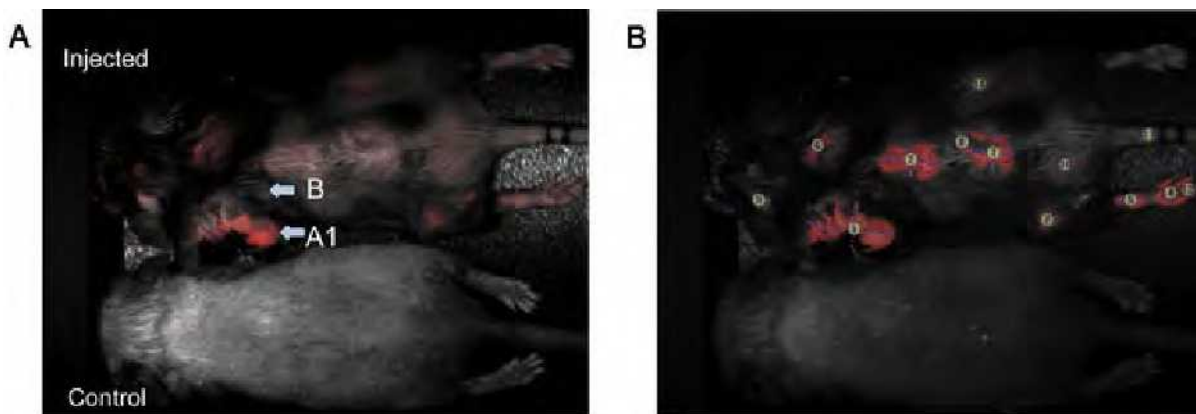
Presentation Number **0810B**

Poster Session 3c: In Vivo Studies & Development/Novel Use of Imaging Probes

COX-2 probe as a Diagnostic Tool for Identifying Basal Cell Carcinoma

Irfan Ali-Khan¹, Christopher Contag¹, Hyejun Ra¹, Jean Y. Tang¹, Kris Chang¹, Jashim Uddin², Lawrence Marnett², ¹Stanford University, Stanford, CA, USA; ²Institute of Chemical Biology, Vanderbilt University, Nashville, TN, USA. Contact e-mail: irfan.alikhan@gmail.com

On average, one in every five caucasians in the United States will suffer from skin cancer at some point in their lives. Basal cell carcinoma (BCC) accounts for approximately 800,000 new cases annually, with 80% of instances on the cosmetically sensitive area of the head and neck. We present promising results that demonstrate the effectiveness of using a COX-2 probe as a diagnostic tool for identifying BCC tumors and microtumors in mouse models. It has been shown that there is an increase in the expression of COX-2 in cancer lesions. A fluorescent molecular probe that preferentially binds to COX-2 has been reported. We inject this COX-2 probe into mouse models of BCC and perform whole-animal fluorescent imaging using the Maestro™ imaging system. Representative images are shown in Figs. 1 (A) and (B). BCC tumors are identified with arrows in Fig.1(A), while potential BCC microtumors are identified as the numbers 1-12 in Fig.1(B). All identified sites are excised and sectioned. H&E staining is performed on the sections and their morphology is examined to check for the presence or absence of BCC tumors. The results of the experiments are shown in Table 1. As seen in Table 1, the COX-2 probe demonstrates high sensitivity as a probe to identify BCC. The low specificity can be improved by optimizing the post-process threshold.



Imaging of BBC tumors (arrows), and (B) potential micro-tumors (numbers). Images obtained with the Maestro, with post-processed unmixing of signal.

	Positive Macro Tumors	Positive Micro Tumors	False Positive Macro Tumors	False Negative Micro Tumors
Expt 1	13/14	11A	11A	0/1
Expt 2	9/9	8/20	12/20	0/2

High sensitivity with low specificity is obtained in the experiment. Specificity can be improved by optimizing post-processing parameters.

Presentation Number **0811B**

Poster Session 3c: In Vivo Studies & Development/Novel Use of Imaging Probes

A fluorescent imaging of the murine orthotopic brain tumor, using new nanocarrier "Lactosome"

Kensuke Kurihara¹, **Fumihiko Yamamoto**^{1,2}, **Makoto Yamaguchi**³, **Yoshiki Arakawa**³, **Isao Hara**⁴, **Eiichi Ozeki**⁴, **Akira Makino**^{4,5}, **Kaori Togashi**⁶, **Akira Shimizu**¹, **Shunsaku Kimura**^{1,5}, ¹Transnational Research Center, Kyoto University Hospital, Kyoto, Japan; ²Department of Radiopharmacy, Tohoku Pharmaceutical University, Sendai, Japan; ³Department of Neurosurgery, Kyoto University, Kyoto, Japan; ⁴Technology Research Laboratory, Shimadzu Corporation, Kyoto, Japan; ⁵Department of Material Chemistry, Graduate School of Engineering, Kyoto University, Kyoto, Japan; ⁶Department of Diagnostic Imaging and Nuclear Medicine, Kyoto University, Kyoto, Japan. Contact e-mail: kurihara@kuhp.kyoto-u.ac.jp

We have developed polymer micelle type nanocarrier "Lactosome" composed of amphiphilic polydepsiptide block polymer [1] for application as molecule imaging probes and DDS probes. We previously reported that indocyanine green labeled lactosome (ICG-lactosome) showed a high escape ability from the reticulo-endothelial system and high contrast liver tumor imaging due to the enhanced permeation and retention (EPR) effect with using near infrared fluorescence (NIRF) optical imaging technique.[2] Furthermore, we developed fluorescein isothiocyanate labeled lactosome (FITC-lactosome) as a NIRF optical imaging probe, ¹⁸F labeled lactosome (¹⁸F-lactosome) as a PET imaging probe, and both ¹³¹I and ¹²³I labeled lactosome (¹³¹I-lactosome and ¹²³I-lactosome) as SPECT imaging probes. In present study, we successfully obtained a fluorescent imaging murine orthotopic brain tumor U87 using ICG-lactosome. We think the local accumulation of lactosome is due to both EPR effect and local failure of blood-brain barrier (BBB). We describe about comparison biodistribution of ¹³¹I-lactosome with histopathological views by using FITC-lactosome. Because this nanocarrier shows good accumulation specificity and retention in the tumor tissue, ¹³¹I-lactosome is expected to be applied for radiotherapy, as well as molecular imaging probes. References [1]A. Makino, et.al., Chem. Lett. 2006, 36, 1220. [2]A. Makino, et.al., Biomaterials 2009, 30, 5156.

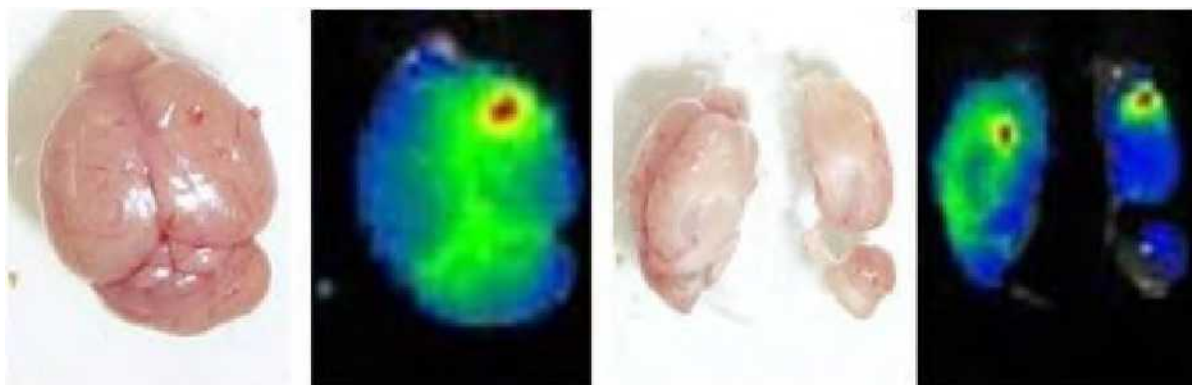


Fig. The part which transplanted brain tumor U87 shows accumulation of ICG-lactosome. We show extracted brain and the section image, and a tumor is divided equally by a section.

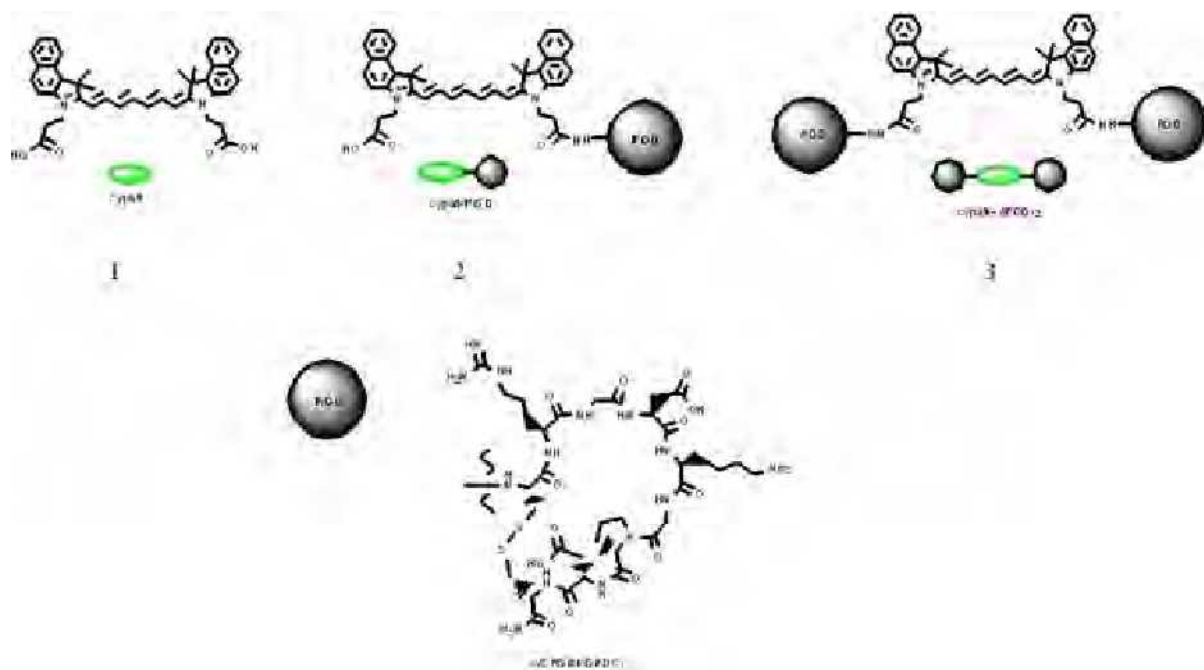
Presentation Number **0812B**

Poster Session 3c: In Vivo Studies & Development/Novel Use of Imaging Probes

Novel Optical Agents Bearing One or Two iRGD Peptides for Integrin-targeted Tumor Imaging: Design, Synthesis, and Evaluation

Yunpeng Ye¹, **Lei Zhu**¹, **Gang Niu**¹, **Ying Ma**¹, **Samuel Achilefu**², **Xiaoyuan Chen**¹, ¹Laboratory of Molecular Imaging and Nanomedicine, NIBIB/NIH, Bethesda, MD, USA; ²Optical Radiology Laboratory, Department of Radiology, Washington University School of Medicine, St. Louis, MO, USA. Contact e-mail: Yunpeng.Ye@nih.gov

Integrin $\alpha\beta_3$ and some other receptors are very attractive targets for molecular imaging and targeted therapy due to their important roles in tumor growth, angiogenesis, and metastasis. We have been interested in discovering novel imaging agents based on a disulfide-based cyclic RGD peptide i.e. CRGDKGPDC or iRGD which can target both integrin and neuropilin-1 receptors with deep tumor penetration. Herein, we report the design, synthesis, and evaluation of a novel dimeric iRGD peptide analog linked by a near-infrared fluorescent dye (cypate,1) for in vivo optical imaging of tumors. The conjugation of 1 and the protected iRGD peptide was performed on solid support and the two final products including 2 and 3 were obtained by TFA cleavage, HPLC purification, and ES-MS identification. The compounds were evaluated in vitro and in vivo, including cell staining, cell binding assay, in vivo tumor imaging in MDA-MB-435 xenograft-bearing mouse models, and ex vivo validation. Our results showed that the divalent iRGD analog 3 is superior to its monovalent counterpart 2. Especially, in vivo optical imaging showed that 3 had better tumor accumulation and retention than 2 due to the possible synergistic effects of the two iRGD motifs. In conclusion, cypate is a powerful scaffold for constructing the novel, near-infrared fluorescent integrin-targeting RGD molecular repertoire. The resulting divalent compound 3 may become a valuable molecular tool for optical imaging of integrin expression and tumor targeting.



Presentation Number **0813B**

Poster Session 3c: In Vivo Studies & Development/Novel Use of Imaging Probes

Development and Application of a Near-Infrared Fluorescence Probe for In Vivo Imaging of Reactive Oxygen Species

Daihi Oushiki^{1,2}, **Hirotsu Kojima**^{2,3}, **Takuya Terai**^{1,2}, **Tetsuo Nagano**^{1,2}, ¹*Graduate School of Pharmaceutical Sciences, The University of Tokyo, Tokyo, Japan;* ²*CREST, Japan Science and Technology Agency, Kawaguchi-shi, Japan;* ³*Chemical Biology Research Initiative, The University of Tokyo, Tokyo, Japan. Contact e-mail: ff097007@mail.ecc.u-tokyo.ac.jp*

Reactive oxygen species (ROS) operate as signaling molecules under various physiological conditions, and overproduction of ROS is involved in the pathogenesis of many diseases. Therefore, several fluorescence probes for ROS have been developed to uncover the molecular mechanisms and widely used for cellular imaging of ROS. However, existing probes have severe limitations for in vivo applications, since they are based on fluorophores emitting in the visible region. Therefore, we attempted to develop a novel fluorescence probe for ROS operating in the physiologically favorable near-infrared (NIR) region, where autofluorescence and interference from hemoglobin absorption are minimal. Cyanine dyes are well-known fluorophores in the NIR region, but their chemical properties have not been thoroughly investigated. Therefore, we set out to establish a novel design strategy to obtain an NIR ROS probe, and found that cyanine dyes react with ROS and their reactivities are correlated with their oxidation potentials, which can be controlled by modifying their chemical structures. We focused on these characteristics and adopted the strategy of utilizing two linked cyanine dyes having differential reactivity with ROS; reaction of the more susceptible dye with ROS releases intramolecular fluorescence quenching of the other dye. Therefore it is possible to follow changes in ROS levels by monitoring the fluorescence emission increase. We developed a novel ROS probe, FOSCY-1, based on the strategy and examined the reactivities with a variety of chemically and enzymatically generated ROS. FOSCY-1 exhibited a high response, showing an immediate fluorescence enhancement. Moreover, the absorbance and fluorescence of FOSCY-1 were sufficiently stable for practical use with respect to photooxidation, indicating that FOSCY-1 can detect ROS with high reliability. We then applied this probe to detect ROS produced by living cells, and the remarkable fluorescence enhancement was observed following stimulation of neutrophils and HL60 cells. We also investigated the ability of this probe to image oxidative stress in a mouse model of peritonitis. Peritonitis mice were given an intraperitoneal injection of FOSCY-1, and the fluorescence intensity of FOSCY-1 in their abdominal region was remarkably increased by stimulation. These experiments demonstrate that FOSCY-1 is practically useful as a biological sensor. On the basis of these results, we anticipate that FOSCY-1 will find wide application as a research tool.

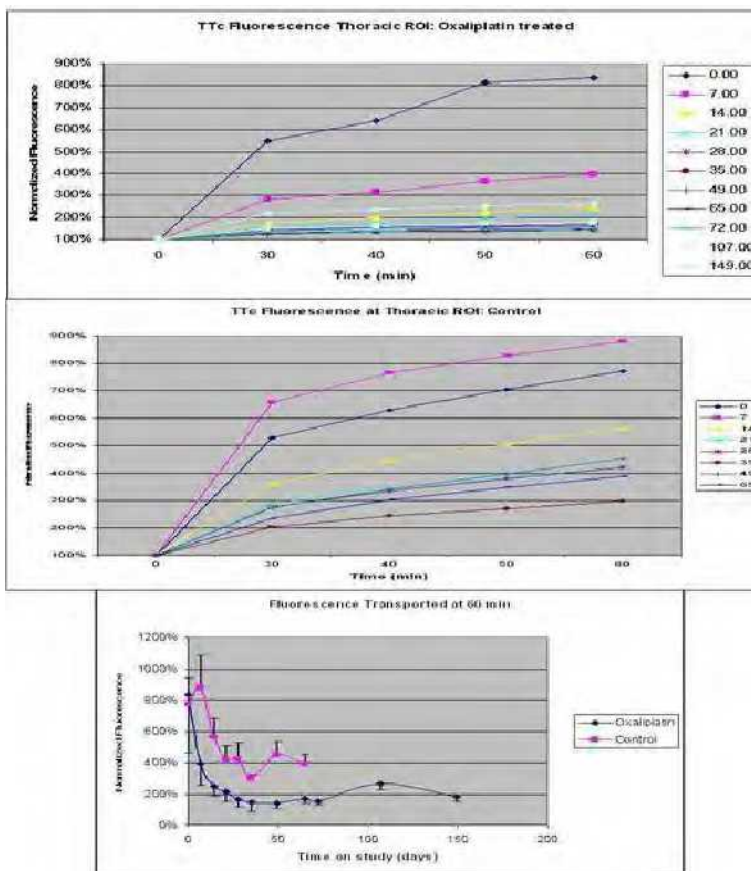
Presentation Number **0814B**

Poster Session 3c: In Vivo Studies & Development/Novel Use of Imaging Probes

In vivo Molecular Neurography Reveals Deleterious Effects of Oxaliplatin Therapy on Retrograde Axonal Transport in Peripheral Nervous System.

Dawid Schellingerhout², Sebastian Bredow¹, Lucia LeRoux¹, Juri G. Gelovani¹, ¹Experimental Diagnostic Imaging, MD Anderson Cancer Center, Houston, TX, USA; ²Radiology, MD Anderson Cancer Center, Houston, TX, USA. Contact e-mail: Dawid.Schellingerhout@mdanderson.org

Objective: The aim of this study was to assess the efficacy of a novel in vivo molecular imaging technology, whole body molecular neurography, which is based on the retrograde neural transport of fluorescently-labeled molecular imaging agent, to determine if oxaliplatin neurotoxicity affects retrograde axonal transport. **Methods:** Female adult BALB/c mice (n=8) were treated with oxaliplatin to a cumulative dose of 30 mg/kg by giving 10 divided intraperitoneal doses using a 5 days of treatment, 5 day rest, 5 day treatment administration paradigm. Animals were imaged at baseline and weekly for 149 days after commencement of therapy. Control animals (n=8 from 8 to 28 days, n=4 from 35 to 65 days) were mock treated with saline and were imaged similarly out to 65 days. All animals received fluorescently labeled TtC-Alexa790 (15 ug in 20 uL) via intramuscular injection into the calf muscles at every imaging session. Fluorescent imaging (Xenogen IVIS 200) was used to image the distribution of TtC over 60 minutes, with ROI measurements taken from the thoracic spine to quantify fluorescence. ROI measurements had background activity subtracted, and normalized to the signal intensity at time = 0. **Results:** With sham treatment, TtC transport through the sciatic nerve and spinal cord causes the fluorescent signal intensity over the thoracic ROI to gradually increase (Figure, legend indicates number of days after start of study). At 60 minutes the grouped mean normalized fluorescence was 562% (+/-210% SD). With oxaliplatin treatment, transport is abruptly and severely impaired with baseline values of 836%+/-375% falling to 396%+/-140%, 247%+/-63%, 213%+/-58%, 162%+/-46%, 147%+/-63% with each successive week and stabilizing around 175% (+/-45%) for grouped means from 6 weeks out to the end of the study. The difference between normalized fluorescence grouped mean values from 6 weeks after oxaliplatin treatment to the end of study, and control animals is highly statistically significant (T-test p<0.0001). **Conclusions:** Oxaliplatin causes a rapid and apparently irreversible (to our current follow-up of 149 days) decrease of retrograde axonal transport in the sciatic nerves and spinal cord, as demonstrated with a neurographic molecular imaging agent.



Presentation Number **0815B**

Poster Session 3c: In Vivo Studies & Development/Novel Use of Imaging Probes

Development of Novel NIR Fluorescent Dyes Based on Rhodamine and Their Application for In Vivo Tumor Imaging

Yuichiro Koide^{1,2}, Yasuteru Urano³, Kenjiro Hanaoka^{1,2}, Takuya Terai^{1,2}, Moriaki Kusakabe^{4,5}, Kiyoshi Okawa⁶, Hisashi Hashimoto⁷, Tetsuo Nagano^{1,2}, ¹Graduate School of Pharmaceutical Sciences, The University of Tokyo, Tokyo, Japan; ²CREST, JST, Tokyo, Japan; ³Graduate School of Medicine, The University of Tokyo, Tokyo, Japan; ⁴Graduate School of Agricultural and Life Sciences, The University of Tokyo, Tokyo, Japan; ⁵Matrix Cell Res. Inst., Inc., Tokyo, Japan; ⁶Department of Biochemistry, The Jikei University School of Medicine, Tokyo, Japan; ⁷Department of Anatomy, The Jikei University School of Medicine, Tokyo, Japan. Contact e-mail: ff087010@mail.ecc.u-tokyo.ac.jp

Near-infrared (NIR) emitting fluorescent dyes are attractive for in vivo imaging and biological applications because of low background autofluorescence from serum, proteins, and other biological macromolecules, and low risk of cell damage by exciting light in this wavelength region. At WMIC 2009, we gave presentation about the photochemical properties and the applications for fluorescence probes of group 14 xanthenes and rhodamines, containing silicon, germanium, or tin at the 10 position of the xanthene chromophore. These group 14 xanthenes and rhodamines showed large bathochromic shifts compared to the original rhodamines, and they retain the advantages of the original rhodamines, including high quantum efficiency in aqueous media ($\Phi_{fl} = 0.3 \sim 0.45$), tolerance to photobleaching, and high water solubility. Although the absorption and fluorescence emission maxima of Si-Rhodamine (SiR), one of the group 14 rhodamines, is as long as around 650 nm, since fluorescent dye emitting over 700 nm is more desirable for in vivo imaging, we developed novel NIR fluorescent dyes, SiR-NIRs, by expanding the xanthene fluorophore of SiR. Then, we introduced succinimidyl ester into SiR-NIR for conjugation with biomolecules, such as antibodies and proteins. As an example of SiR-NIR's application, we tried in vivo tumor imaging that targeted an extracellular matrix glycoprotein tenascin-C (TN-C), which is known to be overexpressed in the extracellular matrices in tumor tissues. After we prepared SiR-NIR-anti-TN-C-antibody conjugates, we intravenously injected them to mouse xenograft tumor models bearing subcutaneous human malignant meningioma HKBMM cells. The fluorescent signals of SiR-NIR were clearly observed 24 h after injection in localized area of the implanted HKBMM cells. In this study, we successfully visualized subcutaneous xenograft tumors in mouse models by novel NIR emitting fluorescent dye-labeled antibodies that targeted TN-C.

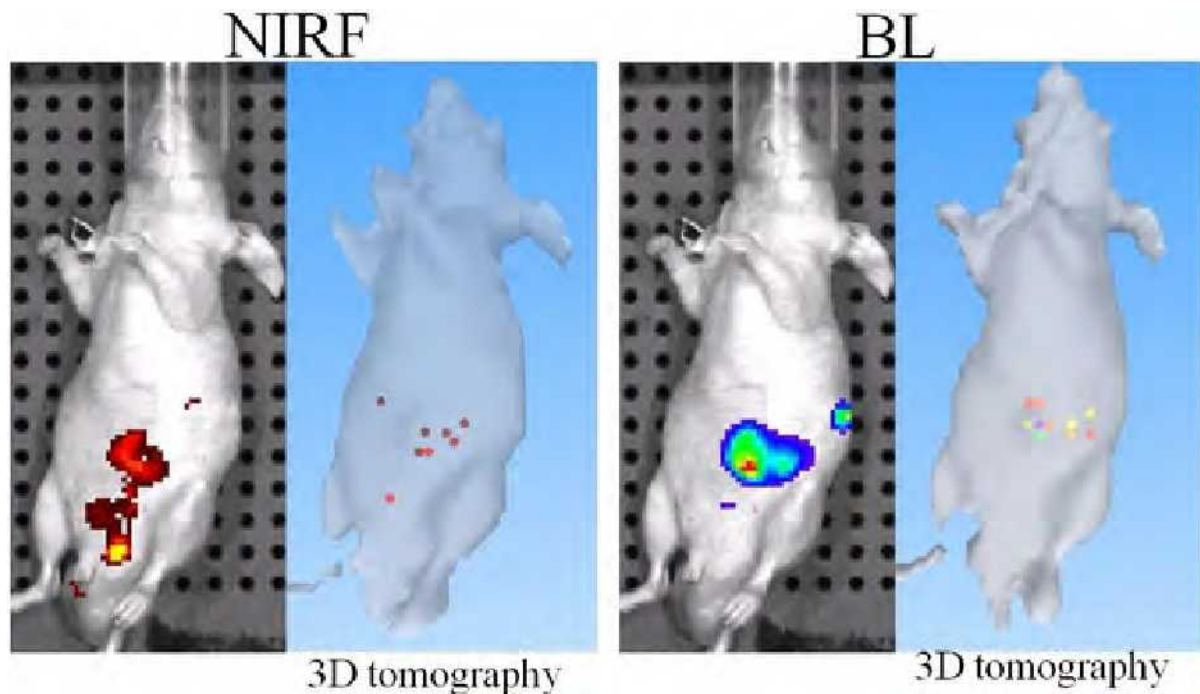
Presentation Number **0816B**

Poster Session 3c: In Vivo Studies & Development/Novel Use of Imaging Probes

Development of fusion protein probes for in vivo imaging of HIF-active cancer cells

Takahiro Kuchimaru¹, Tetsuya Kadosono^{2,3}, Takashi Ushiki⁴, Masahiro Hiraoka^{2,3}, Shinae Kizaka-Kondoh¹, ¹Graduate School of Bioscience and Biotechnology, Tokyo Institute of Technology, Yokohama, Japan; ²Graduate School of Medicine, Kyoto University, Kyoto, Japan; ³Innovative Techno-Hub for Integrated Medical Bio-imaging, Kyoto University, Kyoto, Japan; ⁴Graduate School of Medical and Dental Sciences, Niigata University, Niigata, Japan. Contact e-mail: atuk@kuhp.kyoto-u.ac.jp

Hypoxia-inducible factor-1 (HIF-1) is a master transcriptional regulator for adaptation to hypoxia by inducing more than 100 genes that are involved in proliferation, angiogenesis, apoptosis and energy metabolism. Cancers with more expression of the alpha subunit of HIF (HIF α) tend to become more malignant and treatment-resistant. The fate of HIF α protein is regulated by the oxygen sensor HIF prolyl hydroxylases (HPHDs) through its oxygen-dependent degradation domain (ODD). We recently constructed a fusion protein POH, which consisted of Protein Transduction Domain (PTD), ODD and HaloTag. The PTD was a membrane-permeable peptide, which efficiently delivered fusion proteins into cells. HaloTag was used for labeling the probe with near-infrared fluorescence (NIRF) dyes. POH-NIRF was examined for in vivo dynamic status and its target-specificity by in vivo and ex vivo NIRF imaging. The targets of POH, HIF-active cells, were visualized in vivo by bioluminescence (BL) using a HIF-1-dependent luciferase reporter gene. The NIRF images obtained with POH-NIRF probes overlapped with images of HIF-active region in subcutaneous xenografts and orthotopic pancreatic cancers 9 to 24 h after POH-NIRF injection. Furthermore, immunohistochemical analysis of tumor sections from the mice 6 h after POH-NIRF injection revealed the localization of POH was overlapped with HIF-1 α -positive regions. The regulation of POH probe by HPHDs was confirmed by experiments with a negative control probe P_{OmH}-NIRF, which lacked the HPHDs-target Pro residue in ODD. Overall results demonstrated the specificity of POH-NIRF probe to HIF-active cells and their large potential for imaging and targeting of HIF-related diseases.



In vivo optical imaging of POH probe (NIRF) and HIF-active cells (BL) in pancreatic cancer and their 3D tomography

Presentation Number **0817B**

Poster Session 3c: In Vivo Studies & Development/Novel Use of Imaging Probes

A method to follow tumor induced bone loss over time, in vivo, using whole body fluorescence imaging

Thomas Snoeks¹, **Artem Khmelinski**², **Ivo Que**¹, **Boudewijn Lelieveldt**², **Eric Kaijzel**¹, **Clemens Lowik**¹, ¹Endocrinology, Leiden University Medical Center, Leiden, Netherlands; ²LKEB - Image Processing, Leiden University Medical Center, Leiden, Netherlands. Contact e-mail: t.j.a.snoeks@lumc.nl

In vivo bioluminescence imaging (BLI) of luciferase (Luc) expressing tumor cells has become a well accepted method to quantitatively follow tumor growth. Fluorescence imaging (FLI) can be used to visualize and quantify specific structures and molecules using targeted dyes and enzymatic activity using enzyme activated probes. Traditionally, osteolytic lesions are quantified using x-ray radiographs and μ CT. These procedures are time consuming and irradiate the animal limiting the number of repeated measurements. The aim of this study was to quantify osteolysis by a loss of fluorescent signal after pre-labelling the skeleton with a fluorescent bone probe. In this setup, we compared the performance of various commercially available bone probes. In vivo CT was used as a control method for detecting and quantifying osteolysis. BLI was used to follow tumor growth. BALB/c Nude mice received i.v. OsteoSense-680 or -750 or BoneTag-680 or -800 (n=5), 3 days prior to intra-osseous tumor inoculation with the osteolytic MDA-MB-231-BO2-Luc breast cancer cell line. BLI and FLI were performed using the IVIS Spectrum (Caliper LS). In addition, FLI of the 680 and 800 probes was performed using the Pearl Imager (LI-COR). In the figure the OsteoSense-680 data is shown as representative example. We show that it is possible to visualize osteolysis as a loss of FLI signal and correlate this loss of signal with tumor growth (quantified with BLI) and lesion size (quantified with μ CT). This is valuable tool to non-invasively follow osteolysis in vivo.

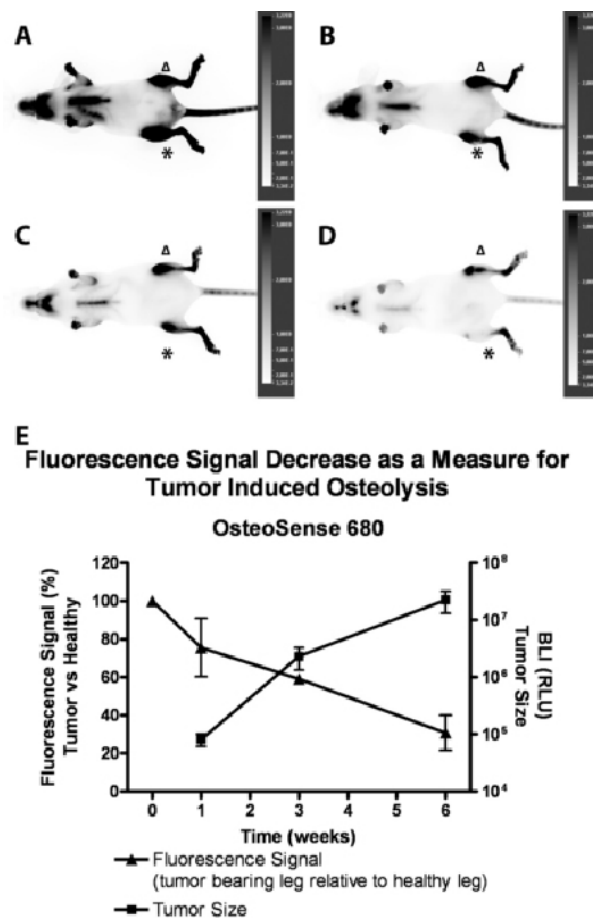


Figure A-D: FLI after OsteoSense-680 pre-labelling and tumor inoculation, images taken at day 0, 8, 21, 42 using the Pearl Imager. The signal of the tumor bearing leg (*) decreases compared to the healthy leg (Δ). Figure E: quantified loss of OsteoSense signal in the tumor bearing leg compared to the healthy control plotted together with the tumor growth at day 8, 21, 42 (n=5). This figure shows the OsteoSense-680 data as representative example.

Presentation Number **0818B**

Poster Session 3c: In Vivo Studies & Development/Novel Use of Imaging Probes

Molecular evaluation of imaging probe specific to HIF-active cancer cells and influence of cell permeable property of fluorescent dye on in vivo optical imaging

Tetsuya Kadonosono¹, **Takahiro Kuchimaru**², **Takashi Ushiki**³, **Masahiro Hiraoka**¹, **Shinae Kizaka-Kondoh**², ¹*Kyoto University, Kyoto, Japan;* ²*Tokyo Institute of Technology, Yokohama, Japan;* ³*Niigata University, Niigata, Japan.* Contact e-mail: tetsuyak@kuhp.kyoto-u.ac.jp

Tumor hypoxia plays a central role in malignant progression and is resistant to both radiotherapy and chemotherapy. Hypoxia-inducible factors (HIFs) are master transcriptional regulators for adaptation to hypoxia by inducing adaptive changes in gene expression for regulation of angiogenesis, proliferation, and metastasis in cancers. Protein stability of the alpha-subunit of HIFs (HIF α) are strictly regulated by the oxygen sensor HIF prolyl hydroxylases (HPHDs). While HPHDs are inactive in hypoxic cells, they hydroxylate the Oxygen-Dependent Degradation (ODD) domain of HIF α s in well-oxygenized cells and the hydroxylated HIF α s are rapidly degraded through the ubiquitin-proteasome system. We recently developed PTD-ODD-HaloTag (POH) probes, which was composed of the PTD domain for cell membrane penetration, the ODD bio-sensing domain for specific stabilization in HIF-active cells as HIF α and the HaloTag domain for covalently binding to HaloTag ligand (HL). In this study, POH protein was bound to HL labeled with near infrared fluorescence dyes (NIRF), AlexaFluora750 (AF750) or IR800. The resultant POH-HL-AF750 (POH-A) and POH-HL-IR800 (POH-I) were then examined their usefulness for imaging probes and analyzed the influence of cell permeable property of fluorescent dye for in vivo imaging. When the cells were treated with POH-A or POH-I, significantly higher levels of the POH protein were detected in cells cultured under hypoxic or hypoxia-mimic conditions than normoxic conditions. This finding revealed that POH probes were efficiently penetrated into cells and specifically stabilized in HIF-active cells. Although POH-A and POH-I showed similar cell membrane permeability, HL-AF750 alone penetrated cell membrane about 16 times less than HL-IR800. Furthermore, POH-I-treated cells showed shorter fluorescence retention time than POH-A-treated cells, indicating that POH-I and/or its pieces diffused away from the cell faster than POH-A. When these probes were applied for in vivo optical imaging of HIF-active hypoxic cells in a subcutaneous xenograft model, POH-I showed significantly higher fluorescent intensity ratio in tumor versus background (T/B) than POH-A and the tissue distribution of probed was different, indicating that the characteristics of NIRF ligand influenced the clearance efficiency and excretion pathway. Overall results demonstrate that POH is a specific probe to HIF-active cells and that high cell permeability of imaging materials conjugated to POH such as fluorescent dyes and isotope-labeled chemicals would improve its in vivo imaging.

Presentation Number **0819B**

Poster Session 3c: In Vivo Studies & Development/Novel Use of Imaging Probes

Imaging of ischemic brain by use of a fusion protein with oxygen-dependent degradation domain of HIF-1

Youshi Fujita¹, Takahiro Kuchimaru², Tetsuya Kadonosono², Masafumi Ihara¹, Ryosuke Takahashi¹, Masahiro Hiraoka³, Shinae Kizaka-Kondoh², ¹Department of Neurology, Kyoto University, Kyoto, Japan; ²Department of Biomolecular Engineering, Tokyo Institute of Technology, Yokohama, Japan; ³Department of Radiation Oncology and Image-applied Therapy, Kyoto University, Kyoto, Japan.
Contact e-mail: fujitauc@kuhp.kyoto-u.ac.jp

INTRODUCTION: Ischemic insult after middle cerebral artery occlusion (MCAO) is known to increase HIF-1 α levels in the brain. HIF-1 is activated in the peri-infarct reversible ischemic penumbra, where blood flow is decreased and oxygen delivery is impaired. HIF-1 α is polyubiquitinated and undergoes proteasomal degradation in normoxic conditions. Hypoxia suppresses the rate of HIF hydroxylation, allowing HIF-1 α to accumulate. We designed a fusion protein (POH-I: PTD-ODD-HaloTag-ligand-NIRF dye (IR800)) consisting of a protein transduction domain (PTD), HaloTag with near-infrared fluorescence (NIRF) dyes, and a portion of the oxygen-dependent degradation domain (ODD) of HIF-1 α that confers the same oxygen-dependent regulation as HIF-1 α on POH-I. The purpose of this study was to evaluate the feasibility of POH-I as an imaging probe for HIF-1-active ischemic brain tissue. **METHODS:** Male C57/BL6 mice (6-7 weeks old) were anesthetized with 1.5 % isoflurane via a snout mask. A 6-mm-diameter hole was made with a fine drill bit in the skull. The dura mater was left intact. An 8-mm cover glass was sealed to the skull with dental cement to cover the hole. Transient focal cerebral ischemia was induced using the intraluminal middle cerebral artery occlusion (MCAO) technique. After occlusion for 60 min, blood flow was restored by withdrawal of the silicon-coated nylon suture. Immediately after inducing MCAO for 60 min, the mice received POH-I via tail vein and the fluorescent signal was monitored for 24 h by using the IVIS Spectrum system (Xenogen). **RESULTS:** Five min after the administration of POH-I, fluorescent signals were lower in the ischemic hemisphere than in the non-ischemic hemisphere, probably reflecting a decreased cerebral blood flow in the ischemic hemisphere. However, 1-3 h after administration of POH-I, the fluorescent intensity increased in the ischemic hemisphere and decreased in the non-ischemic hemisphere. Immunohistochemical analysis of the brain 6 h after POH-I injection showed that the POH protein was mainly localized to the neuronal cytoplasm of cells in the ischemic hemisphere. **CONCLUSIONS:** POH-I provides a novel approach to identify ischemic brain damage, in addition, this PTD-mediated delivery could be used to selectively deliver any drug to the ischemic penumbra.

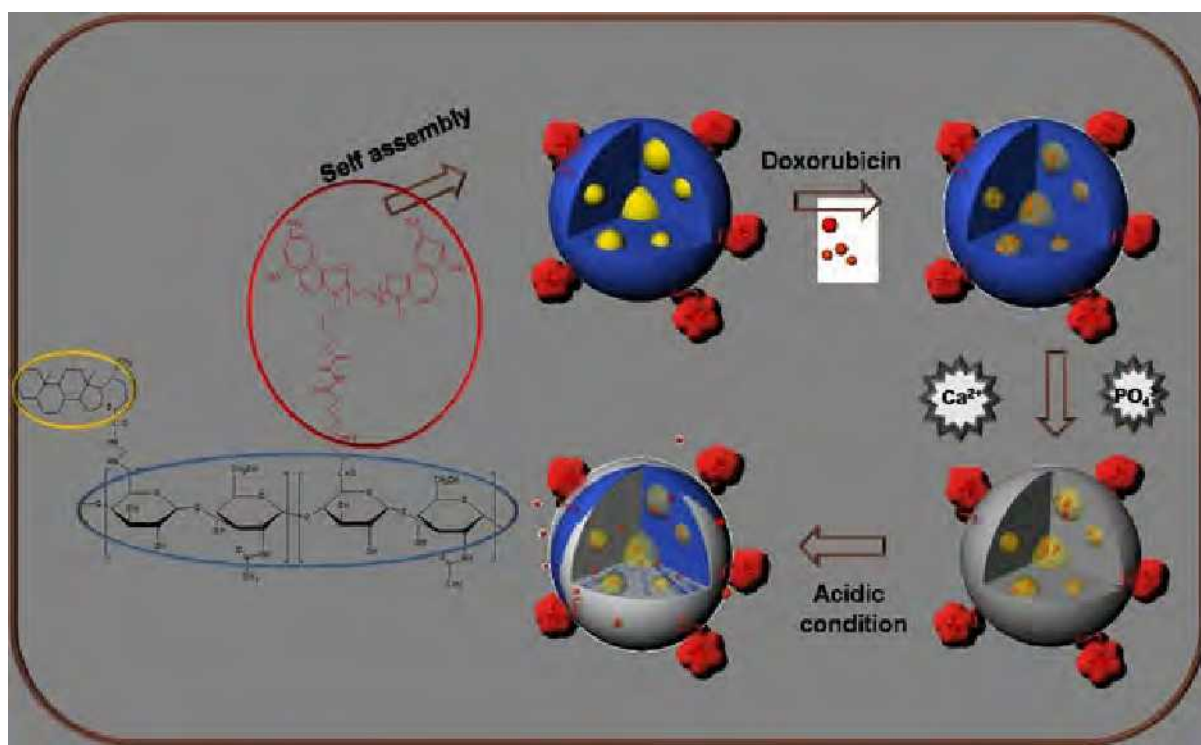
Presentation Number **0820B**

Poster Session 4c: In Vivo Studies & Development/Novel Use of Imaging Probes

Synthesis and Characterization of Theranostic Nanoparticles Based on Mineralized Hyaluronic Acids

Song Yi Han¹, **Hwa Seung Han**¹, **Sang Cheon Lee**², **Jae Hyung Park**^{1,3}, ¹Departments of Advanced Polymer and Chemical Engineering, Kyung Hee University, Gyeonggi-do, Republic of Korea; ²Department of Oral Biology & Institute of Oral Biology, School of Dentistry, Kyung Hee University, Seoul, Republic of Korea; ³Department of Life and Nanopharmaceutical Sciences, Kyung Hee University, Seoul, Republic of Korea. Contact e-mail: chocose@gmail.com

Self-assembled nanoparticles that encompass imaging and therapeutic capabilities provide unique opportunity for the diagnosis and treatment of cancer, since nano-sized particles could passively accumulate tumors via enhanced permeation and retention (EPR) effect. However, poor stability of these particles under dilute in vivo conditions limited their use in clinical applications. In an effort to address the stability of the self-assembled nanoparticulate system, we have prepared novel structurally stable robust doxorubicin-encapsulated hybrid nanoparticles conjugated with Cy5.5, a near-infrared fluorescence dye for optical imaging, via mineralization under ambient temperature. The robustness of the particles were illustrated from the in vivo drug release profile exhibited a delay release under normal physiological condition (pH 7.4) and enhanced drug release at mild acidic pH, due to the dissolution of calcium phosphate under acidic conditions. Furthermore, tumor targetability of the hybrid nanoparticles was investigated using optical imaging technique. When the hybrid nanoparticles were systemically administered into the tumor-bearing mice, enhanced signal intensity was observed at the tumor site, indicating the high tumor-targetability of the hybrid nanoparticles. Overall, the results obtained from the study indicate that these robust hybrid nanoparticles could be useful as potential carrier for cancer diagnosis and therapy.



Presentation Number **0821B**

Poster Session 4c: In Vivo Studies & Development/Novel Use of Imaging Probes

Smart fluorescent caspase-3 probes for molecular imaging of apoptosis : a click chemistry approach

*Christophe Portal¹, Manuelle Debunne^{1,3}, Bruno Delest¹, Pauline Noack¹, Marc Massonneau¹, Anthony Romieu², Christian Thuillez³, Vincent Richard³, **Pierre-Yves Renard^{2,1}**QUIDD, Saint Etienne du Rouvray, France; ²COBRA, University of Rouen, Mont Saint Aignan, France; ³Inserm U644, UFR Médecine-Pharmacie de Rouen, Rouen, France. Contact e-mail: pierre-yves.renard@univ-rouen.fr*

The central role played by apoptosis or programmed cell death in many diseases makes it a very attractive target for molecular imaging in various medical fields. Upon the few molecular imaging modalities, optical imaging is developing exponentially especially because of its ease of use, its high sensitivity and the opportunity to elaborate activable (smart) probes. We developed quenched near-infrared fluorescent probes which become activated upon cleavage by caspase-3, the key regulatory enzyme of apoptosis. A first generation probe was prepared and showed limited cell penetration despite its good selectivity for caspase-3. A versatile and highly adaptive click-chemistry based strategy was then elaborated for the incorporation of additional moieties, not only to tackle cell penetration properties by the addition of a cell penetrating peptide (CPP) but also in vivo half-life by the incorporation of a poly-ethyleneglycol (PEG) spacer additionally to the CPP. The probes were shown to be selectively cleaved by recombinant caspase-3, and to a very small extent by caspase-7, but not by other caspases. We thus demonstrated the potential of this novel approach for the fast preparation of probes with custom pharmacokinetics to detect apoptosis in vitro, allowing for the future elaboration of optical probes aimed at in vivo apoptosis imaging.

Presentation Number **0822B**

Poster Session 4c: In Vivo Studies & Development/Novel Use of Imaging Probes

Fluorescent Nanoparticle Pre-Labeled Tumors Enable Facile Validation of In Vivo NIR Probes

Bryan A. Smith, W. Matthew Leevy, Bradley D. Smith, Notre Dame Integrated Imaging Facility, University of Notre Dame, Notre Dame, IN, USA. Contact e-mail: bsmith23@nd.edu

A common strategy in the tumor probe development community is to utilize cancer cells that are genetically engineered to express a fluorescent or luminescent reporter, such as RFP or Luciferase. When these cells are implanted on a mouse, their genetic reporter provides a convenient way to delineate the tumor as it grows. A tumor probe researcher would then inject their probe with fluorescence in a different filter set, and check for co-registration between images. While this method is great, it does require the genetic engineering of the tumor cell line under study. Further, genetic reporters can be silenced in vivo or influenced by signaling pathways thus complicating the interpretation of such imaging data. We have conceived a facile system for pre-labeling tumor cells for transplantation and longitudinal fluorescence imaging. X-Sight 691 nanospheres were used to pre-label prostate cancer cells to delineate their location in vivo. Next, we injected our near-infrared probe, known as DPA-Cy7, to assess its tumor targeting ability as measured by coregistration with the X691 signal. Strong fluorescence intensities emanated from the palpable xenografts, 14 days after labeling. Spectral unmixing of in vivo fluorescence images showed high colocalization between the X761 labeled prostate xenografts and the near-infrared probe. Ex vivo analysis confirmed the colocalization observed in the in vivo images. X-Sight nanospheres offer a facile and non-invasive method of studying a probe's targeting selectivity in vivo, which could potentially expedite probe development in academia and industry.

Presentation Number **0823B**

Poster Session 4c: In Vivo Studies & Development/Novel Use of Imaging Probes

An improved optical imaging probe targeting integrin $\alpha V\beta 3$ in glioblastoma xenografts*Fulvio Uggeri, Alessandro Maiocchi, Centro Ricerche Bracco, Bracco Imaging, Torino, Italy. Contact e-mail: fulvio.uggeri@bracco.com*

Introduction Optical imaging is emerging as a complement to nuclear imaging since it is highly sensitive and noninvasive, as well as being relatively inexpensive. Integrins are an attractive target for molecular imaging probes, in particular $\alpha V\beta 3$ integrin is the receptor for a variety of extracellular matrix proteins containing an RGD sequence, and serves as a marker of angiogenesis, tumor development and metastasis, since it is barely detectable on quiescent vessels and highly expressed during the angiogenic sprout. In this study we evaluated the sensitivity of a new near-infrared (NIR) fluorescence RGD cyclic probe synthesized by our group (DA364) in noninvasive detection of $\alpha V\beta 3$ -integrin-over-expressing tumors. Methods DA364's binding affinity for $\alpha V\beta 3$ -integrin was first evaluated in vitro by competitive ELISA and confirmed on $\alpha V\beta 3$ -expressing cells. Binding affinity of DA364 to U-87 MG cells was assessed also by cytofluorimetry. Then, U-87 MG human glioblastoma cells were xenografted in nude mice and DA364 injected i.v. to evaluate its in vivo distribution, specificity and sensitivity with an IVIS 200 optical imaging system. The results were compared with those provided by the commercially available probe IntegriSense680 and Cy5.5. Results DA364 bound $\alpha V\beta 3$ integrin on U-87 MG cells with high affinity and specificity, both in vitro and in vivo. This in vivo binding specificity was confirmed by the strong inhibition of tumor uptake of DA364 in the presence of a non-fluorescent cyclic-RGD peptide. Injection of Cy5.5 dye alone only led to a lower nonspecific binding. The results also showed that 1 h after injection DA364 had significantly higher accumulation than IntegriSense680, though this difference disappeared after 24 h. Ex vivo analyses confirmed that DA364 accumulated at tumor site, whereas very low levels were detected in liver and spleen. Conclusions DA364 allows sensitive and specific detection of transplantable glioblastoma by NIR fluorescence, and can thus be considered as a promising candidate for the elaboration of imaging and therapeutic probes for $\alpha V\beta 3$ over-expressing tumors.

Presentation Number **0824B**

Poster Session 4c: In Vivo Studies & Development/Novel Use of Imaging Probes

***In vivo* imaging of MMP-12- and MMP-13- activatable fluorescent near-infrared peptide probes in murine models of arthritis**

Ngee H. Lim¹, Ernst Meinjohanns², George Bou-Gharios¹, Morten Meldal², Hideaki Nagase¹, ¹Kennedy Institute of Rheumatology, Imperial College School of Medicine, London, United Kingdom; ²Carlsberg Laboratory, Valby, Denmark. Contact e-mail: n.lim@imperial.ac.uk

There are currently no reliable methods of detecting the early stages of cartilage destruction that leads to arthritis. Matrix metalloproteinases (MMPs) are a family of zinc metalloendopeptidases which degrade the majority of cartilage components. Optical activity-based probes directed against MMP-12 (macrophage metalloelastase) or MMP-13 (collagenase 3) may be potential early markers for rheumatoid arthritis and osteoarthritis (OA). Here we report the development of MMP-12- and MMP-13-targeted peptide substrates and their deployment in the zymosan-induced model of inflammation and the surgically-induced destabilised medial meniscus model of OA. The substrates were labelled with the near-infrared dye Cy5.5 and the QSY21 quencher flanking the cleavage site. Control substrates with a proline substitution in the P1' position were also synthesised. The substrates were screened against MMP-1, MMP-2, MMP-3, MMP-8, MMP-12 and MMP-13. *In vitro* substrate specificity was confirmed and the control substrates were not cleaved by any of the enzymes tested. In the inflammatory model, the MMP-12- and the MMP-13-directed peptide substrates were preferentially cleaved in the diseased paw compared to the contra lateral paw. Maximum fluorescent signal intensity 4 hours after intravenous injection indicated that the MMP-12-substrate was cleaved more rapidly than the MMP-13-substrate. Co-injection with a general MMP or corresponding MMP-12- or MMP-13-specific small molecule inhibitors abrogated the increase in fluorescence signal. Surprisingly, both control peptides were cleaved more rapidly than the targeted substrates by both control and zymosan-treated animals. Their cleavage was not inhibited by small molecule MMP inhibitors. Thus the degree of MMP-12 and MMP-13 substrate cleavage successfully indicated the sites of inflammation *in vivo*. Preliminary data in the OA model showed a small but significant increase in signal in the operated compared to the contra lateral knee 6 weeks after surgery using the MMP-13-directed substrate. We are continuing our studies in the OA model using the MMP-12-directed substrate. While we have not proven *in vivo* enzyme-specificity, these peptide substrates may be developed further as markers of inflammation and early cartilage degradation. We are in the process of coupling these peptide sequences with dendrimers and other polymers to improve the targeting and retention of these probes to joints. This work was supported by the EU FP6 Strep Project LSHG-2006-018830 "CAMP" and the NIH grant AR40994.

Presentation Number **0825B**

Poster Session 4c: In Vivo Studies & Development/Novel Use of Imaging Probes

Microspheres as novel and versatile cell tracking agents with the ability to deliver cargoes

Manuelle Debunne², Kevin Dhaliwal², Lois Alexander¹, Neil A. McDonald², Haslett Chris², Mark Bradley¹, ¹Department of Chemistry, University of Edinburgh, Edinburgh, United Kingdom; ²Centre for Inflammation Research, University of Edinburgh, Edinburgh, United Kingdom. Contact e-mail: debunne.manuelle@free.fr

Cell tracking is a critical technique and technology that is elucidating both cellular processes and the feasibility of cell therapy. Current cell tracking tools rely on labeling membranes or the cytosol non-specifically. This work describes the utility of using polystyrene microspheres for both adoptive cell tracking and also direct intravenous administration in vivo. Microspheres have the potential to deliver a variety of payloads. METHODS Microspheres were tagged with near infrared fluorophores and imaged in in vitro phantoms using reflectance microscopy. Flow cytometry and confocal analysis showed efficient uptake of microspheres into cells. Toxicology showed no increase in TNF alpha- secretion from primary macrophages and neutrophils. In models of pleural and pulmonary inflammation including fibrosis, microspheres enabled the visualisation of areas of inflammation using both reflectance and tomographic imaging systems CONCLUSION. Given the ability to load microspheres with proteins, small molecule inhibitors and siRNA, they represent a class of agents that may be useful for both cell tracking and therapeutic delivery.

Presentation Number **0826B**

Poster Session 4c: In Vivo Studies & Development/Novel Use of Imaging Probes

Imaging neutrophil specific responses using an optical imaging agent

Nicolaos Avlonitis², *Manuelle Debunne*¹, *Neil A. McDonald*¹, *Kevin Dhaliwal*¹, *Haslett Chris*¹, *Mark Bradley*², ¹*Centre for Inflammation Research, University of Edinburgh, Edinburgh, United Kingdom;* ²*Department of Chemistry, University of Edinburgh, Edinburgh, United Kingdom. Contact e-mail: Nicos.Avlonitis@ed.ac.uk*

Tissue damage caused by trauma, infection or other stimuli triggers a complex sequence collectively known as the inflammatory response. This response includes the direct migration of neutrophils from circulation to the site of injury with the ultimate goal of killing pathogens. Neutrophils are among the first leucocytes to reach a site of injury, and are abundant at local sites of infection. The ability to detect and quantify neutrophilic accumulation could be important not only in locating and identifying inflammatory lesions but also in facilitating the development and testing of anti-inflammatory agents. Currently available clinical nuclear imaging probes for targeting and diagnosing inflammatory lesions include ⁶⁷Ga citrate and ¹¹¹In or ^{99m}Tc leucocytes labelled ex vivo. Another approach involves peptides that have a high affinity for surface receptors on leucocytes. Herein, we report the synthesis and validation of a new highly potent fluorophore-labelled peptide that targets the a specific surface receptor on neutrophils. Using flow cytometry, confocal and in vivo imaging in models of pulmonary inflammation, we show this to be a powerful tool for monitoring neutrophil responses in vivo.

Presentation Number **0827B**

Poster Session 4c: In Vivo Studies & Development/Novel Use of Imaging Probes

Targeting Neutrophil Function Using a New Fluorescent Probe

Nicolaos Avlonitis^{1,2}, Mark Bradley², Kevin Dhaliwal¹, Neil A. McDonald¹, Manuelle Debunne¹, ¹Centre for Inflammation Research, Edinburgh, United Kingdom; ²School of Chemistry, University of Edinburgh, Edinburgh, United Kingdom. Contact e-mail: Nicos.Avlonitis@ed.ac.uk

Tissue damage caused by trauma, infection or other stimuli triggers a complex sequence of events collectively known as the inflammatory response. This response includes the direct migration of neutrophils from circulation to the site of injury with the ultimate goal of killing pathogens. Neutrophils are among the first leucocytes to reach a site of injury, and are abundant at local sites of infection. The ability to detect and quantify neutrophil accumulation could be important not only in locating and identifying inflammatory lesions but also in facilitating the development and testing of anti-inflammatory agents. Currently available clinical nuclear imaging probes for targeting and diagnosing inflammatory lesions include ⁶⁷Ga citrate and ¹¹¹In or ^{99m}Tc leucocytes labelled ex vivo. Another approach involves peptides that have a high affinity for surface receptors (formyl peptide receptors, FMR) on leucocytes. Herein, we report the synthesis and validation of a new highly potent fluorophore-labelled peptide that targets the formyl peptide receptor on leucocytes.

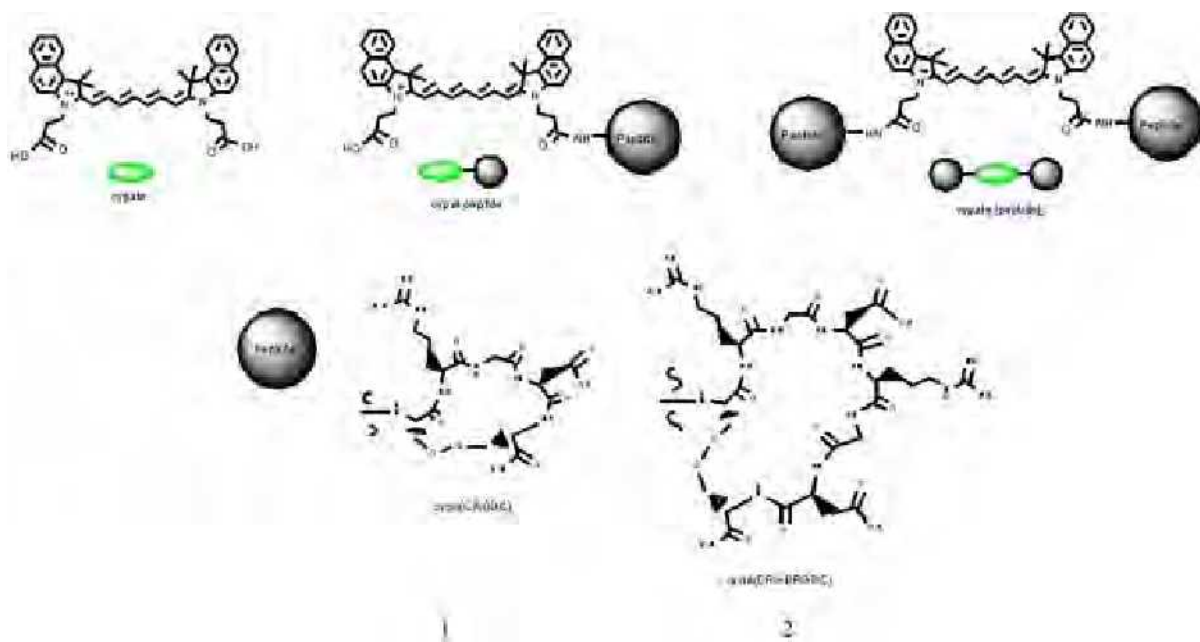
Presentation Number **0828B**

Poster Session 4c: In Vivo Studies & Development/Novel Use of Imaging Probes

Novel Divalent Disulfide-based Cyclic RGD Peptides for Integrin-targeted Tumor Optical Imaging

Yunpeng Ye¹, **Alexandru V. Korotcov**², **Baogang Xu**¹, **Sharon Bloch**¹, **Yue Chen**², **Paul C. Wang**², **Samuel Achilefu**¹, ¹*Optical Radiology Laboratory, Department of Radiology, Washington University School of Medicine, St. Louis, MO, USA;* ²*Molecular Imaging Laboratory, Department of Radiology, Howard University, Washington, DC, USA. Contact e-mail: Yunpeng.Ye@nih.gov*

The RGD peptide motif plays an essential role in the molecular recognition of some integrin receptors. Some cyclic RGD compounds of high affinity and selectivity for $\alpha v \beta 3$, especially some lactam-based cyclic penta-RGD peptide analogs, have been tested as therapeutic agents and molecular imaging agents in clinical trials. Despite much research, many aspects of RGD peptides in tumor imaging and targeting therapy remain unclear. Therefore, it is very significant to explore novel RGD compounds with improved integrin-targeting for tumor imaging. Such compounds should also hold great promise for unraveling the complexity and dynamics of the interactions between RGD peptides and integrin receptors as well as related signal transductions. Over the past years, we have embarked on discovery of novel disulfide-based cyclic RGD peptides for integrin-targeted tumor imaging as such a type of peptides has not been explored fully for molecular imaging, compared with the conventional lactam-based cyclic RGD peptides. This presentation will report the design, synthesis, and evaluation of some novel divalent disulfide-based cyclic RGD peptides for tumor optical imaging. We used a near-infrared fluorescent carbocyanine probe (cypate) as an optical scaffold to prepare some divalent analogs of the two cyclic RGD motifs i.e. cyclo(CRGDC) (1) and cyclo(CRGDRGDC) (2) as showed below. The conjugations of cypate and the protected RGD peptides were performed on solid support to form the desired divalent compounds along with monovalent analogs. The compounds were evaluated in vitro and in vivo, including cellular internalization and localization; receptor binding assays; in vivo tumor imaging; and ex vivo studies. As revealed by in vivo optical imaging, the monovalent analog of 2 showed significant tumor localization with better image contrast than the divalent 1 analog in mouse models of PC3 xenografts. Our work has led to a better understanding of the structure-activity relationship of the disulfide-based cyclic RGD peptides for integrin targeting and tumor optical imaging. Our results suggest the cyclic (CRGDRGDC) peptide motif and related conjugates deserve further studies for their potential in integrin-targeted tumor imaging.



Presentation Number **0829B**

Poster Session 4c: In Vivo Studies & Development/Novel Use of Imaging Probes

Use of Tumor Targeted Raman Nanoparticles for Early Detection of Colon Cancer in Conjunction with a Newly Developed Raman Endoscope

Cristina Zavaleta¹, Jesse V. Jokerst¹, Jonathan T. Liu², Michael J. Mandella², Ellis Garai^{1,2}, Jonathan Hardy^{2,4}, Christopher Contag^{1,2}, Sanjiv S. Gambhir^{1,3}, ¹Radiology, Stanford University, Stanford, CA, USA; ²Pediatrics, Stanford University, Stanford, CA, USA; ³Bioengineering, Stanford University, Stanford, CA, USA; ⁴Microbiology and Immunology, Stanford University, Stanford, CA, USA. Contact e-mail: czavalet@stanford.edu

We have recently developed a new clinical imaging strategy utilizing a customized Raman endoscope in conjunction with locally administered tumor targeting Raman nanoparticles, to be applied during routine colonoscopy. This strategy could offer a new way to sensitively detect and characterize dysplastic flat lesions, which often go undetected within the colon using conventional white light endoscopy. In this study, we evaluated the ability of our surface enhanced Raman scattering (SERS) gold nanoparticles to effectively target fresh human colon cancer tissue after being covalently conjugated with a heptapeptide (VRPMLPQ) sequence previously shown by our group to bind to dysplastic colonocytes in humans. Fresh human colon tissue samples, both malignant and normal adjacent tissue (NAT), were provided to us through our hospital's tissue bank. Tissue sets (malignant and NAT) from each patient (n=4) were analyzed independently. Each of the malignant and NAT samples were cut into two pieces where one was exposed for 10 min to SERS nanoparticles (0.05 nM) conjugated with the tumor targeting (+) heptapeptide sequence and the other SERS nanoparticles (0.05 nM) conjugated with a (-) random heptapeptide sequence (control). The tissue samples were then rinsed with 3% bovine serum albumin for 5 sec and mapped luminal side up using Raman spectroscopy to evaluate binding. Raman imaging revealed a consistent trend where more binding of (+) heptapeptide SERS nanoparticles was seen in malignant versus NAT samples, with an average of 4 times more signal in malignant versus NAT samples of the (+) heptapeptide SERS conjugated nanoparticles. Within the malignant tissue samples themselves, there was also 2 times more signal of the (+) heptapeptide SERS nanoparticles versus the (-) random SERS nanoparticles. These results support the idea of using these heptapeptide labeled SERS nanoparticles as clinical tumor targeting beacons for the early detection of colon cancer in conjunction with our newly developed Raman endoscope.

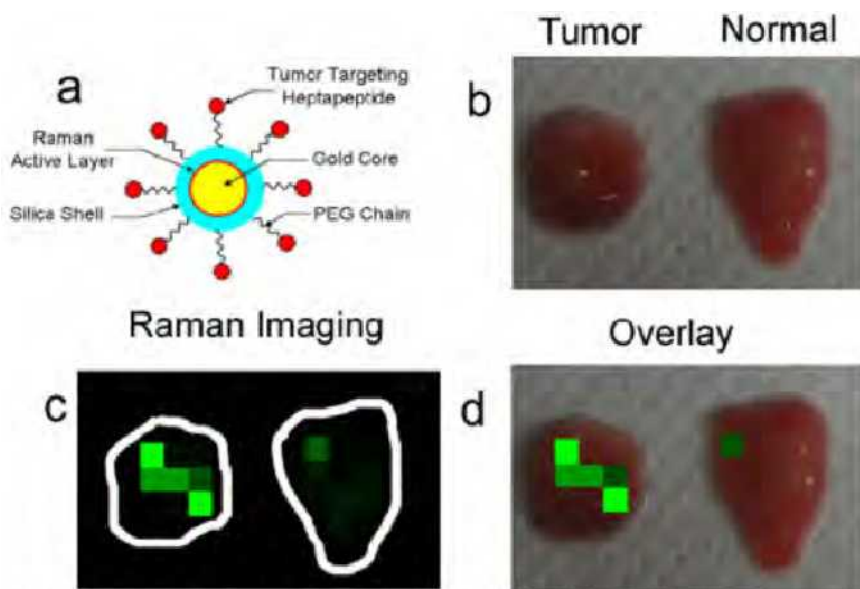


Figure Legend: Binding efficiency of (+) heptapeptide SERS nanoparticles on tumor vs. normal human colon tissue. a) Schematic of SERS nanoparticles conjugated with tumor targeting heptapeptide. b) Digital photo of malignant tumor tissue and normal adjacent tissue. Each tissue was exposed to (+) heptapeptide SERS nanoparticles for 10 min. c) Raman image of the tissues using our Raman mapping system. d) Overlay of Raman intensity map over digital photo of fresh tissue samples. Notice the increased binding of the (+) heptapeptide SERS nanoparticles throughout the entire tumor tissue as opposed to the decreased localized non-specific binding seen in the normal adjacent tissue.

Presentation Number **0830B**

Poster Session 4c: In Vivo Studies & Development/Novel Use of Imaging Probes

Chemiluminescent Probes for Detecting Free Radicals in Inflammation Disease Models

Raj Singh, Ed Lim, Dan Ansaldi, Ali R. Akin, Kshitij Modi, Mark Roskey, Ning Zhang, Caliper Life Sciences, Alameda, CA, USA.
Contact e-mail: raj.singh@caliperls.com

Under physiological conditions, low levels of reactive oxygen and nitrogen species are generated by the cells and play a critical role in cell signaling and maintenance of vascular homeostasis. At pathological inflammatory conditions, elevated levels of free radicals are produced as an innate defense mechanism. A quantitative approach for tracking the extent and longevity of free radical production may shed light on understanding disease progression. A number of chemiluminescent probes have been developed for measuring free radical production in cell based assays. More recently, application of luminol and its analogues for in vivo imaging of the superoxide anion has proven to be successful. In this study, we performed comparative in vivo imaging evaluations of several chemiluminescent agents in inflammation disease models, including LPS induced sepsis, acute arthritis, rheumatoid arthritis, hypersensitive skin reactions and atherosclerosis. Results from live animal imaging to define the utility and optimal conditions of these chemiluminescent agents for tracking disease progression will be presented.

Presentation Number **0831B**

Poster Session 4c: In Vivo Studies & Development/Novel Use of Imaging Probes

In Vivo and in vitro evaluation of Cy5.5 Conjugated Epithelial Growth Factor Receptor Binding Peptide

Min-Hee Jeong^{1,2}, **Eun-Mi Kim**^{1,3}, **DooRye Jang**^{1,2}, **Su-Jin Cheong**^{1,2}, **Chang-Moon Lee**^{1,2}, **Hwan-Jeong Jeong**^{1,2}, **Dong Wook Kim**^{1,3}, **Seok Tae Lim**^{1,2}, **Myung-Hee Sohn**^{1,2}, ¹Nuclear Medicine, Chonbuk national university and hospital, Jeonju, Republic of Korea; ²Research Institute of Clinical Medicine, Chonbuk national university and hospital, Jeonju, Republic of Korea; ³Cyclotron Research Center, Chonbuk national university and hospital, Jeonju, Republic of Korea. Contact e-mail: blue1002@nate.com

Background: Epidermal growth factor receptor (EGFR) is one of four members of the ErbB family of tyrosine kinase receptors. It is overexpressed in a number of tumor types. Apparently, detection of EGFR in clinical practice might influence patient management, including questions of the relevance of the use of EGFR-targeted drugs. Recently, the specific peptide sequence of EGFR (sequence: FPMFNHWEQWPP) was identified using a phage display method. In that study, we choose 8-aminooctanoic acid (AOC) for using linker between EGFR binding peptide and Cy5.5 NIRF probe and evaluated targetability in vitro and in vivo. Methods : Phages were selected for binding to rhEGFR, using a phage display library. The library encoded a random 12 amino acid sequence. Maleimidyl-Cy5.5 was conjugated with thiol group of terminal cystein aminoacid of EBP. After reaction, molecular weight was determined with maldi-tof. In vitro studies were performed in U87MG and CHO cells. We analyzed mRNA levels of EGFR in two cell lines by RT-PCR analysis and performed western blot to confirm EGFR protein expression in the cells. Optical imaging studies were performed in U87MG bearing athymic mice. Results : The exact molecular weight of EBP-AOC-Cy5.5 was 3097 Da. AOC containing EBP-Cy5.5: m/z = 3095.03 for [M]⁺ (calculated MW = 3097.49). The mRNA expression level of EGFR in two cell lines was as follows (UV Abs. ratio): U87MG = 0.66 and CHO = 0.47. The cellular uptake of EBP-AOC-Cy5.5 in U87MG cells exhibited a higher total flux/UV Abs. ratio than CHO cells. EBP-AOC-Cy5.5 was incubated with U87MG and CHO cells. The images were taken with a confocal microscope. EBP-AOC-Cy5.5 was mainly existed in U87MG cell cytoplasm and it was apparently inhibited by free EBP. EBP-AOC-Cy5.5 is mainly shown in the tumor and kidney. On the other hand, the uptake in the muscle was very low. Tumor to muscle ratio at 2 hr was 10. Conclusions : Cy5.5-EBP specifically targets EGFR over-expressed tumor. Cy5.5-EBP might be used potential EGFR target optic probe.

Figure 1. NIR fluorescence images of U87MG cells were obtained after incubation for 30 min in the presence of EBP-AOC-Cy5.5 with (B) or without (A). Cellular uptake was blocked by EBP (C). Blocking image demonstrates EGFR specificity of Cy5.5-conjugated EBP peptide.

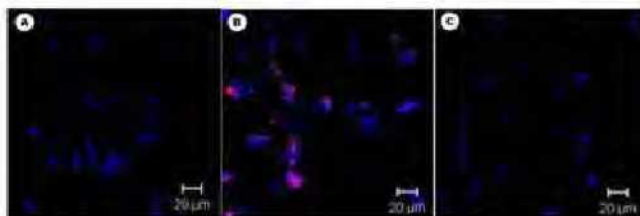
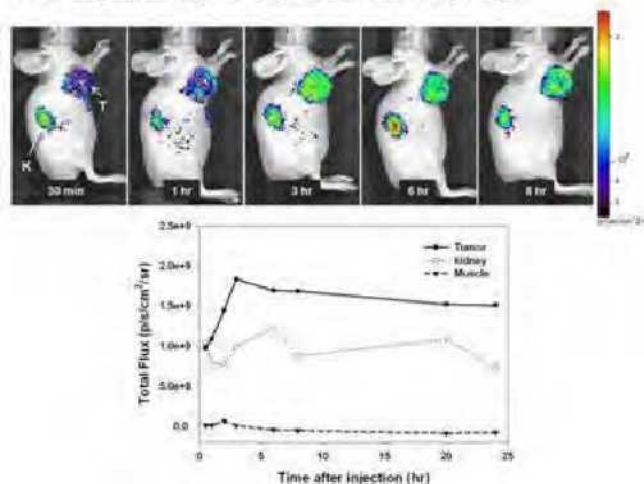


Figure 2. In vivo fluorescence imaging of athymic nude mouse bearing U87MG xenograft after i.v. injection of EBP-AOC-Cy5.5 (A). White arrows indicate the tumor (T) or kidney (K). All time images were acquired with 0.1 sec exposure and background fluorescence was subtracted. Tumor, kidney and muscle uptake curves over time as measured by IVIS (B).



Presentation Number **0832B**

Poster Session 4c: In Vivo Studies & Development/Novel Use of Imaging Probes

Fluorescent NIR Activatable Probes: Lighting up Tumors in vivo

Tao Ji, Sean P. Orton, Yonghong Yang, William McLaughlin, Molecular Imaging, Carestream Health Inc, Woodbridge, CT, USA.
Contact e-mail: jiwendi@yahoo.com

Recent development of activatable probes has drawn significant attention in optical imaging. These probes are designed to have no or very low fluorescence in their native state, but show high fluorescence after enzyme activation. We designed a novel activatable probe based on fluorescent latex nanosphere, NIR quencher dye and enzyme cleavable peptide linker. In this construct, fluorescent nanosphere is quenched by multiple NIR quenchers attached to its surface through enzyme cleavable peptide linkers. Using MMP-2 cleavable peptide linker as an example, we achieved a high fluorescence quenching efficiency (>96%). In vitro study showed that the fluorescence of the MMP-2 activatable probes increased ~5X after enzyme cleavage. A similar result was observed in a mouse model. In vivo imaging in mice showed that the activatable probes successfully detected tumors. The results demonstrate that these activatable probes could be powerful tools for in vivo disease detection and diagnosis.

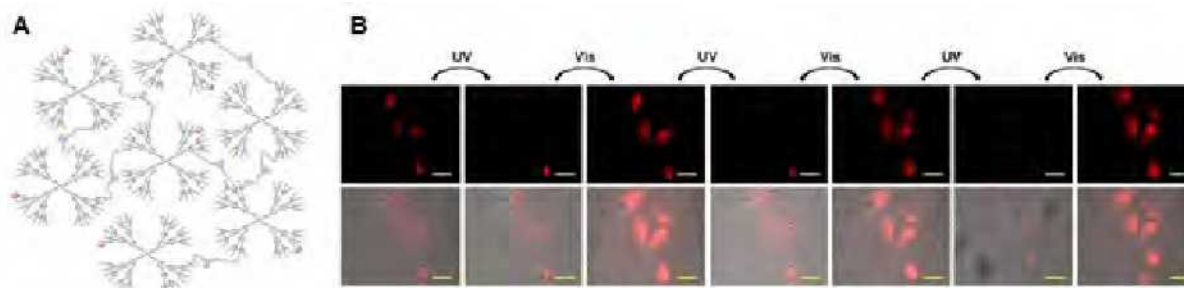
Presentation Number **0834B**

Poster Session 4c: In Vivo Studies & Development/Novel Use of Imaging Probes

Reversible Light Switch for Biological Systems by Photochromic FRET from Dye-Crosslinked Dendritic Nanoclusters

Yoonkyung Kim, Hye-youn Jung, Chaewoon Lee, Bong Hyun Chung, BioNanotechnology Research Center, Korea Research Institute of Bioscience and Biotechnology, Daejeon, Republic of Korea. Contact e-mail: ykim@kribb.re.kr

Diarylethene (DAE) scaffold is known to be one of the most promising photochromic dyes for reversible photoswitching applications, with high thermal stability, high fatigue resistance, high sensitivity, and rapid response time. Furthermore, recent studies reported its use in the reversible quenching of fluorescence by carefully pairing the DAE derivative with one of the fluorescent dyes which has the overlapping emission band with the absorption band of the ring-closed isomer of DAE. Here, a dendritic nanocluster system is prepared which used the DAE moieties as crosslinkers to covalently connect individual poly(amidoamine) dendrimers through the flexible linker arms. Thus, the relatively hydrophobic DAE units are anticipated to be mostly embedded in the interior of the nanocluster while maintaining their original optical properties. Surprisingly, the fluorescence of the Cy3 dye randomly attached to the surface of this DAE-nanocluster was effectively quenched and recovered repeatedly by alternating irradiation with UV (365 nm) and visible (590 nm) light via fluorescence resonance energy transfer (FRET). For biological applications, the amino surface functionality of the Cy3-DAE dendritic nanocluster was modified to either carboxylate groups (anionic) or short methoxy poly(ethylene glycol) (mPEG) chains (neutral). Interestingly, dendritic nanoclusters with either surface modification internalized into the cancer cells, with those having the short mPEG surface being particularly effective. Alternating irradiation of cells containing either type of nanoclusters with UV and visible light reversibly turned the intracellular fluorescence off and on, respectively. This biocompatible dendritic nanocluster-based light switch system may be adopted for certain in vivo applications benefiting from high-contrast optical imaging.



(A) Structure of a dye-crosslinked dendritic nanocluster for photoswitch applications (red: Cy3; blue: DAE derivative). (B) Reversible light switch phenomenon observed from HeLa cells containing internalized Cy3-DAE dendritic nanoclusters (scale bar: 20 μm).

Presentation Number **0835B**

Poster Session 4c: In Vivo Studies & Development/Novel Use of Imaging Probes

Screening of Substrate Targets for Kinases using Phage Peptide Libraries

In-Seop So, Jong-Ho Kim, In-San Kim, school of medicine, Kyungpook National University, Daegu, Republic of Korea. Contact e-mail: soinseop@knu.ac.kr

Protein kinase play pivotal regulatory roles in most cell communication and metabolic pathways. Inhibitors of protein kinases not only hold great promise as therapeutic agents for many diseases, especially cancer, but are also of profound utility in the characterization of signaling pathways because of the centrality of protein phosphorylation as a regulatory process. Therefore, sensitive and widely applicable detection of protein kinase activity will provide a valuable tool to screen protein kinase inhibitors in drug discovery. We previously reported that self-assembled poly-ion complexes (PICs) containing kemptide, protein kinase A specific peptide motif, recognize the phosphorylation of kemptide by protein kinase A by recovery of fluorescence. In this research we found kinase specific substrate peptide with phage display which an efficient primary screening method to detect protein-protein interaction because of its relatively easy, rapid and massive recovery and analysis. Kinase substrate peptide library was made with phage and then library is displayed on capsid protein of phage. After kinase reaction, the phage clones are selected, recovered, and amplified for next round of bio-panning. The candidate clones are selected according for at least 4th round of bio-panning and the resultant peptides are analyzed for specificity. To prepare PICs, found peptide was conjugated with polyethyleneimine (PEI) labeled with cyanine 5.5 (cy5.5). PICs consisting of peptide and cy5.5 chemically conjugated PEI and poly-L-aspartic acid showed significant fluorescent signal recovery in presence of protein kinase while they hardly showed fluorescent signal in absence of protein kinase. In addition, fluorescent signal did not recover with protein kinase inhibitor even though protein kinase was present. We tried to apply highthroughput screening to perform chemical library screening with 384-well plate. While wells without protein kinase showed strong fluorescent signal, wells containing protein kinase inhibitors represented no fluorescent signal, which is fully consistent with previous results and our expects. We conclude that this system is applied to highthroughput screening systems targeting protein kinase inhibitors.

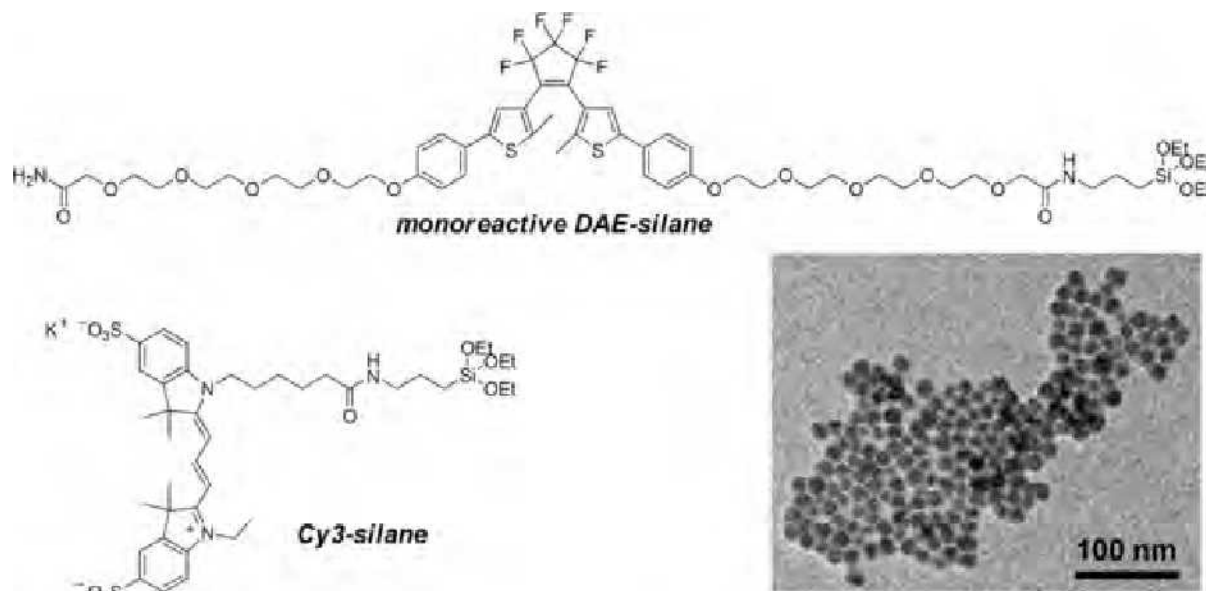
Presentation Number **0836B**

Poster Session 4c: In Vivo Studies & Development/Novel Use of Imaging Probes

Fabrication of Highly Monodisperse Silica Nanoparticles as Reversible Light Switch for Biological Imaging

Hye-youn Jung, Chaewoon Lee, Yoonkyung Kim, Bong Hyun Chung, Korea Research Institute of Bioscience and Biotechnology, Daejeon, Republic of Korea. Contact e-mail: seikotop@kribb.re.kr

Size-control in the fabrication of nanoparticles (NP) is important, particularly when the properties (e.g., physicochemical characteristics, biological responses, etc.) elicited from different size-range groups of NPs vary significantly. Diarylethene (DAE) scaffold is known to be one of the most promising photochromic dyes for the reversible photoswitching applications, with high thermal stability, high fatigue resistance, high sensitivity, and rapid response time. Furthermore, recent studies reported its use in the reversible quenching of fluorescence by carefully pairing the DAE derivative with one of the fluorescent dyes which has the overlapping emission band with the absorption band of the ring-closed isomer of DAE. Here, monofunctionalization of the DAE derivative and that of the Cy3 derivative was carried out respectively, to prepare each silane precursor. Both dye-silane derivatives were mixed and copolymerized with appropriate additives to prepare silica NPs of amino surface. Subsequently, these amine-terminated NPs were further treated with succinic anhydride under basic conditions to modify the surface of silica NPs to a more biocompatible carboxylate group. Effective internalization of the carboxylate-terminated silica NPs into the HeLa cells was observed. The reversible quenching and recovery of the Cy3-fluorescence by the irradiation with UV (365 nm) and visible (590 nm) light is envisioned through the photochromic fluorescence resonance energy transfer (FRET) process. This biocompatible monodisperse silica NP-based light switch system may be adopted for some biological applications requiring reproducible and high-contrast optical imaging.



Chemical structures of DAE- and Cy3-silane used for the fabrication of highly monodisperse silica nanoparticles for biological imaging applications. A TEM image of the corresponding silica nanoparticle with amine surface is shown in the bottom right corner

Presentation Number **0837B**

Poster Session 4c: In Vivo Studies & Development/Novel Use of Imaging Probes

Flamma Fluors™, Fluorescent Probes for Molecular Imaging

Jin Woo Park^{2,1}, YoungSoo Kim¹, Jong Joo Na², Dong Jin Kim¹, ¹Life/Health Division, Korea Institute of Science and Technology, Seoul, Republic of Korea; ²BioActs R&D Center, BioActs, Incheon, Republic of Korea. Contact e-mail: park@bioacts.com

Molecular imaging (MI) is a fast growing and leading technology in life science R&D. MI can visualize and quantify biological phenomena in cellular or sub-cellular levels via various tools such as radioisotopes, magnetic particles and NIR probes. In particular, monitoring pathological routes enables high throughput screening and drug discovery. Among them, optical imaging based on fluorescence molecules is one of the most famous and widely used methods. We introduce Flamma Fluors™ series, which includes fluorescent dyes, indicators and smart probes in a wide range of wavelengths (from 400 to 900 nm). Our preliminary research data confirmed outstanding reactivity and stability of Flamma Fluors™ in in vitro and vivo studies.

Presentation Number **0838B**

Poster Session 4c: In Vivo Studies & Development/Novel Use of Imaging Probes

Biodegradable Near-Infrared Plasmonic Nanoparticles: Clearance and Photoacoustic Imaging In Vivo

Konstantin Sokolov^{1,2}, **Justina O. Tam**², **Avinash Murthy**³, **Soon Joon Yoon**², **Keith P. Johnston**³, **Stanislav Y. Emelianov**^{2, 1}, *Imaging Physics, The UT M.D. Anderson Cancer Center, Austin, TX, USA;* ²*Biomedical Engineering, The University of Texas at Austin, Austin, TX, USA;* ³*Chemical Engineering, The University of Texas at Austin, Austin, TX, USA. Contact e-mail: kostia@mail.utexas.edu*

Nanotechnology can provide unique solutions to diagnosis and treatment of many devastating diseases such as cancer. One specific area of great interest is development of nanoparticles for molecular specific imaging, therapy and combined imaging/therapy. Nanoparticles such as gold and silver with plasmonic resonances in the near-infrared (NIR) optical region, where soft tissue is the most transparent, are of great interest in the biomedical applications. A major roadblock in translation of inorganic nanoparticles to clinical practice is their non-biodegradable nature. The accumulation and potential long-term toxicity of nanoparticles is a major concern. Recently, it was demonstrated that particles with hydrodynamic diameters less than 5.5 nm are efficiently eliminated from the body. However, plasmonic nanoparticles with resonances in the NIR region are approximately 30 nm in size or larger, severely limiting their body clearance rates. Here we present a new class of biodegradable gold nanoparticles with plasmon resonances in the NIR region. The nanoparticles degrade to easily clearable components and, therefore, can provide a crucial missing link between the enormous potential of plasmonic nanoparticles for imaging and therapy and translation into clinical practice. Our synthetic methodology is based on controlled assembly of very small (less than 5 nm) primary gold particles into nanoclusters (NCs) with <100 nm overall diameter. The assembly is mediated by biodegradable polymers and small capping ligands on the primary nanoparticles. The intermolecular interactions of the capping ligands and stabilizing polymer(s) is designed to control cluster growth in order to keep the primary nanoparticles in close proximity, to produce strong NIR absorbance. The degradation in cells was characterized via dark-field reflectance (DR) microscopy, hyperspectral imaging, and transmission electron microscopy, and showed complete degradation of NCs into primary particles after 1 week. NCs were then injected I.V. into Balb/c mice and accumulation of NCs was observed in the liver 1 week post injection. This was followed by a great decrease of NCs in the liver after 1 month, as shown by DR imaging. NCs were cleared through the feces as shown by neutron activation analysis. Control spherical solid 40 nm gold nanoparticles remained in the liver after one month. Current studies include using smaller NCs with varying polymers to study degradation kinetics and evaluating the use of NCs as NIR photoacoustic contrast agents for molecular specific in vivo imaging.

Presentation Number **0948A**

Poster Session 2c: In Vivo Studies & Development/Novel Use of Imaging Probes

Molecular Imaging and Contrast Agent Database (MICAD) - A Free Online Source of Imaging and Contrast Agent Information: Progress and Current Status

Arvind Chopra¹, **Martin Latterner**¹, **Steve Bryant**¹, **Kam Leung**¹, **Liang Shan**¹, **William C. Eckelman**¹, **Anne Menkens**², ¹*National Library of Medicine, National Institutes of Health, Bethesda, MD, USA;* ²*National Cancer Institute, National Institutes of Health, Bethesda, MD, USA. Contact e-mail: chopraa@mail.nih.gov*

The Molecular Imaging and Contrast Agent database (MICAD; www.micad.nih.gov) program is one of the key components of the United States NIH Roadmap. The primary goal of MICAD is to promote research and development in molecular imaging by providing freely accessible, current, online scientific information regarding molecular imaging probes and contrast agents that are under development, in clinical trials or commercially available for use with any modality (PET, SPECT, MRI, optical or ultrasound etc.). The MICAD website, officially launched in September 2005, has detailed information on approximately 850 imaging probes and contrast agents. Recently the following new initiatives have been implemented in MICAD: 1) The MICAD homepage was redesigned so that searches may be performed based on the method of detection, source of signal, agent or target category, available research studies, and text words. Viewing all entries in MICAD is now easier because agents have been categorized and arranged according to the modality used for imaging. Also, a summary of all MICAD entries can be downloaded as a CSV file from the homepage. 2) Each MICAD chapter details the chemical characteristics (including structure e.g. for small molecules) and the in vitro and in vivo (pre-clinical and clinical) activity of an imaging probe or contrast agent. All new chapters in MICAD provide information regarding the nucleotide/protein sequence, gene, ongoing clinical trials, and FDA drug information involving the cellular target of the imaging probe or contrast agent. Each chapter has references that are linked to PubMed. 3) To facilitate rapid expansion of MICAD a Guest Author Program was implemented so that members of the imaging community can write and submit entries (chapters) for publication in the database as guest authors. 4) A Supplemental Information Section was added to each MICAD chapter to facilitate the sharing of cutting-edge, unpublished or as yet unavailable information regarding an agent. This new and largely unrestricted section allows members of the imaging community to deposit images, research data, or other relevant information about the agent in each chapter. 5) An email announcement (eAnnouncement) detailing the new agent chapters added to the database is periodically sent to members of the imaging community registered with MICAD. Individuals interested in receiving the eAnnouncement may register at the MICAD web site (www.micad.nih.gov).

Presentation Number **0949A**

Poster Session 2c: In Vivo Studies & Development/Novel Use of Imaging Probes

Oxidative modification of the novel cysteine-rich cell penetrating peptide CyLoP-1 increases cytosolic delivery

Sven Gottschalk, Deepti Jha, Joern Engelmann, Max-Planck-Institute for Biological Cybernetics, Tuebingen, Germany. Contact e-mail: sven.gottschalk@tuebingen.mpg.de

Intracellular and especially cytosolic delivery with cell penetrating peptides (CPPs) can be severely limited by endocytotic uptake, leading to unwanted vesicular entrapment. A correlation between cell-surface thiols and uptake efficiency of disulfide-containing CPPs was discussed and it was shown that these CPPs possess much better cytosolic targeting capability [1]. Our newly developed, cysteine-rich CPP, CyLoP-1 (Cytosol Localizing Peptide 1, CRWRWKCKK) showed pronounced cytosolic delivery already in its non-oxidized form. Aim of the present study was to evaluate if a controlled oxidation of the cysteines, generating disulfide linkages in CyLoP-1, further increases its cytosolic targeting. To test this hypothesis the pro-apoptotic peptide AVPIAQK (SmacN7) was attached to CyLoP-1. SmacN7 alone can not pass cellular membranes and needs to bind to its cytosolic target to exert a pro-apoptotic action and thus can be used to prove cytosolic delivery of CPP-conjugates. CyLoP-1 (covalently bound to lysine-FITC) was subjected to oxidizing conditions. SmacN7 was covalently conjugated to the N-terminus, yielding the construct SmacN7-K(FITC)-CyLoP-1, which was also oxidized. Internalization of all 4 compounds was evaluated on 3T3 fibroblasts (2.5µM, 18 hours, for method details see [2]). Caspase-3 activity as parameter for apoptosis-induction by the reduced and oxidized SmacN7-K(FITC)-CyLoP-1 was measured in HeLa cells. Intracellular uptake (measured by FITC-fluorescence) was significantly higher for the oxidized versions of both the peptide itself and SmacN7-CyLoP-1. This was confirmed by fluorescence microscopy of the same cells, displaying higher cytosolic fluorescence for the oxidized versions of the compounds. However, cargo-attachment reduced the internalization efficacy of CyLoP-1 in its reduced as well as oxidized form. SmacN7-CyLoP-1 was capable of inducing apoptosis in HeLa cells, while SmacN7 alone had no effect, proving efficient delivery of the bioactive cargo into the cytosol. Oxidation of SmacN7-CyLoP-1 further enhanced the amount of apoptotic cells (i.e. increased Caspase-3 activity). Thereby demonstrating that oxidative modification of cysteine-residues in CyLoP-1 enhances its cytosolic targeting capability. Conclusion: Our results suggest an important role of disulfides in the uptake mechanisms of cysteine-containing CPPs and also in their capability to deliver to the cytosol. The use of disulfide-motifs in CPPs might also be applicable for other types of cargos, like imaging agents. [1]Aubry,FASEB J.23(2009)2956 [2]Mishra,Bioconjug.Chem.2009

Presentation Number **0950A**

Poster Session 2c: In Vivo Studies & Development/Novel Use of Imaging Probes

Usefulness of gold nanocarrier for efficient delivery of anti-oncogenic microRNA in cancer therapy

Do Won Hwang^{1,2}, Hyewon Youn^{1,2}, Keon Wook Kang^{1,2}, Jwa-Min Nam³, Dong Soo Lee^{1,4}, ¹Department of Nuclear Medicine, Seoul National University, Seoul, Republic of Korea; ²Department of Nuclear Medicine, Radiation Medicine, Medical Research Center, Seoul, Republic of Korea; ³Department of Chemistry, College of Natural Sciences, Seoul, Republic of Korea; ⁴Department of Molecular Medicine and Biopharmaceutical Science, WCU Graduate School of Convergence Science and Technology, Seoul, Republic of Korea. Contact e-mail: hdw6592@hanmail.net

Purpose: Development of delivery system of antisense-microRNAs involved in the modulating effect in tumorigenesis will play an important role in supporting an efficient cancer therapy to inhibit oncogenic microRNA in vivo. In this study, we investigated the possibility for efficient delivery of antisense microRNA using gold nanoparticle in vitro. **Methods:** RGD peptide-synthesized gold nanoparticle and SH-tethered microRNA oligomer were mixed and incubated for 15 min in room temperature. U87MG, human glioblastoma (positive cell for RGD) and MCF-7, human breast cancer (negative cell for RGD) were used to test cellular specificity for RGD-gold nanoparticle. The gaussia luciferase vector system containing 3 copy of microRNA binding sequence (CMV/Gluc/miRNA_3XPT) were used to examine the internalization pattern of exogenous microRNA into cells. **Results:** TEM images exhibited that specific internalization of RGD-gold nanoparticle synthesized with microRNA oligomer was detected in U87MG cells. As soon as RGD-gold nanoparticles were mixed with synthetic microRNA oligomer (or scramble microRNAs), the reaction mixture was treated into U87MG cells pre-transfected with CMV/Gluc/miRNA_3XPT vector. Significant reduction pattern of luciferase activity was observed in gold-microRNA treated group. No luciferase signal was detected in gold-scramble microRNA treated group. Confocal microscopy images revealed cellular specificity of RGD-gold/FAM-labeled microRNA complex in U87MG cells, by showing cellular uptake of RGD-gold/FAM-microRNA oligomer in U87MG cells, but not in MCF7 cells. **Conclusion:** We examined the cancer specificity of RGD-gold nanoparticle and usefulness of gold nanoparticle as efficient microRNA delivery carrier in vitro for cancer delivery and therapy. We expect that the developed gold nanomaterial system capable of carrying microRNAs can be applied for microRNA-based cancer therapy.

Presentation Number **0951A**

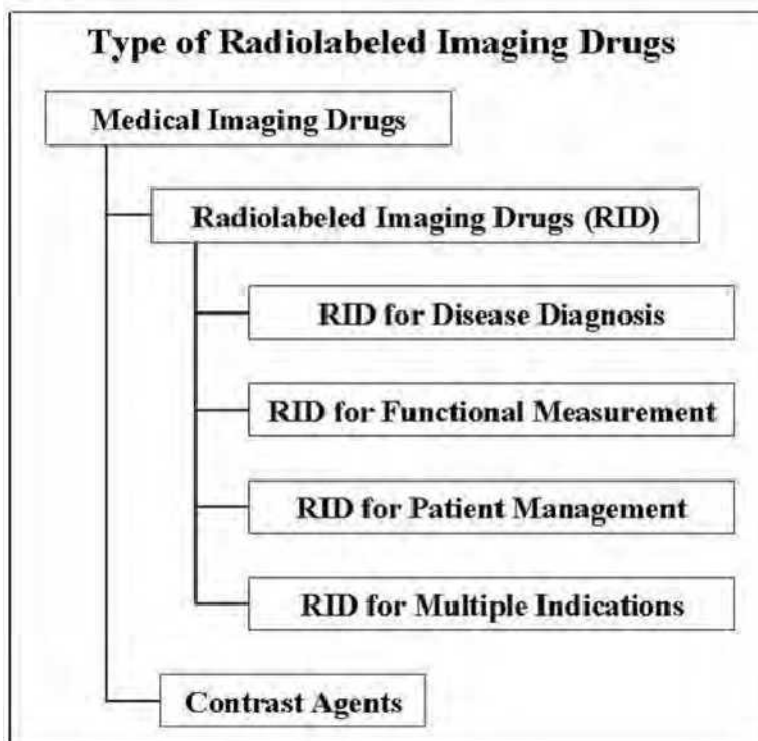
Poster Session 2c: In Vivo Studies & Development/Novel Use of Imaging Probes

Toward Issue of Regulatory Guidance for developing Radiolabeled Imaging Drugs

Tsuneo Yano¹, **Tomio Inoue**², **Michio Senda**³, **Hideo Saji**⁴, **Yasuyoshi Watanabe**¹, ¹Center for Molecular Imaging Science, RIKEN, Kobe, Japan; ²Graduate School of Medicine, Yokohama City University, Yokohama, Japan; ³Institute of Biomedical Research and Innovation, Kobe, Japan; ⁴Graduate School of Pharmaceutical Sciences, Koto University, Kyoto, Japan. Contact e-mail: tyano@riken.jp

Since molecular imaging technology becomes very important in terms of efficacy assessment of therapeutic drugs as well as early diagnosis, it is urgent to formulate the regulatory guidance focusing on the development of radiolabeled imaging drugs (RID) for PET (positron emission tomography) and SPECT (single photon emission computed tomography) under the pharmaceutical affairs law in Japan. Although the guidance of developing medical imaging drugs was issued in June 2004 by the U.S. FDA, 6 years have already passed since then and molecular imaging research has progressed remarkably during that time. We have, therefore, developed “draft guidance for developing RID” while taking up recent regulatory changes and new findings, and we published it on February 2010 in Japan¹. In our published report, we newly proposed “functional measurement” in addition to “disease diagnosis” for the important roles of RID. Our report is composed of four types of RID shown in Figure. Both “RID for functional measurement” and “RID for patient management” are in a new category of functional diagnosis on biochemistry, biology and molecular biology. The former is able to detect and evaluate biomarker which is related to functional abnormality, and the latter is used for selection of patients or their therapeutic regimen based on functional diagnosis. The goal of this report is to offer an effective tool to facilitate the development of and creation of NDAs for RID. The main discussion points are (1) clinical evaluation, (2) pharmacological and toxicological safety, and dosimetry, (3) GMP, manufacturing and quality standards. Toxicological safety standards are discussed under the same standard as the M3(R2) guidance including Microdosing & E-IND studies at the ICH which was issued by the U.S. FDA on January 20, 2010 and by the MHLW on February 19, 2010. Further progress toward issue of regulatory guidance will be discussed at WMIC. 1) Tsuneo Yano, Tomio Inoue, Kengo Ito, Michio Senda, Hideo Saji, Yuichi Sugiyama, Yasuyoshi Watanabe, Chieko Kurihara, Yoshiharu Yonekura, Draft guidance for developing radiolabeled imaging drugs, Rinsho Hyoka, 2010, 37, 473-496.

Figure



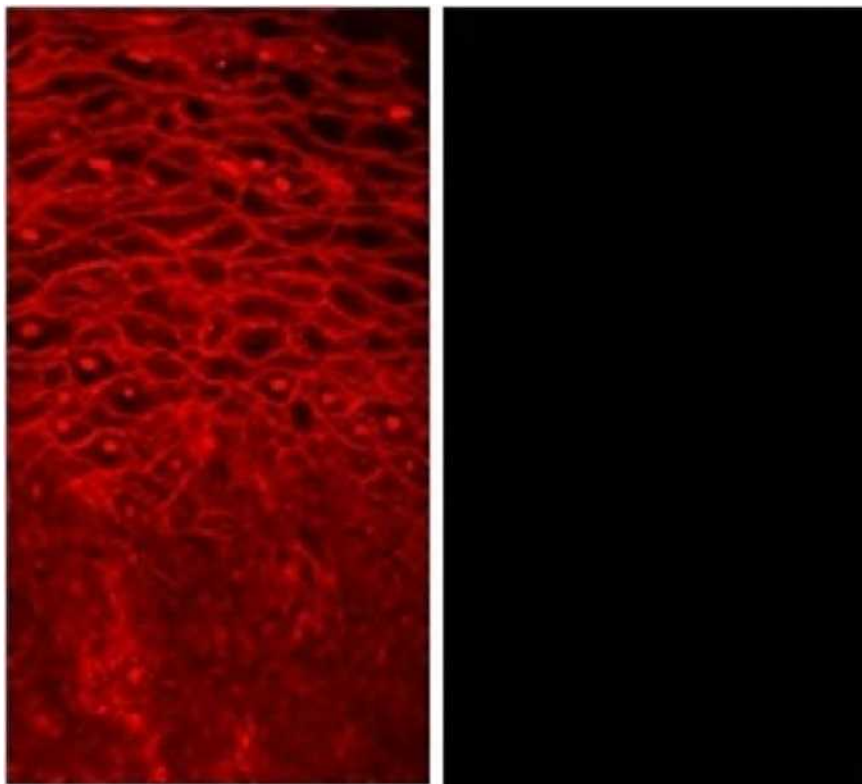
Presentation Number **0952A**

Poster Session 2c: In Vivo Studies & Development/Novel Use of Imaging Probes

Imaging of Molecular Interactions in Live Cells: a Plasmonic Approach

Konstantin Sokolov^{1,2}, Kort Travis³, ¹Imaging Physics, The UT M.D. Anderson Cancer Center, Austin, TX, USA; ²Biomedical Engineering, The University of Texas at Austin, Austin, TX, USA; ³Physics, The University of Texas at Austin, Austin, TX, USA. Contact e-mail: kostia@mail.utexas.edu

One of the major problems in selective detection, monitoring and treatment of cancer is the fact that cancer biomarkers are not unique to cancer cells. Identical molecules are present in normal cells as well; however, their expression is often elevated in cancer. Therefore, selectivity toward cancerous cells can be achieved through development of molecular probes that dramatically change properties in the presence of an over-expressed biomarker. Distance dependant coupling of plasmon resonances between closely spaced metal nanoparticles offers an attractive approach for imaging of molecular interactions. Here we analyzed interactions between molecular specific gold nanoparticles and live cells using a combination of dark-field reflectance and hyperspectral imaging. The results of optical imaging were correlated with transmittance electron microscopy of cell slices and theoretical simulations of optical properties of gold aggregates. We showed that nanoparticles targeted to epidermal growth factor receptor (EGFR) form closely spaced assemblies in the presence of the target molecule. Our experiments with living cells and animal cancer models in vivo showed that receptor mediated assembly and plasmon coupling of gold bioconjugates result in a spectral shift of more than 100 nm in plasmon resonance frequency of the nanoparticles giving a very bright red signal. This approach can allow imaging of molecular interactions ranging from protein pairs to multi-protein complexes with sensitivity and SNR that cannot be currently achieved with any other method. Recently, we have demonstrated that the effect of plasmon resonance coupling can be used for molecular specific cancer imaging in animal cancer models in vivo using confocal reflectance microscopy and spectroscopic optoacoustic imaging. The figure below illustrates contrast between pre-cancerous epithelium (left) and normal epithelial tissue labeled with anti-EGFR gold nanoparticles.



Presentation Number **0839A**

Poster Session 1c: In Vivo Studies & Development/Novel Use of Imaging Probes

A new peptide (PDGFR-P1) for targeting the platelet derived growth factor receptor beta

Vasileios Askoxylakis^{1,2}, Annette Markert², Shoaib Rana³, Annabell Marr³, Annette Altmann², Jurgen Debus¹, Uwe Haberkorn^{2,3},
¹Radiooncology and Radiation Therapy, University of Heidelberg, Heidelberg, Germany; ²Clinical Cooperation Unit Nuclear Medicine, German Cancer Research Center, Heidelberg, Germany; ³Nuclear Medicine, University of Heidelberg, Heidelberg, Germany. Contact e-mail: v.askoxylakis@dkfz.de

The platelet derived growth factor receptor β (PDGFR β) belongs to the family of receptor tyrosine kinases and is known to be overexpressed in a variety of tumors and associated with angiogenesis. We identified a new linear dodecapeptide (PDGFR-P1) binding PDGFR β , using the technology of phage display and evaluated the binding and metabolic properties of it. Phage display was performed with a 12 amino acid phage display library by panning against a recombinant extracellular domain of PDGFR β . The identified peptide (PDGFR-P1) was chemically synthesized by Fmoc solid phase peptide synthesis and labeled with [¹²⁵I] or [¹³¹I]. Binding, kinetic, competition and internalization studies were performed on the human pancreatic cancer cell line BxPC3, the human prostate cancer cell line PC3 and on stable HEK cells permanently over-expressing PDGFR β (HEK-PDGFR β) compared to the wild type HEK 293 cells. Organ distribution studies were carried out in Balb/c nu/nu mice, carrying PC3 and BxPC3 tumors subcutaneously into the trunk. In vitro binding experiments with [¹²⁵I]-labeled PDGFR-P1 revealed an increased uptake of the radioligand in both tumor cell lines BxPC3 and PC3 and in the stable HEK-PDGFR β cells in comparison to the wild type HEK 293 cells. Binding of the radioligand was inhibited up to 90% by the unlabeled PDGFR-P1 peptide but not by other negative control peptides at the same concentration. Internalization experiments revealed an internalization of the radioligand, which could be inhibited by incubation at 4°C. Organ distribution studies in mice carrying BxPC3 and PC3 tumors subcutaneously revealed a higher uptake of [¹³¹I]-labeled PDGFR-P1 in tumors than in most of the organs. The results of our study indicate that PDGFR-P1 might be a promising candidate for the development of a new ligand with affinity for the platelet derived growth factor receptor β that can be used for targeting purposes.

Presentation Number **0841A**

Poster Session 1c: In Vivo Studies & Development/Novel Use of Imaging Probes

A radiolabeled nonapeptide probe targeting bone metastases of prostate cancer in mice

Lu Liu, Qinghua Wu, **Jin Sun**, Zexuan Yang, Hailin Gao, Qi Nie, Radiology, Southeast University, Nanjing, China. Contact e-mail: wander21@126.com

Even today the sensitivity for diagnostic imaging of early bone metastases is still low. Previous investigations have shown interleukin-11(IL-11) and the IL-11 receptor(IL-11R) may play a significant role in the bone metastases. The nonapeptide CGRRAGGSC(IL-11RR) is a phage-display-selected IL-11 mimic binding to IL-11R. The aim of this study was to synthesize radiolabeled-IL-11RR and to assess the interaction between this radioactive probe and a IL-11R positive bone metastatic models of PC-3 prostate cancer. Methods IL-11RR was radiolabeled with ^{99}Tcm using DTPA chelate. Labeling efficiency, radiochemical purity and the stability of ^{99}Tcm -DTPA-IL-11RR were measured by paper chromatograph and HPLC. In vitro immunoreactivity was assessed in PC-3 cells. Biodistribution of ^{99}Tcm -DTPA-IL-11RR was observed in the ICR normal mice. Bone metastatic model were established through $5\mu\text{l}$ PC-3 cells injecting into the right femur of female nude mice. Comparison studies between ^{99}Tcm -DTPA-IL11RR and ^{99}Tcm -MDP were done in this models to compare the dynamic γ imaging after intravenous injection. The same studies were also carried in the standard closed fracture models. Specificity was demonstrated by blocking with the unlabeled nonapeptide. Results The labeling efficiency of ^{99}Tcm -DTPA-IL-11RR reached 90.7% and the radiochemical purity in normal saline was $98.57\pm 1.09\%$. The complex was completely stable to serum challenge for the duration of experiments. Cell-based assays manifested the complex had the specific binding to PC-3 cells. Biodistribution in ICR normal mice revealed the label excreting mainly through the kidneys. The radioactivity in the major organs was quite low, especially in the muscle and brain. The peak values of bone and liver appeared at 4h after injection were $1.910\pm 0.109\% \text{ID/g}$ and $0.366\pm 0.030\% \text{ID/g}$, respectively, coming to background at 24 h postinjection. Dynamic γ images in the metastatic models showed high uptake in tumor regions, mild uptake in the spinal marrow and extremities large joints of mice and a rapid systemic clearance. The T/NT ratios arrived the peak of 5.45 ± 0.37 at 4 h postinjection. In the fracture models, high uptake in fracture bone was observed for ^{99}Tcm -MDP injection, while no obvious uptake for ^{99}Tcm -DTPA-IL11RR injection. The tumor uptake was significantly reduced in the competition study. Conclusion ^{99}Tcm -DTPA-IL11RR had better specificity to PC-3 metastatic tumors in mice compared with ^{99}Tcm -MDP, and may have a good potential for targeted imaging for bone metastatic tumors with IL11R over-expression such as prostate cancer.

Presentation Number **0842A**

Poster Session 1c: In Vivo Studies & Development/Novel Use of Imaging Probes

Evaluation of a second generation annexin V radiotracer labeled with ⁶⁴Cu in the cycloheximide-induced liver apoptosis model

Xiangjun Meng¹, Paul McQuade¹, Marie-Jose Belanger¹, Amy Vanko¹, Brett Connolly¹, Caroline Houde², Huseyin Mehmet², Dinko Gonzalez Trotter¹, Eric Hostetler¹, Ilonka Guenther¹, Jacquelynn J. Cook¹, ¹Imaging, Merck Research Laboratories, West Point, PA, USA; ²Apoptosis, Merck Research Laboratories, Rahway, NJ, USA. Contact e-mail: xiangjun_meng@merck.com

Objectives: This study was designed to evaluate [⁶⁴Cu] labeled wild type annexin V (An-V_I) along with a 2nd generation variant which had been engineered to be radiolabeled site- specifically (An-V_{II}) in a rat model of cycloheximide (CHX) -induced liver apoptosis. A non-binding control variant of 2nd generation annexin V (An-V_{IIINBV}) in which the amino acid sequence had been scrambled to remove phosphatidylserine affinity was also examined. **Methods:** Male SD rats were treated intravenously with CHX (5 or 10 mg/kg, n=15) or normal saline (n=9). Three hours after treatment, rats were imaged dynamically with 0.5-1.0 μCi/g of one of the [⁶⁴Cu] labeled annexin variants for 90 min using positron emission tomography (PET). The livers were harvested at the end of the scan for ex vivo autoradiography and terminal deoxynucleotide end-labeling (TUNEL) staining. **Results:** Liver uptake of both An-V_I and An-V_{II} increased dose dependently after CHX treatment. The uptake ratios (treated/control) were similar with 3.39 and 3.17 (10 mg/kg CHX) for An-V_I and An-V_{II} respectively. Liver uptake of An-V_{IIINBV} did not change after CHX treatment. Ex vivo autoradiography and TUNEL staining showed good agreement of An-V_I and An-V_{II} uptake with TUNEL-positive cells. Liver standardized uptake values (SUVs) at the end of the PET scan increased to a similar extent as the numbers of TUNEL-positive cells for An-V_I and An-V_{II} with both CHX doses; the in vivo liver SUV did not increase for the An-V_{IIINBV} (Figure 1). **Conclusions:** PET studies combined with ex vivo autoradiography and TUNEL staining showed that liver uptake of [⁶⁴Cu] labeled An-V_I and An-V_{II} after CHX treatment is apoptosis specific, with levels of uptake correlating with the total amount of apoptotic cells. No such correlation was observed for the non-binding variant An-V_{IIINBV}.

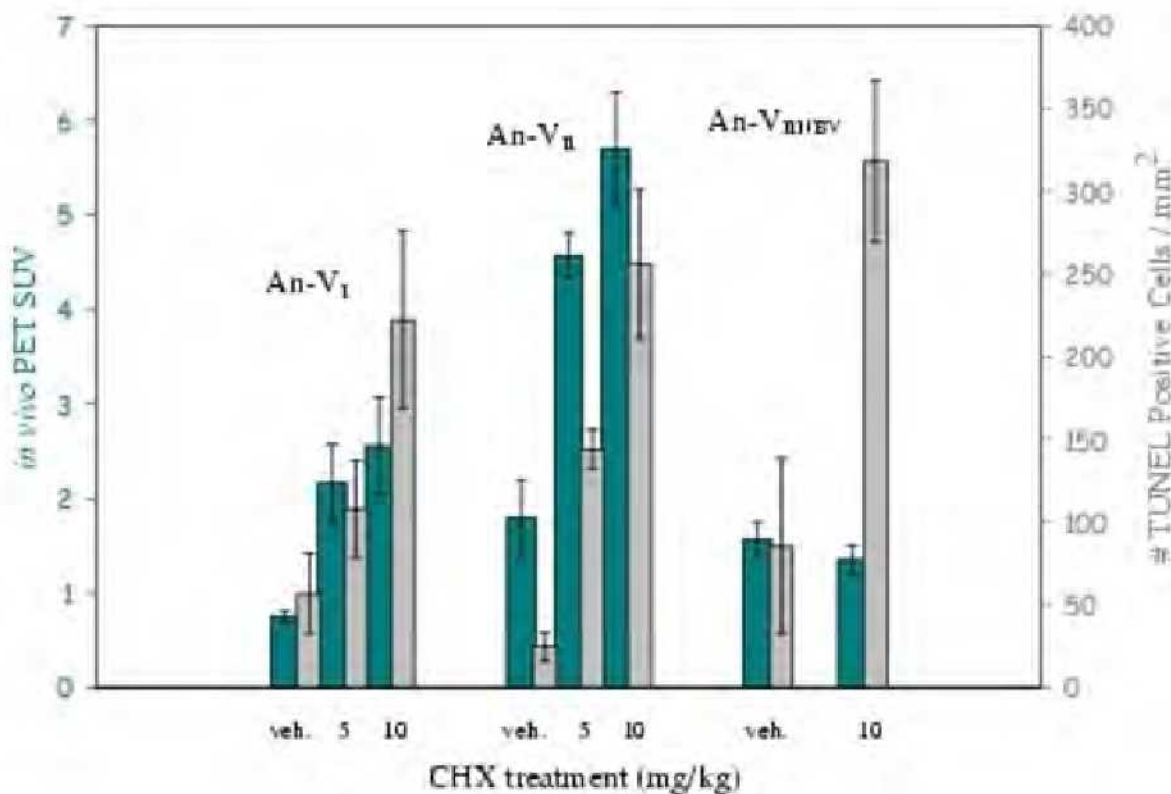


Figure 1. Relationship between in vivo liver SUVs (green bar) at 90min and numbers of the TUNEL staining positive cells (grey bar).

Presentation Number **0843A**

Poster Session 1c: In Vivo Studies & Development/Novel Use of Imaging Probes

A novel tracer for imaging amyloid plaques in human brain tissues: in vitro autoradiography (ARG) and tissue homogenate binding studies

Zhizhen Zeng¹, Patti Miller¹, Stacey O'Malley¹, Tsing-bau Chen¹, Eric Hostettler¹, Sandra Sanabria¹, Brett Connolly¹, John C. Culbertson², Scott Harrison², Jim Mulhearn², Scott Wolkenberg², James Barrow², Jacquelynn J. Cook¹, Richard Hargreaves³, Cyrille Sur¹, David L. Williams¹, ¹Imaging, Merck Research Laboratories, West Point, PA, USA; ²Medicinal Chemistry, Merck Research Laboratories, West Point, PA, USA; ³Neuroscience Franchise, Merck Research Laboratories, West Point, PA, USA. Contact e-mail: zhizhen_zeng@merck.com

The most common cause of dementia in people over age 65 is Alzheimer's Disease (AD). The main components found in two main lesions in AD, senile plaques (SPs) and neurofibrillary tangles (NFTs), are amyloid beta (A β) and tau, respectively. Finding that A β is toxic to neurons supports the hypothesis that A β peptides accumulation in brain plays a pathological role in AD. A β is one of the targets for Disease-Modifying Treatment of AD. The amyloid PET tracer [¹¹C]PIB is valuable for imaging A β plaques in brain, but the short half life (20 min) hampers its use in multicenter clinical trials. Thus, a new tracer with an ¹⁸F label (t_{1/2}=110 min) is highly desirable. Here, we report the in vitro characterization of a novel A β plaque tracer [¹⁸F]MK-3328, using its tritiated version for in vitro ARG and tissue homogenate binding studies. In AD cortex, [³H]MK-3328 binding was saturable and displaceable (K_d=21±10 nM, n=9), similar to that of PIB (K_d=12±4 nM, n=8). [³H]MK-3328 binding sites (B_{max}) in brain homogenates of 9 AD donors ranged from 10-43 pmol/mg protein, giving a mean B_{max}/K_d of 92±15 (n=9) for this sample set. The [³H]MK-3328 binding in brain slices of AD donors was displaceable with a punctate distribution in cortical gray matter that colocalized with the staining for A β plaques (6E10) by IHC in the adjacent slices. [³H]MK-3328 binding was low and homogeneous in non-AD brain slices. In comparison to self block, PIB (0.3 μM) inhibited ~85% of [³H]-MK-3328 binding in AD brain homogenates. The remaining ~15% of [³H]MK-3328 binding could be blocked by lazabemide, a selective MAO-B blocker. Further investigation revealed that [³H]MK-3328 also binds human MAO-B enzyme with good affinity, K_d=4.2±0.8 nM. In non-AD brains, lazabemide fully inhibited [³H]MK-3328 binding, whereas PIB (0.3 μM) showed no inhibition. For the individual brain donors examined (AD and non-AD), MAO-B levels in the cortex were consistently higher (2-fold) than in the cerebellum, but no difference was found in MAO-B levels between AD and age matched control donors (3.5±1.8 and 3.2±1.6 pmol/mg protein in the cortex, respectively, n=12 per group). As the MAO-B levels in AD cortex are significantly lower than the A β plaque levels (21±9 pmol/mg protein), and since there is little difference in brain MOA-B levels between AD and non-AD donors, the MAO-B binding component of [³H]MK-3328 is unlikely to hamper in vivo visualization of amyloid plaques. Altogether, these results support clinical evaluation of this novel amyloid PET tracer.

Presentation Number **0844A**

Poster Session 1c: In Vivo Studies & Development/Novel Use of Imaging Probes

Evaluation of [^{18}F]fluoroethyl GF120918 and XR9576 as a PET probe for evaluating the function of drug efflux transporters

Kazunori Kawamura¹, Tomoteru Yamasaki¹, Fujiko Konno¹, Joji Yui¹, Akiko Hatori¹, Hidekatsu Wakizaka², Masanao Ogawa^{1,3}, Yuichiro Yoshida^{1,3}, Nobuki Nengaki^{1,3}, Kazuhiko Yanamoto^{1,4}, Toshimitsu Fukumura¹, Ming-Rong Zhang¹, ¹Department of Molecular Probes, Molecular Imaging Center, National Institute of Radiological Sciences, Chiba, Japan; ²Department of Biophysics, Molecular Imaging Center, National Institute of Radiological Sciences, Chiba, Japan; ³SHI Accelerator Services, Ltd., Tokyo, Japan; ⁴Division of Health Sciences, Graduate School of Medicine, Osaka University, Osaka, Japan. Contact e-mail: kawamur@nirs.go.jp

Introduction: Drug efflux transporters are expressed on various protective bodies, and play a pivotal role in the absorption, distribution and elimination of xenobiotics. The most extensively characterized drug efflux transporters are ATP-binding cassette transporters including P-glycoprotein (P-gp) and breast cancer resistance protein (BCRP). P-gp and BCRP locate at the blood-brain barrier, and are considered to work together to limit brain penetration of therapeutic agents. We recently developed [^{11}C]GF120918 and [^{11}C]XR9576 as a positron emission tomography (PET) probe for evaluating the function of drug efflux transporters [ref.1,2]. To improve a usability of a probe for evaluating the function of drug efflux transporters, we developed [^{18}F]fluoroethyl GF120918 ([^{18}F]FEGF120918) and [^{18}F]fluoroethyl XR9576 ([^{18}F]FEXR9576), because ^{18}F is longer half life than ^{11}C . Methods: [^{18}F]FEGF120918 and [^{18}F]FEXR9576 were synthesized by the fluoroethylation of these O-desmethyl precursor with [^{18}F]fluoroethyl bromide. PET studies using these PET probes were performed in P-gp and Bcrp knockout, wild-type, and GF120918 (dual P-gp and BCRP inhibitor, 5 mg/kg) treated mice. Results and discussion: [^{18}F]FEGF120918 and [^{18}F]FEXR9576 were successfully synthesized with suitable radioactivity for injection as well as appropriate radiochemical purity and specific activity. In wild-type mice, the radioactivity levels of these PET probes in the brain decreased immediately after initial uptake, and remained constant level. In P-gp and Bcrp knockout mice, the radioactivity levels of these PET probes in the brain were approximately 8-fold higher than that in wild-type mice after initial uptake. In GF120918 (5 mg/kg) treated mice, the radioactivity levels of these PET probes in the brain was approximately 7-fold higher than that in wild-type mice after initial uptake. These results suggest that [^{18}F]FEGF120918 and [^{18}F]FEXR9576 behave as the P-gp and Bcrp substrate, and the increased uptake in the brain relates to P-gp and Bcrp functions. Conclusions: [^{18}F]FEGF120918 and [^{18}F]FEXR9576 showed the P-gp and Bcrp modulation in mice brain. [^{18}F]FEGF120918 and [^{18}F]FEXR9576 may be a potential PET probe for evaluating P-gp and BCRP functions in the brain. Reference: [1] Kawamura, K. et al., (2010) Mol. Imaging. Biol. DOI: 10.1007/s1130701003131. [2] Kawamura, K. et al., (2010) Ann. Nucl. Med. DOI: 10.1007/s121490100373y.

Presentation Number **0845A**

Poster Session 1c: In Vivo Studies & Development/Novel Use of Imaging Probes

Radiosynthesis of [¹¹C]DPA as a small-molecule apoptosis PET tracer

Ganghua Tang^{1,2}, Hongliang Wang¹, Huaiyu Deng¹, ¹Nuclear Medicine, The Affiliated Hospital, Sun Yat-sen University, Guangzhou, China; ²PET Center, Nan Fang Hospital, Southern Medical University, Guangzhou, China. Contact e-mail: gtang0224@yahoo.com.cn

Objectives Fluorescent Zn²⁺-dipicolylamine (DPA) coordination complexes as small molecule annexin mimics have a selective affinity for membrane surfaces that are enriched in anionic phosphatidylserine (PS) to detect apoptosis. Especially, Zinc(II) is now well recognized as an important cofactor in the regulation of apoptosis. A macrocyclic zinc(II) fluorophore can be used as a detector of apoptosis. Therefore, radiosynthesis of [¹¹C]methyl-dipicolylamine ([¹¹C]DPA) as a small molecule apoptosis PET tracer is investigated in this work. Methods Dipicolylamine (DPA) as a precursor was synthesized via multi-step reactions. [¹¹C]DPA was prepared by [¹¹C]methylation of DPA with [11CH₃]triflate and purification with Sep-Pak cartridges. [¹¹C]CH₃OSO₂CF₃ ([11CH₃]triflate) was produced via reaction of [¹¹C]CH₃Br with AgOSO₂CF₃ (silver triflate). Results The uncorrected radiochemical yield of [¹¹C]DPA was 5-10% based on [¹¹C]CH₃Br within a total synthesis time of 40 min and the radiochemical purity of [¹¹C]DPA was greater than 95%. Conclusion [¹¹C]DPA produced from [¹¹C]CH₃Br can be a potential small molecule PET tracer for apoptosis imaging. Research Support: This work was supported by the National Natural Science Foundation (No.30970856), the National High Technology Research and Development Program of China (863 Program, No. 2008AA02Z430), and Sun Yat-Sen University (No. 80000-3126132).

Presentation Number **0846A**

Poster Session 1c: In Vivo Studies & Development/Novel Use of Imaging Probes

Synthesis and evaluation of 2-phenyl-1H-benzo[d]imidazole derivative as a potential SPECT imaging probe for β -amyloid plaques

Mengchao Cui^{1,2}, Masahiro Ono¹, Hiroyuki Kimura¹, Hidekazu Kawashima¹, Boli Liu², Hideo Saji¹, ¹Graduate School of Pharmaceutical Sciences, Kyoto University, Kyoto, Japan; ²Key Laboratory of Radiopharmaceuticals, Ministry of Education, College of Chemistry, Beijing Normal University, Beijing, China. Contact e-mail: cmc1984@mail.bnu.edu.cn

Objective: Imaging agents targeting β -amyloid ($A\beta$) plaques in the living human brain have potential values for early diagnosis of Alzheimer's disease (AD). Recently, great efforts have been put into developing useful $A\beta$ plaque imaging agents for PET. However, the development of imaging agents for SPECT was lagging far behind. In this study, a novel $A\beta$ plaque imaging agent, 4-(6-[¹²⁵I]iodo-1H-benzo[d]imidazol-2-yl)-N,N-dimethylaniline ([¹²⁵I]IMDZ), has been synthesized and its biological characteristics as a potential SPECT imaging probe were evaluated. Method: [¹²⁵I]IMDZ was prepared through an iododestannylation reaction. In vitro binding assay was conducted with aggregated $A\beta$ (1-42) fibrils using [¹²⁵I]IMPY as radioligand. In vitro autoradiography (ARG) was carried out on AD human brain sections. Biodistribution study was performed using ddY mice (5 w). Ex vivo autoradiograms of an APP model mouse brain sections were obtained at 2 h after an i.v. injection of 3.33 MBq of [¹²⁵I]IMDZ. Results: After purification, the radiochemical purity of [¹²⁵I]IMDZ was greater than 98%. High binding affinity of [¹²⁵I]IMDZ was observed with the IC₅₀ value of 10.2 nM. In vitro ARG showed excellent labeling of $A\beta$ plaques in the cortical area of AD brain sections, as evidenced by co-localization with monoclonal $A\beta$ antibody. In vivo biodistribution study showed that [¹²⁵I]IMDZ exhibited a high initial brain uptake in normal mice (4.14% ID/g at 2 min) and a rapid washout (0.15% ID/g at 1 h). The ratio of brain uptake at 2 min to 1 h was 27, which may bring about good signal-to-noise ratio and therefore achieve highly sensitive $A\beta$ plaque detection. Ex vivo ARG of [¹²⁵I]IMDZ clearly displayed a distinct plaque labeling with low background, the localizations of $A\beta$ plaques were confirmed by thioflavine S. Conclusions: These preliminary results suggest that [¹²⁵I]IMDZ demonstrates desirable characteristics for in vivo detecting $A\beta$ plaques. When labeled with ¹²³I, it may be useful as a SPECT imaging agent for $A\beta$ plaques in the brain of living AD patients.

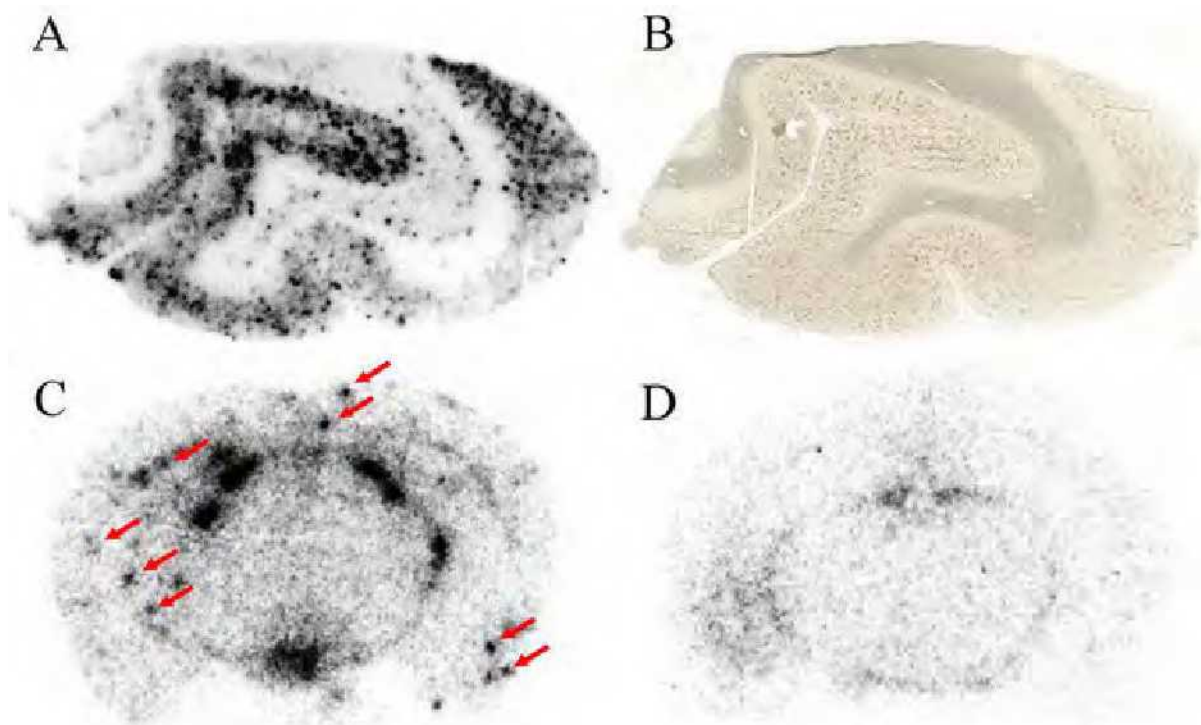


Fig 1. In vitro ARG of [¹²⁵I]IMDZ on AD human brain section (A). Plaques were confirmed by Immunostain (B). Ex vivo ARG of [¹²⁵I]IMDZ using AD model mice (C) and wild control mice (D).

Presentation Number **0847A**

Poster Session 1c: In Vivo Studies & Development/Novel Use of Imaging Probes

Comparative Study of BnAO-derivative and Assess the Effect of Pentoxifylline on Hypoxic Model Imaging

Chien-Chung Hsia^{1,2}, **Fu-Lei Huang**², **Guang-Uei Hung**³, **Wuu-Jyh Lin**¹, **Hsin-ElI Wang**², ¹*Institute of Nuclear Energy Research, Tau-Yen, Taiwan;* ²*Biomedical Imaging and Radiological Sciences, National Yang-Ming University, Taipei, Taiwan;* ³*Nuclear Medicine, Chang-Bing Show Chwan Hospital, Changhua, Taiwan. Contact e-mail: hsiacc@yahoo.com*

Aim: 99mTc-BnAO was the first nonnitro-aryl-based radiotracer used for evaluating hypoxic fraction in neoplasm, stroke and myocardium infarction regions. In this study, 3,3,10,10-tetramethyl-1-(2-nitro-1H-imidazo-1-y1)-4,9-diazadodecane-2,11- dionedioxime (BnAO-NI) was compared with BnAO on stroke bearing mice. Pentoxifylline (PTX), a hemorrheologic methylxanthine derivative for improving the microcirculations, was conducted on stroke and tumor bearing mice for evaluating the effect in the uptake of 99mTc-BnAO-NI on hypoxic region. **Materials and Methods:** BnAO-NI was formulated with stannous chloride and buffer to afford kits. After mixing with 99mTc-pertechnetate, 99mTc-BnAO-NI could be prepared in formulations achieved high radiochemical purity (98.1%). Cellular uptake assays based on KHT cell under normoxic and hypoxic conditions were performed in an oxygen-controlled CO₂ incubator. Brain stroke mouse model was induced by the electrocautery at the middle cerebral artery on C3H mice. Human breast cancer (MDA-MB-231) cells were inoculated subcutaneously into the right thigh of nude mice. After intravenous injection of 99mTc-BnAO-NI or 99mTc-BnAO into the stroke-bearing mice, SPECT images were acquired and autoradiography was conducted. Parallel studies in the effect of pentoxifylline were injected intraperitoneally prior to 99mTc-BnAO or 99mTc-BnAO-NI injection in stroke or tumor-bearing mice. **Results:** Cellular uptake assay showed that 99mTc-BnAO-NI was less selectively retained in hypoxic cells than 99mTc-BnAO. The hypoxic T/N brain ratios of the stroke brains were 3.95±0.07 and 6.08±0.10 (n=3) at 2 h post injection of 99mTc-BnAO-NI and 99mTc-BnAO, respectively. After intraperitoneal treatment of pentoxifylline, the ratios were 3.81±0.08 and 5.18±0.11 (n=3), respectively. In tumor-bearing mice model, there was relatively higher uptake of 99mTc-BnAO-NI in tumor. In addition, the tumor uptake of 99mTc-BnAO-NI had significantly reduced after pentoxifylline treatment. The T/N ratios of 99mTc-BnAO-NI in pentoxifylline treated group and control groups were 1.95 ± 0.34 and 3.53 ± 0.55 (n=3), respectively (P = 0.01). **Conclusions:** This study revealed that 99mTc-BnAO-NI and 99mTc-BnAO could selectively retain in hypoxic region. 99mTc-BnAO had higher cellular and brain hypoxic tissue uptake than 99mTc-BnAO-NI. 99mTc-BnAO-NI could present the specific effect of pentoxifylline in reducing the hypoxic environment on tumor (P=0.01). However, it had no apparent usefulness in improving the severity of hypoxia in brain stroke region (P = 4.66).

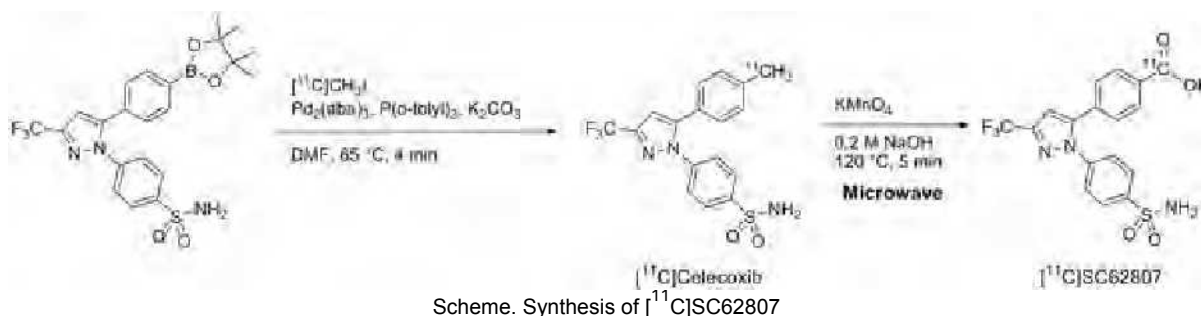
Presentation Number **0848A**

Poster Session 1c: In Vivo Studies & Development/Novel Use of Imaging Probes

Efficient Synthesis of [^{11}C]SC62807 by Sequential Rapid C- ^{11}C Methylation—Microwave-promoted Oxidation Reactions

Misato Takashima-Hirano, Tadayuki Takashima, Yumiko Katayama, Yasuhiro Wada, Yasuyoshi Watanabe, Hisashi Doi, Masaaki Suzuki, Center for Molecular Imaging Science, RIKEN, Kobe, Japan. Contact e-mail: misatot@riken.jp

Objectives: SC62807 is a major metabolite of Celecoxib, a selective cyclooxygenase-2 inhibitor. SC62807 is excreted into bile predominantly via Breast Cancer Resistance Protein (BCRP), therefore, SC62807 would be an efficient probe for the evaluation of biliary excretion.¹ We recently developed the two-step synthesis of [^{11}C]SC62807 via [^{11}C]Celecoxib by successive reactions Pd(0)-mediated rapid C- ^{11}C methylation and rapid oxidation by KMnO_4 .² In order to accelerate the latter oxidation reaction, we adopted microwave technique. **Methods:** [^{11}C]Celecoxib was prepared by rapid C- ^{11}C methylation using the corresponding boron precursor and the crude product was purified by HPLC.² The resulting [^{11}C]Celecoxib was oxidized to [^{11}C]SC62807 by KMnO_4 under microwave conditions. **Results & Discussion:** [^{11}C]Celecoxib was obtained with 91% (av.) radiochemical yield (based on [^{11}C]CH $_3$ I) and >99% radiochemical purity. The following oxidation reaction of [^{11}C]Celecoxib by conventional heating gave [^{11}C]SC62807 in 32 ± 18 % radiochemical yield ($n = 5$) (based on [^{11}C]Celecoxib). On the other hand, the reaction was enhanced to give [^{11}C]SC62807 in 47 ± 11 % radiochemical yield ($n = 5$) under microwave condition with high reproducibility. The total synthetic time was approximately 50 min. The radiochemical purity of [^{11}C]SC62807 was >99% and the isolated radioactivity was applicable to a PET study. The 2 step protocol is now implemented with fully automated system. After intravenous administration of [^{11}C]SC62807 to the rats, the radioactivity was primarily excreted by hepatobiliary transport as unchanged [^{11}C]SC62807. In conclusion we demonstrated the efficient synthesis of [^{11}C]SC62807 by sequential rapid C- ^{11}C methylation with microwave-promoted oxidation reactions and the potential of [^{11}C]SC62807 for the evaluation of BCRP function in biliary excretion. **References:** 1. C. Wu, et al. *Jpn. Pharmacol. Ther.* **2009**, 37(s1), s37-42. 2. M. Takashima-Hirano, et al. *Q. J. Nucl. Med. Mol. Im.* **2010**, 54(s1), s21.



Presentation Number **0849A**

Poster Session 1c: In Vivo Studies & Development/Novel Use of Imaging Probes

Evaluation of ^{18}F -labeled galactose derivative as a novel PET probe for imaging asialoglycoprotein receptor

Hao-Wen Kao¹, Wen-Yi Chang¹, Jenn-Tzong Chen², Wu-Jyh Lin², Ren-Shyan Liu^{3,4}, C. Allen Chang¹, Chuan-Lin Chen¹, Hsin-Ell Wang¹, ¹Department of Biomedical Imaging and Radiological Sciences, National Yang-Ming University, Taipei, Taiwan; ²Department of isotope application, Institute of Nuclear Energy Research, Taoyuan, Taiwan; ³Department of Medicine, National Yang-Ming University, Taipei, Taiwan; ⁴National PET/Cyclotron Center, Veterans General Hospital, Taipei, Taiwan. Contact e-mail: g39620006@ym.edu.tw

Objectives: Asialoglycoprotein receptor (ASGP-R) was expressed exclusively on the surface of parenchymal hepatocyte membrane. ASGP-R has high affinity for the glycoprotein having galactose residues on the terminal position of the saccharide chain. Quantitative evaluation of the expression of ASGP-R could help assess the function of liver and the diagnosis of the liver diseases. We prepared a novel ^{18}F -labeled monomeric galactose derivative (^{18}F -FGal) and conducted the pharmacokinetic studies in a liver fibrosis animal model. Methods: The precursor for F-18 labeling and the authentic standard were prepared from β -D-galactose via a four-step synthesis with a total yield of about 22%. After coupling with ^{18}F -SFB, the ^{18}F -galactose derivative (^{18}F -FGal) was obtained. The radiochemical yield was 25~30% (decay corrected) and the radiochemical purity was $\geq 95\%$. Liver fibrosis in C57BL/6 mouse was induced after multi-dose treatment with dimethylnitrosamine (DMN) for 4 weeks. The biodistribution study and microPET imaging of mouse suffering liver fibrosis were performed after injection with ^{18}F -FGal. The assay of metabolites in urine after radiotracer administration was also conducted. Results: Liver fibrosis of mouse after treating with DMN was validated by histological examination. Though high liver uptakes (in %ID/organ) in both the fibrosis mouse and normal mouse were observed at 5 min after injection of ^{18}F -FGal, significant difference ($P < 0.01$) between the two mouse models was exhibited. Compared with other organs except liver, noted radioactivity accumulation in kidney indicated that the renal clearance is the predominant route of excretion. The retention of radioactivity in the blood and kidney (in %ID/g) of the fibrosis mouse was statistically longer ($P < 0.05$) than that of the normal mouse. The reduced amount of ASGP-R in the fibrosis liver may account for the lower radioactivity accumulation in liver and prolonged retention in the blood and kidney of fibrosis mouse. The results of microPET imaging were consistent with those found in biodistribution studies. The assay of radioactive species in urine indicated that ^{18}F -FGal could either be excreted directly from kidney or metabolized into fluorobenzoic acid (FBA) after i.v. administration. Conclusion: A novel ^{18}F -labeled monomeric galactose derivative (^{18}F -FGal) was successfully prepared and demonstrated as a potent PET probe that can differentiate the fibrosis liver from the normal one. ^{18}F -FGal might have potential for diagnosing the ASGP-related liver diseases.

Presentation Number **0850A**

Poster Session 1c: In Vivo Studies & Development/Novel Use of Imaging Probes

Highly-specific small animal PET imaging of Prostate Specific Membrane Antigen (PSMA) xenografts by an engineered humanized antibody fragment (minibody)

Tove Olafsen², David T. Ho¹, Arye A. Lipman¹, Neil H. Bander⁴, Robert E. Reiter³, Christian P. Behrenbruch¹, **Anna M. Wu²**, Eric J. Lepin², ¹ImaginAb, Inglewood, CA, USA; ²Molecular and Medical Pharmacology, David Geffen School of Medicine at UCLA, Los Angeles, CA, USA; ³Urology, David Geffen School of Medicine at UCLA, Los Angeles, CA, USA; ⁴Urology, Weill Medical College of Cornell University, New York, NY, USA. Contact e-mail: awu@mednet.ucla.edu

PSMA, a transmembrane glycoprotein, is overexpressed in nearly all prostate cancers and in the tumor neovasculature in most cancers. The well characterized humanized anti-PSMA J591 monoclonal antibody (huJ591 mAb) has shown excellent targeting in patients with prostate cancer. In this study, the huJ591 mAb was reformatted into a minibody (Mb; scFv-CH3 dimer; ~80 kDa) by assembling the huJ591 variable regions into single-chain Fv (scFv) and fusion to the hulgG1 hinge and CH3 domain. Four minibody variants that differed in the scFv region were made and expressed in CHO-K1 cells. Specific binding to PSMA was demonstrated by ELISA and flow cytometry. One huJ591 Mb variant, with high expression and PSMA-binding, was selected for protein production, purification, and further evaluation. Confocal microscopy studies of the huJ591 Mb showed increased intracellular staining in CWR22rv1 and LNCaP cells over time, similar to that of the intact huJ591 mAb, suggesting rapid internalization. In order to further evaluate internalization of the huJ591 Mb, two radiolabeling strategies were employed: radioiodination with I-131 and DOTA conjugation for radiometal labelling with In-111. The ¹¹¹In-DOTA huJ591Mb showed a 260% increase in cell-associated radioactivity over a 3 hour time period. In contrast, initial cell binding of ¹³¹I-huJ591 Mb was followed by a significant loss to 80% of the initial activity. The huJ591 Mb was evaluated by small-animal PET following radiolabeling with the positron emitters I-124 (t_{1/2}= 4.2d) and Cu-64 (t_{1/2}= 12.7h), to compare retention of cell-associated radioactivity in vivo. Serial imaging of mice carrying PSMA positive CWR22rv1 and negative PC-3 xenografts resulted in high contrast images and excellent tumor uptakes with both labels. At 19 hours p.i., 8.2(±1.2)%ID/g and 8.8(±2.0)%ID/g were achieved with ⁶⁴Cu-DOTA- and ¹²⁴I-Mb, respectively. At 43 hours p.i., tumor uptake increased to 13.3(±8.3)%ID/g with the ⁶⁴Cu-DOTA-Mb, which declined to 3.25(±0.9)%ID/g with the ¹²⁴I-Mb. Positive to negative tumor ratios were 3.1 and 4.9 at 19 hours and 5.4 and 7.3 at 43 hours for ⁶⁴Cu-DOTA- and ¹²⁴I-Mb, respectively. Persistent high liver uptake [21.4(±3.1)%ID/g at 19hr and 14.4(±2.1)%ID/g at 43hr] was seen with ⁶⁴Cu-DOTA-Mb, whereas ¹²⁴I-Mb exhibited rapid background clearance resulting in higher contrast images. The similar tumor uptakes of both radiolabeled minibodies at 19 hours were unexpected, and suggestive of slower in vivo internalization. Thus, the huJ591 Mb radiolabeled with I-124 is an excellent tracer for detecting PSMA positive cells.

Presentation Number **0851A**

Poster Session 1c: In Vivo Studies & Development/Novel Use of Imaging Probes

Validation of PET probe production in RIKEN CMIS according to GMP for investigational products

Shusaku Tazawa, Akiko Tachibana, Riyo Zochi, Yoko Morimoto, Kazuhiro Takahashi, Tsuneo Yano, Center for Molecular Imaging Science, RIKEN, Kobe, Japan. Contact e-mail: ttsyusaku@riken.jp

We wish to report the validation results of our PET probe production in RIKEN CMIS according to the standards of good manufacturing practice (GMP) for investigational products. In the first step, the qualifications of the design (DQ), the installation (IQ) and the operation (OQ) of production equipments and quality control as well as analytical equipments were conducted. The following equipments concerned with PET probe production were validated; ventilation system of the facility, clean bench of Dalton, hot-cells of Universal Giken, synthetic module of JFE, dispenser of Universal Giken, HPLC, GC of Shimadzu and other analytical equipments. Afterwards, the validation of PET probe manufacturing process (PQ) was started with ^{18}F -FLT (3'-Deoxy-3'- ^{18}F fluorothymidine) production. ^{18}F fluoride was activated by Kryptfix2,2,2 and K_2CO_3 , and was reacted with the protected nosylate precursor. The hydrolysis was performed by hydrochloric acid. ^{18}F FLT was purified by HPLC from the reaction mixture, organic solvent was removed using evaporator. Finally, saline was added and sterile filtration of the product solution was made. The last step was the quality control procedure. Radioactivity of final products were 2.4 - 3.3GBq. Radiochemical purity was over 95% (EOS) and radiochemical yield (EOB) was 7-10%. Three batches of the final products were successfully carried out in all quality control tests as followed; visual inspection, pH determination, chemical and radiochemical purity by HPLC, gamma spectrum, half-life determination, residual solvent, bacterial endotoxin (ratio cloudiness method) and sterility. In addition, we performed the environmental measurement (the suspended particulate examination, the floating microbe examination, the adhesion microbe examination) of the production area. As the result the clean bench and the hot-cells as the important area for process of PET probe production were kept by grade A (class 100). The clean rooms next to grade A (class 100) area were kept by grade B (class 10,000). On the other hand, we made the SOPs about production and the quality control of the PET probe and we established the system of each document and documents administrative provision. The results show that our institution had enough performance for the reliable production of PET probes for the clinical trials. We are planning to deliver a ^{64}Cu -labeled monoclonal antibody to other research institution.

Presentation Number **0852A**

Poster Session 1c: In Vivo Studies & Development/Novel Use of Imaging Probes

Molecular Imaging Using Lung Vascular Endothelium-Targeted Antibody Specific to Aminopeptidase P

Adrian Chrastina, Philippe Valadon, Jan Schnitzer, *Proteogenomics Research Institute for Systems Medicine, San Diego, CA, USA.*
Contact e-mail: achrastina@prism-sd.org

Targeting drugs or imaging agents to a single organ has long been an elusive goal of molecular medicine, further challenged by the lack of accessible, tissue-specific targets. Recent studies have shown that aminopeptidase P (APP) is highly abundant in caveolae of lung vascular endothelium but not in other organs. Antibodies against APP specifically bind pulmonary endothelium within seconds after intravenous injection and are rapidly transcytosed across the endothelial cell layer into lung tissue. In this study we quantitatively analyze temporal and spatial in vivo tissue distribution pattern of the APP-specific recombinant antibody 833c in rats after systemic administration using computed tomography co-registered with single-photon emission computerized tomography (CT-SPECT) imaging, biodistribution and pharmacokinetic analysis. Evaluation of time-activity curves estimated from SPECT acquisition in sequence mode revealed rapid and specific targeting of lungs, gaining maximum uptake at 90 sec after intravenous administration. Quantitative profile of 833c tissue distribution was determined at multiple time points by biodistribution analysis. High level of lung 833c signal was observed over a prolonged time period and declined by first-order kinetics ($t_{1/2} = 110$ h) with substantial levels of 833c still present 30 days after injection. Uptake-based immunospecificity index and localization ratio values confirmed highly specific lung immunotargeting. Pharmacokinetic analysis revealed that cumulative residence ($AUC_{0-\infty}$) of 833c in the lungs was substantially superior compared to all other tissues. Our results, based on the analysis of imaging, biodistribution and pharmacokinetic data indicate that; APP a caveolar marker of pulmonary endothelium is accessible to circulating antibodies; 833c antibody specific to APP rapidly targets lungs in vivo and remains accumulated in lung tissue with significantly extended half-life, suggesting that the 833c antibody after transcytosis persists in the interstitium for an extended period of time without catabolic degradation. Vascular targeting of APP may therefore provide a pathway for rapid and specific delivery of imaging and therapeutic agents into the underlying parenchyma of the lung tissue.

Presentation Number **0853A**

Poster Session 1c: In Vivo Studies & Development/Novel Use of Imaging Probes

Synthesis and evaluation of N-[¹⁸F]fluoroethyl-N-(1-methylpropyl)-1-(2-chlorophenyl) isoquinoline-3-carbamoyl: a new radioligand for PET imaging of peripheral benzodiazepine receptor

Ming Fang Wang^{1,2}, Zhi Fu Luo², Ganghua Tang¹, Baoyuan Li¹, Mingquan Liang¹, ¹Nanfang PET Center, Nanfang Hospital, Southern Medical University, Guangzhou, China; ²China Institute of Atomic Energy (CIAE), Beijing, China. Contact e-mail: drmfwang@126.com

In this study, N-[¹⁸F]fluoroethyl-N-(1-methylpropyl)-1-(2-chlorophenyl) isoquinoline-3-carbamoyl (18F-FEPK11195) was synthesized by reacting 1-bromo-2-[¹⁸F]fluoroethane as alkylating reagent with nor-PK11195, and purified by HPLC in radiochemical yield of 10.7±3.5% (EOS). The total synthesis time was 75min from producing 18F-fluoroethyl bromide to the end of synthesizing of 18F-FEPK11195. Both the radiochemical purity and chemical purity were greater than 98%, and the specific activity was greater than 120 GBq/μmol (EOS). 18F-FEPK11195 injection was placed at room temperature with radiochemical purity being greater than 95% within 6h. 19F-FEPK11195 was synthesized using synthetic nor-PK11195, which was confirmed by 1H NMR. The biodistribution study of 18F-FEPK11195 in mice indicated that the uptake was higher in lung, heart, blood and brain soon after injection. At 20 min post-injection, the uptakes of 18F-FEPK11195 in other tissues such as heart, kidney and liver were increased excepting of lung and blood with the depression of uptake. After 40 min, the radioactivity level in the myocardium and intestines were higher than postinjection 20 min. The radioactivity gradually increased in kidney, which reached a peak value at 20min (4.21±1.56%ID/g). Normal rabbit were scanned with the PET/CT using 18F-FEPK11195. The uptake of 18F-FEPK11195 in liver was highest, followed by kidney, lung, intestine, heart and muscle, but the lowest uptake in brain was found. The metabolites analysis of 18F-FEPK11195 in the plasma found that the labeled metabolites were observed as early as 1 min after injection. The percentage of the un-metabolic 18F-FEPK11195 in plasma was 64.1% at 10 min after injection, 15.5% at 40 min, 7.6% at 60min and 2.3% of the total radioactivity at 120 min post injection. The radiolabeled metabolites were more polar than 18F-FEPK11195. The blocking study found that co-injection with the unlabeled PK11195 exhibited a significant reduction of radioactivity in the brain, kidney and adrenal gland compared with the control group, uptake values in these tissue was 0.38%ID/g, 0.26%ID/g and 0.21%ID/g, respectively. In contrast, 18F-FEPK11195 uptakes in these organs had no significant reduction after co-injection with CBR-selective Flumazenil. The study results indicated that 18F-FEPK11195 was an analogue of PK11195, having similar pharmacological properties with PK11195. In vivo bio-distribution and pre-clinical pharmacology studies proved that 18F-FEPK11195 was a promising PBR PET imaging agent.

Presentation Number **0854A**

Poster Session 1c: In Vivo Studies & Development/Novel Use of Imaging Probes

Affinity, stability and biodistribution studies of [¹⁸F]FBA-FALGEA-NH₂; a potential radiotracer for imaging of EGFRvIII

Charlotte Denholt¹, Tina Binderup^{1,2}, Marie T. Stockhausen³, Hans S. Poulsen³, Paul R. Hansen⁴, Nic Gillings¹, Andreas Kjaer^{1,2},
¹Department of Clinical Physiology, Nuclear Medicine and PET, Copenhagen University Hospital, Rigshospitalet, Copenhagen, Denmark; ²Cluster for Molecular Imaging, Faculty of Health Sciences, University of Copenhagen, Copenhagen, Denmark; ³The Department of Radiation Biology, Copenhagen University Hospital, Rigshospitalet, Copenhagen, Denmark; ⁴IGM-Bioorganic Chemistry, Faculty of Life Sciences, University of Copenhagen, Frederiksberg, Denmark. Contact e-mail: charlotte.lund.denholt@rh.regionh.dk

Introduction We have previously identified H-FALGEA-NH₂ as a potential new tracer for imaging of the cancer specific epidermal growth factor receptor variant III mutation, EGFRvIII, using a Positional Scanning Synthetic Combinatorial Library. This study describes the evaluation of H-FALGEA-NH₂. **Methods** For affinity, stability and PET imaging H-FALGEA-NH₂ was radiolabelled using 4-[¹⁸F]fluorobenzoic acid. The binding affinity of [¹⁸F]FBA-FALGEA-NH₂ was measured on EGFRvIII expressing cells, NR6M. Stability studies were carried out in blood plasma from nude mice, black mice and pigs. PET investigations of [¹⁸F]FBA-FALGEA-NH₂ were performed on a MicroPET scanner, using nude mice (n=11) xenografted subcutaneously with human glioblastoma multiform tumour, expressing the EGFRvIII in this native form. The mice were injected with 5-10 MBq of the radiolabelled peptide. Further, the gene expression of EGFRvIII in the tumours was determined using q-RT-PCR. **Results** The pure radiolabelled peptide was produced with in 180 min., with overall radiochemical yields of 2.6-9.8 % (decay-corrected) and an average specific radioactivity of 6.4 GBq/μmol. The binding affinity (KD) of [¹⁸F]FBA-FALGEA-NH₂ to EGFRvIII was determined to be 23 nM, suggesting moderated to high binding affinity. The peptide was most stable in the plasma from nude mice, where 53 % of the peptide was intact after 60 min of incubation in plasma. For the in vivo stability in nude mice no intact peptide was observed in the plasma 60 min post-injection. In the nude mice, [¹⁸F]FBA-FALGEA-NH₂ accumulated in the human cancer xenografts (T/M up to 30, 60 min post-injection, and up to 15, 240 min post-injection). The biodistribution studies also revealed renal and hepatic elimination of the tracer, with renal elimination being the dominant route. Furthermore, there was a strong correlation (R= 0.86, p= 0.007) between the expression of EGFRvIII in the tumours and the tracer uptake expressed as T/M. **Conclusion** Our results show that [¹⁸F]FBA-FALGEA-NH₂ is a promising tracer for PET imaging of EGFRvIII.

Presentation Number **0855A**

Poster Session 1c: In Vivo Studies & Development/Novel Use of Imaging Probes

Synthesis, Radiofluorination and In Vivo Evaluation of Endothelin-A-Receptor-Ligands

Kristin Michel¹, Simone Maschauer⁴, Carsten Hoeltke², Katrin Büther¹, Stefan Wagner¹, Otmar Schober¹, Olaf Prante⁴, Klaus Kopka^{1,3}, Burkhard Riemann¹, ¹Department of Nuclear Medicine, University Hospital Münster, Münster, Germany; ²Department of Clinical Radiology, University Hospital Münster, Münster, Germany; ³Interdisciplinary Center of Clinical Research, University of Münster, Münster, Germany; ⁴Laboratory of Molecular Imaging, University Hospital Erlangen, Erlangen, Germany. Contact e-mail: kristin.michel@uni-muenster.de

Introduction In papillary thyroid tumors an increased expression of the endothelin (ET) axis has been reported.^[1] The visualization of the ET system by positron emission tomography (PET) in affected tissue would be highly valuable for clinical diagnosis and the prediction of therapy response. Recently we published the synthesis of a ¹⁸F-labeled derivative of the ET_A receptor ligand PD 156707.^[2] In vivo studies revealed an insufficient metabolic stability and high tracer accumulation in liver, bile and intestine. The aim of this study was the development of a subtype-selective ET_A radioligand with improved pharmacokinetics by introduction of a polyethylene glycol spacer, a triazole group or glycosyl moiety as hydrophilic building blocks. **Results and Discussion** We synthesized seven fluoro-substituted analogs of PD 156707 using "click chemistry" and investigated the receptor binding affinities after purification and confirmation of chemical purity by HPLC. The tested compounds revealed high ET_A receptor affinity in the low nanomolar range (1-7 nM) and displayed ET_A/ET_B selectivities of 70-350:1. The radiolabeled derivatives were prepared in a two step synthesis using ¹⁸F-labeled synthons and coupling to the corresponding alkyne or azide. Glycosylation with 2-deoxy-2-[¹⁸F]fluoroglucosyl azide^[3] was successfully accomplished (25 % decay-uncorrected rcy, A_s = 41-138 GBq/μmol, rcy >98 %). The [¹⁸F]FGlc-ET_A radioligand revealed excellent stability in human serum *in vitro* (37°C, 90 min) and *in vivo* (60 min, p.i., mouse blood). In comparison with the fluoroethoxy derivative, that showed polar radiometabolites within 20 min after i.v. injection^[2], the glycosyl derivative revealed improved metabolic stability (>99 %). The [¹⁸F]FGlc-ET_A radioligand was applied to biodistribution studies using nude mice bearing ET_A-receptor-positive thyroid K1 tumors. *In vivo* μPET (Siemens Inveon) imaging studies confirmed specific tumor uptake and ET_A receptor-mediated binding of the glycosylated radioligand 55 min p.i., as demonstrated by coinjection experiments using the high-affinity ET_A antagonist PD 156707 (25 μg/mouse; control: SUV_{mean} = 0.10±0.02, n=4, vs. coinjection: SUV_{mean} = 0.04±0.02, n=4). **Conclusion** Simple hydrophilic modifications of the lead structure PD 156707 improved the pharmacokinetics and offers access to promising radio tracers for the imaging of ET_A receptor expression. **Literature** (1) Donckier et al., Clin Endocrinol (Oxf). **2003**, 59, 354-60. (2) Höltke et al., Bioorg Med Chem **2009**, 17, 7197-7208. (3) Maschauer et al., Carbohydr Res **2009**, 344, 753-761.

Presentation Number **0856A**

Poster Session 1c: In Vivo Studies & Development/Novel Use of Imaging Probes

PET-Imaging of Tumor $\alpha_v\beta_3$ -Integrin Expression with a Novel Probe ^{64}Cu -cyclam-RAFT-c(-RGDfK-)₄

Zhao-Hui Jin¹, Takako Furukawa^{1,2}, Didier Boturyn³, Mathieu Galibert³, Jean-Luc Colf⁴, Toshimitsu Fukumura¹, Tsuneo Saga¹, Pascal Dumy³, Yasuhisa Fujibayashi^{1,2}, ¹Molecular Imaging Center, National Institute of Radiological Sciences, Chiba, Japan; ²Biomedical Imaging Research Center, University of Fukui, Fukui, Japan; ³Département de Chimie Moléculaire, Université Joseph Fourier, Grenoble, France; ⁴INSERM U823, Institut Albert Bonniot & Université Joseph Fourier, Grenoble, France. Contact e-mail: zhaohui@nirs.go.jp

The $\alpha_v\beta_3$ -integrin, a well-known transmembrane adhesion receptor plays important roles in tumor growth, angiogenesis and metastasis. In this work we evaluate a novel multivalent positron emission tomography (PET) probe, ^{64}Cu -cyclam-RAFT-c(-RGDfK-)₄, for $\alpha_v\beta_3$ -targeted imaging. Methods: Cyclam-RAFT-c(-RGDfK-)₄, the conjugate of a chelator, 1,4,8,11-tetraazacyclotetradecane (cyclam) and RAFT-c(-RGDfK-)₄, a tetrameric Arg-Gly-Asp (RGD)-based peptide, was radiolabeled with the positron emitter ^{64}Cu . The resultant ^{64}Cu -cyclam-RAFT-c(-RGDfK-)₄ was evaluated *in vitro* by cell binding and competitive inhibition assays and *in vivo* by biodistribution and receptor blocking studies and PET-imaging. The following cell lines, human embryonic kidney HEK293(β_1) [$\alpha_v\beta_3$ -negative] and HEK293(β_3) [$\alpha_v\beta_3$ -overexpressing] and human glioblastoma U87MG [naturally expressing $\alpha_v\beta_3$], together with their subcutaneous xenografts in athymic nude mice were used for the present study. The levels of $\alpha_v\beta_3$ expression on these cell lines and tumor xenografts were analyzed by flow cytometry and SDS-polyacrylamide gel electrophoresis/autoradiography, respectively. Results: Cyclam-RAFT-c(-RGDfK-)₄ was radiolabeled with ^{64}Cu at 37°C for 1 h with high radiochemical purity (~100%) and biostability. ^{64}Cu -cyclam-RAFT-c(-RGDfK-)₄ targeted the $\alpha_v\beta_3$ *in vitro* and *in vivo* with high affinity and specificity, and displayed rapid blood clearance, predominantly renal excretion, and low-level uptake in nontumor tissues. Tumor uptake of ^{64}Cu -cyclam-RAFT-c(-RGDfK-)₄ (3 h postinjection) in HEK293(β_3) (high levels of $\alpha_v\beta_3$), U87MG (moderate levels of $\alpha_v\beta_3$), and HEK293(β_1) (undetectable levels of $\alpha_v\beta_3$) tumors was 9.35 ± 1.19 , 3.46 ± 0.45 , and $1.18 \pm 0.30\%$ ID/g, respectively [%ID/g is percentage of injected dose per gram], with a strong and positive correlation obtained between the tumor uptake values and tumor $\alpha_v\beta_3$ expression levels. PET images showed that $\alpha_v\beta_3$ -positive tumors were clearly visualized with high tumor-to-background contrast, and agreed well with the biodistribution results. Conclusion: ^{64}Cu -cyclam-RAFT-c(-RGDfK-)₄-based PET is able to visualize $\alpha_v\beta_3$ positive tumor with high imaging quality, and exhibits potential for noninvasively quantifying $\alpha_v\beta_3$ expression.

Presentation Number **0857A**

Poster Session 1c: In Vivo Studies & Development/Novel Use of Imaging Probes

Molecular Orbital (MO) Calculations As A Tool To Predict Nucleophilic Aromatic Fluorination Sites

Ya-Yao Huang, **Chyng-Yann Shiue**, Nuclear Medicine, Tri-Service General Hospital, Neihu, Taipei, Taiwan. Contact e-mail: shiue@ndmctsg.h.edu.tw

Objective: Nucleophilic aromatic fluorination with NCA [^{18}F]fluoride is the only route to prepare NCA [^{18}F]labeled receptor or transporter imaging agents. The purpose of this study was to test the feasibility of using molecular orbital (MO) calculations to predict the radiochemical yield and product distribution in nucleophilic aromatic fluorination before wet chemistry is undertaken. Method: MO calculations were performed according to the reported method (Sun et al., *Angew Chem Int Ed.* 45:2720-25,2006) with some modifications. Briefly, gas-phase structures and energies of 1 and 8 (Fig 1) were optimized using density functional theory (DFT) (B3LYP/6-31G(d)) to obtain the C-N bond lengths of 1 and 8. Vibrational frequency calculations for 1 and 8 were also performed to characterize them as minima and provide thermal (298 K) and zero-point energy (ZPE) corrections for the thermochemical analysis. Self-consistent isodensity polarizable continuum models (SCI-PCM) were employed to model the polar aprotic solvent (DMSO) used in our experiments. Atomic charges at C-4 and C-2 carbons of 1 and 8 were estimated using natural atomic population analysis (NPA) method at B3LYP/6-31G(d) level. 4- ^{18}F -ADAM (2) was prepared as reported previously (Huang et al., *ARI*.67:1063-67, 2009). Results: MO calculations on 1 and 8 in DMSO showed that the atomic charge at C-4 carbon of 1 is lower than that at C-2 carbon (+0.027 vs +0.054 eV) while the bond lengths of C-N at C-2 and C-4 are similar (1.4656 and 1.4667 Å, respectively). In contrast, the atomic charge at C-4 carbon of 8 is higher than that at C-2 carbon (+0.264 vs +0.003 eV) while the bond length of C-N at C-4 is longer than that at C-2 (1.5143 and 1.3781 Å, respectively). Thus, nucleophilic aromatic substitution of 1 with [^{18}F]fluoride will occur predominately at C-2 carbon while nucleophilic aromatic substitution of 8 will occur predominately at C-4 carbon which are in agreement with wet chemistry results. The radiochemical yields of 2 synthesized from 1 and 8 were ~6 and 15%, respectively. Conclusion: The radiochemical yield of 2 synthesized from 1 and 8 correlated well with the prediction of MO calculations. Thus, MO calculations may be a useful tool to predict nucleophilic aromatic fluorination sites and the product yield.

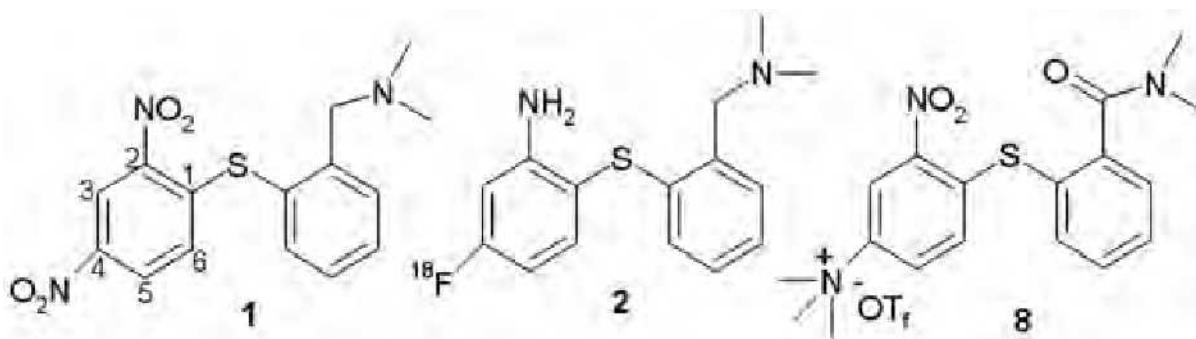


Fig 1. Structures of 1, 8 and 4- ^{18}F -ADAM 2.

Presentation Number **0858A**

Poster Session 1c: In Vivo Studies & Development/Novel Use of Imaging Probes

[¹¹C]Telmisartan as a potential PET molecular imaging probe for human drug transporter OATP1B3

Tomohiko Yamane¹, Keiji Shimizu¹, Masahiro Sasaki¹, Hiromitsu Kageyama¹, Yoshinobu Hashizume², Tadayuki Takashima², Kazuya Maeda³, Yuichi Sugiyama³, Yasuyoshi Watanabe², Michio Senda¹, ¹Division of Molecular Imaging, Institute of Biomedical Research and Innovation, Kobe, Japan; ²RIKEN Center for Molecular Imaging Science, Kobe, Japan; ³Department of Molecular Pharmacokinetics, Graduate School of Pharmaceutical Sciences, The University of Tokyo, Tokyo, Japan. Contact e-mail: yamane@fbri.org

Purpose: Telmisartan, an angiotensin II receptor antagonist used for management of hypertension, is taken up by the liver through the organic anion-transporting polypeptide (OATP) 1B3 transporter and metabolized for bile excretion. Therefore, positron emission tomography (PET) imaging with [¹¹C]telmisartan is expected to provide information about the whole body pharmacokinetics of telmisartan as well as the transport capacity of hepatic OATP1B3. The purpose of this study is to evaluate safety and distribution of [¹¹C]telmisartan in healthy human subjects. Methods: Six healthy male volunteers (20 to 38 years old, median 23.5 years) were enrolled in this study after written informed consent was obtained. PET studies were performed using ECAT EXACT HR+ (Siemens). Dynamic whole-body PET images were acquired starting 0, 11, 22, 33, 44, 55, 66 and 77 min after intravenous injection of 96-120 MBq [¹¹C]telmisartan. As data analysis, uptake percentages of injected dose were calculated for major organs by drawing regions of interest on each PET slice. The radiation dosimetry of [¹¹C]telmisartan was also evaluated using the MIRD methods. In addition, safety of the drug was confirmed using electrocardiogram as well as blood, urine and other medical examinations after the PET scan. Results: Most of the tracer uptake was observed in the liver throughout the scan. Average uptake by the liver increased gradually from 0 to 44-min-scan, and decreased gradually after that. At the 44-min-scan, 55.7% of the injected activity was accumulated in the liver with the other activity being observed in the intestine (7.5%), kidney (2.7%), gall bladder (2.7%), myocardium (1.8%), lung (1.4%) and brain (0.2%). Uptake by the gall bladder and intestine, to which the metabolites of telmisartan were excreted from the liver, increased gradually. Effective dose of [¹¹C]telmisartan was estimated to 4.29μSv/MBq in average. With respect to the safety, no abnormal finding was observed in any subjects. Conclusion: First human PET images with [¹¹C]telmisartan were acquired without any adverse events. More than 50% of the tracer accumulated in the liver, where almost all telmisartan is metabolized and excreted. Acknowledgement: This study is a part of "Research Project for Establishment of Evolutional Drug Development with the Use of Microdose Clinical Trial", sponsored by the New Energy and Industrial Technology Development Organization (NEDO).

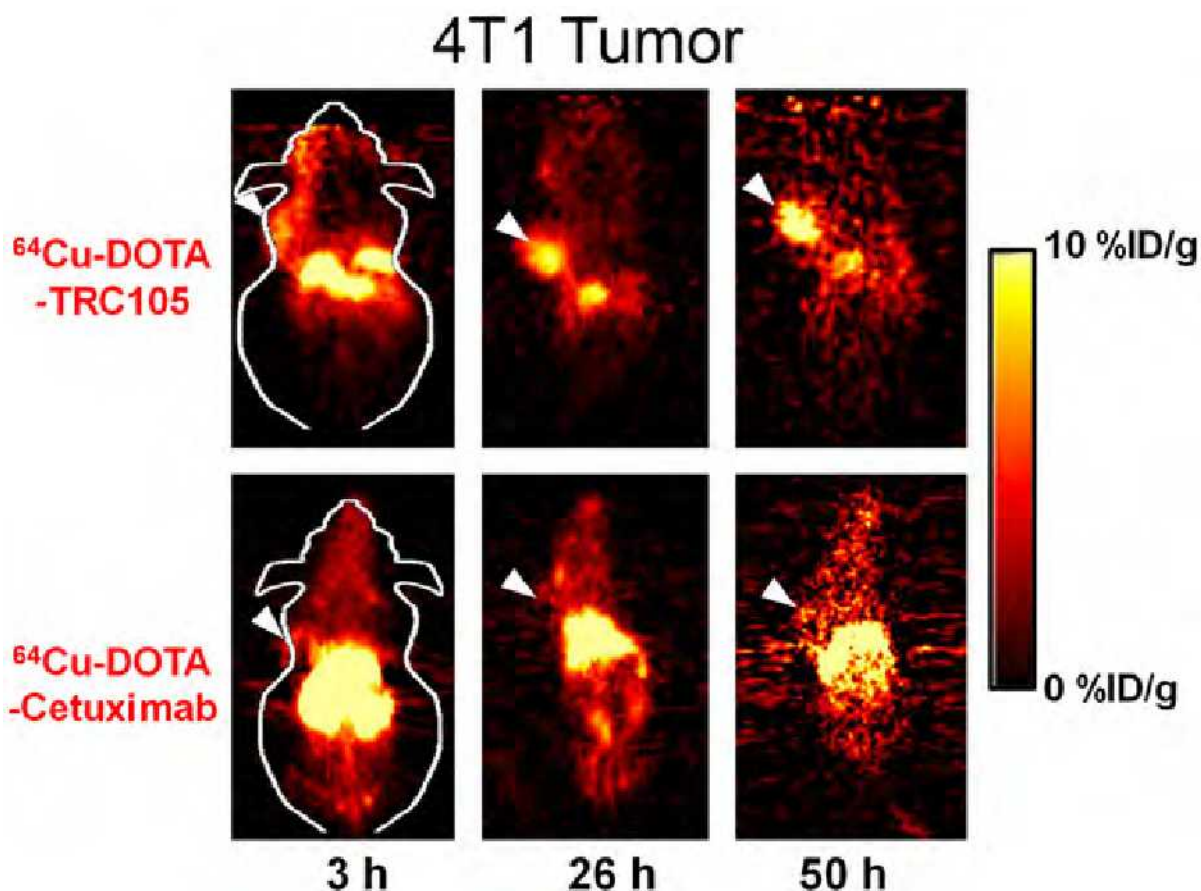
Presentation Number **0859A**

Poster Session 1c: In Vivo Studies & Development/Novel Use of Imaging Probes

Positron Emission Tomography (PET) Imaging of CD105 Expression during Tumor Angiogenesis

Hao Hong¹, **Yunan Yang**¹, **Yin Zhang**¹, **Jonathan W. Engle**¹, **Todd E. Barnhart**¹, **Robert J. Nickles**¹, **Bryan Leigh**², **Weibo Cai**¹,
¹University of Wisconsin - Madison, Madison, WI, USA; ²TRACON Pharmaceuticals, Inc., San Diego, CA, USA. Contact e-mail: hhong@uwhealth.org

Objectives: TRC105, a high-affinity chimeric monoclonal antibody that recognizes CD105 (Endoglin, a marker for tumor angiogenesis), is in a multicenter Phase 1 first-in-human dose-escalation trial. Multiple Phase 2 trials are also planned. Development of a PET tracer based on TRC105 would greatly facilitate its clinical development, such as evaluating its pharmacokinetics, measuring tumor targeting efficacy, guiding anti-angiogenic therapies, and non-invasive imaging of tumor angiogenesis. **Methods:** TRC105 was conjugated to DOTA and labeled with ⁶⁴Cu. FACS analysis and microscopy studies were performed to compare the CD105 binding affinity of TRC105 and DOTA-TRC105. PET imaging, biodistribution, and ex vivo histology studies were performed on 4T1 murine breast tumor-bearing mice to evaluate the tumor angiogenesis targeting effect of ⁶⁴Cu-DOTA-TRC105. Another chimeric antibody, Cetuximab, was used as a negative control. **Results:** FACS analysis of HUVEC cells (CD105-positive) revealed that there is no difference in CD105 binding affinity between TRC105 and DOTA-TRC105, which was further validated by fluorescence microscopy. The ⁶⁴Cu-labeling yield was 71.5±9.4 % (n=4) and the specific activity of ⁶⁴Cu-DOTA-TRC105 was 28.0±2.1 mCi/mg (n=4). Serial PET imaging revealed that the 4T1 tumor uptake of the tracer was 6.5±1.5, 14.8±2.5, and 13.2±4.1 ID%/g (n=3) at 3.2, 25.6, and 48.5 h post-injection (p.i.), respectively, higher than most organs at late time points which provided excellent contrast. Biodistribution data as measured by gamma counting were consistent with the PET findings. Uptake of ⁶⁴Cu-DOTA-Cetuximab in the 4T1 tumor (3.0±0.4 and 3.3±0.3 ID%/g at 5.5 and 50.0 h p.i. respectively; n=4) was significantly lower than that of ⁶⁴Cu-DOTA-TRC105, which confirmed the in vivo target specificity of ⁶⁴Cu-DOTA-TRC105. **Conclusions:** Successful PET imaging of CD105 expression warrants future translation of ⁶⁴Cu-DOTA-TRC105, which can not only facilitate the clinical development of TRC105 but also impact various other facets of cancer patient management such as patient selection and treatment monitoring.



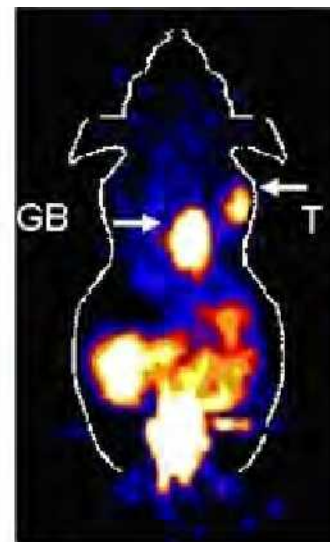
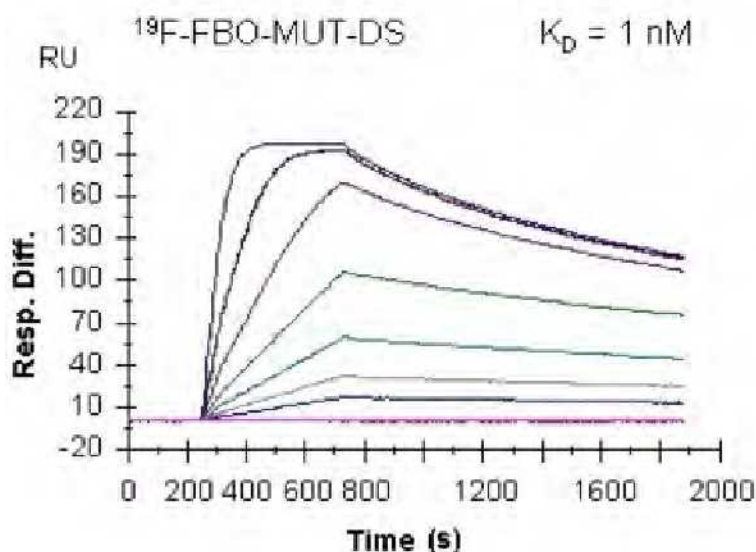
Presentation Number **0860A**

Poster Session 1c: In Vivo Studies & Development/Novel Use of Imaging Probes

Small animal PET imaging of HER2 positive tumors with a novel 18F-labeled two-helix peptide

Zheng Miao^{1,2}, **Gang Ren**^{1,2}, **Lei Jiang**^{1,2}, **Hongguang Liu**^{1,2}, **Jack M. Webster**³, **Rong Zhang**³, **Mohammad Namavari**^{1,2}, **Sanjiv S. Gambhir**^{1,2}, **Faisal A. Syud**³, **Zhen Cheng**^{1,2}, ¹MIPS, Stanford University Medical Center, Palo Alto, CA, USA; ²Radiology, Stanford University Medical Center, Palo Alto, CA, USA; ³Global Research, General Electric Company, Niskayuna, NY, USA. Contact e-mail: zmiao@stanford.edu

Aim: Two-helix peptides (~ 5 KDa) against human epidermal growth factor receptor type 2 (HER2) have been discovered in our previous research. In this research we aimed to develop a 18F labeled 2-helix small peptide for positron emission tomography (PET) imaging of HER2 positive tumors. **Method and Results:** An aminoxy functionalized 2-helix peptide (MUT-DS) with high HER2 binding affinity was synthesized through the conventional solid phase peptide synthesis. The purified linear peptide was cyclized by I2 oxidation to form a disulfide bridge. The cyclic peptide was then labeled with a radiofluorination synthon, 4-18F-fluorobenzaldehyde (18F-FBA), through the aminoxy functional group at the peptide N-terminus (30% yield, non-decay corrected). The resulting PET probe, 18F-FBO-MUT-DS, displayed a high specific activity (20-32 MBq/nmol, 88-140 μ Ci/ μ g, end of synthesis). Cell uptake assays showed high and specific cell uptake (~12 % applied activity at 1 h, 37 oC) by incubation the probe with HER2 high-expressing SKOV3 ovarian cancer cells. The affinities (KD) of MUT-DS and 19F-FBO-MUT-DS as tested by Biacore analysis were 2 and 1 nM, respectively. In vivo small-animal PET imaging demonstrated fast tumor targeting, high tumor accumulation and good tumor-to-normal tissue contrast of 18F-FBO-MUT-DS. Biodistribution studies further demonstrated that the probe had excellent tumor uptake (6.92 %ID/g at 1 h post injection) and was cleared through both liver and kidneys. Co-injection of the probe with 500 μ g of HER2 Affibody protein reduced the tumor uptake (6.92 vs. 1.84 %ID/g). **Conclusion:** 18F-FBO-MUT-DS displays excellent HER2 targeting ability and tumor PET imaging quality. Two helix small proteins are suitable for development of 18F based PET probes.



(A) Biosensor binding studies of 19F-FBO-MUT-DS. Resp. Diff. means respective difference. (B) A representative 18F-FBO-MUT-DS microPET image of a nude mouse bearing SKOV3 tumor on right shoulder at 2 h post-injection. T: tumor, GB: gallbladder.

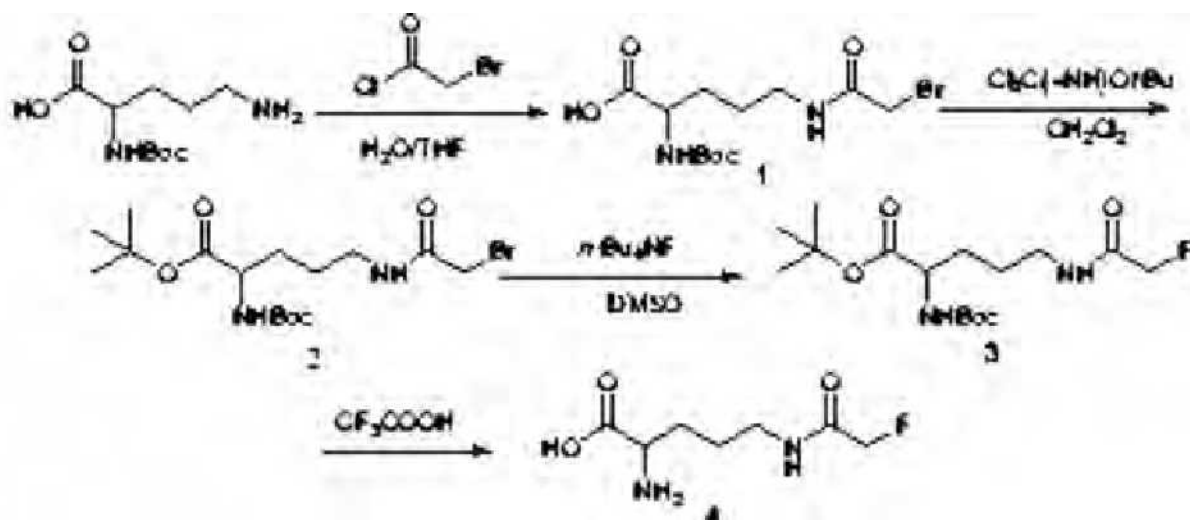
Presentation Number **0861A**

Poster Session 1c: In Vivo Studies & Development/Novel Use of Imaging Probes

Radiosynthesis of N5-^[18F]fluoroacetylornithine (N5-^[18F]FAO) for PET imaging of ornithine decarboxylase (ODC)

Nashaat Turkman, Juri G. Gelovani, Mian Alauddin, Experimental Diagnostic Imaging, The University of Texas MD Anderson Cancer Center, Houston, TX, USA. Contact e-mail: nturkman@mdanderson.org

Introduction: Ornithine decarboxylase (ODC) is the key enzyme that catalyzes the biosynthesis of polyamines. The decarboxylation of ornithine by ODC leads to the route for de novo biosynthesis of putrescine, which is then converted into spermidine and spermine by the concerted actions of down-stream enzymes. ODC is up-regulated in various types of cancer, including breast cancer, melanoma, and neuroblastoma. Difluoromethylornithine (DFMO) is an irreversible inhibitor of ODC and is currently in Phase II clinical trials for therapy of various types of malignancies. With this in mind, we developed a novel derivative of ornithine, the N5-^[18F]fluoroacetylornithine (N5-^[18F]FAO) for PET imaging of ODC expression-activity in tumors, that could be used as a companion diagnostic for selection and monitoring of personalized therapy with DFMO. Methods: The precursor compound N2-Boc-N5-bromoacetylornithine-t-butyl ester **2** was synthesized from 5-amino-2-(tert-butoxycarbonylamino)pentanoic acid by reaction with bromoacetyl chloride followed by esterification with tert-butyl-2,2,2-trichloroacetamide. Fluorination of **2** produced a fluoro-derivative, which was hydrolyzed in acid to obtain the desired compound, N5-FAO. The radiosynthesis of N5-^[18F]FAO was accomplished by reaction of **2** with n-Bu₄N^[18F], followed by high-performance liquid chromatography purification and then by acid hydrolysis. Results: The radiochemical yield was 6-10% (decay corrected) with an average of 8% (n=10) at the end of synthesis. The radiochemical purity was > 99%, and specific activity was > 1,5 Ci/μmol. The synthesis time was 115-120 min from the end of bombardment. Conclusion: N5-FAO and its radiolabeled analogue N5-^[18F]FAO have been synthesized for the first time in good yield, high purity and high specific activity. This method should be applicable for radiosynthesis of α-substituted ornithine, including methyl, fluoromethyl and difluoromethyl derivatives.

Scheme for synthesis of ¹⁸F-FAO

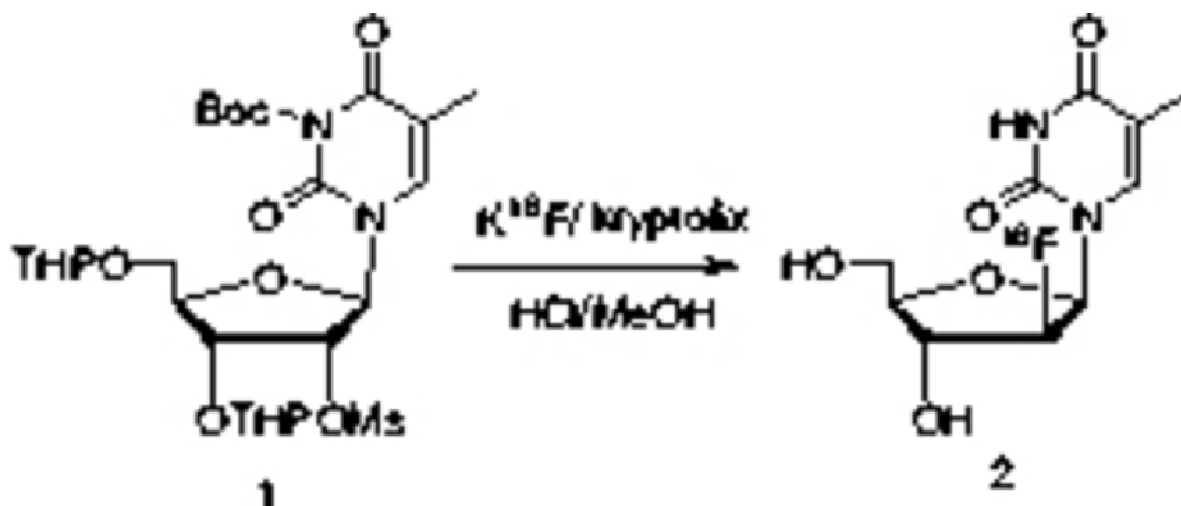
Presentation Number **0862A**

Poster Session 1c: In Vivo Studies & Development/Novel Use of Imaging Probes

Stereospecific fluorination at the 2'-arabino-position of pyrimidine nucleoside analogues: synthesis of [¹⁸F]-FMAU

Nashaat Turkman, Juri G. Gelovani, Mian Alauddin, Experimental Diagnostic Imaging, The University of Texas MD Anderson Cancer Center, Houston, TX, USA. Contact e-mail: nturkman@mdanderson.org

Introduction: Direct fluorination of a pyrimidine nucleoside at the 2'-arabino-position has been deemed to be extremely difficult, if not impossible. The conventional synthesis of 2'-deoxy-2'-fluoro-5-methyl-1-β-D-arabinofuranosyluracil (FMAU) and its 5-substituted analogues involves stereospecific fluorination of the 1,3,5-tri-O-benzoyl-α-D-ribofuranose-2-sulfonate ester followed by bromination at the C1-position, and then coupling with pyrimidine-bis-trimethylsilyl ether. Several radiolabeled nucleoside analogues, including [¹⁸F]FMAU, and other 5-substituted analogues, were developed according to this methodology. However, routine production of these compounds using this multi-step process is inconvenient and limits their clinical application. We developed a novel method for direct fluorination of nucleoside analogues at the 2'-arabino position exemplified by radiosynthesis of [¹⁸F]FMAU. **Methods:** The precursor, 2'-methylsulphonyl-3',5'-O-tetrahydropyranyl-N3-Boc-5-methyl-1-β-D-ribofuranosiluracil **1**, was synthesized from 5-methyluridine in multiple steps. Radiofluorination of **1** with K¹⁸F/kryptofix produced 2'-deoxy-2'-[¹⁸F]fluoro-3',5'-O-tetrahydropyranyl-N3-Boc-5-methyl-1-β-D-arabino-furanosiluracil, which after acid hydrolysis and purification by high-performance liquid chromatography (HPLC) produced the desired product **2** ([¹⁸F]FMAU). **Results:** The average radiochemical yield was 2.0% (decay corrected, n=6), from the end of bombardment. Radiochemical purity was > 99%, and specific activity was > 1.8 Ci/μmol. Synthesis time was 1.5 h from the end of bombardment. **Conclusion:** A novel method for a single-step stereospecific fluorination of pyrimidine nucleoside analogues at the 2'-arabino position has been achieved for the first time. This method is applicable for radiosynthesis of [¹⁸F]FMAU and its 5-substituted analogues, including [¹⁸F]FEAU, [¹⁸F]FIAU, [¹⁸F]FFAU, [¹⁸F]FCAU, [¹⁸F]FBAU and others. Further optimization for improvement on the radiochemical yield is in progress.



Presentation Number **0863A**

Poster Session 1c: In Vivo Studies & Development/Novel Use of Imaging Probes

Effects of the different substituent at 6 position of quinazoline on the uptake in tumor cells with EGFR-TK mutation

Mitsuyoshi Yoshimoto^{1,4}, Masahiko Hirata², Ryuichi Nishii³, Shinya Kagawa³, Keiichi Kawai^{4,5}, Yoshiro Ohmomo², ¹Cancer Prevention Basic Research Project, National Cancer Center Research Institute, Tokyo, Japan; ²Osaka University of Pharmaceutical Sciences, Takatsuki, Japan; ³Research Institute, Shiga Medical Center, Moriyama, Japan; ⁴Graduate School of Medical Science, Kanazawa University, Kanazawa, Japan; ⁵Biomedical Imaging Research Center, University of Fukui, Matsuoka, Japan. Contact e-mail: miyoshim@ncc.go.jp

Introduction: Gefitinib is an EGFR tyrosine kinase (EGFR-TK) inhibitor that binds reversibly to ATP binding sites. Recent reports have revealed that mutations (L858R or L858R + T790M, etc) in EGFR-TK domain modulate the response to gefitinib treatment. We have been developed ¹²⁵I-PHY (4-(3-¹²⁵I-iodophenoxy)-6, 7-diethoxy-quinazoline) and ¹²⁵I-PYK (-(3-¹²⁵I-iodophenoxy)-7-ethoxy-6-(3-morpholinopropoxy) quinazoline) as EGFR-TK imaging agents. In this study, we investigated the effects of the different substituent (ethoxy group and morpholinopropoxy group) at 6 position of quinazoline on the uptake in tumor cells with EGFR-TK mutation.

Methods: Expression of EGFR in A431 (wild type) and H3255 (L858R mutation) was determined using western blotting. To assess the effects of the different substituent at 6 position of quinazoline on growth inhibition, the IC₅₀s of PHY and PYK for growth inhibition was evaluated using MTS assay and compared to PD153035 having methoxy group and gefitinib having morpholinopropoxy group which are conventional EGFR-TK inhibitors. The biodistribution study of ¹²⁵I-PHY and ¹²⁵I-PYK was conducted in tumor bearing mice.

Results: Western blotting revealed the high expression of EGFR in A431 and H3255. IC₅₀s of PHY to A431 and H3255 were 6.9 μM and 2.4 μM, respectively. On the other hand, IC₅₀s of PYK to A431 and H3255 were 12.2 μM and 0.48 μM, respectively. In addition, gefitinib showed more potent growth inhibition in H3255 than PD153035. The IC₅₀ ratios (A431/H3255) of PHY, PYK, PD153035 and gefitinib was 3.1, 25, 5.6 and 90, respectively. In biodistribution study, ¹²⁵I-PHY showed highest uptake at 1 hr after injection in both A431 and H3255, followed by rapid clearance. The uptake of ¹²⁵I-PYK in A431 was highest at 1 hr, whereas that in H3255 was retained to 4 hr.

Conclusion: These results indicated that introduction of morpholinopropoxy at 6 position of quinazoline enhances the affinity to EGFR-TK harboring mutation and suggested that radioiodinated PYK could be a possible EGFR-TK imaging agent which predicts the therapeutic efficacy by EGFR-TK inhibitors.

Presentation Number **0864A**

Poster Session 1c: In Vivo Studies & Development/Novel Use of Imaging Probes

Synthesis of [¹⁸F]fluoroacetate ([¹⁸F]FACE) from butyl {[4-(4-methylphenyl)sulfonyl]oxy}acetate using commercial platform

Obaidur Rahman¹, Johan Ulin¹, Bengt Långström², ¹GE Healthcare, Uppsala Applied Science Laboratory, Uppsala, Sweden;

²Department of Biochemistry and Organic Chemistry, Uppsala University, Uppsala, Sweden. Contact e-mail: obaidur.rahman@ge.com

Objectives: [¹⁸F]Fluoroacetate has been reported to be a potential tracer for imaging prostate cancer metastases [1] and to study the microglial cell metabolism associated with neuroinflammation [2]. This report describes the synthesis of [¹⁸F]fluoroacetate using butyl {[4-(4-methylphenyl)sulfonyl]oxy}acetate and the commercial platform TRACERLab FX-FN (Fig. 1). Method: Potassium carbonate (3.5 mg in 500 μL water), Kryptofix K2.2.2 (10.0 mg in 1 mL acetonitrile), precursor (7.0 mg in 700 μL anhydrous DMF), the HPLC eluent (5 mL), water (10 mL) and sodium hydroxide (1mL, 1M) were loaded into reservoirs 1, 2, 3, 4, 7 and 8 respectively of the platform. The 18F- was separated from target water using QMA and dried with potassium carbonate and kryptofix at 60 °C for 7 min and at 120 °C for 5 min. The mixture of the precursor solution and dried 18F- was heated at 120 °C for 15 min, cooled to 30 °C, diluted with HPLC eluent and loaded into the in-built preparative HPLC system. The separated butyl ester was trapped on a C18 SPE cartridge and treated with sodium hydroxide mixed with ethanol. The hydrolyzed product was eluted with water and the pH was adjusted by adding 0.3 M HCl. The whole procedure was performed with the preprogrammed time sequence of the platform. Results: 18F-Labelled fluoroacetate ([¹⁸F]FACE) was synthesized by one step nucleophilic 18F-fluorination (Scheme 1) with isolated decay corrected radiochemical yield of 32±3% (mean value from four run) after 70-75 min synthesis time. The radiochemical purity was more than 98%. The preparation of [¹⁸F]fluoroacetate has been published previously by several groups including automated synthesis using commercial platform [3]. We report a synthesis using an alternative precursor butyl{[4-(4-methylphenyl)sulfonyl]oxy}acetate. References: [1] E. Ponde, et al J. Nucl. Med. 2007; 48, 420-428. [2] J. Marik, et al J. Nucl. Med. 2009; 50, 982-990. [3] X. Tang, et al J. Label. Compd. Radiopharm. 2008; 51, 297-301.

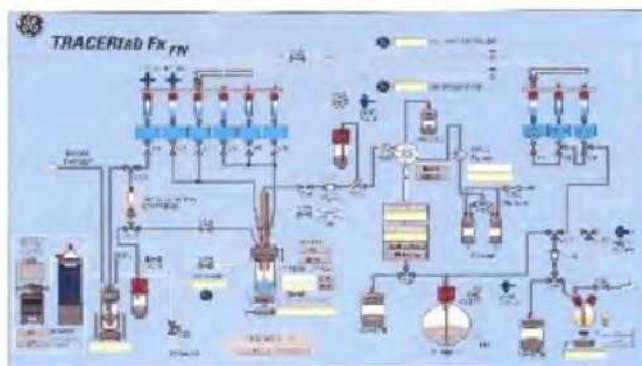
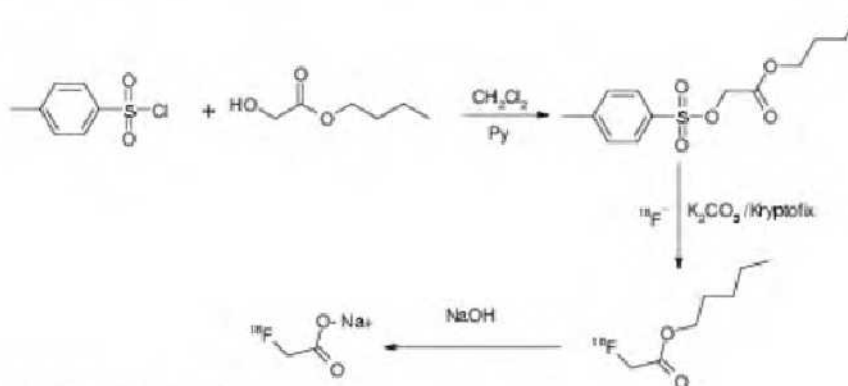


Fig. 1. Graphical display of the platform TRACERLab FX-FN



Scheme 1. Synthesis of [¹⁸F]fluoroacetate

Presentation Number **0865A**

Poster Session 1c: In Vivo Studies & Development/Novel Use of Imaging Probes

Novel Production of Cl-34m and Labeling of Dopamine D1 Agonist, Chloro-SKF 38393

Jonathan W. Engle, Dhanabalan Murali, Todd E. Barnhart, Robert J. Nickles, Onofre T. DeJesus, Medical Physics, University of Wisconsin School of Medicine and Public Health, Madison, WI, USA. Contact e-mail: odejesus@wisc.edu

Cl-34m ($t_{1/2}=32.2$ min) is a positron-emitter with potential as PET label for chlorine-containing drugs. Cl-34m production is currently limited to facilities capable of accelerating alpha particles (Takeia et al. Appl. Radiat. Isot. 65:981, 2007). We previously reported on the S-34(p, n)Cl-34m reaction using a proton-only small cyclotron RDS 11 (DeJesus et al. J. Lab. Comp. Radiopharm., 50:S339, 2007). The poor thermal and electrical properties of sulfur and its compounds, however, limited the yields. The utility of the noble gas target reactions Ne-20(d, α)F-18 (Casella et al. J. Nucl. Med., 21:750, 1980) and Kr-78(d, n α)Br-75 (DeJesus and Friedman, Int. J. Radiat. Appl. Instr., Part A, 39:709, 1988) suggested that an alternative route to Cl-34m would be via the corresponding noble gas reaction Ar-36(d, α)Cl-34m using a PETtrace cyclotron ($E_d = 8.4$ MeV). Irradiations of enriched Ar-36 gas (99.993%, 1 L at STP) with deuteron beam currents between 5 and 20 μ A for 30 minutes were done. Cryotrapping at -196°C recovered >99.5% of the expensive target gas. The average thick-target yield of radionuclidically-pure Cl-34m obtained was 1.8 ± 0.2 mCi/ μ A ($n=12$). The target gas progressively thinned beyond 10 μ A reducing effective yield suggesting that further investment in more enriched Ar-36 (nat. abundance=0.34%) gas will improve recovered yields. Chlorinated derivatives of the dopamine D1 agonist SKF 38393 (1-phenyl-2,3,4,5-tetrahydro-1H-3-benzazepine-7,8-diol) may be useful as PET imaging agents to examine the high affinity state of dopamine D1 receptors. While there are many electrophilic chlorination reactions, e.g., using chloramine-T as oxidant, preparation of [Cl-34m]-labeled SKF 38393 derivatives with high specific activities require no carrier added conditions. To achieve this goal, in situ oxidation of chloride to electrophilic chlorine species was carried out using sodium periodate as the oxidizing agent. Thus, reaction of SKF 38393 with sodium chloride and sodium periodate in aqueous sulfuric acid at room temperature produced a mixture of 2 chlorinated isomers (1-phenyl-2,3,4,5-tetrahydro-1H-3-benzazepine-6-chloro-7,8-diol and 1-phenyl-2,3,4,5-tetrahydro-1H-3-benzazepine-9-chloro-7,8-diol) in 1:1 ratio based on HPLC. Regio-selective starting materials will be prepared in order to obtain single isomer products. Reactions using other oxidation agents and temperatures are currently being investigated in order to optimize the yields and the reaction times.

Presentation Number **0866A**

Poster Session 1c: In Vivo Studies & Development/Novel Use of Imaging Probes

Improved tumor targeting of ^{64}Cu -labeled streptavidin in colorectal xenografts pretargeted with biotinylated bevacizumab

Pramila Paudyal, Bishnuhari Paudyal, Hirofumi Hanaoka, Hideyuki Tominaga, Noboru Oriuchi, Keigo Endo, Gunma University, Maebashi, Japan. Contact e-mail: pramila@med.gunma-u.ac.jp

Introduction: Pretargeting with streptavidin-biotin method has unique characteristics because of the high-affinity binding and the lower molecular weight ligands that are radiolabeled. This strategy is expected to penetrate tumors more rapidly and possibly to overcome the 'binding site barrier' that prevented the full-length antibody to make efficient penetration in the tumor. The present study aimed to evaluate the efficacy of pretargeted ^{64}Cu for imaging of tumor VEGF and compare it with the untargeted radiolabeled antibody. **Methods:** Streptavidin was conjugated with DOTA where DOTA is 1,4,7,10-tetraazacyclododecane-N,N',N'',N'''-tetraacetic acid and radiolabeled with ^{64}Cu . Bevacizumab (Avastin) was labeled with biotin. Nude mice bearing human colorectal cancer HT29 were intravenously injected with biotinylated bevacizumab. The control group were injected with PBS(-). After 24 h, the mice received an intraperitoneal injection of avidin to clear free circulating biotin. Two hours after the avidin injection, the mice received the intravenous injection of ^{64}Cu -DOTA-streptavidin. PET imaging and biodistribution was monitored at 1 h, 6 h and 24 h, 72 h post injection (p.i). The other group received the intravenous injection of ^{64}Cu -DOTA-bevacizumab. **Results:** PET images clearly showed the accumulation of ^{64}Cu -DOTA-streptavidin in the tumor area at 24 h p.i in the mice pretreated with biotinylated bevacizumab. The control group didn't show any specific uptake in the tumor. At 24 h, biodistribution studies showed that the uptake of ^{64}Cu -DOTA-streptavidin in the tumor was 10% ID/g in the pretargeted xenografts while the uptake of ^{64}Cu -DOTA-bevacizumab was 18 %ID/g. The tumor to blood ratio was significantly higher at 24 in the pretargeted group ($p=0.04$). **Conclusion:** This study demonstrates the potential utility of stepwise pretargeting with ^{64}Cu . The excellent tumor visualization in PET and biodistribution and the fast clearance from blood shows the potential clinical translation of this stepwise system for excellent imaging at early time points.

Presentation Number **0867A**

Poster Session 2c: In Vivo Studies & Development/Novel Use of Imaging Probes

Biodistribution of 18F-FP-(+)-DTBZ (AV-133) in rats - imaging studies correlate with quantitative whole body autoradiography

Ko-Ting Chao¹, **Kun-Ju Lin**^{1,2}, **Shiaw-Pyng Wey**^{1,2}, **Hsin-Hsin Tsao**², **Mei-Ping Kung**^{2,3}, **Ing-Tsung Hsiao**^{1,2}, **Daniel M. Skovronsky**⁴, **Tzu-Chen Yen**², ¹*Department of Medical Imaging and Radiological Sciences, Chang Gung University, Tao-Yuan, Taiwan;* ²*Molecular Imaging Center, Department of Nuclear Medicine, Chang Gung Memorial Hospital, Tao-Yuan, Taiwan;* ³*Department of Radiology, School of Medicine, University of Pennsylvania, Philadelphia, PA, USA;* ⁴*Avid Radiopharmaceuticals Inc., Philadelphia, PA, USA.*
Contact e-mail: tpcola26@gmail.com

Objective: 18F-FP-(+)-DTBZ (AV-133) is a novel radiotracer for vesicular monoamine transporter 2 (VMAT2) imaging. To further translate the tracer into human applications, we characterized the biodistribution and dosimetry of this tracer using animal PET. Quantitative whole body autoradiography (QWAR) was also fully examined. Method: Five male Wistar rats were used in the biodistribution study. Six-hour dynamic whole-body animal PET/CT images were acquired immediately after intravenous injection of 25.7 ± 3.09 MBq 18F-FP-(+)-DTBZ. The co-registered PET/CT images were displayed and analyzed using the PMOD image analysis workstation. Volume of interests including brain, lungs, heart, liver, stomach, pancreas, intestine, kidneys, bladder, testes, red bone marrow and whole body were manually delineated on the fused PET/CT images. The animal biodistribution data expressed as the percentage of injected dose (%ID) was extrapolated to model human organs (i.e., Standard Man) according to each organ weight. The OLINDA/EXM application was used to determine the effective doses (EDs) for individual organ. The standard uptake value ratio (SUVR) of region striatum to cerebellum were also been evaluated in another dynamic PET study. Additionally, QWAR was performed at 30 min after tracer injection in five rats. Results: The high-absorbed doses were found in the upper large intestine wall, small intestine, liver and pancreas and correlated well with QWAR results. The critical organ was the upper large intestine wall which received 58.2 ± 6.49 μ Gy/MBq. The 18F-FP-(+)-DTBZ effective dose equivalent and effective dose were 27.10 ± 3.69 μ Sv/MBq and 22.10 ± 2.41 μ Sv/MBq, respectively. These data are similar to those reported in human, which were 32.66 ± 2.97 μ Sv/MBq and 24.58 ± 2.73 μ Sv/MBq, respectively, and comparable to other 18F-labeled radiopharmaceuticals reported in the literatures. SUVR of striatum to cerebellum reached the plateau 7.53 ± 0.61 around 105 minutes after injection. Conclusion: 18F-FP-(+)-DTBZ demonstrated appropriate biodistribution and radiation dosimetry for imaging VMAT2 sites in rats. The results showed that small-animal PET presents an opportunity for providing radiation dose estimates with statistical and logistical advantages.

Presentation Number **0868A**

Poster Session 2c: In Vivo Studies & Development/Novel Use of Imaging Probes

Tissue Factor Imaging to Detect a Key-step toward Thrombus Formation

Takashi Temma¹, Yuki Ogawa¹, Yuji Kuge^{1,2}, Seigo Ishino¹, Kantaro Nishigori¹, Nozomi Takai¹, Masashi Shiomi³, Masahiro Ono¹, Hideo Saji¹, ¹Department of Patho-Functional Bioanalysis, Graduate School of Pharmaceutical Sciences, Kyoto University, Kyoto, Japan; ²Central Institute of Isotope Science, Hokkaido University, Sapporo, Japan; ³Institute for Experimental Animals, Kobe University Graduate School of Medicine, Kobe, Japan. Contact e-mail: ttemma@pharm.kyoto-u.ac.jp

Objectives: Tissue factor (TF), a transmembrane glycoprotein that acts as an essential cofactor to factor VII/VIIa, is an initiator of the exogenous blood coagulation cascade leading to thrombin generation and successive thrombus formation *in vivo*. TF expression is closely related to the plaque vulnerability and high TF expression is shown in the macrophage-rich atheromatous lesions. TF should be a potential target for detecting atheromatous lesions *in vivo*. Thus we prepared ^{99m}Tc-labeled anti-TF monoclonal IgG (mAb) as a molecular probe and evaluated the usefulness to achieve TF specific imaging using myocardial infarction-prone Watanabe heritable hyperlipidemic rabbits (WHHLMI). **Methods:** Anti-TF mAb was established by a standard hybridoma technique and was labeled by ^{99m}Tc with HYNIC as a chelating agent to obtain ^{99m}Tc-TF-mAb. The immunoreactivity of HYNIC-TF-mAb was estimated by flow cytometry method. WHHLMI and control rabbits were injected intravenously with ^{99m}Tc-TF-mAb and *in vivo* planar imaging was performed. Twenty-four hours after the injection, the aorta was removed and radioactivity was measured. Autoradiography and histological studies were performed using serial aorta sections. Subclass matched Ab (IgG₁) was used as a negative control. **Results:** HYNIC-TF-mAb showed 93% immunoreactivity of anti-TF mAb. The radioactivity accumulation in WHHLMI aortas was 6.1-fold higher than that of control rabbits. Autoradiogram showed heterogeneous distribution of radioactivity in the intima of WHHLMI aortas. Regional radioactivity accumulation was positively correlated with TF expression density (R=0.64, P<0.0001). The highest radioactivity accumulation was found in atheromatous lesions (5.2 ± 1.9, %ID x BW/mm² x 10²), followed in decreasing order by fibroatheromatous (2.1 ± 0.7), collagen-rich (1.8 ± 0.7), and neointimal lesions (1.8 ± 0.6). *In vivo* imaging clearly visualized the atherosclerotic lesions. In contrast, ^{99m}Tc-IgG₁ showed low radioactivity accumulation in WHHLMI aortas which was independent of the histologic grade of lesions. **Conclusion:** The potential of ^{99m}Tc-TF-mAb was demonstrated for detecting TF expression and selectively imaging macrophage-rich atheromatous lesions *in vivo*.

Presentation Number **0869A**

Poster Session 2c: In Vivo Studies & Development/Novel Use of Imaging Probes

A novel radiolabeled probe for molecular imaging of thymidine phosphorylase: Suppressed accumulation into tumor cells by target gene knockdown

Hua Li¹, **Songji Zhao**¹, **Yong-Nan Jin**¹, **Ken-ichi Nishijima**¹, **Hiromichi Akizawa**², **Kazue Ohkura**², **Koh-ichi Seki**³, **Nagara Tamaki**^{1,3}, **Yuji Kuge**^{1,3}, ¹Graduate School of Medicine, Hokkaido University, Sapporo, Japan; ²Faculty of Pharmaceutical Sciences, Health Science University of Hokkaido, Ishikari-gun, Japan; ³Central Institute of Isotope Science, Hokkaido University, Sapporo, Japan. Contact e-mail: ri_ka@med.hokudai.ac.jp

Objects: The expression of thymidine phosphorylase (TP) is closely associated with angiogenesis in tumors and activation of anti-tumor agents. Accordingly, a radiolabeled uracil-based TP inhibitor, 5-iodo-6-[(2-iminoimidazolidinyl)methyl]uracil (IIMU) was designed and synthesized by our group. This radioiodinated probe has a high affinity for TP, and exhibited high accumulation in a TP-expressing tumor cell line A431 (a human epidermoid carcinoma cell line). In this study, in order to evaluate specificity of the cellular uptake of IIMU to TP expression, we examined effects of TP-knockdown on the uptake of ¹²⁵I-labeled IIMU (¹²⁵I-IIMU) in the tumor cells. **Methods:** TP-specific siRNA, glyceraldehyde 3-phosphate dehydrogenase (GAPDH) -specific siRNA (positive control) and negative control siRNA were transfected into A431 cells, respectively. Forty eight hours after transfection, reduction of target-mRNA was confirmed using quantitative real time polymerase chain reaction. Seventy two hours after transfection, protein levels of TP and GAPDH were examined by western blot, and the cellular uptake of ¹²⁵I-IIMU was also evaluated two hours after incubation. The results of mRNA expression, protein expression and ¹²⁵I-IIMU uptake were compared after normalization by corresponding negative controls. **Results:** After TP- and GAPDH-specific siRNA transfection, the expression levels of TP and GAPDH mRNA were significantly decreased to 33% and 21%, respectively, compared to the negative control (P<0.001 for both). The expression levels of TP and GAPDH protein were also significantly decreased to 39% and 36%, respectively (P<0.001 for both). By TP-specific siRNA transfection, the cellular uptake of ¹²⁵I-IIMU was significantly decreased to 57% (P<0.01). In contrast, GAPDH siRNA transfection did not significantly affect the cellular uptake of ¹²⁵I-IIMU. **Conclusion:** siRNA-mediated TP-knockdown significantly reduced the cellular uptake of ¹²⁵I-IIMU. These results indicate the specific uptake of IIMU in tumor cells directly corresponding to the TP expression levels. Radioiodinated IIMU deserves further elucidation as a SPECT probe for tumor imaging.

Presentation Number **0870A**

Poster Session 2c: In Vivo Studies & Development/Novel Use of Imaging Probes

Radiosynthesis and evaluation of 11C-CYS as an oncologic PET tracer with report of one human PET study

Ganghua Tang², **Huifu Deng**^{2,1}, Hongliang Wang², Fuhua Wen², ¹Nan Fang Hospital, Guangzhou, China; ²PET-CT Center, Department of Nuclear Medicine, The First Affiliated Hospital, Sun Yat-sen University, Guangzhou, China. Contact e-mail: dengfu77@163.com

Objective: Radiosynthesis and in vivo biodistribution of [S-11C-methyl]-L-cysteine (11C-CYS) as an analogue of 11C-MET, and PET imaging in the hepatocellular carcinoma mice models were undertaken to assess the potential value as a tumor imaging agent. Results of the first human PET study were reported. Methods: 11C-CYS was prepared by one-column [¹¹C]methylation of the precursor L-cysteine with 11CH₃I. Biodistribution in normal mice and uptake studies in the hepatocellular carcinoma mice models and inflammatory mice models of 11C-CYS was determined, and compared with 11C-MET and ¹⁸F-FDG. In a human PET study, a patient with postoperative glioma recurrence was examined with 11C-CYS PET imaging and compared with ¹⁸F-FDG PET imaging. Results: The uncorrected radiochemical yield of 11C-CYS was more than 50% with the synthesis time of 2 minutes, radiochemical purity of 11C-CYS above 99%, and enantiomeric purity over 90%. There was higher accumulation of 11C-CYS, 11C-MET and ¹⁸F-FDG in tumor, but low 11C-CYS uptake in inflammatory tissue, in contrast, high 11C-MET and ¹⁸F-FDG uptake in inflammatory tissue, were observed. PET Images and biodistribution studies showed that the accumulation of 11C-CYS in the tumor was significantly higher than that of ¹⁸F-FDG. For a patient PET imaging, high uptake of 11C-CYS with true-positive result, but low uptake of ¹⁸F-FDG with false-negative result was found in postoperative brain glioma recurrence lesion. Conclusions: 11C-CYS is a potential amino acid tracer for tumors imaging, easy to prepare and superior to 11C-MET and ¹⁸F-FDG in the differentiation of tumor and inflammation. Key Words: 11CH₃I; (S-11C-methyl)-L-cysteine; Automated synthesis; Experimental tumor; Inflammation; PET imaging

Presentation Number **0871A**

Poster Session 2c: In Vivo Studies & Development/Novel Use of Imaging Probes

Synthesis and biological evaluation of novel 4-benzylpiperazine ligands for sigma-1 receptor imaging

Huiying Ren¹, Mengchao Cui¹, Winnie Deuther-Conrad², Ruikun Tang¹, Jörg Steinbach², Peter Brust², Hongmei Jia¹, Boli Liu¹, ¹Key Laboratory of Radiopharmaceuticals (Beijing Normal University), Ministry of Education, College of Chemistry, Beijing Normal University, Beijing, China; ²Neuroradiopharmaceutical Division, Forschungszentrum Dresden-Rossendorf, Institute of Radiopharmacy, Leipzig, Germany. Contact e-mail: cmc1984116@126.com

Sigma-1 (σ_1) receptors are believed to play an important role in the central nervous system. They are linked to a number of brain disorders, including schizophrenia, depression, Alzheimer's disease, as well as ischemia. Development of radiotracers for in vivo imaging of σ_1 receptors may provide much needed diagnostic tools for the above diseases. In the present study, we have synthesized five 4-benzyl-piperazine ligands (BP-CH₃, BP-F, BP-Br, BP-I, and BP-NO₂) and determined their affinity to σ_1 receptors by in vitro radioligand binding assays. Moreover, we synthesized [¹²⁵I]BP-I-(1-(benzo[d][1,3]dioxol-5-ylmethyl)-4-(4-iodobenzyl)piperazine), determined its log D value, and evaluated its potential as a putative SPECT tracer for imaging of σ_1 receptors by biodistribution studies in mice. The synthesized compounds were characterized by IR, NMR, MS, and EA. In vitro competition binding assays showed that all the five ligands exhibit low nanomolar affinity for σ_1 receptors ($K_i = 0.43 - 0.91$ nM) and high subtype selectivity (σ_2 receptor: $K_i = 40 - 61$ nM ; $K_{i\sigma_2}/K_{i\sigma_1} = 52-94$). [¹²⁵I]BP-I was prepared in $50 \pm 8\%$ isolated radiochemical yield, with radiochemical purity of $>99\%$ by HPLC analysis after purification, via iododestannylation of the corresponding tributyltin precursor. The log D value of [¹²⁵I]BP-I was found to be 2.98 ± 0.17 , which is within the range expected to give high brain uptake. In biodistribution studies in female ICR mice [¹²⁵I]BP-I was found to have high initial brain uptake with 5.03%ID/g at 15 min p.i. followed by slow clearance with 2.09 %ID/g at 240 min p.i.. The blood radioactivity levels were low with 1.34 %ID/g at 15 min and 0.72 %ID/g at 240 min p.i., resulting in high brain-to-blood ratios. Moreover, relatively high concentration of radioactivity was observed in organs known to contain σ_1 receptors, including the lung, kidney, heart, and spleen. The accumulation of radioactivity in the thyroid at 240 min p.i. (1.22 %ID/g) was quite low suggesting that [¹²⁵I]BP-I is relatively stable to in vivo deiodination. Administration of haloperidol 5 min prior to injection of [¹²⁵I]BP-I significantly reduced the concentration of radioactivity in organs known to contain σ_1 receptors such as in lung by 37%, kidney by 33%, heart by 32%, spleen by 47%, and brain by 63%. These findings suggest that the binding of [¹²⁵I]BP-I to σ_1 receptors in vivo is specific. The results warrant further evaluation of [¹²⁵I]BP-I as a putative tracer for imaging σ_1 receptors with SPECT.

Presentation Number **0872A**

Poster Session 2c: In Vivo Studies & Development/Novel Use of Imaging Probes

One-Step Automated Synthesis and Biodistribution of [¹⁸F]Bay94-9172

Hongliang Wang^{1,2}, Huaifu Deng¹, Huixian Shi³, Shende Jiang², **Ganghua Tang¹**, ¹Department of Nuclear Medicine, The First Affiliated Hospital, Sun Yat-Sen University, Guangzhou, China; ²School of Pharmaceutical Science and Technology, Tianjin University, Tianjin, China; ³School of Chemical Engineering and Technology, Tianjin University, Tianjin, China. Contact e-mail: gtang0224@yahoo.com.cn

Objectives: [¹⁸F]BAY94-9172 (Florbetaben) is currently used in the phase third clinical trials for in vivo diagnosis of Alzheimer's disease (AD). A novel one-step automated synthesis of [¹⁸F]BAY94-9172 using a new precursor with a high radiochemical yield within a short synthesis time and the biodistribution in normal mice were investigated in this study. Methods: Methanesulfonic acid 2-[2-(2-(4-[2-(4-methylamino-phenyl)-vinyl]-phenoxy)-ethoxy)-ethoxy]-ethyl ester, a new precursor of [¹⁸F]BAY94-9172, was obtained from the nucleophilic reaction of (E)-4-methylamino-4'-hydroxystilbene with methanesulfonic acid 2-[2-(2-methanesulfonyloxy-ethoxy)-ethoxy]-ethyl ester. Automated radiosynthesis of [¹⁸F]BAY94-9172 was carried out by one-step [¹⁸F] fluorination of the new precursor and HPLC purification was performed on the modified PET-MF-2V-IT-1 synthesizer built-in HPLC system made in China. Biodistribution of [¹⁸F]BAY94-9172 was studied in normal mice and PET imaging was also performed in the AD model mice. Results: The uncorrected radiochemical yields of [¹⁸F]BAY94-9172 were 19-35% (based on [¹⁸F]fluoride, n=5) within a total synthesis time of 45-50 min. The radiochemical purities of [¹⁸F]BAY94-9172 were greater than 95%. In the biodistribution study, the uptake ratio of radioactivity in the brain at 2 min and at 60 min postinjection was 5.7. The PET study in the AD model mice showed a high brain uptake and fast wash-out of this compound. Conclusions: An efficient and reliable procedure for [¹⁸F]BAY94-9172 preparation are provided in routine production. The in vivo biodistribution of [¹⁸F]BAY94-9172 in normal mice shows excellent brain uptake and washout. Research Support: This work was supported by Tianjin University, the National Natural Science Foundation (No.30970856), the National High Technology Research and Development Program of China (863 Program, No. 2008AA02Z430), and Sun Yat-Sen University (No. 80000-3126132).

Presentation Number **0873A**

Poster Session 2c: In Vivo Studies & Development/Novel Use of Imaging Probes

Imaging of Translocator Protein (18 kDa) in the Brains of Infarcted Rats Using Small-animal PET and In Vitro Autoradiography with [¹⁸F]FEAC and [¹⁸F]FEDAC

Joji Yui, Akiko Hatori, Katsushi Kumata, Kazunori Kawamura, Kazuhiko Yanamoto, Tomoteru Yamasaki, Nobuki Nengaki, Ming-Rong Zhang, National Institute of Radiological Sciences, Chiba, Japan. Contact e-mail: zhang@nirs.go.jp

Introduction: In the brain, translocator protein 18kDa (TSPO) is mainly located in glial cells, and TSPO expression was increased in microglial cells activated by brain injury or neuroinflammation. Neuropathological evidence has demonstrated that an increase in TSPO and concurrent microglial and astroglial activation accompanies the neurodegenerative process in Alzheimer's disease. In this study, we evaluated two ¹⁸F-labeled PET ligands [¹⁸F]FEAC and [¹⁸F]FEDAC by performing in vitro and in vivo imaging of TSPO in infarcted rat brains. **Methods:** Using each [¹⁸F]ligand, in vitro autoradiography and small-animal PET scan were performed on infarcted rat brains at 7 days after ischemia. Metabolite analysis and distribution was performed on normal mice. **Results and Discussion:** [¹⁸F]FEAC and [¹⁸F]FEDAC were prepared by reacting corresponding precursor with [¹⁸F]fluoroethyl bromide. At EOS, 900-1520 MBq (n = 30) of [¹⁸F]ligand was obtained with a radiochemical purity of ≥97% and specific activity of 330-450 GBq/μmol. Both [¹⁸F]ligands had a high uptake of radioactivity in the heart, lung and other TSPO-rich organs of mice. No significant accumulation of [¹⁸F]- was observed in the mouse bone. In vitro autoradiography showed that the binding of each ¹⁸F-ligand significantly increased on the ipsilateral side of rat brains compared to the contralateral side: the ratios of radioactivity between the two sides were 1.80 for [¹⁸F]FEAC and 1.73 for [¹⁸F]FEDAC, respectively. The difference in radioactivity between contralateral and ipsilateral sides was abolished by incubation with an excess of TSPO-selective AC-5216 or PK11195. In a small-animal PET study, PET summation images showed the contrast of radioactivity between ipsilateral and contralateral sides. Maximum uptakes on the two sides were about 0.87 and 0.49 SUV for [¹⁸F]FEAC, 0.91 and 0.57 SUV for [¹⁸F]FEDAC. The uptake ratios of radioactivity between ipsilateral and contralateral sides reached 3.03 for [¹⁸F]FEAC and 2.76 for [¹⁸F]FEDAC at 20 min after injection. The BPnd values were 1.70 for [¹⁸F]FEAC and 1.37 for [¹⁸F]FEDAC, respectively. Pretreatment with AC-5216 or PK11195 diminished the difference in uptake between the two sides. In the brain homogenate of mice, the percentage of the fraction corresponding to intact [¹⁸F]FEAC and [¹⁸F]FEDAC was 68% and 75% at 30 min after injection. **Conclusion:** [¹⁸F]FEAC and [¹⁸F]FEDAC showed in vitro and in vivo signals to visualize the increase in TSPO expression in infarcted rat brains.

Presentation Number **0874A**

Poster Session 2c: In Vivo Studies & Development/Novel Use of Imaging Probes

Radiosynthesis of [¹¹C]DAC with Ultra-high Specific Activity and Imaging of the Translocator Protein in the Infarcted Rat Brain after Ischemia

Katsushi Kumata¹, Joji Yui¹, Akiko Hatori¹, Kazuhiko Yanamoto¹, Makoto Takei^{1,2}, Nobuki Nengaki^{1,3}, Kazunori Kawamura¹, Tomoteru Yamasaki¹, Kazutoshi Suzuki¹, **Ming-Rong Zhang**¹, ¹National Institute of Radiological Sciences, Chiba, Japan; ²Tokyo Nuclear service, Ltd., , Tokyo, Japan; ³SHI Accelerator Services, Ltd., , Tokyo, Japan. Contact e-mail: zhang@nirs.go.jp

Introduction: Many studies have elucidated the relationship between translocator protein 18kDa (TSPO) and neurodegenerative diseases, such as Alzheimer's disease and stroke-induced brain injury. The aim of this study was to synthesize N-benzyl-N-methyl-2-(7-¹¹C-methyl-8-oxo-2-phenyl-7,8-dihydro-9H-purin-9-yl)acetamide ([¹¹C]DAC) with ultra-high specific activity (SA) and to characterize in vitro and in vivo specific binding to TSPO in infarcted rat brain after ischemia. Using [¹¹C]DAC of high SA (average 3530 GBq/μmol), we expected to acquire higher uptake ratios between the ipsilateral and contralateral sides and higher binding potential for TSPO from autoradiographic and PET images of infarct brains than using [¹¹C]DAC of conventional SA (37 GBq/μmol). Methods: [¹¹C]DAC was prepared by [¹¹C]methylation of desmethyl precursor with [¹¹C]DAC that was produced by iodination of [¹¹C]CH₄ (single pass I2 method). Imaging of TSPO was performed on infarcted rat brains at 7 days after ischemic surgery using in vitro autoradiography and small-animal PET. Results and discussion: [¹¹C]DAC with 3530±1590 GBq/μmol SA and >98% radiochemical purity (EOS, n=40) was prepared in an average synthesis time of 25 min from EOB. At EOS, [¹¹C]DAC of 730-1540 MBq was obtained as an injectable solution starting from [¹¹C]CH₄ of 44 GBq by 30 min proton (14.2 MeV on target) bombardment at a beam current of 20 μA. The final formulated solution was radiochemically pure (≥98%) as detected by analytic HPLC. In vitro autoradiography showed that the binding of high SA [¹¹C]DAC was increased 2.7-fold in the ipsilateral striatum compared to the contralateral side. PET imaging with high SA [¹¹C]DAC showed a high uptake ratio between the ipsilateral and contralateral striatum. The binding potential (BP_{nd}) calculated by the simplified reference-tissue model was 3.1 for high SA, 1.7 for conventional [¹¹C]DAC, respectively. In displacement experiments, the uptake of [¹¹C]DAC in the brain was significantly inhibited by unlabeled TSPO-selective AC-5216 or PK11195. Conclusion: High SA [¹¹C]DAC provided in vitro autoradiographic images with higher uptake and PET images with higher binding potential for the infarction than conventional SA. Specific binding with TSPO is a potent biomarker for brain injury and neuroinflammation. High SA is a powerful tool to characterize receptors in the brain precisely.

Presentation Number **0875A**

Poster Session 2c: In Vivo Studies & Development/Novel Use of Imaging Probes

Molecular Imaging of the Endothelin-A-Receptor Expression in Murine Thyroid Cancer Xenografts using Small Animal PET and Optical Imaging

Katrin Büther¹, Carsten Hoeltke^{1,2}, Kristin Michel¹, Klaus Kopka¹, Otmar Schober¹, Michael Schafers^{1,3}, Burkhard Riemann¹,
¹Department of Nuclear Medicine, University Hospital Münster, Münster, Germany; ²Department of Clinical Radiology, University Hospital Münster, Münster, Germany; ³European Institute for Molecular Imaging EIMI, University Münster, Münster, Germany. Contact e-mail: butherk@uni-muenster.de

Introduction Endothelin (ET) receptor dysregulation has been described in a number of pathophysiological processes, including cancer. A number of human cancer cell lines exhibit an upregulated density of ET-A receptors, influencing tumor growth and aggressiveness. In thyroid cancer, elevated expression of the ET axis is reported for papillary and follicular tumors. Radiolabelled ET receptor antagonists offer the possibility to noninvasively assess ET receptor distribution in vivo by PET. In addition, optical imaging is gaining increasing importance as a powerful technology for the preclinical study of diseases at the molecular level. Therefore, these diagnostic tools are invaluable for the evaluation of disease progression and therapy response. In this study, a radiofluorinated and a fluorescent biomarker, targeted to the ET-A receptor, were used for the evaluation of target expression in thyroid carcinoma xenografts using small animal PET and optical imaging techniques. **Methods** Subcutaneous xenograft models of papillary thyroid carcinoma cells were established in CD-1 nude mice. Western blot and RT-PCR analysis were used to evaluate ET-A receptor expression of the tumor. A radiofluorinated analogue of the known ET-A receptor ligand PD 156707 was designed and applied in small animal PET experiments. Xenografts were evaluated using [¹⁸F]-FDG prior to ET-A receptor imaging. In addition, a fluorescently labelled analogue of PD 156707 was designed and used for optical imaging techniques such as fluorescence reflectance imaging (FRI). **Results** Using western blot and RT-PCR the expression of the ET-A receptor on human papillary thyroid carcinoma was confirmed. Small animal PET experiments showed accumulation of the ET A receptor targeted radiotracer in the tumor after 30-60 min. In optical imaging experiments using FRI, a high fluorescence signal was visible in the tumor. After residual tracer washout via the kidneys and bladder (24-48 hrs) a tumor to muscle ratio of > 5:1 could be observed. Biodistribution studies after 24-48 hrs showed that 30% of total fluorescence was located in the lesion and about 10% in each kidney, the lung and the liver. **Conclusion** Subcutaneous papillary thyroid carcinoma xenografts are a feasible model for the detection of endothelin receptor expression as a benchmark of tumor angiogenesis. Scintigraphic or optical imaging techniques like PET or FRI, respectively, in combination with radioisotope- or fluorescently labelled endothelin receptor ligands can be useful tools for the evaluation of target expression in tumoral lesions.

Presentation Number **0876A**

Poster Session 2c: In Vivo Studies & Development/Novel Use of Imaging Probes

CGMP Synthesis of [¹⁸F]- and [¹¹C]-Labeled Radiopharmaceuticals by Multiple Radiochemical Strategies using Automated Synthesis Modules

Peter J. Scott, Brian G. Hockley, Xia Shao, Radiology, University of Michigan, Ann Arbor, MI, USA. Contact e-mail: pjhscott@umich.edu

After 2011, preparation of clinical doses of radiopharmaceuticals in the United States must be done in accordance with the cGMP regulations recently approved by U.S. FDA. Such preparation is increasingly achieved using automated synthesis modules and presents the challenge of re-configuring synthesis modules for production of radiopharmaceuticals that require non-conventional radiochemistry whilst maintaining full automation and compliance with cGMP regulations. Herein we present simple, fully automated methods for producing a range of carbon-11 and fluorine-18 labeled radiopharmaceuticals by diverse radiochemical techniques using modified General Electric (GE) Tracerlab synthesis modules. Methods : Radioisotopes were prepared using a GE PETTrace cyclotron. Fluoride-18 was produced via the ¹⁸O(p,n)¹⁸F nuclear reaction and carbon-11 was produced via the ¹⁴N(p,α)¹¹C reaction. Fully automated production of [¹⁸F]- and [¹¹C]-labeled radiopharmaceuticals was carried out using Tracerlab FXfn and Tracerlab FXc-pro synthesis modules respectively. Quality control of radiopharmaceuticals was carried out in accordance with the U.S. Pharmacopeia. Results : Simple modifications to GE Tracerlab synthesis modules will be reported that enable production of radiopharmaceuticals using multiple different radiosynthetic strategies. Proof-of-concept will be demonstrated through fully GMP compliant methods for automated production and QC of a range of radiopharmaceuticals including [¹¹C]PIB, [¹¹C] acetate, [¹¹C]choline, [¹⁸F]FLT, [¹⁸F]MPPF and [¹⁸F]sodium fluoride using the modified synthesis modules (see Table). All syntheses have been conducted >10 times to validate the results to be reported. [Table] Conclusions : The Tracerlab family of synthesis modules have proven very efficient in our hands. The results presented demonstrate that through simple modifications, high yielding GMP production of radiopharmaceuticals is possible using a sophisticated array of radiochemical reactions. Research Support : Financial support of this work by the National Institutes of Health and the U.S. Department of Energy, Office of Science is gratefully acknowledged.

Synthesis Data

Radiopharmaceutical	[¹⁸ F]FLT	[¹⁸ F]MPPF	[¹⁸ F]NaF	[¹¹ C]PIB	[¹¹ C]choline
n	>25	>25	>10	>30	>10
Decay-corrected Yield	>10%	>12%	>95%	>3%	>60%

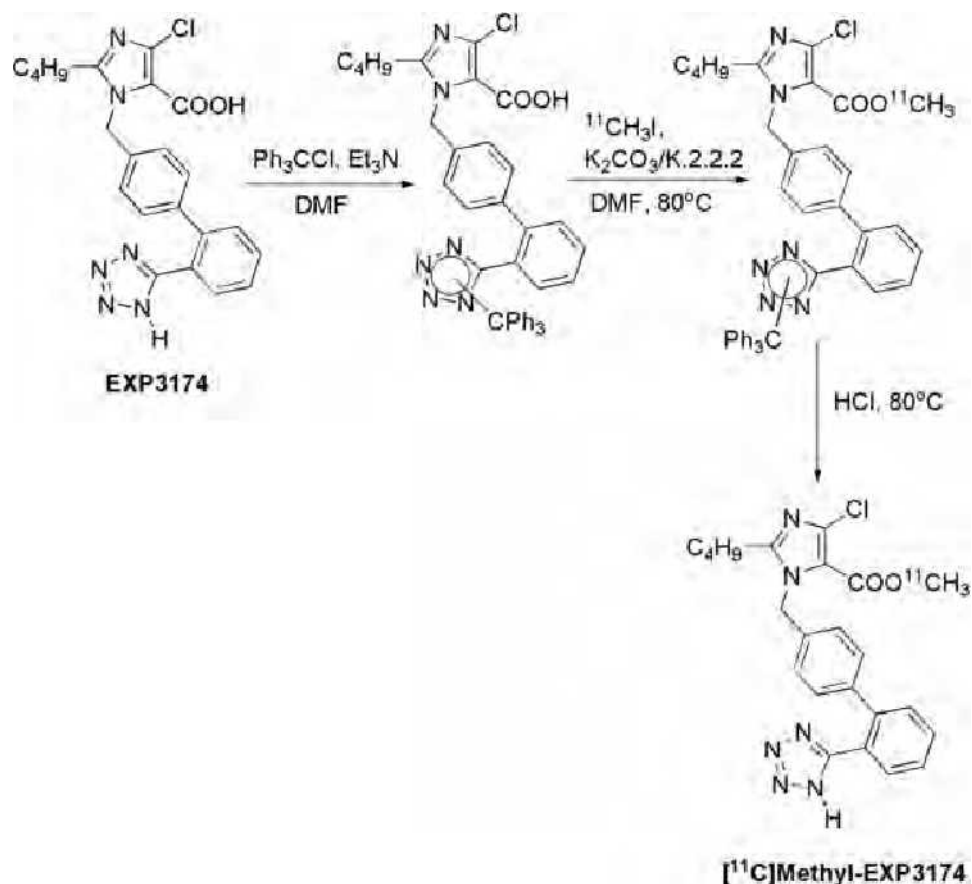
Presentation Number **0877A**

Poster Session 2c: In Vivo Studies & Development/Novel Use of Imaging Probes

Radiosynthesis of [¹¹C]Methyl-EXP3174, a Potential Imaging Agent for Angiotensin AT₁ Receptors

Tayebeh Hadizad, Jeffrey A. Collins, Rob S. Beanlands, Jean N. DaSilva, Cardiac PET Centre, University of Ottawa Heart Institute, Ottawa, ON, Canada. Contact e-mail: thadizad@ottawaheart.ca

Introduction: Angiotensin II (Ang II), a main vasoconstrictor hormone of renin-angiotensin-aldosterone system plays an important role in the pathophysiology of many chronic diseases such as heart failure, atherosclerosis as well as kidney diseases. It can induce physiological functions such as contraction of blood vessel and elevation of blood pressure following stimulation of the Ang II AT₁ receptors. EXP3174, the active metabolite of losartan, was shown to bind with higher affinity and antagonistic activity than the parent compound for AT₁ receptors. Based on previous structure-activity studies and blood pressure measurements in rats, esterification of EXP3174 with [¹¹C]methyl group is expected to maintain the blocking activity for AT₁ receptors, and enhance the lipophilicity (increasing cell membrane penetration) compared to the losartan. We present here the radiosyntheses of the O-[¹¹C]methyl-ester derivative of EXP3174. **Methods:** The [¹¹C]methyl-ester derivative of EXP3174 was synthesized following the route recently published (Hadizad et al, *Bioorg Med Chem*, 2009, 17, 7971) in 3 steps: 1) protection of the tetrazole group with trityl chloride; 2) O-[¹¹C]methylation with [¹¹C]MeI (from [¹¹C]methane and I₂) in the presence of K₂CO₃ and kryptofix (80 °C, 3 min); 3) removal of the protecting group by HCl hydrolysis (80 °C, 2 min) (Scheme 1). [¹¹C]Me-EXP3174 was purified by semi-preparative HPLC (Luna C₁₈, 10μ, 250×10 mm, CH₃CN/0.1M AF solution: 40/60, 7 mL/min) and confirmed by analytical HPLC compared to standard. ¹H and ¹³C NMR, and mass spectrometry were used to identify the structure of the unlabeled standard. **Results:** [¹¹C]Me-EXP3174 was produced in 50-70% radiochemical yield (decay-corrected, based on [¹¹C]MeI), high radiochemical purity (>99%), specific activities of 850-2500 mCi/μmol at EOS, and a synthesis time of 35 min (including QC). **Conclusions:** [¹¹C]Me-EXP3174 is synthesized as a nonpeptide Ang II antagonist and a novel agent with high potential for imaging AT₁ receptors. **Scheme1.** Radiosyntheses of [¹¹C]Me-EXP3174



Presentation Number **0878A**

Poster Session 2c: In Vivo Studies & Development/Novel Use of Imaging Probes

Good reproducibility with the integrin tracer ^{18}F -FP-PRGD₂ in human xenografts

Edwin Chang¹, **Shuanglong Liu**¹, **Gayatri Gowrishankar**¹, **Shahriar Yaghoubi**¹, **Patrick J. Wedgeworth**³, **Frederick T. Chin**¹, **Dietmar Berndorff**², **Volker Gekeler**², **Sanjiv S. Gambhir**¹, **Zhen Cheng**¹, ¹Radiology, MIPS, Stanford University, Palo Alto, CA, USA; ²Global Drug Discovery, Bayer-Schering Pharma AG, Berlin, Germany; ³Radiology, Stanford, Lucas Center, Stanford, CA, USA. Contact e-mail: echangcv@stanford.edu

Serial positron emission tomography (PET) studies may monitor anti-angiogenic therapy response or drug screening; however, the reproducibility of serial scans has not been determined for this PET probe. In our study we study the reproducibility of the integrin $\alpha_v\beta_3$ -targeted PET probe, ^{18}F -FP-PRGD₂, using small animal PET (Figure 1A). Human HCT116 colon cancer xenografts were implanted into nude mice (n = 12) growing to mean diameters of 5-15 mm. A small animal PET scan was done 1 h after tail vein injection of ^{18}F -FP-PRGD₂ (1.9 - 3.8 MBq, 50 - 100 μCi). A second scan was performed 6 h later after re-injection of the probe to assess for reproducibility. Images were analyzed by drawing ellipsoidal regions of interest (ROI) around tumor xenograft activity. Percentage injected dose per gram (%ID/g) values were calculated from the mean or maximum activity in the ROIs. Coefficients of variation and differences in %ID/g values between studies from the same day were also calculated. Coefficient of variation (mean \pm SD) for %IDmean/g- and %IDmax/g-values between ^{18}F -FP-PRGD₂ small animal PET scans performed 6 h apart on the same day were 11.1 \pm 7.6% and 10.4 \pm 9.3% respectively (Figure 1B). First and second scans correlated with one another (R²=0.45, P<0.005 for %IDmean/g; R²=0.68, P<0.001 for %IDmax/g). Corresponding differences in %IDmean/g and %IDmax/g between scans were -0.025 \pm 0.067 and -0.039 \pm 0.426. Immunofluorescence studies revealed a direct relationship between $\alpha_v\beta_3$ integrin expression with tracer uptake. Mouse body weight, injected dose, and fasting state did not contribute to the variability; however, consistent scanning parameters were necessary to ensure accurate studies, in particular, noting tumor volume, and controlling time of imaging after injection plus ROI size. In conclusion, ^{18}F -FP-PRGD₂ small animal PET mouse tumor xenograft studies are reproducible with relatively low variability.

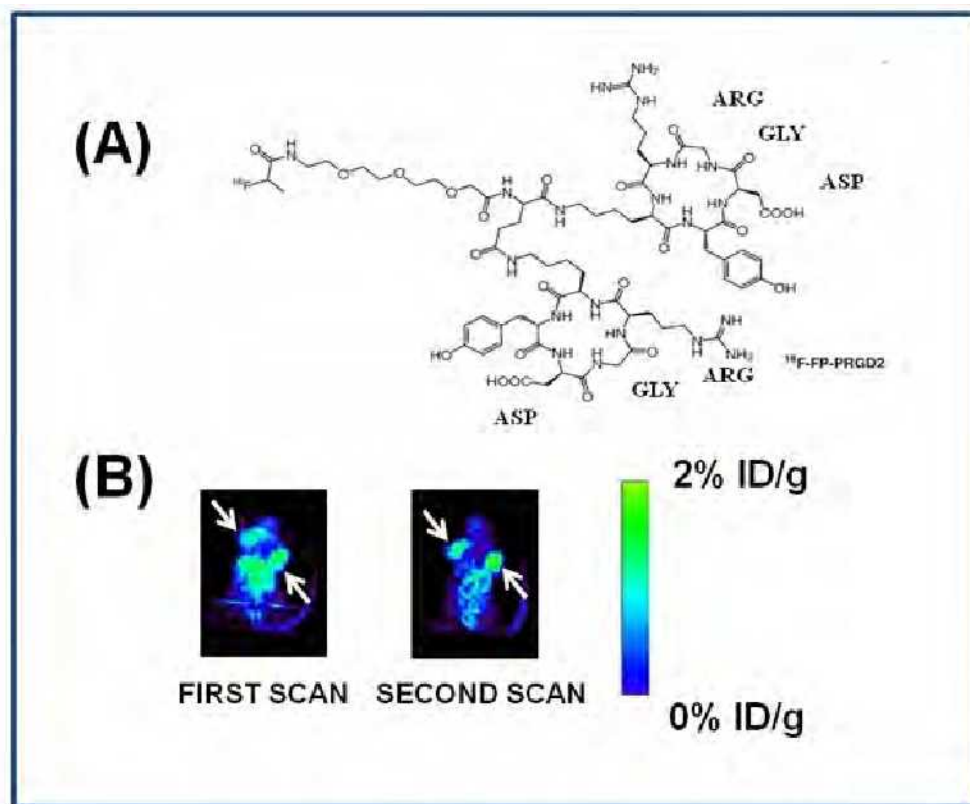


Figure 1: (A) Chemical Structure of ^{18}F -FP-PRGD₂ (B) Representative, 3-dimensional small animal PET images of first and second scan.

Presentation Number **0879A**

Poster Session 2c: In Vivo Studies & Development/Novel Use of Imaging Probes

[¹⁸F]FPTQ: a promising PET Probe for the imaging of mGluR1 in the rodent brain

Masayuki Fujinaga¹, Tomoteru Yamasaki¹, Katsushi Kumata¹, Kazuhiko Yanamoto¹, Joji Yui¹, Kazunori Kawamura¹, Masanao Ogawa^{1,2}, Yuichiro Yoshida^{1,2}, Nobuki Nengaki^{1,2}, Akiko Hatori¹, Toshimitsu Fukumura¹, Ming-Rong Zhang¹, ¹Molecular Imaging Center, National Institute of Radiological Sciences, Chiba, Japan; ²SHI Accelerator Services, Ltd., Tokyo, Japan. Contact e-mail: fujinaga@nirs.go.jp

Introduction: mGluR1 is mainly a postsynaptic receptor and may be related to diseases such as stroke, epilepsy, pain, cerebellar ataxia, Parkinson's disease, anxiety, and mood disorders. The pharmacological role of mGluR1 in the brain has not been fully elucidated. Furthermore, the precise physiological significance of events mediated through mGluR1 in the brain and the therapeutic potential of mGluR1 ligands in the pathology and/or etiology of central nervous system diseases need to be elucidated clearly. We have recently labeled a mGluR1 antagonist YM-202074 with ¹¹C and evaluated the potential of [¹¹C]YM-202074 as a PET ligand for mGluR1 (Yanamoto et al. Nucl. Med. Biol. 2010, In press). In this study, to overcome the disadvantage of [¹¹C]YM-202074, we describe [¹⁸F]FPTQ as a novel PET ligand for the imaging of mGluR1 in the rat brain. Methods: [¹⁸F]FPTQ was synthesized by [¹⁸F]fluorination of bromo precursor with potassium [¹⁸F]fluoride. [¹⁸F]FPTQ was evaluated using in vitro autoradiography and small-animal PET for the rat brain. Results and discussion: [¹⁸F]FPTQ was synthesized with reliable radioactivity, radiochemical purity and stability, and specific activity for animal experiments. In vitro autoradiographic results showed that the distribution pattern of [¹⁸F]FPTQ in brain regions was consistent with the distribution of mGluR1 reported previously. Moreover, in PET study on rat brains, [¹⁸F]FPTQ had a high uptake on the cerebellum, followed by the thalamus, hippocampus, striatum, and cerebral cortex. No observatory radioactivity was found on the medulla, a region with low density of mGluR1. The in vivo uptake of [¹⁸F]FPTQ in the brain was significantly inhibited by mGluR1-selective ligands. Metabolite analysis showed that the percentage of unchanged [¹⁸F]FPTQ was 91% and 72% in the cerebellum and brain except cerebellum at 15 min after injection. Conclusions: [¹⁸F]FPTQ exhibited high in vitro and in vivo specific binding with mGluR1 in the brain regions such as cerebellum and thalamus. Although [¹⁸F]FPTQ was rapidly metabolized in the plasma, main radioactive fraction in the rat brain represented as unchanged [¹⁸F]FPTQ. The biological data indicated that [¹⁸F]FPTQ is a useful PET ligand for the imaging of mGluR1 in brain.

Presentation Number **0880A**

Poster Session 2c: In Vivo Studies & Development/Novel Use of Imaging Probes

Development of novel radioiodine-labeled nanocarrier "Lactosome" and initial evaluation as a tumor imaging probe

Fumihiko Yamamoto^{1,3}, Ryo Yamahara², Kensuke Kurihara³, Eri Takeuchi², Isao Hara², Akira Makino^{2,5}, Shinae Kizaka-Kondoh⁴, Akira Shimizu³, Eiichi Ozeki², Shunsaku Kimura^{3,5}, ¹Radiopharmacy, Tohoku Pharmaceutical University, Sendai, Japan; ²Technology Research Laboratory, Shimadzu Corporation, Kyoto, Japan; ³Translational Research Center, Kyoto University Hospital, Kyoto University, Kyoto, Japan; ⁴Biomolecular Engineering, Graduate School of Bioscience and Biotechnology, Tokyo Institute of Technology, Yokohama, Japan; ⁵Material Chemistry, Graduate School of Engineering, Kyoto University, Kyoto, Japan. Contact e-mail: fyamamot@tohoku-pharm.ac.jp

Objectives: We have developed amphiphilic polydepsipeptide micelle "Lactosome" as a novel nanocarrier with tumor accumulation property by the enhanced permeability and retention effect for cancer imaging probes and anti-cancer reagents. We previously reported that mouse tumors were efficiently detected by ICG labeled lactosome using near infrared fluorescent imaging. In addition, we reported a successful *in vivo* imaging of mouse tumors by ¹⁸F labeled lactosome with small animal PET. In this study, for both *in vivo* imaging by SPECT and internal radiation therapy, a radioiodine-labeled lactosome was synthesized and evaluated. **Methods:** As a containable molecule into the lactosome, ¹³¹I labeled poly-L-lactic acid (¹³¹I-BzPLLA) was synthesized in 6-12 % radiochemical yields by coupling reaction of ¹³¹I-SIB connected at an amino group terminal of poly-L-lactic acid. Micelle assemblies were prepared from a mixture of ¹³¹I-BzPLLA and the amphiphilic block polymer by a film method. More than 96 % of ¹³¹I-BzPLLA radioactivity was composed stably into the lactosome micelle. For biodistribution studies of ¹³¹I-lactosome, we prepared subcutaneous tumor (SUIT2) and various tumor orthotopic graft model mice; brain tumor (U87), lung cancer (H441), pancreas cancer (SUIT2), colorectal cancer (colon26), and liver tumor (HepG2). **Results and Discussions:** ¹³¹I-Lactosome was prepared in good yields (10-31 MBq) enough to biodistribution studies. The radioactivity of ¹³¹I-lactosome was found to be stable in a blood circulation and maintained to higher level during 2 hrs to 48 hrs after injection. Tumor uptake increased gradually after injection. The uptake ratio of subcutaneous tumor/muscle increased from 4.1 at 2 hrs to 13.2 at 48 hrs after injection. The uptake ratio of tumor/brain was 5.9 at 6 hrs after injection. Although the lung cancer/lung ratio was low, it gradually increased from 0.5 at 2hrs to 1.0 at 48 hrs. The tumor/pancreas ratio was increased from 1.3 at 2 hrs to 2.3 at 48 hrs. The relative uptake ratio of colorectal tumor to the large intestine was high (16 at 6hrs). The tumor/liver ratio was low (0.9-1.2 at 24 hrs). These results indicate that SPECT imaging of subcutaneous tumors, brain tumors, pancreas tumors and colorectal cancers are expected to be successfully obtained by the radioiodine-labeled lactosome. We plan SPECT imaging by ¹²³I labeled lactosome.

Presentation Number **0881A**

Poster Session 2c: In Vivo Studies & Development/Novel Use of Imaging Probes

Developmental Changes in P-glycoprotein Function at the Blood-Brain Barrier of Non-Human Primates: PET Study with R -[^{11}C]Verapamil

Tadayuki Takashima¹, Chihiro Yokoyama¹, Hiroshi Mizuma¹, Hajime Yamanaka¹, Yumiko Katayama¹, Yasuhiro Wada¹, Emi Hayashinaka¹, Kayo Onoe¹, Hisashi Doi¹, Hiroyuki Kusahara², Yuichi Sugiyama², Hirotaka Onoe¹, Yasuyoshi Watanabe¹, ¹Molecular Probe Dynamics Laboratory, RIKEN, Center for Molecular Imaging Science, Kobe, Hyogo, Japan; ²Department of Molecular Pharmacokinetics, Graduate School of Pharmaceutical Sciences, the University of Tokyo, Tokyo, Japan. Contact e-mail: ttakashima@riken.jp

[Purpose] Numerous studies indicate that P-glycoprotein (P-gp) plays a pivotal role in limiting the penetration of xenobiotic compounds into the brain at the blood-brain barrier (BBB). Transporter expression changes during the maturation of tissues lead to altered pharmacokinetics of drugs. In this study, we investigated changes in P-gp function at the BBB of non-human primates during development using positron emission tomography (PET) with R -[^{11}C]verapamil, a PET radiotracer useful for evaluating P-gp function. [Methods] PET studies of infant (9 months, n=5), adolescent (24-27 months, n=5), and adult (5 years, n=5) rhesus monkeys (*Macaca mulatta*) were carried out with R -[^{11}C]verapamil. PET images were obtained with arterial blood sampling at frequent intervals up to 60 min following intravenous bolus administration of R -[^{11}C]verapamil. The radiometabolite analysis of R -[^{11}C]verapamil in the blood was performed by HPLC with a coupled NaI(Tl) detector. R -[^{11}C]verapamil penetration mediated by P-gp at the BBB was evaluated by integration plot analysis using dynamic imaging data within the first 2.5 min following administration. [Results and discussion] After the administration of R -[^{11}C]verapamil to the monkeys, the radioactivity highly penetrated into the brain, whereas the blood concentration of intact R -[^{11}C]verapamil decreased rapidly at all stages of development and in adults. The maximum brain uptake value in infants and adolescents was 4.0- and 2.6-fold greater than that in adults, respectively. In addition, the clearance of brain R -[^{11}C]verapamil uptake ($CL_{\text{uptake, brain}}$) in infants and adolescents was significantly greater than in adults. These results revealed developmental changes in P-gp function at the BBB in rhesus monkeys, which may explain some differential response to drug in the brain between younger age and adult.

Presentation Number **0882A**

Poster Session 2c: In Vivo Studies & Development/Novel Use of Imaging Probes

18F-5-fluorouracil Dynamic PET/CT Reveals Decreased Tracer Uptake After Bevacizumab in Colorectal Metastasis

Maurice H. Zissen¹, Pamela L. Kunz², George Fisher², **Andrew Quon¹**, ¹Radiology - Nuclear Medicine, Stanford University School of Medicine, Stanford, CA, USA; ²Medicine, Division of Medical Oncology, Stanford University School of Medicine, Stanford, CA, USA. Contact e-mail: aquon@stanford.edu

In patients with advanced colorectal cancer, chemotherapy regimens incorporating 5-fluorouracil with adjuvant bevacizumab have been established as first-line therapy, however, the physiologic effect of decreasing VEGF-A available to regional vasculature remains uncertain. The aim of this study was to evaluate the potential for 18F-5-fluorouracil (18F-5FU) PET/CT to reveal differences in 5FU uptake in metastatic colorectal cancer before and after treatment with bevacizumab. This was a pilot study of five consecutive patients (4 female, 1 male; mean age, 54.6 years; range, 27-85 years) with newly diagnosed and untreated metastatic colorectal adenocarcinoma. The presence of cancer was confirmed by histopathological analysis and patients served as their own internal control. Each patient underwent baseline 18F-5FU PET/CT scanning prior to treatment with bevacizumab, then received a 90-minute infusion of bevacizumab at a dose of 7.5 mg/kg (mean dose, 437.4 mg; range, 350-518 mg). Approximately 24 hours post-bevacizumab, patients underwent a second 18F-5FU PET/CT. Using CT as an anatomical reference, manually drawn regions-of-interest (ROIs) were drawn around the aorta and all colorectal metastases and time-activity-curves (TAC) were generated at each tumor site. Differences between pre- and post-bevacizumab SUVmax and 5-minute Area Under the Curve ratios (AUC_{tumor}/AUC_{aorta}) were calculated for each lesion as the primary outcome measures. The sizes of the metastatic lesions ranged from the smallest lesion measuring 3.04cm x 1.50cm to the largest measuring 4.19cm x 2.76cm. At baseline, the average SUVmax for 18F-5FU uptake at the metastatic sites 5-minutes after tracer infusion was 3.9 ± 1.4 (range, 0.98 to 8.06) and was not significantly different in patients 24-hours after the administration of bevacizumab, 3.1 ± 1.13 (range, 0.45 to 6.6, $p = 0.125$). In each of the 5 subjects, the 5-minute AUC_{tumor}/AUC_{aorta} ratio decreased 24 hours after treatment. At baseline, the mean AUC_{tumor}/AUC_{aorta} was 1.24 ± 0.30 (range, 0.424 to 2.14) and was significantly lower in patients 24-hours after the administration of bevacizumab, 1.06 ± 0.32 (range, 0.23 to 2.13, $p = 0.04$). This represents an average decline in the AUC_{tumor}/AUC_{aorta} of 20.2%. In this pilot study of five patients with metastatic colorectal cancer, 18F-5FU PET/CT scanning revealed a significant decrease in tumor uptake 24-hours post-bevacizumab. The ability of 18F-5FU PET/CT to demonstrate differential chemotherapy delivery may allow for improved therapy monitoring in patients with advanced colorectal cancer.

Presentation Number **0883A**

Poster Session 2c: In Vivo Studies & Development/Novel Use of Imaging Probes

Development of A Multipurpose Automatic Synthesizer System for Reliable Production of PET Probes

Kazuhiro Takahashi, Shusaku Tazawa, Akiko Tachibana, Riyo Zochi, Yoko Morimoto, CMIS, RIKEN, Kobe, Japan. Contact e-mail: kazu.takahashi@riken.jp

We have developed a multipurpose automatic synthesizer system which has some sterile disposable kits, an exchangeable valve for quantitative HPLC system and an exchangeable evaporator unit for removing organic solvents. The principle design goal is to avoid cross contaminations between each production, to avoid instability based on conditioning after washing equipment and to achieve several kind of labeling reactions, and to provide many saline based injectables which meet regulatory purity requirements. In addition, the system has flexible programming system which is ideal for the routine production of PET probes. This system makes it possible to produce some useful labeling precursors such as [^{11}C]methyl iodide, [^{11}C]methyl triflate, and [^{11}C]acetyl chloride. [^{11}C]methyl iodide is prepared with [^{11}C]CO₂, LAH and HI. [^{11}C]methyl triflate is prepared from [^{11}C]methyl iodide by passing through Ag triflate column. [^{11}C]acetyl chloride is prepared with [^{11}C]CO₂ release from a molecular sieves column into Grignard reagent in diethyl ether. So we can produce [^{11}C]methionine from [^{11}C]methyl iodide, [^{11}C]raclopride from [^{11}C]methyl triflate, [^{18}F]FLT from [^{18}F] fluoride, [^{18}F]FDOPA from [^{18}F] F₂. The reaction mixture is purified with HPLC, and the fraction of the product is collected and transferred into evaporator to remove organic solvents. Each final product is passed through a sterile 0.22 μm filter. The radiochemical yields of some probes are as follows, [^{11}C]acetate in 70-80 %, [^{11}C]methionine in 60-70 %, [^{11}C]raclopride in 30-40 %, [^{18}F]FLT in 10-20 %. The radiochemical purity of each probe is above 95 %. The specific activities at EOS are achieved to 40-100 GBq/ μmol in ^{11}C and 400-1200 GBq/ μmol in ^{18}F , respectively. The production, purification and formulation procedures result in high yield, high purity products with this system constantly. It is expected that this multipurpose system easily meets requirements of GMP for investigational products.

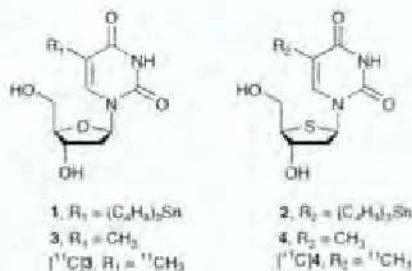
Presentation Number **0884A**

Poster Session 2c: In Vivo Studies & Development/Novel Use of Imaging Probes

Highly Efficient, Practical Syntheses of [Methyl-¹¹C]Thymidine and its Stable Analogue 4'-[Methyl-¹¹C]Thiothymidine by Pd⁰-Mediated Rapid C-[¹¹C]Methylations

Hiroko Koyama¹, **Qin Si**², **Zhouen Zhang**², **Kengo Sumi**¹, **Yuma Hatta**¹, **Hiroko Nagata**², **Hisashi Doi**², **Masaaki Suzuki**², ¹Graduate School of Medicine, Gifu University, Gifu, Japan; ²Center for Molecular Imaging Science, RIKEN, Kobe, Japan. Contact e-mail: hirokok@gifu-u.ac.jp

¹¹C- and ¹⁸F-labelled thymidine and its derivatives have a great potential for the imaging tumor cell proliferation in living systems using Positron Emission Tomography. We investigated Pd⁰-mediated rapid couplings of methyl iodide with excess 5-tributylstannyl-2'-deoxyuridine (**1**) and 5-tributylstannyl-4'-thio-2'-deoxyuridine (**2**) for the syntheses of [methyl-¹¹C]thymidine ([¹¹C]**3**) and its stable analogue, 4'-[methyl-¹¹C]thiothymidine ([¹¹C]**4**), respectively. The previously reported conditions were first attempted using CH₃I/**1**/[Pd₂(dba)₃]/P(o-CH₃C₆H₄)₃ (1:25:0.5:2 in molar ratio) in DMF at 130 °C for 5 min, giving **3** and **4** only in 32 and 30% poor yields, respectively (based on the consumption of methyl iodide). We then intended to adapt the current reaction conditions developed in our laboratory. Consequently, the combination of CH₃I/**1**/[Pd₂(dba)₃]/P(o-CH₃C₆H₄)₃/CuCl/K₂CO₃ (1:25:1:32:2:5 in molar ratio) including the CuCl/K₂CO₃ synergic system at 80 °C for 5 min in DMF gave **3** in 85% yield. Whereas, the reaction under combination of CH₃I/**1**/[Pd₂(dba)₃]/P(o-CH₃C₆H₄)₃/CuBr/CsF (1:25:1:32:2:5 in molar ratio) including another CuBr/CsF synergic system proceeded at a milder temperature (60 °C) for 5 min to give **3** in quantitative yield!. The chemo-response of **2** under the reaction conditions was considerably different from the above thymidine system. Thus, the optimized conditions obtained in thymidine system including the CuBr/CsF synergic system gave **4** in 85% yield, but unexpectedly the reaction was accompanied by a considerable amount of undesired destannylated product. Such destannylation was greatly suppressed by using CH₃I/**2**/[Pd₂(dba)₃]/P(o-CH₃C₆H₄)₃/CuCl/K₂CO₃ (1:25:1:32:2:5 in molar ratio) combination at 80 °C for 5 min to give **4** in 98% yields. The resulting optimized conditions for the reactions of **1** and **2** were successfully applied to the radio labeling to give [¹¹C]**3** and [¹¹C]**4** in 83-95 and 86-93% high yields, respectively (HPLC analytical yields). These radio-labeled compounds were readily isolated by preparative HPLC.



Presentation Number **0885A**

Poster Session 2c: In Vivo Studies & Development/Novel Use of Imaging Probes

EGFR-Binding Radioimmunoconstructs for SPECT Imaging and Molecular Radiotherapy of DNA Double Strand Breaks

Bart Cornelissen, Andrew Waller, Veerle Kersemans, Sean Smart, Katherine A. Vallis, Gray institute for radiation oncology and biology, University of Oxford, Oxford, United Kingdom. Contact e-mail: bart.cornelissen@rob.ox.ac.uk

Background: Many anticancer treatments cause DNA damage. A robust method for imaging DNA damage in vivo in real-time would allow response monitoring following treatment with genotoxic agents. Our goal is to develop tumour-specific, antibody-based radiopharmaceuticals that target the DNA repair protein, γ H2AX, which accumulates at sites of DNA double-strand breaks. In this study the cell penetrating peptide, Tat, and EGF were incorporated into drug design to enhance internalisation and tumour-specific targeting. ^{111}In was used for its possibilities as a SPECT imaging agent as well as an Auger electron emitter for radioimmunotherapy. Methods: Anti- γ H2AX was conjugated to p-SCN-benzyl-DTPA (for ^{111}In -labeling) and to SM(PEO)₆, which results in maleimide-activation. NLS-peptides, containing a cysteine-moiety, were conjugated to EGF using EDC/NHS coupling. EGF-NLS was linked to DTPA-anti- γ H2AX-maleimide and ^{111}In -labeled to yield ^{111}In -anti- γ H2AX-PEG₆-NLS-EGF. A mouse-IgG version was synthesised to act as non-specific control, and a Cy3-labelled version was synthesised for in vitro validation by confocal fluorescence microscopy. Results: In competition binding experiments the affinity of anti- γ H2AX-PEG₆-NLS-EGF for EGFR and γ H2AX was similar to that of EGF and anti- γ H2AX, respectively. Intracellular distribution of Cy3-anti- γ H2AX-PEG₆-NLS-EGF colocalized with that of AlexaFluor-conjugated EGF. Induction of DNA damage in MDA-MB-468 cells using X-irradiation (IR; 4.0 Gy) did not significantly alter the extent of EGFR binding and uptake of ^{111}In -anti- γ H2AX-PEG₆-NLS-EGF compared to untreated cells. However, clonogenic survival of MDA-MB-468 cells was significantly reduced (2.6-fold) following combination treatment with ^{111}In -anti- γ H2AX-PEG₆-NLS-EGF (6 MBq/ μ g) and 4.0 Gy IR, compared to either treatment alone. The biodistribution of ^{111}In -anti- γ H2AX-PEG₆-NLS-EGF was investigated using SPECT/CT imaging of MDA-MB-468 xenograft-bearing mice. ^{111}In -anti- γ H2AX-PEG₆-NLS-EGF uptake in tumour was 5.4% of injected dose(ID)/g at 48h. Co-injection of EGF in 100-fold excess reduced ^{111}In uptake to 0.87%ID/g, confirming that intratumoural accumulation of ^{111}In -anti- γ H2AX-PEG₆-NLS-EGF is EGFR-dependent. Conclusion: ^{111}In -anti- γ H2AX-PEG₆-NLS-EGF is a radioimmunoconstruct, bispecific for the cell membrane target, EGFR, and an intranuclear target, γ H2AX. It is a promising agent for imaging DNA damage response and radioimmunotherapy of EGFR-overexpressing tumours.

Presentation Number **0886A**

Poster Session 2c: In Vivo Studies & Development/Novel Use of Imaging Probes

A New Chelator-Free Multifunctional [64Cu]-CuS Nanoparticle Platform for Simultaneous μ PET/CT Imaging and Photothermal Ablation Therapy

Min Zhou¹, Rui Zhang¹, Miao Huang¹, Wei Lu¹, Marites P. Melancon^{2,1}, Shaoli Song^{1,3}, **Chun Li**^{1,3}, ¹Experimental Diagnostic Imaging, UT-MD Anderson Cancer Center, Houston, TX, USA; ²Imaging Physics, UT-MD Anderson Cancer Center, Houston, TX, USA; ³Nuclear Medicine, Shanghai Jiaotong University, Shanghai, China. Contact e-mail: cli@mdanderson.org

Objectives: Radioisotopes of copper (^{64}Cu , $T_{1/2} = 12.7$ h; ^{67}Cu , $T_{1/2} = 62$ h) have been labeled to antibodies and peptides for positron emission tomography (PET) imaging and targeted radiotherapy. The purpose of this study was to synthesize and evaluate a novel class of chelator-free ^{64}Cu -CuS nanoparticles (NPs) suitable for both PET imaging and as a photothermal coupling agent for photothermal ablation (PTA) therapy. **Methods:** ^{64}Cu -CuS NPs were synthesized and characterized with regard to size, radiolabeling efficiency, stability, and imaging properties. **Results:** ^{64}Cu -CuS possessed excellent stability and were simple to make. Compare to the traditional radiolabeling technique, ^{64}Cu was an integral component of CuS NPs, which obviates the need to introduce radiometal chelators to the surface of NPs. CuS NPs, ~ 11 nm in diameter, displayed strong absorption in the near-infrared region (peak 930 nm), and mediated ablation of U87 tumor cells upon exposure to NIR light both in vitro and in vivo after either intratumoral or intravenous injection. In vivo, polyethylene glycol (PEG)-coated ^{64}Cu -CuS NPs displayed prolonged blood half-life, and was accumulated in subcutaneously inoculated human glioma U87 tumors owing to enhanced permeability and retention effect. **Conclusions:** The combination of small size, strong absorption in NIR region, and integration of ^{64}Cu as one of the structural components of CuS NPs makes ^{64}Cu -CuS NPs ideally suited for multifunctional molecular imaging and PTA therapy applications.

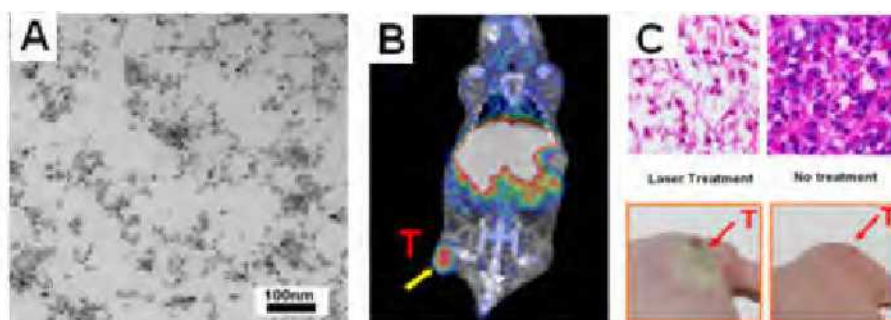


Figure: (A) TEM picture of CuS NPs. (b) *in vivo* microPET imaging, and (C) photothermal therapy effects.

Presentation Number **0887A**

Poster Session 2c: In Vivo Studies & Development/Novel Use of Imaging Probes

Towards Improved Pharmacokinetic Profiles and Increased Metabolic Stability of ^{64}Cu -Labeled Peptides with High Binding Affinity to EphB4 Receptors for Molecular PET Imaging

Chiyi Xiong, **Chun Li**, *Exp. Diagnostic Imaging, U.T. M. D. Anderson Cancer Center, Houston, TX, USA. Contact e-mail: cli@mdanderson.org*

Objectives: Expression of EphB4 receptors is common in a variety of tumors including prostate, colon, ovary, and breast cancers. Radiolabeled peptides that can bind to EphB4 with high affinity represent promising agents for noninvasive imaging of EphB4-expressing tumors, and for monitoring response to targeted therapies directed at EphB4. The purpose of this study was to perform structure-activity studies to further improve the stability and clearance of our first generation EphB4-binding peptides on the basis of our first generation peptides. **Methods:** A battery of methods including introduction of hydrophilic moieties, substitution with D-amino acid, and peptide cyclization were utilized to reduce degradation of peptides in the presence of peptidases and proteinases. Surface plasma resonance (SPR) sensor chip technology was used to screen the resulting peptides with regard to their receptor binding affinity. Lipophilicity measured by octanol-water partition coefficient (LogP). **In vivo** biodistribution and pharmacokinetic data was collected. **Results:** We identified candidate peptides with binding affinity (K_d) in the lower nanomolar range with significantly improved stability in mouse plasma, increased blood circulation time, and reduced retention in the liver and the spleen. **Conclusions:** The improved metabolic stability, along with favorable pharmacokinetic profile and high receptor binding affinity, suggest that these peptides are promising candidate as novel therapeutic and imaging agents targeted to EphB4 receptors.

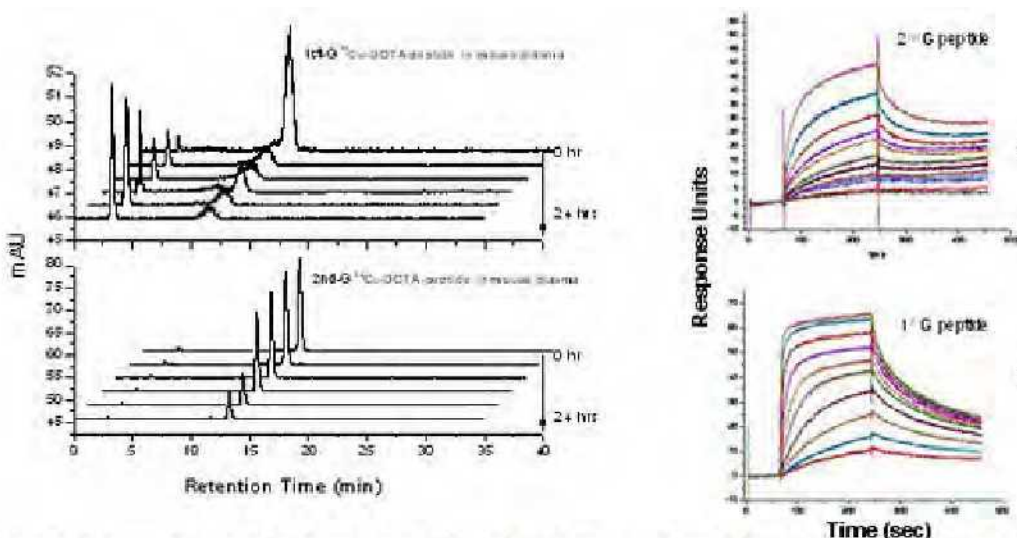


Figure: Comparison of plasma stability of a 1st generation ^{64}Cu -labeled peptide and a 2nd generation ^{64}Cu -labeled peptide targeted to EphB4 receptors (left panel). SPR sensor grams showing increased receptor binding affinity with a 2nd generation peptide as compared to a 1st generation peptide targeted to EphB4 receptors (right panel).

Presentation Number **0888A**

Poster Session 2c: In Vivo Studies & Development/Novel Use of Imaging Probes

18F-LABELING AND RADIOPHARMACEUTICAL EVALUATION OF PHOSHOPEPTIDE-CELL-PENETRATING PEPTIDE DIMERS

Vincent Bouvet¹, **Susan Richter**², **Ines Neundorff**², **Brendan J. Trayner**³, **Melinda Wuest**¹, **Frank Wuest**¹, ¹Department of Oncology, University of Alberta, Edmonton, AB, Canada; ²Institute of Biochemistry, University of Leipzig, Leipzig, Germany; ³Department of Physiology, University of Alberta, Edmonton, AB, Canada. Contact e-mail: bouvet@ualberta.ca

Introduction: Phosphopeptides are useful reagents to study cellular protein phosphorylation/dephosphorylation processes. However, studies of phosphopeptide action in cells are hampered by their poor transport through the cell membrane. The present study describes the synthesis and radiopharmacological evaluation of 18F-labeled phosphopeptide-cell-penetrating peptide (CPP) dimers. CPPs sC18 and hCT(18-32)-k7 we coupled to polo-like kinase-1-binding hexaphosphopeptide H-Met-Gln-Ser-pThr-Pro-Leu-OH to investigate cell uptake of the corresponding phosphopeptide-CPP dimers (CPP-1 and CPP-2). Methods: Phosphopeptide-CPP dimers were synthesized combining manual and automated solid-phase peptide synthesis (SPPS) based on orthogonal Fmoc protection group strategy. Radiolabeling was achieved through acylation of the N terminal end with bifunctional labeling agent [¹⁸F]SFB. Conventional and micro-fluidic methodologies were evaluated for [¹⁸F]SFB labeling of both peptide dimers. Cellular uptake studies were performed in human HT-29, FaDu and MCF-7 tumor cells. Dynamic small animal PET studies of radiolabeled dimers CPP-1 and CPP-2 were carried out in Balb/C mice. Results: The synthesis of the phosphopeptide-CPP dimers combining automated and manual methodology afforded high and reproducible yields. Moreover micro-fluidic methodology significantly improved the yield and the chemoselectivity of the radiolabeling reactions (30% d.c.y. after HPLC) compared the conventional manual methodology (2-4% d.c.y. after HPLC). Both CPP-1 and CPP-2 exhibit comparable cell uptake in all cell lines [30 min: CPP-1 41±7% ID/mg protein (n=3); CPP-2 51±7% (n=4)]. This represents a significant enhancement of cell uptake compared to radiolabeled hexaphosphopeptide alone (<1% ID/mg protein). Preliminary small animal PET studies of radiolabeled peptide dimers CPP-1 and CPP-2 showed distribution pattern as typically found for radiolabeled peptides such as rapid blood clearance and renal elimination. Conclusion: Micro-fluidic methodology significantly improved the radiochemical yield, chemoselectivity and purity of the [¹⁸F]SFB incorporation on the phosphopeptide-CPP dimers compared to the conventional protocols. Cell-penetrating peptides sC18 and hCT(18-32)-k7 are useful drug delivery systems enabling sufficient membrane transport of phosphopeptides to further promote studies on intracellular metabolic pathways involving phosphopeptides.

Presentation Number **0889A**

Poster Session 2c: In Vivo Studies & Development/Novel Use of Imaging Probes

MICRO-FLUIDIC SYNTHESIS OF [¹⁸F]FAZA

Vincent Bouvet, Melinda Wuest, Leonard I. Wiebe, Frank Wuest, Department of Oncology, University of Alberta, Edmonton, AB, Canada. Contact e-mail: bouvet@ualberta.ca

Introduction: [¹⁸F]FAZA is used to determine the presence of hypoxia in solid tumors. Current automated synthesis of [¹⁸F]FAZA involves a 5 min [¹⁸F]fluoride nucleophilic substitution on 1-(2,3-di-O-acetyl-5-O-tosyl- α -D-arabinofuranosyl)-2-nitroimidazole followed by a 2 min hydrolysis step. However, the overall radiochemical yield (RCY) is reported to be low (5-10%). Micro-fluidic technology allows fast reactions in a simple experimental set-up, while using only low amounts of starting material. The present study describes the synthesis of [¹⁸F]FAZA using micro-fluidic technology. Methods: Advion micro-fluidic system was used for [¹⁸F]fluoride drying and radiofluorination. Reaction conditions were optimized by screening the following parameters: temperature (80 °C to 140 °C), flow rate (8 μ L x min⁻¹ to 36 μ L x min⁻¹), reaction time (using different length of reactor) and precursor concentration (1 mg.mL⁻¹ to 5 mg.mL⁻¹). Radiopharmacological evaluation of [¹⁸F]FAZA was performed in EMT-6 tumor bearing mice by means of dynamic small animal PET studies. Results: Conditions for the [¹⁸F]fluoride incorporation were optimal at 120°C with an 18 μ L.min⁻¹ flow rate for 5min20sec in DMSO with a precursor concentration of 2.5mg.mL⁻¹ and afforded 86% d.c. conversion. After hydrolysis 63% d.c. of the purified [¹⁸F]FAZA was obtained. For larger activity reactions (400MBq to 2GBq), the conditions were optimal at 120°C with an 27 μ L.min⁻¹ flow rate for 3min33sec in DMSO with a precursor concentration of 5mg.mL⁻¹ and afforded 40% d.c. conversion and after manual hydrolysis 29% d.c. of the purified [¹⁸F]FAZA was obtained. Dynamic Small animal PET studies for 90 minutes showed tumor uptake in EMT-6 tumor bearing mice reaching maximum uptake (SUV=0.74 \pm 0; n=4) after 25 minutes. Conclusions: Micro-fluidic technology provides [¹⁸F]FAZA in higher radiochemical yields and in significantly shorter reaction times. Micro-fluidic technology represents an interesting alternative synthesis approach for the preparation of [¹⁸F] labeled PET radiotracers.

Presentation Number **0890A**

Poster Session 2c: In Vivo Studies & Development/Novel Use of Imaging Probes

In Vivo Chemistry for Pretargeted Tumor Imaging and Therapy in Mice

Raffaella Rossin¹, Pascal Renart Verkerk¹, Sandra M. van den Bosch¹, Roland C. Vulders¹, Iris Verel², Johan Lub¹, Marc S. Robillard¹, ¹Biomolecular Engineering, Philips Research, Eindhoven, Netherlands; ²Life Science Facilities, Philips Research, Eindhoven, Netherlands. Contact e-mail: marc.robillard@philips.com

A major challenge of radioimmunotherapy (RIT) of cancer is to enhance the nuclear radiation dose delivered to the tumor while minimizing the dose in healthy tissues. Antibodies (mAbs) circulate for a long time and only slowly accumulate in the tumor, which, when used for RIT, leads to dose-limiting side effects in healthy organs. This efficacy-limiting factor can be circumvented by pretargeting (2-step targeting) approaches. The superior image contrast and the ability to administer higher (therapeutic) radiation doses compared to directly labeled mAbs is offset by the drawbacks of the current biological pretargeting systems, involving either immunogenicity issues or extensive re-engineering of the parent mAb. To address this, we designed a novel pretargeting approach based on the bio-orthogonal chemical inverse-electron-demand Diels Alder reaction, employing a trans-cyclooctene (TCO)-conjugated anti-TAG72 mAb CC49 and an ¹¹¹In-labeled DOTA-tetrazine derivative, and we evaluated the in vitro stability and reactivity, and tumor targeting in mice bearing colorectal xenografts.¹ When ¹¹¹In-tetrazine was administered to LS174T-tumored mice 1 day after CC49-TCO, the chemically-tagged tumors reacted rapidly with ¹¹¹In-tetrazine, resulting in pronounced radioactivity localization in the tumor, as demonstrated by SPECT/CT imaging of live mice 3 h post injection: 4.18% ID/g, tumor-to-muscle ratio (T/M)=13.1. In mice treated with unmodified CC49, the tumor could not be discriminated from the surrounding tissue (0.28 %ID/g, T/M=0.5). Mice treated with TCO-modified rituximab, which lacks specificity for TAG72, showed the expected retention of ¹¹¹In-tetrazine in blood and non-target organs, and a much reduced tumor accumulation (1.02 %ID/g, T/M=2.1). Corresponding dual isotope biodistribution experiments confirmed the imaging results and revealed a remarkable 52-57% reaction yield between mAb-TCO and tetrazine moieties present in tumor and blood. This is the first demonstration of an effective chemical reaction between two exogenous moieties in living animals for the non-invasive imaging of low-abundance targets in clinically relevant conditions. To extend this proof of principle to effective RIT, our work next centered on increasing the tumor/non-tumor ratio by optimizing the CC49-TCO modification grade and blood clearance, and improving probe dosing. This contribution will address these and other system and protocol improvements towards pre-targeted RIT in LS174T-tumored mice. [1] Rossin et al. *Angew. Chem. Int. Ed.* 2010, 49, 3375-3378

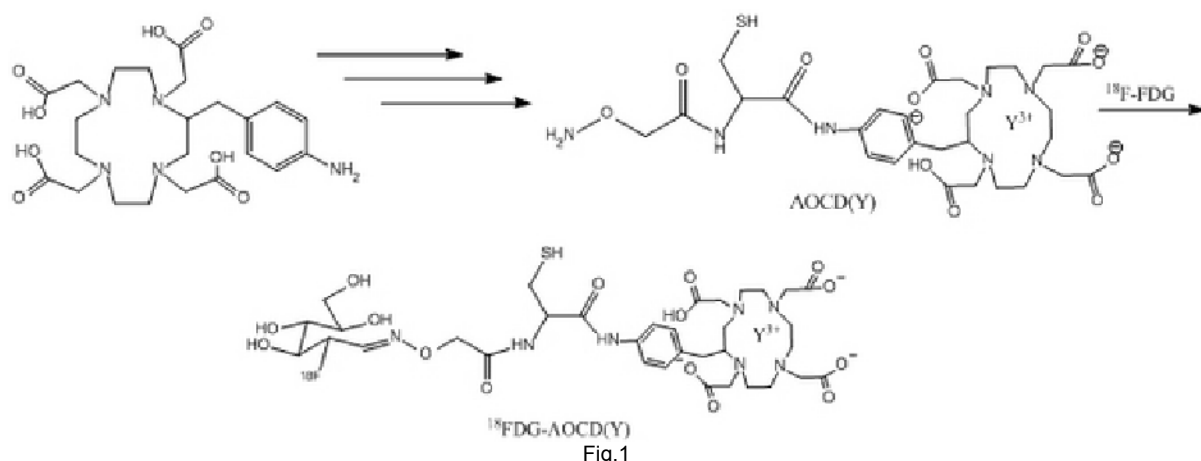
Presentation Number **0891A**

Poster Session 2c: In Vivo Studies & Development/Novel Use of Imaging Probes

18FDG-AOCD(Y) for Imaging DAbR1 Reporter Gene Expression in a Multimodal System

Vahid Eskandari¹, David L. Boucher², Tolulope A. Aweda¹, Heather E. Beck¹, David L. Kukis², Simon R. Cherry², Claude F. Meares¹,
¹Chemistry, University of California, Davis, Davis, CA, USA; ²Center for Molecular and Genomic Imaging, University of California, Davis, Davis, CA, USA. Contact e-mail: veskandari@ucdavis.edu

Objectives: to prepare a probe derived from the common PET radiotracer ¹⁸F-FDG for use with the reporter gene that binds DOTA chelates with infinite affinity (DAbR1) (J Nucl Med 2008;49:1828), and to extend this system to multimodal reporter gene imaging. **Synthesis.** 18FDG-AOCD(Y) was synthesized by sequentially adding protected cysteine and aminoxyacetic acid to aminobenzyl-DOTA, removing the protecting groups and inserting yttrium(III) to produce AOCD(Y) Fig.1. This precursor was radiolabeled with 18FDG by heating in acid (Bioconjugate Chem 2009;20:432, Bioconjugate Chem 2008;19:1202), followed by HPLC purification. The radiochromatogram indicates the elution of unreacted 18FDG after 6 min and the elution of the 18FDG-AOCD(Y) probe after 17 min. **Multimodal Reporters.** A series of DAbR1-based multimodal reporter genes was developed for use in PET and optical imaging applications. Initial versions were composed of DAbR1, mCherry and mTFL (a thermostable mutant of firefly luciferase) arranged in a single reading frame and separated by sequence encoding either serine/alanine rich linkers (to produce multimeric fusions) or 2A peptides ("self-cleaved" during translation to produce three separate polypeptide chains). Preliminary characterization revealed that DAbR1 was unable to bind DOTA as a fusion when transiently expressed; however, binding was not disrupted when 2A peptides were used in place of flexible linkers. The basic DAbR1-2A-mCherry-2A-mTFL structure was thus used to assemble a series of reporters, each with a unique fluorescent component. These reporters were then stably expressed in U-87 glioma cells and separately validated for use with 18FDG-AOCD(Y). **Conclusion.** 18FDG-AOCD(Y) is a viable alternative to rare earth-labeled DOTA complexes for PET imaging and suitable for multimodal imaging when used in conjunction with DAbR1-based multimodal reporters. Grants: NIH CA016861 (CFM) and DOE DE-SC0002294 (SRC)



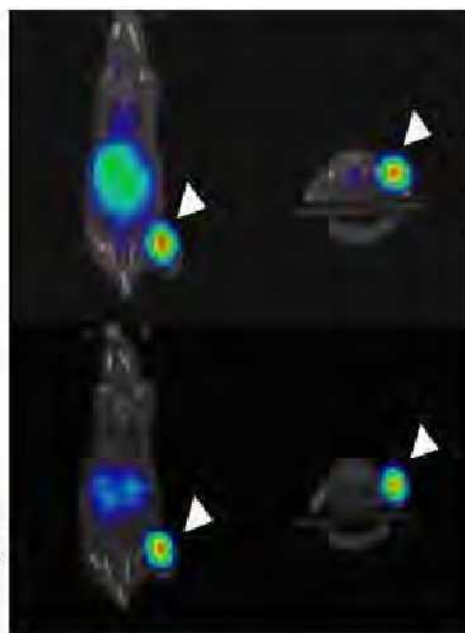
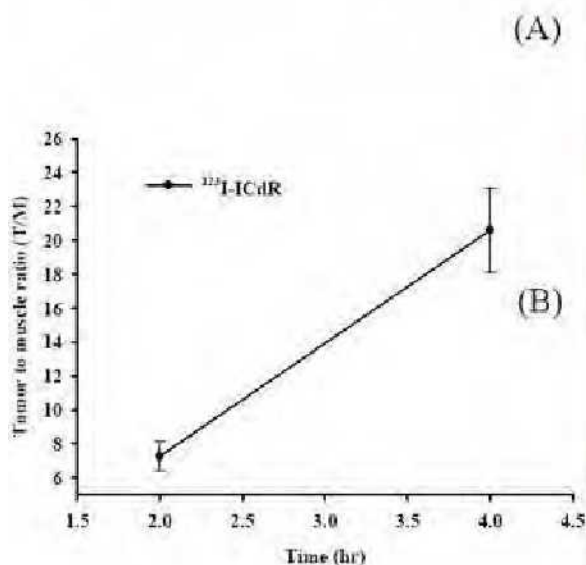
Presentation Number **0892A**

Poster Session 2c: In Vivo Studies & Development/Novel Use of Imaging Probes

Evaluation of ^{123}I -ICdR as a novel SPECT proliferation probe in a mouse tumor model

Pei-Chia Chan¹, **Chih-Yuan Lin**¹, **Chun-Yi Wu**¹, **Chuan-Lin Chen**¹, **Wei-Ti Kuo**², **C. Allen Chang**¹, **Ren-Shyan Liu**^{1,3}, **Chih-Chieh Shen**⁴, **Ming-Hsien Lin**⁵, **Hsin-Ell Wang**¹, ¹Department of Biomedical Imaging and Radiological Sciences, National Yang-Ming University, Taipei, Taiwan; ²Institute of Nuclear Energy Research, Atomic Energy Council, Tao-Yuan City, Taiwan; ³Department of Nuclear Medicine, Faculty of Medicine, National Yang-Ming University, Taipei, Taiwan; ⁴Department of Nuclear Medicine, Cheng Hsin General Hospital, Taipei, Taiwan; ⁵Department of Nuclear Medicine, Taipei City Hospital, Taipei, Taiwan. Contact e-mail: rene1122@gmail.com

Objective: This study aims to evaluate radioiodinated 5-iodo-2'-deoxycytidine (^{123}I -ICdR) as a SPECT probe for detecting tumor in a NG4TL4 sarcoma-bearing mouse model. **Methods:** Starting from 5-tributylstannyl-2'-deoxycytidine, $^{123}\text{I}/^{131}\text{I}$ -ICdR-w and $^{123}\text{I}/^{131}\text{I}$ -ICdR-w/o were prepared in high radiochemical yield (both $\geq 85\%$, decay corrected) and radiochemical purity (both $\geq 95\%$) with and without HPLC purification, respectively. Biological characterization studies of $^{123}\text{I}/^{131}\text{I}$ -ICdR including cellular uptake with and without pyrimidine blocking, DNA incorporation assay, metabolite analysis, and small animal microSPECT/CT imaging were performed. **Results:** The accumulation of ^{131}I -ICdR-w/o in NG4TL4 cell increased with time. The cell-to-medium ratio (C/M) of ^{131}I -ICdR-w/o reached 25.41 ± 4.05 and 75.37 ± 3.23 after 4 and 8 h incubation. However, when $10 \mu\text{M}$ of thymidine or deoxycytidine was added in the culture medium, the C/M of ^{131}I -ICdR-w/o dramatically reduced to 3.16 ± 0.29 or 44.08 ± 6.82 after 8 h incubation. No significant differences in the accumulation of ^{131}I -ICdR-w and ^{131}I -ICdR-w/o in NG4TL4 cell cultures can be observed implied that the small amount of CdR (no more than $0.3 \mu\text{M}$) produced during radioiodine labeling would not influence the cellular uptake. Significant correlation between the C/M ratio and DNA incorporation (in cpm/ μg DNA) in NG4TL4 sarcoma cells ($r^2=0.90$) was noticed. In vivo metabolite assay revealed that the major radioactive component was ^{123}I -ICdR and accounted for 72.2% radioactivity in the blood and 71.0% radioactivity in the urine at 1 h p.i.. MicroSPECT/CT imaging of sarcoma-bearing mouse clearly delineated the tumor lesion with increasing tumor-to-muscle ratio (7.27 ± 0.85 and 20.60 ± 2.49 at 2 and 4 h p.i.). The results of biodistribution studies were in accordance with those observed in SPECT/CT imaging. **Conclusion:** In this study, the $^{123}\text{I}/^{131}\text{I}$ -ICdR was successfully prepared via a one-step reaction in high yield and radiochemical purity. ^{131}I -ICdR is metabolically stable in vivo and is demonstrated a promising SPECT probe for tumor detection in a sarcoma-bearing mouse model.



The MicroSPECT/CT imaging of the mouse bearing with NG4TL4 sarcoma (arrow head) at (A) 2 h and (B) 4 h post intravenous injection of ^{123}I -ICdR ($\sim 600 \mu\text{Ci}$).

Presentation Number **0893A**

Poster Session 2c: In Vivo Studies & Development/Novel Use of Imaging Probes

Can NK Cells Ligands be Targeted for Cancer Diagnosis and Treatment?

Aviv Hagooly¹, Chamutal Gur², Sharon Dotan¹, Samar Dissoki¹, Hana Billauer¹, Galith Abourbeh¹, Smadar Elmachliy¹, Ofer Mandelboim², Eyal Mishani¹, ¹Cyclotron Unit, Department of Nuclear Medicine, Hadassah Hebrew University Hospital, Jerusalem, Israel; ²Lautenberg Center for General and Tumor Immunology, Hebrew University Hadassah Medical School, Jerusalem, Israel. Contact e-mail: hagooly@hadassah.org.il

Natural killing (NK) cells belong to the innate immune system and are capable of identifying and eradicating various malignant cells. A fusion of the extracellular portion of the NK cell receptor, NKp30, with the constant region of human IgG1 (NKp30-Ig) has been previously shown to recognize human malignant cells and effectively treat tumor-bearing mice with prostate carcinoma xenografts. It was hypothesized that the NKp30-Ig specifically recognizes tumor cells through the NK receptor region and that its constant human IgG1 part allows for recruitment of immune components. Labeling the NKp30-Ig with radionuclides can characterize NKp30-Ig pharmacokinetics and facilitate cancer diagnosis *in vivo*. Iodogen tubes were used for direct labeling of NKp30-Ig with ¹²⁴I. For ⁶⁷Ga and ¹¹¹In labeling, the NOTA-Bn-NCS was first conjugated. The *in vitro* activity of the native and NOTA-NKp30-Ig were evaluated by FACS studies using cells containing the ligand for the native NKp30-Ig (colon carcinoma (RKO) and the human hepatoma (Hep3b)). As negative control, the human placental choriocarcinoma Jeg3 cell line was used. The labeled NKp30-Ig was purified on a size exclusion column. Purity of the conjugated and labeled NKp30-Ig was verified by FPLC. The specific activity was 15-25 $\mu\text{Ci}/\mu\text{g}$ with chemical and radiochemical purity of >98%. Cell studies were conducted in 96 well plates. Forty ng of the labeled NKp30-Ig were added, incubated at 4 °C, washed, collected and counted in a gamma counter. Direct labeling with ¹²⁴I/iodogen in Na₂HPO₄ buffer yielded the labeled ¹²⁴I-NKp30-Ig. FACS studies of the conjugated NOTA-NKp30-Ig indicated that the binding efficiency of cancer cells was not hampered. This derivative was labeled with ⁶⁷Ga and ¹¹¹In in NH₄OAc or HEPES buffers, respectively. All labeled NKp30-Ig were stable at 4 °C (>98%). Preliminary *in vitro* studies using labeled NKp30-Ig resulted in a moderate difference in activity uptakes between the positive and negative cells lines. NKp30-Ig and NOTA-NKp30-Ig were labeled with ¹²⁴I, ⁶⁷Ga and ¹¹¹In. The protocols are currently improved in order to evaluate the *in vivo* and *in vitro* properties of the labeled NKp30-Ig, namely, their specific binding, pharmacokinetics and their potential for *in vivo* imaging.

Presentation Number **0894A**

Poster Session 2c: In Vivo Studies & Development/Novel Use of Imaging Probes

Automated Radiosynthesis of [¹⁸F]Fluoroethylazide

Amit Hetsron, Ohad Ilovich, Sassy Cohen, Eyal Mishani, Aviv Hagooley, Cyclotron Unit, Department of Nuclear Medicine, Hadassah Hebrew University Hospital, Jerusalem, Israel. Contact e-mail: hagooley@hadassah.org.il

Copper (I) catalyzed cycloaddition of an alkyne and azide (click) is a convenient synthetic route for PET radiopharmaceuticals. The relative stability of the alkyne and azide moieties, the orthogonal reaction conditions and the stability of the formed 1,2,3 triazole, allow for a wide range of labeling conditions and eliminate the need for any protective group chemistry. Also, the short reaction time and the high radiochemical yields obtained in the click process makes it an excellent approach for ¹⁸F labeling. The limitations of most click protocols are complicated purification steps of the radioactive precursor and considerable exposure to radiation for the radiochemist from manual synthesis. Still, despite the increased popularity of click labeling with ¹⁸F, there is no mention of an automated system for this transformation. [¹⁸F]Fluoroethylazide (FEA) is one of the most frequently used synthons for click labeling, recovered from the reaction of 2-azidoethyl-4-toluenesulfonate and ¹⁸F⁻ by a simple distillation. Automation of this process will simplify the synthesis, decrease radiation exposure and prompt the routine production of such radiolabeled tracers. The automated synthesis of [¹⁸F]FEA was performed on a standard GE Tracerlab® FX-N module. The next step includes manual click labeling of a short sequence peptide (AcFAKAamide) with alkyne moiety that was combined at the Σ amine of the lysine by hexynoic acid succinimidyl ester. Cold FEA and 2-azidoethyl-4-toluenesulfonate were synthesized as previously reported. Validation of precursors and non radioactive standards was done by ¹H NMR and ESI MS. Purity was tested by HPLC chromatography with C-18 columns. Radiochemical purity of all products is >95%. 2-Azidoethyl-4-toluenesulfonate (5 mg) was reacted with 200-300 mCi of ¹⁸F⁻ in the presence of 15 mg kryptofix and 2.5 mg K₂CO₃ for 15 min at 80°C in 1 mL ACN. A short distillation of 150 sec at 75°C furnished the [¹⁸F]FEA with a decay corrected yield (DCY) of 66% ± 8.3 (n=5), total reaction time less than 30 min, in a fully automated process. To test the reactivity of the isolated [¹⁸F]FEA, a manual click step was performed with the peptide in 85% DCY. The automated procedure developed for [¹⁸F]FEA produced higher radiochemical yields and distillation efficiency than the manual synthesis reported so far and enabled the use of higher radioactivity levels per batch. Currently, an automated procedure is developed for the second click step with a biologically active bicyclic RGD peptide.

Presentation Number **0895A**

Poster Session 2c: In Vivo Studies & Development/Novel Use of Imaging Probes

Are Carbon-11 Labeled Ammonium Salts Superior to 99mTc-Mibi as Myocardial Perfusion Imaging Agents?

Ohad Ilovich, Hana Billauer, Sharon Dotan, Moshe Bocher, Nanette Freedman, Galith Abourbeh, Eyal Mishani, Cyclotron/Radiochemistry/Nuclear Medicine, Hadassah Hebrew University, Jerusalem, Israel. Contact e-mail: ilovicho@gmail.com

Coronary artery disease (CAD), a blockage of the coronary arteries, is the most common form of heart disease, and is the leading cause of death in the Western world. Myocardial perfusion imaging (MPI) is a functional imaging tool that can assess coronary perfusion through injection of flow radiotracers and measurement of their uptake into the myocardium. MPI is the most prevailing non-invasive imaging modality for diagnosis and risk-stratification of CAD patients. It has two distinct modes: single photon emission computed tomography (SPECT) and positron emission tomography (PET). Millions of SPECT MPI studies are performed world-wide each year, greatly exceeding PET studies, despite the clear advantages offered by PET. We sought to develop and evaluate in vivo novel carbon-11 labeled ammonium salts as potential MPI PET agents. Four compounds with varying lipophilicities, charges and structures were labeled using either ¹¹CH₃I or ¹¹CH₃OTf. In vivo evaluation of the radiotracers was carried out in mice, rats and rabbits using biodistribution and PET/CT studies. Biodistribution studies in mice were carried out up to 15 min after injection of the radiotracers. Results (Table 1) indicate that whereas compound 1 did not accumulate significantly in cardiac tissue, the more lipophilic compound 2 showed more potential as an MPI tracer. Specifically, it presented high myocardial uptake and low uptake in the liver and lungs, combined with high clearance from the blood pool, prominently via renal excretion. To increase overall positive charge, a dimethylamino group was incorporated into the phenyl ring, yielding compound 3. This compound had enhanced cardiac uptake values, yet with slow washout of activity from the blood pool and increased uptake in the lungs. Finally, substitution of a methyl group in compound 2 with phenyl yielded compound 4. This tracer presented stable cardiac uptake values of ~50% ID/g at all tested time points; having a superior profile over that of 99mTc-MIBI under similar conditions (Table 1). PET/CT scans using rats and rabbits validated the biodistribution results, highlighting the potential use of ammonium salt derivatives as MPI PET agents.

Compound		SUV ^a		Heart/liver b		Heart/blood b		Heart/lung b	
Number	Name	5 min	15 min	5 min	15 min	5 min	15 min	5 min	15 min
1	tert-butylammonium ion	0.2±0.01	0.2±0.04	0.2±0.02	0.2±0.01	1.7±0.6	4.5±1.8	NT ^c	NT ^c
2	tert-butyl-phenylammonium ion	6.7±0.7	3.5±0.4	1.8±0.2	1±0.06	15.5±1.1	10.4±0.7	2.7±0.5	2.8±0.2
3	(4-dimethylamino-phenyl)-tert-butylammonium ion	11.9±0.9	7.1±1.1	3.0±1.1	2.8±0.5	5.3±0.9	4.4±0.5	2.0±0.5	1.9±0.5
4	tert-butyl-diphenylammonium ion	11.5±0.2	10.7±0.5	2.4±0.6	2.8±0.1	4.4±1.2	3.8±1.6	6.6±0.9	12.5±1.9
5	^{99m} Tc-MIBI	5.2±0.5	3.5±0.9	0.9±0.2	1.7±0.7	1.0±1.4	4.5±1.7	5.2±0.9	5.8±1.2

^a SUV = Standardized uptake value.

^b Radioactivity uptake ratios. Results presented as mean±SEM (n=6 for each group).

^c NT = not tested.

Presentation Number **0839B**

Poster Session 3c: In Vivo Studies & Development/Novel Use of Imaging Probes

GE11 Peptide as a Potential Marker for Imaging Epidermal Growth Factor Receptor (EGFR)

Samar Dissoki, Smadar Elmachliy, Sharon Dotan, Hana Billauer, Ohad Ilovich, Galith Abourbeh, Eyal Mishani, Aviv Hagooly, Cyclotron Unit, Department of Nuclear Medicine, Hadassah Hebrew University Hospital, Jerusalem, Israel. Contact e-mail: sdissoki@yahoo.com

The EGFR is involved in proliferation and differentiation of normal and malignant cells and its over-expression may be used as a marker for a variety of human cancers. The peptide sequence YHWYGYTPQNV I (GE11) acts as a ligand for EGFR and was able to bind specifically and efficiently to EGFR competitively with [¹²⁵I]EGF. Labeling GE11 with radionuclides will aid in the noninvasive quantification of EGFR content in tumors and may help in the selection of patients who are expected to benefit from anti-EGFR targeted therapy. For this aim, a GGGK linker was attached to the peptide (GE11') in order to conjugate prosthetic labeling groups such as, [¹⁸F]SFB, [¹²⁴I]SIB and NOTA or DOTA chelators for ⁶⁸Ga and ¹¹¹In labeling. Cold FB-GE11' and IB-GE11' were synthesized in borate buffer pH = 8.4, or DMF/TEA, respectively and purified on a HPLC C-18 preparative column. NOTA-Bn-NCS and DOTA-Bn-NCS chelators were conjugated to the GE11' in NaHCO₃ buffer, pH = 9, and purified as above. All samples were analyzed by MS and purity of >95% was tested by HPLC chromatography. Cold In-NOTA-GE11' was prepared in NH₄OAc buffer, pH = 5.5, and purified as described. All labeled compounds were verified based on the cold samples and their radiochemical purity was >95%. The automated synthesis of [¹⁸F]SFB was performed in two steps on a GE Tracerlab® module. After HPLC purification, the decay corrected radiochemical yield (DCY) was 60% and specific activity (SA) of 844 Ci/μmol was obtained (n=5). [¹²⁴I]SIB was prepared manually with Sep-Pak C18 purification step. The DCY was 65% with SA of 3600 Ci/mmol (n=5). Both [¹⁸F]SFB and [¹²⁴I]SIB were conjugated to GE11' peptide under the conditions mentioned above for 5 min or 1 h, respectively. The DCY of [¹⁸F]FB-GE11' and [¹²⁴I]IB-GE11' was <10% and 30% (n=2) with a total synthesis time of 3.5 h and 2.5 h, respectively. The ¹¹¹In-NOTA-GE11' was prepared in NH₄OAc buffer with >90% radio chemical yields (n=2). The cold derivatives of all the labeled samples were stable at 37 °C for 24 h. Currently, the ⁶⁸Ga-NOTA-GE11' and ¹¹¹In/⁶⁸Ga -DOTA-GE11' are being developed and a screening process to determine which are the best candidates for *in vivo* studies is being done. The GE11' peptide was labeled with ¹⁸F, ¹²⁴I and ¹¹¹In using prosthetic labeling groups and proved to be stable. The binding affinity of the labeled compounds to the receptor and their pharmacokinetics should be tested in order to identify the best candidates to be used as target ligands for cancer diagnostics.

Presentation Number **0840B**

Poster Session 3c: In Vivo Studies & Development/Novel Use of Imaging Probes

Clinical Development of Panitumumab-CHX-A''-DTPA as a Potential SPECT Diagnostic Imaging Agent

Sarah Cheal¹, Olga Vasalatiy¹, Sibaprasad Bhattacharyya², Biying Xu¹, Shannon Cofelli¹, Aaron B. Bate¹, Gary L. Griffiths¹, Agnieszka Sulima¹, ¹NHLBI, NIH, Rockville, MD, USA; ²NCI, NIH, Frederick, MD, USA. Contact e-mail: agnieszks@mail.nih.gov

Panitumumab (Vectibix®, Amgen, Inc., Thousand Oaks, CA), the first fully humanized monoclonal antibody targeting the epidermal growth factor receptor (EGFR), is currently approved for metastatic colorectal cancer with disease progression on or following standard chemotherapy. EGFR overexpression is detected in many human cancers including those of the colon and rectum, but EGFR is also constitutively expressed in many epithelial tissues (e.g. skin follicle). Thus, skin problems including skin swelling, blisters, and abscesses are common following Panitumumab administration, and fatal systemic infections have been reported. Also, there is a low response rate to therapy (10% alone, and 20% when used in combination with chemotherapy) making the risk-benefit estimation vitally important with regard to decisions regarding Panitumumab therapy. There is currently no reliable predictor of EGFR antibody efficacy. To this end, a Panitumumab SPECT imaging agent that demonstrates retained immunoreactivity and tumor localization in vivo will be developed as a predictor of likely efficacy. We chemically conjugated the bifunctional chelate N-[2-amino-3-(p-isothiocyanatophenyl)propyl]-trans-cyclohexane-1,2-diamine-N, N', N'', N''', N''''-pentaacetic acid (CHX-A''-DTPA) to the antibody at well defined and limited substitution ratios. Subsequently we prepared an In-111 [gamma: 0.171 MeV (90%), 0.245 MeV (94%)] radiolabeled Panitumumab in > 98% radiochemical yield. Results establish the feasibility to reproducibly prepare Panitumumab-CHX-A''-DTPA, radiolabel with high efficiency and purity, and maintain in vitro activity following addition of In-111. The agent is under development for preclinical evaluation, and later clinical application as a specific imaging agent for the presence of EGFR positive cancers.

Presentation Number **0841B**

Poster Session 3c: In Vivo Studies & Development/Novel Use of Imaging Probes

μ PET/CT Imaging of EphB4 Receptors in Prostate and Colon Cancer Xenografts Using ^{64}Cu -Labeled Peptide Targeting EphB4 Receptors

Chiyi Xiong, Miao Huang, Rui Zhang, Shaoli Song, Wei Lu, Leo G. Flores, Juri G. Gelovani, **Chun Li**, *Exp. Diagnostic Imaging, U.T. M. D. Anderson Cancer Center, Houston, TX, USA. Contact e-mail: cli@mdanderson.org*

Objectives: Upregulation of EphB4 receptors, a member of a large family of receptor tyrosine kinases, has been found in a variety of tumors including prostate and colon cancers. The widespread expression of EphB4 and other Eph receptors has stimulated interest in exploring these receptors as target for the development of new anticancer therapies. The purpose of this study was to investigate whether radiolabeled peptides that can bind to EphB4 with high affinity represents promising agents for noninvasive imaging of EphB4-expressing tumors. **Methods:** Surface plasmon resonance was used to evaluate the binding affinity of peptides to EphB4. A EphB4-binding peptide was conjugated to the metal chelator 1,4,7,10-tetraazadodecane-N,N',N'',N'''-tetraacetic acid (DOTA) and subsequently labeled with ^{64}Cu for in vitro binding and in vivo PET imaging studies. **Results:** Surface plasmon resonance measurements showed that the targeting peptide and its Cu-DOTA derivatives exhibited high binding affinity ($K_D = 1.98\text{-}23\text{ nM}$) to EphB4, whereas its corresponding scrambled peptide did not bind to the receptors. Both FITC-labeled and ^{64}Cu -DOTA-conjugated peptides were capable of binding to EphB4-expressing PC-3M prostate and CT-26 colon cancer cells in vitro, but not to EphB4-negative A549 lung cancer cells. Moreover, binding of the targeted peptides to PC-3M and CT-26 cells could be quantitatively inhibited in the presence a large excess of cold peptide. After intravenous injection, ^{64}Cu -DOTA-conjugated peptide was selectively taken up by PC-3M prostate and CT-26 colon cancer inoculated subcutaneously in nude mice, but not in receptor-negative A549 lung cancer. μ PET/CT images of tumor bearing mice clearly delineated deposition of ^{64}Cu -DOTA-conjugated peptide in PC-3M and CT-26 tumors but not in A549 tumors. Specificity of EphB4 imaging with ^{64}Cu -DOTA-conjugated peptide was further validated by blocking experiment and ex vivo immunohistochemical staining. **Conclusions:** we demonstrated for the first time noninvasively μ PET/CT imaged of EphB4 receptor expression with a small-molecular-weight peptide based imaging probe.

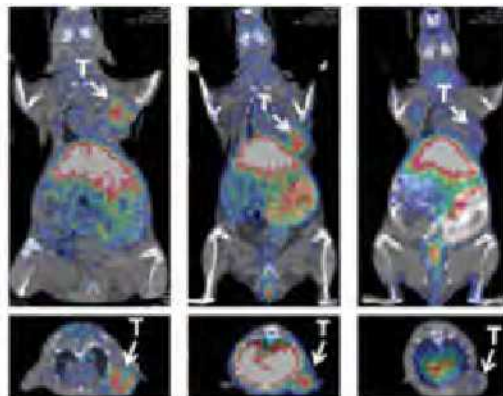


Figure. Representative μ PET/CT imaging of EphB4-expressing PC-3M (left) and CT-26 (middle), and EphB4-negative A649 tumor (right) in nude mice after intravenous injection of ^{64}Cu -DOTA-conjugated peptide directed at EphB4 receptors.

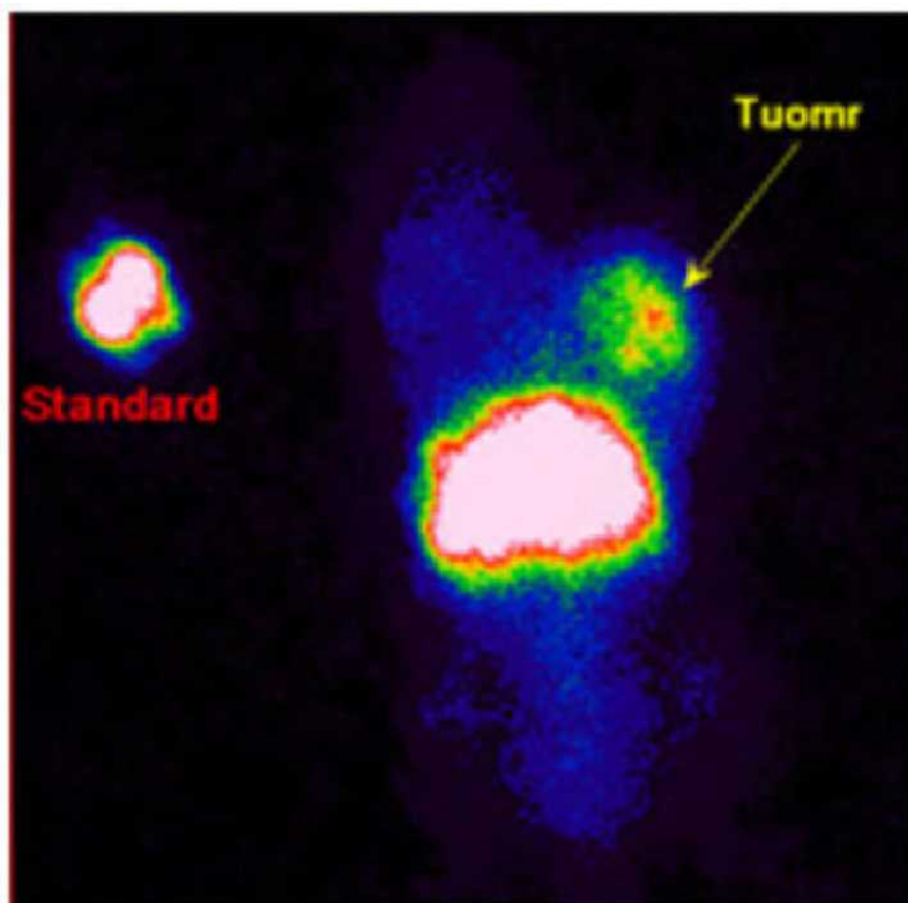
Presentation Number **0842B**

Poster Session 3c: In Vivo Studies & Development/Novel Use of Imaging Probes

γ -Imaging of Systemically Administered Biodegradable, Core-crosslinked Polymeric Micelles as a Potential Drug Carrier

Jun Zhao, Shaoli Song, Jian You, **Chun Li**, *Exp. Diagnostic Imaging, U.T. M. D. Anderson Cancer Center, Houston, TX, USA. Contact e-mail: cli@mdanderson.org*

Objects: It is well known that nanoscale polymeric micelles can preferentially accumulate in tumor after their systematical administration because of the enhanced permeation and retention (EPR) effect. This passive targeting without specific binding ligands enables polymeric micelles to be an effective platform for a variety of contrast agents for tumor imaging and therapeutic agents for cancer therapy. The purpose of this study was to evaluate a biodegradable core-crosslinked polymeric micelle (CCPM) labeled with ^{111}In for in vivo pharmacokinetics and biodistribution studies. Methods: CCPM with average diameter of ~ 20 nm was formed by self-assembly from an amphiphilic block copolymer which consisted of a poly(ethylene glycol) hydrophilic block and a hydrophobic block containing pendent trialkoxysilane functionalities. Core-crosslinking was achieved by the hydrolysis of trialkoxysilane, while the biodegradation was attained by the cleavage of degradable linkage between silica and polymer. Results: ^{111}In was stably chelated to CCPM surface via multi-dentate metal chelators to allow gamma imaging and biodistribution studies. ^{111}In -labeled CCPM was injected intravenously into nude mice bearing s.c. ovarian tumors. The nanoparticles had prolonged blood circulation time with $t_{1/2}$ of ~ 2 hr. Tumors were visualized as soon as 20 min after CCPM injection, and the tumor-to-muscle ratio increased with time over a 24 h period. The Figure below shows representative gamma image obtained at 24 h after intravenous injection of ^{111}In -labeled biodegradable CCPM. Significant activity was observed in the liver and the spleen, and in the tumor owing to EPR effect. Conclusions: Biodegradable CCPM with prolonged blood circulation time and the ability to be modified on its surface is a promising nano-platform for multimodal molecular imaging and targeted drug delivery.



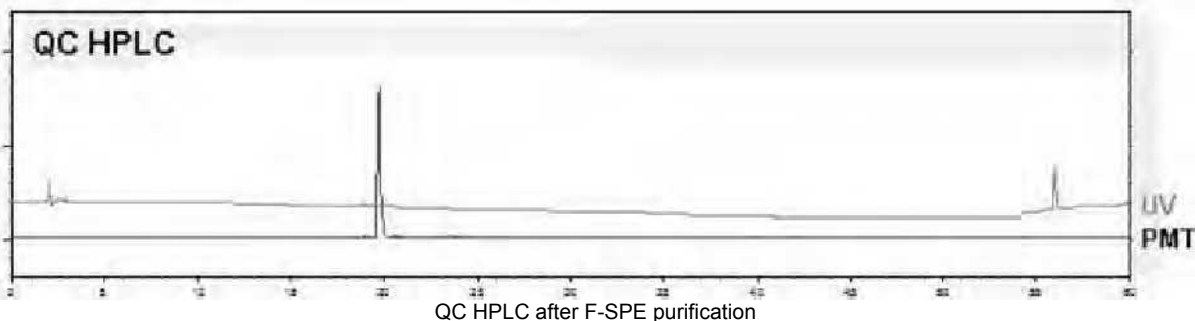
Presentation Number **0843B**

Poster Session 3c: In Vivo Studies & Development/Novel Use of Imaging Probes

Fully HPLC-free Synthesis, Radiolabeling, and Purification of Peptides using Fluorous Extraction Chemistry

Sven H. Hausner¹, Richard D. Carpenter¹, Julie L. Sutcliffe^{1,2}, ¹Biomedical Engineering, UC Davis, Davis, CA, USA; ²Hematology-Oncology, UC Davis, Davis, CA, USA. Contact e-mail: shhausner@ucdavis.edu

Recently, peptides have emerged as attractive PET and SPECT molecular imaging probes. Solid-phase peptide synthesis (SPPS) enables routine preparation of the necessary precursors in excellent crude purity (typically >97%). When combined with solid-phase-radiolabeling (e.g. by using a prosthetic group such as [¹⁸F]fluorobenzoic acid, [¹⁸F]FBA, for PET imaging), only a single HPLC purification is required at the very end of the synthetic process. Thereby, the current solid-phase approach minimizes the amount of precursor required (approx. 3-5 mg resin holding the crude peptide) and facilitates a rapid, simple, and site specific radiolabeling strategy; but, unfortunately, it still requires a lengthy semipreparative HPLC purification. This is necessary to separate the unlabeled precursor (H₂N-peptide) and the radiotracer ([¹⁸F]FBA-peptide). Therefore, a cartridge-based purification approach would be preferable, as it can simplify the setup and make the purification more reproducible and significantly cheaper. Here we present a cartridge-based approach that eliminates the need for HPLC, except for final analytical quality control. By evaluating three model peptides, our initial studies show that when using long-chain perfluoroalkyl (R_F) acids, any H₂N-peptide remaining after solid-phase-labeling can be completely converted to a perfluoroalkyl-tagged R_F-peptide prior to cleavage off the solid support within 5 min (10 equiv F₁₇-acid, 9.8 equiv HATU, 20 equiv DIPEA). By taking advantage of fluorous solid-phase extraction ("F-SPE"), which efficiently retains poly-fluorinated compounds, the R_F-peptide can then be removed completely by simple filtration through a cartridge containing fluorous silica gel (SiO₂-F). The [¹⁸F]FBA-peptide freely passes through the cartridge, ready for final formulation. In preliminary studies, the F-SPE purification yielded competitive results compared to typical HPLC purification in terms of time required (<20 min, including solvent exchange), radiochemical recovery (approx. 50%) and purity (>95%). Thus, using solid-phase-radiolabeling in conjunction with perfluoroalkyl-tagging and F-SPE cartridge filtration can eliminate the need for HPLC purification. Taken together, this approach may offer a broadly applicable and simple, kit-like purification strategy widely applicable for the production of many peptide-based radiotracers.



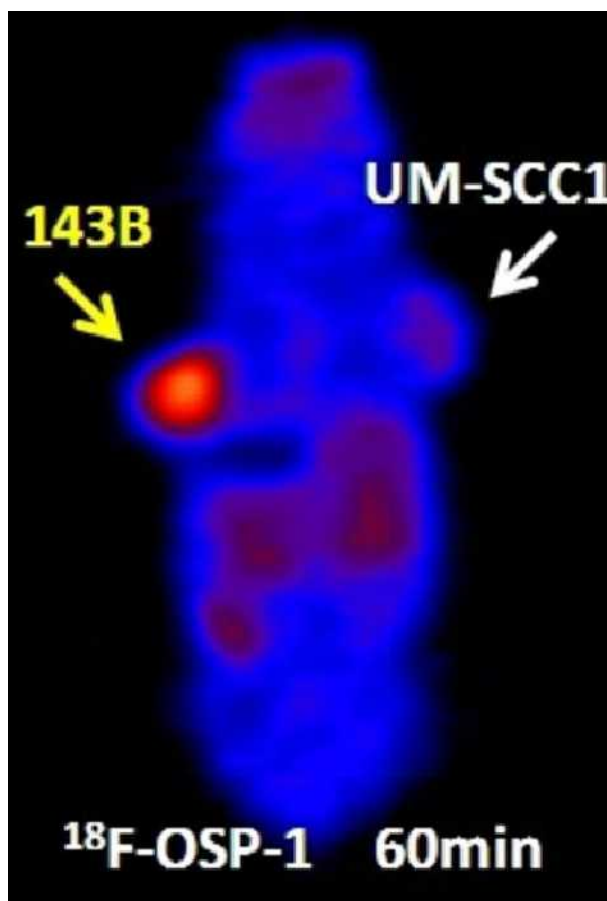
Presentation Number **0844B**

Poster Session 3c: In Vivo Studies & Development/Novel Use of Imaging Probes

Phage Display Derived Peptides for Osteosarcoma Imaging

Xilin Sun^{1,2}, Gang Niu¹, Yongjun Yan¹, Min Yang¹, Ying Ma¹, Baozhong Shen², Xiaoyuan Chen¹, ¹The Laboratory of Molecular Imaging and Nanomedicine (LOMIN), National Institute of Biomedical Imaging and Bioengineering (NIBIB), National Institutes of Health (NIH), Bethesda, MD, USA; ²Department of Medical Imaging and Nuclear Medicine, the Fourth Affiliated Hospital, Harbin, China. Contact e-mail: sunxilin@yahoo.com.cn

To improve existing osteosarcoma diagnosis and treatment methods and broaden the spectrum of imaging agents that can be used for early detection and assessment of tumor response to therapy, we performed a phage-display based screening for peptide sequences that bind specifically to osteosarcoma cells. From the Ph.D.™-12 phage display peptide library, one peptide was enriched after 4 rounds of in vitro selection on 143B osteosarcoma tumor cells with 293T human embryonic kidney cells as a control. Both the peptide and the phage clone displaying the peptide were conjugated with fluorescent dyes for in vitro cell, ex vivo tumor tissue staining and in vivo optical imaging. The peptide was further labeled with ¹⁸F for positron emission tomography (PET) imaging studies. Cell uptake and efflux and ex vivo biodistribution were also performed with ¹⁸F labeled osteosarcoma specific peptide. ASGALSPSRLDT was the dominant sequence isolated from biopanning and named as OSP-1. OSP-1 shares a significant homology with heparinase II/III family protein, which binds and reacts with heparan sulfate proteoglycans (HSPGs). The fluorescence staining showed that FITC-OSP-1-phage or Cy5.5-OSP-1 had high binding with 143B, much less binding with UM-SCC1 human head and neck squamous cell carcinoma cells, and almost no binding with 293T cells; whereas the scrambled peptide OSP-S had virtually no binding to all three cell lines. In optical imaging, the accumulation of Cy5.5-OSP-1 in 143B tumors was clearly visualized and the signal was stronger than Cy5.5-OSP-S in 143B tumors. In PET imaging, ¹⁸F-OSP-1 had significantly higher accumulation in 143B tumor cells both in vitro and in vivo than ¹⁸F-OSP-S. ¹⁸F-OSP-1 also had higher uptake in 143B tumors than UM-SCC-1 tumors. Our data suggest that OSP-1 peptide is osteosarcoma specific, and the binding site of OSP-1 might be related to heparan sulfate proteoglycans. Appropriately labeled OSP-1 peptide has the potential to serve as a novel probe for osteosarcoma imaging.



Presentation Number **0845B**

Poster Session 3c: In Vivo Studies & Development/Novel Use of Imaging Probes

A novel generator for 68Ga-PET radiopharmaceuticals

Ming-Hsin Li, Wuu-Jyh Lin, Isotope Application Division, Institute of Nuclear Energy Research, Longtan, Taoyuan County, Taiwan.
Contact e-mail: mhli@iner.gov.tw

Objectives PET is a powerful diagnostic and imaging technology which requires short-lived positron emitting isotopes. ^{68}Ga coupling to small bio-molecule is potentially an alternative to ^{18}F - and ^{11}C -based radiopharmaceuticals. In particular, ^{68}Ga -peptides coupled receptors on tumor cells have shown pre-clinically and clinically high and specific tumor uptake. The ^{68}Ga generator provides a positron emitter for the synthesis of radiopharmaceuticals for PET independent of a cyclotron. Existed problems: 1. Volatility of GeCl_4 , spread of airborne. 2. Eluted in a large volume of acid ($>5\text{mL}$). 3. Containing metal impurities, such as Zn(II) , Ti(IV) , Fe(III) (high affinity to DOTA). 4. Breakthrough of ^{68}Ge . Methods An innovative $^{68}\text{Ge}/^{68}\text{Ga}$ generator for ^{68}Ga -PET Radiopharmaceuticals was developed. A novel type of a binary enriched- $^{69}\text{Ga}/\text{Ag}$ alloy electrodeposited on silver substrate as a solid target was developed. It was successfully used for the preparation of $^{68}\text{Ge}/^{68}\text{Ga}$ generator. The deposition was carried out in an alkali solution containing gallium, silver and certain electrolytes at controlled current and ambient temperature that the quality of the deposits was proved to be suited for target irradiation. The operational specification of ^{68}Ge was 200 micro-Amperes at 26MeV proton bombardment for 12000 micro-Ampere-Hour on this deposits via the $^{69}\text{Ga}(p,2n)$ reaction. In the chemical process, a macroporous styrene-divinylbenzene copolymer was selected as an adsorbent for 10 mCi $^{68}\text{Ge}/^{68}\text{Ga}$ -generator and eluted by 0.1M sodium citrate. However, the eluate is citrate form and normally contaminated with long-lived ^{68}Ge and other small amounts of Zn(II) , Ti(II) , Fe(III) and residuals. In a method, the citrate form conversion and its concentration and purification of the initial generator eluate are performed using an inorganic/organic column for ion exchanger. Results The retained radioactivity was eluted from the cartridge with 3mL of 0.1M HCl to yield a ^{68}Ga chloride solution free from citrate ion, ready to be used for labeling. It was revealed from long-term elution tests that approximately $>95\%$ of ^{68}Ga could be eluted from the generator column with 10 ml of 0.1M sodium citrate per elution, while the ^{68}Ge leakage was less than 0.0005% of the ^{68}Ge adsorbed on resin. The innovative generator exhibited a better performance in high radio- and chemical purities of the eluates are quite satisfactory for automated labeling applications.

Presentation Number **0846B**

Poster Session 3c: In Vivo Studies & Development/Novel Use of Imaging Probes

¹¹C-Labeled cetrozole and its analogs: excellent PET probes for aromatase

Kayo Takahashi¹, Takamitsu Hosoya², Kayo Onoe¹, Hisashi Doi¹, Hiroko Nagata¹, Yumiko Watanabe¹, Yasuhiro Wada¹, Tadayuki Takashima¹, Yumiko Katayama¹, Hajime Yamanaka¹, Masaaki Suzuki¹, Hiroataka Onoe¹, Yasuyoshi Watanabe¹, ¹Center for Molecular Imaging Science, RIKEN, Kobe, Japan; ²Graduate School of Biomedical Science, Tokyo Medical and Dental University, Tokyo, Japan. Contact e-mail: kayo.takahashi@riken.jp

Aromatase is an enzyme that converts androgens to estrogens. It plays a crucial role in hormone-dependent breast cancer, since breast cancer cells highly express aromatase and local synthesis of estrogen stimulates proliferation of cancer cells. Besides the breast cancer, the enzyme aromatase in the brain is involved in emotional behavior, synaptic plasticity, and neuroprotection. To develop a new diagnosis method for breast cancer and also to investigate the functional activity of aromatase in the brain, we have developed novel PET probes, [¹¹C]cetrozole and its analogs, which allowed to quantify the aromatase level in the living body. [¹¹C]Cetrozole has a superiority as a PET probe in terms of specificity and selectivity as compared with [¹¹C]vorozole, which has been developed for aromatase imaging previously, and none or trace amount of radiolabeled metabolites of [¹¹C]cetrozole was taken up into the brain. Using [¹¹C]cetrozole, we discovered the localization of aromatase in the nucleus accumbens of the nonhuman primate (rhesus monkey). ¹¹C-Labeled cetrozole and its analogs have expanded the possibilities to develop a new diagnosis method for breast cancer and to carry out further research on aromatase in emotional disorders.

Presentation Number **0847B**

Poster Session 3c: In Vivo Studies & Development/Novel Use of Imaging Probes

Biodistribution of $^{99m}\text{Tc}(\text{I})$ -labeled new octreotide derivatives in AR42J pancreatic tumor-bearing mice

Wan-Jou Chen¹, **Shu-Pei Chiu**², **Yu-En Cheng**¹, **Te-Wei Lee**², **Jem-Mau Lo**¹, ¹*Department of Biomedical Engineering and Environment Sciences, National Tsing Hua University, Hsinchu, Taiwan;* ²*Isotope Application Division, Institute of Nuclear Energy Research, Longtan, Taiwan. Contact e-mail: wunjou11@ms65.hinet.net*

Objective: We have prepared three $^{99m}\text{Tc}(\text{I})$ -octreotide complexes conjugated with histidine. The new ^{99m}Tc -octreotide analogs have been investigated for their potential as an imaging agent for the endocrine tumors with overexpression of somatostatin receptor in this work. **Methods:** The three histidine-tagged octreotide derivatives, his-octreotide, his₃-octreotide and his₅-octreotide, were synthesized by a solid phase peptide synthesis method employing Fmoc strategy. The receptor binding affinities of the three octreotide derivatives were tested against human somatostatin sst_{2a} receptor using [¹²⁵I]Tyr¹¹-Somatostatin 14 as the radioligand and octreotide as the control. The three octreotide derivatives were labeled with ^{99m}Tc by using [$^{99m}\text{Tc}(\text{CO})_3(\text{OH}_2)_3$]⁺ as a precursor to obtain $^{99m}\text{Tc}(\text{I})$ -his-octreotide, $^{99m}\text{Tc}(\text{I})$ -his₃-octreotide and $^{99m}\text{Tc}(\text{I})$ -his₅-octreotide. *In vitro* stabilities of the three radioligands were measured in normal saline and rat plasma at room temperature and 37°C by ITLC. The biodistribution study and SPECT/CT imaging of the three radioligands were executed using AR42J pancreatic tumor-bearing SCID mice. **Results:** In *in vitro* receptor binding assay, his-octreotide, his₃-octreotide and his₅-octreotide were found to exhibit similarly high affinities for human somatostatin sst_{2a} receptor with IC₅₀ at 1.83, 2.11 and 1.41 nM, respectively. The three $^{99m}\text{Tc}(\text{I})$ -labeled octreotide analogs were prepared with radiochemical yield greater than 90% and used for subsequent *in vivo* experiments without further purification. All of the three radioligands showed high stability in normal saline. However, $^{99m}\text{Tc}(\text{I})$ -his-octreotide and $^{99m}\text{Tc}(\text{I})$ -his₃-octreotide degraded apparently in rat plasma at 37°C, while $^{99m}\text{Tc}(\text{I})$ -his₅-octreotide maintained its stability in the medium. It was demonstrated from biodistribution study that all of the three radioligands cleared rapidly from the blood and presented significant tumor uptakes in AR42J pancreatic tumor-bearing SCID mice. All of the radioligands were primarily hepatobiliarily eliminated and subsidiarily excreted with kidneys. In SPECT/CT imaging studies, both $^{99m}\text{Tc}(\text{I})$ -his₃-octreotide and $^{99m}\text{Tc}(\text{I})$ -his₅-octreotide showed higher tumor uptakes than $^{99m}\text{Tc}(\text{I})$ -his-octreotide in AR42J pancreatic tumor-bearing SCID mice. **Conclusion:** From the *in vitro* and *in vivo* studies, it is concluded that $^{99m}\text{Tc}(\text{I})$ -his₅-octreotide exhibits higher potential as an imaging agent for somatostatin-receptor expressed endocrine tumors than the other two $^{99m}\text{Tc}(\text{I})$ -labeled histidine-tagged octreotide derivatives and is worthy to be selected for further study.

Presentation Number **0848B**

Poster Session 3c: In Vivo Studies & Development/Novel Use of Imaging Probes

Production of high specific activity [¹¹C]phosgene from [¹¹C]carbon monoxide

Oleksiy Itsenko¹, Gunnar Antoni², Tor Kihlberg³, ¹Uppsala ASL, GE Healthcare, Uppsala, Sweden; ²Department of Oncology, Uppsala University, Uppsala, Sweden; ³Uppsala Imanet, GE Healthcare, Uppsala, Sweden. Contact e-mail: oleksiy.itsenko@ge.com

Introduction. Increasing the specific activity (SA) of PET tracers is imperative from toxicological, biochemical, and regulatory perspectives. [¹¹C]Phosgene is an important labelled building block for the production of [¹¹C-carbonyl]ureas and carbamates, both cyclic and acyclic. Though established over 30 years ago, its synthesis is still evolving, with the focus on improving specific radioactivity and the stability of production. **Methods.** We designed a three-valve unit to complement and utilize the technical advantages of our [¹¹C]carbon monoxide system. First, [¹¹C]carbon dioxide is reduced over zink to [¹¹C]carbon monoxide, which is further photochemically chlorinated to generate [¹¹C]phosgene: $^{11}\text{CO} + \text{Cl}_2 \rightarrow ^{11}\text{COCl}_2$. For increasing SA we sought to minimize isotopic dilution through reducing reaction volumes and associated amounts of reactants: only 200 μL of chlorine gas (STP) was sufficient. **Results and discussion.** To evaluate performance during optimization we used the following test reaction, which is known to be clean and instantaneous at r.t.: $\text{PhNH}_2 + ^{11}\text{COCl}_2 \rightarrow (\text{PhNH})_2^{11}\text{CO}$. The conversion of ^{11}CO to $^{11}\text{COCl}_2$ reached 70–85% in 3 minutes and specific radioactivity – 200 GBq/ μmol and beyond. Separate experiments confirmed that isotopic dilution during the labelling synthesis was negligible. Influence of operational parameters and external factors on conversion and yields has been also studied. **Conclusion.** [¹¹C]Phosgene was reliably produced with high SA from [¹¹C]carbon monoxide using a small-sized remote-controlled unit. Since the process includes handling only gases it is operationally simple.

Presentation Number **0849B**

Poster Session 3c: In Vivo Studies & Development/Novel Use of Imaging Probes

[¹⁸F]FMISO Synthesis on an Integrated Disposable Microfluidic Device

Victor Samper¹, **Stefan Riese**³, Christian Rensch¹, Christoph Boeld¹, Gerald Reischl², Nicole Heumesser², Walter Ehrlichmann², Marko K. Baller¹, ¹GE Global Research, Garching b. München, Germany; ²Radiopharmacy, University Hospital Tuebingen, Tuebingen, Germany; ³GE Healthcare, Muenster, Germany. Contact e-mail: stefan.riese@ge.com

Objectives Miniature fluidic synthesizers promise the advantages of high levels of component and functionality integration in a low-cost, small size, single use format. In addition, performance enhancements are anticipated due to improved process control and higher concentrations. The objective of this work was to investigate a miniature fluidic platform for synthesis of [¹⁸F]FMISO. Methods A TOPAS COC (cyclic olefin copolymer) device consisting of 5 valves, 8 input/outputs, an electrochemical phase transfer element, and 2 thermal reactors, was fabricated by bonding together 3 layers of 2 mm thick COC and one layer of 80µm thick foil. The device was 95 mm x 60 mm x 6 mm and used external heaters, valve actuators, and syringe pumps for performing labeling of <500 µg of NITTP precursor in <100µl of DMSO in 60-120 seconds at 113°C. Heat was applied by a double-side heating arrangement that utilized the stored heat in the plastic structure to achieve rapid heating and good temperature control of the reaction solution*. The septa and input/outputs were designed to provide reliable connections. The valves utilized a deformable membrane that was deflected by an external actuator. The valves were used to steer fluids on the device, selecting waste or product at each step in the synthesis procedure. [¹⁸F]Fluoride in H₂O was used as the input source of activity, K₂222/K₂CO₃ in DMSO was used for phase transfer, and HCl (1M) at 80°C was used for deprotection. Fluids were either moved continuously through the device, or were transported from one process element on the device to the next, stopping at each element for the duration of the process. Results Initial experiments gave an overall phase transfer efficiency of up to 25% using the integrated electrochemical phase transfer block. Labeling was investigated with conventionally (externally) dried fluoride and electrochemically dried fluoride. Both resulted in labeling yields of >80%, followed by near quantitative deprotection using HCl (aq). Conclusion The results reported demonstrate a full synthesis of [¹⁸F]FMISO on an integrated miniature fluidic platform that incorporates all synthesis sub-components. The high labeling yield achieved in 60-120 seconds provides first evidence that a miniature platform may result in performance improvements when compared to conventional scale devices. Acknowledgements Work funded in part by Bavarian State (Germany). Devices produced by RKT GmbH. References *Riese et al, Numerical simulation of heat transfer ..., WMIC 2009

Presentation Number **0850B**

Poster Session 3c: In Vivo Studies & Development/Novel Use of Imaging Probes

Reducing contaminants in thalious (201Tl) chloride for myocardial phantom

Ming-Hsin Li, Isotope Application Division, Institute of Nuclear Energy Research, Longtan, Taoyuan County, Taiwan. Contact e-mail: mhli@iner.gov.tw

Objective With interesting, we review the article of Staelens et al.[2008] and Ensing et al.[2008] on the radionuclidic impurities in 201Tl-Cl3. In these articles, Staelens shows convincingly that the contaminant 200Tl and 202Tl isotopes, when present in levels of 1% at Activity Reference Time (ART), can cause degradation of the contrast obtained in a myocardial phantom. In the discussion, the authors warn against use of 201Tl several days before or after ART because of the relative ingrowth of 200Tl (before ART) and 202Tl (after ART). Ensing et al. concluded that the level of contamination routinely found in the 201Tl produced at the Covidien plant in Petten (The Netherlands) is a factor 10 (200Tl) and 3 (202Tl) lower than the 1% assumed in the calculations of Staelens et al. Method Traditional process for the solid target for 201Tl-Cl3 involves electroplating to stabilize Tl-203 metal on a solid target, irradiating the solid target with by radiation energy 30 MeV for a higher yield, measuring the activity by radioactivity measuring instrument and accordingly calculating the yields. We used the incident energy/cross section relationship (Fig 1, Table 1) to fit our cyclotron infrastructure for maximum synergy about the higher yield and fewer contaminants. Fig 1 incident energy/cross section relationships Result Table 2 Conclusion Our samples from each production of 201Tl have been analysed for both admixtures, and the results from this year and the preceding 4 years are shown in Table 2. We think that it is important to mention that the lower level of contamination routinely found in the 201Tl produced at the TR30 cyclotron in INER(Institute of Nuclear Energy Research) is a factor 25 (200Tl) and 2 (202Tl) lower than the 1% assumed in the calculations of Staelens et al.

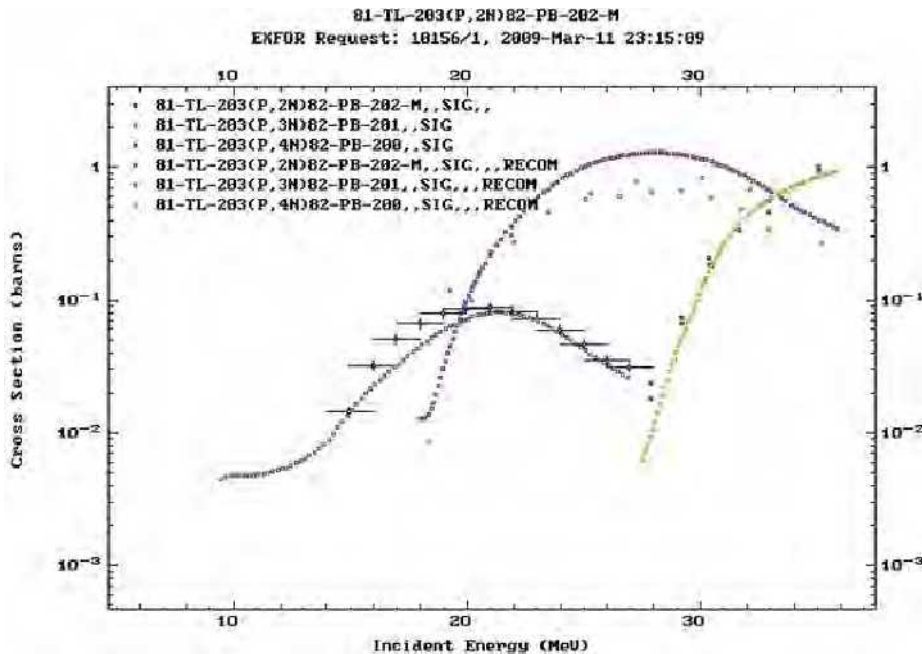


Table 1 Parameters for the production of 201Tl radioisotope

irradiation energy	Beam current	Quantity of Tl-203	Thickness of Tl-203
28.51 MeV	200 uA / 10 hr	2g	0.74mm at a glancing angle of 7 degrees
Table 2 Admixtures (±1 S.D.) of 200Tl at ART, and 201Tl at ART, and 202Tl at ART, for several hundred samples from the 201Tl production produced from 2005 to 2009			
Year	Samples	200Tl admixture (kBq/1MBq 201Tl)	202Tl admixture (kBq/1MBq 201Tl)
2005	282	0.41 ± 0.44	6.70 ± 2.00
2006	297	0.47 ± 0.55	5.02 ± 2.66
2007	286	0.45 ± 0.72	5.06 ± 3.84
2008	297	0.34 ± 0.65	3.15 ± 2.40
2009	254	1.16 ± 1.35	5.54 ± 2.60

Presentation Number **0851B**

Poster Session 3c: In Vivo Studies & Development/Novel Use of Imaging Probes

Synthesis of ApoSense compound [¹⁸F] 2-(5-(dimethylamino)naphthalene-1-sulfonamido)-2-(fluoromethyl)butanoic acid (NST732) via nucleophilic ring-opening of activated aziridine

Falguni Basuli, Haitao Wu, Zhen-Dan Shi, Gary L. Griffiths, **Agnieszka Sulima**, NHLBI, NIH, Rockville, MD, USA. Contact e-mail: agnieszs@mail.nih.gov

2-(5-(dimethylamino)naphthalene-1-sulfonamido)-2-(fluoromethyl)butanoic acid (NST732) is a member of the ApoSense® family of compounds, capable of selective targeting, binding and accumulation within cells undergoing apoptotic cell death. It has application in molecular imaging and blood clotting particularly for monitoring anti-apoptotic drug treatments. We are investigating a fluorine-18-radiolabeled analog for positron emission tomography studies. For its radiosynthesis, reaction of the tosylate precursor methyl 2-(5-(dimethylamino)naphthalene-1-sulfonamido)-2-(tosyloxymethyl)butanoate in 1:1 acetonitrile, dimethylsulfoxide with [¹⁸F] tetrabutyl ammonium fluoride (TBAF) proceeds through an aziridine intermediate to afford two regioisomers [¹⁸F] 2-(5-(dimethylamino)naphthalene-1-sulfonamido)-2-fluorobutanoate and [¹⁸F] methyl 2-(5-(dimethylamino)naphthalene-1-sulfonamido)-2-(fluoromethyl)butanoate. [¹⁸F] 2-((5-Dimethylamino)naphthalene-1-sulfonamido)methyl)-2-fluorobutanoic acid (NST732) was then obtained by the hydrolysis of corresponding [¹⁸F]-labeled ester with 6N hydrochloric acid. The total radiochemical yield was 7% (uncorrected) in a 90 minute synthesis time. In conclusion, we have established a convenient synthetic pathway to prepare both [¹⁸F]-radiolabeled NST732 and its corresponding reference standard compounds for the study of drug-mediated apoptosis.

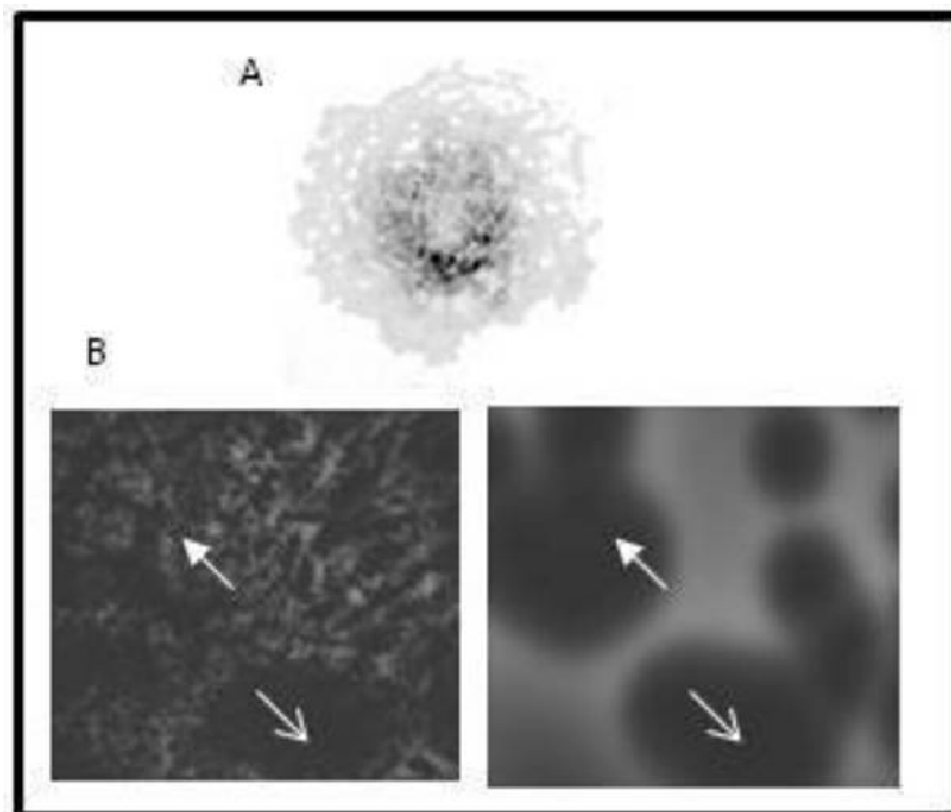
Presentation Number **0852B**

Poster Session 3c: In Vivo Studies & Development/Novel Use of Imaging Probes

Kinetic Modeling of the Hypoxia Marker EF5 in Multicellular Tumour Spheroids and Xenografts

Catherine Kelly¹, **Bart Cornelissen**¹, Sir Michael Brady², Ruth Muschel¹, ¹Gray Institute for Radiation Oncology and Biology, University of Oxford, Oxford, United Kingdom; ²Wolfson Medical Vision Laboratory, University of Oxford, Oxford, United Kingdom. Contact e-mail: bart.cornelissen@rob.ox.ac.uk

Aims: EF5 is a promising dual PET/immunohistochemical hypoxic marker. To fully comprehend its scope as an investigative tool, a quantitative understanding of its biodistribution in tissue is crucial. We use 3D multicellular tumour spheroids (MTS) and kinetic modeling to describe EF5 biodistribution and validate our model using dual-stained xenograft sections. **Methods:** MTS were incubated with EF5 over a timecourse. Adjacent sections were stained for EF5 and cell viability. To obtain kinetic parameters, intensity profiles were fit to a reaction-diffusion model describing binding as a function of oxygen, cell viability and diffusion. The model was validated by comparing real and simulated biodistributions in 2D tumour sections contained with EF5 and the vascular marker CD31, using CD31 to define boundary conditions for delivery. [¹⁸F]-EF5 PET dynamic tissue activity curves (TACs) were simulated from the 2D maps for well and poorly-vascularised tissues. **Results:** EF5 adducts are present in spheroids in regions beyond the theoretical diffusion distance of oxygen, but are reduced in necrotic regions. 2D tissue simulations, obtained using the parameterized model, generally agree with the ground truth, although in some cases vascular and hypoxia staining overlap, suggesting acute hypoxia. [¹⁸F]-EF5 TAC shapes are characteristic for nitroimidazole binding, with well-vascularised TACs following the input function and poorly-vascularised TACs displaying a low initial perfusion peak followed by steep binding. **Conclusion:** Our model adequately describes the binding of the hypoxic marker EF5 in diffusion-limited hypoxia and provides a general tool for analysis of how changes in vasculature affect macroscale PET observations. Discrepancies between predicted and true distributions highlight the issue of temporally varying signals resulting from acute hypoxia.



A: EF5 stained (black) spheroid section B: Real and simulated EF5 distribution showing areas of agreement (thin arrow) and disagreement (solid arrow).

Presentation Number **0853B**

Poster Session 3c: In Vivo Studies & Development/Novel Use of Imaging Probes

Synthesis of a ⁶⁴Cu-labeled peptide and its application for non-invasive PET imaging of uPAR in cancer xenografts in mice

Morten Persson^{1,3}, **Jacob Madsen**², **Søren Østergaard**⁵, **Michael Ploug**^{1,4}, **Andreas Kjaer**^{2,3}, ¹*The Danish-Chinese Center for Proteases and Cancer, , Copenhagen, Denmark;* ²*Department of Clinical Physiology, Nuclear Medicine & PET, Rigshospitalet, Copenhagen, Denmark;* ³*Cluster for Molecular Imaging, University of Copenhagen, Copenhagen, Denmark;* ⁴*Finsen Laboratory, Rigshospitalet, Copenhagen, Denmark;* ⁵*Novo Nordisk A/S, , Copenhagen, Denmark. Contact e-mail: mpersson@mfi.ku.dk*

Background & Aim The urokinase-type plasminogen activator receptor (uPAR) has been shown to facilitate cancer cell invasion and metastasis. uPAR is over-expressed in various human cancers, including breast, prostate and colorectal cancer. With a view to future tailoring of uPAR-targeted therapies, we aimed at developing an in vivo imaging positron-emission-tomography (PET) probe, which could identify cancer patients with high expression levels of uPAR. **Methods** The affinities for human uPAR of a the new PET probe comprising a linear uPAR targeting peptide (AE105) conjugated with macrocyclic chelator DOTA (AE219) and a double-mutated non-binding version (AE254) were measured using surface plasmon resonance. The ⁶⁴Cu-labeled AE219 was further characterized in vivo in four different human cancer xenograft mouse models: H727, HT-29, A2780 and U87MG with a different uPAR expression levels (n=10 mice, 2 tumors/mice). Nude mice each carrying one of these xenografts were injected intravenously with the PET-tracer and 10 min static PET scans were performed 1, 4.5 and 22 hrs post injection, followed by computed-tomography (CT) scan. Another group of mice were probed with ¹⁸F-FDG (n=10) and the results were compared with the results obtained with the uPAR tracer. All tumors were analyzed for uPAR expression using validated ELISA method. In addition, a separate group of tumor-bearing mice were subjected to biodistribution analysis of ⁶⁴Cu-AE219 (n=3 mice) and the control tracer ⁶⁴Cu-AE254 (n=3 mice) using a well-counter. **Results** The IC50-values for AE219 and AE254 were determined to be 7 nM and 78 μM, respectively. To achieve an efficient radiolabeling with ⁶⁴Cu, 10 nmol peptide, pH = 8, 1 hr at 90°C was found to be optimal conditions. No correlation between FDG uptake and uPAR expression was found (p=0.30, r=0.24). In contrast, a significant correlation was found for ⁶⁴Cu-AE219 tumor uptake and uPAR expression after both 1.0 hr (p=0.01, r=0.53), 4.5 hrs (p=0.0075, r=0.57) and 22 hrs (P<0.0001, r=0.76) across all four cancer xenograft models (n=20 tumors). A significant decrease in tumor uptake based on well-counter analysis (n=6 tumors) in the U87MG xenograft was found for ⁶⁴Cu-AE254 compared with ⁶⁴Cu-AE219 tumor uptake after 4.5 hrs post injection (p=0.028), thus validating the specificity of the tracer towards human uPAR. **Conclusion** Our data demonstrate a significant correlation between uPAR expression and tumor uptake of our PET tracer, which highlight ⁶⁴Cu-AE219 as a promising radiotracer for non-invasive and specific detection of uPAR in human cancers.

Presentation Number **0854B**

Poster Session 3c: In Vivo Studies & Development/Novel Use of Imaging Probes

MICROPET IMAGING OF [¹⁸F]-AV-45 IN TRANSGENIC MOUSE BRAIN: A POTENTIAL BIOMARKER OF PATHOGENIC PROCESSES IN ALZHEIMER'S DISEASE

Xuan Zhang¹, Merle G. Paule¹, Glenn D. Newport¹, Fang Liu¹, Natalya V. Sadovova², Marc Berridge³, Scott M. Apana³, Laurence (Larry) C. Schmued¹, William Slikker¹, Cheng Wang¹, ¹NCTR/FDA, Jefferson, AR, USA; ²Toxicologic Pathology Associates, Jefferson, AR, USA; ³3D Imaging, LLC, Little Rock, AR, USA. Contact e-mail: xuan.zhang@fda.hhs.gov

Alzheimer's disease (AD) leads to 2/3 of all age-related human dementias. As a neurodegenerative disease, it has a high incidence in the aged. The defining pathologic characteristic associated with AD is the presence of β -amyloid (A β) plaques in the brain. The TG2576 transgenic mouse, that was developed to mimic human AD pathology, over-expresses the Indiana mutation of human amyloid precursor protein (APP) and develops amyloid plaques by 6-7 months of age. The high-resolution positron emission tomography scanner (microPET), an instrument that can provide in vivo molecular imaging at useful resolution in mouse brain, has been proposed as a minimally-invasive method for detecting A β aggregates in the transgenic mouse using the fluoropegylated tracer (E)-4-(2-(6-(2-(2-(2-18F-fluoroethoxy)ethoxy)ethoxy)pyridine-3-yl)vinyl-N-methyl benzenamine ([¹⁸F]-AV-45). To assess the accumulation of amyloid plaques in brain, both transgenic and wildtype mice were scanned at two time points, 3 and 8 months of age. At both time points, [¹⁸F]-AV-45 (7.5 MBq) was injected into the tail vein of the transgenic and wildtype mice and static microPET images were obtained over 1.5 hours following the injection. Radiolabeled tracer accumulation in the region of interest (ROI) in the frontal cortex was converted into Standard Uptake Values (SUVs). No significant difference was found in radiotracer uptake in the frontal cortex of the brains of 3 month old transgenic mice compared with wildtype controls. In images obtained at 8 months of age, the uptake of [¹⁸F]-AV-45 was significantly increased in the ROI of the transgenic mice. Additionally, the duration required for wash-out of the tracer was prolonged in the transgenic mice. This preliminary study demonstrates that microPET imaging that targets amyloid plaque deposition in vivo can serve as a minimally-invasive assessment tool for monitoring a potential biomarker of pathogenic processes associated with Alzheimer's disease. Avid provides precursor and radiosynthesis methods.

Presentation Number **0855B**

Poster Session 3c: In Vivo Studies & Development/Novel Use of Imaging Probes

PET imaging of integrin expression using fluorine-18 labeled knottin peptides

Shuanglong Liu, Hongguang Liu, Gang Ren, Richard Kimura, Jennifer R. Cochran, Sanjiv S. Gambhir, Zhen Cheng, MIPS, Stanford University, Stanford, CA, USA. Contact e-mail: scottliu@stanford.edu

Knottins peptides 2.5D and 2.5F were engineered, in which 2.5D was successfully ^{18}F -labeled with succinimidyl 4- ^{18}F -fluorobenzoate (18F-SFB). The resulted probe, 18F-FB-2.5D, had been tested in vivo in U87MG glioblastoma xenografts. High liver and gallbladder uptake demonstrated the suboptimal pharmacokinetics of the 18F-FB-2.5D. In this research, our objective is to further optimize and evaluate the radiofluorinated knottins (2.5D, 2.5F) using 4-nitrophenyl 2- ^{18}F -fluoropropionate (18F-NFP) for PET imaging of integrin positive tumors in living subjects. The decay-corrected radiochemical yields of 18F-FP-2.5D and 18F-FP-2.5F based on 18F-NFP are more than 60% with radiochemical purities of >99% and high specific activities (20-40 GBq/ μmol). 19F-FP-2.5D and 19F-FP-2.5F specifically compete with ^{125}I -echistatin for binding to cell surface integrins with an IC_{50} of 79 nM and 107 nM. In vivo microPET imaging of 18F-FP-2.5D and 18F-FP-2.5F exhibits excellent tumor uptake in U87MG glioblastoma mice [4.8 and 5.2 %ID/g, respectively at 30 min post injection (p.i.)] and also rapid clearance through the blood and kidneys, thus leading to excellent tumor-to-normal tissue contrasts. The gallbladder uptake is appreciably lower for 18F-FP-2.5D (0.5%ID/g) compared with 18F-FB-2.5D (3.5%ID/g) at 1 h p.i. Biodistribution studies demonstrate that 18F-FP-2.5D and 18F-FP-2.5F have reduced tumor uptakes at 2 h p.i. when co-injected with c(RGDyK). In conclusions, 18F-NFP radiolabeling significantly improved the overall labeling yield of peptides. 18F-FP-2.5D and 18F-FP-2.5F also show reduced uptakes in some normal organs and similar tumor targeting efficacy as compared with 18F-FB-2.5D. Taken together, 18F-FP-2.5D and 18F-FP-2.5F allow integrin-specific PET imaging of U87MG tumors with high contrast. Knottins are excellent peptide scaffolds for development of PET probes for clinical translation.

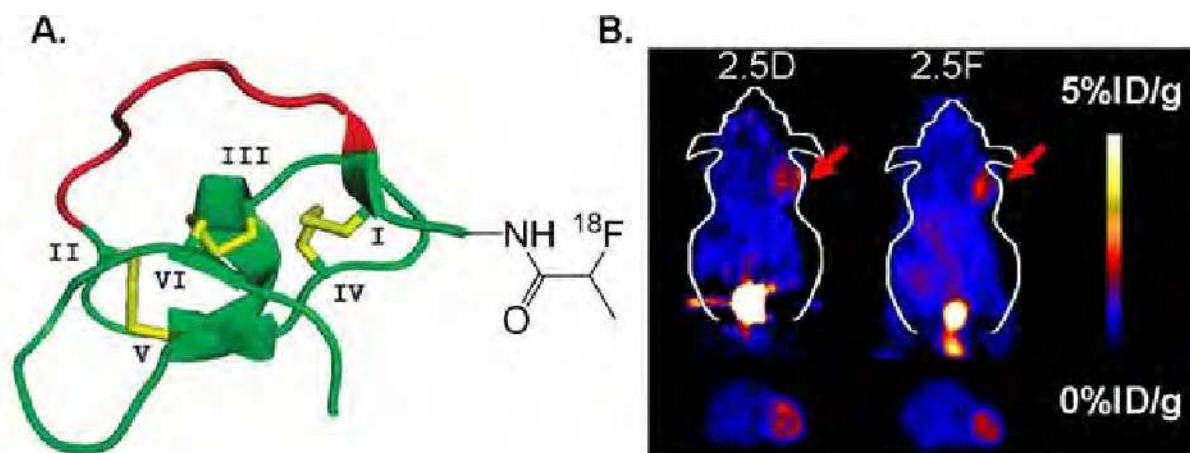


Figure (A). Cartoon representation of knottin peptide scaffold. The imaging label ^{18}F -NFP was site-specifically conjugated to the N terminus amine. (B) Decay corrected coronal (top) and transaxial (bottom) microPET images of nude mice bearing U87MG tumor ($n = 3$ for each group). Images were acquired 2 h after tail vein injection of 18F-FP-2.5D or 18F-FP-2.5F (3.7 MBq, 100 μCi). Red arrows indicate the location of tumors.

Presentation Number **0856B**

Poster Session 3c: In Vivo Studies & Development/Novel Use of Imaging Probes

Rhenium complexes of sugar substituted polypyridyl analogue ligands for the development of radio tracers

Michael Gottschaldt, Justyna A. Czaplowska, Ulrich S. Schubert, *Institute for Organic and Macromolecular Chemistry, Friedrich-Schiller-University of Jena, Jena, Germany. Contact e-mail: michael.gottschaldt@uni-jena.de*

Sugars containing metal complexes are increasingly examined in medicinal inorganic chemistry. Appending a carbohydrate to an active metal complex has the ability to reduce toxicity, increase solubility and to target sugar specific receptors or metabolic pathways.[1, 2] On the other hand polypyridyl derivatives are well-known ligands for the formation of various stable metal complexes such as from ruthenium or rhenium.[3, 4] In order to obtain sugar functionalized polypyridyl analogue ligands the copper catalyzed 1,3-dipolar cycloaddition ("click") reaction was used to prepare bipyridyl or terpyridyl analogue triazoles bearing various protected and unprotected sugar moieties (Figure 1). The ligands containing galactosyl, glucosyl, maltosyl, xylosyl or mannosyl residues were complexed to the Re(I) carbonyl core and the structures of the resulting complexes were examined. The stability of the complexes was determined in a histidine challenge experiment. The complexes were found to have a high in vitro stability over a period of 4.5 h whereas ligand exchange could be observed after 24 h. Furthermore, the complexes were shown to be non-toxic up to a concentration of 100 μM against HepG2 cells. With these results the ligands are promising candidates for further investigations towards the development of 99m-technetium radio tracers. [1] M. Gottschaldt, U. S. Schubert, *Chem. Eur. J.* 2009, 15, 1548-1557. [2] M. Gottschaldt, C. Bohlender, D. Müller, I. Klette, R. P. Baum, S. Yano, U. S. Schubert, *Dalton Trans.* 2009, 5148-5154. [3] M. Gottschaldt, U. S. Schubert, S. Rau, S. Yano, J. G. Vos, T. Kroll, J. Clement, I. Hilger, *ChemBioChem* 2010, 11, 649-652. [4] M. Gottschaldt, D. Koth, D. Müller, I. Klette, S. Rau, H. Görls, B. Schäfer, R. P. Baum, S. Yano, *Chem. Eur. J.* 2007, 13, 10273-10280.

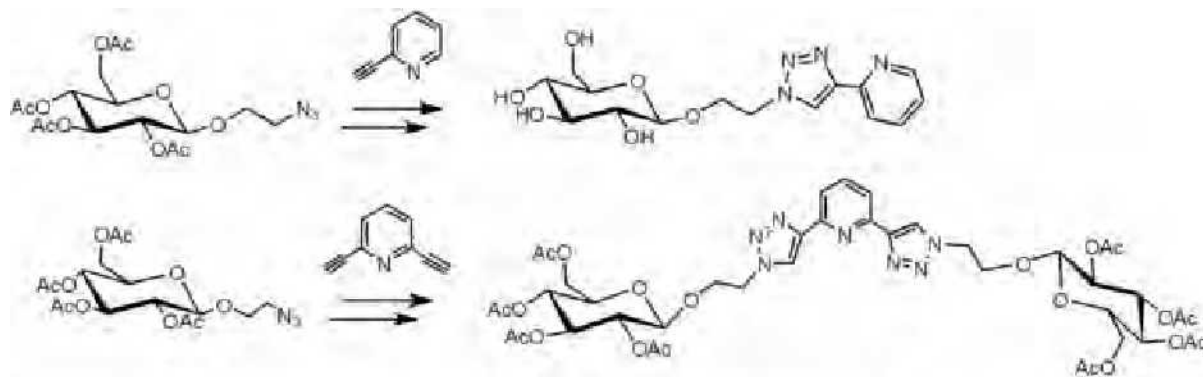


Figure 1: Schematic representation of examples for the 1,3-dipolar cycloaddition ("click") reaction for the synthesis of sugar substituted polypyridyl analogue triazoles.

Presentation Number **0857B**

Poster Session 3c: In Vivo Studies & Development/Novel Use of Imaging Probes

Synthesis and characterization of scVEGF-PEG-[68Ga]NOTA and scVEGF-PEG-[68Ga]DOTA

Elisabeth Blom², Irina Velikyan^{2,3}, Azita Monazzam², Pasha Razifar², Manoj Nair², Arcadius V. Krivoshein¹, Marina Backer¹, Joseph M. Backer¹, Bengt Långström², ¹SibTech, Inc., Brookfield, CT, USA; ²Department of Biochemistry and Organic Chemistry, Uppsala University, Uppsala, Sweden; ³Division of Biomedical Radiation Sciences, Rudbeck Laboratory, Uppsala University, Uppsala, Sweden. Contact e-mail: jbacker@sibtech.com

Angiogenesis is an important process in tumor growth, which is driven by vascular endothelial growth factor (VEGF) acting via its receptors, particularly VEGFR-2. These receptors are overexpressed by endothelial cells in angiogenic vs. quiescent vasculature, and are the target of several approved and many experimental therapeutics. Recent imaging studies (Transl. Oncol. 3:56,2010) indicate that VEGFR-2 prevalence reflects the effects of anti-angiogenic therapy and therefore development of new imaging tracers for VEGFR-2 imaging has a significant translational potential. For positron emission tomography (PET) imaging of VEGFR-2 with ⁶⁸Ga we developed scVEGF-based conjugates with macrocyclic chelator, either 2,2',2''-(1,4,7-triazonane-1,4,7-triyl)triacetic acid (NOTA) or 2,2',2''-2'''-(1,4,7,10-tetraazacyclododecane-1,4,7,10-tetrayl)tetraacetic acid (DOTA), site-specifically conjugated via polyethylene glycol (PEG) linkers of 2.0, 3.4, or 5.0 kDa. The targeting protein, scVEGF is a functionally active single-chain version of VEGF that consists of two 3-112 amino acid fragments of human VEGF₁₂₁ genetically fused head-to-tail and expressed with an N-terminal 15-aa Cys-tag for site-specific conjugation of therapeutic and diagnostic payloads, including radionuclide chelators. scVEGF-based tracers bind to and are internalized by VEGFR, providing for enhanced accumulation of contrast agents in targeted cells. The ⁶⁸Ga-labelling was performed at room temperature with NOTA conjugate or at 90 °C by using either conventional or microwave heating with NOTA and DOTA conjugates. More than 90% radioactivity was incorporated within 5 min at room temperature or using conventional heating or within 2 min under microwave heating. The specific radioactivity of the NOTA tracer at the end of synthesis was 195 ± 15 MBq/nmol when running the radiolabelling with 0.5 nmol conjugate and at elevated temperature. The bioactivity of the NOTA tracer in terms of binding kinetics and saturation was tested in multicellular spheroids (MCS) of 293/KDR cells engineered to express high levels of VEGFR-2. The plateau was achieved within the two-hour incubation time. The B_{max} and K_d values were 508 Bq/Viable Volume of MCS, which is equal to 0.12 million binding sites per cell, and 42 nM, respectively. The NOTA tracer was also tested in an in vivo mouse tumor model. A combination of high specific radioactivity and maintenance of functional activity suggests that scVEGF-PEG-[⁶⁸Ga]NOTA and scVEGF-PEG-[⁶⁸Ga]DOTA might be promising tracers and will be further explored.

Presentation Number **0858B**

Poster Session 3c: In Vivo Studies & Development/Novel Use of Imaging Probes

68Ga-folate-based PET radiotracer for detection and monitoring of ovarian carcinoma

Melpomeni Fani^{1,2}, *Maria Luisa Tamma*², *Guillaume Nicolas*³, *Walter Gonzalez*⁴, *Isabelle Raynal*⁴, *Marc Port*⁴, *Wolfgang A. Weber*¹, *Helmut R. Maecke*^{1,2}, ¹*Clinic for Nuclear Medicine, University Hospital Freiburg, Freiburg, Germany;* ²*Division of Radiological Chemistry, University Hospital Basel, Basel, Switzerland;* ³*Department of Nuclear Medicine, University Hospital Basel, Basel, Switzerland;* ⁴*Research Department, Guerbet, Aulnay sous Bois, France. Contact e-mail: melpomeni.fani@uniklinik-freiburg.de*

Introduction: The folate receptor (FR) is overexpressed in a variety of malignant tumors, including > 90% of ovarian and endometrial carcinomas and therefore represents an attractive molecular target. The aim of our study was to develop and evaluate a new 68Ga-folate-based tracer, as a specific PET tracer for FR-expressing tumors. **Methods:** Three FR-positive tumor models were used for the in vivo evaluation of the new radiotracer, named 68Ga-P3246. Two subcutaneous xenograft tumor models were studied in nude mice, one using the human nasopharyngeal carcinoma cell line KB (most often used for the evaluation of FR-targeting agents) and one using ascites from nude mice implanted with human OVCAR-3 ovarian carcinoma cells. Biodistribution and dose-dependence studies, modulation of kidney radiotracer uptake with antifolates, blocking experiments and PET/CT images were performed in these models. Furthermore, a more realistic, orthotopic ovarian cancer model was evaluated in Wistar rats. The animals were separated in two groups, where one of the groups was treated with cisplatin for two months before PET/CT imaging. Non-tumor bearing rats were imaged as a control. PET/CT images of 68Ga-P3246 were evaluated in this tumor model. **Results:** The biodistribution profile of 68Ga-P3246 is characterized by high uptake in the FR-positive tumors (17.0±2.8 and 11.3±3.7 %ID/g for KB and OVCAR-3 tumors, respectively), fast clearance from the blood, low hepatobiliary clearance and almost negligible background at 1 h p.i. The specificity of the radiotracer was confirmed by blocking experiments. High kidney uptake of 68Ga-P3246 was reduced by pre-injection of antifolates, resulting in an improvement of the tumor:kidney ratio by a factor of 3. No significant differences were observed in the tumor uptake and also tumor-to-non tumor ratios for an injected dose ranging from 10 to 800 pmol. The PET/CT studies, showed high uptake in the kidneys, clear visualization of the tumors and very low background activity. In the orthotopic rat tumor model PET/CT with the new radiotracer visualized the primary tumor as well as peritoneal spread, while reduced tumor growth in the cisplatin treated animals was also detected. **Conclusions:** The new 68Ga-folate-based radiotracer, 68Ga-P3246, showed very good in vivo characteristics in ovarian cancer tumor models. The radiotracer is localized specifically to FR-positive tissues, exhibiting low background activity at 1 h p.i. and was able to monitor the effects of cytotoxic therapy.

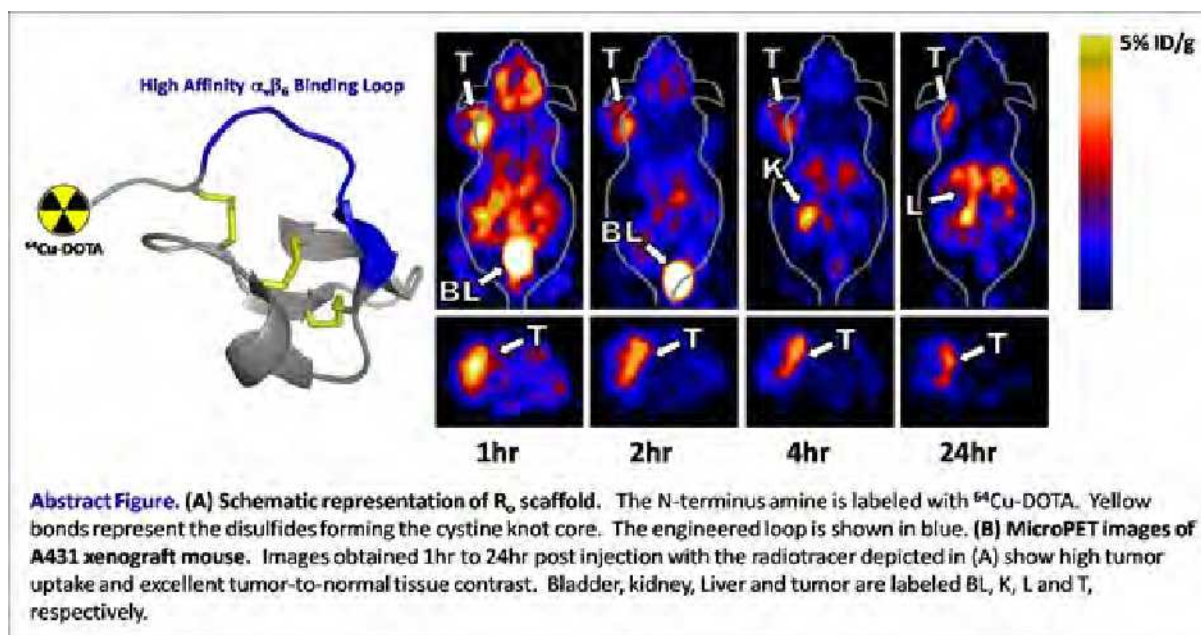
Presentation Number **0859B**

Poster Session 3c: In Vivo Studies & Development/Novel Use of Imaging Probes

Engineering Novel High Affinity Integrin $\alpha_v\beta_6$ Binders in Different Cystine Knot Scaffolds: MicroPET Imaging Reveals Several Promising Candidates for Clinical Translation

Richard Kimura¹, Benjamin J. Hackel¹, Sanjiv S. Gambhir^{1,2}, ¹Radiology, Molecular Imaging Program at Stanford, Canary Center, Stanford University, Palo Alto, CA, USA; ²Bioengineering, Bio-X, Stanford University, Palo Alto, CA, USA. Contact e-mail: rkimura1@stanford.edu

Integrin $\alpha_v\beta_6$ is a cell surface receptor over-expressed on many cancers including breast, colon, lung, ovarian, pancreatic and skin cancer. Moreover, there are currently no imaging agents available for pancreatic cancer. Therefore, integrin $\alpha_v\beta_6$ is an important clinical target for cancer early detection and therapy. Here, we have engineered many new high-affinity integrin $\alpha_v\beta_6$ binders using two different cystine knot scaffolds, which are stabilized by a knotted core of three disulfide bonds. The first knotted scaffold is rich in arginine (Ro) and the second knot is rich in serine (So). Yeast surface display, fluorescence-activated cell sorting, and directed evolution strategies were used to engineer novel binding sequences in the Ro scaffold. These potent bioactivities were then engrafted into the So scaffold. PET imaging of A431 xenograft mouse models revealed that the primary structures of ⁶⁴Cu-DOTA-Ro and -So scaffolds have a profound influence on its pharmacokinetics affecting overall tumor uptake levels as well as clearance rates from target and non-target tissues. In vivo studies showed a Ro peptide's rapid and high accumulation in the tumor occurring to a much greater extent than a So peptide ($5.7 \pm 2.6\%$ ID/g vs. $1.9 \pm 0.3\%$ ID/g, 1 hr). Tumor clearance rates were very slow for both Ro and So radiotracers. ⁶⁴Cu-DOTA labeled Ro and So radiopeptides were also tested using mouse and human serum and show no degradation up to 24 hours. Furthermore, these novel peptides were shown by flow cytometry to be specific for integrin $\alpha_v\beta_6$ and do not bind integrin $\alpha_v\beta_3$. Collectively, these results demonstrate the important pharmacokinetic role predetermined by scaffold primary structure even though they share well-defined cystine knot secondary structure elements. Our imaging studies show that we have successfully engineered potent and highly stable integrin $\alpha_v\beta_6$ binders, which warrant further investigation for clinical translation.



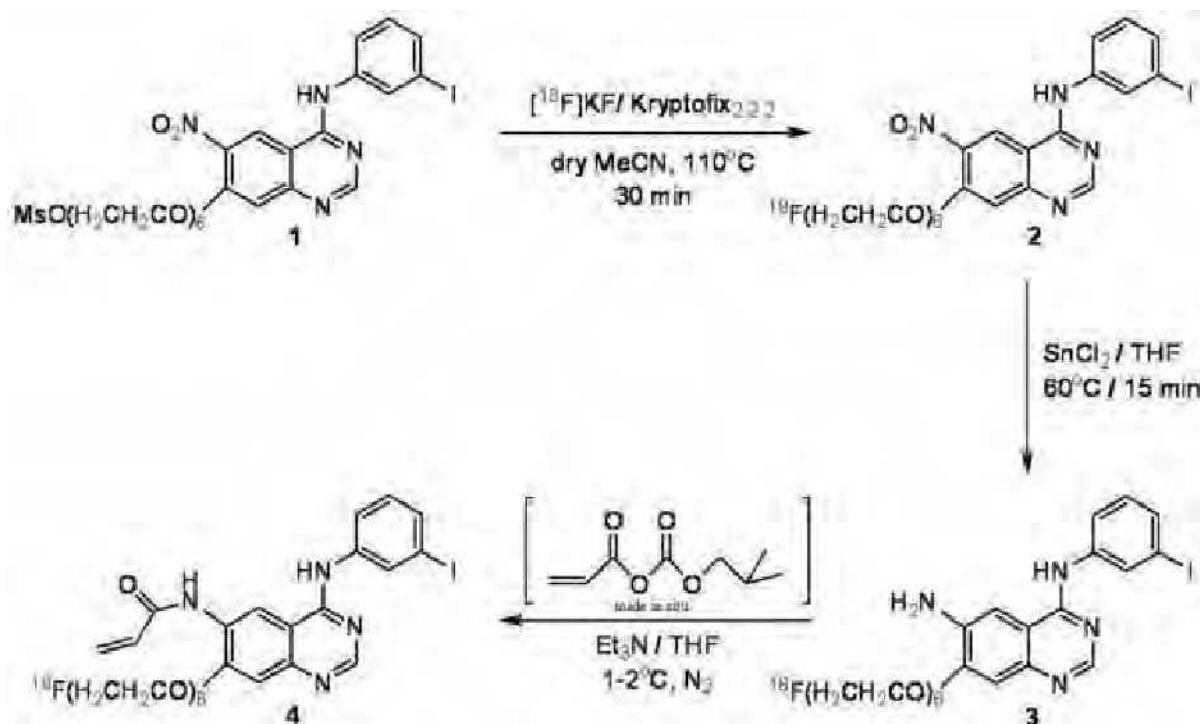
Presentation Number **0860B**

Poster Session 3c: In Vivo Studies & Development/Novel Use of Imaging Probes

Using Two Radiosynthesis Modules in Tandem for Fully Automated Synthesis of ^{18}F -PEG6-IPQA, a Novel PET Imaging Agent for Imaging active mutant EGFR Expression.

Julius A. Balatoni¹, **Uday Mukhopadhyay**¹, **Carlos Gonzalez-Lepera**¹, **Asutosh Pal**¹, **Stefan Riese**², **Mian M. Alauddin**¹, **Juri G. Gelovani**¹, ¹*Experimental Diagnostic Imaging, MD Anderson Cancer Center, Houston, TX, USA;* ²*Radiochemistry Systems, GE Healthcare, Waukesha, WI, USA. Contact e-mail: jbalatoni@mdanderson.org*

Introduction: We have been developing a novel active-mutant EGFR-specific radiotracer termed ^{18}F -PEG6-IPQA for PET imaging of EGFR expression. To perform clinical evaluation of this radiotracer, we developed an automated synthesis of this compound using two GE TracerLab modules, one standard commercial model, and the other, a modified dual reactor model resulting from a collaboration with GE Healthcare. **Methods:** The radiosynthesis of ^{18}F -PEG6-IPQA 4 is a three-step process as shown in the reaction scheme. The first step is a radiofluorination procedure that is performed in a standard, one reactor TracerLab FX F-N module (GE Healthcare). The radiofluorinated intermediate 2 is then transferred to the TracerLab Duo (GE Healthcare), which has been modified with two reaction vessels and an updated computer interface and program. In addition, the compressed air cooling system was enhanced to enable the cooling system to reduce reactor module temperature to 1°C. These changes allowed the reduction step (to prepare compd 3) to be carried out in the first reaction vessel and the acrylamide formation procedure to be conducted at 1-2°C, reproducibly, in the second reaction vessel. The crude mixture of 4 is then filtered into an intermediate glass vial and is transferred to the prep-HPLC injection loop. After injection onto the preparative C8 column, the product fraction is collected and diluted with sterile water. This solution is passed through a C18 solid phase extraction cartridge, which is then washed with sterile water and 4 is eluted off with 95% ethanol/water into a sterile product vial. **Results:** Decay corrected radiochemical yields have averaged about 8.3% for 3 runs so far. Radiochemical purity as determined by analytical HPLC have been >98%. Synthesis time is roughly 2.5 h. **Conclusions:** A successful automated synthesis of ^{18}F -PEG6-IPQA has been accomplished that is CGMP compliant and is suitable for preparation for clinical grade material for PET patient studies.



Presentation Number **0862B**

Poster Session 3c: In Vivo Studies & Development/Novel Use of Imaging Probes

Targeting beta cells for PET imaging using a novel GLP-1-based peptide labeled with Ga-68

Vanessa A. Rota^{1,3}, **Babak Behnam Azad**², **Leonard G. Luyt**^{2,3}, **Savita Dhanvantari**^{1,3}, ¹*Medical Biophysics, The University of Western Ontario, London, ON, Canada;* ²*Chemistry, The University of Western Ontario, London, ON, Canada;* ³*Imaging Program, The Lawson Health Research Institute, London, ON, Canada. Contact e-mail: vrota@lawsonimaging.ca*

Background: In North America, the rise in prevalence of Diabetes Mellitus has prompted a search for a non-invasive technique to image changes in beta cell mass before disease onset and during regenerative therapy. Measuring plasma glucose and insulin secretion both accurately reflect beta cell function, however beta cell function is not directly correlated with beta cell mass since changes in mass occur well before changes in beta cell function can be detected. One suitable target for imaging is the glucagon-like peptide-1 (GLP-1) receptor, which is expressed on the surface of the beta cell. In our previous work, we generated 3 novel GLP-1 derivatives with excellent binding affinity (IC₅₀ = 63-93 nM) for the GLP-1 receptor: 37-Lys-AEEA-DOTA-GLP-1(7-37) [GLP-A], 37 Lys-DOTA-GLP-1(7-37) [GLP-C] and 22Lys-AEEA-DOTA-GLP-1(7-37) [GLP-H]. These peptides also confirmed receptor activation by increasing cAMP levels similar to that of native GLP-1. We have selected GLP-C as a candidate for further characterization by assessing its in vivo biodistribution and ability to image beta cells with Positron Emission Tomography (PET). Methods: For μ PET imaging, a 90 minute dynamic scan was conducted after injection of 10 MBq [68Ga]GLP-C to determine the optimal time for probe uptake. To assess the specificity of probe uptake, euglycemic male CD1 mice were injected with 0.5-3.5 MBq of [68Ga]GLP-C alone or with an excess of unlabelled Exendin-4, a GLP-1 receptor agonist. Mice were euthanized 3 min (n=6), 4 hrs (n=8), or 24 hrs (n=2) post-injection (PI). For each time point, the pancreas and other organs were removed and counted in a high-purity Ge counter. Probe biodistribution was calculated as % injected dose (ID)/g tissue. Results: Upon analysis of μ PET images following a dynamic scan post-[68Ga]GLP-C injection, it was determined that a biodistribution assay should be conducted at two time points: 3 minutes and 4 hours PI. [68Ga]GLP-C biodistribution results revealed ~17% ID/g tissue in the pancreas at both 3 minutes and 4 hours PI; however, there was also significant uptake in the kidneys. Conclusions: While the biodistribution results seem promising in terms of uptake in the pancreas, it will be a challenge to image the beta cells due to the close proximity of the kidneys to the pancreas. We hope to eventually use the peptide to image and quantify changes in beta cell mass in vivo. Future studies will utilize appropriate mouse models to maximize the imaging potential of our novel probe.

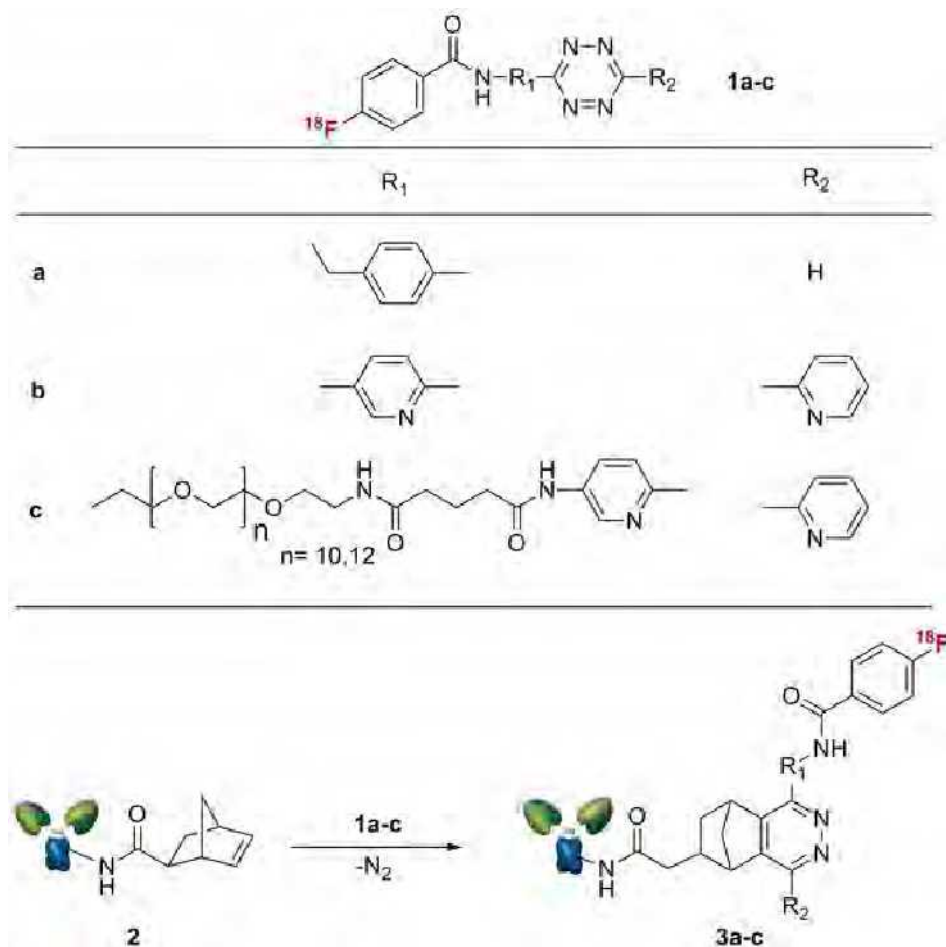
Presentation Number **0863B**

Poster Session 3c: In Vivo Studies & Development/Novel Use of Imaging Probes

Bioorthogonal ¹⁸F-labeling of Biomolecules via Inverse Electron Demand Diels-Alder Cycloaddition

Wei-Yu Lin¹, Kan Liu¹, Hao Wang¹, MingWei Wang¹, Mark M. Girgis^{1,2}, Melissa McCracken¹, Hsian Rong Tseng¹, James S. Tomlinson^{1,2}, Anna M. Wu¹, Clifton K. Shen¹, ¹Department of Molecular and Medical Pharmacology, David Geffen School of Medicine at UCLA, Crump Institute for Molecular Imaging, Los Angeles, CA, USA; ²Department of Surgery, David Geffen School of Medicine at UCLA, Los Angeles, CA, USA. Contact e-mail: weiyulin@mednet.ucla.edu

Bioorthogonal reactions are emerging as a unique research tool for introducing various tags onto target molecules in a complex biological environment. Due to their extremely high selectivity, great functional group tolerance and usually very fast reaction kinetic in aqueous buffer solution, such reactions may become a powerful means for ¹⁸F-labeling biomolecules in vitro or even in vivo. Here we introduce a novel ¹⁸F-tag, N-(4-(1,2,4,5-tetrazin-3-yl)benzyl)-4-[¹⁸F]fluoro-benzamide **1a** ([¹⁸F]TBFB, as a electron-deficient diene) and its oligo-PEGylated derivatives (**1b-c**) to label norbornenyl derivatives of anti-HER3 diabody (**2**) and cyclic RGD peptide (electron-rich dienophile) via an inverse-electron-demand Diels-Alder (IED-DA) cycloaddition. This is the first practical approach to utilize IED-DA method for ¹⁸F-labeling biomolecules. [¹⁸F]TBFB was prepared from N-succinimidyl-4-[¹⁸F]fluorobenzate [¹⁸F]SFB prepared by an one-pot microwave-assisted process developed in our group with the 3-(4-aminomethylphenyl)-1,2,4,5-tetrazine to give a **1a** after HPLC purification. The RCY is ~30 % referred to [¹⁸F]F⁻ after 60 min of synthesis. [¹⁸F]**1a** shows great stability in PBS (pH 7.4) and in 1% FBS/PBS after 2h at 37°C. [¹⁸F]**1a** and **2** successfully underwent IED-DA reaction in buffer solution to give the cycloadduct [¹⁸F]**3a** with high yield and selectively. The conversion was completed within 15 min. The result demonstrated the utility of the [¹⁸F]TBFB/norbornene system, and its potential applications to in vivo experiments. The validation of tumor pre-targeting with our system in xenografted mice is currently underway.



Presentation Number **0864B**

Poster Session 3c: In Vivo Studies & Development/Novel Use of Imaging Probes

Highly Excretable and Specific Gold Nanoparticle Probes with Densely Functionalized I-125 and PEG-RGD for Efficient in vivo Molecular Imaging of Cancer

Young-Hwa Kim¹, Jongho Jeon², Su Hyun Hong², Won-Kyu Rhim², Hyewon Youn¹, Yun-Sang Lee¹, June-Key Chung¹, Dong Soo Lee¹, Jwa-Min Nam², Keon Wook Kang¹, ¹Department of Nuclear Medicine, Seoul National University College of Medicine, Seoul, Republic of Korea; ²Department of Chemistry, Seoul National University, College of Natural Sciences, Seoul, Republic of Korea. Contact e-mail: cine82@snu.ac.kr

Purpose: To develop an in vivo monitoring system targeting integrin $\alpha v \beta 3$ in tumor angiogenesis, we evaluated the versatile carrier system with 125I-labeled gold nanoparticles (AuNPs) conjugated with PEG-RGD peptides for targeting tumor. **Methods:** We developed 13 nm sized PEGylated AuNPs and the cRGD covalently conjugated with amino group on the surface of AuNPs for targeting integrin $\alpha v \beta 3$ expressing cells. 125I was labeled by charge to charge interaction by direct mixing AuNPs with Na125I at room temperature for 5 min. 125I-labeled cRGD-AuNPs were then purified and concentrated. The stability was monitored by ITLC-SG with saline (pH 7) as the solvent for 16 h at 37°C in serum. For the competitive binding assay to the integrin $\alpha v \beta 3$, 125I-echistatin were incubated with $\alpha v \beta 3$ expressing cancer cell (U87MG) and non-expressing cancer cell (MCF7) after pre-treating cRGD-AuNPs or cRGD peptides. Cell uptakes of 125I were measured using γ -counter. To confirm receptor specific internalization of cRGD-AuNPs, TEM image was acquired in U87MG and MCF7 cell lines. The uptake and clearance of 125I-labeled cRGD-AuNPs in vivo was evaluated by serial SPECT/CT studies from 0 h to 6 h after i.v injection of 11.1 MBq 125I-labeled cRGD-AuNPs in a U87MG tumor bearing mouse using an animal SPECT/CT system. Renal clearance of 125I-labeled cRGD-AuNPs was confirmed radio-TLC analysis of urine samples after injection. **Results:** The entire 125I labeling procedure was completed within 20 min including purification and concentration steps. Radio-chemical purity of 125I-labeled cRGD-AuNPs was 97 % at 3 h and 88 % at 16 h during the incubation in serum at 37°C. In competitive binding assay to U87MG cells, IC50 values for cRGD-AuNPs and cRGD peptides were 0.33 nM and 51.34 nM (n=3), respectively. MCF7 cells revealed the same low uptakes while cold formed cRGD peptides were treated or not. TEM images showed intracellular localization of the particles in U87MG cells only, not in MCF7 cells. SPECT/CT image showed uptakes of 125I-labeled cRGD-AuNPs in the U87MG xenografted tumor and blood pool until 1 h after injection, and showed their efficient clearance from the body through renal and urinary excretion route. Radio-chemical yield of urine samples was observed over 50 % of 125I-labeled cRGD-AuNPs. **Conclusion:** In this study, we demonstrated that 125I-labeled cRGD-AuNPs can define $\alpha v \beta 3$ expressing cancer cells both in vitro and in vivo. These functionalized AuNPs have a potential in tumor and angiogenesis targeted imaging which will be useful for various diagnostic and therapeutic applications.

Presentation Number **0865B**

Poster Session 3c: In Vivo Studies & Development/Novel Use of Imaging Probes

Evaluation of CTLA-4 expression as tumor imaging target in colon cancer cells and mouse models

Katsuharu Yagi¹, Kei Higashikawa¹, Keiko Watanabe², Makoto Hiromura², Yousuke Kanayama², Shuichi Enomoto^{1,2}, ¹Graduate School of Medicine, Dentistry, and Pharmaceutical Science, Okayama University, Okayama, Japan; ²Multiple Molecular Imaging Research Laboratory, Center for Molecular Imaging Science, RIKEN Kobe Institute, Kobe, Japan. Contact e-mail: gph421078@s.okayama-u.ac.jp

¹⁸F-fluorodeoxyglucose-positron emission tomography (FDG-PET) is one of the most useful methods for tumor imaging on the basis of increased glucose uptake. However, FDG-PET has difficulty distinguishing between malignant tumors and inflammatory lesions, and diagnosing tumor properties, such as invasiveness and drug sensitivity. Thus, there are requirement for development of novel imaging probes that has specific and functional characters for tumor diagnosis. Recently, it has been reported that Cytotoxic T-lymphocyte-associated protein-4 (CTLA-4) expressed in various types of human tumor cells¹). The regulation of CTLA-4 gene expression has been directly controlled by Wnt/ β -Catenin signaling during tumor development²). In addition, the expressed CTLA-4 on the cell surface of tumor prevents anti-tumor immune response, because of this protein inhibits the activity of T cells that binds with CD80 or CD86 of the antigen-presenting cells. Several clinical studies are reported that anti-CTLA-4 monoclonal antibody, named Ipilimumab, is effective for molecular targeted cancer therapy³). In this study, we investigated whether or not CTLA-4 is available for a tumor-imaging target using cell and mouse models. Two colon cancer cell lines, CT26 and Colon26, were used in this study. The expression level and localization of plasma membrane of CTLA-4 protein were examined by western blotting analysis and immunofluorescence staining, respectively. Next, we established the tumor-bearing mice by subcutaneous transplantation of the CT26 and Colon26 in BALB/c mice. The expression of CTLA-4 in the tumor tissue was confirmed by immunohistochemical staining. In addition, we compared the CTLA-4 expression between tumor and inflammation using dextran sodium sulfate (DSS)-induced colitis in mice. CTLA-4 protein was highly expressed in the Colon26 and CT26 cells and localized at the plasma membrane of both cells. The protein level of CTLA-4 in the tumor tissue was higher than that of the inflamed tissue. From these results, CTLA-4 is able to be used as a targeted molecule for a distinction between colon tumor and colitis. We are investigating the availability of anti-CTLA-4 monoclonal antibody for tumor diagnosis in PET imaging. 1) Contardi E., et al., (2005) *Int. J. Cancer*, 117, 538-550 2) Shah KV., et al., (2008) *J. Invest. Derm.*, 128, 2870-2879 3) O'Mahony D., et al., (2007) *Clin. Cancer. Res.*, 13, 958-964

Presentation Number **0866B**

Poster Session 3c: In Vivo Studies & Development/Novel Use of Imaging Probes

⁶⁴Cu-labeling of octreotide utilizing the N-terminal Cu binding motif (ATCUN)

Koki Hasegawa, Mie Nishimura, Emi Hayashinaka, Yasuhiro Wada, Yosky Kataoka, Yasuyoshi Watanabe, Riken, Kobe, Japan.
Contact e-mail: hkoki@riken.jp

[Introduction] Biological macromolecules including peptides and proteins could be developed as potential imaging agents, but they have complex structures including highly-specific binding sites (active sites) against recognition molecules, such as receptor proteins, etc. It is necessary to keep the active sites intact in the process of radiolabelling of macromolecules. We here demonstrate to radiolabel octreotide, a stable somatostatin analog resistant to metabolism, with ⁶⁴Cu by the N-terminus-specific ⁶⁴Cu labeling method utilizing the N-terminal Cu binding motif (ATCUN). [Method] Octreotide possessing the N-terminal Cu binding motif (Asp-Ala-His-Lys) was synthesized by the Fmoc solid-phase method. Obtained Asp-Ala-His-Lys-octreotide was incubated with ⁶⁴CuCl₂ acetate buffer (pH 6.5) at 40°C for 1 hour. Radiochemical purity of the complex was evaluated by HPLC analysis. PET imaging and biodistribution study were performed in male SD rats. [Result] Specific radioactivity of [⁶⁴Cu]Asp-Ala-His-Lys-octreotide was found to be 79 MBq/nmol at the end of synthesis. Radiochemical purity was better than 99%. Biodistribution study suggested high accumulation of [⁶⁴Cu]DAHK-octreotide in the pituitary and pancreas which express rich somatostatin receptors. In PET study, these organs were visualized by accumulation of [⁶⁴Cu]DAHK-octreotide 15 minutes after the injection. [Conclusion] The N-terminus-specific ⁶⁴Cu labeling method utilizing the N-terminal Cu binding motif realizes easier and efficient labeling of biological macromolecules with ⁶⁴Cu, without deterioration of the biological activities of macromolecules.

Presentation Number **0867B**

Poster Session 3c: In Vivo Studies & Development/Novel Use of Imaging Probes

Effect of P-Glycoprotein Modulators on Brain Uptake of [F-18]Fluoropropylcurcumin in Mice

Choong Mo Kang, Kwang Yup Yoon, Iljung Lee, Yearn Seong Choe, Nuclear Medicine, Samsung Medical Center, Sungkyunkwan University School of Medicine, Seoul, Republic of Korea. Contact e-mail: cm1580.kang@sbsri.co.kr

Objectives: We previously developed 1-[4-(3-[¹⁸F]Fluoropropoxy)-3-methoxyphenyl]-5-hydroxy-7-(4-hydroxy-3-methoxyphenyl)-1,4,6-heptatrien-3-one ([F-18]fluoropropylcurcumin) as a β -amyloid plaque imaging agent. However, its initial brain uptake was relatively low in normal mice. It was reported that P-glycoprotein (P-gp) modulator such as cyclosporin A increases the brain uptake of some radioligands. In this study, therefore, effect of P-gp modulators, cyclosporin A and verapamil on the brain uptake of [F-18]fluoropropylcurcumin was evaluated in mice. **Methods:** [F-18]Fluoropropylcurcumin was synthesized using a known method. Cyclosporin A (15 mg/kg and 50 mg/kg) or verapamil (5 mg/kg) was injected into ICR mice via a tail vein at 30 min prior to the intravenous injection of [F-18]fluoropropylcurcumin. The mice were sacrificed at 2 min post-injection, because β -amyloid plaque imaging agents should have high initial brain uptake at 2 min post-injection and fast brain wash-out by 30 min in normal mice. The tissues were then removed, weighed, and counted. In control experiment, ICR mice were injected with [F-18]fluoropropylcurcumin and treated as above. **Results:** Tissue distribution of [F-18]fluoropropylcurcumin showed high radioactivity accumulation in the liver (42.16 %ID/g) and kidneys (16.16 %ID/g), and relatively low uptake in brain (0.99 %ID/g) at 2 min post-injection in control mice. The initial brain uptake of [F-18]fluoropropylcurcumin increased to 127% (1.26 %ID/g), relative to a value of 100% in control mice, by pre-treatment of high dose cyclosporin A (50 mg/kg). On the other hand, verapamil (5 mg/kg) and low dose cyclosporin A (15 mg/kg) have no effect on the brain permeability of [F-18]fluoropropylcurcumin. Major reduction in the radioactivity uptake was observed in the liver by all P-gp modulators (19-26%). **Conclusion:** This result shows that high dose cyclosporin A increases the brain uptake of [F-18]fluoropropylcurcumin. Further studies are warranted to investigate whether curcumin derivatives may be substrates for *mdr* P-gp.

Presentation Number **0868B**

Poster Session 4c: In Vivo Studies & Development/Novel Use of Imaging Probes

Microdialysis with radiometric monitoring of L- $[\beta\text{-}^{11}\text{C}]\text{DOPA}$ metabolites in rat striatum and plasma

Maki Okada¹, **Ryuji Nakao**¹, **Rie Hosoi**², **Ming-Rong Zhang**¹, **Toshimitsu Fukumura**¹, **Kazutoshi Suzuki**¹, **Osamu Inoue**², ¹Molecular Probe Group, National Institute of Radiological Science, Chiba, Japan; ²Division of Health Science, Graduate School of Medicine, Osaka University, Suita, Japan. Contact e-mail: mokada@nirs.go.jp

The catecholamine, dopamine (DA), is synthesized from 3,4-dihydroxy-L-phenylalanine (L-DOPA) by aromatic L-amino acid decarboxylase (AADC). DA metabolism is regulated by monoamine oxidase (MAO) and catechol-O-methyltransferase (COMT). To measure dopaminergic metabolism, we used microdialysis with radiometric detection to monitor L- $[\beta\text{-}^{11}\text{C}]\text{DOPA}$ metabolites in the extracellular space of the rat striatum and plasma. We also evaluated the effects of AADC, MAO, and COMT inhibitors on striatal metabolite profiles. L- $[\beta\text{-}^{11}\text{C}]\text{DOPA}$ and its radioactive metabolites, $[\text{}^{11}\text{C}]3,4\text{-dihydroxyphenylacetic acid}$ ($[\text{}^{11}\text{C}]\text{DOPAC}$), $[\text{}^{11}\text{C}]\text{homovanillic acid}$ ($[\text{}^{11}\text{C}]\text{HVA}$), L-3-O-methyl- $[\text{}^{11}\text{C}]\text{DOPA}$ ($[\text{}^{11}\text{C}]\text{3-OMD}$) and $[\text{}^{11}\text{C}]\text{3-methoxytyramine}$ ($[\text{}^{11}\text{C}]\text{3-MT}$) were detected, however $[\text{}^{11}\text{C}]\text{DA}$ was not detected in striatal dialysate following intravenous injection of L- $[\beta\text{-}^{11}\text{C}]\text{DOPA}$. The major early species measured after administration of L- $[\beta\text{-}^{11}\text{C}]\text{DOPA}$ were $[\text{}^{11}\text{C}]\text{DOPAC}$ and $[\text{}^{11}\text{C}]\text{HVA}$ in a 1:1 ratio, which shifted toward $[\text{}^{11}\text{C}]\text{HVA}$ with time. An AADC inhibitor increased the uptake of L- $[\beta\text{-}^{11}\text{C}]\text{DOPA}$ and $[\text{}^{11}\text{C}]\text{3-OMD}$ and delayed the accumulation of $[\text{}^{11}\text{C}]\text{DOPAC}$ and $[\text{}^{11}\text{C}]\text{HVA}$. With MAO inhibition, about 80% of total radioactivity was derived from $[\text{}^{11}\text{C}]\text{3-MT}$. The COMT inhibitor increased $[\text{}^{11}\text{C}]\text{DOPAC}$ and decreased $[\text{}^{11}\text{C}]\text{HVA}$. L- $[\beta\text{-}^{11}\text{C}]\text{DOPA}$ and $[\text{}^{11}\text{C}]\text{3-OMD}$ were detected and then achieved equilibrium in plasma with AADC inhibitor. On the other hand, $[\text{}^{11}\text{C}]\text{3-OMD}$ levels in striatal dialysate decreased significantly following intrastriatal administration of L- $[\beta\text{-}^{11}\text{C}]\text{DOPA}$. These results suggest that $[\text{}^{11}\text{C}]\text{3-OMD}$ in striatal dialysate was generated mostly in peripheral tissue and penetrate into brain. Our results reflect the complicated L-DOPA metabolic pathway, suggesting that this method could improve the understanding of the information obtained from an L- $[\beta\text{-}^{11}\text{C}]\text{DOPA}$ PET study or provide an index of dopaminergic metabolism-related neuropsychiatric disorders and evaluation of drug therapies for treatment of the disorder.

Presentation Number **0869B**

Poster Session 4c: In Vivo Studies & Development/Novel Use of Imaging Probes

Novel Positron Emission Tomography Probes Specific for Deoxycytidine Kinase

Caius G. Radu¹, Chengyi J. Shu^{2,1}, Dean O. Campbell¹, Jason T. Lee¹, Michael Phelps¹, N. Satyamurthy¹, Johannes Czernin¹,
¹Molecular & Medical Pharmacology, University of California at Los Angeles, Los Angeles, CA, USA; ²Division of Immunology, The Netherlands Cancer Institute, Amsterdam, Netherlands. Contact e-mail: cradu@mednet.ucla.edu

Deoxycytidine kinase (dCK) is a rate-limiting enzyme in the deoxyribonucleoside salvage pathway and a critical determinant of therapeutic activity for several nucleoside analog pro-drugs. We have previously reported the development of 18F-FAC, (1-(2'-deoxy-2'-18F-fluoro-beta-D-arabinofuranosyl) cytosine), a new probe for PET imaging of dCK activity in immune disorders and certain cancers. The objective of the current study was to develop PET probes with improved metabolic stability and specificity for dCK. Towards this goal, several candidate PET probes were synthesized and evaluated in vitro and in vivo. Methods: High pressure liquid chromatography was used to analyze the metabolic stability of 18F-FAC and of several newly-synthesized analogs with the natural D-enantiomeric sugar configuration or the corresponding unnatural L-configuration. In vitro kinase and uptake assays were used to determine the affinity of the 18F-FAC L-nucleoside analogs for dCK. The biodistribution of selected L- analogs in mice was determined by microPET/CT imaging. Results: Candidate PET probes were selected using the following criteria: low susceptibility to deamination, high affinity for purified recombinant dCK, high uptake in dCK expressing cell lines and biodistribution in mice reflective of the tissue expression pattern of dCK. Amongst the ten newly-developed candidate probes, 1-(2'-deoxy-2'-18F-fluoro-β-L-arabinofuranosyl) (L-18F-FAC) and 1-(2'-deoxy-2'-18F-fluoro-β-L-arabinofuranosyl)-5-methylcytosine (L-18F-FMAC) most closely matched the selection criteria. The selection of L-18F-FAC and L-18F-FMAC was validated by showing that these two PET probes can be used to image animal models of leukemia and autoimmunity. Conclusion: Promising in vitro and in vivo data warrant biodistribution and dosimetry studies of L-18F-FAC and L-18F-FMAC in humans.

Presentation Number **0870B**

Poster Session 4c: In Vivo Studies & Development/Novel Use of Imaging Probes

Development of radiobromine-labeled thymidine analog as a tumor proliferation imaging agent

Yasushi Kiyono¹, Keisuke Sano², Tetsuya Mori¹, Miguel E. Martinez¹, Tatsuya Asai², Hidehiko Okazawa¹, Yasuhisa Fujibayashi^{3,1},
¹Biomedical Imaging Research Center, University of Fukui, Fukui, Japan; ²Graduate School of Engineering, University of Fukui, Fukui, Japan; ³Molecular Imaging Center, National Institute of Radiological Sciences, Chiba, Japan. Contact e-mail: ykiyono@u-fukui.ac.jp

Objectives: The aim of this study was to synthesize and estimate radiobromine-labeled thymidine analogue, 5-bromo-4'-thio-2'-deoxyuridine (BTdU) as a tumor proliferation imaging. **Methods:** The radiolabeling of BTdU with ⁷⁷Br was achieved by a destannylation reaction of tributylstannyl precursor. Using L-M cells and thymidine kinase deficient mutant L-M(TK-) cells, cell uptake and DNA incorporation experiments were performed in vitro. In vivo biodistribution experiments in normal mice and tumor-bearing (L-M and L-M(TK-) cells) mice were also carried out. **Results:** The radiochemical yield of ⁷⁷Br-BTdU was about 30% and the radiochemical purity was more than 99%. The uptake of ⁷⁷Br-BTdU was increased with time in L-M cells (8.4 ± 0.3 %ID/g protein at 30 min, 43 ± 3.6 %ID/g protein at 180 min). On the other hand, there was little uptake of ⁷⁷Br-BTdU in L-M (TK-) cells (1.1 ± 0.3 %ID/g protein at 180 min). In addition, more than 90% of ⁷⁷Br-BTdU was incorporated in DNA at 120 min. These results show that ⁷⁷Br-BTdU is incorporated into DNA via thymidine kinase. In biodistribution experiments, the uptake of ⁷⁷Br-BTdU in proliferating organs was high (spleen: 13 ± 4.8, small intestine: 4.5 ± 1.0 %ID/g at 6 hr) and that in non-proliferating organs was low (brain: 0.18 ± 0.04, muscle: 0.21 ± 0.04, liver: 0.55 ± 0.10 %ID/g at 6 hr). In tumor bearing mice, uptake of ⁷⁷Br-BTdU in tumor was high (5.7 ± 1.0 %ID/g at 3 hr and 2.6 ± 0.9 %ID/g at 24 hr after injection). The ratio of tumor-to-muscle in L-M cells was more than 20 at 3 hr. These results show that ⁷⁷Br-BTdU has suitable characteristics for tumor proliferation imaging. **Conclusion:** Radiobromine-labeled BTdU is potentially useful as a tumor proliferation-imaging agent for PET.

Presentation Number **0871B**

Poster Session 4c: In Vivo Studies & Development/Novel Use of Imaging Probes

Development of a novel radioisotope labeled tumor imaging probe for PET “¹⁸F-Lactosome”

Ryo Yamahara¹, Fumihiko Yamamoto^{2,3}, Kensuke Kurihara², Hideo Tsukada⁴, Eri Takeuchi¹, Isao Hara¹, Akira Makino¹, Akira Shimizu², Shinae Kizaka-Kondoh⁵, Eiichi Ozeki¹, Shunsaku Kimura^{2,6}, ¹Technology Research Laboratory, Shimadzu. corp., Seika-cho, Soraku-gun, Kyoto, Japan; ²Transnational Research Center, Kyoto University Hospital, Kyoto University, Kyoto, Japan; ³Department of Radiopharmacy, Tohoku Pharmaceutical University, Sendai, Miyagi, Japan; ⁴Central Research Laboratory, Hamamatsu Photonics K.K., Hamamatsu, Shizuoka, Japan; ⁵Department of Department of Biomolecular Engineering, Graduate School of Bioscience and Biotechnology, Tokyo Institute of Technology, Yokohama, Kanagawa, Japan; ⁶Department of Material Chemistry, Graduate School of Engineering, Kyoto University, Kyoto, Japan. Contact e-mail: yamahara@shimadzu.co.jp

Objectives: We have developed amphiphilic poly-L-lactic acid-block-polysarcosine polydepsipeptide micelle "Lactosome" as a novel cancer imaging probe utilizing the enhanced permeability and retention (EPR) effect. Lactosome can form stable molecular assembly with polylactic acid (PLA), therefore, radioisotope (RI) labeled Lactosome can be prepared by only mixing RI labeled PLA with the amphiphilic polydepsipeptide. Lactic acid has two optical *D*- and *L*-isomers. In this presentation, effect of the mixed PLA isomers on the Lactosome stability was examined, and strategy of Lactosome modification for the efficient tumor imaging was discussed. **Methods:** ¹⁸F labeled poly-L-lactic acid (¹⁸F-BzPLLA) and poly-DL-lactic acid (¹⁸F-BzPDLLA) were synthesized in 20-37% EOB by coupling reaction of ¹⁸F-SFB to the amino group located at PLA terminal end. Micelle assemblies were prepared from a mixture of ¹⁸F-BzPLLA or ¹⁸F-BzPDLLA with the amphiphilic polymer by a conventional film method (¹⁸F-*L*-Lactosome and ¹⁸F-*DL*-Lactosome, respectively). BALB/cA Jcl-nu/nu mice bearing HeLa cells in right femur region were used for PET studies. PET images of tumor bearing mice were taken by using Clairvivo PET system (Shimadzu Corp. Japan). **Results:** ¹⁸F-Lactosomes were prepared in good RI yields (222-420 MBq). In the bloodstream, radioactivity of ¹⁸F-*L*-Lactosome maintained at higher level for 6 h. By the previous experiments using NIRF labeled PLA, it was revealed that PLA was stably inserted in Lactosome, and its blood circulation time is long. Therefore, background emission observed from blood was persisted, which interferes to increase the contrast between tumor and another femur. On the other hand, ¹⁸F-*DL*-Lactosome was relatively unstable. Owing to the sustained release of ¹⁸F-BzPDLLA from ¹⁸F-*DL*-Lactosome, the background emission was decreased. As the result, the mean uptake ratio of tumor/muscle (left femur) of ¹⁸F-*DL*-Lactosome at 6 h was strengthened to 3.6, compared with that of ¹⁸F-*L*-Lactosome (1.5). **Conclusions:** According to the optical isomers of the mixed radioisotope labeled PLA, stability of radioisotope labeled Lactosome in bloodstream can be controlled. By selecting ¹⁸F-BzPDLLA, the tumor/muscle accumulation ratio of ¹⁸F-Lactosome was improved to 3.6, which is sufficiently high contrast for the tumor imaging.

Presentation Number **0872B**

Poster Session 4c: In Vivo Studies & Development/Novel Use of Imaging Probes

Novel Mitochondrial Voltage Sensor in Rat Myocardial Infarction Model

Dong-Yeon Kim^{1,2}, Uyenchi N. Le¹, Hee Jung Kim², Youn-Do Choi², Byeong-il Lee¹, Kook-Hyun Yu², Hee-Seung Bom¹, Jung-Joon Min¹, ¹Nuclear Medicine, Chonnam National University Medical School, Hwasun, Republic of Korea; ²Chemistry, Dongguk University, Seoul, Republic of Korea. Contact e-mail: blueburr@gmail.com

Despite substantial advances in the diagnosis and treatment of cardiovascular diseases, there are a few radiopharmaceuticals for diagnosis of ischemic heart diseases (IHD) using PET. [¹⁸F] labeled molecular probe for IHD is driving particular interest due to its high clinical applicability. Thus, we synthesized 5-[¹⁸F]fluoropentyltriphenylphosphonium salt (5-[¹⁸F]FPTP), an [¹⁸F] labeled lipophilic cation that specifically accumulates in myocardial cells according to mitochondrial membrane potential. Here, we evaluated the performance of 5-[¹⁸F]FPTP as a mitochondrial voltage sensor in vitro and in vivo. We evaluated cell uptake of 5-[¹⁸F]FPTP in embryonic cardiomyoblast (H9c2) showing over 14-fold higher uptake than in negative control cells (fibroblast, HDF). The uptake of 5-[¹⁸F]FPTP, [³H]tetraphenylphosphonium ([³H]TPP) and [^{99m}Tc]sestamibi was examined after modulation of mitochondrial membrane potential with different concentration of CCCP (carbonyl cyanide m-chlorophenylhydrazone). 5-[¹⁸F]FPTP and [³H]TPP was more sensitive in the change of mitochondrial membrane potential than [^{99m}Tc]sestamibi. We assessed biodistribution of 5-[¹⁸F]FPTP in normal BALB/c mice (n = 12) that showed high accumulation in the heart (12.02 ± 3.63 ID %/g, at 10 min) and very rapid clearance from the blood pool and liver. Dynamic micro PET for 60 min after injecting 1 mCi of 5-[¹⁸F]FPTP showed high accumulation and retention in the heart and very rapid clearance from the liver. Heart-to-Liver ratio was over 1.0, 2.0, and 3.0 after 2 min, 10 min, and 20 min of tracer injection, respectively which was analyzed by time-activity curve of dynamic PET study. Micro PET study in myocardial infarction rats showed decreased uptake of 5-[¹⁸F]FPTP in the region of hypoperfusion confirmed by 2,3,5-Triphenyltetrazolium chloride (TTC) staining. Quantitative analysis revealed high correlation between micro PET image and TTC staining (r²=0.85). 5-[¹⁸F]FPTP might have a potential to be utilized as a novel myocardial agent for PET in IHD. 5-[¹⁸F]FPTP was sensitive in mitochondria membrane potential and allows quantitative assessment of regional myocardial ischemia or infarction. 5-[¹⁸F]FPTP might be useful for clinical cardiac PET/CT applications.

Presentation Number **0873B**

Poster Session 4c: In Vivo Studies & Development/Novel Use of Imaging Probes

Synthesis of [¹⁸F] labeled Novel Mitochondrial Voltage Sensor

Dong-Yeon Kim^{1,2}, Hee Jung Kim², Youn-Do Choi², Kook-Hyun Yu², Uyenchi N. Le¹, Hee-Seung Bom¹, Jung-Joon Min¹, ¹Nuclear Medicine, Chonnam National University Medical School, Hwasun, Republic of Korea; ²Chemistry, Dongguk University, Seoul, Republic of Korea. Contact e-mail: blueburr@gmail.com

Mitochondria was known to important role to cell life and death, which influenced lots of diseases. Lipophilic cations, including tetraphenylphosphonium (TPP) salts, penetrate the hydrophobic barriers of the plasma and mitochondrial membranes and accumulate in mitochondria in response to the negative inner transmembrane potentials. Thus, the development of [¹⁸F] labeled phosphonium cations as a noninvasive imaging agent may serve as a new molecular "voltage sensor" probe to investigate the role of mitochondria in lots of diseases. Here, we report radiosynthesis of 5-[¹⁸F]Fluoropentyltriphenylphosphonium salt (5-[¹⁸F]FPTP) as a new molecular "voltage sensor". We have synthesized a reference compound 5-fluoropentyltriphenylphosphonium salt (5-FPTP) via three step nucleophilic substitution and 5-[¹⁸F]FPTP have labeled via two step nucleophilic substitution of no-carrier-added [¹⁸F]fluoride with the precursor, 1,5-di-tosyloxypentane, in the presence of Kryptofix-2.2.2 and K₂CO₃. The reference compound 5-FPTP was synthesized in 77 % yield. For separation 5-[¹⁸F]FPTP, the last mixture was cooled and injected onto a semi-preparative HPLC column system (the flow rate was 3 ml/min, with the mobile phase distilled water : acetonitrile = 55 : 45, Rt : 19 min). The 5-[¹⁸F]FPTP was synthesized in 15~20% yield. Radiochemical purity was above 98% to determine by analytical HPLC system (same isocratic as used for semi-preparative HPLC system). Specific activity was above 170~200 Ci/umol. 5-[¹⁸F]FPTP was successfully synthesized that might have a potential to be utilized as a novel "voltage sensor".

Presentation Number **0874B**

Poster Session 4c: In Vivo Studies & Development/Novel Use of Imaging Probes

Established the melanoma animal model using HSV1-tk as Positron Emission Tomography reporter gene

Onseok Lee^{1,2}, Gyuchul Hwang³, Gyuman Park², Gunwoo Lee^{1,2}, Seok-Ki Kim⁴, Chilhwan Oh^{1,3}, ¹Biomedical Science of Brain Korea 21, Korea University College of Medicine, Seoul, Republic of Korea; ²Research Institute for Skin Image, Korea University Medical Center, Seoul, Republic of Korea; ³Department of Dermatology, Korea University Guro Hospital, Seoul, Republic of Korea; ⁴Department of Nuclear Medicine, National Cancer Center, Goyang-si, Republic of Korea. Contact e-mail: on-seok@korea.ac.kr

With combination of anatomic imaging method (CT or MRI) and PET technology reflecting the tissue metabolism, the high detection rate and more precise location of the tumor in body was possible. However, PET imaging method based on new radioprobe should be suggested, added to the [¹⁸F]FDG (fluorodeoxyglucose) that is usually incorporated to tissue area of high metabolic rate of glucose other than tumor of interest. Recently, the herpes simplex virus type 1 thymidine kinase (HSV1-tk) positron emission tomography (PET) reporter gene (PRG) are introduced to investigate intracellular molecular events. The expression of these PRGs can be imaged using radiolabeled acycloguanosine analog PET reporter probe (PRP) such as 9-4-[¹⁸F]fluoro-3-(hydroxymethyl) butyl]guanine ([¹⁸F]FHBG). [¹⁸F]FHBG is a substrate for the HSV1-TK enzyme with relatively low affinity for mammalian TK enzymes, accumulating in the cell of HSV1-tk expression. So, specific PET imaging of tumor expressing HSV1-tk is possible by detecting gamma ray emission from PRP. Specific PET imaging of animal melanoma model using the PRG/PRP protocol of HSV1-tk/FHBG can be used as a significant preclinical methodology such as investigation of new anticancer medication.

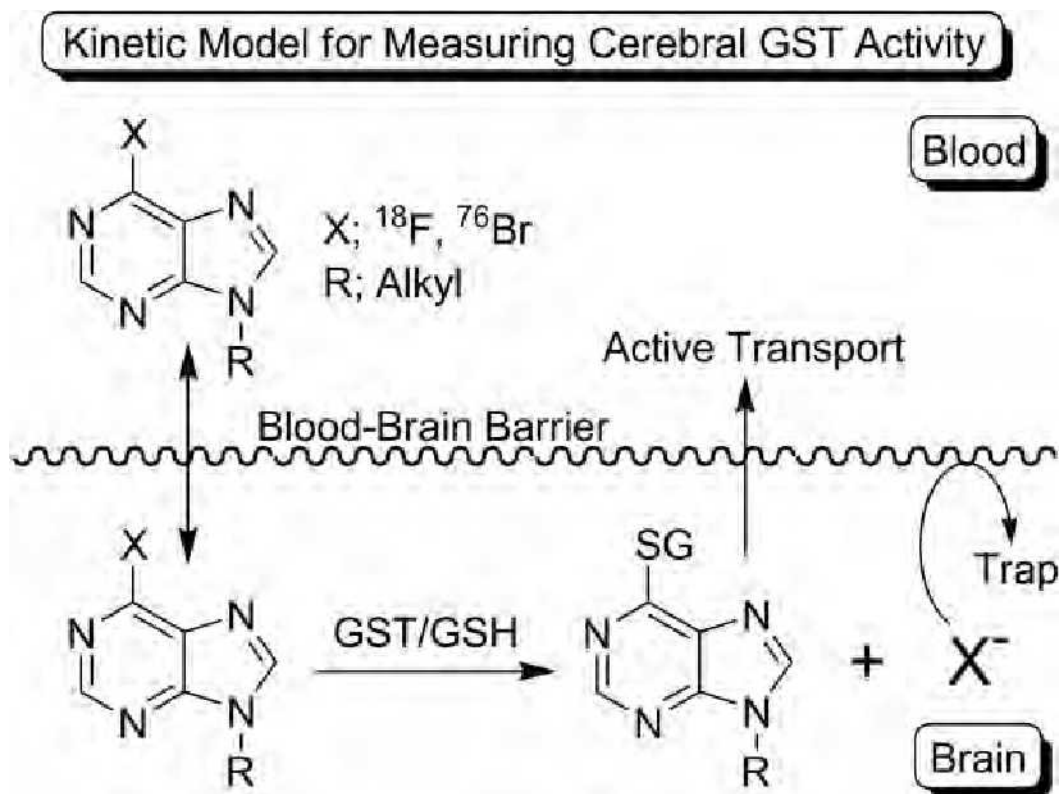
Presentation Number **0875B**

Poster Session 4c: In Vivo Studies & Development/Novel Use of Imaging Probes

Development of a PET probe for in vivo measurement of cerebral glutathione S-transferase activity

Tatsuya Kikuchi, Toshimitsu Okamura, Maki Okada, Hidekatsu Wakizaka, Kiyoshi Fukushi, Toshiaki Irie, Toshimitsu Fukumura, Molecular Imaging Center, National Institute of Radiological Sciences, Chiba, Japan. Contact e-mail: kiku@nirs.go.jp

Glutathione (GSH) and Glutathione S-transferase (GST) are induced by an oxidative stress, which is known to contribute to disease pathogenesis. Especially, GST activity in tissues from patients with neurodegenerative disorders and tumors is widely measured in vitro as an oxidative stress marker. In vivo measurement of GST activity would be useful for the diagnosis of such diseases, whereas the method has not been established. In this study, we evaluated ^{18}F - and ^{76}Br -labeled 9-alkylpurines as a PET probe for in vivo measurement of cerebral GST activity. To measure the cerebral GST activity in vivo, a PET probe should enter the brain followed by retention of the radioactive halogens in the brain depending on GST activity. ^{18}F -labeled alkyl purines were prepared by nucleophilic substitution of 9-methylpurin-6-yl trimethylammonium chloride with ^{18}F in 70% radiochemical yield. ^{76}Br -labeled alkyl purines were prepared by halogen exchange from 9-alkyl-6-iodopurines in 40% radiochemical yield. Dehalogenation by GSH conjugation of all compounds evaluated was specifically mediated by GST. The conjugation rate was increased as the alkyl group enlarges in rat cerebral cortical homogenate. Based on the in vitro evaluation, we selected two compounds, 6- ^{18}F fluoro-9-methyl purine and 6- ^{76}Br bromo-9-ethyl purine, as a potential PET probe, and the compounds were evaluated in vivo using small animal PET. The uptakes of both compounds in the rat brain were high at 1 min after intravenous injection ($> 1\%$ dose/g brain) followed by the elimination of radioactivities by 15 min after injection. Approximately one-third of the high initial radioactivities were completely retained in the brain after the early phase elimination. Chemical form in the extract from rat brain was found to be the corresponding radioactive halogen ion. From these result, the compounds evaluated in vivo would be promising PET probes for measurement of cerebral GST activity.



Presentation Number **0876B**

Poster Session 4c: In Vivo Studies & Development/Novel Use of Imaging Probes

TE2A: a potential bifunctional chelator for ^{64}Cu -labeled biomolecules

Ajit V. Dale¹, **Darpan N. Pandya**¹, **Jung Young Kim**², **Jeong Chan Park**¹, **Wonjung Kwak**¹, **Gwang Il An**², **Jeongsoo Yoo**¹, ¹*Department of Molecular Medicine and Nuclear Medicine, Kyungpook National University School of Medicine, Daegu, Republic of Korea;* ²*Molecular Imaging Research Centre, Korea Institute of radiological and Medical Sciences, Seoul, Republic of Korea. Contact e-mail: ajitvdale@gmail.com*

Objectives: The development of a new bifunctional chelator, which holds radiometals strongly in living systems, is a prerequisite for successful application of disease-specific biomolecules for medical diagnosis and therapy. Recently, TE2A was reported to make kinetically more stable Cu(II) complexes than TETA. Here we report new synthetic route for TE2A, and explore the potential of TE2A as a potential bifunctional chelator. **Methods:** TE2A was synthesized using the regioselective trans-alkyl disubstitution of bisaminal compound with benzyl bromoacetate, followed by successive deprotection of the methylene bridge and benzyl group. Salt-free TE2A was radiolabeled with ^{64}Cu using non-carrier added $^{64}\text{CuCl}_2$ in 0.1 M NH_4OAc buffer solution. The microPET imaging was performed to follow the clearance pattern of the ^{64}Cu -TE2A complex. TE2A was conjugated with c(RGDyK) peptide through one carboxylate group using the standard EDC/SNHS conjugation method. The TE2A-c(RGDyK) conjugate was radiolabeled with ^{64}Cu . **Results:** TE2A was synthesized in salt-free form in an overall yield of 74% starting from cyclam. TE2A was radiolabeled with ^{64}Cu in a quantitative labelling yield at 30°C using NH_4OAc buffer solution at pH 6.5-6.8. The microPET images showed that ^{64}Cu -TE2A was excreted rapidly from the body by the kidney and liver, while no other specific uptake in other organs was observed. Time-activity curve analysis suggested that ^{64}Cu -TE2A was mainly cleared out from body through renal excretion. TE2A was successfully conjugated with c(RGDyK) peptide. The molecular ion peak of the purified conjugate was clearly detected by mass spectrometry. The TE2A-c(RGDyK) conjugate was radiolabeled with ^{64}Cu in 94% yield in 0.1 M NaOAc buffer solution at pH 8 within 30 min at 50°C. **Conclusion:** We report the novel synthetic method for TE2A in salt-free form, overcoming the serious drawbacks of the previous methods. The salt-free TE2A showed a good radiolabeling yield with ^{64}Cu (II) ions. TE2A could be conjugated with the cyclic RGDyK peptide by employing the standard conjugation method and the TE2A-c(RGDyK) conjugate was successfully radiolabeled with ^{64}Cu in high yield, which demonstrates that TE2A can be used as a potential bifunctional chelate without any further structural modification.

Presentation Number **0877B**

Poster Session 4c: In Vivo Studies & Development/Novel Use of Imaging Probes

Reducing renal uptake of radiolabeled DOTA-octreotide by replacing N-terminal amino acid

Fumiaki Takenaka¹, **Yoji Kitamura**², **Shinichiro Kamino**³, **Hikomichi Akizawa**⁴, **Yasushi Arano**⁵, **Yousuke Kanayama**³, **Shuichi Enomoto**^{1,3}, ¹Graduate School of Medicine, Dentistry and Pharmaceutical Sciences, Okayama University, Okayama, Japan; ²Kanazawa University Advanced Science Research Center, Kanazawa University, Kanazawa, Japan; ³Laboratory of Multiple Molecular Imaging Research, Center for Molecular Imaging Science, RIKEN Kobe Institute, Kobe, Japan; ⁴School of Pharmaceutical Sciences, Health Sciences University of Hokkaido, Hokkaido, Japan; ⁵Graduate School of Pharmaceutical Sciences, Chiba University, Chiba, Japan. Contact e-mail: gph422010@s.okayama-u.ac.jp

Objectives: Radiolabeled synthetic somatostatin analogue, the compounds conjugated chelators such as DTPA or DOTA to the N-terminal of octreotide, are used for neuroendocrine tumor scintigraphy and radionuclide therapy. However, the persistent accumulations of radioactivity in kidney after administration of these compounds impair their diagnostic accuracy and cause radiation nephrotoxicity. We have reported that replacement of N-terminal D-phenylalanine of ¹¹¹In-DTPA-D-Phe1-octreotide with negatively charged amino acid, such as aspartic acid or gamma-carboxy-glutamic acid, reduce renal uptake of radioactivity. The aim of this study is to gain insight into the biodistribution of DOTA-octreotide derivatives, which N-terminal amino acid was replaced with negatively charged amino acid, especially accumulation in the kidney and the tumor of tumor bearing mice for molecular imaging of neuroendocrine tumor. **Methods:** The derivatives of DOTA-octreotide, DOTA-D-Phe1-octreotide and DOTA-D-Asp-D-Asp1-octreotide were synthesized by solid-phase synthesis, and radiolabeled with ¹¹¹In. Electrical properties of these compounds were examined by cellulose acetate electrophoresis. Biodistribution studies were performed with BALB c nu/nu mice bearing the AR42J rat pancreatic tumor. **Results:** The result of electrophoresis showed that ¹¹¹In-DOTA-D-Asp-D-Asp1-octreotide was more negatively charged than ¹¹¹In-DOTA-D-Phe1-octreotide. The result indicates that net molecular charge of these octreotide derivatives reflected the number of replaced N-terminal negatively charged amino acid. In biodistribution studies, the renal uptake of ¹¹¹In-DOTA-D-Asp-D-Asp1-octreotide was significantly reduced comparing with ¹¹¹In-DOTA-D-Phe1-octreotide. These results indicated that the renal uptake of radioactivity depends on net charge of the compounds. In addition, accumulation in the tumor was observed in both compounds. Thus, an increase of negative charges in peptide molecules may constitute a strategy for designing radiolabeled peptides with low renal radioactivity levels. We will show the result of PET imaging of radiolabeled DOTA-D-Asp-D-Asp1-octreotide for tumor imaging.

Presentation Number **0878B**

Poster Session 4c: In Vivo Studies & Development/Novel Use of Imaging Probes

MicroSPECT/CT imaging and biological evaluation of ^{111}In -AMBA in PC-3 tumor-bearing SCID mice

Chung Li Ho, I-Hsiang Liu, Yu-Hsien Wu, Liang-Cheng Chen, Chun-Lin Chen, Wan-Chi Lee, Cheng-Hui Chuang, Te-Wei Lee, Chih-Hsien Chang, Isotope Application Division, Institute of Nuclear Energy Research, Taoyuan, Taiwan. Contact e-mail: clho@iner.gov.tw

Bombesin (BBN) is a 14 amino acid peptide with high affinity for the gastrin-releasing peptide receptors (GRPr). Previous studies showed that a variety of tumors including breast, prostate, gastric, colon, pancreatic, and small-cell lung cancer express the GRPr highly. In this study, we synthesized DO3A-CH₂CO-G-4-aminobenzoyl-Q-W-A-V-G-H-L-M-NH₂ (AMBA), a peptide chelated with 1,4,7,10-tetraazacyclododecane-1,4,7,10-tetraacetic acid (DOTA), and radiolabeled this bombesin analogue with $^{111}\text{InCl}_3$. We evaluated the binding affinity of AMBA to BBN type 2 receptor by using ^{125}I -labeled Tyr₄-BBN. MicroSPECT/CT imaging of PC-3 tumor-bearing SCID mice injected intravenously (iv) with ^{111}In -AMBA were performed. We also evaluated pharmacokinetics of ^{111}In -AMBA in PC-3 tumor-bearing SCID mice. **Methods:** A solid phase approach was used to synthesize AMBA. The affinity of AMBA to BBN type 2 receptor was determined by a competitive displacement cell-binding assay using ^{125}I -Tyr₄-BBN. The PC-3 tumor-bearing SCID mice were imaged by microSPECT/CT at 1, 4, 8, 24 and 48 hr after iv injection of ^{111}In -AMBA. The blood was collected at 0.083, 0.25, 1, 4, 8, 24, 48, 72 and 144 hr for pharmacokinetics. **Results:** The purity of synthesized AMBA was greater than 95%. The IC₅₀ and K_i of AMBA in the human bombesin 2 receptor were 0.33 ± 0.09 nM and 0.26 ± 0.07 nM, respectively. The radiolabeling efficiency of ^{111}In -AMBA was 95.43 ± 1.37 %. The microSPECT/CT imaging studies suggested the higher tumor uptake of ^{111}In -AMBA was maintained between 8 and 48 hr post-injection. The maximum concentration of ^{111}In -AMBA was 6.19 %ID/g. The mean residence time of ^{111}In -AMBA was 5.25 h. The area under the time curve of ^{111}In -AMBA was 3.56 g×%ID/h. The clearance rate (Cl) of ^{111}In -AMBA was 29.72 mL/h. **Conclusions:** Our results revealed AMBA has high affinity to BBN type 2 receptor. We also demonstrated a good uptake in the GRPR overexpressed PC-3 tumor-bearing SCID mice. ^{111}In -AMBA is a potential imaging agent for human GRPR-positive tumors.

Presentation Number **0879B**

Poster Session 4c: In Vivo Studies & Development/Novel Use of Imaging Probes

In vivo evaluation of a 18kDa translocator protein (TSPO/PBR) ligand [¹¹C]AC-5216 in Alzheimer's disease mouse models

Jun Maeda¹, **Ming-Rong Zhang**², **Bin Ji**¹, **Takashi Okauchi**¹, **Toshimitsu Fukumura**², **Tetsuya Suhara**¹, **Makoto Higuchi**¹, ¹*Molecular Neuroimaging Group, Molecular Imaging Center, National Institute of Radiological Sciences, Chiba, Japan;* ²*Molecular Probe Group, Molecular Imaging Center, National Institute of Radiological Sciences, Chiba, Japan. Contact e-mail: jun@nirs.go.jp*

Fibrillary lesions composed of amyloid- β peptides (A β) and tau are pathological hallmarks of Alzheimer's disease (AD), and tau aggregates are also characteristic of non-AD tauopathies. These amyloid deposits were inevitably accompanied by microglial activation, which has been noninvasively visualized by recent advances in positron emission tomographic (PET) imaging with the aid of radiolabeled ligands for the peripheral benzodiazepine receptor also known as the 18-kDa translocator protein (TSPO). In the present study, we examined the performance and significance of new TSPO imaging agent, [¹¹C]AC-5216, for pursuing roles of microglia in A β and tau pathogenesis and for diagnostic and therapeutic evaluations of neuroinflammation in AD and related disorders. Immunostaining of TSPO in AD and non-AD tauopathy brains demonstrated an intimate association between TSPO-positive microglia and tau inclusions, and microglial TSPO upregulation antecedent to massive neuronal death was also observed in living tau transgenic mice by means of [¹¹C]AC-5216-PET. A tight correlation between in vitro autoradiographic signals of [¹¹C]AC-5216 and phosphorylated tau burden was found even prior to the emergence of mature tau fibrils detectable with thioflavin-S. Unlike tau-induced TSPO-positive microgliosis, TSPO levels in aged amyloid precursor protein transgenic mice were only modestly increased. This was in sharp contrast with notable A β accumulation in these animals as imaged by an amyloid radioligand, [¹¹C]Pittsburgh Compound-B. These results indicate the usefulness of [¹¹C]AC-5216 in quantitative mapping of tau-provoked toxic neuroinflammation, and support the applicability of PET imaging with this radiotracer to clinical assessments of diverse tauopathies including AD.

Presentation Number **0880B**

Poster Session 4c: In Vivo Studies & Development/Novel Use of Imaging Probes

Comparison of 11C-PiB and 18F-W372 in Alzheimer's disease: a primary human study

Liping Fu¹, Jinming Zhang¹, Xi Zhang², Zengqiang Zhang², Jiahe Tian¹, ¹Nuclear Medicine, General Hospital of the Chinese People's Liberation Army and Military Medical Postgraduate College, Beijing, China; ²Neurology, General Hospital of the Chinese People's Liberation Army and Military Medical Postgraduate College, Beijing, China. Contact e-mail: flp39@163.com

Introduction: The radiotracer Pittsburgh Compound-B (PiB) binds with high affinity to the amyloid- β (A β) peptide, and is clinic used in evaluation the neuropathological changes in AD. But the short half-life time of PiB constricts its clinical usage. A new radioligand 7-Methoxy-2 (6-fluoropyridin-3-yl)imidazo[2,1-b]-8-pyridinothiazol (W372) labeled by 18-fluorine was introduced. The purpose of this study was to compare PiB and W372 in Alzheimer's disease. **Materials and Methods:** Subjects: Five patients with slight to mild AD (1 male and 4 females) and 5 healthy controls (3 males and 2 females) participated in the study, who were matched in age and education. **Acquisition:** All subjects received PiB and W372 scans in random order. 40 and 60-min dynamic PET scans were acquired at a SIEMENS biograph PET-CT scanner. The data were binning into 21 and 25 consecutive frames for PiB and W372. **Data analysis:** Axial images of the 14th frame (9min) for W372 and the 16th frame (15min) for PiB were chose as referential image to draw the volume of interest (VOI). The average counts (Bq/ml) of each VOI were acquired for time-activity curve and for the ratio of each brain region/cerebellum. A univariate of general linear model was performed to assess: 1.at the 40-min time point, regional metabolic difference between PIB and W372 in control; 2.at the final time point (40 and 60-min), regional metabolic difference of W372 and PiB between the groups. **Results:** An increasing trend for both PiB and W372 retention in patients was observed, the univariate analysis revealed that both PiB($F=3.71, P=0.06>0.05$) and W372 ($F=2.49, P=0.12>0.05$) had no obvious difference between groups (Figure 1). No significant difference of PiB and W372 deposit was showed in control at the 40-min time point. **Conclusion:** Consistent with previous reports, PiB is a sensitive molecular probe for plaque imaging. W372 seems to have a similar potential in clinic evaluation of AD.

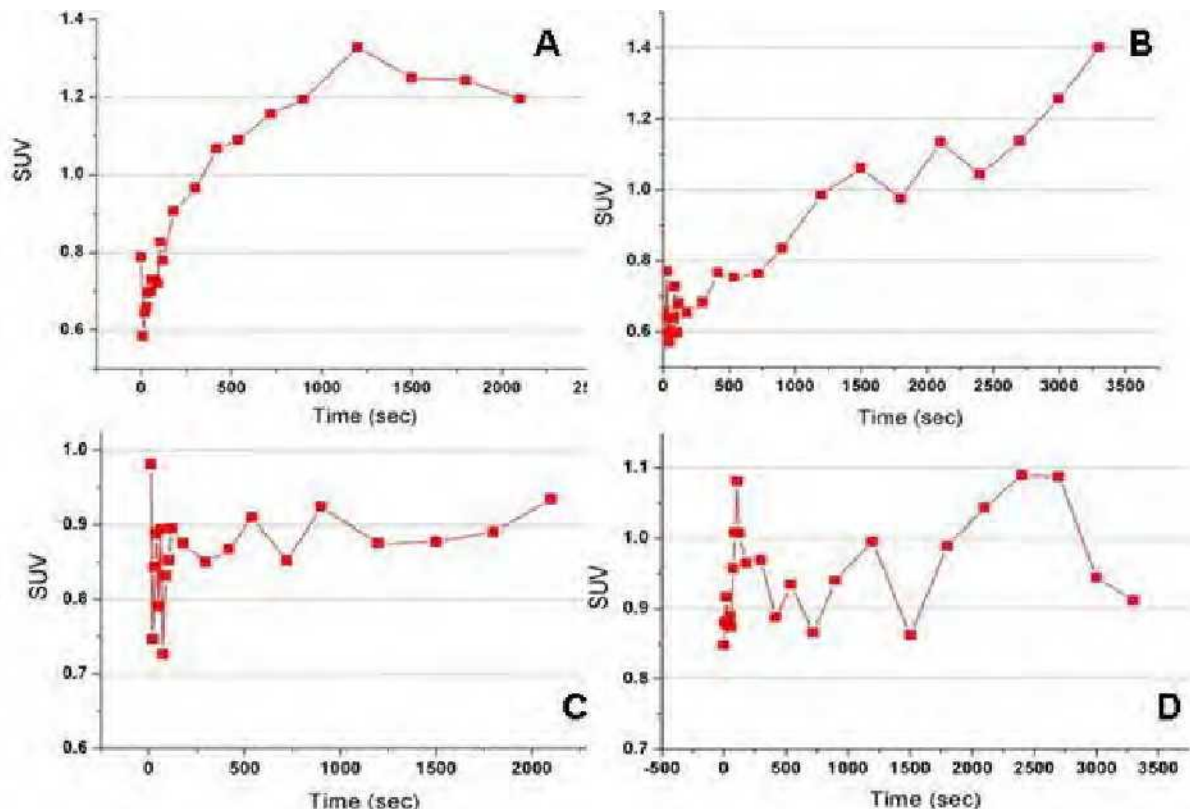


Figure1. The time-activity curves (A: P W372, B: P PiB) revealed a gradually ascending trend of both tracers in AD patient, but a horizontal and descending trend was showed in control (C: C W372, D: C PiB). P= Patient and C=Control.

Presentation Number **0881B**

Poster Session 4c: In Vivo Studies & Development/Novel Use of Imaging Probes

Pre-clinical Evaluation of a New Alpha-2-Adrenoceptor Tracer [¹¹C]ORM-13070 in Rats

Eveliina Arponen¹, Päivi M. Marjamäki², Semi Helin¹, Tove J. Grönroos², Kjell Någren³, Kimmo Ingman⁴, Merja Haaparanta-Solin², Jukka Sallinen⁴, Olof Solin¹, ¹Radiopharmaceutical Chemistry Laboratory, Turku PET Centre, Turku, Finland; ²MediCity/PET Preclinical Laboratory, Turku PET Centre, Turku, Finland; ³Department of Nuclear Medicine, Odense University Hospital, Odense, Denmark; ⁴Research and development, Orion Pharma, Turku, Finland. Contact e-mail: paivi.marjamaki@utu.fi

Purpose: The aim of this study was to develop a PET tracer for α_2 -adrenoceptor imaging and evaluate it using ex vivo methods in rats. α_2 -Adrenoceptors in the human brain are suggested to be involved in various neuropsychiatric diseases, including depression, schizophrenia, and movement disorders. Currently, no PET tracer is available for imaging this receptor system in vivo. **Methods:** [¹¹C]ORM-13070 (1-[(S)-1-(2,3-dihydrobenzo[1,4]dioxin-2-yl)methyl]-4-(3-¹¹C-methoxymethylpyridin-2-yl)-piperazine) was synthesized by ¹¹C-methylation of O-desmethyl-ORM-13070 with [¹¹C]methyl triflate, which was prepared from cyclotron-produced [¹¹C]methane via [¹¹C]methyl iodide. The [¹¹C]methyl triflate was bubbled through a solution of desmethyl-precursor in acetonitrile in the presence of tetrabutylammonium hydroxide. The reaction mixture was heated at 80 °C for 3 min and purified by semi-preparative HPLC. The biodistribution of ¹¹C-radioactivity after [¹¹C]ORM-13070 injection was studied ex vivo in rat brain using photonstimulated luminescence autoradiography. The specificity of [¹¹C]ORM-13070 binding to α_2 -adrenoceptors was estimated in rats that were pre-treated with a dose of atipamezole, a specific α_2 -receptor antagonist. **Results:** The average synthesis time was 32 minutes, including the synthesis of [¹¹C]methyl triflate, methylation, the semi-preparative purification, and formulation. The radiochemical yield calculated from the initial [¹¹C]CH₄ (decay corrected to end of bombardment [EOB]) was $9.6 \pm 2.7\%$ and the radioactivity of [¹¹C]ORM-13070 was 1210 ± 360 MBq at the end of synthesis (EOS). The specific radioactivity measured by analytical HPLC was 640 ± 390 GBq/ μ mol (EOS). The radiochemical purity of all syntheses exceeded 99%. The maximum tracer uptake in rat brain was observed in the caudatus-putamen and olfactory tubercle, brain regions known to contain α_2 -receptors. The ¹¹C-radioactivity uptake ratios at 30 min p.i. were 2.6 for the caudatus-putamen/cerebellum and 3.1 for the olfactory tubercle/cerebellum. The frontal cortex and thalamus exhibited lower radioactivity uptakes. In the rats pre-treated with atipamezole, ¹¹C-radioactivity uptake in the caudatus-putamen and olfactory tubercle decreased to the level of the frontal cortex and thalamus. **Conclusions:** We developed an efficient method for the radiosynthesis of [¹¹C]ORM-13070. Its preliminary pre-clinical evaluation suggest that [¹¹C]ORM-13070 may be a promising PET tracer for α_2 - or α_2C -adrenoceptors.

Presentation Number **0882B**

Poster Session 4c: In Vivo Studies & Development/Novel Use of Imaging Probes

Radiosynthesis of Novel Ligands for Molecular Imaging of Cellular Stress Response

Daniel Y. Lee, Pradip Ghosh, King Li, Radiology, The Methodist Hospital Research Institute, Houston, TX, USA. Contact e-mail: DLee@tmhs.org

Overproduction of heat shock proteins (HSPs) in various solid tumors and the ability to induce these proteins by nonablative heat provide the motivation for targeting this group of critical phylogenetically conserved proteins. There are two ultimate goals for targeting inducible proteins such as the classic 70-kDa molecular chaperone, HSP70: 1) develop new molecular imaging agents capable of evaluating in vivo levels of such proteins as biomarkers for cellular stress response; and 2) to exploit this inducible protein as targets for delivering new pharmaceuticals in a controllable manner. For clinical translation, strategies that target such inducible proteins can be exploited to “create” specific molecular targets simply by localized heating with noninvasive methods such as focused ultrasound. Since HSPs function as molecular chaperones that require ATP for catalysis, a class of adenosine-derived inhibitors have been reported with low micromolar affinities for the inducible HSP70 protein. We have adapted this class of potential HSP70 inhibitors for molecular imaging of the cellular stress response. Here we describe the radiochemical synthesis of a [F-18]fluorinated adenosine-based HSP70 ligand.

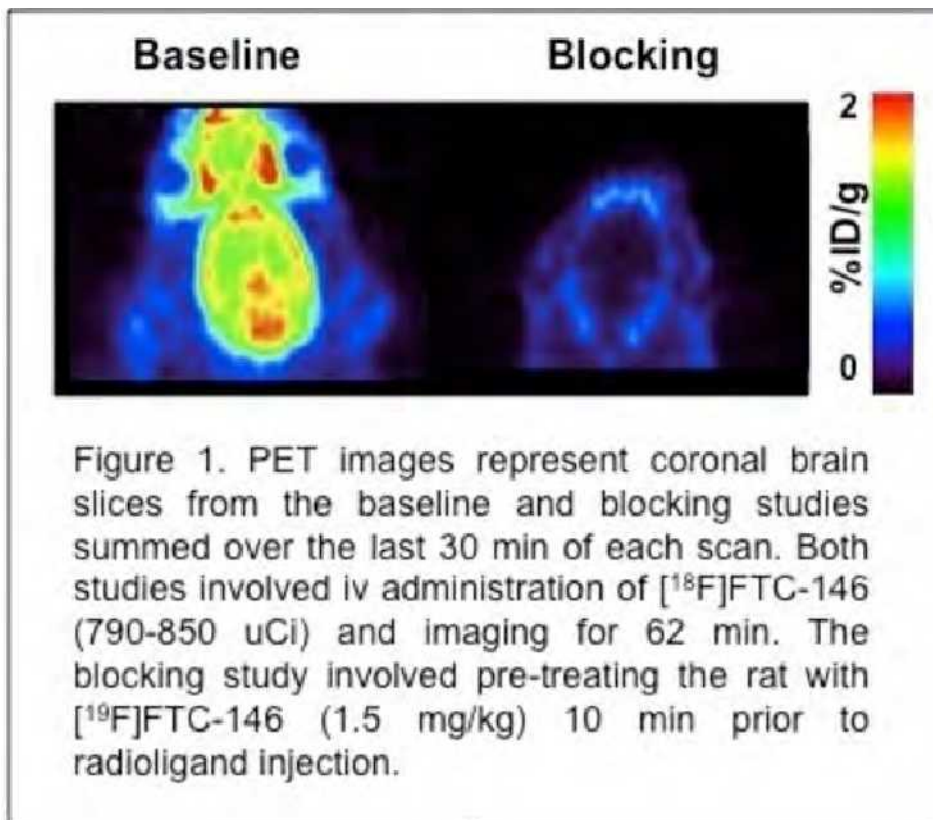
Presentation Number **0883B**

Poster Session 4c: In Vivo Studies & Development/Novel Use of Imaging Probes

A New Ultra Selective PET Probe for Imaging Sigma-1 Receptors in Living Subjects

Michelle L. James¹, **Bin Shen**¹, **Carsten H. Nielsen**^{1,2}, **Cristina Zavaleta**¹, **Rhona A. Berganos**¹, **Christophe Mesangeau**³, **Sanjiv S. Gambhir**^{1,4}, **Christopher R. McCurdy**³, **Frederick T. Chin**¹, ¹Molecular Imaging Program at Stanford (MIPS), Department of Radiology, Stanford University, Palo Alto, CA, USA; ²Cluster for Molecular Imaging & Department of Clinical Physiology, Nuclear Medicine and PET, University of Copenhagen and Rigshospitalet, Copenhagen, Denmark; ³Department of Medicinal Chemistry, The University of Mississippi, Oxford, MS, USA; ⁴Department of Bioengineering, Stanford University, Palo Alto, CA, USA. Contact e-mail: mljames@stanford.edu

Radioligands selective for sigma-1 receptors (S1R) have the potential to non-invasively detect and monitor various pathologies, including cancer and neurodegenerative diseases. This study details the *in vitro* binding, radiosynthesis and evaluation of a new S1R radioligand, [¹⁸F]FTC-146, in living rats using positron emission tomography (PET). *In vitro* binding studies showed that [¹⁹F]FTC-146 has notably high affinity (K_i = 2.5 pM) for S1R, and greater than 140,000-fold selectivity for S1R compared to sigma-2 receptor. [¹⁸F]FTC-146 was synthesized via nucleophilic substitution with a minimum specific radioactivity of 1500 mCi/μmol, radiochemical purity >99% and chemical purity >99%, in total synthesis time of 60 min from end of bombardment (n=9). *In vivo* biodistribution of [¹⁸F]FTC-146 was assessed via 62 min dynamic imaging of normal rats using small animal PET and confirmed by *ex vivo* gamma counting (n=3). PET images and *ex vivo* gamma counting showed significant accumulation of [¹⁸F]FTC-146 in organs known to contain high levels of S1R, including lungs, liver, brain (frontal cortex, thalamus, occipital cortex, cerebellum), and was also seen in bone. Pre-treatment with [¹⁹F]FTC-146 (1.5 mg/kg) reduced the binding of [¹⁸F]FTC-146 in the whole brain at 60 min p.i. by 93% relative to baseline (n=2) (Figure 1). Displacement studies, involving iv administration of [¹⁹F]FTC-146 (1 mg/kg) at 20 minutes p.i. resulted in 38% reduction in whole brain binding at 60 min (n=3). These results indicate that [¹⁸F]FTC-146 accumulation in rat brain most likely represents specific binding to S1R. Imaging baseline rats over a 10-h period demonstrated slow washout of [¹⁸F]FTC-146 uptake in whole brain (1.5 %ID/g at 20 min vs 0.6 %ID/g at 10 h) showing that binding to S1R is reversible. [¹⁸F]FTC-146 shows tremendous potential as a specific radioligand for visualizing S1R *in vivo*. Since [¹⁸F]FTC-146 is the most selective S1R radioligand reported to date, it may be very useful in revealing new information about S1R and hence warrants further investigation.



Presentation Number **0884B**

Poster Session 4c: In Vivo Studies & Development/Novel Use of Imaging Probes

Relationships Between the Uptake of PET Tracers and Hypoxia Markers in HNSCC Mice Xenografts: CA IX, Glut-1 and Hif-1 α Expression vs. the Uptake of [18 F]EF5 and [18 F]FDG

Jonna Sinkkonen¹, Antti Silvonieni^{1,2}, Sarita Forsback¹, Nina Savisto¹, Olof Solin¹, Reidar Grénman², Panu Jaakkola³, Heikki Minn^{1,4}, Tove J. Grönroos¹, ¹Turku PET Centre, University of Turku, Turku, Finland; ²Department of Otorhinolaryngology, University of Turku, Turku, Finland; ³Turku Centre of Biotechnology, University of Turku, Turku, Finland; ⁴Department of Oncology and Radiotherapy, Turku University Hospital, Turku, Finland. Contact e-mail: jmsink@utu.fi

AIM: The abnormal angiogenesis and occasional blocks in blood veins cause hypoxia in tumor tissues. The lack of oxygen radicals in hypoxic tumors has an extreme impact on therapy outcome in the form of resistance to radiotherapy. Hypoxic tumors hence contain aggressive tumor cell populations which decreases the survival of patients. PET combined with [18 F]FDG is increasingly used as a diagnostic and radiotherapy planning tool in cancer. Before PET can be applied for hypoxia related treatment planning, we need a fundamental understanding of the biological processes that affect the uptake of a hypoxia tracer, such as [18 F]EF5. The aim of this study was to examine whether differences in the phenotypes of HNSCC do affect the uptake of [18 F]FDG and [18 F]EF5. **METHODS:** Three cell lines from patients diagnosed with HNSCC were used; UT-SSC-8, -34 and -74. Subcutaneous tumors were created in mice and dynamic whole body PET/CT scans were performed with [18 F]FDG and [18 F]EF5 at two distinct growth stages. The first PET/CT scan was done on tumors with volumes of approximately 500 mm³ and the second scan on tumors with volumes ranging between 2000-3500 mm³. After the second scan mice were sacrificed and paraffine sections of tumors stained against CA IX and Glut-1. In addition, immunoblots against Hif-1 α were determined from cell lysates collected after growing cells under 1% O₂ for 1, 3, 6, 12 and 24h. **RESULTS:** UT-SSC-8 tumors showed a weak membranous CA IX staining and a moderate membranous Glut-1 staining, whereas the staining of CA IX and Glut-1 in UT-SSC-34 tumors was clearly membranous and overlapping. The strongest membranous CA IX and Glut-1 staining was seen in UT-SSC-74 tumors, but some cellular staining could also be seen. Hif-1 α immunoblots for UT-SSC-8 and UT-CC-34 cells showed weakest Hif-1 α expression at the 1 h and strongest at 3 h and 6 h. At later time points the expression of Hif-1 α slightly decreased. The Hif-1 α expression was strongest in UT-SSC-74 cells and did steadily increase over time. ROIs were drawn over whole tumors and the uptake of [18 F]FDG and [18 F]EF5 decay corrected and uptake expressed as percent of injected dose per gram. The uptake of both tracers was two times higher in UT-SSC-34 and UT-SSC-74 tumors compared to that seen in UT-SSC-8 tumors. **CONCLUSION:** Our preliminary results indicate that higher CA IX and Glut-1 staining relates to higher tracer uptakes. We suggested that a relationship exists between differences in cell line phenotypes and the uptake pattern of [18 F]FDG and [18 F]EF5.

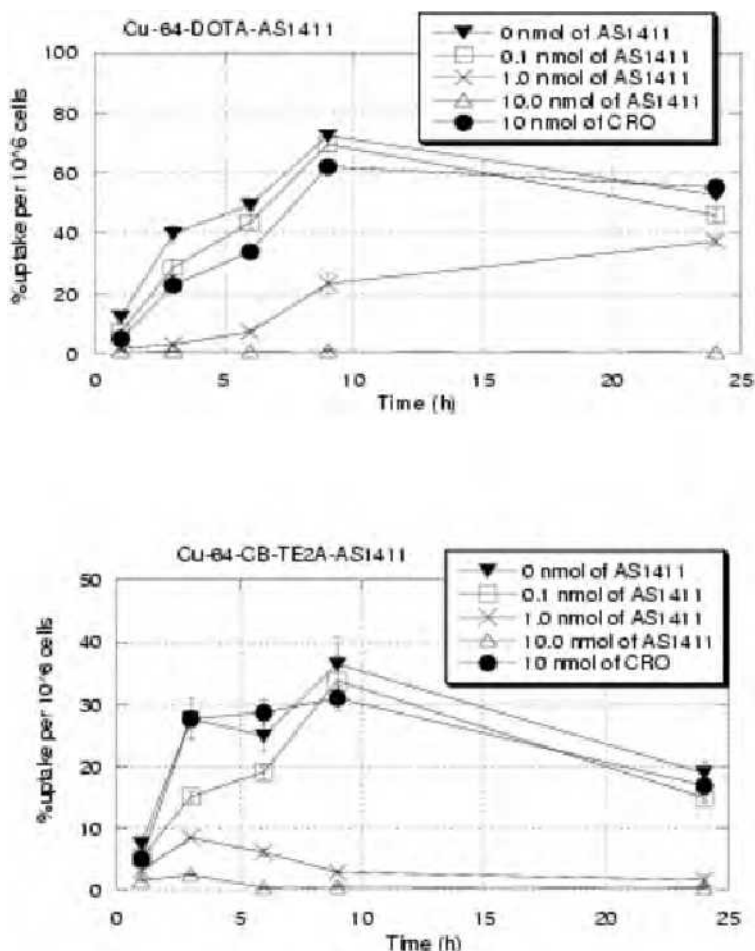
Presentation Number **0885B**

Poster Session 4c: In Vivo Studies & Development/Novel Use of Imaging Probes

Target binding properties of Cu-64 labeled aptamer in lung cancer

Junling Li, Huaiyu Zheng, Xiao-Feng Li, John O. Trent, Paula J. Bates, Chin K. Ng, University of Louisville, Louisville, KY, USA.
 Contact e-mail: junling.li@louisville.edu

Introduction: AS1411, a guanosine-rich oligonucleotide, is an aptamer with specific binding to nucleolin, a protein over-expressed in multiple cancer cells. Studies have indicated that compounds chelated with Cu-64 DOTA could result in high liver accumulation probably due to low in vivo stability of the Cu-64 DOTA complex. On the other hand, compounds chelated with Cu-64 CB-TE2A (4,11-bis(carboxymethyl)-1,4,8,11-tetraazabicyclo[6.6.2]hexadecane) has been shown to reduce liver uptake and enhance target-to-background signal. Thus our objective was to use competition experiments to investigate the effect of these two chelators on target binding properties of Cu-64 labeled AS1411 in lung cancer cell, HTB 177. Methods: A cytosine-rich oligonucleotide (CRO) was used as a control. Either Cu-64 DOTA or CB-TE2A was used to label AS1411 (DA or CBA). HTB177 cells (1×10^5) were seeded into each well. Different amount of AS1411 (0, 0.1, 1 and 10 nmoles) or 10 nmoles of CRO was added with 3 μ Ci of DA or CBA and incubated at 37 oC for 1, 3, 6, 9 and 24 hr respectively (n=4). Uptake was calculated by % (counts in cells)/total counts. Results: All Cu-64 was incorporated into both chelators during the synthesis and specific activity for both DA and CBA was 100-120 and 200-250 mCi/ μ mol respectively. The highest uptake of DA was about 2 times that of CBA when no additional AS1411 was added. Uptake for both DA and CBA was not significantly reduced with CRO added (n=4, p>0.05), but was inversely proportional to the amount of AS1411 present, with >90% reduction at 10 nmoles from 3 to 24 hr. Conclusions: AS1411 was successfully labeled with Cu-64 DOTA and CB-TE2A with high yield and specific activity. A majority of DA and CBA uptake could attribute to targeted protein binding of nucleolin, indicating that DA and CBA might be novel PET imaging probes specifically for lung cancer detection.



Competitive effect of AS1411 or CRO on uptake of Cu-64 DOTA or CB-TE2A AS1411 in lung cancer.

Presentation Number **0886B**

Poster Session 4c: In Vivo Studies & Development/Novel Use of Imaging Probes

Synthesis and initial in vitro and in vivo evaluation of 2'-[¹⁸F]Fluoro-2'-deoxythymidine ([¹⁸F]FT) in TK-expressing tumor cells and tissue

Piyush Kumar¹, **William Sun**², **Melinda Wuest**¹, **Edward E. Knaus**², **Leonard I. Wiebe**¹, ¹*Oncology, University of Alberta, Edmonton, AB, Canada;* ²*Faculty of Pharmacy and Pharmaceutical Sciences, University of Alberta, Edmonton, AB, Canada. Contact e-mail: pkumar@ualberta.ca*

The transmembrane transport, metabolic activation (phosphorylation) and functional properties of nucleosides are strictly dependent upon their stereochemistry, functionality and substitution patterns in their nuclear base and furanose moieties, enabling selective amplification of their antiviral and antitumor properties. Several F-18 labeled nucleosides have been developed for cell proliferation imaging and imaging herpes simplex viral-thymidine kinase (HSV-TK) transgene expression. 3'-Deoxy-3'-[¹⁸F]fluorothymidine([¹⁸F]FLT), a substrate for mammalian TK-1 and TK-2, and HSV-TK, is used for imaging cell proliferation, but not for imaging HSV-TK transgene expression. On the contrary, 5-iodo-2'-fluoro-2'-deoxyuridine (FIRU) and its arabinosyl analogue, FIAU, are poor substrates for TK-1 but have a high affinity for HSV-TK. 2'-Fluoro-2'-deoxythymidine (FT), a structural analogue of FLT, was originally developed as an antiviral agent. Synthesis of ¹⁸F-labeled FT and its initial in vitro and in vivo properties for imaging the HSV-TK transgene are now reported. The radiosynthesis of [¹⁸F]FT was performed in an automated synthesis unit (ASU). In vitro toxicity and cell uptake studies with FT were done in EMT-6, KBALB, 143B tumor cell lines and their counterparts engineered to express HSV-TK (KBALB-STK, 143B-LTK). In vivo tumor uptake was studied in KBALB and KBALB-STK tumor-bearing BALB/C mice using small animal PET and compared to [¹⁸F]FLT. [¹⁸F]FT was synthesized from 3-tert-butoxycarbonyl-1-(3',5'-di-O-benzoyl-2'-O-nosyl-β-D-arabinofuranosyl)thymine using a sequence of reactions adapted to an ASU. [¹⁸F]Fluorination (10 min, 95 °C) of the precursor (5 mg), followed by deprotection (1N HCl, 0.5 mL, 50 °C, 5 min; then 1N NaOMe/MeOH, 1 mL; 50 °C, 3 min), afforded the impure [¹⁸F]FT that, upon reverse phase HPLC purification on a C18 column (Whatman Magnum 9 ODS 9.4 x 250 mm) using water:ethanol (100:8,v/v) as eluent (flow rate, 2 mL/min), gave [¹⁸F]FT (retention time 13.5 min) in 6 ± 2% (uncorrected) radiochemical yield with a radiochemical purity of 94 ± 4% (n=20). In vitro cytotoxicity of FT in 5 murine cell lines was >1 mM. Cell uptake of [³H]FT (per μg protein) was almost equal to thymidine at 24 h in 143B-STK/143B cells, but ~170 times higher in KBALB-STK/KBALB cells. Initial PET imaging data with [¹⁸F]FT in KBALB-STK and KBALB tumors confirmed its preference specifically for HSV-TK expressing tumor. [¹⁸F]FT was developed as a radiotracer and has shown a preferential higher uptake for imaging HSV-TK transgene expression in vitro and in vivo.

Presentation Number **0887B**

Poster Session 4c: In Vivo Studies & Development/Novel Use of Imaging Probes

Radiolabeling and Imaging of ^{212}Pb -TCMC-Trastuzumab

Michael T. Azure¹, Hyunki Kim¹, Sui Shen², Daniel R. Yoder¹, Richard M. Machado³, Gilbert Andreoletti⁴, Patrick L. Maquaire⁴, Martin Brechbiel⁵, Kwamena E. Baidoo⁵, Diane Milenic⁵, Kurt R. Zinn¹, ¹Radiology, University of Alabama/Birmingham, Birmingham, AL, USA; ²Radiation Oncology, University of Alabama/Birmingham, Birmingham, AL, USA; ³Engineering, Canberra AREVA, Grand Rapids, MI, USA; ⁴Chemistry, AREVA NC, Beaumont Hague, France; ⁵Radiation Oncology, NIH, Bethesda, MD, USA. Contact e-mail: mtazure@uab.edu

The potential of ^{212}Pb -TCMC-Trastuzumab as a radiotherapeutic agent was previously reported using the bifunctional chelator TCMC (1,4,7,10-Tetra-(2-Carbamoyl Methyl)-Cyclododecane {*Cancer Biother Radiopharm* 2005; 20:557}. The dual β^- and α particle emanations provide a targeted radiotherapeutic agent with short range and long-range cell destruction. Imaging ^{212}Pb would be advantageous for planned human studies, but thought to be impossible due to the multitude of γ rays and bremsstrahlung associated with the various radioisotopes in the decay of ^{212}Pb . The goal of our research was to image ^{212}Pb with planar (Picker Axis, Philips) and $\mu\text{SPECT/CT}$ (X-SPECT, GammaMedica) imaging. High quality ^{212}Pb eluate (confirmed by HpGe detector) was collected from a $^{224}\text{Ra}/^{212}\text{Pb}$ generator (AREVA Med LLC) for all experiments. Trastuzumab was radiolabeled with ^{212}Pb using TCMC, with the final product composition evaluated by HPLC, gel electrophoresis, ITLC, and Scatchard analyses with purified HER2. Phantom studies were conducted with ^{212}Pb using medium energy collimators optimized for the 238 keV emission. Post acquisition phantom and NHP images were enhanced utilizing a planar standard-spatial filter. Imaging studies were conducted after i.p. injection of ^{212}Pb -TCMC-Trastuzumab in mice and a male cynomolgus primate. Imaging includes planar and μSPECT and with a specially collimated portable HpGe (AREVA Canberra) detector for medium to high energy resolution. Qualitative discernable phantom images were obtained from the phantom studies. The ^{212}Pb -TCMC-Trastuzumab was high purity (>95%) with specific and high affinity binding to HER2 receptors. μSPECT studies in mice with medium energy collimators produced excellent images, showing the ^{212}Pb remained in the peritoneal cavity. A peritoneal distribution was also found for the primate at t0h, t4h, t8h, t24h and t48h. The HpGe detector detected multiple gamma ray emissions, including ^{212}Pb and ^{212}Bi . These data indicate that the ^{212}Pb remained in the peritoneal cavity for up to 48h indicating low probability of dissociation of the ^{212}Pb from the antibody. The imaging methods can easily be applied in the planned clinical studies.

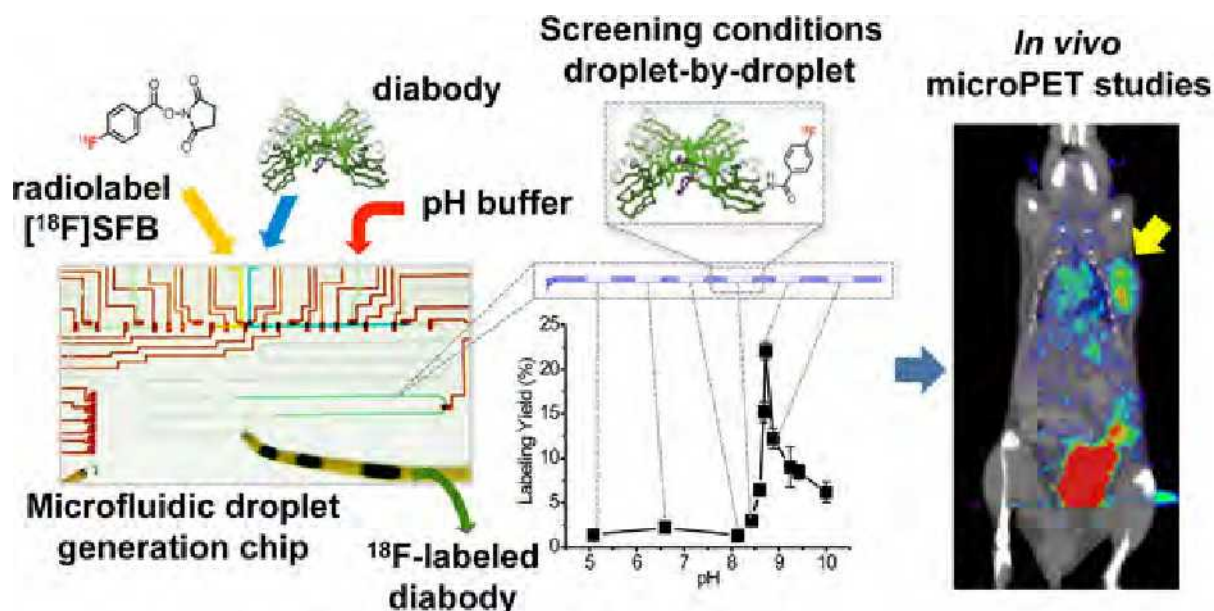
Presentation Number **0888B**

Poster Session 4c: In Vivo Studies & Development/Novel Use of Imaging Probes

Using digital microfluidics to optimize ^{18}F -labeling conditions of diabodies

Kan Liu^{1,2}, Eric J. Lepin¹, MingWei Wang^{1,3}, Wei-Yu Lin¹, Hsian Rong Tseng¹, Anna M. Wu¹, Clifton K. Shen¹, ¹Pharmacology, Crump Institute, Los Angeles, CA, USA; ²College of Electronic and information Engineering, Wuhan Textile University, Wuhan, China; ³Nuclear Medicine, PET center, Cancer hospital, Fudan University, Shanghai, China. Contact e-mail: kshen@mednet.ucla.edu

Biomolecules provide an enormous reservoir for developing specific probes for immunoPET to visualize biological processes and detect biomarkers of interests in vivo. Diabodies (dimers of single-chain Fv antibody fragments) retain the high binding specificity and affinity of their parental antibodies, which can reach maximum uptake in target tissue in 1-2 h post injection, and clear with a terminal half-life of 3-4 h, making them optimal for immunoPET. However, efficient ^{18}F -labeling of diabodies remains challenging. Here we demonstrated the use of a digital microfluidic droplet generator to rapidly scout conditions for radiolabeling diabodies using N-succinimidyl-4- ^{18}F fluorobenzoate (^{18}F SFB). Consuming only small amounts of diabodies and ^{18}F SFB, the optimal reaction parameters (pH, concentration, etc.) can be obtained by screening each individual droplet tailored with different compositions (Figure below). Batches of products can be generated from one single droplet to a mouse-dose scale to match the demand of radioactivity for ^{18}F -labeled diabody evaluation. HER2- and PSCA-expressing xenografts were readily imaged at 4 h post injection with target-to-background ratios over 4:1. Routine ^{18}F -labeling of diabodies provides a practical means for same-day immunoPET using antibody-based imaging probes.



Presentation Number **0889B**

Poster Session 4c: In Vivo Studies & Development/Novel Use of Imaging Probes

Radiopharmacological profile of a potential myocard perfusion tracer - Ga-68 labeled tris(salicylaldimine) analogue

Ralf K. Bergmann¹, Jae Min Jeong³, Jens Pietzsch¹, Jörg Steinbach¹, Richard P. Baum², ¹Institute of Radiopharmacy, Forschungszentrum Dresden-Rossendorf, Dresden, Germany; ²Department of Nuclear Medicine, Zentralklinik Bad Berka GmbH, Bad Berka, Germany; ³Department of Nuclear Medicine, National University Hospital Seoul, Seoul, Republic of Korea. Contact e-mail: r.bergmann@fzd.de

The lipophilic cationic ⁶⁸Ga-complex (Tsang B.W. et al. J Nucl Med 1993; 34; 1127) of Tris(4,6-dimethoxysalicylaldimine)-N,N'-bis(3-aminopropyl)-N,N'-ethylenediamine (BAPEN), showed high accumulation in mice hearts (Nucl Med Biol 2010; 37; 149). The radiopharmacological profile of the ⁶⁸Ga-BAPEN was evaluated in rats, which was produced by a kit formulation and the biodistribution, kinetics and metabolism were studied with small animal PET. The BAPEN was labeled with ⁶⁸GaCl₃ (generator eluate 1 M HCl) in a one step procedure. Before application human serum albumin was added to a final concentration of 1%, and the solution filtrated (22 µm pore size). The biodistribution at 5 and 60 min p.i. (each time point 8 rats) after single intravenous injection, arterial blood clearance over 1 h (n=2), and the in vivo metabolism in Wistar rats were investigated in combination with small animal PET, and the main biokinetic parameters of ⁶⁸Ga-BAPEN were estimated. ⁶⁸Ga-BAPEN was prepared with purity >91% within 20 min. The activity was fast accumulated in the rat heart (values in SUV; 5 min p.i., 1.56 ± 0.19; 60 min, 1.42 ± 0.35) with the following heart-to-tissue ratios at 5 min p.i.: blood 4.2, lung 2.2, liver 0.4, kidneys 0.3, and brain 109.6. No clearance of ⁶⁸Ga-activity from the heart was observed over 1 hour. The arterial blood clearance of the original compound was biphasic with half lifes of 2 min and 23 min respectively; it was metabolized with a half-life of 1.6 min. The ⁶⁸Ga-activity was rapidly excreted into the intestine (5 min p.i. 34.9 ± 4.0%ID; 60 min p.i. 56.7 ± 7.0%ID). ⁶⁸Ga-BAPEN showed a typical perfusion dependent biodistribution pattern in rats, with high accumulation in heart, kidneys, liver, adrenals, and pancreas. The heart was clearly delineated with low background. The increasing liver uptake could complicate the quantitative imaging of the heart apex at late time points. ⁶⁸Ga-BAPEN was fast distributed followed by a slow blood clearance on a low activity level. The fast in vivo metabolism of the ⁶⁸Ga-BAPEN in rats prevented a more distinct perfusion dependent biodistribution pattern. No transport through the blood-brain-barrier into the brain was observed. The ⁶⁸Ga-BAPEN may be useful as radiopharmaceutical for perfusion imaging, particularly, for the heart.

Presentation Number **0890B**

Poster Session 4c: In Vivo Studies & Development/Novel Use of Imaging Probes

Biokinetics, metabolism and PET imaging with Cu-64 and Ga-68 labeled ghrelin analogues in rats

Ralf K. Bergmann¹, Constance Chollet², Jens Pietzsch¹, Anette G. Beck-Sickinger², Jörg Steinbach¹, ¹Institute of Radiopharmacy, Forschungszentrum Dresden-Rossendorf, Dresden, Germany; ²Institute of Biochemistry, Universität Leipzig, Leipzig, Germany. Contact e-mail: r.bergmann@fzd.de

Ghrelin is a gastric peptide involved in food intake control, and growth hormone release. Besides its well-defined orexigenic role, ghrelin is likely involved in tumor development and growth. Therefore, non-invasive imaging agents for determining ghrelin receptors are desirable. However, ghrelin receptors are expressed in low level making detection via imaging difficult. The labeling using activated esters like 4-(F-18-fluoro)benzoyl-succinimide (2) was not possible due to the existence of three primary amino groups per peptide. Therefore, human ghrelin1-28 [Lys16(NODAGA)]-ghrelin1-28 and a short ghrelin inverse agonist NODAGA-KwFwLL-NH₂ were synthesised on solid-phase. Subsequently, radiolabeling yielded Cu-64- and Ga-68-NODAGA-peptides in high radiochemical purity (>98%) with a specific activity >10 GBq/μmol. For basic radiopharmacological characterization biodistribution, small animal PET, and metabolite analysis in arterial blood plasma were carried out in Wistar rats with all 4 radiotracers. The ghrelin analogues were in high amounts taken up by the kidneys. The Cu-64- and Ga-68-NODAGA-KwFwLL-NH₂ were for the most part hepato-biliary eliminated. The metabolite analysis showed the well-known des acyl ghrelin as the main metabolite in vivo reaching 90% in blood plasma after one hour. On the other site the NODAGA-KwFwLL-NH₂ peptides were highly stabile; only 5% metabolites were observed after one hour in rat plasma. Interestingly, the biodistribution and kinetics were similar for the pairs of peptide labeled ether with Cu-64 or Ga-68. This shows the small effect of the different ionization of the Ga-68 (neutral) or Cu-64 (one negative charge) NODAGA complexes on the biodistribution. The blood clearance of these peptides was relative low, with about 50% of starting amount after one hour. The high stability and low blood clearance are important prerequisites for further studies of ghrelin receptor imaging. These results indicate that further in vivo evaluation of radiolabeled ghrelin inverse agonists as potential PET tracers for ghrelin receptors is warranted. Reference: (1) Holst, B., et al. (2003) High constitutive signaling of the ghrelin receptor--identification of a potent inverse agonist. *Mol Endocrinol* 17, 2201-10. (2) Bergmann, R., et al. (2002) Biodistribution and catabolism of (18)F-labeled neurotensin(8-13) analogs. *Nucl Med Biol* 29, 61-72. Acknowledgement: This project was partially supported by FP7 project "GIPIO", Project Reference: 223057

Presentation Number **0891B**

Poster Session 4c: In Vivo Studies & Development/Novel Use of Imaging Probes

A Small Microwave Unit to Enhance Commercial Radiochemistry Modules for Making ^{18}F -labeled Imaging Agents

Bin Shen¹, **Greg LeBlanc**², **Murugesan Subbarayan**¹, **Rhona A. Berganos**¹, **Christophe Mesangeau**³, **Christopher R. McCurdy**³, **Frederick T. Chin**¹, ¹Molecular Imaging Program at Stanford (MIPS), Department of Radiology, Stanford University, Palo Alto, CA, USA; ²CEM Corporation, Matthews, NC, USA; ³Department of Medicinal Chemistry, School of Pharmacy, The University of Mississippi, University, MS, USA. Contact e-mail: binshen@stanford.edu

Objective: Several automated radiochemistry modules (ARMs) are commercially-available to provide PET imaging agents safely and efficiently. However, these modules are generally limited to thermal heating. The use of microwave (MW) heating to speed up chemical kinetics to afford higher yields and cleaner product mixtures is well-known. In this work, we combine a new prototype MW cavity with a commonly-used ARM (Figure 1A) to evaluate this setup. PET tracers, e.g., [^{18}F]FHBG (HSV1-thymidine kinase) [1] and [^{18}F]FTC-146 (ultra-selective to sigma-1) [2], were made by both MW and thermal heating with an ARM and described for comparison. **Method:** The compact MW unit (cavity dimension: 3.5" w x 0.75" h) has features that are suitable for remote control, including temperature feedback control, compressed air cooling system and optional stirring (Figure 1B). The ARM azeotropically dried the [^{18}F]fluoride for the labeling step within 10 min (thermal) vs. 5 min (MW). Dried ^{18}F in DMSO (0.5mL) was mixed with respective tosyl-precursor (0.5mg) and heated to 160 °C to give either [^{18}F]FTC-146 or [^{18}F]FHBG followed by a deprotection step. Subsequent analyses were completed by radio-TLC and HPLC to determine radiochemical yields (RCYs) decay-corrected to end-of-bombardment. **Results:** The use of the MW unit allowed for faster labeling times (7.5 to 10-fold decrease) and offered up to 2.5-fold increase in RCY (see Table 1). **Conclusion:** Preliminary studies clearly show the utility of this new MW cavity to synthesize PET probes more efficiently with an ARM but also its potential suitability to complement other ARMs. Efforts to perform the entire radiosynthesis procedure in the MW cavity for future clinical applications are currently underway. **References:** [1] Chin FT *et al*, *Mol. Imaging Biol.* **2008**, 10(2), 82-91. [2] Shen B *et al*, *manuscript in preparation*

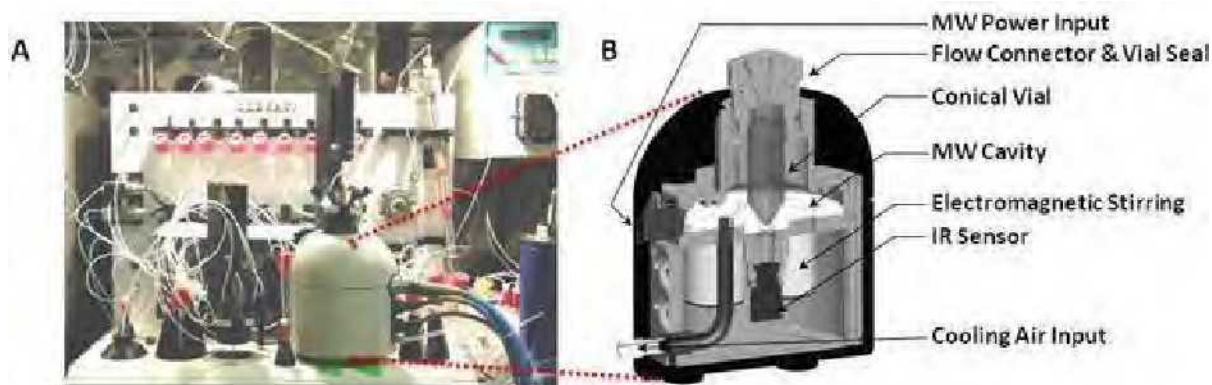


Figure 1. MW unit with ARM (Panel A) and a cut-away view (Panel B) of MW unit
Table 1. Thermal vs. MW-assisted labeling of [^{18}F]FHBG or [^{18}F]FTC-146

Observations	[^{18}F]FHBG		[^{18}F]FTC-146	
	Thermal Δ	MW Δ	Thermal Δ	MW Δ
Labeling Time (min)	10	2	15	2
RCY (decay-corrected)	61%	130.5%	61%	114%

Presentation Number **0892B**

Poster Session 4c: In Vivo Studies & Development/Novel Use of Imaging Probes

PET imaging of somatostatin receptors in the pancreatic endocrine cells with [Ga-68]DOTA-octreotide: A potential biomarker for beta cell mass measurement

Takeo Sako^{1,2}, **Yousuke Kanayama**¹, **Koki Hasegawa**¹, **Mie Nishimura**¹, **Yasuhiro Wada**¹, **Emi Hayashinaka**¹, **Yilong Cui**¹, **Yosky Kataoka**¹, **Michio Senda**^{2,3}, **Yasuyoshi Watanabe**¹, ¹*Center for Molecular Imaging Science, RIKEN, Kobe, Japan;* ²*Graduate School of Medicine, Kobe University, Kobe, Japan;* ³*Division of Molecular Imaging, Institute of Biomedical Research and Innovation, Kobe, Japan.* Contact e-mail: tsako@riken.jp

Introduction: Diabetes mellitus (DM) is a major threat to global public health and its prevalence is dramatically rising all over the world. Preventing or delaying the onsets of DM is an urgent problem. Recent papers have shown loss or dysfunction of beta cells in pre-clinical phase of type 1 and type 2 DM, but current diagnostic methods of beta cell mass (BCM) are invasive and often inaccurate, and can only detect the disease after onset. Non-invasive method to quantify BCM at earlier stages could provide a useful tool for detection and prevention of DM. In the present study, we focused on somatostatin receptors highly expressed in the pancreatic beta cells and developed a positron emission tomography (PET) technique with labeled octreotide, a metabolically stable somatostatin analog. **Method:** We injected [Ga-68]DOTA-octreotide into the tail vein of male Sprague Dawley rats under isoflurane anesthesia and performed emission scans of the abdomen for 90 min after injection. In order to evaluate the specific binding of [Ga-68]DOTA-octreotide to somatostatin receptors, we conducted PET scans with [Ga-68]DOTA-octreotide in rats administered with unlabeled octreotide (1000-folds of the amount of injected labeled octreotide) at 1 min before injection of [Ga-68]DOTA-octreotide. We also performed another PET studies with Streptozotocin (STZ)-induced diabetic rats. After the PET scan, we dissected out tissues and organs from the rats and measured their radioactivity with a gamma counter. **Results:** The PET studies show that [Ga-68]DOTA-octreotide was highly accumulated in the pancreas of normoglycemic rats and that the accumulation was significantly decreased in the rats administered with unlabeled octreotide or after STZ treatment. These results were in good agreement with the tissue biodistribution data. **Conclusion:** PET study in rats showed potent accumulation of [Ga-68]DOTA-octreotide in the pancreas, possibly by the specific binding to somatostatin receptors in the pancreatic islet beta cells. In a STZ-induced DM model rat, the pancreatic accumulation of [Ga-68]DOTA-octreotide was significantly attenuated. These results indicate that [Ga-68]DOTA-octreotide can be a PET probe realizing evaluation of BCM in human including DM patients.

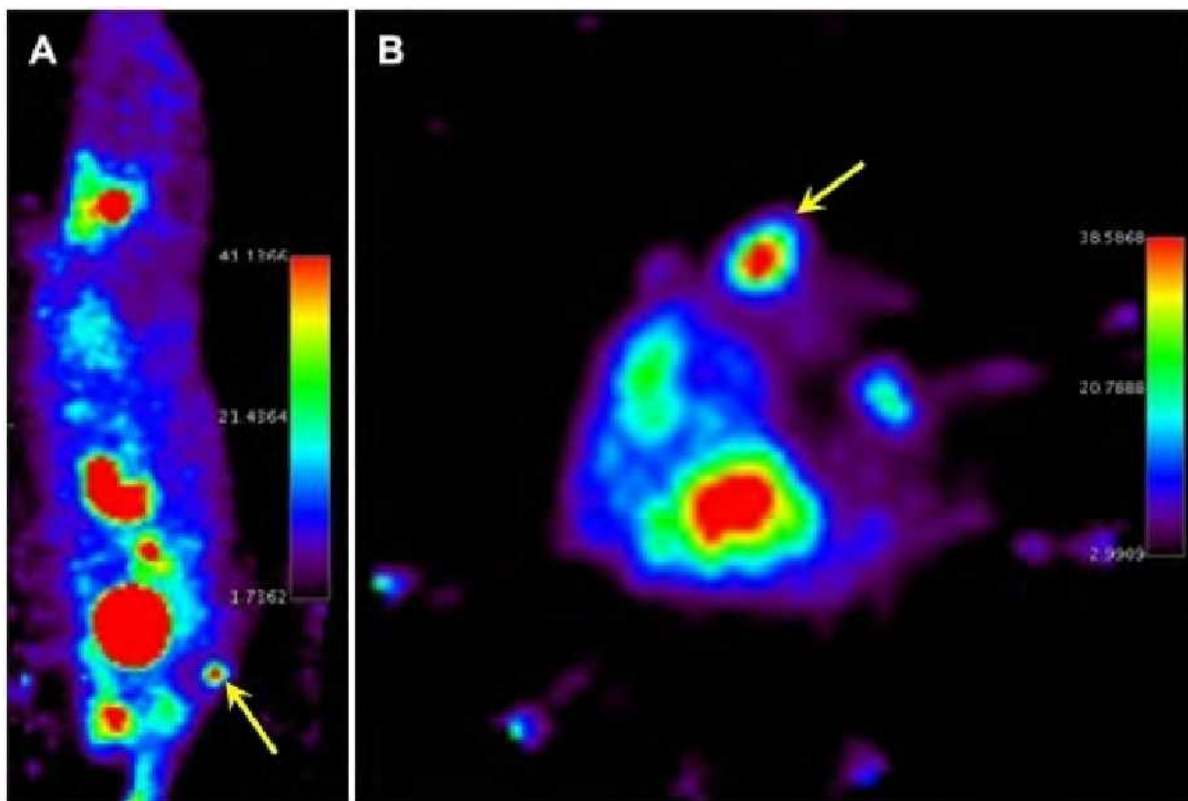
Presentation Number **0893B**

Poster Session 4c: In Vivo Studies & Development/Novel Use of Imaging Probes

125I-labeled PEGylated Dendrimers for Effective SPECT Imaging of Tumor Angiogenesis

Chaewoon Lee¹, Se Hun Kang², Hye-young Jung¹, Bong Hyun Chung¹, Seok-Ki Kim^{2,3}, **Yoonkyung Kim¹**, ¹Bionanotechnology Research Center, Korea Research Institute of Bioscience and Biotechnology, Daejeon, Republic of Korea; ²Molecular Imaging & Therapy Branch, National Cancer Center, Gyeonggi-do, Republic of Korea; ³Department of Nuclear Medicine, National Cancer Center, Gyeonggi-do, Republic of Korea. Contact e-mail: ykim@kribb.re.kr

Dendrimers are treelike monodisperse macromolecular architecture with robust size and shape. Therefore, precise targeting (or intermolecular interactions) is facilitated through the surface-bound ligands on dendritic carriers as opposed to those on the conventional polymer-based nanocarriers commonly adopted for therapy and imaging applications. Nuclear medicine imaging such as single photon emission computed tomography (SPECT) and positron emission tomography (PET) involves the usage of radioisotopes which provides superior image contrast even under microdosing conditions. SPECT imaging is obtained using the radiotracers which adopt longer lived and more easily obtained radioisotopes, whereas PET imaging requires relatively short lived radioisotopes as well as a highly expensive cyclotron facility. In this study, we prepared a new SPECT tracer, 125I-labeled PEGylated poly(amidoamine) dendrimer which is partially modified at its surface with several copies of cyclic RGDyK (c(RGDyK)) peptide, a ligand to target $\alpha v \beta 3$ integrin overexpressed in angiogenesis. Here, the radio-labeling with [125I]NaI was achieved effectively harnessing the D-tyrosine moiety which came as a part of the targeting unit, c(RGDyK). To provide guidelines for the development of a more effective SPECT imaging probe based on dendrimers excluding the issues of polydispersity, PEGylation was proceeded at all remaining surface amino groups using monomolecular PEG derivatives (ca. 2,000 Da). Our preliminary in vivo mouse studies using 125I-labeled dendrimer suggested effective tumor-targeting mediated by surface-bound RGD units.



Animal-SPECT image (A: whole-body sagittal view; B: axial view) of the SCC7 tumor-bearing mouse at 1 hr post-injection treated with 0.7 mCi (100 μ L) of 125I-labeled c(RGDyK)-dendrimer via tail vein injection. The tumor site is indicated with a yellow arrow. Some uptakes are observed at bladder, thyroid, stomach, and intestine, potentially of the free radioactive iodide ion.

Presentation Number **0894B**

Poster Session 4c: In Vivo Studies & Development/Novel Use of Imaging Probes

Development of flexible automatic liquid handling modules for PET probe preparation

Tetsuya Mori¹, Ryo Watanabe², Yukie Yoshii¹, Yasushi Kiyono¹, Tatsuya Asai², Yasuhisa Fujibayashi^{1,3}, ¹BIRC, University of Fukui, Fukui, Japan; ²Graduate School of Engineering, University of Fukui, Fukui, Japan; ³Molecular Imaging Center, National Institute of Radiological Sciences, Chiba, Japan. Contact e-mail: morit@u-fukui.ac.jp

In preliminary steps of PET probe development, radiochemists strongly desire flexible automatic synthesis modules at a low cost without professional engineering knowledge. The automatic modules are realized to bring reproducibility, reduce exposure and prepare the probe on demand without chemists. Commercially-available automated modules are mechanically stable and reliable, however, they have various limitations such as high cost, low flexibility, professional programming, and so on. Recently, microcomputer technology allows us to assemble miniature humanoid robots in hobby level. Using this technology, we developed flexible modules including automatic three-way valves, syringes and I/O unit for controlling external devices. The modules were designed to control a sterilized disposable three-way valve or syringe, to realize sterility even in basic research. In addition, this concept allowed us to prevent cross-contamination of the reagents. A main board which is commercially-available product had a capacity of controlling 24 modules simultaneously. Furthermore, the programming was based on manual positioning and teaching, so that no special engineering knowledge was required. To confirm the usefulness of the system, we developed a ⁶⁴Ni electroplating system for ⁶⁴Cu production and a ⁶⁴Cu purification system from ⁶⁴Ni solid target as an example. The electroplating system was consisted of one syringe, a carbon rod, a power supply and an assembly jig. The purification system consisted of two syringes, 11 three-way valves and three heaters are controlled from temperature controller with timer through I/O unit. The ⁶⁴Cu was produced by ⁶⁴Ni(p, n)⁶⁴Cu reaction at a baby cyclotron (Eclipse RD/HP, 11 MeV, Siemens). In the electroplating, 96±3% of ⁶⁴Ni was plated on gold disc in 12 hours. The results obtained were significantly better than what could be achieved in previous methods with an added advantage of reduced operation time. In the copper purification, we confirmed that this system accomplished to collect and separate the ⁶⁴Cu with sufficient reproducibility. This convenient system may help the research of the PET probe development.

Presentation Number **0895B**

Poster Session 4c: In Vivo Studies & Development/Novel Use of Imaging Probes

Controlled drug delivery systems biodegradation assessment by fluorescence tracking A. Altafaj(1), M. Moreno(2), E. Giralt(2)(3), and X. Cañas(1) (1) Plataforma de Laboratorio Animal Applied Research, Barcelona Science Park, Barcelona Spain. (2) Chemistry and Molecular Pharmacology, Institut for Research in Biomedicine, Barcelona, Spain. (3) Department of Organic Chemistry, Universitat of Barcelona, Barcelona, Spain

Miguel R. Moreno Raja, Institute for Research in Biomedicine of Barcelona, Barcelona, Spain. Contact e-mail: miguel.moreno@irbbarcelona.org

The extremely low availability of peptidic compounds forces pharmaceutical companies to introduce new formulations into the market by modifying them in an appropriate manner to minimize administration interferences. There are well known changes able to be applied without reducing therapeutic efficacy: analogue preparation, chemical modification, conjugations and pharmaceutical formulations, dealing with trapping or encapsulating active principles in a non-covalent way in controlled delivery systems. We have designed novel drug delivery systems to bound high molecular weight therapeutic molecules. These delivery systems have been tested "in vitro" with different cargo types, offering promising cargo delivery kinetics. Experiments have been also performed pointing out that drug delivery is likely to be independent of its degradation in the presence of several cellular membrane enzymes. The aim of this study was monitoring the "in vivo" biodegradation of two different controlled drug delivery systems (Systems 1 and 2) through imaging assays with an IVIS-200® from Xenogen-Caliper. Both systems were labelled with the fluorescent probe dyLight 800. The drug delivery systems (2 mg of each one) were labelled with dyLight 800. They were injected s.c. in 12 male Swiss CD1 mice and images were obtained with the following pattern: 0, 1, 2, 4, 6, 8, 24, 48, 72, and 96 hours, and 7, 9, 11, and 14 days post administration. After 14-days exposition, results were processed to determine the degradation curve of both drug delivery systems (normalized data). In our study, System 1 showed a long life period compared with System 2, which correlates with the treatment period throughout continuously deliver therapeutic agents. We are currently carrying out experiments to elucidate how biodegradation process happens and the involved pathways. In conclusion, fluorescence probes showed as optimal tool to assess drug delivery systems biodegradation.

Presentation Number **0954B**

Poster Session 3c: In Vivo Studies & Development/Novel Use of Imaging Probes

Development of AG73-modified Bubble liposomes as a vascular targeting ultrasound contrast agents

Yoichi Negishi¹, Nobuhito Hamano¹, Yoko Endo-Takahashi¹, Ryo Suzuki², Kazuo Maruyama², Motoyoshi Nomizu¹, Makoto Emoto³, Yukihiko Aramaki¹, ¹School of Pharmacy, Tokyo university of Pharmacy and Life Sciences, Hachioji, Japan; ²School of Pharmaceutical Sciences, Teikyo University, Sagamihara,, Japan; ³Department of Obstetrics & Gynecology, Fukuoka University Medical School, Fukuoka, Japan. Contact e-mail: negishi@toyaku.ac.jp

[Purpose] Endothelial cells (EC) in tumor angiogenesis are characterized by altered expression of molecular markers on their surface. Many types of peptides have been reported that specifically bind tumor angiogenic endothelium, including the AG73 peptide which is considered as a ligand for Syndecan. We hypothesized that echo-contrast gas entrapping liposomes, "Bubble liposome" targeted via linkage with AG73 would specifically adhere to tumor angiogenic endothelium, and that this selective adhesion may enable us to detect tumor angiogenesis ultrasonically. Here, we developed AG73-modified Bubble liposomes (AG73-BL) as a targeted ultrasound contrast agents, which was designed to attach to and allow specific ultrasound detection of angiogenesis. [Methods] AG73-BL was composed of DPPC and DSPE-PEG2000-AG73 and was entrapped with echo-contrast gas (C3F8). Adhesion of AG73-BL to bFGF or VEGF-stimulated HUVEC was examined by a perfusion chamber system and FACS analysis. To detect the ultrasound imaging of AG73-BL binding to HUVEC, a high-frequency ultrasound imaging system (NP60R-UBM, NEPA GENE CO., LTD.) was used. BL, AG73-BL, or AG73T-BL was added into each cultured HUVEC. Ultrasound images of B-mode were detected. Furthermore, colon26 cells were inoculated into BALB/c mice by s.c. AG73-BL was injected into the tumor models by i.v. B-mode images were acquired at a center frequency of 50 MHz. [Results and Discussion] We first observed the interaction between AG73-BL and bFGF or VEGF-stimulated HUVEC in a perfusion chamber system and FACS analysis. As a result, AG73-BL could strongly associate with the HUVEC compared to non-modified BL. The association was blocked by the addition of Heparin which is known as an inhibitor of AG73 peptide binding to Syndecan. Next, we detected the ultrasound imaging of AG73-BL binding to HUVEC. A significantly higher ultrasound echo signal could be detected in the treatment of AG73-BL relative to other treatments. Furthermore, the echo-signal by AG73-BL prolonged in the tumor model compared to other treatments. These data suggest that AG73-BL may be helpful tool as a vascular targeting ultrasound contrast agents. [Acknowledgements] This study was supported by Industrial Technology Research Grand Program (04A05010) from New Energy and Industrial Technology Development Organization (NEDO) of Japan and Grant-in-Aid for Scientific Research (B) (20300179) from the Japan Society for the Promotion of Science.

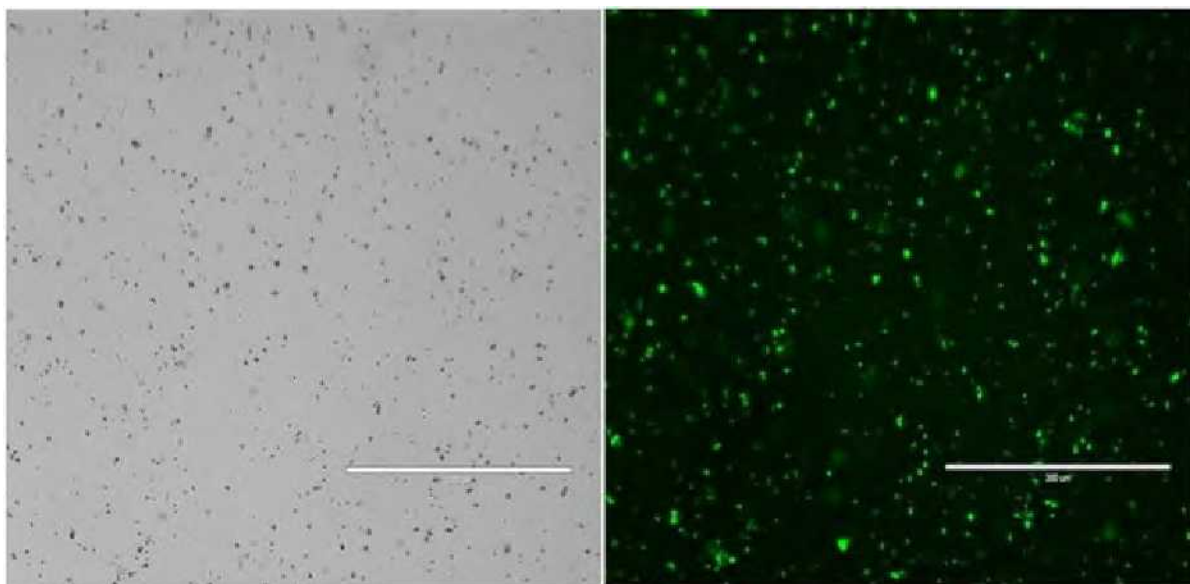
Presentation Number **0955B**

Poster Session 3c: In Vivo Studies & Development/Novel Use of Imaging Probes

Development of Targeted Microbubbles Using Nanobodies

Sophie Hernot¹, Nick Devoogdt^{1,2}, Bernard Cosyns^{1,3}, Geert Stange⁴, Vicky Caveliers^{1,5}, Serge Muyldermans², Alexander L. Klibanov⁶, Tony Lahoutte^{1,5}, ¹ICMI, Vrije Universiteit Brussel, Brussels, Belgium; ²CMIM, Vrije Universiteit Brussel, Brussels, Belgium; ³Department of Cardiology, UZ Brussel, Brussels, Belgium; ⁴Diabetes Research Center, Vrije Universiteit Brussel, Brussels, Belgium; ⁵Department of Nuclear Medicine, UZ Brussel, Brussels, Belgium; ⁶Cardiovascular Division, Department of Medicine, University of Virginia, School of Medicine, Charlottesville, VA, USA. Contact e-mail: sophie.hernot@gmail.com

Introduction: Ultrasound contrast agents or microbubbles (μ B) bearing antibodies or ligands that specifically bind to a molecule of interest, are now used for molecular imaging. Nanobodies are camel-derived heavy chain antibody-fragments (15 kDa), which have nanomolar affinities for their target and they can easily be produced and tailored. Therefore, Nanobodies are suitable for the design of targeted μ B. **Aim:** The development of targeted μ B using biotinylated Nanobodies that are able to bind specifically the model antigens Green Fluorescent Protein (GFP) and Carcino-Embryonal Antigen (CEA). **Materials & Methods:** Nanobodies against GFP or CEA (respectively cAbGFP4 and cAbCEA5) were biotinylated site-specifically in bacteria. The Nanobodies were coupled to the surface of lipid-shelled biotinylated μ B by biotin-streptavidin-biotin bridging chemistry. The ability of μ B-cAbGFP4 to recognize specifically GFP was tested by fluorescent microscopy. FACS with μ B-cAbGFP4 carrying different amounts of Nanobodies on their surface was performed to determine the occupancy of the μ B surface. In vitro binding studies were performed by incubating different amounts of μ B-cAbCEA5 with CEA-transfected CHO cells (CHO-CEA+). After separation of the cells and unbound μ B by floatation, the number of attached μ B per cell was determined. Wild type CHO cells and μ B-cAbGFP4 were used as controls. **Results:** Microscopy images confirmed the specific binding of GFP to μ B-cAbGFP4 (figure 1). FACS profiles showed that maximal occupancy of the μ B surface by Nanobodies is reached with our coupling conditions. The in vitro binding studies demonstrated that the increase in ratio between CEA-targeted μ B and CHO-CEA+ cells resulted in an increase in number of attached μ B per cell. These numbers were significantly higher than those for the controls (all $p < 0.001$). **Conclusions:** The development of targeted μ B using Nanobodies is feasible and they are able to recognize the model antigens GFP and CEA. This study opens opportunities for the development of new targeted μ B against intravascular antigens.



Presentation Number **0956B**

Poster Session 3c: In Vivo Studies & Development/Novel Use of Imaging Probes

Microbubbles targeted to neovasculature with the Shiga-Toxin B-subunit

Olivier Couture^{1,3}, Estelle Dransart², Sabrina Dehay², Ludger Johannes^{2,3}, Mickael Tanter^{1,4}, ¹ESPCI, Paris, France; ²Institut Curie, Paris, France; ³CNRS, Paris, France; ⁴INSERM, Paris, France. Contact e-mail: olicou@gmail.com

The targeting moiety (B-subunit) of the Shiga toxin (STxB) is a very potent ligand for the glycolipid Gb3, which is expressed in ovarian, colorectal and breast carcinomas. It is also present on endothelial cells of tumor neovascularization. STxB binds with high apparent affinity to the plasma membrane of Gb3 expressing cells, and is efficiently internalized. Moreover, STxB has low immunogenicity. The present study demonstrates the targeting of ultrasound contrast agents to human xenograft tumors by exploiting the overexpression of the glycolipid Gb3 in neovasculature. The targeting of Gb3 expressing tumor cells by STxB-microbubbles was first shown by flow cytometry and fluorescence microscopy. A significantly higher proportion of STxB-microbubbles associated with Gb3-expressing tumor cells, as compared to cells in which Gb3 expression was inhibited. Moreover, ultrasonic imaging of culture plates showed a 12 dB contrast enhancement in average backscattered acoustic intensity on the surface of Gb3 expressing cells, as compared to Gb3-negative cells. Also, a 18 dB contrast enhancement was found in favor of STxB-microbubbles, as compared to unspecific microbubbles. Microbubble-signal intensity in subcutaneous tumors in mice was more than twice as high after the injection of STxB-functionalized microbubbles, as compared to the injection of unspecific microbubbles. These in vitro and in vivo experiments demonstrated that STxB-functionalized microbubbles bind specifically to cells expressing the Gb3 glycolipid. The cell binding moieties of toxins thus appear as a new group of ligands for angiogenesis imaging with ultrasound.

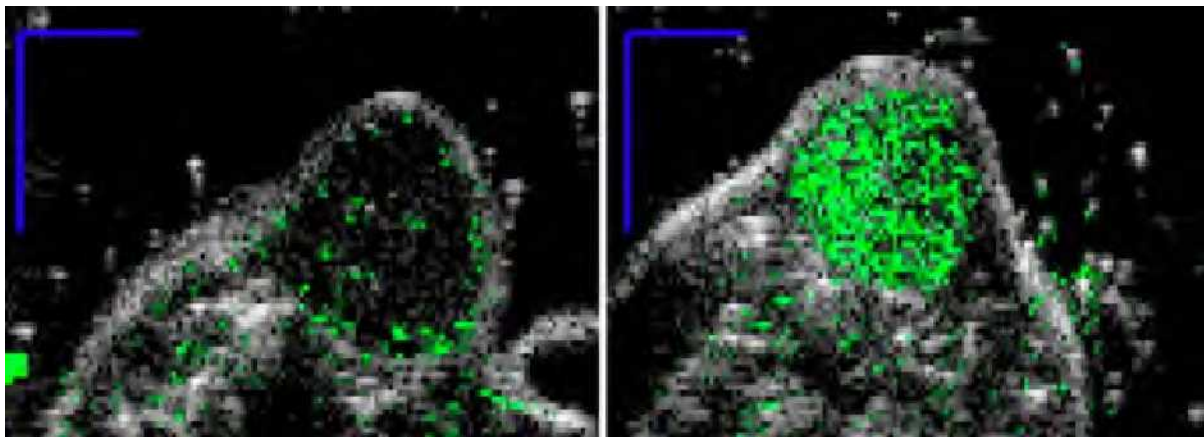


Figure 1: Ultrasound imaging of Gb3-positive HBCX-12 tumours. (Left) Biotin-microbubbles control (Right) STxB-microbubbles. The green overlay is the bubble-specific amplitude-modulation signal.

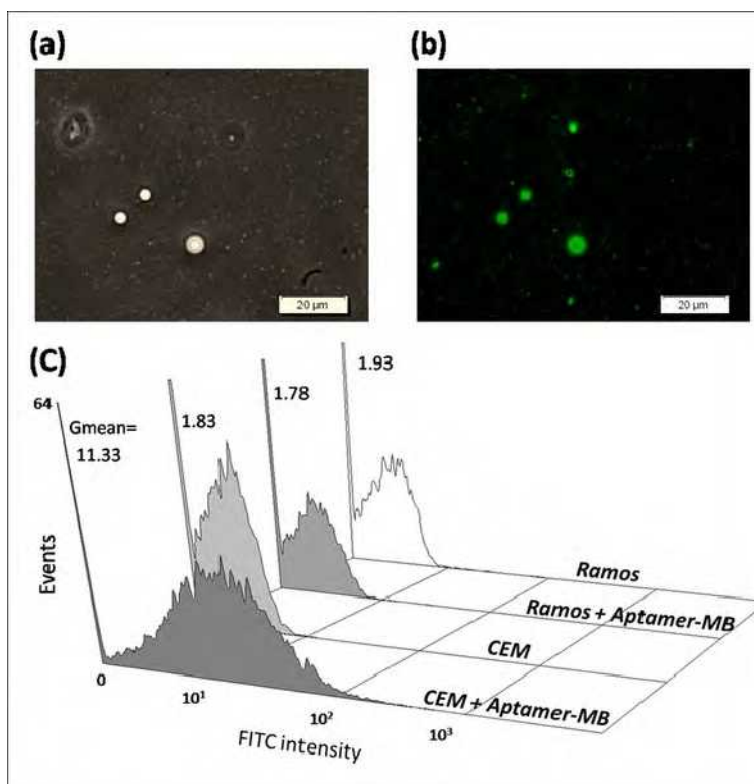
Presentation Number **0957B**

Poster Session 3c: In Vivo Studies & Development/Novel Use of Imaging Probes

One-step Synthesis of Covalently Conjugated Aptamer Microbubbles

Chung-Hsin Wang, Chih-Kuang Yeh, Department of Biomedical Engineering and Environmental Sciences, National Tsing Hua University, Hsinchu, Taiwan. Contact e-mail: jhwg1114@hotmail.com

Targeting ultrasound contrast agents can be prepared by some specific bio-conjugation techniques. The biotin-avidin complex is an extremely useful noncovalent binding system, but the system might induce immunogenic side effects in human bodies. Previous proposed covalently conjugated systems suffered from low conjugation efficiency and complex procedures. In this study, we propose a covalently conjugated microbubbles coupling with nucleic acid ligands (i.e., aptamer) providing a higher specific affinity ($K_d \sim 0.8 \text{ nM}$) for ultrasound targeting studies. The synthesizing aptamer conjugated MBs was achieved by thiol-maleimide crosslinking strategy. The thiol-modified aptamer (sgc8c) could be easily crosslinked with the maleimide functionalized PEG-lipid. The TCEP was used to activate the aptamer by breaking the disulfide bond. Afterward, bubble suspensions were formed with perfluoropropane gas by intense shaking, which yielded bubbles with a mean diameter of 800 nm at a concentration of $10^8 \sim 10^9$ bubbles/mL. Note that purification of aptamer and suitable accelerating sonication are critical procedures to ensure the conjugation efficiency. The efficiency was quantified by calculating the changes of fluorescence intensity using spectrophotometer and the result was 45% at the ratio (functionalized lipid/aptamer) of 80. The cell experiments were performed in two cell lines (CEM for experiment and Ramos for control). The figures (a) and (b) show the optical images in dark field and fluorescence microscopy, respectively. Figure (c) shows the quantitative results of flow cytometry. The GMean value in experiment set was 6.2 folds with respect to control ones. The results indicate that aptamer conjugated microbubbles can be fabricated in one-step synthesis. With *in vitro* selective screening, aptamers can perform higher affinity for specific molecules than those in traditional antibody system. Potential applications include targeting imaging *in vivo* and drug delivery/release.



Presentation Number **0958B**

Poster Session 3c: In Vivo Studies & Development/Novel Use of Imaging Probes

Novel ultrasound contrast agents for therapeutic and imaging applications

Romain P. Berti¹, Lucie Fréret¹, Guillaume Haïat², Emilia Pisan³, Raquel Diaz-Lopez³, Nicolas Tsapis³, Christine Contino Pepin⁴, Bernard Pucci⁴, Elias Fattal³, S. Lori Bridal¹, Wladimir Urbach¹, **Nicolas Taulier**¹, ¹Laboratoire d'Imagerie Paramétrique, UMR 7623, CNRS, Paris, France; ²Laboratoire de Recherches Orthopédiques, CNRS - Université Paris Diderot, Paris, France; ³Laboratoire de Pharmacie Galénique, CNRS - Université Paris 11, Châtenay-Malabry, France; ⁴Laboratoire de Chimie Bioorganique et des Systèmes Moléculaires Vectoriels, Université d'Avignon, Avignon, France. Contact e-mail: nicolas.taulier@upmc.fr

We have developed novel Ultrasound Contrast Agents (UCA) that possess a high stability and that can be used as drug carriers for therapeutic applications. They are of two types. The first one is a nano-emulsion of particles made of a fluorinated liquid (PerFluoro-Octyl Bromide [PFOB]) or gas (PerFluoroPentane and PerFluoroHexane) core encapsulated into an amphiphilic fluorinated telomer derived from Tris(hydroxymethyl) aminomethane. The particles exhibit a radius of 400 nm. The second one is a suspension of capsules made of PLGA (poly(lactide-co-glycolide)) containing a PFOB liquid core [1]. Capsule preparation allows to adjust the particle radius R from 150 nm to 10 μ m and the capsule thickness T through the ratio T/R ($0.2 < T/R \leq 1$). Both types of agents are stable at least over days in solutions. We have tested in vitro the acoustic properties of these agents at ultrasound frequencies of 5 and 50 MHz. Specifically, we have measured the signal-to-noise ratio (SNR) and the backscattered signal of the agent solution, and we have quantified the agent destruction induced by a high intensity ultrasound wave. We demonstrated that the enhanced signal due to the agents is sufficiently high for imaging application and that we control the agent destruction. For targeting purpose, the surface chemistry of the polymeric capsules was modified by incorporating fluorescent, PEGylated, and biotinylated phospholipids [2]. The telomeric particles can be easily functionalized through a γ -aminobutanoic acid or a lysine spacer arm [3]. For a better understanding of the relationship between the physical and acoustic properties of our novel contrast agents, we have performed 2D and 3D time domain simulations of the propagation of ultrasound waves in our agent solution. The physical input parameters of our agents were determined experimentally. The comparison between numerical and experimental results showed a good agreement and gave valuable information about the interaction of ultrasound with agents [4]. Using a commercial echograph, we checked that our agents induce in mice a significant enhancement in the backscattered signal [5]. In conclusion, these results demonstrate that our new particles are suitable as ultrasound contrast agent for targeted therapy and imaging applications. [1] Pisani et al. Adv. Funct. Mater. 18 (2008) 1-9 [2] Diaz-Lopez et al. Biomaterials 30 (2009) 1462-1472 [3] Pucci et al, Curr. Med. Chem.: Anti-Cancer Agents 2 (2002) 645-665 [4] Galaz et al., J. Acoust. Soc. Am. 127 (2010) 148-154 [5] Diaz-Lopez et al. Biomaterials 31 (2010) 1723-1731

Presentation Number **0959B**

Poster Session 3c: In Vivo Studies & Development/Novel Use of Imaging Probes

Systemic delivery of adenovirus (Ad) with cancer targeted microbubbles

Jason M. Warram¹, Anton Borovjagin³, Kurt R. Zinn^{1,2}, ¹Molecular and Cellular Pathology, University of Alabama at Birmingham, Birmingham, AL, USA; ²Radiology, University of Alabama at Birmingham, Birmingham, AL, USA; ³Dentistry, University of Alabama at Birmingham, Birmingham, AL, USA. Contact e-mail: mojack@uab.edu

Safety and efficacy issues have limited the use of recombinant Ad for gene therapy of cancer. While some groups are using genetic approaches to improve the vectors, others are applying alternate delivery vehicles, such as ultrasound contrast agents, or microbubbles, to permit safe and targeted delivery to cancer. Therapy includes the sonification and destruction of microbubbles at the known cancer sites to allow payload release; however, this approach cannot be applied to detect unknown cancer locations. To overcome this limitation, we propose cancer-targeted microbubbles for delivery of a cancer-specific Ad payload to the tumor without the need for external treatment. Streptavidin coated microbubbles were packaged with an Ad encoding luciferase or Ad with surface mCherry, with a protocol that included complement inactivation of unenclosed particles. Packaged microbubbles were then labeled with biotinylated antibodies targeting p-selectin, VEGFR-2, and alpha v integrins. Successful packaging of adenovirus was validated using mCherry coated adenovirus particles which revealed localized mCherry fluorescence in the microbubbles. Preliminary tests have validated complement inactivation to remove unenclosed and partially enclosed particles, and therefore absolute packaging of adenovirus. Microbubbles with packaged Ad encoding luciferase were applied to HEK-293 cells generating dose dependent luciferase expression 24 hrs post microbubble application. Experiments are in progress in a breast tumor mouse model to validate this approach for the early detection of breast cancer using cancer specific Ad and systemic delivery of triple-targeted microbubbles. These targeted receptors are routinely over expressed in tumor vasculature. Once the microbubble is bound to these cancer specific targets, the lipid shell dissipates under the expected hydrostatic pressure of a gas-filled sphere in an aqueous environment leading to lost containment and release of the Ad payload at the target site. Continued success in this project may lead to a widely applicable method for safe and effective systemic delivery of adenoviruses for the purpose of cancer screening.

Presentation Number **0960B**

Poster Session 3c: In Vivo Studies & Development/Novel Use of Imaging Probes

Molecular imaging using targeted ultrasound and adenoviral techniques for receptor density modulation

Reshu Saini¹, Jason M. Warram², Anna Goblirsch Sorace¹, Heidi R. Umphrey³, Kurt R. Zinn³, Kenneth Hoyt^{1,3}, ¹Biomedical Engineering, University of Alabama at Birmingham, Birmingham, AL, USA; ²Molecular and Cellular Pathology, University of Alabama at Birmingham, Birmingham, AL, USA; ³Radiology, University of Alabama at Birmingham, Birmingham, AL, USA. Contact e-mail: mojack@uab.edu

Recently, targeted microbubbles (MB) have been shown to improve ultrasound (US) imaging sensitivity and site specific drug delivery. Antibody (Ab) labeled MB permits binding to receptors typically expressed in the tumor vasculature. The current dogma suggests increased MB binding with increased receptor expression; however this hypothesis has not been fully demonstrated. In order to show that targeted MB accumulation is proportional to receptor density, we validated the relationship between receptor number and targeted MB binding with an adenoviral induced receptor model. 2LMP breast cancer cells were infected with a serotype 5 adenovirus (Ad5-HA-hsSSTR2-GFP) containing GFP and hemagglutinin (HA) tagged hSSTR2 under CMV promoter control. A multiplicity of infection (MOI) of 0, 10, 50, and 100 was used and HA-hSSTR2 receptor density was measured by flow cytometry. MB labeled with anti-HA or isotype control Ab were prepared using a commercially available product (Targestar-B, Targeson) and incubated (~10 MB/cell) with staggered MOI cell groups 15 min before rinsing. Light microscopy determined the number of attached and unattached MB per cell and recorded as mean \pm SD. Lastly, 2LMP tumor bearing mice (n = 9) were sorted into two groups and administered Ad5-HA-hSSTR2-GFP (1×10^9 pfu) intratumorally. On day 1, MB labeled with anti-HA or isotype control Ab were injected in the tail vein (6.2×10^6 MB/mouse) and tumors were imaged 2 min post injection using US (SONIX RP, Ultrasonix). On day 2, targeted and control groups were switched and experiments were repeated. For each tumor, US images of targeted and control MB were paired and assessed by two blinded reviewers to determine greatest degree of intratumoral MB enhancement between the two days. Regression analysis of mean GFP fluorescence revealed a linear relationship between GFP signal (effective gene transfer) and viral MOI ($r^2 > 0.98$), which indicates a positive correlation between infectivity and HA-hSSTR2 expression. For cells incubated with Cy5.5-labeled anti-HA Ab, there was a significant difference between viral MOI and Cy5.5 signal ($p < 0.004$). No difference was observed with Cy5.5-labeled control Ab ($p > 0.21$). MB labeled with anti-HA showed increased cell attachment with increased Ad MOI ($p < 0.005$), indicating targeted MB accumulation was proportional to receptor expression. For the in vivo data, reviewers determined in consensus that 78% of the US images from the targeted MB experimental day exhibited increased enhancement compared to the same animal administered isotype control Ab labeled MB.

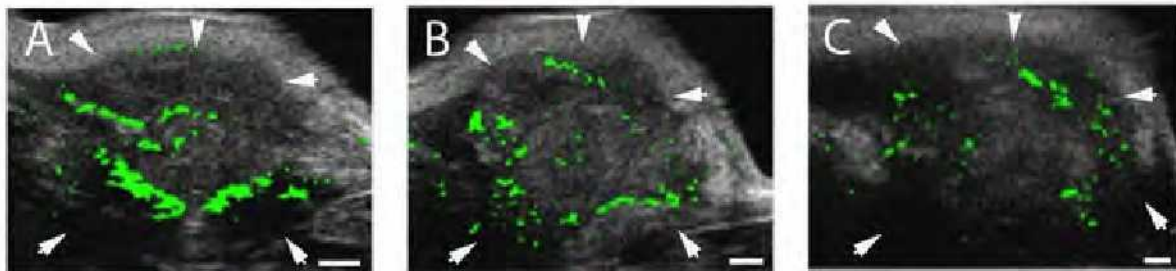
Presentation Number **0961B**

Poster Session 3c: In Vivo Studies & Development/Novel Use of Imaging Probes

Longitudinal Assessment of Expression Levels of Tumor Angiogenic Markers with Molecular Ultrasound Imaging

Nirupama Deshpande, Ying Ren, Kira Foygel, Jarrett Rosenberg, Juergen K. Willmann, Molecular Imaging Program/Radiology, Stanford university, Stanford, CA, USA. Contact e-mail: niru@stanford.edu

The purpose of this study was to evaluate molecular ultrasound (US) to non-invasively assess the temporal expression levels of three angiogenic markers, $\alpha v\beta 3$ integrin, endoglin, and VEGFR2 on tumor vascular endothelial cells in vivo. Three types of targeted microbubbles (MB-Integrin, MB-Endoglin, MB-VEGFR2) were designed and the binding specificity of these MB was tested on endothelial cells (positive and negative for angiogenic marker expression) under flow shear stress conditions (at 100 sec⁻¹) in a flow chamber. In vivo molecular US imaging using the three different MB was performed at three different tumor stages (small, medium, large size) of three different subcutaneous tumor xenografts (breast, ovarian, pancreatic cancer) in mice (n=48) and was correlated with angiogenic marker expression levels as assessed by western blotting. Attachment of all three targeted MB was significantly ($p=0.003$) higher to positive than to negative cells and the attachment was significantly ($p=0.026$) decreased by blocking antibodies. For breast and ovarian cancer, endoglin expression was significantly higher than $\alpha v\beta 3$ integrin ($p=0.005$) and VEGFR2 ($p=0.0003$) expression in small and medium tumors as assessed by in vivo US imaging. In contrast, in pancreatic cancer, $\alpha v\beta 3$ integrin was highest in small tumors compared to endoglin and VEGFR2 ($p=0.05$) and endoglin expression peaked in medium and large tumors. In all tumors types, expression levels of all markers were lowest ($p=0.005$) in large tumors (Figure). In vivo US imaging signal significantly ($R^2>0.6$; $p<.05$) correlated with ex vivo western blotting results for all three markers. In conclusion, molecular US imaging allows non-invasive assessment of the expression levels of different tumor angiogenic markers that vary during tumor growth in various subcutaneous human tumor xenografts. The results provide insights into tumor angiogenesis biology and may help in defining imaging targets for both early cancer detection and treatment monitoring using molecular US imaging.



Transverse contrast-enhanced ultrasound images of a subcutaneous breast cancer tumor graft (arrows) in a nude mouse, imaged longitudinally at small (A), medium (B), and large (C) tumor sizes following intravenous administration of MB-Endoglin. Endoglin expression (shown as green overlay on B-mode images) was highest at small tumor size and decreased at medium and large tumor sizes.

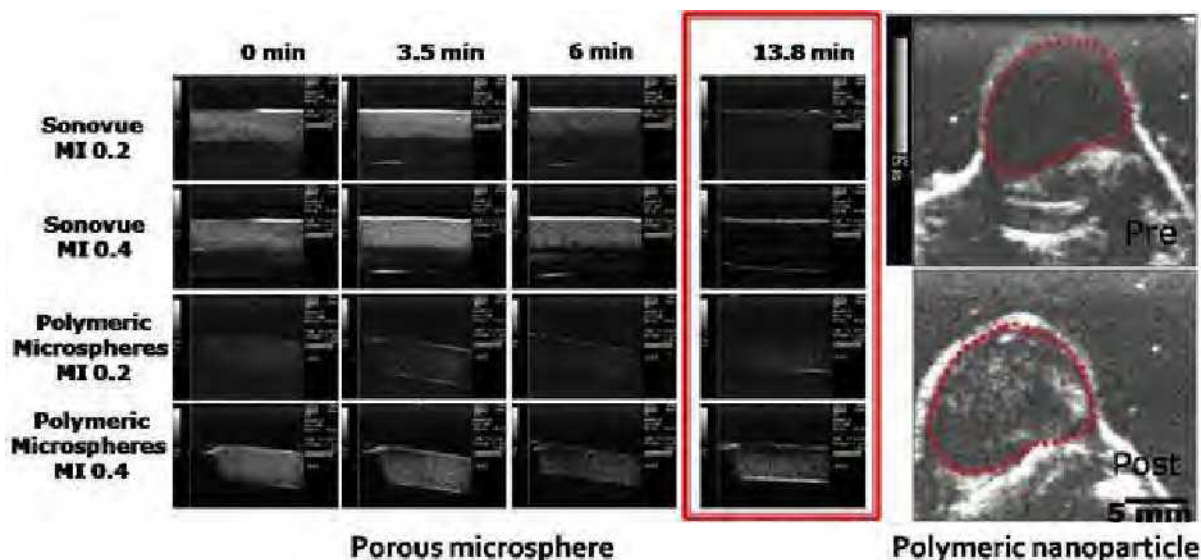
Presentation Number **0962B**

Poster Session 3c: In Vivo Studies & Development/Novel Use of Imaging Probes

Gas-Generating Polymeric Particles for Ultrasound Imaging of Living Subjects

Hyun Su Min^{1,3}, Eunah Kang¹, Kuiwon Choi¹, Kwangmeyung Kim¹, Moon Hee Han², Jae Young Lee², Yongseok Choi³, Ick Chan Kwon¹, ¹Biomedical Research Center, Korea Institute of Science and Technology, Seoul, Republic of Korea; ²Department of Radiology, Seoul National University Hospital, Seoul, Republic of Korea; ³School of Life sciences and Biotechnology, Korea University, Seoul, Republic of Korea. Contact e-mail: hs-min@kist.re.kr

Ultrasound (US) is a noninvasive imaging method that is widely available and provides real time imaging and diagnosis. Traditionally, microbubbles were used as US contrast agents for the blood flow imaging. However these types of US contrast agents have gas on it that causes short half life and the size of particle limits its further application. We prepared polymeric particle for US contrast agents using gas generating polymer which are consist of biodegradable main backbone and carbonate side chain instead of encapsulation of gas on it. And we showed long term US imaging contrast to the commercialized US contrast agents (Sonovue) in vitro by using porous microspheres. We also prepared polymeric nanoparticle coated with hydrophobically modified chitosan. Carbon dioxide nanobubble generated from polymeric nanoparticle in tumor leads to microbubbles that can be visualized by ultrasound.



Presentation Number **0963B**

Poster Session 3c: In Vivo Studies & Development/Novel Use of Imaging Probes

Development of Echogenic Nanobubbles for Ultrasound Molecular Imaging

Tianyi M. Krupka^{1,2}, Hanping Wu¹, Robin Wilson², Yun Zhou³, Ronald E. Kumon³, Cheri Deng³, Agata A. Exner¹, ¹Radiology, Case Western Reserve University, Cleveland, OH, USA; ²Biomedical Engineering, Case Western Reserve University, Cleveland, OH, USA; ³Biomedical Engineering, University of Michigan, Ann Arbor, MI, USA. Contact e-mail: tianyi.krupka@case.edu

Ultrasound contrast agents (microbubbles) can play a pivotal role in molecular imaging and gene and drug delivery. However, the size of microbubbles limits their application, since agents in the range of 1-3 μ m are constrained to the vasculature [Ferrara et al. *Acc Chem Res* 2009]. In contrast, while particles in the 100-400nm size range may be suitable for extravasation in cancer therapy, it is widely accepted that the small size limits echogenicity. We have recently demonstrated simple formulation of stable, echogenic lipid nanobubbles [Krupka et al. *Mol Pharm* 2010]. The objectives of the current study were to 1) optimize formulation parameters for size modulation of nanobubbles and 2) obtain acoustic characterization of the agents. Bubbles were prepared using a cocktail of lipids in chloroform, followed by solvent evaporation and hydration, replacement of air with C3F8 gas and mechanical agitation. Nanobubbles were formed by addition of a tri-block copolymer surfactant (Pluronic). Early acoustic characterization was carried out using the Visualsonics Vevo 770 with scan probes at center frequencies 25-55 MHz. In vivo studies were carried out in a subcutaneous colorectal carcinoma model in rats (50 μ L contrast bolus followed by 0.8 ml saline flush). Contrast harmonic imaging (Aplio XG, Toshiba) was carried out at 6.6 and 8 MHz. Image analysis was done using manufacturer-provided software. Optimization of formulation revealed that bubble diameter (130-1500 nm) is a function of agitation time, Pluronic Mw, and lipid:Pluronic ratio. Optimal combination of these factors produced nanobubbles as small as 130nm. In vitro analysis of frequency response of backscattered signals suggests that 230nm nanobubbles were as echogenic as the commercially available lipid-encapsulated microbubbles. In vivo at 6.6 MHz signal amplitude was 8.2 \pm 4.2 and 14.0 \pm 1.6 dB and the area under the time intensity curve (AUC) was 154.4 \pm 89.3 and 310.7 \pm 40.5 dB for nano- and microbubbles respectively. Both parameters were significantly reduced at 8.0 MHz (p <0.05). Since particle echogenicity is also function of shell thickness and elastic modulus, it is possible that incorporation of Pluronic into the bubble improves shell properties improving contrast visibility. These nanobubbles are able to provide excellent in vivo tumor contrast enhancement at clinically relevant frequencies making them attractive candidates for the design of multifunctional platforms for molecular imaging and gene or chemotherapy.

Presentation Number **0964B**

Poster Session 3c: In Vivo Studies & Development/Novel Use of Imaging Probes

High Frequency Ultrasound Contrast Imaging of Mouse Embryos

Janet M. Denbeigh, Mira Puri, F. Stuart Foster, Medical Biophysics, University of Toronto, Toronto, ON, Canada. Contact e-mail: janet.denbeigh@utoronto.ca

Ultrasound contrast imaging is widespread in adult mice but few studies examine these same contrast agents in the murine embryo. The developing mouse embryo represents a dynamic model for development and angiogenesis. The hemodynamic and molecular expression profiles that arise as part of these processes are of interest to the fields of developmental and cancer biology. We investigated new methodologies to infuse microbubble (MB) contrast agents into living embryos and report preliminary results related to the analysis of MB wash-in kinetics and binding to molecular targets. MicroMarker Microbubbles (Bracco) were reconstituted with saline, with VEGFR-2 (V) or Rat Isotype control (C) antibody added to targeting bubbles. CD-1 mouse embryos were dissected from the mother's belly and kept chilled. Prior to injection, each embryo was removed from its yolk sac and revived using pre-warmed PBS (~57°C), then covered with ultrasound gel. 20 μ L of MB solution was infused at a rate of 0.02 mL/min into a placental artery. A 21 MHz linear array transducer (VisualSonics) was positioned during a 6 minute wait time before a burst pulse was used to disrupt all bubbles in the plane of view. A sequence of nonlinear contrast image frames including both pre and post bubble disruption was obtained at 18 MHz, 4% power, at a frame rate of 9 s⁻¹, and with a contrast gain of 30dB. Preliminary experiments were performed on litters of E15.5-17.5 mice. In a pilot group of embryos (n=3) wash-in and wash-out kinetics of untargeted agents were studied by segmenting nonlinear contrast signals in both hemispheres of the brain, the liver and heart. Molecular imaging studies were then performed in the same 3 tissues for VEGFR-2 in 28 targeted and 26 control embryos. The molecular signal was derived from the difference in contrast enhancement of pre and post bubble destruction values as described previously. Contrast clearance kinetics of embryos appears to differ from those of adult mice. Time to 10% of peak enhancement is reduced from approximately 10 minutes in the embryo to 4 minutes in the adult. Significantly increased binding of the VEGFR2 targeted MBs ($p < 0.001$) compared to controls was demonstrated in the right and left-brain hemispheres (RB_V 4.15±2.60 vs RB_C 2.08±1.04, LB_V 5.01±3.35 vs LB_C 2.10±1.01) as well as in the liver (L_V 5.47±3.70 vs L_C 2.67±2.19). These initial results demonstrate the feasibility of performing molecular imaging with contrast enhanced micro-ultrasound in embryos. Further studies of the time evolution of VEGFR-2 expression are warranted.

Presentation Number **0965B**

Poster Session 3c: In Vivo Studies & Development/Novel Use of Imaging Probes

Ultrasound and Photoacoustic Imaging Enhancement using Nanoscale Dual Contrast Agent

Katheryne Wilson, Kimberly A. Homan, **Stanislav Y. Emelianov**, Biomedical Engineering, University of Texas at Austin, Austin, TX, USA. Contact e-mail: emelian@mail.utexas.edu

Ultrasound (US) is a real time, cost effective, and noninvasive imaging modality widely used to visualize anatomical structures of various organs and tissues. Photoacoustic (PA) imaging maps the optical properties of tissues at a reasonable depth, thus assessing functional properties of organs and tissues. Due to synergistic and complementary features, these imaging technologies are often combined resulting in an ultrasound-guided photoacoustic (USPA) imaging system capable of morphological and physiological imaging of tissue. However, the contrast in USPA imaging can be greatly enhanced with the use of contrast agents. In this report, we introduce acousto-plasmonic nano-sized dual contrast agent for USPA imaging. This contrast nanoagent is based on plasmonic nanoparticles encapsulated inside of perfluorocarbon nanodroplets capped with bovine serum albumin (BSA). During the synthesis, surface modification of gold nanorods (NRs) was performed to allow suspension of NRs in organic perfluorocarbon. This mixture of NRs and perfluorocarbon was then added to a BSA/saline solution and sonicated to emulsify the nanoagent. Sizing of nanoagent was accomplished through a lipid extruder using polycarbonate membranes of the desired size (e.g., 200 nm). To demonstrate the performance of our dual contrast agent in USPA imaging, the agent was incorporated into a 10% polyacrylamide phantom. US images were obtained using a 7 MHz transducer, while PA images were produced using pulsed laser irradiation from an Nd:YAG/OPO laser system (760 nm, 4-6 ns pulse duration, 10 pulse repetition frequency, 5.0 mJ/cm² fluence). The developed hybrid nanoparticles were shown to be effective contrast agents for USPA imaging. The nanoagent remained inactive until remotely triggered with laser irradiation. This activation selectively provided high levels of US and PA signal contrast (up to a 7 fold increase) in the area of irradiated nanoparticles. Therefore, with simple modifications during synthesis, the developed remotely triggered, nanosized contrast agent could be used in many imaging and therapeutic applications including molecular imaging, blood flow imaging, photothermal therapy, vessel occlusion, and drug delivery and release.

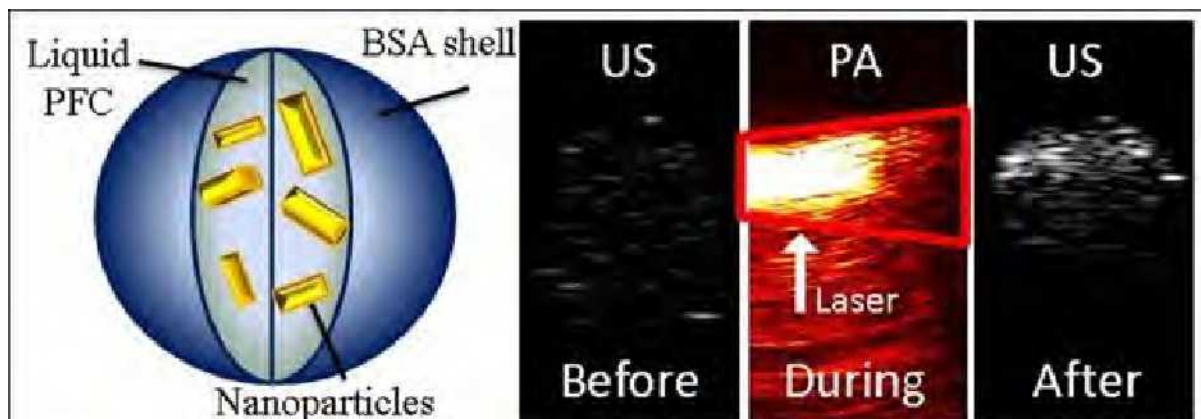


Figure. Left, diagram showing composition of described contrast nanoagent. Right, a series of images (US and PA) showing the progression of activation of the nanoagent and the resulting PA and US contrast enhancement.

Presentation Number **0966B**

Poster Session 3c: In Vivo Studies & Development/Novel Use of Imaging Probes

Role of Blood Rheology in Targeted Ultrasound Contrast Agent Adhesion Behavior

Sunil Unnikrishnan¹, Michael B. Lawrence¹, Klaus Ley³, Alexander L. Klibanov^{2,1}, ¹Biomedical Engineering, University of Virginia, Charlottesville, VA, USA; ²Cardiovascular Medicine, University of Virginia, Charlottesville, VA, USA; ³Inflammation Biology, La Jolla Institute of Allergy and Immunology, San Diego, CA, USA. Contact e-mail: sunil14@virginia.edu

Ligand-bearing microbubble ultrasound contrast agents are being widely studied for potential clinical targeting applications for molecular imaging and drug delivery. In addition to sufficient expression of the cell receptor and high binding specificity of the ligand to the receptor, optimal targeting requires a favorable hydrodynamic environment so the agent can resist the shear forces due to blood flow and bind firmly. In vitro antibody-conjugated microbubbles bind to the targeted receptor only at low wall shear stresses (WSS < 1.5 dyne/cm²), but in vivo binding occurs even at higher WSS (~ 15 dyne/cm²). The presence of red blood cells (RBCs) has been shown to augment leukocyte binding to the vessel wall and could be one of the factors responsible for this discrepancy. We assessed the influence of RBCs on the targeting efficacy of microbubbles in a parallel-plate flow chamber. Experiments were conducted both in an upright configuration, where the microbubble binding to the reactive surface was aided by buoyancy, and an inverted configuration, where buoyancy works against the binding. Targeting was evaluated by fluorescent video microscopy. Biotinylated microbubbles were targeted to streptavidin-coated surface and targeting efficacy was estimated as the adherent fraction of the near-wall microbubble flux. In the upright configuration, at low WSS RBCs did not have a significant effect on binding, but at high WSS (> 1.5 dyne/cm²) presence of RBCs at physiological hematocrit enhanced binding significantly. At a WSS of 4.5 dyne/cm², the binding efficiency increased from < 0.2% in the absence of RBCs to about 12% with 40% hematocrit. This effect persisted at 20% hematocrit and when RBC deformability was modified using glutaraldehyde. In the inverted configuration, binding was virtually absent without RBCs, but was as much as two orders of magnitude greater at high WSS when RBCs were present, effectively abolishing gravity effects. A reduction in the near-wall microbubble flux was observed in the presence of RBCs at high WSS in both configurations, suggesting that enhanced adhesion does not require increased margination of microbubbles. Additionally, in a separate flow assay, using a 100 µm diameter capillary tube, similar increase in attachment was observed with RBCs. In vitro flow assays conducted without RBCs may underestimate the targeting efficacy of microbubble agents. Taking into account the particulate nature of blood would aid in the development of microbubbles that are optimized for targeting and molecular imaging under physiological conditions.

Presentation Number **0500B**

Poster Session 4b: Imaging Molecular and/or Cellular Processes & Drug and/or Radiation Therapy

MicroSPECT/CT imaging and Preclinical evaluation of Human Acidic Fibroblast Growth Factor (haFGF) in rats

Wan-Chi Lee¹, Liang-Cheng Chen¹, Chi-Mou Liu¹, I-Hsiang Liu¹, Chin-Wei Hsu¹, Ming-Jei Lo⁵, Wen-Cheng Huang^{2,3}, Wen-Chi Chang², Henrich Cheng^{2,4}, Te-Wei Lee¹, ¹Institute of Nuclear Energy Research, Taoyuan County, Taiwan; ²Department of Neurosurgery, Neurological Institute, Taipei Veterans General Hospital, Taipei, Taiwan; ³Graduate Institute of Medical Sciences National Defense Medical Center, Taipei, Taiwan; ⁴Department Institute of Pharmacology, National Yang-Ming University, Taipei, Taiwan; ⁵Eusol Biotech Co., LTD, Taipei, Taiwan. Contact e-mail: leewc@iner.gov.tw

Acidic fibroblast growth factor (aFGF) is a potent neurotrophic factor that affects neuronal survival in the injured spinal cord. It could promote the survival of neurons and re-growth of neurites in the injured spinal cord. Recombinant Human Acidic Fibroblast Growth Factor (haFGF) was labeled with ¹³¹I for pharmacokinetics, biodistribution and microSPECT/CT imaging in Sprague-Dawley (SD) rats by intraspinal implantation. ¹³¹I-haFGF was implanted by intraspine and blood samples were collected via heart puncture from 0.25 to 504 hr post-implantation. Biodistribution and microSPECT/CT imaging were performed from 2 to 504 hr in rats. Biodistribution data demonstrated that ¹³¹I-haFGF was major accumulated in T-spine where it was implanted and other organs were low accumulated. The maximum radioactivity (C_{max}) and the area under curve ($AUC_{0 \rightarrow 504 \text{ hr}}$) of ¹³¹I-haFGF were 0.04 %ID/g and $2.05 \pm 0.26 \text{ hr} \times \%ID/g$, respectively. MicroSPECT/CT imaging showed that the radioactivity of ¹³¹I-haFGF mainly retained in T-spine where it was intraspinal implanted until 336 hr after implantation. MicroSPECT/CT imaging confirmed the results of biodistribution studies. Our studies indicated microSPECT/CT imaging with ¹³¹I-haFGF is a good modality to monitor the location and distribution of the haFGF in rats.

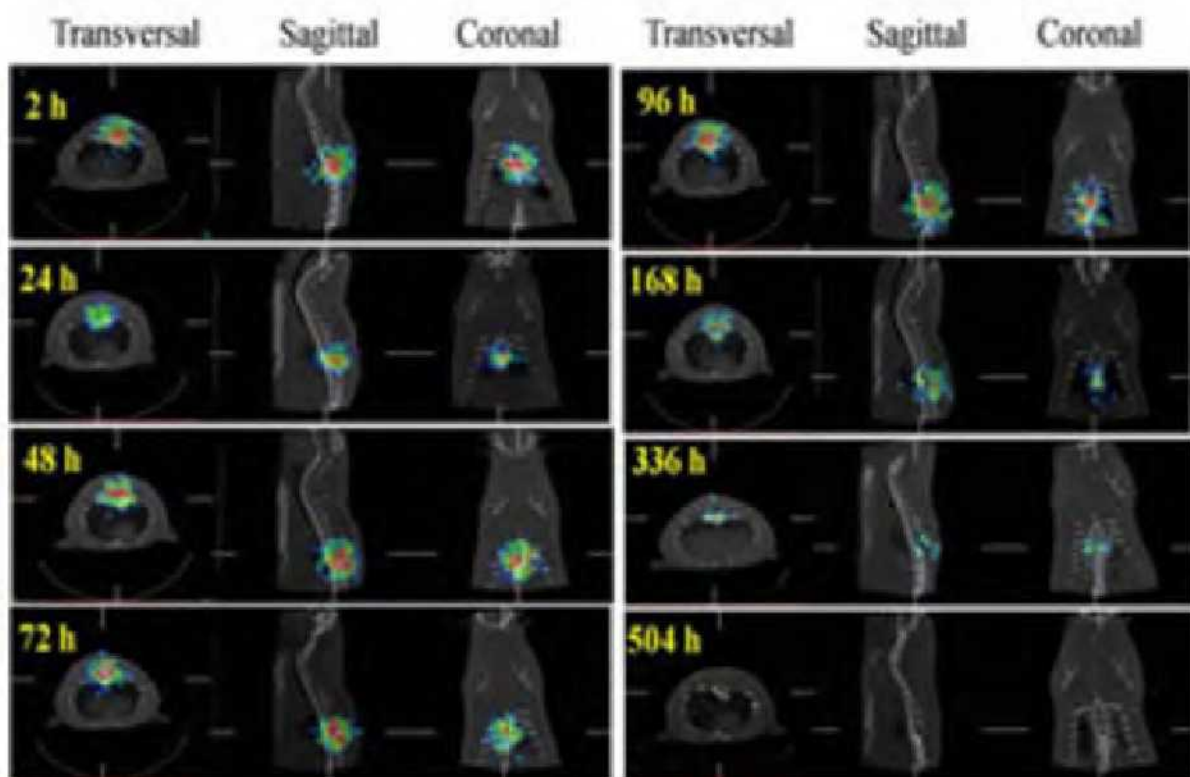


Figure: MicroSPECT/CT imaging of ¹³¹I-haFGF in SD rats by intraspinal implantation performed at 2, 24, 48, 72, 96, 168, 336 and 504 hr.

Presentation Number **0501B**

Poster Session 4b: Imaging Molecular and/or Cellular Processes & Drug and/or Radiation Therapy

MRI-guided p53 Gene Therapy mediated by PEI-functionalized Superparamagnetic iron oxide nanoparticles

Hwa Jeong Lee^{1,5}, Chau Nguyen y toai¹, Myeong Ju Moon², Hieu Vu-Quang^{1,6}, Sangjoon Lee^{1,5}, Hui Lian Che^{1,4}, Yong Yoen Jeong², Il Kwon Lee³, In-Kyu Park^{1,4}, ¹Department of Biomedical Sciences, Chonnam National University Medical School, Gwangju, Republic of Korea; ²Department of Radiology, Chonnam National University Medical School, Gwangju, Republic of Korea; ³Department of Genome Research Center for Hematopoietic Disease, Hwasun Chonnam National University Hospital, Hwasun, Republic of Korea; ⁴Heart Research Center, Chonnam National University Hospital, Gwangju, Republic of Korea; ⁵BioImaging Research Center, GIST, Gwangju, Republic of Korea; ⁶Clinical Vaccine R&D center, Chonnam National University, Hwasun, Republic of Korea. Contact e-mail: hjl1510@gmail.com

Targeting therapeutic drug using Superparamagnetic iron oxide nanoparticles (SPION) as carrier systems gained increased attention in the biomedical field. Generally, particles carrying different core sizes and various coatings were used in in vitro and in vivo. According to their desired purpose, they were also additionally functionalized with drugs, plasmids, peptides or proteins of interest. Tumor gene therapy aims at correcting gene defaults and mutations that are observed in severe hereditary pathologies or cancer tissues. The p53 gene is a tumor suppressor and genome defense. It plays important role in various activities like cell cycle regulation, apoptosis, and DNA repair. Therefore, recovering the normal function in cancer cells by replacement of the aberrant p53 gene with its normal one is one of the most efficient and critical approaches for tumor gene therapy. In this study, we proposed gene carrying SPION for anti-cancer gene therapy. For this purpose, the surface of SPION was functionalized with a random copolymer synthesized from (trimethoxysilyl)propyl methacrylate and PEG methacrylate, denoted as TCL-SPION. With the help of the PEG-silane copolymer, biofouling and aggregation were minimized in physiological conditions. Thereafter, TCL-SPION was conjugated with branched PEI (bPEI) 1800Da by EDC-NHS chemistry for DNA delivery. The presence of bPEI 1800Da was functionalized to bind with DNA due to its electrostatic interaction. The synthesized bPEI 1800Da-conjugated TCL-SPION (bPEI-SPION) was investigated for its potential as an imaging-guided gene carrier. For the first work, transgene delivery with bPEI-SPION was tested in cancer cell lines: 4T1, 4T7 and CT26 compared to original bPEI 1800Da as a control. Particularly, bPEI-SPION achieved higher cell viability compared to bPEI 25kDa and 1800Da. And internalized SPIONs were tracked by Magnetic resonance imaging (MRI). MR contrasts were strong and became more intense with increasing amounts of the bPEI-SPION 1800Da. The shortening of the MR T2 relaxation time was also correlated to increasing amounts of the bPEI-SPION. Finally, delivery of p53 tumor suppressor gene by bPEI-SPION obtained the suppressive effect on CT26, 4T1, Ca46 and Daudi measured by MTS proliferation assay. In conclusion, bPEI-SPION could be used for an efficient gene delivery carrier tracked by MR imaging.

Presentation Number **0502B**

Poster Session 4b: Imaging Molecular and/or Cellular Processes & Drug and/or Radiation Therapy

MRI-Guided Thermal Ablation Using Multimodality, Multifunctional SPIO@Au Nanoshell Targeted to Epidermal Growth Factor Receptors

Marites P. Melancon^{1,2}, Wei Lu², Andrew Elliott¹, Brian A. Taylor¹, Qian Huang², John D. Hazle¹, Chaan S. Ng³, Chun Li², R. Jason Stafford¹, ¹Imaging Physics, UT-MD Anderson Cancer Center, Houston, TX, USA; ²Experimental Diagnostic Imaging, UT-MD Anderson Cancer Center, Houston, TX, USA; ³Radiology, UT-MD Anderson Cancer Center, Houston, TX, USA. Contact e-mail: mmelancon@di.mdacc.tmc.edu

Magnetic resonance imaging (MRI)-guided laser-induced photothermal ablation (PTA) mediated via optically activated nanoparticles is a promising technique in achieving tumor specific heat delivery. In this study, we developed a single agent that can be used for PTA under MRI guidance. Superparamagnetic iron oxide encapsulated with gold was conjugated with C225 monoclonal antibody (C225-SPIO@AuNS) targeted to epidermal growth factor receptors (EGFR). The magnetic and optical properties of C225-SPIO@AuNS were examined both in solution and in agar gel phantoms. C225-SPIO@AuNS has a relaxivity, R2 value of 208 mM⁻¹s⁻¹ at 1.5T and a peak plasmon absorption at 810 nm. The proton resonance frequency of C225-SPIO@AuNS was also determined to be the same as that of water ($\alpha = -0.0097$ ppm/degree C), indicating that SPIO is unlikely to affect temperature measured with MRT1. Irradiation of C225-SPIO@AuNS in solution with near infrared (NIR) laser centered 810 nm at 4 W/cm² had a temperature increase of about 65 degrees C at 0.12 mM equivalent Fe. When incubated with EGFR-positive cells (A431), C225-SPIO@AuNS selectively bound to A431 cells as shown by microscopic and MR imaging data. Selective tumor ablation was induced with C225-SPIO@AuNS when treated with NIR laser as shown in the figure below. In conclusion, targeted C225-SPIO@AuNS is a promising agent for selective PTA of tumors under MRI guidance.

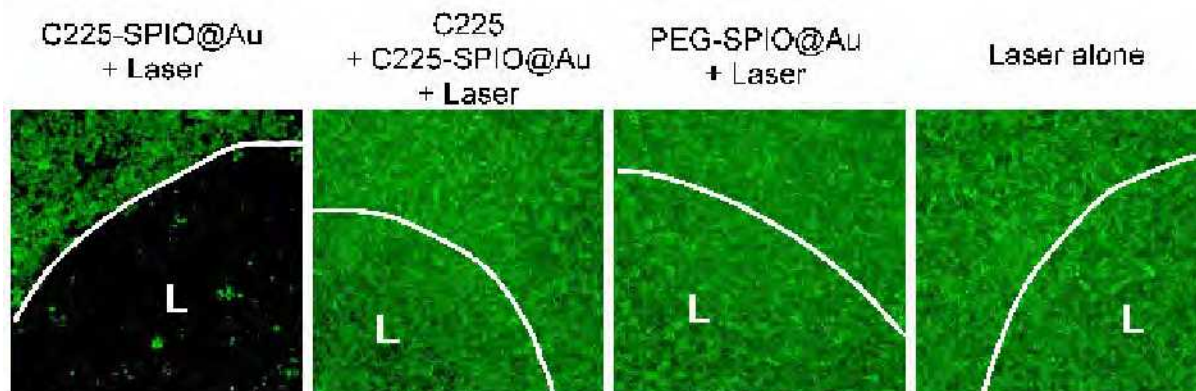


Figure. In vitro ablation of A431 tumor cells with C225-SPIO@AuNS targeted to EGFR, but not with C225-SPIO@AuNS in the presence of a large excess of C225, C225-SPIO@AuNS alone, or laser alone. L, zone of laser exposure.

Presentation Number **0503B**

Poster Session 4b: Imaging Molecular and/or Cellular Processes & Drug and/or Radiation Therapy

Imaging and therapy for EBV-associated nasopharyngeal carcinoma in Vivo*Dexue Fu, Oncology, Johns Hopkins UNiversity School of Medicine, Baltimore, MD, USA. Contact e-mail: dfu1@jhmi.edu*

1De-Xue Fu, 1Yvette Tanhehco, 1Jianmeng Chen, 2James Fox, 2Catherine Foss, 2Sridhar Nimmadda, 2Gibert Green, 2George Sgouros, 1, 2 Martin Pomper and 1Richard Ambinder 1Oncology, Johns Hopkins University, Baltimore, MD, USA 2Radiology, Johns Hopkins University, Baltimore, MD, USA Epstein-Barr virus (EBV) has been identified in a wide variety of lymphomas and carcinomas. The virus encodes kinases that phosphorylate nucleoside analogs such as 2'-deoxy-2'-fluoro-5-iodo-1-beta-D-arabinofuranosyluracil (FIAU). We hypothesized that it might be possible to use the viral enzyme to concentrate [¹²⁵I]FIAU specifically within tumor cells harboring virus and thus deliver imaging and therapeutic radiation. In previous study, we found that bortezomib (Velcade) is a potent stimulator of viral kinase expression in EBV (+) lymphoma cell lines in vitro and EBV-associated lymphoma can be imaged by induction of viral gene expression with bortezomib treatment in vivo (Fu. D., et al. Clin Cancer Res 13, 1453-1458, 2007). Moreover a therapeutic effect was demonstrated with [¹³¹I]FIAU in xenografts derived from EBV (+) human lymphoma and gastric cancer cell lines as well as KSHV (+) primary effusion lymphoma (Fu. D., et al. Nature Medicine, 2008). In this study, we extend those results to targeting of EBV-associated nasopharyngeal carcinoma (NPC). Ex vivo bio-distribution studies with [¹²⁵I]FIAU showed that uptake and retention of [¹²⁵I] FIAU is highly specific for NPC cells that are EBV positive upon lytic infection but not when virus is in the latent state. Planar gamma imaging and SPECT/CT imaging with [¹²⁵I]FIAU of NPC-bearing SCID mice showed selective concentration of radiotracer in tumor tissue in EBV-associated NPC when animals were pretreated with the bortezomib. We found dramatically increased [¹²⁵I]FIAU uptake within EBV (+) NPC at 72 hours after injection of [¹²⁵I]FIAU. Treatment with [¹³¹I]FIAU alone had no effect on EBV-associated NPC xenografts and all tumors increased in volume. However, treatment with bortezomib and [¹³¹I]FIAU led to marked tumor regression in EBV-associated NPC. These results indicate that treatment with bortezomib leads to selective concentration of radiolabeled FIAU in the EBV-associated NPC xenografts and may provide a simple way for the localization, monitoring and therapy of EBV-associated NPC that could be translated to the clinic.

Presentation Number **0504B**

Poster Session 4b: Imaging Molecular and/or Cellular Processes & Drug and/or Radiation Therapy

Identify Optimal Timing for Combining Endostatin with Resveratrol Using HIF-1 Expression Imaging in Vivo

I-Tsang Chiang¹, Ching-Chang Lin¹, Ya-Fang Chang¹, Keng-Li Lan², Jeng-Jong Hwang¹, ¹Department of Biomedical Imaging and Radiological Sciences, National Yang-Ming University, Taipei, Taiwan; ²Cancer Center, Taipei Veterans General Hospital, Taipei, Taiwan. Contact e-mail: cynthialin01@gmail.com

Angiogenesis is theoretically a valid target for cancer treatment. Nonetheless, the survival outcome has far been rather modest, thus development of more effective methods for combining antiangiogenic drugs and chemotherapy is in need. However, the optimal time point for combined therapy to gain higher therapeutic ratio is ambiguous. To determine the optimal time point for resveratrol in combined endostatin, we established constitutively-expressing luc and hypoxia-induced HRE-luc reporters to monitor tumor growth and kinetics of HIF-1 in vivo, respectively. BALB/c mice bearing both CT26/luc and CT26/HRE-luc were treated with 10 mg/kg endostatin by intraperitoneal injection, and 10 mg/kg resveratrol was then gavaged once a wk for 3 wks when vascular normalization occurred in tumor environment, judged by HIF-1 expression. Bioluminescent imaging (BLI) demonstrated that the HIF-1 activity was significantly elevated after the treatment of endostatin ($p < 0.01$ vs. control) at day 4, and attenuated rapidly after day 11 during resveratrol treatment. IHC staining also showed the similar results with micro-vessel density (MVD) dramatically decreased ($p < 0.01$) and HIF-1 positive staining ratio increased after endostatin treatment. The percentages of vascular maturity and apoptotic cells in tumors were both increased in the combined group which received resveratrol at day 11 after endostatin administration. Tumor growth delay time (TGD) and survival were also significantly improved as compared with all other groups ($p < 0.01$). This study indicated that combined chemotherapy of endostatin and resveratrol at the optimal time point could augment the efficacy of resveratrol through the vascular remodeling and improvement of drug accumulation in tumors. In conclusion, this reporter system may not only be a potential tool for imaging HIF-1 kinetics, but also speed up the development of efficient chemotherapies.

Presentation Number **0505B**

Poster Session 4b: Imaging Molecular and/or Cellular Processes & Drug and/or Radiation Therapy

In vivo detection of N-Acetylcysteine (NAC)-induced suppression of Matrix-Metalloproteinase activity in delayed-type hypersensitivity reactions by optical imaging

Johannes Schwenck¹, Christoph M. Griessinger¹, Kerstin Fuchs², Daniel Bukala¹, Bernd J. Pichler¹, Manfred Kneilling², ¹Laboratory for Preclinical Imaging and Imaging Technologies of the Werner Siemens Foundation, Department of Radiology, Eberhard Karls University, Tübingen, Germany; ²Department of Dermatology, Eberhard Karls University, Tübingen, Germany. Contact e-mail: johannes.schwenck@student.uni-tuebingen.de

Angiogenesis plays a major role in organ-specific autoimmune diseases caused by delayed type hypersensitivity reactions (DTHR). NF- κ B regulates the induction of pro-inflammatory mediators such as TNF in DTHR. Importantly, TNF enhances matrix metalloproteinase (MMP) expression which degrades components of the extracellular matrix required for angiogenesis. Our aim was to analyse whether inhibition of NF- κ B induction by NAC is sufficient to suppress DTHR and whether analysis of MMP-activation is applicable to detect anti-inflammatory and anti-angiogenic effects of NAC-treatment in vivo. DTHR was elicited by sensitizing mice at the abdomen and challenging seven days later the right ear repetitively every 48h up to five times with trinitrochlorobenzene (TNCB). To suppress NF- κ B signalling we added continuously 5mg/ml NAC to the drinking water starting two days prior first ear challenge. We analysed ear swelling responses 12-24h after challenge. Furthermore we investigated MMP-activation by MMPsense 680, a MMP-2, 3, 9, and 13 detecting bioactive optical imaging (OI) agent. We injected MMPsense 12h after the first and 5th TNCB-challenge and performed in vivo OI investigations 24h later. Additionally we examined mRNA expression of pro-inflammatory cytokines and MMP-2, 3, 9, 13 as well as sections with H&E-, and pan endothelial adhesion molecule (PECAM-1, CD31) staining of inflamed and control ears. NAC-treatment significantly reduced acute and chronic DTHR. 24h after first challenge (acute DTHR) we detected a strongly suppressed ear swelling response in NAC-treated mice ($60\pm 15\mu\text{m}$) compared to sham-treated mice ($190\pm 40\mu\text{m}$). 12h after the 5th challenge (chronic DTHR) ear thickness in the NAC-treated group was $155\pm 40\mu\text{m}$ compared to $370\pm 150\mu\text{m}$ in sham-treated mice. In the sham-treatment group MMPsense activity in TNCB-challenged ears increased four-fold compared to not challenged control ears. In sham-treated mice MMPsense intensity increased 42% between the first and the 5th ear challenge. MMPsense intensity was 52% lower in NAC-treated mice after the first and 43% after 5th TNCB-ear challenge. In vivo data were confirmed by mRNA expression patterns of MMPs and pro-inflammatory cytokines. H&E- and CD31-staining validated angiogenesis in chronic DTHR. Thus, NAC is a powerful therapeutic tool to minimize detrimental effects of NF- κ B induction during DTHR by suppression of MMP-activation and angiogenesis. Furthermore in vivo imaging of MMP-activity might be an applicable tool control success of anti-angiogenic treatment in autoimmune diseases such as rheumatoid arthritis.

Presentation Number **0506B**

Poster Session 4b: Imaging Molecular and/or Cellular Processes & Drug and/or Radiation Therapy

Theranostic Imaging of Metastatic Prostate Cancer

Zhihang Chen, Marie-France Penet, Sridhar Nimmagadda, Cong Li, Sangeeta Ray, Paul T. Winnard, Dmitri Artemov, Kristine Glunde, Martin Pomper, **Zaver M. Bhujwala**, JHU ICMIC Program, Russell H. Morgan Department of Radiology, Johns Hopkins School of Medicine, Baltimore, MD, USA. Contact e-mail: zaver@mri.jhu.edu

There is a compelling need to find effective treatments for metastatic disease. We are developing prostate specific membrane antigen (PSMA) targeted nanoplexes carrying multimodality imaging reporters together with small interfering RNA (siRNA) and a prodrug enzyme for theranostic imaging of metastatic prostate cancer. Down-regulation of specific pathways using siRNA provide unique opportunities to target cancer cells selectively while sparing normal tissue. Our prototype nanoplexes are synthesized by conjugating: (i) the prodrug-activating enzyme bacterial cytosine deaminase (bcd) that converts 5-fluorocytosine (5-FC) to 5-fluorouracil (5-FU), (ii) the multimodal imaging reporter carrier poly-L-lysine (PLL) that carries [¹¹¹In]DOTA for SPECT or [Gd³⁺]DOTA for MR and a near-infrared fluorescent probe Cy5.5 and, (iii) the siRNA delivery vector: PEI (polyethyleneimine)-PEG (polythethyleneglycol) co-grafted-polymer that carries siRNA targeting choline kinase (Chk). Chk siRNA was selected as it enhances the effect of 5-FU. The incorporation of a low molecular weight PSMA targeting moiety allows specific targeting of the nanoplex to PSMA expressing tumors in vivo as shown with SPECT imaging (Figure 1a) and MRI (Figure 1b). The nanoplexes have the ability to deliver multiple siRNA, that can be extended to downregulate multi-drug resistance pathways or repair enzymes to increase the efficacy of chemo- or radiation therapy.

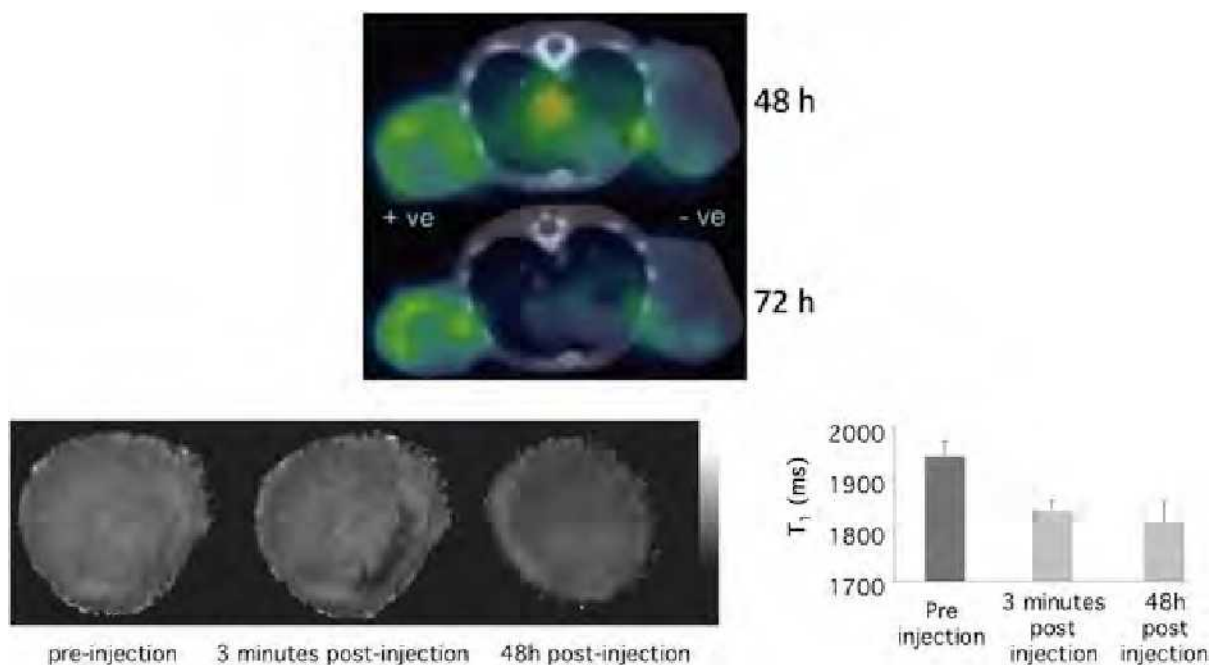


Figure 1: (a) SPECT imaging of SCID mouse bearing PIP (PSMA+ve) and FLU (PSMA-ve) tumor. Mouse was injected i.v. with 1.4 mCi of ¹¹¹In labeled PSMA targeted nanoplex. SPECT images were acquired in 64 projections at 30 sec/projection. CT images were acquired in 512 projections to allow coregistration. Transaxial slices show accumulation of radioactivity in PSMA expressing PIP tumor at 48 and 72 h. (b) Quantitative T1 maps of PSMA expressing LNCaP tumor following administration of PSMA targeted nanoplex labeled with [Gd³⁺]DOTA, demonstrating feasibility of detection with MRI.

Presentation Number **0507B**

Poster Session 4b: Imaging Molecular and/or Cellular Processes & Drug and/or Radiation Therapy

Imaging of High Intensity Focused Ultrasound (HIFU)-induced Heat Shock Response

Yoo-shin Kim, Pradip Ghosh, Daniel Y. Lee, Brian E. O'Neill, King Li, Radiology, The Methodist Hospital Research Institute (Weill medical college of Cornell University), Houston, TX, USA. Contact e-mail: cacophony73@gmail.com

Ultrasound has been used successfully in medical imaging for many years because it is safe, real-time, noninvasive, and cost effective. High intensity focused ultrasound (HIFU) ablation is a highly precise procedure that uses ultrasound to rapidly heat and destroy diseased tissue. Pulsed mode HIFU (pHIFU) has recently been demonstrated to increase the efficacy of a variety of systemically administered chemotherapies. We have attempted to use HIFU study to induce up-regulation of stress response proteins. Classically defined heat shock proteins (HSPs) are over-expressed to high levels in response to various stresses such as hyperthermia, chemical toxins, changes in pH and oxidative states, starvation, and viral infections. It is expressed at elevated levels in a large fraction (up to 50%) of common solid cancers such as malignancies of the breast, lung, and prostate. It also correlates with increased cancer cell proliferation, lymph node metastases, poor clinical response to chemotherapy, and reduced survival. In this work, we have modified a recently described small molecule inhibitor specific for the inducible HSP70 protein as a specific molecular imaging ligand. This adenosine-based compound was modified with a fluorophore (fluorescein) for in vivo imaging following pHIFU treatment of normal tissue in experimental mice. Early preliminary results indicate that this agent accumulates preferentially in otherwise normal muscle tissue that has been pre-treated with pHIFU. In contrast, the fluorescent dye alone or another non-HSP selective agent both demonstrated no significant accumulation. We hypothesize that selective tumor targeting may be achievable by targeting endogenously over-expressed HSPs in tumors or by inducing in vivo targets by HIFU. Ongoing studies are currently underway to further adapt this molecular imaging agent as a targeting ligand for potential drug delivery.

Presentation Number **0508B**

Poster Session 4b: Imaging Molecular and/or Cellular Processes & Drug and/or Radiation Therapy

MR Imageable Gene Delivery to Malignant Breast Cancer mediated by SPION-encapsulated Polymersome

SangJoon Lee^{1,4}, **Hyun Jin Lee**², **Myeong Ju Moon**³, **Hieu Vu-Quang**^{1,6}, **Hwa Jeong Lee**^{1,5}, **Hui Lian Che**^{1,5}, **Yong Yoen Jeong**³, **In-Kyu Park**^{1,4}, ¹*Biomedical Sciences, Chonnam National University Medical School, Gwangju, Republic of Korea;* ²*Chemical and Biomolecular Engineering, Korea Advanced Institute of Science and Technology, Daejeon, Republic of Korea;* ³*Radiology, Chonnam National University Medical School, Gwangju, Republic of Korea;* ⁴*BioImaging Research Center, GIST, Gwangju, Republic of Korea;* ⁵*Heart Research Center, Chonnam National University Hospital, Gwangju, Republic of Korea;* ⁶*Clinical Vaccine R&D center, Chonnam National University, Hwasun, Republic of Korea. Contact e-mail: kg2080@gmail.com*

Development of magnetic materials for diagnosis has been tried for several decades to identify the disease-related tissues as well as the specific anatomical structures. Recently, combination of SPION-based diagnostic properties with accompanying therapeutics such as drugs or genes has been explored to improve their therapeutic efficacy. In this regard, positively charged SPION-loaded polymersome tethering PEG as a hydrophilic corona layer was prepared to deliver therapeutic genes to target sites, which was monitored by MRI concomitantly. To investigate the composition of the particle, nuclear magnetic resonance (NMR) and thermogravimetric analysis (TGA) were used. Cu acetate assay was used for the calculation of N/P molar ratio and the complex formation with plasmid DNA was investigated by agarose gel electrophoresis. Complete nanoparticle formation of SPION-loaded polymersome with plasmid DNA was observed at about 15. Particle size and morphology of the prepared SPION-loaded polymersome were measured by electrophoretic dynamic light scattering (DLS) and transmission electron microscopy (TEM), respectively. Hydrodynamic particle size of SPION-embedded supra-assembly was found to range between 150 and 200 nm, and its surface charge was slightly positive determined by zeta potential measurement. The transfection efficiency in vitro was tested by treating 3T3 fibroblast and 4T1 breast cancer cell line with luciferase or GFP-expressing plasmids/SPION-embedded supra-assembly complex. Bcl-2 Antisense Oligodeoxyribonucleotide G3139 was used to test the cure of the disease. The detectability of SPION in transfected cells by MRI was also checked. This result indicates that the SPION-embedded supra-assembly can be applied to MR imaging guided gene therapy.

Presentation Number **0509B**

Poster Session 4b: Imaging Molecular and/or Cellular Processes & Drug and/or Radiation Therapy

MRI guided Boron Neutron Capture Therapy (BNCT)

Simonetta Geninatti-Crich, Diego Alberti, Antonio Toppino, Annamaria Deagostino, Nicoletta Protti, Saverio Altieri, Paolo Venturello, Silvio Aime, Department of Chemistry, Center for Molecular Imaging, University of Torino, Torino, Italy. Contact e-mail: simonetta.geninatti@unito.it

Since the success of BNCT depends upon the selective delivery of ^{10}B atoms to tumor cells, "in vivo" quantitative visualization of ^{10}B distribution is important. Thanks to its superb spatial resolution MRI appears to be the most appropriate technique to tackle this task. In this work a new compound containing a carborane unit and a Gd-containing complex (Gd-DCL, Figure 1) has been synthesized. The compound contains a palmityl chain that allows its binding to LDL (Low Density Lipoproteins). The supramolecular B/Gd/LDL adduct accumulates in tumor cells that overexpress transporters for these lipoproteins. Furthermore, the presence of the boron and gadolinium in the same compound is beneficial for enhancing the radiation dose to the tumor as also ^{157}Gd (15% natural abundance) owns a good cross-section for neutron capture. Each LDL particle can load up to 250 Gd-DCL probes that correspond to 250 Gd and 2500 B atoms respectively. The size of the adduct, determined by Dynamic Light Scattering, is similar to that of native protein (22 nm). The cellular labelling experiments proved that, after 16 hours of incubation in the presence of 10-40 $\mu\text{g}/\text{ml}$ of Gd/B containing LDL the amount of internalized Gd is sufficient to generate hyper intense signals in the corresponding MR images. The Signal Intensity (SI) measured on cells is directly proportional to the amount of Boron internalized and the B/Gd molar ratio found into tumor cells by ICP-MS measurements remains ca. 10 thus indicating the total absence of Gd-DCL degradation or Gd release upon incubation. The amount of Boron internalized by Hepg2 and B16 cells "in vitro" was of 30 and 36 $\mu\text{g}/\text{g}$ of cell. B16 tumor bearing mice showed a good tumor signal intensity enhancement (30-40%), 6 and 24 hours after the injection of of Gd-DCL. The tumor SI reports about Boron concentration. In order to test the efficacy of the Boron/Gd/LDL adduct B16 tumor bearing have been irradiated by thermal neutrons inside the thermal column of the TRIGA Mark II reactor at the University of Pavia, Italy, 6 and 24 hours after Boron administration. The effect of neutron irradiation has been assessed on control and treated mice by acquiring MR images of the tumor region over two weeks. In conclusion, LDLs act as efficient carriers for the delivery of a new imaging probe containing Gd and Boron. It follows that imaging-guided BNCT appears possible as, from the signal enhancement generated by the paramagnetic Gd(III) complexes, one can assess whether or not the required ^{10}B concentration threshold has been reached.

Presentation Number **0510B**

Poster Session 4b: Imaging Molecular and/or Cellular Processes & Drug and/or Radiation Therapy

Development of X-ray Luminescence Tomography for Intra-operative molecular imaging

Colin M. Carpenter, Guillem Pratx, Conroy Sun, Lei Xing, Radiation Oncology, Stanford University School of Medicine, Stanford, CA, USA. Contact e-mail: colincarpenter@stanford.edu

Objective: A new imaging modality, X-ray Luminescence Tomography (XLT), is being developed for molecular imaging. This modality uses a collimated X-ray source to image the concentration of nano-sized phosphors tagged with molecular targets. This technology utilizes a limited-angle raster-scanned source and a projection-type detection geometry which is amenable to surgical interventions. This study compared the resolution and contrast recovery of XLT and fluorescence molecular tomography (FMT). **Methods:** Simulations and phantom measurements were performed for comparison. An X-ray model was used for excitation modeling (for the XLT case), and a diffuse optical light propagation model for emission (and reflection for the FMT case). Various inclusions with 5x contrast were imaged in a 9 x 5 cm volume. The inclusions were placed at various depths to determine the concentration recovery performance between XLT and FMT. Experimental measurements used a 50 keV X-ray radiotherapy source collimated into a 1mm-wide beam, and an EM-CCD camera. Tissue-simulating solutions of India ink and intralipid solutions were mixed in a 12 x 7cm phantom. Two cylindrical inclusions, 3mm and 9mm, of gadolinium oxysulfide: europium phosphors (625, 705 nm emission), sized between 10 and 25nm, were imaged at various depths. **Results:** For all inclusion sizes tested (2mm to 16mm diameters), recovered inclusion contrast decayed rapidly with depth for the FMT case; recovered contrasts were less than 10% accurate for depths greater than 15mm. XLT was able to distinguish the inclusion with at least 50% accuracy for depths up to 35mm for inclusion sizes greater than 6mm, and at least 25% accuracy for sizes down to 3mm. Image reconstructions from the experimental phantom were able to recover 50% contrast for the 3mm inclusion at depths up to 2.5cm, and the 9mm inclusion was at least 50% accurate at these depths. **Discussion:** X-ray excitation is highly localized due to lack of scatter. This is especially true when compared to FMT, where light is an diffuse field emitting from an isotropic source. Thus, spatial localization at depth is poor in FMT. Similarly, concentration recovery suffers at shallower depths. This could limit its use during surgical procedures, such as lumpectomy, where a spiculated lesion could extend well beyond the surgical margin, or if poorly resolved, could be masked by background heterogeneity. Future work will involve investigation in small-animals.

Presentation Number **0511B**

Poster Session 4b: Imaging Molecular and/or Cellular Processes & Drug and/or Radiation Therapy

Polymeric Nanomedicines for Image-guided Drug Delivery and Tumor-targeted Combination Therapy

Twan Lammers^{1,2}, **Gert Storm**², **Fabian Kiessling**¹, ¹*Experimental Molecular Imaging, RWTH Aachen University, Aachen, Germany;*
²*Pharmaceutics, Utrecht University, Utrecht, Netherlands. Contact e-mail: tlammers@ukaachen.de*

Purpose: To assist i.v. applied anticancer agents in achieving proper circulation times and an appropriate biodistribution, and to thereby improve the balance between their efficacy and their toxicity, a large number of drug delivery systems have been designed and evaluated over the years. Clinically relevant examples of such nanometer-sized carrier materials are liposomes, polymers, micelles and antibodies. In the vast majority of cases, however, and especially in patients, tumor-targeted nanomedicines are only able to attenuate the toxicity of the intervention, and they generally fail to improve the efficacy of the conjugated or entrapped chemotherapeutic drug. To overcome this shortcoming, and to broaden the clinical applicability of tumor-targeted nanomedicines, we have developed several concepts for using image-guided nanomedicine formulations to improve the efficacy of combined modality anticancer therapy. Methods: HPMA copolymers were used as a model macromolecular drug carrier, doxorubicin and gemcitabine as model drugs, and the syngeneic and radio- and chemoresistant Dunning AT1 rat prostate carcinoma as a model tumor model. Magnetic resonance imaging, gamma-scintigraphy, fluorescence microscopy and HPLC were used to monitor the biodistribution of the copolymers, and clinically relevant regimens of radiotherapy and chemotherapy to evaluate their efficacy-enhancing effects. Results: Upon having shown that HPMA copolymers circulate for prolonged periods of time, that they localize to tumors both effectively and selectively, and that they are able to improve the tumor-directed delivery of low molecular weight agents, we have used these passively tumor-targeted polymeric drug carriers to improve the efficacy of surgery, of radiotherapy and of chemotherapy combinations. Regarding surgery, HPMA copolymers were shown to be able to improve the retention of intratumorally injected chemotherapeutic drugs at the pathological site, and to thereby increase their therapeutic index. Regarding radiotherapy, a synergistic interaction was observed, with radiotherapy improving the tumor accumulation of the copolymers, and with the copolymers improving both the efficacy and the toxicity of radiochemotherapy. And regarding chemotherapy, we have for the first time provided in vivo evidence showing that passively tumor-targeted polymeric drug carriers can be used to deliver two different drugs to tumors simultaneously. Conclusion: Image-guided polymeric nanomedicines are highly suitable systems for improving the efficacy of combined modality anticancer therapy.

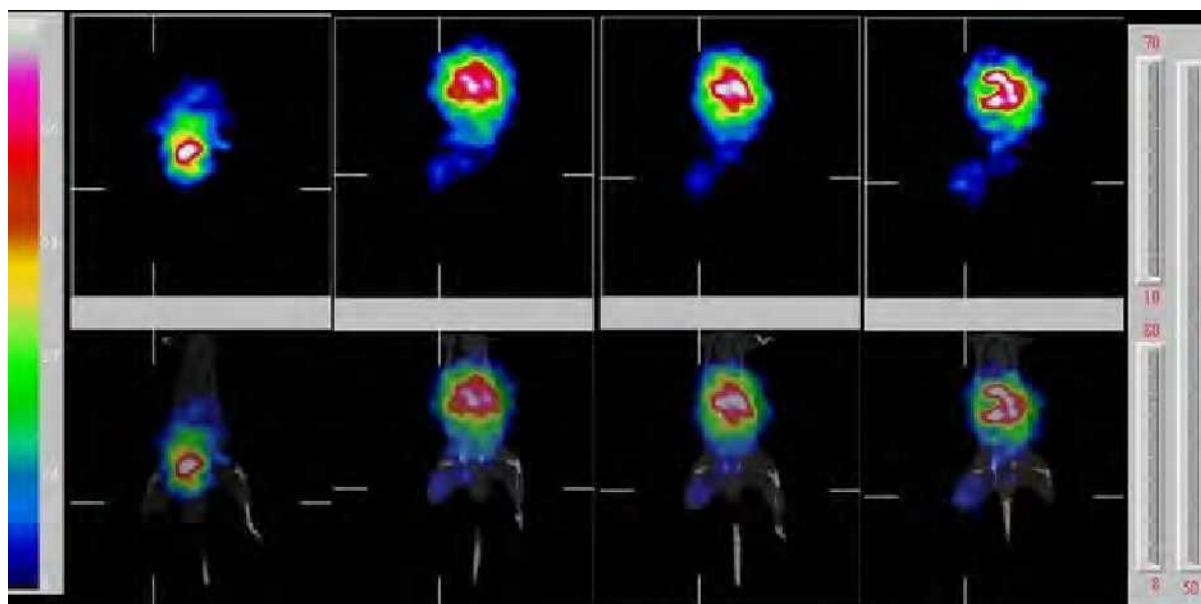
Presentation Number **0512B**

Poster Session 4b: Imaging Molecular and/or Cellular Processes & Drug and/or Radiation Therapy

Multimodality Imaging and Preclinical Evaluation of ^{177}Lu -AMBA in Human Prostate Tumor-bearing Mice

I-Hsiang Liu, Chung Li Ho, Shu-Pei Chiu, Wan-Chi Lee, Tsui-Jung Chang, Liang-Cheng Chen, Yu-Hsien Wu, Te-Wei Lee, Chih-Hsien Chang, Institute of Nuclear Energy Research, Taoyuan County, Taiwan. Contact e-mail: kazuhide@iner.gov.tw

Gastrin-releasing peptide receptors (GRPr) are over-expressed in varieties of tumor including prostate, small-cell lung and breast cancers. AMBA (DO3A-CH₂CO-G- (4-aminobenzoyl)-QWAVGHLM-NH₂) is one kind of Bombesin (BN)-like peptides which has high affinity with GRPr, and ^{177}Lu -AMBA is used to prostate cancer diagnosis and therapy. Bioluminescent imaging (BLI) is often used to application in tumor model system and which can be applied in longitudinally monitoring tumor growth and evaluation of therapeutic efficacy. PC-3M-luc-C6 is one kind of human prostate tumor cell line that can constitutively express luciferase gene for BLI. The cell line could be evaluated the feasibility of modality monitor and ^{177}Lu -AMBA treatment. The result of plasma stability of ^{177}Lu -AMBA could be maintained up to $55.67 \pm 6.07\%$ at 24 h in protection buffer. In tumor size monitoring, there was indicated high positive correlations of PC-3M-luc-C6 tumor growth in SCID mice between caliper measurement and BLI ($R^2=0.999$). Both biodistribution and microSPECT/CT imaging in PC-3M-luc-C6 bearing-tumor mice showed that ^{177}Lu -AMBA in tumor uptake and could be retained for 24 h. The distribution half-life ($t_{1/2\alpha}$) and the elimination half-life ($t_{1/2\beta}$) of ^{177}Lu -AMBA were 0.52 h and 26.63 h, respectively, in mice. Our results indicated that multimodality imaging combining BLI and microSPECT/CT could be used in monitoring tumor growth and uptake of ^{177}Lu -AMBA in the PC-3M-luc-C6 tumor in SCID mice, and high uptake ratio of ^{177}Lu -AMBA in PC-3M-luc-C6 tumor-bearing mice model can further evaluate the potentials of ^{177}Lu -AMBA therapy in PC-3M-luc-C6 tumor by multimodality imaging.



Micro-SPECT /CT images of ^{177}Lu -AMBA were performed in PC-3M-luc-C6 tumor-bearing mice; tumor was intravenously injected with $14.8 \text{ MBq}/0.95 \mu\text{g}$ ^{177}Lu -AMBA. The energy window was set at $113 \text{ KeV} \pm 10\%$ and $209 \text{ KeV} \pm 10\%$.

Presentation Number **0513B**

Poster Session 4b: Imaging Molecular and/or Cellular Processes & Drug and/or Radiation Therapy

Assessment of tumor microvasculature in brain metastasis by pharmacokinetic model using dynamic MRI

YuChun Lin^{1,2}, **Yau-Yau Wai**^{2,3}, **Jiun-Jie Wang**³, ¹*Department of Electrical Engineering, ChangGung University, Taoyuan, Taiwan;* ²*Department of Radiology, ChangGung Memorial Hospital, Taoyuan, Taiwan;* ³*Department of Medical Imaging and Radiological Science, ChangGung University, Taoyuan, Taiwan. Contact e-mail: jack805@gmail.com*

Introduction: Angiogenesis plays a key element in the pathophysiology of tumor growth and metastasis. Dynamic contrast-enhanced magnetic resonance imaging (DCE-MRI) was proposed to investigate the microvascular structure. The pharmacokinetics of injected contrast agents were tracked by MRI as they pass through the tumor vasculature. Quantitative parameters can be derived, which reflected the treatment responses in primary tumors. The purpose of the study was to explore the induced changes from metastatic tumors, such as in patients with brain metastasis from breast cancer. **Methods and Materials:** Patients of breast cancer with evidence of brain metastasis underwent radiotherapy and/or chemotherapy. Imaging of the brain were performed before and one month after treatment using a 3 Tesla MRI scanner (Trio with TIM, Siemens, Germany). Contiguous 3D volumes were obtained with a gradient echo sequence of TR/TE=13.6/3.8 ms, and a rapid intravenous bolus injection (0.1 mmol/kg) of Gadopentetate dimeglumine (Magnevist; Schering, Germany). 120 volumes were acquired with the temporal resolution of 2.6 seconds. Quantitative DCE parametric maps were reconstructed based on two-compartment model, including the vascular plasma volume (Vp), transcapillary contrast agent transfer constant (Ktrans) and extracellular extravascular volume (Ve). The derived parameters at regions of tumors as well as the tumor volumes were compared before and after treatment. **Results and discussion:** The findings showed that the microenvironment from a metastatic tumor can be modified by radiotherapy and/or chemotherapy. The vascular permeability within the tumor could be decreased, as reflected in the reductions in Ktrans immediately after the treatment. It could suggest an early sign of the tumor response to the treatment, because of the disruption of vasculatures. The changes of Ve and Vp could be a reflection of the temporal evolutions from the therapeutic intervention. Decreased tumor volume was expected at a later stage. The findings obtained from the DCE derived indices are consistent with the expected biological effect. The underlying mechanism quarantines the worth of further investigation. **Conclusion:** Dynamic MRI enables quantification of the tumor vascularity and permeability, hence could serve as a potential surrogating biomarker for treatment response for patients with brain metastasis.

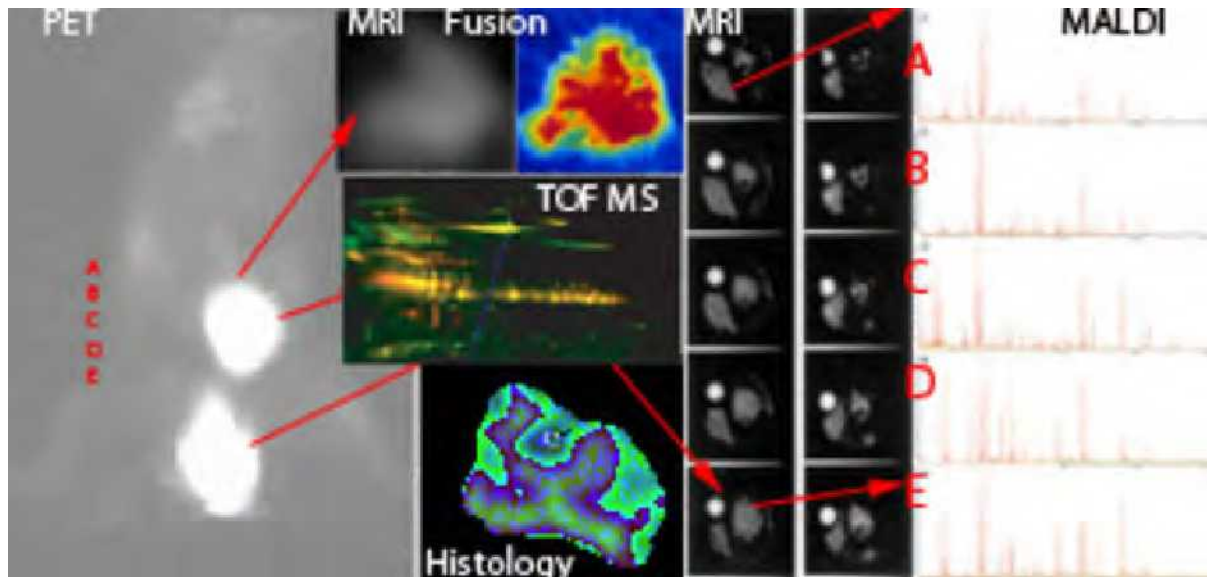
Presentation Number **0514B**

Poster Session 4b: Imaging Molecular and/or Cellular Processes & Drug and/or Radiation Therapy

Integration of MRI-PET and MALDI of MCF-7 Induced Tumor: Taxotere Chemosensitivity Assay

Rakesh Sharma^{1,2}, **Soonjo Kwon**^{3,1}, **Jose Katz**², ¹Computer Science, TCC and Florida State University, Tallahassee, FL, USA; ²Medicine, Columbia University, New York, NY, USA; ³Biological Engineering, Utah State University, Logan, UT, USA. Contact e-mail: rksz2004@yahoo.com

Aim: To integrate increased PET (glycolysis and oxygen contents) and MRI (sodium-pump action) image intensities of rat breast tumors with protein MALDI peaks and histostaining tumor characteristics. **Hypothesis:** Increased μ MRI signal intensities and flouro-2-deoxyglucose utilization by μ PET in apoptosis protein rich regions in tumors evaluate Taxotere. **Methods:** The MCF-7 tumor MRI and PET images, histology slices and proteomic peaks were digitally captured and compared in pre- and post-Taxotere treated tumors. **Results:** A criterion was developed to evaluate malignancy by PET-MRI, histology and proteomics and immunostaining from MCF-7 induced tumor after 24 and 48 hr post-Taxotere treatment. MRI and PET signal intensity distributions at specific locations were measured in tumor tissue regions. In tumors, Taxotere induced an increase in intracellular sodium MRI signal 35% ($p < 0.001$) with decreased tumor size (25%; $p < 0.001$) and micro-PET showed FDG uptake increase 12-15% ($p < 0.001$) with decreased tumor size (12%; $p < 0.001$) than that of control tumors after 24 hours. Histological features indicated tumor risk (high intracellular/extracellular ratio, high mitotic index, apoptotic index with proteomic peak), decreased tumor viability (reduced mitotic figures, reduced diploidy or aneuploidy, and proliferation index) after Taxotere treatment. These features in co-registered intracellular sodium, μ PET hypermetabolic, and proteomic peak visible regions showed (% difference > 10%). Apoptosis rich regions showed characteristic proteomic peak and nuclei with S phase DNA histogram, appearing brighter on IC-Na images and mild active on PET images (sensitivity=65%; specificity=70%). **Conclusion:** MRI and PET multimodal imaging with apoptosis sensitive protein may be non-invasive assay to monitor the drug anticancer effect.



On Left: Tumor by PET; In middle: MRI-PET fusion(top), TOF-MS(middle), digital immunostaining(bottom), NaMRI(right) and MALDI peaks at locations A-E tumor sites(at rightmost).

Presentation Number **0515B**

Poster Session 4b: Imaging Molecular and/or Cellular Processes & Drug and/or Radiation Therapy

Hyperpolarized ¹³C MR Metabolic Imaging for the Detection of Early Response to Temozolomide Treatment in Brain Tumors

Ilwoo Park^{1,2}, **Robert Bok**¹, **Tomoko Ozawa**³, **Daniel B. Vigneron**^{1,2}, **C. David James**³, **Sabrina Ronen**^{1,2}, **Sarah Nelson**^{1,2}, ¹Surbeck Laboratory of Advanced Imaging, Department of Radiology and Biomedical Imaging, University of California San Francisco, San Francisco, CA, USA; ²UCSF/UCB Joint Graduate Group in Bioengineering, University of California San Francisco, San Francisco, CA, USA; ³Brain Tumor Research Center, Department of Neurological Surgery, University of California San Francisco, San Francisco, CA, USA. Contact e-mail: ipark@radiology.ucsf.edu

Introduction: A recent study has shown that tumor metabolism in brain tumor model can be examined using hyperpolarized ¹³C MR metabolic imaging [1]. The purpose of this study was to demonstrate the feasibility of using this technique in measuring early response to Temozolomide (TMZ) therapy in a human glioblastoma xenograft in rat brain. **Methods:** 20 athymic rats with intracranial implantation of human glioblastoma cells were divided into two groups: one group received an oral administration of 100 mg/kg TMZ (n=10) and the other control group received the vehicle only (n=10). All animals underwent ¹³C and ¹H imaging using a 3T scanner with a custom RF coil before the treatment (D0), at D1 (days from treatment) or D2 and at several subsequent time points. 4 treated and 4 control rats were sacrificed at D2 and the tumor tissue from their brains analyzed. ¹³C 3D MRSI data [2] were acquired 20 sec after the injection of 2.5 ml (100 mM) hyperpolarized ¹³C₁-pyruvate through their tail vein. Lactate over pyruvate ratio (Lac/Pyr) was calculated for the assessment of change in tumor metabolism. Tumor volume was estimated from T1 post-Gd images. **Results:** Tumor metabolism as measured by Lac/Pyr was altered at D1 for the group treated with TMZ (Fig 1a) but the tumor volume did not show a reduction until D5 to D7 (Fig1b). The percent change in Lac/Pyr from baseline was statistically different between the two groups at D1 and D2, while percent tumor volume was not (Fig1). Lower NADH level in treated rats compared to control rats at D2 is consistent with the early change in tumor metabolism in the treated group (Fig2). **Conclusions:** We have demonstrated the feasibility of using hyperpolarized ¹³C MR imaging to detect early response to treatment with TMZ in a pre-clinical brain tumor model system. Future studies will examine the application of this technology to monitor response to therapy for patients with brain tumors. **References:** [1] Park et al. *Neuro-Oncology*, 2010. [2] Cunningham et al. *J Magn Reson*, 2007. **Grant support:** ITLBIO04-10148, NIH RO1 EB007588.

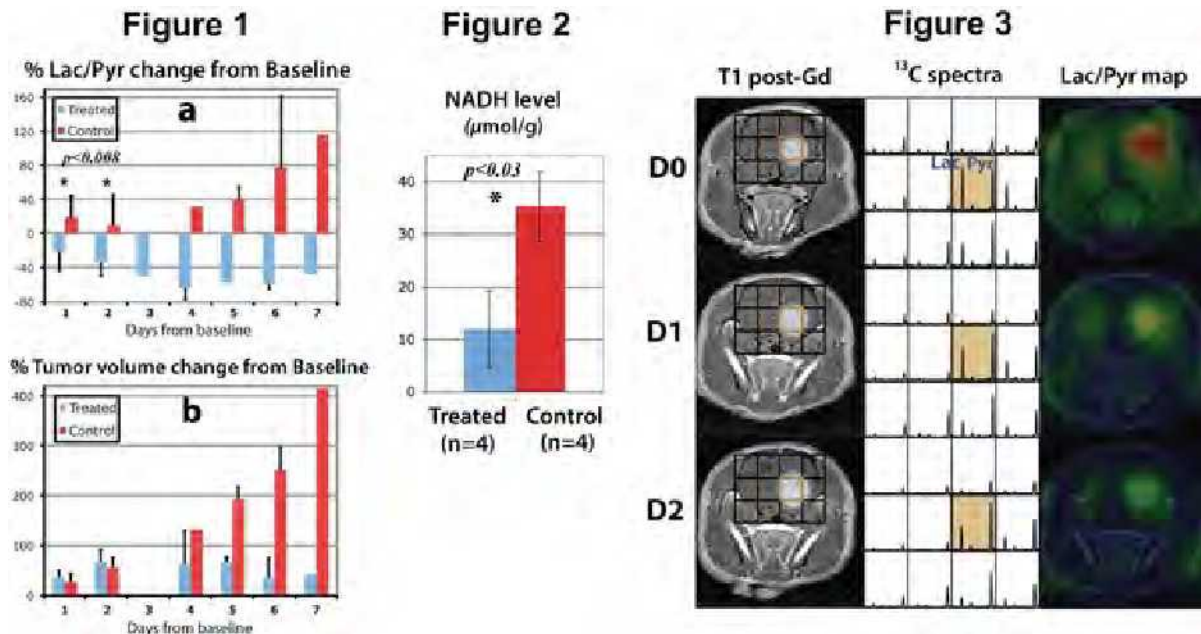


Fig 1: % Lac/Pyr (a) and tumor volume (b) change from baseline in two groups. Fig 2: NADH level. Figure 3: An example of radiographic and metabolic changes at D0, D1 and D2 from a TMZ treated rat.

Presentation Number **0516B**

Poster Session 4b: Imaging Molecular and/or Cellular Processes & Drug and/or Radiation Therapy

Micro-SPECT/CT quantification of ^{188}Re -BMEDA and ^{188}Re -liposome via intraperitoneal injection in a C26 ascites mouse model

Liang-Cheng Chen^{1,2}, Cheng-Hui Chuang¹, Yu-Hsien Wu¹, Chung Li Ho¹, Wan-Chi Lee¹, Ya-Jen Chang¹, Meei-Ling Jan¹, Te-Wei Lee¹, Jui-Hung Shien², Chih-Hsien Chang¹, ¹Isotope Application Division, Institute of Nuclear Energy Research, Taoyuan, Taiwan; ²Department of Veterinary Medicine, National Chung Hsing University, Taichung, Taiwan. Contact e-mail: lcchen@iner.gov.tw

Objectives: Micro-single photon emission computed tomography (micro-SPECT)/computed tomography (CT) is a noninvasive imaging modality for monitor radioisotope-labeling drug distribution. The aim of this study was to investigate the ability of micro-SPECT/CT to quantitate intraperitoneal (i.p.) administration of ^{188}Re -N,N-bis (2-mercaptoethyl)-N',N'-diethylethylenediamine (^{188}Re -BMEDA) and ^{188}Re -BMEDA labeled pegylated liposome (^{188}Re -liposome) and to compare with in vivo biodistribution in the C26 murine colon carcinoma ascites mouse model. **Methods:** Male BALB/c mice were i.p. inoculation with 2×10^5 C26 cells. At 10 days after tumor inoculation, imaging was performed at 4, 24, 48 and 72 h after ^{188}Re -BMEDA or ^{188}Re -liposome injection. Each mouse was i.p. injection 350 $\mu\text{Ci}/200 \mu\text{L}$ ^{188}Re -BMEDA or ^{188}Re -liposome and scanned for 100 min. Percentage injection dose (%ID) per milliliter (%ID/mL) of ^{188}Re -BMEDA or ^{188}Re -liposome with the peritoneal cavity were also calculated from regions of interest analysis of the micro-SPECT/CT images. These values (%ID/mL) of images were compared with biodistribution data (%ID/g). **Results:** Correlations between the peritoneal uptake (%ID/mL) of ^{188}Re -BMEDA and ^{188}Re -liposome in the micro-SPECT/CT imaging (n=3) and biodistribution studies (n=4) were high levels ($R^2 = 0.992$ and 0.986 ; pearson correlation, $r = 0.996$ and 0.993 , respectively). Peritoneal uptake (%ID) of ^{188}Re -BMEDA and ^{188}Re -liposome were from 90.2%ID at 4 h to 38.7%ID at 24 h, and from 87.1%ID at 4 h to 78.5%ID at 24 h postinjection in the tumor-ascites mice, respectively. **Conclusions:** Micro-SPECT/CT can be used a noninvasive tool to localize and follow the radioisotope-labeling drug via intraperitoneal injection in a C26 ascites mouse model.

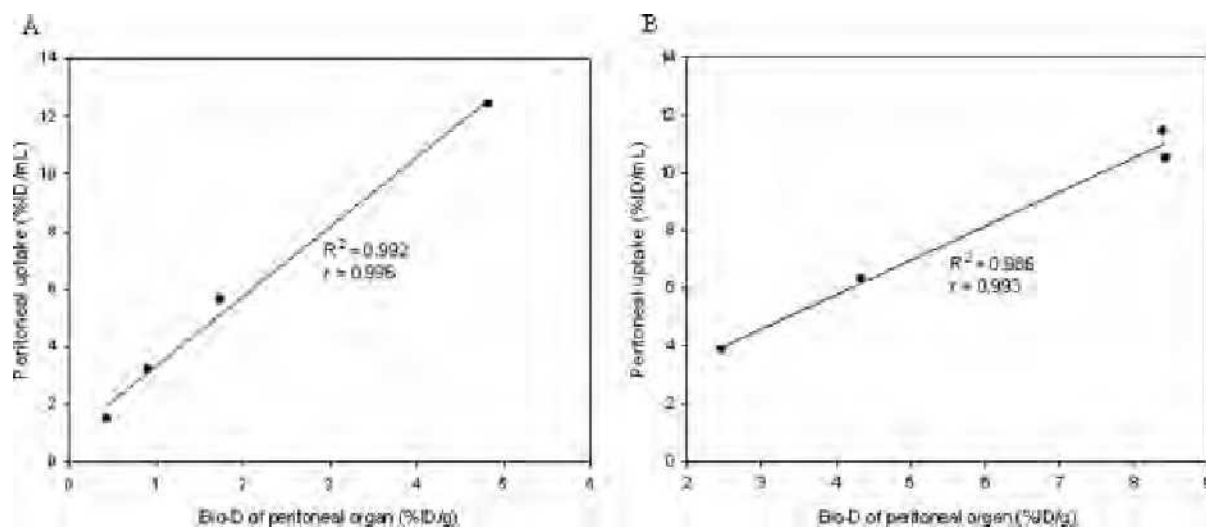


Figure. Correlations between the peritoneal uptake (%ID/mL) of ^{188}Re -BMEDA (A) and ^{188}Re -liposome (B) in the micro-SPECT/CT imaging (n=3) and biodistribution (Bio-D) studies (n=4).

Presentation Number **0517B**

Poster Session 4b: Imaging Molecular and/or Cellular Processes & Drug and/or Radiation Therapy

The proteasome inhibitor Bortezomib affects proliferation, cell cycle and metabolism in rat Morris hepatoma cells

Annette Markert¹, Tilman Schoening², Annette Altmann^{3,1}, Vasileios Askoxylakis^{4,1}, Uwe Haberkorn^{3,1}, ¹Clinical Cooperation Unit Nuclear Medicine, DKFZ, Heidelberg, Germany; ²Clinical Pharmacy, University of Heidelberg, Heidelberg, Germany; ³Nuclear Medicine, University of Heidelberg, Heidelberg, Germany; ⁴Radiooncology and radiation therapy, University of Heidelberg, Heidelberg, Germany. Contact e-mail: a.markert@dkfz.de

Aim: Intracellular protein metabolism involves both synthesis as well as degradation of proteins (1). The 26S proteasome is involved in cell cycle control and tumor growth by degradation of ubiquitinated proteins. Proteasome inhibition constitutes an alternative therapeutic strategy against hematological malignancies and a variety of solid tumors. Bortezomib (PS-341) is a highly selective and reversible inhibitor of the 26S proteasome and the first clinically approved proteasome inhibitor. Bortezomib disrupts the equilibrium between protein biosynthesis and protein degradation which ultimately results in apoptosis triggered through the unfolded protein response (2). Here we determined the effect of a concentration range of Bortezomib on rat Morris hepatoma (MH3924A) cells in vitro and in vivo. **Methods:** MH3924A cells were exposed to different concentrations of Bortezomib (1nM-1µM) for 12, 24 or 48 hours. Proliferation and metabolism studies were performed by uptake experiments employing 3H-thymidine (TdR), 3H-FDG, 14C-aminoisobutyric acid (AIB) and 3-O-Methyl-D-(3H)glucose. The measurement of apoptosis and the cell cycle analysis were performed employing the Annexin V/Propidium Iodide Assay and FACS. FDG metabolism was investigated in ACI rats bearing MH3924A tumors prior and 1 day after Bortezomib therapy employing PET and 18F-fluorodeoxyglucose (18FDG). **Results:** Bortezomib induced a dose-dependent reduction of proliferation in MH3924A cells associated with an increase of the apoptotic cell fraction. Studies concerning metabolic changes revealed a significant dose-dependent decrease of the AIB uptake after Bortezomib treatment for 48h. The uptake of FDG and Glucose was initially increased, but after 48h incubation the uptake decreased by 80% (FDG) and by 4% (Glucose). Furthermore, MH3924A cells exposed to 100nM Bortezomib for 12h and 24h accumulated in the G2/M phase of the cell. In vivo, a dose-dependent decrease of FDG uptake was observed 1 day after Bortezomib therapy. **Conclusions:** Bortezomib induced strong antiproliferative effects on rat Morris hepatoma cells. These effects associated with an induction of apoptosis and cell cycle arrest in vitro and changes in metabolism in vitro and in vivo. **References:** 1. The proteasomal and apoptotic phenotype determine bortezomib sensitivity of non-small lung cancer cells. Vortmann, J. et al. *Molecular Cancer* (2007) 2. Characterization of the ubiquitin-proteasome system in bortezomib-adapted cells. Rückrich, T. et al. *Leukemia* (2009)

Presentation Number **0518B**

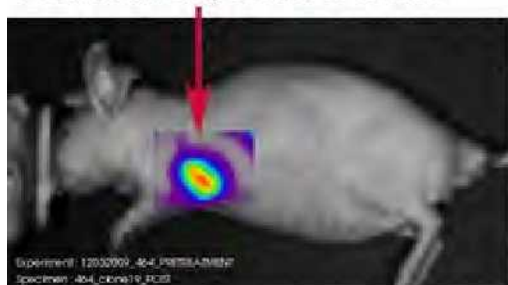
Poster Session 4b: Imaging Molecular and/or Cellular Processes & Drug and/or Radiation Therapy

Optical Imaging with a HER2-targeted Affibody can monitor Hsp90 treatment response in a xenograft mouse model

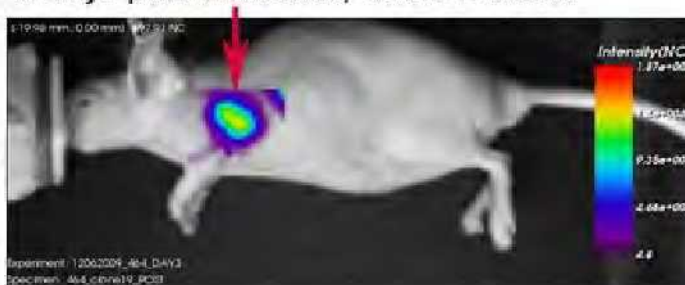
Stephanie M. Van de Ven^{1,3}, **Sjoerd G. Elias**^{5,3}, **Carmel T. Chan**^{2,3}, **Zheng Miao**^{2,3}, **Zhen Cheng**^{2,3}, **Abhijit De**^{2,3}, **Sanjiv S. Gambhir**^{3,4},
¹Radiology, University Medical Center Utrecht, Utrecht, Netherlands; ²Radiology, Stanford University Medical Center, Stanford, CA, USA; ³Molecular Imaging Program at Stanford (MIPS), Stanford University Medical Center, Stanford, CA, USA; ⁴Bioengineering, Stanford University, Stanford, CA, USA; ⁵Julius Center for Health Sciences and Primary Care, University Medical Center Utrecht, Utrecht, Netherlands. Contact e-mail: s.m.w.y.vandeven-2@umcutrecht.nl

Aim: The goal of this study was to determine if fluorescence imaging with a HER2-targeted affibody can be used for non-invasive and repetitive imaging of HER2 expression and monitoring of the Hsp90 treatment effect on HER2 expression in human breast cancer xenografts in mouse models. **Methods:** MCF7 parental cells and two clones (A and B) transfected with HER2 were used for characterization by flow cytometry and western blotting, and to establish human breast cancer xenografts in nude mice. Anti-HER2 affibody (ZHER2:342) was labeled with AlexaFluor680 for optical imaging studies. Mice received either 120 mg/kg of the Hsp90 inhibitor 17-DMAG in 4 doses at 12 hour intervals i.p. (n=10), or PBS as a carrier control in a similar dosing scheme (n=5). Time-resolved fluorescence optical images were obtained at 4 different days: pre-treatment at day -1, and post-treatment at day 3, 6, and 9. On each imaging day optical images were acquired pre- and 5 hours post-injection of 500 pmol of Affibody-AlexaFluor680 in a volume of 150 μ l via tail vein. Mice were sacrificed at day 9 and tumors were excised to correlate in vivo optical imaging signal with ex vivo HER2 levels by western blot. **Results:** Cell culture studies showed that HER2 expression was dependent on 17-DMAG dose. In vivo optical imaging signal was reduced by 21% in Clone B tumors (p=0.016) and by 13% in MCF7 parental tumors (p=0.063) at 3 days after 17-DMAG treatment; optical imaging signal recovered in both tumor types at day 6-9 after 17-DMAG treatment. In the carrier group no significant signal reduction was observed. Pearson correlation coefficient of in vivo optical imaging signal with ex vivo HER2 levels ranged from 0.74 to 0.89. **Conclusion:** Optical imaging with an affibody can be used to non-invasively monitor changes in HER2 expression in vivo in response to treatment with an Hsp90 inhibitor. This work supports the use of pre-clinical models to monitor drug efficacy in a low-cost high-throughput fashion with optical imaging.

Pretreatment; Clone B tumor



3 Days post treatment; Clone B tumor



Presentation Number **0519B**

Poster Session 4b: Imaging Molecular and/or Cellular Processes & Drug and/or Radiation Therapy

Effect of the proteasome inhibitor Bortezomib on gene expression and metabolism of anaplastic thyroid carcinoma

Annette Altmann^{1,2}, **Tilman Schoening**³, **Annette Markert**², **Vasileios Askoxylakis**^{4,1}, **Uwe Haberkorn**^{1,2}, ¹*Nuclearmedicine, University of Heidelberg, Heidelberg, Germany;* ²*Clinical Cooperation Unit nuclearmedicine, DKFZ, Heidelberg, Germany;* ³*Clinical Pharmacy, University of Heidelberg, Heidelberg, Germany;* ⁴*Radiooncology and Radiation Therapy, University of Heidelberg, Heidelberg, Germany.* Contact e-mail: a.altmann@dkfz.de

Aim: The ubiquitin-proteasome pathway plays a critical role in the regulated degradation of proteins involved in cell cycle control and tumor growth. Proteasome inhibition has been proposed as a therapy target for the treatment of solid and haematological malignancies and the anticancer activity of specific proteasome inhibitors is currently under investigation. Among these, the inhibitor Bortezomib (PS-341) has been shown to exhibit substantial cytotoxic effect against a broad range of human tumor cells leading to an increase in the intracellular levels of cell-regulatory proteins including the cyclin-dependent kinase inhibitor p21. Employing the human anaplastic thyroid tumor cell lines SW1736 and C643 we investigated the effect of Bortezomib on metabolism, proliferation and gene expression of anaplastic thyroid carcinoma in vitro. **Methods:** C643 and SW1736 tumor cells were exposed to different concentrations of Bortezomib (1nM-1µM) for 12, 24 or 48 hours. Studies on proliferation and metabolism were performed by uptake experiments employing 3H-thymidine (TdR), 3H-FDG, 14C-aminoisobutyric acid (AIB) and 3-O-Methyl-D-(3H)glucose, respectively. The measurement of apoptosis and the cell cycle analysis was performed employing the Annexin V/Propidium Iodide Assay and FACS, respectively. Gene expression was quantified by the Step one plus Real-time PCR System using gene specific probes. **Results:** Bortezomib induced a time- and concentration dependent reduction of the proliferation in C643 and SW1736. After the incubation with 1µM Bortezomib for 48h an almost 100% decrease of the uptake of FDG and AIB was measured in both cell lines, whereas the Glucose uptake significantly increased by 3.8fold and 6.5fold in C643 and SW1736, respectively. In parallel, the apoptotic cell fraction increased up to 99% in C643 cells and up to 77% in SW1736 cells. Moreover, in both cell lines the incubation with 100nM Bortezomib for 12h and 24h induced an almost 2fold increase the G2/M phase cell fraction associated with a decrease in the G1 and S phase fraction of the cell cycle. Gene expression analysis revealed a 13fold and 8.3fold higher expression of the thyroid-specific transcription factor Pax8 and a 6fold and 7.6fold higher expression of p21CIP1/WAF1 in SW1736 and C643 cells, respectively, treated with 100nM Bortezomib for 24h. **Conclusions:** Bortezomib was shown to provide strong antiproliferative effect on anaplastic thyroid carcinoma cells and, therefore, represents a promising therapeutic agent for the treatment of anaplastic thyroid carcinoma.

Presentation Number **0520B**

Poster Session 4b: Imaging Molecular and/or Cellular Processes & Drug and/or Radiation Therapy

Brachytherapy using nano-submicronic ¹⁶⁶Ho particles

Jacqueline Taleb^{1,5}, Brice Mutelet^{3,2}, Luca Maciocco⁴, Sophie Humbert⁸, Pascal Perriat³, David Kryza^{1,6}, Marc F. Janier^{1,6}, Olivier Tillement², Cedric Louis⁵, Kamel Abbas⁷, Federica C. Simonelli⁷, **Claire Billotey**^{1,6}, ¹Laboratoire Creatis-LRMN, Université Claude Bernard Lyon 1, Lyon, France; ²Laboratoire de Physico-Chimie des Matériaux Luminescents, Université Claude Bernard Lyon 1, Villeurbanne, France; ³INSA, Villeurbanne, France; ⁴Advanced Accelerator Applications, St Genis Pouilly, France; ⁵NanoH, Saint-Quentin Fallavier, France; ⁶Hospices Civils de Lyon, Lyon, France; ⁷Institute for Health and Consumer Protection, Joint Research Centre, European Commission, Ispra, Italy; ⁸CERMA, Archamps, France. Contact e-mail: claire.billotey@univ-lyon1.fr

Introduction: Brachytherapy consists in placing radioactive sources inside or next to the area requiring treatment, especially tumor. In this work we used radioactive sub-micro/nanoparticles as brachytherapy agent to enhance homogeneous and intense radio-effect and consequently improve the anti-tumoral effect and decrease the probability of relapse. The aim of this study, carried out in the framework of the Eureka project INBARCA, was to: i) select from 2 different types of ¹⁶⁶Ho nano or sub-micronic particles which one had the most suited intra-tumoral persistence using in vivo imaging; ii) to evaluate efficacy of the selected radio-activated particle on breast tumor xenografts. Materials and Methods: Animals: 13 Fischer rats with double xenograft of murine breast tumor cells including 6 rats used as control. Particles: i) Colloidal suspension of 1.2 nm diameter oxide holmium coated with 1 nm polysiloxane shell labelled with FITC or cyanine 5; ii) 300 nm diameter particles containing about 90% of Ho oxide. Imaging: T2w. seq. with 7T small animal dedicated MR system (Brucker™)-whole body and ex-vivo organ optical imaging with a CDD-Hamamatsu™ system, in vivo whole-body gamma-scintigraphy (Hi-SPECT system-Bioscan™) and ex-vivo gamma-counting of organs with low level activated particles (INBARCA cyclotron-driven activator in JRC-Ispra). Therapeutic test: Once the selection of particles done, an efficacy evaluation was performed. Each 8-10 mm diameter tumour were injected with high level activated particles (low-flux nuclear reactor in NRG-Petten), at day 7 after tumour grafting, with an activity of 15 to 200 MBq, both with a hypodermic syringe and with a high-kinetic injection system (CERMA™) in 7 rats (14 tumours). The volume of the tumours was daily measured and calculated in all rats. Animals were sacrificed at day 14 after tumour grafting. Results: High leaking of colloidal suspension was observed (rapid elimination by urines, without RES uptake). In contrast, 300 nm particles had a high intro-tumor persistence as confirmed by ex-vivo gamma counting, and were therefore used for the therapeutic test. In 9/12 tumours, growth of tumour after injection of Ho particles at D11 was dramatically inhibited in contrast to control rats. Conclusion: Promising efficacy effects were demonstrated with 300 nm particles in a xenograft tumor of breast cancer. These particles were selected thanks to their high biodistribution evaluated by in vivo imaging. Colloidal ¹⁶⁶Ho particles suspension open perspectives in the field of targeted curietherapy, with a favourable biodistribution.

Presentation Number **0521B**

Poster Session 4b: Imaging Molecular and/or Cellular Processes & Drug and/or Radiation Therapy

The Auger Electron-Emitting Radioimmunoconjugate, ^{111}In -AHT, Causes Satellite DNA Lesions Grouped Around Pre-existing γH2AX Foci

Bart Cornelissen, Philip D. Allen, Sean Smart, Katherine A. Vallis, Gray institute for radiation oncology and biology, University of Oxford, Oxford, United Kingdom. Contact e-mail: bart.cornelissen@rob.ox.ac.uk

Background: ^{111}In -DTPA-anti- γH2AX -Tat (^{111}In -AHT), a radioimmunoconjugate directed against the DNA damage repair protein, γH2AX , has been developed for SPECT imaging and Auger electron radiotherapy. γH2AX accumulates in foci at sites of DNA double-strand breaks (DNA Dsb). We have shown that AHT colocalizes with γH2AX foci that form following exposure of cells to X-irradiation (IR) or bleomycin, resulting in amplification of pre-existing DNA damage and reduced clonogenic survival. We hypothesize that following binding of ^{111}In -AHT to γH2AX , the Auger electrons that it emits, having a range of only a few nm, cause additional DNA damage in the immediate vicinity of the initial γH2AX focus. Methods: MDA-MB-231/H2N cells were exposed to ^{111}In -AHT or ^{111}In -DTPA-mouseIgG-Tat, a non-specific control construct (2.5 $\mu\text{g}/\text{mL}$; 6 MBq/ μg), for 2 h following IR (4 Gy) or in combination with bleomycin (20 mg/mL). Cells were fixed, permeabilized, stained for γH2AX and mounted with the nuclear stain, DAPI. Z-stacks, acquired using confocal fluorescence microscopy, were used to construct 3D images for evaluation of spatial distribution of γH2AX foci within nuclei. Image-analysis was performed using MATLAB. γH2AX foci were segmented using an algorithm for finding local maxima in a 3D environment. Nuclei were segmented by applying a Gaussian blur and an intensity threshold on the DAPI signal. To determine whether γH2AX foci were grouped together, Ripley's K-function was used. This measures how much the distribution of objects differs from a random distribution, in this case by comparing the local density of foci around a γH2AX focus with the overall density, dubbed the "K-value". A correction is built in for edge-effects at the interface of the nucleus with the cytoplasm. Monte-Carlo simulation was used to determine the statistical significance of K-values. Results: ^{111}In -AHT plus IR and ^{111}In -AHT plus bleomycin resulted in a significant reduction in the P-values of K ($P < 0.0001$), indicating that foci are distributed in non-random groups following these combinations. No clustering was observed when cells were exposed to ^{111}In -AHT only or following ^{111}In -DTPA-mouseIgG-Tat in combination with IR or bleomycin ($P > 0.05$). Conclusion: Auger electron therapy with ^{111}In -AHT produces groups of DNA dsb around the target epitope, consistent with the hypothesis that it causes local amplification of pre-existing DNA damage.

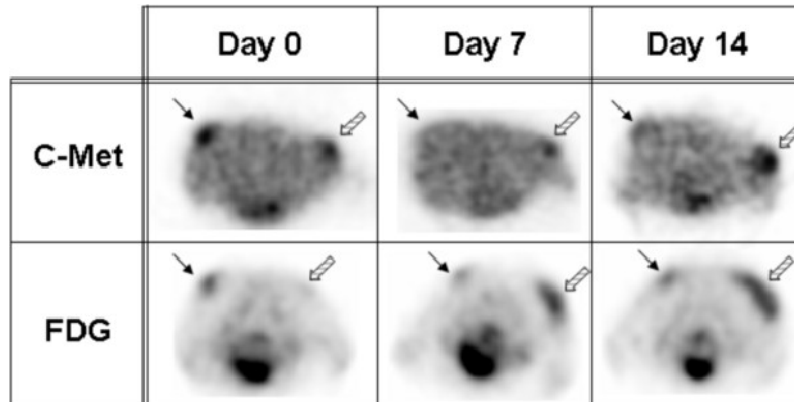
Presentation Number **0522B**

Poster Session 4b: Imaging Molecular and/or Cellular Processes & Drug and/or Radiation Therapy

Quantitative Follow-Up and Resistance Monitoring of ER+/ER α -Knockdown Murine Breast Tumors under Hormonotherapy using ¹⁸F-FDG and ¹¹C-Methionine PET

Michel Paquette¹, Sebastien Tremblay¹, Francois Benard², Roger Lecomte¹, ¹Nuclear Medicine and Radiobiology, Université de Sherbrooke, Sherbrooke, QC, Canada; ²Radiology, University of British Columbia, Vancouver, BC, Canada. Contact e-mail: michel.paquette@usherbrooke.ca

MC7-L1 murine breast adenocarcinoma (Estrogen Receptor +; ER+) received an shRNA sequence targeting the ER α gene by stable lentiviral infection to create a MC7-L1 ER α -Knockdown (ER α -KD) cell line. The new phenotype was confirmed by immunoblotting (~75% protein expression) and saturation curve (~50% binding). Both cell lines (ER+ and ER α -KD) were implanted in the axillary area of Balb-c mice and grown for 19-22 days (up to 3-4 mm diameter). Each mouse was then scanned using a LabPET4 scanner at days 0, 7 and 14 using either ¹⁸F-FDG or ¹¹C-Methionine (C-Met), both tracers at doses between 18 and 30 MBq. A 15-min static image was acquired 30 min after FDG injection, and a 20-min static image was obtained 10 min after C-Met injection. Mice received either 0.5 mg Fulvestrant by subcutaneous injection or 5 mg/kg/day Letrozole per os; a third group received nothing to monitor the normal tumor growth and uptake during the follow-up period. At the end of each scan sequence, a quantitative phantom the approximate size of a mouse (24.6 ml) was filled with 18-25 MBq FDG and scanned for 9 minutes as a calibration standard. Quantitative measurements allowed calculation of the %ID/g of each tumor. While both tumor types showed a similar increase in FDG and C-Met uptake over 14 days without treatment (p > 0.17), there were significant uptake differences at days 7 (p < 0.05) and 14 (p < 0.01) with either Fulvestrant or Letrozole treatments. Uptake stayed stable or increased slightly for ER+ tumors under treatment, but ER α -KD tumors were unaffected by the therapy (p > 0.08). Hence, this ER+/ER α -KD tumor-bearing mouse model could serve as a hormone sensitive/resistant preclinical tool to test new estrogen-dependent therapies. These results suggest that a loss of ER expression as induced by specific knockdown of the ER α gene may be partly responsible for hormone therapy resistance.



Representative transaxial slices of a ER+/ER α KD tumor-bearing mouse scanned with either FDG or ¹¹C-Methionine (C-Met) PET, receiving a 0.5 mg Fulvestrant treatment. → = ER+; ⇨ = ER α KD

%ID/g of FDG and C-Met of ER+ and ER α KD tumors with different treatments

FDG	Control	Fulvestrant	Letrozole	C-Met	Control	Fulvestrant	Letrozole
ER+ Day 0	2.3 ± 0.1%	1.1 ± 0.0%	1.4 ± 0.0%	ER+ Day 0	0.6 ± 0.1%	0.8 ± 0.1%	1.0 ± 0.3%
ER+ Day 7	2.6 ± 0.3%	1.9 ± 0.4%	2.4 ± 0.5%	ER+ Day 7	1.1 ± 0.2%	0.5 ± 0.1%	0.7 ± 0.1%
ER+ Day 14	3.7 ± 0.4%	2.6 ± 0.6%	3.8 ± 0.7%	ER+ Day 14	1.9 ± 0.2%	0.6 ± 0.1%	0.9 ± 0.5%
ER α KD Day 0	2.6 ± 0.1%	2.0 ± 0.1%	1.6 ± 0.4%	ER α KD Day 0	0.6 ± 0.2%	0.8 ± 0.3%	1.3 ± 0.7%
ER α KD Day 7	3.2 ± 0.3%	4.0 ± 0.5%	3.5 ± 0.1%	ER α KD Day 7	1.3 ± 0.4%	0.9 ± 0.1%	1.3 ± 0.5%
ER α KD Day 14	4.1 ± 0.9%	4.6 ± 0.3%	5.0 ± 0.3%	ER α KD Day 14	2.0 ± 0.2%	1.3 ± 0.1%	2.1 ± 0.9%

Presentation Number **0523B**

Poster Session 4b: Imaging Molecular and/or Cellular Processes & Drug and/or Radiation Therapy

Mirtazapine Postpones Tumor Growth and Prolongs Survival via Overexpression of Interleukin-12 and Serotonin in CT26/luc Tumor-Bearing Animal Model

Chieh Yin Tung¹, Chun-Kai Fang^{1,2}, Hong-Wen Chen³, Ya-Fang Chang¹, Jeng-Jong Hwang¹, ¹*Biomedical Imaging and Radiological Sciences, National Yang-Ming University, Taipei, Taiwan;* ²*Dept of Psychiatry & Center of Suicide Prevention, Mackay Memorial Hospital, Taipei, Taiwan;* ³*Dept of Radiation Oncology & Hospice Palliative Care Center, Mackay Memorial Hospital, Taipei, Taiwan.*
Contact e-mail: tung0920@gmail.com

Mirtazapine, a norepinephrine and specific serotonergic antidepressant, is often used in cancer patients for the treatment of depression and related symptoms. The effectiveness of mirtazapine on cancer patients with depression, however, has never been elucidated. A murine colon carcinoma (CT26/luc)-bearing mouse model, as the mimic of cancer patients, was established to explore the mechanism of mirtazapine effect. We hypothesized the tumor growth inhibition by mirtazapine was via evoked immune system and the recovery of serotonin level in the brain. BALB/c mice were treated with 10 mg/kg/d mirtazapine by gavage before (named as 'always' in contrast to 'never', which had no mirtazapine treatment), concurrent and after tumor inoculation, respectively. Tumor growth was monitored with both caliper and bioluminescent imaging. Serum interleukine-12 (sIL-12) was assayed once a week. Brain serotonin (5-HT) level was evaluated with ex vivo autoradiography ([¹²³I]ADAM) at the 3rd week after tumor inoculation. Overall survival was calculated. Significant tumor growth inhibition was found in mice treated with mirtazapine (p<0.001 for always and concurrent v.s. never; after v.s. never, p<0.05). The survival also showed the similar results (p<0.001 for always and concurrent v.s. never; after v.s. never, p<0.01). The sIL-12 level was significantly and rapidly elevated in always, concurrent, and after groups, with the highest expression in the always as compared with never and wild-type (no tumor and mirtazapine). Ex vivo autoradiography also showed high uptake of [¹²³I]ADAM, a serotonin transporter imaging radiopharmaceutical, in mirtazapine-treated mice. This study showed that mirtazapine could postpone the tumor progression effectively and prolong the survival of tumor-bearing mice. The mechanism might via the elevation of IL-12 due to the evoke of immune system and the overexpression of 5-HT in the brain. (This study was supported by a grant VGHUST98-P6-39 from the University System of Taiwan.)

Presentation Number **0524B**

Poster Session 4b: Imaging Molecular and/or Cellular Processes & Drug and/or Radiation Therapy

Metastasis Suppress by Liposomal β -Sitosterol on CT26/luc Colon Carcinoma via Inhibition of MMP-9 and Evoke of Immune System

Chia-Fen Lee¹, Chih-Yuan Lin¹, Yun-Long Tseng², Jeng-Jong Hwang¹, ¹Department of Biomedical Imaging and Radiological Sciences, National Yang-Ming University, Taipei, Taiwan; ²Taiwan Liposome Company, Taipei, Taiwan. Contact e-mail: mini827@hotmail.com

To assess the anticancer effect of liposomal β -sitosterol (LS) on tumor progression and metastasis using mouse CT26/luc-bearing animal model. β -Sitosterol (SITO) was encapsulated in liposomal carrier, and delivered to mice with gavage. The loading capacity of SITO in liposomes was evaluated with HPLC. For in vitro study, cell viability was assessed by MTT, and metastasis ability was determined with invasion assay and western blot. For in vivo study, seven-week-old BALB/c mice were treated with PBS, SITO and LS once a day for 7 days before i.v. injections of CT-26/luc cells, following by twice a week post tumor cell injection. Therapeutic efficacy was monitored with bioluminescent imaging (BLI). On the other hand, both IL-12 and IL-18 cytokines in the intestinal epithelium were determined using a specific ELISA kit. Loading capacity of SITO in liposome was 80%. Surviving fraction of CT26/luc cells treated with 32 μ M free SITO for 72 hr were significantly reduced to 20% vs. 70% of those treated with LS. Both SITO and LS could inhibit MMP-9 expression. In in vivo study, IL-12 and IL-18 levels were significantly increased at 3 h post drug treatment in LS-treated mice as compared with SITO and control groups. BLI also showed significant tumor inhibition in LS-treated group 3 weeks later on post tumor injection as compared with those of control and SITO groups. We concluded that LS significantly reduced lung metastasis of CT26/luc carcinoma in vivo as compared with SITO and control. The mechanism may via the inhibition of mmp-9 expression and evoked immune system.

Presentation Number **0525B**

Poster Session 4b: Imaging Molecular and/or Cellular Processes & Drug and/or Radiation Therapy

Tumor growth inhibition by 111-In octreotide is mediated by the peptide-portion inducing receptor signaling instead of radiation induced injury

Lin Han², Murali K. Ravoori², Sheela P. Singh², Vikas Kundra^{1,2}, ¹Department of Diagnostic Radiology, University of Texas-M.D. Anderson Cancer Center, Houston, TX, USA; ²Department of Experimental Diagnostic Imaging, The University of Texas M. D. Anderson Cancer Center, Houston, TX, USA. Contact e-mail: lhan@mdanderson.org

Objective: To assess whether an 111-In based ligand can be used not only for imaging somatostatin receptor type-2 (SSTR2), but also for therapy of tumors exogenously expressing a SSTR2-based reporter. **Methods:** Mice were injected at three locations with HT1080 tumor cells each consisting of cells transfected with HA-SSTR2, a signaling deficient HA-SSTR2, or control vector. Mice with tumors (N=3) were injected with a large dose of 111-In-octreotide (0.9mCi) and gamma-camera imaging was performed 24 and 48 hours later. Mice were reinjected with 0.9 mCi of 111-In-octreotide and gamma-camera imaging was performed 24 hours later. Tumor size was measured up to day 17. Another group of mice (N=6) was treated daily with a somatostatin analog (octreotide-based, no radioactive label) once tumors became palpable. **Results:** Tumors exogenously expressing HA-SSTR2 had decreased growth upon exposure to 111-In octreotide, as compared to tumors derived from cells transfected with control vector (P<0.05). In contrast, no difference in growth was observed between tumors expressing a signaling deficient HA-SSTR2 compared to tumors derived from cells transfected with control vector. Tumors expressing HA-SSTR2 or signaling deficient HA-SSTR2 were clearly visualized by gamma camera imaging 24 hours after the first dose of 111-In-octreotide and the signal decreased in both tumor types at 48 hours. Signal was greater 24 hours after the second dose of 111-In-octreotide. In contrast, tumors established from cells transfected with a control vector were not detectable by gamma camera imaging. Somatostatin analog (octreotide-based, no radioactive label) treatment significantly inhibited the growth of tumors expressing HA-SSTR2, as compared to tumors derived from cells expressing a signaling deficient HA-SSTR2 or control vector (P<.05). As with 111-In-octreotide, no difference was observed in the growth of tumors derived from cells expressing a signaling deficient HA-SSTR2 versus control vector. **Conclusions:** 111-In octreotide can be used to image exogenous SSTR2-based gene expression. At the high doses of 111-In-octreotide evaluated, tumor growth inhibition was due to the biologic effect of the peptide inducing growth inhibitory signals but not due to radiation from the 111-In label.

Presentation Number **0526B**

Poster Session 4b: Imaging Molecular and/or Cellular Processes & Drug and/or Radiation Therapy

Sorafenib Sensitizes Human Colorectal Cancer to Radiation through inhibition of NF- κ B expression

Ya-Fang Chang¹, Yu-Cheng Kuo^{1,2}, Shih-Hao Su¹, Wei-Chan Lin¹, I-Tsang Chiang¹, Jeng-Jong Hwang¹, ¹Biomedical Imaging & Radiological Sciences, National Yang-Ming University, Taipei, Taiwan; ²Biomedical Imaging & Radiological Science, China Medical University, Taichung, Taiwan. Contact e-mail: d49520006@ym.edu.tw

Radiation therapy plays an important role in neoadjuvant therapy of colorectal cancer. However, only 20% of patients achieved complete response due to radioresistance of the tumor. Several studies suggest that radiation-induced nuclear factor kappa B (NF- κ B) expression is related to tumor tolerance and poor prognosis. Sorafenib is a multikinase inhibitor that can block tumor proliferation and induce apoptosis by inhibition of PI3K and ERK pathways, both have been shown to be linked to NF- κ B pathway. In this study, we investigated whether sorafenib caused enhance the radiosensitivity of colorectal carcinoma, and elucidated the underline mechanism. We established stable clone, HT29/tk-luc, and analyzed the mechanism of radioresistance by colony formation assay, flow cytometry and western blotting assay. For In vivo study, HT29/tk-luc were subcutaneously implanted into the right gluteal back region of NOD/SCID mice. The mice were randomly divided into four groups: control, sorafenib alone (15mg/kg/day), radiation alone (single dose 12Gy), and combination (sorafenib15mg/kg/day + radiation 12 Gy). Bioluminescent imaging (BLI) was performed weekly and microSPECT was used on the 35th day. Mice were then sacrificed and performed immunohistostaining. Sorafenib combined with radiation significantly inhibited the proliferation of tumor growth as compared with sorafenib or radiation alone ($p < 0.001$). Radiation could induced transient elevation of NF- κ B activity, whereas sorafenib suppressed the radiation-induced Bcl-2, Mcl-1, XIAP and MMP-9 through inhibition of NF- κ B expression. BLI and microSPECT/CT further confirmed that the best therapeutic efficacy could be by combination therapy. Our results suggest that sorafenib potentiates the antitumor effects of radiation in colorectal cancer via suppression radiation-induced NF- κ B expression and NF- κ B regulated gene products. Combination treatment of sorafenib and radiation exerted synergistic effect both in vitro and in vivo as shown in this studies.

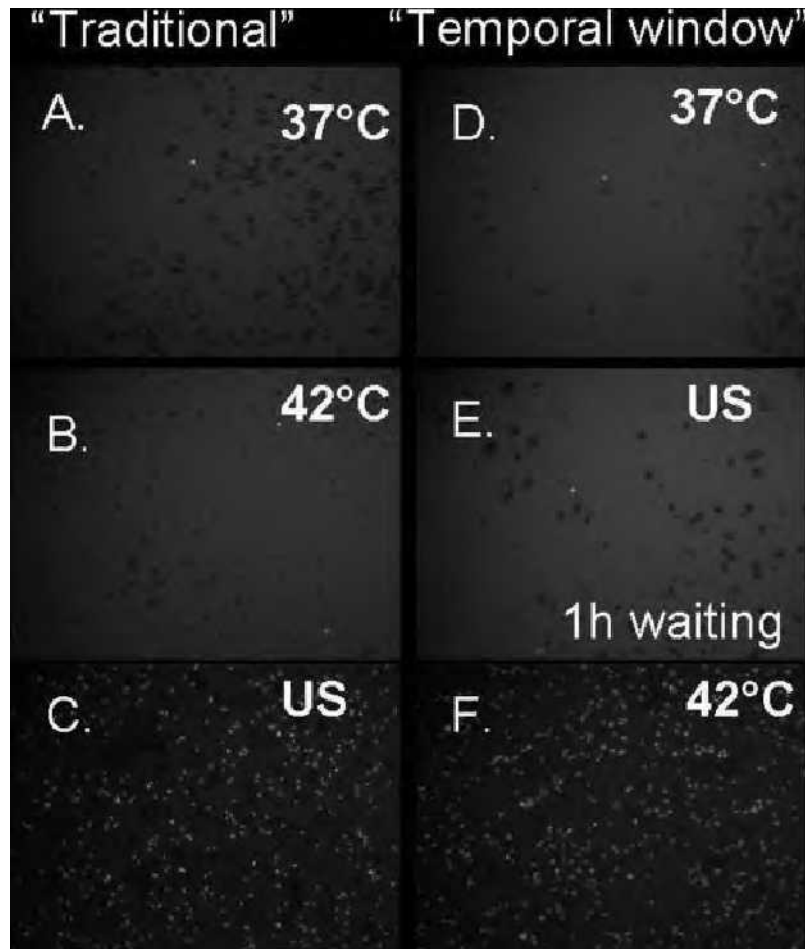
Presentation Number **0527B**

Poster Session 4b: Imaging Molecular and/or Cellular Processes & Drug and/or Radiation Therapy

Long-lasting effect of ultrasound on cell membrane permeability: application to 2-step intracellular small-molecule delivery system using thermosensitive liposomes and cavitation

Anna Yudina¹, **Matthieu Lepetit-Coiffe**¹, Mariska de Smet², Sander Langereis³, Holger Gruell^{2,3}, Chrit Moonen¹, ¹IMF, Bordeaux, France; ²Eindhoven University of Technology, Eindhoven, Netherlands; ³Philips Research Eindhoven, Eindhoven, Netherlands. Contact e-mail: matthieu.lepetit-coiffe@imf.u-bordeaux2.fr

Recent studies have shown the utility of thermosensitive liposomes (TSLs) for local drug release and ultrasound (US) for intracellular delivery via transient pores that are known to spontaneously reseal within seconds. The combination of these two approaches has been validated for the temperature-controlled US-mediated delivery of a cell-impermeable fluorescent model drug. However under certain conditions the effects of US on membrane permeability can last for hours after exposure. The present work confirms the long-lasting impact of US (temporal window) in a 2-step delivery system using TSLs and cavitation. TSLs incorporating 50 μ M TO-PRO-3 (a dye that exhibits fluorescence enhancement upon binding to DNA) were prepared with a phase transition temperature (T_m) of 42°C. C6 rat glioma cells were grown in 2 OptiCell chambers. In OptiCell 1 (traditional) cells were incubated with TSLs and microbubbles at 37°C then heated to 42°C to release TO-PRO-3 (step 1) and US to internalize the dye (step 2). In OptiCell 2 (temporal window) steps 1 and 2 have been reversed and separated in time by 1h. In Opticell 1 the nuclear staining was observed after step 2 only indicating that heating released the dye from the liposomes and US has permeabilized the membrane (Fig. 1, mean intensity 524 \pm 49, 366 \pm 44 cells stained, n=16). Interestingly, similar results regarding dye internalization were obtained when US had preceded the heating (mean intensity 454 \pm 28, 376 \pm 46 cells stained, n=16). Most of the cells were found viable 26h post-US. Thus the long-lasting effect of US on cell membrane permeability has been confirmed by optical read-out for 2-step delivery system (TSLs and cavitation). This may have important implications for in vivo protocols in which membrane permeabilization can be temporally separated from drug carrier administration and drug release to better suit pharmacokinetic / pharmacodynamic properties of liposomes and their cargo.



Presentation Number **0528B**

Poster Session 4b: Imaging Molecular and/or Cellular Processes & Drug and/or Radiation Therapy

[¹⁸F]-FLT PET for non-invasive assessment of tumor sensitivity to chemotherapy: Studies with experimental chemotherapy TP202377 in human cancer xenografts in mice

Mette Munk Jensen^{1,2}, Kamille Dumong Erichsen³, Fredrik Björkling³, Jacob Madsen², Peter Buhl Jensen³, Liselotte Hoejgaard^{1,2}, Maxwell Sehested³, Andreas Kjaer^{1,2}, ¹Cluster for Molecular Imaging, Faculty of Health Sciences, University of Copenhagen, Copenhagen, Denmark; ²Department of Clinical Physiology, Nuclear Medicine & PET, Rigshospitalet, Copenhagen, Denmark; ³TopoTarget A/S, Symbion Science Park, Fruebjergvej 3, Copenhagen, Denmark. Contact e-mail: mettemj@sund.ku.dk

Aim: 3'-deoxy-3'-[¹⁸F]fluorothymidine ([¹⁸F]-FLT) is a tracer used to assess cell proliferation in vivo. The aim of the study was to use [¹⁸F]-FLT positron emission tomography (PET) to study non-invasively early anti-proliferative effects of the experimental chemotherapeutic agent TP202377 in both sensitive and resistant tumors. **Methods:** Xenografts in mice from 3 human cancer cell lines were used: the sensitive A2780 ovary cancer cell line (n=8-12 tumors/group), the induced resistant A2780/Top216 cell line (n=6-8 tumors/group) and the natural resistant SW620 colon cancer cell line (n=10 tumors/group). In vivo uptake of [¹⁸F]-FLT was studied at various time points after TP202377 treatment (40 mg/kg i.v. at 0 hours) was initiated. Baseline FLT scans were made before either TP202377 or vehicle was injected and repeated 6 hours, day 1, and day 5 or 7 after treatment start. Tumor volume was followed with computed tomography (CT) during the experiment. Tracer uptake was quantified using small animal PET/CT. PET scans were acquired over 20 minutes one hour after i.v. injection of [¹⁸F]-FLT and region of interests (ROIs) covering whole tumors were defined on PET/CT images for calculation of standard uptake values (SUV). **Results:** TP202377 (40 mg/kg at 0 hours) caused growth delay at day 7 in the sensitive A2780 tumor model compared to the control group (P=0.001). In the A2780 tumor model TP202377 treatment caused significant decrease in uptake of [¹⁸F]-FLT at 6 hours (-42%; P<0.001) and day 1 (-44%; P<0.001) after treatment start compared to baseline uptake. At day 7 uptake was increased (+16%; P=0.01) compared to baseline. In the control group uptake of [¹⁸F]-FLT did not change. Treatment with TP202377 or vehicle did not influence tumor growth or [¹⁸F]-FLT uptake in the resistant A2780/Top216 and SW620 tumor models. No difference in tumor volume between the TP202377 and control group at day 5 was observed. No changes in [¹⁸F]-FLT uptake following treatment were found. **Conclusion:** Treatment of A2780 xenografts in mice with TP202377 (single dose i.v.) caused a rapid and significant decrease in cell proliferation assessed by [¹⁸F]-FLT PET after 6 hours. Inhibition persisted at day 1; however, cell proliferation had returned to baseline at day 7. In the resistant A2780/Top216 and SW620 tumor models uptake of [¹⁸F]-FLT did not change after treatment. With [¹⁸F]-FLT PET it was possible to distinguish non-invasively between sensitive and resistant tumors already 6 hours after treatment initiation.

Presentation Number **0529B**

Poster Session 4b: Imaging Molecular and/or Cellular Processes & Drug and/or Radiation Therapy

Monitoring Transient Metabolic Processes in Various Photodynamic Therapy Protocols with Dynamic FDG-PET Imaging

Nicole Cauchon, Roger Lecomte, Johan E. van Lier, *Département de médecine nucléaire et radiobiologie, Université de Sherbrooke, Sherbrooke, QC, Canada. Contact e-mail: nicole.cauchon@usherbrooke.ca*

Objectives: Dynamic FDG-PET was used to monitor transient metabolic processes in real-time during tumor treatment by photodynamic therapy (PDT). The tumor response induced by PDT was influenced by critical factors such as physicochemical properties of the photosensitizer (PS) and light dose. The PDT activity of four phthalocyanine-based PS and two different illumination protocols were investigated. **Methods:** Mice (n=4) bearing two mammary tumors received 1 μ mole/kg of four different PS. The following day, the animals were positioned in a LabPET scanner and continuously infused with FDG while dynamic images were acquired for 3 h. Thirty minutes after starting FDG infusion, one tumor was exposed to red light (680 nm, 100 J/cm²) from a laser diode using two light delivery protocols. Images were reconstructed as 2 min frames and tumor, myocardium and blood time-activity curves (TACs) were extracted by ROI analysis. **Results:** FDG TACs during PDT showed distinct transient patterns. Variations in tumor uptake rate and response delay revealed tumor and systemic metabolic response processes that correlate with differences in action mechanism between drugs. TACs were characterized by an initial drop and subsequent recovery of tumor FDG uptake rate except for ZnPcS4. Continuous light delivery induced reduced FDG uptake in the treated tumor after treatment for all drugs. Fractionated light treatment caused no change in FDG uptake pattern in the case of ZnPcS2, but surprisingly, increased FDG tumor uptake rates during and following ZnPcS4-PDT. A steeper drop and lower recovery in FDG TAC was observed during and following the ZnPS3C6-PDT with fractionated light protocol as compare to the continuous protocol. As well, the fractionated light treatment resulted in a 26-day doubling time and 73% tumour cure in contrast to 14 days and 41% for the continuous protocol with ZnPS3C6. Moreover, myocardial FDG TACs showed a reduction in cardiac activity immediately after continuous ZnPcS2- or ZnPcS4-PDT, which correlated with elevated animal mortality. The fractionated light protocol stabilized the cardiac activity during these treatments and increased viability. **Conclusion:** Monitoring real-time tumor response to PDT in mice with dynamic FDG-PET provides a unique means to unveil differences in tumor response mechanisms for different drugs and light delivery protocols. In addition, changes in cardiac FDG uptake rates could serve as an indicator of toxic side-effects due to drug or cancer treatment protocol.

Presentation Number **0530B**

Poster Session 4b: Imaging Molecular and/or Cellular Processes & Drug and/or Radiation Therapy

Early therapy assessment of combined anti-DR5 antibody and abraxane in a triple-negative breast cancer model using diffusion-weighted imaging

Hyunki Kim^{1,4}, Guihua Zhai⁴, Naomi S. Fineberg², Patsy G. Oliver³, Donald J. Buchsbaum³, Kurt R. Zinn^{1,4}, ¹Radiology, University of Alabama, Birmingham, AL, USA; ²Biostatistics, University of Alabama at Birmingham, Birmingham, AL, USA; ³Radiation Oncology, University of Alabama at Birmingham, Birmingham, AL, USA; ⁴Comprehensive Cancer Center, University of Alabama at Birmingham, Birmingham, AL, USA. Contact e-mail: hyunki@uab.edu

Purpose: To measure the early therapy response of an anti-DR5 antibody, TRA-8, in combination with abraxane using diffusion-weighted imaging (DWI) in a triple-negative breast cancer mouse model. Methods: Groups 1-4 of nude mice (n=4 for group 1, n=5 for groups 2-4) bearing subcutaneous triple-negative breast tumors (2LMP) were used; group 1 was untreated (control), while groups 2-4 were treated with abraxane (20mg/kg i.v.), TRA-8 (0.2mg, i.p.), and the combination respectively. TRA-8 was administered on days 0 and 3, while abraxane was administered on days 1 and 5. DWI and anatomical MRI were performed on days 0, 3, and 7, before dosing. Apparent-diffusion coefficient (ADC) of tumor regions and tumor-volume measurements were made among groups 1-4 over 7 days, and analyzed using two-way repeated measures analysis of variance (RM ANOVA). Results: The intra-tumoral ADC changes were $-5\pm 3\%$ (mean \pm SE), $8\pm 5\%$, $5\pm 3\%$, and $12\pm 2\%$ at day 3, and $-4\pm 1\%$, $8\pm 5\%$, $11\pm 6\%$, and $18\pm 3\%$ at day 7, relative to day 0 for groups 1-4, respectively. The tumor-volume changes were $29\pm 21\%$, $66\pm 13\%$, $-7\pm 16\%$, and $6\pm 20\%$ at day 3, and $105\pm 52\%$, $150\pm 38\%$, $19\pm 38\%$, and $-12\pm 42\%$ at day 7, relative to day 0 for groups 1-4, respectively. The ADC increases of groups 2 and 4 were significantly higher than that of the control group ($p=0.047$ and <0.001 , respectively), whereas no difference was detected in tumor-volume change between the control group and any treatment groups ($p>0.05$). Conclusion: DWI measured effective therapy early with combined TRA-8 and abraxane for triple-negative breast-cancer xenografts at 7 days post-treatment, whereas anatomical MRI did not.

Presentation Number **0531B**

Poster Session 4b: Imaging Molecular and/or Cellular Processes & Drug and/or Radiation Therapy

The effect of radionuclide human NIS gene therapy and lentivirus-mediated RNA Interference hexokinase II(HKII) in rat primary aortic vascular smooth muscle cells

Mi-hye Hwang, Jung Eun Kim, Lee You La, Yong Hyun Jeon, Ho Won Lee, Shin Young Jeong, Sang-Woo Lee, Byeong-Cheol Ahn, Jaetae Lee, Department of Nuclear Medicine, School of Medicine, Kyungpook National University, Daegu, Republic of Korea. Contact e-mail: hye6887@nate.com

Objective: Abnormal proliferation and migration of vascular smooth muscle cells are important in pathogenesis of atherosclerosis. Sodium/iodide symporter (NIS) has been used radionuclide therapeutic gene for cancer and RNAi of HKII can be tool inhibit cell proliferation. This study was undertaken to clarify the radionuclide human NIS gene therapy effect of combined lentivirus-mediated HKII-shRNA gene expression on rat primary vascular smooth muscle cells. Methods: Rat vascular smooth muscle cells(VSMCs) were isolated from the thoracic aorta of SD rats and VSMCs were cultured. Cells from the third to fifth passage were used for the experiments. A recombinant adenovirus vector containing hNIS and GFP genes driven by CMV promoter, called Ad-hNIS/GFP, was transduced to VSMCs and VSMC-hNIS/GFP cells. Functional gene expression of hNIS and GFP was confirmed using I-125 uptake and fluorescence microscopy. Recombinant lentivirus producing HKII-shRNA was prepared. The effects of the lentivirus HKII-shRNA on mRNA expression of HKII examined by quantitative RT-PCR analysis. After the adenoviral transduction of NIS gene, VSMCs and cells exposed to I-131 and lentivirus HKII-shRNA, the survival rate of each cells was measured with a clonogenic assay. Result: Cells were infected with Ad-hNIS/GFP at multiplicity of infection (MOI) values of 50. The expression of Ad-NIS/GFP on VSMCs was detected by fluorescence microscopy. Ad-hNIS/GFP was transduced to VSMCs showed 139-fold higher I-125 uptake compared to VSMCs. After transfection of the NIS gene, I-131 treatment resulted decreased survival rate of VSMCs to 30%. The proliferation of VSMCs was further inhibited by the addition of lentivirus HKII-shRNA therapy. Conclusions: Our results suggest that the combined radionuclide hNIS gene therapy and the lentivirus-mediated HKII-shRNA suppressed cell proliferation of VSMC cells. Therefore both therapies can be applied to treat atherosclerosis or prevent recurrence of atherosclerotic process by inhibiting proliferation of vascular smooth muscle cells.

Presentation Number **0532B**

Poster Session 4b: Imaging Molecular and/or Cellular Processes & Drug and/or Radiation Therapy

Volume response of human colorectal cancer after radiation therapy correlated with Ktrans validated by DCE MRI in nude mouse model

Sung Jun Ahn¹, Chan Sik An¹, Woong Sub Koom², Joon Seok Lim¹, Ho-Taek Song¹, Jin-Suck Suh¹, ¹Radiology, College of medicine, Yonsei university, Seoul, Republic of Korea; ²Radiation oncology, College of medicine, Yonsei university, Seoul, Republic of Korea.
Contact e-mail: aahng77@yuhs.ac

Purpose: The purpose of this study was to validate the sequential changes of a MRI perfusion parameter (Ktrans) and volume response of human colorectal cancer after radiation therapy in nude mouse model using dynamic contrast enhanced MRI at 3Tesla. **Material and methods:** Human colon cancer xongraft model was produced by inoculation of DLD-1 cancer cells subcutaneously into the right proximal hind limbs of 5 mice. Tumors were irradiated with 3 fractions of 10 Gy each for 3 weeks. DCE MRI was performed one day before scheduled radiation therapy. Tumor volume response was measured by MRI and calculated at each time point. Toft model analysis was performed for transfer constant Ktrans. Kendall's tau correlation analysis was performed to validate the statistical significance between tumor volume response, Ktrans value, and the range of standard deviation of Ktrans. **Results:** The mean Ktrans value was increased by 2nd radiation therapy, and then decreased. Growing of tumor retarded at the point of peak mean Ktrans value. Pretreatment mean value of Ktrans was significantly correlated with tumor volume response after 2nd radiation therapy ($r=-0.800$, $p=0.0275$). The range of standard deviations of Ktrans is significantly correlated with tumor volume response after 1st radiation therapy ($r=-1.000$, $p=0.0071$). **Conclusion:** The increase of Ktrans values was observed after 2nd radiation therapy and it was correlated with tumor volume response. The evaluation of the pretreatment and serial Ktrans value after radiation therapy would be helpful to validate the tumor response for planning of tailored personal therapy.

Presentation Number **0533B**

Poster Session 4b: Imaging Molecular and/or Cellular Processes & Drug and/or Radiation Therapy

Molecular imaging in evaluation the effect of histone deacetylase (HDAC) inhibitor SAHA in rat glioma

Jung-Wen Kuo¹, **Chun-Yi Wu**¹, **Kuan-Hao Su**¹, **Ren-Shyan Liu**^{1,2}, ¹MAGIC/NRPGM, Nuclear Medicine, Faculty of Medicine, National Yang-Ming University Medical School, Taipei, Taiwan; ²NPCC, Taipei Veterans General Hospital, Taipei, Taiwan. Contact e-mail: g880k13@ym.edu.tw

Objectives: It has been proved that suberoylanilide hydroxamic acid (SAHA), a histone deacetylase (HDAC) inhibitor, can be used as an anticancer drug for brain tumors growth arrest and apoptosis. In this study, 6-(¹⁸F-fluoro-acetamido)-1-hexanoic-anilide (¹⁸F-FAHA) PET imaging is used for monitoring HDAC inhibition efficiency. Furthermore, quantitative estimated constants were used to monitor the progress of the drug treatment. **Methods:** Fischer rats were stereotactically implanted with F98 rat glioma cells into left forebrain. After oral- administrating SAHA (100 mg/kg) twice a day for two days, PET dynamic scans were performed with ¹⁸F-FAHA for 60 min. Arterial blood samples were obtained in 8, 25 min to estimate a input function for quantitative analysis. For estimating the quantitative constants, Image-derived input functions were estimated from the cardiac region from each rat experiment. Three-compartment combined FAHA+FAC (¹⁸F-fluoroacetate) model formed by flux constants, K_1 , k_2 , k_3 and k_4 , was used for quantification. Pathological sections were used to compare the actual anatomical location of the implanting tumors. **Results:** The tumor detected by PET imaging was consistent with the tumor found on the pathological sections. The dynamic uptake curve of the rat brain reached a steady-state quickly after injecting the ¹⁸F-FAHA; whereas the uptake curve of the tumor was still increase. The tumor-to-brain ratio of ¹⁸F-FAHA in vivo was 1.4, respectively. On the other hand, the rate constant k_3 of the tumor decreased from 0.25 min^{-1} to 0.00 min^{-1} substantially when the tumor-to-brain ratio was reduced to 1.2 after SAHA treatment. This reduction can also be found in the uptake activities of other normal tissue. Although the effect of SAHA treatment can be demonstrated as the change of tumor uptake curves or tumor-to-brain ratios, the quantitative results showed a comparatively great magnitude when treating with the SAHA. **Conclusions:** It has been shown that ¹⁸F-FAHA PET imaging can be used for monitoring the HDAC activity quantitatively. The tumor responses monitored by quantitative analysis is more sensitive than monitored using the tumor uptake curve or the tumor-to-brain ratio.

Presentation Number **0534B**

Poster Session 4b: Imaging Molecular and/or Cellular Processes & Drug and/or Radiation Therapy

Monitoring In Vivo behavior of Sonosensitive Liposomes Using Encapsulated Lanthanide MRI Contrast Agents

Robert Fowler¹, **Sigrid L. Fossheim**², **Emannuelle Canet-Soulas**³, **Alexei Moussatov**¹, **Lucie Somaglino**¹, **Sabrina Chesnais**¹, **Cyril Lafon**¹, ¹U556, Inserm, Lyon, France; ²Clavis Pharma ASA, Oslo, Norway; ³Creatis, University Lyon 1, Lyon, France. Contact e-mail: andrew.fowler@inserm.fr

Ultrasound-mediated drug delivery improves the efficacy and safety of anti-tumoral chemotherapeutic drugs such as doxorubicin. The naturally fluorescent properties of doxorubicin make in vitro confirmation of ultrasound-induced drug release straightforward, but this technique is not applicable to in vivo animal models. The aim of this study was to confirm liposomal accumulation and ultrasound triggered release in vivo. PEGylated liposomes with a diameter < 90nm loaded with two different lanthanide-based MRI contrast agents were injected intravenously into rats with subcutaneously implanted tumors. The susceptibility effect of liposomal Dy-DTPA-BMA (Sprodiamide) allows liposome uptake to be monitored by changes in T2 and T2* relaxation times of tumor tissue. The T1 effect of Gd-DTPA-BMA (Gadodiamide) in tumor tissue depends strongly on its accessibility to tissue water and can therefore be used to observe liposomal release by a marked T1 decrease, or an increase in the longitudinal relaxation rate, R1. In these animal experiments, T2* and R1 values calculated from raw MRI data were mapped to images in order to visualize liposomal uptake and release. After injection, the liposomes were allowed to accumulate in the tumor for 48 hours, and the rats were treated with High Intensity Focused Ultrasound (HIFU) to induce the release of contrast agents. HIFU treatment was applied with two stationary confocal transducers, and the rat was passed through the ultrasound focus using a robotic arm controlled by an ultrasonic imaging probe. Figure 1 shows an R1 map of a tumor (A) before HIFU exposure and (B) after. The changes in the R1 maps correspond to a ΔT_1 of ~200ms, and the T2* maps correspond to a ΔT_2^* of approximately ~1ms. The R1 and T2* maps constructed from this series of experiments suggest ultrasound triggered release of contrast agents, and inhomogeneous accumulation in the tumor.

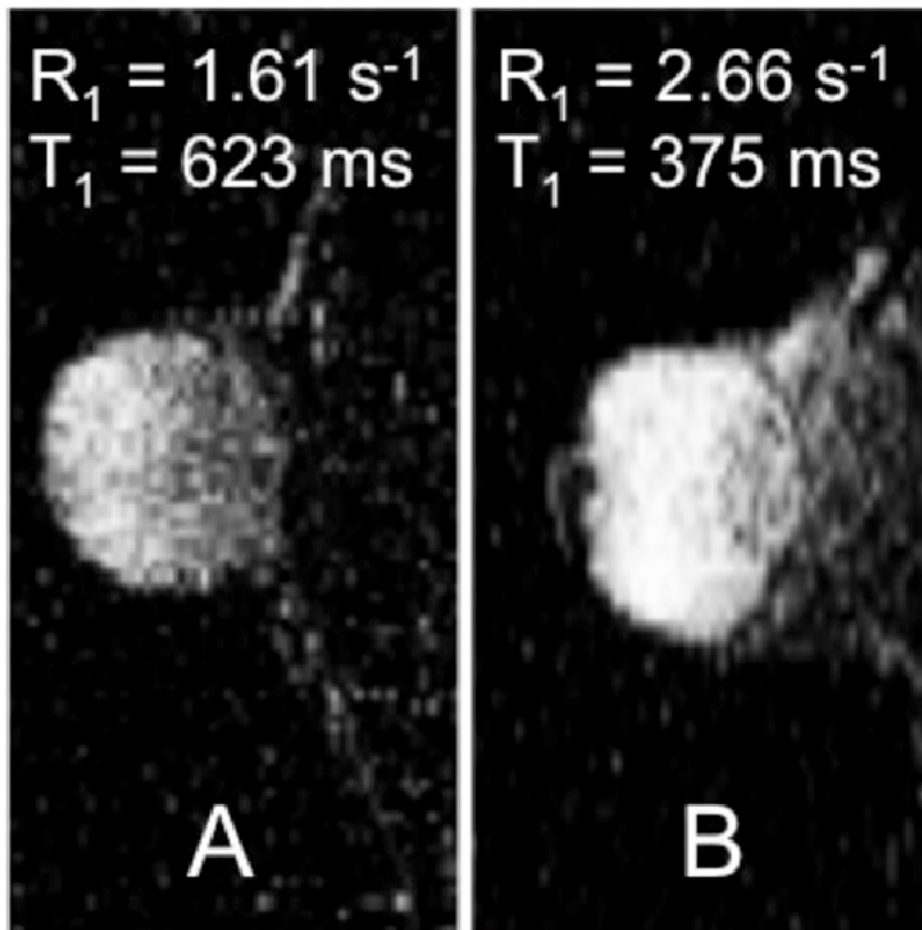


Figure 1: R1 maps of tumor 48 hours post liposome injection (A) before HIFU (B) After HIFU.

Presentation Number **0535B**

Poster Session 4b: Imaging Molecular and/or Cellular Processes & Drug and/or Radiation Therapy

**Impact of FDG PET/CT on management in Takayasu Disease - a clinico-metabolic correlation
Dr Khushboo Gupta, DRM, DNB Nuclear Medicine P.D. Hinduja Hospital***Khushboo Y. Gupta, Nuclear Medicine Dept., P.D.Hinduja Hospital,, Mumbai, India. Contact e-mail: khushg_99@yahoo.com*

AIM The utility of FDG PET in treatment response by assessing intensity of inflammation in aorto-arteritis and its correlation with symptomatic status. **METHOD** We studied a total of 12 patients (age range 9-70yrs, 9females, 3males) within the period April 2005-April 2010 who underwent FDG PET scan at pre treatment stage and during the course of therapy. All 12 patients underwent angiography/ MRI /Doppler studies prior to therapy initiation and prior to PET scans. The active inflammation intensity assessment between the pre and post therapy FDG PET scans was based on qualitative and quantitative methods, with quantitative assessment done using vessel to liver counts ratio and/or SUV method. All 12 patients were also followed up in the post therapy setting with their clinical and symptomatic status, and their drug management protocol. A comparison between metabolic intensity and symptomatic status in pre and post therapy setting was studied. **RESULT** In group I, 5 of the total 12 (35 %) patients demonstrated a decrease in inflammation intensity on FDG PET scan suggesting favorable response to therapy, all of whom also demonstrated relief in symptoms. Drugs were not increased in this group; instead they were either kept at maintenance dose or changed from steroid to immunomodulators. In group II, 3 of 12 (25 %) patients showed persistent inflammation intensity on PET, with persistent symptomatology suggesting no significant response. Steroids and/or immunomodulators were not decreased/stopped in this group. In group III, 3 of 12 (25%) patients PET demonstrated increase in disease status, suggesting no response; with increase in clinical symptoms too. Drugs were stepped up in this group. In group IV, one patient showed a decrease in inflammation on PET with decrease in symptom. However, a different site of disease was demonstrated on PET scan suggesting partial response, for which drugs were not reduced. **CONCLUSION** FDG-PET showed high accuracy in identifying responders from non-responders, correlating well with clinical symptomatic status and aiding the clinician in therapeutic decision. Hence, FDG PET proves to be an useful tool impacting the overall management of Takayasu patients.

Presentation Number **0536B**

Poster Session 4b: Imaging Molecular and/or Cellular Processes & Drug and/or Radiation Therapy

Dynamic Monitoring of Surface Charge-Mediated Sub-Hepatic Distribution of Mesoporous Silica Nanoparticles Using Intravital Multiphoton Microscopy

Shih-Hsun Cheng^{4,1}, Feng Chieh Li³, Chung-Shi Yang², Fan-Gang Tseng⁴, Chen Yuan Dong³, **Leu-Wei Lo**¹, ¹Medical Engineering Research, National Health Research Institutes, "Zhunan Town, Miaoli County", Taiwan; ²Nanomedicine Research, National Health Research Institutes, Zhunan Town, Miaoli County, Taiwan; ³Physics, National Taiwan University, Taipei, Taiwan; ⁴Engineering and System Science, National Tsing Hua University, Hsinchu, Taiwan. Contact e-mail: lwlo@nhri.org.tw

One of the current emerging challenges of nanomedicine in drug delivery is the liver accumulation of nanocarriers. The resided nanoparticles (NPs) in liver post i.v. injection need to be degraded and/or excreted rapidly to avoid detrimental side-effects. Therefore, to define the characteristics of synthetic NPs that govern their biodegradation and/or excretion in vivo would be the prerequisite for advance of nanomedicine in drug delivery for clinic. We hereof report the dynamic monitoring of surface charge-mediated sub-hepatic distribution of mesoporous silica nanoparticles (MSNs) using intravital multiphoton microscopy. MSNs were synthesized with different surface charge by tuning the amount of 3-Aminopropyl-trimethoxysilane (APTMS), to assess the effect of surface charge on sub-hepatic distribution of NPs. Three fluorescent MSNs: FITC-MSN (-12 mV/pH7.4), FITC-MSN-1X (26 mV/pH7.4) and FITC-MSN-3X (45 mV/pH7.4) were synthesized and characterized. With a series of intravital imaging at 3 sec intervals, it clearly demonstrated that within 30 min after i.v. injection, the negative surface-charged FITC-MSNs were uptaken by Kupffer cells, the resident macrophage of the liver; whereas the positive surface-charged FITC-MSN-3X extravasated sinusoid into the hepatic parenchyma for possible hepatobiliary excretion. In current study, we report the dynamic information of sub-hepatic distributions of MSNs, and which could be regulated by surface-charge manipulation.

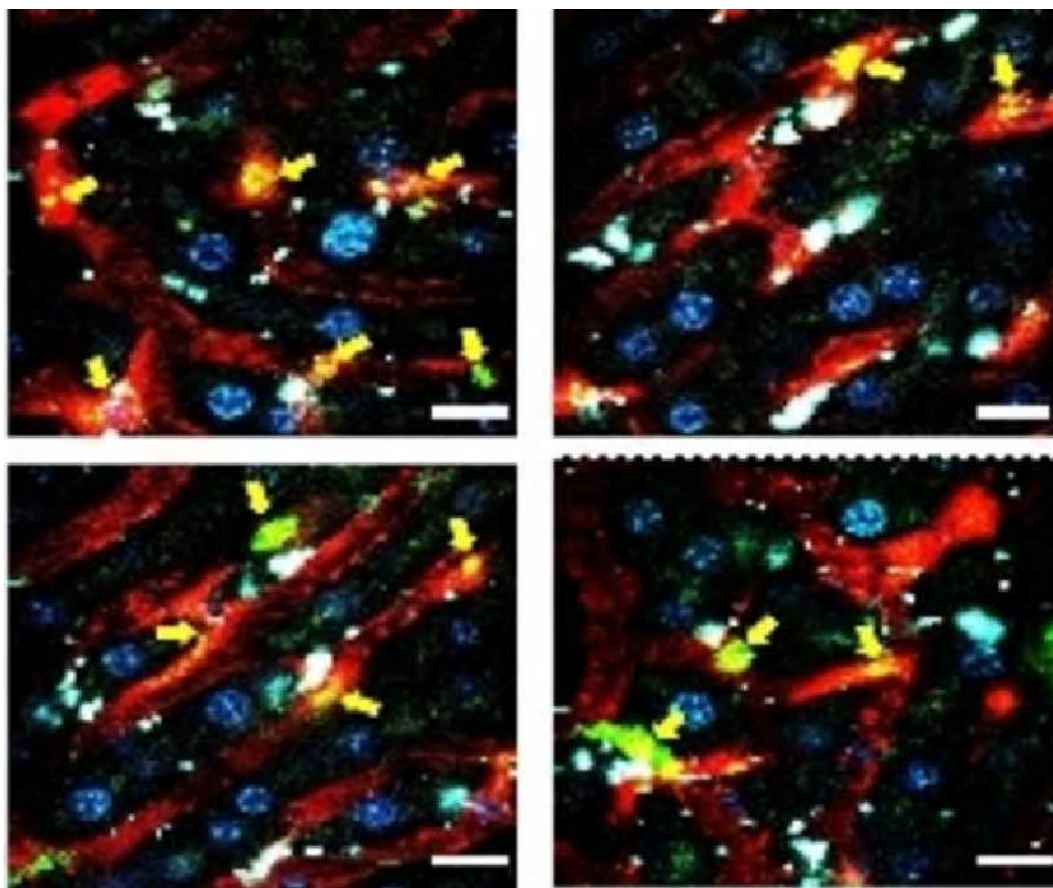


Figure 1. The sub-hepatic distribution of FITC-MSN with negative surface charge at 2 hr post-injection. Yellow arrows indicate the co-localization of FITC-MSN and Kuffer cells. Red: Kupffer cells stained with PE-labeled F4/80 antibody; Green: FITC-MSN; Blue: Nuclei of Hepatocytes stained with Hoechst 33342; Scale bar: 50 micron.

Presentation Number **0500A**

Poster Session 2b: Drug and/or Radiation Therapy & Imaging Molecular and/or Cellular Processes

The therapeutic potential of ^{32}P -chromicphosphate-poly L-lactic acid delayed release seeds on lymph metastases in hepatoma (H22) xenograft models

Lu Liu, Hailin Gao, Jin Sun, Zexuan Yang, Qinghua Wu, Peilin Huang, Radiology, Southeast University, Nanjing, China. Contact e-mail: luliuzhou@sina.com

Objective To investigate the therapeutic potential of ^{32}P -chromicphosphate - poly L-lactic acid (^{32}P -CP-PLLA) delayed release seeds on regional lymph nodes in the KM mice model of hepatoma H22 lymph metastasis. **Methods** Using Chinese KM mice, H22 murine ascites hepatoma cells were injected into right claw pad to establish lymph node metastatic model. Fifty KM mouse models were randomly assigned into groups of two, including ^{32}P -CP-PLLA implantation group and ^{32}P -CP intravenous injection group, with 37 MBq per mouse. In vivo biodistribution was observed from each group. Another thirty models were randomly divided into groups of six through ^{32}P -CP-PLLA implantation or ^{32}P -CP intravenous injection, at doses of 18.5, 37 or 74 MBq per mouse. Dynamic imaging was performed by γ camera and 7.0 T MicroMR. After 16d, all of KM mice were sacrificed to take popliteal lymph node (PLN) and inguinal lymph nodes (ILN). The dose-effect relationship was evaluated by lymph node weighing and LM and electron microscopy scanning. **Results** The results of biodistribution study revealed ^{32}P -CP-PLLA seeds remained inside the tumors. The radioactivity in tumors, right popliteal lymph node (PLN) and right inguinal lymph nodes (ILN) were 17.9 ± 8.3 , 5.8 ± 3.24 and 4.1 ± 3.9 MBq/g, respectively, less in other major organs of a range from 0.0056 to 0.3867 MBq/g. Comparatively, in ^{32}P -CP group, uptake in tumors, right PLN and right ILN were 14.6 ± 5.9 , 16.5 ± 4.0 and 6.1 ± 2.7 MBq/g, respectively, from the range of 0.0547 ~ 0.9501 MBq / g in other major organs. MR imaging in mice showed a oval low signal area. γ imaging demonstrated the seeds were limited and remained in the implantation points in ^{32}P -CP-PLLA group, while in ^{32}P -CP group a initial uptake appeared in tumor and then dispersed with gradually gathered radioactivity in regional lymph nodes (LN). The regional LN in ^{32}P -CP group had higher radioactivity but lower weight than that of ^{32}P -CP-PLLA group at the same dose after 14-day administration. Both groups in these three doses revealed higher doses obtained a better effort to regional LN for showing higher radioactivity and lower weight. **Conclusions** The ^{32}P -CP-PLLA seeds can be lasting inside the tumors and its degradation product ^{32}P -CP can also be used for regional LN treatment. These delayed release seeds may have a good potential for local radionuclide brachytherapy to different tumors and their lymph metastases.

Presentation Number **0501A**

Poster Session 2b: Drug and/or Radiation Therapy & Imaging Molecular and/or Cellular Processes

MicroSPECT/CT Imaging and Comparison of Therapeutic Efficacy between ^{188}Re -Liposomes and Lipo-Dox in a 4T1 Murine Orthotopic Breast Cancer Model

Chi-Mou Liu¹, Wan-Chi Lee¹, Chia-Yu Yu¹, Keng-Li Lan², Gann Ting¹, Te-Wei Lee¹, Chih-Hsien Chang¹, ¹*Institute of Nuclear Energy Research, Taoyuan, Taiwan;* ²*Cancer Center, Taipei Veterans General Hospital, Taipei, Taiwan.* Contact e-mail: chimou@iner.gov.tw

Rhenium-188 (^{188}Re) radiolabeled liposomes (^{188}Re -Liposomes) own the potential in radiotherapy and diagnostic imaging. The Liposome-Doxorubicin (Lipo-DOX) has been widely used for chemotherapy of breast cancer patients. However, there is little information available concerning a comparison of therapeutic efficacy between internal radiotherapy and chemotherapy. This study was to investigate the therapeutic efficacy of ^{188}Re -liposomes versus Lipo-DOX in a 4T1 murine orthotopic breast cancer model by intravenous injection. The highest uptake of ^{188}Re -liposomes in tumor was 3.03 ± 0.29 (%ID/g) at 24 h, and the highest tumor to muscle ratio of ^{188}Re -liposomes was approximately 17.1-fold at 48 h after intravenous administration. MicroSPECT/CT imaging also showed that the highest uptake of ^{188}Re -liposomes was found at 24 h. According to the measurements of body weight and survival rate, the maximum tolerated dose (MTD) of ^{188}Re -liposomes and Lipo-DOX were 37 MBq and 25 mg/kg, respectively. The 4T1 murine tumor-bearing mice ($\sim 300 \text{ mm}^3$) treated with Lipo-DOX (4/5 MTD, 20 mg/kg) showed better tumor growth inhibition and longer survival time than those treated with ^{188}Re -liposomes (4/5 MTD, 29.6 MBq). The median survival time for mice treated with ^{188}Re -liposomes (23 days; $P < 0.05$) and Lipo-DOX (41 days; $P < 0.05$) was better than those from normal saline treated mice (17 days). The results demonstrated that Lipo-DOX is better than ^{188}Re -liposomes for treatment of the breast tumor in the mouse model. Further integration of chemotherapy and radiotherapy is ongoing for treatment of malignant breast cancer in our laboratory.

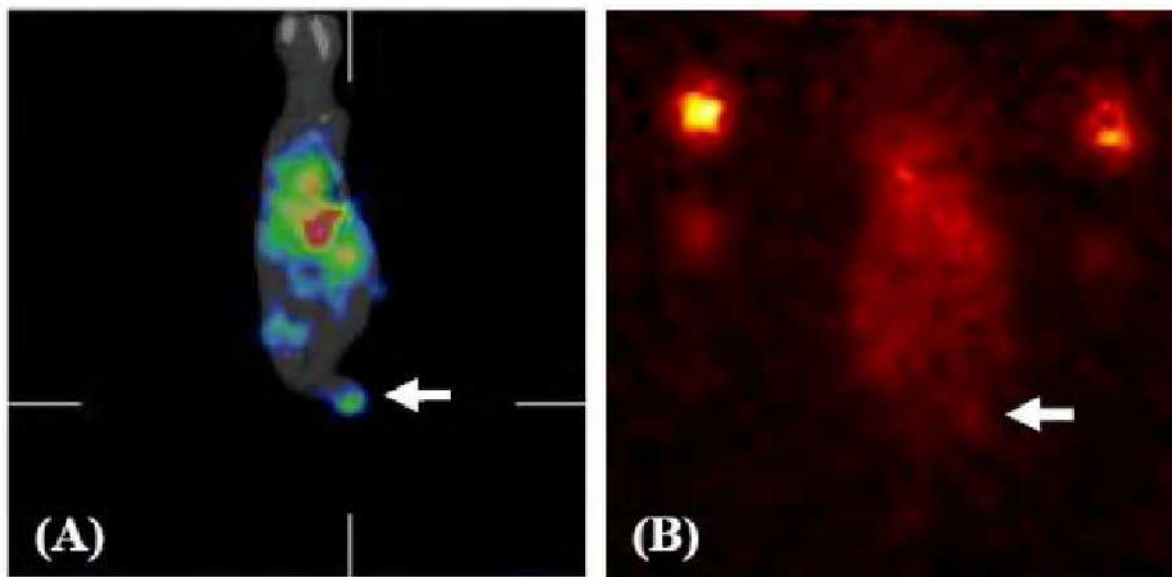


Figure. MicroSPECT/CT images of ^{188}Re -Liposomes targeting 4T1 tumors bearing in BALB/c female mice. The ^{188}Re -Liposomes containing 11.1 MBq of ^{188}Re was administered to each mouse by intravenous injection. The images were acquired at 24 h post injection. (A) tomography; (B) planar image. The arrows indicate the localization of 4T1 tumor in mice.

Presentation Number **0502A**

Poster Session 2b: Drug and/or Radiation Therapy & Imaging Molecular and/or Cellular Processes

Synthesis , Characterization and Application of Polymeric Micelles with pH-Sensitive Surface Charge for Enhanced Theranostics

Yi Li, GuangHui Gao, Seong Woo Kang, Doo Sung Lee, Polymer Science and Engineering, Sungkyunkwan University, Suwon, Republic of Korea. Contact e-mail: liyi@skku.edu

Polymeric micelles as carriers for drugs and imaging agents have been investigated extensively in the past decades. The particles can aggregate passively at the tumor site by the enhanced permeation and retention (EPR) effect due to they are nano-sized. Some smart drug delivery systems (DDS) with PEG as outer shell and pH-sensitive polymer as inner core have been developed based on the fact that the pH at tumor site (6.5-7.0) is lower than that in the blood (7.4). Herein, we designed a nano-sized drug delivery system which has two advantages compared to conventional PEG-based systems. First, the surface of the micelle is neutral at physiological pH and positively charged at tumor pH, that will enhance the uptake of the nanoparticles by cells while reduce the interactions with red blood cell (RBC) during circulation in the blood vessel. Second, compared to PEG, the hydrophilic main chain is biodegradable and the excess hydroxyl group made it possible to be further functionalized by imaging agent and target ligand. The hydrophilic main chain PEG-based Poly(β -amino amine) (PEGAE) is synthesized by the Michael-type addition of PEG diacrylated(PEGDA) and 3-amino-1-propanol(AP). PEGAE is soluble in water and has a pKa value of 6.84 which is between the physiological and tumor pH. Further conjugation of carboxylated PCL (PCL-COOH) and PEGAE resulted in the desired polymer (PEGAE-g-PCL). The polymer was characterized by ^1H NMR and GPC and the micelles were prepared by a film hydration method. Dynamic light scattering (DLS) measurement showed that they are 60nm and 72nm in size at pH 7.4 and 6.5, respectively. Zeta-potential measurement indicated that the micelles are neutral at pH 7.4 and positively charged at pH 6.5. Furthermore, imaging agent (RBITC) and targeting ligand (Folic acid) were conjugated to the backbone. Doxorubicin (DOX) is loaded in the micelle to achieve simultaneous optical imaging and therapy. The multi-functional drug delivery system is promising for enhanced theranostics.

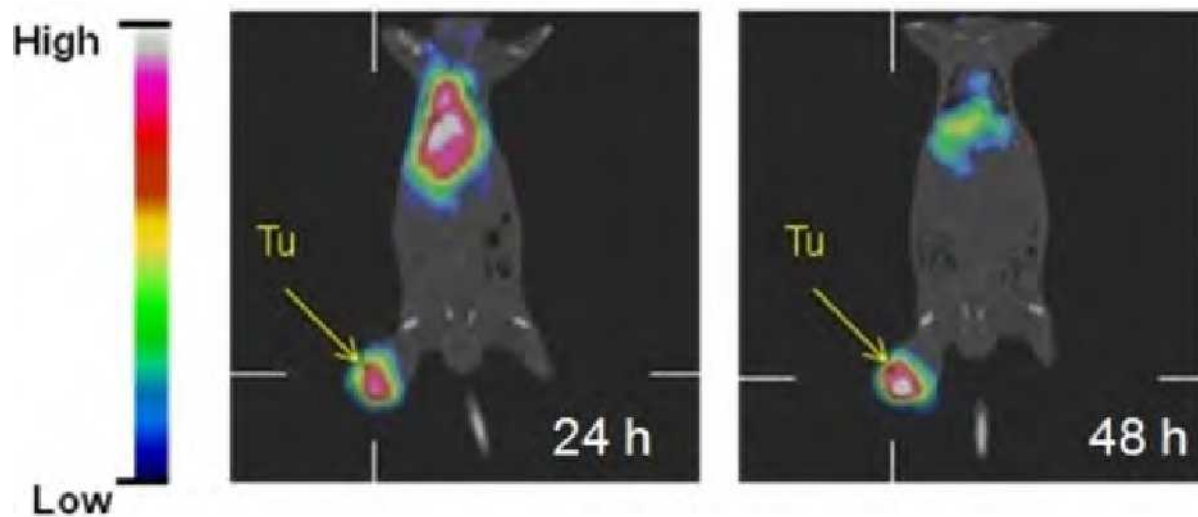
Presentation Number **0503A**

Poster Session 2b: Drug and/or Radiation Therapy & Imaging Molecular and/or Cellular Processes

MicroSPECT/CT imaging and Therapeutic Efficacy of ^{188}Re -Liposomes and 5-FU in LS-174T human Colon Carcinoma Solid Tumor Xenografts

*Chin-Wei Hsu, Chih-Hsien Chang, Ya-Jen Chang, Te-Wei Lee, Gann Ting, Institute of Nuclear Energy Research, Taoyuan, Taiwan.
Contact e-mail: wei0511@iner.gov.tw*

Rhenium-188(^{188}Re) radiolabeled liposomes (^{188}Re -Liposome) own the potential in radiotherapy and diagnostic imaging. The 5-fluorouracil (5-FU) is the first choice of chemotherapy for treating colon cancer patients. However, it has considerable toxicity by intravenous injections or via alimentary treat. The purpose of this study was to investigate the maximum tolerated dose (MTD) of ^{188}Re -Liposome and 5-FU in murine LS-174T human colon adenocarcinoma-bearing nude mice by i.v. injection. MicroSPECT/CT images and biodistribution of ^{188}Re -Liposome were also evaluated. Furthermore, comparison of therapeutic efficacy between ^{188}Re -Liposome and 5-FU in LS-174T colon adenocarcinoma mice was evaluated. The MTD of ^{188}Re -Liposome and 5-FU were 29.6 MBq and 180 mg/kg, respectively. For the biodistribution study, the highest uptake in LS-174T tumor was found to be $11.27\% \pm 0.99\%$ at 24 h, and the tumor to muscle ratio of ^{188}Re -Liposome was $16.07\% \pm 1.91\%$. MicroSPECT/CT imaging indicated the highest uptake of ^{188}Re -liposome in LS-174T tumor in nude mice at 24 h after injection. The imaging analysis showed a positive correlation of tumor targeting of ^{188}Re -liposome between biodistribution and microSPECT/CT imaging. For therapeutic efficacy, the large tumor-bearing mice ($\sim 300 \text{ mm}^3$) treated with radiotherapeutics of ^{188}Re -Liposome (4/5 MTD, 23.7 MBq) showed better tumor growth inhibition and longer survival time than those treated with chemotherapeutics of 5-FU (4/5 MTD, 144 mg/kg). The median survival time for mice treated with ^{188}Re -Liposome (53.78 days; $P < 0.05$) and 5-FU (43.17 days; $P > 0.05$) was better than those from normal saline treated mice (25.88 days). These results suggested the potential and advantage of ^{188}Re - liposomes for imaging and treatment of malignant diseases.



Presentation Number **0504A**

Poster Session 2b: Drug and/or Radiation Therapy & Imaging Molecular and/or Cellular Processes

Development and utilization of a bioluminescent systemic in vivo model of acute lymphoblastic leukemia for the assessment of ABT-263 anti-tumor efficacy

Jonathan Hickson, Scott Ackler, Anatol Oleksijew, Sally Schlessinger, David Frost, Erwin R. Boghaert, Abbott, Abbott Park, IL, USA.
Contact e-mail: jonathan.hickson@abbott.com

To generate preclinical oncology models, murine or human cancer cells can be directly implanted in deep tissues or inoculated intravenously (systemically), allowing cancer cells to disseminate throughout the animal and seed to the organ(s) of preference. The major advantage of these models over subcutaneous inoculation is that for some targets they closer mimic the human disease by allowing for proper microenvironmental interaction and metastasis to clinically relevant sites. Because the tumor is often inaccessible for observation and measurement, such models traditionally require groups of animals to be sacrificed at each time point to determine disease status. As such, routine employment of these types of models is not practical due to the necessary size of the trial and length of the study. Here we report the generation of a human acute lymphoblastic leukemia cell line, RS4;11, that stably expresses the fusion construct of luc2, a firefly luciferase optimized for expression in mammalian cells, and mCherry, a far-red fluorescent protein. Disease burden and progression caused by cells that express this dual reporter can be longitudinally monitored by non-invasive bioluminescent imaging of the animal. Similar to the clinical pathogenesis of acute lymphoblastic leukemia, RS4;11-luc2-mCherry cells engraft in bone marrow, liver, spleen and lung. We have confirmed tumor engraftment at these locations using immunohistochemical techniques. Previously we have shown that RS4;11 cells grown subcutaneously were highly responsive to ABT-263, a small molecule inhibitor of Bcl-2, Bcl-xL, and Bcl-w designed to restore apoptosis, currently in Phase II clinical trials. We utilized the systemic model to assess efficacy of ABT-263 on disseminated cancer cells. While ABT-263 significantly inhibited tumor growth in the bone marrow, the amplitude and durability of the inhibition was reduced in comparison to the response of subcutaneous xenografts. We are currently using this model to gain insight into site-dependent resistance mechanisms to ABT-263, as well as to explore potential synergistic chemotherapy combinations and dosing schedules/regimens in acute lymphoblastic leukemia.

Presentation Number **0505A**

Poster Session 2b: Drug and/or Radiation Therapy & Imaging Molecular and/or Cellular Processes

Chemically Conjugated Affibody-HSA as a Potential Radiotherapeutic Agent for Treatment of HER2-Positive Cancer

Susan Hoppmann, Zheng Miao, Hongguang Liu, Shuanglong Liu, Zhen Cheng, Radiology, Stanford University, Stanford, CA, USA.
Contact e-mail: hoppmann@stanford.edu

Affibody molecules have attracted significant interest as new protein scaffolds for cancer drug development. One major problem with Affibody scaffolds, however, is their extremely high renal uptake when they are labeled with radiometals. The radiation dose to the kidney, a radiation sensitive organ, may likely be a concern for the use of Affibodies as radiotherapeutic agents. To address this issue, the purpose of our study is to explore a simple and generalizable method to chemically conjugate Affibody and human serum albumin (HSA), and to evaluate the potential of the resulting Affibody-HSA bioconjugate for radiotherapy. HSA was thus modified by a site specific conjugation with DOTA-NHS ester and the bifunctional crosslinker Sulfo-SMCC, respectively. The anti-human epidermal growth factor receptor type 2 (HER2) Affibody analog, Ac-Cys-ZHER2:342, was then covalently conjugated with HSA. HER2 Affibody conjugated DOTA-HSA, DOTA-HSA-ZHER2:342, was then radiolabeled with ^{111}In in NH_4OAc buffer (0.25 M, pH=5.5) at 39°C for 1.5 h. In vitro cell uptake studies using SKOV3 cells were performed with and without pre-incubation of Ac-Cys-ZHER2:342 for blocking (n=6). Furthermore ^{111}In -DOTA-HSA-ZHER2:342 (Fig. A) was administered into nude mice bearing SKOV3 tumors via tail-veins for microSPECT-CT imaging (400 μCi ; 24 h and 96 h) and biodistribution studies (50 μCi ; 24 h; n=3). It was found that radiolabeling with ^{111}In resulted in good radiochemical yields (~ 50 %). The radiolabeled protein displayed a significant (1.46 % at 2 h) and specific in vitro cell uptake. MicroSPECT-CT imaging studies showed an excellent tumor uptake and imaging contrast (Fig. B). These results were consistent with the biodistribution data: ^{111}In -DOTA-HSA-ZHER2:342 showed high tumor uptakes (15.41 % ID/g) and liver uptakes (13.32 % ID/g) and very low kidney uptakes (5.76 % ID/g) at 24 h p.i. In conclusion, ^{111}In -DOTA-HSA-ZHER2:342 is a promising SPECT probe for imaging of HER2 cancer. More importantly, DOTA-HSA-ZHER2:342 is suitable for the labeling with radiolanthanides such as ^{177}Lu and ^{90}Y for radiotherapeutic applications.

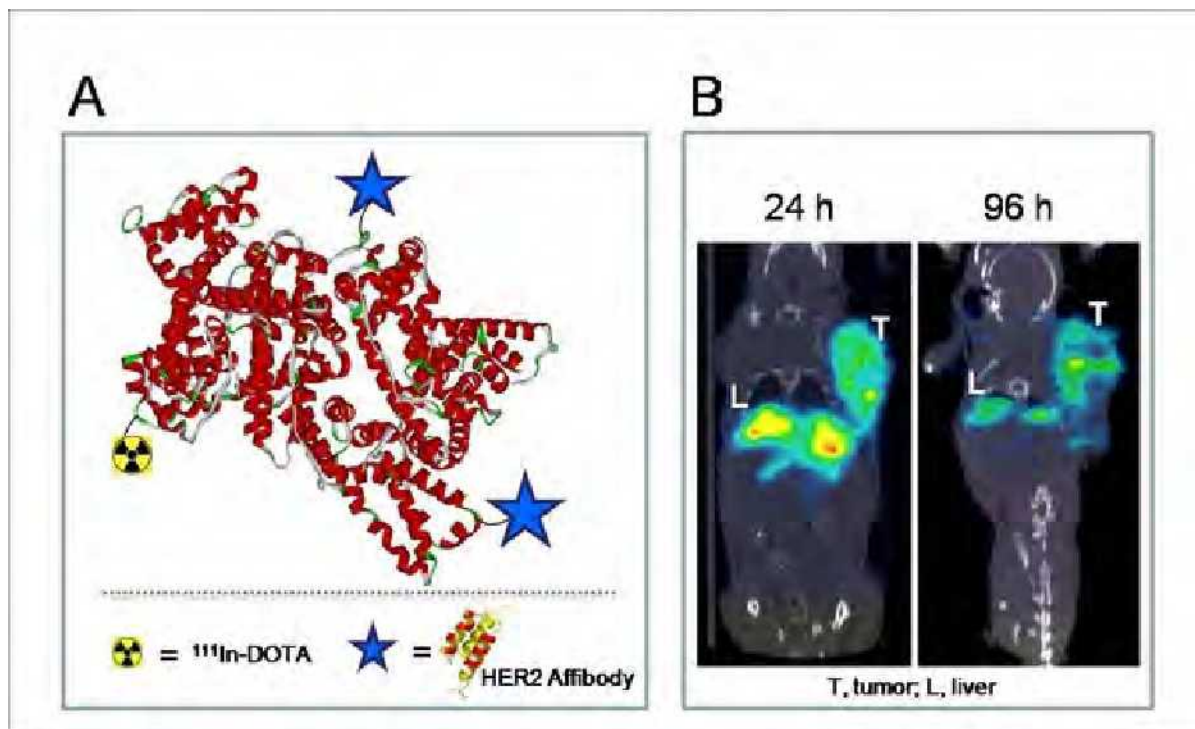


Fig: (A) Illustration of ^{111}In -DOTA-HSA-ZHER2:342. (B) SPECT-CT scan of a SKOV3-tumor bearing mouse.

Presentation Number **0506A**

Poster Session 2b: Drug and/or Radiation Therapy & Imaging Molecular and/or Cellular Processes

Estimation of dosimetry after intravenous and intraperitoneal administration of radiolabeled liposomes in colon carcinoma-bearing mouse models

Yi-Yu Lin¹, **Chih-Hsien Chang**^{1,2}, **Jia-Je Li**¹, **Tsui-Jung Chang**², **Te-Wei Lee**², **C. Allen Chang**¹, **Ming-Hsien Lin**^{1,3}, **Gann Ting**⁴, **Hsin-Ell Wang**¹, ¹Department of Biomedical Imaging and Radiological Sciences, National Yang-Ming University, Taipei, Taiwan; ²Institute of Nuclear Energy Research, Taoyuan, Taiwan; ³Taipei City Hospital Zhongxiao Branch, Taipei, Taiwan; ⁴National Health Research Institutes, Miaoli, Taiwan. Contact e-mail: g39420018@ym.edu.tw

Objective: A dosimetric study was performed to evaluate PEGylated liposomes as carriers of radionuclides (¹⁸⁸Re-liposomes) and radio-chemo-therapeutic drugs (¹⁸⁸Re-labeled doxorubicin (DXR)-encapsulated liposomes, ReDXRL, and ¹¹¹In-labeled vinorelbine (VNB)-encapsulated liposomes, InVNBL) for radionuclide therapy in colon carcinoma-bearing mice. **Methods:** Two CT26 colon carcinoma mouse models, the subcutaneous solid tumor-bearing and tumor/ascites-bearing mice, were employed. Biodistribution studies of ¹⁸⁸Re-liposomes, ReDXRL and InVNBL after intravenous (i.v.) administration in subcutaneous solid tumor mice (protocol A) and intraperitoneal (i.p.) administration in tumor/ascites-bearing mice (protocol B) were performed. The radiation dose to normal tissues and tumors were derived from the results of distribution studies in mice using the OLINDA/EXM program. The maximum administered activity (MAA) of the liposomal drugs considering the radiation dose to the subject was estimated. **Results:** The radiation doses to normal tissues after InVNBL injection in either protocol A or protocol B was lower than those after ¹⁸⁸Re-liposomes and ReDXRL injection, though higher accumulated radioactivity in normal tissues after InVNBL administration was observed. The tumor-to-liver and tumor-to-red marrow radiation dose ratios post InVNBL administration (69 and 164, protocol A; 231 and 210, protocol B) were higher than those post ¹⁸⁸Re-liposomes (8.4 and 66, protocol A; 6.3 and 30, protocol B) and ReDXRL (3.8 and 26, protocol A; 6.5 and 24, protocol B) administration. The critical organ was found red marrow, and thus the red marrow dose defined the MAA of these liposomal drugs. **Conclusion:** Our results suggest that InVNBL may be a safer and more promising radio-chemo-therapeutic liposomal drugs than ¹⁸⁸Re-liposomes and ReDXRL in the two colon carcinoma mouse models.

Estimated radiation doses (mGy/MBq) to tissues post administration of liposomal drugs in colon carcinoma mouse models via treatment protocol A and B.

Tissue	InVNBL		¹⁸⁸ Re-liposomes		ReDXRL	
	Protocol A	Protocol B	Protocol A	Protocol B	Protocol A	Protocol B
Liver	0.091	0.010	0.31	0.24	0.26	0.17
Spleen	0.0029	0.0006	0.26	0.12	0.32	0.26
Kidneys	0.0012	0.0007	0.20	0.09	0.13	0.08
Red Marrow	0.013	0.011	0.039	0.050	0.038	0.046
Total Body	<0.0001	<0.0001	0.096	0.104	0.097	0.100
Tumor	2.1	2.3	2.6	1.5	1.0	1.1
T/LV	69	231	8.4	6.3	3.8	6.5
T/RM	164	210	66	30	26	24

Extrapolated radiation dose for a 70 kg male adult. Tumor-to-normal tissue radiation dose ratios were calculated from the radiation dose in a 300 g tumor weight and tissues. T: tumor; LV: liver; RM: red marrow.

Presentation Number **0507A**

Poster Session 2b: Drug and/or Radiation Therapy & Imaging Molecular and/or Cellular Processes

Securin knockdown enhances fisetin-induced apoptosis in human colorectal cancer cells*Shu-jun Chiu, Chih-Wen Peng, Yi-Chu Yu, Life Science, Life Science, Hualien, Taiwan. Contact e-mail: chiusj@mail.tcu.edu.tw*

Securin has been regarded as a prognostic marker for tumor recurrence as the increased expression of securin correlated with poor prognosis in multiple tumor types, including human colorectal cancer. Fisetin (3, 7, 3, 4-tetrahydroxyflavone), a naturally-occurring flavonoid widely distributed in fruits and vegetables, has previously been shown to exhibit a variety of biological activities, including antioxidant, anti-inflammatory, anti-angiogenic, anti-invasive, and anti-proliferative effects in a wide variety of tumor cells. However, the role of securin on the fisetin-induced apoptosis in human colorectal cancer cells remains unclear. Fisetin treatments (10-100 μM for 24 h) reduced the surviving fraction more significantly in securin-null HCT116 human colorectal cancer cells than securin-wild type cells. The apoptotic hallmarks, the levels of caspase-3 activation and PARP cleavage, were more significantly increased in securin-null HCT116 cells after fisetin treatments as compared with securin-wild type cells. Fisetin treatment (50 μM for 24 h) reduced the cell viability in securin-wild type HCT116 cells after securin knockdown. Transient securin re-expressions reduced fisetin-induced caspase-3 activation and PARP cleavage in securin-null cells. Moreover, securin gene knockdown increased fisetin-induced caspase-3 activation and PARP cleavage in HCT116 p53-null cells. Fisetin treatments (25-100 μM , 24 h) significantly reduced surviving fraction in p53-wild type HCT116 cells as compared with p53-null HCT116 cells. Knockdown of securin decreased the surviving fraction in p53-null HCT116 cells as compared with scrambled siRNA transfected cells. Taken together, we suggest that knockdown of securin could be an effective strategy for the p53-null cancer cells exhibiting highly chemo-resistance and enhance apoptosis in p53-wild type HCT116 colorectal carcinoma cells.

Presentation Number **0509A**

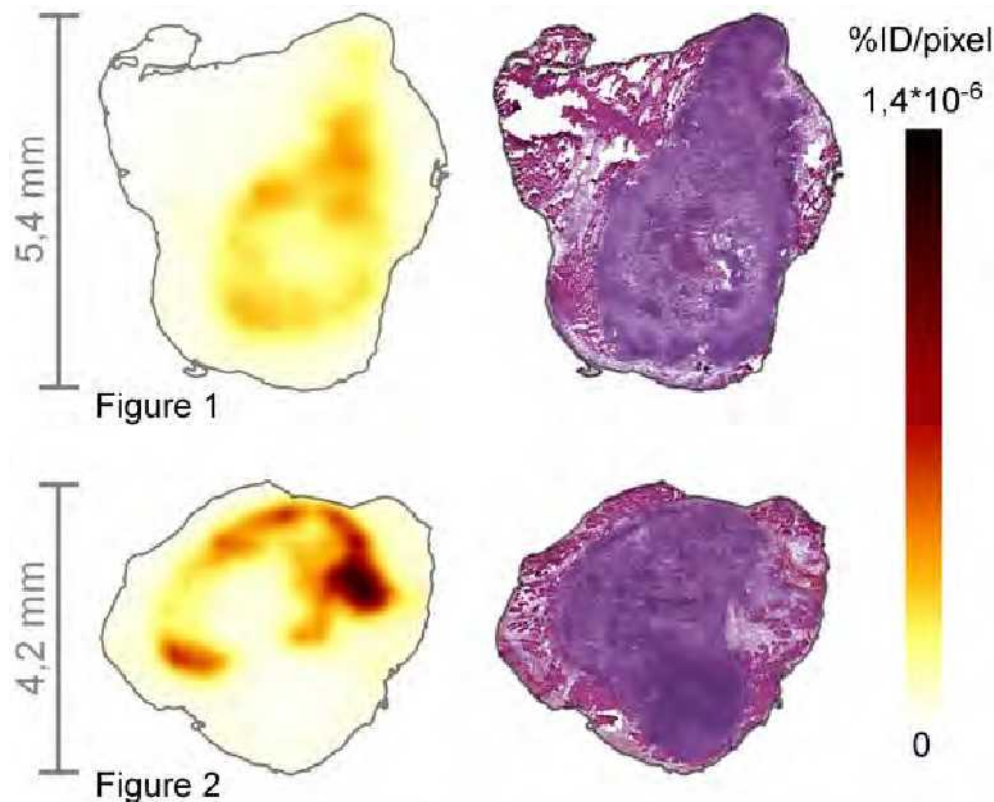
Poster Session 2b: Drug and/or Radiation Therapy & Imaging Molecular and/or Cellular Processes

Ex vivo Imaging of Tumors from a Rat Colon Carcinoma Model for Radioimmunotherapy Using Digital Autoradiography

Anders Orbom¹, Sophie E. Eriksson², Rune Nilsson², Jan Tennvall², Sven-Erik Strand¹, ¹Medical Radiation Physics, Lund University, Lund, Sweden; ²Department of Oncology, Clinical Sciences, Lund University, Lund, Sweden. Contact e-mail: anders.orbom@med.lu.se

Introduction In an ongoing preclinical radioimmunotherapy study, an experimental model has been set up with syngeneic rat colon carcinoma tumors expressing the epitope for the mAb BR96. The intratumoral distribution of the radiolabeled antibody (¹⁷⁷Lu-DOTA-BR96) will have a major impact on the absorbed dose to viable tumor cells and consequently on the therapeutic effect. The purpose of this pilot study was to image the radioactivity distribution in tumor sections from treated animals and compare it to tissue histology.

Methods Thirteen days after inoculation with tumor cells, all animals in the study were injected i.v. with either 50 (n=1), 150 (n=3) or 300 (n=3) MBq/kg ¹⁷⁷Lu-DOTA-BR96. From the two latter cohorts, one animal was sacrificed at each time point (2, 4 and 7 days p.i.). The single animal given 50 MBq/kg was sacrificed at 7 days p.i. Tumors were excised and cryosectioned at 10 μm. The sections were then imaged using a double sided silicon strip detector and subsequently stained with hematoxylin and eosin (H&E). Generated images were scaled to percent of injected dose and stained sections were scanned. **Results** Comparisons between activity distribution and H&E staining revealed very little to no antibody uptake in purely necrotic areas or muscle tissue adjacent to the tumor. Generally, high uptake was seen in the tumor periphery and in areas containing visible vasculature (Fig. 1). Especially at 4 and 7 days p.i., high uptake was seen in areas with sparse and necrotic/apoptotic tumor cells and heavy infiltration of stroma. In some cases, dense areas of viable tumor cells exhibited almost no uptake (Fig. 2). **Conclusion** These preliminary results indicate that ¹⁷⁷Lu-DOTA-BR96 generally distributes to viable tumor cell populations. Vascularization may influence the distribution. The reason why some dense, viable areas have very little uptake will be further investigated in a recently started study using multi isotope imaging to contrast antibody uptake with ¹⁸F-DG and ^{99m}Tc-labelled blood cells.



Digital autoradiography image and H&E staining of tumor section from rat 2 days p.i. of 300 MBq/kg ¹⁷⁷Lu-DOTA-BR96 (Figure 1) or 7 days p.i. of 150 MBq/kg ¹⁷⁷Lu-DOTA-BR96 (Figure 2).

Presentation Number **0510A**

Poster Session 2b: Drug and/or Radiation Therapy & Imaging Molecular and/or Cellular Processes

Therapeutic Effects of Targeted Delivery of Lu-177 to Tumor Vasculature

Zoia Levashova², Arcadius V. Krivoshein¹, Marina Backer¹, **Joseph M. Backer¹**, Francis G. Blankenberg², ¹SibTech, Inc., Brookfield, CT, USA; ²Department of Pediatrics & Division of Nuclear Medicine/Department of Radiology & MIPS, Stanford University, Stanford, CA, USA. Contact e-mail: jbacker@sibtech.com

Our goal is to develop a targeted anti-cancer Lu-177 radiotherapeutic that accumulates in tumor via receptor-mediated uptake by tumor endothelial cells. Due to β -emission with a max depth of 1.5 mm, targeted Lu-177 radiopharmaceutical is expected to be cytotoxic to tumor endothelial cells and to surrounding tumor cells, but not to healthy tissue. In addition to direct killing of tumor cells within a 1.5-mm distance from blood vessels, targeted destruction of tumor vasculature can bring starvation to deeper tumor areas far beyond the areas of Lu-177 uptake, further amplifying the cytotoxic effects of the proposed radiopharmaceutical. Vascular endothelial growth factor receptors (VEGFR) are overexpressed in tumor vasculature, providing opportunities for selective and specific delivery of targeted radiopharmaceuticals. For targeting VEGFR we used scVEGF-PEG-DOTA conjugate, an engineered single-chain (sc) VEGF, site-specifically derivatized with DOTA chelator via a 3.4-kDa PEG linker. The conjugate was previously radiolabeled with Cu-64, Ga-64, and Tc-99m for PET and SPECT imaging of VEGFR (1-3). Biodistribution and clearance studies with scVEGF-PEG-DOTA/Lu-177 indicated that 3.4-kDa PEG linker provides for the optimal ratio of tumor vs. non-specific uptake. ICR-SCID mice, bearing orthotopic human breast cancer xenograft MDA231luc (luciferase-expressing derivative of human MDA-MB-231 breast carcinoma), were injected with 0.5 mCi of scVEGF-PEG-DOTA/Lu-177, given either as bolus dose or as three equal weekly doses. At 4 weeks after the beginning of treatment both regimens resulted in 3 to 4-fold smaller tumors relative to controls. At that time, weight loss (~15%) was observed only for bolus injection. Blood markers of radiotoxicity were within an acceptable range. Further increase in the dose did not lead to larger effects on tumor growth, but increased radiotoxicity. Immunohistochemical analysis indicated that scVEGF-PEG-DOTA/Lu-177 treatment induced widespread apoptosis of tumor cells, virtual elimination of tumor vasculature, and the lack of vascular rebound at the tumor periphery. Taken together, scVEGF-PEG-DOTA/Lu-177 appears to be a promising targeted radiopharmaceutical, deserving further exploration. This work was supported by NIH Grants 1R01 CA131263-01A2 ARRA to FGB, and 1 R43 CA141806-01 to JMB. References 1. Backer et al. Nature Med. 13, 504-9, 2007 2. Levashova et al. Bioconjugate Chem. 19, 1049-54, 2008. 3. Eder et al. Nucl. Med. Biol. In press.

Presentation Number **0511A**

Poster Session 2b: Drug and/or Radiation Therapy & Imaging Molecular and/or Cellular Processes

Both pro-angiogenic and anti-angiogenic cytokines are secreted during radiation-induced senescence of securin-depleted human cancer cells*Yi-Chu Yu, Shu-jun Chiu, Life Science, Life Science, Hualien, Taiwan. Contact e-mail: 98726104@stmail.tcu.edu.tw*

Our previous study showed that depletion of securin induces senescence after irradiation and enhances radiosensitivity in human cancer cells regardless of functional p53 expression. Cellular senescence suppresses cancers by irreversibly arresting cell cycle of damaged cells. Various cellular and environmental factors were known for inducing senescence. Curiously, senescent cells also secrete factors that alter tissue microenvironments. The beneficial and deleterious bystander effects of radiation-induced senescent cancer cells remain unclear. We adopted cytokine antibody arrays to provide a quantitative assessment of factors secreted in the conditioned medium by senescent cells. Radiation-induced senescent securin-null HCT116 human colorectal cancer cell secreted factors associated with pro-angiogenesis and anti-angiogenesis. The cytokine antibody array analysis revealed that radiation-induced senescent cells contained five- to nine-fold higher levels of human angiogenic cytokines and growth factors, VEGF, angiogenin and IGFBP-2, as compared with un-irradiated securin-null HCT116 cells. The senescent cells also showed elevated levels of expression of anti-angiogenic factors, MIF, TIMP-1, TIMP-2, IL-8, GRO- α and TGF- β . Moreover, the gene expression levels of VEGF, GRO- α , IL-8 and TGF- β determined by real-time quantitative RT-PCR were found to be significantly upregulated. Accordingly, TGF- β proteins measured by Western blotting were found to be 1.5-fold upregulated. By using an ELISA-based and a β -galactosidase activity assay, IL-8 and GRO- α were found to have a pro-senescence effect on securin-null HCT116 cells. Our results provide for the first time that radiation-induced senescence of securin-depleted cancer cells produces elevated levels of multiple cytokines, chemokines, growth and angiogenic factors. These findings bring new insight to understand beneficial and deleterious bystander effects exhibited by radiation-induced senescent cancer cells.

Presentation Number **0512A**

Poster Session 2b: Drug and/or Radiation Therapy & Imaging Molecular and/or Cellular Processes

Evaluation of the intra-tumoral accumulation and the radiosensitizer effect of Hybrid Gadolinium Nanoparticles after IV injection

Miladi Imen¹, **Christophe Alric**², **Géraldine Le Duc**³, **Stephane Roux**⁴, **Jacqueline Taleb**¹, **Marc Janier**¹, **Olivier Tillement**², **Claire Billotey**¹, ¹CREATIS-LRMN, Lyon, France; ²LPCML, Lyon, France; ³ESRF, Grenoble, France; ⁴Institut UTINAM, UMR 6213 CNRS-UFC, Besancon, France. Contact e-mail: miladi@creatis.insa-lyon.fr

Purpose: This study aimed to evaluate the radiosensitizer effect of hybrid nanoparticles (NP) with gadolinium oxide core. Thanks to their high density, and their paramagnetic properties, the NP biodistribution after intravenous (IV) injection has been evaluated using MRI in rats, with tumoral grafts of gliosarcoma and breast cancer in order to define which model and which time was the most suited to demonstrate the radiosensitizer effect. **Materials and methods:** Ultrasmall Gadolinium (Gd) hybrid NP, with final size under 5 nm, were suspended in saline. To evaluate the EPR effect in experimental tumors after injection of NP, two animal models were used: -Xenograft: murine model of heterotopic graft of MatBIII Breast cancer -Orthotopic: intra-cerebral graft gliosarcoma 9L murine model Dynamic and static in vivo images were acquired after IV injection using magnetic resonance imaging (MRI 7T for small animals, Bruker™) To evaluate the radiosensitizer effect, rats with gliosarcoma were irradiated after NP IV injection, with Microbeam Radiation Therapy (MRT) at the ESRF with a skin entrance dose of 400Gy. **Results:** -EPR effect: after IV injection, NP were highly accumulated in gliosarcoma tumor (Enhancement contrast ratio EHC= 400%) and for at least 30min. Passive accumulation was observed as early as 4 min after IV injection Passive accumulation of NP was also observed in breast tumors. EHC was about 60% after 3min of IV injection. Accumulation in tumor without necrosis was more important and more sustained than in necrosed tumor (EHC= 50%) -Radiosensitizer effect: after MRT, the IV injection of NP enhances the efficiency of radiotherapy. Survival time after irradiation of rats injected with NP was more prolonged than with rats only irradiated without NP injection **Conclusions and perspectives:** Gd NP can be detected in vivo using dynamic MRI after IV injection. They showed a high tumor to normal tissue ratio. NP accumulation after IV injection is probably related to the neoangiogenesis of the tumor since no accumulation was seen in tumors with necrosis. The EHC in brain tumors was higher than in breast tumors. This passive accumulation provided a "therapeutic window" where the external irradiation could benefit of the maximum of the NP radiosensitizer effect. This permits radiotherapy using these nano-objects, without having recourse to specific targeting of the nanoparticles. Targeting can increase the intra-tumoral concentration of the NP, in particular for the extra-cerebral tumors, and thus probably therapy effectiveness.

Presentation Number **0513A**

Poster Session 2b: Drug and/or Radiation Therapy & Imaging Molecular and/or Cellular Processes

Metallofullerene Nanoparticles Improve Defective Endocytosis to Circumvent Tumor Resistance To Cisplatin

Paul C. Wang¹, Huan Meng², Yuliang Zhao², Xing-jie Liang³, ¹Radiology, Howard University, Washington, DC, USA; ²CAS Key Laboratory for Biomedical Effects of Nanomaterials and Nanosafety, Institute of High Energy Physics, Beijing, China; ³Laboratory of Nanomedicine and Nanosafety, National Center for Nanoscience and Technology of China, Beijing, China. Contact e-mail: pwang@howard.edu

BACKGROUND: As a major chemotherapeutic agent for tumor treatment, cisplatin remains a cornerstone of the present-day chemotherapy regimens against not only epithelial malignancies but also metastatic and advanced malignancies. However, because of high toxicity and easy development of resistance, successful treatment with cisplatin often is limited. To overcome the resistance to cisplatin, we hypothesized, based on our previous findings of mediation of cellular responses by [Gd@C82(OH)22]n nanoparticles, that [Gd@C82(OH)22]n may reverse tumor resistance to cisplatin by reactivating the impaired endocytosis of cisplatin-resistant prostate cancer (CP-r) cells. **MATERIAL AND METHODS:** [Gd@C82(OH)22]n nanoparticles were synthesized and purified. PC-r cells were derived from cisplatin sensitive prostate cancer PC-3-luc cells (PC-s). In vitro, both PC-s and PC-r cells were treated with [Gd@C82(OH)22]n nanoparticles (1-50 μ M) with or without 1 μ g/mL cisplatin. In vivo, both CP-r and CP-s cells were injected in the either side of flanks of athymic nude mice and grew into xenografts. The animals were treated with cisplatin (10 mg/kg, x2/wk) and [Gd@C82(OH)22]n nanoparticles (1.0 μ M/kg, daily), or just cisplatin. **RESULTS:** Exposure of CP-r cells to cisplatin in the presence of nontoxic [Gd@C82(OH)22]n not only decreased the number of surviving CP-r cells but also inhibited growth of the CP-r tumors in mice as measured by optical and MRI methods. Labeling the CP-r cells with transferrin, an endocytotic marker, demonstrated that pretreatment of the CP-r cells with [Gd@C82(OH)22]n enhanced intracellular accumulation of cisplatin in vitro, and formation of cisplatin-DNA adducts by restoring the defective endocytosis of the CP-r cancer cells in vivo. Tumor resistance to cisplatin was circumvented by treatment with a combination of [Gd@C82(OH)22]n with cisplatin both in vitro and in vivo. **CONCLUSION:** The results suggest [Gd@C82(OH)22]n nanoparticles overcome tumor resistance to cisplatin by increasing intracellular accumulation through mechanisms of restoring defective endocytosis. The technology can be extended to other challenges related to multidrug resistance often found in cancer treatments. Using nanomaterials to overcome the drug resistance of malignant tumors could lead to new therapies for cancer patients. This provides a promising chemotherapeutic method to treat tumors at lower, nontoxic dose levels

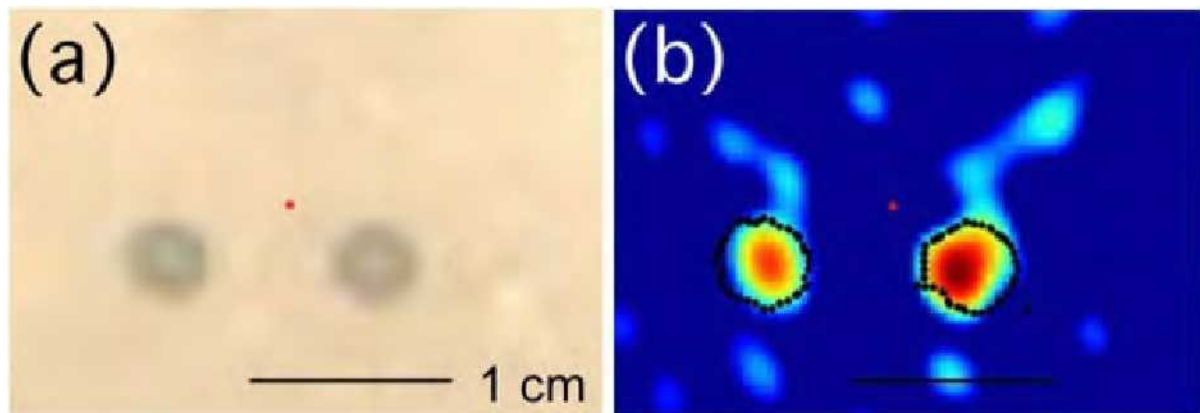
Presentation Number **0514A**

Poster Session 2b: Drug and/or Radiation Therapy & Imaging Molecular and/or Cellular Processes

Adaptive focusing of therapeutic ultrasound on targeted contrast agents

Olivier Couture^{1,3}, **Mathias Fink**^{1,2}, **Mickael Tanter**^{3,1}, ¹Institut Langevin, ESPCI, Paris, France; ²UMR 7587, CNRS, Paris, France; ³ERL979, INSERM, Paris, France. Contact e-mail: olicou@gmail.com

Ultrasound can be used for imaging, but also for therapy through heating, cavitation, local delivery, sonoporation or opening of blood brain barrier. These effects are localized at the focus of the ultrasound system, which is usually determined by the geometry of the acoustic transducers. Using the ability of time-reversal to refocus an amplified ultrasound wave on an arbitrary source, we present a method to restrict energy deposition on zones of specific biomarkers expression. This treatment technique can exploit the various ultrasound contrast agents developed for molecular imaging. Droplets of avidinated-microbubbles were deposited on biotinylated gelatin to mimic targeting. The gel was then immersed in a water tank equipped with an array made of 80 fully-programmable focused transducers working at a 1MHz central frequency. A dedicated disruption imaging sequence was developed to select the echoes from the targeted microbubbles, which were then time-reversed, amplified, elongated and reemitted by the ultrasound array. The resulting pressure field at each point was measured using a scanning hydrophone. Depending on the size of the focal spot, peak pressure field were typically reaching 5 MPa, which is sufficient for therapy. Fig. 1 shows the two colored dots of microbubbles on the gelatin surface. When the time-reversed ultrasound pulses were emitted, the hydrophone scan showed a pressure-increase corresponding to the original pattern formed by the microbubbles. The strong added value of time reversal focusing lies in two key points : first, its ability to focus almost instantaneously (<500 μ s for deep seated targets) a focused therapeutic beam whose shape is automatically mimicking the area containing targeted microbubbles. Secondly, its ability to correct both for tissue aberration along the beam paths and respiratory motion artifacts by simply repeating this adaptive time reversal focusing sequence several thousand times per second. Figure 1: (Left) Photography of the dyed microbubbles dot. (Right) Acoustic field collected by the hydrophone



Presentation Number **0515A**

Poster Session 2b: Drug and/or Radiation Therapy & Imaging Molecular and/or Cellular Processes

MRI evaluation of the neuroprotective effect of a brain-targeting form of docosahexaenoic acid after stroke

Fabien Chauveau¹, **Tae-Hee Cho**¹, **Adrien Riou**¹, **Pierre Aguetzaz**¹, **Michel Guichardant**², **Magali Perez**², **Madeleine Picq**², **Michel Lagarde**², **Yves Berthezène**¹, **Norbert Nighoghossian**¹, **Marlène Wiart**¹, ¹CREATIS, CNRS UMR 5220, INSERM U630, INSA-Lyon, University of Lyon, Lyon, France; ²Multidisciplinary Institute of Biochemistry of Lipids, INSERM UMR 870, INRA 1235, INSA-Lyon, Lyon, France. Contact e-mail: chauveau@creatis.insa-lyon.fr

Introduction Epidemiologic studies report cardio-vascular protection conferred by omega-3 fatty acids, in particular docosahexaenoic acid (DHA) [1]. Few experimental studies have addressed the neuroprotective potential of DHA in acute stroke treatment [2]. In brain, DHA accumulation has been evidenced through a specific uptake of DHA-containing lysophosphatidylcholine (LysoPC) [3]. Our aim was to use multimodal MRI to assess in vivo neuroprotection conferred by DHA and by a stabilized biomimetic form of LysoPC-DHA (AceDoPC) in an animal model of stroke. Methods Rats underwent a sixty-minute proximal middle cerebral artery occlusion (MCAO) with the intraluminal thread model, confirmed by MR angiography. Immediately following reperfusion, animals were randomly and blindly treated by intravenous injection of i) saline (n=8), or ii) plasma from donor rats, or iii) DHA or iv) AceDoPC, both solubilised in plasma (n=10 each). Twenty-four hours after reperfusion, animals were submitted to behavioural tests and sacrificed. MRI was performed on a Bruker Biospec 7T/12-cm magnet at H0 during occlusion and at H24 before sacrifice. The MR exam included a 2D angiography, Diffusion-Weighted Imaging, Dynamic Susceptibility Contrast-enhanced Perfusion-Weighted Imaging, and T2-weighted imaging over the entire MCA territory. Initial and final lesions were defined as hypointense signal on H0 apparent diffusion coefficient (ADC) maps and as hyperintense signal on H24 T2-weighted images. Results Median neuroscores exhibited a non significant trend to decrease in treatment groups (6.5, 6 and 4 in plasma, DHA and AceDoPC groups respectively) compared to the saline group (8), reflecting fewer deficits in treated animals. Mean initial lesion size was comparable in the 4 groups, as well as PWI/DWI mismatch. Between H0 and H24, lesion size increased in the saline group (mean±SD: +18%±20%), was stable in the plasma group (-3%±29%), decreased in the DHA group (-17%±15%, p<0.05), and further decreased in the AceDoPC group (-34%±27%, p<0.05). Discussion The results provide an in vivo evidence of neuroprotection in acute stroke by a biomimetic stable form of LysoPC-DHA solubilised in plasma, AceDoPC. Brain accumulation has to be confirmed by post-mortem tissue dosages of lipid peroxidation. MRI may play an important role for the controlled evaluation of new stroke treatments and thus help translate experimental findings into the clinic. References [1] Iso, et al. *Jama* 2001;285:304-312 [2] Belayev, et al. *Stroke* 2009;40:3121-3126 [3] Picq, et al. *Mol Neurobiol* (In press)

Presentation Number **0516A**

Poster Session 2b: Drug and/or Radiation Therapy & Imaging Molecular and/or Cellular Processes

Brain Tumor Theranostics: Photoacoustic Tomography-Guided Thermal Ablation Mediated with Targeted Hollow Gold Nanospheres (HAuNS)

Wei Lu¹, **Marites P. Melancon**^{2,1}, Chiyi Xiong¹, Qian Huang¹, Andrew Elliott², R. Jason Stafford², Geng Ku¹, Juri G. Gelovani¹, Chun Li¹, ¹Experimental Diagnostic Imaging, UT-MD Anderson Cancer Center, Houston, TX, USA; ²Imaging Physics, UT-MD Anderson Cancer Center, Houston, TX, USA. Contact e-mail: mmelancon@di.mdacc.tmc.edu

Objectives: Local brain tumor therapy under the guidance of noninvasive molecular imaging techniques shows promise for improving treatment outcome. Hollow gold nanospheres (HAuNS) have the unique combination of small size (~40 nm), spherical shape, and a hollow interior with tunable surface plasmon absorption in the near-infrared (NIR) region that mediate highly efficient photothermal conversion. The purpose of this study was to evaluate whether HAuNS could be used to not only mediate effective photothermal ablation of tumor cells, but also generate strong photoacoustic signals upon near-infrared laser irradiation. **Methods:** Cyclic RGD pentapeptide that recognizes integrin $\alpha v \beta 3$ receptors highly expressed in glioblastoma cells and angiogenic blood vessels was conjugated to the surface of HAuNS through a poly(ethylene glycol) (PEG) linker to obtain RDG-PEG-HAuNS. Twenty four hours after intravenous injection of RDG-PEG-HAuNS, human glioblastoma U87-TGL tumors grown in the brain of nude mice were imaged with a prototype photoacoustic tomography (PAT) camera. The presence of tumors was confirmed by MRI and chemiluminescent imaging. The PAT imaging results were used to guide the treatment with NIR laser-induced photothermal ablation. **Results:** Tumors were clearly visualized with PAT at 800 nm. Intracellular distribution of RDG-PEG-HAuNS in the tumor cells was confirmed in cryosectioned brain tissues. Under the guidance of photoacoustic imaging, the tumor-bearing mice were exposed to continuous wave NIR laser (66 W/cm²) for 3 min. The treatment elevated the temperature of the tumor as measured with MR temperature imaging, and significantly reduced bioluminescence signal from U87-TGL tumor cells stably transfected with the luciferase gene. **Conclusions:** We demonstrated molecular photoacoustic imaging and targeted photothermal ablation of brain tumors with RDG-PEG-HAuNS, which simultaneously served as an optical contrast agent and a photothermal coupling agent.

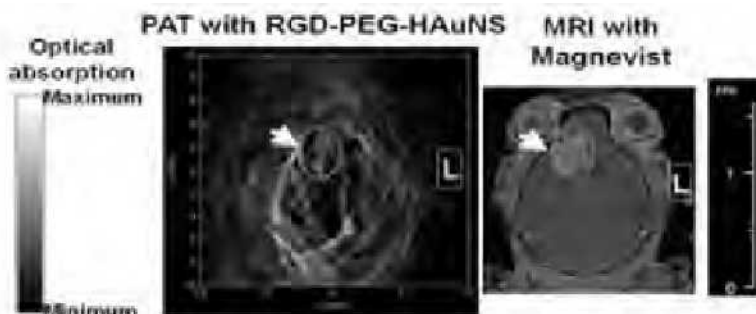


Figure Photoacoustic tomography (PAT) imaging delineated U87 brain tumor in the brain of a nude mouse 24 h after intravenous injection of RGD-PEG-HAuNS. The presence of tumor was confirmed by contrast enhanced MRI.

Presentation Number **0517A**

Poster Session 2b: Drug and/or Radiation Therapy & Imaging Molecular and/or Cellular Processes

Brain Tumor-Selective Imaging and Therapy by Saposin C-Phospholipid Nanovesicles

Xiaoyang Qi¹, Zhengtao Chu¹, Mary B. Palasca², Robert Franco², Vinod Kaimal^{3,4}, Scott K. Holland^{3,4}, Balveen Kaur⁵, Antonio Chiocca⁵, Brian Gray⁶, Koon Y. Pak⁶, Ray Takigiku⁷, ¹Human Genetics, Cincinnati Children's Hospital Research Foundation, University of Cincinnati College of Medicine, Cincinnati, OH, USA; ²the Division of Internal Medicine-Hematology/Oncology, University of Cincinnati College of Medicine, Cincinnati, OH, USA; ³Neuroimaging Research Consortium, Cincinnati Children's Hospital Research Foundation, University of Cincinnati College of Medicine, Cincinnati, OH, USA; ⁴Biomedical Engineering, University of Cincinnati, Cincinnati, OH, USA; ⁵Neurological Surgery, The Ohio State University, Columbus, OH, USA; ⁶Molecular Targeting Technologies, Inc., West Chester, PA, USA; ⁷Bexion Pharmaceuticals, Covington, KY, USA. Contact e-mail: xiaoyang.qi@cchmc.org

Nanovesicles composed of a lysosomal fusogenic protein, saposin C (SapC), and a phospholipid, dioleoylphosphatidylserine (DOPS), selectively target and induce ceramide- and caspase-mediated apoptotic death in a variety of cancerous cells in vitro and in vivo (Qi et al., 2009, Clin. Cancer Res. 15, 5840-5851). In this report, we tested these proteolipid nanovesicles (SapC-DOPS) for delivering fluorescent probes and magnetic resonance (MR) contrast agents selectively to CNS cancers. The nanovesicles were labeled with a far-red fluorescent probe (CellVue® Maroon), or conjugated with a dextran coated MR contrast agent, Ultrasmall Super Paramagnetic Iron Oxide (USPIO), and were in separate experiments, systemically administered into animals bearing human glioblastoma (GBM) xenografts. We demonstrated that labeled nanovesicles enabled cancer-selective optical, or MR detection by targeting and accumulating in deep-seated and diffusely infiltrating brain tumors. Furthermore, using a double-tracking method in living mice, we showed that fluorophore-tagged nanovesicles were specifically targeted and co-visualized to orthotopic bioluminescent GBM tumors. A distinguishing feature of the SapC-DOPS nanovesicles is their high affinity for PS-rich membranes. We observed that CNS cancer cells abnormally express phosphatidylserine (PS) rich domains on their cell membrane. These PS rich domains can be targeted as a novel therapeutic strategy using the SapC-DOPS nanovesicles. Interestingly, the cytotoxic effects of SapC-DOPS correlated to the PS level exposed on the outside of human cancer cells. We determined the relationship of surface exposed PS and SapC-DOPS's cytotoxic response in human CNS cancer cells. Using orthotopically-implanted fluorescent or bioluminescent GBMs in nude mice, we demonstrated that intravenous SapC-DOPS treatment significantly provided survival benefit and extended life. Some of the nanovesicle-treated animals were completely rescued without detectable tumor fluorescence signals. This was confirmed at necropsy. PBS- or DOPS-treated controls had a narrow survival window. Finally, separate toxicity studies in mice showed no adverse behavioral, physical, or histopathologic changes, even at high chronic doses of the SapC-DOPS nanovesicles. Based on these results, we propose that SapC-DOPS nanovesicles offer promise as a novel and robust imaging modality as well as therapeutic agent for CNS cancer-selective diagnosis and treatment.

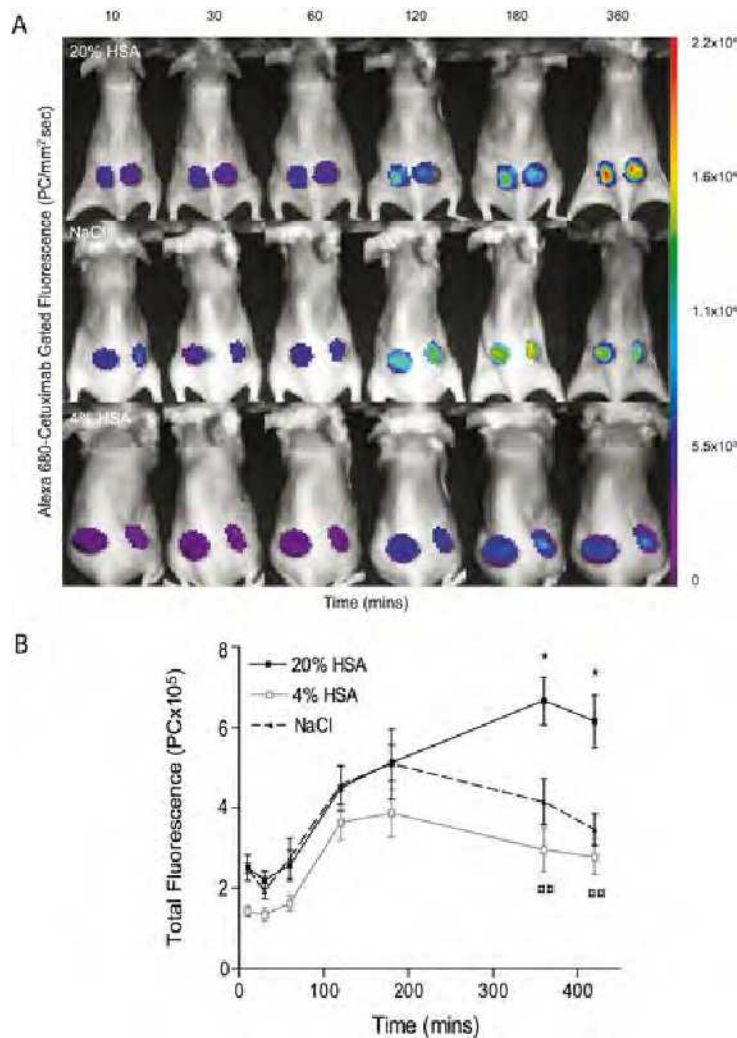
Presentation Number **0518A**

Poster Session 2b: Drug and/or Radiation Therapy & Imaging Molecular and/or Cellular Processes

Time domain optical imaging validates uptake of therapeutic macromolecules after lowering of tumor interstitial fluid pressure in a xenograft tumor model

Matthias Hofmann^{1,2}, Emmet McCormack³, Helge Wiig², Stefan Kippenberger¹, ¹Department of Dermatology, Goethe-University, Frankfurt, Germany; ²Dept. of Biomedicine, University of Bergen, Bergen, Norway; ³Institute of Medicine, University of Bergen, Bergen, Norway. Contact e-mail: matze@tuebingen.mpg.de

Elevated tumor interstitial fluid pressure (TIFP) is a characteristic of most solid tumors. Clinically, TIFP may hamper the uptake of drugs into tumor tissue reducing their therapeutic efficacy. In this study a means of modulating TIFP to increase the concentration of macromolecules into tumor tissue is presented, which is based on the rationale that elevated plasma colloid osmotic pressure (COP) pulls water from tumor interstitium lowering TIFP. Concentrated human serum albumin (20%; HSA) reduced the TIFP time-dependently in xenograft models bearing human A431 carcinomas. To evaluate whether this reduction facilitates the uptake of macromolecules, distribution of fluorescently conjugated dextrans and cetuximab was probed employing novel time-domain near-infrared fluorescence imaging. Co-administration of 20% HSA together with dextrans or cetuximab was found to lower the TIFP significantly and increase the concentration of the substances within the tumor tissue compared to controls. These data demonstrate the usage of time-domain near-infrared fluorescence imaging to monitor the uptake of substances into the tumor interstitium to identify a novel approach of drug delivery of therapeutics into tumor tissue.



Time-domain fluorescence imaging of Alexa680-conjugated cetuximab accumulation 30 min after the i.v. injection of 20% HSA.

Presentation Number **0519A**

Poster Session 2b: Drug and/or Radiation Therapy & Imaging Molecular and/or Cellular Processes

Therapy evaluation of a novel anti-EMMPRIN monoclonal antibody for orthotopic pancreatic cancer xenografts by ultrasonography

Hyunki Kim^{1,4}, **Guihua Zhai**⁴, **Zhiyong Liu**², **Emily E. Helman**², **Tong Zhou**^{3,4}, **Kurt R. Zinn**^{1,4}, **Eben L. Rosenthal**^{2,4}, ¹Radiology, University of Alabama, Birmingham, AL, USA; ²Surgery, University of Alabama at Birmingham, Birmingham, AL, USA; ³Medicine, University of Alabama at Birmingham, Birmingham, AL, USA; ⁴Comprehensive Cancer Center, University of Alabama at Birmingham, Birmingham, AL, USA. Contact e-mail: hyunki@uab.edu

Purpose: To evaluate the therapeutic benefit of a novel monoclonal antibody targeting extracellular matrix metalloproteinase (EMMPRIN) for pancreatic cancer treatment in an orthotopic mouse model. **Methods:** Cytotoxicity of anti-EMMPRIN mAb was assessed in MIA PaCa-2 and PANC-1 human pancreatic-cancer cell lines in vitro. Scatchard analysis was conducted with Tc-99m-labeled anti-EMMPRIN mAb for MIA PaCa-2 cells or those silenced for EMMPRIN gene expression by siRNA. Groups 1-7 of SCID mice (n=5~12 per group) bearing orthotopic MIA PaCa-2 tumors (groups 1, 3-7) or EMMPRIN silenced tumors (group 2) were used. Groups 1-3 were injected with PBS, PBS, and anti-EMMPRIN mAb (0.2mg) respectively twice weekly for 3 weeks after cell implantation, while ultrasound imaging was applied at 15 and 21 days post cell injection. Dosing for groups 4-7 started at 21 days post cell injection; groups 4 and 5 were injected with PBS and anti-EMMPRIN mAb (0.2mg) twice weekly for 3 weeks, while ultrasound imaging was applied at days 21, 28, 35, and 42. Groups 6 and 7 were injected with PBS and anti-EMMPRIN mAb (1mg) twice weekly for 2 weeks, while ultrasound imaging and diffusion-weighted MRI were applied at days 21, 28, and 35. **Results:** No cytotoxic effect was demonstrated in escalating doses of anti-EMMPRIN mAb in either cell line in vitro. Scatchard analysis showed the number of EMMPRIN molecules expressed per MIA PaCa-2 cell was 3.6 million, whereas that per EMMPRIN silenced cell was 0.7 million. Tumor volumes of groups 1-3 were 66±17 (mean±SE), 21±5, and 4±2mm³ at day 15, while those at day 21 were 240±41, 80±15, and 15±4mm³, which represents statistical differences among groups at each day (p<0.05). Tumor-volume increases of group 4 relative to day 21 were 282±33, 495±107, and 725±166% at days 28, 35, and 42, while those of group 5 were 191±7, 263±27, and 429±39%; groups 4 and 5 were statistically different at day 28 (p=0.03), not at the other days. Group 6 showed an increase in tumor-volume of 317±55 and 505±96% at days 28 and 35 respectively, while those in group 7 were 189±27 and 244±41%; groups 6 and 7 were statistically different at day 35 (p=0.04), but not at day 28. Mean intra-tumoral ADC change of group 7 was about 10% higher than that of group 6 at either day, but not statistically significant. **Conclusion:** Significant tumor-growth suppression was detected following anti-EMMPRIN therapy in an orthotopic pancreatic cancer model in early tumorigenesis, supporting the potential benefit of anti-EMMPRIN therapy in the adjuvant setting for pancreatic-cancer patients.

Presentation Number **0520A**

Poster Session 2b: Drug and/or Radiation Therapy & Imaging Molecular and/or Cellular Processes

Tumor diagnosis and photodynamic therapy in live animals via turn-on system with tumoral pH-responsive polymeric micelle

Heebeom Koo¹, Hyejung Lee^{1,2}, Sojin Lee¹, Kuiwon Choi¹, Ick Chan Kwon¹, Seo Young Jeong², Doo Sung Lee³, Kwangmeyung Kim¹,
¹Biomedical Research Center, KIST(Korea Institute of Science and Technology), Seoul, Republic of Korea; ²Department of Life and Nanopharmaceutical Sciences, Kyung Hee University, Seoul, Republic of Korea; ³Department of Polymer Science and Engineering, Sungkyunkwan University, Suwon, Republic of Korea. Contact e-mail: iamac9@kist.re.kr

Photosensitizers could be useful in both diagnosis and therapy, because upon irradiation, they produce strong fluorescence and singlet oxygen simultaneously without additional fluorescence dye. We have synthesized the pH-responsive MPEG poly (β -amino ester) polymeric micelles, and these micelles showed sharp pH-dependent demicellization at the acidic extracellular pH of tumors. We showed that this tumor targeted delivery system have great potential especially in PDT, because photosensitizers encapsulated in micelle core have even weaker fluorescence and singlet oxygen for self-quenching. At tumor site, photosensitizer could be released as dimicellization and recover their ability to produce fluorescence and singlet oxygen and enable tumor site turn-on system with simultaneous diagnosis and therapy. In tumor bearing mice model, these micelles showed high sensitive fluorescent images of tumors and complete ablation of them. Therefore we can conclude that this turn-on system at tumor site with pH-responsive micelle and photosensitizer enables both tumor diagnosis and therapy simultaneously, and have great potential for biological studies and clinical treatments of various tumors.

Presentation Number **0521A**

Poster Session 2b: Drug and/or Radiation Therapy & Imaging Molecular and/or Cellular Processes

Non-invasive imaging of gene silencing efficacy of nano-sized siRNA delivery system in tumor-bearing mice

Sojin Lee¹, **Seung-Young Lee**¹, **Solki Min**¹, **Myung Sook Huh**¹, **Kuiwon Choi**¹, **Ick Chan Kwon**¹, **Yongseok Choi**², **Kwangmeyung Kim**¹,
¹KIST, Seoul, Republic of Korea; ²Korea University, Seoul, Republic of Korea. Contact e-mail: ssojin85@paran.com

Small interfering RNA (siRNA) therapy is good promising tool for treatment of diverse diseases, such as cancer and viral infection etc. But siRNA therapy has a hurdle for its' clinical application due to low stability within physiological environment and poor cellular uptake efficiency. In this study, to overcome these problems, we designed a new nano-sized siRNA carrier system. We used siRNA for red fluorescent protein (RFP) gene, and synthesized it as a poly-siRNA (polymerized siRNA) mediated by disulfide bond at the 5'-ends of both sense and anti-sense strands of siRNA. For the efficient systemic delivery of poly-siRNA, biocompatible/biodegradable glycol chitosan polymer (GC) was introduced and modified, as a Thiolated GC. Thiolated GC was conjugated with poly-siRNA via disulfide bond. In vitro GC-poly-siRNA complexes exhibited good silencing efficiency to the RFP labeled melanoma cells (RFP/B16F10) compared to untreated cells, we confirm that using Kodak Image Station 4000MM Digital Imaging System. And GC-poly-siRNA presented a good targeting efficacy in vivo. In SCC7 tumor-bearing mice, GC-Cy 5.5 labeled poly-siRNA were intravenously injected and exhibit excellent tumor specificities and targeting of GC-Cy 5.5 labeled poly-siRNA were imaged by eXplore Optix System. Also we know GC-poly-siRNA locate in tumor tissues. In tumors from mice administered GC-cy5.5 labeled-poly-siRNA, the cy5.5 signal was observed in tissues outside of the vessels (FITC-dextran). Inhibition of RFP gene expression in RFP/B16F10-bearing mice is good efficacy, due to their higher tumor-targeting ability. These results revealed the promising therapeutic potential of Thiolated GC-poly-siRNA as a stable and effective nano-sized siRNA delivery system for cancer treatment .

Presentation Number **0522A**

Poster Session 2b: Drug and/or Radiation Therapy & Imaging Molecular and/or Cellular Processes

Biodistribution and Therapeutic Potentials of Re-188 MN-16 Lipiodol and Re-188 MN-16ET Lipiodol in Rats with Hepatic Tumors after Intra-arterial Injection via the Hepatic Artery

Shih-Chuan Tsai¹, Tsai-Yueh Luo², Hsin-Yi Wang¹, Wan-Yu Lin¹, ¹Department of Nuclear Medicine, Taichung Veterans General Hospital, Taichung, Taiwan; ²Isotope Application Division, Institute of Nuclear Energy Research, Taoyuan County, Taiwan. Contact e-mail: sctsai@vghtc.gov.tw

Background: Re-188 lipiodol has many advantages for cancer treatment. However, according to the literature, the reported labelling methods were too complicated. In addition, the yield rates for the Re-188 lipiodol were low due to the limitation of labelling methods. In this study, two new monoamine-monoamide-dithiol tetradentate ligands- N-[2-(triphenylmethyl)thioethyl] 3-aza-3-[2-(triphenylmethyl)thioethyl] nonadecane (H3MN-16) and N-[2-(triphenylmethyl)thioethyl] 3-aza-18-ethyloxycarbonyl-3-[2-(triphenylmethyl)thioethyl] octadecanoate (H3LMN-16ET), were developed and conjugated with Re-188 and then dissolved in lipiodol to form the radiopharmaceuticals Re-188 MN-16 lipiodol and Re-188 MN-16ET lipiodol. Biodistribution examination was performed to determine the best lipiodol derivative and its potential for the treatment of liver cancer was evaluated. Methods: Two kinds of Re-188 labelled lipiodol, Re-188 MN-16 lipiodol and Re-188 MN-16ET lipiodol, were developed by Institute of Nuclear Energy Research (INER) in Taiwan. Thirty male rats bearing hepatic tumor were divided into two groups (fifteen rats in each group using one kind of Re-188 compound). The rats were sacrificed at 1 hr, 24 hrs and 48 hrs after injection of 0.1 mCi of Re-188 Lipiodol derivatives via the hepatic artery. Samples of various organs were obtained to calculate the tissue concentration. We also evaluated the survival time after injection of 0.1, 0.3 and 0.5 mCi of Re-188 Lipiodol derivatives, respectively. Results: In these two kinds of Re-188 preparations, Re-188 MN-16ET lipiodol showed better promising result in the biodistribution data and we considered it the most potential one for the treatment of liver cancer. In the group with Re-188 MN-16ET lipiodol, the highest uptake ratios of hepatoma were 13.69 at 1 h, 11.28 at 24 hr, and 6.20 at 48h, respectively. Except for the uptake in the tumour and in the liver, other organs such as kidney, intestine...etc. showed very low concentrations of radioactivity. In the survival test, 100% of rats showed poor results in the control group and 75% of rats showed poor response in the group with 0.1 mCi Re-188 MN-16ET lipiodol. In the groups with 0.3 mCi and 0.5 mCi of Re-188 MN-16ET lipiodol, 100% of rats showed good response to the treatment. Conclusion: We consider Re-188 MN-16ET lipiodol has good therapeutic potentials for the treatment of hepatoma.

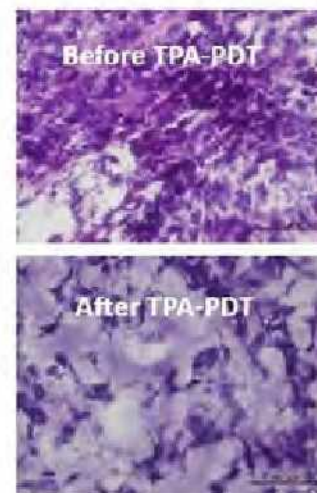
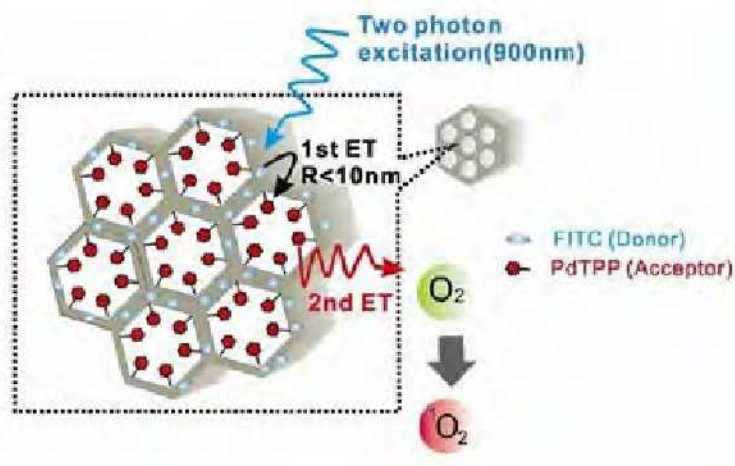
Presentation Number **0523A**

Poster Session 2b: Drug and/or Radiation Therapy & Imaging Molecular and/or Cellular Processes

Intra-Mesoporous Silica Nanoparticle Energy Transfer for Two-Photon Photodynamic Therapy

Shih-Hsun Cheng^{1,2}, Cheng-Chih Hsieh³, Chung-Shi Yang², Fan-Gang Tseng¹, Pi-Tai Chou³, Leu-Wei Lo², ¹Institute of NanoEngineering and MicroSystems, National Tsing Hua University, Taiwan, Kaohsiung, Taiwan; ²National Health Research Institutes, Zhunan, Taiwan; ³National Taiwan University, Taipei, Taiwan. Contact e-mail: smallgi2002@gmail.com

Photodynamic therapy (PDT) has several limitations in treatment of cancer. The limited depth of light penetration in tissue is one of the major challenges that PDT is facing in clinic. Most currently available PDT photosensitizers (PS) absorb visible photons below 700 nm, where light penetration into the skin is less than a few millimeters. However, two-photon activated (TPA)-PDT is one of the promising approaches to surpass such a constraint. The TPA-PDT possesses two advantages: (i) It enables the use of light in the tissue transparent window (750-1000 nm) and (ii) TPA-PDT has higher selectivity than one-photon absorption PDT and enhanced spatial resolution in deeper tumors due to a quadratic dependence on laser intensity of TPA. Herein, we functionalized mesoporous silica nanoparticle (FITC@MSN-PdTPP), comprising moieties of two-photon antenna and PS, for TPA-PDT via an intra-particle energy transfer mechanism (Figure left). The fluorescent dye FITC was incorporated in the frameworks of MSNs serving as two-photon absorber and subsequently transfers the energy to the nearby PS, Pd-porphyrin (PdTPP), that covalently modified onto the nanochannels of MSNs. High efficiency of energy transfer was expected due to the well-ordered mesoporous structure of nanoparticle, by which the two-photon energy harvested by each FITC molecule could be transferred to multiple PS located in the very close proximity less than 2 nm. Thus, the activated PS can further render high amount of single oxygen to induce pronounced cytotoxicity via Type II mechanism of PDT. The two-photon energy transfer efficiency, from FITC to PdTPP, was approximately 90 % determined by fluorescence lifetime measurements. Moreover, the *in vivo* efficacy of TPA-PDT on treating nude mice bearing MDA-MB-231 breast tumor was demonstrated by haematoxylin and eosin stain (H&E stain) of tumor-sections before and after treatments (Figure right). In summary, we developed functional MSNs for highly efficient TPA-PDT via the mechanism of intra-particle energy transfer.



Presentation Number **0524A**

Poster Session 2b: Drug and/or Radiation Therapy & Imaging Molecular and/or Cellular Processes

In Vivo Delivery of Apoptosis-Inducing Peptides by using Attenuated *Salmonella typhimurium* to Suppress Tumors

Vu Hong Nguyen¹, Hye Kyung Chung¹, Yeongjin Hong², Hyon El Choy², Jung-Joon Min¹, ¹Nuclear Medicine, Chonnam National University Medical School, Hwasun, Republic of Korea; ²Microbiology, Chonnam National University Medical School, Gwangju, Republic of Korea. Contact e-mail: nghongvu13@gmail.com

Tumor-targeting bacteria for cancer treatment have been studied for over 100 years. To strengthen the therapeutic effect of bacterial therapy, various kinds of therapeutic agents such as proteins, genes, siRNA or prodrug-converting enzymes have been delivered specifically along with the bacteria. Most of cargo molecules target the cancer cell membrane or their synthesis machinery that usually leads to necrosis or apoptosis. Comparing with the necrosis, the apoptosis with the programmed-cell death might be better with less toxic effect caused by cellular necrotizing process. Therefore, in this study, we are trying to deliver Noxa, apoptosis-inducing peptides to the cancer cells for the purpose of apoptic cell death. To deliver Noxa specifically to tumor cells in vivo, we exploited the tumor targeting attenuated *Salmonella typhimurium* which was defective in ppGpp-synthesis pathway as a delivery system where Noxa expression could be deliberately controlled by P_{BAD} promoter which can be activated by L-Arabinose as an inducer. For intracellular translocation, a short cell-penetrating peptide sequence was conjugated in the proximal gene (Noxa). In addition, to secrete the peptides successfully out of the bacteria, a secretion peptide signal was also conjugated with the gene construction. In order to know kinetic distribution of the bacteria and suitable time for therapeutic gene expression, the bacterial strain was transduced with lux operon in their chromosome. The engineered bacteria were injected intravenously into tumor-bearing mice. The lux signal emitted from the bacteria were detected by cooled CCD-camera in everyday. According to the kinetic distribution of bacteria, gene expression of Noxa was induced when the bacteria confined in the tumor after clearing from the other organs. To evaluate the therapeutic effect, CT-26 expressing Fluc bearing mice were generated as the cancer models. Comparing with the control groups, significant decrease in tumoral size as well as in cellular bioluminescence were observed in the groups administrated the bacteria carrying Noxa. The results indicated that apoptosis-inducing peptides can be successfully delivered to the tumor tissue by using tumor-targeting bacteria.

Presentation Number **0525A**

Poster Session 2b: Drug and/or Radiation Therapy & Imaging Molecular and/or Cellular Processes

Increasing potential of attenuated *Salmonella* as a specific gene delivery vector to infarcted myocardium by hypoxia-inducible promoter system

Uyenchil N. Le, Hee Jung Lee, Jung-Joon Min, Nuclear Medicine, Chonnam National University Medical School, Hwasun, Republic of Korea. Contact e-mail: uyenchile@hanmail.net

Myocardial infarction (MI) is caused by the interruption of blood supply to a part of the heart, which results in the imbalance of oxygen supply and demand, leading to the hypoxia and necrosis in heart. We have been developed a cardiac gene-delivering vector using *Salmonella typhimurium*, which could be monitored by noninvasive bioluminescence imaging technique, with the necessity to design a hypoxia-inducible promoter system that is able to regulate gene expression only inside low oxygen infarcted myocardium. We isolated hypoxia-inducible promoters of *ansB* and *pflE* genes, which were designed to promote expression of *Rluc8* reporter gene inside attenuated *Salmonella* defective in ppGpp molecule synthesis. Murine MI models were received safe dose of engineered *Salmonella*, and systemic distribution of bacteria in host was visualized by luminescence *in vivo* imaging system (IVIS). Specific targeting of bacteria was evaluated by photon measurement based on bacterial viable counting from homogenized tissues. Luminescent signals expressing from hearts demonstrated the accumulation of bacteria at damaged heart, specifically at infarcted region on left ventricle. No signals of *Rluc8* expression were detected in liver, spleen and normoxic myocardium on day 1 despite of high quantities of existing viable bacteria. The new construct hypoxia-inducible promoter system tightly allowed *Salmonella* to express gene of interest only in hypoxic environment. This bacteria model could be used as a potential gene-delivering vector for MI, opening a new trend for selectively transferring therapeutic genes/proteins into ischemic hearts.

Presentation Number **0526A**

Poster Session 2b: Drug and/or Radiation Therapy & Imaging Molecular and/or Cellular Processes

Visualization infarcted tissues using engineered bacteria

Uyenchil N. Le, Ari Chong, Jung-Joon Min, Nuclear Medicine, Chonnam National University Medical School, Hwasun, Republic of Korea. Contact e-mail: uyenchile@hanmail.net

Gene therapy that augments the angiogenesis and muscle regeneration is a promising treatment approach for ischemia in myocardium, cerebral cortex and skeletal muscles. Still, there is no optimal vehicle to deliver therapeutic genes into ischemic tissues. We first time examined the possibility of targeting hypoxic tissue by bacteria based on the observation that certain anaerobic bacteria are capable of targeting hypoxic regions present in solid tumors. Non-pathogenic *Salmonella typhimurium* were defected in ppGpp synthesis to reduce the unwanted bacterial toxicity and transduced with the intact *lux* operon of bacterial luciferase reporter gene to express the luminescence for *in vivo* monitoring. The *Salmonellae* were intravenously injected into murine models of myocardial, cerebral or peripheral ischemia. Bacterial tropism for ischemia was observed by cooled CCD camera. We then assessed the systemic or local toxicity after bacterial injection and measured the infarct size by TTC staining. Bioluminescence imaging revealed the accumulation of the *Salmonellae* in ischemic regions without serious local or systemic inflammation reactions following intravenous administration of attenuated *Salmonellae*. Histological study revealed the selective localization of the *Salmonellae* in the necrotic ischemic regions, not in the normoxic areas of heart, brain or hindlimb. This is a novel finding of bacterial tropism for ischemic/infarcted tissues, and suggests that the *Salmonellae* can be exploited as vehicle for the delivery of therapeutic genes/proteins in patients of coronary/peripheral artery diseases and ischemic strokes. It opens many new avenues for molecular imaging and therapy, including tissue-specific targeting with signal amplification based on bacterial proliferation, *in vivo* tissue-specific drug delivery, and the design of imageable therapeutic probes.

Presentation Number **0527A**

Poster Session 2b: Drug and/or Radiation Therapy & Imaging Molecular and/or Cellular Processes

A comparison between 188Re-MN-16ET and 188Re-MN-16ET/Lipiodol in SD rat models

Tsai-Yueh Luo, I-Chang Tang, Yin-Hsia Shia, Cheng-Liang Peng, Wu-Jyh Lin, isotope Application Division, Institute of Nuclear Energy Research, Taoyuan, Taiwan. Contact e-mail: tylo@iner.gov.tw

Introduction: H3MN-16ET, N-[2-(triphenylmethyl)thioethyl]-3-aza-19-ethyloxycarbonyl-3-[2-(triphenylmethyl)thioethyl] octadecanoate, is a new developed N2S2 tetradentate ligand which has been labeled with 188Re-perrhenate to form the 188Re-MN-16ET and then extracted in Lipiodol phase. In this study, we compare the pharmacokinetic parameters between 188Re-MN-16ET and 188Re-MN-16ET/Lipiodol in Sprague-Dawley rat models to evaluate the potential for hepatoma therapy. Two kinds of rat models were included which were normal rat and the xenotransplanted hepatoma rat models induced by N1S1 cell line. Methods: H3MN-16ET was labeling with 188Re-perrhenate and then extracted by Lipiodol to form 188Re-MN-16ET/Lipiodol. Twenty normal SD rats were used to evaluate distribution pattern of 188Re-MN-16ET by tail vein injection separately. Another twenty rats implanted with hepatoma were injected with 3.7MBq/0.1mL of 188Re-MN-16ET/Lipiodol via transcatheter arterial embolization or tail vein injection respectively. Biodistribution experiment and micro-SPECT/CT images were performed to investigate the tumor accumulation. Results: The radiochemical purity (RCP) of 188Re-MN-16ET was proved to more than 90% by radio-HPLC system with the assistance of tartaric acid and stannous chloride. The major distribution organs of 188Re-MN-16ET and 188Re-MN-16ET/Lipiodol were lung and liver in the normal SD rat study. However, 188Re-MN-16ET/Lipiodol in hepatoma animal model via transarterial administration has selectively retained at the tumor site. The metabolism study also showed that only 1.2 % of injected dose in 188Re-MN-16ET/Lipiodol group was excreted through urinary and feces systems at 72 hours post-injection, compared to 7.5 % in 188Re-MN-16ET group. Conclusion: The animal data demonstrate 188Re-MN-16ET/Lipiodol by transarterial injection has a high tumor accumulation in the hepatoma rat model. We suggest that 188Re-MN-16ET/Lipiodol has potential to be a therapeutic radiopharmaceutical for hepatoma treatment.

Presentation Number **0528A**

Poster Session 2b: Drug and/or Radiation Therapy & Imaging Molecular and/or Cellular Processes

Novel radioimmunotherapy with $^{131}\text{I-E}[\text{c(RGDyK)}]_2$ for Glioblastoma Multiforme

Yi-Hsin Pan¹, Jem-Mau Lo¹, Kun-Ju Lin², Shiaw-Pyng Wey³, Shu-Chi Wang¹, Ling Fan², Hsin-Hsin Tsao², ¹Department of Biomedical Engineering and Environmental Sciences, National Tsing Hua University, Hsinchu, Taiwan; ²Molecular Imaging Center and Department of Nuclear Medicine, Chang Gung Memorial Hospital, Taoyuan, Taiwan; ³Medical Imaging and Radiological Sciences, Chang Gung University, Taoyuan, Taiwan. Contact e-mail: hsin0521@gmail.com

Purpose Glioblastoma multiforme is the most prevalent and malignant primary brain tumor in human. Because of its high proliferation rate, marked neovascularization, central necrosis, and extensive local invasion into normal brain parenchyma, gliomas have developed resistance to traditional radiation and chemotherapy agents. E[c(RGDyK)]₂ is a dimeric RGD peptide specific to bind human integrin $\alpha\beta_3$, a cell adhesion molecule expressing in angiogenesis. Moreover, it had been found that glioblastoma multiforme has highly integrin $\alpha\beta_3$ expression than other tumor types. The purpose of this study is to estimate the radioimmunotherapy efficacy of $^{131}\text{I-E}[\text{c(RGDyK)}]_2$ in glioblastoma models with noninvasive in vivo molecular imaging and histopathology processing. Experimental design Two subcutaneous GL261 and ALTS1C1 murine glioblastoma models were adopted for biodistribution study and SPECT/CT imaging. These two models were also compared for the $^{131}\text{I-E}[\text{c(RGDyK)}]_2$ uptake associated with the degree of integrin $\alpha\beta_3$ expression with micro-autoradiography, qPCR, and immunohistochemistry. Besides, an orthotopic glioblastoma model was used to premaritally estimate the radioimmunotherapy efficacy of $^{131}\text{I-E}[\text{c(RGDyK)}]_2$ under the condition that blood-brain barrier was destroyed. Results Female C57BL/6J mice bearing GL261 tumors were injected subcutaneously with about 50 μCi of $^{131}\text{I-E}[\text{c(RGDyK)}]_2$. The mice were sacrificed and dissected at 0.5, 4, 24, 48, and 72-h postinjection. The tumor uptake was 3.10 ± 0.01 %ID/g at 0.5-h postinjection and the tumor to blood ratio was 12.7 in GL261 murine glioblastoma model. It was found that GL261 expressing higher degree of integrin $\alpha\beta_3$ integrin had higher $^{131}\text{I-E}[\text{c(RGDyK)}]_2$ uptake than ALTS1C1 from the results of micro-autoradiography, qPCR and immunohistochemistry. From the in vivo imaging, either of free iodine-131 and $^{131}\text{I-E}[\text{c(RGDyK)}]_2$ accumulated in the tumor of orthotopic glioblastoma model at first. However, $^{131}\text{I-E}[\text{c(RGDyK)}]_2$ presented remarkably higher retention than free iodine-131 at longer postinjection time. Conclusion It is evidenced that $^{131}\text{I-E}[\text{c(RGDyK)}]_2$ exhibits the potent for radioimmunotherapy for glioblastoma multiforme in this work.

Presentation Number **0529A**

Poster Session 2b: Drug and/or Radiation Therapy & Imaging Molecular and/or Cellular Processes

Engineering HSV1-TK expressing attenuated *Salmonella typhimurium* for monitoring targeted bacterio-therapy

Yoon Wha Oh¹, Vu Hong Nguyen¹, Hyon El Choy², Jung-Joon Min¹, ¹Nuclear Medicine, Chonnam National University Medical School, Hwasun, Republic of Korea; ²Microbiology, Chonnam National University Medical School, Gwangju, Republic of Korea. Contact e-mail: oyoona@hanmail.net

Attenuated *Salmonella typhimurium* has been explored to visualize or treat solid tumors due to their characteristics of selective localization in solid tumors. Therefore, exploiting *Salmonella* to deliver therapeutic genes has been considered for a long time. Here, we have established a multifunctional bacterial system that can suppress tumor growth combined with monitoring power by PET system through expression of HSV1-TK, a suicide gene as well as imaging reporter gene. A truncated thymidine kinase (ttk) was constructed under the control of a constitutive promoter (lac promoter) or a remote controllable promoter (P_{BAD} promoter). The western analysis showed well expression of thymidine kinase (TK) enzyme in *E. coli* such as DH5a or MG1655, or attenuated *Salmonella typhimurium* (Δ ppGpp). The activity of ttk expression in the bacteria was also confirmed by TK enzyme assay. To monitor the HSV1-TK expressing bacteria in vivo by optical imaging system, the lux operon was integrated in the chromosome by P22 phage transduction. By optical imaging, the HSV1-TK expressing bacteria showed specific targeting and proliferation in tumor (CT26 murine colon cancer). TK enzyme assay was also showed high accumulation of ³H-PCV in tumor tissue in targeted tumor tissue. MicroPET imaging study showed specific uptake of ¹⁸F-FHBG in the tumors of mice injected with the ttk expressing Salmonellae as compared to that of non-injected mice. In conclusion, we established the HSV1-TK expressing bacteria which can target tumor effectively. Therefore, it would be a good candidate of multifunctional bacteria that can target and suppress tumors as well as be monitored by both optical and PET imaging system.

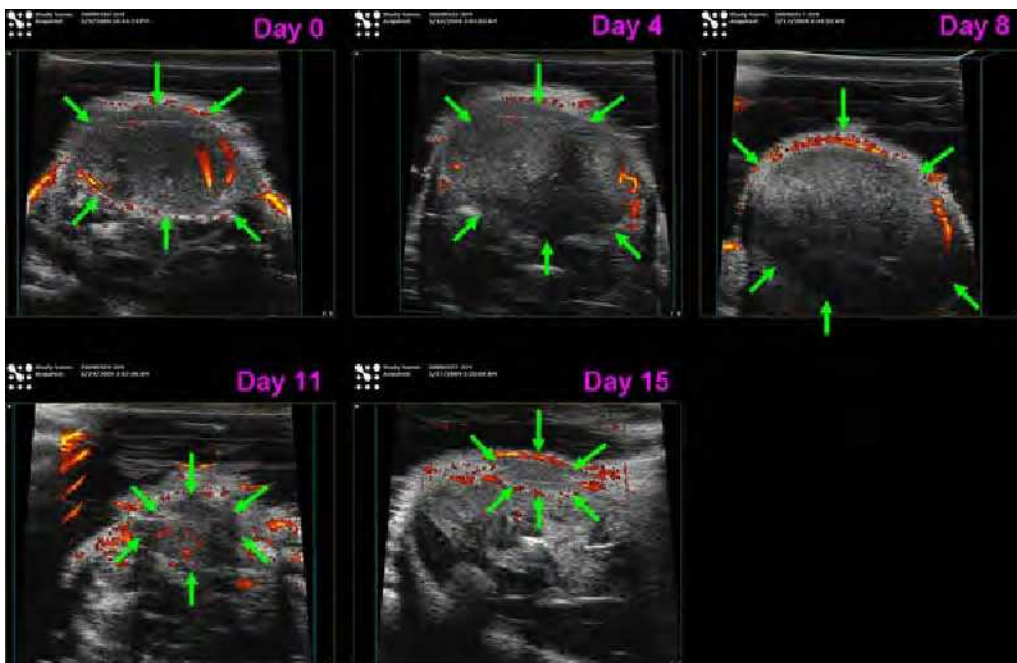
Presentation Number **0530A**

Poster Session 2b: Drug and/or Radiation Therapy & Imaging Molecular and/or Cellular Processes

Therapeutic efficacy of 188Re-liposome in a C26 colon tumor-bearing mouse model

Ya-Jen Chang, Chin-Wei Hsu, Wan-Chi Lee, Chia-Yu Yu, Liang-Cheng Chen, Chih-Hsien Chang, Te-Wei Lee, Gann Ting, Radiation Application, Institute of Nuclear Energy Research, Taoyuan, Taiwan. Contact e-mail: yjchang@iner.gov.tw

Liposomes are good candidates as drug carriers and have been widely investigated for use in drug-delivery systems. The objective of this study is to investigate the therapeutic efficacy of a new radio-therapeutics of 188Re-labeled pegylated liposome in a C26 murine colon carcinoma solid tumor model. The anti-tumor effect of 188Re-liposome was assessed by tumor growth inhibition, survival ratio and ultrasound imaging. In the study on therapeutic efficacy, tumor growth inhibition of mice treated with 188Re-liposome was obviously precisely controlled (Mean tumor size was 245.8 ± 150.23 mm³; Mean growth inhibition rate (MGI) was 0.135) and have longer median survival time (62 d) than those treated with anti-cancer drug 5-FU and untreated control mice(39 d and 30 d, respectively). Noninvasive monitoring of anti-angiogenesis and tumor volume of C26 murine colon tumors treated with 188Re-liposome was performed by serial 3-D power Doppler ultrasound imaging. The imaging showed a decrease in the tumor volume and number of blood vessels. These results were pointed to the potential benefit of the radio-therapeutics 188Re-liposome for adjuvant cancer treatment on oncology applications.



Longitudinal power Doppler ultrasound Imaging. The images were acquired at 0, 4, 8, 11 and 15 days after injection of 188Re-liposome (29.6 MBq). Locations of color signals indicative of blood vessels. The arrow marks an area of tumor. The imaging showed a decrease in the tumor volume and number of blood vessels.

Therapeutic efficacy of 188Re-liposomes on C26 colon tumor-bearing BALB/c mice

Treatment Modality	Tumor Growth Inhibition		Survival	
	MGI	median survival time (d)	P value	Life span (%)
Normal Saline		30		
188Re-liposomes	0.135	62	0.0191	106.7
5-FU	0.201	30	0.0306	30

1.MGI, Mean growth inhibition rate = Growth rate of treated group/Growth rate of untreated group.

2.P values were estimated by log-rank test, P < 0.05 indicates significance.

3.Percentage increase in life span was expressed as (T/C - 1) × 100%, where T is the median survival time of treated mice and C is the median survival time of control mice.

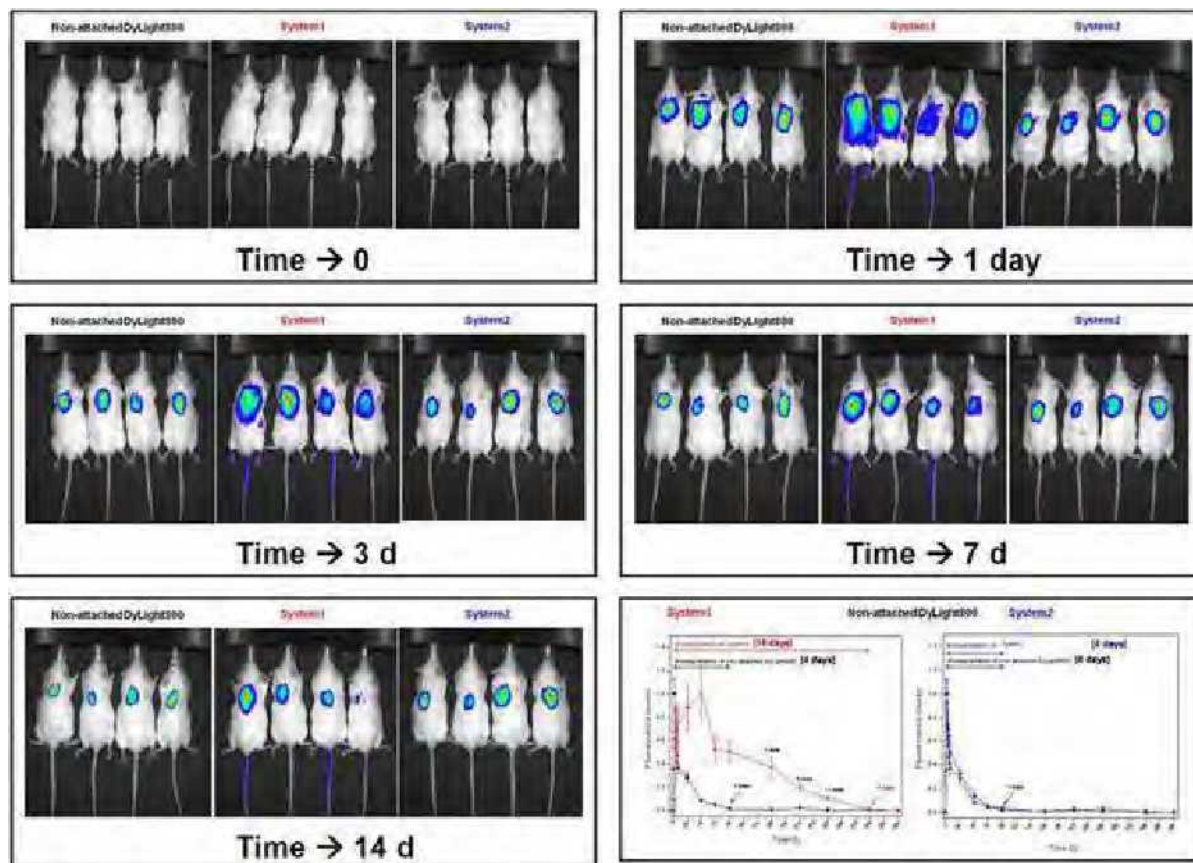
Presentation Number **0531A**

Poster Session 2b: Drug and/or Radiation Therapy & Imaging Molecular and/or Cellular Processes

Controlled drug delivery systems biodegradation assessment by fluorescence tracking

Albert Altafaj¹, Miguel R. Moreno Raja², Ernest Giral^{2,3}, **Xavier Cañas**¹, ¹PRAAL-PCB, Barcelona Science Park, Barcelona, Spain; ²Chemistry and Molecular Pharmacology, Institute of Biomedical Research, Barcelona, Spain; ³Organic Chemistry, University of Barcelona, Barcelona, Spain. Contact e-mail: xcanas@pcb.ub.cat

The extremely low availability of peptidic compounds forces pharmaceutical companies to introduce new formulations into the market by modifying them in an appropriate manner to minimize administration interferences. There are well known changes able to be applied without reducing therapeutic efficacy: analogue preparation, chemical modification, conjugations and pharmaceutical formulations, dealing with trapping or encapsulating active principles in a non-covalent way in controlled delivery systems. We have designed novel drug delivery systems to bound high molecular weight therapeutic molecules. These delivery systems have been tested "in vitro" with different cargo types, offering promising cargo delivery kinetics. Experiments have been also performed pointing out that drug delivery is likely to be independent of its degradation in the presence of several cellular membrane enzymes. The aim of this study was monitoring the "in vivo" biodegradation of two different controlled drug delivery systems (Systems 1 and 2) through imaging assays with an IVIS-200® from Xenogen-Caliper. Both systems were labelled with the fluorescent probe dyLight 800. The drug delivery systems (2 mg of each one) were labelled with dyLight 800. They were injected s.c. in 12 male Swiss CD1 mice and images were obtained with the following pattern: 0, 1, 2, 4, 6, 8, 24, 48, 72, and 96 hours, and 7, 9, 11, and 14 days post administration. After 14-days exposition, results were processed to determine the degradation curve of both drug delivery systems (normalized data). In our study, System 1 showed a long life period compared with System 2, which correlates with the treatment period throughout continuously deliver therapeutic agents. We are currently carrying out experiments to elucidate how biodegradation process happens and the involved pathways. In conclusion, fluorescence probes showed as optimal tool to assess drug delivery systems biodegradation.



Presentation Number **0532A**

Poster Session 2b: Drug and/or Radiation Therapy & Imaging Molecular and/or Cellular Processes

Analysis of a Somatostatin Receptor-Yeast Cytosine Deaminase Construct for Imaging Suicide Gene Therapy

Jesse J. Parry, Kimberly A. Lears, Rebecca Andrews, Buck Rogers, Radiation Oncology, Washington University School of Medicine, St. Louis, MO, USA. Contact e-mail: jparry@radonc.wustl.edu

Introduction. Suicide gene therapy is a process by which cells are administered a gene that encodes a protein capable of converting a nontoxic prodrug into an active toxin. Cytosine deaminase (CD) has been widely investigated as a means of suicide gene therapy due to the enzyme's ability to convert the prodrug 5-fluorocytosine (5-FC) into the toxic compound 5-fluorouracil (5-FU). However, the extent of gene transfer is a limiting factor in predicting therapeutic outcome. The ability to monitor gene transfer, non-invasively, would strengthen the efficiency of therapy. In this regard, we evaluated a replication-deficient adenovirus (Ad) containing the human somatostatin receptor subtype 2 (SSTR2) fused with a C-terminal yeast CD gene for the non-invasive monitoring of gene transfer and therapy. Methods. AdSSTR2 or AdSSTR2-yCD were administered to MCF-7 cells at a multiplicity of infection (MOI) of 10 or 100. Competitive binding assays were performed on membrane preparations of infected cells using ¹²⁵I-Tyr11-SST-14 to determine receptor expression and function. To evaluate yCD activity, 5-FC conversion assays were performed on cell extracts from infected cells. Additionally, cell killing studies were performed using 5-FC in a colorimetric assay to determine IC₅₀ values. Results and Discussion. The B_{max} values for the AdSSTR2-infected cells were found to be 751 and 1595 fmol/mg for 10 and 100 MOI, respectively, as compared to 764 and 1829 fmol/mg for the AdSSTR2-yCD-infected cells at 10 and 100 MOI, respectively. The amount of receptor was not significantly different between the constructs, but there was a significant increase ($P < 0.02$) in expression with the increased MOI for each virus. The CD activity was measured over time by the pmol of 5-FU produced per mg of protein. As expected, neither MOI of AdSSTR2 produced 5-FU above background. As for the AdSSTR2-yCD-infected cells, the enzyme activity was found to be 62 and 386 pmol/min/mg for 10 and 100 MOI, respectively, and there was a significant ($P < 0.001$) increase in yCD activity from 10 to 100 MOI. Cell killing assays were performed on cells infected with AdSSTR2-yCD. The IC₅₀ values were found to be 18 and 3 μ g/mL for 10 and 100 MOI, respectively. In vivo biodistribution and microPET imaging studies will be performed in the immediate future. Conclusion. AdSSTR2-yCD was found to be functional for both the somatostatin receptor and the enzymatic activity of yeast cytosine deaminase in vitro. This suggests the construct is suitable for monitoring suicide gene therapy in an animal model.

Presentation Number **0533A**

Poster Session 2b: Drug and/or Radiation Therapy & Imaging Molecular and/or Cellular Processes

COMPARATIVE ONCOLOGY AND CLINICAL TRANSLATION OF GLYCO PROTEIN CONJUGATED GOLD NANO THERAPEUTIC AGENT (NBI-29)

Kattesh V. Katti^{1,4}, *Nripen Chanda*¹, *Ravi Shukla*¹, *Ajit Zambre*¹, *Kavita K. Katti*^{1,4}, *Cathy S. Cutler*², *Henry W. White*⁴, *Anandhi Upendran*⁴, *Carolyn J. Henry*³, *Sandra M. Axiak*³, *Jimmy C. Lattimer*³, *Carlos H. Souza*³, *Raghuraman Kannan*^{1,4}, ¹Radiology, University of Missouri-Columbia, Columbia, MO, USA; ²Missouri University Research Reactor, University of Missouri, Columbia, MO, USA; ³Veterinary Medicine, University of Missouri, Columbia, MO, USA; ⁴Nanoparticle Biochem Inc, Columbia, MO, USA. Contact e-mail: kattik@health.missouri.edu

As part of our efforts toward clinical translation of NBI-29 (GA-198AuNP), our studies are focused on determination of therapeutic efficacy of nanoparticulate NBI-29 agent in dogs with prostatic carcinoma. The overall goal is to gain clinical insights on therapeutic efficacy of NBI-29 in a large animal model. We have performed a phase I clinical trial in dogs using NBI-29 administered intravenously or intratumorally by injection or infusion. CT scans were performed prior to injection and 24 hours post injection in 3 of the 4 dogs. Following injections, dogs were allowed further treatment as recommended by the primary attending clinician. Four dogs have been treated to date. Complications related to NBI-29 treatment were not observed, and all 4 dogs received adjunctive treatment with radiation therapy and/ or chemotherapy. These preliminary studies have clearly provided compelling evidence on the therapeutic potential of biocompatible NBI-29 for their utility as novel therapeutic agents in treating various types of inoperable solid tumors. Intratumoral and intravenous administration of NBI-29 is safe in dogs with spontaneously occurring tumors. As further therapeutic efficacy studies continue, the outcome of this clinical trial in a large animal model will generate therapeutic efficacy data which will be used for filing IND application for Phase I clinical trial studies. This clinical translation effort provides significant advances in terms of delivering optimum therapeutic payloads into prostate cancers with subsequent reduction in tumor volume, thus may effectively reduce/eliminate the need for surgical resection. This presentation will include details of clinical translation of NBI-29 in prostate tumor bearing dogs.

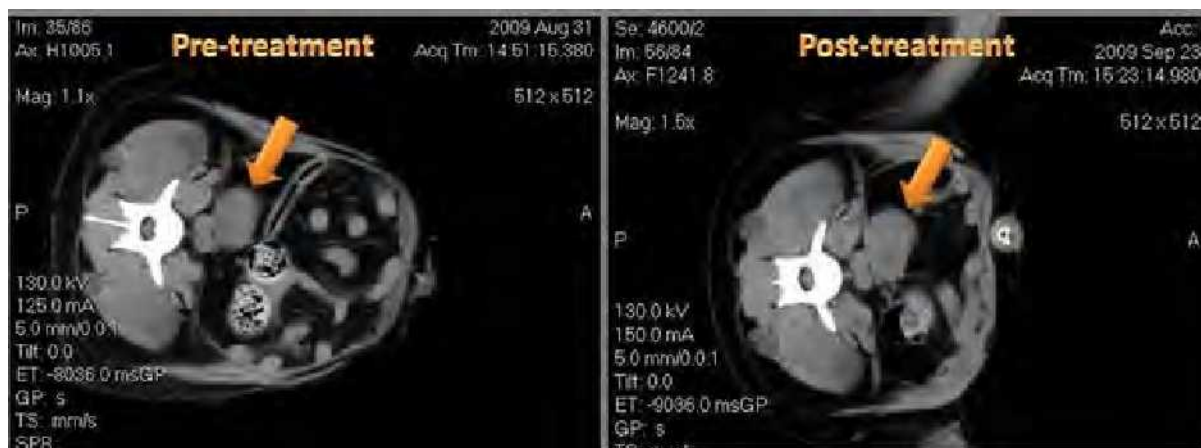


Figure 1 (A) Pre-treatment CT scan; (B) 3 weeks Post-treatment showing stable disease (arrow points to prostatic tumor) in client owned prostate tumor dogs.

Presentation Number **1000A**
Poster Session 1d: Imaging Disease/Organ Processes

The prognostic value of metabolic tumor volume of F-18 fluorodeoxyglucose positron emission tomography for patients with non-small cell lung cancer

Nan-Tsing Chiu¹, **Bi-Fang Lee**¹, **Helen H. Chen**², ¹*Nuclear Medicine, National Cheng Kung University Hospital and College of Medicine, National Cheng Kung University, Tainan, Taiwan;* ²*Radiation Oncology, National Cheng Kung University Hospital and College of Medicine, National Cheng Kung University, Tainan, Taiwan. Contact e-mail: ntchiu@mail.ncku.edu.tw*

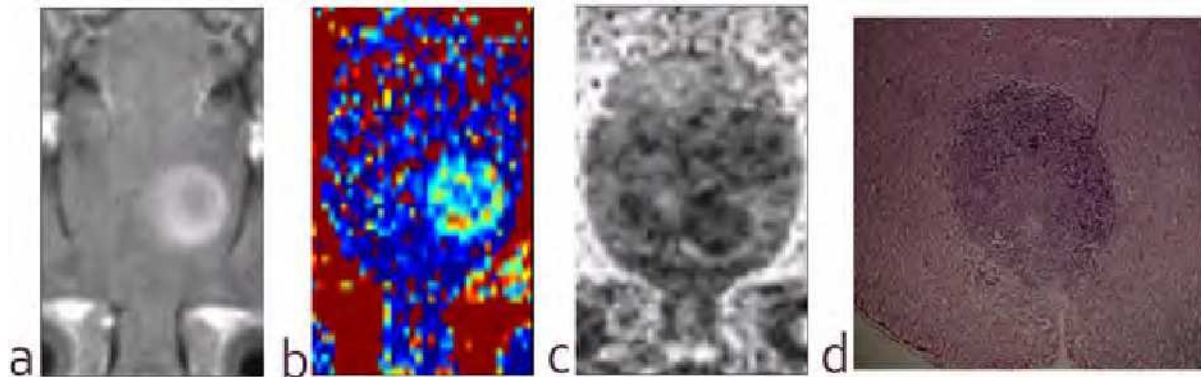
Purpose: The accumulation of F-18 fluorodeoxyglucose (FDG) in non-small cell lung cancer (NSCLC) has been showed to have prognostic value. To determine if the metabolic tumor volume, determined by FDG PET, could predict prognosis of patients with NSCLC, we underwent this study. **Materials and Methods:** A retrospective review of patients with a newly diagnosis of NSCLC was performed. We identified patients who had FDG PET before treatment for NSCLC. Total metabolic tumor volume (MTV), i.e. the summation of all the active tumor volumes including primary lung tumor and metastatic sites, and the highest standardized uptake value (SUV_{hi}) of all the tumor sites, were assessed by FDG PET. Those who had brain metastasis were excluded. Progression-free survival (PFS) was recorded. The prognostic significance was assessed by univariate and multivariate analyses. **Results:** There were totally 105 patients enrolled, including 28 with stage I, 8 patients stage II, 46 patients stage III and 23 patients stage IV disease. The estimated median PFS for the cohort was 10.8 months. The univariate analysis showed that both MTV and SUV_{hi} were significant prognostic factors for PFS ($P < 0.05$). On multivariate Cox proportional hazards regression analysis, MTV ($P = 0.03$) was a significant predictor of PFS after controlling for stage, treatment intent, age, sex, and pathology, while SUV_{hi} ($P = 0.15$) was not. **Conclusion:** MTV, assessed by FDG PET, has a significant independent prognostic value for patients with NSCLC. It has a better predictive value than the highest SUV in tumors of NSCLC.

Presentation Number **1001A**
Poster Session 1d: Imaging Disease/Organ Processes

Multiparametric MRI in characterizing C6 brain tumor with histological validation

Yu-Jung Chiang¹, YuChun Lin^{2,3}, Hao-Li Liu², Li-An Lu², Jiun-Jie Wang^{1,3}, ¹Department of Medical Imaging and Radiological Science, ChangGung University, Taoyuan, Taiwan; ²Department of Electrical Engineering, ChangGung University, Taiwan, ChangGung University, Taoyuan, Taiwan; ³Department of Diagnostic Radiology, ChangGung Memorial Hospital, Taiwan, ChangGung University, Taoyuan, Taiwan. Contact e-mail: jusmile_ul@hotmail.com

Purpose: To monitor the changes in tumour microenvironment by multimodality MRI and the validation with histology Method and material: C6 glioma cells were harvested and injected to the striatum of rat brains (n=10). Longitudinal MRI were scheduled at 10, 17, 24 and 31 days after tumor implantation by a 3.0 Tesla MR scanner (Trio with TIM, Siemens, Germany). Multi-modality MRI was acquired, including diffusion tensor imaging (DTI) and dynamic contrast enhanced (DCE) MRI. The imaging protocols included: (a) T2 and T1 weighted anatomical images by turbo spin echo sequences, TR/TE=4000/90 ms and 400/12 ms, respectively; (b) spin-echo DTI, diffusion gradients in nine orthogonal directions and b-value of 1000 s/mm², TR/TE = 2000/91 ms; (c) DCE, gradient-echo sequence with TR/TE=33 / 4.14 ms, baseline longitudinal-relaxation time calculated from two acquisitions of different flip angles (20° and 40°), 120 consecutive measurements following bolus injection of 0.2ml Gd-DTPA. The temporal resolution was 2.1 second. Indices from the diffusion tensor and maps of permeability (Ktrans) were reconstructed by MATLAB 7.0. Ktrans was calculated using the pharmacokinetic model. Animals were sacrificed after MR image acquisition. Tissues were prepared for histology using Hematoxylin and Eosin (H&E) stain. **Results:** Figure shows the T1WI with Gd(a), Ktrans(b), Fractional Anisotropy(c) and the histology(d) maps of a rat. Peripheral enhancement of the tumor in T1WI was consistent with tumor growth. A significantly high permeability of Ktrans was found in the corresponding region, which suggested angiogenesis. Anisotropic water diffusion could be seen at the central core of the tumor in DTI, indicating a change of water balance due to the reorganization of cytoarchitecture, which was also shown in histology. **Conclusion:** Combined DTI and DCE MRI could be used to characterize the microenvironmental changes in rodent brain tumor.

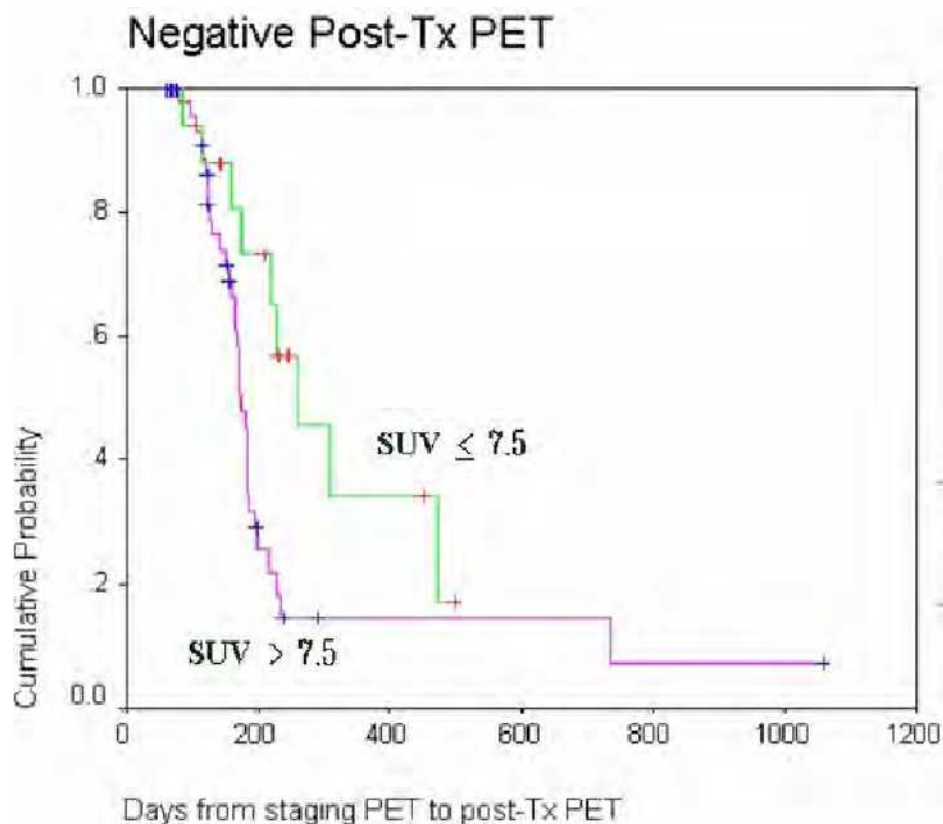


Presentation Number **1002A**
Poster Session 1d: Imaging Disease/Organ Processes

Metabolic phenotypes of lymphomas relate to the rates of treatment response

Regina H. Wong^{1,2}, Bingfeng Tang², Christiana O. Wong², Malaykumar M. Patel², Laura Nadeau², Pek Lan Khong³, Ching Y. Wong²,
¹Biophysics, University of Michigan, Ann Arbor, MI, USA; ²Nuclear Medicine, William Beaumont Hospital, Royal Oak, MI, USA;
³Radiology, University of Hong Kong, Hong Kong, China. Contact e-mail: iregina@umich.edu

Objectives : To investigate the relationship of metabolic phenotype measured by staging PET and the time interval for first metabolic remission of lymphomas. **Methods :** 66 patients with newly diagnosed non-Hodgkin's lymphoma (NHL) and Hodgkin's disease (HD) but without diabetes and other malignancies who had F-18 FDG PET scan performed within 3 months of biopsy were included. Lymphomas were classified using the WHO criteria and graded by the metabolic activity of initial staging PET using maximum standard uptake value (SUV) over the area of biopsy. Cox regression was performed for the duration of post-treatment PET against status of negative PET (otherwise censored) with age, sex, pathologic grade and SUV from staging pre-treatment PET as covariates. Kaplan Meier analysis of the probability of the interval for first negative post-treatment PET was performed in patients with a best discriminating SUV. All PET scans were obtained one hour after injection of 370 MBq F-18 FDG after the patients fasted about 4 hours using a dedicated whole body PET scans. **Results :** The mean interval of the first post-treatment PET was performed after a duration of 198 \pm 153 days of the first staging PET scan. Cox regression analysis suggested that SUV=7.5 stratified the differences in the probability in the interval of the first metabolic remission or negative post-treatment PET. Using this cut-off value SUV, there was a difference in the remission interval as revealed by the first negative PET scans among various lymphomas ($p=0.02$). **Conclusions :** Results suggest that high metabolic phenotype lymphomas by initial staging PET would respond more quickly to treatment as measured by post-treatment PET than those with low metabolic phenotype lymphomas. As there is a high rate of recurrence in NHL, this may impact decision for the follow up interval of lymphomas.



Presentation Number **1003A**
Poster Session 1d: Imaging Disease/Organ Processes

Prognostic Value of Baseline Whole-Body Metabolic Tumor Burden and Their Response Indices on PET/CT in Patients with Non-small Cell Lung Cancer

Yonglin Pu, Kristen Wroblewski, Andrew Hall, Daniel E. Appelbaum, Cassie A. Simon, Kenji Suzuki, Bill C. Penney, The University of Chicago, Chicago, IL, USA. Contact e-mail: ypu@radiology.bsd.uchicago.edu

Purpose: To assess the prognostic value of baseline whole body tumor burden as measured by metabolic tumor volume (MTV), total lesion glycolysis (TLG) and standardized uptake value (SUVmax and SUVmean) of all tumors and the response indices (RIs) of these PET measurements in non-small cell lung cancer (NSCLC). **Material and Methods:** Fifty-one consecutive cases (21 males, 30 females; median age 64 years) with newly diagnosed NSCLC who had (chemo) radiotherapy and FDG PET/CT scans before and after the therapy were retrospectively reviewed. In 19 cases, surgery was performed either before (n=15) or after the start of chemoradiotherapy (n=4). The FDG PET/CT scans were performed in accordance with National Cancer Institute guidelines. The MTV, TLG as well as the SUVmean and SUVmax of whole-body tumors were measured with the PETedge tool on MIMvista workstation with manual adjustment. The median follow-up among survivors is 47.2 months from initial diagnosis (range of 22.5 to 66.1 months). Statistical methods included log-rank tests and Cox regression. **Results:** Mean±SD levels at baseline for log MTV, log TLG, SUVmean, and SUVmax were: 3.8±1.3, 5.1±1.6, 3.9±1.5, and 9.3±4.6, respectively. There were a total of 34 deaths during follow-up. Median overall survival (OS) was 27.6 months (95% CI 21.6 to 37.6 months). There was a statistically significant association, after adjusting for cancer stage and age, between OS and log MTV (Hazard Ratio [HR] for 1 SD increase=1.76, 95% CI (1.11, 2.80), p=0.02) and log TLG (HR for 1 SD increase=1.68, 95% CI (1.04, 2.71), p=0.03) measured on baseline PET/CT but not SUVmax or SUVmean (p=0.91 and 0.56, respectively). Among patients who did not have surgery(n=32), the only statistically significant association between survival from follow-up PET/CT and RIs was for MTV (HR for 20% increase= 0.98, 95% CI (0.96 to 0.99), p= 0.01). Further analysis of this data is ongoing. **Conclusion:** Baseline whole-body metabolic tumor burden as measured with MTV or TLG on PET/CT is an independent prognostic measurement in NSCLC. Only the RI of MTV on PET was a statistically significant predictor of patient's survival.

Presentation Number **1004A**
 Poster Session 1d: Imaging Disease/Organ Processes

**Clinical validation of current FDG PET criteria in characterizing borderline adrenal activity:
 Comparison of multiple criteria in previous literatures**

Sunhee Kim, ¹UPMC, Pittsburgh, PA, USA; ²Diagnostic radiology, Children's hospital of Pittsburgh of UPMC, Pittsburgh, PA, USA.
 Contact e-mail: INDIANA111111@YAHOO.COM

Objectives : The role of F-18 FDG PET in characterizing adrenal lesions has been demonstrated by several previous studies. However, each study used different FDG PET criteria to define positive adrenal lesions. From our clinical experience, these criteria seem to be valid in defining obvious benign or malignant adrenal lesion. However, there seems to be inconsistency in interpretation among readers in defining borderline adrenal activity. Objective consensus of these parameters to characterize adrenal lesions accurately and consistently is critical especially defining borderline adrenal activity. Our study is to compare each parameter with radiologic and clinical correlation and to find the most accurate PET parameter in characterizing borderline adrenal activity in real clinical practice. Methods : Total of 48 adrenal lesions (13 malignant and 35 benign) and 30 patients (mean age 63, M:F=19:21) with F18 FDG PET/CT with IV contrast were collected retrospectively. Except for clearly obvious PET finding (no adrenal activity or definite adrenal activity to suggest malignancy), all studies with adrenal activity were included. Each study was read 5 times using by 5 different parameters and compared with clinical (46/48) and histopathologic (2/48) correlation. Results : Please see a table. Among 5 parameters, the overall accuracy and specificity were the highest using parameter of SUVmax/liver SUVmax >1.5 in characterizing borderline adrenal FDG activity although the sensitivity is low. The highest sensitivity was seen using visual background parameter or quantitative liver SUV mean. Liver SUV max has overall consistent sensitivity, specificity and accuracy compared to other parameter. In contrast to the results of previous literatures on SN and SP of FDG PET in characterizing "general" adrenal lesion using various criteria (sensitivity 93-100% and specificity 80-94%), the SN and SP in characterizing "borderline" adrenal activity using the same criteria is relatively low. Conclusions : Criteria used in previous literatures are less accurate in characterizing borderline adrenal activity than in defining overall adrenal lesions. However, the overall accuracy and specificity were the highest using parameter of SUVmax/liver SUVmax >1.5.

Comparison of criteria from previous literatures in characterizing borderline adrenal activity

	SN%	SP%	PPV%	NPV%	ACC%
Visual assessment using background activity	100	3	28	100	39
Visual assessment using liver activity	83	45	33	88	54
Quantitative assessment using liver SUV mean	100	30	32	100	42
Quantitative assessment using liver SUV max	69	69	43	86	69
Quantitative assessment using adrenal SUV max/liver SUVmax > 1.5	23	97	75	77	77

Presentation Number **1005A**
 Poster Session 1d: Imaging Disease/Organ Processes

New parameter for characterizing borderline adrenal activity

Sunhee Kim, ¹UPMC, Pittsburgh, PA, USA; ²Radiology, Children's hospital of Pittsburgh of UPMC, Pittsburgh, PA, USA. Contact e-mail: INDIANA111111@YAHOO.COM

Objectives : Several previous studies used different criteria in characterizing positive adrenal lesions such as background activity, SUVmean of the liver, SUVmax of the liver and adrenal/liver SUVmax ratio. From our clinical experience, these criteria seem to be valid in defining obvious benign or malignant adrenal lesion. However, there seems to be inconsistency in interpretation among readers in defining borderline adrenal activity. Objective consensus of these parameters to characterize adrenal lesions accurately and consistently is critical especially defining borderline adrenal activity. Our study is to define multiple objective criteria in characterizing borderline adrenal activity for the best differentiation between benign and malignant lesion. **Methods :** Total of 48 adrenal lesions (13 malignant and 35 benign) and 30 patients (mean age 63, M:F=19:21) with F18 FDG PET/CT with IV contrast were collected retrospectively. The mean interval of follow up PET/CT is 125 days. Each adrenal lesion was confirmed by clinical (46/48) and histopathologic (2/48) correlation. Borderline activity is defined by mid FDG activity exceeding background activity but less than moderate to severe degree to suggest definite malignancy by visual analysis. Benign and malignant groups were analyzed and compared on multiple parameters such as adrenal SUVmax, adrenal SUV max/liver SUVmax ratio, % change in adrenal SUVmax in follow up PET and % change in adrenal SUV max/liver SUVmax ratio with statistical p value using t test. **Results :** Please see table **Conclusions :** Overall, there is no significant difference in adrenal SUV max and adrenal SUV max/liver SUV max ratio between benign and malignant groups (p>0.05). However, there is much more significant (p<0.05) difference in % change in adrenal SUVmax in follow up PET and % change in adrenal SUV max/liver SUV max ratio. Our result suggest % change in adrenal SUVmax in follow up PET and % change in adrenal SUV max/liver SUV max ratio would better delineate benign and malignant adrenal lesions with borderline activity compared to parameters such as adrenal SUVmax or adrenal SUV max/liver SUVmax ratio.

Comparison of parameters between benign and malignant lesions

	mean adrenal SUVmax	mean adrenal SUV max/liver SUVmax ratio	mean % change in adrenal SUVmax	% change in adrenal SUV max/liver SUVmax ratio
Malignant (n=13)	4.2±0.8	1.2±0.3	+42.7%	+40.1%
Benign(n=35)	3.0±1.0	1.0±0.3	-31.8%	-30.4%

Presentation Number **1006A**
Poster Session 1d: Imaging Disease/Organ Processes

Comparison of 18F-choline Uptake and Proliferative Activity in Localized Prostate Cancer

Sandi A. Kwee¹, Gregory P. Thibault², Richard S. Stack², Bungo Furusato³, Marc Coel¹, Isabell A. Sesterhenn³, ¹Hamamatsu/Queen's PET Imaging Center, The Queen's Medical Center, Honolulu, HI, USA; ²Urology, Tripler Army Medical Center, Tripler, HI, USA; ³Genitourinary Pathology, Armed Forces Institute of Pathology, Washington, DC, DC, USA. Contact e-mail: skwee@queens.org

PURPOSE: Immunohistochemical labeling for the Ki-67 antigen using MIB-1 antibody has potential prognostic value in localized prostate cancer. To evaluate the possibility of tissue 18F-choline correlating with this marker of tumor proliferation in primary prostate cancer, we compared pre-operative 18F-choline uptake in malignantly involved prostate sextants to the MIB-1 labeling index of prostate tumors assessed after radical prostatectomy. **METHODS:** All subjects gave informed consent in this institutional review board approved study. Pre-operative PET/CT was performed in 24 patients at 10 minutes after intravenous injection of 3.3 to 4 MBq/kg of 18F-choline. The maximum standardized uptake value (SUVmax) of prostate sextants was measured by region of interest analysis. Histopathology involved whole-mount prostate specimens. Markings were applied to the specimen surface before sectioning to maintain spatial orientation and tomographic correspondence with PET/CT. Sections were evaluated by antigen retrieval and immunohistochemical labeling. A MIB-1 labeling index was expressed as the percentage of tumor cells demonstrating nuclear staining. Only macroscopic tumors (diameter > 5mm) were assessed for correlation between sextant SUVmax and MIB-1 index. The accuracy of SUVmax-based diagnosis was estimated by receiver operator characteristic (ROC) analysis based on the histopathologic standard. **RESULTS:** Average weight of prostate specimens was 46 grams (s.d. 23 grams). Average total tumor volume was 8.2 cc (s.d. 9 cc). MIB-1 staining was assessed in 34 tumors (up to 3 per specimen). Median MIB-1 index was 8% (range 1% to 21%). There was no significant correlation between MIB-1 labeling index and sextant SUVmax for the tumors ($r=0.12$, $p=0.5$). There was also no significant correlation between Gleason sum score and SUVmax. The area under the ROC curve (AUC) was 0.80 (sensitivity 82% if specificity 60%). Two patients that received hormonal therapy prior to surgery but after PET/CT were excluded from ROC analysis because the PET/CT scans showed globally decreased prostate activity. **CONCLUSION:** No significant correlation between tumor 18F-choline uptake and MIB-1 staining was found in patients with organ-confined prostate cancer. Tumor 18F-choline uptake may not be a strong indicator of prostate cancer proliferative activity. Acute hormonal therapy administered to hormone-naïve patients may diminish prostatic 18F-choline uptake on PET/CT.

Presentation Number **1007A**
 Poster Session 1d: Imaging Disease/Organ Processes

Pretreatment [¹⁸F] Fluorodeoxyglucose Positron Emission Tomography Standardized Uptake Value of Neck Lymph Nodes and Nodal Staging Predict Prognosis in Patients with Stage IV Hypopharyngeal Cancer

Yasser G. Abd El-Hafez¹, Chien-Yu Lin², Shu-Hang Ng³, Tzu-Chen Yen¹, ¹Nuclear Medicine, Chang Gung Memorial Hospital and Chang Gung University, Taoyuan, Taiwan; ²Dept of Radiation Oncology, Chang Gung Memorial Hospital and Chang Gung University, Taoyuan, Taiwan; ³Department of Diagnostic Radiology, Chang Gung Memorial Hospital and Chang Gung University, Taoyuan, Taiwan. Contact e-mail: yen1110@adm.cgmh.org.tw

The standardized uptake value (SUV), a semi-quantitative measurement of FDG uptake on positron emission tomography (PET) scan, has a proven prognostic value in several different types of cancer. In this study, we sought to assess the prognostic significance of SUV of primary tumor and metastatic neck lymph nodes in patients with stage IV hypopharyngeal cancer (HPC) treated with concurrent chemoradiotherapy (CCRT). Methods: We examined 37 stage IV HPC patients who underwent PET/CT prior to treatment with CCRT. All patients were followed-up till death or at least 24 months. The study outcomes were 3 year local control (LC), neck control (NC), disease free survival (DFS), disease-specific survival (DSS) and overall survival (OS). The Cox proportional hazards model was used to identify independent prognostic factors for the study endpoints. Results: Median follow-up for surviving patients was 30.3 months. Three year LC, NC, DFS, DSS and OS were 42%, 43%, 31%, 52% and 38% respectively.. In multivariate analysis, maximum SUV of the neck lymph nodes (NSUV) > 9.2 was significantly associated with poor DSS and OS. N3 patients had significantly lower LC, NC and DFS. A scoring system using these two covariates defined three distinct prognostic groups, scored 0 to 2. Patients with score 0 (N1-2 with NSUV ≤ 9.2) had significantly better outcome (3 year DSS = 79%) in comparison with patients with score 2 (N3 with NSUV > 9.2) who showed the worst outcomes (3 year DSS = 0%, Hazard ratio [HR] = 13.1, 95% confidence interval [CI] = 2.4-70.7; P = 0.003). Conclusion: Pretreatment FDG uptake in the metastatic neck lymph node together with nodal staging are independent prognostic factors in stage IV HPC patients. The proposed risk scoring system may be useful in risk stratification of HPC patients for future clinical research.

Hazards Model for 3-year Local Control (LC), Neck Control (NC), Disease Free Survival (DFS), Disease Specific Survival (DSS) and Overall Survival (OS) According to the Prognostic Risk Score

Risk score [*]	n	LC HR %95 (CI) P	NC HR %95 (CI) P	DFS HR %95 (CI) P	DSS HR %95 (CI) P	OS HR %95 (CI) P
Score 0#	12	1	1	1	1	1
Score 1	19	2.4 (0.6, 9.3) 0.189	1.7 (0.1, 1.8) 0.370	1.6 (0.6, 4.4) 0.333	3.6 (0.3, 16.3) 0.108	2.1 (0.7, 6) 0.159
Score 2	6	11.1 (2.3, 54.6) 0.003	7.7 (2, 30.2) 0.003	3.7 (1.7, 19.8) 0.006	13.1 (2.4, 70.7) 0.003	6 (1.8, 20.5) 0.004

* Score 0 (N1-2 with NSUV ≤ 9.2), score 1 (N3 or NSUV > 9.2) and score 2 (N3 with NSUV > 9.2).
 # Reference category.

Presentation Number **1008A**
Poster Session 1d: Imaging Disease/Organ Processes

Labeling and In vivo Localization of Ovarian Cancer Cells using a nearIR Probe and a Multi-Modality Imaging System

John Pizzonia¹, Jennie C. Holmberg², Sean P. Orton¹, Oscar Viteri², Jingyi Pan¹, Wenyi Che¹, Gil G. Mor², ¹Molecular Imaging, Carestream Health, Woodbridge, CT, USA; ²Department of Obstetrics, Gynecology, and Reproductive Sciences, Yale University School of Medicine, New Haven, CT, USA. Contact e-mail: john.pizzonia@carestreamhealth.com

Ovarian cancer is the fourth leading cause of cancer related deaths and the leading cause of gynecological cancer deaths. Recurrence and chemoresistance are the major hurdles in the management of patients with ovarian cancer. Ovarian cancer stem cells (OvCSC) have been postulated as the potential source of recurrence and chemoresistance. Persistence of chemoresistant OvCSC after debulking or chemotherapy may "heal" the cancer and lead to recurrence. Therefore identification of OvCSC and their complete removal is a pivotal stage for the treatment of ovarian cancer. Recent advances in reagent chemistry have facilitated the development of near Infra red emitting probes ideal for optical localization of tumor cells in vivo. The objective of the following study was to develop a new in vivo imaging model that allows for the detection and monitoring of OvCSC. We describe here the use of X-Sight 761 Nanospheres to detect intraperitoneal localization and growth of ovarian cancer stem cells. Ovarian cancer spheroid progenitors were labeled with X-Sight 761 Nanospheres (Carestream Health, Woodbridge, CT) and injected both intra-peritoneally (i.p.) and subcutaneously (s.c.) to Athymic nude mice. The Carestream In-Vivo Imaging System FX was used to obtain X-ray and, concurrently, near-infrared fluorescence images. Tumors were imaged for fluorescence at days 7, 14, and 21. Tumors were observed from different angles by automatic rotation of the mouse. On Day 21 the animals were sacrificed and tumor fluorescence was analyzed ex vivo. Nanospheres labeled almost 100% of the cells (verified by FACS). No difference on growth rate was observed between labeled and unlabeled cells. Following s.c. injection, tumors were observed and monitoring revealed strong signaling up to 21 days. A strong signal was also observed in the i.p. model corresponding to metastatic implants. By day 21, the percentage of labeled metastatic implants decreased to approximately 70%. Using the rotation system we were able to follow the location of the i.p. tumors. Labeling did not affect the metastatic capacity of the cells. We describe here the application of X-Sight 761 Nanospheres for labeling ovarian cancer cells and its use for in vitro and in vivo models. The system is highly efficient for labeling cells and it is retained for several passages. Following injection to the mouse, labeled tumors are detected after three weeks. Furthermore, the signal emitted by X-Sight 761 Nanospheres is detectable in intraperitoneal tumors.

Presentation Number **1009A**
Poster Session 1d: Imaging Disease/Organ Processes

Novel internalizing human antibodies targeting all subtypes of malignant mesothelioma

Arun K. Iyer¹, Xiaodong Zhu², Yang Su², Yue Liu², Jinjin Feng¹, Youngho Seo¹, Henry F. VanBrocklin^{1,4}, Courtney Broaddus^{3,4}, Bin Liu^{2,4}, **Jiang He**^{1,4}, ¹Radiology and Biomedical Imaging, University of California San Francisco, San Francisco, CA, USA; ²Anesthesia, University of California San Francisco, San Francisco, CA, USA; ³Lung biology center, University of California San Francisco, San Francisco, CA, USA; ⁴Hellen Dillen Family Comprehensive Cancer Center, University of California San Francisco, San Francisco, CA, USA. Contact e-mail: jiang.he@radiology.ucsf.edu

Background: Human antibodies targeting all subtypes of mesothelioma can be useful for imaging and therapy of this deadly disease. The objective of this study was to evaluate the tumor targeting of a novel rapidly internalizing human single chain antibody fragment (scFv) in a murine model bearing mesothelioma tumors of both epithelioid and sarcomatoid origins. **Methods:** A mesothelioma targeting scFv, M40, was labeled with ^{99m}Tc. For in vitro studies, the radiolabeled M40 was incubated at 37°C for 1 h with M28, VAMT-1 or control cells (BPH-1), to assess the total cellular binding versus intracellular uptake. Cy5.5 labeled M40 was used to monitor the in vitro intracellular uptake employing fluorescence microscopy. For animal studies, the radiolabeled M40 was administered to athymic mice bearing both M28 and VAMT-1 tumors, and imaged with a small animal-SPECT/CT at 1 and 3 h after injection with concomitant biodistribution at 1, 3 or 6 h. **Results:** The M40 scFv was radiolabeled in 70-85 % yield and remained stable in phosphate buffer up to 24 h. The ^{99m}Tc labeled M40 scFv was taken up rapidly and specifically by both M28 and VAMT-1 tumor cells but not by the non-target cells. Incubation of tumor cells with ^{99m}Tc labeled M40 scFv at 37°C resulted in internalization of 68-92% of the total cell-associated scFvs within 1 h; the specificity of binding was evidenced by successful blocking (up to 98%) with 10-fold excess unlabeled scFv. In animal studies, SPECT/CT showed significant tumor uptake in both subtypes of mesothelioma tumors as early as 1 h after injection. At 3 h after injection, tumor uptake was 4.38 and 5.84 percent injected dose per gram (%ID/g) for M28 and VAMT-1 tumors respectively, significantly greater than all other organs or tissues studied (liver, 2.62%ID/g; other organs or tissues <1.7%ID/g), except the kidneys (130.7%ID/g), giving M28 and VAMT-1 tumor-to-blood ratios of 5:1 and 7:1 and tumors-to-muscle ratios of 45:1 and 60:1, respectively. The target-mediated uptake was evidenced by nearly 70% reduction in tumor activity following administration of 10-fold excess unlabeled M40 scFv 1h prior to imaging. **Conclusion:** We showed that ^{99m}Tc-labeled M40 could bind and internalize selectively into both M28 and VAMT-1 tumors in vitro. In vivo studies on animals showed rapid and specific targeting into both epithelioid (M28) and sarcomatoid (VAMT-1) subtypes, demonstrating the potential as a versatile targeting ligand for imaging and therapy of mesothelioma, warranting further investigation.

Presentation Number **1010A**
Poster Session 1d: Imaging Disease/Organ Processes

18F-fluorodeoxyglucose PET/CT in Cholangiocarcinoma - SGH Experience

Winnie W. Lam, Wai Yin Wong, David C. Ng, Ajit K. Padhy, Kelvin S. Loke, Anthony S. Goh, Nuclear Medicine and PET, Singapore General Hospital, Singapore, Singapore. Contact e-mail: lamwinnie@gmail.com

Purpose: This paper aims to evaluate our experience with 18F-fluorodeoxyglucose (FDG) PET/CT in the detection of cholangiocarcinoma and associated distant and regional lymph node metastases. Materials and Method: Between November 2003 and October 2009, a total of 29 patients with biopsy-proved or presumed cholangiocarcinoma underwent PET/CT. Patient followup information and serial imaging were reviewed for progression of lesions detected by PET/CT. Results: Of the 29 study patients, 16 (55%) underwent preoperative staging PET/CT scans. Histologic confirmation of the diagnosis was used as the reference standard with which PET/CT results were compared. The sensitivity and specificity of PET/CT for identifying the primary tumor were 94% and 67% respectively. Distant and regional lymph node metastases were detected by PET/CT in 27% and 31% respectively. Conclusion: Most cholangiocarcinomas are FDG-avid tumors. PET/CT is also valuable in detecting unsuspected distant metastases which are not diagnosed by standard imaging.

Presentation Number **1011A**
Poster Session 1d: Imaging Disease/Organ Processes

In Vivo Imaging of DNA Damages and Repair in Cancer Chemotherapies

Yanming Wang¹, **Chunying Wu**¹, **Lili Liu**², **Stan Gerson**², ¹*Radiology, Case Western Reserve University, Cleveland, OH, USA;*
²*Medicine, Case Western Reserve University, Cleveland, OH, USA. Contact e-mail: yxw91@case.edu*

Background: Efficacy of DNA-targeted chemotherapeutic agents such as temozolomide is often compromised by intrinsic cellular responses such as DNA base excision repair (BER). Previous studies have shown that BER pathway results in formation of abasic or apurinic/apyrimidinic (AP) sites and inhibition of AP sites leads to significant reduction of drug resistance and enhancement of drug sensitivity. Thus, AP-site formation has been identified as an important biomarker in DNA-targeted chemotherapies. The objective of this study is to develop radiotracers for PET to directly quantify DNA damage and repair induced by various chemotherapeutic agents in cancer. Methods: Design, synthesis, and evaluation of PET imaging agents that bind to AP sites with high affinity and specificity. To date, we have developed positron-emitting [C-11]methoxyamine for positron emission tomography (PET) that allows for quantification of AP sites in vivo. Results: [C-11]methoxyamine has been synthesized with high radiochemical yield and purity. Following radiolabelling, microPET studies have been conducted to evaluate their pharmacokinetic profiles in melanoma and glioma xenograft tumor mouse models that are pre-treated with temozolomide to induce AP-site formation. Subsequent quantitative analysis showed that the radioactivity concentration were elevated in proportion to the AP sites induced in tumor regions pre-treated with temozolomide relative to tumor regions without any treatment. In vivo blocking studies based on microPET also showed that the agents bound to AP sites with high specificity. Conclusion: Our studies demonstrated that PET imaging can be used to monitor DNA damages and repair and evaluate efficacy of DNA-targeted therapeutic treatments in cancer. Clinical protocol has been approved by IRB for the first-in-human trial in cancer patients.

Presentation Number **1012A**
 Poster Session 1d: Imaging Disease/Organ Processes

Combined optical, magnetic resonance spectroscopic, and mass spectrometric imaging reveals the metabolic signature of hypoxic breast tumor regions

Lu Jiang¹, Kamila Chughtai², Tiffany R. Greenwood¹, Dmitri Artemov¹, Paul T. Winnard¹, Venu Raman¹, Zaver M. Bhujwala¹, Ron M. Heeren², Kristine Glunde¹, ¹Radiology Department - NMR Research - Oncology Section, Johns Hopkins University, Baltimore, MD, USA; ²FOM-Institute for Atomic and Molecular Physics, Amsterdam, Netherlands. Contact e-mail: ljiang12@jhmi.edu

Introduction: Tumor hypoxia triggers signaling cascades that have significant impact on normal biological processes. So understanding and being able to image the hypoxic response of tumors is critical. We studied links between hypoxia and metabolites in a human breast cancer model by combining in vivo magnetic resonance spectroscopic imaging (MRSI) with ex vivo optical imaging and mass spectrometric imaging (MSI). Methods: Human MDA-MB-231-HRE-tdTomato breast cancer cells, which express red fluorescent tdTomato protein under hypoxic conditions, were grown in female athymic nude mice. 3-dimensional (3D) water-unsuppressed MRSI to determine tumor shape and water-suppressed 3D MRSI to detect metabolites were performed. Each tumor was sectioned to obtain fiducially marked 2 mm-thick slices, which were imaged by bright-field and fluorescence microscopy to visualize hypoxia, and then sectioned to 10 μm-thick slices. Hematoxylin-and-eosin (H&E)-stained images and mass spectrometric images were obtained from sequential sections. We performed 3D reconstruction, registration of MRSI and optical images(Fig 1), and 2D registration of MSI and optical images of tumors(Fig 2). Results: The overlapping region between total choline signal and hypoxia normalized to the hypoxic region was 37.40%, while overlap with the normoxic region was only 14.07%. The glutamate/glutamine and lipid/lactate CH3 overlaps were increased in the normoxic region. The detection of other importantly metabolites included the heme group (m/z 616) and a molecular ion (m/z 734) in the normoxic region, and a molecular ion (m/z 644) in the hypoxic region. Conclusions: We developed a powerful multimodal imaging technology, which provides information on a multitude of metabolites and other biomolecules, to mine for novel biomarkers in hypoxic breast tumor regions. Increased tCho in the hypoxic region can be attributed to the hypoxia-inducible expression of choline kinase as previously reported, while occurrence of the heme group indicates the presence of red blood cells. We are currently further mining the observed changes for novel biomarkers. This work was supported by NIH R01 CA134695.

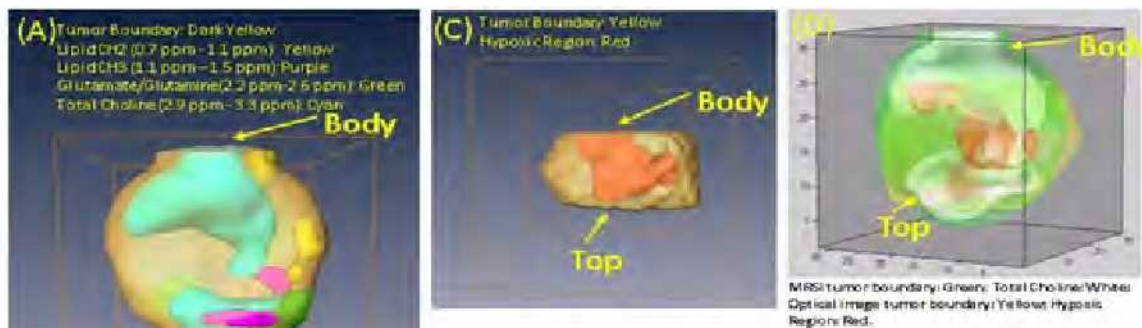


Fig. 1 (A) . 3D reconstruction of MRSI with tumor boundary and metabolites (Lipid CH₂, Lipid CH₃, Glutamate/Glutamine and Total Choline), and (B) corresponding single-voxel MR spectra. (C) 3D reconstruction of optical imaging with hypoxia in red. (D) 3D registration of optical imaging (yellow) and MRSI (green), with corresponding Total Choline (white) and hypoxic region (red).

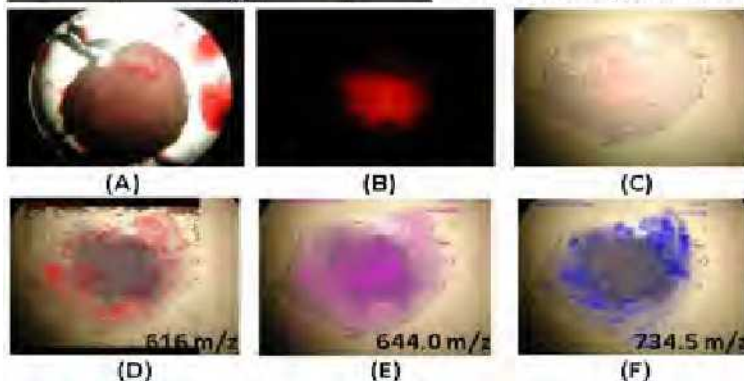


Fig. 2 (A) Bright field image of 2mm serial slice; (B) Fluorescence image of 2mm serial slice; (C) H&E staining of 10um serial slice; (D) overlay of H&E staining, fluorescence image (hypoxia in gray) and MSI (616m/z heme group in red); (E) overlay of H&E staining, fluorescence image (hypoxia in gray) and MSI (644m/z in pink); (F) overlay of H&E staining, fluorescence image (hypoxia in gray) and MSI (734.5m/z in blue).

Presentation Number **1013A**
Poster Session 1d: Imaging Disease/Organ Processes

Targeted delivery of contrast agents to leaky vasculature using sterically stabilized liposomes: implications in screening drugs for tumor and arthritis disease models

Britto S. Sandanaraj^{1,2}, Rainer Kneuer³, Stefan Wacha³, Hans-Ulrich Gremlich³, Janet Dawson², Thomas Krucker¹, ¹Global Imaging Group, Novartis Institutes for Biomedical Research, Inc, Cambridge, MA, USA; ²Autoimmunity, Transplantation and Inflammation, Novartis Institutes for Biomedical Research, Basel, Switzerland; ³Global Imaging Group, Novartis Institutes for Biomedical Research, Basel, Switzerland. Contact e-mail: sandanaraj.selvaraj@novartis.com

Fluorescence microscopy and Near-infrared fluorescence (NIRF) are important research tools in the area of in vivo imaging applications. These techniques can provide information at molecular level thus having a distinct advantage over other imaging modalities such as magnetic resonance imaging, computer tomography and nuclear imaging. Small molecule fluorescent probes have been widely used to address key biological questions in vitro as well as in cellular studies. However, these probes have very limited scope for in vivo applications because of their poor pharmacokinetic (PK) and pharmacodynamic properties (PD). In order to improve the PK and PD of optical probes for in vivo imaging applications, the present study focus on the use of sterically shielded liposomes (SSL) as delivery vehicles carrying probes to their target site. SSL protect the encapsulated materials from the inactivating effect of external conditions and provide the opportunity to encapsulate both hydrophilic and hydrophobic optical probes. These fluorescent nanoparticulate formulations have been found to be long circulating and passively targeting the leaky vasculature of inflamed or tumor tissue due to the enhanced permeation and retention (EPR) effect. Successful in vivo application of this methodology for screening drugs in tumor and arthritis disease models will be demonstrated

Presentation Number **1014A**
Poster Session 1d: Imaging Disease/Organ Processes

Cancer metastasis to lymph node in melanoma bearing mice is accompanied by abnormal lymphatic drainage and function

Sunkuk Kwon, Eva Sevick, *Institute of Molecular Medicine, University of Texas Health Science Center, Houston, TX, USA. Contact e-mail: sunkuk.kwon@uth.tmc.edu*

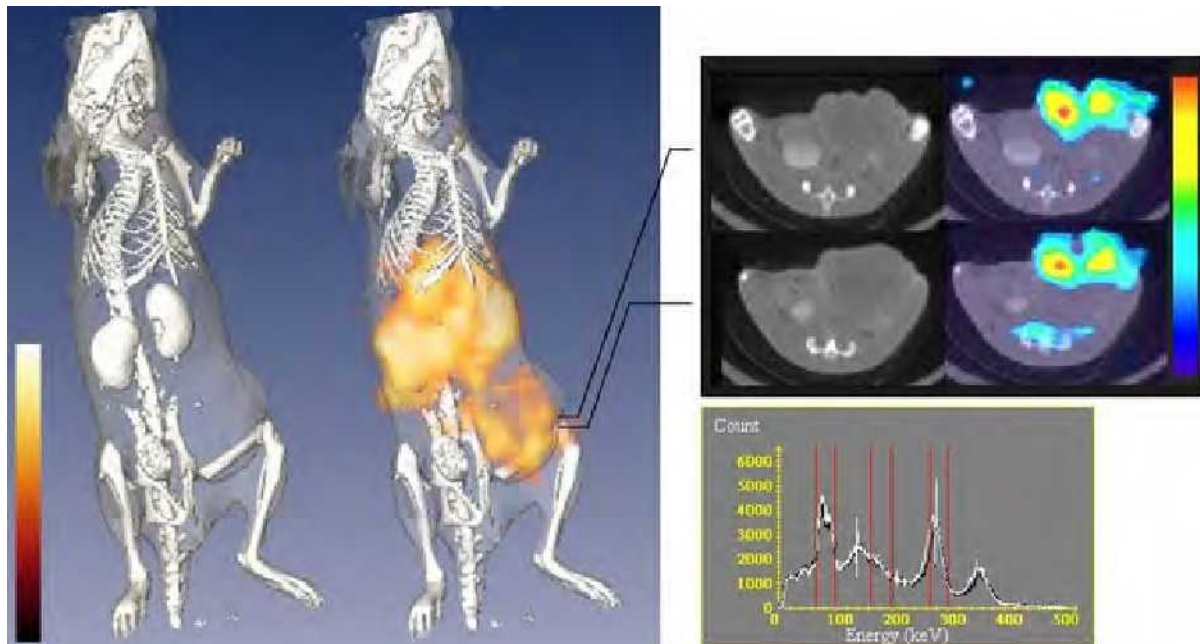
The lymphatic system provides a major route of cancer cell dissemination from the primary tumor to regional draining lymph nodes (LNs). Previously, it has been shown that lymph sinus remodeling/dilation along with LN lymphangiogenesis occurs prior to LN metastasis and LN lymphangiogenesis is required to increase lymph flow through the tumor draining LN. Yet to date there has been no in vivo imaging technique available to demonstrate functional and structural changes within the lymphatic system in response to tumor growth and metastasis. Herein, we employed a dynamic near-infrared (NIR) fluorescence imaging technique and showed spatial and temporal changes in lymphatic function and architecture during tumor progression. C57BL6 mice were injected with 2ul of indocyanine green (ICG) in the second digit of the foot and were dynamically imaged for baseline information before implantation of DsRed-expressing B16F10 melanoma cells to the dorsal aspect of the foot, and every three days for up to 27 days after inoculation. Our NIR fluorescence imaging data show significantly higher fluorescence intensity in the tumor draining popliteal LN (PLN), which is enlarged as confirmed by computed tomography (CT), as compared to the control PLN, indicating increased lymph flow to the tumor-associated PLN. In addition, metastases within lymphatic vessels were detected using red-fluorescence imaging of fluorescent cancer cell trafficking in lymphatics. When tumor involvement to the PLN increases, we observed (i) reduced fluorescent signals in the tumor draining PLN and (ii) abnormal lymphatic drainage and function to the inguinal LN and subsequently to the axillary LN as early as three days after implantation of tumor cells. More importantly, we could not observe altered lymphatic drainage in mice without PLN metastasis during the primary tumor growth. Our imaging results demonstrate that the dilation of the tumor draining LN, due possibly to LN lymphangiogenesis, is the early response to LN metastasis, which in turn increases lymph flow to the LN, and cancer metastasis to the LN is accompanied by abnormal lymphatic drainage and function. NIR fluorescence imaging technology can be used to non-invasively and quantitatively detect functional lymphatic changes associated with cancer, which may enable accurate nodal staging of cancer patients and provide new approaches to diagnose and treat cancer metastasis.

Presentation Number **1015A**
 Poster Session 1d: Imaging Disease/Organ Processes

Single-photon emission computed tomography imaging of Ga-67 citrate accumulation in experimental tumor models

Adrian Chrastina, Jan Schnitzer, Proteogenomics Research Institute for Systems Medicine, San Diego, CA, USA. Contact e-mail: achrastina@prism-sd.org

Ga-67 citrate scanning was extensively used for scintigraphic imaging of tumors, infected lesions and/or inflammatory activity in clinics. Ga-67 scans were largely substituted by 2-FDG based positron emission tomography (PET) imaging. However, recently gallium 67 scintigraphy regained attention as a sensitive indicator of inflammatory activity for identification of acute myocarditis and for imaging of lymphomas. Aim of our study was to analyze accumulation of Ga-67 citrate in experimental rodent tumor models using small animal computed tomography co-registered with single-photon emission computed tomography (CT-SPECT) system as well as to optimize settings of imagery platform. For this purpose, nude mice subcutaneously xenografted with human colorectal carcinoma cell line HT-29, balb/c mice bearing orthotopic murine mammary carcinoma 4T1 and Sprague-Dawley rats with intracranially implanted C6 gliomas were intravenously injected with Ga-67 citrate. CT and SPECT scans were acquired using X-SPECT second generation MicroSPECTR imaging system and tomographic projections were reconstructed by standard filtered backprojection algorithm and processed on AMIRA system. Analysis of CT-SPECT slices and 3D-reconstructed anatomic/functional fusion images showed significant uptake of Ga-67 tracer in HT-29 and 4T1 tumors at 72-96h post administration. Apparent accumulation of Ga-67 was also observed in liver, kidney and bone/bone marrow. Uptake of Ga-67 in the skull bone diminished effective imaging of intracranial C6 gliomas. Our findings suggest utility of Ga-67 as a non-specific marker for tumor imaging and cost-effective alternative to PET imaging in small animal models. Further insight into the molecular mechanism of Ga-67 uptake requires future correlative study with intratumoral inflammation.



CT-SPECT imaging of subcutaneous 4T1 tumor xenograft (96 h after intravenous injection of 20 mCi Ga-67 citrate).

Presentation Number **1016A**
Poster Session 1d: Imaging Disease/Organ Processes

Pretargeted PET imaging of hypoxia-inducible factor-1-active tumors with an oxygen-dependent degradable streptavidin and a ^{18}F -labeled biotin derivative

Masashi Ueda^{1,2}, Takashi Kudo², Hiroaki Konishi², Hidekazu Kawashima^{2,3}, Yuji Kuge⁴, Takahiro Mukai⁵, Masahiro Ono², Shinae Kizaka-Kondoh⁶, Masahiro Hiraoka³, Hideo Saji², ¹Radioisotopes Research Laboratory, Kyoto University Hospital, Kyoto, Japan; ²Graduate School of Pharmaceutical Sciences, Kyoto University, Kyoto, Japan; ³Graduate School of Medicine, Kyoto University, Kyoto, Japan; ⁴Central Institute of Isotope Science, Hokkaido University, Sapporo, Japan; ⁵Graduate School of Pharmaceutical Sciences, Kyushu University, Fukuoka, Japan; ⁶Graduate School of Bioscience and Biotechnology, Tokyo Institute of Technology, Yokohama, Japan. Contact e-mail: uedama@kuhp.kyoto-u.ac.jp

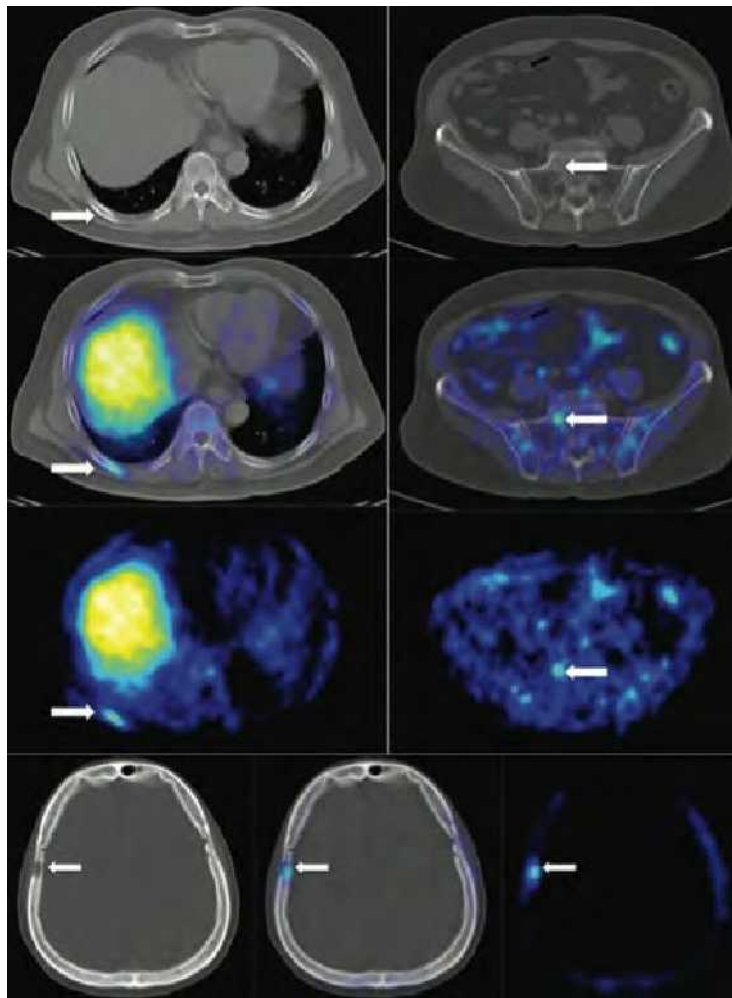
Introduction: Hypoxia-inducible factor-1 (HIF-1) is a master transcriptional activator of various genes related to tumor progression, metastasis, and resistance to therapy. We have developed a protein containing a protein transduction domain (PTD), an essential part of the oxygen-dependent degradation domain (ODD) of HIF-1 α , and a monomeric streptavidin (SAV) (PTD-ODD-SAV; POS). This protein was effectively delivered to and selectively stabilized in HIF-1-active cells. In the present study, we attempted to perform positron emission tomography (PET) imaging by using a pretargeting method based on the streptavidin-biotin system. This study aimed to evaluate the feasibility of POS pretargeting and (4- ^{18}F -fluorobenzoyl)norbiotinamide (^{18}F -FBB) for the PET imaging of HIF-1-active tumor cells. **Methods:** We first examined the biodistribution of ^{18}F -FBB alone and subsequently performed pretargeting studies. Tumor-implanted mice were pretargeted with POS. After 24 h, ^{18}F -FBB was administered and subsequently, the biodistribution of radioactivity was investigated. In addition, we performed an in vivo blocking study involving D-biotin pretreatment. In mice with tumors harboring the HIF-1-dependent luciferase reporter gene, tumoral ^{18}F -FBB accumulation was compared to the HIF-1 activity in the identical tumor. Metabolite analysis, autoradiography, and HIF-1 α immunohistochemical analysis were also performed using the same mice. Further, PET images were acquired. **Results:** The results of the biodistribution study revealed that ^{18}F -FBB alone was rapidly cleared from the mouse bodies with no evidence of tumor targeting (0.11% \pm 0.10% injected dose per gram tissue (ID/g) at 3 h after the administration of ^{18}F -FBB). In contrast, the tumor uptake increased more than 25-fold (2.85% \pm 0.55% ID/g at 3h) in the mice pretargeted with POS. Tumoral ^{18}F -FBB accumulation was significantly inhibited on pretreatment with D-biotin, and 79% of the radioactivity of the tumor was attributable to macromolecules. These results indicate that ^{18}F -FBB bound to POS in vivo. We obtained clear PET images of tumors at 3 h after the administration of ^{18}F -FBB in the pretargeted group. Further, we found that the tumoral ^{18}F -FBB accumulation positively correlated with the HIF-1 activity ($R = 0.72$, $P < 0.05$) and that the majority of ^{18}F -FBB-distributed areas corresponded to HIF-1 α -positive areas in the tumors pretargeted with POS. **Conclusion:** Pretargeting with POS and ^{18}F -FBB is effective for the PET imaging of HIF-1-active tumor cells.

Presentation Number **1017A**
Poster Session 1d: Imaging Disease/Organ Processes

Fluorocholine PET/CT for prostate cancers. Initial experience in a Singapore tertiary facility

Andrew Tan, Kelvin S. Loke, Sidney Yu, Anthony S. Goh, Nuclear Medicine and PET, Singapore General Hospital, Singapore, Singapore. Contact e-mail: andztan@yahoo.com.sg

Purpose: We present our initial experience in utilizing 18Fluorine-Fluorocholine (FCH) Positron Emission Tomography / Computed Tomography (PET/CT) in patients with histologically proven prostate carcinoma, outlining the technical and practical aspects in implementing such a clinical service. **Background:** Prostate cancer is a significant public health issue, being the leading cancer and second leading cause of cancer related death among men in the United States. There exists limitations to current diagnostic imaging techniques in the evaluation of patients with prostate carcinoma, with potential impact on management and outcomes. Molecular imaging techniques can potentially address several of these shortfalls. Of interest is the compound choline, which is a major component of cell membranes. Malignant tumors often show high proliferation and increased cell membrane metabolism, and the choline compound can be labeled with Fluorine-18, creating a positron tracer (FCH) that can potentially target areas of increased cell membrane metabolism and hence tumor cells. **Materials and Methods:** From January 2010, the Department of Nuclear Medicine and PET in the Singapore General Hospital initiated FCH PET/CT imaging as part of a prospective clinical trial evaluating its clinical use in the pre-therapy staging of prostate carcinoma as well as in the post-therapy assessment of patients with suspected recurrent disease. We illustrate our initial experiences with FCH PET/CT imaging, covering FCH radiopharmaceutical preparation and logistical handling, several technical and practical aspects involved in imaging of the patient, and case studies of patients. **Conclusion:** FCH PET/CT is a technically and practically feasible imaging technique that can be quickly and efficiently implemented into a molecular imaging facility, and shows excellent potential in clinical practice.



Axial CT, PET and Fused images of the head, chest and pelvis. White arrows highlight areas of increased FCH uptake, suspicious for tumor

Presentation Number **1018A**
 Poster Session 1d: Imaging Disease/Organ Processes

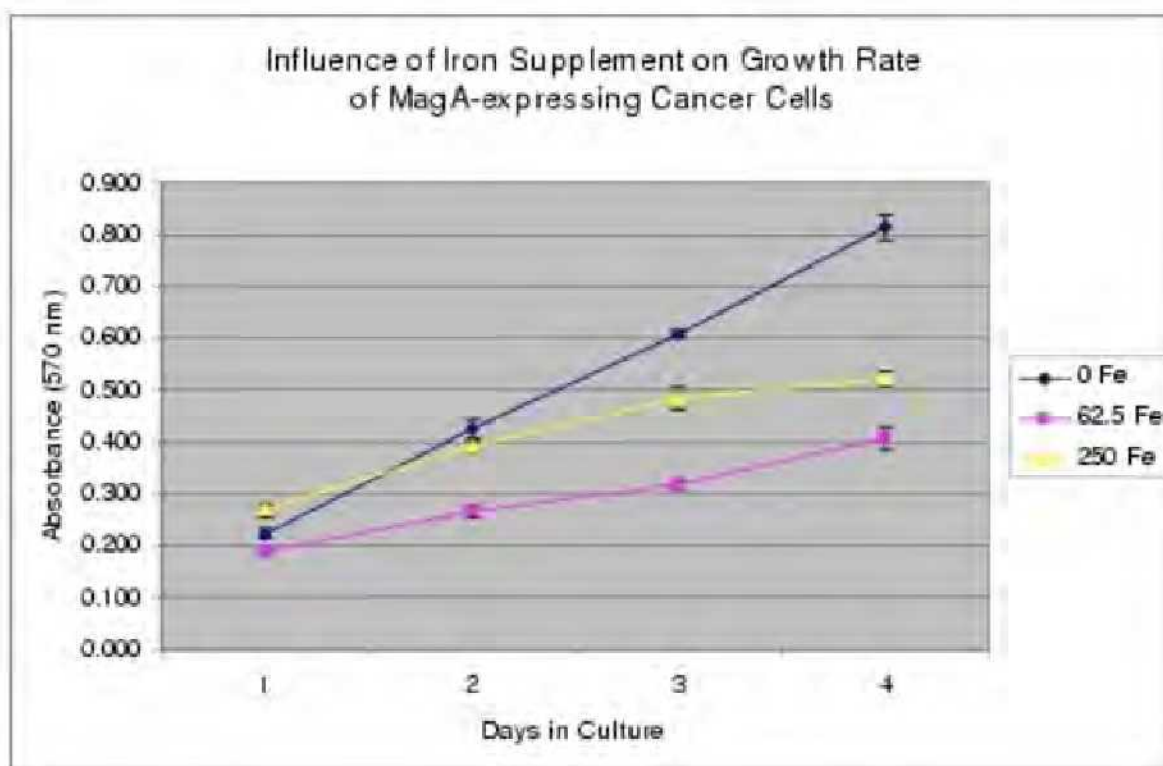
Effect of MagA Expression on Iron Regulation in a Human Cancer Cell Line

Donna E. Goldhawk^{1,4}, **Rene Figueredo**^{2,4}, **Paula Foster**^{3,4}, **James Koropatnick**^{2,4}, **R. Terry Thompson**^{1,4}, **Frank S. Prato**^{1,4}, ¹Lawson Health Research Institute, London, ON, Canada; ²London Regional Cancer Program, London, ON, Canada; ³Robarts Research Institute, London, ON, Canada; ⁴University of Western Ontario, London, ON, Canada. Contact e-mail: Donna.Goldhawk@lawsonimaging.ca

Formation of iron biominerals is a naturally-occurring phenomenon in magnetic bacteria, which produce magnetite in a membrane-enclosed compartment termed the magnetosome. Under the control of numerous genes, the magnetosome serves as a model upon which to (1) develop gene-based contrast in mammalian cells and (2) provide a mechanism for reporter gene expression in magnetic resonance imaging (MRI). We have developed expression vectors using the magnetosome gene MagA and demonstrated contrast enhancement in transfected cells and the tumours they form. However, little is known about the regulation of MagA activity in mammalian cells. To optimize intracellular contrast, we examined the behaviour of MagA-expressing cancer cells in the presence and absence of various iron supplements. Comparison to cells expressing vector or the modified ferritin subunits, lacking iron response elements, provided information about iron uptake and handling by a prokaryotic iron transporter functioning in a eukaryotic environment. Human MDA-MB-435 were transfected to provide a stable, clonal line of MagA-expressing cells. Their growth rate was measured using the MTT assay, monitoring mitochondrial activity subsequent to culture in iron-supplemented media containing either ferric nitrate, ferric ammonium citrate or hemin. We identified a greater decrease in the growth rate of MagA-expressing cells when cultured at lower concentrations of iron supplement: 60 μM versus 250 μM ferric nitrate (Figure). There was no effect of ferric nitrate on the MTT assay. Establishing the growth conditions conducive to optimal iron biomineralization in MagA-expressing cells will enhance the molecular imaging capabilities of MRI for cancer cell tracking.

May 5, 2010

Donna E. Goldhawk



Rate of MagA-expressing Cell Growth Varies with Concentration of Ferric Nitrate. Human MDA-MB-435 cells overexpressing MagA were cultured in the presence (squares, 62.5 μM ; triangles, 250 μM) and absence (diamonds, 0.25 μM) of iron supplemented medium.

Presentation Number **1019A**
Poster Session 1d: Imaging Disease/Organ Processes

Optical imaging of leukemia xenografts with near infrared probe conjugated to a monoclonal antibody

Sabrina Pesnel^{1,2}, Arnaud Pillon², Yoann Menon², Laurent Créancier², Stéphanie Lerondel¹, Alain Le Pape^{1,3}, Nicolas Guilbaud², Christian Bailly², Anna Kruczynski², ¹CIPA, TAAM, UPS44 - CNRS, Orléans, France; ²Centre de Recherche en Oncologie Experimentale, Institut de Recherche Pierre Fabre, Toulouse, France; ³INSERM U618, Tours, France. Contact e-mail: sabrina.pesnel@cncrs-orleans.fr

For experimental oncology with orthotopic models of leukemia in mice, imaging is the only non-invasive resource to assess both tumor progression and to locate tumor foci. When cells are genetically modified to emit light, bioluminescence imaging (BLI) can be used. But in some case it is not possible because either the transfection method does not work or is suspected to modify the characteristics of the tumor cells. The aim of this work was to develop an alternative method to the BLI. The strategy consisted in using a monoclonal antibody (mAb) labeled with a near infrared optical probe suited for fluorescence imaging (FLI). A mouse anti-human mAb against the CD44 human myeloid marker was chosen. It was labeled with Alexa Fluor 750 to get a low in vivo autofluorescence, so as to enhance sensitivity. Scid nod mice were injected intravenously with 5x10⁶ human leukemia HL60 cells stably transfected with a luciferase-expressing gene. The use of bioluminescent cells allowed us to compare BLI and FLI and to determine the minimal mAb dose required to detect all foci. In a second time, mice received three weekly injections of the minimal dose of the AF750-CD44 mAb to determine the impact of the antibody on tumor progression. The results showed a good correlation between BLI and FLI and 1µg of AF750-CD44 was sufficient to detect all foci in mice. However, this low dose of mAb showed a strong impact on cell proliferation when it was injected early after leukemia induction. Indeed, a growth inhibition, calculated as the ratio of the median bioluminescence of mAb-treated versus control group was observed and achieved 1.2% on day 59. In addition, the increase of survival leukemia-bearing mice, treated by multiple injections of AF750-CD44 mAb, was significant, as assessed by the Log-rank test (p=0.009). This study reveals that it is possible to detect leukemic foci with a mAb labeled with a near infrared fluorochrome but another human leukemic marker must be selected to avoid a therapeutic response. The use of labeled mAb fragments is currently under investigation.

Presentation Number **1020A**
Poster Session 1d: Imaging Disease/Organ Processes

Functional Imaging of Neuroendocrine Tumors

Andrew Tan, Sidney Yu, Arthur Ng, Anthony S. Goh, Nuclear Medicine and PET, Singapore General Hospital, Singapore, Singapore.
Contact e-mail: andztan@yahoo.com.sg

Purpose: To illustrate the use of various functional imaging techniques and modalities in the diagnosis, prognostication, management stratification and interval assessment of patients with neuroendocrine tumors. **Background:** Neuroendocrine tumors are a heterogeneous group of tumors that phenotypically are composed of cells that belong to the system of disseminated neuroendocrine cells. These cells are derived from their similarity to neural cells in the expression of certain proteins, such as synaptophysin, neuron-specific enolase and chromogranin A. They can arise from a wide variety of organ systems and locations, with gastroenteropancreatic neuroendocrine tumors being the most common. There are intrinsic limitations in anatomical diagnostic imaging techniques, predominantly related to the non-specific nature of such imaging and the absence of functional information. Molecular imaging techniques potentially address several of these limitations, allowing for more accurate assessments of such tumors. **Materials and Methods:** We present several of the commonly used molecular imaging techniques used for neuroendocrine tumors, including Meta-iodobenzylguanidine (MIBG) scintiscan, Fluorine-18 Fluorodeoxyglucose (FDG) positron emission tomography, and somatostatin receptor scintigraphy using both gamma and positron emission imaging, illustrating the clinical uses of these molecular imaging modalities with selected case studies. **Conclusion:** There exist a variety of molecular imaging techniques available for use in neuroendocrine tumors, the selection of which depending on clinical requirements, and existing technical and professional capabilities.

Presentation Number **1021A**
Poster Session 1d: Imaging Disease/Organ Processes

Non-invasive Imaging of Tumour Cell Death using a Hsp90 Ligand

Danielle Park¹, Anthony Don¹, Tania Massamiri², Amol Karwa², Beth Warner², Christine L. Hemenway², Arati D. Naik², Kah-Tiong Kuan², Pierre J. Dilda¹, Jason Wong¹, Lori K. Chinen², Mary Dyszlewski², Philip J. Hogg¹, ¹Lowy Cancer Research Centre, Prince of Wales Clinical School, University of New South Wales, Sydney, NSW, Australia; ²Covidien, Imaging Solution, , St Louis, MO, USA.
Contact e-mail: danielle.park@student.unsw.edu.au

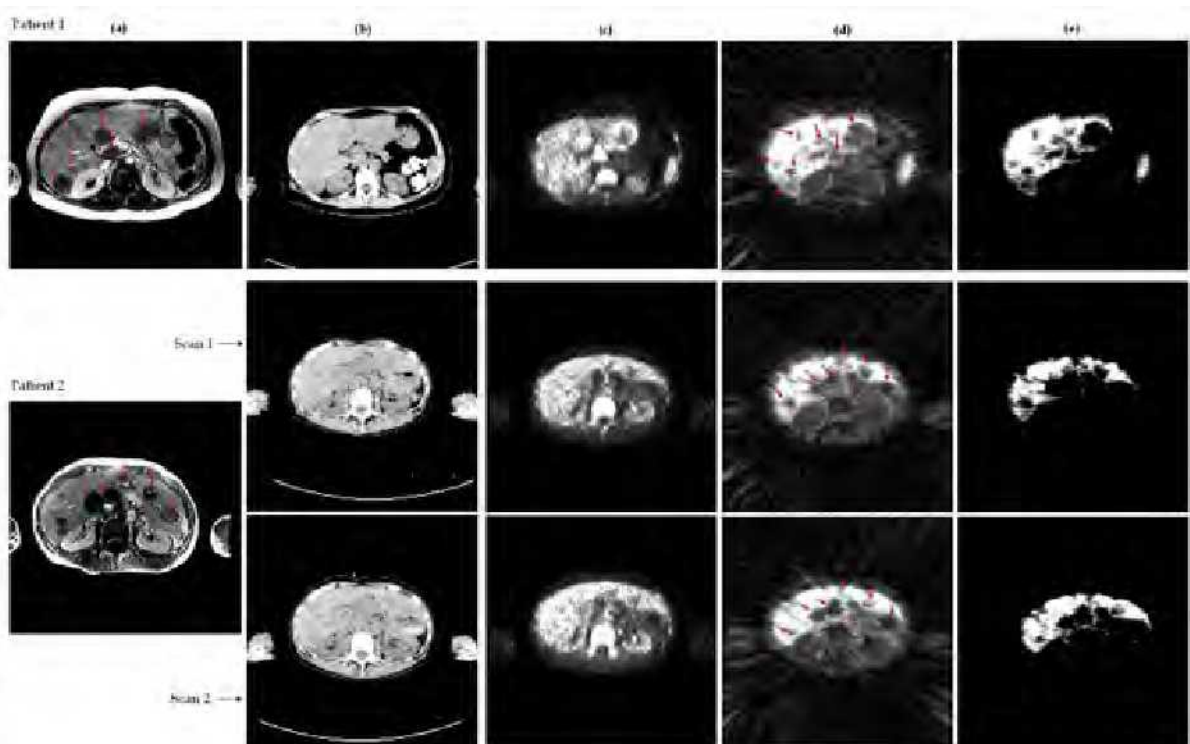
Cell death plays an integral role in turnover of cells in the gastrointestinal tract, the menstrual cycle and the immune system. Imbalance of this process is often associated with disease. Excessive cell death is characteristic of vascular disorders, neurodegenerative diseases, myelodysplastic syndromes, ischaemia/reperfusion injury and organ transplant rejection, among others. Despite our understanding of its molecular basis there are no situations where specific measures of cell death are used in diagnosis or patient management. In particular, solid tumours generally contain a large number of dying or dead cells. Cell death is also central to cancer therapy. Most chemotherapeutics, radiation treatments and anti-hormonal agents act by inducing death of target cells. GSAO (4-(N-(S-glutathionylacetyl)amino) phenylarsonous acid) is a synthetic tripeptide trivalent arsenical that rapidly accumulates in dying and dead tumour cells. Tagging of GSAO with a reporter group allows non-invasive imaging of tumour cell death in rodents. GSAO rapidly accumulates in the cytosol of cells during the mid to late stages of apoptotic cell death, coincident with loss of plasma membrane integrity. The compound is retained in the cytosol predominantly by covalent reaction with the 90-kDa heat shock protein (Hsp90), the most abundant molecular chaperone of the eukaryotic cytoplasm. GSAO tagged with a radioisotope (¹¹¹In-DTPA-GSAO) was used to non-invasively image tumour cell death in murine Lewis Lung carcinoma and human CT26.WT colon carcinoma tumours in mice by SPECT/CT. Treatment of the Lewis Lung tumours with cyclophosphamide or CT26 colon tumours with doxorubicin resulted in significant tumour cell death, which was detected with ¹¹¹In-DTPA-GSAO. The cell death imaging was superior to that achieved using ^{99m}Tc-Annexin V. In conclusion, GSAO is an effective imaging agent for tumour cell death in mice and can be used to monitor the efficacy of chemotherapy.

Presentation Number **1022A**
 Poster Session 1d: Imaging Disease/Organ Processes

Temporal Shape Driven Filtering (TSDF) to enhance contrast of liver against liver metastases and other organs in FLT-PET

Mahbubunnabi Tamal¹, Ioannis Trigonis¹, Marie-Claude Asselin¹, Anne Armstrong², Laura H. Horsley¹, Gordon Jayson², Alan Jackson¹, ¹Wolfson Molecular Imaging Centre, The University of Manchester, Manchester, United Kingdom; ²The Christie NHS Foundation Trust, Manchester, United Kingdom. Contact e-mail: M.Tamal@manchester.ac.uk

High physiological uptake of [¹⁸F]Fluorothymidine (FLT) due to liver glucuronization reduces tumour contrast limiting the utility of FLT-PET in assessing liver metastases. Temporal intensity information based clustering for FLT-PET has previously been applied [1]. Here we propose a temporal shape driven filtering (TSDF) method which enhances contrast between healthy liver and liver metastases in FLT-PET utilizing the shape of each voxel time activity curve independently of voxel intensity. The work is inspired by the work 'Active Shape Model' [2]. Voxels are classified based on the fitting distance of the temporal shape of activity with a particular trained temporal shape model (TSM). The TSM was trained using normal liver FLT uptake temporal data from 2 separate scans of 1 patient. Dynamic images of 3 separate FLT-PET scans of 2 patients with known liver metastases were then used for the test and results were validated with MRI. The proposed TSDF distance map enhances contrast of liver metastases (both hot and cold) that are non-identifiable in original PET images. It also separates liver from other organs with high FLT uptake, e.g., vertebra, kidney, aorta (Figure 1). This method could circumvent the limitations of FLT-PET in assessing liver metastases. Furthermore distance maps generated using different tissue kinetics would help to identify other organs or tissues (e.g. blood vessels). The enhanced image then can be used in accurate co-registration of FLT-PET with other high spatial imaging modalities, e.g. MRI, to delineate tumours. [1] Gray et al, 2010, Kinetic filtering of [¹⁸F]Fluorothymidine in positron emission tomography studies, *Phys. Med. Biol.* (55), 695-709. [2] Cootes et al, 1995, Active shape models- their training and application, *Comp. vis. Imag. Under.* (61), 38-59.



(a) T1-weighted MRI images of two patients with red arrows indicating liver metastases, (b) anatomical CTs of PET-CT, (c) original FLT-PET images at 45-60 minutes (OSEM reconstruction), (d) the distance map images with red arrows indicating liver metastases, (e) segmented healthy liver. 1st row contains images of one patient, 2nd and 3rd rows contain two different scans of another patient taken 5 days apart (images (b)-(e)).

Presentation Number **1023A**
 Poster Session 1d: Imaging Disease/Organ Processes

Changes in Tumor Microenvironment in a Human Colorectal Xenograft model following Cediranib (AZD2171, Recentin) treatment

Khushali Kotedia¹, **Louisa Bokacheva**¹, **Megan Reese**¹, **Sally-Ann Ricketts**², **Jane Halliday**², **Jason A. Koutcher**¹, **Sean Carlin**¹,
¹Medical Physics, Memorial Sloan-Kettering Cancer Center, New York, NY, USA; ²Imaging, AstraZeneca, Macclesfield, United Kingdom. Contact e-mail: kotediak@mskcc.org

Introduction: Optimizing the clinical utility of antiangiogenic drugs requires greater understanding of the specific consequences of their vascular-modifying action. Cediranib (AZD2171, Recentin), is a highly potent inhibitor of tyrosine kinase activity associated with vascular endothelial growth factor (VEGF) receptors-1, -2 and -3, currently in Phase II/III clinical trials. Non-invasive imaging was used to determine a relationship between administration and changes in tumor cellularity/perfusion using diffusion-weighted imaging (DWI), dynamic contrast-enhanced (DCE) MRI and comparing to histological markers of vasculature as surrogates of tumor response to cediranib. **Methods:** Rats bearing human HT29 colorectal tumors at ~1cm³ were imaged at pre-treatment (n=12) and randomized into vehicle control (0.5% methylcellulose w/v, n=6) and cediranib-treated cohorts (3x3mg/kg over 48h, imaging was performed 2h after final dose of cediranib was given, n=6). DWI and DCE-MRI were performed on a 7T spectrometer. For DCE-MRI, Gd-DTPA (0.2mmol/kg) was injected via the tail vein after 2min of baseline acquisition followed by 14min of dynamic acquisition. Apparent diffusion coefficient (ADC) maps, initial area under the curve (IAUC), enhancing fraction (EnF) and the Hoffman-derived Akep (reflecting vascular permeability/perfusion) were determined. Following MRI, rats were injected with the perfusion marker Hoechst 33342, sacrificed and excised for histological analysis of multiple vascular parameters. **Results:** No change in ADC values were observed between pre and post cediranib treated animals, suggesting minimal changes in tumor cellularity (Figure 1A). IAUC, EnF and Akep indicate a drug-dependent reduction in overall tumor perfusion when compared to controls after 48h (Figure 1B-D). These findings were corroborated by histochemical analysis of tumor vasculature and perfusion. **Conclusion:** DCE-MRI can be used to detect changes in perfusion following cediranib treatment. These changes are observed within 48 hours following commencement of treatment. These findings suggest that DCE-MRI may be useful in the early assessment of tumor response to cediranib. Further work is underway to investigate the effect of drug treatment 4 and 7 days post treatment.

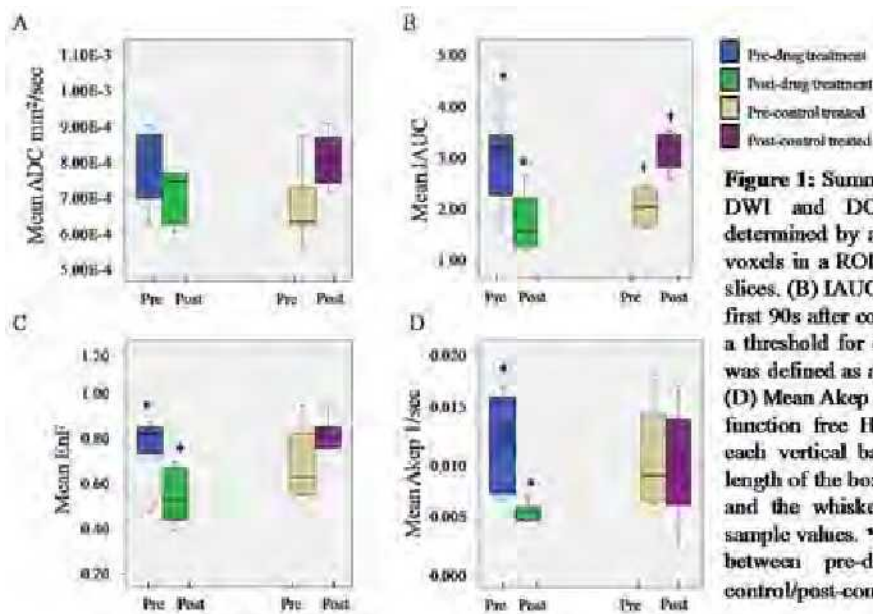


Figure 1: Summary of parameters determined from DWI and DCE-MRI data. (A) Mean ADC determined by averaging the ADC values from all voxels in a ROI drawn around the whole tumor on slices. (B) IAUC determined by integrating over the first 90s after contrast arrival, (C) Mean EnF where a threshold for enhancing pixels in the tumor ROI was defined as a signal change greater than muscle. (D) Mean Akep derived from using the arterial input function free Hoffmann Model. The bold line in each vertical bar indicates the median value, the length of the box show the lower and upper quartile and the whiskers show the smallest and largest sample values. * and | significance taken as $p < 0.05$ between pre-drug/post-drug treated and pre-control/post-control treated, respectively.

Presentation Number **1024A**
Poster Session 1d: Imaging Disease/Organ Processes

Should Gallium 68 labelled somatostatin receptor PET/CT be made the new 'gold' standard for staging gastrointestinal neuroendocrine tumours? A review of the pattern of metastasis and comparison with conventional cross sectional imaging

Tian Yue Kok, Pin Lin Kei, Singapore General Hospital, Singapore, Singapore. Contact e-mail: kok.tian.yue@gmail.com

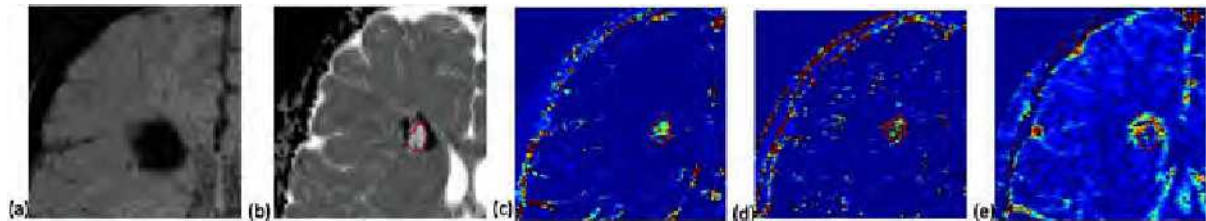
Gastrointestinal neuroendocrine tumours often pose a diagnostic challenge on conventional morphological imaging, which essentially depends on lesion contrast enhancement characteristics. Hence, there has been a long standing role for octreotide or MIBG labelled radionuclide imaging. However, though nuclear medicine technique lends greater specificity, the lack of anatomical detail and poorer spatial resolution often leads to improper staging or hampers treatment decisions e.g extent of surgical resection or metastastectomy. Gallium 68 labelled octreotide derivative tracers are now emerging as an alternative tracer, with demonstrated increased affinity to somatostatin receptors compared to octreotide or MIBG. Coupled with PET/CT, this promises to overcome the noted deficiencies of conventional nuclear medicine techniques. We evaluate our institutional experience in using this new technique to evaluate gastrointestinal neuroendocrine tumours. Through this, we aim to answer the following questions : - whether spread to the liver is mandatory before metastasis elsewhere in the body - what is the best imaging modality to evaluate for neuroendocrine liver metastasis - whether the relative avidity of the tumour for Gallium 68 SRS tracer has prognostic value similar to that noted for some tumours using FDG PET - whether SRS PET/CT has a role in monitoring treatment response

Presentation Number **1025A**
Poster Session 1d: Imaging Disease/Organ Processes

Change in water transport balance in cerebral cavernous malformation as visualized in dynamic contrast enhanced MRI, susceptibility imaging and diffusion maps

Hsiang-Ling Huang¹, YuChun Lin^{2,3}, Yau-Yau Wai^{1,3}, Yih-Ru Wu⁴, Jiun-Jie Wang¹, ¹Medical Imaging and Radiological Science, Chang Gung University, Taoyuan, Taiwan; ²Electrical Engineering, Chang Gung University, Taoyuan, Taiwan; ³Diagnostic Radiology, ChangGung Memorial Hospital, Taoyuan, Taiwan; ⁴Neurology, ChangGung Memorial Hospital, Taoyuan, Taiwan. Contact e-mail: sandralovegreen@hotmail.com

Poupose: To assess the tumor microenvironment of cerebral cavernous malformation (CCM) by incorporating Dynamic contrast-enhanced (DCE) MRI, Susceptibility Weighted Images (SWI) and Diffusion weighted imaging (DWI) Materials and Methods: MRI from 10 patients with CCMs were measured by a 3 Tesla MRI scanner. DCE MRI were acquired by a T1-weighted gradient-echo sequence (TR/TE = 250/2.46 ms, 7 slice of 4-mm, 130 measurements, gadodiamide administration 0.1 mmol/Kg of 3 mL/sec). Other imaging sequences included SWI (TR/TE = 28/20 ms, 8 slice of 1.2-mm) and DWI (TR/TE = 5100/91 ms, 56 slice of 4-mm). Baseline longitudinal-relaxation time was calculated from three acquisitions of different flip angles (2°, 10°, and 35°). DCE MRI was analyzed in a two compartments model. Maps of permeability (Ktrans), volume fraction of extravascular extracellular space (Ve) and capillary vascular plasma space (Vp) were calculated. Apparent diffusion coefficients (ADC) were calculated in a pixelwise manner. Phase mask of SWI was created. Results and Discussion: Figure shows the SWI (a), ADC (b), Ktrans (c) and Ve (d) and Vp (e) from a patient with CCM. SWI showed an extensive region of signal loss, suggesting the existence of excessive blood product inside the lesion. The red circle indicated increases in ADC and the corresponding Ktrans and Ve in the central core of the lesion. The increase of vessel permeability is consistent with the increase of free water in the extracellular space. Reduced ADC was noticed at the peripheral rim of the lesion, which corresponds to the increased Vp and a signal void in SWI. It suggests that a clot with an increased vascular plasma space. Conclusion: DCE MRI combined with diffusion and susceptibility weighted imaging provided complimentary information, which helps to define the underlying physiological changes in blood/water transport balance, for example, in patients with cerebral cavernous malformation.



Presentation Number **1026A**
Poster Session 1d: Imaging Disease/Organ Processes

Bioluminescence reporter gene assay to investigate hypoxic signaling in gliomas

Sandra Bürgi¹, Steffi Lehmann¹, Johannes vom Berg², Markus Rudin^{1,3}, ¹*Institute for Biomedical Engineering, ETH and University of Zurich, Zurich, Switzerland;* ²*Department of Pathology, Experimental Immunology, University of Zurich, Zurich, Switzerland;* ³*Institute of Pharmacology and Toxicology, University of Zurich, Zurich, Switzerland.* Contact e-mail: buergi@biomed.ee.ethz.ch

Tumor hypoxia is a microenvironmental factor that plays a key role in the malignant progression of many types of cancer including gliomas. It triggers the stabilization and activity of the family of oxygen sensitive transcription factors, so called hypoxia inducible factors, HIFs. These have been shown to regulate fundamental processes for the tumorigenesis such as angiogenesis, cell survival, anaerobic glycolysis and cell migration. So far it is not fully understood to which extent hypoxia influences progression of gliomas. To study the role of hypoxic signaling events in the progression of malignant gliomas a bioluminescence reporter gene assay has been used. We have stably transfected different glioma cell lines (LN229, U87, and GL261) with both, a HIF-1 α -firefly luciferase fusion construct and a plasmid driving the expression of luciferase from a HIF responsive promoter (HRE). These constructs have both been established and characterized previously in C51 colon cancer cells and used for longitudinal monitoring of hypoxia signaling in murine tumor xenografts implanted subcutaneously [1]. In vitro experiments have demonstrated oxygen dependent regulation and functionality of the reporter proteins in all three glioma cell lines for both the HIF-1 α fusion and the HRE construct. Initial in vivo experiments were performed by subcutaneous injection of the tumor cells as xenografts into nude mice. In vivo bioluminescence imaging in tumor bearing mice revealed distinct activation of the HIF system in the tested glioma models. The next step we will be monitoring of hypoxia signaling in orthotopic brain tumors. Comparing glioma cell lines of different degree of malignancy should allow studying the role of HIF signaling with regard to cell migratory properties and host tissue infiltration. [1] Lehmann S, et al., Proc Natl Acad Sci USA 2009 Aug 18;106(33):14004-9.

Presentation Number **1028A**
Poster Session 2d: Imaging Disease/Organ Processes

Noninvasive optical imaging of cancers with fluorescent retinoid probes

*Wei Wang, Arlin G. Cameron, Juliet Wendt, Michel E. Mawad, Shi Ke, Radiology, Baylor college of medicine, Houston, TX, USA.
Contact e-mail: shik@bcm.tmc.edu*

Imaging technology plays an important role in early detection of cancers and improved prognoses. Among of the various imaging techniques used near infrared (NIR) optical imaging is an active and promising area for both in vitro and in vivo molecular imaging studies. However, NIR fluorophores normally only possess optical imaging properties without selectivity to diseased tissues. To address this problem, a targeting moiety can be introduced to help to deliver the imaging report to its target. It is know that retinoids, analogs of vitamin A, are assessed for multiple therapeutic uses. In particular, their potential chemopreventive and therapeutic roles in different kinds of cancers have attracted much attention. The cancer types include head and neck, lung, breast, esophagus, colon, kidney, prostate, bladder cancers and so on. Considering the important role of retinoids in cancer treatment, developing retinoid derivatives as targeting imaging agents should be a useful approach for noninvasive detection and characterization of solid tumors. Herein, we demonstrate optical imaging of different kinds of cancers from cell level to whole body with fluorescent retinoid probes generated in house.

Presentation Number **1029A**
Poster Session 2d: Imaging Disease/Organ Processes

Fluorescence-guided real-time endoscopic peritoneal ovarian cancer detection using a gamma-glutamyltransferase sensitive ultra-fast enzyme-activatable imaging probe

Hisataka Kobayashi¹, Nobuyuki Kosaka¹, Masayo Sakabe², Daisuke Asanuma², Makoto Mitsunaga¹, Mikako Ogawa¹, Mako Kamiya³, Tetsuo Nagano², Peter Choyke¹, Yasuteru Urano³, ¹Molecular Imaging Program, National Cancer Institute/NIH, Bethesda, MD, USA; ²Graduate School of Pharmaceutical Sciences, The University of Tokyo, Tokyo, Japan; ³Graduate School of Medicine, The University of Tokyo, Tokyo, Japan. Contact e-mail: Kobayash@mail.nih.gov

From our library of peptidase- or glycosidase-sensitive fluorescence imaging probes we selected a gamma-glutamyltransferase sensitive enzyme-activatable fluorescence imaging probe (gGlu-HMRG), which is based on a chemically quenched rhodamine derivative. This probe exhibits no fluorescence emission before activation but becomes highly fluorescent within seconds to minutes of exposure to gamma-glutamyltransferase expressing cells. In this study, we used 11 different ovarian cancer cell lines and 6 different peritoneal metastasis models to evaluate the *in vitro* and *in vivo* efficacy of this gGlu-HMRG activatable probe. Eleven ovarian cancer cell lines were incubated with this gGlu-HMRG probe for 10 and 60 min and examined with a fluorescence microscope and flow cytometry. Six of 11 cell lines successfully established peritoneal cancer nodules *in vivo* in athymic mice. These tumor models were observed before and after spraying 15 nmol of gGlu-HMRG probe on the surface of the peritoneum using a home-designed miniature fluorescence endoscope system. *In vitro* studies showed nine of 11 ovarian cancer cell lines quickly and strongly activated the gGlu-HMRG probe within 10 min. Two other cell lines (SKOV3 and OVCAR4) emitted moderate fluorescence at 60 min after incubation. Four of 6 peritoneal tumors emitted strong fluorescence signal within 5 min after spraying the gGlu-HMRG probe. Among them, SHIN3 tumors were the most clearly and quickly visualized with fluorescence appearing within 10 seconds after spraying the gGlu-HMRG probe. Moreover, since the normal peritoneal membrane did not activate the gGlu-HMRG probe and minimal leakage of the activated gGlu-HMRG probe was found around the tumor nodules, the tumor-to-background ratio was as high as 50 within 10 min of spraying the gGlu-HMRG probe. Sensitivity and specificity of SHIN3-DsRed tumors (>0.05mm², n=104) was 100% and 100%, respectively, with an appropriate threshold setting. This gGlu-HMRG probe was activated by most ovarian cancer cells within 5 min with minimal background. Therefore, gGlu-HMRG is a promising molecular imaging probe for assisting physicians during endoscopic and surgical evaluation of disseminated ovarian cancer.

Presentation Number **1030A**
Poster Session 2d: Imaging Disease/Organ Processes

Discovery of a Breast Cancer Targeting Peptide for Imaging and Treatment

*Bettina Proneth¹, Wouter H. Driessen¹, Amin Hajitou², Fernanda I. Staquicini¹, Maria Hoh³, Zaver M. Bhujwalla³, Suren Soghomonyan⁴, Leo G. Flores⁴, Mian M. Alauddin⁴, Juri G. Gelovani⁴, Wadih Arap¹, **Renata Pasqualini¹**, ¹David H. Koch Center, The University of Texas M. D. Anderson Cancer Center, Houston, TX, USA; ²Imperial College London, London, United Kingdom; ³The Russell H. Morgan Department of Radiology and Radiological Science, The Johns Hopkins University School of Medicine, Baltimore, MD, USA; ⁴Department of Experimental Diagnostic Imaging, The University of Texas M. D. Anderson Cancer Center, Houston, TX, USA. Contact e-mail: rpasqual@mdanderson.org*

The American Cancer Society estimates 192,370 women will be diagnosed with breast cancer in the United States in 2009, and approximately 40,170 will die of this disease. In working towards a ligand-directed theranostic approach in breast cancer, we have developed an in vivo screening method, where peptides that home specifically to the vascular component of tissues are selected after intravenous administration of an engineered combinatorial peptide phage library. A combinatorial phage library displaying cyclic peptides was injected intravenously in tumor-bearing mice after which phage was recovered from the tumor-tissue in a process termed biopanning. Sequencing of recovered phage revealed several candidate peptides. One breast cancer targeting peptide (BCTP) was recovered from all tumors with the highest frequency. This peptide showed marked tumor homing as verified by immunohistochemistry (IHC). We used peptide affinity chromatography and tandem mass spectrometry to identify the target receptor of BCTP. Strikingly, this newly discovered receptor plays an as yet unrecognized role in the pathology of breast cancer. The BCTP was conjugated to dual-labeled liposomes with fluorescent markers for ex vivo optical imaging and chelated gadolinium for in vivo T1 weighted MR-imaging. To investigate if the BCTP receptor is a relevant candidate drug target in human breast cancer, we obtained biopsy samples of breast cancer patients prior to chemotherapy. Strong immunoreactivity of the BCTP receptor was observed in the tissue sections. Next, mammary tumor-bearing mice were systemically treated twice per week with BCTP and controls. BCTP treated mice demonstrated a marked decrease in tumor size of treated mice, compared to controls. In summary, we have identified, characterized and validated the peptide BCTP, specifically homing to highly aggressive, vascularized breast tumors. In addition to its tumor targeting capabilities this peptide possesses anti-tumor function in itself, inhibiting tumor growth and progression in tumor-bearing mice. The peptide can be used for molecular imaging of receptor-expression using T1-weighted MR-imaging with Gadolinium-containing liposomes. More importantly, the target receptor expression has been verified in human biopsy samples of breast cancer, indicating that this protein might be a promising new drug target.

Presentation Number **1031A**
Poster Session 2d: Imaging Disease/Organ Processes

Radiopharmacological evaluation of 6-deoxy-6-[¹⁸F]fluoro-D-fructose (6-[¹⁸F]FDF) as a new radiotracer for imaging breast cancer

Melinda Wuest¹, **Brendan J. Trayner**², **Grant Tina**³, **Hans-Soenke Jans**¹, **John Mercer**¹, **David Murray**¹, **Frederick West**³, **Alexander J. McEwan**¹, **Frank Wuest**¹, **Chris I. Cheeseman**², ¹*Department of Oncology, University of Alberta, Cross Cancer Institute, Edmonton, AB, Canada;* ²*Department of Physiology, University of Alberta, Edmonton, AB, Canada;* ³*Department of Chemistry, University of Alberta, Edmonton, AB, Canada. Contact e-mail: mwuest@ualberta.ca*

Several clinical studies have revealed low or negative expression of GLUT1 in breast cancer patients which may account for lower clinical specificity and sensitivity of [¹⁸F]FDG-PET in some of those patients. Therefore, it has been proposed that other hexose transporters such as GLUT2 and GLUT5 could be used as targets to develop alternative strategies to detect breast cancer. Here we have studied the *in vitro* and *in vivo* radiopharmacological profile of 6-deoxy-6-[¹⁸F]fluoro-D-fructose (6-[¹⁸F]FDF) as a novel radiotracer for PET imaging of GLUT5 expression in murine and human breast cancer cells. 6-[¹⁸F]FDF was synthesized in an Eckert & Ziegler Modular-Lab. Cell uptake was studied in murine EMT-6 and human MCF-7 breast cancer cells and compared to [¹⁸F]FDG. Biodistribution was determined in Balb/C mice. *In vivo* tumor uptake was studied with dynamic small animal PET in normal and EMT-6 tumor-bearing Balb/C as well as in MCF-7 tumor-bearing NIH-III mice xenografts in comparison to [¹⁸F]FDG. 6-[¹⁸F]FDF metabolism was investigated in mouse blood and urine. 6-[¹⁸F]FDF uptake in EMT-6 and MCF-7 cells was independent of extracellular glucose levels, reaching 24±2%ID/mg protein in EMT-6 and 12±1%ID/mg protein in MCF-7 cells (n=6; 5mM glucose) after 60min. Biodistribution in normal mice showed radioactivity uptake in bone and brain. 3.65±0.30%ID/g (n=3) was found in EMT-6 tumors after 5min p.i., decreasing to 1.75±0.03%ID/g after 120 min p.i. Dynamic small animal PET studies showed significantly lower initial radioactivity uptake in MCF-7 tumors (SUV_{15min}0.76±0.06, n=3) compared to EMT-6 tumors (SUV_{max}1.23±0.09, n=3). Over time, no significant changes in radioactivity level were observed in MCF-7 (SUV_{120min}0.69±0.02), whereas levels in EMT-6 (SUV_{120min}0.54±0.06) decreased within 120 min. [¹⁸F]FDG uptake was completely different in MCF-7 (SUV_{15min}0.74±0.12 to SUV_{120min}0.80±0.15, n=3) versus EMT-6 tumors (0.74±0.12 to 1.80±0.25, n=3). 6-[¹⁸F]FDF was metabolized rapidly *in vivo*. Only 9±4% (n=3) of the intact radiotracer was detected in mouse blood after 30min. In an enzyme reaction 6-[¹⁸F]FDF was shown to be a substrate for recombinant human ketohexokinase *in vitro*. Enzyme reaction afforded 97% of phosphorylated 6-[¹⁸F]FDF after 60min. 6-[¹⁸F]FDF represents a novel PET radiotracer for imaging GLUT5 expression *in vivo*. 6-[¹⁸F]FDF is a substrate for ketohexokinase and it is rapidly metabolized in mice. Small animal PET studies demonstrated radiotracer uptake in murine and human breast cancer xenografts indicating its potential application for imaging breast cancer.

Presentation Number **1032A**
Poster Session 2d: Imaging Disease/Organ Processes

Magnetic Resonance Imaging of Tissue Red/ox Activity in Cancer

Zhivko Zhelev¹, Rumiana Bakalova¹, Ichio Aoki¹, Veselina Gadjeva², Iwao Kanno¹, ¹Department of Biophysics, Molecular Imaging Center, NIRS, Chiba, Japan; ²Department of Chemistry and Biopchemistry, Trakia University, Stara Zagora, Bulgaria. Contact e-mail: zhivko@nirs.go.jp

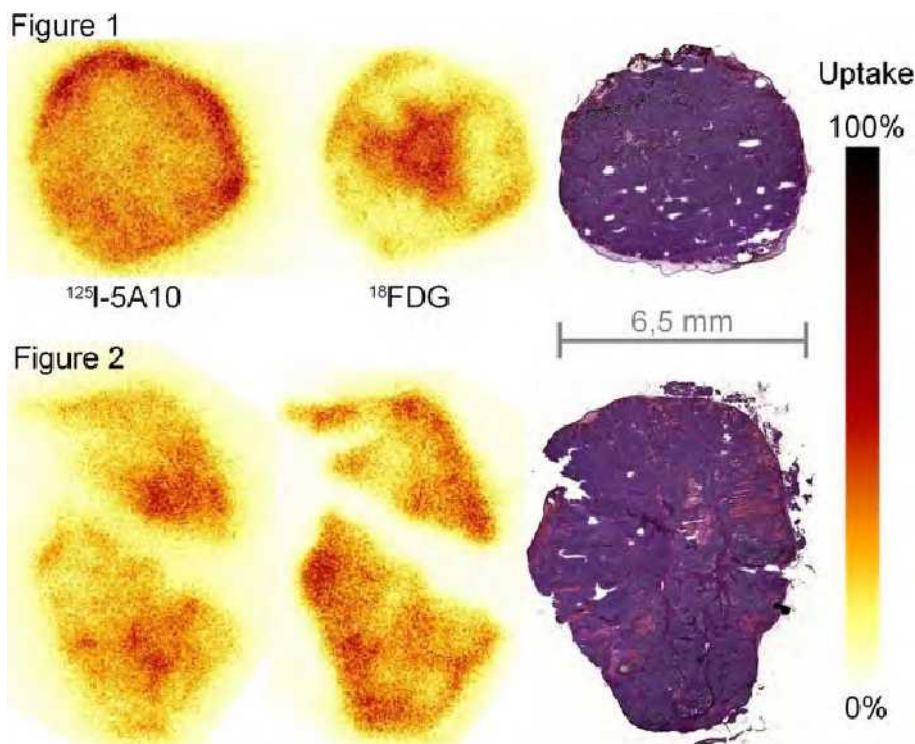
Background: Carcinogenesis provokes strong changes of tissue red/ox activity, resulting in high resistance of cancer tissue and high susceptibility of "normal" surrounding tissues to oxidation. The evaluation of tissue red/ox activity has a large prognostic value for radiotherapy and chemotherapy of cancer and could significantly help planning of tolerant treatment and increasing quality of life of the patients. Our study is directed to development of rapid and simple methodology for non-invasive evaluation of this parameter in vivo (in intact animals), that might be of high clinical impact. The methodology was based on the application of stable nitroxide radicals as red/ox-sensitive probes in magnetic resonance imaging (MRI) of cancer. **Methods:** The mice (Balb6) were separated in two experimental groups - healthy(controls) and cancer-bearing mice (with brain neuroblastoma or glioma). The mice were used 8-9 days after inoculation of cancer cells in the brain. They were subjected to anesthesia (1.5% isoflurane). A hydrophobic, blood-brain barrier permeable and DNA annealing probe (nitroxide-labeled nitrosourea) was injected into the tail vein and T1 weighted (gradient-echo) MRI of mouse brain was performed on 7 Tesla magnet. The imaging was conducted within 25 min. **Results:** The absolute value of MRI signal intensity of nitroxide probe in cancer-bearing brain was much higher than in healthy brain at same experimental and imaging conditions. In the brain of control mice, the dynamics of MRI signal of nitroxide radical was characterized with rapid increase (immediately after injection of the probe), followed by rapid decay to the baseline level with a half-life ~1 min. In the brain of cancer-bearing animals, the dynamics of MRI signal of nitroxide radical was characterized with rapid increase (immediately after injection of the probe), which was constant up to 25 min and without decay. **Conclusions:** The results suggest for a markedly different red/ox activity of the brain tissue in normal and cancer-bearing animals, which could be used as a new diagnostic marker for carcinogenesis. The half-life of MRI signal decay in normal (healthy) brain could be considered as a referent value. The results are discussed in the context of different reduction/oxidation potential of cells in cancer development, diagnostic and therapy.

Presentation Number **1033A**
 Poster Session 2d: Imaging Disease/Organ Processes

Biodistribution and Dual Isotope Ex Vivo Imaging of an Antibody Targeting Secreted Free Prostate Specific Antigen (fPSA)

Susan Evans¹, **Anders Orbom**², **Hans Lilja**³, **Sven-Erik Strand**², **Anders Bjartell**¹, **David Ulmert**³, ¹Department of Clinical Sciences, Lund University, Malmö, Sweden; ²Medical Radiation Physics, Lund University, Lund, Sweden; ³Department of Clinical Laboratory, Memorial Sloan-Kettering Cancer Center, New York, NY, USA. Contact e-mail: susan.evans@med.lu.se

Introduction: Despite recent imaging advances in the diagnosis and staging of prostate cancer, current probes lack accuracy and specificity in detecting advanced and metastatic disease. One strategy is to target fPSA using radiolabelled monoclonal antibodies (mAb). Our objective is to assess if the fPSA specific mAb, 5A10, is a candidate for imaging advanced prostate cancer using an animal model. **Methods:** The 5A10 mAb was labeled with ¹²⁵I and injected intravenously in LNCaP-based xenograft nude mice (n=13). The mice were sacrificed at 4 time-points post injection (p.i.) and the tumor/organs removed. Ab uptake in organs was evaluated by *ex vivo* measuring the radioactivity. In addition, 3 mice were given ¹⁸F-FDG at 47h p.i. of 5A10, sacrificed 1h later and tumors excised and snap frozen for cryosectioning. Thick sections (100 µm) were imaged by digital autoradiography using a silicon strip detector. Thin sections (20 µm) were stained with hematoxylin and eosin or immunostained to detect PSA expression. ¹²⁵I and ¹⁸F-FDG images were produced using energy separation and stained sections were scanned. **Results:** Biodistribution results showed that the ¹²⁵I-5A10 mAb displayed tumor specific uptake and cleared faster from all other organs. The tumor-to-blood ratio grew exponentially and by the last time-point (72h p.i.) had reached 0.8. Autoradiography images and histology showed that for smaller tumor containing dense viable cells, ¹⁸F-FDG uptake corresponds to the viable cell populations whereas 5A10 uptake is mostly around the edges (Fig 1). For larger tumors, 5A10 appears to pool in necrotic areas and stromal compartments while ¹⁸F-FDG is accumulated around the viable edges (Fig 2). **Conclusion:** *Ex vivo* imaging show an inhomogeneous uptake of the Ab not directly correlated to viable cells. Although our preliminary tumor-to-blood ratios are low, we plan to optimize the method with regards to dosing, labeling, molecule size and eventually pre-targeting. A dosing optimization study is planned and will be presented.



Individually normalized uptake of ¹²⁵I-5A10 (48h p.i.) and ¹⁸F-FDG (1h p.i.) in tumor sections. Nearby sections stained with H&E.

Presentation Number **1034A**
Poster Session 2d: Imaging Disease/Organ Processes

Early Treatment Response Evaluation in Patients with Aggressive Non-Hodgkin's Lymphoma - A Comparison of MRI and PET/CT Study

Xingchen Wu^{1,2}, **Prasun Dastidar**^{2,3}, **Hannu Pertovaara**¹, **Pasi M. Korkola**⁴, **Hannu Eskola**^{2,5}, **Pirkko-Liisa Kellokumpu-Lehtinen**^{1,3},
¹Oncology, Tampere University Hospital, Tampere, Finland; ²Radiology, Tampere University Hospital, Tampere, Finland; ³Medical School, University of Tampere, Tampere, Finland; ⁴Nuclear Medicine, Tampere University Hospital, Tampere, Finland; ⁵Biomedical Engineering, Tampere University of Technology, Tampere, Finland. Contact e-mail: Xingchen.Wu@uta.fi

Imaging studies have played an important role in treatment response evaluation of lymphomas, primarily through the use of computed tomography (CT). The integration of positron emission tomography with the use of the fluorine-18 fluorodeoxyglucose (¹⁸F-FDG-PET) into oncologic imaging has facilitated functional evaluation of disease behaviour. Magnetic resonance imaging (MRI) provides excellent tissue contrast and detailed morphological information. This is a pilot study in aggressive non-Hodgkin's lymphoma (NHL) patients undergoing conventional treatment. Aim of the study: To evaluate the predictive value of volumetric MRI and PET/CT early during chemotherapy and further to compare the results from MRI and PET/CT. Patients and Methods: This study included 8 consecutive patients with histologically proven aggressive NHL, clinical stage II to IV. The patients were imaged by MRI and PET/CT before treatment (E1); one week after chemotherapy (E2); and at the end of the second treatment cycle (E3). The volumetric analysis of target tumour on MRI was performed semiautomatically (1). The PET/CT images were analyzed visually and quantitatively. Standardized uptake value (SUV) and functional tumour volume were measured on fused PET/CT images by a 42% maximum SUV (SUVmax) threshold determination algorithms. Results: Eight patients completed E1 and E2. One patient died after E2, the other 7 completed E3. The volume of target tumour on MRI decreased 58% one week after chemotherapy ($p < 0.05$), and it decreased further after two treatment cycles ($p < 0.05$). SUVmax decreased 60% one week after chemotherapy ($p < 0.05$), and it decreased further after two treatment cycles ($p < 0.05$). In accordance, the functional tumour burden decreased 66% one week after the chemotherapy ($p < 0.05$), so did the volume of target functional tumour ($p < 0.05$). Baseline SUVmax correlated with functional tumour burden at E2 ($r = 0.76$, $p < 0.05$). The volumes of target tumour on MRI correlated with the volumes of target functional tumour in the same region of interest both at baseline and after one week's chemotherapy ($r = 0.88$, $p < 0.01$; respectively). Conclusion: The results indicate that pre-therapy SUVmax may be a potential predictor of clinical outcomes. Early assessment of response during the first treatment cycle is important to tailor treatment individually, and volumetric MRI could be used as a radiation free alternative tool to evaluate the early treatment response in patients with aggressive NHL. Reference: 1. Heinonen T, et al. Med Biol Eng Comput 1998; 36:291-6.

Presentation Number **1035A**
Poster Session 2d: Imaging Disease/Organ Processes

Intraoperative detection of the sentinel lymph node in cervical cancer using near-infrared fluorescence imaging: a technical feasibility study

Lucia M. Crane¹, Rick G. Pleijhuis¹, George Themelis³, Niels J. Harlaar¹, Athanasios Sarantopoulos³, Marleen van Oosten¹, Henriette G. Arts², Ate G. van der Zee², Vasilis Ntziachristos³, Gooitzen M. van Dam¹, ¹Surgery, University Medical Center Groningen, Groningen, Netherlands; ²Gynaecology & Obstetrics, University Medical Center Groningen, Groningen, Netherlands; ³Helmholtz Zentrum, Technical University, Munich, Germany. Contact e-mail: l.m.a.crane@chir.umcg.nl

Introduction Treatment of early stage cervical cancer consists of radical hysterectomy and pelvic lymph node (LN) dissection. LN metastases are found in only 20% of patients, while full pelvic LN dissection is frequently associated with lymphedema in the legs. The sentinel lymph node (SLN) method is designed to yield a more selective resection of LNs, thus reducing complications. If the SLN contains no tumor, it is assumed safe to omit the full lymphadenectomy. In this pilot study, we investigate the technical applicability of an intraoperative multispectral fluorescence camera system combined with the fluorescent contrast agent indocyanin green (ICG) for SLN detection in cervical cancer. **Methodology** The pilot study includes ten patients with early stage cervical cancer. Prior to the lymphadenectomy, a mixture of 1 ml of patent blue and 1 ml of the fluorescent agent ICG (0.5 mg/ml) is injected into the cervix uteri. Subsequently, color and fluorescence images and real-time videos of the lymph flow are acquired using an intraoperative multispectral fluorescence camera system. SLNs (the first appearing fluorescent or blue LN) are excised and analyzed ex vivo for fluorescence. Next, all remaining LNs are removed following the standard procedure. These LNs are also analyzed for fluorescence. Routine histopathological examination is performed to reveal possible metastases in SLNs and LNs. **Results** So far, nine patients have been included in the pilot study. In vivo lymphatic mapping with fluorescence was possible in six patients; leading to detection of one or more SLNs in five patients. Disappointing results in four cases were due to either bulky tumor, intra-abdominal fat or deep seated LNs. In total, a number of eight SLNs were detected with fluorescence imaging, of which five also showed blue discoloration. One of the SLNs (12.5%) contained metastatic tumor cells. A number of 178 non-sentinel LNs were taken out, one of which (0.6%) contained metastases. No adverse events were encountered and the surgical procedure was not hindered by using the intraoperative camera system. Fluorescence imaging prolonged the surgical procedure with no more than 30 minutes. **Conclusion** We present first results of detection of the SLN in early stage cervical cancer using ICG and an intraoperative fluorescence camera system. The technique is technically feasible, but detection may be hampered by bulky tumors and/or deep-seated lymph nodes. Future studies are needed to establish the definitive diagnostic accuracy.

Presentation Number **1036A**
Poster Session 2d: Imaging Disease/Organ Processes

Distribution pattern of focal FDG uptake in the mediastinal and symmetrically in bilateral pulmonary hilar regions in FDG PET/CT scan: mimicking malignancy but does not interpret to malignancy

Chih S. Wu¹, Wen T. Huang², Yueh F. Tsai³, Chiang H. Lee⁴, ¹Division of Nuclear Medicine, Department of Medical Image, Chi Mei Medical Center, Liouying,, Tainan County, Taiwan; ²Medical oncology, , Tainan County, Taiwan; ³Chest Surgery, , Tainan County, Taiwan; ⁴Division of Nuclear Medicine, Department of Medical Image, Chi Mei Medical Center, Yung Kang, Tainan County, Taiwan. Contact e-mail: d930811@mail.chimei.org.tw

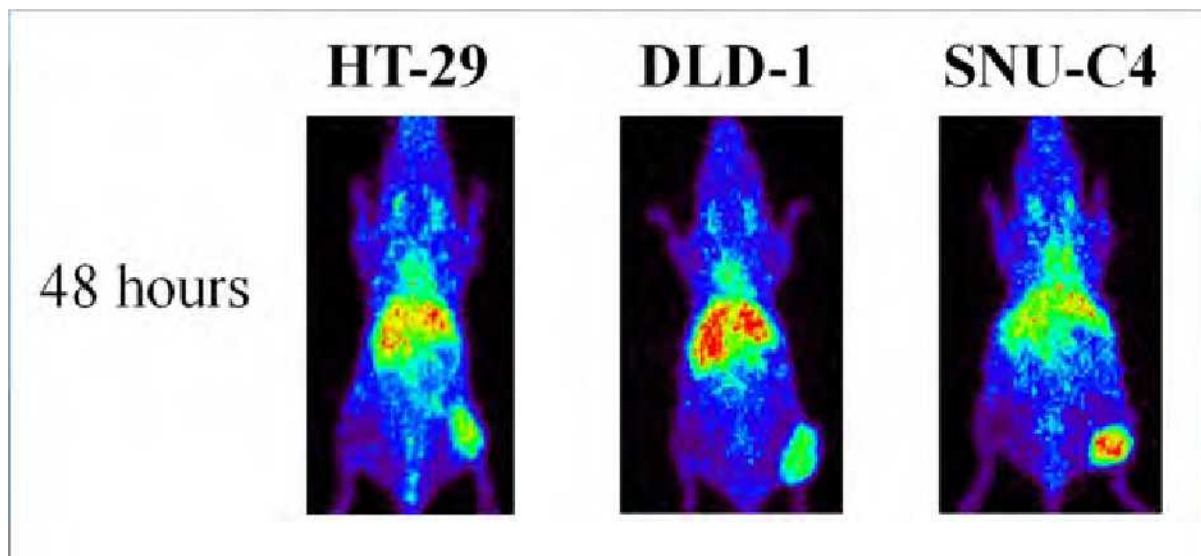
Objective: Focal FDG uptake distributed in the mediastinal and symmetrically in bilateral pulmonary hilar regions in ¹⁸F-FDG PET/CT scan is sometimes noted and it is difficult to ascertain the nature of benign or malignancy. The purpose of this study is to verify the nature of benign or malignancy in those focal FDG uptake presumed lymph nodes distributed in mediastinal and bilateral pulmonary hilar regions. Materials and methods: 8 cases with distribution pattern of focal FDG uptake in the mediastinal and symmetrically in bilateral pulmonary hilar regions in ¹⁸F-FDG PET/CT scan were retrospectively reviewed. These 8 cases are non-small-cell lung cancer (NSCLC) and received surgical nodal staging. Their ¹⁸F-FDG PET/CT scan were performed within one month before operation. Result: A total of 39 node stations (13 mediastinal, 26 hilar regions) distributed in FDG PET/CT scan and 17 node stations were received surgical node staging and the pathological results showed benign in nature. The mean of maximal standardized uptake value corrected with body weight (max.SUVbw) in those node stations is 3.07. There is increased max.SUVbw in 17/29 node stations and decreased max.SUVbw in 12/29 node stations in the delayed film. Calcification of node stations are noted in 7/8 cases. Conclusion: From our data, the distribution pattern of focal FDG uptake in the mediastinal and symmetrically in bilateral pulmonary hilar regions is usually associated with lymph node calcification. Usually it is benign in nature and should not be interpret to malignancy.

Presentation Number **1037A**
Poster Session 2d: Imaging Disease/Organ Processes

Evaluation of ^{64}Cu -labeled Cetuximab for Colorectal Cancer Imaging

Arifudin Achmad¹, **Hirofumi Hanaoka**¹, **Hiroki Yoshioka**¹, **Shinji Yamamoto**¹, **Yasuhiro Ohshima**², **Hideyuki Tominaga**¹, **Pramila Paudyal**¹, **Bishnuhari Paudyal**¹, **Keigo Endo**¹, ¹*Diagnostic Radiology and Nuclear Medicine, Gunma University Graduate School of Medicine, Maebashi, Japan;* ²*Medical Radioisotope Application Group, Quantum Beam Science Directorate, Japan Atomic Energy Agency, Takasaki, Japan. Contact e-mail: deanzification@yahoo.com*

Objective: Cetuximab is widely used for advanced colorectal cancer therapy, but the result is still less than satisfactory. It was reported that tumor uptake does not seem to depend on EGFR expression level in several tumor types. Previously ^{64}Cu -labeled antibodies have been proven as good imaging radiopharmaceutical for antigen expression level. In this study, relation between EGFR expression level and ^{64}Cu -DOTA-cetuximab uptake of colorectal cancer cell are studied. **Methods:** EGFR expression levels of 3 colorectal cancer cell lines (HT-29, DLD-1 and SNU-C4) were studied using flow cytometry. Tumor uptake of ^{64}Cu -DOTA-cetuximab was studied in nude mice bearing colorectal tumor xenograft using small animal PET scanner. Biodistribution study was done using ^{111}In -DOTA-cetuximab. **Results:** Flow cytometry using EGF antibody and Cetuximab showed different EGFR expression level (HT-29 = high, DLD-1 = medium, SNU-C4 = low). ^{64}Cu -DOTA-Cetuximab showed high accumulation in tumors and clearly imaged with PET. Tumor accumulation was much higher in SNU-C4 (low EGFR level) than HT-29 and DLD-1 at 48 hours after injection. Biodistribution study demonstrated high accumulation of Cetuximab after 48 hours in SNU-C4 (23.1 ± 2.6 %dose/g) compared to HT-29 (15.6 ± 2.1 %dose/g) and DLD-1 (13.2 ± 0.9 %dose/g). Radioactivity in blood, liver and other organs at 1, 24 and 48 hours showed no significant difference. **Discussion:** ^{64}Cu -DOTA-Cetuximab can be used for colorectal cancer imaging. In this study, discrepancy between EGFR expression level and tumor accumulation in colorectal tumor was also found. Biodistribution of normal tissue uptake in 1, 24 and 48 hours was unaffected by tumor types differences, suggest that discrepancy may be caused by intrinsic tumor factors. **Conclusion:** High accumulation of Cetuximab in the low EGFR expressing colorectal tumor suggests that EGFR expression level is not enough as the predictor of Cetuximab tumor accumulation. Other factors are important as the predictor of Cetuximab tumor accumulation.



PET image of ^{64}Cu -DOTA-Cetuximab in three colorectal cancer cell lines. Tumor accumulation were high in SNU-C4 tumor which has low EGFR expression level.

Presentation Number **1038A**
Poster Session 2d: Imaging Disease/Organ Processes

Anionic Phospholipid-Targeting Agent for Brain Tumor Imaging

Xiaoyang Qi², Zhengtao Chu², Balveen Kaur³, Antonio Chiocca³, Brian Gray¹, Bradley D. Smith⁴, Koon Y. Pak¹, ¹Molecular Targeting Technologies, Inc., West Chester, PA, USA; ²Human Genetics, Children's Hospital Research Foundation, Cincinnati, OH, USA; ³Neurological Surgery, The Ohio State University, Columbus, OH, USA; ⁴Chemistry and Biochemistry, University of Notre Dame, Notre Dame, IN, USA. Contact e-mail: cpak@mtarget.com

Synthetic bis-zinc(II)-dipicolylamine (Zn-DPA) containing compounds have been shown to have a strong binding affinity for biological membranes enriched with surface anionic phospholipids, and a growing body of evidence has demonstrated that anionic phosphatidylserine (PS) is highly exposed on the surfaces of cancerous cells and tumor blood vessels. Based upon these observations, we set out to determine whether Zn-DPA bearing molecules could be used for selective targeting to brain tumor cells and vessels through specific association with inside-out PS. Zn-DPA complexes conjugated to visible and near-infrared emitting fluorophores were used. In vitro studies using a FITC conjugated Zn-DPA molecule (PSVue™ 480) showed that the conjugate bound to human glioblastoma multiforme (GBM) cells. While in vivo studies using the near-infrared analog (PSVue™ 794) demonstrated that this conjugate selectively stained and accumulated in orthotopically implanted human GBM tumors in live nude mice in a dose-dependent manner using an IVIS fluorescence imaging system. These intriguing observations support the use of the Zn-DPA motif as the targeting component for new imaging agents to improve early diagnosis of brain tumors as well as to assist imaging-guided surgery.

Presentation Number **1039A**
Poster Session 2d: Imaging Disease/Organ Processes

Gaussia Luciferase for Bioluminescence Tumor Monitoring in Comparison with Firefly Luciferase

Yusuke Inoue¹, Fugeng Sheng¹, Shigeru Kiryu¹, Harnprasopwat Ratanakanit², Kiyoko Izawa², Arinobu Tojo², Kuni Ohtomo³,
¹Department of Radiology, Institute of Medical Science, University of Tokyo, Tokyo, Japan; ²Division of Molecular Therapy, Institute of Medical Science, University of Tokyo, Tokyo, Japan; ³Department of Radiology, Graduate School of Medicine, University of Tokyo, Tokyo, Japan. Contact e-mail: inouey-sky@umin.ac.jp

Gaussia luciferase (Gluc) is a secreted reporter and its expression in living animals can be measured by either in vivo BLI or blood assay. We characterized Gluc as an in vivo reporter in comparison with firefly luciferase (Fluc). Tumor cells that express both Fluc and Gluc stably under the control of the same promoters were inoculated subcutaneously in the SCID mice. Gluc BLI using the IV injection of coelenterazine and Fluc BLI using the IV or SC injection of D-luciferin were performed in mice bearing the SC tumors. Images were acquired sequentially after substrate injection, and the time course of bioluminescence was evaluated. Moreover, the tumor growth was assessed 4-28 days after tumor cell inoculation using Fluc BLI, Gluc BLI, blood assay of Gluc activity, and caliper measurement of the tumor volume. Mice received the SC injection of D-luciferin in Fluc BLI, and the peak signal was determined as an indicator of tumor burden. For Gluc BLI, images were acquired sequentially for 4 min after the IV injection of coelenterazine, the peak signal, 1-min area under the curve (AUC), and 4-min AUC were determined. Following the IV injection of coelenterazine, the signal reached a peak immediately and then decreased rapidly. The peak time and half time of light emission were mildly longer for the IV injection of D-luciferin and much longer for the SC injection of D-luciferin. In the longitudinal monitoring, all measures indicated increase in tumor burden early after cell inoculation. However, the increase reached a plateau on Gluc BLI and Fluc BLI despite continuous increase on the caliper measurement and, to a lesser degree, Gluc blood assay. Significant correlations were found between the measures and the correlation between the blood signal and caliper volume was the highest. Variation among mice was generally low for Gluc blood assay and very large for the caliper measurement early after cell inoculation. The 1-min and 4-min AUCs were highly correlated with the peak signal in Gluc BLI. The Gluc allows in vivo quantitative assessment of tumor burden in mice and should be applicable to dual reporter assay in combination with Fluc. The imaging time window is limited for Gluc BLI, and both Gluc BLI and Fluc BLI may underestimate tumor burden in large tumors. Gluc blood assay appears to provide a reliable indicator of viable tumor burden, and the combination of blood assay and in vivo BLI using Gluc would be a promising tool for quantifying and localizing the tumors.

Presentation Number **1040A**
 Poster Session 2d: Imaging Disease/Organ Processes

Evaluation of ¹⁸F-FBAU as a PET probe for Brain Tumor Imaging in F98-tk/luc Glioma-Bearing Rat Model

Yi-Chun Chien^{1,2}, **Chih-Hao K. Kao**³, **Jeng-Jong Hwang**^{1, 1} *Department of biomedical image and radiological sciences, National yang-ming university, Taipei, Taiwan;* ²*Department of medical image and radiological sciences, I-Shou university, Kaohsiung, Taiwan;* ³*Department of Radiopharmaceutical Production, Buddhist Tzu Chi General Hospital, Hualien, Taiwan. Contact e-mail: chienyc@isu.edu.tw*

FDG-PET has been primarily approved for the use in the staging and restaging of several tumors. However, ¹⁸F-FDG PET for the brain lesion imaging is limited due to higher glucose metabolism in the normal brain tissue, and the uptake of ¹⁸F-FDG in the tumor is not specific. ¹⁸F-FBAU is a DNA-incorporable thymidine analogue. The blood clearance of ¹⁸F-FBAU in vivo is very slow. Although ⁷⁶Br-FBAU has been used as PET reporter probe in human glioma mouse xenograft, it has potentially high radiation dose to the patients. ¹⁸F-FBAU, from the aspect of the lower absorbed dose, may be a better PET reporter probe due to its much shorter half-life. In this study, a rat glioma cell line- F98 was transfected with dual reporter genes, herpes simplex virus type 1 thymidine kinase (HSV1-tk) and luciferase (luc), and renamed as F98-tk/luc, and combined with multimodalities of molecular imaging to explore the imaging quality of ¹⁸F-FBAU as compared with that of ¹⁸F-FDG. Fischer 344 male rats (12-14 wks old) were inoculated with 1x10⁶ F98-tk/luc cells in the left brain as previously described. On 13th day post tumor cell inoculation, rats were monitored with PET post i.v. injection with F-18 labeled drugs, and bioluminescent imaging (BLI) post i.p. injection of D-luciferin. Ex vivo autoradiography, MRI and histochemical staining were also performed. The luc activities of F98-tk/luc determined by BLI were well correlated with the volume determined by MRI (R2= 0.7). The significant difference of the ¹⁸F-FBAU uptake was observed in the right brain as compared with the left one. However, no such difference was found from ¹⁸F-FDG PET. In conclusion, ¹⁸F-FBAU could be a potential PET reporter probe for the brain tumor imaging.

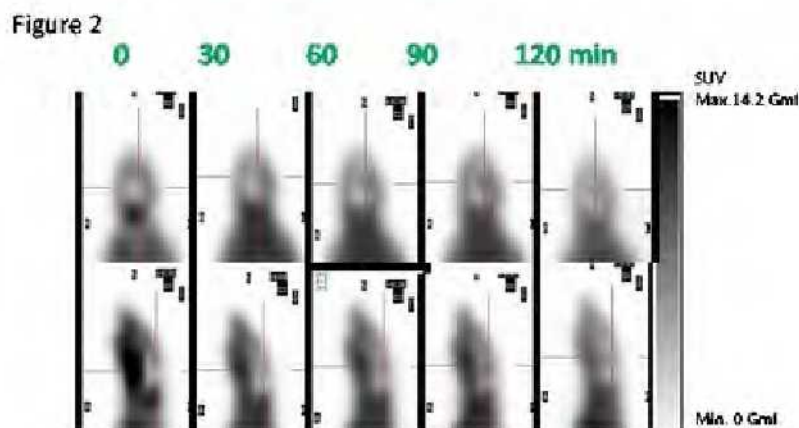
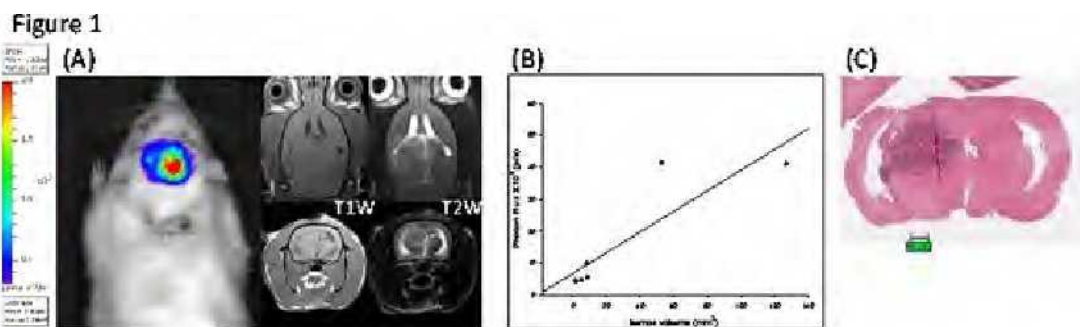


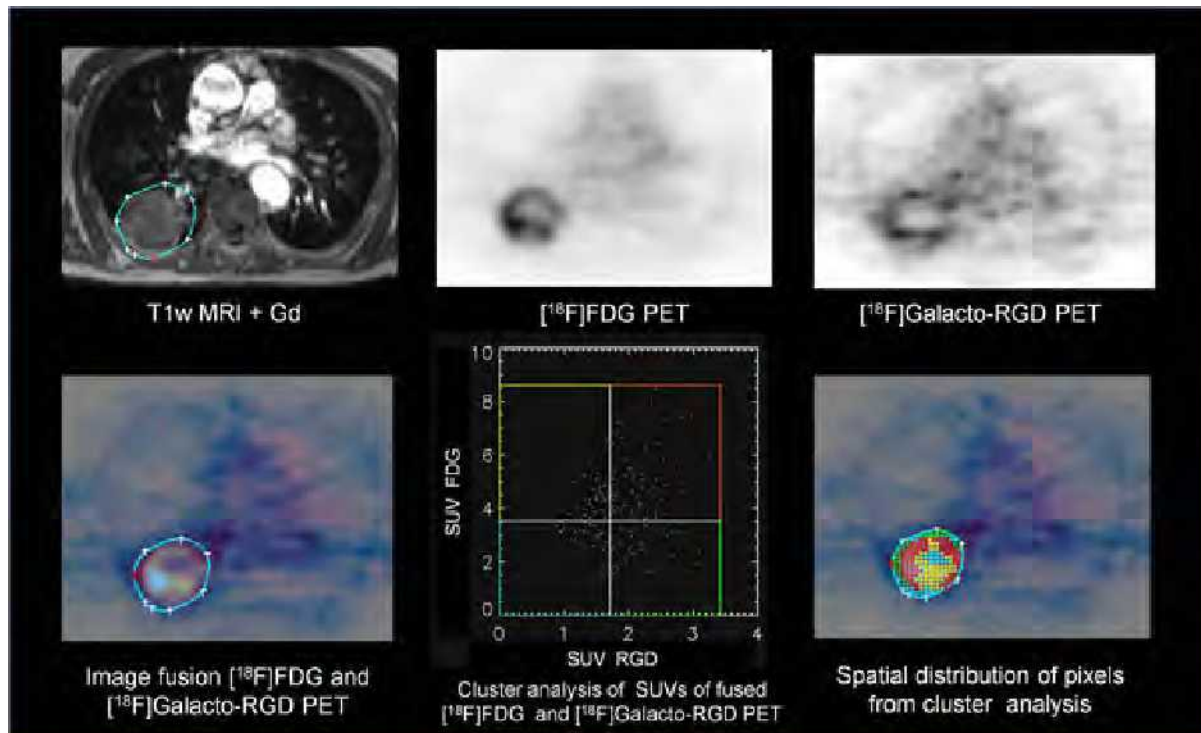
Figure 1. (A) F98-tk/luc brain tumor imaging with BLI and T1-weighted and T2-weighted 3T MRI on 13th days post-tumor cell inoculation. (B) The correlation of BLI photon flux versus tumor volume assayed with 3T MRI (r2 = 0.73). (C) Brain pathological examination stained with H&E. Figure 2. PET imaging of ¹⁸F-FBAU uptake in F98-tk/luc bearing rat model. At 0, 30, 60, 90 and 120 min post i.v. injection of 50 MBq of ¹⁸F-FBAU.

Presentation Number **1041A**
 Poster Session 2d: Imaging Disease/Organ Processes

Multiparametric Evaluation of the Spatial Relationship of $\alpha\beta3$ Expression and Glucose Metabolism in NSCLC

Stephan Metz², Sylvie Lorenzen³, Hans J. Wester¹, Stephan G. Nekolla¹, Markus Schwaiger¹, **Ambros J. Beer¹**, ¹Department of Nuclear Medicine, Technische Universität München, Klinikum rechts der Isar, Munich, Germany; ²Department of Radiology, Technische Universität München, Klinikum rechts der Isar, Munich, Germany; ³Department of Oncology, Technische Universität München, Klinikum rechts der Isar, Munich, Germany. Contact e-mail: ambros.beer@tum.de

Purpose: Positron emission tomography (PET) provides non-invasively quantitative data on tumor biology in living organisms. We analyzed the relationship of $\alpha\beta3$ -expression and glucose metabolism focusing on tumor heterogeneity to gather more insight into the spatial relationship of these important parameters of tumor biology. **Material and Methods:** 12 patients with primary or metastasized non small cell lung cancer (NSCLC) were examined with PET using [¹⁸F]Galacto-RGD and [¹⁸F]FDG. In malignant lesions (n=17), the standardized-uptake-values (SUV's) were correlated on a pixel-by-pixel basis by using dedicated imaging software. To reflect spatial heterogeneity, all tumor sections were divided into pixel rings, starting from periphery to central. For cluster analysis, we used the 25th percentile as threshold for low and high tracer uptake (SUV=1.5 for [¹⁸F]Galacto-RGD and SUV=3.6 for [¹⁸F]FDG). Thus up to four tumor regions of different biologically activity could be defined, which are described as: FDG+/RGD+, FDG-/RGD-, FDG+/RGD- and FDG-/RGD+. **Results:** Considering the entire tumor area, a significant correlation could be noted between the mean SUV values of [¹⁸F]Galacto-RGD and [¹⁸F]FDG (r=0.66, p<0,01). Both tracers showed a decreasing uptake to central. Both FDG+/RGD+ and FDG-/RGD+ pixels were found only in more peripheral tumor zones. In contrast, FDG-/RGD- clusters were predominant in central areas of large tumors. FDG+/RGD- pixels are detectable predominantly in the transitional zone and less frequently in the central parts. **Conclusions:** Based on the cluster analysis, we noted the following spatial distributions of glucose metabolism and $\alpha\beta3$ -expression: Areas with high glucose metabolism and $\alpha\beta3$ -expression (FDG+/RGD+) were found mainly in the tumour periphery. Areas with low glucose metabolism and low $\alpha\beta3$ -expression (RGD-/FDG-) were mainly found in the centre of larger tumors. Areas with high glucose metabolism and but low $\alpha\beta3$ -expression (FDG+/RGD-) were mainly found in the transitional zone and might represent areas with high tumor activity and hypoxia due to low levels of angiogenesis. This hypothesis now has to be proven in future prospective studies with histopathological correlation.

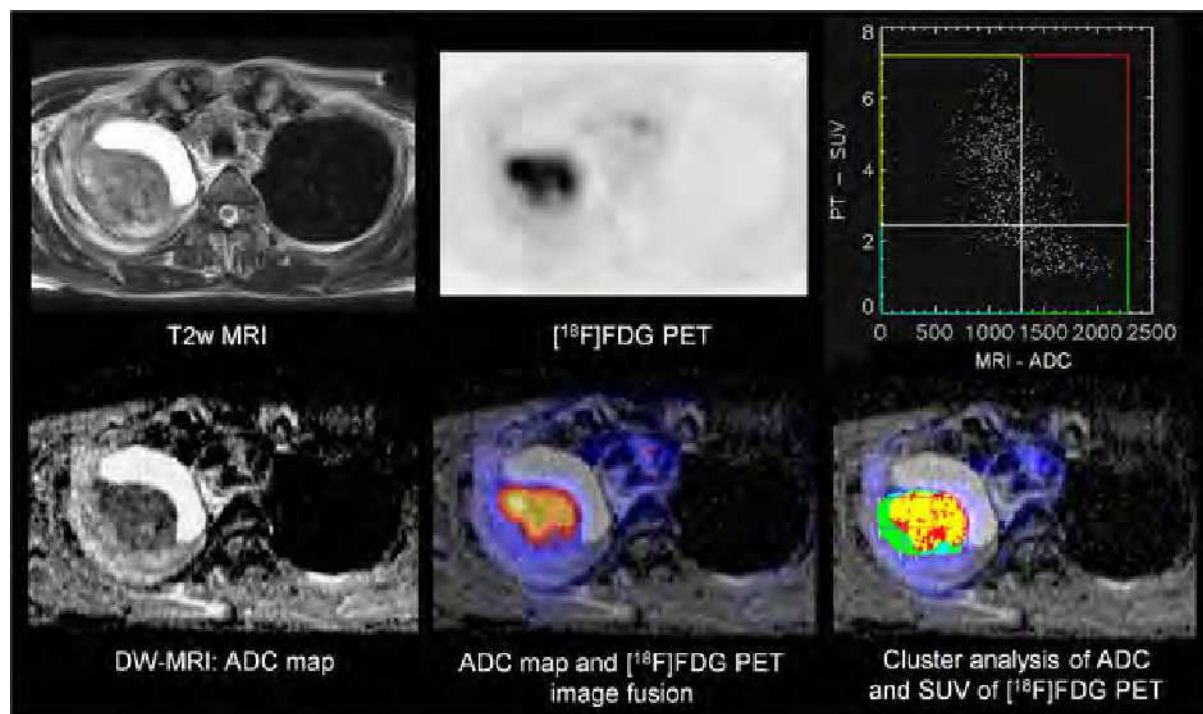


Presentation Number **1042A**
 Poster Session 2d: Imaging Disease/Organ Processes

Multiparametric MRI and PET Imaging: Analysis of the Relationship of Water Diffusivity and Glucose Metabolism in Cancer Patients

Stephan Metz², Sylvie Lorenzen³, Konstantin Holzapfel², Sandra van Marwick¹, Stephan G. Nekolla¹, Markus Schwaiger¹, **Ambros J. Beer**¹, ¹Department of Nuclear Medicine, Technische Universität München, Klinikum rechts der Isar, Munich, Germany; ²Department of Radiology, Technische Universität München, Klinikum rechts der Isar, Munich, Germany; ³Department of Oncology, Technische Universität München, Klinikum rechts der Isar, Munich, Germany. Contact e-mail: ambros.beer@tum.de

Purpose: Diffusion weighted magnetic resonance imaging (DW-MRI) as well as positron emission tomography (PET) with [¹⁸F]FDG provides quantitative data on tumor biology. However, knowledge about the biological correlate of DW-MRI is still incomplete. We therefore evaluated the relationship of DW-MRI and [¹⁸F]FDG-PET in cancer patients. Material and Methods: 16 patients with primary or metastasized cancer (NSCLC n=12; other tumors n=4) were examined with DW-MRI using an echoplanar single-shot (SSEPI) sequence (b-values of 50, 300 und 600 s/mm²) and [¹⁸F]FDG-PET. The apparent diffusion coefficient (ADC) from DW-MRI was correlated with standardized-uptake-values (SUV's) from PET imaging in malignant lesions (n=28) on a pixel-by-pixel basis using dedicated imaging software. For cluster analysis, we used the 25th percentile as threshold for low and high tracer uptake (SUV=3.6 for [¹⁸F]FDG) and 1.5 as threshold for ADC. Thus we could define up to 4 tumor regions of different biological activity (FDG+/ADC+, FDG-/ADC-, FDG+/ADC- and FDG-/ADC+). Results: The mean tumor data showed no significant correlation between ADC and SUVs of [¹⁸F]FDG (r²=0.205). Spatial analysis showed relatively homogeneous ADC values over the mean entire tumor area. In contrast, the mean SUVs decrease from the tumor periphery to the centre. Cluster analysis revealed that 60% of the pixels were located in the FDG+/ADC- cluster. Conclusions: Our data suggest that tissue diffusivity and biological tumor activity as defined by glucose metabolism are not strongly correlated. Based on cluster analysis, we hypothesize that basically four different areas of tumor biology can be defined by combining DW-MRI and PET: Areas with low ADC and high tracer uptake represent vital tumor with high density of viable tumor cells, whereas areas with low ADC and low uptake represent areas of low tumor activity and pronounced stroma density and fibrosis. Areas with high ADC and low uptake probably represent macroscopic tumor necrosis whereas areas with high ADC despite high uptake might represent areas with very high tumor activity and regions of micronecrosis. This hypothesis now has to be proven in future prospective studies with histopathological correlation.



Presentation Number **1043A**
Poster Session 2d: Imaging Disease/Organ Processes

Comparison of Diffusion Weighted Imaging with [¹⁸F]FDG/[¹⁸F]FLT Uptake in Human Tumor Xenograft Models

Valerie S. Honndorf¹, Sally-Ann Ricketts², Carsten Liess², Jane Halliday², Hans F. Wehr¹, Stefan Wiehr¹, Damaris Kukuk¹, Maren K. Koenig¹, Mareike Lehnhoff¹, Julia G. Mannheim¹, Gerald Reischl¹, Heather Keen², Bernd J. Pichler¹, ¹Laboratory for Preclinical Imaging and Imaging Technology of the Werner Siemens-Foundation, Department of Radiology, Eberhard Karls University Tübingen, Röntgenweg 13, 72076 Tübingen, Germany; ²Imaging, Translational Sciences, AstraZeneca, Alderley Park, Macclesfield, Cheshire, United Kingdom. Contact e-mail: Valerie.Honndorf@googlemail.com

Diffusion-weighted magnetic resonance imaging (DWI) enables the in vivo characterization of biologic tissues on the basis of their water diffusion properties and therefore it is a useful diagnostic tool for monitoring cancer therapy. PET imaging with [¹⁸F]FDG and [¹⁸F]FLT provides information on tumour glucose uptake and cell proliferation, respectively. However, the uptake of these tracers can be variable across different tumour types. Here, we investigate the tumor metabolism, functional status and growth of a human colon adenocarcinoma cell line (HCT116) in female SWISS nude mice by PET and MRI. We concentrate on the comparison and correlation between the uptake of [¹⁸F]FDG and [¹⁸F]FLT and the apparent diffusion coefficient (ADC) of the tumors over a period of 8 to 10 days. After s.c. inoculation of 10⁷ HCT116 cells into the upper right flank of the mice a visible tumor appeared after 8 days. For the dynamic and static PET scans mice were administered 350 µCi [¹⁸F]FLT (n=6) or [¹⁸F]FDG (n=6). The uptake times for the static PET scans were 55min for [¹⁸F]FDG and 90min for [¹⁸F]FLT. Following the PET scans, each mouse was transferred on the same bed to the 7T MRI scanner. DWI was performed in sagittal direction (b = 150, 250, 400, 600, 800, 1000 mm²/s, TE = 112ms, TR = 5000ms, Δ = 41 ms, δ = 20 ms). ADC maps were calculated and coregistration of the MRI and PET images was performed using Inveon Research Workplace. For the quantitative analysis of tumor tracer uptake, regions of interest (ROIs) were drawn manually on coronal images. Overall, HCT116 tumors showed no significant change in [¹⁸F]FDG uptake over the measurement period (3.33 %ID/cc ± 0.68 on day 8 and 3.87 %ID/cc ± 0.87 on day 17) whereas [¹⁸F]FLT uptake increased with tumour growth (3.29 %ID/cc ± 1.14 on day 8 and 5.00 %ID/cc ± 1.34 on day 15). The ADC values revealed no remarkable changes or heterogeneity over the measurement period (mean ADC between 0.59*10⁻³mm²/s ± 0.11 and 0.74*10⁻³mm²/s ± 0.13, n=12). However, the ADC images showed highly heterogeneous regions in the tumors after 15 to 17 days of tumor growth. A coregistration of [¹⁸F]FDG or [¹⁸F]FLT images with the corresponding ADC maps revealed an inverse correlation between PET tracer uptake and ADC values, particularly in highly heterogeneous or necrotic tumor regions. Ongoing work is aimed at further quantifying the ADC/PET tracer uptake cross-correlation and other adenocarcinoma cell lines (HCT116, SW620, A549, Calu-6) will be investigated.

Presentation Number **1044A**
 Poster Session 2d: Imaging Disease/Organ Processes

Evaluation of a PET Antibody Tracer for Monitoring Lymphoma Therapy in a Humanized Transgenic Mouse Model

Arutselvan Natarajan¹, **Gayatri Gowrishankar**¹, **Carsten H. Nielsen**^{1,3}, **Sen Wang**¹, **Nicholas van Bruggen**⁴, **Sanjiv S. Gambhir**^{1,2},
¹Molecular Imaging Program at Stanford (MIPS), Radiology, Stanford University, Stanford, CA, USA; ²Bioengineering, Bio-X, Stanford University, Stanford, CA, USA; ³Cluster for Molecular Imaging & Department of Clinical Physiology, Nuclear Medicine and PET, University of Copenhagen, Rigshospitalet, Denmark; ⁴Biomedical Imaging, Genentech, South San Francisco, CA, USA. Contact e-mail: anatarajan@stanford.edu

Positron emission tomography (PET) tracers offer a broad spectrum of clinical applications in oncology, including improved tumor diagnosis, staging, surveillance, monitoring of antitumor therapy, and tumor tissue characterization. Aim: To radiolabel and image in pre-clinical models an antibody based PET tracer, ⁶⁴Cu-DOTA-Rituximab (Rmab). Method: The ⁶⁴Cu was chelated to DOTA-NHS linked Rituximab. QA of the radiotracer was established by HPLC, sterility, and in vitro live cell uptake assay. To validate the study multiple radiolabeling and imaging experiments were carried out in three groups of mice; two groups of mice had huCD20 transgene (CD20TM) that expresses the human CD20 on their B cells. The study groups of mice are as follows; a) control (nude mice, n=2) received Rmab 200 μ Ci/dose, b) negative (CD20TM, n=2): received 2mg/kg pre-dose of cold Rituximab prior to 2h of Rmab dose of 200 μ Ci, and c) positive (CD20TM, n=2): Rmab alone 200 μ Ci/dose. Small animal PET was used to image mice at various time points (0, 1, 2, 4, 24, 48, and 72h) after tracer injection. AMIDE software was used to analyze the images. Results: QA of the Rmab was: DOTA/antibody (>1), specific activity (75-125 μ Ci/ μ g), radiochemical yield (>80%), and purity (>98%). The Rmab immunoreactivity was >80% and sterile. At 24h, Rmab uptake (% ID/g) by spleen and liver of CD20TM were (mean \pm STD): spleen uptake by negative and positive groups was 1.76 ± 0.006 % and 16.5 ± 0.713 % (p value < 0.011); and liver uptake by negative and positive groups was 0.41 ± 0.088 % and 0.55 ± 0.112 % (p value < 0.153). Figure 1 μ PET/CT image shows the specific uptake of Rmab in mice, compared to the liver the spleen specific uptake of Rmab is ~15 times high due to the expression of huCD20. Conclusion: We have optimized and validated Rmab radiochemistry and PET imaging in mice for clinical translation to applications in lymphoma patients.

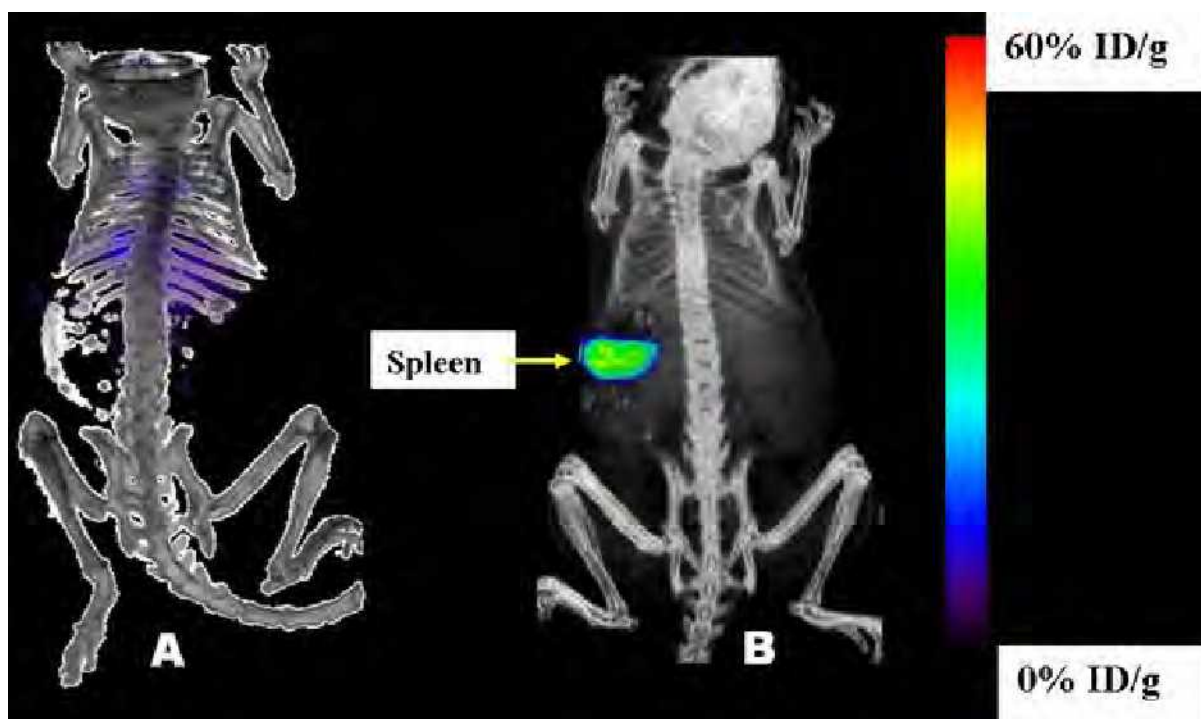


Figure 1. The small animal PET-CT transgenic mice images shows after tracer injection of ⁶⁴Cu-Do-Rituximab (200 μ Ci/2 μ g) at 24h: 1A) received Rituximab pre-dose of 2mg/kg 2h prior to tracer injection; 1B) mouse received only tracer no pre-dose. Figure 1B shows the specific uptake of tracer in the spleen where huCD20 expressing B cells.

Presentation Number **1045A**
Poster Session 2d: Imaging Disease/Organ Processes

Clinical Benefit of 18Fluorocholine PET/CT in Prostate Cancer

Rodolfo Núñez¹, Raquel Jover¹, Miguel A. Pozo¹, Carlos Núñez², Juan Carlos Viera³, Ignacio Duran⁴, Dionisio Lasa-Perez¹, Luis Gorospe-Sarasua¹, Daniel Lourido Garcia¹, Agustina Vicente-Bartulos¹, Javier Garcia-Poza¹, Jose Miguel Alfonso-Alfonso¹,
¹Department of Nuclear Medicine and PET/CT, Instituto Tecnológico de Servicios Sanitarios, Madrid, Spain; ²Urology, Centro Oncológico MD Anderson International España, Madrid, Spain; ³Radiation Therapy, Centro Oncológico MD Anderson International España, Madrid, Spain; ⁴Medical Oncology, Hospital de Madrid Norte Sanchinarro, Madrid, Spain. Contact e-mail: directormedico@petmadrid.com

Objective: To evaluate the clinical usefulness of 18Fluorocholine PET/CT in prostate cancer patients. **Material and Methods:** We present the results of the first 27 patients (pts), ages 49 to 81 (mean of 69 years) with suspected (5 pts) or proven (22 pts) prostate cancer, who had a 18Fluorocholine PET/CT done between July 2009 and April 2010. Of the 27 pts, 17 were referred due to biochemical recurrence of disease, 5 for re-staging purposes and other 5 for initial diagnosis and staging. The serum PSA at the time of the study ranged between 0.42 ng/ml and 72.5 ng/ml (average of 6.2 ng/ml), and the Gleason score from 5 to 9 with a mean of 7. The PET/CT scan was carried out after the intravenous injection of 8 mCi (296MBq) of 18Fluorocholine, starting with an initial dynamic scan of the pelvis at one minute post-injection, and lasting for 8 minutes, followed by additional imaging of the pelvis at 15 and 60 minutes post-injection. At 30 minutes, a whole body scan (from the vertex of the skull to the upper thighs) was also acquired. The CT scan was done without intravenous or oral contrast. Follow up ranged from several weeks to 9 months. Validation of imaging results was obtained from biopsy (directed by PET/CT findings) and/or surgical pathology in 7 cases, conclusive and unequivocal radiological and clinical follow up findings in other 7 cases, and in 2 cases from the highly characteristic and clear cut findings seen mainly in the CT component of the 18Fluorocholine PET/CT scan. **Results:** On a per patient basis, disease was suspected in 21/27 (78 %) scans. Of the other 6 scans, 4 were negative, one had a very questionable and doubtful finding in the lower pelvis and the other patient was thought to have a benign prostatic hyperplasia. All the negative cases had a PSA of less than 2 ng/ml. Of the 16 patients from whom validation of imaging results were available, there were 13 true positive scans (TP), 2 true negative (TN), 1 false negative (FN) and no false positive scans. Therefore, the sensitivity, specificity and accuracy for 18Fluorocholine PET/CT was, 92.8%, 100% and 93.7%, respectively. **Conclusion:** 18Fluorocholine PET/CT in prostate cancer has a high percentage of positive cases, many of them being true positive. It is very useful for the detection of disease in patients with biochemical recurrence, for whom conventional imaging has been negative. In these cases, the PET/CT findings facilitate and guide biopsy sampling to confirm and pinpoint the recurrence of disease, helping -in some cases considerably- with disease management.

Presentation Number **1046A**
Poster Session 2d: Imaging Disease/Organ Processes

Synthesis of Mannose-PEG-Superparamagnetic Iron Oxide Nanoparticles as Magnetic Resonance Contrast Agent for Lymph Node Imaging

Hieu Vu-Quang^{1,2}, Sangjoon Lee^{1,6}, Hwa Jeong Lee^{1,6}, Hui Lian Che^{1,2}, Myeong Ju Moon³, Mi Kyong Yoo⁴, Chong Su Cho⁴, Chang-Moon Lee⁵, Hwan-Jeong Jeong⁵, Yong Yoen Jeong³, In-Kyu Park^{1,6}, ¹Department of Biomedical Sciences, Chonnam National University Medical School, Gwangju, Republic of Korea; ²Clinical Vaccine R&D center, Chonnam National University, Hwasun, Republic of Korea; ³Department of Radiology, Chonnam National University Medical School, Gwangju, Republic of Korea; ⁴Department of Agriculture Biotechnology, Seoul National University, Seoul, Republic of Korea; ⁵Department of Nuclear Medicine, Research Institute of Clinical Medicine, Chonbuk National University Medical School and Hospital, Jeonbuk, Republic of Korea; ⁶BioImaging Research Center, GIST, Gwangju, Republic of Korea. Contact e-mail: vuquanghieu86@gmail.com

The aim of the study is to detect metastatic lymph nodes which are hard to distinguish from normal nodes, because of their same size and shape, by Magnetic Resonance Imaging (MRI). Many contrast agents have been developed to target to Antigen-Presenting Cells (APCs) which migrate to the lymph node and can be detected by MRI. In this study, we synthesized super paramagnetic iron oxide nanoparticles (SPIONs) carrying immobilized mannose sugar on the surface for targeting to APCs through the specific interactions of mannose on the SPIONs with mannose receptor on these cells. The surface of SPIONs were conjugated with 3-aminopropyltriethoxysilane (APTES) and then Mannose-PEG was immobilized onto APTES-modified SPIONs by conventional method using EDC/NHS coupling agents to produce mannose-PEG-coupled SPIONs. We have supposed that hydrophilic PEG corona layer in mannose-PEG-SPIONs can serve to be prevented from aggregation during the systemic circulation and that mannose ligands present on mannose-PEG-SPIONs be targeted effectively to APCs which are then accumulated in lymph nodes. The accumulations of the SPIONs in the lymph nodes lead to decrease signal intensities in MR images. The Mannose-PEG-SPIONs were characterized by TEM, ELS, XRD, SQUID, and uptake of mannose-PEG-SPIONs by macrophage cells was confirmed by FACS analysis and fluorescent microscopy. For in vivo study, rats were intravenously injected with Mannose-PEG-SPIONs and PEG-SPIONs as a control and then scanned by MRI after 1h, 2h, 3h and 24h. MRI studies demonstrated that the accumulation in the lymph nodes of Mannose-PEG-SPIONs was significantly more intense than PEG-SPIONs that is, non-target to macrophage and also lymph nodes, which were also confirmed by Prussian blue staining of lymph nodes. Based on these results, Mannose-PEG-SPIONs have a great potential for lymph node imaging in order to detect metastatic lymph nodes at the early stage. Currently, some studies are under ways to test the detectability of the metastatic lymph nodes in tumor bearing mouse model by mannose-PEG-SPIONs.

Presentation Number **1047A**
Poster Session 2d: Imaging Disease/Organ Processes

THE ROLE OF FDG PET/CT IN SYNOVIAL CARCINOMA

Jyotsna Rao, Kavitha Nallapareddy, Alka A. Chengapa, Sikandar M. Shaikh, Apollo Gleneagles PET CT Ctr, Hyderabad, India.
Contact e-mail: jyotsnael@gmail.com

Synovial sarcomas are rare and form 8-10% of all sarcomas. They are slow growing but can be locally aggressive. MRI is the imaging modality of choice. FDG PET is sensitive in identifying sarcomas. We wish to present data from patients referred to our center for management of synovial sarcoma. Aim: To evaluate the role of FDG PET/CT in the management of synovial sarcoma. Material and method: A retrospective data analysis of PET/CT reports of 16 patients with synovial sarcoma referred to our center between May 2005 and December 2009 was performed. Patients were injected intravenously with 10-15 mCi of F18 FDG after 4 hours of fasting and scanned per standard whole body protocol after giving oral and intravenous contrast. The scans were reported jointly by a radiologist and PET physician. Follow up was obtained where possible. Results: 1/16(7%) patients was referred for staging, 12/16 (75%) patients for restaging and 3/16(12%) to monitor response to therapy. The single patient referred for staging showed primary tumor and nodal metastasis. Of the 12 restaged patients, 3/12(25%) were negative, 3/12(25%) showed only primary tumor recurrence, 3/12(25%) showed primary tumor recurrence and metastases, 2/12(17%) showed lung metastases (more lesions on CT), and 1/12(8%) showed a mildly active lung nodule. Of the 3 patients scanned to monitor response to therapy, 1(34%) patient was negative, 1/3(33%) showed residual viable metastases and 1/3(33%) showed increased viable metabolism in the primary tumor and previous metastases and appearance of new metastases. Conclusion: FDG PET/CT proved useful in the management of the small number of patients referred with synovial sarcoma to our center and may be considered as one of the imaging tools during work up.

Presentation Number **1048A**
Poster Session 2d: Imaging Disease/Organ Processes

THE ROLE OF FDG PET/CT IN BLADDER CANCER

Jyotsna Rao, Kavitha Nallapareddy, Alka A. Chengapa, Sikandar M. Shaikh, Apollo Gleneagles PET CT Ctr, Hyderabad, India.
Contact e-mail: jyotsnael@gmail.com

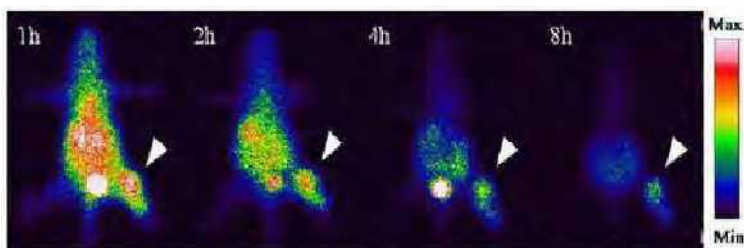
Bladder cancer is most common in industrialized countries. It is frequently multifocal and has a high rate of recurrence. FDG uptake by primary bladder tumor and metastases is known but identifying primary tumor proved difficult due to tracer pooling in the bladder although loco regional and distant spread were identified with high sensitivity. We present our experience in bladder cancer imaging with FDG PET/CT. Aim: To study the role of FDG PET/CT in bladder cancer. Material and method: A retrospective analysis of reports of 24 patients with bladder cancer referred to our center between May 2005 and December 2009 was performed. Patients were injected intravenously with 10-15 mCi of F18 FDG after 4 hours of fasting and scanned per standard whole body protocol after giving oral and intravenous contrast. The scans were reported jointly by a radiologist and PET physician. Follow up was obtained where possible. Patients imaged after 2007 had delayed imaging of the bladder one to one and half hours following intravenous injection of furosemide to identify bladder wall FDG uptake. One patient with sarcoma was referred to monitor response to therapy. One patient had 2 other primaries. Results: 4/24(17%) patients were referred for staging, 16/24(66%) for restaging and 4/24(17%) to monitor response to therapy. 2/4(50%) of the staged patients showed only primary tumor, 2/4(50%) showed primary tumor and nodal metastases. 5/16(31%) of the restaged patients were negative, 6/16(37%) showed only metastases, 2/16(12%) showed primary tumor recurrence and metastases and 3/16(20%) showed only primary tumor recurrence. 2/4(50%) scanned after treatment to evaluate response showed viable primary tumor, 1/4(25%) showed increase in metabolism of primary tumor and metastases and 1/4(25%) was negative. Conclusion: FDG PET/CT proved useful in the management of the small number of patients referred with bladder cancer to our center.

Presentation Number **1049A**
 Poster Session 2d: Imaging Disease/Organ Processes

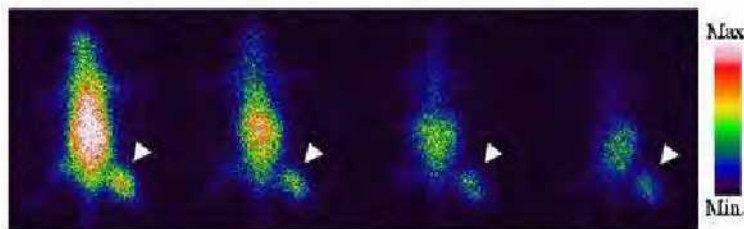
Evaluation of ^{123}I -IUdR as a SPECT probe in sarcoma- and lung carcinoma-bearing mouse models

Chih-Yuan Lin¹, Chun-Yi Wu¹, Pei-Chia Chan¹, Ren-Shyan Liu^{1,2}, C. Allen Chang¹, Jenn-Tzong Chen³, Wu-Jyh Lin³, Ming-Hsien Lin⁴, Hsin-Ell Wang¹, ¹Department of Biomedical Imaging and Radiological Sciences, National Yang-Ming University, Taipei, Taiwan; ²Department of Nuclear Medicine, Faculty of Medicine, National Yang-Ming University, Taipei, Taiwan; ³Institute of Nuclear Energy Research, Atomic Energy Council, Tao-Yuan City, Taiwan; ⁴Department of Nuclear Medicine, Taipei City Hospital, Taipei, Taiwan. Contact e-mail: wcy72210@gmail.com

Objective: This study aims to evaluate radioiodinated 5-iodo-2'-deoxyuridine (^{123}I -IUdR) as a SPECT probe for tumor detection in NG4TL4 sarcoma- and LL/2 lung carcinoma-bearing mice. **Methods:** Starting from 5-tributylstannyl-2'-deoxyuridine, $^{123}\text{I}/^{131}\text{I}$ -IUdR was prepared with high radiochemical yield ($\geq 90\%$, decay corrected) and radiochemical purity ($\geq 98\%$). Biological characterization studies including cellular uptake with and without deoxyuridine (UdR), DNA incorporation assay, pharmacokinetics, metabolite analysis, biodistribution and scintigraphic imaging, were performed. **Results:** The cellular uptake of ^{131}I -IUdR in NG4TL4 and LL/2 cell cultures increased with time. The cell-to-medium ratio (C/M) reached 476.38 ± 36.51 and 277.49 ± 33.41 after 8 h incubation, respectively. However, when $10 \mu\text{M}$ of UdR was added in the culture medium, the C/M in LL/2 cells reduced to 155.12 ± 22.11 , about 55% compared with that without UdR addition. The results suggested that the small amount of UdR (no more than $0.3 \mu\text{M}$) produced during IUdR preparation would only have insignificant effect in the biological study, and HPLC purification would be unnecessary. High correlation between C/M ratio and DNA incorporation (in $\text{cpm}/\mu\text{g}$ DNA) in NG4TL4 sarcoma cells ($r^2=0.96$) was observed. ^{131}I -IUdR is not biologically stable after i.v. injection in the mouse model. The major radioactive component is ^{131}I -iodide and accounts for 71.1% radioactivity in the blood and 88.0% radioactivity in the urine at 5 min p.i. However, the high first pass uptake in all tissues (including tumor) and fast elimination from normal tissues resulted in high tumor-to-muscle ratio (T/M= 19.91 at 8 h p.i.) in NG4TL4 sarcoma-bearing mice, as observed in the biodistribution study. Scintigraphic imaging also showed specific tumor uptakes. The T/M reached 11.49 ± 2.55 for NG4TL4 sarcoma at 8 h p.i., and 7.04 ± 0.97 for LL/2 lung carcinoma at 24 h p.i., respectively. **Conclusion:** This study demonstrated that ^{123}I -IUdR is rapidly deiodinated in the liver and is biological unstable in vivo. However, ^{123}I -IUdR is still a promising SPECT probe for detecting NG4TL4 sarcoma and LL/2 lung carcinoma in the mouse model.



The gamma planar imaging of the mouse bearing with NG4TL4 sarcoma (arrow head) injected with ^{123}I -IUdR (n=4) at each time point.



The gamma planar imaging of the mouse bearing with LL/2 lung carcinoma (arrow head) injected with ^{123}I -IUdR (n=4) at each time point.

Presentation Number **1050A**
Poster Session 2d: Imaging Disease/Organ Processes

PET Study with [¹¹C]Choline and its Derivates in the Human hormone-dependent Prostate Cancer Rat-Xenograft-Tumor-Model PAC120

Damaris Kukuk¹, Olivier Raguin³, Hans F. Wehr¹, Carsten Calaminus¹, Andreas Schmid¹, Valerie S. Honndorf¹, Stefan Wiehr¹, Olivier L. Duchamp³, Walter Ehrlichmann², Julia G. Mannheim¹, Gerald Reischl², Bernd J. Pichler¹, ¹Department of Radiology, Laboratory for Preclinical Imaging and Imaging Technology of the Werner Siemens-Foundation, Eberhard-Karls University Tuebingen, Tuebingen, Germany; ²Department of Radiology, Radiopharmacy, University Hospital of Tuebingen, Tuebingen, Germany; ³Oncodesign - Biotechnology, , Dijon Cedex, France. Contact e-mail: damaris.kukuk@med.uni-tuebingen.de

Prostate cancer is the most prominent oncologic disease in men in the western world. Therefore a big range of biomarkers is available for primary cancer diagnostic as well as therapy monitoring. Prostate cancer is a very heterogeneous disease which ranges between indolent and aggressive states making imaging a challenge. The aim of this work was to validate [¹¹C]Choline, [¹⁸F]FEC and [¹⁸F]FCh, three PET tracers specifically developed for prostate cancer imaging, and compare them with [¹⁸F]FDG and [¹⁸F]FLT pre and post surgical castration in the hormone-dependent PAC120 tumor-xenograft-rat-model. While a previous study revealed neither significant [¹¹C]Choline uptake nor a change of tracer accumulation after therapy in a PAC120 mouse model, we decided to perform identical imaging procedures in rats. Dynamic and static "baseline" PET images of tumor bearing RH/nu- ν rats (mean tumor size 2217mm³, n=10) were acquired on five consecutive days with each tracer. After "baseline" imaging rats were surgically castrated and thereafter measured at two different time points. Tracer uptake was analyzed by acquiring time activity curves, standard uptake values and tumour-to-muscle-ratios (T/M). In addition we measured the apparent diffusion coefficient (ADC) and did chemical shift imaging (CSI) of the hormone-dependent PAC120 tumor-xenograft-rat-model on a 7.2T MRI scanner. The PET image analysis of the PAC120 tumor showed low "baseline" uptake of [¹⁸F]FLT (T/M: 1.14 \pm 0.16). [¹⁸F]FDG showed the highest uptake (T/M: 4.99 \pm 0.84) followed by [¹¹C]Choline (T/M: 2.19 \pm 0.32), [¹⁸F]FEC (T/M: 1.54 \pm 0.29) and [¹⁸F]FCh (T/M: 1.79 \pm 0.38). Nevertheless we found a significant decrease in the T/M ratios three weeks post castration with [¹⁸F]FLT (T/M:0.93 \pm 0.07), [¹⁸F]FDG (T/M: 2.96 \pm 0.64), [¹¹C]Choline (T/M: 1.31 \pm 0.23), [¹⁸F]FEC (T/M: 1.07 \pm 0.12) and [¹⁸F]FCh (T/M: 1.26 \pm 0.26). Analysis of the ADC maps revealed a clear increase of the diffusivity post castration (mean ADC 0.47 \pm 0.02 \rightarrow 0.57 \pm 0.11 10⁻³mm²/sec, n=3) because of a change in tumor microenvironment. These data show for the first time a significant therapy response mimicking an androgen ablation therapy through surgical castration with [¹¹C]Choline and its derivates in a hormone-dependent prostate cancer xenograft rat model. Most importantly, the same studies were previously performed in mice without showing a significant therapy response for choline tracers. This indicates the importance to choose the right animal species. Conclusively the PAC120 tumor rats seem to be a viable animal model to study prostate cancer in vivo.

Presentation Number **1051A**
Poster Session 2d: Imaging Disease/Organ Processes

A Peptide Probe for In Vivo Imaging and Delivery of Liposomal Doxorubicin to Lung Tumor

So-yeon Lee, Xiaofeng He, Moon Hee Na, In-San Kim, Byung-Heon Lee, Department of Biochemistry and Cell Biology and Cell Matrix, Kyungpook National University, Daegu, Republic of Korea. Contact e-mail: lololmoon@naver.com

Targeted delivery of imaging agents and therapeutics to cancer would provide early detection and increased therapeutic efficacy against cancer. Here we have screened a phage-displayed peptide library to identify peptides that selectively bind to lung tumor cells. After incubating with H460 lung tumor cells, the cell-bound phages were enriched. Evaluation of individual phage clones revealed that a phage clone displaying LT-1 (Lung Tumor-targeting peptide-1) bound to H460 cells at higher extent than other clones. LT-1 peptide strongly bound to H460 cells and efficiently internalized into the cells, while little binding of a control peptide was seen. It also preferentially bound to other lung tumor cell lines, such as A549 and H226. In contrast, its binding to other types of tumor cells, such as stomach, breast, and colon, was relatively weak. In vivo imaging of tumor was achieved by homing of LT-1 peptide to H460 tumor in mice. Ex vivo imaging and microscopic analysis further demonstrated the targeting of LT-1 peptide to tumor. Doxorubicin-loaded liposomes coupled with LT-1 peptide inhibited the tumor growth more efficiently than untargeted liposomes and free doxorubicin. These results suggest that LT-1 peptide is a promising targeting probe that can direct imaging agents and therapeutics to lung tumor.

Presentation Number **1052A**
Poster Session 2d: Imaging Disease/Organ Processes

Uveal melanoma and ^{18}F -FDG PET: correlation between primary lesion and metastasis

Arthur Cho¹, Christopher S. Lee², Jun Young Park¹, Won Jun Kang¹, Jong Doo Lee¹, ¹Nuclear Medicine, Severance Hospital, YUMC, Seoul, Republic of Korea; ²Ophthalmology, Severance Hospital, YUMC, Seoul, Republic of Korea. Contact e-mail: artycho@hotmail.com

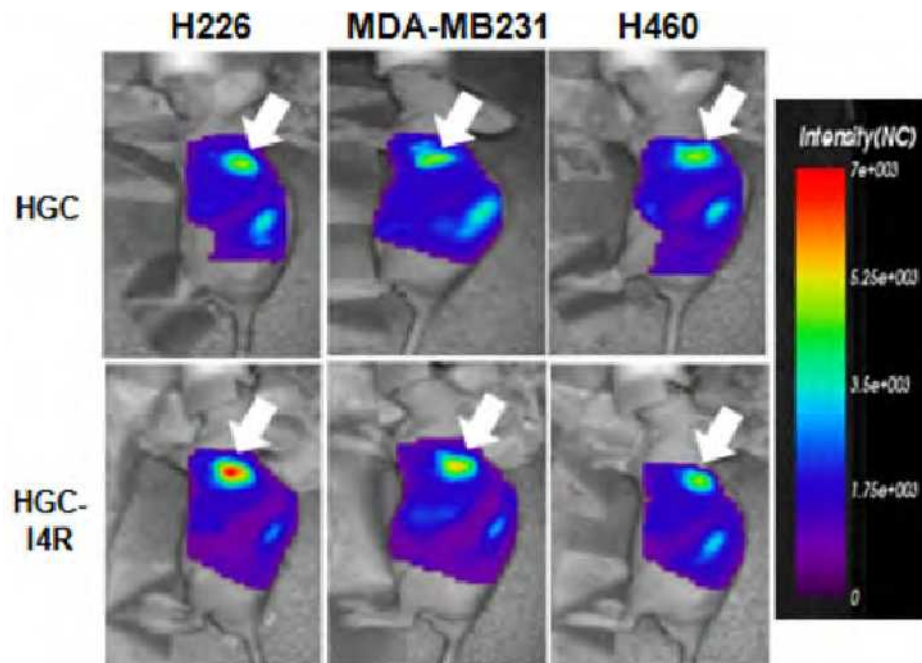
Purpose: Uveal melanoma (UM) is the most common primary intraocular tumor in adults and about 50% metastasize, especially when monosomy 3 or chromosome 8 gain is present. Although ^{18}F -FDG PET is shows low ^{18}F -FDG uptake in the ocular lesion, increased ^{18}F -FDG uptake is frequently seen in distant metastasis. We studied ^{18}F -FDG uptake of the primary lesion with distant metastasis and correlated pathological and cytogenetic analysis. Materials and Methods: A retrospective data analysis of 68 UM patients (average age 47.3 years old, 35 male), who underwent initial ^{18}F -FDG PET from 2004 to 2009 was performed. Tumor size was correlated with ^{18}F -FDG uptake. Patients were treated either by enucleation or brachytherapy using ruthenium-106. Twenty-two patients underwent follow up PET (range 0.7-5.5 years) for clinical suspicion of metastasis. Fluorescence in situ hybridization (FISH) was performed on 10 patients for detection of chromosome 3 loss or chromosome 8 gain. ^{18}F -FDG uptake was evaluated by visual analysis and standard uptake value (SUV). Correlation of ^{18}F -FDG PET findings in initial and follow up scans were correlated with clinical and pathological findings. Results: Twenty-eight of 68 lesions (41.2%) showed increased ^{18}F -FDG uptake, with an average SUV of 1.94. There was a significant correlation between largest basal diameter (LBD) of the tumor and ^{18}F -FDG uptake in the primary lesion ($R^2=0.283$, $p<0.001$). Six patients developed metastasis during the follow up period. These patients showed larger LBD (13.4mm vs 9.0mm, $p<0.01$) compared to patients who did not metastasize. Five patients who developed metastasis underwent ^{18}F -FDG PET for systematic evaluation and all showed intense ^{18}F -FDG uptake in the liver and bone metastasis. There was no statistical correlation between initial ^{18}F -FDG uptake and ^{18}F -FDG uptake in the metastatic lesions. Of the 10 patients who underwent genetic analysis, 8 showed no chromosomal abnormalities, and had no metastasis. Two patients with chromosomal abnormalities developed metastasis with intense ^{18}F -FDG uptake on PET. Conclusion: Although uveal melanoma in the primary lesion shows variable uptake, metastatic lesions shows intense ^{18}F -FDG uptake. Routine ^{18}F -FDG PET follow up is recommended to detect systematic metastasis, especially in patients with monosomy 3 or chromosome 8 gain.

Presentation Number **1053A**
Poster Session 2d: Imaging Disease/Organ Processes

Peptide-guided tumor-targeting nanoparticle for cancer imaging

Jong-Ho Kim¹, Kwangmeyung Kim², Byung-Heon Lee¹, Rang-Woon Park¹, Ick Chan Kwon², In-San Kim¹, ¹School of Medicine, Kyungpook National University, Daegu, Republic of Korea; ²Biomedical Research Center, Korea Institute of Science and Technology, Seoul, Republic of Korea. Contact e-mail: jonghokim@knu.ac.kr

Macromolecular nanoparticles can accumulate and extravasate within tumor tissues because of the prolonged circulation by enhanced permeability and retention effect, passive targeting system. The passive targeting systems show unsatisfactory tumor therapeutic efficacies to apply clinics since extravasated nanoparticles were concentrated around tumor vessels. Therefore, active targeting drug delivery systems have recently gained considerable attention to solve limits about distribution and uptake. Here, we describe chitosan nanoparticles conjugated with interleukin-4 receptor binding peptides, I4R, that target tumors present better therapeutic and imaging efficacy than nonconjugated nanoparticles in mice bearing IL-4R positive tumors. We concluded that I4R facilitated microdistribution and enhanced cellular uptake of nanoparticles in tumor tissues. This study suggests that the microdistribution of nanoparticles in tumors is an essential factor needed to design nanoparticles for tumor targeting drug delivery and imaging.



Non-invasive cancer imaging at 24 hour after intravenous injection through tail vein.

Presentation Number **1054A**
Poster Session 2d: Imaging Disease/Organ Processes

Ga-68 Radiolabeled DOTA-Affibody for Positron Emission Tomography

Nalini Shenoy¹, Gabriela Kramer-Marek², Jacek Capala², Gary L. Griffiths¹, ¹NHLBI/IPDC, NIH, Rockvill, MD, USA; ²National Cancer Institute, National Institutes of Health, Bethesda, MD, USA. Contact e-mail: marekg@mail.nih.gov

Positron emission tomography (PET) is an important imaging modality for preclinical and clinical quantitative imaging in a range of diseases. Biomolecules and small molecules radiolabeled with positron emitting radionuclides are increasingly used as diagnostic tools in disease detection and therapy evaluations. Gallium-68 decays by positron emission with a half-life of 68 minutes and can be obtained from a Ge-68/Ga-68 radionuclide generator. This makes Ga-68 readily available to facilities that lack a cyclotron, and several generators are being developed with intent for clinical application. Affibody molecules® are small targeting proteins with a three helix bundle. The ZHER2:2891 Affibody molecules used in this work have high specificity towards HER2, known to be overexpressed in several types of tumors. The unique cysteine on the C terminal of the Affibody molecule has been derivatized with a DOTA in order to incorporate Ga-68. A modern titanium oxide-based Ge-68/Ga-68 generator was coupled to a remote, automated module for radiolabeling of targeting moieties. Elution of the generator with 0.1 M hydrochloric acid yields Ga-68 in an ionic form. The eluent is subjected to a pre-purification step, which reduces the metallic trace impurities such as Zn²⁺, Fe³⁺, Ti⁴⁺ and germanium breakthrough, which could potentially interfere with the complexation reactions. Reaction parameters such as reaction time, buffer, temperature, and pH were optimized to obtain high radiolabeling efficiencies for the DOTA-derivatized Affibody® molecules and Octreotide®. The optimized conditions used for labeling were found to be 0.25 M ammonium acetate buffer, pH of 3.5-3.9, and heating at 80 °C for 15 minutes. Typically, the radiolabeling yield was in the range of 90-94%. The Ga-68-DOTA-ZHER2:2891 was purified by size-exclusion and its purity assessed by HPLC. The resulting radioconjugate was found to be stable up to 3 hours in PBS, as determined by HPLC. In vivo biodistribution and imaging studies of ⁶⁸Ga-DOTA-ZHER2:2891 were carried out in athymic nude mice bearing subcutaneous tumors with different levels of HER2 expression. The results showed that the tracer was eliminated quickly from the blood and normal tissues (except the kidneys), providing high contrast PET images already 1h post injection. The radioactivity concentration in BT474 tumors (very high HER2 expression) was 19 [%ID/g] at this time point. Our results suggest that the described radioconjugate can be used to assess HER2 expression in vivo by PET imaging.

Presentation Number **1055A**
Poster Session 2d: Imaging Disease/Organ Processes

MR Imaging with new Folate-Receptor targeted Contrast Agents

Rosalinda T. Castaneda¹, **Sophie E. Boddington**¹, **Daniel Golovko**¹, **Dong Zhang**¹, **Zhen J. Wang**¹, **Yanjun Fu**¹, **Claire Corot**², **Lisa M. Coussens**³, **Heike E. Daldrup-Link**¹, ¹Radiology, University of California, San Francisco, San Francisco, CA, USA; ²Research, Guerbet, Paris, France; ³Pathology & CRI, University of California, San Francisco, San Francisco, CA, USA. Contact e-mail: rosalinda.castaneda@radiology.ucsf.edu

Purpose: The FR is over expressed on cancer cells, but not on cells of normal organs. Thus, FR-targeted are expected to provide "cancer-specific" imaging. The purpose of this study was to determine, which of three contrast agent families provided best contrast enhancement of ovarian cancers on MR images. Experimental Procedures: The following contrast agents, developed by Guerbet research (Paris, France), were evaluated: (1) The FR-targeted gadolinium (Gd) chelate P866 and its non-targeted analogue P1001, (2) the FR-targeted iron oxide nanoparticle P1133 and its non-targeted analogue P904 and (3) the FR-targeted emulsion-based Gd-contrast agent P03362 and its non-targeted analogue P03037. FR positive IGROV-1 cells and FR-negative controls were incubated for 24 hrs with FR-targeted contrast agents. Intracellular Gd or iron concentrations were measured by mass spectrometry. Subsequently, athymic rats with implanted IGROV-1 ovarian tumors underwent MR imaging before and after injection of the above mentioned contrast agents. Additional pilot experiments were obtained for group 3 after pre-treatment with an Alk5 inhibitor, designed to improve tumor microvascular permeability. Changes in tumor longitudinal ($\Delta R1$) and transverse ($\Delta R2$) relaxation rates were compared between FR-targeted and non-targeted agents and correlated with histopathology. Summary of Data: IGROV-1 cells showed a significant uptake of FR-targeted contrast agents when compared to unlabeled controls ($p < 0.05$). Mean tumor $\Delta R1$ values with P866 were significantly higher ($\Delta R1 = 0.214 \text{ s}^{-1}$) compared to P1001 ($\Delta R1 = 0.112 \text{ s}^{-1}$) ($p < 0.05$). Mean $\Delta R2$ values for P1133-treated tumors ($\Delta R2 = 0.0027 \text{ s}^{-1}$) were higher compared to P904 ($\Delta R2 = 0.0011 \text{ s}^{-1}$), although this difference was not statistically significant ($p = 0.09$). Likewise, $\Delta R1$ values were higher for P03362 ($\Delta R1 = 0.085 \text{ s}^{-1}$) compared to P03037 ($\Delta R1 = 0.065 \text{ s}^{-1}$), again not significantly different ($p > 0.05$). Alk-5 inhibitor pre-treatment revealed improved tumor delivery of P03362 ($\Delta R1 = 0.149 \text{ s}^{-1}$) compared to untreated tumors ($\Delta R1 = 0.099 \text{ s}^{-1}$). Histopathologic correlations confirmed FR-expression of all investigated tumors. Conclusions: Novel FR-targeted MR contrast agents provide a FR-specific enhancement of ovarian cancers. The tumor delivery of nanoparticulate contrast agents can be increased by pre-treatment with Alk5 inhibitor.

Presentation Number **1056A**
Poster Session 2d: Imaging Disease/Organ Processes

SPECT/CT and MRI of orthotopic pleural mesothelioma with radiolabeled antibodies

Tapan K. Nayak¹, **Marcelino Bernardo**², **Diane Milenic**¹, **Peter Choyke**², **Martin Brechbiel**¹, ¹NCI/NIH, Bethesda, MD, USA; ²Molecular Imaging Program, NCI/NIH, Bethesda, MD, USA. Contact e-mail: tapann@gmail.com

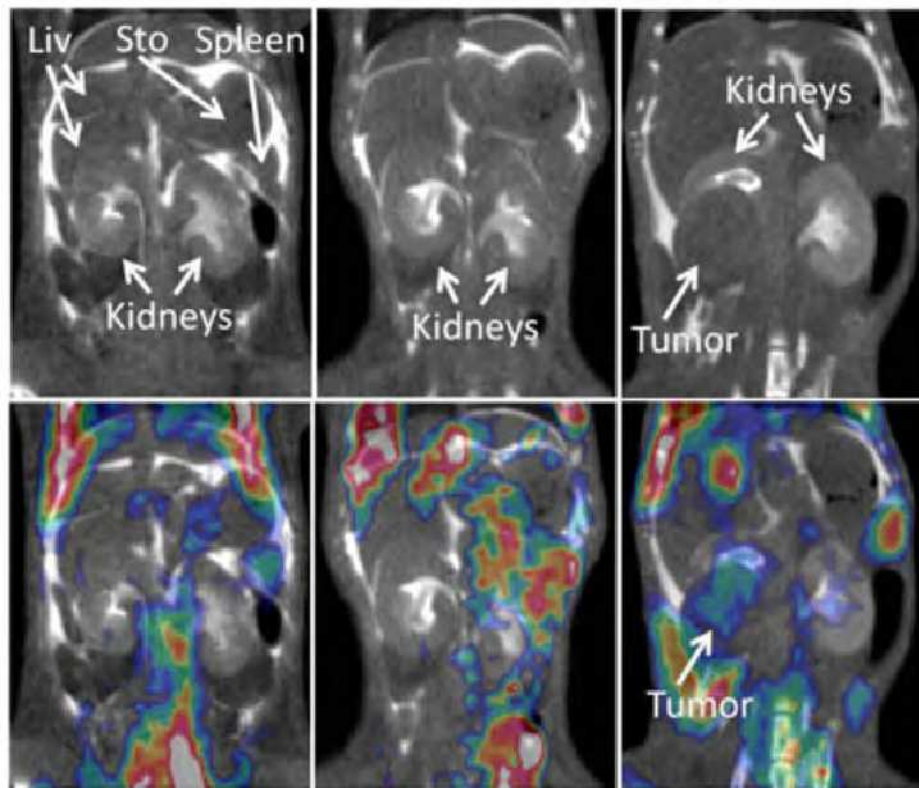
Purpose: Imaging plays an essential role in the evaluation of malignant pleural mesothelioma (MPM). Magnetic resonance (MR) imaging, and more recently, nuclear imaging have emerged as modalities that can provide additional important diagnostic and prognostic information to help further assist in therapeutic intervention. Asbestos exposure, the primary cause of MPM, increases HER1-activity and expression in pre-clinical models. Therefore, in this study we explored the utility of HER1-targeted 111In-panitumumab for SPECT/CT imaging. In addition, MRI studies were performed to monitor the spread of orthotopic MPM. Methods: Flow cytometry studies were performed to evaluate the HER1 expression in NCI-H226 and MSTO-211H cell lines. HER1-targeted 111In or 125I-panitumumab was employed as the positive mAb and HER2-targeted 111In or 125I-trastuzumab was used as the negative mAb. Biodistribution and SPECT/CT imaging studies were performed in mice bearing subcutaneous and orthotopic MPM tumors. Longitudinal MRI studies were performed in mice bearing orthotopic tumors. In addition, at the last imaging time point, SPECT/CT/MRI studies were performed. Results: In vivo studies demonstrated high HER1 tumor uptake of both tumor models. The 111In or 125I-panitumumab tumor uptake was significantly greater than 111In or 125I-trastuzumab, demonstrating uptake in the tumor was HER1 specific. 111In labeled mAbs had more favorable targeting characteristics than 125I labeled mAbs. Orthotopic tumors and effusions were clearly visualized with MRI imaging. In terms of spread and effusion, MSTO-211H model seemed to be more aggressive than NCI-H226 as determined by MRI. MR fusion with SPECT/CT provided more accurate information about 111In-panitumumab localization in the tumor as the tumor was poorly visualized with CT only. Conclusion: This study demonstrates the utility of 111In-panitumumab for non-invasive staging and assessment of the HER1 status of MPM and utility of MRI to study the spread of tumors. The combination of HER1 assessment by SPECT/CT and tumor monitoring by MRI offers an attractive diagnostic and prognostic tool for management of MPM.

Presentation Number **1000B**
 Poster Session 3d: Imaging Disease/Organ Processes

A Novel Model of Renal Tumor in Transgenic Mice: Characterization with Repetitive ^{18}F FDG PET and Dual Contrast-Enhanced CT Imaging.

Leo G. Flores¹, Hsin-Hsien Yeh¹, Suren Soghomonyan¹, Daniel Young¹, Qianghua Hu², Vicki Huff², Juri G. Gelovani¹, ¹Experimental Diagnostic Imaging, MD Anderson Cancer Center, Houston, TX, USA; ²Genetics, MD Anderson Cancer Center, Houston, TX, USA. Contact e-mail: Leo.Flores@mdanderson.org

Background: Wilms' tumor or is the second most common intra-abdominal cancer in children and accounts for more than 95% of all tumors of the kidney in the pediatric age group. A new transgenic model of Wilms' tumor in mice $\text{Wt1}^{\text{fl/fl}}/\text{H19}^{\text{+/m}}; \text{Cre-ER}^{\text{TM}}$ was developed that carries both homozygous inactivation of WT1 and upregulation of IGF2. Due to a strong link of these altered signaling pathways with glucose metabolism, we selected ^{18}F FDG PET/CT as the most suitable imaging modality for detection and monitoring of these transgenic tumors. In this study we aimed to optimize microPET/CT imaging for early detection and monitoring of transgenic Wilms' tumor development in mice. **Methods & Results:** Studies were performed using small animal PET/CT system INVEON (Siemens). CT parameters were: 80kVp, 500 μA , 360 rotational steps 300-350 msec each. CT images were reconstructed using Shepp Logan algorithm. In preliminary studies in normal mice, we determined that i.p. injection of (Ioversol 678 mg/ml, Mallinckrodt) 200 μL i.p. followed by 100 μL intravenously at 20 and 15 minutes prior to imaging, respectively, improves the discrimination of different organs in the abdomen. Because ^{18}F FDG is excreted through kidneys, the most optimal time for PET imaging was found to be 3 hrs after i.v. injection of ^{18}F FDG, which resulted in a clear visualization of ^{18}F FDG accumulation in the renal tumors. Total of 63 mice were imaged with this methodology: 39.1% were imaged once and 52.2% were imaged at least 3-4 times. In $\text{Wt1}^{\text{fl/fl}}/\text{H19}^{\text{+/m}}; \text{Cre-ER}$ tumors were found in 54.3% of animals as early as 50 days, with single lesion found in 34.6% and multifocal lesions in 65.4% of animals. In 35.6% of animals tumors were found on the right side, in 24% on the left side, while 40.4% of animals had bilateral tumors; 15.4% of $\text{Wt1}^{\text{+/-}}; \text{Cre-ER}$ animals had also extrarenal tumors. **Conclusions:** The optimized dual contrast PET CT imaging with delayed ^{18}F FDG provides the most sensitive and reliable methodology for detection and monitoring of this transgenic Wilms' tumor growth in mice. This methodology could also be potentially applicable to orthotopic renal tumor xenograft as well as imaging of primary tumor tissue obtained from surgery and implanted in renal capsule in nude mice, and to monitor renal responses to novel agents and approaches to therapy of renal tumors.

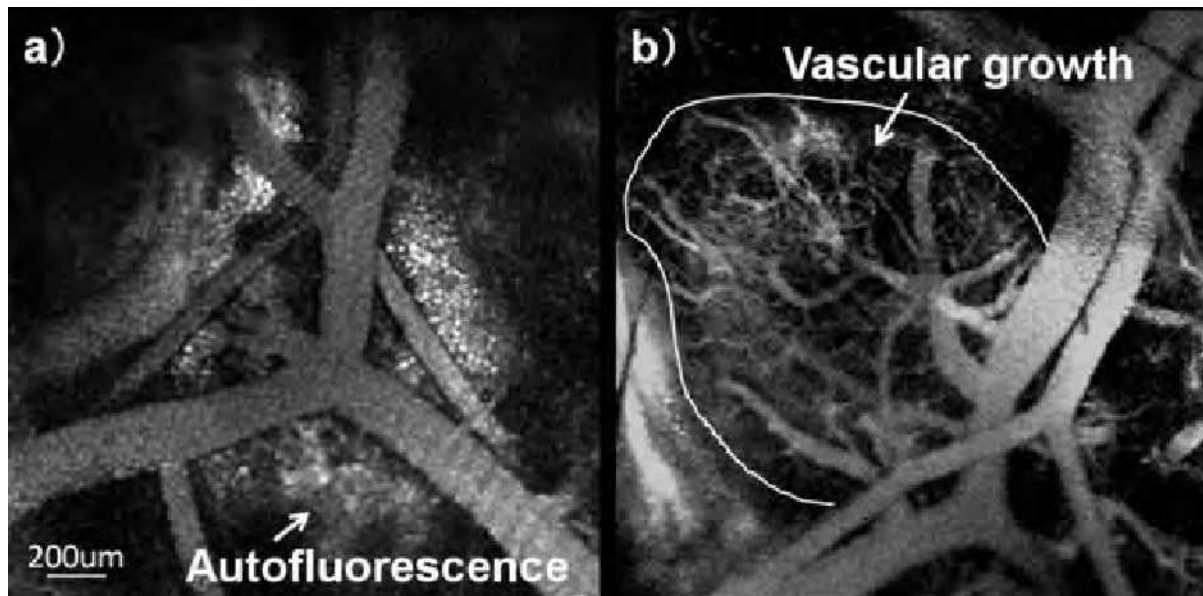


Presentation Number **1001B**
 Poster Session 3d: Imaging Disease/Organ Processes

Imaging of Vascular Progression Within a Lymph Node in a Lymphoma Mouse Model

Ken Ito¹, Bryan R. Smith¹, Natesh Parashurama¹, Cornelius Miething², Scott Lowe², Sanjiv S. Gambhir¹, ¹Department of Radiology and Molecular Imaging Program at Stanford, Stanford University, Stanford, CA, USA; ²Cold Spring Harbor Laboratory, Cold Spring Harbor, NY, USA. Contact e-mail: kenito@stanford.edu

Non-Hodgkin's Lymphoma is a heterogeneous disease with significant mortality. Data we have accumulated indicates that angiogenesis plays an important role in the genesis of lymphoma. We reasoned that intravital microscopy (IVM) could be used to assess the vascular progression of lymphoma in mouse models. We utilized a model of lymphoma in which tail vein-injected murine lymphoma cells undergo homing to the inguinal lymph node. Two types of murine lymphoma cell lines, p53^{-/-} (Doxorubicin (DOX) and Cyclophosphamide (CTX) resistant: IC₅₀= 46.2nM and 84.1μM, respectively) and ARF^{-/-} (DOX and CTX sensitive: IC₅₀= 3.5nM and 10.0μM, respectively) were used. We tail-vein injected 1×10⁶ cells of both groups and PBS as a control into C57BL/6 mice (p53^{-/-} and ARF^{-/-}: N=4, cont.: N=3). On the day of imaging, the inguinal lymph node was exposed by creating a tissue flap. IVM image stacks of blood vessels (using a near infrared intravascular dye) within the inguinal node were obtained and inguinal lymph node size was measured at days 0, 7, 14, and 21 after injection and analyzed using Image J software. We furthermore developed a lymph node window chamber in order to serially image vascularization within the lymph node. We identified that micro vessel number and circulating dye intensity in the inguinal lymph node were significantly higher in p53^{-/-} cell-injected mice compared to ARF^{-/-} cells and control mice at day 7 (p<0.01). Mean vessel length was significantly longer in both p53^{-/-} cells and ARF^{-/-} cells-injected groups compared to control mice at day 7 (cont. vs. p53^{-/-} p<0.001, cont. vs. ARF p< 0.05). At days 14 and 21, vessel growth was higher in both groups compared to control. There is no significant difference in inguinal lymph node size between p53^{-/-} cells and ARF^{-/-} cells-injected mice. These data indicate that inguinal lymph node imaging in an orthotopic murine lymphoma model using IVM is a powerful tool for elucidating unprecedented detail in lymphoma development.(KI and BS contributed equally.)



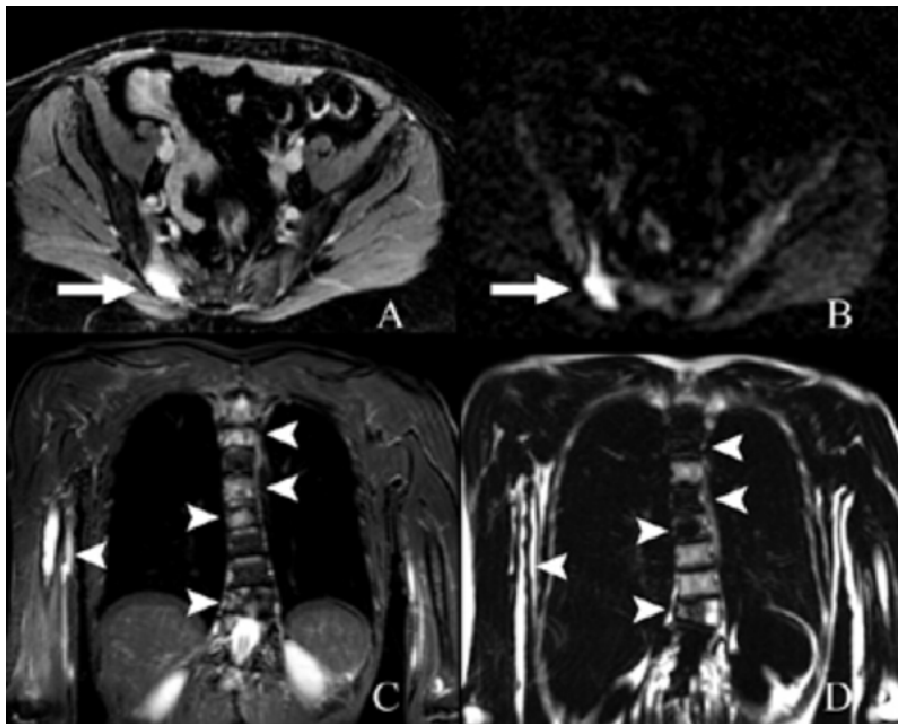
Intravital Microscope (IVM) Images in the Inguinal Lymph Node of a Living Mouse. a) Control mouse. Day 7 after injection of PBS. b) Day 7 after injection of p53^{-/-} lymphoma cells. Enhanced angiogenesis is significantly higher in panel b) as compared to panel a).

Presentation Number **1002B**
 Poster Session 3d: Imaging Disease/Organ Processes

Conspicuity of Bone Lesions on Fast Dixon-Based Whole Body MRI with Diffusion-Weighted Sequences: Estimate of Clinical Utility Per Sequence

Colleen M. Costelloe¹, **Jingfei Ma**², **John E. Madewell**¹, **Robyn K. Harrell**³, **Roland L. Bassett**³, **Vikas Kundra**¹, ¹Radiology, University of Texas MD Anderson Cancer Center, Houston, TX, USA; ²Imaging Physics, University of Texas MD Anderson Cancer Center, Houston, TX, USA; ³Biostatistics, University of Texas MD Anderson Cancer Center, Houston, TX, USA. Contact e-mail: ccostelloe@di.mdacc.tmc.edu

Fast Dixon-based MRI and diffusion-weighted imaging (DWI) have been successfully used for whole body (WB) MRI. Dixon imaging generates 3 sequences per acquisition, resulting in large numbers of images. Limiting the sequences reviewed to the most clinically useful can increase the efficiency of image interpretation. The purpose of this study is to compare the conspicuity of bone metastases on Dixon and DWI WB MRI sequences. Methods: Twenty-nine breast cancer patients with bone metastases prospectively underwent fast Dixon-based WB MRI including coronal T2, axial T1 without and with IV Gd contrast (+C), axial DWI and axial inversion recovery images. The fat only (FO) and fat saturated (FS) images generated with each T1 and T2 acquisition were also reviewed, for a total of 11 different sequences. The skeleton was evaluated in anatomic segments corresponding to image acquisition (head/neck, chest, abdomen/pelvis, thigh, calf). Reviewers were blinded to other imaging studies. Lesion conspicuity, a surrogate of clinical utility, was measured on a 5 point scale, with 5 most and 1 least conspicuous. When multiple lesions existed within a segment, 1 conspicuous lesion was rated per anatomic segment. Segments without bone lesions were excluded. The conspicuity scale was analyzed as a continuous variable; data were combined for all body parts, and sequences were compared using analysis of variance (ANOVA). Tukey's HSD method was used to make pair-wise comparisons to determine differences between sequences. A subsequent analysis compared the 4 highest mean conspicuity values to the remaining 7. Results: There is a statistically significant difference among the conspicuity of the sequences, $p < 0.0001$. The conspicuity values of FS T1+C axial ($n=93$ sequences, mean conspicuity 3.55), DWI axial ($n=89$, mean 3.43), FO T2 coronal ($n=94$, mean 3.40) and FS T2 coronal ($n=96$, mean 3.39) were significantly higher than the others, $p=0.0001$. Conclusion: Among Dixon-based and DWI WB MRI sequences, bone lesions are more conspicuous on FS T1+C, DWI, FO T2 and FS T2 implying these should be primarily used for lesion detection.



Bone metastases (arrows/arrowheads) demonstrate increased signal in the sacrum on FS T1+C axial (A) and DWI axial (B) as well as in the spine and left humerus on FS T2 coronal (C) sequences. The same lesions in the spine have decreased signal on the FO T2 coronal (D) sequence.

Presentation Number **1003B**
Poster Session 3d: Imaging Disease/Organ Processes

Manganese-enhanced MRI as a molecular imaging of mesothelioma

Sumitaka Hasegawa, Shigeyoshi Saito, Yukie Morokoshi, Takako Furukawa, Ichio Aoki, Tsuneo Saga, *Molecular Imaging Center, National Institute of Radiological Sciences, Chiba, Japan. Contact e-mail: shase@nirs.go.jp*

Purpose: To develop a selective diagnostic imaging of mesothelioma by targeting disease-specific biomarkers. **Materials and Methods:** All experiments were approved by the Institutional Animal Care and Use Committee. Manganese-superoxide dismutase (Mn-SOD) expression was evaluated in one human mesothelial cells and five human malignant mesothelioma (MM) cells. Mn accumulation in NCI-H226 and MSTO-211H MM cells was examined when loaded with Mn. Mn-enhanced magnetic resonance imaging (MEMRI) of those cell pellets and subcutaneous tumors were conducted using 7 Tesla-MRI. Signal enhancement of H226 xenografted pleural tumors was determined by MEMRI with manganese dipyridoxyl diphosphate (MnDPDP) as well as manganese chloride (MnCl₂). **Results:** We found that 4 of 5 human MM cells over-expressed Mn-SOD protein compared to mesothelial cells, and that H226 MM cells highly expressed Mn-SOD and augmented Mn accumulation when loaded with MnCl₂. The cells showed marked T1-signal enhancement on in vitro MRI after incubation with MnCl₂. H226 subcutaneous tumors were preferentially enhanced compared to MSTO-211H tumors, which had less Mn-SOD expression, in MnCl₂-enhanced T1-weighted MR image (T1WI). H226 pleural tumors were markedly enhanced and readily detected by MEMRI using MnDPDP as well as MnCl₂. **Conclusion:** We propose that MEMRI can be a potentially powerful method for non-invasive detection of MM with high spatial resolution and marked signal enhancement by targeting Mn-SOD.

Presentation Number **1004B**
Poster Session 3d: Imaging Disease/Organ Processes

Imaging mechanisms of cycling hypoxia-promoted tumor progression in U87 glioma

Chian-Yi Chung¹, Chih-Ling Hsu², Hui-Shan Chien², **Chia-Hung Hsieh**³, ¹Graduate Institute of Clinical Medical Science, China Medical University, Taichung, Taiwan; ²Department of Biomedical Imaging and Radiological Science, China Medical University, Taichung, Taiwan; ³Graduate Institute of Basic Medical Science, China Medical University, Taichung, Taiwan. Contact e-mail: chiahung2004@msn.com

Abstract Cycling hypoxia is a common characteristic of solid tumors due to inadequate blood flow. However, the effects of cycling hypoxia on tumor development remained underestimated and controversial for a long time, because it is difficult to clearly evidence the repetition of hypoxia and reoxygenation cycles within tumors, which characterize cycling hypoxia. Recently, in vitro and in vivo studies have shown that tumor exposed experimentally imposed cycling hypoxic stress could modulate tumour growth, angiogenic processes, and radioresistance. These studies also suggest that reactive oxygen species (ROS) and HIF-1 α are important mediators involved in these process. However, the direct evidence from endogenous cycling hypoxia within tumor has not been established. Furthermore, whether antioxidant therapy is able to inhibit cycling hypoxia-mediated tumor progression is not addressed. The purpose of this study is to explore the impact of cycling hypoxia in glioblastoma multiforme (GBM) progression and document the potential mechanism in this process using molecular imaging approaches. Here, our results showed that the most dynamic changes in R2* (a value represented oxygen level) tended to occur in highly vascular regions with relatively high permeability by following the oxygen-sensitive MRI (BOLD R2*) measurements with a terminal DCE-MRI scan in U87 glioma-bearing mice. Furthermore, in vivo monitoring of tumor ROS and HIF-1 signal transduction activity studies also demonstrated that the perfusion area within tumor had high intracellular ROS level and HIF-1 signal transduction activity, and this effect could be blocked by Tempol, a membrane-permeable radical scavenger. Tempol treatment also suppressed the tumor angiogenesis and growth in U87 glioma-bearing mice. Our studies document a therapeutical approach to cycling hypoxia-induced effects and demonstrate that cycling hypoxia-induced ROS is critical aspect of cancer biology to consider for the therapeutical targeting of HIF-1 activation and cancer progression.

Presentation Number **1005B**
Poster Session 3d: Imaging Disease/Organ Processes

Detection of the sentinel lymph node in vulvar cancer, using near-infrared fluorescence intraoperative imaging: a technical feasibility study

Lucia M. Crane¹, Rick G. Pleijhuis¹, George Themelis³, Niels J. Harlaar¹, Athanasios Sarantopoulos³, Henriette G. Arts², Ate G. van der Zee², Vasilis Ntziachristos³, Gooitzen M. van Dam¹, ¹Surgery, University Medical Center Groningen, Groningen, Netherlands; ²Gynaecology & Obstetrics, University Medical Center Groningen, Groningen, Netherlands; ³Helmholtz Zentrum, Technical University, Munich, Germany. Contact e-mail: l.m.a.crane@chir.umcg.nl

Introduction Treatment of squamous cell carcinoma of the vulva consists of radical excision of the tumor with inguofemoral lymphadenectomy. The sentinel lymph node (SLN) procedure, in which the first draining lymph node from the tumor is identified, has proved safe in vulvar cancer, thus decreasing complications such as lymphedema. Disadvantages of the SLN procedure are the use of radioactivity and preoperative injections in the genital area that pose stress on the patient. Intraoperative imaging using a fluorescent agent can possibly be used to detect the SLN, thus leading to an all-intraoperative procedure. In a pilot study, we investigate the value and applicability of an intraoperative multispectral fluorescence camera system combined with the fluorescent agent indocyanin green (ICG) for SLN detection in vulvar cancer. **Methodology** Ten patients with unifocal squamous cell carcinoma of the vulva will be included in the pilot study. One day prior to surgery, radiocolloid is injected around the primary tumor and a lymphoscintigram is acquired. During surgery, a mixture of 1 ml of patent blue and 1 ml of ICG (at a concentration of 0.5 mg/ml) is injected at the same spots. Subsequently, color and fluorescence images and real-time videos of the lymph flow are acquired using the intraoperative multispectral fluorescence camera system. A gamma probe is used to identify SLNs according to the standard procedure. All SLNs are taken out and analyzed ex vivo for fluorescence. Routine histopathological examination and pathologic ultrastaging is performed to reveal possible metastases in the SLNs. **Results** So far, three patients have been included in the pilot study. In all patients, it was possible to detect the SLN with the aid of fluorescence imaging. In total, a number of seven SLNs were detected, all of which were both radioactive and fluorescent, and six of which were blue. One of the SLNs contained metastatic tumor cells. No adverse events were encountered and the surgical procedure was not hindered by the intraoperative camera system. Fluorescence imaging prolonged the surgical procedure with no more than 15 minutes. **Conclusion** We show first clinical results indicating the technical feasibility of SLN detection in squamous cell carcinoma of the vulva using an intraoperative multispectral fluorescence camera system and ICG. Extended inclusion of patients is necessary to define the diagnostic accuracy.

Presentation Number **1006B**
Poster Session 3d: Imaging Disease/Organ Processes

Indocyanine Green Liposomes for Quantitative Near Infrared Imaging of Lymphatic Function

Steven Proulx, Paola Luciani, Stefanie J. Derzsi, Matthias Rinderknecht, Viviane Mumprecht, Jean-Christophe Leroux, Michael Detmar, Swiss Federal Institute of Technology (ETH) Zurich, Zurich, Switzerland. Contact e-mail: steven.proulx@pharma.ethz.ch

Lymphatic vessels play a major role in cancer progression and in postsurgical lymphedema, and several new therapeutic approaches targeting lymphatics are currently being developed. Thus, there is a critical need for quantitative imaging methods to measure lymphatic flow. Indocyanine green (ICG) is currently used for near infrared optical imaging of the lymphatic system but it is unstable in solution and rapidly enters venous capillaries after local injection. Therefore, we developed a novel ICG liposomal formulation (~60 nm) (LP-ICG) which improved the dye's stability in solution and increased its fluorescence signal with a shift towards longer wavelength absorption and emission. When injected intradermally into C57/Bl6 albino mice, LP-ICG was specifically taken up by lymphatic vessels and allowed improved visualization of deep lymph nodes. In biodistribution studies, there was no evidence of increased retention of LP-ICG compared to free ICG at the injection site or in any other tissues. In a genetic mouse model of lymphatic dysfunction, injection of LP-ICG showed no fluorescent signal enhancement of draining lymph nodes and slower clearance from the injection site. Mice bearing B16-F10 luciferase expressing melanomas transfected with human vascular endothelial growth factor-C (VEGF-C) were used as a model of enhanced lymphatic metastasis. Using bioluminescent imaging, we validated an increased level of metastasis at day 21 post-inoculation to draining lymph nodes in the mice bearing VEGF-C expressing tumors (7/9 positive) compared to pcDNA3.1 control transfected tumors (2/8 positive). Using an exponential decay model, we quantified the flow from sequential near infrared images of intradermally-injected LP-ICG through the tumor draining lymph nodes. Increased flow was observed in mice bearing VEGF-C expressing tumors with low level or no metastases (decay constant $K_{LN} = 0.069 \pm 0.011 \text{ min}^{-1}$) compared to mice bearing pcDNA3.1 control transfected tumors ($K_{LN} = 0.042 \pm 0.016 \text{ min}^{-1}$). Interestingly, in mice bearing VEGF-C expressing tumors with a higher lymph node tumor burden, a decreased flow pattern was seen ($K_{LN} = 0.021 \pm 0.011 \text{ min}^{-1}$) indicating a possible disruption of lymphatic flow by tumor cells. These new methods likely will facilitate quantitative studies of lymphatic function in preclinical studies and may also have potential for imaging of lymphedema or improved sentinel lymph detection in cancer.

Presentation Number **1007B**
Poster Session 3d: Imaging Disease/Organ Processes

Reduction of Radiation Risk in Molecular Breast Imaging

Douglas J. Wagenaar¹, Amanda L. Weinmann², Michael K. O'Connor², Carrie B. Hruska², Samir Chowdhury¹, Bradley E. Patt¹,
¹Research, Gamma Medica-Ideas, Inc., Northridge, CA, USA; ²Radiology, Mayo Clinic, Rochester, MN, USA. Contact e-mail: douglas.wagenaar@gm-ideas.com

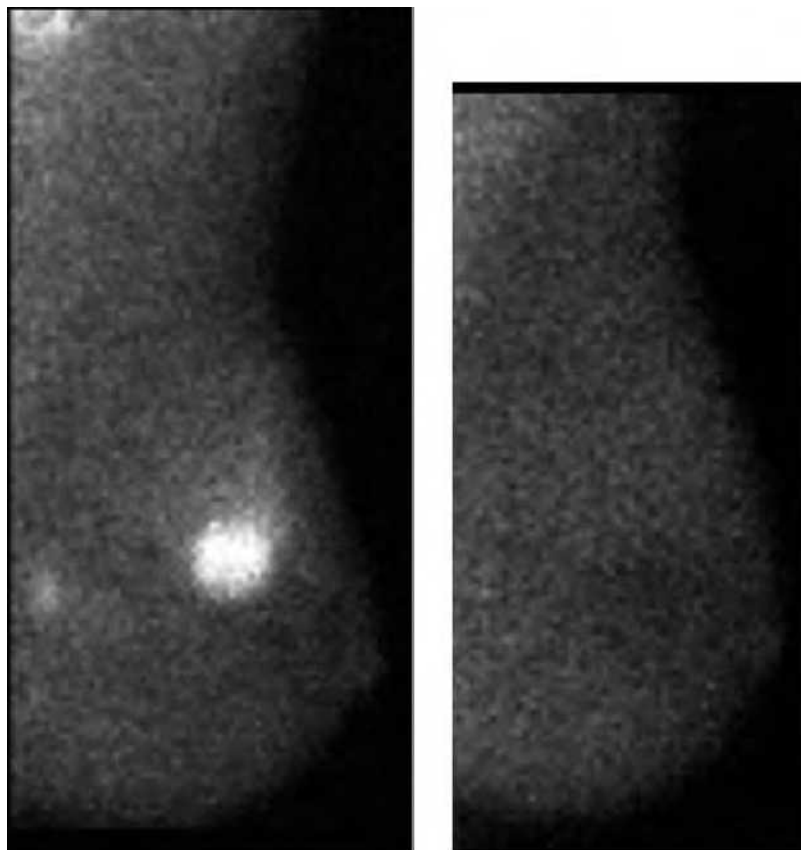
Molecular Breast Imaging (MBI) uses a new semiconductor (CZT) imaging detector in a dual-head configuration to optimize detection of small (<1.0 cm) lesions in early stage breast cancer. CZT has been used in microSPECT research with multiple pinholes. The clinical technique involves the intravenous administration of the radiopharmaceutical Tc-99m-sestamibi (MIBI), which is the contrast agent of choice in more than 15 M nuclear cardiology studies annually worldwide. The combination of enhanced permeability and retention in neovasculature with mitochondrial metabolism produce uptake of MIBI in breast cancer lesions that is generally greater than 10:1 compared with background tissue uptake. Because MBI detects cancers in women with radiographically dense breasts, this new modality has been proposed for use in screening of this population that is underserved by conventional mammography (MMG). Screening MBI requires an analysis of the risk/benefit associated with the study. In comparison with screening MMG, the radiation dose from MBI is systemic, whereas in MMG the dose is concentrated within the breast tissue. The wholebody radiation dose from MBI is well documented due to nearly 20 years of nuclear cardiology with MIBI. The proposed screening application places demands upon the MBI modality to reduce the radioactivity necessary to detect small lesions in asymptomatic women. Our analysis, based on the NCRP BEIR VII risk tables, concludes that a factor of ~7 reduction in radioactivity is necessary in order for MBI screening dose equivalent to match that of MMG. From the standard 25 mCi injection, one must reduce the MBI injected activity to ~3 mCi. Experience with more than 2000 MBI acquisitions tells us that we wish to image for no more than 10 minutes per view to avoid patient discomfort, which is a 40 minute (+ positioning time) session for the standard four-view screening study. In this work we describe a comparison trial with 10 patients who underwent standard injections of 20-30 mCi with two MBI collimators: 1) conventional hexagonal lead; and 2) registered square-hole, near-field collimator. List-mode acquisition was performed, such that 1 mCi injections could be incrementally accumulated (up to 8 mCi). Energy window optimization, dual-head data amalgamation, and denoising algorithms also were employed to lower dose. We conclude that custom-designed collimator in combination with dual CZT heads and dose-reduction algorithms can reduce wholebody dose of MBI to the level comparable to that of screening MMG.

Presentation Number **1008B**
 Poster Session 3d: Imaging Disease/Organ Processes

Molecular Breast Imaging for Neoadjuvant Chemotherapy Assessment

Douglas J. Wagenaar¹, Judy C. Boughey², Carrie B. Hruska³, Michael K. O'Connor³, Dietlind L. Wahner-Roedler⁴, Rex Moats⁵, Samir Chowdhury¹, Bradley E. Patt¹, ¹Research, Gamma Medica-Ideas, Inc., Northridge, CA, USA; ²Surgery, Mayo Clinic, Rochester, MN, USA; ³Nuclear Medicine, Mayo Clinic, Rochester, MN, USA; ⁴Internal Medicine, Mayo Clinic, Rochester, MN, USA; ⁵Radiology, Children's Hospital of Los Angeles, Los Angeles, CA, USA. Contact e-mail: douglas.wagenaar@gm-ideas.com

Molecular Breast Imaging (MBI) is used to assess response to neoadjuvant chemotherapy (NAC) in patients with invasive breast cancer prior to surgery. Also MBI is compared with MRI for NAC assessment. MBI is a nuclear medicine technique that uses a dedicated, dual-head CZT imager to measure the radiotracer uptake in breast lesions. Tc-99m-sestamibi (MIBI) is now the MBI agent of choice for lesion detection; this study reports on a pilot study of the agent for NAC assessment. A total of 11 patients (12 breasts) were imaged with MBI; with 4 of these patients undergoing MRI in addition to MBI. In 8 of the 12 specimens examined by pathology, MBI findings were concordant with pathology. Two discordant cases found <1 mm residual disease in pathology; one MBI with low intensity residual (post-therapy) uptake showed complete pathological response; and one MBI showed uptake throughout a mass that revealed only 3 pockets of invasive disease within fibrotic tissue. MBI was more accurate than MRI in the four cases compared: one case showed MRI-MBI-pathology concordance; two cases showed residual MRI enhancement in fibrosis that was negative on MBI, and one case was negative in MRI-MBI and positive for a 1 mm residual lesion on pathology. The results of this pilot study suggest that MBI with Tc-99m MIBI may be useful for assessment of NAC response prior to surgery. Quantitative evaluation of MBI uptake values are next step to follow this initial pilot trial. Additionally, quantitative uptake of molecular imaging agents other than MIBI, e.g. I-123-labeled estradiol, can be added to MIBI since dual-isotope imaging is enabled by MBI. In conclusion, MBI shows promise as a non-invasive tool for NAC assessment.



MRI showed a 2.3 cm mass in the central breast corresponding to biopsy-proven invasive cancer. MBI (left) showed a 2.3 cm focus of uptake with posterior extension and second area of focal uptake in lower outer quadrant measuring 1.5 cm. After completion of NAC, MBI (right) showed no uptake consistent with no residual disease. Pathology revealed a fibrotic area of 2.1 cm in the central breast with 0% tumor viability.

Presentation Number **1009B**
Poster Session 3d: Imaging Disease/Organ Processes

THE ROLE OF FDG PET/CT IN PANCREATIC CANCER

Jyotsna Rao, Kavitha Nallapareddy, Alka A. Chengapa, Sikandar M. Shaikh, Apollo Gleneagles PET CT Ctr, Hyderabad, India.
Contact e-mail: jyotsnael@gmail.com

Pancreatic cancer incidence has risen slowly worldwide. The five year survival is less than 5%. Early diagnosis is difficult and at the time of diagnosis more than half the patients have regional and distant spread. We wish to present our experience of FDG PET/CT in imaging pancreatic cancer. Aim: To evaluate the role of FDG PET/CT in imaging pancreatic cancer. Material and method: A retrospective analysis of reports of patients with pancreatic cancer referred to our center between May 2005 and December 2009 was performed. Patients were injected intravenously with 10-15 mCi of F18 FDG after 4 hours of fasting and scanned per standard whole body protocol after giving oral and intravenous contrast. The scans were reported jointly by a radiologist and PET physician. Follow up was obtained where possible. Results: 31 patients with pancreatic cancer were referred for various indications. 5/31(16%) were referred for diagnosis, 6/31(19%) for staging, 17/31(55%) for restaging and 3/31(10%) to monitor response to therapy. 3/5(60%) patients referred for diagnosis showed primary tumor and metastases, 1/5(20%) showed only primary tumor and 1/5(20%) showed pancreatic duct activity and active mediastinal nodes. 2/6(33%) of the staged patients showed only primary tumor and 4/6(67%) showed primary tumor and metastases. 5/17(29%) of the restaged patients were negative, 3/17(24%) showed primary tumor recurrence and metastases, 6/17(35%) only metastases, 1/17(4%) only primary tumor recurrence, 1/17(4%) progression of metastases and 1/17(4%) showed a second primary in the duodenum. 2/3(67%) patients scanned after treatment to evaluate response showed viable primary tumor and 1/3(33%) viable primary tumor and FDG uptake in lung atelectasis. Conclusion: FDG PET/CT proved useful in patients referred for various indications of pancreatic malignancy to our center.

Presentation Number **1010B**
Poster Session 3d: Imaging Disease/Organ Processes

THE ROLE OF FDG PET/CT IN ENDOMETRIAL CANCER

Jyotsna Rao, Kavitha Nallapareddy, Alka A. Chengapa, Sikandar M. Shaikh, Apollo Gleneagles PET CT Ctr, Hyderabad, India.
Contact e-mail: jyotsnael@gmail.com

Endometrial cancer is the most common gynecological cancer in the West. In India, cervical cancer is the most common female malignancy but endometrial cancer is next in incidence. FDG PET has high sensitivity in identify endometrial tumor. Aim: To evaluate the role of FDG PET/CT in the management of endometrial cancer. Material and method: A retrospective data analysis of reports of 56 patients with endometrial cancer referred to our center between May 2005 and December 2009 for FDG PET/CT was performed. Patients were injected intravenously with 10-15 mCi of F18 FDG after 4 hours of fasting and scanned per standard whole body protocol after giving oral and intravenous contrast. The scans were reported jointly by a radiologist and PET physician. Follow up was obtained where possible. Results: Of the patients referred with endometrial cancer, 5/56(9%) were referred for staging, 45/56(74%) for restaging and 6/56(17%) to monitor response to therapy (radiation and/or chemotherapy). 1/5(20%) of patients staged showed only the primary, 2/5(40%) showed the primary and nodal metastases, 2/5(40%) showed the primary and nodal activity related to local infection. 25/45(55%) of the patients restaged were negative, 13/45(31%) showed only metastases (which included nodal, peritoneal, lung, splenic and adrenal),3/35(6%) showed active thyroid nodules and axillary nodes only, 2/45(5%) showed primary tumor recurrence, 1/45 showed a breast abnormality on PET alone and 1/45(3%) showed a second primary along with metastases.1/6(17%) patients scanned after treatment to evaluate response was negative, 1/6(17%) patient showed viable primary tumor, 2/6(32%) patients showed decrease in metabolism of nodal metastases, 1/6(17%) was negative but showed increase in size of a lung nodule on CT and 1/6(17%) showed active peritoneal/pelvic nodules and operative site. Conclusion: FDG PET/CT proved useful in the management of patients referred with endometrial cancer for various indications to our center.

Presentation Number **1011B**
Poster Session 3d: Imaging Disease/Organ Processes

Phage Display Selection of a Gastric Tumor Cell-Binding Peptide for Imaging Gastric tumor

Jiyoung Lee, Sangeetha Purushotham, Eun-Joo Lee, Napoleon Bonaparte, Byung-Heon Lee, Department of Biochemistry and Cell Biology, School of Medicine, Kyungpook National University, Daegu, Republic of Korea. Contact e-mail: jylee80@live.co.kr

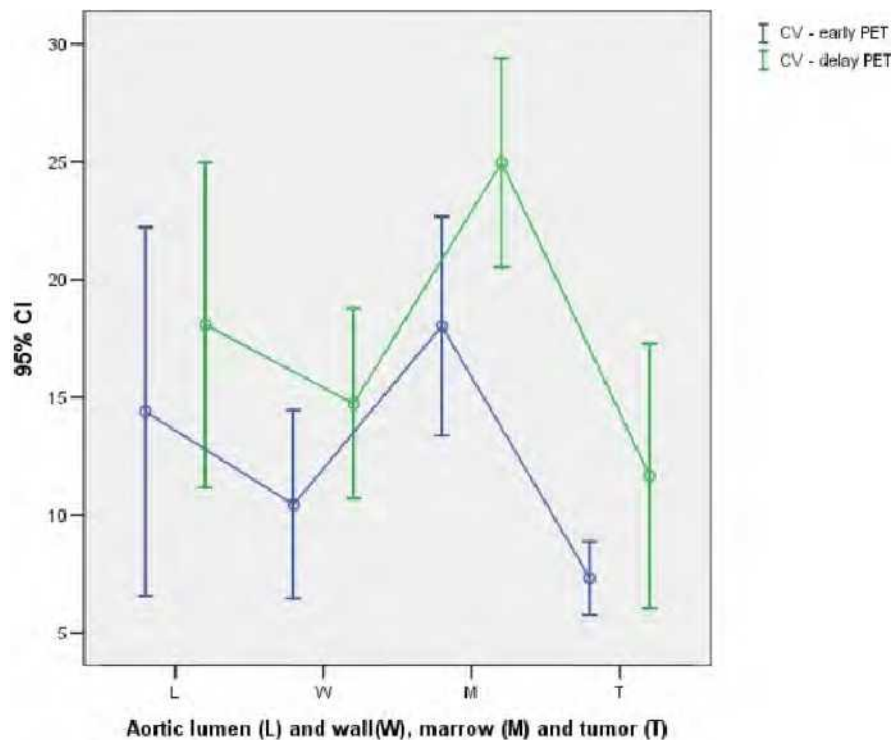
Tumor cells may put unique molecular signatures on their cell surface, which are distinct from their normal counterpart cells. The molecular signatures can be addressed by screening phage displayed-peptide libraries. Such a tumor cell-specific binding peptide would be a useful tool for in vivo imaging of the tumor. Here, we screened a phage library containing random peptides for peptides that bind to a human gastric cancer cell line SNU484 on culture. Of these, we selected the most frequently occurring peptide for further study and named it GT-1 (Gastric Tumor-binding peptide-1). Flow cytometric studies showed the preferential binding of the GT-1 peptide to SNU16 and SNU484 human stomach adenocarcinoma cells compared to a control peptide. On the other hand, the binding of the GT-1 peptide to other types of cells, such as H460 lung tumor cells and BEAS2B normal bronchial cells, was minimal. Selective binding of the GT-1 peptide to SNU484 cells and rapid internalization into the cells were observed by confocal microscopic study. When intravenously injected into SNU484 tumor-bearing mice, the GT-1 peptide homed to and accumulated at tumor tissue in vivo. These results demonstrate that the GT-1 peptide could selectively target gastric tumor and be used as a targeting probe for imaging gastric tumor.

Presentation Number **1012B**
 Poster Session 3d: Imaging Disease/Organ Processes

Which SUV (standard uptake value) can be used in modern respiratory gated PET-CT (GPET): ungated, single phase gated, or averaged gated value and with or without Time of Flight (TOF)?

Regina H. Wong^{1,3}, Joanna Hooten², Christiana O. Wong², Larry Kestin³, Janice Campbell², Inga Grills³, Di Yan³, George D. Wilson³, Alvaro Martinez³, Ching Y. Wong², ¹Biophysics, University of Michigan, Ann Arbor, MI, USA; ²Nuclear Medicine, William Beaumont Hospital, Royal Oak, MI, USA; ³Radiation Oncology, William Beaumont Hospital, Royal Oak, MI, USA. Contact e-mail: iregina@umich.edu

Aim : To investigate the potential differences in SUV of lung cancers by GPET using TOF and dual time early(E) and delayed (D) scans. **Methods :** List mode TOF GPET of the chest with and without gating of the thorax was performed using average of 10 mCi of F-18 FDG at 1 (E) and 2-hour (D) post-injection under fasting condition. The maximum SUV (SUVmax) was measured in 4 regions [ascending aortic lumen (L) and wall (W), marrow in manubrium (M) and tumor (T)] in ungated PET and each of the 10 phases of the GPET. 83 sites [(L,W,M,T)=(16,14,15,38)] were obtained from E and D-GPET. Another 66 pairs of data from ungated E- and D-GPET [(12,10,11,33)] were analyzed. Out of these 66 data pairs, 18 pairs of tumor E and D-SUVmax were obtained in both TOF and non-TOF reconstructions. **Results:** There were good linear correlations among ungated, averaged gated and each respiratory phase SUVmax using TOF with the coefficients of correlation (CV) all over 96% (p<0.0005). But the average gated SUVmax was significantly higher than ungated PET(E-GPET by 14.7%, p<0.0005, and D-GPET by 14.2%, p<0.0005). CV at D-GPET among different phases was significantly higher than that in E-GPET (15.5% vs 10.8%, p<0.0005). Though E and D ungated SUVmax in TOF (9.0+/-5.7 and 10.9+/-6.9) appeared to be slightly lower than that in non-TOF(10.2+/-9.6 and 12.2+/-8.5), it did not reach statistical significance and the trend of higher delayed SUVmax remained similar in both TOF and non-TOF ungated PET. **Conclusions:** Gating procedures increase the signal to noise ratio. The apparent increase in SUVmax determined by gating is very variable, but augmentation of SUVmax on D-GPET is generally consistent with ungated TOF or non-TOF data in dual time PET. However, the use of any single respiratory phase SUVmax is not recommended due to wide variations. Thus for GPET alone, the averaged gated or ungated value should be used with a calibration curve. The retention index can also be calculated using averaged gated or ungated SUVmax and are comparable to non-TOF techniques.



Presentation Number **1013B**
 Poster Session 3d: Imaging Disease/Organ Processes

Collagen Fibers and Macromolecular Transport altered by Hypoxic Environments

Samata Kakkad, Marie-France Penet, Meiyappan Solaiyappan, Arvind P. Pathak, Venu Raman, Kristine Glunde, **Zaver M. Bhujwalla**, JHU ICMIC Program, The Russell H. Morgan Department of Radiology, The Johns Hopkins University School of Medicine, Baltimore, MD, USA. Contact e-mail: zaver@mri.jhu.edu

Solid tumors are characterized by hypoxic environments. Hypoxia stimulates the gene expression of a cluster of hydroxylases used for collagen fiber formation, and may lead to abnormal collagen deposits. In normal tissue collagen fibers direct interstitial fluid into lymphatic channels. In tumors these fibers may not be structured for efficient flow of fluid, especially in hypoxic areas. Our purpose was to understand the role of hypoxia in modifying macromolecular fluid transport using in vivo MRI of macromolecular albumin-GdDTPA, and collagen fiber distribution using second harmonic generation microscopy of corresponding fresh tissue slices. Studies were performed using MDA-MB-231 tumors derived from cells stably expressing tdTomato red fluorescent protein (RFP) under control of the hypoxia response element of VEGF. MRI data (Figure 1A) were related to oxygenation within the imaged slices (Figure 1a). We observed a trend of higher draining voxels in normoxic regions compared to hypoxic regions (Figures 1a and b). Representative SHG images of collagen fiber distribution are shown in Figure 1c. Quantitative analyses of collagen fiber distribution density and volume revealed lower fiber density ($p=0.0149$) and volume ($p=0.0008$) in hypoxic regions. These results suggest that collagen fibers may facilitate macromolecular transport in tumors and their absence in hypoxic regions may reduce this transport.

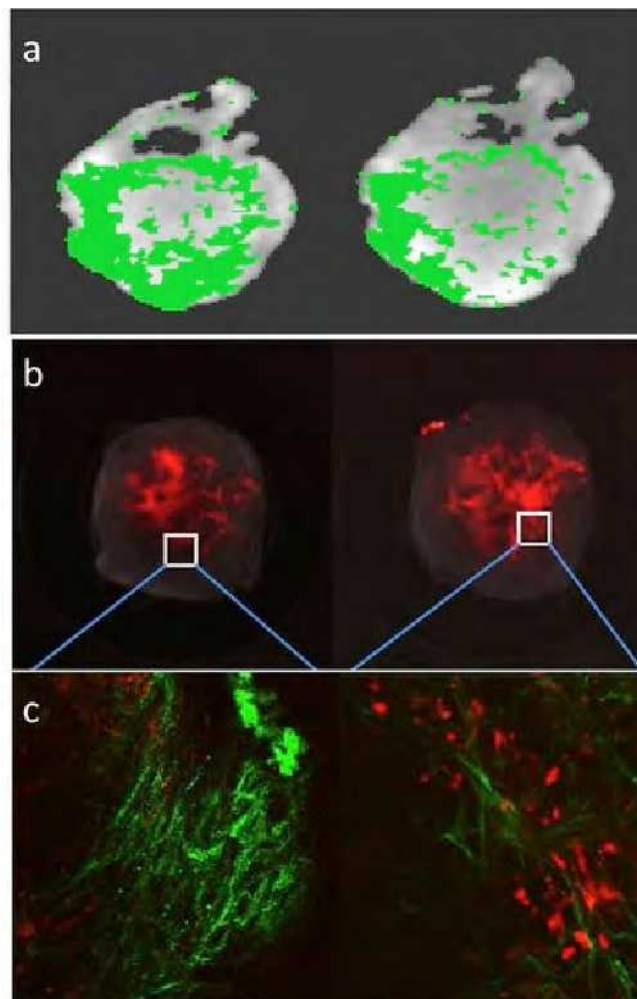


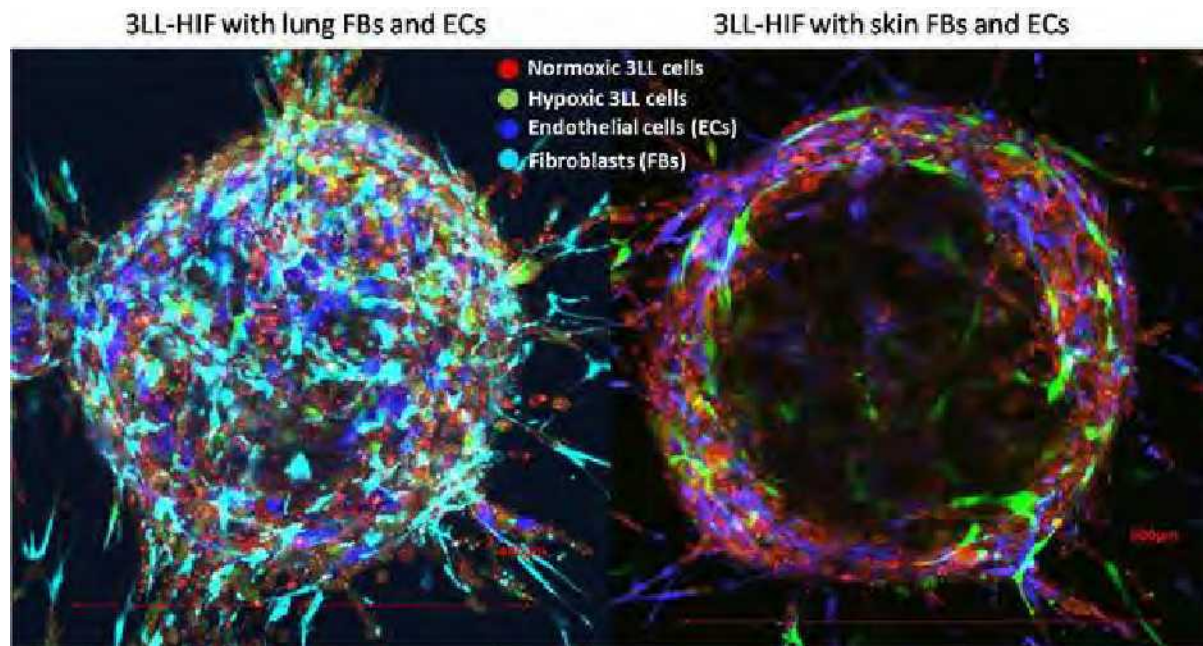
Figure 1: (a) Representative MR images showing voxels draining albumin-GdDTPA. Images from 1 mm slices were acquired with an in-plane spatial resolution of $0.125\text{ mm}\times 0.125\text{ mm}$. (b) Optical images from 1 mm thick fresh tissue slices corresponding to the MR images shown in (a). Red fluorescing regions report hypoxic microenvironments. (c) Collagen I fiber patterns observed in the SHG microscopy images (green) overlaid with the RFP channel reporting on hypoxia (red). Representative images are shown from a normoxic region (left) and a hypoxic region (right) from the corresponding slices.

Presentation Number **1014B**
 Poster Session 3d: Imaging Disease/Organ Processes

DEVELOPMENT OF FUNCTIONAL TUMOR-STROMAL MICROARCHITECTURE DEPENDS ON COMPATIBILITY OF TUMOR CELLS WITH TISSUE-SPECIFIC FIBROBLASTS AND ENDOTHELIAL CELLS AND INVOLVES HIF1 SIGNALING.

Andrei Volgin, Lucia LeRoux, Brian Rabinovich, Juri G. Gelovani, *Experimental Diagnostic Imaging, MD Anderson Cancer Center, Houston, TX, USA. Contact e-mail: andrei.volgin@mdanderson.org*

Background: Intercellular communication and cooperation between tumor cells and stromal-type cells are critical for tumor development. Recruitment of fibroblasts (FBs) and endothelial cells (ECs) within and surrounding the tumor mass is mediated by tissue-specific factors produced by the tumor cells that should match with the surrounding tissue stromal cells. In this study, we aimed to model organ-specific stromal microenvironment matching with the organ-origin of tumor cells and to investigate the role of HIF1 signaling in the development of tumor-stromal architecture and tumor invasion. **Methods and Results:** Organotypic spheroids were generated from the mixture of (a) Lewis lung carcinoma tumor cells (3LL LM) stably expressing a DsRed2/XPRT fusion protein (peak emission of 590 nm) and hypoxia (HIF1 α)-inducible HSV1tk/eGFP, (peak emission of 507 nm), (b) mouse tsA58 (H-2Kb) pulmonary or skin FBs expressing eBFP2 (peak emission of 478 nm), and (c) tsA58 pulmonary or skin ECs expressing mKateS158A (peak emission of 620 nm). Spheroids were generated by mixing tumor cells, FBs and ECs at various ratios in matrigel. Dynamic confocal fluorescence microscopy revealed that co-cultures of metastatic tumor cells with tissue matching (i.e. pulmonary) ECs and FBs (type I spheroids) resulted in the generation of organized spheroids characterized by functional stromo- and vascular tubulo-genesis and migration of ECs towards hypoxic regions. Importantly, we observed the formation of tumor-fibroblast-endothelial cell "invasion complexes", which migrated outside these spheroids and onto the underlying plastic. In contrast, heterotypic tumor (pulmonary) and ECs/FBs (integumentary) co-cultures did not produce organized spheroids (type II spheroids) but instead resulted in migration of EC and FBs to the corona of the tumor cell followed by escape into the surrounding matrix. Cultivation of type I spheroids with inhibitors of HIF1 (YC-1 and Px-478) resulted in a dysfunctional phenotype similar to type II organotypically unmatched spheroids, with "chaotic" distribution of tumor, fibroblast, and endothelial cells. The motility of tumor-fibroblast-endothelial cell complexes towards the outside of such spheroids was significantly inhibited. **Conclusions:** The development of functional tumor-stromal architecture of microscopic (< 1mm) tumors requires (at least in vitro) compatibility of tumor cells derived from a particular organ site with the corresponding organ-specific microvascular endothelial cells and fibroblasts. Tumor invasion and motility requires cooperation of tumor cells, fibroblasts, and endothelial cells that form "invasion complexes". Inhibition of HIF1 signaling disrupts tumor-stromal microarchitecture and suppresses the formation of "invasion complexes".



Multi-spectral confocal microscopy of organotypic multi-cellular tumor spheroids consisting of 3LL lung carcinoma cells transduced with HIF1-inducible GFP (normoxic cells express only RFP) and either lung-derived or skin-derived fibroblasts (light blue) and endothelial cells (dark blue).

Presentation Number **1015B**
Poster Session 3d: Imaging Disease/Organ Processes

Early detection and treatment monitoring of human breast cancer MCF-7 using fluorescence imaging

Dao Chao Huang, Marilyse Piché, Guobin Ma, Muriel Jean-Jacques, Mario Khayat, ART Advanced Research Technologies, Inc., Montreal, QC, Canada. Contact e-mail: gma@art.ca

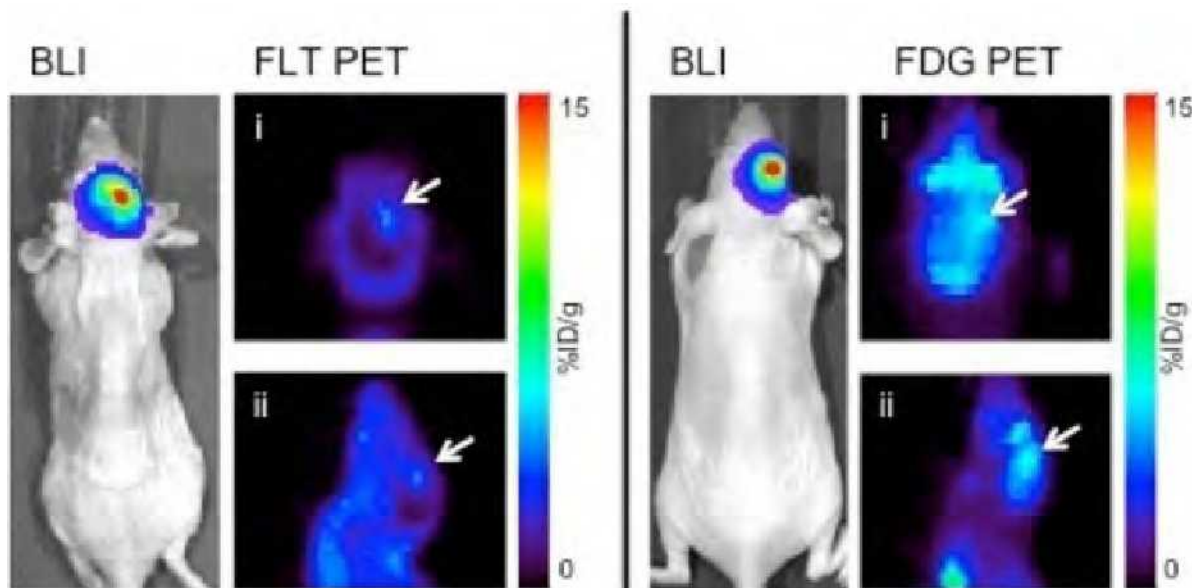
In vivo fluorescence imaging has been increasingly applied in small-animal research because of its quantitative sensitivity, inherent biological safety, and relative ease of use. Epithelial cell adhesion molecule (EpCAM) is highly overexpressed on the cell surface of breast carcinoma. Fluorescently labeled anti-EpCAM antibody (e.g. EpCAM-Cy5.5) as well as cells expressing green fluorescence protein may aid in noninvasive and quantitative screening and treatment monitoring of breast cancer. We present results on the detection of human breast cancer MCF-7 as well as monitoring its treatment in nude mouse using a time-domain in vivo animal fluorescent imaging system. In the first part of our study, we detected non-palpable tumors using the EpCAM-Cy5.5 probe. In the experiment, several mice received subcutaneous injection of either one or five million of MCF-7 cells in the flank, and then tail-vein injection of EpCAM-Cy5.5 probe. Imaging results showed that the antibody was accumulated in both tumor cell spots 24h after injection of the probe although the tumor cells are non-palpable and impossible to be detected by conventional means. In the second part of the study, we quantitatively monitored tumor growth and the effect of treatment using Tamoxifen. In the experiment, one group of mice with GFP expressing MCF-7 tumors was treated by Tamoxifen pellets. The control group was kept in the same condition except no treatment. Treated and non-treated tumors were measured at different time points with both a standard caliper and fluorescent imaging. Analysis of the data revealed that (1) fluorescent signal increased in control mice and decreased in treated mice over time; (2) time domain fluorescence imaging techniques are much more sensitive than conventional manual measurement of tumor volume. At the early stage of tumor formation, fluorescence imaging can detect very small tumors that are not noticeable with manual techniques. Similarly, time-domain fluorescence imaging indicated that there still existed non-palpable tumors after treatment although they were not measurable manually. (3) The weights of Tamoxifen treated tumors were significantly lower than that of the control. Ex vivo fluorescent signals were well correlated to the tumor weight in both treated and non-treated groups. In conclusion, our study demonstrates that fluorescence imaging using either cells expressing GFP or Cy5.5 labeled anti-EpCAM antibody can be used to sensitively, specifically and non-invasively detect non-palpable MCF-7 tumor and effectively monitor their treatment.

Presentation Number **1016B**
 Poster Session 3d: Imaging Disease/Organ Processes

Comparison of ¹⁸F-FDG and ¹⁸F-FLT small-animal PET imaging in an orthotopic glioblastoma mouse model

Erik Mittra¹, Hua Fan-Minogue¹, Frank I. Lin¹, Venkataraman Sriram², Satya Medicherla², Sanjiv S. Gambhir^{1,3}, ¹Radiology-Nuclear Medicine, Stanford University, Stanford, CA, USA; ²Merck Research Laboratories, Palo Alto, CA, USA; ³Bioengineering, Stanford University, Stanford, CA, USA. Contact e-mail: erik.mittra@stanford.edu

Objectives: Pre-clinical orthotopic models of glioblastoma are important for the development of novel therapies. Non-invasive methods to assess response to therapy that can also be used in the clinic are favored, but currently limited. We investigate the utility of ¹⁸F-FDG and ¹⁸F-FLT small-animal PET in an orthotopic glioblastoma model in mice, using bioluminescence (BLI) as a reference. Methods: Fifteen 9 week-old nude mice (7 FDG; 8 FLT) were injected with 3x10⁵ U87 MG-Luc2 cells directly into the right subcortical region. BLI and FDG or FLT PET were performed on these mice weekly for 5 weeks using dedicated small animal imaging apparatus. Region of interest (2D) analysis was used to calculate the photon flux per area (p/s/cm²/sr) and mean percent injected dose per gram (%ID/g), respectively. The BLI and PET signals were compared to assess their relative utility. Results: There was a steady increase in the BLI signal over the course of 5 weeks (Table). Both visually and quantitatively, FLT PET provided a better signal to background ratio than FDG PET within the brain (P = 0.01; Figure). The FLT signal was appreciable when the BLI signal reached ~3x10⁷ which occurred 4 weeks post-implantation. The FDG signal never rose significantly above background levels in the brain. Conclusions: Orthotopic implantation of glioblastoma cells in the mouse brain is feasible and can be imaged non-invasively. BLI is much more sensitive than PET, but FLT PET can be successfully used for this application while FDG PET is not suitable. Subsequent work will evaluate the ability of these models to assess response to therapy.



Whole-body BLI and small animal PET images of the head (coronal (i); sagittal (ii)) showing tumor (white arrows) visibility at 4 weeks. Both mice shown have similar luminescence of 4x10⁷ p/s/cm²/sr. The FLT signal is clearly visible above background while the FDG signal is not. Average and standard deviation (SD) of BLI, FLT PET, and FDG PET signals among all mice over 5 weeks post-implantation.

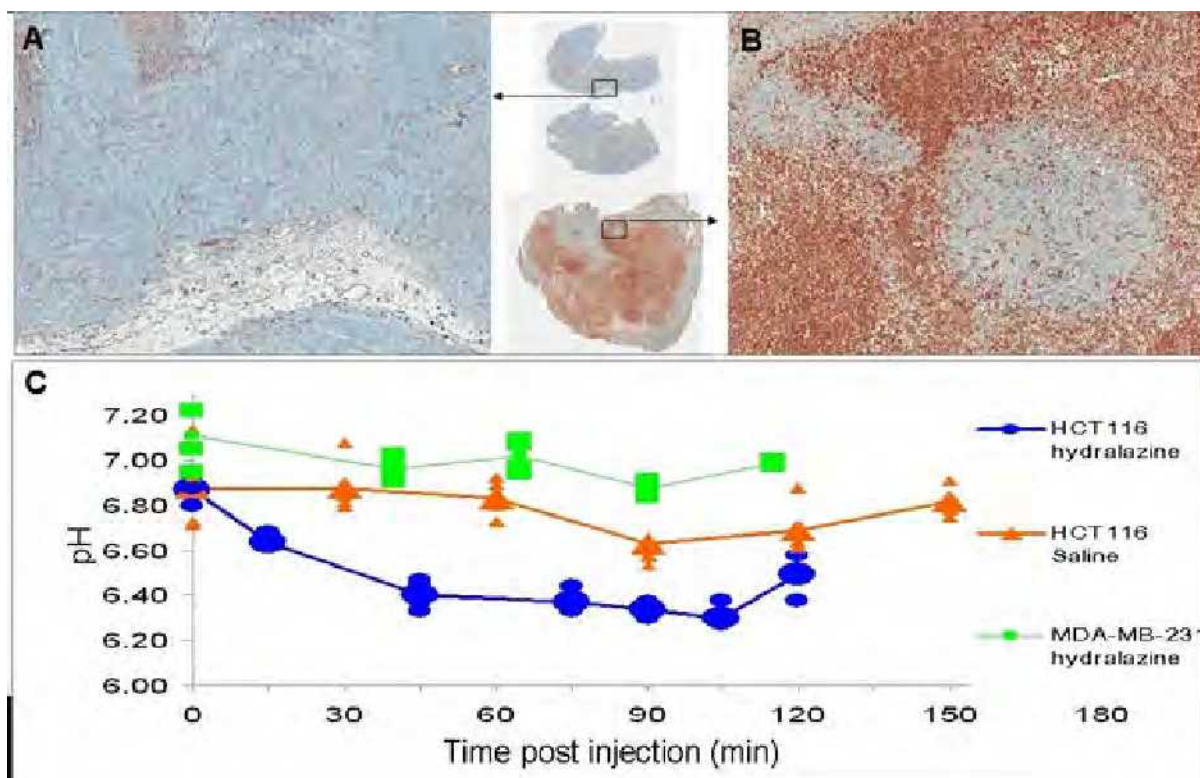
	Bioluminescence (p/s/cm ² /sr)		Lesion : Brain ratio of FLT		Lesion : Brain ratio of FDG	
	Average	SD	Average	SD	Average	SD
Week 1	1.32E+06	2.24E+06	1.3	0.9	0.0	0.5
Week 2	2.62E+06	3.65E+06	1.3	1.3	0.0	0.0
Week 3	4.06E+06	5.53E+06	1.9	1.2	0.0	0.5
Week 4	3.02E+07	3.25E+07	2.6	1.1	0.0	0.5
Week 5	4.06E+07	6.06E+07	1.5	4.0	1.1	1.5

Presentation Number **1017B**
 Poster Session 3d: Imaging Disease/Organ Processes

Manipulating the Tumor Vasculature

Heather Cornell¹, Arig Ibrahim Hashim¹, Gary Martinez³, Amanda F. Baker⁴, **Robert Gillies**^{1,2}, ¹Molecular and Functional Imaging, Moffitt Cancer Research Institute, Tampa, FL, USA; ²Experimental Therapeutics and Diagnostic Imaging, Moffitt Cancer Research Institute, Tampa, FL, USA; ³Small Animal Models and Imaging, Moffitt Cancer Research Institute, Tampa, FL, USA; ⁴Department of Medicine, Arizona Cancer Center, Section of Hematology/Oncology, University of Arizona, Tucson, AZ, USA. Contact e-mail: robert.gillies@moffitt.org

Cancers progress through somatic evolution and this selects for phenotype, not genotype. Thus, although cancers are genetically heterogeneous, there are common phenotypic traits, or “hallmarks”, among all cancers. Therapeutic targeting of hallmarks and their sequelae is an emergent approach that has the possible advantage of treating a variety of cancers in a wide array of patients. One hallmark is sustained angiogenesis, which results in chaotic and immature vasculature that leads to regional hypoxia and acidosis. MR imaging and spectroscopy have documented that the pH of solid tumors is acidic. The focus of this work is to exacerbate tumor acidosis and hypoxia through the use of vasodilators, such as hydralazine. Vasodilators reduce systemic blood pressure and divert blood supply from tumors through the “steal” phenomenon, leading to increased intratumoral hypoxia and acidosis. Preliminary data suggest that lowering pH and pO₂ even further can enhance the activity of acid-induced nanoparticles or hypoxia activated prodrugs. In this study, we have used human tumor xenografts from a variety of cancers with varying degrees of angiogenesis as documented by immunohistochemistry. Two of these are shown below. HCT-116 tumors (A) were much less vascular than MDA-mb-231 tumors (B), and hydralazine caused a dramatic drop in the pH of HCT-116, while MDA-mb-231 tumors were relatively unaffected (C). Furthermore, imaging should provide biomarkers to predict the effects of hydralazine and acid or hypoxia activated agents. The effects of these agents on tumor pH are monitored in vivo using both MRS of IEPA for accuracy and MRI of Gd-DOTA-4AmP for high spatial and temporal resolution, and hemodynamic effects are monitored with ultrasound.



Immunohistochemistry staining for CD31 was much lower in HCT-116 xenograft flank (A) than in MDA-MB-231 mammary fat pad xenograft tumor (B) suggesting that the MDA-MB-231 have greater vascularization. (C) Measurements of pH in animal models after administration of vasodilator indicate a sustained drop in pH in the HCT116 while the MDA-mb-231 remained unaffected.

Presentation Number **1018B**
Poster Session 3d: Imaging Disease/Organ Processes

Development of Targeted Gene Vectors for Tumor Imaging Based on Simian Adenovirus Serotype 24

*Natalya Belousova¹, Galina Mikheeva¹, Chiyi Xiong¹, Suren Soghomonyan¹, Luc Bidaut², Chun Li¹, Juri G. Gelovani¹, **Victor Krasnykh¹**, ¹Experimental Diagnostic Imaging, University of Texas M.D. Anderson Cancer Center, Houston, TX, USA; ²Imaging Physics, The University of Texas M. D. Anderson Cancer Center, Houston, TX, USA. Contact e-mail: vkrasnykh@di.mdacc.tmc.edu*

Development of molecular-genetic imaging approaches promises to improve in vivo imaging of biological processes in norm and disease. These approaches may also improve disease treatment by facilitating surgical and therapeutic interventions, and monitoring of responses to treatment. However, the progress toward these goals is limited by the shortage of gene vectors capable of delivering imaging reporter genes to desired locales safely and efficiently. The objective of our research is to develop adenovirus (Ad)-based gene vectors suitable for safe and efficient molecular-genetic imaging of tumors in humans. Most of the currently used Ad vectors are derived from human Ad serotype 5 (Ad5), which is a suboptimal gene vector prototype because it lacks specificity for tumors, infects normal tissues and causes toxicity, and is neutralized by antibodies found in most humans. To overcome these limitations, we are developing an alternative vector platform using simian Ad serotype 24 (sAd24), to which pre-existing antibodies are rare. We found that, compared to Ad5, sAd24 causes greatly reduced transduction of the liver and other normal tissues, and showed that this low background transduction is due to the instability of complexes formed by sAd24 virions with blood coagulation factor X. To alter the virus' natural tropism, we modified its receptor-binding fiber protein with Her2-specific affibody ligand and showed that the resultant vector infected target human tumor cells in vitro in a Her2-dependent manner. In the presence of neutralizing anti-Ad5 antibodies, Her2-mediated infection by targeted sAd24 in vitro compared favorably to that by the Ad5-derived vector, suggesting more efficient gene delivery by the tropism-modified sAd24 vectors in Ad5-seropositive subjects. The targeted vector retained its infectivity in vivo and was able to express its reporter transgene in Her2-positive tumor cells in circulation. It also achieved higher gene transfer to murine lungs containing Her2-expressing breast tumor metastases, than to tumor-free lungs. The results of this study provide additional justification for development of tumor-targeted sAd24-based vectors for clinical gene delivery of imaging reporter genes.

Presentation Number **1019B**
Poster Session 3d: Imaging Disease/Organ Processes

Multi Modality Molecular Imaging as a Tool Towards Personalizing Met Targeted Therapy

Sari Natan¹, **Miriam Shaharabany**¹, **Yael Zilberstein**¹, **Judith Horev**¹, **Gideon Y. Stein**², **Galia Tsarfaty**³, **Ilan Tsarfaty**¹, ¹*Sackler School of Medicine, Tel Aviv University, Tel Aviv, Israel;* ²*Department of Internal Medicine "B", Beilinson Hospital, Rabin Medical Center, Petah-Tikva, Israel;* ³*Department of Radiology, Sheba Medical Center, Ramat Gan, Israel. Contact e-mail: sazor8@gmail.com*

Breast cancer is the most common malignant disease in western women. In the majority of cases the cause of death in cancer patients is not the primary tumors, but complications derived from metastases at distant sites. The met proto-oncogene product (Met) and its ligand, hepatocyte growth factor/scatter factor (HGF/SF), mediate cell motility and proliferation in vitro and tumorigenicity, angiogenesis and metastasis in vivo. Aberrant Met (a receptor tyrosine kinase) signaling has been widely implicated in most types of human cancers including breast cancer. Over expression of Met and HGF/SF is associated with poor prognosis in several major solid tumor types. Several anti Met targeted therapies are in development and some have entered phase III clinical trials. We have previously shown that activation of Met by HGF/SF induces an increase in tumor blood volume in a dose-dependent manner. The goal of our studies is to further understand the role of Met oncogene in cancer progression and metastasis, and to develop molecular imaging modalities for personalizing targeted Met therapy. To study Met activation by HGF/SF in vivo, we used a xenograft mouse model in which DA3 cells expressing the fluorescent protein mCherry (DA3-mCherry) are injected orthotopically into mice mammary glands. Contrast media ultrasound-based Met functional molecular imaging (FMI) demonstrated that HGF/SF-induced increased hemodynamics upon over expression and dramatically decreased upon down regulation of the receptor and its signaling pathway; Whole animal spectral imaging demonstrated fast developing micrometastatic spread of the tumor enabled detection of sub-millimeter metastases demonstrating fast developing micrometastatic spread of the tumor; Macro to Micro and two photon confocal imaging demonstrated HGF/SF induced changes in blood flow at single vessel resolution, localization of metalloprotease and catapsine activity at the tumor edge and increase in single cell motility. Met molecular imaging demonstrated that Met signaling modulation plays a major role in breast cancer tumor growth and development. These emerging MI modalities may help tailor Met-targeted therapy.

Presentation Number **1020B**
Poster Session 3d: Imaging Disease/Organ Processes

Polymer/Metal Composite Nanoparticles with Magnetic Resonance Imaging and Tumor Targetibility

Keun Sang Oh¹, **Seung Ki Kim**², **Beom Suk Lee**³, **Kuiwon Choi**¹, **Ick Chan Kwon**¹, **Sang Yoon Kim**³, **Soon Hong Yuk**², **Kwangmeyung Kim**¹, ¹*Biomedical Research Center, KIST, Seoul, Republic of Korea;* ²*Department of Advanced Materials, Hannam University, Daejeon, Republic of Korea;* ³*Asan Medical Center, University of Ulsan College of Medicine, Seoul, Republic of Korea.* Contact e-mail: oks5486@nate.com

A novel method for gold-deposited iron oxide/glycol chitosan nanoparticles with heparin has been designed and characterized as a magnetic resonance imaging agent with tumor targeting characteristic. Gold-deposited iron oxide nanoparticles (the mean diameter: 6 ± 2.0 nm) was prepared as a magnetic resonance imaging probe based on the previous method. Iron oxide nanoparticles and glycol chitosan show a cationic characteristic in the aqueous solution. To induce the ionic interaction between iron oxide nanoparticles and glycol chitosan, gold was deposited on the surface of iron oxide nanoparticles. After the immobilization of gold-deposited iron oxide nanoparticles into the glycol chitosan network, the nanoparticles were stabilized with heparin based on the ionic interaction between cationic glycol chitosan and anionic heparin, and were freeze-dried to prepare gold-deposited iron oxide nanoparticles in the powdery state. TEM and ELS were used to observe the size distribution and zeta-potential. With the formation of nanoparticles with glycol chitosan, the stability of gold-deposited iron oxide nanoparticles used a molecular imaging probe in the aqueous media was improved significantly. To observe the MRI contrast characteristic, the nanoparticles were injected into the tail veins of tumor-bearing mice to demonstrate their selective tumoral distribution. MR images were collected with conventional T2-weighted spin echo acquisition parameters. Gold-deposited iron oxide/glycol chitosan nanoparticles in this study can be utilized as a drug delivery system for anti-cancer drug with molecular imaging.

Presentation Number **1021B**
Poster Session 3d: Imaging Disease/Organ Processes

Analysis of False-positive Foci with F-18 FDG Avidity on PET/CT Imaging in Breast Cancer

Soon-Ah Park¹, **UnJong Choi**², **Hye-Won Kim**³, **Hun Soo Kim**⁴, **Sang-Ah Jung**¹, ¹*Nuclear medicine, wonkwang university college of medicine, Iksan, Republic of Korea;* ²*Surgery, wonkwang university college of medicine, Iksan, Republic of Korea;* ³*Radiology, wonkwang university college of medicine, Iksan, Republic of Korea;* ⁴*Pathology, wonkwang university college of medicine, Iksan, Republic of Korea.* Contact e-mail: nmbach@wonkwang.ac.kr

Purpose: The aim of this study was to evaluate the normal physiologic and benign F-18 fluorodeoxyglucose (FDG) avid foci to differentiate them from metastases in patients with breast cancer. **Methods:** Three hundred and nine FDG PET/CT files from 241 women with breast cancer were reviewed retrospectively. The hypermetabolic lesions were defined as those lesions with a higher maximum standardized uptake value (maxSUV) compared to the surrounding normal region. Available reports of other relevant radiological imaging, pathology findings, laboratory test results and follow-up PET/CT were reviewed for explanations of the abnormal uptake. **Results:** Among the 70 physiologic foci, ipsilateral muscular uptake of the lower neck was observed in patients that had a surgical intervention (29%). Non-specific bowel uptake (33%), hypermetabolic ovaries (16%) and uterine (10%) uptake during the late follicular to the early luteal phase was noted during the normal menstrual cycle, and hypermetabolic brown fat in cold-induced thermogenesis (7%), non-specific distal esophagus (1%) and axillary lymph node uptake due to extravasation of radiotracer (1%) were observed. The range for the mean maxSUV of these foci was from 2.0 to 6.3. In the 147 benign lesions, inflammatory sequelae of the chest wall and breasts, after surgical intervention and/or radiation therapy, were often observed (27%). Reactive hyperplasia of lymph nodes associated with pulmonary tuberculosis or inflammation were also observed (32%). Hypermetabolic thyroid glands were noted as adenomas and chronic thyroiditis (18%). Degenerative osteoarthritis and healed fractures showing increased uptake were detected (15%). Focal hypermetabolic lung lesions related to inactive pulmonary tuberculosis and benign solitary pulmonary nodules were observed (6%). The range of the mean maxSUV was from 1.3 to 3.8. **Conclusion:** Knowledge of these findings of the FDG PET/CT might aid in the correct staging and detection of disease recurrence in patients with breast cancer.

Presentation Number **1022B**
Poster Session 3d: Imaging Disease/Organ Processes

Incremental value of FDG PET/CT in carcinoma gall bladder

Rohini Mishra, NUCLEAR MEDICINE, PD Hinduja National Hospital andMRC, Mumbai, India. Contact e-mail: rohini1223@yahoo.co.in

Aim :- A retrospective analysis of 21 patients with carcinoma gall bladder in the post laparoscopic cholecystectomy setting was undertaken to assess utility of FDG PET/CT in detecting occult disease, staging, and institution of therapy. We studied patients from September 2007 to March 2010 (15 females, 6 males, and age range 30-77 years). Results:- In group I (with no disease on post-op CT scan), PET was positive for disease in 5 patients of total 9 (55%). Amongst these, residual disease was revealed in all, additional nodal disease in 2, and distant metastasis in 1. On follow up, chemotherapy was instituted in 4 patients, re-exploration surgery was done in 1, while the patient with distant metastasis was lost to follow up. The remaining 4/9 patients had PET scan negative for disease, and were asymptomatic till follow up of 1 year with no further treatment and subsequent sonography negative. In group II (with CT suspicious for disease), PET upstaged 8 out of 11 patients (72 %) in whom CT scan was positive for only residual or nodal disease, and confirmed liver metastasis in 2 patients. On follow up, treatment was altered in 8 of these 11 patients (72%). In group III (with no prior imaging), PET/CT was negative in 1 patient who remained asymptomatic at 1.5 year follow up, while chemotherapy was instituted for the other with PET positive disease. Conclusion:- PET/CT upstages the disease in 66% of patients. In 50% of the patients early institution of therapy could be done due to detection of occult disease. PET/CT demonstrated high negative predictive value

Presentation Number **1023B**
Poster Session 3d: Imaging Disease/Organ Processes

Imaging marrow cell population change in lymphoma after chemotherapy by FDG-PET scans and its clinical implications

Bingfeng Tang¹, **Regina H. Wong**², **Malaykumar M. Patel**¹, **Christiana O. Wong**¹, **Pek Lan Khong**³, **Ching Y. Wong**¹, ¹*Nuclear Medicine, William Beaumont Hospital, Royal Oak, MI, USA;* ²*Biophysics, University of Michigan, Ann Arbor, MI, USA;* ³*Radiology, University of Hong Kong, Hong Kong, China. Contact e-mail: tangbf@gmail.com*

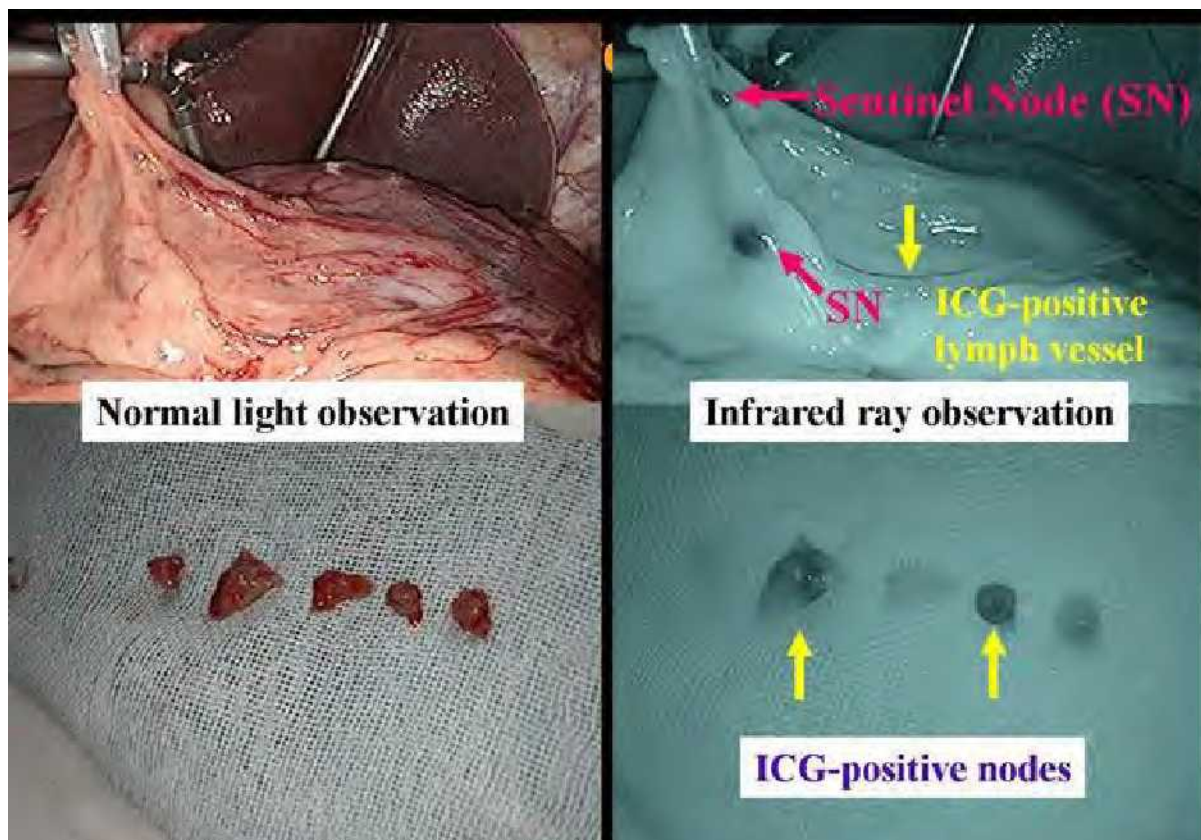
Purpose: It is common to see the pattern of diffusely increased FDG uptake in normal bone marrow after chemotherapy on FDG-PET scans due to change in hematopoietic cell population. Decreased FDG uptake after chemotherapy is noted in the areas with PET evidence of bone marrow involvement due to reduction in tumor population. The aims were to correlate cell population change with SUV change over bone marrow biopsy (BMBx) sites after chemotherapy using bone marrow histopathology as the gold standard and investigate its potential predictive value for occult bone marrow involvement by malignant lymphoma. **Methods:** 26 patients (mean age, 58±15y; 13 female, 13 male) with follicular lymphoma (FL) (Grade I, II, III, n=16) or diffuse large B-cell lymphoma (DLBC) (n=10), referred for FDG-PET/CT scan for initial staging and first restaging after chemotherapy, who had BMBx from unilateral or bilateral iliac crest(s) before chemotherapy, were studied retrospectively. The maximal standardized uptake value (SUV) was measured from BMBx site over the same area on both initial staging and restaging FDG-PET/CT scans. The interval changes of SUV were classified as increase or decrease and correlated with BMBx result of positive or negative for bone marrow involvement by lymphoma. **Results:** 35 BMBx sites in 26 patients were evaluated. 12 of 35 sites were BMBx positive with interval decrease in SUV in 11 of 12 sites (92%). The remaining 23 of 35 sites were BMBx negative with interval increase in SUV in 21 of 23 sites (91%). The correlation between SUV change over the BMBx site before and after chemotherapy and BMBx result was significant (P<0.0001). Among 14 of the 26 patients (FL, n=4; DLBC, n=10) with focal increased FDG uptake (SUV range from 4.3-31.9) in bone marrow indicating involvement by lymphoma on initial staging scans, all (100%) showed significant interval decreased SUV after chemotherapy. **Conclusions:** This study demonstrates a strong correlation between marrow metabolic changes (as determined by FDG PET) after chemotherapy with marrow cell population change. This may provide a retrospective means of predicting occult marrow involvement and may help in deciding to deliver more extended therapy during management of lymphoma patients.

Presentation Number **1024B**
 Poster Session 3d: Imaging Disease/Organ Processes

Lymphatic mapping with indocyanine green (ICG) and infrared ray detection in early gastric cancer: more reliable than ICG alone and a tool for limited nodal dissection

Wendy Kelder¹, Hiroshi Nimura², Naoto Takahashi², Norio Mitsumori², Gooitzen M. van Dam^{1,3}, Katsuhiko Yanaga², ¹Surgical Oncology, University Medical Center Groningen, Groningen, Netherlands; ²Surgery, Division of Digestive Surgery, Jikei University School of Medicine, Tokyo, Japan; ³BioOptical Imaging Center Groningen, University Medical Center Groningen, Groningen, Netherlands. Contact e-mail: wendykelder@gmail.com

Introduction: One of the most important prognostic factors in early gastric cancer is the presence of lymph node (LN)metastases. This lead to the concept of standardized nodal dissection. LN metastases in early gastric cancer patients occur in 5-15 % of patients. This implicates that in the remaining 85-95% of patients an extended LN dissection is unnecessary. The sentinel node (SN) biopsy is an intra-operative diagnostic method to detect lymphatic drainage patterns and possible LN metastases. Different techniques are possible: dye alone (patent blue or ICG), a combination of dye and radio-active colloid, and infrared ray electronic endoscopy (IREE) to detect ICG. The advantage of IREE is the ability to detect light with wavelenghts of around 805 nm which is able to penetrate fatty tissues up to a depth of 3-5 mm. This study compares lymphatic mapping in early gastric cancer with ICG and infrared ray electronic endoscopy (IREE) to ICG alone and describes the optimal method for intra-operative detection of metastasis. **Methods:** 212 patients underwent the SN procedure with IREE and peri-tumoural ICG injection. 0.5ml ICG was injected endoscopically in four quadrants surrounding the tumour. SN's stained with ICG were observed with the naked eye as well as with infrared ray electronic endoscopy (IREE, Olympus Optical, Tokyo, Japan). Evaluated parameters were detection of sentinel nodes with IREE versus ICG alone, intra-operative detection rate of LN metastasis and lymphatic drainage patterns. **Results:** 34 patients had LN metastases. The SN identification rate and sensitivity for IREE versus ICG alone were 99.5 versus 85.8% and 97.0 versus 48.4% respectively. Intra-operative accuracy for detecting LN metastasis was 50% with node picking versus 92.3% with lymphatic basin dissection. LN metastases were always in the SN basin. **Conclusion:** The SN procedure with IREE can detect the SN and is better than ICG alone. LBD of the SN basin is required for accurate intra-operative diagnosis of metastases and, if based on IREE, is a safe method of nodal dissection in early gastric cancer.



Presentation Number **1025B**
Poster Session 3d: Imaging Disease/Organ Processes

Kinetic modeling may improve usefulness of ^{64}Cu -ATSM PET for hypoxia imaging

Fan Li^{1,2}, **Jesper T. Joergensen**^{1,2}, **Jacob Madsen**², **Andreas Kjaer**^{1,2}, ¹*Faculty of Health Sciences, University of Copenhagen, Cluster for Molecular Imaging, Copenhagen N, Denmark;* ²*Department of Clinical Physiology, Nuclear Medicine and PET, Rigshospitalet, Copenhagen OE, Denmark. Contact e-mail: fanli@sund.ku.dk*

Introduction/Aim: Tumor hypoxia is associated with tumor aggressiveness and treatment resistance and of importance for therapy planning. To be clinical useful a non-invasive method is preferred. ^{64}Cu -ATSM is promising radiotracers for visualization of hypoxia in tumors. However, hypoxic areas have poor perfusion that may mask the specific hypoxic binding. This may be circumvented by mathematical kinetic modeling. The aim of our study was to develop and evaluate such a kinetic model for ^{64}Cu -ATSM using gene expression of HIF-1 α as reference. **Methods:** Four 6 weeks old female NMRI nude mice were xenografted with human colorectal cancer (HT29) or human neuroendocrine cancer (H727) (n=7 tumors). A dynamic PET acquisition was started and 20 MBq ^{64}Cu -ATSM injected into the tail vein, while dynamic PET acquisition continued for 1.5 h. Subsequently, 0.2 ml of intravascular contrast was injected into the tail vein the mouse was moved to a CT scanner for a 7 minutes CT scan. The procedure was repeated 9 h after ^{64}Cu -ATSM injection (20 min. static PET and CT without contrast). SUVs and T/M-ratios were calculated based on obtained PET scanning data. An image-based input function derived from left ventricle (LV) was developed by drawing ROIs in the left ventricular cavity on fused PET/CT images in order to obtain noninvasive time activity curves (TACs). The TACs from tumor-bearing regions were also obtained. Tracer kinetics was analyzed using a multi compartment model. The TACs obtained by PET were evaluated with the model by using nonlinear curve fitting based on Levenberg-Marquardt algorithm, to quantify model parameters. To validate the net accumulation (EA) (i.e. $K_{acc} = K_1 \times k_3 / (k_2 + k_3)$) based on Patlak Plot from the model output. SUV, T/M and EA were compared with gene expression of the hypoxia marker HIF-1 α measured by real-time qPCR. Correlations were analyzed by linear regression. **Results:** No correlation was found between SUVmean after 1h ($R^2=0.045$; $P=0.65$) or 9h ($R^2=0.008$; $P=0.85$) and HIF-1 α gene expression. Likewise, no correlation was found between T/M after 1h ($R^2=0.069$; $P=0.57$) or 9h ($R^2=0.003$; $P=0.90$) and HIF-1 α . In contrast EA based on the kinetic model showed a tendency to positive correlation with HIF-1 α gene expression ($R^2=0.31$; $r=0.56$; $P=0.19$). **Conclusion:** Our preliminary results may indicate that EA derived from TACs on dynamic PET imaging is a better measure than SUV or T/M for hypoxic specific binding of ^{64}Cu -ATSM in human tumor xenografts. Further testing of the model is currently undertaken (larger number of animals, wider range of oxygenation).

Presentation Number **1026B**
Poster Session 3d: Imaging Disease/Organ Processes

Peering into the Tumor Microenvironment: Aspects of Multimodal Imaging Methodology for Determining Efficacy of Drug Treatment

Mathew Divine¹, **Carsten Calaminus**¹, **Christoph M. Griessinger**¹, **Christian Kesenheimer**^{1,2}, **Walter Ehrlichmann**², **Nadine Bauer**¹, **Caroline Herrmann**¹, **Bernd J. Pichler**^{1,2}, ¹Radiology, Laboratory for Preclinical Imaging and Imaging Technology of the Werner von Siemens Foundation, Tübingen, Germany; ²Radiopharmacy, University of Tübingen, Tübingen, Germany. Contact e-mail: mathew.divine@gmail.com

The purpose of this study was to assess the feasibility of developing compartmental models in both PET and MR which would offer complementary information to support a mathematical model of tumor therapy. Cetuximab, a monoclonal antibody that targets the Endothelial Growth Factor Receptor to suppress angiogenesis and tumor growth and which was approved for clinical use, was directly labeled with ¹²⁵I for use in SPECT and later with ⁶⁴Cu via the DOTA chelator for use in PET studies. Female NMRI nu/nu mice (n=10) were injected subcutaneously on the right shoulder with one million NCI-H460 tumor cells which were allowed to grow for 2 weeks. The radiolabeled Cetuximab was then injected via the tail vein and then imaged, depending on imaging modality, directly after injection for 90 minutes, 3, 12, 24, 48, and/or 84 hrs post injection. SPECT images were co-registered to CT and/or T2-weighted Turbo Spin Echo (TSE) MR images which were performed directly afterwards. In the case of PET studies, all images were directly co-registered to T2-weighted TSE images. DCE MRI compartmental modeling was performed directly prior to and 24 hrs post injection of ⁶⁴Cu-DOTA-Cetuximab imaging. Imaging studies were followed up with organ and tumor extraction for gamma counting. Microscopy slices of the tumor were stained with either hematoxylin and eosin (H&E) or labeled with pecam CD31 antibody. The ex vivo biodistribution of the SPECT tracer measurements resulted in a Percent Injected Dose per Gram (%ID/g) in the blood of 6.1 and 2.7 and in the tumor of 2.7 and 3.2 at 24 and 84 hrs post injection, and the ex vivo biodistribution of the PET tracer measurements resulted in a %ID/g of 43.2 and 32.4 in blood and in the tumor of 22.5 and 45.6 at 24 and 48 hrs respectively. A 2-tissue, 3-compartmental model of ⁶⁴Cu-DOTA-Cetuximab was calculated with model coefficients K₁, k₂, k₃, and k₄ as being 0.0258 ml/ccm/min, 2.254 min⁻¹, 0.0195 min⁻¹, and 0.0007 respectively. 2-tissue, 2-Compartmental model Coefficients for DCE imaging were as follows: K₁=0.050 +/-0.060 ml/ccm/min, k₂=0.405 +/-0.277 min⁻¹, and a fractional plasma volume (fpv) of 0.291 +/-0.094. ⁶⁴Cu-DOTA resulted in the best radiolabeling technique for this study. SPECT or PET images co-registered to MR rather than CT images provide a vastly more reliable way of quantifying organ uptake of radioactive tracer substance. DCE MRI and PET compartmental modeling provide complementary information about the tumor microenvironment, especially when matched with histological staining.

Presentation Number **1027B**
Poster Session 3d: Imaging Disease/Organ Processes

Assessment of whole body distribution of AS1411 aptamer using in vivo and ex vivo fluorescence imaging

Ye Lim Cho, Ju Ri Chae, Jun Young Park, Jong Doo Lee, Won Jun Kang, Department of Radiology, Division of Nuclear Medicine, Yonsei University College of Medicine, Seoul, Republic of Korea. Contact e-mail: etommi@yuhs.ac

Synthetic nucleotide, aptamer, is a promising targeting agent due to high affinity and low side effect. Of various aptamers, AS1411 targeting nucleolin is most widely investigated, and is expected to be an anticancer agent under clinical trial. However, whole body distribution and tumor targeting property of AS1411 is not well reported. We assessed whole body distribution of AS1411 using in vivo and ex vivo fluorescence imaging. AS1411 aptamer sequence was as follows: H₂N-C₆-5'-TTGGTGGTGGTGGTTGTGGTGGTGGTGG-3'-OH. AS1411 aptamer was labeled with cy3 for in vitro assay or ex vivo assay, and with IR700 dye for in vivo imaging. Breast cancer cell line, MDA-MB231 was cultured and injected into thigh of nude mice. One nmole of IR700 dye labeled AS1411 was injected into nude mouse via tail vein. With excitation wavelength of 640 nmeter and emission wavelength of 720 nmeter, fluorescence image was acquired with IVIS spectrum. After injection of IR700 labeled AS1411, 1, 2, 4, 6, 24 hour images were acquired. MDA-MB231 cell showed high expression of nucleolin, which was assessed by confocal imaging after AS1411 injection. In vivo fluorescence imaging showed that AS1411 aptamer was accumulated in tumor of nude mice. After tail vein injection, AS1411 accumulated highly in liver and spleen up to 2-4 hours. After 4 hours of injection, liver and spleen signal decreased, and kidney and bladder uptake increased. We demonstrated whole body distribution of AS1411 in tumor bearing mouse, and high accumulation of AS1411 in tumor tissue using in vivo and ex vivo fluorescence image. Initial high uptake of liver/spleen and subsequent high uptake in kidney/bladder was suggested normal excretion pattern of AS1411.

Presentation Number **1028B**
Poster Session 4d: Imaging Disease/Organ Processes

Evaluation of ^{64}Cu -TE2A-NCS-c(RGDyK) as a potential PET radiotracer for tumors expressing $\alpha_v\beta_3$ integrin

Darpan N. Pandya¹, Jung Young Kim², Jeong Chan Park¹, Wonjung Kwak¹, Eun Kyung Wang¹, Yeong Su Ha¹, Gwang Il An², Jeongsoo Yoo¹, ¹Department of Molecular Medicine and Nuclear Medicine, Kyungpook National University School of Medicine, Daegu, Republic of Korea; ²Molecular Imaging Research Center, Korea Institute of Radiological and Medical Sciences, Seoul, Republic of Korea. Contact e-mail: darpan2147@gmail.com

Objectives: The choice of bifunctional chelator and radioisotope are crucial for successful tumor imaging using target-specific peptides. ^{64}Cu ($t_{1/2}$ 12.7 h) is both a β^+ and a β^- emitter allowing it to be used for both imaging and radiotherapy. In order not to sacrifice any carboxylate coordination to Cu(II) ions in Cu-TE2A complex, we introduced a third orthogonal pendant arm having $-\text{NH}_2$ or $-\text{NCS}$ functionality suitable for conjugation with peptides or antibody. **Methods:** Initially cyclam was treated with formaldehyde to give a tricyclic cyclam which was trans-dialkylated with t-butyl bromoacetate followed by the cleavage of the bis-aminal bond by treating with 3M NaOH aqueous solution. This product was then selectively alkylated by refluxing with 4-nitro phenethyl bromide in toluene. The nitro group was reduced into the amino group by catalytic hydrogenation. Removal of the t-butyl groups followed by reaction with thiophosgene provided the desired ligand TE2A-NCS. A mixture of TE2A-NCS and c(RGDyK) in 0.1 M sodium carbonate buffer (pH 9.5) was allowed to react for 22 h at room temperature in the dark for thiourea bond formation. The conjugate obtained was purified by semipreparative HPLC. The purified TE2A-NCS-c(RGDyK) was then labeled with ^{64}Cu in 0.1 M NH_4OAc (pH 8) at 30°C for 10 min and the radiolabeled conjugate was purified by analytical HPLC. ^{64}Cu -TE2A-NCS-c(RGDyK) was injected into xenografts bearing U87MG tumor cells. Biodistribution and imaging studies were performed at 1 and 4 h postinjection. **Results:** This preparation of TE2A-NCS is highly efficient in terms of overall yield (57%) and number of synthetic steps (7) as well as facile purification compared to all routes published previously involving other bifunctional chelators with NH_2/NCS linkers. The TE2A-NCS-c(RGDyK) is labeled with ^{64}Cu to greater than 95% purity and 90% yield within 10 min at 30°C. U87MG tumors were clearly visualized by ^{64}Cu -TE2A-NCS-c(RGDyK) with high signal to background ratio at 1 and 4 h postinjection. Biodistribution studies showed that the liver and kidneys were the only organs to have similar or slightly higher uptake of ^{64}Cu -TE2A-NCS-c(RGDyK) than the tumor. **Conclusions:** We have successfully synthesized a new bifunctional chelating agent derived from TE2A backbone. ^{64}Cu -TE2A-NCS-c(RGDyK) was produced rapidly at high yield and purity with a straightforward method. TE2A-NCS might be widely utilized to label many disease-specific peptide and antibody thanks to its easy conjugation with biomolecules and easy radiolabeling with ^{64}Cu (II) ions.

Presentation Number **1029B**
Poster Session 4d: Imaging Disease/Organ Processes

Toad extract treatment show tumorstatic effect in human neuroendocrine tumor xenografts: Studies with ^{18}F -FLT PET

Camilla B. Johnbeck^{1,2}, Rongyao Zhou³, Xin Guan³, Anne Mette F. Hag^{1,2}, Tina Binderup^{1,2}, Mette Munk Jensen^{1,2}, Jacob Madsen², Andreas Kjaer^{1,2}, ¹Cluster for Molecular Imaging, Faculty of health sciences, University of Copenhagen, København N, Denmark; ²Department of Clinical Physiology, Nuclear Medicine and PET, Rigshospitalet, Copenhagen OE, Denmark; ³Shanghai Shuguang Hospital, Shanghai TCM University, Shanghai, China. Contact e-mail: camillabj@sund.ku.dk

Aim: Huachansu Zhusheye is an aqueous extract from the toad *Bufo bufo gargarizans* Cantor. The compound is widely used in Traditional Chinese Medicine for the treatment of various types of cancer. In this pilot study we tested in a longitudinal design the effect of toad extract on the proliferation of neuroendocrine tumors using the proliferation-detecting PET tracer 3-deoxy-3- ^{18}F flourothymidine (FLT). **Methods:** In vivo uptake of FLT in human neuroendocrine xenografts (H727) in mice was studied at baseline when the tumors were on average 110 mm³. One group of mice (n=6 tumors) were then treated with i.p. injections of Huachansu Zhusheye (26.25 ul/g) twice daily for 14 days while the vehicle group (n=6 tumors) was given the same volume of saline i.p.. After 14 days of treatment the mice were FLT-PET scanned again. Each PET scanning was acquired over 20 minutes 1 hour after i.v. injection of 10 MBq of FLT. A CT-scan was performed immediately after the PET scan for calculation of tumor volume. The tumors were defined on PET/CT images and standard uptake values (SUV) were calculated. **Results:** Huachansu Zhusheye treated mice showed a significant stagnation in the SUVmax after treatment relative to SUVmax before treatment (SUVmaxratio) compared to the vehicle group (SUVmaxratio 1.02 ± 0.03 vs. 1.30 ± 0.16 ; p< 0,01 and deltaSUVmax 0.02 ± 0.04 vs. 0.26 ± 0.04; p <0.01). The relative SUVmean values showed same tendency and where borderline significant. (SUVmeanratio 1.12 ± 0.12 vs. 1.38 ± 0.06; p=0.07 and deltaSUVmean 0.07 ± 0.05 vs. 0.20 ± 0.03; p=0,06). The relative tumor volume change between the groups was not significant but showed a trend towards less tumor growth in the treated group than the vehicle group (3.51 ± 0.43 vs. 3.18 ± 0.58 p=0.67). **Conclusion:** Daily injections with toad extract for 14 days showed significant stagnation in tumor proliferation as assessed by FLT PET. Our data underlines, that effects on tumor proliferation may be present and are easily overlooked when only looking at tumor volume. FLT is a promising and sensitive tracer for detecting early signs of effect of Huachansu Zhusheye in neuroendocrine tumors and may in the future be used to predict effect in patients.

Presentation Number **1030B**
 Poster Session 4d: Imaging Disease/Organ Processes

Evaluation of androgen deprivation therapy on [¹⁸F]FDG uptake in xenograft prostate tumor models

Yun Lin, Damaris Kukuk, Daniel Bukala, Martin S. Judenhofer, Bernd J. Pichler, Department of Radiology, Laboratory for Preclinical Imaging and Imaging Technology of the Werner Siemens-Foundation, University of Tuebingen, Tuebingen, Germany. Contact e-mail: yun.lin@med.uni-tuebingen.de

Androgen deprivation therapy (ADT) is one of the widely used treatments in patients with hormone-dependent prostate cancer. However, ADT can also bring metabolic changes in the body. The aim of this study was to investigate the effect of surgical castration on glucose uptake changes in the xenograft models with hormone-dependent prostate tumors CWR22 and PAC120 by [¹⁸F]FDG-PET imaging. A 2x2x1mm³ viable tumor outgrowth was grafted subcutaneously into 6-8 weeks old BALB/c-nude male mice. The mice were imaged with [¹⁸F]FDG-PET at two different times and overnight fasted before imaging. The first imaging was performed after tumor formation. The second imaging was performed 2 (PAC120) or 3 (CWR22) weeks after the surgical castration mimicking ADT. 20min static (1hr after the tracer administration) and 90min dynamic PET data acquisitions were performed with 10-12MBq of [¹⁸F]FDG. The ROIs (region of interest) were delineated on the tumor, the shoulder muscle (s.m.) and the myocardium (myo). A 2-tissue compartment model was applied to estimate the influx constant (Ki) in dynamic analysis. The input function was derived from the ROIs on the left ventricle and corrected for partial volume, spillover effect and metabolites. [¹⁸F]FDG uptake in SUV and the blood glucose level were also measured in both dynamic and static studies. In PAC120 model, the s.m. SUV at 2 weeks post castration (p.c.) was significantly lower than baseline (p=0.006) while the blood glucose level and myo SUV were significantly higher 2 weeks p.c. than baseline (both p<0.05). In CWR22 model, the tumor SUV at 3 weeks p.c. was significantly lower than baseline (p=0.026) while the blood glucose level and myo SUV were significantly higher 3 weeks p.c. (both p<0.05). The myo Ki of CWR22 dynamic studies was significant higher 3 weeks p.c. (0.29± 0.09) than at baseline (0.06±0.03; p=0.013; n=4). Moreover, the myo and s.m. SUV of PAC120 model were significantly higher than CWR22 model (both p <0.05) at baseline, but did not differ significantly p.c.. The [¹⁸F]FDG-PET indicated different glucose uptake between hormone-dependent models. The ADT mimicked by surgical castration was able to reduce the tumor [¹⁸F]FDG uptake, especially in CWR22 model, but also induced higher myo [¹⁸F]FDG uptake in both models. Further studies will concentrate on the differentiation between blood glucose level and myo [¹⁸F]FDG uptake in healthy, non-tumor bearing animals with ADT.

SUV	Baseline - CWR22 n=10; PAC120 n=6				Post castration - CWR22 n=6; PAC120 n=7			
	myo	tumor	s.m.	Glucose(mg/dl)	myo	tumor	s.m.	Glucose(mg/dl)
CWR22	1.43±0.81	0.87±0.27	0.30±0.08	54.56±12.19	1.26±0.99	0.33±0.10	0.26±0.04	67.13±13.34
PAC120	1.98±0.83	0.67±0.18	0.53±0.15	40.33±17.95	4.64±1.55	0.52±0.19	0.26±0.05	87.43±22.43

Presentation Number **1031B**
Poster Session 4d: Imaging Disease/Organ Processes

Are Primary Tumour Standardized Uptake Value (PT SUVmax), Total lesion glycolysis (TLG) and metabolic volume (MV) measured on FDG PET(CT) predictors of survival in advanced Non-Small Cell Lung Cancer (NSCLC)?

Camilo Garcia¹, Vanessa Terrones², Jean Paul Sculier², Patrick Flamen¹, Thierry Berghmans², ¹Nuclear Medicine, Jules Bordet Institute. Brussels. Belgium, Brussels, Belgium; ²Thoracic Oncology, Jules Bordet Institute. Brussels., Brussels, Belgium. Contact e-mail: camilo.garcia@bordet.be

Aim of the study: PT SUVmax measured on FDG-PET(CT) is of prognostic value for survival in early stages NSCLC but its role has to be confirmed in advanced disease. TLG (SUVavg multiplied by tumour volume) and its semiautomatic defined Metabolic Volume (MV) allow assessing the total metabolically active disease burden. We aimed to determine the prognostic value for survival of PT SUVmax, TLG and MV in advanced NSCLC. Methods We retrospectively selected patients with proven NSCLC who underwent FDG PET (CT) before any treatment. Staging was done according to the 2010 classification. Whole body PET(CT) imaging started 60-75 minutes after IV administration of 250-350 MBq FDG. The PET VCAR 4.5 (General Electric) software was used to delineate all volumes of metabolic significant lesions (lesions <1cm³ were excluded) with a gradual segmentation algorithm. For each lesion MV and TLG were calculated. The sum of all lesions resulted in the total body TLG (TBTLG) and MV (TBMV). The survival prognostic role of SUVmax, TBTLG and TBMV was assessed according to their median value. Results: 99 patients with stage III or IV NSCLC were included (IIIA/IIIB/IV: 12, 14, 73). Median PT SUVmax was 11.6 (range: 1.2-83.7). No survival difference was found between patients with low or high SUV (p = 0.71). Median TBTLG and TBMV were 498 (range 1.4-5722) and 85cm³ (range 1-909 cm³), respectively. Low TBTLG and TBMV are associated with better survival (p = 0.003 and p = 0.007). Conclusion In patients with untreated advanced NSCLC, the metabolically active tumour load, measured on FDG PET(CT) by the total body MV and TLG, is significantly associated with overall survival. Further analyses will be performed.

Presentation Number **1032B**
Poster Session 4d: Imaging Disease/Organ Processes

MONOCLONAL ANTIBODIES FOR IN VIVO CANCERS IMAGING

Muriel Busson, Christel Larbouret, Isabelle Teulon, Jean-Pierre Pouget, Pierre-Olivier Kotzki, Andre Pèlerin, IRCM - U896, INSERM, Montpellier, France. Contact e-mail: m.busson@valdorel.fnclcc.fr

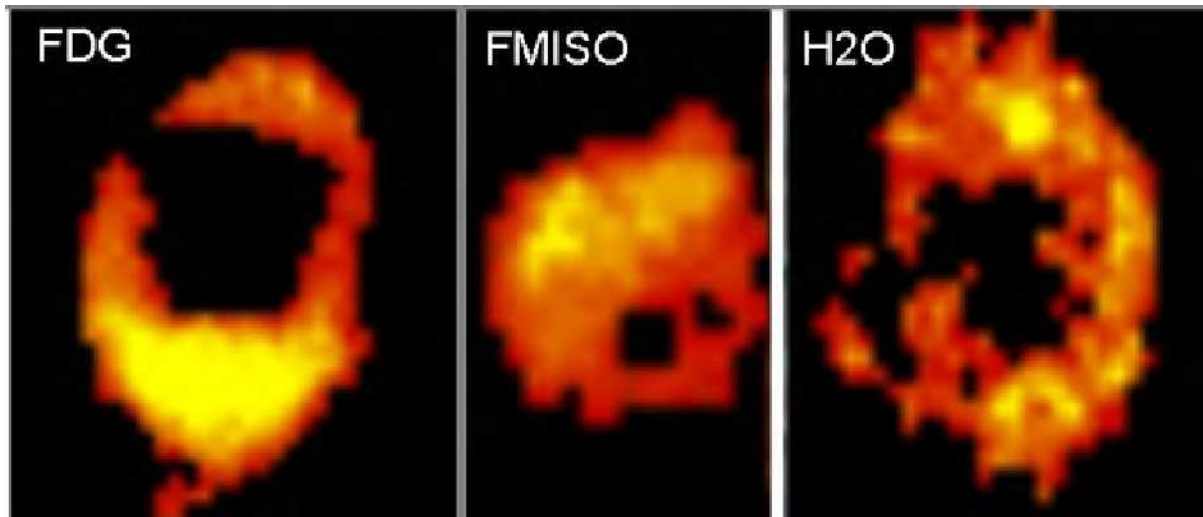
Drug development for cancer therapy needs new tools to detect small amounts of tumor cells, either in the early course of disease or remaining after therapy. Discovery of new radiopharmaceuticals needs also to validate their biodistribution and uptake by the tumor. The combined nanoSPECT/CT (Bioscan Inc.) system is directly derived from the medical imaging technology and allows the acquisition and superposition of functional molecular images (SPECT) and morphological images (CT). It consists of 2 detectors, each outfitted with a 9-pinhole aperture. Scanning mode is helical, and tracers emitting photons range from 24 to 364 keV. We were able to follow biodistribution of molecules with biological half-lives ranging from hours to several days. Small specific regions were imaged for their activity, showing the ability of the tracer to cross the brain barrier. Clinically used therapeutics antibodies, labelled with ^{125}I , allowed us to detect and characterize the tumor. We showed specific uptakes by the tumors, either in transgenic mice developing spontaneous cancer (HER2/neu transgenic line), or in nude mice bearing subcutaneous tumors. We were also able to screen several antibodies for their uptake by the tumor, in order to choose the best radiotracer. We then compared the fixation kinetics of the same tracer delivered by several modes of administration (IP vs IV). For a rapid detection and in order to avoid sacrificing numerous animals, cancer cells expressing luciferase gene were used as models of in vitro and in vivo proliferation. Luciferase gene expression was monitored in intact animals with a CCD camera (Berthold Technologies) and allowed us to follow tumor formation, proliferation rate and metastases location, and to evaluate radioimmunotherapy and immunotherapy strategies in these animals. Last, a multimodal non invasive imaging (SPECT / CT / bioluminescence) allowed us to visualize mouse peritoneal carcinomatosis proliferation but also radiolabeled antibody tumor uptake in radioimmunotherapy trials. These complementary modalities permit to confirm the presence of small metastases with sizes less than a millimetre square. Finally, the use of contrast agents allowed us to enhance CT contrast, which was particularly relevant for the study of small peritoneal carcinomatosis. In conclusion, CT allows the readjustment of SPECT images and engenders a better anatomical localisation of the radiopharmaceuticals. In combination with bioluminescence imaging, these systems constitute a particularly powerful tool to evaluate cancer treatment efficiencies.

Presentation Number **1033B**
Poster Session 4d: Imaging Disease/Organ Processes

Multiparameter PET imaging of the tumor microenvironment: comparison of glucose metabolism, hypoxia and perfusion in rodent glioma model

Sebastien Jan¹, **Philippe Gervais**¹, **Bertrand Kuhnast**¹, **Bertrand Tavitian**^{1,2}, **Régine Trebossen**¹, **Raphael Boisgard**^{1,2}, ¹I2BM, CEA, orsay, France; ²U1023, INSERM, orsay, France. Contact e-mail: sebastien.jan@cea.fr

Introduction: The in-vivo knowledge of the spatial distribution of active, hypoxic, well-perfused and necrotic tumor regions can provide some prognostic information regarding the risk of tumor evolutions, metastasis developments or therapeutic responses. This study aims to characterize the tumor developments by using some relevant functional parameters and quantify their relationships such as perfusion, hypoxia and glucose metabolism by using murine tumor model, PET imaging and dedicated tracers. **Methods and Materials:** Four nude mice were included in this study. Two 9L glioma xenografts were implanted on the posterior area for each mouse. [15O]H₂O was used to measure the tissue perfusion, [¹⁸F]FDG for the glucose metabolism and [¹⁸F]FMISO to evaluate the tumor hypoxia. For each tumor, the tracer uptake and its spatial distribution are evaluated by an analysis voxel by voxel applied on the dynamic functional PET images. This analysis is based on histogram studies to evaluate correlation coefficient and the relationship between each biological parameter associated to the tracer compartment in the tumor. **Dynamic PET acquisitions** are performed with the FOCUS PET system (Siemens). **Results:** Quantitative PET images are obtained with the different tracers. This validates the capabilities to study the tumor microenvironment parameters on the same animal by using [¹⁸F]FDG for glucose metabolism, [¹⁸F]FMISO for the hypoxia response and [15O]H₂O for the perfusion. The quantitative analysis (figure 1) shows a direct correlation between well-perfused and glucose metabolically active tumor regions. In the same way, an anti-correlation is observed regarding hypoxic and perfused tissue. **Conclusion:** This study shows the validity of PET multi-tracer measurements for the tumor microenvironment imaging and to identify regions of tumor necrosis, glucose activity, hypoxia and well-perfused tissue. Finally, this approach should give us information regarding the relationship between critical biologic parameters related to the tissue compartment in the tumor environment.



Images of tracer uptake in the tumor after the voxel analysis to identify correlations between perfusion, hypoxia and metabolism

Presentation Number **1034B**
Poster Session 4d: Imaging Disease/Organ Processes

USEFULNESS OF F-18 FDG PET/CT IN PATIENTS WITH GASTRO-INTESTINAL LYMPHOMA Dr. Khushboo Gupta, DRM, DNB, P.D. Hinduja Hospital, Mumbai, India

Khushboo Y. Gupta, Nuclear Medicine Dept., P.D.Hinduja Hospital,, Mumbai, India. Contact e-mail: khushg_99@yahoo.com

AIM: The extent of the disease involvement and question of gastritis versus disease in gastric lymphomas has been a challenge in follow up post treatment patients. Hence, we undertook a study to evaluate the usefulness of F-18 FDG PET/CT scan in patients with gastro intestinal lymphomas. **METHODS:** A total of 19 patients with histopathologically proven gastro-intestinal NHL were studied in the period from May, 2006 to April, 2010 (age: 10 to 90 years). Histology of 14 of these patients was DLBCL, 3 had Burkitt's NHL, 2 were MALT and one was anaplastic carcinoma. The areas of involvement were gastric in 6 patients, small intestine in 9 and large bowel in 4. We analysed patients in three groups. Group I consisted of patient in post treatment follow up phase and were 9 in number with suspicion of recurrence in 1, and non-specific CT scan findings in two patients. In Group II 7 patients were studied of treatment response post chemotherapy. Group III, including 3 patients, 2 patients for pre-treatment staging and another for post operative small bowel Burkitt's NHL restaging were studied. Whole body FDG PET/CT scan were performed in all the patients. All patients were followed either on biopsy, clinical assessment and / or further institution of therapy. **RESULTS:** In Group I of the total 9 patients in the follow up phase, PET/CT detected true disease recurrence proved on biopsy in two patients where CT was negative and the other in stomach where initially biopsy had revealed gastritis. There was a false positive detection in the liver in 1 patient, and another patient of ileum anastomotic site disease detection was lost to follow up. Rest of the patients with true remission on PET/CT did well clinically. The sensitivity and specificity in this group I patients for disease recurrence was 100% and 75% respectively. In Group II of the total 7 patients studied for treatment response PET/CT showed true responders in 6 and true partial responder in 1 patient. In Group III of total 3 patients PET/CT did upstage 1 patient as compared to CT and the staging of other patients were not changed **CONCLUSION:** PET/CT proves to be valuable in evaluation of the patients with gastro-intestinal NHL, specially the issue of disease recurrence; where conventional modalities are equivocal; and demonstrating early response to therapy, hence yielding information decisive for management.

Presentation Number **1035B**
Poster Session 4d: Imaging Disease/Organ Processes

Non-invasive "E2F sensing" system for monitoring DNA damage alteration in glioma

Parisa Monfared¹, Daniel Rudan¹, Thomas Viel¹, Yannic Waerzeggers¹, Gabriele Schneider¹, Bernd Neumaier¹, Heiko Backes¹, Andreas H. Jacobs^{1,2}, ¹Max-Planck-Institute for Neurological research, Koeln, Germany; ²European Institute for Molecular Imaging (EIMI), Muenster, Germany. Contact e-mail: Parisa.Monfared@nf.mpg.de

Introduction: Non-invasive assessment of the dynamics of gene regulation is of interest for the detection of endogenous disease-specific biological alterations and for monitoring the induction and regulation of therapeutic genes. In our preliminary study, the endogenous expression of E2F, a gene that affects several important biological processes, has been imaged in vivo with bioluminescence imaging (BLI). A retroviral vector Cis-E2F/LUC-IRES-TKEGFP was generated by placing the reporter genes under control of an artificial cis-acting E2F-specific enhancer element. Following retroviral transduction of tumor cells in established xenografts, DNA damage induced alteration of E2F transcriptional activity, which correlated with the expression of E2F-dependent downstream genes as assessed by bioluminescence imaging. Aim: To verify whether the cis-reporter system (Cis-E2F/LUC-IRES-TKEGFP) is sufficiently sensitive to image endogenous transcriptional gene regulation by FHBG PET imaging. We particularly compared FLT-PET with FHBG uptake in response to BCNU treatment. Methods: U87dEGFR-E2F-LITG cells were injected subcutaneously in nude mice and the development of the tumours was followed by Multimodal imaging. Two weeks after implantation BLI, FLT and FHBG were performed before and 24h after treatment with low and high doses of BCNU. Results: Here, we validate the utility of FLT-PET to image proliferation rate of the tumor in response to DNA damage and compare with FHBG uptake which is associated with E2F transcriptional activity. In keeping with in vitro findings, after 24 h post-treatment, low dose of BCNU induced an increase in FHBG uptake as compared to non-treated mice. However, with high dose of BCNU FHBG uptake decreased in E2F xenografts. FLT accumulation in E2F xenografts decreased with low and high doses of BCNU at 24 and 48 hours. Quantitative changes in tumor FLT uptake were associated with decreased tumor proliferation and tumor FHBG uptake correlated with transcriptional gene regulation of E2F in response to DNA damage. Conclusions: We show the utility of FHBG-PET to image DNA damage induced by BCNU and shown the tumor-specific activity of E2F. We propose that these types of reporter systems will allow a detailed insight into the kinetics of cell cycle control and for the development of new cell cycle targeted molecular therapies. Acknowledgement: This work is supported in part by the EC-FP6 European DiMI, (LSHC-CT-2004-503569), LSHB-CT-2005-512146 and Clinigene (LSHB-CT-06-018933).

Presentation Number **1036B**
Poster Session 4d: Imaging Disease/Organ Processes

In vivo NIR fluorescent imaging in various tumor models using tumor homing chitosan nanoparticle

JinHee Na^{1,2}, Heebeom Koo¹, Kuiwon Choi¹, Jae Hyung Park², Ick Chan Kwon¹, Seo Young Jeong², Kwangmeyung Kim¹, ¹Korea Institute of Science and Technology(KIST), Seoul, Republic of Korea; ²Department of Life and Nanopharmaceutical Science, Kyung Hee University, Seoul, Republic of Korea. Contact e-mail: mongtoto@hanmail.net

Hydrophobically modified glycol chitosan nanoparticles exhibited distinguished biocompatibility and tumor-targeting ability in both cell culture system and tumor-bearing mice in our many previous papers. Here, they were examined using the near infrared fluorescence (NIRF) optical imaging technique in various in vivo tumor models. In liver cancer model, we showed distinct difference of NIR intensity between the tumor tissues and surrounding normal liver tissues with nanoparticle, and in lung cancer model, they showed superior detecting ability about wide spread tumor cells in lung organ. In brain cancer, the images showed the possibility of partial disruption of blood-brain barrier (BBB) and penetration of nanoparticles. Finally in colon cancer model, the imaging resolution of our nanoparticle was tested and their great potential in clinical fields for endoscopy was successfully proved.

Presentation Number **1037B**
Poster Session 4d: Imaging Disease/Organ Processes

Tumor Imaging With a Multifunctional Targeted-Reporter Complex via Reporter Enzyme Complementation

Ann-Marie Broome^{1,2}, Gopalakrishnan Ramamurthy^{1,2}, Kari Lavik^{1,2}, Luther A. Liggett^{1,2}, James Basilion^{1,2}, ¹*Biomedical Engineering, Case Western Reserve University, Cleveland, OH, USA;* ²*National Foundation for Cancer Research, Case Western Reserve University, Cleveland, OH, USA. Contact e-mail: Ann-Marie.Broome@case.edu*

Determining the status of cell surface receptors has become routine in the care of patients with cancer and has proven to be helpful in guiding treatment. Mutational events that drive a normal cell to become a cancer cell require the coordinated overexpression of not just one receptor at a time, but rather multiple biomarkers. A growing body of evidence from genomic and proteomic research asserts that several receptors contribute to tumor behavior and these expression patterns are referred to as the cancer signature. Many cancers are characterized by an abnormal increase in the activity of epidermal growth factor receptors (EGFR) and transferrin receptors (TfR). Our data of representative human cancer cell lines demonstrate unique, observable expression patterns for the two receptors. Targeted-reporter imaging agent platforms have real application for noninvasive imaging of the multi-step progression of cancer growth, creating the next frontier in in vivo imaging. To develop imaging tools that take advantage of the diagnostic molecular signature, new technologies must employ a contrast generating agent whose signal is dependent on the presence of multiple markers. To achieve this we have divided β -gal into unique sets of complementing subunit pairs that individually have no enzymatic activity. However, when brought into close proximity, complementing pairs associate, resulting in detectable enzymatic activity. To drive complementation at the site of target expression, we have constructed a targeting complex composed of reporter fragment, linker, and targeting moiety. By targeting each subunit to a different cell surface marker, we can drive enzyme complementation and β -gal activity only on cells that express both markers. Using this strategy, we were able to generate imageable enzyme activity when two cell surface receptors implicated in cancer development, EGFR and TfR, are both expressed simultaneously. Cells expressing only one (or none) of the two receptors do not generate activity or signal. Time course studies indicate that knowledge about receptor cycling is critical for complementation to occur. Further studies to translate this technology to an in vivo setting are under way. [Broome, A-M. et al. (2010) Expanding the functionality of the classic β -galactosidase complementation assay: piece by piece. *Mol Pharmaceuticals* 7:60.]

Presentation Number **1039B**
Poster Session 4d: Imaging Disease/Organ Processes

Multiparametric characterization of diethylnitrosamine (DEN) induced liver damage and liver tumor in rat

Sufyan G. Sayyed¹, Andreas Steingötter⁵, Yvonne Kosanke¹, Jennifer Altomonte², Marcus Settles¹, Irene Esposito³, Markus Schwaiger⁴, Ernst J. Rummeny¹, Oliver Ebert², Rickmer Braren¹, ¹Institute of Radiology, Klinikum rechts der Isar TU Munich, Munich, Germany; ²Department of Internal Medicine, Technical University Munich, Munich, Germany; ³Institute for Pathology, Technical University Munich, Munich, Germany; ⁴Department of Nuclear Medicine, Technical University Munich, Munich, Germany; ⁵Institute for Biomedical Engineering, University and ETH Zurich, Zurich, Switzerland. Contact e-mail: rbraren@roe.med.tum.de

Introduction: constant DEN exposure in rats results in the development of primary liver cancer with underlying liver damage, closely mimicking the human condition, and thus representing a preclinical model for imaging and treatment studies with high predictive value. **Objective:** The objectives of this study were to (1) optimize an oral feeding protocol for DEN, (2) establish a multiparametric long-term imaging protocol for multifocal lesions and (3) correlate imaging findings with histopathological and biochemical analyses. **Materials and Methods:** rats received 2, 4, 6 or 8 weeks of DEN drinking water (0.01%) followed by weekly MRI scans until 24 weeks, including T2-weighted (T2w) imaging, DCE-MRI and multi-slice diffusion weighted imaging (DWI) using a human wrist coil and a 1.5 Tesla clinical MRI system (Achieva 1.5T, Philips Medical Systems). In addition, weekly blood samples were taken at each time point. (18F)-FDG and (18F)-FLT μ PET scans were performed after 16 weeks. Volume was calculated from manual segmentation of T2w image data. ROI and pixel based analysis was performed for DCE-MRI and ADC data respectively. Animals were sacrificed at 24 weeks and livers were processed for histopathology. **Results:** all 8 week and one (20%) 6 week animal developed multifocal liver lesions, histologically confirmed as HCC and CCC with underlying mild liver damage. Liver damage, was further confirmed by elevated CHE and gammGT serum levels as well as elevated perfusion levels. Weekly monitoring of tumor volume and perfusion showed high inter-lesion variation but were consistent over time. In contrast, ADC values showed high inter- and intra-lesion variation over time. ¹⁸F-FDG uptake ratios were only moderately elevated in some lesions; no 18F-FLT positive tumor lesions were identified. **Conclusion:** 8 week oral DEN feeding results in mild liver damage and primary liver cancer, in appearance comparable to the human condition. Longitudinal monitoring of tumor volume and perfusion are promising imaging parameter candidates for long term monitoring of therapy induced changes in this rat tumor model.

Presentation Number **1040B**
Poster Session 4d: Imaging Disease/Organ Processes

Combination of molecular and morphological imaging, for in vivo assessment of head and neck cancer using fibered confocal endomicroscopy

Muriel Abbaci¹, **Odile Casiraghi**², **Stephane Temam**³, **Gian Luca Armas**³, **Jacques Bosq**², **Philippe Vielh**², **Corinne Laplace-Builhé**¹,
¹Cellular Imaging and Cytometry Platform, IR4M, IRCIV, Institut Gustave Roussy, Villejuif, France; ²Department of Pathology, Institut Gustave Roussy, Villejuif, France; ³Department of Otorhinolaryngology and Head and Neck Surgery, Institut Gustave Roussy, Villejuif, France. Contact e-mail: muriel.abbaci@igr.fr

Cancer diagnosis and therapy are primarily based on histological analysis. Resection margins of small head and neck tumours with millimeter-order are difficult to evaluate for surgeons and pathologists. In addition, biopsies can cause local tissue changes like bleeding that may affect the evaluation of tumor extent by the clinician during the resection procedure. In recent years, miniaturization of imaging systems has led to the development of non invasive optical technologies which allow "optical biopsies" at the cellular level. Among them, fibered confocal endomicroscopy (CEM) successfully provides dynamic images of the microarchitecture of tissues during conventional endoscopy. In this study, we assess the potential use of CEM for combined functional and morphological imaging to characterize human head and neck malignant lesions. Non cancerous and cancerous tissue samples were taken from human surgical head and neck specimens after total or partial surgery. Tissues were then processed using fluorescently labelled deoxyglucose (2-NBDG), for glucose uptake activity measurement, and methylene blue for tissue morphology description. En face images were completed using both CEM (CellVizio®, Mauna kea Tech.) and conventional confocal microscopy (Leica SPE). Image pairs were finally compared with the corresponding H&E sections by experimented pathologist. 2-NBDG fluorescence intensity appeared usually higher in cancerous tissue than in non cancerous tissues. But despite the molecular targeting of that contrast agent, basal fluorescence signal in non cancerous tissue close to that expressed by cancerous tissues, was sometimes observed and could led to false positives for the physician. The dual sample staining with methylene blue allows for better comparison of glucose activity with tissue architecture and especially with tissue disorganisation, such as abnormal keratinisation, and nuclear anomalies. In conclusion, the combination of 2-NBDG molecular imaging that "lights up" abnormal tissue areas with morphological information using CEM imaging improves evaluation of the margins of lesions to be removed.

Presentation Number **1041B**
Poster Session 4d: Imaging Disease/Organ Processes

Study of glioblastoma cancer initiating cells on tumorigenesis and metastasis by multiple imaging modalities

Liang-ting Lin¹, Shih-Hwa Chiou², Chiung-Tong Chen³, Yi-Jang Lee¹, ¹Dept. of Biomedical Imaging and Radiological Sciences, National Yang-Ming University, Taipei, Taiwan; ²Dept. of Medical Research and Education, Taipei Veteran General Hospital, Taipei, Taiwan; ³Division of Biotechnology and Pharmaceutical Research, National Health Research Institutes, Miaoli, Taiwan. Contact e-mail: g39720022@ym.edu.tw

CD133 (Prominin-1) have been reported as one of CNS cancer stem cell markers, and is used for isolating cancer stem cells via magnetic-bead cell sorting. However, accumulated evidence showed that CD133 cannot totally indicate to cancer stem cells, and the role of CD133 plays in glioblastoma still remains controversial. Here, we tend to use multiple imaging modalities to investigate CD133-positive and CD133-negative cells on tumorigenesis and recurrence in vivo. We sorted patient tumor-derived GBM cells by FACS with CD133-PE staining, and delivered multicistronic reporter system into each group of cells by lentivirus. The established cells stably expressed green fluorescent protein, firefly luciferase and thymidine kinase, and each of them was assayed in vitro. GFP expression was used for collecting cells with better reporter efficiency. Our in vitro results showed that CD133-positive cells revealed shorter doubling time and better transgene expression than CD133-negative cells. Furthermore, both groups of CD133 expression cells were implanted orthotopically into left brain of nude mice, and the tumorigenesis phenomena were evaluated by magnetic resonance imaging and bioluminescence. Tumor formation was observed in only CD133-negative groups, suggested that CD133 may not play the key role in tumorigenesis of glioblastoma. Moreover, leptomeningeal metastasis of tumor was observed, and one of the cases showed only vertebral tumor occurrence. Western blotting results demonstrated normal p53 expression but relatively lower expression of p-CFL in CD133-negative cells. In addition, immunohistochemistry staining results showed the PTEN expression between tumor and normal brain tissue were significant different. It is hypothesized that PTEN and cytoskeleton-related signal transduction pathway may take the responsibility in tumorigenesis and invasiveness rather than CD133.

Presentation Number **1042B**
Poster Session 4d: Imaging Disease/Organ Processes

Same-session comparison of Fluorocholine and Choline for PET imaging of hepatocellular carcinoma

Jeffrey A. Kolthammer¹, David J. Corn², Chunying Wu², Nathan P. Tenley¹, Yanming Wang², **Zhenghong Lee**^{1,2}, ¹Biomedical Engineering, Case Western Reserve University, Cleveland, OH, USA; ²Radiology, Case Western Reserve University, Cleveland, OH, USA. Contact e-mail: zxl11@po.cwru.edu

[¹⁸F]Fluoroethylcholine (FEC) is a potential longer half-life alternative to [N-methyl(-¹¹C)]-Choline (CHOL) for PET imaging of cancer. In this study, these two radiotracers were compared using a woodchuck model of hepatocellular carcinoma (HCC). Method: PET data using two radiotracers were acquired in consecutive scans in a single imaging session: 1h CHOL, followed by 1h pause and 1h FEC. The study was repeated with the animals fasted. Suspected tumor regions in the liver were identified as regions of increased uptake in the PET image with either tracer and correlated with CT imaging. Time-activity curves from the regions of increased uptake and surrounding hepatic regions were calculated. Results: Of three animals studied, two showed clearly-defined hot spots with characteristics indicative of tumor: positive contrast to surrounding tissue at 60 min post-injection (PI), and a contrast peak at 30-45s PI, associated with tracer kinetics. The two tracers showed similar dynamics in both tumor and surrounding regions, with tissue activity concentration reaching 90% of its 1h value at 25 ± 10 min PI. Contrast was higher with FEC for some tumor regions and with CH for others. Image characteristics and contrast were similar between the fasted and non-fasted acquisitions for both tracers: in one illustrative region, contrast at 1h PI was 1.5 and 1.6 with FEC, and 1.1 and 1.2 with CH; for the animal non-fasted and fasted. Conclusions: As in previous work, suspected tumor regions in the liver are identified using CH and FEC. Comparing the tracers within the same imaging session has mitigated problems with physiologic change between experiments and allowed a more direct comparison of the effect of subject fasting. Contrast provided by CH and FEC varied, with some regions of increased uptake more visible with either tracer; however, fasting did not have a significant effect on the contrast with either choline-based tracer.

Presentation Number **1043B**
Poster Session 4d: Imaging Disease/Organ Processes

The discovery of novel non-RGD-containing $\alpha v \beta 3$ ligands for molecular imaging

Choi-Fong Cho^{1,2}, **Giulio Amadei**³, **Daniel Breadner**³, **Leonard G. Luyt**^{3,4}, **John D. Lewis**^{1,2}, ¹*Medical Biophysics, University of Western Ontario, London, ON, Canada;* ²*Translational Prostate Cancer Research Group, London Regional Cancer Program, London, ON, Canada;* ³*London Regional Cancer Program, Cancer Research Laboratory Program, London, ON, Canada;* ⁴*Chemistry, University of Western Ontario, London, ON, Canada. Contact e-mail: ccho8@uwo.ca*

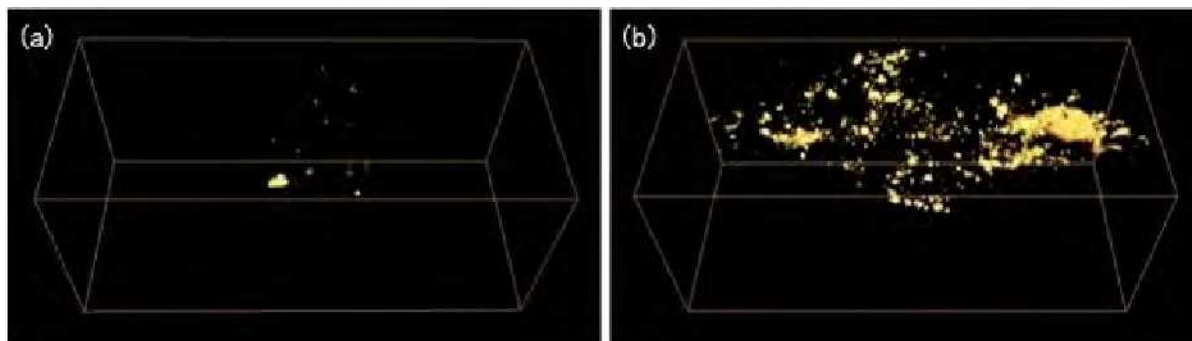
Metastasis is the cause of 90% of cancer deaths. The detection of neoplasms before they metastasize using non-invasive molecular imaging approaches can have a significant impact on patient survival. For many years it has been known that $\alpha v \beta 3$ integrin, which is over-expressed on angiogenic endothelium and many tumours, associates with the extracellular matrix through an RGD tripeptide motif. RGD-mediated targeting has been utilized for a wide variety of peptide and nanoparticle molecular imaging agents that are in various stages of development and in clinical trials. RGD peptides exert an anti-angiogenic effect through their inhibition of $\alpha v \beta 3$ integrin, raising the concern given recent studies (Ebos et. al., 2009, Cancer Cell v15; Paez-Ribes et. al., 2009, Cancer Cell v15) that this anti-angiogenic activity may result in increased tumour invasion and metastasis. We sought, therefore, to discover novel $\alpha v \beta 3$ integrin-targeted peptides that do not contain RGD for the development of new molecular imaging agents. Using a recently developed "beads on a bead" approach, we screened an octapeptide one bead one compound library using purified $\alpha v \beta 3$ integrin. Over one hundred peptides were cleaved and sequenced "on bead" using a novel MALDI-TOF/MS technique and a number of non-RGD containing peptides were identified. Two of these peptides had a higher binding affinity for purified $\alpha v \beta 3$ integrin than RGD peptide (P62, KD = 4.7 nM and P64, KD = 16.3 nM) as determined by surface plasmon resonance. In contrast to peptides containing RGD, these peptides did not impact the morphology and adhesion of $\alpha v \beta 3$ integrin-expressing cells, nor did they inhibit angiogenesis. Uptake of both fluorescein-labeled P62 and P64 in $\alpha v \beta 3$ integrin-expressing breast cancer cells was significantly higher than control peptides, and uptake was effectively blocked by a free excess of unlabeled peptide. These novel $\alpha v \beta 3$ integrin-binding peptides could provide a basis for a new and potentially safer generation of molecular imaging agents for the early diagnosis of cancers.

Presentation Number **1044B**
Poster Session 4d: Imaging Disease/Organ Processes

GI cancer detection in *APC-Min* mouse models with COX-2 probes using a dual-axis confocal fluorescence microscope

Hyejun Ra¹, Jonathan T. Liu¹, Jashim Uddin², Lawrence Marnett², Christopher Contag¹, ¹Clark Center for Biomedical Engineering and Sciences, Molecular Imaging Program at Stanford, Stanford University School of Medicine, Stanford, CA, USA; ²A.B. Hancock Jr. Memorial Laboratory for Cancer Research, Departments of Biochemistry, Chemistry, and Pharmacology, Vanderbilt Institute of Chemical Biology, Vanderbilt-Ingram Cancer Center, Vanderbilt University School of Medicine, Nashville, TN, USA. Contact e-mail: hra@stanford.edu

Cancer diagnoses in patients are mainly performed through histopathology of tissue biopsies. In the case of the gastrointestinal (GI) tract, standard endoscopy screening is used to examine the tissue surface for apparent abnormalities that are then biopsied and analyzed. However, flat lesions and early disease are generally hard to diagnose. We have developed miniaturized dual-axis confocal (DAC) microscopes that fit into the instrument channel of endoscopes and can provide histopathologic data on intact tissues without sampling. A fluorescent molecular probe that preferentially binds to tumor cells can be used to increase the sensitivity of detection, and when coupled with the DAC microscope comprises a powerful *in vivo* screening method for early cancer detection. Cyclooxygenase-2 (COX-2) is found at high levels in inflammatory lesions and tumors, while mainly absent from normal cells. The importance of COX-2 in tumor progression has been documented in a number of cancers including esophagus, stomach, and colon, where COX-2 is detected in premalignant lesions and levels increase through tumor progression. A recently developed fluorescent COX-2 probe has been shown to accumulate in inflamed and tumor tissue, and therefore has the potential to be an effective reagent for cancer detection. We have tested the COX-2 probe and DAC microscope in C57BL/6 *APC-Min* mice that develop intestinal polyps and serve as a model for GI cancer. The *APC-Min* mice were anesthetized prior to intravenous injection of the COX-2 probe into the retro-orbital plexus. The mice were euthanized at 3 hours post-injection, then the intestines were resected and washed with PBS. The fresh tissues were imaged using a tabletop DAC microscope, where three-dimensional images were taken under constant gain conditions. Images from polyps generally show higher expression of the COX-2 probe than tissue from flat regions of the intestine (Fig. 1). There are areas that express higher fluorescence levels in seemingly normal tissue that may be due to inflammation or premalignant tumors hard to see from the surface. This study demonstrates the potential of COX-2 fluorescent probes and the miniaturized DAC microscope for early GI cancer detection.



3-D DAC microscope images of (a) normal tissue and (b) polyp from an *APC-Min* mouse 3 hours after COX-2 probe injection. The volume dimensions are 600 μm x 300 μm x 300 μm .

Presentation Number **1045B**
Poster Session 4d: Imaging Disease/Organ Processes

Imaging Labeled Tumor Cell Growth and Lymphatic Micrometastasis in Mice Xenograft Model with MR

Ting Liu¹, Rui Xia¹, Haijun Zhou², Jichun Liao¹, Feng Bi², Hua Ai³, Hui Wang¹, Fabao Gao¹, ¹Radiology, West China Hospital, Sichuan University, Chengdu, China; ²Oncology, West China Hospital, Sichuan University, Chengdu, China; ³National Engineering Research Center for Biomaterials, Sichuan University, Chengdu, China. Contact e-mail: liuting20072008@yahoo.com.cn

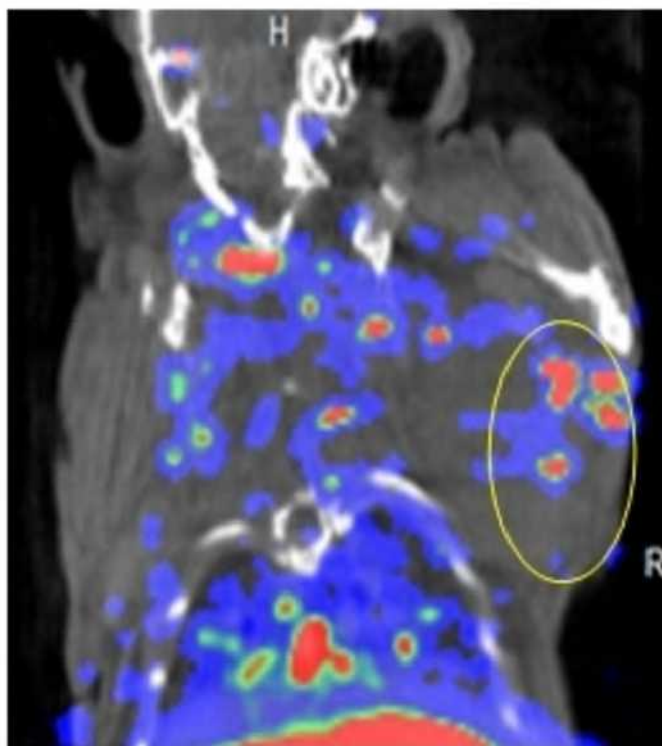
PURPOSE: To investigate primary tumor formation and lymphatic micrometastasis of magnetically labeled tumor cells in nude mouse using magnetic resonance imaging (MRI). **METHOD AND MATERIALS:** Human colorectal cancer LOVO cells were labeled with ultrasmall superparamagnetic iron oxide (USPIO) nanoparticles. The labeling efficiency was evaluated by Prussian blue staining. Then the labeled and unlabeled LOVO cells (108 cells/0.05 ml) were inoculated in axilla area, claw pad and groin area of nude mice. A 7T MR with T1, T2, T2* and T2* parametric mapping of the tumors and surrounding lymph nodes was performed in following 4 weeks. After imaging, tumor tissues and lymph nodes were collected and subjected to immunohistologic analysis, which include hematoxylin and eosin (H&E) staining, Prussian blue (PB) staining, CD68 staining and lymphatic vessel endothelial hyaluronan receptor (LYVE-1) staining. **RESULTS:** The accumulation of the USPIO particles in LOVO cells was rapid and labeling efficiency was 90%. MR imaging demonstrated hypointense regions where USPIO labeled tumor cells located, then the low signal increased gradually. The increase in signal of the periphery was more rapid than central parts of the tumor and unable to distinguish from surrounding tissues since 10 days P.I.. MR T2* weighted image (WI) detected a 1.5 mm lymphatic micrometastasis at 7 days P.I., and lymphatic metastasis of tumor cells was before the exponential growth. Lymph node metastasis was verified by H&E staining and Prussian blue staining. Immunohistochemical analysis of primary tumor sections collected at 8, 28 days P.I. revealed existence of macrophages, lymphangiogenesis and Prussian blue positive tumor cells. **CONCLUSION:** Our preliminary data suggested that the growth of tumor cells can be observed by MRI and lymphatic micrometastasis can be detected as early as 7 days P.I.. MR imaging of USPIO labeled tumor cells might provide important physiopathological information on primary tumor formation and lymphatic micrometastasis.

Presentation Number **1046B**
 Poster Session 4d: Imaging Disease/Organ Processes

RAGE-directed Imaging of Tumor

Yared Tekabe, Vivek Rai, Joane Luma, Ann Marie Schmidt, Lynne Johnson, Columbia University, Yonkers, NY, USA. Contact e-mail: yt2166@columbia.edu

The receptor for advanced glycation endproducts (RAGE) plays a role in tumor development and metastasis. We tested the hypothesis that ^{99m}Tc-labeled monoclonal anti-RAGE F(ab')₂ fragments can be used as a noninvasive tool to access tumor development and progression in SCID mice. Methods: Seven SCID mice, age 6-8 weeks, were subcutaneously injected with 10⁵ C6 glioma cells on right lateral shoulder and on day 21, each mouse was injected with 21.6 MBq (0.5 mCi) ^{99m}Tc-labeled monoclonal anti-RAGE F(ab')₂. Control (n=3) mice were injected with culture medium. All mice were imaged on a SPECT/CT camera (Bioscan) 4 hr after injection (time based on blood pool clearance). At the end of imaging session, animals were sacrificed and the tumor dissected and photographed, counted, and sectioned for immunohistochemical staining. Tumor activity from the scans was quantified in uCi using InVivoScope software. Results: All seven mice injected with ^{99m}Tc-labeled anti-RAGE F(ab')₂ fragments showed tracer uptake in the tumor. Control mice were scan-negative. Values for % injected dose per gram (%ID/g) and scan tumor activity are shown in table. Conclusion: These data show feasibility of noninvasively imaging RAGE in Tumor.



Coronal image showing uptake of radiolabeled anti-RAGE F(ab')₂ in tumor (outline).
 Table

	In vivo scan (uCi)	Camera counts (%ID/g)
Mouse #1	0.1708	0.137
Mouse #2	0.314	0.129
Mouse #3	0.0723	0.158
Mouse #4	0.700	0.163
Mouse #5	0.683	0.147
Mouse #6	0.2912	0.171
Average	0.374	0.15
SD	.26	0.09

Presentation Number **1047B**
Poster Session 4d: Imaging Disease/Organ Processes

THE ROLE OF FDG PET/CT IN PRIMARY BONE TUMOR

Jyotsna Rao, Kavitha Nallapareddy, Alka A. Chengapa, Sikandar M. Shaikh, Apollo Gleneagles PET CT Ctr, Hyderabad, India.
Contact e-mail: jyotsnael@gmail.com

Primary bone tumors are rare. They are difficult to diagnose as they have many entities and different biological behavior. FDG PET/CT is important in the management of bone tumors. We wish to present retrospective PET/CT data from our center regarding our experience. Aim: To evaluate the role of FDG PET/CT in the management of primary bone tumors. Material and method: A retrospective analysis of reports of 68 patients with primary bone tumors referred to our center between May 2005 and December 2009 was performed. Patients were injected intravenously with 10-15 mCi of F18 FDG after 4 hours of fasting and scanned per standard whole body protocol after giving oral and intravenous contrast. The scans were reported jointly by a radiologist and PET physician. Follow up was obtained where possible. Results: Patients with the diagnosis of osteosarcoma, chondrosarcoma, fibrosarcoma, primary neuroectodermal tumor (PNET) and Ewing's sarcoma from both pediatric and adult age groups referred for staging, restaging and monitoring response to therapy were included in the study. 7/68 patients were referred for staging of which 5/7(72%) showed only the primary and 2/7(28%) showed primary tumor and metastases. 54/68(80%) were referred for restaging- 27/54(50%) were negative, 6/54(11%) showed only metastases, 6/54(11%-lung and bone) showed only CT lesions-suspicious for metastases, 3/54(5%) showed only the primary, 5/54(9%) showed primary tumor recurrence and metastases, 2/54(4%) showed primary tumor recurrence on PET/CT and additional PET findings (thigh and breast), 2/54(4%) showed primary tumor recurrence on PET/CT and lungs metastases on CT only, 1/54(2%) showed multiple osteochondromas on CT, 1/54(2%) showed primary tumor recurrence and progression of metastases and 1/54(2%) showed recurrent primary tumor and right breast lesion, probably representing a second primary. 7/68(10%) were referred after treatment to assess response-5/8(72%) were negative, 1/8(14%) showed viable primary tumor and metastases and 1/8(14%) showed decrease in metabolism of the primary tumor. Conclusion: FDG PET/CT proved useful in the management of patients with primary bone tumors referred to our center.

Presentation Number **1048B**
Poster Session 4d: Imaging Disease/Organ Processes

THE ROLE OF FDG PET/CT IN GASTRIC CARCINOMA

Jyotsna Rao, Kavitha Nallapareddy, Alka A. Chengapa, Sikandar M. Shaikh, Apollo Gleneagles PET CT Ctr, Hyderabad, India.
Contact e-mail: jyotsnael@gmail.com

Gastric carcinoma is the second most common cause of death due to cancer after lung although its incidence has decreased. The role of FDG PET/CT in managing gastric carcinoma is well documented and we wish to present our experience. Aim: To evaluate the role of FDG PET/CT in gastric carcinoma. Material and method: A retrospective analysis of reports of 86 patients with stomach cancer referred to our center between May 2005 and December 2009 was performed. Patients were injected intravenously with 10-15 mCi of F18 FDG after 4 hours of fasting and scanned per standard whole body protocol after giving oral and intravenous contrast. The scans were reported jointly by a radiologist and PET physician. Follow up was obtained where possible. Note was made of patients with signet ring/mucinous type of tumor in view of low FDG sensitivity. Results: 27/86 were referred for staging- 14/27((52%) patients showed primary tumor and metastases, 5/27(20%) only primary tumor, 1/27(3%) primary tumor on CT only, 2/27(8%) primary tumor and lung metastases on CT, 2/27 (8%) showed primary tumor on PET, 1/27(3%) primary tumor and metastases on PET/CT and additional metastases on PET, 1/27(3%) primary tumor, metastases and an active thyroid nodule and 1/27(3%) primary tumor, skeletal metastases on PET and nodal metastases on CT. 48/86(56%) patients were restaged-10/48(21%) were negative, 7/48(15%) showed primary tumor recurrence, 11/48(22%) metastases, 4/48(12%) showed primary tumor recurrence and metastases, 3/48(6%) recurrence at the anastomotic site, 2/48(4%) findings suggestive of second primary along with primary tumor recurrence, 3/48(6%) tumor recurrence at primary and anastomotic sites, 3/48 (6%) were positive on CT at the primary site and negative on PET, 1/48(3%) was positive at the operative site, 3/48(6%) was positive at sites other than the primary suggestive of second primaries and 1/48(3%) was positive at the primary sites and showed metastases with CT showing additional metastases. 11/86(13%) patients were scanned after treatment to assess response-3/11(27%) were negative, 2/27(19%) showed viable primary tumor, 3/11(27%) showed viable primary tumor and metastases, 1/11(9%) decrease in metabolism of metastases, 1/11(9%) viable primary tumor and progression of metastases and 1/11(9%) a second primary. 8/86(9%) of patients referred had signet ring type of histopathology. Conclusion: FDG PET/CT proved useful in the management of gastric malignancy in patients referred to our center for various indications.

Presentation Number **1049B**
Poster Session 4d: Imaging Disease/Organ Processes

Detection of N-nitrosodiethylamine-induced Liver Cancer in Living Mice with CT and MR Images

Ju Hui Park^{1,2}, **Joo Hyun Kang**¹, **Yong Jin Lee**¹, **Tae Sup Lee**¹, **Kwang Il Kim**¹, **Yin Ohk Ko**¹, **Kyeong Min Kim**¹, **Sang Soep Nahm**⁴, **Young Seo Park**², **Gi Jeong Cheon**^{1,3}, **Chang Woon Choi**³, **Sang Moo Lim**³, ¹Molecular Imaging Research Center, KIRAMS, Seoul, Republic of Korea; ²Dept. of Food Science & Biotech., Kyungwon university, Soeng-nam, Republic of Korea; ³Department of Nuclear Medicine, KIRAMS, Seoul, Republic of Korea; ⁴Dept. of Veterinary Medicine, Konkuk University, Seoul, Republic of Korea. Contact e-mail: syurey@kirams.re.kr

Micro-computed tomography (CT) and magnetic resonance imaging (MRI) are important equipments for diagnosis and longitudinal development of tumor. Liver cancer is one of the most common malignancies and lethal cancers in the world, especially in eastern Asia and Africa. We aimed to be evaluating micro-CT and MRI as the diagnosis equipment of liver cancer in mice model induced by N-nitrosodiethylamine (DEN) as a chemical carcinogen. The carcinogen-induced mice model was developed by intraperitoneal injection of DEN in C57BL/6 mice. Eight mice of group 1 and twelve mice of group 2 were induced by 20 mg/kg of body weight of DEN at 3 weeks after birth and at 4 day after birth, respectively. The tumor regions were detected with a 3 Tesla MAGNETOM trio (Siemens, PA, USA) with gadolinium based contrast media (Primovist, Bayer HealthCare, Germany). Micro-CT (IVEON, Siemens, PA, USA) imaging was performed with contrast media for CT images was eXIATM160 (Binitio biomedical INC., Ottawa, Canada). After scanning, the animals were sacrificed and histological assessment of liver specimen was performed. Liver cancers were confirmed macroscopically in 3 mice of 20 mice by MRI. These were progressed after 36 weeks (#1 and #2) and 28 weeks (#3) after DEN treatment in group 1 and group 2, respectively. The tumor regions detected by MRI also coincided with those by micro-CT images. One more tumor of #1 and #2 mice were detected by micro-CT than that by MRI. By MRI images, tumor of #1 was located to surface of median lobe (long diameter of tumor: 4.53 mm), the tumor of #2 was long diameter with 17.82 mm. The tumor of #3 was placed between lobes (long diameter: 4.19 mm). From the histological assessment, tumor of #1 was identified as adenoma and tumors of #2 and #3 were carcinoma. The liver cancers induced by DEN treated mice were detected by MRI and micro-CT images with valid contrast media. They could be valuable tools for detecting and monitoring longitudinally liver cancer progression.

Presentation Number **1050B**
Poster Session 4d: Imaging Disease/Organ Processes

Identification of Pancreatic Cancer Stem Cells and Early Detection of Pancreatic Cancer by Optical and New T1/T2-Weighted MR Molecular Imaging

Chia-Chi J. Lee¹, **HongVy Tran**¹, **Zhao Li**¹, **Yung-Ya Lin**^{1,2}, ¹*Chemistry and Biochemistry, UCLA, Los Angeles, CA, USA;* ²*California NanoSystem Institute, Los Angeles, CA, USA. Contact e-mail: jcclee@ucla.edu*

I. Purpose. Pancreatic cancer is the 4th leading cause of cancer-related death in US. Due to difficulties in diagnosis and resistance to chemotherapy and radiotherapy, pancreatic cancer has the worst survival of any solid tumor - 5-year survival rate < 4% in US. Since emerging evidence suggests there are putative pancreatic cancer stem cells (PCSC), we used existing method in optical molecular imaging and developed new approaches to MR molecular imaging to accurately identify and sensitively image pancreatic cancer stem cells in vitro. II. Materials and Methods. The experimental procedures consist of three steps. (i) Bioconjugation chemistry: conjugated quantum dots and magnetic nanoparticles with specific PCSC biomarker antibody. (ii) Material chemistry — synthesized iron-oxide magnetic nanoparticles that exhibit unusual T1/T2 relaxation effects to surrounding water protons; (iii) Spin engineering - developed new MR pulse sequences for T1/T2-weighted imaging to enhance the contrast and detection sensitivity for the magnetic nanoparticles and therefore the PCSC biomarker and PCSC. III. Results and Discussions. In vitro identification of the PCSC is first done by fluorescence microscopy of YAG-AB-quantum dots incubated with PCSC in cell media, using antibody CD24, CD44, and ESA (Figs. A, B). After the binding was confirmed and the PCSC was identified, we then imaged PCSC via MR microimaging with new superparamagnetic nanoparticles that exhibit unique T1/T2 values and new radio-frequency pulse sequences that generated T1/T2-weighted imaging for enhanced imaging contrast and sensitivity of the diluted PCSC (only 0.5% of cell population) (Figs. C, D). It was demonstrated that the proposed new approaches may help make early detection of pancreatic cancers and targeted therapy possible.

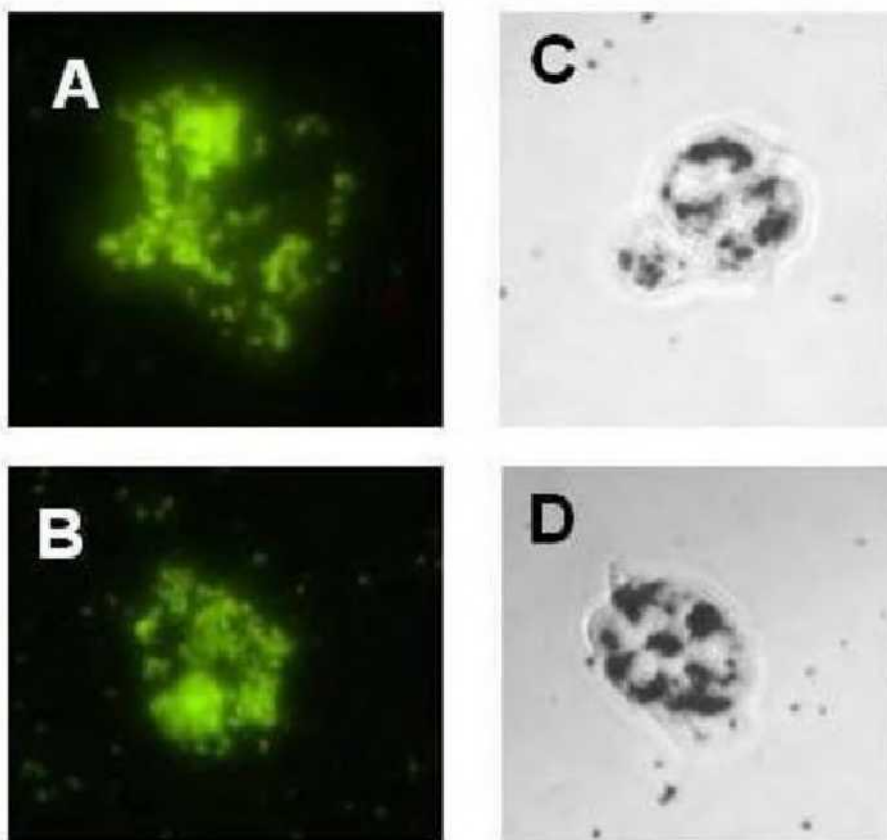


Fig. 1 Fluorescence microimaging of YAG-AB-quantum dots (A,B) and T1/T2-weighted MR microimaging of superparamagnetic nanoparticles (C,D). The nanoparticles are bound to the pancreatic cancer stem cells in cell media through antibody CD24, CD44, and ESA.

Presentation Number **1051B**
Poster Session 4d: Imaging Disease/Organ Processes

Evaluation of ^{18}F -FDG uptake in the renal parenchyma: clinical significance in hydronephrosis

Arthur Cho, Jun Young Park, Won Jun Kang, Jong Doo Lee, Severance Hospital, YUMC, Seoul, Republic of Korea. Contact e-mail: artycho@hotmail.com

Purpose: Hydronephrosis is often encountered in ^{18}F -FDG PET/CT scans, especially in pelvic origin malignancies or periurethral metastasis. Identification of hydronephrosis is clinically important as it can lead to progressive renal failure and can be a source of infection. The purpose of this study is to evaluate for ^{18}F -FDG uptake in normal renal parenchyma and in hydronephrotic kidneys to correlate with clinical findings. **Materials and Methods:** A retrospective review of 91 patients (mean age 53 years old, 30 male) who had ^{18}F -FDG PET/CT for staging for various malignancies and showing unilateral hydronephrosis on CT was performed. ^{18}F -FDG uptake for normal renal parenchyma uptake was evaluated in 59 patients (mean age 55 years old, 28 male) who had ^{18}F -FDG PET/CT for surveillance for non-abdominal origin malignancies. ^{18}F -FDG uptake was evaluated by visual analysis and maximum standard uptake value (SUV) of the renal cortex on coronal images. Clinical findings for urine analysis for pyuria or bacteriuria within 3 days of ^{18}F -FDG PET/CT and serum creatinine analysis were correlated with PET findings. **Results:** Average ^{18}F -FDG uptake in the normal renal parenchyma was 2.36 in the left kidney and 2.37 in the right kidney. Hydronephrotic kidney showed significant ^{18}F -FDG uptake compared to contralateral normal kidney (3.09 vs 2.41, $p < 0.001$). Hydronephrotic kidney also showed significant ^{18}F -FDG uptake compared to kidney uptake in surveillance patients (3.09 vs 2.36, $p < 0.001$). Of the 91 hydronephrosis patients, 35 patients showed pyuria or bacteriuria and 45 patients had no signs of infection on urine analysis. There was a significant increase in ^{18}F -FDG uptake in the renal parenchyma in infection patients compared to hydronephrosis without clinical suspicion of infection (3.48 vs 2.88, $p < 0.009$). There was a significantly higher serum creatinine in hydronephrosis patients compared to surveillance patients (1.06 vs 0.91, $p < 0.009$). **Conclusion:** Increased ^{18}F -FDG uptake is seen in hydronephrotic kidneys compared to non-obstructive kidneys. Hydronephrotic kidneys with infection can show higher uptake compared to hydronephrotic kidney without infection signs. Complicated hydronephrosis should be considered when severe unilateral retention of ^{18}F -FDG uptake is seen in patients with pelvic malignancies.

Presentation Number **1052B**
Poster Session 4d: Imaging Disease/Organ Processes

Dynamic Tumour Hypoxia Imaging in Mice with ^{18}F -FAZA PET-CT

David E. Green¹, *Douglass C. Vines*^{1,2}, *Stephen Chung*³, *Lisa Di Diodato*¹, *Brad Wouters*^{1,3}, ¹*Radiation Medicine Program, Princess Margaret Hospital, Toronto, ON, Canada;* ²*Radiation Oncology, University of Toronto, Toronto, ON, Canada;* ³*Ontario Cancer Institute, Princess Margaret Hospital, Toronto, ON, Canada. Contact e-mail: david.green@rmp.uhn.on.ca*

Purpose: Dynamic imaging of tumour hypoxia with ^{18}F -FAZA was performed in a mouse model of human cancer utilizing a small animal PET and CT. This allowed the optimal imaging timepoint to be determined after the uptake and clearance of unbound tracer. The hypoxic fraction of HCT116 xenografts and tumor volumes were also analyzed from the PET and CT images. Methods: Four female NOD-SCID mice were subcutaneously inoculated with human colon cancer HCT116 cells in the shoulder region and imaged after 15 days. Mice were anesthetized (1.5% isoflurane in medical air) for injection of ^{18}F -FAZA (~7-15 MBq) and scanned for 140 minutes with a Focus 220 microPET followed by an anatomical CT scan (GE Locus Ultra: 80 kV, 70 mA). Tumours were excised, counted and weighed. The dynamic listmode data was binned (12x5s; 12x15s; 8x120s; 12x10 min.), the sinograms were reconstructed (OSEM3D/MAP) and tumour hypoxia was assessed by manually placing 3D regions-of-interest over the entire tumour on fused PET-CT images. The hypoxic fraction within the tumors was determined by thresholding of hypoxic volumes ≥ 1.5 times background muscle mean percent injected dose per gram (%ID/g) from 120-140 min duration p.i. Results: Uptake in the hypoxic fraction and clearance ^{18}F -FAZA from normoxic tumor tissues starts to be discerned 40 minutes p.i. and onwards. The tracer concentration in the hypoxic volume of the tumor leveled after ~100 minutes. Clearance from muscle continued after peak uptake for 10-120 minutes p.i. The mean (\pm SD) gross tumour volumes were determined from CT to be $142 \pm 30 \text{ mm}^3$. The hypoxic fraction for the tumors was determined to be $13.4 \pm 9.2\%$ Conclusions: Dynamic PET imaging of mice bearing HCT116 colon cancer xenografts was utilized to determine the optimal uptake of ^{18}F -FAZA and clearance in this tumor model. The hypoxia-specific uptake of the tracer and rapid blood clearance kinetics allow for static imaging at 120 minutes p.i. Imaging of the hypoxic regions within the tumor provided a non-invasive method to determine the hypoxic fraction in the colon cancer xenografts.

Presentation Number **1053B**
Poster Session 4d: Imaging Disease/Organ Processes

Strong Correlation between Accumulation of ^{64}Cu -ATSM and Gene Expression of HIF-1 α in Human Ovarian Cancer Xenografts

Jesper T. Joergensen^{1,2}, **Jacob Madsen**², **Andreas Kjaer**^{1,2}, ¹Cluster for Molecular Imaging, Department of Biomedical Sciences, University of Copenhagen, Copenhagen, Denmark; ²Department of Clinical Physiology, Nuclear Medicine and PET, Rigshospitalet, Copenhagen, Denmark. Contact e-mail: jtjoergensen@mfi.ku.dk

Aim: To validate the use of the PET radiotracer, ^{64}Cu -diacetyl-bis(N^4 -methyl-thiosemicarbazone) (^{64}Cu -ATSM) for imaging of hypoxia in mice xenografts derived from human ovarian cancer, by comparing tracer uptake and gene expression of molecular marker of hypoxia, hypoxia inducible factor 1 α (HIF-1 α). **Methods:** Six Nude NMRI mice, had approximately 10^7 tumor cell (A2780 human ovarian cancer cell line), implanted in each flank. After 2-3 weeks, a dose of approximately 10 MBq ^{18}F -FDG was administered *i.v.* and the mice were PET scanned for 20 minutes 1 hour after injection using a small animal PET scanner, followed by a 7 minutes small animal CT scan. The following day, each mouse had between 10-20 MBq ^{64}Cu -ATSM administered *i.v.* and was PET scanned for 20 minutes at 1, 9 and 22 hours post injection, again in each case followed by a 7 minutes CT scan. Immediately after the 22 hour scan tumor tissue was collected and measurements of the gene expression of HIF-1 α were performed, using the quantitative real-time PCR with Taqman chemistry. PET data were reconstructed using MAP algorithm, ROIs were drawn on fused PET/CT images, and SUV values and T/M-ratio were calculated. Finally, correlations between SUVmean, SUVmax, T/M-ratios and the gene expression of HIF-1 α were analyzed by linear regression. **Results:** While no correlations between HIF-1 α and SUVmean or SUVmax for ^{18}F -FDG were observed, HIF-1 α showed positive correlations with SUVmean for ^{64}Cu -ATSM 1, 9 and 22 hours after injection ($R^2=0.77$ $P=0.004$; $R^2=0.62$ $P=0.030$; $R^2=0.65$ $P=0.022$, respectively). In the same way HIF-1 α also showed positive correlation with SUVmax 1 hour after injection ($R^2=0.60$ $P=0.040$) and T/M-ratio 1 and 9 hours after injection ($R^2=0.66$ $P=0.019$; $R^2=0.61$ $P=0.037$, respectively). **Conclusion:** A strong correlation between gene expression of HIF-1 α and ^{64}Cu -ATSM accumulation in tumor tissue was found in mice xenografts derived from human ovarian cancer. The correlation was robust over time and already seen 1 hour post injection.

Presentation Number **1054B**
 Poster Session 4d: Imaging Disease/Organ Processes

Quantitative Image Analysis to Predict the Neoplastic Region in Oral Squamous Cell Carcinoma using Multiple Fluorescent Imaging Agents

Kelsey J. Rosbach¹, Michelle D. Williams², Ann M. Gillenwater³, Rebecca Richards-Kortum^{1, 1} *Bioengineering, Rice University, Houston, TX, USA;* ²*Pathology, M. D. Anderson Cancer Center, Houston, TX, USA;* ³*Head and Neck Surgical Oncology, M. D. Anderson Cancer Center, Houston, TX, USA.* Contact e-mail: kelsey.rosbach@gmail.com

Background: Early detection of pre-cancerous lesions and cancer in the oral cavity improves patient survival, but dysplasia is difficult to detect clinically. Non-invasive, molecular-specific optical imaging has the potential to rapidly assess expression of biomarkers that indicate neoplastic changes, which may aid in detection at the point of care and determination of an appropriate surgical margin. Methods: Two imaging agents were used: 2-NBDG (Invitrogen, CA), a glucose tagged with a fluorescent dye to target overexpression and activity of GLUT transporters, and an epidermal growth factor (EGF) protein tagged with a fluorescent dye to target overexpression of the EGF receptor. Both agents were topically applied to freshly resected oral lesions from human patients and imaged with a widefield fluorescence microscope after a 20 minute incubation period. Images were quantitatively analyzed using Matlab 7.1 using intensity to predict the region of disease. This prediction was overlaid onto a histopathology map of the tissue created following analysis of H&E stained slides with an expert Head and Neck Pathologist to serve as our gold standard of comparison. Results: Histopathology maps have been created and compared with predicted regions of disease in 12 different patient samples. Figure 1 shows representative oral specimens, images, histopathology maps and disease predictions. Conclusions: This study demonstrates non-invasive topical delivery of two imaging agents that can be used in combination to provide molecular and morphologic information about tissue to improve detection of oral neoplasia. Predictions are generated not only for samples with invasive cancer, but also for early neoplastic changes. These results suggest that topically applied, targeted optical contrast agents allow non-invasive, rapid assessment of oral tissue that may aid clinicians in early detection, biopsy site selection, and surgical planning.

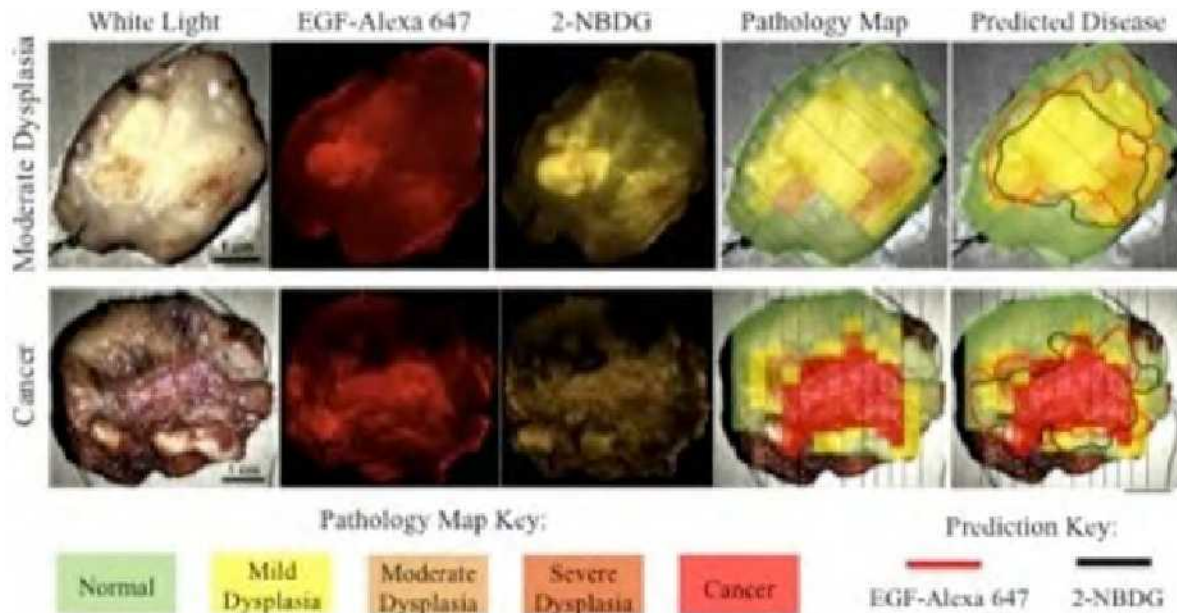


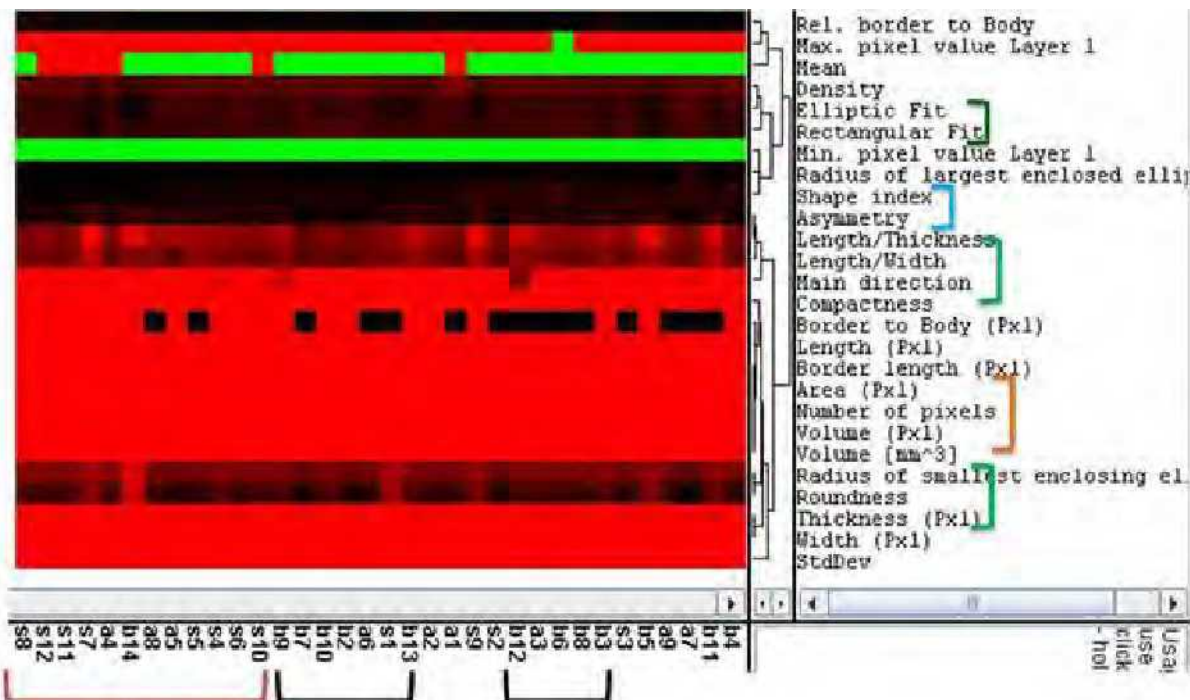
Fig.1. Widefield images of two resected oral lesions. White light images are shown along with fluorescence images taken after incubation with each contrast agent. The pathology map indicates the gold standard diagnosis throughout the tissue. The red and black outlines indicate the predicted region of disease based on analysis of each fluorescence image.

Presentation Number **1055B**
 Poster Session 4d: Imaging Disease/Organ Processes

Radiomics of Non Small Cell Lung Cancer: Association of Quantitative Image Features with histology and outcomes

Virendra Kumar¹, **Yuhua Gu**¹, **Steven Eschrich**², **Edward A. Eikman**³, **Claudia Berman**³, **Dmitry Goldgof**⁴, **Lawrence Hall**⁴, **Robert A. Gatenby**³, **Robert Gillies**¹, ¹Imaging, H Lee Moffitt Cancer Center and Research Institute, Tampa, FL, USA; ²Bioinformatics, H Lee Moffitt Cancer Center and Research Institute, Tampa, FL, USA; ³Radiology, H Lee Moffitt Cancer Center and Research Institute, Tampa, FL, USA; ⁴Computer Science and Engg., University of South Florida, Tampa, FL, USA. Contact e-mail: virendra.kumar@moffitt.org

Conventional radiology has largely utilized qualitative terminology to characterize the appearance of pathological features on radiographic images, e.g. characterizing tumors as having, "irregular borders, central necrosis", etc. However, positron emission tomography (PET) and computed tomography (CT) images can provide objective and quantitative information (features) as well. A large proportion of information contained in currently available imaging data are underutilized and extraction and quantification of these data, may result in improved diagnosis and assessing effect of treatment non-invasively. Automated or semi-automated methods can be developed to efficiently extract quantifiable information from radiologic images, i.e. "radiomics.". In the present study we have extracted quantitative image features from lung cancer CT images to test the hypothesis that these features can be quantitatively related to outcomes. The current work is semi-heuristic in that all features have associated specific hypotheses relating to what is measured and how the features will perform as diagnostic indicators. CT images of lung cancer patients were analyzed using Definiens® software. The present study included data from 44 patients, for all of whom pre-therapy CT scan, gene expression data and clinical outcome are available. CT images were 512 × 512, 16 bit, 5 mm slices. A multidimensional seed growing approach was used to automatically segment the tumor. Following the segmentation of tumor, over 20 image features were quantified. These are being compared to expression and outcomes. Additional features to describe tumor texture are also being developed to test the hypothesis that tumor heterogeneity is of prognostic significance. Analysis is also being extended to PET data as well. We have also identified additional patients with complete data sets (CT-cel-outcomes) that will enter in the analysis.



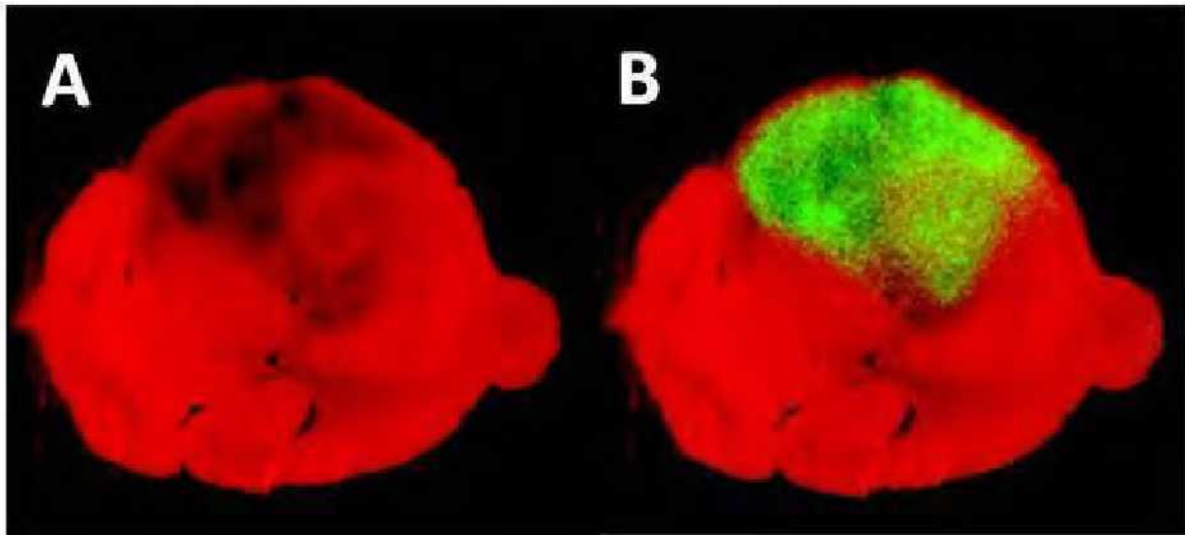
Hierarchical clustering of tumor features among three different histological tumor types. The horizontal axis represents the individual tumor (per patient) and vertical axis represents the tumor features extracted from CT images. a, adenocarcinoma; b, bronchoalveolar carcinoma; s, squamous cell carcinoma.

Presentation Number **1056B**
Poster Session 4d: Imaging Disease/Organ Processes

Multi-Tracer Molecular-Genetic Imaging Reveals Distinct Areas of Coupling and Uncoupling of Blood Flow and HIF1 Signaling in a Rat Brain Glioma Model.

Hwan Jeong, Hsin-Hsien Yeh, Nashaat Turkman, Nobuyoshi Fukumitsu, Andrei Volgin, Daniel Young, Leo G. Flores, Mian M. Alauddin, Juri G. Gelovani, *Experimental Diagnostic Imaging, MD Anderson Cancer Center, Houston, TX, USA. Contact e-mail: jhjeong@mdanderson.org*

Introduction: Tumor development is associated with constant remodeling of neoangiogenic vasculature that heterogeneous and variably affects regional blood flow and the development of hypoxic signaling in different tumor regions. In this study we investigated coupling and uncoupling of perfusion and HIF1 signaling in a rat brain tumor model. **Methods:** C6#4 rat glioma cells express HIF-1-inducible "sensor" reporter gene (HSV1-tk/GFP fusion) and a constitutively expressed "beacon" reporter gene (DsRed2/XPRT). The C6#4 cells were injected intracerebrally (0.5×10^6 in $20 \mu\text{l}$ of PBS) in 6 rnu/rnu rats. Tumor growth was monitored by MRI. microPET/CT imaging with ^{18}F -FEAU was performed 14-28 days after tumor implantation. After PET imaging, $25 \mu\text{Ci}$ of ^{14}C -IAP was infused over 1 min, while the arterial blood was constantly withdrawn through the femoral arterial catheter. Then, animals were sacrificed, brains extracted, frozen and cryosectioned for dual-label QAR. QAR images of ^{18}F -FEAU (HIF1 signaling) and ^{14}C -IAP (blood flow) were co-registered with corresponding H&E stained tissue sections using MCID Elite software (InterFocus Imaging, UK). Regional blood flow (ml/g/min) was calculated from ^{14}C -IAP images as described before (Sakurada, et al. 1978; Oku, et al. 1998). Distribution of CD34+ microvasculature was assessed by immunohistochemistry (IHC). **Results:** A heterogeneous pattern of HIF1 activity was observed in tumors with ^{18}F -FEAU accumulation ranging from 0.5 to 2.5 %ID/g. Blood flow, as measured by ^{14}C -IAP, was significantly decreased below 1 ml/g/min in most hypoxic tumor areas with high ^{18}F -FEAU accumulation. Blood flow and HIF1-signaling were inversely related based on pixel-by-pixel regression analysis. However, in some medium-size tumors a large cluster of pixels with moderate-to high HIF1 signaling (^{18}F -FEAU $>1\%$ ID/g) in the areas of increased regional blood flow (>1 ml/g/min) surrounding regions of impending or fulminant necrosis. Fluorescence microscopy confirmed the presence of GFP-expressing tumor cells in those areas, while IHC revealed multiple enlarged CD34+ hyperplastic microvessels. **Conclusions:** This study demonstrated that some hyper-perfused tumor areas may be hypoxic and have increased HIF1-signaling due to uncoupling of blood flow and oxygen extraction (or utilization) fraction. Such uncoupling develops as the result of overproduction of pro-angiogenic factors (i.e., VEGF), vascular endothelial hyperplasia, enlarged tortuous microvessels, A-V shunts, and "luxury perfusion". Such decompensated stage of angiogenesis leads to tumor necrosis, which explains the proximity of high blood flow and HIF1 signaling to necrotic regions.



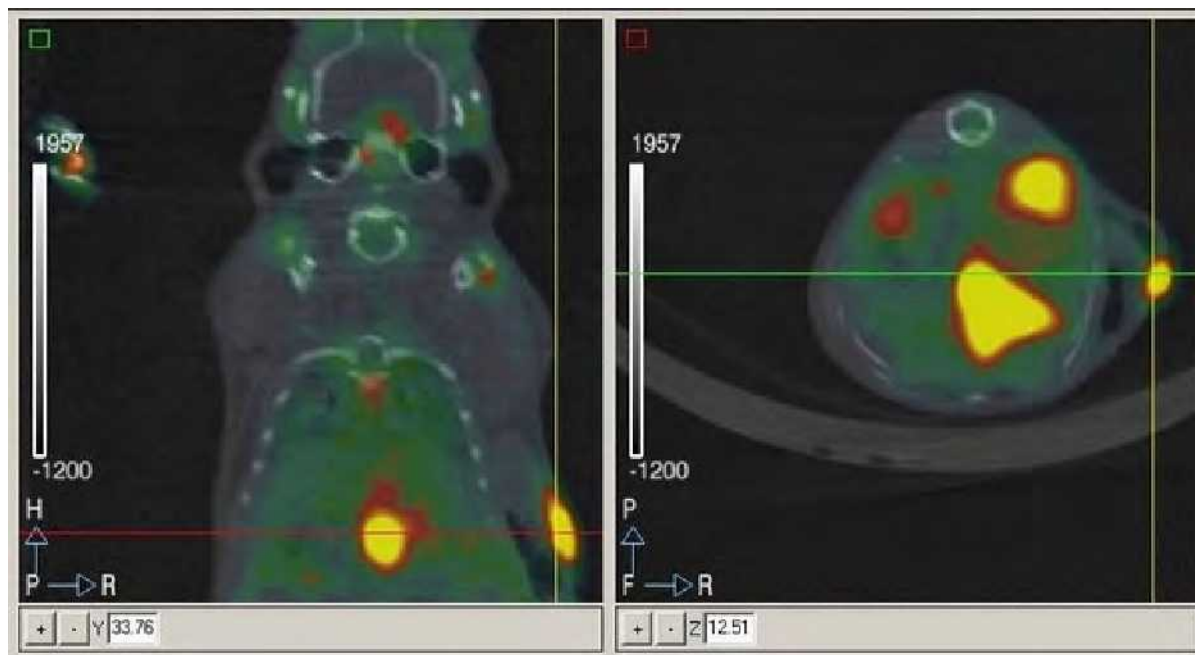
Autoradiographic images of the same brain tissue section: (A) ^{14}C -IAP, blood flow, coded in red; (B) ^{18}F -FEAU, HIF1-signaling, coded in green and co-registered with the corresponding blood flow image.

Presentation Number **1057B**
Poster Session 4d: Imaging Disease/Organ Processes

IMPROVEMENTS OF 18F-PEPTIDES LABELING SYNTHESIS

Mariarosaria Panico^{1,3}, **Lixin Lang**², **Michele Larobina**¹, **Adelaide Greco**³, **Sara Gargiulo**³, **Matteo Gramanzini**¹, **Camillo Palmieri**⁴, **Enrico Iaccino**⁴, **Giuseppe Scala**⁴, **Bruno Alfano**¹, **Marco Salvatore**³, ¹Nuclear medicine, IBB - CNR, Naples, Italy; ²PET Department, Clinical Center, NIH Build 10 Center Drive, Bethesda, MD, USA; ³Dep. of Biomorphological and Functional Sciences and CEINGE, Federico II University, Naples, Italy; ⁴Dep. of Clinical and Experimental Medicine, University "Magna Graecia", Catanzaro, Italy. Contact e-mail: rori.panico@ibb.cnr.it

Objectives: A20 and A20-36 peptides can be labelled with fluorine-18 as a potential radiopharmaceutical for quantitative in vivo mapping of B Cell receptors (BCR) in Murine B-cell lymphoma. We used the F-18 N-succinimidyl 4-fluorobenzoate to label the amino group of terminal aminoacid of A20 and A20-36 peptides and we could obtain radiolabelling yields of >15%. Results: In labelling with fluorine-18 the yield of peptides synthesis showed to be very low. The analysis of every step of radiosynthesis, measuring the activity of every utilized stuff in dose calibrator revealed that a great part of radioactivity stuck in the reactival where both the water was eliminated and the fluorine-18 nucleophilic substitution reaction took place. In addition to this some radioactivity was present in the silica purification cartridge. Finally a loss of fluorine-18 isotope was evident in the first phase of synthesis. This fact, present in every synthesis, excludes the hypothesis of a loss of activity due to the manipulation of radiosynthesis itself, as it takes place in the initial phase. On the basis of my direct experience on cyclotron I have supposed a fault in fluorine-18 production: in particular a loss of Silver cations from target chamber itself during bombardment. The Silver cations effectively can seize a part of fluorine-18 product, in the initial phase eliminating it. The tests have supported our hypotesis: 1) Evaporating the target water at 105°C with argon stream the day after the irradiation, it has been noticed the presence of metal grey residual in the conical bottom of reactival. 2) Filtering the target water by 0.2 mm HPLC filter immediately after irradiation and making the fluorine-18 labelling synthesis there was a 10% increased of yield. 3) Utilizing a scx resin cartridge, which eliminates Silver cations from water, there was a further increase of the yield. In conclusion it is evident the presence of Silver cations in the irradiated water which reduces the final product yield. A20 and A20-36 peptides labelled with 18F-N-succinimidyl 4-fluorobenzoate is presently purified with gradient analytical HPLC in Vydac column (5micron, 250mm, 4.6mm) using ethanol and water as the eluent. This method allows to inject directly the radiocompounds into the animals. References: M.Panico, L.Lang, M.B.Sassman, and W.C.Eckelman. RADIOLABELING OF UNPROTECTED OCTREOTIDE WITH F-18. Journal Lab.Comp.and Radioph.(JLCR) vol.44:pp.922-924(2001). Ed.J.Wiley.



Presentation Number **1070B**
Poster Session 4d: Imaging Disease/Organ Processes

Effect of foam cell formation on [¹⁸F]FDG uptake to macrophages in atherosclerosis

Mikako Ogawa¹, **Satoki Nakamura**², **Mutsumi Kosugi**¹, **Yasuhiro Magata**¹, ¹Photon Medical Research Center, Hamamatsu University School of Medicine, Hamamatsu, Japan; ²Internal Medicine 3, Hamamatsu University School of Medicine, Hamamatsu, Japan. Contact e-mail: mogawa@hama-med.ac.jp

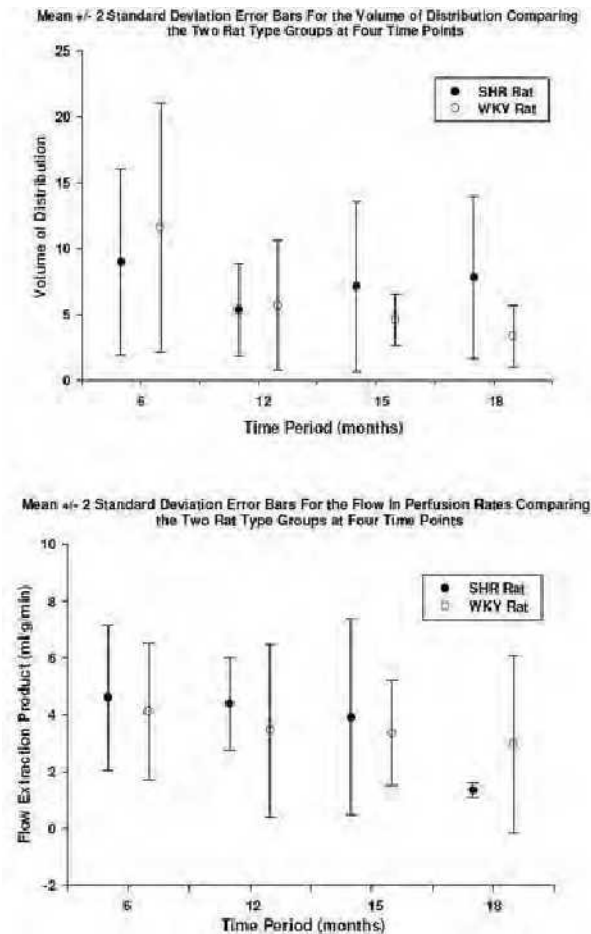
Background: The rupture of atherosclerotic plaque is responsible for the myocardial and cerebral infarctions. Macrophage infiltration and vulnerable plaque formation play an essential role in plaque rupturing. We and other group have shown that a glucose metabolism imaging probe for PET, [¹⁸F]FDG, can specifically detect vulnerable plaque depending on the macrophage infiltration extent to the atherosclerotic lesion since energy metabolism rate is high in macrophages. However, it is still not clear which stage of the lesion can be detected by [¹⁸F]FDG, that is, whether foam cell formation affects the [¹⁸F]FDG uptake or not. **Methods:** Macrophages were isolated from the mice peritoneum following thioglycollate injection, and cultured for 24hrs. Then acetylated LDL (acLDL) was added to form foam cells. For control, PBS was added. After the culture for 12, 24 or 48 hrs, [¹⁸F]FDG was added to each well and incubated for 3hr at 37°C. Then, cells were peeled from the wells and the radioactivity was measured. The protein concentration was measured after homogenization. One culture well was used for Oil-Red-O staining to check the foam cell formation. Furthermore, hexokinase activity was measured in each condition. **Results:** Macrophages were stained with Oil-Red-O and shown to be formed foam cells 24 hr after the incubation with acLDL. The cells were not stained with 12hr acLDL treatments. [¹⁸F]FDG uptake in acLDL treated cells were 45.5 ± 11.8, 82.1 ± 12.0 and 21.0 ± 3.3 %dose/mg protein, at 12, 24 and 48 hr, respectively. The uptake in the control condition was 46.3 ± 9.0, 51.6 ± 1.2 and 20.1 ± 3.7 %dose/mg protein at each incubation time. The significantly higher [¹⁸F]FDG uptake was observed in the 24hr acLDL treated condition compared to the control condition. Hexokinase activities were 0.081, 0.161 and 0.059 U/mg protein for 12, 24 and 48 hr acLDL treatments, respectively. In control conditions, the activities were 0.099, 0.098 and 0.066 U/mg protein. **Discussion:** [¹⁸F]FDG accumulation was increased by foam cell formation, but the uptake was decreased to control level after completely differentiated to foam cells. These findings suggest that [¹⁸F]FDG-PET detects the early stage of forming foam cells in atherosclerosis. And, changes in hexokinase activities were revealed to be one of the causes of alterations in [¹⁸F]FDG uptake in foam cells. The changes in G6Pase activity and glucose transporter expression are under investigation for more detailed investigations.

Presentation Number **1071B**
 Poster Session 4d: Imaging Disease/Organ Processes

Relationship Between Perfusion and Heart Failure Due to Hypertensive Related Pathophysiology Using microPET/CT Imaging of F-18-fluorodihydrorotanol

Hilla Wahnish^{1,2}, **Youngho Seo**², **James P. O'Neil**¹, **Mustafa Janabi**¹, **Kathleen M. Brennan**¹, **Henry F. VanBrocklin**², **Grant T. Gullberg**^{1,2}, ¹Radiotracer Development & Imaging Technology, Lawrence Berkeley National Laboratory, Berkeley, CA, USA; ²Radiology and Biomedical Imaging, University of California San Francisco, San Francisco, CA, USA. Contact e-mail: hilla.wahn@gmail.com

The goal is to develop radionuclide molecular imaging technologies for studying the progression of heart failure using microPET/CT to quantify changes in perfusion as a function of hypertrophy and age in the spontaneous hypertensive rat (SHR). Methods: Normotensive Wistar Kyoto rats (WKY) and SHRs were imaged at 6, 12, 15, and 18 months of age using the microPET/CT Inveon scanner (Siemens). Dynamic gated list mode data of approximately 2-2.5 million counts were acquired over 60 mins immediately after injecting 1-1.5 mCi of F-18-fluorodihydrorotanol (FDHROL). The data were reconstructed as a dynamic sequence of 3D images. Time activity curves for the left ventricle and for the blood sampled from the left ventricular blood pool were fit to a one-compartment perfusion model to obtain estimates of the flow extraction product (K1) and distribution volume (Vd) of FDHROL in the left ventricle. Results: At 6 and 12 months the SHR model showed a higher K1 for FDHROL compared to the WKY model (but not significant). Over time, both the SHR and WKY models showed a general downward trend in K1 with the SHR dropping significantly lower than the WKY at 18 months. The Vd for the SHR and WKY were not significantly different at 6 and 12 months but then showed a significant difference at 15 and 18 months. The affect of age on the results for both groups combined was significant with a linear contrast time factor being significant for both K1 (p=0.018) and Vd (p = 0.001). Conclusion: F-18-fluorodihydrorotanol's excellent extraction versus flow provides an outstanding tracer for analyzing perfusion in small animal models. With the increase in cardiac hypertrophy in the SHR model, the K1 decreases at the onset of heart failure. This decrease is indicative of decreased function of myocytes and overall reduced homeostasis of body systems. An upward trend in the Vd in the last three time points for the SHR may be due to increase in collagen content and a potential decrease in capillary density in the hypertrophied heart.

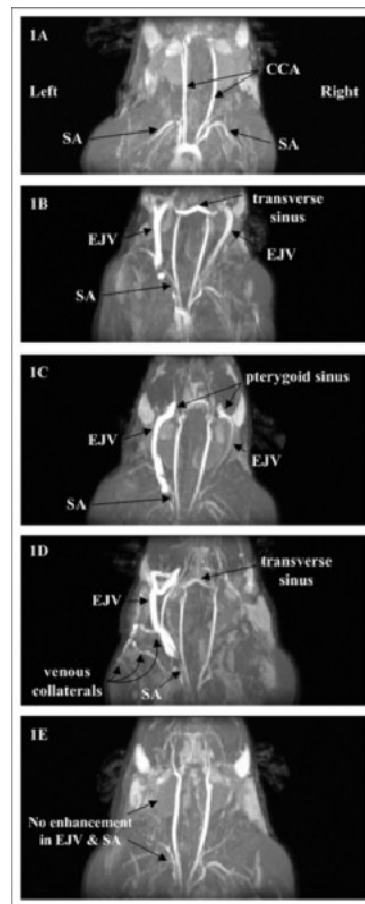


Presentation Number **1072B**
 Poster Session 4d: Imaging Disease/Organ Processes

Neck Time-of-flight MRA in the Jugular Venous Reflux Animal Model

Chang-Chyi Shieh^{1,2}, **Yau-Yau Wai**^{2,3}, **Han-Hwa Hu**^{4,5}, **Chih-Ping Chung**^{4,5}, ¹Graduate Institute of Biomedical Electronic and Bioinformatics, National Taiwan University, Taipei, Taiwan; ²Department of Medical Imaging and Intervention, Linkou Chang Gung Memorial Hospital, Taoyuan, Taiwan; ³Department of Medical Imaging and Radiological Sciences, Chang Gung University, Taoyuan, Taiwan; ⁴Department of Neurology, Taipei Veterans General Hospital and National Yang Ming University, Taipei, Taiwan; ⁵Institute of Clinical Medicine, National Yang Ming University, Taipei, Taiwan. Contact e-mail: chyi.mark@msa.hinet.net

Background and Purpose : A rat model of jugular venous reflux (JVR) is used widely in studies of cerebral arteriovenous fistula, cerebral venous hypertension and chronic cerebral hypoperfusion. However, methods to validate the effectiveness of the operation are needed. **Methods :** We performed neck 3D time-of-flight (TOF) magnetic resonance angiography (MRA) with a clinical scanner in a rat model of JVR before and after the operation. High-resolution arterial angiography of the rat neck was acquired with maximum intensity projection. **Results :** In the JVR model, the success of the operation was validated by enhanced venous structures on MRA. The angiogram also provided information on the height of JVR and the status of other neck vessels. JVR animal model (n = 5) Neck 3D TOF MRA showed the aorta, bilateral common carotid arteries (CCA) and subclavian arteries (SA) before the operation (Fig. 1A). Two weeks after the creation of a left-sided SA- to-external jugular vein (EJV) anastomosis, bilateral EJV were enhanced in four rats, which represented jugular venous reflux (JVR) (Fig. 1B). The height of JVR reached the level of transverse sinus in three rats (Fig. 1B) and the petrygoid sinus in one rat (Fig. 1C). Three months after operation, several venous collaterals developed on the left side, and right-side JVR disappeared (Fig. 1D). The SA-EJV fistula was thrombosed in one rat, and the neck MRA in this animal showed no distal SA and EJV enhancement on the left side (Fig. 1E). **Conclusions :** The neck 3D TOF MRA is a useful noninvasive method for monitoring blood flow in multiple cerebral vessels in this animal model. It also revealed the height of JVR, collateral development, and changes in vessels over time in longitudinal studies. This information should be considered in the evaluation of the animal model.



Presentation Number **1073B**
Poster Session 4d: Imaging Disease/Organ Processes

MULTIMODAL ASSESSMENT OF HEPATOCYTE GROWTH FACTOR ANGIOGENIC GENE THERAPY IN RAT MYOCARDIAL INFARCT MODEL

Yong-Nan Jin, Masayuki Inubushi, Kazuto Masamoto, Kenichi Odaka, Ichio Aoki, Atsushi B. Tsuji, Masashi Sagara, Misturu Koizumi, Tsuneo Saga, Molecular Imaging Center, National Institute of Radiological Sciences, Chiba, Japan. Contact e-mail: jyn921@nirs.go.jp

Hepatocyte growth factor (HGF) has been shown to have a potent angiogenic activity in vitro, however, the in vivo therapeutic effects of angiogenic gene therapy using HGF gene in ischemic heart disease remains controversial. The aim of this study was to investigate the effects of HGF gene therapy in rat myocardial infarct model precisely with multimodal imaging including cine MRI, SPECT/CT, and two-photon excitation fluorescent microscopy (TPEFM). Human sodium-iodide symporter (hNIS) gene was used as a radionuclide reporter gene. Recombinant adenoviruses expressing both HGF and hNIS genes comparably driven by dual constitutive cytomegalovirus promoters (Ad-CMV-HGF-CMV-hNIS; Treatment) and hNIS gene only (Ad-CMV-hNIS; Control) were constructed. Wister rats (10 week-old male) received permanent ligation of the left anterior descending artery, followed by injection of Treatment or Control vector into peri-infarct regions of the left ventricular myocardium. On Day 1, cine MRI was performed using a 7.0T MRI (Bruker Biospin BGA-1) to measure end-diastolic volume (EDV) and ejection fraction (EF). On Days 2 and 4, SPECT/CT images of therapeutic gene expression and myocardial perfusion were obtained with $^{99m}\text{TcO}_4^-$ and ^{99m}Tc -tetrofosmin using a small animal SPECT/CT (Gamma Medica-Ideas FX). Nine (5 Treatment and 4 Control) rats showing similar infarct size and similar gene expression levels were followed for 10 weeks to repeat cine MRI and SPECT/CT. Afterwards, excised hearts were processed for immunohistochemistry with alpha-SMA and CD31 to measure small blood vessels and capillary density, and TPEFM to visualize the three-dimensional microvasculature. The repeated cine MRI demonstrated significantly increased EDV in both Treatment and Control rats without significant difference between the groups. The infarct size was similar after follow-up. Capillary density defined by immunohistochemistry was significantly higher in Treatment rats, while small blood vessels were comparable between the groups. TPEFM revealed very thin ($\approx 2\mu\text{m}$) irregular vessels increased at peri-infarct regions of Treated hearts. TPEFM provided direct evidence that sole HGF gene therapy could induce exclusively immature dysfunctional vessels, which explains other results that increased capillary density didn't lead to cardiac functional recovery. This may contribute to solve the gap between promising results from basic researches and lack in decisive therapeutic effects in clinical researches.

Presentation Number **1074B**
Poster Session 4d: Imaging Disease/Organ Processes

Multimodal Analysis of Lipid-based MR Contrast Agents to detect Atherosclerotic Plaques in the Aortic Arch

Brigit den Adel^{1,5}, *Linda M. van der Graaf*^{1,5}, *Bianca Hogers*¹, *Maaïke de Backer*^{3,5}, *Ivo Que*^{4,5}, *Clemens Lowik*^{4,5}, *Klaas Nicolay*², *Robert E. Poelmann*¹, *Louise van der Weerd*^{1,3}, ¹*Anatomy and Embryology, Leiden University Medical Center, Leiden, Netherlands;* ²*Biomedical Engineering, Eindhoven University, Eindhoven, Netherlands;* ³*Radiology, Leiden University Medical Center, Leiden, Netherlands;* ⁴*Endocrinology, Leiden University Medical Center, Leiden, Netherlands;* ⁵*Molecular Imaging Laboratories Leiden, Leiden University Medical Center, Leiden, Netherlands. Contact e-mail: b.den_adel@lumc.nl*

Introduction: Several MRI studies have shown atherosclerosis can be detected both in humans and animal models. These have shown that uptake of non-targeted contrast agents (CA) in the leaky endothelium of atherosclerotic plaque gives good plaque enhancement, but little is known about the time course of enhancement. In the present study we characterized the in vivo biokinetics of lipid-based MR CA in the aortic arch of ApolipoproteinE deficient (ApoE^{-/-}) mice, using MRI, 3D optical imaging, and histology/relaxivity measurements. **Methods:** Dotarem and Gd-containing NIR664-conjugated micelles and liposomes were applied in 3 groups (n=5/group) of 10 months old male ApoE^{-/-} mice. Mice were imaged using a vertical 9.4T Bruker MRI system. The aortic arch was imaged at baseline and 6-12 hour intervals for 6 days following iv injection of CA (equivalent doses of 50µmol Gd/kg). Retrospectively gated cine-FLASH images with 10 cardiac frames were obtained from 6 cross-sectional slices (TR 31 ms/TE 3 ms, NA 400, MTX 128*128, FOV 18*18, hermite FA 15°, slice 0.4 mm). In 2 separate groups (n=5) CA biodistribution was followed on a Caliper 3D IVIS for 6 days using the NIR664 fluorescence of the CA. Immunohistochemistry and scanning confocal microscopy localized CA within atherosclerotic plaques. Blood half-life was determined by assessing T1 relaxivity of blood samples drawn at different time-points. **Results:** Heterogeneous contrast enhancement (CE) in the aortic wall was observed within 6 hours after Dotarem injection. Both micelle- and liposome-injected mice showed bi-phasic CE, with a 1st peak in contrast-to-noise-ratio (CNR) ~ 12 hours after injection. A 2nd peak CE was observed around 60-72 hours. Relaxivity measurement of blood showed a pattern inversely related to aortic CE, suggestive for organ retention of micelles and liposomes. Organ retention, mainly in liver and kidneys, and release of CA in the circulation was confirmed by in vivo follow-up of NIR664 fluorescence. Histological examination demonstrated a correlation between the site of MRI enhancement and the presence of atherosclerotic plaques. MR signal intensity in the 2nd CE wave after CA injection was predictive for plaque volume. **Conclusions:** Using a multimodal approach we show lipid-based CA have a complex biodistribution involving multiple organ systems and we observe CA retention in several plaque regions. We conclude that the optimal imaging moment may vary for different animal models and contrast agents. **Acknowledgement:** This work is supported by the Dutch Heart Foundation and NWO.

Presentation Number **1075B**
Poster Session 4d: Imaging Disease/Organ Processes

Detecting atherosclerotic plaques using PET and CT targeted P-selectin in mice

Ikuko Nakamura^{1,2}, Koki Hasegawa¹, Riyo Zochi¹, Takeo Sako¹, Mie Nishimura¹, Emi Hayashinaka¹, Yasuhiro Wada¹, Tetsuaki Hirase^{2,3}, Koichi Node², Yasuyoshi Watanabe¹, ¹Center for Molecular Imaging Science, RIKEN, Kobe, Japan; ²Department of Cardiovascular and Renal Medicine, Saga University, Saga, Japan; ³Department of Bioscience and Genetics, National Cerebral and Cardiovascular Center Research Institute, Suita, Japan. Contact e-mail: nakamuraiku@riken.jp

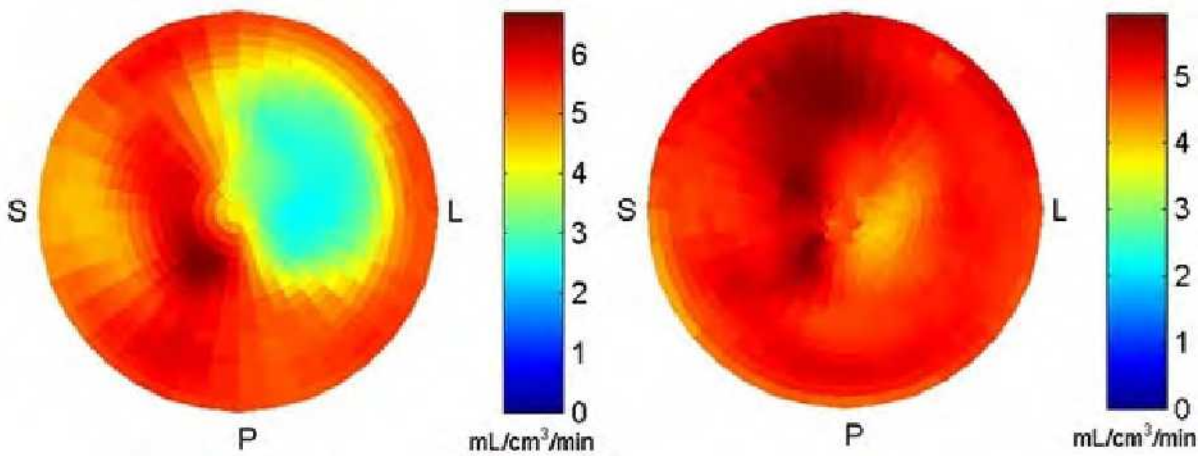
Cardiovascular diseases induced by atherosclerosis are a leading cause of death in the western world. It is postulated that PET and CT imaging using probes based on antibodies against proteins expressed selectively in atherosclerotic plaques enables quantitative and qualitative imaging of atherosclerosis that meets clinical demand. P-selectin is an adhesion molecule that has been implicated in atherothrombosis in human and animals. In this study, we aimed to detect atherosclerotic lesions by PET and CT using probes based on a monoclonal antibody against P-selectin in atherosclerosis-prone low density lipoprotein receptor-deficient (Ldlr^{-/-}) mice in vivo. Anti-P-selectin monoclonal antibody was conjugated with DOTA-OSu and subsequently labeled with ⁶⁴Cu. Thirty six hours prior to PET and CT imaging, 3 MBq/body of ⁶⁴Cu-anti P-selectin monoclonal antibody was intravenously injected to each mouse. Just before CT imaging, 300 µl/body of the contrast agent was injected intravenously. After imaging, we examined the biodistribution of ⁶⁴Cu-anti P-selectin monoclonal antibody using excised aortas. In Ldlr^{-/-} mice fed with a high cholesterol diet so as to develop atherosclerotic plaques, PET and CT imaging revealed selective and prominent accumulation of the probe in the aortic root. The autoradiography of aortas demonstrated uptake of the probe into atherosclerotic plaques confirmed by oil red staining for lipid droplets. In Ldlr^{-/-} mice fed with chow diet that hardly develop atherosclerotic plaques, accumulation of the probes was hardly detectable in aortic root in PET and CT imaging. Biodistribution of the probe in aortas was 5.8-fold higher in Ldlr^{-/-} mice fed with a high cholesterol diet than in Ldlr^{-/-} mice fed with chow diet (5.77% ± 1.10% ID/g vs. 1.00% ± 0.29% ID/g). These data revealed that ⁶⁴Cu-anti P-selectin monoclonal antibody shows accumulation selectively in atherosclerotic plaques of aortas that is detectable by PET and CT imaging in atherosclerosis-prone Ldlr^{-/-} mice, suggesting that P-selectin is a candidate of target molecule for atherosclerosis plaque imaging by PET and CT.

Presentation Number **1076B**
 Poster Session 4d: Imaging Disease/Organ Processes

High-uptake polar map PET segments display increased phosphodiesterase-4 inhibitor (R)-¹¹C]rolipram retention 8-10 weeks post-myocardial infarction

Miran Kenk^{1,2}, **Stephanie Thorn**^{1,2}, **Adam J. Thomas**^{1,2}, **Jennifer M. Renaud**¹, **Ran Klein**¹, **Mireille Lortie**¹, **Rob S. Beanlands**^{1,2}, **Robert A. deKemp**¹, **Jean N. DaSilva**^{1,2}, ¹Cardiac PET Centre, University of Ottawa Heart Institute, Ottawa, ON, Canada; ²Cellular and Molecular Medicine, University of Ottawa, Ottawa, ON, Canada. Contact e-mail: mkenk@ottawaheart.ca

Objectives: Altered myocardial noradrenergic signaling follows the progression of heart failure after myocardial infarction. (R)-¹¹C]Rolipram binds cardiac phosphodiesterase-4 (PDE4) cAMP-catalyzing enzymes. The aim of this study is to evaluate alterations in PDE4 enzyme and, indirectly, cAMP-mediated signaling 8-10 weeks post-infarct with (R)-¹¹C]rolipram and PET, comparing in vivo findings with in vitro techniques. **Methods:** Sprague-Dawley rats underwent left anterior descending coronary artery ligation (n=7) or sham surgeries (n=4). Animals were scanned with [¹³N]NH₃ (30 min, 2.9-4.6 mCi iv) and (R)-¹¹C]rolipram (60 min, 0.5-1.2 mCi iv, cold mass <0.2 µg/kg). Images were re-oriented and tracer uptake was quantified using FlowQuant© software, with infarcted area defined as the percentage of the left ventricle (LV) with [¹³N]NH₃ myocardial blood flow (MBF) below 85% of the maximal value. Logan graphical analysis was utilized to estimate (R)-¹¹C]rolipram distribution volumes (DV) in 17 segments of the polar map. Western blots and enzyme activity assay were used to evaluate changes in PDE4 expression and activity in the non-infarcted LV. **Results:** Infarcted rats showed a MBF defect encompassing 26.3-48.5% of the LV. (R)-¹¹C]rolipram DV values were increased by 15% (p=0.01, t-test) in the non-infarcted portions of the high uptake segments of infarcted rats, compared to sham animals. MBF in the non-infarcted myocardium was unaffected (p=0.2), suggesting that the changes in (R)-¹¹C]rolipram DVs are due to altered PDE4 binding and not pharmacokinetic factors. In vitro techniques detected no change in the activity or expression of PDE4 subtypes. **Conclusions:** In a LAD-ligation heart failure rat model, (R)-¹¹C]rolipram PET imaging detects an increase in PDE4 tracer binding in non-ischemic tissue 8 weeks post-infarct, warranting further studies.



Representative polar maps of (R)-¹¹C]rolipram DVs in infarcted (left) and sham-treated (right) rat.
 MBF and (R)-¹¹C]rolipram DV values for infarcted and sham-treated rats

	[¹³ N]NH ₃ MBF	(R)- ¹¹ C]rolipram DV
MI (n=7)	3.0 ± 0.1	6.24 ± 0.6
Sham (n=4)	2.9 ± 0.3	5.31 ± 0.3* (p=0.01)

Presentation Number **1077B**
 Poster Session 4d: Imaging Disease/Organ Processes

68Ga-Chloride Preferably Delineates Macrophages in Atherosclerotic Plaques of LDLR-/- ApoB100/100 Mice

Johanna Silvola¹, **Iina Laitinen**^{1,2}, **Henri J. Sipilä**¹, **Jukka Laine**³, **Pia Leppänen**⁴, **Seppo Ylä-Herttua**⁴, **Juhani Knuti**¹, **Anne Roivainen**^{1,5}, ¹Turku PET Centre, Turku, Finland; ²Technische Universität München, München, Germany; ³Department of Pathology, Turku University Hospital, Turku, Finland; ⁴A.I. Virtanen Institute, University of Kuopio, Kuopio, Finland; ⁵Turku Centre for Disease Modelling, University of Turku, Turku, Finland. Contact e-mail: johanna.silvola@utu.fi

Introduction: Atherosclerosis is a chronic inflammatory disease of artery wall with infiltration of monocytes into subendothelial space and differentiation into macrophages. Since, the rupture prone plaques commonly contain high amount of activated macrophages, imaging of the macrophage content may provide an excellent tool for the evaluation of plaque vulnerability. 67Ga-citrate SPECT has been used for decades for in vivo imaging of inflammation. 68Ga PET may have advantages e.g. better resolution, for the detection of inflammatory cells, compared to 67Ga. **Methods:** Uptake of intravenously administered 68Ga-chloride (17 ± 2 MBq) was investigated in 9 atherosclerotic LDLR-/-ApoB100/100 mice and 6 control mice at 3 hours after injection. LDLR-/-ApoB100/100 mice were kept on a high fat, Western-type diet for 3-4 months, starting at the age of 7 months. Control mice were fed with regular diet. The biodistribution of 68Ga-radioactivity was evaluated by gamma counting of excised tissue samples and by digital autoradiography of aortic cryosections. Subsequently, the autoradiographs were combined with histological and Mac-3 immunohistochemical analysis of the sections. **Results:** Our results revealed that the 68Ga-radioactivity uptake in atherosclerotic plaques was higher compared to healthy vessel wall (ratio 1.8 ± 0.2, P = 0.0002) and adventitia (ratio 1.3 ± 0.2, P = 0.0011). Autoradiography signal prominently co-localized with macrophages as demonstrated by Mac-3 staining (Figure 1). Some radioactivity was also detected in calcified regions of plaques. In both mice strains, the highest level of radioactivity was found in the urine and blood. **Conclusions:** We observed a moderate but significantly higher 68Ga-chloride uptake in the aortic plaques of atherosclerotic mice, especially at the sites of macrophages. While the uptake of 68Ga-chloride was promising in this animal model, the slow blood clearance may limit the usability of 68Ga-chloride for in vivo imaging of atherosclerotic plaques.

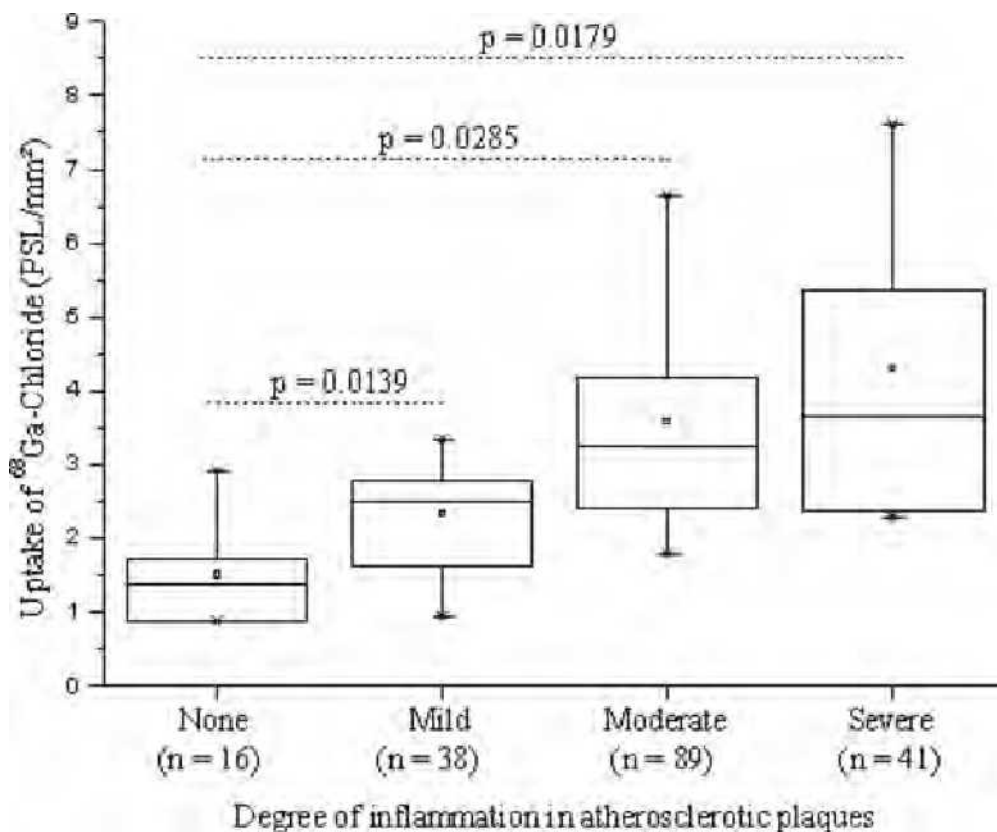


Figure 1.

Presentation Number **1078B**
 Poster Session 4d: Imaging Disease/Organ Processes

In Vivo Assessment of Aortic Wall Stiffness and Degeneration Using Ultrasound Imaging and 3D Optical Imaging in Aneurysmal Fibulin-4 Mice

Jeroen Essers^{1,3}, Paula van Heijningen¹, Miranda Harteveld², Marcia Emmer², Frank Gijzen², Johan G. Bosch², Marcel Vermeij⁴, Ivo Que⁶, Gert V. van Cappellen⁵, Alan Chan⁷, Nico de Jong², Clemens Lowik⁶, Eric Kaijzel⁶, ¹Cell Biology & Genetics, Erasmus MC, Rotterdam, Netherlands; ²Biomedical Engineering, Erasmus MC, Rotterdam, Netherlands; ³Department of Vascular Surgery, Erasmus MC, Rotterdam, Netherlands; ⁴Department of Pathology, Erasmus MC, Rotterdam, Netherlands; ⁵Department of Reproduction and Development, Erasmus MC, Rotterdam, Netherlands; ⁶Department of Endocrinology and Metabolic Diseases, Leiden University Medical Center, Leiden, Netherlands; ⁷Perucuros, Perucuros, Enschede, Netherlands. Contact e-mail: j.essers@erasmusmc.nl

Introduction: Our focus is the early detection and therapeutic treatment of aortic aneurysms. Aneurysmal Fibulin-4 mice (Fibulin-4R/R) show dilatation of the ascending aorta and a tortuous and stiffened aorta, resulting from disorganized elastic fiber networks. Strikingly, already a modest reduction in expression of Fibulin-4 in the heterozygous Fibulin-4+/R mice occasionally resulted in modest aneurysm formation. The aim of the present study is to examine alterations in aortic distensibility and extracellular matrix degradation in the Fibulin-4 mouse models using non-invasive ultrasound imaging and 3D fluorescence imaging/tomography (FLI), respectively. **Methods:** Aortic wall stiffness was assessed by small animal ultrasound imaging using a VisualSonics Vevo 2100 at 25MHz. Systolic and diastolic ascending aortic diameters were recorded in M-mode. In addition, using protease-activatable NIRF probes for activated matrix-metallo proteases (MMPsense 680) and Cathepsins (ProSense 750), we simultaneously monitored and quantified MMP upregulation in Fibulin-4+/R and Fibulin-4R/R animals using 2D and 3D quantitative in vivo optical imaging modules. We determined life-time properties of these dyes using in vivo time domain imaging followed by ex vivo high-resolution 3D confocal imaging. **Results:** Ultrasound imaging revealed an increased aortic stiffness index (β) in Fibulin-4R/R mice. Furthermore, we mapped the differential localization of the protease-activatable sensors for activated MMPs and Cathepsin in vivo during different degrees of aneurysm formation. Subsequent high-resolution 3D confocal imaging allowed accurate analysis of defects in collagen microarchitecture in the aneurysmatic aortic wall. **Conclusion:** Using tomographic non-invasive in vivo imaging methods in combination with protease-activatable NIRF probes, we quantitatively determined the upregulation of key biomarkers and aortic wall stiffness during aneurysm formation and response

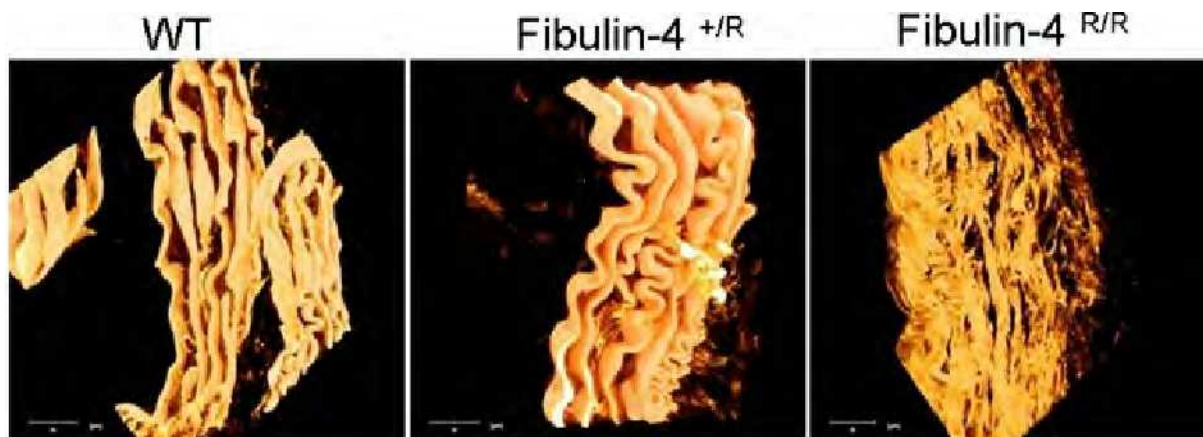


Figure 1. 3D high resolution confocal imaging of defective collagen microarchitecture using protease-activatable sensors for matrix-metallo proteases during various degrees of aortic wall degeneration.

Presentation Number **1079B**
Poster Session 4d: Imaging Disease/Organ Processes

Imaging of Apoptosis in Atherosclerosis using a small peptide probe

Bodhraj Acharya, Kai Wang, Moon Hee Na, In-San Kim, Byung-Heon Lee, Department of Biochemistry and Cell Biology, Kyungpook National University, Daegu, Republic of Korea. Contact e-mail: bodhach@gmail.com

A growing number of evidence shows that atherosclerotic plaque put its molecular signatures on the tissue, such as apoptosis of macrophages, vascular cell adhesion molecule expression, and $\alpha\beta 3$ integrin expression in angiogenic blood vessels. Apoptotic cells may release pro-coagulant and pro-oxidative stimuli that contribute to plaque destabilization and myocardial injury in atherosclerosis. Imaging of apoptosis in atherosclerosis, therefore, may provide a tool for the detection of atherosclerotic lesions and also vulnerable plaques, which is still an unmet medical need. Using phage display, we have previously indentified ApoPep-1 (Apoptosis-targeting Peptide-1), which is a six-amino acid peptide and selectively binds to apoptotic and necrotic cells. Here we used ApoPep-1 to image atherosclerosis plaque in an atherosclerosis mouse model. When injected into Ldlr^{-/-} mice, ApoPep-1 that was labeled with Cy7.5 near-infrared fluorescence dye showed significant fluorescence signals at aorta. In contrast, little signals were observed in Ldlr^{-/-} mice injected with a control peptide and wild-type mice injected with ApoPep-1. ApoPep-1 was localized at inside plaque and overlying endothelial cells, when examined under immunofluorescence microscope. Furthermore, its location at atherosclerotic plaques was co-localized with matrix metalloprotease-9 and TUNEL staining. These results suggest that ApoPep-1 is a promising, small peptide probe for imaging of apoptosis in atherosclerosis and for the detection of vulnerable plaque.

Presentation Number **1080B**
Poster Session 4d: Imaging Disease/Organ Processes

Longitudinal In Vivo Imaging Quantification of Inflammation and Reduction in Vascular Inflammation by Ezetimibe in Atherosclerotic Lesions of apoE^{-/-} Mice Using Fluorescence Molecular Tomography (FMT) and Cathepsin and $\alpha\beta 3$ Integrin Biomarkers

Bohumil Bednar¹, Shu-An Lin¹, Manishkumar Patel¹, Donna L. Suresch¹, Brett Connolly¹, Michael Klimas², Cyrille Sur², ¹Department of Imaging, Merck Research Laboratories, West Point, PA, USA; ²Imaging, Merck Research Laboratories, West Point, PA, USA.
Contact e-mail: bohumil_bednar@merck.com

Atherosclerosis is an inflammatory disease caused by accumulation of LDL and cholesterol in arterial walls leading to the formation of vulnerable plaques characterized by infiltration of circulating inflammatory cells. Development of atherosclerosis associated inflammation results in the activation of cathepsin proteases and expression of $\alpha\beta 3$ integrin receptors. Conventional imaging techniques largely assess luminal narrowing, calcification, or morphological abnormalities of atherosclerotic plaque, which have been shown to be poor indicators of vulnerable plaque and thus poor predictors of heart attack and stroke. Thus, it is desirable to develop molecular imaging biomarkers and noninvasive methods for detection of the vulnerable plaques. In this study, we describe longitudinal quantification of inflammation and reduction of inflammation by Ezetimibe in the atherosclerotic lesions of apolipoprotein E-deficient (apoE^{-/-}) mice using newly developed optical molecular reporters of cathepsin proteases and $\alpha\beta 3$ integrin and FMT. Transgenic, as well as control C57BL/6 mice, were fed a cholesterol enriched diet (9% fat, 0.15% cholesterol) for 35 weeks to induce atherosclerosis. A statistically significant increase ($p < 0.05$) in the inflammation between apoE^{-/-} and control mice was detected using large molecular weight cathepsin probe (LMCP) (24 hours after injection) as well as a newly developed low molecular weight probe (FAST) (6 and 24 hours after injection) after 10 to 12 weeks on the diet, while the $\alpha\beta 3$ integrin agent required mice to be on the diet for 15 weeks. In the prevention studies using Ezetimibe (7 mg/kg) LMCP and FAST detected statistically significant ($p < 0.05$) reduction in inflammation in the treated animals after 31 and 21 weeks, respectively. The localization of FMT signal in the thorax area was confirmed by coregistration with CT and by fluorescence measurements of dissected arteries and histopathology of the sections from different parts of the arteries. Fluorescence of both cathepsin and $\alpha\beta 3$ integrin probes was found to co-localized in the arterial sections with macrophages. This study demonstrated that the cathepsin as well as $\alpha\beta 3$ integrin optical reporters can be used as molecular imaging biomarkers for longitudinal detection of atherosclerosis associated inflammation and reduction of inflammation by Ezetimibe. Such biomarkers can serve in the preclinical testing of therapeutics and potentially for early diagnosis of atherosclerosis in patients.

Presentation Number **1082B**
Poster Session 4d: Imaging Disease/Organ Processes

Induction of Endothelial Dysfunction in Wild-Type Mice on Western Type Diet May Be Studied By ^{18}F -FDG PET of Aorta

Anne Mette F. Hag^{1,2}, Sune F. Pedersen^{1,2}, Andreas Kjaer^{1,2}, ¹Cluster for Molecular Imaging, University of Copenhagen, Copenhagen, Denmark; ²Department of Clinical Physiology, Nuclear Medicine & PET, Rigshospitalet, Copenhagen, Denmark. Contact e-mail: annemette@mfi.ku.dk

Aim: To follow development of endothelial dysfunction in response to Western type diet in wild-type mice non-invasively with ^{18}F -FDG PET. **Methods:** We have previously shown that ^{18}F -FDG PET can be used to visualize inflammation in aorta of ApoE-deficient mice. In the present study, we used the technique to study effect of Western type diet in wild-type mice. Five groups of wild-type mice (C57BL/6NTac) were investigated. All mice were 8 weeks old at the initiation of the experiment. One group was scanned and sacrificed at the beginning of the experiment as a baseline group (n=7, 0 weeks). Two other groups received normal diet for 16 weeks (n=4, 16 weeks) and 32 weeks (n=7, 32 weeks), respectively. The last two groups received a high-fat Western type diet for 16 weeks (n=11, 16 weeks + diet) and 32 weeks (n=3, 32 weeks + diet). Approximately 15 MBq of ^{18}F -FDG was administered to the mice as well as 0.3 mL of a contrast-agent. Three hours later a PET/CT scan was performed in a dedicated animal scanner. After the scan, the animals were sacrificed and the aortas taken out for gene expression studies. SUV-values for the aorta were calculated. Unpaired t-tests were used to compare groups. **Results:** The SUVmean for 0 weeks and the groups on normal diet was not significantly different from each other (0.76±0.10 vs. 0.71±0.13, p=0.72 and 1.00±0.11, p=0.14 for 16 and 32 weeks, respectively). The Western type diet increased FDG SUVmean in the 16 weeks + diet group to 1.75±0.10 (p<0.0001 vs. 0 weeks) indicating inflammatory activity in aorta. The inflammatory effect of the diet seemed to have reached a plateau at 16 weeks, since no further increase in FDG SUVmean was observed at 32 weeks in the diet group (1.80±0.12, p<0.0001 vs. 0 weeks, NS vs. 16 weeks + diet). **Conclusion:** A clear increase in FDG uptake was seen in wild type mice on a Western type diet indicating induction of endothelial dysfunction. Our data support the use of FDG PET and wild-type mice for the study of development of endothelial dysfunction/early atherosclerosis. Comparison of FDG uptake with gene expression of markers characteristic of inflammation and endothelial dysfunction are currently undertaken.

Presentation Number **1083B**
Poster Session 4d: Imaging Disease/Organ Processes

Real-time quantitative fluorescence imaging of atherosclerosis progression in ApoE knockout mice

Dao Chao Huang¹, Marilyse Piché¹, Guobin Ma¹, Muriel Jean-Jacques¹, Mehdi Arbabi², Mario Khayat¹, Abedelnasser Abulrob², ¹ART Advanced Research Technologies, Inc., Montreal, QC, Canada; ²Neurobiology Program, Institute for Biological Sciences, National Research Council of Canada, Ottawa, ON, Canada. Contact e-mail: gma@art.ca

The molecular mechanism of atherosclerosis includes attachment of leucocyte to endothelium and expression of adhesion molecules by activation of endothelial cells to initiate formation of the atherosclerotic lesions. Certain endothelial cell adhesion molecules such as ICAM-1 are up-regulated in early inflammation of atherosclerotic disease which remains a major health problem in western societies and causes 50,000 annual deaths in the United States. The best solution to reduce the death rate is early detection and therapy before plaque erosion and rupture. We hypothesize that fluorescence imaging of ICAM-1 activity in atherosclerosis may serve as a new measure of plaque inflammation. To test this hypothesis, we selected an anti-ICAM-1 single domain antibody and tagged it with NIR fluorophore Cy5.5 to detect atherosclerosis in ApoE^{-/-} mice model using a time-domain in vivo small animal fluorescent imaging system. In the study, anti-ICAM sdAb-Cy5.5 was intravenously injected in high fat diet-fed ApoE^{-/-} and control mice, and imaged before and 24, 48 and 72 hours post-injection. The injection/imaging was repeated each month for 6 months following the start of a high-fat diet for the mice. Fluorescence imaging show that (1) anti-ICAM-1 sdAb accumulated in the thorax centre of ApoE^{-/-} mice but not control mice; (2) the amount of anti-ICAM-1 sdAb in the thorax region were increasing following the atherosclerosis plaques development; (3) using time resolved 3D fluorescence imaging technique, we found that the anti-ICAM-1 sdAb is localized in the heart-aorta region of ApoE^{-/-} mice. Fluorescence results were confirmed by micro-computed tomography imaging, which showed that calcified plaques were present in the heart-aorta location. Ex vivo fluorescence signal analysis revealed that ApoE^{-/-} group has 8-fold higher fluorescence signal than the control group. Extensive colocalization of Cy5.5 with large atherosclerosis plaque lesions were observed in both aortic root and ascending aorta of ApoE^{-/-} mice. In contrast, frozen sections of heart-aorta from control mice showed no Cy5.5 signal. In summary, NIRF-labelled anti-ICAM-1 sdAb specifically recognized early and developed atherosclerotic plaques in large vessels in high-fat diet fed ApoE^{-/-} mice; it was additionally shown that this can be monitored non-invasively by prospective optical imaging in vivo. The distribution of the ICAM-1 sdAb in the plaques was confirmed using microscopic techniques and immunohistochemistry.

Presentation Number **1084B**
 Poster Session 4d: Imaging Disease/Organ Processes

Inverse Correlation of [¹¹C]meta-Hydroxyephedrine Cardiac Retention Measurements to Norepinephrine Concentration in Rats

James T. Thackeray^{1,2}, Jennifer M. Renaud¹, Myra A. Kordos¹, Ran Klein¹, Robert A. deKemp¹, Rob S. Beanlands^{1,2}, Jean N. DaSilva^{1,2}, ¹National Cardiac PET Centre, University of Ottawa Heart Institute, Ottawa, ON, Canada; ²Cellular & Molecular Medicine, University of Ottawa, Ottawa, ON, Canada. Contact e-mail: jthackeray@ottawaheart.ca

Background: Retention of the PET radiotracer and norepinephrine (NE) analogue [¹¹C]meta-hydroxyephedrine (HED) reflects the integrity of neuronal reuptake. The contribution of endogenous NE levels on HED retention has not been fully established. **Methods:** Male Sprague Dawley rats (n=3/group) were implanted with osmotic minipumps containing NE bitartrate (0.05 or 0.15 mg/kg/h) or saline (7.6 µL/h). Serial venous blood samples were taken. After 6 h, rats were injected with 0.42-0.77 mCi HED and a dynamic PET scan was acquired over 60 min using an Inveon™ scanner. Data were reconstructed by OSEM3D/MAP and images analyzed using FlowQuant©. Retention index was calculated as activity in the myocardium at 30-40 min divided by the integral of the input function. Washout rate was determined by fitting a monoexponential curve to the myocardial time activity curve over 10-60 min. Plasma and tissue NE concentrations were measured by column switch HPLC with electrochemical detection. **Results:** Myocardial activity in NE-treated rats showed lower sustained retention resulting in less distinct images (Fig). Cardiac retention index was reduced and washout rate was elevated by NE infusion (Table). Plasma and cardiac NE was significantly elevated in treated rats (0.15 mg/kg/h) to controls: (4.6±0.2 vs 1.1±0.3 ng/mL, p<0.0001; 6.5±2.7 vs 3.0±0.5 ng/mg, p=0.02, respectively). Inverse correlations were established between plasma NE and HED retention index (r=-0.91, p=0.01); cardiac NE and retention index (r=-0.87, p=0.03); plasma NE and washout rate (r=-0.93, p=0.01); and cardiac NE and washout rate (r=-0.96, p<0.01). **Conclusion:** We describe an inverse correlation of HED PET measurements to plasma and cardiac NE following 6 h infusion. HED imaging may be useful for detection of global and regional sympathetic dysfunction and elevated tissue NE in early stages of cardiac pathology.

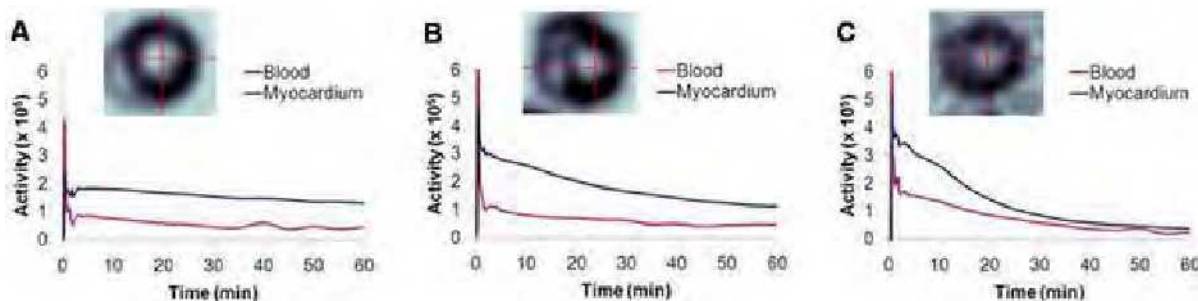


Figure: Short axis HED images with myocardial and blood time activity curves in rats after 6 hour subcutaneous infusion of saline (A), 0.05 mg/kg/h norepinephrine (B), or 0.15 mg/kg/h norepinephrine (C).

Cardiac HED measurements in control and NE-infused rats

	Control	NE 0.05 mg/kg/h	NE 0.15 mg/kg/h
Retention Index	6.31±0.55	4.00±0.70	1.02±0.10*
Washout Rate	-0.67±0.15	-0.88±0.19	-1.31±0.15*

* p<0.001 to controls, one-way ANOVA, Bonferroni post hoc

Presentation Number **1085B**
Poster Session 4d: Imaging Disease/Organ Processes

Discovery of a peptide targeting stabilin-2 homing to atherosclerotic plaque

Gayoung Lee¹, **Jong-Ho Kim**¹, **Goo Taeg Oh**³, **Byung-Heon Lee**¹, **Ick Chan Kwon**², **In-San Kim**¹, ¹*Biochemistry and Cellular Biology, KYUNG POK NATIONAL UNIVERSITY, DAEGU, Republic of Korea;* ²*Biomedical Research Center, Korea Institute of Science and Technology, Seoul, Republic of Korea;* ³*Division of Molecular Life Sciences, Ewha Womans University, Seoul, Republic of Korea.*
Contact e-mail: tube11@gmail.com

A large number of cells including macrophages accumulate in atherosclerotic lesion, and destabilize plaques and drive plaque disruption. Therefore, macrophages would be efficient target for atherosclerosis treatment and imaging. Stabilin 2 is a transmembrane protein which is predominantly expressed in macrophages as well as endothelial cells. In this study, we found that stabilin 2 is widely expressed in atherosclerotic plaques but not in normal vessel wall and localized in not only macrophages but also endothelial cells and smooth muscle cells. We performed phage display to identify peptides that specifically bound to stabilin 2. After four rounds of selection, the most frequent CRTLTVRKC was identified. We confirmed that this peptide specifically binds to stabilin 2 expressing cells in vitro and sinus endothelial cells in the spleen and lymph nodes in vivo. A FITC conjugated synthetic CRTLTVRKC peptide was demonstrated to home to atherosclerotic plaques in Ldlr^{-/-} mouse and to co-localize with endothelial cells, macrophages, and smooth muscle cells in plaques. These results show that the CRTLTVRKC peptide homes to atherosclerotic plaques by targeting stabilin 2 and would be a promising moiety for drug delivery and molecular imaging of atherosclerosis and other inflammatory diseases.

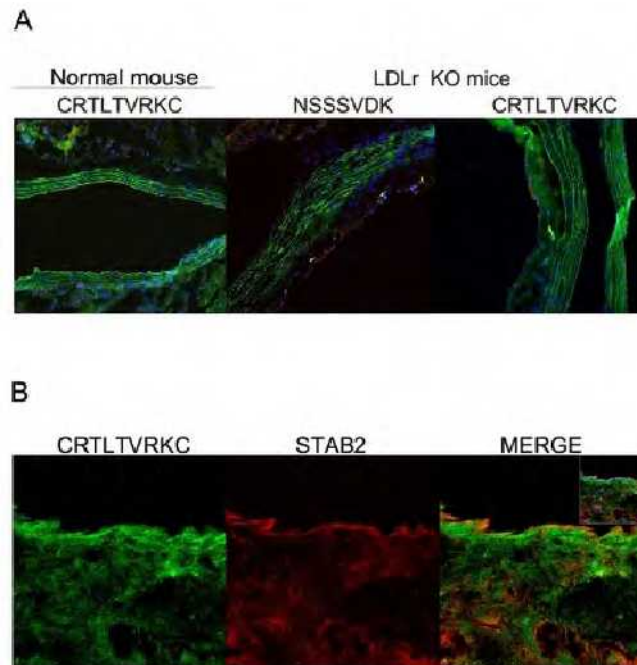


FIGURE 4

Presentation Number **1086B**
Poster Session 4d: Imaging Disease/Organ Processes

Can Aortic MMP Activities on NIRF Molecular Imaging Be Predicted with Visceral Fat Amount on microCT-based Anatomic Imaging?

Soo-Min Shon¹, Dong Kun Lee¹, Jeong-Yeon Kim¹, Jin-yong Park¹, Ju Hee Ryu², Kwangmeyung Kim², Ick Chan Kwon², Dong-Eog Kim¹, ¹Molecular Imaging & Neurovascular Research(MINER) Lab, Neurology, Dongguk Univ. International Hospital, Goyang-si, Republic of Korea; ²Biomedical Research center, Korea institute of science and technology, Seoul, Republic of Korea. Contact e-mail: 83brain@gmail.com

Background: Inflammatory proteolytic enzymes such as matrix metalloproteinases(MMPs) contribute to various pathologic processes of coronary artery disease(CAD), leading to plaque rupture and thromboembolic vascular events. Near-infrared fluorescent(NIRF) MMP imaging is an effective tool for translational preclinical atherosclerosis research by providing molecular information on plaque inflammation. Clinically, it has been shown that intra-abdominal visceral fat correlates with the occurrence of CAD. Among various methods to measure the amount of intra-abdominal fat, CT is regarded as the most accurate diagnostic technique. Objective: To see if MMP-related NIRF signal in mouse atheromata correlate with the extent of intra-abdominal visceral fat amount on microCT. Methods: 8 weeks ApoE knock-out(k/o) mice were fed on either a normal diet(n=10) or a Western diet(n=10) for 21 weeks. For the last 13 weeks, a half of the animals on a Western diet or normal diet were trained(30min/d, 5days/w) to run on a treadmill at a controlled speed(17m/min). During the last week, microCT was performed to measure intra-abdominal visceral fat percentage per abdominal cavity, and the animals' aortas were imaged ex vivo using a NIRF imaging machine four hours after the intra-venous injection of MMP-2/9 activatable NIRF probe. After normalization of the MMP NIRF images, the median NIRF signal intensities of the entire aortic tissue were calculated. Plaque size was quantified by calculating the percentage of oil red O staining of the total aortic surface area. Results: In ApoE k/o mice, 13-week exercise training did not significantly reduce the plaque size either in the normal diet group(32.1±7.7 vs. 28.7±11.8%) or in the Western diet group(48.7±8.5 vs. 49.3±9.1%). However, exercise reduced the MMP activity in the Western diet group(62.0±19.2 vs. 26.8±16.1%, p<0.05, Student's t-test), but not in the normal diet group(19.6±15.7 vs. 20.6±13.5%). Although the normal diet group had less visceral fat(1961.4±756.6mm³) than the Western diet group(4659.4±1130.9mm³, p<0.05, Student's t-test), exercise training did not affect the fat extent in either group. The amount of visceral fat correlated with the plaque size(r²=0.41, p<0.05, Pearson correlation). However, neither visceral fat nor plaque size correlated with the MMP activity in the aorta. Conclusions: Aortic MMP activity in the ApoE k/o mice, which was measured with the help of the NIRF molecular imaging technique, could not be predicted with the visceral fat extent quantified by using the anatomy-based imaging modality, 'microCT'.

Presentation Number **1087B**
Poster Session 4d: Imaging Disease/Organ Processes

Visualization of tenascin-C activity in atherosclerosis using fluorescence labeled aptamer

Ju Ri Chae, Ye Lim Cho, Jun Young Park, Jong Doo Lee, Won Jun Kang, Department of Radiology, Division of Nuclear Medicine, Yonsei University College of Medicine, Seoul, Republic of Korea. Contact e-mail: jjuri1230@yuhs.ac

Tenascin-C is a matrix glycoprotein generally found in tumor or healing wounds. It has been reported that tenascin-C is also expressed in macrophage-rich atheromatous plaque. Recently, aptamer targeting tenascin-C protein was developed and reported to be useful in specific tumor imaging. We investigated the feasibility of fluorescence-labeled aptamer to visualize tenascin-C expression in atheromatous plaque model. Tenascin-C aptamer sequence was as follows: H2N-C6-5'CCTGCACTTGGCTTGGATTTCAGAAGGGAGACCC-3'-OH. Tenascin-C aptamer was labeled with Texas-red for in vitro assay, and with Cy5.5 dye for in vivo imaging. Macrophage cell line, Raw 264.7 was tested for tenascin-C expression after application with Texas-red labeled aptamer using confocal microscopy. Apoprotein E (APOE) knock-out mice were fed with high cholesterol diet over 2 months. One nmole of fluorescence labeled tenascin-C aptamer was injected. With excitation wavelength of 640 nmeter and emission wavelength of 720 nmeter, fluorescence image was acquired with IVIS spectrum. Macrophage cell line, Raw 264.7, showed expression of tenascin-C, which was assessed by confocal imaging after tenascin-C aptamer. In vivo fluorescence imaging showed that tenascin-C aptamer was accumulated in atheromatous plaque of APOE knock-out mice. Tenascin-C aptamer was not accumulated in normal aortic wall. Control aptamer showed no increased uptake in APOE knock-out mice. We demonstrated that tenascin-C was highly expressed in atheromatous plaque of APOE knock-out mice using fluorescence labeled aptamer. Aptamers including tenascin C aptamer targeting atheromatous plaque could be used for specific targeting method to detect atheromatous plaque.

Presentation Number **1088B**
Poster Session 4d: Imaging Disease/Organ Processes

Impact of FDG-PET Myocardial Viability on left ventricular ejection fraction post revascularization

Rohini Mishra, NUCLEAR MEDICINE, PD Hinduja National Hospital andMRC, Mumbai, India. Contact e-mail: rohini1223@yahoo.co.in

Methods & materials- We undertook a study of total 35 patients (35-75 yrs of age , 31 males and 4 females) within the period of Aug'07-Jan'09, with myocardial infarction/ischemic dilated cardiomyopathy in whom FDG PET scan demonstrated myocardial viability. All the patients had severe LV dysfunction on echocardiography with LVEF ranging from 10-35%, and all patients underwent FDG PET scan including myocardial perfusion imaging. 29 of total 35 patients further underwent revascularization. They were followed up with LVEF on echocardiography and symptomatology. The remaining 6 patients were not revascularised and kept on medical management due to non cardiac causes. Results - There was improvement in the left ventricular function with rise in LVEF by 15-20% post revascularization in 20 of total 29 patients (69%). The remaining 9 (31%) patients maintained the same EF post intervention. Symptom wise, there was significant improvement in 16 patients (56%), while 13 (44%) patients were asymptomatic, thus improving the quality of life in all 29 patients. 6 of 35 patients who did not undergo revascularization maintained same EF with rise in EF by 15% post EECF in 2 of them. Conclusion - Demonstration of myocardial viability on FDG PET scan had an significant impact on the out come of revascularization in form of improvement LVEF and quality of life.

Presentation Number **1089B**
Poster Session 4d: Imaging Disease/Organ Processes

New application of optical agent to image angiogenesis in hind limb ischemia

Yared Tekabe, Alexander D. Klose, Joane Luma, Lynne Johnson, Columbia University, New York, NY, USA. Contact e-mail: yt2166@columbia.edu

Peripheral artery disease is a prevalent clinical problem with significant morbidity. We investigated whether optical imaging can identify the molecular mechanisms involved in the angiogenesis using a fluorophore labeled RGD (IntegriSense 750 nm, Visen Medical) that targets avb3 integrin expression occurring during capillary sprouting. Methods: Seven C57BL/6 mice underwent femoral artery ligation. Between 3 and 7 days later under isoflurane a catheter was inserted in a jugular vein and 2 nmol IntegriSense was injected. Six hours later mice underwent optical imaging in the PhotonImager (BiospaceLab, France). The excitation wavelength was set at 660 nm and fluorescence light was collected with a cut-off pass filter above 700 nm. Autofluorescence was removed at an excitation wavelength of 580 nm. After imaging the mice were sacrificed and the anterior tibialis muscles sections and stained for lectin and immunohistochemical staining for RGD. Regions of interest were drawn around the fluorescence signal in the left (ligated) limb and right (control) limb and ratios R of the photon flux [photons s⁻¹cm⁻²sr⁻¹] in the L/R limbs calculated. Results and Discussion: The fluorescence images showed increased signal in the ligated limb in all mice. The ratio of photon flux in the left limb to right limb averaged R=1.86 (range 1.15 to 3.47). Lectin staining showed capillary sprouting in the ischemic limbs and fluorescent staining showed co-localization of the RGD fluorescence to CD 31 positive (endothelial) cells. Conclusion: Fluorescence imaging can be used to follow angiogenic response to hind limb ischemia and may have applications in development of drugs to improve limb perfusion.

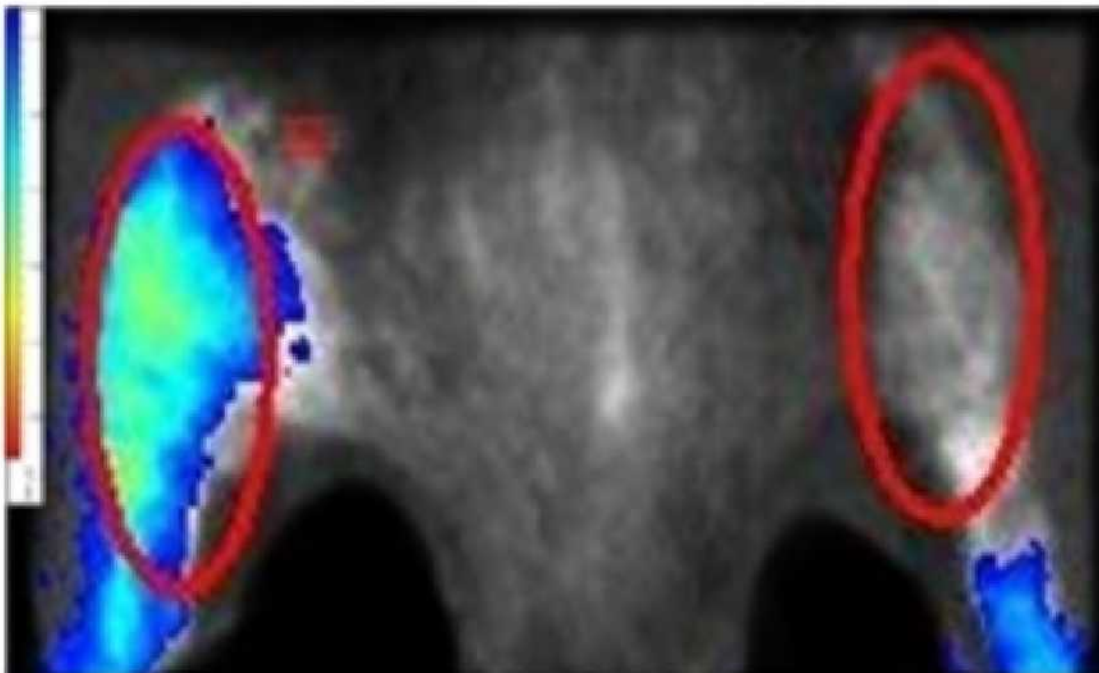


Fig. 1: Image of photon flux [photons s⁻¹cm⁻²sr⁻¹]. Fluorescence image was taken above 700 nm and autofluorescence-corrected. ROI (left: ligated; right: control) is used for calculating R.

Presentation Number **1090B**
 Poster Session 4d: Imaging Disease/Organ Processes

Small Animal Cardiac PET Imaging of Myocardial Blood Flow in Coronary Artery Ligation and Reperfusion

Kumiko C. Mackasey^{1,2}, *Stephanie Thorn*^{1,2}, *Miran Kenk*^{1,2}, *Myra A. Kordos*¹, *Jennifer M. Renaud*¹, *Ran Klein*¹, *Robert A. deKemp*¹, *Rob S. Beanlands*^{1,2}, *Jean N. DaSilva*^{1,2}, ¹*National Cardiac PET Centre, University of Ottawa Heart Institute, Ottawa, ON, Canada;* ²*Cellular and Molecular Medicine, University of Ottawa, Ottawa, ON, Canada. Contact e-mail: kmackasey@ottawaheart.ca*

Introduction: LAD ligation is a commonly used animal model of myocardial infarction (MI). In vivo imaging of receptor expression using PET is limited by tracer delivery to the infarct. Reperfusion following a transient ligation may allow tracer delivery. Using in vivo [¹³N]ammonia PET to assess myocardial blood flow (MBF), this work will show that ligation of the LAD for 3, 5 and 20 min followed by 2 week reperfusion produces no change to the area distal to the ligation. **Methods:** Male Sprague Dawley rats (n=6) were injected with 2.5-3 mCi of [¹³N]ammonia and scanned for 30 minutes to assess baseline MBF. For the transient ligation, a 6-0 suture was passed through the heart close to the proximal end of the LAD. Polypropylene tubing was placed on top of the artery and the suture was ligated around the artery and the tubing. The ligation was held in place for 3, 5 and 20 min and then released. MIs were performed on n=6 additional rats as positive controls. A follow-up [¹³N]ammonia scan was completed 1-2 weeks post-surgery. Dynamic images were reconstructed using OSEM3D/MAP ($\beta=1$). FlowQuant© automated analysis software and a 1-tissue-compartment model was used to create polar maps of MBF. **Results:** Blanching of the myocardium was observed after LAD ligation but disappeared upon release of the suture. Polar maps of reperfusion animals showed uniform flow throughout the heart and values (3.23 ± 0.51 mL/min/g) not significantly different to baseline (3.05 ± 0.38 mL/min/g). 1-2 weeks after permanent occlusion, decreased flow was observed in the infarcted area compared to baseline (1.53 ± 0.38 mL/min/g; $p<0.05$, t-test); while non infarcted regions displayed normal flow (2.63 ± 0.60 mL/min/g). **Conclusions:** LAD occlusion showed a decrease in MBF in the infarcted area, while ligation/reperfusion led to no change as assessed with [¹³N]ammonia PET. This model of transient LAD ligation followed by reperfusion will be used for in vivo serial measurements with PET radioligands to assess changes in the myocardium post injury.

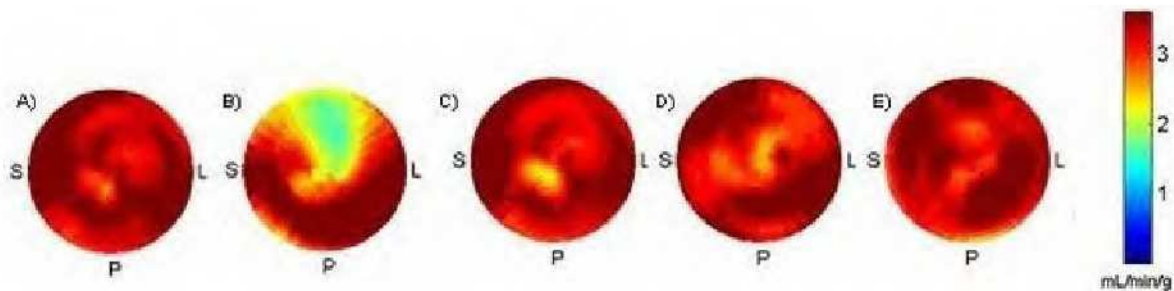


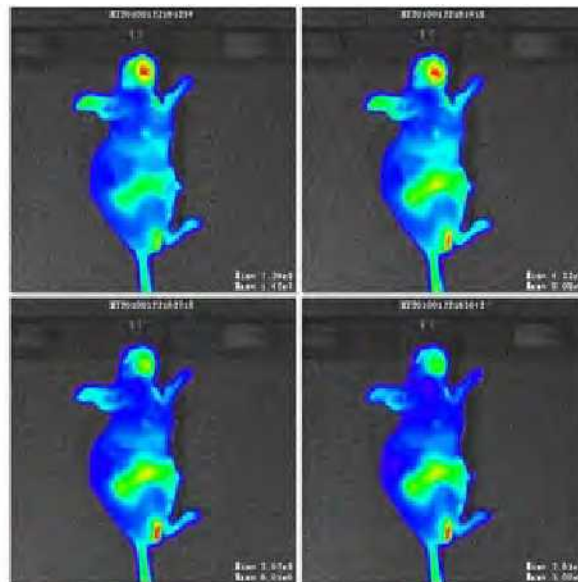
Figure: Polar maps of LV [¹³N] ammonia scans: Baseline flow (A), permanent occlusion with infarcted area (B), and transient ligation/reperfusion groups (C: 3min, D: 5min, E: 20min).

Presentation Number **1091B**
Poster Session 4d: Imaging Disease/Organ Processes

Non-invasive Detection of Angiogenesis of Mycobacterium Tuberculosis by Bioluminescent Imaging in Transgenic Mouse Models

Tao Huang, Baozhong Shen, Kezheng Wang, Lihong Bu, medical imaging center, Harbin, China. Contact e-mail: playno1@sina.com

Materials and Results: Tuberculosis (TB) is a major cause of morbidity and mortality. Angiogenesis is required for the progression of tuberculosis. Vasculature imaging is an attractive method for determining the efficacy of anti-tuberculosis therapy. The vascular endothelial growth factor-2 (VEGF-2) gene is transcriptionally regulated angiogenesis. Given that VEGFR2 plays such an important role in many aspects of blood vessel growth, it would be advantageous to monitor VEGFR2 gene expression noninvasively in real time in vivo in angiogenesis of mycobacterium tuberculosis. A transgenic mouse, Vegfr2-luc, in which a luciferase reporter is under control of the murine VEGFR2 promoter. We have discovered that the Vegfr2-luc model is useful to monitor VEGFR2 expression to angiogenesis of mycobacterium tuberculosis. Mycobacterium tuberculosis was injected into rat head. Angiogenesis in infections were seen until day 9 after injection. Bioluminescent signal was highest in day 14. And VEGFR2 gene expression was not founded until day 26. Optical imaging is an effective method for conducting longitudinal studies of mycobacterium tuberculosis in transgenic mouse models.



Presentation Number **1069B**
Poster Session 4d: Imaging Disease/Organ Processes

Pilot study of a Fab Fragment Targeting Oxidized LDL in a Mouse Model of Atherosclerosis Using *In Vivo* PET/CT and *Ex Vivo* Digital Autoradiography

Anders Orbom¹, Bo Jansson², Gunilla N. Fredrikson³, Anne Mette F. Hag^{4,5}, Henrik Hussein El-Al^{4,5}, Andreas Kjaer^{4,5}, Jan Nilsson³, Sven-Erik Strand¹, ¹Medical Radiation Physics, Lund University, LUND, Sweden; ²BioInvent International AB, Lund, Sweden; ³Clinical Science, Lund University, Malmö, Sweden; ⁴Cluster for Molecular Imaging, Faculty of Health Sciences, University of Copenhagen, Copenhagen, Denmark; ⁵Department of Clinical Physiology, Nuclear Medicine & PET, Rigshospitalet, Copenhagen, Denmark. Contact e-mail: anders.orbom@med.lu.se

Introduction As reported at last years WMIC (Orbom et al.), we have shown that an intact antibody against oxidized low-density lipoprotein (oxLDL) gave better contrast between atherosclerotic plaques and the aorta wall than ¹⁸F-FDG in *ex vivo* imaging of the aorta from Apobec-1^{-/-} LDLr^{-/-} mice. A more rapid uptake and clearance of the tracer would however be preferable and the aim of this study is to study the pharmacokinetics of a Fab fragment targeting a different epitope on oxLDL and compare it to ¹⁸F-FDG using *in vivo* micro-PET/CT imaging. **Methods** ApoE^{-/-} mice were fed western diet for 14 weeks to develop atherosclerosis. All food was removed the morning of the day of imaging. *In vivo* Imaging was done using small animal PET and CT systems with contrast agent given i.v. to visualize the aorta. Eight animals were given ¹⁸F-FDG and contrast and imaged 3 h p.i. for 30 min by PET plus CT. Five to seven days later the animals were given ¹²⁴I labeled anti oxLDL Fab fragments and CT contrast i.v., They were imaged at approximately 2 h p.i. (n=2), 4 h p.i. (n=3) and 15 h p.i. (n=3) for 40 min by PET plus CT. All animals were sacrificed after imaging between 15 and 24 h p.i. and the aorta was opened and mounted on a glass slide after fixation and taken for imaging with digital autoradiography using a double-sided silicon-strip detector. Following imaging, aortas were stained with Oil Red O and scanned. **Results** Images were successfully produced both from PET/CT and digital autoradiography. Analysis of the *in vivo* and *ex vivo* results is currently ongoing. We will present values for the uptake in the aorta for ¹⁸F-FDG as well as for the oxLDL specific Fab fragment.

Presentation Number **1060A**
Poster Session 2d: Imaging Disease/Organ Processes

Noninvasive measurements of cerebral metabolic rates of glucose in rats over time using microPET - a quality assurance study

Hsiao-Ming Wu^{1,2}, *Ilaria M. Brun del Re*³, *Richard L. Sutton*^{4,5}, *Neil G. Harris*^{4,5}, *Michael Phelps*^{1,2}, ¹*Molecular and Medical Pharmacology, University of California, Los Angeles, Los Angeles, CA, USA;* ²*Crump Institute for Molecular Imaging, University of California, Los Angeles, Los Angeles, CA, USA;* ³*Division of Laboratory Animal Medicine, University of California, Los Angeles, Los Angeles, CA, USA;* ⁴*UCLA Brain Injury Research Center, University of California, Los Angeles, Los Angeles, CA, USA;* ⁵*Neurosurgery, University of California, Los Angeles, Los Angeles, CA, USA. Contact e-mail: cwu@mednet.ucla.edu*

In this work, we reported our first experience in performing longitudinal (3 time points), noninvasive brain imaging in the surgically manipulated rats. Our purpose is to evaluate a noninvasive imaging technique for brain injury research. **Surgery:** Six adult male rats underwent sham injury without craniotomy. The animals were anesthetized with 2% isoflurane and a midline incision was made over the skull, and the skin, fascia and temporal muscles were reflected bilaterally. The tissue on skull over the left parietal cortex was scraped down and bleeding was minimized by applying bone wax. The incision was closed by suturing in 30 minutes. **PET scans:** Three microPET sessions were performed on each sham rat 2 days before (baseline), 2 days after and 9 days after the surgery. In addition, the baseline studies were performed on another 10 control rats. The plasma input functions were converted from the heart-image-derived whole blood curves obtained from the FADS method (Wu et al., 1996). Each PET session included a 45-minutes heart scan and a subsequent 30-minutes brain scan under 2% isoflurane immediately after a ~3mCi FDG tail-vein injection. Two minutes before the end of the heart scan, a ~100 μ L blood sample was taken from a tail vein for plasma glucose and the end-time FDG activity measurements. CT scans were performed for attenuation correction. **Data analysis:** The operational equation was used to calculate the cerebral metabolic rates of glucose (CMRG, μ mol/min/100g). The regional CMRG were estimated from the ROI data derived from the consecutive image planes (thickness: 0.8 mm) covering the frontal cortex (3 planes), parietal cortex (6 planes) and cerebellum (3 planes). **Results:** The baseline CMRG (e.g. the right parietal cortex (R): 46 \pm 8; the left parietal cortex (L): 43 \pm 8; n=16) were comparable to the reported CMRG (R: 44 \pm 6; L: 36 \pm 7; n=4) from the DG autoradiography acquired under similar experimental conditions. The CMRG increased globally 2 days after the surgery (e.g. R: 52 \pm 9 vs. 44 \pm 6, p>0.05; L: 50 \pm 7 vs. 41 \pm 6, p<0.05; n=6; Repeated measures analysis of variance). The CMRG (R: 42 \pm 7; L: 42 \pm 6) at 9 days after the surgery returned to the baseline CMRG. There was no significant difference (p>0.1; two-factor study with repeated measures) among the CMRG of the right and left cortex. **Conclusion:** Anesthesia used during PET scans suppressed the CMRG. However, the repeated measurements were reproducible and reflected the CMRG changes as expected. Noninvasive FDG-PET is a reliable tool to study a disease model of brain injury.

Presentation Number **1061A**
Poster Session 2d: Imaging Disease/Organ Processes

Posttraumatic hyperglycolysis was seen consistently in the FDG images of adult rats following traumatic brain injury

Hsiao-Ming Wu, ¹*Department of Molecular and Medical Pharmacology, University of California, Los Angeles, Los Angeles, CA, USA;*
²*Crump Institute for Molecular Imaging, University of California, Los Angeles, Los Angeles, CA, USA. Contact e-mail:*
cwu@mednet.ucla.edu

The acute (e.g. within hours) increase of regional cerebral metabolic rates of glucose (CMRG) is a hallmark of traumatic brain injury and has been demonstrated consistently in animal models autoradiographically. However, the posttraumatic hyperglycolysis seen in the severely injured or comatose patients has never been reported by this technique. Autoradiographic studies were often performed on the post-surgical (e.g. to cannulate a blood vessel) and body-restrained (e.g. to sample the blood) animals. We hypothesized that posttraumatic hyperglycolysis existed in the experimental animals but might have been masked by the increased neural activities due to the awareness, procedure-related pain and stress. In addition to the autoradiography, we studied the sedated (2% isoflurane; a neuroprotective agent), brain-injured rats using noninvasive quantitative FDG-PET imaging to monitor the regional CMRG changes following the controlled cortical impact injury (CCI). **Methods:** Six adult male rats underwent craniotomy and CCI with a pneumatic injury device. After the injury, the craniotomy site was covered by a small piece of gelform and the wound sutured closed. Three FDG-PET sessions were performed on 4 CCI rats 2 days before (baseline), 2 days after and 15 days after the surgery. Two FDG-PET sessions (baseline and 2 days post-injury) were performed on another 2 rats. Autoradiography of each rat was performed immediately after the last PET session. **Data analysis:** The parametric images of CMRG ($\mu\text{mol}/\text{min}/100\text{g}$) were generated from each PET study. The plasma input functions required by the CMRG calculation were converted from the heart-image-derived whole blood curves obtained from the FADS method (Wu et al., 1996). The regional CMRG were compared using the voxel analysis and the histograms generated from the CMRG parametric images. **Results:** The CMRG in cortex were reduced by ~50% under anesthesia. Two days post-CCI, high FDG uptakes were seen in the injured cortical epicenter and near the contusion. Fifteen days post-injury, high FDG uptakes were seen and extended to the ipsilateral subcortical regions, including thalamus and CA3 regions of the hippocampus. Voxel analysis of PET images showed similar patterns of spatial and temporal CMRG changes over time. **Conclusion:** The patterns of CMRG changes seen in the FDG-PET matched and mapped the regional and temporal changes of neuronal degeneration following traumatic brain injury in adult rats. It may serve as a useful quantifiable marker for assessing the pharmacological therapies after head injury.

Presentation Number **1062A**
Poster Session 2d: Imaging Disease/Organ Processes

Proton MR Spectroscopy of the Cerebellum and in Patients with Ataxia

Hung-Chieh Chen^{1,2}, Jiing Feng Lirng^{1,2}, Wan Yuo Guo^{1,2}, Hsiu-Mei Wu^{1,2}, Cheng-Yen Chang^{1,2}, ¹Department of Radiology, Taipei Veterans General Hospital, Taipei, Taiwan; ²School of Medicine, National Yang-Ming University, Taipei, Taiwan. Contact e-mail: hcchen8@vghtpe.gov.tw

Purpose: To investigate the value of proton magnetic resonance spectroscopy (MRS) in the patients with ataxia. **Material and Methods:** This prospective study recruited 143 patients with ataxia and 44 healthy control subjects. Single voxel proton MRS of bilateral cerebellar hemispheres, and vermis were performed. From the MRS several indexes including N-acetylaspartate/creatine (NAA/Cr), choline/Cr (Cho/Cr), and myo-inositol/Cr (ml/Cr) ratios were obtained. Final diagnosis of the patients were spinocerebellar ataxia (SCA) types 1, 2, 3, 6, 17 (N=80) and multiple systemic atrophy (MSA, N=63). Differences of the spectroscopic data among the patients of different types of SCA, MSA and healthy subjects were evaluated with the Mann-Whitney tests. Correlation between clinical disability score (scale for the assessment and rating of cerebellar ataxia, SARA) and spectroscopic data was performed by Spearman's rank test. **Results:** The cerebellar (cerebellar hemisphere and vermis) NAA/Cr ratio were all significantly lower in patients with different types of SCA and MSA as compared to healthy subjects, except for SCA type 6 ($p=.427$ and $.057$), which is the modest form of SCA. The cerebellar Cho/Cr ratio were significantly lower in different types of SCA and MSA, except for SCA types 3 ($p=.239$ and $p=.402$) and 17 ($p=.096$ and $p=.391$), indicating their white matter were better preserved. The cerebellar ml/Cr ratio was also significantly higher in patients with SCA type 2 ($p=.001$ and $p=.002$), SCA type 3 ($p=.002$ and $p=.001$), SCA type 17 ($p=.000$ and $p=.001$) and MSA ($p=.000$ and $p=.000$). Both cerebellar NAA/Cr ratio and cerebellar Cho/Cr ratio were significantly different between SCA and MSA. The cerebellar NAA/Cr ratio and Cho/Cr ratio showed a strong correlation with SARA (all $p < .01$). **Conclusion:** Many diseases present ataxia clinically but their prognoses are different. They are difficult to diagnose until advanced stage, even in hereditary type. MR spectroscopy is a useful early diagnostic tool for patients presenting with ataxia and correlated well with clinical disability score.

Presentation Number **1063A**
Poster Session 2d: Imaging Disease/Organ Processes

siRNA Probes for Stroke Therapy and Imaging

Marytheresa Ifediba, Zdravka Medarova, Anna Moore, Radiology, Massachusetts General Hospital, Charlestown, MA, USA. Contact e-mail: ifediba@nmr.mgh.harvard.edu

OBJECTIVE Neuroprotective approaches to ischemic stroke treatment have been ineffective clinically, due in part to inadequate delivery of therapeutics to injured brain cells. We propose to develop a siRNA-based probe imbued with cell translocation properties through complexation to blood-brain barrier permeable modified poly-arginine peptide (MPAP). Additionally we intend to enable direct monitoring of probe delivery by optical imaging by fluorescently labeling its peptide and siRNA components. We expect that in vitro testing of the probe will result in significant uptake by central nervous system cells and silencing of genes associated with increased tissue damage in cerebral ischemia models. **MATERIALS AND METHODS:** Probe synthesis involved the mixture and incubation of different stoichiometries of MPAP-Cy5.5 and siRNA-Cy3 directed against c-Src, a protein implicated in stroke damage, to optimize complexation of the two components. The resulting MPAP-siRNA probe was tested for serum stability and subsequently evaluated in vitro in primary neurons and astrocytes harvested from C57BL/6 mice. Probe internalization was assessed by flow cytometry and confocal microscopy, and effect on gene expression was evaluated by RT-PCR. **RESULTS** MPAP-siRNA probe was partially protected from serum nuclease degradation and was efficiently internalized by cells following 24-hour incubation (Figure 1). RT-PCR analysis of total mRNA from cells treated with MPAP-siRNA showed statistically significant reduction of endogenous c-src expression. Furthermore, internalized probe led to no significant increase in cytotoxicity. **CONCLUSION** We demonstrate the proof-of-principle that simple complexation techniques can be employed to produce a dual optical imaging and therapeutic probe. We believe that this technique will ultimately aid in managing stroke damage in vivo.

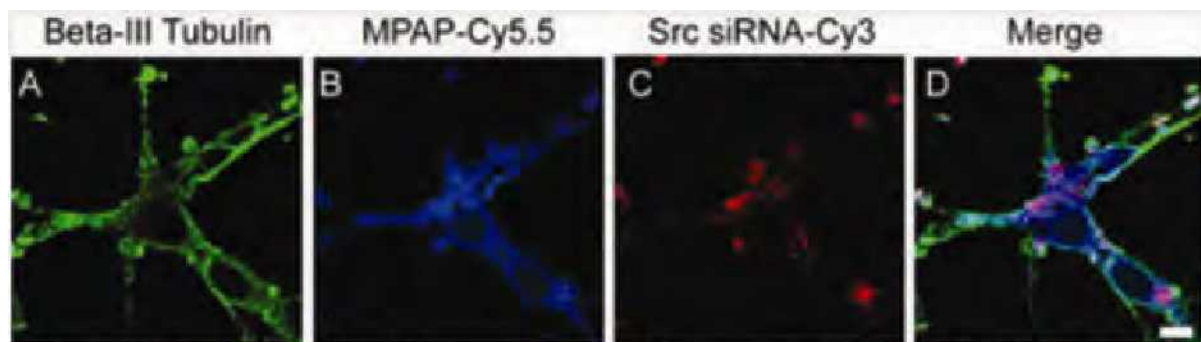


Figure 1. Confocal microscopy of primary neurons stained of neuron-specific marker beta-III tubulin (A). Neurons were incubated with MPAP-siRNA probe complexes consisting of 500 pmoles MPAP (B) and 100 pmoles siRNA (C). MPAP-siRNA was taken up by cells following 24-hour incubation (D). Scale bar = 10 μ m.

Presentation Number **1064A**
Poster Session 2d: Imaging Disease/Organ Processes

Fluorinated Benzofuran Derivatives for PET Imaging of β -Amyloid Plaques in Alzheimer's Disease Brains

Yan Cheng¹, Masahiro Ono¹, Hiroyuki Kimura¹, Shinya Kagawa², Ryuichi Nishii², Hidekazu Kawashima¹, Hideo Saji¹, ¹Department of Patho-Functional Bioanalysis, Graduate School of Pharmaceutical Sciences, Kyoto University, Kyoto, Japan; ²Shiga Medical Center Research Institute, Moriyama City, Japan. Contact e-mail: y.cheng@ky8.ecs.kyoto-u.ac.jp

Objective: Developing radiolabeled agents targeting β -amyloid plaques has provided a window of opportunity to improve the diagnosis of AD. In our study, a series of fluorinated benzofuran derivatives as potential tracers for positron emission tomography (PET) targeting β -amyloid plaques in the brains of patients with AD were synthesized and evaluated. **Method:** The derivatives were synthesized using an intramolecular Wittig reaction. The binding experiments were carried out with $A\beta(1-42)$ aggregates using 125I-IMPY as a radioligand. Biodistribution experiment was performed using ddY mice. In vitro autoradiographic imaging of [¹⁸F]5d was conducted with sections (10 μ m) of Tg2576 mouse brain and β -amyloid plaques were confirmed by thioflavin-S staining. In vivo plaque labeling with [¹⁸F]5d was conducted using Tg2576 transgenic mice and wild-type mice as an Alzheimer's model and an age-matched control, respectively. Ex vivo autoradiograms of brain sections were obtained after an i.v. injection of [¹⁸F]5d. **Results:** In experiments in vitro, all fluorinated benzofuran derivatives displayed high affinity for $A\beta(1-42)$ aggregates with Ki values in the nanomolar range. [¹⁸F]5d, in particular, labeled β -amyloid plaques in a section of Tg2576 mouse brain, and displayed high uptake (5.66%ID/g) at 10 min postinjection, sufficient for PET imaging. [¹⁸F]5d also labeled β -amyloid plaques clearly in APP transgenic mice and showed low background in the wild-type mice. **Conclusions:** We synthesized a series of fluorinated benzofuran derivatives which bind well to $A\beta(1-42)$ aggregates and clearly stain β -amyloid plaques. In vitro and ex vivo studies showed that [¹⁸F]5d labeled β -amyloid plaques clearly. Thus, these benzofuran derivatives provide novel PET tracers for imaging β -amyloid plaques in the brain, which are currently being evaluated for potential clinical use.

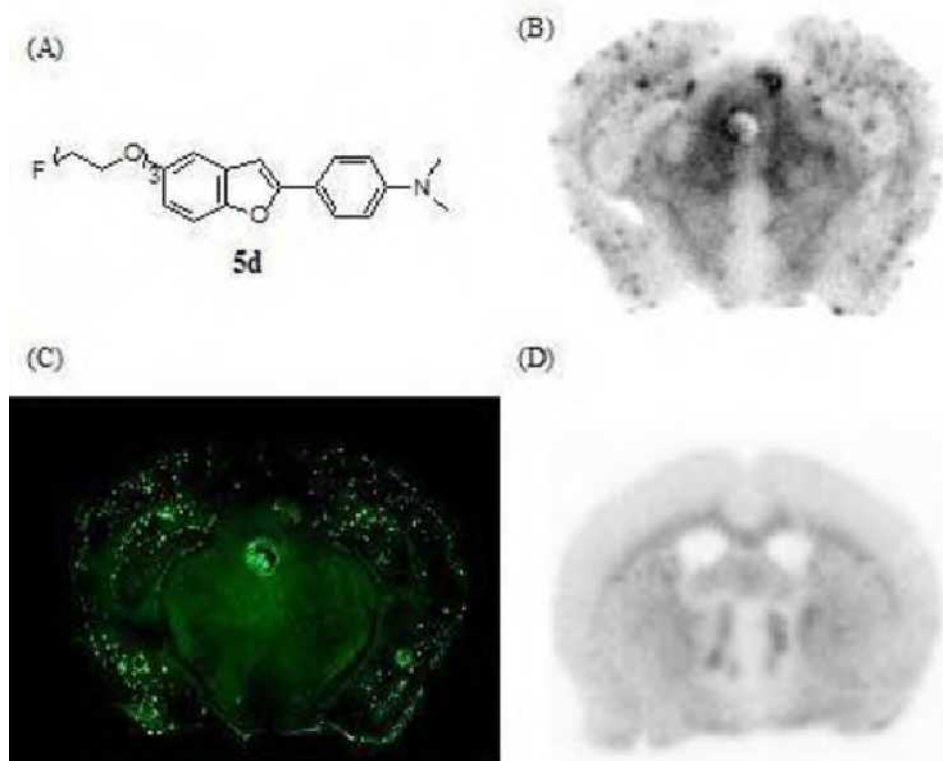


Figure 1. Labeling of β -amyloid plaques in vivo. (A) Chemical form of 5d. (B) Autoradiogram ex vivo with [¹⁸F]5d in a section of Tg2576 mouse brain. (C) Thioflavin-S staining in the same section as (B). (D) Autoradiogram ex vivo with [¹⁸F]5d in a section of wild-type mouse brain.

Presentation Number **1065A**
Poster Session 2d: Imaging Disease/Organ Processes

Functional brain imaging analysis by PET in frontotemporal lobar degeneration (FTLD) model mice

Hiroshi Mizuma¹, Kayo Onoe¹, Taiki Kambe², Yumiko Moto², Hirotaka Onoe¹, ¹RIKEN Center for Molecular Imaging Science, Kobe, Japan; ²Department of Neurology, Juntendo University School of Medicine, Tokyo, Japan. Contact e-mail: mizuma_hiroshi@riken.jp

Recently, we established a method of brain PET imaging in mouse under conscious condition. We assume that it opens new avenues to examine the functional brain imaging by measuring the regional cerebral glucose utilization with [¹⁸F]FDG, which detects regional neural dysfunctions in mouse models of various neurological disorders (e.g. dementia, depression). In this study, we applied for the first time to an imaging analysis using statistical parametric mapping (SPM) of [¹⁸F]FDG-PET in a mouse model of dementia. Tg601 mouse was developed as a model of frontotemporal lobar degeneration (FTLD), which was genetically modified by overexpressing the wild-type human tau protein (2N4R type) under CAMK-II promoter region. FTLD, one of dementia, is clinically characterized by memory impairment, behavioral abnormality, and/or aphasia. In postmortem study, neurofibrillary tangles related to the accumulation of abnormal tau protein were observed in frontal cortical region of FTLD patients. Similarly, Tg601 mice exhibited impaired memory and abnormal anxiety behavior, and showed highly expressed tau protein in neurons in the frontal cortical region in aged period. To clarify whether Tg601 mouse has a loss of regional neural activity, we conducted [¹⁸F]FDG-PET scan for 60 min under conscious condition. Mice were surgically attached a head-holder with dental cement at 1 week prior to the PET scan, and were acclimated to the environment of the experimental condition. SPM analysis was performed using mean SUV image (summed 30 to 60 min after injection of [¹⁸F]FDG) registered on the MR-T1 template image. We also evaluated morphological changes in the brain by immunohistochemical study of postsynaptic density protein (PSD-95) and Drebrin, postsynaptic markers. In Tg601 mice, glucose metabolism was significantly and focally low in the nucleus accumbens (NAc) as compared with that in wild-type mice in aged period ($P < 0.001$), but not in adult period. A synapse loss was also found in only in the NAc of aged Tg601 mice. These finding suggest that the neural dysfunction of NAc which occurred in the aged Tg601 mouse may be involved in the onset of behavioral abnormalities. We conclude that this method is useful for the functional analysis of gene-manipulated mice and for the biological assessment of drug developments.

Presentation Number **1066A**
Poster Session 2d: Imaging Disease/Organ Processes

Modeling glaucomatous neurodegeneration using diffusion tensor imaging

Takuya Hayashi^{1,2}, Masamitsu Shimazawa³, Yuta Inoguchi³, Yasushi Ito³, Hajime Yamanaka¹, Hidehiro Iida², Yasuyoshi Watanabe¹, Hideaki Hara³, Hirotaka Onoe¹, ¹RIKEN Center for Molecular Imaging Science, Kobe, Japan; ²National Cardiovascular Center Research Institute, Osaka, Japan; ³Gifu Pharmaceutical University, Gifu, Japan. Contact e-mail: takuya.hayashi@riken.jp

Prediction of neurodegenerative process is requisite when trying to modify the disease progress. A critical point lines in a model by which we predict how neurons will degenerate when exposed to the risk. A classical interpretation has its basis on a deterministic model in which the neurodegeneration, once initiated, proceeds with an elapsed time at a rate faster than in normal-aging. A more elaborated interpretation has its basis on a stochastic model, whereby neurons degenerate as random events at a probability upon the risk, such as aggregation of neurotoxic molecules. By using diffusion tensor imaging (DTI), we here measure *in vivo* microstructural integrity in animals of glaucomatous neurodegeneration, and show that the kinetics of degrading integrity can be explained by the stochastic model upon the risk, increased intra-ocular pressure. We used five macaque monkeys of glaucomatous neurodegeneration. Glaucoma is known to involve a pathology in which axons of retinal ganglion neurons degenerate due to chronic increase in intra-ocular pressure (IOP) and dysregulated aqueous-fluid circulation. The glaucomatous neurodegeneration was made by surgically inhibiting the aqueous-fluid absorption using laser-photocoagulation of trabecular meshwork and was repeatedly measured the IOP, the risk of glaucomatous pathology. We also performed DTI for *in vivo* assessment of the microstructural integrity in the white matter. We followed up glaucomatous animals from 33 to 168 days after laser-photocoagulation, during which we measured FA and IOP repeatedly. The FA values in the glaucomatous optic nerve measured by DTI were decreased with elapsed time after laser-photocoagulation. This was the same when the FA values of affected optic nerve were expressed as a ratio relative to those in the contralateral non-affected nerve. The deterministic model explained the variance of relative FA values at a coefficient of determination (R^2) of 0.36 ($P < 1.0 \times 10^{-4}$). In contrast, the stochastic model, by calculating the cumulative risk (time-integral of the increase in IOP), better explained the variance of relative FA values ($R^2 = 0.87$, $P < 1.0 \times 10^{-7}$) than in the deterministic model. Our findings indicate that the neurodegeneration proceeds probabilistically upon the risk. This indicates that the process of neurodegeneration is virtually independent among neurons. The model may help to predict the neurodegeneration by identification and repeated measurement of the risk, e.g. using a recently-advanced imaging technique for bio-markers that label neurotoxic molecules.

Presentation Number **1067A**
Poster Session 2d: Imaging Disease/Organ Processes

Fluorescent Real Time Imaging of APP β -secretase (BACE1) Activity in Live Cells

Ke Zhan, Hexin Xie, Jessica Gall, Jianghong Rao, Radiology, Stanford University, Stanford, CA, USA. Contact e-mail: kezhan@stanford.edu

Alzheimer's disease (AD) is an age-related, slowly progressive neurodegenerative disease that leads to specific, degenerative changes in a number of central nervous system (CNS) neuronal populations. A substantial amount of evidence indicates A β is a significant cause of these disease. A β is generated from a sequential proteolysis of amyloid precursor protein (APP). BACE1 (β -site of APP cleaving enzyme 1), also known as β -secretase, initiates the cleavage of APP at the β site mainly in early endosomes, followed by γ -secretase cleavage to produce the A β peptide. BACE1 activity has been the focal point in Alzheimer research for the past decade because of its pivotal role in the A β production pathway. Recent studies indicate that the majority of Alzheimer cases are sporadic, meaning they are not associated with familial mutations in APP or γ -secretase, but rather with increased amount and activity of BACE1. Thus for the purpose of monitoring the production and aggregation of A β in the CNS in order to understand and diagnose the onset and progression of AD, we have successfully developed a BACE1 biosensor for live imaging of BACE1 activity in living cells. This probe aims specifically at the proteolytic process of APP by BACE1. The 12-amino acid probe backbone sequence is derived from the BACE1 cleavage site at APP with point mutations that optimizes BACE1 cleavage efficiency. Fluorophore and specific quencher were added on both N- and C- termini followed by a coupled sterol moiety for plasma membrane anchoring. Our results show that this cell-penetrating, activatable BACE1 activity biosensor increases its fluorescent intensity up to 20 fold by BACE1 cleavage, and penetrates cell membrane and internalizes into early endosomes within 15 min at 37 °C. At 1 μ M concentration, this probe is able to distinguish between cells that have elevated BACE1 and cells that have basal level of BACE1 activity. Cytotoxicity assay demonstrated that this probe is biocompatible and does not cause cell death. Our work advances Alzheimer's disease research as well as molecular imaging technology into the sub-cellular localization resolution with the real time quantification capability. This new type of biosensor opens the door to diagnosing the early onset of neurodegeneration in AD, and monitoring the environmental factors that affect APP amyloidogenic processing in vivo. It has also paved the road towards a venue in which amyloid production and accumulation could be imaged in real time.

Presentation Number **1068A**
Poster Session 2d: Imaging Disease/Organ Processes

Follow up study of amyloid positive and negative MCI with 11C-PiB PET

Suzuka Ataka¹, **Hiroyuki Shimada**¹, **Takami Miki**¹, **Yasuhiro Wada**², **Kazuhiro Takahashi**², **Yasuyoshi Watanabe**², ¹*geriatrics and neurology, osaka city university graduate school of medicine, Osaka, Japan;* ²*RIKEN center for Molecular Imaging Science, Kobe, Japan. Contact e-mail: suzuka126@med.osaka-cu.ac.jp*

Background: Patients with mild cognitive impairment (MCI) represent an important clinical group as they are increased risk of developing Alzheimer disease (AD). PiB positive MCI patients are suggested more likely to convert to AD than PiB negative patients in some previous studies. Objective: To assess the rates of conversion of MCI to dementia during 1.5-2 years follow-up period and to compare levels of amyloid deposition between MCI converters and nonconverters. Methods: Nineteen subjects (Male:5, Female:14 Age: 73±7) with MCI with baseline 11C-PiB PET and neuropsychological examination have been clinically followed up for 1.5 to 2 years. PiB binding was calculated using the Logan graphical analysis method in regions-of-interest to yield regional distribution volume ratio (DVR) with cerebellar gray matter as reference. We used the mean cortical DVR value as an index of amyloid accumulation. Results: Nine of the 19 MCI patients converted to AD (MCI-convert=MCI-c). Seven of 19 MCI patients showed cognitive decline but not fulfilled with Dementia criteria (MCI-progressive=MCI-p). Three MCI patients have no cognitive decline (MCI-stable=MCI-s). Fourteen of 19 (73%) MCI patients have higher PiB retention and five are PiB negative. Eleven of the 14(78%) PiB positive MCIs converted to AD or showed cognitive decline. All five PiB negative MCIs converted to AD or showed cognitive decline. These five PiB negative MCIs had not increased PiB retention during follow-up period. Conclusions: PiB positive MCI subjects are not more likely to convert to AD than PiB negative MCI patients. We suggested that both PiB positive MCIs and PiB negative MCIs have similar risk of convert to dementia. These PiB negative MCIs might be preclinical non AD type dementia which is so called PiB negative dementia that we have been reported in previous study. Further studies are needed to clarify clinical significance of PiB-PET to detect amyloid deposition for the evaluation of the preclinical stage of AD. This work was partly supported by KAKENHI (19390307)(21613007).

Presentation Number **1069A**
Poster Session 2d: Imaging Disease/Organ Processes

Novel fluorescent imaging evaluation of blood-brain-barrier permeability on stroke rat animal model

Jun-ming Shih, Yung-Ruei Huang, Kang W. Chang, Shih-Ying Lee, Chia-Chieh Chen, Institute of Nuclear Energy Research, Taoyuan County, Taiwan. Contact e-mail: jmshih@iner.gov.tw

Purpose : We used Evans blue dye to evaluate the BBB permeability in SD stroke rat animal model by detecting fluorescent signals with IVIS Imaging System. This study attempts to acquire images of the change of BBB permeability on stroke rat brain after occlusion. **Material& method:** SD rats were used in this study. Transient focal ischemia was induced by occlusion of the right middle cerebral artery (MCA). Evans blue dye in saline was injected intravenously at 24 hours after MCA occlusion and allowed to circulate for 15 minutes. Rats were anesthetized and transcardially perfused to remove the intravascular dye. The brain were obtained and taken pictures, then put into the chamber of IVIS 100(Caliper). Evans blue dye content was evaluated by IVIS 100 at an excitation wavelength of 620 nm and emission wavelength of 680 nm. **Result:** Stroke rats injected intravenously with Evans blue, leakage of the dye into right hemisphere parenchyma was observed at 24 hr after ischemia. Fluorescent signals were detected on the same side of ischemia compared with left hemisphere. Merging the optical and fluorescent images, the data strongly demonstrated that the fluorescent signals of the dye were co-localized with the occlusive region, indicated that ischemia disrupt BBB permeability and Evans blue leak into brain tissue and distribute in infarct area. **Conclusion:** We successfully established the platform to evaluate the BBB permeability of brain tissue on stroke rat by using novel fluorescent technique. Our platform make it possible to detect exactly where BBB was not in the integrity by merging the optical and fluorescent images.

Presentation Number **1070A**
Poster Session 2d: Imaging Disease/Organ Processes

Influence of propofol anesthesia on regional functional state of brain serotonin transporter; PET study with [¹¹C]DASB in macaque monkeys

*Hajime Yamanaka, Kayo Onoe, Chihiro Yokoyama, Hirotaka Onoe, RIKEN, Center for Molecular Imaging Science, Kobe, Japan.
Contact e-mail: hajimey@riken.jp*

Propofol, an intravenous anesthetic, is often used when light surgical procedures are required. However, several psychological effects such as mood-alteration, hallucination, euphoria, and psychomotor dysfunctions have been also reported. Although propofol acts as a positive modulator of gamma-aminobutyric acid (GABA) A receptor, its actions on other neurotransmissions in the brain are still unclear. Serotonin is involved in several psychological functions, of which abnormalities have been implicated in a wide variety of neuropsychiatric disorders. In this study, we examined whether propofol influences the regional functional states of the serotonin transporter (SERT) in macaque monkey brain using positron emission tomography (PET) technique with [¹¹C]DASB, a specific PET tracer for SERT. Four male adult rhesus monkeys (*Macaca mulatta*) were studied by PET under both conscious and propofol anesthetized (10~20 mg/kg/h, i.v.) conditions. Parametric images of binding potential (BP) were generated by the two-parameter linearized reference tissue model 2 (MRTM2). Regional differences in BP values between consciousness and propofol anesthesia were analyzed by voxelwise statistical parametric mapping (SPM08). Test-retest variability was also investigated in two conditions. While k₂ showed poor reproducibility (variability 36.5%) under propofol anesthesia, BP values calculated using k₂ value obtained from the corresponding scan represent high reproducibility (variability 17.2%). By the SPM analysis, significant increases of BP value were observed in the prefrontal cortex (PFC), anterior cingulate cortex (ACC), insular cortex (Ins), and putamen (Pu) ($P < 0.001$, uncorrected for multiple comparisons). The result indicates that propofol alters the brain serotonergic neural activities by affecting functional states of SERT in the PFC, ACC, Ins, and Pu, which could be involved in its psychological effects.

Presentation Number **1071A**
Poster Session 2d: Imaging Disease/Organ Processes

PET imaging of neurogenic inflammation with [¹¹C]PK11195 in the rat model of migraine

Yilong Cui¹, Misato Takashima-Hirano², Tadayuki Takashima³, Kaori Okuyama¹, Miho Shukur⁴, Emi Hayashinaka³, Yasuhiro Wada³, Hisashi Doi², Hirota Onoe⁴, Yasuyoshi Watanabe³, Yosky Kataoka¹, ¹Cellular Function Imaging Laboratory, RIKEN Center for Molecular Imaging Science, Kobe, Japan; ²Molecular Imaging Labeling Chemistry Laboratory, RIKEN Center for Molecular Imaging Science, Kobe, Japan; ³Molecular Probe Dynamics Laboratory, RIKEN Center for Molecular Imaging Science, Kobe, Japan; ⁴Functional Probe Research Laboratory, RIKEN Center for Molecular Imaging Science, Kobe, Japan. Contact e-mail: cuiyl@riken.jp

Migraine is a recurring neurological disorder characterized by unilateral, intense, and pulsatile headaches. The neurogenic inflammation triggered by extravasation of plasma protein has been hypothesized to be a key process of pain sensation of migraine. In order to evaluate the neurogenic inflammation in the migraine etiology, we focused on the microglia, which is a principal immune cell responding to such an inflammatory process in the central nervous system. Using positron emission tomography (PET) imaging with [¹¹C]PK11195, a PET ligand for peripheral type-benzodiazepine receptor which is well known to be up-regulated in the activated microglia, we evaluated the neurogenic inflammation in the rat brain after generation of unilateral cortical spreading depression (SD), a stimulation used for making an experimental animal model of migraine. Here we provide a new line of evidence that 1) a significant increase in brain uptake of [¹¹C]PK11195, which was completely displaceable by excess amounts of unlabeled ligands, was observed in the ipsilateral hemisphere of the SD-generated rats, 2) binding potential for [¹¹C]PK11195 in the SD-generated rats was significantly higher compared to that in the sham-operated control rats, 3) predominant microglia activation in the ipsilateral cerebral hemisphere was also confirmed by immunohistochemical study. These results suggest that as an inflammatory reaction, microglia are activated in response to the nociceptive stimuli induced by cortical SD in the rat brain. Therefore, the [¹¹C]PK11195-PET technique could be a useful tool for diagnostic and therapeutic monitoring of neurological disorders related to neuroinflammation such as migraine.

Presentation Number **1072A**
 Poster Session 2d: Imaging Disease/Organ Processes

Datscan Quantification Images - Attempt For Normal Reference Values

Guilhermina Cantinho^{1,2}, **Helena Pena**^{1,2}, **Sergio Figueiredo**¹, **Pedro Gonçalves**¹, **Fernando Godinho**^{1,2}, ¹Atomedical, SA, Lisboa, Portugal; ²Instituto de Medicina Nuclear, Faculdade de Medicina de Lisboa, Lisboa, Portugal. Contact e-mail: gcantinho@atomedical.pt

Aim: 123I-FP-CIT is an important tool in the investigation of movement disorders. The images analysis is qualitative by visual assessment. In borderline cases or when assessment of disease progression is required, quantification of the imaging data is important. Quantification involves the differentiation of normal and abnormal distribution, based on the striatum and the occipital cortex uptake mean counts' ratios. No normal ranges are currently available. We tried to obtain our own normal references. **Material & Methods:** We evaluated 53 patients, submitted to SPECT 180 minutes after e.v. 210-230 MBq 123I-ioflupane, rotation 360°, matrix 128X128, 60+60 views, 35 s/view. FBP reconstruction with Butterworth filter, frequency 0.4 and power 8, was applied. For quantification, we used 5 ROIs: 2 for the caudate, 2 for the putamen and one for the occipital cortex. Each region's counts result from the mean counts of the 3 consecutive slices with highest uptake. The mean counts and two sets of indexes were obtained. The non-specific uptake index (NSUI) is the ratio between the caudate as well as the putamen (right and left separately) and the occipital cortex mean counts. The specific uptake index (SUI) is obtained by each striatum region minus the occipital cortex, divided by the occipital cortex mean counts. Each index was compared with the visual analysis, according to the classification of normal or abnormal studies, considering the four striatum regions (uptake level and striatum's morphology). **Results:** There is a 100% correlation between NSUI and SUI in all cases (SUI=NSUI-1). We obtained a mean NSUI <2.1 and <1.8 on abnormal caudates and putamens. There were no significant differences between left and right indexes in normal or abnormal bilateral cases (p>0.7). In studies classified with asymmetrical abnormalities, we found significant differences between left and right indexes (p<0,00005) [tables]. **Conclusions:** Visual assessment of 123I-ioflupane SPECT images is easily performed to evaluate striatum's dopamine transporters uptake. Our results show significant differences between normal and abnormal studies. This helps as a second insight in difficult studies and allows patients follow-up. The two indexes analyzed methods don't show differences in the separation of the two populations, which makes the choice of the method unimportant, as long as the same method is adopted and reported.

NSUI Caudate and Putamen (mean±dp)

	Normal Caudate	Abnormal Caudate	p	Normal Putamen	Abnormal Putamen	p
Left	2.73±0.73 (n=42)	2.09±0.61 (n=11)	0.0096	2.32±0.51 (n=19)	1.71±0.45 (n=34)	0.000002
Right	2.62±0.77 (n=36)	2.17±0.63 (n=15)	0.0222	2.46±0.61 (n=23)	1.62±0.53 (n=30)	0.000008

Presentation Number **1073A**
Poster Session 2d: Imaging Disease/Organ Processes

Tractography in a Saporin Alzheimers Disease Mouse Model

Marianne D. Keller¹, Georg Kerbler², Adam S. Hamlin², Ian Brereton¹, Elizabeth J. Coulson², ¹Centre for Advanced Imaging, The University of Queensland, St. Lucia, QLD, Australia; ²Queensland Brain Institute, The University of Queensland, St. Lucia, QLD, Australia. Contact e-mail: m.keller@uq.edu.au

Loss of cholinergic basal forebrain neurons (cBFN) is an early and key feature of Alzheimer's disease. Early detection of this neurodegeneration will be critical for the timely treatment of this disease including improving efficacy of the currently prescribed acetylcholine esterase inhibitors. The aim of this study was to determine if cBFN loss could be detected using MR tractography in a mouse model. A widely used marker of cBFN is the p75 neurotrophin receptor. To selectively ablate cBFN in mice, animals were injected i.c.v. with the ribosomal inactivating protein saporin conjugated to either a p75 antibody (mu-p75-SAP, 0.4µg), or to a rabbit IgG (IgG-SAP; Advanced Targeting Systems). Five, 14 or 35 days following saporin injections groups of mice were perfused. The formalin-fixed brains were imaged in a 700MHz wide bore Bruker system at 100µm isotropic resolution. A 3D DTI (30 directions) sequence, (TR/TE=400ms/22.3 ms) NEX=1 was used. Diffusiontoolkit and trackvis were used for postprocessing of DTI images to selectively measure the of septal-hippocampal cBFN projections. Following imaging, brains were sectioned at 40µm and choline acetyltransferase, p75 and parvalbumin immunohistochemistry were performed to determine the extent and specificity of the lesion. In mice injected with mu-p75-SAP, the number of streamlines decreased significantly over the 5 week experiment, suggesting a degeneration of cBFN axons. In contrast, the number and integrity of septo-hippocampal streamlines of IgG-SAP injected animals were consistent across groups. The streamline number of corpus collosal axons, which are not expected to be targeted by the p75 antibody, were found to be unchanged between mu-p75-SAP and IgG-SAP conditions. Our findings were validated by histology, with mu-p75-SAP producing a specific lesion of up to 50% of BFCN in the medial septum, vertical and horizontal limbs of the diagonal band of broca, and significant loss of terminal projections in the hippocampus and prefrontal cortex in both 14 and 35 day mu-p75-SAP treatment groups. This study demonstrates that a 50% loss of cBFN can be detected by measuring the streamlines of the septo-hippocampal tracts, despite this representing only an ~25% loss of all septo-hippocampal axons. Our study further demonstrates the feasibility of using an MRI technique to image cholinergic basal forebrain degeneration in vivo which might be utilised as an early diagnostic of onset of Alzheimer disease. Acknowledgments Queensland Government Smart Futures NIRAP(Australia)

Presentation Number **1074A**
 Poster Session 2d: Imaging Disease/Organ Processes

In vivo use of fluorescently and radiolabeled single chain antibody fragments for the detection of A β in an Alzheimer's disease mouse model

Rob Nabuurs^{1,2}, **Kim Rutgers**⁴, **Mick Welling**^{1,2}, **Maaïke de Backer**^{1,2}, **Mark A. van Buchem**^{1,2}, **Silvere van der Maarel**⁴, **Louise van der Weerd**^{1,3}, ¹Radiology, LUMC, Leiden, Netherlands; ²Molecular Imaging Laboratories Leiden, LUMC, Leiden, Netherlands; ³Anatomy & Embryology, LUMC, Leiden, Netherlands; ⁴Human Genetics, LUMC, Leiden, Netherlands. Contact e-mail: r.j.a.nabuurs@lumc.nl

Introduction Single chain antibody fragments (V_HH) were selected against A β . Selection yielded V_HH targeting all human brain A β deposits (2H) or specifically only vascular deposits (3A).¹ Their size, high specificity, and possible blood-brain barrier (BBB) passage² makes them promising tools for early detection of A β deposits in vivo. Here we studied biodistribution and ability to detect A β in vivo in AD mice. **Materials&Methods** Following direct radiolabeling of V_HH 3A and 2H, aged APP-PS1 mice and wildtype littermates were injected i.v. with $\pm 2.0 \mu\text{g}$ 99mTc-labeled V_HH. Affinity was not affected by labeling conditions. At t=1-3-6-24h four Tg and four Wt animals were sacrificed. Blood, urine and various organs including brain and cerebellum were excised, weighed and counted for radioactivity. For blood clearance, 2 μl blood samples were collected at several time points up to 3hr. BBB was disrupted with carotid injection of 600 μl 15% mannitol in PBS mixed 100 μl of Alexa594-2H at 60 $\mu\text{l}/\text{min}$. 2hrs p.i. animals (n=4) were perfused/fixated and brain sections were stained with ThT or immunofluorescent antiA β . **Results & Conclusion** For both 99mTc-labeled V_HHs, blood clearance was slower in Tg compared to Wt mice. Compared to 3A, 2H had a slower clearance in all genotypes. Clearance occurred via the kidneys and urine. At t=24, 2H brain uptake in Tg was slightly higher. Other time points showed no apparent brain uptake for either the animals or the V_HHs. Following BBB disruption, Alexa594-2H detects A β plaques in vivo confirmed by ThT and immunostaining. (fig.1) Although thus far no specific in vivo BBB passage has been determined, both V_HHs show good affinity to allow in vivo detection of A β and possibly differential detection of vascular and parenchymal deposits in humans. Further research is ongoing to develop clinical labeling strategies combined with improved brain delivery of these V_HHs. ¹Rutgers Neurobiol.Aging(2009) ²Rutgers (submitted) This research was supported by the Center for Translational Molecular Medicine (LeARN).

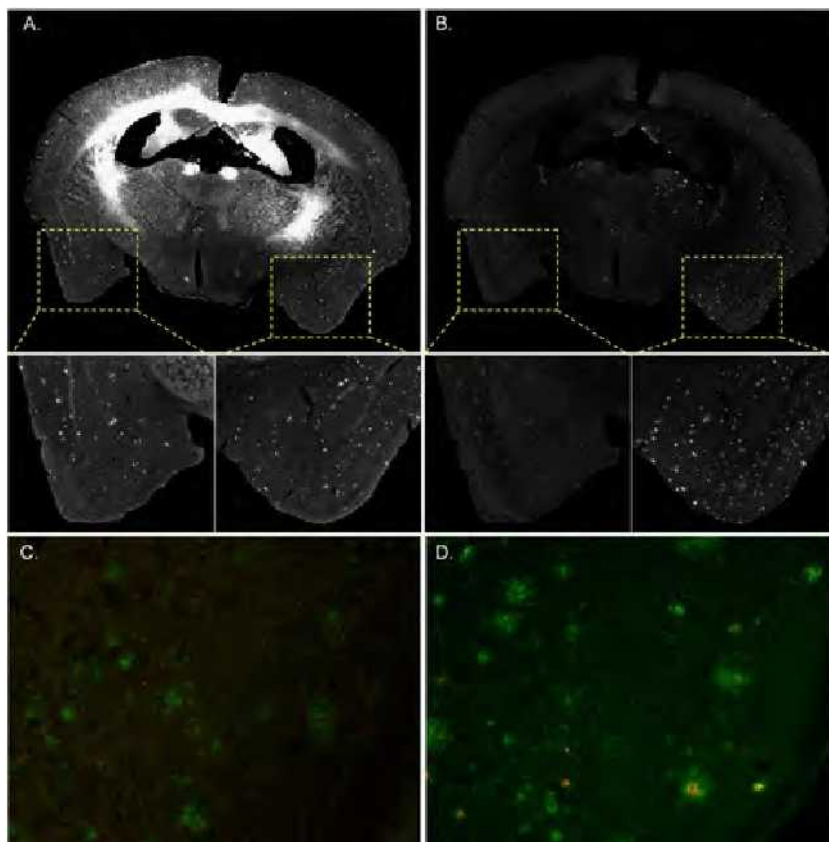


Figure 1. Following BBBd with 15% mannitol coinjected with Alexa594-2H into the right carotid artery of an aged APP-PS1 mouse, amyloid plaques are clearly depicted in both hemispheres using a ThT staining (A), while the Alexa594 signal is only detected in the right hemisphere (B). More careful shows all Alexa594 signal colocalizes with ThT in the right hemisphere, while in the left shows only autofluorescence. Furthermore, immunofluorescence A β staining of the plaques within the left hemisphere (C) results only in green signal, while within the right hemisphere the red signal from Alexa594-2H nicely colocalizes within the plaques.

Presentation Number **1075A**
 Poster Session 2d: Imaging Disease/Organ Processes

In vivo NIR imaging of amyloid- β deposits in APP-PS1 mice: a spatial-temporal and lifetime profile of AOI987

Rob Nabuurs^{1,4}, Ivo Que^{2,4}, Alan Chan⁵, Guobin Ma⁶, Clemens Lowik^{2,4}, Louise van der Weerd^{1,3}, ¹Radiology, LUMC, Leiden, Netherlands; ²Endocrinology, LUMC, Leiden, Netherlands; ³Anatomy & Embryology, LUMC, Leiden, Netherlands; ⁴Molecular Imaging Laboratories Leiden, LUMC, Leiden, Netherlands; ⁵Percurus B.V., Enschede, Netherlands; ⁶ART Advanced Research Technologies, Montreal, QC, Canada. Contact e-mail: r.j.a.nabuurs@lumc.nl

Introduction Alzheimer's disease (AD) is a disorder characterized by extracellular amyloid- β (A β) deposits that are increasingly found in the demented brain. This makes it an attractive target for optical imaging and for therapy monitoring. A number of NIR dyes, e.g. AOI987¹, have been developed for use in vivo. However, the low plaque-to-background contrast, due to non-specific binding and slow washout, has meant that planar optical imaging does not give a complete window into the disease. New whole animal NIR imaging systems are now available that include 3D volume and lifetime measurements. In this study, we looked at whether such systems could yield additional data on the in vivo properties of NIR probes, in AD. **Method** Six 12-14 month old APP-PS1 mice (Tg) and six wildtype (Wt) littermates were injected i.v. with 150 μ l saline, with/without 0.1mg/kg AOI987, and imaged in groups of 4 at t=5h and t=24h at 670nm laser excitation (Optix MX3, ART, Canada). A pre-injection scan was obtained for one animal. Some mice were extinguished and 30 μ m brain sections were stained with Thioflavin T to confirm the presence of A β plaques. Intensity and lifetime ROI images were determined and 3D volume was reconstructed using MatLab. **Results & Conclusion** Consistent with previous reports¹, signal intensity was indeed higher in Tg mice compared to Wt. (fig.A) 3D reconstructed images confirmed this spatially, where significantly more AOI987 was detected in the Tg mice.(fig.C) Also fluorescence lifetime differed significantly between Tg and Wt genotypes(fig.B), which indicates different binding properties of AOI987. Moreover, the higher lifetime in Tg mice may reflect binding specificity of the dye to A β plaques. Thus in vivo lifetime measurements may provide a more sensitive parameter in distinguishing bound from unbound probe and therefore a better indicator of A β load. Furthermore, time domain lifetime measurements also established that binding of AOI987 decreased significantly between t=5h and t=24h. This confirmed earlier findings that showed AOI987 was washed out within 24h.¹ We thank Novartis/ART for the gift of AOI987 and the loan of the MX3. ¹Hintersteiner 2005

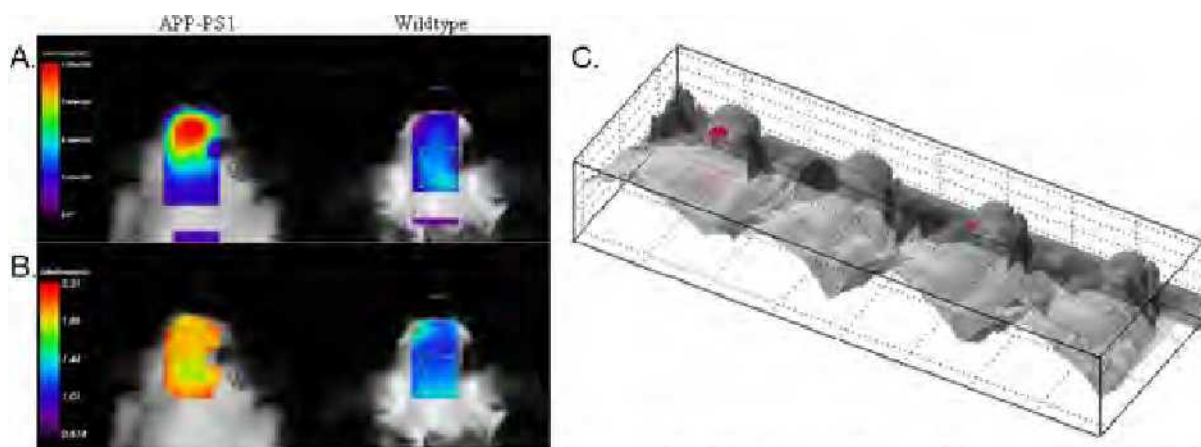


Figure A. Raw signal intensities of APP-PS1 and wildtype littermate 5hrs following i.v. injection of 0.1 mg/kg AOI987 with their associative lifetime images shown in **B**. Corresponding 3D reconstruction images of this group including the transgenic and wildtype controls are shown in **C**.

Presentation Number **1076A**
Poster Session 2d: Imaging Disease/Organ Processes

Comparative assessment of two novel 18 kDa translocator protein (TSPO) ligands ^{18}F -PBR111 and ^{18}F -PBR102 after excitotoxin-induced acute neuroinflammation

Paul D. Callaghan, Catriona Wimberley, Gita L. Rahardjo, Paula Berghofer, Tien Pham, Tim Jackson, David Zahra, Thomas Bourdier, Naomi Wyatt, Ivan Greguric, Filomena Mattner, Christian Loch, Marie-Claude Gregoire, Andrew Katsifis, ANSTO Life Sciences, ANSTO, Kirrawee, Sydney, NSW, Australia. Contact e-mail: pcn@ansto.gov.au

Objective: Quantify the in vivo binding of two novel TSPO ligands, ^{18}F -PBR111 and ^{18}F -PBR102 and compare the binding potential with in vitro assessment of TSPO density and microglial activation in a rodent model of acute neuroinflammation. Methods: Acute neuroinflammation was assessed 7 days after unilateral stereotaxic administration of (R,S)-a-amino-3-hydroxy-5-methyl-4-isoxazolopropionique (AMPA) in anaesthetised adult Wistar rats (326±7g, mean±SEM) (1). Anaesthetised rats were implanted with a femoral arterial canula then injected with a low mass of ^{18}F -PBR111 (0.12±0.03 nmol) or ^{18}F -PBR102 (0.09±0.01 nmol) and dynamic images acquired over 60 minutes using an INVEON microPET/CT camera. Another population of rats underwent the same PET protocol, after a pre-treatment with a saturating mass of the same cold compound (1mg/kg). Arterial blood was sampled during imaging, allowing pharmacokinetic determination of radiotracer concentration. Plasma activity concentration-time curves were corrected for unchanged tracer based on metabolic characterisation experiments in a separate cohort of Wistar rats (radiometabolites by HPLC, TLC and SPE analyses). Binding potential values of each ligand were assessed for the two cohorts of lesioned animals, using both Simplified Reference Tissue Model (as in [1]) and a two-compartment fit using the arterial parent compound concentration, coupled with results from the pre-saturation cohort. Post mortem confirmation of microglial activation was assessed with OX-42 immunohistochemistry on unfixed frozen sections, with consecutive sections assessed using Fluorjade C staining (neurodegeneration) and ^{125}I -CLINDE autoradiography (PBR density). Results: In vivo: BP as assessed by both methods did not show any significant results between the two compounds. The BP values obtained for ^{18}F -PBR111 and ^{18}F -PBR102 are respectively 5.28±1.7 and 4.68±1.21. In vitro: Discrete lesions were localised to rostrocaudal striatum in all subjects. No differences were seen in the ipsilateral:contralateral striatum TSPO specific binding ratios between ^{18}F -PBR111 and ^{18}F -PBR102 groups (7.0±0.8 vs. 8.6±0.1 respectively). We will also report the full correlation between the in vivo BP and the in vitro ratios). Conclusion: We could not find any significant difference between our compounds in this rodent model. However, we have showed that our two compounds are highly specific of TSPO expressed in microglial activation after excitotoxic lesions. 1. Van Camp et al., Eur J Nucl Med Mol Imaging. 2010, 37:962-72

Presentation Number **1077A**
Poster Session 2d: Imaging Disease/Organ Processes

Antipsychotic-induced mental side effects and their relationship to dopamine D2 receptor occupancy in striatal subdivisions: A high resolution PET study with [¹¹C]raclopride

Jong-Hoon Kim¹, **Young-Don Son**², **Sang-Yoon Lee**², **Young-Bo Kim**², **Zang-Hee Cho**², ¹*Psychiatry, Gachon University of Medicine and Science, Incheon, Republic of Korea;* ²*Neuroscience Research Institute, Gachon University of Medicine and Science, Incheon, Republic of Korea. Contact e-mail: jhnp@chol.com*

Background: The subjectively experienced mental adverse effects of antipsychotics have been well known since their introduction into clinical practice; however, the precise mechanism is still unclear. In the present study, we comprehensively examined the relationship between antipsychotic-induced mental side effects and dopamine D2 receptor occupancy in striatal subdivisions using high resolution positron emission tomography (PET) instrumentation with [¹¹C]raclopride to better characterize the neurochemical mechanism underlying these adverse effects. **Materials and Methods:** Twenty-five schizophrenic patients receiving stable doses of atypical antipsychotics for at least 2 weeks and 25 age- and gender-matched normal controls completed an MRI on a 3-Tesla scanner and a high resolution PET scan with [¹¹C]raclopride to measure D2 binding potential in the striatum. The D2 receptor binding potential (BP_{ND}) was calculated using a Logan graphical analysis and receptor occupancy was calculated as the percentage reduction of receptor BP_{ND} with drug treatment relative to baseline. The data obtained from age- and gender-matched normal controls, using the same PET and MRI protocols, were used as an estimate of the patients' unmedicated baseline, as previously proposed. Patients' psychopathology and adverse drug effects were comprehensively evaluated. Antipsychotic-induced subjective side effects were assessed using the Liverpool University Neuroleptic Side Effect Rating Scale (LUNSERS). **Results:** The LUNSERS total score was significantly positively associated with D2 receptor occupancy in the ventral striatum (VST) ($r=0.42$, $P<0.01$) and pre-commissural dorsal caudate (preDCA) ($r=0.35$, $P=0.02$). The mental side effects as assessed by the psychic side effect subscale of the LUNSERS were significantly positively associated with D2 receptor occupancy in the VST ($r=0.35$, $P=0.02$). **Conclusion:** The results of the present study suggest that the mental adverse effects of antipsychotics are significantly and specifically associated with D2 receptor blockade in the ventral portion of the striatum, which is considered to play a crucial role in reward and motivation. Considering the significant negative impact of mental side effects on drug compliance, future drug development may focus on antipsychotics with a different mechanism of action. **Acknowledgments:** This work was supported by the Korea Science and Engineering Foundation (KOSEF) grant funded by the Korea government (MEST) (No. 2009-0075839).

Presentation Number **1078A**
Poster Session 2d: Imaging Disease/Organ Processes

Imaging diagnosis of Parkinson's disease using FMT-PET

Junichi Saitou, Toshihiko Sato, Utsunomiya Central Clinic, Utsunomiya, Japan. Contact e-mail: junichi_saitou@ucc.or.jp

Purpose Parkinson's disease is thought to be caused by decrease of dopamine or dopaminergic neurons in the substantia nigra. Levodopa (L-dopa) is one of the effective therapeutic agents for the disease. It is metabolized into dopamine with aromatic L-amino acid decarboxylase (AADC), and dopaminergic nerves have high activity of AADC. However, its efficacy is weakened as the disease progresses, because AADC gradually decreases in activity. 6-[¹⁸F] fluoro-meta-tyrosine (FMT) is an analogue of dopa and has affinity to AADC as well as L-dopa. The purpose of this study is to establish imaging findings of Parkinson's disease. Materials and methods We performed 3-tesla MRI upon patients with Parkinson's disease and normal volunteers, and excluded the cases with basal ganglia abnormalities such as infarction or hemorrhage. After that, we performed FMT-PET upon 20 cases of Parkinson's disease patients (male:10,female:10) and 10 cases normal volunteers.(male:5,female:5) We injected Carbidopa intravenously to each case to prevent accumulation except brain. Sixty minutes after that, we injected FMT intravenously. We performed scanning 80 minutes after FMT injection. We also classified the patient's stages according to Hoehn-Yahr's classification, and examined the correlation with the imaging appearances. Accumulation is evaluated by putamen/cerebellum ratio with software (Putamen Analyzer). Result 20 out of 20 cases with Parkinson's disease (100%) demonstrated decreased accumulation of bilateral basal ganglia, whereas 10 out of 10 normal volunteers (100%) ,good accumulation. Symmetrical and asymmetrical decrease of accumulation had good correlation with the symptom. The decrease of the accumulation had tendency to correlated with Hoehn-Yahr's classification. Conclusion FMT-PET is useful for diagnosis of Parkinson's disease.

Presentation Number **1079A**
Poster Session 2d: Imaging Disease/Organ Processes

Activity-related Changes in Brain HDAC using [¹⁸F]FAHA PET in Rats and Monkeys

Ryuichi Nishii¹, **Hiroshi Mizuma**², **Shinya Kagawa**¹, **Akiko Tachibana**², **Kazuhiro Takahashi**², **Hajime Yamanaka**², **Tatsuya Higashi**¹, **Juri G. Gelovani**³, **Hirota Onoe**², ¹Division of PET Imaging, Shiga Medical Center Research Institute, Shiga, Japan; ²RIKEN Center for Molecular Imaging Science, Kobe, Japan; ³Department of Experimental Diagnostic Imaging, University of Texas MD Anderson Cancer Center, Houston, TX, USA. Contact e-mail: nishii@shigamed.jp

Purpose: We have investigated activity-related changes of brain PET imaging with or without anesthesia, and have reported the importance of brain PET imaging under physiological conscious condition (*J. Nucl. Med.*, *in press*). 6-([¹⁸F]fluoroacetamide)-1-hexanoicanilide ([¹⁸F]FAHA), an analog of suberoylanilide hydroxamic acid (SAHA), is known as a novel PET probe of histone deacetylase (HDAC). In order to study the functional role of HDAC in the central nervous system, we try to perform the in vivo brain imaging of PET with [¹⁸F]FAHA in rats and monkeys under the conscious and anesthetized states. Methods: [¹⁸F]FAHA was synthesized according to the method developed in our group with high specific activity (>2 Ci/μM). Brain dynamic PET-imaging with [¹⁸F]FAHA was performed for 60 min in rats (Wistar, 8 weeks of age) and monkeys (Macaca mulatta, 6 years of age). Brain HDAC activity measured by PET under the conscious condition was compared with that under the condition of propofol (10 mg/kg/hr, i.v.) or ketamine (3.3 mg/kg, i.m.) anesthesia. We also conducted [¹⁸F]FDG PET imaging to monitor brain activity. Results: [¹⁸F]FAHA specifically accumulated in the rat brain by blocking [¹⁸F]FAHA uptake using SAHA. We here examined the influence of consciousness level on HDAC activity in brain measured by PET with [¹⁸F]FAHA. By either propofol or ketamine anesthesia, standardized uptake value (SUV) of [¹⁸F]FAHA in the brain was 20-30% higher than that under the conscious condition, while SUV of [¹⁸F]FDG was low compared with that under conscious condition. Conclusion: We have performed PET imaging with [¹⁸F]FAHA and [¹⁸F]FDG under conscious and anesthetized conditions, and results suggest the neural activity related changes in the HDAC activity of the brain in rats and monkeys.

Presentation Number **1080A**
Poster Session 2d: Imaging Disease/Organ Processes

[¹¹C]PIB Shows Increased Binding in the Brain of the Transgenic APP23 Mice Even With Modest Specific Radioactivity

Annina Pakkanen¹, Johanna Rokka¹, Francisco Lopez¹, Gianluigi Forloni³, Mario Salmona², Olof Solin¹, Juha Rinne¹, Merja Haaparanta-Solin¹, ¹Turku PET Centre, University of Turku, Turku, Finland; ²Department of Molecular Biochemistry and Pharmacology, Mario Negri Institute for Pharmacological Research, Milan, Italy; ³Department of Neurosciences, Mario Negri Institute for Pharmacological Research, Milan, Italy. Contact e-mail: aepakk@utu.fi

PET imaging of transgenic mouse models of Alzheimer's disease (AD) is valuable for the pre-clinical evaluation of novel anti-amyloid pharmaceuticals and their effects on ongoing amyloidogenesis in the brain. [¹¹C]Pittsburgh Compound B ([¹¹C]PIB) is a β -amyloid (A β) binding PET imaging agent, used to detect amyloid deposits in AD patients. However, transgenic mouse PET imaging has shown promising results only with [¹¹C]PIB with very high specific radioactivity (>200GBq/ μ mol at the time of injection). We performed a longitudinal PET imaging study using [¹¹C]PIB to evaluate its in vivo binding to A β in the brain of the APP23 mouse model of AD. The detection of mouse amyloid with [¹¹C]PIB with modest specific radioactivity and relatively young animals was considered unlikely based on previously published results. Two APP23 mice were imaged with [¹¹C]PIB repeatedly, one at the age of 7 and 12 months, the other at 7, 12 and 15 months. An additional evaluation at 18 months is yet to be performed for the second mouse. The specific radioactivity of [¹¹C]PIB at the time of injection ranged from 20 to 85 GBq/ μ mol and injected masses from 50 to 160 ng. Dynamic 60 minutes PET scans were performed for isoflurane anesthetized mice using an Inveon Multimodality PET/CT -scanner and an injected dose of 8.2 \pm 2.3 MBq. Tracer uptake in and clearance from the whole brain, frontal cortex, neocortex, and cerebellum was investigated using the cerebellum as a reference region. At 12 months, one mouse was sacrificed and ongoing A β deposition evaluated using thioflavin-S staining and immunohistochemistry. The frontal cortex-to-cerebellum radioactivity ratio of [¹¹C]PIB measured from the last imaging frame (50-60 min) was elevated from 0.9 and 1.2 (7 months) to 1.1 and 1.3 (12 months), and finally to 1.6 (15 months). In C57BL/6N wild-type mice, the ratio at 50-60 min was 1.1 (n=2). At 12 months, A β deposits were detected in the brain using the two staining techniques. Our study continues with a larger number of animals and different transgenic strains to further evaluate the binding potential of [¹¹C]PIB to mouse amyloid.

Presentation Number **1081A**
Poster Session 2d: Imaging Disease/Organ Processes

Evaluation of serotonin dynamics in the brain of functional somatic syndrome using positron emission tomography

Kei Mizuno¹, Kayo Takahashi¹, Kazunari Tominaga², Chikako Tsumoto², Suzuka Ataka³, Yasuyoshi Watanabe^{1,4}, ¹Molecular Probe Dynamics Laboratory, RIKEN Center for Molecular Imaging Science, Kobe, Japan; ²Department of Gastroenterology, Osaka City University Graduate School of Medicine, Osaka, Japan; ³Department of Geriatrics and Neurology, Osaka City University Medical School, Osaka, Japan; ⁴Department of Physiology, Osaka City University Graduate School of Medicine, Osaka, Japan. Contact e-mail: keimizuno@riken.jp

The term functional somatic syndrome has been applied to several related syndromes characterized more by symptoms, suffering, and disability than by consistently demonstrable tissue abnormality. These syndromes include chronic fatigue syndrome (CFS) and functional dyspepsia (FD). Symptoms common to the functional somatic syndromes include fatigue; weakness; sleep difficulties; visceral pain; headache; muscle aches and joint pain; and cognitive problems. Although these common symptoms are partly associated with serotonergic neurotransmitter system, common or different serotonin dynamics in the brain between the CFS and FD patients are unclear. Thus, we investigated the serotonin dynamics in the brain of the CFS and FD patients by using positron emission tomography (PET). We previously reported that the density of serotonin transporters in the brain, as determined by using [¹¹C]-(+)-6beta-(4-Methylthiophenyl)-1,2,3,5,6alpha,10beta-hexahydropyrrolo[2,1-a]isoquinoline ([¹¹C](+)McN5652), was significantly reduced in the rostral subdivision of the anterior cingulate in the CFS patients as compared with that in healthy volunteers (Yamamoto, S. et al., 2004). Recently, we investigated the density of serotonin transporters in the brain of the FD patients, as determined by using [¹¹C]-3-amino-4-(2-dimethylaminomethyl-phenylsulfanyl)-benzonitrile ([¹¹C]DASB). Binding potentials of [¹¹C]DASB of the thalamus and midbrain in the FD patients were significantly higher than those in the healthy volunteers. In addition, the binding potentials of the central gray of midbrain in the healthy volunteers and FD patients were well correlated with score of pain derived from gastrointestinal symptom rating scale. These results suggest that depletion of the serotonin release of the FD patients is induced in order to palliate the pain. These PET studies demonstrate the difference of serotonin dynamics in the brain regions between CFS and FD patients.

Presentation Number **1082A**
Poster Session 2d: Imaging Disease/Organ Processes

Development of genetic methods to image dynamic structural and functional changes in the mammalian blood brain barrier in health and disease

Dritan Agalliu¹, Axel Nimmerjahn^{2,3}, Ahmet Arac⁴, Mark Schnitzer^{2,3}, Ben A. Barres¹, ¹Neurobiology, Stanford University, Stanford, CA, USA; ²Biological Sciences, Stanford University, Stanford, CA, USA; ³Applied Physics, Stanford University, Stanford, CA, USA; ⁴Neurosurgery, Stanford University, Stanford, CA, USA. Contact e-mail: dagalliu@stanford.edu

The endothelial cells in the Central Nervous System (CNS) form a barrier to blood-borne molecules that is essential for CNS function by three mechanisms: a) presence of tight junctions (TJs); b) a small number of caveolae with a low rate of transcytosis; and c) passive and active transporters. Abnormalities in blood brain barrier (BBB) permeability are found in many CNS diseases such as stroke or multiple sclerosis. However, it is unclear which structural components of the BBB are predominantly affected in various CNS diseases with a compromised BBB function. Furthermore, since BBB undergoes rapid changes in permeability in response to CNS insults, it has been difficult to correlate the timing and extent of BBB structural changes with its functional impairment during disease progression. To address these questions, we have generated two novel lines of transgenic mice that label two components necessary for BBB integrity namely, TJs and caveolae. These mice express either the fusion protein green fluorescent protein eGFP with Claudin5, an essential component of the BBB TJs, or the red fluorescent protein pmKate2 with Caveolin1, a transmembrane protein present in caveolae, under the control of the Tie2 promoter in all endothelial cells. We have imaged TJs in CNS endothelium of Tie2p::eGFP::Claudin5 transgenic mice using a two-photon laser microscope and combined it with injection of fluorescently-labeled molecular tracers, to correlate structural changes in TJ protein localization within the CNS endothelium with diffusion of tracers across the BBB. We have found that TJs are very stable structures in the CNS endothelium of healthy transgenic mice and the tracers are retained within the CNS capillaries. We have also examined the structural integrity of TJs in transgenic mice that have undergone middle cerebral artery occlusion, a mouse model for stroke. We have found that, although BBB functional integrity is impaired in stroke, TJs seem very stable at least within 24 hours post-lesion. We plan to use this imaging method to analyze dynamic changes in TJs and BBB permeability in the Experimental Allergic Encephalomyelitis (EAE), the mouse model for multiple sclerosis. We also plan to image the Tie2::pmKate2::Caveolin1 transgenic mice and analyze changes in the rate of transcytosis in CNS capillaries with BBB permeability during disease progression either in stroke or in the EAE mouse model. This will allow us to elucidate the mechanisms that impair the structural and functional BBB integrity during various CNS diseases and develop therapies to restore it.

Presentation Number **1083A**
Poster Session 2d: Imaging Disease/Organ Processes

In Vivo Dual Isotope SPECT to Determine Brain Trauma Extent in Mice

Domokos Mathe¹, Krisztian Szigeti¹, Katalin Fekete², Ildiko Horvath¹, Zoltan Benyo², ¹Nanobiotechnology&In Vivo Imaging Centre Faculty of Medicine Semmelweis University, Budapest, Hungary; ²Human Physiology Exp. Clinical Medicine, Faculty of Medicine Semmelweis University, Budapest, Hungary. Contact e-mail: krisztian.szigeti@eok.sote.hu

We applied dual isotope SPECT/CT in detecting and quantifying the extent of mouse blood-brain barrier disruption. Methods: Mice were subjected to a standardized freezing method transcranially. We imaged 5 hours post trauma. We used a dedicated, quantitative multiplexed multipinhole SPECT imaging system. X-ray CT of brain was also performed together with SPECT data acquisition. We applied ^{99m}Tc-DTPA to detect the disruption of the BBB. Blood perfusion of the brain was assessed using ^{99m}Tc-HMPAO. ²⁰¹Tl was used to track K⁺ uptake changes quantitatively. ²⁰¹Tl ions were taken up by brain tissues by means of diethyl-dithiocarbamate (DDC) complex that redistributes to ionic ²⁰¹Tl after being taken up. Uptake volumes (in mm³) and lesion radioactivities (in kBq) were quantified in treated mice (n=5 per group) and a non-treated group. Besides imaging of single tracers (3 groups), multi-channel imaging was used in two other groups of mice having received ^{99m}Tc-DTPA plus ²⁰¹Tl-DDC or, ^{99m}Tc-HMPAO plus ²⁰¹Tl-DDC. Histological control of the brain trauma size and localization was performed. Results: The uptake of ^{99m}Tc-DTPA correlated well with the size and localization of the lesion whereas the cold spot of the lesion at the perfusion image was evident in all animals having received ^{99m}Tc-HMPAO. When comparing with ²⁰¹Tl-DDC images, a penumbra was seen, especially in the animals imaged with ^{99m}Tc-HMPAO and ²⁰¹Tl-DDC simultaneously. The area of non-active glial and neuronal potassium uptake was significantly larger than the non-perfused area. SPECT/CT identified the dislocation of brain due to increased intracranial pressure in all treated animals. Conclusions: In vivo whole-animal imaging using quantitative SPECT is a very promising method to dissect different activation patterns and regulation of different mechanisms behind the events following neurotrauma. Using a unique dual-isotopic approach to detect multiple events in the same time in the same animals, the size and presence of a penumbral region could be identified. Acknowledgement: We are grateful for Dr. Jürgen Goldschmidt (Magdeburg) and Roberto Pasqualini (Orsay) for valuable advice and kind hints in ²⁰¹Tl-DDC application and preparation. References: Goldschmidt et al. NeuroImage 49 (2010) 303-315

Presentation Number **1084A**
Poster Session 2d: Imaging Disease/Organ Processes

Potential PET Imaging Agents for Early Diagnosis of Alzheimer's Disease

YoungSoo Kim, Dong Jin Kim, Life/Health Division, Korea Institute of Science and Technology, Seoul, Republic of Korea. Contact e-mail: yskim@kist.kr

Alzheimer's disease (AD) is a neurodegenerative brain disorder accompanying progressive memory loss and decline of cognitive functions. At present, clinical diagnosis of AD is performed via mental status tests, physical exam, diagnostic tests, neurological exam, and brain imaging. In this study novel chemical probes for beta-amyloid-specific binding agents is described. Twelve compounds were synthesized and evaluated via a competitive binding assay with [(125)I]TZDM against beta-amyloid 1-42 (Abeta42) aggregates. Two new [(18)F]-labeled isoindole derivatives were synthesized and evaluated as potential beta-amyloid imaging probes based on the in vivo pharmacokinetic profiles. The preliminary results suggest that these probes are promising positron emission tomography (PET) imaging probes for studying accumulation of Abeta fibrils in the brains of AD patients.

Presentation Number **1060B**
Poster Session 3d: Imaging Disease/Organ Processes

Evaluation of Fluorescence Proteins for Study of Tuberculosis in-vitro and in Live Animals

Ying Kong¹, *Suat L. Cirillo*¹, *Ali R. Akin*², *Kevin P. Francis*², *Jeffrey D. Cirillo*¹, ¹*Texas A&M Health Science Center, College Station, TX, USA;* ²*Caliper Life Sciences, Alameda, CA, USA. Contact e-mail: ykong@medicine.tamhsc.edu*

Tuberculosis is one of the leading causes of mortality worldwide. The slow growth of *Mycobacterium tuberculosis*, the causative agent of tuberculosis, hinders development of rapid diagnostics, novel therapeutics and improved vaccines for the eradication of tuberculosis. The ability to use non-invasive real-time imaging technologies to monitor the disease process in live animals would facilitate research on pathogenesis by tuberculosis, efficacy of anti-tuberculosis therapies and vaccines. We cloned six fluorescent proteins, designated tdTomato, mCherry, mPlum, mKate, Katushka and mKeima, into mycobacteria under the control of either a mycobacterial Hsp60 or L5 promoter, and compared their signal strength for in-vitro and in-vivo quantification of bacteria. We were able to use fluorescent proteins to obtain real-time images of pulmonary *Mycobacterium* infections in living mice and rapidly determine the number of bacteria present during disease. This system also allowed efficacy testing for rifampicin and isoniazid therapy in-vitro and in-vivo. The potential for rapid therapeutic efficacy testing was demonstrated by differences observed in treatment groups as early as 24 h post-treatment. Application of fluorescent proteins to detection and imaging of tubercle bacilli demonstrates that these reporters represent a valuable tool for the rapid evaluation of therapeutics, vaccines and virulence in mycobacterial research.

Presentation Number **1061B**
Poster Session 3d: Imaging Disease/Organ Processes

Significant differences in migration properties of ovalbumin (OVA) specific-Th1 cells into OVA-B16- and B16-melanomas due to the mode of T cell administration

Christoph M. Griessinger¹, Kerstin Fuchs², Ralph Meyer¹, Daniel Bukala¹, Susanne Kaesler², Martin Röcken², Bernd J. Pichler¹, Manfred Kneilling², ¹Department of Radiology, Eberhard Karls University Tübingen, Laboratory for Preclinical Imaging and Imaging Technology of the Werner Siemens-Foundation, Tübingen, Germany; ²Department of Dermatology, Eberhard Karls University Tübingen, , Tübingen, Germany. Contact e-mail: christoph.griessinger@med.uni-tuebingen.de

Tumor-associated-antigen (TAA)-specific interferon-gamma producing CD4⁺ T cells (Th1) play an important role in upcoming T cell based immunotherapy of cancer. Besides TAA-cytotoxic T cells, TAA-Th1 cells can deploy strong antitumoral effects. Until now only little is known about the migration behaviours of TAA-Th1 cells and the basic mechanisms of tumor rejection. The first goal of our study was to investigate the migration properties of Cy5-labelled OVA-specific Th1 cells in B16-melanoma and OVA-B16-melanoma bearing C57/Bl6 mice by optical imaging (OI). A second goal was to analyse the dependency of the OVA-Th1 cell administration routes (intravenous (i.v.) versus intra-peritoneal (i.p.)). We intra-cutaneously injected 2E+05 B16-melanoma cells into the left flank and 2E+05 OVA-B16-melanoma cells into the right flank of C57Bl/6 mice. CD4⁺ T cells were isolated from the spleens and lymph nodes of OVA-T cell receptor transgenic (OT-2) C57Bl/6 mice, and cultured together with irradiated antigen presenting cells, OVA peptide, CpG-oligonucleotide 1668, anti-IL-4, and IL-2 for 12-14 days to generate a Th1 phenotype. OVA-Th1 cells were labelled intracellular with Cy5 vibrant dye solution for 2 minutes. 1E+07 Cy5-labelled OVA-Th1 cells were injected i.p. or i.v. into littermates four days after melanoma-inoculation and investigated in vivo by OI on the following 4 consecutive days. We sacrificed mice on day 4 after OVA-Th1 cell administration for ex vivo OI-investigation and flow cytometric (FACS) analysis of the OVA-B16-melanomas, B16-melanomas, lymph nodes, spleen, thymus, and other organs of interest. We detect a strong accumulation of the OVA-Th1 cells in lymph nodes, thymus and the tumours after i.p. administration, but not after i.v. administration. Almost no OVA-Th1 cell migration was observable into lymph nodes and tumors four days after i.v. administration. Intra-venous administered OVA-Th1 cells predominantly accumulated in the lung, spleen and liver. OI data were confirmed by FACS analysis. Surprisingly, we could not detect specific migration of OVA-Th1 cells into OVA-B16-tumors for both administration routes. Our data indicate that it is necessary to reveal suitable administration routes for T cell based immunotherapy as treatment success might be dependent on the location and nature of the tumor. Future experiments will focus on Th1 cell-based treatment schemes for B16 melanomas. Also, we will compare the results in the B16 tumor model to the RIP1-Tag2 mouse model where the i.v. administration of Tag-Th1 cells was more effective.

Presentation Number **1062B**
Poster Session 3d: Imaging Disease/Organ Processes

Bioluminescent Mouse Models for Monitoring NF-kappaB Activation in the Lungs and Effect of Therapeutic Agents on Disease Progression

Ning Zhang, Dan Ansaldi, Ed Lim, Ali R. Akin, Jae-Beom Kim, Kevin P. Francis, Mark Roskey, Raj Singh, Caliper Life Sciences, Alameda, CA, USA. Contact e-mail: ning.zhang@caliperls.com

NF-kappaB activation is a critical signaling event of inflammation and has been indicated under a number of pathological conditions of lung diseases, including asthma, chronic bronchitis, and chronic obstructive pulmonary disease (COPD). Intervention of this pathway may hold promises to clinical therapy of these diseases. To enable assessment of NF-kappaB activity in the lungs, we established a mouse model through delivery a luciferase based NF-kappaB reporter to the lung tissues. NF-kappaB activation can be monitored through bioluminescent imaging of the transfected mice, allowing sensitive quantification of the response kinetics to inflammatory stimuli. Using this model, we validated NF-kappaB activation in a TNFalpha mediated acute response. We were able to observe a dose dependent induction of NF-kappaB activity in the lungs. In an LPS induced experimental COPD model, induction of NF-kappaB activity in the lungs correlated with phagocyte accumulation in the bronchoalveolar lavage. Further assessment of this model for examining NF-kappaB activation will include Streptococcus pneumonia mediated acute exacerbations of chronic bronchitis as well as the effect of NF-kappaB inhibitor and antibiotic treatment on disease progression.

Presentation Number **1063B**
Poster Session 3d: Imaging Disease/Organ Processes

In vivo ¹⁸F-Fluoromisonidazole (FMISO) PET-Imaging Confirms Therapeutic Inhibition of Hypoxia by Methylene Blue-treatment in a Small Animal Model of Rheumatoid Arthritis

Kerstin Fuchs^{1,2}, **Stefan Wiehr**², **Gerald Reischl**³, **Martin Röcken**¹, **Bernd J. Pichler**², **Manfred Kneilling**¹, ¹Department of Dermatology, Dermatology, Eberhard Karls University of Tuebingen, Tuebingen, Germany; ²Departement of Radiology, Laboratory for Preclinical Imaging and Imaging Technology of the Werner Siemens-Foundation, Eberhard Karls University of Tuebingen, Tuebingen, Germany; ³Department of Radiology, Radiopharmacy, Eberhard Karls University of Tuebingen, Tuebingen, Germany. Contact e-mail: kerstin.fuchs@med.uni-tuebingen.de

Auto-antibodies against Glucose-6 phosphate-isomerase (GPI) induce arthritis in mice that closely resembles human rheumatoid arthritis (RA). Angiogenesis and hypoxia play a major role in organ-specific autoimmune diseases such as GPI triggered arthritis. Hypoxia induces angiogenesis via stabilization of the transcription factor hypoxia inducible factor (HIF)-1 α and induction of pro-angiogenic mediators. The aim of our study was to analyze whether inhibition of hypoxia may minimize inflammation, angiogenesis and joint destruction in GPI-arthritis. Methylene blue (Mb), a derivate of hemoglobin should inhibit hypoxia by interfering the nitric oxide activation synthase pathway and inhibition of nitric oxide synthase and guanylate cyclase. In experiments, we injected GPI-serum or control-serum in BALB/c mice to induce joint inflammation. We started daily Mb-treatment (0,23mg/kg body weight (BW)) or sham-treatment (PBS) two days later. To investigate effects of Mb-treatment we measured ankle swelling and hypoxia in arthritic joints by [¹⁸F]FMISO and PET. Additionally we analyzed mRNA expression of HIF-1 α /2 α , pro-angiogenic, and pro-inflammatory mediators as well as H&E-, and pimonidazol-stained slices of arthritic- and healthy joints. Mb-treatment significantly suppressed GPI-arthritis and protected mice from angiogenesis, pannus formation and joint destruction. At early time points of Mb treatment ankle thickness still increased from 2.5 \pm 0.04 mm at day 0, to 2.8 \pm 0.15 mm at day 2 after GPI-arthritis induction. Therapeutic inhibition of arthritis was detected already one day later, as ankle swelling in Mb-treated mice was reduced to 2.7 \pm 0.15 mm compared to 3.2 \pm 0.16 mm in sham treated mice. Four days after beginning of Mb-application, mice still displayed an ankle thickness of 2.7 \pm 0.13 mm compared to an impaired swelling of 3.6 \pm 0.06 mm in sham-treated mice. Investigating hypoxia in vivo using [¹⁸F]FMISO-PET we detected a 15% reduced [¹⁸F]FMISO uptake (2,43%ID/cc sham treatment vs. 2,06%ID/cc Mb-treatment) one day and a significant 55% reduced uptake, four days after initiation of Mb-treatment (1,52%ID/cc) when compared to sham treated mice (3,06%ID/cc). In vivo [¹⁸F]FMISO-PET-data were further confirmed by histology and real-time PCR analysis of gene expression patterns (HIF-1 α /2 α , pro-angiogenic, and pro-inflammatory mediators). Thus, anti-hypoxic Mb-treatment is a powerful tool to suppress hypoxia-induced angiogenesis and to protect mice from joint destruction. [¹⁸F]FMISO-PET provides an early detection of treatment response in RA.

Presentation Number **1064B**
Poster Session 3d: Imaging Disease/Organ Processes

Low dose whole body irradiation has no therapeutic effect on pancreatic cancer progression but opens the gate for tumorantigen-specific CD4+ T cells in immunotherapy

*Ralph Meyer¹, Christoph M. Griessinger¹, Kerstin Fuchs², Daniel Bukala¹, Maren Koenig¹, Mareike Lehnhoff¹, Heidi Braumüller², Martin Röcken², Bernd J. Pichler¹, **Manfred Kneilling²**, ¹Laboratory for Preclinical Imaging and Imaging Technology of the Werner Siemens-Foundation, Department of Radiology, Eberhard Karls University, Tuebingen, Germany; ²Department of Dermatology, Eberhard Karls University, Tuebingen, Germany. Contact e-mail: manfred.kneilling@med.uni-tuebingen.de*

Immunotherapy with intra-peritoneal (i.p.) injected tumor antigen (TA) specific IFN- γ producing CD4+ T cells (Th1) prolonged life of pancreatic cancer bearing RIP1-Tag2 mice two-fold. In this endogenous model, where the large and small T antigen (Tag2) oncoproteins are expressed tissue-specific in beta cells under control of the rat insulin promoter (RIP1), mice start to develop pancreatic tumors at 6 weeks and die at 14-16 weeks of age. Interestingly, immunotherapy is only successful in combination with 2Gy low dose whole body irradiation every six weeks, starting one day prior to the first Th1 cell administration, while irradiation alone does not display any therapeutic effect. The aim of our study was to clarify the role of irradiation on the migration properties of TA-specific Th1 cells. Additionally we wanted to analyze whether irradiation displays its effects through TNFR1-signalling. In our studies CD4+ T cells were isolated from spleens and lymph nodes of Tag2 T cell receptor transgenic (TCR-tg) mice or ovalbumin (OVA)-TCR-tg (OT-2) mice, and specifically cultured to generate a Th1 phenotype. Tag2-Th1/OT2-Th1 cells were labeled using Cy5 vibrant dye solution and injected i.p. (5×10^6) into 2Gy-irradiated and non-irradiated RIP1-Tag2/ TNFR1^{-/-} or control mice, 7-20 weeks of age. We investigated migration behaviour and biodistribution of TA-specific Th1 cells for up to 24 days in vivo and organs ex vivo using optical imaging (OI). Additionally we performed flow cytometry (FACS)-analysis of lymphatic organs. OI-in vivo and ex vivo examination of adoptively transferred Cy5-labelled Tag2-Th1 cells revealed migration into lymph nodes, omentum majus and the thymus. 2Gy whole body irradiation enhanced Tag2-Th1 cell accumulation into all lymph nodes and spleens, but not into the thymus. FACS-analysis confirmed an up to 3.5-fold increase of adoptively transferred Cy5-labeled Tag2-Th1 cells in the pancreatic ($14.0 \pm 2.2\%$ vs. $4.0 \pm 1.7\%$), mesenteric ($9.5 \pm 0.7\%$ vs. $2.9 \pm 0.3\%$), inguinal lymph nodes ($5.3 \pm 1.0\%$ vs. $2.3 \pm 0.6\%$) and the spleen ($10.4 \pm 3.1\%$ vs. $7.1 \pm 1.7\%$) of 2Gy-irradiated C3H mice compared to non irradiated control mice. Similar data were observed in RIP1-Tag2 mice. Interestingly, we observed an impaired OT2-Th1 cell migration into pancreatic lymph nodes in irradiated but also non irradiated TNFR1^{-/-} mice compared to wild-type mice. Thus, low dose whole body irradiation may enhance the effects of T cell based immunotherapy through enrichment of adoptively transferred T cells in lymph nodes and spleen in a TNFR1-independent manner.

Presentation Number **1065B**
Poster Session 3d: Imaging Disease/Organ Processes

In Vivo Monitoring of Graft-versus-leukemia Effect using Bioluminescence Imaging in Murine Bone Marrow Transplantation Model

So Won Oh^{1,2}, **Hyewon Youn**^{1,3}, **Myoung Geun Song**^{1,4}, **Ji-Young Lim**⁵, **Chang-Ki Min**⁵, **Myung Chul Lee**¹, **Dong Soo Lee**^{1,6}, **June-Key Chung**¹, ¹Department of Nuclear Medicine, Seoul National University College of Medicine, Seoul, Republic of Korea; ²Department of Nuclear Medicine, Seoul National University Boramae Hospital, Seoul, Republic of Korea; ³Institute of Radiation Medicine, Seoul National University Medical Research Center, Seoul, Republic of Korea; ⁴Tumor Immunity Medical Research Center, Seoul National University Cancer Research Institute, Seoul, Republic of Korea; ⁵Department of Internal Medicine, The Catholic University of Korea St.Mary's Hospital, Seoul, Republic of Korea; ⁶Department of Molecular Medicine and Biopharmaceutical Science, Seoul National University WCU Graduate School of Convergence Science and Technology, Seoul, Republic of Korea. Contact e-mail: excellent99@naver.com

BACKGROUND: Since critical links between graft-versus-host-disease (GVHD) and graft-versus-leukemia (GVL) were reported, numerous studies have been done to minimize risks of GVHD and to enhance beneficial effects of GVL. To objectively investigate the GVL effect, we established efficient in vivo monitoring system using bioluminescence imaging in mouse model with bone marrow transplantation (BMT). **METHODS:** Lethal dose total body irradiation (TBI) were given to all recipient mice (BDF1, n=26). Within 6 hours from TBI, T-cell depleted bone marrow cells (5x10⁶ cells/each) and splenic T-cells (1x10⁶ cells/each) from MHC mismatched donor C57B6 (H-2b) mice were intravenously administered to BDF1 (H-2 b/d) mice (allogeneic group, n=14). For controls, syngeneic BMT was performed to BDF1 mice (syngeneic group, n=12). To make a xenograft, mouse mastocytoma cell line P815 transfected with an enhanced firefly luciferase (p815-effLuc) was subcutaneously injected into both the allogeneic and syngeneic groups (5x10⁵cells/each). The tumor growth rate was monitored using optical imaging system (Xenogen IVIS 100, Caliper Life Sciences) at a 6-day interval, and final bioluminescence imaging follow-up was done on day 21. **RESULTS:** In the allogeneic group, all mice developed significant acute GVHD and 64% (n=9/14) were alive until day 33. In contrast, 83% (n=10/12) of the syngeneic group was survived without features of GVHD on day 33, but the tumor progression was evident even by visual inspection. The difference of tumor growth rate, estimated by a fold increase of bioluminescence activity, began to increase on day 18; the tumor growth rate in the allogeneic group was significantly lower than in the syngeneic group (26,710 vs. 59,381; p < 0.001). Finally, the tumor increase of the allogeneic group was 39,905 folds in average; the syngeneic group was 109,824 folds in average (p < 0.001) on day 21. **CONCLUSION:** We successfully demonstrated the GVL effect in mouse BMT model, and the quantitative measurement of the GVL effect was possible with in vivo bioluminescence imaging. In vivo monitoring system based on molecular imaging is expected to facilitate further investigations in the field of GVL and GVHD.

Presentation Number **1066B**
Poster Session 3d: Imaging Disease/Organ Processes

Longitudinal relative quantification of inflammation in a DSS-induced colitis model using μ PET/CT

Steven G. Staelens¹, **Pieter Hindryckx**², **Steven Deleyle**¹, **Stefaan Vandenberghe**¹, **Martine De Vos**², ¹*Ibitech-Medisip, Ghent University - IBBT, Gent, Belgium;* ²*Hepatology and Gastroenterology, Ghent University,, Ghent, Belgium. Contact e-mail: steven.staelens@ugent.be*

INTRODUCTION: This study investigates whether μ PET/CT can serve as a non-invasive monitoring and quantification tool for an acute model of colitis. Such animal models are essential in pathophysiological research and preclinical evaluation of potential therapeutic compounds for inflammatory bowel disease in humans. **METHODS:** Acute distal colon damage was induced by administering dextran sodium sulphate (DSS) through the drinking-water of four CD-1 mice. These animals were scanned with μ PET/CT at day 0, 3, 5, 7, 11 and 14 each time anesthetised with an 1,5% isoflurane mixture. The mice were fasted overnight, after which they received an oral gavage with 200 μ l of gastrografin and 30 min later an IV injection with 1mCi 2-Deoxy-2-[¹⁸F]Fluoro-d-Glucose (FDG). Another half hour later, a gastrografin mixture was administered rectally just before a CT and PET scan of these animals was acquired with the Flex Triumph PET/CT (Gamma Medica Ideas, Northridge, LA, USA). The aforementioned CT scan was acquired in 2x2 binning mode, with a 50 μ m spot size, at 70kVp and 145 μ A in 512 projections using a magnification of 1.3 followed by a 2 bed position static PET scan of 20 min during which the animal's bladder was continuously flushed using a double-lumen urethral catheter. ROIs for the colon and the brain (as a reference region for vasculature) were determined in VIVID (GMI) on a sagittal, coronal and transversal reconstructed CT plane and automatically wrapped to 3D VOIs encompassing the colon and the brain respectively. The ratio of the mean voxel count of the PET images in these 2 VOIs was then compared with the MPO data for the final timepoint of these animals and evaluated versus the histological inflammation score for alle timepoints of a separate experiment on mice with the same genetic background. **RESULTS:** The comparison with the histological inflammation score shows that the evolution over time (day 0-14) is well reproduced by μ PET/CT and the evaluation versus the MPO data at the final timepoint illustrates a good agreement of the relative quantification. We learned that it is mandatory to continuously flush the bladder in μ PET studies to be able to evaluate (distal) colon inflammation. Also, to delineate the colon as the exact VOI, rectal administration of a contrast agent is required to deliver sufficient soft tissue μ CT contrast. **CONCLUSION:** μ PET-CT is a feasible non-invasive method to evaluate DSS induced colitis provided that a μ CT contrast agent is administered and a bladder flushing procedure is in place.

Presentation Number **1067B**
Poster Session 3d: Imaging Disease/Organ Processes

A longitudinal evaluation of terminal ileal inflammation using μ PET/CT

Steven G. Staelens¹, **Pieter Hindryckx**², **Steven Deleeye**¹, **Stefaan Vandenberghe**¹, **Martine De Vos**², ¹*Ibitech-Medisip, Ghent University - IBBT, Gent, Belgium;* ²*Hepatology and Gastroenterology, Ghent University, Ghent, Belgium.* Contact e-mail: steven.staelens@ugent.be

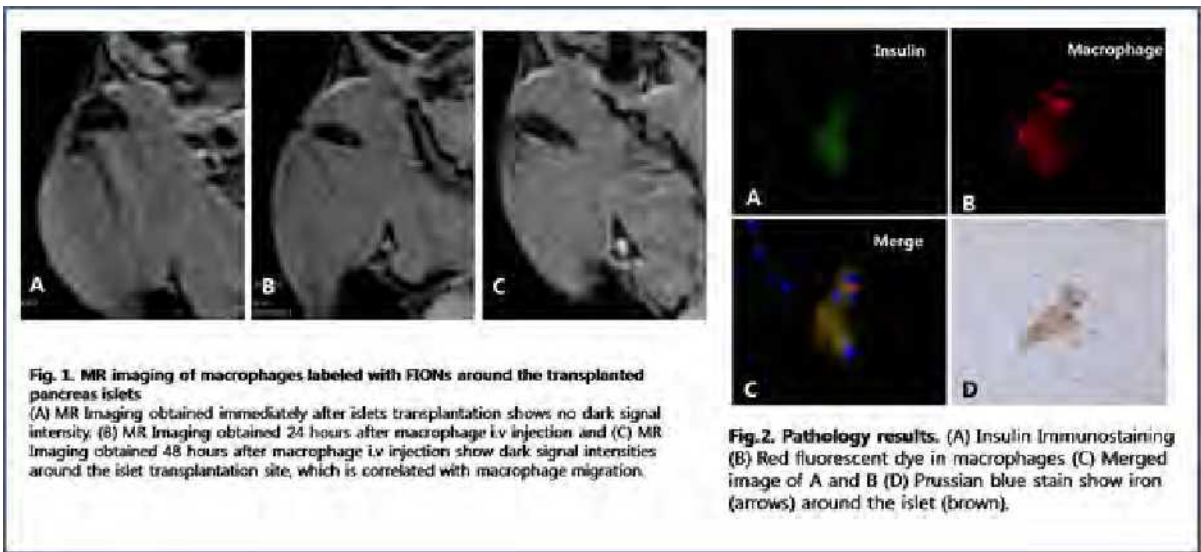
INTRODUCTION: TNF Δ ARE/+ mice spontaneously develop a chronic terminal ileitis which is strikingly similar to human Crohn's disease (CD). As such, they represent an unique model to study promising new therapeutics for intestinal CD. However, animal studies are hampered by several problems such as inter-animal variability and timing or sampling errors. Small animal molecular imaging is an expanding and promising technology that may largely overcome the aforementioned problems. **METHODS:** TNF Δ ARE/+ mice and corresponding healthy controls were scanned with μ PET/CT at 16 and 24 weeks each time anesthetised with a 1,5% isoflurane mixture. These animals were fasted overnight, after which they received an IV injection with 1mCi 2-Deoxy-2-[¹⁸F]Fluoro-d-Glucose and an oral gavage with 200 μ l of gastrografin. After \pm 50 min the animals were positioned under the X-ray tube of the μ CT in continuous scout view mode to accurately and dynamically monitor the progress of the contrast agent in the gastro-intestinal tract in order to exactly determine the point when the ileal-caecal transition is reached. At that time (typically after 55 min to 65 min) a μ CT and a μ PET scan of these animals was acquired with the Flex Triumph PET/CT (Gamma Medica Ideas, Northridge, LA, USA). First a CT scan was acquired in 2x2 binning mode, with a 50 μ m spot size, at 70kVp and 175 μ A in 2048 projections using a magnification of 1.3 followed by a 30 min PET scan in 2 bed positions. A Volume-of-Interest (VOI) encompassing the ileum was delineated slice-by-slice on the contrast-enhanced reconstructed μ CT images using VIVID (GMI). The mean voxel count of the μ PET images in this VOI was corrected for injected activity and was then compared between the animal groups and the two timepoints. **RESULTS:** Quantification of inflammation using μ PET/CT delivers significant differences between healthy and diseased populations and between different time points in the TNF series. The evolution of the disease as determined with μ PET/CT corresponds to ex vivo histological predictions. The timing for the μ CT scan after administration of the contrast agent in order to exactly pinpoint the ileal-caecal transition appeared to be crucial and animal-specific. **CONCLUSION:** μ PET-CT is a feasible non-invasive method to longitudinally evaluate terminal ileitis provided that a μ CT contrast agent is administered intra-gastrically and provided that the timing of the μ CT scan is determined on an animal specific basis using the μ CT 's scout view.

Presentation Number **1068B**
 Poster Session 3d: Imaging Disease/Organ Processes

The evaluation of the effect of thalidomide to macrophages labeled with ferromagnetic iron oxide nanocubes (FIONs) after pancreas islet xenogeneic transplantation in a mouse model

Shunmei Lin¹, Seung Hong Choi¹, Nohyun Lee², Taeghwan Hyeon², Woo Kyung Moon¹, ¹Department of Diagnostic Radiology, Seoul National University Hospital, Seoul, Republic of Korea; ²National Creative Research Initiative Center for Oxide Nanocrystalline Materials and School of Chemical and Biological Engineering, Seoul National University, Seoul, Republic of Korea. Contact e-mail: bee606@gmail.com

INTRODUCTION Acute immune rejection is one of the major problems in islet xenogeneic transplantation, in which macrophages are known to play an important role. Thalidomide has been reported as an anti-inflammatory drug for its inhibitory effect on macrophages [1]. Iron-oxide-based cellular MR imaging has been used to assess immune rejection after transplantation by monitoring the accumulation of immune cells at the rejection site [2]. To increase the sensitivity of MR imaging, specific cells such as macrophages were isolated and labeled with MRI contrast agent such as iron nanoparticles. After injection of macrophages labeled with iron nanoparticles via veins, the migration of macrophages can be monitored by MR imaging in vivo [3]. In this study, we investigated the migration and accumulation of the macrophages around the transplanted xenograft islets, which were labeled with ferromagnetic iron oxide nanocubes (FIONs). **MATERIALS AND METHODS** Peritoneal macrophages were harvested from thioglycolate-treated Balb/c mice, and labeled with FIONs in vitro. For labeling macrophages, they were incubated with 50µg iron/ml for 2 hours. To confirm whether the macrophages were the identical ones that we injected, they were co-labeled with NEO-STEMTM fluorescent particles. Pig islets were transplanted to Balb/c mice at the left thigh muscle. Macrophages of 2x10⁶ labeled with both FIONs and NEO-STEMTM fluorescent particles were injected intravenously (n=5) into the xenogeneic transplanted Balb/c mice immediately after islets transplantation. In vivo MR imaging was performed immediately, and approximately 24, 48 and 72 hours after macrophages injection. 3D GRE MR imaging was obtained by using 1.5 T MR scanner (GE health care). At the end of experiment, the mice were sacrificed and both left and right thigh muscles were harvested. Pathological analysis was performed to correlate MR imaging results. **RESULTS AND DISCUSSION** FION-labeled macrophages were observed in vivo MR imaging around the xenogeneic graft 24 hours later after islets transplantation, and showed maximum migration after 48 hours (Fig 1), but were not observed in the mice treated with thalidomide. The same results were confirmed by histopathology (Fig 2). We demonstrated that FIONs-labeled macrophages can be monitored on 1.5T MR imaging and the anti-immune rejection effect of thalidomide can be monitored by in vivo MR imaging. **REFERENCES** (1) Chunguang Chen et al., PLOS ONE 20;4(7):e6312(2009), (2) Kanno et al., J Thorac Cardiovasc Surg 120:923-34 (2000), (3) Terrovitis J et al., Circulation 117:1555-62 (2008)



Presentation Number **1057A**
Poster Session 1d: Imaging Disease/Organ Processes

¹⁸F-fluoroacetate PET imaging for bacteria-induced inflammation

Chin-Ho Tsao^{1,2}, **Chun-Yi Wu**², **Hsin-Ell Wang**², **Kuo Wei-Ying**², **Bing-Fu Shih**¹, **Ren-Shyan Liu**^{2,3}, ¹*Nuclear Medicine, Mackay Memorial Hospital, Taipei, Taiwan;* ²*MAGIC/NRPGM, Nuclear Medicine, Faculty of Medicine, National Yang-Ming University Medical School, Taipei, Taiwan;* ³*NPCC, Taipei Veterans General Hospital, Taipei, Taiwan.* Contact e-mail: tsao.souzay@msa.hinet.net

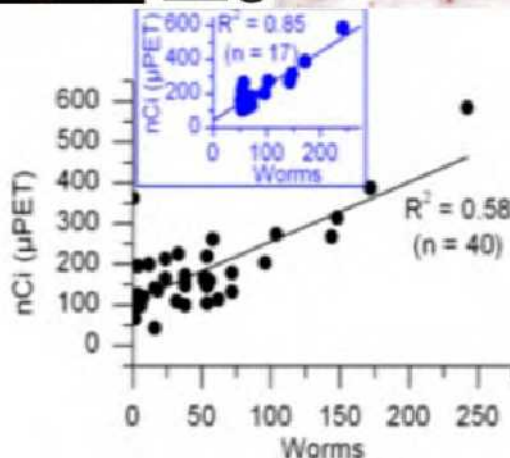
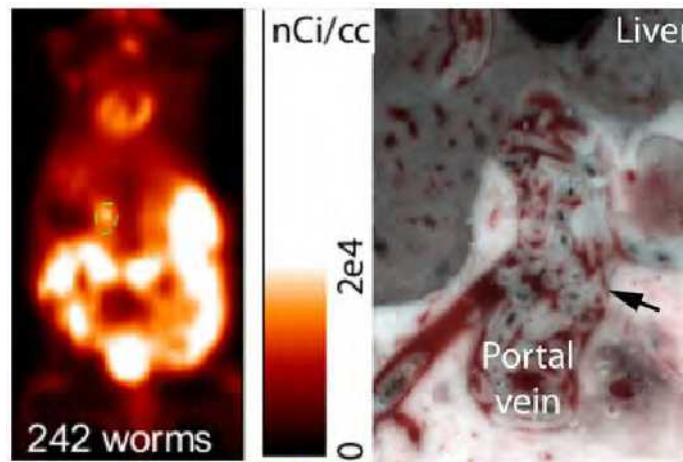
Objective: Our previous study showed that ¹⁸F-fluoroacetate (FAC) accumulated in the turpentine oil induced non-infectious inflammation (Nucl Med Biol 2009;36:305-12). FAC is also a non-invasive index of glial cell metabolism and appears to be a useful diagnostic tool to assess central nervous system (CNS) inflammation in human. This study aimed to assess the use of FAC in imaging bacteria induced infectious inflammation in mouse model. **Methods:** Escherichia coli (E. coli), Staphylococcus aureus (S. aureus) and Mycobacterium bovis bacillus Calmette-Guérin (BCG) were inoculated in the axillary region of six months-old Balb/c mice. MicroPET imaging of FAC and FDG were performed at day 5 on the acute infection animal model, and at day 18 on the granulomatous infection animal model. Per cent injected dose (%ID) of FAC and FDG within the regions of interest (ROI) was calculated. The uptake ratio was defined by %ID of lesion/%ID of contralateral soft tissue. **Results:** FAC and FDG PET imagings showed increased uptake in all infectious lesions. The uptake ratios of FAC and FDG were 3.69/4.75 (mean) for E. coli and 3.26/3.61 for S. aureus, respectively. The relative accumulation of FAC was slightly lower than FDG. Different from high uptake of FDG (10.07) in the granulomatous lesion, FAC uptake is low (1.68). **Conclusion:** Our study suggests that FAC imaging is not only useful in evaluating the lesions of both non-infectious inflammation (turpentine oil induced) and infectious inflammation (E. coli and S. aureus), but not in granulomatous infection (BCG). The accumulation of FAC appears to contribute to active immune cells and bacteria-induced inflammatory cells. We suggest that assessing gliolysis with FAC in CNS inflammation and tumors should be careful for associated non-infectious or infectious inflammation.

Presentation Number **1058A**
 Poster Session 1d: Imaging Disease/Organ Processes

In vivo imaging of schistosomes to assess disease burden using PET

Nicolas Salem¹, Jason D. Balkman², Jing Wang¹, David L. Wilson³, Zhenghong Lee^{2,3}, Christopher L. King^{4,5}, James Basilion^{1,3},
¹Radiology, Case Western Reserve University, Cleveland, OH, USA; ²Radiology, University Hospitals Case Medical Center, Cleveland, OH, USA; ³Biomedical Engineering, Case Western Reserve University, Cleveland, OH, USA; ⁴Center for Global Health and Disease, Case Western Reserve University, Cleveland, OH, USA; ⁵Veterans Affairs Medical Center, Cleveland, OH, USA. Contact e-mail: nxs90@case.edu

Schistosomiasis is a well-studied parasitic disease that is far from eradication despite the development of an effective treatment. The lack of an efficacious vaccine and high re-infection rates are major factors in its intractable worldwide prevalence. A non-invasive imaging technique could give clinicians and researchers a quantitative and visual tool to characterize the worm burden in infected individuals, determine the efficacy of a candidate vaccine, and provide information about parasite migration patterns and basic biology. We are proposing the application of PET imaging to schistosomiasis to advance the management and research of this infectious disease. Athymic nude mice infected with *S. mansoni* 5-6 weeks earlier were used in the imaging studies. Fluorescence molecular tomography (FMT) imaging with Prosense 680 was first performed. Accumulation of the imaging probe in the lower abdomen correlated with the number of worms, but only in mice with low infection burden. The total FDG uptake in the common portal vein and/or regions of elevated FDG uptake in the liver linearly correlated to the number of worms perfused from infected animals, but the correlation was stronger in mice with high infection burdens. Cryomicrotome imaging confirmed that most of the worms in a mouse with high infection burden were in the portal vein. In a mouse with a low infection burden, worms were not found in the portal vein. The total FDG uptake as measured by scintillation counting in perfused schistosomes linearly correlated with the number of worms. Infected mice showed a 41% average decrease in total FDG uptake after praziquantel treatment. FDG PET may be useful to non-invasively quantify the worm burden in schistosomiasis-infected animals. Future investigations will aim at minimizing non-specific FDG uptake to improve the recovery of signal from worms located in the lower abdomen. More specific radiotracers will simultaneously be investigated.



FDG uptake in portal vein (dotted green line) correlated with worm burden.

Presentation Number **1059A**
Poster Session 1d: Imaging Disease/Organ Processes

Combined siRNA Therapy and in vivo Imaging in Islet Transplantation

Ping Wang, Mehmet V. Yigit, Zdravka Medarova, Guangping Dai, Anna Moore, Radiology, Massachusetts General Hospital, Charlestown, MA, USA. Contact e-mail: amoores@helix.mgh.harvard.edu

OBJECTIVE Two major scientific obstacles hamper broad clinical application of islet transplantation (Tx): 1) inability to follow islet fate directly and 2) significant graft loss shortly after transplantation. We propose to address both issues by utilizing a dual purpose therapy/imaging siRNA-nanoparticle probe targeting apoptotic related gene caspase-3. We expect that treatment with the probe will result in significantly better survival of transplanted islets, which will be evaluated by in vivo MRI. **MATERIALS AND METHODS:** Synthesis of the probe (MN-NIRF-siRNA) consisted of three steps: synthesis of dextran-coated magnetic nanoparticles (MN); conjugation of the near infrared fluorescent (NIRF) dye Cy5.5 to MN and conjugation of siRNA to caspase-3 to MN. The control probe contained scrambled siRNA. Human islets were obtained from the Islet Cell Resource Center (ICR). In vitro testing of the probe included serum starvation of the islets followed by treatment with the probe ([Fe]=25mg; [siRNA]=105pmole). Caspase-3 gene and protein silencing were determined by RT-PCR and western blot respectively. For in vivo studies NOD-SCID mice (n=8) were transplanted with MN-NIRF-siCaspase-3-labeled human islets under the left kidney capsule, and MN-treated islets were transplanted under the right kidney capsule. In vivo MRI was performed using a 9.4T scanner (Billerica, MA) equipped with ParaVision 3.0.1 software. Animals were sacrificed at 2, 4, 7 and 14 days post Tx. Histology was performed to confirm imaging results. **RESULTS** As a result of incubation with the probe caspase-3 mRNA and protein expression decreased in treated islets compared to the islets treated with the scrambled probe. After transplantation, a hypointense area under the left kidney capsule was significantly larger than the control side. Histology revealed decreased apoptosis in MN-NIRF-siCaspase-3-treated islets compared to the control side. **CONCLUSION** We observed a protective effect of MN-NIRF-siCaspase-3 in treated islets both in vitro and in vivo. This study could potentially aid in increasing the success of clinical islet transplantation.

Presentation Number **1058B**
Poster Session 3d: Imaging Disease/Organ Processes

Value of ^{18}F -FDG PET in diagnosing vasculitis and vascular stent graft infection in comparison to CT and MRI

Sedat Alibek¹, Ulrich Gärtner², Rainer Linke², Torsten Kuwert², Michael Uder¹, Alexander Cavallaro¹, ¹Radiology Institute, University of Erlangen, Erlangen, Germany; ²Nuclear Medicine, University of Erlangen, Erlangen, Germany. Contact e-mail: sedat.alibek@uk-erlangen.de

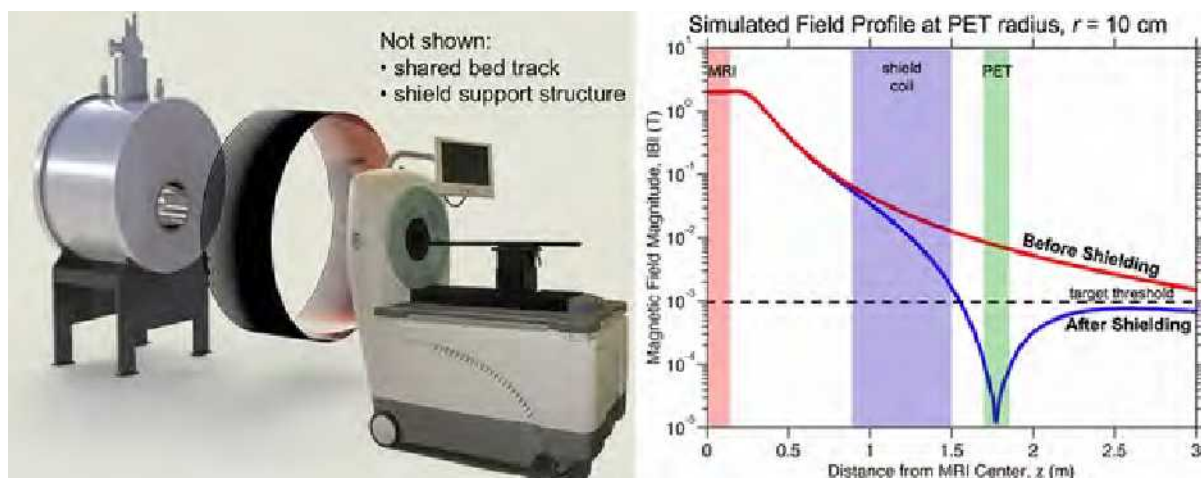
METHOD AND MATERIALS A retrospective database search with the logical keyword combination ["vasculitis" or "takayasu" or "arteritis" or "graft infection"] regarding imaging diagnosis revealed a total of 13 patients who were referred from January 2006 to April 2010 to Positron Emission Tomography in our institution. All patients were examined on a hybrid PET-CT system. In addition to ^{18}F -FDG PET scan additional non contrast enhanced low dose CT scans (n=6) or non contrast enhanced diagnostic CT scans (n=2) or a Magnetic Resonance Angiography (n=6) was performed if vasculitis was suspected, whereas a contrast enhanced diagnostic CT scan was performed in addition if "fever of unknown origin" was the referring diagnose (n=5). Diagnose of vasculitis or vascular stent graft/prosthesis infection was based on the detection of high accumulation of radiopharmaceuticals in vessel/stent graft/prosthesis walls and significantly higher SUV values compared to average liver SUV in PET and thickening as well as contrast media enhancement in CT or MRI. **RESULTS** In 13/13 patients (100%), ^{18}F -FDG PET findings were positive for vasculitis or vascular stent graft/prosthesis infection with SUV values ranging from 3,4-17,1 (mean: 7,0) in comparison to average liver SUV values ranging from 1,7-3,2 (mean: 2,4), thus being significantly increased. Findings of comparative imaging studies were suggestive of vasculitis in 1/6 MR exams (Sensitivity 16,7 %, Specificity 100%) and in 2/13 CT exams regardless of contrast administration, diagnostic or low dose scan protocols (Sensitivity 15,4%, Specificity 100%). **CONCLUSION** Positron emission tomography using ^{18}F -FDG is a valuable and effective tool to detect vasculitis and vascular stent graft/prosthesis infection in patients. ^{18}F -FDG PET can detect vasculitis and vascular stent graft/prosthesis infection where other cross-sectional imaging methods fail

Presentation Number **0300B**
 Poster Session 4a: Imaging Instrumentation and Methodology

Collinear PET/MRI: External Magnetic Field Limits and Magnetic Shield Design for a Small-Animal PET System

Geron Bindseil¹, **Chad Harris**¹, **William B. Handler**¹, **Timothy J. Scholl**^{1,2}, **Blaine A. Chronik**^{1,2}, ¹Department of Physics and Astronomy, University of Western Ontario, London, ON, Canada; ²Department of Medical Biophysics, The University of Western Ontario, London, ON, Canada. Contact e-mail: gbindsei@uwo.ca

One approach to combining PET and MRI into hybrid systems is to place conventional PMT-based PET detectors in a region with very low magnetic field. The authors describe an approach in which a small-animal PET system (Siemens Inveon) operates collinear with an MRI system (MagneX 2.0T/310), as in PET/CT, with the addition of active magnetic shielding of PET detectors. This approach would enable the use of highly optimized PET systems with no physical modification. The authors determined the requirements for magnetic shielding by testing the robustness of the PET system during and after exposure to various magnetic field strengths, and then designed an appropriate shielding coil. Position reproducibility and count-rate experiments were performed on the PET system using phantoms to test changes in gain and efficiency. Two tests were conducted: (1) Count-rate during PET acquisition in the presence of weak magnetic fields of various magnitudes, and (2) count-rate & position measurement of a point source immediately after a strong magnetic field exposure (11 mT) was turned off. Results: Test (1). PET coincidence count-rate fell gradually as magnetic field increased. Count-rate was reduced by 10% at 1 mT and by 85% at 3 mT. Test (2). Coincidence counts increased from $(2.95 \pm 0.01) \times 10^7$ before to $(2.97 \pm 0.01) \times 10^7$ after strong field exposure (11 mT). The coordinates of the reconstructed point-source position experienced a maximum shift of 0.01 mm, much less than the resolution of this PET system (> 1 mm). These results suggest that the PET system should suffer almost no performance hit so long as: (a) The axial field during PET acquisition is below 1 mT, and (b) axial field exposures are limited to less than 11 mT between acquisitions. Next, a resistive electromagnet shield was designed to null the MRI fringe field to below 1 mT in the detectors when the systems are separated by 1.8 m. Various coil geometries and positions were investigated. One candidate coil (Fig. left) has length 60 cm and radius 75 cm, dissipates 7.3 kW and reduces the field within the PET detectors to below 0.08 mT, much better than required (Fig. right). These results show that a simple active magnetic shield can enable collinear small-animal PET/MRI. More efficient geometries are currently being explored, and construction will begin shortly.



Presentation Number **0301B**
Poster Session 4a: Imaging Instrumentation and Methodology

A bimodal ultrasound and optical endorectal probe for prostate cancer diagnosis adapted to the clinical environment

Jerome Boutet¹, *Mathieu M. Debourdeau*¹, *Lionel Herve*¹, *Aurélie Laidevant*¹, *Didier Vray*², *Jean-Marc Dinten*¹, ¹*CEA-LETI-MINATEC, Grenoble, France;* ²*INSA Lyon-CREATIS, Villeurbanne, France. Contact e-mail: jerome.boutet@cea.fr*

Fluorescence tomography techniques are widely used for preclinical studies of new drugs, and for obtaining a better understanding of the development of certain diseases. Nowadays, studies subject to clinical constraints and reaching clinical trial level are not that numerous and are mainly limited to certain easily accessible organs. The protocol for prostate cancer diagnosis, currently based on PSA determination and ultrasound guided biopsy, is criticized for its lack of relevance and high false negative rate. To improve this protocol, a new approach was recently proposed combining optical and ultrasound measurements. However, use of these systems has been limited to phantom and canine prostate studies. The adaptation of such a highly complex bimodal system to the clinical environment is challenging. The laser radiation must be harmless; the housing of the probe must be resistant to the corrosive fluids used for sterilization and the optical measurements must be taken through a condom-like protection layer covering the probe. Moreover, the overall size of the detection and excitation modules should not exceed a given dimension so as to fit the operative environment. Finally, examination of the entire prostate should not take more than 15 min. to avoid any complication for the patient. This paper will indicate how a combined ultrasound and optical endorectal probe has been designed to comply with the constraints of the sterilization protocols, the examination duration and required compactness. Therefore a totally innovative pulsed laser source has been designed to meet compactness requirements while providing accurate time-resolved measurements. A dedicated multi-channel photon counting system has been optimized to decrease the examination duration. A fast reconstruction method was used to provide 3D localization of fluorescent dots almost immediately after acquisition. The optical components are capable of withstanding the sterilization procedures thanks to the addition of a protection layer covering the probe. The design of this layer has a limited impact on the signal-to-noise ratio. The performance of this compact laser source was comparable to that of a standard laboratory Ti:Sa laser. Finally, combined with a dedicated photon counting solution, this source is capable of acquiring optical data in less than one minute. To evaluate the overall performance of the system in dealing with a realistic background signal, measurements and reconstructions were conducted on a combination of phantoms and small animals with ovarian tumors.

Presentation Number **0302B**

Poster Session 4a: Imaging Instrumentation and Methodology

Topographic diagnosis of parathyroid adenoma by imaging modalities

Kenichi Sakurai, *Breast and Endocrine Surgery, Nihon University School of Medicine, Tokyo, Japan. Contact e-mail: ksakurai@med.nihon-u.ac.jp*

Primary hyperparathyroidism is characterized by hypercalcemia, which is easily diagnosed through a routine blood test. However, the topographic diagnosis of affected gland(s) with non-invasive imaging studies is sometimes difficult. We evaluated the degree of confidence and the detection limit of imaging modalities, including ultrasound, contrast-enhanced CT, and 201Tl minus 99mTc subtraction scintigram. We evaluated the degree of confidence of imaging modalities including ultrasound, contrast-enhanced computerized tomography (CT), and parathyroid scintigram in identifying the localization of parathyroid adenoma. The study was conducted on 36 patients with known primary hyperparathyroidism. All 36 patients underwent all three tests. In ultrasound, the overall sensitivity in detecting parathyroid adenoma was 86.1%. If confined to the adenomas bigger than 500 mg in weight and 13 mm in diameter, ultrasound could detect 100% adenomas. In contrast-enhanced CT, the overall sensitivity was 83.3%. CT was thought to be reliable if adenomas were bigger than 500 mg in weight and 10 mm in size. In 201Tl - 99mTc subtraction scintigram, the overall sensitivity was 86.1%. Subtraction scintigram seemed to be able to detect adenomas bigger than 500 mg in weight and 10 mm in size, though it could not detect one adenoma with 600 mg in weight and 20 mm in size. There was only one patient in whom the affected gland could not be identified through all three tests, but was successfully detected with MIBI scintigram. At present it is suggested to be necessary to combine multiple imaging modalities for the topographic diagnosis of parathyroid adenoma.

Presentation Number **0303B**
 Poster Session 4a: Imaging Instrumentation and Methodology

Machine learning model for molecular and metabolic pattern classification of recurrent brain gliomas

Farzin Imani¹, **Fernando Boada**¹, **Frank S. Lieberman**², **Erin L. Deeb**¹, **James M. Mountz**¹, ¹Radiology, University of Pittsburgh Medical Center, Pittsburgh, PA, USA; ²Neurology, University of Pittsburgh Medical Center, Pittsburgh, PA, USA. Contact e-mail: fimani@nucmed.com

Objectives: The aim of this study was to systematically combine multimodal imaging data to improve diagnostic accuracy of glioma progression from postradiation necrosis using Support Vector Machine (SVM) learning model. We demonstrate that SVM outperforms single-parameter cutoffs obtained from receiver operating characteristic (ROC) plot analysis of proton magnetic resonance spectroscopy (MRS) and FDG PET data. **Methods:** 12 post-therapy patients (5 m, 7 f, 25-70y), initially with histology proven gliomas (6 grade II and 6 grade III) who presented with contrast enhancing lesions on MRI and clinical symptoms suggestive but not conclusive of recurrence were selected. FDG uptake of lesions was rated 0 (no uptake), 1 (<WM), 2 (=WM), 3 (>WM, <GM), 4 (=GM), 5 (>GM). Choline (Cho) over Creatine (Cr) ratios of the lesions were normalized to the contralateral hemisphere. Clinical follow-up (>12mo) and sequential MRI studies were used as the reference standard. An SVM with linear classifier was computed using quadratic programming to maximize the distances between the hyperplane to the closest points of either class (supporting vectors). The ROC plots and optimal cutoff values for FDG uptake and Cho/Cr were calculated. **Results:** The SVM with 4 supporting vectors was able to classify all recurrent cases (n=8) without false results (accuracy 100%). The equation of maximal margin separating hyperplane was $0.5F+0.86C=2.23$, where F and C represent FDG uptake and normalized Cho/Cr ratio, respectively. The accuracy of PET and MRS based on optimal cutoff values (FDG 2.5 and Cho/Cr 1.455) using ROC analyses were 83% and 75% respectively. **Conclusion:** SVM technique, in spite of small number of cases, was able to effectively combine MRS and FDG PET data and successfully classify recurrent gliomas more accurately than single-parameter cutoffs.

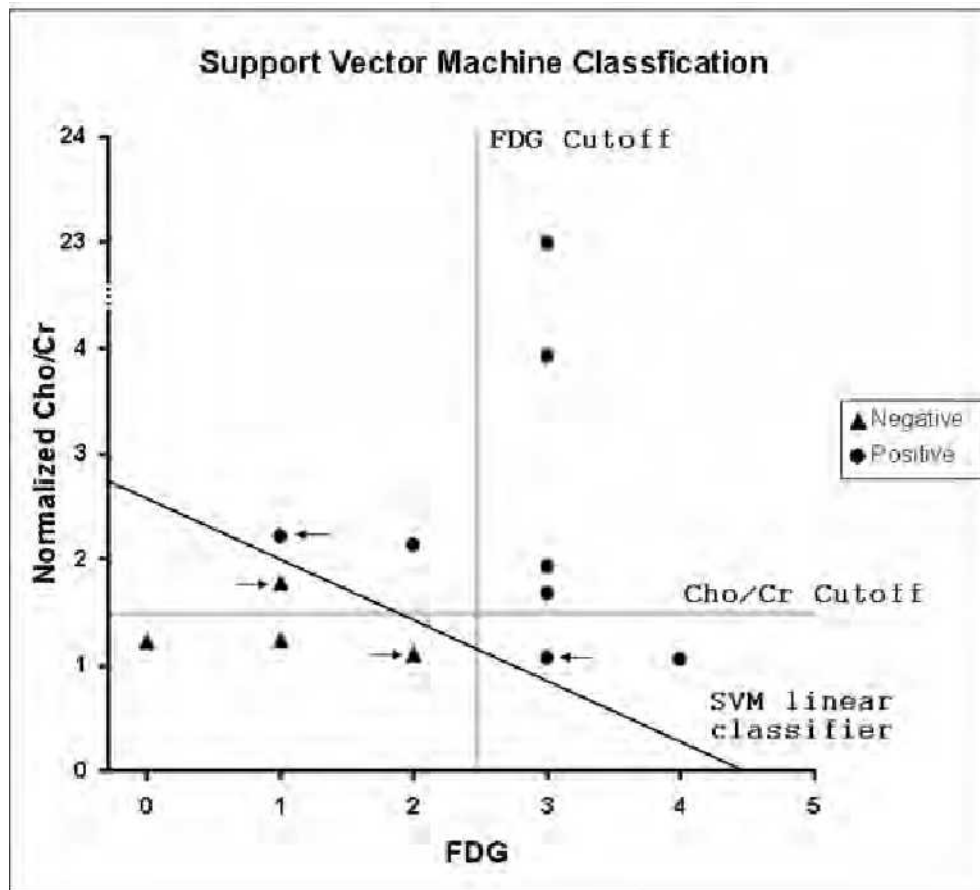


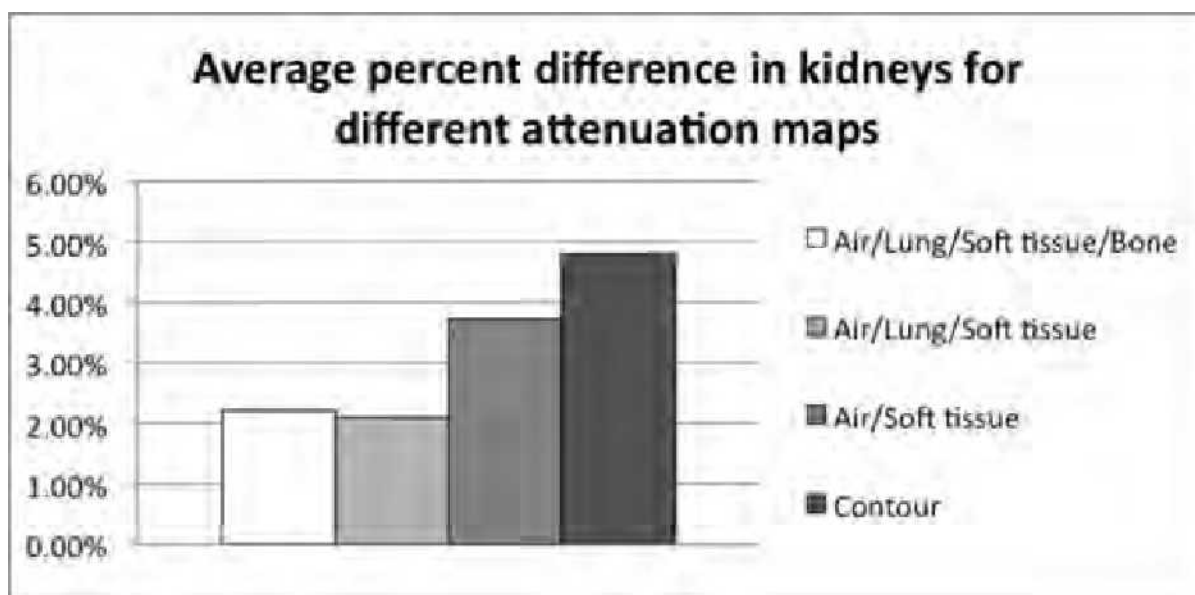
Figure 1. Recurrent glioma classification by calculated cutoff values from ROC analysis of FDG PET and normalized Cho/Cr MRS data, as well as SVM classification of the combined data. The arrows point to the supporting vectors.

Presentation Number **0304B**
 Poster Session 4a: Imaging Instrumentation and Methodology

Whole-body MR-based Attenuation Correction for microSPECT-MR

Vincent Keereman¹, **Yves Fierens**², **Christian Vanhove**^{3,4}, **Tony Lahoutte**^{3,4}, **Yves De Deene**⁵, **Stefaan Vandenberghe**¹, ¹MEDISIP, Ghent University, Ghent, Belgium; ²Radiology/BEFY, UZ Brussel, Brussels, Belgium; ³In-Vivo Cellular and Molecular Imaging, UZ Brussel, Brussels, Belgium; ⁴Nuclear Medicine, UZ Brussel, Brussels, Belgium; ⁵Laboratory for Quantitative NMR, ECNURAD, Ghent University, Ghent, Belgium. Contact e-mail: Vincent.Keereman@ugent.be

INTRODUCTION In the past we have demonstrated the feasibility of performing MR-based attenuation correction (AC) for μ SPECT of the rat brain. A UTE sequence was used to visualize bone, because it is invisible in conventional MRI. Whole-body AC gives the extra problem of segmenting lung tissue, which is also invisible in conventional MRI. We propose the use of UTE images for whole-body μ SPECT attenuation correction. **METHODS** A rat was injected with Tc99-DMSA and fixed in a plastic holder. μ SPECT images were acquired on a Siemens e.cam with 3 1.5 mm pinholes. A μ CT was acquired on a SkyScan 1178 (0.083 mm resolution). MR images were acquired on a Philips Achieva 3T, using a dual-echo UTE sequence with TE1=0.12 ms and TE2=2.3 ms (0.7 mm resolution). 6 cobalt point sources and 2 water tubes were fixed to the holder for μ CT- μ SPECT and μ CT-MR registration. The R2-map was derived from both echo's of the UTE data set. As was expected, lung tissue has a very high R2. Very high R2 values were also seen in parts of the abdomen that also had a lower density on μ CT. This probably relates to air/water mixture inside the bowel. Bone has a high and soft tissue a medium/low R2. All voxels containing air were set to 0 by applying a mask derived from the first echo image. Four attenuation maps were then derived from the R2-map: air/lung/soft tissue/bone, air/lung/soft tissue, air/soft tissue and a contour attenuation map, which is derived by assigning a soft tissue attenuation coefficient to all voxels inside the body. The μ SPECT images were reconstructed with these four attenuation maps and the μ CT attenuation map. The average percent difference between the μ CTAC and the different MRAC reconstructions was calculated in a ROI containing the kidneys. **RESULTS** The figure shows that the average percent difference is below 5% for all of the images. The map containing air/lung/soft tissue performs best. Including bone yields slightly worse results. This is probably caused by segmentation errors in the bone. The largest errors are found using the contour attenuation map. **CONCLUSION** The feasibility of whole-body rat MR-based attenuation correction was shown. Using MRAC leads to small errors (< 5%) in the reconstructed images, even when using an attenuation map that simply defines the contours of the animal.

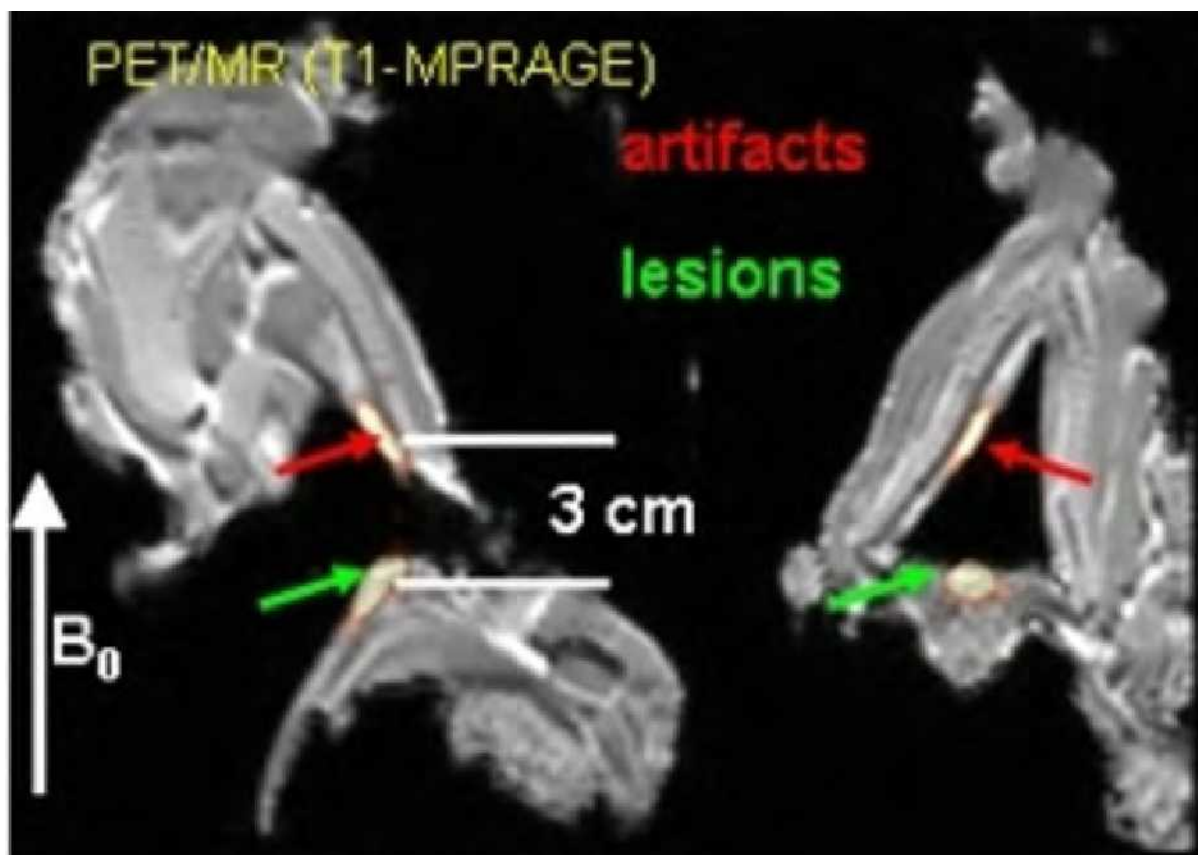


Presentation Number **0305B**
 Poster Session 4a: Imaging Instrumentation and Methodology

Inhomogeneous Positron Range Effects in High Magnetic Fields might Cause Severe Artefacts in PET/MRI

Armin Kolb¹, **Matthias Hofmann**^{1,2}, **Alexander Sauter**^{1,4}, **Chih-Chieh Liu**¹, **Lars A. Eriksson**³, **Bernd J. Pichler**¹, ¹Laboratory for Preclinical Imaging and Imaging Technologies of Werner Siemens Foundation, University of Tuebingen, Tuebingen, Germany; ²Cybernetic Research, Max Planck Institute, Tuebingen, Germany; ³Molecular Imaging, Siemens Healthcare, Knoxville, TN, USA; ⁴Department of Radiology, University of Tuebingen, Tuebingen, Germany. Contact e-mail: armin.kolb@med.uni-tuebingen.de

The combination of PET and MRI is an emerging field of current research. It is known that the positron range is shortened in high magnetic fields (MF), leading to an improved resolution in PET images. Interestingly, only the fraction of positron range (PR) orthogonal to the MF is reduced and the fraction along the MF is not affected and yields to a non-isotropic count distribution. We measured the PR effect with PET isotopes like F-18, Cu-64, C-11, N-13 and Ga-68. A piece of paper (1 cm²) was soaked with each isotope and placed in the cFOV of a clinical 3T BrainPET/MR scanner. A polyethylene board (PE) was placed as a positron (β^+) stopper with an axial distance of 3 cm from the soaked paper. The area under the peaks of one pixel wide profiles along the z-axis in coronal images was compared. Based on these measurements we confirmed our data in organic tissue. A larynx/trachea and lung of a butchered swine were injected with a mixture of NiSO₄ for T1 MRI signals and Ga-68, simulating tumor lesions in the respiratory tract. The trachea/larynx were aligned in 35° to the MF lines and a small mass lesion was inserted to imitate a primary tracheal tumor whereas the larynx was injected submucosally in the lower medial part of the epiglottis. Reconstructed PET data show that the annihilated ratio of β^+ at the origin position and in the PE depends on the isotope energy and the direction of the MF. The annihilation ratios of the source and PE are 52.4/47.6 (F-18), 57.5/42.5 (Cu-64), 43.7/56.7 (C-11), 31.1/68.9 (N-13) and 14.9/85.1 (Ga-68). In the swine larynx measurement, an artefact with approximately 39% of the lesion activity formed along MF lines 3cm away from the original injected position (fig.1). The data of the trachea showed two shine artefacts with a symmetric alignment along the MF lines. About 58% of the positrons annihilated at the lesion and 21% formed each artefact. The PR effects are minor in tissue of higher or equal density to water (0.096 cm⁻¹). However, the effect is severe in low density tissue or air and might lead to misinterpretation of clinical data.



Presentation Number **0306B**
 Poster Session 4a: Imaging Instrumentation and Methodology

Fluorescence Microendoscopy of Peripheral Lung Cancer Using Indocyanine Green Dye

Miguel Valdivia y Alvarado, Tian Cheng He, Zhong Xue, Stephen T. Wong, **Kelvin Wong**, Center of Bioinformatics, The Methodist Hospital Research Institute., Houston, TX, USA. Contact e-mail: kwong@tmhs.org

Introduction: Fluorescent imaging using microendoscopy probes is a promising tool for tumor vessel visualization. The benefits of this technique could be further enhanced using image-guided interventional procedures that enable the use of the microendoscope non-invasively. **Materials and Methods:** A lung tumor model was created using VX2 carcinoma in ten New Zealand White Rabbits. After an incubation period (14 days) the animals were anesthetized and underwent a chest CT scan, from the first scan a thoracic puncture was planned using a minimally invasive multimodality image-guided (MIMIG) system that allows 3D needle path planning in real time. Once the desired path was chosen, the needle was introduced, and a second scan was recorded to verify the needle location. Indocyanine Green (ICG) was administered I.V. and after 15 minutes the needle was withdrawn and a microendoscope (Cellvizio 660, Mauna Kea) was introduced through the needle. Videos from the tumor were recorded for 10 minutes. **Results:** All tumors were targeted accurately using MIMIG system and needle adjustment was necessary in one case only. Two pneumothorax cases were seen at the second scan (20%); no other complications were seen after the procedure. Tumor leaky vasculature visualization was possible in all the tumors. **Conclusion:** Intravenous labeling using ICG dye allows lung tumor identification using CT image-guided microendoscopy. **Discussion:** Fluorescent imaging allows the visualization of tumors with leaky microvasculature in real time. One problem to overcome is the access to organs safely. MIMIG facilitate this task by overlaying real time instrument tracking information on a prior CT images. This approach is faster, safer, and gives less radiation exposure than repeatedly CT scan punctures.

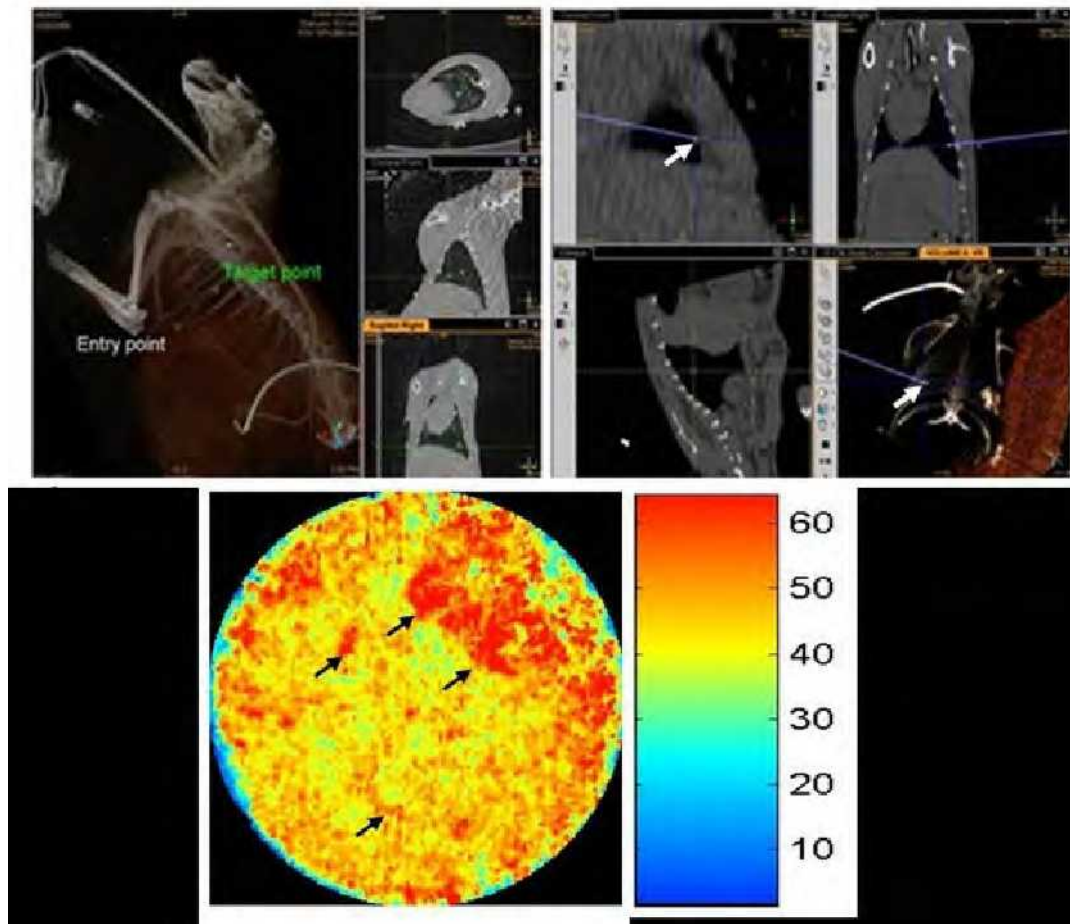


Fig. 1. A: Real time navigation provided by MIMIG system. The purple line in the top-right figure represents the needle. B: Microendoscopic fluorescent image in the tumor showing a high contrast uptake. A tubular structure (~100 micron) is seen in the center of the tumor indicated by black arrows.

Presentation Number **0307B**
 Poster Session 4a: Imaging Instrumentation and Methodology

Improved quantification in multiple-pinhole SPECT by anatomy-based reconstruction using μ CT information

Christian Vanhove^{1,3}, **Michel Defrise**^{2,3}, **Axel Bossuyt**^{1,3}, **Tony Lahoutte**^{1,3}, ¹*Nuclear Medicine, UZ Brussel, Jette, Belgium;* ²*Experimental Medical Imaging, Vrije Universiteit Brussel, Jette, Belgium;* ³*In-vivo Cellular and Molecular Imaging, Vrije Universiteit Brussel, Jette, Belgium. Contact e-mail: Christian.Vanhove@uzbrussel.be*

The aim of this study was to evaluate the potential of anatomy-based reconstruction, using μ CT information, to improve quantitative accuracy in multiple-pinhole SPECT. Multiple-pinhole SPECT and μ CT images were acquired of the Micro Deluxe Phantom using both, hot and cold rods inserts. The phantoms were filled with 3.7MBq/ml of Tc-99m. To improve μ CT contrast, the phantoms were also filled with clinical contrast agent. Emission images were reconstructed using a One Step Late (OSL) modification of the OSEM algorithm for incorporation of μ CT information, to encourage smoothing within but not across boundaries. To allow quantification, the OSL-OSEM algorithm takes into account imperfect camera motion, collimator response, angular variation of the sensitivity, intrinsic camera resolution, attenuation, and scatter. For comparison, the SPECT images were also reconstructed by OSEM using a post-reconstruction filtering, and by OSL-OSEM using a quadratic prior (QP) and a median root prior (MRP). In each rod of the phantom the recovery coefficient (RC), defined as measured divided by the true activity concentration, was expressed as a function of the noise. Different noise levels were obtained by varying the amount of spatial filtering during or after reconstruction. Results are summarized in Table1. Compared to OSEM using post-reconstruction filtering and to OSL-OSEM using a QP, our study demonstrated that the use of anatomical information during reconstruction significantly improved the quantitative accuracy in cold and hot rods with a diameter ≥ 2.4 mm. When compared to the MRP, the anatomic prior (AP) performs significantly better in hot rods with diameters ≥ 2.4 mm. In conclusion, anatomy based reconstruction using μ CT information has the potential to improve quantitative accuracy in multiple-pinhole SPECT.

Table1

Rod diameter	Post-Gauss	QP	MRP	AP
4.8mm hot rod	0.62±0.07	0.67±0.04	0.70±0.02	0.74±0.03
4.0mm hot rod	0.54±0.08	0.60±0.04	0.64±0.02	0.67±0.02
3.2mm hot rod	0.47±0.08	0.52±0.06	0.56±0.03	0.61±0.02
2.4mm hot rod	0.37±0.09	0.40±0.07	0.44±0.03	0.50±0.03
1.6mm hot rod	0.21±0.03	0.22±0.02	0.23±0.02	0.24±0.02
1.2mm hot rod	0.18±0.02	0.19±0.02	0.19±0.02	0.19±0.02
4.8mm cold rod	0.62±0.07	0.62±0.08	0.68±0.03	0.70±0.02
4.0mm cold rod	0.54±0.07	0.57±0.08	0.60±0.03	0.61±0.03
3.2mm cold rod	0.46±0.08	0.44±0.10	0.50±0.06	0.52±0.05
2.4mm cold rod	0.36±0.06	0.34±0.08	0.37±0.06	0.39±0.06
1.6mm cold rod	0.24±0.04	0.23±0.04	0.23±0.04	0.23±0.04
1.2mm cold rod	0.17±0.04	0.16±0.05	0.16±0.04	0.16±0.05

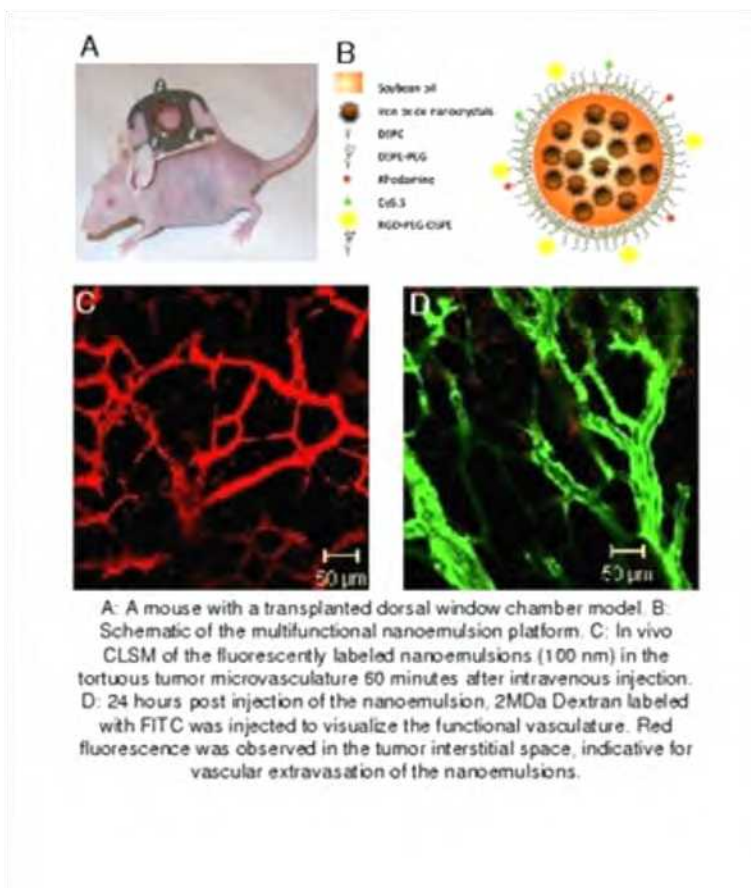
RC averaged over different noise levels for all the rods of the Micro Deluxe Phantom. Results are show for 4 different reconstruction algorithms: OSEM with post-reconstruction filtering (Post-Gauss), OSL-OSEM using a quadratic prior (QP), a median root prior (MRP), and using μ CT information (AP).

Presentation Number **0308B**
 Poster Session 4a: Imaging Instrumentation and Methodology

Combined In Vivo MRI and In Vivo CLSM to Study the In Vivo Behavior of Multifunctional Nanoemulsions

Sjoerd Hak¹, Peter A. Jarzyna², Willem J. Mulder², Marte Thuen¹, Nina K. Reitan³, Olav Haraldseth¹, Catharina D. Davies³,
¹Department of Circulation and Medical Imaging, Norwegian University of Science and Technology, NTNU, Trondheim, Norway;
²Department of Radiology, Translational and Molecular Imaging Institute, Mount Sinai School of Medicine, New York, NY, USA;
³Department of Physics, Norwegian University of Science and Technology, NTNU, Trondheim, Norway. Contact e-mail: sjoerd.hak@ntnu.no

Oil-in-water emulsions are increasingly being employed as drug delivery and molecular imaging agents. To that end, Jarzyna et al. recently developed a multifunctional nanoemulsion contrast agent platform and demonstrated its tumor targeting potential in a cancer mouse model. The nanoemulsion consists of soybean oil stabilized by a monolayer of ordinary and PEGylated phospholipids and it can be prepared in sizes ranging from 25 to 100 nm (fig). In the current study, the in vivo behaviour of this agent is investigated as a function of size and targeting ligand with both magnetic resonance imaging (MRI) and confocal laser scanning microscopy (CLSM) in tumors grown in a MRI compatible mouse dorsal window chamber model. RGD-peptides were conjugated to target the angiogenic endothelium, while a folate functionalized lipid can be incorporated to acquire specificity for tumor cells that upregulate the folate receptor. To allow high resolution MRI using a 7 Tesla animal scanner, we have designed a Helmholtz receive only coil to fit the window chamber (fig). This setup will be exploited to study the particle dynamics with dynamic contrast enhanced MRI as well as to show particle targeting. CLSM will be utilized to study the in vivo dynamics and the localisation of the nanoemulsions in tumor and healthy tissues at subcellular resolution in real time. In vivo CLSM of the nanoemulsions in the window chamber model was demonstrated in a pilot experiment. Directly after injection of untargeted 100 nm sized nanoemulsions they were visible in the vasculature (fig). 24 hours after injection, fluorescence was observed in the tumor interstitial space, indicative for vascular extravasation of this agent (fig). Ultimately, the unique combination of in vivo CLSM and MRI is anticipated to validate and better understand the clinically relevant MRI observations and to facilitate particle design optimization for enhanced target specificity and tumor delivery of our nanoparticle and its cargo.

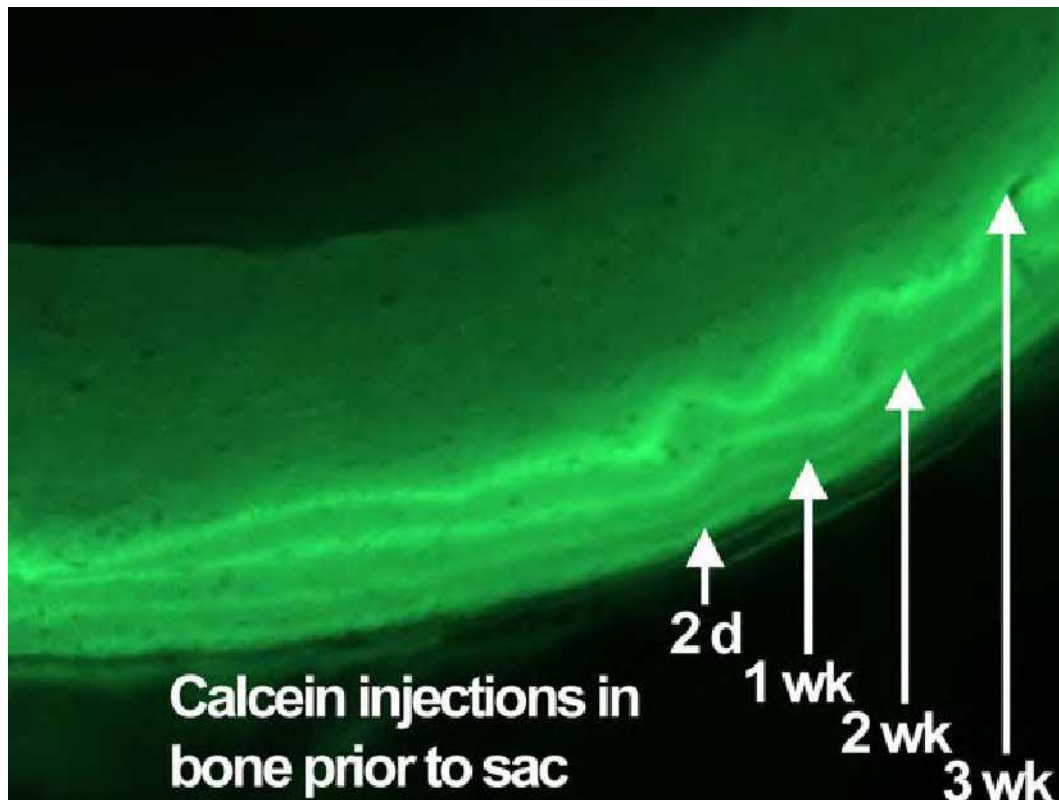


Presentation Number **0309B**
Poster Session 4a: Imaging Instrumentation and Methodology

Fluorescence-Guided Micron-Level Mechanical Testing Of Bone Reveals Patterns Of Tissue Mineralization And Age

Benjamin P. Sinder^{1,2}, Grant C. Goulet¹, Neil R. Halonen¹, David J. Vodnick³, Ron F. Zernicke^{1,2}, **Kenneth M. Kozloff^{1,2}**, ¹Orthopaedic Surgery, University of Michigan, Ann Arbor, MI, USA; ²Biomedical Engineering, University of Michigan, Ann Arbor, MI, USA; ³Hysitron, Inc., Minneapolis, MN, USA. Contact e-mail: kenkoz@umich.edu

Traditional predictors of skeletal fragility are based on bone mineral density (BMD), however BMD alone is insufficient to directly predict fracture risk. Bone quality measures such as material or compositional changes may provide additional information describing fracture susceptibility and require alternate techniques to locally quantify tissue properties. Nanoindentation can be used to directly probe bone tissue with high spatial and mechanical resolution. Traditional nanoindentation relies on bright field microscopy to select indent location based on microstructural features alone. Here, we describe a new indentation device which couples epifluorescence microscopy, to visualize fluorescent bone turnover markers embedded in the bone matrix, with traditional nanoindentation testing to determine material properties as a direct function of tissue age. A Hysitron TI950 TriboIndenter nanomechanical instrument was equipped with an epifluorescence source and filters selected to optimize wavelengths for traditional bone fluorescent turnover markers, providing the capability to position tests within +/-500nm of the desired test site. Mice (5 wk) were administered 4 bouts of calcein (30 mg/kg ip) to label the bone mineralization front 2d, 1, 2 and 3 wks prior to sac (Fig). 2 days after the final injection, femora were dissected, sectioned, and polished to a mid-diaphyseal surface. Selection of test points based on inter-calcein label visualization was performed under epifluorescence microscopy (480/30nm exc. 535/40nm em.) and tissue elastic modulus was directly assessed as a function of tissue age by indenting to 500 nm depth. Elastic modulus was calculated with standard analysis techniques using the initial slope of the force-displacement unloading curve. Results suggest site-specific differences in tissue elastic modulus directly related to a pattern of progressive mineralization from periosteal to mid-cortical, and endosteal-to mid-cortical bone surfaces reflected by in situ fluorescent bone turnover markers.



Presentation Number **0310B**
Poster Session 4a: Imaging Instrumentation and Methodology

Prospective study of truncation artifacts in simultaneous whole-body PET/MR

Gaspar Delso, Rebekka Kraus, Sibylle Ziegler, TU Muenchen, Munich, Germany. Contact e-mail: gaspar.delso@tum.de

The development of an integrated PET/MR tomograph for whole-body imaging has already been announced by two major manufacturers. However, quantitative PET imaging requires information about the attenuation properties of the tissue being scanned. Current estimates indicate that the field-of-view diameter of a combined scanner will oscillate around the 450 mm. MR images will therefore be unable to encompass the entire patient breadth, leading to truncation artifacts. This study was performed to estimate the location, frequency and severity of these artifacts. A database of 300 adult oncology patients having undergone thoracic FDG PET/CT was collected. The profile of all patients was segmented and the transaxial span at the hips, abdomen, chest and shoulders measured. Patients scanned with one or both arms resting along the body were processed separately. The amount of tissue that would be lost with field-of-view diameters ranging from 400 to 500 mm was measured and its frequency distribution computed. The intensity and extent of the truncation artifacts was estimated by comparing the standard PET/CT reconstruction with offline reconstructions using the truncated attenuation data. The results were validated using simulated data: First by means of simple forward/backprojection and posteriorly with Monte-Carlo simulation of focal lesions. Our sample population had an average age of 60 and 22% of it was above the 90 kg. Given a PET/MR field-of-view diameter of 400mm, 65% of this population would suffer from truncation artifacts in more than 10% of the reconstructed slices. This figure is reduced to 16% for a 450mm diameter and to <1% for a 500mm diameter. For a field of view of 450 mm, 27% of the patients scanned with their arms up would present truncation artifacts in the hips, 2% on the abdomen, 4% on the breast region and 55% on the shoulders. The reconstructed images show that truncation artifacts generate locally strong deviations (2% for 1 cm³ of soft-tissue) that could lead to false positives. The results obtained with simulated data are in agreement with the previous values. These results prove that truncation artifacts, especially in the hips and shoulders, if left uncorrected, can be a major issue in PET/MR whole-body imaging, affecting a large percentage of patients even if arms-up protocols could be imposed. Unfortunately, truncation correction techniques currently in use for PET/CT are not applicable to MR-based attenuation correction. New approaches based on PET segmentation are currently being investigated.

Presentation Number **0311B**

Poster Session 4a: Imaging Instrumentation and Methodology

The Relationship between the Arterial Input Function Obtained with Gd-DTPA / MRI and ¹⁸F-FDG / PET: a New Multimodality Approach

Éric Poulin, Réjean Lebel, Etienne Croteau, Roger Lecomte, M'hamed Bentourkia, Martin Lepage, Department of Nuclear Medicine and Radiobiology, Université de Sherbrooke, Sherbrooke, QC, Canada. Contact e-mail: eric.poulin3@usherbrooke.ca

Introduction: MRI-PET multimodality scanners for fundamental and clinical research are already available. Exploitation of the full potential of such hybrid systems will require new methodology that uses the advantages of one modality to compensate for the limitations of the other. The arterial input function (AIF) is commonly used for several types of MRI and PET pharmacokinetic analyses, but measurement of the AIF remains a challenge for both modalities. The most commonly used contrast agent, Gd-DTPA, and radiotracer, ¹⁸F-FDG, respectively in MRI and PET are both subjected to extravasation and excretion. The aim of our study was to evaluate the correspondence between the AIF used in MRI and PET and to determine if the AIF obtained by one modality can be substituted for pharmacokinetic modeling of data acquired with the other modality. **Methods:** Fisher rats (n = 7) were scanned in a μ PET scanner during an intravenous co-injection of ¹⁸F-FDG and Gd-DTPA and dynamic PET images of the myocardium were acquired for 50 min in list mode. The metabolic rate of glucose (MRGlc) was extracted from the myocardium tissue. Blood samples were collected at several time points and the blood concentration of ¹⁸F-FDG and Gd-DTPA was determined with a gamma counter and by induced coupled plasma mass spectroscopy, respectively. These AIF curves were fitted with a 4-parameter bi-exponential model [TOFTS, P.S.; MRM 17,357-367 (1991)]. The parameters represent a fast and a slow decay, each with independent amplitude. A Student's t-test was performed on each fitting parameter. **Results:** While the fast decay parameters were similar, the slow elimination time and amplitude parameters were statistically different (p<0.05). Phosphorylated ¹⁸F-FDG accumulates in cells and may return more slowly to the blood circulation. It was noted that the ratios between the MRI and PET AIF parameters were similar in all rats. Using these ratios, it was possible to calculate the ¹⁸F-FDG AIF from the Gd-DTPA AIF, and vice versa, for each animal. The MRGlc values calculated with the ¹⁸F-FDG AIF and the corrected Gd-DTPA AIF were identical within experimental uncertainties (p>0.05). Using an uncorrected Gd-DTPA AIF, however, yielded statistically higher MRGlc values (p<0.05). **Conclusion:** It is possible to use the AIF obtained by manual blood sampling of Gd-DTPA or FDG to calculate the AIF of the other and to use the Gd-DTPA AIF to evaluate MRGlc from PET data in the myocardium of rats.

Presentation Number **0312B**

Poster Session 4a: Imaging Instrumentation and Methodology

High resolution isotropic non-contrast 3D MR of carotid artery can supplement CT in PET/CT for characterization of atherosclerosis plaque

Ravi T. Seethamraju¹, Michael Jerosch-Herold², Yiu-Cho Chung⁵, Peter Libby³, Marcelo Di Carli⁴, Raymond Y. Kwong³, ¹MR R and D, Siemens Medical Solutions, USA Inc., Malden, MA, USA; ²Radiology, Brigham and Women's Hospital, Boston, MA, USA; ³Cardiovascular Medicine, Brigham and Women's Hospital, Boston, MA, USA; ⁴Nuclear Medicine, Brigham and Women's Hospital, Boston, MA, USA; ⁵MR R & D, Siemens Medical Solutions, USA Inc., Columbus, OH, USA. Contact e-mail: ravi.seethamraju@siemens.com

Currently CT provides morphology for localization of metabolically active carotid plaques in PET/CT, but the ability to characterize plaque is limited to calcification [1]. With the advent of MR-PET scanners [2], the ability to detect and characterize vulnerable plaque components is highly enhanced, with excellent spatial resolution for morphological imaging. High resolution non-contrast 3D MR sequences, MPRAGE and T2 black-blood SPACE [3] can provide adequate characterization of plaque and with MR UTE imaging [4] calcification can both be visualized and quantified, so we demonstrate here that MR-PET fusion would provide enhanced plaque component characterization, hitherto missing in PET/CT. In an IRB approved study cohort of 6 patients with confirmed carotid stenosis, imaging was performed on MR(3 Tesla) and PET/CT standard clinical scanners. 0.7mm 3D Isotropic coronal slabs were acquired in MR for maximum coverage of the two vessels to determine stenosis severity. MR images were coregistered using custom software [5] to PET using CT as reference, as PET is inherently co-registered to CT. Simple rigid registration was sufficient in most cases, failing which a non-rigid registration was applied. The co-registered PET, CT and MR data allowed extraction of complimentary information on plaque composition, metabolism and neovascularization. T2W SPACE images (fig 1) were precisely registered to the PET/CT data to the point that the carotid bifurcation can even be clearly localized on PET images which is difficult with just PET/CT. Edemic plaque is clearly visible in MR while activated on PET and not visible in CT. The vessel wall in MR is very clearly delineated due to which precise stenosis measurements can be made. Initial findings show good correlation of PET activation to T2 enhancement in MR, so we hypothesize that MR-PET imaging alone could help in better characterization of atherosclerosis plaque. References 1 S. Silvera et.al, Atherosclerosis. 2009 Nov;207(1):139-43 2 Catana C. et.al., J Nucl Med. 2006 Dec;47(12):1968-76. 3 Seethamraju RT et al., #1439 Proc. ISMRM, 2010. 4 Chan CF et.al., J Cardiovasc Magn Reson. 2010 Mar 26;12:17. 5 Azar FS et. Al., #0673, Proc JMIMC 2007

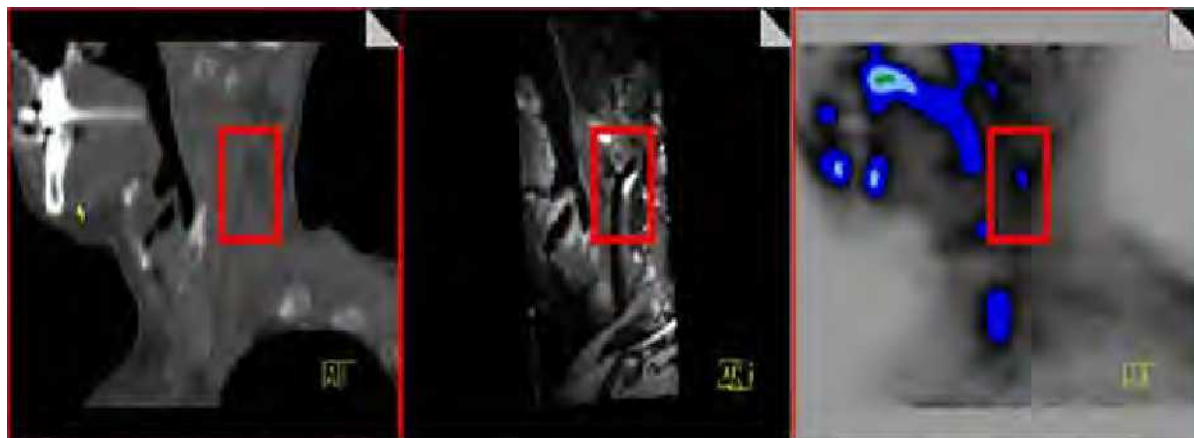


Fig 1. CT, MR and PET respectively co-registered showing the carotid bifurcation clearly on a T2 weighted black blood SPACE MR image with edemic plaque and as activation in PET.

Presentation Number **0314B**
Poster Session 4a: Imaging Instrumentation and Methodology

A X-ray/fluorescence bi-modal tomographer to reconstruct fluorophore distribution in pre-clinical studies : in vivo evaluation

Anne Planat-Chretien¹, Anne Koenig¹, Jean-Guillaume Coutard¹, Lionel Herve¹, Marco Brambilla¹, Véronique Josserand², Jean-Luc Coll², Jean-Marc Dinten¹, ¹LETI-CEA, Grenoble Cedex 9, France; ²IAB - INSERM U823, Grenoble Cedex 9, France. Contact e-mail: vaplanatchretien@gmail.com

We present a demonstrator of a new tomographic system that couples, in a cylindrical acquisition geometry, fluorescence diffuse optical tomography (fDOT) and micro X-Ray CT (XCT). The advantage of this bi-modal system is to provide accurate morphological (XCT) and functional information (fDOT) on the same gantry. A dedicated calibration and acquisition protocol associated to a specific reconstruction algorithm have been developed. Our fDOT algorithm takes into account the exact external shape of the animal provided by X-ray tomography to reconstruct both the heterogeneities map from the excitation signal and then the fluorescence distribution, using Greens functions corrected from optical properties heterogeneities [1]. The reconstruction performances of our bi-modal instrument are characterized on phantoms in terms of repeatability (less than 1% of variation), linearity (excellent between 0.2 and 5 pmol with a detection limit of 0.1pmol) and resolution in X/Y and Z plane (2 mm in any direction). "In vivo" characterization has been carried out on 6 mice: capillaries filled with a solution of fluorophores (Alexa 750) are inserted either in the lungs via the trachea and the bronchi or in the abdomen of sacrificed healthy nude mice. We show that we localize the fluorophore in the morphology of the animal with a tolerance of 1mm (Fig 1). We discuss the concentration of fluorophores required to get out non specific fluorescence for each region of interest - [2.5 to 5] pmol for the lung region and [5 to 10] pmol for the abdomen region and present reconstructions with the same mice reconstructed without any capillary inside for comparison purpose. We point out the different detection limit for the lung - absorbent region - and the abdomen - very heterogeneous region. Next step will be to show the benefit of bi-modal imaging on longitudinal studies of real lung or peritoneal tumours bearing mice. [1] Koenig A. and all, Bios 2010.

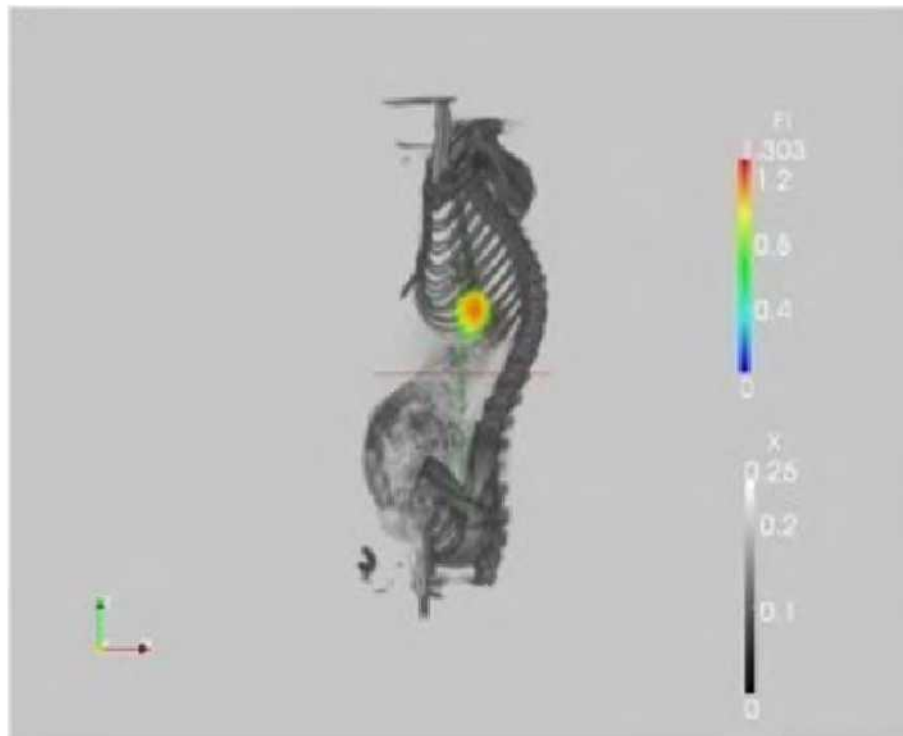


Fig 1: Reconstruction of a capillary filled with 2.5 pmol AlexaFluor 750 inserted in the lungs via the trachea and the bronchi

Presentation Number **0315B**

Poster Session 4a: Imaging Instrumentation and Methodology

In Vivo Imaging of Hypoxia: Hemodynamic Model of Tumor Oxygenation

Keith Stantz^{1,2}, **Ning Cao**¹, **Michael Shaffer**¹, **Bo Liu**¹, **Ling Chen**¹, **Kathy D. Miller**⁴, **Song-Chu Ko**³, ¹*School of Health Sciences, Purdue University, West Lafayette, IN, USA;* ²*Radiology, Indiana University School of Medicine, Indianapolis, IN, USA;* ³*Radiation Oncology, Indiana University School of Medicine, Indianapolis, IN, USA;* ⁴*Hematology/Oncology, Indiana University School of Medicine, Indianapolis, IN, USA.* Contact e-mail: kstantz@iupui.edu

Purpose: The objective is to develop and validate a multivariate in vivo hemodynamic model of tissue oxygenation (MiHMO2). **Introduction:** Clinical studies targeting hypoxia or tumor angiogenesis have demonstrated significant enhancement in local progression free survival when concurrent reduction in acute and chronic types of hypoxia are addressed. This distinction has been shown to initiate differing molecular pathways associated with DNA repair and cellular motility, and is believed to have a varying longitudinal response to anti-angiogenic drugs as well as radiation and chemotherapies. To understand this link between tumor microenvironment and cellular response, an in vivo imaging model (MiHMO2) to noninvasively measure tumor hypoxia, identify its type, and monitor its heterogeneity is devised. **Mathematic Model:** Our model fuses parameters of hemoglobin status (hemoglobin concentration, CtHb, and oxygen saturation, SaO2) and vascular physiology (perfusion, permeability, fractional plasma, fp, and interstitial volumes) to assess tumor oxygen concentration, pO2, or hypoxic fraction, HF, and the hemodynamic factors delineating the form of hypoxia. **Material and Methods:** Simulations are performed to compare tumor pO2 levels and hypoxic fraction based on physiology and hemoglobin parameters based on in vivo photoacoustic spectroscopic and dynamic contrast-enhanced measurements of breast (MCF7neo and MCF7VEGF) and pancreatic (BxPC-3) tumors in mice. Local measurements of tumor CtHb, SaO2, perfusion, and fp, are compared to pO2 and hypoxia measurements using photoluminescence-quenching and pimonidazole immunofluorescence. **Results:** Presented will be line plots of pO2 across the diameter of each tumor are compared to CtHb, SaO2, perfusion and fp measurements. MCF7VEGF tumors demonstrate a uniform distribution of pO2 values (40-50mmHg) consistent with elevated perfusion, fp, CtHb, and SaO2. MCF7neo tumors demonstrate a radial heterogeneity of pO2 which tracks SaO2 and perfusion. BxPC-3 demonstrates a heterogeneous pO2 pattern, where pO2 strongly tracks SaO2 and perfusion in most regions but not all. Results are in line with simulated data. Changes in perfusion or fp can have the largest effect on pO2 or HF, for example varying fp from 2.5 to 15% (MCF7neo versus MCF7VEGF) decreases HF5 from 1.0 (hypoxic) to 0.1 (anoxic). **Conclusions:** The combination of photoacoustic CT spectroscopy and physiological imaging provides a unique ability to monitor tumor hypoxic due to aberrant tumor hemodynamics, which is corroborated by oxygen probe measurements.

Presentation Number **0316B**

Poster Session 4a: Imaging Instrumentation and Methodology

TOPEM: a PET TOF probe, compatible with MRI and MRS for diagnosis and follow up of prostate cancer

Franco Garibaldi¹, Raffaele De Leo², Paolo Musico⁵, Roberto Perrino⁷, Antonio Ranieri², Maurizio Foresta², Flavio Loddo², Camillo Tamma², Alessandro Gabrielli³, Franco Meddi^{1,8}, Filippo M. Giorgi³, Roberto Fonte⁴, Francesco Librizzi⁴, Paolo Finocchiaro⁶, Bruno Maraviglia^{8,1}, Luigi Cosentino⁶, Federico Giove⁸, Tommaso Gilli⁸, Francesco Cusanno¹, Angelo Rivetti¹¹, Neal Clinthorne⁹, Stan Majewski¹⁰, Sam Huhss⁹, ¹INFN Roma1, Rome, Italy; ²INFN Bari, Bari, Italy; ³INFN Bologna, Bologna, Italy; ⁴INFN Catania, Catania, Italy; ⁵INFN Genova, Genova, Italy; ⁶INFN LNS, Catania, Italy; ⁷INFN Lecce, Lecce, Italy; ⁸Physics, University of Rome, Rome, Italy; ⁹Radiology, University of Michigan, Ann Arbor, MI, USA; ¹⁰Radiology, University of West Virginia, Morgantown, WV, USA; ¹¹INFN Torino, Torino, Italy. Contact e-mail: franco.garibaldi@iss.infn.it

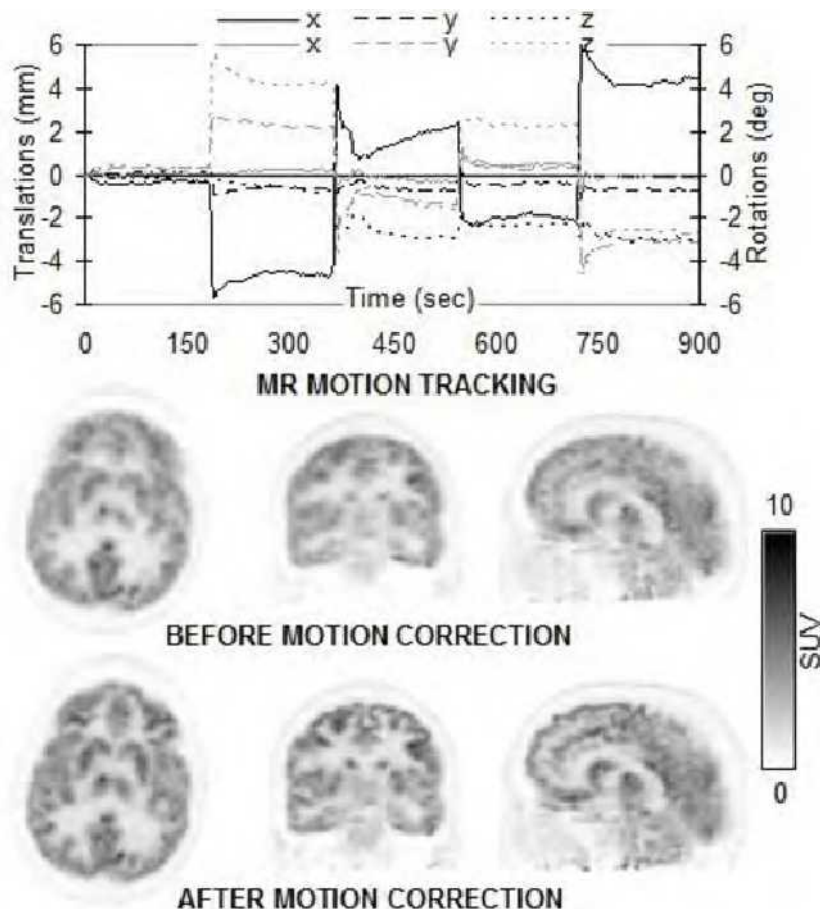
Prostate cancer (PC) is the most common disease and a leading cause of cancer death. The current standard for diagnosing PC is transrectal biopsy; however, it is far from perfect. Multimodality imaging can play a significant role by merging anatomical and functional details from simultaneous PET and MRI (and MRS) scans for guiding biopsy, diagnosis and follow up. Due to sub-optimal prostate imaging geometries, generic scanners prevent separation of the signal from surrounding organs with sensitivity, spatial resolution and contrast inferior to what is achievable with dedicated prostate imagers. Our project (TOPEM) is developing an endorectal PET-TOF MRI probe. Exploiting the TOF capability allows an increase in the SNR/NECR and also permits elimination of bladder background. The internal probe is used in coincidence with an external dedicated detector and/or a standard PET ring. Performance is dominated by the endorectal detector with improvements in both spatial resolution and efficiency. The electronics must measure coincidences with a precision of 300 ps or less, and be small enough to be connected to the internal detector. For compactness and MRI compatibility, Silicon Photomultipliers (SiPM) are used. Their time jitter is negligible so the expected time resolution is a direct function of the sqrt of photoelectron number related to the PDE. Extensive ongoing simulation by Geant4 allows study of the scintillator geometry, coupling to the SiPMs and their pixel dimensions. Measurements for characterization of the performance of different SiPMs (temperature behavior, PDE etc) are ongoing. A discrete electronics system has been built to perform measurements until the dedicated electronics system, namely the challenging ASIC (the design of it is ongoing), is available. Simulation results show spatial resolution of 1.5 mm - 2 mm for source distances of 10-20 mm, with improved efficiency over external PET. Depending on the reconstructed resolution desired, noise can be reduced by up to ~7x over external ring PET alone giving improvements of effective NEC of ~50x. Timing resolution (only the electronics) of 100 ps has been obtained with the discrete electronic system. A minidetector prototype (LYSO coupled to a SiPM array) has been built and will be tested in a 3 T MRI soon. We have preliminary results of measurements and simulations; results from a more advanced stage of the project will be presented at the conference.

Presentation Number **0317B**
 Poster Session 4a: Imaging Instrumentation and Methodology

MR-assisted PET Motion Correction for Neurological Studies on an Integrated MR-PET Scanner

Ciprian Catana¹, **Andre van der Kouwe**¹, **Thomas Benner**¹, **Larry Byars**², **Michael Hamm**³, **Daniel B. Chonde**¹, **Christian J. Michel**², **Matthias Schmand**², **Gregory A. Sorensen**¹, ¹Radiology, Massachusetts General Hospital, Charlestown, MA, USA; ²Siemens Healthcare USA, Inc, Knoxville, TN, USA; ³Siemens Healthcare USA, Inc, Charlestown, MA, USA. Contact e-mail: ccatana@nmr.mgh.harvard.edu

Subject head motion is difficult to avoid in long neurological PET studies, degrading the image quality and offsetting the benefit of using a high-resolution scanner. As a potential solution in an integrated MR-PET scanner, the simultaneously acquired MR data could be used for tracking the motion. In this work, a novel data processing and rigid-body motion correction (MC) algorithm for the MR-compatible BrainPET prototype scanner was developed and tested using 3 different MR-based motion tracking methods. First, an image-based approach was used to derive motion estimates by spatially co-registering the simultaneously acquired MR volumes. Using this method, the proposed MC algorithm was tested and validated for a wide range of translations and rotations in phantoms. Next, human volunteer studies were performed and motion estimates were obtained from EPI data every TR (e.g. every 3 s). This method is particularly attractive because it allows the simultaneous acquisition of fMRI and PET data. Finally, motion estimates were obtained every 20 ms using cloverleaf navigators. Similar to the previous method, this has the advantage of not interfering with the standard MR data acquisition. Furthermore, the high temporal resolution motion estimates can be used to correct the PET data in very short frames (e.g. 1 s). Our results suggest that MR-based MC has the potential to improve PET as a quantitative method. First, the nominal spatial resolution of the current state-of-the-art scanners can be achieved. Second, the mismatch between the attenuation and emission volumes can be eliminated. Third, better estimates of the radiotracer AIF can be obtained using image based approaches. Together these methods could increase the reliability and reproducibility of the PET data and this could potentially benefit a number of neurological applications that require precise quantification (e.g. neuroreceptor studies, therapy monitoring) or that involve uncooperative subjects (e.g. AD, movement disorders or pediatric patients).



Presentation Number **0318B**
 Poster Session 4a: Imaging Instrumentation and Methodology

Localization of Subcutaneous, Intraperitoneal and Secondary Tumor Sites Utilizing an animal rotation device and a Multimodal Imaging System

Sean P. Orton¹, Gilbert D. Feke¹, **John Pizzonia¹**, Gil G. Mor², Jingyi Pan¹, Rao V. Papineni¹, Douglas Vizard¹, William McLaughlin¹,
¹Molecular Imaging, Carestream Health, Woodbridge, CT, USA; ²OB/GYN, Yale University, New Haven, CT, USA. Contact e-mail: john.pizzonia@carestreamhealth.com

Non-invasive in-vivo optical imaging has been increasingly used in the pre-clinical arena. Tumorigenesis studies, in particular, have lent themselves to fluorescent tracking as a means of tumor detection, growth monitoring, and for determining the efficacy of treatment(s). Monitoring the growth and early detection of tumors at both the primary and secondary sites is of principle concern to the researcher. Light scattering, narrow visualization windows in deep tissue, and inability of fluorescent signal to penetrate completely through animal models further compounds the difficulties of the researcher. As a result, optimal detection of signal often requires the animal to be positioned at an optimal orientation; one in which the origin of the fluorophore is positioned so that the excitation and emission light has to travel through less tissue. Furthermore, in many studies tumors originate from an unknown location, making it difficult for the researcher to properly position the mouse for optimal detection of tumors. To overcome these issues, we have developed a murine rotation device for use in a commercially available Multimodal Imaging System that enhances detection through visualization of the mouse at multiple angles. To enhance detection of optical signal originating from tumors, 360 degree rotations on mice were completed, with multimodal (Near-Infrared, X-ray, reflectance) images taken at every 10 degrees. Acquiring images at these precise angles enhanced quantitation and detection of tumors. This novel animal rotation device was demonstrated to be a useful system for detection and longitudinal tracking of subcutaneous, intraperitoneal, and secondary tumor sites non-invasively in live mice.

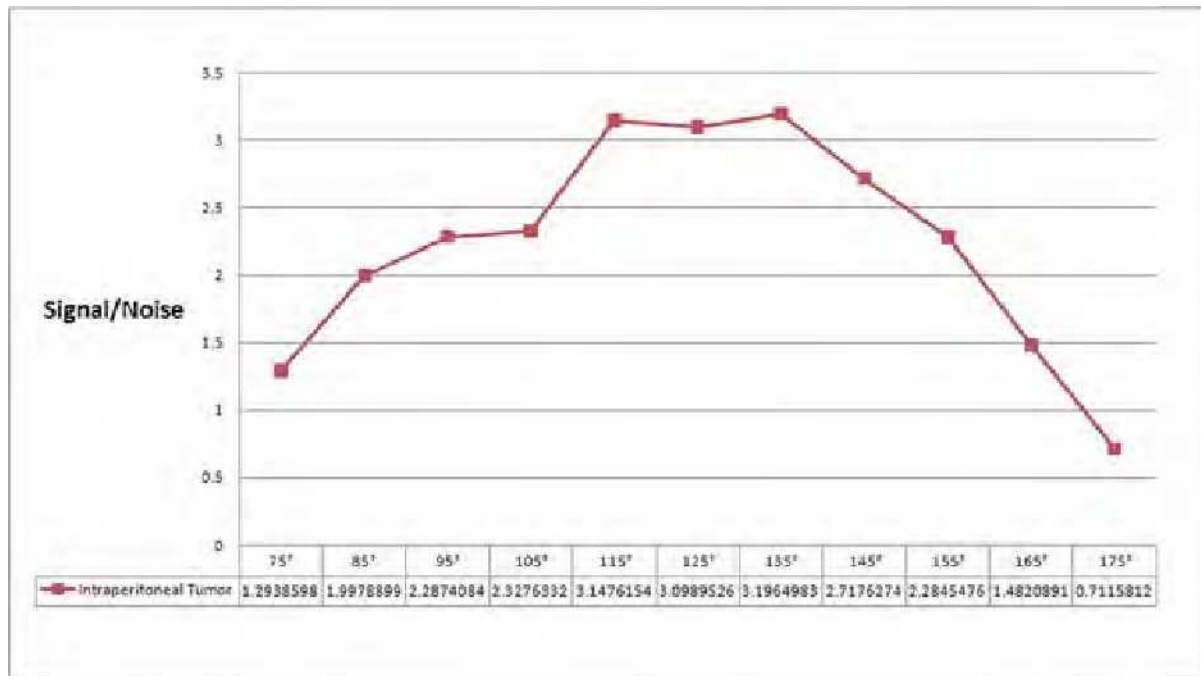


Figure 1: Signal/Noise ratio of intraperitoneal (i.p.) tumor as a mouse is driven to precise angles of rotation. IP tumor site would not be visualized at prone or supine positions and non-optimally at lateral position. (i.p. tumor site confirmed ex-vivo).

Presentation Number **0319B**
 Poster Session 4a: Imaging Instrumentation and Methodology

A phantom design for fully automatic image co-registration for combined hybrid imaging systems

Thomas S. Ng¹, Daniele Procissi^{2,1}, Hargun Sohi¹, Yibao Wu³, Simon R. Cherry³, Russell Jacobs¹, ¹Biology, Caltech, Pasadena, CA, USA; ²Radiology, Northwestern University, Chicago, IL, USA; ³Biomedical Engineering, UC Davis, Davis, CA, USA. Contact e-mail: thomasn@caltech.edu

Increasing efforts are being devoted to develop and validate hybrid techniques for multimodality imaging of biological processes in vivo. Several dual modality platforms have been successfully developed and tested. For example, positron emission tomography (PET) has been combined with computed tomography (CT), magnetic resonance imaging (MRI) and optical tomography. The major advantage of these methods lies in the possibility of imaging the same living subject in a single session, in some cases simultaneously. A vital component for multimodal imaging is the requirement of accurate spatial co-registration of the separate image spaces. Significant efforts have been devoted to cross-modal registration in small animal imaging, based upon optimizing animal holders and utilizing manually segmented phantom designs. Hybrid imaging systems adds an extra complexity; the geometry constraints of integrated systems along with the disparate field of view between the individual modalities require a modification to previous approaches. A registration phantom design that can be adapted for different hybrid systems and can perform image registration automatically is highly desirable. Here, we evaluate a phantom design adapted for use in a MR-compatible PET insert for simultaneous PET/MR imaging. The phantom design allows simple image acquisition, fully automatic segmentation of the phantom components and subsequent image co-registration. We compare the registration error of this fully automated strategy with our previous semi-automatic alignment strategy. Both strategies aligned the PET and MR image spaces to within single voxel accuracy throughout the whole field of view of the combined scanner with no significant difference of registration errors (two-sample t test: $p = 0.2$). In addition to providing equivalent co-registration results the automatic alignment strategy guarantees a non biased, fast and versatile tool which could be adapted easily for other types of combined imaging systems.



MRI of phantom PET of phantom co-registered phantom

MR, PET images of alignment phantom (left, center). Overlaid aligned images after automatic alignment (right).
 Alignment error comparison between automated and semi-automated alignment methods

Method	Alignment error (mm)
Semi-automated	0.12016
Full-automated	0.11301

Presentation Number **0320B**

Poster Session 4a: Imaging Instrumentation and Methodology

Simultaneous SPECT-MRI System Design for Human Brain and Pediatric Research

James W. Hugg¹, Douglas J. Wagenaar¹, Dirk Meier², Benjamin M. Tsui³, Orhan Nalcioglu⁴, Samir Chowdhury¹, Bradley E. Patt¹,
¹Research, Gamma Medica-Ideas, Northridge, CA, USA; ²Research, Gamma Medica-Ideas, Oslo, Norway; ³Radiology, Johns Hopkins University, Baltimore, MD, USA; ⁴Radiology, University of California, Irvine, CA, USA. Contact e-mail: james.hugg@gm-ideas.com

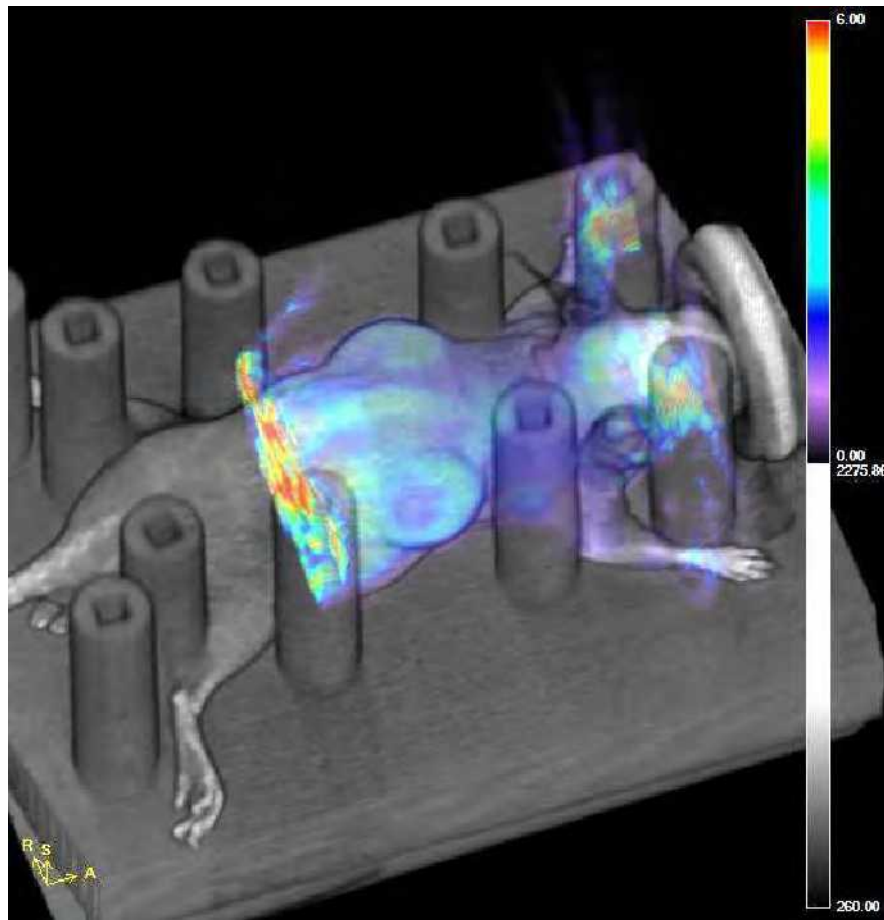
Feasibility studies with our simultaneous SPECT-MRI prototype systems for mouse studies have validated the design concepts and subsystem components. We now present a scaled-up design intended for use in both human brain and pediatric whole-body research. Our mouse prototype system was designed for 3T - 9.4T magnets with a 20 cm diameter warm bore. The insertable magnet field gradient provides a 12 cm inner diameter for the MR-compatible SPECT system. The MR-compatible gamma detector uses our pixellated CZT semiconductor modules with custom-designed electronics and packaging. In one prototype, three rings of eight detectors have an azimuthal offset between rings to increase angular coverage. Collimation is provided by a stationary tungsten-compound cylinder with multiple-pinholes. We have designed a larger detector ring system that will also accommodate rats, requiring a 30 cm magnet warm bore and 20 cm gradient bore. In a second prototype for use in larger animal or human whole-body MRI systems, multiple small gamma cameras with flat-panel CZT arrays are collimated by parallel-hole or converging collimators. The small gamma cameras can be rotated around the field of view to acquire angular samples for SPECT imaging. The collimated gamma detectors can be integrated into the RF coil. One advantage for the stationary full-ring system is the demonstrated ability to acquire rapid (3 second bins) dynamic images, useful for pharmacokinetic studies. Our iterative image reconstruction accounts for detector interactions with the magnetic field, including the Lorentz displacement of the semiconductor charge cloud. There is no significant degradation of spin-echo MR images when the SPECT system is stationary. Although gradient-echo images are sensitive to the proximity of metal, cylindrical symmetry minimizes this effect. MR imaging can be paused when SPECT system motion is required by the modular cameras. We designed a full detector ring system for use in human whole-body MRI systems to simultaneously image human brain or small pediatric patients. We are optimizing the design by using computer modeling. The 3T design integrates a birdcage RF coil and a cylindrical multiple-pinhole collimator. The SPECT-MRI system will provide simultaneous multiple-isotope and dynamic molecular imaging contrast, co-registered in space and time with high-resolution anatomic MRI. This hybrid system will be first applied to diagnosis, drug development, and therapy monitoring in neurodegenerative and psychiatric diseases, as well as oncology and pediatric cardiology.

Presentation Number **0321B**
Poster Session 4a: Imaging Instrumentation and Methodology

Multi-modal Immobilization Bed for Mice for Serial Imaging

Geoffrey S. Nelson^{1,2}, *Magdalena Bazalova*², *Marta Vilalta*², *Jessica R. Perez*², *Rehan Ali*², *Edward E. Graves*², ¹*Bioengineering, Stanford, Stanford, CA, USA;* ²*Radiation Oncology, Stanford, Stanford, CA, USA.* Contact e-mail: geoffsn@stanford.edu

Purpose: To make an immobilization bed for mice which will facilitate longitudinal PET studies. Given the nature of such studies the bed needed to be capable of not only immobilizing, but keeping the mouse in the same position as previous scans. It also needed to be capable of both imaging mice of various sizes and registering the PET images with CT. **Method and Materials:** The bed was with acrylic to enable use with optical imaging including 3d optical imaging. Measurements of multiple mice of various ages and species were made in order to find the optimal size for the bed and for the immobilizing pegs. The pegs are in stationary positions which effectively immobilize most mice and enables high throughput imaging by avoiding adjustments for every mouse. The pegs are placed such that the front legs of the subject are each placed between two pegs as are the hind legs. An additional set of pegs are placed laterally and posteriorly to guide the hind legs in a reproducible direction. Na-22 PET/CT fiducials were put in the pegs at unique depths to enable fast and accurate image registration. **Results:** The fiducials have allowed for easy CT registration. Two users registering the same images were able to quickly and very accurately register images acquired with the bed relative to each other ($6\text{min} \pm 1\text{min}$ & $0.5\text{mm} \pm 0.5\text{mm}$) as compared to registration without the bed ($16\text{min} \pm 6\text{min}$ and $2.2\text{mm} \pm 2\text{mm}$). Various fused images show instances of common pitfalls in PET/CT registration which are avoided with the use of this bed. A worst-case scenario motion artifact scan was acquired with a mouse after the anesthesia wore off. The mouse was only capable of moving 2.7mm vertically and no movement was made in the horizontal plane. **Conclusion:** The bed is effective in immobilization and image registration. Its use in pre-clinical work will improve image registration and temporal resolution in longitudinal PET studies. This will be vital in many studies including the elucidation of minute changes in serial PET scans.



Presentation Number **0322B**

Poster Session 4a: Imaging Instrumentation and Methodology

Dual Mouse Parallel Coil Array and Transportable Bed for Sequential Multimodality MR, PET, and SPECT/CT Imaging

Marcelino Bernardo^{1,2}, **Gabriela Kramer-Marek**³, **Jurgen Seidel**^{1,2}, **Michael Green**^{1,2}, **Jacek Capala**³, **Peter Choyke**², ¹*Imaging Physics, SAIC-Frederick, Frederick, MD, USA;* ²*Molecular Imaging Program, National Cancer Institute, Bethesda, MD, USA;* ³*Radiation Oncology Branch, National Cancer Institute, Bethesda, MD, USA. Contact e-mail: bernardom@mail.nih.gov*

Mice are commonly scanned in pairs during pre-clinical PET and SPECT imaging studies in order to increase throughput and efficiently utilize the short-lived radioactive tracer isotopes. In tumor model studies involving mouse xenografts where the tumor cells are injected subcutaneously, registration to anatomic CT images that are common in hybrid systems are usually sufficient but not always required to confirm and determine agent uptake in the tumor. When the studies involve orthotopic or genetically engineered mouse models, however, registration to MR is more effective due to the superior soft tissue contrast. However, hybrid preclinical PET/MR or SPECT/MR systems are not widely available, and they often require a compromise in performance from either modality. A more practical method is to perform the scans sequentially and transport the mouse bed into the MR after completion of the PET or SPECT scans. We found this scheme to be necessary in a F-18 imaging study of a lung tumor metastasis model where we used a full mouse 44 mm OD receiver coil for a clinical 3.0 T MR scanner that can accommodate the PET and SPECT/CT single mouse bed. Since the bed can only hold one mouse, the PET study took more than twice as long as PET only studies where we can scan two mice simultaneously. In order to increase throughput of the sequential PET-MR study, we designed and constructed a Dual Mouse Parallel Coil Array and Transportable Bed (DUMPCART) that is compatible with our existing PET and SPECT/CT animal bed system. The dual coil array is comprised of a four-element array that covers the mouse abdomen while the double bed provides for gas anesthesia, air heating, and respiration sensor. Corregistration of the PET or SPECT images to the MR images were easily performed using a freely available DICOM viewer (Osirix). This method will facilitate the testing of novel targeted PET and SPECT diagnostic and therapeutic agents.

Presentation Number **0323B**

Poster Session 4a: Imaging Instrumentation and Methodology

Co-registration of in vivo Optical Tomography and Micro-CT for Longitudinal Studies

Heng Xu, Anna Christensen, Chaincy Kuo, David Nilson, Ed Lim, Jay Whalen, Jae-Beom Kim, Ning Zhang, Raj Singh, Stephen J. Oldfield, Tamara L. Troy, Brad Rice, Caliper Life Sciences, Alameda, CA, USA. Contact e-mail: heng.xu@caliperls.com

In vivo optical molecular imaging is a powerful tool to study pre-clinical animal models. While it can provide 3D distribution of bioluminescent or fluorescent probes quantitatively, the utility can be strengthened by incorporating high resolution anatomical information from other modalities, such as micro-CT. Standalone optical imaging systems offer the best quantitative analysis and dedicated micro-CT imaging systems offer the best resolution, but present the challenge of accurate and robust co-registration between two modalities. A novel co-registration scheme that involves an animal restraining bed and manual or fiducial registration methods is presented for combining in vivo optical tomography and micro-CT modalities. The bed equipped with gas anesthesia connections helps maintain the animal position during the transition between the systems. An innovative fiducial design using a position encoded pattern allows accurate registration of the CT volume to optical coordinates even when only a portion of the subject is scanned at high resolution. 3D reconstructions of optical and x-ray modalities can be performed, visualized and finally co-registered within the same software. A dedicated high sensitivity optical imaging instrument optimized for in vivo detection of both fluorescent and bioluminescent probes is used with a stand-alone micro-CT system. The micro-CT system uses a fast and low-dosage CT technology suitable for non-invasive longitudinal studies and typical imaging time is 17s with the dose of 11mGy. We applied this optical and micro-CT multimodal imaging scheme to assess tumor development and osteolytic activities in mice that were intra-cardiacally delivered with MDA-MB-231 D3H2 LN-Luc cells. Optical imaging allows functionally sensitive and longitudinal detection of tumor metastases. As tumors progressed, high resolution CT scans tracked morphological changes and showed the presence of osteolytic lesions at the site of metastases. 3D reconstruction of bioluminescence signals were nicely correlated with the bone degradation induced by the osteolysis. The combined multi-modal imaging scheme provides an exquisite platform for longitudinal assessment of disease development in aspect of both biological functionality and anatomical location.

Presentation Number **0324B**

Poster Session 4a: Imaging Instrumentation and Methodology

Assessment technology of a rat myocardial infarct size using ^{18}F -FDG PET and contrast enhancement CT polar map

Sang-Keun Woo, Gi Jeong Cheon, Kyeong Min Kim, Yong Jin Lee, Ji-Ae Park, WonHo Lee, Yin Ohk Ko, Jin Su Kim, Jong Guk Kim, Young Hoon Ji, Chang Woon Choi, Sang Moo Lim, Molecular Imaging Research Center, KIRAMS, Seoul, Republic of Korea. Contact e-mail: skwoo@kcch.re.kr

The aim of this study was to improve quantitative assessment of rat myocardial infarct size using attenuation corrected PET polar map with gated CT image and contrast enhanced CT polar map. The PET/CT images obtained with a small animal PET/CT scanner (InveonTM, Siemens). The experimental conditions were feeding, warming, and 2% isoflurane anesthesia. Gating was realized with the help of an external trigger device (BioVET). PET imaging was started 60 min after the administration of 30 MBq of ^{18}F -FDG via tail vein injection. The three bed CT images for attenuation map were acquired with following settings: X-ray voltage of 70 kVp, anode current of 400 μA , an exposure time of 200 milliseconds for each of 360 rotational steps. Contrast enhanced CT images of heart were obtained at second bed after injection of contrast agent using catheter. The pixel size of PET/CT image was being converted to automated myocardial wall detection by the QGS software used to process the gated image series. The SUV PET image pixel size was Percent variation was calculated anterior wall (ANT), septal wall (SEP), inferior wall (INF) and lateral wall (LAT) in polar map. Homogeneity was calculated no corrected PET (NC), attenuation corrected PET with CT image (AC-CT), attenuation corrected PET with gated CT image (AC-gCT) and attenuation corrected gated PET with gated CT image (gAC-gCT). The contrast enhanced CT images show the better image quality in myocardium. The contrast of no gating and gating CT image was 4.99 and 2.77, respectively. The SNR of no gating and gating CT image was 4.9 and 5.4, respectively. The NC and AC-CT image percent variation of ANT, SEP, INF and LAT was -0.42%, 1.61%, -0.41% and -0.86%, respectively. The gAC-gCT image percent variation of ANT, SEP, INF and LAT was 3.74%, 1.21%, 3.28% and 4.29%, respectively. The homogeneity of NC, AC-CT, AC-gCT and gAC-gCT was 0.054, 0.062, 0.112 and 0.049, respectively. The gated CT attenuation corrected gated PET polar map homogeneity was improved myocardial activity in anterior, inferior and lateral region. Contrast enhanced CT image based polar map will be a useful method for measurement of myocardial infarction size.

Presentation Number **0325B**
Poster Session 4a: Imaging Instrumentation and Methodology

¹⁸F-FDG PET-MRI can be Used to Identify Injured Peripheral Nerves in a Model of Neuropathic Pain

Deepak Behera, Kathleen E. Jacobs, Subrat Behera, Sandip Biswal, Radiology, Stanford University, Stanford, CA, USA. Contact e-mail: biswals@stanford.edu

Purpose: Increased spontaneous neural activity and metabolic changes are known to occur in injured nerves and contribute to the symptoms of neuropathic pain. Using ¹⁸F-Fluorodeoxyglucose (¹⁸F-FDG) positron emission tomography-magnetic resonance imaging (PET-MRI), we wanted to determine whether increased ¹⁸F-FDG uptake is observed in injured peripheral nerves in a rat model of neuropathic pain. Methods: Animal experiments were approved by Stanford IACUC. Neuropathic pain model of Spared-Nerve Injury (SNI) and control sham-operated animals were created (adult male Sprague-Dawley rats; n=3 each group). SNI was created by ligating and transecting branches of the left sciatic nerve. The right sciatic nerve served as an internal control. Rats were allowed 4 weeks to heal and develop pain. Presence of pain was confirmed by testing for allodynia. Rats were given 500 μ C of ¹⁸F-FDG IV under anesthesia. Animals were held rigidly in a transportable holder with attached MR- and PET-compatible fiducials. Ten minute static scans of the thighs were obtained using a small animal PET (microPET; R4 microPET, Siemens). T1-weighted FSE images were obtained using a 7T small-animal MRI (microMRI; Magnex). MicroPET-MR image fusion was performed using Amide software. MicroMR images were used to define the anatomic localization of the peripheral nerves and placement of volumetric ROIs containing 2 mm segments of either sciatic nerve, proximal to the level of injury. Radioactivity counts were then recorded from the fused images. Additionally, background ROIs were placed in the adjacent muscle on each side and a signal-to-background ratio (SNR) was obtained. Data were analyzed using paired t-tests (significance is p<0.05). Results: In SNI rats, allodynia in the operated limb was confirmed. The 50% paw withdrawal threshold 2.6 ± 0.1 and 4.3 ± 0.2 on the SNI and control side, respectively (p<0.01). Significantly increased ¹⁸F-FDG SNR was seen in the SNI nerve (1.7 ± 0.3) compared to control side (1.0 ± 0.3) (p<0.03). In sham-operated rats, no allodynia was seen in the operated limb (50% paw withdrawal threshold 4.9 ± 0.0 and 4.9 ± 0.1 on the operated and control side, respectively). In sham-operated animals, ¹⁸F-FDG SNR in the left sciatic nerve is not statistically significant compared to the control, (1.2 ± 0.2 vs. 1.0 ± 0.1 , respectively; p>0.05). Conclusion: Animals with neuropathic pain show significantly increased ¹⁸F-FDG uptake in the injured nerve. The hybrid ¹⁸F-FDG PET-MRI method can potentially be used to accurately localize injured peripheral nerves in neuropathic pain.

Presentation Number **0300A**
Poster Session 1a: Imaging Instrumentation and Methodology

The effect of Mild Hyperthermia on Extravasation of USPIO Particles in a murine tumor model

Claus Tvedesoe¹, **Thomas Nielsen**^{3,2}, **Esben Larsen**⁴, **Michael Horsman**³, **Steffen Hokland**^{2,3}, ¹orthopaedic research center, Aarhus University Hospital, Aarhus, Denmark; ²MR research center, Skejby Hospital, Aarhus, Denmark; ³Department of Clinical Experimental Oncology, Aarhus University Hospital, Aarhus, Denmark; ⁴Interdisciplinary Nanoscience Center, University of Aarhus, Aarhus, Denmark. Contact e-mail: tvedesoe@ki.au.dk

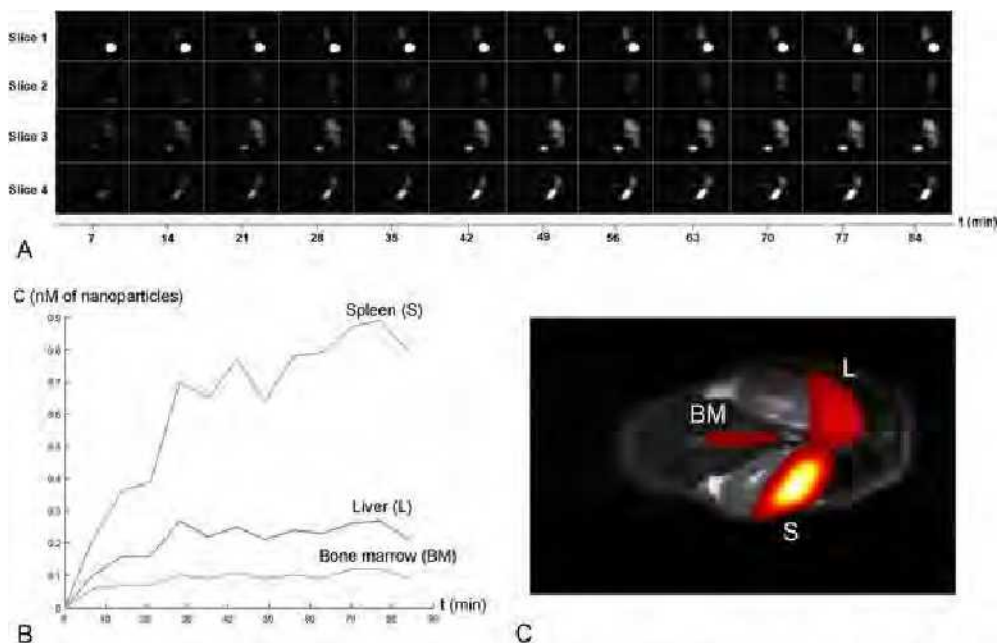
INTRODUCTION Tumor vasculature is highly disorganized and many solid tumors contain significant fractions of hypoxic and acid regions. This complicates treatment with chemotherapeutics. Ultrasmall Iron Oxide (USPIO) particles have super-paramagnetic characteristics. It is possible to attach various compounds to USPIO particles such as chemotherapy and silencing RNA sequences. Mild hyperthermia can disrupt tumor vessel endothelial barrier allowing USPIO particles to diffuse into the interstitial space of tumor. In this study we have investigated the effect of various lengths of localized mild hyperthermia on the extravasation of i.v injected USPIO particles in a murine tumor. **METHODS:** Mammary carcinoma tumors were grown in the rear right foot of 10-14 weeks old female CDF1 mice. Hyperthermia Heat treatment was performed locally by submerging the tumor bearing foot in a circulating water bath mo. The water temperature was set to 41.5 °C. Animals were randomized into four groups receiving either 1, USPIO particles only; 2, USPIO particles and 5 min of hyperthermia; 3, USPIO particles and 30 min of hyperthermia and 4, USPIO particles and 60 min of hyperthermia. N=9 in each group. Animals were MR scanned prior to injections and again after 90-, 390- and 1140 min. **RESULTS SECTION:** Change in T2* in response to heating length shows a significant difference between animals heated for 30- and 60 minutes compared to animals heated for only 5 minutes and controls having received only USPIO particles and no heat ($p < 0.05$). T2* decreases rapidly by the time of the first scan (90min) and incline slightly on scans 390, 1140 min. After 1140 min (24h) the T2* value in the control group, is 39.5 +/-4.3 compared to 27 +/-3.2 in the group receiving heat for 60 minutes and after 90 min the values are 31+/- 5.6 and 10 +/-2.1. There is a fine relationship between heating length and T2* value throughout the data. **DISCUSSION:** The heating length seems to be of great importance when it comes to the amount of USPIO particles being trapped in the tumor. We expect that the mechanism behind the retention in tumor is the enhanced permeability and retention effect that is being further potentiated by the localized mild hyperthermia leading to increasingly permeable tumor vessels. The optimal heating length seems to be 30 minutes, with very little benefit of going up to 60 minutes.

Presentation Number **0301A**
 Poster Session 1a: Imaging Instrumentation and Methodology

Dynamic and quantitative assessment of the biodistribution of a perfluorooctylbromide emulsion in mice by *in vivo* ^{19}F MRI

Céline Giraudeau¹, Benjamin Marty¹, Julien Flament¹, Sébastien Mériaux¹, Fawzi Boumezbear¹, Boucif Djemaï¹, Sidi Mohamed Ould Ahmed Ghaly¹, Caroline Robic², Marc Port², Philippe Robert², Franck Lethimonnier¹, Denis Le Bihan¹, Julien Valette¹, ¹NeuroSpin, I2BM, Commissariat à l'Energie Atomique, Gif-sur-Yvette, France; ²Guerbet, Research Division, Aulnay-sous-Bois, France. Contact e-mail: celine.giraudeau@cea.fr

Introduction Perfluorooctylbromide (PFOB) emulsion is a promising tracer for ^{19}F MRI. Thanks to its biocompatibility, it has potential medical applications including oxygen carrying and sensing, tumor imaging, atherosclerotic plaques detection and cell tracking. After intravenous injection, PFOB emulsion is known to localize in the reticuloendothelial system, mainly the liver and spleen where it accumulates within macrophages, before being excreted by the lungs. However, the kinetics of this emulsion is unknown within the minutes following injection, which can be critical when PFOB is coadministered with drugs. We show here that ^{19}F MRI is an efficient technique to monitor the biodistribution of PFOB emulsion, with no need to sacrifice animals at successive time intervals. **Method** The low concentration of PFOB in tissues and the need to acquire images fastly requires a high sensitivity acquisition method. Therefore our recent multi spin-echo sequence allowing *in vivo* imaging of PFOB with an excellent sensitivity (Magn Res Med 63:1119-24, 2010) was used. After a bolus injection of a PEGylated PFOB emulsion (200 μL , 20% w/w) in the tail vein, ^{19}F images were acquired every seven minutes. The concentration of nanoparticles was quantitatively derived using an internal reference with known concentration. **Results** ^{19}F signal appears in the liver, spleen and bone marrow from the first minutes, reflecting an immediate activation of the macrophages in these organs. Concentrations in PFOB rapidly level off in the liver and bone marrow, whereas the kinetics is slower in the spleen, but reaches a higher level. **Discussion and conclusion** Our method allows non-invasive, quantitative assessment of the kinetics of PFOB emulsions in the reticuloendothelial system, despite probable uptake by macrophages. One of our objectives is now to assess the stealth of these emulsions for different levels of PEGylation, in order to optimize pharmaceutical targeting.



(A) Evolution of ^{19}F signal as a function of time in coronal images of a mouse injected with 200 μL of our PFOB emulsion and superposition. Four 5-mm-slices are displayed from belly (slice 1) to back (slice 4). The big white spot seen in slice 1 is the reference of emulsion placed for signal calibration. Images were performed at 7T with a Bruker PharmaScan and a $^1\text{H}/^{19}\text{F}$ linear birdcage coil.

(B) Corresponding concentration curves in the different organs (slice 4)

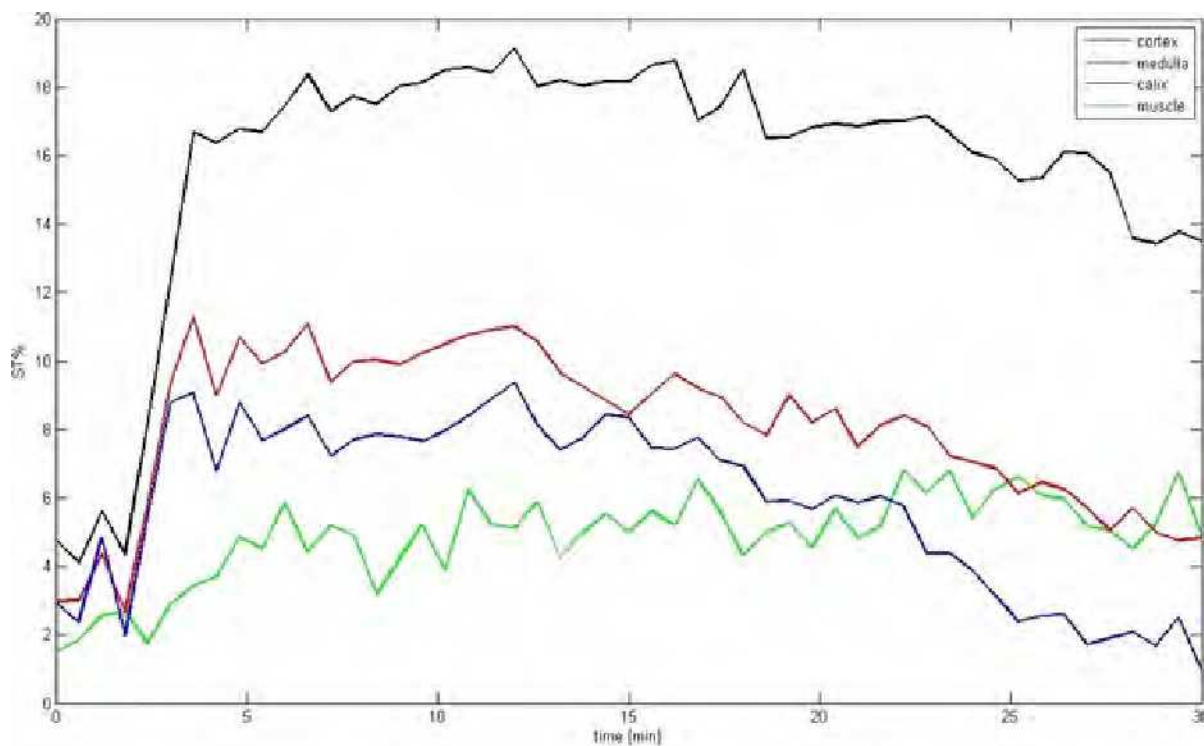
(C) Superposition of ^{19}F image (in red, slice 4) with anatomical ^1H image at $t=84$ min

Presentation Number **0302A**
Poster Session 1a: Imaging Instrumentation and Methodology

A fast acquisition scheme for dynamic CEST detection

Dario L. Longo, Evelina Cittadino, Enzo Terreno, **Silvio Aime**, Department of Chemistry IFM / Molecular Imaging Center, University of Torino, Torino, Italy. Contact e-mail: silvio.aime@unito.it

Chemical Exchange Saturation Transfer (CEST) is an emerging MRI method covering a wide range of in vivo imaging application. For Diamagnetic CEST contrast molecules, a correct saturation transfer (ST%) quantification requires long and selective irradiation pulses of the mobile proton pool and the acquisition of many images at different frequency offsets (Z-spectrum), thus making a CEST experiment a time-consuming procedure depending on the number of sampled frequency offsets. Many efforts have been addressed to reduce the k-space acquisition time, even though most of the scan time is spent on the long saturation step. In this study we developed a fast acquisition scheme, by i) optimizing the number of frequency offsets centered around the resonant frequency of the mobile proton pool and ii) acquiring first a complete Z-spectrum followed by the sampling of a limited number of frequency offsets and then replacing these points in the first Z-spectrum, for an accurate ST% quantification. This new acquisition scheme allows to distinguish the characteristic ST% time course for individual voxels in different anatomical regions, thus improving the temporal resolution without sacrificing the ST% accuracy. ST% accuracy was compared on simulated Z-spectra (interpolated with B-splines) by taking into account: the number of points around the resonant frequency, the frequency width, the line width of the DIACEST peak and the presence of zero shifts. In in vivo CEST images were acquired first with a complete Z-spectrum (single-shot RARE spin-echo, TR 6 s, centric encoding, MTX 64) followed, upon injection of a Diacest agent by the dynamic acquisition of only 3 points around the resonant frequency (both at positive and negative offsets) for 30 min (50 scans). The optimized acquisition scheme displayed mean ST errors lower than 1%, in comparison with a full Z-spectrum. In in vivo the dynamic acquisition allowed to differentiate pixels in kidneys and other anatomical regions according to their ST% time course. The application of the above described methodology allowed also to follow pH changes of mouse kidney upon the administration of a ratiometric pH responsive agent.



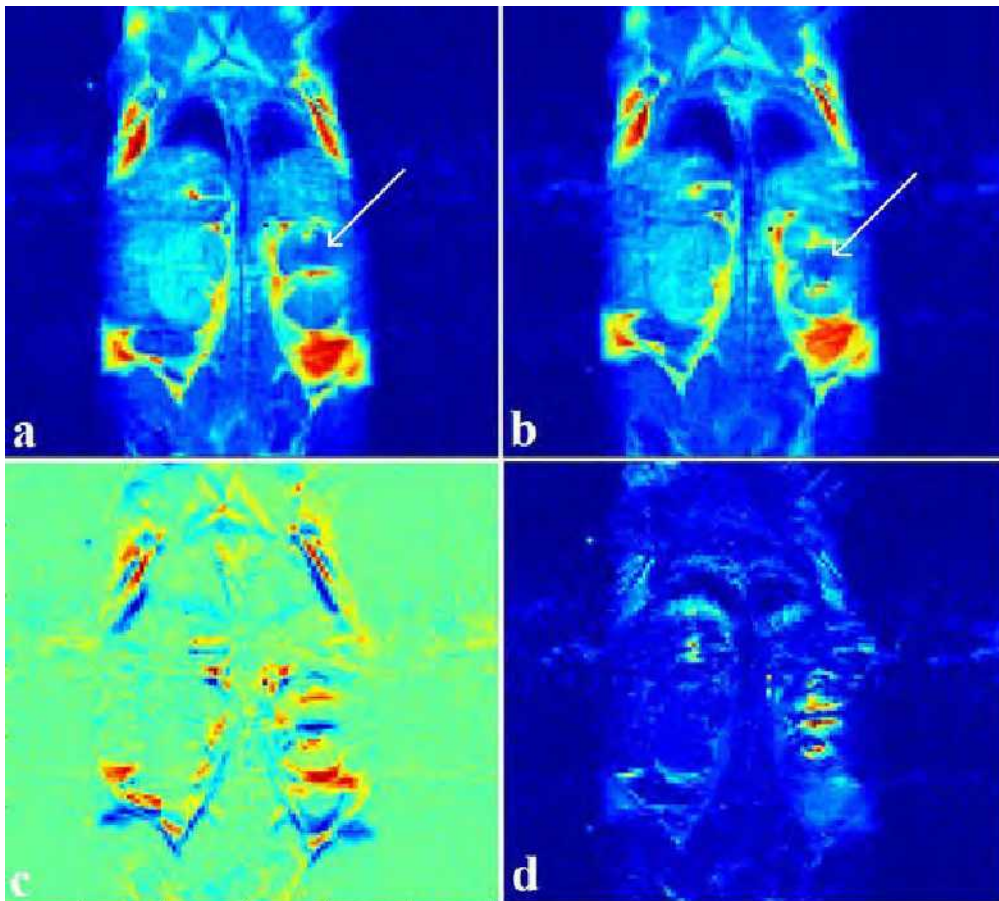
ST% time course for different anatomical region

Presentation Number **0303A**
Poster Session 1a: Imaging Instrumentation and Methodology

Enhanced MRI of SPIO-labeled Tumor by Images from Opposite Readout Gradients

Haitao Zhu, Kazuyuki Demachi, Department of Nuclear Engineering, The University of Tokyo, Tokyo, Japan. Contact e-mail: htzhu@nuclear.jp

Cells labeled by superparamagnetic iron oxide nanoparticles (SPIOs) produce dark signal with conventional imaging methods as a result of decreased effective transverse relaxation time T_2^* . It is a challenge to differentiate the dark signals of SPIOs from other dark components such as voids, calcification or water/lipid interface. In this work, an enhancing method is proposed to magnify the signal from SPIOs by two images from opposite readout gradients. **Method:** Coexistence of readout gradient and magnetic field distortion leads to a positional shift in the reconstructed image based on Fourier transform theory, $\sigma = \Delta B / G_{\text{read}}$. Therefore, if two images scanned with opposite readout gradients are subtracted, signal from uniform magnetic field get canceled but the signal from SPIOs are preserved because their positional shifts are toward opposite directions. A problem of this subtracting method comes from the chemical shift effect that leads to misregistration of water and lipid. In this work, misregistration is corrected in k-space using "energy of image" as a criterion to determine the optimal value to compromise the influence from both water and lipid. In vivo experiments were performed at 6 nude mice with a 4.7 Tesla Varian MRI system. BxPC-3 cells were labeled by SPIOs (Resovist) at iron concentration of 50 $\mu\text{g}/\text{ml}$ and implanted subcutaneously into the nude mice. MRI scanning was performed one week after implantation by spin echo protocol with opposite readout gradients. **Result:** Fig. *a* and *b* are the spin echo images with opposite readout gradients. Tumor region labeled by SPIOs (arrow position) appears low signal but it is less recognizable at the presence of other low-signal components. Fig. *c* is the subtraction between *a* and *b*, where lipid signal cannot get fully canceled due to chemical shift misregistration. Fig. *d* is the subtracted image after correcting misregistration, where the signal from uniform magnetic field is suppressed and the signal from SPIO-labeled tumor gets enhanced.



Presentation Number **0304A**
 Poster Session 1a: Imaging Instrumentation and Methodology

Apparent diffusion coefficient of Gd-based contrast agents assessed in vivo in the rat brain using MR dynamic T1 mapping

Benjamin Marty¹, Julien Flament¹, Céline Giraudeau¹, Boucif Djemai¹, Caroline Robic², Marc Port², Denis Le Bihan¹, Fawzi Boumezbeur¹, Julien Valette¹, Franck Lethimonnier¹, Sébastien Mériaux¹, ¹CEA/DSV/I2BM/Neurospin, Gif-Sur-Yvette, France; ²Research Division, Guerbet, Roissy-Charles de Gaulle, France. Contact e-mail: sebastien.meriaux@cea.fr

INTRODUCTION. Gadolinium-based contrast agents (Gd-based CA) have been used for many years for various MRI applications including more recently molecular imaging with targeted compounds. One of the most important factors to consider for brain applications is the diffusivity of these probes through the blood-brain barrier and the cerebral tissue to their target. This study proposes a highly sensitive methodology allowing in vivo quantification of Gd-based CA concentration based on the acquisition of MR dynamic T1 maps. This approach has been applied to estimate in the rat brain in vivo the apparent diffusion coefficients (ADC) of five compounds with different hydrodynamic diameters. **MATERIALS AND METHODS.** Anesthetized rats were injected in the brain parenchyma with 2µL of different Gd-based CA. MRI experiments were performed on a 7T preclinical scanner using birdcage 1H coil. T1 maps were acquired before and every 10' after injection with an IR-TurboFLASH sequence (TE/TR=2.4/4.8ms, 30 inversion times spaced by 96.6ms) to produce quantitative concentration maps of the contrast agent. Each concentration map was adjusted with a 2D-Gaussian function (model consistent with a 2D free or tortuous diffusion) to determine an ADC in two orthogonal directions. In vitro experiments were carried out in agar gel in order to validate the model and measure the free diffusion coefficient (D_{free}) and the hydrodynamic size of each compound using Stokes-Einstein law. **RESULTS AND DISCUSSION.** Figure 1 shows the calculated quantitative concentration maps of one Gd-based CA along the 2h acquisition after injection revealing its diffusion through the cerebral tissue. Mean apparent diffusion coefficients of the five Gd-based CA are given in Table 1. They are in good agreement with studies performed using other techniques (optical imaging, radiotracers, ...) and show a consistent behavior with the inverse of hydrodynamic diameter as predicted by Stokes-Einstein law (Fig.3). **CONCLUSION.** In this study, we have demonstrated that diffusion of Gd-based CA with size up to 25nm can be investigated in vivo using dynamic T1 mapping in the rat brain. MRI seems to be a promising tool in order to understand diffusion mechanisms of supra-molecular probes in brain tissues, particularly in deep regions which are more difficult to access using other techniques such as optical imaging.

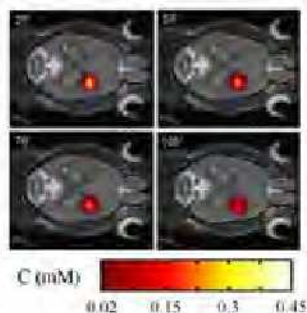


Fig. 1 Concentration maps of P792 27', 53', 79' and 105' after injection

PCA	D _{free} (x10 ⁻¹⁰ m ² /s)	d _{hydro} (nm)	ADC (x10 ⁻¹⁰ m ² /s)	z
Diamrom	40.5	1.1	4.6	3.33
P1152	30.5	2.15	1.5	4.0
TB46	15.5	4.2	1.35	3.38
P792	8.75	6.7	0.83	3.43
P904	3.2	21.2	0.24	3.65
TR-dex3	32.2	2.95	3.4	2
TR-dex70	4.67	14.1	0.6	2.8

Table 1 Measured diffusion parameters for the contrast agents (* Thorne et al. PNAS. 2006)

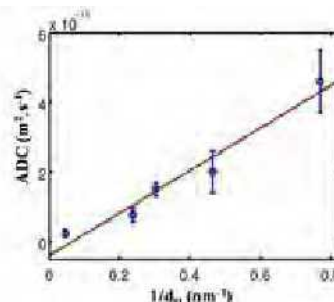


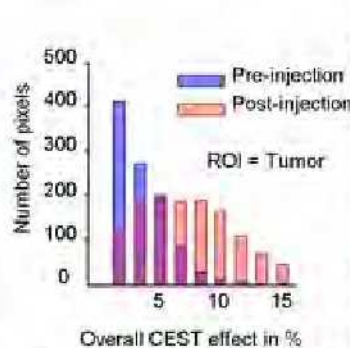
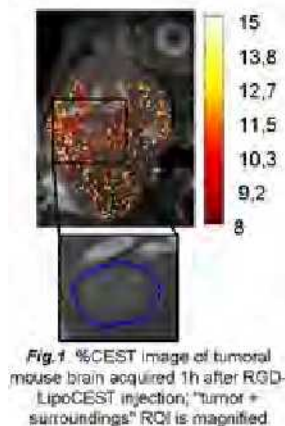
Fig. 2 In vivo verification of Stokes-Einstein law for small molecules

Presentation Number **0305A**
 Poster Session 1a: Imaging Instrumentation and Methodology

In vivo $\alpha_v\beta_3$ CEST-based molecular imaging using RGD-LipoCEST in U87 mice brain tumor

Julien Flament¹, Boucif Djemai¹, Françoise Geffroy¹, Benjamin Marty¹, Céline Giraudeau¹, Sébastien Mériaux¹, Julien Valette¹, Christelle Medina², Caroline Robic², Marc Port², Franck Lethimonnier¹, Gilles Bloch¹, Denis Le Bihan¹, **Fawzi Boumezbeur¹**,
¹NeuroSpin, CEA/DSV/I2BM, Gif-sur-Yvette, France; ²Research Division, Guerbet, Roissy-Charles de Gaulle, France. Contact e-mail: fawzi.boumezbeur@cea.fr

Introduction Recently, LipoCEST were introduced as a new class of paramagnetic contrast agents for CEST-MRI. They provide a tremendous amplification factor and a high biocompatibility and can be easily functionalized by grafting specific peptide targeting pathology specific biomarker. We aim at imaging the integrin $\alpha_v\beta_3$ which is expressed by platelets involved in tumor growth by the mean of a RGD-functionalized LipoCEST. **Subjects and Methods** Animal preparation. Tumor was induced by i.c. injection of U87 cells in four nude mice brain. MRI acquisition. CEST images were acquired using a MSME sequence preceded by a CW saturation pulse ($T_{sat}=400ms$, $B_{1sat} \sim 7\mu T$, $\delta_{sat}=\pm 9ppm$) on a 7T small animal MRI scanner. Images were acquired before (pre-injection) and 1-hr (post-injection) after i.v injection of 200 μ L of RGD-LipoCEST in the tail vein. Image analysis. %CEST images were obtained by the subtraction of images acquired with saturation applied at 9 and -9ppm normalized by the reference image without saturation. %CEST contrast was analyzed in different regions-of-interest (Fig.1). **Results** The average %CEST contrast before injection in the "tumor" is 3.9% (endogenous MT background effect) and rise to 7.2% after injection which corresponds to an 84% elevation of the %CEST contrast following the RGD-LipoCEST injection (Fig.2). In the "controlateral" and "brain" ROIs, elevation of the %CEST contrast are detected as well (+47% and +61%, Tab.1). For mouse #3, no pre-injection acquisition was acquired thus CEST effect was arbitrary set to 6% which corresponds to the maximum MT effect observed. **Discussion and conclusion** %CEST effect increases overall in the brain following i.v. injection. Secondly, the preliminary comparison of %CEST contrast elevations in the tumor and in other part of the brain leads us to think that a majority of the %CEST contrast elevation is due to non-specific binding or distribution of our RGD-LipoCEST CA excepted for mouse #4 which had the smallest tumor. Yet, the higher %CEST contrast elevation in the tumor and its surroundings is a promising result. This study constitutes to our knowledge the first attempt towards brain tumor detection using LipoCEST contrast agents *in vivo*. In a future work, we will try to quantify RGD-LipoCEST associated with specific tumor receptors.



Mouse		Brain	Tumor	Controlateral
# 1	Pre-injection	4.1 ± 2.2	3.9 ± 1.9	4.5 ± 2.3
	Post-injection	6.9 ± 3.4	7.2 ± 3.2	6.6 ± 3.4
	Relative variation	61	84	47
# 2	Pre-injection	4.9 ± 3.9	4.7 ± 4.1	4.8 ± 4.9
	Post-injection	8.6 ± 5.2	7.1 ± 3.9	5.4 ± 3.8
	Relative variation	98	53	34
# 3	Pre-injection	6*	6*	6*
	Post-injection	12.3 ± 6.2	16.3 ± 5.8	7.9 ± 4.7
	Relative variation	105	172	32
# 4	Pre-injection	3.1 ± 2.4	3.1 ± 2.5	2.8 ± 2.3
	Post-injection	4.5 ± 2.8	3.3 ± 2.3	4.1 ± 2.6
	Relative variation	45	6	46

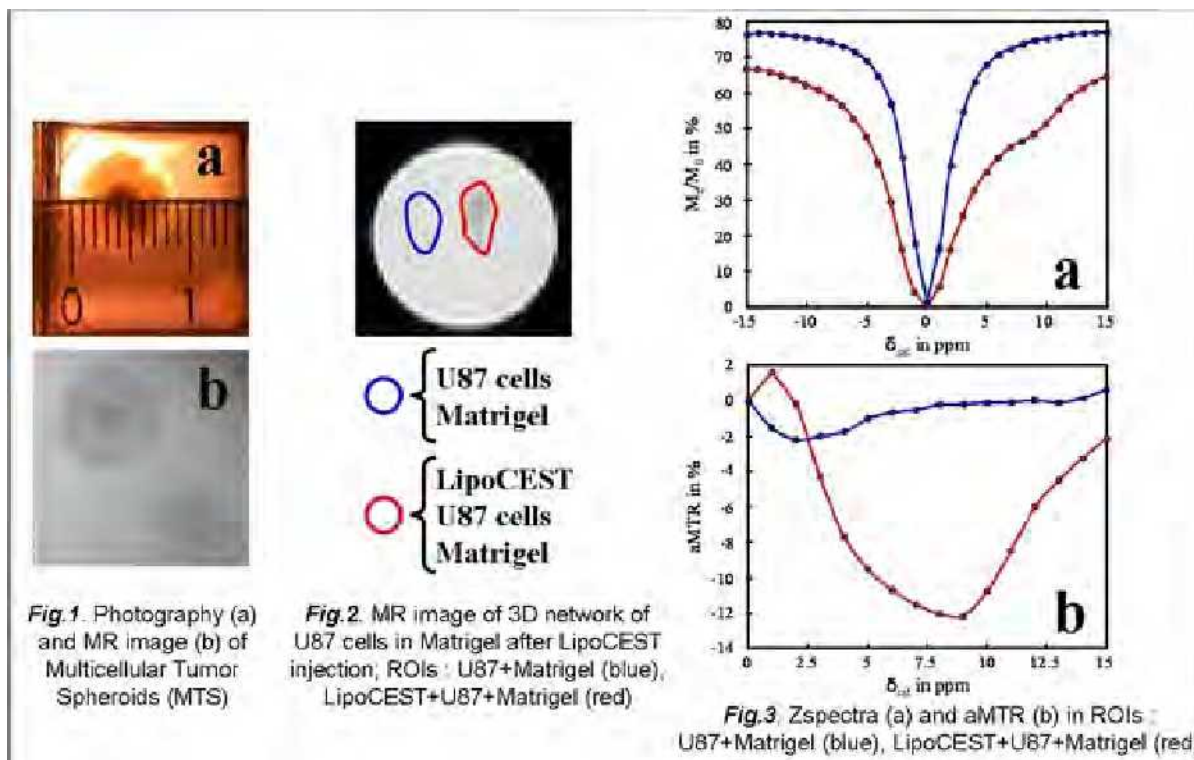
Tab. 1. Mean, standard deviation and relative variation of %CEST contrast in "all brain" (yellow), "tumor+ surroundings" (blue) and "controlateral" (red) ROIs

Presentation Number **0306A**
 Poster Session 1a: Imaging Instrumentation and Methodology

Novel 3D cell culture medium for characterization of contrast agent in the MRI environment

Françoise Geffroy¹, Julien Flament¹, Gaëlle Jestin², Boucif Djemai¹, Benjamin Marty¹, Céline Giraudeau¹, Sébastien Mériaux¹, Julien Valette¹, Franck Lethimonnier¹, Gilles Bloch¹, Denis Le Bihan¹, **Fawzi Boumezbeur¹**, ¹NeuroSpin, CEA/DSV/I2BM, Gif-sur-Yvette, France; ²Research Division, Guerbet, Roissy-Charles de Gaulle, France. Contact e-mail: fawzi.boumezbeur@cea.fr

Introduction *In vitro* MR studies are frequently performed to characterize contrast agent (CA) properties in model biological surroundings. In order to improve the stability/simplicity of such studies, we developed large phantoms of still growing cells using Becton Dickinson Matrigel Basement Membrane as a matrix. Two different 3D cell cultures are presented as illustrations for this novel biological medium for CA characterization compatible with the MRI environment. **Materials and Methods** 3D network of growing cells. U87-MG cells culture was performed as usual. To create 3D networks, cells were collected and re-suspended (2.105 cells/mL) in DMEM/10%FBS+Matrigel (25%), and kept 3 days in culture before MR imaging. Multicellular Tumor Spheroids (MTS). U87-MG cells were used as well. The hanging droplet method was used to obtain spheroids. Matrigel solution was prepared (25% in DMEM/10%FBS) in a 24 wells plate and spheroids were carefully positioned on the surface of the Matrigel, followed by the addition of 1mL of DMEM/10% FBS. MTS were transferred one by one in a new plate filled with a 25% Matrigel solution, and a 15% Matrigel was added on the MTS (Fig.1). Phantom preparation. 5µL of LipoCEST was added at the core of 3D cell culture using a Hamilton syringe (Fig.2). MR Acquisitions. Zspectra (Fig.3.a) were acquired on a 7T Bruker Pharmascan scanner with stabilized temperature (T~37°C) using MSME sequence (TE/TR=54/5000ms) preceded by a CW saturation pulse ($B_{1sat} \sim 7\mu T$, range=[-15;15]ppm). The asymmetric Magnetization Transfer Ratio (aMTR) is calculated following $(I_{on}-I_{off}) / I_{ref} * 100$. **Results** After 3 hours of MRI measurement, the % of living cells in the 3D network of growing cells was very good at 93%, whereas it was closer to 65% for MTS. Both endogenous MT effect and LipoCEST effect are visible (Fig.3.b respectively blue curve at 2ppm and red curve at 9ppm). **Conclusion** We propose a novel method to characterize CA properties *in vitro* in model biological surroundings. It allows for long MR experiments with a good survival rate of the cells without a complex setup. This method could be particularly interesting to explore biological interactions between functionalized contrast agents and targeted cells.

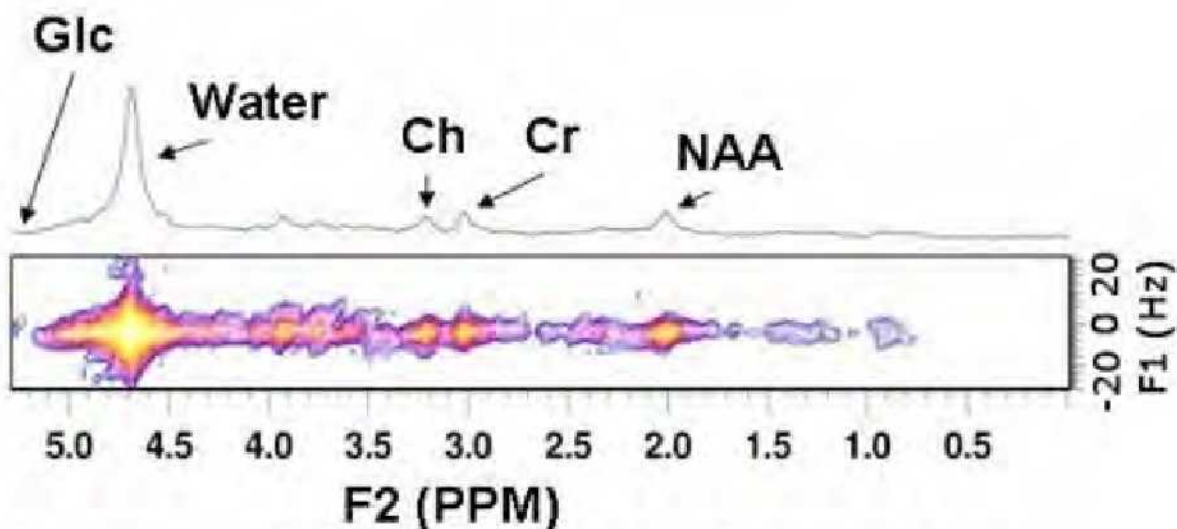


Presentation Number **0307A**
 Poster Session 1a: Imaging Instrumentation and Methodology

Implementation and Validation of Localized Turbo 2D JPRESS on a 7T MRI/MRS scanner

Bhaskaran David Prakash, Terry Yew Shze Keong, S. Sendhil Velan, Singapore Bioimaging Consortium, Singapore, Singapore.
 Contact e-mail: bhaskaran_david@sbic.a-star.edu.sg

Introduction: Localized 2D JPRESS has been demonstrated to achieve improved spectral resolution and quantitation [1] of brain metabolites. There is a great interest in reducing the acquisition speed of this technique for several in vivo applications. Here we implemented a turbo version of the localized J PRESS to perform multiple acquisitions within a TR for reducing the total scan time. Methods: Localized Turbo 2D J PRESS was implemented on a 7T MRI/MRS scanner equipped with a 72mm volume resonator for RF transmit in combination with four channel phased array receive coil. The sequence begins with the conventional water suppression and outer volume suppression modules followed by $[90^\circ - a - 180^\circ - (a + bi) - 180^\circ - bi \{-c - 180^\circ - (c + bi+1) - 180^\circ - bi+1\}n]$ where $a =$ constant delay, $c =$ constant delay, $n \geq 0$ and $bi =$ incremental delay. This version has an additional 180° pulse in the turbo module which is used to maintain bi with a small initial value and gave a decent spectrum as compared to another version using $[90^\circ - a - 180^\circ - (a + bi) - 180^\circ - bi \{-bi+1 - 180^\circ - bi+1\}n]$ which requires a large initial bi . Validation: The method was validated with a brain phantom of 20 metabolites and also applied to few healthy Wister rats weighing about 300g. A voxel size of $0.4 \times 0.4 \times 0.4 \text{ cm}^3$ ($64 \mu\text{l}$) from the thalamus of the brain was used for in vivo studies. The TR was 2s, 50 t_1 increments, and 16 averages per experiment. For turbo factor of 2, the total acquisition time was halved to ~ 16 minutes. Discussion: Our technique reduces the experimental time by the turbo factor. With higher turbo count, a compromise on the spectral resolution is needed due to reduction in acquisition duration permitting higher bandwidth to complete the turbo module within the repetition time. Conclusion: Our turbo 2D JPRESS technique permits faster acquisition while maintaining reliable detection of several metabolites including Glu, Glc. and Ala. References: [1] MR Biomed. 2009 Aug;22(7):762-9. [2] Magn Reson Med. 2006 Aug;56(2):386-94.



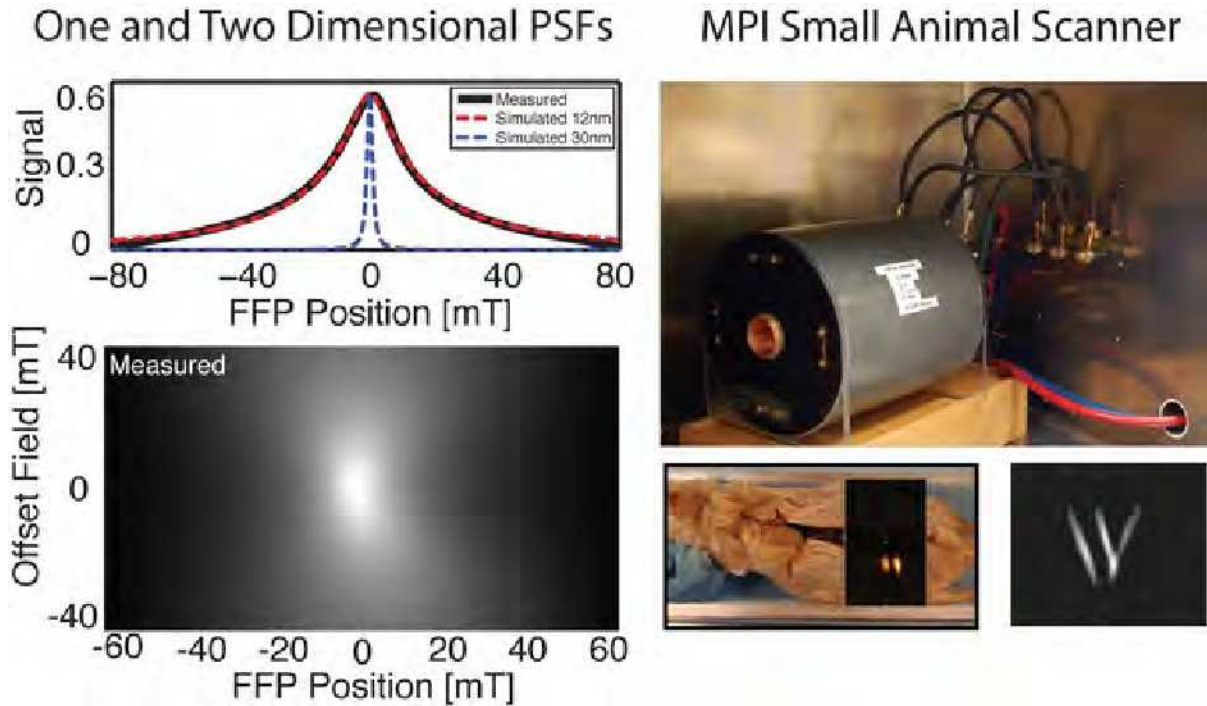
2D Localized Turbo JPRESS spectrum from a rat brain thalamus using turbo factor of 2, ADC bandwidth of 3500hz and TR=2000ms

Presentation Number **0308A**
 Poster Session 1a: Imaging Instrumentation and Methodology

Experimental Demonstration of x-Space Magnetic Particle Imaging

Patrick Goodwill, Steven Conolly, Bioengineering, University of California, Berkeley, San Francisco, CA, USA. Contact e-mail: goodwill@berkeley.edu

Magnetic Particle Imaging (MPI) is a new imaging modality that promises nano-molar detection of iron oxide SPIO tracers deep in tissue [1]. MPI does not rely on magnetic resonance and detects the electronic magnetic moment of iron oxide nano-particles, which is a million times larger than the nuclear moment detected by NMR at 7T. MPI hardware is similar to Magnetic Resonance Imaging hardware, but all magnets have 1% tolerances. There has been excellent work to describe the MPI imaging process in frequency space [2], but this formulation has proven difficult to use in practice. <p> We show that MPI can be understood as a x-domain scanning process and, as such, reconstructed quickly and simply. We begin by approaching MPI as a one-dimensional system and solve for the point spread function (PSF). The PSF gives us resolution and bandwidth requirements, which we use to derive the signal-to-noise ratio. We then separately discuss SAR and Magneto-stimulation, which give surprising results regarding excitation slew rates and excitation frequencies. <p> We then describe instrumentation to test x-space MPI theory, which we use to measure the one-d and two-d MPI spread functions for commercially available SPIO tracer agents. Our experimental results show that the main limitation to MPI resolution and sensitivity is the magnetic domain size of the SPIO tracer, which are typically ~12 nm. <p> [1] B Gleich, et. al. Nature, 435:1214-17, 2005. [2] J Rahmer, et. al. BMC Med. Img.,9(1):4, 2009.



[Left] Measured and Simulated Point Spread Functions in one dimension and two dimensions for a 12 nm particle. A 30 nm particle would have 15 times better resolution than a 12 nm particle. [Right] MPI mouse imager, and two images acquired using the scanner. We are working to incorporate x-space theory into our scanner.

Theoretical Properties of a Human Scale Scanner

Signal	Resolution [mm]	BW [MHz]	SHR [L ng Fe]	SAR [4W/kg]	MagnStim
Linear, Space-Invariant	1 x 2 x 2	0.3-0.8	~1	Link to SHR	Limits Resolution Scan Region

*assumptions: 30 nm particles, 2.6 T/m gradient strength.

Presentation Number **0309A**
 Poster Session 1a: Imaging Instrumentation and Methodology

T₂-Mapping vs ORS imaging to visualize *in vivo* liposomal superparamagnetic Dy-based Contrast Agent

Julien Flament¹, Benjamin Marty¹, Céline Giraudeau¹, Boucif Djemai¹, Françoise Geffroy¹, Sébastien Mériaux¹, Julien Valette¹, Christelle Medina², Caroline Robic², Marc Port², Franck Lethimonnier¹, Gilles Bloch¹, Denis Le Bihan¹, **Fawzi Boumezbeur¹**,
¹NeuroSpin, CEA/DSV/I2BM, Gif-sur-Yvette, France; ²Research Division, Guerbet, Roissy-Charles de Gaulle, France. Contact e-mail: fawzi.boumezbeur@cea.fr

Introduction Recently, liposomes loaded with paramagnetic lanthanide complex were introduced as a new class of contrast agents (CA) for MR-based molecular imaging due to their impressive water-shifting ability or their r_2 relaxivity. In order to estimate which properties would be more interesting to exploit for visualization of our new liposomal superparamagnetic Dy-based CA, we tested T₂-mapping and Off-Resonance Saturation (ORS) imaging and compared them based on their normalized Contrast-to-Noise Ratio (nCNR) measured *in vivo*. **Materials and Methods** r_2 measurement was performed using a 4-tube phantom containing 0/8/16/33 nM of CA. Animal preparation. Anesthetized rat was injected intra-cerebrally with 3 μ L of Dy-based CA 1hr prior imaging. MRI acquisition. T₂-mapping and ORS images were acquired both using a MSME sequence on a 7T small animal MRI scanner (T_{2m2}:TE/TR=5.6/3000ms, 36 echoes; ORS: TE/TR=8/5000ms, T_{sat}=400ms, B_{1sat}~1 μ T, δ_{sat} =0.3ppm). **Results** The r_2 relaxivity was 4.0x10⁶ mM⁻¹.s⁻¹ (see Fig.1). nCNR were measured between two ROIs: injection site & contralateral zone. nCNR = 6.0 mm⁻³.s^{-1/2} for T₂-mapping (Fig.2.b) whereas its value was 2.0 mm⁻³.s^{-1/2} using ORS (Fig.2.c). **Discussion and conclusion** Besides the huge r_2 relaxivity of our Dy-based liposomal CA, we note that both contrast modalities allow for an easy visualisation of the CA. Interestingly, T₂-mapping is the most sensitive modality in our conditions (high local CA concentration at injection site). Even if this preliminary result seems to challenge recent work with superparamagnetic CA and ORS, we aim at keeping comparing both modalities in the future. In particular, we would like to evaluate their sensibility threshold hoping it to be picomolar. Finally, in the perspective of MR-based targeted molecular imaging, both modalities could be combined in a multimodal imaging approach to probe cellular compartmentation as proposed recently by Delli Castelli *et al.*

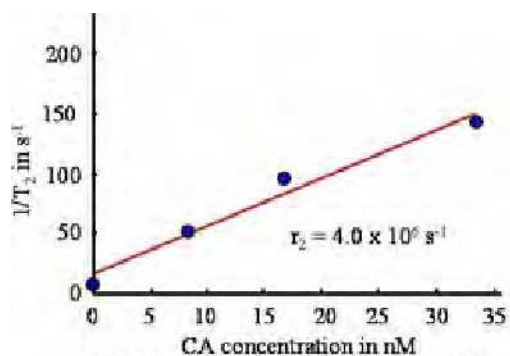


Fig.1 *in vitro* measure of r_2 relaxivity of Dy-based CA, blue dots: experimental data, red line: fitting ($R^2 = 0.93$)

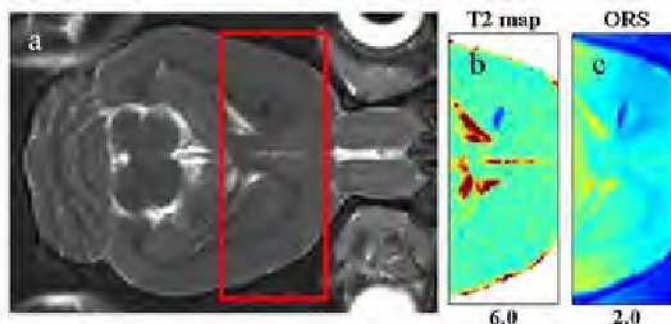


Fig.2 a: Anatomical image of CA injection (in rat brain), b: T₂ map, c: ORS contrast. Normalized Contrast to Noise Ratio (nCNR) is expressed in mm⁻³.s^{-1/2}

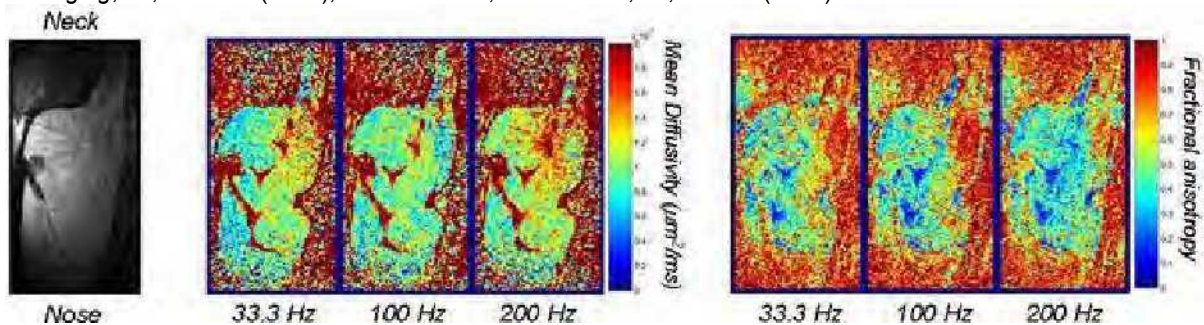
Presentation Number **0310A**
Poster Session 1a: Imaging Instrumentation and Methodology

Apparent diffusion anisotropy in rat cerebellum is altered at short effective diffusion-times using oscillating-gradient diffusion-tensor MRI

Jeff Kershaw¹, Christoph Leuze², Joonas Autio^{1,3}, Sayaka Shibata¹, Takayuki Obata¹, Iwao Kanno¹, Ichio Aoki¹, ¹Molecular Imaging Centre, National Institute of Radiological Sciences, Chiba, Japan; ²Department of Neurophysics, Max Planck Institute for Human Cognitive and Brain Sciences, Leipzig, Germany; ³National Bio-NMR Facility, Aalto University, Kuopio, Finland. Contact e-mail: len@nirs.go.jp

It has long been hypothesised that restricted (or hindered) motion of water molecules is responsible for the anisotropic image contrast in diffusion-tensor MRI, in particular in white matter. It has also been recognised that in that case, by varying the length or separation of the motion-probing gradients (MPGs), it should be possible to alter the contrast of in vivo images and thus common measures of diffusion anisotropy to probe tissue microstructure. Most previous efforts were unable to find in vivo evidence for the restricted-diffusion hypothesis (eg Clark [1]), but recent work using a technique that utilises rapidly oscillating MPGs added to a standard spin-echo sequence, has demonstrated some of the characteristics of restricted diffusion for in vitro samples, and normal and diseased rat brain [2-4]. However, the technique has never been applied to examine alterations to apparent diffusion anisotropy as the MPG frequency is increased (or, equivalently, the diffusion-time is decreased). In this study, an oscillating MPG sequence was applied to investigate changes to the apparent diffusion tensor, fractional anisotropy and mean diffusivity in rat cerebellum. The gradient frequencies were in the range 30-200 Hz and corresponded to effective diffusion times of 1-8 ms [2]. The results clearly showed that the mean diffusivity increased with MPG frequency, which is a characteristic expected of the restricted/hindered diffusion model (see figure). Other indices of diffusion anisotropy were also visibly altered by changes to the MPG frequency. Given sufficient gradient-set performance, it is anticipated that normal and pathological in vivo tissue structure can be probed with this technique to frequencies of at least 1-2 kHz.

References: 1. Clark et al, *Magn Reson Med*, 45, 1126-9 (2001); 2. Does et al, *Magn Reson Med*, 49, 206-215 (2003); 3. Parsons et al, *Magn Reson Imaging*, 21, 279-285 (2003); 4. Colvin et al, *Cancer Res*, 68, 5941-7 (2008).



Presentation Number **0311A**
Poster Session 1a: Imaging Instrumentation and Methodology

Quantitative assessment of radiation-induced CNS disorder models using T2, diffusion and manganese-enhanced MRI

Shigeyoshi Saito^{1,2}, **Ichio Aoki**¹, **Kazuhiko Sawada**³, **Iwao Kanno**¹, **Tetsuya Suhara**^{1,2}, ¹*Molecular Imaging Center, NIRS, Chiba, Japan;* ²*Graduate School of Medicine, Tohoku University, Sendai, Japan;* ³*Physical Therapy, Tsukuba International University, Tsuchiura, Japan. Contact e-mail: saito@nirs.go.jp*

We quantitatively assessed the central nervous system (CNS) of a developmental disorder induced by prenatal X-ray exposure with T2, diffusion and manganese-enhanced MRI (MEMRI). During childhood, radiological examinations like abdominal X-ray or CT during pregnancy have in some studies been associated with increased risk of brain tumor. Also, animal studies have found that the animal embryo is sensitive to radiation. Especially, prenatal radiation-exposure can induce various CNS disorders depending on the dose, affected gestation-period. We used quantitative MRI and histological experiment to clarify the alterations of quantitative MRI parameters. We observed changes in T1 induced by intracellular Mn²⁺ contrast agents in the CNS of normal and radiation-exposed rats. Moreover, the apparent diffusion coefficient (ADC) and transverse relaxation time (T2) were also compared to histological results obtained using Hematoxylin-Eosin (to estimate cell density), Activated Caspase-3 (to detect number of apoptotic cells), and Glial fibrillary acidic protein (to assess proliferation of astrogliosis). We found that: a decreased MnCl₂ uptake for radiation-exposed rats as indicated by longer MEMRI T1 and a significant increase of apoptotic cells were correlated with a decrease of cell viability after prenatal radiation exposure; larger T2 and ADC were associated with a decrease in CNS cell density after radiation exposure. In addition to a slight proliferation of astroglia (+58%), a substantial decrease in cell density (-78%) and increase of apoptotic cells (+613%) was observed in our prenatal radiation-exposure model. The results suggest that MEMRI predominantly reflected the decrease in cell density and viability in the prenatal x-ray exposure model rather than the proliferation of astroglia. In conclusion, quantitative MRI (such as T1-mapping with MEMRI, ADC and T2-mapping) provides information useful for the evaluation and diagnosis of prenatal radiation exposure in the CNS.

Presentation Number **0312A**
Poster Session 1a: Imaging Instrumentation and Methodology

Contrast enhancement effects of iDQC MR images for detecting contrast agent-labeled cells

Jee H. Cho^{1,2}, **Janggeun Cho**^{1,2}, **Kee-Choo Chung**², **Sangdoon Ahn**², **Chulhyun Lee**¹, ¹Div. of Magnetic Resonance Research, Korea Basic Science Institute, Ochang, Republic of Korea; ²Dept. of Chemistry, Chung-Ang Univ., Seoul, Republic of Korea. Contact e-mail: jhcho@kbsi.re.kr

As a new method for contrast enhancement in MRI, the intermolecular double quantum coherences (iDQCs) MR imaging both in vitro and in vivo has been reported recently. This imaging method is strongly depending on the local magnetic properties of samples which can be modified by appropriate contrasting agents. In this study, the iDQC and conventional MR images of the labeled cells with contrast agents were obtained at 14.1 T micro-MR imaging system. To investigate the cell detection efficiency of the iDQC imaging, we have obtained the MR images of the iron-labeled cells by varying the MR experimental conditions like spatial resolution, slice thickness and the concentration of contrast agents. The results showed the iDQC images could visualize the labeled cells more effectively with high contrast-to-noise ratio than the conventional images at the common conditions. Some numerical analyses of iDQC signals have also been conducted to understand how to enhance contrast in iDQC images of iron-labeled cells.

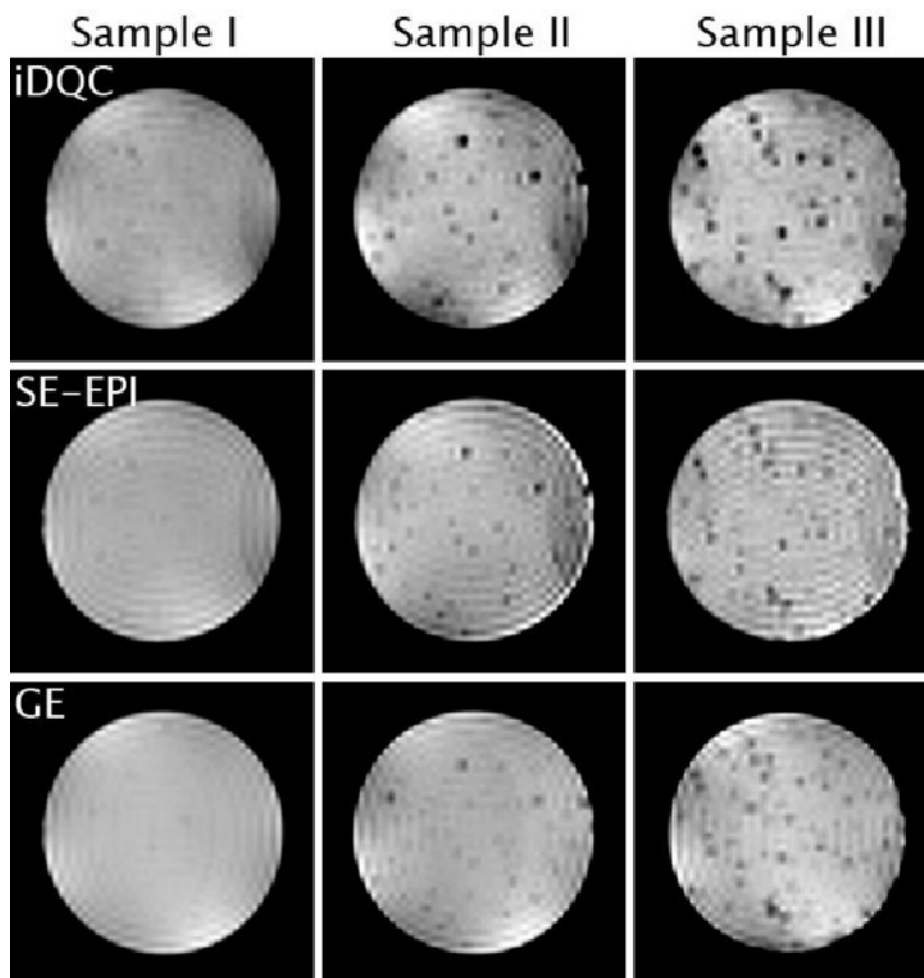


Fig 1. Comparison of MR images from different cell samples: iron unlabeled cell sample (Sample I), iron labeled cell samples with low and high concentrations of contrast agents (Sample II and III, respectively).

Presentation Number **0313A**
 Poster Session 1a: Imaging Instrumentation and Methodology

Anisotropic diffusion phantom - application for DTI

Artur T. Krzyzak¹, Leszek R. Jaroszewicz², ¹IFJ PAN, Cracow, Poland; ²Military University of Technology, Warsaw, Poland. Contact e-mail: artur.krzyzak@ifj.edu.pl

Introduction DTI allows to determine diffusion tensor **D** for phantoms[1]. The evaluation of **D** for an anisotropic diffusion model provides possibilities to calculate the b-matrix for any DTI sequence[2]. In this study, potential applications of anisotropic diffusion phantom in DTI field is reported. **Subject&methods** DTI measurements of the phantom were performed on 9.4T Bruker scanner using PGSE sequence (Fig.1). The calculated tensor **D** was then used as a norm to evaluate the b-matrix for an analogous SE sequence on 4.7T scanner (Bruker magnet, DRX Maran console). The b-matrix for selected ROIs was carried out using Stejskal-Tanner equation[1]. In order to determine the b-matrix for any direction of the diffusion gradient vector, a system of at least six equations was solved for distinct tensors **D_i**. The required different **D_i** were obtained by rotation of the phantom (tensor **D**) with various sets of Euler's angles. Data for different ROIs were statistically compared using the ANOVA test. **Results** The reference **D** eigenvalues (Tab.1) of the phantom were received on 9.4T scanner. The experiments on 4.7T showed the existence of the statistically significant alterations ($p < 0.05$) between b-matrix components for different ROIs in certain directions of diffusion gradient vectors. This outcome suggests the occurrence of gradient field inhomogeneity. **Conclusions** The phantom can be used to achieve the b-matrix for any direction of diffusion gradients and for any DTI sequence. This method should be especially useful for sequences for which the b-matrix calculation is difficult or impossible. It also seems to be valuable for verification of calculated b-matrix and for numerical correction of gradient field inhomogeneity. **References** 1. Basser PJ et al JMR(1994)103:247-254 2. Krzyzak AT WO/2009/145648 **Acknowledgments** Ministry of Science and Higher Education of Poland for grant N518413238 & POIG.01.03.01-14-016/08

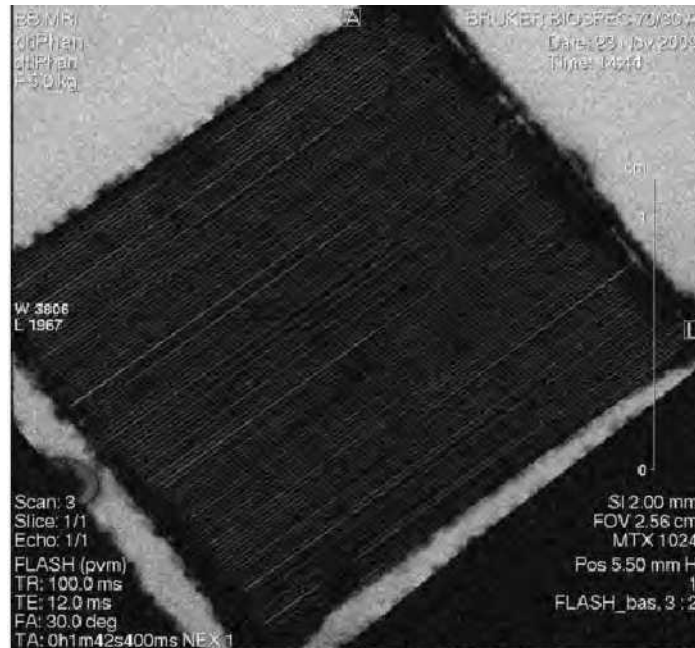


Fig. 1 MR image of the anisotropic diffusion phantom built in the form of a brick (2.5cm²x2cm) composed as an array of thin glass plates (100 um) separated with H₂O layers (20 um). The phantom was placed in a tube filled with water – light environment.

DTI measurements were performed on 9.4T Bruker scanner using PGSE sequence with $b=500s/mm^2$ for 30 directions and $\delta=4ms, \Delta=40ms, RT=3s, TE=50ms$

Tab.1 The eigenvalues of **D** and fractional anisotropy FA.

$L1=2.12 \pm 0.15 [\times 10^{-3} mm^2/s]$	$L2=1.81 \pm 0.14 [\times 10^{-3} mm^2/s]$	$L3=0.7 \pm 0.19 [\times 10^{-3} mm^2/s]$	$FA=0.45 \pm 0.07$
--	--	---	--------------------

Presentation Number **0314A**
 Poster Session 2a: Imaging Instrumentation and Methodology

Monitoring glucose in vivo using 2D J PRESS on a 7T MRI/MRS scanner: Implications for neurodegeneration in diabetes

Loyola DSilva, Bhaskaran David Prakash, Terry Yew Shze Keong, Nikita Agarwal, David W. Townsend, George K. Radda, S. Sendhil Velan, Singapore Bioimaging Consortium, Singapore, Singapore. Contact e-mail: loyola_dsilva@sbic.a-star.edu.sg

Introduction: An increasing interest is directed to develop methods for improving spectral resolution and quantification of cerebral metabolites to understand neurodegenerative diseases. To achieve this, we implemented the 2D JPRESS technique on a 7 Tesla Bruker MRI scanner. Since diabetes is linked to neurodegeneration, detection of abnormal glucose levels in the hippocampus could be significant for understanding neurodegeneration. Methods: The 2D JPRESS sequence utilizes three slice-selective RF pulses [90°-180°-(t1/2)-180°-(t1/2)] to achieve localization. For our studies, a voxel size of 0.4x0.6x0.3cm³ (72µl) predominantly from the hippocampus, with TR/TE of 2s/13ms, 64 t1 increments, and 16 averages lasting ~40 minutes was used. Results: Figure 1, top panel shows the voxel location in the rat brain. The middle panel shows the 2D J PRESS spectrum from a fasting rat. Clearly glucose is not seen due to hypoglycemia. The bottom panel shows the 2D-JPRESS spectrum in a normal rat, with Glucose resonance at 5.2ppm being detected. Other detected metabolites are shown in Table 1. Conclusions: With 2D J PRESS it is possible to detect resonances like Glu and Glc that are not detected by conventional 1D methods. This technique exhibits higher spectral resolution at 7T and permits to monitor the concentration of metabolites under different pathological conditions, specially glucose, that could be significant in differentiating euglycemia from hypo or hyperglycemia. Currently, these data are being used to quantify different brain metabolites for understanding neurodegeneration in the hippocampus and developing new techniques for spectroscopic imaging.

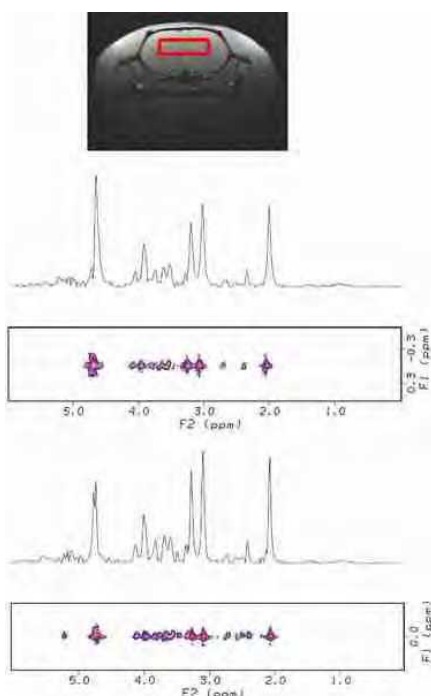


Figure 1
 Table 1:

PPM	Assignment
2.03	HAA (Acetyl moiety)
2.34	Glu+GABA
2.61	Asp
3.02	PCr+Cr
3.24	GPC+PCho
3.42	Tau
3.71	Glu
3.9	Cr+GPC
5.2	Glc

Presentation Number **0315A**
Poster Session 2a: Imaging Instrumentation and Methodology

Influence of Different Anaesthetics on MR Contrast Enhanced Imaging in Mice

Nadine Bauer, Daniel Bukala, Damaris Kukuk, Julia G. Mannheim, Andreas Schmid, Martin S. Judenhofer, Bernd J. Pichler, Laboratory for Preclinical Imaging and Imaging Technology of the Werner Siemens-Foundation, Eberhard Karls University, Department of Radiology, Tuebingen, Germany. Contact e-mail: Nadine.Bauer@med.uni-tuebingen.de

In preclinical research, MR imaging of mice provides important information about morphology and function. In the field of oncology MR contrast agents (CA) are often used to enhance tumour visualization and, if dynamic acquisitions are performed, to show perfusion characteristics. Since anaesthesia, physiological parameters or exact scan times might vary for different studies a direct comparison of contrast agent kinetic might not be possible. This study investigates the influence of different anaesthetics on MR contrast agent kinetics and blood parameters. Nude Balb/c mice were injected with 6×10^6 PC-3 cells in the right shoulder yielding tumours of approximately 350 mm^3 after 14 days. Animals were randomly split in four groups ($n=4$) measured with isoflurane/O₂, isoflurane/air, Ketamine/Xylazine or Pentobarbital as anaesthesia. MRI measurements (7T) with T1 weighted sequences pre and post administration of Gadolinium-CA as well as dynamic contrast enhancement sequences (FLASH) were performed on the animals. In addition, blood samples were taken after measurements to obtain parameters like pO₂, pCO₂, sO₂, pH-value, different forms of haemoglobin and glucose as well as liver parameters (GGT, ALT, AST) and kidney parameters (BUN, Creatine). To investigate the influences of repeated CA administrations a second cohort of 12 animals with PC-3 cells tumours (270 mm^3 after 14 days) was split in three groups ($n=4$). Group one received three doses of saline, group two received two doses of saline and one dose CA (for MRI) and group three received three doses of CA on three consecutive days. MRI was performed on the last day. The analysis of pre and post (5 min post) CA images showed no significant differences for the used anaesthetics and also no difference when CA was administered multiple times. Dynamic MRI-CA curves were normalized to the baseline and showed no differences in the equilibrium state. However, for pentobarbital a slightly faster perfusion slope was observed. The blood glucose level for Ketamin/ Xylazine (190 mg/dL) was increased compared to the other anaesthetics (110-120 mg/dL). Blood oxygenation values like pO₂ were increased for the gas anaesthetics (110 mmHg vs. 50-80 mmHg). Values for liver and kidney did not show alterations due the anaesthesia or CA. Overall, MRI in combination with CA is not influenced by different anaesthetics. Multiple CA does not seem to change expected image results.

Presentation Number **0316A**

Poster Session 2a: Imaging Instrumentation and Methodology

Assessment of tissue shrinkage caused by different histological fixatives using in vivo MRI and ex vivo CT

Mareike Lehnhoff¹, Alexander Sauter^{1,2}, Kerstin Fuchs^{1,3}, Manfred Kneilling³, Leticia Quintanilla-Fend⁴, Bernd J. Pichler¹, ¹Laboratory for Preclinical Imaging and Imaging Technology of the Werner Siemens-Foundation, Department of Radiologie, Eberhard Karls University Tübingen, Röntgenweg 13, 72076 Tuebingen, Germany; ²Department of Diagnostic and Interventional Radiology, Eberhard Karls University Tübingen, Röntgenweg 13, 72076 Tuebingen, Germany; ³Department of Dermatology, Eberhard Karls University Tübingen, Röntgenweg 13, 72076 Tuebingen, Germany; ⁴Department of Pathology, Eberhard Karls University Tübingen, Röntgenweg 13, 72076 Tuebingen, Germany. Contact e-mail: mareike.lehnhoff@med.uni-tuebingen.de

Purpose: It is well known that histological fixatives alter the tissue characteristic and cause shrinkage. The assessment of the shrinkage degree is crucial for the correlation between in vivo imaging and histology. Without this knowledge, comparisons are questionable and corrective registration algorithms cannot be implemented. Material and Methods: We have performed brain scans with a 7T MRI (Bruker) and a t2 tse 3d sequence on 36 C57/BL6 mice. Subsequently, the animals were sacrificed, brains were dissected and immediately placed in different fixatives for 48h: 10 brains in zinc fixative, 8 brains in paraformaldehyde/lysine/periodate fixation, 8 brains in Bouin-Hollande fixation and 10 in 4% paraformalin. The fixation was continued with an ascending alcohol gradient and finally the tissues were embedded in paraffin. Due to the loss of water signal required for MR imaging, the embedded tissues were scanned with a microCT (Siemens). The brain volume and density of the MRI and CT scans were assessed with Amira (Visage Imaging). Results: The mean brain volume assessed with MRI was 475.2 mm³ (SD ± 20.4). After zinc fixation the volume was 303 mm³ (SD ± 18) yielding a density of 740.9 HU (SD ± 22). Paraformaldehyde/lysine/periodate fixation provided a volume of 150.9 mm³ (SD ± 34.4) and a density of 567.3 HU (SD ± 57.5). After Bouin-Hollande fixation the volume was 289.5 mm³ (SD ± 9.8) and the density 720.1 HU (SD ± 11.8). With paraformalin the volume was 197.3 mm³ (SD ± 17) and the density 561.9 mm³ (SD ± 8.1). Conclusion: We conclude that zinc fixation causes only a moderate tissue shrinkage followed by Bouin-Hollande fixation. Paraformalin and Paraformaldehyde/lysine/periodate fixation reduce the tissue volume dramatically. With this knowledge registration algorithms can be implemented to overlay histology and imaging data.

Presentation Number **0317A**
Poster Session 2a: Imaging Instrumentation and Methodology

Automated selection and segmentation of normally appearing white matter for Glioma grading from RelCBV maps

Ravi T. Seethamraju¹, Hui You^{3,2}, Jinrong Qu^{4,5}, Geoffrey Young², ¹MR R and D, Siemens Medical Solutions, USA Inc., Malden, MA, USA; ²Neuro Radiology, Brigham and Women's Hospital, Boston, MA, USA; ³Radiology, Peking Union Medical College Hospital, Beijing, China; ⁴Radiology, Tiantan Hospital, Beijing, China; ⁵Radiology, Henan Tumor Hospital, Zhengzhou, China. Contact e-mail: ravi.seethamraju@siemens.com

Identification of normal appearing white matter (NAWM) is crucial in glioma grading for normalization of relCBV maps. In the hot spot technique, the current standard several ROIs have to be drawn in regions that are assumed to be contralateral NAWM [1,2]. Choosing contralateral NAWM ROIs is very subjective, time consuming and requires expert operator time. Automated approaches for normalization have been proposed using both histograms [2] and DSC first-pass [3] with varying complexity. It was also hypothesized that the highest peak of the histogram after excluding noise and vascular pixels [4], essentially represented the NAWM for a slice, however in many instances a unique peak is not observed leading to ambiguity, so we propose a simple approach to identify NAWM pixels and thereby to provide whole brain normalization. The first step of involves normalizing the histogram of the relCBV for each slice with the value of the highest frequency occurring within that slice whether or not a unique peak is present after excluding noise and vascular pixels. The resulting normalized histograms are then averaged for the whole brain to create a unique whole brain histogram. Pixel values which have >80% of the maximum frequency of this unique histogram are then used as the threshold for NAWM. With these limits the NAWM can be segmented out from the whole brain. The average of all of the pixel intensities of the segmented NAWM for the whole brain is then a measure for the normalization of the relCBV maps. Data from a validated cohort of 12 patients enrolled after resection of pathologically confirmed HGG for treatment with whole brain radiation were tested with the approach. 3 experts were asked to pick 4 ROIs for each patient. The mean NAWM for each of the operator was then compared to the automated value. The Pearson correlation coefficient varied from $R=0.5$ ($P<0.07$) to $R=0.86$ ($P<0.0003$) amongst all raters including the automated one, suggestion operator variance. A segmented sample of the NAWM from the automated tool is shown in fig 1., demonstrating the efficacy of the tool. 1.Hakyemez B et.al. Clin Radiol 2005;60(4):493-502. 2.Emblem KE et.al., Radiology 2008: 247:(3):808-817 3.Emblem K.E. et.al., AJNR Am J Neuroradiol 30:1929-32 4.Seethamraju R. et.al.. #1254 proc of WMIC,2009.

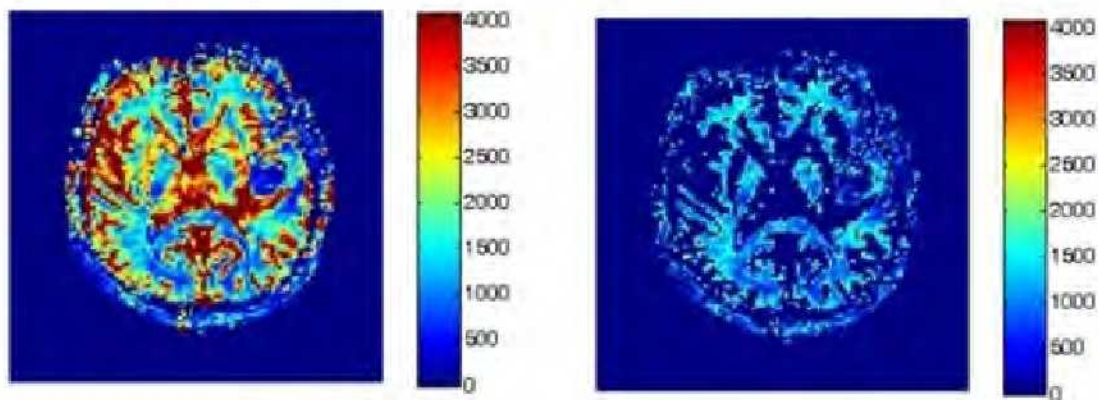


Fig. 1 Unsegmented and segmented NAWM relCBV maps demonstrating the efficacy of the segmentation algorithm

Presentation Number **0318A**
 Poster Session 2a: Imaging Instrumentation and Methodology

Optimizing the nanomolar sensitivities of positive contrast sequences for iron oxide nanoparticles detection

Ravi T. Seethamraju^{1,2}, David M. Grodzki⁵, Sonia Nielles-Vallespin⁴, Ralph Weissleder³, David E. Sosnovik^{2,3}, ¹MR R and D, Siemens Medical Solutions, USA Inc., Malden, MA, USA; ²Radiology, Martinos Center for Biomedical Imaging, Charlestown, MA, USA; ³Radiology, Center for Molecular Imaging Research, Boston, MA, USA; ⁴Cardiovascular MR, Royal Brompton Hospital, London, United Kingdom; ⁵MR Application Development, Siemens AG, Erlangen, Germany. Contact e-mail: ravi.seethamraju@siemens.com

Introduction In the current clinical context sensitivity of MR to Monodisperse Iron Oxide Nanoparticles contrast agents (MION) falls short of PET activation, especially through negative contrast. It is known that off resonance techniques like IRON show promise at clinical field strengths via positive contrast [2,3], recent studies have shown that Ultra Short TE (UTE) imaging exhibits positive contrast mainly by leveraging the inherent T1 contrast of MION [1]. In this abstract we wish to optimize both UTE and IRON sequences to measure the positive contrast via the T1 of MION at 1.5T and 3T, so as pick the best positive contrast sequence for nanomolar sensitivity. Method A phantom with 6 tubes containing MION (Size 30nm, R1@ 0.47T ~26.4 & R2 ~74.9) diluted in water to concentrations of 0,10,50,100,200 and 400 nmols immersed in a beaker filled with water was scanned at 1.5 and 3T with a 12 channel head coil. GRE-UTE, GRE-IRON and TSE-IRON sequence were tested with 3D isotropic voxels of 0.8mm. For all sequences the TE was set to the shortest possible value (UTE-70µs, GRE-IRON-2ms, and TSE-IRON-8ms) at both field strengths, TR, water suppression flip angle and water suppression band width were all optimized to provide maximum signal at 400 nmols while maintaining a fairly linear relationship between signal intensity and concentration. Results Fig 1 show the sample concentration ratio curves at 1.5T. It can be seen from the curves that UTE performs better than either of the IRON sequences in terms of sensitivity and linearity. TSE-IRON has similar performance to UTE below 100nmols but quickly saturates beyond that. Overall GRE-IRON has the least performance. Conclusion In the current context UTE seems to offer best sensitivity over IRON sequences for the detection of nanomolar concentrations of MION. Further studies are needed to explore the possibility of a hybrid UTE-IRON sequence to enhance the sensitivity. 1 Seethamraju RT et.al., Proc ISMRM 2010;#3743 2 Farrar CT et.al., NMR Biomed. 2008 June ; 21(5): 453-463 3 Stuber M et.al., MRM 58:1072-1077 (2007)

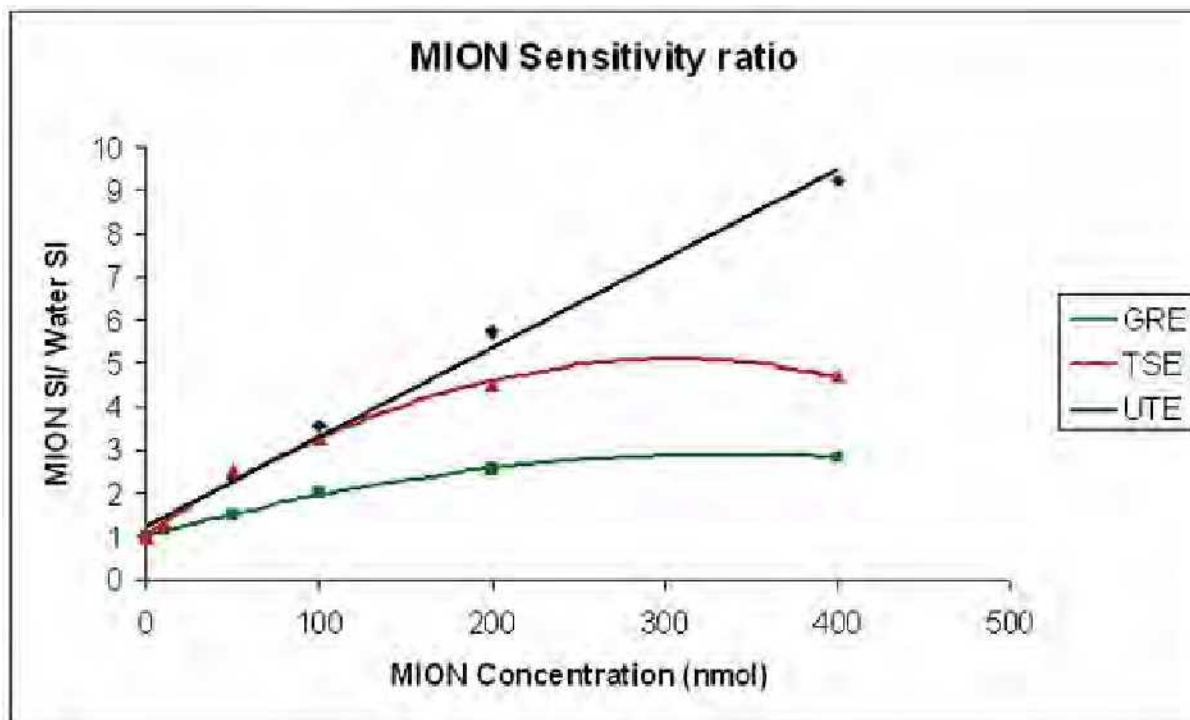


Fig 1. Concentration ratio curves demonstrating the sensitivity of MION for UTE and IRON sequences. Ratios are calculated with respect to SI of water.

Presentation Number **0319A**

Poster Session 2a: Imaging Instrumentation and Methodology

Evaluation of tumor angiogenesis by MRI study using iron nanoparticles

Fatemeh Rahimi, ¹*Nuclear Engineering, Science and Research Azad university, Tehran, Islamic Republic of Iran;* ²*Noor Medical Imaging Center, , Tehran, Islamic Republic of Iran. Contact e-mail: Fatima_rahimii@yahoo.com*

Abstract: Angiogenesis is the growth of new blood vessels from existing ones and it is a prerequisite for the growth, invasion and metastasis of solid tumors. Tumors lay dormant yet viable, unable to grow beyond 2-3 mm³ in size without angiogenesis. For some imaging modalities, methods have been developed to measure blood volume, blood flow, and several other semi quantitative and quantitative kinetic hemodynamic parameters like vascular permeability. MRI and DCE-MRI is a practical modality for evaluating angiogenesis. Paramagnetic contrast agents (SPIO) by making non homogeneity among them enhance the images and we can measure the rCB, CBV, MTT by measuring the IUAC and time to peak in signal intensity - time curve. We utilize the paramagnetic characteristics of SPIO to improve the contrast of the image in MRI. Perfusion imaging is another method for assessing these parameters. The difference in magnetic susceptibility between the tissue and the blood results in local magnetic field lead to large signal loss. The CBF calculated from T1 techniques was lower than the expected CBF. one cause could be change in MRI signal intensity due to blood flowing into the measurement slice therefore for quantifying the effects of inflow on perfusion measurements we use phantom. For the first time we introduce a method for evaluating angiogenesis by iron nanoparticles in clinical research and we also assess some mathematical models of angiogenesis and define an applicable model for using iron nanoparticles in MRI. By defining mathematical model we can predict the progress of tumor growth and also we can assess the antiangiogenic therapy by evaluating the flow (drug and blood) in vasculature. Our proposed model both eliminate the need for estimating the Arterial Input function (AIF) and normalizes analysis so that comparisons across patients can be performed. The method is viewing anatomical structures as filters, pharmacokinetic analysis tells us that simulator structures will be similar filters. By cascading the inverse filter at a reference region with the filter at the voxel being analyzed, we obtain a transfer function relating the concentration of a voxel to that of the reference region. By evaluating input and output of function we get such a beneficial results about angiogenesis. Cascading filters in the frequency domain allows us to manipulate more complex models, like accounting for the vascular tracer component. We demonstrate that the negative contrast of nanoparticles in MRI for detecting angiogenesis has a beneficial results.

Presentation Number **0320A**

Poster Session 2a: Imaging Instrumentation and Methodology

High-Efficiency Continuous Production of Hyperpolarized Xe-129 using Line-Narrowed Diode Lasers and Optimized Cell for High Concentration of Optically Pumped Rubidium

*Mineyuki Hattori, Takashi Hiraga, photonics RI, National Institute of Advanced Industrial Science and Technology, Tsukuba, Japan.
Contact e-mail: m-hattori@m.aist.go.jp*

The hyperpolarization of Xe gas is usually performed by the spin-exchange method. Here, we present a compact flow-through-type apparatus for the high-efficiency continuous production of hyperpolarized Xe-129 using line-narrowed diode lasers and an optimized cell for obtaining a higher rubidium vapor concentration at a higher temperature. In the flow-mode generation of a hyperpolarized noble gas, it has been difficult to increase polarization and the generation rate (flow rate) simultaneously. When the amount of light absorption is increased, the proportion of ineffective gas, which flows in the region with low light intensity, can be decreased by decreasing the optical-path length of the optical pumping cell. In our study on the structure of the pumping cell, the following conditions have been found to be essential for increasing the generation efficiency of the hyperpolarized noble gas:(1) using a flat flow cell with a thin gap, a mixture of the noble gas and vaporized rubidium is introduced into the flow cell along one direction;(2) excitation light is irradiated inside the flow cell and a magnetic field is created by placing a magnet in the flow cell in such a way that the lines of magnetic force are perpendicular to the surface of the flow cell;(3) linear laser diode arrays are used as light sources, and the arrays are arranged so that all the gas flowing through the cell passes through the region where the pumping light is sufficiently intense. A flow-through-type apparatus for the polarization of Xe-129 using four line-narrowed high-power diode laser arrays (Coherent), with fast and slow axis collimation lenses (Ingeneric) and a volume holographic grating (Ondax PowerLocker)(794.73±0.15nm, 40W×4=160W) was constructed. The mixed gas was introduced into a quartz cell (~50mm×70 mm×1mm) set at the center of the assembled permanent magnet. The polarization rates of hyperpolarized Xe-129 were calculated using the accumulated thermally polarized Xe-129 NMR signal intensity. The obtained maximum polarization of Xe-129 for the natural abundance of Xe gas was 20% when the temperature of the cell was ~220oC and the flow rate of the mixture gas was 40-100 sccm. In this equipment, to increase the laser adsorption coefficient, heating temperatures in the polarization cell are set at 180 to 300oC. Heating causes the vapor pressure of Rb to increase. The newly developed equipment makes it possible to realize the continuous production of hyperpolarized Xe-129 with high productivity.

Presentation Number **0321A**

Poster Session 2a: Imaging Instrumentation and Methodology

Repeatability and Reproducibility of Transverse Relaxation Time Measurements in Magnetic Resonance Imaging

Michael G. Kaul, Gerhard Adam, Department of Diagnostic and Interventional Radiology, University Medical Center Hamburg-Eppendorf, Hamburg, Germany. Contact e-mail: mkaul@uke.uni-hamburg.de

PURPOSE The measurement of the transverse relaxation times T_2 and T_2^* gain importance for the quantification of contrast agents in vivo. Accurate measurements are necessary for the assessment of perfusion changes due to tumor therapy or for more advanced techniques like vessel size imaging. In this work the repeatability and reproducibility of the T_2^* estimation process is systematically analysed. **MATERIAL AND METHODS** A dilution series in 15 steps of Gadobenate Dimeglumine in distilled water was pipetted to aim relaxation times of 2, ..., 10, 17.5, 25, 50, 75, 100 and 150ms. Measurements were performed on a 3T MR scanner at 21°C in a water bath. A multiecho gradient echo sequence (95 echoes, echo spacing 1.34ms, voxel size 1x1x1mm³) delivering real and imaginary images was repeated 200 times. $SNR = 0.65 \cdot \text{signal}(\text{sample}) / \text{standard deviation}(\text{air})$ was measure for each sample in the first images of the echo train. T_2^* maps were calculated with different fitting settings to exam the impact of 2- or 3-parameter exponential fitting [2-parameter: baseline is zero], bias correction and/or noise thresholding. All regions-of-interest were standardized for position and size. Finally, 8 magnitude images were calculated each out of 25 consecutively achieved measurements to simulate an improved SNR. [Variation coefficient = standard deviation (SD)/mean] **RESULTS** For the single measurements SNR ranged from 3 to 26 in the samples due to the different gadolinium contents. SNR variation coefficients were for most of the samples less than 1%. Using a 2-parameter fit, bias correction and 1xSD-thresholding the r_2^* relaxivity in water was 6.9/mMs which is smaller than reported in blood. The T_2^* variation coefficients were for samples with a longer T_2 than 5ms smaller than 5%. The T_2^* variation coefficient of the 2ms sample (SNR=3) was 67%. The 3-parameter fit with 2xSD-thresholding showed an at least 3-fold increase in the T_2^* variation coefficients compared to the 2-parameter fit. When the sampling interval was shorter than the underlying T_2^* time, which was the case for the 150ms sample, the 3-parameter fit revealed 58±7ms in contrast to the 2-parameter fit with 145±4 ms. Adding 25 measurements produced a SNR improvement of factor five as theoretically predicted. This reduced the T_2^* variation coefficients for 3-parameter fits, but also for 2-parameter fits in samples with a previous SNR less than 20. **CONCLUSION** The SNR is a major critical parameter to assure small statistical variations in the calculated T_2^* times. 2-parameter fitting is more robust than 3-parameter fitting.

Presentation Number **0322A**

Poster Session 2a: Imaging Instrumentation and Methodology

Measurement of Polyunsaturated Fatty acids in Fish using 3T MR Spectroscopy: Options for metabolic MRS?

Jin Yamamura, Nina Raabe, Alexander Laatsch, Klaus[^] Toedter, Gerhard Adam, Ulrike Wedegaertner, Diagnostic and Interventional Radiology, University Medical Center Hamburg-Eppendorf, Hamburg, Germany. Contact e-mail: j.yamamura@uke.de

Purpose: To assess the concentration of polyunsaturated fatty acids (PUFA) in fishes by using MR spectroscopy (MRS) and comparing the results with gas chromatography. **Materials and Methods:** Six different fish subjects were examined with MRS and gas-chromatography(GC). The first and the second subjects were commercially available fried sea salmon from the supermarket, of which the second one claimed to be enriched with omega-3-fatty acid by the manufacturer. The third and the fourth subject were the same fried salmons but without the coating (breadcrumbs). The last two subjects were fresh wild and farm salmons. They were examined with MRS and GC. All examinations were performed on a 3.0 T whole body scanner with a six element body array. The ¹H MR Spectroscopic Imaging was performed with the single-voxel spectroscopic software provided by the MR scanner, using only the body phased-array coil. After extracting dilutions from the fish tissue toluene was added preliminarily to the sodium carbonate, and GC-analyses were performed using an HP 5890 gas chromatography equipped with flame ionization detectors. The so obtained results of both MRS and GC were compared to each other by calculating the ratio of the polyunsaturated fatty acids (PUFA) to each other. **Results:** Both GC and MRS showed the biggest amount of total lipids in farm salmon followed by wild salmon. MRS signals for water and different proton species present in fatty acids could be observed. Due to the sample size available, best signal to noise ratios were achieved in salmon samples. PUFA content of total lipids was estimated as the ratio of sp³-hybridised protons between C-C double bonds (at 2.8 ppm) to the general lipid peak (around 1.3 ppm, containing mostly methylen and methyl protons). The relation of PUFA content measured by MRS between the two salmon species was comparable to the GC reference measurement. **Conclusion:** This study demonstrates the capability of clinical MRS to differentiate different groups of fatty acid and determine their abundance in tissues. **Clinical Relevance:** Currently, radiologists take an important role in detection of several diseases, e.g. coronary heart diseases. In future radiology might even play an important role in determining the quality of nutrition and metabolic patterns in human beings and thus move from detection to prevention of diseases.

Presentation Number **0323A**

Poster Session 2a: Imaging Instrumentation and Methodology

Statistical and Systematic Errors in T2 and T2* Relaxation Time Measurements: Assessment by Monte Carlo Simulations

Michael G. Kaul, Gerhard Adam, Department of Diagnostic and Interventional Radiology, University Medical Center Hamburg-Eppendorf, Hamburg, Germany. Contact e-mail: mkaul@uke.uni-hamburg.de

PURPOSE The assessment of expected statistical and systematic errors in a quantitative MR-relaxation time determination procedure would be of great help to judge whether a measurement protocol is sufficient for the applied purposes. The underlying problem is the complex relation between measurement-analysis parameters. In this work Monte Carlo simulations of MR sequences providing mono exponential signal decay are presented to assess statistical and systematic errors in dependence of the signal-to-noise ratio (SNR), sequence parameters as well the data processing strategies. **MATERIAL AND METHODS** Software modules for the generation and analysis of the relaxation process with underlying noise with Gaussian and Rayleigh distribution were implemented as well as different fit strategies that can be tested in combination with thresholding for noise exclusion and bias correction procedures. The errors of various T2(*) and SNR combinations can be visualised in quantitative colour maps for given echo-spacing (ES) and echo-train-length (ETL). For a fixed SNR the additional information will be provided how many echoes are used minimally and maximally for fitting and for which T2(*) the numerical analysis process becomes efficient indicating a lower limit. **RESULTS** SNR affects the post processing strategies and the resultant aberrations. Non-linear regression with 2 degrees of freedom (baseline is set to zero) is often favourable over 3 degrees of freedom or logarithmic regression. When relaxation times of the order of the ES shall be measured it will be difficult if not impossible when SNR is lower than 20. Thresholding will decrease the systematic error but increases the minimal detectable T2(*). A bias correction which can be applied additionally will reduce systematic errors more significantly especially in low SNR (<10) situations but also in better SNR conditions. A higher SNR will reduce the variance. **CONCLUSION** Monte Carlo simulations are a helpful tool to optimize relaxation measurements and to depict limitations on repeatability and reproducibility before the measurement is performed. The SNR is as critical as a sufficient short ES. Rayleigh noise correction procedures are advisable.

Presentation Number **0324A**

Poster Session 2a: Imaging Instrumentation and Methodology

Comparative Study of Rodent DSC-MRI using FLASH and EPI

Josiane Yankam Njiwa¹, Aileen Schroeter¹, Markus Rudin^{1,2}, ¹ETH-University Zurich, Institute for Biomedical Engineering, Zurich, Switzerland; ²University of Zurich, Institute of Pharmacology & Toxicology, Zurich, Switzerland. Contact e-mail: njiwa@biomed.ee.ethz.ch

Functional capacity of cerebral vessels is important in establishing diagnosis and prognosis. This implies that chosen experimental parameters do not corrupt image representation of physiologic alterations associated with a signal intensity change. Action of dynamic susceptibility contrast(DSC)-MRI on the intravoxel magnetic field distribution is independent of the imaging technique. Thus, any suitable MRI sequence should yield similar results. Several groups advocate using EPI instead of FLASH for DSC-MRI. For further clarification, our work compares FLASH and gradient echo(GE)-EPI sequences. Imaging was performed using a 9.4T Bruker scanner, using a 4 element phased array surface coil. The CA Endorem was injected i.v. to rats (12.5mg/kg, 1.5ml/min). T²*-weighted images (NR:150, temporal resolution:1s) were acquired using FLASH and GE-EPI with the same FOV, matrix dimension, and slice thickness. A comparative analysis for a cortical brain ROI comprised the computation of regional CBV(rCBV), MTT, regional CBF(rCBF) and SNR at max. concentration value. Fig.1 shows that FLASH and GE-EPI yield similar concentration time curves. However, differences appear when computing quantitative values. FLASH/EPI: rCBV±Std=0.54±0.047/0.79±0.09, rCBF±Std=1.13±0.31/9.37±4.89, MTT±Std=0.32±0.15/0.1±0.03, SNR±Std=17.42±1.47/23.85±2.69. EPI yields higher rCBF and MTT values when computing comparable rCBV values - probably due to higher sensitivity of EPI vs. FLASH. It is known that the degree of T²*-weighting in GE images, i.e. the visibility of magnetic field inhomogeneities and susceptibility differences is mainly controlled by echo time and voxel size. Thus, not only the chosen spatial resolution but also the duration of the acquisition period relative to T²* may affect the 'functional' SNR of an image. We are currently studying other reasons possibly contributing to the difference regarding CBF and MTT quantification.

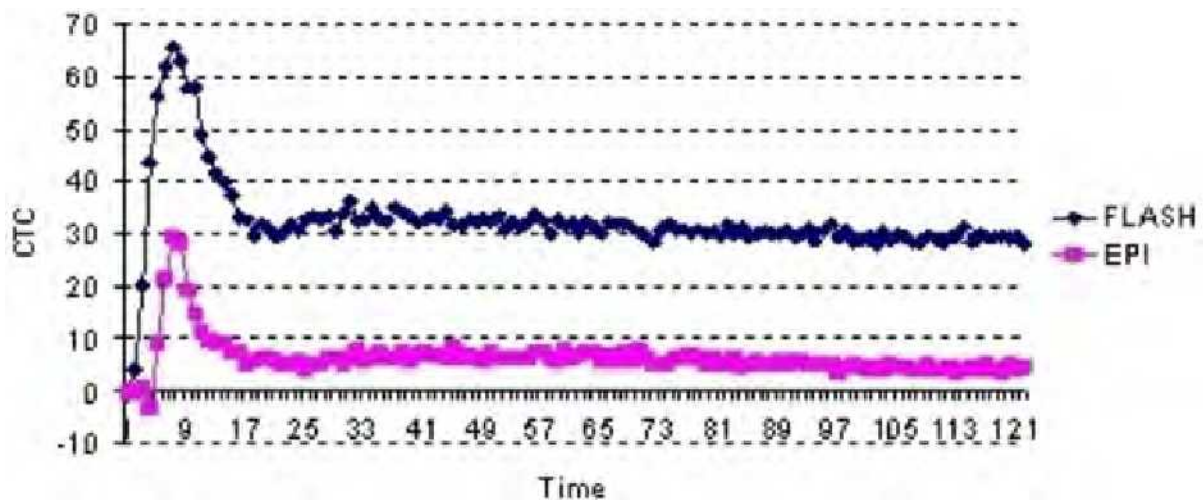


Fig.1: Concentration time curve (CTC) of FLASH and GE-EPI sequences.

Presentation Number **0325A**

Poster Session 2a: Imaging Instrumentation and Methodology

Amyloid Plaque Detection by using Clinical Magnetic Field Strength MRI

Tetsuya Yoneda¹, Hiroshi Toyoda², Kei Mizuno², Terumasa Takemaru³, Motohira Mio³, Yasuyoshi Watanabe⁴, ¹Department of Medical Physics in Advanced Biomedical Sciences, Kumamoto University, Kumamoto, Japan; ²Molecular Probe Dynamics Laboratory, RIKEN Center for Molecular Imaging Science, Kobe, Japan; ³Graduate School of Health Sciences, Kumamoto University, Kumamoto, Japan; ⁴RIKEN Center for Molecular Imaging Science, Kobe, Japan. Contact e-mail: tyoneda@kumamoto-u.ac.jp

In high field magnetic field MRI, Amyloid Plaque (AP) detections have been reported by using T2* weighed imaging. In the lower magnetic field such as 3 Tesla, detection of AP has not been perfectly realized because of lower signal intensity compared to one at 7 Tesla. In this couple of years, phase information of MRI is used for generating high contrast image at 3 Tesla and much lower magnetic field MRI in the clinical sites. Phase imaging technique is now thought of as a strong tool to create contrast of a tissue having tiny signal like the AP. One of realizations of phase imaging is Susceptibility Weighted Imaging (SWI) which enhances phase information related to deoxygenated blood or iron content materials on the magnitude image. Although SWI had created excellent contrast, targeted tissue had been restricted because of restricted phase selection to enhance. Recently, we have developed a new phase imaging technique called "Phase Difference Enhanced Imaging (PADRE)" which have created much higher contrasted phase image compared to SWI due to variable enhancement and phase selection. Thanks to this high signal sensitivity of PADRE, we could make contrast of AP in the brain of amyloid precursor protein transgenic mouse models with Alzheimer disease-like pathology at clinical magnetic field strength 2.89 Tesla (Allegra; Siemens Healthcare, Germany). Scan time was about 80 min which is much shorter than ordinary scan time reported about 10 hrs at 7 Tesla. This shorter scan time at clinical magnetic field strength without any contrast agent implies a possibility to detect AP at the present clinical sites. We are to report and discuss these preliminary results with histologic images in order to apply PADRE as a clinical application.

Presentation Number **0326A**

Poster Session 2a: Imaging Instrumentation and Methodology

Manganese-Enhanced Magnetic Resonance Imaging (MEMRI) Highlights Injured Peripheral Nerves in Neuropathic Pain (Chronic Constrictive Injury)

Deepak Behera, Kathleen E. Jacobs, Subrat Behera, Sandip Biswal, Radiology, Stanford University, Stanford, CA, USA. Contact e-mail: biswals@stanford.edu

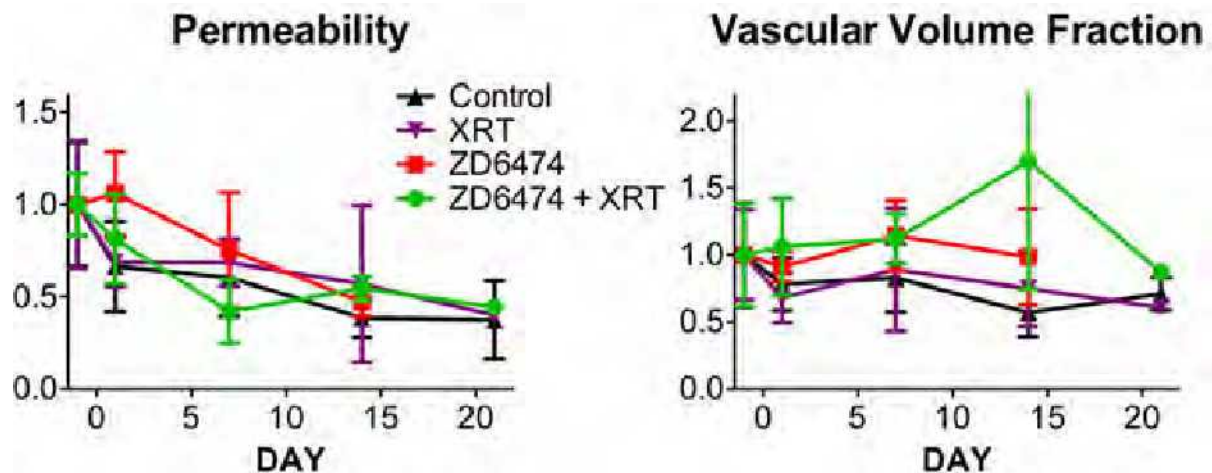
Objective: Manganese-enhanced MRI (MEMRI) is a surrogate method to interrogate calcium fluxes in nervous system since Mn²⁺ physiologically follows calcium and is a T1 shortening agent. Our purpose is to validate MEMRI for detection of changes in lumbar nerves related to neuropathic nociception in a model of Chronic Constrictive Injury. Methods: Animal experiments were approved by Stanford IACUC. A neuropathic pain model was created by Chronic Constrictive Injury (CCI) of the left sciatic nerve of Sprague-Dawley rats by placing four interrupted loose ligatures on the nerve. Rats were allowed to heal for four weeks. Rats with CCI (n=5) and uninjured animals (control; n=3) were evaluated for allodynia in the hind paws using von-Frey's filaments. All MRI experiments were performed on a small animal MR imaging unit (7T, Microsigna) and T1 weighted Fast Spin Echo images were obtained of the lumbosacral region. Baseline scans were obtained on all rats before MnCl₂ administration. Then all rats were injected with MnCl₂ (30mM; 1 ml/100 gm; IP) and scanned again 24 hours after injection. ROIs (RT_Image image analysis software) were placed on sciatic nerves bilaterally, just inferior to L6 vertebra, at the level of sacral promontory to quantify the degree of manganese enhancement, which were normalized to background signal in the muscle (normalized signal). Statistical analysis of normalized MEMRI signal intensities was done with ANOVA with variable sample sizes (n=5 in CCI group; n=3 in control group). Von-Frey test results were assessed by paired t-test for difference in mean 50% threshold values of the left and right paws of CCI rats. Data are reported at mean±standard deviation. Results: Allodynia was illustrated in left hindpaws of CCI rats (50% paw withdrawal thresholds; mean log stiffness: left paw 4.35±0.46, right paw 5.00±0.19; p<0.0117). No difference was seen between the right and left paws of control rats (left paw 5.07±0.05, right paw 5.02±0.10; p<0.42) Increased normalized MEMRI signal is seen in the CCI rats (baseline 1.31±0.04; post-MnCl₂ 1.8±0.08) compared to control rats (baseline 1.32±0.10; post-MnCl₂ 1.56±0.23); p<0.0082. No statistical difference was seen in normalized signal between left and right sides. Conclusion: Rats with neuropathic pain show increased manganese uptake on MEMRI in vivo. MEMRI Functional Neurography can be used to assess pain-activated neural pathways.

Presentation Number **0327A**
 Poster Session 2a: Imaging Instrumentation and Methodology

Comparing response to therapy using a multi-animal dual-tracer DCE-MRI platform

Stephen Y. Lai¹, Yunyun Chen¹, Maria Gule¹, Robert Lemos², Jeffrey N. Myers¹, David L. Schwartz³, **James A. Bankson**^{5,4}, ¹Head & Neck Surgery, The University of Texas M.D. Anderson Cancer Center, Houston, TX, USA; ²Experimental Therapeutics, The University of Texas M.D. Anderson Cancer Center, Houston, TX, USA; ³Radiation Medicine, North Shore-LIJ Health System, New Hyde Park, NY, USA; ⁴Biomedical Engineering, The University of Texas, Austin, TX, USA; ⁵Imaging Physics, The University of Texas M.D. Anderson Cancer Center, Houston, TX, USA. Contact e-mail: jbankson@mdanderson.org

Dynamic contrast-enhanced (DCE)-MRI is a functional imaging method that is often used to quantify changes in tumor microvasculature in small animal models of cancer. We have previously demonstrated a multi-animal imaging system to enable simultaneous DCE-MRI measurements from up to four animals at a time [1] with no sacrifice in image quality when compared to serial single-animal imaging. This platform has been used to compare response to vandetanib (a dual-kinase inhibitor for EGFR and VEGFR2) in combination with radiation therapy (XRT) in a murine orthotopic xenograft model of anaplastic thyroid carcinoma. Four groups of athymic nude mice with orthotopic thyroid xenograft tumors (Hth83) were administered either: 3 Gy XRT daily for 3 days; 25 mg/kg vandetanib daily for 3 days; concurrent vandetanib+XRT with vandetanib (as above) given 1 hours before XRT daily for 3 days; or sham irradiation. A dual-tracer DCE-MRI protocol [2,3] was used to evaluate changes in tumor microvasculature on four animals at a time using a four-channel, 4.7T Biospec imaging system. Dynamic measurements were performed at baseline (day -1) before therapy, on day 3 when treatment was completed and weekly thereafter. DCE-MRI estimates of permeability significantly decreased from baseline (day -1) to one week post-treatment ($p = 0.0286$). Permeability was decreased in vandetanib+XRT as compared to control animals ($p = 0.0571$). Vascular volume fraction was significantly different at one week post-treatment ($p = 0.026$), preceding statistically significant differences in tumor growth curves. Preclinical assessment of vandetanib in combination with XRT demonstrates significant tumor growth inhibition and alteration of vascular characteristics. These results also suggest that DCE-MRI may provide an early indication of response to therapy. References: [1] Ramirez MS, et al. Magn Reson Med 58(3):610-5, 2007. [2] Weissleder R, et al. Eur J Cancer 34(9):1448-54,1998. [3] Orth R, et al. Magn Reson Med 58(4):705-16, 2007.



Presentation Number **0359A**
Poster Session 1a: Imaging Instrumentation and Methodology

Quantitative Second Harmonic Imaging of Renal Fibrosis in Rat CKD Tissues

Hu Sheng Qian¹, Ryan Wirtes², Damian Matera¹, Michael Thibodeau², Steven Weldon¹, Magdalena Alonso-Galicia¹, Silvia Pomposiello¹, ¹CardioMetabolics Disease Research, Boehringer Ingelheim Pharmaceuticals, Inc, Ridgefield, CT, USA; ²Experimental Pathology, Boehringer Ingelheim Pharmaceuticals, Inc, Ridgefield, CT, USA. Contact e-mail: husheng.qian@boehringer-ingelheim.com

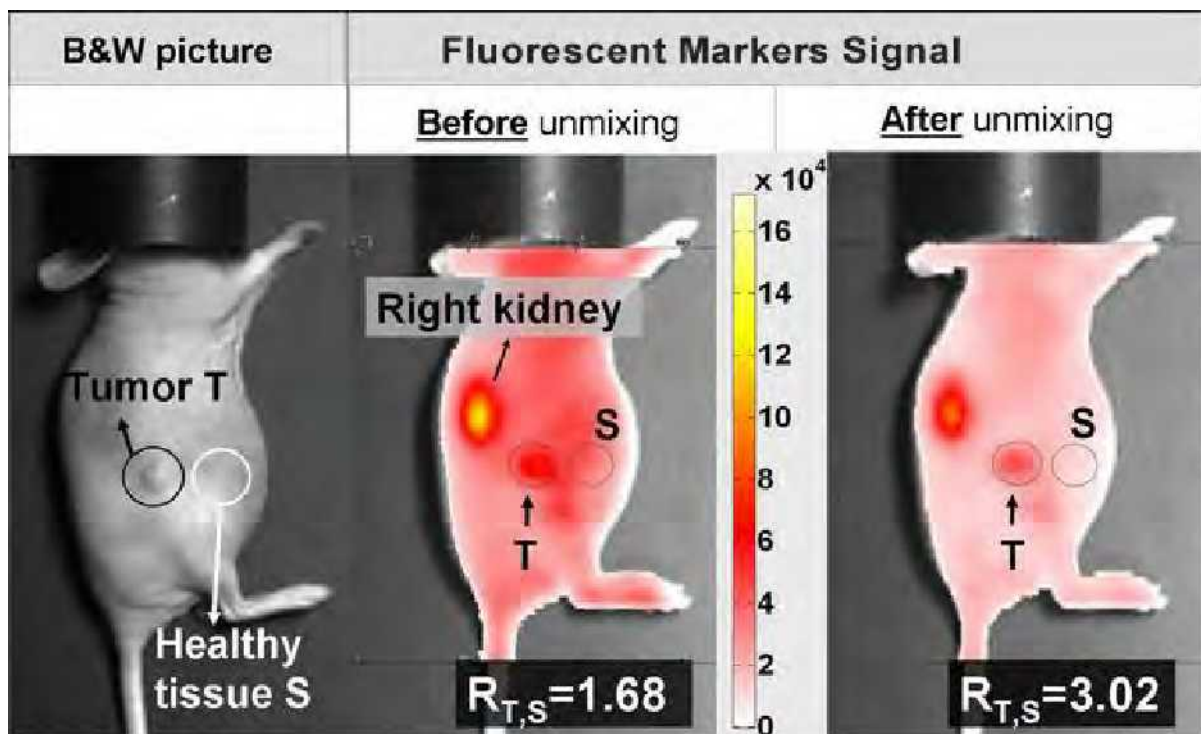
Interstitial fibrosis is a powerful predictor of progression of nephropathies in a variety of chronic kidney diseases (CKD). It is characterized by the depletion of normal kidney architecture and replacement by extracellular matrix, in particular, type-I fibrillar collagen, a protein scarce in normal interstitium. However, assessment, especially for quantitative analysis of fibrosis remains a challenge in research. Our aim was to establish an imaging technique that would enable us, without any staining, to easily assess and quantify fibrillar collagen in kidney tissues as an alternative to standard histological techniques. In this study, based on the imaging of Second Harmonic Generation (SHG) with Zeiss Multiphoton System, we first developed a novel methodology for imaging renal fibrosis in the kidney tissues from ZSF1 diabetic rats or rats surgically induced unilateral ureteral obstruction (UUO). The Two Photon Excitation Fluorescence (TPEF) allows for the visualization of kidney background and tubular organization, while SHG is used for the display of the three dimensional architecture of fibrillar collagen. To validate the specificity of the fibrillar components detected by the SHG in renal fibrosis which is mainly formed by fibrillar collagens I and III, immunohistochemistry was then performed, and the relationship between SHG signal and immunohistochemistry for collagens Type I, III, and IV was closely observed. Our results showed that the SHG signal strongly co-localized with fibrillar collagens I and III, whereas no significant correlation was found for collagen IV. These results demonstrated that SHG imaging can be used for specific detection of the main types of fibrillar collagens involved in renal fibrosis. Finally, to achieve the maximal information from SHG imaging in unstained paraffin-embedding sections, we developed and optimized the imaging processing for thicker rat kidney tissues samples (up to 60 μ m). This approach allows quantitative 3-D imaging of interstitial fibrosis and arterial remodeling with a high degree of accuracy. We conclude that the combination of SHG and TPEF imaging of unstained kidney tissues can be used as a powerful tool for the visualization and quantitative assessment of renal fibrosis in preclinical CKD models.

Presentation Number **P0360A**
 Poster Session 1a: Imaging Instrumentation and Methodology

In vivo autofluorescence and specific fluorescence unmixing by Non-negative Matrix Factorization

Anne-Sophie Montcuquet^{1,3}, **Lionel Herve**¹, **Véronique Josserand**², **Jean-Marc Dinten**¹, **Jérôme I. Mars**³, ¹DTBS, CEA Léti Minatec, Grenoble, France; ²OPTIMAL, Institut Albert Bonniot, INSERM U823, La Tronche, France; ³Signal Image Physics, Gipsa-lab, Grenoble, France. Contact e-mail: anne-sophie.montcuquet@cea.fr

Fluorescence imaging locates fluorescent markers that specifically bind to tumors: markers are injected to a patient, and optimally excited with near infrared light. To investigate thick media, as the fluorescence signal decreases with the light travel distance, the autofluorescence of biological tissues becomes a limiting factor. To remove autofluorescence and isolate specific fluorescence, a spectroscopic approach, based on Non-negative Matrix Factorization (NMF), is explored. A murine breast cancer cell line (5.106 TS/Apc cells in 200 µL sterile DPBS) was implanted subcutaneously in female nude mouse. Twelve days after tumor cells implantation, fluorescent markers (AngioStamp, Fluoptics-Grenoble-France) were injected intravenously (50 nmol, 200 µL). Two days after marker injection, a spectral acquisition is performed. The animal is illuminated with a laser at 690 nm and the emitted back fluorescence signal is collected by an imaging spectrometer coupled with a CCD camera. At this point, the ratio between non-specific fluorescence (marker everywhere but in the tumor) and specific fluorescence (marker in the tumor) is supposed to be optimal for biological analysis, but a non-negligible autofluorescence signal (with a distinct fluorescence spectrum) still remains. We process our NMF algorithm on the spectrally resolved acquisition: the algorithm successfully separated fluorescent markers from autofluorescence despite their overlapping fluorescence spectra. Unmixing results are presented on figure 1: non-specific fluorescent markers signal still remains in kidneys and everywhere else the marker has traveled, but autofluorescence has been removed. Ratio between skin and tumor has been noticeably increased. Comparable results have been obtained from two hours after injection, with only 5 nmol (200µL) of marker: tumor localization was already sensibly improved. We found that in vivo spectrally resolved acquisition combined to NMF processing successfully filters fluorescence contributions of interest from measurements impaired by unwanted signals. Autofluorescence removal is a fundamental pre-processing step to get accurate FDOT reconstructions.



Presentation Number **0361A**
Poster Session 1a: Imaging Instrumentation and Methodology

Near-infrared optical imaging of 3D-breast model with diffuse photon-pair density waves

Yu-Ching Ni¹, Meei-Ling Jan¹, Fan-Pin Tseng¹, Sheng-Ju Yu¹, Wen-Bin Lin¹, Hsien-Ming Wu², ¹Radiation Application Technology Center Physics Department, Institute of Nuclear Energy Research, Taoyuan, Taiwan; ²Material and Electro-Optics Research, Chung-Shan Institute of Science and Technology, Taoyuan, Taiwan. Contact e-mail: janet@iner.gov.tw

Aim Near-infrared Diffuse Optical Tomography has unique capabilities for imaging functional parameters such as hemoglobin concentration and oxygen saturation of the tissue. It is a promising technique applied to breast and brain imaging. And the instrumentation is noninvasive, non-ionizing, inexpensive, and portable. In this study the feasibility of diffuse photon-pair density waves (DPPDW) and MRI-breast model were simulated using ASAP® BIO Toolkit (Breault Research Organization, Inc.). The SNRs and the signal differences between normal and abnormal breast tissue were discussed. **Methods** The system includes a $210 \times 150 \text{mm}^2$ pixelized planar detector and a DPPDW NIR source. Each pixel size is $5.92 \times 5.88 \text{mm}^2$. The DPPDW source is produced by two NIR lasers at wavelength 800nm, which generate a laser beam with two frequency components that are orthogonally polarized, and offset by 80MHz. Passing through an analyzer make these two waves become parallel. Then a beam splitter divides this beam into a signal and a reference beam. MR breast images were utilized to build a 3D CAD model and loaded into ASAP. The μ_a of breast tissue is 0.0017mm^{-1} , the μ_s of breast tissue and tumors are 7.2mm^{-1} ; various μ_a s of tumors (0.3, 0.75, 1mm^{-1}) were considered. Two kinds of breast thicknesses (54 and 42 mm) and four kinds of tumor sizes (5, 10, 15 and 20 mm) were also analyzed. First the irradiance differences between normal and abnormal breast tissue at each detector pixel were recorded. The global SNR was defined as the average SNR of every detector pixels. And the global SNRs were calculated for each situation mentioned above. **Results** The initial results shown that the global SNR was found to be greater when the breast thickness was 42mm (SNR=5 for 15mm tumor at $\mu_a=0.3 \text{mm}^{-1}$) than 54mm (SNR=3.66 for 15mm tumor at $\mu_a=0.3 \text{mm}^{-1}$). The global SNRs were 6.75, 5, 3.66 with 42mm breast thickness for 20mm, 15mm and 10mm tumor size respectively. **Conclusion** We set up a flexible diffuse optical simulation platform for breast imaging researches, specifically using DPPDW concept and 3D-breast model. In the current simulation model the coherent property can not be preserved when the DPPDW NIR rays propagate in the breast tissue. If the simulation model considers the amplitude and phase in the breast tissue, the global SNR should be better and the detectable tumor size would be smaller.

Presentation Number **0362A**
 Poster Session 1a: Imaging Instrumentation and Methodology

Evaluation of the simplified spherical harmonics approximation in heterogeneous bioluminescence tomography through mouse models

Kai Liu, Jie Tian, Chenghu Qin, Xin Yang, Shouping Zhu, Dong Han, Xibo Ma, Medical Image Processing Group, Institute of Automation, Chinese Academy of Sciences, Beijing, 100190, China. Contact e-mail: tian@ieee.org

In vivo bioluminescence imaging (BLI) has played a more and more important role in biomedical research of small animals. Bioluminescence tomography (BLT) further translates the BLI optical information into bioluminescent source distribution, which could greatly facilitate applications in related studies. Although the diffusion approximation (DA) is one of the most widely-used forward models, higher-order approximations are still needed for in vivo small animal imaging. In this work, as a relatively accurate a higher-order approximation theory, the performance of the simplified spherical harmonics approximation (SPN) in image reconstruction is investigated detailedly in heterogeneous small animals. In the numerical validations, the proposed method demonstrates better imaging quality compared with diffusion approximation heterogeneously over wide optical domain. The numerical validations are shown in Figure 1. It is apparent that, the results of SP3 more accurately reflect the information for actual source not only in the position but also in the distribution than that of DA. It is also worth highlighting that, in all the cases for the SP3 model, the artefactual sources do not exist, but it is not the case of DA. In what follows, heterogeneous experimental BLT reconstructions using in vivo mouse further evaluate the capability of the proposed reconstruction method (Figure 2). The experiment was performed on the optical/micro-CT in vivo imaging system developed in our lab. Although both the reconstructed sources only had a little difference from the actual position, artifacts appeared near the reconstructed source in the DA-based results, whereas its counterpart not. Moreover, in the mouse experiment, as one of the simulations with the source located in the narrow interspace of liver, the assumptions for diffusion approximation is not completely sufficed in such small geometry any more. The experimental reconstructions in vivo further demonstrates the capability of higher-order method.

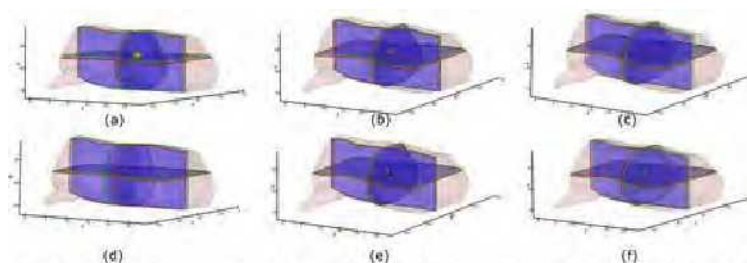


Figure 1: The reconstruction comparisons between SP3 and DA approximation in heterogeneous background. (a)-(c) are the SP3-based reconstruction results of 800, 670, and 620nm optical domains. (d)-(f) are the corresponding DA-based reconstruction results. The source is located at (21.45, 33.65, 14.50).

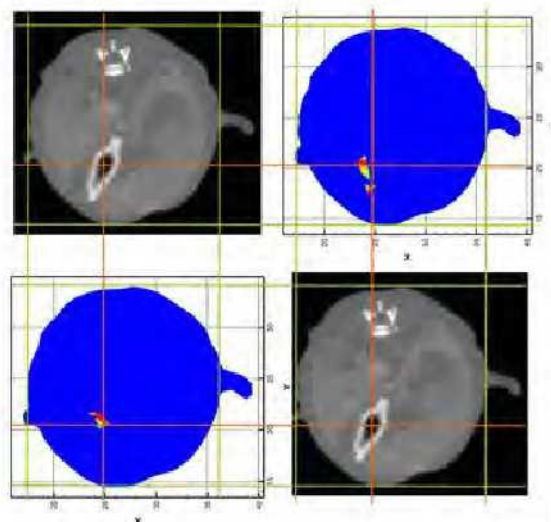


Figure 2: Reconstruction comparisons between the SP3 and DA based results. The left-bottom and right-top figures are the results of SP3 and DA models in lateral cross sectional views respectively, compared with the source location in the corresponding CT slices.

Presentation Number **0363A**
 Poster Session 1a: Imaging Instrumentation and Methodology

A Novel Class of Caged Fluorescent Dyes for Optical Imaging in Microscopy

Kirill Kolmakov¹, **Vladimir N. Belov**¹, **Christian A. Wurm**¹, **Vadim P. Boyarskiy**², **Stefan Jakobs**¹, **Stefan W. Hell**¹, ¹NanoBiophotonics, Max Planck Institute for Biophysical Chemistry, Goettingen, Germany; ²Chemistry, Saint Petersburg State University, St. Petersburg, Russian Federation. Contact e-mail: kkolmak@gwdg.de

Caged fluorescent dyes are very important in optical microscopy and nanoscopy, protein tracking, and multicolor imaging of biological objects. We invented a new class of caged dyes - Rhodamines NN and Carbopyronines NN with a 2-diazoketone (COC=N=N) caging group incorporated to the dye core (see Fig. 1 for an illustrative example).[1,2] This very simple and small functional group (2-diazoketone) is the key feature of these compounds. Upon irradiation with UV or blue light (at wavelengths ≤ 420 nm) they are rapidly photolyzed to form highly fluorescent dyes and nitrogen gas, which is neither toxic nor colored. Specific conjugation via linkers with reactive groups is also an important option. Moreover, the uncaging scheme works in aqueous buffers and in various embedding media normally used in microscopy. The novel caged dyes (spiro diazoketones) are stable in the dark, and their synthesis is straightforward. They can be used in microscopy either as single labels or in combination with the conventional fluorescent dyes and photo-switchable rhodamine spiroamides[1,2]. The "compact" structure and the very small size of the caging group facilitate their penetration through the membranes of living cells. References: [1] V. N. Belov, C. Wurm, V. P. Boyarskiy, S. Jakobs, and S. W. Hell: Rhodamines NN: a novel class of caged fluorescent dyes. *Angew. Chem. Int. Ed.* 2010, 122, DOI: 10.1002/ange.201000150. [2] S. W. Hell, V. N. Belov, V. P. Boyarskiy, C. A. Wurm, S. Jakobs, and C. Geisler (Max-Planck-Innovation GmbH), PCT/EP/2009/006578 (10.09.2009).

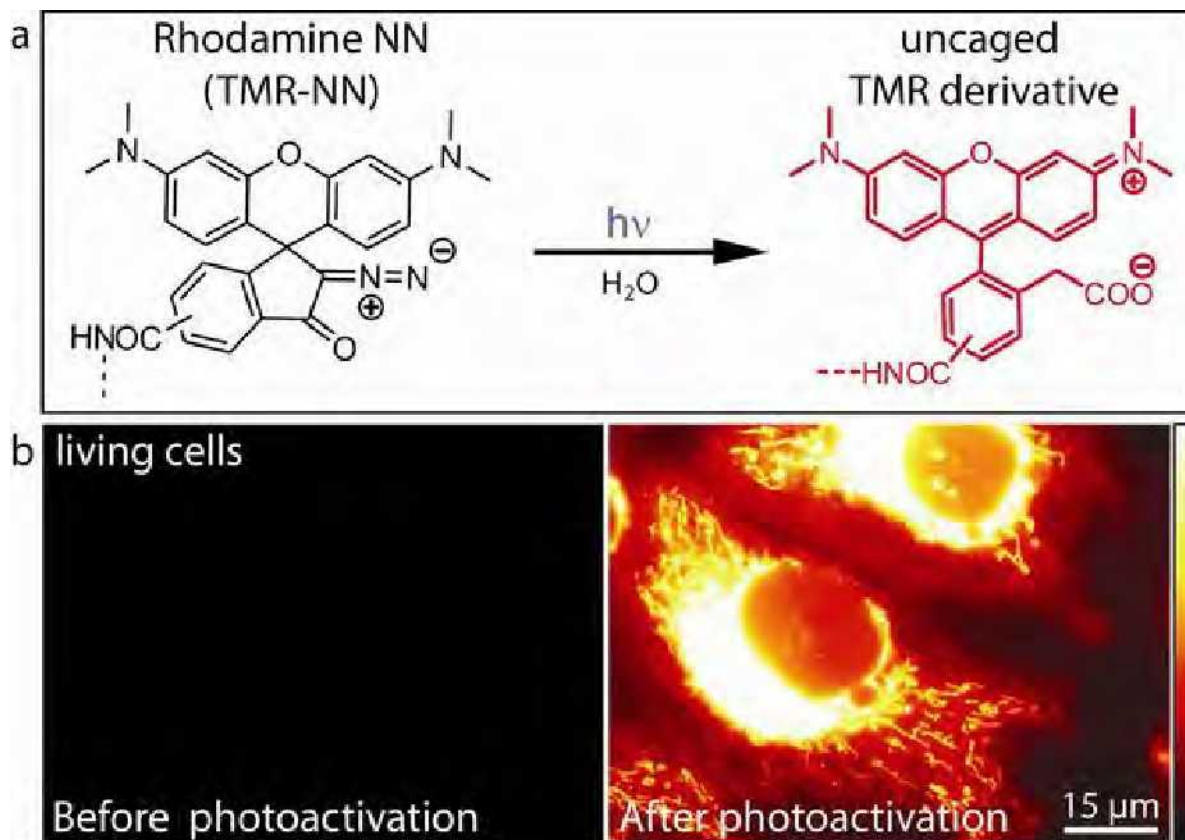


Figure 1. Rhodamine NN: structure and uncaging. (a) Non-fluorescent caged compound TMR-NN (left) is uncaged upon irradiation with UV or visible light ($\lambda \leq 420$ nm) liberating a brightly fluorescent TMR derivative (right). (b) TMR-NN penetrates through cellular membranes and can be used for imaging not only in fixed but also in living cells. After irradiation, the fluorescence signal increases by a factor of 40 and more.

Presentation Number **0364A**
Poster Session 1a: Imaging Instrumentation and Methodology

Imaging and Non-Invasive Measurement of Capsaicin Induced Dermal Blood Flow

Rao V. Papineni¹, Sunil K. Reddy², Sean P. Orton¹, William McLaughlin¹, Douglas Vizard¹, John Pizzonia¹, M.u R. Naidu²,
¹Carestream Molecular Imaging, Carestream Health, Inc., Woodbridge, CT, USA; ²Clinical Pharmacology & Therapeutics, Nizam's
Institute of Medical Sciences, Hyderabad, India. Contact e-mail: rao.papineni1@carestreamhealth.com

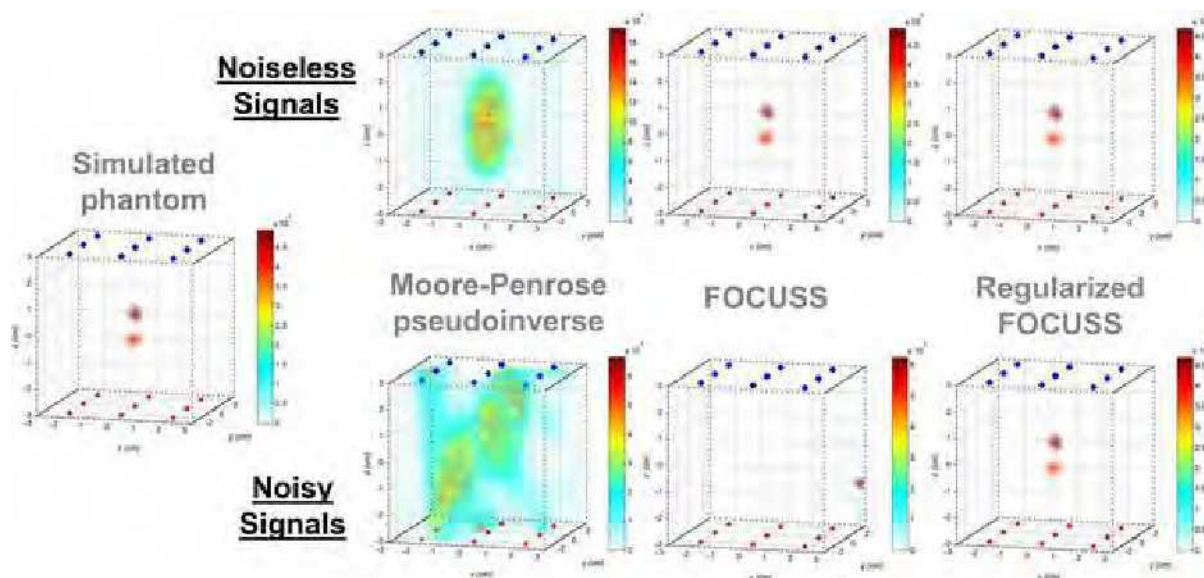
Capsaicin effects neurogenic inflammation and a localized vasodilation by activating transient receptor potential vanilloid type 1 receptor (TRPV1). Topical application of capsaicin on the human forearm results in increased dermal blood flow (DBF). Capsaicin induced changes in the microvascular dynamics at the dermis, is mainly driven through the calcitonin gene-related peptide (CGRP) receptor activation. There is growing evidence suggesting that endothelial dysfunction is an important and an early event in the pathogenesis of major cardiovascular diseases. Novel sensitive and robust methodologies are becoming essential in clinics to determine endothelial function in dermal circulation non-invasively. Here, we have utilized two approaches to both compare and validate the methodologies in determination of the DBF. In the method-1, RBC perfusion was carried out in healthy human subjects using Laser Doppler Flowmetry. Measurements were made after 30 min of topical application of capsaicin (0.075%) on one arm and saline on the other arm (control). Significant change in the DBF was observed in the arm applied with capsaicin- the mean blood flow increased from 25.7 bpu to 83.5 bpu. The mean blood flow change in the control arm however showed negligible changes (26.1 bpu to 26.6 bpu). In the second method, we determined the dermal blood flow in response to the topical application of capsaicin using a planar optical imaging setup. Multispectral fluorescence images were captured using excitation filters between 420 nm and 650 nm to unmix the capsaicin-induced dermal blood flow from the skin autofluorescence. The results indicate the possibility of utilizing inexpensive optical imaging in the clinical and pharmaceutical fields in microvascular dynamic analysis and testing endothelial function in clinical studies. Also, provides opportunity for rapid screening of novel compound antagonists of CGRP receptor that block the capsaicin-induced DBF.

Presentation Number **0365A**
 Poster Session 1a: Imaging Instrumentation and Methodology

Sparse reconstruction for fluorescence diffuse optical tomography: a FOCUSS-based algorithm with noise regularization

Ludovic Lecordier^{1,2}, Lionel Herve¹, Jean-Marc Dinten¹, Françoise Peyrin^{2, 1}CEA-LETI, Minatec, Grenoble, France; ²CREATIS, INSERM U 630; CNRS UMR 5220; INSA Lyon; Université de Lyon, Villeurbanne, France. Contact e-mail: ludovic.lecorder@cea.fr

Fluorescence Diffuse Optical Tomography (FDOT) provides a promising approach for targeted cancer diagnosis using near infrared light. Formally, it consists in localizing fluorescent markers in a diffusive medium by solving an inverse problem. Unfortunately, FDOT is known to be an ill-posed problem, which implies noise sensitivity and non-uniqueness of solution. Prior information about medium properties or fluorescent yield shape is injected to get satisfying solution. In most cases, tumors we are trying to detect represent a small part of the entire volume of the medium and that is not taken into account by common reconstruction algorithms such as conjugate gradient method or Moore-Penrose pseudoinverse. Sparse solutions - that is to say solutions with a minimized number of non-zero values - seem well adapted to the problem. The FOCal Underdetermine System Solver algorithm (FOCUSS) is a recursive algorithm developed for electroencephalography which converges to a sparse solution. Yet, in its original form this algorithm remains still noise-sensitive. We developed a regularized FOCUSS-Based algorithm for FDOT. Tikhonov regularization with an optimization of the regularization parameter is performed for each iteration of the algorithm. It has been tested on different sets of simulated data with Poisson noise for decreasing signal-to-noise ratio. We have shown that we were able to localize punctual fluorophores separated by only a few millimeters, whereas reconstruction with Moore-Penrose pseudoinverse did not give a satisfying solution and basic FOCUSS could not reach convergence.

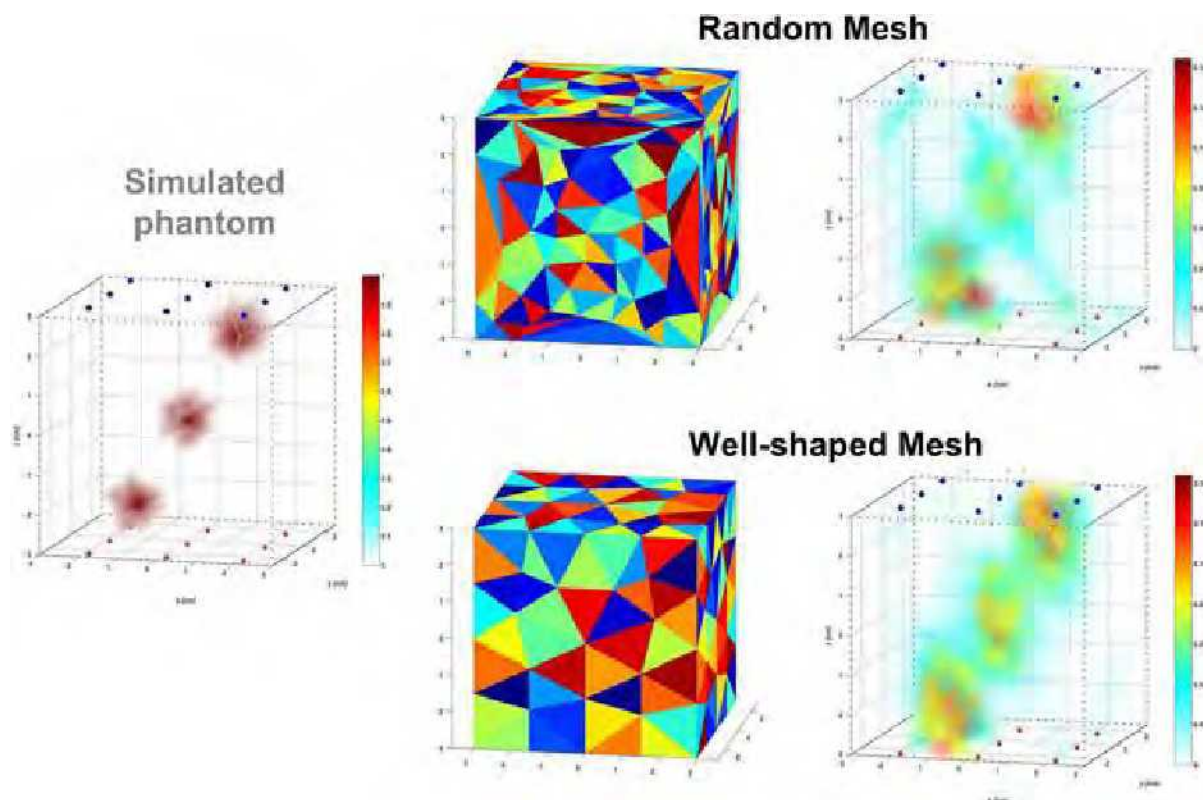


Presentation Number **0366A**
 Poster Session 1a: Imaging Instrumentation and Methodology

Fluorescence diffuse optical tomography: Influence of the discretization mesh on forward and inverse problems

Ludovic Lecordier^{1,2}, Lionel Herve¹, Jean-Marc Dinten¹, Françoise Peyrin², ¹CEA-LETI, Minatec, Grenoble, France; ²CREATIS, INSERM U 630; CNRS UMR 5220; INSA Lyon; Université de Lyon, Villeurbanne, France. Contact e-mail: ludovic.lecorder@cea.fr

Fluorescence diffuse optical tomography (FDOT) is an optical imaging technique which consists in exploring biological tissues using near-infrared light and localizing fluorescent markers. The 3-D fluorescence yield map is reconstructed from a set of measurements by solving an inverse problem. It is based on comparing prediction with a forward model of the light behavior from a determined fluorescence distribution with measurements. In this work, we assume that the forward model of light propagation is approximated by the diffusion equation. While analytical solutions are available for simple geometries, numerical methods are required to solve the equation for arbitrary geometries representative of experimental situations. Furthermore numerical methods imply the use of discretized volumes and compromises have to be made between numerical solutions accuracy and calculation complexity. In this work, we present a dedicated Finite Volume Method to solve the diffusion equation on tetrahedral meshes. The 3-D fluorescence map reconstructions of a simulated phantom is compared with the one obtained from randomly-generated meshes. Influence of the mesh size and geometrical quality is assessed. As we can see on the figure, we obtained a better fluorescence reconstruction using a mesh with good geometrical quality. In order to be able to compare our results this study has been carried out in a homogenous infinite medium to have reference solutions given by analytical expressions.



Presentation Number **0367A**
 Poster Session 1a: Imaging Instrumentation and Methodology

Classification of Skin Lesion Progression with Optical Spectroscopy

Asad A. Safi, Victor Castaneda, Tobias Lasser, Nassir Navab, Fakultät für Informatik, Technische Universität München, Garching bei München, Germany. Contact e-mail: safi@in.tum.de

Skin cancer is one of the common cancer types in humans and its incidence is on the rise. The correct and timely diagnosis of suspicious skin lesions is one of the most important factors in the therapeutical outcome. At present most dermatologists rely on their experience of visual assessment to distinguish benign and malign skin lesions in addition requiring biopsies of the affected skin. Cutaneous T-Cell Lymphoma is a blood cancer type with symptoms that are exhibited as skin lesions which is hard to distinguish. New technologies to assist in identifying and diagnosing skin lesion and to minimize invasive biopsies have been developed, like hand-held magnification devices and computer-aided image analysis. Most technologies focused on non-constant visual information of skin lesions. Optical spectroscopy provides non-visual information such as physiological changes like those associated with increased vasculature, cellular structure, oxygen consumption or edema in tumors. We propose a framework using optical spectroscopy and a multi-spectral classification scheme using support vector machines to assist dermatologists in diagnosis of normal, benign and malign skin lesions. As a first step we show successful classification (95.8%) of skin moles from regular skin in 4 patients based on 80 measurements. Before classification, PCA was applied to each data vector for dimension reduction to yield our classification input. The eigenvalue cut-off C_{PCA} was empirically chosen as one of $C_{PCA} \in \{2,3,4,5\}$. To achieve best results different SVM kernels were used.



CTCL classification of inner lesion is significant for dermatologist
 Classification accuracy results

	Linear Kernel	Poly Kernel	RBF Kernel	Sigmoid Kernel
$C_{PCA}=2$	90.6%	92.3%	92.1%	91.6%
$C_{PCA}=3$	91.3%	93.0%	93.3%	93.1%
$C_{PCA}=4$	93.1%	94.7%	94.3%	94.6%
$C_{PCA}=5$	93.3%	94.6%	95.3%	95.6%

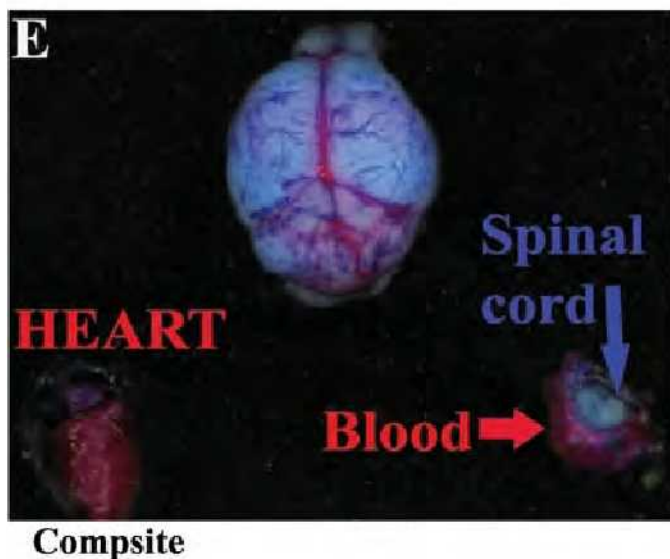
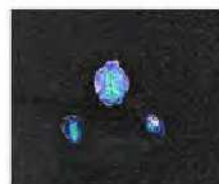
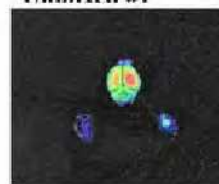
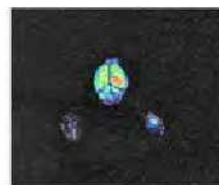
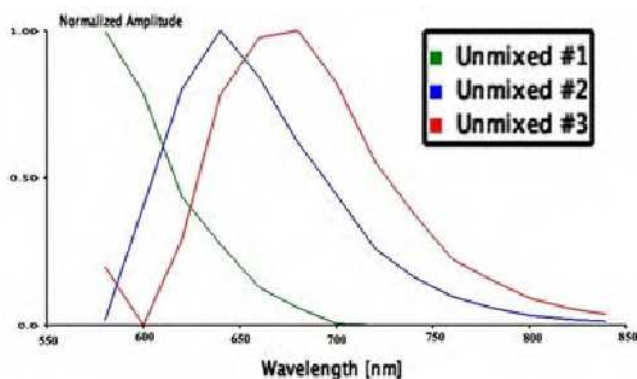
The accuracy of validation dataset V . We compared the manual ground truth labeling $l(y_i)$ for data point y_i and compute the accuracy as $Accuracy = (\# \text{ of correctly predicted data} \div \# \text{ of total data}) \times 100\%$

Presentation Number **0368A**
 Poster Session 1a: Imaging Instrumentation and Methodology

Imaging of amyloid beta species by using spectral unmixing with a “smart” fluorescence probe

Chongzhao Ran, Anna Moore, Radiology, Massachusetts General Hospital, Charlestown, MA, USA. Contact e-mail: cran@nmr.mgh.harvard.edu

Quantifying the concentration of bound fluorescent probe in vivo involves the evaluation of probe signal after a finite wash-out period of free, unbound probe. This process is complicated by the tendency for partially-bound probe to wash away with free probe, leading to an underestimation of bound probe and target quantities. We investigated a method for the real-time assessment of target concentration in vivo using a combination of a commercial spectral unmixing technique and a “smart” fluorescent probe for A β species, CRANAD-3. With our approach we were able differentiate bound from unbound probes in phantoms, in vitro tissues, in vivo transgenic mice and ex vivo brains. In phantom studies the fluorescence intensity of the unmixed bound signal is tightly correlated with the concentration of A β and not with the amount of probe added. Tissue staining of transgenic APP/PS1 mouse brain slices revealed that bound CRANAD-3 specifically distributed across cortical regions, while unbound CRANAD-3 was randomly deposited throughout the whole tissue. Remarkably, the unmixing imaging results from a 24-month old APP/PS1 mouse showed that the signals of bound CRANAD-3 were unchanged for different injection dosages, a finding that is consistent with the phantom results. In addition, ex vivo unmixing imaging clearly showed that bound probe was primarily located in the cortex while unbound probe was diffusely present in blood vessels, across the whole brain and in the heart (Figure E). We believe that this method will be a useful tool for more reliable detection and monitoring of A β species in vivo. To the best our knowledge, this is the first demonstration that a real-time assessment of a target concentration is feasible in vivo.



Presentation Number **0369A**
 Poster Session 1a: Imaging Instrumentation and Methodology

Simulating the response of arbitrary-shape acoustic detectors for optoacoustic imaging

Amir Rosenthal^{1,2}, **Daniel Razansky**², **Vasilis Ntziachristos**², ¹Cardiovascular Research Center (CVRC) and Cardiology Division, Massachusetts General Hospital and Harvard University, Boston, MA, USA; ²Institute for Biological and Medical Imaging (IBMI), Helmholtz Zentrum München, Neuherberg, Germany. Contact e-mail: eamir@gmail.com

One of the major challenges of optoacoustic imaging is that it involves relatively weak acoustic signals, which need to be detected with high signal-to-noise ratio (SNR). Because the SNR is generally proportional to the area of the detector's face, large detectors are commonly used. Although the use of such detectors improves the SNR, it may lead to significant signal distortion resulting in artifacts in the reconstructed optoacoustic image. In this work we developed a method for simulating the spatially dependent frequency response of acoustic detectors with arbitrary surface shapes. The frequency response is incorporated into a forward model for optoacoustic propagation [1]. Our method can be used for designing detectors with desired qualities and reducing reconstruction artifacts caused by the response of finite-size detectors. In order to obtain the response of an arbitrary-shape detector, we approximate its surface by a series of flat detectors, to which the responses were calculated analytically, and sum their respective contributions. We demonstrate this approach for a 2D focused detector, approximated by 30 flat detectors. The geometry of the problem is shown in Fig. 1a. Figure 1b shows the bandwidth of the detector's frequency response over the grid. Clearly, the detector exhibits a wider bandwidth around its focal point. We used the obtained response to calculate the signal produced by the detector for 100- μm wide targets in various locations. Figure 1c shows the targets in the imaged plane, whereas Fig. 1d shows the corresponding signal produced by the focused detector (solid curve) and by a point detector (dashed curve). The figure shows that the focusing of the detector leads to significant attenuation and distortion of the signal from the out-of-focus target. References: [1] Amir Rosenthal et al., "Fast semi-analytical model-based acoustic inversion for quantitative optoacoustic tomography", accepted to IEEE Trans. Med. Imag.

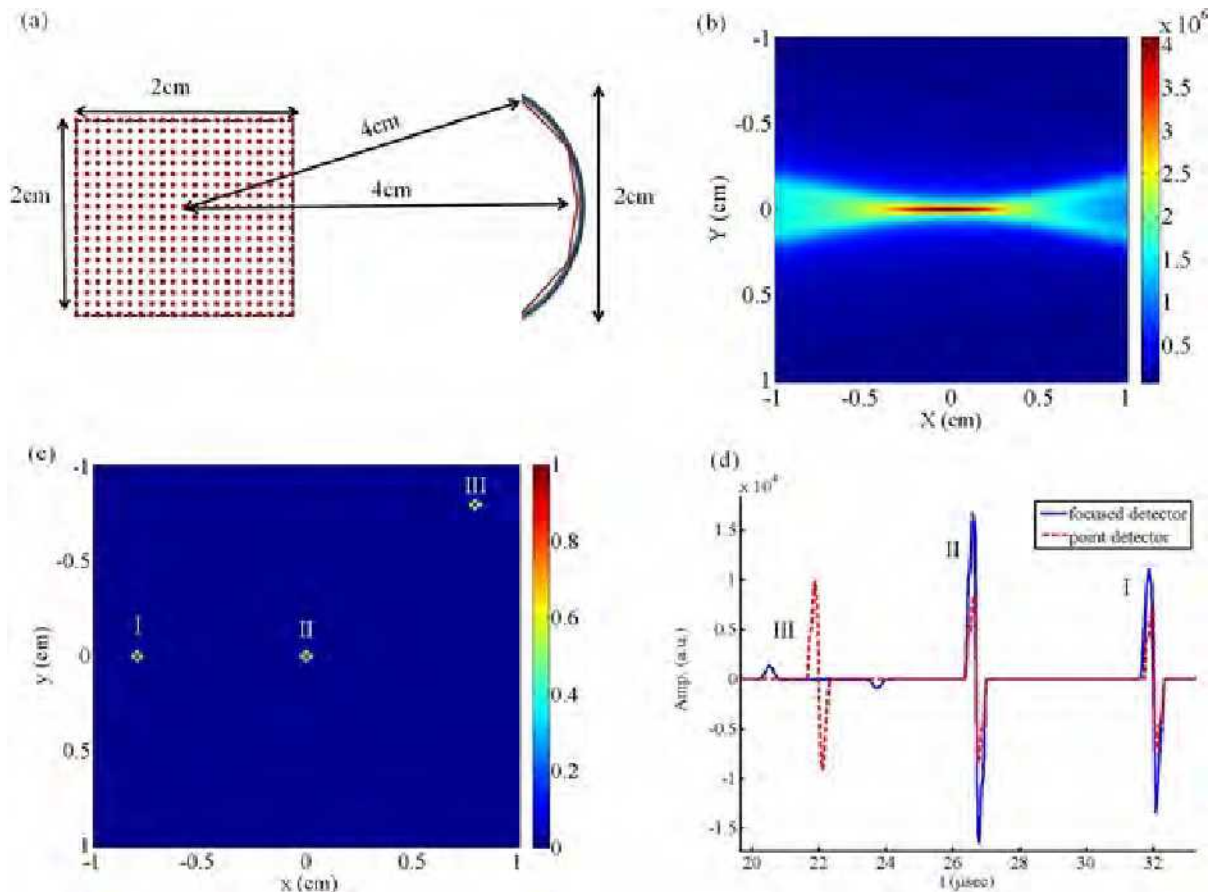


Fig. 1. (a) Simulated geometry; (b) the bandwidth of the detector's frequency response over the grid; (c) optoacoustic targets and (d) their corresponding detected signals.

Presentation Number **0370A**
Poster Session 1a: Imaging Instrumentation and Methodology

Terahertz Imaging and Spectroscopy: Advances in Power and Tunability

Boris G. Tankhilevich, Yehiel Korenblit, and Thomas F. Budinger, Terahertz Technologies, Walnut Creek, CA, USA. Contact e-mail: tfbudinger@lbl.gov

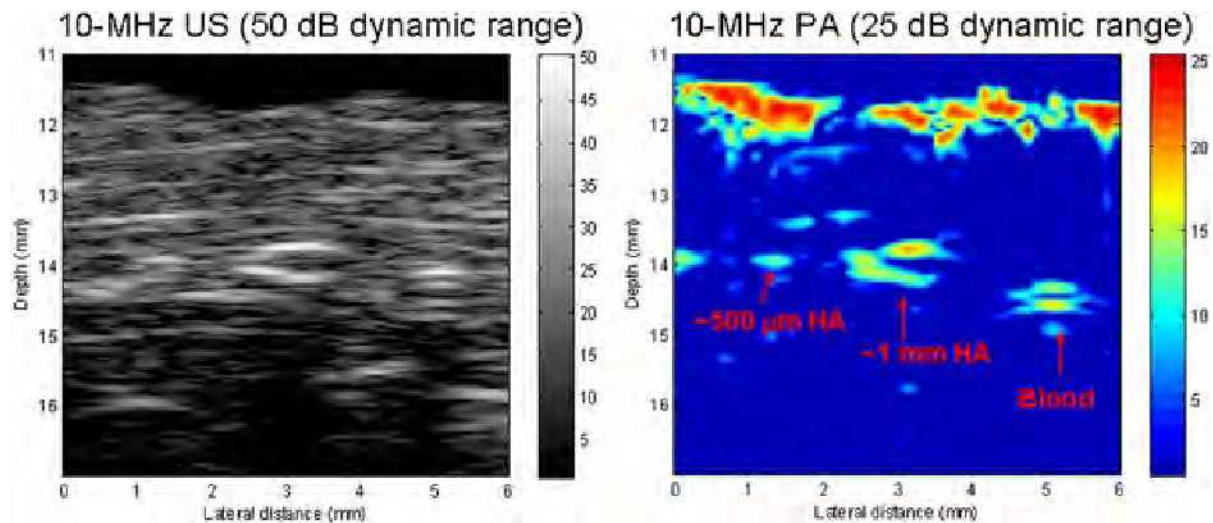
Terahertz frequencies for spectroscopy and imaging are between the microwave band and far infrared (e.g. in a wavelength band around 300 micrometers). The frequency range allows interrogation of unique molecular vibrations. Heretofore the applications to molecular spectroscopy (1) have been limited by insufficient power and poor tunability of the transmitted photons. The new approach (2-4) involves generation of magnons (spin waves)* within a solid state material such as europium oxide (doped with Gd or oxygen vacancies) using short pulses of high current density electrons. The generating substrate is placed in a static magnetic field. The electrons in a ferromagnetic semiconductor can be divided into two groups: free electrons, which determine the electrical conductivity; and d- or f-shell electrons, which determine the magnetic properties. The main interaction between these two groups is the exchange interaction, which lifts the spin degeneracy of the electrons. The conduction band splits into two sub-bands: a lower one with electron spin in the direction of the magnetization ("spin up") and an upper one with spin down, separated by the exchange gap. If a spin-down electron is injected into the upper sub-band, it rapidly flips its spin and emits a non-equilibrium magnon (spin-wave), with a typical frequency in the THz region. When the electron pumped into the spin-down sub-band reaches a threshold value, the magnon system becomes a three-level magnon laser. When two non-equilibrium magnons collide, they annihilate, generating a THz photon. Thus, a magnon laser becomes a THz magnon laser, the generated power being of the order of mW vs. μ watt power generated by contemporary systems. The mechanism of the magnon generation by spin-down electrons in a ferromagnetic semiconductor has been verified in a low power tunneling experiment (5). We show alternative configurations for transmitting terahertz photons and the expected intensity up to tissue penetrations of 50mm. * Magnons are the spin waves associated with electron spins within the crystalline lattice somewhat analogous to the phonons associated with elastic vibrations of an excited lattice (6). 1. C. A. Schmuttenmaer. *Chemical Reviews* 104: 1759 (2004). 2.Y. Korenblit and B. G. Tankhilevich. *Phys. Lett. A.* 64, 307 (1977) 3..Y. Korenblit, B. Tankhilevich, US Patent No. 7,430,074. (2008).4.Y. Korenblit, B.Tankhilevich, US Patent No. 7,508,578 (2009). 5.Guo-Xing Miao, et al. *Physical Review Letters* 102, 076601 (2009). 6. C. Kittel. *Intr. Solid State Physics*, John Wiley & Sons, Inc. p. 330 (2005).

Presentation Number **0371A**
 Poster Session 1a: Imaging Instrumentation and Methodology

Photoacoustic Imaging of Micro-calcifications

Meng-Lin Li¹, **Tsai-Chu Hsiao**^{2,3}, **Po-Hsun Wang**¹, **Yao-You Cheng**¹, **Chih-Tai Fan**¹, ¹Dept. of Electrical Engineering, National Tsing Hua University, Hsinchu, Taiwan; ²Electronics and Optoelectronics Research Laboratories, Industrial Technology Research Institute, Hsinchu, Taiwan; ³Institute of Photonics Technologies, National Tsing Hua University, Hsinchu, Taiwan. Contact e-mail: mlli@ee.nthu.edu.tw

Breast microcalcifications are one of the important indicators for early breast cancer detection. Currently, X-ray mammography and ultrasound imaging are routine diagnostic tools in clinics for breast cancer; however, X-ray mammography is with ionizing radiation and thus there is inevitably carcinogenic risk. Ultrasound (US) imaging also suffers speckle noises, resulting in low contrast between breast tissues and micro-calcifications. In this paper, we report on the first demonstration of photoacoustic (PA) imaging for micro-calcification detection. Compared with X-ray mammography and US imaging, PA imaging owns the features of non-ionizing radiation, speckle free, high optical absorption contrast given an optimal wavelength, and good ultrasonic resolution as well. A 10-MHz confocal PA imaging system was employed to verify our idea in this study. A chicken breast tissue phantom with granulated calcium hydroxyapatite (HA) embedded was imaged. The HA particles were served as calcification particles because HA is the major chemical composition of the breast calcification associated with malignant breast cancers. Optimal excitation wavelengths at the near infrared window for PA imaging of HAs were also analyzed. The imaging results showed that the distribution of $\sim 500 \mu\text{m}$ HAs could be clearly revealed in the PA image (right panel in the figure) while it was hardly identified in the US B-mode image (left panel in the figure) because of speckle noise. In summary, from our results, PA imaging show its promise as a new imaging modality for breast micro-calcification detection. In addition, co-registration of the PA and US images can further render the locations of micro-calcifications within anatomical landmarks of the breast tissue, which is clinically useful for biopsy and diagnosis of breast cancer staging.



10-MHz US (left) and PA (right) B-mode images of a chicken breast tissue phantom with HA particles and a blood loaded tube embedded.

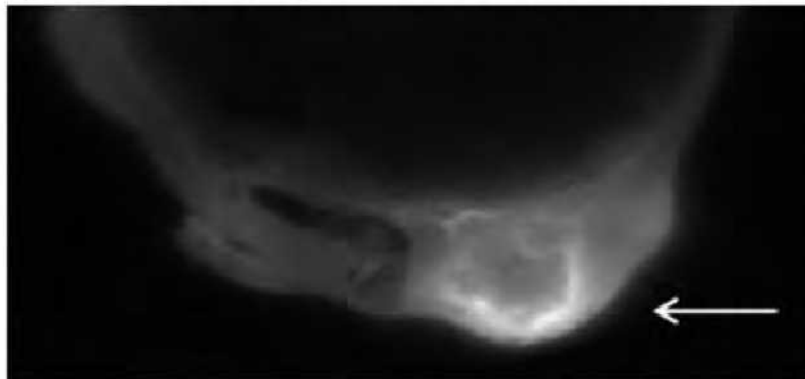
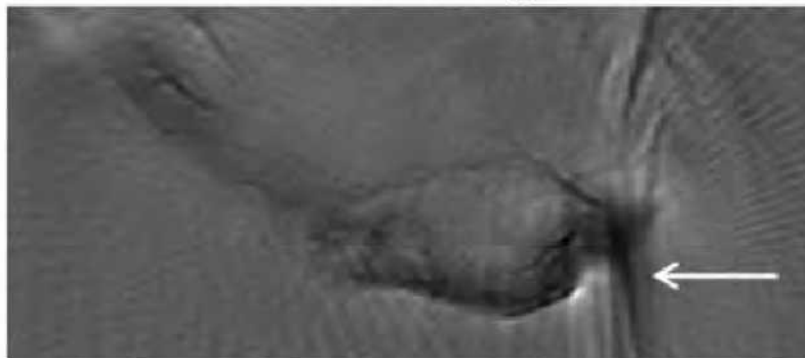
Presentation Number **0372A**

Poster Session 1a: Imaging Instrumentation and Methodology

Molecular Oncologic Imaging using Multi-Spectral Opto-acoustic Tomography

Vladimir Ermolayev¹, Nikolaos Deliolanis¹, Athanasios Sarantopoulos¹, Daniel Razansky¹, Susanta K. Sarkar², Marina Backer³, Joseph M. Backer³, Vasilis Ntziachristos¹, ¹Institute for Biological and Medical Imaging, Technical University and Helmholtz Zentrum Munich, Neuherberg, Germany; ²Medicines Development, Oncology R&D, GlaxoSmithKline, Collegeville, PA, USA; ³SibTech, Inc., Brookfield, CT, USA. Contact e-mail: volodymyr.ermolayev@helmholtz-muenchen.de

We explored the potential of Multispectral Opto-Acoustic Tomography (MSOT) to visualize in high resolution the development of tumor vasculature using a scVEGF/Cy tracer. The study relates to angiogenesis, a process that requires the coordination of complex and redundant molecular pathways, a key component being the vascular endothelial growth factor (VEGF). VEGF and its receptors (VEGFRs) are involved in the proangiogenic signaling causing formation of tumor vasculature where endothelial cells overexpress VEGFRs. The role of VEGF/VEGFR inspired drug design to selectively inhibit this pathway. Several drugs, such as antibodies against VEGF and VEGFRs or small molecule inhibitors of VEGFR, are approved for clinical use, either as monotherapy or as part of a combination therapy. The treatment benefits, however, remain limited due to the lack of reliable ways for drug evaluation or clear definition of target patient group. Moreover, mechanisms of sensitivity and resistance to anti-angiogenic drugs are poorly understood. The scVEGF/Cy is an engineered single-chain VEGF, labeled with fluorescent dye Cy5.5. scVEGF/Cy specifically binds to and is internalized by VEGFRs providing new opportunities for imaging VEGFR dynamics in tumor vasculature. The tracer was injected in the tail vein of CD-1 nude mice bearing subcutaneous HT-29 human colon xenografts, a model for colorectal adenocarcinoma. Near-Infrared fluorescence imaging revealed selective scVEGF/Cy accumulation in HT-29 tumors with maximal fluorescence at 22 hours post-injection. Subsequently, the mice were imaged in the MSOT system in vivo 22 hours post scVEGF/Cy injection. The tumor area was scanned with excitation wavelengths spanning the 680 to 820 nm spectral window and slice thickness of 1 mm. The MSOT analysis provided tumor molecular images that correlated with epi-fluorescent of tumor cryosections. Our results demonstrate the ability of the MSOT method to offer high resolution and fidelity imaging of optical contrast and impact biological research and drug discovery in oncology.

Cryosection, epi-fluorescence, 710 nm**MSOT image**

Presentation Number **0373A**
Poster Session 1a: Imaging Instrumentation and Methodology

Development of vignetting correction method for expanding useful FOV of optical imaging equipment

YoonOh Tak^{1,2}, **Hyeon Sik Kim**¹, **Hyeong Ju Park**¹, **Heung-Kook Choi**³, **Byeong-il Lee**¹, ¹*Nuclear Medicine, Chonnam National University Hwasun Hospital, Hwasun-gun, Republic of Korea;* ²*Medical Imaging Science, Inje University, Gimhae-si, Republic of Korea;* ³*Computer Science, Inje University, Gimhae-si, Republic of Korea. Contact e-mail: takuno7@gmail.com*

Purpose: ALIS (animal lighting imaging system) what we made in prior study is an equipment to measure of bioluminescence radiance from small animal models. Although it uses LN (liquid nitrogen)-cooled CCD, some errors and optical distortion caused by vignetting. It is a reason why ALIS has small useful FOV (field of view). In this study, we describe a method to correct vignetting distortion of ALIS by using a reference image. **Methods:** A raw image of ALIS follows the model $R=(U+T+N_s+N_r)*A+N_q$ (where R : raw image, U : the useful signal image, T : the thermal signal, N_s : shot noise, N_r : readout noise image, A : analog gain, N_q : Quantization noise). At first, we extracted U image from R to measure of vignetting distortion of ALIS more exactly. U can be written, $U=(R-N_q)/A-T-N_s-N_r$. We acquired 200 images with zero exposure time and summarize it in order to obtain a mean image of readout noise. We assumed as N_r because readout noise follows a Gaussian distribution. And then we made 25 rectangle ROIs (5 rows and 5 cols) on the image ($R-N_r$) to find proper value of T . And we chose the minimum mean value of ROIs as T . We defined a reference image to correct vignetting as V . To generate V image, we used a calibrated light source and acquired 25 images with 5 second exposure time. Each image has different light position of 5 rows and 5 cols. We measured a photon count of light source from each image and made the reference image by using 2D spline interpolation method. By multiply the reference image to U , we got a result image with less noise and distortion. We investigated uniformity and reproducibility to evaluate our method. **Results:** By using proposed method, we could correct vignetting distortion satisfactory. Uniformity to evaluate result is 97.4% before correction but after correction, it increased to 99.5%. Cronbach's alpha to investigate reproducibility was .99 at the .05 significance level. And ICC (Intraclass Correlation Coefficient) was .78 for single measurement and .99 for average measurement. It shows there is no significant difference between the measurements ($p<.001$). **Conclusion:** We proposed the method to correct vignetting distortion of the optical imaging equipment ALIS. By using proposed method, we expanded useful FOV of ALIS and its reliability and reproducibility is also increased. Thus, it is expected that ALIS equipment can be used for molecular imaging research as a useful tool with proposed method.

Presentation Number **0374A**

Poster Session 2a: Imaging Instrumentation and Methodology

Development of background noise elimination method of bioluminescence image for advancing accuracy

*Hyeon Sik Kim*¹, *Eun Seo Choi*², *YoonOh Tak*¹, *Hyeong Ju Park*¹, *Byeong-il Lee*¹, ¹*Nuclear Medicine, Chonnam National University Hwasun Hospital, Hwasun-gun, Republic of Korea;* ²*Physics, Chosun Unibersity, Gwangju, Republic of Korea. Contact e-mail: dewpapa@hanmail.net*

Purpose: The background noise in optical molecular imaging is mainly given by electric noise and noise from cosmic ray. Electric noise provides uniform and continuous background noise and cosmic rays that are high energy particle from the space makes random spike noise. In this research, we developed background noise elimination method to improve accuracy of bioluminescence signal. **Materials and Methods:** When a bioluminescence image is obtained with a CCD, the established cosmic ray noise cancelation method is to perform averaging of eight pixels around a target pixel. The value of the target pixel is compared with reference value, which is the 1.5 times the average value. If the target pixel's value is bigger than the reference value, we replaced the value to minimum of 8 neighbor pixels. When the reference value is the bigger than the value of the target pixel, we excluded that and the average value was inserted instead of the target pixel's value. From the acquired image containing the background noise except the noise contribution from the comic ray, flux (count/cm²/sec) of noise is obtained and the variation of noise depending on exposure time is observed. We applied to fitting function to a bioluminescence image of luminous bacteria, and the effect of the proposed method was analyzed in the average and the standard deviation. **Results:** After the elimination of cosmic ray's contribution in the image, we obtained the fitting function of background noise, $P_{B,N} = 0.0279t + 112.79$ ($R^2=0.9973$), where t is the exposure time and R^2 is the coefficient of determination. In the luminous experiment, flux of an original image was decreased along exposure time exponentially. The average flux was changed from 63.02 in the original image into 32.12 in the corrected image resulting in the decrease of the standard deviation from 41.63 in the original image to 4.77 in the corrected image, respectively. **Conclusion:** In this research, we eliminated the background noise coming from electric reason and cosmic rays by using background noise fitting function. The proposed method reduced the deviation in flux value although the exposure time was elapsed. The method could contribute to the accurate quantitative analysis in bioluminescence imaging.

Presentation Number **0375A**

Poster Session 2a: Imaging Instrumentation and Methodology

Development of dual CCD system for effective fluorescent targeting

Hyeong Ju Park¹, **Hyeon Sik Kim**¹, **YoonOh Tak**¹, **Yoon Wha Oh**¹, **Eun Seo Choi**², **Byeong-il Lee**¹, ¹*Nuclear Medicine, Chonnam National University Hwasun Hospital, Hwasun-gun, Republic of Korea;* ²*Physics, Chosun University, Gwangju, Republic of Korea.*
Contact e-mail: piotex@nate.com

Purpose: The improvement of optical imaging system utilizing fluorescent proteins is recently achieved. In this research, we demonstrated a dual-CCD optical imaging system for fluorescent targeting, which performs both monitoring in-vivo imaging and enlarged specific imaging. **Materials and Methods:** We implemented AFIS (Animal Fluorescence Imaging System) for observation of fluorescence two different image signals at the same time. System consists of two CCD cameras; one (SENTECH, STC-630CT) is for the monitoring imaging, and the other (OLYMPUS, DP71) is for specific imaging. We observed fluorescence imaging with fluorescent proteins these are Salmonella typhirium transformed by GFP (Green Fluorescent Protein) expression vector, FM Red (Fast Maturing Red fluorescent protein) and ARO (The thyroid carcinoma-derived cell line ARO) cells. The cells were cultured on the plate and the plate itself was used as a specimen of fluorescence imaging. Two excitation wavelengths (453 nm or 545 nm) were used and related tunable filter (570 nm or 630 nm) were selected. Commercialized lens (RAYMAX, RHV2Z0614G) was used as monitoring imaging, which is called by reference lens. For the magnification, zoom lens (Navitar, Zoom 6000, ×6.5) and different two lens (Navitar, 1-60112, ×1.5 (1.5 lens), Navitar, 1-60113, ×2.0, (2.0 lens)) were used. Magnification factor of each lens was examined with metal wire, which has thickness of 0.13 mm. The measured FWHM at enlarged images was compared and used to get an exact magnification of the 5 enlarged images. **Results:** The monitoring and specific fluorescence images of the cells smeared on the plate were successfully obtained. The thickness of metal wire was corresponding to pixel numbers in different magnifications, which was calculated after 5 times averaging of measured values; 61.4pixel, 191.6pixel, and 252.5pixel. **Conclusion:** Appropriate monitoring image and specific image were obtained simultaneously by using dual CCD camera imaging system. The proposed dual imaging system will enhance the effectiveness in the molecular imaging research field.

Presentation Number **0376A**

Poster Session 2a: Imaging Instrumentation and Methodology

Fluorescent inclusion localizing precision of a time-resolved diffuse optical prostate probe

*Lionel Herve, Aurélie Laidevant, Mathieu M. Debourdeau, Jerome Boutet, Jean-Marc Dinten, CEA, LETI-MINATEC, Grenoble, France.
Contact e-mail: lionel.herve@cea.fr*

Prostate cancer diagnosis relies on biopsies taken on patients with suspected tumors. As the biopsy sampling pattern is either systematic or random, the procedure may miss small and medium size tumors of early-stage cancer. To increase the diagnosis accuracy, a tool combining fluorescence and ultrasound methods is proposed to guide such biopsies: the ultrasound method provides morphological information and the optical method detects and locates fluorophore-marked tumors. This paper will focus on the optical method. In order to guide a biopsy tool reliably, the optical method must locate the fluorescence with a precision of around 1 mm, corresponding to an early-stage tumor size. However, optical measurements performed on prostate are challenging because of the high absorption coefficient ($\mu_a=0.3 \text{ cm}^{-1}$ at 800 nm), depth of the potential fluorescent inclusion (up to 3 cm) and reflection geometry leading to high background noise levels. Moreover, despite the low fluorescence signal, to ensure patient comfort, measurements must be completed in less than two minutes. Since such precision cannot be reached with continuous optics, notably in terms of depth direction, a time-resolved acquisition chain was needed: a femtosecond laser and photomultipliers were used to probe the medium at six source locations and with four detector points. The fluorescence yield was reconstructed by processing the acquired time-resolved signal of each source-detector combination. These computations were based on 48 measurements of intensity and mean time of flight. To solve the fluorescence yield of each prostate mesh point (3000), a matching pursuit algorithm introduced a sparsity constraint to force a single solution. By simulation, it was shown that the above experimental set-up can reconstruct fluorescent dots with a precision better than 1 mm despite photon noise. This finding is validated from a feasibility experiment performed on a dedicated bimodal phantom [1]. A 5 μl fluorescent (IndoCyanine Green) ICG inclusion with 1 $\mu\text{M/L}$ concentration was inserted at a depth of 2 cm to simulate a marked tumor. Acquisitions were performed several times and for varying fluorescent inclusion positions in order to test the localizing precision of the device. The localizing precision of the measurement on the prostate mimicking phantom is around 1 mm which is compatible with early-stage tumor size and biopsy constraints. Therefore, this study shows that the fluorescence method shows great promise to significantly improve prostate cancer screening. [1] Boutet, JBO,2009(14), 064001

Presentation Number **0377A**
Poster Session 2a: Imaging Instrumentation and Methodology

Fast, robust and efficient algorithm for determination of optimal targeted scan path for sparsely distributed cells examined by precise two-photon molecular imaging with high temporal resolution

Tomasz Soltysinski, *Warsaw University of Technology, Institute of Metrology and Biomedical Engineering, Warsaw, Poland. Contact e-mail: tomasz_s@vp.pl*

Two photon microscopy is one of the most advanced tools to investigate neural processes. Due to their nature fast 2p scanning of single neurons is required with very high precision. This is still beyond the scope of present 2p technology as only few solutions for precisely controlled rapid scanning of selected neurons along a given path has been proposed, like targeted scan path (TSP) or application of acousto-optic deflectors (AOD's). The currently used algorithms to scan, for instance, selected neurons along an optimal path with high speed suffer from a number of limitations like either low speed or low accuracy (TSP), low field of view or degraded resolution (AOD's), long optimization time while looking for best trajectory to chosen set of neurons, large amplitude of accelerations and decelerations along the path. Throughout this study a new algorithm is proposed and discussed that overcomes some of current limitations. The algorithm automatically determine optimal low inertia path suitable to drive galvo mirrors with their highest possible speed. Proposed solution does not calculate any cost function providing smooth path along all selected points corresponding to neurons. The algorithm allows to generate either the path with evenly distributed samples of trajectory what determine the constant scan speed leading to low inertial scanning or densified, uneven distribution of points what leads to more accurate scanning of particular cells keeping the overall movements between cells optimal. To validate the algorithm a number of simulations of its performance on randomly generated sparse spatial configurations of cells represented as a set of points has been done. Each simulation provides a set of descriptors like scan path length, estimated time and speed of scan, curvature of trajectory and hence the inertia given as a function of number of points (cells). Through discussion of previously reported results and presented simulations done with new algorithm it is shown that proposed solution overcomes some of current limitations and has real potential for scanning of freely selected cells to monitor their activities with high temporal resolution and accuracy. Preliminary implementation within currently used 2p setup will be demonstrated. Provided theoretical analysis of such a class of algorithms proves its robustness and flexibility to any coplanar and sparsely distributed set of cells opening a wide range of applications in molecular imaging, from neuronal calcium waves monitoring to molecular neuroimaging with high temporal resolution.

Presentation Number **0378A**

Poster Session 2a: Imaging Instrumentation and Methodology

Time-resolved two-photon spectra of short and long fluorescent lifetime dyes - auramine O and fluorescein solved in water and ethanol

Tomasz Soltysinski, ¹Warsaw University of Technology, Institute of Metrology and Biomedical Engineering, Warsaw, Poland; ²Polish Academy of Sciences, Institute for Biocybernetics and Biomedical Engineering, Warsaw, Poland. Contact e-mail: tomasz_s@vp.pl

Introduction Multi-photon spectra of most dyes remain unknown and differ when obtained due to one- or two-photon (2p) excitation. Novel imaging technologies make possible effective exploration of fluorescent dyes lifetime after 2p excitation. Two dyes, fluorescein and auramine O, differing by fluorescent lifetimes have been investigated in time and spectral domain. A new study is presented with use of technology of spectral multi-channel (multi-wavelength) time-resolved single fluorescent photon counting. Materials and methods Fluorescein (FL) is a standard used in microimaging with a long lifetime (~4 ns). Auramine O (AO) is used for imaging of cells and their structures or for Pb detection. It has short solution-dependent sub ns lifetime. Both dyes have been dissolved in distilled water and ethanol (up to 95 % of C₂H₅OH in water) until solution filled. Both dyes have large cross section for multi-photon excitation. Spectra were obtained with fs Ti:Sapphire laser source working at 80MHz with tunable emission wavelength between 720 and 900 nm. PC-based instrumentation was used to control the cards, DCC-100 for driving the power supply of photomultiplier tubes (PMTs) and SPC-830 or SPC-150 for photon counting with sub ns time resolution (Becker & Hickl). PMTs are integrated with polychromator (PMLSpec) that allows for simultaneous observation of arrival of single photons on 16 spectral channel of width 12.5 nm and the range of 208 nm for any region between 300-850 nm. Registered photons allow to recombine histograms of times of arrivals of photons. The grating was set to cover the range 435-643 nm. Integration time of measurement was varying up to 300s in static or dynamic mode of spectra detection. Results Time-resolved spectra have been investigated for different wavelength of excitation with interval of 20 nm, within range of 720 to 840 nm providing normalized matrices of the most dominant part of histograms obtained for differing excitation wavelength. It is found that maximal levels of emission for AO takes place for excitation at 740 and 760 nm. Instrument response function has been determined. Maxima of emission found: AO, H₂O - 550nm, FL, H₂O - 537-550nm. Lifetime changes found: AO, H₂O - decreasing with excitation wavelength, decreasing with amount of ethanol in solution, stable for FL dissolved in water or solution with ethanol. Conclusions Presented study shows the proposed technology and pipe able to characterize all available dyes excited in two-photon regime. Examined dyes lifetimes are a subject of change under controlled conditions.

Presentation Number **0379A**

Poster Session 2a: Imaging Instrumentation and Methodology

Using Single Molecule Imaging to Quantify and Characterize Fluorophores on Multi-Modal Nanoprobes

Ambika Bumb¹, **Susanta Sarkar**², **Keir C. Neuman**², **Martin Brechbiel**¹, ¹*Radiation Oncology Branch, National Cancer Institute, Bethesda, MD, USA;* ²*Biochemistry and Biophysics Center, National Heart Lung and Blood Institute, Bethesda, MD, USA. Contact e-mail: Bumba@mail.nih.gov*

While it is always possible to know the molar equivalence of dye being reacted to nanoparticle, precisely quantifying the amount that attached is a true challenge that many struggle with in molecular imaging. Typically, dye content is analyzed by quantum yield characterization of fluorescence. The method for measuring quantum yield involves comparing absorbance and integration of fluorescence curves of the test sample to well characterized standard samples. The technique requires an assumption that the solvents of the two samples behave similarly, which is not the case when the nanoprobe has a core structure such as iron oxide that has its own absorbance spectrum, refractive index, and light scattering. Additionally, near infrared (NIR) fluorophores are frequently chosen for in vivo imaging applications because of their ability to penetrate tissue the farthest. Choosing the appropriate NIR standard dye to compare to is difficult because most have very low quantum yield values that vary in literature. We synthesized a number of dual-reporting (magnetic resonance and optical imaging) nanoparticles by encasing ultrasmall superparamagnetic iron oxide nanoparticles in a thin ~3nm layer of silica containing different conjugated fluorophores. During each phase of development, the nanoparticles were characterized for size, surface charge, structure, and magnetic properties. To study their optical properties in comparison to free dye, single molecule measurements were performed using a home-built prism-type total internal reflection fluorescence microscope. Fluorescence intensity of individual particles and photobleaching of individual dye molecules as a function time was observed and recorded. Using this information it was possible to analyze the number of fluorophores per particle, and the results demonstrated that encapsulating dye in silica increased its brightness and prolonged its photobleaching lifetime.

Presentation Number **0380A**

Poster Session 2a: Imaging Instrumentation and Methodology

A new computational method for multispectral bioluminescence tomography

Yanbin Hou¹, **Jie Tian**^{1,2}, Xiaopeng Ma¹, Xiangsi Li¹, Qian Zhang¹, Yuanyuan Zhou¹, Xiuduan Lin¹, ¹Life Sciences Research Center, School of Life Sciences and Technology, Xidian University, Xi'an, China; ²Medical Image Processing Group, Institute of Automation, CAS, "Beijing, 100190", China. Contact e-mail: tian@ieee.org

Bioluminescence tomography (BLT) is able to in vivo localize and quantify the underlying light-emitting probes in non-invasive manner, thus providing a valuable tool for characterizing and measuring physiological and pathological processes at cellular and molecular levels in living small animals. Because of the wavelength-dependence of the biological tissue in terms of optical coefficients, it tends to result in undesirable ill-posed problem when BLT source reconstruction is performed based on boundary measurement with a mixed or a single spectrum. A large number of studies have shown that multispectral approach can significantly improve the accuracy and stability of BLT source reconstruction, especially for deep sources. However, multispectral approach increases not only data acquisition time but also computation burden. According to available multispectral algorithms, it need set up and solve a group of simultaneous partial differential equations (PDEs), e.g. the most widely used diffusion equation. It means that the computation cost will rise with the square of the number of spectra, so no more than three spectral bands are generally used in existing studies. We develop a new computational method for multispectral BLT on the basis of theoretical analysis and formula derivation, which introduces equivalent achromatic optical coefficients to establish system matrix of the same size as that in a single spectrum. The equivalent achromatic optical coefficients are determined by considering the contribution of each unmixed spectral band to the gross boundary measurement. Numerical simulations are designed and performed to evaluate the accuracy and efficiency of this new method. The relevant results demonstrate that the proposed method can provide comparative accuracy as available multispectral method, while at a much lower computation cost. What is even more important, we can deal with an infinite number of spectral bands, i.e. at any desirable wavelength in practice.

Presentation Number **0381A**

Poster Session 2a: Imaging Instrumentation and Methodology

A general simulation platform for light propagation in turbid tissues with irregular shapes

Nunu Ren¹, **Jie Tian**^{1,2}, Xiaohui Zhao¹, Man Shen¹, Jianfeng Li¹, Hongliang Liu¹, Xiaomin Shen¹, ¹Life Sciences Research Center, School of Life Sciences and Technology, Xidian University, Xi'an, China; ²Medical Image Processing Group, Institute of Automation, CAS, "Beijing, 100190", China. Contact e-mail: tian@ieee.org

Among the techniques for molecular imaging, optical molecular imaging, including diffuse optical tomography (DOT), fluorescence molecular tomography (FMT) and bioluminescence tomography (BLT), is an important one because of its special advantages of high efficiency, high sensitivity and nonionizing radiation. At the same time, some simulation platforms based on Monte Carlo method have been developed for simulating light propagation in biological tissues. However, those platforms cannot catch up with the development of the researches on optical molecular imaging. Herein, the platform MOSE (Molecular Optical Simulation Environment) previously developed to simulate near-infrared light propagation in turbid tissues and free-space is updated for a better simulation. The latest version is improved from the following several aspects: simulation algorithm, graphic visualization, overall framework and software operation. For a good consistence with the real experiment, the structural information of the light source and tissue can be described by regular or irregular shapes. The regular shapes include cube, cylinder and ellipsoid, while the irregular shape is constructed by triangle meshes which can be reconstructed from the data provided by MRI or CT. The new version can be used for investigating fluorescence interaction with the biological tissues. In addition, both the continuous wave (CW) and time-domain (TD) Monte Carlo codes are included to meet the requirements of the researchers. In addition, the graphic visualization and software operation are also improved to facilitate the analysis of the simulation results (absorption, transmittance and detection results) in CW or TD. With the help of MOSE, the researchers could flexibly and efficiently implement the simulation of light propagation and data analysis.

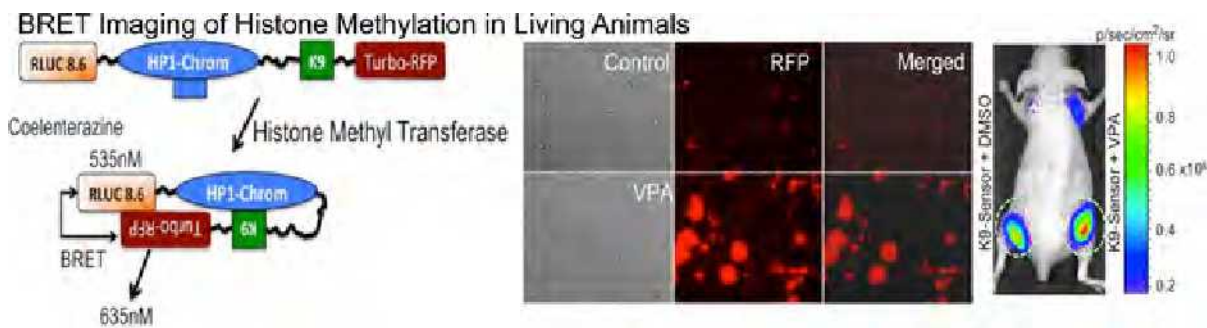
Presentation Number **0382A**

Poster Session 2a: Imaging Instrumentation and Methodology

Imaging Histone Methylation in Living Animals

Ramasamy Paulmurugan^{1,2}, **Veerapazham S. Thillai**^{1,2}, ¹Radiology, Stanford University, Palo Alto, CA, USA; ²Molecular Imaging Program at Stanford, Stanford University, Palo Alto, CA, USA. Contact e-mail: paulmur8@stanford.edu

Histone modifications, including histone methylation and histone acetylation, are two important epigenetic processes that play a key role in maintaining the chromatin structure and regulate gene expression. The methylation of amino acids lysine and/or arginine residues occurs at NH₂- terminal tail of histones (H3: Lys 4, 9, 27 and 36, and H4: Lys 20) by histone methyltransferases (HMTs), which recruits chromodomain from heterochromatin-associated proteins, and forms a complex that functionally remodel chromatin structure and regulate gene expression. If an in vivo imaging method can be developed for monitoring this cellular process, it may accelerate drug development for different diseases, including cancer, by targeting this regulatory process. From this study, we developed a bioluminescence resonance energy transfer (BRET) sensor that can optically image histone-methylation in cells and in living animals. A mutant renilla luciferase (RLUC 8.6, Ex:535nm), in combination with Turbo-RFP-FP635 (Ex:588nm), was used to construct a vector expressing fusion protein with the histone methylation domain (H3-K9) and chromodomain (HP1) connected by specific linker peptides (RL8.6-Link-HP1-Link-K9-Link-Turbo-RFP-FP635). A similar sensor with Lys-27 peptide that normally interacts with the chromodomain from polycomb protein was used as control. The 293T-cells stably expressing the K9 sensor was studied by inducing with different epigenetic modulators [valproic acid (VPA), TSA, and 5-Aza] known to inhibit HDAC activity in cells and in living animals, showed an increase in the BRET signal (~1.5±0.5 fold). Fluorescent microscopy imaging of cells showed a significant (P<0.5) increase in the level of Turbo-RFP signal due to histone methylation. The cell implants in animals imaged after the cells were pre-exposed to VPA, showed a similar level of signal increase as in the cells. The BRET signal is estimated to be ~10% of the total RLUC signal, which we imaged in animals. The cells stably expressing K27-peptide showed no BRET signal. The western blot analysis of H3 protein showed no change in endogenous level of its expression, further confirming the specificity of the system. The developed BRET system is sensitive and has the advantage of having been used for the screening and pre-clinical evaluation of new drugs targeting this epigenetic regulator to test for different therapeutic applications.



Presentation Number **0383A**

Poster Session 2a: Imaging Instrumentation and Methodology

Compare Non- Negative Matrix Factorization with Singular Value Decomposition method for obtaining the unmixed fluorescence spectra of a mouse tissue using FRI

Ebrahim Najafzadeh^{1,2}, **Marjaneh Hejazi**^{1,2}, **Divya Vats**³, ¹*Medical Physics, Tehran University of medical sciences, Tehran, Islamic Republic of Iran;* ²*laser lab, Research Center for Science and Technology in Medicine, Tehran University of Medical Sciences, Tehran, Islamic Republic of Iran;* ³*biomedical engineering, 3 Institute for Biomedical Engineering, Zurich, Switzerland. Contact e-mail: najafzadeh@razi.tums.ac.ir*

Introduction. Reflectance fluorescence imaging (FRI) is a powerful modality for detecting simultaneously different fluorophores attached to target proteins. The common fluorophores used in FRI have overlapping emission spectra which makes them difficult to separate by just using optical filtering methods. The emission spectra can be unmixed by applying methods such as singular value decomposition (SVD) into orthogonal and negative basis matrices. Recently a blind source separation algorithm called non-negative matrix factorization (NMF) was proposed for FRI imaging using of non-negativity constraints. The aim of this work is to compare NMF with the SVD algorithm for obtaining the unmixed fluorescence spectral of a mouse tissue using FRI. Materials and Methods. Our FRI setup is consisted of three Lasers (Coherence Ltd, USA) at wavelength from 473nm up to 787nm. The near-infrared quantum dot (QD 705 ITK, Invitrogen) and Qdot(800, Invitrogen) spectra measured with a commercial fluorimeter then injected percutaneously into a mouse. The FRI images were acquired by a cooled CCD camera using band pass filters centred at 705nm and 800 nm for QD705 and QD800 respectively. The unmixed images of the QDs were proceeded on a pixel-by-pixel using SVD and NMF. We used NMF based Lee and Seung's algorithm because of its easiness of implementation and its guarantee of convergence properties. The aim of this work is comparing SVD performance with that of NMF on the same data by means of Peaks Signal to noise ratio (PSNR): where RMSE is the mean squared-error between the original and unmixed images. Results. The results of applying the SVD and NMF for obtaining the separated sources by unmixing the QDs spectra were obtained. The evaluation shows that PSNR of FRI images obtained by SVD is 103 db that of the NMF is 94 db. Discussion and conclusion. Tissue spectral unmixing can be used as powerful tool for choosing the most appropriate target proteins as well as fluorophores for biological applications. SVD and NMF were used to perform a quantitative unmixing of the QDs spectra in FRI. However NMF is an iterative algorithm which may provide a local optimum solution and unmixed even no priori information of spectra of the fluorophores were available. The NMF is more suitable for our non-negative data however its PSNR is 1.1 lower than that of SVD. In conclusion, our results showed that the non-negativity constraints in NMF are much better suited for the unmixing spectral problem than the orthogonality constraints in traditional decompositions, such as SVD.

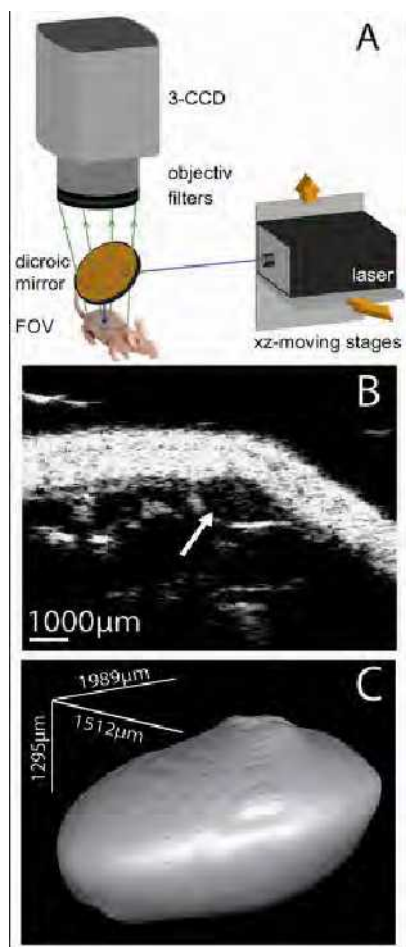
Presentation Number **0384A**

Poster Session 2a: Imaging Instrumentation and Methodology

Reconstruction of Fluorescent Protein Distribution in vivo using Mesoscopic Epifluorescence Tomography

Saskia Bjoern¹, **Lotfi Abou-Elkacem**², **Wiltrud Lederle**², **Vasilis Ntziachristos**¹, **Fabian Kiessling**², **Ralf B. Schulz**¹, ¹*Institute for Biological and Medical Imaging, Helmholtz Zentrum München, München, Germany;* ²*Department of Experimental Molecular Imaging, Medical Faculty, RWTH Aachen University, Aachen, Germany. Contact e-mail: saskia.bjoern@helmholtz-muenchen.de*

Mesoscopic Epifluorescence Tomography (MEFT) is a technique derived from Lamellar Optical Tomography, determining fluorescence biodistribution by tomographic means in reflectance geometry. Herein, a pencil beam (473 nm) is scanned over the region of interest to excite fluorophores hidden within the tissue, while a 3-CCD camera acquires an image of the fluorescence emission for each source position (A). This configuration is advantageous whenever transillumination of the specimen is not feasible, e.g. in the presence of skin chambers or when using wavelengths in the visible range where absorption is high. The reconstruction algorithm is similar to the one used in Fluorescence Molecular Tomography; however diffusion theory cannot be employed, since the source-detector separation for most image pixels is comparable to or below the scattering length of the tissue. Instead Monte Carlo simulations are employed for a semi-infinite layered medium to predict the sensitivity functions. Initial in vivo studies were performed imaging subcutaneously injected HCT-116 human colon cancer cells that express green fluorescent protein (GFP) in the nucleus and red fluorescent protein (RFP) in the cytoplasm. Prior to the MEFT measurements the animal was scanned with ultrasound for reference and comparison purposes (B). The reconstructed fluorescence distribution precisely correlates with the ultrasound measurements (1260 μ m x 3300 μ m x 2480 μ m), while the segmented tumor volume (C) compares well with the measured tumor size. Future work will include combined GFP and RFP measurements using excitation light at 473 nm and 532 nm. Acknowledgement: The cells were kindly provided by Dr. Robert Hoffman, AntiCancer Inc., San Diego



Presentation Number **0385A**

Poster Session 2a: Imaging Instrumentation and Methodology

High resolution detection of Chromophoric Agents in the Murine Heart by Multispectral Optoacoustic Tomography (MSOT)

Adrian Taruttis^{1,2}, Daniel Razansky^{1,2}, Vasilis Ntziachristos^{1,2}, ¹*Institute for Biological and Medical Imaging, Technische Universität München, Munich, Germany;* ²*Institute for Biological and Medical Imaging, Helmholtz Zentrum München, Neuherberg, Germany.*
Contact e-mail: adrian.taruttis@helmholtz-muenchen.de

Multispectral Optoacoustic Tomography (MSOT) enables spectral differentiation of multiple molecules in tissues with high resolution. It has already been shown capable of resolving, with high specificity, fluorochromes, gold nanoparticles and other chromophores with unique spectral signatures. In this work we examine the feasibility of MSOT detection of chromophoric agents in the mouse heart, thus proving the potential of the technique for molecular imaging of cardiac disease. Results from mice are validated with data from simulations, tissue realistic phantom studies and excised heart measurements. Our simulations are based on employing light diffusion models and a realistic multispectral tissue model of wavelength dependent absorption and scattering to investigate target detection in the myocardium. We show the feasibility of detecting a range of available agents (fluorescent dyes, gold nanorods) with absorption peaks in the near-infrared. In a further step, MSOT measurements on excised hearts imbedded in optically scattering and absorbing backgrounds confirm the ability to resolve exogenously administered chromophores inside the heart chambers. Finally, experimental results from mice show that MSOT can tomographically capture cardiovascular structures and produce transverse (axial) anatomical and molecular images at high spatial resolution (~ 100-200 μm). In conclusion MSOT shows high potential as an imaging approach to facilitate in-vivo quantitative imaging investigations of cardiovascular disease.

Presentation Number **0386A**

Poster Session 2a: Imaging Instrumentation and Methodology

Infarct Size Prediction Using a Combined Technique of Cerebral Blood Flow Monitoring and Near-infrared Fluorescent Thrombi Imaging in a Mouse Model of Embolic Stroke

Jeong-Yeon Kim¹, Jin-yong Park¹, Byeong-Teck Kang¹, Ju Hee Ryu², Dong Kun Lee¹, Kwangmeyung Kim², Ick Chan Kwon², Dong-Eog Kim¹, ¹Molecular Imaging & Neurovascular Research (MINER) Lab, Neurology, Dongguk Univ Ilsan Hospital, Goyang, Republic of Korea; ²Biomedical Research Center, Korea Institute of Science and Technology, Seoul, Republic of Korea. Contact e-mail: dr.neurovascular@gmail.com

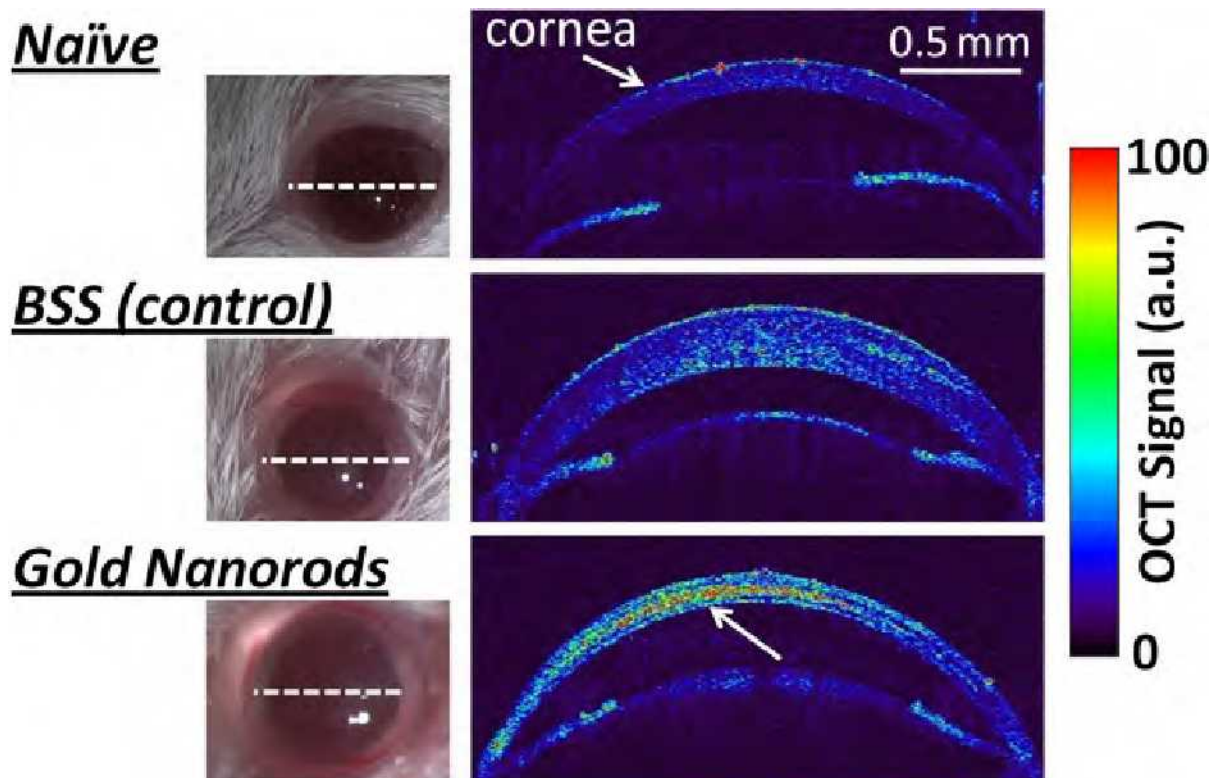
Background & Objective: When making an embolic stroke model, the change of the cerebral blood flow (CBF) in the middle cerebral artery (MCA) is monitored by using a laser Doppler flowmeter (LDF). However, not only CBF change but also thrombi extent could affect final infarct size, which is one of the most important research outcomes. Here, we present a new combined technique of in vivo LDF monitoring and ex vivo NIRF imaging of cerebral thrombi in C57BL/6 mice, and show its usefulness in predicting infarct volumes. **Methods:** Autologous blood clots were labeled with a Cy5.5 NIRF imaging agent (2nM or 20nM) that could sense the activity of the factor XIII coagulation enzyme. In 10-week-old mice (n = 40), the fluorescent labeled clot emboli (3.70mm³) were injected as previously reported into the proximal portion of the MCA, while monitoring the CBF using a LDF. 24hr later, the animals were euthanized, and the brains were removed and imaged ex vivo by using a NIRF imaging machine. The brains were then used for immediate TTC staining to delineate the infarct area. After normalization, pixel counts of Cy5.5 NIRF signals in the MCAs, which represent thrombi extents, were calculated. The infarct volumes were measured and expressed as a percentage of the total brain volume. Statistical analyses including Pearson correlation and multiple regression analyses were performed using a software package (R version 2.11.0). **Results:** Immediately after the thromboembolism was induced, the CBF was decreased to about 40% of the baseline (39.1% in the 2nM group, n = 22; 40.2% in the 20nM group, n = 17). At 24 hr, the thrombi extents were non-significantly lower in the 2nM group (88.6 ± 78.6) than in the 20nM group (149.5 ± 138.9, p = 0.11, Student's t-test). Moreover, infarct size did not differ between the two groups (27.8% vs. 29.6%, p = 0.50, Student's t-test). The CBF decrease was positively correlated with the infarct size (r² = 0.28, p < 0.01). The thrombi extent was also positively correlated with the infarct size (r² = 0.13, p = 0.02). The multiple regression analysis revealed that both CBF decrease (p < 0.01) and thrombi extent (p = 0.02) could independently (and better when combined) predict the infarct size (r² = 0.39, p < 0.01): every 10% decrease of the CBF or 100 pixels increase of the thrombi extent was estimated to produce about 2.5 fold increase of the infarct size. **Conclusion:** In vivo CBF monitoring combined with ex vivo NIRF imaging of thrombi is more accurate for predicting cerebral infarct volumes than either CBF monitoring or thrombi imaging alone.

Presentation Number **0387A**
 Poster Session 2a: Imaging Instrumentation and Methodology

Optical Coherence Molecular Imaging using Gold Nanorods in Living Mice Eyes

Adam de la Zerda^{1,2}, Jianhua Wang⁴, Victor Perez⁴, Marco Ruggeri⁴, Sanjiv S. Gambhir^{2,3}, Richard Awdeh⁴, ¹Electrical Engineering, Stanford University, Stanford, CA, USA; ²Radiology Department and the Molecular Imaging Program at Stanford, Stanford University, Stanford, CA, USA; ³Bioengineering, Stanford University, Stanford, CA, USA; ⁴Bascom Palmer Eye Institute, University of Miami, Miami, FL, USA. Contact e-mail: adlz@stanford.edu

Optical Coherence Tomography (OCT) is a powerful imaging modality to visualize various structures in the eye at very high spatial resolution. Here we demonstrate for the first time an OCT nanoparticle imaging agent in living mice. The imaging agent is a gold nanorod 15 nm in diameter and 45 nm in length. These dimensions resulted in a peak absorbance at 780 nm, which matches well with the laser source in our custom made OCT imaging system. The gold nanorods were coated with polyethylene-glycol-5000 (PEG₅₀₀₀) to render water-solubility to the gold nanorods. We injected 5 μ l of gold nanorods at concentration of 50 nM into mice corneas (n = 3) and acquired OCT cross sectional images of the mice corneas. Control mice were either injected with 10 μ l of balanced saline solution (BSS) or not injected with anything (naïve). The gold nanorods have created a strong contrast in the OCT image, over 6-fold higher than in control mice (p < 0.01) (see Figure). OCT images of the mice corneas were acquired over the following 4 days post-injection. At 4 days post-injection, a strong OCT signal, 5-folds higher than control mice (p < 0.05) was observed from the corneas of the mice injected with gold nanorods, despite the possible diffusion of the gold nanorods in the corneal space. Finally, we measured the minimal detectable concentration of the gold nanorods by injecting decreasing concentration of particles into the mice corneas. The lowest detectable concentration was determined to be 50 pM. At this concentration, the OCT signal from the gold nanorods was equivalent to the tissue background OCT signal. OCT imaging of gold nanoparticles was demonstrated for the first time in living subjects at exquisite pico-molar sensitivity.



Mice corneas were injected with 5 μ l of gold nanorods at 50 nM (lower mouse), while control mice corneas were injected with 10 μ l of balanced saline solution (middle mouse) or not injected at all (upper mouse). OCT cross-sectional images through the mice eyes (white dotted line) visualized the high contrast created by the gold nanorods in the cornea (lower white arrow) as compared with control mice.

Presentation Number **0388A**

Poster Session 2a: Imaging Instrumentation and Methodology

Time-Gated Fluorescence Mediated Tomography: Resolution, Noise and Sensitivity

Mark Niedre, Niksa Valim, Zhi Li, Electrical and Computer Engineering, Northeastern University, Boston, MA, USA. Contact e-mail: mniedre@ece.neu.edu

Small animal fluorescence mediated tomography (FMT) is increasingly recognized as an important tool in biomedical research. Among the important technical challenges in FMT is the limited imaging resolution which results from the high degree of light scatter in biological tissues. Temporal gating of transmitted photon fields has been shown to effectively reduce light scatter and improve resolution. In particular, 'early-transmitted' photons propagate along less diffusive paths between source and detector pairs versus un-gated photons, but this requires rejection of more than 99% of incident photons. While this principle has been demonstrated previously, the degree of resolution improvement obtainable under typical small animal imaging conditions is still poorly understood, as is the impact on imaging noise performance and detection sensitivity. In the first part of this study we investigated the influence of time-gating on paths of photon propagation in diffusive media. Absorption and fluorescence photon density sensitivity functions (PDSFs) were explicitly measured using a perturbation method with a picosecond pulsed laser and time-resolved photon counting detection. Noise performance at different time gates was also recorded. Measurements were made in optical phantoms over a range of optical properties and pathlengths, and the optimal imaging time gate was determined. It was found that by using early-photons, imaging PDSFs with central radii as small as 1.5 mm were obtainable with typical small animal dimensions and optical properties, corresponding to a 4-6 fold reduction in the PDSF volume versus constant intensity (CW) measurements. These findings were supported with Monte Carlo simulation studies. In the second part of the study, we investigated the influence of time-gating on the tomographic image reconstruction problem. We determined that while smaller PDSFs resulted in significantly improved resolution with early photons, the signal to noise ratio was correspondingly reduced compared to CW measurements, primarily due to rejection of large numbers of photons. This reduced the imaging sensitivity by approximately an order of magnitude. Finally, to solve this problem, we developed a novel image reconstruction strategy that combined early arriving and CW photons in a 'hybrid' approach. We demonstrate that by using this approach the respective advantages of both - i.e. resolution and sensitivity - were retained. This was demonstrated in both simulation studies and experimentally in nude mice with fluorescent (Alexa-Fluor 750) inclusions.

Presentation Number **0356B**
Poster Session 3a: Imaging Instrumentation and Methodology

Quantification of hemoglobin status using Photoacoustic Computed Tomography Imaging: from phantom to tumor study

Bo Liu, Keith Stantz, Minsong Cao, Michael Shaffer, School of Health Sciences, Purdue University, West Lafayette, IN, USA. Contact e-mail: liu@purdue.edu

Purpose: The purpose of this study is to develop a methodology to calibrate the photoacoustic computed tomographic spectroscopic (PCT-S) small animal scanner, to quantify the hemoglobin status (hemoglobin concentration and oxygen saturation) based on the PCT intensities extracted from reconstructed 3D PCT images, and to identify intra-tumor hemoglobin status variations for breast tumors with different angiogenic phenotypes. **Material and Methods:** Calibration procedure was developed using India ink solutions filled in FEP phantom tube to evaluate the performance of the scanner system. Phantom studies were first conducted to acquire the PCT spectrum of blood which was used to determine the optical to acoustic conversion efficiency for red blood cells, Kappa. This Kappa model was built up to convert the PCT intensity to optical absorption property of hemoglobin in RBCs. Then the hemoglobin status for blood samples of different hemoglobin concentrations and oxygen saturations levels were measured and compared to co-oximeter measurements (Gold Standard). These techniques were tested in vivo by scanning the artery and veins in a mouse tail while exposed to different levels of oxygen. Mice were sacrificed, blood extracted from the aorta, and hemoglobin concentration measured by co-oximeter and compared to PCT-S measurements. Lastly, PCT-S scans of three breast tumor models (MCF7, MCF7/VEGF and MDA231) were spectrally analyzed to obtain the intra-tumor hemoglobin status. **Results:** The Kappa value of hemoglobin molecule in RBCs was calculated to be $1.89 \times 10^{11} \text{ pu/J}$, where pu is an arbitrary unit of PCT intensity calibrated to acoustic energy (e.g., Pascal). The combined statistical and systematic errors of hemoglobin status in phantom study between PCT and co-oximeter was less than 5%, which was consistent with in vivo mouse tail study of 3.8%. The tumor analysis result showed a significant intra-tumor oxygen saturation distribution difference among three different tumor types, where MCF7 have low SaO₂ levels (0.68 ± 0.1) and MCF7/VEGF have high SaO₂ levels (0.82 ± 0.16) throughout the tumor, and MDA231 had high levels at the periphery and very low values interior to the tumors. **Conclusion:** This study has shown the feasibility to quantify the hemoglobin status in mouse tumor model using photoacoustic imaging technique. Results demonstrate significant differences in intra-tumor heterogeneity and thus oxidative stresses. As an innovative non-invasive imaging modality, PCT could provide hypoxia and anemia information inside the tumor for therapy response evaluation.

Presentation Number **0357B**

Poster Session 3a: Imaging Instrumentation and Methodology

Automatic surface extraction algorithm for optical tomography utilizing 360° projection photographic images

Xiaopeng Ma¹, **Jie Tian**^{1,2}, Xiangsi Li¹, Xueli Chen¹, Yuanyuan Zhou¹, ¹Life Sciences Research Center, School of Life Sciences and Technology, Xidian University, Xi'an, China; ²Medical Image Processing Group, Institute of Automation, CAS, "Beijing, 100190", China. Contact e-mail: tian@ieee.org

Optical imaging has attracted much more attention in recent years due to its reasonable spatial and temporal resolution, high imaging contrast and sensibility and affordable cost. In particular, its tomographic counterpart, optical tomography has become a valuable tool for the noninvasive detection because of its significant advantages in recovering three-dimensional spatial distribution and depth information of the internal abnormalities of biological tissues. In tomographic imaging, surface extraction of arbitrary geometries is needed for further acquiring the flux distribution on the surface from measurements. Although some structure imaging techniques, such as computed tomography and magnetic resonance imaging can achieve surface structure of arbitrary geometries, they are hampered from radiation hazards and higher cost. Thus, to develop a simple and effective method to automatically extract surface of arbitrary geometries using optical images has become a significant problem. In this contribution, we developed a simple and effective method to extract surface of arbitrary geometries using 360° projection photographic images. This method was implemented by adding all the projections of research object considering the projection angle. Firstly, image for each projection was thresholded and converted to a binary image. Thus, the border of research object in each image was obtained. Secondly, a Cartesian coordinate system referring to the arbitrary geometries was established utilizing the first projection image, where the origin was the center of the image, X and Y axes were the horizontal and vertical direction of the image, and Z axis was obtained using the Right-hand rule. Thirdly, the coordinate of each point on the surface of arbitrary geometries can be calculated by considering the pixel numbers from the point on the border to X or Z axis, the pixel size, the magnification factor of imaging system and the rotation angle of each projection. Finally, triangle meshes were generated from the calculated points using octree surface rendering method. This method has been implemented with MATLAB language and preliminarily demonstrated. Some useful results have also been obtained and further improvements will go on in future.

Presentation Number **0358B**
 Poster Session 3a: Imaging Instrumentation and Methodology

A practical parameter selection method for Tikhonov regularization in Bioluminescence tomography

Xiaowei He^{1,2}, Jie Tian^{1,3}, Jimin Liang¹, Xiaochao Qu¹, Duofang Chen¹, Yanbin Hou¹, ¹Life Sciences Research Center, School of Life Sciences and Technology, Xidian University, Xi'an, China; ²School of Information Science and Technology, Northwest University, Xi'an, China; ³Medical Image Processing Group, Institute of Automation, CAS, "Beijing, 100190", China. Contact e-mail: tian@ieee.org

Reconstruction of the bioluminescent source distribution in small animals is the inverse problem of bioluminescence tomography (BLT), which is proved to be severely ill-posed. Hence, it is necessary to incorporate some a priori information about the exact solution to stabilize the problem and to single out a meaningful and stable solution, which is the purpose of regularization. Through the most well-known Tikhonov regularization method, a well-posed optimization problem to approximate the original BLT problem is obtained. In this process, regularization parameter is a crucial factor which influences the properties of the regularized solution, and should therefore be chosen with care. It is well known that parameter selection method (PCM) is generally problem-dependent. Additionally, automated PCMs for Tikhonov regularization in BLT have not been sufficiently considered to date. In this contribution, we present a practical PCM that can adaptively adjust the parameter during the calculating process by comparing the thresholded residual norm iteratively. The proposed method is validated by numerical simulations with a heterogeneous phantom. In order to evaluate the performance of the proposed method, two commonly used PCMs in other inverse problems, namely L-Curve and generalized cross-validation (GCV) serve as the counterparts in the comparison. The reconstructed results suggest that the proposed parameter choosing method performs best and combined with Tikhonov regularization it can achieve accurate localization of bioluminescent source even if the initially selected parameter is not optimal.

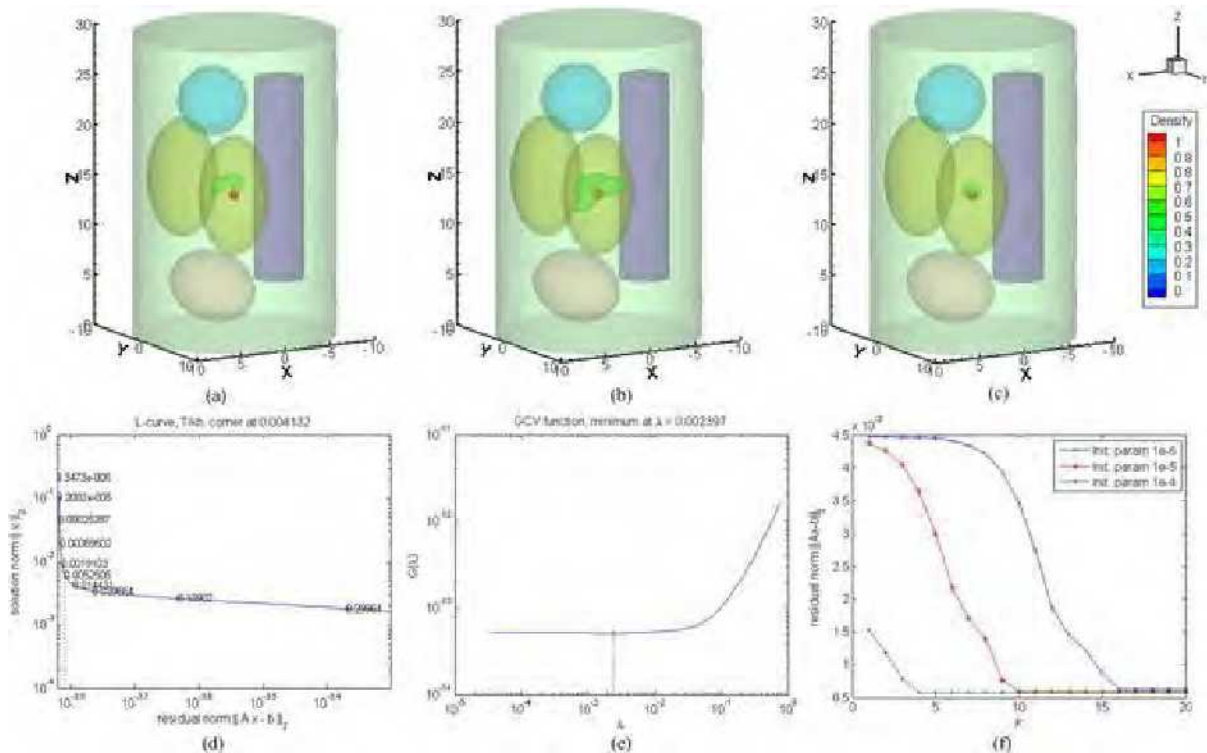


Figure 1. Reconstruction results of (a) L-Curve, (b) GCV and (c) the proposed method. Regularization parameter determined by (d) L-Curve and (e) GCV, (f) the residual vector norms vary with k under different initial parameter λ .

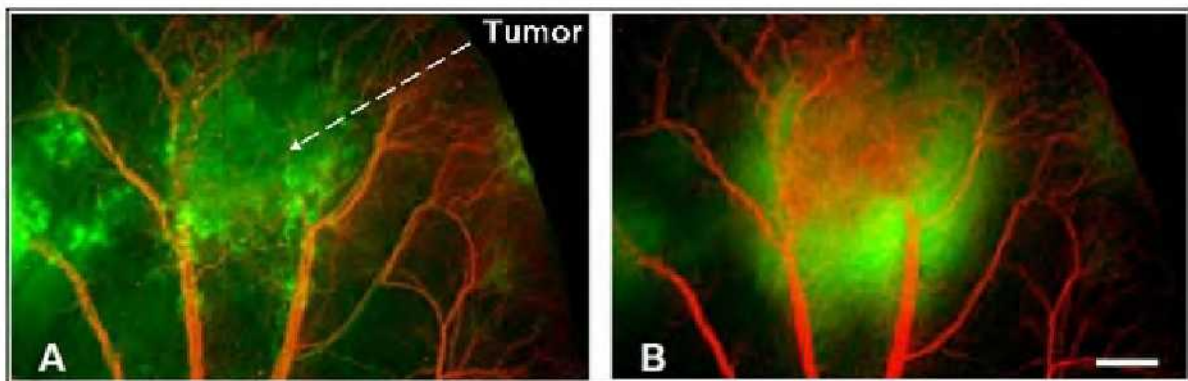
Presentation Number **0359B**

Poster Session 3a: Imaging Instrumentation and Methodology

Multimodal Optical Imaging of Microvascular Network and Tumor Angiogenesis

Vyacheslav Kalchenko¹, **Igor Meglinski**², **Alon Harmelin**¹, ¹*Veterinary Resources, Weizmann Institute of Science, Rehovot, Israel;*
²*Department of Physics, University of Otago, Dunedin, New Zealand. Contact e-mail: a.kalchenko@weizmann.ac.il*

Angiogenesis is a fascinating and rapidly developed research area dedicated to the study of tumor growth and metastases progression, whereas studying tumor microvascular network aims to improve drug delivery that is likely to lead to grant tumor regression. In addition, recent studies of tumor development demonstrated that malformations of microvascular blood circulation can noticeably affect the tumor growth and metastasis evolution. Therefore, understanding the basic mechanisms and key influence factors of tumor angiogenesis and blood micro-circulation are ultimately required. Small animal models are widely used in this purpose. In order to achieve high resolution imaging of tumor and tumor micro-vascular network in mouse external ear we developed a new multimodal (dual CCD camera) optical diagnostic system. System utilizes combined use of Temporal Laser Speckle Contrast Imaging (TLSCI) approach for label-free visualization of blood vessels and blood flow characterization, and Fluorescent Intravital Microscopy (FIVM) for screening blood vessels permeability. The obtained results demonstrate that such a multimodal combined application of TLSCI and FIVM has a great potential and can significantly expand the capabilities of tumor angiogenesis studies and notably contribute to the development of cancer treatment.



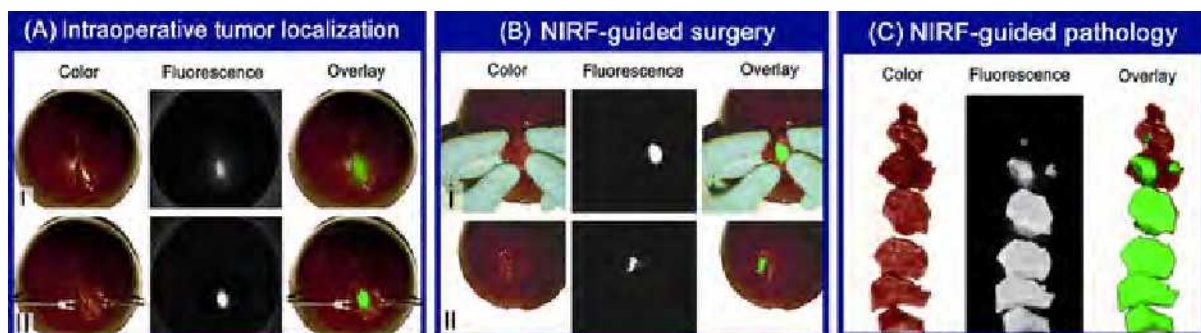
Images of mouse ear tumor: A - just after intravenous injection of FITC-Dextran, B - 20 minutes later. The blood microvascular network is obtained by label-free TLSCI mode (red), whereas the tumor seeing in FIVM mode (green). Bar is 1mm.

Presentation Number **0360B**
 Poster Session 3a: Imaging Instrumentation and Methodology

Near-Infrared Fluorescence (NIRF) Imaging Applications in Breast-Conserving Surgery: Assessing Intra-operative Techniques in Tissue-Simulating Breast Phantoms

Rick G. Pleijhuis¹, **Gerrit C. Langhout**¹, **Wijnand Helfrich**¹, **George Themelis**², **Athanasios Sarantopoulos**², **Johannes S. de Jong**¹, **Vasilis Ntziachristos**², **Gooitzen M. van Dam**¹, ¹*Department of Surgery / Surgical Research Laboratory / BioOptical Imaging Center Groningen, University Medical Center Groningen, Groningen, Netherlands;* ²*Institute for Biological and Medical Imaging/Helmholtz Center, Technical University Munich, Munich, Germany. Contact e-mail: r.g.pleijhuis@chir.umcg.nl*

Introduction: Breast-conserving surgery (BCS) still results in positive surgical margins in 20-40% of the patients. Currently, the only tools available to the surgeon for intra-operative localization of the primary tumor are tactile information and common visual inspection. There is great demand for imaging techniques that provide real-time feedback on tumor location and surgical margin status. In this study, the potential of pre- and intra-operative NIRF imaging applications for lumpectomy in BCS was assessed in tissue-simulating breast phantoms. **Methods:** Four breast phantoms with uniform optical properties were produced, based on the optical characteristics of breast tissue. Additionally, two fluorescent tumor-like inclusions containing indocyanine green were integrated in all breast phantoms. A state-of-the-art NIRF intra-operative camera system was applied to simulate real-time NIRF-guided i) pre-operative tumor localization, ii) tumor resection, and iii) intra-operative and *ex vivo* margin assessment. **Results:** All fluorescent inclusions placed ≤ 2.0 cm depth in phantom tissue could be retrieved pre-operatively with the NIRF intra-operative camera system. Real-time NIRF-guided resection enabled radical excision of 4 out of 4 tumor-like inclusions. Additionally, surgery was performed on 4 tumor-like inclusions without NIRF guidance, resulting in radical excision of 2 out of 4 inclusions. Intra-operative NIRF imaging revealed the existence of positive surgical margins and enabled instant re-excision of 2 out of 2 inadequately excised tumor-like inclusions. **Conclusion:** In this study, we have evaluated potential NIRF imaging applications for BCS in a simulated clinical setting with tissue-like phantoms and tumor-like inclusions. Although the value of pre-operative tumor localization seems limited, NIRF optical imaging could complement BCS by offering the surgeon intra-operative tumor localization, detection of remnant disease and finally, intra-operative and *ex vivo* margin status assessment (Figure 1). Clinical studies are needed in order to further validate these results.



Presentation Number **0361B**

Poster Session 3a: Imaging Instrumentation and Methodology

Near-Infrared Fluorescence (NIRF) Optical Imaging for the Detection of the Sentinel Lymph Node (SLN) in Breast Cancer Patients: Feasibility and Future Perspectives

Rick G. Pleijhuis¹, George Themelis², Niels J. Harlaar¹, Wendy Kelder¹, Lucia M. Crane¹, Liesbeth Jansen¹, Jakob de Vries¹, Barbara L. van Leeuwen¹, Athanasios Sarantopoulos², Johannes S. de Jong¹, Vasilis Ntziachristos², Gooitzen M. van Dam¹, ¹Department of Surgery / Surgical Research Laboratory / BioOptical Imaging Center Groningen, University Medical Center Groningen, Groningen, Netherlands; ²Institute for Biological and Medical Imaging/Helmholtz Center, Technical University Munich, Munich, Germany. Contact e-mail: r.g.pleijhuis@chir.umcg.nl

Introduction: The sentinel lymph node (SLN) procedure is widely accepted as a method for lymph node staging in cT1-2 N0 breast carcinoma. In the case of a positive SLN, additional axillary lymph node (ALN) dissection is performed. However, in 50-80% of the patients, these ALNs do not contain metastases. Consequently, non-affected ALNs are often needlessly removed, inducing significant morbidity. A minimally invasive technique which could indicate or exclude the presence of lymph node metastases, could prevent unnecessary surgical interventions and morbidity. Near-infrared fluorescence (NIRF) optical imaging combined with a tumor-targeted fluorescent contrast agent seems suitable for this purpose. For this feasibility study, NIRF imaging was applied in combination with a non-specific optical contrast agent for the intra-operative detection of the SLN. As a next step, NIRF imaging will be evaluated for the detection of lymph node metastases. **Methods:** Five (5) women with primary cT1-2 N0 breast carcinoma underwent a standard SLN procedure, consisting of preoperative lymphoscintigraphy with radiolabeled colloid and intra-operative injection with patent blue. Additionally, all patients received a peritumoral injection with 1 ml (0.5 mg/ml) non-specific fluorescent contrast agent (indocyanine green), which accumulates in the SLN. The SLN was visualized with a state-of-the-art NIRF camera system during the surgical procedure. **Results:** A total of 11 SLNs could be identified intra-operatively in all five patients. The number of lymph nodes identified with indocyanine green, patent blue and radiolabeled colloid was 10, 6 and 11, respectively. Several minutes after the peritumoral injection of ICG, both lymph vessels and SLNs could be visualized intra-operatively with the NIRF camera system. The use of the camera system did not interfere with the standard operative procedure. None of the patients developed wound infections. The total duration of the surgical procedure was prolonged with 15-30 minutes. **Conclusion:** The intra-operative detection of the SLN with a state-of-the-art NIRF camera system is technically feasible. The definitive value of this technique will be addressed in a concordance study. In the near future, tumor-targeted optical contrast agents may allow for the intra-operative evaluation of lymph node status of both the SLN and the ALNs.

Presentation Number **0362B**

Poster Session 3a: Imaging Instrumentation and Methodology

Longitudinal optical measurement of cerebral hemodynamics in awake mice

Hiroyuki Takuwa¹, Kazuto Masamoto^{1,2}, Joonas Autio^{1,3}, Takayuki Obata¹, Iwao Kanno¹, ¹Molecular Imaging Center, National Institute of Radiological Science (NIRS), Chiba-shi, Japan; ²Center for Frontier Science and Engineering, University of Electro-Communications, Chouhu-shi, Japan; ³Department of Neurobiology, University of Kuopio, Kuopio, Finland. Contact e-mail: takuwa@nirs.go.jp

Background: It is necessary to track the longitudinal effects of neurovascular coupling and pathogenesis of neurodegeneration in the same single animal. However, stability and reproducibility of vascular response in repeated longitudinal experiments remain undetermined specifically in awake mice whose behavioral activity is daily variable. We therefore focused on the behavior and its effect on the cerebral hemodynamics during spontaneous and stimulation-induced changes. Materials and Methods: We used custom-made apparatus which consisted of a styrofoam ball floated by air, and a metal rod to hold a head plate. This allows for the animal to walk on the ball, while the head was securely fixed with the apparatus. A total of fifteen male C57BL/6J mice were prepared for the experiments. The head plate was attached to the animal skull. Cerebral blood flow (CBF) was measured in the somatosensory cortex with laser-Doppler flowmetry, whereas animal locomotion was monitored with optical motion sensor that detects a rotation distance of the ball. Whisker stimulation (frequency 10 Hz and duration 20 sec) to the contra-lateral side of the measurement site was induced to evoke neural activity at the measurement site. Two experiments were conducted to determine the effect of locomotion on CBF measurement, i.e. i) Stimulation-induced CBF response and locomotion were compared between daytime and nighttime, ii) Longitudinal CBF and locomotion were measured over seven days. Results and Discussion: The comparison between daytime and nighttime measurements showed no significant differences in CBF response (24% and 23% relative to baseline, respectively), but 22% higher locomotion under nighttime. Longitudinal measurements showed consistent CBF response in spite of day-to-day variations in locomotion. These results indicated that CBF measurement is stable and reproducible. In conclusion, we developed a feasible method to allow the chronic experiment of cerebral hemodynamics with awake mice.

Presentation Number **0363B**

Poster Session 3a: Imaging Instrumentation and Methodology

Fast reflection-mode scanning system for 3D in-vivo optoacoustic molecular imaging

Marc Fournelle¹, Wolfgang Bost¹, Eike C. Weiss³, Robert Dinser², **Robert M. Lemor¹**, ¹Ultrasound Department, Fraunhofer IBMT, Sankt Ingbert, Germany; ²Abteilung für Rheumatologie, Kerckhoff-Klinik, Bad Nauheim, Germany; ³kibero GmbH, Saarbrücken, Germany. Contact e-mail: robert.lemor@ibmt.fhg.de

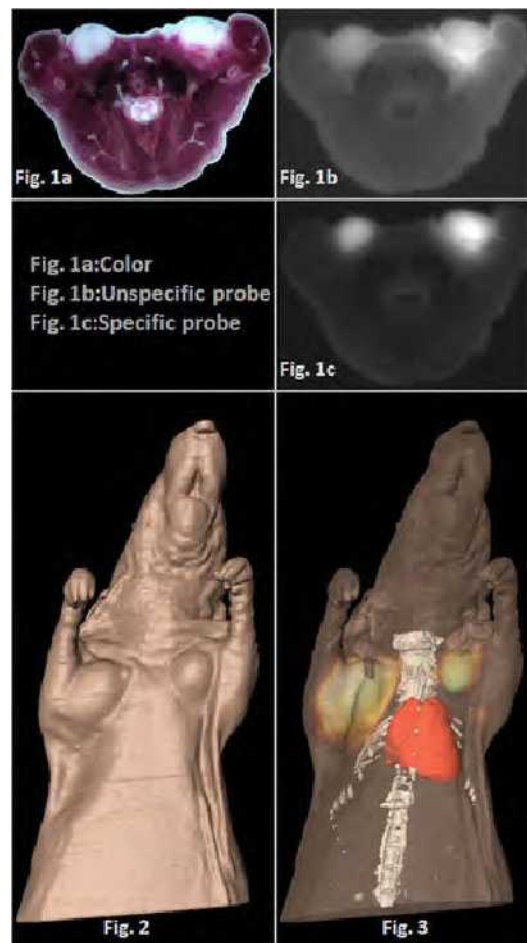
Optoacoustic molecular imaging can provide spatially resolved information about the presence of molecular markers in vivo with high sensitivity. While tissue types having high optical absorption (blood vessels) or local agglomerations of contrast agents can easily be recognized in optoacoustic images, only poor signals are generated by anatomical structures (skin, bones) when a NIR laser is used. When compared with classical ultrasound, optoacoustic imaging is therefore more challenging in terms of image interpretation and recognition of structures. Nevertheless, this technique has already shown its suitability in a variety of applications (imaging of vasculature anatomy, nanoparticle extravasation, gene expression). However, in order to overcome the limitation related to limited access to anatomical information, we developed a hybrid system for high resolution 3D imaging based on conventional ultrasound and optoacoustic techniques. This image approach allows easy interpretation of optoacoustic data since optical absorption images can be placed in the anatomical context provided by high resolution ultrasound. Optoacoustic signals can be generated by two different Nd:YAG lasers at the fundamental wavelength. While high-contrast structures can easily be detected with the 1 kHz system, a higher sensitivity is obtained with the 20 Hz laser providing higher pulse energies. With a 30 MHz focused PZT transducer, the resolution of the system was characterized to 50 μm using adequate phantoms. For data acquisition and scan control, a single channel hardware platform with 800 MHz digitization rate (kibero GmbH) is used. This set-up allows acquisition of 3D ultrasound data in less than 2 min and of 3D optoacoustic data in 2 to 15 min depending on the used laser system. For proof of concept of the systems usability as in-vivo molecular imaging platform, we investigated the knee joints of mice affected with a collagen-induced arthritis. Ultrasound images were performed prior to optoacoustic measurements for identification of the region of interest and thus allowing a reproducible positioning of the animals. Gold Nanorods were synthesized for absorption maximum at 1064 nm and modified with an antibody against TNF-alpha. Optoacoustic and ultrasound data were acquired pre- and post-injection (1h and 15h) of antibody-modified or pegylated control particles. While only early (1h post-injection) signal enhancement was shown using control particles, antibody modified nanorods lead to strong optoacoustic signal enhancement in the ROI after 1 and 15h.

Presentation Number **0364B**
 Poster Session 3a: Imaging Instrumentation and Methodology

Imaging multiple molecular contrast agents with a novel multispectral cryoslicing method

Athanasios Sarantopoulos, George Themelis, Vasilis Ntziachristos, Chair for Biological Imaging & Institute for Medical and Biological Imaging, Technische Universität München and Helmholtz Zentrum, Neuherberg, Germany. Contact e-mail: sarantopoulos@helmholtz-muenchen.de

In the last decade progress in optical contrast agents' development has boosted fluorescence imaging, both planar and tomographic. So far only few tried to address the ex-vivo imaging of anatomical features and/or fluorescent biological markers inside animals in a systematic way [1-2]. We report the development of a novel multispectral imaging method that captures μm -resolution color and fluorescence volumes of multiple fluorophores (up to 5 concurrently) in small animals. The custom epi-illumination and imaging setup can be coupled to virtually any commercial cryotome. To attest the system's capabilities a nude mouse was implanted with 4T1 tumor cells in two places subcutaneously in the mammary fat pad. The animal was injected with one fluorescent probe targeting the avb3-receptor and another unspecific, was euthanized after 24h and imaged transversely every 125 μm (Fig.1). The figure of the animal (Fig.2) is the outcome of an automatic segmentation procedure, which applies a threshold on the fluorescent signal coming from the mouse skin. It is evident that the segmentation perfectly reconstructs the original shape and appearance of the animal with elaborate details. Thresholding can additionally be used to render the geometry of internal organs (Fig.3) that either have a distinctly different fluorescence signal from their surrounding (heart) or have a discrete color appearance (spinal cord). The 3D fluorescence bio-distribution of both probes is shown in (Fig.3) using maximum intensity projection, where one can observe how two agents (green:specific, orange:unspecific) differ in tumor targeting (contrast) and localization (specificity). The presented setup can obtain quantitative, high-res volumes of multiple biological markers at the molecular level and therefore is highly appropriate for assisting basic and translational research in any 'targetable' disease. 1. Weninger WJ, Nat Genet, 2002. 30(1): p. 59-65. 2. Wilson, D, Proc. of SPIE, 2008: p. 6916: 69161I-5.

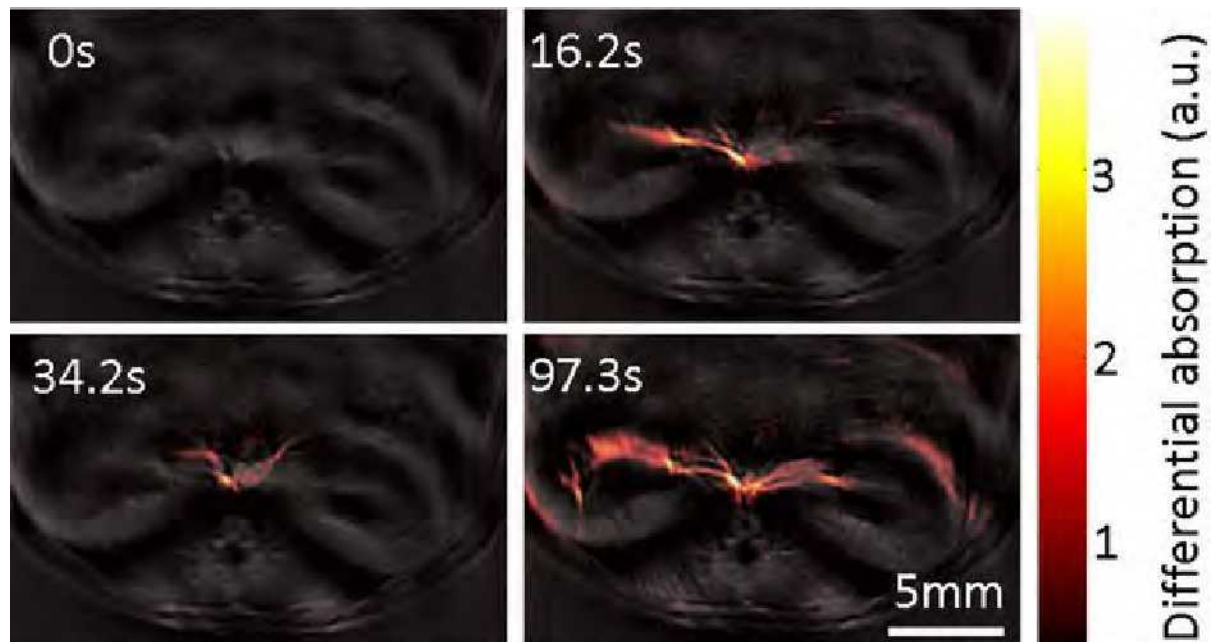


Presentation Number **0365B**
Poster Session 3a: Imaging Instrumentation and Methodology

Video rate optoacoustic tomography of mouse kidney perfusion

Andreas Buehler, Daniel Razansky, Vasilis Ntziachristos, Helmholtz Center Munich and Technical University of Munich, Institute for Biological and Medical Imaging (IBMI), Munich, Germany. Contact e-mail: andreas.buehler@helmholtz-muenchen.de

Small animal imaging plays an important role in basic research, drug discovery and clinical translation due to the widespread use of animal models of human disease in understanding systemic responses. An emerging imaging modality is optoacoustic (photoacoustic) tomography, a hybrid imaging approach that can resolve optical contrast through several centimeters of tissue with the resolution achieved by ultrasound imaging. It has the capacity to simultaneously visualize structural, functional and molecular information non-invasively. We report on a novel non-contact optoacoustic tomography system for whole body imaging of small animals at video rate with high spatial resolution in the range of 150 microns. We demonstrate the previously undocumented ability of optoacoustics to deliver anatomical and functional images from deep tissues in real time by in-vivo visualization of kidney perfusion using Indocyanine Green (ICG). Multi-spectral capabilities are also showcased by resolving externally administered contrast agent based on its unique spectral signature without using background measurements made prior to the probe's administration. The system paves the way for high resolution in-vivo visualization of fast dynamic phenomena including whole-body longitudinal molecular imaging studies.



Optoacoustic image before administration of the probe, superposed with the ICG location (shown in color) at different time points after injection.

Presentation Number **0366B**

Poster Session 3a: Imaging Instrumentation and Methodology

Improved in vivo fluorescence tomography and quantitation in small animals using a novel multiview, multispectral imaging system

James R. Mansfield¹, Craig Gardner¹, Joyita Dutta², Gregory S. Mitchell³, Changqing Li³, Peter Harvey¹, Russ Gershman¹, Sangtae Ahn², Steve Sheedy¹, Simon R. Cherry³, Richard M. Leahy², Richard Levenson^{1,4}, ¹CRi, Woburn, MA, USA; ²Dept. of Electrical Engineering Systems, University of Southern California, Los Angeles, CA, USA; ³Dept. of Biomedical Engineering, UC-Davis, Davis, CA, USA; ⁴Brighton Consulting Group, Brighton, MA, USA. Contact e-mail: jmansfield@cri-inc.com

Fluorescence-based molecular imaging in small animals is having a major impact on drug development and disease research. There have been a number of stages in the development of systems for fluorescence imaging in vivo, ranging from simple monochrome epi-fluorescent imaging systems, to multispectral imaging systems which can separate fluorophores of interest from the interference of tissue autofluorescence, to systems which attempt to determine three-dimensional information about the distribution and concentration of fluorophores. Although useful in a wide range of experiments, epi-fluorescence imaging systems can overemphasize the contributions of fluorophores nearer the surface and under-emphasize signals from deeper tissues. Transillumination methodologies can aid in the detection and quantitation of deeper signals, and combining single-side images with fluorescence spot transillumination can provide data from which a tomographic reconstruction can be obtained. However, images of a single side of an animal, whether in conjunction with epi- or trans-illumination are limited in the accuracy of their tomographic reconstructions. Multiple views of the animal can aid in the determination of the three-dimensional distribution of fluorophores and tomographic reconstructions. However, to date, no system combines multispectral imaging for both excitation and emission spectroscopy with an ability to image multiple views of the animal along with control of the direction of the excitation light. We describe here a multi-view, multispectral 3D tomographic small animal in vivo fluorescence imaging system that is designed around a multi-view mirror system which allows the simultaneous viewing of four sides of a mouse. The excitation light, under control of a digital micromirror device, can be directed sequentially onto each of four sides of the animal while simultaneously imaging all four sides. In addition, the system is equipped to perform both excitation and emission imaging spectroscopy, resulting in an excitation-emission map of the animal at each pixel on each of the sides of the animal. These data are then combined with a sophisticated system for determining the position of the surface of the animal and a three-dimensional tomographic reconstruction of the distribution of fluorophores inside the animal. This novel tomographic instrument and algorithm set provides greatly improved volumetric localization, resolution and contrast over single-view tomographic systems.

Presentation Number **0367B**

Poster Session 3a: Imaging Instrumentation and Methodology

High-sensitivity, high-resolution multispectral fluorescence imaging of small (and very small) animals

James R. Mansfield¹, Farid Sari-Sarraf², Allison Curtis², Abhiruchi Agarwal², Thomas Krucker², ¹CRi, Woburn, MA, USA; ²Novartis Institutes for BioMedical Research, Cambridge, MA, USA. Contact e-mail: jmansfield@cri-inc.com

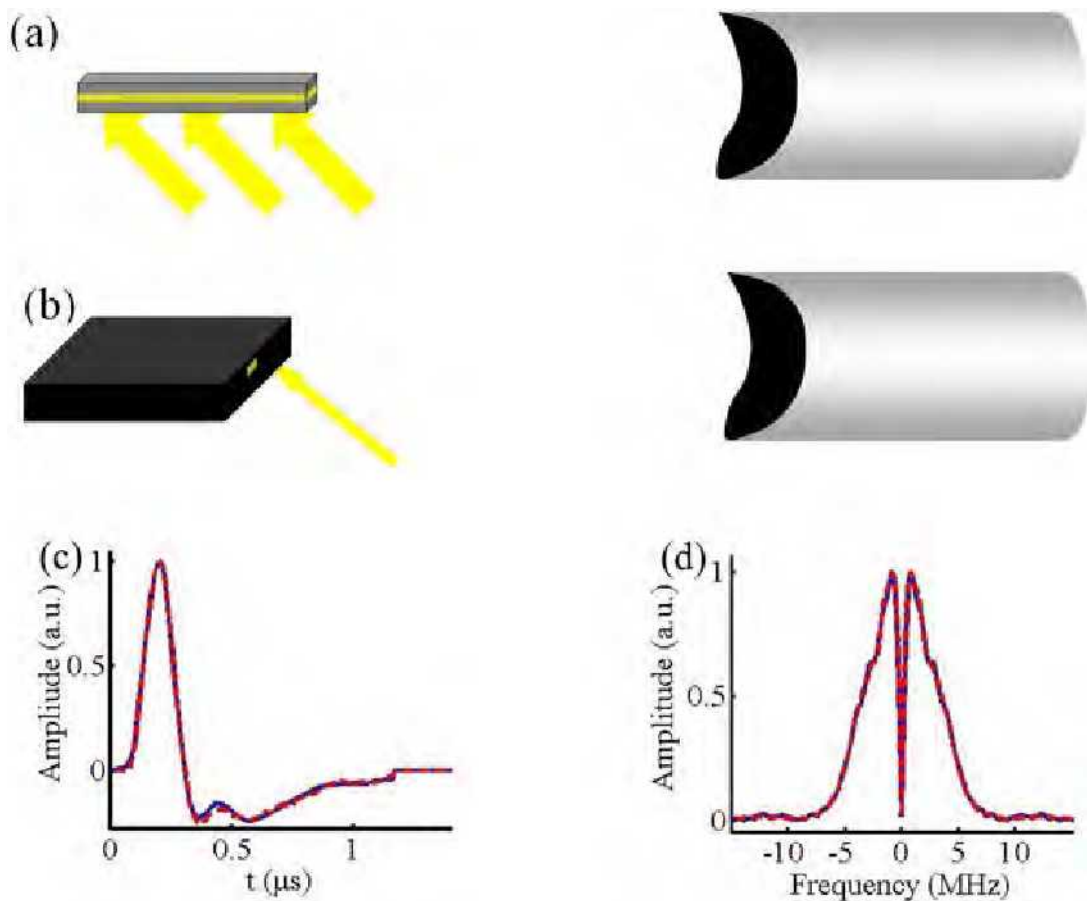
in vivo multispectral imaging (MSI) increases the sensitivity and usefulness of small animal models of development and disease, including the most popular and promising experimental systems. In mice, MSI can essentially eliminate autofluorescence that otherwise limits sensitivity, reducing detection limits by as much as 100-fold. Fluorescence imaging is a key technology for determining the where, the when and the how much of gene expression. However, the ability to image and quantitate fluorescently labeled markers *in vivo* has typically been limited by the bright autofluorescence of animal tissues. Small-animal imaging, which often means the imaging of mouse or rat models, encounters autofluorescence primarily from components in skin (collagen, which fluoresces green) and food (chlorophyll, which fluoresces red). However, other small animal model systems, such as nematodes (*C. elegans*), zebrafish (*D. rerio*) embryos or adult fish, and *drosophila* (*D. melanogaster*) pose similar problems due to the presence of autofluorescent structures that may render common labeling strategies, including the use of green fluorescent protein (GFP) labels, problematic. Various solutions have been proposed for the reduction or elimination of autofluorescence. The most prevalent is simply to use narrow bandpass emission filters in an effort to isolate the desired fluorescence signal [1]. More recently, there has been a move to use infrared-emitting labels that are excited at wavelengths that are much less likely to induce autofluorescence signals. However, autofluorescence still limits sensitivity. Fortunately, the low signal-to-background contrast created by autofluorescence can be substantially eliminated using MSI techniques. Moreover, MSI permits the simultaneous use of multiple labels, such as GFP and RFP, even when they spectrally overlap [2]. Presented here are the results of applying a multispectral imaging strategy to the whole-animal imaging of mice, *C. elegans*, *D. rerio* and *D. melanogaster* at a variety of magnifications, ranging from the imaging of three whole mice simultaneously down to microscopic images. [1] Niswender K.D. et al., *J Microsc* 180, 109-116 (1995) [2] Levenson, Mansfield, *Cytometry A*. 2006 Aug; 69(8):748-58.

Presentation Number **0368B**
 Poster Session 3a: Imaging Instrumentation and Methodology

Optoacoustic methods for frequency calibration of ultrasonic sensors

Amir Rosenthal^{1,2}, **Vasilis Ntziachristos**², **Daniel Razansky**², ¹*Cardiovascular Research Center (CVRC) and Cardiology Division, Massachusetts General Hospital and Harvard Medical School, Boston, MA, USA;* ²*Institute of Biological and Medical Imaging (IBMI), Helmholtz Zentrum München, Neuherberg, Germany. Contact e-mail: eeamir@gmail.com*

Ultrasonic detectors are commonly calibrated by finding their response to incident plane waves [1]. However, in optoacoustics, the response to broadband point sources is required. To induce such sources using the optoacoustic effect, the illuminated object's dimensions must be smaller than the resolution achievable by the optoacoustic system. The main difficulty in such measurements is that the magnitude of the field emitted by such sources is proportional to their dimensions, and thus may be weak compared to parasitic sources in the setup. In this work we experimentally demonstrate two methods for calibrating acoustic detectors. In both methods, acoustic sources are optoacoustically induced in large optically absorbing slabs. Despite the large dimensions of the illuminated objects, the geometry used yields wide-band acoustic fields, which are perceived by the detectors as originating from point sources. Figures 1a and 1b show the two geometries used in our experiments, in which the illuminated part of the proximal face of the phantoms had the dimensions of 0.5mm x 2mm. However, the orientation of the phantoms lead to the creation of acoustic signals comparable to targets with a typical dimension of 40 μ m. In geometry I, the phantom was semi-transparent, leading to the creation of short positive- and negative-pressure pulses from its proximal and distal faces, respectively. In geometry II, the phantom was highly absorbing, leading to the creation of a bipolar signal from its proximal face. Figure 1c and 1d respectively show the amplitude and phase of the frequency response of the transducer. In geometry I (solid curve), the response was obtained by Fourier transforming the signal obtained from the proximal edge, whereas in geometry II, the signal was integrated prior to the transformation. The figure shows an excellent match between the two methods. Reference: 1)G. Ludwig et al., IEEE Trans. Ultrason. Ferroelec. Freq. 35, 168-174, 1988.



A schematic description of geometry (a) I and (b) II used and the corresponding (c) impulse and (d) frequency responses.

Presentation Number **0369B**
 Poster Session 3a: Imaging Instrumentation and Methodology

A truncated conjugated gradient method for trust region subproblem in bioluminescence tomography

Bo Zhang¹, Jie Tian^{1,2}, Xin Yang², Chenghu Qin², Dong Han², Xibo Ma², ¹Sino-Dutch Biomedical and Information Engineering School, Northeastern University, Shenyang, China; ²Medical Image Processing Group, Institute of Automation, CAS, "Beijing, 100190", China. Contact e-mail: zhangbo@fingerpass.net.cn

Bioluminescence tomography (BLT) is an effective optical molecular imaging modality due to its low cost, high sensitivity and non-ionizing radiation properties. As the inverse problem of BLT is ill-posed, it is still open now. And the regularization is usually adopted to overcome the ill-posedness. The trust region method (TRM) has just been applied in the adaptive finite element (AFE) framework for the BLT inverse problem, as TRM is also a kind of regularization. When solving the trust region subproblem (TRS), the "TRUST" function that is provided by the Matlab tool box is used in the literature. However the "TRUST" function is meant to be applied to very small dimensional problems. So we propose a truncated conjugated gradient (TCG) method for the TRS. We've successfully carried out a BLT reconstruction comparison experiment on a nude mouse with an implanted light source. The distance between the actual source position and the reconstructed source position is reduced from 2.025 to 1.134. The comparison of the reconstruction results between the TCG for TRS and the "TRUST" function for TRS is shown in Fig. 1. The result of the experiment can convince us that the proposed TCG method works very well in the AFE framework for BLT.

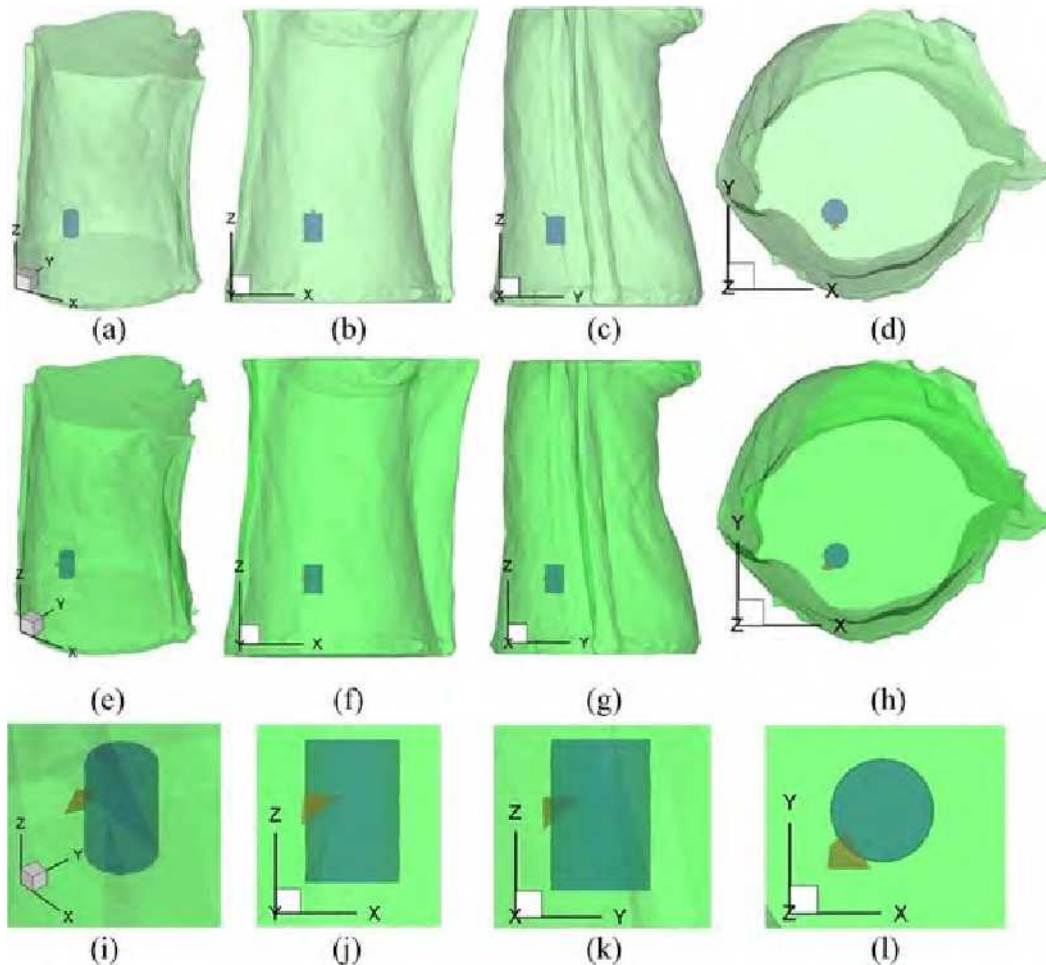


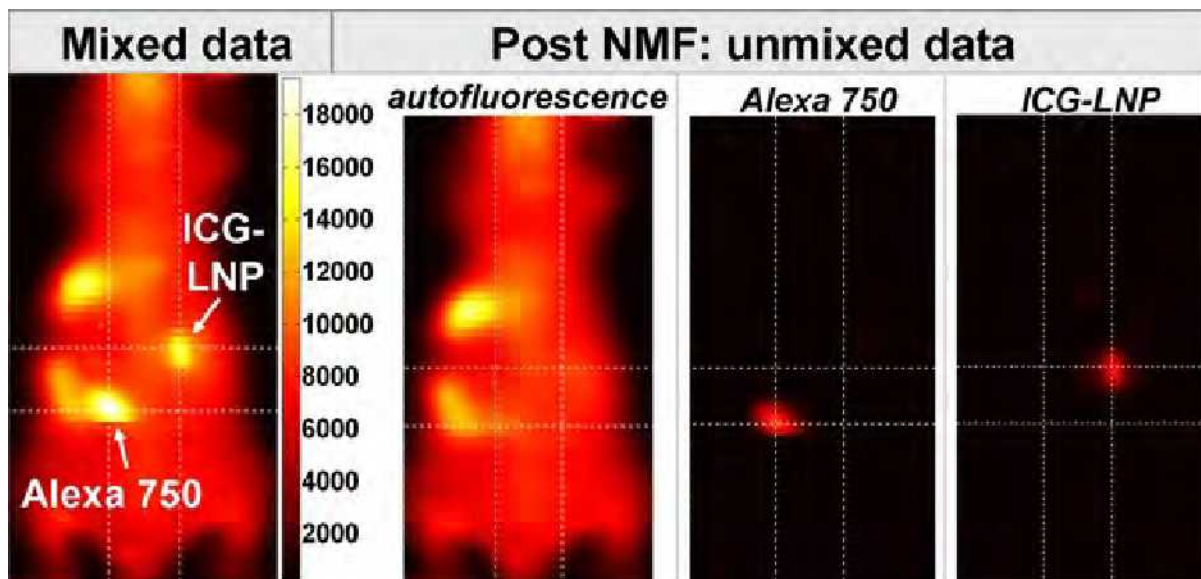
Fig. 1. Reconstruction results comparison between TRUST function for TRS (sub figures (a) to (d)) and TCG for TRS (sub figures (e) to (l)) in single source heterogeneous nude mouse case. Sub figures (a), (e) and (i) are 3D views; (b), (f) and (j) are front views; (c), (g) and (k) are side views; (d), (h) and (l) are top views. Sub figures (i) to (l) are zoom in images of sub figures (e) to (h) around the real source, respectively. The blue cylinder in each sub figure denotes the real source and the red tetrahedron denotes the reconstructed source with the maximum density. For concision, only the real source and the reconstructed source are displayed.

Presentation Number **0370B**
Poster Session 3a: Imaging Instrumentation and Methodology

New Non-negative Matrix Factorization algorithm with sparsity constraints and application to in vivo spectrally resolved data unmixing

Anne-Sophie Montcuquet^{1,2}, Lionel Herve¹, Fabrice P. Navarro¹, Jean-Marc Dinten¹, Jérôme I. Mars², ¹DTBS, CEA Grenoble, Grenoble, France; ²Signal Image Physics, Gipsa-lab, Grenoble, France. Contact e-mail: anne-sophie.montcuquet@cea.fr

Fluorescence imaging in diffusive media is an emerging diagnosis modality which locates specific targets (e.g tumors) thanks to injected fluorescent markers. The region of interest is illuminated with near infrared light and the emitted back fluorescence is analyzed to locate the fluorescence sources. Since the fluorescence signal decreases with the light travel distance, while the autofluorescence of biological tissues signal remains constant, autofluorescence removal is necessary to explore thick media. We propose a spectroscopic approach, based on a new Non-negative Matrix Factorization (NMF) algorithm with sparsity constraints, to unmix several fluorescence sources, including autofluorescence. An experiment is performed on a mouse to test our method: two capillary tubes respectively filled with 5 μ l of Indocyanine Green loaded into nanoparticles (ICG-LNP) at 0.35 μ M and 5 μ l of Alexa 750 at 0.1 μ M are inserted subcutaneous to simulate marked targets. The animal is illuminated at 690 nm with a laser and the emitted back fluorescence signal is collected by an imaging spectrometer coupled with a CCD camera (Andor Technologies): a scanning of the animal is obtained (Figure 1, left). The spectrally resolved acquisition is processed with our NMF algorithm, which approximates data as the product of two non-negative matrices, one carrying the spectra information and the other the weighting factors of the fluorescence sources. A sparse constraint is imposed on specific markers weight factors, expected sparse enough to represent a local fluorescence signal. Link can be made between size of tumor and corresponding sparsity value imposed to the algorithm. On figure 1 (right), the separated fluorescence contributions of the three sources (Autofluorescence, ICG-LNP, Alexa 750) obtained are presented: the algorithm successfully filters fluorescence contributions of interest from in vivo spectrally resolved measurements impaired by unwanted signals. Sparsity constraints allowed getting more accurate unmixing results (previous studies on simulated data have illustrated that consequence).



Left: mixed data; right: unmixing results

Presentation Number **0371B**
Poster Session 4a: Imaging Instrumentation and Methodology

L1-Regularized Cerenkov Luminescence Tomography with Adaptive Finite Element: Methodology and Simulation

Jianghong Zhong, Jie Tian, Xin Yang, Chenghu Qin, Bo Zhang, Medical Image Processing and Analyzing Group, Institute of Automation, Chinese Academy of Sciences, Beijing, China. Contact e-mail: tian@ieee.org

Cerenkov luminescence tomography (CLT) is a molecular imaging technique with its high throughput and cost-effective detection for imaging beta particles-emitting radionuclides in small animals. The key issue is how to quantitatively model the in vivo complex photon propagation in tissues based on the Vavilov-Cerenkov effect and fast re-establish the light source inside a medium. Focusing on the core theory of CLT, our work is supposed to offer an effective approach, which is the l1-regularized CLT with adaptive finite element. In this approach, the simplified spherical harmonics approximation (SPN) is developed to model the photon transportation via heterogeneous phantoms. Taking into account the spectral characteristics of Cerenkov photons, SPN is an accurate and computational-efficient higher-order approximation contrast to the diffusion approximation (DA). Coupled with the SPN, a specialized interior point method is presented for solving l1-regularized least-squares inverse problem with no negativity constraints that used the Euclidean projection onto the l1-ball to compute the best search direction. The l1-regularized CLT should be fast come true compared with the general Tikhonov regularization method, because of the sparse nature of the light source distribution inside the small animal or the phantom. In order to improve the solution accuracy, the mesh is adaptively refined according to a posteriori error estimation. The results of simulation experiments demonstrate the capability of the l1-regularized CLT algorithm based on the refined mesh.

Presentation Number **0372B**

Poster Session 4a: Imaging Instrumentation and Methodology

Development of a Combined Photoacoustic Micro-Ultrasound System for Estimating Blood Oxygenation

Andrew Needles¹, **Pinhas Ephrat**¹, **Corina Bilan**¹, **Anna Trujillo**¹, **David Bates**¹, **Catherine Theodoropoulos**¹, **Desmond Hirson**¹, **F. Stuart Foster**^{1,2}, ¹VisualSonics, Toronto, ON, Canada; ²Sunnybrook Health Sciences Centre, Toronto, ON, Canada. Contact e-mail: aneedles@visualsonics.com

Photoacoustic (PA) imaging can estimate the spatial distribution of oxygen saturation (SO₂) in blood, and be co-registered with B-Mode images of the surrounding anatomy. This talk will focus on the development of a PA imaging mode on a commercially available array based micro-ultrasound (μUS) system that is capable of creating such images. Beamforming techniques, mode-interleaving, digital sampling and signal processing will be described, along with *ex vivo* and *in vivo* results. A modified μUS system (Vevo 2100, VisualSonics) was operated with a linear array transducer (MS-250, f_c = 21 MHz). The array was retrofitted with a housing that held rectangular fiber optic bundles (25.4 x 1.25 mm) to either side, at an angle of 30° relative to the imaging plane. The rectangular bundles were bifurcated ends of a single bundle that was coupled to a tunable laser (Rainbow NIR, OPOTEK Inc., Carlsbad CA, 680-950 nm). The μUS system was synchronized with the laser and PA signals were acquired with a fluence < 20 mJ/cm², beamformed in software, and displayed at 5 Hz. For SO₂ estimates, PA images were collected at 700 and 800 nm and parametric maps of SO₂ were processed offline with a two-wavelength approach. *Ex vivo* imaging was conducted with venous blood drawn into 500 μm diameter tubing from the tail vein of an adult mouse. The animal first inhaled isoflurane mixed with room air before *ex vivo* imaging. The room air was then replaced with 100% oxygen for 10 minutes, before a second round of *ex vivo* imaging. For the *in vivo* experiments, hepatocarcinoma cells (Hep3B-Luc-C4) were injected subdermally in mice (n = 5) 4-5 weeks prior to imaging. The tumors were imaged in 3-D by linearly translating the transducer/fiber with a stepper motor. When the animal inhaled a mixture of room air with isoflurane, the SO₂ of the venous blood was in the range of 65-75%. Switching to 100% inhaled O₂, the SO₂ in the blood increased to > 95%. 3-D stacks of *in vivo* tumor images were co-registered with B-Mode and rendered into a 3-D surface view. Analyzing a 3-D region within the tumors gave average SO₂ values of 75-85%. A new combined PA/μUS system with linear array based technology has been demonstrated. Single wavelength (680-950 nm) imaging was possible at 5 Hz. The PA images correlated well with B-Mode images, and the system showed promise for imaging SO₂. Further validation of *ex vivo* data with gold standard techniques for measuring SO₂, such as blood gas analysis, will allow more conclusions to be made related to the hypoxic state of the tumors and their response to treatment.

Presentation Number **0373B**
 Poster Session 4a: Imaging Instrumentation and Methodology

The application of optical molecular imaging in detecting the tumor proliferative and metastasis in vivo

Xibo Ma¹, Jie Tian¹, Xin Yang¹, Chenghu Qin¹, Shouping Zhu¹, Qiujuan Gao¹, Bo Zhang², Dong Han¹, Kai Liu¹, ¹Medical Image Processing Group, Institute of Automation, CAS, "Beijing, 100190", China; ²Sino-Dutch Biomedical and Information Engineering School, Northeastern University, Shenyang, China. Contact e-mail: Maxibo@fingerpass.net.cn

Bioluminescent is credible and sensitive in detecting the tumor proliferation and metastasis in vivo. In this paper, we clearly detected the curvilinear growth characteristic of hepatocellular carcinoma cells in vivo by bioluminescent imaging (BLI) (Developed by Guangzhou Zhongke Kaisheng Medical Technology Co. Ltd and molecular imaging research group of institute of Automation, Chinese Academy of Science). Xenograft tumor model were created by subcutaneously injection of HCC-LM3-Fluc cells suspensions into the right flanks of BALB/c nude mice. HCC-LM3-Fluc cells were kindly provided by Prof. Jian Zhao in Shanghai Second Military Medical University. All animal experiments were performed in accordance with guidelines of Institutional Animal Care and Use Committee (IACUC). At about 0-6 day the bioluminescent intensity weakened and at about 6-12 day the bioluminescent intensity swelled gradually. In the following 10 days, the tumor showed an trait of exponential proliferation and afterwards the tumor enter the date of slow growth (shown in Figure1). At the 50th day, the micro-PET can not discern the position of tumor transfer (Figure not shown) by injection of ¹⁸F-FDG through the tail vein. Contrast with micro-PET we detect the tumor metastasis clearly using BLI and the pathology results also testify the conclusion (Figure not shown).

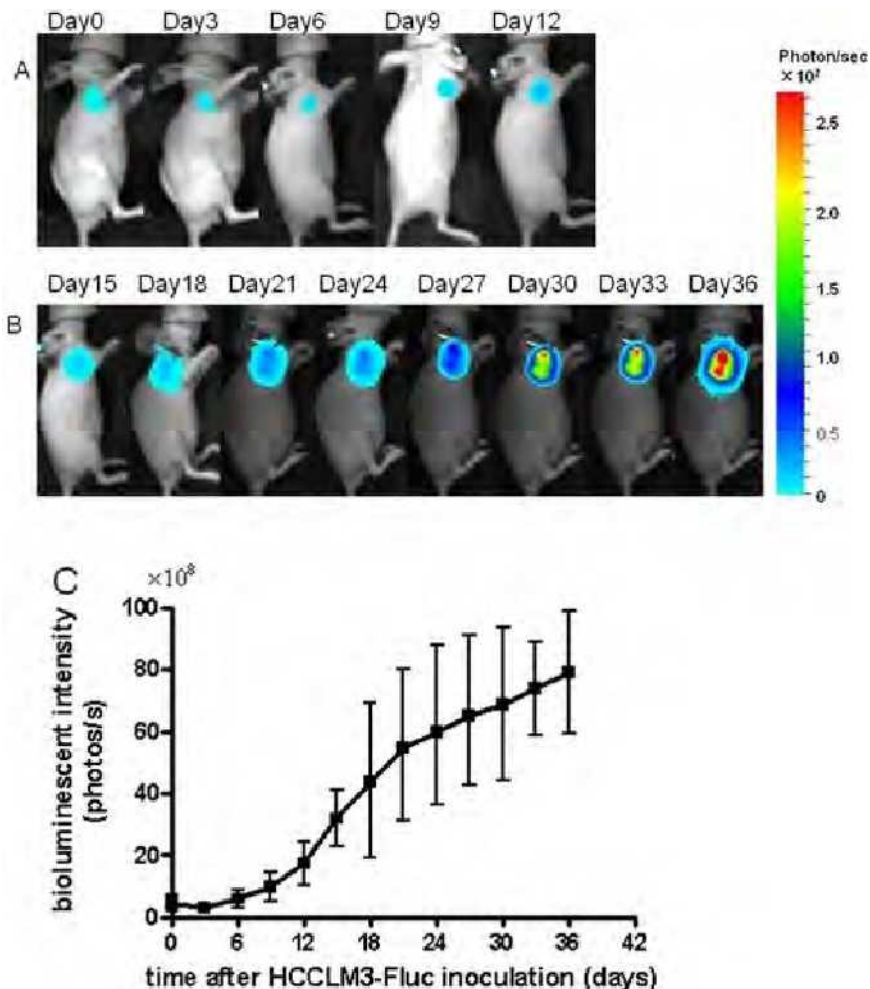


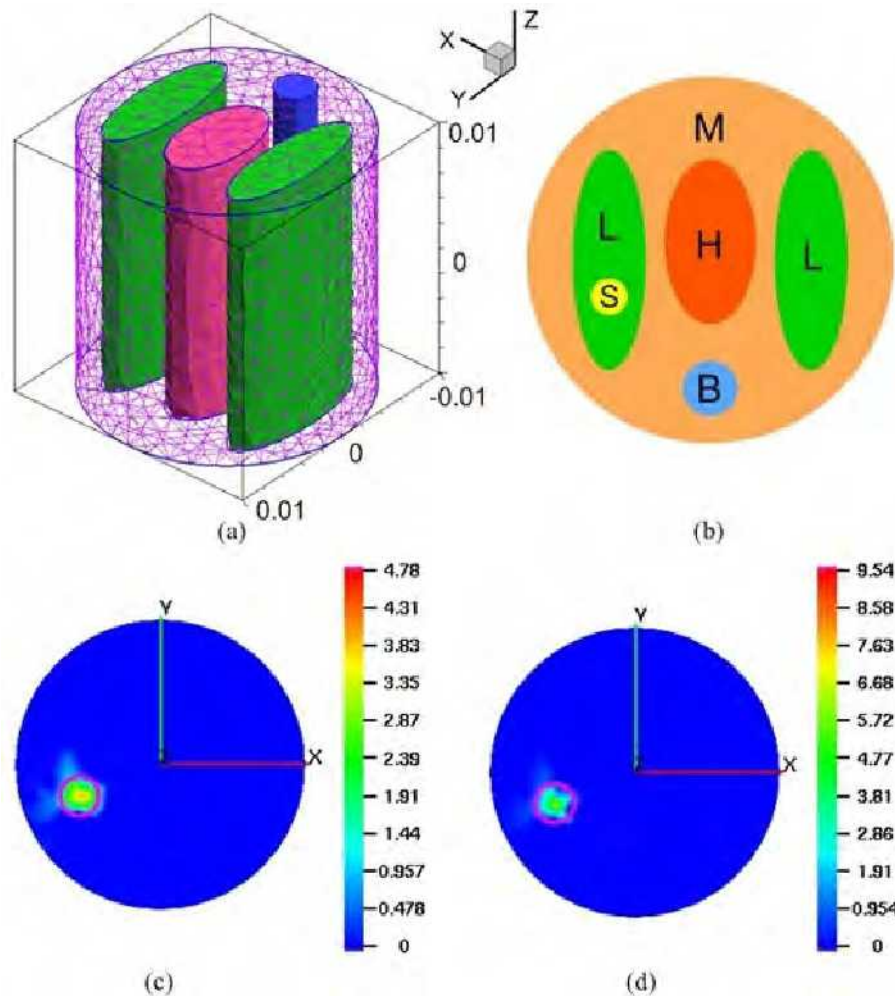
Fig1. A)&B) Serial bioluminescence images of the HCC-LM3-fluc tumor-bearing nude mice. A) Decline and increase proliferation after inoculation of HCC-LM3-fluc cells. B) Exponentially and gradually increase proliferation after inoculation of HCC-LM3-fluc cells. C) The quantified BLI intensity of the HCC-LM3-fluc tumors in the nude mice.

Presentation Number **0374B**
 Poster Session 4a: Imaging Instrumentation and Methodology

Fluorescence Molecular Tomography with Adaptive Tikhonov Regularization

Dong Han¹, Jie Tian¹, Kai Liu¹, Bo Zhang², Xibo Ma¹, ¹Medical Image Processing Group, Institute of Automation, CAS, "Beijing, 100190", China; ²Sino-Dutch Biomedical and Information Engineering School, Northeastern University, Shenyang, China. Contact e-mail: tian@ieee.org

Through the reconstruction of the fluorescent probe distributions, fluorescence molecular tomography (FMT) can three-dimensionally resolve the molecular processes in small animals in vivo. Due to the ill-posed and the ill-conditioned nature of the FMT problem, Tikhonov regularization is usually incorporated to stabilize the problem. However, the solution is often over-smoothed with reduced fluorescence intensities. In this study, an adaptive regularization method is proposed for FMT reconstructions. This method is based on the adaptive finite element framework. When entering a new mesh refinement level, elements with values no less than 40% of the maximum value are selected to be refined. To make the FMT problem less ill-posed, a posteriori permissible region strategy is utilized. Specifically, elements with values no less than 10% of the maximum value are selected to be permissible. For a new mesh level, the L2-norm penalty function of the solution is replaced with another penalty function, which is proportional to the distance between the current solution and the solution from the previous mesh. Simulation experiments were conducted. Compared with the traditional Tikhonov regularization, the proposed method can obtain more accurate fluorescence intensities.



Mouse-mimicking heterogeneous phantom experiment. (a) is the 3D view of the phantom. (b) is the slice image of the phantom in $z=0$ plane. This phantom consists of four kinds of materials to represent muscle (M), lung (L), heart (H) and bone (B), respectively. A spherical fluorescent source centered in $z=0$ plane is placed in the left lung. (c) and (d) are the reconstruction results from the traditional Tikhonov regularization and the adaptive regularization method, respectively. The true intensity of the fluorescent source is 10. The small circles in (c) and (d) denote the real positions of the fluorescent sources.

Presentation Number **0375B**

Poster Session 4a: Imaging Instrumentation and Methodology

A new method to eliminate auto-fluorescence for fluorescence molecular imaging

Zhenwen Xue, **Jie Tian**, Dong Han, Chenghu Qin, Medical Image Processing Group, Institute of Automation, CAS, "Beijing, 100190", China. Contact e-mail: tian@ieee.org

Tissue auto-fluorescence can limit the ability to image fluorescent probes in fluorescence molecular imaging. Especially in the blue and green spectral range, auto-fluorescence signal is even stronger than useful fluorescent signal. In this paper, we propose an algorithm to eliminate the interference of auto-fluorescence, which can extract expected fluorescence signal. First, we collect two emission fluorescent images by different excitation wavelength bands. One is used as the normal excitation, while the other is selected as the background excitation signal. Next, we discretize these two images into groups of identical number regions respectively, and further we calculate the ratio of each group. We distinguish fluorescent groups from the others on the premise that the ratio of the former is significantly larger than the latter. Therefore, we can get the scaling parameters depending on the corresponding regions' gray values. Finally, the images can be corrected and improved a lot using the parameters to eliminate the auto-fluorescence.

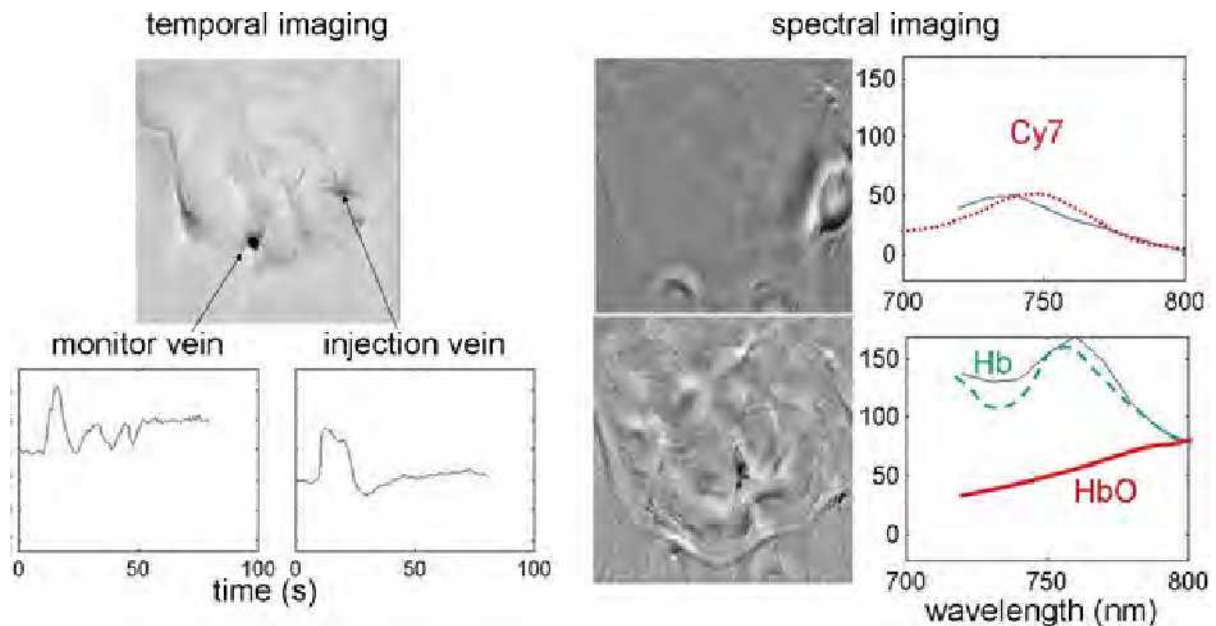
Presentation Number **0376B**

Poster Session 4a: Imaging Instrumentation and Methodology

Blind Spectral and Temporal Unmixing in Optoacoustic Tomography

Nikolaos C. Deliolanis, Juergen Glatz, Andreas Buehler, Daniel Razansky, Vasilis Ntziachristos, Institute for Biological and Medical Imaging, Helmholtz Zentrum and Technical University of Munich, Munich, Germany. Contact e-mail: ndeliolanis@yahoo.com

Optoacoustic (or photoacoustic) tomography is an emerging imaging technology that employs the optoacoustic effect to create 3D images of the optical absorption in tissue. In Multispectral Optoacoustic Tomography (MSOT) the images are acquired at different wavelengths and are used to resolve tissue components that have distinct spectral profiles. The different components can be simply separated by fitting with their known spectral absorption coefficients, however this approach has significant disadvantages, such as the assumptions that the spectral profile of every component is accurately known, that the reconstructed images are free of artifacts, and that the light attenuation through tissue is wavelength independent. As a result, there is a cross talk between the unmixed components and loss of quantization. On the other, several blind source separation techniques developed for signal processing can alternatively unmix the components with higher accuracy and sensitivity. We examine the use of principle and independent component analysis in optoacoustic tomography to resolve the geometrical location of components and their distinct spectral or temporal responses. We demonstrate the capabilities of this method in in-vivo experiments by imaging at video-rate the temporal dynamics of blood circulation in mice and the spectral unmixing of subcutaneous fluorochrome concentrations (Fig. 1).



In-vivo temporal and spectral unmixing in mice.

Presentation Number **0377B**

Poster Session 4a: Imaging Instrumentation and Methodology

In vivo mouse studies with bioluminescence tomography combined with micro-CT for early tumor detection

Junting Liu¹, Jie Tian^{1,2}, Xiangsi Li¹, Xiaopeng Ma¹, Weiwei Fan³, Congye Li³, Xiaochao Qu¹, Jimin Liang¹, Feng Cao³, ¹Life Sciences Research Center, School of Life Sciences and Technology, Xidian University, Xi'an, China; ²Medical Image Processing Group, Institute of Automation, CAS, "Beijing, 100190", China; ³Department of Cardiology, Xijing Hospital, Fourth Military Medical University, Xi'an, China. Contact e-mail: tian@ieee.org

Bioluminescence tomography (BLT) is an emerging optical molecular imaging modality, which can monitor both physiological and pathological processes using light-emitting probes in small living animal. Furthermore, this technology possesses great potential in drug development, early detection, and therapy monitoring in preclinical research. In present study, we evaluated the feasibility of early tumor detection using our developed dual-modality BLT prototype system with micro-CT registration approach. We developed a spectrum modulation quantitative reconstruction algorithm based on energy and hp-FEM frame. 1×10^5 PC3-Luc cells were mixed with Matrigel (BD Matrigel™ Basement Membrane Matrix, BD Biosciences, NJ) were injected into the right hepatic lobes in deep tissue to establish tumor-bearing mouse model. Multi-view multi-spectral images of bioluminescence were acquired by CCD camera from four directions with 90 degree intervals at the time point of day 1 after inoculation. The measurement data was used to reconstruct the source of tumor cells with firefly luciferase reporter gene; and the reconstructed total power of the tumor is 2.4 nW, which can reflect the total cell number accurately. The 3D reconstruction results of the source of tumor were shown in Fig. 1. Our experimental data suggest that BLT technology is feasible both for the localization and quantification of very small number of tumor cells utilizing appropriate reconstruction algorithm. Overall, BLT/micro-CT imaging method offers the advantages of cost-effectiveness, good molecular specificity and sensitivity for noninvasive 3D imaging, and consequently enormous potential in drug development and preclinical oncological investigations.

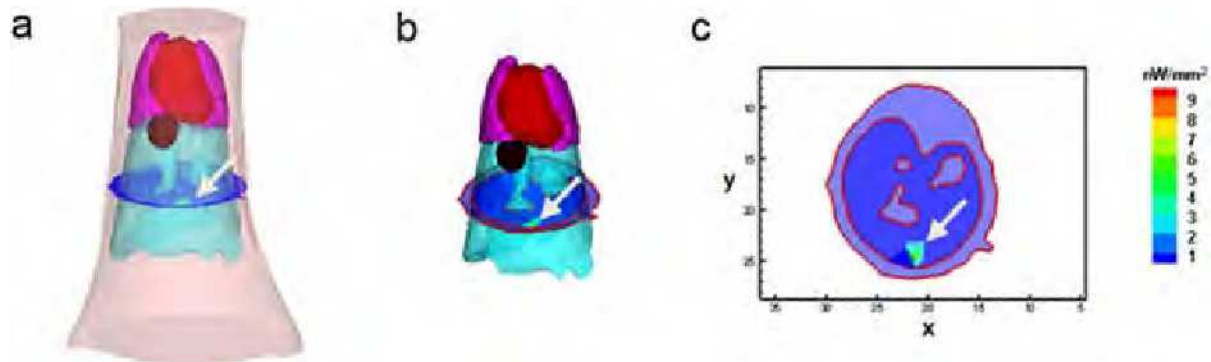


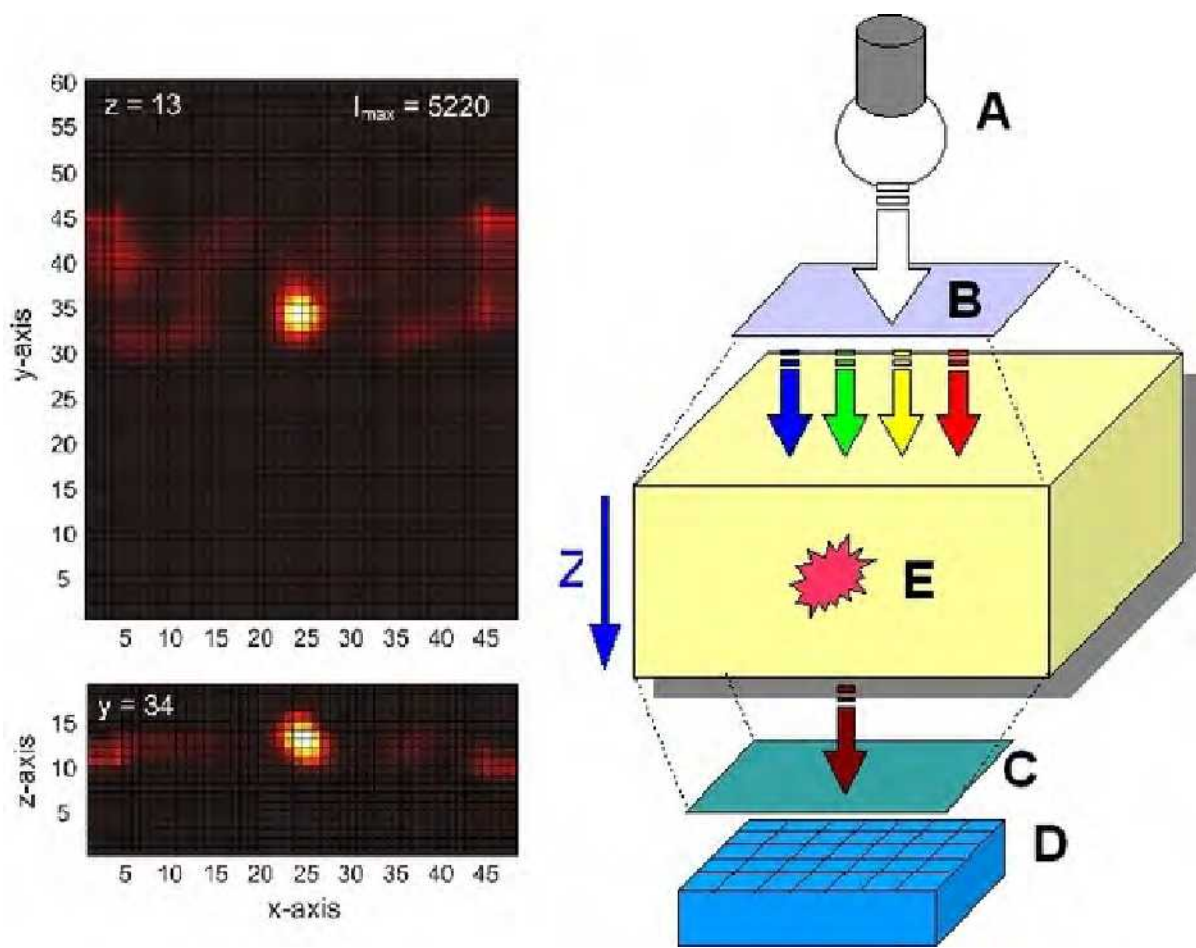
Fig.1 3D reconstruction of the source of tumor cells with firefly luciferase report gene (arrow) (a) The mouse body and anatomical structure of main organs. (b) Anatomical structure of main organs. (c) One slices in the Z-axis direction of reconstructed tumor center.

Presentation Number **0378B**
 Poster Session 4a: Imaging Instrumentation and Methodology

Hyperspectral excitation-resolved fluorescence tomography

Alexander D. Klose¹, **Yared Tekabe**², **Lynne Johnson**², ¹*Department of Radiology, Columbia University, New York, NY, USA;*
²*Department of Medicine, Columbia University, New York, NY, USA. Contact e-mail: ak2083@columbia.edu*

Most work in clinical and pre-clinical optical imaging has been limited to direct or planar imaging of light that escapes through the tissue surface. Planar surface images of optical reporter probes in small animals, however, contain little information about the actual depth and strength of the source of light emission. Hyperspectral excitation-resolved fluorescence tomography (HEFT), on the other hand, reconstructs the three-dimensional (3D) spatial distribution and concentration of fluorescent reporter probes in tissue by using planar fluorescence images and a wavelength tunable white light source for fluorescence stimulation. In Fig. 1 (right), the tissue surface is illuminated with light at different wavelengths between 580 nm and 700 nm and fluorescent nanoparticles, e.g. quantum dots (QDs), are stimulated for fluorescence light emission. QDs have a broad absorption spectrum, which coincides with the large varying extinction spectrum of (oxy-)hemoglobin in tissue. In fact, the optical properties of QDs and hemoglobin are exploited for 3D image reconstruction. Moreover, the QDs can be conjugated to antibodies or peptides for targeting specific cell surface receptors (VEGF, integrin) and, hence, serve as a beacon. Next, the fluorescence light is measured by a camera on the tissue surface. Using different excitation wavelengths, a computer algorithm based on a light propagation model (SPN equations), calculates the 3D location of the QDs in vivo. Fig. 1 (left) shows the reconstructed spatial location of fluorescent QDs in tissue. This work was supported in part by Columbia University's CTSA grant UL1 RR024156 from NCRR/NIH, and by grants NCI-4R33CA118666 and 5U54CA126513-029001 from the National Institutes of Health (NIH).



Left: horizontal (top) and vertical (bottom) cross-sections of fluorescent QD reconstruction in chicken tissue. Right: schematic of HEFT method, (A) white light source, (B) wavelength-tunable emission filter, (C) bandpass filter, (D) optical camera, (E) light emitting probe inside tissue.

Presentation Number **0379B**

Poster Session 4a: Imaging Instrumentation and Methodology

Quantitative Assessment of Nipple Perfusion using Near-Infrared Fluorescence Imaging

Yoshitomo Ashitate^{1,2}, **Bernard T. Lee**^{1,3}, **Rita Laurence**¹, **Hak Soo Choi**¹, **Rafiou Oketokoun**¹, **John V. Frangioni**^{1,4}, ¹*Departments of Medicine, Beth Israel Deaconess Medical Center, Boston, MA, USA;* ²*Department of Surgical Oncology, Hokkaido University Graduate School of Medicine, Sapporo, Japan;* ³*Department of Surgery, Beth Israel Deaconess Medicine Center, Boston, MA, USA;* ⁴*Department of Radiology, Beth Israel Deaconess Medicine Center, Boston, MA, USA. Contact e-mail: yashitat@bidmc.harvard.edu*

Background: Nipple-sparing mastectomy (NSM) is thought to be superior to standard mastectomy in terms of cosmetic outcome and patient satisfaction. However, necrosis of the nipple areola complex (NAC) remains a devastating complication of NSM. Many factors contribute to the blood supply of the NAC, and although the skin incision is a primary factor, the most suitable choice of incision is not yet known. In this study, we quantified nipple perfusion in three different nipple incision models using near-infrared (NIR) fluorescence imaging methods. Materials and Methods: Methylene blue (MB) and indocyanine green (ICG), both clinically available fluorophores, were injected intravenously into n = 6 pigs. Three skin incision models were created: Model 1 was created using a circular incision with the perforator preserved, Model 2 a mastopexy incision, and Model 3 with a radial incision. Because perforators are typically dissected in NSM, Model 1 was used as an internal control. The Fluorescence-Assisted Resection and Exploration (FLARE™) NIR fluorescence imaging system was employed to assess the models. Images were recorded pre-operatively (0 h) and 72 h after survival surgery. The NIR fluorescence contrast-to-background ratio (CBR) curve was measured for 2 min following IV injection of contrast agents and processed for analysis. Results: CBR analysis revealed that MB has much lower variance than ICG and provides a more reliable measure of tissue perfusion. At 72 h, the CBR curve of MB showed significant differences between all pairs of control and experimental models. Model 1 exhibited the best blood supply due to preservation of perforators. Model 3 proved to have statistically higher perfusion than Model 2, although the difference between the two was not dramatic. Conclusions: For quantitative assessment of tissue perfusion using NIR fluorescence, MB is an excellent choice. Our data suggests that during nipple-sparing mastectomy, a radial incision (Model 3) is more effective than a mastopexy incision (Model 2) for maintaining nipple perfusion, although preservation of the perforators (Model 1) provides superior perfusion.

Presentation Number **0380B**

Poster Session 4a: Imaging Instrumentation and Methodology

Techniques to Improve 3D Optical Imaging Quantification and Sensitivity

Tamara L. Troy, Ali R. Akin, Ed Lim, Ning Zhang, Jae-Beom Kim, Jay Whalen, Chaincy Kuo, Heng Xu, Brad Rice, Caliper Life Sciences, Alameda, CA, USA. Contact e-mail: tamara.troy@caliperls.com

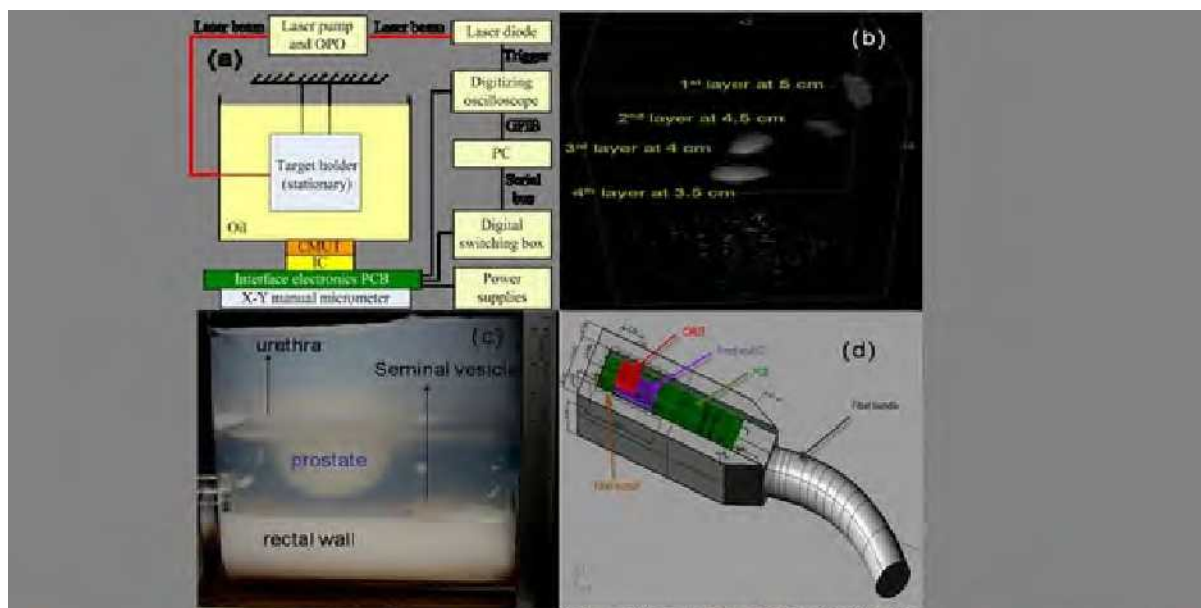
Optical tomography of bioluminescent and fluorescent reporters in pre-clinical animal models is an important technology for the study of disease and drug development. However, the quality of 3D reconstructions can be limited by the sensitivity of detection and 3D results often lack quantification with biologically relevant units. Therefore, new methods to improve detection and to quantify the results in terms of absolute cell number or dye molecules will be discussed. To enhance signal levels and support multi-modality imaging, a mouse bed has been developed which slightly compresses an animal thereby reducing the amount of tissue light propagates through. Comparisons show that compression can pick up deep-tissue signals that were previously undetectable. The compression bed also reduces the complexity of the boundary condition (rough fur, etc.) leading to more accurate 3D reconstructions. Reconstructions for compressed and uncompressed animal models will be shown co-registered to microCT data for cross validation. Sensitivity of fluorescence detection can further be improved through an imaging method called normalized transmission fluorescence (NTF) efficiency. Since the sensitivity of fluorescent imaging is limited by autofluorescence, transillumination is used to trap the autofluorescent signal on the opposite side from the detector. However for transillumination imaging, the pattern of the emission light includes contributions from tissue heterogeneity and animal surface topography. To reduce this contribution from the detected signal the fluorescent emission image is normalized by a transfer function comprised of a transmission image measured with the same emission filter and open excitation filter. Eliminating the excitation light contribution from the measurement improves the robustness of the algorithm by reducing artifacts and giving better signal localization and sensitivity. These improvements will be illustrated with several animal models. We also describe a technique to absolutely quantify 3D images in terms of biological activity using well plate calibration. In this technique measurements of known serial dilutions of luminescent or fluorescent cells, or fluorescent dye molecules, are used in order to generate quantification databases of photons per second per cell or extinction coefficients per cell or per molecule. These databases are then used to determine the number of cells or dye molecules from the tomographic sources reconstructed inside an animal. We present validation of this technique with calibrated sources.

Presentation Number **0381B**
 Poster Session 4a: Imaging Instrumentation and Methodology

Transrectal Photoacoustic Imaging of the Prostate using Capacitive Micromachined Ultrasound Transducers

Sri Rajasekhar Kothapalli¹, **Te Jen Ma**², **Srikant Vaithilingam**², **Omer Oralkan**², **Butrus Khuri-Yakub**², **Sanjiv S. Gambhir**^{1,3},
¹Radiology, Stanford University, Palo Alto, CA, USA; ²Electrical Engineering, Stanford University, Palo Alto, CA, USA; ³Bioengineering, Stanford University, Palo Alto, CA, USA. Contact e-mail: ksraj@stanford.edu

Standard screening methods for prostate cancer - such as blood screening for prostate specific antigen (PSA), digital rectal examination (DRE), and transrectal ultrasound (TRUS) guided prostate biopsy - have limited capacity (sensitivity and specificity) in the early diagnosis of prostate cancer. Photoacoustic (PA) imaging is an emerging hybrid medical imaging modality that combines optical and ultrasound imaging modalities to achieve high optical contrast imaging at ultrasonic resolution. To improve diagnostic accuracy of TRUS, we developed transrectal photoacoustic (TRPA) imaging of prostate with sub-millimeter spatial resolution and high soft tissue contrast based on both endogenous (blood vasculature) and exogenous molecular agents. A transrectal photoacoustic probe that integrates a fiber optic light guide and Capacitive Micromachined Ultrasound Transducers (CMUT) has been developed. We also developed a prostate phantom that mimics both optical and ultrasound properties of the prostate tissue. Nano-second pulsed laser light (800nm wavelength, 6ns pulse width, 10Hz repetition rate, energy density of 15mJ/cm²) was delivered to the prostate phantom using the fiber optic light guide and PA signals were detected using a state of art 16x16 element CMUT array with a center frequency of 5.5MHz. The CMUT array was mechanically scanned in the x and y directions to simulate the aperture of a 64x64-element CMUT array and 3D volumetric images were reconstructed by applying synthetic aperture focusing. The phantom images clearly show pieces of horse tail hair oriented in different directions at different depths (up to 5cm) inside the phantom. Our results show that at similar center frequency, CMUT has the ability to image much deeper than conventional piezoelectric transducers, which are the most common photoacoustic imaging detectors used today. Thanks to its low noise floor, wide fractional bandwidth, and high sensitivity, the 2D CMUT array with integrated frontend circuits proved to be an attractive candidate for transrectal photoacoustic volumetric imaging of the prostate.



Photoacoustic Imaging using a CMUT. a) Schematic of the experimental setup b) 3-D volume rendered image of an optically scattering slab phantom. Four single strands of horsehair with different orientations embedded at different depths (3.5 cm, 4 cm, 4.5 cm, and 5 cm) can be clearly resolved; c) Home built prostate phantom that mimics ultrasound and optical properties of prostate; d) skeleton view of CMUT based TRPA probe.

Presentation Number **0382B**

Poster Session 4a: Imaging Instrumentation and Methodology

Simultaneous Assessment of the Biliary Tract and Arterial Anatomy in Real-Time using Dual-Channel NIR Fluorescence Imaging

Yoshitomo Ashitate^{1,2}, **Hak Soo Choi**¹, **Rita Laurence**¹, **Alan Stockdale**¹, **John V. Frangioni**^{1,3}, ¹*Departments of Medicine, Beth Israel Deaconess Medical Center, Boston, MA, USA;* ²*Department of Surgical Oncology, Hokkaido University Graduate School of Medicine, Sapporo, Japan;* ³*Department of Radiology, Beth Israel Deaconess Medical Center, Boston, MA, USA. Contact e-mail: yashitat@bidmc.harvard.edu*

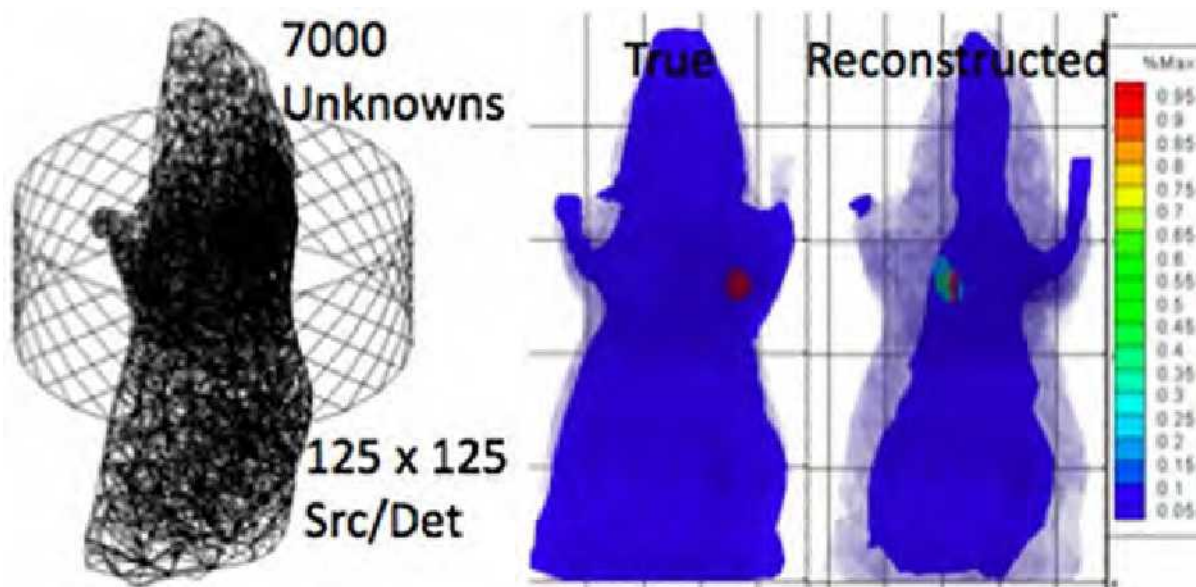
Background: Bile duct injury is a major complication of hepatobiliary surgery. To develop methods to prevent this complication, we focused this study on intraoperative identification of both bile duct lumens and arterial anatomy using the dual-channel capabilities of the Fluorescence-Assisted Resection and Exploration (FLARE™) near-infrared (NIR) imaging system. **Materials and Methods:** Three different combinations of 700 nm and 800 nm fluorophores were injected in twelve 35-kg female Yorkshire pigs. Combination 1 (C-1) was methylene blue (MB) for arterial anatomy and indocyanine green (ICG) for bile duct imaging. Combination 2 (C-2) was ICG for arterial anatomy and MB for bile duct imaging. Combination 3 (C-3) was a newly developed NIR fluorophore ZW-1 for arterial imaging and MB for bile duct imaging. Bile ducts and hepatic arteries were visualized using FLARE™. In addition, experiments were repeated using a new minimally-invasive FLARE system (m-FLARE™) that accommodated a standard 10 mm laparoscope. **Results:** Using all three combinations, both bile ducts and hepatic arteries could be visualized simultaneously and in real-time. Since ZW-1 is completely eliminated by the kidney, it did not cause high background after injection. In C-3, the arterial image could be completely separated from the bile duct image. On the other hand, ICG and MB caused high background of bile ducts or liver, which complicated multiple injections for arterial imaging. The m-FLARE™ system provided images similar to those gathered during open surgery with FLARE™. **Conclusions:** We demonstrate that the combination of two kinds of NIR fluorophores provide sufficient identification of the bile ducts and arterial anatomy simultaneously. This technique could be used in both open and laparoscopic surgery. Although the ideal combination of C-3 is not currently available for clinical use, combinations C-1 and C-2 are clinically available and can be translated rapidly to human investigational studies.

Presentation Number **0383B**
Poster Session 4a: Imaging Instrumentation and Methodology

A Nonlinear Block ART Algorithm for Radiative Transport Based Fluorescence Optical Tomography

Alexander E. Maslowski², John McGhee², Amit Joshi¹, ¹Radiology, Baylor College of Medicine, Houston, TX, USA; ²Transpire Inc., Gig Harbor, WA, USA. Contact e-mail: amitj@bcm.edu

We report a novel nonlinear Block-ART algorithm for radiative transport equation (RTE) based fluorescence optical tomography. We demonstrate commercial quality software for solving the inverse problem in small animals geometries, with optical properties varying from ballistic transport to diffusion-dominated regimes. METHODS: RTE based optical tomography approaches can handle all configurations encountered in nude mice imaging including the presence of internal voids, absorption dominated tissue (e.g. liver) and non-contact free space measurements. Current approaches are constrained by the high computational cost of numerical solutions, unsatisfactory convergence behavior of numerical differencing schemes, and failure to demonstrate the diffusion limit for optically thick cases. We solve the above problems by proposing the following advancements: (i) Discretization with discrete Ordinates method in angle, and Linear Discontinuous Finite Elements in space, (ii) Solving the free space propagation with ray tracing coupled with a low order angular discretization in optically thick regions with diffusion synthetic acceleration, (iii) Implementing the nonlinear block-ART scheme with an adjoint-based on the fly Jacobian matrix calculation simplified with the iterative Born approximation, and (iv) shared memory parallelization to exploit the multi-core computer architectures. The performance of the algorithm is demonstrated on a micro-MRI derived nude mouse phantom imaged in frequency domain. RESULTS: Fig.1 depicts the simulation geometry with ICG like fluorescence target in the thorax of the mouse. Measurements are acquired on 125 detectors for 125 modulated (100MHz) sources in a free space mode. The reconstruction after five nonlinear iterations is depicted in Fig.1. Over 95% accuracy in magnitude reconstruction was obtained. Overall 625 forward and 625 adjoint simulations along with 78125 ART updates were performed on a 7000 unknown tetrahedral mesh within 1hr on a quad core workstation.



Presentation Number **0384B**
Poster Session 4a: Imaging Instrumentation and Methodology

Fluorescence Tomographic Image Reconstruction Using Joint L1 and Total Variation Norm Penalties

Joyita Dutta¹, Sangtae Ahn¹, Changqing Li², Simon R. Cherry², Richard M. Leahy¹, ¹Electrical Engineering - Systems, USC, Los Angeles, CA, USA; ²Department of Biomedical Engineering, University of California-Davis, Davis, CA, Davis, CA, USA. Contact e-mail: jdutta@usc.edu

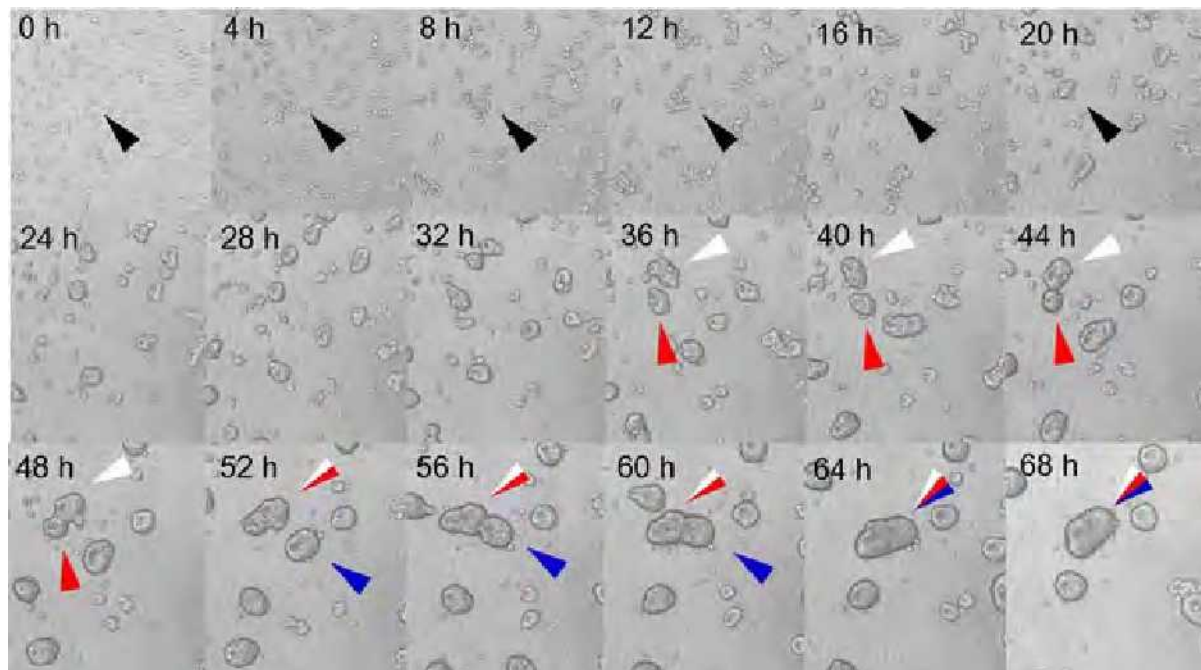
Fluorescence molecular tomography (FMT) is an imaging modality that exploits the specificity of fluorescent biomarkers to enable 3D visualization of molecular targets and pathways in vivo in small animals. Owing to the high degrees of absorption and scattering of light through tissue, the FMT inverse problem is inherently ill-posed. Approaches for alleviating this problem and improving source localization include multispectral illumination and/or detection (which exploit the spectral variation of tissue optical properties) and the use of multiple spatial patterns of illumination to increase the information content in the collected data. While these approaches improve the conditioning of the FMT system matrix to a great degree, image reconstruction continues to be highly susceptible to the effects of noise and numerical errors. Appropriate priors or penalties are needed to facilitate reconstruction and to restrict the search space to an specific solution set. The most widespread method for handling the ill-conditioning of the FMT inverse problem is Tikhonov regularization, in which the cost function contains an L2 norm penalty term in addition to the data-fitting term. The L2 norm penalty generates the minimum energy solution, which tends to be spread out in space. Typically, fluorescent probes are locally concentrated within specific areas of interest (e.g., inside tumors). Hence, reconstructed fluorescence images tend to be sparse. Alternatively, an L1 norm penalty can be used to enforce sparsity in reconstructed fluorescence images. Another sparsifying penalty extensively used in the area of compressed sensing is the total variation norm which tends to preserve the piecewise constant nature of images. Our approach is to use a combination of the L1 and total variation norm penalties to suppress spurious background signals and generate reconstructed images that are spatially sparse yet smooth. We compare this approach with the L1, L2, and total variation norm penalty based approaches. For validation, we perform realistic simulations on the Digimouse atlas, a labeled atlas based on co-registered CT and cryosection images of a nude mouse. For further validation, we use experimental data to compare the reconstruction results obtained using the four different regularization schemes. The data is acquired using a tissue phantom with embedded fluorescent sources placed inside a multi-view 3D imaging setup with a CCD camera for detection.

Presentation Number **0389A**
 Poster Session 1a: Imaging Instrumentation and Methodology

3D tumor spheroids constructed with nano-sized pattern scaffoldings: a novel model for molecular imaging research

Yukie Yoshii¹, **Atsuo Waki**^{4,1}, **Kaori Yoshida**⁴, **Anna Kakezuka**⁴, **Maki Kobayashi**⁴, **Yusei Kuroda**², **Yasushi Kiyono**¹, **Hiroshi Yoshii**³, **Takako Furukawa**⁵, **Hidehiko Okazawa**¹, **Yasuhiro Fujibayashi**^{5,1}, ¹Biomedical Imaging Research Center, University of Fukui, Eiheiji, Fukui, Japan; ²Faculty of Engineering, University of Fukui, Fukui, Japan; ³Faculty of Medical Sciences, University of Fukui, Eiheiji, Fukui, Japan; ⁴SCIVAX Corporation, Kawasaki, Japan; ⁵Molecular Imaging Center, National Institute of Radiological Sciences, Chiba, Japan. Contact e-mail: yukiey@u-fukui.ac.jp

3D multicellular spheroid (MCS) of tumor cells is expected to be a useful *in vitro* model reflecting characteristics of *in vivo* tumors, in tumor research. However, conventional methods to form 3D MCSs have problems in convenience and cell viability. Here we propose a method to acquire 3D MCSs, which are constructed from spontaneous migration and gathering of tumor cells and sustain high proliferation and viability, by simply culturing cells on the plates with nano-sized pattern scaffoldings on surface of the bottom (nano-pattern culture). In this study, we examined detailed characteristics of 3D MCSs constructed with nano-pattern culture to evaluate its utility in molecular imaging research. Morphology and formation process of the MCSs were examined with an inverted light microscope and SEM and with time-lapse analysis, respectively. Proliferation, viability, gene expression profile and response to hypoxia of the MCSs were also investigated. Transcription of hypoxia-inducible factor 1 (HIF-1) was examined with GFP reporter assay. Our observations showed that tumor cells elongated foots to grasp nano-sized pattern scaffoldings, migrated and gathered each other, which results in formation of adherent MCSs. On the other hand, gene expression profile of the cells on nano-sized pattern scaffoldings was mostly similar to that of 2D monolayer cells in cell adhesion and motility, which indicates that nano-pattern culture can liberate latent potential of tumor cells in cell adhesion and motility rather than 2D culture. Additionally, the mature MCSs constructed with nano-pattern culture were up-regulated in gene expression of multicellular organismal development and response to hypoxia. Transcription of HIF-1 and gene expression of HIF-1 target genes were also activated and there were hypoxic regions detected by pimonidazol binding, in the MCSs from this culture. These facts demonstrate that 3D culture system with nano-sized pattern scaffoldings can provide a model for cell migration, construction of organizational structure and hypoxia in 3D formation, which are linked with characteristics of *in vivo* tumors. Therefore, the nano-pattern culture system could be useful in development of molecular imaging probes.



Time-lapse analysis

Presentation Number **0390A**
Poster Session 1a: Imaging Instrumentation and Methodology

Study of 3D Imaging Performance Of A Two-Head Electron-Tracking Compton Gamma-Ray Camera

Shigeto Kabuki¹, **Hiroyuki Kimura**², **Hiroo Amano**², **Hidetoshi Kubo**¹, **Kentaro Miuchi**¹, **Hidekazu Kawashima**³, **Masashi Ueda**⁴, **Hideo Saji**², **Toru Tanimori**¹, ¹*Department of Physics, Kyoto University, Kyoto, Japan;* ²*Department of Patho-functional Bioanalysis, Kyoto University, Kyoto, Japan;* ³*The Advanced Medical Engineering Center, Department of bio-medical imaging, National Cerebral engineering Center, Osaka, Japan;* ⁴*Radioisotopes Research Laboratory, Kyoto University Hospital, Kyoto, Japan. Contact e-mail: kabuki@cr.scphys.kyoto-u.ac.jp*

Positron Emission Tomography (PET) and Single Photon Emission Computed Tomography (SPECT) achieved great success at a molecular imaging. These detector, however, have the energy limitation (PET : 511keV, SPECT : < 360 keV), which is a problem in a design of new imaging reagents. We have developed an Electron-Tracking Compton Camera (ETCC) for medical imaging. Because ETCC has a wide energy dynamic range (200 - 1500 keV) and wide field of view (FOV, 3 steradian), this camera has a potential of developing the new reagents for molecular imaging. The ETCC can reconstruct the initial gamma-ray direction using the Compton scattering phenomenon. Using this physics process, ETCC does not need a coincidence of two annihilation gamma rays and also does not need a collimator. For this reason, ETCC has no energy limitation of hardware and wide FOV. ETCC consists of two detectors. An initial gamma ray is Compton scattered in a first detector, which is a micro Time Projection Chamber (μ -TPC) based on a micro P1xel gaseous Chamber (μ -PIC). The μ -TPC (size $10 \times 10 \times 10 \text{ cm}^3$) filled with Ar-C₂H₆ (9:1) gas can catch a 3D Compton-recoil electron track and energy. The position resolution of the μ -TPC is less than 200 μm . Because conventional Compton camera (CC) can't take the recoil electron track, CC requires the many statistics for imaging. The scattered gamma ray is absorbed by a pixel scintillator arrays (PSAs). Whole PSAs area is $15 \times 15 \text{ cm}^2$ and which pixel size is $6 \times 6 \text{ mm}^2$. PSA materials are LaBr₃ or GSO crystal. The ETCC can reconstruct the 3D image using only one-head camera system. However the resolution of transverse is inferior to coronal or sagittal direction. To improve the resolution of depth direction, we have developed the two-head ETCC. Second ETCC head located at the front of first ETCC head. This geometry can easily reconstruct the gamma ray direction. First, we checked the detector performance and 3D spatial resolution using the point source. The resolution of transverse improved about two times (70mm), and coronal or sagittal direction keep the resolution of one head system (16mm). In this presentation, we will report the three-dimensional reconstruction results of phantom and small-animal data which are imaged by the two-head ETCC.

Presentation Number **0391A**
Poster Session 1a: Imaging Instrumentation and Methodology

Improved Imaging Performance of Semiconductor Compton Camera GREI for Multiple Molecular Simultaneous Imaging

Shinji Motomura¹, Tomonori Fukuchi¹, Shin'ichiro Takeda¹, Yousuke Kanayama¹, Hiromitsu Haba¹, Yasuyoshi Watanabe², Shuichi Enomoto^{1,3}, ¹Multiple Molecular Imaging Research Laboratory, RIKEN Center for Molecular Imaging Science, Kobe, Japan; ²Molecular Probe Dynamics Laboratory, RIKEN Center for Molecular Imaging Science, Kobe, Japan; ³Department of Pharmaceutical Analytical Chemistry, Graduate School of Medicine, Dentistry and Pharmaceutical Sciences, Okayama University, Okayama, Japan. Contact e-mail: motomura@riken.jp

We have developed various technologies to put our semiconductor Compton camera GREI into practical use for nuclear medicine. We had already succeeded in demonstrating the concept of multiple molecular simultaneous imaging, and showing the feasibility of three-dimensional (3D) tomographic imaging with a single Compton camera unit [1]. One of our ambitions was to extend the energy range of gamma rays to lower than 200 keV, which had been limited due to the characteristics of germanium semiconductor detector, and another was to improve the image quality of the three-dimensional tomographic images. For low-energy gamma-ray imaging with the semiconductor Compton camera GREI, we have integrated a double-sided orthogonal-strip lithium-drifted silicon [Si(Li)] detector into the imaging system. Monolithic Si(Li) detector can have more than 1 cm thickness, and this enables compact implementation of high-sensitivity Compton camera. Moreover, our Si(Li) detector is designed to achieve an excellent energy resolution of higher than 1 keV for 60 keV incident gamma rays. The use of high-sensitivity and high-energy-resolution Si detector is desirable especially for low-energy gamma-ray imaging with Compton camera, to efficiently perform the correction of Doppler broadening. One measure to improve the 3D image quality is to add more Compton camera units around the subject and construct a Compton camera array. We have constructed an array of two Compton camera units, and succeeded in demonstrating the improvement of 3D tomographic imaging performance. Two spherical gamma-ray sources of Mn-54 positioned along the axis of one Compton camera were clearly separated in the image of the array system, while they were not separated in the image of the single Compton camera unit. Recent progress in life science research has revealed that various common diseases, including cancer, cranial nerve disease, and other lifestyle-related diseases, are multi-factorial diseases that are complicatedly related to some genetic and environmental factors. If we can realize simultaneous imaging of multiple molecular probes that specifically trace each factor related to the diseases, and make simultaneous use of these factors for advanced imaging analysis, ultimately accurate and specific medical diagnosis is possible, and this will cause innovative advancement in new drug development and study of diagnosis of diseases by use of molecular imaging technology. [1] S. Motomura et al., J. Anal. Atom. Spectrom., 23, pp. 1089-1092, 2008.

Presentation Number **0328A**
Poster Session 1a: Imaging Instrumentation and Methodology

Feasibility studies of a four-layer high-resolution DOI detector using MPPCs for PET

Ryoko Yamada, Takahiro Moriya, Tomohide Omura, Mitsuo Watanabe, Central Research Laboratory, Hamamatsu Photonics K.K., Hamamatsu, Japan. Contact e-mail: ryoko@crl.hpk.co.jp

Positron emission tomography (PET) systems in molecular imaging are required to have high spatial resolution while keeping high sensitivity. To achieve sub-millimeter resolution, most small animal PET systems have adopted finely pixellated scintillators coupled to a position-sensitive photomultiplier tube (PS-PMT) as the detector. However, in such high-resolution systems with small ring diameter, the parallax error becomes dominant over the other errors like positron range or angular deviation. Therefore, the scheme to acquire depth of interaction (DOI) information is immensely desired in order to suppress the rapid degradation of the spatial resolution in the peripheral region of the field of view. We have designed a new DOI detector composed of four layers of detector unit. Each detector unit consists of a LYSO scintillator array finely segmented by the laser processing technique and an 8×8 array of multi-pixel photon counters (MPPCs), which are one of the products of silicon photomultiplier (SiPM) family. The MPPC is so compact and insensitive to gamma-rays that the detector units can be piled up with small gaps between each scintillator array in the depth direction. In order to obtain uniform sensitivity at the unit of the different layer, the scintillator thickness was designed at 3 mm, 4 mm, 5 mm and 8 mm toward the bottom respectively, and the total thickness is 20 mm. We adopted an internal focused laser processing technique to the fabrication of scintillator arrays. The technique can realize a finely segmented array to a monolithic scintillator block without the deterioration of primary scintillation properties and detection efficiency. We fabricated a 2D segmented array of 32×32 with 1.2 mm pitch in 38.4 mm square cross-sectional area of monolithic LYSO scintillator. In this feasibility studies, the performance of the new four-layer DOI detector was evaluated and demonstrated by the Monte Carlo simulation as well as experiments, i.e. energy spectra, spatial resolution and the behavior of gamma-ray interactions. We perform the simulation studies by using Geant4 of simulation tool kit that enables to track and record the passages of particles through matter. In addition, the characteristics of the ideal DOI detector composed of multi-layers of the thinner plate on various materials were also studied by the simulation to investigate the limitation of spatial resolution.

Presentation Number **0329A**
 Poster Session 1a: Imaging Instrumentation and Methodology

Organ segmentation of mouse using intraperitoneal injection of iohexol contrast agent

Xiangsi Li¹, **Jie Tian**^{1,2}, Xiaopeng Ma¹, Junting Liu¹, Man Shen¹, Xiuduan Lin¹, Xiaochao Qu¹, ¹Life Sciences Research Center, School of Life Sciences and Technology, Xidian University, Xi'an, China; ²Medical Image Processing Group, Institute of Automation, CAS, "Beijing, 100190", China. Contact e-mail: tian@ieeee.org

In the area of computer-aided diagnosis, accurate and robust organ segmentation from medical images is a prerequisite for disease diagnosis and surgery planning. CT volume data is often used for organ segmentation. Due to the similar absorption coefficients of the soft tissues to the X-ray, the contrast of the CT volume is usually low, which makes organ segmentation a challenging task. This paper presents a distinct intraperitoneal (IP) injection method using the common iohexol contrast agent (GE Healthcare) to improve the contrast of the CT volume. In this method, about 15 hours before the data acquisition, iohexol contrast agent (300 mg I/ml) was injected into the nude BALB/c mouse by IP injection; and about 6 hours before the data acquisition, another iohexol contrast agent was injected into the mouse by IP injection. A cone-beam micro-CT prototype system developed by our group for small animal imaging was used to acquire the 2D multi-view projection data of the mouse. FDK algorithm is adopted for 3D reconstruction with GPU acceleration. The slice images of the reconstructed volume are shown in Fig. 1 (a). Then, the threshold segmentation and improved live wire segmentation methods were used to segment the main organs (muscle, heart, lungs, gallbladder, liver, stomach, spleen, kidneys and bone) sequentially through segmenting each organ in each slice. The segmented organs were extracted after being smoothed using Gaussian method. The slice images of segmented volume are shown in Fig. 1 (b) and Fig. 1 (c) presents the registration images of micro-CT reconstructed images and segmented images. The IP injection method increases the contrast of micro-CT volume, which significantly improves the efficiency of the organ segmentation with the improved live wire segmentation method.

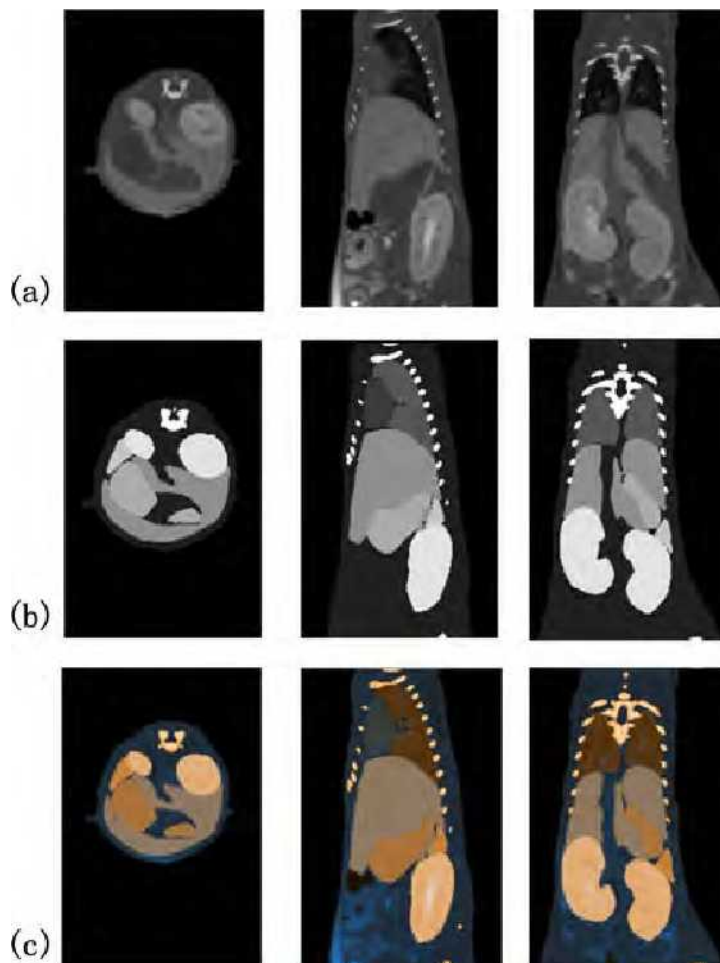


Fig. 1. Micro-CT reconstructed, segmented and registration images of the mouse in horizontal, sagittal and coronal views. (a) reconstructed images; (b) segmented images; (c) registration images.

Presentation Number **0330A**
Poster Session 1a: Imaging Instrumentation and Methodology

Towards standardization and quantification of PET/CT imaging in multi-centre trials

Thomas Beyer^{1,2}, **Bernd Klaeser**², **Frederic Corminboeuf**², **Thomas Krause**², **Thilo K. Weitzel**², ¹*cmi-experts GmbH, Zurich, Switzerland;* ²*Nuclear Medicine, Inselspital Bern, Bern, Switzerland. Contact e-mail: thomas.beyer@cmi-experts.com*

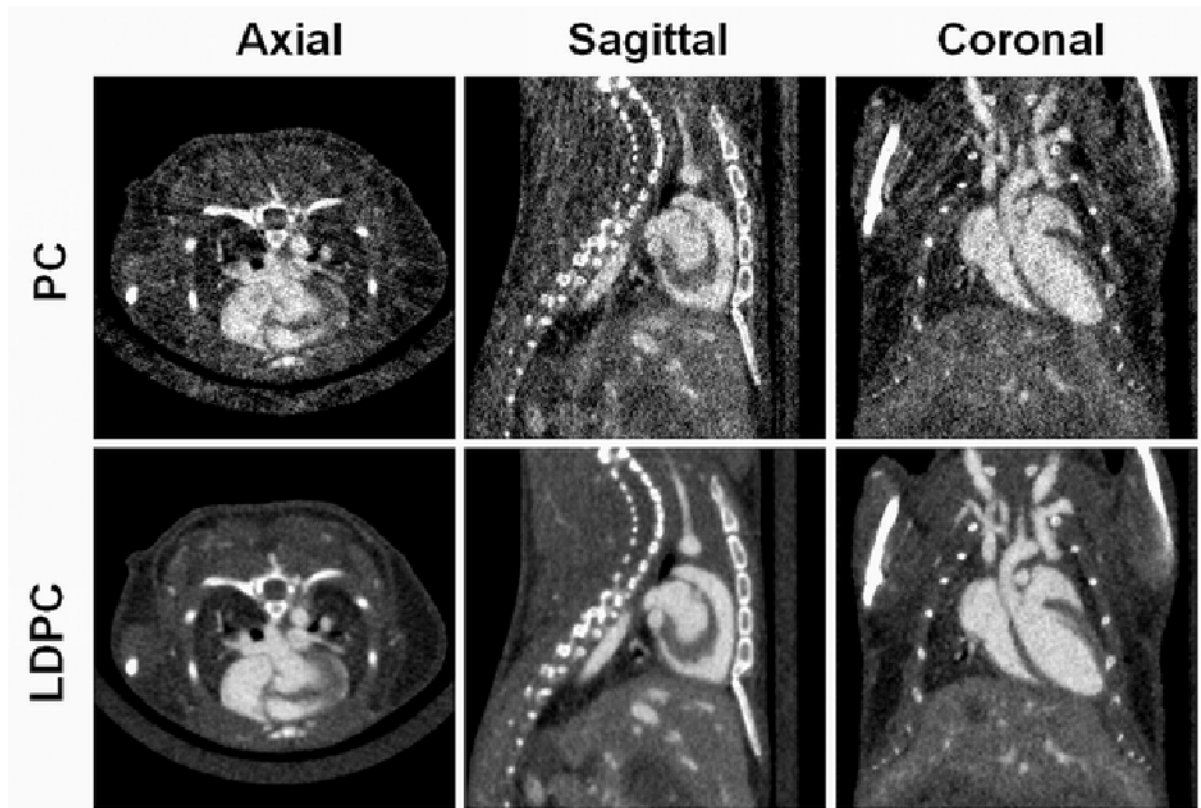
INTRODUCTION Combined PET/CT has become a standard in clinical imaging and is increasingly used in pharmaceutical trials since it provides both anatomical and metabolic endpoints. Metabolic endpoints are based on measuring changes of tumour uptake (EORTC) expressed as standardized uptake values (SUV). SUV's are affected by a range of protocol and analysis parameters. In multi-centre trials SUV analysis can be dominated by properties of the PET system despite the use of standardized protocols across trial sites. We present an approach to correcting for PET recovery effects (RC) in multi-centre imaging trials involving different PET systems. **METHODS** We employ a novel recovery phantom made of a 20cm plastic cylinder in which two sets of in-plane, plastic spheres are arranged in two concentric circles (13cm and 5cm). Sphere diameters d are 2.5-8mm and 10-31mm for hot spheres in the inner and outer circle, respectively. All lesions are filled with ⁶⁸Ge-resin (0.1MBq/ml). Each lesion can be unscrewed and scanned individually within specific surroundings to estimate RC in other tissues, e.g. lungs or bone. RC for all spheres are calculated on CT-based attenuation-corrected PET images using an IDL-based software (QuantScan). We consider all lesions as strictly circumscribed homogeneous ellipsoids. Through the use of an iterative approximation of the 3D activity concentration in each sphere using local intensity maxima the size and the concentration of each lesion can be obtained with high accuracy. Phantom-based RC are used to correct patient-based RC. The RC phantom was filled with water and scanned on a Siemens HiRez16-PET/CT, a GEHC Discovery STE and a Philips Gemini-TF64 following standard whole-body imaging protocols. **RESULTS** This study is work in progress. Cross-comparison of the lesion phantom scanned without and with water on the HiRez16 against a similar scan with a NEMA contrast phantom using ¹⁸F-filled spheres (d :10-31mm) demonstrated the validity of using ⁶⁸Ge-based RC estimates. Cross-system quantification of phantom-based soft tissue lesions was shown to be improved to 3-5% for lesions with d :10-32 mm. **CONCLUSION** We present a concept for multi-centre RC and standardization of PET imaging results using a novel phantom. Through the use of long-lived isotope ($T_{1/2}$ ~270d) complex preparation of phantoms on-site is avoided and exposure of the technical staff is limited. Based on properly calibrated PET systems, repeated quality control scans and a base recovery scan using above phantom PET results across trial sites can be standardized.

Presentation Number **0331A**
 Poster Session 1a: Imaging Instrumentation and Methodology

Dedicated Low-Dose Small Animal Cardiac Micro-CT Image Reconstruction

Stefan Sawall¹, Frank Bergner¹, Michael Knaup¹, Marc Kachelriess¹, Andreas Hess², ¹Institute of Medical Physics, Friedrich-Alexander University Erlangen-Nürnberg, Erlangen, Germany; ²Institute of Experimental and Clinical Pharmacology and Toxicology, Friedrich-Alexander-University Erlangen-Nürnberg, Erlangen, Germany. Contact e-mail: stefan.sawall@imp.uni-erlangen.de

The reconstruction of a given cardiac and respiratory phase in functional CT imaging of rodents typically utilizes only a small amount of the total projections acquired (1 to 2%). Hence, conventional double gating requires a high dose (typically around 2 Gy) to obtain images with acceptable noise levels. We propose a new method that allows to reduce dose by an order of magnitude without compromise in image quality. In a standard micro-CT scan the respiratory motion and ECG signals are extracted from the rawdata and used to select the projections appropriate for the given heart and respiratory phases (kymogram). The conventionally double gated phase-correlated (PC) images suffer from a high noise level as only a small number of the total projections match the desired motion phase. We implemented an iterative approach using a priori information from all projections combined with 5D (spatial, cardiac and respiratory) anisotropic edge-preserving filtering to overcome this drawback and improve the image quality. Our low-dose phase-correlated (LDPC) reconstruction method is evaluated using contrast-enhanced, retrospectively gated micro-CT scans of mice. A typical scan comprises 7200 projections acquired within 10 rotations over 5 minutes at a tube voltage of 65 kV and a dose of 200 to 500 mGy. Ten respiratory phases and five cardiac phases are reconstructed, thus each reconstruction only uses 2% of the acquired data. Using LDPC reconstruction the voxel noise is reduced from 170 HU to 30 HU, on average, and artifacts are almost removed. The dose of our standard protocol is about 500 mGy. Reducing the number of rotations available for image reconstruction shows that we can get comparable image quality with only 200 mGy. Compared to other publications, that apply 1840 to 2400 mGy dose and use PC reconstruction, our LDPC approach therefore achieves a more than ten-fold dose usage improvement. LDPC enables high fidelity low-dose double-gated imaging of free breathing rodents without compromises in image quality. Compared to the PC reconstruction image noise is significantly decreased with LDPC, and the administered dose can be reduced accordingly.



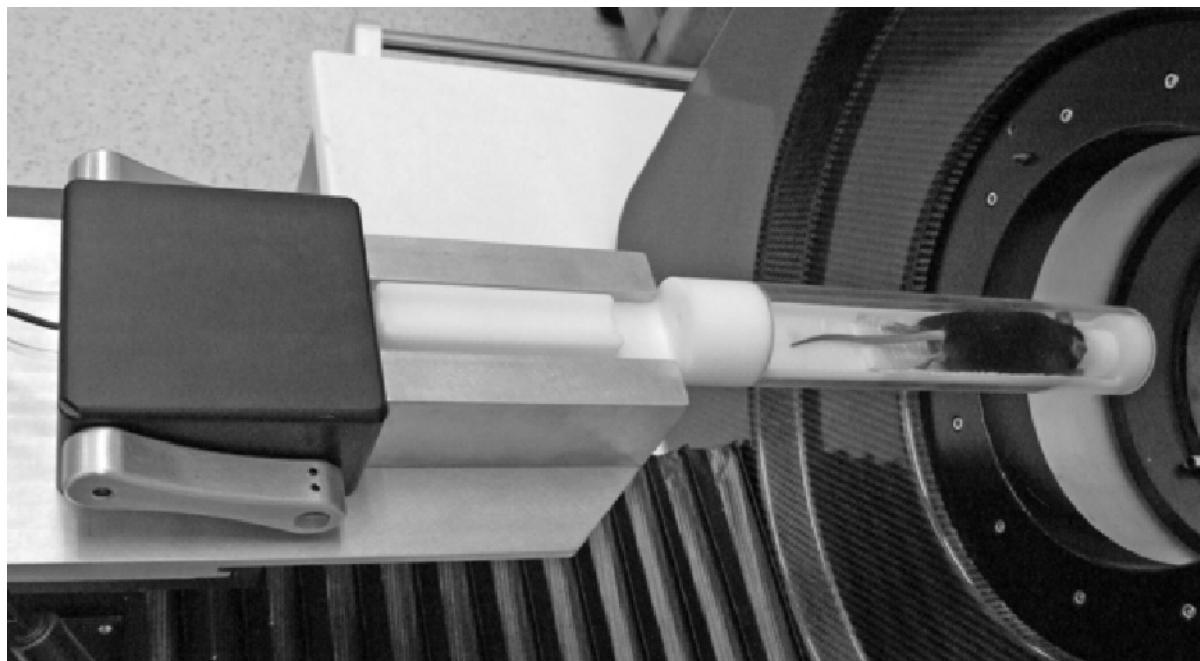
Dose: 500 mGy, c/w: 0 HU / 300 HU

Presentation Number **0332A**
Poster Session 1a: Imaging Instrumentation and Methodology

Environmental Control Chamber for coregistered mouse PET-CT imaging

David Stout, Waldemar Ladno, Darin Williams, Dirk A. Williams, *Molecular and Medical Pharmacology, Crump Institute for Molecular Imaging, Los Angeles, CA, USA. Contact e-mail: dstout@mednet.ucla.edu*

Introduction: A new mouse environmental control chamber has been created to enable coregistered PET and CT imaging. This improved version has a simplified connection scheme, with an enclosure to facilitate use with biohazardous and carcinogenic agents. We compared the ability to position, inject, maintain temperature, anesthetize and image with our previous chamber design. **Methods:** Temperature rise and stability were tested using both thermocouple and infrared measurement systems. Anesthesia stability was evaluated by flow meter verification from a calibrated vaporizer and observation of mouse respiration. Reproducibility of the chamber and mouse were assessed using landmark locations in the CT images acquired with 100 micron voxel size (n=5): in vivo locations were top of skull and spine, hip and shoulder joints and distal mediastinum. Distance from each mean location was computed in mm. We verified coregistered mouse FDG PET and CT images could be acquired from 2 separate imaging systems. **Results:** Temperature rapidly rose to over 35C within 2 min and stabilized to the set point of 37 C within 5 min. Animal access for catheterization, positioning and anesthesia stability was equal or better than our older design due to added space for the animal. Based on the CT scans, there was no measureable difference in the images for changing the base plate plus chamber or repositioning only the chamber and leaving the base plate in place, thus reproducibility of the chamber was less than the 100 um voxel size. Mouse imaging measurements showed positional variability on average of ~0.55 mm, max distance of 1.2 mm. Our old design had an average of 0.79 mm, max of 1.8 mm. **Conclusions:** The imaging chamber provides an improved closed and controlled environment for working with immune compromised mice and potentially enables working with infectious or hazardous agents. We have integrated the heating and anesthesia lines together with the docking system to eliminate the need to handle wire, tubing, alignment pins or screws. Positioning and physiology support are well managed for PET-CT imaging of metabolic processes. We anticipate validating further design improvements, including our plans for a sealed environment, in the near future.



Presentation Number **0333A**
 Poster Session 1a: Imaging Instrumentation and Methodology

Quantitative evaluation of a new flat panel PET scanner with mouse FDG and FAC images

David Stout, Richard Taschereau, Arion Chatziioannou, Molecular and Medical Pharmacology, Crump Institute for Molecular Imaging, Los Angeles, CA, USA. Contact e-mail: dstout@mednet.ucla.edu

Introduction: A new desktop PET system has been designed for high throughput imaging of mice and well plates. It has a simple user interface, integrated animal handling, anesthesia support and respiratory monitoring. This dual head BGO-based system provides spatial resolution of ~1.6 mm in-plane and ~ 2.6 mm between the detectors with ~4% sensitivity. We evaluated its ability to quantify PET probe uptake, comparing it to two conventional full ring systems. Methods: Five nude mice were injected with FDG and the following day with FAC (marker of immune system activation). These mice were irradiated and had various treatments affecting the immune system, creating signals in bone, spleen, liver, thymus, along with activity in the bladder, heart, brain and GI tract. Mice were injected with ~100 uCi, unconscious uptake for 60 min, followed by 10 min sequential imaging in CT and three PET systems. Data was corrected for decay, normalization, deadtime, randoms and CT-based attenuation. Images were created using OSEM for the ring based systems and MLEM for the planar system. 3D Regions of interest were drawn and percent injected dose (%ID) calculated based on total activity in a whole body region based on the CT image. Results: Coronal images were comparable and showed very similar uptake patterns when scaled to the same percent maximum image intensity. Correlation coefficients of %ID between the planar and ring based systems ranged from 0.994 to 1.0 for each region. Small but statistically significant differences were found (paired 2 tailed T test <0.05) for the %ID values only in the spleen and brain for FDG, and thymus and bone for FAC. Conclusions: This new PET system acquires and processes data to create images and biodistribution data very similar to commercial ring-based systems. Small differences in uptake values were found in a few organs; however the measured %ID tracked variations in uptake due to treatment that were highly correlated with the ring-based systems.

	Spleen %ID			Thymus %ID		
	Ring-F	Ring-1	Planar-G	Ring-F	Ring-1	Planar-G
FAC #1	2.0%	2.0%	2.6%	0.32%	0.36%	0.31%
FAC #2	0.34%	0.34%	0.73%	0.36%	0.40%	0.33%
FAC #3	1.7%	1.7%	1.5%	0.10%	0.11%	0.09%
FAC #4	2.7%	2.8%	2.2%	0.02%	0.02%	0.04%
FAC #5	1.2%	1.1%	1.2%	0.27%	0.28%	0.23%
Correlation	0.993	0.989		0.997	0.997	
T Test P	0.189	0.023		0.038	0.024	
	Spleen %ID			Liver %ID		
	Ring-F	Ring-1	Planar-G	Ring-F	Ring-1	Planar-G
FDG #1	2.4%	2.4%	2.1%	0.39%	0.41%	0.33%
FDG #2	0.16%	0.16%	0.20%	0.07%	0.07%	0.09%
FDG #3	1.1%	1.1%	1.0%	0.35%	0.44%	0.44%
FDG #4	0.17%	0.16%	0.14%	0.11%	0.11%	0.13%
FDG #5	1.7%	1.4%	1.1%	0.13%	0.15%	0.14%
Correlation	0.999	0.998		0.993	0.970	
T test P	0.030	0.019		0.581	0.569	

Presentation Number **0334A**
 Poster Session 1a: Imaging Instrumentation and Methodology

Design and Validation of a Baffle for Multiple Pinhole Small Animal SPECT

Peter L. Kench^{1,2}, Jianyu Lin¹, Marie-Claude Gregoire³, Steven Meikle^{1,2}, ¹Ramaciotti Imaging Centre, The Brain and Mind Research Institute, The University of Sydney, Camperdown, NSW, Australia; ²The Discipline of Medical Radiation Sciences, The Faculty of Health Sciences, The University of Sydney, Lidcombe, NSW, Australia; ³LifeSciences, Australian Nuclear Science and Technology Organisation, Lucas Heights, NSW, Australia. Contact e-mail: peter.kench@sydney.edu.au

Multiple pinhole collimation (MPC) increases detection efficiency compared to single pinhole collimation (SPC) for small animal SPECT. However, the quality of the reconstructed volume is dependent upon the degree of projection multiplexing and the benefit of higher efficiency may be offset by the need for increased iterations to reduce artifacts. Reconstruction artifacts are particularly strong when imaging elongated objects (such as animals) through axially displaced pinholes. We designed an attenuating baffle positioned between the object and MPC to minimise axial multiplexing and hypothesised that this would reduce reconstruction artifacts and improve quantitative accuracy. A tungsten alloy MPC and baffle were constructed and SPECT performed on a rat sized elongated phantom. The MPC incorporated four knife edged pinholes with an aperture of 1.0mm and acceptance angle 30° positioned 17mm apart in a square configuration centred over the detector. A rectangular baffle was positioned adjacent to the outer edge of pinholes perpendicular to the axis of rotation. The phantom was created using Tc-99m in gelatine and comprised a 50ml conical tube with 3 internal cylindrical structures of known activity, 1 axially displaced with respect to the others. SPECT was acquired for 360° and 64 steps with SPC and MPC with and without the baffle in place. All acquisitions were reconstructed using an OS-EM algorithm for 40 iterations. Bias was calculated for ROIs drawn on the two central internal structures as (MPC-SPC)*100/SPC. The reconstructed contrast phantom with the MPC and baffle was free of artefacts with a bias of -8% and -8% whereas the MPC study without baffle produced marked artifacts as illustrated in figure 1 and a bias of -29% and -24%. We conclude that an appropriately designed baffle for MPC substantially eliminates axial multiplexing and associated reconstruction artefacts, thus improving quantitative accuracy.

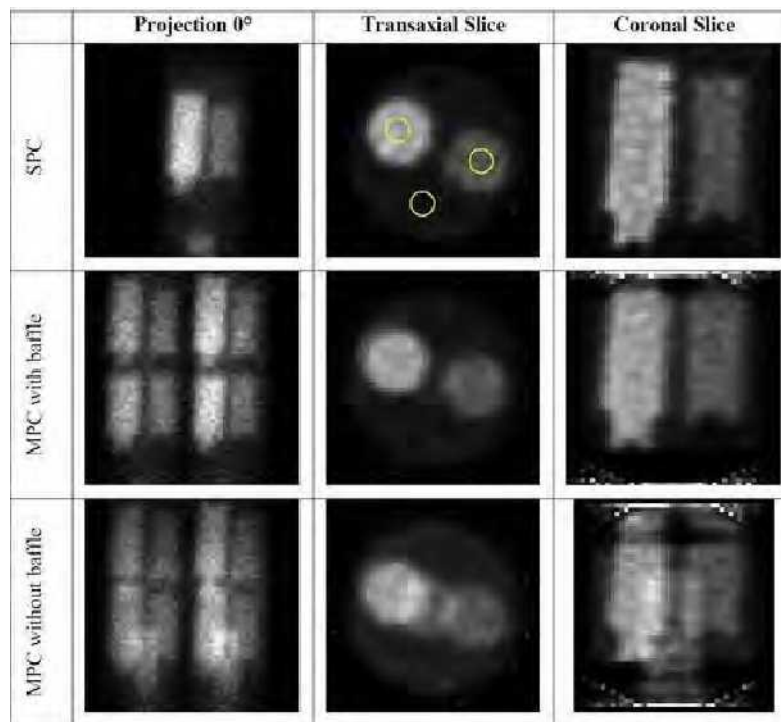


Figure 1. Projections and reconstructed slices of a rat phantom acquired with the single (SPC) and multiple pinhole (MPC) collimators with and without the baffle. The region of interest locations for the bias calculation are displayed on the SPC transaxial slices as the two yellow circles within the two adjacent internal structures.

Presentation Number **0335A**
 Poster Session 1a: Imaging Instrumentation and Methodology

Half Dose MIBG Cardiac SPECT Clinical Evaluation of Resolution Recovery Methods

Guilhermina Cantinho^{1,2}, **Helena Pena**^{1,2}, **Deolinda Cerqueira**¹, **João Clemente**¹, **Fernando Godinho**^{1,2}, ¹Atomedical, SA, Lisboa, Portugal; ²Instituto de Medicina Nuclear, Faculdade de Medicina de Lisboa, Lisboa, Portugal. Contact e-mail: gcantinho@atomedical.pt

Introduction: The tomographic reconstruction by iterative methods, as WBR, allows acquisition's time or activity reduction in perfusion scans, issues with an increasing importance in NM departments. We've also been witnessing a growing interest in the use of 123I-MIBG cardiac SPECT, especially in familiar amyloid polyneuropathy (FAP). To process tomographic studies, we used WBR methodology and the more recently developed Xpress3, itself an improvement of WBR. We evaluated the possibility of performing the 123I-MIBG cardiac SPECT studies, using lower activity than the usually recommended. Material & Methods: 50 patients (pts) with FAP or high blood pressure (HBP) were randomly studied. We sequentially acquired tomographic studies at 30 minutes and at 3 hours after e.v. 185-222 MBq 123I-MIBG: A1 (30 s/view/60 views) and A2 (15 s/view/60 views). A1 studies were processed by FBP and A2 by WBR and Xpress3. The 100 studies were analyzed by two independent observers who classified the slices in very good (VG), good (G) and sufficient (S) quality. For quantification purposes, we analyzed all studies and then, separately: abnormal studies, FAP studies and HBP patients' studies. To quantify LV radiopharmaceutical distribution, the 3 main vascular territories were considered, using Germano's QPS method to assess lesions score, severity and area. Paired Student t test (p) and Pearson correlation coefficient analysis (r) were used for statistical purposes. Results: In none of the studies did the visual analysis modify the final report. On the qualitative analysis of the tomographic slices, the two observers always found a better quality when WBR or Xpress3 was used, compared to the FBP processed studies, with an inter-observer agreement >96%. Half of the FBP studies were classified as S, while none of the WBR or Xpress3 was. On the quantitative lesion and score analysis, the correlation coefficients was always > or = 0.96 for the all patients group. On the 21 abnormal studies (FBP score > 4), the quantitative analysis didn't show any statistically significant difference [table]. On FAP abnormal studies, the results were similar. All the HBP studies were normal and statistically similar. Conclusions: We can conclude that the use of WBR and Xpress3 for 123I-MIBG cardiac SPECT doesn't affect the results, with important advantage on time and administered activity reduction and at last, but not less importantly, less expensive.

Score Comparison - Abnormal Studies

	FBP vs WBR	FBP vs Xpress3	WBR vs Xpress3
p	0.50	0.95	0.05
r	0.91	0.91	0.99

Presentation Number **0336A**
 Poster Session 1a: Imaging Instrumentation and Methodology

XPRESS3 – Half-Dose / Half-Time GATED Cardiac SPECT Validation

Guilhermina Cantinho^{1,2}, **Helena Pena**^{1,2}, **Lorena Pereira**¹, **Inês Magno**¹, **Fernando Godinho**^{1,2}, ¹*Atomedical, SA, Lisboa, Portugal;*
²*Instituto de Medicina Nuclear, Faculdade de Medicina de Lisboa, Lisboa, Portugal. Contact e-mail: gcantinho@atomedical.pt*

Introduction: Over conventional FBP, WBR tomographic reconstruction methodology has the advantage of improving image resolution with shorter time acquisitions or, even more useful, with reduced radiopharmaceutical dose. From the improvement of this technique, a new software was developed: Xpress3. We've been invited by UltraSPECT to test this new software that allows acquisitions with WBR time and half the administered activity dose. Material & Methods: 53 patients underwent stress and rest gated-SPECT with half the usual injected activity (407-481 MBq at stress and 185-222 MBq at rest) We acquired 2 sequential studies: A1 (20 s/view/60 views) and A2 (10 s/view/60 views). A1 was processed by WBR and A2 by Xpress3. Cedars-Sinai QGS and QPS was used for LVEF, EDV, ESV and perfusion quantification (by vascular territories), represented by scores, lesions area and severity (%). Paired Student t test (p) and Pearson's correlation coefficient (r) were used for statistical analysis (A1/A2). Tomographic slices were qualitatively analyzed and classified as better, worse or similar. Results: The 106 studies gave this work a 98% power (ES=0.5; a-level=0.05) Qualitative appreciation didn't show significant differences. 72 studies were considered identical and classified with very good quality. With Xpress3, 16 (15%) studies were considered of better quality and 18 (17%) of worse quality. On none of the cases, the images reevaluation altered the final report. For the quantitative analysis by vascular territories, there weren't statistically significant differences between scores (p>0.5) at rest (r=0.82), as well as at stress (r=0.9) On the statistical analysis of lesions' area and severity, small differences were found at rest, on LAD and RC territories, but in patients with normal perfusion studies. We also found worse correlation on the rest studies, compared with the stress statistical analysis. The remaining analyzed parameters didn't show statistically significant differences [table]. Conclusions Half-time and half-dose protocols are important goals in Nuclear Medicine cardiac procedures and nowadays a good solution to the technetium shortage. The good results obtained increase our confidence on the use of this new methodology that is more comfortable for the patients and lightens the departments' routine, time wise as well as for technetium management.

WBR vs Xpress3

	LVEF	EDV	ESV
p	>0.5	>0.05	>0.5
r	0.98	0.98	0.97

Presentation Number **0337A**
Poster Session 1a: Imaging Instrumentation and Methodology

First Quantified Images of a Unique and Dedicated Breast PET

*Antonio J. González Martínez^{1,2}, Carlos Correcher Salvador¹, Julio Barbera Ballester¹, Carlos Vazquez¹, Jose M. Benlloch², Tjeerd S. Aukema³, Renato A. Valdés Olmos³, **Luis Caballero Ontanaya¹**, ¹Oncovision, Valencia, Spain; ²Instituto de Física Corpuscular, Valencia, Spain; ³Nuclear Medicine, National Cancer Institute, Amsterdam, Netherlands. Contact e-mail: Luis.Caballero@oncovision.es*

In this work we present the most relevant aspects of the highest clinical spatial resolution PET, best focus on early breast cancer detection. Breast cancer is the second leading cause in the world of cancer death in woman. In particular, it is a dedicated breast PEM with a ring geometry avoiding any type of uncomfortable breast compression. The detector has a ring shape where the breast of the woman is inserted being the woman lying down in prone position on a special hanging breast device. This design has several advantages. From the clinical point of view, it makes possible to scan the breasts up to zones very close to the base of the pectoral. From the image quality point of view, it allows one to reach a spatial resolution up to 1.5 mm at the time that reduces scatter events as only the breast is scanned compared with whole body equipments. The ring aperture is 186 mm with a transaxial field of view of 170 mm. Axially, the system can cover up to 170 mm too recording several frames which are internally overlapped. The ring is composed of 12 detector heads, each containing a single monolithic LYSO crystal, a position sensitive photomultiplier tube and readout electronics. The use of monolithic crystals allows us not only to measure the planar XY coordinate of the photon impact, but also its depth of interaction (DOI) by measuring the width of light distribution collected in the PSPMT. Due to the selected crystal and sensor types, the system reaches an average energy resolution of about 14%, which increases locally up to 9%. The new and dedicated breast PET has demonstrated to acquire images with good agreement when compared with standard PET. Up to date about 30 patients have been successfully scanned and 3D images fused with whole body PET ones at the National Cancer Institute in Amsterdam. Both PET-CT and the PEM prototype measures were carried out with the special hanging breast devices. Quantification data has been accurately extracted and SUV values obtained. Absolute SUV values (SUVmax) between standard PET and PEM showed a small discrepancy in the order of a factor 2 higher for PEM data. However, relative values deviated just a factor 1.5. Summarizing, an innovative and dedicated breast PET has shown to have an increased spatial resolution to look for small and early breast tumors. Prone position is suitable for PET breast imaging. This device is intended to work in both early breast cancer screening and therapy response.

Presentation Number **0338A**

Poster Session 1a: Imaging Instrumentation and Methodology

Multi-Resolution Restoration for Micro-SPECT

Sih-Yu Chen¹, **Kuan-Hao Su**¹, **Tat-Wei Tan, David**¹, **Ren-Shyan Liu**², **Jyh-Cheng Chen**^{1,3}, ¹*Dept. of Biomedical Imaging and Radiological Sciences, National Yang-Ming university, Taipei, Taiwan;* ²*Dept. of Nuclear Medicine, Taipei Veterans General Hospital, Taipei, Taiwan;* ³*Dept. of Education & Research, Taipei City Hospital, Taipei, Taiwan. Contact e-mail: sy1004@iyw.tw*

Purpose: The nuclear medicine images from micro SPECT are usually reconstructed by ordered subsets expectation maximization (OSEM) algorithm. Its image quality depends on OSEM's iteration number and spatial frequency content, higher spatial frequency will cause lower convergent rate. If the iteration number is small, image will be blurred. Thus, large iteration number is usually chosen, and then the reconstructed images are further processed by some smoothing filter for the noise reduction. However, it is time-consuming and will decrease spatial resolution. The purpose of this study was to use wavelet transform (WT) to decompose images to different spatial frequency bands with less iteration number and to deblur the wavelet approximated image to get better image quality with faster convergent rate. **Methods:** In this study, we compared different wavelets, including discrete wavelet transform (DWT), stationary wavelet transform (SWT), dual-tree complex wavelet transform (CWT), with different deblurring methods such as constrained least squares filter (CLSF), Lucy-Richardson algorithm (LR), and fast total variation de-convolution (FTVd). We use a physical resolution phantom with 0.35~0.75 mm hot spot areas to acquire images from the micro SPECT with 0.5 mm single pinhole collimator. Then, the images were reconstructed by OSEM algorithm with 10 iterations of 8 subsets. To restore images, we applied different wavelet transform to decompose the image to wavelet domain, and then deblurred the wavelet approximated image with three deblurring methods. Finally, we applied the inverse WT to the deblurred approximated image to obtain its spatial domain image. The coefficient of variation (CV) and contrast recovery coefficient (CRC) were used to evaluate noise and contrast of the images. **Results:** The best CRC value of CLSF with CWT is five times than that of the original image, and it is comparable to over 80 iterations of 8 subsets of the original image which spends eight times longer in processing time. In addition, the CRC values of the deblurred image using CLSF with three WTs and FTVd with DWT are higher than that without wavelet transform and the CV values are lower than that without wavelet transform. In comparison with the original image, in which 0.75 mm hot spot area can be distinguished barely, our best result among above mentioned methods is CLSF with CWT and even the 0.6 mm hot spot area can be distinguished clearly on the image. **Conclusion:** Our results show that the image quality and convergent rate can be improved by our deblurring methods.

Presentation Number **0339A**
 Poster Session 1a: Imaging Instrumentation and Methodology

Ultra-Low-Dose Computed Tomography Provide Adequate Attenuation Correction for 18F-fluoride Bone PET/CT: A Phantom Study

Nai-Ming Cheng¹, **Hui-Yu Tsa**^{2,1}, **Tzu-Chen Yen**^{1,2}, **Kun-Ju Lin**^{1,2}, ¹*Nuclear medicine, Chang Gung Memorial Hospital at Linkou, Guishan Shiang, Taiwan;* ²*Medical Imaging and Radiological Sciences, Chang Gung university, Guishan Shiang, Taiwan. Contact e-mail: med8611023@yahoo.com.tw*

We performed a phantom study by different computed tomography (CT) settings to find parameters with adequate diagnostic utility and lower radiation in 18F-fluoride PET/CT. Methods: Point sources of 18F-fluoride were positioned in skull base, T5, L2 spines, right ilium, and right rib of a medium adult anthropomorphic phantom. CT scans were done with 80/100/120 kVp and 30/70/110/150/180/250/300 mA, respectively, with 0.5 second per rotation and pitch of 1.5:1. Volume-of-Interest (VOI) of each point source was drawn and radiation count was measured. Ratio of counts quantified from images to true counts (by calibrator before scanning with time correction) was used for the wellness of attenuation correction. We selected T5, T9, L2 and right ilium for CT noises evaluation. CT effective dose was estimated according to the tube current per slice showing in the whole image series, using ImPACT dose calculation with Monte Carlo based database. Tissue weighting factors were recommended by International Commission on Radiological Protection publication number 60 (ICRP 60). Results: For attenuation correction, significant different ratios were found among CT scans of different voltage and current ($p < 0.001$). But, post hoc tests revealed no difference among tube currents in CT of 100 and 120kVp ($p = 0.999$ in 100kVp, and $p = 0.979$ in 120kVp). In order to maintain adequate image quality as our current standard CT (120kVp/300mA) in PET/CT and minimize radiation dose, CT scan of 120kVp/30mA was favored. However, significant more CT noise was found in this setting ($p < 0.001$). Therefore, CT of 120kVp/70mA was favored due to its adequate attenuation correction and compatible CT noise ($p = 0.401$). The effective dose for 120kVp/70mA and conventional CT were 1.03 and 4.30mSv, respectively. Conclusion: We conclude that adequate attenuation correction can be obtained with 120 kVp/70 mA CT, which leads to a 4-fold dose reduction without deterioration of image quality.

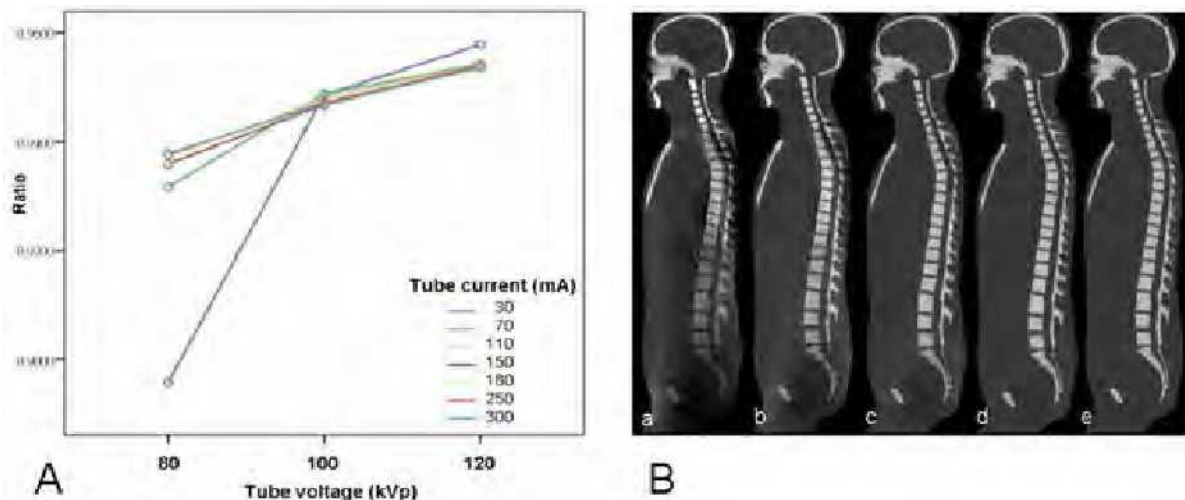


Figure A showed the effects of CT tube voltage and current to the wellness of attenuation correction. Significant variances were noted in the 80kVp, but not in the 100 and 120kVp groups. Figure B showed CT images of (a)80kVp/30mA, (b)100kVp/30mA, (c)120kVp/30mA, (d)120kVp/70mA, and (e)120kVp/300mA. Deterioration of spine and pelvic areas was noted in (a), (b), and (c) but not in (d).

Presentation Number **0340A**
 Poster Session 1a: Imaging Instrumentation and Methodology

Comparison of Planar and Single Photon Emission Computed Tomography Quantification based on different reference model

An-Jim Long, Chih-Hsien Chang, Liang-Cheng Chen, Cheng-Hui Chuang, Meei-Ling Jan, Isotope Application Division, Institute of Nuclear Energy Research, Taoyuan County, Taiwan. Contact e-mail: jimlong@iner.gov.tw

SPECT has been widely accepted for quantification of radioisotope. Comparison of quantification from planar and SPECT were proposed and evaluated. However, comparison of planar and SPECT based on different references model has not yet been conducted. Phantom was prepared by glass bottles filled with 50, 100, 200, 400, and 800(uCi) 111In. 1-ref/1-target (800 and 400uCi) and 4-ref/1-target phantom was imaged with CT and planar and SPECT. Phantom and SPECT detector remain unmoved during the entire scan. Accuracy of SPECT quantification, compared with dose calibrator measurements, for determining radioisotope uptake was conducted by image analysis using PMOD. ROI and ROI segmentation was done by circle based on CT. Radius was defined in 5 and 15mm. Automatic detection was set as absolute value threshold to 40. Time-activity frames and randomized segmentation of regions ROI/VOI were analyzed for gage repeatability. Linear regression was used to analyze 400uCi target activity from the rest of four. Agreement and reproducibility of radioactivity measurements were assessed by Lin's concordance correlation coefficient (CCC). GRR varies from 0.49%-0.63% on 15mm and automatic segmentation of ROI/ VOI and 1.47%-2.23% on 5mm segmentation of ROI/VOI, while GRR varies from 0.4%-2.89% based on time-activity frames. All studies were examined (CCC=0.987-1). Size of segmentation is key performance factor of radioactivity quantification. Automatic segmentation showed worst performance than the rest of methods. Exact size with CT landmark showed best quantification performance. SPECT and planar did not show difference on quantification performance. Since planar is a lot faster than SPECT, planar with CT supported accurate size and position of segmentation are highly suggested for targets with distinguishable ROI/VOI. Too many references with one target seem to be possible to interfere the representation of target hence analysis performance cannot be enhanced. 1-ref quantification or longer distance between reference and target is highly suggested.

Radioactivity measured by dose calibrator and ROI/VOI image analysis using tomography SPECT, planar via different segmentation techniques.

	R=1.5mm, 1 Ref	R=1.5mm, 5 Ref	R=5mm, 1 Ref	R=5mm, 5 Ref	Auto-segmentation
800uCi SPECT	3918.1	2888.4	591.7	913.2	2427.7
400uCi SPECT	1477.1	1575.8	43.40	455.7	1000.0
Estimated activity	404.9	393.0	390.2	378.0	329.8
Distance to 400uCi	1.23%	-1.76%	-2.46%	-5.51%	-17.54%
CCC	1.000	0.995	1.000	1.000	0.987
800uCi Planar	2800.7	2873.4	903.0	936.2	2309.6
400uCi Planar	1490.3	1597.7	448.4	459.1	1033.4
Estimated activity	412.5	402.9	397.0	376.8	345.3
Distance to 400uCi	3.11%	0.72%	-0.74%	-5.80%	-13.68%
CCC	0.999	0.995	1.000	1.000	0.992

Presentation Number **0341A**
Poster Session 1a: Imaging Instrumentation and Methodology

Feasibility of Different Scatchard Approaches For Quantitative in vivo [¹¹C]Raclopride PET Imaging in Mice: Comparison with the True Equilibrium Approach

Kristina Fischer¹, **Andreas Schmid**¹, **Walter Ehrlichmann**², **Julia G. Mannheim**¹, **Florian C. Maier**¹, **Maren K. Koenig**¹, **Vesna Sossi**³, **Bernd J. Pichler**¹, ¹Laboratory for Preclinical Imaging and Imaging Technology of the Werner Siemens Foundation, University of Tuebingen, Tuebingen, Germany; ²Radiopharmacy, University of Tuebingen, Tuebingen, Germany; ³Physics and Astronomy, University of British Columbia, Vancouver, BC, Canada. Contact e-mail: kristina.fischer@med.uni-tuebingen.de

High resolution small animal PET has emerged as a valuable tool to study receptor expression in rodents. We investigated the relationship between specific activity (SA), tracer mass and receptor occupancy (OCC) for [¹¹C]raclopride (RAC) imaging in mice and performed test-retest experiments to determine reproducibility and reliability. Moreover, we used the multiple ligand concentration receptor assay (MLCRA) and the bolus plus constant infusion protocol (BI) to determine receptor density Bmax and apparent affinity Kdapp at true equilibrium. We further aimed to identify a bolus analysis approach that meets the requirements of technical simplicity and greatest possible accuracy. Therefore we tested the following bolus scatchard approaches towards its applicability in mice by comparing it to the equilibrium approach (EA): the MLCRA at transient and peak equilibrium (PEA) and the single injection approach at partial saturation (PSA). We further used the PSA to identify the affect of DA release on Bmax and Kdapp 15min and 4h after 3mg/kg d-amphetamine (AMPH). 12 mice underwent a total of 3-4 scans with decreasing SA and an additional high SA scan for the test retest experiments, either using the bolus injection approach (n=6) or the BI protocol (n=7). Injected activity was 458±33 MBq/kg and SA ranged from 190-1.8 GBq/μmol, corresponding to injected masses of 0.02-0.5μg. For the PSA an injected mass of 4.5μg was chosen. The average Bmax was 22±4 pmol/ml and Kdapp was 11±3 pmol/ml using the BI protocol, which was defined as gold standard. If the tracer was injected by bolus, estimation of bound (B) tracer concentration by the Ratio method and B/F using the Logan graphical approach was found to agree best with the EA (Bmax=23±5; Kdapp=10±2) (p>0.05). Higher values were obtained using the PEA (Bmax=46±5; Kdapp=23±2 pmol/ml) and the PSA (Bmax=35±8; Kdapp=15±6 pmol/ml) (p<0.05). The receptor occupancy curves showed that an injected tracer mass of 2 μg/kg yielded approximately 10%OCC with corresponding SA values of 1973 Ci/mmol. Reproducibility was found to be 8% and reliability 53% using the Logan graphical analysis. 15min after AMPH challenge we found a 100% increase in Kdapp with no change in Bmax, while 4h after AMPH both Kdapp and Bmax revealed unchanged, although Bmax was expected to decrease due to receptor internalization. However further experiments are planed with more mice and different challenges. Our data showed that separate determination of Bmax and Kd in mice using in vivo PET is feasible; however tracer mass has to be taken into account.

Presentation Number **0342A**
Poster Session 1a: Imaging Instrumentation and Methodology

Evaluation of gastrointestinal drug absorption process after oral administration using positron emission tomography (PET) with 2- ^{18}F fluoro-2-deoxy-D-glucose (^{18}F FDG) and its rate limiting steps under anesthesia

Tadayuki Takashima¹, Makoto Kataoka², Yumiko Katayama¹, Tomotaka Shingaki³, Yilong Cui¹, Yasuhiro Wada¹, Emi Hayashinaka¹, Shinji Yamashita², Yasuyoshi Watanabe¹, ¹RIKEN Center for Molecular Imaging Science, Kobe, Japan; ²Faculty of Pharmaceutical Sciences, Setsunan University, Hirakata, Japan; ³ADME research Inc., Mino, Japan. Contact e-mail: ttakashima@riken.jp

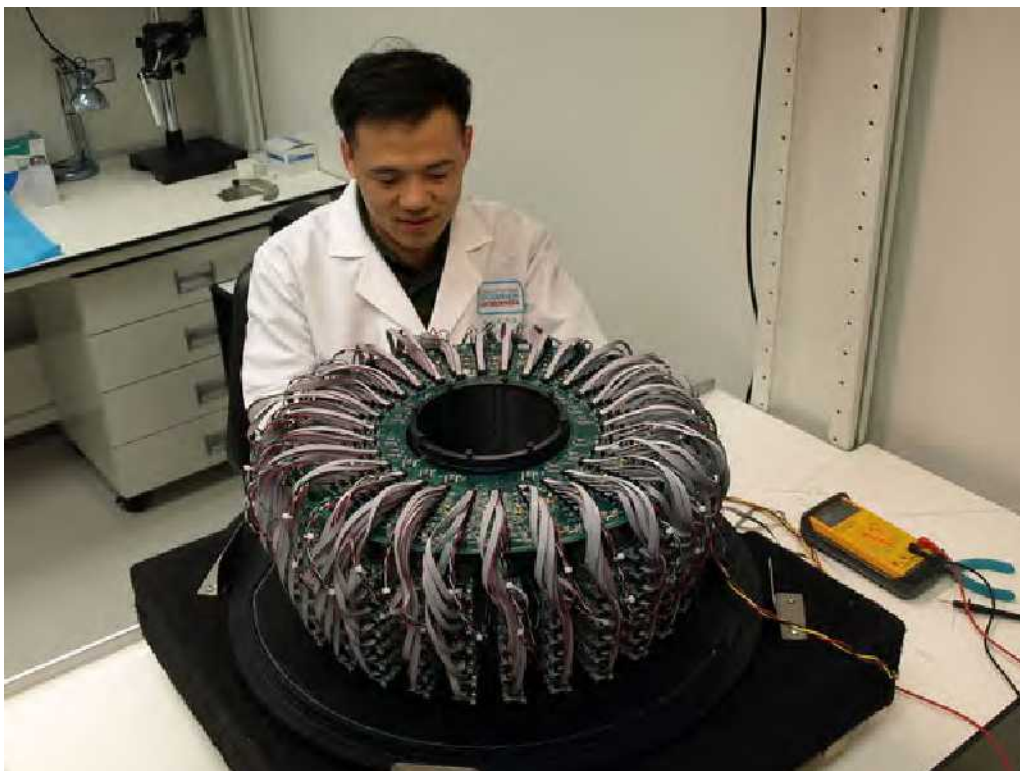
[Purpose] In order to develop potent drugs for oral use, information on their pharmacokinetic (PK) properties after oral administration are required. Also, oral absorption processes should be understood to verify their absorbability and to consider appropriate oral formulations. It has been desired the methods that enables to quantitatively determine the drug concentration in the gastrointestinal (GI) tract and fully elucidate the drug absorption behavior, since PK analysis based on the plasma profile in clinical studies provides only the overall parameter of absorption. In this study, PET image analysis was applied to investigate oral absorption processes by visualizing the time-course of drug disposition in the GI tract after oral administration. The rate limiting steps of drug absorption in anesthetized rats were also determined by the PET analysis. [Method] A quantitative PET study with ^{18}F FDG was done in conscious and anesthetized rats with 1.5% isoflurane inhalation or propofol continuous IV infusion (20 mg/h/kg). After oral administration of ^{18}F FDG, a 90-minute PET scan was performed as well as continuous blood sampling, and then the disposition of radioactivity in each part of GI tract was calculated. The radiometabolite analysis of ^{18}F FDG in the intestine, blood and urine were performed by TLC-autoradiography. The mechanism of intestinal absorption of ^{18}F FDG was also investigated using *in situ* closed loop method. [Results and Discussion] PET study showed that after oral administration of ^{18}F FDG, radioactivity was rapidly passed through the stomach, periodically migrated along to the intestinal tract, and then gradually disappeared from the intestinal tract in conscious rats. During its transit, the radioactivity, supposed to be absorbed to the systemic circulation, appeared in the blood and then in the urinary bladder. In contrast, the radioactivity in the stomach strongly remained and its transit to the intestine was significantly slower under anesthesia. Blood PK analysis also showed slower T_{max} in the anesthetized rats. These results suggest that the GI absorption in the anesthetized rats is rate limited by the gastric emptying. The metabolite analysis showed that radioactivity in intestinal mucosal tissues, blood and urine were mainly derived from parent ^{18}F FDG. Moreover, *in situ* loop studies showed the high FDG permeability to intestinal membrane that mediated mainly by GLUTs. In conclusion, we demonstrated the high potency of PET imaging technique to elucidate the GI absorption behavior *in vivo* after oral administration.

Presentation Number **0343A**
Poster Session 1a: Imaging Instrumentation and Methodology

Development of a lower-cost animal PET-CT with 1.25-mm LYSO detectors and 11.6-cm axial Field of View

Wai-Hoi Wong, *Experimental Diagnostic Imaging, University of Texas M.D. Anderson Cancer Center, Houston, TX, USA. Contact e-mail: gwong@mdanderson.org*

OBJECTIVE: This paper presents the design and engineering of a lower-cost, large axial-field micro PET-CT. The system has been assembled and being tested. **SYSTEM DESIGN:** The PET has 30420 LYSO detectors (180 blocks) in a 16.5-cm detector ring and a large 11.6-cm axial field for high detection sensitivity. The average detector size is 1.25-mm transaxial x 1.4-mm axial x 10-mm deep. The 30240 crystals are precisely glued together into a solid crystal ring consisting 78 detector rings and 390 detectors/ring, with a 90% volumetric packing fraction. This solid crystal ring with 30420 crystals are decoded by only 210 PMT (19-mm round PMT) using our PMT-Quadrant-Sharing scheme, with each PMT coupling to 169 crystals. The 180 position-decoding detector blocks were produced by an efficient slab-sandwich-slice method that incorporates mirror film of different sizes and shapes between crystals for position-decoding. This detector design and production engineering allow very high resolution to be achieved with large low-cost round PMT. The front-end electronics use our digital HYPER crystal-decoding electronic design (High-Yield-Pileup-Event-Recovery). The electronics can process 25 million random "singles"/sec with a 10% loss. The system coincidence-timing window is 3-ns. The preliminary timing resolution is 700-800 ps, despite using non-time-of-flight PMT and very narrow crystals. The electronics has an online-baseline correction and automatic PMT-gain control using LED for stabilizing detector decoding and minimizing the effects of room temperature variation. The CT section is a cone-beam CT using a flat panel detector with 43-micron pitch and 80KVp (0.5 mA) x-ray generator. Monte Carlo simulations using GEANT (GATE) were preformed. The projected reconstructed image resolution using 2-D filtered backprojection is 1.2 mm and 1.6 mm at the center and 2.5 cm off center, respectively. With resolution-recovery reconstruction, resolution less than 1.0 mm can be achieved at the center. The absolute sensitivity is estimated to be 7.3% for a point source at the center of the PET for a 300-750 KeV window.



Presentation Number **0344A**

Poster Session 2a: Imaging Instrumentation and Methodology

TeraTomo project: a fully 3D GPU based reconstruction code for exploiting the imaging capability of the NanoPET™/CT system

Milán Magdics¹, László Szirmay-Kalos¹, Ákos Szlavecz¹, Gábor Hesz¹, Balázs Benyó¹, Áron Cserkaszkó², Judit Lantos², Szabolcs Czifrus², Dávid Légrády², András Wirth^{3,2}, Béla Kári^{3,4}, Tamás Bükki⁴, Gergely Patay⁴, Dávid Völgyes⁴, Péter Major⁴, Gabor Nemeth⁴, Balázs Domonkos⁴, ¹Control Engineering and Information Technology, Budapest University of Technology and Economics, Budapest, Hungary; ²Nuclear Techniques, Budapest University of Technology and Economics, Budapest, Hungary; ³Clinics of Radiology and Oncotherapy, Semmelweis University of Budapest, Budapest, Hungary; ⁴R&D, Mediso Ltd., Budapest, Hungary. Contact e-mail: gumi@inf.elte.hu

Introduction: The TeraTomo project is dedicated to the development of a fully 3D iterative reconstruction code for multi-modality (PET/SPECT/CT) imaging. The NanoPET™/CT is an ultra-high resolution, high sensitivity pre-clinical PET-CT system using the most advanced, commercially available components, i.e. an 18 cm diameter PET-detector polygon with 12 detector modules, each consisting of 81×39 LYSO crystals (1.12mm×1.12 mm×13 mm) tightly packed and coupled to two 256-channel PS-PMTs. The imaging capability of this system can only be exploited by using a fully 3D reconstruction algorithm modeling the detector response, positron range, and gamma attenuation and scatter effects. Methods: Recently we have been employing the EM/OSEM scheme for reconstruction of PET images; we have decided to focus on the on-the-fly calculation of the system matrix elements as precisely as possible taking the following physical effects into account: 3D geometry, detector response, positron-range effect, attenuation, and scatter in the medium. The reconstruction algorithms have been tailored to the massively parallel GPU platform (using CUDA technology), enabling to execute the code in parallel on multiple graphics cards. The reconstruction algorithm employs Monte Carlo (MC) techniques for sampling line of responses (LOR) and voxels in forward- and back-projection steps. Results: We have applied GATE simulated mathematical phantoms to verify the 3D reconstruction code and real measured data in order to demonstrate the achievable imaging capability of NanoPET™/CT system. Reconstruction results of phantom simulations and measurements will be presented. Significant improvement in resolution, SNR and image contrast is achieved comparing to 2D reconstruction methods. Due to the multi-GPU architecture, the run time of the fully 3D reconstruction software decreases into the acceptable range.

Presentation Number **0345A**

Poster Session 2a: Imaging Instrumentation and Methodology

Performance Characteristics of a Small Animal PET Scanner Based on Continuous LYSO Crystals

Laura Moliner Martinez¹, Antonio Soriano Asensi¹, Abel Orero¹, Filomeno Sanchez Martinez¹, Carlos Correcher Salvador², Antonio J. Gonzalez Martinez², Jose M. Benlloch¹, ¹Nuclear, Atomic, Molecular, IFIC, Valencia, Spain; ²ONCOVISION (GEM-Imaging Group), Valencia, Spain. Contact e-mail: moliner@ific.uv.es

Positron emission tomography (PET) dedicated to imaging of small laboratory animals has been developed rapidly in recent years and has showed up as an essential technique in biomedical research. With the increasing number of animal models of human diseases, e.g., transgenic mice, PET represents an essential non-invasive tool to assess biological functions [1-4]. We have developed a small animal PET scanner based on continuous LYSO crystals coupled to Position Sensitive Photomultiplier Tubes (PSPMTs). The scanner consists of eight compact modules forming an octagon with a scanner aperture of 105 mm while an axial Field of View (FoV) of 40 mm and a transaxial FoV of 80 mm diameter is achieved. By measuring the width of light distribution collected in the PSPMT we are able to determine Depth of Interaction (DOI), thus making it possible the proper identification of LORs with large incidence angles. Its most innovative feature is that the scintillating crystals are continuous (non-pixelated) with a special truncated pyramid shape in order to minimize compression of the image at the borders. Moreover, our design drastically simplifies the requirements of the data acquisition electronics. Since only 5 signals are read from each detector module (4 for the spatial X and Y information, and an additional one for the depth of interaction information), a single ADC electronic card is used to read two opposite modules (each ADC card supports 10 signals). Therefore, the eight modules are read-out only with 4 ADCs. The integration time of each ADC card may vary from 100 to 400 ns. In order to fully determine its performances, recently issued NEMA protocol [5], specifically developed for small animal PET scanners, has been followed. The PET spatial resolution, sensitivity, scatter fraction, image quality, and counting rate performances have been measured and compared with those obtained with currently commercially available small animal PET scanners. [1] M. E. Phelps "PET: the merging of biology and imaging into molecular imaging," J. Nucl. Med. 41 661-81 (2000). [2] S.R. Cherry et al, "MicroPET: a high resolution PET scanner for imaging small animals," IEEE Trans. Nucl. Sci. 44, 1161-1166 (1997). [3] R. Myers, "The biological application of small animal PET imaging," Nucl. Med. Biol. 28, 585-593 (2001). [4] A.F. Chatziioannou, "Molecular imaging of small animals with dedicated PET tomographs," Eur. J. Nucl. Med. 29, 98-114 (2002). [5] Performance Measurements of Small Animal Positron Emission Tomographs, NEMA Standards Publication NU 4-2008.

Presentation Number **0346A**

Poster Session 2a: Imaging Instrumentation and Methodology

Comparison of 99mTc-TRODAT SPECT and 18F-AV-133 PET Imaging in Healthy Controls and Parkinson's Disease Patients

Chia-Ju Hsieh¹, **Kun-Ju Lin**^{1,2}, **Ing-Tsung Hsiao**^{1,2}, **Wey-Yil Lin**³, **Yi-Hsin Weng**³, **Chin-Song Lu**³, **Mei-Ping Kung**⁴, **Daniel M. Skovronsky**⁵, **Tzu-Chen Yen**^{1,2}, ¹*Medical Imaging and Radiological Sciences, Chang Gung University, Tao-Yuan, Taiwan;* ²*Molecular Imaging Center and Nuclear Medicine, Chang Gung University and Memorial Hospital, Taoyuan, Taiwan;* ³*Neurology, Chang Gung Memorial Hospital, Taoyuan, Taiwan;* ⁴*Radiology, University of Pennsylvania, PA, PA, USA;* ⁵*Avid Radiopharmaceuticals, PA, PA, USA. Contact e-mail: funnybobo@gmail.com*

Introduction: 18F-AV-133 is a novel PET radiotracer of vesicular monoamine transporter type 2 (VMAT2) imaging that was proposed to detect monoaminergic terminal reduction in Parkinson's disease (PD) patients. The aim of this study is to compare neural images with 18F-AV-133 to dopamine transporter tracers - 99mTc-TRODAT in same subjects. **Methods:** Fourteen subjects (3 healthy control and 9 PD subjects) were recruited for 99mTc-TRODAT SPECT, 18F-AV-133 PET, and MRI within two weeks. The SPECT images were performed at 4h post-injection for 1h, and PET images were performed at 90min post-injection for 10 min. Region of interest (ROI) analysis were performed in all PET and SPECT images with co-registered MRI. ROI of occipital cortex (OCC), caudate, and putamen were manually defined by two well trained nuclear medicine physicians. The uptake ratios (UR) to OCC were determined for comparison. The nonparametric Mann-Whitney U test was used to evaluate the ability of differentiating control from PD subjects in both image modalities. The correlation between quantitative parameters of image studies, and clinical characteristics (Hoehn and Yahr stage and clinical laterality index) were examined. All statistical analyses were performed using SPSS 15.0. **Results:** As expected, The UR of caudate and putamen correlate well between two image modalities ($r = 0.72$, $P < 0.001$). 18F-AV-133 PET and 99mTc-TRODAT SPECT UR of PD subjects were significant different from those of the controls ($p < 0.05$). 18F-AV-133 PET UR demonstrated similar correlation to PD clinical stage as compared to 99mTc-TRODAT SPECT ($r=0.669$ vs. $r=0.633$). Of noted, the clinical laterality index correlate better to putamen UR asymmetry of 18F-AV-133 than 99mTc-TRODAT ($r=0.90$ vs. $r=0.74$). **Conclusion:** 18F-AV-133 PET can differentiate control from PD as good as 99mTc-TRODAT SPECT in a shorter time frame (100 min vs. 5h). Moreover, the quantitative analysis showed better correlation of 18F-AV-133 PET to clinical characteristics than 99mTc-TRODAT SPECT. In this regards, 18F-AV-133 PET is promising for clinical use of detecting monoaminergic terminal reduction in PD patients.

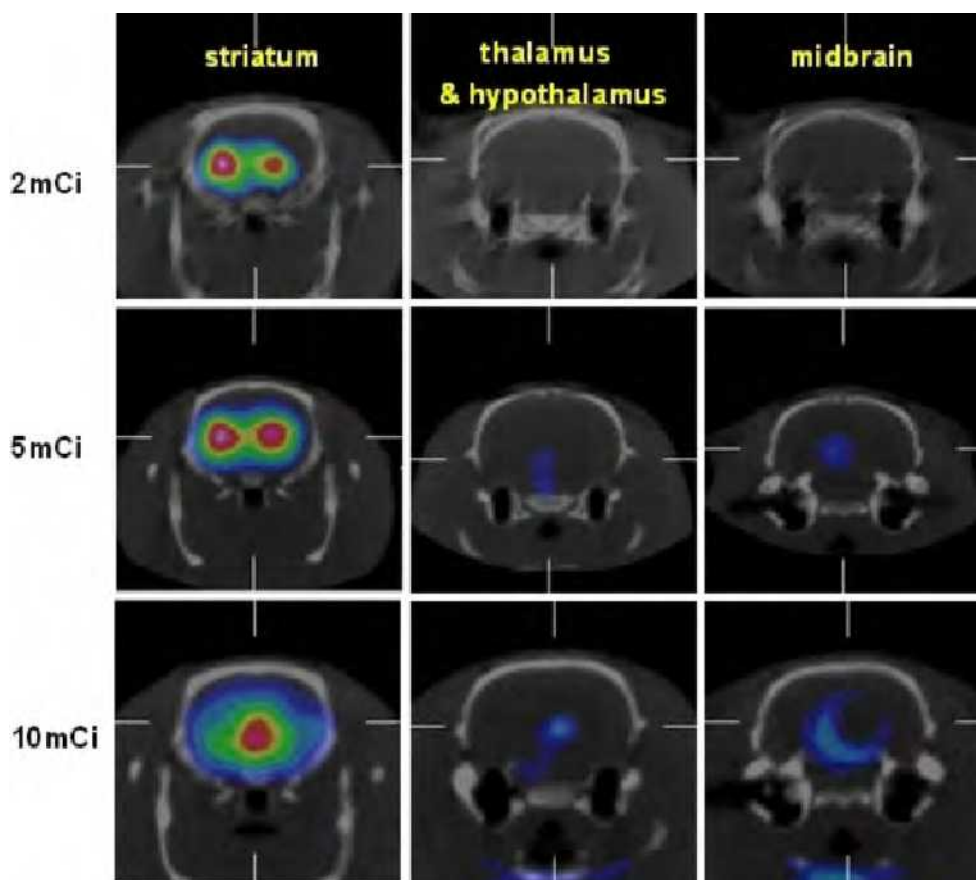
Presentation Number **0347A**

Poster Session 2a: Imaging Instrumentation and Methodology

Evaluating Adequate Dose of Iodine-123-Epidopride for Dopamine D2/D3 Receptors microSPECT Imaging in Rat Brain

Yung-Ruei Huang, Shih-Ying Lee, Jun-ming Shih, Chia-Chieh Chen, Wu-Jyh Lin, Isotope Application, Institute of Nuclear Energy Research, Taoyuan County, Taiwan. Contact e-mail: yuanruei@iner.gov.tw

Background: Epidopride is a compound derived from benzamide with high affinity for dopamine D2/D3 receptor. The affinity of Iodine-123 form of epidopride is in picomolar range that makes it useful for microSPECT imaging of the D2/D3 receptors in brain, including the low density extrastriatal receptors. Our aim of the study was to evaluate an adequate dose of I-123-epidopride for microSPECT imaging in rat brain. Method(s): Radiochemical purities of I-123-epidopride were analyzed by Radio-Thin-Layer Chromatography (chloroform/methanol, 9:1, v/v). microSPECT images were acquired by a dual-head gamma camera with multi-pinhole collimators from normal rat brains after 30min distribution of I-123-epidopride (2mCi, 5mCi and 10mCi, respectively), which all of the results were reconstructed and fused with CT imaging. Result(s): Radiochemical purity of I-123-epidopride was >95% as determined by radio-TLC. In microSPECT study of I-123-epidopride, images with there different doses all presented relative strong radioactivities in striatum, respectively. But by using 10mCi, images of two striatums merged. Meanwhile, the microSPECT study also performed radioactivities in extrastriatal regions (thalamus, hypothalamus and midbrain) except the images with injection of 2mCi I-123-epidopride. Conclusion: In the report, we acquired microSPECT images with different doses of I-123-epidopride in rat brain. Images obtained with 2mCi only performed the radioactivity in striatum, not in extrastriatal regions. Meanwhile, there showed radioactivities in striatum and extrastriatal regions by intravenous injection of 5mCi and 10mCi I-123-epidopride. But 10mCi was too strong that made images of two striatums merged, which could not represent the actual condition. Overall, the results showed I-123-epidopride from our procedure was available for tracing the dopamine D2/D3 receptors, and we considered the adequate dose of I-123-epidopride for microSPECT imaging in rat brain was about 5 mCi.



Presentation Number **0348A**

Poster Session 2a: Imaging Instrumentation and Methodology

Performance evaluation of a novel dual head SPECT scanner for small animal imaging

Abel Orero^{1,2}, Antonio Soriano Asensi¹, Montserrat Carles¹, Laura Moliner Martinez¹, Carlos Correcher Salvador², Vicente Carrilero², Michael Seimetz², Filomeno Sanchez Martinez¹, Jose M. Benlloch¹, ¹Instituto de Fisica Corpuscular, Consejo Superior de Investigaciones Cientificas, Valencia, Spain; ²ONCOVISION, Valencia, Spain. Contact e-mail: aorero@ific.uv.es

Recent advances in molecular imaging have motivated a growing interest in in-vivo imaging techniques to study biochemical processes at molecular level for pharmacology, genetics and pathologic research. Positron Emission Tomography (PET) and Single Photon Emission Computed Tomography (SPECT) have represented a valuable approach in such a field [1]. The advent of multimodality PET/CT and SPECT/CT scanners facilitates the fusion of functional and morphological information, thus improving the accuracy in the interpretation of experimental results. Molecular imaging of small animals requires the development of imaging systems with improved spatial resolution with respect to those obtained with human body scanners. Moreover, for SPECT systems using pinhole collimators, the choice of the optimum configuration must be selected as a trade off between the spatial resolution, desired Field of View (FoV) and the sensitivity of the system. Therefore, an accurate characterization of SPECT performance in each possible configuration is essential in order to optimize the design and main parameters of the SPECT scanner. In this work we present the design and performance evaluation of a dual head SPECT scanner, conceived to be a part of a PET/SPECT/CT multimodality system for small animal molecular imaging. Two highly precise actuators permit a fine adjust of the radial position of the SPECT detector heads mounted on a rotating gantry. Therefore, a selectable axial and transaxial FoV as big as 100 mm can be achieved with the SPECT scanner design presented in this work. Each detector head consists of a single monolithic CsI(Na) scintillating crystal coupled to a flat-panel type multianode Position Sensitive Photomultiplier Tube (PSPMT), together with their associated electronic [2], [3]. The system energy resolution is about 13% at 140 keV with spatial resolution smaller than 1 mm. In order to improve the sensitivity of the SPECT scanner, a multipinhole collimator was also designed. The comparison of SPECT scanner performances with pinhole and multipinhole collimator is also presented in this work. Reference [1] A. Del Guerra, N. Belcari "State-of-the-art of PET SPECT and CT for small animal imaging" Nuclear Instruments and Methods in Physics Research A 583 (2007) 119-124. [2] F. Sanchez, et al. "Design and tests of a portable mini gamma camera" Medical Physics, Vol 31 (6), 1384-1397. (June 2004). [3] F. Sanchez, et al. "Performance tests of two portable gamma cameras for medical applications" Medical Physics, Vol 33 (11), 4210-4220. (November 2006).

Presentation Number **0349A**

Poster Session 2a: Imaging Instrumentation and Methodology

Quantification of Skeletal Blood Flow and Fluoride Metabolism in Rodents

Ryan Tomlinson^{1,2}, Matthew J. Silva^{1,2}, **Koresh I. Shoghi**³, ¹Biomedical Engineering, Washington University in St. Louis, St. Louis, MO, USA; ²Orthopaedic Surgery, Washington University in St. Louis, St. Louis, MO, USA; ³Radiology, Washington University in St. Louis, St. Louis, MO, USA. Contact e-mail: shoghik@wustl.edu

Angiogenesis is an important factor in osteogenesis, although its role in osteogenesis induced by mechanical loading is unknown. Previous studies have evaluated vascular outcomes with postmortem techniques, but no *in vivo* studies have been performed. Here, we present techniques for evaluating these outcomes in bone after loading-induced osteogenesis. Lamellar or woven bone formation was induced by forelimb compression in adult rats using established methods. Right limbs were loaded, and left limbs were used as controls. PET scans were obtained 0, 1, 3, 7, and 14 days after loading and analyzed at the mid-forelimb. Each rat was imaged with ¹⁵O water to evaluate blood flow, followed by ¹⁸F fluoride to determine fluoride kinetics and provide anatomical landmarks. Cylindrical 3D ROIs were created with 1.5 times the diameter of the bone and 1/3 the length of the bone on ¹⁸F images and overlaid onto ¹⁵O images. The kinetics of ¹⁵O was modeled using a one-compartment, two-parameter model. A two-compartment, three-parameter model was used to model the kinetics of ¹⁸F near the site of bone formation. Both models include a parameter to represent the underlying vascular fraction. Image-derived input functions (IDIF) were created from the left ventricle using cylindrical 3D ROIs (r=0.5mm, l=1mm). The IDIF was convolved with a Gaussian function to account for the diffusion of the injected bolus. A stochastic search algorithm was implemented to provide initial parameter values in conjunction with a Levenberg-Marquardt optimization algorithm. 100 trial fits were conducted for each PET scan. The five fits with the lowest residuals were averaged to find the final solution. The results show significant differences in vascular outcomes between these two osteogenic scenarios. Specifically, there is an immediate and persistent 25-35% increase in flow rate to the limbs producing woven bone. Limbs producing lamellar bone show no increase in flow rate until a 15% increase on day 14. Additionally, there is decreased fluoride clearance (2-4%) on days 0 and 1, as well as increased incorporation of fluoride into bone at all time points (5-15%). All results were significant (p<0.05). The results from this *in vivo* method agree with the results of previous studies, confirming this technique is suitable for evaluating the vascular response and mineral kinetics of osteogenic mechanical loading.

Presentation Number **0350A**

Poster Session 2a: Imaging Instrumentation and Methodology

High-Resolution CT Imaging of Single Breast Cancer Microcalcifications In Vivo

Kazumasa Inoue^{1,3}, Fangbing Liu¹, Jack Hoppin⁴, Elaine P. Lunsford¹, Christian Lackas⁴, Jacob Hesterman³, Robert Lenkinski², Hirofumi Fujii⁵, John V. Frangioni^{1,2}, ¹Department of Medicine, Beth Israel Deaconess Medical Center, Boston, MA, USA; ²Department of Radiology, Beth Israel Deaconess Medical Center, Boston, MA, USA; ³Bioscan, Inc., Washington, DC, USA; ⁴inviCRO, LLC, Boston, MA, USA; ⁵Functional Imaging Division, National Cancer Center Hospital East, Kashiwa, Japan. Contact e-mail: kinoue@bidmc.harvard.edu

Background: Microcalcification, a hallmark of the breast cancer, is a key diagnostic marker on mammograms. Benign breast calcifications are mainly composed of calcium oxalate, and malignant breast calcifications (microcalcifications) are typically composed of hydroxyapatite (HA) deposited in specific patterns. HA deposits range in size from 100 μm single crystals to clusters that can be several centimeters in diameter. We recently described the first robust animal model of breast cancer microcalcification. In this study, we hypothesized that high-resolution computed tomography (CT) could potentially detect the genesis of a single microcalcification in vivo and quantify its growth over time. Materials and Methods: We systematically optimized acquisition and reconstruction parameters using a commercial CT scanner (NanoSPECT/CT, Bioscan, Washington, DC). Two ray-tracing image reconstruction algorithms were tested, a voxel-driven "fast" cone beam algorithm (FCBA), and a detector-driven "exact" cone beam algorithm (ECBA). The acquisition parameters, including CT detector pixel size, exposure time, voxel size on the reconstructed image, and reconstruction parameters, were optimized for single microcalcification in vivo imaging. We also quantified calcification volume over time on optimized parameters ($n = 3$). Results: We selected a detector pixel size of 48 μm , an exposure time of 3000 ms/projection, the ECBA with sampling number of 6 and a reconstruction voxel size of 50 μm in order to achieve the highest possible resolution and image quality for in vivo imaging. By optimizing acquisition and reconstruction parameters, we were able to achieve a resolution of 104 μm full-width at half maximum (FWHM). At an optimal detector sampling frequency, ECBA provided a 28 μm (21%) FWHM improvement in resolution over FCBA. In vivo, we were able to image a single 300 μm by 100 μm hydroxyapatite crystal. We were also able to quantify calcification volume over time on high-resolution CT. Conclusion: In a syngeneic rat model of breast cancer, we were able to detect the genesis of a single microcalcification in vivo and follow its growth longitudinally over several weeks. Taken together, this study provides an in vivo "gold standard" for the development of calcification-specific contrast agents and a model system for studying the mechanism of breast cancer microcalcification.

Presentation Number **0351A**

Poster Session 2a: Imaging Instrumentation and Methodology

Evaluation of Solid- State Photomultiplier Arrays for PET Block Detectors with Finely Pixelated Crystals

Emilie Roncali¹, Jeffrey P. Schmall¹, Yibao Wu¹, Christopher Stapels², James Christian², Kanai Shah², Simon R. Cherry², ¹Dept. of Biomedical Engineering, UC Davis, Davis, CA, USA; ²Radiation Monitoring Devices Inc., Watertown, MA, USA. Contact e-mail: eroncali@ucdavis.edu

The need for high sensitivity and high spatial resolution imaging has initiated numerous developments in combined positron emission tomography (PET) and magnetic resonance imaging. Because of their insensitivity to magnetic fields, solid-state photomultipliers (SSPMs) constitute a promising alternative to photomultiplier tubes for this application. In addition, the next generation of preclinical PET scanners may include depth of interaction information via dual-ended readout of scintillators and have a reduced ring diameter for improved sensitivity, which requires compact detectors. SSPMs have dimensions comparable to that of avalanche photodiodes (APDs) but their operating conditions are much less challenging. SSPMs are therefore a good candidate for small animal PET scanners. SSPMs are not mature photodetectors yet, although important progress in manufacturing has been made. The technology still suffers from fabrication challenges, especially in terms of sensitive area, which is generally 10 mm² whereas the sensitive area of APDs goes up to ~ 400 mm². To overcome this limitation, development of SSPMs arrays has led to commercially available devices with a sensitive area greater than 100 mm². However, SSPMs arrays introduce manufacturing and operational issues. Firstly, an ideal photodetector would present uniform detection performances, and this becomes challenging as more individual SSPM elements are combined within an array. Secondly, working with arrays raises practical issues such as a larger number of output signals, and non-uniformity between the elements that complicates the data acquisition and analysis. This indicates that SSPM array performance should be thoroughly characterized before the devices are integrated in PET detectors. Several 4 x 4 SSPMs arrays, with individual element sizes of 1.5 x 1.5 mm², developed by Radiation Monitoring Devices Inc. (Watertown, MA), were studied. Our investigation focused on the comparison of the different SSPMs in the array. Flood histograms from various LSO arrays (pixels ranged from 1.5 x 1.5 x 20 mm³ to 0.5 x 0.5 x 10 mm³) were acquired through a position sensitive readout. Signals from each single element were compared to corresponding signals extracted from flood histograms. Current - voltage characteristics were measured for all individual elements. The breakdown voltage was found to be very uniform (variation of 0.5 %) and the overall uniformity is promising for the integration of these SSPM arrays in PET block detectors.

Presentation Number **0352A**

Poster Session 2a: Imaging Instrumentation and Methodology

Performance evaluation of NanoSPECT/CT by imaging phantom and small animal

Tsutomu Zeniya, Hidekazu Kawashima, Noboru Teramoto, Kazuhiro Koshino, Hajime Fukuda, Yoshiko Hashikawa, Akihide Yamamoto, Yoshiyuki Hirano, Yoshinori Miyake, Hidehiro Iida, Department of Investigative Radiology, Advanced Medical Engineering Center, National Cerebral and Cardiovascular Center Research Institute, Suita, Japan. Contact e-mail: zeniya@ri.ncvc.go.jp

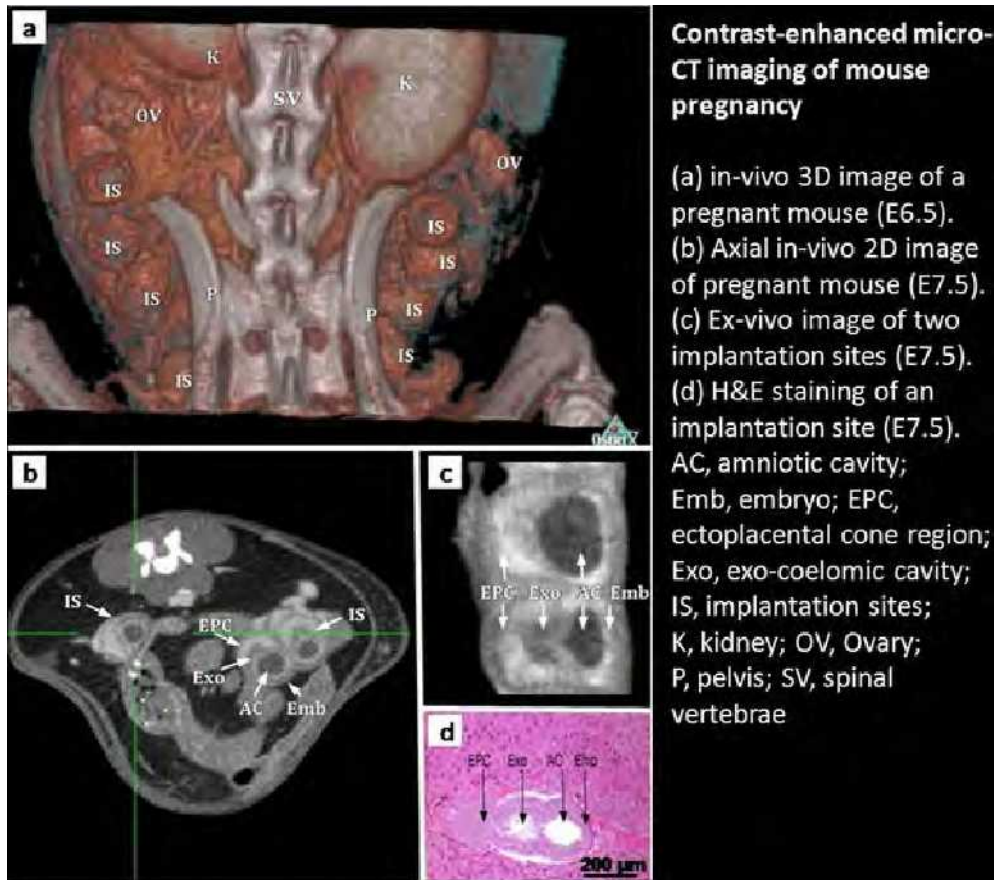
Objectives: NanoSPECT/CT system (Bioscan) with four detectors and multi-pinhole collimators was recently installed. This system images physiological functions of small animals with high spatial resolution and high sensitivity. We also expect quantitative measurement in this system. This study was aimed at evaluating the performance of this system for small animal imaging. **Methods:** We have three kinds of collimators with 9 pinholes per detector: APT3 (ϕ 1.0mm) and APT11 (ϕ 2.0mm) for mouse; APT5 (ϕ 1.5 mm) for rat. For APT3 the spatial resolution of the reconstructed image was measured using Tc-99m filled mini-Jaszczak phantom with a series of columns ranging in diameter from 0.7 to 1.2 mm. The uniformity and the linearity between radioactivity and image counts in the reconstructed image are required for quantitative measurement. The uniformities for three radioisotopes (Tc-99m, I-123, Tl-201) and three collimators were evaluated using cylindrical phantoms with 23-mm or 46-mm diameters. For APT3 the linearity of count was evaluated using a series of syringes filled with Tc-99m solution ranging in radioactivity from 0.7 to 34.5 MBq. Three mice studies were performed using APT3: cerebral perfusion study with I-123-IMP; myocardial perfusion study with Tl-201; whole body bone scan with Tc-99m-HMDP. Anesthetized mice were fixed on the bed dedicated to NanoSPECT/CT. Mice fixed on the bed were scanned using MRI scanner (Signa 3T, GE) before SPECT/CT scan. SPECT scan was performed following CT scan. MRI, CT and SPECT images were automatically co-registered. **Results:** The spatial resolution was 0.8 mm. The relationship between radioactivity(x) and image counts(y) was plotted. The linearity was good in the range from 0.7 to 34.5 MBq because $y=1.01x$ was obtained and correlation coefficient was 0.99. Clear images were obtained in the cerebral perfusion, myocardial perfusion and bone scan studies. SPECT, CT and MR images were successfully co-registered. However, in some case, the images were not uniform and had geometrical artifacts, when cylindrical phantoms were imaged. The ring-like artifact appeared, when the 23-mm diameter phantom was imaged using APT3. Especially severe spiral artifact appeared, when the 46-mm diameter phantom was imaged using APT5. **Conclusions:** We confirmed that NanoSPECT/CT has high spatial resolution and good linearity of image count required for quantitative measurement, and provides clear images for a variety of small animal imaging studies. However, further investigation will be needed for artifacts in the images of cylindrical phantoms.

Presentation Number **0353A**
 Poster Session 2a: Imaging Instrumentation and Methodology

Contrast-enhanced micro-CT as a tool for in-vivo and ex-vivo imaging of embryo implantation and placentation in the mouse

Tal Raz¹, **Inbal E. Biton**², **Nava Dekel**¹, **Michal Neeman**¹, ¹*Department of Biological Regulation, Weizmann Institute of Science, Rehovot, Israel;* ²*Department of Veterinary Resources, Weizmann Institute of Science, Rehovot, Israel. Contact e-mail: talrazg@gmail.com*

Successful embryo implantation followed by the development of a functional placenta are crucial in mammalian pregnancy. Although there are obvious differences between human and mouse implantation and placentation, the use of mouse models has significantly advanced our understanding of the normal path as well as the pathological disorders of these biological processes. Micro-computed tomography (micro-CT) offers high-resolution volumetric imaging of the inner anatomy of living small animals; however, the contrast between the different soft tissues is inherently poor. Our objective was to develop techniques for in-vivo and ex-vivo micro-CT imaging of embryo implantation and placentation in the mouse. Female wild type ICR mice on different pregnancy stages (E6.5 - E18.5; vaginal plug = E0.5) were scanned in the TomoScape® 30S Duo micro-CT. For in-vivo scan, anesthetized animals were injected with Iohexol (Omnipaque®) through an IV catheter placed in the tail-vein; animals were scanned immediately after Iohexol administration, and again after 5 min. For ex-vivo scan, an additional dose of Iohexol was administered, the ovarian and uterine arteries were surgically ligated, and the reproductive tract was removed; after short fixation (5 min) in 4% formaldehyde, the reproductive tract was scanned. In-vivo and ex-vivo micro-CT imaging after Iohexol administration resulted in high spatial 3-dimensional resolutions of the implantation sites and the placentas. We found that an in-vivo scan 5 min after Iohexol administration provided a better image than a scan immediately after Iohexol injection. Implantation sites were detected as early as E6.5, and different structures in the pregnancy progression, such as the ectoplacental cone region, the amniotic cavity, the exo-coelomic cavity, the embryo, and later the placenta, could be detected with high resolution. Validation was done by H&E histology. We concluded that contrast-enhanced micro-CT can be a valuable research tool for in-vivo and ex-vivo imaging of embryo implantation and placenta development in the mouse.



Presentation Number **0354A**

Poster Session 2a: Imaging Instrumentation and Methodology

Improved spatial resolution of the X'tal cube: a 3D crystal array covered with MPPCs

Naoko Inadama¹, **Mitsuhashi Takayuki**^{2,1}, **Hideo Murayama**¹, **Fumihiko Nishikido**¹, **Eiji Yoshida**¹, **Mikio Suga**^{2,1}, **Mitsuo Watanabe**³, **Taiga Yamaya**¹, ¹*Molecular Imaging Center, National Institute of Radiological Sciences, Chiba-shi, Japan;* ²*the Graduate School of Science and Technology, Chiba university, Chiba-shi, Japan;* ³*Hamamatsu Photonics K.K., Hamamatsu-shi, Japan.* Contact e-mail: inadama@nirs.go.jp

The “crystal (X’tal) cube” is our new PET detector, which is composed of a segmented scintillation crystal block covered with Multi-Pixel Photon Counters (MPPCs). For a proof-of-concept, in the last year, we developed the first prototype detector having 3 mm isotropic resolution with 3 mm × 3 mm aperture MPPCs. In this paper, we succeeded to obtain 2 mm isotropic detector resolution (i.e., each crystal whose volume was reduced to 8/27 was identified) with the same MPPCs. In PET, it is important to get information of radiation detected location in PET detectors 3-dimensionally to achieve both high spatial resolution and high sensitivity. A photomultiplier tube (PMT) which generally used as a photo-detector of a PET detector provides the 2-dimensional information and additional idea is always required to obtain depth of interaction (DOI) information. Fig. 1a) shows a typical structure of X’tal cube in which MPPCs are used instead of PMTs. Unlike a PMT, a MPPC is small enough and will not interfere in radiation detection even if it is set on the path of the radiation. In X’tal cube, MPPCs are then set on the all six surfaces of the segmented crystal block and detect scintillation photons in 3-dimension. Since always some MPPCs are placed near originated position of scintillation photons, the photons can be detected before attenuation and sufficient amount of detected photons creates clear responses, which allow fine segmentation of the crystal block for high spatial resolution. In this study, we made the X’tal cube composed of a cubic crystal block 18.0 mm on a side and 96 MPPCs (Hamamatsu Photonics K.K., Japan, sensitive area: 3 mm × 3 mm, micro cell: 50 μm), 16 MPPCs on each surface of the crystal block. The crystal block consists of a 9 × 9 × 9 array of cubic Lu_{2x}Gd_{2(1-x)}SiO₅ (LGSO, x = 0.9) crystals 2 mm on a side. Fig.1b) shows the results of crystal identification performance. Each peak is crystal response. All responses were discriminated sufficiently and that means the X’tal cube achieved 2 mm isotropic spatial resolution.

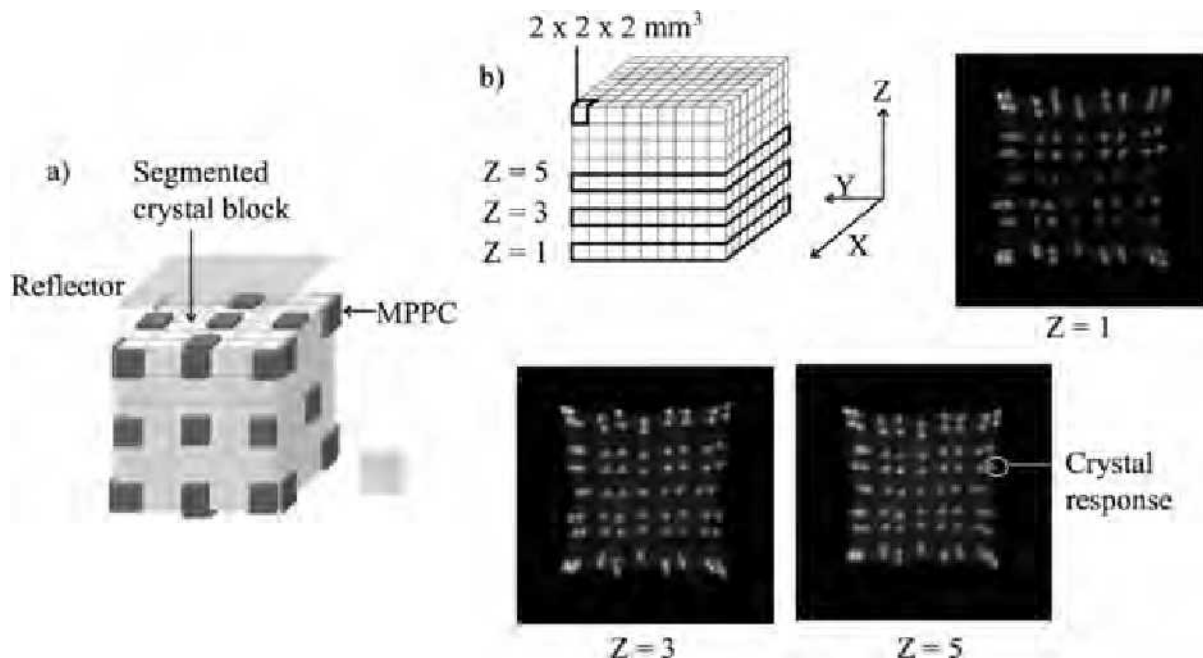


Fig. 1. a) Structure of X'tal cube. b) Results of crystal identification performance of the X'tal cube composed of cubic LGSO crystals 2 mm on a side.

Presentation Number **0355A**

Poster Session 2a: Imaging Instrumentation and Methodology

3D Molecular Simulation of Fmiso Dynamic PET

Wang Po¹, Catherine Kelly², Sir Michael Brady¹, ¹University of Oxford, Oxford, United Kingdom; ²Gray Institute for Radiation Oncology and Biology, Oxford, United Kingdom. Contact e-mail: wangpo@robots.ox.ac.uk

Abstract: This paper proposes a 3D in vivo fmiso delivery simulation framework. A spatiotemporal model of oxygen and fmiso in vivo delivery process was developed by augmenting conventional compartmental models with spatial diffusion. The model takes 3D microscope vessel images as input and simulates oxygen and fmiso distributions through time. Fmiso time activity curves (TAC) have been produced based on the simulation results and are found to be consistent with TACs observed in real PET imaging. We propose that this framework could be employed to predict dynamic PET TACs in the development of new tracers. Introduction: TACs in dynamic PET imaging are clinically useful to infer cell functional status in regions of interest. Since the resolution in current PET imaging is ca. 1 mm³, conventional compartmental models assume spatial independence in TAC modelling. Focussing on fmiso, a clinically used PET tracer, we developed our model at micron scale and considered inter-voxel dependence. The integration of models at different scales could help us better understand the biochemical information conveyed in dynamic PET TACs. Method: Compartmental models were used to model oxygen and fmiso distribution. The spatial diffusion effects of diffusible oxygen and fmiso were considered and the distribution of oxygen and fmiso were described using partial differential equations. The simulation was conducted on spatial grids on a 256 x 256 x 60 volume. The PDEs were converted to ODEs by assuming diffusion effect constant during a short period. A Runge Kutta method with adaptive step size control was then utilized to solve the resulting ODEs. GPU technology was used to accelerate the simulation 6 times faster than normal CPU computation. Results: We used model parameters published in the relevant literatures and found that the simulated diffusible oxygen concentration is in the physiological range of 2.322 and 39.994 mmHg (assuming plasma oxygen 40 mmHg) . The fmiso binding kinetics were calculated from a reaction model as a function of diffusible oxygen concentration proposed by [1] and was found between 0.0057 and 0.0599 min⁻¹, which agrees with the value proposed in related research [1]. The average total fmiso concentration was calculated through simulation and plotted against time. It has been found that TAC produced by molecular simulation is similar with that calculated based on compartmental models. [1] Casciari, J. et al. Medical Physics, 22, 1127.

Presentation Number **0356A**

Poster Session 2a: Imaging Instrumentation and Methodology

Progress in TOF-PET Scintillation Detectors Based on Silicon Photomultipliers

Dennis R. Schaart¹, **Stefan Seifert**¹, **Herman van Dam**¹, **Ruud Vinke**², **Peter Dendooven**², **Herbert Löhner**², **Frederik J. Beekman**¹,
¹Applied Sciences, Delft University of Technology, Delft, Netherlands; ²KVI, University of Groningen, Groningen, Netherlands. Contact e-mail: d.r.schaart@tudelft.nl

The use of time-of-flight (TOF) information in positron emission tomography (PET) enables significant improvement in image noise properties and, therefore, lesion detection. Silicon photomultipliers (SiPMs) are solid-state photosensors that have several advantages over photomultiplier tubes (PMTs). SiPMs are small, essentially transparent to 511 keV gamma rays, and insensitive to magnetic fields. This enables novel detector designs aimed at e.g. compactness, high resolution, depth-of-interaction (DOI) correction, and MRI-compatibility. We are studying the timing performance of SiPMs in combination with LYSO:Ce and LaBr₃:Ce scintillators. Using 3 mm × 3 mm × 5 mm LaBr₃:Ce(5%) crystals coupled to 3 mm × 3 mm Hamamatsu MPPC-S10362-33-050C SiPMs, a coincidence resolving time (CRT) of ~100 ps FWHM has previously been demonstrated. Recently, experiments using 3 mm × 3 mm × 5 mm LYSO:Ce crystals coupled to the same SiPMs were conducted, yielding a CRT of ~160 ps. In all cases, pulse height spectra showed well-resolved full-energy peaks. These results obtained with small crystals indicate that SiPM-based PET detectors may perform at least as good as detectors based on conventional PMTs. In larger crystals the variation of the scintillation photon transit time with the position of interaction will affect the timing resolution. To study this effect, experiments on prototype detectors consisting of 18 mm × 16 mm × h monolithic LaBr₃:Ce(5%) crystals coupled to a Hamamatsu S11064-050P(X) 4 × 4 array of SiPMs are being performed. In preliminary measurements a detector timing resolution of ~225 ps FWHM was obtained for a crystal height of $h = 10$ mm, but further improvement is expected from optimization of the measurement setup. Crystals with heights of $h = 15$ mm and $h = 20$ mm will also be studied. Furthermore, methods to correct for the photon transit time, based on the independently measured position of interaction, are under investigation. At the conference, the status of this work in progress will be presented in more detail.

Presentation Number **0357A**

Poster Session 2a: Imaging Instrumentation and Methodology

Performance Evaluation of a MultiModality SPECT/CT Scanner

Julia G. Mannheim, Martin S. Judenhofer, Thomas Schlichthärle, Bernd J. Pichler, *Departement of Radiology, Laboratory for Preclinical Imaging and Imaging Technology of the Werner Siemens-Foundation, Eberhard Karls University Tuebingen, Tuebingen, Germany. Contact e-mail: julia.mannheim@med.uni-tuebingen.de*

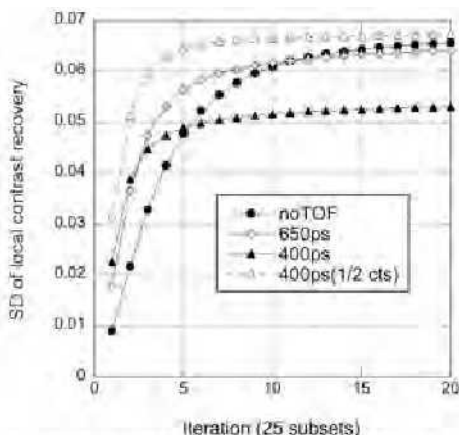
This study concentrates on the performance evaluation of the Siemens Inveon MultiModality SPECT/CT scanner using phantom measurements. For the CT, several parameters like the binning factor and exposure time as well as different acquisition modes, like continuous rotation or use of sum and average frames, were investigated. The image quality was evaluated based on measurements with a cylindrical phantom, equipped with six tubes of materials with different densities. SNR was calculated for the materials acquired with different binning factors (4, 2, 1) as well as varying exposure times (10-100ms). The continuous rotation mode was investigated using a binning factor of 4 with exposure times between 10ms and 500ms. Sum and average frame modes were evaluated using exposure times of 10ms, 15ms, 25ms & 50ms with total frames of 1, 2, 4, 6, 8 & 10. As expected, the SNR is increased with higher binning and exposure times until over-exposition occurs. The continuous rotation mode showed slightly degraded quality and increased the acquisition time by 33%. The use of sum frames showed a slight reduction of ring artifacts compared to an equivalent one-exposure scan, which, however, suffered from a reduced SNR. The CT provides over all the option for short exposition times which are required for gating applications. For the SPECT evaluation, phantom measurements were performed with a multi pinhole-collimator with 5 holes (\varnothing 1mm) and radius of rotations (ROR) of 30, 35 & 40mm. For determining the quantification accuracy three different sized cylindrical phantoms (small, medium and large) were filled with ~ 4MBq of Tc-99m. Data were calibrated to the smallest phantom for each ROR. Deviations from the true to the measured activity were determined. They increase with the size of the phantom from 34% to 38% for the 30mm ROR, from 37% to 38% for the 35mm ROR, and from 10% to 14% for the 40mm ROR. These effects are partially due to attenuation but may also result from the field of view being smaller than the imaged object. To determine the partial volume effect, a small sphere with a 3.2 mm inner diameter located in a cylindrical phantom was filled with an 8:1 contrast-ratio of Tc-99m. The recovery was 82% for a ROR of 30mm degrading to 69% and 62% for 35 and 40mm ROR. Ongoing tests concentrate on a comparison between one and five pin-hole collimators and image quality for different isotopes. Even though the normalization and calibration of SPECT data seems to be an unsolved problem this small animal SPECT/CT system yields an overall good performance and image quality.

Presentation Number **0358A**
 Poster Session 2a: Imaging Instrumentation and Methodology

Impact of TOF PET on variability in lesion uptake estimation

Suleman Surti¹, Amy E. Perkins², Enrico Clemente³, Margaret E. Daube-Witherspoon¹, Joel Karp¹, ¹Radiology, University of Pennsylvania, Philadelphia, PA, USA; ²Philips Healthcare, Philadelphia, PA, USA; ³MEDISIP-IBBT, University of Ghent, Ghent, Belgium. Contact e-mail: surti@mail.med.upenn.edu

Previous phantom studies showed that improved timing resolution in TOF PET leads to a reduced variability in the contrast estimation for hot spheres in a uniform cylinder. Compared to a phantom study that is performed in a controlled environment, a clinical study will be affected by variable amounts of scatter and attenuation, as well as the impact of local activity distribution near the lesion. In this study we aim to evaluate the variability in estimation of lesion uptake for TOF and Non-TOF PET in a patient background for two different local regions (liver and lung). For our study we use a prototype TOF PET scanner (LaBr₃ crystals) with a system timing resolution of 375ps. Three normal volunteer patients were imaged after the injection of ¹⁸F-FDG. Separately, we imaged 1cm spheres in air at various positions in the scanner FOV corresponding to lung and liver locations. Sphere data were appropriately attenuated and merged with patient data to produce fused list data files. All list files were reconstructed with full corrections and with or without the TOF kernel. Lesion contrast was measured by drawing ROIs in the patient and fused images. Preliminary results show that with TOF information we achieve higher contrast, and reduced variability in the lesion contrast over multiple locations within the lung or liver when compared to Non-TOF reconstruction (at similar noise). While the phantom study uses multiple sphere replicates to estimate the variability in sphere contrast, this is not practical in a patient study. Instead, we are generating multiple, bootstrap list files for the patient and fused list data sets in order to estimate the variability in lesion uptake estimation in a patient for each lesion location. Variability in lesion contrast estimation will be estimated over the multiple bootstrap copies for each lesion location in the liver or the lung, as well as over multiple lesion locations, to better understand the impact of TOF PET on the precision of lesion estimation in a clinical environment.



Standard deviation over replicate spheres of contrast recovery as a function of iteration for hot spheres for TOF reconstructions of 400 ps and 650 ps data and non-TOF reconstruction from 54 Mct studies; the result from the 27 Mcts study for the 400 ps timing resolution is also shown (open triangles). The data were measured with 1-cm diameter spheres placed in a 35-cm diameter water-filled cylinder. This shows that, for phantom data, TOF has less variability in the measured contrast.



Transverse image of a normal patient study acquired on the LaPET scanner (left) and reconstructed after insertion of 4 spheres in the liver (right).

Presentation Number **0326B**
Poster Session 3a: Imaging Instrumentation and Methodology

Validation of the “Octamouse” Holder for Simultaneous microPET [¹⁸F]fallypride Recordings from Eight Mice

Axel Rominger, Erik Mille, Guido Boening, Björn Wängler, Peter Bartenstein, Paul Cumming, Dept. of Nuclear Medicine, University of Munich, Munich, Germany. Contact e-mail: axel.rominger@med.uni-muenchen.de

Introduction: Data collection in preclinical microPET studies has been hindered by the small number of recordings typically obtained for a single radiosynthesis. Therefore, we tested procedures for obtaining eight simultaneous brain microPET recordings from mice using a Plexiglas anaesthesia distributor (Octamouse), with the dopamine D2/3 ligand [¹⁸F]fallypride serving as a test substance for brain receptor imaging. Methods: The effect of scatter-correction on the microPET recordings was first evaluated in phantom studies in which sources of different radioactivity concentration were placed within the chambers of the Octamouse holder. Next, potential effects of mass on the [¹⁸F]fallypride binding potential (BPND) in striatum were tested in groups of mice receiving [¹⁸F]fallypride at two different specific activities (140 and 50 GBq/μmol), with and without scatter-correction. Finally, the relationship between BPND and injected dose of [¹⁸F]fallypride (3.5 - 17 MBq/mouse) was tested. Results: Scatter-correction improved the contrast between sources and air-space within the Octamouse phantom. The magnitude of [¹⁸F]fallypride BPND in mouse striatum was invariant across the tested range of specific activities, and scatter-correction increased BPND by a mean of 6%; covariances of the inter- and intraoperator variability of BPND were 10%. There was a positive correlation between radiochemical dose and BPND with (R2 = 0.53) and without (R2 = 0.63) scatter-correction, which was driven by increasing area under the %ID curve in striatum. Conclusions: The quantitation of emission sources placed within Octamouse is linear over a wide range of source activities. In striatum of living mice, the magnitude of [¹⁸F]fallypride BPND was highly reproducible between operators, and was constant over a three-fold range of specific activities, indicating lack of significant occupancy. Scatter-correction improved quantitation, but did not entirely correct for the dependence of BPND on injected dose, which was deemed to arise due to effects propagating from detector deadtime when the total radiochemical dose in the field of view exceeded 50 MBq. Given this consideration, we were still able to quantify [¹⁸F]fallypride BPND in 16 mice from a single radiosynthesis, an economy which should be generalizable to brain studies of diverse radioligands.

Presentation Number **0327B**

Poster Session 3a: Imaging Instrumentation and Methodology

Performance characteristics of the Inveon micro-CT scanner in small animal imaging

Magdy M. Khalil, Willy Gsell, Melvyn Myers, *Biological imaging Centre, Medical research Council, Clinical Sciences Centre, Faculty of Medicine, Hammersmith Campus, London, United Kingdom. Contact e-mail: magdy.khalil@imperial.ac.uk*

Micro-Computed Tomography (μ CT) has become an indispensable tool for morphological in vivo as well as ex vivo preclinical imaging. Its role is not only confined for attenuation correction in addition to anatomical localization but its benefit has been extended to include CT angiography. Inveon is a tri-modality (PET/SPECT/CT, Siemens Medical Solutions) imaging system designed to image rodents such as mice and rats. The objective of this study was to characterize the performance of the CT component in terms of image noise, uniformity, spatial resolution as well as image quality. Effects of beam hardening correction, ring/noise reduction and number of projections were also examined. Furthermore, the system was tested in a number of studies including in vivo and ex vivo samples. Methods: A clinically relevant water phantom was used for the measurement of image noise and uniformity. Spatial resolution was measured by calculating the modulation transfer function (MTF) using the slanted edge method. Image noise was estimated under several conditions of beam amperage (50-500 μ A) and x-ray CT voltages (40-80 kVp) at an exposure time of 200 ms. The CT number for different tissues was measured using a manufacturer-supplied phantom of different densities (0,50,250 and 750 mg/cc). System linearity was assessed using a wide range of iodine concentrations (Ultravist 370) ranging from 5 to 70 mg/cc. To further assess the system performance, a variety of studies were acquired on animal models including contrast CT agents as well as ex vivo samples. Results: No significant change was noticed for image uniformity across the whole range of tube currents at a voltage of 80 kVp (On average, 25 ± 0.41 HU). However, a significant reduction of the noise was noticed when the current increased from 50 to 500 μ A and also with gradual increment of the tube voltage. The best noise measure was obtained at 500 μ A and 80 kVp (40.4 ± 1.8 HU). Noise or ring reduction option showed a significant reduction of the noise from 90 HU to 55 HU when using 40 kVp at 500 μ A. The relationship between noise and the current was shown to be dominated by the photon statistics with less contribution from the system noise. The MTF calculated showed a resolution of 198 μ m at 10% modulation. A good linear correlation was found between the CT number and iodine concentrations and data were fitted using linear regression with high statistical significance. Conclusion: The system has good CT performance measures for uniformity, spatial resolution, image noise and linearity versus wide range of contrast concentrations. Clinical results showed the capability of the system in acquiring anatomical images with high spatial resolution. One of the shortcomings is disability to perform 4D CT which might be solved by the manufacture improving the overall system features. An additional engineering work has been requested to further enhance the spatial and temporal resolution of the scanner.

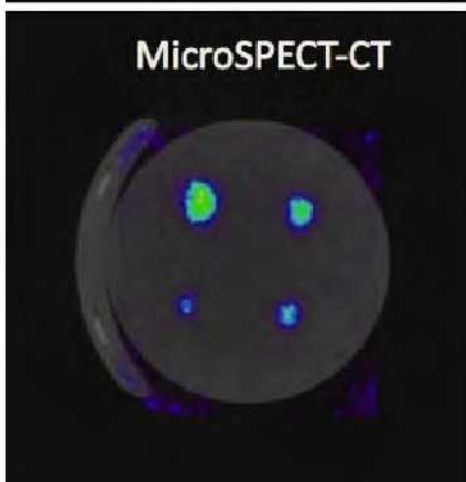
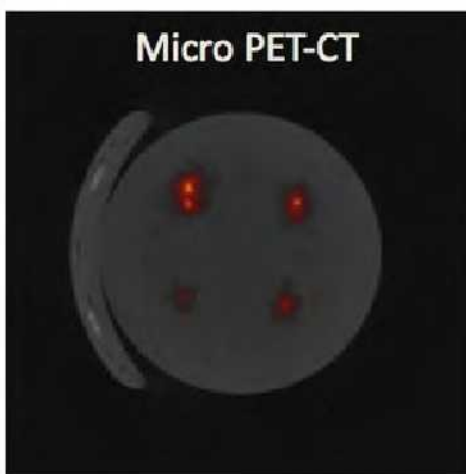
Presentation Number **0328B**

Poster Session 3a: Imaging Instrumentation and Methodology

Imaging Y-90 with microSPECT and microSPECT

Stefaan Vandenberghe¹, **Steven Deleye**¹, **Jan De Beenhouwer**¹, **Larry van Elmbt**³, **Steven G. Staelens**¹, **Bieke Lambert**², **Stephan Walrand**³, ¹MEDISIP-IBITECH, Ugent-IBBT, Gent, Belgium; ²Department of nuclear medicine, Ugent, gent, Belgium; ³Department of nuclear medicine, UCL, Brussels, Belgium. Contact e-mail: Stefaan.Vandenberghe@ugent.be

INTRODUCTION: Y-90 is one of the most popular isotopes for radionuclide therapy. PET imaging is only possible using the low fraction (32 per million decays) of the annihilation photons generated after internal pair production. SPECT imaging can be performed based on the indirect x-rays generated after bremsstrahlung in the object. Here we investigate the performance of both imaging methods on microSPECT and microPET. **METHODS:** A line source, a phantom with 4 hotspots (3.9 -7.8mm diameter) and a small animal NEMA phantom filled with Y-90 were scanned on the U-SPECT II and the labPET. Additionally a countrate measurement from 0-50 mCi was performed on the labPET to determine the suitable range for imaging. Monte Carlo simulations with Gate enabled to determine the average distance of production of x-rays and to explain the spatial resolution obtained in microSPECT. Images were reconstructed with MLEM (20 iterations). **RESULTS:** All spheres were visible on both modalities, the smallest sphere has about 50 % contrast loss compared to the biggest sphere. The spatial resolution on microPET and microSPECT is respectively 1.9 and 2 mm. The spatial resolution on the U-SPECT was close to the results predicted by Monte Carlo simulations (1.9 mm). The NEMA phantom did not give acceptable image quality on both PET and SPECT. MicroSPECT has higher sensitivity but suffers more from contamination than microPET. Countrate performance on the PET scanner shows that imaging should be performed with activities below 10 mCi to limit the amount of randoms. The intrinsic activity of LYSO adds a significant contamination background. **CONCLUSION:** Both microPET and microSPECT imaging can be used for imaging Y-90 concentrated in small areas and spatial resolution is relatively good for both imaging modalities. Therefore it may be used for imaging the dose delivered by Y-90 DOTATOC radionuclide therapy. MicroSPECT has higher sensitivity than microPET but has more contamination from high energies.



Presentation Number **0329B**
 Poster Session 3a: Imaging Instrumentation and Methodology

Bone Structure Changes in Hypertensive Rats using MicroCT Imaging

Bryan J. Hermansson¹, Andrew J. Burghardt¹, Youngho Seo¹, Sharmila Majumdar¹, Kathleen M. Brennan², Grant T. Gullberg^{2,1},
¹Radiology, University of California San Francisco, San Francisco, CA, USA; ²Radiotracer Development & Imaging Technology, Lawrence Berkeley National Laboratory, Berkeley, CA, USA. Contact e-mail: bryanh@radiology.ucsf.edu

Purpose: The goal of this project is to quantify the effects of hypertension on bone quality and structure using microCT imaging techniques. **Materials and Methods:** For this study, we used 8 spontaneous hypertensive rats (SHR), born with high blood pressure and 4 age-matched Wistar Kyoto (WKY) rats as controls. Ages ranged from 6 to 18 months. The left tibia from each specimen was excised and imaged at the proximal metaphysis using a desktop microCT system (μ CT-40, Scano Medical) at 8 μ m- isotropic resolution. Trabecular and cortical regions of interest (ROI) were drawn semi-manually for each specimen, starting adjacent to the proximal growth plate and extending distally 2 mm. Trabecular and cortical morphological parameters were calculated from binary images created by applying a single grayscale. **Results:** Overall tibial trabecular bone structure was robust in SHR specimens, while cortical bone was compromised as compared with the WKY controls. As seen in Fig 1, the SHRs were found to have statistically significant greater bone volume/total volume (BV/TV), trabecular number (Tb.N), and lower trabecular spacing (Tb.Sp). In contrast they showed a significantly lower cortical thickness (Ct.Th) and tissue mineral density (Ct.TMD). These cortical and trabecular differences are visualized in Fig 2. **Conclusions:** Despite their poor cardiovascular health, SHRs were found to have trabecular bone structure normally associated with greater bone strength including greater BV/TV, Tb.N, and Connectivity Density (Conn.D). However, the higher trabecular bone volume was offset by cortical bone deficits, which likely resulted in altered load distribution and may lead to compromised bending strength. The decrease in the load-bearing cortex often results in an increase of trabeculae to compensate for the loss.

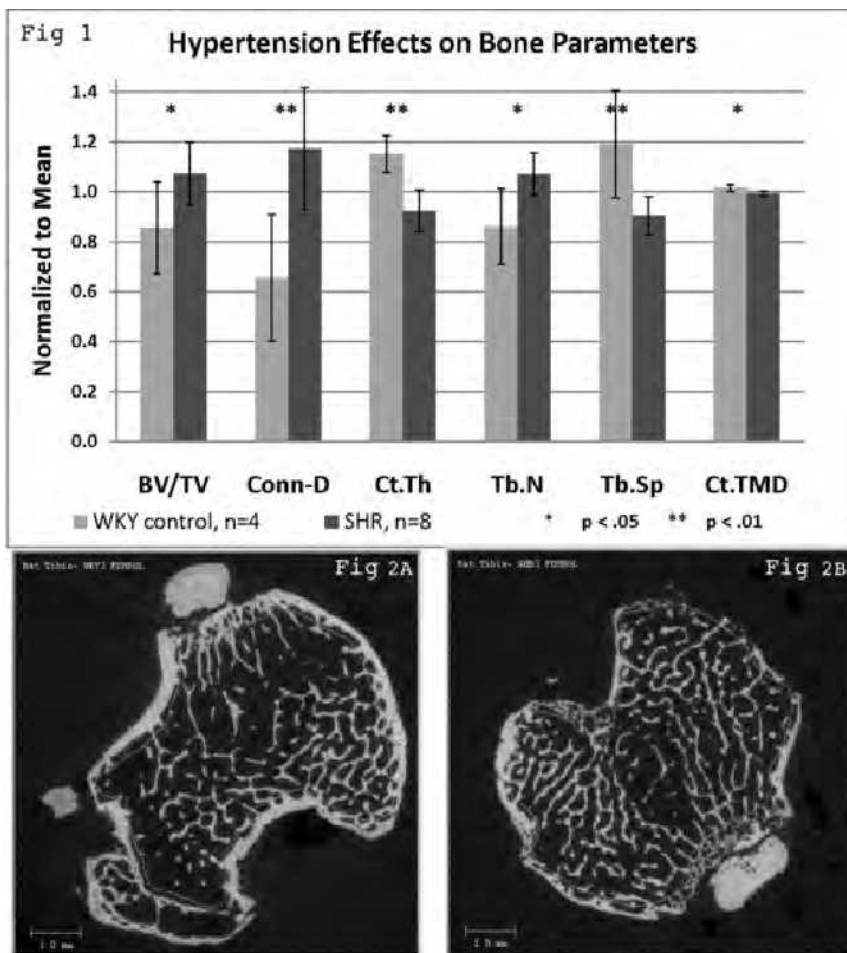


Fig 1: Bone parameter differences in hypertensive rats. Error bars show ± 1 StDev. Fig 2: Slice and age matched microCT images. 2A: WKY control, low Tb.N, high Ct.Th 2B: SHR, high Tb.N, low Ct.Th

Presentation Number **0330B**

Poster Session 3a: Imaging Instrumentation and Methodology

Imaging ^{125}I labelled nanoparticle distribution in Mice with PILATUS II

Graeme J. O'Keefe^{1,2}, David W. Pook², Vivien Lee³, Glenn Cartwright², Uwe Ackermann¹, F. T. Lee², Angela Rigopoulos², Diana Cao², Sylvia J. Gong¹, Bryn A. Sobott³, Roger P. Rassool³, Andrew M. Scott², ¹Centre For PET, Austin Health, Heidelberg, VIC, Australia; ²Ludwig Institute for Cancer Research, Melbourne, VIC, Australia; ³School of Physics, University of Melbourne, Melbourne, VIC, Australia. Contact e-mail: graeme.okeefe@petnm.unimelb.edu.au

Objectives Nano-engineered particles are an area of intense interest as a means of selective delivery of chemotherapy to tumours. These are created by depositing various layers of biodegradable polymers onto a silica core. They vary in size from 300-100 nm and their biodistribution properties as a function of physical characteristics such as size require investigation. By labelling nano-particles of interest with ^{125}I or ^{18}F , the biodistribution properties of the nano-particles can be explored to investigate their suitability as vectors for oncology treatment. ^{125}I has a dominant x-ray emission in the energy range 27 - 35 keV and is commonly used as a radioactive label in ex-vivo biodistribution studies in small animal models. ^{125}I based imaging lends itself readily to translation into human imaging and/or treatment using other isotopes such ^{131}I and ^{124}I . **Methods** The PILATUS detector is a single photon counting hybrid-pixel detector with pixels of size 172x172 μm and a silicon substrate thickness of 300 μm . A typical detector module is 8x5 cm and contains 100,000 pixels. The excellent spatial resolution of this detector, together with its compact design make it a suitable choice for a ^{125}I small animal imaging system. Preliminary measures are presented in which a PILATUS 100K module was used to image mice injected with ^{125}I labelled nano-particles with a radioactivity ranging from 12.5 μCi to 500 μCi to determine the in-vivo biodistribution of nano-particles in mouse. **Results** A case is presented which revealed the trapping of the nano-particles in the liver, this was subsequently confirmed with ^{18}F labelled nano-particles using a Philips Mosaic microPET scanner. Results revealed the trapping of the nano-particles in the liver and spleen during the first-pass and was conjectured to be due to the size of the nano-particle and aggregation effects. **Conclusions** The Imaging with PILATUS provided a real-time, non-invasive way to image for nano-particle distribution. In the case study presented, the observed focal uptake in liver / spleen that was identified in the ^{18}F -nano-particle study is conjectured from the ^{125}I -nano-particle study as being due to first-pass trapping within liver / spleen. As a result, before anti-body labelling strategies are adopted, nano-particle size and aggregation issues be addressed. Further developments are underway for the construction of a pin-hole based imaging system with a thicker Si substrate so as to allow high-sensitivity / high-resolution tomographic measurement of ^{125}I labels.

Presentation Number **0331B**
 Poster Session 3a: Imaging Instrumentation and Methodology

Micro-liter Order Blood Sampling System for Small Animal Molecular Imaging Using PET — Validation with Animal Study—

Nobuya Hashizume¹, Yuichi Kimura², Chie Seki², Hidekatsu Wakizaka², Takahiro Nishimoto¹, Keishi Kitamura¹, Iwao Kanno²,
¹Technology Research Laboratory, Shimadzu Corp., Kyoto, Japan; ²Molecular Imaging Center, National Institute of Radiological Sciences, Chiba, Japan. Contact e-mail: hasizume@shimadzu.co.jp

Introduction Quantitative molecular imaging using PET requires radioactivity concentrations in whole blood and plasma to estimate a behavior of an administered isotope labeled molecules in target tissues. However, a small size of rodent restricts an amount of blood sample to a few micro-liters, and a rapid change in a time activity curve requires a frequent sampling, every 5 sec. Therefore we designed Microfluidic Mouse Plasma Counting System (μ FmPC, patent pending) to overcome these issues. **Method** μ FmPC had following functions: a precise micro-liter ordered blood sampling (minimum 1 μ L blood sampling, 5 sec interval), maximally 33 blood samplings, centrifugation to separate plasma from blood, and radioactivity and volume measurements in whole blood and plasma. Fig.1 is the block diagram. Blood was sampled into an acrylic disc named CD-Well and in-house software was applied to calculate the radioactivity concentration. CD-Well had 36 U-shaped channels with a precise cross-section area (0.1 mm²), hydrophilic inside walls and a tapered inlet. The accurate volume was measured by the extracted region from the image acquired from an ordinary flatbed scanner, and a radioactivity was derived using an imaging plate (BAS-5000, Fujifilm Corp., Japan). An animal study was conducted using a rat. Fifty-MBq of ¹⁸F-FDG in 500 μ L was injected into the tail vein. A catheter (PE-10) was inserted into the femoral artery, and blood was dropped onto an inlet on CD-Well. Its volume was around 3 μ L for each. For validation, 100 μ L blood was also sampled manually and the radioactivity concentration was measured. **Result and Conclusion** Fig.2 shows time histories measured activity concentration. The bias of whole blood and plasma between manual blood sampling and μ FmPC were within 5 % and 20 %, respectively, and the time histories could be obtained. We concluded that μ FmPC had a potential to be useful for fully quantitative molecular imaging using rodent. This work was supported by Grant-in-Art for Scientific Research (B) (20390333) by JSP, Japan.

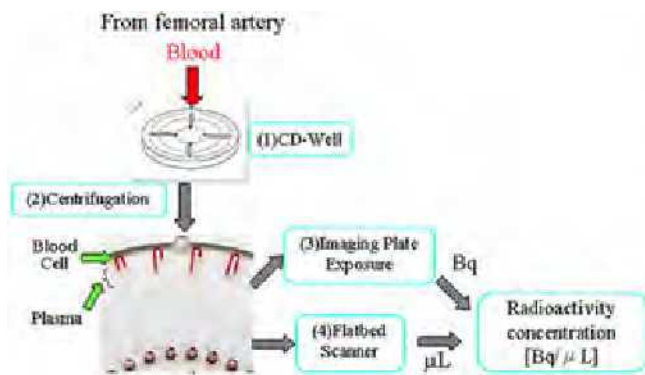


Fig 1 Block diagram of radioactivity measurement

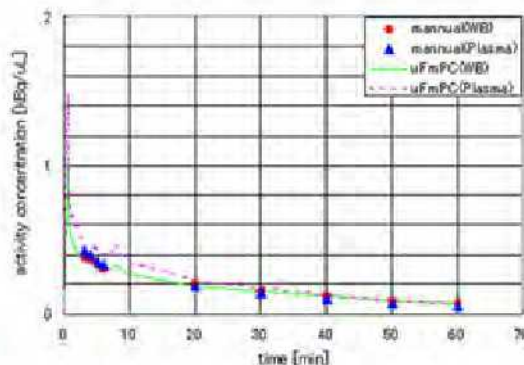


Fig 2 Radioactivity concentration of whole blood (WB) and plasma of the rat experiment

Presentation Number **0332B**

Poster Session 3a: Imaging Instrumentation and Methodology

Absolute quantitative assessment for micro-SPECT images of ^{188}Re -BMEDA-Liposome in a C26 murine colon carcinoma solid tumor model

Fan-Pin Tseng, Meei-Ling Jan, Shiang-Lin Hsu, Yu-Ching Ni, Ya-Jen Chang, Wen-Bin Lin, Te-Wei Lee, Institute of Nuclear Energy Research, Taiwan, Taiwan. Contact e-mail: ecyor@iner.gov.tw

Micro-SPECT/CT pre-clinical experiment is a powerful tool for quantifying the distribution of a radioactive compound in living animals. The conventional method of absolute quantification uses a known-activity source as reference, however the reference may cause unexpected crosstalk to the imaging results. In this study, multiple reference radiation sources were scanned to obtain a relation between activity concentrations and pixel values. After restoration being applied on tumor-bearing mice images, it substituted activity/pixel-value equation with recovered pixel value, finds the more accurate activity quantitation. Various activity concentrations of ^{188}Re (four groups of 1600, 800, 400, 200, 100 and 50 $\mu\text{Ci}/\text{cc}$.) were injected into well plates. The plates were the same distance apart. It were scanned by X-SPECT/CT (Gamma-Medica-Ideas Inc.) with high resolution parallel hole collimator at 0, 42, 60, and 72 h after injection. Twenty-seven BALB/c mice were subcutaneously inoculated with 2×10^5 tumor cells in the right hind flank, and then the ^{188}Re -BMEDA-labelled pegylated liposomes ($\sim 0.5\text{mCi}/0.2\text{cc}$) was administered to each mouse by intravenous injection. SPECT imaging was performed using high resolution parallel collimators at 1, 4, 24, 48, 72 h after injection ($n=2$). The other mice were sacrificed at selected times for bio-distribution. And the Lucy Richardson algorithm was used to recover the micro-SPECT mice images. After drawing the region of interest (ROI) on the tumor, activity/pixel-value equation was used to transform the correlation between real activity concentrations and the mean pixel value of ROI. Standardized uptake values (SUV) of tumor were respectively estimated from original and recovered images with activity/pixel-value equation and reference source. The results were compared with bio-distribution (5 mice for each time point). It is conducted that the absolute quantitative results with activity/pixel-value equation can provide better correlation of bio-distribution. The results are expected to benefit the analysis of pre-clinical animal experiments for drug development.

Presentation Number **0333B**
 Poster Session 3a: Imaging Instrumentation and Methodology

X-Ray tomography goes to nano and reveals glioma microvasculature

Cyril Petibois¹, **Yeukuang Hwu**², ¹University of Bordeaux, CNRS UMR 5248, Pessac, France; ²Academia Sinica, Institute of Physics, Nankang-Taipei, Taiwan. Contact e-mail: c.petibois@cbmn.u-bordeaux.fr

We demonstrate that X-Ray nano-tomography now allows a 50-nm spatial resolution imaging of brain vasculature in situ and thus opens the way to fundamental research on tumor angiogenesis. Intracranial implantation of U87Ctrl and U87IRE1dn cells developing solid and diffuse forms of gliomas, respectively, were used for short-term tumor development. X-Ray synchrotron radiation source was used to image brain vascular system using gold (diameter 25 nm) and BaSO₄ (diameter 500 nm) nanoparticles injected in vascular system to reveal both healthy and tumor blood micro-vasculature as well as diffusion properties of tumor leaky blood vessels. Solid and diffuse models of mice glioma could be identified down to tumor volumes as small as 1 mm³ and with all vasculature details. BaSO₄-NP provided sufficient X-Ray attenuation contrast for a quantitative analysis of tumor vasculature (number of capillaries and junctions, diameter and morphological aberrations of capillaries...). Au-NP allowed imaging diffusion space around tumor blood vessels, which was larger ($85 \pm 32 \mu\text{m}$, $n = 120$) in coopted blood vessels of diffuse tumors than in neoformed capillaries ($62 \pm 23 \mu\text{m}$, $n = 120$; $P < 0.01$) of solid tumors (see figure). This study has revealed that both solid and diffuse forms of glioma tumors may be investigated at early stage on tumor development, and with unprecedented spatial resolution on the tomographic image. Issuing the biocompatibility of NP used as contrast agent as well as the X-Ray dose to apply in brain, the next step for X-Ray nano-tomography is imaging tumor vasculature in vivo. Our results mark the advent of nanoscale biological X-Ray nano-tomography with Au-NP imaging agents.

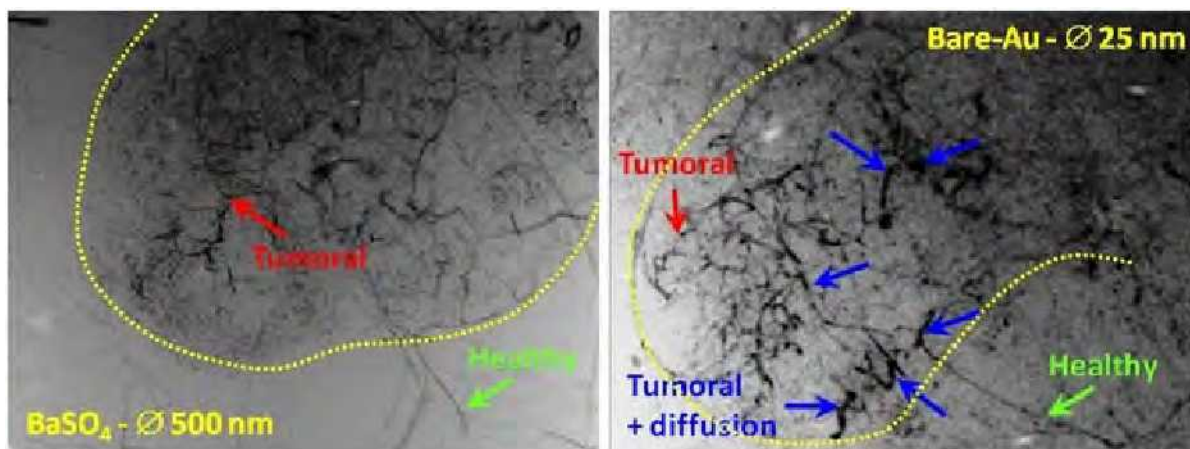


Figure: 3*2.5 mm images extracted from X-Ray nano-tomography analysis of solid forms of gliomas developed in mice brain at 50-nm spatial resolution. Tomographic image acquisition = 200 shots (1° angle change) of 100 msec at 7 KeV with X-Ray synchrotron radiation at Taiwan NSRRC (Hsinchu).

Presentation Number **0334B**

Poster Session 3a: Imaging Instrumentation and Methodology

Comparison of the Quantification Accuracy and the Partial Volume Effect of three state-of-the-art small animal PET Scanners

Julia G. Mannheim¹, Martin S. Judenhofer¹, Julia Tillmanns², Thomas Kull³, Sven N. Reske³, Detlef Stiller², Bernd J. Pichler¹,
¹Laboratory for Preclinical Imaging and Imaging Technology of the Werner Siemens-Foundation, University of Tuebingen, Tuebingen, Germany; ²Drug Discovery Support, Boehringer Ingelheim Pharma GmbH and Co. KG, Ingelheim, Germany; ³Department of Nuclear Medicine, University of Ulm, Ulm, Germany. Contact e-mail: julia.mannheim@med.uni-tuebingen.de

This study concentrates on quantification accuracy and partial volume effects (PVE) of three state-of-the-art small animal PET scanners, the microPET Focus 120, the Inveon Dedicated PET (DPET) and the Inveon MultiModality (MM) PET/CT. Quantification accuracy was determined using a homogeneous phantom which was measured over an activity range of 37MBq-0MBq. Transmission measurements (either by a rotating Co-57 source or by the CT) were done before, during and after the scan to determine an influence of the emission activity on the transmission scan. The PVE was investigated in dependence of the object size and location within the PET FOV. The NEMA micro hollow sphere phantom including four different sphere sizes was measured with a sphere to background ratio of 8:1 centered in the FOV. To determine the variation in PVE in dependence of the location, a single sphere (\varnothing 3.2mm), centered in a cylindrical phantom (8:1), was moved axially and transaxially through the FOV. All data were reconstructed using FBP with attenuation and scatter correction. The Inveon DPET showed smallest quantification deviations when including the transmission measurement acquired at 37 MBq for attenuation correction. Using a transmission scan with a lower emission activity the attenuation correction showed higher deviations. The same characteristics were seen for the Focus 120. This behavior is related to the scanner calibration procedure where the transmission scan is performed with a hot emission phantom. However, for the Inveon MM the emission activity did not influence the quantification results since the CT was used for attenuation correction. The recovery of the biggest sphere (\varnothing 7.86mm) was 69% for the Focus 120, 59% for the Inveon DPET and 61% for the Inveon MM. The smallest sphere (\varnothing 3.95mm) had a recovery of 42%, 30% and 29%, respectively. For the Focus 120 the recovery values changed by 13% from the center to the axial edge and 45% to the transaxial edge. For the DPET the recovery values changed by 18% and 9%, respectively. For the Inveon MM a misalignment between CT and PET FOV was observed which leads to wrong recovery values. Therefore, the recovery changed by 46% to the axial & 30% to the transaxial edge. The CT-based attenuation map seems to be much less biased from an emission activity in the FOV than a source-based transmission scan. However there was a misalignment between the PET and CT FOV observed which lead to inaccuracies in the attenuation correction. The Focus 120 showed slightly improved recovery values in axial direction due to a better spatial resolution.

Presentation Number **0335B**
Poster Session 3a: Imaging Instrumentation and Methodology

Design and implementation of a single chip FPGA-based coincidence unit for Positron Emission Mammography

Tzong-Dar Wu¹, Chung-Hung Chang², Meei-Ling Jan², ¹*Electrical Engineering, National Taiwan Ocean University, Keelung, Taiwan;*
²*Institute of Nuclear Energy Research, Atomic Energy Council, keelung, Taiwan. Contact e-mail: tdwu@mail.ntou.edu.tw*

The design of modern Positron Emission Mammography has been toward to modular, flexible, and compact. The use of Field Programmable Gate Arrays (FPGA) and Digital Signal Processing (DSP) provide enough reprogrammable flexibility and expandability in the evolution of modern PEM scanners. One of the core technologies suited for the FPGA implementation is the detection circuits for coincidence events. In this paper, a compact low dead-time coincidence system for the PEM camera is proposed and implemented on a single FPGA chip. The Pulse-AND logic method is chosen firstly to be realized in the coincidence detection because of its simplicity. The hardware simulation results show that the dead time of our system is less than 15 ns. However, the drawback of the Pulse-And method is sensitive to noise. A new hybrid coincidence approach combining Pulse-And logic and the traditional timing mark methods is also proposed and implemented on a single FPGA chip. The block diagram of the proposed system is shown in Fig.1. By using Pulse-And method for the rough coincidence detection and the timing-mark method for the final coincidence decision, the proposed hybrid system has the advantage of less noise sensitivity, and in the same time, reduce the complexity of the timing mark system. In our simulation, the 16 possible pair combinations of modules are derived from 4 detector modules in coincidence with 4 opposite modules. In order to test the capability of the single chip coincidence system, the possible pair combinations of modules are extended to 144, which derived from 12 detector modules in coincidence with 12 opposite modules. In order to reduce the circuit complexity in the 144 pair combination realization, the grouping and encoding techniques are used to divide the modules into different group before the detection of coincidence. Hardware simulations show that the resource of the FPGA can be reduced and the system dead time can be decreased.

Presentation Number **0336B**

Poster Session 3a: Imaging Instrumentation and Methodology

Kinetic modelling of 18F-fallypride binding to dopamine receptors - a comparison between beta microprobe and microPET

Geoff I. Warnock¹, Mohamed-Ali Bahri¹, David Goblet¹, Christian Lemaire¹, Fabrice Giacomelli¹, Xavier Langlois², Andre Luxen¹, Alain Plenevaux¹, ¹Cyclotron Research Center, University of Liege, Liege, Belgium; ²Johnson & Johnson Pharmaceutical Research & Development, A Division of Janssen Pharmaceutica N.V., Beerse, Belgium. Contact e-mail: gwarnock@ulg.ac.be

Beta microprobes are a recently developed, affordable alternative to microPET scanners for the quantification of radiotracer uptake and binding in the rodent brain (Zimmer et al., 2002; Weber et al., 2003). We have studied the compatibility of radiotracer binding data from a beta microprobe system (Swisstrace) with matching data from a Focus 120 microPET scanner (Siemens). 18F-fallypride is a high affinity tracer for dopamine D2/D3 receptors in the brain, and is of use in the quantification of these receptors in models of diseases such as Parkinson's, psychosis and addiction. Both microPET and microprobe studies were performed in male Sprague-Dawley rats under isoflurane anesthesia. For the microprobe studies probes were inserted stereotactically into the striatum and cerebellum for the measurement of tracer binding. Input function was measured using a system previously described (Warnock et al., 2009) which places a beta microprobe directly into the blood flow of an arteriovenous shunt. The same system was used for input function in both PET and microprobe studies. The input function was corrected for metabolites using a predetermined parent fraction function. All PET scanning was performed in the Focus 120 MicroPET scanner, in list mode. The data was histogrammed and reconstructed using filtered back projection with all corrections except scatter. 18F-fallypride was injected intravenously via the arteriovenous shunt. PET VOIs were selected for striatum and cerebellum to match the microprobe studies. A two compartment kinetic model in PMOD was used to measure binding parameters from both microPET and microprobe data. Rate constants and distribution values were compared between the two methods. The rate constants k_1 , k_2 and k_3 were significantly reduced in the microprobe studies (PET: $k_1=1.29\pm 0.17$, $k_2=0.44\pm 0.04$, $k_3=0.26\pm 0.02$; probe: $k_1=0.71\pm 0.07$, $k_2=0.15\pm 0.01$, $k_3=0.15\pm 0.01$), while the specific and total distribution volumes were unaffected (PET: $V_s=35.1\pm 1.8$, $V_t=38.0\pm 1.7$; probe: $V_s=36.5\pm 2.9$, $V_t=41.4\pm 3.1$). A simulation of microprobe placement in the striatum in PET data was made using a VOI sphere (17 μ l volume) located at the implant coordinates. The rate constants were unaffected by this change in VOI volume. These results indicate that the invasive implantation of beta microprobes in the rat brain for tracer studies may influence tracer transport compared to intact studies in PET. References Zimmer et al. (2002) J Nucl Med 43:227-233. Weber et al. (2003) JCBFM 23:1455-1460. Warnock et al. (2009) JCBFM 29(S1):S329-S345.

Presentation Number **0337B**

Poster Session 3a: Imaging Instrumentation and Methodology

A New Method for Linear Transmission Attenuation Correction in Cardiac SPECT Images

Alireza Karimian¹, Mahan Mohamadrezaee², Fariba Saddadi³, Ghasem Forozani⁴, ¹Biomedical Engineering, University of Isfahan, Isfahan, Islamic Republic of Iran; ²Physics, Booali Sina University of Hamedan, Hamedan, Islamic Republic of Iran; ³Nuclear Medicine, Nuclear Science and Technology Research Institute, Karaj, Islamic Republic of Iran; ⁴Physics, Booali Sina University of Hamedan, Hamedan, Islamic Republic of Iran. Contact e-mail: karimian@eng.ui.ac.ir

In nuclear medicine studies of important tissues such as cardiac, the emitted photons from the cardiac before reaching the gamma detectors are attenuated and scattered by other tissues inside the thorax. Therefore the quality and contrast of the image will be reduced. In this research work, to improve the quality of cardiac images by SPECT system, in the first step the most convenient algorithms for attenuation correction were studied and assessed. Then the best method which was using from a line source for Transmission Attenuation Correction (TAC), was modified in hardware and software algorithm, in a way to use a fill able line source of Tl-201 instead of using from expensive and not easy available Gd-153. Then the experimental data by using from this new and modified method, cardiac phantom (simulates the cardiac and thorax) that was filled with about 2 mCi of Tc-99m, GE (General Electric) Dual Head SPECT system and a line source of Tl - 201 with the activity of about 0.5 mCi were acquired. The data acquisition was done in two steps: I. Scanning the cardiac phantom and line source which was beside the cardiac phantom, this step means we used from emission and transmission simultaneously and II. Scanning the cardiac phantom in the absence of the line source which means using from emission data. Then the suggested attenuation correction formula in this research work, was used and the attenuation coefficient for each pixel was calculated and applied to each pixel. Our results showed a nice improvement in contrast and visibility of the images by this simple and not expensive method. These improvements in the cardiac SPECT images were approved by nuclear medicine doctors. The advantages of this method in comparison with the conventional TAC methods are: its simplicity, using the available radionuclide instead of using from expensive Gd-153 that is not homemade, improvement in the accuracy, quality and contrast of the final image and finally, it is economic. These advantages may help the nuclear medicine centers to improve their ability to detect the physiological and functional defects of the cardiac especially in the elder and women patients. The only shortcoming of our suggested method is, in the re-construction and processing steps it takes a little more time because we have done this correction method for each pixel separately and not for a group of pixels.

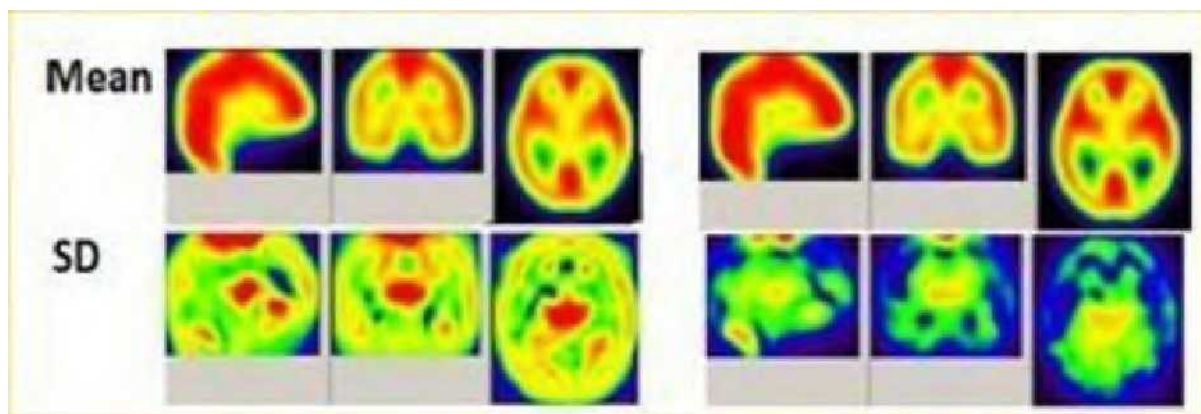
Presentation Number **0338B**

Poster Session 3a: Imaging Instrumentation and Methodology

Three-dimensional realistic brain phantom containing bone and detailed grey matter structures for evaluating inter-institutional reproducibility of PET/SPECT images

Hidehiro Iida, Tsutomu Zeniya, Department of Biomedical Imaging, National Cerebral and Cardiovascular Center, Suita City, Japan.
Contact e-mail: iida@ri.ncvc.go.jp

Recently, a physical 3-dimensional phantom simulating realistic head model has been developed. This study was intended to evaluate adequacy of using this phantom for quality assessment of PET/SPECT images obtained from different institutions with different reconstruction programs. The phantom was made of transparent photo-curable polymer of density at 1.07 g/mL (TSR-829, CMET Inc., Yokohama City, Japan) constructed with a laser-modeling technique. The 3-dimensional fine grey matter structure was defined by tracing a high-resolution MRI on a young healthy volunteer. Additional component was for bone, in which bone-equivalent solution of K₂HPO₄ can be inserted. Reproducibility of volumes for grey matter and bone compartments, as well as X-ray CT structures were assessed for 5 phantoms. SPECT images were acquired with I-123 at 5 institutions using cameras from 3 different manufacturers, fitted with 4 different collimator sets. Volumes of grey-matter and bone compartments (552 \pm 0.8 and 305 \pm 1.2 mL, respectively), and geometric sizes (< 0.5 mm) were reproducible. X-ray CT images of each phantom visually agreed with digital design. The apparent attenuation coefficient for the whole brain was 0.173 cm⁻¹ for Tc-99m, slightly higher than a typical value averaged over human brain (0.168 cm⁻¹), attributed to the higher density of polymer material. Air bubbles can be avoided easily from each compartments, as confirmed by X-ray CT. SPECT images obtained with a recently developed QSPECT package showed a good agreement among the 5 institutions, but showed greater variations if reconstructed with on-site reconstruction programs (Figure 1). The brain phantom appeared to be feasible to use for quality assessment of PET/SPECT images and maybe of use for future multicenter studies.



Averaged and standard-deviation images of the 3D brain phantom reconstructed at each institution (left) and by a recently-developed QSPECT reconstruction package (right)

Presentation Number **0339B**

Poster Session 3a: Imaging Instrumentation and Methodology

Assessment of brain glucose metabolism with input function determined from PET images by means of independent component analysis and Markov Chain Monte Carlo method

Khadidja Berradja¹, **Nabil Boughanmi**¹, **M'hamed Bentourkia**², ¹*Électronique, Université des Sciences et de la Technologie d'Oran, Oran, Algeria;* ²*Nuclear Medicine and Radiobiology, Université de Sherbrooke, Sherbrooke, QC, Canada. Contact e-mail: berradja2@yahoo.fr*

Positron emission tomography (PET) imaging has the capability to produce regional or parametric images of physiological aspects in a tissue of interest. Apart from the acquired PET data, the concentration of the radiotracer supplied to the tissue through the vascularisation has to be known as the input function (IF). IF can be obtained by manual or automatic blood sampling and cross calibrated with PET. These procedures are cumbersome, invasive and generate uncertainties, and in some patients and small animals, the blood sampling is inefficient. IF derived from images suffers from partial volume effect and spillover from neighboring tissues. In the present work, we determine IF from coronal slices of blood arteries in fluorodeoxyglucose (FDG) brain images by means of independent component analysis (ICA) based on Bayesian theory and Markov Chain Monte Carlo (MCMC) sampling method. This model assumes a mixture of two independent components, tissue and blood, with weights varying as a function of time, by generating samples from the posterior distribution from which statistical estimates are calculated. ICA-MCMC allows extraction of blood image sequence from which the blood time course (BC) is determined. BC is directly used in the kinetic model to account for the tissue blood volume, while IF is defined from BC by a scaling factor accounting for the concentration of the radiotracer in plasma. This scaling factor is obtained from a single blood sample. Since the partial volume affects the artery image depending on its size, the scaled BC providing IF is then corrected for partial volume effects. The present method is applied in the calculation of regional brain glucose metabolism (rCMRG) in ten brain structures from normal volunteers (n = 7), in comparison to rCMRG obtained with sampled IF. The results show comparable calculated and sampled IFs. The slight difference arises from the difference in time sampling of the sampled and calculated IFs. In this work, the blood samples were withdrawn at every 4 sec while the images were reconstructed in frames of 10 sec at the first 2 min of the PET scan. Accordingly, the peaks of the IFs do not match in time and amplitude, and consequently, rCMRG values differ by approximately 3%. In conclusion, ICA-MCMC allows to decompose a sequence of PET images in a number of desired components and to produce the input function in a simple, reproducible and non-invasive fashion.

Presentation Number **0340B**

Poster Session 3a: Imaging Instrumentation and Methodology

FDG-PET study of brain glucose metabolism variability in young and elderly

Wassila Benabbas¹, **Otman Sarrhini**², **M'hamed Bentourkia**², ¹*Medical imaging, Université de Batna, Batna, Algeria;* ²*Nuclear Medicine and Radiobiology, Université de Sherbrooke, Sherbrooke, QC, Canada. Contact e-mail: bwassila@hotmail.com*

FDG-PET has been established as an efficient imaging modality to diagnose dementia. The advantage of PET in comparison to conventional approaches was associated with a reduced rate of false-negative and false-positive cases (3.1% vs. 8.2% and 12.0% vs. 23.0%, respectively) (Silverman et al. J Nucl Med, 43:253-266, 2002). The most appropriate and precise approach in calculating regional cerebral metabolic rates of glucose (rCMRG) is the non-linear compartmental pharmacokinetic modeling. Generally, any PET study has to include control measurements as for Alzheimer disease where normal aged volunteers are used for comparison. Actually, there are discrepancies between repetitive measurements. These divergences are due more to the protocols of measurements and data corrections and analyses than to the differences in types of PET scanners (Maquet et al., Eur J Nucl Med, 16:267-273, 1990). rCMRG values could be only slightly affected by scanner detection efficiency, sensitivity and spatial resolution. Obviously the recovery factors to correct images for partial volume effect depend on the spatial resolution of the scanner, and omitting this correction generates variations in rCMRG from different scanners. Even the state of the subject affects the rCMRG values. These values could vary in the same subjects measured in different sessions due to behavioral mental status (Stapelton et al., J cereb blood flow metab, 17:704-712, 1997). In this work, where we used brain FDG images in young (n = 8) and aged (n = 8) healthy volunteers, we demonstrate the effects of the standardisation of the input function and the effects of blood sampling versus image derived input functions and found a variation of about 3%. We report also the effects of the measurement durations from 20 min to 60 min at steps of 10 min, and time framing that should be optimal in terms of noise and accuracy in the time-activity curves. The global drop of rCMRG values for a 60 min scan in aged relative to young subjects was 13%, this value shifted to 9% when normalising to cerebellum, while normalising to the whole brain generated in some regions higher values in aged than in young. In conclusion, we report in this work the impact of the determination of the principle factors affecting the accuracy of the rCMRG values, which depend on scanner operation and data analyses, in order to reduce variability in rCMRG values.

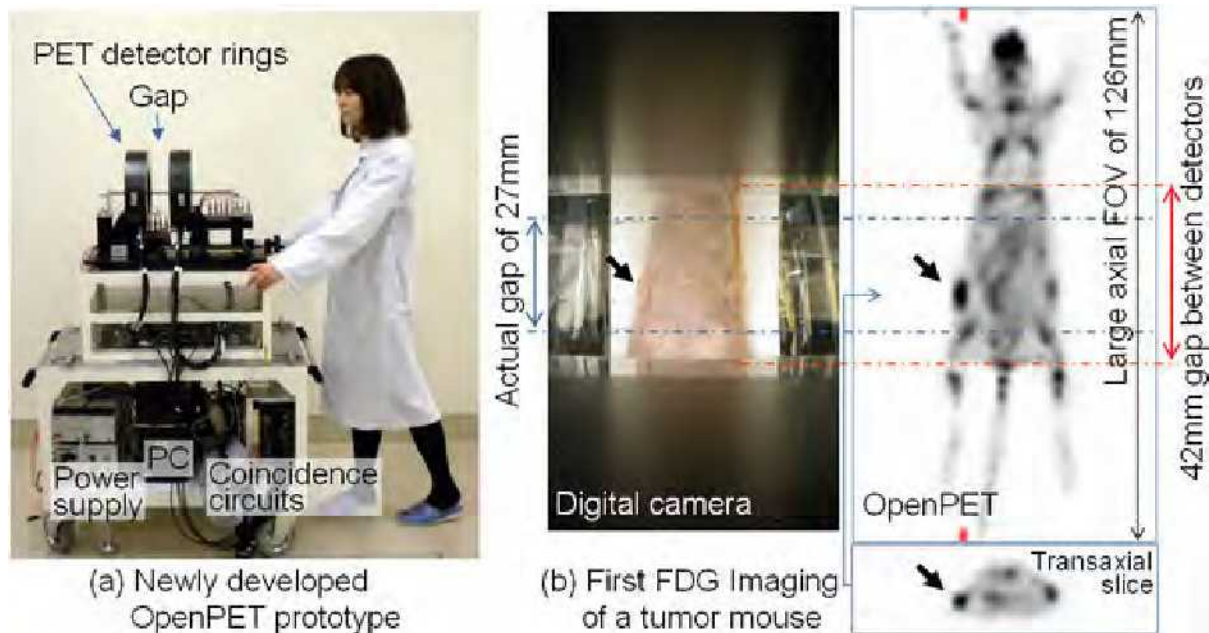
Presentation Number **0341B**

Poster Session 4a: Imaging Instrumentation and Methodology

First Imaging Tests of an OpenPET Prototype for Small Animals

Taiga Yamaya¹, Eiji Yoshida¹, Shoko Kinouchi^{2,1}, Mikio Suga², Daisuke Kokuryo¹, Ichio Aoki¹, Atsushi B. Tsuji¹, Hidekatsu Wakizaka¹, Hideaki Tashima¹, Fumihiko Nishikido¹, Naoko Inadama¹, Hideo Murayama¹, ¹Molecular Imaging Center, National Institute of Radiological Sciences, Chiba, Japan; ²Chiba University, Chiba, Japan. Contact e-mail: taiga@nirs.go.jp

Introduction: The OpenPET geometry is our new idea to visualize a physically opened space between two detector rings (Yamaya, PMB 757, 2008). The OpenPET is expected to enable 1) PET image-guided radiation therapy by letting the beams pass through the gap, 2) real-time multimodal imaging by inserting another imaging device in the gap, and 3) extension of an axial field-of-view with the limited number of detectors. In this paper, we developed the first prototype for small animals to show a proof-of-concept of OpenPET imaging. Methods: The prototype was designed as a compact system so as to be easily carried between PET areas and therapy areas such as the Heavy Ion Medical Accelerator in Chiba (HIMAC) (figure (a)). Two detector rings of 110 mm in diameter composed of 8 block-detectors were placed with a gap of 42 mm. Actual gap was limited to 27 mm by the gantry structure (but the gap will become over 20 cm, which is enough for radiation therapy, if the gantry is extended to the human size in scale). Each block-detector, which had 4-layer depth-of-interaction capability based on our method (Tsuda, IEEE TNS 2537, 2004), was composed of 2.9 x 2.9 x 5 mm³ LGSO crystals and a Hamamatsu H8500 PMT. Colon-26 cancer cells (2.0×10^5) were inoculated subcutaneously into a female BALB/c nude mouse (16.5 g weight) and allowed to grow for 7 days. ¹⁸F-FDG (1.6 MBq) was injected intravenously via tail vein. After 70min, the animal was placed so that the tumor located in the gap, and measured for 10 min. For an initial proof-of-concept of real-time multimodal imaging, an optical image of the surface was taken during PET imaging by inserting a digital camera in the gap. Results: As shown in figure (b), the tumor in the gap was clearly visualized. In addition, the large axial FOV of 126 mm was obtained with the detectors originally covering only an 84 mm axial FOV. Conclusion: Our initial imaging studies showed promising performance of the OpenPET prototype. In a molecular imaging field, we expect novel applications of the OpenPET which make the best use of the gap.



A newly developed OpenPET prototype (a) and the first FDG Images of a tumor mouse (b)

Presentation Number **0343B**

Poster Session 4a: Imaging Instrumentation and Methodology

SPECT System Design Flexibility: a New Paradigm Emerges

James W. Hugg¹, Douglas J. Wagenaar¹, Dirk Meier², Benjamin M. Tsui³, David R. Gilland⁴, Gunnar E. Maehlum², Samir Chowdhury¹, Bradley E. Patt¹, ¹Research, Gamma Medica-Ideas, Northridge, CA, USA; ²Research, Gamma Medica-Ideas, Oslo, Norway; ³Radiology, Johns Hopkins University, Baltimore, MD, USA; ⁴Radiology, University of Florida, Gainesville, FL, USA. Contact e-mail: james.hugg@gm-ideas.com

The gamma camera of the 1950's has changed only at a slow evolutionary pace and the detector still usually comprises a large monolithic scintillator crystal and photomultiplier tubes. The PMT signal is now digitized and the number of camera heads in a typical clinical system is two or three. Since the 1980's traditional gamma cameras have been applied to tomographic (SPECT) in addition to planar imaging. With the rapid increase in computer power during the last two decades, iterative reconstruction has replaced filtered back-projection (FBP), yet the requirements of complete, regular angular sampling associated with FBP have remained in common use. During just the last few years, several commercial products have been offered featuring semiconductor gamma detectors in the form of direct-conversion pixellated CZT crystals. Many of the limitations of SPECT system design have now been removed. Small CZT imaging modules (2.5 cm or 4 cm squares) with no edge dead-space enable designs with contiguous curved detector surfaces (e.g., rings, arcs, hemispheres) or multiple small cameras. Iterative reconstruction enables designs with incomplete or irregular angular sampling, or designs that mix and match detectors with different collimator resolutions, different fields of view, or different degrees of multiplexing. The sleek solid-state detectors can be positioned and operated inside an MRI system, presenting exciting new applications and additional design freedom within a confined volume. Multiple-pinhole collimation has been rediscovered, along with other collimator designs outside of the conventional resolution-efficiency tradeoff performance bounds. Energy resolution < 5% enables simultaneous multiple-isotope studies. We will present examples from the literature and from patent art to support our contention that most SPECT system design constraints no longer apply: many of the standard design guidelines can now be challenged as a new paradigm emerges. Dedicated, organ-specific limited-angle SPECT units that provide optimum performance in resolution and sensitivity as well as quantitative molecular imaging can be designed as cost-effective alternatives to large, whole-body molecular imaging systems with comparatively conservative performance.

Presentation Number **0344B**

Poster Session 4a: Imaging Instrumentation and Methodology

Analysis of the SharpIR Reconstruction Algorithm on the Discovery(TM) PET/CT 690

Steven Ross¹, *Timothy Deller*¹, *Charles Stearns*¹, *Sharon M. Hamblen*¹, *Alex Ganin*¹, *Brad Kemp*², ¹*Molecular Imaging, GE Healthcare, Waukesha, WI, USA;* ²*Department of Radiology, Mayo Clinic, Rochester, MN, USA.* Contact e-mail: steven.ross@med.ge.com

Due to the significant improvement provided in image quality, iterative reconstruction methods such as OSEM (Ordered Subsets Expectation Maximization) have now generally replaced analytic methods such as filtered backprojection for PET imaging. A key factor to effective iterative reconstruction is an accurate model of system physics. Advancements in computing power and algorithm design have allowed more accurate models to be utilized in the reconstruction algorithms, such as accurate projectors based on the detector geometry, fully 3D scatter estimates, and low noise estimates of random coincidences. The SharpIR reconstruction algorithm is based on a further improvement to the system model to include the measured detector response of the PET scanner in the iterative system model. The detector response is modeled as a one-dimensional blurring in projection space; the detector response is measured at several points across the field of view and parameterized to be applied everywhere in projection space. This paper analyzes clinical and phantom images from VUE Point HD and VUE Point FX (time-of-flight) iterative reconstruction incorporating the SharpIR algorithm on the Discovery PET/CT 690 Scanner. Clinical data was analyzed by drawing ROIs on hot anatomical regions to measure contrast (ROI mean) and in the liver to assess noise (ROI standard deviation). Phantom results were obtained with the NEMA Image Quality Phantom, a cylinder phantom with a Hot Spot Insert(TM) (Data Spectrum Corporation, Hillsborough, NC), and a line source. The resulting reconstructed images show improvement in image SNR and resolution (as measured by small object recovery), although in some instances, these occur at the expense of convergence rate due to the more sophisticated system model.

Presentation Number **0345B**
 Poster Session 4a: Imaging Instrumentation and Methodology

Test-retest Reproducibility and Reliability of FDG PET imaging in Mice and Rats using Different Kinetic Modeling Approaches

Stephanie Thorn, Jennifer M. Renaud, Ran Klein, Julia Lockwood, Myra A. Kordos, Michael Gollob, Rob S. Beanlands, Jean N. DaSilva, Robert A. deKemp, University of Ottawa Heart Institute, Ottawa, ON, Canada. Contact e-mail: sthorn@ottawaheart.ca

Background Measurement of mouse rMGU with microPET is variable due to myocardial spillover and camera spatial resolution. Methods for quantification of FDG myocardial uptake were investigated using blood sampling vs non-invasive imaging to measure the arterial input function (AIF). **Methods** Rat FDG PET (n=2) imaging was completed with simultaneous blood sampling (counted in a γ -counter) from a carotid artery. Dynamic images were reconstructed with OSEM3D/MAP ($\beta=1$). Image-derived blood VOIs (LV cavity, right atrium, left atrium, aortic arch) were compared to blood sampling data. This methodology was applied to rat FDG test-retest data (n=4) to validate reproducibility of quantification methods and then repeated in n=6 test-retest mice. **Results** Blood sampled and first-pass AIF curves are similar (Figure), but spillover from the LV myocardium increases the late VOI values by 17-56% at 60 min compared to blood sampling. In test-retest (Table), repeatability coefficients were lowest in the rat using LV cavity data, however in mice a combined LV cavity (first-pass) and right atrium (2-60 min) AIF produced the best reproducibility. Application of a mono-exponential fit to the myocardial uptake curve (excluding AIF) shows the lowest repeatability coefficients for both rats and mice. **Conclusions** These results suggest that measurements of myocardial FDG uptake are greatly influenced by the animal size and regions used for the AIF. In all cases, the use of a mono-exponential fit to the myocardial uptake curve provided the best reproducibility and repeatability data and should be sensitive to detect MGU changes of 10 and 20 % in rats and mice.

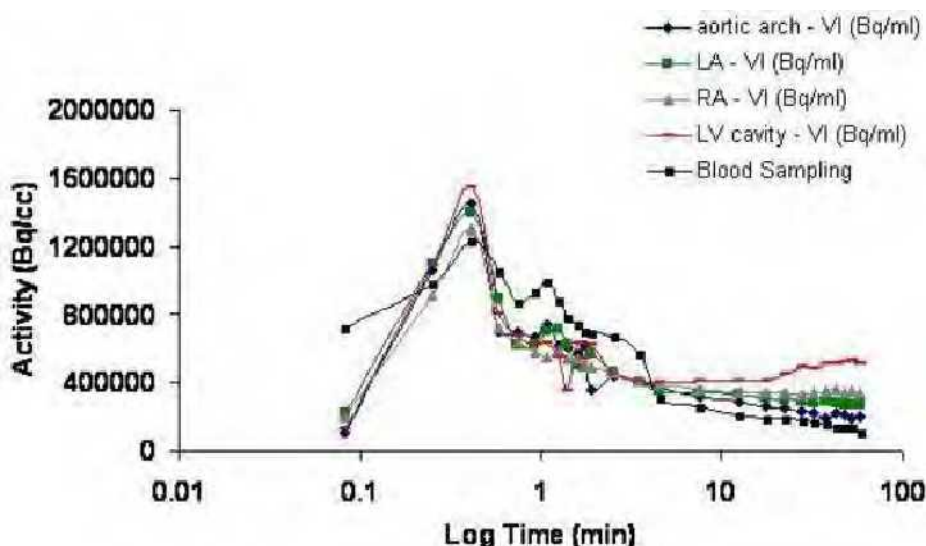


Figure : Rat FDG blood time activity curve using different regions of interest compared to blood sampling
 Table: Test-Retest in Rats and Mice

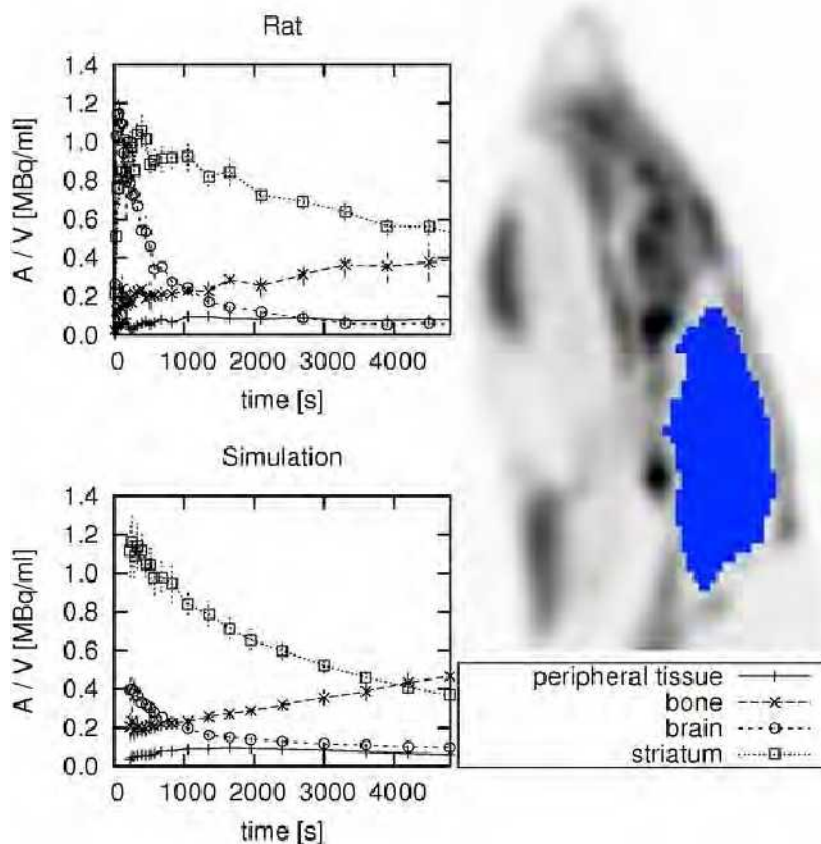
	rMGU using various AIF (nmol/mg)				Mono (L/min)
	LV Cavity	RA	Aortic Arch	Combined LV/RA	
Rat (n=4) Mean	1.32	1.35	1.15	1.38	0.09
CV %	23.01	27.64	54.91	22.82	62.3
Test-retest Difference %	29.08	39.28	67.82	30.50	4.33
Repeatability Coefficient % of mean	34.49	42.66	129.75	40.33	9.78
Mouse (n=6) Mean	17.98	5.68	18.39	5.97	0.08
CV %	81.67	97.93	29.24	101.10	10.10
Test-retest Difference %	61.14	60.22	39.59	55.67	10.61
Repeatability Coefficient % of mean	267.35	237.45	88.93	223.10	20.72

Presentation Number **0346B**
 Poster Session 4a: Imaging Instrumentation and Methodology

Automatic tissue segmentation in dynamic PET based on voxel-wise fitting of pseudo-pharmacokinetic functions to time-activity curves

Erik Mille, Peter Bartenstein, Guido Boening, Department of Nuclear Medicine, Hospital of the University of Munich, Munich, Germany. Contact e-mail: erik.mille@med.uni-muenchen.de

This work aims for a general approach of tissue segmentation in dynamic PET data by voxel-wise fitting of time activity curves (TAC). The ROOT library (Cern, CH) was used for fitting, filtering and segmentation were performed with the Insight toolkit (ITK). This method was evaluated for the segmentation of brain in dynamic ¹⁸F-desmethoxyfallypride (DMFP) PET scans (Siemens Inveon DPET) of rats. Voxel size in all data was 0.2 μl. A numerical phantom representing a simplified rat head consisted of co-centered spheres for peripheral tissue (r: 12.0 mm), skull (r: 9.5 mm), brain (r: 8.0 mm) and striatum (r: 1.5 mm). Dynamic data were simulated from empirical pseudo-pharmacokinetic functions with 20 frames using a simplified Bateman function (peripheral tissue), a linear function multiplied by mono-exponential function (bone), and bi-exponential functions with individual parameters for brain and striatum. To match a realistic scan situation, data were blurred and Poisson noise applied. Original (S0), blurred (S1), noisy (S2) and noisy and blurred (S3) data were analyzed. The dynamic scan (47.5 MBq, 90 min) of a rat was reconstructed in 28 time frames and also analyzed. Object boundaries were segmented by applying a histogram-based threshold to the summed and filtered image (3D median) followed by a hole-filling filter. Within the object a bi-exponential function was fit onto each TAC. On success the fit parameters were combined and weighted by the correlation coefficient into a score map which showed increased signal within the brain. The above segmentation was applied to this map, areas smaller than 5000 voxels were removed using a shape-opening filter. The resulting segmented brain volumes were 2% (S0), 5% (S1), 11% (S2) and 14% (S3) smaller than the original brain template. The distances between the center of mass of the segmented volumes and their true location were less than 0.02 mm in all 4 cases.



TACs of 4 VOIS positioned into rat and S3 together with the segmented rat brain.

Presentation Number **0347B**
 Poster Session 4a: Imaging Instrumentation and Methodology

Retrospective replacement of ECG trigger events in PET listmode data by an offline reprocessing approach for stored ECG data

Andrei Todica, Guoming Xiong, Erik Mille, Peter Bartenstein, Marcus Hacker, Guido Boening, Dept. of Nuclear Medicine, Ludwig-Maximilians University of Munich, Munich, Germany. Contact e-mail: Andrei.Todica@med.uni-muenchen.de

The physiological monitoring of the subject during positron emission tomography (PET) measurements is routine in small animal studies. Electro-cardiogram (ECG) devices can be utilized to automatically generate trigger events to reconstruct gated images for the assessment of heart wall motion. Although ECG is an established method, online ECG processing can fail e.g. in case of a poor signal due to complex measurement conditions. To overcome this problem and to allow for advanced ECG post-processing, we simultaneously acquired PET listmode data (Siemens Inveon DPET 120) and the ECG signal (BioVet, m2m Imag. Corp.). Offline synchronization was achieved by analyzing the trigger events stored in both files. New trigger events were determined by a robust search for the R-peaks in the ECG. After removing the existing trigger events from the listmode file the new trigger events were inserted. We carefully maintained the structure and format of the listmode file so that it was processable with the Inveon software. We have evaluated our method by selecting 2 groups of ¹⁸F-FDG PET animal measurements from our archive. All acquisitions were performed over 30 min. (60 min p.i., 17.3±5.4 MBq). High ECG quality and successful online ECG processing was available in group 1 (9 mice, BALB/c, 38.2±2.4 g) whereas online ECG processing yielded unacceptable trigger events in group 2 (8 mice, SWR, 26.3±2.0 g). For both groups, new trigger events were generated and gated images reconstructed from original and modified listmode files (3DOSEM/MAP). Image analysis was performed with QGS (Cedars-Sinai) to assess the end diastolic (EDV), the end systolic (ESV), the stroke (SV) volume and the ejection fraction (EF). A paired t-test showed no significant difference between original and modified data in group 1. In group 2 where ECG online processing failed, the wall motion information was significantly improved after inserting new trigger points. This study shows that ECG offline reprocessing and retrospective gating is feasible when the full ECG signal is recorded together with the PET listmode data. The results of quantitative wall motion analysis were not altered when online ECG processing was successful, but significantly improved in case of false initial online ECG processing.

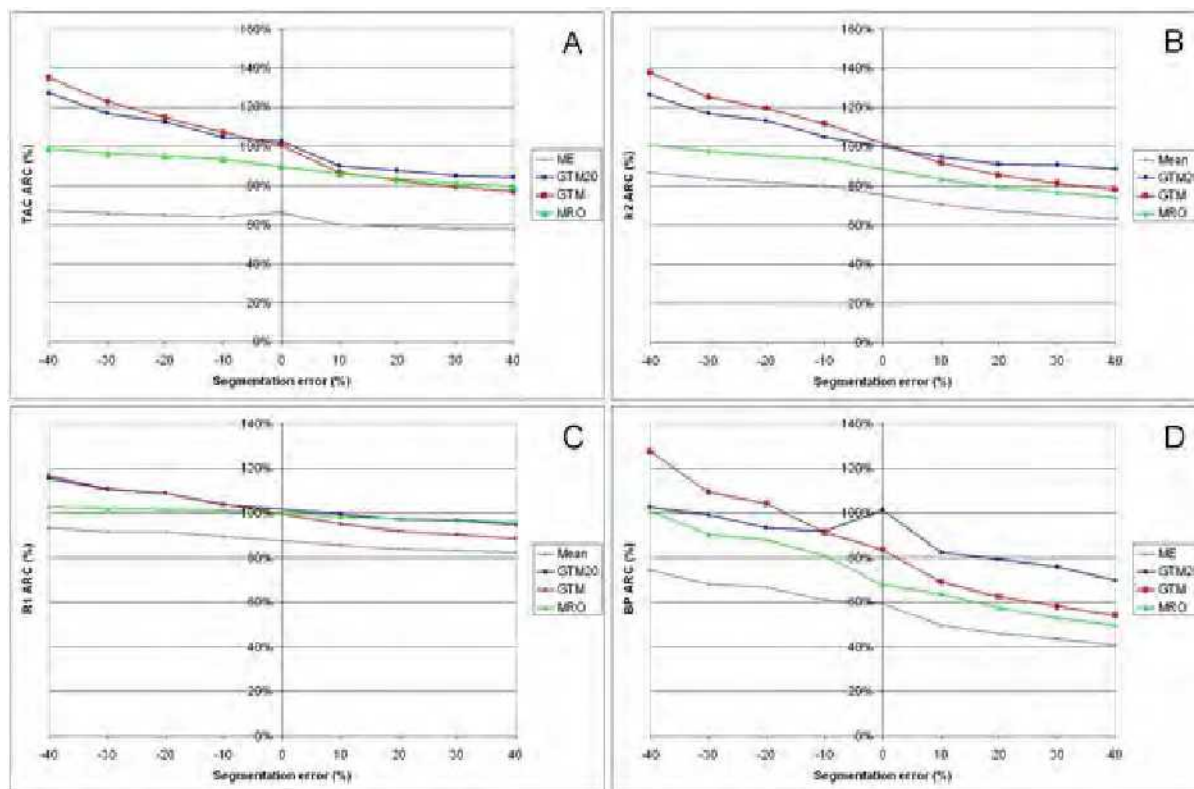
Trigger	Group 1			Group 2		
	Original	New	p	Original	New	p
EDV (µl)	69±11	69±11	0.17	40±10	47±10	< 0.05
ESV (µl)	11±5	10±5	0.39	13±9	19±9	< 0.05
SV (µl)	43±6	44±6	0.47	17±7	27±6	< 0.05
EF (%)	64±5	64±7	0.35	41±10	60±13	< 0.05

Presentation Number **0348B**
 Poster Session 4a: Imaging Instrumentation and Methodology

Partial volume effect for binding potential estimation in 11C-PE2I PET brain striatal images using a simplified tissue model

Renaud Maroy, Elodie Dusch, Claude Comtat, Claire Leroy, Régine Trebossen, DSV/SHFJ, CEA, Orsay, France. Contact e-mail: renaud.maroy@cea.fr

Objectives: Numerous methods have been proposed for the correction of the Partial Volume Effect (PVE) that hampers striatal PET studies. While their quantification accuracy is known for most, their ability to recover correct pharmacokinetic parameters in case of segmentation errors is less clear. The work proposes to compare the binding potential estimations using 4 distinct Time Activity Curve (TAC) estimation methods. Method: A phantom based on the Zubal phantom of a 11C-PE-2I PET exam with kinetics generated using the simplified tissue model of Lammertsma[1] ($R1=1.28$, $k2=.09$, $BP=17$) was analytically simulated on a ECAT HRRT (Siemens, 2.4mm intrinsic resolution). PET images were reconstructed with $1.2 \times 1.2 \times 1.2 \text{mm}^3$ voxels and 20 frames using both RM-OP-OSEM[2], which compensate for PVE, and OP-OSEM. Twenty realizations of caudate segmentations containing errors ranging between 40% volume underestimation (-40%) and 40% volume overestimation (40%) were defined[3]. Four TAC estimation methods were compared for the caudate: the mean TAC measurement in the standard OP-OSEM image (ME) and in the RM-OP-OSEM image (MRO), the Geometric Transfer Matrix method (GTM) and an improved GTM3 method using voxel selection (GTM20). The $R1$, $k2$ and binding potential (BP) estimated with the estimated TACs using[1] were compared based on the Apparent Recovery Coefficient (ARC). Results: Unlike $k2$ and $R1$, the BP is globally underestimated by the methods. The lowest performances are obtained without correction. The best ARC for the TACs (Fig 1.A) and $R1$ (Fig 1.C) are achieved using MRO, but the use of MRO leads to suboptimal BP (Fig 1.D), which is the model parameter of major interest. The best ARC for BP and $k2$ (Fig 1.B) are achieved using GTM20, which provides better TACs than GTM, leading also to better ARC than GTM. Conclusion: Our improved GTM method with voxel selection achieves the TAC estimation in terms of binding potential and $k2$ recovery. 1 A A Lammertsma et al. Neuroimage, 1996 2 F C Sureau et al. JNM, 2008 3 R Maroy et al. SNM, 2009



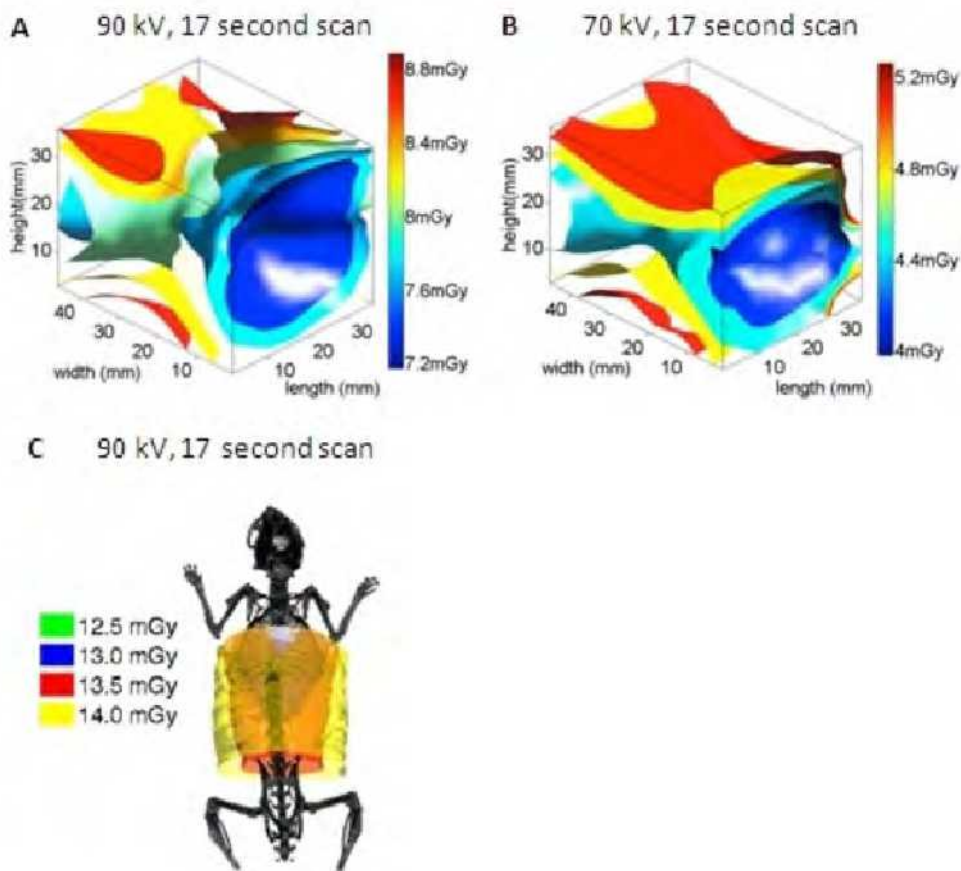
Apparent recovery coefficient for the pharmacokinetic parameters depending on the percentage of segmentation errors. A. TAC. B. $k2$. C. $R1$. D. BP.

Presentation Number **0349B**
 Poster Session 4a: Imaging Instrumentation and Methodology

Evaluation of the Imaging Performance and Dosimetry of the Quantum FX microCT scanner

Magdalena Bazalova¹, **Steven Jones**², **Jay Whalen**², **Stephen J. Oldfield**², **Edward E. Graves**¹, ¹Stanford University, Palo Alto, CA, USA; ²Caliper Life Sciences, Alameda, CA, USA. Contact e-mail: bazalova@stanford.edu

Introduction: Micro CT is commonly used in longitudinal studies of small animals to monitor disease and assess the response to therapy, but biological results can display artifacts caused by the high radiation imaging dose. In this abstract, a new microCT scanner is evaluated for longitudinal studies by measuring the imaging dose using EBT Gafchromic films. Methods and materials: The Quantum FX microCT scanner Quantum FX (Caliper Life Sciences, Hopkinton, MA) is equipped with a novel efficient flat panel detector and a micro-focus x-ray tube allowing for fast low-dose imaging at high image resolution. First, the image quality was quantified in terms of signal-to-noise ratio, $SNR=20 \times \log_{10}(\mu/\sigma)$, using a mouse phantom. CT images were acquired at 58 μm resolution with 90kV, 160 μA , and 17s and 3min scan times. Next, the imaging dose was measured using EBT Gafchromic films sandwiched between 3mm thick solid water slabs. The phantom was imaged with 160 μA , 70 and 90kV with 2min scan time. The phantom was also irradiated with a stationary x-ray tube for 25min with 200 μA and 90kV. Finally, the stationary x-ray tube dose distribution together with CT images of a mouse was used for analytical calculation of imaging dose to a small animal for a 17s scan. Results: The SNR for 90kV images is 30.2dB and 23.0dB for a 3min and a 17s scan, respectively, qualifying for excellent and acceptable image quality. The 3D dose distributions in the rectangular phantom for 17s scans at 90kV and 70kV are shown in Fig A and B. The mean dose for the 90kV scan is 8.0mGy and it is 4.6mGy for the 70kV scan. The skin doses are 8.8mGy and 5.2mGy, respectively. The mean and the skin doses for the mouse 90kV 17s scan (Fig C) are 13.2 and 14.0mGy. Conclusions: The imaging dose of the Quantum FX microCT scanner is significantly lower than the dose from other microCT systems reported in the literature. Quantum FX is therefore a suitable imaging apparatus for longitudinal animal studies.

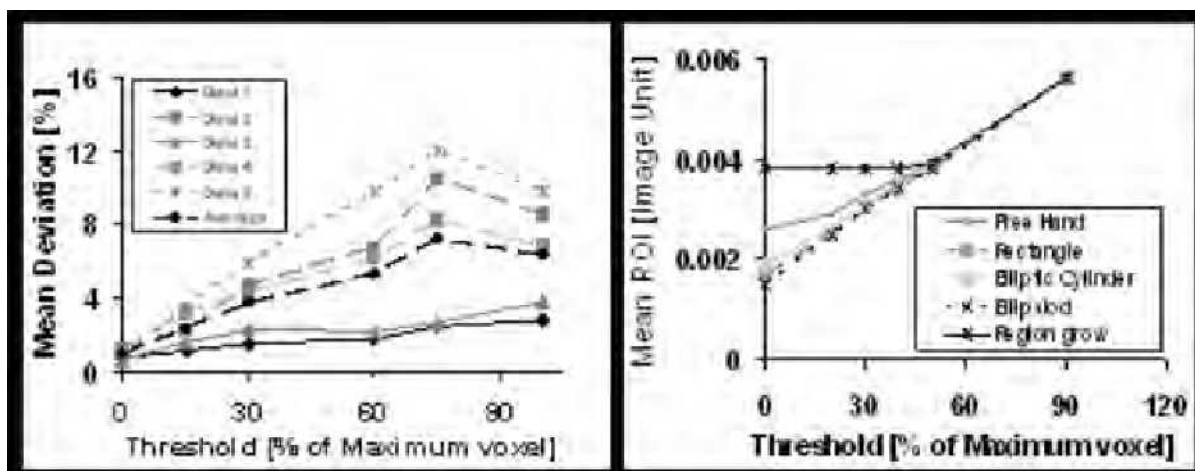


Presentation Number **0350B**
 Poster Session 4a: Imaging Instrumentation and Methodology

Reduction of variability in microPET quantitation using ROI_{max}-based statistics

Frezghi Habte^{1,3}, Timothy Doyle^{2,3}, David Paik^{2,3}, ¹Radiology, Stanford University, Stanford, CA, USA; ²Pediatric, Stanford, Palo Alto, CA, USA; ³Molecular Imaging Program at Stanford, Stanford, Palo Alto, CA, USA. Contact e-mail: fhabte@stanford.edu

Quantitation of ROI using the maximum pixel value is frequently used in order to nearly eliminate variation due to differences in hand-drawn ROIs. An alternative technique is to utilize multiple pixel values while minimizing the effect of hand-drawn ROIs. This technique thresholds the ROI above a percent of the maximum value and returns the mean of those values (where 100% is simply ROI_{max}). In order to study the repeatability of ROI measurements on the same lesion in the same subject, we examined dynamic microPET images, restricting the analysis to the washout phase. We removed the variation due to tracer kinetics by comparing the ROI value to a second order polynomial fitted to this relatively flat section of the time activity curve. We computed mean percent deviation from fitted polynomial line to determine variability across multiple time points within the same dynamic data for each threshold. The result demonstrates that the variability due to different threshold values generally increases as the threshold is dropped from 100% to 75% of max and then decreases below a threshold of 75%. Non-intuitively, this means that thresholds between 70-90% of max actually increase variability rather than reduce it. While values below 60% are an improvement over ROI_{max}, this requires reasonable signal to noise ratio. For very low activity lesions relative to background, ROI_{max} is recommended.



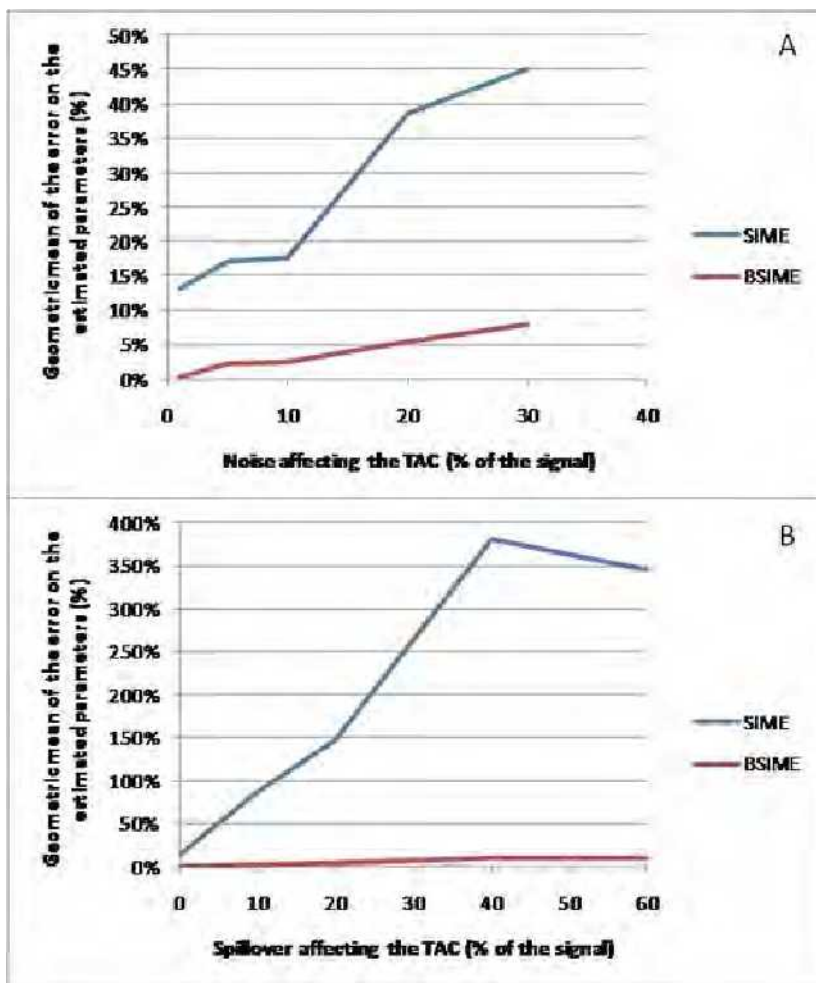
Variability of mean ROI value across different time point of dynamic images of microPET during washout phase (Left) and quantitation comparison of different type of ROIs (Right) as function of threshold levels set as percent of Maximum pixel value.

Presentation Number **0351B**
 Poster Session 4a: Imaging Instrumentation and Methodology

Non-invasive input function estimation for ¹⁸F-FDG PET studies in the human brain

Segolene de Gavriloff, **Renaud Maroy**, DSV/SHFJ, CEA, Orsay, France. Contact e-mail: renaud.maroy@cea.fr

Objectives: In multi-compartments modeling for ¹⁸F-FDG PET, the knowledge of the input function (IF) is required for the access to the pharmacokinetic parameters (PK). Among the works proposed for image derived IF, the SIME method [1] seems to allow the access to individual parameters but proved very sensitive to noise without venous blood sampling. The present method reduces the noise impact on the IF estimation using a bootstrap approach. Method: Fifty sets of realistic TACs for 15 structures were generated in a random way according to a 3-compartments model with k4=0. Realistic noise was added to the TACs with 1% to 30% of the signal. Spillover was also simulated for the TACs with 1% of noise with a spillover of 0% to 60% of the signal. The SIME method estimates the IF and the PK for a given set of N TACs. The present method, called Bootstrap SIME (BSIME) proposes (1) to generate all possible sets of 3 TACs (2) to order these sets by an increasing mean noise affecting the set TACs (3) to estimate the IF for the 30% best sets of TACs according to this order (4) to compute as final parameters of the TAC the mean of the estimated parameters weighted by the corresponding objective function value on all 15 structures TACs. Results: The use of our BSIME method allowed a precision gain of a mean factor 23 as compared to SIME. The error on the estimated parameters was increasing with noise (Fig 1.A) and with spillover (Fig 1.B) for both methods. It was lower than 10% for BSIME and higher than 12% for SIME whatever the noise. Both SIME and BSIME seem equally affected with spillover, the difference seen on the curves (Fig 1.B) being due to the higher robustness of BSIME to noise. Conclusion: Our bootstrap SIME method reduces considerably the error on the IF parameter estimation, enabling its use without resort to venous blood sampling if Partial Volume Correction is applied to the TACs. Results on clinical datasets will be presented. 1 D Feng et al. IEEE Trans Inf Technol Biomed, 1997 2 V Frouin et al. JNM, 2002



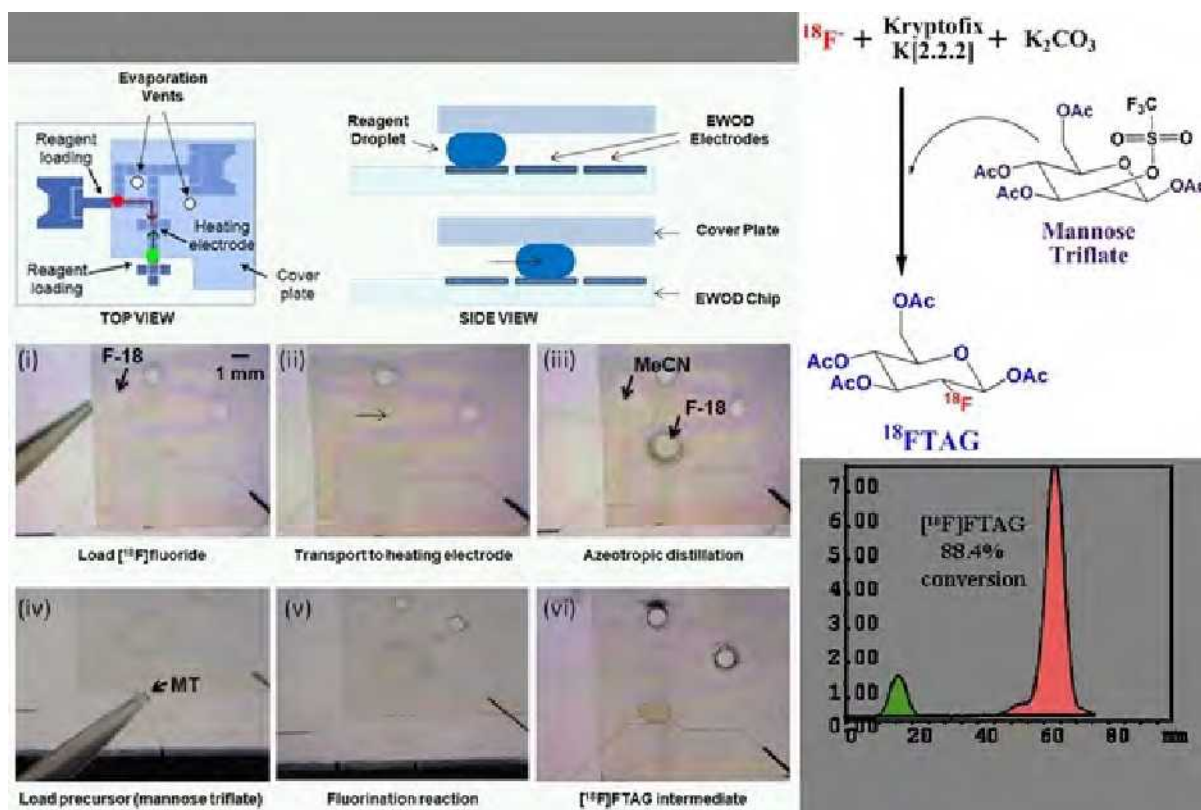
Comparison of the SIME and BSIME IF methods based on the estimation error dependency on A. Noise. B. Spillover

Presentation Number **0352B**
 Poster Session 4a: Imaging Instrumentation and Methodology

All-Electronic Microfluidic Chips for Radiosynthesis of Diverse Molecular Probes

Pei Yuin Keng^{1,2}, **Supin Chen**³, **Huijiang Ding**^{1,2}, **Saman Sadeghi**^{1,2}, **Michael Phelps**^{1,2}, **N. Satyamurthy**^{1,2}, **Chang-Jing Kim**^{3,4}, **R Michael van Dam**^{1,2}, ¹Department of Molecular and Medical Pharmacology, University of California Los Angeles, Los Angeles, CA, USA; ²Crump Institute for Molecular Imaging, University of California Los Angeles, Los Angeles, CA, USA; ³Biomedical Engineering Department, University of California Los Angeles, Los Angeles, CA, USA; ⁴Mechanical and Aerospace Engineering Department, University of California Los Angeles, Los Angeles, CA, USA. Contact e-mail: pkeng@mednet.ucla.edu

The limited availability and difficulty in the development of molecular probes has remained a critical bottleneck in the wide-spread use of positron emission tomography to advance cancer research. Due to the complexity of the syntheses of PET radiotracers, which require specialized facilities, equipment and personnel, only [¹⁸F]FDG and a few other probes are routinely available, produced at commercial radiopharmacies, and delivered to the lab or clinic. To enable increased use of PET imaging by more scientists, we are developing microfluidic platform technologies for the next-generation, compact, user-friendly radiosynthesizers that could produce molecular probes on-demand in the imaging center. Herein, a dedicated radiosynthesis chip based on the technology of electrowetting on dielectric (EWOD) is described and the multistep radiosyntheses of 2-[¹⁸F]fluorodeoxyglucose ([¹⁸F]FDG) and 1-[¹⁸F]fluoro-4-nitrobenzene ([¹⁸F]FNB) are demonstrated, with radiolabeling efficiencies up to 80% and 95%. Compared to other types of microfluidic devices, EWOD chips are particularly attractive for the radiosyntheses of diverse molecular probes due to their high temperature stability, chemical inertness toward a wide range of organic solvents, and the electronic manipulation of reagents instead of valves and pump, which simplifies control and increases reliability. The basic principle of EWOD is the use of patterned electrode arrays for control of sub-microliter droplets of reagents, each serving as a discrete micro-vessel, to be transported, split, merged, and mixed by applying appropriate voltages. Additionally, the EWOD chip dedicated for radiosynthesis that is developed in our c chips group is enhanced with localized on-chip heating and feedback control that allows efficient drying of initial [¹⁸F]fluoride solution, and performing radiolabeling reactions at elevated temperatures. Ultimately, microfluidic could be the revolutionary approach for probe-specific "kits" for the production of probes by non-specialized personnel.



Presentation Number **0353B**

Poster Session 4a: Imaging Instrumentation and Methodology

Dual-isotope SPECT: advantage in Molecular Breast Imaging with CZT

Douglas J. Wagenaar¹, James W. Hugg¹, Dirk Meier², Gunnar E. Maehlum², Rex Moats³, Alan Waxman⁴, Michael K. O'Connor⁵, Samir Chowdhury¹, Bradley E. Patt¹, ¹Research, Gamma Medica-Ideas, Inc., Northridge, CA, USA; ²Research, Gamma Medica-Ideas, Inc., Oslo, Norway; ³Radiology, Children's Hospital of Los Angeles, Los Angeles, CA, USA; ⁴Nuclear Medicine, Cedars-Sinai Medical Center, Los Angeles, CA, USA; ⁵Radiology, Mayo Clinic, Rochester, MN, USA. Contact e-mail: douglas.wagenaar@gm-ideas.com

Molecular Imaging techniques utilize the tracer principle to probe and report on cellular and molecular processes non-invasively in vivo. Single photon emission computed tomographic imaging (SPECT) can use energy discrimination properties of imaging detectors to create separate images for each gamma or x-ray photon energy emitted from the subject. The new room-temperature semiconductor CZT has shown superior energy resolution of <4% at 140 keV compared with >9% for conventional NaI/PMT gamma cameras. CZT's superior energy resolution allows better separation of monoenergetic photon emissions - for example 140 keV (99mTc) distinguished from 159 (123I) or 170 and 250 keV (111In). The energy resolution of CZT is sufficient to clearly separate K α from K β characteristic x-rays from heavy metals such as lead and tungsten (used for SPECT shielding), as well as the mercury x-rays from 201Tl decay. Fluorescence x-ray imaging is another form of dual-isotope SPECT in which separate images are formed from individual energy windows. For example, fluorescent x-ray emission from bismuth, gold, or other heavy elements can be employed as a position marker for biopsy needles or other surgical instruments, using the photons from the primary injection of 99mTc to stimulate the fluorescence. Early dual isotope SPECT applications from the Anger camera era distinguished anatomical features from targeted molecular processes. We analyze breast cancer patient management, in particular, with the new molecular imaging contrast agents and CZT's superior energy resolution, which enables simultaneous, non-invasively, quantitative probing of two (or more) biological processes associated with the disease and response to therapy. Although screening with Molecular Breast Imaging must be held to a single, low-dose injection of 99mTc-sestamibi (MIBI) to minimize whole-body radiation dose, dual-isotope SPECT can be used later in patient management: the first opportunity is when the core needle biopsy is obtained. Two contrast agents - one of MIBI to localize the lesion(s) and the other to quantify the receptor status (e.g., hormone or somatostatin receptors) or a biological process (e.g., sodium-potassium pump with 201Tl) can be used. Another opportunity for Molecular Breast Imaging to utilize dual-isotope imaging is in therapy planning by using dynamic MIBI uptake together with labeled tamoxifen or endoxifen to probe therapeutic response. Quantitative multi-isotope SPECT can also be used for therapy guidance, evaluation, and follow-up.

Presentation Number **0354B**
 Poster Session 4a: Imaging Instrumentation and Methodology

Advantages for Sensitivity of Knife-edge Multi-pinhole Collimation in microSPECT

Brent J. Coco¹, Joann Zhang¹, Koji Iwata¹, Richard Tabassi², James W. Hugg², Samir Chowdhury², Bradley E. Patt², Douglas J. Wagenaar², ¹Molecular Imaging, GE Healthcare, Waukesha, WI, USA; ²Pre-clinical Imaging, Gamma Medica-Ideas, Northridge, CA, USA. Contact e-mail: brent.coco@ge.com

Introduction: The GE Healthcare Triumph tri-modality small animal scanner has the distinct advantage of being a fully digital system for single photon emission computed tomography (SPECT), positron emission tomography (PET) and computed tomography (CT) imaging. The 1, 2, 3 or 4 gamma camera configurable SPECT modality utilizes the advanced Cadmium Zinc Telluride (CZT) crystal technology offering greater energy resolution and improved response time over the older Sodium Iodine (NaI) variety. To offer further flexibility in use of the SPECT gamma cameras, pinhole collimation can be used to improve image results via higher resolution. Two-millimeter multi-pinhole (5) collimators provide greater sensitivity necessary in applications with less radioactivity over the Triumph System standard 1 mm multi-pinhole arrangement. Modification of the 2mm multi-pinhole collimator from 'tunnel' to 'knife-edge' style pinholes further increases sensitivity by ~20% while showing no visible degradation to resolution. Materials and Methods: Sensitivity measurements were performed using the same hardware at a radius of rotation of 25 mm with a 500 µCi 99mTc source in ~50 µL volume. Events were processed and calculated through GE Healthcare VIVID visualization software and reported as counts per second per MBq. Results: Sensitivity measurements for both mouse and rat multi-pinhole 2 mm collimators (4 head system) demonstrated a 22% and 20% increase, respectively, in sensitivity for the new 'knife-edge' style pinhole (see table). An "Ultra micro" resolution phantom (Data Spectrum Corporation) was used for resolution testing at a radius of rotation of 30mm on a two-head SPECT CZT GE Triumph scanner. Resolution results show the 1.7 mm hot spot resolved with little variation between knife-edge and tunnel pinhole collimator types. Conclusion: The newer knife-edge 2mm pinhole design allows for greater gamma camera sensitivity without sacrificing image quality or resolvable detail for the ultra-micro phantom with hot spot insert. Customers concerned with sensitivity in SPECT while imaging rat or mouse subjects would do well opt for the new knife-edge multi-pinhole collimator design as it provides leading sensitivity in a wide array of applications.

2mm multi-pinhole sensitivity in 4-camera Triumph microSPECT

	Tunnel multi-pinhole collimator	Knife-edge multi-pinhole collimator
'tunnel' pinhole design	5180 cps/MBq	4580 cps/MBq
'knife-edge' pinhole design	6000 cps/MBq	5700 cps/MBq

Measurements at 25mm radius of rotation with 500 µCi in ~50 µL volume. "cps" = counts per second.

Presentation Number **0355B**

Poster Session 4a: Imaging Instrumentation and Methodology

Differences in postoperative bone mineralization rates between cortical and spongy bones detected by 99mTc-MDP SPECT/CT and its use as a bone implant material screening tool

Krisztian Szigeti¹, Ildiko Horvath¹, Domokos Mathe^{1,3}, Gabor Nemeth³, Kinga Karlinger⁴, Eszter Pankota², Miklos Wesszl², Zsombor Lacza², ¹Biophysics & Rad.Biol., Nanobiotechnology & In Vivo Imaging Centre Faculty of Medicine Semmelweis University, Budapest, Hungary; ²Human Physiology Exp. Clinical Medicine, Faculty of Medicine Semmelweis University, Budapest, Hungary; ³Translational Imaging, Mediso Ltd., Budapest, Hungary; ⁴Radiology, Faculty of Medicine Semmelweis University, Budapest, Hungary. Contact e-mail: krisztian.szigeti@eok.sote.hu

Measurement of implant-related osteoblast activation in animal models bearing implants carries the possibility of “screening” for implant materials with the most intense osteoblast activation effect. Scintigraphy and SPECT using 99mTc-MDP has sometimes already been applied in implant research. However, a systematic longitudinal in vivo animal study could still well contribute to define the role of bone SPECT in defining in vivo osteoblast activation biomarkers. Methods: For spongy bone model, Male Sprague-Dawley rats were subjected to constant size burr hole in the 6th tail vertebra. For cortical bone healing the same animal strain was performed a cut in the left femur with the insertion of a spacer. All animals were scanned using a quantitative multiplexed multipinhole SPECT/CT system in a longitudinal way for 4 weeks in a row. Imaging started 2 weeks post surgery and was performed weekly until week 6. Animals were injected intravenously with ~80 MBq of 99mTc-MDP and imaged with the SPECT-CT at 2h post injection. During image processing, appropriate cylindrical volumes of interest (VOI) were defined (in mm³) around the lesions and in bone remodeling reference regions in articulation of the nontreated adjacent bone and the femoral greater trochanter. Radioactivity was determined in the uptake VOIs. Activity concentration using summarized VOI activity and volume was determined and it was normalized to the radioactive concentration of 99mTc-MDP by the whole body weight of the animals. Proportions of healing VOI vs. remodeling VOI were set. One group of animals (n=3) was operated and sham-treated, another 3 animals were implanted with a known inactive material, polymethyl-metacrylate and a group of 5 animals was implanted with bone implants in the lesion in both femur-operated and vertebra-operated rats. Results: The lesion radioactive uptake concentration (a SUV-like measure) was 3-fold higher in the first 4 weeks in the test group than in the sham or the control group. The increase change was significantly slower in vertebra-operated than in femur-operated rats. Conclusions: In vivo longitudinal whole-body imaging using quantitative SPECT screens animals to choose the most activating bone implant material. To our surprise a clear slower and lower bone mineralization rate was seen in cortical bone. The results of MDP uptake patterning in time are in line with previous studies published measuring ex vivo bone activity.

Presentation Number **0385B**

Poster Session 3a: Imaging Instrumentation and Methodology

Localization and Characterization of Tumors by Ultrasound-Induced Release of Multiple Biomarkers

Aloma L. D'Souza^{1,2}, Sanjiv S. Gambhir^{1,2}, Gary M. Glazer¹, ¹Radiology, Stanford University, Stanford, CA, USA; ²Molecular Imaging Program, Stanford University, Stanford, CA, USA. Contact e-mail: adsouza@stanford.edu

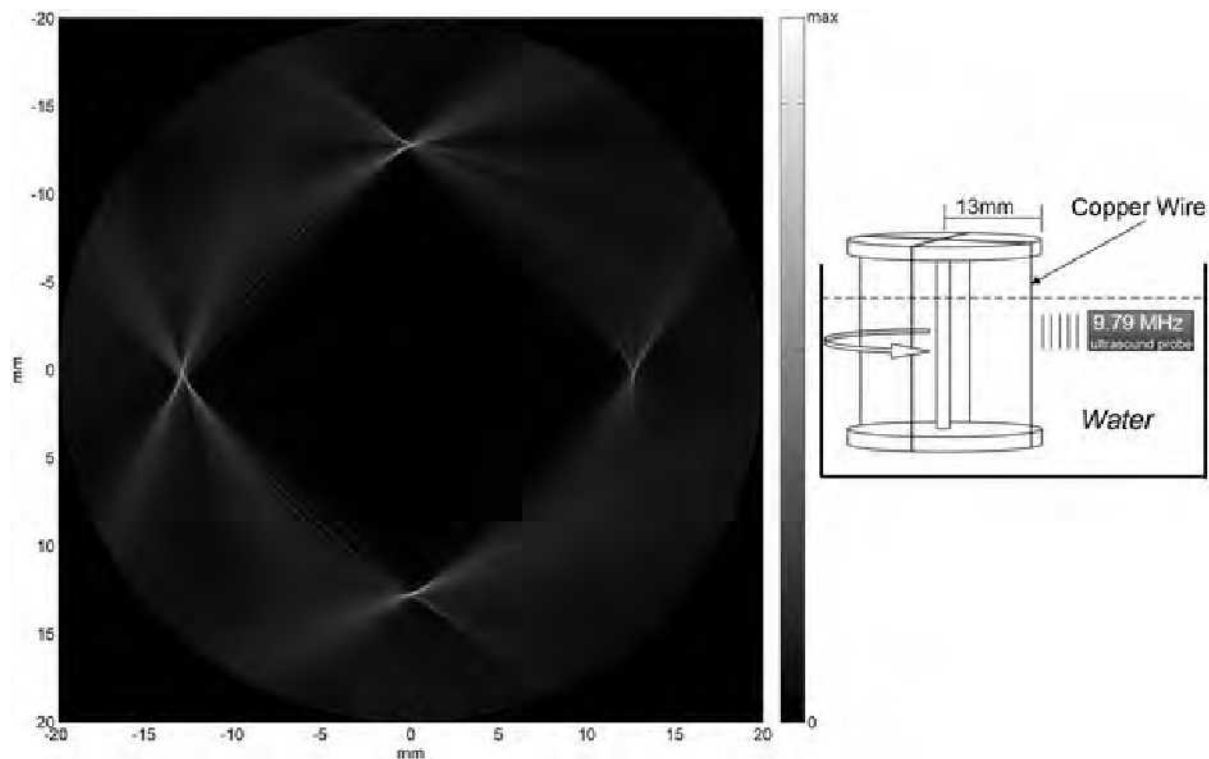
Ultrasound at low frequencies has been used for drug delivery due to its effect of permeabilization of cellular membranes. We hypothesize and prove that this bioeffect of ultrasound also causes the extracellular release of multiple biomarkers from cells in culture and in living mice. The increased release of biomarkers could lead to the identification of incidental lesions and earlier detection of cancer and other disease. The ability to focus ultrasound and confine it to a defined area, allows for localization of the source of the biomarker release. Materials/Methods: Cancer cell lines (colon-LS174T; prostate-LNCaP) that produce biomarkers (CEA, CA19-9; PSA) were exposed to varying intensities and time of low frequency (1 MHz) ultrasound in culture and in subcutaneous tumors of the cells in living mice. The released biomarkers in the cell culture supernatants or serum of the mice were detected using an enzyme-linked immunosorbant assay. Results: LS174T cells treated with 1 MHz ultrasound at a low intensity of 0.3 W/cm² was shown to release CEA and CA19-9 with an increase in time (0, 10, 30 min; p<0.05). These cells were also shown to increase the release of the biomarkers in serum of mice when ultrasound at 2 W/cm² was applied to subcutaneous tumors (CEA p<0.04; CA19-9 p<0.002). Controls treated with ultrasound on non-tumor sites of tumor-bearing mice did not show any increase in the release of biomarkers. The prostate cancer cell line, LNCaP, in culture also showed a substantial increase in the release of PSA with ultrasound treatments. Conclusions: Low frequency ultrasound releases multiple biomarkers only when directly applied to cells or tumors. This allows for the spatial localization of tumors expressing the biomarkers as well as characterization of unknown tumor mass due to the biomarker amplification. This has further implications for monitoring the therapy of lesions. The clinical applications for the use of MR image-guided focused ultrasound for this method of biomarker localization and release would be straightforward and bring together the fields of imaging and in vitro diagnostics.

Presentation Number **0386B**
 Poster Session 3a: Imaging Instrumentation and Methodology

Coherent Ultrasonic Doppler Tomography (CUDT): Simulated and Real Experiment results

Chun Sing L. Tsui¹, **Haidong Liang**¹, **Mike Halliwell**¹, **Michael Shere**³, **Jeremy Braybrooke**², **Elisabeth Whipp**², **Peter Wells**⁴, ¹*Medical Physics and Bioengineering, University Hospitals Bristol NHS Foundation Trust, Bristol, United Kingdom;* ²*Bristol Haematology and Oncology Centre, University Hospitals Bristol NHS Foundation Trust, Bristol, United Kingdom;* ³*Breast Care Centre, Frenchay Hospital, Bristol, United Kingdom;* ⁴*Medical Engineering & Medical Physics, Cardiff University, Cardiff, United Kingdom.* Contact e-mail: chun_sing_tsui@hotmail.com

Ultrasonic imaging based on the pulse-echo principle is widely employed in medical imaging applications. However, its poor spatial resolution (around 2 times the wavelength, or 0.2mm at 15 MHz) is limiting its ability to detect small but clinically important lesions, such as micro calcifications in breast cancer. In contrast to the traditional approach, we present a method based on continuous-wave ultrasound and synthetic aperture technique to obtain tomographic images of the scanned object. When a rotating object (or stationary object with an ultrasound probe orbiting it) is insonated by continuous-wave, the reflected and scattered waves are Doppler shifted. By processing the amplitude and phase of the returned signal coherently, tomographic images of the object's backscatter field can be reconstructed. The spatial resolution is very high at around 0.19 wavelengths that can be demonstrated via simulation of infinitely small point scatters. Real experiments, as illustrated by the diagram, were performed to scan various forms of phantom. Here a Coherent Ultrasonic Doppler Tomography (CUDT) image of a phantom consisting of 4 very thin copper wires with thickness of 0.05mm is presented. Each copper wire was approximately 13mm away from the centre of rotation, parallel to each other, and orthogonal to the transmitted wave's direction. Two 9.79MHz ultrasound elements were used, one for transmission and the other for reception. The result was a 2D image of the backscatter cross-section, showing clearly the locations of each copper wire in respect to the centre of rotation.



CUDT image of 4 copper wires (left). Experimental set-up (right).

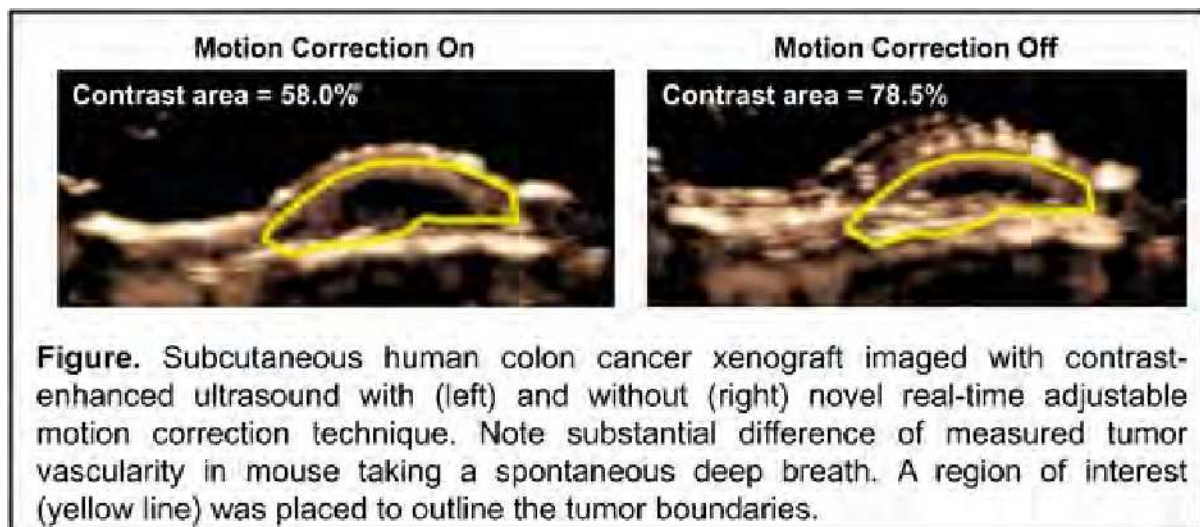
Presentation Number **0387B**

Poster Session 3a: Imaging Instrumentation and Methodology

Assessment of a Novel Real-Time Motion Correction Technique for Contrast-enhanced Ultrasound Imaging of Tumor Vascularity

Marybeth A. Pysz¹, Ismayil Guracar², Kira Foygel¹, Juergen K. Willmann¹, ¹MIPS, Radiology, Stanford University, Stanford, CA, USA; ²Siemens Medical Solutions, Mountain View, CA, USA. Contact e-mail: mpysz@stanford.edu

The purpose of our study was to develop and test a real-time adjustable motion correction algorithm for contrast-enhanced ultrasound (US) imaging in human colon cancer xenografts in mice receiving vascular disruptive tumor treatment. A motion correction technique that measured horizontal and vertical B-mode pixel displacements using sum of absolute difference in a size- and location-adjustable tracking box, was incorporated into the software of a clinical US scanner (Sequoia Acuson 512, Siemens). Contrast-enhanced US imaging in the maximum intensity projection mode (14 MHz, MI=0.26) was performed on subcutaneous human colon cancer xenografts (implanted on backs of mice). Extent of tumor vascularity (expressed as % contrast area) was calculated in real-time with and without motion correction in tumors with different grades of vascularity (low, moderate, high; n=16), and in mice with (n=5) and without (n=5) treatment with a vascular disrupting agent (VDA). In moderately vascularized tumors, the effect of motion correction on the measured tumor vascularity was significantly ($P<.001$) higher (mean differences, $13.3\% \pm 2.3\%$) compared with tumors with low (mean differences, $3.2\% \pm 2.7\%$) or high (mean differences, $4.8\% \pm 2.5\%$) vascularity. The differences in tumor vascularity measurements with and without motion correction were also highest in animals taking a spontaneous deep breath when the tumors were moderately vascularized (mean differences, $25.4\% \pm 5.2\%$; Figure) compared to low (mean differences, $13.4\% \pm 7.2\%$) and highly (mean differences, $12.0\% \pm 10.0\%$) vascularized tumors. Following VDA treatment, tumor vascularity significantly ($P=.003$) decreased on motion-corrected images ($51.7\% \pm 25.1\%$ to $19.7\% \pm 11.4\%$), whereas vascularity minimally increased ($P=.03$) in non-treated mice (from $64.0\% \pm 15.4\%$ to $70.7\% \pm 18.9\%$; Figure). In conclusion, the effects of real-time motion correction for contrast-enhanced US imaging of tumor vascularity substantially depend on the grade of tumor vascularity and the extent of motion. Real-time capabilities of motion correction may improve the practicality and reliability of contrast-enhanced US imaging of tumor vascularity in patients receiving novel cancer treatments such as VDA or anti-angiogenic drugs.



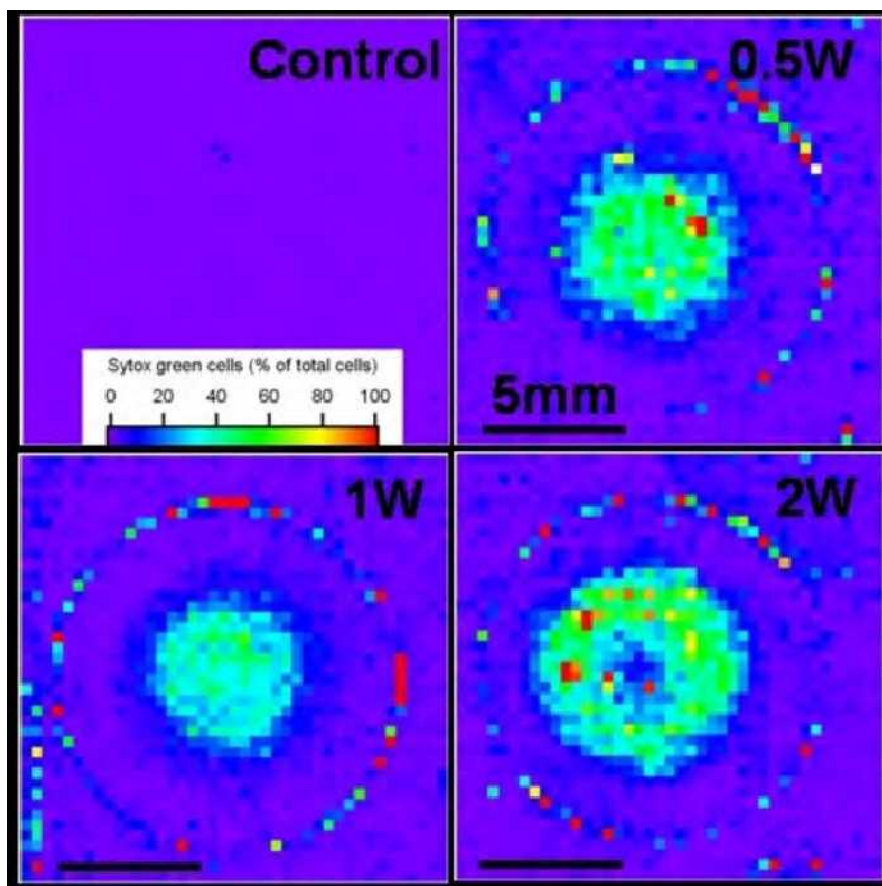
Presentation Number **0388B**

Poster Session 3a: Imaging Instrumentation and Methodology

2D uptake percentage maps for evaluation of US mediated fluorescent model drug delivery

Matthieu Lepetit-Coiffe¹, Anna Yudina¹, Christel Poujol², Philippe Lourenco de Oliveira¹, Franck Couillaud¹, Chrit Moonen¹,
¹Laboratoire IMF CNRS UMR 5231 / Universite Bordeaux 2, Bordeaux, France; ²Bordeaux Imaging Center, Institut Francois Magendie /
 Universite Bordeaux 2, Bordeaux, France. Contact e-mail: matthieu.lepetit-coiffe@imf.u-bordeaux2.fr

The purpose of this study is to visualise and quantify the ultrasound-mediated internalization of a 'smart' model drug by means of mosaic video-microscopic imaging and correlate it with acoustical properties of the transducer. C6 rat glioblastoma cells were cultured in Opticell chambers up to confluence. 2 μ M cell-impermeable Sytox Green, a dye that exhibits a 1000-fold increase upon binding to nucleic acids was co-injected with 3x10⁷ SONOVUE microbubbles (10mL total volume). An active surface of the 5.8 mm diameter mono-element US transducer was positioned 8mm with regard to the Opticell membrane in water at 37°C because it corresponded to the maximum of acoustical pressure (0.88MPap-p for 1.0W electrical power at 1.5MHz) after hydrophonic measurement. Duration, electrical power and duty cycle of pulsed US exposure were varied from 1s-3min, from 0.5-2.0W and from 1%-30% respectively. Control area corresponded to the area not exposed to US. After 15 min of recovery, for quantitation, the nuclei of all cells were stained with Hoechst 33258; An acquisition of 22 x 22 mosaic images covering the entire field of view (FOV = 15mm x 15mm) of each US exposed areas was performed with epifluorescence Leica DMR video-microscope. Each large FOV was analyzed by Metamorph to evaluate cell density as well as uptake percentage, given by the ratio of Sytox positive cells and total number of cells. These maps were then compared to acoustical pressure data. To our knowledge, it is the first time that Sytox Green positive- and Hoechst positive- cell density 2D maps and corresponding uptake percentage maps were obtained for such US application. The size of acoustical field of the transducer closely matches with the spatial profile of the model drug internalized into the cells by US. Maximum of uptake percentage was found at 1W. With such method, correlation between the large FOV macroscopic fluorescent images with microscopic resolution and acoustical pressure map was found.



2D uptake % maps for control (No US), 0.5W, 1W & 2W

Presentation Number **0389B**
 Poster Session 3a: Imaging Instrumentation and Methodology

A Maleimide-Based Phantom Model for Ultrasound Targeted Imaging

Shih-Tsung Kang, Chih-Kuang Yeh, Department of Biomedical Engineering and Environmental Sciences, National Tsing Hua University, Hsinchu, Taiwan. Contact e-mail: charly81509@gmail.com

Intricate variations and poor visual access result in the difficulties in studying ultrasound targeted imaging using an animal model. Here, we propose a simple phantom model based on the maleimide-cysteine interaction between maleimide bubbles and natural gelatin, as depicted in Fig. 1(a). DSPE-PEG2000-maleimide (3 mol%) were used to fabricate maleimide bubbles. Porcine gelatin (4% w/v) was used to prepare flat phantoms and flow phantoms. The flat phantoms were used to quantify the relationship between the densities of adherent maleimide bubbles and their acoustic responses. The flow phantoms were used to study the adhesion behaviors of flowing maleimide bubbles with and without applying an acoustic radiation force. An optical microscope and a 40-MHz ultrasound imaging system were adopted in the experiments. The optical image and corresponding ultrasound image (C-scan mode) presented in Fig. 1(b) and (c), respectively, indicate that abundant maleimide bubbles anchored to the surface of a flat phantom without losing their acoustic activity. The intensity of ultrasound backscattered signal can achieve 40 dB at a density of 1.47×10^5 adherent-bubbles/mm². The adherent bubbles exposed to 300-kPa ultrasound pulses can be disrupted rapidly. However, increasing the adhesion density to 3.62×10^5 adherent-bubbles/mm² can prolong their lifetime by up to 40 minutes. The maleimide bubble in a 1-mm diameter chamber with a flow rate of 3 mL/h can adhere to the chamber wall, as shown in Fig. 1(d). Applying one acoustic radiation force substantially increases the bubble adhesion efficiency, as shown in Fig. 1(e). In this work we propose a simple phantom model providing the flowing bubbles, adherent bubbles, and tissue mimicking structure for studying ultrasound targeted imaging. Potential applications of this model include evaluating the performances of different ultrasound targeted imaging strategies, as well as the efficacies of various acoustic radiation forces applied for enhancing targeting efficiency.

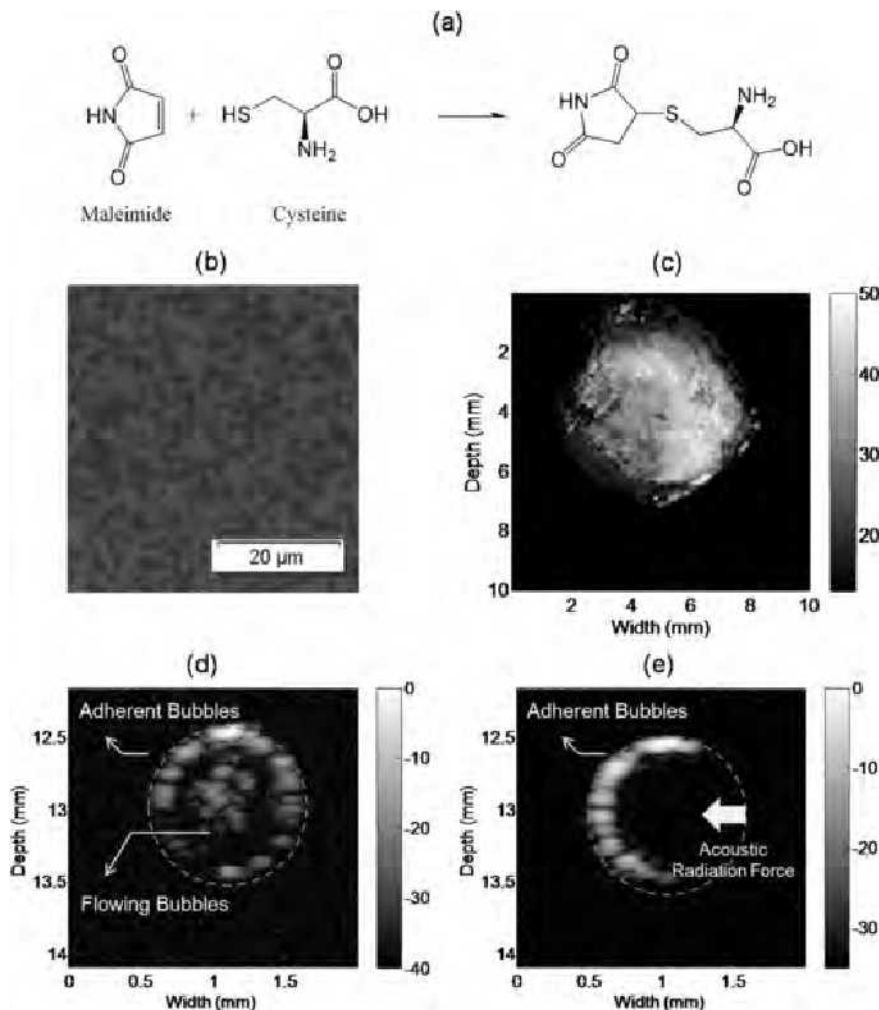


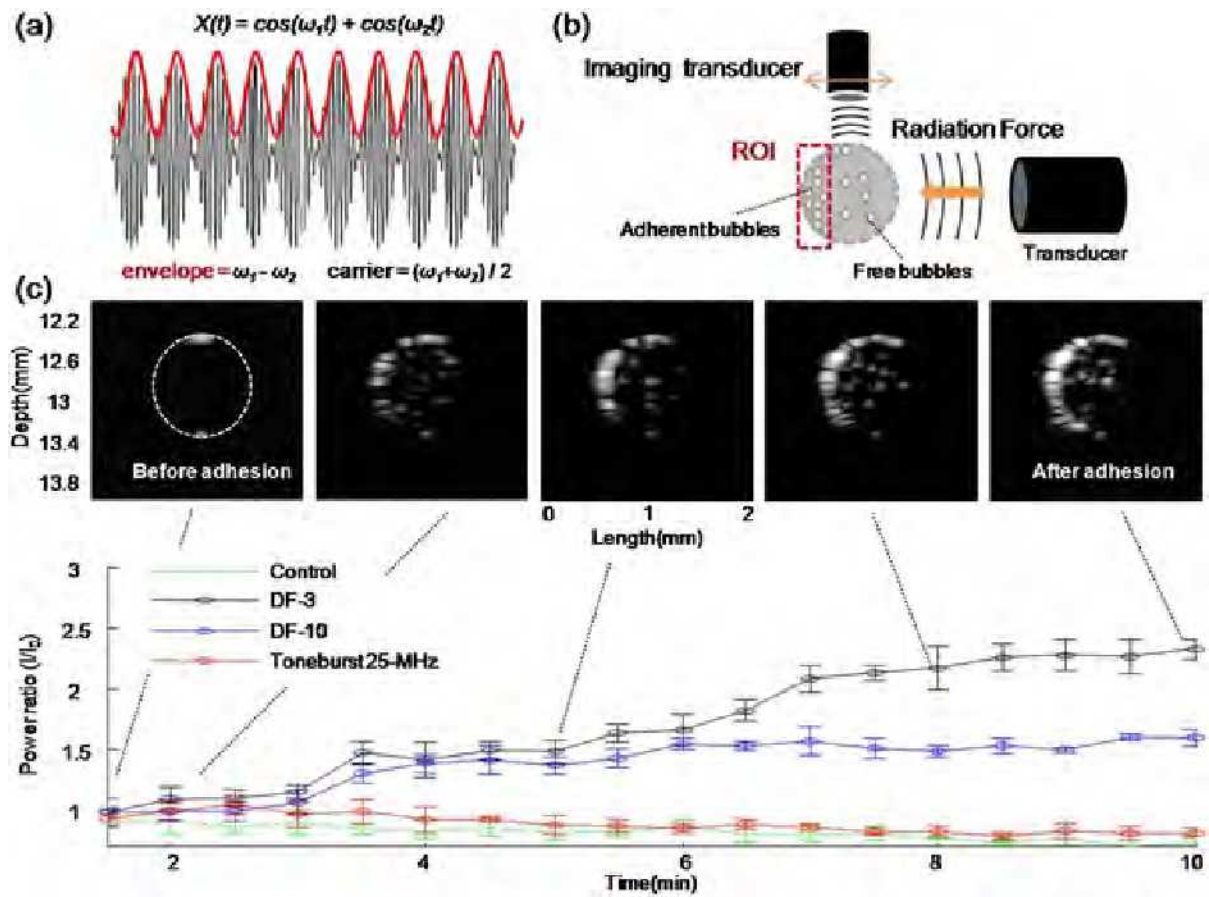
Figure 1

Presentation Number **0390B**
 Poster Session 3a: Imaging Instrumentation and Methodology

Enhancement of microbubbles targeting efficiency by dual-frequency excitation

Ting-Yu Huang, Chih-Kuang Yeh, Biomedical Engineering and Environmental Science, National Tsing Hua University, Hsinchu, Taiwan. Contact e-mail: mich501501@gmail.com

Ultrasound radiation force (USRF) is commonly used to facilitate the efficiency of targeted bubble adhesion. Previous reports showed that USRF provides better performance as USRF frequency close to bubbles' resonant frequency (e.g., several megahertz). However, USRF in low-frequency ultrasound suffers from a large sample volume such that USRF cannot be pinpointed to a specified region of interest. In this study, we proposed a high-frequency dual-frequency (DF) excitation with a low frequency envelope component as USRF while retaining a high spatial resolution. DF pulse is an amplitude modulated wave comprising two sinusoids (Fig. (a)). We fabricated lipid-based bubbles with mean sizes of 2 μm and their resonant frequency was close to 3-MHz. To investigate the targeting efficiencies, two DF pulses with envelope frequencies of 3 MHz (DF-3) and 10 MHz (DF-10) at 25-MHz carrier frequency, and a 25-MHz toneburst waveform with acoustic pressure of 50 kPa and PRF of 2 kHz were adopted. The experimental setup was illustrated in Fig. (b). We used a flow phantom for mimicking receptor-ligand mediated bubbles adhesion and monitored targeted bubbles adhesion simultaneously by a 40-MHz ultrasound imaging system. Figures (c) show the time course images of bubbles adhesion with the quantitative results. The efficiency of bubbles adhesion was calculated the intensity changes in ROI. The DF-3 and DF-10 waveforms performed 2.44 and 1.56 folds enhancement with respect to the cases without USRF, respectively. However, 25-MHz toneburst only had 1.1 folds. The results indicate that high-frequency DF excitation indeed produces a strong USRF and enhances the efficiency of bubbles adherent as its envelope frequency close to bubbles' resonant frequency. In addition, high-frequency DF excitation provides a narrower sample volume and hence it can generate more localized bubbles adherent by USRF.



Presentation Number **0391B**
Poster Session 3a: Imaging Instrumentation and Methodology

Attachment of ultrasound contrast microbubbles to SkHep1 cells under varying flow conditions

Adele Edgeworth, James A. Ross, Tom Anderson, Mairead Butler, William N. McDicken, Carmel M. Moran, University of Edinburgh, Edinburgh, United Kingdom. Contact e-mail: carmel.moran@ed.ac.uk

Aim To determine the conditions which enhance antibody-targeted ultrasound microbubble cellular attachment. **Background** An in-house, lipid-based, microbubble ultrasound contrast agent has been manufactured (Moran et al 2006). Previous investigations have shown that the strength of the streptavidin-biotin bond, used to attach the targeting ligand (CD31 antibody) to the microbubble, is 75 times stronger than the equivalent electrostatic attachment (Edgeworth 2010). Attachment and visualisation of these microbubbles to specific markers may permit molecular imaging with ultrasound. **Method** A volume of 200 μ L of cells, in a 3.5×10^5 /ml concentration were seeded into an Ibidi microslide flow cell with a flow channel of 50x 5x0.8mm. Tubing with an internal diameter of 1.6mm was connected to the flow slide and to a pump and reservoir of warm medium maintained at 37⁰C. The slide was placed on a warm plate on the microscope platform. Images of the cells being subjected to varying wall shear stress (WSS) were recorded at volume flow rates of 1ml/min, rising in 1ml/min increments up to 6ml/min, corresponding to WSS of 0.03, 0.06, 0.09, 0.12, 0.15 and 0.17Pa. In addition a control in which the cells were subjected to 0Pa WSS was prepared for comparison. For attachment under low WSS, positively charged fluorescent microbubbles were added to the reservoir in a 1.3×10^6 /ml concentration. The cells on the slides were exposed to microbubbles at each wall shear stress for 10 minutes. Following this, the reservoir was replaced by one containing medium with no microbubbles and the cells washed for a further 10 minutes at the same WSS. The slides were then imaged. In order to determine the influence of ultrasound on the attachment process, microbubbles and cells were subjected to an ultrasound beam from an L10-22 ultrasound probe (Dynamic Imaging, Livingston, UK) held above the flow cell with a measured downward force of 15.6(\pm 3.3) nN. **Results** Targeted microbubbles were successfully attached to a cellular monolayer in the flow slides under static conditions with a mean 29.1(\pm 10.0)mm⁻² of microbubbles attached. Under WSS of 0.03PA, this number reduced to 4.0(\pm 2.4)mm⁻² increasing by 15.5(\pm 7.9) mm⁻² for ultrasound mediated enhancement. Increasing wall shear stress resulted in a decreasing number of attached microbubbles. **Conclusion** Positively targeted in-house microbubbles have been shown to actively target SK-Hep-1 cells. Acoustic radiation force has been shown to significantly enhance this attachment process.

Presentation Number **0600A**

Poster Session 1b: Imaging Molecular and/or Cellular Processes & Drug and/or Radiation Therapy

Quantitative determination of apoptosis of pancreatic beta cells using ^{99m}Tc -annexin A5 in streptozotocin-induced diabetic mice

Ayahisa Watanabe^{1,2}, Ken-ichi Nishijima¹, Songji Zhao¹, Yan Zhao¹, Yoshikazu Tanaka², Hiroshi Takemoto², Nagara Tamaki¹, Yuji Kuge¹, ¹Central Institute of Isotope Science, Hokkaido University, Sapporo, Japan; ²Shionogi Innovation Center for Drug Discovery, Shionogi & Co., Ltd., Sapporo, Japan. Contact e-mail: ayahisa@med.hokudai.ac.jp

Introduction: Both type 1 and type 2 diabetes mellitus are characterized by a significant deficit in pancreatic beta cell mass, presumably caused by apoptosis of pancreatic beta cells. However, no methods exist for continuous monitoring of apoptosis of pancreatic beta cells. ^{99m}Tc -labeled hydrazinonicotinamide-annexin A5 (^{99m}Tc -annexin A5) is a single photon emission computed tomography tracer, which can noninvasively image apoptotic cells. In this study, we evaluated the possibility of ^{99m}Tc -annexin A5 on quantitative determination of apoptosis of pancreatic beta cells in streptozotocin-induced diabetic mice. **Methods:** Recombinant human annexin A5 derivatized with hydrazinonicotinamide was labeled with ^{99m}Tc by use of tricine as the coligand. As a diabetic model, male Balb/c mice were intraperitoneally injected with streptozotocin (STZ, 200 mg/kg). Diabetic and control mice (n=4-5/group) were injected with ^{99m}Tc -annexin A5 (3.7-18.5 MBq/mouse) and sacrificed 6 hour later for tissue distribution and autoradiography. Pancreatic islets were identified using insulin immunostaining, and apoptotic cells in pancreas were determined by terminal deoxynucleotidyl transferase mediated fluorescein-dUTP Nick-end-labeling (TUNEL) staining. **Results:** Uptake of ^{99m}Tc -annexin A5 in the pancreas of diabetic mice was significantly higher as compared with that of control mice (0.025 ± 0.002 vs 0.018 ± 0.003 %ID/g of tissue/kg, $p < 0.05$), while uptake of ^{99m}Tc -annexin A5 in the blood and excretory tissues (kidney and liver) showed no significant differences between the two groups. In the autoradiographic study, uptake of ^{99m}Tc -annexin A5 was specific to pancreatic islets of diabetic mice. Uptake of ^{99m}Tc -annexin A5 was significantly higher in pancreatic islets of diabetic mice as compared with those of control mice (2.47 ± 0.72 vs 0.74 ± 0.11 %ID/mm² of pancreatic islets /kg, $p < 0.0001$). In the TUNEL staining, TUNEL-positive cells were specific to pancreatic islets of diabetic mice. The number of TUNEL-positive cells significantly increased in pancreatic islets of diabetic mice as compared with those of control mice ($1.2 \times 10^3 \pm 0.5 \times 10^3$ vs 5.3 ± 5.7 cells/mm² of pancreatic islets, $p < 0.0001$). Uptake of ^{99m}Tc -annexin A5 correlated with the number of TUNEL-positive cells in pancreatic islets ($r = 0.821$, $p < 0.001$). **Conclusion:** These results suggest that ^{99m}Tc -annexin A5 is a promising tracer for quantitative detection of apoptosis of pancreatic beta cells associated with diabetes mellitus.

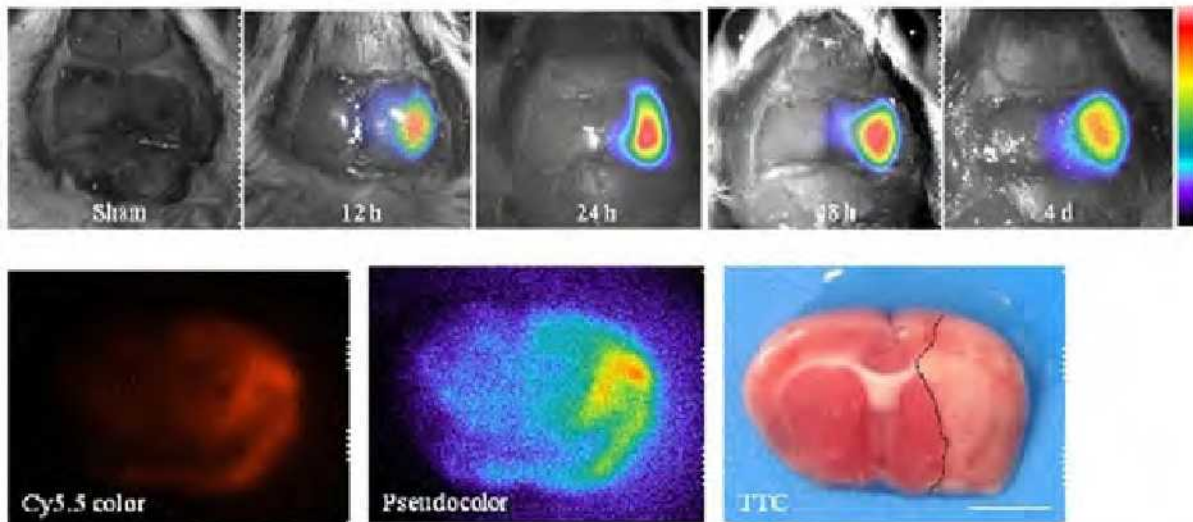
Presentation Number **0601A**

Poster Session 1b: Imaging Molecular and/or Cellular Processes & Drug and/or Radiation Therapy

In vivo optical imaging of early stage apoptosis in mice brain after transient cerebral ischemia

Ning Liu, Kentaro Deguchi, Jingwei Shang, Xuemei Zhang, Feng-Feng Tian, Toru Yamashita, Yasuyuki Ohta, Yoshio Ikeda, Koji Abe, Department of Neurology, Okayama University Graduate School of Medicine, Okayama, Japan. Contact e-mail: liuning@cc.okayama-u.ac.jp

Apoptosis is one of the mechanisms contributing to neuronal degeneration in ischemic stroke. In vivo imaging of annexin V was performed at 12 h, 24 h, 48 h and 4 d after 90 min transient middle cerebral artery occlusion (tMCAO) in mice with a fluorescent protein Cy5.5. Immunohistochemistry for heat shock protein 70 (HSP70), annexin V and terminal deoxynucleotidyl transferase-mediated dUTP-biotin in situ nick end labeling (TUNEL) were also performed with brain sections after the tMCAO. With time dependent examinations, the fluorescent signals with removal of both head skin and skull bone were observed over the ischemic hemisphere at 12 h, 24 h, 48 h and 4 d after the tMCAO with the strongest signal at 48 h. The slice of the brain at 48 h after tMCAO showed a remarkable signal with 2 mm thickness. The characteristics of ex vivo imaging was not diffuse fluorescent signal but zonal signal surrounding the ischemic core. 2, 3, 5-Triphenyl tetrazolium chloride (TTC) staining showed an infarction of the involved MCA territory with the 2 mm thickness slice including the lesion area corresponding to the Cy5.5 signal. While HSP70 was observed at the peak time of 24 h, annexin V became detectable at 12 h with increasing numbers until 48 h. The number of TUNEL positive cells increased at 24 h and kept the level until 4 d, showing dissociating temporal pattern with annexin V. Double positive cells for annexin V/TUNEL became the peak at 48 h. This study shows that in vivo Cy5.5 fluorescence represents annexin V signal spatially surrounding the ischemic core, and that the annexin V fluorescence temporally detects an early stage apoptosis after cerebral ischemia.



Presentation Number **0602A**

Poster Session 1b: Imaging Molecular and/or Cellular Processes & Drug and/or Radiation Therapy

Imaging Cancer Cell Dynamics of UV Light Therapy In Vitro and In Vivo

Hiroaki Kimura^{1,3}, Hiroyuki Tsuchiya³, Katsuro Tomita³, Robert M. Hoffman^{1,2}, ¹AntiCancer, Inc., San Diego, CA, USA; ²Department of Surgery, University of California San Diego, San Diego, CA, USA; ³Department of Orthopedic Surgery, Kanazawa University School of Medicine, Kanazawa, Japan. Contact e-mail: all@anticancer.com

Our laboratory pioneered dual-color cancer cells, in which red fluorescent protein (RFP) is expressed in the cytoplasm and green fluorescent protein (GFP) in the nucleus (Cancer Research 64, 4251-4256, 2004; Nature Protocols 1, 928-935, 2006). Total cellular dynamics can be visualized in the living dual-color cells in real time. In this study, we investigated the cancer-cell-killing efficacy of UV light using the dual-color cancer cells. For UV irradiation experiments, a Benchtop 3UV transilluminator, which emits UVC with an emission peak at 254 nm; UVB with an emission peak at 302 nm; and UVA with an emission peak at 365 nm; was used. After exposure to various doses of UVA, UVB, or UVC, apoptotic, necrotic and viable cells were quantitated under fluorescence microscopy using dual-color 143B human osteosarcoma cells (143B). UV-induced cancer cell death was wave-length and dose dependent. After UVA exposure, most cells were viable even if the UV dose was increased up to 200 J/m². In the UVB group, cell death began to appear when irradiated at 50 J/m². For UVC, the rate of cell killing was proportional to increased UVC irradiation. 25 J/m² UVC irradiation killed over 40% of the 143B dual-color cells. However, the rate of cell killing plateaued at 100 J/m². We also tested 50J/m² UVC and 100J/m² of UVB on four types of dual-color cancer cell lines. UV-induced cancer cell death varied among the cell lines. Cell death began about 4 hours after irradiation and continued until 10 hours after irradiation. Real-time movies were made of cells undergoing UV-induced cell death. Most cells died via apoptosis and only a small portion of them died via necrosis. We will develop UV irradiation for treatment of fluorescent-protein-expressing minimal residual cancer remaining after resection.

Presentation Number **0603A**

Poster Session 1b: Imaging Molecular and/or Cellular Processes & Drug and/or Radiation Therapy

Peptide-Based Imaging Agents Targeting Phosphatidylserine for the Detection of Apoptosis

Chiyi Xiong, Shaoli Song, Rui Zhang, Wei Lu, Xiaoxia Wen, **Chun Li**, *Exp. Diagnostic Imaging, U.T. M. D. Anderson Cancer Center, Houston, TX, USA. Contact e-mail: cli@mdanderson.org*

Externalized phosphatidylserine (PS) on the cell surface is commonly detected using annexin V coupled with radioactive, optical, or magnetic molecular probes. However, this approach may not be optimal for solid-tumor imaging. The purpose of this study was to identify PS-binding peptides (PSBPs) with high PS binding affinity suitable for molecular imaging of apoptosis. Methods: Targeted peptide libraries were synthesized and screened for their binding affinity to PS using surface plasmon resonance technology. The lead peptides were chelated to ^{99m}Tc and evaluated for their ability to bind to apoptotic cells *in vitro* and *in vivo*. Results: Scanning of a consensus 14-residue peptide shared by protein kinase C and PS decarboxylase (FNRLKAGQKIRFG; PSBP-0) and testing of PS binding affinity using surface plasmon resonance showed that substitution of Gln6 with Ala significantly elevated the binding affinity of the resulting peptide, PSBP-6, to PS ($K_d \sim 100$ nM). Introduction of a lipophilic amino acid derivative (single-amino acid chelate, SAAC) chelated with Re to the N-terminus of PSBP-6 further increased the binding affinity of the resulting peptide, SAAC(Re)-PSBP-6 ($K_d \sim 26$ nM). Fluorescein-labeled SAAC(Re)-PSBP-6 colocalized with annexin V in apoptotic cells. Moreover, radiolabeled SAAC(^{99m}Tc)-PSBP-6 bound to apoptotic cells in a dose-dependent manner. After intravenous injection, SAAC(^{99m}Tc)-PSBP-6 located to B16/F10 melanoma tumors treated with taxanes that induced significant apoptotic response, but not to untreated tumors. Conclusions: PSBP-6-based imaging probes with high binding affinity to PS are promising for imaging of therapy-induced apoptosis.

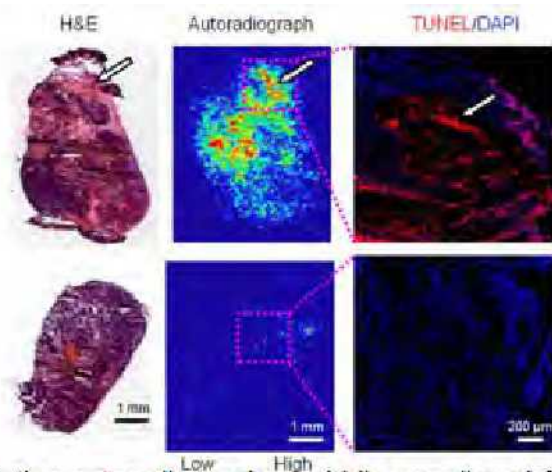


Figure. Representative autoradiographs (middle panel) and fluorescence microphotographs of tumor sections stained with TUNEL (right panel) 4 hr following intravenous injection of SAAC- ^{99m}Tc -PSBP-6 in nude mice bearing B16/F10 melanoma. Top row: tumor from a mouse treated with taxane; bottom row: untreated tumor.

Presentation Number **0604A**

Poster Session 1b: Imaging Molecular and/or Cellular Processes & Drug and/or Radiation Therapy

Annexin A5-Functionalized Nanoparticle for in Vivo Dual Modality Imaging of Apoptosis

Rui Zhang, Wei Lu, Xiaoxia Wen, Qian Huang, Miao Huang, Min Zhou, **Chun Li**, *Exp. Diagnostic Imaging, U.T. M. D. Anderson Cancer Center, Houston, TX, USA. Contact e-mail: cli@mdanderson.org*

Objectives: Noninvasive detection of apoptosis may play an important role in the evaluation of therapy efficiency and disease progression. In this study, we aim to develop Annexin A5-functionalized nanoparticles for dual optical/nuclear imaging of apoptosis. **Method:** Poly (ethylene glycol) (PEG)-coated, core-crosslinked polymeric micelles (CCPM) were dual-labeled with a near-infrared fluorescence fluorophores (Cy7) and a radioisotope (^{111}In). CCPM nanoparticles were conjugated with Annexin A5. To evaluate the specificity of Annexin A5-CCPM to apoptotic cells, both in vitro cell binding experiments and in vivo animal studies were carried out in a liver apoptosis model and a tumor apoptosis model. **Results:** In vitro, Annexin A5-CCPM exhibited high-affinity binding to apoptotic cells. This binding affinity could be efficiently blocked by Annexin A5. In liver apoptosis model, the apoptotic liver induced by anti-Fas antibody was clearly visualized by both nuclear and optical images after i.v. administration of ^{111}In -labeled Annexin A5-CCPM. In contrast, significantly lower signals were detected in healthy livers of untreated mice after i.v. injection of ^{111}In -labeled Annexin A5-CCPM and in apoptotic livers after i.v. injection of ^{111}In -labeled CCPM (without Annexin A5). The uptake values of ^{111}In -labeled Annexin A5-CCPM in apoptotic liver and healthy liver were 35% and 10%, respectively after injection. Similarly, ^{111}In -labeled Annexin A5-CCPM showed a significantly higher uptake in EL4 lymphoma in mice treated with cyclophosphamide/etoposide (8.0%) than in EL4 tumor in mice received no chemotherapy (3.2%). Histological analysis revealed colocalization between radioactivity and fluorescence signals from the nanoparticles, and therapy-induced apoptosis. **Conclusion:** Polymeric micelle targeted to apoptotic cells is a promising imaging probe for dual nuclear and optical imaging of apoptosis.

Presentation Number **0605A**

Poster Session 1b: Imaging Molecular and/or Cellular Processes & Drug and/or Radiation Therapy

 μ PET Imaging of Tumor Necrosis Induced by Photothermal Ablation Therapy

Shaoli Song^{1,2}, Chiyi Xiong¹, Min Zhou¹, Qian Huang¹, **Chun Li**¹, ¹Exp. Diagnostic Imaging, U.T. M. D. Anderson Cancer Center, Houston, TX, USA; ²Nuclear Medicine, Shanghai Jiaotong University, Shanghai, China. Contact e-mail: cli@mdanderson.org

Purpose: To investigate the potential application of small molecular weight ⁶⁴Cu-labeled hypericin in noninvasive assessment of response to photothermal ablation therapy. Methods: Hypericin was labeled with ⁶⁴Cu with high efficiency (>95% without purification). Eight mice bearing human mammary BT474 tumors were used. Four mice were injected intratumorally with semiconductor CuS nanoparticles followed by near-infrared (NIR) laser irradiation 2 h later (12 W for 5 min), and 4 mice were not treated to be used as a control. ⁶⁴Cu-DOTA-hypericin was injected intravenously 24 h after the laser treatment. μ PET images were acquired at 1, 6, 24, and 48 h after radiotracer injection. Results: CuS nanoparticles with diameter of ~11 nm absorbed NIR light, and mediated extensive tumor necrosis upon NIR light irradiation. Significant increases in ⁶⁴Cu-DOTA-hypericin uptake were found at 6, 24, 48 h after radiotracer injection in the treatment group while no uptake was observed in the control group at all time points. Tumor-to-muscle ratio in the treated group was ~20, which was >4 times higher than that in the control group at 6-48 h. Autoradiography and histology results were consistent with selective uptake of the radiotracer in the necrotic zone of the tumor induced by photothermal ablation therapy. Conclusions: ⁶⁴Cu-DOTA-hypericin is a promising agent in imaging therapy-induced necrosis.

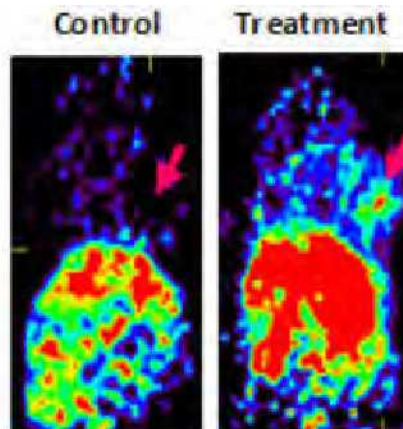


Figure 1. Representative μ PET images of mice in treatment and control groups 24 h after intravenous injection of ⁶⁴Cu-hypericin. High uptake of ⁶⁴Cu-hypericin was seen in tumors of treated mice but no of the control mice.

Presentation Number **0606A**

Poster Session 1b: Imaging Molecular and/or Cellular Processes & Drug and/or Radiation Therapy

Fluorescence imaging of tumor cell death using C2Am

Israt S. Alam¹, **Andre Neves**¹, **Kevin M. Brindle**^{1,2}, ¹University of Cambridge and Cancer Research UK Cambridge Research Institute, Cambridge, United Kingdom; ²Department of Biochemistry, University of Cambridge, Cambridge, United Kingdom. Contact e-mail: israt.alam@cancer.org.uk

The detection of phosphatidylserine (PS), exposed on the plasma membrane during apoptosis, is an established strategy for the detection of cell death. Annexin V (AnxV) is a PS-targeting probe, used extensively in vitro and in human studies. The C2A domain of Synaptotagmin I, like AnxV also binds PS in calcium dependent manner with nanomolar affinity. We have produced a site-directed mutant of the C2A domain (C2Am) with a single cysteine residue, providing a unique site for chemical modification with contrast agents (CA). We have recently shown that a fluorescent derivative of C2Am is a more specific probe for the detection of cell death in vitro than AnxV, due to C2Am's reduced background binding to viable cells. We show here, using fluorescence imaging that murine lymphoma tumors, treated with a chemotherapeutic drug, showed a 52% higher accumulation of the CA than control tumors treated with vehicle ($P < 0.05$, $n = 5/\text{group}$; see Figure 1). Ex vivo imaging of tumor necropsies also showed 82% higher signal in treated v. control tumors. Moreover, the probe showed favorable biodistribution with minimal liver accumulation and rapid kidney clearance (up to 86% in 24 hours). These preclinical results further highlight the potential of C2Am as a targeted CA for the detection of cell death, and consequently for monitoring tumour response to therapy, in the clinic. Comparative in vivo studies with AnxV are currently being undertaken.

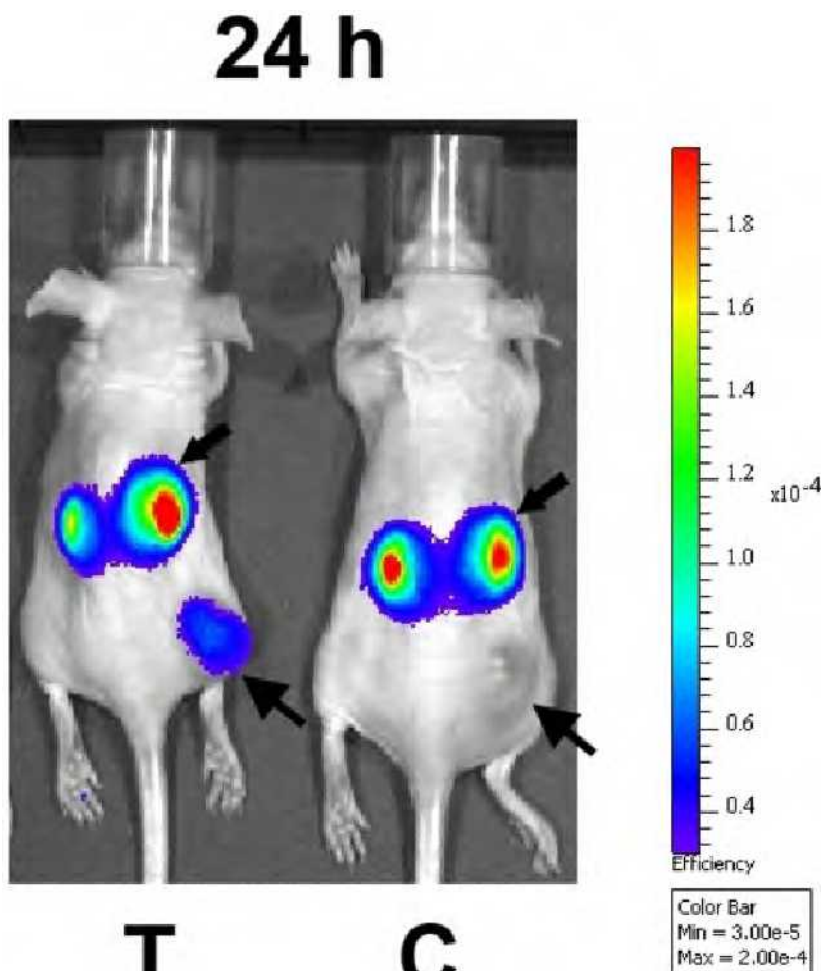


Figure 1: In vivo imaging of EL-4 murine lymphoma tumours implanted subcutaneously in the flank of nu/nu mice (indicated by thin arrows). The image above shows a representative mouse from the drug treated group (T) and from an untreated control group (C) at 24 hours post injection of the fluorescent derivative of C2Am. At 24 hours, signal from C2Am is only observed in the tumour of the treated mouse. Signal from the kidneys can be observed in both mice (thick arrows). The colour scale bar is in fluorescence efficiency units ($3E-05:2E-04$)

Presentation Number **0607A**

Poster Session 1b: Imaging Molecular and/or Cellular Processes & Drug and/or Radiation Therapy

Comparisons between mutant C2A, Apo-TRACE™ and other members of the Apo-SENSE family for the detection of cell death

Sarah L. Fawcett^{1,2}, **Israt S. Alam**^{1,2}, **Andre Neves**^{1,2}, **Jean-Frédéric Salazar**³, **Kevin M. Brindle**^{1,2}, ¹*Cambridge Research Institute, Li Ka Shing Centre, Cambridge, United Kingdom;* ²*Department of Biochemistry, University of Cambridge, Cambridge, United Kingdom;* ³*GSK Clinical Imaging Centre, Imperial College, Hammersmith Hospital, London, United Kingdom. Contact e-mail: slf43@cam.ac.uk*

The exposure of phosphatidylserine (PS) by dying cells has been exploited for imaging cell death in vitro and in vivo using Annexin V, including in clinical trials. Another PS-targeted agent, a site-directed mutant of the C2A domain of synaptotagmin I (C2Am) has recently been demonstrated to show more specific binding than Annexin V to apoptotic and necrotic cells in vitro (In press). Other imaging probes of cell death include the Apo-SENSE family of small molecules, which respond to apoptosis related membrane acidification, depolarisation, changes in electric potential and phospholipid scrambling. One member of this family, ML-10, is currently in human trials as a PET tracer. Another member, Apo-TRACE™, which has a UV fluorescent dansyl group, has been used for fluorescence-based in vitro studies. Using flow cytometry, the capability of C2Am labelled with Alexa-Fluor647 to identify cell death was compared with Apo-TRACE™. Both molecules labelled early apoptotic (EA) and late apoptotic/necrotic (LAC/N) murine lymphoma (EL4) cells following treatment with 5µM etoposide. C2Am-AF647 showed better differentiation between LA/N and viable cells and between the EA cells and the viable cells than Apo-TRACE™. For Apo-TRACE™ the fluorescence intensity of the LA/N cells fell below that of EA cells, suggesting reduced, or loss of, labelling of LA/N cells. This was not observed with C2Am. ML-10 accumulates in apoptotic but not in necrotic cells and its uptake can be increased upon depolarisation of viable cells with high K⁺ buffer. However, these characteristics were not shared by its "sister" Apo-TRACE™. The exact mode of action and the specific target of these molecules are unknown. Different members of the family appear to behave very differently. In conclusion, Apo-TRACE™ and C2Am-AF647 identify the same dead and dying cell populations but the C2Am-AF647 gives better differentiation from viable cells. Further comparisons are needed using PET/SPECT imaging to assess the ability of these molecules to identify cell death in vivo.

Presentation Number **0608A**

Poster Session 1b: Imaging Molecular and/or Cellular Processes & Drug and/or Radiation Therapy

Real Time Imaging of Apoptosis with a Polymeric Nanoprobes in live cells and animals

Sangmin Lee^{1,2}, **Seulki Lee**³, **Ki-Young Choi**^{1,2}, **Seo Young Jeong**², **Xiaoyuan Chen**³, **Kuiwon Choi**¹, **Ick Chan Kwon**¹, **Kwangmeyung Kim**¹, ¹*Biomedical Research Center, Korea Institute of Science and Technology (KIST), Seoul, Republic of Korea;* ²*Department of Life and Nanopharmaceutical Sciences, Kyung Hee University, Seoul, Republic of Korea;* ³*National Institute of Biomedical Imaging and Bioengineering, National Institutes of Health, Bethesda, MD, USA. Contact e-mail: basillio0902@hanmail.net*

Caspases are potentially useful direct markers for apoptosis and the real-time imaging of apoptosis would be valuable for both preclinical and clinical applications. In this study, we developed a biocompatible, cell-permeable, polymeric nanoparticle-based and caspase-3-sensitive nanoprobe (NP) capable of revealing early signs of apoptosis. Using a TRAIL and doxorubicin-induced apoptosis system, caspase-3 activity could be directly visualized in real time at the single cell level and in mouse models. Combination of near-infrared (NIR) fluorophore (Cy5.5) and dual-quenching mechanism provided low background and strong fluorescence signal amplification, thereby enabling clear optical imaging of intracellular processes. This system can be used to monitor dynamic changes in caspase activity, facilitating screening of apoptotic drugs in cell-based systems and in vivo models. The NP design platform is flexible and can be extended to the development of other specific caspase probes for real-time imaging of caspase-cascade reaction.

Presentation Number **0609A**

Poster Session 1b: Imaging Molecular and/or Cellular Processes & Drug and/or Radiation Therapy

Changes of ^{18}F -FDG and ^{18}F -FLT uptake by radiation induced senescence in human lung cancer cells

Kwang Il Kim¹, Joo Hyun Kang¹, Jin Kyung Rho², Yong Jin Lee¹, Tae Sup Lee¹, Jae Cheol Lee², Jae-Seon Lee³, Su Cheol Park², Gi Jeong Cheon¹, ¹Molecular Imaging Research Center, Korea Institute of Radiological and Medical Sciences, Seoul, Republic of Korea; ²Department of Internal Medicine, Korea Cancer Center Hospital, Korea Institute of Radiological and Medical Sciences, Seoul, Republic of Korea; ³Division of Radiation Cancer Research, Korea Institute of Radiological and Medical Sciences, Seoul, Republic of Korea.
Contact e-mail: kikim@kiram.s.re.kr

Purpose: Recently, it has been reported that radiotherapy or chemotherapy could induce premature senescence in cancer treatment. The evaluation of senescent cancer cells is indispensable for cancer treatment by induction of premature senescence. To develop imaging technique for evaluation of radiation induced senescence in cancer, we performed comparative analysis between the changes of ^{18}F -FDG/ ^{18}F -FLT uptake, and cellular senescence marker after radiation in human lung cancer cells. **Methods:** Two human lung cancer cell lines (A549 and H460) were plated with 5×10^4 cells per well in 6-well plates and were irradiated with 6 Gy the next day. After 72 hr, ^{18}F -FDG and ^{18}F -FLT uptake assay were performed, and these results were corrected with viable cell numbers. Also, cellular senescence was verified using senescence-associated β -galactosidase (SA- β -Gal) staining in the same batch. Gene expressions associated with glucose metabolism or cell proliferation were evaluated by RT-PCR. **Results:** The SA- β -gal positive cells as representative senescent cell marker were observed in irradiated A549 and H460 cells. ^{18}F -FDG uptake of irradiated cells was 2 fold increased than that of non-irradiated cells. ^{18}F -FLT uptake was decreased in irradiated A549 cells, but not changed in irradiated H460 cells. The increase of ^{18}F -FDG uptake seemed to be results in increase of glucose metabolism by radiation-induced senescence, and the decrease or constancy of ^{18}F -FLT uptake seemed to be results in inhibition of cell proliferation for typical phenotype of senescence. These results were supported with increase of hexokinase 2 and decrease of thymidine kinase 1 in gene expression level. **Conclusions:** In vitro model, radiation-induced senescence was able to be evaluated by the changes of ^{18}F -FDG/ ^{18}F -FLT uptake. These findings suggest that ^{18}F -FDG/ ^{18}F -FLT PET can be a useful imaging technique for in vivo evaluation of premature senescence.

Presentation Number **0610A**

Poster Session 1b: Imaging Molecular and/or Cellular Processes & Drug and/or Radiation Therapy

Simulation of the oxidative metabolism of 5-pyrrolidinylsulfonylisatins by online electrochemistry-HPLC-MS

Andreas Faust¹, **Anne Baumann**³, **Marilyn P. Law**¹, **Otmar Schober**¹, **Michael Schafers**², **Uwe Karst**³, **Klaus Kopka**¹, ¹*Nuclear Medicine, University Hospital Münster, Münster, Germany;* ²*European Institute for Molecular Imaging, University of Muenster, Muenster, Germany;* ³*Institute of Inorganic and Analytical Chemistry, University of Muenster, Muenster, Germany. Contact e-mail: faustan@uni-muenster.de*

Pyrrolidinylsulfonylisatins are of particular interest due to their specific inhibition of activated effector caspases, which execute the programmed cell death, called apoptosis. Therefore an ¹⁸F-labelled 5-pyrrolidinylsulfonylisatin ([¹⁸F]-AF-110) has been proposed as a potential caspase-targeted radiotracer for the molecular imaging of apoptosis in vivo. In addition to the evaluation of specific binding as well as pharmacokinetic properties the metabolic stability of the parent compound has to be examined to correct for signals arising from radioactive metabolites during the in vivo experiment. To refine the susceptibility of a radioligand to metabolism detailed structural information about its metabolites are needed. As reactive metabolites tend to undergo covalent binding to cellular macromolecules, the isolation and identification of the metabolites in these experiments are often hampered. Due to low amounts of the radiotracer and its radioactive metabolites down to the picomolar range a direct measurement of prepared blood samples by mass spectrometry cannot be realized. A purely instrumental method has thus been developed using an electrochemical cell coupled online to a HPLC-TOF/MS system to imitate the oxidative phase-I metabolism of AF-110 thereby identifying its metabolites. The oxidative metabolism of AF-110 has been investigated using online electrochemical oxidation as well as in vitro experiments based on incubation with liver cell microsomes. The electrochemical simulation resulted in a number of metabolites, including hydroxylation and N-dealkylation products. In comparison to the microsomal approach, some additional potential metabolites were detected. In a subsequent experiment [¹⁸F]-AF-110 was intravenously injected in mice, and then samples of organs and blood were taken and characterized ex vivo by radio-HPLC. HPLC traces indicate one main radioactive metabolite of [¹⁸F]-AF-110. The idea is to compare the different metabolites formed in vivo (mice), in vitro (rat liver microsomes) and electrochemically thereby gathering the desired structural information of the metabolites. These observations should result in a corresponding refinement of the parent AF-110 by introducing substituents that prevent and reduce oxidative phase-I metabolism and increase metabolic stability. The electrochemical approach is a valuable complementary tool and adds on existing methods already exploring metabolism of drugs. Finally, this approach can provide structural information of any metabolites very fast and in the end will reduce animal experiments.

Presentation Number **0611A**

Poster Session 1b: Imaging Molecular and/or Cellular Processes & Drug and/or Radiation Therapy

Apoptosis Targeting Peptides and Application to Molecular Imaging

Kiweon Cha, Mei Lan Piao, Byung-Heon Lee, In-San Kim, *Biochemistry and Cell Biology, Kyungpook National University, School of Medicine, Daegu, Republic of Korea. Contact e-mail: kwcha@knu.ac.kr*

Apoptosis has an essential role in controlling cell number in many developmental and physiological settings. Recently, the induction of apoptosis has been used in cancer treatments, including irradiation and chemotherapy. Therefore, the detection and monitoring of apoptotic cells is an extensively used molecular marker in noninvasive apoptosis imaging under certain clinical conditions, including the myocardial infarction, cerebral stroke and assessment of clinical diagnosis and therapeutic anti-cancer agents. Apoptosis targeting peptides have been identified by the screening of the phage display peptide library, which may be developed into a molecular probe for the apoptosis both in vitro and in vivo. Here, we lay particular emphasis on the quantitative and qualitative analysis of these peptides to apoptotic cells and the application to molecular imaging by a quantitative FACS analysis, fluorescence microscope and histological examination. The binding of peptides to apoptotic cells was evaluated via FACS analysis and histological examination. Molecular imaging analysis show that NIR fluorescent dye labeled apoptosis targeting peptides efficiently detect H460 tumor cells in xenografted animal model.

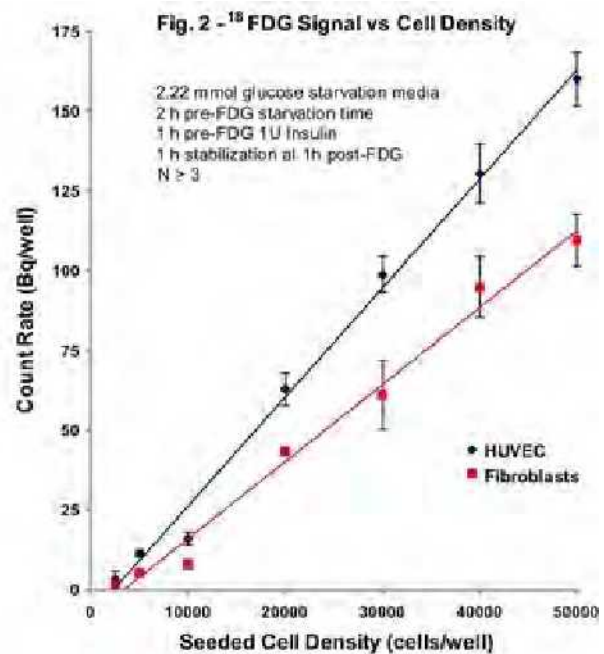
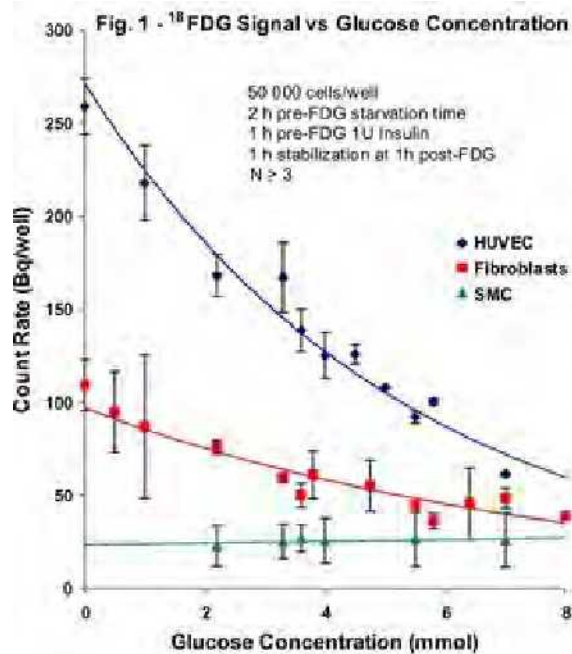
Presentation Number **0612A**

Poster Session 1b: Imaging Molecular and/or Cellular Processes & Drug and/or Radiation Therapy

18FDG PET Signal Optimization in Vascular Cells: A First Step Toward Bioreactor Cultures Monitoring

Julie A. Chouinard^{1,2}, Jacques A. Rousseau¹, Jean-François Beaudoin¹, Patrick Vermette², Roger Lecomte¹, ¹Médecine Nucléaire et Radiobiologie, Université de Sherbrooke, Sherbrooke, QC, Canada; ²Génie chimique et Génie biotechnologique, Université de Sherbrooke, Sherbrooke, QC, Canada. Contact e-mail: j.a.chouinard@gmail.com

Microenvironment strongly influences cell growth and function. One of the challenges in tissue engineering is to recreate and modulate such a complex in vivo setting within a bioreactor. Proper knowledge of the hydrodynamic, biochemical and mechanical factors influencing cell behavior in a controlled 3D environment is essential to generate tissue constructs suitable for clinical applications. Other significant challenges faced by tissue engineers include the lack of adequate tissue vascularization to ensure tissue oxygenation, nutrient delivery and waste removal, and the non-invasive assessment of tissue growth. Positron Emission Tomography (PET) provides a powerful mean for real-time monitoring of 3D cell or tissue cultures, allowing non-destructive, almost continuous, follow-up of the same samples. Various PET tracers are also available to potentially evaluate cell metabolism, proliferation, angiogenesis, perfusion, hypoxia, or apoptosis without hindering normal tissue development. In this study, living monolayer cell cultures were imaged with PET to investigate glucose metabolism in three human vascular cell types that are critical for micro-vessel network formation: endothelial (HUVEC), smooth muscle (SMC) and fibroblasts. The following 18FDG uptake parameters were optimized: insulin exposure and concentration, glucose starvation, incubation time, cell density and cell culture stabilization. Results (Fig. 1) show that glucose starvation combined with insulin stimulation greatly enhanced PET signal from HUVEC and fibroblasts, while insulin was found to hinder FDG uptake by SMC. Optimal factors were then used to correlate PET signal vs cell density starting with only a few thousand cells (Fig. 2). With the current settings, detection thresholds of 2300 seeded HUVEC and 3400 fibroblast cells were estimated. Briefly, cell FDG uptake parameters have been optimized by directly imaging living cells with PET. Future plans include the extension of the established method to a more realistic 3D model using a perfusion bioreactor.



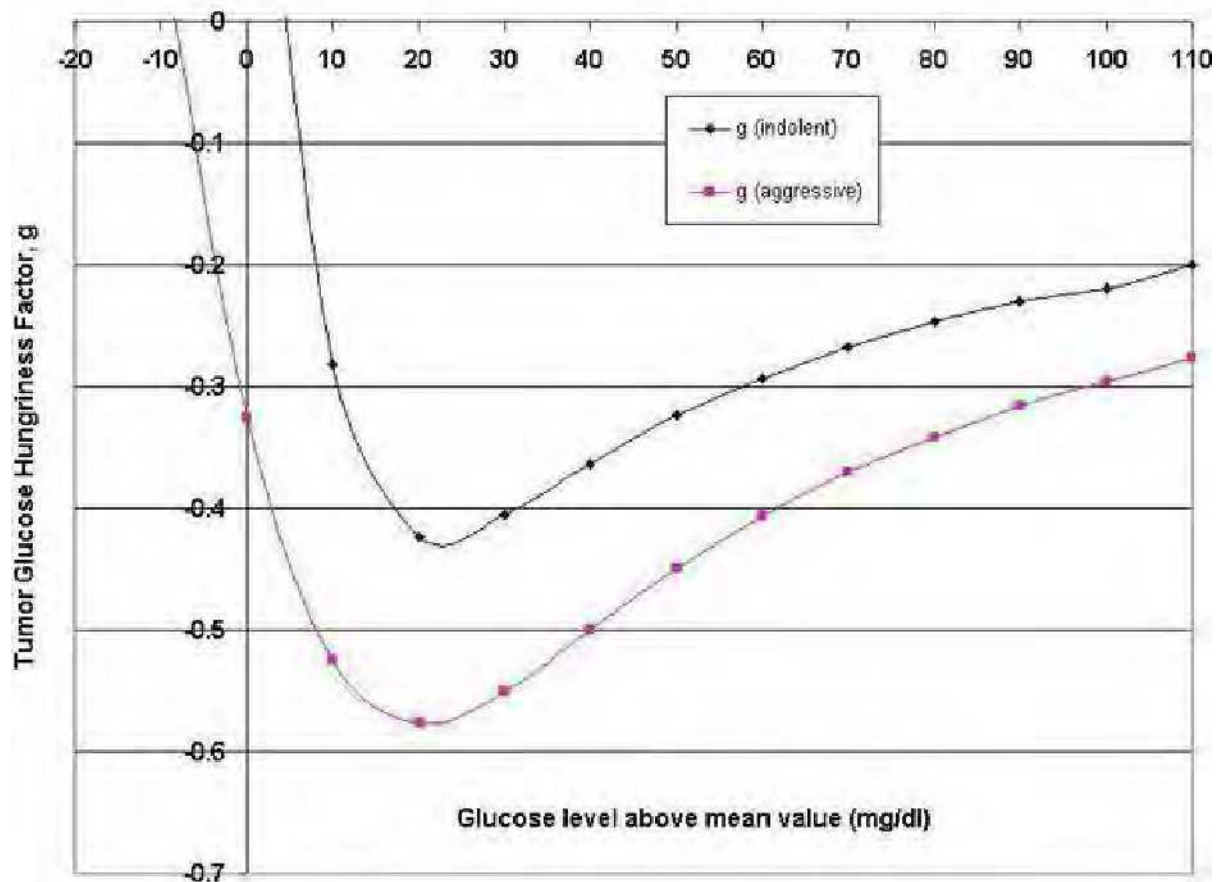
Presentation Number **0613A**

Poster Session 1b: Imaging Molecular and/or Cellular Processes & Drug and/or Radiation Therapy

Biostatistical investigation of tumor hungriness for glucose in lymphomas and its clinical implications

Regina H. Wong^{1,4}, **Christiana O. Wong**^{2,4}, **Bingfeng Tang**⁴, **Malaykumar M. Patel**⁴, **Joseph Thie**³, **Ching Y. Wong**⁴, ¹*Biophysics, University of Michigan, Ann Arbor, MI, USA;* ²*Cranbrook Education Community, Bloomfield Hills, MI, USA;* ³*University of Tennessee, Knoxville, TN, USA;* ⁴*Nuclear Medicine, William Beaumont Hospital, Royal Oak, MI, USA. Contact e-mail: iregina@umich.edu*

Objectives : To investigate tumor hungriness for lymphoma using biostatistical analysis of PET-CT data in aggressive and indolent lymphomas. **Methods :** 84 patients with aggressive (diffuse large B-cell, n=70) and indolent (follicular grade 1, n=14) grade lymphomas with FDG PET imaging were studied. The serum glucose level, [Glc], just before FDG injection, was recorded for each patient and the highest maximum SUV(standard uptake uptake) of the body were measured. The tumor hungriness for glucose was measured by g as defined by: $SUVc = SUV * (Gls / Glc)^g$ where [Gls] is the standard glucose level intended to be used for correction of SUV (SUVc). The various g values at different [Gls] in these two groups were separately calculated by minimizing the sum of square errors from the mean SUV of each group. Then the g values were plotted against [Gls] for these groups. **Results :** The mean [Glc] for aggressive and indolent lymphoma were similar (100±26 vs 98±12 mg/dl, p=ns). Both lymphoma types had a negative g value when [Gls] increased above mean value, which was consistent with physiologic response of tumor to ambient glucose changes. But the aggressive lymphoma had a more negative g value than that of indolent lymphoma for all ranges of [Gls], indicating different degree of tumor hungriness (g-negativity) for glucose in lymphoma subtypes. The g values achieved their minimum (most negative) value at [Gls] around 20 mg/dl above the mean value of [Glc]. **Conclusions :** There exists different degree of tumor hungriness for glucose in indolent and aggressive types of lymphoma. In order to obtain a more uniform SUV for tumor comparison among individuals, the SUV from PET imaging may need to be corrected with a tumor sub-type specific g-factor depending on the aggressiveness of lymphomas.



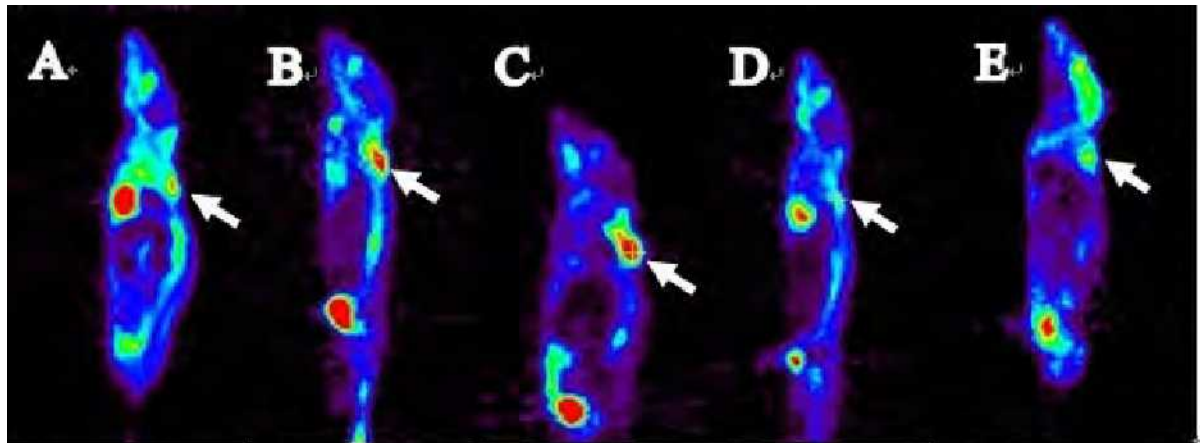
Presentation Number **0614A**

Poster Session 1b: Imaging Molecular and/or Cellular Processes & Drug and/or Radiation Therapy

Stimulation and inhibition of ^{18}F -FDG uptake in brown adipose tissue of mouse

Chenxi Wu^{1,2}, **Wuying Cheng**², **Zhaohui Zhu**², ¹*Nuclear Medicine, PUMC & CAMS, Beijing, China;* ²*Nuclear Medicine, Peking Union Medical College Hospital, Beijing, China. Contact e-mail: cicikitten@yahoo.com.cn*

Purpose: This study aims to investigate the physical (temperature) and pharmacological interventions to stimulate or inhibit ^{18}F -FDG uptake in brown adipose tissue (BAT) of mouse using MicroPET. **Method:** 5-10 weeks old female Kunming mice were enrolled. In physical intervention, 6 mice were exposed to cold (6-7 centigrade) for 1h before ^{18}F -FDG injection, 6 were exposed to cold for 1h and then kept in warm (35 centigrade) for 1h, 6 without cold exposure were kept in warm for 1h, and 12 controls were examined under room temperature (21 centigrade). For pharmacological stimulation, the mice received intraperitoneal injection of norepinephrine (NE, 2g/kg, n=3), isoprenaline (0.02g/Kg, n=6), epinephrine (0.025g/kg, n=5), and both cold and NE (n=7). For pharmacological inhibition, 6 cold pre-exposed mice received intragastric administration of propranolol (17g/kg, n=3) and 0.3ml saline (n=3) under 21 centigrade 1h before FDG injection. ^{18}F -FDG of 3.7 MBq was injected into peritoneal cavity for each mouse 40min before anesthesia with isoflurane. MicroPET scan under Siemens Inveon system was performed 50min after FDG injection. The uptake ratio (R) between interscapular BAT and brain was calculated and compared. Student's t-test was used for statistical analysis and $P < 0.05$ was considered significance. **Result:** Compared to controls, BAT uptake was significantly higher under cold exposure ($R: 10.22 \pm 4.13$ vs 4.08 ± 1.32 , $P = 0.01$) and highest with both cold and norepinephrine stimulations ($R: 15.64 \pm 5.58$ vs 4.08 ± 1.32 , $P = 0.001$). A stimulation with only NE, isoprenaline or epinephrine under room temperature all increased BAT uptake but with no significance ($p = 0.655$, 0.643 and 0.459). Warming could significantly reduce BAT uptake in mice with cold pre-exposed ($R: 2.13 \pm 0.43$ vs 10.22 ± 4.13 , $P = 0.005$) and without cold exposure ($R: 2.48 \pm 0.88$ vs 4.08 ± 1.32 , $P = 0.017$). In addition, propranolol could significantly reduce BAT uptake in cold pre-exposed mice ($R: 1.30 \pm 0.16$ vs 3.09 ± 0.90 , $P = 0.027$). **Conclusion:** Norepinephrine can generate a synergy effect with cold stimulation in increasing ^{18}F -FDG uptake in BAT. Warm intervention and Propranolol administration can inhibit the activation of BAT to different degrees. ^{18}F -FDG MicroPET scanning is useful to study BAT activation status under various interventions.



MicroPET images showing interscapular BAT FDG uptake (arrow) of control mouse (A), mouse under cold exposure (B), cold+NE (C), cold+warm (D) and cold+ propranolol (E).

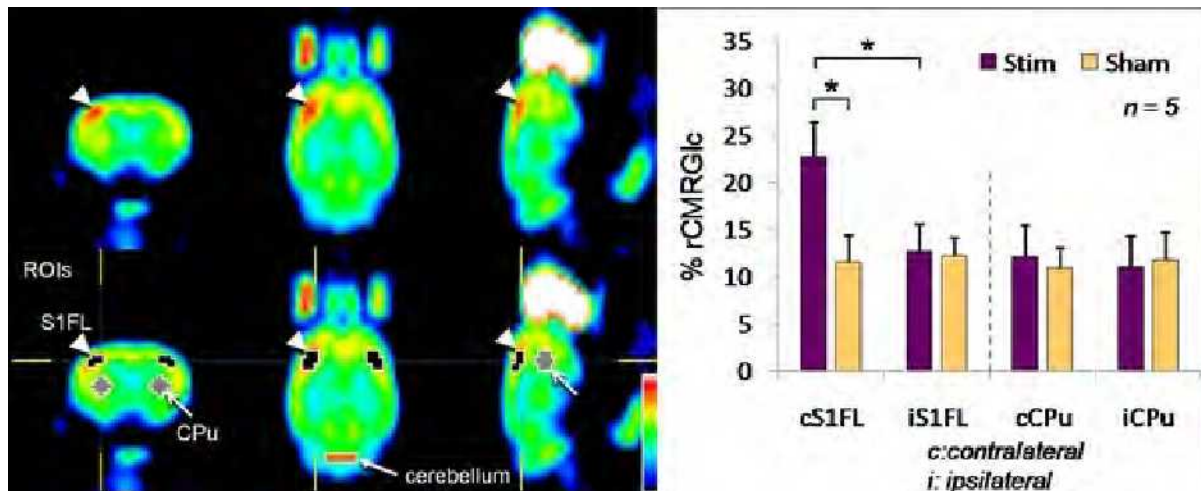
Presentation Number **0615A**

Poster Session 1b: Imaging Molecular and/or Cellular Processes & Drug and/or Radiation Therapy

¹⁸F-FDG microPET responses to the noxious forepaw stimulation

Yen-Yu Shih, Bryan H. De La Garza, Hsiao-Ying Wey, Timothy Q. Duong, *Research Imaging Institute, UT Health Science Center at San Antonio, San Antonio, TX, USA. Contact e-mail: shihy@uthscsa.edu*

Background: Forepaw electrical stimulation is the most widely used model in the field of fMRI. However, to our knowledge, this model has not been previously studied using microPET. Our group recently reported that noxious forepaw electrical stimulation not only activated the sensory cortex, but also specifically evoked sustained vasoconstriction in the rat striatum, together with increased neuronal spike activity [1]. This particular neurovascular uncoupling pattern prompted us to further investigate the metabolic responses to this stimulation model using ¹⁸F-FDG microPET. **Methods:** Ten SD rats were anesthetized with α -chloralose (60 mg/kg), mechanically ventilated (60 breaths/min), paralyzed with pancuronium bromide (3 mg/kg). Stimulation was applied to the right forepaw at 10 mA, 3 Hz, and 10 ms pulse duration. microPET scans were performed on a Focus 220 system. Three dimensional list-mode data were collected for 70 mins after the ¹⁸F-FDG injection (2.0-2.2 mCi, 0.5 ml). Typical OFF-ON stimulation paradigm was performed throughout the entire data acquisition period, where OFF = 1 min and ON = 1 min (n = 5). Another group of rats without stimulation was used as sham control (n = 5). Image reconstruction was performed by the MAP-OSEM algorithm. Data were analyzed by MANGO and the methods proposed previously [3]. Percent-relative cerebral metabolic rate of glucose (%rCMRglc) was computed by normalizing the microPET signal intensity to the cerebellum. Paired t-test and independent t-test were used to compare the difference between two hemispheres and two groups, respectively. Significance level was p < 0.05. Error bars were SEM. **Results & Discussion:** Increase in rCMRglc was predominantly localized in the contralateral primary somatosensory cortex of the forelimb (S1FL), but not in the ipsilateral side. Our findings demonstrated for the first time that ¹⁸F-FDG microPET can detect robust metabolic activation of the S1FL in the noxious forepaw electrical stimulation model. No significant change was observed in the striatum (CPu), indicating the vasoconstrictive pattern that we found previously [1] is independent of the neuronal (glucose) metabolism. References: [1] Shih et al., J Neurosci, 2009, 29:3036. [2] Shih et al., Neuroscience, 2008, 155:1221.



Presentation Number **0616A**

Poster Session 1b: Imaging Molecular and/or Cellular Processes & Drug and/or Radiation Therapy

Early Variable Time Point MicroPET/CT Modeling of Tumor Metabolic Kinetics in Xenograft Models of Murine Carcinoma

John L. Chunta¹, **Ching Y. Wong**², **Brian Marples**¹, **Sean Park**¹, **Alvaro Martinez**¹, **George D. Wilson**¹, ¹*Radiation Oncology, William Beaumont Hospital, Royal Oak, MI, USA;* ²*Nuclear Medicine, William Beaumont Hospital, Royal Oak, MI, USA.* Contact e-mail: John.Chunta@beaumont.edu

Objective: Early variable time point ¹⁸F-FDG PET imaging (VPET) may characterize tumor biology more completely than standard single time point scans. The aim was to investigate a sensitivity factor (S-factor) from VPET in human xenograft tumors for enhanced in vivo tumor characterization for the biostaging and ongoing evaluation of treatment (Tx) of novel and existing Tx protocols. Method: UT-14a (n=5)/UT16a (n=6) head & neck, and HT-29 (n=6) colon carcinomas were established in the flank of 17 surviving nude mice. Tumors were grown to a minimum diameter of 8mm before being imaged twice 7 days apart (PET0 and 7) using a FLEX Triumph™ PET-SPECT-CT system (GE/Gamma Medica, Waukesha, WI). Mice were fed on standardized diet and anesthetized with 1-2% isoflurane before injecting 22.9 MBq (±10%) of ¹⁸F-FDG into tail vein. PET were dynamically acquired for 2 hours with a CT scan. Data was analyzed using PMOD (PMOD Technologies, Zurich, Switzerland) to generate tumor time activity curves and volumes were derived from CT images using VIVID (GE/Gamma Medica). With the dynamic tumor activity (Q) from VPET, the S factor was calculated by $d\{\ln(Q)/d\{\ln(t)\}$ using regression of log-transformed data with 70% weighing on time from 0 to 33 min. A p-value <0.05 was considered significant by two-tailed t-tests. Procedures were approved by the institutional IACUC. Results: Faster growing tumors demonstrated a higher PET0 S-factor (HT-29 = 0.215±0.091, UT14a = 0.293±0.064) than slower growing tumors (UT16a = 0.132±0.046, p=0.0002). In HT-29 tumors, PET0 S-factor values were significantly higher than PET7 values (0.208±0.073, p=0.007), and this temporal difference nearly approached statistical significance in UT14a tumors (0.117±0.055, p=0.086). In contrast, the slower growing UT16a tumors proved to have a significantly lower S-factor on PET0 (0.132±0.046) than that derived from PET7 (0.241±0.062, p=0.006). Conclusions: S-factor variability was related to tumor growth rate. Faster growing tumors (HT-29, UT14a) characteristically had higher initial S-factor values than the slower growing tumors (UT16a). Additionally, the S-factor of aggressive tumors decreased with further growth, which was the opposite in the less aggressive tumors. Therefore, the S-factor reflects the time-dependent uptake activity of a tumor cell population. This metabolic kinetic parameter may be useful in studying post-Tx tumor response and characterizing remaining cell population, as well as in the “biostaging” of untreated tumors for optimal Tx planning during imaged guided adaptive cancer Tx.

Presentation Number **0617A**

Poster Session 1b: Imaging Molecular and/or Cellular Processes & Drug and/or Radiation Therapy

Molecular Imaging of Alterations in Cellular Bioenergetics and Met-HGF/SF Signaling induced by Mimp/Mtch2, a Mitochondrial Carrier Homologue

*Yamit Abargil Bar-Lev, Orly Cohen-Neeman, Ilan Tsarfaty, Microbiology and clinical immunology, Tel Aviv University, Tel Aviv, Israel.
Contact e-mail: yamit_abr@walla.co.il*

Mimp/Mtch2, a mitochondrial carrier homologue, induced by Met-HGF/SF signaling cloned in our lab, is involved in metabolic and bioenergetic processes. Mimp/Mtch2 is a target of tBID in cells signaled to die by TNF- α , and was recently shown to be a genetic marker for obesity. Mimp/Mtch2 reduces cells proliferation in vitro and tumor growth in vivo. Here we demonstrate the sub-cellular localization of Mimp in the mitochondrial outer membrane, using confocal microscopy and Imaris 3-D image visualization software. Over expression of Mimp alters mitochondrial structure. Using confocal based molecular imaging we show that Mimp/Mtch2 reduces the levels of reactive oxygen species ROS and prevents the HGF/SF induced increase in ROS. Mimp/Mtch2 also reduces the polarization of the mitochondrial membrane potential. Using cell array analysis we demonstrate that Mimp reduce the levels of Met signaling proteins or their activity (MAPK, pErk, Akt, pAkt, Myc, Ras, cJun and Src), in parallel to preventing the up-regulation of the transcription factors AP1, SRE, CRE and GRE. Advanced Network Analysis Tool (ANAT), was used to construct a protein network leading from Met to the proteins altered by Mimp. The putative signaling pathways are: Met-Ctnnb1(β -catenin)-Cnd1-Cdkn1A(p21), Met-Ctnnb1(β -catenin)-Gsk3B-Myc/Akt, Met-Cbl-Syk-TubA1A(Tubulin), Met-Cbl-Abl1-Rb1, Met-Cbl-PIK3R3, Met-RanBP9-Nr3c1(GRE)-Mapk1/CREB1/Jun, Met-Grb2-Src-Raf1-KRas, Met-Grb2-Src-SRF(SRE) and Met-Grb2-Shc. Several of the putative pathways such as β -catenin were validated using biochemical analysis. These recent results show a link between Mimp/Mtch2, an outer membrane mitochondrial carrier homologue, alterations of cellular metabolism and a tyrosine kinase growth factor receptor activity. Better understanding of this interplay between Met receptor tyrosine kinase and Mimp induced metabolic deregulation can improve the search for new targeted therapy in cancer and obesity.

Presentation Number **0618A**

Poster Session 1b: Imaging Molecular and/or Cellular Processes & Drug and/or Radiation Therapy

Exploring and Differentiating Early and Late Time Sensitivity Factors by MicroPET/CT Imaging of Indolent and Aggressive Head and Neck Carcinomas (HNCa) in Murine Xenograft Models

Ching Y. Wong¹, John L. Chunta², Brian Marples², Sean Park², Regina H. Wong^{3,1}, Alvaro Martinez², George D. Wilson², ¹Nuclear Medicine, William Beaumont Hospital, Royal Oak, MI, USA; ²Radiation Oncology, William Beaumont Hospital, Royal Oak, MI, USA; ³Biophysics, University of Michigan, Ann Arbor, MI, USA. Contact e-mail: owong@beaumont.edu

Objective: A previous study by Wong, et al. 2009 using late time point variable dual ¹⁸F-FDG PET scans has defined a time (t) sensitivity factor from any dynamic PET measurement Q as $S = d\{\ln(Q)/d\{\ln(t)\}$ to be a useful parameter for tumor kinetics in HNCa. The aim was to explore and compare an early time point S (ES) with the late time S (LS) in differentiating indolent and aggressive tumors using xenograft HNCa models. Method: Aggressive UT14a (n=5) and indolent UT16a (n=6) HNCa were established in the flank of 11 surviving nude mice. Tumors were grown to a minimum diameter of 8mm before being imaged two to three times at 7 days apart using a FLEX Triumph™ PET-SPECT-CT system (GE/Gamma Medica, Waukesha, WI). Mice were fed on standardized diet and anesthetized with 1-2% isoflurane before injecting 22.9 MBq (±10%) of ¹⁸F-FDG into tail vein at fasting condition. A total of 24 PET scans were dynamically acquired for 2 hours with a CT scan. Data was analyzed using PMOD (PMOD Technologies, Zurich, Switzerland) to generate tumor time activity curves and volumes were derived from CT images using VIVID (GE/Gamma Medica). The S factors was calculated by logarithmic regression of ln(Q) and ln(t) using time intervals from 0 to 33 min for ES and 60-120 min for LS. The transfer constant, Ki was also calculated using Patlak analysis from 12 to 70 min with the input function derived from aorta. A p-value <0.05 was considered significant by two-tailed t-tests. Procedures were approved by the institutional IACUC. Results: Aggressive tumors demonstrated significant higher ES than indolent tumors (0.250±0.078 vs 0.182±0.076, p=0.04) like the Ki (/min)(0.026±0.018 vs 0.012±0.009, p=0.04). The LS failed to reach a significant discrimination (0.021±0.199 vs, 0.168±0.193, p=0.08 for aggressive and indolent HNCa). Paired t-tests suggested significantly lower LS than ES in aggressive tumors (p=0.002) but not in indolent tumors (p=0.8), indicating that most of the FDG uptake in aggressive tumor occurred in early time points. Conclusions: S-factors in early time points appear to reflect the aggressiveness of tumors in the HNCa murine xenograft models. Aggressive tumors (UT14a) characteristically had higher ES than LS while there was no such difference in indolent tumors (UT16a). Therefore, the S-factor is time-dependent and ES may be used to indicate a tumor phenotype in a tumor cell population. This metabolic kinetic parameter may be useful in the "biostaging" for optimal Tx planning.

Presentation Number **0619A**

Poster Session 1b: Imaging Molecular and/or Cellular Processes & Drug and/or Radiation Therapy

Determination of Metabolic Biomarkers of Fatty Acid Synthase Inhibition with Orlistat in Non Small Cell Lung Carcinoma Cells In Vitro using NMR Spectroscopy.

Madhuri Sankaranarayanapillai, Juri G. Gelovani, *Experimental Diagnostic Imaging, MD Anderson Cancer Center, Houston, TX, USA. Contact e-mail: madhuri.pillai@mdanderson.org*

Introduction: Abnormal fatty acid synthesis is one of the common features of human cancer. Fatty acid synthase (FAS) is the key enzyme responsible for the de novo fatty acid biosynthesis and is over expressed in several cancers such as breast, prostate and lung. Limited data are available on the consequences of FAS inhibition in lung carcinomas. This study was aimed to elucidate the changes in metabolic characteristics of two non small cell lung carcinoma (NSCLC) cells, following inhibition of FAS with Orlistat using magnetic resonance spectroscopy (MRS). **Methods:** In vitro cultures of two human NSCLC cells, H441 and H1975 were treated for 24 hrs with 30 μ M of Orlistat; controls were treated with vehicle (DMSO). Culture medium contained equal concentrations of unlabeled and 1-¹³C D-glucose, and 64 μ M of 1,2-¹³C₂ Choline chloride. Water-soluble and lipid metabolites were extracted from the cells by dual phase method. ¹³C and ³¹P MRS was performed on a 600-MHz spectrometer. Metabolite levels were normalized to total cellular protein levels. Student's t-test was used to determine the statistical significance ($p < 0.05$) of the differences between control and Orlistat treated groups. **Results:** ¹³C MRS of water soluble metabolites showed no significant difference in de novo phosphocholine (PC) levels in H441 cells whereas in H1975 cells, the de novo PC levels are slightly increased (129% of control) in Orlistat treated group compared to control. The ¹³C labeled glucose was significantly higher in Orlistat treated group (156% of control in H441 and 186% of control in H1975), compared to control. Treatment with Orlistat resulted in a statistically significant drop in the de novo synthesis of fatty acids (43% of control in H441 and 42% in H1975) and phosphatidylcholine (PtdCho) (38% of control in H441 and 28% in H1975) as shown by ¹³C MRS of lipid-soluble metabolites. ³¹P MRS of water-soluble metabolites showed 340 & 160% increase in total PC levels following FAS inhibition in H441 and H1975 cells respectively. However, ³¹P MRS of lipid-soluble metabolites demonstrated a 63 and 72% decrease in total cellular PtdCho levels following Orlistat treatment, in H441 and H1975 cells respectively, as compared to control. **Conclusions:** The observed increase in PC levels following FAS inhibition by Orlistat in H441 and H1975 could be due to upregulation of PC synthesis and/or a decrease in PC utilization. The absence of changes in de novo synthesis of PC and a significant drop in de novo PtdCho levels following FAS inhibition also suggests a possibility of marked decrease in the Cytidylyltransferase (CTP) activity and/or a marked increase in choline kinase activity in these cells and could be used as non-invasive pharmacodynamic biomarkers.

Presentation Number **0600B**

Poster Session 3b: Imaging Molecular and/or Cellular Processes & Drug and/or Radiation Therapy

In vivo bioluminescence reporter gene imaging of the olfactory bulb in the mouse brain

Toshiyuki Hamada, Sato Honma, Ken-ichi Honma, *Advanced Photonic bioimaging center, Hokkaido University Graduate School of Medicine, Sapporo, Japan. Contact e-mail: toshi-ha@med.hokudai.ac.jp*

Bioluminescence by means of reporter enzyme firefly luciferase (luc) and substrate luciferin enables optical imaging of living animals with high sensitivity. In present study, we measured bioluminescence reporting clock gene expression in the olfactory bulb (OB) of the brain after systemic administration of D-luciferin without anesthesia under mild restriction. Period 1 (Per1) and Bmal1 are the clock genes which compose an autoregulatory feedback loop to generate circadian rhythms. Deficiency or mutation of the clock genes results in altered or loss of circadian rhythms in behavior and physiology. Per1 and Bmal1 are highly expressed in the OB and show robust circadian rhythms which are antiphasic to each other. Using Per1::luciferase (Per1::luc) and Bmal1::luciferase (Bmal1::luc) transgenic mice, we examined the time course of bioluminescence in the OB by an EM-CCD camera and the concentration of plasma D-luciferin by HPLC. Bioluminescence imaging revealed significant day-night differences in the OB 1h after the D-luciferin administration, which were antiphasic to each other in Per1::luc and Bmal1::luc mice. However, the plasma D-luciferin levels were not different between them and showed exponential decay after the injection. We also demonstrated that the circadian rhythms of bioluminescence in cultured OB and of mRNA levels are in accord with the in vivo imaging studies. These results suggest the bioluminescence of Per1 and Bmal1 expressions in the OB of conscious mice reflect the transcriptional activity of Per1 and Bmal1 genes in vivo.

Presentation Number **0601B**

Poster Session 3b: Imaging Molecular and/or Cellular Processes & Drug and/or Radiation Therapy

***In vivo* imaging of tumor transduced with bimodal lentiviral vector encoding human ferritin and green fluorescence protein on a 1.5T clinical MR scanner**

Hoe Suk Kim^{1,2}, Hye Rim Cho¹, Seung Hong Choi¹, YoonSeok Choi¹, Hyun Jung Joo¹, Woo Kyung Moon^{1,2}, ¹Radiology, Seoul National University Hospital, Seoul, Republic of Korea; ²Institute of Radiation Medicine, Medical Research Center, Seoul National University, Seoul, Republic of Korea. Contact e-mail: hoeskim@gmail.com

The aim of this study was to develop molecular imaging technology to be applied in studies to monitor tumor using lentivirus to simultaneously generate MRI and fluorescent imaging via expression of both myc-tagged human ferritin heavy chain (myc-hFTH) and green fluorescent protein (GFP). The transgene construct was stably transfected into MCF-7 and F-98 cells. After transplantation of the cells expressing myc-hFTH and GFP into mice or rats, serial MRI and fluorescent imaging of the transplanted cells were identified at locations corresponding to injection sites for 4 weeks, both using a 1.5T clinical MR scanner and using optical imaging analyzer. Cellular toxicity by overexpression of myc-hFTH and GFP evaluated by MTT and trypan blue exclusion assays was not observed. A large amount of accumulated iron in myc-hFTH cells and tumors was observed by Prussian blue staining and an iron binding assay. MRI analysis of the myc-hFTH cells and tumors showed significant signal drops in T2- and T2*-weighted images compared to mock ($p \leq 0.05$). Our study here represents the direct evidence that myc-hFTH expression can indeed be visualized non-invasively on a 1.5T clinical MR scanner. The success of this bimodal imaging technique using lentiviral vector may allow to monitor tumor growth, metastasis and regression with a high degree of accuracy and to provide further insight into the molecular mechanisms of cancer. Acknowledgements: This work was supported by the National Research Foundation of Korea(NRF) grant funded by the Korea government(MEST) (2010-0000423), by Basic Science Research Program through the National Research Foundation of Korea(NRF) funded by the Ministry of Education, Science and Technology (2009-0070356), by a grant from the Innovative Research Institute for Cell Therapy, Republic of Korea(Grant no. A062260) and by the Seoul R&D Program. Y. Choi and H. J. Joo are fellowship awardees of the Brain Korea 21 (BK21). Corresponding Author: Woo Kyung Moon

Presentation Number **0602B**

Poster Session 3b: Imaging Molecular and/or Cellular Processes & Drug and/or Radiation Therapy

Noninvasive assessment of regulable transferred-p53 gene expression and evaluation of therapeutic response with FDG-PET in tumor model

Winn Aung, Sumitaka Hasegawa, Michiko Koshikawa-Yano, Atsushi B. Tsuji, Chizuru Sogawa, Hitomi Sudo, Aya Sugyo, Misturu Koizumi, Takako Furukawa, Tsuneo Saga, Diagnostic Imaging Group, Molecular Imaging Center, National Institute of Radiological Sciences, Chiba, Japan. Contact e-mail: winn@nirs.go.jp

The use of tumor-suppressor gene p53 as an anticancer therapeutic has been vigorously investigated. However, progress has met with limited success to date. Some major drawbacks are the difficulty in achieving controllable and efficient gene transfer as well as in analyzing the transferred gene expression in real time and the treatment response in a timely manner. Thus, development of novel gene transfer vector with a regulative gene expression system coupled with the reporter gene, by which transgene can be monitored simultaneously, is critical. Moreover, noninvasive imaging-based assessment of the therapeutic response to exogenous wild-type p53 gene transfer is crucial for refining treatment protocols. In this study, as a simple preclinical model, we constructed a doxycycline-regulated bidirectional vector harboring a reporter gene encoding red fluorescence protein (RFP) and p53. Then, we determined the controllable and simultaneously coordinated expression of both proteins and the p53-mediated anticancer effects *in vitro* and *in vivo*. Next, we evaluated glucose utilization in cells with and without exogenous p53 expression by measuring the cellular uptakes of [¹⁴C]FDG, a PET radiotracer analogue, indirectly verified the transferred p53 overexpression in xenograft tumor via simultaneous expression of RFP detectable with an *in vivo* optical imaging system, and subsequently performed FDG-PET imaging in mice. We observed that cells or tumors with induced p53 overexpression exhibited decreased uptake of [¹⁴C]FDG in cellular assay and [¹⁸F]FDG in PET imaging. Thus, by coupling with novel bidirectional vector, controllable p53 transfer and the assumption that FDG-PET could be used as a surrogate imaging tool to assess the therapeutic response to p53 gene therapy was evidently confirmed, and this may favorably influence the improvement of p53 gene therapy.

Presentation Number **0603B**

Poster Session 3b: Imaging Molecular and/or Cellular Processes & Drug and/or Radiation Therapy

Improved Method of Lentiviral Based Gene Transduction in Human Hematopoietic Stem Cells (hHSCs)

Nadimpalli Ravi S Varma, Branislava Janic, Asm Iskander, M. M. Ali, Ali S. Arbab, Cellular and Molecular Imaging Laboratory, Henry Ford Hospital, Detroit, MI, USA. Contact e-mail: saali@rad.hfh.edu

Background: Human hematopoietic stem cells (hHSCs) have enormous potential as gene delivery vehicles in cell-based therapies. Successful delivery of therapeutic genes requires robust foreign gene expression in these cells. Therapeutic genes can be expressed in stem cells via Lentiviral transduction. However, Lentiviral transduction in stem cells is very often associated with low transduction efficiency and low levels of foreign gene expression. Therefore, the objective of this study was to optimize the conditions that will improve transduction efficiency and the expression levels of GFP protein. These results indicate cell growth factor stimulation of stem cells improved the transduction rate of Lentivirus carrying GFP gene. Methods and Results: Human cord blood was collected with an approved IRB protocol and cord blood AC133+ hHSCs were isolated by immunomagnetic positive selection using the MidiMACS system (Miltenyi, Auburn CA). To improve the transduction efficiency, prior to transduction AC133+ hHSCs were stimulated by using the concentration of growth factors that was 2 fold higher than the concentration used in standard AC133+ hHSC growth media. Specifically, AC133 cells were incubated for 10 hrs in Stemline II media (Sigma, MO) supplemented with 80 ng/ml of stem cell factor (SCF), 80 ng/ml of FLT3 and 20 ng/ml of thrombopoietin (TPO) (all from CellGenix, IL). After stimulation with the growth factors cells were transduced with Lentivirus as follows: hHSCs and Lentivirus were added to sterile 1.5 ml microcentrifuge tube in the 1: 2000 ratio and incubated for 1 hour at 37°C, 5% CO₂. After one hour, 500 µl of fresh media was added and transferred to a 6-well plate and further incubated for 24 hours. The GFP expression in transduced cells was analyzed by flow cytometry and 73% of transduced cells exhibited expression of GFP protein. At the same time, 41% of control cells that were incubated under standard growth conditions were positive for GFP. Conclusion: AC133+ hHSCs stimulated with higher concentration of growth factors exhibited improved transduction efficacy. The results indicate that a total of 32 % overall improvement of transduction rate was achieved with this improved transduction method. Cell growth factor stimulation of stem cells improved the transduction rate of Lentivirus carrying GFP gene and improved the transgene expression in the stem cells.

Presentation Number **0604B**

Poster Session 3b: Imaging Molecular and/or Cellular Processes & Drug and/or Radiation Therapy

Possibility of translocator protein (TSPO) as a PET reporter gene in the brain

Tsuyoshi Tahara, Atsuko Tamamoto, Kumiko Kobayashi, Hirotaka Onoe, Functional Probe Research Lab., RIKEN, CMIS, Kobe, Japan. Contact e-mail: tsuyoshi.tahara@riken.jp

Gene therapy and cell transplantation are expected to be breakthrough of therapeutic approach for neurodegenerative disorders, such as Parkinson's and Alzheimer's diseases. Though it is critically important to monitor the functionality and safety of virus vectors and survival of engrafted cells in the brain during the therapeutic period, there are a few methods to estimate those aspects under the living condition. Therefore, it is quite useful to monitor the effectiveness of these therapies by noninvasive imaging method, such as positron emission tomography (PET) or magnetic resonance imaging (MRI). Translocator protein (TSPO), also known as a peripheral benzodiazepine receptor (PBR), has been studied in vivo by PET using [^{11}C]PK11195 to detect the activated glial cells in inflammation and cancer. In PET study under the normal condition, [^{11}C]PK11195 is known to enter but hardly accumulate in the brain, because its low level of the expression in the neuronal cells. To investigate the possibility of TSPO as a reporter gene for monitoring of availability of engrafted cells after transplantation and function of virus vector after infection in the brain, we constructed the expression vector of TSPO. In addition, we also constructed the expression vectors of TSPO mutants (Y153S, R156L and both) in CRAC sequence, which is known as a binding domain of cholesterol in C-terminus, to lose the physiological function of cholesterol transportation. Using expression vectors, wild type TSPO (WT) and 3 mutant proteins were able to be expressed in the mouse neuroblastoma cell, neuro2a and rat glioma cell, C6. To examine the binding activity of these mutant proteins [3H]PK11195, we carried out binding assay of C6 glioma cells transfected with TSPO and its mutant. As similar to WT transfected cell, other 3 transfected cells with mutant proteins showed higher binding activities as compared with that of untransfected cells. To investigate whether TSPO gene could be used as a PET reporter gene in the brain, first, we performed [^{11}C]PK11195 PET study of rat, which was engrafted C6 cells with WT gene (C6-WT) in the brain. By the PET imaging, we observed higher accumulation of [^{11}C]PK11195 in the engrafted C6-WT cells than those in engrafted normal C6 cells. These results indicate that TSPO gene has the potency as tool of in vivo imaging of cell availability of engrafted cells in the brain.

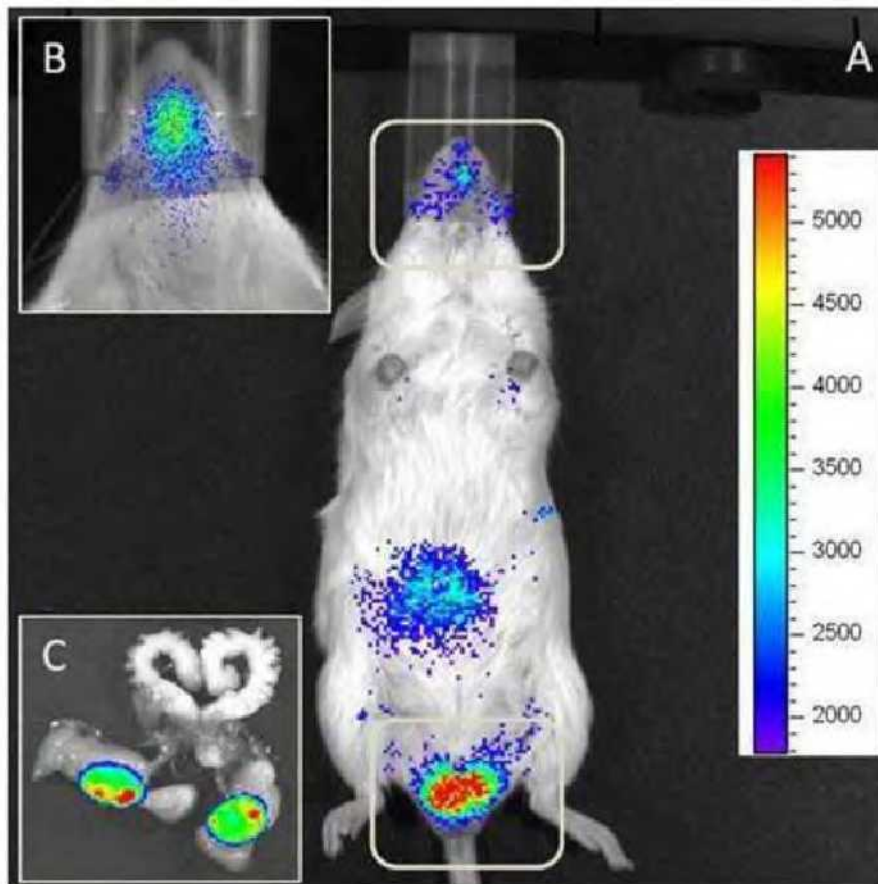
Presentation Number **0605B**

Poster Session 3b: Imaging Molecular and/or Cellular Processes & Drug and/or Radiation Therapy

In vivo Imaging Reveals Tissue-Specific Fibroblast Growth Factor 1.B (FGF1.B) Promoter Activity in Trimodal Reporter Mice

Shan-Wen Liu^{1,2}, **Mei-Ru Chen**², **Tzu-Chin Wu**², **Ching-Han Hsu**^{1,2}, **Kurt M. Lin**², ¹*National Tsing Hua University, Hsinchu County, Taiwan;* ²*National Health Research Institutes, Miaoli County, Taiwan.* Contact e-mail: jwniffliu@gmail.com

The objective of this study was to develop a trimodality imaging reporter (abbreviated as TMIR) transgenic mouse driven by fibroblast growth factor 1B promoter (FGF1.B or F1B) and to visualize the expression of imaging reporters as a marker for endogenous F1B promoter activity in a living animal. In this study we established a trimodal imaging reporter gene, including components from firefly luciferase, enhanced green fluorescent protein, and truncated herpes simplex virus type 1 thymidine kinase (HSV1 tk). This single fused reporter was placed under the control of 540-bp human F1B promoter that along with other three promoters (1.A, 1.C and 1.D) controls FGF1 expression in a tissue-specific manner. F1B was previously shown to enhance the FGF1 expression in brain and retina. Using in vivo non-invasive imaging including bioluminescence and HSV1 tk- specific PET/SPECT, expression of TMIR in mice was revealed not restricted in the brain and eyes, but also in the nasopharynx, skull, and spine. A high level of TMIR expression was also found in the testes (Fig. A and the amplified Figs. B & C). We validated our findings by analyzing the bio-distribution of HSV1tk probes in isolated organs and by immunohistochemical staining for TMIR, of which the expression was confirmed in the above tissues and in the Leydig cells of testes. Moreover, we analyzed the expression pattern of FGF1 exons and confirmed that the endogenous F1B promoter activity in tissues was in agreement with a high level of reporter expression in F1B-TMIR mice. In summary, we demonstrated in this study that the reporter transgene expression could be imaged in vivo by various imaging platforms with corresponding probes. Our results demonstrate the advantages and challenges of employing multimodal reporter mice driven by endogenous promoter in biomedical research; in particular, the imaging results of F1B-TMIR mice have led to the novel discovery of FGF1B promoter activity in the Leydig cells of testes.



Presentation Number **0606B**

Poster Session 3b: Imaging Molecular and/or Cellular Processes & Drug and/or Radiation Therapy

Localized imaging and blood-based detection of breast cancer

Jason M. Warram¹, Anton Borovjagin³, Kurt R. Zinn^{1,2}, ¹Molecular and Cellular Pathology, University of Alabama at Birmingham, Birmingham, AL, USA; ²Radiology, University of Alabama at Birmingham, Birmingham, AL, USA; ³Dentistry, University of Alabama at Birmingham, Birmingham, AL, USA. Contact e-mail: mojack@uab.edu

Improvements are needed for the early detection of breast cancer, as current imaging methods lack sensitivity to detect small tumors and account for differences in patient phenotype. New imaging technologies include genetic strategies for improved diagnostic screening. It would be advantages to link an easy screening method with imaging. We propose a system where early diagnostic and monitoring of breast cancer can be achieved with a dual-reporter adenovirus (Ad) that includes a human secreted embryonic alkaline phosphatase (SEAP) reporter for blood-based screening and a fluorescent reporter (mCherry) for imaging, both under the control of the cancer-specific Id1 promoter. Id1 is a member of the inhibition of differentiation gene family that encodes helix-loop-helix proteins which inhibit transcription by forming inactive heterodimers with basic helix-loop-helix (bHLH) proteins. Id1 is up regulated in association with breast tumor progression. SEAP is not expressed in adults, expression will not induce an immune response since it is of human origin, and it can be detected specifically in blood with high sensitivity. Toward this goal, the cancer-specific diagnostic Ad vector (Ad5/3-Id1-SEAP-Id1-mCherry) was produced, with an Id1 promoter driving expression of each reporter to permit optimal levels along with a 5/3 fiber modification to improve targeting and overall infectivity. Breast cancer cell lines (MDA-MB-231 and MCF7) infected with Ad5/3-Id1-SEAP-Id1-mCherry produced SEAP levels that were at least 10-fold above background by 2 days and the absolute levels were correlated via western blot with the varying levels of Id1 protein in the cell lines. As expected for the Id1 promoter, a drop in serum to 2% in the growth media significantly ($p < 0.05$) decreased both SEAP and mCherry. A bolus of Ad5/3-Id1-SEAP-Id1-mCherry infected cells (MDA-MB-231, MOI=10) and uninfected cells implanted in the mammary fat pad of athymic nude mice to evaluate sensitivity produced blood SEAP levels (0.36ug/ml +/- 0.05) that were significantly ($p < 0.05$) elevated over baseline (0.03ug/ml +/- 0.002), with as little as 2.5% (5×10^4) Ad-infected cells constituting the total tumor. Imaging easily detected mCherry in tumor xenografts on day 2 post implantation. This diagnostic system that combines screening with imaging can easily be manipulated to include other reporters/modalities and cancer-targeting methods leading to a continuous progression in the field of breast cancer detection and monitoring.

Presentation Number **0607B**

Poster Session 3b: Imaging Molecular and/or Cellular Processes & Drug and/or Radiation Therapy

In vivo tracking of fibroblast trans-differentiation to myofibroblasts in the tumor microenvironment*Yoseph Addadi, Michal Neeman, Biological regulation, weismann institute, Rehovot, Israel. Contact e-mail: yosepha@weizmann.ac.il*

The tumor microenvironment has a crucial role in the process of tumor development and its interaction with the surrounding tissue, affecting processes such as angiogenesis, lymphangiogenesis and metastatic spread. One of the major components of the tumor stroma are fibroblast cells originating from the surrounding tissue and recruited from distant locations. Once at the tumor site, fibroblasts are known to trans-differentiate to myofibroblasts, acquiring properties of smooth muscle cells. Previous studies performed in our lab and by others led to the suggestions that myofibroblasts at the tumor - host interface guide endothelial sprouts. Fibroblast activation can be monitored through the expression of alpha smooth muscle actin (α -SMA). This can be easily done ex vivo by immunohistochemical staining on processed tissue. In order to study the trans-differentiation process in vivo with high specificity and high resolution, we cloned the α -SMA promoter from genomic DNA and inserted it in front of a red fluorescent protein. This reporter was utilized to transfect a fibroblasts cell line. Upon injection of these cells into tumor bearing mice, they are recruited to the tumor, where they differentiate. Following differentiation the promoter is activated and red fluorescent signal can be detected. Introducing these cells to mice in which tumors develop in a dorsal skin chamber imaged by two photon microscopy, enabled us to follow the differentiation process at high resolution in real time, study its relations to the blood vasculature, tumor cells and tumor progression kinetics. In order to validate our results we performed immunohistochemical staining for α -SMA in the experiment end point, without destroying the signal from the differentiated cells. This stain adds the detection of α -SMA positive cell that does not originate from the transfected fibroblast injected by us, therefore, does not create a signal in vivo. Differentiation of fibroblast to myofibroblast is of a high functional significance; incorporation of this data into the available knowledge of the 3D arrangement and dynamic of fibroblast in the tumor area will improve our understanding of fibroblasts function and their contribution to the overall angiogenic and lymphangiogenic processes.

Presentation Number **0608B**

Poster Session 3b: Imaging Molecular and/or Cellular Processes & Drug and/or Radiation Therapy

Development of monitoring system for activation of neuronal differentiation induced by Neurogenin 1 gene in human neural stem cell

Hyun Jeong Oh¹, **Do Won Hwang**^{1,2}, **Hyewon Youn**^{1,2}, **Dong Soo Lee**^{1,2}, ¹*Department of Nuclear Medicine, Seoul National University College of Medicine, Seoul, Republic of Korea;* ²*Institute of Radiation Medicine, Medical Research Center, Seoul, Republic of Korea.*
Contact e-mail: holyhiphop@lycos.co.kr

Purpose: Neurogenin1 (Ngn1) which is known as a basic helix loop helix neurogenic factor has been used as an activator of neuronal differentiation. The aim of this study is to confirm the functional effect of Ngn1 during the induction of neuronal lineage from human neural stem cell and develop the reporter-based monitoring system for neural differentiation induced by Ngn1. **Methods:** Neuron specific enolase (NSE) promoter-coupled luciferase reporter system (pNSE-Gluc) was used to confirm NSE activity during neural differentiation. G2, human neural stem cell was maintained in general culture medium containing doxycycline. Gaussia luciferase activity was acquired using luminometer for examining pNSE-Gluc reporter activity and normalized by BCA (bicinchoninic acid) assay. **Results:** Ngn1-induced neuronal differentiation was successfully monitored by pNSE-Gluc reporter system. After induction of neuronal differentiation for 2 days by removal of doxycyclin, a morphological change such as neurite outgrowth was observed. Immunofluorescence staining exhibited that MAP2, neuronal marker expression was seen in 4 days after induction of neuronal differentiation. Moreover, 4 days after induction of neuronal differentiation, we were able to observe that G2 cells carrying luciferase gene regulated by NSE promoter exhibited the enhanced luciferase signal when it compared to that of undifferentiated G2 cells. However, transient transfection of Ngn1 showed that the elevated luciferase expression was observed in undifferentiated condition. **Conclusions:** In this study, we confirmed the functional effect of Ngn1 and established the condition of neurogenesis in G2 cells. Ngn1 factor is sufficient to induce neuronal differentiation of human neural stem cell G2. Moreover, our reporter system could provide feasible study to monitor the activation pattern of the neuronal differentiation by Ngn1.

Presentation Number **0609B**

Poster Session 3b: Imaging Molecular and/or Cellular Processes & Drug and/or Radiation Therapy

Visualization of hNIS activity enhancement via heat shock using hNIS/tdTomato fusion reporter gene for nuclear imaging and red fluorescence imaging

Chan Joo Yeom¹, Hyewon Youn¹, Keon Wook Kang¹, Dong Soo Lee^{1,2}, June-Key Chung¹, ¹*Department of Nuclear Medicine and Cancer Research Institute, Seoul National University College of Medicine, Seoul, Republic of Korea;* ²*Department of Molecular Medicine and Biopharmaceutical Science, WCU graduate School of Convergence Science and Technology, Seoul, Republic of Korea.*
Contact e-mail: cj.yeom@gmail.com

Thyroid cells have a unique ability to accumulate radioiodine due to the expression of sodium-iodide symporter (NIS) protein, consequently permitting radioiodine therapy. However, the iodide uptake is lost in 10-30% of thyroid cancers and this causes the failure of radioiodine therapy. Researches have been focused to elevate NIS activity for improving the efficacy of radioiodine therapy. Heat stress has been reported to activate heat shock proteins which play central roles in folding and assembly of proteins. In this study, we hypothesized that heat shock may contribute to produce functional hNIS protein, and evaluated whether heat shock enhances the hNIS activity in cancer cells using a fluorescence imaging reporter gene named tdTomato. We established HeLa cells expressing hNIS/tdTomato fusion proteins under CMV promoter (HeLa-hNIS/tdTomato). We measured the activity of NIS/tdTomato using I-125 uptake assay and a fluorescence imaging system before and after heat stress. To validate the successful use of fusion protein for reflecting functional NIS activity, we evaluated the changes of hNIS activity when the cells were treated with siRNA for hNIS. An inhibitor of transcription, actinomycinD (AMD) and an inhibitor of protein synthesis, cycloheximide (CHX) were treated before heat shock for monitoring the effective level of NIS expression. In vivo images of HeLa-hNIS/tdTomato xenografts were acquired using a gamma camera for nuclear imaging and Maestro instrumentation for fluorescence imaging. In confocal microscopy imaging, tdTomato fluorescence signal in stable cells decreased depending on the concentrations of siRNA for hNIS, indicating hNIS/tdTomato fusion proteins successfully represent hNIS. The radioactivity or fluorescent signal increased in HeLa-hNIS/tdTomato cells after heat shock compared to that in stable cells incubated at 37°C for 24 h without heat treatment. In live cell imaging, the signal intensity of hNIS/tdTomato which is localized in cell membrane, gradually increased up to 24 h after heat shock. In vivo imaging, scintigraphy and fluorescence signal were observed in xenografts. These results indicate that heat stress induces the enhancement of the hNIS/tdTomato activity and our gene fusion system can be useful for monitoring change of hNIS expression in the cellular levels (by fluorescence) as well as in the whole animal (by scintigraphy).

Presentation Number **0610B**

Poster Session 3b: Imaging Molecular and/or Cellular Processes & Drug and/or Radiation Therapy

Remote control of gene expression in *Salmonella typhimurium* with doxycycline and Tet repressor

Sheng Nan Jiang¹, Seung-Hwan Park¹, Yeongjin Hong², Hyon El Choy², Jung-Joon Min¹, ¹Nuclear Medicine, Chonnam National University Medical School, Hwasun, Republic of Korea; ²Microbiology, Chonnam National University Medical School, Gwangju, Republic of Korea. Contact e-mail: quanjz@hanmail.net

We previously reported that bacteria carrying cytotoxic protein such as cytolysin A (ClyA) showed high tumor suppression effect in tumor-bearing mice. Because the bacteria might show severe toxic effect on normal organ when therapeutic protein is expressed constitutively, we need to develop the controllable system that is able to be turned on gene expression only in the tumor tissue. We employed the bacterial Tet promoter which is a potential remote controllable systems by tetracycline or doxycycline. The Tet system is composed of Tet operator and Tet repressor. Without inducer doxycycline, Tet repressors binds to Tet operator and repress the two divergent Tet promoters. Upon binding doxycycline, conformation of Tet repressor is changed and released from Tet operator thus the Tet promoters are activated. In this study, we constructed bacterial Tet plasmid (pTet) system in which two different genes could be controlled simultaneously and cloned reporter gene Rluc8 under TetA promoter and Fluc under TetR (pTet-Rluc8/Fluc) respectively. When the pTet-Rluc8/Fluc of *Salmonella typhimurium* Δ ppGpp strain was induced by doxycycline (0.5 μ g/ml) in vitro, the expression of Rluc8 and Fluc increased > 1000 -fold and 11-fold, respectively. When the pTet-Rluc8/Fluc was assayed in tumor bearing mice, two reporter genes was expressed only after feeding doxycycline (475 μ g/day). Based on the result, we are constructing pTet-ClyA/GFP and transformed *Salmonella typhimurium* (Δ ppGpp) expressing lux operon in their chromosome to develop multifunctional bacteria expressing diverse diagnostic and therapeutic signals; (1) noninvasive whole body bioluminescence, (2) cellular fluorescence, and (3) therapeutic cancer agent. In conclusion, we successfully engineered bacteria to deliver and express diagnostic or therapeutic molecules specifically in tumor.

Presentation Number **0611B**

Poster Session 3b: Imaging Molecular and/or Cellular Processes & Drug and/or Radiation Therapy

MRI detection of mouse-ferritin transgenic mice

Sunup Park^{1,2}, Gunwoo Lee^{1,2}, Gyuman Park², Onseok Lee^{1,2}, Kwan S. Hong³, Hyeonseung Lee³, Yu Dae-Yeul⁴, Chilhwan Oh^{1,5},
¹Biomedical Science of Brain Korea 21, Korea University College of Medicine, Seoul, Republic of Korea; ²Research Institute for Skin Image, Korea University Medical Center, Seoul, Republic of Korea; ³MRI Team, Korea Basic Science Institute(KBSI), Chungbuk, Republic of Korea; ⁴Aging Research Center, Korea Research Institute of Bioscience and Biotechnology, Taejeon, Republic of Korea; ⁵Department of Dermatology, Korea University Guro Hospital, Seoul, Republic of Korea. Contact e-mail: sunup72@naver.com

Ferritin is a ubiquitous protein which serves to store iron in cytoplasmic part of cell as a non-toxic form. Recently, it has been developed for new methodology for tracking the cell by endogenous MRI reporter, ferritin. In this study, we generated TET:AcGFP-mFth1(tet-mFth1) transgenic mice from a bidirectional expression cassette containing AcGFP and hemagglutinin-tagged mouse ferritin heavy chain protein coding region. We induced transgene expression in double-transgenic (dTG) offspring derived by crossing tet-hfer mice with CMV:tTA mice. We further bred one founder family, found to express both AcGFP and mFth1, to establish a homozygous transgenic tet- mFth1 line. By RT-PCR, we found that mFth1 was over-expressed in liver by tetracycline treatment. We also performed magnetic resonance image of transgenic mice at 4.7 Tesla. We acquired R2 values from multi-slice-spin-echo (MSME) images (TR 2,000ms, 8 echo times 11-88 ms, slice thickness 1 mm, matrix 128 x 128) by single exponential fit of the signal intensity decay with echo time. In double-transgenic transgenic mice, elevated relaxation rates are detected in liver with tetracycline treatment. We propose that this transgenic mouse could be useful animal model for monitoring the hepatologic diseases.

Presentation Number **0612B**

Poster Session 3b: Imaging Molecular and/or Cellular Processes & Drug and/or Radiation Therapy

Establishment of tightly IR switch for cancer genetic therapy

AI Huang¹, Luen Hwu¹, Ren-Shyan Liu^{1,2}, ¹MAGIC/NRPGM, Nuclear Medicine, Faculty of Medicine, National Yang-Ming University Medical School, Taipei, Taiwan; ²NPCC, Taipei Veterans General Hospital, Taipei, Taiwan. Contact e-mail: s19204005@hotmail.com

Aim: Traditionally, radiotherapy provides a first frontline management of cancer. However, the shortage of radiotherapy could be resulted from the radio-resistant and damage to normal tissues. To manipulate endogenous expression and applicant in cancer therapy, we focused on certain immediately early genes that codes for transcriptional factors were induced by IR. To achieve tightly ionizing radiation (IR) switch, we constructed several synthetic CArG promoterless constructs that control therapeutic/reporter gene expression with the spatial and temporal manner in the radiation-induced genetic therapy on tumor. In the present study, we showed that the tandem repeated CArG element could be function as IR switch to image reporter gene expression in vivo by using two-step transcriptional amplification (TSTA) system. **Method:** We acquired three constructs that contain 9, 18, and 31 tandem repeated CArG element, respectively, linking with the luciferase reporter gene to evaluate these constructs activity in the presence of IR triggering. Furthermore, we choose the E9 promoter as IR switch model, pE9nlsCRE and the loxP flanked stop cassette reporter construct (pCMV-stop-luc), to validate IR inducible activity by TSTA system. Then we established pCMV-stop-luc stable clones were used for in vivo and in vitro study of E9 IR switch. **Result:** All constructs showed transcription activation increased above 1.5 folds after radiation triggering. The reporter activity obtained from transient transfection pE9nlsCRE into the pCMV-stop-luc reporter clone showed that significant amplified about 100 folds in the absence of irradiation. Besides, under IR triggering, radiation enhancement transcription expression still retain in Cre/loxP system. In addition, we used mouse xenograft of pCMV-stop-luc stable clone as in-vivo animal model to test E9 function. Bioluminescence image showed that the pE9nlsCRE could activate luciferase gene expression remarkable by directly injection of pE9nlsCRE- in vivo-jetPEITM mixture into the xenograft of mouse in the presence of IR triggering. **Conclusion:** Base on our results, we applied tandem repeated CArG element directly as a radio-responsive promoter and which could be activated in the spatial and temporal manner. However, we believe this promoter combines with TSTA system that could result in significantly amplified reporter/therapeutic gene expression and will be benefit to cancer genetic therapy.

Presentation Number **0613B**

Poster Session 3b: Imaging Molecular and/or Cellular Processes & Drug and/or Radiation Therapy

Use of the piggyBac Transposon Based Gene Delivery System for Dual Reporter Gene Imaging

Shiau-yi Wang, Ren-Shyan Liu, Hsin-Ell Wang, Jeng-Jong Hwang, Yi-Jang Lee, Department of Biomedical Imaging and Radiological Sciences., Taipei, Taiwan. Contact e-mail: yi9530338@hotmail.com

Background and Purpose: Compared with viral-based vectors, non-viral gene delivery systems are usually less efficient transgenesis. Transposon is a mobile gene that can move and integrate to another gene. The piggyBac transposon for gene delivery has been reported to be an efficient non-viral system for sustained gene expression in vivo and in vitro. Here we investigated if the piggyBac transposon system is an ideal method for reporter gene imaging in experimental animals. **Methods:** PB[Act-RFP]DS or PB[Act-RFP, HSV-tk] was transfected or co-transfected with Act-PBase (piggyBac transposase) to 293T cells or H1299 lung cancer cells using polyethylening (PEI) reagent. Expression of monomeric red fluorescent (RFP) was detected by fluorescence microscopy. Chromosomal integration of the RFP reporter genes was confirmed by genomic PCR. HSV-tk expression was detected by immunoblot analysis and cell uptake assay. Subsequently, H1299 cells transfected with PB[Act-RFP, HSV-tk] alone or co-transfected with Act-PBase were collected 2 days post-transfection, and 5X10⁶ cells were subcutaneously seeded in NOD-SCID mice (N=4). RFP signal and HSV-tk activity expressing in xenograft tumors were detected by IVIS50 system and SPECT/CT, respectively. **Results:** Compared to single transfection of PB [Act-RFP, HSV-tk] or PB [Act-RFP] DS, co-transfection of the recombinant constructs with Act-PBase exhibited sustained RFP and HSV-tk reporter gene activity over 6 weeks in cultured cells. The similar results were visualized in xenograft tumors derived from H1299 lung cancer cells formed co-transfected with PB [Act-RFP, HSV-tk] and Act-PBase constructs. **Conclusion:** Recombinant plasmid PB [Act-RFP, HSV-tk] indeed work and thymidine kinase (TK) also expressed in the 293T and H1299 cells. Our data suggests that the piggyBac transposon based vector is an ideal tool for non-viral gene delivery of reporter genes that can be uses for non-invasively molecular imaging.

Presentation Number **0614B**

Poster Session 3b: Imaging Molecular and/or Cellular Processes & Drug and/or Radiation Therapy

Induction of Epstein-Barr virus thymidine kinase expression in nasopharyngeal carcinoma by histone deacetylase inhibitors in vitro and in vivo

Ren-Shyan Liu^{1,2}, **Fu-Hui Wang**¹, ¹MAGIC/NRPGM, Nuclear Medicine, Faculty of Medicine, National Yang-Ming University Medical School, Taipei, Taiwan; ²NPCC, Taipei Veterans General Hospital, Taipei, Taiwan. Contact e-mail: rslu@vghtpe.gov.tw

Purpose: Nasopharyngeal carcinoma (NPC) is an Epstein-Barr virus (EBV) associated malignancy with high prevalence in Southern Chinese. Like most other herpesviruses such as herpes simplex virus type1 (HSV-1), HSV-2, and Kaposi's sarcoma herpesvirus (KSHV), EBV encodes a virus-induced protein with thymidine kinase (TK) activity. This study aimed to assess that treatment of EBV-associated NPC cell lines with histone deacetylase inhibitors (HDACI) led to induction of the EBV lytic gene expression, including expression of the EBV-TK. **Method:** The in vitro cell uptake study was performed with EBV-positive NPC cell line, NA and the parental EBV-negative NPC cell line, TW01. To induce EBV lytic cycle, cells were treated with either trichostatin A (TSA), valproic acid (VPA) or suberoylanilide hydroxamic acid (SAHA) for 4 and 16 hours and then incubated with [³H]2'-fluoro-2'-deoxyarabinofuranosyl-5-ethyluracil ([³H]FEAU). Cell uptake was expressed as the accumulation ratio [i.e., counts per minute per milligram (cpm/mg) of total proteins divided by the cpm/g (ml) of medium]. For tumor generation, cells (5×10^6) were resuspended in 100- μ l Matrigel matrix and injected s.c. in the shoulder of 4- to 5-week-old male severe combined SCID mice. The microPET imagings of [¹⁸F]FEAU were done when tumors reached a size of ~1 cm in diameter. **Results:** In vitro cellular studies revealed highly uptake of [³H]FEAU in the EBV-positive NPC cell line treated with SAHA (1.15~1.35-fold) and VPA (1.22~1.45-fold) at 4 and 16 hours after incubation. The uptake of [¹⁸F]FEAU in EBV- positive NPC tumor (NA) was higher than that of EBV-negative NPC tumor (TW01) at 1 h p.i.. The tumor accumulation ratio increased with SAHA and VPA treatment in EBV- positive NPC tumor. **Conclusion:** HDACI such as SAHA and VPA can activate viral lytic gene (EBV-TK) expression and trigger the switch of EBV from latent to lytic cycle. Strong induction of EBV lytic cycle, may lead to development of novel targeted therapeutic strategies (e.g. treating with anti-viral drug such as ganciclovir) against EBV-associated malignancies.

Presentation Number **0615B**

Poster Session 3b: Imaging Molecular and/or Cellular Processes & Drug and/or Radiation Therapy

MRI monitoring of intra-arterial bone marrow-derived macrophages delivery after transient ischemia

Adrien Riou¹, **Fabien Chauveau**¹, **Tae-Hee Cho**¹, **Marilena Marinescu**¹, **Serge Nataf**², **Yves Berthezène**¹, **Norbert Nighoghossian**¹, **Marlène Wiat**¹, ¹CREATIS-LRMN - Université Lyon 1 - INSA Lyon, CNRS UMR 5220 - INSERM U630, Bron, France; ²NeuroOncologie and NeuroInflammation, Inserm U842, Lyon, France. Contact e-mail: adrien.riou@creatis.insa-lyon.fr

Introduction: It is well established that cerebral ischemia results in a complex inflammatory cascade that mainly involves cells from the mononuclear phagocyte system [1], although the beneficial or deleterious effect of this activation following stroke is still a matter of controversy. Furthermore, therapeutic benefits gained from cell-based therapy depend on migration and localization of grafted cells within the target tissue that is closely related to the cell delivery route [2] and therapeutic time window [3] chosen for the therapy. Methods: Male Sprague Dawley rats (n=15) were subjected to 1-h intraluminal transient middle cerebral artery occlusion (tMCAO) (n=10) or sham procedure (n=5). IA administration of labeled cells was performed at the time of reperfusion in 9 tMCAO animals and in 3 shams animals (4 million in 1-ml except for one sham: 1 million in 1-ml). MRI was performed on a Bruker Biospec 7T/12cm magnet at D0 just after cells administration and from D1 to D9. The MR exam included T2-, T2*-, diffusion- and perfusion-weighted imaging and multi-echo 3D imaging. Results: IA administration in tMCAO group lead to heterogeneous results: 3 rats died following injection, 3 animals were excluded from analysis because of atypical striatal lesions and 3 had a widespread persistent hypointense signal distribution. Furthermore, IA administration in the sham group caused lesion formation on follow-up scans in all injected animals (n=3), even when cell number was decreased, as opposed to the non-injected sham rats that did not have any lesions. Immunohistological analysis is in progress to ascertain iron-labeled macrophage localization (Prussian blue for iron detection and Ox-42 for macrophage detection). Conclusions: Our results were consistent with that of previous studies [2,4] showing that IA delivery route efficiently brought a large number of cells to the brain soon after transplantation, but severely increased mortality. More importantly, lesions observed in the sham group (undemonstrated to date to our knowledge) suggested that this high mortality rate resulted from cell embolisation in cerebral vessels leading to formation or worsening of the ischemic lesion. This result points out a serious limitation for the translation of this cell delivery route into the clinics. References: 1. Huang J, et al. *Surg Neurol.*;66:232-45 (2006). 2. Li L, et al. *J Cereb Blood Flow Metab* (2009). 3. de Vasconcelos Dos Santos A, et al. *Brain Res.*1306:149-58 (2010). 4. Walczak P, et al. *Stroke.* 2008;39:1569-74 (2008).

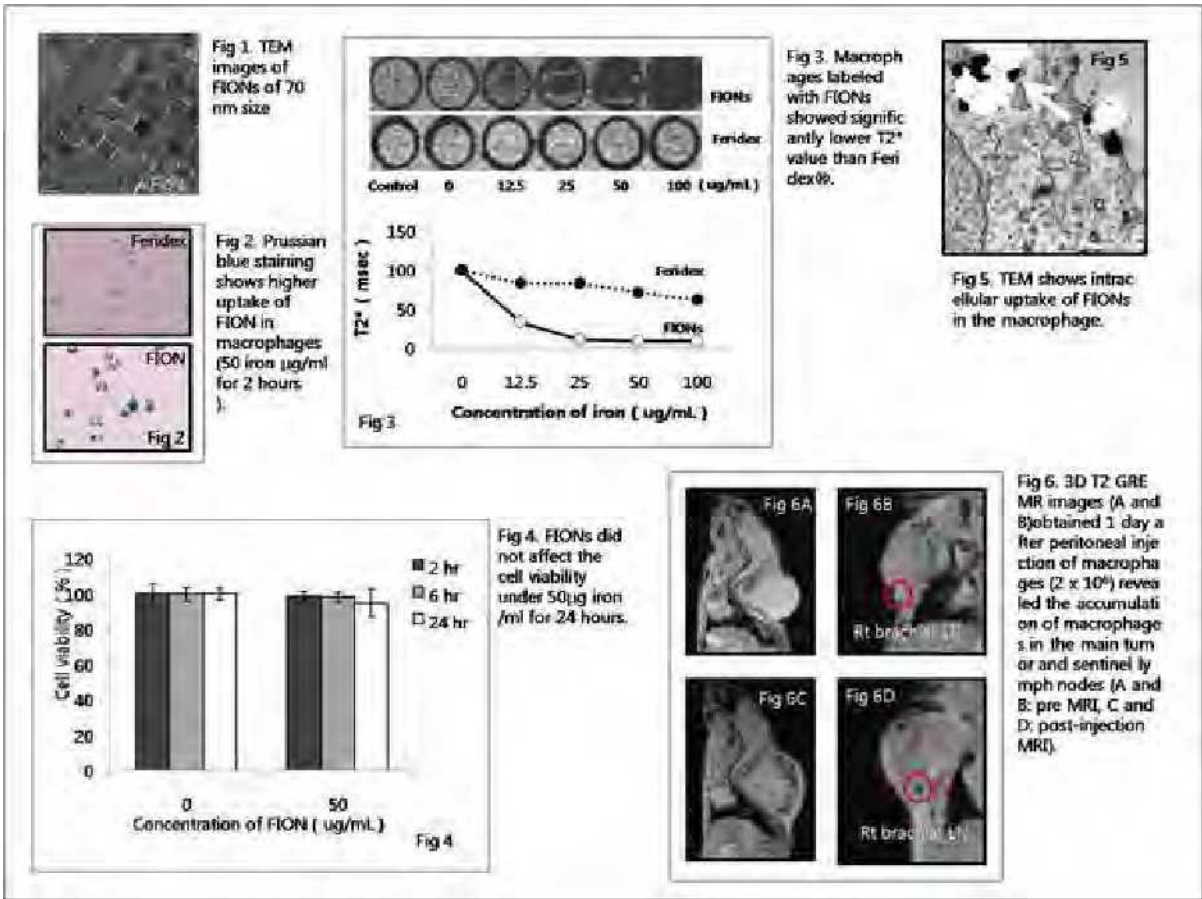
Presentation Number **0616B**

Poster Session 3b: Imaging Molecular and/or Cellular Processes & Drug and/or Radiation Therapy

Targeting sentinel lymph nodes with macrophages labeled with FIONs on 1.5 T MR imaging

Hye Rim Cho, Seung Hong Choi, Woo Kyung Moon, Department of Radiology, Seoul National University Hospital, Seoul, Republic of Korea. Contact e-mail: hyerimcho1030@gmail.com

To our knowledge, there was no report concerning the possibility of delivery of therapeutic agent to metastatic lymph nodes using macrophages. To monitor the fate of injected macrophages on MR imaging, we labeled them with ferromagnetic iron oxide nanocubes (FIONs) (Fig 1). The purpose of the present study was to confirm if metastatic lymph nodes can be targeted by macrophages labeled FIONs by using a mouse melanoma model. Materials and Methods Peritoneal macrophages were harvested from thioglycolate-treated Balb/c nude mice, cultured, labeled with FIONs in vitro. For labeling macrophages, they were incubated with 50µg iron/ml for 2 hours. To compare the cell labeling efficacy of FIONs with that of Feridex®, macrophages were labeled with Feridex® under same condition, and T2* values were measured for 1 x 10⁵ macrophages labeled with FIONs and Feridex® by using 1.5 T MR scanner, respectively. We used a MGRE sequence. Cell viability was measured by MTT assay. TEM was performed to confirm the phagocytosis of FIONs. Macrophages of 2x10⁶ labeled with FIONs were injected intraperitoneally (n = 5) and intravenously (n=5) into the Balb/c nude mice with melanoma tumor induced by B16F10 cell line. 3D T2 GRE MR images were obtained prior to and 1 day after the injection of macrophages. Hematoxylin/eosin staining and Prussian blue staining were performed for the main melanoma tumor and lymph nodes. Results and Discussion Prussian blue staining revealed higher uptake of FIONs than Feridex® in macrophages (Fig 2). Macrophages labeled with FIONs showed significantly lower T2* value than Feridex® (Fig 3). FIONs did not affect the cell viability under 50µg iron/ml for 24 hours (Fig 4). TEM showed intracellular uptake of FIONs in the macrophage (Fig 5). 3D T2 GRE MR images obtained 1 day after peritoneal injection of macrophages revealed the accumulation of macrophages in the main tumor and sentinel lymph nodes (Fig 6). We believe that macrophages have the potential for the application of targeting the main tumor as well as sentinel lymph node, which was easily monitored by using FIONs and 1.5T MR scanner.



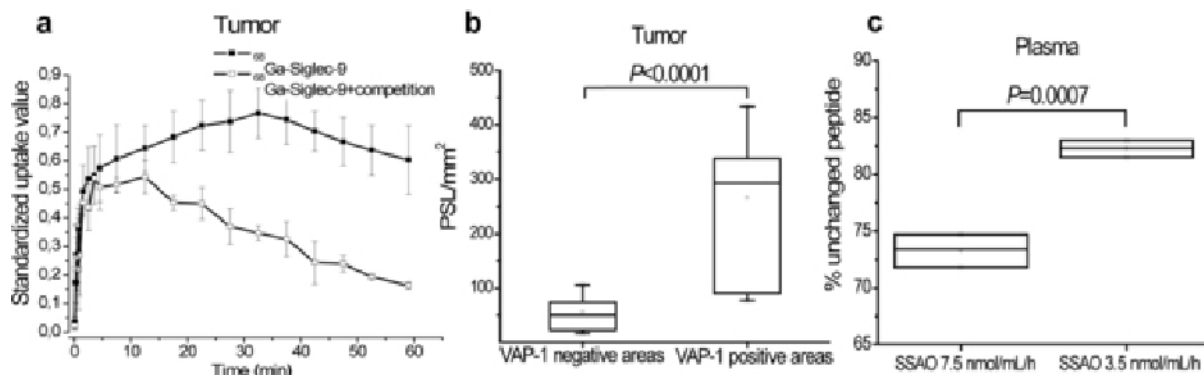
Presentation Number **0617B**

Poster Session 3b: Imaging Molecular and/or Cellular Processes & Drug and/or Radiation Therapy

A Leukocyte Ligand of Vascular Adhesion Protein-1 as an Imaging Tool in PET

Anu K. Autio¹, Kristiina Aalto³, Tiina Saanijoki¹, Henri J. Sipilä¹, Sirpa Jalkanen³, **Anne Roivainen**^{1,2}, ¹Turku PET Centre, University of Turku, Turku, Finland; ²Turku Center for Disease Modeling, University of Turku, Turku, Finland; ³MediCity Research Laboratory, University of Turku, Turku, Finland. Contact e-mail: anne.roivainen@utu.fi

Introduction: Vascular adhesion protein-1 (VAP-1) is both an endothelial glycoprotein and a semicarbazide-sensitive amine oxidase (SSAO) enzyme playing a critical role in leukocyte trafficking to the sites of inflammation. Although VAP-1 was identified more than 15 years ago, the leukocyte ligand has remained unknown until very recently. Last year it was shown that Siglec-10 (sialic acid-binding immunoglobulin-like lectin) expressed on a subpopulation of lymphocytes can bind to VAP-1 and serve as its substrate [1]. According to phage display screening and structural modeling also Siglec-9 expressed on granulocytes and monocytes interacts with VAP-1. In this study, we investigated a Siglec-9 peptide as a potential imaging tool in positron emission tomography (PET). **Methods:** A cyclic peptide binding to recombinant human VAP-1 was conjugated with DOTA-chelator through PEG-linker and ⁶⁸Ga-labeled for PET studies as previously described [2]. The interaction between VAP-1 and ⁶⁸Ga-Siglec-9 peptide was evaluated *in vitro* in human plasma samples possessing different SSAO levels. The VAP-1 specificity was further tested with competition assay in mice bearing melanoma xenografts by PET imaging and autoradiography. *In vivo* imaging of inflammation was examined in a rat model. All *in vivo* studies were confirmed by *ex vivo* measurements. **Results:** The Siglec-9 peptide binding to the enzymatic groove of VAP-1 could specifically detect inflammation in rat and tumor in mouse. Competition experiments with excess of unlabeled Siglec-9 peptide revealed 3-fold lower tumor uptake in mice. According to autoradiography of the tumor cryosections, the radioactivity co-localized notably with VAP-1 as demonstrated by immunohistochemistry ($P < 0.0001$). In a rat model, the Inflammation-to-muscle ratio of ⁶⁸Ga-Siglec-9 peptide was 5.9 ± 2.3 . Moreover, in radio-HPLC analyses, the amount of intact ⁶⁸Ga-Siglec-9 peptide in human plasma was significantly different between low and high levels of SSAO activity ($P = 0.0007$). **Conclusions:** Our results show that the Siglec-9 peptide detects VAP-1 in inflammation and tumor vasculature in animal models and it may also have potential in imaging of these diseases in patients. **References:** [1] Kivi E et al; Blood. 114:5385-5392 (2009) [2] Ujula T et al; Nucl Med Biol. 36:631-641 (2009)



(a) PET study (b) Autoradiography study (c) HPLC study.

Presentation Number **0620A**

Poster Session 1b: Imaging Molecular and/or Cellular Processes & Drug and/or Radiation Therapy

BLI to non-invasively quantify anti-fungal activity against in vivo *Candida albicans* biofilm formation in a rodent model

Greetje Vande Velde¹, **Sona Kucharikova**², **Helene Tournu**², **Patrick Van Dijck**², **Uwe Himmelreich**¹, ¹Radiology/ MoSAIC, Katholieke Universiteit Leuven, Leuven, Belgium; ²VIB, Molecular Microbiology, KULeuven, Leuven, Belgium. Contact e-mail: greetje.vandevelde@med.kuleuven.be

Biofilm formation by fungal pathogens is a major problem in hospitals. Especially *C. albicans* biofilms are formed on the surface of many medical implants. Being often resistant to the classical antifungal drugs, they are difficult to treat. For testing antifungal drugs against *C. albicans* biofilm formation, a subcutaneous catheter rat model system has been developed (1). Fungal load in biofilms is traditionally analyzed post mortem, requiring host sacrifice and enumeration of microorganisms from individual biofilms to evaluate the efficacy of antifungal treatment. We aim to make this model compatible for bioluminescence imaging (BLI), where detecting a quantifiable in vivo BLI signal from biofilms formed on the inside of catheters will be challenging. Wild-type *C. albicans* (SC5314) was engineered to express *C. albicans* codon-optimized *Gaussia princeps* luciferase (gLuc) at the cell wall, under the control of biofilm growth phase specific promoters (2). gLuc activity from *Candida* cells and biofilms is measured and correlated with cell counts. Catheters are implanted on the back of mice and rats and in vivo biofilm formation was followed up with BLI. In vivo MR images are acquired and coregistered to the BL images to verify the site of catheter implantation. To validate the model for antifungal testing, rats are treated with different antifungals and imaged with BLI. At different time points post implantation, cfu counts from biofilms on explanted catheters are then compared to the in vivo BLI data for validation. We report significant gLuc activity from *Candida* cells and biofilms, where the signal is corresponding to the specific yeast or hyphal cell stage. The BLI signal was proportional to the amount of yeast or hyphal cells in vitro and in biofilms. We could detect a significant BLI signal above background (control biofilm) from in vitro and in vivo formed biofilms in live animals, and compared this signal with biofilm analysis and cfu from explanted catheters. To the best of our knowledge, this is the first study that quantifies in vivo biofilm formation by BLI. The so developed multi-temporal non-invasive imaging assay for quantifying in vivo biofilm formation is suitable for the validation of antifungal drugs under in vivo conditions. 1. Ricicova, M., Kucharikova, S. et al. *Candida albicans* biofilm formation in a new in vivo rat model. *Microbiology* 156, 909-919 (2010). 2. Enjalbert, B., et al. A multifunctional, synthetic *Gaussia princeps* luciferase reporter for live imaging of *Candida albicans* infections. *Infect Immun* 77, 4847-4858 (2009).

Presentation Number **0621A**

Poster Session 1b: Imaging Molecular and/or Cellular Processes & Drug and/or Radiation Therapy

MicroCT quantification of LPS-mediated calvarial bone resorption

Jie Zheng, Diane Thome, Lore Gruenbaum, Debra Klatte, Gerald Nabozny, Aruna K. Behera, Boehringer Ingelheim Pharmaceuticals, Inc, Ridgefield, CT, USA. Contact e-mail: jie.zheng@boehringer-ingelheim.com

Bone destruction and resorption is a hallmark feature of rheumatoid arthritis. The lipopolysaccharide (LPS) mediated calvarial bone resorption model in mice provides a valuable tool to understand cellular mechanisms involved in inflammatory mediated bone resorption. Our goal was to develop a non-invasive approach to quantify bone changes in this model with microCT. Methods: C57Bl/6 mice were challenged subcutaneously over the calvaria with LPS and orally dosed once daily with either dexamethasone or water. The treatment groups as follow: LPS, 50µg/calvaria; LPS, 100µg/calvaria; LPS, 100µg/calvaria +3mg/kg and 10mg/kg Dexamethasone, and naïve. On the fifth day after challenge, animals were euthanized. Calvariae were scanned under the Scanco Medical MicroCT-40 with a voxel size of 20 µm. Image quantitative analysis was performed with the software in the system. Results: MicroCT images of the calvariae revealed the presence of irregularly distributed erosions in the surface of the calvariae in LPS treated mice. The PBS treated control mice demonstrated smooth calvarial surfaces. The lesions were more prevalent on the right frontal part of the skull at the site of LPS injection. The most severe erosions were seen in mice treated with 100 µg LPS. Mice treated with either 3mg or 10mg/kg of dexamethasone exhibited much less erosions compared to the group which received 100µg LPS alone. Quantification of osteolysis, indicated as a loss in bone volume (BV) and increased roughness of the bone surface (surface density BS/BV), was performed with both the entire calvariae and the right frontal part of skull. There was significant loss in bone volume ($p < 0.003$), an increase in bone surface density ($p < 0.006$), a reduction in bone thickness ($p < 0.001$), and bone mineral density ($p < 0.001$) in LPS-treated mice compared to naïve mice. All parameters (BV, BS/BV, BMD, and bone thickness) were significantly improved ($p < 0.05$) in mice that were co-administration with either 3mg or 10mg/kg dexamethasone with 100µg LPS compared to mice treated with 100µg LPS alone. In this study, we demonstrated the use of MicroCT to quantify BV/TV, BS/BV, and bone thickness as biomarkers for the evaluation of bone erosions and drug treatment response. In conclusion, the main advantage of MicroCT technology for evaluation of calvarial osteolysis include 1), a fully automated means to quantify bone destruction within the entire specimen or a region of interest and 2), accurate 3-D reconstruction based on numerous slices allows detection of small changes.

Presentation Number **0622A**

Poster Session 1b: Imaging Molecular and/or Cellular Processes & Drug and/or Radiation Therapy

Imaging MMP Expressions and Proteoglycans in Human Osteoarthritic Knees

David C. Miller, Joseph Schooler, Hilla Wahnishe, Sarmad Siddiqui, Xiaojuan Li, Sharmila Majumdar, Ella F. Jones, Radiology, University of California, San Francisco, San Francisco, CA, USA. Contact e-mail: dcmill@gmail.com

Background: Osteoarthritis (OA) is the most common form of arthritis. Owing to the lack of sensitivity and specificity, standard magnetic resonance (MR) or computed tomography (CT) imaging techniques have met with difficulties to detect early biochemical events that lead to cartilage degeneration. More recently, T1 ρ relaxation mapping by MR has been proposed to detect the loss of proteoglycan (PG) macromolecules at early stages of OA. Although such a clinical technique has shown great promise for measurements of macromolecular changes in early cartilage failure, the direct link from the earliest pathological signaling pathway to the change of macromolecules that leads to structural and functional degradation is still missing. Matrix metalloproteinases (MMPs) are known to be involved in early events of arthritic diseases. In particular, active MMP-9 and -13 are key enzymes that are responsible for the degradation of collagens and PG at early stages of OA. In this work, we successfully demonstrate the utility of optical and MR imaging to account for the MMP activities and their correlation with PG content in knee specimens from OA patients. Methods: Human femoral condyles were collected from patients diagnosed with severe osteoarthritis during total knee replacement surgeries at the UCSF Dept. of Orthopedic Surgery. Specimens were immediately placed in specimen cups and frozen at -80 oC. For imaging, specimens were thawed overnight and incubated in 0.2 μ M of MMPsense680 and incubated in the dark at 37 oC for 2 h. The specimens were removed and washed with PBS followed by optical imaging and histology. The corresponding T1 ρ MR measurements were collected from a 3T whole body MR scanner using spin-lock techniques and an SPGR image acquisition. Results: All osteoarthritic knee specimens showed intense signal for MMP activities after 2 h incubation. The corresponding T1 ρ values were in the range of 48 to 75 ms indicating a severe loss of PG macromolecules and cartilage degeneration. The overall MMP activity measured by optical imaging (normalized in efficiency) directly correlates to the T1 ρ measurements, showing high MMP activities in specimens with severe loss of PG. Conclusion: We have successfully demonstrated the upregulation of MMP expressions in OA cartilage from knee specimens in patients. Through the combination of optical and MR imaging, we have now established the correlation of the upstream MMP molecular events to the downstream macromolecular PG changes that ultimately lead to the degradation of cartilage integrity in OA patients.

Presentation Number **0623A**

Poster Session 1b: Imaging Molecular and/or Cellular Processes & Drug and/or Radiation Therapy

PET Imaging of the 18 kDa Translocator Protein (TSPO) Reveals Inflammation in Mouse Models of Breast Cancer

Jinzi Zheng^{1,2}, **Raphael Boisgard**^{1,2}, **Karine Siquier-Pernet**^{1,2}, **Didier Decaudin**³, **Frederic Dolle**^{1,2}, **Bertrand Tavitian**^{1,2}, ¹*Biomedical Imaging, Commissariat à l'énergie atomique, Orsay, France;* ²*Laboratoire d'Imagerie Moléculaire Expérimentale, INSERM U1023, Orsay, France;* ³*Laboratoire d'investigation préclinique, Institut Curie, Paris, France.* Contact e-mail: jinzi.zheng@cea.fr

Rationale: Tumor-associated inflammation has been linked to angiogenesis, metastasis and poor prognosis. The 18 kDa translocator protein (TSPO) is over-expressed in activated immune cells such as macrophages. Reports also suggest TSPO over-expression in a number of cancers. For example, in breast cancer (BC) cell lines, TSPO density has been correlated with aggressiveness, and TSPO expression in BC patients has been proposed as a prognostic factor for survival. This study aims to assess of the feasibility of employing the neuroinflammation radiotracer [¹⁸F]DPA-714 for PET imaging of TSPO in mouse models of BC, and investigate the relative contribution in tracer uptake by the neoplastic and inflammatory components of the tumor. Methods: Female nude mice were s.c. inoculated with MDA-MB-231, MCF-7, a patient-derived breast tumor HBCx-12B and a transgenic mouse-derived mammary carcinoma PyMT. [¹⁸F]FDG and [¹⁸F]DPA-714 PET imaging were conducted 3-6 weeks post-inoculation. Autoradiography, immunohistochemistry (IHC) and western blot were performed on the excised tumors. Results: The 4 breast tumors showed varied expressions of TSPO as well as uptake of [¹⁸F]DPA-714 (Table 1). There was no correlation between the tumor uptake of [¹⁸F]FDG and [¹⁸F]DPA-714 (Figure 1a). Ex-vivo autoradiography with displacement confirmed that the [¹⁸F]DPA-714 binding was specific (Figure 1b). A positive correlation was seen between the in-vivo [¹⁸F]DPA-714 PET signal and the expression of murine TSPO in HBCx-12B tumors, while no correlation was found between the tracer uptake and the human TSPO expression (Figure 1c). IHC showed significant localization of the mouse TSPO within cells which are positively stained for the F4/80 pan-macrophage marker (Figure 1d). Conclusion: Macrophage-associated TSPO is the dominant factor for [¹⁸F]DPA-714 uptake in the BC models investigated. This supports the potential use of this tracer for imaging tumor-associated inflammation.

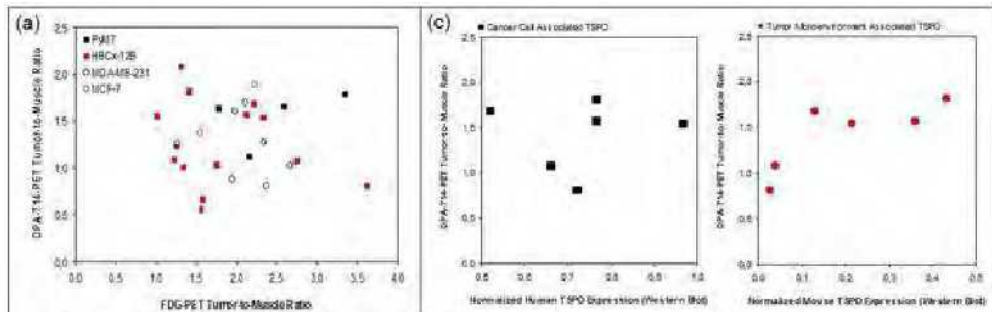


Figure 1a. There is no clear correlation between the uptake of [¹⁸F]DPA-714 and [¹⁸F]FDG in the 4 models of breast cancer. This suggests that the 2 tracers target independent processes.

Figure 1c. The tumor uptake of [¹⁸F]DPA-714 in the HBCx-12B model correlates with the TSPO expression in the tumor stromal cells (of mouse origin, right graph), but there is no clear correlation to the TSPO expression in cancer cells (of human origin, left graph).

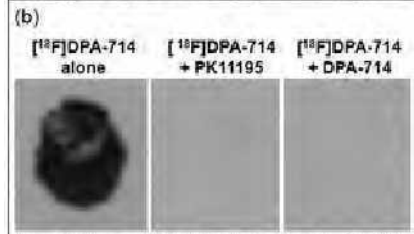


Figure 1b. Ex-vivo [¹⁸F]DPA-714 binding (left, 2 mCi in 200 µL) in a tumor section (10 µm thick) from a PyMT mouse. Co-incubation with PK11195 (middle, 20 µM) or DPA-714 (right, 20 µM) results in complete displacement of [¹⁸F]DPA-714.

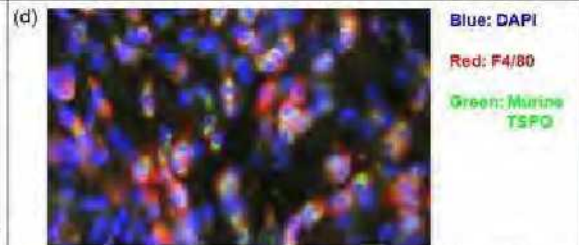


Figure 1d. Immunohistochemical staining of a tumor section (10 µm thick) from an HBCx-12B mouse displaying co-localization of the murine TSPO antibody (green) with the F4/80 macrophage marker (red).

Tumor Models in Nude Mice	Human TSPO Expression by Western Blot	[¹⁸ F]DPA-714 PET Tumor Uptake (% ID/g)	[¹⁸ F]DPA-714 PET Tumor-to-Muscle Ratio
MDA-MB-231	++	0.6 ± 0.1 (n=7)	1.2 ± 0.3 (n=7)
MCF-7	-	1.0 ± 0.2 (n=3)	1.5 ± 0.4 (n=3)
HBCx-12B	+++	0.5 ± 0.3 (n=15)	1.1 ± 0.4 (n=15)
PyMT	Murine tumor	0.6 ± 0.1 (n=4)	1.0 ± 0.3 (n=4)

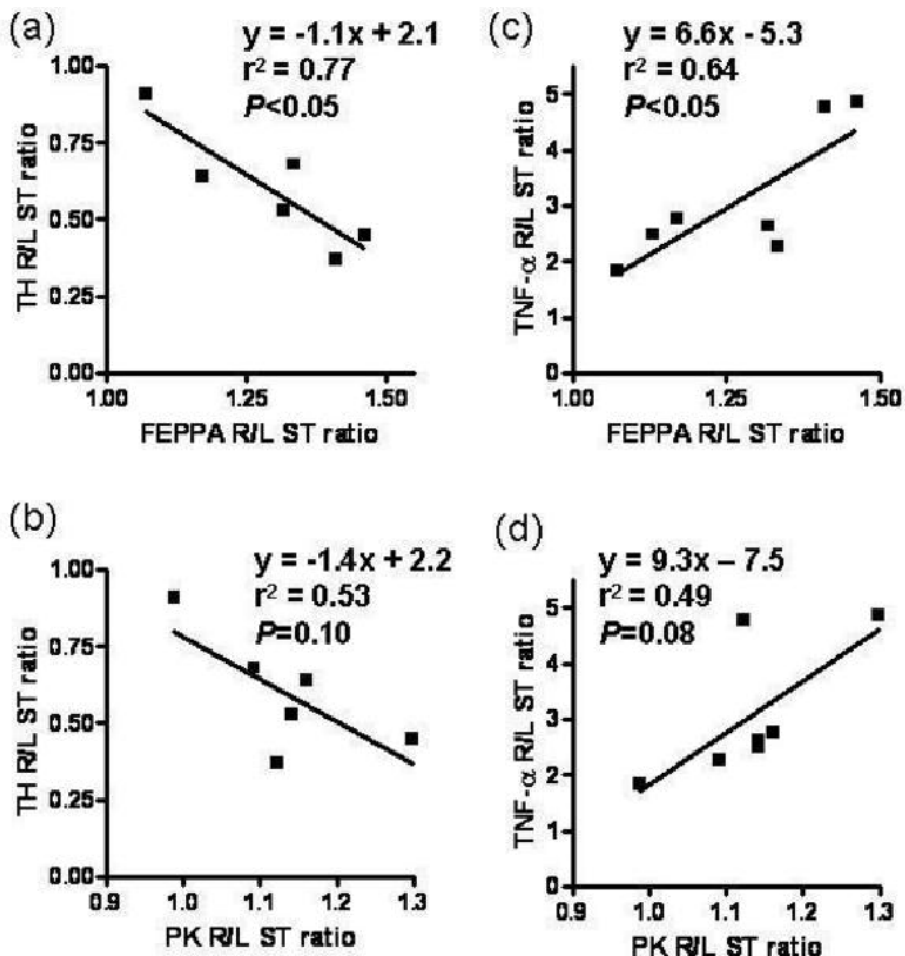
Presentation Number **0624A**

Poster Session 1b: Imaging Molecular and/or Cellular Processes & Drug and/or Radiation Therapy

Detection of fully activated microglia with novel translocator protein (18 kDa) ligand, [¹⁸F]FEPPA PET

Hiroshi Toyama¹, Gen Kudo¹, Kentaro Hatano², Hiromi Suzuki³, Takashi Yamada², Masahiko Nomura¹, Masanori Ichise⁴, Alan A. Wilson⁵, ¹Radiology, Fujita Health University, Toyoake, Japan; ²National Center for Geriatrics and Gerontology, Obu, Japan; ³Brain Science, Nagoya University, Nagoya, Japan; ⁴Radiology, Columbia University, New York, NY, USA; ⁵Centre for Addiction and Mental Health, Toronto, ON, Canada. Contact e-mail: htoyama@fujita-hu.ac.jp

Objectives: Activated microglia (AMG) exist in two functionally different states, cytotoxic and protective states. The former is referred to as a "fully activated form". It is worthwhile to distinguish between the two states for diagnosis and treatment. However, there is no reliable method to evaluate the different states. AMG is known to increase the expression of translocator protein (18 kDa) (TSPO), formerly called the peripheral benzodiazepine receptors. A TSPO ligand, [¹¹C]PK11195, suffers low brain uptake and specific binding. We evaluated if a novel TSPO ligand, [¹⁸F]FEPPA can detect "fully AMG" in comparison with tyrosine hydroxylase (TH) stain and inflammatory cytokines in a rat 6-hydroxydopamine (OHDA) model. Methods: Under anesthesia, 6-OHDA was injected into the rat right striatum (ST). On day 4, PET imaging was performed for 60 min after injection of [¹¹C]PK11195 and then [¹⁸F]FEPPA under anesthesia. Seven 6-OHDA rats were then euthanized and immunohistochemical staining (TH) and RT-PCR for inflammatory cytokines (TNF α) was performed for confirmation of the cytotoxic damage. Right/left ST [¹¹C]PK11195 and [¹⁸F]FEPPA uptake ratios were evaluated. Results: TH staining ratios showed significantly negative correlation with [¹⁸F]FEPPA PET ratios ($r^2=0.77$, $P<0.05$). TH staining ratios tended to correlate negatively with [¹¹C]PK-11195 ratios. TNF α ratios showed significantly positive correlation with [¹⁸F]FEPPA PET ratios ($r^2=0.64$, $P<0.05$). TNF α ratios also showed a positive correlation with [¹¹C]PK11195 PET ratios. However, [¹⁸F]FEPPA PET and TNF α were more closely correlated. Conclusions: [¹⁸F]FEPPA appears a promising alternative to [¹¹C]PK11195 for PET brain imaging of "fully AMG".



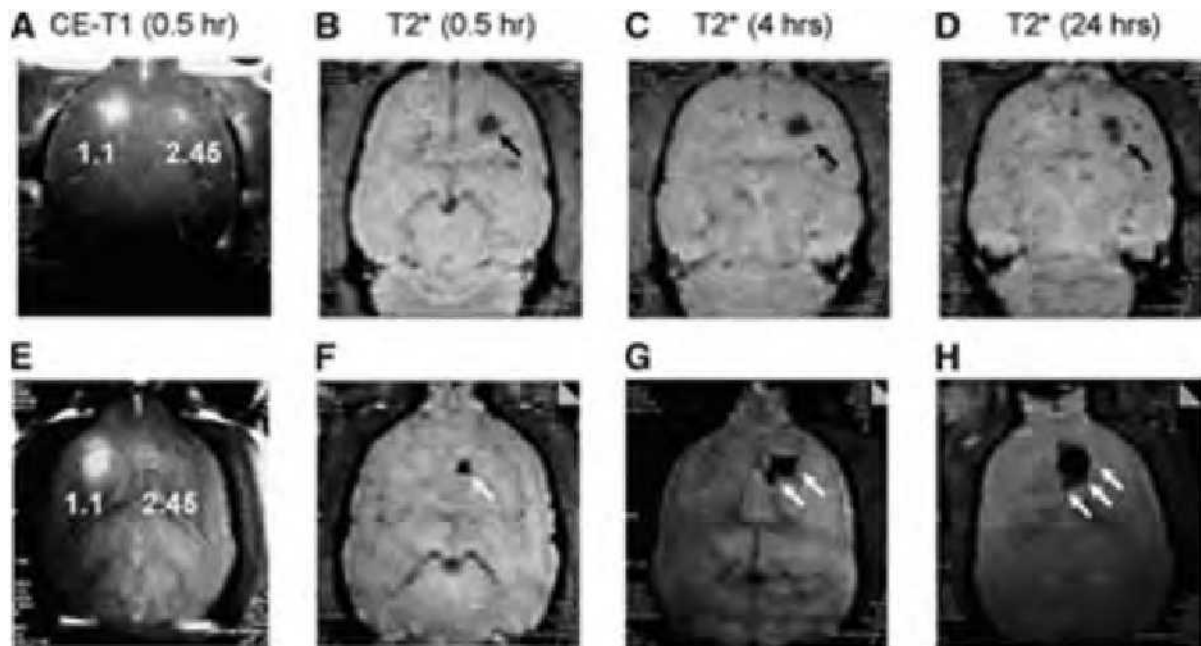
Presentation Number **0625A**

Poster Session 1b: Imaging Molecular and/or Cellular Processes & Drug and/or Radiation Therapy

CNS infiltration of macrophage labeled with superparamagnetic iron oxide indicated the inflammatory response during disruption of the blood-brain barrier with focused ultrasound

Jiun-Jie Wang, Hao-Li Liu, Tzu-Chen Yen, ChangGung University, Kweishan, Taoyuan, Taiwan. Contact e-mail: jwang@mail.cgu.edu.tw

Introduction The endocytotic loading of circulating macrophages with superparamagnetic iron oxide (SPIO) was used to monitor inflammatory response after ultrasound-induced blood-brain barrier (BBB) disruption in vivo using MRI. Focused ultrasound was used to locally disrupt BBB. The phagocytic capacity of activated macrophages and their ability to migrate to inflammation sites was examined up to 24 hours. **Materials and methods** Craniotomy was performed on 6 adult SD rats 3 days before sonications. Monocytes were labeled with SPIO (Resovist, Schering AG, Germany), in a dose of 15 mmol/kg 24 hours before sonication. A focused ultrasound transducer (Imasonics, France) was used. Sonications at 1.1MPa were applied in the left forebrain and 2.45MPa in the right, in the presence of an ultrasound microbubble agent (SonoVue, Bracco, Italy). Each bolus injection contained 0.025 mL/kg microbubbles. Images were acquired using a 3-T scanner (Trio with Tim, Siemens, Germany), including a contrast-enhanced T1 turbo spin-echo (TR/TE = 534/11 msec) and a series of heavy T2* 3D Gradient Echo (TR/TE/flip angle = 28 msec/ 20 msec/151) sequences. Images were acquired at (1) 30 mins before sonication, (2) 4 h, (3) 24 h after sonication. **Results** Figure showed images of rat brains with (upper) /without(lower) SPIO. MRI showed hemorrhage at 0.5 h at 2.45MPa, which persisted for 24h. The inflammatory response was clear (lower) by the continuous expansion of the signal dropout region, (white arrows), which was due to the aggregation of SPIO laden macrophages, causing a susceptibility induced signal loss. **Discussion** This study showed that SPIO laden monocyte activity was evident at the hemorrhagic site as early as 4 h after sonication. It subsequently increased until 24 h, suggesting that monocyte activity was instantly activated by sonication. The results showed the occurrence of brain macrophage infiltration produced by focused ultrasound stimulation, resulting in phagocyte infiltration into the brain parenchyma.



Presentation Number **0626A**

Poster Session 1b: Imaging Molecular and/or Cellular Processes & Drug and/or Radiation Therapy

Migration of Bone-Marrow Derived Macrophages as a Function of their Polarization in an Inflammatory Animal Model: a High Resolution MRI Study

Achraf Al Faraj^{1,2}, Nathalie Luciani¹, Claire Wilhelm¹, Olivier Clément², Florence Gazeau¹, ¹University Paris 7, CNRS 7057, MSC, Paris, France; ²Paris Cardiovascular Research Center - PARCC, Université Paris 6, INSERM U970, Paris, France. Contact e-mail: achraf.al-faraj@univ-paris-diderot.fr

MR tracking of cells labeled with iron oxide nanoparticles offers novel perspectives for both noninvasive diagnostic purposes and therapeutic interventions because of the high spatial resolution of three-dimensional MRI in deep tissue and the ability to label many different cell types with MR contrast agents. Recently, macrophages have been presented to display remarkable plasticity by giving rise to different subpopulations with distinct functions in response to environmental conditions. Bone-marrow derived stem cells were differentiated *in vitro* in proinflammatory M1 or immunodulator M2 macrophages, labeled with anionic USPIO and intravenously injected to mice developing muscle inflammation in the right calf 5h after endotoxin bacterial inoculation. A positive control, injected with free USPIO, was also included in this study. In order to discriminate the migration dynamic of macrophages subpopulations, a noninvasive high resolution MRI protocol was performed on a 4.7T magnet to evaluate the biodistribution of macrophages in organ of interest (liver, spleen and kidneys) and to detect single macrophages in the inflammatory site using a cryogenic probe which allows high resolution 3D images. Following injection, macrophages (10^6 cells labeled at 10 pg Fe/cells) were mainly detected in the spleen with a 2 fold attenuation of signal assessed using a susceptibility weighted Gradient Echo sequence during the 3 days follow-up. No kinetic variation was observed between the macrophages subpopulations (M0, M1 and M2). However, free USPIO was found in both the liver and the spleen. Single macrophages were also detected in the infected calf using a cryogenic probe with a 3D 50 μ m spatial resolution images acquired in only 10 min. Leg muscles were finally removed for immunohistology and flow cytometry analyses to assessed macrophages polarization in the inflammatory site.

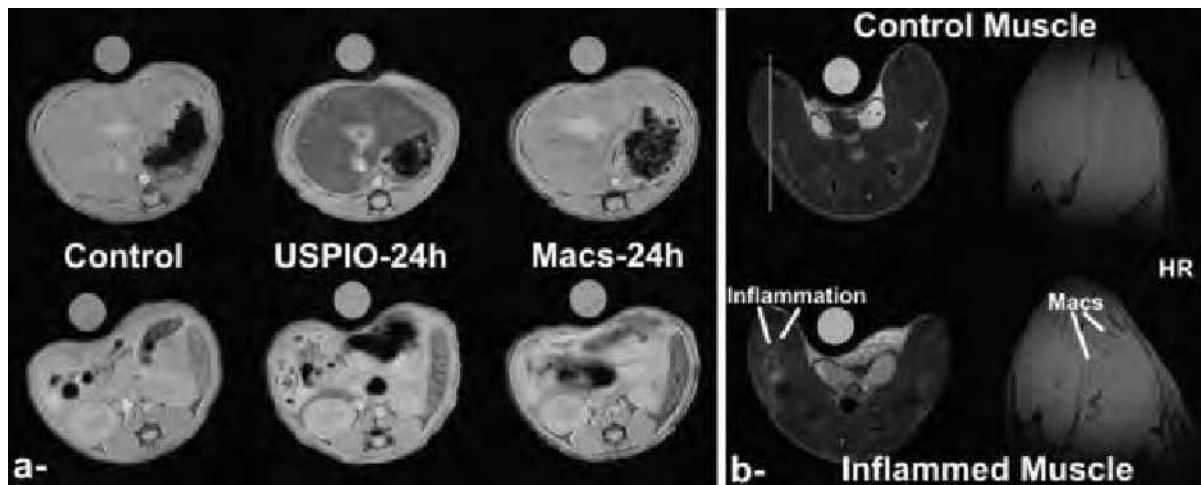


Figure 1: MR images of (a) the organ of interest (liver, spleen and kidneys) of a control, USPIO and macrophages injected mouse and (b) of the muscle using both volumic (inflammation evaluation) and cryogenic probe (high resolution: single cell detection).

Presentation Number **0627A**

Poster Session 1b: Imaging Molecular and/or Cellular Processes & Drug and/or Radiation Therapy

In vivo monitoring of experimental arthritis using [¹¹C]PK11195 and [¹¹C]Ketoprofen before joint destruction

Satoshi Nozaki¹, **Shinobu Suzuki**², **Naoko Ozaki**², **Misato Takashima-Hirano**³, **Miki Goto**³, **Emi Hayashinaka**¹, **Jeffrey Encinas**², **Hisashi Doi**³, **Yasuhiro Wada**¹, **Yasuyoshi Watanabe**¹, ¹Molecular Imaging Dynamics Laboratory, RIKEN Center for Molecular Imaging Science, Kobe, Japan; ²Dept. of Molecular & Cellular Biology, Nippon Boehringer Ingelheim Co., Ltd, Kobe, Japan; ³Molecular Imaging Labeling Chemistry Laboratory, RIKEN Center for Molecular Imaging Science, Kobe, Japan. Contact e-mail: satoshi.nozaki@riken.jp

In vivo detection of pathological insults during early stages of rheumatoid synovitis is essential to allow early anti-inflammatory treatment and prevention of joint destruction. Several PET studies have been reported using [¹⁸F]fluorodeoxyglucose ([¹⁸F]FDG); however, [¹⁸F]FDG is not a biomarker specific for inflammation. We undertook this study to investigate whether rheumatoid synovitis can be visualized by PET using tracers specific for the inflammatory process. During early stages of a collagen-induced experimental rat model of rheumatoid arthritis, we performed in vivo imaging using the activated glial cell PET tracer (R)- [¹¹C]PK11195, which binds to the peripheral benzodiazepine receptor (PBR), and the newly developed PET tracer [¹¹C]Ketoprofen, used for cyclooxygenase (COX) imaging (See Ref). Arthritis was induced with an emulsion of complete Freund's adjuvant and collagen injected intradermally at the base of the tail. Paw swelling was scored as an indicator of disease severity. The rats were injected with 50 MBq (R)- [¹¹C]PK11195 or [¹¹C]Ketoprofen and then scanned for 90 min using a small-animal PET system. Regions of interest for each hind paw were drawn on the summed (R)- [¹¹C]PK11195 or [¹¹C]Ketoprofen image and a standardized uptake value (SUV) was calculated. All experiments were approved by the animal ethical committee of RIKEN (Approval number. MAH21-20). As a result, (R)- [¹¹C]PK11195 and [¹¹C]Ketoprofen uptake on inflamed paw PET scans was significantly higher than control. The resulting data enabled a correlation analysis between SUV and paw swelling to be performed. As compared with the results from parallel PET study with [¹⁸F]FDG, both tracers accumulated much more specific to the region of inflammation occurs. Thus, by using (R)- [¹¹C]PK11195 and [¹¹C]Ketoprofen, noninvasive in vivo PET imaging for rheumatoid synovitis could provide diagnostic evidence of early synovitis and allow monitoring of synovitis activity during treatment. [Reference] M. Takashima, and M. Suzuki, et. al., Chem. Eur. J., 16(14) 4250-4258, 2010

Presentation Number **0628A**

Poster Session 1b: Imaging Molecular and/or Cellular Processes & Drug and/or Radiation Therapy

Microautoradiographic studies with ^{18}F -FDG, combined with immunohistochemistry

Masanori Yamato¹, Sachi Sugita³, Hiroshi Mizuma², Yasuhiro Wada³, Yosky Kataoka¹, Yasuyoshi Watanabe³, ¹Cellular Function Imaging Laboratory, RIKEN Center for Molecular Imaging Science, Kobe, Japan; ²Functional Probe Research Laboratory, RIKEN Center for Molecular Imaging Science, Kobe, Japan; ³Molecular Probe Dynamics Laboratory, RIKEN Center for Molecular Imaging Science, Kobe, Japan. Contact e-mail: yamatomasa@riken.jp

PET with ^{18}F -FDG is widely used for imaging tumor or inflammation. PET imaging, however, can not show ^{18}F -FDG accumulation in cellular level. In order to identify cells showing accumulation of ^{18}F -FDG, we have developed the microautoradiographic method combined with histochemical techniques including immunohistochemistry (Yamato M. et al., J Nucl Med. 50;266-273, 2009). We will here report the further progressed method applied for the accumulation of ^{18}F -FDG in indomethacin-induced intestinal ulceration and healing processes. In rats with intestinal ulcer, the accumulation was observed in inflammatory cells containing peroxidase on day 1 and in cells forming granulation tissue (α -smooth muscle actin-positive myofibroblasts and ED2-positive macrophages) on days 2-4 in and around ulcers. The study also revealed heavy accumulation of ^{18}F -FDG in proliferating (Ki67-immunopositive) intestinal crypt cells in the intact intestinal tissue. These observations indicate that marked ^{18}F -FDG uptake is brought about by cells involved in inflammation, tissue repair, and cell proliferation.

Presentation Number **0629A**

Poster Session 1b: Imaging Molecular and/or Cellular Processes & Drug and/or Radiation Therapy

Effects of different in vivo imaging modalities on the expression of pro-inflammatory mediators in lymphatic and radiosensitive organs on mRNA level

Daniel Bukala¹, Christoph M. Griessinger¹, Bernd J. Pichler¹, Manfred Kneilling², ¹Departement of Radiology, Laboratory for Preclinical Imaging and Imaging Technology of the Werner Siemens-Foundation, Eberhard Karls University Tuebingen, Tuebingen, Germany; ²Department of Dermatology, Eberhard Karls University, , Tuebingen, Germany. Contact e-mail: daniel.bukala@med.uni-tuebingen.de

Non-invasive in vivo imaging using high sensitive emission tomography (PET), computed tomography (CT), and magnet resonance tomography (MRT) is an important tool for preclinical studies. No valid data exist about the effects of these modalities on lymphatic and radiosensitive organs. Therefore, the aim of our study was to examine whether these modalities impair genomic expression of pro-inflammatory cytokines and adhesion molecules in lymphatic tissue and radiosensitive organs on mRNA-level. In experiments BALB/c mice underwent anesthesia prior to tail vein injection of 13 MBq (volume: 150µl) [¹⁸F]FDG or [¹⁸F]FLT and were kept anesthetized for one hour before mice were PET-imaged for 15 minutes. CT-, MRT- as well as control mice were sham injected (sodium chloride) and anesthetized for 75 minutes. Positive controls received a 2Gy whole body irradiation (caesium-137, n = 4). For CT-imaging we scanned mice 12 minutes (360 projections, 300ms, 80kV, 500µA) at a micro CT, and for MRT-investigations 24 minutes in a T2-weighted 3D-space-sequence (two scans, TR: 300ms, TE: 205ms, FoV 35x57mm, matrix size: 161x256) on a 7T MRT. We killed mice four hours after tracer/sham injection or whole body irradiation to remove, homogenize, and lyse organs. We normalized relative mRNA expression levels of IL-6, TNF, IL-1β, VCAM-1, and P-selectin with the expression level of aldolase. [¹⁸F]FDG induced an enhanced mRNA expression of TNF and IL-1β in the kidneys and of IL-6 in the ovaries, while [¹⁸F]FLT did not. Similarly [¹⁸F]FDG enhanced mRNA expression of TNF, IL-1β and IL-6 in the liver. Importantly, [¹⁸F]FDG and [¹⁸F]FLT displayed no significant influence on lymph nodes, spleen, and thymus. Low dose (2 Gy) whole body irradiation induced strongly enhanced mRNA levels of TNF, IL-1β, IL-6, and P-selectin in the thymus. Moreover 2Gy irradiation enhanced mRNA levels of VCAM-1 and P-selectin in the kidneys, and of IL-1β, VCAM-1 and P-selectin in the liver. MRT-imaging slightly increased TNF mRNA expression in the thymus and IL-6 mRNA in the ovaries. Interestingly, we could not detect any influence on mRNA expression of pro-inflammatory cytokines or adhesion molecules due to CT investigations. In summary we conclude that [¹⁸F]FDG/[¹⁸F]FLT-PET, CT and MRT displayed no effects on secondary lymphatic organs such as spleen and lymph nodes. Interestingly, [¹⁸F]FDG-PET investigations induced genomic mRNA-expression of TNF and IL-1β in kidneys and livers while [¹⁸F]FLT-PET did not. Importantly, CT and MRT seem to have no influence on lymphatic and radiosensitive organs.

Presentation Number **0630A**

Poster Session 1b: Imaging Molecular and/or Cellular Processes & Drug and/or Radiation Therapy

Longitudinal MRI follow-up of anti-inflammatory treatment using two magnetic labeling strategies for macrophage assessment

*Monica Sigovan¹, Amine Bessaad¹, Magali Breisse³, Claire Corot², Eric Lancelot², Nicolas A. Provost³, Zouher Majd³, Christine Menager⁴, Serge Nataf⁵, Norbert Nighoghossian¹, **Emmanuelle Canet-Soulas¹**, ¹Lyon1 University, Creatis-LRMN, Lyon, France; ²Guerbet, , Paris, France; ³Genfit, , Lille, France; ⁴PECSA Laboratory, , Paris, France; ⁵INSERM, U842, Lyon, France. Contact e-mail: emmanuelle.canet@univ-lyon1.fr*

Introduction The objective of the study was to evaluate the effect of an angiotensin II receptor antagonist, Irbesartan on atherosclerosis development in ApoE-deficient mice. Two strategies were used to assess macrophages non-invasively using iron-enhanced MRI. **Materials and Methods** 26 animals were divided into 4 groups and started on a high fat diet. Irbesartan was added to the diet of two groups. Animals were investigated at three time points: 10, 24 and 38 weeks of diet. At each point, after baseline MRI, the animals were administered either 1 mmolFe/kg of an USPIO agent (Guerbet, France) (1) or 10 million labeled macrophages with anionic iron nanoparticles (2). A second MRI was performed 48h post contrast. A gradient echo sequence was used for iron accumulation assessment in the vessel wall by T2* mapping. The temporal variation of the vessel wall areas and mean T2* values at both baseline and post-contrast was analyzed with an ANOVA test. Student's t-test was used to assess the statistical significance of the differences between vessel wall areas and mean T2* values of the two groups. All animals were sacrificed after MR session at the last imaging point. Lesion formation was validated by histology on aortic arch samples, serially cut into 10µm sections, stained with Oil Red O and counterstained with hematoxylin. **Results** Animal weight showed no significant difference between the groups throughout the study. Histological analysis of the vessel wall area showed a statistically significant difference between the treated and not treated groups. Thinner vessel walls were observed for the treated animals with MRI at the last imaging point. Direct injection of USPIO lead to large signal loss regions in the aortic wall. Focal signal loss was observed on post-macrophage injection images, however of lesser spatial extent. No significant differences were found between the groups for both strategies based on the calculated T2* values. **Conclusions** Irbesartan lead to a marked reduction in the plaque formation. Concerning iron-enhanced MRI, the study did not highlight differences between the two groups based on the post-contrast plaque T2* values. The high blood levels of VCAM indicate activation of endothelial cells of the treated group. A consequence of this could be the migration of immune cells inside the lesion which would explain the similar T2* values obtained by MRI. A limitation of the study is that only one image of the ascending aorta was acquired, hence the obtained information may not be fully representative of the general effect of the drug.

Presentation Number **0631A**

Poster Session 1b: Imaging Molecular and/or Cellular Processes & Drug and/or Radiation Therapy

Noninvasive Molecular Imaging of USPIO Uptakes in Atherosclerotic Aorta using Nonlinear Raman Microscopy

Lina Machtoub, *Universitätsklinik für Radiodiagnostik I, Innsbruck Medical University, Innsbruck, Austria. Contact e-mail: lina.machtoub@lycos.com*

The ultra small paramagnetic iron oxide nanoparticles (USPIO) a potent new class of magnetic resonance imaging (MRI) contrast agents have drawn much attention for its wide diverse diagnostic and potential therapeutic applications particularly in monitoring the inflammatory responses in various central nervous system (CNS) diseases such as cerebral ischemia, multiple sclerosis and acute disseminated encephalomyelitis. Recent in vivo MRI studies on hyperlipidemic rabbits have shown that ultra small superparamagnetic particles of iron oxide (USPIOs) accumulate in plaques with a high macrophage content that induces magnetic resonance (MR) signal changes correlated to the absolute iron content in the aortic arch. The scope of this work encompasses investigating USPIO uptakes in atherosclerosis experimental models using nonlinear Raman microscopy-based on Surface Enhanced Coherent anti-Stokes Raman Scattering (SECARS) microscopy. Like MRI, SECARS microscopy can be tuned to provide a wide variety of possible tissue contrasts, but with sub-cellular spatial resolution and near real time temporal resolution. Previously we have investigated USPIO uptakes in brain tissues taken from neurodegenerative disorder rat model. In this work experiments are performed on USPIO treated tissue sections taken from aortic arch of animal model of experimental atherosclerosis. Significant CARS intensity enhancement has been observed in regions highlighting the distribution of USPIO nanoparticles. The results presented shows the potential of nonlinear Raman microscopy in investigating USPIO uptakes in atherosclerotic models which can be promising for future studies on in vivo detection of macrophages in human plaques and early detection of atherosclerotic diseases.

Presentation Number **0633A**

Poster Session 1b: Imaging Molecular and/or Cellular Processes & Drug and/or Radiation Therapy

Monitoring the secretory compartments in mastocytes with cyanine-doped mesoporous nanoparticles

*Maneerat Ekkapongpisit¹, Giuseppina Nicotra¹, Matteo Ozzano¹, Roberta Castino¹, Ildiko Bojtos², Ivana Miletto³, Giuseppe Caputo², **Ciro Isidoro¹**, ¹Scienze Mediche, Università del Piemonte Orientale, Novara, Italy; ²Cyanine Technologies Spa, , Torino, Italy; ³NIS Centre of Excellence, University of Turin, Torino, Italy. Contact e-mail: isidoro@med.unipmn.it*

Basophils and mast cells play a central role in immediate allergic and inflammatory responses. These cells contain a peculiar class of inflammatory granules that discharge their content upon antigen-mediated crosslinking of IgE-membrane receptors. We have shown that mast cell inflammatory granules belongs to the family of secretory lysosomes, since their biogenesis pathway shares several features with that of true endosomes and lysosomes (Dragonetti et al., 2000). Recently, it has been shown that mastocytes possess two different subpopulation of inflammatory granules. Whether the two subpopulations of mast cell granules follow identical or different pathways for calcium-regulated exocytosis is still largely obscure. In this study, we employed two different types of fluorescent nanoparticles (NP) to trace the calcium-regulated exocytosis of inflammatory secretory granules in rat basophilic/mast cells (RBL). We used cyanine-doped silica mesoporous MCM-41 IRIS-3 NPs of 10 nm (produced by Cyanine Technologies, Turin - Italy; Gianotti et al., ACS Appl Mater Interfaces. 2009) and the FITC-conjugated polystyrene Latex beads of 30 nm (purchased from Sigma-Aldrich). Acidic compartments were identified by Lysosensor labeling. True endosomes and lysosomes were recognized by transgenic expression of Green Fluorescent Protein (GFP)-linked chimeric cathepsin D, a lysosomal resident protein. MCM-41 IRIS-3 NPs were rapidly internalized by RBL and, at least temporarily, they co-localized with Lysosensor. At steady-state, MCM-41 IRIS-3 NPs did not colocalize with CD-GFP, which marked endosomes and lysosomes. Latex beads also were internalized, though less efficiently, by RBL cells. MCM-41 IRIS-3 NPs and Latex beads showed only temporarily colocalization. The intracellular compartments of final destination were clearly distinct for the two types of NPs. Granule exocytosis was stimulated by means of A23187, a calcium ionophore, and by specific IgE-receptor stimulation with appropriate antigen (DNP-BSA). Kinetic study of induced exocytosis revealed that Latex beads were promptly extruded by the cells, whereas MCM-41 IRIS-3 NPs were exocytosed at a much later time. This study demonstrate the usefulness of fluorescent NPs for monitoring exocytosis in living cells. NPs could be exploited as a tool to reveal alterations in the secretory pathway of mastocytes.

Presentation Number **0634A**

Poster Session 1b: Imaging Molecular and/or Cellular Processes & Drug and/or Radiation Therapy

MRI Assessment of Focally Involved Monocyte Infiltration with Magnetic Nanoparticles in Myocarditis Rats

Hyeyoung Moon^{1,3}, **Hyo Eun Park**², **Kiyuk Chang**², **Kwan S. Hong**^{1,4}, ¹MR division, Korea Basic Science Institute, ChungcheongBuk-Do, Republic of Korea; ²Department of Internal Medicine, Catholic University, Seoul, Republic of Korea; ³Bio-Analytical Science, University of Science and Technology, Daejeon, Republic of Korea; ⁴Graduate School of Analytical Science and Technology, Chungnam National University, Daejeon, Republic of Korea. Contact e-mail: hymoon@kbsi.re.kr

We investigated whether long-vascular circulating MNP (magnetic nanoparticle) combined with CMR (cardiac magnetic resonance) imaging could detect inflammation area and estimated the possibility of guidance where biopsy samples should be collected in a rat model of experimental autoimmune myocarditis (EAM). We used home-made MNPs that provide fluorescent and magnetic properties in cells and tissues. We performed MRI in EAM (n=35) and control rats (n=5), and compared the MR images obtained before and 24 hr after the intravenous injection of MNP (10 mg Fe/kg) in order to determine whether the MNP could provide MRI contrast in the inflamed myocardium. MRI was performed using a 4.7 T MRI system with dual ECG and respiratory gating. After in vivo MR imaging, all hearts were extracted, sectioned, and stained for H&E and immunohistochemistry (IHC) studies. And we separately processed FACS analyses from extracted whole hearts of EAM (n=10) and control (n=3) rats. Immune cells with MNPs were collected, and classified as granulocytes (G), B cells, T cells, and monocytes/macrophages (M). The amount of iron per cell was also measured for the four different cells by ICP-AES. Comparing the CNRs (contrast-to-noise ratios) in the myocardium before and 24 hr after the MNP injection, there is shown significant difference between the control and EAM rats. There was a dramatic CNR change (~75%) in the myocardium of EAM rats, while it was ~20% in the control rats. From the H&E-, IHC-stained images and fluorescence images, the regions of M cells infiltrated in heart myocardium were precisely measured, and which were in good correlation with the negative contrast areas in MR images obtained in the EAM rats. From the FACS results, M cells were the major sources (>87%) that resulted in negative contrast in MR images. About 70% of the immune cells were indicated as M cells, whereas granulocytes, B cells, T cells were about 14, 10, and 7%, respectively. The amount of iron per cell in M cells was more than three times those in other cells. We demonstrated that the noninvasive imaging of myocardial inflammation is feasible in autoimmune myocarditis rats by using the MNP-contrasted CMR imaging. This approach provided the feasibility and efficiency to noninvasively image and track heterogeneous and focal involvement of macrophage infiltration in EAM rats. We expect that the MNP-contrasted CMR imaging could give us a guide where to take biopsy samples from the heart suspecting myocarditis, which will reduce making an error in diagnosis of human myocarditis.

Presentation Number **0635A**

Poster Session 1b: Imaging Molecular and/or Cellular Processes & Drug and/or Radiation Therapy

Multispectral Optoacoustic Tomography for High Resolution Visualization of Inflammation-Related Bio-markers in Vulnerable Human Carotid Plaques

Daniel Razansky¹, Niels J. Harlaar^{1,2}, Jan-Luuk Hillebrands³, Adrian Taruttis¹, Eva Herzog¹, Clark J. Zeebregts², Gooitzen M. van Dam², Vasilis Ntziachristos¹, ¹Technical University of Munich and Helmholtz Center Munich, Institute for Biological and Medical Imaging (IBMI), Neuherberg, Germany; ²Department of Surgery and Bio-optical Imaging Center Groningen, University Medical Center Groningen, Groningen, Netherlands; ³Department of Pathology & Medical Biology, University Medical Center Groningen, Groningen, Netherlands. Contact e-mail: daniel.razansky@helmholtz-muenchen.de

High activity levels of tissue biomarkers, such as cathepsins, integrins, and matrix metalloproteinases (MMPs), have been associated with atherosclerotic plaque instability, thus can potentially be used for highly specific diagnosis. However, high fidelity imaging of those markers is challenging due to intense scattering of light in biological tissues, limiting the ability to deliver accurate information on structure and molecular activity in large tissue volumes. We developed a multispectral optoacoustic tomography (MSOT) method suitable for simultaneous high-resolution visualization of morphology and molecular activity in human carotid plaque. Human carotid plaque sample from a symptomatic patient was incubated with a MMP-sensitive activatable fluorescent probe (MMPsense 680, VisEn, Medical, Boston, MA) directly after endarterectomy. An intact sample was subsequently imaged in the MSOT scanner to acquire 200 micron resolution three-dimensional images of plaque anatomy and distribution of MMP activity. The hot and cold spot regions, identified by MSOT in an intact specimen, had a good correspondence to epi-fluorescence imaging of cryosliced plaque, and was further validated by observing macrophage and smooth muscle cells appearance in immunohistochemistry and immunofluorescence. Here we demonstrate, for the first time to our knowledge, the ability of multispectral optoacoustic tomography to deliver volumetric images of activatable molecular probe distribution deep from optically opaque tissues. High resolution mapping of MMP activity in the vulnerable plaque of human carotid specimen was demonstrated. This ability directly relates to clinical potential as it can allow highly specific visualization and staging of plaque vulnerability in atherosclerosis during surgical intervention or by intravascular or potentially non-invasive imaging; thus impacting therapeutic clinical decision.

Presentation Number **0636A**

Poster Session 2b: Drug and/or Radiation Therapy & Imaging Molecular and/or Cellular Processes

Formation of focal adhesion mediates primary cilia-involved mechanotransduction in MC3T3-E1 pre-osteoblastic cells

Ok Hee Jeon, Yeong-Min Yoo, Chi Hyun Kim, Department of Biomedical Engineering, Yonsei university, Wonju, Republic of Korea.
Contact e-mail: junohki1004@Hotmail.com

Fluid flow-induced shear stress (FSS) is an important anabolic mechanical signal that results in the increase of cyclooxygenase2 (COX2) and prostaglandin E2 (PGE2) in bone cells. Primary cilium is a microtubule-based structure that may play a mechanosensory role in bone cells. It has been shown that primary cilia are required for FSS-induced COX2 and PGE2 release in bone cells. In this study, we hypothesized that primary cilia regulate FSS-induced COX2 release in osteoblasts via increases in focal adhesion. MC3T3-E1 pre osteoblastic cells were treated with 4mM chloral hydrate for 72 hours to abrogate primary cilia and allowed to adhere in glass slides for 1 hour in fresh medium. Then cells were subjected to FSS of 1 Pa for 2 hours. First, mRNA levels of COX2 and focal adhesion kinase (FAK) were determined using real-time RT-PCR. Second, FAK was assessed using immunofluorescence microscopy. Cells were fixed in 4% formalin for 20 min, permeabilized in 0.2% Triton, and stained with anti-vinculin antibody to visualize focal adhesion. When FSS loading was applied, both COX2 and FAK mRNA decreased by over 90% in cells without cilia (No-Cilia/Load) compared to cells with cilia (Cilia/Load). Immunofluorescence images confirmed these results by displaying a significant lack of focal adhesion in the No-Cilia/Load group compared to the Cilia/Load group (Figure 1). Our results suggest that primary cilia may mediate upregulation of COX2 gene expression and bone mechanotransduction via the focal adhesion in osteoblastic cells.

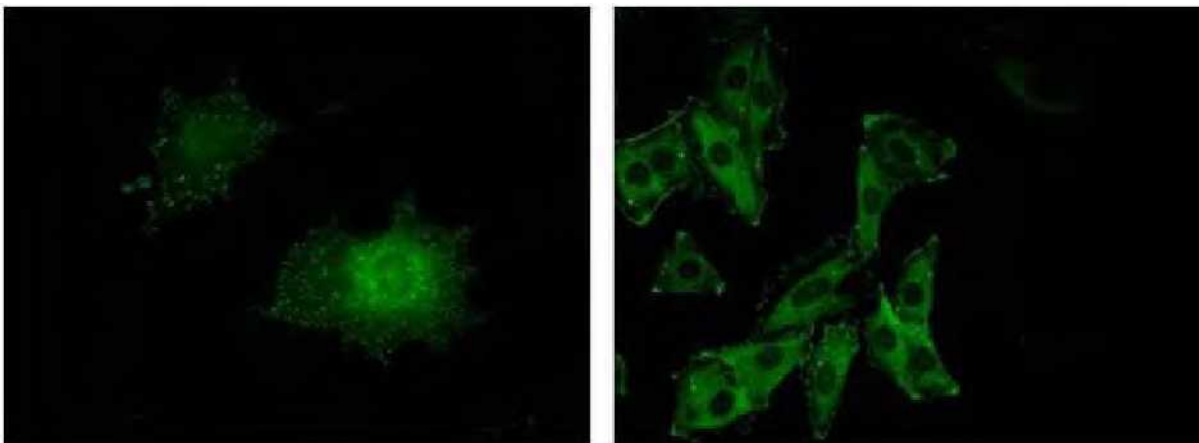


Fig 1. Anti-vinculin staining of FAK in cells with primary cilia (left) and without primary cilia (right). FSS was applied to both groups.

Presentation Number **0638A**

Poster Session 2b: Drug and/or Radiation Therapy & Imaging Molecular and/or Cellular Processes

Monitoring down-regulation of TERT promoter activity by anti-miR-21 induced PTEN expression

Myoung Geun Song¹, **Seung Hoo Kim**¹, **Hyewon Youn**^{1,2}, **Keon Wook Kang**¹, **Dong Soo Lee**^{1,3}, **June-Key Chung**^{1,2}, ¹*Nuclear Medicine, Seoul National University College of Medicine, Seoul, Republic of Korea;* ²*Institute of Radiation Medicine, Medical Research Center, Seoul, Republic of Korea;* ³*Molecular Medicine and Biopharmaceutical Science, WCU Graduate School of Convergence Science and Technology, Seoul National University, Seoul, Republic of Korea. Contact e-mail: bororia@hanmail.net*

Purpose: microRNA 21 (miR-21) is expressed in many tumors and the expression of human telomerase reverse transcriptase (hTERT) also shows tumor specificity. As a tumor suppressor, phosphatase and tensin homolog (PTEN) has been reported to have miR-21 targeting site on the 3' untranslated region (UTR) of mRNA, and the level of PTEN was down-regulation by binding of miR-21 on the 3'UTR. Recently, a possible use of antisense miR-21 (anti-miR21) for blocking miR-21 activity was suggested as a therapeutic agent to induce PTEN tumor suppressor. To study the relationship between miR-21 and hTERT expression, we developed two reporter systems visualizing the changes of PTEN and hTERT expression by treatment of miR-21 and anti-miR21. Materials and Methods: Two reporter gene constructs, PTEN binding promoter/luciferase fusion reporter (PTEN-luci) and hTERT promoter/hNIS with 5 repeated copy of c-myc binding site (5mm-hTERT-NIS), were constructed for visualizing the expression of PTEN or hTERT. PTEN expression was measured by western blot and an IVIS imaging system using PTEN-luci. After treatment with anti-miR21 in Hep3B cells, mRNA levels or reporter gene activity of PTEN was evaluated. The elevated level of hTERT promoter activity by miR21 was also observed using I-125 uptake assay. The mRNA and protein levels were measured by RT-PCR and western blot, respectively. Results: Higher PTEN expression was observed by western blot in PTEN-positive Du145 and Hep3B but not in PTEN-negative PC3 cells. In Hep3B cells, the mRNA levels of PTEN were increased when anti-miR21 was added. The luciferase activity was also significantly increased in the anti-miR21 treated Hep3B cells. Changes of PTEN expression by anti-miR21 were also visualized using luciferase reporter by transfection with PTEN-luci construct. Interestingly, the promoter activity of hTERT was decreased by anti-miR21, and which down-regulates the level of c-Myc, a major activator of hTERT. Conclusion: Our research demonstrated that the increased PTEN expression by inhibition of miR-21 can modulate signaling pathways associated with hTERT gene expression. We expect that our system can contribute to evaluate of the therapeutic effect of anti-miR21 by monitoring the modulation of PTEN and/or hTERT expression using reporter imaging.

Presentation Number **0639A**

Poster Session 2b: Drug and/or Radiation Therapy & Imaging Molecular and/or Cellular Processes

Regulation of RhoA by Arhgap12 as a novel partner of GULP during Stabilin-2-mediated cell corpse engulfment

Sang-Yeob Kim, Jae-Hoon Pyo, In-San Kim, Department of Biochemistry and Cell Biology, Kyungpook National University, School of Medicine, Daegu, Republic of Korea. Contact e-mail: sykimbear@gmail.com

Phagocytosis is the activity performed by phagocytes to engulf large particles. Stabilin-2 is a phosphatidylserine receptor that mediates the clearance of apoptotic cells. An adaptor protein, GULP, directly interacts with the NPXY motif of stabilin-2 via its PTB domain and plays a key role in stabilin-2-mediated phagocytosis. However, mechanisms that control the stabilin-2-mediated engulfment of cell corpse through actins rearrangement are largely unknown. Here, we identified ArhGAP12 as a novel partner of GULP. ArhGAP12 interacted with the proline-rich motif of GULP via its Src homology 3 domain and was dissociated from GULP upon stimulation of stabilin-2. Knockdown of ArhGAP12 decreased stabilin-2-mediated phagocytosis whereas overexpression of ArhGAP12 increased phagocytosis. The ArhGAP12 specifically controlled the activity of RhoA GTPase, but not Rac1. Inhibition of RhoA activity by ArhGAP12 could lead to enhancement of stabilin-2-mediated phagocytosis as the dominant negative form of RhoA did. Taken together, these results indicate that ArhGAP12 as a novel partner of GULP regulates RhoA activity to enhance stabilin-2-mediated cell corpse engulfment.

Presentation Number **0640A**

Poster Session 2b: Drug and/or Radiation Therapy & Imaging Molecular and/or Cellular Processes

Is [¹⁸F]FAHA feasible for assessing drug resistance of histone deacetylase inhibitor in leukemia?

Ren-Shyan Liu^{1,2}, Chieh-Ling Kao¹, Liang-Tsai Hsiao¹, Chueh-Chuan Yen², Chun-Yi Wu¹, Hsin-Ell Wang¹, Po-Min Chen², Juri G. Gelovani³, ¹MAGIC/NRPGM, Nuclear Medicine, Faculty of Medicine, National Yang-Ming University Medical School, Taipei, Taiwan; ²NPCC, Taipei Veterans General Hospital, Taipei, Taiwan; ³Experimental Diagnostic Imaging, MD Anderson Cancer Center, Houston, TX, USA. Contact e-mail: rslu@vghtpe.gov.tw

Objectives: 6-([¹⁸F]-fluoro-acetamido)-1-hexanoic-anilide ([¹⁸F]FAHA) is a radiolabeled histone deacetylase (HDAC) substrate which can be used for monitoring HDAC activity in tumors by PET imaging. Suberoyl anilide hydroxamic acid (SAHA) is one kind of HDAC inhibitor. HL-60/LR and HL-60 are leukemia cells having different HDAC expression and different drug resistance of HDAC inhibitor. The former (HL-60/LR) is resistant to HDAC inhibitor, the latter (HL-60) is not. This study was to investigate if [¹⁸F]FAHA is feasible for assessing these two types of leukemia cells before/after SAHA treatment. **Methods:** Nude mice were subcutaneously transplanted with 1×10^6 HL-60 and 1×10^6 HL-60/LR cells on right and left shoulders respectively. On 15th day, small animal PET imaging was performed at 1 hour after injecting [¹⁸F]FAHA ($50 \pm 10 \mu\text{Ci}$) through the tail vein. Three mice were oral administrated SAHA (50mg/kg) once a day for 3 days and scanned on 18th day again. 20-min static images were obtained by the reconstruction methods of OSEM 3D and MAP. ROIs were then carefully drawn on tumors and muscle. Maximum %ID/gram and mean %ID/gram of ROIs were measured. Tumor to muscle ratio ($T_{\text{max}}/M_{\text{mean}}$) was used to estimate the different uptake of [¹⁸F]FAHA in HL-60 and HL-60/LR cells. One-tailed Student's t-test was applied to determine the significant difference ($\alpha=0.05$). **Results:** The [¹⁸F]FAHA uptake in HL-60/LR was 20% higher than HL-60 (6.435 ± 0.81 vs 5.404 ± 1.02 ; $p < 0.001$). Furthermore, it was also shown higher $T_{\text{max}}/M_{\text{mean}}$ in HL-60/LR (3.81 ± 0.88 vs 3.17 ± 0.72 ; $p < 0.05$). In SAHA-treated group, it demonstrated that $T_{\text{max}}/M_{\text{mean}}$ is significantly increased in HL-60 (3.07 vs 4.94; $p < 0.05$) but not in HL-60/LR (4.58 vs 4.95). **Conclusions:** [¹⁸F]FAHA PET imaging may differentiate leukemia with drug resistance of HDAC inhibitor from that without drug resistance. The former has higher [¹⁸F]FAHA uptake than the latter. In addition, the binding of [¹⁸F]FAHA in drug resistant type of leukemia was not altered by SAHA. The mechanisms need to be elucidated.

Presentation Number **0641A**

Poster Session 2b: Drug and/or Radiation Therapy & Imaging Molecular and/or Cellular Processes

Relaxivity and Invitro Cytotoxicity of Positive MRI Contrast Agent Based on Gd2O3 Nanomagnetic Particles for Cell Tracking

Nader Riyahi Alam¹, **Soheila Haghighi**², **Zahleh Behrouzki**¹, ¹Medical Physics & Biomedical Engineering, Tehran university of medical sciences(TUMS), Tehran, Islamic Republic of Iran; ²Pharmaceutical Department, Food & Drug Laboratory Research Center, Ministry of Health, tehran, Islamic Republic of Iran. Contact e-mail: riahinad@sina.tums.ac.ir

The aim of this study by performing the development of gadolinium(III) oxide(Gd2O3) nanoparticles with diethylene glycolpolymer (DEG) and also by achievement of the contrast enhancement evaluation of Gd loaded nanoparticles in comparison with Magnevist(Gd-DTPA), was to indicate that Gd2O3 nanoparticles with diethylene glycol polymer could produce a good MR signal and therefore could be a useful potential contrast medium for cell tracking in magnetic resonance molecular imaging(MRMI). This study would be complicated with nanoparticles composed gadolinium (III) oxide (Gd2O3) with diethylene glycol polymer. The size and morphological structure of this Nano particle determined by particle size analysis device(zeta sizer) and Transmission Electronic Microscope(TEM). Proton relaxation times were measured with a 1.5-T MRI scanner. The measurements were performed in aqueous solution. Other purpose of this study was to assess cytotoxicity of polymerized gadolinium oxide nanoparticles. The effects of nanoparticles on 3 cell lines of U-87 MG, THP_1 and SK_MEL were evaluated by light microscopy, and also by standard cytotoxicity assays. The results showed a significantly higher incremental relaxivity for Gd2O3 nanoparticles compared to Gd-DTPA. The slope of R1 relaxivity(1/T1) vs. concentration curve of Gd-DTPA and Gd2O3 were 4.33, 13.37s⁻¹ mM⁻¹. The slope of R2 relaxivity(1/T2) vs. concentration curve of Gd-DTPA and Gd2O3 were 5.06, 9.05s⁻¹ mM⁻¹. Viability results indicate that U-87 MG, THP_1 and SK_MEL 3 cells endure treatment with Gd2O3 nanoparticles for an wide-ranging stage of time and it is therefore concluded that results in this study are founded on viable cells. The study indicates the possibility of obtaining high relaxivity compared to Gd-DTPA using Gd2O3 as contrast agent. Results: Figure 1 shows The signal had higher intensity for Gd2O3 samples compared with Gd-DTPA. Fig.2 signal intensity for Gd2O3 samples compared with Gd-DTPA. In Vitro Cytotoxicity of Gd2O3 Nanoparticles-Cell Morphology-The general morphology of the U-87 MG, THP_1 and SK_MEL 3 cells incubated with nanoparticles in phase-contrast microscopy is shown in Figure 2.(a)(b)(c) Discussion Gadolinium based nanoparticles(1-2)have the potential to greatly enhance the sensitivity, and therefore clinical usefulness of MRI by enabling imaging at cellular and subcellular levels. Cell viability observed in this study did not decrease to any significant level. References 1- A. Klasson, M. Ahren, E. Hellqvist, et al. "Positive MRI contrast enhancement in THP-1 cells with Gd2O3 nanoparticles". Contrast Media Mol. Imaging. 2008. Vol 3. 106-111. 2- G.M. Lanza, P.M. Winter, S.D. Caruthers, et al, "Magnetic resonance molecular imaging with nanoparticles". Nucl Cardiol 2004;No 11,733- 743.

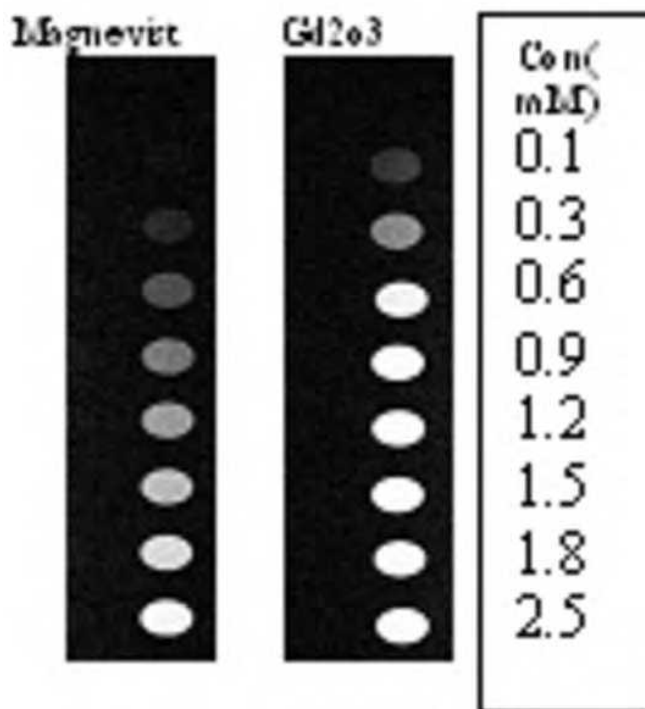


Fig.1 signal intensity for Gd2O3 samples compared with Gd-DTPA.

Presentation Number **0618B**

Poster Session 3b: Imaging Molecular and/or Cellular Processes & Drug and/or Radiation Therapy

Poly-L-lysine/Resovist complexes for cellular imaging in a rat spinal cord injury model

Gang Liu¹, Yun Zeng¹, Pu Yu², ¹Department of pharmacology, North Sichuan Medical College, Nanchong, China; ²Department of Radiology, Affiliated Hospital of North Sichuan Medical College, Nanchong, China. Contact e-mail: gangliu@nsmc.edu.cn

The therapeutic application of mesenchymal stem cells (MSCs) in central nervous system is still in its early stages. It is necessary to understand how MSCs will migrate and function in vivo, which will provide important information for designing better therapeutic strategies. In the present study, we evaluated poly-L-lysine/Resovist complexes for MSCs tracking in a rat spinal cord injury model. MSCs were labeled with poly-L-lysine/Resovist complexes and the viability, proliferation and differentiation of MSCs were determined. The cellular labeling efficiency was detected by electron microscopy and atomic absorption spectroscopy. 27 spinal cord injured rats were randomly selected for injection of PBS, unlabeled MSCs and labeled MSCs. Hind limb motor function was assessed using the open field Basso-Beattie-Bresnahan (BBB) scoring system and the test was carried out before injury and once a week after injury up to 5 weeks. Serial magnetic resonance imaging was performed after implantation and correlated with prussian blue staining. The results showed that MSCs labeled with poly-L-lysine/Resovist complexes were unaffected in their viability, apoptosis, and differentiation capacities. The poly-L-lysine/Resovist complexes were found mostly in cytoplasm and the uptake of complexes by MSCs displayed a dose-dependent behavior. After local administration into injured rat spinal cord, the labeled MSCs could be detected by the definite decreased signal intensity on T2-weight imaging until 14 days and the histology study identified the MRI results. BBB scores of labeled MSCs and unlabeled MSCs-treated rats were significantly higher than controls after injury. Our study describes a highly efficient and nontoxic method to label MSCs and it can provide a useful tool for tracking transplanted MSCs after intraslesional administration in spinal cord and in other intraparenchymal models.

Presentation Number **0619B**

Poster Session 3b: Imaging Molecular and/or Cellular Processes & Drug and/or Radiation Therapy

Stem cells-mediated delivery of magnetic nanoparticles to tumors for imaging and targeted hyperthermia

Lyubov Ostrovsk¹, Mohammad Hedayati², Christine Cornejo², Jana Mihalic³, Alison Geyh³, Dmitri Artemov¹, Theodore L. DeWeese², Robert Ivkov², ¹The Russell H. Morgan Department of Radiology and Radiological Science Division of MR Research, The Johns Hopkins University School of Medicine, Baltimore, MD, USA; ²Department of Radiation Oncology and Molecular Radiation Sciences, The Johns Hopkins University School of Medicine, Baltimore, MD, USA; ³Department of Environmental Health Sciences, Bloomberg School of Public Health, The Johns Hopkins University, Baltimore, MD, USA. Contact e-mail: lostrov1@jhmi.edu

Introduction: Stem cells loaded with magnetic nanoparticles are increasingly used for clinical applications, such as MRI and drug delivery. Previously, we demonstrated that in mouse models of prostate cancer intravenously injected mesenchymal stem cells (MSCs) migrate to tumors, home to the hypoxic areas, undergo endothelial differentiation, and participate in neovasclogenesis in growing tumors. Here, we aim to develop methods for stem cell-based delivery of magnetic nanoparticles to hypoxic areas in tumors to sensitize those areas with hyperthermia to subsequent irradiation. **Methods and Results:** In the current study, we optimized loading conditions and determined loading capacity of the mouse mesenchymal stem cells (MSCs) with magnetic bionized nanoferrite (BNF)-nanoparticles that generate heat in an alternating magnetic field (AMF). The iron concentration in BNF-loaded MSCs was quantified with inductively-coupled mass spectrometry (ICP-MS). Our data demonstrate that BNF-loaded stem cells differentiate according to differentiation media and do not change their growth characteristics. They can be successfully imaged with MRI. We measured the heating characteristics of BNF-loaded stem cells and determined dose-dependent decrease in survival via clonogenic and proliferation ability after exposure to AMF. Our data indicate that stem cells can be used to deliver BNF nanoparticles to hypoxic areas in tumors for targeted hyperthermia. **Significance:** We hypothesize that AMF will cause local hyperthermia at the sites of neovascularization in hypoxic tumor regions. This will sensitize those regions to irradiation and cause vascular disruption and tumor cell death, yielding tumor regression. Stem cells loading with bi-functional iron oxide nanoparticles permits tracking cells migration with MRI and heating with AMF. When combined with irradiation, this technique may provide new insights into stem cell physiology and enable new tools for cancer therapy.

Presentation Number **0620B**

Poster Session 3b: Imaging Molecular and/or Cellular Processes & Drug and/or Radiation Therapy

Visualizing of the proliferation and survival of dermal apilla cell using in vivo bioluminescence imaging

Jung Eun Kim, Hwang Mi Hye, Lee You La, Yong Hyun Jeon, Ho Won Lee, Young Kwan Sung, Sang-Woo Lee, Byeong-Cheol Ahn, Jaetae Lee, Kyungpook National University School of Medicine, Daegu, Republic of Korea. Contact e-mail: gene7302@hotmail.com

Objective: The purpose of this study is to investigating the trafficking of dermal papilla cell expressing enhanced green fluorescent protein(EGFP) and enhanced firefly luciferase(effluc) using non-invasive in vivo bioluminescence imaging. **Methods:** SV40ThTERT-EGFP-effluc cell line was established by infected with a retrovirus expressing the EGFP driven by respiratory syncytial virus(RSV) promoter and another retrovirus effluc reporter genes driven by cytomegalovirus (CMV) promoter and Thy1.1 linked with the IRES2 sequence. The cells with double expression of eGFP proteins and Thy1.1 were sorted out with flow cytometry. In RT-PCR analysis, mRNA expressions of EGFP were evaluated and confirmed gene expression of EGFP in cell cytoplasm using confocal microscopy. The function of effluc gene was verified by luciferase assay. Non-invasive bioluminescence imagings with D-luciferin were performed in mice having 1×10^4 of SV40ThTERT-EGFP-effluc cells at right flank. **Results:** Compared with untransfected SV40ThTERT cells, SV40ThTERT-EGFP-effluc cells had EGFP mRNA expression and confirmed the gene expression in cytoplasm using confocal microscopy. The luciferase activity from SV40ThTERT-EGFP-effluc cells showed increase higher compare to untransfected SV40ThTERT cells. We obtained positive bioluminescence signal at implantation site of SV40ThTERT-EGFP-effluc cells in nude mice. **Conclusions:** We have established SV40ThTERT cells expressing both EGFP and effluc biomluminescence reporter genes. Hair regeneration study can be done feasibly and this molecular imaging technique would be a great help for further hair research fields.

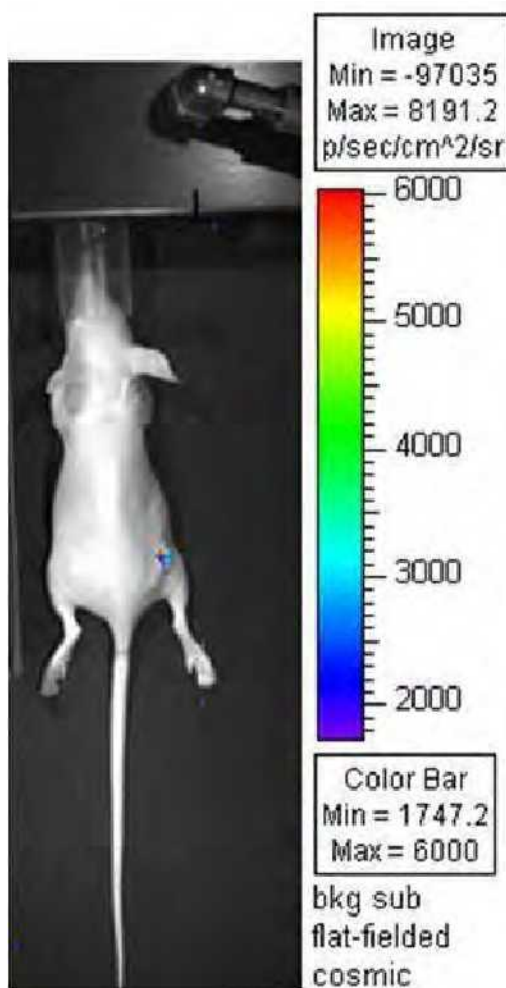


Fig 1. In vivo imaging of s.c. implanted SV40ThTERT-EGFP-Effluc cells. One day after injection, mice were imaged at 10 min after intraperitoneal injection of luciferin (5 mg/mouse). (Lt flank : 1×10^4 , SV40ThTERT cells Rt flank: 1×10^4 , SV40ThTERT-EGFP-Effluc cells)

Presentation Number **0621B**

Poster Session 3b: Imaging Molecular and/or Cellular Processes & Drug and/or Radiation Therapy

Labeling Human iPS Cells with the USPIO Nanoparticle Ferumoxytol

Rosalinda T. Castaneda¹, **Sophie E. Boddington**¹, **Edward Hsiao**², **Tobias D. Henning**¹, **Michael F. Wendland**¹, **Daniel Golovko**¹, **Heike E. Daldrup-Link**¹, ¹University of California, San Francisco, San Francisco, CA, USA; ²Endocrinology, University of California, San Francisco, San Francisco, CA, USA. Contact e-mail: rosalinda.castaneda@radiology.ucsf.edu

Purpose: FDA-approved Ferumoxides are not produced any more and, thus, are no longer available for clinical cell tracking studies. Ferumoxytol is a new USPIO that has recently been approved by the FDA. The purpose of this study was to optimize a labeling protocol for human induced pluripotent stem (hiPS) cells with this new iron oxide compound for translational cell tracking applications. Materials and Methods: Human iPS (hiPS) cells were labeled with Ferumoxytol by either (I) simple incubation or (II) transfection with protamine sulfate, using different iron oxide doses and incubation times. Triplicate samples from different experimental groups were imaged on a 7T MR scanner using T2-weighted spinecho and T2*-weighted gradient echo sequences. Trypan blue assays were performed to assess viability. T2- and T2* relaxation times and iron content, as measured by inductively coupled plasma atomic emission spectrometry, were compared between cells labeled with different labeling protocols and non-labeled controls, using a non-parametric Kruskal-Wallis ANOVA. Results: hiPS cells labeled by simple incubation techniques did not show significant T2*-effects, while all hiPS cells labeled with Ferumoxytol-Protamine demonstrated significant T2- and T2* effects. The optimal labeling protocol, which resulted in maximal iron oxide uptake and preserved cell viability was achieved with doses of 200 µg Fe/ml Ferumoxytol + 10 µg/ml Protamine and a 24 hr incubation period. This protocol resulted in significantly shortened T2*-relaxation times of labeled cells (10.27 ms +/-1.25 SD) compared to controls (65.70 ms +/-9.80 SD). Conclusion: Efficient labeling of hiPS cells with Ferumoxytol requires Protamine Sulfate transfection. To our knowledge this is the first study to successfully label stem cells with Ferumoxytol.

Presentation Number **0622B**

Poster Session 3b: Imaging Molecular and/or Cellular Processes & Drug and/or Radiation Therapy

In vivo PET imaging of NG2 cells in the adult brain

Yasuhisa Tamura, Akiko Tachibana, Yasuhiro Wada, Kazuhiro Takahashi, Yosky Kataoka, Center for Molecular Imaging Science, RIKEN, Kobe, Japan. Contact e-mail: tamuray@riken.jp

NG2-immunopositive cells (NG2 cells), ubiquitously distributed throughout the gray and white matter, undergo cell division and can generate oligodendrocytes and astrocytes as well as neurons even in the adult brain. NG2 cells become rapidly activated with their morphological changes including hypertrophy of the cell body and processes, and facilitate the proliferation in response to several brain insults including traumatic injury, excitotoxic lesions and viral infections. Establishment of in vivo imaging technique of NG2 cells could help us to evaluate the extent of brain injury and repair processes. In this study, we generated a transgenic rat strain overexpressing human estrogen receptor- α ligand binding domain (hERL) in the NG2 cells (NG2-hERL Tg rat). We performed PET imaging using 16α -[18 F]fluoro- 17β -estradiol (FES) in NG2-hERL Tg and the wild-type (WT) rats. In the wild-type rats, FES accumulation was observed in the hypothalamus and amygdala where original estrogen receptors are expressed under physiological condition. In the NG2-hERL Tg rats, FES uptake was observed in the cerebral cortex and striatum where NG2 cells abundantly exist, besides those regions. In this study, we evaluated biological usefulness of the FES-hERL PET reporter system in the in vivo imaging of neural stem/progenitor cells in the experimental animal brain.

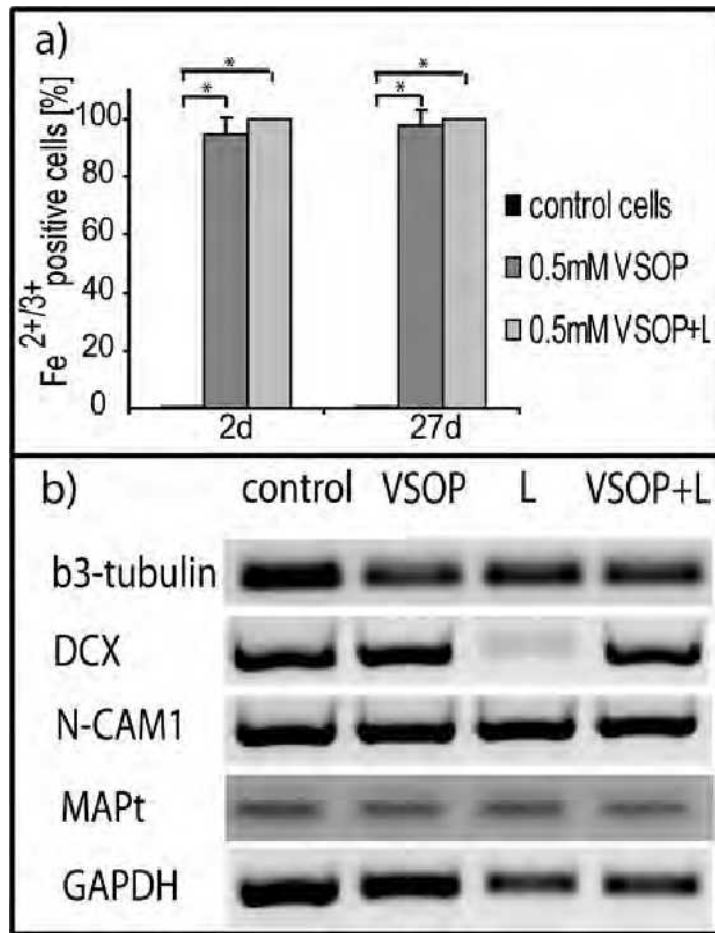
Presentation Number **0623B**

Poster Session 3b: Imaging Molecular and/or Cellular Processes & Drug and/or Radiation Therapy

Long term VSOP labeling: Human adult progenitors differentiate into mature neurons

Jenny Kressel^{1,2}, **Roland Coras**³, **Ingmar Blümcke**³, **Saida Zoubaa**⁴, **Jürgen Schlegel**⁴, **Claus Zimmer**¹, **Albrecht Stroh**¹, ¹Department of Neuroradiology, Klinikum rechts der Isar, Technische Universität München, Munich, Germany; ²Institute for Biological and Medical Imaging, Helmholtz Zentrum München, Munich, Germany; ³Department of Neuropathology, University Hospital Erlangen, Erlangen, Germany; ⁴Division of Neuropathology, Klinikum rechts der Isar, Technische Universität München, Munich, Germany. Contact e-mail: jenny.kressel@lrz.tum.de

Magnetic resonance imaging (MRI) is a unique non-invasive technique to monitor in vivo procedures with non-limited depth penetration. High-resolution imaging requires a sufficient cytoplasmatic incorporation of magnetic contrast agents into the cells. Commonly used and safe contrast agents are very small superparamagnetic iron oxide particles (VSOPs). However the effects of VSOP incorporation on stemness and neuronal differentiation potential of human adult neural stem cells (haSCs) remain unknown. The haSCs were isolated from surgical specimens obtained from patients with intractable temporal lobe epilepsy. Application of an efficient labeling protocol resulted in a stable uptake of high amounts of magnetic contrast agent, even at low VSOP concentrations sufficient for in vivo applications. Histological staining for iron-oxide revealed a stable vesicular incorporation for at least one month. By advising tailored labeling strategies, cellular viability remained unaffected, a prerequisite towards clinical application of this method. Transcriptional analysis (RT-PCR) of pluripotency markers (Oct4, Sox2) revealed no impact of VSOP incorporation on stemness. Subsequent neuronal differentiation of the labeled populations resulted in a neuronal phenotype, expressing various neuronal markers (β 3-tubulin, DCX, N-CAM1, MAPt) as measured by RT-PCR.



a) Stable VSOP uptake into 90-100% of human adult neural stem cells, following simple incubation with 0.5mM VSOP or lipofection. Data were analyzed and presented as means \pm s.e.m. Differences were considered significant at P < 0.01. b) Transcriptional analysis following neuronal differentiation.

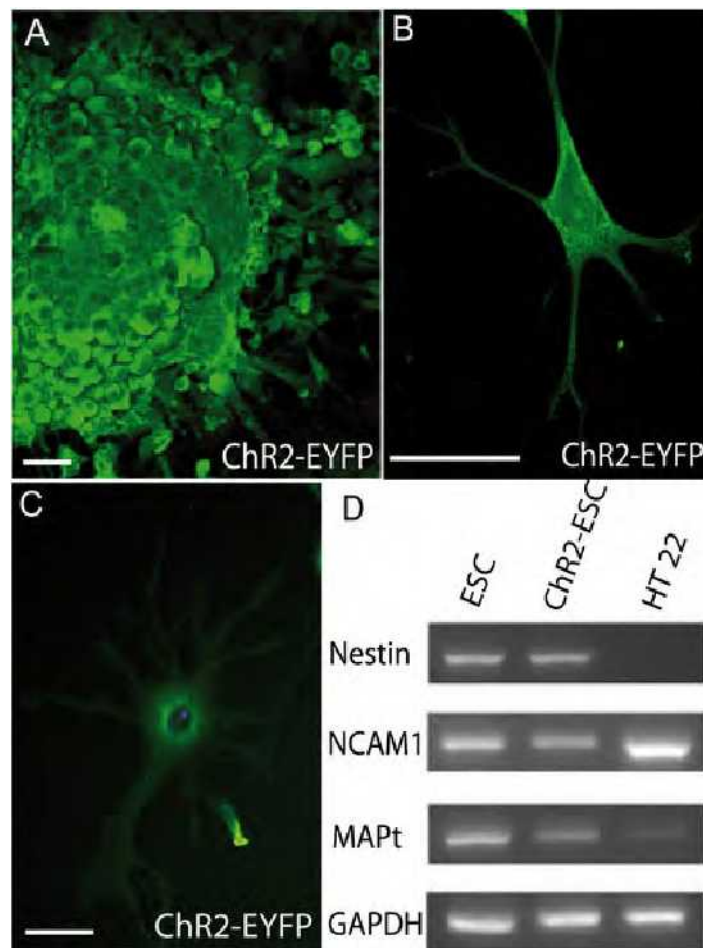
Presentation Number **0624B**

Poster Session 3b: Imaging Molecular and/or Cellular Processes & Drug and/or Radiation Therapy

Combining MRI and Optogenetics: Expression of Channelrhodopsin-2 in stem cells

Jenny Kressel^{1,2}, **Benedikt Berninger**³, **Vasilis Ntziachristos**², **Claus Zimmer**¹, **Albrecht Stroh**¹, ¹Department of Neuroradiology, Klinikum rechts der Isar, Technische Universität München, Munich, Germany; ²Institute for Biological and Medical Imaging, Helmholtz Zentrum München, Munich, Germany; ³Institute for Stem Cell Research, Helmholtz Zentrum München, Munich, Germany. Contact e-mail: jenny.kressel@lrz.tum.de

Magnetic resonance imaging (MRI) is a unique non-invasive technique to monitor in vivo procedures with high-resolution and a non-limited depth penetration. It requires a cellular non-genetic targeting with very small superparamagnetic iron oxide particles (VSOPs). For specific intervention we aim at combining this powerful technique with targeted optogenetic stimulation. Therefore, we introduced the genetically targeted optogenetic construct Channelrhodopsin-2 (ChR2) into stem cells. Following illumination with blue light (470nm) ChR2 leads to a high-speed depolarization, fast enough to drive precisely timed light-evoked spikes in neurons. Lentiviral integration of ChR2-EYFP into stem cells has the perspective of non-invasive control of cells both in vitro as well as after transplantation. Even in non-excitabile cells, optogenetic stimulation may result in alterations in gene expression due to activation of voltage gated calcium channels. Magnetically labelled embryonic stem cells (ESCs), as well as neural precursor cells from the adult mouse subventricular zone (SVZ), were transduced with a lentiviral ChR2-EYFP construct. Transcriptional analysis (RT-PCR) of pluripotency markers revealed no impact on stemness. Subsequent neuronal differentiation resulted in a neuronal phenotype expressing various neuronal markers. Fluorescence microscopy indicates strong membranous expression of ChR2 in mature neurons.



Membrane-bound expression of Channelrhodopsin-2 (ChR2-EYFP) in A) embryonic stem cells, B) embryonic stem cell derived neurons, and C) adult SVZ neural stem cells. D) Transcriptional analysis following neuronal differentiation.

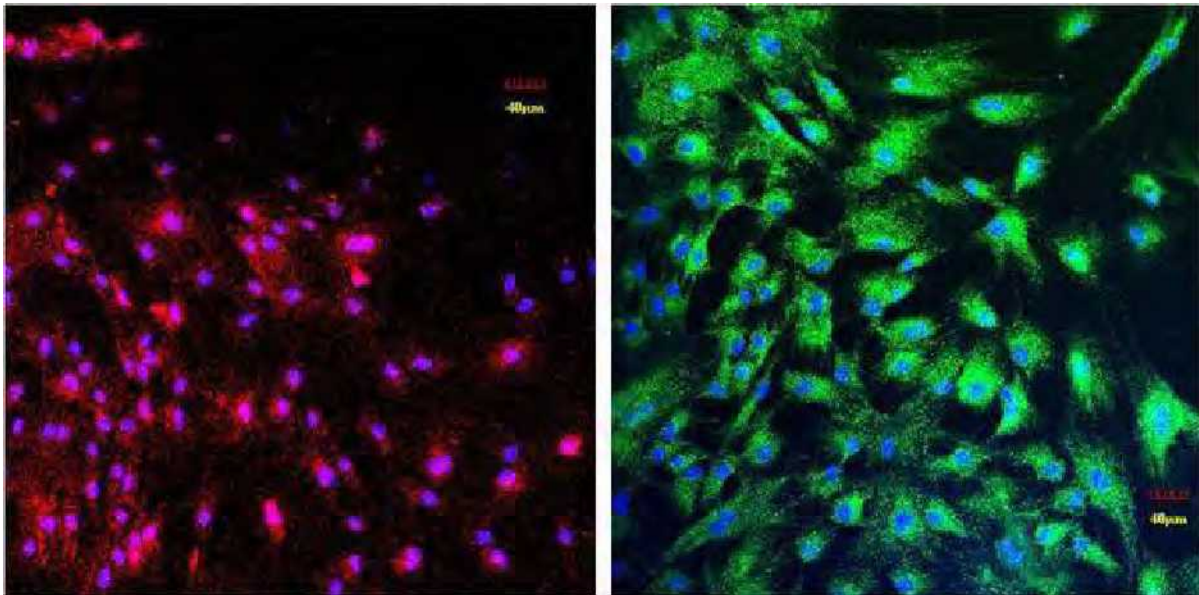
Presentation Number **0625B**

Poster Session 3b: Imaging Molecular and/or Cellular Processes & Drug and/or Radiation Therapy

MESENCHYMAL STEM CELLS DIFFERENTIATE INTO LYMPHATIC ENDOTHELIAL CELLS IN RESPONSE TO INFLAMMATORY AND LYMPHOANGIOGENIC STIMULI.

Andrei Volgin¹, Daniel Young¹, Brian Rabinovich¹, William Decker², Simon Robinson¹, Elizabeth J. Shpal², Juri G. Gelovani¹,
¹Experimental Diagnostic Imaging, MD Anderson Cancer Center, Houston, TX, USA; ²Stem Cell Transplantation, MD Anderson Cancer Center, Houston, TX, USA. Contact e-mail: andrei.volgin@mdanderson.org

Background: Mesenchymal stem cells (MSCs) have the capacity to differentiate into a variety of cell types including mesodermal (adipocyte, chondrocyte, hematopoietic support, myocyte, osteoblast, tenocyte), ectodermal (epithelial, glial, neural), and endodermal (hepatocyte, islet cell) lineages. Previously, we used autologous MSCs for intramyocardial transplantation for treatment of cardiac infarction in a porcine model of myocardial infarction (MI). We observed that a significant fraction of MSCs migrates through the cardiac lymphatic system and contributes to formation of lymphatic microvasculature in the area of infarct. Therefore, in the current in vitro study, we assessed the capacity of primary swine MSC lines to differentiate into lymphatic endothelial cells and acquire lymphatic endothelial biomarkers when exposed to inflammatory and lymphoproliferative factors. **Methods and Results:** MSCs were isolated from bone marrow of adult pig *S.scrofa* using conventional methods. MSCs were cultured with or without ligands for CCR7 and VEGFR3, expressed on the lymphoid vasculature (i.e. recombinant Human CCL19/MIP-3 β , recombinant Mouse CCL 21/6CKine and recombinant Human VEGF-C). Swine MSCs grew as adherent monolayers with a fibroblast-like morphology characterized by long podocytic protrusions, typical of endothelial differentiation. With or without treatment with mitogens, MSCs organized into tube like structures (indistinguishable from endothelial cells) when cultured on Matrigel. Immunohistochemical analysis and flow cytometry indicated that early-passage MSCs already expressed lymphoendothelial markers LYVE-1, VEGFR-3 and CD-90, the expression of which increased after treatment with lymphoendothelial mitogens (described above). In contrast, CCR-7 was not expressed in early-passage MSCs, but was expressed by approximately 40% of MSCs after 10 passages, independent of mitogen treatment. **Conclusions:** This in vitro study demonstrated that under the influence of inflammatory and lymphoangiogenic stimuli in vitro, porcine MSCs can differentiate into lymphoendothelial-like cells as evidenced by expression of key lymphoendothelial-specific biomarkers and tubulogenic phenotype. These results are in support of our previous in vivo studies that demonstrated the ability of MSCs to migrate through the cardiac lymphatic system upon intramyocardial injection and to contribute to the formation of lymphatic microvasculature in the area of infarct.



Expression of VEGFR-3 (red) and LYVE-1 (green) in porcine MSCs after 10 passages in presence of inflammatory and lymphoangiogenic factors. Cell nuclei (blue).

Presentation Number **0626B**

Poster Session 3b: Imaging Molecular and/or Cellular Processes & Drug and/or Radiation Therapy

In vitro specific monitoring cardiomyogenic differentiation of bone marrow derived mesenchymal stem cells (BMSCs) from α -myosin heavy chain (α -MHC) promoter driven sodium iodide symporter (NIS) transgenic mouse

Min Hwan Kim^{1,2}, **Yong Jin Lee**¹, **Joo Hyun Kang**¹, **Kwang Il Kim**¹, **Tae Sup Lee**¹, **Chan Wha Kim**², **Gi Jeong Cheon**¹, **Chang Woon Choi**¹, **Sang Moo Lim**¹, ¹Molecular Imaging Research Center, Korea Institute of Radiological And Medical Sciences, Seoul, Republic of Korea; ²School of Life Sciences and Biotechnology, Korea University, Seoul, Republic of Korea. Contact e-mail: bluecorps23@naver.com

Purposes: Development of a cell trafficking system for the transplanted stem cells enable us to image cellular differentiation in vivo. Although, bone marrow derived mesenchymal stem cells (MSCs) may be useful cell therapeutic agents in heart disease, there are still exist major obstacles to monitor their ability to differentiate into functional cardiomyocytes. In our previous study, the transgenic mouse model expressing sodium iodide symporter (NIS) driven by α -myosin heavy chain (α -MHC) promoter was developed to image cardiomyocyte with γ -camera and microPET in vivo (Kang et al. J Nucl Med 2005). In this study, we monitoring effect of α -MHC driven NIS gene of bone marrow derived mesenchymal stem cells (BMSCs) from the transgenic mouse during cardiomyogenic differentiation in vitro. **Methods:** BMSCs were isolated from bone marrow of femur and tibia of transgenic mouse. BMSCs specific surface markers including stem cell antigen 1 (Sca-1) and CD44, was investigated by flow cytometry (FACS) analysis. To differentiated into cardiomyogenic lineage, 1 μ M all-trans retinoic acid was treated to BMSCs for 3 weeks in vitro. Expression of cardiomyocyte specific gene was analysis by RT-PCR. According to cardiomyogenic differentiation, expression of NIS gene was tested by I-125 uptake assay. **Results:** Isolated BMSCs were showed up-regulated expression of stem cells specific surface markers including Sca-1 and CD44. But, majority of these cells negative for specific markers for hematopoietic and endothelial cells, such as CD34 and CD45. Differentiation properties of BMSCs committed to cardiomyocyte like cells after all trans-retinoic acid treatment. Cardiomyocyte like morphological change was observed in all trans-retinoic acid treated BMSCs. In RT-PCR analysis, the cardiomyogenic differentiated BMSCs were increased gene expression of α -MHC at the time of 3 weeks. In the I-125 uptake assay, the differentiated BMSCs accumulated 197.30 pmol/ mg protein at 60 min. But undifferentiated cells did not uptake iodide. **Conclusions:** The cardiomyocyte differentiated BMSCs from our established transgenic mouse showed that the high level of cardiac specific gene expression and increased reporter gene activity. Our results provided that the BMSCs expressing NIS under controlled by α -MHC promoter, can be used for imaging and monitoring agents for cellular differentiation into cardiomyocytes after stem cell transplantation.

Presentation Number **0627B**

Poster Session 3b: Imaging Molecular and/or Cellular Processes & Drug and/or Radiation Therapy

Mesenchymal Stem Cell could be differentiated into neuron after superparamagnetic iron oxide labeling

Jongkai Hsiao^{1,2}, Dong-Ming Huang³, KunEng Lim¹, Hon-Man Liu², ¹Medical Imaging, Taipei Tzu Chi General Hospital, Sindian, Taiwan; ²Medical Imaging, National Taiwan University Hospital, Taipei, Taiwan; ³Center for Nanomedicine Research, National Health Research Institutes, Zhunan Town, Taiwan. Contact e-mail: jongkai@gmail.com

Mesenchymal stem cells (MSCs) that has variable differentiation capacity plays important role in tissue engineering. Labeling mesenchymal stem cells with magnetic resonance imaging (MRI) contrast medium such as superparamagnetic iron oxide (SPIO) is beneficial for guidance of implantation of stem cells into living organism. We previously developed SPIO (Ferucarbotran) labeling technique without the assistance of transfecting agent. We could still visualize each mesenchymal stem cells under 1.5 Tesla clinical MRI system at single cell level. We currently developed differentiation technique that enables MSCs differentiate into astrocytes under variable growth factors such as beta fibroblast growth factor, platelet derived growth factor, epidermal growth factor, brain-derived growth factor and hormones including hydrocortisone and progesterone with the assistance of all-trans retinoic acid. These mesenchymal stem cells develop synapse like connection between cells 2 days after treatment. After treatment with growth factor cocktail, these cells becomes network like mesh no matter SPIO labeling or not. The labeling efficiency was determined by technique we developed previously and we can visualize identical signal intensity change between neuron differentiation and non-differentiation groups under 1.5 T MRI. The labeling efficiency could further proved microscopically by Prussian blue staining. The neuron differentiation capacity was proved by identifying neuron markers including glial fibrillary acidic protein, NeuN and beta-III-tubulin. Under flow cytometry, MSCs labeled with or without SPIO were differentiated into astrocytes and observed one and two weeks later. There is identical amount of new onset expression of these proteins. Under fluorescent microscopy, these cells with or without SPIO labeling show similar fluorescent signal. The finding represents neuron differentiation. We conclude that MSCs could be differentiated into neurons and SPIO will not alter the differentiation capacity. In the coming future, the technique might be beneficial for image guided cell therapy in face of stroke.

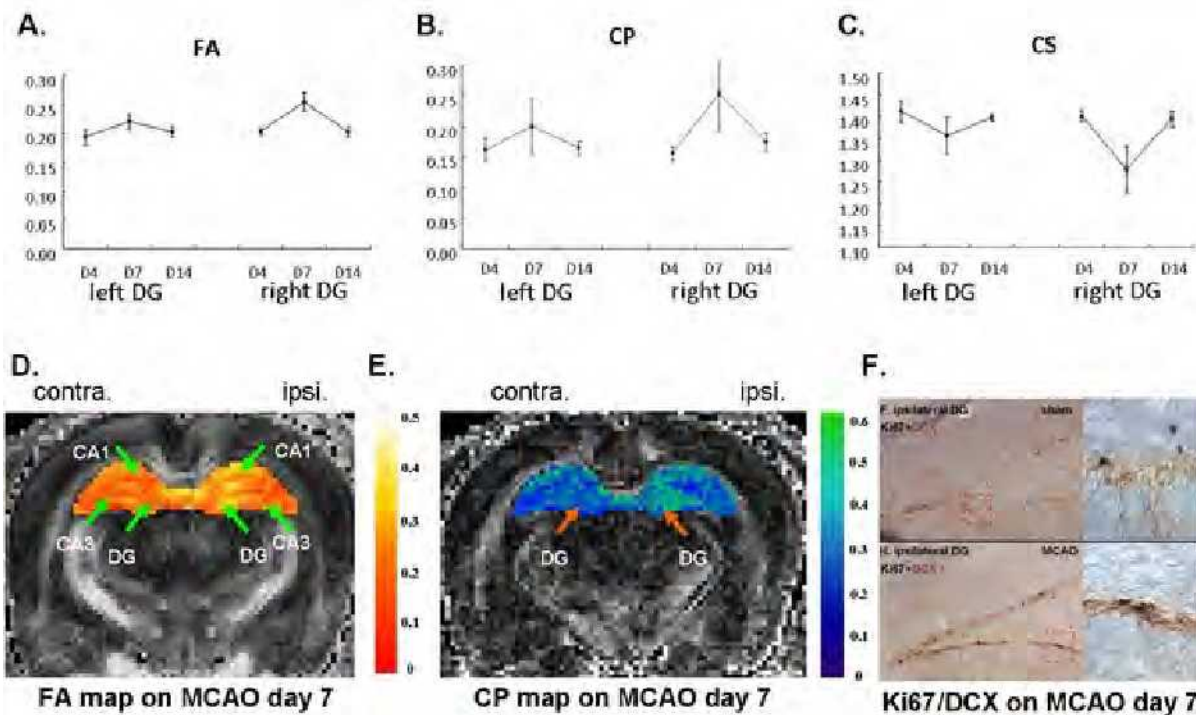
Presentation Number **0628B**

Poster Session 3b: Imaging Molecular and/or Cellular Processes & Drug and/or Radiation Therapy

Diffusion tensor imaging reveals longitudinal changes in hippocampal neurogenesis

Chiao-Chi V. Chen, Kuan-Chi Mo, Chen Chang, Functional and Micromagnetic Resonance Imaging Center, Institute of biomedical sciences, Academia Sinica, Taipei, Taiwan. Contact e-mail: ccchentw@ibms.sinica.edu.tw

Hippocampal neurogenesis involves the addition of newly generated neural cells into the existing neuroarchitecture. The distribution of the new cells is specific along the directions parallel and perpendicular to the dentate gyrus layer(DG). This imposes an influence on the directionality of water diffusion in the region, and thus the process is reported to be detectable in vivo by diffusion tensor imaging(DTI). The goal of the present study is to examine whether DTI is capable of detecting the different levels of hippocampal neurogenesis with time occurring in a stroke model, middle carotid artery occlusion (MCAO). MCAO mainly causes cortical ischemia ipsilateral to the ligation side. This model is known to enhance ipsilateral hippocampal neurogenesis peaking at the 7th day after MCAO. Nine week-old rats were used, each of which was repeatedly scanned for DTI on D4, D7, and D14 after MCAO. A spin echo imaging sequence was employed for acquiring the required series of axial diffusion-weighted images (DWIs) with b values=1100 mm²/s applied along the six directions with repetition time=1.5 s, spin echo time=31 ms, time between diffusion gradient pulses=15 ms, duration time of diffusion gradient=7.5 ms, slice thickness=1 mm, field of view=2.56 cm, data matrix=128x128, and four averages. Following scanning, the rat was immediately perfused and the brain tissue was processed for staining against Ki67 and doublecortin X(DCX) for histological confirmation. Results showed that the fractional anisotropy(FA) and the case of planar(CP) tensor shape in the DG peaked at day 7. In line with this, the case of spherical(CS) tensor shape was the lowest at day 7. These directional changes were related to the specific distribution of the processes/extensions of the newly generated cells along the DG layer revealed by Ki67/DCX double staining. This is the first report revealing longitudinal neurogenesis changes in vivo. The results also demonstrate the sensitivity of DTI in detecting subtle neural activity such as neurogenesis.



Presentation Number **0629B**

Poster Session 3b: Imaging Molecular and/or Cellular Processes & Drug and/or Radiation Therapy

PET imaging using [¹¹C]GF120918 (elacridar): to evaluate P-glycoprotein- and breast cancer resistance protein-mediated multidrug resistance in Caco-2 bearing mice

Tomoteru Yamasaki¹, Kazunori Kawamura¹, Fujiko Konno¹, Akiko Hatori¹, Joji Yui¹, Hidekatsu Wakizaka¹, Yuichiro Yoshida^{1,2}, Masanao Ogawa^{1,2}, Nobuki Nengaki^{1,2}, Kazuhiko Yanamoto³, Toshimitsu Fukumura¹, Ming-Rong Zhang¹, ¹Molecular Imaging Center, National Institute of Radiological Sciences, Chiba, Japan; ²SHI Accelerator Services, Tokyo, Japan; ³Division of Health Sciences, Graduate School of Medicine, Osaka University, Osaka, Japan. Contact e-mail: yamato@nirs.go.jp

Objective: Multidrug resistance (MDR) is a major problem in chemotherapy against cancers. P-glycoprotein (Pgp) and breast cancer resistance protein (BCRP) belong to ATP binding cassette (ABC) transporter super families and are mainly involved in MDR in tumors. GF120918 (elacridar) was developed as an acridonecarboxamide derivative and was widely used as a specific inhibitor against Pgp and BCRP. Recently, it is reported that some specific inhibitors to ABC transporters, such as verapamil, laniquidar, and GF120918, act in a substrate-like way when present in radiotracer amounts. In this study, we performed an in vitro cellular uptake study and a small animal PET study using [¹¹C]GF120918 to evaluate Pgp- and BCRP-mediated MDR in human colon adenocarcinoma. Methods: [¹¹C]GF120918 was synthesized by methylation of 5-O-desmethyl GF120918 with [¹¹C]methyl iodide [Kawamura, et al. Mol. Imaging. Biol. doi: 10.1007/s1130701003131.]. In vitro cellular uptake study was performed in human colon adenocarcinoma (Caco-2) and canine kidney epithelial (MDCK) cell lines. In vivo distribution study was determined in Caco-2-bearing mice by a small animal PET scanner. Metabolite analysis of [¹¹C]GF120918 in the plasma and tumor was performed using radio-HPLC. Results: Coincubation with unlabeled GF120918 in Caco-2 cells expressing Pgp and BCRP caused an approximately 2-fold increase in [¹¹C]GF120918 uptake, compared to the control ([¹¹C]GF120918 only). In PET study using Caco-2-bearing mice, [¹¹C]GF120918 uptake in the tumor was low but was significantly increased by treatment with unlabeled GF120918. Metabolite analysis showed that [¹¹C]GF120918 in the plasma and tumor was almost unchanged form at 60 min after a intravenous injection. Conclusion: A PET study by combining administration of [¹¹C]GF120918 with unlabeled GF120918 is a useful tool to evaluate Pgp and BCRP-mediated MDR in tumors.

Presentation Number **0630B**

Poster Session 3b: Imaging Molecular and/or Cellular Processes & Drug and/or Radiation Therapy

Amino acid esters could increase the transport of artificial amino acids into cells by trans-stimulation

Masato Ogura^{1,3}, **Syuichi Nakajima**^{1,2}, **Shinya Nakazawa**¹, **Masato Kobayashi**^{3,4}, **Naoto Shikano**¹, **Keiichi Kawai**^{3,4}, ¹*Radiological Sciences, Ibaraki Prefectural University of health sciences, Inashiki-gun, Japan;* ²*Radiology, Ibaraki prefectural central hospital, Kasama, Japan;* ³*Clinical laboratory, Kanazawa University, Kanazawa, Japan;* ⁴*Biological Imaging Research Center, University of Fukui, Fukui, Japan. Contact e-mail: oguram@jpu.ac.jp*

Introduction: To diagnose the malignancy of tumors by a labeled artificial amino acid, the tracer accumulation should be associated to not only localization but function (e.g., transport activity). One of the interesting features of system L1 amino acid transporters is "obligatory exchange" when amino acids accumulate in cells. In this study, we attempted to i) validate natural amino acids as the influx substrates, ii) establish an ¹²⁵I-3-iodo-alpha-methyl-L-tyrosine (IMT) uptake stimulation method, and iii) clarify the process of generating efflux substrates from an amino acid ester using Chinese hamster ovary (CHO-K1) cells. Methods: IMT uptake inhibition and pre-/co-loading studies were conducted with both inhibitors and esters. To confirm de-esterification of esters in the cells (e.g., by enzymatic attack), the concentration of de-esterified amino acids in the cell homogenates was analyzed by high-performance liquid chromatography. Results: The contribution of systems L and ASC on IMT uptake was 70% and 20%, respectively. Using L-Tyr methyl ester (L-Tyr-OMe), the esterified form of L-Tyr, we found that both the pre- and co-loading of L-Tyr-OMe with IMT significantly increased IMT uptake; however, the time-course curves of pre-loading and co-loading differed in shape. In cells exposed to bis(p-nitrophenyl) phosphate, an esterase inhibitor, this increase in IMT uptake was reduced slightly. Time-dependent de-esterification of L-Tyr-OMe and production of L-Tyr was observed in the cytosolic fractions, corresponding to the IMT uptake results. Temperature- and enantiomeric-dependent de-esterification was also observed. Discussion: With the precursor L-Tyr-OMe as the substrate provided to cells, IMT uptake into the cells was increased compared with the control. Moreover, L-Tyr could be generated by hydrolysis of esters using any enzyme. Unlike that for pre-loading natural amino acids, L-Tyr-OMe loading did not appear to inhibit IMT uptake. Such features of transport activity will allow us to establish an in vivo or ex vivo method for diagnosis of tumor malignancy.

Presentation Number **0631B**

Poster Session 3b: Imaging Molecular and/or Cellular Processes & Drug and/or Radiation Therapy

Differential effects of isoflurane and ketamine anesthesia on dopamine transporter function; PET study in mice with [¹¹C]PE2I

Toshiyuki Kawasaki¹, Hiroshi Mizuma¹, Hiroko Nagata², Hisashi Doi², Hirotaka Onoe¹, ¹Functional Probe Research Laboratory, RIKEN, Center for molecular imaging science, Kobe, Japan; ²Molecular Imaging Labeling Chemistry Laboratory, RIKEN, Center for molecular imaging science, Kobe, Japan. Contact e-mail: t.kawasaki@riken.jp

Studies with mice are useful for elucidation of pathophysiological mechanisms in several diseases, since many kinds of gene-manipulated models have been developed. Recently, positron emission tomography (PET) system has been dramatically improved its performance, which enable to perform noninvasive *in vivo* molecular imaging in rodents. We have recently established the PET [¹⁸F]FDG imaging method for mice without anesthesia, and have evaluated the brain regional glucose utilization in conscious state, which was significantly high as compared with that in isoflurane anesthesia. With PET, the imaging of central dopamine transporter (DAT) would be useful for elucidation of diagnosis in several neurological diseases and for developments of psychotropic drugs. Here, we have reported DAT imaging using PET with (*E*)-*N*-(3-iodoprop-2-enyl)-2 β -carbo[¹¹C]methoxy-3 β -(4-methylphenyl) nortropine (PE2I) in the mouse under conscious, isoflurane (1.5%) anesthetized and ketamine (100 mg/kg) anesthetized conditions. Male 10-12 week-old C57BL/6 mice were used in this study. To keep the head in immobilized state during PET scan, the mouse was pre-attached the acryl-made holder on the skull. [¹¹C]PE2I was administered via indwelling venous catheter, and then, the emission data were acquired for 90 min with a small animal PET scanner (microPET focus220). The binding potential (BP) of [¹¹C]PE2I in the striatum, which was calculated by simplified reference tissue model using cerebellum as a reference, was significantly high under isoflurane and also under ketamine anesthetized states as compared with that under the conscious state. Calculation of striatal *K_d* and *B_{avail}* values by *ex vivo* saturation study revealed that isoflurane anesthesia significantly increased *B_{avail}* but not *K_d*, suggesting the increased the numbers of functional DATs at cell surface, and ketamine anesthesia, in contrast, significantly decreased *K_d*, suggesting the increase of the affinity of the DAT for dopamine. These results strongly indicate that functional state of DAT *in vivo* is affected by isoflurane and ketamine anesthesia via different mechanisms, and imply that this novel brain PET imaging system for mouse under unanesthetized condition is useful for evaluating DAT function in several gene-manipulated mice models.

Presentation Number **0632B**

Poster Session 3b: Imaging Molecular and/or Cellular Processes & Drug and/or Radiation Therapy

Functional associations of aromatase and serotonin transporters with social behavior: PET studies with [¹¹C]cetrozole and [¹¹C]DASB in common marmosets

Chihiro Yokoyama¹, Akihiro Kawasaki¹, Kayo Takahashi², Takamitsu Hosoya³, Yasuyoshi Watanabe², Hirota Onoe¹, ¹Functional Probe Research Laboratory, RIKEN CMIS, Kobe, Japan; ²Molecular Probe Dynamics Laboratory, RIKEN CMIS, Kobe, Japan; ³Graduate School of Biomedical Science, Institute of Biomaterials and Bioengineering, Tokyo Medical and Dental University, Tokyo, Japan. Contact e-mail: chihiro@riken.jp

Aromatase, an enzyme that converts androgens to estrogens, is located not only in the female reproductive organ but also in the brain, and regulates sex steroid hormone level, which has been reported to alter the serotonin transmission including the functions of serotonin transporters (SERT) and receptors. Serotonin is involved in social and emotional behaviors including social stress responses, impulsive aggression, depression and anxiety. Relationship between serotonin and sex steroid hormone level in these behaviors, however, is not yet well known. In this study, we performed the functional imaging of aromatase and SERT in brain, and investigated their associations with individual variations of social behavior using common marmosets (*Callithrix jacchus*), which is considered as valuable animal models for examining in the cooperative aspects of social behaviors. Twelve male common marmosets were used for behavioral analysis and in vivo imaging by positron emission tomography (PET) with specific PET tracers for aromatase and SERT, [¹¹C]cetrozole and [¹¹C]DASB, respectively. We tested a social challenge between two unfamiliar males in a direct encounter with each other, and performed a factor analysis of behaviors, which resulted in represented individual characteristics of social behavior in three dimensions, 'sociability', 'aggression' and 'social anxiety'. The specific binding of [¹¹C]cetrozole were localized in the amygdala, hypothalamus, and nucleus accumbens, which were implicated as a part of the neuronal circuits for emotional processing. In the amygdala, [¹¹C]cetrozole binding sites partly overlapped with [¹¹C]DASB binding sites. Furthermore, binding potentials of [¹¹C]cetrozole and [¹¹C]DASB in the amygdala were associated with the representative factor scores of individuals for 'social anxiety', but not for 'sociability' or 'aggression'. The present results revealed that aromatase closely located in serotonin nerve terminals of the amygdala may be involved in serotonergic functional activities associated with 'social anxiety' behaviors in common marmosets.

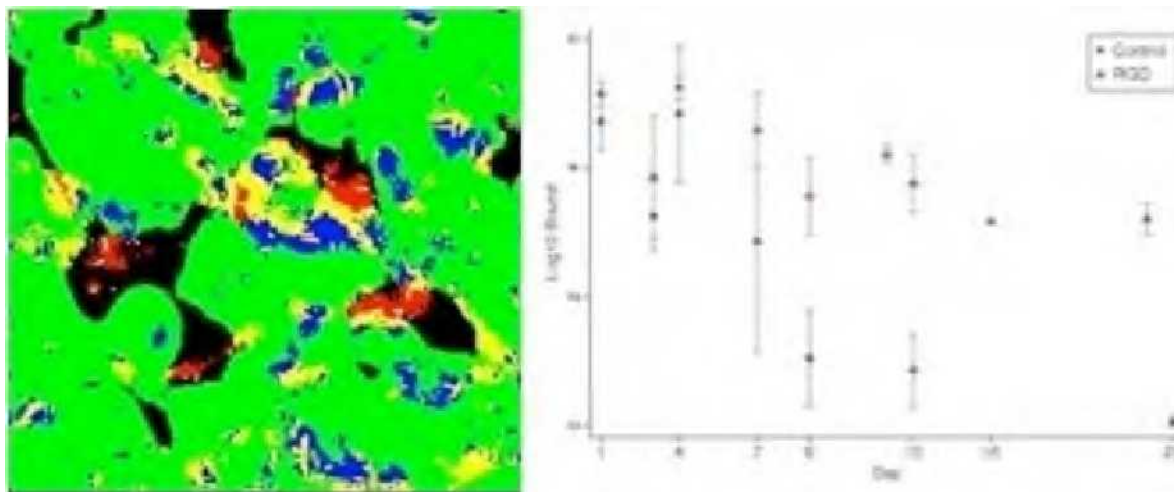
Presentation Number **0633B**

Poster Session 3b: Imaging Molecular and/or Cellular Processes & Drug and/or Radiation Therapy

How Do Nanoparticles Target Cancer? Real-time Microscopic Imaging with Carbon Nanotubes in Mouse Tumor Models

Bryan R. Smith¹, **Cristina Zavaleta**¹, **Zhuang Liu**², **John Ramunas**³, **Jarrett Rosenberg**¹, **Ricky Tong**⁴, **Hongjie Dai**², **Sanjiv S. Gambhir**^{1,4}, ¹Radiology/Molecular Imaging, Stanford University, Stanford, CA, USA; ²Chemistry, Stanford University, Stanford, CA, CA, USA; ³Neuroscience, Stanford University, Stanford, CA, CA, USA; ⁴School of Medicine, Stanford University, Stanford, CA, CA, USA.
Contact e-mail: brsmith@stanford.edu

While nanoparticles have become invaluable in the molecular imaging toolkit, little is known about the mechanisms by which they target diseased tissues. Single-walled carbon nanotubes (SWNTs) were previously demonstrated to display among the highest tumor uptake across nanoparticle constructs (12-15% ID/g). We thus carefully examined the modes of uptake by directly observing SWNTs entering tumor vasculature, specifically binding luminal targets, extravasating from vessels, and binding to tumor cells over time. To understand the fundamental mechanisms underlying SWNT tumor uptake, we confirmed and correlated our intravital microscopy (IVM) results with macroscopic Raman imaging, which quantifies SWNTs' intrinsic Raman signal. We used RGD peptide-bound SWNTs and controls to study the kinetics and routes of SWNT uptake and the ability of integrin targeting to enhance SWNT uptake and retention. We prepared targeted SWNTs by conjugating RGD (targeting $\alpha\beta3$ -integrins expressed on tumor neovasculature and some tumor cells, ~60/SWNT) and Cy5.5 dye (22/SWNT). Dorsal window chambers were surgically implanted into mice and EGFP-U87MG (expressing $\alpha\beta3$ -integrins) or EGFP-SKOV3 tumor cells were inoculated. 25 mice (U87MG, SKOV-3, no tumor) were imaged with RGD-SWNTs (~60 pmol) and RAD and no peptide controls. Mice were imaged during tail-vein injection and frequently over the following two months with Raman and IVM. Unlike controls, RGD-SWNTs were observed to bind tumor blood vessels. Within hours, all SWNT conjugates extravasated in U87MG tumor beds, but not SKOV-3 as quantified using 10-50 fields-of-view per mouse per time point. RGD-SWNTs were observed associated with tumor cells in U87MG tumors significantly more than RAD-SWNT controls ($P < 0.0001$). Furthermore, RGD-SWNTs differentially bound tumor cells over time compared with controls ($P < 0.007$) and they persisted in tumor for more than a month. Control SWNTs cleared within ~1 week. In summary, IVM allowed detailed exploration of the mechanisms of SWNT uptake in tumor. This work offers unprecedented understanding of the mechanisms/temporal framework of nanoparticle dynamics in tumors, which should translate into superior properties for pre-clinical and clinical utility.



Using an algorithm, we binarized our tumor cell image data from living mice (left), obtaining an image showing cell (green) and bound SWNTs (yellow). On the right, a graph shows the behavior of SWNTs depending on if the ligand is specific (RGD) or non-specific (RAD). Over the first week, SWNT association is similar between the two, but afterward RGD-SWNTs tend to remain bound over 3 weeks post-injection.

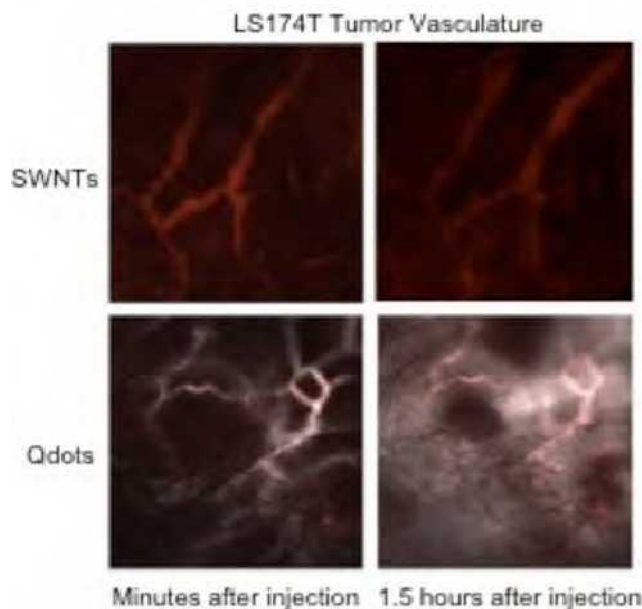
Presentation Number **0634B**

Poster Session 3b: Imaging Molecular and/or Cellular Processes & Drug and/or Radiation Therapy

Intravital Microscopy Reveals Surprising Differential Extravasation of Quantum Dots and Nanotubes Across Multiple Tumor Models in Living Subjects

Bryan R. Smith¹, **Scott Tabakman**², **Hongjie Dai**², **Sanjiv S. Gambhir**¹, ¹Radiology/Molecular Imaging, Stanford University, Stanford, CA, USA; ²Chemistry, Stanford University, Stanford, CA, USA. Contact e-mail: brsmith@stanford.edu

Nanoparticles (nps) comprising various materials, shapes, and sizes are becoming ubiquitous within molecular imaging, particularly for cancer diagnosis/treatment. Because nps are typically introduced via intravenous injection and expected to localize in tumor, a deeper understanding of how and why these nps extravasate from tumor neovasculature into interstitium is critical. It is essential to the field to characterize shape- and size-dependent np behavior across multiple tumor varieties in order to provide researchers with the ability to design the appropriate np for its purpose. This will also help optimize np formulations and decrease the time for clinical translation. We probed the extravasational behavior of two np types with three different tumor types using intravital microscopy (IVM) in 30 living mice. We used nude mice with an ear tumor model. We employed near-infrared (800nm) emitting quantum dots (qdots) (~20 nm diameter) and single-walled carbon nanotubes (SWNTs, 2 nm X 200 nm) conjugated to Cy5.5. Three different tumor cell lines were employed, all transduced with EGFP for visualization: SKOV3, LS174T, and U87MG cells. Long-circulating dye was injected to visualize the vasculature. No extravasation occurred in SKOV-3 with either np. In U87MG tumors, SWNTs extravasated rapidly (35.1% average fluorescence increase in interstitium from 2 to 30 minutes post-injection) while qdots extravasated minimally (12.7% increase from 2 minutes to 1.5 hours). However, intriguingly in LS174T tumors the opposite occurred: qdots extravasated rapidly (294% increase from 2 minutes to 1.5 hours), while SWNTs extravasated minimally. This role reversal reveals unanticipated complexity in np extravasational behavior and we quantified it using a region of interest analysis to better understand the underlying mechanisms. We thus directly visualized np extravasation from tumor blood vessels and demonstrated surprising np- and tumor-dependent differences, which will aid in the design of nps for optimal tumor uptake.



Displays regions of LS174T tumors in mice injected with SWNTs and with Qdots and imaged over time. Tumor signal (fluorescent green) was removed from the merged images shown above to clarify the extravasation signal. In the top set of images, no SWNTs have extravasated from the vasculature over a period of 1.5 hours. On the bottom, qdots have clearly extravasated from the vasculature within 1.5 hours of injection.

Presentation Number **0635B**

Poster Session 3b: Imaging Molecular and/or Cellular Processes & Drug and/or Radiation Therapy

Accumulation mechanism of 3- 123 I]iodo- α -methyl-L-tyrosine using human colon cancer DLD-1 cells

Takahiro Nadamura¹, Naoto Shikano², Masato Ogura^{2,1}, Fumiya Takahashi¹, Kazuyo Ohe¹, Masato Kobayashi^{1,3}, Keiichi Kawai^{1,3},
¹School of Health Sciences, Kanazawa University, Kanazawa, Japan; ²Department of Radiological Science, Ibaraki Prefectural University of Health Sciences, Ibaraki, Japan; ³Biomedecal Imaging Research Center, University of Fukui, Fukui, Japan. Contact e-mail: nada@stu.kanazawa-u.ac.jp

Introduction: 3- 123 I]iodo- α -methyl-L-tyrosine (123 I]IMT) has been clinically used for SPECT tumor imaging. However, the gene expression of neutral amino acid transporters has not been fully clarified even in those cell lines. In this study, we examined 123 I]IMT uptake and inhibition by amino acid-like drugs using the human colon cancer cell line, DLD-1. **Methods:** We investigated the time course of 18.5 kBq 125 I]IMT uptake, contributions of transport systems in Na⁺-free or Na⁺-containing medium and Na⁺-free medium containing 2-amino-bicyclo[2,2,1]heptane-2-carboxylic acid (BCH) and the effects of natural amino acids on 125 I]IMT uptake. 1 mM natural amino acid and amino acid-like drug inhibition of 125 I]IMT transport into DLD-1 cells in Na⁺-containing uptake medium was examined. Twenty D- and L-natural amino acids, tyrosine analogues, tryptophan analogues and p-halogeno-L-phenylalanines were used as the inhibitors. In addition, amino acid-like drugs such as 3,4-dihydroxy-L-phenylalanine (L-DOPA), threo- β -(3,4-dihydroxyphenyl)-DL-serine (DOPS), R(+)- and S(-)-baclofen, 1-(aminomethyl)cyclohexaneacetic acid (gabapentin) were selected as the substrates of system L, 2-(methylamino)isobutyric acid (MeAIB) and N-methylglycine (sarcosine) were used as ones of system A. Kinetic parameters with 125 I]IMT uptake were determined based on the results of the concentration-dependence study. Expression of relevant neutral amino acid transporters was examined by real-time PCR with DLD-1 cells. **Results:** 125 I]IMT uptake into DLD-1 cells was inhibited by natural L- and D-amino acids. Na⁺-independency and little stereoselectivity were observed in the strong inhibitory effects of phenylalanine, methionine and tyrosine. Tyrosine analogues, tryptophan analogues, p-halogeno-L-phenylalanines, L-DOPA, DOPS and gabapentin inhibited 125 I]IMT uptake, except for L-tyrosine methyl ester and R(+)/S(-)-baclofen. The substrates of system ASC and system A did not inhibit 125 I]IMT uptake, except for L-serine and D/L-cysteine. None of the tested cationic or anionic amino acids inhibited 125 I]IMT transport into DLD-1 cells. Expression of system L (LAT1, LAT2 and 4F2hc), system A and system ASC was strongly detected, while LAT3, LAT4 and B⁰AT1 were weakly detected by real-time PCR. **Conclusions:** Since 125 I]IMT was transported into the DLD-1 cells via LAT1, substrates of system L inhibit 125 I]IMT uptake. Whether transport of amino acid-like drugs is involved in LAT1 depends on the structure of the group corresponding to the amino acid residue.

Presentation Number **0636B**

Poster Session 3b: Imaging Molecular and/or Cellular Processes & Drug and/or Radiation Therapy

Selective polyplex delivery system of NGR-PEI: prospective tumor targeting agent

Jaeho Jang¹, **Do Won Hwang**^{2,3}, **Sejin Son**⁴, **Hyewon Youn**^{2,5}, **Won Jong Kim**⁴, **Dong Soo Lee**^{1,2}, ¹*Department of Molecular Medicine and Biopharmaceutical Science WCU Graduate school of Convergence science and Technology, Seoul National University, Seoul, Republic of Korea;* ²*Department of Nuclear Medicine, Seoul National University College of Medicine, Seoul, Republic of Korea;* ³*Institute of Radiation Medicine, Medical Research Center, Seoul, Republic of Korea;* ⁴*Laboratory of Molecular Imaging and Therapy, Cancer Research Institute, Seoul National University, Seoul, Republic of Korea;* ⁵*Department of Chemistry, Pohang University of Science and Technology, Pohang, Republic of Korea. Contact e-mail: asakura14@hotmail.com*

Purpose The peptides containing the Asn-Gly-Arg (NGR) motif have been shown to specifically bind to aminopeptidase N (CD13) which is selectively over-expressed in some tumor cells and implicated in angiogenesis and tumor growth. The cationic polymer, polyethylenimine (PEI) has been widely explored in gene delivery research. In this study, we investigated the tumor targeting characteristics of NGR-PEI polymer nanoparticle using luciferase reporter system. Methods HT1080, human fibrosarcoma as CD13/aminopeptidase positive cells and Hep3B, human hepatoma as CD13/aminopeptidase negative cells were used. With those cells, polyplex-mediated transfection with NGR-PEI and CMV-Fluc plasmid DNA was performed. Confocal fluorescence microscopy was used to monitor NGR-mediated cancer specific uptake using eGFP (Enhanced Green Fluorescence Protein) vector transfection system. In this experiment, HT1080 and Hep3B cells were stained with CellTracker™ CM-Dil and DiD (Invitrogen) respectively to track individual cellular pattern in co-culture system. Those two dyes are detected in different wavelength (549/565 nm, 644/663 nm). Result In vitro polyplex-mediated transfection with NGR-PEI and CMV-Fluc plasmid DNA demonstrated that definitely specific luciferase signal was observed in HT1080, but not in Hep3B. Significantly higher luciferase activity was found in HT1080 cell lysates, compared with luciferase activity in Hep3B. Confocal fluorescence microscopy data show that GFP signal intensity was specifically detected in HT1080 under co-culture condition after treatment of NGR/eGFP vector. **Conclusion** These results demonstrate the prospects of selective gene delivery system. This study could provide some clues for developing therapeutic gene delivery system for efficient cancer therapies.

Presentation Number **0637B**

Poster Session 3b: Imaging Molecular and/or Cellular Processes & Drug and/or Radiation Therapy

The possibility of combined therapy of siTERT virus and I-131 therapy following NIS gene expression in 5mmTERT-NIS expressing cells

Seung Hoo Kim^{1,2}, Hyewon Youn^{3,4}, Joo Hyun Kang⁶, Keon Wook Kang^{1,2}, Dong Soo Lee^{1,5}, June-Key Chung^{1,2}, ¹Department of Nuclear Medicine, Seoul National University College of Medicine, Seoul, Republic of Korea; ²Department of Tumor Biology, Seoul National University College of Medicine, Seoul, Republic of Korea; ³Laboratory of Molecular Imaging and Therapy of Cancer Research Institute, Seoul National University College of Medicine, Seoul, Republic of Korea; ⁴Institute of Radiation Medicine, Medical Research Center, Seoul National University College of Medicine, Seoul, Republic of Korea; ⁵Department of Molecular Medicine and Biopharmaceutical Science, WCU Graduate School of Convergence Science and Technology, Seoul National University College of Medicine, Seoul, Republic of Korea; ⁶Laboratory of Nuclear Medicine, Korea Institute of Radiological and Medical Sciences, Seoul, Republic of Korea. Contact e-mail: mid98@hanmail.net

Objectives: siRNA system can be used as a powerful tool for gene silencing. Human telomerase reverse transcriptase (hTERT) has been reported to involve in cancer progression by activating telomerase. Possible use of hTERT-specific siRNA (siTERT) by inhibiting TERT expression in cancer cells has been suggested as a therapeutic option, and NIS gene transfer has been tested for radioiodine gene therapy. In this study, we investigated the possibility of combined gene therapy of siTERT virus and I-131 in TERT positive-NIS expressing cells. Materials and methods: Human hepatocellular carcinoma (Hep3B) cells having TERT promoter/NIS gene (Hep3B-5mmTERT-NIS) were produced for radioiodine gene therapy, and a retrovirus having siTERT was produced for viral gene therapy. Reduced expression of hTERT mRNA, protein and its activity by infection of the siTERT virus was confirmed by RT-PCR, Western blotting and TRAP assay. The down regulation of hTERT expression was also visualized by IVIS imaging system and luciferase assay in vitro. Induced apoptosis was determined by annexin V-PI staining. Therapeutic effect of I-131 and/or siTERT was evaluated by clonogenic assay and visualization of tumor growth in animal xenograft model. Results: The siTERT virus infection successfully reduced the levels of hTERT mRNA and protein as well as hTERT activity. After siTERT virus treatment, the viability of cancer cells was significantly decreased to 50%, compared with control. It is confirmed that the early apoptotic cell population can be also increased by siTERT virus treatment and the apoptotic population was reached up to $13.9 \pm 2.9\%$. Tumor specific expression of hNIS gene or luciferase gene by 5mmTERT promoter was confirmed by micro-SPECT/CT and IVIS bioluminescence imaging. We also visualize the siTERT virus-induced the change of hTERT expression in vitro using 5mmTERT-luci system. Combined gene therapy with siTERT virus and hNIS based I-131 radioiodine therapy showed the synergistic effect in vivo as well as in vitro. Conclusion: This system can be used for visualization of target gene silencing by siRNA and monitoring the effect of combination therapy using radioiodine and siRNA.

Presentation Number **0638B**

Poster Session 3b: Imaging Molecular and/or Cellular Processes & Drug and/or Radiation Therapy

The accumulation mechanisms of *anti*-1-amino-3-^[18F]fluorocyclobutane-1-carboxylic acid and gene expression patterns of amino acid transporters in human derived tumor cell lines

Kazuyo Ohe¹, Fumiya Takahashi¹, Hiroyuki Okudaira¹, Shinya Kagawa², Ryuichi Nishii², Naoto Shikano³, Masato Kobayashi¹, Keiichi Kawai^{1,4}, ¹Graduate School of Medical Sciences, Kanazawa University, Kanazawa, Japan; ²Division of PET Imaging, Shiga Medical Center Research Institute, Moriyama, Japan; ³Department of Radiological Sciences, Ibaraki Prefectural University of Health Sciences, Inashiki, Japan; ⁴Biomedical Imaging Research Center, University of Fukui, Yoshida-gun, Japan. Contact e-mail: popo-rat@mhs.mp.kanazawa-u.ac.jp

[Introduction] *Anti*-1-amino-3-^[18F]fluorocyclobutane-1-carboxylic acid (^[18F]FACBC) is an artificial cyclic amino acid as L-leucine analog. Since ^[18F]FACBC has metabolic stability and high affinity to tumor cell, the ^[18F]FACBC is undergoing initial human clinical trials to validate it as a valuable imaging agent for the diagnosis and management of treatment of cancer as a positron emission tomography (PET) tracer. The purpose of this study is to define the relationship between ^[18F]FACBC accumulation and gene expression levels of amino acid transporters in several tumor cells. Also we aimed to evaluate the clinical utilities of ^[18F]FACBC as a PET tumor imaging agent. **[Method]** [¹⁴C]FACBC(^{[14}C]FACBC) transport assay was performed in vitro using 5 kinds of human cancer derived cell lines, such as MDA-MB435 (breast cancer), A431 (epidermal carcinoma), H441 and PC14 (adenocarcinoma derived from lung), LS180 (adenocarcinoma derived from colon). To investigate the contribution of transport systems, we used several buffer conditions of sodium-free phosphate-buffered saline (PBS) and sodium-containing PBS. In inhibition studies, 2-aminobicyclo-(2,2,1)-heptane-2-carboxylic acid (BCH) or 2-(methylamino)isobutyric acid (MeAIB) was added as a system L and system A specific amino acid transport inhibitor, respectively. The correlation between the accumulation of [¹⁴C]FACBC and the expression levels of the candidate transporters was evaluated using microarray gene expression profiling assay. Subsequently, we validated the expression levels by quantitative polymerase chain reaction (qPCR). **[Result]** In all cells, highly accumulation level of [¹⁴C]FACBC was shown under the condition of sodium-containing PBS. It revealed that [¹⁴C]FACBC worked well as a substrate in this condition. In the presence of BCH, [¹⁴C]FACBC accumulation was strongly inhibited especially in A431, H441 and MDA-MB435 cell lines. The expression levels of LAT1 and 4F2 mRNA were shown to be up-regulated in A431, H441 and MDA-MB435 with microarray and following qPCR. **[Conclusion]** High accumulation of [¹⁴C]FACBC and its inhibition by BCH suggest that system L transporter or some of sodium-dependent transporters might be main contributor to ^[18F]FACBC transport system. The up-regulation of expression levels of LAT1 and 4F2hc in those human derived tumor cells showed that they are strong contributors to [¹⁴C]FACBC transport system. These results suggest that, in a transporter expression-dependent manner, ^[18F]FACBC is useful as a potential metabolically based radiotracer for PET tumor imaging.

Presentation Number **0639B**

Poster Session 3b: Imaging Molecular and/or Cellular Processes & Drug and/or Radiation Therapy

Differential uptake and intracellular destination of silica Mesoporous and Latex nanoparticles in ovarian cancer cells

Maneerat Ekkapongpisit¹, Roberta Castino¹, Marilena D'Aquino¹, Ildiko Bojtos², Angela Mesiti², Giuseppe Caputo², **Ciro Isidoro**¹,
¹Scienze Mediche, Università del Piemonte Orientale, Novara, Italy; ²Cyanine Technologies Spa, , Torino, Italy. Contact e-mail:
isidoro@med.unipmn.it

Nanoparticle (NP) biocompatibility, cellular uptake mechanisms and intracellular localization are of particular relevance in live cell imaging studies, as well as for drug targeting and delivery applications in disease therapy. Toxicity/biocompatibility and mechanisms of cellular uptake depend on the cell type and the size, material and surface charge of the NP used. NPs can enter the cell via clathrin-mediated endocytosis, micro/macro-pinocytosis or phagocytosis. In this work we compared the biocompatibility and the mechanism(s) of internalization of two types of fluorescent NPs: the cyanine-doped silica mesoporous MCM-41 IRIS-3 NP of 10 nm (produced by Cyanine Technologies, Turin - Italy; Gianotti et al., ACS Appl Mater Interfaces. 2009) and the FITC-conjugated polystyrene Latex beads of 30 nm (purchased from Sigma-Aldrich). We also studied the intracellular trafficking and attempted to characterize the compartment(s) of final destination of the two NPs. The study was conducted in cultured human ovarian cancer OVCAR3 cells. Based on kinetic studies, MCM-41 IRIS-3 NPs were internalized more efficiently than polystyrene beads. The two types of NPs followed different pathways of internalization, as demonstrated by the separate and distinct fluorescent signals. Pre-treating the cells with 5 mM methyl-beta-cyclodextrin, an inhibitor of caveolae/clathrin-mediated endocytosis, impaired the internalization of MCM-41 IRIS-3 NPs, not that of latex beads. A2780 ovarian cancer cells, which are genetically devoid of caveolae, showed impaired uptake of MCM-41 IRIS-3 NPs. The fate of the NPs after entry into the cells was studied by pulse exposure to NPs and chase at different time points. No co-localization of the two types of NPs was observed at any time-point. With time, polystyrene Latex NPs accumulated beneath the plasmamembrane and thereafter were extruded by the cell. By contrast, MCM-41 IRIS-3 NPs rapidly reached and accumulated within compartments localized in the perinuclear region for several days. Co-localization studies with Lysosensor, a tracer of acidic vacuolar compartments, revealed that silica MCM-41 IRIS-3 NPs temporarily entered the endosomal-lysosomal pathway, but soon reached compartments not labeled with Lysosensor. The present data, demonstrating great differences in the uptake and intracellular fate of silica mesoporous and polystyrene NPs, underscore the importance of choosing NPs of appropriate material and size for in cell imaging and drug delivery depending on the genetic and functional endocytosis properties of the target cell.

Presentation Number **0640B**

Poster Session 3b: Imaging Molecular and/or Cellular Processes & Drug and/or Radiation Therapy

Compared with gene expression levels of amino acid transporter and accumulation of [¹⁴C]MeAIB and [³H]MET in human carcinomas

Shinya Kagawa^{1,2}, **Ryuichi Nishii**¹, **Tatsuya Higashi**¹, **Kazuyo Ohe**², **Hiroyuki Okudaira**², **Masato Kobayashi**², **Tomoya Uehara**³, **Yasushi Arano**³, **Keiichi Kawai**², ¹Shiga Medical Center Research Institute, Shiga, Japan; ²Graduate School of Medical Science, Kanazawa University, Kanazawa, Japan; ³Chiba University, Graduate School of Pharmaceutical Sciences, Chiba, Japan. Contact e-mail: kagawa@shigamed.jp

[Objective] To clarify the difference between system A and L amino acid transport imaging in clinical amino acid PET, we particularly focused on [*N*-methyl-¹⁴C]α-methylaminoisobutyric acid ([¹⁴C]MeAIB), compared with [*S*-methyl-¹⁴C]-L-methionine ([¹⁴C]MET). Our previous studies using five types of human carcinoma cells have been indicated that the main transport mechanism of [*S*-methyl-³H]-L-methionine ([³H]MET) takes place via Na⁺-independent system L. The main transport mechanism of α-[1-¹⁴C]-methylaminoisobutyric acid ([¹⁴C]MeAIB) takes place via system A with high specificity. The aim of this study was to assess the relativity of gene expression levels of amino acid transporter and accumulation of radiopharmaceuticals in tumor cells *in vitro*. [Methods] Uptake experiments of amino acid radiotracers, [¹⁴C]MeAIB and [³H]MET were performed in five types of human carcinoma cells (epidermal carcinoma: A431, colorectal carcinoma: LS180, lung carcinoma: PC14/GL, H441/GL, breast carcinoma: MDA-MB435). Inhibition studies of system A and L were also performed using MeAIB in Na⁺-containing solution as a specific inhibitor of system A, and BCH in Na⁺-free solution as a specific inhibitor of system L. Also, we investigated gene expression profiles of amino acid transporter in five types of human carcinoma cells by microarray analysis and quantitative polymerase chain reaction (qPCR), compared with accumulation of [¹⁴C]MeAIB and [³H]MET in human carcinomas. [Results and Conclusions] On accumulation of [³H]MET, the high contribution rate of system L amino acid transport were observed 76.3% (A431), 48.9% (H441) and 54.7% (MDA-MB435), respectively. These results were concerted the major amino acid transporter gene expression levels detected by microarray and qPCR analysis: system L (LAT1, 4F2hc). However, similar correlative patterns were not found in the contribution of system A amino acid transport in the five types of human carcinomas. It was considered that there were the participation of transporter systems other than amino acid transporters and further experiments are needed.

Presentation Number **0700A**

Poster Session 1c: In Vivo Studies & Development/Novel Use of Imaging Probes

Long-Term Toxicity Studies on ³²P-Chromic Phosphate-Poly-L Lactic Acid Seeds Interstitial Delivery of Beagle Dogs

*Lu Liu, Jin Sun, Qi Nie, Hailin Gao, Zexuan Yang, Qinghua Wu, Peilin Huang, Radiology, Southeast University, Nanjing, China.
Contact e-mail: luliuzhou@sina.com*

Objective To explore the possibility and safety of ³²P-CP-PLLA seeds administrated through interstitial implantation. **Methods** Thirty Beagle dogs were randomly divided into groups of ten according to different implants (³²P-CP-PLLA seeds or ³²P-CP colloids), different doses (185, 370 or 740 MBq), and different injection sites (gluteus or liver). Dynamic observation was performed including dogs weighting, blood, blood biochemistry and liver fibrosis detection, SPECT imaging and histology examination. The radioactivity of body surface, blood and daily urine and faeces were measured. **Result** γ imaging demonstrated both of ³²P-CP-PLLA groups and ³²P-CP groups had radioactivity congregating in the implantation field, without liver intake. In ³²P-CP group, amounted to 794.28MBq/m² administration, obvious liver damage appeared with 56Gy absorbed dose and systemic toxicity. In ³²P-CP-PLLA groups, up to 1588.89MBq/m², no obvious liver damage was observed with 89.83-178.68Gy absorbed dose in implantation liver area and 1.09-2.18Gy absorbed dose in the rest liver area. Dogs in high-dose ³²P-CP group appeared weight lost progressively and PLT and Hb obviously reduced. AST and ALT sharply increased before dying and the values of liver fibrosis indicators were higher than that of other groups (FPCIII =3.727, PPCIII =0.002; FHA =9.856, PHA =0.000; FCG =18.988, PCG =0.000; FPCIV =4.598, PPCIV=0.000). The results of blood and blood biochemistry among other groups showed no significant differences. Effective half-life of ³²P-CP-PLLA was 11.78 d, while ³²P-CP was 6.82 d through liver implantation, and 8.73 d through gluteus implantation. Within 4 weeks, moderate to serious liver injuries were found in high-dose ³²P-CP group, while mild to moderate liver injury in other liver implantation groups. Gluteus implantation groups had no significant pathological liver changes. All groups showed no abnormalities in heart, lung, spleen and kidneys. The blood radioactivity showed slowly jagged decreasing in ³²P-CP-PLLA groups and exponential decreasing in ³²P-CP groups. The mean accumulated radioactivity in urine / faeces after 30-day liver or gluteus implantation were 7.31% /9.86% or 6.75% /8.46% in ³²P-CP-PLLA group, while 23.69%/8.86% or 36.85%/10.93% in ³²P-CP groups. **Conclusion** ³²P-CP-PLLA seeds have a higher tolerated dose in dogs which can even endure double doses of ³²P-CP lethal dose, with mild and reversible injury to target organs and no obvious systemic toxicity. The ³²P-CP-PLLA seeds may have better therapy potential to solid tumors than traditional ³²P-CP colloids.

Presentation Number **0701A**

Poster Session 1c: In Vivo Studies & Development/Novel Use of Imaging Probes

Preliminary in vivo study on ^{32}P -chromic phosphate-poly (L-lactic) acid seeds in experimental mice

Lu Liu, Jin Sun, Hallin Gao, Zexuan Yang, Qinghua Wu, Qi Nie, Radiology, Southeast University, Nanjing, China. Contact e-mail: luliuzhou@sina.com

Objective Targeted positioning is one of the important characteristics of radionuclide brachytherapy. This study was to investigate the feasibility of preparation of ^{32}P -chromic phosphate (CP) with polymer materials poly (L-lactic) acid (PLLA) seed and to observe its in vivo degradation and metabolism in experimental mice. Methods ^{32}P -CP-PLLA seeds (with radioactivity of 20.44 - 25.14 kBq) were implanted into 72 KM mice through laparotomy or percutaneous puncture to the liver, abdominal cavity or limb muscles. The experimental mice were executed within 30 days at different time points. The seeds were taken out. ^{32}P radioactive counting rate (min-1) in main organs was determined and the percentage of injection dosage in one gram tissue (%ID/g) was calculated. The morphological change of seeds was observed by electron microscopy scanning. The seeds were also implanted into the liver of five SD rats bred in metabolic cage, the radioactive counting rate in 24 h feces and urine was determined and the 30d ^{32}P excretion rate was also calculated. Results The biodistribution in KM mice revealed no displacement of seeds occurred. The released radioactivity of ^{32}P in main organs or tissues was slightly higher than that of background level. The culminated counting rate in organs or tissues within 30 days changed in different phases: the aggregated uptake in liver was very low during 1-5 d, slightly increased during 6-10 d, decreased during 11-20 d and increased again during 21-25 d to reach its peak value, and then slightly decreased during 26-30 d; the changes in muscle were similar to those in liver but the peak appeared earlier (15 d) with relatively lower value. In abdominal cavity group, the uptake value in feces and urine appeared on 16 d and 19 d, the rates of whole 30-day excretion were 4.08% and 1.33%, respectively. Conclusions ^{32}P -CP-PLLA seeds can be newly prepared implants for the potential treatment of malignant tumor. The seeds remained inside the implantation organs with slowly phased degradation, excreting through feces and urine different from colloid implantation with high liver intake. ^{32}P -CP-PLLA seeds presented fairly stability and targeting orientation.

Presentation Number **0702A**

Poster Session 1c: In Vivo Studies & Development/Novel Use of Imaging Probes

In vivo monitoring of therapeutic efficacy of Cy5.5 labeled polymeric micelle containing doxorubicin for treatment of human breast cancer bone metastasis in nude mouse model by dual optical imaging

Young Jin Park^{1,2}, Eun Hye Song^{1,3}, Soul Hwa Kim¹, Ho-Taek Song¹, Kyung Taek Oh⁴, Jin-Suck Suh^{1,2}, ¹Department of Radiology, Yonsei University, College of Medicine, Seoul, Republic of Korea; ²National Core Research Center, Yonsei University, Seoul, Republic of Korea; ³Brain Korea 21 Project for Medical Sciences, Yonsei University, Seoul, Republic of Korea; ⁴Physical Pharmacy, Chung-Ang University, College of Pharmacy, Seoul, Republic of Korea. Contact e-mail: yjp@yuhs.ac

Background: Bone metastasis is frequently found in breast cancer patients and it cause severe pain and disabilities. Finding an effective therapy and a monitoring modality to validate the efficacy of treatment in vivo for the early therapeutic intervention to choose appropriate therapeutic option is challenging. Thus, we developed a model system to monitor the drug delivery in real time and to validate the therapeutic efficacy of Cy5.5 labeled polymeric micelle containing doxorubicin for the treatment of breast cancer. Methods: The luciferase expressing MDA-MB-231 2x10⁵ human breast cancer cells were injected into the left ventricle of ten 6-week-old female nude mice under ultrasonography guidance. The development of metastatic bone tumor was monitored by bioluminescent imaging every week. At week 2, control group A 5 mice underwent IV injection of 2mg/kg doxorubicin and study group B underwent Cy5.5 labeled polymeric micelle containing equivalent dose of doxorubicin. Each group was treated every other day by 4 times. In vivo bioluminescence imaging was performed to monitor the tumor and efficacy of therapy, and near infrared fluorescence imaging was performed to validate the drug delivery to the tumor after the injection. Statistical analysis was performed using Student t-test with significance of p<0.05. Results: Decreasing photon flux intensity at bioluminescence imaging was observed in the group A treated with polymeric micelle containing doxorubicin by week 5. Control group showed continued increase in the photon flux intensity. Efficacy of treatment was statistically significant (<0.05). Near infrared fluorescence imaging proved the Cy5.5 conjugated drug delivery vehicle co-localized to the metastatic bone tumor. Conclusion: In vivo dual optical monitoring system using bioluminescence imaging and near infrared fluorescence imaging successfully demonstrated the metastatic bone tumor development and efficacy of drug delivery. Polymeric micelle would be a promising drug delivery vehicle to treat metastatic bone tumor.

Presentation Number **0703A**

Poster Session 1c: In Vivo Studies & Development/Novel Use of Imaging Probes

In vivo imaging on bile-chemotactic migration of juvenile *Clonorchis sinensis* in rabbits

*Tae Im Kim*², *Won Gi Yoo*², *Hye Lim Kang*³, *Ji Sung Jung*³, *Byung Kook Kwak*³, ***Ju-Won Seok***¹, *Sung-Jong Hong*², ¹*Nuclear Medicine, College of Medicine, Chung-Ang University, Seoul, Republic of Korea;* ²*Medical environmental biology, College of Medicine, Chung-Ang University, Seoul, Republic of Korea;* ³*Radiology, College of Medicine, Chung-Ang University, Seoul, Republic of Korea. Contact e-mail: ethmoid@hanmail.net*

The metacercariae of *Clonorchis sinensis* excyst in the duodenum and migrate with chemotaxis to bile in the bile duct. We were curious about how fast the *C. sinensis* newly excysted juveniles (CsNEJs) migrate up through the ampulla of Vater. The CsNEJs were labeled with 18F-fluorodeoxyglucose (18FDG) by incubating in a maintaining media containing 2 mCi 18FDG at 37°C. After washing, radioactivity was measured using a gamma counter. Labeling efficiency was highest at 15 min incubation. Sensitivity of rabbits to cholecystikinin-8 (CCK-8), gallbladder contracting agent, was determined using 99mTc-mebrofenin cholescintigraphy. After injecting 2 mCi 99mTc-mebrofenin in 0.5 ml volume to the rabbits starved rabbits for 16 hrs, bile secretion was derived by intravenously injecting CCK-8 at dosage 20 ng/kg every 1 min, then dynamic image was taken every 1 min for 1 hr. The gallbladder was contracted 50% volume within 12 min of CCK-8 injection. A catheter was positioned in middle duodenum of the rabbit under anesthesia and 20 ng/kg CCK-8 was injected every 1 min over this experiment. In vivo images were collected using positron emission tomography- computed tomography (PET-CT). One CT image was scanned at starting point and dynamic PET scan was performed for 90 min with a 3-min acquisition per frame. Twelve min after CCK-8 injection, about 3,000 18FDG-labeled CsNEJs were placed in duodenum through catheter. The CsNEJs were detected in the common bile duct 9 - 10 min after the CsNEJ injection, and kept migrating up peripheral capillary bile duct during early 30 min. A large number of adult *C. sinensis* were recovered from the rabbit livers 4 weeks after the CsNEJ infection. Collectively, the CsNEJs sensed bile in the duodenum and migrated up quickly with bile-chemotaxis into the bile duct.

Presentation Number **0704A**

Poster Session 1c: In Vivo Studies & Development/Novel Use of Imaging Probes

Evaluation of Tc-99m mebrofenin cholescintigraphy with cholecystokinin in rabbits

Ju-Won Seok¹, **Tae Im Kim**², **Won Gi Yoo**², **Ji Sung Jung**³, **Byung Kook Kwak**³, **Sung-Jong Hong**³, **Hye Lim Kang**², ¹*Nuclear Medicine, College of Medicine, Chung-Ang University, Seoul, Republic of Korea;* ²*Medicel Environmental Biology, College of Medicine, Chung-Ang University, Seoul, Republic of Korea;* ³*Radiology, College of Medicine, Chung-Ang University, Seoul, Republic of Korea.* Contact e-mail: ethmoid@hanmail.net

Purpose : This study evaluated the utility of non-invasive assessment of hepatobiliary function by Tc-99m mebrofenin cholescintigraphy with cholecystokinin in a rabbit. Our purpose was to determine the appropriate infusion time of cholecystokinin in a rabbit. **Methods :** 8 Male new Zealand white rabbits (2.2-2.3kg) underwent Tc-99m mebrofenin cholescintigraphy to evaluate the hepatocyst mebrofenin uptake rate, the time of maximum hepatic uptake (Tmax) and the time required for peak activity to decrease by 50%(T1/2max) with cholecystokinin. **Results :** A scintigraphic study in rabbits showed that most of the administrated radioactivity accumulated in the liver and was rapidly excreted through the hepatobiliary system, visualizing the gallbladder within 15 min. Tmax of Tc-99m mebrofenin cholescintigraphy in rabbit is 2.93min. **Conclusion :** Tc-99m mebrofenin cholescintigraphy enables the identification of hepatobiliary function and the appropriate infusion time of cholecystokinin in rabbit.

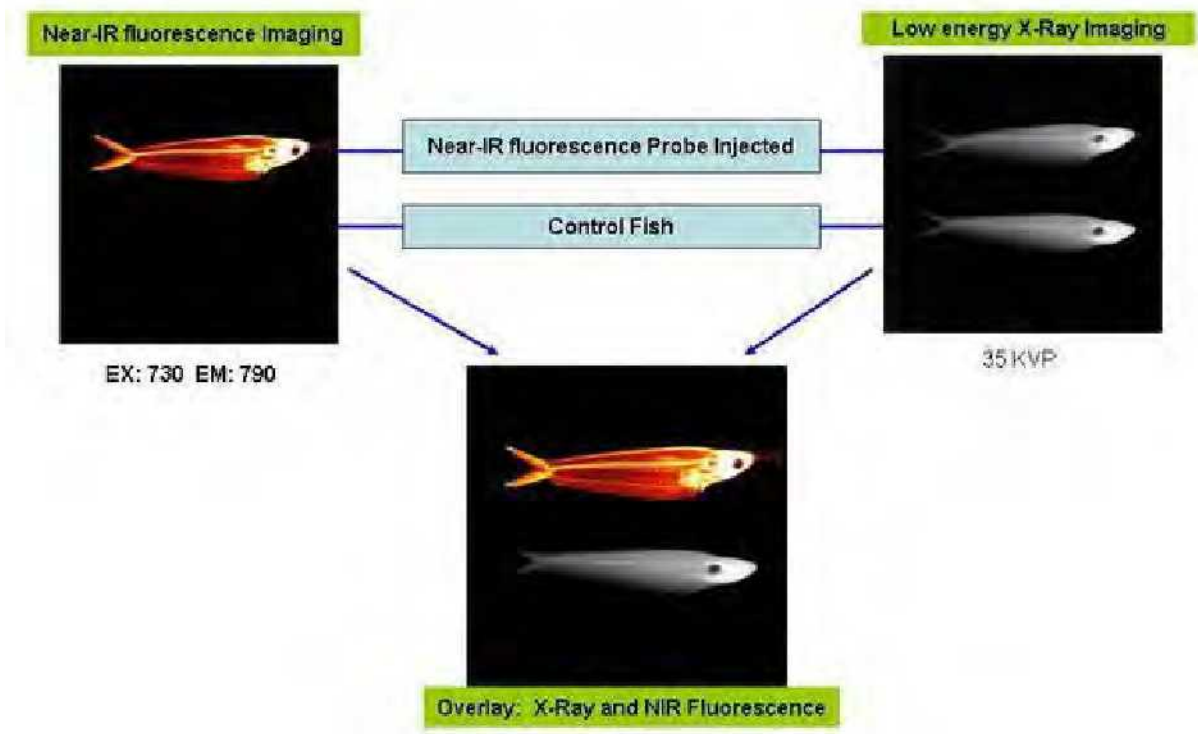
Presentation Number **0706A**

Poster Session 1c: In Vivo Studies & Development/Novel Use of Imaging Probes

NONINVASIVE NEAR-INFRARED FLUORESCENCE AND X-RAY IMAGING OF FISH SKELETON

Rao V. Papineni¹, **Jingyi Pan**¹, **Mayur Danny I. Gohe**³, **Doris W. Au**², ¹Carestream Molecular Imaging, Carestream Health, Inc., Woodbridge, CT, USA; ²Biology and Chemistry, City University, Hong Kong, Hong Kong; ³Health Technology & Informatics, Hong Kong Polytechnic University, Hong Kong, Hong Kong. Contact e-mail: rao.papineni1@carestreamhealth.com

Extensive homology in Telomerase Reverse Transcriptase (TERTs) exists between various species of fish and humans. This conserved telomerase function, and the fast and consistent growth pattern of fish allows it to be a vertebrate model for studying various mechanisms related to aging, cancer, and tissue regeneration. In particular, a model to screen compounds clinically relevant for bone growth, osteoarthritis, fracture-healing, and other age-related bone changes. Here, we describe the mode of probe administration and noninvasive visualization methods of fish skeleton using both low energy X-ray, and near-infrared fluorescence (NIRF) imaging. *Kryptopterus bicirrh*, as an example was administered (i.m) with the NIRF-bone binding agent. Non-invasive X-ray and NIRF images of the fish skeleton (figure) were obtained using a commercially available multimodal imaging system. Similar methodology was applied to several other species in this work. The vertebrate model and the imaging methodology provided here describes the potential in pharmaceutical research, where rapid screening of large candidate drug libraries can be facilitated in a short time span and lowered costs.



Presentation Number **0707A**

Poster Session 1c: In Vivo Studies & Development/Novel Use of Imaging Probes

In vivo micro-CT imaging of hepatic tumor in small animal model

Xiang Yang^{1,2}, Jie Tian^{2,3}, Junting Liu³, Xiangsi Li³, Maojie Ran¹, Yanqun Liu¹, ¹Guangzhou Zhongke Kaisheng Medical Technology Co., Ltd, Guangzhou, China; ²Medical Image Processing Group, Institute of Automation, CAS, "Beijing, 100190", China; ³Life Sciences Research Center, School of Life Sciences and Technology, Xidian University, Xi'an, China. Contact e-mail: tian@ieee.org

Micro-computed tomography (CT) is a useful tool for monitoring the construction of animal models and longitudinal imaging of tumor development. It is a challenge to monitor accurately tumor and its volume in the liver in living animals using micro-CT. In present study, We evaluated the feasibility of high-resolution micro-CT (ZKKS-MCT-III, Guangzhou Zhongke Kaisheng Medical Technology Co., Ltd, Guangzhou, China) enhanced with a hepatocyte-selective contrast agent (Fenestra VC, Advanced Research Technologies Inc., QC, Canada) for detecting hepatic tumor proliferation in small animal model. Firstly, two hepatic tumor models in situ with 1×10^6 hepa 1-6 cells and 50 μ l Matrigel (BD Matrigel Basement Membrane Matrix, BD Biosciences, NJ) were established. Secondly, micro-CT imaging was performed at 3.5 hours after distal tail intravenous administration of blood pool contrast agent containing iodine with a concentration of 130 mg/mL (Fenestra VC). Finally, we obtained high-resolution anatomical information of the tumor in vivo in rodents, the 3D tumor architecture is revealed in exquisite detail at 50 μ m resolution. In addition, the accurate shape (Fig. 1(b)) and volume (1.0631 cm³ and Fig. 1(c) 13.0107 mm³) of the tumors can be calculated through our software. The actual volume was verified through water displacement volume of tumor mass (Fig.1 (a) showed the tumor mass and liver). The scanning volume error is less than 2% in our experiments for the first tumor mouse model monitoring. Pathological section of another C57 tumor mouse model (fig.1(c)) showed the volume of tumor is identical with our software measured value (13.0107 mm³). Overall, our data suggest that this imaging approach could be used to understand tumor proliferation better and be the basis for evaluating anti-tumor therapies.

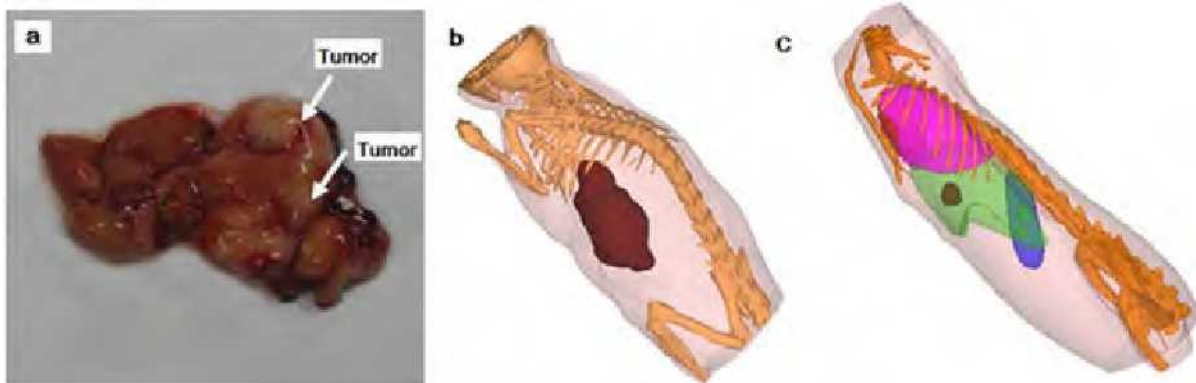


Fig. 1. In vivo micro-CT imaging of hepatic tumor in small animal model. (a) Tumor mass after dissecting the first C57 mouse model, (b) 3D tumor figure of the first C57 mouse model was obtained by micro-CT, (c) 3D tumor figure and anatomical structure of the second C57 mouse model.

Presentation Number **0708A**

Poster Session 1c: In Vivo Studies & Development/Novel Use of Imaging Probes

The effect of P-gp blockade on the binding of 18F-fallypride to dopamine receptors in the rat brain

Geoff I. Warnock¹, Mohamed-Ali Bahri¹, David Goblet¹, Christian Lemaire¹, Fabrice Giacomelli¹, Xavier Langlois², Andre Luxen¹, Alain Plenevaux¹, ¹Cyclotron Research Center, University of Liege, Liege, Belgium; ²Johnson & Johnson Pharmaceutical Research & Development, A Division of Janssen Pharmaceutica N.V., Beerse, Belgium. Contact e-mail: gwarnock@ulg.ac.be

Radiotracers penetrate the brain as only a small fraction of the injected dose. The ability of a radiotracer to cross the blood-brain-barrier is influenced by the multi-drug transporter P-glycoprotein (P-gp), and inhibition of its function has been shown to increase the amount of tracer reaching the brain (Ishiwata et al., 2007; Lacan et al., 2008). It has been shown that uptake of the dopamine receptor radiotracer 11C-raclopride is significantly increased after treatment with the P-gp blocker cyclosporin A (Ishiwata et al., 2007). 18F-fallypride is a high affinity tracer for dopamine D2/D3 receptors in the brain, and is of use in the quantification of these receptors in models of diseases such as Parkinson's, psychosis and addiction. Using a within-subject design we have investigated the effect of cyclosporin A on the uptake of 18F-fallypride in the rat brain. In addition to the standard measures of uptake %ID/cc and brain:blood ratio, the effect of P-gp blockade on binding potential and other kinetically modeled parameters was studied. Detailed kinetic modeling was made possible using a system developed in our lab for the measurement of input function simultaneously with PET. All PET scanning was performed in a Focus 120 MicroPET scanner (Siemens), in list mode. The data was histogrammed and reconstructed using filtered back projection with all corrections except scatter. Catheters were inserted into the femoral artery and vein of 7 male Sprague-dawley rats to allow measurement of input function using an arteriovenous shunt and beta microprobe. After scanning on the first day, these catheters were removed, then re-implanted contralaterally for the second scan one week later. For the first scan the animals were pretreated with saline. For the second scan 50 mg/kg cyclosporin A was injected subcutaneously 4 hours prior to scanning. A comparison of reference tissue and input function-based kinetic models was possible via the input function obtained from the arteriovenous shunt and beta microprobe. While neither kinetic modeling or dose-ratio methods revealed changes in 18F-fallypride uptake after blockade of P-gp, clear differences in the measured binding potential were found between reference tissue and input function-based modeling methods. These data suggest that 18F-fallypride is not a substrate for P-gp, but indicate that care should be taken in selecting kinetic models for this tracer. References Ishiwata et al. (2007) J Nucl Med 48:81-87. Lacan et al. (2008) Eur J Nucl Med Mol Imaging 35:2256-2266.

Presentation Number **0709A**

Poster Session 1c: In Vivo Studies & Development/Novel Use of Imaging Probes

The effect of beta microprobe implantation on the blood brain barrier

Geoff I. Warnock¹, *Stefanie Dedeurwaerdere*², *Mohamed-Ali Bahri*¹, *David Goblet*¹, *Christian Lemaire*¹, *Fabrice Giacomelli*¹, *Xavier Langlois*², *Andre Luxen*¹, *Alain Plenevaux*¹, ¹*Cyclotron Research Center, University of Liege, Liege, Belgium;* ²*Johnson & Johnson Pharmaceutical Research & Development, A Division of Janssen Pharmaceutica N.V., Beerse, Belgium. Contact e-mail: gwarnock@ulg.ac.be*

Beta microprobes are a recently developed, affordable alternative to microPET scanners for the quantification of radiotracer uptake and binding in the rodent brain (Zimmer et al., 2002; Weber et al., 2003). However, in contrast to microPET, implantation of beta microprobes in specific regions of the brain is an invasive procedure. This raises questions about the normal functioning of the brain after implantation and the integrity of the blood brain barrier (BBB). We selected two methods to test the integrity of the BBB in the hours immediately after probe implantation. In the first of these methods we examined the ability of the dopamine receptor antagonist domperidone to displace binding of the dopamine receptor tracer 18F-fallypride in the striatum of SD rats. Under normal conditions, peripherally administered domperidone does not penetrate the BBB. Displacement of 18F-fallypride by haloperidol was used as a positive control. Under isoflurane anesthesia, beta microprobes were stereotactically implanted in the striatum and cerebellum, and 18F-fallypride injected IV. After 60 minutes domperidone (0.63 mg/kg IV) or haloperidol (0.05 mg/kg IV) was injected. Haloperidol displaced specific binding of 18F-fallypride in the striatum by 75%, while domperidone had no significant effect. In the second test of BBB integrity, Evan's blue dye (1% in saline, 4ml/kg) was injected IV 1 hour after probe implantation in the striatum. After removal of the probe the brain was frozen and sectioned for histological examination. The presence of Evan's blue in the tissue around the probe site was measured by fluorescence. No specific Evan's blue staining was detected. The results of these two studies indicate that the integrity of the BBB is not compromised under the acute conditions of beta microprobe implantation. Further studies will investigate the effect of chronic implantation and effects on brain function such as glucose metabolism. References Zimmer et al. (2002) J Nucl Med 43:227-233. Weber et al. (2003) JCBFM 23:1455-1460.

Presentation Number **0710A**

Poster Session 1c: In Vivo Studies & Development/Novel Use of Imaging Probes

Lentiviral Transduction of the Mammary Intraepithelial Neoplasia Outgrowth (MIN-O) Transplant Lines for in Vivo Molecular Imaging

David L. Boucher¹, Jane Q. Chen², Alexander D. Borowsky², Simon R. Cherry¹, ¹Biomedical Engineering, University of California, Davis, Davis, CA, USA; ²Center for Comparative Medicine, University of California, Davis, Davis, CA, USA. Contact e-mail: dlboucher@ucdavis.edu

Introduction. The Mammary Intraepithelial Neoplasia Outgrowth (MIN-O) series of transplant lines is well characterized as a biologically relevant model of Ductal Carcinoma in situ (DCIS) with consistent periods of latency and metastatic potential. These lines are propagated in cleared fat pads of immune-intact genetically identical FVB mice which allows for studies of the progression of breast cancer to be completed in the presence of a microenvironment that more closely recapitulates that which is found in normal disease. This feature is the significant advantage of utilizing the MIN-O model rather than xenografts or cell lines; however, it has complicated imaging studies which have been previously limited by an inability to complete genetic modifications (i.e., insertion of imaging reporter constructs) in the lines. In this report, we describe a protocol for the efficient lentiviral transduction, in vitro culture and retransplantation of positively transduced "MIN-O-spheres" to generate genetically modified sublines more suited for imaging studies. **Method and Results.** Briefly stated, our protocol is divided into four subtasks as follows: a) dissociation of MIN-O tissue and isolation of MIN-O cells to create a slurry of "single" cells in suspension, b) "spinduction" (centrifugation-aided transduction) of the those cells with concentrated lentiviral particles, c) in vitro culture of transduced MIN-O cells until spherical, clonal populations develop, and d) transplantation of the cultured "MIN-O-spheres" into pre-cleared fat pads of FVB mice. As validation of this protocol, we describe the establishment of the MIN-O/mCherry transplant line. This novel line is a clonal derivation of MIN-O line D which stably and constitutively expresses the mCherry fluorescent protein. MIN-O/mCherry spheres (approximately 150-200 cells) cultured in vitro were transplanted into pre-cleared fat pads of FVB mice and yielded mCherry-positive lesions in vivo that could be detected via fluorescent imaging as early as two weeks post-transplantation. **Conclusion.** The ability to generate genetically modified MIN-O sublines further enhances the appeal of this model to study the progression of breast cancer, particularly when used in conjunction with molecular imaging techniques.

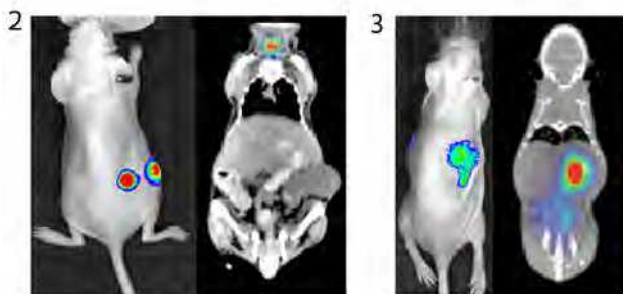
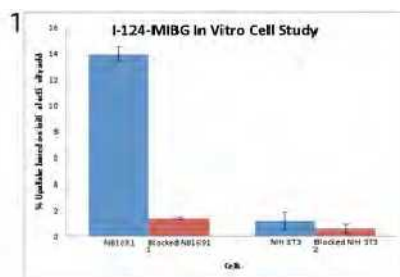
Presentation Number **0711A**

Poster Session 1c: In Vivo Studies & Development/Novel Use of Imaging Probes

In vivo tracking of ¹²⁴I-metaiodobenzylguanidine (MIBG) uptake in animal models of neuroblastoma using microPET/CT

Youngho Seo^{1,2}, **Hilla Wahnische**¹, **Shorouk F. Dannon**¹, **Henry F. VanBrocklin**¹, **Miguel Hernandez Pampaloni**¹, **Xiaodong Yang**², **Daphne A. Haas-Kogan**², **Melissa Itsara**³, **Willam Weiss**^{4,3}, **Katherine Matthey**³, ¹Department of Radiology and Biomedical Imaging, University of California, San Francisco, San Francisco, CA, USA; ²Department of Radiation Oncology, University of California, San Francisco, San Francisco, CA, USA; ³Department of Pediatrics, University of California, San Francisco, San Francisco, CA, USA; ⁴Department of Neurology, University of California, San Francisco, San Francisco, CA, USA. Contact e-mail: youngho.seo@radiology.ucsf.edu

Objectives: ¹²⁴I-MIBG has a strong potential to be used for pretherapy imaging and dosimetry prior to ¹³¹I-MIBG therapy of neuroblastoma. Unlike ¹²³I (T_{1/2}=13.2h), ¹²⁴I (T_{1/2}=4.2d) has a similar half-life to that of ¹³¹I (T_{1/2}=8.02d), and can be imaged by PET for more accurate quantification of the radiotracer distribution. Hence, we investigated microPET/CT imaging methods to track tumor uptake of ¹²⁴I-MIBG in animal models of neuroblastoma. **Methods:** NB1691-luc, a neuroblastoma cell line that expresses high levels of human norepinephrine transporter (hNET), was used in xenograft models of neuroblastoma. We first performed in vitro assay of NB1691 cells with nonneuroal NIH 3T3 cells as control using ¹²⁴I-MIBG. Then, a cohort of athymic mice subcutaneously (SQ) implanted with NB1691 cells (n=6) and the other cohort with NB1691 cells administered intravenously (IV) (n=2) were imaged by microPET/CT at five time points (2, 4, 24, 48, and 96h). Ordered subsets expectation maximization (OS-EM) algorithm was used for PET reconstruction with photon attenuation correction using attenuation map derived from the coregistered CT. Bioluminescence imaging to track where NB1691-luc cells were localized was performed prior to microPET/CT. **Results:** Although high specific uptake of MIBG was demonstrated in vitro, the SQ tumors did not take up ¹²⁴I-MIBG at a level that was distinguishable from background. In contrast, IV models showed avid ¹²⁴I-MIBG uptake in tumors. The tumor uptake was distinguishable only at 48h and 96h time points because of the slow clearance of ¹²⁴I-MIBG from the liver and kidneys. **Conclusion:** The tumor microenvironment (SQ versus IV) was a crucial determinant of uptake by NB1691 cells in xenograft models. The relatively long half-life of ¹²⁴I and the capacity to combine with PET/CT makes ¹²⁴I-MIBG a promising modality with the potential for quantitative monitoring of tumor uptake and background clearance in the animal models of neuroblastoma, and for future planning of ¹³¹I-MIBG therapy in patients.



1: ¹²⁴I-MIBG in vitro evaluations of NB1691 (left) and 3T3 cells (right)
 2: Subcutaneous xenograft of NB1691-luc seen by bioluminescence (left) and microPET/CT at 96h postinjection (right)
 3: Intravenous xenograft of NB1691-luc seen by bioluminescence (left) and microPET/CT at 96h postinjection (right)

Presentation Number **0712A**

Poster Session 1c: In Vivo Studies & Development/Novel Use of Imaging Probes

Real-Time Functional Imaging of Tumor Vascular Normalization by Antiangiogenic Agents

Qingbei Zhang¹, Vytas Bindokas⁴, Jikun Shen², **Robert M. Hoffman**^{5,6}, H. Rosie Xing^{1,3}, ¹Department of Pathology, The University of Chicago, Chicago, IL, USA; ²Section of Genetic Medicine and Center for Biomedical Informatics, Department of Medicine, The University of Chicago, Chicago, IL, USA; ³Department of Cellular and Radiation Oncology, The University of Chicago, Chicago, IL, USA; ⁴Integrated Microscopy Core, The University of Chicago, Chicago, IL, USA; ⁵AntiCancer, Inc., San Diego, CA, USA; ⁶Department of Surgery, University of California, San Diego, CA, USA. Contact e-mail: all@anticancer.com

We have developed and optimized non-invasive in vivo imaging to continuously visualize and characterize tumor angiogenesis and vascular response to anticancer therapies in real time in live mice. Tumor vessels could be monitored longitudinally undergoing vasculogenesis and angiogenesis the same mouse. Morphometric changes of the same vessel prior to and after drug treatment were captured with high resolution. Differences in vascular responses to the mTOR inhibitor rapamycin and to an anti-VEGF antibody were imaged. The multi-channel imaging capability of the OV100 small animal imaging system (Olympus) enabled visualization of the functional integrity (permeability) of tumor vessels before and after anti-angiogenic therapies using the near-infrared blood pool reagent Angiosense750. We observed real-time tumor vessel normalization as demonstrated by significantly reduced leakiness and subsequent improved delivery of BODPY-Paclitaxel upon administration of low-dose and short-term anti-angiogenic therapy. Further, alterations in Angiosense750 tumor retention in response to different treatments were confirmed and quantified using noninvasive fluorescent molecular tomography (VisEN FMT). Histological, and immunofluorescence staining (CD31, lectin, SMA, NG2) along with confocal microscopy, confirmed the in vivo imaging observations. Thus, imaging is a powerful tool for investigating tumor angiogenic progression and for preclinical drug screening of anti-angiogenic agents.

Presentation Number **0713A**

Poster Session 1c: In Vivo Studies & Development/Novel Use of Imaging Probes

Development of effective cancer therapy by the combination of ultrasound-mediated mild hyperthermia and immunotherapy

Ryo Suzuki, Yusuke Oda, Risa Koshima, Naoki Utoguchi, Kazuo Maruyama, Biopharmaceutics, Sch. of Pharm. Sci., Teikyo Univ., Sagamihara, Japan. Contact e-mail: r-suzuki@pharm.teikyo-u.ac.jp

[Objective] Recently, we developed novel liposomal bubbles (Bubble liposomes (BLs)) containing ultrasound (US) imaging gas, perfluoropropane. We reported that BLs have a function as US imaging agent. On the other hand, disruption of BLs by exposure of high intensity US could induce serious damages to adjacent cells by high temperature and shock waves, and antitumor effects utilized this phenomenon was observed. In the tumor tissue, tumor associated antigens and danger signal for dendritic cells(DCs) from damaged tumor cells would be released. Therefore, strong tumor-specific immunity would be induced by intratumoral injection of DCs after US therapy. In this study, we examined about activation of effective antitumor effects by the combination of US therapy and DC-based immunotherapy. [Methods] Colon 26 cells were inoculated into the backs of mice. After 8 days, BL were intratumorally injected and US was transdermally exposed toward tumor tissue (1 MHz, 4 W/cm², 120 sec). DCs were intratumorally immunized on days 9, 10, 11, and 13 after tumor inoculation. [Results & Discussion] In either US therapy with BLs or DC-based immunotherapy, we obtained only slight anti-tumor effects. On the other hand, the combination of US therapy with BLs and DC-based immunotherapy efficiently suppressed tumor growth (Fig. 1). This result suggests that this combination therapy prime antitumor immune system and result in obtaining effective antitumor effect. [Conclusions] It seems that US therapy with BLs support induction of effective antitumor immunity. Therefore, the combination of US therapy with BLs and DC-based immunotherapy might be a useful therapeutic strategy for cancer. [Acknowledgements] This work was supported by MEXT KAKENHI (21700511) and JSPS KAKENHI (21650131).

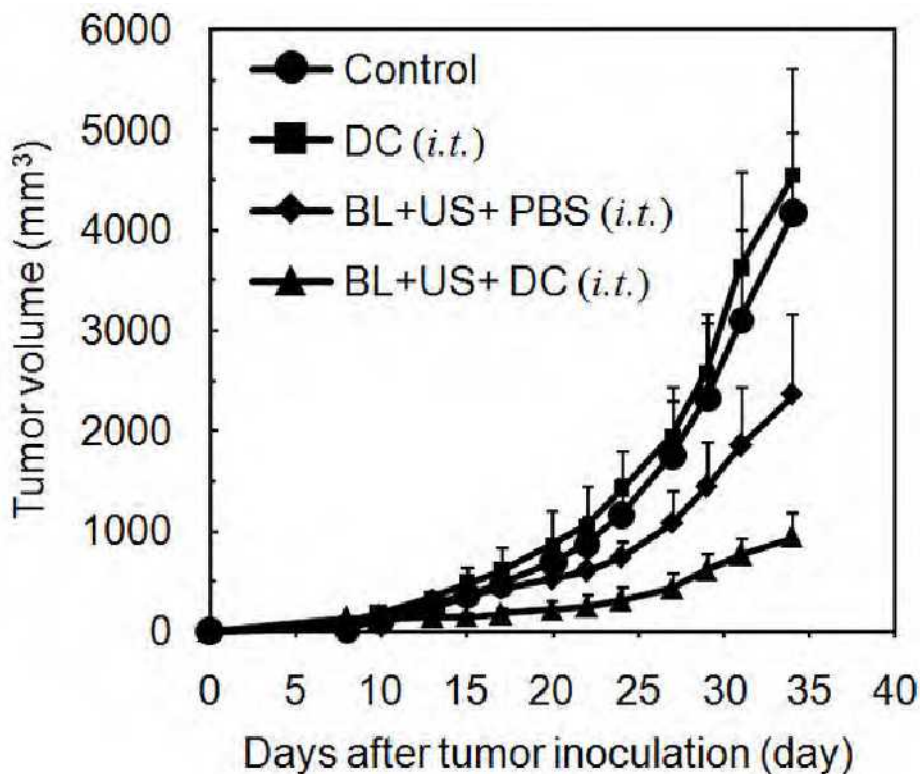


Fig.1 Antitumor effect by ultrasound therapy and/or DC based immunotherapy

Presentation Number **0714A**

Poster Session 1c: In Vivo Studies & Development/Novel Use of Imaging Probes

1H-MRI and 1H-MRS in ferritin transgenic mice

Yukie Morokoshi¹, **Sumitaka Hasegawa**¹, **Shigeyoshi Saito**^{1,2}, **Jun-ichi Takanashi**^{1,3}, **Takako Furukawa**¹, **Tsuneo Saga**¹, **Ichio Aoki**¹,
¹National Institute of Radiological Sciences, Chiba, Japan; ²Tohoku University, Sendai, Japan; ³Kameda Medical Center, Kamogawa, Japan. Contact e-mail: moro-y@nirs.go.jp

Iron homeostasis is tightly regulated by iron-binding proteins, as iron excess exhibits toxicity in cells. Ferritin is an intracellular iron storage protein that plays various roles such as controlling iron concentration in vivo. It is well-known that ferritin is involved in the pathogenesis of some human disorders, for example, aberrant ferritin expression has shown to be involved in neurodegenerative diseases. We generated transgenic (Tg) mice of human ferritin heavy chain (FTH) gene and investigated the effects of ferritin overexpression by 1H-MRI and 1H-MRS. The mice displayed no apparent neurological symptoms, no specific morphological and T2 alterations in the brain were found in MRI, and not even in histological studies. 1H-MRS, however, revealed that some metabolic markers were significantly altered in FTH-Tg brains compared to wild-type brains, such as decreases in myo-inositol and glutamine, and an increase in lactate. Our findings provide the evidence that ferritin overexpression affects brain metabolism.

Presentation Number **0715A**

Poster Session 1c: In Vivo Studies & Development/Novel Use of Imaging Probes

In vivo capillary imaging of spinal anterior horn in ALS model mice

Kazunori Miyazaki¹, **Kazuto Masamoto**^{2,3}, **Nobutoshi Morimoto**¹, **Yasuyuki Ohta**¹, **Tomoko Kurata**¹, **Yoshio Ikeda**¹, **Tohru Matsuura**¹, **Takayuki Obata**², **Iwao Kanno**², **Koji Abe**¹, ¹*Department of Neurology, Graduate School of Medicine, Dentistry and Pharmaceutical Sciences, Okayama University, Okayama, Japan;* ²*Molecular Imaging Center, National Institute of Radiological Sciences, Chiba, Japan;* ³*The University of Electro-Communications, Chohu, Japan. Contact e-mail: gmd20021@s.okayama-u.ac.jp*

Introduction: Amyotrophic lateral sclerosis (ALS) is a progressive and fatal disease that is caused by the selective death of motor neurons. The underlying mechanism of ALS has not yet been fully clarified. Recently, abnormality of the micro vessels in the anterior horn of the spinal cord has been reported in ALS model mice, but there is no previous report on vivo imaging of capillary structures and the real-time blood flow of the anterior horn. In this report, we attempted to develop in vivo imaging system in the anterior horn of the spinal cord in ALS model mice using multi-photon excitation microscopy. **Methods:** We used ALS model transgenic (Tg) mice and non-Tg (WT) mice as controls. The 10-week-old (W) Tg mice were considered to be at the pre-symptomatic stage, the 16 W mice to be at the early-symptomatic stage, and the 19 W mice to be at the end stage of the disease. Physiological parameters of each mouse were monitored throughout all experiments. For in vivo imaging, laminectomy of the lumbar vertebrae at the level of (L4-5) was performed in mice anesthetized with isoflurane. After intravenously injection of Qdot, spinal column was stabilized and the image was captured. **Results:** With multi-photon excitation fluorescence microscopy, we approached and monitored anterior horn of the spinal cord in ALS model Tg mice and WT controls. In vivo capillary ultra structures were successfully visualized, and the diameter was measured. We also visualize red blood cell flow that appears as shadows against bright background and could measure average velocity. We could compare the fluxional microvascular condition between WT and Tg mice. **Discussion:** Some reports showed the in vivo imaging of the dorsal horn of the spinal cord. In the present study, we focused on anterior horn and successfully visualized capillary structure and red blood cell flow. In vivo imaging of anterior horn may be useful to understand underlying mechanisms of the disorders that anterior horn is the main focus of disease such as ALS.

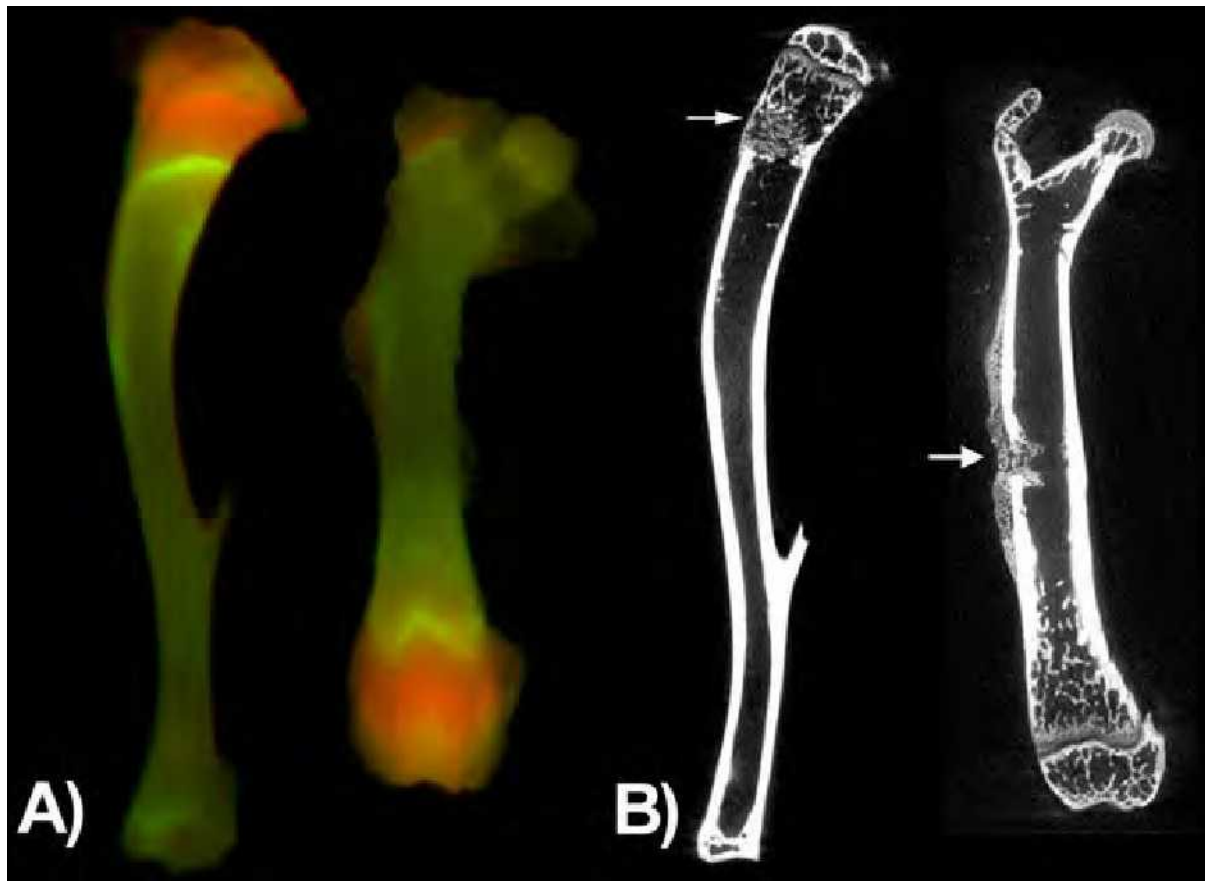
Presentation Number **0716A**

Poster Session 1c: In Vivo Studies & Development/Novel Use of Imaging Probes

Local Bisphosphonate Heterogeneity Revealed By Fluorescence Imaging Is Correlated With Impaired Bone Healing In Pediatric Model Of Disuse Osteoporosis

Kenneth M. Kozloff^{1,2}, Benjamin P. Sinder^{1,2}, Michelle S. Caird¹, ¹Orthopaedic Surgery, University of Michigan, Ann Arbor, MI, USA; ²Biomedical Engineering, University of Michigan, Ann Arbor, MI, USA. Contact e-mail: kenkoz@umich.edu

Bisphosphonates (BP) induce osteoclast apoptosis and reduce bone turnover. While typically used to treat adult low bone mass, BP use has expanded to pediatric conditions. The effect of resident BP on tissue repair is unknown and has led to concern for long-term treatment. We hypothesize that spatial differences in tissue healing will reflect differences in local BP concentration. Here, we demonstrate BP heterogeneity in a model of pediatric disuse osteoporosis by visualization of a fluorescent BP compound (FRFP). With BP heterogeneity established, focal skeletal defects were created at sites of high and low drug concentration and BP effects on repair were quantified using μ CT imaging and histology. To mimic pediatric disuse osteoporosis, 4 wk mice were subject to hindlimb suspension (HLS) for 3 wks with or without weekly alendronate (ALN 0.219 mg/kg). Ground controls (GRND) were also divided into ALN or untreated groups. BP localization was monitored by two spectrally distinct versions of a far-red fluorescent pamidronate (Osteosense) given at the start and end of the 3 wk period. FRFP revealed high BP in the proximal tibia and distal femur while mid-diaphyseal regions were low (Fig A). To assess bone healing dependency on BP, focal defects were created in proximal tibial metaphyses and mid-femoral diaphyses and mice recovered for 2 wks without additional treatment (Fig B). μ CT of regenerate bone revealed reduced tissue mineral density (TMD) in proximal tibiae of GRND mice, while mid-femoral TMD remained unchanged, suggesting impaired tissue mineralization at sites of high BP concentration. In HLS, a significant increase in regenerate bone volume fraction was found in the proximal tibia but not in the mid-femur, suggesting altered tissue remodeling. Significant reductions in osteoclast number suggest impaired recruitment or activity of cells in HLS sites of high BP concentration. These findings suggest that history of BP treatment may impair healing of skeletal defects dependent on local BP concentration.



Presentation Number **0717A**

Poster Session 1c: In Vivo Studies & Development/Novel Use of Imaging Probes

Longitudinal three-dimensional noninvasive imaging analysis and quantification of anti-tumor effects of TNF-alpha gene for small tumor

Sachiko Horie¹, Yukiko Watanabe¹, Yoko Yagishita^{2,1}, Nicolas Sax¹, Rui Chen¹, Li Li^{3,1}, Takanori Kojima^{4,1}, Hidehiro Morikawa⁵, Maya Sakamoto⁶, Masao Ono⁷, Shiro Mori⁸, Tetsuya Kodama¹, ¹Biomedical Engineering, Tohoku University, Sendai, Japan; ²Dentistry, Tohoku University, Sendai, Japan; ³Radiology, Tohoku University, Sendai, Japan; ⁴Engineering, Tohoku University, Sendai, Japan; ⁵Oral Surgery, Tohoku University Hospital, Sendai, Japan; ⁶Oral Diagnosis, Tohoku University Hospital, Sendai, Japan; ⁷Histopathology, Tohoku University, Sendai, Japan; ⁸Maxillofacial Surgery, Tohoku University Hospital, Sendai, Japan. Contact e-mail: horiesachiko@bme.tohoku.ac.jp

Noninvasive imaging can be helpful for diagnosing cancer in its earliest stages as well as for developing therapeutic agents to treat cancer and monitoring whether treatment is working. In this study, tumor necrosis factor (TNF- α) plasmid DNA is transfected into solid tumor of luciferase-expressing EMT-6 (breast carcinoma) using nanobubbles and ultrasound (frequency: 1MHz, intensity: 0.01-3W/cm², duration time: 1min, duty ration: 20%, pulse: 200) two times a week for two weeks. The anti-tumor effects were longitudinally assessed using three noninvasive imaging modalities: (1) high-frequency ultrasound imaging system (40MHz) and mechanical caliper to measure volumetric changes, (2) bioluminescent imaging system to quantify the growth of the tumor, and (3) high-intensity ultrasound imaging system (40MHz) and microbubbles to construct tumor vessels three-dimensionally and quantify changes in the density in tumor area. After two times of TNF- α gene transfection, vessel density in tumor is significantly decreased (control group: 26.1 \pm 3.4%, treatment group: 14.8 \pm 3.0%, P<0.05) while there was no significant differences between the volume of each group (control group: 10.4 \pm 1.1mm³, treatment group: 10.2 \pm 2.5mm³). After four times of treatment, the volume and the luciferase activity of group transfected with nanobubbles and ultrasound became 2.6 times and 2.1 times lower than that of control group, respectively. Noninvasive imaging strategies for small cancer would be an enabling tool to predict disease development, progression, and clinical outcomes in early stage and improve the chances for successful treatment.

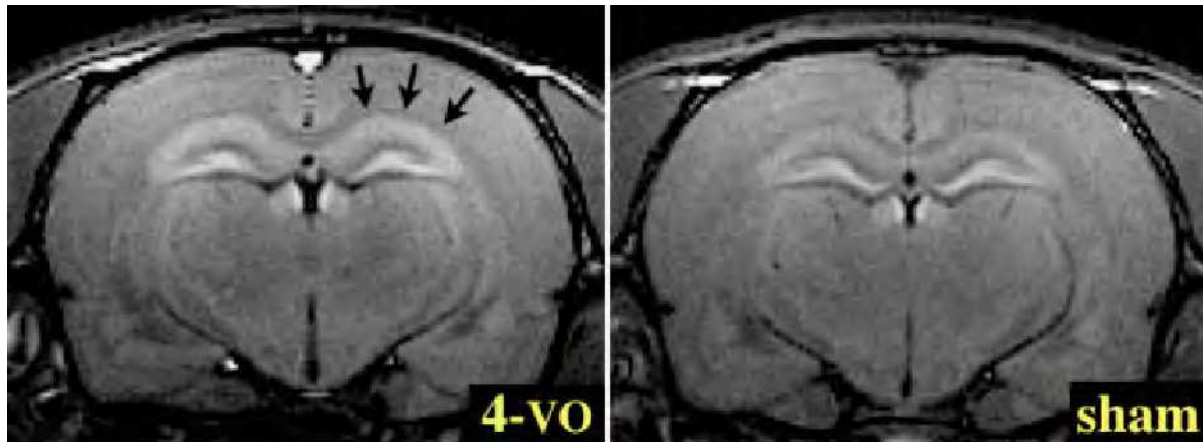
Presentation Number **0718A**

Poster Session 2c: In Vivo Studies & Development/Novel Use of Imaging Probes

Detection of Signal Enhancement in the Hippocampus after Transient Forebrain Ischemia using Manganese-enhanced MRI

Yuko Kawai¹, **Yuko Yasuda**², **Narito Tateishi**², **Masahiro Umeda**¹, **Yasuharu Watanabe**¹, **Toshihiro Higuchi**³, **Seiichi Furuya**^{4,2}, **Shoji Naruse**^{5,2}, **Setsuya Fujita**², **Chuzo Tanaka**³, ¹Medical Informatics, Meiji University of Integrative Medicine, Kyoto, Japan; ²Basic Research, Louis Pasteur Center for Medical Research, Kyoto, Japan; ³Neurosurgery, Meiji University of integrative Medicine, Kyoto, Japan; ⁴Radiology, Japanese Red Cross Kyoto Daiichi Hospital, Kyoto, Japan; ⁵Radiology, Kyoto Prefectural University of Medicine, Kyoto, Japan. Contact e-mail: kawai@meiji-u.ac.jp

Introduction The four-vessel occlusion (4-VO) is famous as forebrain ischemia model that cause delayed neuronal cell death in the CA1 region of the rat hippocampus. Brain injury after ischemia is caused by a complex signaling cascade which comprises depolarization of neurons and glial cells and the release of excitatory amino acids. Manganese is good T₁ contrast agent for MRI. The manganese administration with intravenous injection can find unique contrast change that is dependent on the cell activity or cell density, it is known as Manganese-enhanced MRI (MEMRI). MEMRI is taken notice as useful molecular imaging technique for nervous system. We reported the possibility of detection of signal enhancement caused by the manganese accumulation using MEMRI in the gliosis area after temporary middle cerebral artery occlusion cerebral ischemia. The purpose of this study is in vivo detection of glial function at the hippocampus after the 4-VO in the rodent. **Materials and Methods** Male Wistar rats (300.4 ± 15.6 g, n = 30) were divided into six groups consisting with 2 days, 3 days, and 10 days after 4VO group and same time course of sham group. Twenty-four hours before the induction of ischemia, rats were anesthetized with pentobarbital sodium and the bilateral vertebral arteries were heat-cauterized at both vertebral arteries using a soldering iron. Both common carotid arteries were then gently isolated and a silicon tube placed around each vessel. The following day, both common carotid arteries were occluded with vascular clamps for 10 min under the 2.5 % isoflurane. T₁-weighted images and inversion recovery images were acquired at 2 days, 3 days and 10 days after the 4-VO using 4.7T MRI (Bruker, Germany). 50 mM MnCl₂ solution was infused via the tail vein before 24 hour scanning of the MRIs. **Results and Discussion** Signal enhancement was observed in the CA1 and CA2 legion by the MEMRI at 72 hour after 4-VO. It is suggested that a lot of manganese was taken in the hippocampus, and shortened T₁ relaxation time. On the other hand, sham operated group was not shown the significant signal change. MEMRI will detect glial activity which related with about of the neural death.



The typical images of Manganese-enhanced MRI

Presentation Number **0719A**

Poster Session 2c: In Vivo Studies & Development/Novel Use of Imaging Probes

An Orthotopic Pancreatic Cancer Xenograft Model via Ultrasound Guided Injection of Cells

Amanda Shanks Huynh¹, David L. Morse¹, Dominique Abrahams³, Monica Torres³, Hartmut Berns², Margi K. Baldwin³, Robert Gillies¹, ¹Functional & Molecular Imaging, H. Lee Moffitt Cancer Center & Research Institute, Tampa, FL, USA; ²Small Animal Modeling & Imaging Core, H. Lee Moffitt Cancer Center & Research Institute, Tampa, FL, USA; ³Comparative Medicine, H. Lee Moffitt Cancer Center & Research Institute, Tampa, FL, USA. Contact e-mail: amanda.huynh@moffitt.org

Subcutaneous xenograft models are well-established and have been used for many years in cancer research (Fig. 1A). However, there is great interest in use and development of orthotopic models that more closely resemble human cancers. Typically, an invasive surgical orthotopic implantation (SOI) procedure is used for orthotopic models. In this study, we developed an orthotopic pancreatic cancer xenograft model by ultrasound guided injection (USGI) technique. HCT-116 cells engineered to express the δ -opioid receptor (DOR+) were injected into the pancreas of nude mice guided by ultrasound, VisualSonics Vevo 2100 Imaging Station. Animals under anesthesia were placed on imaging stage, Ultrasound gel put on abdomen, and the transducer located the pancreas, with the spleen as a reference. A syringe with 30g needle on a mechanical holder moved into the pancreas and 1×10^6 HCT-116 DOR+ cells injected (1B). The physiological status was monitored using sensors. Mice with SOI were used for comparison. The abdomen is cut open, pancreas pulled out, cells injected, pancreas replaced, and incision site sutured. Mice imaged by ultrasound for 4 weeks to monitor tumor growth. Tumors imaged using a fluorescent probe, Dmt-Tic-Lys(Cy5)-OH, with high affinity (3 nM Ki) for the human DOR using a Caliper Lifesciences IVIS 200 Imaging System. Tumor presence was confirmed by visual inspection, ex vivo fluorescence imaging and histology. For orthotopic models, there was a strong correlation between the ultrasound detected tumor volume and fluorescence associated with the orthotopic tumors (1C). We demonstrated a non-invasive, rapid, and reproducible method for developing orthotopic pancreatic cancer xenograft models.

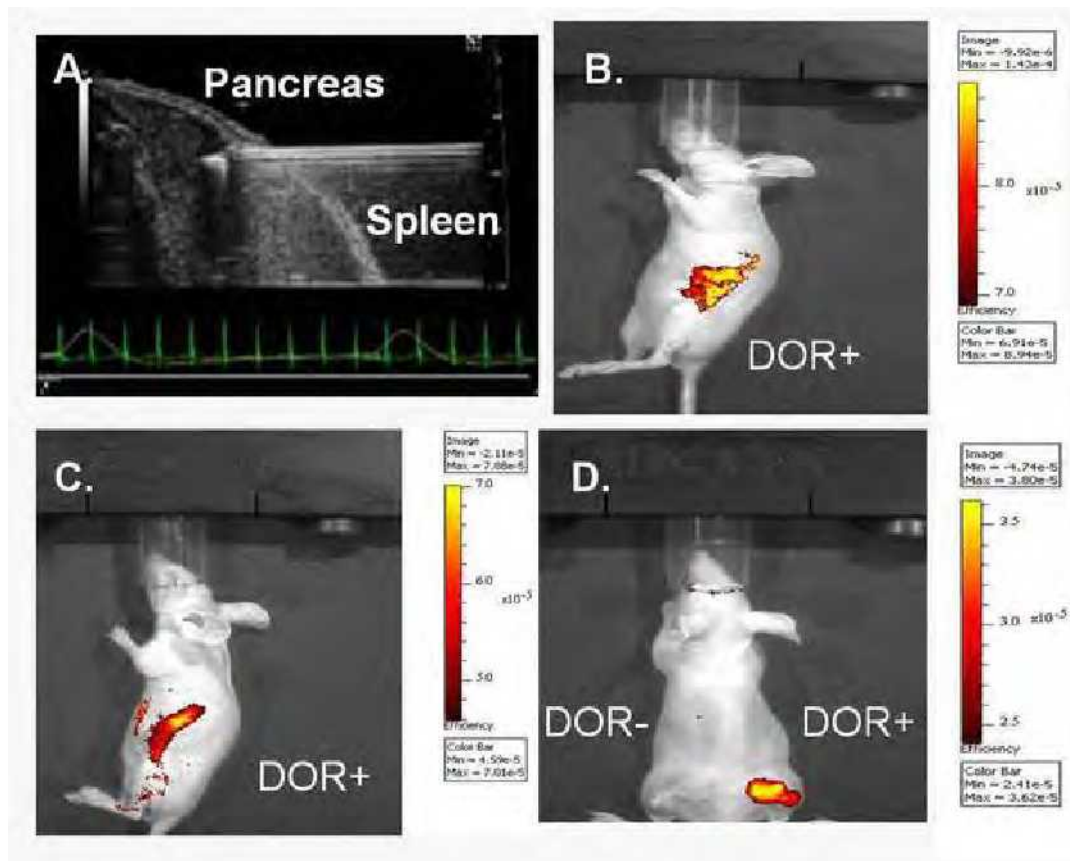


Figure 1. A) Ultrasound image of 1×10^6 HCT-116 DOR+ cells injected into the pancreas of nude mice. B) Fluorescence image of USGI orthotopic model at 6 h shows signal in pancreas. C) Fluorescence image of SOI orthotopic model at 6 h shows signal in pancreas. D) Fluorescence image of subcutaneous model at 6 h, signal is only observed in DOR+ tumor showing specificity of the probe.

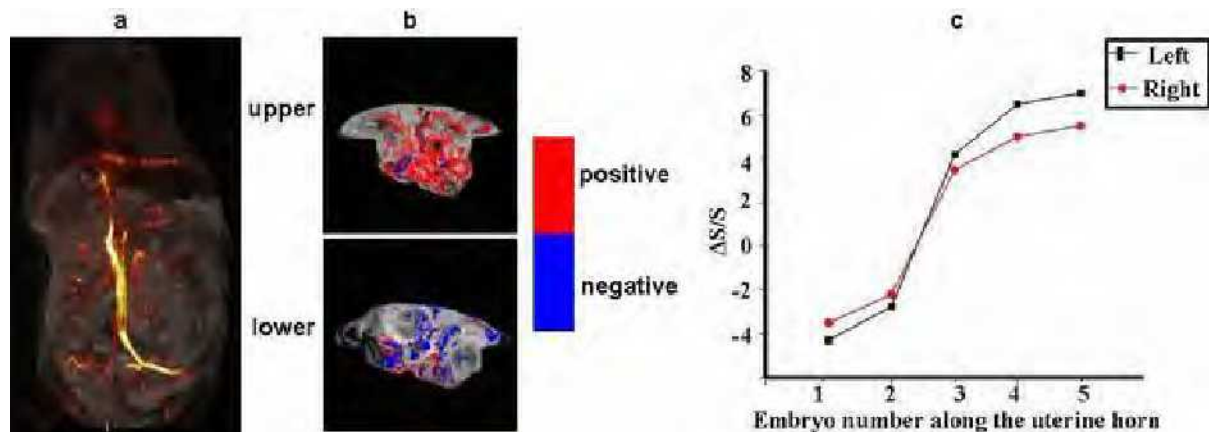
Presentation Number **0720A**

Poster Session 2c: In Vivo Studies & Development/Novel Use of Imaging Probes

Who is Who? Non-Invasive Identification of Fetal Order in Pregnant Mice by ASL-MRI

Reut Avni¹, Tal Raz¹, Joel R. Garbow², Michal Neeman¹, ¹*Biological Regulation, Weizmann Institute of Science, Rehovot, Israel;* ²*Radiology, Washington University, St. Louis, MO, USA. Contact e-mail: reut.avni@weizmann.ac.il*

One of the obstacles to longitudinal in vivo imaging studies of fetuses is the accurate identification of specific embryos, often with different genetic status, in utero. Currently, no direct approach to identify uniquely each embryo throughout gestation exists. The aim of this study was to develop a non-invasive MRI tool to determine the fetal order along the uterus horn in vivo. For that we employed Arterial Spin Labeling (ASL) MRI methodology which measures perfusion and water exchange within different tissues. The mouse uterus is duplex, composed of two independent uterine horns which end at the cervix. The origin of the blood vessels feeding the upper portion of each horn is the ovarian artery, whereas blood enters the lower end from the uterine artery. Thus, blood reaches the embryos from both directions. 3D Angiography protocol (Figure a) was used to identify the major blood vessels, followed by the collection of two sequential images: one with cardiac tagging of ovarian arterial water and the second with tagging of arterial water in the uterine artery. Changes in signal intensities of the images represent water exchange between the blood and the embryo/placenta. The normalized difference between the two acquired images produced saturation transfer maps, which were color coded to generate maps of flowing blood that are directionality dependent. Histogram plots maps were then generated for each embryo (numbered from 1 to 5 according to their order along the horn), showing a correlation between the embryo position along the uterine horn and the peak of the histogram. For embryos positioned at the lower end, a negative ASL signal was observed (Figure b lower), suggesting blood flow mainly from the uterine artery. In the middle and upper parts of the uterus, ASL signal was positive (Figure b upper) and increased gradually, with the embryo closest to the ovarian artery showing the largest positive signal in each of the horns (Figure c). This suggests that ASL is a tool that can provide information about the order of fetuses in the uterus, and could assist, in the future, in distinguishing and following each embryo in utero.



Presentation Number **0721A**

Poster Session 2c: In Vivo Studies & Development/Novel Use of Imaging Probes

Evaluation of intratumoral ^{18}F -FDG distribution using small animal PET: Comparison with autoradiography

Songji Zhao^{1,2}, Toshiyuki Hatano³, Yan Zhao^{1,2}, Ken-ichi Nishijima⁴, Wataru Takeuchi⁵, Norihito Kuno⁵, Yuichi Morimoto⁵, Hiroko Hanzawa⁵, Takeshi Sakamoto⁵, Nagara Tamaki², Yuji Kuge³, ¹Tracer Kinetics & Bioanalysis, Hokkaido University Graduate School of Medicine, Sapporo, Japan; ²Nuclear Medicine, Hokkaido University Graduate School of Medicine, Sapporo, Japan; ³Central Institute of Isotope Science, Hokkaido University, Sapporo, Japan; ⁴Molecular Imaging, Hokkaido University Graduate School of Medicine, Sapporo, Japan; ⁵Central Research Laboratory, Hitachi, Ltd, Tokyo, Japan. Contact e-mail: zsi@med.hokudai.ac.jp

Objectives: Accurately evaluating intratumoral ^{18}F -FDG (FDG) distribution is strongly required in clinical PET studies, because the intratumoral heterogeneity is an important indicator of tumor malignancy and radiotherapy planning. On the other hand, recent advance in PET technology enabled us apply it to the various fields of animal studies. If intratumoral FDG distribution can be accurately evaluated using small animal PET, it may provide important information that can be translated into patient studies. Therefore, to clarify the applicability of small animal PET for imaging intratumoral FDG distribution in rats, the PET images were visually and semi-quantitatively evaluated in comparison with autoradiography (ARG). **Methods:** Rats were implanted with C6 glioma cells (n=3). When the tumors reached ca. 20 mm in diameter, rats were injected with FDG. Tumor tissues were excised after PET scans and sectioned into slices for ARG and HE studies. Referring to the HE staining, viable and necrotic regions were determined on the ARG images. Regions of interest (ROIs, 1.7 x 1.7 mm, n=46) were placed on the viable and necrotic regions. FDG uptake in each ROI was expressed as the ratio of radioactivity in each ROI to the average value in the ROIs on viable regions. The ROIs on viable regions were further assigned to high and low FDG uptake regions (FDG_{high}, FDG_{low}, respectively). Every ROI on the ARG images were transferred to PET images. **Results:** Heterogeneous FDG distribution was visualized with the PET and the patterns were consistent with the ARG images. The necrotic area of 1.7 x 3.4 mm could be visually discriminated on the PET image. In the PET images, the FDG uptake ratios were 1.09 ± 0.12 , 0.90 ± 0.14 and 0.34 ± 0.18 , respectively, in the FDG_{high}, FDG_{low} and necrotic regions, and the differences were significant (p<0.001). The FDG uptake ratios in the FDG_{high} and FDG_{low} regions were consistent with those in the ARG images (ARG FDG_{high}: 1.10 ± 0.07 , FDG_{low}: 0.88 ± 0.10 , FDG_{high}/FDG_{low}: 1.25). The FDG uptake ratio in the necrotic regions was significantly higher in PET images than that in ARG images (p<0.001), indicating "spill over" from the surrounding tissues. **Conclusion:** In small experimental tumors (i.d. < 20 mm), intratumoral heterogeneity in FDG distribution was visualized with small animal PET and the patterns were consistent with ARG images. PET imaging could detect a 25% of difference in FDG uptake. Small animal PET can be applied for imaging intratumoral FDG distribution, and may provide fundamental data for patient studies.

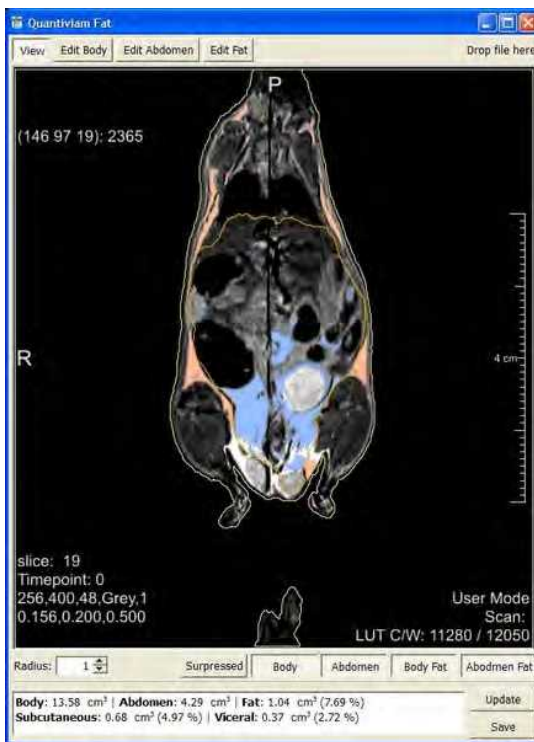
Presentation Number **0722A**

Poster Session 2c: In Vivo Studies & Development/Novel Use of Imaging Probes

Automated Quantification of Adipose Tissue in Whole Body Small-Animal Micro MRI Images

Dirk Loeckx¹, **Tom Dresselaers**^{2,3}, **Bianca Hemmeryckx**⁴, **Bart De Dobbelaer**¹, **Frederik Maes**¹, **H. Roger Lijnen**⁴, **Uwe Himmelreich**^{2,3}, **Paul Suetens**¹, ¹Medical Image Computing, ESAT/PSI, K.U.Leuven, Leuven, Belgium; ²Biological NMR unit, K.U.Leuven, Leuven, Belgium; ³Molecular Small Animal Imaging Centre (MoSAIC), K.U.Leuven, Leuven, Belgium; ⁴Center for Molecular and Vascular Biology, K.U.Leuven, Leuven, Belgium. Contact e-mail: Dirk.Loeckx@uz.kuleuven.ac.be

AIM: The amount of adipose tissue is generally considered as a comorbidity for a multitude of diseases, for which various small-animal models have been developed. We present a method for the in vivo quantification of the amount of fat using micro MRI, distinguishing visceral and subcutaneous pads. **METHODS:** First, two consecutively recorded images are acquired using RARE sequence on a 9.4 Tesla scanner: image *N* without and image *FS* with fat suppression. Next, an initial fat percentage image *FP* is created as $FP = 1 - (FS / (FS + 1.5 (N - FS)))$. Automated image processing is used to segment the 3D mouse body, the fat pads and - starting from an atlas - the abdomen. Dedicated software was developed to perform the segmentation and allow manual corrections. **RESULTS:** The method was applied to 10-weeks, 12- and 24-months old C57BL6J male mice to study the natural ageing process. Visual inspection showed good delineation of the adipose tissue and abdomen, although some manual correction was required. Total, subcutaneous, and visceral fat volume increases between the age of 10-weeks and 12-months and drops significantly between the age of 12- and 24-months, illustrating that old age is accompanied with a reduction of fat volume in both regions of the body. **CONCLUSION:** Micro MRI and advanced image processing allow for the automated localization and quantification of adipose tissue in rodents. Although the values obtained will deviate from the 'absolute' fat content, e.g. as we did not correct for the T2 of fat, the values can be indicative for the longitudinal study of the amount of fat.



Yellow: body contour; orange: abdomen contour; red: subcutaneous fat, blue: visceral fat. Quantitative results are shown at the bottom.

Adipose tissue volume

(n=10)	10 weeks	12 months	24 months	p-value
Body volume (ml)	20.53±0.25	21.54±0.36	23.40±0.64†	<0.0001
Total fat volume (ml)	1.38±0.24	3.27±0.35	1.33±0.30‡	0.0011
SC fat volume (ml)	0.83±0.14	1.51±0.19	0.59±0.14‡	0.0040
ABD fat volume (ml)	0.70±0.11	1.75±0.17	0.74±0.17‡	0.0005

● p<0.05 10 wks to 12 mo; † p<0.015 10 wks to 24 mo; ‡ p<0.05 12 to 24 mo

Presentation Number **0723A**

Poster Session 2c: In Vivo Studies & Development/Novel Use of Imaging Probes

Reporter mice and modified luciferin: the passe-partout to study apoptosis, drug metabolism and many other molecular events in the same living organism

Andrea Biserni¹, Nicoletta Rizzi¹, Chiara Roncoroni¹, Dieter H. Klaubert², **Adriana C. Maggi**³, Paolo Ciana³, ¹TOP (Transgenic Operative Products) srl, Lodi, Italy; ²Promega Biosciences, San Luis Obispo, CA, USA; ³Depart. Pharmacological Sciences, University of Milan, Milan, Italy. Contact e-mail: adriana.maggi@unimi.it

Bioluminescence imaging of reporter genes in transgenic mice enables the spatio-temporal study of molecular events in the pathophysiology of a living system and in response to a drug treatment. Ubiquitous expression of the reporter gene is fundamental for the pharmacological use of these models. To this aim we developed a technology granting the generalized and reliable expression of reporter-based biosensors in transgenic mice. Here, we show that the ubiquitous luciferase expression in repTOP™ mice when coupled with the in vivo use of modified luciferase substrates provides an innovative tool for the study of multiple biological events and molecular pathways in the same reporter mouse. As a proof-of-principle, we have demonstrated first, that apoptosis can be measured in vivo by the administration of VivoGlo™ Caspase-3/7 substrate (Z-DEVD-Aminoluciferin, Sodium Salt) to luciferase reporter mice in which liver apoptosis was induced by a single i.p. injection of D-galactosamine (800 mg/kg) and Lipopolysaccharide (100 mg/kg) (Nakama T et al. 2001). In these mice i.p. administration of increasing doses of the modified luciferin (17-150 mg/kg), produced a clear dose-dependent induction of photon emission selectively in the liver area as detectable by in vivo imaging and also confirmed by ex vivo imaging analysis of dissected tissues. The presence of apoptotic cells in the photon emitting tissues was also confirmed by the assay of Caspase 3/7 enzymatic activity and by western blot analysis in protein extracts. As a second application of the in vivo use of Glo technology, we have measured the activity of Cytochrome P450, one of the most important metabolizing enzymes responsible for oxidation of 50-60% of clinical drugs (Li AP et al., 1995). repTOP™ mice were injected i.p. with dexamethasone (50 mg/kg), a potent inducer of CYP3A, and we measured P450 activity in vivo after the administration of VivoGlo CYP3A4: selectively in treated animals, we have detected by in vivo imaging a bright photon emission in the chest area. The increased activity of CYP3A was also confirmed in liver protein extracts by P450-Glo Cyp3A4 in vitro assay. The current study showed for the first time the possibility to measure apoptosis, drug metabolism and potentially many other molecular events in living reporter mice providing an important advancement over current imaging methodologies: virtually null background, high sensitivity and simple instrumentation needed for the in vivo imaging measurement thus opening a new avenue to study multiple pathways within the same living organism.

Presentation Number **0724A**

Poster Session 2c: In Vivo Studies & Development/Novel Use of Imaging Probes

Head to head comparison of pinhole ^{99m}Tc-sestamibi gated SPECT and contrast-enhanced 3D echocardiography for determining left ventricular function in normal rats

Bram Roosens^{1,2}, *Sophie Hernot*¹, *Steven Droogmans*^{1,2}, *Guy Van Camp*^{1,2}, *Tony Lahoutte*^{1,4}, *Patrizio Lancellotti*³, *Bernard Cosyns*¹,
¹*In Vivo Cellular and Molecular Imaging (ICMI), Vrije Universiteit Brussel (VUB), Brussels, Belgium;* ²*Department of Cardiology, UZ Brussel, Brussels, Belgium;* ³*Department of Cardiology, CHU Sart Tilman, Liège, Belgium;* ⁴*Department of Nuclear Medicine, UZ Brussel, Brussels, Belgium. Contact e-mail: broosens@vub.ac.be*

Background: The determination of the global left ventricular (LV) function and cardiac volumes remains one of the most important issues in the everyday practice of the cardiologist. The study of cardiomyopathies in small animals may contribute to our understanding of the pathophysiology and to evaluate experimental treatment strategies. Using pinhole collimators and advances in dataprocessing, gated SPECT was recently validated to estimate rat LV function. More recently, it has been shown in patients that contrast (microbubbles) combined with 3D-echocardiography (3DC) decreased geometric assumptions compared to bidimensional echocardiography and provided an accurate estimation of LV function compared to reference methods. Aim : Therefore we sought to examine the feasibility and the accuracy of 3DC for the evaluation of LV function in rats relative to ^{99m}Tc-sestamibi gated SPECT as an independent reference. Methods : We prospectively performed scintigraphy and 3DC with a 3D-pediatric probe in random order at one day intervals in 6 male Wistar rats. For echocardiography, 3D-guided biplane tracings were performed manually. Data were analyzed with dedicated software for both techniques. Results : There was no significant difference between SPECT and 3DC for LV end systolic volume and end diastolic volume respectively (0.33±0.03 vs 0.32±0.05 and 0.88±0.05 vs 0.85±0.08 microL/g). There was also a good correlation for LV ejection fraction measured by both methods (r=0.65, p<0.01). Conclusions : 3DC is feasible and provides an accurate estimation of LV volumes and function in normal rats with pinhole gated SPECT as reference. Pending technical improvement, 3DC would be the method of choice for rapid, repeatable and reproducible evaluation of LV function in small animal models of cardiomyopathies.

Presentation Number **0725A**

Poster Session 2c: In Vivo Studies & Development/Novel Use of Imaging Probes

Bioluminescence-based imaging for the study and classification of drugs on the basis of their spatio-temporal action*Adriana C. Maggi, Depart. Pharmacological Sciences, University of Milan, Milan, Italy. Contact e-mail: adriana.maggi@unimi.it*

For more than one century, the measure of drug structure-activity relationships has been based on mathematical equations describing the interaction of the drug with its biological receptor. The understanding of the multiplicity of biological responses induced by the drug-receptor interaction demonstrated the limits of current approach and the necessity to develop novel concepts for the quantitative analysis of drug action. Using a systematic study of spatio-temporal effects is proposed as a measure of drug efficacy for the classification of pharmacologically active compounds. The application of this methodology is expected to simplify the identification of families of molecules functionally correlated and to speed up the process of drug discovery. The study was carried out using a mouse model engineered to measure estrogen receptor (ER) transcriptional activity in living organisms. We investigated the effect of long term (21 days) hormone replacement on ER signaling by whole body, in vivo, imaging. Estrogens and SERMs were administered daily at doses equivalent to those used in humans as calculated by the allometric approach. As controls, ER activity was measured also in cycling and ovariectomized mice. The study demonstrated that ER-dependent transcriptional activity oscillated in time and the frequency and amplitude of the transcription pulses was strictly associated with the target tissue and the estrogenic compound administered. Our results indicate that the spatio-temporal activity of Selective Estrogen Receptor Modulators (SERMs) is predictive of their structure demonstrating that the analysis of the effect of estrogenic compounds on a single surrogate marker of ER transcriptional activity is sufficient to classify families of compounds structurally and functionally related.

Presentation Number **0726A**

Poster Session 2c: In Vivo Studies & Development/Novel Use of Imaging Probes

Metabolic alterations during visual stimulation in 6-hydroxydopamine rat model for Parkinson's disease - *in vivo* small animal positron emission tomography study -

Naoya Oishi, Manabu Inoue, Hidenao Fukuyama, Human Brain Research Center, Kyoto University Graduate School of Medicine, Kyoto, Japan. Contact e-mail: noishi@kuhp.kyoto-u.ac.jp

Objective: To evaluate the dopaminergic modulation of visual function using a well-accepted selective nigrostriatal dopamine deficit animal model for Parkinson's disease (PD). Background: Several stages of the visual processing system are proposed to be involved in PD, which could be related to visual dysfunction or clinical symptoms like visual hallucination. Although several studies suggest the importance of nigrostriatal dopamine system for visual dysfunction, it's difficult to exclude effects of other neurotransmitter systems, such as cholinergic or serotonergic, which are concurrently affected in PD. The 6-hydroxydopamine (6-OHDA) rat model is suitable for evaluating the effect of dopamine system on visual function. Methods: Sixteen male Sprague-Dawley rats were divided into two groups: 8 rats that received stereotactically and unilaterally administered 6-OHDA (15µg/2µl) in the left medial forebrain bundle (MFB), and 8 control rats that similarly received saline solution. Both groups were also received saline solution in the right MFB. 11C-2β-carbomethoxy-3β-(4-fluorophenyl)tropane (11C-CFT), a selective dopamine transporter (DAT) ligand, images were obtained in the 6-OHDA-lesioned rats by small animal positron emission tomography and parametric binding potential (BP) images were calculated. 18F-fluoro-2-deoxy-D-glucose (¹⁸F-FDG) images were also obtained in the both groups during two conditions (5Hz photic stimulation and resting condition) in an awake state. DAT BP and relative glucose metabolism images were anatomically normalized to the Paxinos stereotaxic space and analyzed on a voxel-basis using Statistical Parametric Mapping and by template-based predefined volumes-of-interests. Results: The 6-OHDA-lesioned group showed a significant decrease of DAT BP in the ipsilateral caudate-putamen compared with the contralateral one ($p < 10^{-6}$). ¹⁸F-FDG images revealed visual stimulation caused an increase of glucose uptake in visual-related areas, such as the bilateral primary and secondary visual cortices, superior colliculus (SC), and lateral geniculate nucleus (LGN) and a significant glucose hypometabolism in the bilateral primary and secondary visual cortices of the 6-OHDA-lesioned group compared with the control group during visual stimulation. Conclusions: Nigrostriatal dopaminergic dysfunction induces metabolic alterations by visual stimulation mainly in the cortical visual-related areas rather than the subcortical ones. The alteration can be related to characteristic visual dysfunction and related symptoms in PD.

Presentation Number **0727A**

Poster Session 2c: In Vivo Studies & Development/Novel Use of Imaging Probes

In Vivo MR Imaging of the Breast Tumor-Initiating Cells

YoonSeok Choi^{1,2}, **Mulan Li**^{1,2}, **KyungMin Lee**^{3,4}, **Seung Hong Choi**¹, **Hyung-Joon Noh**⁵, **Hoe Suk Kim**¹, **Hyeonjin Kim**⁵, **DongYoung Noh**^{3,4}, **Woo Kyung Moon**^{1,2}, ¹Radiology, Seoul National University, Seoul, Republic of Korea; ²Biomedical Science, Seoul National University, Seoul, Republic of Korea; ³Surgery, Seoul National University, Seoul, Republic of Korea; ⁴LeeGunHee Cancer institute, Seoul National University, Seoul, Republic of Korea; ⁵Institute of LeeGilYeo Cancer and Diabetes Center, Gachon University of Medical Science, Incheon, Republic of Korea. Contact e-mail: yschoi21@snu.ac.kr

Based on cell surface marker analysis and xenotransplant study, many evidences seem to support that highly tumorigenic subpopulations are existed in cancer with the abilities to form tumors in immune compromised mice. In breast cancer, CD44 positive/CD24 negative/Lineage negative (CD44+/CD24-/Lin-) populations are considered as stem cell-like cancer cells. Furthermore, aldehyde dehydrogenase (ALDH) which seems to have an important role in stem cells becomes a candidate marker of tumor-initiating cells because ALDH maintains stem cell properties by oxidizing retinol to retinoic acid. Recently, researches on stem cell-like cancer cells are rapidly progressing being based on traditional stem cell biology but the roles of stem cell related genes in stem cell-like cancer cells still need to be figured out. In particular, animal models of stem cell-like cancer cells seemed to be necessary considering the importance of microenvironments and stem cell niches. Here, we report the MR reporter gene, ferritin, induced tumor-initiating cells and show their potential for tumor initiating cells in vivo studies. Heavy chain subunit of human ferritin (hFTH) and EGFP for the MR and fluorescent images were induced by lenti-viral vector. No significant changes between control tumor-initiating cells and ferritin induced cells were observed in cell growth assay and mammosphere forming abilities. Also, analysis of cell surface markers (CD44+/CD24-/CD133-/CD49f+) and ALDH expression showed that ferritin induced cells retained the markers of breast tumor-initiating cells. MR evaluations of ferritin gene on cellular level study (TR/TE=43/10ms) and animal level study (TR/TE=34/4.4ms) were performed with a 9.4 T MR scanner. Cells were cultured with 20 uM ferric ammonium sulfate for 5 days and hFTH induced cells (10.98±0.21ms) showed decreased T2* relaxation times compared to control cells(14.73±0.34ms). In animal study, cells were subcutaneously injected in immune compromised mice and MRI scans were performed after 3 weeks of transplantation. Similar results were obtained with cell study and decreased T2* relaxation times in hFTH induced tumors were observed (10.44±0.28ms) compared to control (13.73±0.58ms)

Acknowledgement This work was supported by the National Research Foundation of Korea(NRF) grant funded by the Korea government(MEST 2010-0000423) and the second stage of brain korea 21 program in 2010

Presentation Number **0728A**

Poster Session 2c: In Vivo Studies & Development/Novel Use of Imaging Probes

In Vivo Optical Imaging of Hetero-Bivalent Ligand for Potential Cancer Targeting Therapy

Liping Xu¹, **Jatinder S. Josan**², **Josef Vagner**², **David L. Morse**¹, **Victor J. Hruby**², **Robert Gillies**¹, ¹*Imaging, H.Lee Moffitt cancer center & research institute, Tampa, FL, USA;* ²*Chemistry, University of Arizona, Tucson, AZ, USA.* Contact e-mail: liping.xu@moffitt.org

Effective treatment of cancer requires delivery of drug specifically to cancer cells sparing normal cells. We have proposed the use of hetero-multivalent ligands (htMVL) as specific targeting agents. htMVLs can carry imaging or therapeutic moieties directed against receptor combinations that are unique to targeted cells. As proof of concept, we describe the use of an htMVL-Cy5 conjugate as an in vivo optical imaging probe in an HCT116 xenograft model. The probe contained a version of [Nle4, D-Phe7]- α -melanocyte stimulating hormone (MSH7) and cholecystokinin-6 (CCK-6) connected via a linker made of 3 proline-glycine repeats flanked by 20-atom PEG, with Cy5 attached to an intervening lysine bridge. In vitro, this ligand preferentially bound to cells expressing both melanocortin (MC4R or MC1R) and cholecystokinin (CCK2R) receptors compared to cells that expressed only one of the two receptors. To investigate the specificity of this agent for targeting in vivo, HCT116 cell lines were engineered to express the MC1R alone, the CCK2R alone, or both and grown as flank xenografts in nude mice. In vivo fluorescence imaging showed that the dual receptor tumors were clearly visualized from 1 to 4 hours after tail vein injection of the conjugate (Figure 1). At 4 h post injection of 90 nmol/kg agent, a 5.9 ± 1.1 fold ($n = 3$) enhancement in fluorescence signal was observed in the dual receptor tumor (right flank) versus a single receptor tumor (left flank), suggesting specificity of the htMVL for the target tumor. This is the first in vivo evidence suggesting that htBVLs can distinguish tumors with 2, as compared to only 1, target receptors. This study shows the feasibility of specifically targeting receptor combinations for delivery of imaging or therapeutic agents.

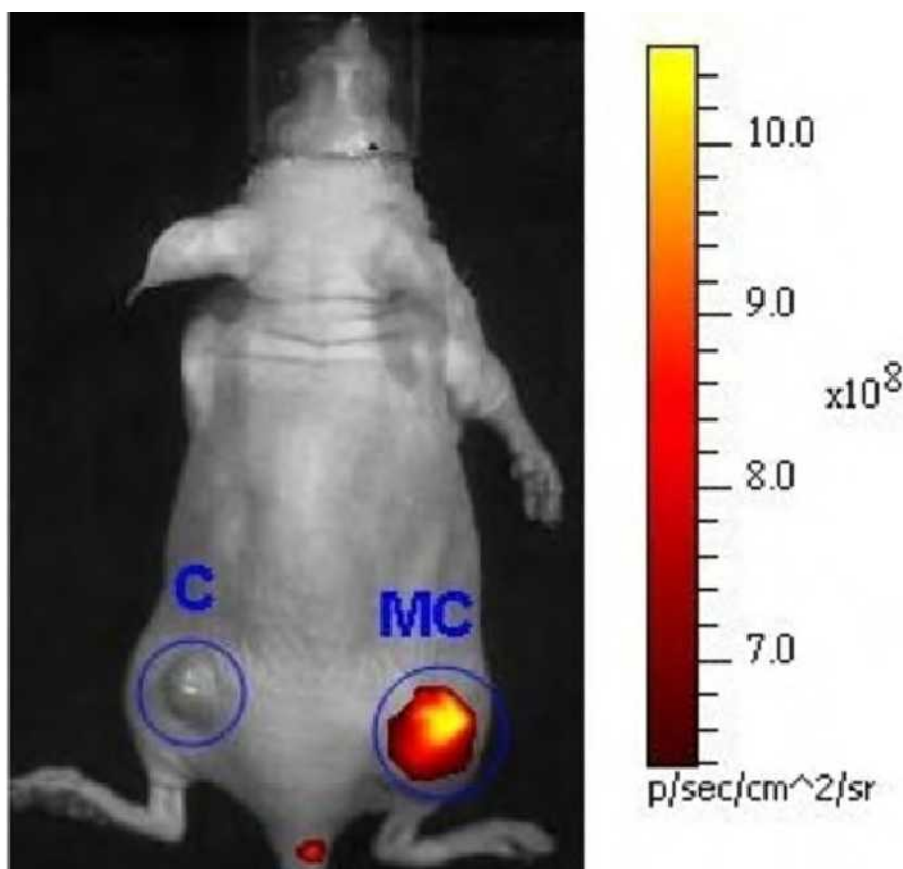


Figure 1. Fluorescence image of nude mouse bearing HCT-116 tumor xenografts that express both MC1R and CCK2R (MC) on the right flank; or only express CCK2R (C) on the left flank. Image was taken 4 hr post-injection of Cy5 CCK-MSH heterodimer.

Presentation Number **0729A**

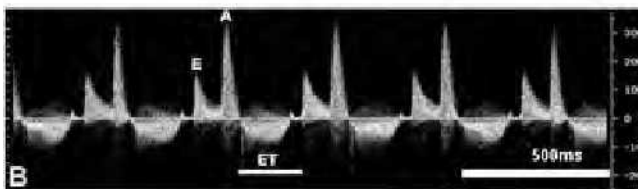
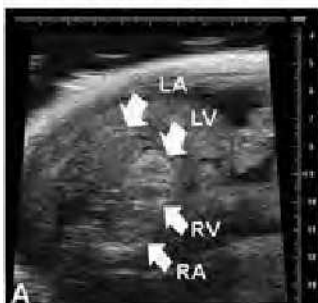
Poster Session 2c: In Vivo Studies & Development/Novel Use of Imaging Probes

The role of Akt1/PKBalpha signaling in fetal and adult cardiac growth

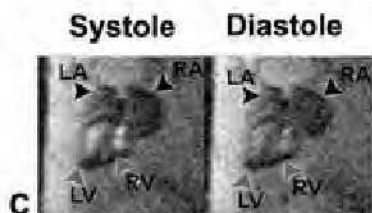
Katrien Vandoorne¹, Inbal E. Biton², Brian A. Hemmings³, Alon Harmelin², Michal Neeman¹, ¹Biological Regulation, Weizmann Institute, Rehovot, Israel; ²Veterinary Resources, Weizmann Institute, Rehovot, Israel; ³Friedrich Miescher Institute for Biomedical Research, Basel, Switzerland. Contact e-mail: Katrien.Vandoorne@weizmann.ac.il

Akt1/PKBalpha is an intracellular protein kinase regulating cellular growth, proliferation, survival and metabolism, and controls cardiac size and function. In an attempt to discover the basis of the higher fetal mortality and reduced body weight of Akt1/PKBalpha deficient (-/-) mice and the intermediate phenotype of Akt1/PKBalpha heterozygous (+/-) mice, we studied fetal and adult hearts. Left ventricular (LV) function of Akt1/PKBalpha -/-, +/- and wild type (+/+) littermates was examined during embryonic day (E) 14.5 and E16.5 using non-invasive in utero high-frequency ultrasound (Fig. A; RV=right ventricle; RA=right atrium; LA=left atrium). Pulsed-waved Doppler elucidated significantly shortened isovolumetric relaxation time of Akt1/PKBalpha -/- embryos and increased mitral valve E/A ratio (Fig. B; ET=ejection time). Mineralization of the skeleton in late stage fetuses (E18.5) hindered non-invasive in utero cardiography, therefore +/+ fetuses were imaged using in utero MRI (Fig. C), as a first step to also image late stage Akt1/PKBalpha -/- and +/- hearts in utero. Adult cardiac MRI (n=7 for each group) confirmed that left ventricular (LV) mass in adult -/- mice was reduced, consequently also cardiac output was reduced (Fig. D). Relative to the body mass, LV mass was not reduced in these mice, since the -/- mice are smaller in general. Additionally, heart monitoring during anesthesia showed a lower heart rate in -/- and +/- mice. LV Mass/body mass was significantly increased in +/- mice, which indicated modest hypertrophy, validated using histology. Here, we showed in vivo, during development and in adulthood, slight alterations of Akt1/PKBalpha deficient and heterozygous hearts, both structurally and functionally. These results raise the possibility for a compensatory role for Akt2 and 3 under conditions of total Akt1 deficiency.

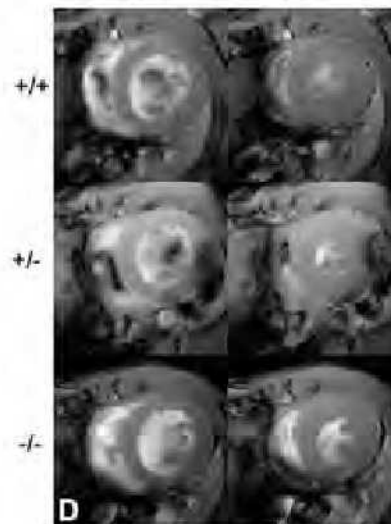
In utero cardiography E16.5



In utero cardiac MRI E18.5



Adult cardiac MRI



Presentation Number **0730A**

Poster Session 2c: In Vivo Studies & Development/Novel Use of Imaging Probes

Effects of anesthetics and contrast media in MRI-SPECT multimodality imaging

Joost Haeck^{1,2}, **Marleen de Poel**², **Sander Bison**^{2,1}, **Sandra van Tiel**¹, **Magda Bijster**², **Jan de Swart**², **Jifke Veenland**^{3,1}, **Monique R. Bernsen**^{1,2}, **Marion De Jong**^{2,1}, ¹Radiology, Erasmus Medical Centre, Rotterdam, Netherlands; ²Nuclear Medicine, Erasmus MC, Rotterdam, Netherlands; ³BIGR-Biomedical Imaging Group Rotterdam, Erasmus MC, Rotterdam, Netherlands. Contact e-mail: j.haeck@erasmusmc.nl

Introduction: Neuro-endocrine tumors originating from various organs are known to over-express somatostatin receptors (sst). The CA20948 rat pancreatic sst-positive tumor model is used in targeted imaging and treatment studies using radiolabelled somatostatin analogues, e.g. the SPECT tracer ¹¹¹In-DTPA-octreotide. Using this model to investigate tracer distribution we also use MRI to study tumor morphology and functional characteristics, such as tumor perfusion. The MRI facilities do not have the possibility of using gas anesthetics, and during perfusion measurements gadolinium contrast agent is used. To do both SPECT and MRI measurements to relate MRI characteristics to tracer distribution, the effects of the anesthetics and MRI contrast agent on the distribution was studied. **Methods:** 8 Lewis rats were inoculated with CA20948 tumor cells in both flanks which grew to approximately 2 cm² before imaging. Prior to i.v. injection of the tracer (50 MBq, 0.5 µg) the animals were anesthetized with either inhalant-anesthetic isoflurane (n=4) or intra-peritoneally injectable anesthetic mixture consisting of sufentanil (300µg/kg) and medetomidine (300µg/kg) (n=4), the latter is applied in our MRI studies. After SPECT imaging the rats were euthanized. Tumor and organs were removed to study peptide biodistribution ex vivo. The influence of MRI contrast agent on tracer uptake was examined in vitro. CA20948 cells were pre-incubated for 30 minutes in six-wells plates with either Gadovist or Magnevist (0.015mmol/ml). Afterwards the cells were incubated 1h at 37 degrees with the tracer (100MBq in 1 µg) in the presence or absence of the contrast agents. **Results:** A higher tumor uptake of ¹¹¹In-DTPA-octreotide was measured when rats were anesthetized with isoflurane than with medetomidine/sufentanil anesthesia, p<0,05. In other sst-positive organs, such as pancreas and stomach, the extent of tracer uptake was also dependent on the type of anesthesia used. There was a significant lowering of tumor tracer uptake (20-30%) when MRI contrast agents were present in the media prior to the tracer (p<0.05), even when the agents were washed off just before tracer addition. **Conclusion:** When conducting a study on tracer uptake in sst-positive tumors, the results can be influenced by anesthetics. Isoflurane has higher tracer uptake in tumors as opposed to sufentanil/medetomidine. MRI contrast agents should be allowed to washout prior to SPECT imaging to avoid interference in tumor tracer uptake. SPECT imaging prior to MRI imaging could also avoid the lower tracer uptake.

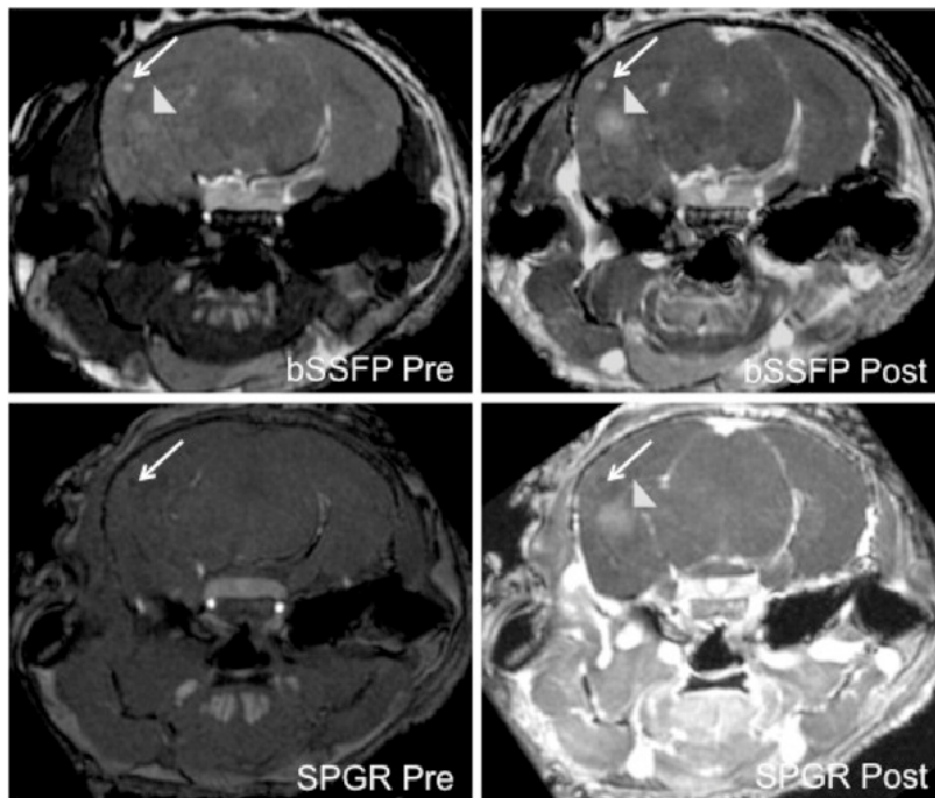
Presentation Number **0731A**

Poster Session 2c: In Vivo Studies & Development/Novel Use of Imaging Probes

In vivo visualization of differential blood-tumour-barrier permeability among developing metastases in a mouse model of breast cancer metastasis using gadolinium contrast MRI

Dean Percy^{1,2}, **Carmen Simedrea**³, **Catherine Ramsay**¹, **Emeline J. Ribot**¹, **Ann Chambers**², **Paula Foster**^{1,2}, ¹*Imaging Laboratories, Robarts Research Institute, London, ON, Canada;* ²*Medical Biophysics, The University of Western Ontario, London, ON, Canada;* ³*London Regional Cancer Program, London, ON, Canada. Contact e-mail: dpercy@imaging.robarts.ca*

Here we use high resolution MRI of the mouse brain to detect breast cancer metastases to the brain and to monitor blood-tumor barrier (BTB) permeability. Methods: Brain metastatic human breast cancer cells were injected into the left ventricle of the beating heart in nude mice for delivery to the brain. Imaging was performed using a clinical 3T MRI system, with a high performance gradient coil insert. Three sequences were compared: T1w spoiled gradient recovery (SPGR), balanced steady state free precession (bSSFP) and magnetization transfer (MT). Images were acquired before and after intraperitoneal Gd-DTPA injection (5mmol/kg). Results: All imaging sequences reveal substantial heterogeneity in the leakiness of the BTB. In T1w-SPGR brain images three types of metastases are detected: those which are hypointense in T1w images and enhance after Gad, those which are isointense in T1w images and enhance after Gad, and those which are hypointense in T1w images and do not enhance after Gad. The hypointensity of many metastases in T1w images is suggestive of tumors with high water content. bSSFP provides excellent visualization of brain metastases, appearing hyperintense to the surrounding brain tissue in precontrast images. Two types of metastases are detected in bSSFP images: those which are visible as regions of signal hyperintensity pre Gad and enhance after Gad, and those which are visible pre Gad and do not enhance after Gad. The nonenhancing tumors in SPGR and bSSFP images are the same tumors. In MT images the signal intensity of the normal brain tissue is reduced enhancing visibility of metastases even without Gad. Greater numbers of metastases were visible in the whole brain of the same animal in bSSFP images compared to either SPGR or MT. MRI is a valuable tool for investigating the evolution of brain metastases and for understanding differences in the BTB which is crucial in developing treatment strategies to heterogeneous populations of brain metastases.



MR images of the same mouse showing two types of brain metastases: enhancing (arrowhead) and nonenhancing (arrow).

Presentation Number **0732A**

Poster Session 2c: In Vivo Studies & Development/Novel Use of Imaging Probes

Non-invasive quantitative in vivo assessment of tumor vitality, necrosis and haemorrhage using MRI

Joost Haeck^{1,3}, **Lejla Alic**^{2,1}, **Sandra van Tiel**¹, **Magda Bijster**³, **Piotr A. Wielopolski**¹, **Gyula Kotek**¹, **Jifke Veenland**^{2,1}, **Marion De Jong**^{3,1}, **Monique R. Bernsen**^{1,3}, ¹Radiology, Erasmus Medical Centre, Rotterdam, Netherlands; ²BIGR - Biomedical Imaging Group Rotterdam, Erasmus MC, Rotterdam, Netherlands; ³Nuclear Medicine, Erasmus MC, Rotterdam, Netherlands. Contact e-mail: j.haeck@erasmusmc.nl

Introduction: MRI is a non-invasive imaging technique with numerous possibilities to see contrast within tissues. MRI contrast is governed by tissue composition and physiology by which it has the potential to provide in vivo histology. To validate the value of "MRI-histology" accurate validation by traditional histology is necessary. In this study we investigated which MRI parameters are representative for viable, haemorrhagic and necrotic tissue using the CA20948 rat pancreatic tumor, known for its heterogeneous tumor composition. Methods: Lewis rats were inoculated with CA20948 cells in the flank. Several contrast weighted images as well as T1, T2 or T2* maps were acquired. After imaging, the tumors were dissected and marked with dye to track original in vivo orientation during further processing. Tumors were fixed and paraffin-embedded. 5 μ sections were cut and H&E stained for histological assessment. The sections were digitized, and using the marked edges, registered to the appropriate MRI slice. On the digitised histological sections ROI corresponding to areas of necrosis, haemorrhage and viable tissue were drawn. Results: Due to the hemorrhagic and necrotic nature of the CA20948 tumor T2* weighted images give a large intra-tumor contrast range. The co-registered T2* value from the T2* map was calculated using a mono-exponential fit. An R-square value of greater than 0.85 was considered to be reliable. The three annotated tissue areas in histology were compared according to their T2* value. An unpaired t-test was performed on the T2* values of the different regions. The T2* value of viable areas (13.7 \pm 7.2) are significantly different ($p < 0.05$) than the T2* value of necrotic areas (6.36 \pm 2.8). There is no significance between hemorrhagic (7.4 \pm 15.7) and either necrotic or viable areas. The mean of hemorrhagic regions is similar to that of necrotic areas, which is explained by the fact that both hemorrhagic and necrotic areas have blood deposits and thus iron load, lowering the T2* value. The spread in the hemorrhagic areas could be explained by the large areas of viable cells between intracellular blood pools, so there is a mixture of cellular components in the regions drawn. Conclusion: It is possible to use MRI as a tool to characterise regions within the CA20948 tumor. Bright T2* contrast coincides with viable tissue and dark T2* contrast coincides with haemorrhage or necrosis. When the T2* value is calculated it is possible to differentiate viable from necrotic tissue, which is validated by histological findings.

Presentation Number **0733A**

Poster Session 2c: In Vivo Studies & Development/Novel Use of Imaging Probes

In Vivo Subcellular Imaging of Cancer Cell Dynamics in the Brain

Masashi Momiyama^{1,3}, Itaru Endo³, **Robert M. Hoffman**^{1,2}, ¹AntiCancer, Inc., San Diego, CA, USA; ²Department of Surgery, University of California San Diego, San Diego, CA, USA; ³Department of Gastroenterological Surgery, Yokohama City University School of Medicine, Yokohama, Japan. Contact e-mail: all@anticancer.com

We have developed a novel in vivo mouse model to image cancer cell nuclear-cytoplasmic dynamics in the brain in real-time and to visualize UV-C light killing of these cells. We used dual-color fluorescent cancer cells that express green fluorescent protein (GFP) linked to histone H2B in the nucleus and retroviral red fluorescent protein (RFP) in the cytoplasm. In order to visualize metastatic single cancer cell nuclear-cytoplasmic dynamics in the brain, dual-color Lewis Lung carcinoma (LLC) cells were injected into the right internal carotid artery of nude mice. A craniectomy open window was made over the right parietal bone. Metastatic dual-color LLC cells were irradiated with a 3.6-watt hand held UV-C light source for 60 seconds. The cells were then observed over 24 hours at 3 hour intervals through the open craniectomy window. The cancer cells were observed in the brain with the Olympus OV100 Small Animal Imaging System under high magnification. Metastatic dual-color LLC cells were visualized at the subcellular level in the brain enabling apoptosis to be imaged by nuclear morphology. UV-C light induced apoptosis of the dual-color LLC cells in the brain. Aggregation of chromatin at the nuclear membrane and fragmented nuclei of the cancer cell were followed in real time in the brain. More than 90% of the cancer cells irradiated with UV-C light died and disappeared without overt toxicity of the host. The novel mouse model used here will enable a deeper understanding of cancer cell dynamics in the brain. UV-C light may be a powerful tool for treatment of cancer cells expressing fluorescent reporters which now can be effected in vivo (Proc. Natl. Acad. Sci. USA, 1-6, 14514-14517, 2009 and Molecular Cancer Therapeutics 8, 3001-3008, 2009).

Presentation Number **0734A**

Poster Session 2c: In Vivo Studies & Development/Novel Use of Imaging Probes

High-Resolution Fluorescence Laparoscopy of Metastatic Cancer in an Orthotopic Mouse Model

*Hop S. Tran Cao*¹, *Sharmeela Kaushal*¹, *Claudia Y. Lee*³, *Cynthia S. Snyder*², *Kari Thompson*¹, *Santiago Horgan*¹, *Mark A. Talamini*¹, ***Robert M. Hoffman***^{1,4}, *Michael Bouvet*^{1,2}, ¹*Department of Surgery, University of California San Diego, San Diego, CA, USA;* ²*Moores Cancer Center, University of California San Diego, San Diego, CA, USA;* ³*UVP, LLC, Upland, CA, USA;* ⁴*AntiCancer, Inc., San Diego, CA, USA. Contact e-mail: all@anticancer.com*

We report here the development of fluorescence laparoscopy to image green fluorescent protein (GFP)-expressing pancreatic tumors in an orthotopic mouse model. An orthotopic mouse model of human pancreatic cancer was established by injecting GFP-expressing MiaPaca-2 human pancreatic cancer cells into the pancreas of 6-week old female athymic mice. On post-operative day 14, the animals underwent a diagnostic laparoscopy using both white and fluorescent light. The fluorescence laparoscope was constructed by modifying a standard laparoscopic system in the following manner: a 480-nm short pass excitation filter was placed between the light cable and the laparoscope, and a 2-mm thick emission filter that allows leakage of 1% of the background light was placed between the laparoscope and the camera. The camera and recording system were replaced with a MultiCam 310C (UVP, Upland, CA) that allows variable exposure time and gain setting in the controlling software. The exposure time was set to 110 msec and the gain to 97. A 3-mm 0-degree laparoscope was used in the mice. The mouse's abdomen was gently insufflated to 2 mm Hg via a 22-gauge angiocatheter that was secured via a suture. After fluorescence laparoscopy, the animals were sacrificed, and the identified tumors were collected and processed for histology. The experiments were performed in triplicate. Fluorescence laparoscopy allowed facile and rapid identification of the bright fluorescent tumors in the pancreatic body. By employing the specific parameters above mentioned, a clear background was visible along with the fluorescent tumor under the fluorescent light mode. This could proffer an advantage in allowing exact localization of the lesions, eliminating the need to flip back and forth between white and fluorescent lighting, under which the background is usually so darkened that it is difficult to maintain spatial orientation. In summary, the use of fluorescence laparoscopy permits the facile, clear, and rapid identification and localization of tumors that are labeled with fluorescent proteins or other fluorophores. Fluorescence laparoscopy may thus play a useful role in the diagnosis and staging of pancreatic and other aggressive gastrointestinal cancers.

Presentation Number **0700B**

Poster Session 3c: In Vivo Studies & Development/Novel Use of Imaging Probes

Non-Invasive Real-Time Imaging of Thyroid Cancer Progression in an Orthotopic Model

*Hop S. Tran Cao¹, Sharmeela Kaushal¹, Cynthia S. Snyder², Weg M. Ongkeko¹, **Robert M. Hoffman**^{1,3}, Michael Bouvet^{1,2},
¹Department of Surgery, University of California San Diego, San Diego, CA, USA; ²Moore's Cancer Center, University of California San Diego, San Diego, CA, USA; ³AntiCancer, Inc., San Diego, CA, USA. Contact e-mail: all@anticancer.com*

We report here a novel orthotopic mouse model of human thyroid cancer that can be imaged non-invasively with the use of red fluorescent protein (RFP). Human thyroid cancer cell lines NPA (papillary) and KAK-1 (anaplastic) were stably transfected to express RFP or the green fluorescent protein (GFP). The cells were then injected into the thyroid glands of 8-week old athymic mice. The animals were noninvasively imaged weekly, and sacrificed when premorbid. Their tumor was subsequently resected en bloc with the respiratory system for further processing and analysis. H&E staining was performed to confirm the pathological diagnosis. Both anaplastic and papillary thyroid cancer cell lines led to the robust development of orthotopic fluorescent tumors in nude mice. While RFP-expressing tumors were easily identified transcutaneously, autofluorescence of the skin prevented visualization of GFP-expressing tumors, making GFP a suboptimal model. Injection of 5×10^5 cells was as efficacious in allowing tumor development as 5×10^6 cells. Tumors were first visualized for both cell lines via whole-body noninvasive imaging as early as four weeks post-implantation and could be monitored over time. The time to premorbid conditions varied greatly between mice and seemed to be associated with the tumor growth pattern rather than tumor size. The earliest appearance of morbidity was five weeks post-implantation in an animal with cachexia due to local compression of the esophagus by the tumor. Other mice died at later stages from metastatic disease. The bright fluorescence of the tumors allowed identification of multiple micrometastases at necropsy in the lungs, lymph nodes, and the vascular system, lesions that were not visible under white light. In summary, we have developed a novel orthotopic fluorescent mouse model of thyroid cancer that should serve a valuable role in the understanding of this disease and in the evaluation of new therapeutics, allowing assessment of the tumor response over time.

Presentation Number **0701B**

Poster Session 3c: In Vivo Studies & Development/Novel Use of Imaging Probes

Color-Coded Imaging of Cancer Cell-Immune Cell Interaction In Vivo

*Hiroaki Kimura^{1,2}, Katsuhiko Hayashi², Hiroyuki Tsuchiya², Katsuro Tomita², Ryoichi Aki^{1,3}, Hiroyuki Kishimoto^{1,3}, Atsushi Suetsugu^{1,3}, Masashi Momiyama^{1,3}, Michael Bouvet³, **Robert M. Hoffman**^{1,3}, ¹AntiCancer, Inc., San Diego, CA, USA; ²Department of Orthopedic Surgery, Kanazawa University School of Medicine, Kanazawa, Japan; ³Department of Surgery, University of California San Diego, San Diego, CA, USA. Contact e-mail: all@anticancer.com*

We imaged the interaction between osteosarcoma cells and splenocytes using fluorescent proteins during chemotherapy or dendritic-cell (DC) therapy. GFP-expressing splenocytes (5 x 10⁶), derived from GFP transgenic BALB/c mice, were transplanted to BALB/c nude mice. Then, RFP-143B human osteosarcoma cells (5 x 10⁵) were injected in a skin flap raised in these mice. The mice were treated with doxorubicin (5 mg/kg), i.p. three days in a row. The RFP-expressing 143B tumor and the GFP splenocytes accumulation around the tumor were imaged for three days. Dendritic cells (1x10⁶), which were activated with a 143B cells lysate, were injected into the inguinal lymph node of the mice. The tumor grew gradually in the control group, whereas in the chemotherapy group, the tumor became progressively smaller. In the DC group, the tumor regressed and was almost eradicated 12 days after treatment. In the DC group, GFP splenocytes accumulated in large numbers around the tumor three days after DC treatment. The accumulation of DC cells was diminished as the tumor became smaller. In the chemotherapy group, in contrast, accumulation of splenocytes gradually increased even though the tumor became progressively smaller. Future experiments will be on syngeneic models to determine the influence of an intact immune system on the interaction of splenocytes and DC cells with cancer cells.

Presentation Number **0702B**

Poster Session 3c: In Vivo Studies & Development/Novel Use of Imaging Probes

Hypoxia in Models of Lung Cancer and its Implications for targeted Therapeutic Studies

Marta Vilalta¹, **Alejandro Sweet-Cordero**², **Dean W. Felsher**³, **Quynh-Thu Le**¹, **Amato Giaccia**¹, **Edward E. Graves**¹, ¹*Division of Radiation Oncology, Molecular Imaging Program at Stanford, Stanford University, Stanford, CA, USA;* ²*Pediatric Cancer Biology Program, Molecular Imaging Program at Stanford, Stanford University, Stanford, CA, USA;* ³*Medicine, Molecular Imaging Program at Stanford, Stanford University, Stanford, CA, USA.* Contact e-mail: mvilalta@stanford.edu

Hypoxia is a common phenomenon in human tumors with important prognostic implications; therefore many efforts have focused on targeting hypoxic tumor cells for treatment. In order to optimize these therapies, different experimental models of cancer have been used in preclinical studies. The most common is the subcutaneous tumor growth model, even though orthotopic and spontaneous models exhibit properties more closely related to human cancer. Our goal was to investigate potential discrepancies in the hypoxic tumor microenvironment between different preclinical models of lung cancer in order to establish the appropriateness of each model for studies of tumor biology and therapeutic response. Subcutaneous and orthotopic human A549 lung carcinomas, as well as spontaneous lung tumors initiated by tissue-specific activation of the K-ras and Myc oncogenes, growing in mice were studied using both the standard clinical radiotracer [¹⁸F]-fluorodeoxyglucose (FDG) and the hypoxia-specific radiotracer [¹⁸F]-fluoroazomycin arabinoside (FAZA) imaged with positron emission tomography (PET), in order to measure both the metabolic activity and oxygen status of each model. The hypoxia marker pimonidazole was used post-mortem in order to compare macroscopic and microscopic patterns. In addition the sensitivity of these lung tumor models in vitro and in vivo to DNA damage induced by the hypoxia-activated prodrug PR-104 was assessed by measuring the formation of γH2AX foci. While all tumors studied exhibited elevated metabolism activity as observed by FDG PET imaging, minimal FAZA and pimonidazole accumulation was seen in orthotopic xenografts and spontaneous murine tumor, suggesting that these tumors are well oxygenated. Interestingly subcutaneous A549 tumors showed substantial trapping of both hypoxia probes. These measures of tumoral hypoxia correlated with the response to PR-104 treatment under hypoxic conditions where only the subcutaneously A549 tumor model exhibited a response to this treatment in vivo. Observations from a large multi-institutional study where measurements of oxygenation of human lung tumors were done showed that the incidence of hypoxia in these cancers is less than in other solid tumor types. These results show that the appropriateness of each model type for the therapeutic investigations depends on which model is most reflective of the human cancer and suggest judicious selection of preclinical tumor models for the study of both hypoxia imaging and anti-hypoxic therapies.

Presentation Number **0703B**

Poster Session 3c: In Vivo Studies & Development/Novel Use of Imaging Probes

Isoflurane, Desflurane and Sevoflurane gas Anesthesia Inhibit Firefly Luciferase in a Dose-Dependent Way: Relevance for In Vivo Bioluminescence Imaging

Marleen Keyaerts^{1,2}, **Isabel Remory**^{1,3}, **Vicky Caveliers**^{1,2}, **Pierre-Alix Dancer**⁴, **Jan I. Poelaert**³, **Axel Bossuyt**^{1,2}, **Tony Lahoutte**^{1,2}, ¹*In vivo Cellular and Molecular Imaging Lab, Vrije Universiteit Brussel, Brussel, Belgium;* ²*Nuclear Medicine, UZ-Brussel, Brussel, Belgium;* ³*Anesthesiology, UZ-Brussel, Brussel, Belgium;* ⁴*Biospace Lab, Paris, France. Contact e-mail: mkeyaerts@gmail.com*

Rodents are anesthetized during Bioluminescence imaging (BLI) and BLI cameras are routinely provided with an isoflurane anesthesia unit. Isoflurane is animal- and user-friendly because of its fast induction and recovery. However a direct inhibition of the Firefly luciferase (Fluc) enzyme by anesthetics has been described and might influence in vivo quantification. **Aim:** 1. To assess the impact of isoflurane, desflurane and sevoflurane anesthesia on the bioluminescent signal intensity in vitro. 2. To evaluate the effect of isoflurane anesthesia in vivo. **Methods:** For in vitro assessment, 10E6 Fluc+ R1M cells were plated in 25 cm² flasks. Cells were exposed to O₂/anesthesia mixtures starting 10 min before and continuously throughout BLI. D-luciferin was added to reach a 0.15 mg/ml concentration. Experiments were performed in triplicate with in each replica at least 3 samples per condition and expressed relatively to control conditions (100% O₂). For in vivo analysis, 10 mice bearing Fluc+ 293T cells in matrigel were imaged awake and under 2% Isoflurane with a 48 h interval (cross-over design, 150 mg/kg D-luciferin). Kinetic BLI data were acquired using the in actio intensified CCD-camera. **Results:** For all three gasses, a dose-dependent inhibition of the bioluminescent signal was observed in vitro. The average bioluminescent signal at 1.3x the minimum alveolar concentration (MAC) was reduced to 67.4±6.8%, 53.7±12.9% and 62.4±13.2% for isoflurane, sevoflurane and desflurane respectively (p=.0093 between isoflurane and sevoflurane). There was a significant reduction of BLI signal in mice anesthetized with 2% Isoflurane compared to awake mice, on average to 45±13% of control values for the peak intensity and to 70±16% of control values for the area under the curve. The shape of the time profile was also different, with a fast rise and a more rapid decline in awake animals, and a slower evolving kinetic profile in anesthetized mice. **Conclusion:** Isoflurane anesthesia significantly reduces the intensity of the BLI signal in vitro with 33%. Other candidate gas anesthetics show equal (desflurane) or worse (sevoflurane) inhibition of the BLI signal and are therefore no good alternatives. For isoflurane, in vivo comparison between awake mice and anesthetized mice showed a reduction of the BLI peak signal of 55%, probably due to both a direct inhibitory effect and changes in physiologic parameters, as reflected in altered kinetic profiles.

Presentation Number **0704B**

Poster Session 3c: In Vivo Studies & Development/Novel Use of Imaging Probes

Quantitative correlation of DCE-MRI parameters with microvessel density and the size of human colorectal cancer in xenograft mouse model with 3T

Sung Jun Ahn, Ho-Taek Song, Chan Sik An, Young Jin Park, Joon Seok Lim, Jin-Suck Suh, departement of radiology, yonsei university, college of medicine, Seoul, Republic of Korea. Contact e-mail: aahng77@yuhs.ac

Purpose: The aim of this study was to correlate the quantitative dynamic contrast enhanced MRI (DCEMRI) parameters with microvessel density (MVD) and the size of human colon cancer in nude mouse model with 3T. **Material and methods:** Human colon cancer xenograft model was produced by inoculating 1x10⁶ DLD-1 human colon cancer cells subcutaneously into the right hind limbs of total 10 mice. MRI was performed when the tumor reached predetermined size. Tumors were grouped according to the diameter. Group A: 6-9 mm, group B: 10-15 mm, group C: >16 mm. DCEMRI was performed by tail vein injection of 0.3 mmol/kg of gadolinium. ROI was drawn at the midpoint along the z-axis of the tumor. Toft model analysis was performed. Mean, median, and upper 10% value of Ktrans were calculated. Microvessels staining was performed at the MRI corresponding sections. MVD was analyzed according to Weidner criterion. Both maximum and mean value of three hot spots were used for MVD. Correlation between MVD, Ktrans, and tumor size was analyzed by Spearman's rho correlation. **Results:** Mean, median and upper 10% values of Ktrans in designated ROI are not significantly correlated with mean or maximum microvessel counts of three hot spots. ($r > 0.5$). Size of the tumor was linearly correlated with MVD score ($p = 0.041$). Size of the tumor was not correlated with the Ktrans values ($P > 0.05$). Necrosis in the tumor was prominent in larger tumors (group C). **Conclusion:** Transfer constant 'Ktrans' obtained from DCEMRI was not correlated with MVD in this study. MVD of the tumor reflected the status of growing tumor. Averaged Ktrans was probably underestimated due to the necrosis in the tumor. Hot pixel of DCEMRI correlated with hot spot in MVD would provide reliable information.

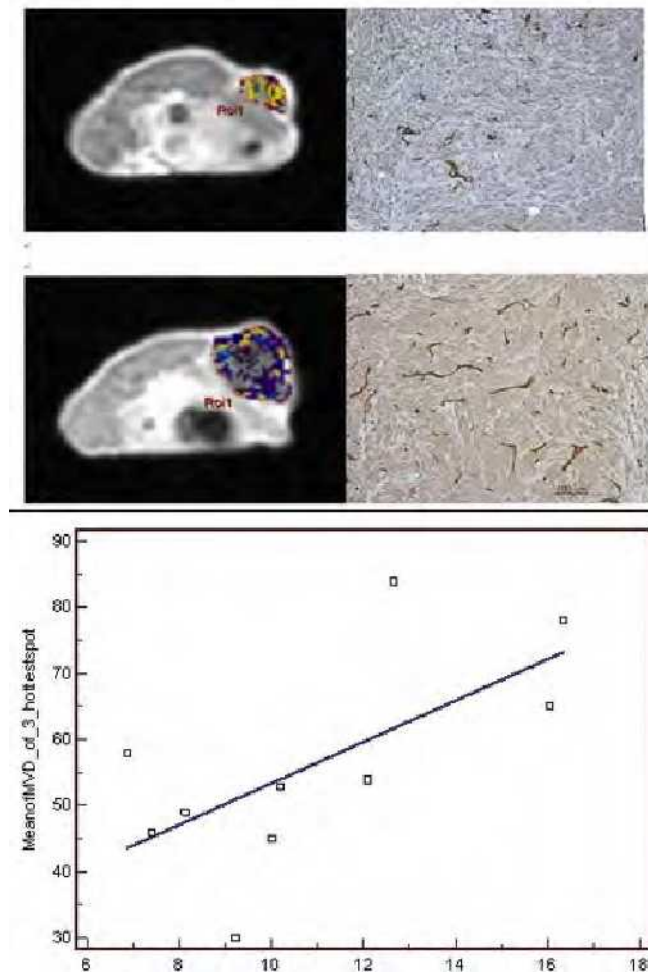


Figure 1. Pixel by pixel analysis of Ktrans and MVD correlation. Figure 2. Correlation between tumor size and MVD

Presentation Number **0705B**

Poster Session 3c: In Vivo Studies & Development/Novel Use of Imaging Probes

Influence of different anesthetics and air or oxygen breathing on the vital parameters, blood glucose levels, and blood oxygenation of BALB/c mice

Maren K. Koenig¹, Mareike Lehnhoff¹, Kerstin Fuchs², Florian C. Maier¹, Damaris Kukuk¹, Julia G. Mannheim¹, Stefan Wiehr¹, Manfred Kneilling², Bernd J. Pichler¹, ¹Laboratory for Preclinical Imaging and Imaging Technology of the Werner Siemens-Foundation, Department of Radiology, Eberhard Karls University Tübingen, Röntgenweg 13, 72076 Tübingen, Germany; ²Department of Dermatology, Eberhard Karls University Tübingen, Liebermeisterstr. 25, 72076 Tübingen, Germany. Contact e-mail: Maren.Koenig@med.uni-tuebingen.de

In [¹⁸F]FLT-PET studies we unexpectedly observed significant differences in [¹⁸F]FLT uptake in inflamed joints and tumors when comparing dynamic and static PET scans. Thus, we suspected that short or long-term anesthesia together with different breathing protocols (air/oxygen) and anesthetics can impair cell functioning and subsequently tracer uptake. Validating this, mice underwent 1.5% Isoflurane, Midazolam/Medetomidine (5mg/kg body weight (BW)/0.5mg/kg BW) or Ketamine/Xylazine (100mg/kg BW/5mg/kg BW) anesthesia with air or oxygen breathing. To simulate dynamic PET-scans mice were kept anaesthetized for 30 minutes and placed on a temperature feedback control unit with a rectal probe on the PET-scanner bed to keep the body temperature at a constant level (36.6 - 37.1°C). To simulate static PET-scans mice were kept conscious for 30min and then anaesthetized for 15min. During anesthesia we continuously monitored the heart and breathing rate and the rectal temperature. Additionally, we collected blood from the retro-bulbar venous plexus to determine pO₂, pCO₂, pH, and blood glucose levels at two time points (0min, 45min). All three anesthetics induced an increase in blood glucose level during anesthesia, regardless of the breathing protocol, albeit mice were anaesthetized for only 15 minutes. Blood glucose levels varied between 128-183mg/dl at the beginning and between 181-334mg/dl at the end of anesthesia. Isoflurane anesthesia caused the lowest increase in blood glucose levels (max.: 260mg/dl). We detected the lowest heart rate under Ketamine/Xylazine anesthesia (185-273 beats per minute (bpm)), the highest heart rate under Isoflurane anesthesia (304-424bpm), and the most constant heart rate under Midazolam/Medetomidine anesthesia (236-280bpm). Lowest breathing rate was measured under Isoflurane (118-197 respiration per minute (rpm)) and between 111-266rpm under Midazolam/Medetomidine and Ketamine/Xylazine anesthesia. Sleeping and conscious mice denote quite constant venous pO₂-level in a range from 103-142mmHg (0min, 45min). O₂-breathing mice displayed pCO₂-levels between 29.5-63.5mmHg with a tendency to increase during anesthesia, regardless whether mice were sleeping or conscious. Mice that underwent air breathing surprisingly displayed lower pCO₂ levels between 18.5-40.5mmHg. In conclusion, different anesthetics together with different breathing protocols (air/oxygen) impair vital parameters, cell functioning and biomarker uptake dramatically. Thus, anesthesia protocols should be chosen carefully due to the significant impact to the animal model.

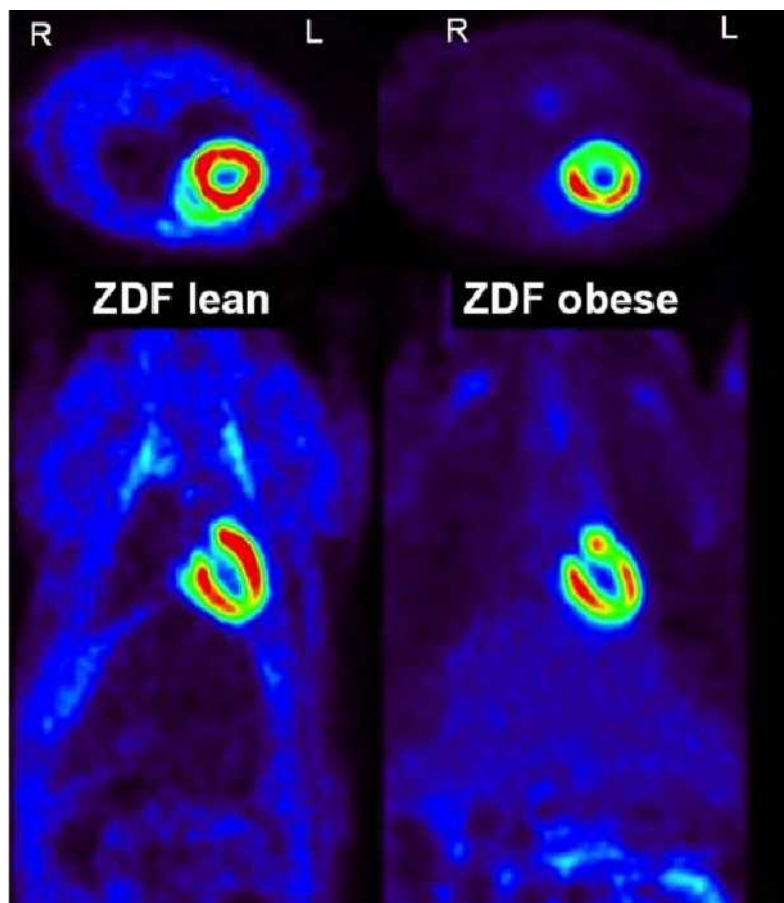
Presentation Number **0706B**

Poster Session 3c: In Vivo Studies & Development/Novel Use of Imaging Probes

Euglycemic-hyperinsulinemic clamp & small animal PET: Noninvasive assessment of glucose uptake rates in Zucker diabetic fatty rats

Michael C. Kreissl¹, Paula Arias², Franz R. Kaiser¹, Andreas Schirbel¹, Ina Israel¹, Samuel Samnick¹, Christoph Reiners¹, Theo Pelzer², ¹Nuclear Medicine, University Hospital Wuerzburg, Wuerzburg, Germany; ²Internal Medicine I, University Hospital Wuerzburg, Wuerzburg, Germany. Contact e-mail: kreissl_m@klinik.uni-wuerzburg.de

Aim: The aim of this study was to combine euglycemic-hyperinsulinemic with small animal PET using 2-deoxy-2-(18F)fluoro-D-glucose (FDG) and to assess glucose uptake rates in a model of Type 2 diabetes mellitus (ZDF rat). **Methods:** 11 obese and 9 lean animals (~14 weeks old) were fasted over night and anesthetized using pentobarbital. After an insulin primer followed by a continuous infusion, blood glucose levels were titrated using glucose solution. FDG (~ 25 MBq) was injected i.v. after start of a 60-minute list mode acquisition. Data were corrected for attenuation and scatter and binned into 22 frames. FDG uptake rates (Ki) were determined using organ VOIs, patlak plot and a hybrid input function. **Results:** Obese animals displayed a lower whole body glucose disposal rate as reflected by a lower glucose infusion rate (7.3 ± 1.2 vs 17.3 ± 3.1 mg/(kg*min); $p < 0.001$). Ki values in the myocardium and the skeletal muscle were found to be lower in diabetic animals (5.9 ± 4.0 vs 15.0 ± 4.4 ml/(min*100g); $p < 0.001$ and 0.9 ± 0.3 vs. 2.3 ± 0.2 ml/(min*100g); $p < 0.001$). Assuming a lumped constant of 1 glucose metabolic rates for obese and lean animals were calculated to be 6.3 ± 5.0 and 13.4 ± 3.2 mg/(ml*100g) ($p = 0.004$) for the myocardium and 0.97 ± 0.37 and 2.09 ± 0.40 mg/(ml*100g) for the skeletal muscle. Upon ex-vivo western blot analysis a significant reduction GLUT-4 but not GLUT-1 expression was found; this observation was confirmed by the results of the Real Time PCR arrays. **Conclusions:** We were able combine clamping and small animal PET to study diabetic rats using 2-FDG. Peripheral insulin resistance was quantified and correlated with ex-vivo assays. The reduced glucose uptake rate in diabetic animals may at least in part be attributed to a reduction of GLUT-4.



Coronal & transverse views (50-60 min post FDG): Obese rats show a much lower tracer accumulation in the insulin dependant organs (skeletal muscle and myocardium) as compared to leans.

Presentation Number **0707B**

Poster Session 3c: In Vivo Studies & Development/Novel Use of Imaging Probes

Magnetic resonance imaging and Pattern analysis in the study of tumor angiogenesis

Marco Dominietto, Steffi Lehmann, Ruth Keist, Markus Rudin, Institute for Biomedical Engineering, ETHZ, Zurich, Switzerland.
Contact e-mail: dominietto@biomed.ee.ethz.ch

Various image techniques are available to monitor tumor angiogenesis including magnetic resonance imaging (MRI), which allows investigating angiogenesis-related parameters such as tumor blood volume (TBV) and blood flow (TBF), the average vessel diameter in a voxel (vessel size index, VSI) and vascular permeability noninvasively in vivo. As tumor tissue is highly heterogeneous comprising areas with different degree of vascularization, an analysis procedure such as pattern analysis, which accounts for shape and texture of the structures to be analyzed is promising. In this study we applied principles of pattern analysis to quantitatively assess angiogenesis/vascularity in a murine subcutaneous tumor model. Ten balb/c nude mice were injected subcutaneously with 10⁶ C51 cells (colon carcinoma). A first group (N=5) was treated with dimethylxalylglycine (DMOG), a compound that has been reported to increase tumor vascularisation through activation of HIFs. A second group (N=5) was treated with NaCl. MR experiments assessing TBV, TBF, VSI and permeability were performed before and after 6 days of treatment. Data were analyzed with a standard image analysis, and subsequently with pattern analysis technique. We did not find any significant differences between the two groups of animals regarding TBV, VSI or permeability readout averaged over the whole tumor volume. When applying pattern analysis, there was no difference in shape between the two groups. In contrast, analysis of texture showed significant differences in the spatial distribution of TBV (fractal dimension) and of non-perfused regions (lacunarity). In view of the heterogeneity of tumors, analysis relying on values averaged of the whole tumor volume are insensitive in picking up differences among treatment groups. In contrast, pattern analysis is particularly sensitive to changes in tissue texture.

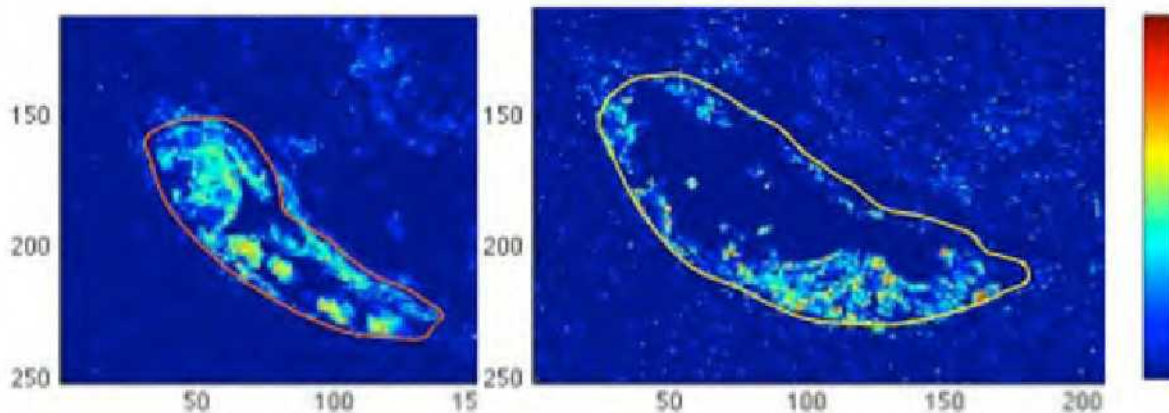


Fig 1: TBV maps at the end of the treatment period with different values of lacunarity: DMOG (left), NaCl (right).

Presentation Number **0708B**

Poster Session 3c: In Vivo Studies & Development/Novel Use of Imaging Probes

Effect of anesthesia and hypothermia on the hepatic kinetics of Gd-EOB-DTPA: Evaluation using MR imaging of conscious mice

Shigeru Kiryu¹, Yusuke Inoue¹, Makoto Watanabe¹, Kuni Ohtomo², ¹Radiology, Institute of Medical Science, University of Tokyo, Tokyo, Japan; ²Radiology, Graduate School of Medicine, University of Tokyo, Tokyo, Japan. Contact e-mail: kiryu-ty@umin.ac.jp

Magnetic resonance (MR) imaging of small animals is usually performed under anesthesia, which may change physiological conditions and affect the experimental results including the pharmacokinetics of a contrast agent. We aimed to develop a method for body MR imaging of conscious mice and investigate the effect of isoflurane anesthesia and hypothermia on the hepatic kinetics of a hepatobiliary contrast agent gadoxetate disodium (Gd-EOB-DTPA). Conscious or anesthetized mice were restrained on an imaging holder, and the rectal temperature was measured serially inside or outside the magnet. Serial MR imaging of the liver was performed after intravenous injection of Gd-EOB-DTPA with or without temperature control, and the time course of liver enhancement was assessed. Moreover, the time course was evaluated in anesthetized mice at various degrees of hypothermia. Outside the magnet, the rectal temperature decreased rapidly in anesthetized mice. The decline was less prominent, but still evident in conscious mice. The environment temperature was slightly higher inside the magnet than outside the magnet, and the rectal temperature decreased less in anesthetized mice and remained constant in conscious mice. With the aid of the restraining technique, the liver in conscious mice was visualized by serial MR imaging after contrast injection, which allowed quantitative evaluation of temporal changes in the liver signal. The washout of Gd-EOB-DTPA from the liver was slower in anesthetized hypothermic mice than in conscious normothermic mice. When anesthetized mice were warmed to attain normothermia, the washout was accelerated and became as fast as that in conscious normothermic mice. When cooling decreased the rectal temperature in conscious mice to the level in anesthetized mice without temperature control, the washout was delayed, as in anesthetized hypothermic mice. Severer hypothermia in anesthetized mice resulted in lower peak enhancement and more prominent prolongation of washout. By separately manipulating the presence or absence of anesthesia and hypothermia, we demonstrated that washout of Gd-EOB-DTPA from the liver was delayed under hypothermia, regardless of the use of anesthesia. Serial body MR imaging of conscious mice was feasible and allowed the kinetics of a contrast agent to be evaluated, while excluding the possible effects of anesthesia.

Presentation Number **0709B**

Poster Session 3c: In Vivo Studies & Development/Novel Use of Imaging Probes

In vivo biodistribution of the anti $\alpha 4$ integrin antibody Natalizumab in a longitudinal study of multiple sclerosis using an EAE mouse model

Carsten Calaminus¹, Christian Kesenheimer¹, Christoph M. Griessinger¹, Stefan Wiehr¹, Julia G. Mannheim¹, Arthur Melms², Bernd J. Pichler¹, ¹Laboratory for Preclinical Imaging and Imaging Technology of the Werner Siemens-Foundation, University of Tuebingen, Tuebingen, Germany; ²Department of General Neurology, Hertie Institute for Clinical Brain Research, University of Tuebingen, Tuebingen, Germany. Contact e-mail: carsten.calaminus@med.uni-tuebingen.de

Multiple sclerosis (MS) remains one of the most popular but also most mysterious neuronal diseases in the industrial world despite intense effort took place in investigating the cause of this immune mediated disease. Although recent research has focused on options for therapy, only few promising approaches achieved clinical relevance. One drug which is currently used as a therapeutic agent is the humanized anti- $\alpha 4$ integrin antibody Natalizumab. This is an effective but also controversially discussed treatment for relapsing-remitting multiple sclerosis. Natalizumab is thought to exert its therapeutic efficacy by blocking the $\alpha 4$ integrin-mediated binding of circulating immune cells to the blood-brain barrier (BBB). By means of intravital microscopy it could recently be shown, that Natalizumab specifically inhibit the firm adhesion but not the rolling or capture of human T cells on the inflamed BBB in mice with acute experimental autoimmune encephalomyelitis (EAE). As $\alpha 4$ integrins control other immunological processes, Natalizumab may, however, execute its beneficial but also harmful effects like the progressive multifocal leukoencephalopathy (PML) or melanoma elsewhere. For following the biodistribution in a longitudinal study using transgenic SJL-mice simulating an anti-MS therapy in humans and for identifying potential unknown sites of pharmaceutical action of Natalizumab we inject the [64Cu]labelled antibody in SJL transgenic mice expressing EAE. Immediately after EAE-induction and the onset of characteristic behavioural EAE symptoms we acquire static images (10min) in a small animal PET. We could demonstrate that Natalizumab persists in the organism for at least 72h. As expected we could not observe an accumulation of activity in the brain before the induction of EAE (brain: $0.49 \pm 0.12\%$ ID/cc; muscle: $0.44 \pm 0.26\%$ ID/cc). Interestingly after EAE induction the intracranial signal does not increase as it would be suggested for an inflamed BBB (brain: $1.39 \pm 0.11\%$ ID/cc; muscle: $1.44 \pm 0.23\%$ ID/cc). In conclusion we were able for the first time to follow the biodistribution of Natalizumab in a longitudinal study using transgenic SJL mice simulating a long lasting MS therapy in patients. It could be observed that despite progressive disease [64Cu]labelled Natalizumab does not infiltrate the brain permanently as it could be suspected assuming an EAE induced cranial accumulation of inflammatory T-cells. Therefore future studies will follow the biodistribution of Natalizumab daily after EAE induction to visualize the T-cell infiltration preceding an EAE attack.

Presentation Number **0710B**

Poster Session 3c: In Vivo Studies & Development/Novel Use of Imaging Probes

59Fe labeled SPIO for quantification of particle concentration in vivo at 3T

Evelyn Grabowski¹, Nina Raabe¹, Barbara Freund², Oliver T. Bruns³, Markus Heine⁴, Gerhard Adam¹, Harald Ittrich¹, ¹Department for Diagnostic and Interventional Radiology, University Medical Center Hamburg-Eppendorf, Hamburg, Germany; ²Department of Biochemistry and Molecular Biology II, University Medical Center Hamburg-Eppendorf, Hamburg, Germany; ³Heinrich-Pette-Institute for Experimental Virology and Immunology of the University of Hamburg, University of Hamburg, Hamburg, Germany; ⁴Department of Anatomy II: Experimental Morphology, University Medical Center Hamburg-Eppendorf, Hamburg, Germany. Contact e-mail: e.grabowski@uke.uni-hamburg.de

Background: There is an intense interest in the use of superparamagnetic iron oxide nanoparticles (SPIO) as a contrast agent in medicine and especially in human imaging. The in vivo application unfortunately does not allow direct quantification of SPIO concentration in tissue. Being able to exactly quantify concentration of SPIO in tissue is an elemental requirement for quantitative susceptibility MRI and future preclinical and clinical SPIO applications. Therefore the purpose of our study was to use 59Fe-labeled SPIO* as a tool to exactly quantify the concentration of injected SPIO in different tissue. Material and methods: Polymere coated, monodisperse 59Fe-labeled SPIO* (core size 10 nm) were injected at concentrations of 20 µg/100 µl (n = 3), 40 µg/100 µl (n = 2) and 60 µg/100 µl (n = 3). MR measurements were performed at a 3.0T whole body scanner (Intera; Philips, Netherlands) with a custom made small solenoid animal coil. In vitro r2 and r2* relaxivities of SPIO* were determined before in vivo application. T2* was measured in liver, spleen, kidneys, muscle and brain before and after SPIO* administration. R2* and ΔR2* were calculated for all tissues and r2* was assessed for the liver. 59Fe activity measurements of SPIO* in whole mice and all tissues were performed immediately after MRI by whole body radioactivity counter. We estimated liver r2* by correlating the results of the activity measurements with ΔR2* to define the dependency of ΔR2* and SPIO* concentration in vivo. Samples of liver, spleen and kidneys were analyzed by transmission electron microscopy (TEM) and histology (Prussian blue). Results: ΔR2* revealed a concentration dependent particle incorporation of SPIO* in the liver. SPIO* activity measurements showed that 70 % - 88 % of injected SPIO* accumulated in the liver, followed by the spleen with 0.7 % - 2 %. All other organs showed no significant SPIO* activity. Percentage SPIO* accumulation showed no difference between the applied SPIO* concentrations. ΔR2* in liver showed a linear correlation to SPIO* activity measurements for all concentrations (R2 = 0.84). Calculation of r2* [in mM-1s-1] in the liver results in a value of 483 compared to in vitro value of r2* = 47.0 ± 1.3. Conclusion: The use of 59Fe-labeled SPIO* offers a method for a direct quantification of signal changes caused by SPIO* via in vivo MR Relaxometry.

Presentation Number **0711B**

Poster Session 3c: In Vivo Studies & Development/Novel Use of Imaging Probes

Development of an animal model of pulmonary embolism for the evaluation of a new starch-based radiotracer for lung perfusion scintigraphy

Sidonie Jouaneton¹, Franck Lacoeyille^{1,2}, Francis Bouchet², Benoit Denizot³, Marie-Christine Rousselet⁴, Olivier Couturier^{1,2}, Jean-Pierre Benoit^{1,5}, Serge Askiénazy⁶, François Hindré¹, Jean-Jacques Le Jeune^{1,2}, ¹INSERM U646, IFR 132, University of Angers, 49100, France, Angers, France; ²Nuclear Medicine Department, Academic Hospital, Angers, 49933, France, Angers, France; ³Nuclear Medicine Department, Hospital of Annemasse-Bonneville, 74107, France, Annemasse-Bonneville, France; ⁴Cell and Tissue Pathology Department, Academic Hospital, Angers, 49933, France, Angers, France; ⁵Pharmacy Department, Academic Hospital, Angers, 49933, France, Angers, France; ⁶Laboratoires Cyclopharma., Biopôle Clermont-Limagne, France, Clermont-Limagne, France. Contact e-mail: franck.lacoeyille@univ-angers.fr

Objectives: New starch-based microparticles labeled with technetium-99m were developed and tested in vitro and in vivo on healthy animals. For further evaluation of the radiotracer we have developed an animal model of pulmonary embolism in rodent. This model was assessed by histopathological studies and scintigraphy. **Materials & Methods:** In order to induce a pulmonary embolism in Male Wistar Rat, 300µL of polyvinyl acetate (PVA) microspheres (300-500 µm) solution (Contour SE®) diluted in saline (1/10) were injected in penis vein. Following induction of pulmonary embolism, scintigraphic studies were performed using starch-based microparticles labeled with technetium-99m (15MBq). Acquisitions consisted in static anterior, posterior and oblique views realized either with parallel or pin-hole collimator. After 48 hours, animals were euthanized; their lungs were removed and fixed with a 4% paraformaldehyde. Lungs lobes were separated and treated with alcohol baths before paraffin fixation. Paraffin blocks were then cut with a rotary microtome in 5µm sections for microscopic analysis. **Results:** Histopathological analysis of the lung sections revealed the presence of vascular PVA microspheres surrounded by macrophages blocked in the small lung arteries. Despite evidence of pulmonary embolism no sign of necrosis was observed. Scintigraphic studies showed heterogeneous distribution of the starch-based microparticles, especially on anterior and posterior acquisitions, in adequacy with the pulmonary embolism revealed by histopathological analysis of the lung sections. **Conclusion:** We have successfully developed a model of pulmonary embolism on male Wistar rat. In pathological condition, new starch-based radiotracer succeeded to diagnose abnormal perfusion of the lung.

Presentation Number **0712B**

Poster Session 3c: In Vivo Studies & Development/Novel Use of Imaging Probes

Comparison of T2* relaxation changes and dynamic susceptibility contrast MRI in vivo at 3T with use of two different core-size SPIO

Nina Raabe¹, Evelyn Grabowski¹, Barbara Freund², Oliver T. Bruns³, Markus Heine⁴, Michael G. Kaul¹, Gerhard Adam¹, Harald Ittrich¹,
¹Department of Diagnostic and Interventional Radiology, University Medical Center Hamburg-Eppendorf, Hamburg, Germany;
²Department of Biochemistry and Molecular Biology II, University Medical Center Hamburg-Eppendorf, Hamburg, Germany; ³Heinrich-Pette-Institute for Experimental Virology and Immunology, University of Hamburg, Hamburg, Germany; ⁴Department of Anatomy II: Experimental Morphology, University Medical Center Hamburg-Eppendorf, Hamburg, Germany. Contact e-mail: ninaraabe@alice-dsl.net

Background: The purpose of our study was to compare $r2^*$ relaxometry and dynamic susceptibility contrast MRI (DSC-MRI) for estimation of SPIO concentration in tissue and dose optimization. Materials and methods: Superparamagnetic iron oxide nanoparticles (SPIO) with same anionic charged polymere coating but different core size (6 nm, 10 nm) were injected in mice ($n = 18$ and $n = 17$ including control mice) in five different concentrations (10, 25, 50, 75 and 100 $\mu\text{gFe}/100\mu\text{l}$ saline). DSC-MRI and quantitative T2* relaxometry were performed on a clinical 3T scanner using a small animal solenoid coil by measurement of SPIO distribution and uptake in liver, spleen, muscle and kidneys. T2* measurement were performed before and after DSC imaging (15 min, 2.9 s/measurement) followed by calculation of relative SNR changes (rSNR) and $\Delta R2^*$. Local tissue concentration of SPIO segmented area under (sAUC) (last 100 values of DSC) and $\Delta R2^*$ was calculated. $\Delta R2^*$ and sAUC were tested for statistical significance between the different SPIO and different dose groups (t-test). MR data of all tissues were matched with transmission electron microscopy (TEM) and histology (H&E, Prussian blue). Results: $\Delta R2^*$ calculations showed a significant uptake of 6 nm SPIO only in the liver for all concentrations, 10 nm SPIO only on 25 μg and above. Methodically measurable limit of relaxometry was reached at 50 μg for both particles. Core size had no significant influence on $\Delta R2^*$. DSC-MRI showed a perfusion peak in the vena cava and aorta, a first pass perfusion in kidneys, a blood pool effect in spleen and a final uptake of SPIO in liver and spleen for both particles. Comparison of sAUC and rSNR revealed a detection limit in liver above 50 μg (6 nm) but 75 μg (10 nm). rSNR and $\Delta R2^*$ showed a close correlation with injection doses. Uptake of SPIO in macrophages of liver (Kupffer cells) and spleen was proven by TEM and histology. Conclusion: Our study shows that both, MR relaxometry and DSC-MRI, should be used to evaluate SPIO distribution and uptake in tissues after application, but calculating the sAUC seems to be more sensitive. $\Delta R2^*$ seems to be a reliable parameter for estimation of SPIO tissue concentration. We conclude that in vivo MR characterization of SPIO properties is necessary for minimization of injection dosages and successful preclinical and future clinical applications, e.g. in targeted SPIO approaches.

Presentation Number **0713B**

Poster Session 3c: In Vivo Studies & Development/Novel Use of Imaging Probes

 ^{18}F -FP-PRGD₂ uptake tracks effect of drugs on murine ischemic infarcts

Edwin Chang^{1,2}, Evgenios Neofytou³, Shuanglong Liu¹, Patrick J. Wedgeworth², Xi Wang³, Ramin E. Beygui³, Xiaoyuan Chen⁴, Joseph C. Wu³, Sanjiv S. Gambhir¹, Zhen Cheng¹, ¹Radiology, MIPS, Stanford University, Palo Alto, CA, USA; ²Radiology, Canary Institute, Palo Alto, CA, USA; ³Medicine, Falk Cardiovascular Research Institute, Stanford, CA, USA; ⁴NIBIB, NIH, Bethesda, MD, USA. Contact e-mail: echangcv@stanford.edu

Ischemic myocardial infarction triggers collateral neovascularization which is driven by hypoxia inducible factor (HIF-1 α) and results in endothelial $\alpha_v\beta_3$ integrin stabilization. Thus, the integrin tracer, ^{18}F -FP-PRGD₂, may track ischemic wound healing via integrin expression of the infarcted and ischemic tissue. HIF-1 α -stabilizing drugs (deferioxamine or DFO) accelerate ischemia-driven wound healing and should reflect positive ^{18}F -FP-PRGD₂ uptake. To test, female FvB Mice (14-18 week, N=7 per experiment) were used. Infarcted areas were confirmed with triphenyl tetrazolium chloride. ^{18}F -FP-PRGD₂ uptake into infarcts was measured via small animal positron emission tomography (PET). Area (85-620 mm³) and intensity of uptake (%ID/g =0.15-1.67) were assessed up to 3 weeks post-operation. Hypoxia was examined by: ^{18}F -fluoroazomycin arabinoside (^{18}F -FAZA) and ^{18}F -fluoro-deoxy-glucose (^{18}F -FDG). ^{18}F -FP-PRGD₂ uptake was compared to immunofluorescent integrin expression. RESULT: LAD ligation produces infarcts with enhanced ^{18}F -FP-PRGD₂ uptake. This continued 30 days post-operation. Regions of high ^{18}F -FP-PRGD₂ uptake coincided with high ^{18}F -FAZA but low ^{18}F -FDG uptake. Total area of uptake peaked at around 9 days (~600 mm³) post-operation but declined afterwards, however, %IDmean/g and %IDmax/g still persisted (0.15 and 0.9 respectively). Intraperitoneal injections (every two days, 200mg/kg) of deferioxamine (DFO) accelerated decline of the infarcts (N=7 per cohort, P<0.02). But those same regions had significantly augmented %ID/g values compared to saline-injected controls (N=7 per cohort, P<0.05, %IDmean/g: 0.35 \pm 0.03 vs 0.65 \pm 0.05, Control vs DFO, Figure 1A-B). Positive ^{18}F -FP-PRGD₂ uptake corresponded to expression of the integrin $\alpha_v\beta_3$. Thus our studies show that tracking of ^{18}F -FP-PRGD₂ may reveal early assessment of MI-related drug efficacy.

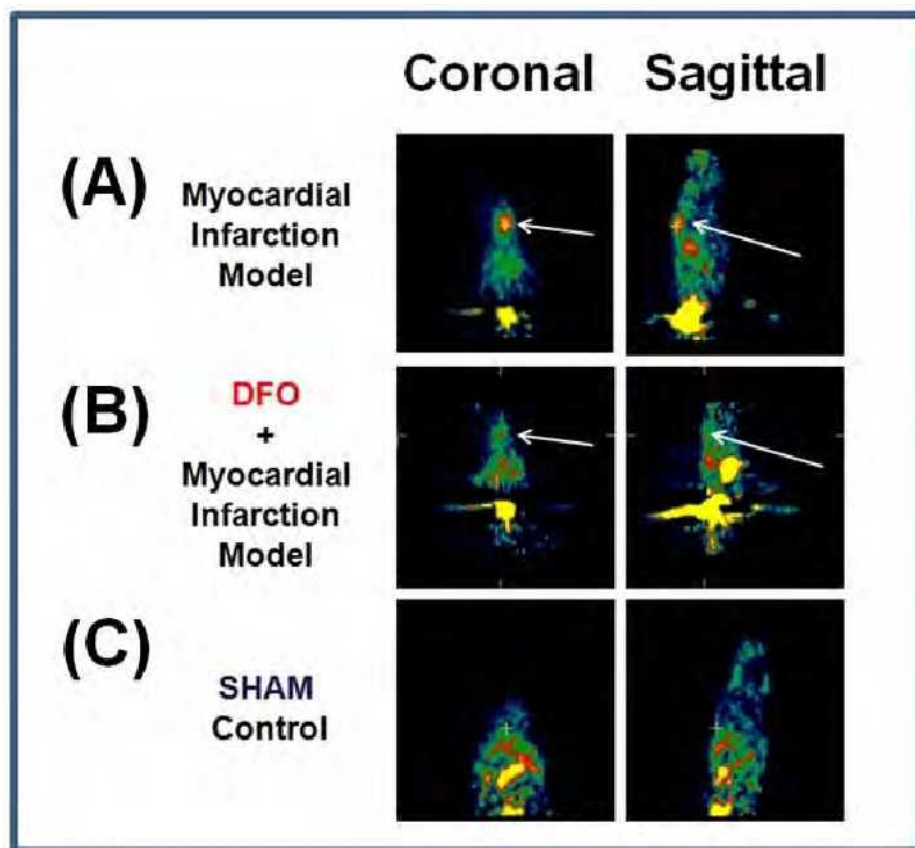


Figure 1: Small animal PET of Myocardial Infarction (MI) for (A) Saline, (B) DFO and (C) Sham treatment

Presentation Number **0714B**

Poster Session 3c: In Vivo Studies & Development/Novel Use of Imaging Probes

Evaluation of different imaging parameters for therapy response prediction and non-invasive quantification of tumor necrosis after transarterial embolization (TAE) in orthotopic rat hepatocellular carcinoma (HCC)

Rickmer Braren¹, Jennifer Altomonte², Yvonne Kosanke¹, Irene Esposito⁴, Neff Frauke⁴, Markus Schwaiger³, Ernst J. Rummeny¹, Oliver Ebert², Andreas Steingötter^{5,6}, ¹Institute for Radiology, Technical University Munich, Munich, Germany; ²Department of Internal Medicine, Technical University Munich, Munich, Germany; ³Department of Nuclear Medicine, Technical University Munich, Munich, Germany; ⁴Institute for Pathology, Technical University Munich, Munich, Germany; ⁵Institute for Biomedical Engineering, University and ETH Zurich, Zurich, Switzerland; ⁶Division of Gastroenterology, University Hospital Zurich, Zurich, Switzerland. Contact e-mail: rbraren@roe.med.tum.de

Objectives: The objectives of this study were (1) to integrate short-term multiparametric imaging in an orthotopic rat HCC tumor model and (2) to test the value of the individual imaging parameters tumor volume (VolMRI), apparent diffusion coefficient (ADC), permeability and perfusion (Ktrans), extracellular extravascular space (ve) and [¹⁸F]-FDG tracer uptake (FDGRatio) to predict response to TAE treatment and to serve as marker of induced necrosis. **Methods and Materials:** HCC bearing rats underwent serial imaging before and after (day -1, 1 and 3) TAE with degradable starch microspheres (DSM), receiving T2-weighted (T2w), DCE-MRI, DWI (1.5T Achieva, Philips) and [¹⁸F]-FDG-μPET (Inveon, Siemens). An affine image fusion algorithm was applied to MRI and PET imaging data. ROI based analyses of imaging data were performed. VolMRI was derived from manual segmentation of T2w images. ADC values were calculated from b value images (b20, b200, b600). Ktrans and ve were calculated from DCE-MRI data using open 2 compartment model. FDGRatio was calculated as tumor to muscle uptake ratio. Parameter values of each time point and of the relative changes were correlated with quantitative histological analysis. **Results and Conclusion:** Tumors were easily identified on MRI and PET derived images at each time point. DSM treatment resulted in a wide range of necrosis with remaining vital tumor (vTu) ranging from 0 to 96% and vital tissue (vTi = vTu + inflammatory tissue, connective tissue within tumor capsule) ranging from 5 to 98%. Multiparametric imaging of orthotopic rat HCC is feasible. pre VolMRI was the only predictive marker, indicating higher responsiveness in larger tumors. post2 ADC values showed highest sensitivity and specificity, respectively, of all tested parameters. Only for FDGRatio specificity was higher compared to sensitivity. Ktrans, ve and FDGRatio showed only moderate correlation with detected necrosis level.

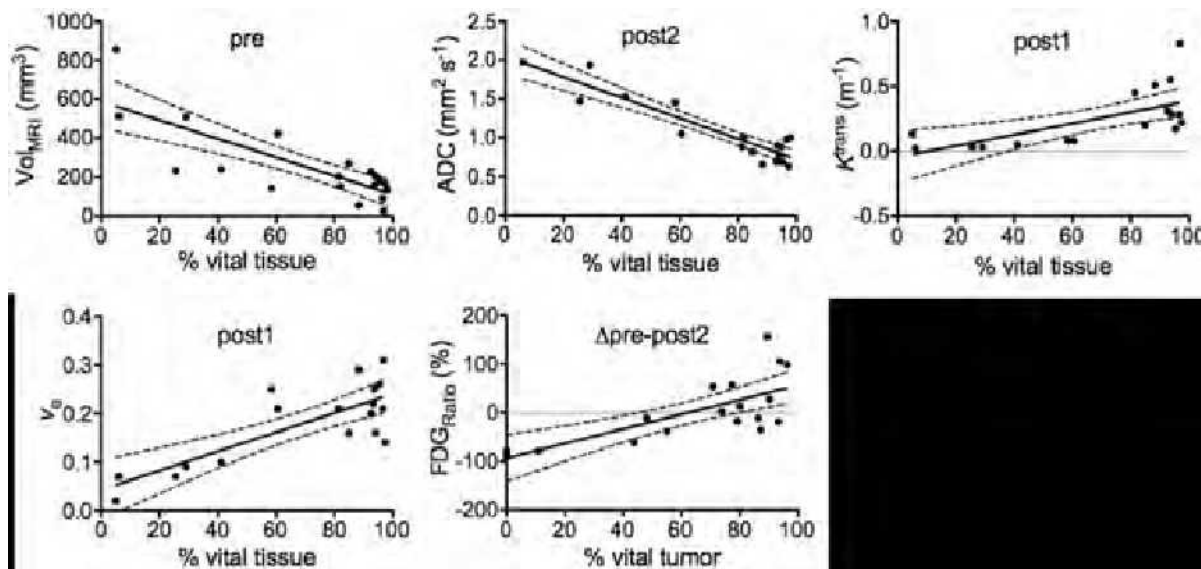


Figure 1: Linear regression plots of each parameter and histology. Only time point or interval of highest correlation r2 is shown for each parameter (VolMRI: 0.63, ADC: 0.86, Ktrans: 0.43, ve: 0.63, FDGRatio: 0.56)

Presentation Number **0715B**

Poster Session 3c: In Vivo Studies & Development/Novel Use of Imaging Probes

Dynamic observation of single spheroids from a malignant mesenchymal stromal cell with stemness properties: proliferation, migration and neoangiogenesis in vivo by vital microscopy and bioluminescence imaging in nude mice

Mengyu Wang, Gunnar Kvalheim, Department of Cellular Therapy, Oslo University Hospital, Oslo, Norway. Contact e-mail: meng@rr-research.no

Cancer cells with stemness characteristics have been found in many solid tumors including breast, brain, lung colorectal, melanoma, prostate, ovarian, and soft tissue. The cancer stem cells (CSC) have been defined in vitro for their surface markers expression and the gene profile but less is known how CSC grow, proliferate and migrate in vivo. We, therefore, used a transformed rat mesenchymal stem cells (Blood Abstract 2006 108. 4256) as CSC model for in vivo assays. TrMSC over-expressed TGF-beta and TGF-beta related proteins, such as bone morphogenetic protein. Based on these findings we concluded that the TrMSC bear some characteristics resembling tumor stem cells. (To further study the in vivo growth properties of the TrMSC, with special emphasis on migration and angiogenesis, we used a previously developed in-growth chamber model for vital microscopy in Balb/c nu/nu athymic nude mice (Falkvoll et al Exp.Cell.Biol. 52,1984). A unique 0,2 plastic chamber with two optical windows was implanted in a skin fold on the neck of the anesthetized mouse). The chamber was specially designed in thickness allowing only capillary blood vessels to grow into the chamber. A single TrMSC sphere with cells transduced with EGFP reporter gene was introduced into the chamber and the growth was studied by vital microscopy employing a fluorescence microscope equipped with a camera. As a control normal EGFP positive MSCs from the same animal was used. Twenty four hours after implantation the TrMSCs proliferated and migrated from the center of the sphere to the blood vessel area. At the same time the vessel started to increase in diameter and shape. After 48 hours the cells invaded the capillary blood vessel area resulting in a further enlargement of the existing vessels along with a significant formation of new vessels. When the normal MSC were tested in the same model no detectable migration and vessel formation could be detected during a 72 hour observation time. We conclude that vital microscope imaging of our malignant TrMSCs is a unique model for dynamic observations of cell proliferation, migration and angiogenesis. To assay real time imaging of TrMSCs growth pattern in vivo dual gene modified TrMSCs with Luc-eGFP are directly injected into left heart ventricle of nude mice. The animals developed metastasis in the lung; abdominal cavity; bone and skin. Data showed that 500 dual reporter marked Side Populating(SP+) cells, highly enriched of CSC, gave tumor growth in animals while 105 SP- cell was required to give tumor growth.

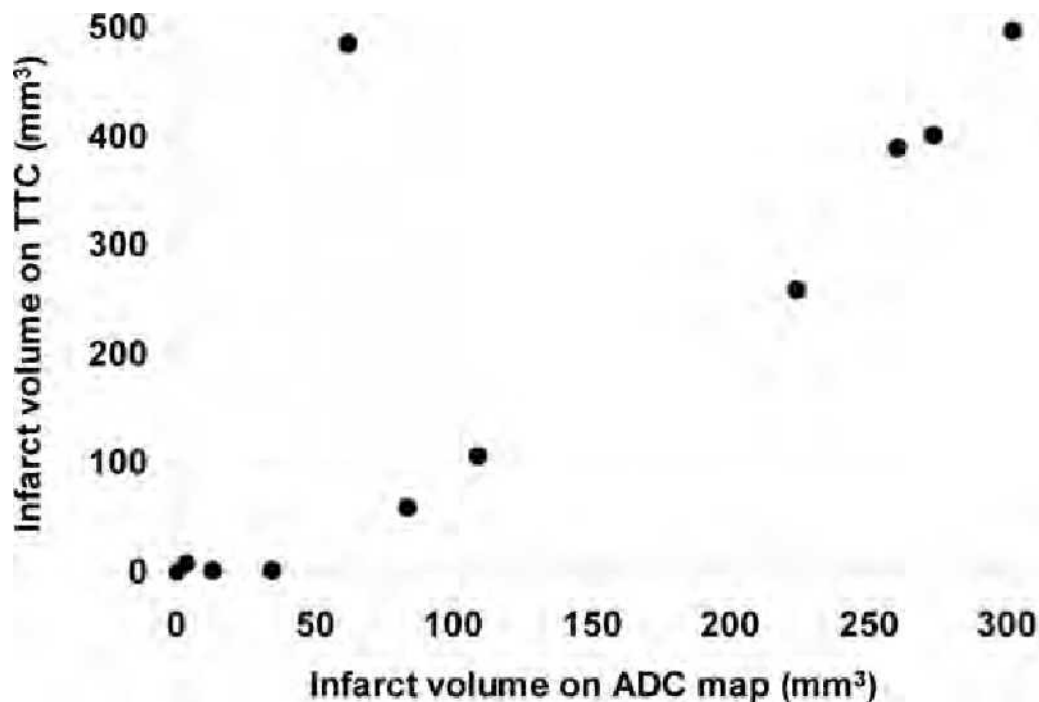
Presentation Number **0716B**

Poster Session 3c: In Vivo Studies & Development/Novel Use of Imaging Probes

Multiparametric MRI at the acute stage of ischemic stroke: improved subject selection for preclinical trials of neuroprotective drugs

Tae-Hee Cho¹, Fabien Chauveau¹, Adrien Riou¹, Jean-Baptiste Langlois², Yves Berthezène¹, Norbert Nighoghossian¹, Marlène Wiat¹, ¹Cerebral Imaging team, CREATIS - CNRS UMR 5220 - INSERM U630 - University Lyon 1 - INSA Lyon, BRON, France; ²CERMEP-Animage, Lyon, France, LYON, France. Contact e-mail: chauveau@creatis.insa-lyon.fr

Background and purpose Models of intraluminal middle cerebral artery occlusion (MCAO) are known to present an intrinsic variability in infarct size, which is a potential confounding factor in drug-testing studies. In this study, we sought to assess whether multiparametric MRI performed during the occlusion was more effective than behavioral examination to include successfully operated rats for experimental assessment of neuroprotective drugs. **Methods** All animals (including sham-operated ones) were tested back-to-back with behavioral assessment (using a 0-20 neuroscore) and MRI (including Magnetic Resonance Angiography, Diffusion-Weighted Imaging and Dynamic Susceptibility Contrast-enhanced Perfusion-Weighted Imaging), both performed during the two hours of middle cerebral artery occlusion using the intraluminal suture model in rats. Twenty-four hours after reperfusion, animals were re-submitted to behavioural tests and sacrificed. Final infarct volume was measured on TTC staining of brain tissue. **Results** Final TTC infarct volume strongly correlated with acute ADC lesion volume ($r^2=0.61$, $p<0.05$, Fig. 1) and with behavioral assessment performed 24 hours after reperfusion ($r^2=0.92$, $p<0.05$). On the other hand, no significant correlation was found between behavioral examination performed during arterial occlusion and respectively final infarct ($r^2=0.29$, $p=0.09$), ADC lesion volume ($r^2=0.38$, $p=0.05$) or hypoperfusion volume ($r^2=0.42$, $p=0.08$). **Conclusions** In conclusion, unlike behavioral testing, the presence of a cortico-striatal lesion on DWI appears to be a valid inclusion criterion for preclinical trials of stroke therapies.



Presentation Number **0717B**

Poster Session 3c: In Vivo Studies & Development/Novel Use of Imaging Probes

Non-invasive In Vivo Monitoring of Bone Metastasis in Mouse Models Using CT, PET, and Optical Imaging

Deanne Lister, Michael Woolliscroft, Vinod Kaimal, **Patrick McConville**, Discovery and Imaging Services, Charles River Laboratories, Ann Arbor, MI, USA. Contact e-mail: patrick@molecularimaging.com

The ability to visualize and quantify early stages of bone involvement in mouse models of bone metastasis would provide a platform for development of new agents targeted at inhibition or treatment of bone metastases. While μ CT imaging provides a semi-quantitative assessment of bone erosion and bioluminescence imaging using luciferase expressing tumor lines enables monitoring of tumor burden, there is a need to track bone lesion progression as well. Two approaches enabling this are optical imaging using biphosphonate fluorescent probes such as Osteosense 750 and ^{18}F -NaF PET imaging; both target hydroxyapatite (HA), a biomarker for osteoblastic activity. In this work, MDA-MB-231-luc-D3H2LN human mammary adenocarcinoma cells were injected into the left ventricle of female nu/nu mice. Bioluminescence scans were used to determine successful injections by distribution of light throughout the bodies. All mice were imaged using bioluminescence and enrolled on study based on incidence of signals at bone sites. Subsequent serial bioluminescence images were used to determine incidence and monitor growth of bone metastases. μ CT was used to qualitatively assess the extent of bone lesions associated with the metastases. Serial whole body PET scans and fluorescence images were used to characterize HA activity. Both ^{18}F -NaF PET imaging and fluorescent imaging using highlighted localized bone signals that could be correlated with bioluminescent measurement of tumor burden and μ CT visualized bone lesions. Bioluminescence imaging showed the greatest sensitivity to disease progression. The PET and fluorescence imaging approaches showed progressive bone involvement, presumably through HA, indicating osteoblastic bone disease progression. The combination of PET and fluorescent imaging of bone remodeling mechanisms coupled with bioluminescent imaging of tumor growth enables a non-invasive, quantifiable method for tracking early bone disease progression which may facilitate development of novel agents for inhibition of tumor growth and/or bone lesion progression.

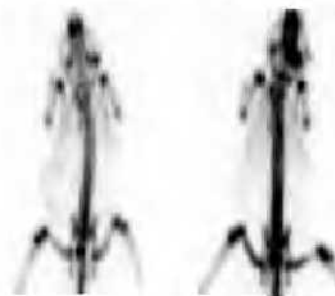
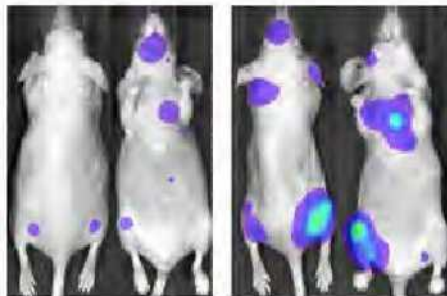
Bioluminescence Imaging 18F-NaF PET Imaging

Day 19

Day 35

Day 22

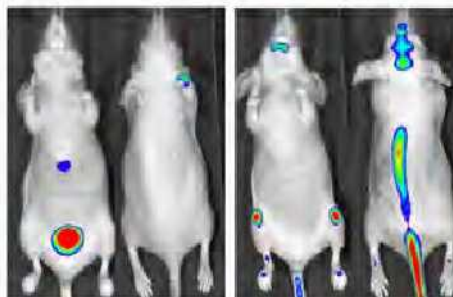
Day 36



Osteosense 750 Imaging

Day 23

Day 36



CT Imaging

Disease Progression
Early Mid Advanced



Presentation Number **0718B**

Poster Session 4c: In Vivo Studies & Development/Novel Use of Imaging Probes

Changes in Cardiac Deformation during the Development of Cardiac Hypertrophy Using microPET imaging

Alexander Veress^{1,2}, **Hilla Wahnische**^{3,4}, **Youngho Seo**⁴, **James P. O'Neil**³, **Mustafa Janabi**³, **Kathleen M. Brennan**³, **Henry F. VanBrocklin**^{3,4}, **Grant T. Gullberg**^{3,4}, ¹Mechanical Engineering, University of Washington, Seattle, WA, USA; ²Department of Bioengineering, University of Washington, Seattle, WA, USA; ³Radiotracer Development & Imaging Technology, Lawrence Berkeley National Laboratory, Berkeley, CA, USA; ⁴Radiology, University of California San Francisco, San Francisco, CA, USA. Contact e-mail: averess@u.washington.edu

The goal of this project is to document the temporal changes in function due to hypertension up to and including heart failure. The work involves molecular imaging of the spontaneous hypertensive rat (SHR) as a model of hypertensive related pathophysiology, utilizing a microPET scanner and analyzing the images with Hyperelastic Warping to quantify the changes in deformation as a function of hypertrophy and age. Methods: Normotensive Wistar Kyoto rats (WKY) and SHR rats were imaged using the microPET/CT Inveon scanner (Siemens). Dynamic gated list mode data of approximately 2 - 2.5 million counts were acquired over 60 mins immediately after injecting 1-1.5 mCi of F-18-fluorodihydrorotenol. The data were reconstructed into 8 separate gates of 3D images. Hyperelastic Warping was conducted on the image data sets from end-systole to end-diastole to document changes in diastolic filling. Results: The image analyses indicated that there were differences in the average LV strains in the first and second imaging points. The SHR rats had higher average strains compared with the normal controls. However by the third image acquisition this had changed, the WKY rats had statistically significantly higher average first principal strain values compared with the SHR subjects ($p < 0.01$) indicating that the SHR subjects LV function had decreased. This was confirmed by the deaths within three weeks of this acquisition of two of the SHR subjects. These rats had died of complications associated with heart failure and exhibited pulmonary edema as well as enlarged livers. Conclusion: The change in LV function determined by Hyperelastic Warping documented the decompensation phase associated with end-stage hypertension and heart failure. The first principal strains suggested that the change in LV function likely occurs in advance of the weight loss and other symptoms associated with heart failure. It may show some predictive value in the determination of the onset of symptoms.

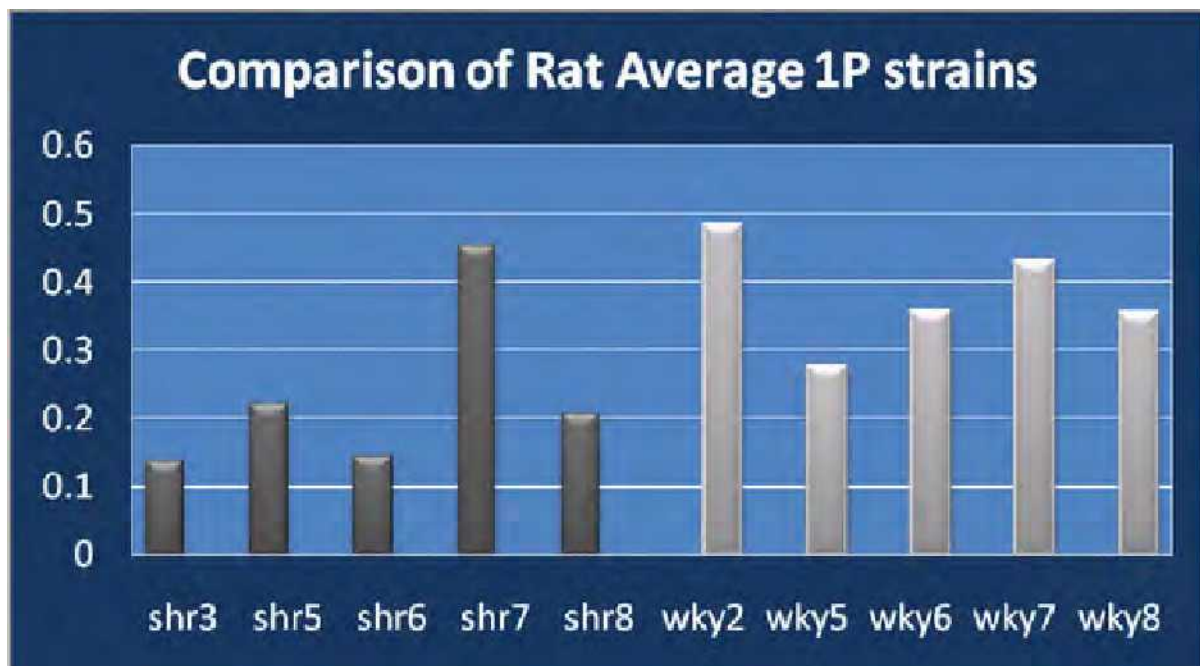


Figure 1: Comparison of first principal strains indicate that the SHR subjects had lower average strain values than the WKY controls. The difference is statistically significant ($p < 0.01$). The SHR and WKY subjects were 16 months in age.

Presentation Number **0719B**

Poster Session 4c: In Vivo Studies & Development/Novel Use of Imaging Probes

***In vivo* tracking of ferritin over-expressing human neural progenitor cells in rodent CNS**

Ksenija Bernau^{1,2}, **Jered V. McGivern**³, **Brandon C. Shelley**⁴, **Allison D. Ebert**³, **Ian J. Rowland**¹, **Genevieve Gowing**⁴, **Bernard L. Schneider**⁵, **Masatoshi Suzuki**⁶, **Mary E. Meyerand**¹, **Clive N. Svendsen**⁴, ¹Medical Physics, University of Wisconsin - Madison, Madison, WI, USA; ²Biomedical Engineering, University of Wisconsin - Madison, Madison, WI, USA; ³Neurology, University of Wisconsin - Madison, Madison, WI, USA; ⁴Regenerative Medicine Institute, Cedars-Sinai Medical Center, Los Angeles, CA, USA; ⁵Brain Mind Institute, EPFL, CH-1015 Lausanne, Switzerland; ⁶Comparative Biosciences, University of Wisconsin - Madison, Madison, WI, USA. Contact e-mail: kbujanovic@wisc.edu

Amyotrophic lateral sclerosis (ALS) is a neurodegenerative disease manifested through the deterioration and loss of function of motor neurons in the spinal cord and brain stem. While drug treatments have shown moderate inhibition of the disorder, stem cell therapy, such as using human neural progenitor cells (hNPC), has become increasingly attractive for treatment of this disease. Still, one of the major roadblocks in these efforts arises from the dynamic nature of hNPC proving it hard to predict their homing *in vivo*. Therefore, having the ability to track hNPC in the central nervous system would allow researchers to better monitor cell behavior once transplanted. So far, superparamagnetic iron oxide (SPIO) has been the gold standard for tracking cells *in vivo* using magnetic resonance imaging (MRI). While this method provides high signal strength, it decays significantly within one month, making long term tracking difficult. For this reason, we have explored over-expression of ferritin, an intracellular iron-storage protein, which by binding endogenous iron molecules allows for detection of hNPC using MRI. We show here that hNPC can be visualized via MRI *in vitro* and *in vivo* following transient transfection of ferritin. As a proof of concept, we transplanted 6×10^5 hNPC transiently transfected with ferritin by nucleofection unilaterally into the striatum of adult rats. As a positive control, we injected SPIO incubated hNPC into the contralateral striatum of the same rats. Using a T2* weighted gradient echo MRI sequence, we detected ferritin-bound iron from the transplanted cells in the striatum of adult rats 24hrs post-transplantation, as well as SPIO incubated cells in the contralateral striatum. In confirmation of the *in vivo* data, *in vitro* protein expression was found to decrease from approximately 90% on the day following transfection to less than 20% ten days later due to its transient expression. Therefore, since this proof of concept held a theoretical value, we can proceed with methods inducing stable over-expression (e.g. viral transduction) in hNPC. This would permit evaluation of long-term tracking of transplanted cells and the effects of continual production of ferritin on hNPC and surrounding tissues *in vivo*. Since MRI provides high resolution but relatively low sensitivity, we are also exploring the sensitivity benefits of optical imaging by over-expressing luciferase in hNPC. Altogether, these studies may be expanded by using different cell lines and may have important clinical applications for ALS and other neurodegenerative disorders.

Presentation Number **0720B**

Poster Session 4c: In Vivo Studies & Development/Novel Use of Imaging Probes

15O-H2O PET and 99Tc-HMPAO SPECT demonstrate a compensatory increase in cerebral perfusion after experimental cerebral ischemia in rats

Abraham Martin^{1,2}, **Raphael Boisgard**^{1,2}, **Benoit Theze**^{1,2}, **Philippe Gervais**², **Catherine Vuilleumard**², **Bertrand Tavitian**^{1,2}, ¹CEA, DSV, I2BM, SHFJ, Orsay, France; ²Inserm, U1023 ; Université Paris Sud, Orsay, France. Contact e-mail: abraham.martin-munoz@cea.fr

Introduction: Brain activity is highly dependent on blood supply and interruption of blood flow during stroke leads to a loss of the function ensured by the cerebral region undergoing ischemia. To a certain extent, brain plasticity may allow functional recovery, through compensatory mechanisms that have been correlated with biological processes such as compensatory growth of blood vessels to supply metabolic demand, inflammation and angiogenesis. Here, we explored the changes in cerebral blood flow after experimental ischemic stroke in rats using PET and SPECT. Methods: PET imaging with [15O]-H₂O and SPECT imaging with [99mTc]-HMPAO were performed during, and immediately (reperfusion) and 1, 2, 4 and 7 days after a 2-hour transient middle cerebral artery occlusion (tMCAO) in rats. All animals (n≥5 per each time point) underwent both PET and SPECT; [15O]-H₂O and [99mTc] HMPAO radioactivity concentrations were correlated (r²=0.7218). Results: In the cerebral territory irrigated by the MCA, both PET and SPECT demonstrated a significant decrease (ca. 50%) of the signal during occlusion with respect to signals in the normal cerebral tissue. This was followed by a return to quasi-normal values during early reperfusion, after what signals dropped to 60% of control at day 1 and then rose steadily, reaching control values around day 2-4, and overshooting to twice the control values at day 7. This suggests a late compensatory increased perfusion in the ischemic area. Surprisingly, the same camel-shaped time course was observed in the contralateral, non-ischemic area, i.e. reduced during occlusion, returning to normal during reperfusion, dropping again at day 1 and increasing thereafter with an overshoot at day 7. As a result, the ratio of PET and SPECT signals in the ischemic to contralateral areas varied from .5 at occlusion to 1.0 at day 4-7. Conclusion: Cerebral blood flow/perfusion after experimental stroke follows a triphasic time course: reduction during occlusion, normal in early reperfusion, reduced at day 1 and rising steadily thereafter. One week after ischemia, both [15O]-H₂O and [99mT]-HMPAO evidence hyperperfusion over the whole brain, including non ischemic areas, likely reflecting the importance of increased blood supply as a compensatory mechanism after cerebral ischemia.

Presentation Number **0721B**

Poster Session 4c: In Vivo Studies & Development/Novel Use of Imaging Probes

Effect of the Cellular Irradiation on Neuro-behavior of Mice after Acute Exposure

Neeraj Kumar^{1,2}, *Rajnish K. Chaturvedi*², *Raees A. Khan*¹, ¹*SIST-DIT, Babasaheb Bhimrao Ambedkar University, Lucknow, India;*
²*DTD, Indian Institute of Toxicology Research, Lucknow, India. Contact e-mail: neerajmtech@gmail.com*

Extension of the mobile phone technology raises concern about the implications of electromagnetic radiation (EMR) on the central nervous system (CNS). Children are more sensitive to EMR due to developing phase of their brain. Generally Mobile phone radiates an average power of 0.2-0.6 watts when hand-held and operated close to the head, background levels are sharply distorted, with likely 40-50 percent of radiated phone energy absorbed into the brain. Our previous study has concluded that the extensive users, they hold cell phone for a period above 3 years, were more attentive for 'headache' symptom in comparison to normal users. In this study we assessed the spontaneous locomotors activity (SLA) of the mice after the acute exposure of cellular telephone (CDMA). 10 mice of the 30 days old (average weight 30gm) were grouped as control and EMR and they were habituated for one week prior to start the experiment in well designed circular cellphone exposure (CCPE) cage. CCPE cage was specially designed for EMR exposure through the cellular phone over the mice in the natural environment and it was placed inside the exposure room where no electric appliances were exist. In the cage, cellular phone was placed in the center and mice were allowed to move around the device within 10 cm. radius. 3 hours/day exposure was applied to the mice of EMR group by the cellular phone in CCPE cage. Locomotor activity was assessed using computerized Optovarimax animal activity monitor, following the method Ali et. al., (1990). In this study Distance traveled, Time resting, Time moving and Stereotypic Time was measured with the help of the activity monitor. No significant changes were found in the EMR exposed mice in comparison of control mice. More laboratory research is essential to clarify the contradictions

Presentation Number **0722B**

Poster Session 4c: In Vivo Studies & Development/Novel Use of Imaging Probes

The multimodal imaging strategy of mesenchymal Stem Cell trafficking for tumor cells

Yeona Jin^{1,2}, **Do Won Hwang**^{1,3}, **Hyewon Youn**^{1,4}, **Dong Soo Lee**^{1,5}, ¹*Department of Nuclear Medicine and Cancer Research Institute, Seoul National University College of Medicine, Seoul, Republic of Korea;* ²*Interdisciplinary Course of Radiation Applied Life Science, Seoul National University College of Medicine, Seoul, Republic of Korea;* ³*Institute of Radiation Medicine, Medical Research Center, Seoul National University College of Medicine, Seoul, Republic of Korea;* ⁴*Laboratory of Molecular Imaging and Therapy, Cancer Research Institute, Seoul National University College of Medicine, Seoul, Republic of Korea;* ⁵*Department of Molecular Medicine and Biopharmaceutical Science, WCU Graduate School of Convergence Science and Technology, Seoul National University College of Medicine, Seoul, Republic of Korea. Contact e-mail: zizzizlove@nate.com*

Purpose: Many studies have reported that stem cells have tropism effect to tumor cells, which can be a possible candidate as a tumor targeting vehicle for the cancer therapy. In this study, we developed a multimodal nanoparticle-carried stem cell system for monitoring stem cell trafficking to the brain tumor. **Methods:** U87MG glioma cells and mouse mesenchymal stem cells (mMSC) were used to visualize the tropism of mMSC in vivo. A retroviral gene transfer system was used for labeling mMSC with a luciferase reporter gene, named by mMSC-Effluc. Silica coated magnetic fluorescence (MF) nanoparticles were treated in the mMSC-Effluc cells for the acquisition of multimodal images. U87MG cells were implanted in mouse brain at a specific coordinate with Stereotaxic frame. Xenografted glioma cell population was examined by magnetic resonance image (MRI) imaging system. **Results:** Luciferase-expressing MSC cells (MSC-Effluc) was isolated by FACS sorter after retroviral transduction, showing gradual increase pattern of luciferase signal in cell number dependent manner. MSC-Effluc transferred with magnetic fluorescence nanoparticle showed that both fluorescence and MR signal were found as the increased concentration of MF nanoparticle. Significant MR contrast signal in the tumor area was clearly observed 7 days after injection. **Conclusion:** This study suggested the possibility for nanoparticle-based multimodal trafficking system of stem cells to the brain tumors. We expect that this technique could be applied for a potential cancer therapy using drug-loaded stem cells as a delivery carrier in the near future.

Presentation Number **0723B**

Poster Session 4c: In Vivo Studies & Development/Novel Use of Imaging Probes

Time-Volume Imaging of Brain Cells and Microcirculation Plasticity with Two-Photon Microscopy

Kazuto Masamoto^{1,2}, **Hiroyuki Takuwa**², **Hiroshi Kawaguchi**², **Takayuki Obata**², **Iwao Kanno**², ¹*Center for Frontier Science and Engineering, University of Electro-Communications, Chofu, Japan;* ²*Molecular Imaging Center, National Institute of Radiological Sciences, Chiba, Japan. Contact e-mail: masamoto@mce.uec.ac.jp*

Introduction: Repeated longitudinal imaging of cellular activity and cerebral microcirculation would provide valuable information on physiologic mechanism of metabolic-vascular plasticity and pathogenesis of neurodegenerative disorder. The present study aimed to visualize structural and functional plasticity of brain cells and microcirculation in mouse cerebral cortex. **Methods:** Animal use and experimental protocols were approved by the Institutional Animal Care and Use Committee. Male C57BL/6J mice (20-30 g) were anesthetized with isoflurane (2-3%), and a custom-made attachment device was fixed on the skull. Craniotomy was performed over the somatosensory area, and astroglial cells and microvessels were fluorescently labeled with intraperitoneal injection (0.1 ml) of sulforhodamine 101 (SR 101) that was preliminarily dissolved in physiologic saline (5-10 mM). Two-photon microscope (TCS SP5 MP, Leica Microsystems) equipped with titanium-sapphire laser (Mai Tai HP, Spectra-Physics) was used to obtain volume images of brain cells and microcirculation concurrently. Time-lapse tomographic imaging was performed every 5 to 30 minutes until 8 hours from when the dye was injected. After all measurements were completed, the animal was allowed to recover from anesthesia, and the experiments were repeatedly performed over multiple days. **Results and Discussion:** Soon after intraperitoneal injection of SR 101, a bright signal appeared at a vascular area in the image obtained at somatosensory cortex. The signal intensity of vessels increased over time and a strong contrast between intra- and extra-vascular spaces was resolved. In small vessels, a typical strip of red blood cell flow in inside of the vessel was also detected. The labeled astroglial cell was identifiable after one hour from the injection. Also, imprint of neural cells was observed as unlabeled dark spots in the extravascular tissue area. Our results of the repeated longitudinal time-volume imaging revealed plasticity changes in neuro-glial structure and microvascular networks. These results demonstrate the capability of time-volume imaging of brain cells and microcirculation for health and disease model animals.

Presentation Number **0724B**

Poster Session 4c: In Vivo Studies & Development/Novel Use of Imaging Probes

In vivo imaging of transplanted mesenchymal stem cells in pancreatectomized mouse model

Song Lee^{1,2}, **Do Won Hwang**^{1,2}, **Hyewon Youn**^{1,3}, **Dong Soo Lee**^{1,4}, ¹*Nuclear Medicine, Seoul National University College of Medicine, Seoul, Republic of Korea;* ²*Radiation Medicine, Medical Research Center, Seoul National University, Seoul, Republic of Korea;* ³*Laboratory of Molecular Imaging and Therapy, Cancer Research, Seoul National University, Seoul, Republic of Korea;* ⁴*Molecular Medicine and Biopharmaceutical Science, WCU Graduate school of Convergence science and Technology, Seoul National University, Seoul, Republic of Korea. Contact e-mail: ssong277@hanmail.net*

Objectives: The non-invasive tracking of engrafted stem cells in disease model plays an important role in figuring out survival time and pattern of engrafted stem cells repetitively in vivo. We monitored enhanced luciferase expressing mesenchymal stem cells (mMSCs-effLuc) in partial pancreatectomized nude mouse in order to chase survival pattern in terms of stem cell-based therapy. **Methods:** We obtained primary mouse bone marrow-derived mMSCs and established luciferase expressing stable MSCs cells (mMSCs-effLuc) by retroviral infection. Mixture of mMSCs-effLuc and matrigel was directly injected to remained pancreas of partial pancreatectomized (PPx) nude mice for monitoring the effect of transplanted mMSCs on the recovery of glycometabolism. In vivo bioluminescence activity was conducted using IVIS optical imaging device. The glycometabolism by intraperitoneal glucose tolerance test (IPGTT) and fasting glucose levels was examined for functional analysis. We also confirmed morphological change of pancreas and detected transplanted mMSCs-effLuc by immunofluorescence. **Results:** In vivo bioluminescence imagings of the grafted mMSCs-effLuc were continually monitored during pancreas regeneration till day 28. This imaging was detected in only grafted mMSC-effLuc of pancreas. Grafted mMSCs-effLuc was stained with immunofluoresce by anti-luciferase in regenerating pancreatic tissue at day 6 and day 28. Mice having transplanted mMSCs-effLuc showed a moderate glucose tolerance levels than only PPx mouse models at day 3 and day 6 post-PPx. **Conclusions:** Our results showed long term monitoring of grafted mesenchymal stem cells in pancreatectomized model to survival pattern in vivo. These studies indicate that transplanted mMSC-effLuc survived and might led normal glycometabolism.

Presentation Number **0725B**

Poster Session 4c: In Vivo Studies & Development/Novel Use of Imaging Probes

Improved *in vivo* Tumor Visualization using Novel ^{99m}Tc-Carrying Liposomes in Mice

Izumi O. Umeda¹, **Mayumi Ogata**^{1,2}, **Emi Kaneko**², **Keisuke Tsuda**¹, **Tomoya Uehara**², **Kunikazu Moribe**², **Masayuki Yamaguchi**¹, **Yasushi Arano**², **Keiji Yamamoto**², **Hirofumi Fujii**¹, ¹Functional Imaging Division, National Cancer Center East, Kashiwa, Japan; ²Graduate School of Pharmaceutical Sciences, Chiba University, Chiba, Japan. Contact e-mail: ioumeda@east.ncc.go.jp

Objectives: Radiolabeled liposomes are promising radiopharmaceuticals for tumor imaging and radionuclide therapy because of their high affinity to tumors. But, conventional liposomes also accumulate in reticuloendothelial systems (RES), such as liver and spleen, even though they are PEGylated. This has hindered their clinical application. The aim of this study was to produce novel ^{99m}Tc-carrying liposomes that are expected to bring about rapid clearance of radionuclide from RES. For this purpose, we investigated a method to encapsulate ^{99m}Tc-ethylenedicycysteine (EC) in liposomes with high efficiency. **Methods:** Liposomes were composed of DSPC and cholesterol. First, ^{99m}Tc was chelated to N-[2(1H-pyrolylmethyl)]-N'-(4-pentene-3-one-2) ethane-1, 2- diamine (MRP20), a lipophilic chelating ligand. Then, ^{99m}Tc was transported from outside to inside of liposomes by transchelation between MRP20 and EC. Biodistribution of obtained ^{99m}Tc-EC liposomes in sarcoma-180-bearing ddY mice were studied, comparing to conventional liposomes encapsulating ¹¹¹In-nitritoltriacetic acid (NTA). *In vivo* images were acquired using a small animal SPECT/CT scanner (Bioscan). **Results:** Formation of ^{99m}Tc-MRP20 complexes and undesired byproducts highly depended on MRP20 and SnCl₂ concentrations. Under the optimal condition, labeling efficiency of liposomes with ^{99m}Tc using transchelation between MRP20 and EC reached 74.1 %, and HPLC analysis confirmed that all of ^{99m}Tc inside liposome was combined with EC. ^{99m}Tc-EC liposomes showed similar distribution to ¹¹¹In -NTA liposomes until 6 hrs after the intravenous injection. After that, ^{99m}Tc-EC was rapidly washed out from liver (2.8 %injected dose/g at 24hrs) and spleen (13.1 %/g) while good retention was shown in the tumor (4.8%/g). On the contrary, ¹¹¹In remained in liver (12.3%/g) and spleen (33.5%/g) as well as tumor (11.5%/g). *In vivo* SPECT imaging at 24hrs after the injection successfully visualized these different biodistribution. ^{99m}Tc-EC liposomes well depicted tumors with low uptake of liver and spleen while ¹¹¹In -NTA liposomes failed to selectively image tumors due to high uptake of liver and spleen. **Conclusions:** ^{99m}Tc-EC carrying liposomes could be produced with high efficiency. It could be excellent tumor imaging agents because they selectively accumulate in tumors with low RES uptake. Radionuclide therapy using ^{186/188}Re-EC liposomes would be also promising.

Presentation Number **0726B**

Poster Session 4c: In Vivo Studies & Development/Novel Use of Imaging Probes

Assessment of therapeutic effect of sunitinib to renal cell carcinoma using animal model

Yoko Hasegawa¹, **NOBUYUKI OYAMA**¹, **Noriko Takahara**¹, **Yoshiji Miwa**¹, **Hironobu Akino**¹, **Yasushi Kiyono**², **Yasuhisa Fujibayashi**³, **Osamu Yokoyama**¹, ¹*Urology, University of Fukui, Eiheiji, Japan;* ²*Biomedical Imaging Research Center, University of Fukui, Eiheiji, Japan;* ³*Molecular Imaging Center, National Institute of Radiological Sciences, Chiba, Japan. Contact e-mail: uromory@u-fukui.ac.jp*

Objectives: Monitoring the early therapeutic effect of sunitinib, a multi-targeted receptor tyrosine kinase inhibitor, in renal cell carcinoma (RCC) is important for better managing of cancer patients. This study was undertaken to determine whether 18F-Fluorothymidine (FLT) is useful for early response assessment in RCC following sunitinib therapy using in vivo biodistribution studies and animal PET of tumor-bearing mice. **Method:** ACHN tumor a well established human RCC cell line, was implanted in athymic male mice. Approximately 4 weeks after tumor implant, the mice were treated with oral sunitinib once daily (sunitinib group) or vehicle only (control group), and tumor volume was calculated. After the treatment, FLT was administered via tail vein and tracer uptake was determined in selected tissues at 1h after injection. To establish the non-invasive assessment of FLT uptake in those mice, animal PET imaging was also performed. The tumors were immunohistochemically assayed for proliferation (PCNA), vascular density (CD34) and apoptosis (TUNEL). Thymidine kinase 1 (TK1) expression of the tumors was also determined with real-time RT-PCR simultaneously. All these parameters of the two groups were compared. **Results:** There was a significant increase of implanted tumors in control group, while there was a minimal change of the tumors in sunitinib group. The biodistribution study showed a marked reduction of FLT uptake in tumors after 5-day-treatment with sunitinib. The tumors could be visualized clearly by FLT animal PET. Animal PET showed the same tendency of biodistribution study. Immunohistochemical analysis of the tumors revealed that the changes of FLT uptake were well correlated with those of proliferation, apoptotic status and vascular density. TK1 expression of the tumors was also correlated with FLT uptake. **Conclusions:** These results of in vivo studies indicate that FLT is a promising tracer in monitoring early therapeutic effects of sunitinib to renal cell carcinoma. 18F-FLT PET imaging may have a potential to visualize early-phase changes in proliferation activity of renal cell carcinoma after sunitinib therapy.

Presentation Number **0727B**

Poster Session 4c: In Vivo Studies & Development/Novel Use of Imaging Probes

ON-LINE VISUALIZATION OF SYNOVIAL MICROCIRCULATORY EVENTS IN NEUTROPHIL LEUKOCYTE-DEPENDENT ACUTE ARTHRITIS IN RATS

Petra Hartmann, Andrea Szabo, Mihaly Boros, Institute of Surgical Research, University of Szeged, Szeged, Hungary. Contact e-mail: boros@expsur.szote.u-szeged.hu

Examinations involving intravital microscopy (IVM) have clearly revealed that the polymorphonuclear leukocytes (PMNs) are the first major cell population recruited to the tissues during the early phase of inflammation. Our primary aim was to develop a standardized rodent model of PMN-driven monoarthritis in order to achieve a precise characterization of the intravital reactions in the synovial membrane. It should be noted that previous research protocols did not allow an assessment of inflammatory reactions in the synovial membrane itself, but only in the surrounding Hoffa's fatty body, an intraarticular fatty tissue containing synovial cells on the interior surface of the joint. In this model, arthritis was induced by injection of a mixture of 2% λ -carrageenan and 4% kaolin into the knee joints, and then we set out to characterize PMN-associated dynamic alterations in the synovium to ascertain the anti-inflammatory properties of different compounds commonly used to treat knee joint inflammation. Male Wistar rats were treated orally with phosphatidylcholine (150 mg kg⁻¹ twice daily), sodium diclofenac (0.5 mg kg⁻¹ twice daily) or saline vehicle. The synovial membrane over the medial condyle of the proximal tibia was exposed with an atraumatic surgical technique, and fluorescence IVM was used to investigate the leukocyte-endothelial interactions (rolling and sticking, by Rhodamine 6G staining) and microhemodynamics (red blood cell velocity (RBCV) by FITC-labeled erythrocytes) in the postcapillary venules at 6 h after the challenge. The development of arthritis (as evidenced by the significant decrease (45%) in the thermal nociceptive latency, the 3-fold increase in the mechanical touch sensitivity and the 35% increase in the knee cross-sectional area) was accompanied by a significant increase in the number of adherent PMNs in the synovial postcapillary venules. Although the PMN-endothelial interactions were notably enhanced, the baseline RBCV was not augmented further by local inflammation. The increased PMN adherence was reduced significantly (40%) by PC, and slightly (by 22%) by diclofenac treatment. In conclusion, the methodology here allowed direct visualization of the microcirculation of the synovial membrane. The anti-inflammatory treatments did not affect the red blood cell velocities at the microcirculatory level, and hence the effects of PC on the PMN-endothelial interactions do not seem to be based on microhemodynamic differences, but rather on adhesion molecule expressions.

Presentation Number **0728B**

Poster Session 4c: In Vivo Studies & Development/Novel Use of Imaging Probes

MRI is a powerful tool for in vivo monitoring of T cell based immunotherapy in mice with endogenous pancreatic cancer

Andreas Schmid¹, Christoph M. Griessinger¹, Daniel Bukala¹, Maren K. Koenig¹, Mareike Lehnhoff¹, Heidi Braumüller², Martin Röcken², Manfred Kneilling², Bernd J. Pichler¹, ¹Laboratory for Preclinical Imaging and Imaging Technology of the Werner Siemens-Foundation, Eberhard Karls University of Tübingen, Tübingen, Germany; ²Dermatology, Eberhard Karls University of Tübingen, Tübingen, Germany. Contact e-mail: a.schmid@med.uni-tuebingen.de

In vivo detection of small abdominal tumors in mouse models is challenging but of major interest as it allows longitudinal studies to investigate tumor progression and to develop novel therapy strategies. Our work focuses on detection of pancreatic tumors and monitoring of therapeutic intervention by MRI in the RIP1-Tag2 mouse model. As recently published treatment with intra-peritoneal (i.p.) administered tumor antigen (TA)-specific IFN- γ producing CD4⁺ T cells (Th1) arrest multistage carcinogenesis and angiogenesis and prolonged life of pancreatic cancer bearing RIP1-Tag2 mice two-fold. In this endogenous mouse model mice start to develop pancreatic tumors at 6 weeks of age and die at approximately 14-16 weeks of age because of hypoglycemia. One aim of our study was to determine whether i.p. administration of tumor antigen specific (Tag2)-Th1 cell is more effective than intra-venous (i.v.) administration. A second aim was to investigate whether MRI is appropriate for therapy monitoring of endogenous pancreatic tumors. In studies we i.p. or i.v. injected 1E+7 Tag2-Th1 cells into RIP1-Tag2 mice starting at 6 weeks of age (\pm 1 week) once weekly. Additionally, the control group was sham treated with physiological saline once a week. CD4⁺ T cells were isolated from the spleens and lymph nodes of large and small T antigen (Tag2) T cell receptor transgenic C3H mice and cultured together with irradiated antigen presenting cells to generate a Th1 phenotype. Specific immunotherapy was monitored by measurement of the blood glucose level and MRI. MRI scans were performed on a 7 T dedicated small animal scanner; a T2-weighted 3D space sequence with isotropic resolution of 220 μ m was used for anatomical information. While the sham treated control group had to be sacrificed at an age of approximately 14 weeks because of the low glucose level (< 30 mg/dl), we measured blood glucose levels of 69 (\pm 18) mg/dl in the i.p. treated group and surprisingly absolutely normal blood glucose of 129 (\pm 4) mg/dl in the i.v. treated group. At an age of approximately 13-14 weeks, average tumor volume was 88.0 mm³ in the sham treated control group and 7.4 mm³ in the i.p. treatment group. No tumors were detectable by MRI in the i.v. treated group. Our data clearly indicate that i.v. administration of Tag2-Th1 cells is much more efficient than i.p. administration and might completely block tumor progression as we could not detect a decrease of blood glucose level or tumors at an age of up to 17 weeks. Furthermore we conclude that MRI is a powerful tool to monitor therapy of pancreatic cancer in mice.

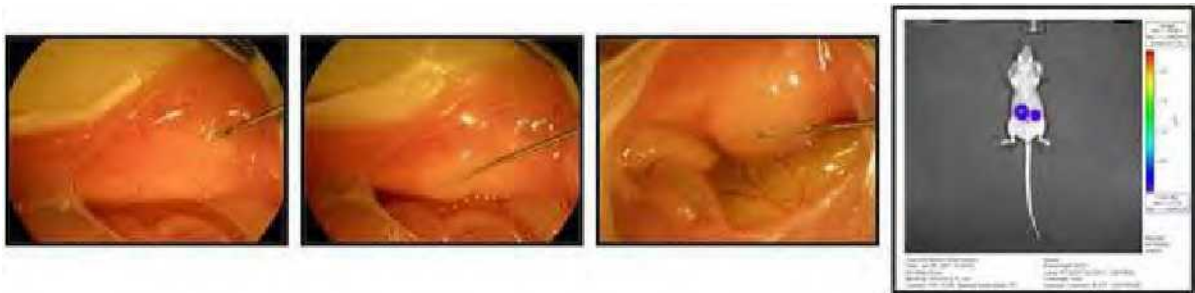
Presentation Number **0729B**

Poster Session 4c: In Vivo Studies & Development/Novel Use of Imaging Probes

Alternative approaches in the study of the tumorigenesis in a xenograft murine model

Albert Altafaj¹, Elena Sancho², Eduard Batlle², **Xavier Cañas**¹, ¹PRAAL-PCB, Barcelona Science Park, Barcelona, Spain; ²Colorectal Cancer, Institute of Biomedical Research, Barcelona, Spain. Contact e-mail: xcanas@pcb.ub.cat

The study of a target gene (EphB2) of the signaling pathway involved in the aetiology of colon cancer involves making xenotransplantation from tumor cell lines and colon tumor cells of patients diagnosed and operated. In both cases the tumor cells are inoculated at different locations in Balb/C nude and SCID mice, in order to assess and compare the resulting tumorigenesis in two types of cell populations. Likewise, depending on the characteristics of the resulting tumour we can determine which model of xenotransplantation offers the best quality of both histopathological results and animal welfare. We have developed different methods of inoculation for the generation of xenotransplanted mice. The route of inoculation used in previous studies was the subcutaneous layer, valuing the resulting tumor two weeks post transplant. This study describes the different methodologies used to inoculate the same type of tumor cells. The selected routes were the subcapsular space of the kidney and the subperitoneal space at the inner wall of the abdomen. In both cases the surgical approach was performed by laparotomy, followed by inoculation of cells in the target organ with a 29-30G needle, followed by standard stitching of the abdominal cavity. Xenografted mice were kept under observation for three weeks to assess their postoperative evolution (body condition) and the tumour growth in the area of inoculation. In all cases, tumor growth was assessed by different techniques: direct observation and measurement, histopathology and noninvasive techniques (bioluminescence with an IVIS-200® system, from Caliper). The resulting tumours showed consistent similarities comparable to those inoculated subcutaneously, causing no paraneoplastic signs in the operated mice. The subsequent histopathological analysis confirmed the presence of tumor cells and the suitability of both models for the study of colonic cancer tumorigenesis. Inoculation of tumoral cells within the subperitoneal layer was considered the easiest method technically and with less risk of postoperative complications. The bioluminescence system was optimal to identify successful xenograft and to track tumorigenesis development.



Bioluminescence IVIS 200
15' post inoculation

Presentation Number **0730B**

Poster Session 4c: In Vivo Studies & Development/Novel Use of Imaging Probes

Advanced Imaging strategies for translational research in lung cancer therapy by aerosolized drugs

*Laura Brullé¹, Guillaume Réveillon¹, Sabrina Pesnel¹, Nathalie Heuzé-Vourc'h², Etienne Lemarié², Patrice Diot², Julien Sobilo¹, Stéphanie Lerondel¹, **Alain Le Pape**^{1,2}, ¹CIPA - TAAM UPS44, CNRS, Orléans, France; ²INSERM U618, Tours, France. Contact e-mail: lepape@med.univ-tours.fr*

Airways are an attractive route to systemic administration for local delivery of drugs to lung tumors in order to increase the dose actually deposited to the target while preserving systemic toxicity. Herein we describe how in vivo imaging can be used as an invaluable tool to accelerate innovation in animal models then transfer to clinical research. The need for relevant orthotopic models of bronchial carcinoma (non small cells, small cells or bronchoalveolar) with suitable stably transfected bioluminescent cells led us to select NCI-H460, NCI-H209 and A549 cells. In male Balb/c nude mice, interventional X ray imaging allowed to position a catheter via the trachea to a given bronchial location in the right lung. The inoculum containing 2.5×10^6 cells traced by 3MBq ^{99m}Tc was injected, the animal being submitted to scintigraphy to check the deposit and determine the equivalent number of tumor cells. Bioluminescence imaging was performed weekly to assess tumor progression and when necessary, high resolution X CT with respiratory gating was used for tumor sizing. Due to current limitations of fluorescence for a quantitative determination in lung, imaging of the expression of biomarkers is preferentially performed using PET or SPECT using tracing dose of ^{64}Cu -DOTA or ^{111}In -DTPA labelled cetuximab® for VEGFR expression and monomeric-RGD-mimetic for $\alpha\beta 3$ integrins. Multimodal imaging was used to determine the tumor response towards aerosolized therapies (gemcitabine, mAb, nano-formulations...). Such an administration route requires optimized delivery and biodistribution in lung so, Pen Century® endotracheal nebulizer was used to deliver the drug traced by ^{99m}Tc -SnF₂ colloids. Extemporaneous scintigraphy allowed determination of the actual dose delivered to the lung for each treatment session. Applied to mAb cetuximab®, this multimodal imaging strategy demonstrated that aerosol delivery results in increasing its concentration within the target organ, limiting its passage into the blood stream and reducing lung tumor formation.

Presentation Number **0731B**

Poster Session 4c: In Vivo Studies & Development/Novel Use of Imaging Probes

A non invasive experimental protocol for fMRI studies: Investigation of the Basal Ganglia-cortex circuit in a rat model

Boussida Salem¹, Amidou Traoré¹, Franck Durif², ¹UR370 QuaPA/NMR plateforme, INRA, Saint Genès Champanelle 63122, France; ²Service de Neurologie, CHU Clermont-Ferrand, Clermont-Ferrand 63000, France. Contact e-mail: salem.boussida@clermont.inra.fr

Basal ganglia (BG) are involved in sensorimotor neural network of the rat. BG have direct connections to the sensorimotor cortex and thalamic nuclei. Most fMRI studies are limited to cortical investigation. The lack of BOLD fMRI studies in deep brain regions could be explained by (i) neuronal activity depression due to anesthesia, (ii) a low Signal to Noise Ratio (SNR) in these regions. Improving these two crucial parameters, we expect that electric hindpaw stimulation could induce a detectable BG activation. T2*-weighted GE-EPI (TEs=18ms/30ms, TR=2s, FA=30°, FOV=2.56cmx2.56cm; Matrix=64x64) were acquired for fMRI experiments on a 4.7 T Bruker scanner using a quadrature surface coil. Wistar rats were continuously anesthetized with 1% isoflurane, mechanically ventilated and Nimblex®(5mg/ml, i.v) was continuously administrated (2.38ml/hr) for muscle relaxation. Right hindpaw stimulation was performed using rectangular pulses (2mA; 8Hz; 10ms) in a 4 x [ON80s-OFF160s] blocs. By computing the spatial distribution of temporal SNR (tSNR) we can identify brain regions where BOLD effects can be detected and assign a degree of confidence to the measured activations. Functional images were processed using SPM8b software (<http://www.fil.ion.ucl.ac.uk/spm>). Based on the spatial distribution of tSNR, BOLD sensitivity map was generated and used as a mask to help removing false positive activations. Statistical activation maps were generated using a combination of two threshold levels, a high level ($p < 0.01$) to ensure the specificity and a lower level ($p < 0.05$) to maximize the sensitivity of activations. Brain activation was reproducibly observed in the contralateral sensorimotor cortex (yellow in fig1). A robust negative BOLD response was observed in the caudate putamen (CPu) region (blue in fig1) with a spatial variability between animals. Experiments are still on going to improve the actual results and the goal of developing a rodent fMRI model to investigate BG activations appears within reach. These findings may have relevance in fMRI studies dealing with physiopathology of neurodegenerative such as Parkinson disease.

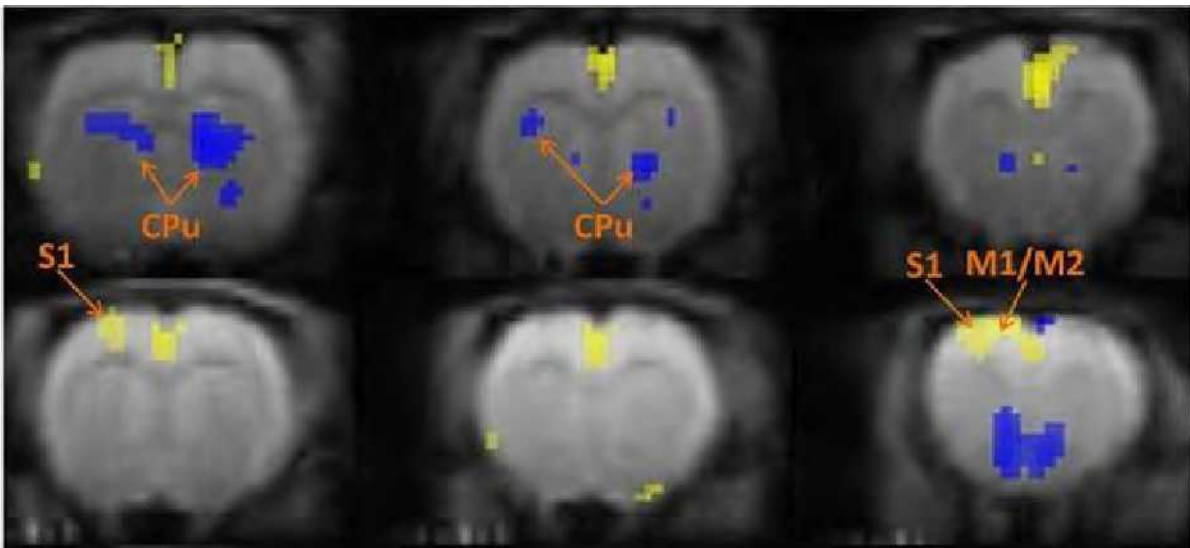


Fig.1: Positive cortical activation (S1/M1/M2; yellow color) and Negative subcortical activation (Caudate Putamen; blue color)

Presentation Number **0732B**

Poster Session 4c: In Vivo Studies & Development/Novel Use of Imaging Probes

In vivo PET Imaging of Stroke-Induced Neuroinflammation in Mice using a Novel Radioligand 18F-PBR06

Frederick M. Lartey¹, Keith-Travis Cord¹, Bin Shen², Joshua Y. Chua³, Rabindra Tirouvanziam⁴, Theo Palmer³, Raphael Guzman³, Frederick T. Chin², Edward E. Graves¹, Billy W. Loo¹, ¹Radiation Oncology, Stanford University, Stanford, CA, USA; ²Radiology, Stanford University, Stanford, CA, USA; ³Neurosurgery, Stanford University, Stanford, CA, USA; ⁴Pediatrics, Stanford University, Stanford, CA, USA. Contact e-mail: fmlartey@stanford.edu

Background: Activated microglia underlie many neuroinflammatory processes and represent a potential imaging target for monitoring neuroinflammation. [¹⁸F]N-fluoroacetyl-N-(2,5-dimethoxybenzyl)-2-phenoxyaniline (18F-PBR06) is a novel radioligand that targets the microglial biomarker, translocator protein 18 kDa (TSPO). The objective was to image stroke-induced neuroinflammation in mice using 18F-PBR06 and Positron Emission Tomography (PET). Methods: 18F-PBR06 [1] was synthesized on a commercial automated radiochemistry module. Stroke was induced using the middle cerebral artery suture occlusion model (MCAO) in 3 Balb/c mice. Three days after stroke, the mice were anesthetized with 2% isoflurane in 100% oxygen and injected with 18F-PBR06 intravenously. PET images were acquired every minute for 2-hours. The mice were then sacrificed and IHC was performed using antibodies to biomarkers of microglial activation (TSPO and CD68). Results: 18F-PBR06 was provided with >99 % purities (radiochemical & chemical) and specific radioactivity of 2574±1039 mCi/μmol (n=5). Mean tracer concentrations in the stroke and non-stroke hemispheres were 0.35 and 0.2 %ID/g respectively (Figure 1A). 18F-PBR06 uptake in the brain peaked within 10 minutes post injection, then remained relatively constant, and was about 70% higher in the stroke vs. non-stroke hemispheres (Figure 1B). TSPO and CD68 expression were also higher on IHC in the stroke vs. non-stroke sections, reflecting an increase in activated microglia. Conclusion: Stroke-induced neuroinflammation can be effectively imaged in mice using 18F-PBR06 and PET. Ongoing studies involve monitoring of the neuroinflammation and effects of various anti-inflammatory interventions over time. Reference [1] E Briard et al., J Med Chem 2009, 52, 688-699

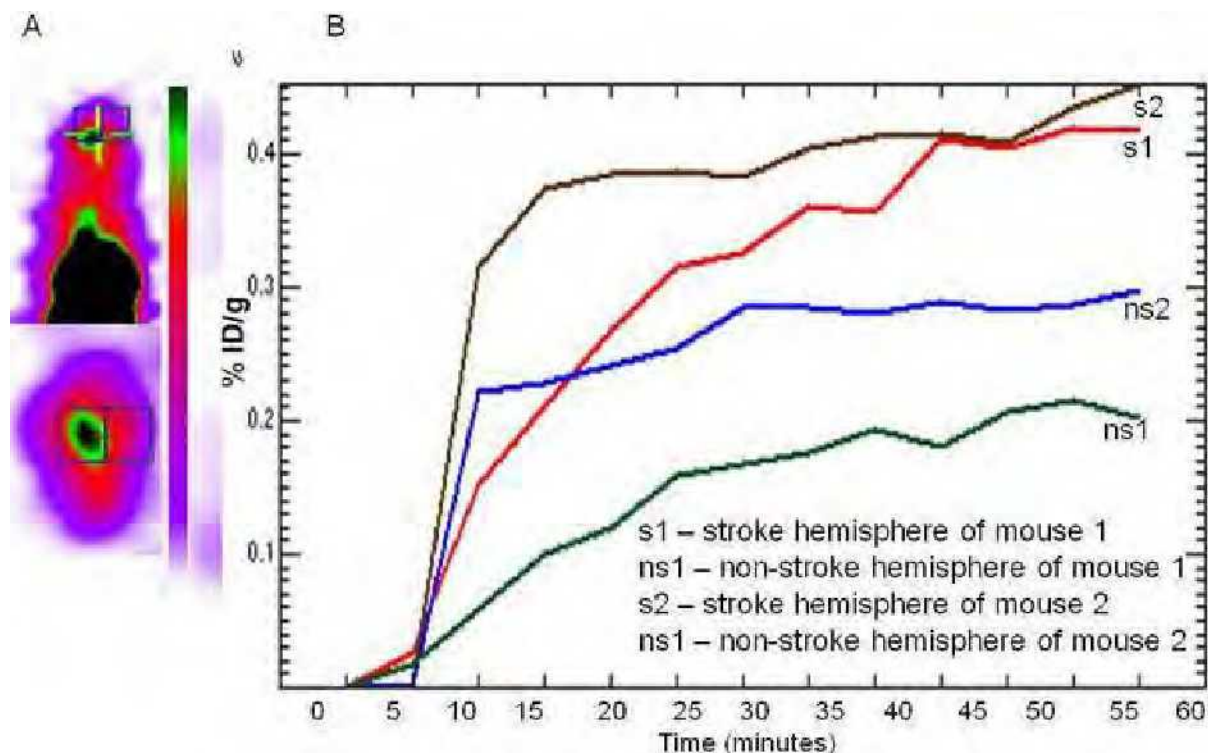


Figure 1. Representative mPET images (axial and coronal views) of the stroke (left) and non-stroke (right) hemispheres of the brain (A) and their change in intensity over 60 minutes (B) in a stroke mouse model (n=2) injected with 18F-PBR06.

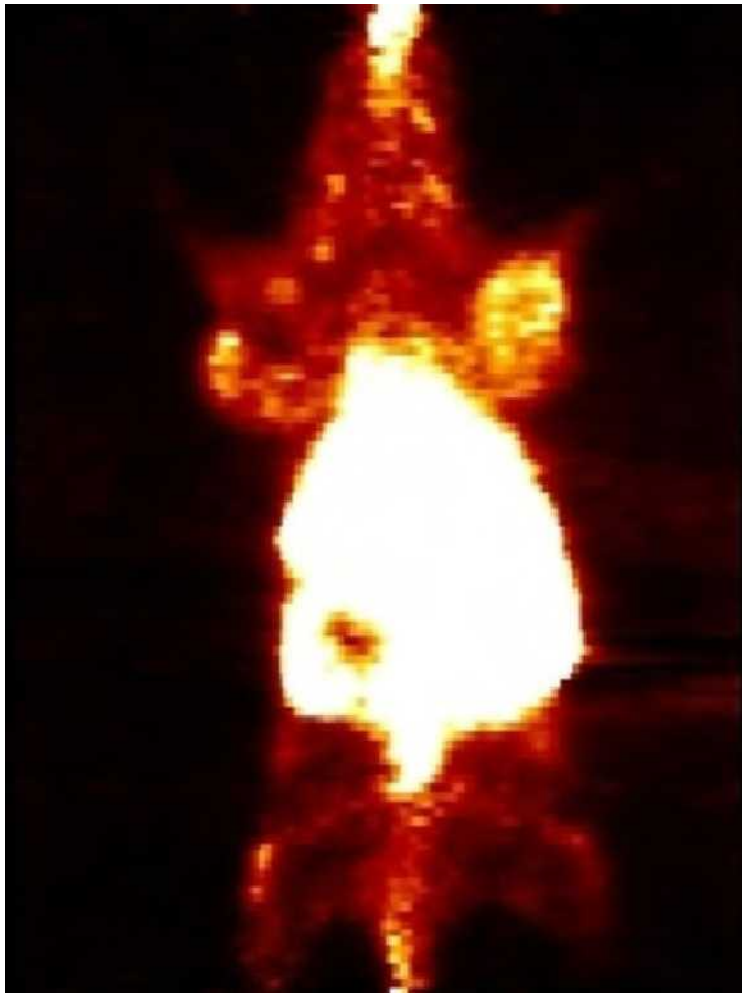
Presentation Number **0733B**

Poster Session 4c: In Vivo Studies & Development/Novel Use of Imaging Probes

Small-animal PET of endothelin A receptor expression in human tumor xenografts

Jinsong Xia¹, Yan Xiang², Eram Zaidi¹, Majid Chalian¹, Zsolt Szabo¹, ¹Radiology, Johns Hopkins Hospital, Baltimore, MD, USA; ²Medicine, Johns Hopkins Hospital, Baltimore, MD, USA. Contact e-mail: jxia5@jhmi.edu

The objective of this study was to evaluate [¹⁸F]FBzBMS as a potential positron emission tomography (PET) probe to quantify the endothelin A receptor subtype (ETAR) in subcutaneous xenograft mouse models. METHODS: Human cancer cell lines with high ETAR expression (E3) and low ETAR expression (CRL-2119) were implanted subcutaneously into the right and left shoulder regions of SCID mice 14-21 days before PET imaging to create ETAR positive and negative tumor models. [¹⁸F]FBzBMS (200 μ Ci in 0.2 cc) was injected through a tail vein into SCID mice for in vivo small-animal PET and ex vivo autoradiography imaging. RESULTS: Small-animal PET showed rapid and clear tumor localization of the radioligand in receptor positive tumors. The radioligand exhibited fast clearance from the circulation, predominantly hepatobiliary way of elimination, moderate uptake in heart and lungs, and only background level activity in muscles. Quantitative analysis of both PET images and ex vivo autoradiography revealed more than two times higher activity in receptor "positive" than "negative" xenografts. The advantage of this technology is that for the first time it permitted in vivo investigation of endothelin A receptor expression in cancer.



Presentation Number **0734B**

Poster Session 4c: In Vivo Studies & Development/Novel Use of Imaging Probes

In Vivo Bioluminescence Imaging of Transplanted Neural Stem Cells in Mouse Model of Parkinson's Disease

Hyung Jun Im^{1,4}, **Do Won Hwang**¹, **Han Kyu Lee**², **Yong Sik Kim**², **Hyewon Youn**^{1,3}, **Dong Soo Lee**^{1,4}, ¹*Department of Nuclear Medicine, Seoul National University College of Medicine, Seoul, Republic of Korea;* ²*Department of Pharmacology, Seoul National University College of Medicine, Seoul, Republic of Korea;* ³*Institute of Radiation Medicine, Medical Research Center, Seoul, Republic of Korea;* ⁴*Department of Molecular Medicine and Biopharmaceutical Science, WCU Graduate School of Convergence Science and Technology, Seoul National University, Seoul, Republic of Korea. Contact e-mail: iihjji@gmail.com*

Purpose: Neural stem cells (NSC) have been proposed to be potential sources to treat Parkinson's disease (PD) due to high potencies of self-renewal and neuronal differentiation. Fate of the transplanted NSCs, however, has not been clearly identified. We established in vivo bioluminescence imaging system of transplanted NSCs (HB1.F3) in mouse model of PD. **Materials and Methods:** To induce PD in C57BL/6 mice (n=4), 6-OHDA was stereotactically injected into the right medial forebrain bundle. Apomorphine induced rotation test and dopamine transporter (DAT) imaging using small animal positron emission tomography with F-18 FP-CIT (FP-CIT) were performed to confirm the establishment of PD. For bioluminescence imaging, HB1.F3 cells that were transduced with an enhanced firefly luciferase retroviral vector (F3-effLuc) were transplanted in the right striatum of the mice (2 x 10⁵ cells/2 ul of PBS). In vivo bioluminescence imaging was serially followed up until day 10. **Results:** By DAT imaging and behavioral test, all mice were proved to develop PD; markedly decreased uptake of FP-CIT was seen in the right striatum, and significant side-biased motor impairments were demonstrated. Transplanted F3-effLuc cells were successfully visualized in the right side of the brain in all mice by bioluminescence imaging on day 3. The bioluminescence activity of the transplanted F3-effLuc cells gradually decreased and then disappeared on day 10. **Conclusion:** We successfully established in vivo bioluminescence imaging system of transplanted NSCs in mouse model of PD, which enabled to longitudinally monitor the fate of the NSCs without sacrificing the animals. In vivo stem cell trafficking method using bioluminescence imaging could be valuable in mouse model of PD.

Presentation Number **0735A**

Poster Session 1c: In Vivo Studies & Development/Novel Use of Imaging Probes

Diagnostic value of dual time point imaging of 18FDG PET/CT for the detection of extrapulmonary tuberculous lesions

Hairil Rashmizal Abdul Razak^{1,4}, Moshi Geso¹, Noraini Abdul Rahim², Abdul Jalil Nordin³, ¹Discipline of Medical Radiations, School of Medical Sciences, RMIT University, Melbourne, VIC, Australia; ²Diagnostic Imaging Department, Serdang Hospital, Kajang, Malaysia; ³Nuclear Imaging Unit, Faculty of Medicine & Health Sciences, University Putra Malaysia, Serdang, Malaysia; ⁴Medical Imaging Department, Faculty of Health Sciences, University Technology MARA, Puncak Alam, Malaysia. Contact e-mail: rashmizal@yahoo.co.uk

Purpose: To evaluate the diagnostic value of Dual Time Point Imaging (DTPI) of 18F-fluorodeoxyglucose (FDG) Positron Emission Tomography/Computed Tomography (PET/CT) for the detection of extrapulmonary tuberculous lesions. Methods: Seven consecutive patients with the final diagnosis of Extrapulmonary Tuberculosis (EPTB) infection were enrolled. All patients underwent FDG PET/CT imaging at two time points: early scan at 51.1 ± 14.7 (30-75) min and delayed scan at 129.0 ± 15.0 (113-158) min after intravenous injection of 359.2 ± 136.3 (145.4-592.4) MBq of FDG. All images were semi-quantitatively interpreted using Maximum Standardized Uptake Value (SUVmax). Results: A total of 21 lesions were evaluated (Table 1). The average SUVmax in extrapulmonary tuberculous lesions was 6.70 ± 2.49 on early scans and 7.86 ± 3.23 on delayed scans. There was a significant difference between these two time points (P<0.05). The calculated percentage difference of SUVmax (Δ%SUVmax) was 16.45% ± 16.43%, indicating a significant increase in SUVmax between the two time points for the entire lesion population. Conclusion: The results of the present study provide additional diagnostic value of DTPI of FDG PET/CT in detecting the extrapulmonary tuberculous lesions. The Δ%SUVmax could potentially be used for the evaluation of lesion activity.

Patients and lesions characteristics

Patient no.	Age	Sex	Weight (kg)	Height (cm)	Location of the lesion	SUVmax1	SUVmax2	Δ%SUVmax
1	26	Female	93.5	159	Right base of the neck	8.0	10.4	30.0
					Right parathyroid	8.1	11.8	35.8
					Right infraclavicular	8.3	11.6	30.8
					Right paratracheal	11.7	15.7	34.2
2	40	Male	72	164	T12 and L1 vertebral bodies	7.2	9.5	31.9
3	22	Female	60.5	148	Left submandibular node	9.7	11.2	15.1
4	19	Female	53	154	Right supraclavicular fossa	2.8	2.3	-17.9
					Right anterior chest wall	5.8	6.8	17.2
					Right subscapular soft tissue space	11.7	8.8	-24.8
5	24	Female	50.8	153.5	Right axillary node	4.3	4.8	11.6
					Left hilar lymphatic node	5.3	6.2	17.0
					Right hilar lymphatic	5.4	4.0	-17.6
					Paracolic node	7.0	7.1	1.4
					Left renal vein node	5.7	6.7	17.1
					Left retroaxillary node	4.8	3.3	-10.4
					Right cervical node	4.7	3.7	-21.3
					L3-L4 intervertebral disc space	8.5	10.7	25.9
6	31	Female	56.4	160	Left psoas muscle at level L4	6.7	8.1	20.9
					Right retroaxillary node	6.0	6.0	0.0
7	17	Male	44	162	Right subpharyngeal node	5.3	4.3	-22.9
					Parapancreatic node	7.1	8.1	14.1
					MEAN	6.7	7.9	16.5
					SD	2.5	3.2	16.4

T12: twelfth thoracic vertebra, L1: first lumbar vertebra, L3: third lumbar vertebra, L4: fourth lumbar vertebra

SUVmax1: Maximum Standardized Uptake Value at early scan

SUVmax2: Maximum Standardized Uptake Value at delayed scan

Δ%SUVmax: The percentage difference of SUVmax; [(SUVmax1 - SUVmax2)/ SUVmax1] x 100

SD: standard deviation

Presentation Number **0736A**

Poster Session 1c: In Vivo Studies & Development/Novel Use of Imaging Probes

Investigation of Intratumoral Heterogeneity in Nasopharyngeal Carcinoma: A Distinct Role of PET-CT from MRI

Bingsheng Huang¹, **Pek Lan Khong**¹, **Dora Lai Wan Kwong**², **Winnie Kit Sum Chan**¹, ¹*Diagnostic Radiology, The University of Hong Kong, Hong Kong Island, Hong Kong;* ²*Clinical Oncology, The University of Hong Kong, Hong Kong Island, Hong Kong.* Contact e-mail: huangbs@gmail.com

Tumors are heterogeneous due to cellular proliferation, necrosis, noncellular accumulations and physiologic characteristics, etc. It has been reported that heterogeneity is related to outcome, and studying its evolution may help to optimize treatment planning. We aimed to study the role of tumor heterogeneity reflected by PET-CT in the diagnosis of Nasopharyngeal Carcinoma (NPC), a leading cancer type in South China, and the correlation with MRI findings. It was hypothesized that tumor heterogeneity reflected by PET-CT correlated with both NPC diagnosis (SUVmax, tumor volume, stage, etc) and heterogeneity reflected by MRI scanning. A total of 26 newly-diagnosed NPC patients who had received both PET-CT and MRI examinations (interval between PET-CT and MRI scans not longer than two weeks) with the tumor size bigger than 1.5cm in any direction were studied. Intratumoral heterogeneity was calculated by taking the derivative (dV/dT) of the volume-threshold function in PET-CT images of the whole tumor. The relationship between intratumoral heterogeneity and NPC diagnosis (SUVmax, tumor volume, staging, etc) was determined for this cohort. To study the correlation between the findings of MR and PET, MR images, including T1W, T2W, post-contrast T1W images were registered to PET images by using the software SPM 5 or FSL. Voxel-based correlation between signal intensity in registered MR and PET images was performed for each patient within the ROI automatically drawn in PET applying a threshold of 40% SUVmax. It was found that the heterogeneity reflected by PET significantly correlated with tumor volume, M-stage, AJCC stage, and SUVmax ($p < 0.05$); but not with T-stage ($p = 0.069$) and N-stage ($p = 0.063$). However, only in part of this cohort, significantly positive or negative correlation was found (9 in 26 cases, between T1W and PET; 19 in 26, between T2W and PET; 13 in 26, between post-contrast T1W and PET), with weak correlation coefficients (-0.206~0.439). In conclusion, the intratumoral heterogeneity of FDG uptake has significant correlation with tumor volume, SUVmax and staging, but no or weak relationship with heterogeneity of MRI signal intensity and contrast enhancement. This finding may help to improve the characterization of NPC, while the value of intratumoral heterogeneity in NPC prognosis remains to be studied.

Presentation Number **0737A**

Poster Session 1c: In Vivo Studies & Development/Novel Use of Imaging Probes

MOLECULAR IMAGING IN EMERGING ECONOMIES

Jyotsna Rao², **Rao V. Papineni**¹, ¹*Carestream Molecular Imaging, Carestream Health, Inc., Woodbridge, CT, USA;* ²*Apollo Gleneagles PET-CT Centre, Hyderabad, India. Contact e-mail: jyotsnael@gmail.com*

Emerging economies like India are planning their resources and infrastructure with a focus on health care that includes prevention, early diagnosis and timely treatment with cost effective measures. We evaluate here the importance and role of molecular imaging (MI) in Healthcare with a scientific perspective. A compilation of the commonly prevalent disease, their incidence, available imaging facilities and projected needs in India are shown with an emphasis to share with the imaging community in facilitating rapid development of new technologies. Currently, 80600 new cases of cancer are diagnosed in India every year with lung, pharynx, esophagus, tongue and stomach most common in men and cervix, breast, ovary, esophagus and oral cancers, most common in women in the given order. With one fifth of the world's cervical cancer coming from India and one third of all cancers in India originating in the head and neck region, the above figure has direct relevance for the planners in development of novel molecular imaging technologies. New radiation techniques and new chemotherapeutic regimens targeting processes such as angiogenesis and hypoxia will need tracers apart from FDG. Imaging modalities such as optical imaging utilizing near-infrared molecular probes will have to play a crucial role in oral cancer detection of both emerging economies and also developing nations in the vicinity. Regarding other diseases in India relevant to MI, Ischemic cardiovascular disease forms 31% of noncommunicable disease in India with inflammatory myocarditis due to sarcoidosis. Recent estimates indicate that India will soon have the largest number of cardiovascular patients with one third of deaths occurring due to it. Neurodegenerative disorders incidences have risen, contributed directly by longer survival rates and aging of the population. Although, there is improved management of infection, tuberculosis still contributes to 3.7 million deaths every year and forms a fifth of the world's incidence. Molecular imaging particularly PET has started becoming important in managing neurological and cardiovascular disease with its role in infection/inflammation imaging starting to get established. Currently, India has 200 gamma and 20 PET/CT cameras with 10 cyclotrons- F18 FDG, N13 ammonia and F18 NaF are in use. We show here that complementing the development of clinical diagnosis infrastructure, the preclinical imaging arm needs to be strengthened. New tracers and multi modality imaging probes needed in cancer, infectious and cardiovascular diseases are described.

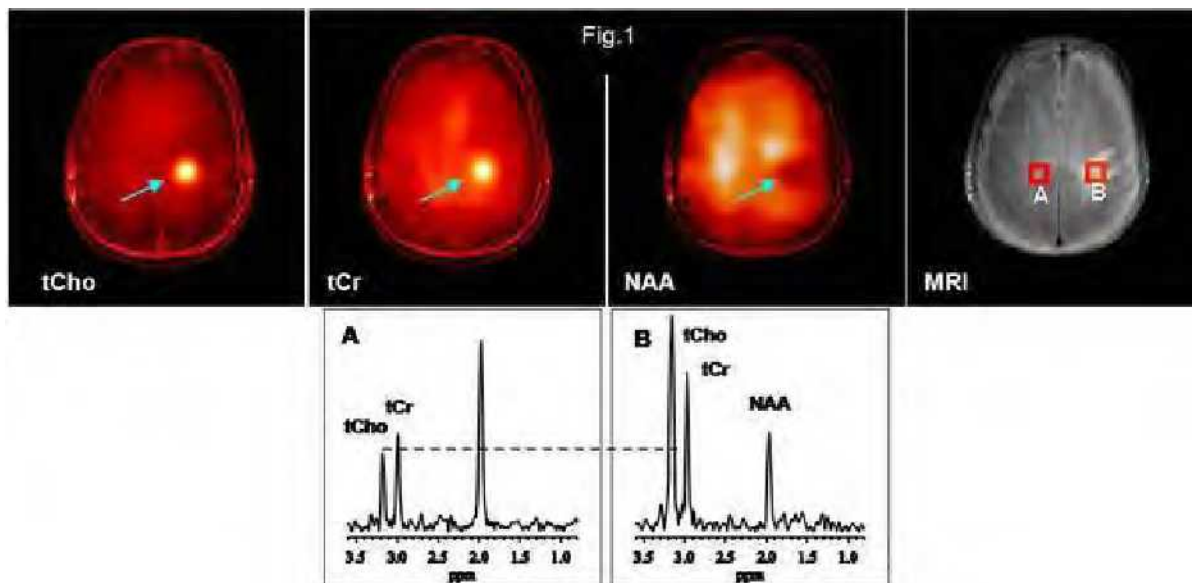
Presentation Number **0738A**

Poster Session 1c: In Vivo Studies & Development/Novel Use of Imaging Probes

¹H MRSI Detection of Elevated Total Creatine in Glioblastoma Multiforme: A Potential Biomarker and a Cautionary Tale

Dikoma C. Shungu¹, Xiangling Mao¹, Apostolos J. Tsiouris¹, Carl E. Johnson¹, Jonathan P. Dyke¹, Linda A. Heier¹, Joseph P. Comunale¹, John A. Boockvar², Theodore H. Schwartz², Susan C. Pannullo², ¹Radiology, Weill Cornell Medical College, New York, NY, USA; ²Neurological Surgery, Weill Cornell Medical College, New York, NY, USA. Contact e-mail: dcs7001@med.cornell.edu

Introduction. Levels of major brain metabolites (e.g., NAA and tCho) detected *in vivo* by ¹H MRS have generally been reported as ratios relative to tCr (ie, Cr+PCr), under the assumption that its intensity remains constant due to the creatine kinase-catalyzed interconversion of Cr and PCr. Here, we report four clear-cut cases of MRS detection of dramatic elevations of tCr in brain tumors, which both suggests its potential utility as a brain cancer biomarker, and adds incontrovertible evidence to the growing body of literature data that has challenged the common practice of using tCr as an internal concentration reference for assessing changes in brain metabolites on the assumption that its integrated peak area remains constant under most conditions. **Methods:** Four patients with focal contrast-enhancing intracranial lesions were referred for examination by multislice ¹H MRSI to rule out multiple sclerosis, cerebral infarction or a brain neoplasm. The ¹H MRSI data were recorded on a GE 3T MR system with TE/TR 280/2300 ms, FOV 240 mm, four 15-mm slices and 3.5-mm gaps, 512 sample points, 32x32 phase-encoding gradients, and a 2.5-kHz spectral width. **Results and Discussion:** Examination of the spectra from all the lesions revealed dramatic increases in the signal intensity of **both** tCho and tCr, and a decrease in the signal intensity of NAA compared to a similar location in the contralateral hemisphere (eg, Fig. 1). Histopathological analyses of the lesions revealed each to be a highly cellular glial neoplasm composed of pleomorphic, hyperchromatic cells, with a final diagnosis of glioblastoma multiforme (GBM). While increased tCho concentration is now an established marker of cancer, our finding of clear and dramatic elevations of tCr in these GBM cases was unanticipated, suggesting a potential role for tCr as a biomarker for brain cancer, while urging caution in using its spectral intensity as an internal concentration reference, especially in highly cellular and rapidly growing glial neoplasms.



Presentation Number **0739A**

Poster Session 1c: In Vivo Studies & Development/Novel Use of Imaging Probes

Malignant and non-malignant lesions incidentally detectable with PET/CT

Masao Ono¹, **Katsuyuki Kobayashi**¹, **Yoshiko Miyatake**¹, **Tatsuya Katoh**¹, **Weijey Ko**¹, **Takashi Ushimi**¹, **Toyoyuki Kojima**¹, **Seiei Yasuda**², ¹*Yotsuya Medical Cube, Tokyo, Japan;* ²*Gastroenterological Surgery, Tokai University School of Medicine, Kanagawa, Japan.*
Contact e-mail: m-ono@mcube.jp

Objectives: Various lesions are incidentally detected during PET/CT study. This study was conducted to determine the types and frequency of carcinoma and clinically meaningful nonmalignant lesions detectable with PET/CT. **Methods:** Subjects were 2937 asymptomatic individuals (1790 men, 1147 women, 53.7±12.3 years old) who underwent PET/CT studies at our institution as part of a cancer screening program from August 2005 to December 2009. PET/CT was performed 60 min after injection of 145 to 260 MBq FDG. PET/CT images were visually evaluated and prospectively recorded. The PET/CT findings were compared with final diagnoses obtained by other imaging modalities, laboratory studies, and clinical follow-up. **Results:** A total of 29 malignant lesions were detected in 29 (1.0 %) of the 2937 subjects. Of the 29 malignant lesions, 27 lesions (93.1%) were PET positive, and 2 lesions (6.9%) were PET negative and detected on CT images. Most subjects with carcinoma underwent potentially curative treatments. A total of 411 nonmalignant lesions were detected in 382 (13.0%) of the 2937 subjects. Of the 411 nonmalignant lesions, 202 lesions (49.1%) were PET positive, and 209 lesions (50.9%) were PET negative and detected on CT images. The nonmalignant lesions were classified into the following three sites. 1) Head & neck: 175 lesions were found, including chronic thyroiditis (120), maxillary sinusitis (27), and benign thyroid tumor (17). 2) Thorax: 25 lesions were found, including atypical mycobacteriosis of the lung (7), sarcoidosis (4), and emphysema (4). 3) Abdomen: 226 lesions were noted, including cholecystolithiasis (116), urinary tract stone (40), adrenal tumor (19), colorectal polyp (7), and abdominal aneurysm (7). **Conclusion:** A wide variety of carcinomas and clinically important benign lesions can be found incidentally at a substantial rate during PET/CT study.

Presentation Number **0740A**

Poster Session 1c: In Vivo Studies & Development/Novel Use of Imaging Probes

The Value of ^{18}F -FDG PET/CT in Predicting Residual Tumor after Conization for Cervical Intraepithelial Neoplasia III and Microinvasive Cervical Carcinoma

Jong-Ryool Oh, Ari Chong, Ja-Hye Kim, Su-Ung Yoo, Byung Hyun Byun, Sun-pyo Hong, Ho-chun Song, Hee-Seung Bom, Jung-Joon Min, Nuclear Medicine, Chonnam National University Hospital, Gwangju, Republic of Korea. Contact e-mail: letzgroove@hanmail.net

Purpose: Focusing on the hypothesis that metabolic focality could differentiate tumoral FDG uptake from post-procedural hypermetabolism, we investigated the value of ^{18}F -FDG PET in predicting residual tumor after conization for cervical intraepithelial neoplasia III (CIN III) and microinvasive cervical carcinoma (MIC). Materials and Methods: A total of 35 patients who underwent ^{18}F -FDG PET/CT within 5 weeks after conization were enrolled in this prospective study. The presence of residual tumor was assessed by hysterectomy in 30 patients and clinical follow-up in 5 patients. The metabolic parameters - maximum standardized uptake value (SUV_{max}), metabolic volume in a 90% threshold of SUV_{max} (MV_{90}), and metabolic volume in a 40% threshold of SUV_{max} (MV_{40}) - were compared according to the presence of residual tumor. Demographic, pathologic and metabolic parameters were evaluated with univariate and multivariate analyses for predicting residual tumor after conization. Result: Out of the 35 patients, 19 had residual tumor and 16 had no residual tumor. While the PET/CT to conization interval (12.8 ± 7.2 vs. 13.0 ± 5.7 days, $p = 0.944$), SUV_{max} (4.56 ± 1.04 vs. 4.68 ± 1.05 , $p = 0.730$), and MV_{40} (11.06 ± 6.85 vs. $14.09 \pm 6.42 \text{ cm}^3$, $p = 0.189$) were not significantly different between the patients with and without residual tumor, MV_{90} of residual group was significantly lower than that of no residual group (0.21 ± 0.12 vs. 0.37 ± 0.25 , $p = 0.021$). Univariate analysis showed that SUV_{max} , MV_{40} , age, menopausal state, HPV test, and severity of disease were not predictive for residual disease, but resection margin ($p = 0.006$, OR = 23.1) and $\text{MV}_{90} < 0.35 \text{ cm}^3$ ($p = 0.011$, OR = 18.0) were significant factors associated with residual tumor. These factors were also significant in a multivariate analysis; resection margin ($p = 0.006$, OR = 29.8) and MV_{90} ($p = 0.012$, OR = 23.9). MV_{90} and resection margin could predict residual tumor with a sensitivity, specificity, diagnostic accuracy, positive predictive value, and negative predictive value of 89%, 81%, 86%, 85%, and 87%, respectively. Conclusion: Metabolic focality represented by a lesser extent of MV_{90} could predict residual tumor after conization for CIN III and MIC by differentiating it from post-procedural hypermetabolism.

Presentation Number **0741A**

Poster Session 1c: In Vivo Studies & Development/Novel Use of Imaging Probes

Utility of FDG-PET and CT for the prediction of liver lesion progression in patients undergoing Y-90 radioembolization

Karam Badran¹, **Anthony Balistreri**³, **Steven C. Rose**², **Carl K. Hoh**², **Sebastian Obrzut**², ¹*Biological Sciences, University of California, San Diego, La Jolla, CA, USA;* ²*Nuclear Medicine, University of California, San Diego, La Jolla, CA, USA;* ³*Biological Sciences, Santa Clara University, San Jose, CA, USA. Contact e-mail: karambadran@gmail.com*

PURPOSE: To assess the predictive value of PET and CT in identifying lesion progression in patients with liver metastases undergoing Y-90 radioembolization. **METHODS:** Sixteen patients (4 females, 12 males; median age, 70; range, 45-82 years) with 29 malignant liver lesions treated with Y90 radioembolization underwent CT and FDG PET imaging and 24 patients (8 females, 16 males; median age, 66 years; range, 27-88 years), with 44 treated liver lesions underwent CT imaging alone. CT lesion measurements were recorded uni- and bi-dimensionally on pre and post therapy scans and were categorized based on RECIST 1.1 and WHO criteria. Post therapy PET scans were assessed visually and semiquantitatively based on maximum lesion SUV. The predictive value of PET and CT in identifying lesion progression was assessed using Kaplan-Meier estimates (Logrank test). **RESULTS:** PET was able to predict lesion progression in lesions labeled as metabolically stable and metabolically progressive disease (MSD/MPD - nonresponding) ($p = .0048$ for visual PET, $p = 0.0497$ for semiquantitative PET with $SUV \Rightarrow 4.25$). CT did not predict lesion progression in lesions labeled as stable disease and progressive disease (SD/PD - nonresponding) ($p = 0.7644$ single diameter, $p = 0.2679$ double diameter). However, CT was able to predict lesion progression in lesions labeled as progressive disease (PD) ($p = 0.0034$ single diameter, $p = 0.0007$ double diameter). **CONCLUSION:** In patients undergoing Y-90 radioembolization PET was better able to predict lesion progression than CT in liver lesions labeled as nonresponding, while CT was only able to identify lesion progression in lesions labeled as progressive.

Presentation Number **0742A**

Poster Session 1c: In Vivo Studies & Development/Novel Use of Imaging Probes

Increased detectability after glucose loading in differentiating recurrent brain tumor from radiation necrosis with F-18 FDG PET/CT

Young-Soon Seo², **Su-Ung Yoo**¹, Seong-Young Kwon³, Byung Hyun Byun¹, Sun-pyo Hong¹, Jung-Min Ha⁴, Ari Chong¹, Jong-Ryool Oh¹, Ja-Hye Kim¹, Byeong-il Lee¹, Ho-chun Song¹, Hee-Seung Bom¹, Jung-Joon Min¹, ¹Nuclear Medicine, Chonnam National University Hospital, Gwangju, Republic of Korea; ²Nuclear medicine, Veterans hospital, Gwangju, Republic of Korea; ³Korea Health Industry Development Institute, Seoul, Republic of Korea; ⁴Nuclear Medicine, Chosun National University Hospital, Gwangju, Republic of Korea. Contact e-mail: ysu2519@nate.com

Introduction: F-18 FDG PET/CT is the widely used method to differentiating tumor recurrence from radiation necrosis in patients with brain tumor. However, because of a high glucose metabolism in normal gray matter, discrimination may be ambiguous. In this study, we evaluated the effect of glucose loading on improvement of diagnostic accuracy. **Materials and Methods:** We included four patients with suspicious recurred lesions on brain MRI after gamma knife surgery (GKS) or radiation therapy for brain tumors. All patients underwent F-18 FDG PET/CT using both conventional and glucose loading methods within 1 week. Glucose loading was performed by infusion of 50 cc 50% D/W for 3 minutes using infusion pump. We analyzed the lesions by visual inspection and by quantifying the lesion-to-background ratio (LBR). All patients underwent magnetic resonance spectroscopy (MRS) to correlate with PET results. **Results:** Three patients out of 5 determined to have recurrence and underwent chemotherapy. On visual inspection, the radioactivity of the recurrent lesion looked more prominent after glucose loading. The mean value of the LBR between conventional and glucose-loading method was 1.54 ± 0.53 and 1.84 ± 0.49 , respectively and showed significant difference ($p < 0.05$). The mean value of the LBR between two methods in radiation necrosis group was 1.22 ± 0.58 and 1.33 ± 0.56 , and showed no significant difference ($p = 0.058$). Percent increase of LBR after glucose loading was two-fold higher in recurrent lesion as compared to the lesion of radiation necrosis (19.5 vs. 9.0%). **Conclusion:** In differentiating recurrent brain tumor and radiation necrosis, glucose loading before FDG injection is simple and useful procedure that suppress background FDG uptake in the normal cerebral cortex leading to improving lesion-to-background ratio.

Presentation Number **0743A**

Poster Session 1c: In Vivo Studies & Development/Novel Use of Imaging Probes

For determination of remnant malignancy after preoperative chemoradiation for rectal cancer; threshold of maxSUV and SUV reduction rate

Ari Chong, Ho-chun Song, Ja-Hye Kim, Su-Ung Yoo, Jong-Ryool Oh, Jung-Min Ha, Hee-Seung Bom, Byung Hyun Byun, Sun-pyo Hong, Jung-Joon Min, Nuclear medicine, Chonnam National University Hospital, Gwang-ju, Republic of Korea. Contact e-mail: aricori@naver.com

Purpose: The purpose of our study is to determine the threshold of maxSUV and SUV reduction ratio in detecting remnant malignancy after preoperative chemoradiation therapy (CRT) in rectal cancer. **Materials and Methods:** Rectal cancer patients (n=25) who underwent F-18 FDG PET/CT (PET/CT) before and after CRT were included. All of them underwent operation after second PET/CT. Complete regression and remnant malignancy groups were pathologically determined after surgery. The threshold of maxSUV (on PET after preoperative CRT) and SSR (SUV reduction ratio = (staging SUV-restaging SUV)/staging SUV) were measured by the areas under the ROC curve. **Results:** Complete remissions were showed in four patients. Twenty-one patients had remnant malignancies on operation. For detecting remnant malignancy, maxSUV threshold of >4 showed sensitivity 66.7%, specificity 100%, positive predictive value 100% and negative predictive value 36.4% (p=0.0031). However, SSR dose not show an ability to distinguish between complete remission and remnant lesions (p=0.77). **Conclusion:** In restaging PET/CT after preoperative CRT in rectal cancer, maxSUV threshold over 4 can be used to determine remnant malignancy.

Presentation Number **0744A**

Poster Session 1c: In Vivo Studies & Development/Novel Use of Imaging Probes

Comparison study among new developed breast specific gamma imaging, PET and MRI in patients with pathologically proven primary breast lesion

Bom Sahn Kim, Nuclear Medicine, Ewha Womans University College of Medicine, Seoul, Republic of Korea. Contact e-mail: kbomsahn@hanmail.net

Introduction The purpose of our study was to evaluate the results of new developed breast specific gamma imaging (BSGI; Dilon), FDG PET(=PET) and breast MRI in patients with pathologically proven primary breast lesion. **Material and Methods** 39 female patients (51.7±8.4 years old) who undergoing BSGI, PET, breast MRI were enrolled, retrospectively. The imaging findings were classified as positive and negative and diagnostic nature among studies was analyzed with 59 pathologic proven breast lesions. Results From 59 breast lesion, 47 lesions were malignant tumor (IDC: 38, DCIS: 5, other malignancy: 4) and the others were benign tumor. BSGI and MRI had 93.6% and 91.5% of sensitivity, 66.7% and 33.3% of specificity. The sensitivity and specificity of PET was 87.2% and 83.3%. Positive predictive value (PPV) of BSGI, MRI and PET was 91.7%, 84.3% and 95.3%. From PET, four lesions were detected on additional delayed regional image. There was no different size between malignant tumor and benign tumor (20.9±13.8 vs. 12.4±8.7 mm; p=0.081). The maximal SUV of malignant tumor was 4.3±3.8 and just two benign tumor had mild metabolism (maxSUV was 1.3 and 1.5). Though, BSGI and MRI detected all of two patients with bilateral breast cancer, but PET just found unilateral lesion in the one patient. **Conclusion** BSGI had better sensitivity and PET had better PPV and specificity than any other exams. From all of exams, post test referral bias could make low specificity. BSGI is an effective discriminating study that should be used to evaluate in patients with suspected breast cancer. This is a preliminary comparison study among the new developed BSGI (Dilon) and the other exams and another large group study including more patients should have to be followed.

Presentation Number **0745A**

Poster Session 1c: In Vivo Studies & Development/Novel Use of Imaging Probes

Imaging water diffusion and quantification of the non-gaussian distribution in kidney

Yu-Jen Lin¹, Koon-Kwan Ng², Hsiang-Yang Ma³, YuChun Lin^{2,3}, Jiun-Jie Wang¹, ¹Department of Medical Imaging and Radiological Science, ChangGung University, Tao-Yuan, Taiwan; ²Department of Diagnostic Radiology, ChangGung Memorial Hospital, Tao-Yuan, Taiwan; ³Department of Electrical Engineering, ChangGung University, Tao-Yuan, Taiwan. Contact e-mail: aron15116@hotmail.com

Purpose: To image the anisotropic water diffusion in Kidney and quantify the extent of deviation from gaussianity. Material and Method: Diffusion weighted images were acquired from 3 healthy volunteers on a 3T-MR scanner (Trio with TIM, Siemens, Germany) with respiration triggering. The diffusion weighting gradient was applied in 20 directions with 11b-values (0 to 3000 sec/mm² in step of 300 sec/mm²). The diffusion tensor (1) and the diffusion kurtosis tensor (2) were calculated in MATLAB 7.5 (MathWork, USA), including Fractional Anisotropy (FA), and mean Kurtosis (MK). Regions of Interest were selected in renal cortex and medulla on a non-diffusion weighted image. Result and Discussion: The figure showed images of FA (a) and MK (b). The averages from the ROIs were plotted against the b-values(c), for cortex (red) and medulla (blue) respectively. Previous study showed that the use of a monoexponential function for renal diffusion measurement plays a substantial role in causing the variability in Apparent Diffusion Coefficient. The current study showed that visualization of the water diffusion process in kidney is feasible using MRI. Diffusion in kidney is anisotropic and deviated from gaussian distribution. FA showed increased anisotropy in the renal medulla, as a result of the radially orientated structures, like vessels, tubules, and collecting ducts. MK is used to quantify the extent of non-gaussianity in water diffusion. Strong deviation from mono-exponential decay in renal diffusion is noticed. Increased MK in medulla can result from many interacting factors, such as restriction from organelles. MK decreases as the diffusion weighting increases, probably because of the selective suppression on components of fast diffusion. Our study demonstrated that visualization of renal diffusion using tensor and kurtosis is possible, which can be of clinical interest. Reference: (1) Basser et. al. MRM 1997; 37(2):292-300 (2) Helpert et. al. MRM 2005; 53:1432-1440

Presentation Number **0746A**

Poster Session 1c: In Vivo Studies & Development/Novel Use of Imaging Probes

The metabolic changes within a month after radiation therapy of cervix cancer; in F-18 FDG PET/CT, compared by MRI

Ari Chong, Ho-chun Song, Jong-Ryool Oh, Su-Ung Yoo, Ja-Hye Kim, Sun-pyo Hong, Byung Hyun Byun, Hee-Seung Bom, Jung-Joon Min, Nuclear medicine, Chonnam National University Hospital, Gwang-ju, Republic of Korea. Contact e-mail: aricori@naver.com

Purpose: Numerous studies about the F-18 FDG PET/CT (PET/CT) after the radiation therapy (RTx) of cervix cancer have been reported. In most of the studies, PET/CT after at least three months was evaluated and recommended. We report the result of early follow-up PET/CT after RTx (at ± 1 month from the end of the RTx) of cervix cancer, through comparison with MRI. Methods: Twenty-eight cervix cancer patients underwent follow-up PET/CT and pelvic MRI about one month after RTx of cervix cancer. In every cases, they also had PET/CT and MRI for staging before radical RTx of cervix cancer. We compared between the changes of metabolic activity of primary tumor on PET and the changes of size measured on MRI. Significant hypermetabolic activity is defined like these; in the lesion of primary lesion, not be considered as urine activity. Results: 10 patients underwent follow-up PET/CT before the completion of RTx (average interval: -13.30 ± 8.98 days), others had follow-up PET/CT after RTx with average time interval of 10.11 ± 9.19 days. Histologic types are squamous cell carcinoma (in 23 patients), adenocarcinoma (2), adenosquamous cell carcinoma (1) and poorly differentiated carcinoma (2). In 21 patients (75% of all cases), short-term follow-up PET/CT after RTx well correlated with the tumor response demonstrated on MRI. Among them, in 13 patients, both follow-up PET/CT and MRI showed no evidence of primary tumor anymore. In 8 patients, the size and metabolic activity of primary lesions were both decreased. The percentage of SUV changes (average $71.06 \pm 7.0\%$) was higher than size changes of MRI (average 62.17 ± 6.60). Higher metabolic activity was detected in the cases with earlier PET/CT than the later PET/CT. PET/CT and MRI mismatched cases were seven (25% of all cases). In these cases, significant hypermetabolic activity was shown in cervix, but MRI could not delineate a remnant malignant lesion. Conclusion: Early follow-up of PET/CT within a month after radiation therapy of cervix cancer can reflect the regression of cervix cancer. Also, it is correlated with the changes of MRI. PET/CT is considered to be available to evaluation of early response of radiation therapy of cervix cancer. Mismatched 7 cases need further follow-up study.

Presentation Number **0747A**

Poster Session 1c: In Vivo Studies & Development/Novel Use of Imaging Probes

Quantitative Measurement of Optic Radiation in the Human Brain using Normalization-Based Diffusion Tensor Tractography

Donghoon Lee¹, **Cheolpyo Hong**¹, **Bongsoo Han**¹, **Sungho Jang**², **Jiwon Park**³, ¹*Radiological Science, Yonsei University, Wonju, Republic of Korea;* ²*Physical Medicine and Rehabilitation, Yeungnam University, Daegu, Republic of Korea;* ³*Physical Therapy, Catholic University of Daegu, Daegu, Republic of Korea. Contact e-mail: ldhdaum@yonsei.ac.kr*

The portion of the optic radiation (OR) is the important pathway for visual function. OR emerges from the lateral geniculate nucleus (LGN) to the posterior cortex. In this study, we extracted individual tract of OR using diffusion tensor tractography (DTT) to measure the fractional anisotropy (FA) and volumetric information of tract without personal brain variation. We studied thirteen healthy subjects and they had no history of neurological disease and optic nerve pathology. DTI data were obtained 1.5-T MRI system (Philips Gyroscan Intera) and image parameters as follow: TR/TE = 10,726/76 ms, matrix = 128 × 128, FOV = 221 mm, b = 800 s/mm², slice thickness = 2.3 mm and using 32 diffusion-sensitizing gradients. Eddy current distortions and subject motion in the diffusion-weighted images were removed by a twelve-parameter affine registration using FSL (Analysis Group, FMRIB, Oxford, U.K.). DTI data were analyzed using the DtiStudio 2.40 (Department of Radiology, Johns Hopkins University, USA) with the termination criteria for fiber tracking : (FA < 0.2, angle change > 70°). The ROI were drawn in the both LGN, on the axial slice at the level of the transition from the posterior limb of the internal capsule to the cerebral peduncle on color-coded FA map. After both optic radiations were reconstructed, the non-diffusion images of DTI were normalized to the standard MNI space by using an EPI template with SPM2 (Wellcome Department of Cognitive Neurology, London, UK). The same transformation parameters were then applied to normalize the OR tract to the MNI space. After this, we measured the value of FA in the extracted tract and counted the voxels through which the OR tract passed. According to our results, the volumetric values of each subject OR was in the range of 259 ~ 482 and percentage values were in the range of 0.108 ~ 0.201. The mean ± standard deviation of FA values from each subject OR tract was 0.5274 ± 0.017. Based on these results, the OR tract volume was about 0.1% within the range of human brain according to the normalized group mapping. Moreover, OR pathway probability measurement of DTT-based group mapping can detect relatively accuracy location in a variety of individual OR pathway. Although our results has limitation of user-dependent ROI setting and not considered cerebral fluid, lipid and heart movement, our result will be useful the quantitative and normalized values of OR tract information. And also it can be provide the preliminary data for OR in the disease treatment related the visualization pathway in the brain.

Presentation Number **0748A**

Poster Session 1c: In Vivo Studies & Development/Novel Use of Imaging Probes

Somatotopic Localization of Corticospinal Tract in the Internal Capsule without Individual Variation: Combined DTT-fMRI Study

Donghoon Lee¹, **Cheolpyo Hong**¹, **Sungho Jang**², **Bongsoo Han**¹, ¹*Radiological Science, Yonsei University, Wonju, Republic of Korea;*
²*Physical Medicine and Rehabilitation, Yeungnam University, Daegu, Republic of Korea. Contact e-mail: ldhdaum@yonsei.ac.kr*

The corticospinal tract (CST) is the most important pathway which was related to movement of human body such as hand or foot. Recently, diffusion tensor tractography (DTT) is the best way to research the location or visualization of CST. However, these studies had some problems due to user dependant ROI setting and crossing fiber effect. In this study, we obtained the normalized CST and analyzed in the internal capsule (IC) to confirm the location of hand/foot fiber. We also used functional magnetic resonance imaging (fMRI) to except from user dependant ROI setting and probabilistic fiber tractography to avoid the crossing fiber effect. Ten right-handed normal volunteers with no history of a neurological disorder. The fMRI data were acquired with following parameters: TR/TE = 2000/60 ms, FOV = 210 mm, matrix = 64×64, slice thickness = 5 mm and using a block paradigm (hand/foot grasp-release movements at 1Hz frequency). The fMRI data was analyzed using SPM2. DTI data were acquired with following imaging parameters: the number of slices = 67, TR/TE = 10726/75 ms, FOV = 221 mm, matrix = 128×128, slice thickness = 2.3 mm, b = 1000mm²s⁻¹ and 32 diffusion sensitizing gradients. Fiber tracking was performed with FSL. The ROIs were drawn in the fMRI activation area and lower portion of pons. After the CSTs were reconstructed, the b=0 images were normalized to the MNI EPI template. The same transformation parameters were then applied to CST. And then, each individual normalized CST overlaid in b=0 images. The innermost locations of hand/foot fiber in the IC were measured based on the x, y coordinate of each normalized b=0 image. We also measured the separation angle between hand/foot fibers in the IC based on 0 degree of foot fiber point. According to our results, the mean ± standard deviation values of hand fiber x, y coordinate locations were 35.84±0.75 / 55.77±0.65. The foot fibers were 35.07±0.99 / 54.54±0.90. The x, y coordinate locations of normalized b=0 image was 182 and 218. The separation angle between hand and foot fibers in the range of 26.56 ~ 63.43 degree. According to our results, the hand fibers were located anteromedial to foot fibers in the IC and hand fibers , relatively. Although we used the tract normalization to above the effects of individual variation, somatotopic localization of the CST in the IC was well matched with well-known knowledge of the organization in the IC. In conclusion, our results seems to be providing the good directions for correlation investigation of the cerebral white matter lesion study with motor symptoms in the IC.

Presentation Number **0749A**

Poster Session 1c: In Vivo Studies & Development/Novel Use of Imaging Probes

The results of Dopamine D2 receptors measurement using [¹¹C]raclopride with ultra-high specific radioactivity in living human brain

Yota Fujimura^{1,3}, Hiroshi Ito¹, Hidehiko Takahashi¹, Fumihiko Yasuno¹, Yoko Ikoma¹, Ming-Rong Zhang², Shinichiro Nanko³, Kazutoshi Suzuki², Tetsuya Suhara¹, ¹Molecular Neuroimaging Group, Molecular Imaging Center, National Institutes of Radiological Sciences, Chiba, Japan; ²Molecular Probe Group, National Institutes of Radiological Sciences, Chiba, Japan; ³Dept. of Psychiatry, School of Medicine, Teikyo University, Itabashi, Japan. Contact e-mail: fyota@yahoo.co.jp

Introduction: Ultra high specific radioactivity is preferable in the measurement of neuroreceptor bindings with positron emission tomography (PET) because receptor occupancy by mixed cold ligand hampers the accurate estimation of receptor binding. Recently, we succeeded in synthesizing [¹¹C]raclopride, a dopamine D2 receptor ligand, with ultra-high specific radioactivity, i.e., several thousand GBq/micromol. In the present study, we compared the [¹¹C]raclopride bindings to dopamine D2 receptors between radioligands with ultra-high specific radioactivity and ordinary high specific radioactivity in healthy human subjects. Methods: Two PET studies using [¹¹C]raclopride with ultra-high specific radioactivity (4302-7222 GBq/micromol) or ordinary high specific radioactivity (133-280 GBq/micromol) were performed on different days in 14 healthy men. Binding potential (BP) was calculated by the simplified reference tissue method, peak equilibrium method, and area-under-the-curve method for each region-of-interest using time-activity data in the cerebellum as a reference brain region. Results: BP values for radioligands with ultra-high specific radioactivity and ordinary high specific radioactivity calculated by the simplified reference tissue method were 4.06 ± 0.29 and 4.10 ± 0.25 in the putamen, 0.44 ± 0.07 and 0.47 ± 0.07 in the thalamus, and 0.37 ± 0.06 and 0.38 ± 0.06 in the temporal cortex, respectively (mean \pm SD). No significant difference in BP was observed between ultra-high specific radioactivity and ordinary high specific radioactivity in any of the brain regions. Conclusion: BP values of [¹¹C]raclopride with ultra-high specific radioactivity did not differ from those with ordinary high specific radioactivity in the measured brain regions, including striatal and extrastriatal regions.

Presentation Number **0750A**

Poster Session 1c: In Vivo Studies & Development/Novel Use of Imaging Probes

Prognostic value of pretreatment splenic FDG uptake in patients with diffuse large B-cell lymphoma

Byung Hyun Byun¹, **Jung-Joon Min**¹, **Ari Chong**², **Jong-Ryool Oh**¹, **Ja-Hye Kim**², **Su-Ung Yoo**¹, **Sun-pyo Hong**¹, **Ho-chun Song**², **Hee-Seung Bom**¹, ¹*Departments of Nuclear Medicine, Hwasun Chonnam National University Hospital, Hwasun, Republic of Korea;*
²*Departments of Nuclear Medicine, Chonnam National University Hospital, Gwangju, Republic of Korea. Contact e-mail: kal-issma@hanmail.net*

The aim of this study is to evaluate the splenic involvement using pretreatment FDG PET/CT and conventional enhanced CT scans, and to investigate its prognostic role in diffuse large B-cell lymphoma (DLBL) patients. Methods: FDG PET was performed in 65 newly diagnosed DLBL patients (42 men, 23 women, age: 64.0±12.3 years) before chemotherapy. On each FDG PET/CT scan, the maximum SUV of the spleen (SUVmax-spleen) and liver (SUVmax-liver) were measured. The ratio of SUVmax-spleen to SUVmax-liver (SL ratio) and areas under the ROC curves were calculated for the recurrence or disease progression. Positive splenic index measured on FDG PET/CT scan (>480 mm³), focal hypermetabolism or focal hypointensity of the spleen were defined as positive criteria for splenic involvement. Time to treatment failure (TTF) was compared with SUVmax-spleen (median), SL ratio, other positive criteria, and International Prognostic Index (IPI) score by Kaplan-Meier survival analysis. Results: Initial stages of DLBL patients were stage I in 12, II in 23, III in 24, and IV in 6 by Ann Arbor system. Median follow-up period was 24.1 months, and estimated mean TTF was 40.7 months. TTF was statistically significantly reduced in those with SL ratio > 1.19 (p=0.000), focal hypermetabolism (p=0.019), focal hypointensity (p=0.041), and higher IPI score (p=0.000). TTF did not correlate with SUVmax-spleen (p=0.112) or splenic index (p=0.455). Both SL ratio>1.19 (p=0.010) and higher IPI score (p=0.034) were associated with reduced TTF. Conclusion: Pretreatment splenic FDG uptake greater than hepatic uptake is suggestive of an independent prognostic factor in patients with DLBL.

Presentation Number **0751A**

Poster Session 1c: In Vivo Studies & Development/Novel Use of Imaging Probes

Diagnostic accuracy of preoperative intrathoracic lymph node staging on ¹⁸F-FDG PET/CT in patients with non-small cell lung cancer

Sun-pyo Hong¹, Ho-chun Song², Ari Chong², Jong-Ryool Oh², Ja-Hye Kim¹, Su-Ung Yoo¹, Jung-Joon Min¹, Hee-Seung Bom¹,
¹Department of Nuclear Medicine and Molecular Imaging, Hwasun Chonnam National University Hospital, Hwasungun Jeonnam, Republic of Korea; ²Nuclear Medicine, Chonnam National University Hospital, Gwangju, Republic of Korea. Contact e-mail: sunmark@nate.com

Purpose We investigated the diagnostic accuracy of preoperative intrathoracic lymph node staging on ¹⁸F-FDG PET/CT and relationship between metabolic volume(MV) and lymph node staging in patients with non-small cell lung cancer. **Methods** Thirty patients with NSCLC (male : female=24:6, mean age 62±10) underwent FDG PET/CT before surgery. Lymph node staging was pathologically confirmed on tissue specimens. The maxSUV, symmetry for lymph node staging, and meanSUV, maxSUV, MV (cm³, threshold 80%) of primary tumor were measured. The difference of meanSUV, maxSUV, meanSUV*MV, maxSUV*MV of primary tumor among lymph node groups were analyzed. Diagnostic characteristics of PET/CT were assessed on a per-patient and on a per-nodal-station basis. **Results** The Sensitivity, specificity and accuracy of PET/CT for detecting metastatic lymph nodes were 47.4%, 90.9% and 63.3% on a per-patient basis, 43.6%, 96.7% and 88.4% and on per-nodal-station basis, respectively. The maxSUVs of primary tumor by lymph node staging group were 11.1 (N0, n=12), 13.3 (N1, n=10), and 10.3 (N2, n=10). There was no significant difference (p=0.98). MVs of lymph node staging groups were 31.4±25.4 cm³ (N0), 36.0±10.3 cm³ (N1) and 36.0±10.3 cm³ (N2) (p=0.80). Mean value of MVs*maxSUV were 425±443 cm³ SUV (N0), 751±950 cm³ SUV (N1), and 323±497 cm³ SUV (N2) (p=0.71). Mean value of MVs*meanSUV were 199±216 cm³ SUV (N0), 323±414 cm³ SUV (N1), and 140±231 cm³ SUV (N2) (p=0.84). **Conclusion** PET/CT provides high specificity and accuracy in intrathoracic lymph node staging in patients with NSCLC. However, maxSUV, mean SUV, metabolic volume and other parameters of primary tumors were not useful for lymph node staging.

Presentation Number **0752A**

Poster Session 1c: In Vivo Studies & Development/Novel Use of Imaging Probes

Radiological protection of human subjects and informed consent: Proposal of basic principles for molecular imaging clinical research

Chieko Kurihara¹, **Yoshiko Fukushima**², ¹*Molecular Imaging Center, National Institute of Radiological Sciences, Chiba, Japan;*

²*Department of Planning and Management, National Institute of Radiological Sciences, Chiba, Japan. Contact e-mail:*

chieko.kurihara@nifty.ne.jp

Background: The issue of essential information to be provided to study subject candidates has been well discussed in the field of general clinical research but from the point of radiological protection of human subjects, there has not been enough discussed. Objectives: To clarify basic principles of informed consent for radiological protection of human subjects, for the conduct of molecular imaging clinical research. Method: (1) Review on several questionnaire surveys on study subjects or laypersons and on literatures of communication issues with study subjects, concerning general points of participating in clinical researches as well as specific points related to radiation exposure; (2) Survey and analysis on information sheet for study subjects participating in research including radiation exposure; (3) Discussion with the members of several study groups and study review members concerned in radiological protection of human subjects. Findings: Healthy young volunteers participating in clinical research are not well aware of the risk of radiation exposure, nevertheless, international standard for radiation dose constrains or limitations are not well discussed in the context of informed consent of research volunteers, and additionally, in many of information sheet there is only explanation on radiation comparing ordinary diagnostic examination, therefore, we would like to propose basic principles of informed consent for radiological protection of human subjects as follows; (1) Radiation dose should be explained numerically even if the dosimetry data is numeric value estimated from animal data; (2) Comparing with ordinary diagnostic examination may be useful but not enough because the risk of radiation in each examination is not well understood by lay person, therefore, relative risk of incidence of fatal diseases should be explained comparing with baseline; (3) Explanation to avoid over-volunteering is necessary from view of dose constrains or limitations of annual total dose of radiation exposure, referring to international or national standards; (4) Follow-up and continuous communication is necessary for better understanding of subjects participating in clinical research involving radiation exposure.

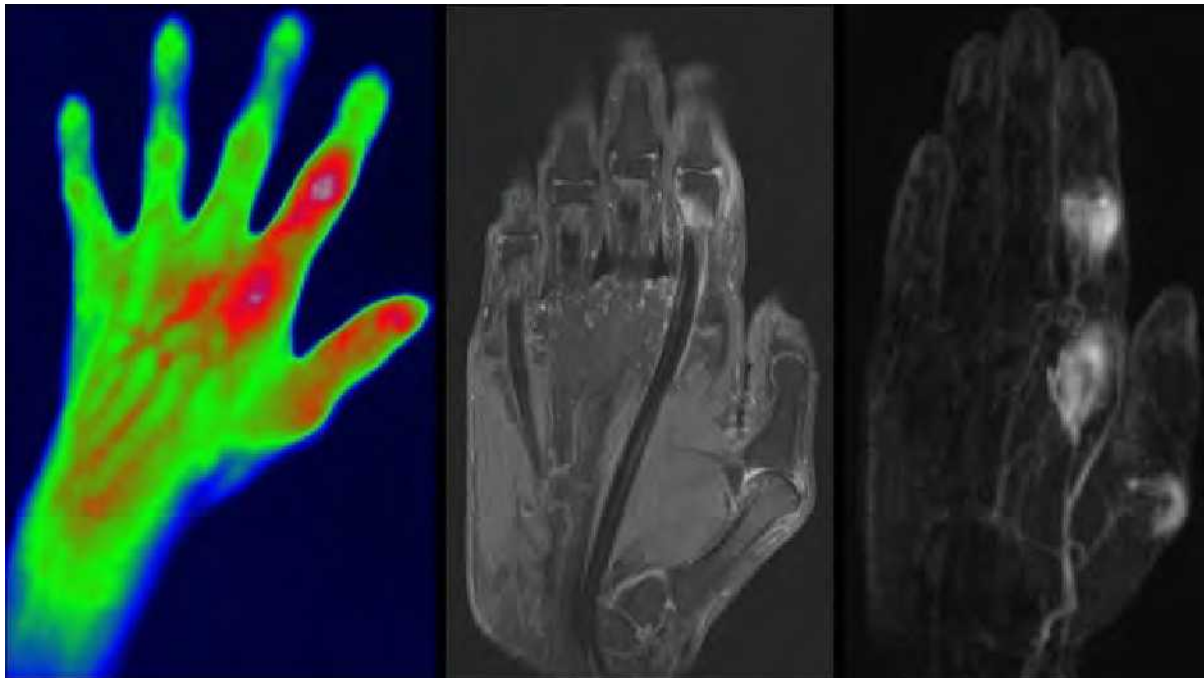
Presentation Number **0753A**

Poster Session 1c: In Vivo Studies & Development/Novel Use of Imaging Probes

Preliminary Results: Detection of active inflammation in rheumatoid arthritis by means of a 2D optical imaging system in comparison to MRI

Reinhard Meier¹, Klaus Thürme², Peter Noel¹, Franziska Dorn¹, Philipp Moog², Martin Henninger¹, Ernst J. Rummeny¹, Klaus Wörtler¹, ¹Department of Radiology, Klinikum rechts der Isar, Technical University Munich, Munich, Germany; ²II. Medizinische Klinik und Poliklinik, Klinikum rechts der Isar, Technical University Munich, Munich, Germany. Contact e-mail: reinhardt.meier@gmail.com

Purpose: To evaluate an Indocyanine Green (ICG)-enhanced optical imaging (OI) system for detection of active inflammation in patients with rheumatoid arthritis in comparison to MRI. Methods and Materials: 10 Patients (70% female, mean age = 52.2) with clinical suspicion of active inflammation in rheumatoid arthritis were examined with a clinically new available ICG-enhanced optical imaging system (mivenion GmbH, Germany). The degree of inflammation in the metacarpophalangeal, proximal and distal interphalangeal joints of both hands was graded objectively by three independent radiologists on a 4-point-ordinate scale (0: no inflammation, 1: mild, 2: moderate, 3: severe) according to the OMERACT RAMRIS score. Results were correlated with MRI (3T Verio, Siemens, Erlangen, Germany) as standard of reference. Results: Of the 280 joints of the 10 patients evaluated, 253 (89.3%) joints showed in OI no inflammation, while 27 (10.7%) joints showed mild, moderate and severe inflammation. In MRI 255 (90.2%) joints showed no inflammation, while 25 (9.8%) joints showed active inflammation (grade 1-3). Using MRI as standard of reference, OI had a sensitivity of 84%, a specificity of 97.6%, an accuracy of 96.4%, a positive predictive value of 77.8% and a negative predictive value of 98.4% for detection of active inflammation in patients with RA. Conclusion: Our preliminary data shows, that optical imaging allows for detection of active inflammation in patients with rheumatoid arthritis. While the performance of OI up to now is slightly inferior to MRI, it might be nevertheless of substantial added value to clinical examination due to its non-invasiveness, low costs and easy availability.



Optical and MR (cor T1 fs +Gd, MIP twist) images of a patient with rheumatoid arthritis with synovial hyperperfusion in the proximal interphalangeal and the metacarpophalangeal joint D2.

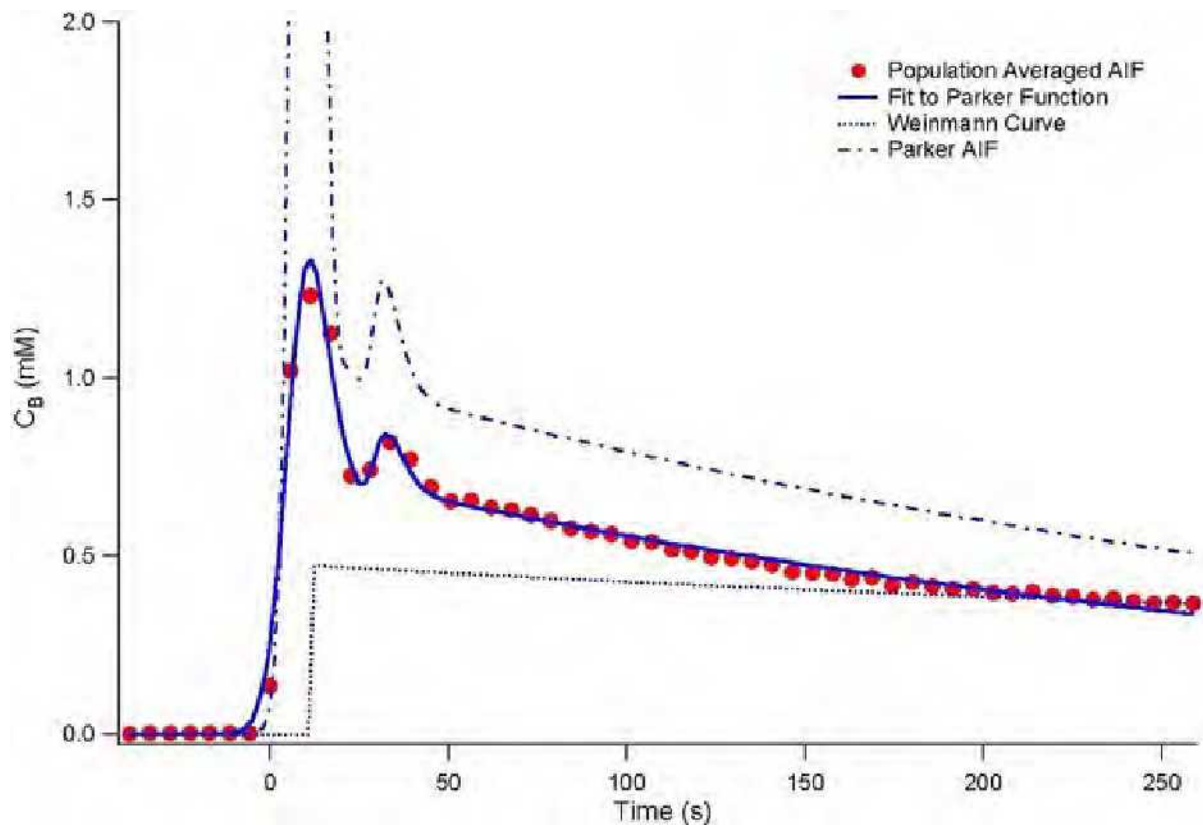
Presentation Number **0754A**

Poster Session 1c: In Vivo Studies & Development/Novel Use of Imaging Probes

Population-Averaged Arterial Input Function for Dynamic Contrast-Enhanced MRI Obtained with Inflow Suppression and B1 Correction

Vijay P. Shah^{1,2}, Baris Turkbey², Yuxi Pang³, Wei Liu⁴, Peter Choyke², **Marcelino Bernardo**^{1,2}, ¹Imaging Physics, SAIC-Frederick, Bethesda, MD, USA; ²Molecular Imaging Program, National Cancer Institute, Bethesda, MD, USA; ³Philips Healthcare, Cleveland, OH, USA; ⁴Clinical Sites Research Program, Philips Research North America, Briarcliff Manor, NY, USA. Contact e-mail: bernardom@mail.nih.gov

In prostate cancer DCE-MRI studies, the femoral arteries are commonly used to measure the arterial input function (AIF). An accurate determination of the AIF is important in order to obtain quantitative pharmacokinetic parameters from the dynamic data. However, the arteries are susceptible to a large inflow effect that shortens the apparent blood T1 and results in an overestimation of the contrast agent concentration. To eliminate this effect, we used a non-selective excitation pulse in a 3D SPGR dynamic sequence with 4x slice oversampling, a large SENSE factor of 5 and a 16-channel surface array coil combined with an endorectal coil. The nonselective pulse polarized the blood outside the imaging volume, while slice oversampling prevented aliasing and SENSE kept the temporal resolution below 6 seconds. A semi-automatic method was used to extract volume-averaged AIF from each patient. An ROI is manually drawn on the dynamic image to select a seed curve. Voxels matching the seed curve were selected from all slices using two different metrics - correlation coefficient and spectral angle mapper. From the selected voxels, the patient's AIF was calculated using the average T1 and B1 values. The resulting PA-AIF from 31 patients matched Wienmann's AIF after 200s, but it is significantly lower than the Parker's AIF (see figure). The parameters obtained when fitted to Parker's function were A1, A2, T1, T2, sig1, sig2, alpha, beta, s and tau of 0.23, 0.24, 0.16, 0.35, 0.09, 0.14, 0.76, 0.19, 29.64 and 0.49, respectively. We generated a simulated phantom data using the PA-AIF and fitted them to a two-compartment model using the Parker's or Weinmann's AIF to determine the error that would result if those functions are used.



Comparison of newly determined population-averaged arterial input function to previously reported input functions.

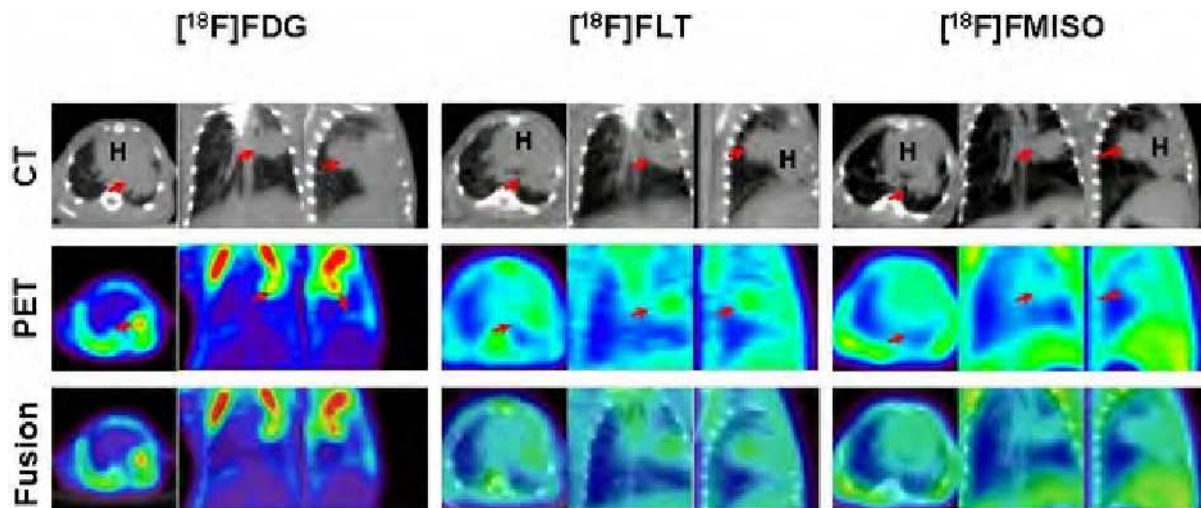
Presentation Number **0755A**

Poster Session 2c: In Vivo Studies & Development/Novel Use of Imaging Probes

Early assessment of drug response using fluoro-L-thymidine positron emission tomography imaging in a clinically relevant orthotopic mouse model of lung cancer

Hiroshi Fushiki^{1,2}, **Sosuke Miyoshi**^{1,2}, **Akihiro Noda**^{1,2}, **Yoshihiro Murakami**^{1,2}, **Hiroshi Sasaki**^{1,2}, **Makoto Jitsuoka**^{1,2}, **Keisuke Mitsuoka**^{1,2}, **Shintaro Nishimura**^{1,2}, ¹Bioimaging Research Laboratories, Astellas Pharma Inc., Tsukuba, Japan; ²The Medical and Pharmacological Research Center Foundation, Hakui, Japan. Contact e-mail: hiroshi.fushiki@jp.astellas.com

Lung cancer causes the major cancer-related death across the globe. Despite the various types of novel agents developed to treat lung cancer, however, its mortality remains high. Determination and classification of responders to treatment in early phases is considered essential to improving patients' benefits and therapeutic outcomes, as well as early detection of tumors. With the recent development of imaging technology, detection of tumor burden using positron emission tomography/computed tomography (PET/CT) imaging has greatly aided not only clinical assessment but also pre-clinical drug development. While clinically relevant animal models such as orthotopic implantation models and genetically engineered mouse models are complex enough to allow observers to monitor tumor burden, other non-invasive and longitudinal evaluations using imaging technologies have also come into use. Here, we demonstrated that microPET imaging using several 18F tracers (fluorodeoxyglucose [FDG], fluoro-L-thymidine [FLT], and fluoromisonidazole [FMISO]) was useful in monitoring a pulmonary tumor nodule in an orthotopic mouse model of lung cancer. Further, early assessment of docetaxel's efficacy using microFLT-PET imaging more clearly demonstrated success than did microCT imaging in orthotopic mouse model of lung cancer. Despite these findings, however, Response Evaluation Criteria In Solid Tumors (RECIST) criteria in combination with CT imaging is widely used in clinical diagnosis of lung cancer. While relatively few pre-clinical studies have applied RECIST criteria, a number of cancer models using CT imaging have been reported. In the present study, we clearly demonstrated the appropriateness of applying RECIST criteria to orthotopically implanted pulmonary tumors in mice. Our results highlight the clinical relevance of PET/CT imaging of pulmonary tumors and potential strategies for drug development using a clinically relevant lung cancer model.



Presentation Number **0756A**

Poster Session 2c: In Vivo Studies & Development/Novel Use of Imaging Probes

In vivo molecular imaging for translational research on antitumor therapy by mAbs: use of a syngeneic bioluminescent murine model of diffuse B lymphoma expressing human CD20

Sabrina Pesnel¹, Julien Sobilo¹, David Daydé², Stéphanie Lerondel¹, Guillaume Cartron^{2,4}, Alain Le Pape^{1,3}, ¹CIPA, TAAM, UPS44 - CNRS, Orléans, France; ²UMR 5235, CNRS, Montpellier, France; ³U618, INSERM, Tours, France; ⁴Service d'hématologie et biothérapies, CHU Lapeyronie, Montpellier, France. Contact e-mail: sabrina.pesnel@cns-orleans.fr

The anti-CD20 monoclonal antibody (mAb) rituximab (Mabthera®) is effective in the treatment of patients with B-cell non Hodgkin's lymphoma. In addition, in the case of refractory or relapsed lymphoma, another CD20-directed radiotherapeutic antibody can be used: mAb ibritumomab tiuxetan (Zevalin®) labeled with Yttrium 90. The aim of this work was to develop a murine model of lymphoma expressing human CD20 and transfected with the luciferase reporter gene to study the tumor exposure and response to rituximab together with biodistribution of ibritumomab in a representative clinical situation of relapsed lymphoma. So, C57Bl6 mice were intravenously injected with murine lymphoma EL4-CD20-Luc cells. On day 13, mice were treated with intravenous infusion of rituximab at dose of 6, 12, 20 or 40mg/kg and the tumor burden was assessed by bioluminescence imaging (BLI). An imaging of apoptosis was equally performed. In a second experiment, we studied the biodistribution of ibritumomab: on day 13 mice were imaged in BLI to locate the tumor foci and were allocated in 2 homogenous groups. Then, a group was treated with rituximab (20mg/kg mouse). The following day, all the mice received ibritumomab labeled with Indium 111 (5.5MBq/mouse). 24h after, mice were imaged in SPECT and mAb amounts linked to each tumor focus and expressed as a percent of the injected dose were determined. The results showed that the 20mg/kg rituximab dose was adequate to achieve a transient response while the 40mg/kg dose resulted in almost complete regression. With SPECT imaging, we showed that in control mice all the foci detected in BLI linked the 111In-ibritumomab while in rituximab treated mice the fixation was significantly inhibited. This study shows that this in vivo model is representative of the clinical situation and that pre-treatment with rituximab has a strong impact on the biodistribution of the ibritumomab; considering the pharmacokinetic of rituximab in blood, that should be taken into account to reconsider the therapeutic schedule for patients with relapsed lymphoma treated by ibritumomab.

Presentation Number **0757A**

Poster Session 2c: In Vivo Studies & Development/Novel Use of Imaging Probes

In vivo PET imaging of the effect of the NMDA antagonist memantine on glucose metabolism in the rodent brain

Geoff I. Warnock¹, **Stefanie Dedeurwaerdere**², **Mohamed-Ali Bahri**¹, **David Goblet**¹, **Christian Lemaire**¹, **Fabrice Giacomelli**¹, **Xavier Langlois**², **Andre Luxen**¹, **Alain Plenevaux**¹, ¹*Cyclotron Research Center, University of Liege, Liege, Belgium;* ²*Johnson & Johnson Pharmaceutical Research & Development, A Division of Janssen Pharmaceutica N.V., Beerse, Belgium. Contact e-mail: gwarnock@ulg.ac.be*

The administration of NMDA antagonists in rodents is used as a model for schizophrenia (Bubeníková-Valesová et al., 2008), and for the development of novel antipsychotic compounds. Further to the behavioral effects of these compounds in rodents, low doses are reported to increase cerebral glucose metabolism (MRGlu) in specific brain regions (Davis et al., 1988). When evaluating different NMDA antagonists using [¹⁴C]2-deoxyglucose autoradiography, we found that memantine induces more robust brain activation than ketamine, a long standing model for pharmacologically induced psychosis. To demonstrate the translational aspect of the memantine test we measured MRGlu non-invasively using FDG PET in mice (C57Bl/6) and rats (SD), comparing baseline with memantine treatment in the same animal. On the first scan day, the animals were pretreated with saline vehicle (SC) followed 15 minutes later by ¹⁸F-fluorodeoxyglucose (~10 MBq per mouse, ~20 MBq per rat, IP). 45 minutes after FDG administration, the animals were anesthetized with isoflurane and a 10 minute static scan was performed on a Focus 120 MicroPET scanner (Siemens). Two days later, the animals were pretreated with memantine (20 mg/kg SC) before undergoing the same FDG and scan protocol. Images were reconstructed using the filtered back projection method (using all corrections except scatter) and co-registered to an MRI template. Uptake of FDG standardized by weight and dose (SUV) was measured in the hippocampus. SUV was significantly increased in the hippocampus of both mice and rats, by 51.8 and 48.3 percent, respectively. These results indicate that the effects of memantine on MRGlu are similar to those reported with other NMDA antagonists in post-mortem autoradiography assays. Further studies will examine the ability of antipsychotic compounds to block the MRGlu response to memantine. These results are an encouraging step towards a truly translational model for testing antipsychotic drugs. References Bubeníková-Valesová et al. (2008) *Neurosci Biobehav Rev.*; 32(5):1014-23. Davis et al. (1988) *Anesthesiology* 69:199-205.

Presentation Number **0758A**

Poster Session 2c: In Vivo Studies & Development/Novel Use of Imaging Probes

Tracking T cells in vivo via Cu-64 PET imaging

Zheng Li¹, Diana Lo¹, Yoonsu Cho², Daniel Y. Lee¹, Feng Li¹, Guoting Qin¹, Laurence J. Cooper², King Li¹, ¹Radiology, The Methodist Hospital Research Institute, Houston, TX, USA; ²Division of Pediatrics, M. D. Anderson Cancer Center, Houston, TX, USA. Contact e-mail: zli@tmhs.org

Adoptive transfer of antigen-specific T cells for cancer shows encouraging results with disease stabilization and remissions in early- and late-stage clinical trials. However, the fate of the infused T cells in vivo requires additional study. Conventional techniques based upon intermittent sampling of peripheral blood and histology from biopsies provide evidence of T-cell persistence and trafficking, but do not provide real time information regarding biodistribution. Imaging is an excellent modality for tracking T cells in vivo non-invasively. Gold nanoparticles (GNPs) have been widely studied because of their biocompatibility, low toxicity, controllable size, and surface modifications well suited for molecular imaging. Introducing radiolabeled GNPs into T cells may allow them to be tracked in vivo by PET imaging. In this study, 7 nm GNPs were successfully radiolabeled with Cu-64 (half life: 12.7h) via a radiometal chelator, 1,4,7,10-tetraazacyclododecane-1,4,7,10-tetraacetic acid (DOTA) anchored with a thioctic acid (TA), covalently attached to GNPs by forming gold-thiol bond. The labeling efficiency was determined by radio thin layer chromatography (radioTLC). The radiolabeled GNPs were introduced into T cell by cell electroporation. Transmission electron microscopy (TEM) confirmed the GNPs loading in T cell and radioTLC established that Cu-64 labeled GNPs were stable under current electroporation conditions. The PET imaging study of Cu-64 GNPs loaded T cell in a mouse model is under investigation.

Presentation Number **0759A**

Poster Session 2c: In Vivo Studies & Development/Novel Use of Imaging Probes

Positron Emission Tomography of Copper Metabolism: Gastrointestinal Absorption and Biodistribution of Copper-64 (II) Chloride in Living Mice

Degang Shi¹, Michael Long¹, Xiankai Sun^{1,2}, **Fangyu Peng**^{1,2}, ¹Radiology, University of Texas Southwestern Medical Center, Dallas, TX, USA; ²Advanced Imaging Research Center, University of Texas Southwestern Medical Center, Dallas, TX, USA. Contact e-mail: fangyu.peng@utsouthwestern.edu

OBJECTIVES: To assess gastrointestinal absorption and metabolism of copper in mice with positron emission tomography (PET) using copper-64(II) chloride ($^{64}\text{CuCl}_2$) as a probe. **METHODS:** Dynamic PET imaging was performed with an Inveon PET/CT Multimodality System (Siemens, Inc) to assess gastrointestinal absorption and biodistribution of ^{64}Cu radioactivity in Balb/c mice (N = 5), immediately after administration of $^{64}\text{CuCl}_2$ by oral gavage (O.G.) at a dose of $2\mu\text{Ci/g}$ body weight contained in 200 μL of orange juice. Subsequently, static PET imaging was performed to assess biodistribution of ^{64}Cu radioactivity at 2 and 24 hours post administration of the tracer respectively. Another group of Balb/c mice (N = 5) were injected with $^{64}\text{CuCl}_2$ intravenously (I.V.) at the same dose and subjected to the same PET-CT imaging procedure. Quantitative analysis of PET was performed to compare the biodistribution of ^{64}Cu radioactivity in the tissues of these two groups of mice, followed by confirmative radioactivity assay of postmortem tissues. **RESULTS:** Dynamic PET imaging demonstrates gastrointestinal absorption of ^{64}Cu radionuclide following O.G. administration of $^{64}\text{CuCl}_2$, with a gradual increase of ^{64}Cu radioactivity in the liver and kidney. In contrast, there was a gradual decrease of ^{64}Cu radioactivity in the blood and brain following initial uptake of the tracer. Comparative PET analysis demonstrates a significant difference in the biodistribution of ^{64}Cu radioactivity between the group of mice which received $^{64}\text{CuCl}_2$ by O.G. and the group of mice which received $^{64}\text{CuCl}_2$ by I.V., as confirmed by the data from the radioactivity assay of postmortem tissues. Hepatic ^{64}Cu radioactivity in the mice injected with $^{64}\text{CuCl}_2$ by I.V. (12.2 ± 1.7 %ID/g) is significantly higher than that of the mice administered with $^{64}\text{CuCl}_2$ by O.G. (3.0 ± 0.2 %ID/g). **CONCLUSIONS:** Gastrointestinal absorption and biodistribution of ^{64}Cu radionuclide were assessed by PET and radioactivity assay of postmortem tissues, following oral gavage administration of $^{64}\text{CuCl}_2$ as a probe. The data from this study suggests that PET is useful for study of copper metabolism in humans and pathophysiology of human diseases associated with disorders of copper metabolism such as Wilson's disease caused by a mutation of *ATP7B* gene.

Presentation Number **0760A**

Poster Session 2c: In Vivo Studies & Development/Novel Use of Imaging Probes

Optical imaging and cancer: from mice to man

Jean-Luc Coll, Sandrine Dufort, Lucie Sancey, Véronique Josserand, Michelle Kéramidas, Christian A. Righini, Jean-Marc Dinten, Isabelle Texier, Stéphane Roux, Catherine Passirani, Pascal Dumy, Didier Boturyn, Institut Albert Bonniot, INSERM U823, La tronche, France. Contact e-mail: Jean-Luc.Coll@ujf-grenoble.fr

Early and accurate detection of tumors, like the development of targeted treatments, are major fields of research in oncology. The generation of specific vectors, capable of transporting a drug or a contrast agent to the primary tumor site as well as to the remote (micro-) metastasis would be an asset for early diagnosis and cancer therapy. Our goal is to develop new treatments based on the use of tumor-targeted delivery of large biomolecules (DNA, siRNA, peptides), able to induce apoptosis while dodging the specific mechanisms developed by tumor cells to resist this programmed cell death. Nonetheless, the insufficient effectiveness of the vectorization systems is still a crucial issue. In this context, we generated new targeting vectors (as the RAFT-RGD) and nanoparticles for drug and biomolecules delivery. To undertake this work, we also developed several optical imaging systems allowing the follow-up and evaluation of our vectorisation systems in mice, large animals and human patients. Based on our recent work, an image guided surgery protocole was initiated in animals. The results demonstrated the very significant improvement in primary tumours resection: higher number of tumour nodules removed, sane margins on the removed fragments and surgery time divided by 2. In addition, using the RAFT-RGD delivery system we were able to target and transfer an active cytotoxic peptide as well as several therapeutic nanoparticles with curative effects on animal models. Our results demonstrate the crucial importance of generating small, PEGylated nanoparticles if one want to be able to gain a targeting efficiency when a specific antitumor ligand like RGD is then added on the particle surface. Finally, in order to translate these applications into the clinic, a new optical laboratory is being installed within the hospital. This will allow deep imaging of prostate using a tomographic bench (in collaboration with CEA-LETI, Grenoble), but also of lymph nodes and prostate biopsies.

Presentation Number **0761A**

Poster Session 2c: In Vivo Studies & Development/Novel Use of Imaging Probes

Evaluation of tumor angiogenesis in a xenograft mouse model of human prostate cancer using dynamic contrast enhanced ultrasonography

Hak Jong Lee^{1,2}, **Sung Il Hwang**^{1,3}, **Jin-Haeng Chung**⁴, ¹Radiology, Seoul National University, Seoul, Republic of Korea; ²Nanoconvergence, Graduate School of Convergence Science and Technology, Suwon, Republic of Korea; ³Radiology, Seoul National University Bundang Hospital, Seongnam-si, Republic of Korea; ⁴Pathology, Seoul National University, Seoul, Republic of Korea.
Contact e-mail: hakjlee@snu.ac.kr

PURPOSE : To evaluate tumor angiogenesis in a xenograft mouse model with human prostate cancer cell with a second-generation US contrast agent. **MATERIALS AND METHODS** : 21 nude mice were injected with human prostate cancer cells (PC3 17, LNCaP 4) on hind limbs. Mean interval between inoculation and imaging was 21 days. Gray scale, color and power doppler ultrasonography of grown tumors were performed before the administration of contrast media. 500 μ l bolus (1×10^8 microbubbles) of second-generation US contrast agent (SonoVue) was injected to the retroorbital vein. Region of interest was drawn over the entire tumor and time-intensity curve was acquired and exported to the workstation. The curves were then fitted to a gamma variate function using weighted nonlinear least square estimation. The maximal intensity, area under the curve up to 50 sec, time to peak, shape parameter (α) and scale parameter (β) were derived from the parameters of the gamma variate fit. Immunohistochemical staining for VEGF and CD31 was performed. Tumor volume, area percentage of VEGF stained in a field and count of CD31 positive vessels were correlated with the parameters from the time intensity curve. Mean parameters from different cancer cells (PC3 and LNCaP) were also compared. **RESULTS** : There were positive correlation between tumor volume and AUC ($r=0.519$) and maximal intensity ($r=0.494$). CD31 count also showed positive correlation with AUC ($r=0.573$) and maximal intensity ($r=0.577$). Area of VEGF percentage did not have any correlation with calculated data from the curve. Mean AUC and VEGF percentages were statistically different between PC3 and LNCaP. **CONCLUSION** : Area under the curve and maximal intensity from the time intensity curve showed correlation between histological data. Two different cell types of prostate cancer showed different histological and dynamic features.

Presentation Number **0762A**

Poster Session 2c: In Vivo Studies & Development/Novel Use of Imaging Probes

In vivo Micro-CT of Multiple Myeloma Mice

Inneke Willekens^{1,2}, Tony Lahoutte², Axel Bossuyt², Johan de Mey¹, ¹Radiology, UZ Brussel, Brussels, Belgium; ²In vivo Cellular and Molecular Imaging - ICMI, Vrije Universiteit Brussel, Brussels, Belgium. Contact e-mail: inneke.willekens@gmail.com

Purpose: The aim of this study was to estimate skeletal defects in mice with multiple myeloma using micro-CT. **Method and Material:** The 5T2MM model was used in this study. Anesthesia was induced with 5% isoflurane and maintained at 2% during the scan with spontaneous breathing via a mask. Serial micro-CT imaging of 5 mice was conducted with a weekly scan during 5 weeks. Micro-CT (Skyscan 1178) was performed using 2 digital X-ray cameras which scanned over 180° at a resolution of 83 µm, a rotation step of 1.08, 50 kV, 615 mA, and 121-second image acquisition time. Images were reconstructed using filtered backprojection and viewed in 3D using CT-Volume software. **Results:** The in vivo micro-CT scans of mice with multiple myeloma revealed osteolytic lesions. At the terminal stage of the illness, cortical perforations were discovered. **Conclusion:** The evaluation of the micro-CT images demonstrated that osteolytic lesions due to multiple myeloma could be discerned visually. This objective opens up the opportunity for preclinical analysis of new therapeutic approaches for multiple myeloma.

Presentation Number **0763A**

Poster Session 2c: In Vivo Studies & Development/Novel Use of Imaging Probes

Establishment of an 18FDG PET-CT imaging protocol of dogs with naturally-occurring malignant cancer

*Debra Gibbons¹, Stewart Ryan², Susan Lana², Susan LaRue¹, **Susan Kraft¹**, ¹Environmental and Radiological Health Sciences, Colorado State University, Fort Collins, CO, USA; ²Clinical Sciences, Colorado State University, Fort Collins, CO, USA. Contact e-mail: skraft@colostate.edu*

Introduction: Spontaneously-occurring neoplasia in dogs represents an excellent translational model. Evaluation of tumor response with PET-CT is a potentially important in vivo endpoint during longitudinal assessment of experimental therapeutics, but little is known about PET-CT imaging of spontaneous canine cancer. Our veterinary institute has recently installed a PET-CT instrument on site, and we have developed an imaging protocol in an initial set of canine cancer-bearing patients. The goals were to minimize radiation exposure to personnel as well as reduce false positive radioisotope uptake from muscle activity, and to begin evaluating the applicability of PET-CT for a variety of canine cancers including prognostic relevance of maximal standard uptake values (SUV). **Methods:** 18FDG-PET/CT imaging was performed on 8 dogs with a primary malignant tumor, and one dog for metastasis of a known primary tumor, with a Philips Gemini TF Big Bore PET-CT instrument. Patients had normal blood glucose levels and were fasted for 12 hours. Induction of general anesthesia, placement of an indwelling urinary catheter, and patient positioning in the PET-CT instrument were performed prior to intravenous injection of 18FDG (0.14 mCi/kg). Whole body CT was acquired for attenuation correction and at 1 hour post-injection, the PET study was acquired. Urine was collected in a small lead-lined containment system for decay in storage. Dogs were housed in a shielded nuclear medicine ward until releasable radioactivity levels were achieved, generally within 6-7 hours post-injection. PET-CT images were evaluated for CT lesions and areas of abnormal radiopharmaceutical uptake. Tumor volume and mSUVs were derived from commercial software (Extended Brilliance Workstation, Phillips Medical Systems). **Results:** Tumor types included osteosarcoma, melanoma, thymoma and thyroid carcinoma (n = 9). Ten metastatic lesions were detected in regional lymph nodes, lung, liver and pleura/mediastinum. Primary tumor volumes had a mean of 64.6 cm³. Maximum SUVs of the primary tumors and metastatic lesions had a mean of 10.6 and 4.2 respectively. **Discussion/Conclusions:** The developed protocol resulted in excellent image quality and met our radiation safety standards. Tumor volumes and mSUVs were comparable to those reported for human cancers. The lower mSUVs of metastatic lesions related, at least in part, to small lesion volume relative to PET spatial resolution. We are now in the process of investigating the potential prognostic value of canine mSUVs.